

351 78

Physics Abstracts

ISSN 0036-8091

Science Abstracts Series A
1st December 1983

Abstracts 111295-116909

U. T. G. L.
JAN 23 1984
LIBRARY

PAMPHLET B

inspec

The Institution of Electrical Engineers

Q
-
S3
v. 86
1983

111295-116909

Sci. 16

PHYSICS ABSTRACTS

Physics Abstracts is one of a series of abstracts publications produced by INSPEC. Published twice monthly by the Institution of Electrical Engineers, it forms the world's major English-language abstracting service for the physics community.

SUBJECT SCOPE & COVERAGE

Physics Abstracts covers the whole field of physics. An impression of its scope can be gained from the classification scheme. The information contained in *Physics Abstracts* is derived from a wide range of sources including journals, reports, books, dissertations and conference papers published in all countries and languages of the world.

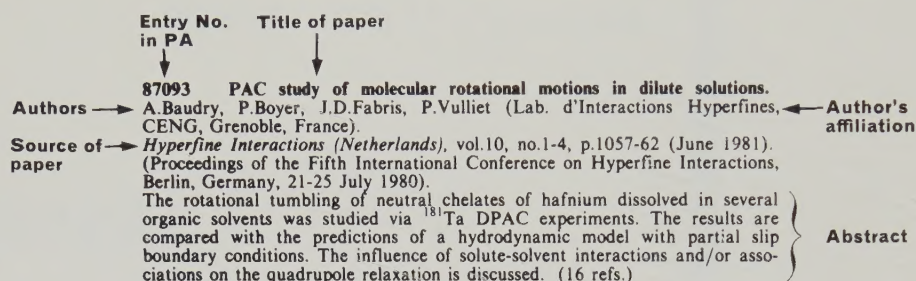
The number of items included is currently running at over 100,000 per year.

JOURNALS SCANNED

A list of the journals scanned for the INSPEC services is published with the twice-yearly author indexes to *Physics Abstracts*. Additions and amendments to this list are included in *Physics Abstracts* towards the end of the first issue for each month.

FORM OF ENTRY

All entries in *Physics Abstracts* follow the same basic pattern. The following example identifies the individual parts of a typical entry for an article from a journal.



Entries for other types of material differ mainly in the reference to the source, e.g., a report will refer to the report series and the number of the individual report. A conference paper on the other hand will normally refer to the title, place and date of the conference at which the paper was given.

SUBJECT ARRANGEMENT & SUBJECT GUIDE

The abstracts are arranged by subject in accordance with the scheme in the CLASSIFICATION and CONTENTS which appears opposite. The page number for the start of each subject section is given. An alphabetical index to the scheme—the SUBJECT GUIDE—follows the CLASSIFICATION and CONTENTS.

SUBJECT INDEXES

Detailed twice-yearly subject indexes to the individual entries are provided separately, covering the periods January-June and July-December. In these SUBJECT INDEXES each major concept occurring in each paper abstracted is indexed under headings drawn from the INSPEC Thesaurus.

AUTHOR INDEX

At the end of each issue, an alphabetical index of authors is provided showing the entry number of the items written by them. These indexes are cumulated every six months and, with the addition of the title of the individual papers, are published separately to cover the periods January-June and July-December of each year.

SUBSIDIARY INDEXES

Where appropriate, the following subsidiary indexes are included for the convenience of users:

Bibliography index of articles where a significant list of references or bibliography is contained.

Book index of books received and abstracted.

Corporate Author index where a corporate organisation rather than an individual is responsible for publication. This index includes all reports.

Conference index with reference to individual papers.

Subscription prices and ordering procedure are shown on the inside back cover.

PHYSICS ABSTRACTS is published twice monthly by the Institution of Electrical Engineers in association with the Institute of Electrical and Electronics Engineers Inc. Printed by Unwin Brothers Limited, The Gresham Press, Old Woking, Surrey. 2nd Class postage paid at Piscataway, N.J. 08854, USA. POSTMASTER: Send address changes to INSPEC/IEEE SERVICE CENTER, 445 Hoes Lane, Piscataway, N.J. 08854.

© 1983. THE INSTITUTION OF ELECTRICAL ENGINEERS. All rights reserved. No part of this publication may be reproduced, stored in a retrieval system, or transmitted, in any form or by any means, electronic, mechanical, photocopying, recording or otherwise without the prior permission of the Institution of Electrical Engineers.

Physics Abstracts

CLASSIFICATION AND CONTENTS

The abstracts are arranged by subject in accordance with the following scheme. The page number for each section is given. The CLASSIFICATION AND CONTENTS is followed by an alphabetical guide to the scheme, the SUBJECT GUIDE.

The classification scheme is the result of cooperation between INSPEC, the American Institute of Physics, the European Physical Society and the Physics Working Group of the ICSU-AB.

	page		page
0000 GENERAL	8899	0620H Measurement standards and calibration	8922
0100 COMMUNICATION, EDUCATION, HISTORY, AND PHILOSOPHY	8899	0620J Determination of fundamental constants	8922
0110 Announcements, news, and organizational activities	—	0630 Measurement of basic variables	8922
0130 Physics literature and publications	8899	0630C Spatial variables measurement	8922
0130B Publications of lectures (advanced institutes, summer schools, etc.)	8899	0630E Mass and density measurement	8923
0130C Conference proceedings	8899	0630F Time and frequency measurement	8924
0130E Monographs, and collections	8900	0630G Velocity, acceleration and rotation measurement	8924
0130K Handbooks, dictionaries, tables and data compilation	8900	0630L Measurement of basic electromagnetic variables	8924
0130M Textbooks for graduates and researchers	8901	0650 Data handling and computation	8924
0130P Textbooks for undergraduates	8901	0660 Laboratory techniques	8924
0130R Surveys and tutorial papers; resource letters	8901	0670 General instrumentation	8924
0130T Bibliographies	8902	0690 Other topics in measurement science, general laboratory techniques and instrumentation systems	—
0140 Education	8902	0700 SPECIFIC INSTRUMENTATION AND TECHNIQUES OF GENERAL USE IN PHYSICS	8926
0150 Educational aids	8903	0710 Mechanical instruments and measurement methods	8926
0155 General Physics	—	0720 Thermal instruments and techniques	8926
0160 Biographical, historical, and personal notes	—	0720D Thermometry	8926
0165 History of science	8905	0720F Calorimetry	8926
0170 Philosophy of science	8905	0720H Furnaces	—
0175 Science and society	—	0720K High-temperature techniques and instrumentation; pyrometry	8926
0190 Other topics of general interest	8905	0720M Cryogenics	8927
0200 MATHEMATICAL METHODS IN PHYSICS	8905	0725 Hygrometry	8927
0210 Algebra, set theory, and graph theory	8905	0730 Vacuum production and techniques	—
0220 Group theory	8905	0730C Vacuum pumps	—
0230 Function theory, analysis	8906	0730D Vacuum meters	—
0240 Geometry, differential geometry, and topology	8907	0735 High pressure production and techniques	8927
0250 Probability theory, stochastic processes, and statistics	8907	0750 Electrical instruments and techniques	8927
0260 Numerical approximation and analysis	8907	0755 Magnetic instruments and techniques	8928
0270 Computational techniques	8908	0758 Magnetic resonance spectrometers, auxiliary instruments and techniques	8928
0290 Other topics in mathematical methods in physics	—	0760 Optical instruments and techniques	8929
0300 CLASSICAL AND QUANTUM PHYSICS; MECHANICS AND FIELDS	8908	0760D Photometry and radiometry	8930
0320 Classical mechanics of discrete systems: general mathematical aspects	8908	0760F Polarimetry and ellipsometry	8930
0330 Special relativity	8909	0760H Refractometry and reflectometry	8930
0340 Classical mechanics of continuous media: general mathematical aspects	8909	0760L Interferometry	8931
0340D Mathematical theory of elasticity	8909	0760P Optical microscopy	8932
0340G Fluid dynamics: general mathematical aspects	8910	0762 Detection of radiation (bolometers, photoelectric cells, i.r. and submillimetre waves detection)	8932
0340K Waves and wave propagation: general mathematical aspects	8910	0765 Optical spectroscopy and spectrometers	8933
0350 Classical field theory	8911	0765E UV and visible spectroscopy and spectrometers	8933
0365 Quantum theory; quantum mechanics	8912	0765G IR spectroscopy and spectrometers	8933
0370 Theory of quantized fields	8913	0768 Photography, photographic instruments and techniques	8934
0380 General theory of scattering	8913	0775 Mass spectrometers and mass spectrometry techniques	8934
0400 RELATIVITY AND GRAVITATION	8914	0777 Particle beam production and handling; targets	8935
0420 General relativity	8914	0780 Electron and ion microscopes and techniques	8936
0430 Gravitational waves and radiation: theory	8915	0785 X-ray, gamma-ray instruments and techniques	8937
0440 Continuous media; electromagnetic and other mixed gravitational systems	8915	0790 Other topics in specialised instrumentation	8938
0450 Unified field theories and other theories of gravitation	8915	1000 THE PHYSICS OF ELEMENTARY PARTICLES AND FIELDS	8939
0460 Quantum theory of gravitation	8915	1100 GENERAL THEORY OF FIELDS AND PARTICLES	8939
0465 Supergravity	8915	1110 Field theory	8939
0480 Experimental tests of general relativity and observations of gravitational radiation	8916	1120 S-matrix theory	8942
0490 Other topics in relativity and gravitation	8916	1130 Symmetry and conservation laws	8942
0500 STATISTICAL PHYSICS AND THERMODYNAMICS	8916	1140 Currents and their properties	8943
0520 Statistical mechanics	8916	1150 Dispersion relations and sum rules	8943
0530 Quantum statistical mechanics	8916	1160 Complex angular momentum; Regge formalism	8943
0540 Fluctuation phenomena, random processes, and Brownian motion	8917	1180 Relativistic scattering theory	—
0550 Lattice theory and statistics; Ising problems	8920	1190 Other topics in general field and particle theory	—
0560 Transport processes: theory	8921	1200 SPECIFIC THEORIES AND INTERACTION MODELS; PARTICLE SYSTEMATICS	8943
0570 Thermodynamics	8921	1210 Unified field theories and models	8943
0590 Other topics in statistical physics and thermodynamics	—	1220 Models of electromagnetic interactions	8944
0600 MEASUREMENT SCIENCE, GENERAL LABORATORY TECHNIQUES, AND INSTRUMENTATION SYSTEMS	8921	1220D Specific calculations and limits of quantum electrodynamics	8944
0620 Metrology	8921	1220F Experimental tests of quantum electrodynamics	8944
0620D Measurement and error theory	8921	1225 Models for gravitational interactions	—
0620F Units	8922	1230 Models of weak interactions	8944
		1235 Composite models of particles	8945
		1235C General properties of quantum chromodynamics (dynamics, confinement, etc.)	8945
		1235E Applications of quantum chromodynamics to particle properties and reactions	8945
		1235H Phenomenological composite models of particle structure and reactions (partons, bags, etc.)	8946
		1235K Other composite models	8946

	page		page
1240 Models of strong interactions	8946	2360 alpha decay	8960
1240E Statistical models	8946	2390 Other topics in nuclear decay and radioactivity	—
1240F Bootstrap models	—		
1240H Duality and dual models	8947	2400 NUCLEAR REACTIONS AND SCATTERING: GENERAL	8960
1240K Hadron classification schemes	—	2410 Nuclear reaction and scattering models and methods	8960
1240M Complex angular momentum plane; Regge poles and cuts (Reggeons)	8947	2410H Optical and diffraction models	8961
1240P Absorptive, optical, and eikonal models	—	2430 Resonance reactions and scattering	8962
1240Q Potential models	8947	2450 Direct reactions	8963
1240R Peripheral models (one or more particle exchange)	—	2460 Statistical theory and fluctuations	8963
1240S Multiperipheral and multi-Regge models	8947	2470 Polarization in reactions and scattering	8964
1240V Vector-meson dominance	8947	2475 General properties of fission	8964
1270 Hadron mass formulas	8947	2490 Other topics in nuclear reactions and scattering, general	—
1290 Miscellaneous theoretical ideas and models	8947		
1300 SPECIFIC REACTIONS AND PHENOMENOLOGY	8947	2500 NUCLEAR REACTIONS AND SCATTERING: SPECIFIC REACTIONS	8964
1310 Weak and electromagnetic interactions of leptons	8947	2510 Nuclear reactions and scattering involving few-nucleon systems	8964
1315 Neutrino interactions	8947	2520 Photonuclear reactions and photon scattering	8964
1320 Leptonic and semileptonic decays of mesons	8948	2530 Lepton-induced reactions and scattering	8964
1325 Hadronic decays of mesons	8948	2540 Nucleon-induced reactions and scattering	8965
1330 Decays of baryons	8948	2550 ^2H - and ^3H -induced reactions and scattering	8968
1335 Decays of leptons	8948	2560 ^3He - and ^4He -induced reactions and scattering	8969
1340 Electromagnetic processes and properties	8948	2570 Heavy ion induced reactions and scattering	8969
1340D Electromagnetic mass differences	8948	2580 Meson- and hyperon-induced reactions and scattering	8972
1340F Electromagnetic form factors; electric and magnetic moments	8948	2585 Fission reactions	8972
1340H Electromagnetic decays	8948	2588 Fusion reactions	8973
1340K Electromagnetic corrections to strong and weak interaction processes	8949	2590 Other topics in nuclear reactions and scattering: specific reactions	—
1360 Photon and charged-lepton interactions with hadrons	8949		
1360F Elastic and Compton scattering	8949	2700 PROPERTIES OF SPECIFIC NUCLEI LISTED BY MASS RANGES	8973
1360H Total and inclusive cross sections	8949	2710 $A \leq 5$	8973
1360K Meson production	—	2720 $6 \leq A \leq 19$	8973
1360M Meson-resonance production	—	2730 $20 \leq A \leq 38$	8974
1360P Baryon and baryon resonance production	8949	2740 $39 \leq A \leq 58$	8974
1365 Hadron production by electron-positron collisions	8949	2750 $59 \leq A \leq 89$	8974
1375 Hadron-induced low- and intermediate-energy reactions and scattering, energy ≤ 10 GeV	8950	2760 $90 \leq A \leq 149$	8975
1375C Nucleon-nucleon interactions, including antinucleon, deuteron, etc. (energy ≤ 10 GeV)	8950	2770 $150 \leq A \leq 189$	8975
1375E Hyperon-nucleon interactions (energy ≤ 10 GeV)	—	2780 $190 \leq A \leq 219$	8975
1375G Pion-baryon interactions (energy ≤ 10 GeV)	—	2790 $220 \leq A$	8975
1375J Kaon-baryon interactions (energy ≤ 10 GeV)	—		
1375L Meson-meson interactions (energy ≤ 10 GeV)	—	2800 NUCLEAR ENGINEERING AND NUCLEAR POWER STUDIES	8976
1385 Hadron-induced high- and super-high-energy interactions, energy > 10 GeV	8950	2820 Neutron physics	8976
1385D Elastic scattering (energy > 10 GeV)	8950	2841 Fission reactor theory and design	8976
1385F Inelastic scattering, two-particle final states (energy > 10 GeV)	—	2842 Fission reactor materials	8977
1385H Inelastic scattering, many-particle final states (energy > 10 GeV)	8950	2842H Fuel preparation and reprocessing	8980
1385K Inclusive reactions, including total cross sections, (energy > 10 GeV)	8950	2843 Fission reactor operation	8980
1385M Cosmic ray interactions	—	2844 Fission reactor protection systems, safety and accidents	8983
1388 Polarisation in interactions and scattering	8950	2850 Fission reactor types and applications	8986
1390 Other topics in specific reactions and phenomenology of elementary particles	8951	2852 Fusion reactors	8986
		2858 Integrated reactor systems	8987
1400 PROPERTIES OF SPECIFIC PARTICLES AND RESONANCES	8951	2870 Nuclear explosions	8988
1420 Baryons and baryon resonances	8951	2880 Radiation technology, including shielding	8988
1440 Mesons and meson resonances	8951	2890 Other topics in nuclear engineering and nuclear power studies	8989
1460 Leptons	8951		
1480 Other and hypothetical particles	8951	2900 EXPERIMENTAL METHODS AND INSTRUMENTATION FOR ELEMENTARY-PARTICLE AND NUCLEAR PHYSICS	8989
2000 NUCLEAR PHYSICS	8952	2910 Preacceleration (injection)	8989
2100 NUCLEAR STRUCTURE	8952	2915 Electrostatic and linear particle accelerators	8989
2110 General and average properties of nuclei; properties of nuclear energy levels	8952	2920 Cyclic accelerators and storage facilities	8991
2110D Binding energy and masses	8953	2925 Particle sources and targets, preparation and technology	8991
2110F Shape, charge, radius and form factors	8953	2930 Radiation spectrometers and spectroscopic techniques	8993
2110H Spin, parity, and isobaric spin	8954	2940 Radiation detectors	8994
2110J Spectroscopic factors	8955	2960 Counting circuits and nuclear electronics	8997
2110K Electromagnetic moments	8955	2970 Radiation measurement, detection and counting	8998
2110M Level density and structure	8955	2975 Polarization analysis	—
2130 Nuclear forces	8955	2980 Nuclear information processing	8999
2140 Few-nucleon systems	8956	2990 Other topics in high-energy and nuclear experimental methods and instrumentation	8999
2160 Nuclear-structure models and methods	8956		
2160C Shell model	8956	3000 ATOMIC AND MOLECULAR PHYSICS	8999
2160E Collective models	8957		
2160F Models based on group theory	8957	3100 THEORY OF ATOMS AND MOLECULES	8999
2160G Cluster models	8958	3110 General theory of structure, transitions and chemical binding	8999
2160J Hartree-Fock and random-phase approximations	8958	3115 General mathematical and computational developments	9000
2165 Nuclear matter	8958	3120 Specific calculations and results	9000
2180 Hypernuclei	8958	3120D Complete <i>ab initio</i> calculations (exact or nearly exact calculations on small species)	—
2190 Other topics in nuclear structure	—	3120E <i>Ab initio</i> LCAO and GO SCF calculations	—
2300 RADIOACTIVITY AND ELECTROMAGNETIC TRANSITIONS	8958	3120G Other accurate, or nearly <i>ab initio</i> calculations (DIM method, SAMO method, etc.)	9002
2320 Electromagnetic transitions	8958	3120L Statistical model calculations (Thomas-Fermi and Thomas-Fermi-Dirac models)	9002
2320C Lifetimes and transition probabilities	8959	3120N Semi-empirical NDO calculations (CNDO, INDO, MINDO, PCILO methods, etc.)	9002
2320N Internal conversion and extranuclear effects	8960		
2340 beta decay; electron and muon capture	8960		

3120P	Other semi-empirical calculations (Hückel, generalized Hückel, PPP methods, etc.)	9003	3500	PROPERTIES OF ATOMS AND MOLECULES; INSTRUMENTS AND TECHNIQUES	9021
3120R	Valence bond calculations (ab initio or not)	9003	3510	Atoms	9021
3120T	Electron correlation and CI calculations	9003	3510B	Atomic masses, mass spectra, abundances, and isotopes	9021
3120W	Empirical methods (nonquantum methods for conformations, as Wiberg method, Westheimer method, etc.)	—	3510D	Electric and magnetic moments, polarizability	9021
3130	Corrections to electronic structure	9004	3510F	Relativistic corrections, fine- and hyperfine-structure constants	9021
3150	Excited states	9004	3510H	Ionization potentials, electron affinities	9021
3170	Effects of molecular interactions on electronic structure	9005	3510W	Weak Interactions	9021
3170D	Environmental and solvent effects	9005	3520	Molecules	9021
3170F	Potential-energy surfaces for collisions	9005	3520B	General molecular conformation and symmetry; stereochemistry	9021
3170H	Time-dependent phenomena: excitation and relaxation processes, and reaction rates	—	3520D	Interatomic distances and angles	9022
3170K	Molecular solids	—	3520G	Bond strengths, dissociation energies, hydrogen bonding, etc	9022
3190	Other topics in the theory of atoms and molecules	9005	3520J	Barrier heights (internal rotation, inversion); rotational isomerism, conformational dynamics	9022
3200	ATOMIC SPECTRA AND INTERACTIONS WITH PHOTONS	9005	3520M	Electric and magnetic moments (and derivatives), polarizability, and magnetic susceptibility	9023
3220	Atomic spectra grouped by wavelength ranges	9005	3520P	Rotation, vibration, and vibration-rotation constants	9023
3220B	Radiofrequency, microwave, and infrared spectra	9005	3520S	Hyperfine and fine-structure constants	9023
3220J	Visible and ultraviolet spectra	9005	3520V	Ionization potentials, electron affinities, molecular core binding energy	9023
3220R	X-ray spectra	9005	3520W	Weak interactions	—
3250	Fluorescence, phosphorescence	9005	3520X	Mass spectra	9023
3260	Zeeman and Stark effects	9005	3520Y	Correlation times in molecular dynamics	—
3270	Spectral line shapes and intensities	9006	3580	Atomic and molecular measurements and techniques	9023
3280	Photon interactions with atoms	9006			
3280B	Level crossing and optical pumping	9006			
3280D	Autoionization	—			
3280F	Photoionization and photodetachment	9006	3600	STUDIES OF SPECIAL ATOMS AND MOLECULES	9024
3280H	Auger effect and inner-shell ionization	—	3610	Exotic atoms and molecules (containing mesons, muons, and other abnormal particles)	9024
3280K	Multiphoton processes	—	3620	Macromolecules and polymer molecules	9024
3290	Other topics in atomic spectra and interactions with photons	9006	3640	Atomic and molecular clusters	9025
			3690	Other special atoms and molecules	—
3300	MOLECULAR SPECTRA AND INTERACTIONS WITH PHOTONS	9006	4000	CLASSICAL AREAS OF PHENOMENOLOGY	9025
3310	Calculation of molecular spectra	9006			
3320	Molecular spectra grouped by wavelength ranges	9008	4100	ELECTRICITY AND MAGNETISM; FIELDS AND CHARGED PARTICLES	9025
3320B	Radiofrequency and microwave spectra	9008	4110	Classical electromagnetism	9025
3320E	Infrared spectra	9009	4110D	Electrostatics, magnetostatics	9025
3320F	Raman and Rayleigh spectra	9010	4110F	Steady-state electromagnetic fields; electromagnetic induction	9025
3320K	Visible spectra	9010	4110H	Electromagnetic waves: theory	9025
3320L	Ultraviolet spectra	9011	4170	Particles in electromagnetic fields: classical aspects	9026
3320N	Vacuum ultraviolet spectra	—	4180	Particle beams and particle optics	9027
3320R	X-ray spectra	—	4180D	Electron beams and electron optics	9027
3325	Nuclear magnetic resonance and relaxation; nuclear quadrupole resonance (NQR)	9011	4180G	Ion beams and ion optics	9027
3330	Electron paramagnetic resonance and relaxation	9011	4190	Other topics in electricity and magnetism	—
3335	Double resonances and other multiple resonances	9012			
3335H	MODR and PMDR (microwave optical double resonance and phosphorescence microwave double resonance)	9012	4200	OPTICS	9027
3340	Mössbauer spectra	9012	4210	Propagation and transmission in homogeneous media	9027
3345	Magneto-optical and electro-optical spectra; dichroism	9012	4220	Propagation and transmission in inhomogeneous media	9028
3345B	Zeeman and Stark effects	9012	4230	Optical information, image formation and analysis	9029
3345C	Magnetic circular dichroism	9012	4240	Holography	9030
3350	Fluorescence, phosphorescence; radiationless transitions (intersystem crossing, internal conversion)	9013	4250	Quantum optics	9030
3365	Photoelectron spectra	9014	4252	Masers	9031
3370	Intensities and shapes of molecular spectral lines and bands	9014	4255	Lasing processes	9031
3380	Photon interactions with molecules	9015	4255B	General theory of lasing action	9031
3380B	Level crossing and optical pumping	9015	4255D	CO ₂ lasers	9031
3380E	Autoionization, photoionization, and photodetachment	9015	4255F	Inert gas lasers	9031
3380G	Diffuse spectra; predissociation, photodissociation	9015	4255H	Lasing action in other gas lasers	9031
3380K	Multiphoton processes	9015	4255K	Chemical lasers	9032
3390	Other topics in molecular spectra and interactions with photons	—	4255M	Lasing action in liquids and organic dyes	9032
			4255P	Lasing action in semiconductors with junctions	9032
3400	ATOMIC AND MOLECULAR COLLISION PROCESSES AND INTERACTIONS	9016	4255R	Lasing action in other solids	9033
3410	General theories and models	9016	4255T	Free electron lasers	9033
3420	Interatomic and intermolecular potentials and forces	9016	4260	Laser systems and laser beam applications	9033
3440	Elastic scattering of atoms and molecules	—	4260B	Design of specific laser systems	9033
3450	Inelastic scattering of atoms and molecules	9016	4260D	Laser resonators and cavities	9034
3450E	Rotational and vibrational energy transfer	9017	4260F	Laser beam modulation	9034
3450H	Electronic excitation and ionization (inc. beam-foil excitation and ionization)	9018	4260H	Optical problems related to properties and interactions of laser beams	9035
3450L	Chemical reactions, energy disposal, and angular distribution, as studied by atomic and molecular beams	9019	4265	Nonlinear optics	9035
3470	Charge transfer	9019	4265B	General theory	9036
3480	Electron scattering	9020	4265C	Stimulated Raman, Brillouin and Rayleigh scattering; parametric oscillations and harmonic generation	9036
3480B	Elastic scattering of electrons by atoms and molecules	9020	4265F	Phase conjugation	9037
3480D	Atomic excitation and ionization by electron impact	9020	4265G	Photon echoes, self-induced transparency, optical saturation and related effects	9037
3480G	Molecular excitation, ionization, and dissociation by electron impact	9020	4265J	Beam trapping, self focusing, thermal blooming, and related effects	9037
3490	Other topics in atomic and molecular collision processes and interactions	9021	4270	Optical materials	9037
			4270C	Glass	9038
			4270G	Light-sensitive materials	9038
			4272	Optical sources and standards	9038
			4278	Optical lens and mirror systems	9038
			4278H	Coatings	—
			4280	Optical devices, techniques and applications	9038

		page			page
4280B	Spatial filters, zone plates	9038	4755K	Multiphase flows	9068
4280C	Spectral and other filters	9039	4755M	Flow through porous media	9069
4280D	Monochromators	9039	4760	Flows in ducts, channels, and conduits	9069
4280E	Shutters, windows, diaphragms, deflectors, choppers	9039	4765	Magnetohydrodynamics and electrohydrodynamics	9070
4280F	Gratings, echelles	9039	4770	Reactive, radiative, or nonequilibrium flows	9070
4280K	Optical beam modulators	9039	4775	Relativistic fluid dynamics	—
4280L	Optical waveguides	9039	4780	Instrumentation for fluid dynamics	9070
4280M	Fibre optics	9040	4790	Other topics in fluid dynamics	—
4280Q	Image detectors, convertors, and intensifiers	9042			
4280S	Optical communications devices	9043	5000	FLUIDS, PLASMAS AND ELECTRIC DISCHARGES	9072
4282	Integrated optics	9043			
4285	Optical testing and workshop techniques	9043	5100	KINETIC AND TRANSPORT THEORY OF FLUIDS; PHYSICAL PROPERTIES OF GASES	9072
4290	Other topics in optics	—	5110	Kinetic and transport theory	9072
			5120	Viscosity and diffusion: experimental	9072
4300	ACOUSTICS	9044	5130	Thermal properties of gases	9072
4320	General linear acoustics	9044	5140	Acoustical properties of gases; ultrasonic relaxation	—
4325	Nonlinear acoustics and macrosonics	9045	5150	Electrical phenomena in gases	9072
4328	Aeroacoustics and atmospheric sound	—	5160	Magnetic phenomena in gases	—
4330	Underwater sound	9045	5170	Optical phenomena in gases	9073
4335	Ultrasonics, quantum acoustics, and physical effects of sound	9046	5190	Other topics in the physics of fluids	9073
4340	Mechanical vibrations and shock	9046			
4345	Statistical studies of acoustical response	—	5200	THE PHYSICS OF PLASMAS AND ELECTRIC DISCHARGES	9073
4350	Noise, its effects and control	9046	5220	Elementary processes in plasma	9073
4355	Architectural acoustics	9047	5220F	Electron collisions	—
4360	Acoustic signal processing	9047	5220H	Atomic, molecular, heavy-particle collisions	9073
4363	Acoustic holography	9048	5225	Plasma basic properties	9073
4370	Speech communication	9048	5225F	Transport properties	9074
4375	Music and musical instruments	9049	5225P	Emission, absorption, and scattering of radiation	9075
4385	Acoustical measurements and instrumentation	9049	5230	Plasma flow; magnetohydrodynamics	9075
4388	Transduction; devices for the generation and reproduction of sound	9050	5235	Waves, oscillations, and instabilities in plasma	9075
4390	Other topics in acoustics	—	5235R	Plasma turbulence	9077
			5235T	Shock waves	9078
4400	HEAT FLOW, THERMAL AND THERMODYNAMIC PROCESSES	9051	5240	Plasma interactions	9078
4410	Heat conduction (models, phenomenological description)	9051	5240D	Electromagnetic wave propagation in plasma	9078
4425	Convective and constrained heat transfer	9051	5240F	Antennas in plasma; plasma-filled wave guides	9078
4430	Heat transfer in inhomogeneous media and through interfaces	9051	5240H	Solid-plasma interactions	9078
4440	Radiative heat transfer	9051	5240K	Sheaths	9078
4450	Thermal properties of matter (phenomenology, experimental techniques)	9052	5240M	Beam interactions in plasma	9078
4460	Thermodynamic processes (phenomenology, experimental techniques)	9052	5250	Plasma production and heating	9079
4490	Other topics in heat flow, thermal and thermodynamic processes	9052	5250J	Plasma production and heating by laser beams	9079
			5250L	Plasma production and heating by shock wave and wire explosion	9079
4600	MECHANICS, ELASTICITY, RHEOLOGY	9052	5255	Plasma equilibrium and confinement	9079
4610	Mechanics of discrete systems	9052	5260	Relativistic plasma	9080
4620	Continuum mechanics	9053	5265	Plasma simulation	9080
4630	Mechanics of solids and rheology	9054	5270	Plasma diagnostic techniques and instrumentation	9081
4630C	Static elasticity	9054	5275	Plasma devices and applications	9082
4630J	Viscoelasticity, plasticity, viscoplasticity, creep, and stress relaxation	9055	5280	Electric discharges	9082
4630L	Static buckling and instability	9056	5290	Other topics in plasma physics and electric discharges	—
4630M	Vibrations, aeroelasticity, hydroelasticity, mechanical waves, and shocks	9057			
4630N	Fracture mechanics, fatigue, and cracks	9058	6000	CONDENSED MATTER: STRUCTURE, THERMAL AND MECHANICAL PROPERTIES	9084
4630P	Friction, wear, adherence, hardness, mechanical contacts	9059			
4630R	Measurement methods and techniques	9060	6100	STRUCTURE OF LIQUIDS AND SOLIDS; CRYSTALLOGRAPHY	9084
4660	Rheology of fluids and pastes	9061	6110	X-ray determination of structures	9084
4690	Other topics in mechanics, elasticity, and rheology	—	6110D	Theories of diffraction and scattering	9084
			6110F	Experimental techniques	9084
4700	FLUID DYNAMICS	9061	6112	Neutron determination of structures	9085
4710	General theory	9061	6114	Electron determination of structures	9085
4715	Laminar flows	9062	6114D	Theories of diffraction and scattering	—
4715C	Laminar boundary layers	9062	6114F	Experimental diffraction and scattering	—
4715F	Stability of laminar flows	9062	6114H	Low-energy electron diffraction (LEED) and reflection High-energy electron diffraction (RHEED)	9085
4720	Hydrodynamic stability	9062	6116	Other determination of structures	9085
4725	Turbulent flows, convection, and heat transfer	9063	6116D	Electron microscopy determinations	9085
4725C	Isotropic turbulence	9063	6116F	Field-ion microscopy determinations	9085
4725F	Boundary layer and shear turbulence	9064	6116N	EPR and NMR determinations	9085
4725J	Turbulent diffusion	9064	6120	Classical, semiclassical, and quantum theories of liquid structure	9085
4725M	Noise (turbulence generated)	—	6125	Studies of specific liquid structures	9086
4725Q	Convection and heat transfer	9064	6125M	Liquid metals	9087
4725R	Wakes	9065	6130	Liquid crystals	9087
4730	Rotational flow and vorticity	9065	6140	Amorphous and polymeric materials	9088
4735	Waves	9066	6140D	Glasses	9088
4740	Compressible flows; shock and detonation phenomena	9066	6140K	Polymers, elastomers, and plastics	9089
4740D	General subsonic flows	—	6150	Crystalline state	9091
4740H	Transonic flows	9067	6150C	Physics of crystal growth	9091
4740K	Supersonic and hypersonic flows	9067	6150E	Crystal symmetry; models and space groups, and crystalline systems and classes	9092
4740N	Shock-wave interactions	9067	6150J	Crystal morphology and orientation	9092
4745	Rarefied gas dynamics	—	6150K	Crystallographic aspects of polymorphic and order-disorder transformations	9092
4750	Non-Newtonian dynamics	9067	6150L	Crystal binding	9093
4755	Nonhomogeneous flows	9067	6155	Specific structure of elements and alloys	9093
4755B	Cavitation	9068	6155D	Nonmetallic elements	9093
4755C	Jets	9068	6155F	Metallic elements	—
4755E	Nozzles	—	6155H	Alloys	9093
4755H	Stratified flows	9068	6160	Specific structure of inorganic compounds	9093
			6165	Specific structure of organic compounds	9096
			6170	Defects in crystals	9097

		page			page
6170B	Interstitials and vacancies	9098	6630D	Theory of diffusion and ionic conduction in solids	9135
6170D	Colour centres	9102	6630F	Self-diffusion in metals, semimetals, and alloys	9135
6170E	Other point defects	9102	6630H	Self-diffusion and ionic conduction in nonmetals	9135
6170G	Dislocations: theory	9102	6630J	Diffusion, migration, and displacement of impurities	9136
6170J	Etch pits, decoration, transmission electron-microscopy and other direct observations of dislocations	9102	6630L	Diffusion, migration, and displacement of other defects	9138
6170L	Slip, creep, internal friction and other indirect evidence of dislocations	9103	6630N	Chemical interdiffusion	9138
6170N	Grain and twin boundaries	9104	6630Q	Electromigration	9139
6170P	Stacking faults, stacking fault tetrahedra and other planar or extended defects	9104	6660	Thermal conduction in nonmetallic liquids	9139
6170R	Crystal impurities: general	9105	6670	Nonelectronic thermal conduction and heat-pulse propagation in nonmetallic solids	9139
6170T	Doping and implantation of impurities	9105	6690	Other topics in nonelectronic transport properties	—
6170W	Impurity concentration, distribution, and gradients	9106	6700	QUANTUM FLUIDS AND SOLIDS; LIQUID AND SOLID HELIUM	9139
6170Y	Interaction between different crystal structure defects	9107	6720	Quantum effects on the structure and dynamics of nondegenerate fluids	—
6180	Radiation damage and other irradiation effects	9109	6740	Boson degeneracy and superfluidity of helium-4	9139
6180B	Laser beams	9110	6750	Fermi fluids; liquid helium-3	9139
6180C	X-rays	9112	6760	Mixed systems; liquid helium 3-4 mixtures	9139
6180E	Gamma rays	9112	6770	Films	—
6180F	Electrons and positrons	9112	6780	Solid helium and related quantum crystals	9139
6180H	Neutrons	9114	6790	Other topics in quantum fluids and solids (e.g. neutron-star matter)	—
6180J	Ions	9115	6800	SURFACES AND INTERFACES; THIN FILMS AND WHISKERS	9140
6180L	Atoms and molecules	9116	6810	Fluid surfaces and interfaces with fluids	9140
6180M	Channelling, blocking and energy loss of particles	9116	6815	Liquid thin films	9140
6190	Other topics in structure of liquids and solids	—	6820	Solid surface structure	9140
6200	MECHANICAL AND ACOUSTIC PROPERTIES OF CONDENSED MATTER	9116	6825	Mechanical and acoustical properties of solid surfaces and interfaces	9141
6210	Mechanical properties of liquids	9116	6830	Dynamics of solid surfaces and interface vibrations	9142
6220	Mechanical properties of solids (related to microscopic structure)	9117	6840	Surface energy of solids; thermodynamic properties	9142
6220D	Elastic constants	9117	6845	Solid-fluid interface processes	9142
6220F	Deformation and plasticity	9117	6848	Solid-solid interfaces	9145
6220H	Creep	9118	6855	Thin film growth, structure, and epitaxy	9146
6220M	Fatigue, brittleness, fracture, and cracks	9119	6860	Physical properties of thin films, nonelectronic	9150
6220P	Tribology	9120	6870	Whiskers and dendrites: growth, structure, and nonelectronic properties	9150
6230	Mechanical and elastic waves	9121	6890	Other topics in the structure and nonelectronic properties of surfaces and thin films	—
6240	Anelasticity, internal friction, and damping	9121	7000	CONDENSED MATTER: ELECTRONIC STRUCTURE, ELECTRICAL, MAGNETIC, AND OPTICAL PROPERTIES	9150
6250	High-pressure and shock-wave effects in solids	9121	7100	ELECTRON STATES	9150
6260	Acoustic properties of liquids	9121	7110	General theories and computational techniques	9150
6265	Acoustic properties of solids	9121	7120	Electronic density of states determinations	9150
6280	Ultrasonic relaxation	9121	7125	Nonlocalized single-particle electronic states	9151
6290	Other topics in mechanical and acoustical properties of condensed matter	9122	7125C	Techniques of band-structure calculation (general theory, applications of group theory, analytic continuation, etc)	9151
6300	LATTICE DYNAMICS AND CRYSTAL STATISTICS	9122	7125H	Measurement of Fermi surface parameters	9151
6310	General theory	9122	7125J	Effective mass and g-factors	9151
6320	Phonons and vibrations in crystal lattices	9122	7125L	Electron energy states in liquid metals	9151
6320D	Phonon states and bands, normal modes, and phonon dispersion	9122	7125M	Electron energy states in amorphous and glassy solids	9151
6320H	Phonon-phonon interactions	9123	7125P	Band structure of crystalline metals	9151
6320K	Phonon-electron interactions	9123	7125R	Band structure of crystalline elemental semiconductors	9151
6320M	Phonon-defect interactions	9123	7125T	Band structure of crystalline semiconductor compounds and insulators	9152
6320P	Localized modes	9123	7130	Metal-insulator transitions	9152
6350	Vibrational states in disordered systems	9123	7135	Excitons and related phenomena	9152
6370	Statistical mechanics of lattice vibrations	9124	7136	Polaritons	9153
6375	Statistical mechanics of displacive phase-transitions	9124	7138	Polarons and electron-phonon interactions	9153
6390	Other topics in lattice dynamics and crystal statistics	9124	7145	Collective effects	9153
6400	EQUATIONS OF STATE, PHASE EQUILIBRIA, AND PHASE TRANSITIONS	9124	7145G	Exchange, correlation, dielectric and magnetic functions, plasmons	9153
6410	General theory of equations of state and phase equilibria	—	7145J	Fermi-Thomas model	9154
6430	Equations of state of specific substances	9124	7145N	Calculations of total electronic binding energy	—
6460	General studies of phase transitions	9124	7150	Localized single-particle electronic states	9154
6470	Phase equilibria, phase transitions, and critical points	9125	7155	Impurity and defect levels	9154
6470D	Solid-liquid transitions	9125	7155J	Localization in disordered structures	9156
6470F	Liquid-vapour transitions	9127	7165	Positron states	9156
6470H	Solid-vapour transitions	9127	7170	Level splitting and interactions	9156
6470J	Liquid-liquid transitions	9127	7170C	Crystal and ligand fields	9156
6470K	Solid-solid transitions	9127	7170E	Spin-orbit coupling, Zeeman, Stark and strain splitting	9157
6470M	Transitions in liquid crystals	9129	7170G	Exchange interactions	9158
6470P	Glass transitions	9129	7170J	Nuclear states and interactions	9158
6475	Solubility, segregation, and mixing	9129	7190	Other topics in electron states	—
6480	Other phase properties of systems	9131	7200	ELECTRONIC TRANSPORT IN CONDENSED MATTER	9158
6490	Other topics in equations of state, phase equilibria, and phase transitions	—	7210	Theory of electronic transport; scattering mechanisms	—
6500	THERMAL PROPERTIES OF CONDENSED MATTER	9132	7215	Electronic conduction in metals and alloys	9158
6520	Heat capacities of liquids	9132	7215C	Electrical and thermal conduction in amorphous and liquid metals and alloys	9158
6540	Heat capacities of solids	9132	7215E	Electrical and thermal conduction in crystalline metals and alloys	9158
6550	Thermodynamic properties and entropy	9132			
6570	Thermal expansion and thermomechanical effects	9133			
6590	Other topics in thermal properties of condensed matter	9133			
6600	TRANSPORT PROPERTIES OF CONDENSED MATTER (NONELECTRONIC)	9133			
6610	Diffusion and ionic conduction in liquids	9133			
6620	Diffusive momentum transport	9134			
6630	Diffusion in solids	9135			

Classification and Contents		page		page	
7215G	Galvanomagnetic and other magnetotransport effects	9159	7510J	Heisenberg and other quantized localized spin models	9173
7215H	Thermomagnetic effects	—	7510L	Band and itinerant models	9173
7215J	Thermoelectric effects	9159	7520	Diamagnetism and paramagnetism	9173
7215L	Relaxation times and mean free paths	9159	7520C	Nonmetals	9173
7215N	Collective modes, e.g. in one-dimensional conductors	9159	7520E	Metals and alloys	9174
7215Q	Scattering mechanisms and Kondo effect	9159	7520H	Local moment in dilute alloys; Kondo effect	9174
7220	Conductivity phenomena in semiconductors and insulators	9159	7525	Spin arrangements in magnetically ordered materials (neutron studies, etc)	9174
7220D	General theory, scattering mechanisms	9159	7530	Magnetically ordered materials, other intrinsic properties	9174
7220F	Low-field transport and mobility; piezoresistance	9159	7530C	Saturation moments and magnetic susceptibility	9174
7220H	High-field and nonlinear effects	9160	7530D	Spin waves	9175
7220J	Charge carriers: generation, recombination, lifetime, and trapping	9160	7530E	Exchange and superexchange interactions	9175
7220M	Galvanomagnetic and other magnetotransport effects	9162	7530G	Anisotropy	9175
7220N	Thermomagnetic effects	—	7530H	Magnetic impurity interactions	9175
7220P	Thermoelectric effects	—	7530K	Magnetic phase boundaries	9176
7230	High-frequency effects; plasma effects	9163	7530S	Magnetocaloric effect	9176
7240	Photoconduction and photovoltaic effects; photodielectric effects	9163	7540	Critical-point effects, specific heats, short-range order	9176
7250	Acoustoelectric effects	9164	7540D	Ising and other classical spin models	9176
7255	Magnetoacoustic effects	—	7540F	Heisenberg and other quantized spin models	9176
7260	Mixed conductivity and conductivity transitions	9164	7550	Studies of specific magnetic materials	9176
7270	Noise processes and phenomena	9164	7550B	Ferromagnetism of Fe and its alloys	9176
7280	Conductivity of specific semiconductors and insulators	9164	7550C	Ferromagnetism of other metals	9177
7280C	Elemental semiconductors	9165	7550D	Ferromagnetism of nonmetals	9177
7280E	III-V and II-VI semiconductors	9165	7550E	Antiferromagnetics	9177
7280G	Transition-metal compounds	9165	7550G	Ferrimagnetics	9177
7280J	Other crystalline inorganic semiconductors	9165	7550K	Amorphous magnetic materials	9177
7280L	Organic semiconductors	9165	7550M	Magnetic liquids	—
7280N	Amorphous and glassy semiconductors	9165	7560	Domain effects, magnetization curves, and hysteresis	9177
7280P	Liquid semiconductors	—	7560C	Domain walls and domain structure	9177
7290	Other topics in electronic transport in condensed matter	9165	7560E	Magnetization curves, hysteresis, Barkhausen and related effects	9177
			7560G	High coercivity materials	9178
			7560J	Fine-particle systems	—
			7560L	Magnetic aftereffects	9178
			7560N	Magnetic annealing and temperature-hysteresis effects	9178
7300	ELECTRONIC STRUCTURE AND ELECTRICAL PROPERTIES OF SURFACES, INTERFACES, AND THIN FILMS	9166	7570	Magnetic films and plates	9178
7320	Electronic surface states	9166	7570K	Domain structure (magnetic bubbles)	9178
7325	Surface conductivity	9166	7580	Magnetomechanical and magnetoelectric effects, magnetostriction	9178
7330	Surface double layers, Schottky barriers, and work functions	9166	7590	Other topics in magnetic properties and materials	9179
7340	Interfaces	9167	7600	MAGNETIC RESONANCES AND RELAXATION IN CONDENSED MATTER; MÖSSBAUER EFFECT	9179
7340B	Static electrification	—	7620	General theory of resonances and relaxation	9179
7340G	Tunnelling: general	9167	7630	Electron paramagnetic resonance and relaxation	9179
7340J	Metal-to-metal contacts	9167	7630D	Ions and impurities: general	—
7340L	Semiconductor-to-semiconductor contacts, p-n junctions, and heterojunctions	9167	7630F	Iron group (3d) ions and impurities (Ti-Cu)	9179
7340M	Semiconductor-electrolyte contacts	9168	7630H	Platinum and palladium group (4d and 5d) ions and impurities (Zr-Ag and Hf-Au)	—
7340N	Metal-nonmetal contacts	9168	7630K	Rare-earth ions and impurities	9179
7340Q	Metal-insulator-semiconductor structures	9168	7630L	Other ions and impurities	9180
7340R	Metal-insulator-metal structures	9169	7630M	Colour centres and other defects	9180
7340S	Metal-semiconductor-metal structures	—	7630P	Conduction electrons	—
7360	Electronic properties of thin films	9169	7630R	Free radicals	9180
7360D	Metallic thin films	9169	7640	Diamagnetic and cyclotron resonances	9180
7360F	Semiconductor films	9170	7650	Ferromagnetic, antiferromagnetic, and ferrimagnetic resonances; spin wave resonance	9180
7360H	Insulating thin films	9170	7660	Nuclear magnetic resonance and relaxation	9180
7360K	Superconducting films	—	7660C	Chemical and Knight shifts	9181
7390	Other topics in electrical properties of surfaces, interfaces, and thin films	9170	7660E	Relaxation effects	9181
			7660G	Quadrupole resonance	—
7400	SUPERCONDUCTIVITY	9170	7660L	Spin echoes	9181
7410	Occurrence, critical temperature	9170	7670	Magnetic double resonances and cross effects	9181
7420	Theory	—	7670D	Electron-nuclear double resonance (ENDOR)	9181
7420F	BCS theory and its applications	—	7670E	Dynamical nuclear polarization	—
7430	General properties	9171	7670F	Double nuclear magnetic resonance (DNMR)	—
7430C	Magnetization curves, Meissner effect, penetration depth	9171	7670H	Optical double magnetic resonance (ODMR)	9181
7430E	Thermodynamic properties; thermal conductivity	9171	7670K	Electron double resonance (ELDOR)	—
7430G	Response to electromagnetic fields, nuclear magnetic resonance, ultrasonic attenuation	—	7680	Mössbauer effect; other gamma-ray spectroscopy	9182
7440	Fluctuations and critical effects	9171	7690	Other topics in magnetic resonances and relaxation	9182
7450	Proximity effects, tunnelling phenomena, and Josephson effect	9171	7700	DIELECTRIC PROPERTIES AND MATERIALS	9183
7455	Type-I superconductivity	—	7720	Permittivity	9183
7460	Type-II superconductivity	9172	7730	Polarization and depolarization effects	9183
7460E	Mixed state, H_{c2} , surface sheath	9172	7740	Dielectric loss and relaxation	9183
7460G	Flux pinning; fluxon-defect interactions	9172	7750	Dielectric breakdown and space-charge effects	9184
7460J	Critical currents	9172	7755	Dielectric thin films	9184
7470	Superconducting materials	9172	7760	Piezoelectricity and electrostriction	9184
7470D	Material effects on T_c , K , critical currents	9172	7770	Pyroelectric and electrocaloric effects	9185
7470G	Type-I superconductors (non transition metals)	9172	7780	Ferroelectricity and antiferroelectricity	9185
7470L	Type-II superconductors (transition metals, alloys and compounds)	9172	7780B	Transitions and Curie point	9185
7470N	Dirty superconductors	—	7780D	Domain structure and effects; hysteresis	9185
7470P	Materials for high-field applications	9172	7785	Electrical resonances	—
7490	Other topics in superconductivity	9172	7790	Other topics in dielectric properties and materials	9186
			7800	OPTICAL PROPERTIES AND CONDENSED MATTER SPECTROSCOPY AND OTHER INTERACTIONS OF MATTER WITH PARTICLES AND RADIATION	9186
7500	MAGNETIC PROPERTIES AND MATERIALS	9172	7820	Optical properties and materials	9186
7510	General theory and models of magnetic ordering	9172	7820B	General theory (for pure homogeneous materials)	9186
7510D	Crystal-field theory and spin Hamiltonians	9172			
7510H	Ising and other classical spin models	9172			

	page		page		
7820D	Optical constants and parameters	9186	8140E	Cold working, work hardening; annealing, recovery and recrystallisation; textures	9218
7820E	Optical rotatory power	9187			
7820F	Birefringence	9187	8140G	Other heat and thermomechanical treatments	9219
7820H	Piezo-, elasto- and acousto-optical effects	9188	8140J	Elasticity and anelasticity	9220
7820J	Electro-optical effects	9188	8140L	Deformation, plasticity and creep	9221
7820L	Magneto-optical effects	9188	8140N	Fatigue, embrittlement, and fracture	9225
7820N	Thermo-optical effects	—	8140P	Friction, lubrication, and wear	9230
7830	Infrared and Raman spectra and scattering	9188	8140R	Electrical and magnetic properties (related to treatment conditions)	9231
7835	Brillouin and Rayleigh scattering	9191	8140T	Optical properties (related to treatment conditions)	9231
7840	Visible and ultraviolet spectra	9191	8160	Corrosion, oxidation and surface treatments	9231
7845	Stimulated emission	9192	8160B	Metals and alloys	9233
7850	Impurity and defect absorption in solids	9192	8170	Materials testing	9237
7855	Photoluminescence	9193	8190	Other topics in materials science	9240
7860	Other luminescence spectra and radiative recombination	9196			
7860F	Electroluminescence	9196	8200	PHYSICAL CHEMISTRY	9241
7860H	Cathodoluminescence, ionoluminescence	9196	8220	Chemical kinetics	9241
7860K	Thermoluminescence	9197	8220K	Potential energy surfaces for chemical reactions	9241
7860M	Sonoluminescence, triboluminescence	—	8220M	Nonequilibrium kinetics	9241
7860P	Chemiluminescence	—	8220R	Energy distribution and transfer, relaxation	—
7865	Optical properties of thin films	9197	8230	Specific chemical reactions; reaction mechanisms	9241
7870	Other interactions of matter with particles and radiation	9198	8235	Polymer reactions and polymerization	9244
7870B	Positron annihilation	9198	8240	Chemical kinetics and reactions: special regimes	9244
7870C	X-ray scattering	9199	8240D	Atomic and molecular beam reactions	—
7870D	X-ray absorption and absorption edges	9199	8240T	Chemiluminescence and chemical laser kinetics	9245
7870E	X-ray emission threshold and fluorescence	9199	8245	Electrochemistry and electrophoresis	9245
7870G	Microwave and radiofrequency interactions	9199	8250	Photochemistry and radiation chemistry	9245
7890	Other topics in optical properties of condensed matter and other interactions of matter with particles and radiation	—	8250E	Photodissociation, photoionization as studied by luminescence and radiationless transitions	—
			8255	Radiochemistry	9246
			8260	Chemical thermodynamics	9246
			8265	Surface processes	9246
			8270	Disperse systems	9247
7900	ELECTRON AND ION EMISSION BY LIQUIDS AND SOLIDS; IMPACT PHENOMENA	9200	8280	Chemical analysis and related physical methods of analysis	9248
7920	Impact phenomena	9200	8290	Other topics in physical chemistry	—
7920D	Laser-light impact phenomena	9200			
7920F	Electron impact: Auger emission	9200	8600	ENERGY RESEARCH AND ENVIRONMENTAL SCIENCE	9249
7920H	Electron impact: secondary emission	—	8610	Energy resources and their utilisation	9249
7920K	Other electron impact phenomena	9200	8610B	Fossil and other fuels	—
7920N	Atom, molecule, and ion impact	9201	8610D	Wind energy	9249
7920R	Atomic and molecular beam interactions	9202	8610F	Tidal and flow energy	9249
7940	Thermionic emission	9202	8610H	Geothermal energy	—
7960	Photoemission and photoelectron spectra	9202	8610K	Solar energy	9249
7970	Field emission and field ionization	9203	8610N	Nuclear energy	—
7975	Exoelectron emission	—	8610Z	Other topics	—
7980	Resonance tunnelling	9204	8630	Energy conversion	9250
7990	Other topics in emission and impact phenomena in condensed matter	—	8630D	Electrochemical conversion: general	9250
			8630E	Primary cells	9250
8000	CROSS-DISCIPLINARY PHYSICS AND RELATED AREAS OF SCIENCE AND TECHNOLOGY	9204	8630F	Secondary cells	9250
8100	MATERIALS SCIENCE	9204	8630G	Fuel cells	9251
8110	Methods of crystal growth and purification	9204	8630J	Photoelectric conversion: solar cells and arrays	9251
8110B	Growth from vapour	9204	8630K	Photoelectrochemical conversion	9253
8110D	Growth from solutions	9204	8630L	Electrostatic and magnetohydrodynamic conversion	9253
8110F	Growth from melts	9204	8630M	Thermoelectric conversion	—
8110H	Zone melting and zone refining	9205	8630N	Thermionic conversion	—
8110J	Growth from solid phases	9205	8630P	Photosynthesis	—
8115	Methods of thin film deposition	9205	8630Q	Chemical energy conversion	9253
8115C	Deposition by cathodic sputtering	9205	8630R	Thermal energy conversion (heat engines and heat pumps)	9253
8115G	Vacuum deposition	9206	8630S	Photothermal conversion	9254
8115H	Chemical vapour deposition	9206	8630Z	Other topics	9255
8115J	Ion plating and other vapour deposition	9209	8640	Energy storage (secondary energy)	9255
8115L	Deposition from liquid phases (melts and solutions)	9210	8640C	Storage in mechanical energy	—
8120	Other methods of preparation of materials	9210	8640F	Storage in thermal energy	9255
8120C	Vacuum methods	—	8640H	Storage in chemical energy	—
8120E	Powder techniques, compaction and sintering	9211	8640K	Hydrogen storage and technology	9256
8120G	Specific metals and alloys (compacts, pseudoalloys)	9212	8640Z	Other topics	—
8120J	Dispersion-fibre-, and platelet-reinforced metal-based composites	9213	8660	Requirement for energy: ecological aspects	—
8120L	Ceramics and refractories	9213	8670	Environmental science	9256
8120N	Cermets, ceramic and refractory composites	9214	8670C	Soil	9256
8120P	Glasses	9214	8670E	Water	9256
8120Q	Glass-based composites, vitroceraics	—	8670G	Atmosphere	9256
8120S	Polymers	9214	8670J	Noise	—
8120T	Reinforced polymers and polymer-based composites	9214	8670L	Measurement techniques in environmental science	9257
8130	Phase diagrams and microstructures developed by solidification and solid-solid phase transformations	9214	8670Z	Other topics	9257
8130B	Phase diagrams of metals and alloys	9214	8690	Other topics in energy research and environmental science	—
8130D	Phase diagrams of other materials	9215	8700	BIOPHYSICS, MEDICAL PHYSICS, AND BIOMEDICAL ENGINEERING	9257
8130F	Solidification	9215	8710	General, theoretical, and mathematical biophysics	9257
8130H	Constant-composition solid-solid phase transformations: polymorphic, massive, and order-disorder	9216	8715	Molecular biophysics	9258
8130K	Martensitic transformations	9216	8715B	Structure, configuration, conformation, and active sites at the biomolecular level	9258
8130M	Precipitation	9217	8715M	Interactions with radiations at the biomolecular level	9259
8140	Treatment of materials and its effects on microstructures and properties	9217	8716	Biothermics	9260
8140C	Solid solution hardening, precipitation hardening, dispersion hardening	9218	8720	Membrane biophysics	9260
			8725	Cellular biophysics	9261
			8725D	Biological transport; cellular and subcellular transmembrane physics	9262
			8730	Biophysics of neurophysiological processes	9262

	page		page
8732	Physiological optics, vision	9263	9460 Interplanetary space
8732C	<i>Anatomy and optics of the eye</i>	9263	9480 Aerospace facilities and techniques; space research
8732E	<i>Physiology of the eye; nerve structure and function</i>	9263	9490 Other topics in space physics
8732L	<i>Light detection; adaptation and discrimination</i>	9263	
8732N	<i>Colour detection; adaptation and discrimination</i>	9263	9500 FUNDAMENTAL ASTRONOMY AND
8732S	<i>Psychophysics of vision, visual perception, binocular vision</i>	9263	ASTROPHYSICS, INSTRUMENTATION AND
8734	Audition	9264	TECHNIQUES AND ASTRONOMICAL
8736	Speech	9264	OBSERVATIONS
8738	Mechano- and chemio-ceptions	9265	9311 Fundamental astronomy
8740	Biomagnetism	9265	9311 <i>Celestial mechanics</i>
8745	Biomechanics, biorheology, biological fluid dynamics	9266	9312 Fundamental aspects of astrophysics
8750	Biological effects of radiations	9266	9314 Observatories
8750B	<i>Interactions of biosystems with radiations</i>	9267	9315 Astronomical instruments
8750C	<i>Bioacoustics (sonic and ultrasonic effects on living matter)</i>	9267	9315 Auxiliary and recording instruments
8750E	<i>Bio-optics (effects of microwaves, light, laser and other electromagnetic waves)</i>	9267	9315 Other instrumentation and techniques
8750G	<i>Ionizing radiations (u.v., X-ray, gamma-ray; particle radiation effects)</i>	9268	9316 Techniques of observation and reduction
8760	Medical and biomedical uses of fields, radiations, and radioactivity	9270	9316 Astronomical observations (listed by techniques of observation)
8760B	<i>Sonic and ultrasonic radiation</i>	9270	9316 <i>Radio and radar</i>
8760D	<i>Electric and magnetic fields (d.c. and pulsed)</i>	9271	9316 <i>Far infrared (bolometric, photoconductive)</i>
8760G	<i>Laser beams, microwaves, and other electromagnetic waves</i>	9271	9316 <i>Photographic region (near infrared, visible, and normal ultraviolet)</i>
8760J	<i>Corpuscular radiation and radioisotopes</i>	9272	9317 <i>Space ultraviolet</i>
8760L	<i>Preparation of radioactive materials for medical and biomedical uses</i>	9273	9318 <i>X-ray</i>
8760M	<i>Radiation dosimetry</i>	9274	9318 <i>gamma-ray and elementary particle</i>
8760P	<i>Radiation protection</i>	9274	9318 <i>Other (inc. gravitational radiation, magnetograms, etc)</i>
8760R	<i>Radioactive pollution</i>	9274	9318 Catalogues, atlases etc
8765	Aerospace biophysics and medical physics (effects of accelerations, weightlessness and environment)	9276	9318 Other topics in astronomy and astrophysics
8770	Biomedical engineering	9276	9600 SOLAR SYSTEM
8770E	<i>Diagnostic methods and instrumentation</i>	9276	9610 General, solar nebula, and cosmogony
8770G	<i>Patient care and treatment</i>	9277	9620 Moon
8770J	<i>Prosthetics and other practical applications</i>	9278	9630 Planets and satellites
8780	Biophysical instrumentation and techniques	9278	9630D <i>Mercury</i>
8790	Other topics in biophysics, medical physics, and biomedical engineering	9279	9630E <i>Venus</i>
9000	GEOPHYSICS, ASTRONOMY AND ASTROPHYSICS	9279	9630G <i>Mars</i>
9100	SOLID EARTH GEOPHYSICS	9279	9630H <i>Asteroids</i>
9110	Geodesy and gravity	9279	9630K <i>Jupiter</i>
9125	Geomagnetism and palaeomagnetism; geoelectricity	9280	9630M <i>Saturn</i>
9130	Seismology	9281	9630T <i>Other planets</i>
9135	Earth's interior structure and properties	9282	9650 Other objects in the planetary system
9140	Volcanology	9284	9650D <i>Interplanetary matter, magnetic and electric fields</i>
9145	Physics of plate tectonics	9284	9650G <i>Comets</i>
9150	Marine geology and geophysics	9285	9650K <i>Meteors, showers and meteoroids</i>
9160	Physical properties of rocks and minerals	9285	9650M <i>Meteorites, micrometeorites</i>
9165	Geophysical aspects of geology, mineralogy and petrology	9286	9660 Solar physics
9190	Other topics in solid Earth geophysics	9286	9690 Other topics on the solar system
9200	HYDROSPHERIC AND ATMOSPHERIC GEOPHYSICS	9287	9700 STARS
9210	Physics of the oceans	9287	9710 Stellar characteristics
9220	Interdisciplinary aspects of oceanography	9290	9720 Normal stars (by class): general or individual
9240	Hydrology and glaciology	9291	9730 Variable and peculiar stars
9260	Meteorology	9292	9760 Late stages of stellar evolution
9260S	<i>Climatology</i>	9298	9760B <i>Supernovae</i>
9265	Atmospheric optics	9298	9760G <i>Pulsars</i>
9290	Other topics in hydrospheric and atmospheric geophysics	9299	9760J <i>Neutron stars</i>
9300	GEOPHYSICAL OBSERVATIONS, INSTRUMENTATION, AND TECHNIQUES	9299	9760L <i>Black holes</i>
9330	Information related to geographical regions	9299	9780 Binary and multiple stars
9355	International organizations, national and international programs	9301	9790 Other topics in stellar astronomy
9365	Data acquisition and storage	9301	9800 STELLAR SYSTEMS; GALACTIC AND
9385	Instrumentation and techniques for geophysical research	9301	EXTRAGALACTIC OBJECTS AND SYSTEMS;
9400	AERONOMY AND SPACE PHYSICS	9304	THE UNIVERSE
9410	Physics of the neutral atmosphere	9304	9335 Stellar dynamics
9410Q	<i>Airglow and nightglow</i>	9304	9335 Stellar clusters and associations
9410S	<i>Aurora</i>	9305	9336 Interstellar matter; and nebulae
9420	Physics of the ionosphere	9305	9338 The Galaxy, extragalactic objects and systems
9430	Physics of the magnetosphere	9307	9342 <i>Groups, clusters, superclusters</i>
9440	Cosmic rays	9310	9342 Other objects and background radiations of unknown origin and distances
9440C	<i>Origin and propagation outside the solar system</i>	9310	9342 <i>Discrete radio sources</i>
9440E	<i>Interplanetary propagation and effects</i>	9310	9343 <i>Quasars</i>
9440H	<i>Energetic solar particles and photons</i>	9310	9343 <i>IR sources</i>
9440K	<i>Solar modulation and geophysical effects</i>	9310	9343 <i>X-ray and gamma-ray sources</i>
9440L	<i>Composition and energy spectra</i>	9310	9343 <i>Cosmic ray sources</i>
9440N	<i>Extensive air showers</i>	9310	9344 <i>Background radiations</i>
9440R	<i>High-energy interactions</i>	9310	9344 Cosmology
9440T	<i>Muons and neutrinos</i>	9310	9344 Other topics in galactic and extragalactic astronomy
9440V	<i>Cosmic-ray effects in meteorites and terrestrial matter</i>	9310	

AUTHOR INDEX

xvii

followed by

SUBSIDIARY INDEXES

SUBJECT GUIDE

The SUBJECT GUIDE is an alphabetical index to subjects covered in the classification scheme, by which the abstracts are arranged. The numbers given are classification codes. The CLASSIFICATION AND CONTENTS, which precede the Guide, gives the page number for each section.

	Classification		Classification		Classification
A mesons	1440	Atomic polarisability	3510D	Boson systems	0530
Ab initio calculations	3120	Atomic spectra	32	Boundary layer flow	4715C, 4725F
Aberrations	4180, 4230, 4278	Atomic structure	31, 3510	Boundary layer turbulence	4725F
Abrasion	4630P, 6220P, 8140P	Atomic transitions	3110	Brain	87
Absorptive models	1240P	Atoms	30	Bremsstrahlung	0350, 41, 7870
Acceleration measurement	0630G	Audition	8734	Brillouin spectra	3320F, 4265C, 5170, 7835
Accumulation layers	7320, 7340Q	Auger effect	3280H, 7920F, 7920N, 7960, 8260	Brillouin zones	6320, 7125
Acoustic devices	4385	Aurora	9410S	Brink model	2160G
Acoustic holography	4363	Autoionisation	3280D, 3380E	Brittleness	4630N, 6220M, 8140N
Acoustic noise	4350, 4360, 4388, 8670J	Axial vector currents	1140	Brownian motion	0540
Acoustic nuclear magnetic resonance	7660	Axiomatic field theory	1110	Bubble chambers	2940
Acoustic paramagnetic resonance	7630			Buckling	4630L, 6220F, 8140L
Acoustic properties of gases	5140				
Acoustic properties of liquids	6260				
Acoustic properties of solids	6265				
Acoustic signal processing	4360				
Acoustic wave propagation	4320, 4325, 5140, 6260, 6265				
Acoustics	43	B mesons	1440	C invariance	1130
Acousto-optical effects	5140, 5170, 7820H	Background radiation	9870V	Calibration	0620H
Acoustoelectric effects	4388, 5140, 5150, 7250	Band model of magnetism	7510L	Calorimetry	0720F
Adaptive optics	42	Band structure	7125	Cameras	0768
Adherence	4630P	Barkhausen effect	7560E	Capillarity	6810
Adhesion	4630P, 6825, 8190	Barrier heights	3520J	Carbon dioxide lasers	4255D, 4260
Adsorption	6845, 8265	Baryon-baryon interactions	1375C, 1375E, 1385	Cardiology	87
Aerodynamics	4740	Baryon-baryon scattering	1375C, 1375E, 1385	Carrier density	7220
Aeroelasticity	4630C, 4630M	Baryon decays	1330	Carrier lifetime	7220J
Aeronomy	94	Baryon electric moment	1340F, 1420	Carrier mobility	7220
Aerosols	4755K, 8270, 92	Baryon-kaon interactions	1375J, 1385	Casting	8120, 8130F
Aerospace	9480, 9555	Baryon-kaon scattering	1375J, 1385	Catalogues	9585
Aerospace biophysics	8765	Baryon magnetic moment	1340F, 1420	Cathodochromism	7820
Ageing	8140Q	Baryon mass	1420	Cathodoluminescence	7860H
Airglow	9410Q	Baryon parity	1420	Cavitation	4755B
Algebra	0210	Baryon-pion interactions	1375G, 1385	Celestial mechanics	0320, 9510C
Alpha decay	2360	Baryon-pion scattering	1375G, 1385	Cells (electric)	8630D
Alpha particle-nucleus reactions	2560	Baryon production	1360P, 1365, 1375, 1385	Cellular biophysics	8725
Alpha particle-nucleus scattering	2560	Baryon resonance production	1360P, 1365, 1375, 1385	Ceramic preparation	8120L, 8120N
Alpha particle spectroscopy	2930	Baryon resonances	1420	Ceramics	81
Alpha particles	2140, 2710	Baryon spin	1420	Cermets	81
Amorphous semiconductors	6140, 7125M, 7220, 7280N	Baryons	1420	CESR	7630P
Amorphous state	6140, 81	BCS theory	2160, 7420F	Chalcogenide glasses	6140D, 7280N
Anderson model	7110, 7125M, 7155	Beam-foil excitation	3450H	Channel flow	4760
Anelasticity	4630J, 6240, 8140J	Beam-foil ionisation	3450H	Channelling	6180M
Anemometers	4780, 9385	Beam handling equipment	2925	Chaos	0540
Angular measurement	0630C	Beam handling techniques	2925	Charge density waves	7145, 7215N
Annealing	8140E, 8140G	Bending	4630J, 6220F, 8140L	Charge exchange	3470
Anodisation	8160, 8245	Beta decay	2340	Charge ordered states	7145, 7150
Antiferromagnetism	7530	Beta ray spectroscopy	2930	Charge transfer	3470
Antiferroelectric materials	7780	Betatrions	2920	Charge transfer reactions	8230
Antiferromagnetic properties of substances	75, 7550E	Bethe-Salpeter equations	1110	Charge transfer states	31, 7170C
Antiferromagnetic resonance	7650	Bi-metric gravity theories	0450	Charm particles	1420, 1440
Antiphase boundaries	81	Bibliographies	0130T	Chemical analysis	8280
Antiphase domains	81	Binary stars	9780	Chemical binding	3110, 3520G
Antireflection coatings	4270, 4278H, 4280	Binding energy	31, 3520V, 6150L	Chemical energy conversion	8630Q
Appearance potential spectroscopy	0785, 7870E	Bio-optics	8750E, 8760G	Chemical energy storage	8640H
APW calculations	7110, 7125C	Bioacoustics	8738, 8750B, 8750C, 8760B	Chemical kinetics	8220
Architectural acoustics	4355	Biocommunications	87	Chemical lasers	4255K, 4260, 8240
Artificial limbs	8770J	Biocontrol	8710	Chemical reactions	3450L, 8230, 8235, 8240
Artificial organs	8770J	Biocybernetics	8710	Chemical shifts	3325, 7660C
Association	6120, 6125, 8230	Bioelectric phenomena	8730, 8732E	Chemical thermodynamics	8260
Asteroids	9630H	Bioenergy conversion	8630Z	Chemical vapour deposition	6855, 8115H
Astroarchaeology	9590	Biography	0150	Chemiluminescence	5170, 7860P, 8240
Astrometry	95, 9555	Biological effects of radiation	8750	Chemoception	8738
Astronomical instruments	95	Biological fluid dynamics	8745	Chemisorption	6845, 8265
Astronomy and astrophysics	95, 96, 97, 98	Biological techniques and instruments	8780	Cherenkov detectors	2940
Atlases	9585	Biology	87	Cherenkov radiation	41
Atmospheric acoustics	4328	Biomagnetism	8740, 8760D	Chiral symmetries	1130
Atmospheric optics	9265	Biomass	8630Z	Cholesteric liquid crystals	6130, 6470M
Atmospherics	9260, 94	Biomechanics	8745	CI calculations	3120T
Atom beam reactions	8240D	Biomedical engineering	8770	CIDEP	3330
Atom-surface impact	34, 7920N, 7920R	Biomedical equipment	8770	CIDNP	3325
Atomic beams	3440, 3450, 3580, 8240D	Biomedical measurement	8770	Cinematography	0768
Atomic clusters	3640	Biomedical ultrasonics	8760G	Claddings	8160
Atomic collisions	34	Biomedical uses of radiation and radioactivity	8760	Classical field theory	0350
Atomic electric moments	3510D	Biomembrane transport	8720, 8725D	Classical mechanics	0320, 0340
Atomic electron correlations	3120T	Biomembranes	8720	Classical statistical mechanics	0520
Atomic electron impact excitation	3480	Biomolecular effects of radiation	8715M, 8750	Clebsch-Gordon coefficients	0365
Atomic electron impact ionization	3480	Biomolecular structure	3620, 8715B	Climatology	9260
Atomic excited states	3150	Biophysical techniques and instruments	8780	Cloud chambers	2940
Atomic fine structure	3510F	Biophysics	87	Clouds	9260
Atomic fluorescence	3250	Biorheology	8745	Cluster approximation	7110, 7125M
Atomic forces	3420	Biothermics	8716	CNDO calculations	3120N
Atomic hyperfine interactions	3130	Biotransport	8725D, 8745	CO ₂ lasers	4255D, 4260
Atomic hyperfine structure	3510F	Birefringence	4210, 4220, 7820F	Coal	8610B
Atomic inelastic collisions	3450	Black holes	9760L	Coating techniques	6855, 8115, 8160
Atomic magnetic moments	3510D	Blood	87	Coatings	6855, 8115, 8160
Atomic mass	3510B	Bolometers	0720, 0762	Coercivity	7560, 7780
Atomic orbital calculations	3120	Boltzmann equation	0560	Coherent antiStokes Raman scattering	3320F, 4265C, 7830
Atomic orbitals	3120	Bond angles	3520D	Cold working	8140E
Atomic phosphorescence	3250	Bond lengths	3520D	Collective accelerators	2915
Atomic physics	30	Bond strength	3520G	Colloids	4755K, 8270
		Bonds (chemical)	31, 3520G, 6150L	Colorimetry	0760D
		Bone	87	Colour centre lasers	4255R, 4260, 6170D
		Bootstrapping	1150, 1240F	Colour centres	6170D, 7155, 7630M, 7850
		Bose-Einstein statistics	0530	Colour model	1235C
				Colour vision	8732N
				Comets	9650G

	Classification
Commensurate-incommensurate transformations	0570, 6460, 6470K, 7780B
Compaction	8120E
Complex angular momentum plane	1160
Composite material preparation	8120J, 8120N, 8120Q, 8120T
Composite materials	81
Composite particle models	1235
Compressibility	4630J, 51, 6210, 6220F, 8140L
Compressible flow	4740
Compton effect	1360F, 6180C, 6180E, 7870
Computerised tomography	8760J, 8770E
Configuration interactions	3120T
Conformational dynamics	3520J
Conservation laws	1130
Constrained heat transfer	4425
Contact lenses	8732, 8770J
Continuous media mechanics	4620, 4630
Convection	0560, 4425, 4725Q, 5130
Conversion electron spectra	2320N
Correlation times	3520Y
Corrosion	8160, 8160B
Corrosion protective coatings	8160, 8160B
Corrosion testing	8170
Cosmic dust	9840
Cosmic ray interactions	1385M, 9440
Cosmic ray-nucleus reactions	2590, 9440R
Cosmic rays	9440, 9870S
Cosmogony	9610
Cosmology	9880
Cottrell atmospheres	6170G, 6170J, 6170L
Couette flow	4730
Coupled channel theory	2410
CP invariance	1130
CPA calculations	6350, 7110, 7125
CPT invariance	1130
Crack detection	8170
Cracks	4630N, 6220M, 8140N
Crazing	6220M, 8140N, 8160
Creep	4630J, 6170L, 6220H, 8140L
Creep testing	8170
Critical points	0570, 6460, 6470, 8260
Crossing symmetries	1150
Cryogenics	0720M
Crystal binding	6150L
Crystal defects	6170
Crystal field theory	7170C, 7510D
Crystal growth	6150C, 8110
Crystal growth from melt	6150C, 8110F
Crystal growth from solution	6150C, 8110D
Crystal growth from vapour	6150C, 8110B
Crystal hyperfine field interactions	7170, 7510D
Crystal inclusions	6170, 8130, 8140
Crystal microstructure	6170, 6480, 8130, 8140
Crystal morphology	6150J
Crystal purification	8110
Crystal structure	61
Crystal structure of alloys	6155H
Crystal structure of elements	6155D, 6155F
Crystal structure of inorganic compounds	6160
Crystal structure of organic compounds	6165
Crystal surface and interface vibrations	6830
Crystal symmetry	6150E
Crystallisation	6140, 6150C, 6470D
Crystallographic shear	6170P
Crystallography	61
Curie temperature	7530K, 7540, 7780B
Current algebra	1140
CVD coatings	6855, 8115H, 8160
Cyclic accelerators	2920
Cyclotron resonance	7125, 7640
Cyclotrons	2920
D mesons	1440
De Haas-van Alphen effect	7125
Debye temperature	6370
Debye-Waller factors	6370
Decomposition	6475, 8130
Deep levels	7155
Defect electron energy states	7155
Defibrillators	8770G, 8770J
Deformation	0340, 4630, 6220F, 8140L
Degenerate semiconductors	7220, 7280
Dendrites	6870
Dendritic structure	8130, 8140
Densitometry	0768
Density measurement	0630E
Density of liquids	6210
Density of solids	6220, 8190
Desorption	6845, 8265
Detonation	4740, 8240
Deuteron-nucleon interactions	1375C, 1385
Deuteron-nucleon scattering	1375C, 1385
Deuteron-nucleus reactions	2550
Deuteron-nucleus scattering	2550
Deuterons	2140, 2710
Diamagnetic properties of substances	5160, 7520
Dibaryons	1420
Dichroism	3345, 7820F

	Classification
Dictionaries	0130K
Dielectric function	7145G, 7820D
Dielectric hysteresis	7780D
Dielectric losses	7740
Dielectric measurement	0750
Dielectric polarisation	5150, 7730
Dielectric properties of substances	77
Dielectric relaxation	5150, 7740
Dielectric resonance	7785
Dielectric thin films	7755
Differential geometry	0240
Diffraction gratings	4280F
Diffraction models	1240S
Diffuse spectra	3380G
Diffusion	0560
Diffusion in gases	5110, 5120
Diffusion in liquids	6610
Diffusion in solids	6630
DIM method	3120G
Dingle temperature	7125, 7520
Diode lasers	4255P, 4260
Dirac equation	0365
Direct nuclear reactions	2450
Discharges (electric)	5280
Disclinations	6130, 6170G, 6170J, 6170L
Discrete system mechanics	4610
Dislocations	6170G, 6170J, 6170L
Disperse systems	8270
Dispersion hardening	8140C
Dispersion relations	0210, 1120, 1150
Displacive transformations	6375, 6470K, 7780B
Dissociation	3380G, 3480G, 8230
Dissociation energies	3520G
Distorted wave Born approximations	2410
Distributed Bragg reflector lasers	4260, 4282
Distributed feedback lasers	4260, 4282
Domains	8130, 8140
Doping profiles	6170W
Dosimeters	2940, 2970
Dosimetry	2880, 8760M
Double NMR	3335, 7670F
Double resonances	3335, 7670
Drawing (mechanical)	6220F, 8120, 8140L
Drift chambers	2940
Dual models	1240H
Duct flow	4760
Ductility	4630J, 6220F, 8140L
Dye lasers	4255M, 4260
Dynamic nuclear polarisation	3335, 7670E
Dynamic testing	8170
Dynamical symmetries	1130
Dynamics	0320
Ear	8734
Earth	90
Earthquakes	9130
ECG	8730, 8770
Echelles	4280F
Eclipses	95, 9620, 9660
Ecology	8660
Education	0140, 0150
Educational aids	0150
Educational computer use	0150
EEG	8730, 8770
Eikonal models	1240P
Einstein equation	0420
Einstein-Maxwell fields	0440, 0450
Elastic constants	6220D
Elastic deformation	4630C, 6220F, 8140J
Elastic waves	0340K, 4630M, 6230
Elasticity	0340D, 4630C, 6220, 8140J
Elastomers	3620, 6140K, 81
ELDOR	3335, 7670K
Electron correlations	3120T
Electrets	7730
Electric breakdown	5280, 7750
Electric charge	4110D
Electric discharges	5280
Electric domains	7780D
Electric fields	4110
Electric moments	2110K
Electrical conductivity of gases	5150
Electrical conductivity of liquids	6610, 72
Electrical conductivity of solids	72
Electrical conductivity transitions	7260
Electrical phenomena in gases	5150
Electrical properties of substances	5150, 72, 8140R
Electrical variables measurement	0750
Electricity	41
Electro-optical effects	3345, 5170, 7820J
Electrocardiography	8730, 8770
Electrochemical analysis	8280
Electrochemical energy conversion	8630D
Electrochemistry	8245
Electrodeposition	6855, 8115L, 8160, 8245
Electrodynamics	0350, 4170
Electroencephalography	8730, 8770
Electroforming	8120, 8245
Electrogasdynamic conversion	8630L
Electrohydrodynamics	4765

	Classification
Electrojet	94
Electroluminescence	7860F
Electrolysis	8245, 8630D
Electrolytic polishing	8160, 8170
Electromagnetic corrections	1340H
Electromagnetic decays	1340H
Electromagnetic fields	4110
Electromagnetic induction	4110F
Electromagnetic interaction models	1220
Electromagnetic wave propagation	4110H
Electromagnetic waves in plasma	5240D
Electromagnetism	0350, 4110
Electromigration	6610, 6630Q
Electron affinity	3510H, 3520V
Electron beam deposition	8155G
Electron beam effects	51, 6180F
Electron beams	4180D
Electron capture decay	2340
Electron diffraction crystallography	6114
Electron-electron interactions	1310, 1365
Electron-electron scattering	1310
Electron emission	79
Electron energy states (condensed matter)	71
Electron field emission	7970
Electron gas	0530, 7145
Electron-hadron interactions	1360
Electron-hadron scattering	1360F
Electron-hole drops	7135, 7855
Electron-hole recombination	7220J
Electron impact	3480, 7920
Electron lenses	4180D
Electron microscopes	0780
Electron microscopy	0780, 6116D
Electron-nucleus reactions	2530
Electron-nucleus scattering	2530
Electron optics	4180D
Electron-phonon interactions	6320K, 7138, 72, 7420
Electron-positron interactions	1310, 1365
Electron-positron scattering	1310
Electron probe analysis	8280
Electron radiation	41
Electron ring accelerators	2915
Electron scattering	3480
Electron sources	2925
Electron spectra	3365, 3480, 79
Electron spectroscopy	0780, 2930, 3365, 79, 8280
Electron spin polarisation	75
Electron traps	7155, 7220J
Electronic conduction in thin films	7360
Electronic density of states	7120
Electronic excitation	3450H
Electronic ionisation	3450H
Electrons	1460
Electrophoresis	8245
Electrophoretic coatings	6855, 8115L, 8160
Electrophysiology	8730, 8732E
Electroplating	8115L, 8160
Electropolishing	8160, 8170
Electrostatic accelerators	2915
Electrostatic coatings	8115, 8160
Electrostatic lenses	4180
Electrostatics	4110D
Electrostriction	7760
Electroviscous effect	6210, 6620, 8270
Elemental abundance	3510B
Elemental semiconductors	7220, 7280C
Elementary particle electric moments	1340F
Elementary particle form factors	1340F
Elementary particle inclusive interactions	1310, 1360H, 1365, 1385K
Elementary particle magnetic moments	1340F
Elementary particle polarisation	1388
Elementary particle symmetries	1130
Ellipsometry	0760F
Embrittlement	6220M, 8140N
Emissivity	6590
ENDOR	3335, 7670D
Energy conversion	8630
Energy gap	7125, 74
Energy loss of particles	2970, 6180M
Energy range relationships	2970
Energy research	86
Energy resources	8610
Energy storage	8640
Enthalpy	0570, 6550, 8260
Entropy	0570, 5130, 6550
Epitaxial growth	6855, 8115
Epitaxial layers	6855, 6860
EPR	3330, 7630
Equations of state	0570, 5110, 6410, 6430
Eta meson resonances	1440
Eta mesons	1440
Etching	6170J, 8160, 8170
Euclidean field theory	1110
Eutectic structure	8130, 8140
Evaporation	6470F
Evolution (biological)	8790
EXAFS	3220R, 3320R, 7870D
Exchange interactions (electron)	7170G, 7530E
Excimer lasers	4255F, 4255H, 4260

Classification		Classification	
Excitons	7135	Gamma-ray sources	2925
Exoelectron emission	7975	Gamma-ray sources (astronomical)	9870Q
Exosphere	94	Gamma-ray spectra	2320, 7680
Exotic atoms	3610	Gamma-ray spectroscopy	2930
Exotic molecules	3610	Gamma ray transitions	2320
Explosions	4740, 4770, 8240	Garnets	7550G
Extraterrestrial life	8790, 9590	Gas lasers	4255D, 4255F, 4255H, 4260
Eye	8732	Gases	50
Eye anatomy and optics	8732C	Gauge field theory	1110
Eye physiology	8732E	Gegenschein	9650D
		Geiger counters	2940
		Gels	8270
F mesons	1440	General relativity	0420
Faddeev equation	1180	Generalised Huckel calculations	3120P
Fallout	2870, 2880, 9260, 94	Generator coordinate method	2160E
Faraday effect	7820L	Geodesy	9110
Fatigue	4630N, 6220M, 8140N	Geoelectricity	9125
Fatigue testing	8170	Geographical regions	9330
Fermi-Dirac statistics	0530	Geology	9165
Fermi level	7125	Geometrical optics	42
Fermi surface	7125H	Geometry	0240
Fermion systems	0530	Geophysical equipment	9385
Ferrimagnetic properties of substances	75, 7550G	Geophysics	91, 92, 93
Ferrimagnetic resonance	7650	Geothermal energy	8610H
Ferrites	7550G	Giant stars	9720
Ferroacoustic resonance	7125, 7255, 7580	Ginzburg-Landau theory	7420
Ferroelectric semiconductors	7220, 7780	Glaciology	9240
Ferroelectricity	7780	Glass	4270C, 6140D, 81
Ferromagnetic properties of substances	75, 7550B, 7550C, 7550D	Glass preparation	8120P, 8120Q
Ferromagnetic resonance	7650	Glass transitions	6470P
Few nucleon systems	2140	Glauber model	2410H
Fibre optics	4280M	Glauber scattering	1180
Fibre reinforced composites	81	Gluons	1480
Field emission electron microscopy	0780, 6116D	GO calculations	3120
Field emission ion microscopy	0780, 6116F	Graded Lie algebras	1130
Field ion emission	7970	Grain boundaries	6170N, 8130, 8140
Filtration	4755M	Grain size	8130, 8140
Fission breeder reactors	2850	Granular structure	81
Fission counters	2940	Graph theory	0210
Fission-fusion reactor systems	2858	Gravimeters	9385
Fission power reactors	2850	Gravitation	04, 9530
Fission reactor design	2841	Gravitational collapse	0440, 9530, 9760
Fission reactor fuel	2842	Gravitational constants	0490
Fission reactor fuel preparation	2842H	Gravitational experiments	0480
Fission reactor fuel reprocessing	2842H	Gravitational interaction models	1225
Fission reactor materials	2842	Gravitational radiation	0430, 0480
Fission reactor operation	2843	Gravitational waves	0430, 0480
Fission reactor safety	2844	Gravity	0320, 9110
Fission reactor theory	2841	Grinding	4285, 8120, 8160
Fission reactor waste	2842	Group theory	0220, 0365, 1130
Fission research reactors	2850	Guided electromagnetic wave propagation	0320, 4110H
Flames	8240	Guided light propagation	4280L
Flexoelectricity	6130, 7760	Gunn effect	7220H
Flow	47	H I regions	9840
Flow birefringence	5170, 7820F	H II regions	9840
Flow instrumentation	4780	Hadron calorimeters	2970
Flow measurement	4780	Hadron classification schemes	1240K
Flow separation	4755	Hadron-electron interactions	1360
Flow stability	4720	Hadron-electron scattering	1360F
Flow through porous media	4755M	Hadron-hadron interactions	1375, 1385
Flowmeters	4780	Hadron-hadron scattering	1375, 1385
Fluctuations	0540	Hadron-muon interactions	1360
Fluid dynamics	0340G, 47	Hadron-muon scattering	1360F
Fluid kinetic theory	5110	Hadron-nucleus reactions	2540, 2580
Fluid mechanics	0340G, 47	Hadron-nucleus scattering	2540, 2580
Fluid rheology	4660	Hadron-photon interactions	1360
Fluid transport theory	5110	Hadron-photon scattering	1360F
Fluorescence	3250, 3350, 7855	Hadronic decays	1325, 1330
Fluxmeters	0755	Haemodynamics	8745
Foams	8270	Half lives	23
Folding models	2410H	Hall effect	7215G, 7220M
Forming processes	8120	Hardening	8140C, 8140E, 8160
Fossil fuels	8610B	Hardness	4630P, 6220M, 6825, 8140N
Fourier transform optics	4230	Hardness testing	8170
Fracture	4630N, 6220M, 8140N	Harmonic generation	4265C, 4325, 4360
Fracture toughness testing	8170	Harmonic oscillators	0365
Fragmentation reactions	2450	Hartree-Fock approximation	2160J, 3120D, 3120G, 7110
Free-electron approximation	7110, 7125C	Hawking effects	0460
Free electron lasers	4255T, 4260	Health hazards	8750, 8760R, 8790
Free energy	0570, 5130, 64, 6550	Health physics	8760
Free molecular flows	4745	Hearing	8734
Free radicals	30, 7630R, 8230, 8250	Hearing aids	8734, 8770J
Frenkel defects	6170B	Heat capacity	4450
Friction	4630P, 6220P, 8140P	Heat conduction	4410
Fuel cells	8630G	Heat engines	8630R
Functional analysis	0230	Heat exchanges	8630R
Functions	0230	Heat flow	44
Fusion reactions	2588	Heat pumps	8630R
Fusion reactor plasma confinement	5255	Heat radiation	4440
Fusion reactors	2852	Heat transfer	44, 4725Q
		Heat treatment	8140G
Galaxies	9850	Heavily doped semiconductors	7220, 7280
Galaxy	9850	Heavy ion-nucleus reactions	2570
Galvanomagnetic effects	7215G, 7220M	Heavy ion-nucleus scattering	2570
Gamma ray angular distributions	2320	Heavy leptons	1460
Gamma ray astronomy	95	Heavy particle spectroscopy	2930
Gamma-ray effects	5170, 6180E	Heisenberg model	7510J, 7540F
Gamma-ray lasers	4255	Helicity	1130
Gamma ray mixing ratios	2320	Helicons	7230
		Helium 3-nucleus reactions	2560
		Helium 3-nucleus scattering	2560
		Higgs bosons	1480
		High-energy cosmic ray interactions	1385M, 9440
		High field effects	7220H
		High-frequency effects	7230
		High pressure effects in solids	6250
		High pressure techniques	0735
		High temperature techniques	0720K
		History	0160, 0165
		Hodoscopes	2970
		Hole traps	7155, 7220J
		Holography	4240
		Hopping conduction	7220F
		Hot carriers	7220H, 7230
		Hot working	8140G
		Hubbard model	7110, 7510L
		Huckel calculations	3120P
		Humidity	51, 9260
		Hybrid reactors	2858
		Hydroelasticity	4630C, 4630M
		Hydroelectric power	8610F
		Hydrogen bonds	3520G
		Hydrogen economy	8640K
		Hydrogen embrittlement	6220M, 8140N, 8160
		Hydrogen power	8640K
		Hydrogen production	8640K
		Hydrogen storage	8640K
		Hydrology	9240
		Hydrosphere	92
		Hygrometry	0725
		Hypernuclei	2180
		Hyperon decays	1330
		Hyperon-kaon interactions	1375J, 1385
		Hyperon-kaon scattering	1375J, 1385
		Hyperon-nucleon interactions	1375E, 1385
		Hyperon-nucleon scattering	1375E, 1385
		Hyperon-nucleus reactions	2580
		Hyperon-nucleus scattering	2580
		Hyperon-pion interactions	1375G, 1385
		Hyperon-pion scattering	1375G, 1385
		Hyperon resonances	1420
		Hyperons	1420
		Hypersonic flows	4740K
		Hypothetical particles	1480
		II-VI semiconductors	7220, 7280E
		III-V semiconductors	7220, 7280E
		III-VI semiconductors	7220, 7280
		Image convertors, detectors & intensifiers	4280Q
		Image processing	4230, 9575
		Impact ionisation	7220H
		Impurities	6170R, 6170T, 6170W
		Impurity and defect absorption spectra of solids	7850
		Impurity electron states	7155
		Inclusions	6170, 8130, 8140
		Indeterminacy	0365
		INDO calculations	3120N
		INDOR	3335
		Inert gas lasers	4255F, 4260
		Infrared astronomy	95
		Infrared detectors	0730, 0762
		Infrared imaging	0720, 4280Q, 8760G
		Infrared sources (astronomical)	9870L
		Infrared spectra	3220B, 3320E, 7830
		Injection lasers	4255P, 4260
		Injector acceleration	2910
		Inner-shell ionisation	3280H
		Instrumentation	06, 07
		Insulating thin films	7360H
		Integral radiation detectors	2970
		Integrated optics	4282
		Interacting boson model	2160E, 2160F
		Interatomic angles	3520D
		Interatomic distances	3520D
		Interatomic forces	3420
		Interatomic potentials	3420
		Interface phenomena	68, 7340
		Interferometry	0760L, 9575
		Intergalactic matter	9850
		Intermediate boson decay	1390
		Intermediate bosons	1230, 1480
		Intermediate state	7455
		Intermolecular forces	3420
		Intermolecular mechanics	3420
		Intermolecular potentials	3420
		Internal conversion	3250
		Internal friction	6170L, 6240, 8140J
		Internal rotation	3520J
		Internal stresses	4630, 6220, 8140
		Internal symmetries	1130
		Interplanetary matter	9460, 9650D
		Interstellar matter	9840
		Interstitials	6170B
		Inversion	3520J
		Inversion layers	7320, 7340Q
		Ion-atom collisions	34
		Ion beam effects	6180J
		Ion beams	4180G

	Classification
Ion emission	79
Ion implantation	6170T, 6180J
Ion lasers	4255F, 4255H, 4260
Ion microscopes	0780
Ion microscopy	0780, 6116F
Ion-molecule collisions	34
Ion optics	4180G
Ion plating	8115J, 8160
Ion pumps	0730C
Ion recombination	34
Ion sources	0777, 2925
Ion-surface impact	7920N
Ionic conduction in solids	6630
Ionisation	52, 5280, 79
Ionisation counters	2940
Ionisation gauges	0730D
Ionisation potentials	3510H, 3520V
Ionoluminescence	7860H
Ionosphere	9420
Irreversible thermodynamics	0570
Ising lattices	0550
Ising model	7510H, 7540D
Isobaric analog resonances	2430
Isobaric analog states	2430
Isotope effects	3130
Isotope enrichment	2842H
Isotope separation	2842H, 3510B
Isotopes	30, 3510B
Isotropic turbulence	4725C
IV-VI semiconductors	7220, 7280
Jahn-Teller effect	3130, 7170C
Jets	4755C
Josephson effect	7450
Joule-Thomson effect	5130
Junction lasers	4255P, 4260
Jupiter	9630K
K-harmonics model	2160G
Kaon absorption	2580
Kaon-baryon interactions	1375J, 1385
Kaon-baryon scattering	1375J, 1385
Kaon capture	2580
Kaon decays	1320, 1325
Kaon-nucleus reactions	2580
Kaon-nucleus scattering	2580
Kaons	1440
Kapitza resistance	6740, 6830
Kidney	87
Kinetic theory	0520
KKR calculations	7110, 7125C
Knight shift	7660C
Knock-on reactions	2450
Knudsen flow	4745
Kondo effect	7215Q, 7520H
Kronig-Penney model	7110, 7125C
Laboratory apparatus and techniques	0150, 0660, 0670, 07
Laminar flows	4715
Laminates	81
Landau levels	7145
Laser accessories	4260
Laser beam applications	4260K
Laser beam effects	4260H, 6180B, 7920D
Laser beam modulation	4260F
Laser beam properties	4260H
Laser cavity resonators	4260D
Laser system design	4260B
Laser theory	4255B
Laser velocimeters	0630G, 4260K, 4780
Lasers	4255, 4260
Latent heat	0570, 64, 6550, 8260
Lattice constants	6150, 6155, 6160, 6165
Lattice dynamics	63
Lattice energy	6150L
Lattice field theory	1110
Lattice localised modes	6320P
Lattice phonons	6320
Lattice theory and statistics	0550
LCAO calculations	3120, 7110
Least squares analysis	0250
Lee model	1110
Lenses	4278
Lepton decays	1335
Lepton electromagnetic interactions	1310
Lepton-lepton scattering	1310
Lepton mass	1460
Lepton-nucleus reactions	2530
Lepton-nucleus scattering	2530
Lepton parity	1460
Lepton spin	1460
Lepton weak interactions	1310
Leptonic decays	1320, 1330, 1335
Leptons	1460
Level crossing	3280B, 3380B
Light	42
Light absorption	4210, 4220, 5170, 78
Light coherence	4210, 4220, 4250

	Classification
Light interference	4210, 4220
Light interferometry	0760L
Light modulation	4260F, 4280K
Light polarisation	4210, 4220
Light propagation	4210, 4220
Light scattering	4210, 4220, 5170, 78
Light sensitive materials	4270G
Light sources	4272
Light transmission	4210, 4220
Lightning	9260
Linear accelerators	2915
Lipid bilayers	8720, 8725
Liquid crystal phase transformations	6130, 6470M
Liquid crystals	6130
Liquid helium 3-4 mixtures	6760
Liquid helium-3	6750
Liquid helium	67
Liquid lasers	4255M, 4260
Liquid metal embrittlement	6220M, 8140N, 8160
Liquid phase epitaxial growth	6855, 8115L
Liquid semiconductors	6125, 7120, 7220, 7280P
Liquid structure	6120, 6125
Liquid theory	6120, 6130
Liquid-vapour transformations	6470F
Liver	87
Localized electron states	7150
Lorentz invariance	1130
Lorentz transformation	0330
Low energy electron diffraction	6114H, 6820
Low mass nuclear reactions	2510
Low temperature techniques	0720M
LPE	6855, 8115L
Lubrication	4630P, 6220P, 8140P
Luminescence	3250, 3350, 7855, 7860
Lung	87
Mach number	4740
Macromolecules	3620
Magnetic aftereffect	7560L
Magnetic anisotropy	7530G
Magnetic annealing	7560N, 8140E
Magnetic breakdown	7125H
Magnetic bubbles	7570K
Magnetic circular dichroism	3345C, 7820L
Magnetic cooling	0720M, 7530S
Magnetic domains	7560C, 7570K
Magnetic fields	4110
Magnetic hysteresis	7560E
Magnetic lenses	4180
Magnetic materials	75, 7550
Magnetic monopoles	1480
Magnetic phenomena in gases	5160
Magnetic properties of substances	5160, 75, 8140R
Magnetic relaxation	5160, 76
Magnetic resonance	3220B, 3325, 76
Magnetic resonance spectrometers	0758
Magnetic semiconductors	7220, 75
Magnetic storms	9430
Magnetic thin films	7570
Magnetic transitions	7530K, 7540
Magnetic traps	5255
Magnetic variables measurement	0755
Magnetisation	7430C, 7560
Magnetism	41, 5160, 75
Magneto-optical effects	3345, 5160, 5170, 7820L
Magnetoacoustic effects	5140, 5160, 7125, 7255, 7580
Magnetocaloric effects	7530S
Magnetocardiography	8740, 8760D
Magnetoelastic effects	7580
Magnetolectric effects	5150, 5160, 7580
Magneto hydrodynamic conversion	5230, 8630L
Magneto hydrodynamic waves	4765, 5235, 7230
Magneto hydrodynamics	4765, 5230
Magnetomechanical effects	7580
Magnetometers	0755, 9385
Magnetoresistance	7215G, 7220M
Magnetosphere	9430
Magnetostatic waves	75
Magnetostatics	4110D
Magnetostriiction	7580
Magnetrons	0750
Magnons	7530D, 7650
Majorana-Weyl fields	0450
Mandelstam representation	1150
Many-body problems	05, 9510C
Many-body reaction theory	2410
Marine geology	9150
Markov processes	0540
Mars	9630G
Martensitic transformations	6470K, 8130K
Masers	4252
Mass differences	1340D
Mass formulae	1240K, 1270
Mass spectra	3510B, 3520X
Mass spectrometers	0775

	Classification
Mass spectroscopic chemical analysis	8280
Mass transfer	0560
Materials preparation	8120
Materials science	81
Materials testing	8170
Mathematical computing	0270
Mathematics	02
Maxwell equations	0350, 4110
MBE	6855, 8115G
Measurement	06
Mechanical birefringence	4210, 7820F
Mechanical contact	4630P
Mechanical energy storage	8640C
Mechanical impact	4630P
Mechanical properties of substances	4630, 4660, 62, 8140
Mechanical property measurement	4630R
Mechanical strength	4630, 6220, 8140
Mechanical testing	8170
Mechanical waves	4630M, 6230
Mechanics	0320, 0340, 46
Mechanoception	8738
Medical diagnosis	8770E
Medical effects of radiation	8750
Medical physics	87
Medical uses of radiation and radioactivity	8760
Medicine	87
Meissner effect	7430C
Melting	6470D
Membrane biophysics	8720
Membranes	5120, 6610, 8265, 8720, 8725
Mercury (planet)	9630D
Meson absorption	2580
Meson capture	2580
Meson decays	1320, 1325
Meson electric moments	1340F, 1440
Meson magnetic moments	1340F, 1440
Meson mass	1440
Meson-meson interactions	1375L, 1385
Meson-meson scattering	1375L, 1385
Meson-nucleon interactions	1375, 1385
Meson-nucleon scattering	1375, 1385
Meson-nucleus reactions	2580
Meson-nucleus scattering	2580
Meson parity	1440
Meson production	1360K, 1365, 1375, 1385
Meson resonance production	1360M, 1365, 1375, 1385
Meson resonances	1440
Meson spin	1440
Mesons	1440
Mesosphere	9260
Metal corrosion	8160B
Metal-insulator boundaries	7340N
Metal-insulator-metal structures	7340R
Metal-insulator-semiconductor structures	7340Q
Metal-insulator transition	7130
Metal oxidation	8160B
Metal-semiconductor-metal structure	7340S
Metallurgy	8170
Metallurgy	81
Metamagnetism	7530K
Meteorites	9650M
Meteorology	9260
Meteors	9650K
Microphones	4385, 4388
Microscopes	0760P
Microtrons	2920
Microwave-optical double resonance	3335H, 7670H
Microwave spectra	3220B, 3320B, 7870G
Microwave spectrometers	0758, 0765
Mictomagnetism	7540
MINDO calculations	3120N
Mineralogy	9160
Mirrors	4278
Mixed conductivity	7260
Mixed state	7460E
Mixed valence states	7170C
Mixing	6475
Moderators	2842
Moire fringes	0760, 4210
Molecular beam epitaxial growth	6855, 8115G
Molecular beam reactions	8240D
Molecular beams	3440, 3450, 3580, 8240D
Molecular biophysics	8715
Molecular clusters	3640
Molecular collisions	34
Molecular configurations	3520B
Molecular dissociation	3380G, 3480G
Molecular dynamics	3520Y
Molecular electric moments	3520M
Molecular electron correlations	3120T
Molecular electron impact ionisation	3480G
Molecular electronic states	31
Molecular fine structure	3520S
Molecular fluorescence	3350
Molecular hyperfine interactions	3130
Molecular hyperfine structure	3520S
Molecular inelastic collisions	3450
Molecular magnetic moments	3520M

	Classification
Molecular magnetic susceptibility	3520M
Molecular moments	3520M
Molecular nuclear coupling	3325
Molecular orbitals	3120
Molecular orbitals calculations	3120
Molecular phosphorescence	3350
Molecular photodissociation	3380G
Molecular physics	30
Molecular polarisability	3520M
Molecular predissociation	3380G
Molecular rotation	3310, 3520P
Molecular rotation-vibration	3310, 3450E, 3520P
Molecular solids	3170K
Molecular spectra	3320
Molecular structure	31, 3520B
Molecular symmetry	3520B
Molecular transitions	3110
Molecular vibration	3310, 3520P, 6320, 7830
Molecule-surface impact	34, 7920N, 7920R
Molecules	30
Monochromators	0785, 4280D
Monolayers	6845, 8265
Monte Carlo methods	0250
Moon	9620
Morin temperature	7530K, 7540
Mossbauer effect	2430, 2520, 3340, 7680
Muffin-tin potential	7110, 7125C
Multi-Regge models	1240S
Multiperipheral models	1240S
Multiphase flow	4755K
Multiphoton spectra	3280K, 3380K
Multiple stars	9780
Multiwire proportional chambers	2940
Muon absorption	2530
Muon capture	2340, 2530
Muon-hadron interactions	1360
Muon-hadron scattering	1360F
Muon-nucleus reactions	2530
Muon-nucleus scattering	2530
Muon spin rotation	7690
Muons	1460
Muscle	87
Musical acoustics	4375
N/D method	1150
NDT	8170
Nebulae	9840
Neel temperature	7530K, 7540
Negative resistance	7220H
Nematic liquid crystals	6130, 6470M
Neptune	9630T
Neurophysiology	8730, 8732E
Neutral currents	1140, 1230
Neutrino interactions	1315
Neutrino-nucleus reactions	2530
Neutrino-nucleus scattering	2530
Neutrino scattering	1315
Neutrinos	1460
Neutron absorption	2540, 2820
Neutron diffraction crystallography	6112
Neutron diffraction examination of materials	6112, 7525
Neutron diffusion	2820
Neutron effects	51, 6180H
Neutron-hyperon interactions	1375E, 1385
Neutron-hyperon scattering	1375E, 1385
Neutron induced fission	2540, 2585
Neutron-kaon interactions	1375J, 1385
Neutron-kaon scattering	1375J, 1385
Neutron-meson interactions	1375, 1385
Neutron-meson scattering	1385
Neutron moderation	2820
Neutron-neutron interactions	1375C, 1385
Neutron-neutron scattering	1375C, 1385
Neutron-nucleus reactions	2540
Neutron-nucleus scattering	2540
Neutron physics	2820
Neutron-pion interactions	1375G, 1385
Neutron-pion scattering	1375G, 1385
Neutron-proton interactions	1375C, 1385
Neutron-proton scattering	1375C, 1385
Neutron radiative capture	2540
Neutron radiography	8170, 8760J
Neutron scattering	2820
Neutron sources	2925
Neutron spectroscopy	2930
Neutron stars	9760J
Neutron transport	2820
Neutrons	1420
Nightglow	9410Q
Nilsson model	2160C
NMR	3220B, 3325, 7430G, 7660
Nomenclature and symbols	01
Nomograms	0260
Non-Abelian fields	1110
Non-Newtonian dynamics	4750
Non-Newtonian flows	4750
Noncollisional ionisation	3490
Noncrystalline state structure	6140
Nondestructive testing	8170
Nonequilibrium flows	4770

	Classification
Nonhomogeneous flows	4755
Nonlinear acoustics	4325
Nonlinear field theory	1110
Nonlinear optics	4265
Nonlinear optics theory	4265B
Nonlinear symmetries	1130
Nonlocal field theories	1110
Normalising	8140G
Novae	9730
Nozzles	4755E
NQR	3325, 7660G
Nuclear backbending	2110, 2110H
Nuclear binding energy	2110D
Nuclear bombardment target	2925
Nuclear charge	2110F
Nuclear chemistry	8255
Nuclear cluster model	2160G
Nuclear collective levels	2110
Nuclear collective models	2160E
Nuclear collective resonances	2430
Nuclear Coulomb effects	2110
Nuclear cranking model	2160E
Nuclear decay	23
Nuclear deformation	2110F
Nuclear electric moments	2110K
Nuclear electromagnetic transitions	2320
Nuclear electronics	2960
Nuclear emulsions	2940
Nuclear energy	8610N
Nuclear energy level lifetimes	2320C
Nuclear energy level schemes	2110, 2110M
Nuclear energy level transitions	2320
Nuclear energy levels	2110, 2110M
Nuclear energy states	2110, 2110M
Nuclear engineering	28
Nuclear engineering computing	2841, 2980
Nuclear explosions	2870
Nuclear fireballs	2460
Nuclear fission	2475, 2585
Nuclear forces	2130
Nuclear form factors	2110F
Nuclear g-factors	2110K
Nuclear giant resonances	2430
Nuclear hole states	2110
Nuclear information processing	2980
Nuclear instrument control	2980
Nuclear instrumentation	2880, 29
Nuclear isobaric spin	2110H
Nuclear magnetic moments	2110K
Nuclear magnetic resonance	3320B, 3325, 7430G, 7660
Nuclear mass	2110D
Nuclear matrix elements	2320
Nuclear matter	2165
Nuclear medicine	8760J, 8770
Nuclear models	2160
Nuclear optical model	2410H
Nuclear Overhauser effect	3335
Nuclear parity	2110H
Nuclear physics	20
Nuclear polarisation in liquids and solids	7660
Nuclear power	28
Nuclear pumped lasers	4255, 4260
Nuclear quadrupole resonance	3325, 7660G
Nuclear radius	2110F
Nuclear reaction models	2410
Nuclear reactions	24, 25
Nuclear resonance reactions	2430
Nuclear resonances	2430
Nuclear rotational bands	2110
Nuclear shape	2110F
Nuclear shell model	2160C
Nuclear single particle levels	2110
Nuclear size	2110H
Nuclear spectroscopic factors	2110J
Nuclear spin	2110H
Nuclear statistical models	2460
Nuclear structure	21
Nuclear structure models	2160
Nuclear transition probabilities	2320C
Nucleation	6150C, 64, 6855, 8140
Nucleon decays	1330
Nucleon-hyperon interactions	1375E, 1385
Nucleon-hyperon scattering	1375E, 1385
Nucleon-kaon interactions	1375J, 1385
Nucleon-kaon scattering	1375J, 1385
Nucleon-meson interactions	1375, 1385
Nucleon-meson scattering	1375, 1385
Nucleon-nucleon interactions	1375C, 1385
Nucleon-nucleon scattering	1375C, 1385
Nucleon-nucleus reactions	2540
Nucleon-nucleus scattering	2540
Nucleon-pion interactions	1375G, 1385
Nucleon-pion scattering	1375G, 1385
Nucleons	1420
Numerical analysis	0260
Numerical methods	0260
Observatories	9545
Occultations	9510
Oceanography	9210
Ohmic contacts	7340

	Classification
Oil	8610B
Omega mesons	1440
One-dimensional conductivity	7215N
One-meson exchange models	1240R
Opalescence	7820
Optical beam splitters	4280
Optical bistability	4265, 4280
Optical choppers	4280E
Optical coatings	4270, 4278H, 4280
Optical coherent transients	4265G
Optical collimators	4280
Optical communication devices	4280S
Optical constants	5170, 7820D
Optical couplers	4280L, 4280M
Optical deflectors	4280E
Optical design techniques	4278, 4280
Optical diaphragms	4280E
Optical dispersion	4210, 4220, 5170, 7820
Optical double resonance	3335, 7670H
Optical elements	4278, 4280
Optical fabrication	4285
Optical fibres	4280M
Optical films	4270, 4278, 4280, 7865
Optical filters	4280B, 4280C
Optical frequency conversion	4265C
Optical glass	4270C
Optical gratings	4280F
Optical harmonic generation	4265C
Optical images	4230
Optical information processing	4230
Optical instruments	0760, 4278, 4280
Optical Kerr effect	4265J
Optical materials	4270
Optical model	1240P
Optical modulation	4260F, 4280K
Optical monochromators	4280D
Optical parametric devices	4265C
Optical phase conjugation	4265F
Optical phenomena in gases	5170
Optical prisms	4278, 4280
Optical projectors	4278
Optical properties of substances	5170, 78, 8140T
Optical pumping	3280B, 3380B, 4255, 7845
Optical rangefinders	4280
Optical resolving power	4230
Optical rotation	4210, 7820E
Optical saturable absorption	4265G
Optical saturation	4265G
Optical self-focusing	4265J
Optical self-induced transparency	4265G
Optical shutters	4280E
Optical sources	4272
Optical storage	4230, 4240
Optical susceptibility	77, 78
Optical systems	0760, 4278, 4280
Optical telescopes	0760, 4278, 9555
Optical testing	4278, 4285
Optical transfer function	4230
Optical waveguide components	4280L
Optical waveguides	4280L
Optical windows	4280E
Optical workshop techniques	4285
Optical zone plates	4280B
Optics	0760, 0765, 42
OPW calculations	7110, 7125C
Orbital calculation methods	3120
Order-disorder transformations	6150K, 6460, 6470K, 8130H
Orthotics	8770J
Otology	8730
Overhauser effect	3325
Oxidation	8160, 8160B, 8230
Ozonosphere	9260
P invariance	1130
p-n junctions	7340L
Pacemakers	8770J
Pade scattering	1180
Palaeomagnetism	9125
Paramagnetic properties of substances	5160, 7520
Paramagnetic resonance	3330, 7630
Partially conserved currents	1140
Particle beam diagnostics	2925
Particle beams	4180
Particle optics	4180
Particle telescopes	2970
Particle track visualisation	2940
Parton models	1235H
Passivation	8160
Paste rheology	4660
Patient care	8770G
Patient diagnosis	8770E
Patient monitoring	8770
Patient treatment	8770G
PCILO calculations	3120N, 3120T
Peculiar stars	9730
Peierls instability	7130, 7215N
Peripheral models	1240R
Permittivity	5150, 7720
Petrology	9160, 9165

	Classification		Classification		Classification
Phase diagrams	6470, 8130B, 8130D	Plasma waves	5235	Quantum fluids	0530, 67
Phase equilibrium	0570, 64, 8130B, 8130D	Plasmons	7145G, 7230	Quantum gravity	0460
Phase transformations	0570, 64, 8130	Plastic crystals	6150, 7660	Quantum measurement theory	0365
Phi mesons	1440	Plastic deformation	4630J, 6220F, 8140L	Quantum mechanics	0365
Philosophy of science	0170	Plastic detectors	2940	Quantum optics	4250
Phonon interactions	6320	Plasticity	4630J, 6220F, 8140L	Quantum statistical mechanics	0530
Phosphorescence	3250, 3350, 7855	Plastics	6140K, 81	Quark confinement	1235C
Phosphorescence microwave double resonance	3335H, 7670H	Plate tectonics	9145	Quark models	1235
Photoacoustic effect	4388, 6265	Pleochroism	3345, 7820F	Quarks	1480
Photocapacitance	7240	Pluto	9630T	Quasars	9870J
Photocathodes	79C0	Pneumodynamics	8745	Quenching (thermal)	8140G
Photochemistry	8250	Poincare invariance	1130		
Photochromism	7820	Point contacts	7340		
Photoconductivity	7240	Point defects	6170B, 6170D, 6170E, 7850	Radiation angular correlations	2970
Photodetachment	3280F, 3380E	Poiseuille flow	4760	Radiation belts	9430
Photodielectric effect	7240	Poisson ratio	6220D, 8140J	Radiation chemistry	8250
Photodisintegration	2520	Polar semiconductors	7220, 7280	Radiation coincidence measurements	2970
Photoelasticity	4630C, 4630R, 7820F, 8140J	Polarimeters	0760F, 2975	Radiation detectors	0762, 2940, 2970
Photoelectric conversion	8630J	Polarimetry	2975	Radiation effects	5190, 6180
Photoelectricity	7240	Polarised bombardment targets	2925	Radiation gas dynamics	4770
Photoelectrochemical conversion	8630K	Polarised nuclear reactions	2470	Radiation hardening	8140C
Photoelectromagnetic effects	7240	Polarised sources	2925	Radiation measurement	2970
Photoelectron spectra	3280F, 3365, 7960	Polaritons	6320, 7136, 7830	Radiation monitoring	2880, 2940, 2960, 2970, 8760P
Photoemission	7960	Polarography	8280	Radiation monitoring electronics	2960
Photofission	2520, 2585	Polarons	7138	Radiation protection	2880, 8760P
Photography	0768, 8250, 9575	Polishing	4285, 8160, 8170	Radiation spectrometers	2930
Photoionisation	3280F, 3380E	Pollution	8670, 9220, 9260	Radiation spectroscopy	2930
Photoluminescence	3250, 3350, 7855	Polymer films	6140K, 6855, 81	Radiation therapy	8760B, 8760G, 8760J, 8770G
Photolysis	8250	Polymer melts	4750, 6125	Radiative effects	3130
Photomagnetic effect	7520, 7590	Polymer molecules	3620	Radiative flows	4770
Photometry	0760D, 9575	Polymer preparation	8120S, 8120T	Radiative transfer	0560, 4440, 9265, 9530, 9710
Photomultipliers	0760D, 2940	Polymer reactions	8235	Radioactive dating	0790, 9385
Photon counting	0762, 4250	Polymer solutions	4750, 6125	Radioactive decay periods	23
Photon echo	4265G	Polymerisation	8235	Radioactive decay schemes	23
Photon-hadron interactions	1360	Polymers	3620, 6140K, 81	Radioactive pollution	8670, 8760R
Photon-hadron scattering	1360F	Polymorphic transformations	6150K, 6470K, 8130H	Radioactive sources	2925
Photon-nucleus scattering	2520	Polymorphism	6150K, 6155, 6160, 6165	Radioactive tracers	2925, 8760J, 8760L
Photon sources	2925	Pomeranchuk poles	1240M	Radioactive waste	2842
Photons	1480	Population II stars	9720	Radioactivity	23, 2880
Photonuclear reactions	2520	Population inversion	3280B, 3380B, 4250, 4255, 7845	Radioactivity measurement	2970
Photoplasticity	4630J, 6220F, 8140L	Porous materials	4755M, 81	Radioastronomy	95
Photorefractive effect	4240, 4270G, 7820	Position sensitive detectors	2940	Radiobiology	8750G
Photosphere	9660	Positron annihilation in liquids and solids	6180F, 7125, 7870B	Radiochemistry	8255
Photosynthesis	8630P, 8725	Positron states	7165	Radiofrequency spectra	3220B, 3320B, 7870G
Photothermal conversion	8630S	Positrons	1460	Radiofrequency spectrometers	0758, 0765
Photovoltaic effects	7240	Potential energy curves	3190	Radiography	0785, 8170, 8760J, 8770E
Physical chemistry	82	Potential energy surfaces	3170F, 8220K	Radioisotope scanning and imaging	8760J, 8770E
Physical optics	42	Potential models	1240Q	Radiometry	0760D
Physiological models	8710	Potts model	0550	Radiosources (astronomical)	9870D
Physiological optics	8732	Powder metallurgy	8120E, 8120G	Rain	9260
Physiology	87	Powder spraying	8115, 8160	Raman lasers	4255, 4260, 4265C
Pick-up reactions	2450	Powder technology	8120E	Raman spectra	3320F, 7830
Piezoelectricity	7760	Powders	4755K, 8120	Random noise	0250, 7270
Piezorefractance	7820H	PPP calculations	3120P	Random phase approximations	2160J, 7110, 7145
Piezoresistance	7220F	Pre-equilibrium model	2460	Random processes	0540
Pinch effect	5255	Preacceleration	2910	Rarefied gas dynamics	4745
Pion absorption	2580	Precipitation	6475, 8130M, 8260	Rayleigh scattering	3320F, 4265C, 7835
Pion-baryon interactions	1375G, 1385	Precipitation hardening	8140C	Reaction kinetics	8220, 8240
Pion-baryon scattering	1375G, 1385	Primary cells	8630E	Reactive flows	4770
Pion capture	2580	Probability theory	0250	Recrystallisation	6150C, 8110J, 8140E
Pion decays	1320, 1325	Proportional counters	2940	Reflection high energy electron diffraction	6114H
Pion-nucleus reactions	2580	Prosthetics	8770J	Reflectivity	42, 4210, 4220, 5170, 78
Pion-nucleus scattering	2580	Protective coatings	8160	Reflectometry	0760H
Pions	1440	Proteins	3620, 8715	Refractive index	4110H, 4210, 4220, 5170, 7820D
Pipe flow	4760	Proton absorption	2540	Refractometers	0760H
Plane wave Born approximations	2410	Proton-hyperon interactions	1375E, 1385	Refractories	81
Planetary nebulae	9840	Proton-hyperon scattering	1375E, 1385	Refractory preparation	8120L, 8120N
Planets	9630, 9780	Proton-kaon interactions	1375J, 1385	Regge poles	1160, 1240M
Plasma	52	Proton-kaon scattering	1375J, 1385	Relativistic band structure calculations	7110, 7125C
Plasma antennas	5240F	Proton magnetic resonance	3325, 7660	Relativistic effects	3130, 3510F
Plasma applications	5275	Proton-meson interactions	1375, 1385	Relativistic field theory	1110
Plasma arc spraying	5275, 8115, 8160	Proton-meson scattering	1375, 1385	Relativistic flows	4775
Plasma beam interactions	5240M	Proton-neutron interactions	1375C, 1385	Relativistic mechanics	0330
Plasma collision processes	5220F, 5220H	Proton-neutron scattering	1375C, 1385	Relativistic plasmas	5260
Plasma confinement	5255	Proton-nucleus reactions	2540	Relativistic scattering theory	1180
Plasma deposited coatings	6855, 8115J, 8160	Proton-nucleus scattering	2540	Relativity	04, 9530
Plasma deposition	8115J	Proton-pion interactions	1375G, 1385	Remote sensing	8670L, 9385
Plasma devices	5275	Proton-pion scattering	1375G, 1385	Renormalisable fields	1110
Plasma diagnostics	5270	Proton-proton interactions	1375C, 1385	Replica techniques	0780, 6116, 68
Plasma electromagnetic wave propagation	5240D	Proton-proton scattering	1375C, 1385	Resistance thermometers	0720D
Plasma elementary processes	5220	Proton radiative capture	2540	Resource letters	0130R
Plasma equilibrium	5255	Protons	1420	Reverberation	4355
Plasma-filled waveguides	5240F	Pseudopotential methods	7110, 7125C	Reviews	0130R
Plasma flow	5230	Psi mesons	1440	Rheopexy	4660
Plasma heating	5250	Pulsars	9760G	Rho mesons	1440
Plasma heating by laser beam	5250J	Pulsatile flow	4760	Ring lasers	4260D
Plasma heating by shock wave	5250L	Pulse amplifiers	2960	Rock magnetism	9160
Plasma heating by wire explosion	5250L	Pulse counting	2960	Rotational energy transfer	3450E
Plasma magnetohydrodynamics	5230	Pulse height analysers	2960	Rotational flow	4730
Plasma oscillations	5235	Pulse shaping circuits	2960	Rotational isomerism	3520J
Plasma production by laser beam	5250J	Pyroelectricity	7770	RPA calculations	2160J, 7110, 7145
Plasma production by shock wave	5250L	Pyrometers	0720, 0762	S-matrix theory	1120
Plasma production by wire explosion	5250L			SAMO method	3120G
Plasma radiation	5225P				
Plasma sheaths	5240K				
Plasma shock waves	5235T				
Plasma simulation	5265				
Plasma sources	5250				
Plasma transport processes	5225F				
Plasma turbulence	5235R				
Plasma-wall interactions	5240H				
		Q-switching	4260F		
		QCD	1235C		
		QED	1220		
		Quadrupole moments	2110K, 3520M, 7660		
		Quantum electrodynamics	1220		
		Quantum field theory	0370, 1110		

	Classification		Classification		Classification
Satellites	9480, 9630	Spin-spin relaxation	3325, 3330, 76	Thermal conductivity	0570, 0720, 4450, 5130, 6660, 6670, 7215C, 7215E, 7430E
Saturn	9630M	Spin waves	7530D, 7650	Thermal diffusion in gases	5110, 5120
Scaling phenomena	1130	Spinoidal decomposition	6475, 8130	Thermal diffusion in liquids	4725J, 6610
Scanning radiography		Spontaneous fission	2585	Thermal energy conversion	8630R
Scattering	0785, 8170, 8760J, 8770E	Spontaneous symmetry breaking	1130	Thermal energy storage	8640F
SCF calculations	0365, 0380	Spray coating techniques	8115, 8160	Thermal expansion	5130, 6570
Schlieren devices	3120, 7110, 7125, 7170	Sputter etching	8160	Thermal processes	44
Schottky defects	4280	Sputtered coatings	6855, 8115C	Thermal properties	4450
Schottky effect	6170B	Sputtering	7920, 8115C	Thermal properties of gases	5130
Schrodinger equation	7330, 7940	Stacking faults	6170P	Thermal property measurement	4450
Schwinger source theory	0365	Stark effect	3260, 3345B, 7170E, 7820J, 7830, 7840	Thermal quenching	8140G
Scintillation counters	1110	Stars	97	Thermally stimulated currents	7220J, 7730
Second sound	2940	Statistical models	1240E	Thermionic conversion	8630N
Secondary cells	67	Statistical physics	05	Thermionic emission	7940
Secondary emission	8630F	Statistics	0250	Thermo-optical effects	5130, 5170, 7820P
Segregation	7920	Stellar clusters	9820	Thermochemistry	8
Seismology	6475, 8130M	Stellar motion	9810	Thermocouples	0720, 0762
Self-diffusion	9130	Stellarators	5255, 5275	Thermodynamic properties	6550
Self-focusing	51, 66	Stereochemistry	3520B	Thermodynamics	0570, 4460
Self-induced transparency	4265J	Stimulated Brillouin scattering	4265C	Thermoelectricity	4630C, 4660, 6220D, 8140J
Semiconductor counters	4265G	Stimulated emission	4250, 4255, 7845	Thermoelectric conversion	8630M
Semiconductor doping	2940	Stimulated light scattering	4265C	Thermoelectricity	7215J, 7220P
Semiconductor-electrolyte boundaries	6170T	Stimulated Raman scattering	4265C	Thermoluminescence	7860K
Semiconductor growth	7340M	Stochastic processes	0250, 0540	Thermoluminescent dating	0790, 9385
Semiconductor-insulator boundaries	6150C, 6855, 8110, 8115	Storage rings	2920	Thermoluminescent dosimeters	2940, 2970
Semiconductor junction lasers	7340Q	Strain gauges	0710, 4630R	Thermomagnetic effects	7215H, 7220N
Semiconductor junctions	4255P, 4260	Strange particles	1420, 1440	Thermomechanical treatment	8140G
Semiconductor materials	7340L	Stratified flow	4755H	Thermometers	0720D
Semiconductor metal boundaries	7280	Stratons	1480	Thermopiles	0720, 0762
Semiconductor thin films	7340N	Stratosphere	9260	Thickness measurement	0630C
Semiempirical NDO calculations	7360F	Streamer chambers	2940	Thin films	6855, 6860, 7360, 7570, 7755, 7865
Semi-leptonic decays	3120N	Stress corrosion cracking	6220M, 8160, 8160B	Thixotropy	4660
Semimetallc thin films	1320, 1330, 1335	Stress relaxation	4630J, 6240, 8140J	Thomas-Fermi-Dirac model	3120L
Sensory aids	7360F	Stress/strain relations	46, 6220F, 8140L	Thomas-Fermi model	2160, 3120L, 7145J
Sets	8770J	Stripping reactions	2450	Tidal energy	8610F
Shape memory effects	0210	Strong gravity	0460	Tides	9110, 9210, 9410
Shear modulus	6220F, 8130K, 8140L	Strong interaction models	1240	Time measurement	0630F
Shear turbulence	6220D, 8140J	Structure functions	1340F	Time-of-flight spectrometers	0775, 2930
Shielding	4725F	SU ₂ theory	1130	Tokamaks	5275
Shock waves	2842, 2880	SU ₃ theory	1130	Topology	0240
Sintering	4630M, 4740N, 6250	SU ₄ theory	1130	Track chambers	2940
Size effect	8120E	Sublimation	6470H	Transducers	0670, 4388
Skin effect	7230, 7360	Subsonic flows	4740D	Transition radiation	41, 6180, 7870
Slip	7230	Substrates	6855, 6860, 8115	Transits	9510
Slip flows	4630J, 6170L, 6220F, 8140L	Sum rules	1150	Transonic flows	4740H
Slip flow	4745	Sun	9660	Transport processes	0560
Smectic liquid crystals	4755K	SU _N theory	1130	Triboelectricity	7340B
Societal aspects	6130, 6470M	Superconducting materials	7470	Triboluminescence	7860M
Societal aspects	0175	Superconducting semiconductors	7470	Triplet state	3150, 7135
Solar absorbers	8630S	Superconducting thin films	7360K	Triton-nucleus reactions	2550
Solar cells	8630J	Superconductive tunnelling	7450	Triton-nucleus scattering	2550
Solar collectors	8630S	Supercooling	64	Tritons	2140, 2710
Solar energy	8610K	Superexchange interactions	7530E	Troposphere	9260
Solar energy concentrators	4278, 8610K	Superfluidity	0530, 67	Tube flow	4760
Solar nebula	9610	Supergiant stars	9720	Tunnelling	7340, 7450
Solar system	96	Supergravity	0465	Turbidity	4220, 8270, 9210, 9265
Solar wind	9440H, 9460, 9660	Superionic conducting materials	6630	Turbulence generated noise	4725M
Solid helium	6780	Superlattices	6155, 6160, 6165, 7340L, 8130, 8140	Turbulent diffusion	4725J
Solid instability	4630L	Supernova remnants	9840	Turbulent flows	4725
Solid lasers	4255R, 4260	Supernovae	9760B	Twilight	9260, 94
Solid-liquid transformations	6470D	Superparamagnetism	75	Twinning	6170N
Solid rheology	4630	Superradiance	3290, 4250, 7845	Two-phase flow	4755K
Solid solubility	6475, 8130	Supersonic flows	4740K		
Solid solution hardening	8140C	Supersymmetry	1130	Ultrasonic absorption	43, 5140, 6260, 6265
Solid state detectors	2940	Surface acoustic wave devices	4360, 4385, 4388	Ultrasonic applications	43
Solid state phase transformations				Ultrasonic relaxation	5140, 6280
Solid-state plasma	6470K, 8130H	Surface acoustic waves	4320, 4325, 4360, 4388, 6825	Ultrasonic velocity	43, 5140, 6260, 6265
Solid-vapour transformations	7230	Surface carrier scattering	7325	Ultrasonic waves	43, 5140, 6260, 6265
Solidification	6470H	Surface electron states	7320	Ultraviolet spectra	3220J, 3320L, 3320N, 7840
Sols	6470D, 8130F	Surface energy	6810, 6840	Umklapp process	6320H, 6320K
Solubility	4755K, 8270	Surface hardening	8160, 8160B	Underwater sound	4330, 9210
Solutions	6475, 8130	Surface ionisation	7330, 79	Undulator radiation	4170
Solvent effects	3170D	Surface reactions	8270	Unified field theories	0450, 1210
Sonar	6120, 6125, 6475	Surface structure	6820	Units (measurement)	0620F
Sonoluminescence	3170D	Surface tension	6810	Upsilon mesons	1440
Sorption	7860M	Surface texture	6820	Uranus	9630T
Space charge	6845, 8265	Surface treatment	8160, 8160B		
Space groups	52, 5280, 7750	Surgery	8770G	Vacancies (crystal)	6170B
Space physics	6150E	Suspensions	8270	Vacuum apparatus	0730
Space research	94	Synchrocyclotrons	2920	Vacuum deposited coatings	6855, 8115G
Space-time configurations	9480	Synchrotron radiation	4170, 4272	Vacuum deposition	8110B, 8115G, 8120C
Spallation breeder reactors	04	Synchrotrons	2920	Valence bond calculations	3120R
Spallation reactions	2858	Synergetic fission reactor systems	2858	Van de Graaff accelerators	2915
Spallation reactions	2450, 2540			Van de Graaff generators	0750
Spark chambers	2940			Van der Waals forces	3420
Spatial filters	4280B			Vaporisation	6470F
Special relativity	0330			Vapour deposited coatings	6855, 8115C, 8115G, 8115H, 8115J
Specific heat	4450, 5130, 6520, 6540, 7430E, 7540			Vapour deposition	8110B, 8115C, 8115G, 8115H, 8115J
Speckle	4220			Vapour phase epitaxial growth	6855, 8115G, 8115H, 8115J
Spectra	32, 3320, 78			Variable stars	9730
Spectrochemical analysis	8280			Vector meson dominance model	1240V
Spectrophotometers	0760D, 0765			Velocity measurement	0630G
Spectroscopy	0758, 0765, 0775, 9575			Veneziano model	1240H
Speech	4370, 8736			Venus	9630E
Speech communication	4370			Vibrating bodies	4630N
Spheroidizing	8140G				
Spin density waves	75				
Spin glasses	7540				
Spin-lattice relaxation	76				
Spin-orbit interactions	2110, 2160, 31, 7170E				
Spin-phonon interactions	6320, 75, 76				

	Classification
Vibrational energy transfer	3450E
Vibrational states of disordered systems	6350
Vibrations	0320, 0340K, 4340, 4630M
Viscoelasticity	4630J, 4660, 6240, 8140J
Viscometers	4780
Viscoplasticity	4630J, 6220F, 8140L
Viscosity	5110, 5120, 6210, 6620
Viscosity of gases	5120
Visible spectra	3220J, 3320K, 7840
Vision	8732
Visual perception	8732S
Visual pigments	8732L, 8732N
Vitreous state	6140, 81
Vlasov equation	5220, 5225F
Voids (solid)	6170, 6180
Volcanology	9140
Volume measurement	0630C
Vorticity	4730, 6740
VPE	6855, 8115G, 8115H, 8115J

Wakes	4725R
Water wave energy	8610F
Wave energy	8610F
Wave equations	0340K, 0365
Waves	0340G, 0340K, 4735, 4740N
Weak interaction models	1230
Weak interactions (atomic)	3510W

	Classification
Weak interactions (molecular)	3520W
Wear	4630P, 6220P, 8140P
Wear resistant coatings	6220P, 8140P, 8160
Weather analysis	9260
Weighing	0630E
Weinberg-Salam model	1210
Westheimer method	3120W
Wetting	6810, 6845, 81
Whiskers (crystal)	6870
White darfs	9720
Wiberg method	3120W
Wigner functions	0365
Wind	9260, 9410
Wind energy	8610D
Woods-Saxon potentials	2160C
Work function	7330, 7340, 79
Work hardening	8140E

X-ray absorption spectra	3220R, 3320R, 7870D
X-ray apparatus	0785
X-ray astronomy	95
X-ray crystallography	6110
X-ray diffraction	6110
X-ray diffraction examination of materials	6155, 6160, 6165, 6170
X-ray effects	6180C

	Classification
X-ray emission spectra	3220R, 3320R, 7870E
X-ray lasers	4255
X-ray monochromators	0785, 6110F
X-ray scattering	6110, 7870C
X-ray sources	2925
X-ray sources (astronomical)	9870Q
X-ray spectra	3220R, 3320R, 7870D, 7870E
X-ray spectroscopy	2930
Xalpha calculations	3120G

Yang-Mills fields	1110
Yield point	4630J, 6220F, 8140L
Young's modulus	6220D, 8140J
Yrast states	2110

Zeeman effect	3260, 3345B, 7170E, 7820L, 7830, 7840
Zener effect	7220H
Zener relaxation	4630J, 6240, 8140J
Zero sound	67
Zodiacal light	9460, 9650D
Zone melting	8110H
Zone refining	8110H
Zoology	87

Physics Abstracts

1st DECEMBER 1983

Volume 86

Number 1221

00.00 GENERAL

01.00 COMMUNICATION, EDUCATION, HISTORY, AND PHILOSOPHY

01.30 PHYSICS LITERATURE AND PUBLICATIONS

01.30B Publications of lectures (advanced institutes, summer schools, etc.)

111295 Symmetries in Nuclear Structure. Proceedings of a NATO Advanced Study Institute on Symmetries in Nuclear Structure. New York, USA: Plenum Press (1983), ix+301 pp. [0 306 41341 8] Conference held at: Dronten, Netherlands. Date 16-28 Aug. 1982. Sponsors: NATO; Netherlands' Min. Educ. & Sci.; Found. Physica; Netherlands' Phys. Soc. The following topics were dealt with: electromagnetic and weak currents in nuclei; unification of weak and electromagnetic forces; breaking of fundamental symmetries in nuclei; microscopic basis of collective symmetries; symmetry aspects of the shell model; energy of a nucleon in a nucleus; general principles of statistical spectroscopy; search for neutrino masses and oscillations; electron scattering; Δ dynamics; and parity non-conservation in muonic He atoms.

01.30C Conference proceedings

111296 Workshop on Positron-Electron Pairs in Astrophysics. AIP Conf. Proc. (USA), no.101 (1983). Conference held at: Greenbelt, MD, USA. Date Jan. 1983. The following topics were dealt with: solar flare gamma ray lines, positron annihilation spectra, cosmic gamma ray burst energy spectra, burst optical counterparts, fireball model, pulsars, pair production, galactic centre, Galaxy, Sun, supernovae, active galaxies, galactic nuclei, X-ray background, black holes, accretion discs, plasmas, relativistic winds, magnetic fields, radio stars, polar regions, spinless hadron pairs and proton exchange.

111297 Proceedings of Helsinki International Summer School on Semiconductors 1982. Acta Polytech. Scand. Electr. Eng. Ser. (Finland), no.EL50 (1983). Conference held at: Espoo, Finland. Date 14-18 June 1982. The following topics were dealt with: small devices; noncrystalline semiconductors; dynamical conductivity and dielectric function; hot carrier physics and higher order electron phonon dynamics; electronic correlations in magnetic semiconductors and functional integral approach to Hubbard model; dielectric semiconductor systems; electronic transport in tetrahedral amorphous semiconductors; magnetic ordering phenomena in rare earth semiconductors. 8 papers were presented, of which 7 are published in full in the present proceedings, and 1 as abstract only. Abstracts of individual papers can be found under the relevant classification codes in this or future issues.

111298 Proceedings of the International Workshop on Cross Sections for Fusion and Other Applications. Nucl. Instrum. & Methods Phys. Res. (Netherlands), vol.214, no.1 (1983). Conference held at: College Station, TX, USA. Date 4-6 Nov. 1982. The following topics were dealt with: magnetically confined fusion; multicharged ion interactions with hydrogen; inner shell ionisation; deuterium-induced L-shell X-ray production; L-shell Coulomb ionisation; L-shell ion-input ionisation; direct ionisation and capture in inner-shell processes; K-shell ionisation and capture by light ions; charge change in atomic collisions; charge transfer from molecules to bound and continuum states; ion-atom collisions; impact parameter dependence of electron capture; long-range couplings in collisional charge transfer; collisions involving hydrogen atoms; spectra of np-1s transitions excited during the passage of the Mg ions through carbon targets; ion induced electron ejection from solids; and electron-ion collision of fusion interest. Abstracts of individual papers can be found under the relevant classification codes in this or other issues.

111299 Metallogeny and Tectonics of the North American Cordillera GAC/MAC/CGU Symposium. Can. J. Earth Sci. (Canada), vol.20, no.6 (1983). Conference held at: Calgary, Alta., Canada. Date 13 May 1981. The following topics were dealt with: displaced terrains, metal deposits in British Columbia, and mineral deposits in the United States and Mexico.

111300 1st European Conference on Cineradiography with Photons or Particles. Proc. SPIE Int. Soc. Opt. Eng. (USA), vol.312 (1983). Conference held at: Paris, France. Date 18-21 May 1981. Sponsors: CEA. The following topics were dealt with: cineradiography in technology; cineradiography in experimental physics; cineradiography in biophysics; image processing-3D reconstruction; X-ray and particle generators; image detectors and cameras. 40 papers were presented, of which 39 are published in full in the present proceedings. Abstracts of individual papers can be found under the relevant classification codes in this or future issues.

111301 SPIE Proceedings on Wavefront Sensing. Proc. SPIE Int. Soc. Opt. Eng. (USA), vol.351 (1983). [received: Sept. 1983] Conference held at: San Diego, CA, USA. Date 24-25 Aug. 1982. The following topics were dealt with: wavefront measurement and interpretation; wavefront sensing by phase retrieval; development and applications of wavefront sensing technology. 21 papers were presented, all of which are published

in full in the present proceedings. Abstracts of individual papers can be found under the relevant classification codes in this or future issues.

111302 SPIE Proceedings on Microscopy Techniques and Capabilities. Proc. SPIE Int. Soc. Opt. Eng. (USA), vol.368 (1983). [received: Sept. 1983] Conference held at: London, England. Date 21-22 Sept. 1982. Sponsors: IOP; IEE. The principal aim of the meeting was to describe the method of operation of a selection of the most recently developed techniques used in microscopy and to illustrate their practical capabilities by discussing a variety of applications. A total of 4 sessions, extending over 2 days, covered X-ray microscopy, electron microscopy, acoustic microscopy and infrared and visible microscopy. Abstracts of individual papers can be found under the relevant classification codes in this or future issues.

111303 American Geophysical Union Chapman Conference on Waves in Magnetospheric Plasma. Geophys. Res. Lett. (USA), vol.10, no.8 (1983). Conference held at: Kona Coast, HI, USA. Date 7-11 Feb. 1983. The following topics were dealt with: whistlers in the VLF range, electron loss, effect of man-made transmissions, the interaction of heavy ions and waves with frequencies around the ion gyrofrequency, auroral zone processes, long-period pulsations, and plasma modification.

111304 Proceedings of the Sixteenth Rare Earth Research Conference. J. Less-Common Met. (Switzerland), vol.93, no.1 (1983). Conference held at: Tallahassee, FL, USA. Date 18-21 April 1983. The following topics were dealt with: lanthanide and actinide chemistry and physics; surface spectroscopy; organometallic chemistry; magnetic superconductors and spin glasses; bioinorganic chemistry; crystal fields and spectroscopy; industrial applications of rare earths; lanthanide-transition metal intermetallics and hydrides; inorganic structures and low valent compounds; structure-property relationships. 28 papers are published in full in the present proceedings, and 14 as abstracts only. Abstracts of individual papers can be found under the relevant classification codes in this or future issues.

111305 Nordic Conference on Surface Science. Phys. Scr. (Sweden), vol.T4 (1983). Conference held at: Tampere, Finland. Date 18-20 Aug. 1982. The following topics were dealt with: surface physics and biological phenomena; physisorption interaction; adsorbed atoms and adsorption layer superstructure formation; LEED measurement; surface phase transitions; photoelectron diffraction; surface electronic structure; photoelectron spectroscopy; surface catalysis; positron surface states; surface reactions; oxidation; electron spectroscopy; low temperature surface phase; spin-orbit coupling; crystal symmetry; Auger spectra; interface states; chemisorption and corrosion. 48 papers were presented, of which all are published in full in the present proceedings. Abstracts of individual papers can be found under the relevant classification codes in this or future issues.

111306 Proceedings of the 4th Nordic Meeting on Nuclear Physics. Phys. Scr. (Sweden), vol.T5 (1983). Conference held at: Fuglso, Denmark. Date 16-20 Aug. 1982. Sponsors: NORDITA; Danish Natural Sci. Res. Council; Niels Bohr Inst. The following topics were dealt with: high spin phenomena; Gamow-Teller states; heavy-ion collisions; JET project; LEAR project; electromagnetic transitions; nuclear shape transitions; fragmentation reactions. 44 papers were presented, of which all are published in full in the present proceedings. Abstracts of individual papers can be found under the relevant classification codes in this or future issues.

111307 Proceedings of the International Conference on Order in Chaos. Physica D (Netherlands), vol.7D, no.1-3 (May 1983). Conference held at: Los Alamos, NM, USA. Date 24-28 May 1982. The following topics were dealt with: order in chaos; chaotic systems; turbulence; nonlinear systems; superfluid ^4He ; bifurcations; dimensions; fractal structures; coherence; solitons; maps; fluids; vortices; Lie algebras; quantum chaos. 29 papers were presented, of which 27 are published in full in the present proceedings, and 2 as abstracts only. Abstracts of individual papers can be found under the relevant classification codes in this or future issues.

111308 Transactions of the 4th International Meeting on Radiation Processing. Radiat. Phys. & Chem. (GB), vol.22, no.3-5 (1983). Conference held at: Dubrovnik, Yugoslavia. Date 4-8 Oct. 1982. The following topics were dealt with: optichromic dosimetry; radiation processing of wires and cables, urban solid wastes, polymers, hides, rubber-insulated wires, effluents from livestock farms, liposomes, medical products, peat carriers for legume seed inoculants, herbal tea, onions, tomatoes, unfermented grape juice, poultry meat, fresh fish, pork, rice, white wine, pressure-sensitive adhesives, coating materials, sawdust-clay composites, archaeological artifacts and hydrogels; dosimetry; radiation safety; low energy accelerators and electron accelerators; depth-dose curves; electrochromism; gammagraphy; Isu and bremsstrahlung generators; corrosion; radiation-induced polymerisation; radiation sterilisation; regulation; radiation curing; radiation grafting; radiation polymerisation for preservation and radiation processing centres. 87 papers were published in the present proceedings.

111309 Proceedings of the 1983 RCNP International Symposium on Light Ion Reaction Mechanism. Osaka, Japan: Osaka University (1983), x+929 pp. Conference held at: Osaka, Japan. Date 16-20 May 1983. The following topics were dealt with: nuclear optical potential, phenomenological and microscopical; effective interactions and microscopic descriptions of nuclear reactions; inelastic and charge exchange scatterings; single step and multistep processes, breakup and transfer reactions; equilibrium and preequilibrium processes. 101 papers were presented, all of which are published in full in the present proceedings. Abstracts of individual papers can be found under the relevant classification codes in this or future issues.

111310 Symmetries and Properties of Non-Rigid Molecules. A Comprehensive Survey. Proceedings of an International Symposium. Amsterdam, Netherlands: Elsevier (1983), xvi+520 pp. [0 444 42174 2]. Conference held at: Paris, France. Date 1-7 July 1983. Sponsors: CNRS; Direction de la Recherche du Ministère Educ. Nat. The following topics covering the symmetries and properties of nonrigid molecules were dealt with: nonrigid molecule theory; classical molecular structure; symmetry operations; category theory; semi-direct product structure; induced representations; hyperfine structure; isometric groups; group theory; energy level classification; molecular vibrations and spectra; Jahn-Teller effect; permutational analysis; potential energy surfaces; rovibrational and rovibronic spectra. Applications to chemical reactions, liquid, crystal and nuclear physics are also discussed. 33 papers were presented, all of which are published in full in the present proceedings. Abstracts of individual papers can be found under the relevant classification codes in this or future issues.

111311 Polymer Alloys III Blends, Blocks, Grafts and Interpenetrating Networks. Proceedings of a Symposium. New York, USA: Plenum (1983), ix+302 pp. [0 306 41138 5]. Conference held at: New York, USA. Date 23-28 Aug. 1981. Sponsors: American Chem. Soc. The following topics were dealt with: fracture toughness of polymer blends; plastic-rubber composites; morphology; mechanical properties; melt rheology; dimensional stability; microphase segregation; block and graft polymers; interpenetrating polymer networks. Abstracts of individual papers can be found under the relevant classification codes in this or future issues.

111312 Role of the Polymeric Matrix in the Processing and Structural Properties of Composite Materials. Proceedings of a Joint US-Italy Symposium. New York, USA: Plenum (1983), xii+684 pp. [0 306 41134 2]. Conference held at: Capri, Italy. Date 15-19 June 1981. The following topics were dealt with: the role of the matrix in fibrous composite structures; composites in commercial aircraft and current research needs in aircraft structure; materials; chemical and environmental effects; short fibre reinforcement effects; interface effects; and continuous fibre reinforcements and design. 37 papers were presented, all of which are published in full in the present proceedings. Abstracts of individual papers can be found under the relevant classification codes in this or future issues.

111313 Proceedings of Four Contractors' Meetings on Heat Pumps (EUR 8077 EN). Luxembourg: Comm. European Communities (1982), 390 pp. Conference held at: Brussels, Belgium. Date 28-29 April & 12-13 May 1982. The following topics were dealt with: heat pump systems, industrial heat pumps, ground as heat source and advanced heat pumps.

111314 Proceedings of the Eighteenth General Assembly of the IAU. Dordrecht, Netherlands: Reidel (1983), x+603 pp. [90 277 1563 7]. Conference held at: Patras, Greece. Date 17-26 Aug. 1982. Sponsors: IAU. Presents a report of the inaugural ceremony and the General Assembly (sessions 1 and 2). Reports of the meetings of 40 commissions of the IAU are discussed.

111315 Defects in Semiconductors II, Symposium Proceedings. New York, USA: North-Holland (1983), xv+582 pp. [0 444 00812 8]. Conference held at: Boston, MA, USA. Date Nov. 1982. The following topics were dealt with: defects in Si, general and O-related; defects in III-V semiconductors; dislocations and interfaces; defects in relation to device properties; laser beam annealing and other special processes and materials. 61 papers are published in full in the present proceedings. Abstracts of individual papers can be found under the relevant classification codes in this or future issues.

111316 Proceedings of the 4th European Conference on Chemical Vapour Deposition. Eindhoven, Netherlands: Philips Centre Manuf. Technol. (1983), 586 pp. Conference held at: Eindhoven, Netherlands. Date 31 May-2 June 1983. The following topics were dealt with: analysis and theory; metals and superconductors; electronic materials; carbides and nitrides; oxides. 76 papers were presented, of which 59 are published in full in the present proceedings, and 5 as abstracts only. Abstracts of individual papers can be found under the relevant classification codes in this or future issues.

111317 Extended Abstracts from the 164th Electrochemical Society Technical Meeting. Pennington, NJ, USA: Electrochem. Soc. (1983), xxvi+786 pp. Conference held at: Washington, DC, USA. Date 9-14 Oct. 1983. The following topics were dealt with: batteries; corrosion; dielectrics and insulation; thin film interfaces; electrodeposition processes; contacts, connectors and interconnections; semiconductor industry; semiconductor technology; high-temperature materials; industrial electrolytics; luminescence and display materials; experimental electrochemistry.

01.30E Monographs, and collections

111318 Elastic media with microstructure II. Three-dimensional models. I.A.Kunin. Berlin, Germany: Springer-Verlag (1983), viii+272 pp. [0 387 12078 5]. Crystals and polycrystals, composites and polymers, grids and multibeam systems can be considered as examples of media with microstructure. A characteristic feature of all such models is the existence of scale parameters which are connected with microgeometry or long-range interacting forces. As a result the corresponding theory must essentially be a nonlocal one. This treatment provides a systematic investigation of the effects of microstructure, inner degrees of freedom and nonlocality in elastic media. The propagation of linear and nonlinear waves in dispersive media, static, deterministic and stochastic problems, and the theory of local defects and dislocations are considered in detail. Especial attention is paid to approximate models and limiting transitions to classical elasticity. The book forms the second part of a revised and updated edition of the author's monograph published under the same title in Russian in 1975. The first part (vol.26 of Springer Series in Solid-State Sciences) presents a self-contained theory of one-dimensional models. The theory of three-dimensional models is considered in this volume. (368 refs.)

111319 Perturbative quantum chromodynamics. M.Jacob [Ed.]. Amsterdam, Netherlands: North-Holland (1982), viii+836 pp. [0 444 86420 2]. Over the past decade quantum chromodynamics (QCD) has developed into a very serious contender for a theory of strong interactions. As a theory of quarks and gluons interacting through their colour degree of freedom, it has the remarkable property of implying an effective coupling constant which decreases with momentum transfers or when interactions are probed at very short distances. While many problems remain to be solved, this remarkable property has allowed one to develop perturbative calculation techniques which have met with some definite success studying a wide array of phenomena

where large momentum transfers are involved. This perturbative approach has presently reached a level which is such that it is deemed appropriate to review it altogether, combining into a single volume several Physics Reports articles which provided timely reviews of QCD as it developed. Such a book could be used by the particle physicist not yet acquainted with QCD. It provides a self-teaching text. It should also be useful to the specialist by providing thorough discussions of questions which are still at the forefront of research and easy references to a large amount of material. Subjects discussed include: deep inelastic lepton-hadron scattering, hadron production in electron-positron annihilations, large mass lepton pair formation in hadron interactions and hadron or photon production at large transverse momentum. (1466 refs.)

Self-study manual on optical radiation measurements: Part I - Concepts, chapter 10. Introduction to coherence in radiometrySee Entry 111382

Self-study manual on optical radiation measurements: Part III - Applications, chapter 1. Measurement of solar terrestrial spectral irradiance in the ozone cut-off regionSee Entry 111383

01.30K Handbooks, dictionaries, tables and data compilation

111320 Shape functions for atomic-field bremsstrahlung from electrons of kinetic energy 1-500 keV on selected neutral atoms $1 \leq Z \leq 92$. L.Kissel (Sandia Nat. Labs., Albuquerque, NM, USA), C.A.Quarles, R.H.Pratt. *At. Data & Nucl. Data Tables (USA)*, vol.28, no.3, p.381-460 (May 1983). A tabulation is presented of theoretical predictions for the shape functions for atomic-field bremsstrahlung for 24 atoms with atomic number Z ranging from 1 to 92 for six incident electron energies T_1 from 1 to 500 keV. The shape function is defined as the ratio of the bremsstrahlung cross section differential in photon energy and angle to the photon energy spectrum. Shape functions have been tabulated for photon angles from 0° to 180° in 5° intervals of 12 values of the fraction of energy radiated k/T_1 from 0 to 1.0. The tables for $2 \leq Z \leq 92$ result from interpolations in atomic number and fraction of energy radiated from a set of benchmark data calculated by treating the bremsstrahlung process as a single-electron transition in a relativistic self-consistent screened potential. The table for $Z=1$ is calculated using a screened Born approximation. (7 refs.)

111321 Differential bremsstrahlung cross sections for collisions of electrons with unscreened nuclei of low atomic numbers. K.Bernhardt (Inst. für Experimentalphys. AG, Ruhr Univ. Bochum, Bochum, Germany), E.Haug, K.Wiesemann. *At. Data & Nucl. Data Tables (USA)*, vol.28, no.3, p.461-75 (May 1983).

Differential bremsstrahlung cross sections for unscreened nuclei are calculated using Sommerfeld-Maue eigenfunctions for the electronic continuum states. The photon energy spectrum and the shape function, defined as the ratio of the differential bremsstrahlung cross section to the photon energy spectrum, are tabulated for incident electron kinetic energies $T_1=5, 10, 50$, and 100 keV and for atomic numbers $Z=8, 18, 26$, and 36. For sufficiently low Z and for incident electron kinetic energies and emitted photon energies greater than the K -shell binding energy of the target atom, the present results for unscreened nuclei are in reasonable agreement with and easier to compute than the atomic-field bremsstrahlung cross sections. (10 refs.)

111322 Hartree-Fock momentum expectation values for atoms and ions. S.R.Gadre, P.S.Geji, S.J.Chakravorty (Dept. of Chem., Univ. of Poona, Pune, India). *At. Data & Nucl. Data Tables (USA)*, vol.28, no.3, p.477-91 (May 1983). Nonrelativistic (p^n) values are calculated for $n=-2, -1, 1, 2, 3$, and 4 from the analytic Roothaan-Hartree-Fock atomic wave functions of Clementi and Roetti. Results are tabulated for the ground and certain excited states of the atoms helium through xenon and their singly charged positive and negative ions. (12 refs.)

111323 Backscattering coefficients of H, D, and He ions from solids. T.Tabata (Inst. of Plasma Phys., Nagoya Univ., Nagoya, Japan), R.Ito, Y.Iitaka, N.Itoh, K.Morita. *At. Data & Nucl. Data Tables (USA)*, vol.28, no.3, p.493-530 (May 1983). Experimental data on the number-backscattering coefficient R_N , the energy-backscattering coefficient R_E , and the mean fractional energy r_E of backscattered particles are tabulated for H, D, and He ions normally incident on elemental solids. References through 1981 are covered. The dependence of R_N and R_E on incident energy is shown graphically for energies from about 10 eV to 100 keV by plotting the experimental data and the empirical formulas of Tabata et al. (1981). Graphs are provided for 36 elemental targets of atomic numbers from 6 to 92. (27 refs.)

111324 Single-particle Glauber matrix elements. E.Oset (Dept de Fisica Atomica y Nuclear, Univ. de Valladolid, Valladolid, Spain), D.Strottman. *At. Data & Nucl. Data Tables (USA)*, vol.28, no.3, p.531-55 (May 1983). The single-particle matrix elements of the Glauber profile function are tabulated for harmonic oscillator single-particle wave functions. The tables are presented in such a manner as to be applicable if the hadron-nucleon elementary scattering amplitude is specified by either a partial wave expansion or a Gaussian in momentum transfer squared. The table is complete through the $1g_{9/2}$ orbital and contains entries for the $3s_{1/2}$ orbital for use if realistic wave functions are expanded in terms of harmonic oscillator functions. (9 refs.)

111325 Calculated oscillator strengths and wavelengths for allowed transitions within the third shell for ions in the Al-like isoelectronic sequence between Cl V and Ni XVI. B.C.Fawcett (Rutherford Appleton Lab., Chilton, Didcot, England). *At. Data & Nucl. Data Tables (USA)*, vol.28, no.3, p.557-78 (May 1983). Theoretical wavelengths and weighted oscillator strengths are tabulated for spectral emission lines of the ions Cl V, Ar VI, Ca VIII, Ti X, Cr XII, Fe XIV and Ni XVI, together with available measured wavelengths. The computations are made in a theoretical framework which includes all configuration-interactions within the complex of principal quantum number $n=3$ and involves the scaling of ab initio values of Slater radial energy integrals based on empirical data. The empirical scale factors and the adopted Slater parameters are listed along with derived energy levels and wave functions. Racah reduced radial dipole matrix elements are also given. (30 refs.)

111326 Calculated oscillator strengths and wavelengths for allowed transitions within the third shell for ions in the Mg-like isoelectronic sequence between S V and Ni XVII. B.C.Fawcett (Rutherford Appleton Lab., Chilton, Didcot, England). *At. Data & Nucl. Data Tables (USA)*, vol.28, no.3, p.579-96 (May 1983). Weighted oscillator strengths, energy levels, and wavelengths are calculated for the $3s^2-3s3p$, $3s3p-3p^2$, $3s3p-3s3d$, $3p^2-3p3d$, and $3s3d-3p3d$ transition arrays for Mg-like ions in the sequence from S V to Ni XVII. Their values are tabulated along with Slater radial integrals, Racah reduced radial dipole matrix elements, and level compositions. The theoretical procedure involves the computation of ab initio values for the Slater radial energy integrals and

their subsequent optimization in accordance with dependent measured wavelengths. Published energy levels are improved on the basis of new calculations of wavelengths of the $3s^2\ ^1S_0-3s3p\ ^3P_1$ intercombination lines. Observational wavelength and energy-level data are tabulated. (31 refs.)

111327 Nuclear data sheets for A=79. B.Singh, D.A.Viggars (Kuwait Inst. for Sci. Res., Kuwait). *Nucl. Data Sheets (USA)*, vol.37, no.3, p.393-485 (Nov. 1982). [received: Sept. 1983]

The 1975 version of Nuclear Data Sheets (75Ur03) has been revised. Nuclear spectroscopic information for known nuclides of mass number 79 (Zn, Ga, Ge, As, Se, Br, Kr, Rb, Sr) has been evaluated and presented together with adopted level energies level J^π s and γ -rays in these nuclei. No data are yet available for excited states in ^{79}Zn and ^{79}Ga . (153 refs.)

111328 Nuclear data sheets for A=153. M.A.Lee (Idaho Nat. Engng. Lab., EG&G Idaho Inc., Idaho Falls, ID, USA). *Nucl. Data Sheets (USA)*, vol.37, no.3, p.487-594 (Nov. 1982). [received: Sept. 1983]

The experimental results from the various reaction and decay studies leading to nuclides in the A=153 mass chain have been reviewed. These data are summarized and presented, together with the adopted level schemes and properties. (203 refs.)

111329 Recent References, January through April 1983 [nuclear data sheets]. S.Ramavataram (Brookhaven Nat. Lab., Upton, NY, USA). *Nucl. Data Sheets (USA)*, vol.37, no.4, p.595-717 (Dec. 1982). [received: Sept. 1983]

Gives nuclear data references for levels, J^π and transitions for various nuclei received in the period January to April 1983. (506 refs.)

111330 Optical fiber systems: Technology, design, and applications. C.K.Kao.

New York, USA: McGraw-Hill (1982), xi+204 pp. [0 07 033277 0]

The book is written to give the readers a glimpse of the range of application and the impact of this technology, as well as to introduce the associated technology of optical fiber systems in a concise and, hopefully, clear manner. The reader can see the interrelationship of the technology and its implications, construct the basis of a system design and perceive the relative advantages and disadvantages.

111331 Selected tables of atomic spectra. Atomic energy levels and multiplet table. O IV. Data derived from the analyses of optical spectra. C.E.Moore.

Report NSRDS-NBS-3-Sect.10, Nat. Bur. Stand., Washington, DC, USA (March 1983), viii+14 pp.

The present publication is the tenth section of a series being prepared in response to the need for a current revision of two sets of the author's tables containing data on atomic spectra as derived from analyses of optical spectra. Part A contains the atomic energy levels and Part B the multiplet tables. Data for O IV are included.

Effect of excited states on thermonuclear reaction ratesSee Entry 116631

01.30M Textbooks for graduates and researchers

111332 Radiation effects computer experiments. J.R.Beeler, Jr.. Amsterdam, Netherlands: North-Holland (1982), xviii+873 pp. [0 444 86315 X]

This book is intended as an introductory handbook, and as a guide for people wishing to learn how to develop and use computer experiment programs to simulate defect production and annealing in solids. Each particular computer experiment approach described has been proven in practice by several competing computer experimenters. Both the functional structure and procedure for the use of these approaches is easily understood. Historically, radiation effects theory has tended to concentrate on either the primary production of Frenkel pairs by a collision cascade or the diffusion of 'free' defects to various sinks long after the primary defect production events have occurred. The intermediate regime is seldom treated. During the intermediate regime, (1) some defects collect into clusters, (2) a large fraction of the defects produced is annihilated, and (3) a small minority emerges as mobile (free) defects, sufficiently far from their origins to have forgotten their native regions. This regime, called short-term annealing ion implantation, is covered in detail in this book and is held as being equal in importance to the primary defect production process. (257 refs.)

111333 Laser annealing of semiconductors. J.M.Poate, J.W.Mayer [Ed.]. London, England: Academic Press (1982), xi+564 pp. [0 12 558820 8]

The laser annealing of semiconductors deals with the materials science of surfaces that have been subjected to ultrafast heating by intense laser beams. The time scale is such that layers can melt and recrystallize in a few hundred nanoseconds. This rapid resolidification of semiconductors has led to novel regimes of phase formation and has served as a means of removing implantation damage. It was this latter aspect that stimulated the field. The chapters in this book follow a logical sequence from basic concepts to device structures. The topics covered include: crystallisation processes; fundamentals of energy deposition; heat flow calculations; supersaturated alloys, solute trapping and zone refining; microstructure and topography; epitaxial growth; surface properties; solid phase regrowth; compound semiconductors; silicides and metastable phases; applications.

01.30P Textbooks for undergraduates

111334 Advances in Mossbauer spectroscopy. Applications to physics, chemistry and biology. B.V.Thosar, P.K.Iyengar, J.K.Srivastava, S.C.Bhargava [Ed.].

Amsterdam, Netherlands: Elsevier (1983), xxiv+924 pp. [0 444 42186 6]

The resonance spectroscopy of gamma-radiation, conventionally known as Mossbauer spectroscopy, after its discovery a quarter of a century ago has developed into an important and versatile tool for the study of solid state properties. The book reviews the experimental method and describes its applications to problems in the general domain of solid state physics. The book is intended to serve as an introductory text to students and to researchers who are new in the field, as well as to provide the specialist with information outside of his immediate field of interest.

111335 Surface physics. Second edition. M.Prutton.

Oxford, England: Clarendon (1983), 138 pp. [0 19 851855 2]

This book emphasizes the physical aspects of surface physics and should have a wide interdisciplinary appeal. It reviews the physical techniques that are now available to give reliable diagnostics of crystal surfaces. Case studies of the application of these techniques to important technological surfaces convey clearly the present state of the art. There are chapters on surface chemical composition, surface structure, surface electronic properties, atomic motion on surfaces, and adsorption of atoms and molecules on surfaces. The book is

suitable as a text for a final-year undergraduate course in physics, chemistry, materials science or electrical engineering. A general background of solid-state physics or chemistry is a necessary prerequisite, but no sophisticated mathematics is needed. (107 refs.)

01.30R Surveys and tutorial papers; resource letters

Self-study manual on optical radiation measurements: Part I -Concepts,

chapter 10. Introduction to coherence in radiometrySee Entry 111382

Self-study manual on optical radiation measurements: Part III - Applications,

chapter 1. Measurement of solar terrestrial spectral irradiance in the ozone

cut-off regionSee Entry 111383

Persistence properties of bifurcationsSee Entry 111570

The dimension of chaotic attractorsSee Entry 111573

The twist map, the extended Frenkel-Kontorova model and the devil's staircase

.....See Entry 111577

Balances of powerSee Entry 111649

Ion sources (recent topics)See Entry 111812

Negative ion sourcesSee Entry 111813

High-resolution scanning transmission electron microscopySee Entry 111827

X-ray microscopy: recent developments and practical applications

.....See Entry 111848

Reassessment of fission fragment angular distributions from continuum states

in the context of transition-state theorySee Entry 112291

Post-critical heat flux heat transfer: a survey of current correlations and their

applicabilitySee Entry 112367

The ignition and burning behaviour of sodium metal in airSee Entry 112401

Transient cooldown in a model cold leg and downcomerSee Entry 112427

Summary report on development of an integral model of a radioactive jet [from

a reactor accident]See Entry 112448

Some remarks concerning triple angular correlationsSee Entry 112597

Historical survey and recent progress in the theory of non-rigid molecules

.....See Entry 112618

The semi-direct product structure of nonrigid molecule groups

.....See Entry 112624

The use of induced representations in nonrigid moleculesSee Entry 112625

Nonempirical calculations of molecular characteristicsSee Entry 112642

The Jahn-Teller effect as a case of electronic non-rigidity. Application to the

ground state of the symmetric $\text{C}_6\text{F}_5\text{H}_3^+$ ionSee Entry 112674

L-shell Coulomb ionizationSee Entry 112830

Future prospects in the development of gaseous electron diffraction

.....See Entry 112853

Electron-ion collisions of fusion interestSee Entry 112855

Molecular structure from the viewpoint of the experimenter—the evolution of

the concept and the problems arisingSee Entry 112866

Optical image processing in coherent and incoherent light: a short comparative

reviewSee Entry 112947

Generation of coherent far-infrared radiation using lasersSee Entry 113059

Review of fiber optic gyroscopesSee Entry 113101

Optical fibre sensors: principles and applicationsSee Entry 113104

Origins and control of polarization effects in single-mode fibers

.....See Entry 113118

Scanning acoustic microscopy: review of recent developments

.....See Entry 113233

Hybrid experimental-numerical stress analysisSee Entry 113290

The turbulence problem: a surveySee Entry 113422

Soliton experiments in plasmasSee Entry 113602

Dynamic methods in plasma physicsSee Entry 113633

Microstructure and topography [laser annealing of semiconductors]

.....See Entry 113709

The application of neutron scattering methods to aqueous electrolyte solutions

.....See Entry 113720

Melt flow of polymer blendsSee Entry 113722

Phase domain size and continuity in sequential IPNs: a review

.....See Entry 113772

Creation of point defects in superconductors. A short review

.....See Entry 113859

Interaction of dislocations with impurities and its influence on the mechanical

properties of silicon crystalsSee Entry 113981

Fundamentals of energy deposition [laser annealing of semiconductors]

.....See Entry 114003

Compound semiconductors [laser and electron beam annealing]

.....See Entry 114007

Structural transformations and their precursorsSee Entry 114154

Clean and adsorbate-induced surface phase transitions on $\text{W}\{100\}$

.....See Entry 114310

Analysis of surfaces and thin filmsSee Entry 114317

Electrical properties of dislocations and boundaries in semiconductors

.....See Entry 114481

Crystal field theory: past, present and futureSee Entry 114498

Nonlinear and frequency-dependent transport phenomena in low-dimensional

conductorsSee Entry 114514

Polyacetylene: A perspective in scientific and technological research of con-

densed matter physicsSee Entry 114515

Transport properties of nearly magnetic alloys and metalsSee Entry 114653

The effect of the microscopic structure of metal surfaces on their optical

propertiesSee Entry 114807

Surface physics with slow positronsSee Entry 114953

Ion-induced sputteringSee Entry 114993

Chemical vapor deposition of group IVB, VB, and VIB elements with nonme-

talts. A literature reviewSee Entry 115076

Siloxanes, silanes, and silazanes in the preparation of ceramics and glasses

.....See Entry 115144

The role of the matrix in fibrous composite structuresSee Entry 115160

Characterization of high performance composite matrices	See Entry 115361
Creep and fracture initiation in fibre reinforced plastics	See Entry 115363
Some aspects of improving abrasive resistance	See Entry 115373
Rust formation on iron - a model	See Entry 115405
Anodic oxidation of iron and cathodic reduction of the anodic film: a review	See Entry 115442
Determination of longevity under a two-frequency load (review), I	See Entry 115468
Acoustic emission in the deformation of concrete (review)	See Entry 115480
Acoustic emission: Past experience within ECSC contracts and future trends	See Entry 115494
The preparation and properties of metallic optically transparent electrodes	See Entry 115565
Absorber surfaces and durability of solar heat collectors	See Entry 115700
Future of biomagnetism	See Entry 115813
The effects of infrasound on human health	See Entry 115830
Measurement of blood flow	See Entry 115880
Image processing for medicine	See Entry 115881
Medical NMR spectroscopy and intoscropy: progress and prospects	See Entry 115895
The biomedical laser	See Entry 115897
The prospects of instrumentation in medical radiology and problems of clinical dosimetry	See Entry 115902
Nuclear medicine	See Entry 115913
Recent advances in medical imaging	See Entry 115914
Cancer and radiotherapy. VI. Present status of radiation therapy	See Entry 115915
Indoor radiation exposures from ²²² Rn and its daughters: a view of the issue	See Entry 115938
Background atmospheric ²²² Rn concentrations outdoors and indoors: a review	See Entry 115939
Airborne radionuclides and radiation in buildings: a review	See Entry 115940
Indoor radon progeny exposure in the Florida phosphate mining region: a review	See Entry 115943
Biomedical telemetry: the formative years	See Entry 115953
Overview of biomedical telemetry techniques	See Entry 115954
Transducers	See Entry 115956
Electrocardiography	See Entry 115957
The recent trend of biomedical signal processing research	See Entry 115958
Safety and reliability in medical equipment and systems	See Entry 115974
Artificial organs	See Entry 115978
Sensory prosthesis	See Entry 115980
Wildlife biotelemetry	See Entry 115983
The seismology of Greece	See Entry 116033
The dynamic Earth	See Entry 116047
The Earth's core	See Entry 116048
The Earth's mantle	See Entry 116049
The oceanic crust	See Entry 116050
The continental crust	See Entry 116051
The Long Valley/Mono Basin volcanic complex in eastern California: status of present knowledge and future research needs	See Entry 116056
The benthic boundary layer and sediment transport	See Entry 116077
An overview of the physical oceanography report	See Entry 116135
Mid-latitude mesoscale variability	See Entry 116136
Subsurface subtropical gyre of the North Atlantic and Pacific oceans	See Entry 116137
Polar oceanography	See Entry 116138
Poleward heat transport by the ocean	See Entry 116139
Equatorial oceanography	See Entry 116140
Physical oceanography of continental shelves	See Entry 116141
Small-scale physics of the ocean	See Entry 116142
Internal waves in the ocean: a review	See Entry 116143
Advances in satellite oceanography	See Entry 116144
Paleoceanography: global ocean evolution	See Entry 116145
Models of the oceanic internal wave field	See Entry 116146
Marine chemistry and paleoceanography in the United States—1978-82—an overview	See Entry 116147
Advances in marine chemistry 1979-82	See Entry 116148
Review of marine organic geochemistry	See Entry 116149
The ocean	See Entry 116150
Progress in cloud physics 1979-1982	See Entry 116252
Cloud electrification	See Entry 116253
Lightning	See Entry 116254
The dynamics of large scale atmospheric motions	See Entry 116255
Mesoscale meteorology	See Entry 116256
Atmospheric boundary layers	See Entry 116257
Polar meteorology and climatology 1979-1982	See Entry 116258
Progress in weather modification research: 1979-1982	See Entry 116259
Advances in short term climate prediction	See Entry 116260
The atmospheric aerosol system: an overview	See Entry 116261
The atmosphere	See Entry 116263
Atmospheric radiation: 1975-1983	See Entry 116277
The Global Atmospheric Research Program: 1979-82	See Entry 116279
Advances in remote sensing of the atmosphere	See Entry 116305
The expansion of a plasma into a vacuum: basic phenomena and processes and applications to space plasma physics	See Entry 116470
Results of astrophysical investigations of asteroids (survey). II	See Entry 116516
Magnetic field lines in the Galaxy (Review of the interstellar magnetic field)	See Entry 116796

The determination of cloud masses and dust characteristics from submillimetre thermal emission	See Entry 116808
Tracing the gas in galaxies	See Entry 116809
Gamma ray bursts	See Entry 116875
Gamma-ray astronomy	See Entry 116886

01.30T Bibliographies

111336 Recent bibliography on analytical and sampling problems of a PWR primary coolant. Supplement II. H. Illy. Report KFKI-1983-81, Hungarian Acad. Sci., Budapest (1983), 22 pp. The first two bibliographies on Analytical and Sampling Problems of a PWR Primary Coolant (KFKI Report-1980-48 and KFKI Report-1981-97) were published in 1980 and 1981, and covered the literature published in the previous 8-10 years. The present Supplement II reviews the subsequent literature up till June 1983. It also includes some references overlooked in the first two volumes. The serial numbers are continued from the first two bibliographies. Cross-referencing was not intended. (178 refs.)	
The seismology of Greece	See Entry 116033
The benthic boundary layer and sediment transport	See Entry 116077
Mid-latitude mesoscale variability	See Entry 116136
Subsurface subtropical gyre of the North Atlantic and Pacific oceans	See Entry 116137
Polar oceanography	See Entry 116138
Equatorial oceanography	See Entry 116140
Physical oceanography of continental shelves	See Entry 116141
Small-scale physics of the ocean	See Entry 116142
Internal waves in the ocean: a review	See Entry 116143
Advances in satellite oceanography	See Entry 116144
Paleoceanography: global ocean evolution	See Entry 116145
Advances in marine chemistry 1979-82	See Entry 116148
Review of marine organic geochemistry	See Entry 116149
Progress in cloud physics 1979-1982	See Entry 116252
Cloud electrification	See Entry 116253
Lightning	See Entry 116254
The dynamics of large scale atmospheric motions	See Entry 116255
Mesoscale meteorology	See Entry 116256
Atmospheric boundary layers	See Entry 116257
Polar meteorology and climatology 1979-1982	See Entry 116258
Progress in weather modification research: 1979-1982	See Entry 116259
Advances in short term climate prediction	See Entry 116260
Atmospheric radiation: 1975-1983	See Entry 116277
The Global Atmospheric Research Program: 1979-82	See Entry 116279
Advances in remote sensing of the atmosphere	See Entry 116305

01.40 EDUCATION

111337 Procedure for written test follow-ups in large sections of university physics. R.R.Boedeker (Dept. of Phys., Southern Illinois Univ., Edwardsville, IL, USA). <i>Am. J. Phys. (USA)</i> , vol.51, no.9, p.859-60 (Sept. 1983). In an earlier article (1978) the author discussed the use of oral follow-ups to written tests. These orals offer students some incentive to improve their understanding of concepts which caused trouble on the written exam. By concentrating on the weak area immediately, they can fill in gaps in knowledge which may be essential to subsequent material. That article outlined an alteration of an earlier approach found in the literature (1975) and the purpose of this note is to present a written follow-up alternative to the oral method. The author believes that the oral method is better and still uses it in small sections (mostly upper level and graduate physics courses), but because of time pressures caused by heavy work loads and large enrollments in sections of University Physics, he has used the written follow-up method recently in these large sections. (4 refs.)	
111338 Biomedical engineering course development for health care delivery. A.Ambardar (Dept. of Electrical Engng., Michigan Technol. Univ., Houghton, MI, USA). <i>IEEE Trans. Educ. (USA)</i> , vol.E-26, no.3, p.111-15 (Aug. 1983). A new program of courses in biomedical engineering has been initiated at Michigan Technological University, both at the graduate and undergraduate level. The rationale for the development of these courses stems from the rapid growth in technology which has permeated almost all areas of health care delivery. The major goals of each course are described in terms of (1) establishing a required level of technical competence and literacy in the field, (2) developing those communication skills that will typically be required of the students after graduation, and (3) developing a sense of challenge which will last the students beyond their formative years. The philosophy underlying the choice of topical content, course organization, and student evaluation are all considered within the broader framework of establishing a modern foundation which the student, as well as the industrial and clinical community, can readily appreciate and identify with. (21 refs.)	
111339 The crisis in high-school physics education: overview of the problem. J.W.Layman. <i>Phys. Today (USA)</i> , vol.36, no.9, p.26-30 (Sept. 1983). The present situation is the culmination of a long trend—interrupted only weakly in the Sputnik era—of declining enrollments in physics, but the state of the economy may provide a new context. (16 refs.)	
111340 The crisis in high-school physics education: why physicists leave teaching. B.F.Porter (American Inst. of Phys., New York, NY, USA), W.H.Kelly. <i>Phys. Today (USA)</i> , vol.36, no.9, p.32-7 (Sept. 1983). A host of problems leads one to wonder who will be there to teach the coming generation of students to work and to succeed in the technological society. (5 refs.)	
111341 The crisis in high-school physics education: paths to a solution. J.R.Franz, B.G.Aldridge, R.B.Clark. <i>Phys. Today (USA)</i> , vol.36, no.9, p.44-9 (Sept. 1983). How local, state and national initiatives are addressing the need for improved financial benefits, better training and greater recognition for science teachers, and for programs to attract more science students. (5 refs.)	

111342 The crisis in high-school physics education: places where things are right. J.M.Wilson (American Assoc. of Phys. Teachers, New York, NY, USA), T.C. Ingoldsbey.

Phys. Today (USA), vol.36, no.9, p.52-7, 60 (Sept. 1983). Analysis of the reasons for the success of a number of outstanding high-school programs in physics suggests a set of conditions for creating successful programs at other schools. (1 ref.)

111343 Experimental physics courses at the Universidad Autonoma Metropolitana, Unidad Iztapalapa. M.A. Patron (Dept. de Fisica, Univ. Autonoma Metropolitana, Mexico City, Mexico).

Rev. Mex. Fis. (Mexico), vol.29, no.3, p.409-17 (May 1983). In Spanish. [received: Sept. 1983]

The criteria and objectives that were used to design the curriculum of experimental physics of the UAM Iztapalapa are briefly discussed. The contents of each course is presented as well as its relationship with the original aims. (no refs.)

01.50 EDUCATIONAL AIDS

111344 The physics of karate. S.R. Wilk, R.E. McNair, M.S. Feld (Dept. of Phys., MIT, Cambridge, MA, USA).

Am. J. Phys. (USA), vol.51, no.9, p.783-90 (Sept. 1983).

This study analyzes physical aspects of a karate strike and its interaction with a target, examining some heretofore unexplored dynamical and biomechanical questions. (22 refs.)

111345 Periodic boundary conditions in special relativity. P.C. Peters (Dept. of Phys., Univ. of Washington, Seattle, WA, USA).

Am. J. Phys. (USA), vol.51, no.9, p.791-5 (Sept. 1983).

The imposition of periodic boundary conditions on the space-time of special relativity is shown to lead to the existence of a preferred frame of reference. One characteristic of the preferred frame is that it is the frame in which the resulting finite universe has the smallest size. In a frame moving with respect to the preferred frame, global synchronization of clocks cannot be carried out and the transit time to traverse the universe depends on the direction of travel. As measured in a moving frame, a person at rest in the preferred frame can be found at two or more different places at the same time, although the age of the person will be different at each of those places. A 'pole in the universe' paradox is presented, the resolution of which requires use of some of these bizarre properties of the universe of periodic boundary conditions. (3 refs.)

111346 Clock synchronization, a universal light speed, and the terrestrial red-shift experiment. A.L. Macdonald (Luther Coll., Decorah, IA, USA).

Am. J. Phys. (USA), vol.51, no.9, p.795-7 (Sept. 1983).

This paper (i) gives necessary and sufficient conditions that clocks in an inertial lattice can be synchronized, (ii) shows that these conditions do not imply a universal light speed, and (iii) shows that the terrestrial red-shift experiment provides evidence that clocks in a small inertial lattice in a gravitational field can be synchronized. (8 refs.)

111347 Under \$100 home computers as laboratory devices. F.J. Wunderlich, D.E. Shaw (Dept. of Phys., Villanova Univ., Villanova, PA, USA).

Am. J. Phys. (USA), vol.51, no.9, p.797-801 (Sept. 1983).

The purpose of this article is to alert physics educators to an important new application of inexpensive home computers in the undergraduate laboratory. These computers can be used to establish cost effective yet versatile experimental laboratory stations which directly measure physical parameters and control experiments, as do their more expensive computer counterparts. As specific examples, the authors illustrate how the computer with minimal circuitry can function as digital voltmeter and pulse counter. (26 refs.)

111348 Home-experimental demonstrations of Hart's frictional force rotor. F.S. Crawford (Dept. of Phys., Univ. of California, Berkeley, CA, USA).

Am. J. Phys. (USA), vol.51, no.9, p.804-6 (Sept. 1983).

A block, pushed steadily across the slope of a plane inclined to the horizontal at less than the critical angle, describes a straight-line trajectory having a direction independent of velocity. If instead the block is projected across the slope and then allowed to slide freely, it stops after describing a curved trajectory. For different initial velocities the stopping points all lie on the same straight line. For small inclinations of the plane this stopping-point line makes an angle with the direction of constant elevation that is just half the angle that the trajectory of the steadily pushed block makes with that direction. (1 ref.)

111349 Nonionizing radiation: appropriate topic in a physics curriculum. A.J. Adams (Graduate Inst. of Technol., Univ. of Arkansas, Little Rock, AR, USA).

Am. J. Phys. (USA), vol.51, no.9, p.807-10 (Sept. 1983).

A three-hour, one-semester course in nonionizing radiation for students in the interdisciplinary field of electronics and instrumentation is outlined. Electromagnetic radiation extending from the ultraviolet to the 60-Hz power frequency and ultrasonic radiation were discussed. Emphasis was placed on the nature and sources of the radiation, the biophysical interaction mechanisms, and the instrumentation used to measure nonionizing radiation. (17 refs.)

111350 Electron impact excitation and UV emission in the Franck-Hertz experiment. W. Buhr, W. Klein (I. Phys. Inst., Univ. Koln, Koln, Germany), S. Pressler.

Am. J. Phys. (USA), vol.51, no.9, p.810-14 (Sept. 1983).

With the Franck-Hertz experiment described the inelastic collision of electrons with mercury atoms and the ultraviolet emission of the excited atoms can be observed simultaneously. The Franck-Hertz tube is a four electrode tube with a concentric system and a quartz window. An electron current stabilization allows the observation of a stepwise increase in light intensity by means of a photomultiplier. The emission spectrum shows the Hg 2536-Å line and two molecular emission bands arising from Hg dimer and trimer transitions. The light emission from the trimer state reveals the influence of geometrical factors of the tube at different accelerating potentials. (17 refs.)

111351 An optimal speed for traversing a constant rain. S.A. Stern (Dept. of Civil Engng., Univ. of Texas, Austin, TX, USA).

Am. J. Phys. (USA), vol.51, no.9, p.815-18 (Sept. 1983).

Whether it is better to walk or run through a rain shower is a question often posed by adult and child alike. The answer to this question requires careful physical analysis and provides an instructive even illuminating exercise for high school as well as undergraduate introductory physics classes. The author derives a rule for the optimal travel speed which minimizes the number of rainstrikes on a given surface element over a given course. He also investigates the speed versus intensity relationship. Methods of extending these results to include rainfalls with horizontal velocity relative to the travel path and for surfaces of arbitrary geometry are presented. (4 refs.)

111352 A criterion for stationary states in quantum mechanics. M.R. Aub

(Dept. of Math., Univ. of the West Indies, Kingston, Jamaica), H. Niederreiter.

Am. J. Phys. (USA), vol.51, no.9, p.818-19 (Sept. 1983).

The authors show a criterion for a vector ϕ in a complex inner product space V to be an eigenvector of a Hermitian operator A in V in terms of the values of inner products $\langle X\phi, A\phi \rangle$ for Hermitian operators X . This result can be applied to the characterization of stationary states in quantum mechanics. (7 refs.)

111353 A spherical viewing screen for diffraction patterns. R.D. Ayers (Dept. of Phys.-Astron., California State Univ., Long Beach, CA, USA).

Am. J. Phys. (USA), vol.51, no.9, p.820-3 (Sept. 1983).

Fraunhofer diffraction from a planar diffracting object is explained in terms of spatial Fourier transforms and the Ewald sphere construction from solid-state physics. It is found that the most meaningful view of such a diffraction pattern is obtained by letting it fall on a spherical screen centered upon the diffracting object and then observing the pattern from a distance along the normal to the plane. This visual projection yields a circular portion of the two-dimensional spatial transform of the diffracting object without any geometrical distortion. A classroom demonstration using a laser and crossed gratings of good quality illustrates clearly the superiority of this viewing technique over the standard procedure of simply allowing the pattern to fall directly on a flat screen. (9 refs.)

111354 Measurements on the He-Ne laser lines near 633 nm. D.W. Steinhilber (Dept. of Phys., Southwestern at Memphis Coll., Memphis, TN, USA).

Am. J. Phys. (USA), vol.51, no.9, p.824-5 (Sept. 1983).

The red line from an inexpensive He-Ne laser is made up of several closely spaced lines. To separate these lines very high spectral resolution is required. This apparatus requirement can be met by a simple modification of a student Fabry-Perot interferometer. Laboratory measurements can then be made to verify the expected number, spacing, and polarization of these lines during a single afternoon laboratory session. (12 refs.)

111355 Some novel delta-function identities. C.P. Frahm (Illinois State Univ., Normal, IL, USA).

Am. J. Phys. (USA), vol.51, no.9, p.826-9 (Sept. 1983).

Two novel identities arising from the second- and third-order derivatives of the reciprocal radial distance and involving delta functions are introduced, proven, and illustrated. A general procedure is described for establishing similar identities for higher-order derivatives of the reciprocal radial distance. (9 refs.)

111356 How batteries work: a gravitational analog. D. Roberts (Dept. of Phys., MIT, Cambridge, MA, USA).

Am. J. Phys. (USA), vol.51, no.9, p.829-31 (Sept. 1983).

There is a region in any battery where the charges move in a direction opposite to that of the electric force on them. A 'gravitational cell' is used to show that this motion is a diffusion analogous to that against pressure gradients in osmotic pressure situations. The driving mechanism for the diffusion is the existence of lower lying states in one region compared to an adjacent region, and it is relaxation into these low lying states that is the source of energy for the circuit. (8 refs.)

111357 Optical correlator using the incoherent light of a slide projector. A. Hairie, J. Provost (Inst. des Sci. de la Matiere, Univ. de Caen, Caen, France).

Am. J. Phys. (USA), vol.51, no.9, p.832-6 (Sept. 1983).

The simple apparatus based on geometrical optics described allows both qualitative and quantitative verification of the main properties of convolution, correlation, or autocorrelation. These concepts are of considerable interest in several areas of physics and engineering. Qualitative verifications are easily made by projection of convolution or correlation function on a screen. Quantitative verifications have been performed in the case of functions of one coordinate by recording convolution or correlation on an X-Y recorder. (8 refs.)

111358 The Born centenary: remarks about classical thermodynamics. P.T. Landsberg (Dept. of Electrical Engng., Univ. of Florida, Gainesville, FL, USA).

Am. J. Phys. (USA), vol.51, no.9, p.842-5 (Sept. 1983).

Max Born (1882-1970) advocated Caratheodory's approach to thermodynamics in 1921 and 1949, and it was expounded by various authors in the intervening years, but it did not come into general use. Some historical remarks are made concerning the discussions between Born and Caratheodory. Although the Caratheodory approach continues to be regarded as 'difficult', it is noted that his principle (as contrasted with what is called his theorem) is really straightforward in concept. It is emphasized that there was a need to push Caratheodory's approach further since it did not cover the third law of thermodynamics, and that set theory and simple topological concepts provided the ideal tools to achieve this aim. This led to a more complete geometrization of thermodynamics. Although specialized and mathematical work on the axiomatization of thermodynamics continued in the 1960s and 1970s, there also emerged a reasonably simple way of combining elements of the geometrical approach and the approach via thermodynamic cycles, as it is recalled. When Born died in 1970 this work was essentially complete. (27 refs.)

111359 General solution of the classical Schwinger model. F.J. Carbajo, E. Sanchez-Velasco.

Am. J. Phys. (USA), vol.51, no.9, p.845-7 (Sept. 1983).

The general solution of the massless Maxwell-Dirac equations in 1+1 dimensions, the classical version of the Schwinger model, is found. This solution serves as a good introduction in an intermediate course of mathematical physics to the study of concentrated propagating waves. (3 refs.)

111360 Rubens flame tube demonstration: a closer look at the flames. G.F. Spagna, Jr. (Rensselaer Polytech. Inst., Troy, NY, USA).

Am. J. Phys. (USA), vol.51, no.9, p.848-50 (Sept. 1983).

The author studies how structure and behavior of flames is affected by the sound driving the tube by examining the individual flames using a variety of techniques and instruments. Specifically, they deal with photocell, microphone, television, film and schlieren projection observations. The television and schlieren studies were done with a stroboscopic disk, the photocell and microphone studies employed a dual trace oscilloscope, and the film study was done with a high-speed rotating prism camera. (8 refs.)

111361 Teaching first-year kinematics via the scalar product. T.H. Chyba (Dept. of Phys., Randolph-Macon Coll., Ashland, VA, USA).

Am. J. Phys. (USA), vol.51, no.9, p.851 (Sept. 1983).

A systematic development of vector mathematics in a calculus-based physics course constrains the teacher to introduce the cross and dot products during the first two weeks. Unfortunately, their application to physics is forsaken until later discussions of work (6th week) and torque (11th week). Several texts offer geometrical interpretations of these products, which, though instructive, are not germane to the development of mechanics. The problem is how to reinforce these concepts quickly within the natural presentation of

mechanics. The author describes one application of the scalar product to kinematics (3rd week) which is not mentioned in common texts. (2 refs.)

111362 The range of a data set: a quick estimator of the standard deviation. G.C.Kyker, Jr. (Kose-Hulman Inst. of Technol., Terre Haute, IN, USA).

Am. J. Phys. (USA), vol.51, no.9, p.852 (Sept. 1983).

One of the concepts most stressed in the elementary physics laboratory is the need to assess the uncertainty in each measurement of a physical quantity, as the measurement is made. In practice, one of the most usual ways in which students are taught to do this is by making repeated trials of a measurement and calculating a standard deviation. There are good practical reasons for knowing the precision of a set of data while one is working in the laboratory—to signal the need for more or different measurements, to flag a malfunctioning piece of equipment, and so on. On the other hand, frequent pauses to calculate out a standard deviation during the work in a student lab are annoying, distracting, and error prone. It turns out that the range of a set of numbers provides an estimate of the standard deviation that is available literally at a glance, and is nearly as good an estimate as the usual calculation. (7 refs.)

111363 A simple demonstration of spherical aberration. A.R.Lachaine, P.Rochon (Dept. of Phys., Royal Military Coll., Kingston, Ontario, Canada).

Am. J. Phys. (USA), vol.51, no.9, p.853-5 (Sept. 1983).

The study of geometrical optics has long been an integral part of any course in elementary physics. Indeed, the introduction of the paraxial rays approximation and Snell's law make the study of thin lenses tractable in easy and concise mathematical form. In the laboratory, however, the student quickly becomes aware of the limitations of the theory and finds that the aberrations, often just mentioned in the lectures, are very important and are the origin of many errors in measurement. The failure of all rays from a point object on the optic axis to converge to a single point image is due, in part, to spherical aberration, i.e. to the spherical form of the lens surfaces. Although, in general, calculations of spherical aberrations in lenses can be quite complicated, requiring in many instances use of numerical methods, a particular case, described by the authors, involving a plano-concave diverging lens, permits comparison between experiment and a simple analytical theory. (6 refs.)

111364 More on two-dimensional scattering. P.A.Maurone (Dept. of Phys., Villanova, Univ., Villanova, PA, USA), T.K.Lim.

Am. J. Phys. (USA), vol.51, no.9, p.856-7 (Sept. 1983).

The authors have given a derivation of the optical theorem in two dimensions and shown its consistency with the standard partial wave analysis. One should notice that this presentation is more difficult in the two-dimensional case than it was in the three-dimensional case. The study of this two-dimensional problem as an introduction to the three-dimensional case is probably not a good pedagogical tool. However, the authors feel there is justification for studying two-dimensional dynamics since there are a wealth of physical applications. (5 refs.)

111365 Newton's law of cooling with finite reservoirs. P.A.Maurone, C.Shiomos (Dept. of Phys., Villanova Univ., Villanova, PA, USA).

Am. J. Phys. (USA), vol.51, no.9, p.857-9 (Sept. 1983).

A compact analysis of both theory and experiment that the authors find very appropriate for an introductory laboratory course is presented. Students surmise that when one has two finite samples in a cooling experiment, the samples should both exhibit some sort of exponential behavior toward final equilibrium. In this paper they are shown how to derive and verify this intuition. The apparatus described is inexpensive, easy to construct, and experimental results are easily reproducible. (12 refs.)

111366 Galactic lens. J.Higbie (Dept. of Phys., Univ. of Queensland, Brisbane, Queensland, Australia).

Am. J. Phys. (USA), vol.51, no.9, p.860-1 (Sept. 1983).

It is well known that light rays are 'bent' in the vicinity of a gravitating object such as the Sun or a black hole. Earlier, a plastic lens has been described which simulates this action and demonstrates quite convincingly the visual distortions which arise and in particular the generation of visual double images of a single source (1980, 1981). One of these lenses was constructed in response to the recently announced discovery of a double quasar which is thought to be a gravitational double image. In the Scientific American article discussing this phenomenon, Frederick Chaffee (1980) mentions the possibility of three images being produced if the gravitating object has an extended mass distribution. In order to see how this can come about and to appreciate how the various images differ from one another, the authors have constructed yet another plastic lens which simulates the action of an extended (transparent) mass distribution. (4 refs.)

111367 Spectroscopically silent fundamental vibrations. R.L.Keiter (Univ. of Illinois, Urbana, IL, USA).

J. Chem. Educ. (USA), vol.60, no.8, p.625 (Aug. 1983).

Nonlinear polyatomic molecules will have 3N-6 fundamental vibrations is readily understood, and that these vibrations may be infrared or Raman active is common knowledge. The student is led to see that a fundamental vibration will be infrared active only if it is accompanied by a change in dipole moment and Raman active only if there is a change in polarizability (symmetry selection rules). Furthermore, for a centrosymmetric molecule a given vibration cannot be both infrared and Raman active (rule of mutual exclusion). Unless these concepts are taught carefully certain extensions of thought are implied which are not true. While most chemists know that a fundamental vibration may be both infrared and Raman active and that it may be either infrared or Raman active, few appear to be aware that it may be neither. It also appears that many nonspectroscopists who deal with these topics in their teaching have not considered the spectroscopically silent vibration. It is the purpose of this communication to explore the reasons for this pedagogical blind spot. (3 refs.)

111368 Adiabatic lapse rates of planet atmospheres. H.F.Blanck (Austin Peay State Univ., Clarksville, TN, USA).

J. Chem. Educ. (USA), vol.60, no.8, p.637-8 (Aug. 1983).

It has recently been suggested by Blanck (1982) and Earl (1982) that derivations of the equation for the dry adiabatic lapse rate and related equations which give the temperature and pressure of planet atmospheres as a function of altitude be included in undergraduate physical chemistry class discussions and textbooks. Using the hydrostatic equation $dp = -\rho g dh$, the ideal gas law, and an adiabatic change of state equation for an ideal gas, a straightforward derivation yields $-dT/dh = Mg/C_p$, $T = T_0 - Mgh/C_p$, and $p = p_0 [1 - Mgh/C_p T_0]^{C_p/R}$ provided the heat capacity is treated as being constant. While these derivations are certainly worthwhile additions to physical chemistry material, it is equally important to discuss the consequences of these equations and relate them to actual planet atmospheres where possible. (12 refs.)

111369 Bond angles and hybridization indices in AX₂YZ and AX₂Y systems. G.Gilli, V.Bertolasi (Istituto Chimico, Univ. di Ferrara, Ferrara, Italy).

J. Chem. Educ. (USA), vol.60, no.8, p.638-9 (Aug. 1983).

The authors discuss the solution of the bond angles and hybridisation indices for the AX₂YZ or AX₂YE (where E denotes a lone pair) systems of C_s symmetry and, for the particular case of the AX₂Y system of C_{2v} symmetry. (11 refs.)

111370 Note on a simple derivation of Planck's formula from special relativity. J.B.Dence (Washington Univ., St. Louis, MO, USA).

J. Chem. Educ. (USA), vol.60, no.8, p.645-6 (Aug. 1983).

Textbooks of physical chemistry and of general physics still present the events of the period of the old quantum theory (1900-25) in a historical manner. For example, the Planck formula, $E = h\nu$, for the quantization of electromagnetic radiation is usually presented as a bold and ground-breaking proposal, which it was in 1905. The authors present a simple alternative way of introducing the important Planck formula. While the treatment here does not pretend to be an original idea, it is to be found in very few textbooks and, therefore, may not be too well known. The authors show how the equation may be deduced from ideas of special relativity and the hypothesis of wave-particle duality. (no refs.)

111371 Kinetic models for adiabatic reversible expansion of a monatomic ideal gas. On-Kok Chang (Univ. of California, Davis, CA, USA).

J. Chem. Educ. (USA), vol.60, no.8, p.647-8 (Aug. 1983).

The model contains a fixed amount of an ideal gas confined in an adiabatic cylinder and piston device. The piston is moved outward slowly with a constant speed u by an external device, with u much smaller than the average velocity of gas molecules. In this process, the gas expands reversibly and adiabatically. (2 refs.)

111372 Measurement of mass. R.W.Zimmerer (Univ. of Colorado, Boulder, CO, USA).

Phys. Teach. (USA), vol.21, no.6, p.354-9 (Sept. 1983).

Many examples of mass measurement depend on basic physics which has been known and understood since Newton first proposed it. Adapting these physical laws to construct instruments for the measurement of mass has depended on mechanical and electronic apparatus of ever increasing complexity and sophistication. Various techniques become practical or obsolete according to the ever changing state of the art. The author considers the impact modern technology has had in this small field of mass measurement and speculates on what future developments might be. (3 refs.)

111373 More bicycle physics. T.B.Greenslade, Jr. (Dept. of Phys., Kenyon Coll., Gambier, OH, USA).

Phys. Teach. (USA), vol.21, no.6, p.360-3 (Sept. 1983).

The author presents several examples drawn from experience in cycling, for use in teaching mechanics. These include: a West Indian Rastafarian broom seller carrying brooms on his head, turning a corner while riding a bicycle; the problems of riding a Penny-farthing (known as an Ordinary bicycle in the US); and a model for bicycle dynamics. (3 refs.)

111374 Bernoulli on a large scale. A.A.Bartlett (Dept. of Phys., Univ. of Colorado, Boulder, CO, USA).

Phys. Teach. (USA), vol.21, no.6, p.376-7 (Sept. 1983).

The author describes the rising air currents over the press box at a football stadium, traced by the movements of litter from a football game. The circulation of large pieces of paper indicates clockwise circulation of air from the field, up the inclined row of seats, up the side of the press box, into a low pressure region, round and down to the field again. This appears to be a large-scale manifestation of the Bernoulli principle. (1 ref.)

111375 Practical mechanics: raising a mast. R.L.Neman (Dept. of Chem., East Central Univ., Ada, OK, USA).

Phys. Teach. (USA), vol.21, no.6, p.379-80 (Sept. 1983).

The author discusses the mechanics of raising a long pole, ladder, post, antenna support tower, or basketball goal support by 'walking' the object from a horizontal position to a vertical one. The first few steps are not bad, but as the mast is raised further into the air, the job becomes increasingly more difficult; even the lightest structure can be deceiving. There comes a point, however, at which the job becomes easy once again, and finally, at vertical, the 'weight' of the mast is apparently zero; all one has to do is keep it balanced until it is secured. The analysis of the situation is an excellent example of practical physics for the students of mechanics. (1 ref.)

111376 Kinematics of a student. J.H.Nelson (Harrington High School, Rosemont, PA, USA).

Phys. Teach. (USA), vol.21, no.6, p.386-7 (Sept. 1983).

Describes experiments that involve the student as the object of the experiment. Other such experiments include measuring: student reaction time; horsepower generated by a student. Such experiments generate student interest and thus increase understanding of the physics principles involved. (2 refs.)

111377 Homemade rainbows: a backyard experiment. R.W.Robinett (Dept. of Phys., Univ. of Wisconsin-Madison, Madison, WI, USA).

Phys. Teach. (USA), vol.21, no.6, p.388-90 (Sept. 1983).

The natural phenomenon of the rainbow has fascinated man throughout history; it has appeared in literature since at least Biblical times and intrigued scientists since Aristotle. The history of man's attempts to understand the rainbow has been admirably reviewed by Boyer (1959) while many sources treat the optics of its formation in detail. Primary and secondary bows can be easily seen using the fine mist of a garden hose. Such a 'homemade' rainbow not only makes a good demonstration, but the quantitative predictions of its location and size can be verified with the absolute minimum of equipment, making it useful for a simple home project or outdoor experiment. The author briefly reviews the physics of the rainbow using only the ideas of reflection and refraction. (9 refs.)

111378 Standing waves—a new twist. C.J.Roddy (North Carolina State Univ., Raleigh, NC, USA).

Phys. Teach. (USA), vol.21, no.6, p.408-9 (Sept. 1983).

In order to demonstrate standing waves to a large lecture audience or even a moderate one, it has been traditional to use a small string vibrator and line or to shake a rubber rope. Both of these are adequate demonstrations; however, the vibrating string is hard for students to see, and the rubber rope is difficult for the lecturer to operate effectively. The author presents a new apparatus that alleviates these problems while keeping costs to a minimum. (no refs.)

111379 Resonance demonstrator. T.A.Scott (Missouri Western State Coll., Saint Joseph, MO, USA).

Phys. Teach. (USA), vol.21, no.6, p.409 (Sept. 1983).

The author describes a resonance demonstrator with ball-bearing and wire oscillators, mounted on a wooden frame and driven by a variable speed rotator. By changing the speed of the variable rotator, the different oscillations can be excited separately. (no refs.)

111380 Conversations with Avogadro. D.Moreno (Dept. de Fisica, Facultad de Ciencias, Univ. Nacional Autonoma de Mexico, Mexico City, Mexico). *Rev. Mex. Fis. (Mexico)*, vol.29, no.3, p.401-8 (May 1983). In Spanish. [received: Sept. 1983]
A criticism is made of the most usual type of teaching laboratory practice. It is shown that experiments designed for measurements of fundamental constants are specially dangerous. As an example, an analysis is made of an 'experiment' to determine Avogadro's number and the argument is presented that probably the only one to learn some physics from this type of experiment, is the physicist who wrote it. A proposal is made to turn around this drawback and to produce some laboratory activities with more educational value. (2 refs.)

111381 Physics in Xalapa. C.R.de la Cruz (Facultad de Fisica, Univ. Veracruzana, Xalapa, Mexico). *Rev. Mex. Fis. (Mexico)*, vol.29, no.3, p.449-60 (May 1983). In Spanish. [received: Sept. 1983]
A brief history of the development of physics in the state of Veracruz is presented. This account is mainly based on the activities centered at the Universidad Veracruzana. (no refs.)

111382 Self-study manual on optical radiation measurements: Part I - Concepts, chapter 10. Introduction to coherence in radiometry. J.B.Shumaker. **Report NBS-TN-910-6**, Nat. Bur. Stand., Washington, DC, USA (March 1983), viii+60 pp.
The manual is a comprehensive tutorial treatment of the measurement of optical radiation that is complete enough for self instruction. Detailed chapter summaries make it also a convenient authoritative reference source. In this chapter the reader is introduced to the basic field quantity of the theory of partial coherence, the cross-spectral density function, and shown how it is used to describe radiation fields. The propagation of cross-spectral density along a beam is discussed and this propagation illustrated with calculations of diffraction effects in a number of simple aperturing and imaging examples. For instance, the author treats in considerable detail one of the most common radiometric situations in which coherence effects can manifest themselves, the measurement of the slit-scattering function of a monochromator. Among other things, this treatment shows that laser illumination of a monochromator entrance slit must be nearly on-axis to avoid serious slit-scattering function distortions. Finally, the relationships between the cross-spectral density function and the classical radiometric quantities, such as spectral radiance are presented. (21 refs.)

111383 Self-study manual on optical radiation measurements: Part III - Applications, chapter 1. Measurement of solar terrestrial spectral irradiance in the ozone cut-off region. H.J.Kostkowski, R.D.Saunders, J.F.Ward, C.H.Popenoe, A.E.S.Green. **Report NBS-TN-910-5**, Nat. Bur. Stand., Washington, DC, USA (Dec. 1982), xii+80 pp.
Material developed in earlier chapters is used to perform state-of-the-art measurements in Gainesville, Florida, of solar terrestrial spectral irradiance between 290 and 340 nm. The measurement equation is used to design the experiment and to address the effects of polarization, non-linearity, spectral scattering, distortion, slit-scattering function, spectral irradiance calibration, and wavelength calibration. Estimates are made of the uncertainties associated with all these factors. The total uncertainty is estimated to be about 10 percent. An appendix includes details for computing the solar terrestrial spectral irradiance between 280 and 310 nm. Suggestions are made for reducing the uncertainty by about one third and for further research in UV solar terrestrial measurements. (26 refs.)

01.65 HISTORY OF SCIENCE

111384 Transuranium research in Germany 1939 to 1945. K.Starke (Philips-Univ., Marburg, Germany). *Atomkernenerg. Kerntechnik. (Germany)*, vol.41, no.4, p.264-6 (1982). [received: Sept. 1983]
The first nuclear reactor became self-sustaining in Chicago on December 2, 1942. The 40th anniversary of this event gives occasion to recollect the German reactor project. The failure to achieve, after a promising beginning, a uranium-graphite pile also in Germany is discussed. (29 refs.)

111385 Computers and philosophical lexicography: the activities of the Lessico Intellettuale Europeo. A.Lamarra (Lessico Intellettuale Europeo, Rome, Italy). *Comput. & Hum. (Netherlands)*, vol.16, no.4, p.223-8 (Dec. 1982).
Discusses some activities of the research institute, Lessico Intellettuale Europeo in text analysis of philosophical and scientific works. The use of computers in two distinct areas is noted: the integrated analysis of texts so that lexicons can be compiled, of an author's complete works or of a single text; the establishment of a database to support the Thesaurus Mediae et Recentioris Latinitatis and the Dizionario Filosofico del Seicento e del Settecento. (18 refs.)

111386 October 8, 1958—first pacemaker implantation: a milestone in medical history. G.Bartels. *Electromedica (Germany)*, vol.51, no.3, p.119-21 (1983).
The first implantable cardiac pacemaker was developed by Siemens-Elema, Stockholm (then Elema-Schonander), and implanted in a patient on October 8, 1958. Dr. Rune Elmqvist, Elema, developed this cardiac pacemaker at the suggestion of Dr. Ake Senning, surgeon at the Karolinska Hospital in Stockholm. The pacemaker had silicon transistors and a nickel-cadmium battery. (no refs.)

111387 The relics of physics. B.Elbek (Niels Bohr Inst., Copenhagen, Denmark). *Phys. Scr. (Sweden)*, vol.T5, p.143-4 (1983). (Proceedings of the 4th Nordic Meeting on Nuclear Physics, Fuglso, Denmark, 16-20 Aug. 1982).
Discusses the lack of relics from famous discoveries in physics such as Newton's apple and Archimede's bathtub. (no refs.)

111388 The introduction of wave optics: the Fresnelian explanation of diffraction. J.J.Saldana (Facultad de Filosofia y Letras, Univ. Nacional Autonoma de Mexico, Mexico City, Mexico). *Rev. Mex. Fis. (Mexico)*, vol.29, no.3, p.419-47 (May 1983). In Spanish. [received: Sept. 1983]
The paper is concerned with the historical and scientific context in which the wave theory of light was introduced in the early 19th century in France. In particular, the political and scientific activity is analyzed to understand the emergence of Fresnel's undulatory explanation of diffraction phenomena. The opposition of the partisans of the 'theorie de l'emission' is analyzed too. The aim of the paper is to show the methodological relevance of the social history of science, in the historical explanation of science. (58 refs.)

01.70 PHILOSOPHY OF SCIENCE

Computers and philosophical lexicography: the activities of the Lessico Intellettuale Europeo See Entry 111385

01.90 OTHER TOPICS OF GENERAL INTEREST

111389 Structure of system rule of structure formation in steps, application of the new rule, and primary design of data center system. H.Kato, Y.Hori, T.Hata, T.Yamamoto, Y.Yamada, T.Muta. *Rep. Gov. Ind. Res. Inst. Nagoya (Japan)*, vol.32, no.5-6, p.105-16 (May-June 1983). In Japanese.
The authors propose a new concept of structure formation of science and technology. And the history of science and technology was analyzed by applying the new concept. As a result, a new rule on the structure formation of science and technology was found out. The new method that was applied to formulate the structure of science and technology in steps was developed by applying the new rule and primary design of data center system for ceramic studies was finished. (23 refs.)

111390 Mechanics of maneuvering aircraft by rotation of the thrust vector. I.F.Obraztsov, V.F.Pavlenko, A.I.Nelyubov (N.E. Zhukovskii Air Force Engng. Acad., Moscow, USSR). *Sov. Phys.-Dokl. (USA)*, vol.27, no.12, p.1027-9 (Dec. 1982). Translation of: *Dokl. Akad. Nauk SSSR*, vol.267, no.4-6, p.1327-30 (Dec. 1982). [received: Sept. 1983]
Technical progress in constructing aircraft and especially in constructing engines has permitted the production of vertical takeoff and landing aircraft (VTOLA) with useful flight characteristics, whose propulsion unit includes, as a rule, extra-lift engines (ELE) with rotation of the thrust vector upward from the longitudinal axis of the aircraft through an angle greater than $\pi/2$. With some modifications of the turning system, the rotation of the ELE thrust vector can be used not only to provide for vertical takeoff and landing but also to improve maneuverability in flight. (2 refs.)

02.00 MATHEMATICAL METHODS IN PHYSICS

02.10 ALGEBRA, SET THEORY, AND GRAPH THEORY

111391 [n,n-1] Pade' approximants=N term borel integral for frequency dependent polarizability. G.C.Shukla (Dept. of Biophys., AIIMS, New Delhi, India). *Indian J. Phys. Part B*, vol.57B, no.3, p.264-6 (June 1983).
Dispersion force computations take recourse to Pade' approximants to construct a converging sequence of Pade' bounds (lower and upper) i.e. $[n,n-1]$, knowing its Cauchy moments. Also a related method the method of Borel (Langhoff and Karplus 1970) and numerical methods to solve the relevant set of equations were provided by the authors (Yousif and Shukla 1980, Yousif 1979). In earlier work (Yousif and Shykla 1980), the equivalence of $n=3$ term Borel integral has been established with $[3,2]$ Pade' approximants numerically. The aim of the present note is to give an algebraic proof for such an equivalence for $n=3$. Nevertheless, the proof can be extended to any order of n . (8 refs.)

111392 On the inversion of the commutation operator. M.Bruschi, O.Ragnisco (Istituto di Fisica, Univ. di Roma, Rome, Italy). *Lett. Nuovo Cimento (Italy)*, vol.38, ser.2, no.2, p.41-4 (10 Sept. 1983).
The authors display the explicit form of the inverse of the commutation operator $[A, \cdot]$, A being a matrix of arbitrary dimension with simple characteristic roots. (1 ref.)

111393 Lie algebras whose maximal subalgebras are modular. V.R.Varea (Dept. of Algebra, Univ. of Zaragoza, Zaragoza, Spain). *Proc. R. Soc. Edinburgh Sect. A (GB)*, vol.94, pt.1-2, p.9-13 (1983).
A subalgebra M of a Lie algebra L is called modular in L if M is a modular element in the lattice of the subalgebras of L . The author studies the finite-dimensional Lie algebras, all of whose maximal subalgebras are modular. The author characterizes these algebras over any field of characteristic zero. (11 refs.)

ILUCG2: subprograms for the solution of a linear asymmetric matrix equation arising from a 9-point discretization See Entry 111396

ICCG2: subprograms for the solution of a linear symmetric matrix equation arising from a 9-point discretization See Entry 111397

ILUCG3: subprograms for the solution of a linear asymmetric matrix equation arising from a 7, 15, 19 or 27 point 3D discretization See Entry 111398

ICCG3: subprograms for the solution of a linear symmetric matrix equation arising from a 7, 15, 19 or 27 point 3D discretization See Entry 111399

Almost asymptotic stability of system of processes See Entry 111426

The recursion method of a linear operator inversion. III See Entry 111480

On field algebras in quantum theory with indefinite metric ... See Entry 111905

Linear theory of thin shells on the basis of the concept of added vectors See Entry 113287

02.20 GROUP THEORY
(for algebraic methods in quantum mechanics, see 03.65; for symmetries in elementary particle physics, see 11.30)

111394 Method of recurrent construction of Lowdin spin-adapted wave functions. III. Lowdin basis and its permutation symmetry: evaluation of overlap integrals. A.I.Panin (Chem. Dept., Leningrad State Univ., Leningrad, USSR). *Int. J. Quantum Chem. (USA)*, vol.24, no.3, p.279-306 (Sept. 1983).
For pt.II see *ibid.*, vol.22, p.1177 (1982). The Lowdin basis functions are introduced and their permutation symmetry is studied in detail. A simple relation between the Lowdin basis and the orthogonal basis constructed by means of Young-Yamanouchi units is established. Both analytical and recurrence formulas for the overlap integrals of the Lowdin and some relevant auxiliary functions are derived. The symmetry of the overlap matrix of the Lowdin basis functions is briefly discussed. (26 refs.)

111395 Site symmetry, interchange symmetry, and projection operators in non-rigid symmetry groups. R.L.Flurry,Jr. (Dept. of Chem., Univ. of New Orleans, New Orleans, LA, USA). *Symmetries and Properties of Non-Rigid Molecules. A Comprehensive Survey. Proceedings of an International Symposium, Paris, France, 1-7 July 1983* (Amsterdam, Netherlands: Elsevier 1983), p.113-32. Groups involving more than one generating element can be constructed as products of groups defined by independent generators. The use of the Frobenius reciprocity theorem allows the correlation of the irreducible representations of the subgroups with those of the full group. Projection operators within the full group can be constructed as products of the projection operators of the subgroups. The correlations and the projection operators are independent of the types of product involved in the group structure. A particularly useful factorization for point groups involves factoring the group into the site symmetry group and the interchange symmetry. Symmetry-adapted functions can be constructed by applying the projection operators of the site symmetry group to the basis functions centered on a site to obtain functions adapted to the site symmetry, and then by applying the projection operators from the interchange symmetry to these, to obtain functions adapted to the full group. When the site and interchange symmetries are properly defined, the procedure works equally well for non-rigid systems, even though the interchange symmetry may not define a group. The technique is presented in detail and applied to the construction of symmetry-adapted functions for several non-rigid molecules. (7 refs.)

Proceedings of the International Conference on Order in Chaos See Entry 111307

Symmetries and Properties of Non-Rigid Molecules. A Comprehensive Survey. Proceedings of an International Symposium See Entry 111310

Lie algebras whose maximal subalgebras are modular See Entry 111393

Nonsteady waves in distributed dynamical systems See Entry 111461

On dual spaces of differential Lie algebras See Entry 111582

Universal properties of the transition from quasi-periodicity to chaos in dissipative systems See Entry 111586

The breadth of the lattice of those varieties of inverse semigroups which contain the variety of groups See Entry 111604

Counterexamples to some results on the existence of field copies See Entry 111865

Difficulties with massless particles? See Entry 111988

Historical survey and recent progress in the theory of non-rigid molecules See Entry 112618

Group theory of non-rigid molecules and its applications See Entry 112809

Coadjoint orbits, vortices, and Clebsch variables for incompressible fluids See Entry 113455

Noncanonical Hamiltonian formulation of ideal magnetohydrodynamics See Entry 113517

02.30 FUNCTION THEORY, ANALYSIS

111396 ILUCG2: subprograms for the solution of a linear asymmetric matrix equation arising from a 9-point discretization. A.I.Shestakov, D.V.Anderson (Lawrence Livermore Nat. Lab., Univ. of California, Livermore, CA, USA). *Comput. Phys. Commun. (Netherlands)*, vol.30, no.1, p.31-6 (July-Aug. 1983).

Elliptic and parabolic partial differential equations which arise in plasma physics applications (as well as in others) are solved in two dimensions. Plasma diffusion, equilibria and phase space transport (Fokker-Planck equation) have been treated by these methods. These problems share the common feature of being stiff and requiring implicit solution techniques. Generally, the resulting matrix equations are asymmetric; the authors solve them here with the ILUCG2 program. (9 refs.)

111397 ICCG2: subprograms for the solution of a linear symmetric matrix equation arising from a 9-point discretization. D.V.Anderson, A.I.Shestakov (Lawrence Livermore Nat. Lab., Univ. of California, Livermore, CA, USA). *Comput. Phys. Commun. (Netherlands)*, vol.30, no.1, p.37-42 (July-Aug. 1983).

Elliptic and parabolic partial differential equations which arise in plasma physics applications (as well as in others) are solved in two dimensions. Plasma diffusion, equilibria and phase space transport (Fokker-Planck equation) have been treated by these methods. These problems share the common feature of being stiff and requiring implicit solution techniques. Sometimes, the resulting matrix equations are symmetric; the authors solve them here with the ICCG2 coding. (8 refs.)

111398 ILUCG3: subprograms for the solution of a linear asymmetric matrix equation arising from a 7, 15, 19 or 27 point 3D discretization. D.V.Anderson (Lawrence Livermore Nat. Lab., Univ. of California, Livermore, CA, USA).

Comput. Phys. Commun. (Netherlands), vol.30, no.1, p.43-9 (July-Aug. 1983). Elliptic and parabolic partial differential equations which arise in plasma physics applications (as well as in others) are solved in three dimensions. Plasma diffusion, equilibria and phase space transport (Fokker-Planck equation) have been treated by similar methods in two dimensions using the codes ICCG2 and ILUCG2. These problems share the common features of being stiff and requiring implicit solution techniques. Generally, the resulting matrix equations are asymmetric; the authors solve them here with the ILUCG3 program. (8 refs.)

111399 ICCG3: subprograms for the solution of a linear symmetric matrix equation arising from a 7, 15, 19 or 27 point 3D discretization. D.V.Anderson (Lawrence Livermore Nat. Lab., Univ. of California, Livermore, CA, USA). *Comput. Phys. Commun. (Netherlands)*, vol.30, no.1, p.51-7 (July-Aug. 1983).

Elliptic and parabolic partial differential equations which arise in plasma physics applications (as well as in others) are solved in three dimensions. Plasma diffusion, equilibria and phase space transport (Fokker-Planck equation) have been treated by similar methods in two dimensions using the codes ICCG2 and ILUCG2. These problems share the common features of being stiff and requiring implicit solution techniques. Sometimes, the resulting matrix equations are symmetric; the authors solve them here with the ICCG3 program. (8 refs.)

111400 On a local hidden-variable model with unusual properties. G.C.Scalera (Istituto Nazionale di Geofisica, Roma, Italy).

Lett. Nuovo Cimento (Italy), vol.38, ser.2, no.1, p.161-8 (3 Sept. 1983). Shows that a local hidden-variable model exists which violates Bells inequality (1964). The correlation function depends on the definition of the time of coincidence, are obtained for arbitrarily small times of coincidence. (no refs.)

111401 On the isospectral-eigenvalue problem and the recursion operator of the Harry-Dym equation. M.Leo, R.A.Leo, G.Soliani, L.Solombrino (Dipartimento di Fisica, Univ. di Lecce, Lecce, Italy).

Lett. Nuovo Cimento (Italy), vol.38, ser.2, no.2, p.45-51 (10 Sept. 1983). The isospectral-eigenvalue problem for the Harry-Dym equation is derived using a prolongation technique. The eigenvalue equation is then exploited to find a recursion operator. (21 refs.)

111402 A study of fast Laplace transform. K.Kanematsu, A.Ametani (Dept. of Electrical Engng., Doshisha Univ., Kyoto, Japan). *Sci. & Eng. Rev. Doshisha Univ. (Japan)*, vol.24, no.1, p.41-9 (May 1983). In Japanese.

The weighting function and shifting constant of integral path of the FLT (fast Laplace transform) were investigated. As the result, the meanings of the weighting function and the characteristic of the error due to the shifting constant of the integral path have been made clear. The reason why the FLT does not show an aliasing error was studied, and it became clear that because time functions used in the FLT are causal function, no aliasing error appears. Furthermore, the error of the FLT was investigated. The pair of the FLT was studied, and a linear-approximation Laplace transform (LLT) has been developed as the pair of the FLT. The FLT-LLT pair is not a perfect transform-pair. But, because both transforms have no aliasing error, the error due to the FLT-LLT pair is very small. (6 refs.)

111403 Lattice theoretic properties of Carleson measures. C.Matsuoka (Dept. of Mech. Engng., Doshisha Univ., Kyoto, Japan). *Sci. & Eng. Rev. Doshisha Univ. (Japan)*, vol.24, no.1, p.63-8 (May 1983). In Japanese.

On a given compact Hausdorff space, the author investigates the decomposition property of measures with respect to an arbitrary max-stable convex subcone of continuous functions. The result can be applied to Carleson measures on the unit disk, which leads to another proof of Pehr Beurling's theorem. (8 refs.)

111404 The method of spherical harmonics for the transfer equation. V.Yu.Plyashkevich (I.V. Kurchatov Inst. of Atomic Energy, Acad. of Sci., Moscow, USSR).

Sov. Phys.-Dokl. (USA), vol.27, no.12, p.1018-24 (Dec. 1982). Translation of: *Dokl. Akad. Nauk SSSR*, vol.267, no.4-6, p.1098-102 (Dec. 1982). [received: Sept. 1983]

The author discusses the result of an investigation of a system of equations by the method of spherical harmonics, formulates for the system correct boundary conditions that correspond to the general laws of boundary reflection of radiation emerging from the region, and establishes convergence of the method. (4 refs.)

111405 Complex geometry and integral representations in the future tube in C^1 . A.G.Sergeev.

Theor. & Math. Phys. (USA), vol.54, no.1, p.62-70 (Jan. 1983). Translation of: *Teor. & Mat. Fiz. (USSR)*, vol.54, no.1, p.99-110 (Jan. 1983). [received: Sept. 1983]

It is shown that the boundary of the future tube in C^3 cannot be holomorphically rectified along complex light rays lying on the boundary. From the general Cauchy-Fantappie representation the Cauchy-Bochner, Jost-Lehmann-Dyson, Leray, and other integral representations for holomorphic function and solutions of the $\bar{\alpha}$ equation in the future tube are derived. (16 refs.)

Optimization of a quadratic performance index on solutions of nonlinear two-point boundary-value problems See Entry 111432

Analyses of large quasistatic deformations of inelastic bodies by a new hybrid-stress finite element algorithm See Entry 111443

New splitting-up schemes for solving hyperbolic and parabolic non linear problems: applications to Euler and Navier-Stokes equations See Entry 111450

Classical and quantal supersymmetric Liouville theory See Entry 111470

Intensity moments of semiclassical wavefunctions See Entry 111496

Fermionic lifting of variational self-adjointness See Entry 111549

Exact solutions of simple nonlinear difference equation systems that show chaotic behavior See Entry 111554

One-dimensional Brownian motion near an absorbing boundary: solution to the steady state Fokker-Planck equation See Entry 111555

Persistence properties of bifurcations See Entry 111570

On the attracting set for Duffing's equation. II. A geometrical model for moderate force and damping See Entry 111571

A renormalisation approach to invariant circles in area-preserving maps See Entry 111579

Quasiperiodicity in dissipative systems: a renormalization group analysis See Entry 111580

A simple dynamical system with stochastic behaviour See Entry 111587

Amplitude equations for systems with competing instabilities See Entry 111593

Stability of nonlinear modes and chaotic properties of 1D Fermi-Pasta-Ulam lattices See Entry 111609

Solution of the axisymmetric problem of the torsion of an inhomogeneous layer See Entry 113271

Axisymmetric stress state of thick-walled elastic near-spherical shells See Entry 113283

Numerical solution of axisymmetric problems of the dynamics of thin orthotropic shells of revolution See Entry 113289

Conservation laws for material exhibiting power-law creep See Entry 113313

Nonlinear oscillations of weakly asymmetric elastic systems with several degrees of freedom See Entry 113347

Calculation of the static crack propagation trajectory See Entry 113360

Local regularity, boundary values and maximum principles for pseudoparabolic equations See Entry 113401

Limits of regions of strict hyperbolic and composite type for nonlinear equations of two-layer shallow water See Entry 113415

Transitions to chaos in the Ginzburg-Landau equation See Entry 113419

Local existence theorems for the first and second initial-boundary value problems for a weakly non-Newtonian fluid See Entry 113479

Variational functional for a rigid-plastic porous material See Entry 115279

02.40 GEOMETRY, DIFFERENTIAL GEOMETRY, AND TOPOLOGY

(see also 04. Relativity and gravitation)

Quantum mechanics of predictive Poincare-invariant systems. II. Mixed spin ($\frac{1}{2},0$) two-particle systems	See Entry 111430
The conserved currents for the Maxwellian field	See Entry 111466
A critique of relativity and localization	See Entry 111504
The positivity of gravitational energy and global supersymmetry	See Entry 111505
Material and electromagnetic sources of the Kerr-Newman geometry	See Entry 111523
Spontaneous compactification of $D=10$ Maxwell-Einstein theory leads to $SU(3)\times SU(2)\times U(1)$ gauge symmetry	See Entry 111529
Emission of relativistic particles in a strong gravitational field	See Entry 111531
A simple dynamical system with stochastic behaviour	See Entry 111587
The discrete Frenkel-Kontorova model and its extensions. I. Exact results for the ground-states	See Entry 111608
Counterexamples to some results on the existence of field copies	See Entry 111865
Dynamical gauge symmetry breaking as the Casimir effect ..	See Entry 111889
Topological charge distribution in $SU(N)$ gauge theories	See Entry 111890
The existence of a black hole due to condensation of matter	See Entry 116464
Stellar collapse without singularities?	See Entry 116644
Rotating black hole in asymptotic de Sitter space: perturbation of the space-time with spin fields	See Entry 116738
Homogeneity of Riemannian space-times of Godel type	See Entry 116906
Feynman propagator in a linearly expanding Universe	See Entry 116907

02.50 PROBABILITY THEORY, STOCHASTIC PROCESSES, AND STATISTICS

(see also 05. Statistical physics)

111406 Parsimonious asymptotics. D.Ludwig. <i>SIAM J. Appl. Math. (USA)</i> , vol.43, no.4, p.664-72 (Aug. 1983). There appears to be a connection between parsimony in construction of an asymptotic approximation, and robustness of the result. This point is illustrated by two examples from widely different fields: (1) Keller's geometric theory of diffraction, with special reference to approximations for eigenvalues, and (2) maximum likelihood estimators for simple vs. complex models of fishery dynamics. (7 refs.)	
111407 Transformations to linearity in binary regression. A.S.White-moore (Dept. of Family, Community & Preventive Medicine, Stanford Univ. School of Medicine, Stanford, CA, USA). <i>SIAM J. Appl. Math. (USA)</i> , vol.43, no.4, p.703-10 (Aug. 1983). A one-parameter family of transformations for binary response probabilities is introduced. The family is used to explore relationships between response and explanatory variables by assuming that the transformed probabilities depend linearly on the known variables and on unknown parameters reflecting the variables' effect on response. The family includes the logistic and one-hit transformations, which form the bases for two popular notions of 'no interaction' between explanatory variables. Maximum likelihood methods are used to determine those transformations in the family that provide acceptable fits to data, and the methods are illustrated with data from an animal cancer bioassay. The paper concludes with a comparison of probabilistic and statistical properties of logistic and one-hit transformations. (18 refs.)	
A statistical physics model	See Entry 111544
Comment on 'Monte Carlo evaluation of functional integrals using coherent-state Slater determinants' [and reply]	See Entry 111550
Stochastic theory of adiabatic explosion	See Entry 111557
A simple dynamical system with stochastic behaviour	See Entry 111587
Long-time correlations in the stochastic regime	See Entry 111588
On the representation of solutions of nonlinear equations as an integral over the set of trajectories of a random process	See Entry 111590
Stationary probability distribution for one of the simplest strange attractors	See Entry 111591
On the non-linear dynamical power-reactor model with temperature feedback	See Entry 112299
Onefold photoelectron-counting statistics for non-Gaussian light: scattering from an arbitrary number of weak scatterers	See Entry 112939
A scattering on an adsorbed layer. IV. Scattering function ..	See Entry 115004
Statistical analysis of some gas chromatography measurements	See Entry 115601

02.60 NUMERICAL APPROXIMATION AND ANALYSIS

111408 Economical stiffness formulations for nonlinear finite elements. R.A.Brockman (Res. Inst., Univ. of Dayton, Dayton, OH, USA). <i>Comput. & Struct. (GB)</i> , vol.18, no.1, p.15-22 (1984). Element-level calculations often represent a significant part of the computing effort in a nonlinear finite element solution, especially when three-dimensional, higher-order elements are used. This paper explores some possibilities for increasing the efficiency of element computations within the general framework of a Newton-Raphson solution technique. A modified tangent stiffness formulation is introduced which provides relatively fast convergence without the extreme computational effort sometimes associated with the usual Newton-Raphson interaction. Numerical examples are used to illustrate the behavior of the method. The use of different types of element formulations within a single finite element mesh, according to the expected or observed degree of nonlinearity, is also identified as a means of reducing solution cost. (14 refs.)	
--	--

111409 On the choice of a cost function for the reconstruction of surfaces by triangulation between contours. W.R.J.Funnell (Dept. of Otolaryngology, McGill Univ., Montreal, Quebec, Canada). <i>Comput. & Struct. (GB)</i> , vol.18, no.1, p.23-6 (1984). Methods for the reconstruction of three-dimensional objects by triangulating between pairs of two-dimensional contours are discussed. Alternative cost functions for optimizing the triangulation are considered, and new cost functions are proposed that measure the narrowness of the triangles. These narrowness functions are particularly well suited to the generation of finite-element meshes. (15 refs.)	
111410 Anchorage plates for Cable-Stayed bridges. C.P.Heins, K.Kano (Dept. of Civil Engng., Univ. of Maryland, College Park, MD, USA). <i>Comput. & Struct. (GB)</i> , vol.18, no.1, p.47-54 (1984). The design of Cable-Stayed bridges requires the engineer to examine in detail the local force distribution in the plates which transfer the cable force to the main structure. It is therefore the intention of this paper to present the response of these plate elements, when subjected to the cable forces, using the finite element method. The results are presented such that rapid evaluation of their strength can be determined. (7 refs.)	
111411 Automatic node resequencing with constraints. L.V.Quoc, J.R.O'Leary (Dept. of Civil Engng., Illinois Inst. of Technol., Chicago, IL, USA). <i>Comput. & Struct. (GB)</i> , vol.18, no.1, p.55-69 (1984). Presented here is an algorithm for finite element node resequencing to reduce the bandwidth and profile of the resulting matrices while taking into account node constraints. Particular attention is given to the fluid-solid interaction problem with added-mass, the analysis with linear constraint equations, and the static condensation by partial decomposition. In the aforementioned applications, additional relationships (constraints) between the degrees of freedom must be considered in the renumbering process since they usually lead to an increase in the matrix configuration. A description of the above mentioned applications is presented as well as the implementation of the proposed algorithm to these problems on a small rectangular mesh in order to clearly illustrate its functioning. Finally, the algorithm is applied to larger, more realistic examples; these results show that the algorithm performs remarkably well, chiefly in achieving an optimal configuration for both the mass (augmented) and the stiffness matrices in the context of the fluid-solid interaction analysis. (29 refs.)	
111412 Harmonic acceleration method for dynamic structural analysis. I.Senjanovic (Faculty of Mech. Engng. & Naval Architecture, Univ. of Zagreb, Zagreb, Yugoslavia). <i>Comput. & Struct. (GB)</i> , vol.18, no.1, p.71-80 (1984). The harmonic acceleration is assumed in each time step of integration of the dynamic equilibrium equation of a structure and its modal transformation. As a result of this two different numerical integration methods have been derived. Both the methods are unconditionally stable and very accurate compared to some other commonly used methods. (16 refs.)	
111413 Finite strip method with X-spline functions. H.Y.Yang (Dept. of Basic Sci., Tianjin Univ., Tianjin, China), K.P.Chong. <i>Comput. & Struct. (GB)</i> , vol.18, no.1, p.127-32 (1984). An alternative method of finite strip is developed by using cubic X-spline functions in the y-direction instead of trigonometric series. The main advantage of the method is to be able to solve the problems defined in some irregular shaped regions. Numerical examples have shown that the new method, as well as the original one developed by Cheung, is superior to the Finite Element Method in saving the computational labor. (8 refs.)	
A simple algorithm for the nonlinear dynamic analysis of networks	See Entry 111433
A partitioned finite element method for dynamical systems ..	See Entry 111434
Galerkin method as a tool to investigate the planar and nonplanar behavior of curved beams	See Entry 111435
A stress versus compliance constraint in a minimum weight design	See Entry 111439
Dynamic finite element analysis of nonaxisymmetric structures	See Entry 111440
Solutions of plates on a heterogeneous elastic foundation	See Entry 111441
Application of the quadratic functional to nonconservative problems of elastic stability	See Entry 111442
Analyses of large quasistatic deformations of inelastic bodies by a new hybrid-stress finite element algorithm	See Entry 111443
An improved treatment of transverse shear in the Mindlin-type four-node quadrilateral element	See Entry 111444
Mechanical analysis of 18 ϕ piston-cylinder type high pressure apparatus by the finite element method	See Entry 111699
Finite element Hamiltonian Monte Carlo of $SU(2)$	See Entry 111893
Diffraction of an EM wave by an absorbing circular cylinder	See Entry 112900
An updated Lagrangian formulation for Timoshenko beams including non-conservative loads for divergence-type systems	See Entry 113282
Numerical solution of axisymmetric problems of the dynamics of thin orthotropic shells of revolution	See Entry 113289
Hybrid experimental-numerical stress analysis	See Entry 113290
Dynamic response of orthotropic curved bridge decks due to moving loads	See Entry 113293
Alternate stress and conjugate strain measures, and mixed variational formulations involving rigid rotations, for computational analyses of finitely deformed solids, with application to plates and shells. I. Theory	See Entry 113294
Variation of stress resultants in concrete structures due to time-dependent creep and shrinkage strains of concrete	See Entry 113295
Nonlinear viscoelastic stress analysis—a finite element approach	See Entry 113296
Minimum mass design of elastic frames subjected to multiple load cases	See Entry 113297
A direct solution of the equivalent frame for two-way slabs ..	See Entry 113298
Finite element model simulation of creep crack growth in low-ductility material	See Entry 113371
Domain decomposition methods for nonlinear problems in fluid dynamics	See Entry 113403
Limits of regions of strict hyperbolic and composite type for nonlinear equations of two-layer shallow water	See Entry 113415
Calculation of transient heat transfer in channels with Neumann boundary conditions	See Entry 113505

- Finite analysis of the control of interface shape in Bridgman crystal growth See Entry 113780
- Determination of certain elastic characteristics of materials with the use of parabolic interpolation of strain curves See Entry 115478

02.70 COMPUTATIONAL TECHNIQUES

(for data handling and computation, see 06.50)

- Solution of the inverse spectral problem by variable metric methods See Entry 112879

03.00 CLASSICAL AND QUANTUM PHYSICS; MECHANICS AND FIELDS

03.20 CLASSICAL MECHANICS OF DISCRETE SYSTEMS: GENERAL MATHEMATICAL ASPECTS

(for applied classical mechanics of discrete systems, see 46.10; for celestial mechanics, see 95.10)

- 111414 Formulation of equations of motion for multi-rigid-body systems.** Shen Qianruo (Peking Inst. of Aeronautics & Astronautics, Peking, China). *Acta Mech. Sin. (China)*, no.3, p.259-66 (1983). In Chinese. Deals with the formulation of dynamical equations for multi-rigid-body systems in a topological tree configuration. The author briefly analyses and compares various methods, vectorial and analytical, for deriving these equations. A new method is presented. Its feature is that the equations of motion are formulated by a series of matrix transformations. There are two key points in this method, the 'partial derivative of matrix' by means of which the application of equations of analytical dynamics in their matrix format becomes possible, and two basic matrices called the 'Incidence Matrix' and 'Mass-center-vector Matrix' which describe the structure of the system. The Kane-Wang quasi-coordinate formula is adapted. The general format of rotational equations appearing as a matrix equation has been established. The attitude equations of a multi-rigid-body satellite are given as an example. (9 refs.)
- 111415 Generalized dynamical equations for tree-shaped multi-rigid-body systems.** Zhou Qizhao (Peking Univ., Peking, China). *Acta Mech. Sin. (China)*, no.3, p.267-77 (1983). In Chinese. Following Wittenburg (1977) and utilizing the viewpoint of graph theory, the author analyses the structure for a tree shaped system of an arbitrary number of interconnected rigid bodies. The author describes a dynamical model of overlapping subtreeshaped structures and a definition of the so-called artery graph and modifies the idea of augmented bodies so that the equivalent dynamical decomposition of the system can be carried out. By specifying certain symbols and rules of calculation, generalized dynamical equations for the tree-shaped multi-rigid-body system are set up in a rather compact matrix form. Thus, after introducing the hinge matrix, both the constraint relations and the kinematics of the system are written in matrix form. Finally the dynamical equations are expressed in terms of generalized coordinates so that they can be used for computer programming. (5 refs.)
- 111416 First integrals for one-dimensional particle motion in a non-linear, time-dependent potential field.** W.Sarlet (Inst. voor Theoretische Mech., Rijksuniv. Gent, Gent, Belgium). *Int. J. Non-Linear Mech. (GB)*, vol.18, no.4, p.259-68 (1983). Following a direct ad hoc procedure for the construction of first integrals established previously (see *ibid.*, vol.15, p.133-46, 1980) all potentials $V(q,t)$ are derived for which an equation of type $\ddot{q} + \partial V / \partial q = 0$ has a first integral, quadratic in \dot{q} . Polynomial non-linearities are focussed on and a characterization of all admissible equations is given in terms of an arbitrarily assigned coefficient of the highest order term. Adiabatic invariants are discussed for which the unusual feature is that the highest nonlinear term again is dominating and linear terms are comparatively small. (11 refs.)
- 111417 Torsional vibrations of a non-shallow spherical sandwich shell.** C.Prasad, A.P.Gupta (Dept. of Maths., Univ. of Roorkee, Roorkee, India). *Proc. Natl. Acad. Sci. India Sect. A*, vol.52, pt.1, p.89-94 (1982). [received: Aug. 1983] Free torsional vibrations of a non-shallow spherical sandwich shell are considered by taking into account the effects of transverse shear and rotatory inertia for the core as well as for the facings. The equations of motion derived by the Hamilton energy principle are solved in terms of a Legendre function with the aid of auxiliary variables. Frequencies computed for the first four normal modes of vibrations of sandwich shells are compared with those of monocoque shells. (10 refs.)
- 111418 Stability of collinear solutions in the restricted problem of three bodies with variable mass.** A.K.Srivastava, B.Ishwar (Dept. of Math., Bihar Univ., Muzaffarpur, India). *Proc. Natl. Acad. Sci. India Sect. A*, vol.52, pt.2, p.163-7 (1982). [received: Aug. 1983] The authors have examined the stability of collinear solutions of the restricted problem of three bodies with variable mass by the method adopted by Moulton. The authors have found three variational equations. The last equation is independent of the first two equations. The characteristic equation for the first two equations is biquadratic. The authors have discussed the different cases which give the condition for the collinear solution to be stable or unstable. They come to the conclusion that the collinear solutions are, in general, unstable. (7 refs.)
- 111419 A theory of exact and approximate configurational invariants.** L.S.Hall (Lawrence Livermore Nat. Lab., Univ. of California, Livermore, CA, USA). *Physica D (Netherlands)*, vol.8D, no.1-2, p.90-116 (July 1983). A theory of integrable Hamiltonian systems in two dimensions is formulated and applied. The four-dimensional phase-space problem that is the vanishing of the Poisson bracket between another invariant and the Hamiltonian is reduced to the solution of a series of two-dimensional configuration-space equations. (The theory is also applicable to more than two dimensions.) The constraints are found which admit to integrability of the orbits for magnetic or Coriolis forces as well as for forces derivable from a potential. When a system admits a given invariant, the invariant is found—for example, by quadrature. A number of examples including known and apparently previously unknown invariants are given. The theory of exact integrals of the motion

also can be extended to the derivation of approximate invariants. The orbital structure of integrable or approximately integrable systems correlates with the degree (maximum power of the velocity) of a standardized invariant. The theory admits a variational principle, among other approximation techniques, for the computation of a 'best' approximate invariant. The problem of the general cubic potential with one symmetric coordinate, $V = \frac{1}{2}Ax^2 + \frac{1}{2}By^2 + Cx^2y + \frac{1}{3}Dy^3$ (of which the well-studied Henon-Heiles potential is the special case for $A=B$ and $C=-D$), is examined in detail. (19 refs.)

- 111420 Infinite bifurcations, gaps and bubbles in Hamiltonian systems.** G.Contopoulos (European Southern Obs., Garching, Germany). *Physica D (Netherlands)*, vol.8D, no.1-2, p.142-56 (July 1983). The author studies the bifurcations, gaps and bubbles along the characteristics of families of periodic orbits in Hamiltonian systems of two degrees of freedom. Bubbles (closed characteristics) appear when the rotation number along a family does not vary monotonically. There are infinite bifurcations, appearing when the rotation number along a family is rational, n/m . The most important bifurcations have $m=1$, or $m=2$ (equal period and double period bifurcations). In a rotating system the central family of periodic orbits is the family of direct circular orbits of the axisymmetric case. At each bifurcation $n/1$ there is either a change of stability (if n is odd), or a gap (if n is even) of the central family; this phenomenon is explained theoretically. In cases of infinite transitions from stability to instability along the same family, the successive intervals between bifurcations do not follow the universal Feigenbaum ratio. But the author also found several cases of infinite pitchfork period doubling bifurcations, and in all cases the Feigenbaum ratio is consistent with the universal value $\delta=8.72$. All Feigenbaum sequences in rotating systems are followed by inverse Feigenbaum sequences, i.e. they form infinite bubbles. An explanation of this effect is given. (16 refs.)
- 111421 The Benettin-Strelcyn oval billiard revisited.** M.Henon (Obs. de Nice, CNRS, Nice, France), J.Wisdom. *Physica D (Netherlands)*, vol.8D, no.1-2, p.157-69 (July 1983). The wall of the oval billiard defined by Benettin and Strelcyn (1978) has a discontinuous curvature; the associated mapping has a discontinuous derivative. The authors find that invariant curves of the mapping are generally destroyed when they cross a line of discontinuity. They can survive, however, in particular cases where two successive discontinuities cancel each other. (9 refs.)
- 111422 The analytic structure of dynamical systems and self-similar natural boundaries.** Y.F.Chang, J.M.Greene, M.Tabor, J.Weiss (Center for Studies of Nonlinear Dynamics, La Jolla Inst., La Jolla, CA, USA). *Physica D (Netherlands)*, vol.8D, no.1-2, p.183-207 (July 1983). The authors investigate the analytic, complex-time structure of the movable singularities for several dynamical systems. In general, it is found that there exists a direct connection between the occurrence of a certain type of multiple-valuedness of the singularities and the existence of a class of remarkable, 'self-similar' natural boundaries for these systems. An asymptotic description of the distribution of singularities in the natural boundary is developed. This provides a description of the fine-scale structure of these natural boundaries that agrees closely with the numerical calculations. (12 refs.)
- 111423 Some symmetric, two-dimensional, dissipative maps.** J.Froyland (Inst. of Phys., Univ. of Oslo, Oslo, Norway). *Physica D (Netherlands)*, vol.8D, no.3, p.423-34 (Sept. 1983). A class of simple, symmetric, two-dimensional maps have been studied theoretically, and one finds periodic N doubling at values of a parameter of the form $\cos(\pi k/N)$. A computer simulation confirms this, and it is also found that in general there are only a finite number of successive period doubling generations. Finite jump (first order) transitions are shown to take place. (6 refs.)
- 111424 Shock and transition layers for singularly perturbed second-order vector systems.** R.E.O'Malley, Jr. (Dept. of Math. Sci., Rensselaer Polytech. Inst., Troy, NY, USA). *SIAM J. Appl. Math. (USA)*, vol.43, no.4, p.935-43 (Aug. 1983). Considers boundary value problems for certain vector systems of the form $\Omega(\epsilon)y' + f(x,y)y' + g(x,y) = 0$ with $y(0)$ and $y(1)$ prescribed, in the limit as the coefficient matrix Ω tends to zero. Emphasis is on specific two-dimensional examples with limiting solutions displaying jumps at interior points which are not obvious prior to analysis. (17 refs.)
- 111425 A transformation method of non-Hamiltonian system and its application.** Liu Lin, Zhang Shenpan (Dept. of Astron., Nanjing Univ., China). *Sci. Sin. (China)*, vol.26, no.8, p.861-73 (Aug. 1983). A transformation method of non-Hamiltonian systems was presented by Liu Lin (*Acta Astron. Sin.*, vol.23, p.255, 1982). In this paper, this method is concretized, and the principle, process and forms of two kinds (the forms of the implicit function and the explicit function) of the method are discussed in detail, with the motion solution of a small celestial body under the oblateness perturbation of a principal celestial body given as an example. (4 refs.)
- 111426 Almost asymptotic stability of system of processes.** A.A.Martynyuk, V.D.Podil'chuk (Inst. of Mech., Acad. of Sci., Kiev, Ukrainian SSR). *Sov. Appl. Mech. (USA)*, vol.19, no.1, p.74-9 (Jan. 1983). Translation of: *Prikl. Mekh. (USSR)*, vol.19, no.1, p.89-94 (Jan. 1983). [received: Sept. 1983] The study is a continuation of one begun earlier (see A.A. Martynyuk, *Prikl. Mekh.*, vol.16, no.6, p.104-9, 1980). The state of a system of processes is characterized by a multidimensional functional (vector measure) and the problem of an almost asymptotic stability of such a system with respect to two vector measures is considered on this basis. An essential distinguishing feature of this study is that the components of a vector measure can have positive as well as negative values. The concept of vector measure is a generalization of the concept of measure and, as far as these authors know, has not been used before in the problem of practical stability. (7 refs.)
- Home-experimental demonstrations of Hart's frictional force rotator** See Entry 111348
- Teaching first-year kinematics via the scalar product** See Entry 111361
- Resonance demonstrator** See Entry 111379
- Universal properties of the transition from quasi-periodicity to chaos in dissipative systems** See Entry 111586
- Stationary probability distribution for one of the simplest strange attractors** See Entry 111591
- Diffusion across characteristics boundaries with critical points** See Entry 111592
- Symmetric rectilinear periodic orbits of three bodies** See Entry 116429
- A noncanonical analytic solution to the J_2 perturbed two-body problem** See Entry 116430

An analytic solution for the J_2 perturbed equatorial orbit See Entry 116431

Theory of the Trojan asteroids. IV See Entry 116432

Three-dimensional regions of stability about the triangular equilibrium points See Entry 116433

Existence of the solution of Szebehely's equation in three dimensions using a two-parametric family of orbits See Entry 116434

03.30 SPECIAL RELATIVITY

111427 Energy conserving non-relativistic guiding center mechanics and the Galilean principle of relativity. H.K.Wimmel (Max-Planck-Inst. fur Plasma-phys., EURATOM Assoc., Garching, Germany). *Z. Naturforsch. Teil A (Germany)*, vol.38A, no.8, p.841-7 (Aug. 1983). Arguments and representative examples are given that exact energy conservation and Galilei invariance are incompatible in non-relativistic guiding-center mechanics. Provided that this is true in general it also follows that exact energy conservation and Lorentz invariance are incompatible in relativistic guiding-center mechanics. It would furthermore follow that every guiding-center mechanics with exact energy conservation is a non-unique theory owing to the principle of relativity. The paper also presents a Galilei invariant guiding-center mechanics that does not conserve energy. (9 refs.)

111428 Lie-isotopic lifting of the special relativity for extended deformable particles. R.M.Santilli (Inst. for Basic Res., Cambridge, MA, USA). *Lett. Nuovo Cimento (Italy)*, vol.37, ser.2, no.16, p.545-55 (20 Aug. 1983). The author recalls the variation of the speed of light with the local physical conditions of the material media in which it propagates, and identify a corresponding class of generalised metrics. The underlying group of isometries is constructed via a Lie-isotopic lifting of the envelope, algebra and group structure of Lorentz transformations. It is shown that the generalised transformations, called Lorentz-isotopic, are apparently capable of characterizing an isotopic lifting of the special relativity for extended, and therefore deformable particles. The current experimental information on the apparent approximate character of the conventional Lorentz transformations in particle physics are reviewed, and a number of direct tests suitable for the resolution of the issue are indicated. (28 refs.)

111429 A myth for special relativity. L.Epstein. *New Sci. (GB)*, vol.99, no.1374, p.690-2 (8 Sept. 1983). The author states that the ultimate reality in physics is not an equation but a myth. He points out that even expert physicists think in terms of various myths; for example, the Second Law of Thermodynamics interpreted as a natural tendency for things to get messed up. A good myth, in the sense meant by the author, must be easy to understand. It must explain what is found in nature, and what is deduced from the myth must also be found in nature. The author presents a myth to explain time dilation and the twins paradox: he describes a situation in which a clock properly moves through time, not space. If it also moves through space, it has to divert some of the energy used for travelling through time, and so a clock travelling in space at sufficiently high speed will stop travelling in time. (no refs.)

111430 Quantum mechanics of predictive Poincare-invariant systems. II. Mixed spin ($1/2,0$) two-particle systems. L.Bel (Inst. Henri Poincare, Paris, France). *Phys. Rev. D (USA)*, vol.28, no.6, p.1308-25 (15 Sept. 1983). The author discusses the problem of quantizing mixed spin (0 and $1/2$) two-particle systems in the framework of predictive relativistic mechanics. They propose a general scheme for quantization, but a detailed analysis is given only for the linearized scalar or vector interactions (with short or long ranges). Approximate wave equations are derived for the electromagnetic interaction in the cases where the particles are slowly moving or have very different masses. (26 refs.)

111431 Problems in special relativity. I.McCausland (Dept. of Electrical Engng., Univ. of Toronto, Toronto, Ontario, Canada). *Wireless World (GB)*, vol.89, no.1573, p.63-5 (Oct. 1983). Arguments have been used to defend the special theory of relativity against criticism contain many inconsistencies. These problems should be thoroughly and objectively examined by scientists and philosophers to attempt to ascertain the truth of the matter. (19 refs.)

Periodic boundary conditions in special relativity See Entry 111345

Clock synchronization, a universal light speed, and the terrestrial red-shift experiment See Entry 111346

Note on a simple derivation of Planck's formula from special relativity See Entry 111370

The original Ampere force and Biot-Savart and Lorentz forces See Entry 111468

03.40 CLASSICAL MECHANICS OF CONTINUOUS MEDIA: GENERAL MATHEMATICAL ASPECTS

111432 Optimization of a quadratic performance index on solutions of nonlinear two-point boundary-value problems. V.V.Vanisovich. *Appl. Math. & Mech. (USA)*, vol.46, no.4, p.556-8 (1982). Translation of: *Prikl. Mat. & Mekh. (USSR)*, vol.46, no.4, p.697-9 (1982). [received: Sept. 1983]

A problem of optimizing nonlinear systems with boundary conditions of general form and a quadratic performance index is examined. Conditions for the existence of an optimal control are formulated. The optimal controls are written in explicit form as functions of the phase coordinate and the solutions of auxiliary boundary-value problems. Various applied problems of mechanics lead to the determination of optimal modes of the systems examined. (10 refs.)

111433 A simple algorithm for the nonlinear dynamic analysis of networks. P.G.Papadopoulos (Faculty of Structural Engng., Univ. of Thessaloniki, Thessaloniki, Greece). *Comput. & Struct. (GB)*, vol.18, no.1, p.1-8 (1984). A simple and economical algorithm is presented for the nonlinear dynamic analysis of networks, with lumped masses on the nodes, bars obeying uniaxial stress-strain laws and no damping. The step-by-step algorithm of the trapezoidal rule is used, combined with the predictor-corrector technique, with only two corrections per step. The prediction of an upper-bound for the eigenfrequencies permits the use of a constant steplength throughout the whole algorithm. An example problem and an error analysis of the algorithm are presented. (5 refs.)

111434 A partitioned finite element method for dynamical systems. A.Maher, P.G.Kessel, R.D.Cook (Univ. of Wisconsin, Madison, WI, USA). *Comput. & Struct. (GB)*, vol.18, no.1, p.81-91 (1984). A new analytical method is described for deriving the equations of motion of dynamical systems. The concept is to consider the displacements of the domain to be composed of rigid and elastic components. In contrast to other reduction methods, the domain modeled by finite number of degrees of freedom is discretized into two distinctive types of subdomains. Rigid and elastic subdomains are generated by consistent lumping of the domain properties under unique kinematic constraint relations. Equations of motion of the disjoint subdomains are derived by Lagrange's equations, in conjunction with the shape function matrix represented in partitioned form. This allows reduced size of matrices and avoids their possible singularities. Based on the invariance of energies under a compatible partitioned procedure, a simple analytical method is introduced for building the equations of motion of the whole domain from those of the subdomains. The dynamic analysis of a two-node domain with application to a blade-shaft combination is presented to illustrate the method. (15 refs.)

111435 Galerkin method as a tool to investigate the planar and nonplanar behavior of curved beams. A.Rosen, H.Abramovich (Dept. of Aeronaut. Engng., Technion-Israel Inst. of Technol., Haifa, Israel). *Comput. & Struct. (GB)*, vol.18, no.1, p.165-74 (1984). The equations of equilibrium which describe the three-dimensional behavior of curved beams are derived. These equations include first order geometric non-linear influences. The equations are solved by the Galerkin method. The method is very general and allows general variation of the geometric and structural properties along the beam. Any combination of boundary conditions is possible and the most general distribution of loads along the beam can be treated. Numerical results for a few examples are presented and compared to other theoretical and experimental results. The agreement between the results is generally good. It is shown that Galerkin method is an efficient method which enables one to solve the problem using small number of unknowns compared to other methods which are in use. (17 refs.)

03.40D Mathematical theory of elasticity (see also 46.20 Continuum mechanics, and 46.30 Mechanics of solids)

111436 The effective field method in linear problems of statics of composite media. S.K.Kanaun. *Appl. Math. & Mech. (USA)*, vol.46, no.4, p.520-8 (1982). Translation of: *Prikl. Mat. & Mekh. (USSR)*, vol.46, no.4, p.655-65 (1982). [received: Sept. 1983]

A composite material consisting of a homogeneous matrix containing a random, spatially homogeneous set of ellipsoidal inclusions with different physical and mechanical properties is investigated. Statics are studied (such as electric, elastic, stationary temperature, etc.), induced in such a medium by the action of various specified external fields. The problem consists of determining the statistical moments of the random tensor-type functions of the flux density and field strength in the composite material in question. The problem of describing many important physical and mechanical properties of the heterogeneous materials can be reduced to that of solving the above problem. (17 refs.)

111437 Effective rigidities of composite plates. A.G.Kolpakov. *Appl. Math. & Mech. (USA)*, vol.46, no.4, p.529-35 (1982). Translation of: *Prikl. Mat. & Mekh. (USSR)*, vol.46, no.4, p.666-73 (1982). [received: Sept. 1983]

A problem of constructing the effective rigidities of composite plates, i.e. of the rigidities ensuring that the solutions of the initial problem of the three-dimensional theory of elasticity for an inhomogeneous body are close to a solution of some problem in the theory of quasihomogeneous plates, is investigated. The homogenization method is used to obtain the solution. The theory of plates employed has the following significant characteristic feature, namely the fact that mechanical hypotheses are used to execute the passage from the three-dimensional problem of the theory of elasticity to the two-dimensional problem of the theory of plates. The methods used explain the discrepancies occurring in various methods of constructing the effective characteristics. (15 refs.)

111438 Program to calculate elastic Green's functions, displacement fields and interaction energies in cubic materials. J.W.Deutz, H.R.Schober (Inst. fur Festkorperforschungsanlage Kernforschung Julich, Julich, Germany). *Comput. Phys. Commun. (Netherlands)*, vol.30, no.1, p.87-91 (July-Aug. 1983).

In linear elasticity theory a continuous medium is characterized by its Green's function. In the static case this Green's function can be calculated by a one-dimensional integration. Also calculated are the first two derivatives yielding displacement fields and interaction energies of point defects. (13 refs.)

111439 A stress versus compliance constraint in a minimum weight design. A.Zochowski (Systems Res. Inst., Warsaw, Poland), K.Mizukami. *Comput. & Struct. (GB)*, vol.18, no.1, p.9-13 (1984). The paper contains a study of the stress-constrained minimum-weight design of the beam in the framework of Zochowski et al. (ibid., vol.17, p.365, 1983). The existence of optimal shape is considered. The numerical examples are given and stress-constrained designs are compared to compliance-constrained ones. (8 refs.)

111440 Dynamic finite element analysis of nonaxisymmetric structures. A.R.Zak, A.D.Antartis (Dept. of Aeronaut. & Astronaut. Engng., Univ. of Illinois, Urbana, IL, USA). *Comput. & Struct. (GB)*, vol.18, no.1, p.33-9 (1984). A dynamic finite element method of analysis is developed for structural configurations which are derived from axisymmetric geometries but contain definite nonaxisymmetric features in the circumferential direction. The purpose of the analysis is to develop a method which will take into consideration the fact that the stress and strain conditions in these geometries will be related to the corresponding axisymmetric solution. This analysis is an extension of previously published work, Zak et al. (1978, 1979), in which a similar approach was developed for static structural problems. The analysis is developed in terms of a cylindrical coordinate system r, θ and z . As the first step of the analysis, the geometry is divided into several segments in the $r-\theta$ plane. Each segment is then divided into a set of quadrilateral elements in the $r-z$ plane. The axisymmetric displacements are obtained for each segment by solving a related axisymmetric configuration. A perturbation analysis is then performed to match the solutions at certain points between the segments, and obtain the perturbation displacements for the total structure. The total displacement is then the axisymmetric displacement plus the perturbation displacement. The analysis allows for elastic-plastic materials with orthotropic yield criterion based on Hill's yield function and kinematic strain hardening. The finite element dynamic equations are solved by finite differences by dividing the

time domain into incremental steps. The solution has been programmed on a computer and applied to a number of examples. (5 refs.)

111441 Solutions of plates on a heterogeneous elastic foundation. M.Witt (Inst. of Civil Engng., Wrocław Tech. Univ., Wrocław, Poland). *Comput. & Struct. (GB)*, vol.18, no.1, p.41-5 (1984). The solution of the problem of interaction of a plate with a two parameter elastic foundation is presented. Vertical displacements of rectangular plates having free edges resting on a heterogeneous elastic foundation have been analysed by using the finite element method. The heterogeneity of the foundation caused by the orthotropy has been taken into account when forming the equations of equilibrium and variable thickness of the foundation by approximating it by Haar's functions. The obtained results have been compared with the results for a homogeneous foundation. (6 refs.)

111442 Application of the quadratic functional to nonconservative problems of elastic stability. W.Altman (Inst. Tecnol. de Aeronautica, Sao Paulo, Brazil), A.M.de Oliveira. *Comput. & Struct. (GB)*, vol.18, no.1, p.141-5 (1984). Two methods for solving nonconservative problems by applying the quadratic functional are presented. The corresponding approximate methods of solution are obtained by using suitable polynomial trial functions and are illustrated by solving Beck's and Leipholz's rods. (4 refs.)

111443 Analyses of large quasistatic deformations of inelastic bodies by a new hybrid-stress finite element algorithm. K.W.Reed, S.N.Atluri (Center for the Advancement of Computational Mech., Georgia Inst. of Technol., Atlanta, GA, USA). *Comput. Methods Appl. Mech. & Eng. (Netherlands)*, vol.39, no.3, p.245-95 (Sept. 1983). The finite element algorithm is based upon a generalization of de Veubeke's (1972) complementary energy principle. The principal variables in the formation are the nominal stress rate and spin, and the resulting finite element equations are discrete versions of the equations of compatibility and angular momentum balance. The algorithm produces true rates, time derivatives, as opposed to 'increments'. There results a complete separation of the boundary value problem (for stress rate and velocity) and the initial value problem (for total stress and deformation); hence, their numerical treatments are essentially independent. After a fairly comprehensive discussion of the numerical treatment of the boundary value problem, the authors launch into a detailed examination of the numerical treatment of the initial value problem, covering the topics of efficiency, stability and objectivity. The paper is closed with a set of examples, finite homogeneous deformation problems, which serve to bring out important aspects of the algorithm. (70 refs.)

111444 An improved treatment of transverse shear in the Mindlin-type four-node quadrilateral element. A.Tessler (Structural Life Assurance Res., Northrop Corp., Hawthorne, CA, USA), T.J.R.Hughes. *Comput. Methods Appl. Mech. & Eng. (Netherlands)*, vol.39, no.3, p.311-35 (Sept. 1983). An improved displacement methodology based on Mindlin theory is developed and applied to a four-node, twelve degrees-of-freedom quadrilateral element. Special attention is directed toward enhancement of the transverse shear energy representation. Particularly, a nonuniform order kinematic interpolation scheme is accompanied by what is termed element appropriate shear correction factors. The element matrices are consistently derived from Hamilton's variational principle using exact numerical integration throughout. The element stiffness matrix possesses correct rank and is well conditioned over the entire Mindlin theory range of thickness-to-length ratios. Exceptionally good element performance is demonstrated by solutions to a set of static and vibrational problems. (21 refs.)

111445 On differential equations of nonlocal elasticity and solutions of screw dislocation and surface waves. A.C.Eringen (Princeton Univ., Princeton, NJ, USA). *J. Appl. Phys. (USA)*, vol.54, no.9, p.4703-10 (Sept. 1983). Integropartial differential equations of the linear theory of nonlocal elasticity are reduced to singular partial differential equations for a special class of physically admissible kernels. Solutions are obtained for the screw dislocation and surface waves. Experimental observations and atomic lattice dynamics appear to support the theoretical results very nicely. (15 refs.)

111446 Nonlinear eigenvalue problems for the whirling of heavy elastic strings. II. New methods of global bifurcation theory. J.C.Alexander, S.S.Antman (Dept. of Math., Univ. of Maryland, College Park, MD, USA), Shi-tao Deng. *Proc. R. Soc. Edinburgh Sect. A (GB)*, vol.93, pt.3-4, p.197-227 (1983). For pt.1 see Arch. Rational Mech. Anal., vol.74, p.339-54 (1981). The authors treat the global qualitative behaviour of all bifurcating configurations of whirling nonlinearly elastic strings with ends fixed on the axis of rotation. (30 refs.)

111447 Continuous data dependence in linear elastodynamics on unbounded domains without definiteness conditions on the elasticities. G.P.Galdi, S.Rionero (Istituto di Matematica 'R. Caccioppoli', Naples, Italy). *Proc. R. Soc. Edinburgh Sect. A (GB)*, vol.93, pt.3-4, p.299-306 (1983). By suitably coupling convexity and weight function methods, the authors prove uniqueness and continuous dependence theorems in linear elastodynamics in unbounded domains without definiteness conditions on the elasticities. The class of solutions considered allows the 'growth' at large spatial distances. (9 refs.)

111448 Estimates for solutions of the Dirichlet problem for the biharmonic equation in a neighbourhood of an irregular boundary point and in a neighbourhood of infinity: Saint-Venant's principle. V.A.Kondratiev, O.A.Oleinik (Moscow Univ., Moscow, USSR). *Proc. R. Soc. Edinburgh Sect. A (GB)*, vol.93, pt.3-4, p.327-43 (1983). Energy estimates for solutions of the Dirichlet problem for the biharmonic equation, expressing Saint-Venant's principle in elasticity, are proved. From these integral inequalities, estimates for the maximum modulus of solutions and the gradient of solutions with homogeneous Dirichlet's boundary conditions in a neighbourhood of an irregular boundary point or in a neighbourhood of infinity are derived. These estimates characterize the continuity of solutions and their gradients at these points. (9 refs.)

Nonlinear vector waves in a mechanical model of a molecular chain See Entry 111606

Analogies of 6 classic properties of materials See Entry 113264

Note on the applications of the Frechet derivative See Entry 113309

03.40G Fluid dynamics: general mathematical aspects (see also 47. Fluid dynamics)

111449 A rigorous study of periodic orbits by means of a computer. S.De Gregorio (Istituto di Math., Università dell'Aquila, Aquila, Italy), E.Scoppola, B.Tirozzi. *J. Stat. Phys. (USA)*, vol.32, no.1, p.25-33 (July 1983). The authors apply a modified version of the method of Sinai and Vul (1980) in order to study, by means of a computer, a closed orbit which appears in the five-mode model of bidimensional incompressible fluid on the torus. (7 refs.)

111450 New splitting-up schemes for solving hyperbolic and parabolic non linear problems: applications to Euler and Navier-Stokes equations. P.Laval (ONERA, Chatillon, France).

Rech. Aerosp. (France), no.4, p.257-309 (July-Aug. 1983). In French. The most significant results obtained at ONERA over the last few years from the theoretical and numerical study of the splitting-up (disintegration) explicit method are presented. A general class of second-order splitting-up schemes is introduced for solving hyperbolic nonlinear problems. An 'optimal' scheme (defined as dissipative with minimal dissipation) is derived for solving a shock problem. It yields a numerically stable solution for this problem without any artificial viscosity. The results obtained from the computations of two-dimensional transonic flows with shocks show the significant improvements that can be expected from the sub-class of schemes, dissipative with minimal dissipation in each direction. The method is extended to the computations of three-dimensional unsteady non uniform flows in a turbo-machine. New classes of second order 'optimal' time splitting schemes (which allow optimal time steps) are also introduced for solving the Euler equations and the full time-dependent compressible viscous Navier-Stokes equations in fluid mechanics. The stability of the newly-derived schemes which is determined analytically shows that the present 'optimal' method should lead to considerably shorter computation times than the other existing explicit methods. (60 refs.)

111451 Logarithmic self-similar solutions. A.L.Brezhnev, I.A.Chernov (M.I. Kalinin Inst. of Agricultural Mechanization & N.G. Chernyshevskii State Univ., Saratov, USSR). *Sov. Phys.-Dokl. (USA)*, vol.27, no.12, p.1011-12 (Dec. 1982). Translation of: *Dokl. Akad. Nauk SSSR*, vol.267, no.4-6, p.1331-3 (Dec. 1982). [received: Sept. 1983] Self-similar solutions of equations containing partial derivatives play an important role in various branches of fluid mechanics. The authors demonstrate a means of constructing solutions close to self-similar in three classical models: (1) in transonic gas dynamics; (2) in the theory of one-dimensional, nonstationary gas flows; (3) in boundary-layer theory. (3 refs.)

Singular filaments organize chemical waves in three dimensions. I. Geometrically simple waves See Entry 111460

Applications of exponential splines in computational fluid dynamics See Entry 113397

Pseudospectral approximation in a three-dimensional Navier-Stokes code See Entry 113398

The real and complex Lorenz equations and their relevance to physical systems See Entry 113405

03.40K Waves and wave propagation: general mathematical aspects

(see also 46.30M Mechanical and elastic waves, 43.20 General linear acoustics)

111452 Propagation reflection and transmission of waves under initial shear stresses. S.Dey, S.P.Mukherjee (Dept. of Phys. & Math., Indian School of Mines, Dhanbad, India). *Int. J. Non-Linear Mech. (GB)*, vol.18, no.4, p.269-77 (1983). Deals with the study of propagation of Love waves and reflection as well as transmission of SH waves under initial shear stresses. The results have been computed taking two real media and presented graphically to compare with the initial stress-free cases. (16 refs.)

111453 Acceleration waves in elastic dielectrics with polarization gradient effects. S.Dost (Dept. of Mech. Engng., Univ. of Calgary, Calgary, Alberta, Canada). *Int. J. Eng. Sci. (GB)*, vol.21, no.11, p.1305-11 (1983). Investigates the propagation of acceleration waves of arbitrary form in a deformed elastic dielectric with polarization effects. An acceleration wave is defined as a second order propagating surface of discontinuity on which the position vector, the polarization vector and Maxwell potential, and their first order derivatives with respect to time and space coordinates are continuous while the second order derivatives of these quantities may suffer jumps but are continuous everywhere else. By computing the jumps of the balance equations on the singular surface implicit equations for wave speeds corresponding to non-zero amplitudes of the acceleration wave are obtained. It is noteworthy that the second order derivatives of Maxwell potential are also continuous across the acceleration wave. The same equation for wave speeds are also derived for isotropic elastic dielectrics. The wave speeds for longitudinal and transverse waves are obtained in explicit forms and the conditions of existence for real wave speeds are investigated. (17 refs.)

111454 Nonlinear lattice and soliton theory. M.Toda. *IEEE Trans. Circuits & Syst. (USA)*, vol.CAS-30, no.8, p.542-54 (Aug. 1983). Since the notion of stable pulses, known as solitons, plays a central role in the phenomena of wave propagation in nonlinear systems, an exposition of this topic is developed in some detail. It is known that the equations of motion of the one-dimensional lattice of particles with exponential interaction are integrable, namely, they admit exact solutions, and this system is equivalent to an LC circuit with certain nonlinear capacitance. In addition, a closely related partial differential equation called the Korteweg-de Vries (KdV) equation is also integrable. Special emphasis is placed on these integrable systems. (27 refs.)

111455 On the method for solving the complex sine-Gordon equation. Hang Nian-Ning (Istituto Nazionale di Fisica Nucleare, Torino, Italy). *Lett. Nuovo Cimento (Italy)*, vol.38, ser.2, no.2, p.60-4 (10 Sept. 1983). A general form of the Lax pair equation is found to be reduced to the Zakharov and Sabat (ZS) form by using a similarity transformation whose existence is guaranteed by the compatibility conditions. Through the ZS solutions, two solutions of the complex Sine-Gordon equation in the one soliton case corresponding to different initial conditions, are easily found. (3 refs.)

- 111456 Hybrid mode technique yields waveguide dispersion analysis.** A.M.Pavio (Texas Instruments Inc., Dallas, TX, USA). *MSN Microwave Syst. News (USA)*, vol.13, no.4, p.106-11 (April 1983). Describes a numerical solution method which allows the evaluation of planar circuit structures for monolithic circuit applications. The dispersion characteristics of a coplanar waveguide in the direct presence of a ground plane surface is investigated using a full-wave analysis technique. Classical electromagnetic theory, applied to the illustrated boundary value problem, forms the basis of the solution method. This application of Galerkin's method in the Fourier-transform domain is commonly referred to as spectral domain analysis. A frequency dependent hybrid-mode analysis in the space domain generates a set of coupled integral equations which are transformed to a coupled set of algebraic equations. An accurate determination of the propagation constant is obtained by solving the eigenvalue equation of a low-order matrix equation. (6 refs.)
- 111457 Admissibility criteria for shock wave solutions of a system of conservation laws of mixed type.** M.Shearer (Dept. of Math., Duke Univ., Durham, NC, USA). *Proc. R. Soc. Edinburgh Sect. A (GB)*, vol.93, pt.3-4, p.233-44 (1983). The following system of conservation laws is considered: $u_t - v_x = 0$, $v_t - \sigma(u)_x = 0$ where $\sigma: \mathbb{R} \rightarrow \mathbb{R}$ is a smooth function monotonically increasing except in an interval. Two criteria for the admissibility of shocks are shown to be independent in the sense that there are shocks satisfying each and violating the other. This contrasts with the corresponding situation for strictly hyperbolic systems ($\sigma'(u) > 0$ for all u), for which the two criteria are equivalent. (6 refs.)
- 111458 Almost-periodic forcing for a wave equation with a nonlinear, local damping term.** A.Haraux (Univ. Pierre et Marie Curie, Paris, France). *Proc. R. Soc. Edinburgh Sect. A (GB)*, vol.94, pt.3-4, p.195-212 (1983). (27 refs.)
- 111459 On a Dirichlet-Neumann-Third mixed boundary value problem for the Helmholtz equation.** M.David (Sci. Dept., Min. of Defense, Tel Aviv, Israel). *Proc. R. Soc. Edinburgh Sect. A (GB)*, vol.94, pt.3-4, p.221-33 (1983). Existence and uniqueness theorems are proved for the solution of a Dirichlet-Neumann-Third mixed boundary value problem for the Helmholtz equation in \mathbb{R}_3 . The proofs make use of an equivalent system of two integral equations of the second kind. (5 refs.)
- 111460 Singular filaments organize chemical waves in three dimensions. I. Geometrically simple waves.** A.T.Winfree, S.H.Strogatz (Dept. of Biological Sci., Purdue Univ., West Lafayette, IN, USA). *Physica D (Netherlands)*, vol.8D, no.1-2, p.35-49 (July 1983). This is the first of a series of papers on the anatomy of three-dimensional dissipative structures in excitable media. The Belousov-Zhabotinsky reagent provides examples. The authors describe the propagation of chemical waves in such media first in terms of 'phase' in a cycle of excitation and relaxation, then in terms of chemical concentration surfaces. Phase singularities are shown to arise in a natural way as ring-like filaments in three dimensions. They describe the known methods of creating singularities and the simplest wave structure organized by a singular filament: the experimentally demonstrated scroll ring. (30 refs.)
- 111461 Nonsteady waves in distributed dynamical systems.** B.A.Malomed (Inst. of Biological Phys., Acad. of Sci., Moscow, USSR). *Physica D (Netherlands)*, vol.8D, no.3, p.353-9 (Sept. 1983). The author studies one-dimensional and two-dimensional transient wave regimes in nonlinear systems of the reaction-diffusion type. In a one-dimensional case the process of collision of two travelling waves is considered. It is demonstrated that in the case of a nondispersive nonlinear system, where a steady regime of the collision is not possible, the process can be described by means of an approximation which is nonuniform in a spatial coordinate. The collision results, in a general case, in formation of an oscillatory shock moving with varying velocity. In a two-dimensional situation the transition of a rotating vortex into a rotating spiral wave in the case of dispersive systems and the inverse transition in the case of nondispersive systems are considered. (15 refs.)
- 111462 Scattering and nonscattering obstacles.** V.Twersky (Math. Dept., Univ. of Illinois, Chicago, IL, USA). *SIAM J. Appl. Math. (USA)*, vol.43, no.4, p.711-25 (Aug. 1983). Two problems of Helmholtz's equation for a wave incident on an obstacle are considered. For the first, the scattering problem, the obstacle's response satisfies Sommerfeld's outgoing wave radiation condition, and the net radiative response is positive; for the second, the response satisfies a standing wave condition (an appropriate combination of outgoing and incoming waves) such that the net radiative response is zero. The essential features of the solutions are exhibited in terms of amplitude functions g (the usual scattering amplitude) and g' , and the interrelation of the functions are stressed in the derivation of integral equations $g[g']$ (introduced earlier in multiple scattering contexts). The scattering amplitude g is always complex, but the simpler function g' is shown to be imaginary for nonabsorbing obstacles having inversion symmetry. Long-wavelength approximations for g' may be obtained from potential theory and perturbation procedures, and corresponding approximations for g then follow from $g[g']$. (12 refs.)
- 111463 Low frequency scattering by local inhomogeneities.** G.A.Kriegsmann, E.L.Reiss (Dept. of Engng. Sci. & Appl. Math., Northwestern Univ., Evanston, IL, USA). *SIAM J. Appl. Math. (USA)*, vol.43, no.4, p.923-34 (Aug. 1983). An asymptotic expansion which is uniformly valid space is obtained for the low frequency scattering of a plane wave incident on a localized inhomogeneity. The scattering region, which may be simply of multiply (collection of scatterers) connected, has a characteristic length which is small compared with the wave length of the incident wave. The index of refraction n is unity outside the scattering region and it is arbitrary inside the region. The method of matched asymptotic expansions is used in the analysis. The Born approximation is shown to agree with the uniform expansion in the far and the near fields. The leading term in the uniform expansion is a linear functional of $1-n^2$. Thus, statistics of the scattered field are easily evaluated from the statistics of n , when n is a random process. The method is then applied to the low frequency of an acoustic plane wave by localized inhomogeneities in the density and the index of refraction. Finally, the scattering by a plane which is acoustically hard except for a small impedance spot, is analyzed by the same method. (15 refs.)
- 111464 Equipartition of energy in scattering theory.** G.Dassios (Dept. of Math., Univ. of Patras, Patras, Greece), M.Grillakis. *SIAM J. Math. Anal. (USA)*, vol.14, no.5, p.915-24 (Sept. 1983). It is shown that the difference between the kinetic and the potential energy of a solution of the wave equation in the exterior of a star-shaped body, which vanishes on the surface of the body and has Cauchy data with compact support, decays to zero as time tends to infinity. Therefore asymptotic equi-

partition of energy occurs even in the presence of a scatterer. An upper bound for the rate of decay has been found. An extension of Morawetz's local energy decay result (1961) for the case of an expanding sphere is also obtained. (11 refs.)

- Proceedings of the International Conference on Order in Chaos** See Entry 111307
- Standing waves—a new twist** See Entry 111378
- On differential equations of nonlocal elasticity and solutions of screw dislocation and surface waves** See Entry 111445
- Lectures on the inverse scattering method** See Entry 111500
- Influence of solitons in the initial state of chaos in the driven damped sine-Gordon system** See Entry 111578
- Nonlinear vector waves in a mechanical model of a molecular chain** See Entry 111606
- Scattering of lattice solitons from a mass interface—A synergetic approach** See Entry 111607
- Quantitative maximum principles and strongly coupled gradient-like reaction-diffusion systems** See Entry 111614
- Thermal waves in an absorbing and convecting medium** See Entry 111615
- Solitons and numerical experiments** See Entry 111903
- Energy balance equations describing point sources of elastic waves in a continuously varying medium** See Entry 113345
- Cyclic gravity waves in deep water** See Entry 113458
- Water waves, nonlinear Schrödinger equations and their solutions** See Entry 116114
- Scattering analysis and synthesis of wave trains** See Entry 116115

03.50 CLASSICAL FIELD THEORY

- 111465 The classical electromagnetic field and the vacuum.** A.B.Datzeff (Dept. of Theoretical Phys., Univ. of Sofia, Sofia, Bulgaria). *Bulg. J. Phys. (Bulgaria)*, vol.10, no.3, p.239-55 (1983). An attempt to build up a microtheory of the electromagnetic field has been made on the basis of the hypothesis of a material field carrier. This carrier is called subvac and has a discrete structure. Without the use of the formal method with a test body to introduce the basic notions of the field (E, H, ϕ, A, e, m), these notions are defined by the internal subvac's properties. These notions yield the known relations for the classical electromagnetic field, as well as the Maxwell equations. Some logical difficulties of the classical theory are thus removed. The problem of the structure of the elementary charge (the electron) which requires a non-linear generalization of the Maxwell equations admittedly remains open. (9 refs.)
- 111466 The conserved currents for the Maxwellian field.** R.Arens (Dept. of Maths., Univ. of California, Los Angeles, CA, USA). *Commun. Math. Phys. (Germany)*, vol.90, no.4, p.527-44 (1983). The author classifies the conserved currents for the Maxwellian field. There are four families: (1) the classical currents derived using Noether's theorem from conformal invariance (2) certain Noetherian currents based on translations in field space, (3,4) two more kinds not equivalent to any Noetherian form. (7 refs.)
- 111467 Lagrangian dynamics of a classical spinning particle with dipole moments.** G.Cognola, R.Soldati, L.Vanzo, S.Zerbini (Dipartimento di Fisica, Univ. di Trento, Trento, Italy). *Nuovo Cimento B (Italy)*, vol.76B, ser.2, no.2, p.109-29 (11 Aug. 1983). A singular Lagrangian formulation for the motion of a spinning particle (Dirac-Pauli electron) with general dipole moments in the presence of external electromagnetic and gravitational fields is given. The Dixon-Souriau equations are derived. The Lagrangian gives the transversality condition as primary constraint and leads to a phase space of minimal dimension. The Lagrangian approach is then extended to include a torsion field and the equations of motion for the classical counterpart of the Dirac electron in such a field are obtained. They are in full agreement with those derived by some authors using semi-classical approximations of the Dirac equation. The necessity to consider a mass dipole moment for such a particle is stressed. The Hamiltonian formulation for a spinning particle with anomalous magnetic moment in a pure electromagnetic field is also treated. Finally, the possibility of including nonAbelian gauge fields is briefly outlined and the Wong equations for a spinning particle are obtained. (23 refs.)
- 111468 The original Ampere force and Biot-Savart and Lorentz forces.** P.T.Pappas (Dept. of Phys., Univ. of Athens, Athens, Greece). *Nuovo Cimento B (Italy)*, vol.76B, ser.2, no.2, p.189-97 (11 Aug. 1983). The author presents the results of a very simple experiment, which favours the original Ampere force and unambiguously disproves the Biot-Savart force of relativity, or its approximation in a covariant relativistic form, namely the Lorentz force. This experiment with its extra degree of freedom has the advantage over the many other similar ones, including Ampere's original experiment, which have been performed in the past and recently by Graneau (1982), of giving results which are both qualitative and quantitative, as well as unambiguous. Due to the strong association of the Biot-Savart and Lorentz force to relativistic theories, the experiment can also be considered as limiting the generality of these theories. (33 refs.)
- 111469 Shortcut for constructing any Lagrangian from its equations of motion.** R.Hojman (Dept. de Física, Univ. de Santiago de Chile, Santiago, Chile), S.Hojman, J.Sheinbaum. *Phys. Rev. D (USA)*, vol.28, no.6, p.1333-6 (15 Sept. 1983). The authors show how to construct the Lagrangians for any regular mechanical system. The Lagrangians are a linear combination of the left-hand sides of their own equations of motion (up to a total derivative). The examples suggest that the same holds even for singular systems in field theory. (6 refs.)
- 111470 Classical and quantal supersymmetric Liouville theory.** E.D'Hoker (Dept. of Phys., MIT, Cambridge, MA, USA). *Phys. Rev. D (USA)*, vol.28, no.6, p.1346-57 (15 Sept. 1983). The classical supersymmetric Liouville theory is shown to be invariant under the supersymmetric extension of the conformal group. Lax pair and Backlund transformations are derived and the general classical solution is obtained. The isotropy group for every solution is constant on the solution manifold and equal to an $N=1$ conformal supersymmetry. For the quantum theory, the effective potential is computed exactly. The spectrum of the theory is continuous, bounded from below by zero, but no translationally invariant ground state exists. Translational invariance may be broken without the appearance of a Goldstone boson and a consistent perturbation theory in the coupling constant is obtained. The constant $N=1$ supersymmetry is also broken to a constant $N=1/2$ supersymmetry, and no Goldstone fermion arises. Space is

spontaneously reduced to the half-line. $N=1$ conformal supersymmetry remains exact to all orders of perturbation theory. (17 refs.)

111471 Null strings and null solutions of Maxwell's equations. K.Nagatomo (Dept. of Math., Osaka Univ., Osaka, Japan). *Proc. Jpn. Acad. Ser. A (Japan)*, vol.59, no.4, p.136-8 (April 1983). [received: Sept. 1983]

Establishes a relation between null strings and null solutions of Maxwell's equations (null electromagnetic fields). The author expresses Plucker's coordinates of the 2-dimensional surface swept out by a null string by means of a null electromagnetic field. (5 refs.)

Some novel delta-function identities See Entry 111355

On the significance of the axial Newtonian gravitational force of the finite cylinder See Entry 111538

New and old symmetries of the Maxwell and Dirac equations See Entry 111902

03.65 QUANTUM THEORY; QUANTUM MECHANICS

(see also 05.30 Quantum statistical mechanics; for relativistic wave equations, see 11.10)

111472 Elliptical orbits in quantum mechanics. D.R.Snider (Dept. of Phys., Univ. of Wisconsin-Milwaukee, Milwaukee, WI, USA). *Am. J. Phys. (USA)*, vol.51, no.9, p.801-3 (Sept. 1983).

Solutions are found to Schrodinger's equation with an inverse- r potential which well approximate the classical solution, an elliptical orbit. (2 refs.)

111473 Nonlinearly coupled oscillators: dynamics and statistical mechanics. Ta-You Wu (Inst. of Phys., Acad. Sinica, Taipei, Taiwan). *Annu. Rep. Inst. Phys. Acad. Sin. (Taiwan)*, vol.12, p.1-9 (Dec. 1982). [received: Sept. 1983]

In connection with the principle of equipartition of energy, the distinction between strict dynamics and statistical theory is illustrated by an example of two oscillators coupled by anharmonic potentials. Instead of solving an initial value problem in dynamics (such as in the work of Fermi-Pasta-Ulam), an element of randomness is introduced by the use of two independent time scales, a fast time for the oscillations and a slow time for the energy transfer due to the non-linear coupling. The non-linear equations of motions have been solved by numerical integration. The result is that an initial state of excitation does not recur as in Fermi-Pasta-Ulam's work, but approaches asymptotically (logarithmically) a redistributed state. (4 refs.)

111474 One-electron relativistic molecules with Coulomb interaction. I.Daubechies, E.H.Lieb (Dept. of Maths. & Phys., Princeton Univ., Princeton, NJ, USA).

Commun. Math. Phys. (Germany), vol.90, no.4, p.497-510 (1983).

As an approximation to a relativistic one-electron molecule, the authors study the operator $H = (-\Delta + m^2)^{1/2} - e^2 \sum_{j=1}^N |Z_j| x = R_j|^{-1}$ with $Z_j \geq 0$, $e^2 = 137.04$. H is bounded below if and only if $e^2 Z_j \leq 2/\pi$, all j . Assuming this condition, the system is unstable when $e^2 Z_j > 2/\pi$ in the sense that $E_0 = \inf \text{spec}(H) \rightarrow -\infty$ as the $R_j \rightarrow 0$, all j . They prove that the nuclear Coulomb repulsion more than restores stability; namely $E_0 + 0.069e^2 \sum_{j=1}^N Z_j |R_j - R_i|^{-1} \geq 0$. They also show that E_0 is an increasing function of the inter-nuclear distances $|R_i - R_j|$. (14 refs.)

111475 A new approach to the determination of good action-angle variables for coupled oscillator systems. L.C.Geiger, G.C.Schatz (Dept. of Chem., Northwestern Univ., Evanston, IL, USA).

Chem. Phys. (Netherlands), vol.79, no.3, p.431-47 (15 Sept. 1983).

A theory of action-angle variables for coupled oscillator systems is developed which involves solving the Schrodinger equation using a basis of WKB eigenfunctions, then using the logarithm of the resulting wavefunction to define the generator for the canonical transformation which determines the action-angle variables. This theory is based on the marriage between Miller's method for solving the Hamilton-Jacobi equation using the logarithm of the generating function, and the Ratner-Buch-Gerber method for solving the Schrodinger equation using WKB basis functions. A perturbation-theory analysis of this theory indicates that the semiclassical eigenvalues and canonical transformations obtained from it should become identical to their exact classical counterparts in the limit of large actions for each vibrational mode. Two methods for systematically improving the theory for the lower eigenstates are also proposed. Numerical applications of the theory are presented for two systems, the Morse oscillator and the Henon-Heiles two-mode hamiltonian. (24 refs.)

111476 Constraints on boundary conditions for enclosed systems due to real energy eigenvalues. R.J.Swenson (Phys. Dept., Montana State Univ., Bozeman, MT, USA).

Int. J. Quantum Chem. (USA), vol.24, no.3, p.333-4 (Sept. 1983).

The quantum mechanics of enclosed systems is of considerable interest. The consequences of various boundary conditions (BC) on the wave function have been treated recently (1981). The author discusses constraints on the types of BC which are imposed by requiring that the energy eigenvalues be real. (2 refs.)

111477 Bound-state energies for the superposed screened Coulomb potential. A.P.Kajwadkar, L.K.Sharma (Dept. of Appl. Phys. Government Engng. Coll., Jabalpur, India).

Indian J. Phys. Part B, vol.57B, no.3, p.209-14 (June 1983).

The bound-state eigenenergies for all angular momenta for the superposition of two static screened Coulomb potentials (SSCP) having different coupling constants and screening parameters have been evaluated by approximating it to the Eckart potential. The eigenenergy values for the single SSCP are found to have been enhanced considerably due to this superposition. (15 refs.)

111478 A new uniform semiclassical wave function for single surface and multisurface scattering. M.F.Herman (Dept. of Chem., Tulane Univ., New Orleans, LA, USA).

J. Chem. Phys. (USA), vol.79, no.6, p.2771-8 (15 Sept. 1983).

A procedure for the evaluation of one-dimensional uniform semiclassical wave functions is explored. This form of the approximate wave function is tested for the case of an exponential potential and is compared to the exact quantum mechanical and WKB wave functions. It is found that the uniform approximation provides a very accurate representation of the exact wave function, even at the turning points of the classical motion, where the WKB approximation diverges. It is demonstrated how correction terms can be constructed, leading to a formal expansion for the exact wave function. The individual terms of this expansion each involve a finite number of reflection points with uniform semiclassical propagation between these reflections. The analysis is extended to multisurface (nonadiabatic) problems, removing the turning point singularities which are generally present in semiclassical formulations of nonadiabatic problems. (15 refs.)

111479 A comparison of some lower bounds for eigenvalues of Schrodinger's equation. P.G.Hornby, M.N.Barber (Dept. of Appl. Math., Univ. of New South Wales, Kensington, NSW, Australia).

J. Phys. A (GB), vol.16, no.14, p.3291-311 (1 Oct. 1983).

A method proposed recently by Singh (1981) of finding lower bounds to the eigen-energies of Schrodinger's equation is reviewed and compared with the methods of Bazley and Fox (1961) and of Lowdin (1965). Numerical results for an anharmonic oscillator suggest that the Singh method is less accurate than the others, but unlike the Lowdin single bracketing function technique does not suffer from any eigenvalue ordering problems. (22 refs.)

111480 The recursion method of a linear operator inversion. M.Znojil (Inst. of Nuclear Phys., Czechoslovak Acad. of Sci., Rez, Czechoslovakia).

J. Phys. A (GB), vol.16, no.14, p.3313-23 (1 Oct. 1983).

For pt.II see *ibid.*, vol.11, p.1501 (1978). Suggests constructing an inverse of the infinite-dimensional matrix Q by means of its recurrent algebraic decomposition into the easily invertible two-diagonal factors. The merits and feasibility of the method are illustrated on the five-diagonal matrices. Quartic and decadic-decadic anharmonic propagators are chosen as examples of the application. (13 refs.)

111481 Quantum tunneling with dissipation. A.I.Larkin, Yu.N.Ovchinnikov (L.D. Landau Inst. of Theoretical Phys., Acad. of Sci., USSR). *JETP Lett. (USA)*, vol.37, no.7, p.382-5 (5 April 1983). Translation of: *Pis'ma v Zh. Eksp. & Teor. Fiz. (USSR)*, vol.37, no.7, p.322-5 (5 April 1983). [received: Oct. 1983]

Dissipative processes reduce the probability for quantum tunneling. The temperature dependence of the probability for the decay of a metastable state is analyzed. (5 refs.)

111482 On the law of composition of probabilities. E.Eberle (Istituto Dipartimentale di Fisica, Univ. di Catania, Catania, Italy).

Lett. Nuovo Cimento (Italy), vol.38, ser.2, no.1, p.24-6 (3 Sept. 1983).

A general formula for the composition of probabilities is derived, by means of few general assumptions, which is an evident generalization of the quantum formula. (5 refs.)

111483 Magnetic-field effects on the polarization correlation of photon couples emitted in an atomic cascade. F.Falciglia (Istituto di Fisica, Univ. di Catania, Catania, Italy), A.Garuccio, G.Iaci, L.Pappalardo.

Lett. Nuovo Cimento (Italy), vol.38, ser.2, no.2, p.52-4 (10 Sept. 1983).

A modification of the experiments for verifying the Einstein locality is proposed. It is possible to study the effects of an external magnetic field on the polarization correlation function of photon couples emitted in an atomic cascade of calcium. (4 refs.)

111484 The Aharonov-Bohm effect: how the switching-on procedure helps to understand it better. P.Frolov, V.D.Skarzhinsky (P.N. Lebedev Phys. Inst., Moscow, USSR).

Nuovo Cimento B (Italy), vol.76B, ser.2, no.1, p.35-46 (11 July 1983).

The procedure of switching on the magnetic field in a solenoid is considered in order to investigate its influence on quantum states of an electron for a wave packet scattering and for a finite motion. It allows one to separate the classical action of the induced electric field on the electron from a pure quantum-mechanical effect connected with the appearance of a vector potential (Aharonov-Bohm effect). (10 refs.)

111485 Minimal constraints for a joint-probability distribution associated to microsystems. D.Evrard (Lab. de Mecanique Quantique, UER Sci., Reims, France).

Nuovo Cimento B (Italy), vol.76B, ser.2, no.2, p.139-52 (11 Aug. 1983).

A general continuity equation in the (\mathbf{q}, \mathbf{p}) -space is stated for virtual flows from Liouville's complete theorem, i.e. not reduced to a Hamiltonian form. The comparison with the Schrodinger equation permits one to disclose the minimal imposed by this equation upon a joint-probability distribution function $P(\mathbf{q}, \mathbf{p}, t)$ associated to a microsystem. (11 refs.)

111486 On the occurrence of multiple spectra of eigenvalues in the one-dimensional complex scaled Schrodinger equation. O.Atabek, R.Lefebvre (Lab. de Photophys. Moleculaire, CNRS, Univ. de Paris-Sud., Orsay, France).

Nuovo Cimento B (Italy), vol.76B, ser.2, no.2, p.176-88 (11 Aug. 1983).

Numerical experiments performed on the complex scaled one-dimensional radial Schrodinger equation with an exponential wall show that different rotation angles may produce different spectra. An explanation is given from a study of the analytic solutions and the relation with the Stokes phenomenon is pointed out. However, the spectra predicted by this analysis are not always obtained numerically. This is shown to be due to a self-correction effect which erases the memory of the boundary conditions. (18 refs.)

111487 Topology of two-dimensional autowaves. G.T.Gurija, M.A.Livshits (Inst. of Molecular Biology, Acad. of Sci., Moscow, USSR).

Phys. Lett. A (Netherlands), vol.97A, no.5, p.175-7 (29 Aug. 1983).

A two-dimensional waves classification based on the topology of the wave-vector distribution is suggested. The conservation laws for two topological quantum numbers impose restrictions on the possible wave transformations. The predictions are in full agreement with observations. (5 refs.)

111488 Moment method and the Schrodinger equation in the large N limit. J.P.Ader (Lab. de Phys. Theorique, Bordeaux, France).

Phys. Lett. A (Netherlands), vol.97A, no.5, p.178-82 (29 Aug. 1983).

A new technique is presented for solving the Schrodinger equation in the framework of the $1/N$ expansion. Based on recursion relations satisfied by moments of the coordinate operator, this method which allows to compute energy levels and wavefunctions is applied to four examples: the harmonic oscillator, the rotating harmonic oscillator, a linear plus Coulomb potential and a logarithmic one. (9 refs.)

111489 On the existence of bound states of N -particle systems in one and two dimensions. F.A.B.Coutinho, C.P.Malta, J.Fernando Perez (Inst. de Fisica, Univ. de Sao Paulo, Sao Paulo, Brazil).

Phys. Lett. A (Netherlands), vol.97A, no.6, p.242-4 (5 Sept. 1983).

The authors give sufficient conditions for the existence, in one and two dimensions, of bound states of a system of N -particles interacting via two-body potentials. (7 refs.)

111490 Time-dependent superposition of spinors. G.Badurek, H.Rauch, J.Summhammer (Atominst., Osterreichischen Univ., Wien, Austria).

Phys. Rev. Lett. (USA), vol.51, no.12, p.1015-18 (19 Sept. 1983).

Inverting the spin state of one of the two coherent waves propagating within a neutron interferometer by means of a radio-frequency spin-flip device leads to a nonstationary interference pattern. By using stroboscopic neutron detection one can resolve this to demonstrate the nonclassical behavior of spinor superposition. (11 refs.)

111491 Comment on 'Direct measurement of the longitudinal coherence length of a thermal neutron beam' [and reply]. G.Comsa (Inst. für Grenzflächenforschung und Vakuumphys., KFA Jülich GmbH, Jülich, Germany), H.Kaiser, S.A.Werner, E.A.George. *Phys. Rev. Lett. (USA)*, vol.51, no.12, p.1105-6 (19 Sept. 1983). In a recent letter, Kaiser, Werner and George (KWG) (*ibid.*, vol.50, p.560, 1983) present a beautiful neutron interference experiment and claim to have observed 'the detailed longitudinal shape of a neutron wave packet'. It is shown here that the KWG experiment only confirmed the already known value of the incident-beam wave-number spread, σ_n , but did not supply any new information, i.e. it was simply an alternative way to measure the wave-number spread. KWG then reply to this. (5 refs.)

111492 Quantum tunneling in multidimensional systems. S.Y.Lee, N.Takigawa (Inst. Phys., Acad. Sinica, Taipei, Taiwan). *Phys. Rev. C (USA)*, vol.28, no.3, p.1123-35 (Sept. 1983). The effects of coupling to a harmonic oscillator on the quantum tunneling of a macroscopic motion are studied through the influence functional formalism of Feynman's path integral method for the general coupling form factor. As an example, the authors consider the model in which the potential barrier is parabolic and the coupling Hamiltonian is linear in both coordinates of the macroscopic motion and of the intrinsic harmonic oscillator. The results are then compared with the exact solution obtained through the canonical transformation into normal coordinates in the limiting cases when the normal coordinates reduce to the original coordinates. They found that: (1) In the adiabatic case, i.e. when the recurrence time π/ω of the oscillator is much shorter than the transmission time through the macroscopic potential barrier, the effect of oscillator coupling can be well represented by an effective potential. The coupling enhances the tunneling probability on the whole. (2) There exists a critical energy, above which the tunneling probability is reduced because of the linear oscillator coupling. In the weak coupling limit and when $\omega \rightarrow 0$, the critical energy becomes $-\infty$, so that the coupling to the oscillator always reduces the tunneling probability. (20 refs.)

111493 Absence of singular continuous spectrum for two-body Schrödinger operators with long-range potentials (a new proof). H.L.Cycon (Courant Inst. of Math. Sci., New York Univ., New York, NY, USA). *Proc. R. Soc. Edinburgh Sect. A (GB)*, vol.94, pt.1-2, p.61-9 (1983). The author proves the absence of singular continuous spectra for Schrödinger operators $-\Delta + V$ with long-range potential V such that V and $(1+r)^{1+\epsilon}(\partial/\partial r)V$ is $(-\Delta)$ -compact by using a modified 'Mourre type' estimate and by Kato-Lavine's H -smoothness theory. (14 refs.)

111494 Stochastic behavior in quantum scattering. M.C.Gutzwiller (IBM Thomas J. Watson Res. Center, Yorktown Heights, NY, USA). *Physica D (Netherlands)*, vol.7D, no.1-3, p.341-55 (May 1983). (Proceedings of the International Conference on Order in Chaos, Los Alamos, NM, USA, 24-28 May 1982). A 2-dimensional smooth orientable, but not compact space of constant negative curvature with the topology of a torus is investigated. It contains an open end, i.e. an exceptional point at infinite distance, through which a particle or a wave can enter or leave, as in the exponential horn of certain antennas or loudspeakers. In the Poincaré model of hyperbolic geometry the solutions of Schrödinger's equation for the reflection of a particle which enters through the horn are easily constructed. The scattering phase shift as a function of the momentum is essentially given by the phase angle of Riemann's zeta function on the imaginary axis, at a distance of $1/2$ from the famous critical line. This phase shift shows all the features of chaos namely the ability to mimic any given smooth function, and great difficulty in its effective numerical computation. A plot shows the close connection with the zeros of Riemann's zeta function for low values of the momentum (quantum regime) which gets lost only at exceedingly large momenta (classical regime?) Some generalizations of this approach to chaos are mentioned. (14 refs.)

111495 Quantum-classical correspondence for the Fourier spectrum of a trajectory. E.J.Heller (Theoretical Div., Los Alamos Nat. Lab., Los Alamos, NM, USA). *Physica D (Netherlands)*, vol.7D, no.1-3, p.356-61 (May 1983). (Proceedings of the International Conference on Order in Chaos, Los Alamos, NM, USA, 24-28 May 1982). Using a displaced localized wavepacket (coherent state) as a quantum analog to a classical trajectory, the author examines the Fourier spectrum of the expectation value of position X_t^Q and compare it with the classical Fourier spectrum of position X_t . In both the quasiperiodic and chaotic regimes, a strong classical-quantum correspondence exists in the Fourier spectrum. However, the quantum spectrum has certain interesting features not present in the classical case. (4 refs.)

111496 Intensity moments of semiclassical wavefunctions. M.V.Berry, J.H.Hannay, A.M.Ozorio de Almeida (H.H. Wills Phys. Lab., Bristol, England). *Physica D (Netherlands)*, vol.8D, no.1-2, p.229-42 (July 1983). For normalized wavefunctions $\psi(q)$ of N coordinates q , the authors obtain semiclassical approximations to the moments $I_m = \int dq |\psi(q)|^{2m}$, as a measure of the intensity variations of ψ . If ψ is a regular state, associated with an N -dimensional phase-space torus T , I_m diverges as $\hbar \rightarrow 0$ because of strong and rapidly-varying intensities at caustic singularities C , as follows: if C is a fold catastrophe, $I_m \sim F_m/\hbar^{(m-2)/3}$ if $m \geq 3$ and $I_2 \sim F_2 \ln(B/\hbar)$; if C is a cusp point, $I_m \sim C_m/\hbar^{(3m/2-1/4)}$; if C is a hyperbolic umbilic 'corner' point, $I_m \sim H_m/\hbar^{(2m-2)/3}$ if $m \geq 3$ and $I_2 \sim H_2 [\ln(B/\hbar)]^2$, the constants F_m , C_m and H_m are evaluated explicitly in terms of diffraction catastrophe integrals and the geometry of T . If ψ is a chaotic state, associated with a phase-space region of dimensionality $> N$ (e.g. the energy surface of an ergodic system), $I_m \sim \text{constant}$ as $\hbar \rightarrow 0$ because the (moderate) intensity fluctuations arise not from caustics but from incoherent interference of many de Broglie waves. (19 refs.)

111497 The calculations of an inverse potential problem. C.S.Morawetz (Courant Inst. of Math. Sci., New York Univ., New York, NY, USA), G.A.Kriegsmann. *SIAM J. Appl. Math. (USA)*, vol.43, no.4, p.844-54 (Aug. 1983). A method is developed for solving an inverse problem for the wave equations with potential where the object is to find the potential given Cauchy data on a time-like surface. The computation is carried out with one space variable by an iterative procedure. The point of this method is that it can be extended to higher dimensions in principle. A coarse mesh finite difference scheme is used which yields fair accuracy. (8 refs.)

111498 Conservative difference scheme for generalized nonlinear Schrödinger equations. Chang Qianshun (Inst. of Appl. Math., Acad. Sinica, Beijing, China). *Sci. Sin. (China)*, vol.26, no.7, p.687-701 (July 1983). The conservative difference schemes for two mixed initial-boundary value problems of generalized nonlinear Schrödinger equations are considered. Using the Sobolev inequality for the difference operator, Gronwall's inequality, and the imbedded theorem, the author makes prior estimates of the difference solution and proves the stability and convergence of the difference

schemes. The difference schemes belong to transcendental equations. In order to solve it, computation formulae for the catch-ran iterative method are presented and the iterative convergence is proved. (6 refs.)

111499 Application of inverse scattering method to singular solutions of nonlinear equations. II. V.A.Arkad'ev, A.K.Pogrebkov, M.K.Polivanov (V.A. Steklov Math. Inst., Acad. of Sci., USSR). *Theor. & Math. Phys. (USA)*, vol.54, no.1, p.12-22 (Jan. 1983). Translation of: *Teor. & Mat. Fiz. (USSR)*, vol.54, no.1, p.23-37 (Jan. 1983). [received: Sept. 1983] For pt.1, see *ibid.* vol. 53, p.163, (1982). The inverse scattering method is generalized to the case of the Zakharov-Shabat system with singular potentials. (6 refs.)

111500 Lectures on the inverse scattering method. V.E.Zakharov. Report KFKI-1983-71, Hungarian Acad. Sci., Budapest (1983), 58 pp. In a series of six lectures an elementary introduction to the theory of inverse scattering is given. The first four lectures contain a detailed theory of solitons in the framework of the KdV equation, together with the inverse scattering theory of the one-dimensional Schrödinger equation. In the fifth lecture the dressing method is described, while the sixth lecture gives a brief review of the equations soluble by the inverse scattering method.

A criterion for stationary states in quantum mechanics See Entry 111352

Quantum mechanics of predictive Poincaré-invariant systems. II. Mixed spin ($1/2, 0$) two-particle systems See Entry 111430

Remote quantum mechanical detection of gravitational radiation See Entry 111522

An uncertainty principle for fermions with generalized kinetic energy See Entry 111546

Expectation values for Morse oscillators See Entry 112806

Walking on potential energy surfaces See Entry 112807

Collisionless cyclotron absorption of photons by electrons in a laser beam See Entry 112969

Classical statistical mechanics of a lattice model of superradiance See Entry 112970

03.70 THEORY OF QUANTIZED FIELDS

(see also 11.10 Field theory)

111501 New quantum treatment of Liouville field theory. J.-L.Gervais, A.Neuve (Lab. de Phys. Théorique, Ecole Normale Supérieure, Paris, France). *Nucl. Phys. B, Part. Phys. (Netherlands)*, vol.B224, no.2, p.329-48 (12 Sept. 1983). The authors exhibit a new treatment of the quantum Liouville theory in a box. In this treatment, the central charge of the Virasoro algebra is finite at the critical dimension of the associated string model and show how to reconstruct conformally covariant quantum field operators, in terms of a set of equally spaced harmonic oscillators. (7 refs.)

111502 Self-adjointness of the Fourier expansion of quantized interaction field Lagrangians. S.M.Paneitz, I.E.Segal (Dept. of Math., MIT, Cambridge, MA, USA). *Proc. Natl. Acad. Sci. USA*, vol.80, no.14, p.4595-8 (July 1983). Regularity properties significantly stronger than were previously known are developed for four-dimensional nonlinear conformally invariant quantized fields. The Fourier coefficients of the interaction Lagrangian in the interaction representation—i.e. evaluated after substitution of the associated quantized free field—is a densely defined operator on the associated free field Hilbert space K . These Fourier coefficients are with respect to a natural basis in the universal cosmos M , to which such fields canonically and maximally extend from Minkowski space-time M_0 , which is covariantly a submanifold of M . However, conformally invariant free fields over M_0 and M are identifiable. The k th Fourier coefficient of the interaction Lagrangian has domain inclusive of all vectors in K to which arbitrary powers of the free hamiltonian in M are applicable. Its adjoint in the rigorous Hilbert space sense is a_{-k} in the case of a hermitian Lagrangian. In particular ($k=0$) the leading term in the perturbative expansion of the S -matrix for a conformally invariant quantized field in M_0 is a self-adjoint operator. Thus, for example, if $\phi(x)$ denotes the free massless neutral scalar field in M_0 , then $\int_{M_0} \phi(x)^4 dx$ is a self-adjoint operator. No coupling constant renormalization is involved here. (15 refs.)

Classical and quantal supersymmetric Liouville theory See Entry 111470

03.80 GENERAL THEORY OF SCATTERING

(see also 11.20 S-matrix theory, and 11.80 Relativistic scattering)

111503 Recovery of spherically symmetric density distribution from a small-angle scattering curve. D.I.Svergun, L.A.Feigin, B.M.Shchedrin (Inst. of Crystallography, Acad. of Sci., USSR). *Sov. Phys.-Crystallogr. (USA)*, vol.28, no.2, p.147-50 (March-April 1983). Translation of: *Kristallografiya (USSR)*, vol.28, no.2, p.252-9 (March-April 1983). [received: Sept. 1983] The authors discuss an algorithm for determining the signs of the scattering amplitudes of a system of identical spherically symmetrical particles of finite size. The method recovers the distribution of the scattered intensity from the particles without the need of any additional information. The authors discuss the application of the algorithm to the characteristic density distributions. They show that the method is stable against errors in determining the size of the particles, to cutoff of the scattering curve, and to deviations from spherical symmetry. (10 refs.)

Equipartition of energy in scattering theory See Entry 111464

04.00 RELATIVITY AND GRAVITATION

(for special relativity, see 03.30; for relativistic astrophysics, see 95.30; for relativistic cosmology, see 98.80)

04.20 GENERAL RELATIVITY

(see also 02.40 Geometry and topology)

111504 A critique of relativity and localization. E.T.Gendlin (Dept. of Behavioral Sci., Univ. of Chicago, Chicago, IL, USA), J.Lemke. *Math. Modelling (USA)*, vol.4, no.1, p.61-72 (1983).

A new philosophical model makes particles and information at single points derivative. Space-time grids are not events but only ideal comparisons made by observers. Therefore the identity of space-time points and also of single particles is inherently a speculative assumption. The conservation of units can be derived and is not a foundation for events. An interaction is an actual change and can determine changed particles and a changed space-time grid from itself, both forward and backward in time. In contrast, relativity theory still retains the classical unit model in which information is localized at single points, merely positing more than one observer. One implication of the new model is that quantummechanical solutions need not be limited by the requirements of relativity as is currently done. The model correctly predicts where difficulties should be found, and relates and explains many puzzles which are otherwise separated and inexplicable. (14 refs.)

111505 The positivity of gravitational energy and global supersymmetry. C.M.Hull (Dept. of Appl. Maths. & Theoretical Phys., Univ. of Cambridge, Cambridge, England).

Commun. Math. Phys. (Germany), vol.90, no.4, p.545-61 (1983). The concept of gravitational energy and the proof of its positivity are reviewed. The relationship between Witten's proof of the positivity of mass and supergravity is explained with reference to the group of global supersymmetries of a spacetime. A formula for the mass is given, in terms of the change of the supercharge under global supersymmetry, which has a simple positivity theorem and which reduces to Witten's expression. An interpretation of Witten's constraint on the spinors used in his proof is given. (26 refs.)

111506 Finding space-time geometries without using a metric. A.Karlhede, U.Lindstrom (Inst. of Theoretical Phys., Univ. of Stockholm, Stockholm, Sweden).

Gen. Relativ. & Gravitation (USA), vol.15, no.7, p.597-610 (July 1983). A new method for obtaining solutions to Einstein's field equations is presented. It is based on the description of a geometry in terms of the curvature tensor and a number of its covariant derivatives. These entities are used instead of the metric. Physical requirements, such as symmetries, are easily imposed in this picture. An example, including the Schwarzschild geometry, is discussed in detail, but no attempts to find new solutions are made. (10 refs.)

111507 Dual interpretation of electromagnetic fields in general relativity. A.K.Raychaudhuri, S.K.Saha (Dept. of Phys., Presidency Coll., Calcutta, India).

Gen. Relativ. & Gravitation (USA), vol.15, no.7, p.611-23 (July 1983). An energy stress tensor satisfying Rainich's algebraic relations along with a specified metric tensor sometimes admits two alternative Maxwell fields—one with a nonvanishing current vector as source and the other without any source. The authors investigate the conditions for the existence of a source-free interpretation when a 'with source' solution with various types of the source current vector (i.e. timelike, null, or spacelike) is known and illustrate the results with some examples. It turns out that in the case of timelike currents a dual interpretation requires this to be a purely convection current, while in other cases a dual interpretation is possible only if the conductivity is infinite and the 'conduction' current is in the direction of the magnetic field. (12 refs.)

111508 Real structures in asymptotically flat \mathcal{U} spaces. N.Kamran (Dept. of Appl. Maths., Univ. of Waterloo, Waterloo, Ontario, Canada), E.T.Newman.

Gen. Relativ. & Gravitation (USA), vol.15, no.7, p.655-60 (July 1983). A real structure is defined in asymptotically flat \mathcal{U} spaces and investigated in connection with the equations of motion in \mathcal{U} space. (8 refs.)

111509 Curvature collineations for type-N Robinson-Trautman space-times. E.G.L.R.Vaz, C.D.Collinson (Dept. of Appl. Maths., Univ. of Hull, Hull, England).

Gen. Relativ. & Gravitation (USA), vol.15, no.7, p.661-71 (July 1983). The metric of type-N Robinson-Trautman space-times (1962) is generated by a real function P satisfying certain field equations. Canonical forms for P are obtained under the assumption that at least one curvature collineation exists. In order to give an example of the improper subgroup structure of a group of curvature collineations all the curvature collineations are determined for the space-times corresponding to one of the two canonical forms. (12 refs.)

111510 On the global geometry of the Stephani universe. A.Krasinski (Max-Planck-Inst. fur Phys. und Astrophys., Garching, Germany).

Gen. Relativ. & Gravitation (USA), vol.15, no.7, p.673-89 (July 1983). A preliminary investigation of global properties of the Stephani solution (1967) of the Einstein field equations is presented. This solution generalizes those of Friedman-Robertson-Walker (FRW) in such a way that the spatial curvature index k (a constant in the FRW models) is a function of the time coordinate. The de Sitter solution, which is also a special case of the Stephani solution, is analyzed in the Stephani coordinates to gain insight into the global structure of the manifold and its foliation. The general metric is found to have several properties in common with this example. It has singularities which can be avoided either by matching the solution to an (as yet unknown) empty-space solution or confining the curvature index to be positive at all times. (17 refs.)

111511 Multipole moments for stationary systems: the equivalence of the Geroch-Hansen formulation and the Thorne formulation. Y.Gursel (W.K. Kellogg Radiation Lab., California Inst. of Technol., Pasadena, CA, USA).

Gen. Relativ. & Gravitation (USA), vol.15, no.8, p.737-54 (Aug. 1983). It is proved that the multipole moments of a stationary asymptotically flat system in general relativity theory as defined by Thorne (1980) are identical, aside from normalization, to those defined by Geroch (1970) and Hansen (1974). The mathematical techniques of Thorne are combined with those of Geroch and Hansen to prove several new theorems about multipole moments, and to give new proofs to some of the old theorems. (13 refs.)

111512 Exterior fields can have different sources—even empty ones. G.Lawitzky (Max-Planck-Inst. fur Phys. und Astrophys., Inst. fur Astrophys., Garching bei Munchen, Germany).

Gen. Relativ. & Gravitation (USA), vol.15, no.8, p.755-9 (Aug. 1983). Using York's formulation (1971) of the constraint equation in general relativity, the author proves the existence of a pair of solutions on \mathbb{R}^3 which coincide outside a compact set and have finite ADM-mass, one with material sources, the other one purely gravitational. (9 refs.)

111513 A rotating mass embedded in an Einstein-Godel universe. M.D.Patel, P.C.Vaidya (Dept. of Math., Sardar Patel Univ., Vallabh Vidyanagar, India).

Gen. Relativ. & Gravitation (USA), vol.15, no.8, p.777-83 (Aug. 1983). A metric containing a parameter ϵ ($\epsilon^2=1$) has been obtained which represents a Kerr metric in the background of a static Einstein universe when ϵ is put equal to +1. The same metric will represent the external field of a mass embedded in a rotating Godel universe when ϵ is set equal to -1. (4 refs.)

111514 Non-Einsteinian gravitational Lagrangians assuring cosmological solutions without collapse. J.P.Duruisseau, R.Kerner (Dept. de Mécanique, Univ. Pierre et Marie Curie, Paris, France), P.Eysseric.

Gen. Relativ. & Gravitation (USA), vol.15, no.8, p.797-807 (Aug. 1983). The authors discuss a method of determining the form of the hypothetical gravitational Lagrangian $f(R)$ replacing the Einsteinian Lagrangian R in order to avoid the singularity in cosmological solutions. Instead of supposing some form of $f(R)$ as an unknown function while inserting the cosmological solution coinciding with Friedmann solution everywhere except for the singularity, which is replaced by a regular minimum of the scale factor $a(t)$ (a regular maximum of curvature). Then they find $f(R)$ by numerical integration. The Lagrangians thus obtained for different cases ($k=0, \pm 1$, and with the equation of state corresponding to pure radiation) have some common properties, among which $|f(R)| < |R|$ (concavity), and the absence of asymptotes. (11 refs.)

111515 An inequality relating total mass and the area of a trapped surface in general relativity. M.Ludvigsen (Dept. of Math., Univ. of Canterbury, Christchurch, New Zealand), J.A.G.Vickers.

J. Phys. A (GB), vol.16, no.14, p.3349-53 (1 Oct. 1983). Let M be a space-time which is asymptotically flat at past null infinity \mathcal{I}^- , satisfies the dominant energy condition and contains a trapped surface \mathcal{T} . The authors show that if \mathcal{T} can be connected to \mathcal{I}^- by means of a nonsingular null-hypersurface \mathcal{N} , then $m^2 \geq A/16\pi$ where m is the Bondi mass with respect to \mathcal{N} and A in the area of \mathcal{T} . (12 refs.)

111516 Canonical general relativity: the primary constraint algebra. J.M.Charpap, J.E.Nelson (Dept. of Phys., Queen Mary Coll., London, England).

J. Phys. A (GB), vol.16, no.14, p.3355-60 (1 Oct. 1983). Discusses the canonical treatment of general relativity in a vierbein formulation. The authors derive the primary constraints, and find that they satisfy an algebra the same as that of the generators of local Poincaré transformations, namely the Poincaré algebra. (5 refs.)

111517 Einstein equations as identities in the theory of direct gravitational interaction. A.Yu.Turygin (Dept. of Theoretical Phys., Moscow Univ., Moscow, USSR).

Moscow Univ. Phys. Bull. (USA), vol.37, no.5, p.131-4 (1982). Translation of: *Vestn. Mosk. Univ. Ser. 3 (USSR)*, vol.37, no.5, p.110-13 (1982). Specific form is given to the action and, correspondingly, the effective metric for a trial particle constructed in an earlier work. It is shown that this metric identically satisfies the Einstein equations at each step of the iteration. (4 refs.)

111518 Absorber theory for the Einstein equations in the first approximation. A.Yu.Turygin (Dept. of Theoretical Phys., Moscow Univ., Moscow, USSR).

Moscow Univ. Phys. Bull. (USA), vol.38, no.1, p.101-4 (1983). Translation of: *Vestn. Mosk. Univ. Ser. 3 (USSR)*, vol.38, no.1, p.84-7 (1983). The validity of absorber theory for the Einstein equations in the first approximation, within the framework of a static model of the Universe, is shown. (5 refs.)

111519 Einstein equation solutions related to the Weyl metric through Ehlers Method. R.Balbinot, R.Bergamini (Istituto di Radioastronomia, CNR, Bologna, Italy), B.Giorgini.

Nuovo Cimento B (Italy), vol.76B, ser.2, no.1, p.1-8 (11 July 1983). The Ehlers theorem is applied to produce internal solutions corresponding to a rigidly rotating pressureless body. (5 refs.)

111520 Covariant concept of gravitational energy. E.Gliner (Joint Inst. for Lab. Astrophys., NBS, Boulder, CO, USA).

Phys. Rev. D (USA), vol.28, no.6, p.1278-84 (15 Sept. 1983). The covariant approach is proposed for the energy description of matter integrated with gravitation. The approach is based on the generalization of the special relativity stress-energy tensor up to the fourth tensor rank which introduces the anisotropies of mass, impulse, and their fluxes. The components describing anisotropies form an 'energy deviator' which is a traceless fourth-rank tensor corresponding to Weyl's part of gravitation. (6 refs.)

111521 Stationary vacuum fields with a conformally flat three-space III. The conformal condition. B.Lukacs, Z.Perjes, A.Sebestyen, G.A.J.Sparling.

Report KFKI-1983-31, Hungarian Acad. Sci., Budapest (1983), 6 pp. For pt.II see KFK preprint KFKI-1982-19 (1982). The general solution is obtained for the conformal equation of the three-space of a stationary vacuum space-time in general relativity. There are three classes of solutions, characterized by the parameter values $k=\pm 1$ and 0, respectively. All explicitly known conformastat space-times fall into the class with $k=+1$. (7 refs.)

Material and electromagnetic sources of the Kerr-Newman geometry See Entry 111523

Relativistic inert-mass tensor See Entry 111527

On calculation of magnetic-type gravitation and experiments See Entry 111535

Uniformly valid amplitude expansions for non-Abelian gauge theories See Entry 111876

The existence of a black hole due to condensation of matter See Entry 116464

On the dynamics of a thin spherically symmetric radiating shell, its classical model, and relativistic effects See Entry 116465

Softening effects in the equation of state and influence of general relativity on the outcome of stellar collapse See Entry 116708

Rotating black hole in asymptotic de Sitter space: perturbation of the space-time with spin fields See Entry 116738

Cosmic censorship and curvature growth See Entry 116899

The cosmological constant and classical tests of general relativity See Entry 116901

Modeling in chaotic relativity See Entry 116903

Homogeneity of Riemannian space-times of Godel type See Entry 116906

04.30 GRAVITATIONAL WAVES AND RADIATION: THEORY

111522 Remote quantum mechanical detection of gravitational radiation. T.K.Leen, L.Parker, L.O.Pimentel (Dept. of Phys., Univ. of Wisconsin-Milwaukee, Milwaukee, WI, USA). *Gen. Relativ. & Gravitation (USA)*, vol.15, no.8, p.761-76 (Aug. 1983). The presumed existence of atomic hydrogen in the vicinity of sources of gravitational radiation suggests its use as a radiation detector. Curvature-induced atomic energy level shifts carry a unique signature and could thus provide from remote detection of gravitational radiation. The authors investigate the shifts induced by space-time curvature arising from gravitational waves. The effect is studied for both low-lying and highly excited states of atomic hydrogen. Numerical results are quoted for radiation from various sources, including binary star systems, binary neutron stars, binary black holes, collapsing stars and pulsars. In addition, they provide a theoretical upper limit to the magnitude of the effect. For completeness, they examine the shifts induced in a harmonic oscillator as well as a rigid rotator. (12 refs.)

Emission of relativistic particles in a strong gravitational field See Entry 111531

04.40 CONTINUOUS MEDIA; ELECTROMAGNETIC AND OTHER MIXED GRAVITATIONAL SYSTEMS

111523 Material and electromagnetic sources of the Kerr-Newman geometry. C.A.Lopez (Dept. de Fisica, Facultad de Ciencias Fisicas y Matematicas, Univ. de Chile, Santiago, Chile). *Nuovo Cimento B (Italy)*, vol.76B, ser.2, no.1, p.9-27 (11 July 1983). A method based on the theory of distributions, introduced by the author to analyse Kerr's singularity, is extended to the study of the Kerr-Newman geometry. In this case both the metric tensor and the electromagnetic potential are considered to be distributions defined all over space-time. The second partial derivatives of these quantities, when inserted into the coupled Einstein-Maxwell equations, give distributions with support on the singular ring and equatorial disk. It is verified that the material stress-energy tensor, as well as the electromagnetic-current vector, correctly reproduces the known asymptotic values of mass, charge and angular momentum of the collapsed object, provided due account is taken of the energy and angular momentum lying outside the source. Furthermore, a mapping of the electromagnetic field in the vicinity of the singularity is achieved by drawing the electric and magnetic lines of force. (7 refs.)

Lagrangian dynamics of a classical spinning particle with dipole moments See Entry 111467

Dual interpretation of electromagnetic fields in general relativity See Entry 111507

Spontaneous compactification of $D=10$ Maxwell-Einstein theory leads to $SU(3)\times SU(2)\times U(1)$ gauge symmetry See Entry 111529

Softening effects in the equation of state and influence of general relativity on the outcome of stellar collapse See Entry 116708

Black holes See Entry 116739

04.50 UNIFIED FIELD THEORIES AND OTHER THEORIES OF GRAVITATION

111524 A bimetric Machian approach to gravitation. R.Goldoni (Dipartimento di Matematica, Univ. of Pisa, Pisa, Italy). *Gen. Relativ. & Gravitation (USA)*, vol.15, no.7, p.691-9 (July 1983). Proposes a bimetric Machian approach to gravitation with a mathematical structure much simpler than the one of Rosen's bimetric theories. The author obtains two cosmological models based on the simplest assumption that the Universe be filled of pure dust matter. One of the two cosmological models is compatible with the currently observed value of the density of dust matter, and provides an age of the Universe which is of the order of the inverse of the present Hubble parameter. One also obtains the Schwarzschild-like solution and its Newtonian limit together with the modified three Kepler laws which allows the author to find that presently $0.5\times 10^{-10} \text{ (yr)}^{-1} \delta(\dot{A}/A)\delta 0.625\times 10^{-10} \text{ (yr)}^{-1}$, a denoting the semimajor axis of the orbit of the test particle. Lastly the author obtains the Newtonian limit of the theory. (12 refs.)

111525 Topological maxima and the dynamics of an axial vector torsion field. W.Drechsler (Max-Planck-Inst. fur Phys. und Astrophys., Werner-Heisenberg-Inst. fur Phys., Munich, Germany). *Gen. Relativ. & Gravitation (USA)*, vol.15, no.8, p.703-23 (Aug. 1983). A generalized theory of gravitation is discussed which is based on a Riemann-Cartan space-time, U_4 , with an axial vector torsion field. Besides Einstein's equations determining the metric of the U_4 a system of nonlinear field equations is established coupling an axial vector source current to the axial vector torsion field. The properties of the solutions of these equations are discussed assuming a London-type condition relating the axial current and torsion field. To characterize the solutions use is made of the Euler and Pontrajagin forms and the associated quadratic curvature invariants for the U_4 space-time. It is found that there exists for a Riemann-Cartan space-time a relation between the zeros of the axial vector torsion field and the singularities of the Pontrajagin invariant, which is analogous to the well-known Hopf relation between the zeros of vector fields and the Euler characteristics. (13 refs.)

111526 Electric and magnetic monopole solutions free from singularities in the nonsymmetric unified field theory. Min-Guang Zhao (Phys. Dept., Sichuan Teachers' Coll., Chengdu, China). *J. Phys. A (GB)*, vol.16, no.14, p.3341-8 (1 Oct. 1983). By introducing a physically acceptable, supplementary condition for the field functions in unified field theory, the electric and magnetic monopole solutions free from singularities everywhere were deduced. This indicates that the divergence difficulties of a point particle can be removed by utilising a reasonable Boal-Moffat condition (1975). (12 refs.)

111527 Relativistic inert-mass tensor. G.Yu.Bogoslovskii (Sci. Res. Inst. of Nuclear Phys., Moscow, Univ., Moscow, USSR). *Moscow Univ. Phys. Bull. (USA)*, vol.38, no.1, p.81-3 (1983). Translation of: *Vestn. Mosk. Univ. Ser. 3 (USSR)*, vol.38, no.1, p.70-1 (1983). Within the framework of the relativistic theory of anisotropic space-time, an explicit expression is found for the relativistic inert-mass tensor in terms of the field values determining the local spatial anisotropy and the isolated direc-

tion. In accordance with the initial idea of Dicke, the dependence of the inertia on the localization of the body and the direction in space is found to be universal, and identical for all bodies that are in identical states. (7 refs.)

111528 Chaotic inflation. A.D.Linde (Lebedev Phys. Inst., Moscow, USSR). *Phys. Lett. B (Netherlands)*, vol.129B, no.3-4, p.177-81 (22 Sept. 1983). A new scenario of the very early stages of the evolution of the universe is suggested. According to this scenario, inflation is a natural (and may be even inevitable) consequence of chaotic initial conditions in the early universe. (15 refs.)

111529 Spontaneous compactification of $D=10$ Maxwell-Einstein theory leads to $SU(3)\times SU(2)\times U(1)$ gauge symmetry. S.Watamura (Inst. of Phys., Univ. of Tokyo, Tokyo, Japan). *Phys. Lett. B (Netherlands)*, vol.129B, no.3-4, p.188-92 (22 Sept. 1983). Solutions of ten-dimensional Maxwell-Einstein theory and a bosonic part of $N=2$, $D=10$ supergravity theory are examined. It is shown that there is a solution for which six-dimensional internal space is compactified into $CP_2\times S_2$. The gauge symmetry of the effective four-dimensional theory is $SU(3)\times SU(2)\times U(1)$. The introduction of fermions is also considered. The requirement of consistency in introducing a spin^c structure on CP_2 results in a $U(1)$ charge quantization condition. (14 refs.)

Towards a realistic SUGRA-GUT See Entry 111937

Bianchi-I universes of the Brans-Dicke theory for the vacuum See Entry 116896

Spatially homogeneous and anisotropic cosmological solution in Brans-Dicke theory See Entry 116898

04.60 QUANTUM THEORY OF GRAVITATION

111530 Various aspects of the time-gauge in Poincare gauge theory. M.Bлагоjevic (Dept. of Theoretical Phys., Kidric Inst., Belgrade, Yugoslavia), I.A.Nikolic. *Lett. Nuovo Cimento (Italy)*, vol.38, ser.2, no.3, p.77-82 (17 Sept. 1983). The procedure for using the time gauge at an early stage of the Poincare gauge theory is precisely defined, and the equivalence with the standard Hamiltonian approach is shown. (6 refs.)

111531 Emission of relativistic particles in a strong gravitational field. A.A.Sokolov, A.N.Aliev, D.V.Gal'tsov (Dept. of Theoretical Phys., Moscow Univ., Moscow, USSR). *Moscow Univ. Phys. Bull. (USA)*, vol.37, no.5, p.102-5 (1982). Translation of: *Vestn. Mosk. Univ. Ser. 3 (USSR)*, vol.37, no.5, p.88-91 (1982). The local-coordinate method is used to investigate the synchrotron radiation of ultrarelativistic particles moving in a magnetic field in curved space-time. General covariant formulas are obtained for the radiation spectrum in the classical and quantum cases. It is shown that the radiation intensity and the relative values of the quantum corrections increase when the particle moves close to the event horizons in the Schwarzschild metric. The limiting transition to conditions of geodesic synchrotron radiation is considered. (4 refs.)

Einstein equations as identities in the theory of direct gravitational interaction See Entry 111517

04.65 SUPERGRAVITY

111532 Gravity with extra gauge symmetry. I.Bars, S.W.MacDowell (J.W. Gibbs Lab., Yale Univ., New Haven, CT, USA). *Phys. Lett. B (Netherlands)*, vol.129B, no.3-4, p.182-4 (22 Sept. 1983). In addition to the tangent space Lorentz gauge invariance, the authors introduce an extra gauge principle in the gauge formulation of gravity, in any dimension. The connection ω_{μ}^{ij} , which starts out as an elementary field, undergoes a gauge transformation which mixes tangent space indices (i,j) with base indices (μ). The equations of motion determine ω_{μ}^{ij} as the sum of usual riemannian connection and a completely antisymmetric torsion piece. In 11 dimensions the theory reproduces the bosonic sector of supergravity if they identify torsion with the 3-index potential $A_{\mu\nu\lambda}$. This generalizes Englert's recent observation, since the formulation torsion= $A_{\mu\nu\lambda}$ for any field configuration, not just a solution. (5 refs.)

111533 Inequivalence between gauged $O(8)$ supergravities. J.-P.Hurni, B.Morel (Dept. de Phys. Theorique, Univ. de Geneve, Geneva, Switzerland). *Phys. Lett. B (Netherlands)*, vol.129B, no.3-4, p.185-7 (22 Sept. 1983). The authors analyze the geometrical structure of the de Wit and Nicolai $SO(8)_{loc}\times SU(8)$ supergravity. They conclude that $SO(8)$ is non-linearly realized down to $SU(4)$. (7 refs.)

111534 How does anticommutator $\{Q_{\alpha}Q_{\beta}\}$ realize energy-momentum P_{μ} in quantum supergravity? Particular properties of global gauge transformation charges in gauge theories. T.Kugo, T.Kuramoto, S.Uehara (Dept. of Phys., Kyoto Univ., Kyoto, Japan). *Z. Phys. C (Germany)*, vol.19, no.3, p.241-50 (1983). It is investigated to what extent the well-known algebra $\{Q^s, \bar{Q}^s\} = \gamma^{\mu} P_{\mu}$ in the rigid supersymmetry theory holds in quantum supergravity. The anticommutator $\{Q_{\alpha}^s, \bar{Q}_{\beta}^s\} \equiv (\gamma^{\mu})_{\alpha\beta} P_{\mu}$ defines an 'internal' translation generator P_{μ} , quite another from the 'external' translation generator P_{μ} . It is, however, shown that those two operators give the same matrix elements between any two physical states aside from a proportional factor. Such a 'miracle' is caused by some particular properties of global gauge transformation charge universal in gauge theories. These properties are fully clarified in a general manner. (12 refs.)

The positivity of gravitational energy and global supersymmetry See Entry 111505

Chaotic inflation See Entry 111528

Spontaneous compactification of $D=10$ Maxwell-Einstein theory leads to $SU(3)\times SU(2)\times U(1)$ gauge symmetry See Entry 111529

Non-linear representations of extended supersymmetry with central charges See Entry 111918

Elimination of unitarily nonequivalent vacua in supersymmetric grand unified theories by gravity See Entry 111922

Electron-positron annihilation cross section in $SU(2)_L\times U(1)$ supergravity See Entry 112010

04.80 EXPERIMENTAL TESTS OF GENERAL RELATIVITY AND OBSERVATIONS OF GRAVITATIONAL RADIATION

111535 On calculation of magnetic-type gravitation and experiments. Peng Hui (Inst. of Appl. Math., Acad. Sinica, Beijing, China). *Gen. Relativ. & Gravitation (USA)*, vol.15, no.8, p.725-35 (Aug. 1983). The linearized Einstein equations are written in the same form as the Maxwell equation. In the case of a weak stationary field and low velocity, the geodesic equations are written in the form of the Lorentz equation of motion. The author suggests that the existence of the magnetic-type gravitation predicted by GR is equivalent to the existence of the gravitational wave predicted by GR. The Schiff effect is explained as one of the magnetic-type gravitation and the new effect is given. The Hall-type gravitational experiment is studied. (8 refs.)

111536 Matching of high-Q gravitational antenna with the resonator of a capacitive oscillation transducer. A.D.Kochubei, V.P.Mitrofanov (Dept. of Oscillation, Moscow Univ., Moscow, USSR). *Moscow Univ. Phys. Bull. (USA)*, vol.38, no.1, p.84-6 (1983). Translation of: *Vestn. Mosk. Univ. Ser. 3 (USSR)*, vol.38, no.1, p.72-4 (1983).

A capacitive oscillation transducer of parametric type with VHF pumping is used to measure the limiting small antenna oscillations in a gravitational-wave experiment. A matching scheme for a high-Q antenna and a transducer resonator that is stable to seismic perturbation is considered. (4 refs.)

111537 A proposed back action evading read-out for a gravitational wave detector. M.F.Bocko, L.Narici, D.H.Douglass, W.W.Johnson (Dept. of Phys. & Astron., Univ. of Rochester, Rochester, NY, USA). *Phys. Lett. A (Netherlands)*, vol.97A, no.6, p.259-62 (5 Sept. 1983).

The authors propose a Back Action Evasion read out to improve the sensitivity of a capacitively coupled resonant transducer for gravitational wave detectors. They show that the noise can be reduced by factors 10 to 100 over the standard amplifier limit using detector parameters already achieved. (9 refs.)

Parametric detector as a tunable antenna for continuous gravitational radiation See Entry 116485

Gravitational radiation reaction in the binary pulsar and the quadrupole-formula controversy See Entry 116731

04.90 OTHER TOPICS IN RELATIVITY AND GRAVITATION

111538 On the significance of the axial Newtonian gravitational force of the finite cylinder. Chen Yingtian, Wang Qing (Huazhong Univ. of Sci. & Technol., Wuhan, China). *Sci. Sin. (China)*, vol.26, no.7, p.732-8 (July 1983).

The general expression of the axial Newtonian force of a right circular cylinder is given; the behaviour of the gravitational field of a hollow cylinder in the proximity of the stationary points is derived and discussed. (9 refs.)

05.00 STATISTICAL PHYSICS AND THERMODYNAMICS

(see also 02.50 Probability theory, stochastic processes, and statistics)

05.20 STATISTICAL MECHANICS

111539 Density functionals for Coulomb systems. E.H.Lieb (Dept. of Math. & Phys., Princeton Univ., Princeton, NJ, USA). *Int. J. Quantum Chem. (USA)*, vol.24, no.3, p.243-77 (Sept. 1983).

Discusses some of the mathematical connections between N -particle wave functions ψ and their single-particle densities $\rho(x)$. The author establishes some of the mathematical underpinnings of 'universal density functional' theory for the ground state energy as begun by Hohenberg and Kohn. He shows that the HK functional is not defined for all ρ and presents several ways around this difficulty. Since the functional mentioned is not computable, the author reviews examples of explicit functionals that have the virtue of yielding rigorous bounds to the energy. (30 refs.)

111540 Expansions of the kinetic hierarchy for a massive particle: the repeated ring and Fokker-Planck equations. J.Mercer, T.Keyes (Sterling Chem. Lab., Yale Univ., New Haven, CT, USA). *J. Stat. Phys. (USA)*, vol.32, no.1, p.35-51 (July 1983).

The tagged particle BBGKY hierarchy is systematically expanded in inverse powers of the square root of the particle mass. In the Brownian limit, for fixed Knudsen number, the hierarchy reduces to the Brownian limit of the repeated ring equation which itself reduces to the Fokker-Planck equation. The friction coefficient of the Fokker-Planck equation is found to be a functional of the solution of Dorfman, van Beijeren, and McClure's (1976) extended Boltzmann equation for a fixed object in a flowing gas. As a consequence, the tagged particle diffusion coefficient calculated in the Brownian limit of the repeated ring equation is valid for all particle sizes. (15 refs.)

111541 Comments on the Grad procedure for the Fokker-Planck equation. J.Meyer, J.Schroter (AG Theoretische Phys., Univ. Paderborn, Paderborn, Germany). *J. Stat. Phys. (USA)*, vol.32, no.1, p.53-69 (July 1983).

If the kinetic equation of a macroscopic system is expanded with respect to the velocity in terms of orthogonal functions, e.g. in terms of Hermite functions one obtains an infinite hierarchy of equations for the expansion coefficients. Grad's method consists in truncating this hierarchy and investigating the remaining finite system. The authors set up conditions under which this procedure is rigorously justified in case of the Fokker-Planck equation. (6 refs.)

111542 Equilibrium theory for the hard-core systems. S.Shinomoto (Dept. of Phys., Faculty of Sci., Tohoku Univ., Sendai, Japan). *J. Stat. Phys. (USA)*, vol.32, no.1, p.105-13 (July 1983).

It is found that the density expansion in the argument of the exponential function gives a fine convergence on the equation of state of the hard-sphere system. The pair distribution function and the equation of state is constructed by an intuitive kinetic theoretical method. The equation of state of the hard-core system with attractive potential is constructed semiempirically with the aid of this simple analytical result, and Kammerling-Onnes' constant of the critical point is obtained analytically. (10 refs.)

111543 Perturbation expansions in statistical physics. I.P.Bazarov, P.N.Nikolaev (M.V. Lomonosov State Univ., Moscow, USSR). *Sov. Phys.-Dokl. (USA)*, vol.27, no.12, p.1021-2 (Dec. 1982). Translation of: *Dokl. Akad. Nauk SSSR*, vol.267, no.4-6, p.1344-5 (Dec. 1982). [received: Sept. 1983]

In the determination of the configurational free energy of a system of N identical particles interacting via central forces with interaction potential $\Phi(r)$, the free energy is defined as $F = -\theta \ln[Q/N]$, where Q is the configurational integral. In the case $N \gg 1$ the free energy is additive in the number of particles. Therefore, $F = F_0 + F_1$, where $F_0 = -\theta \ln[qe/N] + o(N)$, $q = Q^{1/N}$. Thus, the central task of the statistical theory of many particles is the determination of $q(\theta, v)$, where $\theta = kT$ and v is the volume per particle. This paper is devoted to solving this problem. (5 refs.)

111544 A statistical physics model. V.S.Vladimirov, I.V.Volovich (V.A. Steklov Math. Inst., Acad. of Sci., USSR). *Theor. & Math. Phys. (USA)*, vol.54, no.1, p.1-12 (Jan. 1983). Translation of: *Teor. & Mat. Fiz. (USSR)*, vol.54, no.1, p.8-22 (Jan. 1983). [received: Sept. 1983]

A Gaussian model on a half-axis with interaction given by a Toeplitz form is considered. The free energy and correlation functions are calculated. A new method of inverting Toeplitz matrices and solving the generalized Wiener-Hopf problem is used. The asymptotic behaviour of the correlation functions is studied and the conditions for the presence or absence of long-range order are established. The free energy and correlation functions are calculated for a Gaussian model with external field. An expression is obtained for the free energy of a multidimensional Gaussian model. (29 refs.)

111545 On random fields corresponding to the BBGKY, Vlasov, and Boltzmann hierarchies. V.P.Maslov, A.M.Chebotaev (Moscow Inst. of Electronic Engng., Moscow, USSR).

Theor. & Math. Phys. (USA), vol.54, no.1, p.48-55 (Jan. 1983). Translation of: *Teor. & Mat. Fiz. (USSR)*, vol.54, no.1, p.78-88 (Jan. 1983). [received: Sept. 1983]

A correspondence is established between the creation and annihilation operators introduced by Maslov and Tariverdiev (1982) for the densities of the Bogolyubov and Boltzmann hierarchies and the transformations of the measures of the random fields associated with the hierarchies. Bogolyubov's equation (1962) in variational derivatives for the moment functional of the hierarchies is replaced by an equation for the characteristic functional, which is an infinite-dimensional Fourier transform of a measure. The measures of the random fields of the hierarchies satisfy infinite-dimensional analogs of the known equations. These equations are written down by means of creation and annihilation operators acting on functionals and measures. (15 refs.)

Untersuchungen zur statistischen Mechanik von linearen Polymeren unter verschiedenen physikalischen Bedingungen (Investigation of the statistical mechanics of linear polymer molecules under various physical conditions) See Entry 111611

Classical statistical mechanics of a lattice model of superradiance See Entry 112970

05.30 QUANTUM STATISTICAL MECHANICS

(see also 67. Quantum fluids, and 71. Electron states in condensed matter)

111546 An uncertainty principle for fermions with generalized kinetic energy. I.Daubechies (Phys. Dept., Princeton Univ., Princeton, NJ, USA). *Commun. Math. Phys. (Germany)*, vol.90, no.4, p.511-20 (1983).

The author derives semiclassical upper bounds for the number of bound states and the sum of negative eigenvalues of the one-particle Hamiltonians $h = (-\nabla^2) + V(x)$, acting on $L^2(\mathbb{R}^N)$. These bounds are then used to derive a lower bound on the kinetic energy $\sum_{i=1}^N \langle \psi, f(-\nabla^2) \psi \rangle$ for an N -fermion wavefunction ψ . The author discusses two examples in more detail: $f(p) = |p|$ and $f(p) = (p^2 + m^2)^{1/2} - m$, both in three dimensions. (8 refs.)

111547 Towards a comprehensive semiclassical ergodic theory. K.G.Kay (Dept. of Chem., Univ. of Toronto, Toronto, Ontario, Canada). *J. Chem. Phys. (USA)*, vol.79, no.6, p.3026-50 (15 Sept. 1983).

The authors identify quantum dynamical conditions that tend, as $\hbar \rightarrow 0$, to the classical conditions of ergodicity, weak mixing, mixing, and absolutely continuous spectrum. They use these conditions to derive asymptotic properties of wave functions, matrix elements, and energy levels of systems with various ergodic properties in the classical limit. Some of these properties are new while others modify older predictions of 'quantum ergodic properties'. Thus, the present work serves to extend, unify, and refine a number of previous theories. One new prediction is that weak mixing leads to the Van Hove diagonal singularity condition for a certain class of operators. This result may have significant implications for the applicability of nonequilibrium statistical mechanics to finite systems. (54 refs.)

111548 Monte Carlo calculation of the radial distribution function of quantum hard spheres at finite temperatures using path integrals with boundary conditions. G.Jacucci (Dipartimento di Fisica, Univ. di Trento, Trento, Italy), E.Omert.

J. Chem. Phys. (USA), vol.79, no.6, p.3051-4 (15 Sept. 1983). The two body contribution to the radial distribution function of quantum hard spheres is calculated using the Monte Carlo method based on path integrals. Hard core boundary conditions are taken into account by means of an 'image' approximation obtaining accurate numerical results. (7 refs.)

111549 Fermionic lifting of variational self-adjointness. R.Trostel (Inst. fur Theoretische Phys., Tech. Univ. Berlin, Berlin, Germany). *Lett. Nuovo Cimento (Italy)*, vol.38, ser.2, no.1, p.19-23 (3 Sept. 1983). Variational principles, Helmholtz's variational self-adjointness conditions and Santilli's method (1977, 1978, 1983) of the indirect analytic representation factors are extended to the case of dealing with fermionic systems described by Grassmann variables. (9 refs.)

111550 Comment on 'Monte Carlo evaluation of functional integrals using coherent-state Slater determinants' [and reply]. T.Troudet, S.E.Koonin (W.K. Kellogg Radiation Lab., California Inst. of Technol., Pasadena, CA, USA), Y.Avishai, J.Richert. *Phys. Rev. Lett. (USA)*, vol.51, no.12, p.1103-4 (19 Sept. 1983).

In a recent letter, Avishai and Richert (ibid., vol.50, p.1175, 1983) proposed a Monte Carlo evaluation of many-fermion functional integrals using real coherent-state Slater determinants. Troudet and Koonin present briefly the results of their own investigations of this problem. First, they have obtained the computer code used in the calculations and have verified that they can reproduce the results presented there. However, further calculations with this code (such as changing the step in x used in the Metropolis algorithm) indicated that the original step size used was far too small, resulting in a sampling of Slater determinants only in a small neighborhood about the state

from which the random walk was initiated. Avishai and Richert then reply to this. (6 refs.)

111551 Green's functions in the Dicke model. I. Evolution equation. N.N.Bogolyubov, Jr., A.R.Kazaryan, A.M.Kurbatov, V.N.Neskoromnyi (V.A.Steklov Math. Inst., Acad. of Sci., USSR). *Theor. & Math. Phys. (USA)*, vol.54, no.1, p.93-7 (Jan. 1983). Translation of: *Teor. & Mat. Fiz. (USSR)*, vol.54, no.1, p.147-53 (Jan. 1983). [received: Sept. 1983]

A system of two-level emitters interacting with a photon field in the 'rotating wave' approximation is investigated. For the Green's function of such a system an exact equation in which the variables of the photon field are eliminated is obtained. The self-consistent field approximation and the small value of the coupling constant are used to obtain a closed system of equations. (15 refs.)

Formation of large groups of recombining particles of the same type of excitation (two- and three-dimensional continuous models)See Entry 111610

Two-dimensional electron fluid at high temperatureSee Entry 113564

On the statistical distribution of massive fermions and bosons in a Friedmann UniverseSee Entry 116893

05.40 FLUCTUATION PHENOMENA, RANDOM PROCESSES, AND BROWNIAN MOTION

111552 Brownian motion lifetime and curvature conditions. J.-L.Ducourtieux (Univ. de Clermont, Aubiere, France). *C.R. Seances Acad. Sci. Ser. I (France)*, vol.296, no.18, p.769-72 (16 May 1983). In French.

The author discusses what conditions insure that the Brownian motion of a complete Riemannian manifold be conservative. (5 refs.)

111553 Mass dependence of the Kolmogorov-Arnold-Moser stability and low-order resonances in the kinetically coupled two-degree-of-freedom Morse system. T.Matsushita (Dept. of Chem., Keio Univ., Hiyoshi, Yokohama, Japan), T.Terasaka.

Chem. Phys. Lett. (Netherlands), vol.100, no.2, p.138-44 (2 Sept. 1983). The dependence of the mass ratio of the stability of Kolmogorov-Arnold-Moser surface around the central fixed point is numerically analyzed for the escape energy region in the kinetically coupled symmetric Morse system with two degrees of freedom. Strong third-order resonances, together with other weak resonances of higher order, are found for the approximate mass ratio $\delta=(1+\gamma)^{-1}=0.263$ at the dissociation threshold $E=1.0$ (in units of the dissociation energy) and for $\delta=0.293$ at $E=0.7$, an approximate lowest energy for a globally widespread chaos to develop. (20 refs.)

111554 Exact solutions of simple nonlinear difference equation systems that show chaotic behavior. T.Tsuchiya, A.Szabo (Lab. of Chem. Phys., Nat. Inst. of Arthritis, Diabetes & Digestive & Kidney Diseases, Bethesda, MD, USA), N.Saito.

Z. Naturforsch. Teil A (Germany), vol.38A, no.9, p.1035-9 (Sept. 1983). Exact solutions are given for May's simple difference equation and the broken linear model, both for extreme values of the parameters, and the relation between these two systems for the solvable cases is clarified. The invariant measure and the correlation function for each case are calculated using the exact solutions. The initial-value dependence of the behavior of the solutions, chaotic or periodic, is completely determined. By using the exact solution, encounters of any two nonperiodic orbits can be precisely analyzed. (9 refs.)

111555 One-dimensional Brownian motion near an absorbing boundary: solution to the steady state Fokker-Planck equation. Y.S.Mayya (Health Phys. Div., Bhabha Atomic Res. Center, Bombay, India), D.C.Sahni.

J. Chem. Phys. (USA), vol.79, no.5, p.2302-7 (1 Sept. 1983). The problem of steady, one-dimensional Brownian motion under prescribed flux in the presence of an infinite plane absorbing boundary is discussed from the point of view of the eigenfunction expansion solution to the relevant Fokker-Planck equation. The expansion coefficients are determined by reducing it to a problem of the initial value type, using a parametrized Maxwellian for the velocity distribution of incoming particles only at the boundary. The number density function expressed in the form of an infinite series of exponentials is cast into a rapidly convergent form at the boundary layer. While some of the physical quantities obtained by this method are in essential agreement with those obtained by certain previous investigators, the following new results are to be noted: (i) the fractional power law variation of the number density in the vicinity of the boundary; and (ii) the complete vanishing of the space dependent diffusion coefficient at the boundary. The results are further discussed. (11 refs.)

111556 Exact results for diffusion on a disordered chain. P.J.H.Denteneer, M.H.Ernst (Inst. for Theoretical Phys., Utrecht, Netherlands).

J. Phys. C (GB), vol.16, no.27, p.L961-9 (30 Sept. 1983). The authors study diffusion on a chain with static disorder, characterised by random transition rates $\{w_n\}$ using an expansion in powers of the fluctuation $\delta_n=(w_n^{-1}-\langle w^{-1}\rangle)/\langle w^{-1}\rangle$ around the exact diffusion coefficient $D=1/\langle w^{-1}\rangle$ (low-frequency behaviour), or in powers of the fluctuation $\delta_n=(w_n-\langle w\rangle)/\langle w\rangle$ around the bare diffusion coefficient $D_0=\langle w\rangle$ (high-frequency behaviour). The former method yields a systematic expansion of the frequency-dependent diffusion coefficient $U_0(z)$, the single-site Green function $\langle \hat{p}_0(z) \rangle$ (spectral properties) and related quantities in powers of $\sqrt{z}(z\rightarrow 0)$; the latter method yields a systematic $1/z$ expansion ($z\rightarrow\infty$). The exact results for the transport properties show that the approximate results of effective medium or hypernetted chain approximations are incorrect at low frequencies beyond the \sqrt{z} terms. The results for the spectral properties of the chain agree with exact results for low and high frequencies. (13 refs.)

111557 Stochastic theory of adiabatic explosion. F.Baras, G.Nicolis, M.Malek Mansour, J.W.Turner (Univ. Libre de Bruxelles, Faculte des Sci., Bruxelles, Belgium).

J. Stat. Phys. (USA), vol.32, no.1, p.1-23 (July 1983). A stochastic description of an exothermic reaction leading to adiabatic explosion is set up. The numerical solution of the master equation reveals the appearance of a long tail and of multiple humps of the probability distribution which subsist for a certain period of time. During this interval the system displays a markedly chaotic behavior, reflecting the random character of the ignition process. An analytical description of this transient evolution is developed, using a piecewise linear approximation of the transition rates. A comparison with other transient phenomena observed in stochastic theory is carried out. (23 refs.)

111558 Critical fluctuations in a thermochemical instability. I. Mean field description. C.Van den Broeck (Dept. Natuurkunde, Vrije Univ. Brussel, Brussels, Belgium).

J. Stat. Phys. (USA), vol.32, no.1, p.153-68 (July 1983). The author calculates the temperature and concentration fluctuations in a homogeneous thermochemical model in the vicinity of a transition point

towards a multiple steady state regime. Enhanced fluctuations of 0.1% are predicted at a distance of 10^{-3} K from the critical point in a volume element of 10^{-3} mm³. (13 refs.)

111559 Relaxation time and randomness in phase space. M.Casartelli (Istituto di Fisica, Univ. di Parma, Parma, Italy).

Nuovo Cimento B (Italy), vol.76B, ser.2, no.2, p.97-108 (11 Aug. 1983). The stochastic region in the phase space of a classical nonlinear system, a Lennard-Jones chain, is proven to be nonuniform with respect to a random access, through the sensitivity of the relaxation time to initial conditions. The dependence on various parameters is analysed and the results are interpreted geometrically as the effect of residual invariant tori in the stochastic domain. (11 refs.)

111560 Fractal dimension of the strange attractor in a piecewise linear two-dimensional map. T.Tel (Fachbereich Phys., Univ. Essen GHS, Essen, Germany).

Phys. Lett. A (Netherlands), vol.97A, no.6, p.219-23 (5 Sept. 1983). The author calculates the fractal dimension of the strange attractor in the map $x'=ax-\text{sgn}(x)+bx, z'=x$. The method is based on the construction of the unstable manifolds of period-two points. The critical case characterized by heteroclinic tangents is investigated. (22 refs.)

111561 On the fractal dimension of the Henon attractor. P.Grassberger (Dept. of Phys., Univ. of Wuppertal, Wuppertal, Germany).

Phys. Lett. A (Netherlands), vol.97A, no.6, p.224-6 (5 Sept. 1983). The author has re-measured the fractal dimension of the Henon attractor by direct box-counting. He has paid special attention to (a) optimal speed and use of storage, and (b) systematic corrections due to the finiteness of the number of iterations. Covering with grids of up to 9600×9600 boxes, he observes that the number $N(e,n)$ of boxes visited after n iterations obeys a scaling law $N(e,\infty)-N(e,n)\approx\text{const}\times e^{-\alpha}n^{-\beta}$ (for $n\rightarrow\infty$) with $\alpha=2.42\pm 0.15$, $\beta=0.89\pm 0.03$. Using this to extrapolate to $n\rightarrow\infty$, he obtains $D=1.28\pm 0.01$ in disagreement with previous box-counting estimates, but in agreement with a recent indirect evaluation. (11 refs.)

111562 Generalized dimensions of strange attractors. P.Grassberger (Dept. of Phys., Univ. of Wuppertal, Wuppertal, Germany).

Phys. Lett. A (Netherlands), vol.97A, no.6, p.227-30 (5 Sept. 1983). It is pointed out that there exists an infinity of generalized dimensions for strange attractors, related to the order- q Renyi entropies. They are monotonically decreasing with q . For $q=0, 1$ and 2 , they are the capacity, the information dimension and the correlation exponent, respectively. For all q , they are measurable from recurrence times in a time series, without need for a box-counting algorithm. For the Feigenbaum map and for the generalized Baker transformation, all generalized dimensions are finite and calculable, and depend nontrivially on q . (20 refs.)

111563 Observation of a noise-induced phase transition with an analog simulator. J.Smythe, F.Moss (Dept. of Phys., Univ. of Missouri, St. Louis, MO, USA), P.V.E.McClintock.

Phys. Rev. Lett. (USA), vol.51, no.12, p.1062-5 (19 Sept. 1983). The first measurements are presented of the phase diagram of a noise-induced phase transition for a model, nonlinear system with multiplicative noise proposed by Horsthemke and Lefever (1977-80). Measurements of two of the critical exponents are also presented. The present results are in good agreement with theoretical predictions based on the Stratonovic treatment of the stochastic evolution equation. (13 refs.)

111564 Observations of order and chaos in nonlinear systems. H.L.Swinney (Dept. of Phys., Univ. of Texas, Austin, TX, USA).

Physica D (Netherlands), vol.7D, no.1-3, p.3-15 (May 1983). (Proceedings of the International Conference on Order in Chaos, Los Alamos, NM, USA, 24-28 May 1982).

Experiments on nonlinear electrical oscillators, the Belousov-Zhabotinskii reaction, Rayleigh-Benard convection, and Couette-Taylor flow have revealed several common routes to chaos that have also been found in numerical studies of models with a few degrees of freedom. Experimental results are presented illustrating the following transition sequences: period doubling and the U -sequence, intermittency, the periodic-quasiperiodic-chaotic sequence, frequency locking, and an alternating periodic-chaotic sequence. (101 refs.)

111565 Universal behavior in nonlinear systems. M.J.Feigenbaum (Center for Nonlinear Studies, Los Alamos Nat. Lab., Los Alamos, NM, USA).

Physica D (Netherlands), vol.7D, no.1-3, p.16-39 (May 1983). (Proceedings of the International Conference on Order in Chaos, Los Alamos, NM, USA, 24-28 May 1982).

A semipopular account of the universal scaling theory for the period doubling route to chaos is presented. (10 refs.)

111566 Five turbulent problems. D.Ruelle (Inst. des Hautes Etudes Sci., Bures-sur-Yvette, France).

Physica D (Netherlands), vol.7D, no.1-3, p.40-4 (May 1983). (Proceedings of the International Conference on Order in Chaos, Los Alamos, NM, USA, 24-28 May 1982).

Five questions which involve strange attractors in one way or another are discussed. These are: the choice of probability measures to describe turbulence, the Hausdorff dimension of Julia sets for rational maps of the Riemann sphere, the existence of nonperiodic 'turbulent' crystal structure, the mechanism intermittency in developed hydrodynamic turbulence, the distribution of characteristic exponents in a turbulent fluid. (25 refs.)

111567 Oscillations and chaos in chemical systems. I.R.Epstein (Dept. of Chem., Brandeis Univ., Waltham, MA, USA).

Physica D (Netherlands), vol.7D, no.1-3, p.47-56 (May 1983). (Proceedings of the International Conference on Order in Chaos, Los Alamos, NM, USA, 24-28 May 1982).

The chemical community today views chemical chaos much as it did chemical oscillation 20 to 30 years ago. There are a number of 'enlightened' students of and believers in the phenomenon, but the vast majority of chemists are either ignorant or skeptical about the possibility of genuine chaos in a well-controlled chemical system. Major developments in the understanding of periodic chemical oscillation, including the recent systematic design of a new family of oscillators, are reviewed. The question of how closely linked periodic and chaotic behavior are in chemical systems is considered briefly, and implications for the design of chaotic systems are noted. Two systems are considered in some detail. The first, earlier reported as a photochemical oscillator and/or chaotic reaction, is shown to be a system of hydrodynamic rather than chemical interest. The second, one of the newly designed family of chlorite oscillators, exhibits many of the features found in experiments on chaos in the Belousov-Zhabotinskii reaction. It illustrates the close relation between complex periodic oscillations and chaos. Both examples serve to point out the origin of the present controversy over the existence of chemical chaos. (43 refs.)

111568 Experimental studies of bifurcations leading to chaos in the Belousov-Zhabotinsky reaction. J.-C.Boux (Dept. of Phys., Univ. of Texas, Austin, TX, USA).

Physica D (Netherlands), vol.7D, no.1-3, p.57-68 (May 1983). (Proceedings of the International Conference on Order in Chaos, Los Alamos, NM, USA, 24-28 May 1982).

A review is presented of the experimental evidence of chemical chaos in the Belousov-Zhabotinsky reaction, with special emphasis on the bifurcations leading to the chaotic dynamics. It is shown that a simple 1D map can account for most of the exceptional observations. (30 refs.)

111569 Bifurcation and chaos in a periodically stimulated cardiac oscillator. L.Glass, M.R.Guevara, A.Shrier (Dept. of Physiology, McGill Univ., Montreal, Quebec, Canada), R.Perez.

Physica D (Netherlands), vol.7D, no.1-3, p.89-101 (May 1983). (Proceedings of the International Conference on Order in Chaos, Los Alamos, NM, USA, 24-28 May 1982).

Periodic stimulation of an aggregate of spontaneously beating cultured cardiac cells displays phase locking, period-doubling bifurcations and aperiodic 'chaotic' dynamics at different values of the stimulation parameters. This behavior is analyzed by considering an experimentally determined one-dimensional Poincaré or first return map. A simplified version of the experimentally determined Poincaré map is proposed, and several features of the bifurcations of this map are described. (53 refs.)

111570 Persistence properties of bifurcations. J.Guckenheimer (Div. of Natural Sci., Univ. of California, Santa Cruz, CA, USA).

Physica D (Netherlands), vol.7D, no.1-3, p.105-10 (May 1983). (Proceedings of the International Conference on Order in Chaos, Los Alamos, NM, USA, 24-28 May 1982).

Reviews results about bifurcations which occur in families of differential equations. Persistent properties are defined to be those which remain when the family of equations is perturbed. The author provides a list of such properties which is relevant for numerical studies of dynamical systems. (23 refs.)

111571 On the attracting set for Duffing's equation. II. A geometrical model for moderate force and damping. P.Holmes, D.Whitley (Dept. of Theoretical & Appl. Mech., Cornell Univ., Ithaca, NY, USA).

Physica D (Netherlands), vol.7D, no.1-3, p.111-23 (May 1983). (Proceedings of the International Conference on Order in Chaos, Los Alamos, NM, USA, 24-28 May 1982).

After a brief review of some earlier work on Duffing's equation in the small force and damping regions, the authors use the results of numerical integrations to construct a geometrically defined Poincaré map which captures the qualitative features of the attracting set of larger force and damping levels. This map has a (small) constant Jacobian determinant and can be regarded as a perturbation of a non-invertible one-dimensional map. They give a partial analysis of the map and pose some important open questions regarding perturbations of one-dimensional maps and the reaction of 'strange attractors' during bifurcation in horseshoes. (42 refs.)

111572 Period doubling in one and several dimensions. O.E.Lanford (Inst. for Math. & its Applications, Univ. of Minnesota, Minneapolis, MN, USA).

Physica D (Netherlands), vol.7D, no.1-3, p.124-5 (May 1983). (Proceedings of the International Conference on Order in Chaos, Los Alamos, NM, USA, 24-28 May 1982). (3 refs.)

111573 The dimension of chaotic attractors. J.D.Farmer (Center for Nonlinear Studies & Theoretical Div., Los Alamos Nat. Lab., Los Alamos, NM, USA), E.Ott, J.A.Yorke.

Physica D (Netherlands), vol.7D, no.1-3, p.153-80 (May 1983). (Proceedings of the International Conference on Order in Chaos, Los Alamos, NM, USA, 24-28 May 1982).

Dimension is perhaps the most basic property of an attractor. The authors discuss a variety of different definitions of dimension, compute their values for a typical example, and review previous work on the dimension of chaotic attractors. The relevant definitions of dimension are of two general types, those that depend only on metric properties, and those that depend on the frequency with which a typical trajectory visits different regions of the attractor. Both this example and the previous work that they review support the conclusion that all of the frequency dependent dimensions take on the same value, which we call the 'dimension of the natural measure', and all of the metric dimensions take on a common value, which they call the 'fractal dimension'. Furthermore, the dimension of the natural measure is typically equal to the Lyapunov dimension, which is defined in terms of Lyapunov numbers, and thus is usually far easier to calculate than any other definition. Because it is computable and more physically relevant, they feel that the dimension of the natural measure is more important than the fractal dimension. (46 refs.)

111574 Crises, sudden changes in chaotic attractors, and transient chaos. C.Grebogi, E.Ott (Lab. for Plasma & Fusion Energy Studies, Univ. of Maryland, College Park, MD, USA), J.A.Yorke.

Physica D (Netherlands), vol.7D, no.1-3, p.181-200 (May 1983). (Proceedings of the International Conference on Order in Chaos, Los Alamos, NM, USA, 24-28 May 1982).

The occurrence of sudden qualitative changes of chaotic dynamics as a parameter is varied is discussed and illustrated. It is shown that such changes may result from the collision of an unstable periodic orbit and a coexisting chaotic attractor. The authors call such collisions crises. Phenomena associated with crises include sudden changes in the size of chaotic attractors, sudden appearances of chaotic attractors (a possible route to chaos), and sudden destructions of chaotic attractors and their basins. They present examples illustrating that crisis events are prevalent in many circumstances and systems, and that, just past a crisis, certain characteristic statistical behavior (whose type depends on the type of crisis) occurs. In particular the phenomenon of chaotic transients is investigated. The examples discussed illustrate crises in progressively higher dimension and include the one-dimensional quadratic map, the (two-dimensional) Henon map, systems of ordinary differential equations in three dimensions and a three-dimensional map. In the case of our study of the three-dimensional map a new route to chaos is proposed which is possible only in invertible maps or flows of dimension at least three or four, respectively. Based on the examples presented the following conjecture is proposed: almost all sudden changes in the size of chaotic attractors and almost all sudden destructions or creations of chaotic attractors and their basins are due to crises. (21 refs.)

111575 Symbolic dynamics of noisy chaos. J.P.Crutchfield, N.H.Packard (Phys. Board of Studies, Univ. of California, Santa Cruz, CA, USA).

Physica D (Netherlands), vol.7D, no.1-3, p.201-23 (May 1983). (Proceedings of the International Conference on Order in Chaos, Los Alamos, NM, USA, 24-28 May 1982).

One model of randomness observed in physical systems is that low-dimensional deterministic chaotic attractors underlie the observations. A phenomenological theory of chaotic dynamics requires an accounting of the

information flow from the observed system to the observer, the amount of information available in observations, and just how this information affects predictions of the system's future behavior. In an effort to develop such a description, the authors discuss the information theory of highly discretized observations of random behavior. Metric entropy and topological entropy are well-defined invariant measures of such an attractor's 'level of chaos', and are computable using symbolic dynamics. Real physical systems that display low dimensional dynamics are, however, inevitably coupled to high-dimensional randomness, e.g. thermal noise. They investigate the effects of such fluctuations coupled to deterministic chaotic systems, in particular, the metric entropy's response to the fluctuations. They find that the entropy increases with a power law in the noise level, and that the convergence of the entropy and the effect of fluctuations can be cast as a scaling theory. They also argue that in addition to the metric entropy, there is a second scaling invariant quantity that characterizes a deterministic system with added fluctuations: I_0 , the maximum average information obtainable about the initial condition that produces a particular sequence of measurements (or symbols). (46 refs.)

111576 On the quadratic mapping $z \rightarrow z^2 - \mu$ for complex μ and z : the fractal structure of its M set, and scaling. B.B.Mandelbrot (IBM Thomas J. Watson Res. Center, Yorktown Heights, NY, USA).

Physica D (Netherlands), vol.7D, no.1-3, p.224-39 (May 1983). (Proceedings of the International Conference on Order in Chaos, Los Alamos, NM, USA, 24-28 May 1982).

For each complex μ , denote by $\mathcal{A}(\mu)$ the largest bounded set in the complex plane that is invariant under the action of the mapping $z \rightarrow z^2 - \mu$. Mandelbrot (1980, 1982) reported various remarkable properties of the M set (the set of those values of the complex μ for which $\mathcal{A}(\mu)$ contains domains) and of the closure M^* of M . The goals of the present work are as follows. A) To restate some previously reported properties of $\mathcal{A}(\mu)$, M and M^* in new ways, and to report new observations. B) To deduce some known properties of the mapping f for real μ and z , with $\mu \in [-1/4, 2]$ and $z \in [-1/2, 1/2] \sqrt{1+4\mu}$, $f_{1/2} + 1/2 \sqrt{1+4\mu}$. In many ways, the properties of the transformation f are easier to grasp in the complex plane than in an interval. (This exemplifies the saying that 'when one wishes to simplify a theory, one should complicate the variables'.) C) To serve as introduction of some recent pure mathematical work triggered by Mandelbrot 1980. Further pure mathematical work is strongly urged. (13 refs.)

111577 The twist map, the extended Frenkel-Kontorova model and the devil's staircase. S.Aubry (Center for Nonlinear Studies, Los Alamos Nat. Lab., Los Alamos, NM, USA).

Physica D (Netherlands), vol.7D, no.1-3, p.240-58 (May 1983). (Proceedings of the International Conference on Order in Chaos, Los Alamos, NM, USA, 24-28 May 1982).

Reviews exact results which the author obtained on the discrete Frenkel-Kontorova (FK) model and its extensions, during the past few years. These models are associated with area preserving twist maps of the cylinder (or a part of it) onto itself. The theorems obtained from the FK model thus yields new theorems for the twist maps. The author describes the exact structure of the ground-states which are either commensurate or incommensurate and assert the existence of elementary discommensurations under certain necessary and sufficient conditions. Necessary conditions for the trajectories to represent metastable configurations which can be chaotic, are given. The existence of a finite Peierls-Nabarro barrier for elementary discommensurations is connected with a property of non-integrability of the twist map. He next proves that the existence of KAM tori corresponds to 'undefectible' incommensurate ground-states and give a theorem which asserts that when the phonon spectrum of an incommensurate ground-state exhibits a finite gap, then the corresponding trajectory is dense on a Cantor set with zero measure length. These theorems, when applied to the initial FK model, allow one to prove the existence of the transition by 'breaking of analyticity' for the incommensurate structure when the parameter which describes the discrepancy of the model from the integrable limit varies. These theorems also allow one to obtain a series of rigorous upper bounds for the stochasticity threshold of the standard map which for the fifth order approximation already approaches within 25% the value which is numerically known. Finally, he describes a theorem proving the existence of a devil's staircase for the variation curve of the atomic mean distance versus a chemical potential, for certain properties of the twist map which are generally satisfied. (27 refs.)

111578 Influence of solitons in the initial state of chaos in the driven damped sine-Gordon system. A.R.Bishop, K.Fesser, P.S.Lomdahl (Center for Nonlinear Studies & Theoretical Div., Los Alamos Nat. Lab., Los Alamos, NM, USA), S.E.Trullinger.

Physica D (Netherlands), vol.7D, no.1-3, p.259-79 (May 1983). (Proceedings of the International Conference on Order in Chaos, Los Alamos, NM, USA, 24-28 May 1982).

The appearance of chaos in the a.c. driven, damped sine-Gordon equation is studied numerically. Several transitions from periodic to chaotic behavior are investigated in detail for flat initial conditions. Spatial structures (breather, kink) in the initial conditions smooth out many of these transitions and give rise to an interesting symbiosis of time and spatial intermittency. This symbiosis appears to be due to the competition between the background tendency towards chaos and the system's preference to maintain a spatial pattern. The way that this competition is relieved is also found to depend very strongly on symmetry in the initial conditions. (15 refs.)

111579 A renormalisation approach to invariant circles in area-preserving maps. R.S.Mackay (Plasma Phys. Lab., Princeton Univ., Princeton, NJ, USA).

Physica D (Netherlands), vol.7D, no.1-3, p.283-300 (May 1983). (Proceedings of the International Conference on Order in Chaos, Los Alamos, NM, USA, 24-28 May 1982).

Kadanoff and Shenker (1982) introduced a renormalisation approach to invariant circles in area-preserving maps. The present author makes more precise the connection between invariant circles and the renormalisation operator. Restricting attention to noble rotation numbers, the stability of a simple fixed point of the renormalisation is analysed, corresponding to a linear twist map. It is found to be essentially attracting, so that noble circles persist under perturbation, giving a new view on KAM theory. Shenker and Kadanoff found evidence for another fixed point, corresponding to a map with a non-smooth noble circle. Further evidence is given. It has essentially only one unstable direction, and its stable manifold is believed to give the boundary of the set of twist maps with a noble circle. Finally, noble circles are shown to be locally most robust, in an important sense. (34 refs.)

111580 Quasiperiodicity in dissipative systems: a renormalization group analysis. S.J.Shenker (James Franck Inst., Univ. of Chicago, Chicago, IL, USA). *Physica D (Netherlands)*, vol.7D, no.1-3, p.301 (May 1983). (Proceedings of the International Conference on Order in Chaos, Los Alamos, NM, USA, 24-28 May 1982).
Abstract form only given. Dynamical systems with quasiperiodic behavior, i.e. two incommensurate frequencies, may be studied via discrete maps which show smooth continuous invariant curves with irrational winding number. These curves are followed using renormalization group techniques which are applied to a one-dimensional system (circle) and also to an area-contracting map of an annulus. Two fixed points are found representing different types of universal behavior: a trivial fixed point for smooth motion and a nontrivial fixed point. The latter represents the incipient breakup of a quasiperiodic motion with frequency ratio the Golden Mean into a more chaotic flow. Fixed point functions are determined numerically and via an ϵ -expansion and eigenvalues are calculated. (8 refs.)

111581 A universal transition from quasi-periodicity to chaos. E.D.Siggia (Dept. of Phys., Cornell Univ., Ithaca, NY, USA). *Physica D (Netherlands)*, vol.7D, no.1-3, p.302 (May 1983). (Proceedings of the International Conference on Order in Chaos, Los Alamos, NM, USA, 24-28 May 1982).
Abstract form only given. A common route to chaos in dissipative systems proceeds from periodic to quasi-periodic flow (with two independent frequencies). Then, in the absence of rotational symmetry, the system generally mode locks before becoming turbulent. Beyond these qualitative features, the numerous experiments that have examined this regime differ in detail. Dynamical system theory had made the occurrence of the above transitions plausible but has provided no nontrivial quantitative and model independent information. This situation, on the theoretical side, has recently changed with a proposal on how to modify the experiments so as to make the transition to chaos occur in a quantitatively universal manner. The essence of the proposal follows from K.A.M. theory which is the weak coupling limit of the strong coupling problem relevant to the turbulent transition. In addition to the Rayleigh number, the experimenter must control a second parameter so as to maintain the frequency ratio in the quasi-periodic state at a fixed irrational value. (2 refs.)

111582 On dual spaces of differential Lie algebras. B.A.Kupersmidt (Center for Nonlinear Studies, Los Alamos Nat. Lab., Los Alamos, NM, USA). *Physica D (Netherlands)*, vol.7D, no.1-3, p.334-7 (May 1983). (Proceedings of the International Conference on Order in Chaos, Los Alamos, NM, USA, 24-28 May 1982).
Presents a mathematical scheme which serves as an infinite-dimensional generalization of Poisson structures on dual spaces of finite-dimensional Lie algebras which are well known and widely used in classical mechanics. These structures have recently appeared in the theory of Lax equations, long waves in hydrodynamics, and various other physical models: compressible hydrodynamics, magnetohydrodynamics, multifluid plasmas, elasticity, superfluid ^4He and $^3\text{He-A}$, Ginzburg-Landau theory of superconductors, and classical chromohydrodynamics (the generalization of plasma physics to Yang-Mills interactions). (9 refs.)

111583 Correlation function behaviour in quantum systems which are classically chaotic. G.P.Berman, A.R.Kolovsky (L.V. Kirensky Inst. of Phys., Acad. of Sci., Krasnoyarsk, USSR). *Physica D (Netherlands)*, vol.8D, no.1-2, p.117-41 (July 1983).
The time behaviour of a phase correlation function for dynamical quantum systems which are classically chaotic is considered. It is shown that under certain conditions there are three time regions of the quantum correlations behaviour; the region of classical stochasticity (exponential decay of quantum correlations); the region of the correlations decay with a power law; the region of the constant level of the quantum correlations. The boundaries of these time regions are presented. The estimation of a remaining level of the quantum correlations is given. (20 refs.)

111584 Some statistical properties of simple classically stochastic quantum systems. D.L.Shepelyansky (Inst. of Nuclear Phys., Novosibirsk, USSR). *Physica D (Netherlands)*, vol.8D, no.1-2, p.208-22 (July 1983).
Numerical studies are made of simple one- and two-dimensional quantum models which are stochastic in the classical limit. It is shown that the correlation properties of the quantum and corresponding classical motions are only similar for very short time intervals t_0 , and that the evolution of the quantum system, unlike the classical one, is stable. The diffusive excitation of the quantum system under a periodic perturbation is limited to a specific time interval $t^* \gg t_0$, during which the diffusion rate is similar to the corresponding classical diffusion rate. For the two-dimensional model, a continuous component in the correlation spectrum survives for an indefinite period $t_0 \gg t^*$. It is shown that the perturbation is quasiperiodic the interval t^* increases sharply. (18 refs.)

111585 Observation of a strange attractor. J.-C.Roux, R.H.Simoyi, H.L.Swinney (Dept. of Phys., Univ. of Texas, Austin, TX, USA). *Physica D (Netherlands)*, vol.8D, no.1-2, p.257-66 (July 1983).
Phase space portraits have been constructed and analyzed for noisy (non-periodic) data obtained in an experiment on a nonequilibrium homogeneous chemical reaction. The phase space trajectories define a limit set that is an 'attractor'—following a perturbation, the trajectory quickly returns to the attracting set. This attracting set is shown to be 'strange'—nearby trajectories separate exponentially on the average. Moreover, the Poincare sections exhibit the stretching and folding that is characteristic of strange attractors. (23 refs.)

111586 Universal properties of the transition from quasi-periodicity to chaos in dissipative systems. S.Ostlund, D.Rand, J.Sethna, E.Siggia (Inst. for Theoretical Phys., Univ. of California, Santa Barbara, CA, USA). *Physica D (Netherlands)*, vol.8D, no.3, p.303-42 (Sept. 1983).
An exact renormalization group transformation is developed for dissipative systems which describes how the transition to chaos may occur in a continuous and universal manner if the frequency ratio in the quasi-periodic regime is held at a fixed irrational value. The approach is a natural extension of KAM theory to strong coupling. Most of our analysis is for analytic circle maps. The authors have found a strong coupling fixed point where invertibility is lost, which described the universal features of the transition to chaos. They find numerically that any two such critical maps with the same winding number are C^1 conjugate. It follows that the low frequency peaks in an experimental spectrum are universal and they determine how their envelope scales with frequency. When the winding number has a periodic continued fraction, their renormalization transform has a fixed point and spectra are self similar in addition. For a set of non-periodic winding numbers with full measure their renormalization transformation yields an ergodic trajectory in a sub-space of all critical maps. Physically they find singular and universal spectra that do not scale. (40 refs.)

111587 A simple dynamical system with stochastic behaviour. B.A.Malomed (Inst. of Biological Phys., Acad. of Sci., Moscow, USSR). *Physica D (Netherlands)*, vol.8D, no.3, p.343-52 (Sept. 1983).
The author treats a dynamical system consisting of two quasiharmonic limit cycles cut off by stall lines. A phase trajectory inside a cycle jumps infinitely quickly to another cycle after having reached the stall line. This dynamical system can be interpreted as an asymptotical form of a system of three differential equations admitting separation of fast and slow motions. The explicit conditions on parameters of the system providing its stochastic behaviour, i.e. local instability of all trajectories, are obtained by means of investigation of the Poincare mapping. A lower estimate for the topological entropy of the system is also obtained. The appendix concerns investigation of some properties of a system consisting of stochastic oscillators of the most simple kind connected by diffusion. (5 refs.)

111588 Long-time correlations in the stochastic regime. C.F.F.Karney (Plasma Phys. Lab., Princeton Univ., Princeton, NJ, USA). *Physica D (Netherlands)*, vol.8D, no.3, p.360-80 (Sept. 1983).
The phase space for Hamiltonians of two degrees of freedom is usually divided into stochastic and integrable components. Even when well into the stochastic regime, integrable orbits may surround small stable regions or islands. The effect of these islands on the correlation function for the stochastic trajectories is examined. Depending on the value of the parameter describing the rotation number for the elliptic fixed point at the center of the island, the long-time correlation function may decay as t^{-5} or exponentially, but more commonly it decays much more slowly (roughly as t^{-1}). As a consequence these small islands may have a profound effect on the properties of the stochastic orbits. In particular, there is evidence that the evolution of a distribution of particles is no longer governed by a diffusion equation. (16 refs.)

111589 The infinite number of generalized dimensions of fractals and strange attractors. H.G.E.Hentschel, I.Proccaccia (Dept. of Chem. Phys., Weizmann Inst. of Sci., Rehovot, Israel). *Physica D (Netherlands)*, vol.8D, no.3, p.435-44 (Sept. 1983).
The authors show that fractals in general and strange attractors in particular are characterized by an infinite number of generalized dimensions D_q , $q > 0$. To this aim they develop a rescaling transformation group which yields analytic expressions for all the quantities D_q . They prove that $\lim_{q \rightarrow 0} D_q = \text{fractal dimension } (D)$, $\lim_{q \rightarrow 1} D_q = \text{information dimension } (q)$ and $D_{q=2} = \text{correlation exponent } (v)$. D_q with other integer q 's correspond to exponents associated with ternary, quaternary and higher correlation functions. They prove that generally $D_q > D_{q'}$ for any $q' > q$. For homogeneous fractals $D_q = D_{q'}$. A particularly interesting dimension is $D_{q=\infty}$. For two examples (Feigenbaum attractor, generalized baker's transformation) they calculate the generalized dimensions and find that D_{∞} is a non-trivial number. All the other generalized dimensions are bounded between the fractal dimension and D_{∞} . (22 refs.)

111590 On the representation of solutions of nonlinear equations as an integral over the set of trajectories of a random process. V.Vagner, S.M.Ermakov (A.A. Zhdanov State Univ., Leningrad, USSR). *Sov. Phys.-Dokl. (USA)*, vol.27, no.12, p.1022-4 (Dec. 1982). Translation of: *Dokl. Akad. Nauk SSSR*, vol.267, no.4-6, p.1346-9 (Dec. 1982). [received: Sept. 1983]
Let $\phi = P(\phi)$ be a functional equation where P is a continuous operator in a certain Banach space B of functions ($\phi \in B$). The authors consider the problem of representing a solution of the equation as an integral over a (probability) measure on the trajectories of a Markov process. Representations of this type are of interest from both a theoretical and an applied point of view in connection with the construction of algorithms of the Monte Carlo method and other algorithms which can conveniently be used on multiprocessor computers. (4 refs.)

111591 Stationary probability distribution for one of the simplest strange attractors. P.S.Landa, R.L.Stratonovich (M.V. Lomonosov State Univ., Moscow, USSR). *Sov. Phys.-Dokl. (USA)*, vol.27, no.12, p.1032-4 (Dec. 1982). Translation of: *Dokl. Akad. Nauk SSSR*, vol.267, no.4-6, p.832-6 (Dec. 1982). [received: Sept. 1983]
It is well known that stochastic self-oscillations occur in many dynamical systems over a wide range of parameters, even in the absence of random external actions. In phase space these self-oscillations in the steady state correspond to an entire domain, which is called a strange attractor. The indicated stochastic oscillations can be described by a stationary probability distribution for the points of phase space in the attractor domain. In contrast with the case of periodic or almost periodic oscillations, this distribution does not have the nature of a delta function. (8 refs.)

111592 Diffusion across characteristics boundaries with critical points. B.J.Matkowsky (Dept. of Engng. Sci. & Appl. Math., Northwestern Univ., Evanston, IL, USA), Z.Schuss, C.Tier. *SIAM J. Appl. Math. (USA)*, vol.43, no.4, p.673-95 (Aug. 1983).
The authors consider the problems of the effect of small white noise perturbations on a deterministic dynamical system in the plane with (i) an asymptotically stable equilibrium point or limit cycle and (ii) an equilibrium point surrounded by closed trajectories. The mean exit time and the distribution of exit points for each problem is determined by solving singularly perturbed elliptic boundary value problems in domains with closed characteristic boundaries with critical points. Uniformly valid asymptotic solutions are constructed for each of the problems. For the asymptotically stable equilibrium point, the method of matched asymptotic expansions with the integral condition of Matkowsky and Schuss is (1977) is employed. A method of averaging combined with boundary layer analysis is used for the problem of an equilibrium point surrounded by closed trajectories. The influence on the solutions, of the critical points on the boundary, is exhibited and explained. An application to the physical pendulum is given. Finally the authors' results are shown to be in close agreement with simulations. (13 refs.)

111593 Amplitude equations for systems with competing instabilities. P.H.Couillet, E.A.Spiegel (Astron. Dept., Columbia Univ., New York, NY, USA). *SIAM J. Appl. Math. (USA)*, vol.43, no.4, p.776-821 (Aug. 1983).
The authors describe how to derive ordinary differential equations to predict the time dependence of a system governed by partial differential equations when that system is near to the polycritical condition for the onset of several instabilities. The method is illustrated for the general case of two competing instabilities and then a specific physical example of this case is worked out in detail. The basic idea is to extend the Krylov-Bogolyubov-Mitropolsky method of nonlinear mechanics to bifurcation problems. (72 refs.)

111594 Dynamic theory of suspensions with Brownian effects. R.Caflisch (Dept. of Math., Stanford Univ., Stanford, CA, USA), G.C.Papanicolaou. *SIAM J. Appl. Math. (USA)*, vol.43, no.4, p.885-906 (Aug. 1983).
The authors consider a suspension of particles in a fluid settling under the influence of gravity and dispersing by Brownian motion. A mathematical description is provided by the Stokes equations and a Fokker-Planck equation

for the one-particle phase space density. This is a nonlinear system that depends on a number of parametric functions of the spatial concentration of the particles. These functions are known only empirically or for dilute suspensions. The authors analyze the system, its stability, is asymptotic behavior under different scalings and its validity from more microscopic description. They summarize their conclusions at the end. (25 refs.)

111595 Propagation of chaos and the Burgers equation. E.Gutkin (Columbia Univ., New York, NY, USA), M.Kac. *SIAM J. Appl. Math. (USA)*, vol.43, no.4, p.971-80 (Aug. 1983).

The authors establish a connection between the Burgers equation and the limit of an N -body problem when $N \rightarrow \infty$. Then they use this connection to linearize the Burgers equation. (3 refs.)

Proceedings of the International Conference on Order in Chaos See Entry 111307

Stochastic behavior in quantum scattering See Entry 111494

Quantum-classical correspondence for the Fourier spectrum of a trajectory See Entry 111495

Expansions of the kinetic hierarchy for a massive particle: the repeated ring and Fokker-Planck equations See Entry 111540

A new candidate for the universality class of disordered electron models? See Entry 111598

The thermodynamic limit for long-range random systems See Entry 111600

Stability of nonlinear modes and chaotic properties of 1D Fermi-Pasta-Ulam lattices See Entry 111609

Untersuchungen zur statistischen Mechanik von linearen Polymeren unter verschiedenen physikalischen Bedingungen (Investigation of the statistical mechanics of linear polymer molecules under various physical conditions) See Entry 111611

The real and complex Lorenz equations and their relevance to physical systems See Entry 113405

Transitions to chaos in the Ginzburg-Landau equation See Entry 113419

Two-parameter study of the routes to chaos See Entry 113443

Coadjoint orbits, vortices, and Clebsch variables for incompressible fluids See Entry 113455

Bifurcation of stationary vortex configurations. II. Topology and integrability See Entry 113456

Noncanonical Hamiltonian formulation of ideal magnetohydrodynamics See Entry 113517

Bifurcation and the universal sequence for first-sound subharmonic generation in superfluid helium-4 See Entry 114297

Phase space analysis of convection in a ^3He -superfluid ^4He solution See Entry 114299

05.50 LATTICE THEORY AND STATISTICS; ISING PROBLEMS

(see also 75.10H Ising models)

111596 Algebraic structure of Toda systems. D.I.Olive, N.Turok (Dept. of Math. & Phys., Univ. of Virginia, Charlottesville, VA, USA). *Nucl. Phys. B, Field Theory & Stat. Syst. (Netherlands)*, vol.B220(FS8), no.4, p.491-507 (5 Sept. 1983).

Following the Leningrad school an operator P is constructed which guarantees the classical complete integrability of the Toda molecule and Toda lattice equations. This quantity depends in a uniform way upon the root system of the underlying algebra, respectively the simple Lie algebras and the affine euclidean Kac-Moody algebras. (20 refs.)

111597 Invasion percolation: a new form of percolation theory. D.Wilkinson, J.F.Willemsen (Schlumberger-Doll Res., Ridgefield, CT, USA). *J. Phys. A (GB)*, vol.16, no.14, p.3365-76 (1 Oct. 1983).

A new kind of percolation problem is described which differs from ordinary percolation theory in that it automatically finds the critical points of the system. The model is motivated by the problem of one fluid displacing another from a porous medium under the action of capillary forces, but in principle it may be applied to any kind of invasion process which proceeds along a path at least resistance. The name invasion percolation is proposed for this new process. Similarities to, and differences from, ordinary percolation theory are discussed. (17 refs.)

111598 A new candidate for the universality class of disordered electron models? J.E.Green (Dept. of Theoretical Phys., Univ. of Manchester, Manchester, England). *J. Phys. C (GB)*, vol.16, no.27, p.5245-53 (30 Sept. 1983).

The authors consider for the behaviour of disordered electrons which has the Hamiltonian $H = \sum_{ij} (\delta_{ij} \sum_k J_{ik} J_{kj}) |i\rangle \langle j|$ where J_{ij} is a random variable. It is shown that to first order in perturbation theory this model is in the same universality class as the Anderson tight-binding model and the random matrix ensemble model. (14 refs.)

111599 Impurity dynamics in a one-dimensional chain. D.F.Calef (Dept. of Chem., MIT, Cambridge, MA, USA). *J. Stat. Phys. (USA)*, vol.32, no.1, p.81-94 (July 1983).

The behavior of an impurity spin in a one-dimensional chain is investigated using the Glauber model. Two different types of impurities are considered and exact expressions for the average spin of the impurity, given that the impurity was initially excited out of equilibrium, are found. The behavior of these models is discussed in detail and their relevance to other physical situations is considered. (10 refs.)

111600 The thermodynamic limit for long-range random systems. A.C.D.van Enter, J.L.van Hemmen (Univ. Heidelberg, Heidelberg, Germany). *J. Stat. Phys. (USA)*, vol.32, no.1, p.141-52 (July 1983).

Long-range spin systems with random interactions are considered. A simple argument is presented showing that the thermodynamic limit of the free energy exists and depends neither on the specific random configuration nor on the sample shape, provided there is no external field. The argument is valid for both classical and quantum spin systems, and can be applied to (a) spins randomly distributed on a lattice and interacting via dipolar interactions, and (b) spin systems with potentials of the form $J(x_1, x_2)/|x_1 - x_2|^{\alpha d}$, where the $J(x_1, x_2)$ are independent random variables with mean zero, d is the dimension, and $\alpha > 1/2$. The key to the proof is a (multidimensional) subadditive ergodic theorem. As a corollary the authors show that, for random ferromagnets, the correlation length is a nonrandom quantity. (18 refs.)

111601 Critical behaviour of the hard-core lattice gas on the honeycomb lattice. J.-M.Debierre, L.Turban (Lab. de Phys. du Solide, ENSMIM, Nancy, France).

Phys. Lett. A (Netherlands), vol.97A, no.6, p.235-8 (5 Sept. 1983).

The hard triangle lattice-gas model (lattice-gas on the honeycomb lattice with first neighbour exclusion) is studied by the phenomenological renormalization method. The critical activity is found to be $z = 7.85$ and the critical exponents suggest that this model belongs to the 2-D Ising universality class. (10 refs.)

111602 Domain walls and shape dependence in the two-dimensional Ising-model critical region. P.Kleban, G.Akinci (Dept. of Phys. & Astron., Univ. of Maine, Orono, ME, USA).

Phys. Rev. Lett. (USA), vol.51, no.12, p.1058-61 (19 Sept. 1983).

Ferdinand and Fisher (1969) have discovered some unusual lattice-shape effects on the finite size-induced specific heat peak shift in the two-dimensional Ising-model critical region. It is shown that they are well approximated by keeping only the two largest eigenvalues of the transfer matrix, and may be expressed entirely in terms of a one-dimensional Ising array of domain walls. Approximate expressions for the effective coupling and number of spins are given. It is also pointed out that in general domain walls should be thermodynamically important for such finite-size effects. (14 refs.)

111603 New spontaneous symmetry breaking for the cubic XY model. S.Galam, J.L.Birman (Dept. of Phys., City Coll., City Univ. of New York, New York, NY, USA).

Phys. Rev. Lett. (USA), vol.51, no.12, p.1066-8 (19 Sept. 1983).

A Landau expansion including sixth- and eighth-degree terms is studied for the cubic XY model. A new ordered phase with 'generic symmetry' is found. The angle of rotation θ of the associated order parameter depends continuously on temperature. The transition from the disordered phase into this new phase must always be first order, irrespective of both the sign of the quartic term and the inclusion of higher-degree terms in the expansion. This prediction can be verified experimentally by studying the temperature dependence of θ . $\text{Tb}_2(\text{MoO}_4)_3$ should be a good candidate. (9 refs.)

111604 The breadth of the lattice of those varieties of inverse semigroups which contain the variety of groups. N.R.Reilly (Dept. of Math., Simon Fraser Univ., Burnaby, BC, Canada).

Proc. R. Soc. Edinburgh Sect. A (GB), vol.93, pt.3-4, p.319-25 (1983).

The author defines two sublattices on a lattice of varieties of inverse semigroups. The breadth of one of the sublattices is determined, from which it follows that the other sublattice has the same breadth. Some consequences concerning varieties generated by fundamental inverse semigroups are also considered. (8 refs.)

111605 Renormalization-group study of the Hamiltonian version of the Potts model. III. Improved results for larger cells. F.Igloi, J.Solyom (Central Res. Inst. for Phys., Budapest, Hungary).

Phys. Rev. B (USA), vol.28, no.5, p.2792-9 (1 Sept. 1983).

For pt.II see *ibid.*, vol.28, no.5, p.2785 (1983). The renormalization-group transformation, applied earlier to the Hamiltonian Potts model to study the crossover from second-order to first-order transition as the number of states q increases, is extended by taking larger cells in the block transformation. The results improve systematically with increasing block size. The critical value of q above which the transition is of first order, seems to converge to 5 instead of the exactly known value $q_c = 4$. The classical equivalents of the new couplings, which drive the system to the first-order transition, are discussed. (9 refs.)

111606 Nonlinear vector waves in a mechanical model of a molecular chain. O.B.Gorbacheva, L.A.Ostrovsky (Inst. of Appl. Phys., Acad. of Sci., Gorky, USSR).

Physica D (Netherlands), vol.8D, no.1-2, p.223-8 (July 1983).

Transverse nonlinear waves in a one-dimensional lattice with elastic bonds under longitudinal stress are investigated taking into account a possibility of lattice rotations. The main types of wave motion are found in the continuum approximation including helical waves and rotation discontinuities, as well as solitons in the form of plane displacements of the lattice and local 'contractions' of the helical wave. The simplest estimates of possible parameters of such waves in molecular chains are given for a polyacetylene molecule. (8 refs.)

111607 Scattering of lattice solitons from a mass interface—A synergetic approach. T.Klinker, W.Lauterborn (Third Phys. Inst., Univ. of Gottingen, Gottingen, Germany).

Physica D (Netherlands), vol.8D, no.1-2, p.249-56 (July 1983).

A special mathematical method—a synergetic approach combining analytical and numerical procedures—is developed to study how a Toda lattice soliton is scattered from a mass interface. The method is based on the inverse scattering transform and the spectral theorem for self-adjoint operators. The laws for the scattering processes are given in a series of diagrams. (11 refs.)

111608 The discrete Frenkel-Kontorova model and its extensions. I. Exact results for the ground-states. S.Aubry, P.Y.Le Daeron (Center for Nonlinear Studies, Los Alamos Nat. Lab., Los Alamos, NM, USA).

Physica D (Netherlands), vol.8D, no.3, p.381-422 (Sept. 1983).

The authors present a rigorous study of the classical ground-states under boundary conditions of a class of one-dimensional models generalizing the discrete Frenkel-Kontorova model. The extremalization equations of the energy of these models turn out to define area preserving twist maps which exhibits periodic, quasi-periodic and chaotic orbits. For all boundary conditions, they select among all the extremum solutions of the energy of the model, those which correspond to the ground-states of the infinite system. They prove that these ground-states are either periodic (commensurate) or quasi-periodic (incommensurate) but are never chaotic. They also prove the existence of elementary discommensurations which are minimum energy configuration of the model for certain special boundary conditions. The topological structure of the whole set of ground-states is described in detail. In addition to physical applications, consequences for twist map homeomorphisms are mentioned. (35 refs.)

111609 Stability of nonlinear modes and chaotic properties of 1D Fermi-Pasta-Ulam lattices. N.Budinsky, T.Bountins (Inst. for Nonlinear Studies, Clarkson Coll. of Technol., Potsdam, NY, USA).

Physica D (Netherlands), vol.8D, no.3, p.445-52 (Sept. 1983).

The stability properties of certain simple periodic solutions (nonlinear modes) of the equations of motion of one-dimensional, N -particle FPU lattices, are obtained analytically by uncoupling the N linear variational equations. The energy per particle E_c/N at which these modes first become unstable is calculated and its asymptotic behavior as $N \rightarrow \infty$ is determined. The authors find that for lattices which experience strong energy sharing $E_c/N \rightarrow 0$ as $N \rightarrow \infty$, while for a lattice where little energy sharing is observed $E_c/N \rightarrow \text{const} > 0$, as N increases. Certain possible connections between the local stability results and some global chaotic properties of FPU lattices are discussed. (23 refs.)

111610 Formation of large groups of recombining particles of the same type of excitation (two- and three-dimensional continuous models). V.V.Antonov-Romanovskii (P.N. Lebedev Phys. Inst., Acad. of Sci., Moscow, USSR). *Sov. Phys.-Solid State (USA)*, vol.25, no.2, p.341-2 (Feb. 1983). Translation of: *Fiz. Tverd. Tela (USSR)*, vol.25, no.2, p.599 (Feb. 1983). [received: Sept. 1983]
Calculations within a one-dimensional continuous model indicate that prolonged excitation due to recombination between two types of particle A and B leads to the formation of groups of particles of the same type containing on the average about 100 particles. The aforementioned treatment is based on the calculation of the probability w_0 of finding a particle of type B to be the nearest particle lying to the right of a particle of type A. It is also necessary to determine the distance X between groups of alternate particles. The author uses the same method. However, he can no longer classify particles as lying to the 'right' or 'left' since neighboring particles can lie along arbitrary directions relative to the initial particle. Consequently, he is faced with the problem of a 'reasonable' restriction of all possible directions. (2 refs.)

111611 Untersuchungen zur statistischen Mechanik von linearen Polymeren unter verschiedenen physikalischen Bedingungen (Investigation of the statistical mechanics of linear polymer molecules under various physical conditions). K.Kremer.
Report JUL-1832, Kernforschungsanlage, Julich, Germany (March 1983), 214 pp. In German.
The statistical mechanics of chain molecules is investigated for various physical conditions. As a model for such chain molecules the author uses the self-avoiding-walk (SAW) on a diamond lattice. Because mainly numerical methods are used, various Monte Carlo techniques are tested and analysed. (143 refs.)

111612 Critical behaviour of a quantum spin problem with three-spin coupling. F.Igloi, D.Kapor, J.Solyom, M.Skrinjar.
Report KFKI-1983-62, Hungarian Acad. Sci., Budapest (1983), 13 pp.
The critical behaviour of an Ising like model with three-spin coupling is studied in a transverse field. A self-dual renormalisation group transformation can be applied which gives well converging results for the critical exponents when large enough cells are taken. Finite size scaling on the same model gives comparable results. (8 refs.)

Nonlinear lattice and soliton theorySee Entry 111454
Relaxation time and randomness in phase spaceSee Entry 111559
The twist map, the extended Frenkel-Kontorova model and the devil's staircaseSee Entry 111577
Mathematical theory of phase transitions [Ising model]See Entry 111617
Distribution of zeros in Ising and gauge modelsSee Entry 111871
On cellular instability in the solidification of a dilute binary alloySee Entry 114142
Floating phase in the chiral Potts model. A Monte Carlo renormalization-group analysisSee Entry 114349
Phase diagrams of multilayer films and the Potts lattice-gas model of adsorptionSee Entry 114350
Spin excitations in a Hubbard chainSee Entry 114429
Phase diagram of the ANNNI model in a field using a low-temperature series techniqueSee Entry 114697

05.60 TRANSPORT PROCESSES: THEORY

111613 On the limiting law solution of the cylindrical Poisson-Boltzmann equation for polyelectrolytes. T.Odijk (Dept. of Phys. & Macromolecular Chem., Univ. of Leyden, Leyden, Netherlands).
Chem. Phys. Lett. (Netherlands), vol.100, no.2, p.145-50 (2 Sept. 1983).
Upper and lower bounds are given for the behaviour of the Poisson-Boltzmann potential of a highly charged, cylindrical polyelectrolyte in excess salt solution as the salt concentration or cylinder radius tends to zero. The exact singular behaviour of the potential very close to the cylinder is given in terms of a delta function. (16 refs.)

111614 Quantitative maximum principles and strongly coupled gradient-like reaction-diffusion systems. N.D.Alikakos (Dept. of Math., Heriot-Watt Univ., Edinburgh, Scotland).
Proc. R. Soc. Edinburgh Sect. A (GB), vol.94, pt.3-4, p.265-86 (1983).
The author considers a system of reaction-diffusion equations with general diffusion matrix and establishes the stabilization of all solutions at $t \rightarrow \infty$. The interest of this problem derives from two separate facts. First, the sets that are useful for localizing the asymptotics cease to be invariant as soon as the diffusion matrix is not a multiple of the identity. Secondly, the set of equilibria is connected. (33 refs.)

111615 Thermal waves in an absorbing and convecting medium. P.Rosenau (Faculty of Mech. Engng., Technion-Israel Inst. of Technol., Haifa, Israel), S.Kamin.
Physica D (Netherlands), vol.8D, no.1-2, p.273-83 (July 1983).
The quasi-linear parabolic equation $\partial_t u = a \partial_{xx} u^a + b \partial_x u^b - cu^c$ exhibits a wide variety of wave phenomena, some of which are studied in this work; and some solvable cases are presented. The motion of the wave front is characterized in terms of α , β and γ . Among the interesting phenomena the authors note the effect of fast absorption ($b=0$, $0 < \gamma < 1$) that causes extinction within a finite time, may break the evolving pulse into several sub-pulses and causes the expanding front to reverse its direction. In the convecting case ($c=0$, $b \neq 0$) propagation has many features in common with Burgers equation, $\alpha=1$; particularly, if $0 < a \leq 1$, a shock-like transit layer is formed. (15 refs.)

111616 Singular problems in the theory of stress-assisted diffusion. V.Alexiades (Dept. of Math., Univ. of Tennessee, Knoxville, TN, USA), E.C.Aifantis.
SIAM J. Math. Anal. (USA), vol.14, no.5, p.925-33 (Sept. 1983).
A recently developed stress-assisted diffusion theory is further substantiated by establishing the well-posedness of relevant (degenerate parabolic) initial-boundary value problems for a plane with a slit. (12 refs.)

On random fields corresponding to the BBGKY, Vlasov, and Boltzmann hierarchiesSee Entry 111545
Exact results for diffusion on a disordered chainSee Entry 111556
Effectiveness of the model of volume backscattering in the theory of radiation transfer in media with axisymmetric scattering indicesSee Entry 113260
Analogies of 6 classic properties of materialsSee Entry 113264
The discrete Boltzmann equation for gas mixtures. A regular space model and a shock wave problemSee Entry 113544

05.70 THERMODYNAMICS
(see also 44.60 Thermodynamic processes, 64. Equations of state, phase equilibria and phase transitions, 65. Thermal properties of condensed matter; for chemical thermodynamics, see 82.60)

111617 Mathematical theory of phase transitions [Ising model]. S.Mukhopadhyay (S.N. Bose Inst. of Phys. Sci., Univ. of Calcutta, Calcutta, India).
Indian J. Phys. Part A, vol.57A, no.3, p.164-9 (May 1983).
In an effort to make operator algebraic methods available for the treatment of cooperative phenomena, the Ising model of ferromagnetism is investigated. Von Neumann's statistical operator U has been computed in each case. Finally the forms of U have been suggested for the respective cases. Applications of U to other thermodynamic inequalities relevant to phase transitions are discussed. (8 refs.)

111618 On the derivation of $dQ=T dS$. J.Dunning-Davies (Dept. of Appl. Math., Univ. of Hull, Hull, England).
J. Phys. A (GB), vol.16, no.14, p.3377-83 (1 Oct. 1983).
The traditional approach using Carnot cycles to the problem of establishing the existence of absolute temperature and entropy and to deriving $dQ=T dS$ is shown to remain valid for systems whose entropy is non-extensive as well as for systems whose entropy is extensive. However, it is seen that the analytical approach to this problem is valid only for systems whose entropy is extensive. Two methods for resolving this difficulty are presented. (11 refs.)

111619 The entropy of the BKW solution. C.J.Tourenne (Phys. Dept., Maharishi Internat. Univ., Fairfield, IA, USA).
J. Stat. Phys. (USA), vol.32, no.1, p.71-80 (July 1983).
The entropy of the d -dimensional generalization of the BKW solution of the homogeneous Boltzmann equation is calculated and expressed for $d=3$ in terms of error functions. It is verified that the McKean (1966) conjecture cannot hold in most of the time domain where the d -dimensional BKW solution is defined. (21 refs.)

111620 Metricization of thermodynamic state space and the renormalization group. L.Diosi, G.Forgacs, B.Lukacs, H.L.Frisch.
Report KFKI-1983-53, Hungarian Acad. Sci., Budapest (1983), 14 pp.
After introducing a suitable Riemannian metric in thermodynamic state space, with a simple statistical thermodynamic interpretation, it is shown that the existence of scaling must imply the existence of a conformal Killing vector field in the neighbourhood of a critical point. (9 refs.)

The Born centenary: remarks about classical thermodynamicsSee Entry 111358
Equilibrium theory for the hard-core systemsSee Entry 111542
A statistical physics modelSee Entry 111544
Critical fluctuations in a thermochemical instability. I. Mean field descriptionSee Entry 111558
Observation of a noise-induced phase transition with an analog simulatorSee Entry 111563
Invasion percolation: a new form of percolation theorySee Entry 111597
The thermodynamic limit for long-range random systemsSee Entry 111600
Critical behaviour of the hard-core lattice gas on the honeycomb latticeSee Entry 111601
Domain walls and shape dependence in the two-dimensional Ising-model critical regionSee Entry 111602
New spontaneous symmetry breaking for the cubic XY modelSee Entry 111603
Renormalization-group study of the Hamiltonian version of the Potts model. III. Improved results for larger cellsSee Entry 111605
Hard-sphere fluid-to-solid transition and the virial expansionSee Entry 114123
Order parameter for tricritical phenomenaSee Entry 114128

06.00 MEASUREMENT SCIENCE, GENERAL LABORATORY TECHNIQUES, AND INSTRUMENTATION SYSTEMS

06.20 METROLOGY

06.20D Measurement and error theory

111621 On the problem of estimating the mean value, correlation function and the spectral density of a stationary random function on the basis of single realisation. L.Kubackova, L.Kubacek.
Elektrotech. Cas. (Czechoslovakia), vol.34, no.5, p.370-8 (1983). In Slovak.
In processing experimental results, it is often necessary to carry out statistical evaluation of the mean value, correlation function and spectral density of a random function. Necessary and sufficient conditions for the evaluation of these variables on the basis of a single realisation are presented. Using as an example a periodic normal stationary signal, it is shown which statistical characteristics can and which cannot be determined from a single measurement. (8 refs.) E.D.

111622 Error analysis of measurement results. M.Mojzis.
Elektrotech. Cas. (Czechoslovakia), vol.34, no.6, p.449-50 (1983). In Slovak.
Simplified formulas and diagrams which can be used for statistical evaluation of measurement errors are presented. The diagrams enable determination of an error on the basis of the known probability and number of experiments. Alternatively, for a predetermined value of probability, it is possible to determine the number of experiments which will ensure that the maximal error required will not be exceeded. (1 ref.) E.D.

111623 Determination of limits for a linear regression or calibration curve. W.H.Swallow (North Carolina State Univ., Raleigh, NC, USA), J.R.Trout.
J. Qual. Technol. (USA), vol.15, no.3, p.118-25 (July 1983).
Trace analysis has become increasingly more important because of its connection with recent environmental, chemical, and biological concerns; therefore, measurement techniques often must be evaluated particularly for their ability to measure low concentrations with acceptable accuracy and precision. A methodology is presented here for determining objectively the lower (or upper) limit associated with a linear regression; that is, the point below (or above) which a regression model fails. Methods are also given for determin-

ing, provided the data include multiple observations at some x values, whether problems observed beyond the limit are due to increased variability of the breakdown of the linear relationship. The methodology is applied to calibration curve data from four chlorine measurement techniques, to estimate lower limits and to show that the principal problem found below the lower limit is dramatically increased variability. (9 refs.)

111624 Progress in metrological support of measuring-computing means. E.I.Tsvetkov, V.N.Ivanov (All-Union Res. Inst. of Electromeasuring Instruments, Leningrad, USSR), G.I.Kavalerov. Technological and Methodological Advances in Measurement. Acta IMEKO 1982. Proceedings of the 9th IMEKO Congress of the International Measurement Confederation, Berlin, Germany, 24-28 May 1982 (Amsterdam, Netherlands: North-Holland 1983), p.21-35 vol.1. The important trends in the development of procedures and means for determining the characteristics of errors in measurement results are discussed. On the basis of an adequate formal description of a measurement procedure, four types of measuring problems are considered as applied to a case when the execution is obtained with the aid of measuring-computing means. The structure of appropriate errors is determined. Three procedures for obtaining the error and error component characteristics are brought into comparison: the analytical, experimental and computer-aided. Type structures of the reference measuring-computing means are given for the experimental procedure. (no refs.)

Lattice theoretic properties of Carleson measuresSee Entry 111403
A further development in error reduction modelsSee Entry 111708

06.20F Units

111625 Legal physical units. J.M.Massalski (Akad. Gorniczo-Hutnicza, Krakow, Poland). *Postępy Fiz. (Poland)*, vol.34, no.3, p.293-301 (1983). In Polish. Definitions of the SI units and the legal status of these units in Poland are presented. (9 refs.)

06.20H Measurement standards and calibration

111626 A note on the interpretation of activation measurements on the Princeton large torus. J.D.Strachan (Plasma Phys. Lab., Princeton Univ., Princeton, NJ, USA), G.Zankl. *Nucl. Instrum. & Methods Phys. Res. (Netherlands)*, vol.214, no.2-3, p.551-2 (1 Sept. 1983).

Foil orientation is found to be unimportant in the interpretation of ^{113}In activation measurements around the PLT fusion experiment. (3 refs.)

111627 Calculating scaling factors—it's easy once you know how. A.L.Nuaimi (Gulf Canada Products Co., Toronto, Ontario, Canada). *Can. Controls & Instrum. (Canada)*, vol.22, no.4, p.16-17 (July 1983). Computational devices are used extensively in combustion control and generally whenever a control or measurement network is required to implement a mathematical process equation. The accurate evaluation of the scaling factors is essential for the controls to perform as intended. This paper describes three methods for calculating these factors. (no refs.)

111628 Estimation of parameters in models for cesium beam atomic clocks. P.V.Tryon, R.H.Jones (NBS, Boulder, CO, USA). *J. Res. Natl. Bur. Stand. (USA)*, vol.88, no.1, p.3-16 (Jan.-Feb. 1983). [received: Sept. 1983]

The authors present an introduction to the use of the Kalman filter in modelling atomic clocks and obtaining maximum likelihood estimates of the model parameters from data on an ensemble of clocks. Tests for the validity of the model and confidence intervals for the parameter estimates are discussed. Techniques for dealing with unequally spaced and partially or completely missing multivariate data are described. The existence of deterministic frequency drifts in clocks is established and estimates of the drifts are obtained. (9 refs.)

111629 Estimating time from atomic clocks. R.H.Jones, P.V.Tryon (NBS, Boulder, CO, USA). *J. Res. Natl. Bur. Stand. (USA)*, vol.88, no.1, p.17-24 (Jan.-Feb. 1983). [received: Sept. 1983]

A Kalman recursive algorithm for estimating time from an ensemble of atomic clocks has been developed. The algorithm allows for the addition or deletion of clocks at any time, and provides automatic error detection and correction. The observations consist of time differences between clocks and may be taken at unequally spaced time points. Maximum likelihood estimates of the unknown parameters are obtained with confidence intervals as well as hypothesis tests to determine whether the estimated parameters are significantly different from zero. (4 refs.)

111630 Transducer calibration supported by a computer and a data bank system. O.Krull, A.Happe, P.-D.Reif (Res. & Dev. Volkswagenwerk AG, Wolfsburg, Germany). Technological and Methodological Advances in Measurement. Acta IMEKO 1982. Proceedings of the 9th IMEKO Congress of the International Measurement Confederation, Berlin, Germany, 24-28 May 1982 (Amsterdam, Netherlands: North-Holland 1983), p.515-24 vol.2

There is an important reason to support the transducer calibration procedure by a computer system, if the number of transducers to be calibrated per day is high and the calibration laboratory staff is relatively small. The computer leads the operator of the calibration system through the calibration procedure, takes care for the correct status of the calibration system and gives information about each step. The new calibration data are automatically transferred to a data bank system from which each user can recall them. This results in an output of approximately 10 calibrations per day. (no refs.)

111631 Macroscopic quantum phenomena in metrology. Yu.V.Tarbee (Mendeleyev Inst., Leningrad, USSR). Technological and Methodological Advances in Measurement. Acta IMEKO 1982. Proceedings of the 9th IMEKO Congress of the International Measurement Confederation, Berlin, Germany, 24-28 May 1982 (Amsterdam, Netherlands: North-Holland 1983), p.571-5 vol.2

Macroscopic quantum phenomena have a special significance for further development of metrology as their use makes possible the change-over to natural standards in a number of fields. Apart from theoretical considerations some of the experiments performed at VNIIM are described. Among these are efforts aimed at the establishment of new standards of electrical resistance and force and improvement of a number of fundamental physical constants. (5 refs.)

Uncertainty of measurements made by laser interferometerSee Entry 111647

Measurement philosophy for the calibration of a set of mass standardsSee Entry 111650

Reception and application of standard frequency- and time-signal emissionsSee Entry 111651

Analysis of small cesium beam tubeSee Entry 111652

The flat spring as a means for producing very small movements [electric sensor calibration]See Entry 111664

New devices for the static calibration of force transducers up to 10 N and for torque dynamometers up to 50 NmSee Entry 111671

Josephson-element voltage standardsSee Entry 111701

Measurement Assurance Program transmittance standards for spectrophotometric linearity testing: preparation and calibrationSee Entry 111781

Use of BPS-75+ 'Elektronika-100I' scanning-measuring system for analysis of photographs from wide-gap chambersSee Entry 112576

The development of radioactive gas standards at LMRISee Entry 112603

The optical target. A new five dimensional transducer using laser holographySee Entry 112965

Acoustic wave calibration for CO₂ laser scattering experimentsSee Entry 113034

Nonlinear optical indication in frequency stabilization systemsSee Entry 113046

New electrostatic method for absolute pressure calibration of pressure sensorsSee Entry 113244

The practical calibration of water flowmeters under realistic temperature conditionsSee Entry 113538

A new primary rig for accurate flowmeter calibrationSee Entry 113540

A high accuracy micro hardness testerSee Entry 115497

Statistical analysis of some gas chromatography measurementsSee Entry 115601

06.20J Determination of fundamental constants

Conversations with AvogadroSee Entry 111380

06.30 MEASUREMENT OF BASIC VARIABLES

111632 Behaviour of manganin gauges in solid pressure-transmitting media. T.Yamamoto, T.Kozuka, R.Kaneda (Nat. Res. Lab. of Metrology, Tokyo, Japan). *Rep. Gov. Ind. Res. Inst. Nagoya (Japan)*, vol.32, no.5-6, p.92-6 (May-June 1983). In Japanese.

The electrical resistance of a manganin coil embedded in solid pressure-transmitting media was measured under pressures up to about 6 GPa at room temperature. The relation between resistance and pressure was nearly linear, having the positive sign, at pressures higher than about 2 GPa, whereas a sharp drop in resistance was observed at an initial stage of loading. The volume discontinuities accompanying pressure-induced phase transitions both of NH_4F and Bi were observed by the corresponding drops in resistance of the manganin coil. (13 refs.)

Use of dielectric sensors in recording pressure pulsesSee Entry 111665

06.30C Spatial variables measurement

(inc. measurement of all variables extending in space e.g. diameter, height, thickness, displacement, surface topography, particle size, area of disperse systems)

111633 Technique for quantitative analysis of specimen microtopography using computer control of a scanning electron microscope. D.M.Holburn (Westfield Coll., Univ. of London, London, England). *Proc. SPIE Int. Soc. Opt. Eng. (USA)*, vol.368, p.35-40 (1983). [received: Sept. 1983] (SPIE Proceedings on Microscopy Techniques and Capabilities, London, England, 21-22 Sept. 1982).

An automated method for quantitative determination of specimen topography is described in which a computer-controlled range finding technique is employed to measure the distance between the objective lens of a scanning electron microscope (SEM) and a set of distinct features on the specimen surface. Computations based on the spatial derivative of the image intensity allow the objective lens setting corresponding to the optimum focus for each feature to be determined, and this can be related to the feature height. Experimental results and theoretical analysis indicate that the sensitivity for discrimination of height differences is of the order of 1 μm . (13 refs.)

111634 Interferometric determination of slow movements. M.Bertolotti, A.Ferrari (Istituto di Fisica Ingegneria, Univ. di Roma, Roma, Italy), P.Jani, C.Sibilia.

Proc. SPIE Int. Soc. Opt. Eng. (USA), vol.369, p.182-5 (1983). (SPIE Proceedings of the Max Born Centenary Conference OPTICS 82, ECOSA 82, Edinburgh, Scotland, 7-10 Sept. 1982).

A simple compact interferometric method is described which allows one to measure very slow movements. Application to the measurement of thermal dilatation of a semiconductor surface heated by a laser is discussed. (1 ref.)

111635 Surface coordinate measurement using high resolution TV cameras. L.J.Robinson (Blackett Lab., Imperial Coll., London, England). *Proc. SPIE Int. Soc. Opt. Eng. (USA)*, vol.369, p.211-17 (1983). (SPIE Proceedings of the Max Born Centenary Conference OPTICS 82, ECOSA 82, Edinburgh, Scotland, 7-10 Sept. 1982).

Describes a system capable of measuring and storing the cylindrical coordinates describing the surface of a small object (<10 mm). Two TV cameras are used to view an illuminated section of the surface and the z and r coordinates are extracted from the video signals and stored on floppy disc. The resolution of these coordinates is $\sim 32 \mu\text{m}$. The θ coordinate is supplied by rotating the object so that a new section of the surface is analysed. The process is repeated until the whole surface has been covered. (2 refs.)

111636 Enhanced-displacement measurement using a generalized formulation for double-aperture specklegrams. M.A.Sutton (Dept. of Mech. Engng., Columbia, SC, USA), A.K.Wong, Y.J.Chao. *Exp. Mech. (USA)*, vol.23, no.3, p.348-53 (Sept. 1983).

A generalized form for the intensity distribution at the observation plane of a spatially filtered double-aperture specklegram is derived using classical Fresnel diffraction theory. The simplified formulas obtained by previous authors are found to be a special case of the general formula. In addition, both analytical and experimental results show that a variation in sensitivity of the double-aperture method exists within any given halo in the filter plane, even in the central DC halo. Also, in the DC halo analytical and experimental work has shown that displacements can be measured parallel to the embedded

grid present on the image, thereby demonstrating that a moire analogy is inadequate to fully describe the phenomena. Finally, a comparison of experimental data to theoretical results based on the generalized formulation demonstrates (a) that the limits proposed by the authors for measuring displacements by use of the double-aperture method are valid, and (b) that the double-aperture method can be extended to measure displacements beyond those predicted by a moire interpretation. (15 refs.)

111637 The validity of the Hertz equations when using mechanical sensing methods in length measuring equipment. F.Ludicke. *Feinwerktech. & Messtech. (Germany)*, vol.91, no.5, p.242-4 (July-Aug. 1983). In German.

The author explains that the sensing components in length measuring equipment are usually spherical while the surfaces to be measured are usually plane. He therefore pays special attention to the important instance where a ball touches a plane. The results can be transferred to curved surfaces. When a sphere touches a plane, Hertz produced an equation for the flattening (oblateness) of the ball at the point of contact which is an approximation to the undeformed regions of the ball and plane. This equation depends on five idealised assumptions. In actual situations the ideal smoothness of the ball and plane can only be approximately achieved by polished or very finely machined metal. From measurements made by this method the author concludes that the theory of Hertz is valid with only trivial deviations for all pairs of surfaces, even if the surfaces have slight errors in shape, provided that these surfaces have been polished. (11 refs.) *G.W.*

111638 Comparison of optical depth-measurement methods on real metal surfaces with sine-phase-gratings. K.D.Stock (Inst. fur Phys., Tech. Univ. Braunschweig, Braunschweig, Germany). *Optik (Germany)*, vol.65, no.2, p.85-96 (1983). In German. Using a special growth technique smooth copper crystals with sine-phase-gratings were prepared with line densities of 50 1/mm to 200 1/mm and profile depths up to 250 nm. These reflection gratings showed up imperfections caused by the preparation technique. To these real metal surfaces the following measurement methods were applied, two-beam-interference-microscopy with evaluation using equidensities; multiple-beam-interference-microscopy according to Tolinsky and diffraction of laser radiation. The author presents the theory and experimental measurement limits of the three methods. (22 refs.)

111639 A method for the estimation of micropore volume and micropore surface area. J.E.Shields, S.Lowell (Quantachrome Corp., Syosset, NY, USA). *Powder Technol. (Switzerland)*, vol.36, no.1, p.1-4 (Sept.-Oct. 1983). Micropore volumes have been estimated by comparing the results of mercury intrusion with helium displacement in porous samples. Differences in the surface area measured by gas adsorption and mercury porosimetry afford an estimation of micropore surface area and the micropore surface to volume ratio gives a mean micropore radius. (6 refs.)

111640 A study on the sizing process of an instrument based on the electrical sensing zone principle. I. The influence of particle material. G.van der Plaats, H.Herps (Corporate Res. & Patents Dept., DSM, Geleen, Netherlands). *Powder Technol. (Switzerland)*, vol.36, no.1, p.131-6 (Sept.-Oct. 1983). Although in principle the use of an instrument based on the electrical sensing zone principle is limited to insulating particles, in practice conductive particles can also be measured. The material of which the particle consists, however, strongly influences the response of such an instrument. The results are presented of a detailed study on the influence of the particle material on the response of an esz instrument. It is confirmed that the apparent resistance of a conductive particle is dependent on the voltage drop over the particle when it passes the orifice. Below a critical value, all particles act as insulators and particle sizes are measured correctly; above this value particles may act as a conductor, causing large deviations in the measured sizes. It is shown that for carbon this critical value is about 1-2 V, for noble metals (palladium) about 3 V and for base metals (nickel) about 9 V. (13 refs.)

111641 A performance test of a microphonic raindrop-sizemeter. K.Tohma, T.Ihara, H.Yamamoto, T.Manabe, Y.Furuhashi, K.Kitamura, Y.Imai. *Rev. Radio Res. Lab. (Japan)*, vol.28, no.147, p.503-19 (Sept. 1982). In Japanese. [received: Sept. 1983] A microphonic measuring system of raindrop size distribution and the shape of raindrops is discussed in connection with the millimeter wave attenuation caused by rainfall. A moving coil microphone with strong damping measures the raindrop size by sensing the momentum of drops falling into its vibration cone. It has shown remarkable performance for a broad region of drop sizes in drop-by-drop experiments, whereas in natural rain experiments it has shown rather reduced accuracy for small drops because of the shock absorbing role of the thick water film on the vibration cone. Waterdrops falling in stagnant air have been photographed, and they have proved to be of the shapes of the Pruppacher-Pitter type (1971). (9 refs.)

111642 Determination of the film thickness in localized epitaxial structures. D.I.Bilenko, N.P.Kazanova, V.P.Polyanskaya. *Sov. Microelectron. (USA)*, vol.12, no.1, p.43-8 (Jan.-Feb. 1983). Translation of: *Mikroelektronika (USSR)*, vol.12, no.1, p.70-5 (Jan.-Feb. 1983). [received: Sept. 1983] Modern complex multilayer structures for microelectronics, optoelectronics, and SHF electronics with pronounced patterns both in the plane and in the volume can be regarded as reflecting amplitude-phase gratings. Measurement of the parameters for such structure can be related to analysis of the radiation diffracted by the structure. The authors show that the diffraction ellipsometry method, which allows one to determine the thickness (d_2), of protective coatings in periodic structures and the depth (d_1) of the roughness between the protective coatings and the local epitaxial formation, has a high resolving power. It is effective in the region of variation of the phase thickness of the protective coating from 0.3 π to 0.7 π and has a good measurement precision of d_2 to 2-3 nm and d_1 to 5-9 nm. (9 refs.)

111643 Multi-function digital readout caliper. E.E.Carrico (Western Electric, Kansas City, KS, USA). *Tech. Dig. (USA)*, no.71, p.5-6 (July 1983). A digital readout caliper features a modified jaw having a special reference extension in addition to standard inside measurement tabs. A foreshortened length on one of the jaws relative to the other, together with the reference extension on the foreshortened jaw increase the measuring capabilities of the caliper. (no refs.)

111644 Application of surface acoustic waves for measuring linear and angular displacement. V.Snitko, A.Zabbarov, K.Ragulska (Vibrotech. Lab., Kaunas Polytech. Inst., Kaunas, Lithuanian SSR). Technological and Methodological Advances in Measurement. Acta IMEKO 1982. Proceedings of the 9th IMEKO Congress of the International Measurement Confederation, Berlin, Germany, 24-28 May 1982 (Amsterdam, Netherlands: North-Holland 1983), p.85-90 vol.1 The possible application of surface acoustic waves for measuring linear and angular displacement has been discussed. The displacement transmitters have been developed and investigated. Theoretical and experimental investigations of transmitter measuring accuracy have been presented. Different methods of measuring on surface acoustic waves (SAW) have been discussed. (2 refs.)

111645 Surface finish measurements and surface characterizing parameters. J.Peters, P.Vanherck (Dept. of Mech. Engng., Katholieke Univ. Leuven, Heverlee, Belgium). Technological and Methodological Advances in Measurement. Acta IMEKO 1982. Proceedings of the 9th IMEKO Congress of the International Measurement Confederation, Berlin, Germany, 24-28 May 1982 (Amsterdam, Netherlands: North-Holland 1983), p.99-108 vol.1 About 12 different surface characteristic parameters have been measured on 90 samples and computed by means of digital methods. A critical assessment shows the superiority of numerical methods above analogous ones and concludes to the necessity and the possibility to base the surface characterisation upon three major parameters. Recommendations are made for future standardisation and instrument design. (5 refs.)

111646 An investigation on capacitive methods for contact free surface measurement. W.Rimkus (Inst. fur Allgemeine Elektrotech., Tech Univ. Berlin, Berlin, Germany). Technological and Methodological Advances in Measurement. Acta IMEKO 1982. Proceedings of the 9th IMEKO Congress of the International Measurement Confederation, Berlin, Germany, 24-28 May 1982 (Amsterdam, Netherlands: North-Holland 1983), p.109-14 vol.1 The present investigation on capacitive displacement sensors with high resolution shows, that by using a guard ring and integrating the sensor and the transducer electronics the measurement range can be considerably expanded. By using a sensor with an electrode diameter 2 $r=1$ mm and a displacement $d_0=100 \mu\text{m}$ a resolution less than 0.2 μm can be reached. The frequency encoded output signal makes this sensor advantageous to the use in digital processing. (4 refs.)

111647 Uncertainty of measurements made by laser interferometer. P.Boloni (Nat. Office of Measures, Budapest, Hungary). Technological and Methodological Advances in Measurement. Acta IMEKO 1982. Proceedings of the 9th IMEKO Congress of the International Measurement Confederation, Berlin, Germany, 24-28 May 1982 (Amsterdam, Netherlands: North-Holland 1983), p.503-8 vol.2 Discusses the sources of uncertainties of length measurements made by laser interferometer. Effects and typical ranges of uncertainties are briefly discussed, as well as a simple method of calibration of laser interferometers. (3 refs.)

RF-transducer for mechanical vibration	See Entry 111661
The flat spring as a means for producing very small movements [electric sensor calibration]	See Entry 111664
Instrumentation for the measurement of thermal expansion of materials at low temperatures	See Entry 111702
Polynomial fit of subaperture interferograms	See Entry 111749
Particle size analysis by automated optical microscopy	See Entry 111764
Method of determining the thickness of nuclear photoemulsions in autoradiography	See Entry 112575
Coherent detection of scattered light from submicron aerosols	See Entry 112938
Methods for the investigation of laser mirrors for laser gyroscopes	See Entry 113075
A fibre optic displacement sensor	See Entry 113139
Noncontact measurement of vibrating membrane and plate parameters	See Entry 113190
Design of an experiment to determine deformations using holographic interferometry	See Entry 113390
Hybrid processing for phase measurement in metrology and flow diagnostics	See Entry 113522
Procedure for measuring the thickness and wave characteristics of the surface of the liquid film in annular-mist flows of steam and water	See Entry 113528
Determination of the particle-size distributions of powders by mercury porosimetry	See Entry 115467
Comparative size distribution measurements on chain aggregates	See Entry 115588
Transducer system for absolute intravascular angiometry	See Entry 115969

06.30E Mass and density measurement

111648 Measurement of the virtual mass of a circular cylinder placed in a resonance tube at a distance from its center. K.Matsuzawa, N.Inoue, T.Hasegawa (Dept. of Phys., Ehime Univ., Ehime, Japan). *Jpn. J. Appl. Phys. Part 1 (Japan)*, vol.22, no.6, p.1072 (June 1983). In previous papers, a method of measuring the inertia coefficient of a cylinder in a resonance tube (the ratio of the virtual mass of the cylinder to the mass of fluid displaced by the cylinder) and some experimental results were reported. In these studies, the cylinder was placed exactly at the center of the resonance tube so as to place it about the loop of the fundamental vibration. In the present paper, we describe an experiment in which the cylinder is placed at a small distance from the center. (4 refs.)

111649 Balances of power. *Lab. Pract. (GB)*, vol.32, no.8, p.40-8 (Aug. 1983). This comprehensive tabular survey of electronic balances is prefaced by a short article illustrating the power and versatility of these instruments in a wide range of environments. The table gives details on the performance of individual balances, together with information on special functions made possible by the electronics. (no refs.)

111650 Measurement philosophy for the calibration of a set of mass standards. M.Kochsiek, H.Kunzmann (Phys.-Tech. Bundesanstalt, Braunschweig, Germany). Technological and Methodological Advances in Measurement: Acta IMEKO 1982. Proceedings of the 9th IMEKO Congress of the International Measurement Confederation, Berlin, Germany, 24-28 May 1982 (Amsterdam, Netherlands: North-Holland 1983), p.523-32 vol.2
The uncertainty of a mass linkup and for a decadic representation of a mass scale is calculated taking the uncertainty of the reference standard(s) into account. The optimum weighing schemes with column orthogonality lose their significance owing to correlation of measuring results. The mathematical details are not elaborated. (8 refs.)

Measurement of massSee Entry 111372

06.30F Time and frequency measurement

(for astronomical aspects see 95.70)

111651 Reception and application of standard frequency- and time-signal emissions. P.Wirz (Zentralschweizerisches Tech. Luzern, Luzern, Switzerland).

Elektroniker (Switzerland), no.15-16, p.74-7 (10 Aug. 1983). In German.
A general description of the special receivers at the ZTL Institute at Lucerne, concerned with the processing of standard frequency and time signals, broadcast from the Swiss HBG transmitter in Prangins and the German source DCF 77 in Mainflingen, both based on caesium clocks in the 75.000... kHz range and holding to 10^{-12} of the nominal. Brief qualitative information is supplied on the aerials, receiver type (both 'straight' and superheterodyne), digitization of receiver readings and routine application for calibration both of precision-pendulum and quartz clocks. (no refs.) A.L.

111652 Analysis of small cesium beam tube. M.Kihara (Yokosuka Electrical Communication Lab., NTT, Yokosuka, Japan), H.Jumonji. *Trans. Inst. Electron. & Commun. Eng. Jpn. Part B (Japan)*, vol.J66B, no.7, p.916-23 (July 1983). In Japanese.

In the cesium beam frequency standard, frequency stability and longevity depend on the cesium beam tube. The authors present an analysis of the cesium beam tube operation and a method which simulates its operation. Assuming two-dimensional deflection, the method considers the tube component characteristics and layout which determine the tube performance. Because the Ramsey pattern is directly calculated by the simulation, the method is practical for the cesium beam tube design. Ramsey pattern shape parameters and velocity distribution obtained by the simulation are compared with experimental results. The data are generally consistent with the calculated results. (12 refs.)

Estimation of parameters in models for cesium beam atomic clocksSee Entry 111628

Estimating time from atomic clocksSee Entry 111629

06.30G Velocity, acceleration and rotation measurement

(for flow velocity measurement see 47.80)

A method of increasing the accuracy of an accelerometerSee Entry 111662

A method for liquid velocity measurement by using two interdigital transducersSee Entry 113527

06.30L Measurement of basic electromagnetic variables

(see also 07.50 Electrical instruments and techniques)

111653 Electric-field measurements over a ground plane. R.Southwick (IBM General Products Div., Tucson, AZ, USA). *R.F. Des. (USA)*, vol.6, no.4, p.60-8 (July-Aug. 1983).

States that the imposition of FCC Regulation Part 15 Subpart J has generated renewed interest in measuring \vec{E} fields over a conducting ground plane, which is required by this regulation. The use of the E-field model described with an automated measurement system is a useful tool in the analysis of site attenuation. One advantage of this method is that sweep-frequency, site-attenuation and antenna-gain measurements can be easily made without either a standard antenna or a standard field. A second advantage is that a computer simulation using the given equation will provide a convenient method to analyze the effects of site geometry on measurement errors. (11 refs.)

06.50 DATA HANDLING AND COMPUTATION

(see also 02.70 Computational techniques; 29.80 Nuclear information processing; for optical data processing, storage and retrieval see 42.30; for geophysical data acquisition and storage see 93.65)

111654 The determination of X-ray spectra from attenuation data. I. The potentials of various methods. H.H.Kramer, H.von Seggern (Phys.-Tech. Bundesanstalt, Braunschweig, Germany). *Nucl. Instrum. & Methods Phys. Res. (Netherlands)*, vol.213, no.2-3, p.373-80 (1 Aug. 1983).

The value of the analysis of so-called ideal attenuation curves for obtaining X-ray spectral information is investigated. Various methods are critically examined. Limitations with respect to their accuracy, the maximum number of energy intervals and the useful energy range are presented for two absorber materials. The influence of various types of errors and uncertainties, which are associated with experimental attenuation data and its analysis, is quantitatively examined. This allows requirements as to the accuracy of the input data to be derived. (15 refs.)

111655 Interfacing a Unicam SP800 spectrophotometer to a microcomputer. M.G.Johnston (Dept. of Phys. Sci. & Technol., Polytech. of the South Bank, London, England). *Lab. Microcomput. (GB)*, vol.2, no.2, p.3-6 (1983).

A simple analogue-to-digital card and its operating software which were used to interface a Unicam SP800 ultraviolet spectrophotometer to an Apple II microcomputer are described. Although a specific application is cited, the technique is quite general and indeed the paper concentrates more on the technique of data accumulation rather than the details of the programming used for spectral analysis. The software required to actually read the digital

data from the converter card is minimal and is easily incorporated into a BASIC program using the PEEK and POKE commands. (1 ref.)

111656 System for acquisition, processing, and recording of experimental data using an 'Elektronika DZ-28' microcomputer. A.I.Fradkov, G.P.Zimin, O.A.Katsyuba (Kuibyshev Polytech. Inst., Kuibyshev, USSR). *Instrum. & Exp. Tech. (USA)*, vol.25, no.6, pt.1, p.1363-8 (Nov.-Dec. 1982). Translation of: *Prib. & Tekh. Eksp. (USSR)*, vol.25, no.6, p.47-52 (Nov.-Dec. 1982). [received: Sept. 1983]

A system is described that permits input of four analog signals with a timer code into a microcomputer, output of processed data to an analog two-coordinate PDP4-002 recorder and a 'Consul-260' alphanumeric printer, and which controls the experimental apparatus. The maximum interrogation rate on one channel is 1 kHz, and the minimum input signal amplitude is $10 \mu\text{V}$. Graphic data output is achieved to 0.1% precision. (4 refs.)

111657 Automated comparison of discrete spectra. P.N.Zaikin, M.V.Ufimtsev. *Moscow Univ. Comput. Math. & Cybern. (USA)*, no.4, p.22-9 (1982). Translation of: *Vestn. Mosk. Univ. Ser. 15 (USSR)*, no.4, p.21-7 (1982). [received: Sept. 1983]

The problem of comparing two discrete spectra specified with different resolution is considered. A method of comparing one-dimensional and multidimensional spectra on the basis of a criterion is proposed. (6 refs.)

111658 Field data logger with EPROM storage. A.W.Robb, W.W.Nazaroff (Lawrence Berkeley Lab., Univ. of California, Berkeley, CA USA). *Rev. Sci. Instrum. (USA)*, vol.54, no.9, p.1252-3 (Sept. 1983).

A data logger using electrically programmable read-only memory for data storage is described. The storage capacity is sufficient to record measurements from eight instruments at 30-min intervals for almost ten days. This approach provides a moderately priced alternative to data loggers using magnetic tape or floppy disks when only modest data-storage capacity is needed. (4 refs.)

Radiation effects computer experimentsSee Entry 111332

On the problem of estimating the mean value, correlation function and the spectral density of a stationary random function on the basis of single realisationSee Entry 111621

Transducer calibration supported by a computer and a data bank systemSee Entry 111630

Surface finish measurements and surface characterizing parametersSee Entry 111645

A simple microcomputer-controlled calorimeter: the heat capacity of copper, Invar and RbNiCl_3 in the range 2-20KSee Entry 111681

Particle size analysis by automated optical microscopySee Entry 111764

System of conversational image processing with two independent control-operator boardsSee Entry 111841

A multi-microprocessor neutron spectrometer computer interface systemSee Entry 112526

Use of BPS-75+'Elektronika-1001' scanning-measuring system for analysis of photographs from wide-gap chambersSee Entry 112576

INS real-time data processing composite system using large scale general purpose computersSee Entry 112609

A digital processing method for structural analysis of atom clusters from high resolution electron micrographsSee Entry 112892

Plotting stress-strain diagrams by recalculation of the computer diagramSee Entry 115477

Simultaneous recording of analyte and background absorbance from the Perkin-Elmer Model 5000 spectrometer using the Model 3600 Data StationSee Entry 115595

06.60 LABORATORY TECHNIQUES

111659 A novel sample preparation technique for cross-sectional TEM investigation of integrated circuits. J.Vanhellemont, H.Bender, C.Claeys, J.Van Landuyt, G.Declercq, S.Amelinckx, R.Van Overstraeten (Univ. Antwerpen, Antwerpen, Belgium). *Ultramicroscopy (Netherlands)*, vol.11, no.4, p.303-5 (1983).

A novel specimen preparation technique which allows cross-sectional TEM investigation of the structure, the geometry and the interfaces of the structures used for the production of integrated circuits is explained. By using a sawing technique no further mechanical thinning is required and one has the freedom to put the periodic structure in any direction on the surface. The same preparation technique also allows the study of the lattice defects at the interface and in the silicon substrate both by HVEM and HREM. (6 refs.)

High resolution spectroscopy using picosecond pulse trainsSee Entry 111775

Picosecond photoinduced dichroism detected by photothermal deflectionSee Entry 111776

Picosecond continuum generation and spectroscopySee Entry 111785

An improved transfer module and variable temperature control for a simple commercial cooling holderSee Entry 111829

High speed cineradiography of projectilesSee Entry 111840

Facility for cineradiography at high energy: the ARTEMIS projectSee Entry 111844

Magnetic focus/deflection image converter camera for cineradiographySee Entry 111846

X-ray visualisation of high speed phenomena: application to the behavior of materials under high explosives loadingSee Entry 113525

Time resolved photoacoustic spectroscopy applied to properties of picosecond transientsSee Entry 115566

Development of an automatic sample-changer and control instrumentation for isotope-source neutron-activation analysisSee Entry 115608

06.70 GENERAL INSTRUMENTATION

111660 On the transfer function of an electromechanical transducer: an application to the Mossbauer velocity drive. P.Yadagiri Reddy, P.Narayan Reddy, C.Seshakumari, K.Rama Reddy (Dept. of Phys., Osmania Univ., Hyderabad, India). *Nucl. Instrum. & Methods Phys. Res. (Netherlands)*, vol.213, no.2-3, p.381-5 (1 Aug. 1983).

A mathematical model has been proposed for the design characterisation of velocity transducers used for Mossbauer drives. Analytical properties of the transfer function representing the dynamical behaviour reproduce all the aspects of empirical measurements. Transducers of symmetrical configuration

have been fabricated and the results of model calculations are verified. The transducer design parameters can thus be quantitatively specified for improving the velocity servo system stability and for fixing the higher mechanical resonance at the desired position with minimal effect on system stability. (14 refs.)

111661 RF-transducer for mechanical vibration. K.Kuroda, H.Hirakawa (Dept. of Phys., Univ. of Tokyo, Tokyo, Japan). *Jpn. J. Appl. Phys. Part 1 (Japan)*, vol.22, no.6, p.1005-8 (June 1983).

A RF-transducer for mechanical vibration is described. A small variable capacitance (~ 50 pF) works in a 1 MHz resonant circuit. A sensitivity of 4×10^{-14} m/ $\sqrt{\text{Hz}}$ is obtained which is limited by FM noise of the pumping oscillator. (10 refs.)

111662 A method of increasing the accuracy of an accelerometer. M.Mojzis.

Elektrotech. Cas. (Czechoslovakia), vol.34, no.6, p.451-2 (1983). In Slovak. An accelerometer employing an EM induction transducer is considered. The principle of the equipment is described and it is shown that by maintaining the linear dependency between the magnetic induction and the voltage at the inputs of the comparing elements of the equipment, the accuracy of the equipment can be increased. Measurement errors due to the nonlinearity of the equipment are evaluated. (1 ref.) E.D.

111663 Sensor for non-optical measuring quantities using optical principles and outputs. I. H.Hart (Sektion Elektronik, Humboldt-Univ. zu Berlin, Berlin, Germany).

Feingeräteechnik (Germany), vol.32, no.7, p.312-15 (1983). In German. Sensors with modulated light output and optical fibre coupling can be used in many applications. The various solution possibilities are discussed. (no refs.)

111664 The flat spring as a means for producing very small movements [electric sensor calibration]. P.Krischker, G.Thurn.

Feinwerktech. & Messtech. (Germany), vol.91, no.5, p.221-3 (July-Aug. 1983). In German.

The authors explain that the calibration of high resolution electric sensors for small displacements requires a means of producing displacements within the micrometre and nanometre ranges. The suitability of leaf springs is discussed and it is shown that if a force is applied to one side of a leaf spring set up as a cantilever, the displacement of the spring can be remarkably accurately determined by a law relating its displacement at the point of measurement to its total displacement at the extreme end. A required very small displacement can thus be determined by focussing a light beam at the required point on the beam and sensing in a second optical system the shape of the reflected spot. Besides discussing the factors affecting the resolving power of such a system, the author discusses the materials used, the construction of the meter and the results obtained. Some information on measurement errors is provided and it is concluded that this method is the most reliable for producing very small displacements. (2 refs.) G.W.

111665 Use of dielectric sensors in recording pressure pulses. V.V.Astanin, G.V.Stepanov.

J. Appl. Mech. & Tech. Phys. (USA), vol.23, no.6, p.817-20 (Nov.-Dec. 1982). Translation of: *Zh. Prikl. Mekh. & Tekh. Fiz. (USSR)*, vol.23, no.6, p.88-92 (Nov.-Dec. 1982). [received: Sept. 1983]

Dielectric pressure sensors are presently used by many researchers to record the profiles of pressure pulses in solids produced by shock or explosive loading. A lack of understanding of the physical principles of sensor operation and unique features of sensor application may be the cause of conflicting estimates of sensor capability and reports of unreliability of measurements performed with such sensors. The present authors review and present results from the latest studies performed on design and application of dielectric sensors for pressure pulse recording in solids. (8 refs.)

111666 Monolithic integrated sensors in I²L technique. H.J.Hwang, H.Reichl (ITF, Munchen, Germany).

Technological and Methodological Advances in Measurement. Acta IMEKO 1982. Proceedings of the 9th IMEKO Congress of the International Measurement Confederation, Berlin, Germany, 24-28 May 1982 (Amsterdam, Netherlands: North-Holland 1983), p.53-62 vol.1

Monolithic integrated frequency-analog pressure sensors were developed. For the application of I²L-ring oscillators in integrated sensors, different pressure-frequency conversion methods were investigated. The sensitivities and temperature coefficients of the fabricated pressure sensors were measured. (7 refs.)

111667 Thin film strain gauge pressure transducers for low-cost mass applications. K.Bethe (Tech. Univ. Braunschweig, Braunschweig, Germany).

Technological and Methodological Advances in Measurement. Acta IMEKO 1982. Proceedings of the 9th IMEKO Congress of the International Measurement Confederation, Berlin, Germany, 24-28 May 1982 (Amsterdam, Netherlands: North-Holland 1983), p.63-73 vol.1

Thin film strain gauges consist of an about 5 micron thick sandwich of an inorganic insulation layer, a strain-sensing resistive layer and a conductor layer, all these being vacuum deposited onto a metallic elastic element. Strain sensing can be accomplished by a ternary metal alloy or by polycrystalline semiconductor films of Si or Ge. Together with individually designed elastic elements, a whole family of mechanical sensors for pressure, force acceleration or flow can be built up. Low-cost fabrication can be realized by the exclusive use of sheet metal, which, being handled in 3'-slices, allows highly automated parallel processing of numerous sensors at once. Two principles of low-cost/low-precision pressure sensors are outlined covering the range of 0,1 to 500 bar. (no refs.)

111668 Very high resistance bonded foil strain gages. J.Dorsey (Micro-Measurements Div., Measurements Group Inc., Raleigh, NC, USA).

Technological and Methodological Advances in Measurement. Acta IMEKO 1982. Proceedings of the 9th IMEKO Congress of the International Measurement Confederation, Berlin, Germany, 24-28 May 1982 (Amsterdam, Netherlands: North-Holland 1983), p.125-31 vol.1

In the transducer and transmitter field the need for smaller bonded foil strain gages with higher resistance has led to work with semiconductor and deposited metal film sensors. Very small, high-resistance bonded foil gages have been developed with two important advantages over their devices: an extremely low temperature effect on zero, and the ability to compensate for loaded time effects in the transducer spring element. These new gages and their performance parameters are described. (no refs.)

111669 Sensors using strain gages. W.J.Ort (Hottinger Baldwin Messtechnik, GmbH, Darmstadt, Germany).

Technological and Methodological Advances in Measurement. Acta IMEKO 1982. Proceedings of the 9th IMEKO Congress of the International Measurement Confederation, Berlin, Germany, 24-28 May 1982 (Amsterdam, Netherlands: North-Holland 1983), p.151-6 vol.1

The authors presents a survey of strain sensitive materials and gives an evaluation of the different types. It is suggested that the best strain gage for precision sensor applications is a foil strain gage using a Ni-Cr alloy with special features like intrinsic compensation of thermal coefficient of Young's

modulus of spring materials used, integrated resistor networks for quick and easy zero balancing and calibration and integrated creep compensation techniques. Thin film strain gages may find more frequent use as their characteristics continue to improve. Some sensors developed for measurement of mechanical quantities using these technologies are introduced. (6 refs.)

111670 Methods of deflection and compensation applied to the pressure transducer. A comparative study. P.Krischker, T.Gast (Inst. fur Mess- und Regelungstechnik, Tech. Univ. Berlin, Berlin, Germany).

Technological and Methodological Advances in Measurement. Acta IMEKO 1982. Proceedings of the 9th IMEKO Congress of the International Measurement Confederation, Berlin, Germany, 24-28 May 1982 (Amsterdam, Netherlands: North-Holland 1983), p.163-7 vol.1

A comparative study of the methods of deflection and compensation will be made with a pressure transducer designed for the measurement of pressure differences from 0 to 500 μ bar (usable resolution is ca. 0.06 μ bar). It turned out that without exception the measurements carried out with the aid of the compensation method are better than those without compensation. This can be particularly observed in connection with the errors of linearity and hysteresis. By means of a volume open-loop control the compensation method offers the opportunity to eliminate the breathing of the diaphragm. (4 refs.)

111671 New devices for the static calibration of force transducers up to 10 N and for torque dynamometers up to 50 Nm. N.Fintinaru, I.Matkovits (Lab. Metrologie, Timisoara, Rumania).

Technological and Methodological Advances in Measurement. Acta IMEKO 1982. Proceedings of the 9th IMEKO Congress of the International Measurement Confederation, Berlin, Germany, 24-28 May 1982 (Amsterdam, Netherlands: North-Holland 1983), p.173-82 vol.1

The first device is aimed at the calibration of force transducers with a measuring margin of 10 N, using the technique of direct deadweight loading. Tensile or compressive loads can be applied in steps of 1 N each, in loading and unloading, with estimated accuracy being $5 \times 10^{-3} = 0.005\%$. The second device is used for the calibration of torque-dynamometers up to 50 Nm. Load steps of 5 Nm each are embodied by direct loading with the deadweights of a double-lever arm provided for positive or negative torques, both for loading and unloading. The overall accuracy ensured is $5 \times 10^{-4} = 0.05\%$. (16 refs.)

111672 An overview on integrated sensors. L.A.Murray (Electro-Optic Integrated Controls Inc., San Diego, CA, USA).

Electro/82 Conference Record, Boston, MA, USA, 25-27 May 1982 (El Segundo, CA, USA: Electron. Conventions 1982), p.19-0/1-5

Sensor for a host all determinant parameters (length, time pressure, temperature, voltage, etc.) and their rates of change can be selected from a wide range of disciplines, materials and technologies. However to address the various applications, the sensor output has to be fed into a silicon integrated circuit to prepare the signal for sensible employment. Because the IC is silicon and because many advantages accrue to integrating the sensor monolithically (cost, reduced size, relaxed sensitivity et al. specifications), silicon based sensors possess advantages over the other competing sensor technologies in meeting volume sales. The author examines the various sensor families and discusses some of the problems encountered in their integration. Finally, the developing integrated sensor markets are looked at. (no refs.)

111673 Integrated circuit sensors. H.Guckel (Dept. of Electrical & Computer Engng., Univ. of Wisconsin, Madison, WI, USA).

Electro/82 Conference Record, Boston, MA, USA, 25-27 May 1982 (El Segundo, CA, USA: Electron. Conventions 1982), p.19-3/1-2

Summary form only given. Viable integrated circuit-sensor technologies are typically the results of positive solutions to certain compatibility problems. Compatibility difficulties are traceable to two sources: interdisciplinary skills and associated misunderstandings, and, rigid IC-processing techniques. The author discusses the experiences at Wisconsin in developing ion sensor technology. The preliminary conclusion from this design effort include the realization that a modest building block library together with a suitable CAD technique provides the needed flexibility to handle most sensor inputs. Compatibility with sensor construction techniques is very difficult to achieve. Moreover, sensor tolerances cause problems for a general circuit design approach. Thus, sensor and system improvements are needed if commercial viability is to be achieved. (no refs.)

Transducer calibration supported by a computer and a data bank system See Entry 111630

The validity of the Hertz equations when using mechanical sensing methods in length measuring equipment See Entry 111637

Application of surface acoustic waves for measuring linear and angular displacement See Entry 111644

An investigation on capacitive methods for contact free surface measurement .. See Entry 111646

Multimode optical fiber sensors See Entry 111674

Mechanical stresses and thermo-EMF stability See Entry 111678

Development of a pneumatically operated cryorefrigerator See Entry 111691

Performance of the pneumatically operated Gifford-McMahon cryorefrigerator See Entry 111694

Measurement of the hydrostatic pressure by means of the manganin gauge up to 100 kbar See Entry 111698

Fast, versatile, and inexpensive pulse sequence generator See Entry 111720

A real-time active vibration controller [for Michelson interferometry] See Entry 111756

The investigation of image formation in a large-area solid state X-ray receptor with electrophoretic display See Entry 111850

Semiconductor detector for the selective detection of atomic hydrogen See Entry 112880

The optical target. A new five dimensional transducer using laser holography .. See Entry 112965

A fibre optic displacement sensor See Entry 113139

A method for liquid velocity measurement by using two interdigital transducers See Entry 113527

Procedure for measuring the thickness and wave characteristics of the surface of the liquid film in annular-mist flows of steam and water .. See Entry 113528

A two-component optomechanical speed transducer for use with turbulent flows of liquid metal See Entry 113529

Characteristics of a film-type heat-flux transducer See Entry 113530

Transducer system for absolute intravascular angiometry See Entry 115969

Measurement of spatial forces by the 'matrix'-method [prosthetics application] See Entry 115981

07.00 SPECIFIC INSTRUMENTATION AND TECHNIQUES OF GENERAL USE IN PHYSICS

(see also within each subdiscipline for specialized instrumentation and techniques)

07.10 MECHANICAL INSTRUMENTS AND MEASUREMENT METHODS

(for measurement in the mechanics of solids and rheology, see 46.30R; for materials testing, see 81.70)

New devices for the static calibration of force transducers up to 10 N and for torque dynamometers up to 50 NmSee Entry 111671

07.20 THERMAL INSTRUMENTS AND TECHNIQUES

(see also 44.50 Thermal properties of matter, 44.60

Thermodynamic processes; for radiometry and detection of thermal radiation see 07.60D and 07.62)

Thermal conductivity measurements on fluids under microgravity using holographic interferometrySee Entry 114291

Change in structure of chromel-alumel thermoelectric transducers used in a medium of natural gasSee Entry 114512

07.20D Thermometry

111674 Multimode optical fiber sensors. M.Brenci, R.Falciai, A.M.Scheggi (IROE, CNR, Firenze, Italy).

Alta Freq. (Italy), vol.52, no.3, p.206-8 (May-June 1983). (4th Italian National Meeting on Applied Electromagnetics, Florence, Italy, 4-6 Oct. 1982).

Fiber optic sensors utilizing induced changes in the transmission characteristics of an optical fiber are being used for different purposes. After a short review on the state of the art on sensors based on multimode fibers this contribution presents the scheme and measurements carried out on a temperature sensor where the transducer is constituted by a liquid which matches a very short section of an unclad multimode step index fiber. The refraction index variations of such a liquid give rise to amplitude variations at the exit of the fiber and depending on the type of liquid may allow the scanning of different temperature ranges which correspond to different fields of application. (14 refs.)

111675 Max/min thermometer. S.Kirby.

Radio & Electron. World (GB), p.9-15 (Sept. 1983).

The author describes a sophisticated, yet practical unit for monitoring temperature. (2 refs.)

111676 Temperature sensors. F.Maderbacher.

Elektronikschau (Austria), vol.59, no.8, p.17-20 (Aug. 1983). In German.

Reviews the operating principles of resistance thermometers, semiconductor temperature sensors, and thermocouples. The market for such devices is briefly indicated and types available in Austria are catalogued with details of manufacturer, operating range, applications, etc. (no refs.) C.C.B.

111677 Need a T/C or RTD in a hurry? [thermocouples and resistance temperature detectors]. H.L.Trietley (Yellow Springs Instrument Co. Inc., Yellow Springs, OH, USA).

I&CS-Ind. & Process Control Mag. (USA), vol.56, no.7, p.43-4 (July 1983).

The 'do-it-yourself' probe systems described allow users to quickly assemble a wide variety of temperature probes. Both have unique advantages: the mineral oxide insulated T/Cs provide the highest operating temperatures, and the adjustable insertion depth probes provide a simple system for longer thermowells at moderate temperatures. Both can help users avoid long, costly downtime while waiting for custom-built probes. (no refs.)

111678 Mechanical stresses and thermo-EMF stability. A.N.Gordov, I.I.Novikov, B.I.Stadnyk, I.I.Fedik (Termopribor Organizatsion, Leningrad, USSR).

High Temp. (USA), vol.20, no.6, p.936-40 (Nov.-Dec. 1982). Translation of: *Templotiz. Vys. Temp. (USSR)*, vol.20, no.6, p.1176-81 (Nov.-Dec. 1982). [received: Sept. 1983]

Experimental data are used in establishing the main reason for thermoelectric inhomogeneity: mechanical stresses in the thermoelectrodes which play the main part in distorting temperature measurement for multicomponent systems. (15 refs.)

111679 Principles of successful use of contactless thermometers. H.Roetschi.

Neue Tech. (Switzerland), vol.24, no.10, p.42-5 (Oct. 1982). In German.

The principles of temperature measurement via infrared energy per unit time are explained, with special attention paid to absorption (emission), reflection and transmission coefficients. The receiver must have an adjustment for its true emission factor, but the error of reading is much smaller than the misestimate of this factor. Metal surfaces present no transmission problems, glass needs an instrument which operates only above 3 μm , and plastics need instruments sensitive only to narrow bands around 3.5 and 7 μm . (no refs.) J.M.S.

111680 Stability of some cryogenic carbon resistance thermometers.

L.M.Besley (CSIRO Div. of Appl. Phys., Sydney, Australia).

Rev. Sci. Instrum. (USA), vol.54, no.9, p.1213-17 (Sept. 1983).

The stability of 12 commercial carbon resistance thermometers has been tested at three temperatures, 12.6, 20.3, and 30K, when the sensors were exposed to cycling between 12.6 and 293K. The resistances of the thermometers changed markedly over 20 such cycles by amounts equivalent to temperature changes of between 0.07 and 0.57K at 20.3K. Both abrupt and gradual changes were observed. A few measurements were made at 4.2K to explore the correlation between changes in resistance at various temperatures. A two-point recalibration method is shown to be accurate to 1 mK over the range 12.6 to 30K and can be used to 4.2K. (9 refs.)

Thermometric and calorimetric methods in electrochemical and corrosion studiesSee Entry 111686

Resistance thermometer for ion-beam calorimetrySee Entry 112515

Fiber-optic temperature sensorSee Entry 113130

Characteristics of a film-type heat-flux transducerSee Entry 113530

07.20F Calorimetry

111681 A simple microcomputer-controlled calorimeter: the heat capacity of copper, Invar and RbNiCl₃ in the range 2-20K. S.J.Collocott (Div. of Appl. Phys., CSIRO, Lindfield, New South Wales, Australia).

Aust. J. Phys. (Australia), vol.36, no.4, p.573-81 (1983).

A simple inexpensive microcomputer has been used to control an adiabatic pulse-type calorimeter. The data acquisition control system incorporates a Rockwell AIM65 microcomputer to control all aspects of the thermometry and the injection of the heat pulse into the sample. Details of the hardware and software requirements are discussed, including the interface of the system with a host computer that uses the UNIX operating system. The performance of the apparatus was evaluated by measuring the heat capacity of 1965 Calorimetry Conference copper between 2 and 20K. The results show a total RMS deviation of less than 0.4% and agree well with the copper reference equation (RMS deviation 0.4%). Measurements are also presented of the heat capacity of Invar (Nilo 36) and RbNiCl₃ over the same temperature range. In the case of RbNiCl₃ the heat capacity anomaly associated with the paramagnetic-antiferromagnetic transition is observed at 11.1K. (21 refs.)

111682 An automated calorimeter for heat-capacity measurements from 5 to 300K. The heat capacity of cadmium sulfide from 5.37 to 301.8K and the relative enthalpy to 1103.4K. R.P.Beyer, M.J.Ferrante, R.V.Mrazek (Albany Res. Center, Bur. of Mines, US Dept. of the Interior, Albany, OR, USA).

J. Chem. Thermodyn. (GB), vol.15, no.9, p.827-34 (Sept. 1983).

An automated adiabatic calorimeter that operates over the range 5 to 300K is described. The heat capacity of cadmium sulfide, CdS, has been measured from 5.37 to 301.8K. A copper-block drop calorimeter was used to measure relative enthalpies to 1103.4K. The values at 298.15K for the molar quantities $C_{p,m}^{\circ}$, $\{S_m^{\circ}(T) - S_m^{\circ}(0)\}$, $-\{G_m^{\circ}(T) - H_m^{\circ}(0)\}/T$, and $\{H_m^{\circ}(T) - H_m^{\circ}(0)\}$, were found to be (47.29 \pm 0.03), (72.18 \pm 0.26), (39.31 \pm 0.33) J.K⁻¹.mol⁻¹, and (9802 \pm 19) J.mol⁻¹, respectively. These functions were calculated to 1100K. (13 refs.)

111683 A semi-micro rotating-bomb combustion calorimeter. R.M.Metzger, C.S.Kuo, E.S.Arafat (Dept. of Chem., Univ. of Mississippi, University, MS, USA).

J. Chem. Thermodyn. (GB), vol.15, no.9, p.841-51 (Sept. 1983).

A semi-micro rotating-bomb combustion calorimeter is described. It is designed on the model of the Bartlesville stirred-water system, but is built into a Parr 1243 adiabatic calorimeter. Quartz thermometers are used to measure temperature. The 29 cm³ bomb is platinum-lined, and requires 50 mg samples. The calorimeter constant is (4168.98 \pm 2.23) J.K⁻¹. For five crystalline substances studied previously the derived standard molar enthalpies of formation at 298.15K are $\Delta_f H_m^{\circ}$ (kJ.mol⁻¹): naphthalene, (87.17 \pm 1.53); anthracene, (125.54 \pm 5.59); 7,7,8,8-tetracyanoquinodimethane (TCNQ), (666.09 \pm 5.91); (1:1)-(N,N,N',N'-tetramethyl-p-phenylenediamine.TCNO), (624.10 \pm 8.63); and diphenyldisulfide, 151.06. (35 refs.)

111684 High-temperature calorimeter for the measurement of vapor pressure and enthalpy of vaporization. G.Natarajan, D.S.Viswanath (Dept. of Chem. Engng., Univ. of Missouri, Columbia, MO, USA).

Rev. Sci. Instrum. (USA), vol.54, no.9, p.1175-9 (Sept. 1983).

An adiabatic calorimeter for the simultaneous measurement of enthalpies of vaporization and vapor pressures of certain coal chemicals is described. The calorimeter was tested using benzene for which accurate experimental data exists in the literature. Benzene is one of the substances recommended by IUPAC as a reference substance for calorimetric studies. The uncertainty in the benzene data is ± 5 J/mole in the temperature range of 350K (very close to the boiling point) to 480K (around 0.85 times the critical temperature). Both vapor pressure and enthalpies of vaporization of benzene showed excellent agreement with the available literature data. (27 refs.)

111685 AC calorimeter for liquid including suspension of biological materials. S.Imaizumi (Dept. of Phys., Suzuka Coll. of Technol., Suzuka, Japan), K.Suzuki, I.Hatta.

Rev. Sci. Instrum. (USA), vol.54, no.9, p.1180-5 (Sept. 1983).

An AC calorimeter is developed for the measurement of heat capacity in liquid including the aqueous suspension of biological materials in the temperature range between 270 and 400K. Using this apparatus the authors performed the measurement of heat capacity at the main phase transition of lipid suspended in water. Additionally a new method to determine the absolute value of the heat capacity is proposed. (24 refs.)

111686 Thermometric and calorimetric methods in electrochemical and corrosion studies. A.T.Kuhn (Dept. of Biomaterials Sci., Eastman Dental Hospital, London, England), A.M.Shams El Din.

Surf. Technol. (Switzerland), vol.20, no.1, p.55-69 (Sept. 1983).

Calorimetric and thermometric techniques have been used sometimes to measure the electrochemical Peltier heat and sometimes to promote understanding of a reaction mechanism or of the nature of complexes from which metals are deposited. In what appears to be an entirely separate branch of study, the 'Mylus method' is used to monitor corrosion or the working of inhibitors by thermometric measurements. A review of the above work and a brief description of the instrumentation used, which ranges from a simple mercury-in-glass thermometer to microwatt calorimeters and thermistor measurement circuits detecting changes of 10⁻³°C or less, are given. (66 refs.)

Resistance thermometer for ion-beam calorimetrySee Entry 112515

Study of low temperature specific heat and DC electrical conductivity of NH₄Cl in pure powder form and in crystalline form grown from urea solutionSee Entry 114205

07.20K High-temperature techniques and instrumentation; pyrometry

111687 Rotational Raman interferometric measurement of flame temperatures. E.J.Burlaw, R.L.Armstrong (Phys. Dept., New Mexico State Univ., Las Cruces, NM, USA).

Appl. Opt. (USA), vol.22, no.18, p.2860-6 (15 Sept. 1983).

The rotational Raman scattered light from the nitrogen present in a flame is analyzed with a Fabry-Perot interferometer whose free spectral range is matched to the frequency separation of the Raman lines. The resulting interferograms are fit to theoretical interferograms using a least- χ^2 technique. Flame temperatures obtained from this analysis are compared to in situ thermocouple measurements with reasonable agreement. The measured temperatures are compared to other published data, and sources of error are discussed. (31 refs.)

111688 Unsteady method of measuring the thermal conductivity of gases at high temperatures. Yu.K.Vinogradov, N.I.Sidorov (S. Ordzhonikidze Moscow Aviation Inst., Moscow, USSR).

High Temp. (USA), vol.20, no.6, p.921-5 (Nov.-Dec. 1982). Translation of: *Teplofiz. Vys. Temp. (USSR)*, vol.20, no.6, p.1158-63 (Nov.-Dec. 1982). [received: Sept. 1983]

The authors describe the theoretical basis of the monotonic heating method relevant to investigation of the thermal conductivity of gases where the heating rate of the measurement cell depends nonlinearly on the temperature. Theoretical relations are obtained for the thermal conductivity of gases, with corrections for nonlinearity of heating rate and nonuniformity of the temperature field. (3 refs.)

111689 Reactive scattering cell for atomic hydrogen and deuterium. J.T.Park, E.Redd, T.J.Kvale, E.Rille (Phys. Dept., Univ. of Missouri-Rolla, Rolla, MO, USA).

Rev. Sci. Instrum. (USA), vol.54, no.9, p.1247-8 (Sept. 1983).

A design for a high-temperature reactive scattering cell for atomic hydrogen and atomic deuterium is described. At approximately 2700K a dissociation of the molecular target species of over 95% has been obtained. The lifetime of 340 h of operation is sufficient for precision, long-time, differential cross-section measurements. (7 refs.)

07.20M Cryogenics

111690 Sensors for cryogenic thermometry. W.G.Pierce, D.J.Bartos. *InTech (USA)*, vol.30, no.7, p.53-6 (July 1983).

Sensors for cryogenic temperature measurement include germanium and carbon-glass resistance, platinum and other metallic resistance, gallium arsenide and silicon diode, strontium titanate capacitance, and thermocouple devices. The elements offer different combinations of range, sensitivity, accuracy, immunity from magnetic field effects, and other properties. (16 refs.)

111691 Development of a pneumatically operated cryorefrigerator. K.G.Narayankhedkar (Dept. of Mech. Engng., Indian Inst. of Technol., Bombay, India).

Indian J. Cryog., vol.6, no.4, p.171-5 (1981).

A pneumatically operated Gifford McMahon cryorefrigerator has been successfully developed. Since the unit is pneumatically operated, it obviates the necessity of an electric motor, gearbox, etc. Air is used as the working substance. Temperatures down to 140K could be obtained under no load conditions using compressed air at 8 ata. The refrigerating capacity at 160K is about 2 watts with the inlet pressure of 8 ata. (4 refs.)

111692 A simple J-T system for testing small heat exchangers. G.Klip-ping (Dept. of Phys., Freie Univ. Berlin, Berlin, Germany), H.Walter, G.Ran-garajan, V.Sankaranarayanan, R.Srinivasan.

Indian J. Cryog., vol.6, no.4, p.176-83 (1981).

Describes a simple Joule-Thomson system to test small heat exchangers. Such heat exchangers are integral parts of cooling systems providing refrigeration of about a watt at 77K. The use of the system is illustrated with results of tests on two small heat exchangers. (2 refs.)

111693 Development of a cryostat for AC Josephson effect studies. V.S.Tomar, N.D.Kataria, M.Prasad, A.K.Gupta (Nat. Phys. Lab., New Delhi, India).

Indian J. Cryog., vol.8, no.1, p.9-12 (1983).

A cryostat is designed to facilitate mounting of Josephson junctions in the resonant RF field in order to study AC Josephson effects. The cryostat consists of a circular brass cap incorporating a stainless steel X-band waveguide welded with the cap at about 10 cm length. The lower end of the waveguide is connected to a junction holder with a moveable short arrangement. The junction holder is also made from a stainless steel waveguide and has a slot milled in its broad wall to facilitate the mounting of the Josephson junction. The short at the bottom of the sample holder can be moved from outside the cryostat using a stainless steel shaft gear arrangement. The moveable short arrangement helps in securing improved microwave coupling with the junctions and they require very low microwave power. Microwave induced steps are observed in *I-V* characteristics of both thin film tunnel junctions and solder-blob (SLUG) junctions. (11 refs.)

111694 Performance of the pneumatically operated Gifford-McMahon cryorefrigerator. P.H.Parmar, K.G.Narayankhedkar (Dept. of Mech. Engng., Indian Inst. of Technol., Bombay, India).

Indian J. Cryog., vol.8, no.1, p.64-6 (1983).

Presents performance details of the pneumatically operated Gifford-McMahon cryorefrigerator. Regenerator is one of the most important components of the cryorefrigerator which influences the performance of the unit. The valve mechanism should also satisfy the requirements of the cycle of operation. Use of the pneumatically operated valve block makes the unit compact. A no load temperature of 140K has been obtained using compressed air at 8 ata. The unit has a refrigerating capacity of 2 watts at 160K with the inlet pressure of 8 ata. (2 refs.)

Stability of some cryogenic carbon resistance thermometers .See Entry 111680

Josephson-element voltage standardsSee Entry 111701

Instrumentation for the measurement of thermal expansion of materials at low temperaturesSee Entry 111702

Apparatus for the measurement of the magnetic susceptibility of liquids in high magnetic fieldsSee Entry 111711

Dewar design for optically pumped semiconductor ring laserSee Entry 113022

Helium acoustic microscopySee Entry 113236

Ten-channel grating chromator for electron cyclotron emission plasma diagnosticsSee Entry 113665

Study of low temperature specific heat and DC electrical conductivity of NH₄Cl in pure powder form and in crystalline form grown from urea solutionSee Entry 114205

Helium-II application in space cooling systemsSee Entry 116475

07.25 HYGROMETRY

111695 Low power consumption solid state humidity sensor. K.Yuuki, T.Sakano, Y.Yokomizo (Marcon Electronic Co. Ltd., Yamagata, Japan).

IEEE Trans. Consum. Electron. (USA), vol.CE-29, no.3, p.305-9 (1983). (1983 IEEE International Conference on Consumer Electronics. ICCE, Des Plaines, IL, USA, 8-10 June 1983).

A new ceramic humidity sensor composed of ZnCr₂O₄-LiZnVO₄ was developed. This high reliability sensor has excellent stability in environments of air and corrosive gas atmospheres. An equivalent circuit of the sensor in the complex impedance method is represented by a parallel combination of resis-

tance and capacitance as a first approximation. The resistance changes linearly from 340 KΩ to 3.4 KΩ in 30 to 90% RH range at 25°C-120 Hz as a logarithmic function. (5 refs.)

111696 Absolute humidity measurement utilizing α-ray absorption. S.Matsumoto, H.Kobayashi (Lab. of Appl. Phys., Saitama Univ., Saitama, Japan).

Radioisotopes (Japan), vol.32, no.9, p.399-403 (Sept. 1983). Changes in the air density due to humidity were measured by a scintillation detector with α-particles. The distance between the scintillator and an α-ray source of ²⁴¹Am, 3.7 MBq (100 μCi), was fixed at 25 mm which was a little shorter than the range of α-particles from the source. The measured absolute humidities were in a range of 7.9 g/m³ to 52.2 g/m³ at temperatures of 35°C and 45°C and under atmospheric pressure. The counting rate of α-particles in an absolute humidity of 31.7 g/m³ (80% in relative humidity) at 35°C increased 28% compared with that in dry air. From experimental results and theoretical calculation, the counting rate difference between humid air and dry air was shown to be almost proportional to the absolute humidity in air. The absolute humidity can be measured with an accuracy of ±3 g/m³, that is ±5% in relative humidity at 45°C. (6 refs.)

07.35 HIGH PRESSURE PRODUCTION AND TECHNIQUES

(inc. pressures above 1 atmosphere)

111697 Improved X-ray collimation system for diamond-anvil high-pressure cells. D.Schiferl, B.Olinger, R.Livingston (Los Alamos Nat. Lab., Los Alamos, NM, USA).

Rev. Sci. Instrum. (USA), vol.54, no.9, p.1250-1 (Sept. 1983).

An improved X-ray collimation system for diamond-anvil high-pressure cells is described. The usual practice of mounting the collimator directly in the diamond-anvil cell is not followed. Instead, the collimator is mounted and aligned in a fixture which can be removed from the diamond-anvil cell. The end of the collimator furthest from the sample can be fitted with a set of removable plugs, each with a different aperture. This collimation system is easily aligned, can be removed from the high-pressure cell with no loss of alignment, and is inexpensive to construct. (3 refs.)

111698 Measurement of the hydrostatic pressure by means of the manganin gauge up to 100 kbar. M.Nomura.

Solid State Phys. (Japan), vol.18, no.6, p.333-8 (June 1983). In Japanese.

The method to measure the hydrostatic pressure up to 100 kbar using the manganin pressure gauge is described. Its applications are also presented. (16 refs.)

111699 Mechanical analysis of 18ϕ piston-cylinder type high pressure apparatus by the finite element method. S.Tamura.

Solid State Phys. (Japan), vol.18, no.6, p.339-43 (June 1983). In Japanese.

Mechanical analysis of the piston, the pedestal of the piston and the cylinder were carried out. The reason why the pressure could be increased when the cylinder was end-loaded was clarified. (16 refs.)

Nitrite and nitrate ions as infrared pressure gauges for diamond anvilsSee Entry 112734

Intense proton beam excitation of the high pressure Ar/N₂ laserSee Entry 113014

Flowmetering in a long-distance pipeline grid for ethylene under high pressureSee Entry 113539

Diamond-anvil system for the investigation of phase equilibria in mixtures at high pressuresSee Entry 113551

07.50 ELECTRICAL INSTRUMENTS AND TECHNIQUES

111700 A new design and experimental testing of a carbon monoxide sensor. A.A.Al-Najar, A.M.Ibraheem (Dept. of Chem., Coll. of Education, Univ. of Basrah, Basrah, Iraq).

Iraqi J. Sci., vol.22, no.4, p.505-19 (1981). [received: Aug. 1983]

A new limiting current sensor for the determination of carbon monoxide at different ambient conditions is considered. The efficiency of this sensor based on electrochemical principles is critically dependent upon the relationship between the CO oxidation current and the electrode potential. The rapid changes of cell current to concentration change in CO, in air samples, suggests that the sensor could be developed further into a useful practical device. (13 refs.)

111701 Josephson-element voltage standards. L.Grimm, J.H.Hinken.

Elektronik (Germany), vol.32, no.13, p.105-8 (1 July 1983). In German.

Josephson effect physical principles where DC current in point contact or tunnel elements at superconducting temperatures is accompanied by alternating current with frequency related precisely to DC voltage through electron charge and Planck's constant, are described. Voltage standards synchronise the Josephson effect frequencies using injected microwave frequencies, with about 72 GHz corresponding to 150 μV applied DC. Typical millivolt DC levels are interpreted at 1 V level by bridge and resistive voltage divider methods. Practical cryo voltage standards and high accuracy performance, with Josephson element, waveguide, voltage divider and superconducting quantum interference device null detector all in liquid helium, are explained. (17 refs.) *H.V.H.*

111702 Instrumentation for the measurement of thermal expansion of materials at low temperatures. P.P.Krishnapur, S.V.Subramanyam, M.V.Lele (Indian Inst. of Sci., Bangalore, India).

Indian J. Cryog., vol.8, no.1, p.43-7 (1983).

A bath type cryostat incorporating the three terminal capacitance technique has been designed and fabricated for the measurement of thermal expansion of materials between 350K and 80K. With a slight modification in the arrangement of capacitor plates the cryostat can also be used conveniently to explore the dielectric properties of materials. The thermal expansion cell made purely with copper is the important part of this. The constructional details and performance characteristics of the cryostat are discussed. Since the method of measurement requires a Ratio Transformer impedance bridge having two inductive arms, and the other two three-terminal capacitors, the Ratio Transformer having six decades fabricated here has been used. The accuracy of comparison is 2 ppm. For standardisation of the cryostat, measurements have been made on high purity copper, TGS and KDP. The data have been found to agree with those of others. (12 refs.)

111703 Improved differential photocurrent method for measurement of optical-absorption coefficient and minority-carrier diffusion length in a semiconductor. S.Hasegawa (Graduate School of Electronic Sci. & Technol., Shizuoka, Univ., Hamamatsu, Japan), T.Watanabe, A.Tanaka, T.Sukegawa. *Rev. Sci. Instrum. (USA)*, vol.54, no.9, p.1165-8 (Sept. 1983). This paper describes an improved differential photocurrent method of measurement of optical-absorption coefficient α and minority-carrier diffusion length L . A prototype instrument can detect signals of the photocurrent I_p , the differential photocurrent ΔI_p , and the depletion-layer width W of sample diode, and plot automatically two linear relationships: $\log(\Delta I_p/\Delta W)$ vs W and I_p vs $\Delta I_p/\Delta W$. From these plots, α and L are readily obtained. Performance of the instrument is demonstrated using a Au-GaAs_{0.62}P_{0.38} Schottky-barrier photodiode. (3 refs.)

111704 Pulse technique for measuring magnetoresistance of metals in high magnetic fields. P.Czarnecki, M.Surma (Inst. of Phys., A. Mickiewicz Univ., Poznan, Poland). *Rev. Sci. Instrum. (USA)*, vol.54, no.9, p.1202-4 (Sept. 1983). A method for measuring magnetoresistance of metals and metallic alloys in a pulse magnetic field of high intensity is presented. The accuracy of the sample magnetoresistance $\Delta\rho/\rho_0$ is $\pm 12\%$ and $\pm 5\%$ for $\Delta\rho/\rho_0$ values of 10^{-3} and 10^{-1} , respectively. This accuracy can be achieved for sample resistances of the order of 10^{-1} - $10^2\Omega$. (6 refs.)

111705 Drift reduction of the incident signal in time domain reflectometry. R.Chahine, T.K.Bose (Dept. de Phys., Univ. du Quebec a Trois-Rivieres, Quebec, Canada). *Rev. Sci. Instrum. (USA)*, vol.54, no.9, p.1243-6 (Sept. 1983). Modification of a 1811 A Hewlett-Packard time domain reflectometry (TDR) system is described for long-time drift reduction. Triggering methods for single-channel as well as dual-channel TDR systems are discussed. It is shown that the long-time drift of the 1024-point incident signal is reduced to less than one discrete point over a period of several hours. This modification extends the upper frequency limit of a TDR system to about 10 GHz for precision permittivity measurements. (14 refs.)

111706 Field-strength measuring probe for appraising the danger to man in the near-field of high-power radio transmitters. D.Hoff, K.-H.Turkner. *Rundfunktech. Mitt. (Germany)*, vol.27, no.4, p.171-8 (July-Aug. 1983). In German.

For the conception of a measuring method, values are derived for appraising the danger due to strong electromagnetic fields. It appears that, in general, all the field-strength components at the point of measurement must be taken into account. For application in the near-field of high-power radio transmitters in the LF, MF and HF bands, certain constraints, in particular regarding isotropy, bandwidth, dynamic, radiation resistance and facility of manipulation, must be made on a universally-applicable measuring installation. The article discusses the problems of development arising from those constraints; the solutions found give rise to a direct-indicating measuring installation which is suitable for practical application. (7 refs.)

111707 Methods and standard apparatus for reproduction and measurement of electrical signals of infrasonic frequencies. E.D.Koltik, S.A.Kravchenko, V.I.Fomenko (D.I. Mendeleev Res. Inst. of Metrol., Leningrad, USSR).

Technological and Methodological Advances in Measurement. Acta IMEKO 1982. Proceedings of the 9th IMEKO Congress of the International Measurement Confederation, Berlin, Germany, 24-28 May 1982 (Amsterdam, Netherlands: North-Holland 1983), p.311-14 vol.2

Presents new methods of designing precise apparatus for reproduction of electrical signals in the frequency range from 0.001 to 1000 Hz and their accurate measurement. It is shown that the apparatus reproduces two voltages of 10 V with an accuracy of 0.01%, the frequency instability being 10^{-3} when the phase angle is adjusted within 0 to 360° at discrete steps of 10° with an error of 0.05°. Voltage is measured with an accuracy of 0.03%, the phase shift measurement has a sensitivity of 0.01°. The harmonic factor is 0.07%. (4 refs.)

111708 A further development in error reduction models. R.Dearnley, A.Barel, J.Renneboog (Dienst voor Algemene Electriciteit, Vrije Univ. Brussel, Brussel, Belgium).

Technological and Methodological Advances in Measurement. Acta IMEKO 1982. Proceedings of the 9th IMEKO Congress of the International Measurement Confederation, Berlin, Germany, 24-28 May 1982 (Amsterdam, Netherlands: North-Holland 1983), p.315-20 vol.2

With the continual increase in computing capabilities and possibilities to use automatic measurement systems, a sixteen term error model was developed. Results are obtained from an automatic microwave measurement system which uses this model. A comparison is made with a twelve-term 'universal' model which has been used in the past. (4 refs.)

Macroscopic quantum phenomena in metrologySee Entry 111631

Reception and application of standard frequency- and time-signal emissionsSee Entry 111651

Charge-density measurement for single nanosecond electron-beam pulsesSee Entry 111824

A note on the correct evaluation of junction capacitance of a solar cellSee Entry 115644

07.55 MAGNETIC INSTRUMENTS AND TECHNIQUES

111709 Dynamic range of a superconducting quantum magnetic-flux measuring instrument. A.V.Filimonov. *Meas. Tech. (USA)*, vol.25, no.11, p.961-3 (Nov. 1982). Translation of: *Izmer. Tekh. (USSR)*, vol.25, no.11, p.63-4 (Nov. 1982).

The results of measurements of the single-signal and two-signal dynamic range of a superconducting quantum instrument for measuring magnetic flux over a frequency band are presented. These results show that the dynamic range is mainly determined by the parameters of the integrator in the circuit. The values obtained for the dynamic range (~ 100 dB at a frequency of 20 Hz) can be used to estimate the dynamic possibilities of measuring instruments using superconducting quantum magnetic-flux measuring instruments. (4 refs.)

111710 Apparatus for measuring the magnetic susceptibility of a diamagnetic or paramagnetic material in the solid or molten state. L.V.Borodin, M.V.Smirnov, V.Ya.Kudakov. *Meas. Tech. (USA)*, vol.25, no.11, p.967-9 (Nov. 1982). Translation of: *Izmer. Tekh. (USSR)*, vol.25, no.11, p.66-7 (Nov. 1982).

The authors consider an apparatus for determining the magnetic susceptibility of a solid or molten substance, which has been used in systematic measurements on the susceptibilities of MeCl-FeCl₃ systems, where Me is K, Na, Rb, Cs. The apparatus consists of a magnet with shaped poletips, a balance placed

in a glass cover, and measurement and control apparatus. The balance enables one to make measurements on solid molten diamagnetic specimens of a specific susceptibility more than -2×10^{-8} cm³g⁻¹, and paramagnetic ones with susceptibilities not more than 4.0×10^{-3} cm³g⁻¹. (10 refs.)

111711 Apparatus for the measurement of the magnetic susceptibility of liquids in high magnetic fields. J.S.Brooks, G.O.Zimmerman (Boston Univ., Boston, MA, USA), R.Meservey. *Rev. Sci. Instrum. (USA)*, vol.54, no.9, p.1234-7 (Sept. 1983).

The authors describe an apparatus capable of measuring the magnetic force on small liquid samples in high magnetic fields. The apparatus has been used to measure the magnetic susceptibility χ of liquid He at pressures up to 3 MPa in high magnetic fields and has a sensitivity in such measurements comparable to superconducting magnetometers in lower fields. The performance was tested by measuring the atomic diamagnetism of liquid ⁴He and liquid ³He as well as the nuclear paramagnetism of liquid ³He at 1.2 K in fields up to 15 T. (8 refs.)

111712 The VUZORT optical magnetometer. I.Soudek. *Sdelovaci Tech. (Czechoslovakia)*, vol.31, no.7, p.263-5 (July 1983). In Czech.

Describes the principle and realisation of an optical magnetometer based on the utilisation of the Kerr magneto-optical effect. The individual components of the system, i.e. the light sources, light polariser, optical system, radiation detector, a magnetisation circuit and the measuring circuits are outlined and the mechanical and functional solution of the system is described. The magnetometer is particularly suitable for measuring the properties of vapour deposited magnetic films on glass. For magneto-optical sensing of signals or for analogue sound recordings, several constructional modifications would be required. (9 refs.) E.D.

111713 Differential measuring instrument of magnetic characteristics. M.N.Mikheev, E.S.Gorkunov, A.V.Antonov, M.I.Shirobokov, V.V.Nikitin (Inst. of Metal Phys., Acad. of Sci., USSR).

Sov. J. Nondestr. Test. (USA), vol.18, no.12, p.982-4 (Dec. 1982). Translation of: *Defektoskopiya (USSR)*, vol.18, no.12, p.62-5 (Dec. 1982). [received: Sept. 1983]

Describes the operating principle of the prototype of the instrument DIMKh-1. With the aid of a differential magnetic transducer the instrument makes it possible to compare magnetic fluxes in relation to a standard specimen in the region of saturation induction, remanent induction, and coercive force, and it can be used under production conditions for the nondestructive determination of the structural state of products, their phase composition, and for estimating the degree of porosity. (7 refs.)

111714 Widening the range of constant magnetic fields which can be measured with impedance-type ferroprobe transducers. A.G.Alekseev, E.I.Zenin, Yu.A.Kovyazin, B.V.Patramanskiy, P.A.Khalileev (Inst. of Metals Phys., Acad. of Sci., USSR).

Sov. J. Nondestr. Test. (USA), vol.18, no.12, p.991-5 (Dec. 1982). Translation of: *Defektoskopiya (USSR)*, vol.18, no.12, p.71-5 (Dec. 1982). [received: Sept. 1983]

Impedance-type transducers for measuring magnetic fields with a wide measurement range in comparison with the existing transducers are examined. (2 refs.)

Critical field measurements in superconductors using AC inductive techniquesSee Entry 114650

Magnetic inspection of the hardness of steel ShKh15 pipesSee Entry 115490

A solid-state compass with microprocessor controlled data acquisitionSee Entry 116315

07.58 MAGNETIC RESONANCE SPECTROMETERS, AUXILIARY INSTRUMENTS AND TECHNIQUES

(see also 61.16N EPR and NMR determinations)

111715 Spin-pattern recognition in high-resolution proton NMR spectroscopy. M.H.Levitt, R.R.Ernst (Lab. fur Phys. Chem., Eidgenossische Tech. Hochschule, Zurich, Switzerland).

Chem. Phys. Lett. (Netherlands), vol.100, no.2, p.119-23 (2 Sept. 1983).

Techniques are introduced for the recognition of specific spin patterns in complex overlapping proton NMR spectra. They are based on the efficient and selective excitation of high-order multiple quantum coherence in systems of specified coupling network topology, and allow the suppression of undesired spin patterns. (30 refs.)

111716 A wide-band power amplifier for a pulsed NQR spectrometer. A.S.Azhaganov, A.V.Danilov (Perm Univ., Perm, USSR).

Instrum. & Exp. Tech. (USA), vol.25, no.5, pt.1, p.1162-4 (Sept.-Oct. 1982). Translation of: *Prib. & Tekh. Eksp. (USSR)*, vol.25, no.5, p.109-11 (Sept.-Oct. 1982). [received: Sept. 1983]

A description is given of an output power amplifier for a pulsed NQR spectrometer. The amplifier develops a pulse power of 2 kW at a load of 75 Ω in the frequency band 2-50 MHz with a nonuniformity of 3 dB. The power gain is 30 dB. (9 refs.)

111717 NMR relaxometer transducer with magnetic-field pulse gradient coil. V.A.Sevryugin, V.D.Skirda (Kazan State Univ., Kazan, USSR).

Instrum. & Exp. Tech. (USA), vol.25, no.5, pt.1, p.1165-7 (Sept.-Oct. 1982). Translation of: *Prib. & Tekh. Eksp. (USSR)*, vol.25, no.5, p.112-13 (Sept.-Oct. 1982). [received: Sept. 1983]

The construction of an NMR relaxometer transducer with magnetic field pulse gradient coil is described, in which the distortion of the self-diffusion coefficient caused by mechanical vibration is eliminated. The combination of a transceiver coil and thermocouple enables the temperature-regulation properties of the transducer to be improved and increases the accuracy with which the temperature of the sample can be monitored, the preset temperature being maintained with an accuracy of $\pm 0.2^\circ\text{C}$ over the range -160°C to 200°C with a lengthwise temperature gradient of $\leq 0.1^\circ\text{C}/\text{cm}$. (4 refs.)

111718 Nuclear-resonance teslameter for use in superconducting solenoids. Yu.I.Kazantsev, S.V.Rypalev, G.K.Yagola. *Meas. Tech. (USA)*, vol.25, no.11, p.959-60 (Nov. 1982). Translation of: *Izmer. Tekh. (USSR)*, vol.25, no.11, p.62-3 (Nov. 1982).

A teslameter that implements the nuclear-magnetic resonance NMR method in flowing water (see *ibid.*, no.10, 1975), enables one to measure magnetic induction over a wide range for fields with considerable inhomogeneity, but the probe is of diameter ~ 25 mm and operates only at room temperature. The authors have devised a flowing-water teslameter which is suitable for measurements on superconducting solenoids at room temperature and in liquid helium. The probe described has the following features relative to those described previously: the flow channel lies along the axis, which enables one to reduce the transverse dimensions; thermal insulation is provided by the

evacuated cavity, which means measurements can be made in the range 4.2-300K. (5 refs.)

111719 NMR-spectroscopic investigation of the distribution of a constant magnetic field. K.L.Zakharov, Yu.S.Konstantinov, A.M.Smirnov (Dept. of VHF Radiophys., Moscow Univ., Moscow, USSR). *Moscow Univ. Phys. Bull. (USA)*, vol.37, no.5, p.98-101 (1982). Translation of: *Vestn. Mosk. Univ. Ser. 3 (USSR)*, vol.37, no.5, p.85-8 (1982). The application of a variant of the sensitive-point method in studying the distribution of a constant magnetic field in the gap of a high-resolution NMR spectrometer is considered. A method of producing two sensitive points is developed and theoretically verified: a motionless point which is used for internal proton stabilization and point scanning over the investigated volume. The following-receiver method is used to derive the NMR signal from the scanning sensitive point. The experimental apparatus is described. (5 refs.)

111720 Fast, versatile, and inexpensive pulse sequence generator. G.A.Mohr, C.M.Edwards (Dept. of Phys., Washington Univ., St. Louis, MO, USA). *Rev. Sci. Instrum. (USA)*, vol.54, no.9, p.1238-42 (Sept. 1983).

A fast, versatile, and inexpensive programmable digital pulse sequence generator (PSG) suitable for use in broadband pulsed NMR has been developed. Its features include 20 ns resolution of pulse duration, operation without direct computer supervision, and enough flexibility to produce essentially any pulse sequence. The architecture and construction of the PSG are discussed, and an example of its programming is presented. (11 refs.)

07.60 OPTICAL INSTRUMENTS AND TECHNIQUES

(for radiation detection, see 07.62; for spectroscopy and spectrometers, see 07.65; for holography, see 42.40; for optical sources and standards, see 42.72; for optical lens and mirror systems, see 42.78; for optical devices, techniques and applications, see 42.80; for optical testing and workshop techniques, see 42.85; for radiation spectrometers and spectroscopic techniques, see 29.30; for radiation measurement, detection and counting, see 29.70)

111721 Edge scan wave-front analyzer for low order aberrations. J.S.Nichols, D.C.Duneman (US Air Force Weapon Lab., Kirtland Air Force Base, NM, USA).

Appl. Opt. (USA), vol.22, no.18, p.2836-43 (15 Sept. 1983). The principles and concepts of a wave-front analyzer based on spot edge scanning techniques and rising and falling illuminance slope comparisons are reviewed. An analyzer implementing these techniques and designed to be used with an adaptive optics element for the real time correction of low order aberrations is described. An evaluation of the tilt output channels of the analyzer shows a linear operating range exceeding $\pm 500 \mu\text{rad}$, frequency response exceeding 250 Hz, and a noise equivalent tilt angle of $4 \mu\text{rad}$. For the focus and astigmatism channels, the analyzer output is linear over an $\sim 2.5\text{-}3\text{-}\mu\text{m}$ range of aberration input for a diffraction-limited (DL) spot. The instrument gain falls from $\sim 8.5 \text{ V}/\mu\text{m}$ for a $1\times\text{DL}$ spot to $\sim 4 \text{ V}/\mu\text{m}$ for a $6\times\text{DL}$ spot. The noise equivalent aberration increases from $0.025 \mu\text{m}$ for a $1\times\text{DL}$ spot to $\sim 0.05 \mu\text{m}$ for a $6\times\text{DL}$ spot. (7 refs.)

111722 Optimal post detection phase estimation for wavefront sensing. R.M.Gagliardi (Dept. of Electrical Engng., Univ. of Southern California, Los Angeles, CA, USA).

Proc. SPIE Int. Soc. Opt. Eng. (USA), vol.351, p.34-41 (1983). [received: Sept. 1983] (SPIE Proceedings on Wavefront Sensing, San Diego, CA, USA, 24-25 Aug. 1982).

The use of optical heterodyne wavefront sensors (HWFS) to estimate and correct distorted optical beams is presently under consideration. The HWFS theoretically allows simultaneous measurements of the phase differences across the received beam. These phase estimates can then be used to phase correct the waveform, for example, by adjustment of segmented mirrors or by differential path length control. A perfect phase estimate and adjustment over the beamfront will bring the corrected wavefront into perfect phase alignment, producing an ideal phase coherent plane wave beam. Several forms of signal processing in order to make the phase measurements following the interferometer. Procedures for frequency locking the local heterodyning laser and for measuring the phase of the photo-detected wavefront samples are discussed. Signal processing models are derived from basic analyses of frequency control and phase estimation subsystems. These models are then used to suggest system design and predict performance. The models are then extended to parallel processors involving arrays of photodetectors which have direct application to the HWFS system. (2 refs.)

111723 Comparison of wavefront sensor configurations using optimal reconstruction and correction. E.P.Wallner (Itek Optical Systems, Itek Corp., Lexington, MA, USA).

Proc. SPIE Int. Soc. Opt. Eng. (USA), vol.351, p.42-53 (1983). [received: Sept. 1983] (SPIE Proceedings on Wavefront Sensing, San Diego, CA, USA, 24-25 Aug. 1982).

Recent work on optimal reconstruction of wavefronts from slope measurements has developed methods based on more realistic models of sensor devices. These methods also resolve certain ambiguities present in earlier reconstruction methods. The author applies these methods to sensor configurations which have been proposed in the literature and compares the errors involved in estimating and correcting the wavefronts. (9 refs.)

111724 Fundamentals of wavefront sensing by phase retrieval. R.A.Gonsalves (EIKONIX Corp., Bedford, MA, USA).

Proc. SPIE Int. Soc. Opt. Eng. (USA), vol.351, p.56-65 (1983). [received: Sept. 1983] (SPIE Proceedings on Wavefront Sensing, San Diego, CA, USA, 24-25 Aug. 1982).

Phase retrieval implies extraction of the phase of a complex signal from its modulus. In the context of wavefront sensing, the unknown wavefront is represented as a phase across an aperture and the observable is the modulus of the diffracted light, measured in a convenient image plane. The author gives a concise statement of the problem, reviews some proposed solutions, discusses the question of uniqueness, gives elementary examples of phase retrieval, and shows how the concept might be used in an imaging context. (15 refs.)

111725 Fundamental performance limitations for the phase retrieval problem. S.R.Robinson (Radar & Optics Div., Environmental Res. Inst. of Michigan, Ann Arbor, MI, USA).

Proc. SPIE Int. Soc. Opt. Eng. (USA), vol.351, p.66-70 (1983). [received: Sept. 1983] (SPIE Proceedings on Wavefront Sensing, San Diego, CA, USA, 24-25 Aug. 1982).

Precomputable (Cramer-Rao) lower bounds for the integrated mean-square error are presented for the phase retrieval problem. The results are based

upon the assumption that the phase is a sample function of a Gaussian random process and that the intensity measurements include additive white Gaussian noise. The bound, which is obtained from an information kernel which is the solution to a Fredholm integral equation, clearly demonstrates the effect of prior statistics, measurement noise and the nature of the linear transformation introduced prior to detection. Several examples are given; in particular, the role of diffraction is shown to be quite important for successful phase retrieval. Finally, the results are extended to include independent measurements of intensity in several planes. (6 refs.)

111726 Phase retrieval by optical phase differentiation. J.C.Bortz, B.J.Thompson (Inst. of Optics, Univ. of Rochester, Rochester, NY, USA).

Proc. SPIE Int. Soc. Opt. Eng. (USA), vol.351, p.71-9 (1983). [received: Sept. 1983] (SPIE Proceedings on Wavefront Sensing, San Diego, CA, USA, 24-25 Aug. 1982).

A phase retrieval technique utilizing a differentiation filter in a coherent processing system has been developed and tested. The image irradiance produced in this system is quadratic in the partial derivative of object phase with respect to an object coordinate parallel to the transmittance gradient of the filter. Given a properly chosen set of such image irradiances it is possible to solve for the object phase. (2 refs.)

111727 Role of diffraction in phase retrieval from intensity measurements. J.T.Foley, M.A.Abdul Jalil (Dept. of Phys., Mississippi State Univ., Mississippi State, MS, USA).

Proc. SPIE Int. Soc. Opt. Eng. (USA), vol.351, p.80-9 (1983). [received: Sept. 1983] (SPIE Proceedings on Wavefront Sensing, San Diego, CA, USA, 24-25 Aug. 1982).

The role played by diffraction in the question of the uniqueness of phase retrieval from intensity measurements in the aperture plane and focal plane of a thin lens is investigated. It is shown for a specific example that diffraction from the lens aperture stop reduces the nonuniqueness which is present if this diffraction is ignored. (13 refs.)

111728 Linear methods in phase retrieval. B.Ellerbroek, D.Morrison (Hughes Aircraft Co., El Segundo, CA, USA).

Proc. SPIE Int. Soc. Opt. Eng. (USA), vol.351, p.90-5 (1983). [received: Sept. 1983] (SPIE Proceedings on Wavefront Sensing, San Diego, CA, USA, 24-25 Aug. 1982).

On-orbit wavefront sensing and active alignment control are essential features of many spaceborne optical systems currently being developed. Phase retrieval is an especially appropriate wavefront sensing technique for this application, because it directly monitors system image quality and eliminates or reduces the need for auxiliary wavefront sensors. Although the general phase retrieval problem is highly complex and requires sophisticated nonlinear estimation techniques, properly selected linear methods provide satisfactory and efficient solutions to a number of important special cases. The authors discuss the performance of several such linear phase retrieval algorithms. One method yields noise-optimal estimates of small wavefront errors, while a second approach can be used with arbitrarily large errors but is much more sensitive to noise. These two phase retrieval algorithms are actually special cases of a general linear algorithm that can be tuned as a function of wavefront error characteristics, measurement noise statistics, and focal plane detector geometry. (5 refs.)

111729 Wavefront sensors for turbulence correction. D.W.Hanson (Rome Air Dev. Center, Griffiss AFB, NY, USA).

Proc. SPIE Int. Soc. Opt. Eng. (USA), vol.351, p.104-7 (1983). [received: Sept. 1983] (SPIE Proceedings on Wavefront Sensing, San Diego, CA, USA, 24-25 Aug. 1982).

Adaptive optics is gaining acceptance as a method of reducing the degrading effects imposed on optical signals by atmospheric turbulence. One of the critical components of an adaptive optical system is the wavefront sensor, the device which measures the aberrations on the wavefront. The wavefront sensor specifications depend on the mission for which the adaptive optical system will be used and the conditions under which it will operate. Typical missions and operating conditions in which adaptive optics can be used are presented. The error sources in a wavefront sensor are discussed in relation to mission and operating conditions. Desirable properties of wavefront sensors are also presented. (1 ref.)

111730 Linear-scanned-array (LSA) outgoing wavefront sensor. N.Bareket (Lockheed Palo Alto Res. Lab., Palo Alto, CA, USA).

Proc. SPIE Int. Soc. Opt. Eng. (USA), vol.351, p.115-20 (1983). [received: Sept. 1983] (SPIE Proceedings on Wavefront Sensing, San Diego, CA, USA, 24-25 Aug. 1982).

The linear-scanned-array wavefront sensor extends the applicability of imaging centroid trackers to Hartmann-type outgoing wave beam-control systems. Oscillating mirrors are used to produce optical integration of the irradiance distribution along one axis while the centroid is measured along the orthogonal axis. The use of linear detector arrays reduces the total detector-element count and increases the measurement bandwidth in comparison to area array sensors. Experiments with a four-beam laboratory model of the sensor have demonstrated centroiding of $150\text{-}\mu\text{m}$ diameter Hartmann spots to an accuracy of better than $0.6 \mu\text{m}$ at 4-kHz bandwidth. Optimal thresholding can improve the measurement accuracy considerably. The linearity of the sensor was measured to be better than $0.2 \mu\text{m}$ over an $80\text{-}\mu\text{m}$ range. (4 refs.)

111731 Experimental verification of an image-based alignment technique for optical systems in space. N.Wu, B.L.Ellerbroek, S.G.Williams (Hughes Aircraft Co., Culver City, CA, USA).

Proc. SPIE Int. Soc. Opt. Eng. (USA), vol.351, p.121-30 (1983). [received: Sept. 1983] (SPIE Proceedings on Wavefront Sensing, San Diego, CA, USA, 24-25 Aug. 1982).

The authors have developed two alignment techniques for optical systems in space, i.e. OYSTER and EEOD. The OYSTER technique is based on wavefront slope. The EEOD technique is based on a star image. The authors discuss the basic algorithms used and the experimental results obtained. (2 refs.)

111732 Use of the superheterodyne wavefront analyzer for ground-to-space power transfer. N.A.Massie (Western Res., San Diego, CA, USA).

Proc. SPIE Int. Soc. Opt. Eng. (USA), vol.351, p.132-40 (1983). [received: Sept. 1983] (SPIE Proceedings on Wavefront Sensing, San Diego, CA, USA, 24-25 Aug. 1982).

Transfer of optical power from ground-to-space at short wavelengths requires an adaptive wavefront corrector and a sensitive wavefront analyzer. In the several applications envisioned, coherent radiation from a laser beacon or retroreflector and ground based illuminator will be available for wavefront sensing. The superheterodyne wavefront analyzer can therefore be employed for performance approaching the quantum limit. The basics of the superheterodyne approach are discussed and its performance as a wavefront analyzer reviewed. (6 refs.)

111733 Point image focus sensing using an automated Foucault test. D.G.Kocher (Lincoln Lab., MIT, Lexington, MA, USA). *Proc. SPIE Int. Soc. Opt. Eng. (USA)*, vol.351, p.148-54 (1983). [received: Sept. 1983] (SPIE Proceedings on Wavefront Sensing, San Diego, CA, USA, 24-25 Aug. 1982).

An electromechanical focus sensing technique for isolated point or small spot images is described. The technique is a mechanisation of the Foucault knife-edge test, and it works with either laser or white light. The focus sensor provides an output voltage vs. focus discriminant which is linear in the vicinity of the best focus and monotonic over a wide range, making it suitable as a sensor for servo focus control applications. The focus sensor uses a chopping wheel at the optical focus and a field lens and bicell photodetector behind the focus. The relative phase of the zero-crossings of the AC-coupled bicell signals is detected electronically to obtain the voltage vs. focus discriminant. Two electronic detection algorithms are described and discriminants obtained with them in a typical implementation of the technique are presented. Also described are two techniques that have been used to compensate the detector signals for rapid fluctuations in the source intensity, if the fluctuations are rapid enough to interfere with the phase detection process. This focus sensing technique is sensitive primarily to focus, but some sensitivity to certain other wavefront aberrations also exists. These sensitivities have been computed for two particular cases, the resolved spot source (with a geometrical analysis) and the unresolved point source (with a diffraction analysis). These results are tabulated for the Zernike aberrations up to $m=n=8$. (3 refs.)

111734 Resonator technique for absolute reflection and transmission measurements. M.A.Bukhshtab. *J. Appl. Spectrosc. (USA)*, vol.37, no.5, p.1330-5 (Nov. 1982). Translation of: *Zh. Prikl. Spektrosk. (USSR)*, vol.37, no.5, p.852-9 (Nov. 1982). [received: Sept. 1983]

The author considers the possibility of making measurements of the absolute value of the specular reflection (transmission) coefficient close to 1.000 with an error better than 0.001-0.002 in the case of normal incidence of light at some given point of a sample under inspection. The main requirement to the new technique is that no standards should be needed so that a dependence upon the storage conditions of the standards and measurements of even greater accuracy cannot affect the results. (10 refs.)

SPIE Proceedings on Wavefront Sensing See Entry 111301

Minimum variance estimation of wavefront aberration See Entry 112946

Fiber optic scattering monitor for application on bulk biological tissue, paper, and plastic See Entry 113103

Near-field measurements in monomode fibres: determination of chromatic dispersion See Entry 113114

Hybrid processing for phase measurement in metrology and flow diagnostics See Entry 113522

An optical technique for measuring fiber orientation in short fiber composites See Entry 115504

07.60D Photometry and radiometry

(inc. colorimetry; see also 07.62 Detection of radiation)

111735 Evaluation and optimization by colorimetry of polarizers for liquid crystal display. R.Mizoguchi, K.Kobayashi (Sanritsu Electric Co. Ltd., Tokyo, Japan), T.Shimomura, S.Kobayashi.

Disp. Technol. & Appl. (GB), vol.4, no.4, p.201-6 (Oct. 1983). Describes the development of useful polarizers for LCD application, their optimization and evaluation based on colorimetry. Figures of merit are suggested for the characterization of LCDs and polarizers using this technique. More than 50 polarizers were used in the experiment, which also evaluated their use for both twisted nematic black-and-white LCDs and guest-host colour LCDs. Their optical properties and the associated display legibility were shown to be best expressed colorimetrically. (18 refs.)

111736 Conditions under which Schrodinger object colors are optimal. G.West (Ziegler-Instruments GmbH, Monchengladbach, Germany), M.H.Brill.

J. Opt. Soc. Am. (USA), vol.73, no.9, p.1223-5 (Sept. 1983). Schrodinger colors are optimal if and only if the spectrum locus in a chromaticity diagram in convex and well ordered in wavelength. The human spectrum locus has this property, but the bee spectrum locus does not. A general algorithm is described for generating the optimal colors for any tristimulus space. (8 refs.)

111737 Statistical analysis of measurement results obtained by pulse laser electron photometry methods. B.P.Klim, R.F.Fedorov.

Otbor & Peredacha Inf. (USSR), no.67, p.20-2 (1983). In Russian. Investigates the statistical properties of a pulse of light, containing measured information after conversion into electrical signals by a photomultiplier. Analytical expressions are derived for the mathematical expectation of the number of the electrons in the output pulse of the photomultiplier, and for the relative statistical error. The accuracy of a numerical estimation of the mathematical expectation of the photons in the light pulse is dependent on results of measurements of the number of the electron in the output pulse. (4 refs.) Z.F.V.

Self-study manual on optical radiation measurements: Part I -Concepts, chapter 10. Introduction to coherence in radiometry See Entry 111382

Silicon photodiode device with 100% external quantum efficiency See Entry 111766

Estimate of the parameters of photomultipliers operating in the photon-counting regime See Entry 111767

Excitation pulse-shape mimic technique for improving picosecond-laser-excited time-correlated single-photon counting deconvolutions See Entry 111771

Detonic research infrared radiometer with nanosecond response See Entry 111772

Spectroscopy by photothermal radiometry See Entry 111774

Measurement Assurance Program transmittance standards for spectrophotometric linearity testing: preparation and calibration See Entry 111781

Drying of porous granular materials See Entry 115507

Improved atmospheric path-length correction by a dual-frequency microwave radiometer See Entry 116264

07.60F Polarimetry and ellipsometry

111738 Polarimetric strain gauges using high birefringence fibre. M.P.Varnham, A.J.Barlow, D.N.Payne, K.Okamoto (Dept. of Electronics, Univ. of Southampton, Southampton, England).

Electron. Lett. (GB), vol.19, no.17, p.699-700 (18 Aug. 1983). When a highly-birefringent fibre is stretched, the birefringence changes. The phenomenon is shown to result from a difference in Poisson's ratio of the two glasses from which the fibre is constructed. Experimental verification is given and a simple polarimetric strain gauge made from bow-tie fibre is demonstrated. (9 refs.)

111739 Spectroscopic ellipsometry. M.-H.Debroux, P.Ged, A.Vareille (CNET, Issy-les-Moulineaux, France).

Echo Rech. (France), no.113, p.61-8 (1983). In French. In silicon microelectronics, the characterization of thin film materials and their interfaces requires analysis tools featuring a depth resolution of about 50 Å. Spectroscopic ellipsometry techniques respond to certain demands such as this, with the added advantage of being non-destructive. Following a brief description of the formalities and tools used in the handling of a polarized light ray, several examples of analysis are given: silicon surface states, oxide thin film, Si-SiO₂ interfaces, implanted silicon. (no refs.)

111740 Recording linear dichroism spectra with the Spectropol-1 spectropolarimeter. A.S.Prishchepov (Phys. Inst., Acad. of Sci., Minsk, Belorussian SSR).

Instrum. & Exp. Tech. (USA), vol.25, no.6, pt.2, p.1464-6 (Nov.-Dec. 1982). Translation of: *Prib. & Tekh. Eksp. (USSR)*, vol.25, no.6, p.134-6 (Nov.-Dec. 1982).

A method is proposed for measuring the linear dichroism of a weakly anisotropic liquid for a solid polymer using the Spectropol 1 spectropolarimeter provided that the linear birefringence is zero or small. Examples are given of measurements on linear-dichroism spectra for solutions of an aggregated pigment partially ordered by the Earth's gravitational field and also for polymer matrices activated by a dye, where the accuracy is 6×10^{-3} optical-density units. (2 refs.)

111741 A simple optical electron polarimeter. T.J.Gay (J.W. Gibbs Lab., Yale Univ., New Haven, CT, USA).

J. Phys. B (GB), vol.16, no.18, p.L553-6 (28 Sept. 1983). It is pointed out that heavy atoms (i.e. those which have spectroscopically resolvable fine structure) are not required for optical measurements of electron polarisation. A polarimeter which uses helium gas instead of heavy-metal vapour is proposed, and several experimental details are discussed. (15 refs.)

111742 Linear and circular polarisation modulation for measuring complex magneto-optical rotation. I. Principles and performance. J.Metzdorf (Inst. für Halbleiterphys. und Optik und Hochmagnetfeldanlage, Tech. Univ. Braunschweig, Braunschweig, Germany).

Optik (Germany), vol.65, no.2, p.103-13 (1983). In German. A dual-purpose polarization modulation method for the measurement of both magneto-optical rotation and ellipticity without a change of the calibration factor is described and discussed. As a polarization modulator a vibrating halfshade polarizer has been developed which allows continuous recording of both the complementary spectra. (32 refs.)

Determination of the film thickness in localized epitaxial structures See Entry 111642

Ellipsometric evaluation of various pretreatments on zircaloy-2 See Entry 115422

High precision spectropolarimetry of stars and planets. I. The ROE spectropolarimeter See Entry 116484

07.60H Refractometry and reflectometry

111743 A new type of receiver for optical time-domain reflectometry. P.Bassi, M.Zoboli (Dipartimento di Elettronica Informatica e Sistemistica, Univ. di Bologna, Bologna, Italy), A.Ragni, C.G.Someda.

Alta Freq. (Italy), vol.52, no.3, p.200-2 (May-June 1983). (4th Italian National Meeting on Applied Electromagnetics, Florence, Italy, 4-6 Oct. 1982).

A new receiver has been envisaged, designed and tested for OTDR. Its key feature is the use of an integrate-and-dump front-end section. The resulting equivalent noise bandwidth is such that a p-i-n photodiode can be conveniently used as a photodetector. The resulting instrument is simple, potentially inexpensive and rugged; therefore it looks attractive for applications in the field. Experimental results of laboratory tests are reported. (4 refs.)

111744 Quantitative shadow method for measuring a one-dimensional refractive index distribution. R.W.Lewis (Phys. Dept., GM Res. Labs., Warren, MI, USA).

Proc. SPIE Int. Soc. Opt. Eng. (USA), vol.351, p.155-63 (1983). [received: Sept. 1983] (SPIE Proceedings on Wavefront Sensing, San Diego, CA, USA, 24-25 Aug. 1982).

A quantitative shadow method was developed and tested by measuring the one-dimensional refractive index distribution of a polished slab of gradient index glass. Tests made on the known glass sample showed that a one-dimensional index distribution can be measured by shadowgraphy to better than one percent accuracy. The method uses simple optics and can easily be automated to perform rapid measurements. Extension of the shadow method to more general distributions requires making many traverses of the refractive index distribution with a narrow sheet of light. (13 refs.)

111745 The resolving power of a reflectometer with compensation of background reflections. V.V.Moiseyev, V.T.Potapov, V.A.Sviridov, A.A.Sokolovskiy.

Telecommun. & Radio Eng. Part 2 (USA), vol.37, no.10, p.68-9 (Oct. 1982). Translation of: *Radiotekhnika, Moskva (USSR)*, vol.37, no.10, p.29-30 (Oct. 1982). [received: Sept. 1983]

Discusses some characteristics of the design of fiber-optic sensors which operate on the 'reflection' principle. The variation of the optical characteristics of the medium which surrounds the end of a fiber changes the signal reflected from the fiber end. The values of this signal depends on the external perturbation and is registered by a measuring photoreceiver (PR). The extraction of the useful signal in such a sensor is usually a problem if no special measures are taken for the optical compensation of the signal caused by Fresnel reflection from the fiber end because the useful signal level is normally much lower than the background level, caused by the initial Fresnel reflection. (1 ref.)

111746 Refractive index measurement using an optical fiber. I.Sankawa, N.Kashima, T.Satake, S.Sumida (Ibaraki Electrical Communication Lab., NTT, Ibaraki, Japan). *Trans. Inst. Electron. & Commun. Eng. Jpn. Part C (Japan)*, vol. J66C, no. 7, p.535-6 (July 1983). In Japanese.
Refractive index measurement using step-index optical fiber as a sensor is investigated. A flat fiber end-face is found to be needed for small measurement errors. Refractive index in the high temperature region and its distribution can be easily measured by this method. (4 refs.)

Measurement of the core diameter of multimode graded-index fibers: a comparison of transmitted near-field and index profiling techniques
See Entry 113117

07.60L Interferometry

111747 Fringe pattern recognition and interpolation using nonlinear regression analysis. J.B.Schemm, C.M.Vest (Dept. of Mech. Engng. & Appl. Mech., Univ. of Michigan, Ann Arbor, MI, USA). *Appl. Opt. (USA)*, vol.22, no.18, p.2850-3 (15 Sept. 1983).
Least-square error criteria are used to fit 1-D interference fringe pattern irradiance data to a physically meaningful function of the form $I(x) = B(x) + E(x) \cos[P(x)]$, where $B(x)$, $E(x)$, and $P(x)$ are low-order polynomials. This procedure is intended to complement digital fringe recognition by providing a method for smoothing and interpolating among fringe position data when the number of fringes is small, there are more than ten irradiance measurements per fringe, and accurate phase values are needed at arbitrary locations in the field. (8 refs.)

111748 Analysis of two-beam interferometry for bulk wave measurements. H.M.South, C.H.Palmer (Appl. Phys. Lab., Johns Hopkins Univ., Laurel, MD, USA). *Appl. Opt. (USA)*, vol.22, no.18, p.2854-9 (15 Sept. 1983).

The application of differential interferometry to bulk wave measurements can be analyzed using the kinematic formulation of the photoelastic effect. For isotropic linearly elastic materials a standing longitudinal wave changes the indicatrix from a sphere to an ellipsoid revolution with axes parallel and perpendicular to the direction of propagation of the acoustic wave. If the probing light is linearly polarized, differential interferometry produces a maximum signal when the polarization of the light is perpendicular to the direction of propagation. This prediction is confirmed by experiment. The case of standing transverse waves can be analyzed in a similar manner. (17 refs.)

111749 Polynomial fit of subaperture interferograms. C.J.Kim (Optical Sci. Center, Univ. of Arizona, Tucson, AZ, USA). *Proc. SPIE Int. Soc. Opt. Eng. (USA)*, vol.351, p.28-33 (1983). [received: Sept. 1983] (SPIE Proceedings on Wavefront Sensing, San Diego, CA, USA, 24-25 Aug. 1982).

A method of obtaining surface figure error information from several subaperture interferograms is analyzed, and the effects of roundoff error, digitization error and fit error are presented. A computer simulation for testing a large flat is shown. This method is applied to average several undersampled interferograms and to analyze lateral shearing interferograms. (4 refs.)

111750 Self-referencing wavefront sensor. K.Underwood, J.C.Wyant, C.I.Koliopoulos (Optical Sci. Center, Univ. of Arizona, Tucson, AZ, USA). *Proc. SPIE Int. Soc. Opt. Eng. (USA)*, vol.351, p.108-14 (1983). [received: Sept. 1983] (SPIE Proceedings on Wavefront Sensing, San Diego, CA, USA, 24-25 Aug. 1982).

A modified Smartt point-diffraction interferometer employing phase-shifting electronic phase measurement techniques is described. Special techniques making it possible for the interferometer to give good visibility interference fringes for a large range of input wavefront tilts are discussed. A trade-off between acceptable values of wavefront tilt and light efficiency is presented. (5 refs.)

111751 Flow field testing with a 64 parallel channel heterodyne interferometer. N.A.Massie (Western Res., San Diego, CA, USA), D.M.Swain, M.R.Dunn, S.E.Muenter. *Proc. SPIE Int. Soc. Opt. Eng. (USA)*, vol.351, p.141-7 (1983). [received: Sept. 1983] (SPIE Proceedings on Wavefront Sensing, San Diego, CA, USA, 24-25 Aug. 1982).

A sensor system capable of simultaneously measuring phase at 64 discrete points has been developed for use with the digital heterodyne interferometer. With this, two dimensional optical path difference maps of high speed phenomena can be obtained. Featured in this system are 64 channels of phase detection with each channel being provided with a dedicated memory 16 bits wide and 4096 words deep. The system operates at a 100 kHz sample rate and has a sensitivity of 1/300 of a wave RMS. A novel method of post priori removal of the corrupting motions of the interferometer optics was demonstrated, allowing high fidelity measurements to be obtained in an unstabilized environment. (6 refs.)

111752 TV based system for interferogram analysis. K.G.Birch, K.Jackson, D.J.Pugh, P.D.West (NPL, Teddington, England). *Proc. SPIE Int. Soc. Opt. Eng. (USA)*, vol.369, p.186-93 (1983). (SPIE Proceedings of the Max Born Centenary Conference OPTICS 82, ECOSA 82, Edinburgh, Scotland, 7-10 Sept. 1982).

Describes the use of a TV based system to measure the position of fringes in the interferograms of OTF standard lenses, as formed in a Twyman-Green interferometer. The core of the system is the transfer, under computer control, of sampled image signals from the TV to the buffer store of a desk-top computer. Data recovered from this memory is then analysed to determine the exact position of fringes within the interferogram pupil. Details of the computer subroutines used to evaluate fringe positions and to automatically renumber the fringes are followed by a brief description of data fitting routines used to derive aberration polynomials and thence the lens Optical Transfer Function. (5 refs.)

111753 Interferometer detection system for optical testing. D.S.Brown (NEI Grubb Parsons, Newcastle upon Tyne, England), M.J.Smyth. *Proc. SPIE Int. Soc. Opt. Eng. (USA)*, vol.369, p.194-8 (1983). (SPIE Proceedings of the Max Born Centenary Conference OPTICS 82, ECOSA 82, Edinburgh, Scotland, 7-10 Sept. 1982).

The production of large precise optical components is usually a cyclical process of measurement and optical working which is repeated many times before the desired accuracy is achieved. The precision of testing limits the accuracy attainable in manufacture and reduces the efficiency of production cycles if the residual errors are comparable in size with the error of testing. To minimise cost it is important that the test equipment should be able to provide an adequate description of the errors in the system under test in a fairly small fraction of the total cycle time. Wavefront shearing interferometry is one of the test methods that has been effective in the past, but its efficiency has been limited by the data recording methods employed. Desirable improvements are: firstly, the ability to handle a larger volume of data,

secondly, reduction in testing time and finally, improved precision of phase measurement. The substitution of a detector which can be interfaced directly with a computer and the adoption of a scanning mode of operation should allow all three of these objectives to be achieved. (2 refs.)

111754 Advances in optical metrology of complex objects. C.Wykes (Dept. of Mech. Engng., Loughborough Univ. of Technol., Loughborough, England), R.Jones. *Proc. SPIE Int. Soc. Opt. Eng. (USA)*, vol.369, p.200-5 (1983). (SPIE Proceedings of the Max Born Centenary Conference OPTICS 82, ECOSA 82, Edinburgh, Scotland, 7-10 Sept. 1982).

It has been shown previously that Electronic Speckle Pattern Interferometry can be used to compare the shape of nominally identical components. The authors for calibrating the measurements and for converting the fringe data to surface shape information are discussed here and the accuracy of the measurements has been established. (5 refs.)

111755 Twyman Green interferometer with curved mirrors. M.V.R.K.Murty, R.P.Shukla (Spectroscopy Div., Bhabha Atomic Res. Centre, Bombay, India). *Indian J. Pure & Appl. Phys.*, vol.21, no.7, p.432-3 (July 1983).

Twyman Green interferometer with curved mirrors is described. It is found that the end mirrors in the Twyman Green interferometer need not be necessarily plane but must be identical in figure. (1 ref.)

111756 A real-time active vibration controller [for Michelson interferometry]. M.R.Serbyn, W.B.Penzes (Center for Mfg. Engng., NBS, Boulder, CO, USA). *ISA Trans. (USA)*, vol.21, no.3, p.55-9 (1982).

The Michelson interferometer is viewed as a noisy system whose noise input results from unwanted changes in the optical path lengths of its beams, and whose desired output is a constant optical path-length difference. A technique for maintaining this quality at a value equal to a multiple of a quarter wavelength of the light is described. (5 refs.)

111757 Contribution to the automatic fringe analysis using Zernike polynomials. F.M.Kuchel, T.Schneider, H.J.Tiziani (Inst. fur Tech. Optik, Univ. Stuttgart, Stuttgart, Germany).

Optik (Germany), vol.65, no.2, p.123-42 (1983). In German.
When measuring wavefront differences in two-beam interferometers the distribution problem of the sampling points arises. The mean square of the coefficients of a Zernike polynomial fit is strongly influenced by the number and location of sampling points. Wavefronts with big gradients demand high density of sampling point distribution. A combination of local and global interpolation is proposed, where the coefficients are determined with high precision and short computing time. (17 refs.)

111758 Theory of Fabry-Perot interferometer with statistically rough mirrors. I.V.Bogatyreva, V.P.Danil'chenko, L.A.Pospelov ('Metrologiya' Sci.-Industrial Assoc., USSR).

Radiophys. & Quantum Electron. (USA), vol.26, no.1, p.49-54 (Jan. 1983). Translation of: *Izv. VUZ Radiofiz. (USSR)*, vol.26, no.1, p.58-63 (Jan. 1983). [received: Sept. 1983]

Results of a theoretical study are presented pertaining to the effect of statistical roughness of mirror surfaces in a Fabry-Perot interferometer on the amplitude-frequency characteristics of H-polarized electromagnetic fields excited in it. (4 refs.)

111759 Optical amplitude and polarization multistability in a nonlinear interferometer. I.P.Areshnev, V.K.Subashiev (A.F. Ioffe Physicotech. Inst., Acad. of Sci., Leningrad, USSR). *Sov. Tech. Phys. Lett. (USA)*, vol.8, no.11, p.588-9 (Nov. 1982). Translation of: *Pis'ma v Zh. Tekh. Fiz. (USSR)*, vol.8, no.21-22, p.1368-72 (Nov. 1982). [received: Sept. 1983]

Discusses a polarizational optical bistability in a nonlinear medium for the case in which the nonlinear increment in the electrical induction is comparable to the linear component. The authors examine the steady-state transmission of arbitrarily polarized monochromatic light by a nonlinear ring interferometer filled with an isotropic medium exhibiting a cubic nonlinearity. They take into account the change in the nature of the polarization of the light as it passes through the interferometer. They discuss in detail the case of linearly polarized incident light. They show that there is a pronounced polarizational multistability here, while the amplitude bistability acquires some completely new features. The hysteresis loop turns out to be complex. (7 refs.)

Measurements on the He-Ne laser lines near 633 nm See Entry 111354

Interferometric determination of slow movements See Entry 111634

Enhanced-displacement measurement using a generalized formulation for double-aperture specklegrams See Entry 111636

Uncertainty of measurements made by laser interferometer See Entry 111647

Rotational Raman interferometric measurement of flame temperatures See Entry 111687

Interferometrical processing of electron microscopic holograms. III. Investigation of special features of the differential interferometry including noise problems See Entry 112918

Self-imaging through a Fabry-Perot interferometer See Entry 112954

Low-noise multicolor archival storage with broad source interferometric imaging See Entry 112955

Direct observation of visibility curve of semiconductor lasers See Entry 113030

Vernier fringe-counting device for laser wavelength measurements See Entry 113032

Optical extinction theorem in the nonlinear theory of optical multistability See Entry 113048

Self-pulsing and transients of a Fabry-Perot interferometer with quadratic nonlinear medium See Entry 113049

Review of fiber optic gyroscopes See Entry 113101

Feasibility of fiber optical hydrophone See Entry 113102

Application of fiber optics to speckle metrology - a feasibility study See Entry 113115

Measurement of the core diameter of multimode graded-index fibers: a comparison of transmitted near-field and index profiling techniques See Entry 113117

Broad-band ultrasonic sensor based on induced optical phase shifts in single-mode fibers See Entry 113125

Design of an experiment to determine deformations using holographic interferometry See Entry 113390

A far-infrared interferometer for the measurement of electron concentration in flames and plasmas with high spatial resolution See Entry 113562

Holographic plasma interferometry in the infrared spectrum. II. Using non-linear effects to increase the sensitivity See Entry 113667

Optical investigation of critical behaviour in simple fluids at reduced gravity See Entry 114131

07.60P Optical microscopy

111760 Applications of scanning optical microscopy. C.J.R.Sheppard (Dept. of Engng. Sci., Univ. of Oxford, Oxford, England). *Proc. SPIE Int. Soc. Opt. Eng. (USA)*, vol.368, p.88-95 (1983). [received: Sept. 1983] (SPIE Proceedings on Microscopy Techniques and Capabilities, London, England, 21-22 Sept. 1982). The scanning optical microscope (SOM) provides new information concerning a wide range of specimens. It is particularly advantageous for study of materials and devices, including semiconductors. The image is built up on a TV-type display by mechanically scanning the object across a focused laser spot. (21 refs.)

111761 Advances in the infrared microscopy of electronic materials. C.R.Elliott, J.C.Regnauld (British Telecom Res. Labs., Martlesham Heath, Ipswich, England), B.T.Meggitt. *Proc. SPIE Int. Soc. Opt. Eng. (USA)*, vol.368, p.96-103 (1983). [received: Sept. 1983] (SPIE Proceedings on Microscopy Techniques and Capabilities, London, England, 21-22 Sept. 1982). Crystalline semiconductor materials often contain structural defects which can influence adversely both the behaviour during processing and the ultimate performance of devices fabricated from them. Traditionally structural perfection has been assessed by the optical microscopy of chemically etched surfaces and augmented by X-ray and electron microscopic techniques when detailed analyses are required. Polarised infrared microscopy (PIM) is emerging as a non-destructive technique for the real time imaging of defects ranging in size from locally strained regions several millimetres across, down to single dislocations. The authors discuss the present state of PIM development, with examples taken principally from the field of opto-electronic materials. The performance of a polarizing microscope operating at near-infrared wavelengths is described for three distinctive imaging modes. In these modes, defects which absorb the illumination or cause stress birefringence or non-radiative carrier recombination in photoluminescent materials respectively are revealed with an optimum resolution of about 1 μm . (20 refs.)

111762 Holography applied to stereomicroscopy. R.W.Smith, T.R.Empson (Blackett Lab., Imperial Coll. London, London, England). *Proc. SPIE Int. Soc. Opt. Eng. (USA)*, vol.368, p.104-9 (1983). [received: Sept. 1983] (SPIE Proceedings on Microscopy Techniques and Capabilities, London, England, 21-22 Sept. 1982). The application of holography to microscopy is outlined with special reference to the identification of fossil ostracods using a stereomicroscope. The effect of laser speckle on the image quality is demonstrated and a speckle reduction technique based on the incoherent superposition of many differently-speckled reconstructions of the same object is discussed. A holographic attachment for a standard stereomicroscope is described in which this speckle reduction technique is implemented by means of a holographic lens array, and results are shown. (7 refs.)

111763 Interference film microscopy for metal phase identification. K.W.Raine, P.N.Quested (NPL, Teddington, England). *Proc. SPIE Int. Soc. Opt. Eng. (USA)*, vol.368, p.110-18 (1983). [received: Sept. 1983] (SPIE Proceedings on Microscopy Techniques and Capabilities, London, England, 21-22 Sept. 1982). Constituents in metal alloys and rocks may be seen as different colours using interference film microscopy. The thin films which produce the interference colours may be deposited either by vacuum evaporation or reactive sputtering. The technique is used in a wide range of investigations which require identification of phases quickly and easily, e.g. in nickel-base superalloys and hard metals. The theory, techniques for optimising the performance and a method of quantifying the results by microspectrophotometry discussed and a case study presented. (10 refs.)

111764 Particle size analysis by automated optical microscopy. L.C.Kenny, A.P.Rood (Health & Safety Executive, London, England). *Proc. SPIE Int. Soc. Opt. Eng. (USA)*, vol.368, p.119-23 (1983). [received: Sept. 1983] (SPIE Proceedings on Microscopy Techniques and Capabilities, London, England, 21-22 Sept. 1982). Recent developments in technology have led to the wide availability of image analysis systems suitable for particle size analysis, and one such system is described. Image analysis offers a significant advantage over manual microscopy as it allows large numbers of particles to be measured consistently and accurately. The image presented to the image analyser must be carefully prepared in order to reduce measurement errors to a minimum. Good sample preparation techniques are much more important here than for manual microscopy, and the greatest care must be taken when setting up the microscope/TV camera imaging system. Many more measurements can be made on each particle than would be possible manually, and several methods of calculating the particle size are described. The use of automated focus, slide transport and slide changing mechanisms under the control of the image analyser can eliminate the need for manual intervention in the system, allowing it to be run overnight. (no refs.)

111765 Reflex microscope: measurement in three dimensions. P.J.Scott (Dept. of Photogrammetry & Surveying, Univ. Coll. London, London, England). *Proc. SPIE Int. Soc. Opt. Eng. (USA)*, vol.368, p.124-8 (1983). [received: Sept. 1983] (SPIE Proceedings on Microscopy Techniques and Capabilities, London, England, 21-22 Sept. 1982). A new three dimensional measuring instrument is described which uses a stereoscopic microscope. Objects of up to 100 \times 100 \times 60 mm can be measured without physical contact, with repeatability spreads of 20 μm . Proposed improvements are described which could reduce the spreads to 10 μm . (1 ref.)

SPIE Proceedings on Microscopy Techniques and Capabilities See Entry 111302

Comparison of optical depth-measurement methods on real metal surfaces with sine-phase-gratings See Entry 111638

X-ray microscopy: recent developments and practical applications See Entry 111848

Methods for the investigation of laser mirrors for laser gyros See Entry 113075

07.62 DETECTION OF RADIATION (BOLOMETERS, PHOTOELECTRIC CELLS, I.R. AND SUBMILLIMETRE WAVES DETECTION)

111766 Silicon photodiode device with 100% external quantum efficiency. E.F.Zalewski (US NBS, Washington, DC, USA), C.R.Duda. *Appl. Opt. (USA)*, vol.22, no.18, p.2867-73 (15 Sept. 1983). A device utilizing four inversion layer photodiodes in a light-trapping arrangement was constructed and tested. The device was found to have a photon-to-electron conversion efficiency of 0.999 for short wavelength and low power visible radiation. It was found that applying a reverse bias voltage extended the high quantum efficiency response over the entire visible spectrum and up to the highest radiant power level studied (several milliwatts). Several radiometrically important characteristics were studied and the results presented: spectral reflectance; polarization sensitivity; quantum efficiency vs. wavelength, photon flux density, and reverse bias voltage; and dark current vs. reverse bias. (19 refs.)

111767 Estimate of the parameters of photomultipliers operating in the photon-counting regime. L.V.Granitskii, N.I.Bukach, L.I.Andreeva, Z.M.Semichastnova, B.M.Stepanov (All-Union Res. Inst. for Optical-Phys. Measurements, Moscow, USSR). *Instrum. & Exp. Tech. (USA)*, vol.25, no.6, pt.2, p.1456-8 (Nov.-Dec. 1982). Translation of: *Prib. & Tekh. Eksp. (USSR)*, vol.25, no.6, p.127-9 (Nov.-Dec. 1982).

The time required to register a given flux at a stipulated accuracy is used as a criterion for estimating the efficiency of photomultipliers operating in the photon-counting regime and recording superweak and weak fluxes. By way of example, the proposed method is used to compare two experimental models of 28ELU-F15 photomultiplier with the EM1-6256B photomultiplier. (4 refs.)

111768 Apparatus for measurement of amplitude-frequency and phase-frequency characteristics of infrared phototransducers in the 1 MHz to 1 GHz frequency range. P.V.Biryulin, M.I.Volubuev. *Instrum. & Exp. Tech. (USA)*, vol.25, no.6, pt.2, p.1468-70 (Nov.-Dec. 1982). Translation of: *Prib. & Tekh. Eksp. (USSR)*, vol.25, no.6, p.138-9 (Nov.-Dec. 1982).

An apparatus is described for measurement of amplitude-frequency and phase-frequency characteristics of infrared phototransducers at a wavelength of 10.6 μm in the 1 MHz to 1 GHz frequency range with electrooptical modulation of CO₂ laser emission and recording of the signal by means of a combined FK2-12 phase-difference meter. (4 refs.)

111769 Advantages of obliquely cut pyroelectric crystals for infrared detectors. A.Shaulov (Philips Labs., Briarcliff Manor, NY, USA). *Laser Focus (USA)*, vol.19, no.9, p.216-18 (Sept. 1983).

The author's previous work has shown that in pyroelectric crystals with strong dielectric anisotropy, a significantly higher figure of merit can be obtained by using cuts at oblique angles to the pyroelectric axis. The oblique cut can be optimized to provide the maximum figure of merit attainable for the particular material used in the chosen temperature of operation. Some basic quantitative results of this effect are reviewed and their importance for IR detector and device improvements discussed. (5 refs.)

111770 Digital radiation temperature sensor using surface acoustic waves. Y.Kasahara, R.Inaba (Central Res. Lab., Matsushita Electrical Industrial Co. Ltd., Osaka, Japan).

Natl. Tech. Rep. (Japan), vol.29, no.3, p.377-86 (June 1983). In Japanese. A study of infrared detectors using the interaction of a surface acoustic wave with a surface region heated by radiation is presented. A phase change of the surface wave is induced by the thermal effect of absorption of infrared radiation from an object. An analysis regarding the sensitivity of the frequency change and time response of the detector is described. An experiment was carried out on the Y cut Z propagation of lithium niobate. The sensitivity of the detector with a frequency change at 170 MHz was found experimentally to be approximately 3.3-8.4 Hz per degree temperature change of the object. (13 refs.)

111771 Excitation pulse-shape mimic technique for improving picosecond-laser-excited time-correlated single-photon counting deconvolutions. D.R.James, D.R.M.Demmer, R.E.Verrall, R.P.Steer (Dept. of Chem., Univ. of Saskatchewan, Saskatoon, Saskatchewan, Canada). *Rev. Sci. Instrum. (USA)*, vol.54, no.9, p.1121-30 (Sept. 1983).

The determination of accurate subnanosecond fluorescence lifetimes by the time-correlated single-photon counting technique is often limited by difficulties in obtaining the correct instrumental response function $f(\lambda, t)$ to the excitation pulse. These difficulties are increased when a grating monochromator is used to disperse the emission due to the introduction of an additional temporal broadening of $f(\lambda, t)$. A technique for determining the correct $f(\lambda, t)$ at the wavelength of sample emission, λ_{em} , is described. The technique consists of using a very short-lived fluorophore to 'mimic' the excitation pulse shape at λ_{em} , yielding the convoluted mimic decay function $C_m(\lambda_{em}, t)$, and then to computationally extract $f(\lambda_{em}, t)$ from $C_m(\lambda_{em}, t)$. The technique is experimentally and computationally simple and yields the desired instrumental response function at λ_{em} which eliminates problems due to the sensitivity of $f(\lambda, t)$ to λ (color shift artifact). The photomultiplier tube receives spatially equal illumination when both the sample decay and $C_m(\lambda_{em}, t)$ are determined because both the mimic and sample emission are spectrally broad, eliminating the problem of the variation of $f(\lambda, t)$ with position of incident light on the photomultiplier tube photocathode (targeting artifact). Artifacts due to monochromator temporal broadening are eliminated since both the mimic and sample emission are monitored at constant wavelength. (34 refs.)

111772 Detonic research infrared radiometer with nanosecond response. W.G.Von Holle, R.A.McWilliams (Lawrence Livermore Nat. Lab., Univ. of California, Livermore, CA, USA). *Rev. Sci. Instrum. (USA)*, vol.54, no.9, p.1218-21 (Sept. 1983).

Two infrared radiometers were constructed for use in shock wave and detonation research. Fast detectors were combined with wide-band amplifiers to achieve an overall response of about 5 ns, which was confirmed by experiments on planar shocked copper plates. Detonation experiments show the merits of a new optical technique for probing detonation wave structure and for reactive and nonreactive shock wave research. (11 refs.)

Self-study manual on optical radiation measurements: Part I -Concepts, chapter 10. Introduction to coherence in radiometry See Entry 111382

Principles of successful use of contactless thermometers See Entry 111679

Performance characteristics of a small side-window photomultiplier in laser single-photon fluorescence decay measurements See Entry 111783

AGA infrared techniques See Entry 113141

Radiative lifetime in semiconductors for infrared detection See Entry 114899

07.65 OPTICAL SPECTROSCOPY AND SPECTROMETERS

(inc. photoacoustic spectroscopy)

111773 Photodisplacement spectroscopy of solids: theory. L.C.M.Miranda (Centro Tecnico Aeroespacial, Inst. de Estudos Avancados, Sao Paulo, Brazil).

Appl. Opt. (USA), vol.22, no.18, p.2882-6 (15 Sept. 1983).

A quantitative derivation is presented for the production of the photodisplacement signal of a sample that is periodically heated by the absorption of modulated light. Numerical estimates are presented for the surface displacement of typical solids; they show that one may get signals well above the thermal noise. (17 refs.)

111774 Spectroscopy by photothermal radiometry. S.O.Kanstad, P.E.Nordal (Laser & Appl. Optics Lab., Oslo, Norway).

Proc. SPIE Int. Soc. Opt. Eng. (USA), vol.369, p.357-60 (1983). (SPIE Proceedings of the Max Born Centenary Conference OPTICS 82, ECOSA 82, Edinburgh, Scotland, 7-10 Sept. 1982).

When a sample is illuminated by pulsed radiation, the concurrent heating at the surface gives rise to a pulsating component in the specimen's thermal infrared radiation. It appears possible to observe surface temperature oscillations as small as 10^{-4} - 10^{-6} K, using current technology in infrared detection; this corresponds to the absorption in less than a monolayer. With monochromatic irradiation, absorption spectra of opaque objects can be obtained; it also becomes possible to examine subsurface structures. The authors review briefly the background of photothermal radiometry, and present some experimental results to demonstrate the technique's versatility, including some new results from studies of photosynthesis in live plants. (9 refs.)

111775 High resolution spectroscopy using picosecond pulse trains. A.I.Ferguson, R.A.Taylor (Clarendon Lab., Univ. of Oxford, Oxford, England).

Proc. SPIE Int. Soc. Opt. Eng. (USA), vol.369, p.366-73 (1983). (SPIE Proceedings of the Max Born Centenary Conference OPTICS 82, ECOSA 82, Edinburgh, Scotland, 7-10 Sept. 1982).

The use of picosecond pulse trains in performing high resolution atomic spectroscopy is described. Methods which rely on producing Hertzian coherence and optical coherence in atoms are compared and contrasted. (23 refs.)

111776 Picosecond photoinduced dichroism detected by photothermal deflection. A.I.Ferguson, C.N.Ironside (Clarendon Lab., Univ. of Oxford, Oxford, England).

Proc. SPIE Int. Soc. Opt. Eng. (USA), vol.369, p.374-8 (1983). (SPIE Proceedings of the Max Born Centenary Conference OPTICS 82, ECOSA 82, Edinburgh, Scotland, 7-10 Sept. 1982).

A technique which uses photothermal deflection spectroscopy to detect photoinduced dichroism is described. Some preliminary results are presented and discussed. The major advantages of the technique are the absence of a coherence spike and that there appear to be no spurious effects due to birefringence of the optical components. (7 refs.)

111777 Anomalous enhancement of photoacoustic signal in metal-film/metal-foil system. K.Azuma, H.Miyamoto, H.Inoue, T.Yamada (Dept. of Precision Engng., Osaka Univ., Osaka, Japan).

Jpn. J. Appl. Phys. Part 1 (Japan), vol.22, no.6, p.1067 (June 1983).

Photoacoustic spectroscopy (PAS) is a new technique for studying solid surfaces having various 'imperfections' that is both sensitive and useful. It enables one to measure the nonradiative absorption even in samples with irregular or granular surfaces. In this experiment, the authors constructed an apparatus to make in situ measurement possible in a vacuum evaporator and observed anomalous enhancement of the photoacoustic effect in the surface layer of metal foils on which an ultra-thin film of the same metal was evaporated. (5 refs.)

111778 Frequency modulation coherent anti-Stokes Raman spectroscopy (FM-CARS): a novel sensitive nonlinear optical method. H.Lotem (Nuclear Res. Center-Negev, Beer Sheva, Israel).

J. Chem. Phys. (USA), vol.79, no.5, p.2177-80 (1 Sept. 1983).

A frequency modulation coherent anti-Stokes spectroscopy (FM-CARS) is proposed. Using phase-modulated Stokes input field, a frequency modulated CARS output is generated. Raman resonances are detected by a CARS heterodyne signal generated in a square-law photodetector. Theoretical estimations show that a high signal-to-noise ratio which is shot-noise limited and effective background suppression are expected with the proposed method independent of the lasers polarization. In typical solvents the sensitivity estimated is $\chi_R^{(3)} = 4.8 \times 10^{-18}$ esu, which corresponds to the detection of 1.2×10^{-4} M benzene in cyclohexane. (13 refs.)

111779 Phase-polarization laser spectroscopy. V.P.Voitovich.

J. Appl. Spectrosc. (USA), vol.37, no.6, p.1427-40 (Dec. 1982). Translation of: *Zh. Prikl. Spektrosk. (USSR)*, vol.37, no.6, p.996-1010 (Dec. 1982). [received: Sept. 1983]

The index of refraction of the medium affects the phase of the wave passing through the medium. The change in phase of the wave in the optical region of the spectrum can be measured by interference methods. Other methods for measuring the phase seemed difficult to realize. This held up the development of appropriate spectroscopic methods. Searches for methods of increasing the sensitivity of high resolution nonlinear spectroscopy led to the development of phase polarization (PP) methods. Such methods of high-resolution LS were first analyzed using methods based on measurements of the change in the polarization characteristics of a wave passing through a medium having an anisotropy induced by an external field or intrinsic anisotropy were classified with it. At the early stage of development of these methods, the phase anisotropy (birefringence) was used. At the present time, there also exist variants that use the amplitude anisotropy (dichroism). The author examines high resolution PP nonlinear spectroscopy and PP laser methods for determining optical constants. (78 refs.)

111780 Nonlinear Zeeman spectroscopy of ultrahigh resolution. N.I.Kaliteevskii, E.N.Kotlikov, V.I.Tokarev.

J. Appl. Spectrosc. (USA), vol.37, no.6, p.1451-7 (Dec. 1982). Translation of: *Zh. Prikl. Spektrosk. (USSR)*, vol.37, no.6, p.1022-9 (Dec. 1982). [received: Sept. 1983]

An original method of nonlinear Zeeman spectroscopy of ultrahigh resolution is outlined, based on an analysis of the fluorescence of the medium interacting with a standing laser wave. Different aspects of the application of this method are presented which permit conducting an investigation of the structure of the transition line and the effect of different kinds of collisions on this structure. The authors consider the fluorescence of an ensemble of atoms which is interacting with a standing laser wave. Linear and nonlinear interference signals are observed in the fluorescence of such an ensemble of atoms in the vicinity of null magnetic fields. As the magnetic field increases, a central saturation resonance caused by the spacing of 'Bennett' gaps in the magnetic

field appears, depending on the intensity of the spontaneous emission from the magnetic field. The width of this resonance is determined in the first approximation by the uniform width of the transition line Γ_{ab} . As the magnetic field increases more, the Bennett gaps from waves traveling in the opposite direction overlap, and one more 'shifted' saturation resonance is observed in spontaneous emission whose width is determined as previously by the uniform width of the transition line and whose position is determined by the difference between the generation frequency and the center frequency of line absorption. (17 refs.)

111781 Measurement Assurance Program transmittance standards for spectrophotometric linearity testing: preparation and calibration. K.L.Eckerle, V.R.Weidner, J.J.Hsia, K.Kafadar (NBS, Washington, DC, USA).

J. Res. Natl. Bur. Stand. (USA), vol.88, no.1, p.25-36 (Jan.-Feb. 1983). [received: Sept. 1983]

The authors describe the preparation and calibration of neutral density glass filters for checking the linearity of photometric response, as applied to spectral transmittance measurements. Several sets of filters were prepared from suitable neutral glass to provide nominal transmittances of 92, 70, 50, 25, 10, 1, and 0.1% at a wavelength of 548.5 nm. The filters were calibrated for spectral transmittance on the NBS Reference Spectrophotometer for high accuracy transmittance measurements. Measurements were made with a 1.5 nm passband collimated sample beam. The filters were checked for uniformity and measurements were made to determine the effects of sample beam polarization. (11 refs.)

111782 Number fluctuation spectroscopy in standing-wave fringes. M.Drewel, P.N.Pusey (Royal Signals & Radar Establ., Malvern, England).

Opt. Acta (GB), vol.30, no.10, p.1483-500 (Oct. 1983).

Considers photon correlation spectroscopy of spontaneous fluctuations in the number of particles in a small scattering volume containing interference fringes formed by counterpropagating laser beams. The 'fringe number fluctuation' contribution to the correlation function of the scattered intensity is predicted to decay exponentially in time. The particle diffusion constant can be obtained directly from the measured decay time and the easily calculated fringe spacing. Experiments were performed on both quasi-elastic and fluorescent scattering from dyed polystyrene particles of diameter 0.109 μ m in aqueous suspension. For the quasi-elastic scattering reasonable agreement with theory was found. Some difficulties were encountered with the fluorescent scattering; nevertheless, the experimentally derived value of the diffusion constant was close to the expected value. Thus the fringe number fluctuation technique appears to provide a useful modification of the usual fluorescence correlation spectroscopy. (14 refs.)

111783 Performance characteristics of a small side-window photomultiplier in laser single-photon fluorescence decay measurements. W.R.Ware, M.Pritidhi, R.K.Bauer (Dept. of Chem., Univ. of Western Ontario, London, Ontario, Canada).

Rev. Sci. Instrum. (USA), vol.54, no.9, p.1148-56 (Sept. 1983).

The performance characteristics of the Hamamatsu R928 side-window photomultiplier tube have been evaluated in the picosecond time domain. This phototube is proposed as an attractive solution to the problem of high time resolution when a sync-pumped dye laser is combined with the single-photon time correlation method for determining fluorescence lifetimes and measuring time-resolved emission spectra and polarization anisotropy. It combines excellent timing characteristics in the single-photon mode and a small-to-negligible wavelength effect with high gain, low noise, and low cost. Twice the resolution previously reported has been obtained. (35 refs.)

111784 Accuracy in analytical spectrophotometry. R.W.Burke, R.Mavrodineanu.

Report NBS-SP-260-81, Nat. Bur. Stand., Washington, DC, USA (April 1983), xiii+126 pp.

Describes activities undertaken since 1969 within the Center for Analytical Chemistry of the National Bureau of Standards (NBS) in the field of high accuracy spectrophotometry. The first part of this work presents a summary of the standard reference materials (SRMs) that have been developed for checking the proper functioning of ultraviolet and visible spectrophotometers and includes a description of the high-accuracy spectrophotometer specially constructed in the Center for Analytical Chemistry and subsequently used for performing all of the transmittance measurements. The second part of this publication is devoted to a critical discussion of the analytical factors that can affect the accuracy of selected spectrophotometric procedures that have been widely used at NBS in the characterization of various SRMs. (39 refs.)

Automated comparison of discrete spectra See Entry 111657

Excitation pulse-shape mimic technique for improving picosecond-laser-excited time-correlated single-photon counting deconvolutions See Entry 111771

Stigmatic systems with concave spherical holographic diffraction gratings See Entry 113082

Photoacoustic spectra of MoS₂ See Entry 114873

Time resolved photoacoustic spectroscopy applied to properties of picosecond transients See Entry 115566

Light sources for fluorescein fluorophotometry See Entry 115893

07.65E UV and visible spectroscopy and spectrometers

111785 Picosecond continuum generation and spectroscopy. A.I.Ferguson, B.A.Taylor (Clarendon Lab., Univ. of Oxford, Oxford, England).

Proc. SPIE Int. Soc. Opt. Eng. (USA), vol.369, p.379-84 (1983). (SPIE Proceedings of the Max Born Centenary Conference OPTICS 82, ECOSA 82, Edinburgh, Scotland, 7-10 Sept. 1982).

Picosecond continua generated by focusing amplified picosecond pulses into various media have been studied. The authors have measured both spectral and temporal characteristics of these continua and discuss the implications of such continuum sources to spectroscopy. The characteristics of the dye amplifier used to generate such continua are also discussed. (10 refs.)

Interfacing a Unicam SP800 spectrophotometer to a microcomputer See Entry 111655

Spectroscopic ellipsometry See Entry 111739

07.65G IR spectroscopy and spectrometers

111786 Rapid infrared multicomponent control analyses. W.L.Truett, M.A.Bayliss (Foxboro Analytical, South Norwalk, CT, USA).

Appl. Spectrosc. Rev. (USA), vol.18, no.3, p.329-71 (1982-1983). [received: Sept. 1983]

Over the past 5 years the authors have carried out a wide variety of control-type analyses in the liquid, solid, and gas phase by utilizing a single beam microcomputer controlled filter instrument. The applications discussed include those performed with the MIRAN 80 or MIRAN 980. Applications

performed using other types of spectrophotometers are also discussed. There are several types of IR instruments in commercial use today which enable one to perform multicomponent analyses with speed and accuracy. Among these types are microcomputer controlled single beam instruments, microcomputer controlled optical-null or ratio-recording double beam spectrophotometers, microcomputer controlled optical-null double beam spectrophotometers with stepping motor control for wavelength positioning, Fourier transform IR spectrophotometers of several types, and tuned laser diode instruments. Within the past 5 years there has been considerable progress in this field, and new developments in instrumentation are constantly occurring. The types noted above are discussed and contrasted. (40 refs.)

111787 Elimination of scintillation noise in dual-beam Fourier spectrometry for optical difference-reflectivity measurements. H.Krenn (Inst. fur Phys., Montanuniv. Leoben, Leoben, Austria). *Infrared Phys. (GB)*, vol.23, no.3, p.161-70 (May 1983).

The problems arising from imbalance in a double-input, double-output interferometer are treated extensively. Optical misalignments, source fluctuation and thermal distortions cause scintillation noise effects which are particularly important in the low frequency region in the far-infrared. By using a new method of double chopping in dual-beam slow-scan interferometers, ratio measurements of interferograms and spectra without scintillation noise are obtained. In addition, difference reflectivity measurements can be performed without the necessity of interchanging sample and reference. (13 refs.)

111788 FTIR photothermal deflection spectroscopy. J.S.Wong (IBM Corp., Armonk, NY, USA). *IBM Tech. Disclosure Bull. (USA)*, vol.26, no.1, p.345-6 (June 1983).

Describes how by means of Fourier transform infrared (FTIR) spectroscopy, solids in the presence of non-corrosive or corrosive liquids or gases and optically transparent solids, liquids and gases can be detected. (no refs.)

Stress activated Raman scattering and microcrack detection See Entry 115461

Diode array versus photomultiplier for measuring the UV-excited resonance Raman spectra of enzyme-substrate transients See Entry 115985

07.68 PHOTOGRAPHY, PHOTOGRAPHIC INSTRUMENTS AND TECHNIQUES

(for light sensitive materials see also 42.70)

111789 Stereo with a modern SLR. G.A.Williams.

Br. J. Photogr. (GB), vol.130, no.28, p.728-31 (15 July 1983).

Whilst specialised equipment for stereoscopic recording is available for larger undertaking, e.g. ophthalmic research, the desirable search is for a camera which without modification, is universal and fully usable for conventional or stereo photography. For extended tests and development experiments the author chose the Mamiya M645 camera as providing an eminently practical solution to the provision of a modern SLR outfit which can cover most requirements of conventional and stereo photography. This additional versatility is accomplished through convenient accessory equipment requiring no alteration or modification to the standard camera. Following a brief outline of the camera features the author goes on to look at split-image stereo theory, image inversion, 120/20 film capacity and action close-up stereo all with reference to the Mamiya system. (no refs.)

111790 Ilfocolor 100—a review. G.Ashton.

Br. J. Photogr. (GB), vol.130, no.34, p.904-5, 909 (26 Aug. 1983).

Ilfocolor 100 is described as a fine-grain, medium-speed colour negative film ideally suited to general purpose photography. It is a very competitive product in all its characteristics and is a film which is capable of giving colour prints with extremely pleasing and attractive qualities; as the manufacturer claims, it has wide exposure latitude and a good neutral overall colour latitude and a good neutral overall colour balance. Although Ilfocolor 100 film does not claim to incorporate any novel emulsion-making technology as do some of the other recently introduced colour negative films, and it is clearly intended by Ilford Ltd. to appeal to the mass market, its qualities are such that it can be used very well in professional practice when a 35 mm material with an ASA100 speed rating is required. (no refs.)

111791 Agfapan 25, 100 and 400. G.Ashton.

Br. J. Photogr. (GB), vol.130, no.36, p.947-8, 959 (9 Sept. 1983).

These newly re-introduced Agfa professional black-and-white films provide a very useful alternative range of materials with well and logically spaced speed ratings. The image quality the films provide is in keeping with their respective speeds and in all cases they would appear to be materials manufactured so as to take advantage of contemporary techniques. When used with the recommended processing solutions development times are reasonably, but not uncontrollably, short and those films which are intended for studio use have the handling characteristics which are generally thought to be essential. (no refs.)

111792 Improved Eastman Colour print films. J.A.G.Clifton (Motion Picture Sales, Kodak Ltd., London, England).

BKSTS J. (GB), vol.65, no.8, p.436-44 (Aug. 1983).

Eastman Colour print film 5384 and 7384 combine improved colour reproduction, reduced sensitivity to process variations and significantly improved dark-keeping dye stability. Eastman Colour low contrast print film 5380 and 7380 designed for making optimum-contrast prints for television use is introduced. The sensitometric characteristics, performance and processing of the new films are discussed. (2 refs.)

111793 Lenses: the angle of coverage. R.Jegerings.

Ind. Photogr. (USA), vol.32, no.8, p.25-6, 29 (Aug. 1983).

Presents some charts and a few simple calculations to help eliminate 'diagonal error'. Charts have been made up giving angles for the most used professional formats and camera lenses common to those formats. The charts are for the following formats: 35 mm full frame, 6×4.5 cm and 6×6 cm, 6×7 cm, 6×9 cm, 4×5" and 8×10", and 5×7". In some cases two formats have been combined in one chart. For the 35 mm format, horizontal angles have also been given for the format cropped to fit a sheet of 8×10" paper because many use their 35 mm cameras in this 'ideal format' manner. (no refs.)

111794 High quality, electron beam sound recording on film. N.Kihara, Y.Ozaki, H.Shirai (Advanced Engng. Div., Sony Corp., Tokyo, Japan).

IEEE Trans. Consum. Electron. (USA), vol.CE-29, no.3, p.383-7 (1983).

(1983 IEEE International Conference on Consumer Electronics, ICCE, Des Plaines, IL, USA, 8-10 June 1983).

In the project of developing a method of transferring pictures from the high definition video system (HDVS) to 35 mm motion picture film, a new audio recording method was sought which would match the quality of HDVS. This objective was achieved with a new system that produces a stereo soundtrack of the variable area type directly on the film by an electron beam. (2 refs.)

111795 Error range calculations of average gradient measurement. I.Galfi.

KeP- & Hangtech. (Hungary), vol.29, no.4, p.109-10 (Aug. 1983).

Measurement of average gradient is very important in checking film processing and in testing photographic substances. This paper deals with error range calculations of this measuring method. (2 refs.)

111796 Function of printers in the recent photofinishing industry. A.Kegy.

KeP- & Hangtech. (Hungary), vol.29, no.4, p.121-4 (Aug. 1983). (3 refs.)

111797 Special effects on film at the Moving Picture Company. I.Chisholm.

Television (J. R. Telev. Soc.) (GB), vol.20, no.3, p.101-3 (May-June 1983).

The author describes his work in the field of computer animation. For outputting the animated sequence onto film the Moving Picture Company use a conventional plotter, except the pen has been replaced by a light source. An animation camera is pointed at the plotter and focused on the plane of the light source. Driving the plotter from a computer means writing directly onto the film emulsion. Colours, diffusion and other effects are achieved with filters, which are also selected and positioned by the computer, and by multiple exposures. (no refs.)

1st European Conference on Cineradiography with Photons or Particles See Entry 111300

Four-dimensional reconstruction problems in cineradiography from space-time integrated projections See Entry 111835

Some applications of cineradiography to gas turbines See Entry 111836

Basic phenomena in high energy-density beam welding and cutting See Entry 111837

Facility for cineradiography at high energy: the ARTEMIS project See Entry 111844

Magnetic focus/deflection image converter camera for cineradiography See Entry 111846

Streak camera for picosecond X-ray diagnostics See Entry 111852

Investigation of material movement within steel test sections by means of high speed X-ray photography See Entry 112319

Effect of pre-exposure of films on radiographic sensitivity See Entry 112365

Method of determining the thickness of nuclear photoemulsions in autoradiography See Entry 112575

High-frequency holographic transmission gratings in photoresist See Entry 112960

Galactic profiles and the point spread function See Entry 116488

07.75 MASS SPECTROMETERS AND MASS SPECTROMETRY TECHNIQUES

(for mass spectroscopic chemical analysis, see 82.80)

111798 A secondary-ion mass-spectrometer system with high depth resolution. V.V.Yagzhev, V.V.Marusin (Inst. of Solid-State Chem. & Mineral Raw Material Processing, Acad. of Sci., Novosibirsk, Ukrainian SSR).

Instrum. & Exp. Tech. (USA), vol.25, no.6, pt.2, p.1458-61 (Nov.-Dec. 1982). Translation of: *Prib. & Tekh. Eksp. (USSR)*, vol.25, no.6, p.129-32 (Nov.-Dec. 1982).

A description is given of an apparatus based on a MKh-1303 mass spectrometer that provides a sensitivity either at the level of 10^{-4} with an average rate of ion etching less than 1 Å/sec when working into a KSP-4 potentiometer, or 10^{-3} in high-speed mass spectrum recording, with a K-121 light-beam oscillograph with cyclic scanning and a wide mass range (12-150 or 150-600 amu). (9 refs.)

111799 Ion-beam scanning circuit for the MI-1305 mass spectrometer. N.N.Korobkov, O.P.Ninburg, P.G.Umantsev.

Instrum. & Exp. Tech. (USA), vol.25, no.6, pt.2, p.1462-3 (Nov.-Dec. 1982). Translation of: *Prib. & Tekh. Eksp. (USSR)*, vol.25, no.6, p.133-4 (Nov.-Dec. 1982).

An ion-beam scanning device is described that is used in the MI-1305 mass spectrometer with an ion probe to produce sputtering craters with flat bottoms. The circuit produces triangular voltage pulses with frequencies of about 1.5 kHz and 50 Hz and amplitudes of 0-500 V, which are applied to two pairs of deflecting plates. The maximum dimensions of a crater are 3×3 mm for a bombarding ion energy of 9 keV. (3 refs.)

111800 A stabilized controlled generator for a quadrupole mass spectrometer. S.A.Shubotenko, A.A.Evstifeev (Moscow Engng. Phys. Inst., Moscow, USSR).

Instrum. & Exp. Tech. (USA), vol.25, no.5, pt.1, p.1160-2 (Sept.-Oct. 1982). Translation of: *Prib. & Tekh. Eksp. (USSR)*, vol.25, no.5, p.107-9 (Sept.-Oct. 1982). [received: Sept. 1983]

A generator in a quadrupole mass spectrometer is described. The range in the amplitude of the high-frequency voltage is 120-2400 V. The amplitude instability is $\leq 1.3 \times 10^{-3}$, while the instability in the ratio of the DC voltage to the amplitude is $\leq 0.5 \times 10^{-3}$ for amplitude of the output voltage of 2400 V and a temperature change of $\pm 10^\circ\text{C}$. Maximum power drawn ≤ 30 W, working frequency 1 MHz. (4 refs.)

111801 Analysis of insulating materials by negative ionmicroprobe. H.Tamura (Central Res. Lab., Hitachi Ltd., Tokyo, Japan).

J. Vac. Soc. Jpn. (Japan), vol.26, no.2, p.179-88 (1983). In Japanese.

Summarizes recent insulator analysis methods using a secondary ion mass spectrometer (SIMS), sometimes called an ion probe, in which a beam of primary ions bombards a small spot on the surface of a sample, and positive and negative secondary ions sputtered from the surface are analyzed in a mass spectrometer. The application of secondary ion mass spectrometry is described to the analysis of inorganic insulators, plants and living things. (8 refs.) K.B.

111802 Application to bio-organic compounds [ion physics]. H.Kambara, S.Seki (Central Res. Lab., Hitachi Ltd., Tokyo, Japan).

J. Vac. Soc. Jpn. (Japan), vol.26, no.2, p.207-17 (1983). In Japanese.

For ionizing organic matter there are the plasma deposition method (PD), field deposition method (FD), laser deposition method (LD), molecular secondary ion mass spectrometry method (molecular SIMS) and fast atom bombardment method (FAB). This paper centres around the molecular SIMS; it describes dry surface molecular SIMS, matrix assisted molecular SIMS, and FAB mass spectrometry; and it makes comparison between dry surface SIMS and matrix assisted SIMS. Furthermore, the SIM spectrum of some materials is shown and molecular structure information obtained from daughter-ion spectrum measurement is given. (22 refs.) K.B.

111803 Plasma source mass spectrometry. J.Cantle (V.G. Isotopes, Winsford, England). *Lab. Pract. (GB)*, vol.32, no.8, p.31-2 (Aug. 1983).
Describes the ICP (inductively coupled argon plasma) source mass spectrometry technique with reference to the Plasma Quad system. The system was initially developed by Alan Gray (University of Surrey) and Alan Date (Institute of Geological Sciences). The features of this technique can be summarised as follows: wide range of elements determined with sub ng/ml limits of detection; automatic operation; multi-element capability; high dynamic range with linearity over six orders of magnitude; minimal matrix effects; fast sample throughput—typically a few minutes; direct analysis of solutions; simple spectra, unambiguous data; rapid isotope ratio determination; isotope dilution capability for high accuracy determinations. (3 refs.)

111804 Ion current measurement channel in single-collector mass spectrometers. M.E.Sluts'kii, M.A.Pushkina. *Meas. Tech. (USA)*, vol.25, no.12, p.991-2 (Dec. 1982). Translation of: *Izmer. Tekh. (USSR)*, vol.25, no.12, p.61-2 (Dec. 1982).
The authors consider a circuit for simultaneous measurement of five ion current components in a radio-frequency mass spectrometer used in medical, biological, and physiological research. To improve the signal/noise ratio the circuit uses automatic level adjustment and signal integration. The scanning period of mass spectrometer peaks in the analyzer is 100 msec and is synchronized with the line frequency of 50 Hz. The electrometer with a pass band up to 1000 Hz consists of a K284UD1B operational amplifier with a 2.2-G Ω input resistor. An active filter suppresses noise outside the operating frequency band. The scaling amplifier provides a variable transfer constant of 3-30 for each of the five ion current components. (1 ref.)

111805 Refraction of an ion beam by the fringe electric field in a mass spectrometer with a laser ion source. A.I.Boriskin, A.S.Bryukhanov, Yu.A.Bykovskii, V.M.Eremenko, V.M.Ivanchenko, I.D.Laptev (Fiftieth Anniversary of VLKSM Electron Microscope Factory, Sumy, USSR). *Sov. Phys.-Tech. Phys. (USA)*, vol.28, no.2, p.215-17 (Feb. 1983). Translation of: *Zh. Tekh. Fiz. (USSR)*, vol.53, no.2, p.351-4 (Feb. 1983). [received: Sept. 1983]
Experimental results are reported on the effects of ion beam refraction by the fringe electric field in a double-focusing mass spectrometer with a laser ion source. The results are compared with data obtained by numerically solving a mathematical model. It is shown that the change in the potential of the point at which the ion beam is injected into the electric field results in a 2-3-fold drop in the mass spectrometer resolution and a simultaneous displacement of the mass lines in the focal plane of the mass analyzer. The mass peak for singly charged ions occurs at the position of maximum spectrometer resolution and the relative number of multiply charged ions is reduced. An electrical method for reducing aberrations caused by ion beam diffraction by the fringe fields is tested. (10 refs.)

111806 Use of the 'large particle' method to calculate parameters of ion sources which employ electron impact ionization. A.S.Mal'kov (Inst. of Analytical Instrumentation, Sci.-Tech. Union, Acad. of Sci., Leningrad, USSR). *Sov. Phys.-Tech. Phys. (USA)*, vol.28, no.2, p.217-20 (Feb. 1983). Translation of: *Zh. Tekh. Fiz. (USSR)*, vol.53, no.2, p.355-60 (Feb. 1983). [received: Sept. 1983]
An algorithm using the 'large particle' method is developed for calculating the parameters of ion sources used in a quadrupole mass spectrometer. The technique includes electron and ion space charge effects and can be used to analyze transient behavior in ion sources until steady-state operation is reached. The use of the algorithm is illustrated through numerical results obtained from computer calculations for a specific source model. (6 refs.)

111807 An energy/mass analyzer with two flat capacitors. V.V.Zashkvara, V.P.Shestakov (S.M. Kirov State Univ., Alma-Ata, Kazakh SSR). *Sov. Phys.-Tech. Phys. (USA)*, vol.28, no.2, p.221-3 (Feb. 1983). Translation of: *Zh. Tekh. Fiz. (USSR)*, vol.53, no.2, p.361-4 (Feb. 1983). [received: Sept. 1983]
The parameters of an energy/mass charged particle beam analyzer consisting of two flat capacitors are analyzed. The particle energy is analyzed under static conditions and the mass is determined in the time-of-flight regime. The time of flight is focused with respect to both the beam energy and divergence angle. Various operating conditions of the energy/mass analyzer are examined. (7 refs.)

Atom-probe field ionmicroscope mass spectrometerSee Entry 111825

07.77 PARTICLE BEAM PRODUCTION AND HANDLING; TARGETS
(see also 29.25 in elementary-particle and nuclear physics, 41.80 Particle beams and particle optics)

111808 A pulsed surface muon beam/pion beam for the Rutherford Appleton Laboratory Spallation Neutron Source. G.H.Eaton, A.Carne, D.H.Reading, E.G.Sandels (Rutherford Appleton Lab., Chilton, Didcot, England). *Nucl. Instrum. & Methods Phys. Res. (Netherlands)*, vol.214, no.2-3, p.151-67 (1 Sept. 1983).
The design and estimated performance of a versatile pulsed surface muon/pion beam for the Rutherford Appleton Laboratory Spallation Neutron Source (SNS) are presented. The characteristics of the SNS extracted proton beam are discussed with reference to their implications on the design of the muon beam and the effect on the neutron source itself. The pulsed nature of the muon beam will allow typically up to two orders of magnitude increases in the data-taking rates for μ SR experiments compared with those which are normally tolerable at the continuous-current meson factories. The versatile features of the beam are described and comparisons made with existing muon sources. Construction of the muon beam for μ SR studies has been proposed at the SNS with first operation expected in late 1984. (36 refs.)

111809 A novel design for a fast intense neutron beam. A.Bol, P.Leleux, P.Lipnik, P.Macq, A.Ninane (Inst. de Phys., Univ. Catholique de Louvain, Louvain-la-Neuve, Belgium). *Nucl. Instrum. & Methods Phys. Res. (Netherlands)*, vol.214, no.2-3, p.169-73 (1 Sept. 1983).
A novel design for the production of fast (40-75 MeV) and intense mono-kinetic neutron beam from the Li(p,n) reaction is described. The primary charged beam is dumped in a Faraday cup immediately behind the Li target. Both the production target and Faraday cup are enclosed inside a compact shielding. With respect to the conventional method where the primary beam is deflected, the advantage of this design is twofold: the neutron beam intensity is enhanced and the background is decreased. The properties of this neutron beam, i.e. its intensity, time width and spatial profile are reported. (4 refs.)

111810 Compact metal-ion beam source using thermal contact ionizer. Y.Sakai (Dept. of Appl. Phys., Osaka City Univ., Osaka, Japan), I.Katsumata, T.Oshio. *Jpn. J. Appl. Phys. Part 1 (Japan)*, vol.22, no.6, p.1048-56 (June 1983).
A small, compact ion beam source which can function in an external magnetic field has been developed for use with a heavy ion beam probe for plasma diagnostics. The source consists of a thermal contact ionizer with a beam material reservoir and an electrostatic lens system for beam acceleration and focusing. The beam can be modulated by means of a beam-extracting electrode. An alkali or an alkali earth metal ion beam was produced at energies up to 3 keV. The source functioned sufficiently well in a magnetic field up to 2 kG. The operating parameters for Cs⁺ and Ba⁺ ion beams were investigated in detail. A beam current up to 10 μ A and a small diameter of 1 mm at the focusing point were obtained. (17 refs.)

111811 Study of beam divergence of a low-energy (1-3 keV) ion source. K.Yatsu, S.Aoki, A.Horie, S.Miyoshi (Inst. of Phys., Univ. of Tsukuba, Ibaraki, Japan), K.Ota, K.Okano, N.Inoue, T.Uchida. *Jpn. J. Appl. Phys. Part 1 (Japan)*, vol.22, no.6, p.1071 (June 1983).
A low-energy large-current ion source is useful in many plasma experiments. One method of obtaining a large beam current at a low energy is to use a strong accel-decel grid system for ion extraction. The authors have carried out a two-dimensional computer simulation of such systems and found that the divergence angle has a minimum when the ratio α is around 10. The simulation results were confirmed by experiment. (3 refs.)

111812 Ion sources (recent topics). T.Ishitani (Central Res. Lab., Hitachi Ltd., Tokyo, Japan). *J. Vac. Soc. Jpn. (Japan)*, vol.26, no.2, p.99-107 (1983). In Japanese.
Ion beams exhibit mass and energy transport phenomena and cover a wide range of applications, e.g. surface-analyzing probes, ion implantation, ion etching, ion lithography and surface modification. There are three major ion sources: (1) plasma discharged source, (2) surface ionization source, and (3) intense field applied source. The topical areas in this review paper include: (1) The description of liquid-metal-ion sources, (2) the operational principle and structure of ion sources, (3) properties of field ionization, duoplasmatron and field emission ion sources, (4) the description and characteristics of gas field ionization ion sources, (5) ion implantation and its ion sources, and (6) the structure and characteristics of microwave ion sources. (65 refs.) K.B.

111813 Negative ion sources. J.Ishikawa, T.Takagi (Dept. of Electronics, Kyoto Univ., Kyoto, Japan). *J. Vac. Soc. Jpn. (Japan)*, vol.26, no.2, p.108-19 (1983). In Japanese.
The need for use with tandem electrostatic accelerators has been reflected in the development of negative ion sources, which can provide negative ion currents between hundreds nA and several μ A. There are the following typical negative ion sources: PIG negative ion source and its modification, duoplasmatron and its modification, the hollow discharge duoplasmatron (HDD), surface plasma source, Aarhus negative ion source (ANIS), universal negative ion source (UNIS), and neutral and ionized cesium bombardment type negative ion source (NICBNIS). The authors discuss: (1) hydrogen negative ion generation in low-electron-temperature plasma, (2) negative ion generation on a metal surface, (3) the theory of secondary negative ion emission, and (4) the description of each negative ion source. (54 refs.) K.B.

111814 Fine-focus ion beam technology for microfabrication. N.Anazawa (JEOL Ltd., Tokyo, Japan). *J. Vac. Soc. Jpn. (Japan)*, vol.26, no.2, p.196-206 (1983). In Japanese.
The fine-focus ion beam refers to an ion beam capable of focusing through a lens system because the beam is emitted from an extremely small spot. The author describes an ion optical system for high-luminance ion sources and reviews recent microstructure fabrication techniques; using the optical system. The topical areas include: (1) maskless ion injection using a 57-kV gallium ion beam equipment, (2) ion beam etching using a 35-kV Ga⁺ ion probe, and (3) ion beam lithography using PMMA resist (Dupont Elvacite 2008). (22 refs.) K.B.

111815 Effect of magnetic field on the characteristics of a hollow cathode ion source. S.Tanaka, M.Akiba, H.Horiike, Y.Okumura, Y.Ohara (Div. of Thermonuclear Fusion Res., JAERI, Ibaraki-ken, Japan). *Rev. Sci. Instrum. (USA)*, vol.54, no.9, p.1104-12 (Sept. 1983).
The effect of magnetic field on the performance of a hollow cathode ion source was experimentally studied. The field strength and the field distribution around the hollow cathode were changed step by step and the source parameters were recorded for each step. The result showed that with the optimum field configuration the discharge was stabilized even at low-operating gas pressures and the arc efficiency of the source was improved. Examination of the field and the neutral gas density distributions along the hollow cathode axis made it clear that the optimum field configuration was such that electrons emitted from the hot cathode surface might easily go out of the cathode cavity through the orifice being guided by the lines of force. Beam extraction from an intensively water-cooled small bucket source with the hollow cathode was carried out and hydrogen ion beams of up to 3 A at 50 keV were successfully obtained for the pulse length of up to 10 s. (8 refs.)

111816 High-current pulsed proton source. V.I.Davydenko, G.I.Dimov, I.I.Morozov, G.V.Rosylakov (Inst. of Nuclear Phys., Acad. of Sci., Novosibirsk, USSR). *Sov. Phys.-Tech. Phys. (USA)*, vol.28, no.2, p.160-3 (Feb. 1983). Translation of: *Zh. Tekh. Fiz. (USSR)*, vol.53, no.2, p.258-63 (Feb. 1983). [received: Sept. 1983]
The design of a pulsed proton source is discussed. The source generates the proton beam by extracting ions from a plasma emitter which consist mainly (>95%) of protons. Beams are produced with current >30 A and energy 25 keV, pulse duration 200 μ s, and pulse repetition frequency 0.2 Hz. The emission diameter of the beams is 9 cm and the angular divergence 10⁻² rad \times 2.10⁻² rad. (9 refs.)

Analysis of small cesium beam tubeSee Entry 111652
Refraction of an ion beam by the fringe electric field in a mass spectrometer with a laser ion sourceSee Entry 111805
Use of the 'large particle' method to calculate parameters of ion sources which employ electron impact ionizationSee Entry 111806
An energy/mass analyzer with two flat capacitorsSee Entry 111807
Charged particle beam envelopesSee Entry 112499
Envelope equation for a beam accelerated by a rotationally symmetric electrostatic fieldSee Entry 112500
Neutralizer for Hall-current acceleratorSee Entry 112512
Charged particle ray simulator and monitorSee Entry 112916
Neutron radiography facility using ²⁵²Cf neutron sourceSee Entry 115498
Improvement of efficiency of n, α converters to realize NR with relatively low n flux sourcesSee Entry 115501

07.80 ELECTRON AND ION MICROSCOPES AND TECHNIQUES

(see also in condensed matter 61.16D Electron microscopy, 61.16F Field ion microscopy)

111817 A fast-response EBIC system. C.J.Rossouw, F.J.Maher, A.A.Panjkov (Div. of Chem. Phys., CSIRO, Clayton, Victoria, Australia). *Aust. J. Phys. (Australia)*, vol.36, no.4, p.565-72 (1983).

The application of the EBIC technique in the study of electrical activity of defects in semiconductors is discussed, with particular reference to instrumentation. A fast-response current amplifier is shown to be more than adequate for most EBIC applications. Some examples of EBIC analysis are presented. (15 refs.)

111818 Use of gold/palladium surface replicas for high kV (30), SEM examination of low Z materials. R.M.Pradhan (Hindustan Lever Res. Centre, Bombay, India). *Bull. Mater. Sci. (India)*, vol.5, no.1, p.49-60 (March 1983). [received: Sept. 1983]

A procedure for making high fidelity gold/palladium surface replicas of various low atomic number (Z) materials for SEM examination has been developed. The procedure facilitates simultaneous replication of a number of SEM specimens. These replicas provide improved image quality, elimination of charging and beam penetration artifacts and microtopographical information, often not available by direct SEM examination of low Z materials at 30 kV. (5 refs.)

111819 Applications of high voltage electron microscopy in materials science. M.J.Goringe (Dept. of Metall. & Sci. of Materials, Univ. of Oxford, Oxford, England).

Proc. SPIE Int. Soc. Opt. Eng. (USA), vol.368, p.41-8 (1983). [received: Sept. 1983] (SPIE Proceedings on Microscopy Techniques and Capabilities, London, England, 21-22 Sept. 1982).

The principal advantages of the high voltage electron microscope, higher resolution, penetrating power, decreased radiation damage and the special effects of critical voltage and displacement damage are outlined. Some application of increased penetration and radiation damage to studies in materials science are then discussed in more detail. (31 refs.)

111820 Magnetic-field-free objective lens around a specimen for observing fine structure of ferromagnetic materials in a transmission electron microscope. K.Tsuno, T.Taoka (JEOL Ltd., Tokyo, Japan).

Jpn. J. Appl. Phys. Part 1 (Japan), vol.22, no.6, p.1041-7 (June 1983).

In order to observe the fine structures of ferromagnetic materials or to observe their magnetic domain structures special magnetic-field-free lenses in which specimens are set in the upper pole-piece have been developed. In these objective lenses, the spherical aberration depends largely on the shape of the lens, especially, (1) the distance between the positions of the specimen and the peak of the lens field, (2) the diameters of the pole-piece bores and the top face of the upper pole-piece, and (3) the gap length. In a lens with a pole-piece of optimum dimensions, the resulting resolution reached 0.7 nm and the leakage field strength was 0.35 mT. Complicated domain structures of ferromagnetic materials could be clearly observed. (5 refs.)

111821 High-voltage long-focus electron gun. N.N.Veniaminov, A.K.Kuzakov, N.G.Rambidi (All-Union Res. Inst. for the Study of Surface Properties in Vacuum, USSR).

Instrum. & Exp. Tech. (USA), vol.25, no.6, pt.2, p.1433-5 (Nov.-Dec. 1982). Translation of: *Prib. & Tekh. Eksp. (USSR)*, vol.25, no.6, p.108-10 (Nov.-Dec. 1982).

A long-focus electron gun is described, capable of producing beams of intensity up to 230 μ A at accelerating voltages 25 and 50 kV. The minimum beam half-width is ~ 0.2 mm at a distance ~ 0.8 m from the directly heated tungsten cathode. The power supply is based on blocks of the EMMA-2 electron microscope. (8 refs.)

111822 Instrument for examining the polarization of low-energy electrons interacting with a solid. I.A.Pchelkin, G.K.Zyryanov (Phys. Res. Inst., Leningrad Univ., Leningrad, USSR).

Instrum. & Exp. Tech. (USA), vol.25, no.6, pt.2, p.1446-7 (Nov.-Dec. 1982). Translation of: *Prib. & Tekh. Eksp. (USSR)*, vol.25, no.6, p.119-20 (Nov.-Dec. 1982).

An instrument is described for examining the polarization of low-energy electrons interacting with a solid, which consists of an electron source, a beam polarizer, and an analyzer. The analyzer can be applied in various ways. When PbS is used, the polarization at an incident electron energy of 125 \pm 5 eV attains 70%. (4 refs.)

111823 Electron-optical recording of nonstationary adsorption on a metal surface. V.I.Zhavoronkov, S.P.Manokhin, A.A.Antonov, V.V.Vedernikov, B.V.Filippov (Kirov Pedagogic Inst., Kirov, USSR).

Instrum. & Exp. Tech. (USA), vol.25, no.6, pt.2, p.1447-50 (Nov.-Dec. 1982). Translation of: *Prib. & Tekh. Eksp. (USSR)*, vol.25, no.6, p.120-3 (Nov.-Dec. 1982).

An apparatus is described for the recording of pulse field-emission images of the surface of a solid by a three-camera electronoptical converter (e.o.c.) U-72-M. Electronoptical recording permitted diminution of the electrostatic forces responsible for migration of the electropositive adsorbate over the surface, and the field-emission current governing the thermal regime of emitter operation, which affords a possibility for investigating nonstationary adsorption under a single delivery of pulses of 1 μ sec duration to the emitter. Application of the e.o.c. permitted observation of the evolution of adsorbed filler on a tungsten emitter surface during interaction with potassium and sodium ion beams. (6 refs.)

111824 Charge-density measurement for single nanosecond electron-beam pulses. V.I.Voroshen', N.M.Chirkin (Minsk Electronics Inst., Minsk, Belorussian SSR).

Instrum. & Exp. Tech. (USA), vol.25, no.5, pt.1, p.1147-9 (Sept.-Oct. 1982). Translation of: *Prib. & Tekh. Eksp. (USSR)*, vol.25, no.5, p.97-9 (Sept.-Oct. 1982). [received: Sept. 1983]

A probe is described together with an electrometer follower circuit for measuring the density of the charge (current) in single electron-beam pulses by integrating the current with a standard capacitor and recording the voltage. The measurement range is from 0.4×10^{-9} to 1×10^{-7} Cu/cm². The measurement accuracy is not worse than 5% for a beam energy of 0.2-3 keV. A limiting density of 4×10^{-6} Cu/cm² and steady current of 3 mA/cm² are due to the breakdown voltage (200 V) of the input capacitor and the insulation of the probe. (2 refs.)

111825 Atom-probe field ion microscope mass spectrometer. O.Nishikawa (Tokyo Inst. of Technol., Yokohama, Japan).

J. Vac. Soc. Jpn. (Japan), vol.26, no.2, p.147-78 (1983). In Japanese.

Atom-probe field ion microscope mass spectrometers, simply called APFIM or atom probes, utilize field evaporation phenomena exhibited from a field ion

microscope. In the atom probe, atoms are removed from the specimen by pulsed field evaporation, fly through the probe hole, and are detected in the built-in mass spectrometer. There are time-of-flight type, fan magnetic-field type and four-pole type atom probes. The author describes his developed time-of-flight type atom probe having high analysis resolution and presents its application to the analysis of TiC and TiSi₂. (17 refs.) K.B.

111826 Statistics of the atom-by-atom dissection of planes in an atom-probe field-ion microscope: the number of atoms detected per plane. A.T.Macrauder, M.Yamamoto, D.N.Sidman (Dept. of Materials Sci. & Engng., Cornell Univ., Ithaca, NY, USA).

Rev. Sci. Instrum. (USA), vol.54, no.9, p.1077-84 (Sept. 1983).

The statistics of the atom-by-atom dissection of planes, in the atom-probe field-ion microscope, have been investigated. Tungsten specimens oriented in the [110] direction, with the probe hole over the center of the plane, were slowly pulsed field-evaporated on a plane-by-plane basis, and statistical-analyses were made on the number of tungsten atoms detected per plane; 30 separate slow dissection experiments were performed. Observed fluctuations in the number of atoms power plane are used to infer a range of allowable values for the detection efficiency. The authors found that, in some cases, the number of atoms per plane can be described as following a binomial distribution. From these results detection efficiencies in the range 0.11 to 0.54 were inferred. This range of efficiencies can be understood with the aid of field-ion desorption images. In addition, a value for the detection efficiency of 0.2 was obtained under the assumption that all atoms in the area projected by the probe hole, along the specimen radius, were analyzed. Thus, it was found that this geometrical procedure, a first-order approach to the problem, yields a reasonable result. Also, the results of a Monte Carlo simulation of atom-by-atom field evaporation of a large number of planes are presented. The Monte Carlo simulation shows that if a binomial distribution is obtained, the uncertainty in concentrations determined by the atom-probe technique will have only a small component owing to the uncertainty in the number of solvent specimen atoms—this is subject to the caveat that there are no special problems with the field-evaporation behavior of the solvent atoms. Although the statistical analyses were applied to a specific crystallographic plane and position, the methodology is reasonably general and can be applied to other situations. (28 refs.)

111827 High-resolution scanning transmission electron microscopy. A.V.Crewe (Enrico Fermi Inst., Univ. of Chicago, Chicago, IL, USA).

Science (USA), vol.221, no.4608, p.325-30 (22 July 1983).

The high-resolution scanning transmission electron microscope is being used in a growing number of laboratories. This article provides a general overview of the instrument and its capabilities. (27 refs.)

111828 Direct observation of microscopic electromagnetic fields by means of electron holography. A.Tonomura.

Solid State Phys. (Japan), vol.18, no.6, p.307-14 (June 1983). In Japanese.

Recently developed techniques of electron holography have opened the way to direct observation of microscopic electromagnetic fields in interference micrographs. (17 refs.)

111829 An improved transfer module and variable temperature control for a simple commercial cooling holder. G.Perlov, Y.Talmon (Dept. of Chem. Engng., Technion-Israel Inst. of Technol., Haifa, Israel), A.H.Falls.

Ultramicroscopy (Netherlands), vol.11, no.4, p.283-8 (1983).

A new cold stage transfer module was designed for the commercially available cooling holder of the JEOL JEM 100CX electron microscope. In the new CSTM the entire loading of the specimen is carried out under liquid nitrogen. This gives a frost-free transfer during which the temperature of the sample does not exceed 120K. Straightforward modifications to the commercial cooling holder permit continuous selection of specimen temperature between 100 and 450K. The sample can be heated or cooled at rates of up to 7K/s. These modifications do not impair the resolution of the holder which is better than 1.5 nm. This work illustrates a relatively simple way of modifying a commercial cooling holder into a true cold stage system. (9 refs.)

111830 A new high-angle annular detector for STEM. S.J.Pennycook, D.McMullan (Cavendish Lab., Cambridge Univ., Cambridge, England).

Ultramicroscopy (Netherlands), vol.11, no.4, p.315-19 (1983).

A channel plate multiplier mounted in a specimen cartridge can form an efficient high-angle detector for any STEM in which the electron gun is below the cartridge while the normal imaging and microanalysis facilities for the microscope are maintained. Such a high-angle detector minimises diffraction contrast effects from crystalline particles or supports and allows thick samples to be penetrated. It is particularly useful for catalyst studies. (15 refs.)

SPIE Proceedings on Microscopy Techniques and Capabilities See Entry 111302

Technique for quantitative analysis of specimen microtopography using computer control of a scanning electron microscope See Entry 111633

Analysis of insulating materials by negative ionmicroprobe ... See Entry 111801

Ion current measurement channel in single-collector mass spectrometers See Entry 111804

Resistance thermometer for ion-beam calorimetry See Entry 112515

A digital processing method for structural analysis of atom clusters from high resolution electron micrographs See Entry 112892

Charged particle ray simulator and monitor See Entry 112916

Interferometrical processing of electron microscopic holograms. III. Investigation of special features of the differential interferometry including noise problems See Entry 112918

Investigation of a double-beam linear high-voltage electron-optic system with centrifugal electrostatic shaping and recovery of electron energy See Entry 112919

Scanning electron acoustic microscopy See Entry 113235

Real space image simulation in high resolution electron microscopy See Entry 113708

Magnetic domain structure observation by electron holography See Entry 114717

Techniques in surface microscopy and analysis See Entry 115596

Analytical capabilities of transmission electron microscope (TEM) systems See Entry 115597

Material analysis by means of high energy ion beams See Entry 115600

Schlieren optical imaging of weak objects See Entry 115992

07.85 X-RAY, GAMMA-RAY INSTRUMENTS AND TECHNIQUES

111831 Magnetic Compton scattering with circularly polarised synchrotron radiation. R.S.Holt, M.J.Cooper (Dept. of Phys., Univ. of Warwick, Coventry, England).

Nucl. Instrum. & Methods Phys. Res. (Netherlands), vol.213, no.2-3, p.447-52 (1 Aug. 1983).

The Compton cross-section contains a term which couples the electron spin to the circularly polarised radiation field making it possible, in principle at least, to study the spin-dependent momentum distribution of electrons in ferromagnetic materials. The intensity of circularly polarised synchrotron radiation, emitted at a small angle to the orbital plane of the circulating electrons has been calculated for the three-pole wiggler magnet on the new Synchrotron Radiation Source (SRS) at the Daresbury Laboratory. The feasibility of a magnetic Compton scattering experiment, in which this component of the beam is selected, has been evaluated for wavelengths in the range 0.1 Å to 1.0 Å. The results, calculated for a 5 mm thick magnetised iron sample, show that, within the life-time of the stored synchrotron beam (≈ 8 h) more than 10^6 counts should be accumulated under the spin-dependent Compton profile. This intensity approaches that of conventional Compton experiments with unpolarised gamma-ray sources and clearly indicates that studies of ferromagnetic materials in the wavelength region 0.25-0.5 Å should be possible on the SRS and other similar machines. (20 refs.)

111832 A simple experimental technique for very small Mossbauer line shifts using resonance detectors. I.G.Mandjukov, B.V.Mandjukova, V.G.Jelev, N.V.Markova (Dept. of Atomic Phys., Sofia Univ., Sofia, Bulgaria).

Nucl. Instrum. & Methods Phys. Res. (Netherlands), vol.213, no.2-3, p.477-81 (1 Aug. 1983).

The composite line resulting from experiments with a fixed resonance sample placed in front of a resonance detector has been studied. An 'inversion' of the composite line at high effective thicknesses of the sample has been observed. The parameter asymmetry of the composite line which is a very sensitive linear function of the relative shift between the sample and detector lines has been defined. As a test of the method the temperature red shifts of SnO_2 and CaSnO_3 have been observed. The isomer shift of CaSnO_3 line relatively to SnO_2 unresolved doublet of $+(0.028 \pm 0.0024)$ mm/s has been measured by temperature shift compensation. Some features and possible applications of the new method have been listed and commented on. (12 refs.)

111833 Self-absorption effect for low energy X-rays. M.Sarkar (Dept. of Phys., Univ. of Dhaka, Dhaka, Bangladesh).

Nucl. Instrum. & Methods Phys. Res. (Netherlands), vol.214, no.2-3, p.557-9 (1 Sept. 1983).

A method for calculating the self-absorption effect for low energy (1 keV $\leq E \leq 3$ keV) X-rays is described. The factor due to self-absorption was calculated for the M_α line of different elements ($62 \leq Z \leq 79$). For Sm ($Z=62$) and Au ($Z=79$), its value varies from 0.957 to 0.977 for a target thickness of $50 \mu\text{g}/\text{cm}^2$. The dependence of this factor on target thickness was also investigated. (4 refs.)

111834 Automatic X-ray inspection system. A.Edwards.

Process Eng. (Australia), vol.11, no.2, p.27 (Feb. 1983).

An interesting concept in automatic inspection, which uses a minicomputer to scan, interpret and sentence the results of an X-ray examination, is now available from a British company, Peerless Control Systems. The system, ART (automatic radiographic testing), has applications in many industries and can inspect at virtually any point or points in a processing line. The system combines a specially matched television camera with an image intensifier. By controlling the X-ray equipment from the computer, high quality television pictures are displayed for immediate visual inspection and for computer comparison with known standard components. Designated inspection programs can be stored on floppy disk or read only memory and test results can be taped for future analysis or reference. (no refs.)

111835 Four-dimensional reconstruction problems in cineradiography from space-time integrated projections. J.Marilleau (CEA, Sevrans, France).

Proc. SPIE Int. Soc. Opt. Eng. (USA), vol.312, p.3-14 (1983). (1st European Conference on Cineradiography with Photons or Particles, Paris, France, 18-21 May 1981).

The author illustrates the principles involved in achieving reconstruction of a space-time dependent object from cineradiography, i.e. from space-time integrations on the object. (no refs.)

111836 Some applications of cineradiography to gas turbines. D.A.W.Pullen (Nondestructive Testing Centre, AERE Harwell, England), P.A.E.Stewart.

Proc. SPIE Int. Soc. Opt. Eng. (USA), vol.312, p.40-9 (1983). (1st European Conference on Cineradiography with Photons or Particles, Paris, France, 18-21 May 1981).

The paper is presented in two parts. The first part deals with the investigation of basic parameters of image intensifier performance with X-ray inputs when applied to the study of dynamic events. The use of a cold neutron beam to study oil flows inside a running gas turbine is also discussed. The second part deals with the application of the developed image intensifier systems to specific studies of various problems related to gas turbines, both in the manufacturing process and in development testing. (5 refs.)

111837 Basic phenomena in high energy-density beam welding and cutting. Y.Arata (Welding Res. Inst., Osaka Univ., Yamadakami, Osaka, Japan).

Proc. SPIE Int. Soc. Opt. Eng. (USA), vol.312, p.50-7 (1983). (1st European Conference on Cineradiography with Photons or Particles, Paris, France, 18-21 May 1981).

Essential features in the dynamic behaviour of welding and cutting processes with high energy density beams are reviewed and clarified by the efficient use of various cineradiography diagnostic techniques. Formation of a deep beam hole in the weld pool are described and the important effect of the front wall characters in the beam hole is demonstrated on the natures of deep penetration and defect formations such as spiking and porosity. The cutting process is also interpreted in the frame of the same physical viewpoint with the welding. A new and efficient suppression method by spiking, porosity and humping are examined and confirmed using a Tandem Electron Beam developed by the author. (7 refs.)

111838 Pulsed high-energy radiographic machine emitting X-rays (PHERMEX): applications to study high-pressure flow and detonation waves. R.D.Dick (Los Alamos Nat. Lab., Los Alamos, NM, USA).

Proc. SPIE Int. Soc. Opt. Eng. (USA), vol.312, p.66-81 (1983). (1st European Conference on Cineradiography with Photons or Particles, Paris, France, 18-21 May 1981).

PHERMEX has been used as a diagnostic tool to make quantitative measurements from radiographs of inert materials under dynamic high-pressure conditions and of explosives during the detonation process. In some experiments,

radiography is the best method to study complicated hydrodynamic flow occurring in a dynamic experiment. To demonstrate the versatility and uniqueness of PHERMEX and the radiographic method, several experiments on inert solids having high and low atomic numbers are discussed with some particulars. This includes the observation of the 11.0-GPa-pressure phase transition for antimony and the accompanying two-shock structure and the off-Hugoniot data for lead using regular reflection. Also, by careful design of a radiographic experiment, the Hugoniot state behind a shock front can be completely and precisely specified. Aluminium is an example of a material studied in this manner. PHERMEX is useful in studying some detonation properties of explosives. As an illustration, the discussion includes radiographic results of divergence characteristics of a detonation wave in sensitive and insensitive explosives as it propagates past a corner and the effect of preshocking on the detonation process of insensitive explosives when the detonation wave interacts with a region that has been shock-compressed at a pressure too low to cause detonation. (16 refs.)

111839 Flash X-ray of shot exit from gun muzzles. D.M.Blake (Central Sci. Services Proof & Experimental Establ., Shoeburyness, England).

Proc. SPIE Int. Soc. Opt. Eng. (USA), vol.312, p.82-5 (1983). (1st European Conference on Cineradiography with Photons or Particles, Paris, France, 18-21 May 1981).

Describes the development and use of flash X-ray system to radiograph the dynamic behaviour of projectiles on exit from gun muzzles. Details of equipment, equipment protection, films, cassettes and system triggering are presented. (2 refs.)

111840 High speed cineradiography of projectiles. R.J.Bracher (Magnacine Corp., Kettering, OH, USA).

Proc. SPIE Int. Soc. Opt. Eng. (USA), vol.312, p.86-92 (1983). (1st European Conference on Cineradiography with Photons or Particles, Paris, France, 18-21 May 1981).

Describes a camera that was developed specifically for high speed cineradiography and was designed to be used both in laboratory and field trials. The camera is programmable by digital controls and can drive flash X-ray units synchronously with framing up to a rate of 250000 FPS. An image format of nine frames 24×30 mm. A gain of times 10000 is incorporated to give amplification of low light level, short exposure X-ray flashes. (4 refs.)

111841 System of conversational image processing with two independent control-operator boards. P.Betremieux (CEA, Sevrans, France).

Proc. SPIE Int. Soc. Opt. Eng. (USA), vol.312, p.230-8 (1983). In French. (1st European Conference on Cineradiography with Photons or Particles, Paris, France, 18-21 May 1981).

The Laboratory of Image Processing was founded in 1975. Its main goal was to contribute to the reading and processing of radiographic films. The author describes the present state of the Laboratory and presents some examples of image processing in the field of nondestructive testing. (no refs.)

111842 Flash X-ray generator at high energy: GREC. J.Buchet, H.Biero, G.Fourrier (CEA, Sevrans, France).

Proc. SPIE Int. Soc. Opt. Eng. (USA), vol.312, p.240-5 (1983). In French. (1st European Conference on Cineradiography with Photons or Particles, Paris, France, 18-21 May 1981).

GREC, an acronym for 'Générateur de Radiographie Eclair' was designed for visualisation, measurements and studies on dynamic behavior of materials under high explosive loading. Since the first operating time, 1975, this facility has been improving, taking advantage of progress in the techniques involved, especially focusing and transport of intense electron beams. The authors describe the X-ray machine and give some details on the image detection device. The pulse generator, a 80 stage Marx generator can deliver a peak voltage of 9 MV in $1.2 \mu\text{s}$ by series erection of 2×80 capacitors charged at ± 60 kV. The pulse-forming network, a tri-axial Blumlein, delivers a 80 ns-pulse via a 26 ohms impedance transmission line to the transport section. This transport section is a 24 cm diameter, 2 meters long, magnetic-insulated coaxial line. At the end, the X-ray radiation is emitted by bremsstrahlung of the electrons impinging the tantalum anode of the discharge diode. The image acquisition device has been designed for X-raying of objects under loading of up to 50 kg of high explosives. Some details are given on the experimental arrangement used. Despite the severe environmental shock constraints, reasonable measurements of line-integrated density are possible. (2 refs.)

111843 PHERMEX—pulsed high energy radiographic machine emitting X-rays. R.D.Dick (Los Alamos Nat. Lab., Los Alamos, NM, USA).

Proc. SPIE Int. Soc. Opt. Eng. (USA), vol.312, p.246-56 (1983). (1st European Conference on Cineradiography with Photons or Particles, Paris, France, 18-21 May 1981).

The PHERMEX facility used to provide flash radiographs of explosives and explosive-driven metal systems is described. With this facility, precision radiographs of large objects containing materials with high atomic number and high density are attainable. PHERMEX encompasses the high-current, three-cavity, 30-MeV linear electron accelerator; the 50-MHz radiofrequency power source to drive the cavities; timing, and signal detection system; and a data-acquisition system. Some unique features of PHERMEX are reliability; very intense submicrosecond bremsstrahlung source rich in 4- to 8-MeV X-rays; less than 1.0-mm-diam spot size; precision determination of edges, discontinuities, and areal-mass distribution; and flash radiographs of large explosive systems close to the X-ray target. Some aspects of the PHERMEX-upgrading program are discussed. The program will result (1) in an increased electron-beam energy to about 50 MeV, (2) the use of an electron-gun pulser that is capable of producing three-time-adjustable pulses for obtaining three 'radiographic' pictures of a single explosive event, (3) an increased electron injection energy of 1.25 MeV, (4) the capability for recording high-speed signals, and (5) the use of computers to assist the monitoring and control of the data-acquisition system and the PHERMEX accelerator. (6 refs.)

111844 Facility for cineradiography at high energy: the ARTEMIS project. A.Hauducœur, J.Buchet (CEA, Sevrans, France), C.Perraudin, J.L.Pourre, J.Aucouturier.

Proc. SPIE Int. Soc. Opt. Eng. (USA), vol.312, p.257-61 (1983). In French. (1st European Conference on Cineradiography with Photons or Particles, Paris, France, 18-21 May 1981).

The ARTEMIS Project, a facility for high speed cineradiography will allow spatial and temporal analysis of physical phenomena in streak or framing operation. The facility will include two parts: a linear electron accelerator (45 to 55 MeV) and an opto-electronic recording system formed by 1 to 3 cameras depending on the observation mode (streak or framing). The linear electron accelerator built by CGR-MeV, will have to deliver a radiation dose at 1 meter higher than: 10 R/μs during a 15 μs pulse, 20 R for each of three 50 ns short pulses in a 15 μs period. The main desired characteristics of the X-ray source for the authors' radiographic purposes are given. The chosen source, a L-band linear electron accelerator is described. Finally the projected image recording system is presented. (2 refs.)

111845 Flash X-ray systems. A.Mattsson (Instrument AB Scanditronix, Uppsala, Sweden).

Proc. SPIE Int. Soc. Opt. Eng. (USA), vol.312, p.270-4 (1983). (1st European Conference on Cineradiography with Photons or Particles, Paris, France, 18-21 May 1981).

The design and performance characteristics of a set of high intensity flash X-ray systems are discussed. At present, six systems are available with output voltages in the range of 75 kV to 1200 kV. Peak current is 10 kA and exposure time 20 ns. Demountable X-ray tubes are being used to increase flexibility and reduce operating costs. Typical applications are found in areas such as ballistics, detonics, quality control, etc. (no refs.)

111846 Magnetic focus/deflection image converter camera for cineradiography. R.J.Bracher (Magnacine Corp., Kettering, OH, USA).

Proc. SPIE Int. Soc. Opt. Eng. (USA), vol.312, p.286-9 (1983). (1st European Conference on Cineradiography with Photons or Particles, Paris, France, 18-21 May 1981).

This camera was developed specifically for high speed cine radiography and was designed to be used both in laboratory and field trials. The camera is programmable by digital controls and can drive flash X-ray units synchronously with framing up to a rate of 250000 fps. An image format of nine frames 24X30 mm and a gain of 10000 is incorporated to give amplification of low light level short exposure X-ray flashes. (3 refs.)

111847 Image converter tubes for radiology and neutronography used in nondestructive testing. M.Verat, H.Rougeot (Thomson-CSF Div. Tubes Electroniques, Paris, France).

Proc. SPIE Int. Soc. Opt. Eng. (USA), vol.312, p.290-7 (1983). In French. (1st European Conference on Cineradiography with Photons or Particles, Paris, France, 18-21 May 1981).

Describes the basic structure and the fabrication process of radiation-sensitive image-converter-tubes; these tubes are self-sensitive for 10 keV to 10 MeV photons or cold and thermal neutrons. In most general use, these tubes have an effective field aperture of 22 or 30 cm but it is also possible to make smaller (15 cm) or larger (40 cm) tubes. Data and application characteristics of these tubes are given. The conversion factor (the output image luminance corresponding to a given input radiation) is high enough to allow real-time acquisition of the image, as with a TV camera or a high speed camera for example. Typical conversion factors are $100 \text{ cd.m}^{-2}.\text{mR}^{-1}.\text{s}$ for X-rays and $3 \times 10^{-10} \text{ cd.s.n}^{-1}$ for neutrons. The spatial resolution is 2.5 to 5 lp.mm⁻¹ depending on the kind of tube; density steps of 2% are detected. Applications of these tubes are illustrated by examples in medicine (cine-angiography and televised-surgery) as well as in ballistics. (no refs.)

111848 X-ray microscopy: recent developments and practical applications. B.Niemann, G.Schmahl, D.Rudolph (Univ. Sternwarte, Göttingen, Germany).

Proc. SPIE Int. Soc. Opt. Eng. (USA), vol.368, p.2-8 (1983). [received: Sept. 1983] (SPIE Proceedings on Microscopy Techniques and Capabilities, London, England, 21-22 Sept. 1982).

X-ray microscopy using soft X-rays has progressed successfully during the past years. The authors discuss the atomic cross sections, the photoelectric absorption and the radiation damage for soft X-rays. Results of contact microradiography are summarized. X-ray optics, which can be used for microscopy are zone plates, grazing incidence mirrors and normal incidence multilayer mirrors, yet this has only been shown in practice with high resolution for zone plates. Details of the 'Göttingen X-ray microscope' are given and a photographic image, showing 50 nm resolution, is shown. The future work of several groups is concentrated on the development of scanning X-ray microscopes. (32 refs.)

111849 Application of synchrotron radiation to X-ray microscopy. P.J.Duke (Daresbury Lab., Sci. & Engng. Res. Council, Warrington, England).

Proc. SPIE Int. Soc. Opt. Eng. (USA), vol.368, p.21-5 (1983). [received: Sept. 1983] (SPIE Proceedings on Microscopy Techniques and Capabilities, London, England, 21-22 Sept. 1982).

Describes work currently going on or under development at the Daresbury Laboratory at shorter X-ray wavelengths, where shorter in this instance means wavelength $< 4 \text{ \AA}$. (11 refs.)

111850 The investigation of image formation in a large-area solid state X-ray receptor with electrophoretic display. K.H.Yang (General Electric Corporate Res. & Dev., Schenectady, NY, USA).

J. Appl. Phys. (USA), vol.54, no.9, p.4711-21 (Sept. 1983).

The image formation and the resolution of a self-contained electrophoretic X-ray imager have been investigated. The electrophoretic suspension contained pigments and counterions, ionic surfactants, and extraneous charges. Rate equations have been formulated to describe the transport properties of the ionic surfactants from the low to high field regions. The electrical transport properties of the electrophoretic suspension were investigated in relation to X-ray image formation using three different modes of operation: the pulse, the biased-pulse, and the universal modes. The reflectance versus charge curves of the X-ray images were qualitatively explained. Both negative- and positive-mode X-ray images of $22 \times 22 \text{ cm}^2$ have been demonstrated with two different electrophoretic suspensions. The imager can achieve X-ray images of high resolution and large area at the same time. (19 refs.)

111851 Square wave gratings for screen-film-combination modulation transfer function determination. D.Hoeschen (Phys.-Tech. Bundesanstalt, Braunschweig, Germany).

Optik (Germany), vol.65, no.2, p.97-101 (1983). In German.

Square wave gratings of lead are often used for the determination of the modulation transfer function of screen-film-combinations. Model calculations show how square wave gratings with continuously changing frequencies should be designed. (4 refs.)

111852 Streak camera for picosecond X-ray diagnostics. P.A.Jaanimagi, M.C.Richardson (Div. of Phys., Nat. Res. Council of Canada, Ottawa, Canada).

Rev. Sci. Instrum. (USA), vol.54, no.9, p.1095-9 (Sept. 1983).

The authors report details of an X-ray sensitive streak camera with an estimated time resolution of less than 10 ps. The streak camera is based on a modified RCA 73435 image tube and features a large photocathode area and high sensitivity. A direct comparison of the relative quantum efficiency of Au and CsI photocathodes for 1-10 keV X-rays is also presented. (17 refs.)

111853 Investigation on the real-time pseudocolor display of three-dimensional X-ray image. Zhang Sen, Zhang Guangzu (Hangzhou Univ., China).

Sci. Sin. (China), vol.26, no.7, p.777-84 (July 1983).

On the basis of the principle of binocular stereoscopy and the principle of pseudocolor display with intensity slicing, a method of the real-time pseudocolor display of three-dimensional X-ray image is proposed. One X-ray stereo-source composed of two triode X-ray tubes, one image intensifier, and one plumbicon camera are used as TV camera system. By means of processing the electronic image with the pseudocolor technique, the authors have

successfully transformed the invisible X-ray image into a visible pseudocolor image which is of clear three-dimension and enhanced contrast. (9 refs.)

1st European Conference on Cineradiography with Photons or Particles See Entry 111300

SPIE Proceedings on Microscopy Techniques and Capabilities See Entry 111302

The determination of X-ray spectra from attenuation data. I. The potentials of various methods See Entry 111654

On the transfer function of an electromechanical transducer: an application to the Mossbauer velocity drive See Entry 111660

Improved X-ray collimation system for diamond-anvil high-pressure cells See Entry 111697

Investigation of material movement within steel test sections by means of high speed X-ray photography See Entry 112319

Effect of pre-exposure of films on radiographic sensitivity See Entry 112365

A multi-microprocessor neutron spectrometer computer interface system See Entry 112526

An automatic gamma spectrometer for activation analysis See Entry 112527

A microprocessor controlled spectrometer for frequency modulation Mossbauer measurements See Entry 112529

Background estimation for gamma-ray spectrometry See Entry 112531

A pseudorandom pulser technique for the correction of dead-time and pile-up losses in γ -ray spectrometry See Entry 112532

Stabilized scintillation spectrometer for scattered low-energy gamma radiation See Entry 112537

Use of BPS-75 + 'Elektronika-100I' scanning-measuring system for analysis of photographs from wide-gap chambers See Entry 112576

Two-stage integrator for an X-ray tomograph See Entry 112605

X-ray visualisation of high speed phenomena: application to the behavior of materials under high explosives loading See Entry 113525

Ray tracing of a concave-curved-crystal spectrometer and its detailed characteristics for X-ray spectroscopic diagnostics of high-temperature plasmas See Entry 113659

Electron temperature monitor for laser-produced plasmas See Entry 113666

Sensitivity of X-ray computer tomography in the inspection of thin layers, glued joints, cracks, laminations, and coatings See Entry 115486

Automatic device for establishing the specified regime of X-ray flaw detectors and frequency doubler for electronic stopwatch See Entry 115488

Neutron and gamma simultaneous radiography using a ^{252}Cf isotopic neutron source See Entry 115499

Quantitative microfocal radiography in medicine, biological research, and the quality control industry See Entry 115906

Soft X-ray imaging microscopy using zone plates and nonsynchrotron sources See Entry 115982

An imaging gas scintillation proportional counter for use in X-ray astronomy See Entry 116472

A proportional counter with one dimensional position sensitivity for image scanning in the soft X-ray region See Entry 116473

07.90 OTHER TOPICS IN SPECIALISED INSTRUMENTATION

111854 The Australian high resolution neutron powder diffractometer. C.J.Howard, C.J.Ball (Lucas Heights Res. Labs., Australian Atomic Energy Commission Res. Establ., Sutherland, New South Wales, Australia), R.L.Davis, M.M.Elcombe.

Aust. J. Phys. (Australia), vol.36, no.4, p.507-18 (1983).

The high resolution neutron powder diffractometer installed on the AAEC HIFAR reactor at Lucas Heights is described. The resolution is in good agreement with predictions and, although below the most optimistic estimates, the intensities are usable. Examples are given of problems solved using the diffractometer which could not have been solved either by X-ray diffraction or by use of a conventional neutron powder diffractometer. Plans for diffractometer development are outlined. (24 refs.)

111855 Goniometer for pole figure measurement by means of neutron diffraction method. M.Dlouha, J.Jerabek, S.Vratilav (Fakulta Jaderna a Fyzikalne Inzenyrská CVUT, Praha, Czechoslovakia).

Jad. Energ. (Czechoslovakia), vol.29, no.8-9, p.316-18 (Aug.-Sept. 1983). In Czech.

The article describes a goniometer which was constructed and made in neutron Diffraction Laboratory of Faculty of Nuclear Science and Physical Engineering. The most important application is texture analysis of different materials after cold-worked or thermal treatment. The instrument is operated together with a neutron diffractometer, a control unit assures automatic measurements. Characteristic parameters and examples of utilization are given. (3 refs.)

111856 Sample-size determination in the certification of suspensions of monodisperse particles. I.I.Kravchenko.

Meas. Tech. (USA), vol.25, no.11, p.964-6 (Nov. 1982). Translation of: *Izmer. Tekh. (USSR)*, vol.25, no.11, p.64-6 (Nov. 1982).

Suspensions of monodisperse particles are used extensively in the testing of aerosol equipment and in a number of research programs. The basic characteristics of such suspensions determined in certification are the average particle size (diameter) and the degree of monodispersity (the entire discussion of this article refers to spherical particles). The suitability of a particular suspension of a specific application depends on the error of estimation of its parameters. The error of determination of the characteristics of the suspension, in turn, depends on the sample size, i.e. on the number of particles in the suspension subjected to analysis. A procedure used for the certification of suspensions is presented. (no refs.)

111857 Cold neutron fluoroscopy of operating automotive engines. P.A.E.Stewart (Rolls-Royce Ltd., Bristol, England), J.Heritage.

Neutron Radiography. Proceedings of the First World Conference, San Diego, CA, USA, 7-10 Dec. 1981 (Dordrecht, Netherlands: Reidel 1983), p.635-42.

The application of neutron fluoroscopy in the automotive industry is a natural extension of previous studies with aircraft engines. The paper describes investigations with two subcompact car engines. The extent and manner in which lubricants reached the various parts of the engines are compared and contrasted. The paper goes on to describe a study of the deposits inside turbochargers and postulates future topics worthy of investigation. The authors

confirm that there is a place for neutron fluoroscopy both as a design tool and for investigations of 'in-service' phenomena. (5 refs.)

111858 High frame-rate neutron radiography of dynamic events. R.H.Bossi, A.H.Robinson, J.P.Barton (Oregon State Univ., Corvallis, OR, USA).

Neutron Radiography. Proceedings of the First World Conference, San Diego, CA, USA, 7-10 Dec. 1981 (Dordrecht, Netherlands: Reidel 1983), p.643-51. A system has been developed to perform neutron radiographic analysis of dynamic events having a duration of several milliseconds. The system has been operated in the range of 2000 to 10000 frames/second. Synchronization has provided high-speed-motion neutron radiographs for evaluation of the firing cycle of 7.62 mm munition rounds within a steel rifle barrel. The system has also been used to demonstrate the ability to produce neutron radiographic movies of two phase flow. Special studies have been performed on the scintillator conversion screens and on the effects of statistical limitations on the image quality. Modulation transfer function analysis has been used to assist in the evaluation of the system performance. (13 refs.)

111859 Performance of the Mound Facility Californium Multiplier. J.D.Hastings (Monsanto Res. Corp., Miamisburg, OH, USA). Neutron Radiography. Proceedings of the First World Conference, San Diego, CA, USA, 7-10 Dec. 1981 (Dordrecht, Netherlands: Reidel 1983), p.695-7. The Californium Multiplier (CFX) is a subcritical fission system which supplies neutrons for neutron radiography and neutron activation analysis. Such a unit has been built by IRT Corporation for use with approximately 20 mg Cf-252, was installed at the Mound Facility in September 1977, and has been operating since October 1977. The Mound CFX is primarily used for neutron radiography and is capable of producing neutron radiographs nearly similar in quality to those obtained by reactor facilities. Approximately 65000 parts have been radiographed in the more than three year period from October 1977 to June 1981. The description and performance of the CFX facility are presented. (1 ref.)

111860 A new accelerator-based neutron radiography system. J.Stokes, L.Parks, C.Preskitt, J.John, H.R.Lukens,Jr., J.MacKenzie, R.Voigt, J.Wilson, N.Lurie, A.P.Trippe (Nuclear Systems Div., IRT Corp., San Diego, CA, USA), W.Davis.

Neutron Radiography. Proceedings of the First World Conference, San Diego, CA, USA, 7-10 Dec. 1981 (Dordrecht, Netherlands: Reidel 1983), p.717-24. A new neutron radiography system capable of accommodating an accelerator source of neutrons has been developed at IRT Corporation. The new system, consisting of a shielded moderator with a specially designed thermal neutron beam port and an access port for an accelerator beam tube, was transported to an available 4-MeV Van de Graaff accelerator for system evaluation. A suitable beam tube extension contained a water-cooled Be target. The target was bombarded with 5-150 μ A of 3 MeV deuterons, and for some tests the deuteron energy was varied from 1.5 to 4.0 MeV. The system was found to be capable of producing a thermal flux of 1.3×10^6 n cm⁻² sec⁻¹ at a collimation ratio of 20:1, for a 300 μ A current of 3.0-MeV deuterons on target. The neutron-to-gamma ratio of the beam was found to be 1.0×10^5 n cm⁻² mR⁻¹, and the measured cadmium ratios were 3.5 and 18.3 for Au foils and ²³⁵U detectors, respectively. Several excellent-quality radiographs of ordinance items were obtained. (8 refs.)

111861 Optimisation of etching conditions and shortening of the etching time of cellulose nitrate films. M.Fantini, G.Renard (Kodak-Pathe Res. Labs., Paris, France).

Neutron Radiography. Proceedings of the First World Conference, San Diego, CA, USA, 7-10 Dec. 1981 (Dordrecht, Netherlands: Reidel 1983), p.737-44. The light depolarization method for the measurement of the optical densities of a picture on cellulose nitrate film was used to plot the precise sensitometric curves of these films. It is found that the apparent sensitivity decreases when the film is over etched or overexposed. By means of these curves, it is possible to select optimal conditions. Results of the research work to minimize etching time are described. The purpose is to permit the routine use of neutron radiography and heavy ion radiography by making an access to the image in a reasonable time. (1 ref.)

Californium-252 as a source of subthermal neutrons	See Entry 112521
Multiple filament plug-in module for use on the Tara neutral beam source	See Entry 113632
Neutron and gamma simultaneous radiography using a ²⁵² Cf isotopic neutron source	See Entry 115499
Simple apparatus for concentration determinations in binary-gas mixtures	See Entry 115604

10.00 THE PHYSICS OF ELEMENTARY PARTICLES AND FIELDS

(for cosmic rays, see 94.40; for high energy-experimental techniques and instrumentation, see 29.)

11.00 GENERAL THEORY OF FIELDS AND PARTICLES

(see also 03.65 Quantum mechanics, 03.70 Theory of quantized fields, 03.80 General theory of scattering)

11.10 FIELD THEORY

111862 Multidyon solutions in SU(2) gauge group. Jiin Chang Shaw (Dept. of Appl. Maths., Chiao Tung Univ., Hsinchu, Taiwan), Jiunn Chuu Chen. *Annu. Rep. Inst. Phys. Acad. Sin. (Taiwan)*, vol.12, p.37-53 (Dec. 1982). [received: Sept. 1983] Recently, Prasad described a systematic framework for the construction of axially symmetric multimonopole solution of arbitrary topological charge. The authors found that these solutions can be transformed into axially symmetric multidyon solutions easily. They write down the multidyon solutions in Yang's K-gauge also. (17 refs.)

111863 The group theoretical aspects of infinitesimal Riemann-Hilbert transform and hidden symmetry. Wu Yong-Shi (Centre de Phys. Theorique, CNRS, Marseille, France). *Commun. Math. Phys. (Germany)*, vol.90, no.4, p.461-72 (1983). The author obtains explicit expressions for infinitesimal regular Reimann-Hilbert (RH) transforms. Using them, the group theoretical aspects of infinitesimal RH transforms are discussed with an eye to the comparison with the hidden symmetry transformations proposed before. The author finds that the RH transforms have very rich group structure; e.g. in the 2-d principal chiral models, their group contains two Kac-Moody algebras as subalgebras. But not all of them are nontrivial hidden symmetries of the theory. (17 refs.)

111864 Classical equations $dN_i/dr = 1/2\epsilon_{ijk}[N_j,N_k]$. N.Ganoulis (Dept. of Theoretical Phys., Univ. of Thessaloniki, Thessaloniki, Greece). *Commun. Math. Phys. (Germany)*, vol.90, no.4, p.493-6 (1983). The author studies the first order system of equations $dN_i/dr = 1/2\epsilon_{ijk}[N_j,N_k]$, where the n_i are classical, 'nonabelian' gauge-Higgs fields with spherical symmetry. Exact solutions are constructed. (5 refs.)

111865 Counterexamples to some results on the existence of field copies. M.A.Mostow (Dept. of Maths., North Carolina State Univ., Raleigh, NC, USA), S.Shnider. *Commun. Math. Phys. (Germany)*, vol.90, no.4, p.521-6 (1983). Several criteria are known for determining which connections A are determined uniquely by their curvature F , or by F and its covariant derivatives. On a principle bundle with semi-simple gauge group G over a 4-manifold M , a sufficient condition for F to determine A uniquely is that the linear map $B \rightarrow [F \wedge B]$ from Lie algebra-valued 1-forms to 3-forms (pulled back to M via a local gauge) be invertible on an open dense set in M . Recently F.A. Doria has claimed that this condition is also necessary. The authors present counterexamples to this claim, and also to his assertion that F determines A uniquely if the restriction of the bundle to every open subset of M has holonomy group equal to G and F is 'not degenerate as a 2-form over space-time'. (18 refs.)

111866 Wilson loop calculations in four-dimensional lattice gauge theory on the CDC CYBER 205. D.Barkai (Center for Appl. Vector Technol., Colorado State Univ., Fort Collins, CO, USA), M.Creutz, K.J.M.Moriarty. *Comput. Phys. Commun. (Netherlands)*, vol.30, no.1, p.13-19 (July-Aug. 1983). Pure SU(4) gauge theory is simulated by Monte Carlo methods on an 8⁴ lattice. The method of Metropolis et al. (1953) is used to equilibrate the space-time lattice. All Wilson loops up to size 4 \times 4 are calculated. Because of memory requirements the authors work on the 2 Mword CDC CYBER 205 at Colorado University and take full advantage of the parallel processing capabilities of this vector machine. (15 refs.)

111867 Halliday-Suranyi expansion for lattice ϕ^4 theory. J.M.Rabin (J.W. Gibbs Lab. of Phys., Yale Univ., New Haven, CT, USA). *Nucl. Phys. B, Part. Phys. (Netherlands)*, vol.B224, no.2, p.308-28 (12 Sept. 1983). The Halliday-Suranyi perturbation expansion for the anharmonic oscillator is generalized and applied to ϕ^4 field theory on a spatial lattice. This expansion is believed to converge for any value of the coupling constant. It also serves as a model of renormalization-scheme dependence in QCD in that physical quantities depend on an arbitrary parameter at finite order but not when the series is summed. The propagator is computed through second order and the single-particle dispersion relation is extracted at strong and weak coupling. The results test both the expansion itself and Stevenson's principle of minimal sensitivity (PMS) for determining the arbitrary parameter. The author shows that use of the PMS prescription can alter the convergence properties of the expansion. (10 refs.)

111868 Fermi-Bose gas equivalence, non-Abelian symmetry groups, phase transitions and all that. S.A.Bulgadaev (L.D. Landau Inst. for Theoretical Phys., Moscow, USSR). *Nucl. Phys. B, Part. Phys. (Netherlands)*, vol.B224, no.2, p.349-78 (12 Sept. 1983). The equivalence triad of the two-dimensional massive Thirring model, sine-Gordon theory and the Coulomb gas is generalized to theories with non-Abelian symmetry groups. The group and field theoretical properties of the resulting bosonic theories, connected with the characters of the corresponding groups, are investigated. (40 refs.)

111869 Ising lattice gauge theory in three dimensions. P.P.Martin (Dept. of Phys., Queen Mary Coll., London, England). *Nucl. Phys. B, Field Theory & Stat. Syst. (Netherlands)*, vol.B220(FS8), no.4, p.366-82 (5 Sept. 1983). By raising the transfer matrix to a finite power the partition function for a finite lattice Z(2) gauge model is obtained exactly. The zeros of the resultant polynomial are found and some plaquette-plaquette expectation values are extracted. An exponential fit for the inverse correlation length matches onto both strong-and weak-coupling results but breaks down close to the second-order phase transition point. Similar calculations for the three-dimensional Ising model are also discussed. (19 refs.)

111870 Dynamical fermions in lattice gauge theories: Metropolis and Langevin techniques in two dimensions. T.Burkitt (Phys. Dept., Univ. of Edinburgh, Edinburgh, Scotland). *Nucl. Phys. B, Field Theory & Stat. Syst. (Netherlands)*, vol.B220(FS8), no.4, p.401-14 (5 Sept. 1983). A variety of techniques for the inclusion of dynamical fermions in lattice gauge theory is examined. Three pseudo-fermionic techniques that have the characteristics desirable for an unquenched simulation of four-dimensional QCD are studied in detail. Langevin and Metropolis pseudo-fermionic techniques are implemented for a 64 \times 64 lattice on the Distributed Array Processor and their relative merits examined both for free fermions and the lattice Schwinger model. (33 refs.)

111871 Distribution of zeros in Ising and gauge models. C.Itzykson, R.B.Pearson, J.B.Zuber (Service de Phys. Theorique, CENS, Gif-sur-Yvette, France). *Nucl. Phys. B, Field Theory & Stat. Syst. (Netherlands)*, vol.B220(FS8), no.4, p.415-33 (5 Sept. 1983). The authors discuss some features of Ising and gauge systems in the complex temperature plane. The distribution of zeros of the partition function enables one to study critical properties in a way complementary to the methods using real values. Data on small lattices confirm this picture. Nearby complex singularities seem to exhibit a universal behaviour which might have some relation with a model of random surfaces. (17 refs.)

- 111872 Loss of continuum Lorentz invariance in gauge theories on a triangular lattice.** W.Celmaster, F.Krausz (Northeastern Univ., Boston, MA, USA). *Nucl. Phys. B, Field Theory & Stat. Syst. (Netherlands)*, vol.B220(FS8), no.4, p.434-46 (5 Sept. 1983).
On a triangular lattice, a weakly chiral lagrangian of interacting bosons and fermions is constructed to be naturally invariant under the triangular symmetry. The continuum limit of the resulting field theory is not Lorentz invariant. The authors explicitly show this for the propagator of the massive Schwinger model. (13 refs.)
- 111873 Flavours of Lagrangian Susskind fermions.** H.Kluberg-Stern, A.Morel, O.Napoly (Service de Phys. Theorique, CENS, Gif-sur-Yvette, France), B.Petersson. *Nucl. Phys. B, Field Theory & Stat. Syst. (Netherlands)*, vol.B220(FS8), no.4, p.447-70 (5 Sept. 1983).
The authors show how to write the Susskind fermionic action explicitly in terms of flavour Dirac fields defined on hypercubes in position space. The remnant continuous global symmetry is identified with a $U(1)_A \otimes U(1)_A$ group, where the axial symmetry is flavour non-singlet. This construction allows us to identify the quantum numbers of states found in dynamical calculations for $SU(N)$ gauge theories, and the currents associated with the above global symmetry. It is also used in the strong-coupling limit to compute the decay constant of the pseudo-scalar Goldstone boson associated with the spontaneous breakdown of the $U(1)_A$ symmetry. The authors stress that the construction of flavours leads to a quark propagator which is continuous on the edges of the Brillouin zone, unlike the one obtained by assigning different flavours to different parts of this zone. (21 refs.)
- 111874 An improved mean field approach to the phase structure in Z_N gauge theory in four dimensions.** K.Odaka, M.Fukugita (Nat. Lab. for High Energy Phys., Tsukuba, Ibaraki, Japan). *Nucl. Phys. B, Field Theory & Stat. Syst. (Netherlands)*, vol.B220(FS8), no.4, p.471-8 (5 Sept. 1983).
The authors extend the mean field approximation scheme to include the effect of a fluctuation of the gauge field. As a consequence, they successfully obtain for the Z_N theory ($N > 5$) the phase transition which separates the Coulomb phase for the ordered phase as well as that separating the Coulomb and disordered phases. The former transition shows characteristics of higher-order phase transitions. (8 refs.)
- 111875 The accuracy of the pseudo-fermion method.** S.Otto, M.Randeria (California Inst. of Technol., Pasadena, CA, USA). *Nucl. Phys. B, Field Theory & Stat. Syst. (Netherlands)*, vol.B220(FS8), no.4, p.479-90 (5 Sept. 1983).
The pseudo-fermion method for dynamical fermions is studied using Monte Carlo techniques. Various approximations are tested by calculating the mass gap of the Schwinger model and by comparing it with results obtained with an exact algorithm. The mass found is consistent with that obtained from the exact algorithm, implying that the systematic errors are small. In addition, the mass is almost independent of the number of pseudo-sweeps used, implying that the statistical error inherent in the Monte Carlo of the pseudo-fermion field does not have a strong effect on the observable. Numerical evidence is presented to show that the algorithm gives the correct answer for even a single pseudo-sweep in the limit that the Metropolis hit size goes to zero. (12 refs.)
- 111876 Uniformly valid amplitude expansions for non-Abelian gauge theories.** J.L.Anderson (Dept. of Phys., Stevens Inst. of Technol., Hoboken, NJ, USA). *Gen. Relativ. & Gravitation (USA)*, vol.15, no.8, p.785-95 (Aug. 1983).
The imposition of a particular gauge condition in a non-Abelian gauge theory may lead to large- r nonuniformities in an amplitude expansion when used in the construction of an approximate solution of the field equations of the theory. The author shows that for both the Yang-Mills theory and general relativity it is always possible to find a class of gauge conditions that do not suffer from this defect and at the same time lead to solvable equations in each order of the approximation employed. The author further shows how one can construct such gauge conditions by a method similar to Lighthill's method of strained coordinates. An example of such a construction is given for the Yang-Mills theory. (5 refs.)
- 111877 Local conservation laws for the two-dimensional periodic $SU(n+1)$ Toda lattices.** R.S.Farwell (Blackett Lab., Imperial Coll., London, England), M.Minami. *J. Phys. A (GB)*, vol.15, no.11, p.3405-10 (Nov. 1982).
An infinite number of local conservation laws are derived for the two-dimensional periodic $SU(n+1)$ Toda lattice equations following the well known method for the sine-Gordon equation. (9 refs.)
- 111878 Auxiliary 'fields' for the massive spinning relativistic particle.** K.Sundermeyer (Inst. fur Theorie der Elementarteilchen Annimallee, Freie Univ. Berlin, Berlin, Germany). *Lett. Nuovo Cimento (Italy)*, vol.37, ser.2, no.16, p.556-60 (20 Aug. 1983).
The author considers the massive spinning relativistic particle formulated in terms of Grassman variables. The Lagrangian action and auxiliary fields are studied. (8 refs.)
- 111879 Conformal symmetry and new exact solutions of SU_2 Yang-Mills theory.** W.I.Fushchich, W.M.Shtelen (Math. Inst., Kiev, USSR). *Lett. Nuovo Cimento (Italy)*, vol.38, ser.2, no.2, p.37-40 (10 Sept. 1983).
Conformally invariant and some others exact solutions of the SU_2 Yang-Mills (YM) theory are found. The final conformal transformations for the YM potentials and the formulae of generating new solutions from known ones are presented. (7 refs.)
- 111880 The field with spin 2. I.** M.H.Nous (CRN, Univ. Louis Pasteur, Strasbourg, France). *Lett. Nuovo Cimento (Italy)*, vol.38, ser.2, no.3, p.65-71 (17 Sept. 1983).
From the theory of higher-spin fields as proposed by Bargmann-Wigner, (1948), the author presents and discusses the formulation of the fourth-rank symmetric spinor $\psi_{abcd}(x)$ which describes the massive spin-2 field. This spinor is then used for the formulation of the Lagrangian and the derivation of the field equation and all the additional conditions. (17 refs.)
- 111881 The field with spin 2. II.** M.H.Nous (CRN, Univ. Louis Pasteur, Strasbourg, France). *Lett. Nuovo Cimento (Italy)*, vol.38, ser.2, no.3, p.72-6 (17 Sept. 1983).
For pt.I see *ibid.*, vol.38, p.65 (1983). Discusses the plane-wave solution for the fourth-rank spinor $\psi_{abcd}(x)$ which represents the massive spin-2 field. The relativistic transformations of this field and the bilinear combinations of the components of the wave function are considered. (4 refs.)
- 111882 Renormalization scheme-invariant perturbation theory.** A.Dhar (Tata Inst. of Fundamental Res., Bombay, India). *Phys. Lett. B (Netherlands)*, vol.128B, no.6, p.407-10 (8 Sept. 1983).
A complete solution to the problem of the renormalization scheme dependence of perturbative approximations to physical quantities is presented. An equation

is derived which determines any physical quantity implicitly as a function of only scheme independent variables. (4 refs.)

- 111883 Quantization of nonlinear sigma model in constrained hamiltonian formalism.** J.Maharana (Inst. of Phys., Bhubaneswar, India). *Phys. Lett. B (Netherlands)*, vol.128B, no.6, p.411-14 (8 Sept. 1983).
The canonical structure and quantization of the $O(N)$ nonlinear sigma model is investigated in the constrained hamiltonian formalism due to Dirac. The explicit form of the quantum hamiltonian of the $O(3)$ nonlinear sigma model is obtained. (6 refs.)
- 111884 String tension in $SU(3)$ gauge theory on a 16^4 lattice.** F.Gutbrod (DESY, Hamburg, Germany), P.Hasenfratz, Z.Kunszt, I.Montvay. *Phys. Lett. B (Netherlands)*, vol.128B, no.6, p.415-17 (8 Sept. 1983).
Wilson loop expectation values are measured with improved statistics at $\beta=5.40$ and 5.70 by the Monte Carlo method. In this coupling constant region the (dimensionless) string tension drops more rapidly than required by the one-loop renormalization formula. (6 refs.)
- 111885 The Eguchi-Kawai model in two dimensions.** G.Maiella (Istituto di Fisica Teorica, Naples, Italy), P.Rossi. *Phys. Lett. B (Netherlands)*, vol.128B, no.6, p.421-4 (8 Sept. 1983).
The strong coupling expansions of the free energy for the Eguchi-Kawai model in two dimensions is evaluated by the use of the character expansion for the two-matrix model. The analyticity domain of the formal series in the complex β plane is smaller than the entire complex plane showing quite a pathological behaviour. (10 refs.)
- 111886 An improved renormalization group transformation in four dimensions.** R.Cordery, R.Gupta, M.A.Novotny (Phys. Dept., Northeastern Univ., Boston, MA, USA). *Phys. Lett. B (Netherlands)*, vol.128B, no.6, p.425-30 (8 Sept. 1983).
A new transformation for Monte Carlo renormalization group analysis of four-dimensional gauge theories is developed. This RG transformation has a scale factor of $\sqrt{3}$. In addition no gauge fixing is required in the construction of the link variables on the renormalized lattice. The $Z(2)$ theory is analyzed as a test case. (14 refs.)
- 111887 Large N reduced models and stochastic quantization.** G.Aldazabal, N.Parga (Centro Atómico de Bariloche, Bariloche, Argentina), M.Okawa, A.Gonzalez-Arroyo. *Phys. Lett. B (Netherlands)*, vol.129B, no.1-2, p.90-4 (15 Sept. 1983).
The authors study the reduction of degrees of freedom for large N matrix models, by means of the stochastic quantization procedure. This provides a simple proof of the validity of the reduction in perturbation theory. In addition, a large class of reduced models are constructed which contain as particular cases those considered previously in the literature. (13 refs.)
- 111888 Improved lattice actions and physical quantities.** R.Musto, F.Nicodemi, R.Pettorino (Istituto di Fisica Teorica, Univ. di Napoli, Naples, Italy). *Phys. Lett. B (Netherlands)*, vol.129B, no.1-2, p.95-8 (15 Sept. 1983).
The authors compare for the usual and for an 'improved' action the approach to the continuum limit of physical quantities in the lattice $O(N)$ nonlinear σ -model using large N techniques. They find a definitely improved behaviour, which for the renormalized coupling constants is due to the absence of all $O(a^2 \ln a)$ terms. The results fit nicely with those obtained recently for $N=3$ in a Monte Carlo simulation. (7 refs.)
- 111889 Dynamical gauge symmetry breaking as the Casimir effect.** Y.Hosotani (Dept. of Phys., Univ. of Pennsylvania, Philadelphia, PA, USA). *Phys. Lett. B (Netherlands)*, vol.129B, no.3-4, p.193-7 (22 Sept. 1983).
A new mechanism of dynamical gauge symmetry breaking is found in a class of higher dimensional theories. A system consisting of non-abelian gauge fields and fermions with minimal gauge interactions on a spacetime $M^n \times S^2$ is considered, where M^n and S^2 are an n -dimensional Minkowski spacetime and a surface of a sphere, respectively. Full analysis is given for odd n . By integrating fermion fields first, the author finds that gauge symmetry is dynamically broken for $n=4p+3$ ($p=0, 1, 2, \dots$), provided that there exists a sufficiently heavy fermion. The phenomenon originates from a shift in fermion zero point energies due to compactness of the extra dimensional space S^2 , being quite similar to the Casimir effect in electrodynamics. (23 refs.)
- 111890 Topological charge distribution in $SU(N)$ gauge theories.** C.M.Bishop, P.V.D.Swift (Phys. Dept., Univ. of Edinburgh, Edinburgh, Scotland). *Phys. Lett. B (Netherlands)*, vol.129B, no.3-4, p.198-200 (22 Sept. 1983).
The probability distribution function for topological charge contained in a sphere of finite radius is calculated. The authors find no need to introduce an arbitrary cutoff on instanton scale sizes as this is controlled by the size of the sphere. Recent Monte Carlo calculations reflect qualitatively all the features of the results. (5 refs.)
- 111891 An exact solution of the Jackiw-Rebbi equations for a Fermion-monopole-Higgs system.** A.M.Din (Inst. of Theoretical Phys., Univ. of Lausanne, Lausanne, Switzerland), S.M.Roy. *Phys. Lett. B (Netherlands)*, vol.129B, no.3-4, p.201-4 (22 Sept. 1983).
The authors present an exact solution for arbitrary partial waves to the Jackiw-Rebbi equations for an isospinor fermion in the background of a non-abelian singular magnetic monopole and a Higgs field. The Higgs coupling produces a centrifugal barrier making the Hamiltonian self-adjoint with ordinary conditions at the origin. There are infinitely many bound states, each doubly degenerate. The scattering is charge conserving. (15 refs.)
- 111892 Infinite N phase transitions in one-plaquette $(2+1)$ -dimensional models of lattice gauge theory with Manton's action.** O.Trinhammer (Inst. of Theoretical Phys., Goteborg, Sweden). *Phys. Lett. B (Netherlands)*, vol.129B, no.3-4, p.234-8 (22 Sept. 1983).
Pure gluon $U(N)$ lattice gauge theory is solved by the transfer matrix method in a semiclassical approximation for Manton's action showing a third order phase transition at $\lambda_c = g^2 N = \pi^2/2$. (21 refs.)
- 111893 Finite element Hamiltonian Monte Carlo of $SU(2)$.** D.Sen (Dept. of Phys., Princeton Univ., Princeton, NJ, USA). *Phys. Lett. B (Netherlands)*, vol.129B, no.3-4, p.239-45 (22 Sept. 1983).
Following Bender et al., the author applies the finite element method to a compact non-abelian system. The author does a Hamiltonian Monte Carlo on a $0+1$ dimensional lattice and compares the results with those obtained by a finite difference method. For the kinetic energy, the Feynman-Hell prescription is followed and the finite element method is shown to be distinctly superior. (10 refs.)
- 111894 Generalized Koba-Nielsen-Olesen scaling.** C.S.Lam (Dept. of Phys., McGill Univ., Montreal, Quebec, Canada). *Phys. Rev. D (USA)*, vol.28, no.5, p.1228-31 (1 Sept. 1983).
Implications for generalized Koba-Nielsen-Olesen (KNO) scaling, namely KNO scaling at a fixed pseudorapidity interval, are discussed. Predictions can be obtained for semi-inclusive pseudorapidity distributions and vice versa. These predictions agree very well with the CERN ISR and $\bar{p}p$ collider data

and they should be tested against e^+e^- , lepton-nucleon, and other hadronic data. A theorem about the relative magnitudes of the moments for different generalized KNO curves is proven. Consequences and validity of a 'strong scaling hypothesis' are discussed. (14 refs.)

111895 New generalization of Dirac's positive-energy relativistic wave equation. Liu Zhe-ming (Peking Feng-Yuan Inst. of Mech. & Electric Engng., Peking, China).

Phys. Rev. D (USA), vol.28, no.6, p.1326-32 (15 Sept. 1983). The relativistic wave equation for a spinless massive particle, suggested by Dirac ten years ago, has only positive-energy solutions. However, this new system of wave equations becomes inconsistent when electromagnetic interactions are included. This is a defect. In this paper, Dirac's work is generalized for cases in which the symmetry of interchangeability among the subparticles in each group contained in a particle satisfied. The inconsistency of Dirac's positive-energy wave equation is avoided either by having a more complex internal structure for a particle or by increasing the degrees of freedom of motion for the internal subparticles involved in this same particle. (6 refs.)

111896 Supersymmetric particles in $N=2$ superspace: phase-space variables and Hamiltonian dynamics. J.A.de Azcarraga, J.Lukierski (Internat. Centre for Theoretical Phys., Trieste, Italy).

Phys. Rev. D (USA), vol.28, no.6, p.1337-45 (15 Sept. 1983). The authors consider a reparametrization-invariant model recently proposed based on the N -extended super-Poincaré group with central charges, which leads to trajectories on the N -extended Salam-Strathdee superspace. The case $N=2$ is discussed in detail. They show that the $N=2$ model is invariant under four real supergauge transformations generated by first-class odd constants which imply the Dirac equation. They introduce one bosonic (which fixes the reparametrization) and four real spinorial (which fix the supergauge) gauge conditions and calculate the Dirac brackets for the remaining unconstrained variables ($\tilde{x}, \tilde{p}, \tilde{\theta}, \tilde{\theta}^c$). The equations of motion are written in Hamiltonian form, with $H \propto \text{Tr}\{Q_{\alpha i} Q_{\beta i}\}$ and correspond to the Heisenberg equations of the (first) quantized theory. (28 refs.)

111897 Symmetry breaking and phase transitions in general statistics. R.Y.Levine, Y.Tomozawa (Dept. of Phys., Univ. of Michigan, Ann Arbor, MI, USA).

Phys. Rev. D (USA), vol.28, no.6, p.1358-63 (15 Sept. 1983). A Higgs-type symmetry-breaking mechanisms with general statistics is described in scalar ϕ^4 theories. It is shown that the minimum of the potential depends upon statistics and the parameter space is subdivided into separate regions, each with a particular statistics as a phase variable. In the model the authors describe, a phase diagram is constructed in parameter space, suggesting new type of phase transition between domains of different statistics. (3 refs.)

111898 Operator-product expansion and the asymptotic behavior of spontaneously broken field theories. C.Taylor, B.McClain (Dept. of Phys., MIT, MA, USA).

Phys. Rev. D (USA), vol.28, no.6, p.1364-71 (15 Sept. 1983). The authors reexamine a recent study of the operator-product expansion in spontaneously broken scalar field theories. First, the asymptotic behaviour of the propagator in a spontaneously broken $\lambda\phi^4$ theory is calculated to lowest nontrivial order. The use of the operator-product expansion in the 'naive' vacuum, with operators developing nonvanishing vacuum expectation values, is found to correctly reproduce the usual perturbative analysis of the shifted theory when carried out to the same order. The renormalization-group improvement of this result is studied. They find that $\lambda_{g(2)}$, the renormalization-group coefficient of the operator ϕ^2 , is nonzero as first order in λ . This contradicts the results of the study of Gupta and Quinn. The generalization of this analysis to all Green's functions at all orders in perturbation theory is outlined. They argue that the renormalization-group improvement of the perturbation theory should yield the same answer for the two methods of calculating the asymptotic limit. Finally, they discuss the implications of this study for gauge theories. (13 refs.)

111899 Phase structure of the $O(N)$ vector model. W.A.Bardeen, M.Moshe (Fermi Nat. Accelerator Lab., Batavia, IL, USA).

Phys. Rev. D (USA), vol.28, no.6, p.1372-85 (15 Sept. 1983). In a large- N analysis of the $O(N)\phi^4$ theory in four dimensions, the authors find that the $O(N)$ -symmetric lowest-lying state is a metastable state. The decay rate of this false vacuum into a broken-symmetry state is, however, suppressed [$\sim \exp(-N)$]. Nevertheless, at finite temperature, they find that above a critical temperature T_c the only existing phase is a broken-symmetry phase with $N-1$ Goldstone bosons. This phase reflects the intrinsic instability of this theory, and the large- ϕ_c structure indicates that the renormalization $\lambda\phi^4$. The only acceptable version of this theory is its regularized form which becomes a free-field theory as the regularization is removed. (27 refs.)

111900 Exact solution of the infrared problem. H.P.Stapp (Lawrence Berkeley Lab., Univ. of California, Berkeley, CA, USA).

Phys. Rev. D (USA), vol.28, no.6, p.1386-418 (15 Sept. 1983). A simple but rigorous solution of the infrared problem is obtained. The basis of this solution is a factorization of the operator corresponding to the Feynman coordinate space plus all electromagnetic corrections to it into a product of two operators. The first is a unitary operator that represents precisely the contribution corresponding to classical electromagnetic theory. The second is a residual operator that is free of infrared problems. This factorization is exact: no soft-photon approximation, or any other approximation, is used. Both the unitary operator and the residual operator are expressed in simple forms amenable to rigorous mathematical analysis. The central technical results of this work, namely the exact yet simple organization of all contributions corresponding to classical physics into unitary factors, may have other important uses. (13 refs.)

111901 Self-dual gauge field, its quantum fluctuations, and interacting fermions. C.A.Flory (Stanford Linear Accelerator Center, Stanford Univ., Stanford, CA, USA).

Phys. Rev. D (USA), vol.28, no.6, p.1425-33 (15 Sept. 1983). The quantum fluctuations about a self-dual background field in $U(2)$ are computed. The background field consists of parallel and equal uniform chromomagnetic and chromoelectric fields. Determination of the gluon fluctuations about this field yields zero modes, which are naturally regularized by the introduction of massless fermions. This regularization makes the integrals over all fluctuations convergent, and allows a simple computation of the vacuum energy which is shown to be lower than the energy of the configuration of zero field strength. The regularization of the zero modes also facilitates the introduction of heavy test charges which can interact with the classical background field and also exchange virtual quanta. The formalism for introducing these heavy test charges could be a good starting point for investigating the relevant physics of the self-dual background field beyond the classical level. (12 refs.)

111902 New and old symmetries of the Maxwell and Dirac equations. V.I.Fushchich, A.G.Nikitin (Inst. of Math., Acad. of Sci., Kiev, Ukrainian SSR).

Sov. J. Part. & Nucl. (USA), vol.14, no.1, p.1-22 (Jan.-Feb. 1983). Translation of: *Fiz. Elem. Chastits & At. Yadra (USSR)*, vol.14, no.1, p.5-57 (Jan.-Feb. 1983). [received: Sept. 1983]

The symmetry properties of Maxwell's equations for the electromagnetic field and also of the Dirac and Kemmer-Duffin-Petiau equations are analyzed. In the framework of a 'non-Lie' approach it is shown that, besides the well-known invariance with respect to the conformal group and the Heaviside-Larmor-Rainich transformations, Maxwell's equations have an additional symmetry with respect to the group $U(2) \otimes U(2)$ and with respect to the 23-dimensional Lie algebra A_{23} . The transformations of the additional symmetry are given by nonlocal (integro-differential) operators. The symmetry of the Dirac equation in the class of differential and integro-differential transformations is investigated. It is shown that this equation is invariant with respect to an 18-parameter group, which includes the Poincaré group as a subgroup. A 28-parameter invariance group of the Kemmer-Duffin-Petiau equation is found. Finite transformations of the conformal group for a massless field with arbitrary spin are obtained. The explicit form of conformal transformations for the electromagnetic field and also for the Dirac and Weyl fields is given. (64 refs.)

111903 Solitons and numerical experiments. V.G.Makhan'kov (Joint Inst. for Nuclear Res. Dubna, USSR).

Sov. J. Part. & Nucl. (USA), vol.14, no.1, p.50-75 (Jan.-Feb. 1983). Translation of: *Fiz. Elem. Chastits & At. Yadra (USSR)*, vol.14, no.1, p.123-80 (Jan.-Feb. 1983). [received: Sept. 1983]

The properties of one- and two-dimensional solitons are discussed. Particular attention is paid to qualitative results obtained by computer simulation. Where possible, a brief description of the computational method is given. (142 refs.)

111904 A method of approximate calculation of Feynman diagrams. I. O.I.Zav'yalov (V.A. Steklov Math. Inst., Acad. of Sci., USSR).

Theor. & Math. Phys. (USA), vol.54, no.1, p.23-31 (Jan. 1983). Translation of: *Theor. & Mat. Fiz. (USSR)*, vol.54, no.1, p.38-51 (Jan. 1983). [received: Sept. 1983]

A method is proposed for elementary approximate calculation of massless Feynman amplitudes on the basis of the so-called loop tables of the corresponding diagrams. A new formulation of the theory is given in terms of the loop tables. (3 refs.)

111905 On field algebras in quantum theory with indefinite metric. K.Yu.Dadashyan, S.S.Khoruzhii (V.A. Steklov Math. Inst., Acad. of Sci., USSR).

Theor. & Math. Phys. (USA), vol.54, no.1, p.35-48 (Jan. 1983). Translation of: *Theor. & Mat. Fiz. (USSR)*, vol.54, no.1, p.57-77 (Jan. 1983). [received: Sept. 1983]

The authors discuss the problem of formulating the algebraic approach directly in a space with indefinite metric. One of the possible ways of constructing a net of local field algebras $\mathcal{A}(O)$ in the J space (Krein space) is considered; it is based on the Bisognano-Wichmann formalism. The authors then establish a number of properties of 'WJ' algebras (weakly closed algebras with J involution and unit in the J space); the algebras $\mathcal{A}(O)$ belong to this class. The methods of the proof use generalizations of the fundamental concepts of Tomita-Takesaki theory for algebras with J involution. (22 refs.)

111906 On super-self-duality equations. I.V.Volovich (V.A. Steklov Math. Inst., Acad. of Sci., USSR).

Theor. & Math. Phys. (USA), vol.54, no.1, p.55-62 (Jan. 1983). Translation of: *Theor. & Mat. Fiz. (USSR)*, vol.54, no.1, p.89-98 (Jan. 1983). [received: Sept. 1983]

Super-self-duality equations in supersymmetric Yang-Mills gauge theory are proposed. Solutions to them are found by means of super-twistors. (24 refs.)

111907 Use of the distribution function method in field theory. V.F.Tokarev (Inst. of Nuclear Res., Acad. of Sci., USSR).

Theor. & Math. Phys. (USA), vol.54, no.1, p.70-8 (Jan. 1983). Translation of: *Theor. & Mat. Fiz. (USSR)*, vol.54, no.1, p.111-23 (Jan. 1983). [received: Sept. 1983]

The distribution function method is used to study the Georgi-Glashow model in 2+1 space-time. Values are calculated for the quark-antiquark and gluon condensates. The masses of mesons and their wave functions taken at the origin are also calculated. The PCAC identity is proved in this model. (9 refs.)

111908 Calculation of many-loop diagrams of perturbation theory. N.I.Usyukina (Sci.-Res. Inst. of Nuclear Phys., Moscow State Univ., Moscow, USSR).

Theor. & Math. Phys. (USA), vol.54, no.1, p.78-81 (Jan. 1983). Translation of: *Theor. & Mat. Fiz. (USSR)*, vol.54, no.1, p.124-9 (Jan. 1983). [received: Sept. 1983]

Some identities are formulated for semi-unique vertices and semi-unique triangles that occur in the diagrams of perturbation theory with massless scalar particles. The use of these identities makes it possible to develop a reduction scheme by means of which the result can be obtained for many-loop diagrams without expansion in infinite series in Gegenbauer polynomials and without the use of the operation of differentiation, which leads to additional kinematic complications. As a result the calculation of many-loop diagrams of the perturbation theory is significantly simplified. (4 refs.)

111909 Quantum field theory models with a large number of colours and the statistical physics of disordered systems. I.Ya.Aref'eva (V.A. Steklov Math. Inst., Acad. of Sci., USSR).

Theor. & Math. Phys. (USA), vol.54, no.1, p.97-101 (Jan. 1983). Translation of: *Theor. & Mat. Fiz. (USSR)*, vol.54, no.1, p.154-60 (Jan. 1983). [received: Sept. 1983]

An analogy is noted between $N \times N$ matrix models of quantum field theory in the limit $N \rightarrow \infty$ and models of disordered spin systems in statistical physics. The replica method is used to establish the existence in the large N limit for the matrix model ϕ_D^4 of a new phase analogous to the spin glass phase in disordered spin systems. (14 refs.)

111910 Continuous regularizations in strong coupling expansions from a generalised inverse propagator method. J.P.Ader, B.Bonnier, M.Hontebeyrie, C.Meyers (Lab. de Phys. Theorique, Univ. de Bordeaux I, Gradignan, France).

Z. Phys. C (Germany), vol.19, no.3, p.233-9 (1983).

A strong coupling expansion is derived in terms of a generalized inverse propagator and is used to construct a regularization scheme which, for some regulators, differs from the canonical one. In particular, the Gaussian cut-off is shown to induce unbiased results, in contrast to a previous analysis using this regulator in the standard way. Several continuous and discrete regulations are then compared through a numerical example which suggests their equivalence. (11 refs.)

111911 Manifestly-covariant canonical formalism of Poincare gauge theories. I. General formulation. S.Hamamoto (Blackett Lab., Imperial Coll. London, London, England).

Z. Phys. C (Germany), vol.19, no.4, p.353-60 (1983).

Presents a general framework for manifestly-covariant canonical formulation of Poincare gauge theories. The author constructs a general class of action that is invariant under two kinds of BRS transformations—translation and internal Lorentz—and suitable for manifestly-covariant canonical quantization. This theory contains a great number of conserved quantities, which are investigated systematically. It is also pointed out that a canonical formulation of higher-derivative theories may be obtained as a limiting case of this framework. (14 refs.)

A critique of relativity and localization See Entry 111504

Spontaneous compactification of $D=10$ Maxwell-Einstein theory leads to $SU(3) \times SU(2) \times U(1)$ gauge symmetry See Entry 111529

Gravity with extra gauge symmetry See Entry 111532

Inequivalence between gauged $O(8)$ supergravities See Entry 111533

How does anticommutator $\{Q_\alpha, \bar{Q}_\beta\}$ realize energy-momentum P_μ in quantum supergravity? Particular properties of global gauge transformation charges in gauge theories See Entry 111534

Supersymmetry breaking by instantons See Entry 111913

Hidden local supersymmetry in the supersymmetric particle action See Entry 111914

One loop corrections of the fermion masses and the CP-violation calculations of the strong and weak interactions See Entry 111916

A $SU(3)$ theory for leptons, quarks and electroweak interactions See Entry 111917

Elimination of unitarily nonequivalent vacua in supersymmetric grand unified theories by gravity See Entry 111922

The weak mixing angles in gauge models with horizontal symmetry—a new approach to quark and lepton masses See Entry 111924

A three-dimensional model with a kink and a Higgs mechanism See Entry 111925

The Lipkin-Weisberger-Peshkin difficulties in abelian and non-abelian gauge theories See Entry 111928

Rapid phase transitions in local SUSY GUT See Entry 111929

The existence of a dual transformation in the Migdal-Kadanoff recursion equations See Entry 111930

Conditions of local gauge and relativistic invariance of universal nonlinear first-order equations in the theory of fundamental interactions See Entry 111935

Phenomenological electromagnetism with magnetic poles See Entry 111942

Neutral currents in the gauge model $SU(3)_F \times U(1)$ See Entry 111944

Supercomplementarity in massless supersymmetric QCD See Entry 111947

A measurement of the string tension near the continuum limit See Entry 111948

A simple interpolation for high and low momentum transfers in QCD See Entry 111949

Relationship between proper time and dimensional regularization of QCD See Entry 111953

Glueball mass calculations on an array of computers See Entry 111958

Static hadron properties in lattice QCD See Entry 111959

Calculation of the glueball mass spectrum of $SU(2)$ and $SU(3)$ non-abelian lattice gauge theories. I. Introduction and $SU(2)$ See Entry 111969

Dirac bound-state spectra of $Q\bar{Q}$, $q\bar{q}$, and $Q\bar{q}$ systems See Entry 111987

Ratio of lifetimes for the D^+ and D^0 mesons See Entry 111995

Bound state wavefunctions and anomalous magnetic moments of leptons See Entry 112004

Monopoles in the inflationary Universe See Entry 116902

11.20 S-MATRIX THEORY

Exact solution of the infrared problem See Entry 111900

Phase-integral formulae in the complex angular momentum (CAM) pole analysis See Entry 111979

On the completeness of the family of eigenfunctions of double-sided Regge problem See Entry 111980

11.30 SYMMETRY AND CONSERVATION LAWS

(see also 02.20 Group theory)

111912 Effect of the fourth-order Casimir invariants on $U_{6/4}$ and $U_{6/2}$ dynamical supersymmetries in nuclei and baryons. S.Iwao (Dept. of Phys. Coll. of Liberal Arts, Kanezawa Univ., Kanezawa, Japan).

Lett. Nuovo Cimento (Italy), vol.38, ser.2, no.2, p.55-9 (10 Sept. 1983).

The relative contribution arising from the fourth-order Casimir invariant in the subgroup B_2 is investigated for the dynamical super-symmetry $U_{6/4}$ proposed by Balantekin, Bars and Iachello (1981) for nuclei in the Os-Pt region, by making use of the data quoted by them. A similar method is applied to the linear and quadratic masses of baryons in the $U_{6/2}$ dynamical supersymmetry for hadrons suggested by the present author in order to find an additional clue. (11 refs.)

111913 Supersymmetry breaking by instantons. I.Affleck (Joseph Henry Labs., Princeton Univ., Princeton, NJ, USA), M.Dine, N.Seiberg.

Phys. Rev. Lett. (USA), vol.51, no.12, p.1026-9 (19 Sept. 1983).

It is shown that instantons generate a superpotential in supersymmetric QCD with N colors and $N-1$ flavors. (16 refs.)

111914 Hidden local supersymmetry in the supersymmetric particle action. W.Siegel (Dept. of Phys., Univ. of California, Berkeley, CA, USA).

Phys. Lett. B (Netherlands), vol.128B, no.6, p.397-9 (8 Sept. 1983).

The action for a massless supersymmetric particle in terms of superspace coordinates $x^\mu(\tau)$ and $\theta^\mu(\tau)$ is found to be invariant under a local supersymmetry which allows half of θ to be gauged away. (4 refs.)

111915 Domain walls. II. Baryon-number generation. B.Holdom (Dept. of Phys., Stanford Univ., Stanford, CA, USA).

Phys. Rev. D (USA), vol.28, no.6, p.1419-24 (15 Sept. 1983).

Domain walls present in the early universe due to a spontaneous breakdown of charge conjugation can leave behind net baryon number. $SU(2)$ instantons provide baryon nonconservation and the proton is effectively stable. Density

perturbations (on scales large enough for galaxy formation) and monopole suppression can occur if walls dominate the energy density. Mechanisms for wall removal are discussed. (11 refs.)

111916 One loop corrections of the fermion masses and the CP-violation calculations of the strong and weak interactions. Li Chong-sheng (Normal Univ. of East China, China), Hu Shi-ke.

Phys. Eng. Fortis & Phys. Nucl. (China), vol.7, no.3, p.333-41 (May 1983). In Chinese.

In a renormalizable gauge theory of spontaneously broken symmetry, using the path integral method, the authors derive a formula for calculating the one loop corrections of the effective potentials in the general case and the expressions for the one loop corrections of the fermion masses. Using these results, they calculate the contributions of the one loop corrections of the fermion masses to the QCD CP-violation, and obtain more general results than V. Goffins (1980), they also discuss the weak CP-violation. (8 refs.)

111917 A $SU(3)$ theory for leptons, quarks and electroweak interactions. R.Montemayor (Dept. de Fisica, Facultad de Ciencias, Univ. Nacional Autonoma de Mexico, Mexico City, Mexico), M.Moreno.

Rev. Mex. Fis. (Mexico), vol.29, no.3, p.369-85 (May 1983). [received: Sept. 1983]

The gauged version of the $SU(3)$ model for vector interactions of leptons and quarks is developed. After reviewing the main features of the global-spontaneously broken $SU(3)$ scheme for leptons, the authors conclude that the gauged version of the theory is incompatible with phenomenology. When the quark sector is included in the picture the problems of gauge theory are overcome. This is so provided that the quark and lepton mass matrices cannot be simultaneously diagonalized. The scheme therefore presents a natural link of the electroweak angles, the existence of two fermion multiplets and the gauge structure of the theory. (10 refs.)

111918 Non-linear representations of extended supersymmetry with central charges. S.Ferrara (CERN, Geneva, Switzerland), L.Maiani, P.C.West.

Z. Phys. C (Germany), vol.19, no.3, p.267-73 (1983).

A new class of nonlinear representations of N extended supersymmetry is found. These nonlinear realizations extend the Volkov-Akulov nonlinear realizations to include central charges which can also be nonlinearly realized. The general construction of the corresponding nonlinear Lagrangians is presented. The coupling to N extended supergravity provides the simultaneous occurrence of the Higgs and super-Higgs effects. The corresponding formulae for spin- $3/2$ gravitinos and spin-1 vector boson masses are derived. (15 refs.)

111919 Lepton number violation with quasi-Dirac neutrinos. J.W.F.Valle, M.Singer.

Report RL-83-018, Rutherford Appleton Lab., Chilton, Oxon., England (March 1983), 24 pp.

Investigates lepton number violation in weak interactions with massive Dirac neutrinos. In the framework of a simple $SU(3)_L \times U(1)$ electroweak model the authors find that neutrinos naturally acquire only Dirac masses at tree level, and for an odd number of lepton families, one neutrino remains massless. After a spontaneous breakdown of symmetry they find that the $SU(2) \times U(1)$ effective theory has lepton number violating currents which couple to the standard gauge bosons. Flavor conserving $|\Delta I|=2$ processes such as neutrinoless double β decay are forbidden in the simplest model, but processes such as $\mu^- + (A, Z) \rightarrow e^+ + (A, Z-2)$ and $K^- \rightarrow \pi^+ e^- \mu^-$ are allowed. (11 refs.)

Symmetries in Nuclear Structure. Proceedings of a NATO Advanced Study Institute on Symmetries in Nuclear Structure See Entry 111295

Classical and quantal supersymmetric Liouville theory See Entry 111470

The positivity of gravitational energy and global supersymmetry See Entry 111505

How does anticommutator $\{Q_\alpha, \bar{Q}_\beta\}$ realize energy-momentum P_μ in quantum supergravity? Particular properties of global gauge transformation charges in gauge theories See Entry 111534

Multidyon solutions in $SU(2)$ gauge group See Entry 111862

The group theoretical aspects of infinitesimal Riemann-Hilbert transform and hidden symmetry See Entry 111863

Classical equations $dN_i/dr = 1/2 \epsilon_{ijk} [N_j, N_k]$ See Entry 111864

Fermi-Bose gas equivalence, non-Abelian symmetry groups, phase transitions and all that See Entry 111868

Loss of continuum Lorentz invariance in gauge theories on a triangular lattice See Entry 111872

Local conservation laws for the two-dimensional periodic $SU(n+1)$ Toda lattices See Entry 111877

Auxiliary 'fields' for the massive spinning relativistic particle See Entry 111878

Conformal symmetry and new exact solutions of SU_2 Yang-Mills theory See Entry 111879

String tension in $SU(3)$ gauge theory on a 16^4 lattice See Entry 111884

Topological charge distribution in $SU(N)$ gauge theories See Entry 111890

Infinite N phase transitions in one-plaquette $(2+1)$ -dimensional models of lattice gauge theory with Manton's action See Entry 111892

Finite element Hamiltonian Monte Carlo of $SU(2)$ See Entry 111893

Supersymmetric particles in $N=2$ superspace: phase-space variables and Hamiltonian dynamics See Entry 111896

Symmetry breaking and phase transitions in general statistics See Entry 111897

Operator-product expansion and the asymptotic behavior of spontaneously broken field theories See Entry 111898

Phase structure of the $O(N)$ vector model See Entry 111899

Self-dual gauge field, its quantum fluctuations, and interacting fermions See Entry 111901

New and old symmetries of the Maxwell and Dirac equations See Entry 111902

On super-self-duality equations See Entry 111906

Elimination of unitarily nonequivalent vacua in supersymmetric grand unified theories by gravity See Entry 111922

Low energy tests of unification See Entry 111923

A grand unified composite model See Entry 111927

The Lipkin-Weisberger-Peshkin difficulties in abelian and non-abelian gauge theories See Entry 111928

Rapid phase transitions in local SUSY GUT See Entry 111929

Left-right symmetry, K_L - K_S mass difference, and heavy quarks See Entry 111931

Lepton spectroscopy See Entry 111934

Chiral Lagrangian calculation of nucleon decay modes induced by $d = 5$ supersymmetric operatorsSee Entry 111936
Towards a realistic SUGRA-GUTSee Entry 111937
 $SU_3 \times SU_2 \times U_1$ next to leading corrections for proton decay in SU_5 modelSee Entry 111938
Unification of weak and electromagnetic forcesSee Entry 111939
Neutral currents in the gage model $SU(3)_F \times U(1)$ See Entry 111944
Supercomplementarity in massless supersymmetric QCDSee Entry 111947
The effective lagrangian for supersymmetric QCDSee Entry 111951
On the breakdown of chiral symmetries in supersymmetric OCDSee Entry 111952
A neutron electric dipole moment from supersymmetric QCDSee Entry 111957
Glueball mass calculations on an array of computersSee Entry 111958
The use of finite energy sum rules for the description of the hadronic properties of QCDSee Entry 111968
Calculation of the glueball mass spectrum of $SU(2)$ and $SU(3)$ non-abelian lattice gauge theories. I. Introduction and $SU(2)$ See Entry 111969
Modified Gell-Mann-Okubo mass formula in the (8,8) modelSee Entry 111984
Photoproduction of selectrons in linear e^+e^- collidersSee Entry 111989
Leading order gluino pair production in heavy quarkonium decaysSee Entry 111993
Possibility of CP violation in the cascade non-leptonic decaysSee Entry 111997
Measurements of hyperon semileptonic decays at the CERN super proton synchrotron IV tests of the Cabibbo modelSee Entry 111998
Charmed baryon magnetic moments in broken $SU(8)$ modelSee Entry 112001
Electron-positron annihilation cross section in $SU(2)_L \otimes U(1)$ supergravitySee Entry 112010
Consequence of isospin conservation in nucleon-nucleon scatteringSee Entry 112018
Energy dependence of the rotational enhancement factor in the level densitySee Entry 112032
Breaking of fundamental symmetries in nucleiSee Entry 112065
Microscopic basis of collective symmetriesSee Entry 112098
Role of finite boson number in the interacting boson approximation description of γ -g transitions in deformed nucleiSee Entry 112100
Parity violation in neutron elastic scattering around compound nucleus resonancesSee Entry 112191
Higher-order field effects in pion absorption on two nucleonsSee Entry 112284
Parity non-conservation in muonic helium atomsSee Entry 112885
Monopoles in the inflationary UniverseSee Entry 116902

11.40 CURRENTS AND THEIR PROPERTIES

Symmetries in Nuclear Structure. Proceedings of a NATO Advanced Study Institute on Symmetries in Nuclear StructureSee Entry 111295
Use of the distribution function method in field theorySee Entry 111907
Lepton number violation with quasi-Dirac neutrinosSee Entry 111919
Electromagnetic and weak currents in nucleiSee Entry 112179

11.50 DISPERSION RELATIONS AND SUM RULES

111920 A P-wave sum rule and quark confinement. M.G.Olsson (Dept. of Phys., Univ. of Wisconsin, Madison, WI, USA). *Phys. Rev. D (USA)*, vol.28, no.5, p.1223-4 (1 Sept. 1983). A sum rule valid to order $(v/c)^2$ for an arbitrary spin-dependent interaction relates the P-wave hyperfine splitting to the spin-orbit contribution due to confinement. A measurement of a 3P_1 level when combined with the spin-triplet splittings would provide an insight into the Lorentz structure of the confinement interaction. (11 refs.)
The use of finite energy sum rules for the description of the hadronic properties of QCDSee Entry 111968

11.60 COMPLEX ANGULAR MOMENTUM; REGGE FORMALISM

(see also 03.80 General theory of scattering, 12.40M in strong interactions)
Phase-integral formulae in the complex angular momentum (CAM) pole analysisSee Entry 111979
On the completeness of the family of eigenfunctions of double-sided Regge problemSee Entry 111980

12.00 SPECIFIC THEORIES AND INTERACTION MODELS; PARTICLE SYSTEMATICS

12.10 UNIFIED FIELD THEORIES AND MODELS

111921 Magnetic bremsstrahlung of a neutrino pair in the Weinberg-Salam model, taking account of the polarizational states of the electron. I.M.Ternov, V.N.Rodionov, A.I.Studenikin (Dept. of Quantum Theory, Moscow Univ., Moscow, USSR). *Moscow Univ. Phys. Bull. (USA)*, vol.37, no.5, p.122-5 (1982). Translation of: *Vestn. Mosk. Univ. Ser. 3 (USSR)*, vol.37, no.5, p.104-7 (1982). The magnetic bremsstrahlung of a neutrino pair is considered, taking account of the initial or final electron polarization within the framework of the Weinberg-Salam weak-interaction model. In the case of ultrarelativistic particle

energies, the transition to crossed fields is made, and expressions are obtained for the probability of the process in the two limiting cases: $\chi = \text{Hep}_0/m^3 \ll 1$ and $\chi \gg 1$. (7 refs.)
111922 Elimination of unitarily nonequivalent vacua in supersymmetric grand unified theories by gravity. J.Kubo (Inst. fur Theoretische Phys., Univ. Dortmund, Dortmund, Germany), S.Sakakibara. *Phys. Lett. B (Netherlands)*, vol.128B, no.6, p.389-92 (8 Sept. 1983). In globally supersymmetric grand unified theories, there may be unitarily nonequivalent vacua which are not present in ordinary theories, reflecting the invariance of the Higgs potential under the complex extension of the gauge group. The authors show that such vacua are eliminated in the presence of $N=1$ supergravity coupling, if local supersymmetry is broken and the cosmological constant vanishes. (9 refs.)
111923 Low energy tests of unification. S.M.Barr (Phys. Dept., Univ. of Washington, Seattle, WA, USA). *Phys. Lett. B (Netherlands)*, vol.128B, no.6, p.400-2 (8 Sept. 1983). The author points out that there may be simple low energy tests of grand unification. In particular in the event that there turn out to be multiple light Z^0 bosons the consequent deviations from standard model neutral current scattering predictions must satisfy certain very simple relations if the world has an $SU(5)$ symmetry (or some larger symmetry). These relations are true even in the Z^0 bosons mix in arbitrarily complicated ways. (4 refs.)
111924 The weak mixing angles in gauge models with horizontal symmetry—a new approach to quark and lepton masses. Z.G.Berezhiani (Inst. of Phys., Acad. of Sci., Tbilisi, Georgian SSR). *Phys. Lett. B (Netherlands)*, vol.129B, no.1-2, p.99-102 (15 Sept. 1983). A generation mechanism of the quark and lepton masses in gauge models with horizontal symmetry is proposed. It is based on the mixing of quark-lepton families with heavy horizontal fermions, acquiring large masses directly after breaking of horizontal symmetry. A simple implementation of this mechanism for the $SU(3)_H \times SU(2)_L \times SU(2)_R \times U(1)$ model is given. The following results are obtained for the Kobayashi-Maskawa mixing angles: $s_1 \approx (m_d/m_s)^{1/2}$, $s_2 \approx (m_c/m_t)^{1/2}$, $s_3 \approx (m_b/m_\tau)^{1/2}$. The extension of this mechanism to GUTs is discussed. (18 refs.)
111925 A three-dimensional model with a kink and a Higgs mechanism. F.Gurse, C.-H.Tze (Phys. Dept., Yale Univ., New Haven, CT, USA). *Phys. Lett. B (Netherlands)*, vol.129B, no.3-4, p.205-18 (22 Sept. 1983). In a conformally invariant scalar field theory on the three-sphere, a scalar-spinor theory with Yukawa interaction, Higgs mechanism and fixed couplings is shown to arise from the curved geometry. This model admits a threefold description and an exact one-link solution. Implications are discussed. (23 refs.)
111926 Monopole chemistry. T.W.Ruijgrok, J.A.Tjon (Inst. voor Theoretische Fysica, Utrecht, Netherlands), Tai Tsun Wu. *Phys. Lett. B (Netherlands)*, vol.129B, no.3-4, p.209-12 (22 Sept. 1983). Possible chemical binding of the magnetic monopole is discussed. The interaction of a monopole with a hydrogen atom is investigated in the Born-Oppenheimer approximation with the electron described by the Dirac equation. The effective potential between the monopole and the proton is determined together with the resulting bound states. (14 refs.)
111927 A grand unified composite model. D.Gonzales (Dept. of Phys., MIT, Cambridge, MA, USA). *Phys. Lett. B (Netherlands)*, vol.129B, no.3-4, p.213-17 (22 Sept. 1983). If certain unusual assumptions about chiral symmetry breaking and dynamical mass generation are valid the gauge hierarchy problem is solved naturally and all elementary particle forces are unified into a single semi-simple gauge group. Three ordinary and two exotic families of fermions exist below 1 TeV. (13 refs.)
111928 The Lipkin-Weisberger-Peshkin difficulties in abelian and non-abelian gauge theories. M.Kamata (Dept. of Phys., Tokyo Metropolitan Univ., Tokyo, Japan). *Phys. Lett. B (Netherlands)*, vol.129B, no.3-4, p.218-22 (22 Sept. 1983). The question is raised on the validity of the usual derivation of the Lipkin-Weisberger-Peshkin (LWP) difficulty. It is shown that the LWP difficulty can be derived legitimately in the framework of the Wu-Yang formalism. A non-abelian version of the LWP difficulty is presented in a Wu-Yang solution of the pure $SU(2)$ Yang-Mills theory, showing a failure of the Jacobi identity at one point through the term $-i4\pi(\vec{r})\delta^3(x)$. A nonrelativistic treatment of the $SU(2)$ doublet particle with spin 1/2 around this solution is given. Some remarks are made also on a possible LWP difficulty in the 't Hooft-Polyakov monopole. (16 refs.)
111929 Rapid phase transitions in local SUSY GUT. C.Kounnas, D.V.Nanopoulos, M.Quiros (CERN, Geneva, Switzerland). *Phys. Lett. B (Netherlands)*, vol.129B, no.3-4, p.223-8 (22 Sept. 1983). The authors propose a class of $SU(5)$ local SUSY GUTs exhibiting the following properties: (i) local SUSY and the $SU(5)$ gauge group are spontaneously broken when a field in the adjoint representation of $SU(5)$ takes a VEV of the order of the grand unification scale M_X ; (ii) the non-zero VEV of that field follows because of finite temperature effects independently of possible confining properties of the GUT; (iii) the phase transition is extremely fast and the critical temperature is of the order of 10^9 GeV; and (iv) the monopole production is suppressed. (20 refs.)
111930 The existence of a dual transformation in the Migdal-Kadanoff recursion equations. S.Matsuda (Dept. of Phys., Kyoto Univ., Kyoto, Japan). *Phys. Lett. B (Netherlands)*, vol.129B, no.3-4, p.229-33 (22 Sept. 1983). A dual transformation is found to exist between the Migdal (M-) and Kadanoff-Migdal (K-) recursion relations. Consequently, a generic form of the Z_L -functionals can be obtained to describe both the M- and K-approximations in a single unified analytic expression. The proof for the claim is given and some implications of the discovered dual transformation are discussed. (10 refs.)
111931 Left-right symmetry, K_L - K_S mass difference, and heavy quarks. M.Denis (Inst. de Phys. Theorique, Univ. Catholique de Louvain, Louvain-la-Neuve, Belgium). *Phys. Rev. D (USA)*, vol.28, no.5, p.1219-22 (1 Sept. 1983). Shows that the lower limit for M_R , the mass of the right-handed bosons, computed from the K_L - K_S mass difference in an $SU(2)_L \times SU(2)_R \times U(1)$ model, strongly depends on the mass of the top quark and on the quark mixing angles. For reasonable choices of these parameters, $\beta = (M_L/M_R)^2$ can be as large as $1/6$. (10 refs.)
111932 Neutrino-induced pion production and proton decay. D.Rein (Phys. Inst., RWTH Aachen, Aachen, Germany). *Phys. Rev. D (USA)*, vol.28, no.7, p.1800-1 (1 Oct. 1983). A quantitative account of the reaction $\bar{\nu}_e + p \rightarrow e^+ + n + \pi^0$ is given and its implications with regard to proton-decay experiments are discussed. (10 refs.)

111933 Proton decay catalyzed by a monopole: the ratio of e^+ to $e^+\pi^0$ final states. C.Schmid (Inst. fur Theoretische Phys., Eidgenossische Tech. Hochschule, Zurich, Switzerland). *Phys. Rev. D (USA)*, vol.28, no.7, p.1802-3 (1 Oct. 1983). The author computes the ratio $\sigma(p+M \rightarrow M+e^++\pi^0) : \sigma(p+M \rightarrow M+e^+)$ using pole dominance for P-wave pion emission from the proton and soft-pion techniques for S-wave pion emission. In this paper the author neglects the form factor of the baryon-number-violating condensate, and concludes that the purely hadronic factors together with phase space enhance the e^+ over the $e^+\pi^0$ final state by a factor of $\simeq 4$. (3 refs.)

111934 Lepton spectroscopy. F.W.Bullock (Dept. of Phys. & Astron., Univ. of Coll. London, London, England), R.C.E.Devenish. *Rep. Prog. Phys. (GB)*, vol.46, no.9, p.1029-191 (Sept. 1983). The complete body of knowledge of the lepton spectrum as it is known today is presented and critically examined. Whilst the emphasis is primarily on the experimental determination of leptonic properties, the authors also summarise the many theoretical endeavours that have enriched and guided the field, and continue so to do. Complete accounts are given of the current situation on neutrino mass determination, on neutrino oscillations and on the properties of the tau and search for its associated neutrino. The subject of lepton conservation is discussed and all the experimental evidence for non-conservation collected together. The search for leptons other than those belonging to the three familiar generations is reviewed. Finally, a brief account is given for the limits on leptonic properties imposed by cosmological arguments. (560 refs.)

111935 Conditions of local gauge and relativistic invariance of universal nonlinear first-order equations in the theory of fundamental interactions. A.A.Babich, V.I.Kuvshinov, F.I.Fedorov (Inst. of Phys., Acad. of Sci., Minsk, Belorussian SSR). *Sov. Phys.-Dokl. (USA)*, vol.27, no.12, p.1015-17 (Dec. 1982). Translation of: *Dokl. Akad. Nauk SSSR*, vol.267, no.4-6, p.1093-7 (Dec. 1982). [received: Sept. 1983] The authors formulate a method for obtaining an explicit form of matrices $(\alpha^a\partial_\mu + \alpha^a\Psi + (g/2)\Lambda\Psi\Psi=0$ from the requirement that the equation be invariant under local gauge and Lorentz transformations for a given structure of the unified field (Ψ_A). They state the form of these matrices for electromagnetic and strong interactions as well as for the unified Weinberg-Salam theory and the grand-unification scheme (without the Higgs mechanism). (11 refs.)

111936 Chiral Lagrangian calculation of nucleon decay modes induced by $d = 5$ supersymmetric operators. S.Chadha, M.Daniel. **Report RL-83-056**, Rutherford Appleton Lab., Chilton, Oxon., England (June 1983), 18 pp. Considers the general baryon number violating operators which are produced by dressing the supersymmetric dimension five operators by gaugino exchanges. The authors then use chiral dynamics to calculate the widths for the decay modes $p \rightarrow K^+ \bar{\nu}_d$, $K^0 e^+ \bar{\nu}_d$, and $n \rightarrow K^0 \bar{\nu}_d$. The resulting branching ratios are rather sensitive to the precise admixture of the various baryon number violating operators involved. In particular the decay mode $p \rightarrow K^+ \bar{\nu}_d$ is generally dominant in qualitative agreement with previous quark model results. (17 refs.)

111937 Towards a realistic SUGRA-GUT. L.E.Ibanez, G.G.Ross. **Report RL-83-060**, Rutherford Appleton Lab., Chilton, Oxon., England (June 1983), 11 pp. Constructs a grand unified model based on $(N=1 \text{ local supersymmetry}) \times SU(5)$ in which the only fundamental mass scale is $0(M_{\text{Planck}})$. The model predicts $\sin^2 \theta_w = 0.22$, and has two new scales induced by gravitational effects $M_X \approx M_{\text{Planck}} / \sqrt{8\pi}$, $M_{\text{SUSY}} \approx 10^{11}$ GeV. $SU(2) \times U(1)$ is broken by radiative corrections for a top quark mass in the range $30 < m_t < 130$ GeV and the colour triplets of Higgs scalars are automatically superheavy. (12 refs.)

111938 $SU_3 \times SU_2 \times U_1$ next to leading corrections for proton decay in SU_5 model. M.Daniel, J.A.Penarrocha. **Report RL-83-042**, Rutherford Appleton Lab., Chilton, Oxon., England (Feb. 1983), 57 pp. Computes in the standard model of $SU_3 \times (SU_2 \times U_1)$ with massless quarks and leptons the two-loop anomalous dimensions of the four-fermion operators relevant to proton decay in processes involving (u,d,e,ν_e) . The calculation is carried out by the use of dimensional reduction, a variant of dimensional regularisation. The aim is to give a complete calculation within the SU_5 GUT model of the next to leading enhancement-suppression factor for nucleon decay due to renormalisation effects arising from hard gluons, W 's and B 's in processes which involve (u,d,e,ν_e) . It turns out that the result is sensitive to the ratios $x_i = M_{H(i)} / M_X$ where $M_{H(i)}$ are the masses of the twelve superheavy Higgs scalars in the 24 multiplet which breaks $SU_5 \rightarrow SU_3 \times SU_2 \times U_1$. (20 refs.)

111939 Unification of weak and electromagnetic forces. D.Atkinson (Inst. for Theoretical Phys., Groningen, Netherlands). Symmetries in Nuclear Structure. Proceedings of a NATO Advanced Study Institute on Symmetries in Nuclear Structure, Dronten, Netherlands, 16-28 Aug. 1982 (New York, USA: Plenum Press 1983), p.35-54 The author introduces the modern theory of the electroweak interaction, and applies it to β -decay. Quantum electrodynamics is reviewed, in a fully relativistic notation, and the theory is illustrated by a calculation of Bhabha scattering in lowest order. A treatment of the weak interaction, in which the photon is replaced by the charged W -boson, is then applied to electron-neutrino scattering. The leptonic sector of the $SU(2)_L \times U(1)$ electroweak theory is introduced; and the spontaneous symmetry-breaking phenomenon is explained in detail. Electron-neutrino scattering is briefly reconsidered. The semileptonic electroweak interactions, in which quarks as well as leptons interact, are treated in the manner of Glashow, Iliopolous and Maiani (1970), in which the charmed quark is used to suppress unwanted strangeness-changing neutral current effects. The application here is to nuclear β^+ -decay, in which a distinction is made between the pure Fermi and pure Gamow-Teller cases. An extension of the above theory to a left-right symmetrical $SU(2)_L \times SU(2)_R \times U(1)$ model, in which low-energy parity violation is a consequence of spontaneous symmetry breakdown, is explained; and β^+ -decay is reconsidered in this light. The result of a recent Groningen experiment that tests this theory is given. (5 refs.)

111940 Search for neutrino masses and oscillations. P.Vogel (California Inst. of Technol., Pasadena, CA, USA). Symmetries in Nuclear Structure. Proceedings of a NATO Advanced Study Institute on Symmetries in Nuclear Structure, Dronten, Netherlands, 16-28 Aug. 1982 (New York, USA: Plenum Press 1983), p.203-22 The author discusses the various aspects of the neutrino mass problem. This has been an interesting story for several reasons. First, if neutrinos are massive one has to modify the 'standard' (Weinberg-Salam-Glashow) theory of weak interactions. A nonvanishing neutrino mass would represent a strong argument for grand unification with its tremendous mass scale. Second, the search for neutrino mass involves an interplay of very different, and often

isolated, subfields of physics. The author mentions astrophysics, particle physics, nuclear physics, and even geophysics. (34 refs.)

Symmetries in Nuclear Structure. Proceedings of a NATO Advanced Study Institute on Symmetries in Nuclear Structure See Entry 111295

Electric and magnetic monopole solutions free from singularities in the non-symmetric unified field theory See Entry 111526

Chaotic inflation See Entry 111528

Auxiliary 'fields' for the massive spinning relativistic particle See Entry 111878

A $SU(3)$ theory for leptons, quarks and electroweak interactions See Entry 111917

Lepton number violation with quasi-Dirac neutrinos See Entry 111919

Neutral currents in the gage model $SU(3)_F \times U(1)$ See Entry 111944

Proton decay: is it fast enough? See Entry 111996

Electron-positron annihilation cross section in $SU(2)_L \otimes U(1)$ supergravity See Entry 112010

Production of a single heavy quark in e^+e^- collisions See Entry 112013

Parity non-conservation in muonic helium atoms See Entry 112885

Upper limit for mediation of baryon decay by slow magnetic monopoles See Entry 116416

Monopoles in the inflationary Universe See Entry 116902

Viscosity and the monopole density of the Universe See Entry 116909

12.20 MODELS OF ELECTROMAGNETIC INTERACTIONS

111941 Random electrodynamics of nonlinear system. I. Quartic anharmonic oscillator. S.Sachidanandam, I.V.V.Raghavacharyulu (Bhabha Atomic Res. Centre, Bombay, India). *Indian J. Pure & Appl. Phys.*, vol.21, no.7, p.408-12 (July 1983). A successful extension of the classical techniques of random electrodynamics to nonlinear microsystems is still not obtained in the literature. A beginning is made in this direction in this paper. The authors study the quartic anharmonic oscillator as an illustrative example. By extending one of the approximation methods employed in the study of deterministic nonlinear systems to stochastic nonlinear systems, properties quite close to those given by the quantum mechanical description are obtained. The results partly dispel the doubts raised by Claverie et al. (1980) in the validity of random electrodynamics in the description of nonlinear microsystems. (17 refs.)

111942 Phenomenological electromagnetism with magnetic poles. G.Calucci (Istituto di Fisica Teorica, Univ. di Trieste, Trieste, Italy). *Lett. Nuovo Cimento (Italy)*, vol.37, ser.2, no.16, p.573-5 (20 Aug. 1983). A qualitative discussion of the feature of the phenomenological electromagnetism in the presence of magnetic poles is presented together with the possible suggestion that one can derive for the combined renormalization of charges and poles. (7 refs.)

Unification of weak and electromagnetic forces See Entry 111939

12.20D Specific calculations and limits of quantum electrodynamics

General solution of the classical Schwinger model See Entry 111359

Lagrangian dynamics of a classical spinning particle with dipole moments See Entry 111467

Conditions of local gauge and relativistic invariance of universal nonlinear first-order equations in the theory of fundamental interactions See Entry 111935

Pair production and annihilation in strong magnetic fields See Entry 116453

12.20F Experimental tests of quantum electrodynamics

111943 An exotic decay of orthopositronium? J.Cleymans, P.S.Ray (Dept. of Theoretical Phys., Univ. of Bielefeld, Bielefeld, Germany). *Lett. Nuovo Cimento (Italy)*, vol.37, ser.2, no.16, p.569-72 (20 Aug. 1983). A discrepancy is apparent between the higher-order QED calculations and a recent experiment on the decay rate of the orthopositronium. It is conjectured here that this can be due to a possible pseudoscalar interaction of the electron-positron field. (4 refs.)

12.30 MODELS OF WEAK INTERACTIONS

111944 Neutral currents in the gage model $SU(3)_F \times U(1)$. M.N.Dubinin (Dept. of High Energy Phys., Moscow Univ., Moscow, USSR). *Moscow Univ. Phys. Bull. (USA)*, vol.38, no.1, p.108-10 (1983). Translation of: *Vestn. Mosk. Univ. Ser. 3 (USSR)*, vol.38, no.1, p.90-2 (1983). A model of electrically weak interactions satisfying presently known experimental data on the process, neutral currents into account, is considered. Two neutral gage bosons with masses of the same order are introduced in the model. (5 refs.)

111945 Higher order exchange contributions to $\Delta S=2$ amplitudes in a dynamical scenario for weak interactions. M.A.B.Beg (Rockefeller Univ., New York, NY, USA). *Phys. Lett. B (Netherlands)*, vol.129B, no.1-2, p.113-16 (15 Sept. 1983). Higher order contributions to $\Delta S=2$ amplitudes, involving the exchange of two gauge bosons are calculated in the framework of a recently described hypercolor-based dynamical scenario for weak interactions. Also calculated are quark masses in a manner that avoids any reference to scaling relationships that relate different QCD-like theories. The result that emerges is that one may generate the masses of the heavier quarks yet keep these contributions to $\Delta S=2$ at a level comparable to that in the canonical theory. The paper concludes with a description of a possible mechanism for generating lepton masses. (8 refs.)

Lepton number violation with quasi-Dirac neutrinos See Entry 111919

Physical null zones and radiation representation See Entry 111956

12.35 COMPOSITE MODELS OF PARTICLES

111946 Remarks on the possible origin of quark charges. K.Koike (Div. of Principles of Natural Sci., Kagawa Univ., Takamatsu, Japan). *Lett. Nuovo Cimento (Italy)*, vol.38, ser.2, no.1, p.1-6 (3 Sept. 1983). The problem concerning the origin of fractional quantum numbers is summarized. Then, possibilities to resolve this problem are investigated. (17 refs.)

A SU(3) theory for leptons, quarks and electroweak interactions See Entry 111917

The weak mixing angles in gauge models with horizontal symmetry—a new approach to quark and lepton masses See Entry 111924

Inclusive production of electrons and muons in multihadronic events at PETRA See Entry 112016

Probing phase transitions via energetic nuclear collisions See Entry 112274

12.35C General properties of quantum chromodynamics (dynamics, confinement, etc.)

111947 Supercomplementarity in massless supersymmetric QCD. T.R.Taylor (Fermi Nat. Accelerator Lab., Batavia, IL, USA). *Phys. Lett. B (Netherlands)*, vol.128B, no.6, p.403-6 (8 Sept. 1983). The presence of at least one supersymmetric phase is established for the strongly interacting SU(N) gauge theory with *n* flavors of massless matter in the *N*+*N* representation of the gauge group. (6 refs.)

111948 A measurement of the string tension near the continuum limit. G.Parisi (Dipartimento di Fisica, Univ. di Roma II, Rome, Italy), R.Petronzio, F.Rapuno. *Phys. Lett. B (Netherlands)*, vol.128B, no.6, p.418-20 (8 Sept. 1983). The string tension has been measured at $\beta=6$ in the quenched approximation using a new technique for minimizing the statistical errors. (12 refs.)

111949 A simple interpolation for high and low momentum transfers in QCD. J.A.Mignaco, I.Roditi (Centro Brasileiro de Pesquisas Fisicas, CBPF/CNPq, Rio de Janeiro, Brazil). *Phys. Lett. B (Netherlands)*, vol.128B, no.6, p.445-7 (8 Sept. 1983). It is shown that a simple rational approximation for the function $\beta(g)$ of the renormalization group provides a useful expansion parameter for the perturbative regime in QCD and, simultaneously, allows for confinement in the functional integral approximation to this problem. (14 refs.)

111950 Consequences of gluon condensation. J.Chakrabarti (Dept. of Phys. & Astron., Univ. of Rochester, Rochester, NY, USA). *Phys. Lett. B (Netherlands)*, vol.128B, no.6, p.448-52 (8 Sept. 1983). The author argues that the present estimates of gluon condensation may indicate that the bound states of gluons could be light. He pursues this line of reasoning to see if such a possibility is phenomenologically consistent. (12 refs.)

111951 The effective lagrangian for supersymmetric QCD. H.P.Nilles (CERN, Geneva, Switzerland). *Phys. Lett. B (Netherlands)*, vol.129B, no.1-2, p.103-7 (15 Sept. 1983). The author constructs an effective lagrangian for supersymmetric QCD with *N* colours and *M* flavours including the gauge fermion bound state. This lagrangian predicts the breakdown of supersymmetry for *M*<*N* in its massless limit, whereas for *M*≥*N* supersymmetry and certain chiral symmetries remain unbroken. (12 refs.)

111952 On the breakdown of chiral symmetries in supersymmetric OCD. J.-M.Gerard, H.P.Nilles (CERN, Geneva, Switzerland). *Phys. Lett. B (Netherlands)*, vol.129B, no.3-4, p.243-7 (22 Sept. 1983). The authors investigate the breakdown of chiral symmetries in supersymmetric QCD with *N* colours and *M* flavours, using anomaly consistency conditions and an effective lagrangian approach. For *M*<*N*, they obtain completely broken chiral symmetries. In the case of *M*>*N*, however, one needs at least unbroken SU(*N*)_V×SU(*M*−*N*)_R×SU(*M*−*N*)_L×U(1)×U(1) to arrive at a consistent picture. (19 refs.)

111953 Relationship between proper time and dimensional regularization of QCD. D.Sen (Dept. of Phys., Princeton Univ., Princeton, NJ, USA). *Phys. Lett. B (Netherlands)*, vol.129B, no.3-4, p.248-50 (22 Sept. 1983). The gluon propagator is renormalized to one loop in two different ways—dimensional regularization and by introducing a proper time parametrization. By comparing the two results, the ratio of the proper time mass parameter to the minimal subtraction mass is calculated. This is a renormalization-point independent and therefore physically interesting number. Using this ratio, the scale mass appearing in the one-loop constant abelian field effective action is calculated in terms of the standard QCD scale mass $\Lambda_{\overline{MS}}$. (7 refs.)

111954 A dynamical model for the gluon distribution function. Zhu Wei (Phys. Dept., Normal Univ. of East China, Shanghai, China), Shen Jian-guo. *Phys. Energy. Fortis & Phys. Nucl. (China)*, vol.7, no.3, p.316-22 (May 1983). In Chinese. The forms of the gluon distribution function at different *Q*² are discussed with the aid of the three-quark model associated with dynamical calculations of QCD (the LLA approximation). The Buras-Gaemers parametrization is improved and the gluon distribution functions are obtained. (12 refs.)

111955 Hadronization of quark systems. J.Dias de Deus, M.Pimenta (CFMC-INIC, Lisboa, Portugal). *Z. Phys. C (Germany)*, vol.19, no.4, p.365-9 (1983). Hadronization in simple models of quark systems is discussed with emphasis on the combinatorial aspects. The number *N*_q of quarks and the number *N*_c of colours are the relevant variables. In one-dimension and in the meson and baryon sector the problem is completely soluble. When multi-quark hadrons are included an iterative procedure still allows a complete solution. Higher dimensions are difficult to treat but global hadronization, without dimensionality constraints, is again soluble. As a general result the baryon/meson ratio is, for large quark densities, rather large, $\approx 1/3$, and may grow without limit as *N*→∞. (3 refs.)

Perturbative quantum chromodynamics See Entry 111319

Halliday-Suranyi expansion for lattice ϕ^4 theory See Entry 111867

Renormalization scheme-invariant perturbation theory See Entry 111882

String tension in SU(3) gauge theory on a 16⁴ lattice See Entry 111884

Infinite *N* phase transitions in one-plaquette (2+1)-dimensional models of lattice gauge theory with Manton's action See Entry 111892

Quantum field theory models with a large number of colours and the statistical physics of disordered systems See Entry 111909

Supersymmetry breaking by instantons See Entry 111913

One loop corrections of the fermion masses and the CP-violation calculations of the strong and weak interactions See Entry 111916

Hadronic-energy correlations in high-energy e^+e^- annihilation See Entry 112014

The LEAR project and physics with low energy antiprotons at CERN. A summary See Entry 112026

The design and calibration of precision drift chambers for use in a gluonium search experiment at the CERN ISR See Entry 112549

12.35E Applications of quantum chromodynamics to particle properties and reactions

111956 Physical null zones and radiation representation. G.Passarino (Linear Accelerator Center, Stanford Univ., Stanford, CA, USA). *Nucl. Phys. B, Part. Phys. (Netherlands)*, vol.B224, no.2, p.265-88 (12 Sept. 1983). General conditions for reconstructing physical null radiation zones in single photon tree amplitudes are given. The systematic analysis has been carried out using invariant quantities. For arbitrary values of masses and charges these zones are always smaller than in the massless and equal charges case. As an application the radiative W boson decay into heavy quarks is studied. This process turns out to be a rather sensitive test of the current quark masses *m_q*(*M_W*²), as well as of the $\bar{q}qW$, $q\bar{q}\gamma$ and *W*⁺*W*[−] γ vertices. This is due to the presence of a null line in the photon phase space with a location which strongly depends on *m_q*. A recently proposed radiation representation for single photon tree amplitudes is analyzed. Explicit examples are given for a number of cases including fermion and vector boson lines. (7 refs.)

111957 A neutron electric dipole moment from supersymmetric QCD. M.J.Duncan (Dept. of Theoretical Phys., Univ. of Oxford, Oxford, England). *Nucl. Phys. B, Part. Phys. (Netherlands)*, vol.B224, no.2, p.289-307 (12 Sept. 1983). Supersymmetric QCD naturally contains CP-violating interactions which can contribute to a neutron electric dipole moment. An analysis of the two-loop graphs results in a non-zero EDM whose magnitude is estimated and found to be compatible with experiment. (19 refs.)

111958 Glueball mass calculations on an array of computers. E.Brooks,III, G.Fox, S.Otto, M.Randeria (Caltech High Energy Phys. Group, Pasadena, CA, USA), B.Athas, E.DeBenedictis, M.Newton, C.Seitz. *Nucl. Phys. B, Field Theory & Stat. Syst. (Netherlands)*, vol.B220(FS8), no.4, p.383-400 (5 Sept. 1983). The authors have calculated the mass of the 0⁺ glueball in SU(2) pure gauge theory in 4 dimensions with very high statistics. The computation was done on an array of microprocessors with nearest-neighbour connections which run concurrently. They discuss, in detail, the implementation of the pure gauge algorithm for SU(2) and SU(3) and also the algorithm for calculating arbitrarily shaped Wilson loops on the array. The extension of these algorithms to the inclusion of dynamical fermions is also discussed. Finally, they present the results of the variational calculation of glueball masses which are in agreement with published results. (27 refs.)

111959 Static hadron properties in lattice QCD. C.Bernard, T.Draper, K.Olynyk (Dept. of Phys., Univ. of California, Los Angeles, CA, USA), M.Rushton. *Nucl. Phys. B, Field Theory & Stat. Syst. (Netherlands)*, vol.B220(FS8), no.4, p.508-32 (5 Sept. 1983). The authors calculate hadron masses and magnetic moments in the quenched approximation to lattice QCD, using Monte Carlo and Gauss-Seidel methods. For the mass computation, they have quite good statistics; in addition, the lattice is long enough in the 'time' direction to make a rather clear separation of the lowest lying hadrons from their radical excitations. They find mass ratios which are far from the experimental values; there is evidence that this may be due to the small spatial size of the lattice (which, however, is as large or larger than that used in most previous computations). For the magnetic moments, the situation is somewhat better, presumably because the moment calculation is really a qualitative test of the constituent quark model. (23 refs.)

111960 Quantum chromodynamics radiation and KNO scaling. G.Pancheri, Y.N.Srivastava (Lab. Nazionali, INFN di Frascati, Frascati, Italy). *Phys. Lett. B (Netherlands)*, vol.128B, no.6, p.433-8 (8 Sept. 1983). The authors obtain the KNO scaling function from the parton model and QCD, after averaging the microscopical system of quarks and gluons over the hadronic matter coordinates. Energy conservation and soft-gluon emission distribution functions are used to derive an expression which exhibits scaling violations and fits the charged multiplicity very well. (12 refs.)

111961 Local quark-hadron duality and nucleon form factors in QCD. V.A.Nesterenko, A.V.Radyushkin (Lab. of Theoretical Phys., JINR, Dubna, USSR). *Phys. Lett. B (Netherlands)*, vol.128B, no.6, p.439-44 (8 Sept. 1983). Quark-hadron duality is incorporated to estimate the non-perturbative $O(\alpha_s^0)$ -contribution to the nucleon form factors $G_{E,N,M}(t)$. For $1 < t < 20 \text{ GeV}^2$ the results are in satisfactory agreement with the existing data. This means that the observed dipole behaviour of $G^N(t)$ has nothing to do with the short distance dynamics. (16 refs.)

111962 The behaviours of $F_2^{ep}(X, Q^2)$ - $F_2^{en}(X, Q^2)$ and the scale-breaking parameter. Shen Qi-xing, Wu Ji-min, Lu Jing-xian, Zhao Pei-ying (Inst. of High Energy Phys., Acad. Sinica, Peking, China). *Phys. Energy. Fortis & Phys. Nucl. (China)*, vol.7, no.3, p.301-8 (May 1983). In Chinese. The scale-breaking parameter $\partial F_2^{ep}(X, Q^2)/\partial \ln Q^2$ of non-singlet component $F_2^{ep}-F_2^{en}$ and some other quantities in the electro-production process are discussed using the analytic expression for the distribution function of valence quarks in hadrons up to the leading log approximation. Comparisons with data are also given. (15 refs.)

111963 The QCD behaviour of the XF₃(X, Q²) up to the leading log in the neutrino deep-inelastic processes. Shen Qi-xing, Wu Ji-min, Lu Jing-xian, Zhao Pei-ying (Inst. of High Energy Phys., Acad. Sinica, Peking, China). *Phys. Energy. Fortis & Phys. Nucl. (China)*, vol.7, no.3, p.309-15 (May 1983). In Chinese. The QCE behaviour of the structure functions XF₃ in the neutrino deep-inelastic processes are discussed using the analytic expression for the distribution function of valence quarks in hadrons up to the leading log approximation. The theoretical predictions are in good agreement with experimental data. The error arising from an approximation in solving the A-P equation is discussed. The calculation shows that relative error remains smaller than 1% even in the case of *Q*²=200 GeV and *X*=0.1. (12 refs.)

111964 Analysis of hard inclusive processes in quantum chromodynamics. A.V.Radyushkin (Joint Inst. For Nuclear Res., Dubna, USSR). *Sov. J. Part. & Nucl. (USA)*, vol.14, no.1, p.23-49 (Jan.-Feb. 1983). Translation of: *Fiz. Elem. Chastits & At. Yadra (USSR)*, vol.14, no.1, p.58-122 (Jan.-Feb. 1983). [received: Sept. 1983]
The two simplest inclusive processes, namely, e^+e^- annihilation into hadrons and deep inelastic lepton-hadron scattering, are used to illustrate one of the approaches to the investigation of hard processes in QCD based on systematic analysis of the asymptotic behavior of the Feynman diagrams in the α representation. (131 refs.)

111965 Constituent quark model for hadron-hadron collisions and multiplicity distributions. F.Takagi (Dept. of Phys., Tohoku Univ., Sendai, Japan). *Z. Phys. C (Germany)*, vol.19, no.3, p.213-20 (1983).
Mean charged multiplicities and multiplicity distributions in proton-proton collisions at high energies are calculated using a class of models including constituent quark model (CQM), quark-parton model (QPM) and leading proton model (LPM). QPM is found to have an unrealistic feature about the mean multiplicity of low mass central components. LPM with the universality hypothesis that the central component in p - p collisions has the same distribution as the final state in e^+e^- annihilation into hadrons at the same effective energy tends to predict too narrow multiplicity distributions. CQM with a simple parametrization of inelastic quark-quark collisions can explain most easily and most naturally the multiplicity distributions in both p - p and π - p collisions, including their approximate KNO scaling. Also studied during the course of those analyses are the conditions under which an exact KNO scaling is realized. (29 refs.)

111966 Quark statistics and hadron spectra in e^+e^- annihilation and deep inelastic scattering. V.V.Anisovich, M.N.Kobrinisky (Leningrad Nuclear Phys. Inst., Leningrad, USSR), P.E.Volkovitski. *Z. Phys. C (Germany)*, vol.19, no.3, p.221-31 (1983).
Predictions of quark combinatoric calculus (QCC, alias quark statistics) for baryon-to-meson ratio in quark jets are compared with hadron production data e^+e^- annihilation and deep inelastic μp collisions. It is shown that charm production data in e^+e^- annihilation provide the impressive evidence confirming QCC which predicts that in the jet formed by c -quark the probability to produce charmed baryons is equal to 1/3. The possibility of successful description of secondary hadron spectra $(s/\beta).d\sigma(e^+e^-\text{-hadrons})/dx_E$ in the region $0.2 < x_E < 0.9$ in the framework of QCC approach is demonstrated. It is also shown that QCC agrees reasonably well with μp data for p/h^+ and p/h^- ratios in the current fragmentation region. (51 refs.)

111967 On the influence of hadronic decay on the properties of hadrons. E.van Beveren, C.Dullemond, T.A.Rijken (Inst. for Theoretical Phys., Univ. of Nijmegen, Nijmegen, Netherlands). *Z. Phys. C (Germany)*, vol.19, no.3, p.275-81 (1983).
In a multichannel treatment of the $q\bar{q}$ -system it is shown that the impact of decay on the spectra, and wavefunctions of hadrons is substantial. Some consequences for potential models are worked out in detail. The authors conclude that an 'equivalent' confining $q\bar{q}$ -potential to be used in an effective single-channel treatment might deviate significantly from the $q\bar{q}$ -potential in a realistic multichannel treatment. (15 refs.)

111968 The use of finite energy sum rules for the description of the hadronic properties of QCD. N.V.Krasnikov (CERN, Geneva, Switzerland), A.A.Pivovarov, N.N.Tavkhelidze. *Z. Phys. C (Germany)*, vol.19, no.4, p.301-9 (1983).
The authors use finite energy sum rules, taking into account nonperturbative corrections, for the calculation of hadron masses within QCD. As a rule, they obtain reasonable agreement with experimental data. They also estimate the proton lifetime in the $SU(5)$ model to be $\tau_p = 10^{28} (M_x/10^{14} \text{ GeV})^4$ years. (23 refs.)

111969 Calculation of the glueball mass spectrum of $SU(2)$ and $SU(3)$ non-abelian lattice gauge theories. I. Introduction and $SU(2)$. K.Ishikawa (City Coll., City Univ. of New York, New York, NY, USA), G.Schierholz, M.Teper. *Z. Phys. C (Germany)*, vol.19, no.4, p.327-52 (1983).
The authors describe a direct method for calculating the glueball mass spectrum in QCD and apply it to the $SU(2)$ non-Abelian gauge theory. The method involves the application of Monte Carlo methods to the lattice regulated theory. They calculate the masses of states of various spins and parity. They check for the absence of finite size effects, for the desired renormalization group dependence and that the higher mass states do not merely reflect a continuum cut. Finally they repeat the calculation in the 'Hamiltonian' limit and in the high temperature deconfining phase of QCD. (44 refs.)

Perturbative quantum chromodynamics See Entry 111319
A simple interpolation for high and low momentum transfers in QCD See Entry 111949
Leading log approximation for parton showers See Entry 111970
 $q\bar{q}g$ hybrid mesons in the MIT bag model See Entry 111971
Leading order gluino pair production in heavy quarkonium decays See Entry 111993
Ratio of lifetimes for the D^+ and D^0 mesons See Entry 111995
Photoproduction of hermaprodite baryons See Entry 112009
Energy moments for quark jets at PETRA See Entry 112015
Total cross sections, additivity, and two-gluon exchange See Entry 112017
Hadronic collisions: A quarkonium factory See Entry 112027

12.35H Phenomenological composite models of particle structure and reactions (partons, bags, etc.)

111970 Leading log approximation for parton showers. M.P.Shatz (California Inst. of Technol., Pasadena, CA, USA). *Nucl. Phys. B, Part. Phys. (Netherlands)*, vol.B224, no.2, p.218-28 (12 Sept. 1983).
The author corrects and extends the leading log parton shower formalism, which is widely used to compute the predictions of QCD for high-energy experiments, by including the information carried by the polarization of the partons. For observables that do not depend on the spins of the final state particles, this introduces a correlation between the azimuthal angles that is not included in current calculations. It also allows one to compute parton showers for observables that do depend on the final state spins. (4 refs.)

111971 $q\bar{q}g$ hybrid mesons in the MIT bag model. T.Barnes, F.E.Close (Rutherford Appleton Lab., Chilton, Didcot, England), F.de Viron. *Nucl. Phys. B, Part. Phys. (Netherlands)*, vol.B224, no.2, p.241-64 (12 Sept. 1983).
The authors suggest that hybrid ($q\bar{q}g$) mesons could exist with rather light masses. The spectrum of the ground state nonets, $J^{PC} = (0,1,2)^{--}; 1^{--}$ is

calculated in the MIT bag model including $O(\alpha_s)$ energy shifts. They discuss hadronic transitions among these states, consider their possible production at LEAR and SPEAR and indicate some interesting decay signatures. (42 refs.)

111972 Comment on 'Quark indistinguishability and the structure functions of the nucleon in a field-theoretic quark model'. M.Gupta (Dept. of Phys., Panjab Univ., Chandigarh, India). *Phys. Rev. D (USA)*, vol.28, no.5, p.1225-6 (1 Sept. 1983).
As a test of the valence contribution of quarks to structure functions, $\Delta^{pp} (=F_2^{pp} - F_2^{pn})$ is calculated in a quark-parton model proposed recently by Misra (1978). Agreement with data is fairly good. (11 refs.)

111973 Calculations of q^2q^2 states in potential theory. R.Aaron, M.H.Friedman, C.P.Jargocki (Dept. of Phys., Northeastern Univ., Boston, MA, USA). *Phys. Rev. D (USA)*, vol.28, no.7, p.1783-6 (1 Oct. 1983).
A model proposed by Aaron and Friedman (1982) is used to study q^2q^2 states. The results lead to speculations concerning the nature of the $\epsilon(1300)$. (9 refs.)

111974 Infrared singularities of the gluon propagator and quark confinement in the limit of an infinite number of colors. A.A.Slavnov (V.A.Steklov Math. Inst., Acad. of Sci., USSR). *Theor. & Math. Phys. (USA)*, vol.54, no.1, p.31-4 (Jan. 1983). Translation of: *Teor. & Mat. Fiz. (USSR)*, vol.54, no.1, p.52-6 (Jan. 1983). [received: Sept. 1983]

An exact solution is obtained for the quark propagator in chromodynamics with neglect of the gluon-gluon interaction in the limit $N \rightarrow \infty$ for different asymptotic behaviours of the gluon propagator as $k \rightarrow 0$. It is shown that a singularity of the type $1/k^{2n}$, $n \leq 2$, leads to quark confinement. (8 refs.)

111975 WKB solutions to relativistic quarkonium model with the potential $V(r) = \mu^2 r + \beta \ln r/r_0$. P.Cea, G.Nardulli, G.Paiano (Dipartimento di Fisica, Univ. di Bari, Bari, Italy). *Z. Phys. C (Germany)*, vol.19, no.4, p.321-6 (1983).
The authors apply WKB techniques to a Schrodinger equation modified for relativistic kinematics. They show that a potential consisting of linear and logarithmic terms accounts for different aspects of quarkonium phenomenology. Using an extended vector meson dominance model they calculate $R_{e^+e^-}$ and derive the quark parton model result. (16 refs.)

Use of the distribution function method in field theory See Entry 111907
A P-wave sum rule and quark confinement See Entry 111920
Quantum chromodynamics radiation and KNO scaling See Entry 111960
Constituent quark model for hadron-hadron collisions and multiplicity distributions See Entry 111965
Hadron production from quark fireballs and CERN SPS Collider results See Entry 111978
Modified Gell-Mann-Okubo mass formula in the (8,8) model See Entry 111984
Heavy baryons as bound states of three quarks See Entry 111985
Baryons with charm and strangeness in potential models See Entry 111986
Dirac bound-state spectra of $Q\bar{Q}$, $q\bar{q}$, and Qq systems See Entry 111987
Proton decay: is it fast enough? See Entry 111996
Measurements of hyperon semileptonic decays at the CERN super proton synchrotron IV tests of the Cabibbo model See Entry 111998
Charmed baryon magnetic moments in broken $SU(8)$ model .. See Entry 112001
Recoil corrections to the nucleon magnetic moment in the bag model See Entry 112003
Theory for a hybrid quark-baryon model for the nucleon-nucleon system See Entry 112080
 Δ dynamics See Entry 112083
Quarkochemistry of the heavy ion reactions See Entry 112266
Higher-order field effects in pion absorption on two nucleons See Entry 112284

12.35K Other composite models

(inc. composite quarks and leptons)

111976 Phenomenologically compatible solutions to 't Hooft's equations for composite models. Y.Meurice (Inst. de Phys. Theorique, Univ. Catholique de Louvain, Louvain-la-Neuve, Belgium). *Phys. Lett. B (Netherlands)*, vol.128B, no.6, p.393-6 (8 Sept. 1983).
A general method is given for building subconstituent models with a spectrum which satisfies 't Hooft's equations and wherein at least three generations of quarks and leptons can be identified. Some applications are given. (12 refs.)

111977 Some experimental constraints on the possible substructure model of leptons and quarks. Huang Tao, Xie Yicheng (Inst. of High Energy Phys., Acad. Sinica, Beijing, China). *Sci. Sin. (China)*, vol.26, no.8, p.848-60 (Aug. 1983).
The authors have obtained general formulations of electromagnetic form factor and effective weak charged currents for leptons (or quarks) in a substructure model, in which, leptons (or quarks) and weak bosons are composed of massive preons (fermions and scalar bosons). It has been shown that, internal structure of leptons (or quarks) will probably contribute anomalous magnetic moment and $(V+A)$ weak charged current to leptons (or quarks), these contributions will become zero, if $H = -1$ and the truncated wavefunction of leptons (or quarks) has a spinor structure $(1-p/m_f)\gamma$. One can make the predicted anomalous magnetic moments and anomalous weak charged currents for leptons (or quarks) smaller than the limitation of experimental data by choosing suitable parameters even if the second condition is not satisfied. (10 refs.)

12.40 MODELS OF STRONG INTERACTIONS

Connection between Koba-Nielsen-Olesen distributions in totally inclusive and single-proton semi-inclusive reactions See Entry 112025

12.40E Statistical models

111978 Hadron production from quark fireballs and CERN SPS Collider results. T.R.Mongan. *Phys. Rev. D (USA)*, vol.28, no.5, p.1210-12 (1 Sept. 1983).
The hadron-production model developed in Phys. Rev. D, 23, 2554 (1981) gives a charged-hadron multiplicity in reasonable agreement with the CERN SPS Collider results at $E_{cm} = 540 \text{ GeV}$, if the production of particles heavier than pions during fireball decay is considered. (9 refs.)

The correlation between $\langle p_{\perp} \rangle$ and the central multiplicity in the hydrodynamical modelSee Entry 112023

Bose-Einstein correlations in $\alpha_s\alpha$, pp and pp interactionsSee Entry 112024

12.40H Duality and dual models

String tension in SU(3) gauge theory on a 16^4 latticeSee Entry 111884

A measurement of the string tension near the continuum limitSee Entry 111948

Local quark-hadron duality and nucleon form factors in QCDSee Entry 111961

12.40M Complex angular momentum plane; Regge poles and cuts (Reggeons)

(see also 11.60 for general theory)

111979 Phase-integral formulae in the complex angular momentum (CAM) pole analysis. K.-E.Thylwe (Inst. of Theoretical Phys., Univ. of Uppsala, Uppsala, Sweden). *J. Phys. A (GB)*, vol.16, no.14, p.3325-40 (1 Oct. 1983). Formulae for calculating CAM pole positions and corresponding S -matrix residues are derived within the framework of the phase-integral method of Froman and Froman (1965, 1974). The formulae allow for the use of higher-order approximations with rigorous error estimates. The contributions from two and three isolated tuning points are considered, which allows applications in the study of rainbow and diffraction features as well as orbiting phenomena in elastic scattering processes. (21 refs.)

111980 On the completeness of the family of eigenfunctions of double-sided Regge problem. I.Yu.Popov, A.V.Strepetov. *Vestn. Leningr. Univ. Ser. Mat. Mekh. & Astron. (USSR)*, no.3, p.25-31 (July 1983). In Russian. Let k_n , $Im\ k_n > 0$, be the zeros of analytic continuation of S -matrix $S(k)$ associated with the operator $Lu = -u'' + q(x)u$, where $q(x) = 0$ for $|x| > a$. Let $f_1(x, k_n)$ be the solutions of the equation $-f_1''(x, k_n) + q(x)f_1(x, k_n) = k_n^2 f_1(x, k_n)$ obeying the conditions: $f_1'(b, k_n) + ik_n f_1(b, k_n) = 0$, $f_1(-b, k_n) - ik_n f_1(-b, k_n) = 0$, $b \geq a$. The completeness of the family $\{f_1(x, k_n)\}$ in $L_2(-b, b)$, when $b \leq 2a$, is proved. (6 refs.)

12.40Q Potential models

111981 A folded diagram method for deriving an energy-independent nucleon-nucleon (N-N) potential from meson exchanges. II. Application. Li Guang-lie (Inst. of High Energy Phys., Acad. Sinica, Peking, China), K.K.Ng, T.T.S.Kuo. *Phys. Energ. Fortis & Phys. Nucl. (China)*, vol.7, no.3, p.342-5 (May 1983). In Chinese. For pt.I see ibid., vol.7, p.67 (1983). Using the method proposed in pt.I, the authors investigate the potential between two neutral scalar nucleons by exchanging neutral scalar mesons. The results show that the contribution of mesonic folded diagrams to this potential is not negligible. (2 refs.)

On the influence of hadronic decay on the properties of hadronsSee Entry 111967

Baryons with charm and strangeness in potential modelsSee Entry 111986

12.40S Multiperipheral and multi-Regge models

(inc. diffraction and diffractive production models)

111982 Construction of diffractive amplitudes. M.Giffon (Inst. de Phys. Nucleaire, Univ. Claude Bernard Lyon-1, Villeurbanne, France), Y.Hama, E.Predazzi. *Z. Phys. C (Germany)*, vol.19, no.4, p.311-20 (1983). Starting from a simple parametrization of production amplitudes an explicit construction of the diffractive elastic amplitude through multiparticle unitarity is given. It is shown that the phase cancellation effect is essential in order to obtain an elastic amplitude which displays a diffractive peak in qualitative agreement with the data. (15 refs.)

Diffractive proton fragmentation in 16, 32, and 110 GeV/c K^-p interactions and the diffractive production of heavy quarks ($s\bar{s}, c\bar{c}$)See Entry 112028

12.40V Vector-meson dominance

111983 Virtual-photon shadowing in nuclei and photon structure. J.A.Alonso, J.L.Sanchez-Gomez (Dept. de Fisica Teorica, Univ. Autonoma de Madrid, Madrid, Spain). *Phys. Lett. B (Netherlands)*, vol.129B, no.1-2, p.121-4 (15 Sept. 1983). The 'standard' two-component (point-like plus VMD) model for the structure of photons seems to be in conflict with recent measurements of total hadronic cross sections for virtual photons incident on several nuclei. The authors show that the model works provided that certain off-shell effects, suggested within the framework of QCD, are properly taken into account. (8 refs.)

WKB solutions to relativistic quarkonium model with the potential $V(r) = \mu^2 r + \beta \ln r / r_0$ See Entry 111975

12.70 HADRON MASS FORMULAS

111984 Modified Gell-Mann-Okubo mass formula in the (8,8) model. T.N.Tiwari, C.V.Sastry (Dept. of Phys., Regional Engng. Coll., Rourkela, India), S.Sharma. *Indian J. Pure & Appl. Phys.*, vol.21, no.7, p.425-6 (July 1983). A modified version of the famous Gell-Mann-Okubo mass formula for the pseudoscalar mesons has been derived from the (8,8) model of the broken chiral SU(3) \otimes SU(3) symmetry. This modified formula agrees with the experimental data to within 0.4%, which is much better compared to 6.3% for the original formula. (10 refs.)

111985 Heavy baryons as bound states of three quarks. A.B.D'Oliveira (Instituto de Fisica, Univ. Fed. Fluminense Outeiro de S.J. Batista, Rio de Janeiro, Brazil), H.F.De Carvalho, E.C.Gerck. *Lett. Nuovo Cimento (Italy)*, vol.38, ser.2, no.1, p.27-32 (3 Sept. 1983). The authors calculate the mass spectrum of heavy baryons as nonrelativistic bound states of three quarks, using phenomenological potentials for the quark-quark interactions derived from QQ effective potentials obtained from fits of the J/ψ and Υ families. They solve Schrodinger's equation according to Flugge (1961) and Zickendraht's (1965) prescription, using a method deve-

loped especially for confining potentials. Results are compared for several types of confining potentials. (9 refs.)

111986 Baryons with charm and strangeness in potential models. J.M.Richard (Div. Phys. Theorique, Inst. de Phys. Nucleaire, Orsay, France), P.Taxil. *Phys. Lett. B (Netherlands)*, vol.128B, no.6, p.453-6 (8 Sept. 1983). The authors use various interquark potentials to calculate the masses of heavy baryons (QSC) and (SSC) with charm and strangeness. In particular the mass of the recently discovered A^+ baryon (USC) can be extrapolated from the masses of the already known baryons. (15 refs.)

111987 Dirac bound-state spectra of $Q\bar{Q}$, $q\bar{q}$, and Qq systems. S.N.Jena, T.Tripati (Dept. of Phys., Aska Sci. Coll., Aska, India). *Phys. Rev. D (USA)*, vol.28, no.7, p.1780-2 (1 Oct. 1983). The mass spectra of $Q\bar{Q}$, $q\bar{q}$, and Qq systems are studied in a unified manner in the Dirac equation with an equally mixed four-vector and scalar power-law potential of the form $V(r) = Ar^{0.1} + V_0$. It is found that with this potential, which describes the ψ , Υ , and ϕ systems reasonably well, the current-mass values for the light quarks give an excellent fit to the spectra of D, F, and B mesons. (9 refs.)

12.90 MISCELLANEOUS THEORETICAL IDEAS AND MODELS

111988 Difficulties with massless particles?. M.Flato (Phys. Math., Faculte des Sci. Mirande, Dijon, France), D.Sternheimer, C.Fronsdal. *Commun. Math. Phys. (Germany)*, vol.90, no.4, p.563-73 (1983). Some difficulties with sharp momentum (one-particle) states for massless particles are indicated, in the framework of unitary irreducible representations of the Poincare group. It is shown that a Poincare covariant set of such states requires the introduction, in the spatial direction opposite to the point stabilized, of momentum generalized eigenstates which (when the helicity is non-zero) have a nontrivial orbital transformation. The relevance of these generalized momentum eigenstates for massless theories is then shown. (15 refs.)

Simulation of angular distributions and correlations in the decay of particles with spinSee Entry 112030

13.00 SPECIFIC REACTIONS AND PHENOMENOLOGY

13.10 WEAK AND ELECTROMAGNETIC INTERACTIONS OF LEPTONS

111989 Photoproduction of selectrons in linear e^+e^- colliders. M.Gluck (Inst. fur Phys., Univ. Dortmund, Dortmund, Germany). *Phys. Lett. B (Netherlands)*, vol.129B, no.3-4, p.255-6 (22 Sept. 1983). It is suggested to observe photoproduced selectrons in linear e^+e^- colliders. The energetic photons are provided by an intense laser photon beam colliding with the electron beam. The observability of selectrons is then essentially limited by phase space, i.e. by $m_{\tilde{e}} + m_{\tilde{s}} \lesssim \sqrt{s}$. (7 refs.)

111990 Measurement of the processes $e^+e^- \rightarrow e^+e^-$ and $e^+e^- \rightarrow \gamma\gamma$ at PETRA. W.Bartel, L.Becker, C.Bowdery, D.Cords, R.Eichler, R.Felst, D.Haidt, H.Krehbiel, B.Naroska, J.Olsson, P.Steffen, P.Warming (DESY, Hamburg, Germany), G.Dietrich, E.Elsen, G.Heinzelmann, H.Kado, K.Meier, A.Petersen, U.Schneekloth, G.Weber, S.Bethke, A.Dieckmann, J.Heintze, K.H.Hellenbrand, R.D.Heuer, S.Komamiya, J.von Krogh, P.Lennert, H.Matsumura, H.Rieseberg, A.Wagner, A.Bell, A.Finch, F.Foster, G.Hughes, T.Nozaiki, H.Wriedt, J.Allison, A.H.Ball, G.Bamford, R.Barlow, I.P.Duerdoh, I.Glendingning, F.K.Loebinger, A.A.Macbeth, H.McCann, H.E.Mills, P.G.Murphy, P.Rowe, K.Stephens, D.Clarke, R.Marshall, G.F.Pearce, J.B.Whittaker, J.Kanzaki, T.Kawamoto, T.Kobayashi, M.Koshiha, M.Minowa, M.Nozaiki, S.Odaka, S.Orito, A.Sato, H.Takeda, T.Takeshita, Y.Totsuka, Y.Watanabe, S.Yamada, C.Yanagisawa. *Z. Phys. C (Germany)*, vol.19, no.3, p.197-203 (1983). Cross sections for the reactions $e^+e^- \rightarrow e^+e^-$ (Bhabha scattering) and $e^+e^- \rightarrow \gamma\gamma$ are measured for center-of-mass (c.m.) energies \sqrt{s} between 12.0 and 34.6 GeV. The results agree with the predictions of Quantum Electrodynamics (QED) and the cut-off parameters are determined. From Bhabha scattering at the highest energy, $\langle \sqrt{s} \rangle = 34.6$ GeV, the σ limits $0.12 < \sin^2 \theta_w < 0.38$ are obtained for the weak mixing angle. The higher order (α^3) QED processes $e^+e^- \rightarrow e^+e^- \gamma$ and $e^+e^- \rightarrow \gamma\gamma\gamma$ are also studied and are found to agree with the α^3 QED predictions. A search for excited electrons is carried out by investigating the $(e^+ \gamma)$ invariant mass distribution in the reaction $e^+e^- \rightarrow e^+e^- \gamma$. (12 refs.)

Fundamental processes in pair plasmasSee Entry 116448

Monte Carlo calculations of pair annihilation and its inverseSee Entry 116451

The particle and photon spectrum of an optically thick relativistic windSee Entry 116452

Pair production and annihilation in strong magnetic fieldsSee Entry 116453

Annihilation lines from confined plasmasSee Entry 116455

Electron-positron pair annihilation and creation in superstrong magnetic fieldsSee Entry 116456

Conditions for stimulated-annihilation in a degenerate e^-e^+ fluid at the surface of pulsarsSee Entry 116458

The production of spinless hadron pairs via virtual photon exchange in uniform magnetic fieldsSee Entry 116459

Criteria for gasar action in astrophysical sourcesSee Entry 116884

13.15 NEUTRINO INTERACTIONS

(inc. interactions involving cosmic rays)

Symmetries in Nuclear Structure. Proceedings of a NATO Advanced Study Institute on Symmetries in Nuclear StructureSee Entry 111295

Neutrino-induced pion production and proton decaySee Entry 111932

Unification of weak and electromagnetic forcesSee Entry 111939

Search for neutrino masses and oscillationsSee Entry 111940

The QCD behaviour of the X_F3 (X, Q^2) up to the leading log in the neutrino deep-inelastic processesSee Entry 111963

13.20 LEPTONIC AND SEMILEPTONIC DECAYS OF MESONS

111991 Constraints on heavy quark-antiquark states. A.K.Common (Math. Inst., Univ. of Kent, Canterbury, England). *Nucl. Phys. B, Part. Phys. (Netherlands)*, vol.B224, no.2, p.229-40 (12 Sept. 1983).

The author improves on and extended previous constraints on the radii and kinetic energies of heavy quark-antiquark systems. Meaningful bounds are placed on corrections to the Van-Royen Weisskopf formula for the leptonic decay rates of these systems. Bounds on the position and width of the peak of the ground state wave functions are also derived. (10 refs.)

111992 Lifetime of particles containing b quarks. E.Fernandez, W.T.Ford, A.L.Read,Jr., J.G.Smith (Dept. of Phys., Univ. of Colorado, Boulder, CO, USA), R.De Sangro, A.Marini, I.Peruzzi, M.Piccolo, F.Ronga, H.T.Shalk, H.B.Wald, R.Weinstein, H.R.Band, M.W.Gettner, G.P.Goderre, B.Gottschalk, R.B.Hurst, O.A.Meyer, J.H.Moromisato, W.D.Shambroom, E.von Goeler, W.W.Ash, G.B.Chadwick, S.H.Clearwater, R.W.Coombes, H.S.Kaye, K.H.Lau, R.E.Leedy, H.L.Lynch, R.L.Messner, S.J.Michalowski, K.Rich, D.M.Ritson, L.J.Rosenberg, D.E.Wiser, R.W.Zdarko, D.E.Groom, Hoyun Lee, E.C.Loh, M.C.Delfino, B.K.Heltsley, J.R.Johnson, T.L.Lavine, T.Maruyama, R.Prepost. *Phys. Rev. Lett. (USA)*, vol.51, no.12, p.1022-5 (19 Sept. 1983).

From a sample of hadronic events produced in e^+e^- collisions, semileptonic decays of heavy particles have been isolated and used to obtain a measurement of the bottom-quark lifetime of $[1.8 \pm 0.6 \text{ (stat.)} \pm 0.4 \text{ (syst.)}] \times 10^{-12}$ sec. (14 refs.)

111993 Leading order gluino pair production in heavy quarkonium decays. M.Gluck (Inst. fur Phys., Univ. Dortmund, Dortmund, Germany). *Phys. Lett. B (Netherlands)*, vol.129B, no.3-4, p.257-9 (22 Sept. 1983).

Leading order gluino production rates in heavy quarkonium (QQ) decays are calculated and compared to the standard gluon production rates. The dependence of this ratio of production rates on the masses of the heavy quark (Q) and the gluino provides a tool for their determination. (5 refs.)

Inclusive production of electrons and muons in multihadronic events at PETRASee Entry 112016

13.25 HADRONIC DECAYS OF MESONS

111994 A model for baryon enhancement in T decay. A.Snyder (Rutgers Univ., New Brunswick, NJ, USA), C.G.Trahern. *Phys. Lett. B (Netherlands)*, vol.129B, no.1-2, p.117-20 (15 Sept. 1983).

The authors present a model based on the three-gluon annihilation of quarkonia which accounts for the baryon enhancement observed in T decays. (7 refs.)

111995 Ratio of lifetimes for the D^+ and D^0 mesons. B.F.L.Ward (Internat. Centre for Theoretical Phys., Trieste, Italy). *Phys. Rev. D (USA)*, vol.28, no.5, p.1215-18 (1 Sept. 1983).

Using the SLAC lattice QCD theory, the author derives an effective interaction density for the process $c+\bar{u} \rightarrow s+G$, where G is a gluon. In this way, the author calculates the ratio of lifetimes for the D^+ and D^0 mesons. The result for this ratio is close to unity. (16 refs.)

On the influence of hadronic decay on the properties of hadronsSee Entry 111967

13.30 DECAYS OF BARYONS

111996 Proton decay: is it fast enough?. A.N.Mitra, R.Ramanathan (Dept. of Phys., Univ. of Delhi, Delhi, India). *Phys. Lett. B (Netherlands)*, vol.128B, no.6, p.381-4 (8 Sept. 1983).

A comprehensive Bethe-Salpeter model for qq and qq \bar{q} systems under harmonic confinement, which has provided an impressive set of agreements in respect of (i) qq, qq \bar{q} mass spectra, (ii) electromagnetic properties of mesons and baryons the proton charge radius and (iii) strong couplings of hadrons, all with basic parameters (universal spring constant $\bar{W}=0.15$ GeV and quark mass $m_q=0.28$ GeV), is employed for the calculation of proton decay rates (inclusive and exclusive). Keeping the GUT parameters fixed at the 'standard' values listed, e.g. in Langacker's review, the decay rates for the inclusive and exclusive modes are: $\Gamma(p \rightarrow e^+ \pi^0)=0.540$, $\Gamma(p \rightarrow e^+ \pi^+)=0.1824$, in 10^{-33} yr $^{-1}$ units. These values (which are mutually consistent) are smaller by about a factor 100 than several contemporary calculations, but do yet seem to be ruled out by the available data. (26 refs.)

111997 Possibility of CP violation in the cascade non-leptonic decays. K.Gavroglou (Phys. Lab., Nat. Tech. Univ., Athens, Greece). *Z. Phys. C (Germany)*, vol.19, no.4, p.361-3 (1983).

There is more than one parameter expressing CP violation in the non-leptonic hyperon decays. The recent experimental results provide us with indications that CP conservation may not be valid for the Ξ decays. Especially for the Ξ decays this is not due to the deviations from the exact $\Delta I=1/2$ rule. (7 refs.)

111998 Measurements of hyperon semileptonic decays at the CERN super proton synchrotron IV tests of the Cabibbo model. Report RL-83-054, Rutherford Appleton Lab., Chilton, Oxon., England (June 1983), 32 pp.

Pt.III ref. unobtainable. Results on five different hyperon semileptonic decays from the WA2 experiment, performed in the CERN SPS charged hyperon beam, have been analysed within the framework of the Cabibbo model. For the first time, the inconsistencies, which inevitably occur when the results from different experiments are combined, have been avoided in these comprehensive fits to high statistics data from a single hyperon decay experiment. Excellent agreement with the basic Cabibbo model has been obtained using the WA2 data either alone or together with neutron lifetime measurements. These results contrast strongly with other recent Cabibbo analyses which have indicated the presence of SU(3) breaking effects. Including radiative corrections the authors have obtained the results, $F=0.477 \pm 0.012$, $D=0.756 \pm 0.011$ and $\sin \theta_C=0.231 \pm 0.003$. (27 refs.)

Neutrino-induced pion production and proton decaySee Entry 111932

Proton decay catalyzed by a monopole: the ratio of e^+ to $e^+ \pi^0$ final statesSee Entry 111933

Chiral Lagrangian calculation of nucleon decay modes induced by $d = 5$ supersymmetric operatorsSee Entry 111936

SU $_3$ x SU $_2$ x U $_1$ next to leading corrections for proton decay in SU $_5$ modelSee Entry 111938

The use of finite energy sum rules for the description of the hadronic properties of QCDSee Entry 111968

Lifetime of particles containing b quarksSee Entry 111992

Dependence of the experimentally obtained age of the Am-Be neutrons ($\tau_{1,ab}$) in water on the source-foil geometrySee Entry 112495

Upper limit for mediation of baryon decay by slow magnetic monopolesSee Entry 116416

13.35 DECAYS OF LEPTONS

111999 Does the positron from muon decay have transverse polarization?. F.Corriveau (Lab. fur Hochenergiephys., Eidgenossische Tech. Hochschule Zurich, Villigen, Switzerland), J.Egger, W.Fetscher, H.-J.Gerber, K.F.Johnson, H.Kaspar, H.J.Mahler, M.Salzmann, F.Scheck. *Phys. Lett. B (Netherlands)*, vol.129B, no.3-4, p.260-4 (22 Sept. 1983).

The transverse polarization of the e^+ in μ^+ decay has been measured for the first time. This measurement allows the initial determination of the four μ decay parameters: α/A and β/A [with their linear combination $\eta=(\alpha-2\beta)/A$] plus, as the first direct measurement of time reversal noninvariant parameters in a purely leptonic interaction α'/A and β'/A . The results are consistent with zero and in agreement with the standard V-A form of the charged leptonic weak interaction. (14 refs.)

112000 Upper bound on the decay constant of familons. D.A.Dicus (Center for Particle Theory, Univ. of Texas, Austin, TX, USA), V.L.Teplitz. *Phys. Rev. D (USA)*, vol.28, no.7, p.1778-9 (1 Oct. 1983).

For massive neutrinos that can decay by emission of a familon (f), a flavor-changing axion, the upper bound on the cosmic energy density of the decay products yields (1) an upper bound on the familon decay constant, and consequently (2) a lower bound on other f emission rates. By comparing the K $\rightarrow \pi f$ lower bound with the experimental upper bound, the authors rule out neutrinos that decay by familon emission and have masses between 5×10^{-5} and 0.1 MeV. (6 refs.)

Direct comparison between the γ -ray fluxes from proton beam dumps at LAMPF and SINSee Entry 112006

A wire-chamber spectrometer for muon spin rotationSee Entry 112535

13.40 ELECTROMAGNETIC PROCESSES AND PROPERTIES

13.40D Electromagnetic mass differences

Left-right symmetry, K $_L$ -K $_S$ mass difference, and heavy quarksSee Entry 111931

13.40F Electromagnetic form factors; electric and magnetic moments

112001 Charmed baryon magnetic moments in broken SU(8) model. K.P.Tiwari, C.P.Singh (Dept. of Phys., VSSD Coll., Kanpur, India). *Indian J. Pure & Appl. Phys.*, vol.21, no.7, p.427-9 (July 1983).

The magnetic moments of charmed baryons are studied in the broken SU(8) framework, including the additional symmetry-breaking effects due to quark masses. The results so obtained differ from those of the conventional quark model incorporating quark-mass breaking in magnetic moment operator only. (27 refs.)

112002 An upper limit on neutrino electric dipole moments. J.A.Morgan, D.B.Farrant (Astron. Centre, Sussex Univ., Brighton, England). *Phys. Lett. B (Netherlands)*, vol.128B, no.6, p.431-2 (8 Sept. 1983).

An upper limit of 2.5×10^{-22} e cm for a possible neutrino electric dipole moment is found from a cosmological argument. (10 refs.)

112003 Recoil corrections to the nucleon magnetic moment in the bag model. P.A.M.Guichon (CERN, Geneva, Switzerland). *Phys. Lett. B (Netherlands)*, vol.129B, no.1-2, p.108-12 (15 Sept. 1983).

It is shown that the recoil correction to the value of the nucleon magnetic moment computed in the static bag model is small and negative. This is due to an over-cancellation of the spin precession effect by the retardation effect. The latter has been ignored in previous calculations, leading to a large positive correction. (15 refs.)

112004 Bound state wavefunctions and anomalous magnetic moments of leptons. Chao Kuang-Tn (Dept. of Phys., Peking Univ., Peking, China). *Phys. Energ. Fortis & Phys. Nucl. (China)*, vol.7, no.3, p.323-32 (May 1983). In Chinese.

Assuming that leptons are composed of a heavy fermion and a heavy scalar boson and using the Bethe-Salpeter equation, the author concludes that in the non-relativistic limit the radius and, in particular, the anomalous magnetic moment of leptons can be sufficiently small provided that the interaction of the constituents is of a vector type and that the fermion is much heavier than the scalar boson. Whereas the scalar type interaction can only give wavefunctions with large radius and anomalous magnetic moment. (10 refs.)

Static hadron properties in lattice QCDSee Entry 111959

Local quark-hadron duality and nucleon form factors in QCDSee Entry 111961

The behaviours of $F_2^{ep}(X, Q^2)$ - $F_2^{en}(X, Q^2)$ and the scale-breaking parameter \dots See Entry 111962

The QCD behaviour of the XF $_3$ (X, Q 2) up to the leading log in the neutrino deep-inelastic processesSee Entry 111963

Comment on 'Quark indistinguishability and the structure functions of the nucleon in a field-theoretic quark model'See Entry 111972

Virtual-photon shadowing in nuclei and photon structureSee Entry 111983

13.40H Electromagnetic decays

112005 Further evidence for the radiative decay of a light, penetrating particle. H.Faissner, W.Heinrigs, A.Preussger, D.Samm (III. Phys. Inst., Tech. Hochschule Aachen, Aachen, Germany). *Phys. Rev. D (USA)*, vol.28, no.5, p.1198-201 (1 Sept. 1983).

Photons and photon pairs from the 590-MeV proton beam dump at SIN have been observed in a counter-triggered spark chamber, placed behind 7.5 m of iron-concrete and 2 m of free space. Nineteen 1 γ events and twelve 2 γ events were found at angles $\alpha \leq 7^\circ$ from the beam-dump direction, whereas a background of, respectively, 4.8 and 2.3 events had been expected. The effect was unchanged by 20 cm of iron in front of the decay region, but vanished when the iron was moved to the end of this region, suggesting these surplus photons stem from a decay. (26 refs.)

112006 Direct comparison between the γ -ray fluxes from proton beam dumps at LAMPF and SIN. H.Faissner, E.Frenzel, W.Heinrigs, A.Preussger, D.Samm (Phys. Inst., RWTH Aachen, Aachen, Germany). *Phys. Rev. D (USA)*, vol.28, no.7, p.1787-9 (1 Oct. 1983). A direct comparison is made between the limit of γ -ray flux obtained at LAMPF, and the rate of 2γ (and 1γ) events found traveling along the beam-dump direction at SIN. The two experiments are not at variance with each other. The LAMPF result is shown to imply limits on axion properties. In turn a limit on muon-neutrino decay of $\tau_\nu/m_\nu > 0.07$ sec/eV is derived from the SIN 1γ data. (16 refs.)

112007 Reply to 'Direct comparison between the γ -ray fluxes from proton beams dumps at LAMPF and SIN'. J.S.Frank, R.L.Burman, D.R.F.Cochran (Los Alamos Nat. Lab., Los Alamos, NM, USA), P.Nemethy, S.E.Willis, V.W.Hughes, R.P.Redwine, J.Duclos, H.Kaspar, C.K.Hargrove, U.Moser. *Phys. Rev. D (USA)*, vol.28, no.7, p.1790-2 (1 Oct. 1983). From the analysis of their own data, the authors find an upper limit of $a \leq 0.35$ (95% confidence level) on the χ^0 -decay photon flux in the LAMPF neutrino experiment when normalized to the observed photon flux $a = 1.0 \pm 0.6$ (95% confidence level) of the SIN experiment. With the relativistic-phase-space model of χ^0 production the 95%-confidence-level limits of the two experiments do not overlap. (9 refs.)

13.40K Electromagnetic corrections to strong and weak interaction processes

Measurements of hyperon semileptonic decays at the CERN super proton synchrotron IV tests of the Cabibbo modelSee Entry 111998

13.60 PHOTON AND CHARGED-LEPTON INTERACTIONS WITH HADRONS

(for neutrino interactions, see 13.15)

Virtual-photon shadowing in nuclei and photon structureSee Entry 111983

13.60F Elastic and Compton scattering

Electromagnetic and weak currents in nucleiSee Entry 112179

13.60H Total and inclusive cross sections

(inc. deep-inelastic processes)

112008 Measurement, parametrization and fast simulation of hadronic showers in lead. M.De Palma, C.Favuzzi, G.Maggi, E.Nappi, A.Ranieri, P.Spinelli.

Report INFN/AE-83/4, Ist. Naz. Fis. Nucl., Bari, Italy (12 April 1983), 17 pp.

Measurements on longitudinal and lateral hadronic shower development in lead at 13 and 20 GeV are presented. It is shown that the longitudinal shower profile can be parametrised by a two component formula. A fast hadronic shower simulation method based on parametrisation is described together with a possible method to introduce fluctuations in the shower development. A comparison between the simulation and data is also presented. (12 refs.)

Perturbative quantum chromodynamicsSee Entry 111319

Generalized Koba-Nielsen-Olesen scalingSee Entry 111894

Analysis of hard inclusive processes in quantum chromodynamicsSee Entry 111964

Quark statistics and hadron spectra in e^+e^- annihilation and deep inelastic scatteringSee Entry 111966

Fundamental processes in pair plasmasSee Entry 116448

13.60P Baryon and baryon resonance production

112009 Photoproduction of hermaphrodite baryons. T.Barnes, F.E.Close. **Report RL-83-020, Rutherford Appleton Lab., Chilton, Oxon., England (Feb. 1983), 13 pp.**

Shows that photoexcitation of the lightest hermaphrodite baryons is strongly suppressed from proton targets but allowed from neutrons, a result that is reminiscent of a quark model selection rule due to Moorhouse (1966). This is consistent with suggestions that the $P_{11}(1710)$ is the lightest $q\bar{q}G$ baryon and eliminates the possibility that the Roper resonance is dominantly an hermaphrodite state. Magnetic moments do not constrain the possibility of considerable mixing of $q\bar{q}G$ into the nucleon and delta's Fock space wavefunctions. (17 refs.)

13.65 HADRON PRODUCTION BY ELECTRON-POSITRON COLLISIONS

112010 Electron-positron annihilation cross section in $SU(2)_L \otimes U(1)$ supergravity. D.A.Dicus, S.Nandi, W.W.Repko, X.Tata (Center for Particle Theory, Univ. of Texas, Austin, TX, USA). *Phys. Rev. Lett. (USA)*, vol.51, no.12, p.1030-3 (19 Sept. 1983).

For a wide range of masses the W superpartners and the supersymmetric scalars it is shown that a measurement of the total electron-positron annihilation cross section is sufficient to demonstrate the existence or nonexistence of supersymmetry. (9 refs.)

112011 Limits on J/ψ and Υ production in e^+e^- interactions at $\sqrt{s}=29$ GeV. C.Matteuzzi, G.S.Abrams, D.Amidei, C.A.Blocker, A.M.Boyarski, M.Breidenbach, D.L.Burke, W.Chinowsky, W.E.Dieterle, J.B.Dillon, J.M.Dorfan, M.W.Eaton, G.J.Feldman, M.E.B.Franklin, G.Gidal, L.Gladney, M.S.Gold, G.Goldhaber, L.J.Golding, G.Hanson, R.J.Hollebeek, W.R.Innes, J.A.Jaros, A.D.Johnson, J.A.Kadyk, A.J.Lankford, R.R.Larsen, B.LeClaire, M.Levi, N.Lockyer, V.Luth, M.E.Nelson, J.F.Patrick, M.L.Perl, B.Richter, P.C.Rowson, T.Schaad, H.Schellman, D.Schlatter, R.F.Schwitters, P.D.Sheldon, J.Strait, G.H.Trilling, C.de la Vaissiere, J.M.Yelton, C.Zaiser (Stanford Linear Accelerator Center, Stanford Univ., Stanford, CA, USA). *Phys. Lett. B (Netherlands)*, vol.129B, no.1-2, p.141-4 (15 Sept. 1983).

A search has been made for the inclusive production of J/ψ (3.1) and Υ (9.4) mesons e^+e^- interactions at 29 GeV via their decay into two leptons. No signal is observed in the J/ψ region, nor in the Υ region. The limits on the cross sections are $\sigma(e^+e^- \rightarrow \psi X) < 4.4 \times 10^{-36}$ cm², and $\sigma(e^+e^- \rightarrow \Upsilon X) < 4.7 \times 10^{-36}$ cm². The same data yields limits on the branching

ratios for the b quark BR ($b \rightarrow \psi X$) < 4.9% and BR ($b \rightarrow \Upsilon X$) < 0.8%. (11 refs.)

112012 Precise measurement of total cross sections for the process $e^+e^- \rightarrow$ multihadrons in the CM energy range between 12.0 and 36.4 GeV. W.Bartel, L.Becker, C.Bowdery, D.Cords, R.Fichler, R.Felst, D.Haidt, H.Krehbiel, B.Naroska, J.Olsson, P.Steffen, P.Warming (DESY, Hamburg, Germany), G.Dietrich, E.Elsen, G.Heinzelmann, H.Kado, K.Meier, A.Petersen, U.Schneekloth, G.Weber, S.Bethke, A.Dieckmann, J.Heintze, K.H.Helbrand, R.D.Heuer, S.Komamiya, J.von Krogh, P.Lennert, H.Matsumura, H.Rieseberg, A.Wagner, A.Bell, A.Finch, F.Foster, G.Hughes, T.Nozaki, H.Wriedt, J.Allison, A.H.Ball, G.Bamford, R.Barlow, I.P.Duerdort, I.Glenn-dinning, F.K.Loebinger, A.A.Macbeth, H.McCann, H.E.Mills, P.G.Murphy, P.Kawe, K.Stephens, D.Clarke, R.Marshall, G.F.Pearce, J.B.Whittaker, J.Kanzaki, T.Kawamoto, T.Kobayashi, M.Koshiha, M.Minowa, M.Nozaki, S.Odaka, S.Orito, A.Sato, H.Takeda, T.Takeshita, Y.Totsuka, Y.Watanabe, S.Yamada, C.Yanagisawa.

Phys. Lett. B (Netherlands), vol.129B, no.1-2, p.145-52 (15 Sept. 1983).

The total cross section for the process $e^+e^- \rightarrow$ hadrons has been measured in the CM energy range between 12.0 and 36.4 GeV using the JADE detector with a typical systematic error of $\pm 3\%$. The ratio $R(\sigma(e^+e^- \rightarrow \text{hadrons})/\sigma_p)$ is found to be constant over this range with an average value of 3.97 ± 0.05 (statistical and point-to-point systematic error) ± 0.10 (normalization error). The data were compared with the standard electro-weak interaction model including QCD corrections. (16 refs.)

112013 Production of a single heavy quark in e^+e^- collisions. G.Eilam (Fermi Nat. Accelerator Lab., Batavia, IL, USA). *Phys. Rev. D (USA)*, vol.28, no.5, p.1202-5 (1 Sept. 1983).

Cross sections for the flavor-changing neutral transition $e^+e^- \rightarrow \bar{t}c$ are calculated in the standard model with three generations, and found to be unmeasurable; $e^+e^- \rightarrow b\bar{s}$ is a few orders of magnitude larger. Experimentalists should nevertheless look for these processes since an increase in the number of generations, strong-interaction effects, and mainly nonstandard models may lead to observable rates. Z^0 decays into a single heavy quark plus a light one are also briefly discussed. (16 refs.)

112014 Hadronic-energy correlations in high-energy e^-e^+ annihilation. F.Csikor, G.Pocsik, A.Toth (Inst. for Theoretical Phys., Eotvos Univ., Budapest, Hungary). *Phys. Rev. D (USA)*, vol.28, no.5, p.1206-9 (1 Sept. 1983).

Extending Brown and Li's calculations (1982), energy-energy correlations in $e^+e^- \rightarrow \gamma, Z^0 \rightarrow \Sigma$ hadrons are investigated off and on the Z^0 peak. The authors establish that while this process measures exactly the same hadronic structure functions as $e^+e^- \rightarrow \gamma \rightarrow \Sigma$ hadrons, the two processes result in different dependences on external angles in the energy-energy correlation at arbitrary initial-state polarizations. The angle-integrated and normalized energy-energy correlations are also studied and found to be independent of initial-state polarization and the details of the γ and Z^0 exchanges (coupling constants and Z^0 mass and width). (6 refs.)

112015 Energy moments for quark jets at PETRA. C.Berger, H.Genzel, W.Lackas, J.Pielorz, F.Raupach, W.Wagner (I. Phys. Inst., RWTH Aachen, Aachen, Germany), L.H.Flolo, A.Kloving, E.Lillestol, J.M.Olsen, J.Burger, L.Criegee, Ch.Dehne, A.Deuter, A.Eskreys, G.Franke, M.Gasparo, Ch.Gerke, U.Jacobs, G.Knies, B.Lewendel, U.Maurus, J.Meyer, U.Michelsen, K.H.Pape, B.Stalla, U.Timm, G.G.Winter, S.T.Xue, M.Zachara, P.Waloschek, W.Zimmermann, P.J.Bussey, S.L.Cartwright, J.B.Dainton, B.T.King, C.Raine, J.M.Scarr, I.O.Skillicorn, K.M.Smith, J.C.Thomson, O.Achterberg, L.Boesten, D.Burkart, K.Diehlmann, V.Hepp, H.Kapitzka, B.Koppitz, M.Kruger, W.Luh-rsen, M.Poppe, H.Spitzer, R.van Staa, C.Y.Chang, R.G.Glasser, R.G.Kellogg, S.J.Maxfield, R.O.Polvado, B.Sechi-Zorn, J.A.Skard, A.Skujia, A.J.Tylka, G.E.Welch, G.T.Zorn, F.Almeida, A.Backer, F.Barreiro, S.Brandt, K.Derik-um, C.Grupen, H.J.Meyer, H.Muller, B.Neumann, M.Rost, K.Stupperich, G.Zech, G.Alexander, G.Bella, Y.Gnat, S.Grunhau, J., H.J.Daum, H.Junge, K.Kraski, C.Maxeiner, H.Maxeiner, H.Meyer, D.Schmidt.

Z. Phys. C (Germany), vol.19, no.3, p.205-12 (1983). Measurements of energy moments for single quark jets at c.m. energies between 12 and 31.6 GeV are presented. The data, corrected for detector effects and initial state radiation, are compared to QCD predictions in the leading log approximation. Nonperturbative effects are found to be moderate, and they strongly decrease with increasing c.m. energy. Once partly corrected for the presence of these fragmentation effects, the data agree well with all features of the leading log prediction, and in particular with the variation of the strong coupling constant over a wide range of energies and momentum transfers. (17 refs.)

112016 Inclusive production of electrons and muons in multihadronic events at PETRA. H.J.Behrend, H.Fenner, M.-J.Schachter, V.Schroder, H.Sindt (DESY, Hamburg, Germany), G.D'Agostini, W.-D.Apel, J.Engler, G.Flugge, D.C.Fries, W.Fues, K.Gamerdinger, G.Hopp, H.Kuster, H.Muller, H.Randoll, G.Schmidt, H.Schneider, W.de Boer, G.Buschhorn, G.Grindhammer, P.Grosche-Wiesmann, B.Gunderson, C.Kiesling, R.Kotthaus, U.Kruse, H.Lierl, D.Luers, H.Oberlack, P.Schacht, P.Colas, A.Cordier, M.Davier, D.Fournier, J.F.Grivaz, J.Haissinski, V.Journe, F.Laplanche, U.Mallik, J.-J.Veillet, J.H.Field, R.George, M.Goldberg, B.Grossetete, O.Hamon, F.Kapusta, F.Kovacs, G.London, L.Poggioli, M.Rivoal, R.Aleksan, J.Bouchez, G.Carnesecci, G.Cozzika, Y.Ducros, A.Gaidot, Y.Lavagne, J.Pamela, J.P.Pansart, F.Pierre.

Z. Phys. C (Germany), vol.19, no.4, p.291-9 (1983). The production of prompt leptons at PETRA has been measured for c.m. energies of 14, 22 and 34 GeV. The rate of prompt electrons and muons is presented, including a determination of the semileptonic branching ratio of the c and b quarks. The authors obtain

$B(c \rightarrow \mu \nu X) = 12.3 \pm 2.9$ (stat.) ± 3.9 (syst.)%,
 $B(b \rightarrow \mu \nu X) = 8.8 \pm 3.4$ (stat.) ± 3.5 (syst.)%,
 $B(b \rightarrow e \nu X) = 14.1 \pm 5.8$ (stat.) ± 3.0 (syst.)%. Systematic effects due to changes in fragmentation and other model parameters have been studied. (25 refs.)

Perturbative quantum chromodynamicsSee Entry 111319

Generalized Koba-Nielsen-Olesen scalingSee Entry 111894

Analysis of hard inclusive processes in quantum chromodynamicsSee Entry 111964

Quark statistics and hadron spectra in e^+e^- annihilation and deep inelastic scatteringSee Entry 111966

Hadron production from quark fireballs and CERN SPS Collider resultsSee Entry 111978

Lifetime of particles containing b quarksSee Entry 111992

Hadron polarization in e^+e^- annihilationSee Entry 112029

Monte Carlo calculations of pair annihilation and its inverseSee Entry 116451

The production of spinless hadron pairs via virtual photon exchange in uniform magnetic fieldsSee Entry 116459

13.75 HADRON-INDUCED LOW- AND INTERMEDIATE-ENERGY REACTIONS AND SCATTERING, ENERGY ≤ 10 GEV

(for higher energies, see 13.85)

112017 Total cross sections, additivity, and two-gluon exchange. P.W.Ensign, J.Randa (Dept. of Phys., Univ. of Colorado, Boulder, CO, USA).

Phys. Rev. D (USA), vol.28, no.7, p.1796-9 (1 Oct. 1983).

All the measured hadron total cross sections are calculated using the two-gluon-exchange model with Gaussian wave functions for the hadrons. Predictions for the light hadrons agree very well with experiment. (11 refs.)

13.75C Nucleon-nucleon interactions, including antinucleon, deuteron, etc. (energy ≤ 10 GeV)

(for N-N interactions in nuclei, see 21.30)

112018 Consequence of isospin conservation in nucleon-nucleon scattering.

A.Gersten (Dept. of Phys., Ben Gurion Univ. of the Negev, Beer-Sheva, Israel).

Phys. Rev. C (USA), vol.28, no.2, p.933-4 (Aug. 1983).

Isospin conservation in nucleon-nucleon scattering leads to an extension of the optical theorem to backward angles. The total neutron-proton and proton-proton cross sections are related to the imaginary parts of the neutron-proton amplitudes at backward angles. The author suggests to incorporate the above relations in the phase shift analysis, especially above 600 MeV lab energy where dibaryons are suspected to exist. (11 refs.)

Further evidence for the radiative decay of a light, penetrating particle See Entry 112005

Coulomb plus separable potential in coupled channels See Entry 112081

13.85 HADRON-INDUCED HIGH- AND SUPER-HIGH-ENERGY INTERACTIONS, ENERGY > 10 GEV

(for low energies, see 13.75)

Quantum chromodynamics radiation and KNO scaling See Entry 111960

Total cross sections, additivity, and two-gluon exchange See Entry 112017

13.85D Elastic scattering (energy > 10 GeV)

112019 Elastic scattering at CERN collider energy and the geometrical picture. T.T.Chou (Dept. of Phys., Univ. of Georgia, Athens, GA, USA), Chen Ning Yang.

Phys. Lett. B (Netherlands), vol.128B, no.6, p.457-60 (8 Sept. 1983).

Recent UA1 and UA4 experimental results for $\bar{p}p$ collisions at 540 GeV center of mass energy are analyzed in the geometrical picture. (14 refs.)

13.85H Inelastic scattering, many-particle final states (energy > 10 GeV)

112020 Search for new $S\bar{S}$ states in the K^- induced K^+K^- system.

T.Armstrong (LPNHE, Univ. Paris VI, Paris, France), M.Baubillier, J.C.Brient, W.Beusch, I.J.Bloodworth, G.Boca, M.Bonesini, D.Bortoletto, A.Burns, J.N.Carney, G.Cecchet, G.Costa, C.Evangelista, B.Ghidini, J.B.Kinson, V.Lenti, L.Mandelli, F.Navach, A.Palano, L.Perini, Y.Pons, E.Quercigh, Z.Strachman, M.Tamborini, M.F.Worsell, G.Zito, R.Zitoun.

Nucl. Phys. B, Part. Phys. (Netherlands), vol.B224, no.2, p.193-217 (12 Sept. 1983). Results from the first PWA of the K^+K^- system produced by incident K^- are presented in the mass range from the threshold to 1.70 GeV. In the P and D waves only the ϕ and f' mesons are observed and their production mechanism studied. A broad S wave peaking at 1.4 GeV is observed but the lack of information about its phase makes the search for new 0^{++} mesons inconclusive. (26 refs.)

112021 Study of resonance production in the multiparticle exclusive K^-p channels at 32 GeV/c. M.Yu.Bogoljubsky, V.V.Brysgalov, A.I.Kotova, S.G.Kiseleva, M.S.Levitsky, A.M.Moisev, D.I.Patalakha (IHEP, Serpukhov, USSR), U.Gensch, J.MacNaughton.

Z. Phys. C (Germany), vol.19, no.3, p.189-96 (1983). The cross sections for ρ^0 , $K^{*0}(890)$, Δ^{++} , Δ^0 and ϕ^0 -production are measured for the 6, 8 and 10 particle exclusive channels in a K^-p experiment at 32 GeV/c. For the channel $K^-p \rightarrow K^-2\pi^+2\pi^-p$ this study is done separately for the diffractive and non-diffractive components, separated by a rapidity gap method. It was found that the proportion of K^* , ρ and π^\pm , coming from resonance decay is a decreasing function of the channel multiplicity. (6 refs.)

13.85K Inclusive reactions, including total cross sections, (energy > 10 GeV)

112022 Evidence for $Z^0 \rightarrow e^+e^-$ at the CERN $\bar{p}p$ collider. P.Bagnaia (CERN, Geneva, Switzerland), M.Banner, R.Battiston, P.Bloch, F.Bonaudi, K.Borer, M.Borghini, J.-C.Chollet, A.G.Clark, C.Conta, P.Darriulat, L.Di Lella, J.Dines-Hansen, P.-A.Dorsaz, L.Fayard, M.Fraternali, D.Froidevaux, G.Fumagalli, J.-M.Gaillard, O.Gildemeister, V.G.Goggi, H.Grote, B.Hahn, H.Hanni, J.R.Hansen, P.Hansen, T.Himel, V.Hungerbuhler, P.Jenni, O.Kofoed-Hansen, E.Lancon, M.Livan, S.Loucatos, B.Madsen, P.Mani, B.Mansoulie, G.C.Mantovani, L.Mapelli, B.Merkel, M.Mermikides, R.Mollerud, B.Nilsson, C.Onions, G.Parroux, F.Pastore, H.Plochow-Besch, M.Polverel, J.-P.Repalli, A.Rimoldi, A.Rothenberg, A.Roussarie, G.Sauvage, J.Schacher, J.L.Siegrist, H.M.Steiner, G.Stimpfl, F.Stocker, J.Teiger, V.Vercesi, A.R.Weidberg, H.Zaccane, J.A.Zakrzewski, W.Zeller.

Phys. Lett. B (Netherlands), vol.129B, no.1-2, p.130-41 (15 Sept. 1983). From a search for electron pairs produced in $\bar{p}p$ collisions at $\sqrt{s}=550$ GeV the authors report the observation of eight events which they interpret as resulting from the process $\bar{p}+p \rightarrow Z^0 + \text{anything}$, followed by the decay $Z^0 \rightarrow e^+e^-$ or $Z^0 \rightarrow e^+\tau^- + \gamma$, where Z^0 is the neutral Intermediate Vector Boson postulated by the unified electroweak theory. They use four of these events to measure the Z^0 mass $M_Z = 91.9 \pm 1.3 \pm 1.4$ (systematic) GeV/ c^2 . (16 refs.)

112023 The correlation between $\langle p_\perp \rangle$ and the central multiplicity in the hydrodynamical model. Y.Hama, F.S.Navarra (Istituto de Fisica, Univ. de Sao Paulo, Sao Paulo, Brazil).

Phys. Lett. B (Netherlands), vol.129B, no.3-4, p.251-4 (22 Sept. 1983).

It is shown that the recently observed growth of $\langle p_\perp \rangle$ when the central multiplicity increases may be interpreted as a natural consequence of the hydrodynamical expansion of highly dense hadronic matter which is formed during multiparticle production processes. (11 refs.)

112024 Bose-Einstein correlations in $\alpha\alpha$, pp and $\bar{p}p$ interactions. T.Akeson (CERN, Geneva, Switzerland), M.G.Albrow, S.Almehed, R.Batley, O.Benary, H.Boggild, O.Botner, H.Breuker, H.Brody, V.Burkert, A.A.Carter, J.R.Carter, P.Cecil, S.U.Chung, W.E.Cleland, D.Cockerill, S.Dagan, E.Dahl-Jensen, I.Dahl-Jensen, P.Dam, G.Damgaard, S.Eidelman, W.M.Evans, C.W.Fabjan, P.Frandsen, S.Frankel, W.Frati, M.Gibson, U.Goerlach, H.Gordon, K.H.Hansen, B.Heck, V.Hedberg, J.Hiddleston, H.J.Hilke, J.Hooper, G.Jarkskog, P.Jeffreys, A.Kalinovsky, G.Kesseler, T.Killian, R.Kroeger, K.Kulka, J.van der Lans, J.Lindsay, D.Lissauer, B.Lorstad, T.Ludlam, A.Markou, N.A.McCubbin, U.Mjornmark, R.Moller, W.Molzon, B.S.Nielsen, A.Nilsson, L.H.Olsen, Y.Oren, L.Rosselet, E.Rosso, A.Rudge, R.Schindler, M.Sullivan, G.Thorstenon, E.Vella, J.Williamson, W.J.Willis, M.Winik, W.Witzeling, C.Woody, W.A.Zajc.

Phys. Lett. B (Netherlands), vol.129B, no.3-4, p.269-72 (22 Sept. 1983).

Bose-Einstein correlations between pions produced in the central region of rapidity in $\alpha\alpha$, pp and $\bar{p}p$ interactions have been studied at the ISR. The parameters r and τc —often interpreted as the radius and depth of the π -emitting region—are found to be independent of incident particle type but to depend on the mean charged multiplicity. In high multiplicity events, the pions appear to originate from a larger space-time region. (17 refs.)

112025 Connection between Koba-Nielsen-Olesen distributions in totally inclusive and single-proton semi-inclusive reactions. C.S.Lam, P.S.Yeung (Phys. Dept., McGill Univ., Montreal, Quebec, Canada).

Phys. Rev. D (USA), vol.28, no.5, p.1213-14 (1 Sept. 1983).

The authors obtain Koba-Nielsen-Olesen multiplicity distributions for $p+p$ —anything from a model relating them to the multiplicity distributions and the proton spectrum in $p+p \rightarrow p + \text{anything}$. The agreement with data for $100 \leq P_{\text{lab}} \leq 1000$ GeV/c is good; comparison with a similar model of Goulianos, Slicker, and White (1982) and the validity of such models at $\sqrt{s}=540$ GeV are discussed. (11 refs.)

112026 The LEAR project and physics with low energy antiprotons at CERN. A summary. R.Klapisch (CERN, Geneva, Switzerland).

Phys. Scr. (Sweden), vol.T5, p.140-2 (1983). (Proceedings of the 4th Nordic Meeting on Nuclear Physics, Fuglo, Denmark, 16-20 Aug. 1982).

The programme of LEAR, the new facility for low energy antiprotons at CERN, is described. Sixteen initial experiments will explore: states in the proton-antiproton system, annihilation, search for glueballs, structure of the proton and interaction antiproton with nuclei. (3 refs.)

112027 Hadronic collisions: A quarkonium factory. R.Baier (Fakultat fur Phys., Univ. Bielefeld, Bielefeld, Germany), R.Ruckl.

Z. Phys. C (Germany), vol.19, no.3, p.251-66 (1983).

Hadronic collisions are quite efficient in producing new quark flavours due to the large gluon content of ordinary hadrons. In particular, one may expect sizable yields of heavy quark-antiquark bound states with various spin and orbital quantum numbers. Using perturbative QCD in combination with the nonrelativistic quarkonium model the authors present a fairly complete and detailed picture of charmonium and bottomonium production. They compare their results on inclusive J/ψ and γ distributions with high energy pp data and make predictions on η_c and χ production. (32 refs.)

112028 Diffractive proton fragmentation in 16, 32, and 110 GeV/c K^-p interactions and the diffractive production of heavy quarks ($s\bar{s}, c\bar{c}$). R.Gottgens, J.M.Kohli, P.Sixel (III. Phys. Inst., Tech. Hochschule Aachen, Aachen, Germany), U.Gensch, H.Vogt, Y.Goldschmidt-Clermont, D.R.O.Morrison, R.T.Ross, S.Squarcia, J.Chwastowski, M.W.Krasny, L.Suszycki, W.Zielinski, P.Girtler, D.Kuhn, K.W.J.Barnham, P.R.S.Wright, M.Zomorrodian, D.I.Patalakha, A.M.Moisev, J.MacNaughton, F.Mandi, M.Markytan, J.Mitendorf, M.Bardadin-Otinowska, A.Jacholkowska, M.Szczekowski.

Z. Phys. C (Germany), vol.19, no.4, p.283-90 (1983).

The inclusive proton diffraction dissociation cross sections in 16, 32, and 110 GeV/c K^-p interactions are determined from the spike near $x=1$ in the inclusive negative particle spectra and are compared to those obtained in K^-p interactions using other selection methods at various energies. The same procedure is applied to events containing a V^0 in order to obtain the cross section for diffractive $s\bar{s}$ production. While the total cross section for proton diffraction is found to be approximately constant in the energy range studied here, proton diffraction yielding an $s\bar{s}$ -pair is found to increase significantly. In particular it is almost constant at 85 μb for Λ^0 and Σ production but for NKK it rises from zero at 16 GeV/c to about 200 μb at 110 GeV/c. From the result for $s\bar{s}$ diffractive production an estimate for the $c\bar{c}$ diffractive production cross section of approximately 1-10 μb at 110 GeV/c is obtained.

Generalized Koba-Nielsen-Olesen scaling See Entry 111894

Constituent quark model for hadron-hadron collisions and multiplicity distributions See Entry 111965

Hadron production from quark fireballs and CERN SPS Collider results See Entry 111978

13.88 POLARISATION IN INTERACTIONS AND SCATTERING

112029 Hadron polarization in e^+e^- annihilation. H.S.Mani, R.Ramachandran (Dept. of Phys., Indian Inst. of Technol., Kanpur, India).

Phys. Rev. D (USA), vol.28, no.7, p.1775-7 (1 Oct. 1983).

The authors show that while the polarization of the charmed quark produced in e^+e^- annihilation is of the order of 3% at $\sqrt{s}=5$ GeV, it gets washed out in subsequent decays. This should therefore cause the polarization of Λ^0 produced in $e^+e^- \rightarrow \Lambda^0 X$ to show a sharp fall as the energy crosses the charm threshold. They discuss ways of measuring charmed-quark polarization in the decays of charmed hadrons. (5 refs.)

Leading log approximation for parton showers See Entry 111970

Does the positron from muon decay have transverse polarization? See Entry 111999

13.90 OTHER TOPICS IN SPECIFIC REACTIONS AND PHENOMENOLOGY OF ELEMENTARY PARTICLES

112030 Simulation of angular distributions and correlations in the decay of particles with spin. C.Amsler (Phys. Inst., Univ. Zurich, Zurich, Switzerland), J.C.Bizot. *Comput. Phys. Commun. (Netherlands)*, vol.30, no.1, p.21-30 (July-Aug. 1983).

A general method to calculate the angular distributions in a chain of decaying particles is described. A computer program has been developed to simulate events that can be compared with experimental data. (6 refs.)

112031 Further evidence for charged intermediate vector bosons at the SPS collider. G.Arnison, A.Astbury (Rutherford Appleton Lab., Chilton, England), B.Aubert, C.Bacci, G.Bauer, A.Bezague, R.Bock, T.J.V.Bowcock, M.Calvetti, P.Catz, P.Cennini, S.Centro, F.Ceradini, S.Cittolin, D.Cline, C.Cochet, J.Colas, M.Corden, D.Dallman, D.Dau, M.DeBeer, M.Della Negra, M.Demoulin, D.Denegri, A.Di Ciaccio, D.DiBitonto, L.Dobrzynski, J.D.Dowell, K.Eggert, E.Eisenhandler, N.Ellis, P.Erhard, H.Faissner, M.Fincke, G.Fontaine, R.Frey, R.Fruhwith, J.Garvey, S.Ge, C.Ghesquiere, P.Ghez, K.Giboni, W.R.Gibson, Y.Giraud-Heraud, A.Givernaud, A.Gonidec, G.Grayer, T.Hansl-Kozanecka, W.J.Haynes, L.O.Hertzberger, C.Hodges, D.Hoffmann, H.Hoffmann, D.J.Holthuizen, R.J.Homer, A.Honma, W.Jank, G.Jorat, P.I.P.Kalmus, V.Karimaki, R.Keeler, I.Kenyon, A.Kernan, R.Kinnunen, W.Kozanecki, D.Kryn, F.Lacava, J.-P.Laugier, J.-P.Lees, H.Lehmann, R.Leuchs, A.Leveque, D.Linglin, E.Locci, J.-J.Malosse, T.Markiewicz, G.Maurin, T.McMahon, J.-P.Mendiburu, M.-N.Minard, M.Mohammadi, M.Moricca, K.Morgan, H.Muirhead, F.Muller, A.K.Nandi, L.Naumann, A.Norton, A.Orkin-Lecourtois, L.Paoluzi, F.Pauss, G.Piano Mortari, E.Pietarinen, M.Pimia, A.Placci, J.P.Porte, E.Radermacher, J.Ransdell, H.Reithler, J.-P.Revol, J.Rich, M.Rijssenbeek, C.Roberts, J.Rohlf, P.Rossi, C.Rubbia, B.Sadoulet, G.Sajot, G.Salvi, G.Salvini, J.Sass, J.Saudraix, A.Savoy-Navarro, D.Schinz, W.Scott, T.P.Shah, D.Smith, M.Spiro, J.Strauss, J.Streets, K.Sumorok, F.Szoncs, C.Tao, G.Thompson, J.Timmer, E.Tscheslog, J.Tuominen, B.Van Eijk, J.-P.Vialle, J.Vrana, V.Vuillemin, H.D.Wahl, P.Watkins, J.Wilson, R.Wilson, C.Wulz, Y.G.Xie, M.Yvert, E.Zurfluh. *Phys. Lett. B (Netherlands)*, vol.129B, no.3-4, p.273-82 (22 Sept. 1983).

A sample of 52 Intermediate Vector Boson decays in the ($\nu_e e$) channel are described. They were produced at the CERN SPS Collider for an integrated luminosity of 0.136 pb⁻¹. Both production and decay properties fit well with expectations from the Standard Model of weak interactions. An improved value for the W mass is given and compared with the previously published value for the Z⁰ mass. (13 refs.)

Lifetime of particles containing b quarks See Entry 111992
 Production of a single heavy quark in e⁺e⁻ collisions See Entry 112013
 Evidence for Z⁰→e⁺e⁻ at the CERN pp collider See Entry 112022
 Fundamental processes in pair plasmas See Entry 116448
 Pair production in thermal plasmas: a computer model See Entry 116450
 Monte Carlo calculations of pair annihilation and its inverse See Entry 116451
 The particle and photon spectrum of an optically thick relativistic wind See Entry 116452
 Pair production and annihilation in strong magnetic fields See Entry 116453
 Equilibrium pair density in a relativistic plasma with magnetic fields See Entry 116454
 Electron-positron pair annihilation and creation in superstrong magnetic fields See Entry 116456
 Comparison of photon-photon and photon-magnetic field pair production rates See Entry 116457
 The production of spinless hadron pairs via virtual photon exchange in uniform magnetic fields See Entry 116459
 Electron positron pairs in radio pulsars See Entry 116724
 Pair production near threshold in pulsar magnetic fields See Entry 116725
 Positrons from gamma bursts See Entry 116882
 Pair production and non-thermal radio stars See Entry 116885

14.00 PROPERTIES OF SPECIFIC PARTICLES AND RESONANCES

14.20 BARYONS AND BARYON RESONANCES

(inc. antiparticles)

Effect of the fourth-order Casimir invariants on U_{6/4} and U_{6/2} dynamical supersymmetries in nuclei and baryons See Entry 111912
 Neutrino-induced pion production and proton decay See Entry 111932
 Proton decay catalyzed by a monopole: the ratio of e⁺ to e⁺π⁰ final states See Entry 111933
 Chiral Lagrangian calculation of nucleon decay modes induced by d = 5 supersymmetric operators See Entry 111936
 SU₃ x SU₂ x U₁ next to leading corrections for proton decay in SU₃ model See Entry 111938
 A neutron electric dipole moment from supersymmetric QCD See Entry 111957
 Local quark-hadron duality and nucleon form factors in QCD See Entry 111961
 The use of finite energy sum rules for the description of the hadronic properties of QCD See Entry 111968
 Comment on 'Quark indistinguishability and the structure functions of the nucleon in a field-theoretic quark model' See Entry 111972
 Heavy baryons as bound states of three quarks See Entry 111985
 Baryons with charm and strangeness in potential models See Entry 111986
 Lifetime of particles containing b quarks See Entry 111992
 Proton decay: is it fast enough? See Entry 111996
 Possibility of CP violation in the cascade non-leptonic decays See Entry 111997

Measurements of hyperon semileptonic decays at the CERN super proton synchrotron IV tests of the Cabibbo model See Entry 111998
 Charmed baryon magnetic moments in broken SU(8) model .. See Entry 112001
 Photoproduction of hermaphrodite baryons See Entry 112009
 Hadron polarization in e⁺e⁻ annihilation See Entry 112029
 Dependence of the experimentally obtained age of the Am-Be neutrons (τ_{1,46}) in water on the source-foil geometry See Entry 112495

14.40 MESONS AND MESON RESONANCES

Use of the distribution function method in field theory See Entry 111907
 Glueball mass calculations on an array of computers See Entry 111958
 Calculation of the glueball mass spectrum of SU(2) and SU(3) non-abelian lattice gauge theories. I. Introduction and SU(2) See Entry 111969
 qq̄ hybrid mesons in the MIT bag model See Entry 111971
 Calculations of q²q² states in potential theory See Entry 111973
 Dirac bound-state spectra of QQ, q̄q, and Qq systems See Entry 111987
 Constraints on heavy quark-antiquark states See Entry 111991
 Lifetime of particles containing b quarks See Entry 111992
 A model for baryon enhancement in T decay See Entry 111994
 Ratio of lifetimes for the D⁺ and D⁰ mesons See Entry 111995
 Direct comparison between the γ-ray fluxes from proton beam dumps at LAMPF and SIN See Entry 112006
 Reply to 'Direct comparison between the γ-ray fluxes from proton beams dumps at LAMPF and SIN' See Entry 112007
 Limits on J/ψ and T production in e⁺e⁻ interactions at √s=29 GeV See Entry 112011
 Search for new SŜ states in the K⁻ induced K⁺K⁻ system .. See Entry 112020
 The LEAR project and physics with low energy antiprotons at CERN. A summary See Entry 112026
 The design and calibration of precision drift chambers for use in a gluonium search experiment at the CERN ISR See Entry 112549

14.60 LEPTONS

Symmetries in Nuclear Structure. Proceedings of a NATO Advanced Study Institute on Symmetries in Nuclear Structure See Entry 111295
 A SU(3) theory for leptons, quarks and electroweak interactions See Entry 111917
 Magnetic bremsstrahlung of a neutrino pair in the Weinberg-Salam model, taking account of the polarizational states of the electron See Entry 111921
 The weak mixing angles in gauge models with horizontal symmetry—a new approach to quark and lepton masses See Entry 111924
 Lepton spectroscopy See Entry 111934
 Search for neutrino masses and oscillations See Entry 111940
 Phenomenologically compatible solutions to 't Hooft's equations for composite models See Entry 111976
 Upper bound on the decay constant of familons See Entry 112000
 An upper limit on neutrino electric dipole moments See Entry 112002
 Bound state wavefunctions and anomalous magnetic moments of leptons See Entry 112004
 Direct comparison between the γ-ray fluxes from proton beam dumps at LAMPF and SIN See Entry 112006
 Inclusive production of electrons and muons in multihadronic events at PETRA See Entry 112016
 Search for mixing of heavy neutrinos in the β⁺ and β⁻ spectra of the ⁶⁴Cu decay See Entry 112124
 Neutrino emission from a hot, dense, plane-parallel atmosphere in hydrostatic equilibrium. III. The three-flavored atmosphere See Entry 116706
 Neutrino-gaseous 'Pancakes' and the problem of hidden mass See Entry 116861
 On the statistical distribution of massive fermions and bosons in a Friedmann Universe See Entry 116893
 Constraints on neutrino-dominated cosmologies from large-scale streaming motion See Entry 116894

14.80 OTHER AND HYPOTHETICAL PARTICLES

Electric and magnetic monopole solutions free from singularities in the non-symmetric unified field theory See Entry 111526
 Multidyon solutions in SU(2) gauge group See Entry 111862
 A SU(3) theory for leptons, quarks and electroweak interactions See Entry 111917
 Low energy tests of unification See Entry 111923
 The weak mixing angles in gauge models with horizontal symmetry—a new approach to quark and lepton masses See Entry 111924
 Left-right symmetry, K_L-K_S mass difference, and heavy quarks See Entry 111931
 Proton decay catalyzed by a monopole: the ratio of e⁺ to e⁺π⁰ final states See Entry 111933
 Towards a realistic SUGRA-GUT See Entry 111937
 Phenomenological electromagnetism with magnetic poles See Entry 111942
 Neutral currents in the gage model SU(3)_F×U(1) See Entry 111944
 Remarks on the possible origin of quark charges See Entry 111946
 Physical null zones and radiation representation See Entry 111956
 Phenomenologically compatible solutions to 't Hooft's equations for composite models See Entry 111976
 Virtual-photon shadowing in nuclei and photon structure See Entry 111983
 Lifetime of particles containing b quarks See Entry 111992
 Upper bound on the decay constant of familons See Entry 112000
 Further evidence for the radiative decay of a light, penetrating particle See Entry 112005
 Production of a single heavy quark in e⁺e⁻ collisions See Entry 112013

- Hadronic-energy correlations in high-energy e^+e^- annihilation See Entry 112014
- Inclusive production of electrons and muons in multihadronic events at PETRA See Entry 112016
- Evidence for $Z^0 \rightarrow e^+e^-$ at the CERN $\bar{p}p$ collider See Entry 112022
- Diffractional proton fragmentation in 16, 32, and 110 GeV/c K^-p interactions and the diffractional production of heavy quarks ($s\bar{s}, c\bar{c}$) See Entry 112028
- Further evidence for charged intermediate vector bosons at the SPS collider See Entry 112031
- Test of a superconducting magnetic-monopole detector for spurious events due to sea-level cosmic rays See Entry 112578
- Upper limit for mediation of baryon decay by slow magnetic monopoles See Entry 116416
- Monopoles in the inflationary Universe See Entry 116902
- Viscosity and the monopole density of the Universe See Entry 116909

20.00 NUCLEAR PHYSICS

21.00 NUCLEAR STRUCTURE

21.10 GENERAL AND AVERAGE PROPERTIES OF NUCLEI; PROPERTIES OF NUCLEAR ENERGY LEVELS

(for properties of specific nuclei listed by mass ranges, see 27.)

112032 Energy dependence of the rotational enhancement factor in the level density. G.Hansen, A.S.Jensen (Inst. of Phys., Univ. of Aarhus, Aarhus, Denmark).

Nucl. Phys. A (Netherlands), vol.A406, no.2, p.236-56 (19 Sept. 1983). The one-shell SU(3) energies are given and the corresponding level density is calculated approximately by use of a distribution function for the SU(3) quantum numbers. The calculation is extended to include many shells by a renormalization procedure and an effective one-shell interaction. The traditional level density is then obtained from the related mean-field hamiltonian which corresponds to a deformed harmonic oscillator potential. Various rotational enhancement factors are considered. Numerical results are obtained and comparisons between the SU(3) and the traditional level densities allow the first computation of the energy dependence of the rotational enhancement factor. A transition from axial to spherical level density is found. A simple parametrization is suggested in terms of a deformation-dependent half-value energy and a transition width. (26 refs.)

112033 Large transient magnetic fields for rare-earth ions recoiling in gadolinium and g-factors of high-spin states in $^{156,158,160}\text{Gd}$. O.Hauser, H.R.Andrews, D.Ward (Chalk River Nuclear Labs., AECL, Chalk River, Ontario, Canada), N.Rud, P.Taras, R.Nicole, J.Keinonen, P.Skensved, C.V.Stager.

Nucl. Phys. A (Netherlands), vol.A406, no.2, p.339-68 (19 Sept. 1983). The authors have determined the transient magnetic field for Coulomb-excited rare-earth nuclei recoiling with velocities in the range between $0.7v_0$ and $6v_0$ into ferromagnetic gadolinium cooled to a temperature $T=80\text{K}$. Measured and calculated g-factors in ^{169}Tm have been used as calibration standards. The transient field is found at first to increase with increasing recoil velocity, and then to level off, approaching a nearly constant value of $5.5\text{ kT at }v=6v_0$. At the higher velocities ($3v_0 < v < 6v_0$) the transient fields for ^{169}Tm recoils in gadolinium are a factor of 1.42 ± 0.12 larger than those in iron, whereas the densities of polarized electrons are the same in both ferromagnets. The transient field calibration has been corroborated making use of known g-factors of low-spin states in $^{156,158,160}\text{Gd}$ populated by Coulomb excitation of thick Gd single crystals. For the high-spin states in these nuclei, the g-factors are found to decrease slightly, with the ratio $g(10^+)/g(2^+)$ reduced to 0.89 ± 0.12 , 0.83 ± 0.11 , and 0.93 ± 0.13 , respectively. Similar decreases have been observed previously for other $N=90-96$ nuclei. (53 refs.)

112034 Odd Ni isotopes in the Lipkin-Nogami approach. R.Raj, M.L.Rustgi (Phys. Dept., Kurukshetra Univ., Kurukshetra, India).

Phys. Rev. C (USA), vol.28, no.2, p.935-7 (Aug. 1983). The modified Tamm-Dancoff approximation is applied to odd Ni isotopes after incorporating the Lipkin-Nogami procedure to improve the nonconservation of number of particles. The numerical calculations are performed employing the Kuo-Brown effective interaction. The Lipkin-Nogami procedure is found to give a general improvement in the agreement with data. (15 refs.)

112035 High-spin states in $^{201,203}\text{At}$ and the systematic behavior of $Z=85$ isotopes. K.Dybdal, T.Chapuran, D.B.Fossan, W.F.Piel, Jr. (Dept. of Phys., State Univ. of New York, Stony Brook, NY, USA), D.Horn, E.K.Warburton.

Phys. Rev. C (USA), vol.28, no.3, p.1171-80 (Sept. 1983). A spectroscopic investigation of high-spin states in $^{201,203}\text{At}$ was performed by means of the reactions $^{192,194}\text{Pt}(^{14}\text{N},\text{Sn})^{201,203}\text{At}$ with ^{14}N energies between 85 and 100 MeV. In-beam measurements of γ -ray excitation functions, γ - γ coincidences, γ -ray angular distributions, and pulsed-beam- γ timing were made to determine the decay scheme, level energies, γ -ray multipolarities, spin-parity assignments, and isomeric lifetimes. The yrast and near-yrast level structures were established up to $J \sim 25/2$, and several isomers with mean lifetimes around 20 ns were observed. The systematic trends of level energies of the odd-mass astatine ($Z=85$) isotopes are discussed in terms of proton-particle configurations of $^{211}\text{At}_{126}$ coupled to neutron-hole configurations of the corresponding even-mass lead isotopes. (15 refs.)

112036 Rotation-aligned bands in ^{196}Hg . H.Helppi, S.K.Saha, P.J.Daly (Dept. of Chem., Purdue Univ., West Lafayette, IN, USA), S.R.Faber, T.L.Kho.

Phys. Rev. C (USA), vol.28, no.3, p.1382-4 (Sept. 1983). Levels in ^{196}Hg have been studied by the $^{196}\text{Pt}(\alpha, n)$ reaction and the high-spin level scheme of ^{196}Hg has been considerably extended. Backbending in both positive and negative parity yrast level sequences is discussed within the cranked shell model description. (13 refs.)

112037 Properties of nuclei at high spins. F.S.Stephens (Lawrence Berkeley Lab., Univ. of California, Berkeley, CA, USA).

Phys. Scr. (Sweden), vol.T5, p.5-9 (1983). (Proceedings of the 4th Nordic Meeting on Nuclear Physics, Fuglso, Denmark, 16-20 Aug. 1982). Nuclei generate high spins by two methods, alignment of single particle angular momentum and collective rotation. The competition of these two modes is discussed for the highest spins $40 \leq I \leq 65\hbar$. Evidence is presented that alignment of the $h_{9/2}$ and $i_{13/2}$ proton orbitals from the next higher major shell produces large effects at high spins in rotational nuclei in the $A=160-166$ region. It is suggested that such major shell effects produce the still larger irregularities known to occur in the lighter nuclei of this region. (10 refs.)

112038 Single-particle and collective aspects of rotating nuclei. I.Hamamoto (Niels Bohr Inst., Copenhagen, Denmark).

Phys. Scr. (Sweden), vol.T5, p.10-15 (1983). (Proceedings of the 4th Nordic Meeting on Nuclear Physics, Fuglso, Denmark, 16-20 Aug. 1982). Some features and quantum-numbers of one-particle motion in rotating potentials are summarized for 'high- J ' orbits and 'normal-parity' orbits, respectively. As an example of collective aspects of rotating nuclei, the disappearance of pair-correlation at high-spin states is discussed especially in connection with available experimental information. (24 refs.)

112039 Recent developments in the interpretation of the discrete line spectroscopy of deformed rare-earth nuclei. J.D.Garrett (Niels Bohr Inst., Univ. of Copenhagen, Copenhagen, Denmark).

Phys. Scr. (Sweden), vol.T5, p.21-8 (1983). (Proceedings of the 4th Nordic Meeting on Nuclear Physics, Fuglso, Denmark, 16-20 Aug. 1982). Recent developments in the interpretation of high-spin discrete-line data in terms of independent-particle motion in a rotating deformed nucleus are discussed. Particular attention is given to the interpretation of the residual interactions derived from a comparison of routhians corresponding to multiple-quasineutron configurations and those constructed from 'experimental' values of the constituent single-quasineutron configurations. Similarly, the correlation between band-crossing frequencies in odd- N nuclei corresponding to the alignment of an $i_{13/2}$ pair of neutrons, and the shape of the valence quasineutron orbit is established for a variety of configurations. The correspondence between the residual-interactions and band-crossing frequencies is discussed, and the extracted estimate of the pairing reduction associated with the 'blocking' of a single quasi-neutron is compared with BCS estimates for constant level spacing. Finally, some suggestions are made concerning the physical basis of the shift in the $h_{9/2}$ proton alignment frequencies between $v_n=2$, $\pi=+$ and $v_n=4$, $\pi=-$ bands in ^{180}Os . (34 refs.)

112040 Aligned bands and nuclear shapes in the $N=90$ region. L.L.Riedinger (Phys. Dept., Univ. of Tennessee, Knoxville, USA).

Phys. Scr. (Sweden), vol.T5, p.36-44 (1983). (Proceedings of the 4th Nordic Meeting on Nuclear Physics, Fuglso, Denmark, 16-20 Aug. 1982). The $N=90$ transition region is studied by gauge-space systematics for Nd through Yb nuclei and by the trend of transition quadrupole moments for ground-state bands. Lifetime measurements on quasiparticle bands in $^{160,161}\text{Yb}$ indicate a systematic decrease in the collectivity at higher rotational frequencies, indicating triaxial shapes. Spectroscopy measurements on ^{159}Tm are described. A change in the order of the signatures of the $h_{11/2}$ and after, compared to before, the backbend is used to extract qualitative information on shape triaxiality. The systematics of 2 and 3 quasiparticle bands in $N=90$ and 91 nuclei is presented and used to deduce the occurrence of a large-interaction crossing in ^{160}Yb and ^{162}Hf due to the alignment of negative-parity neutrons ($h_{9/2}+f_{7/2}$). (35 refs.)

112041 'Non-rotating' yrast states. K.Neergard.

Phys. Scr. (Sweden), vol.T5, p.51-4 (1983). (Proceedings of the 4th Nordic Meeting on Nuclear Physics, Fuglso, Denmark, 16-20 Aug. 1982). Calculations for nuclei in the vicinity of ^{146}Gd based on a version of the deformed independent particle model are discussed. Particular attention is paid to systematic trends in the calculated deformations, deformation energies and pairing energies. (16 refs.)

112042 Collective vibrations as doorway states in the damping of nuclear motion. R.A.Brogli (Niels Bohr Inst., Univ. of Copenhagen, Copenhagen, Denmark).

Phys. Scr. (Sweden), vol.T5, p.80-3 (1983). (Proceedings of the 4th Nordic Meeting on Nuclear Physics, Fuglso, Denmark, 16-20 Aug. 1982). The damping of single-particle and giant resonances is studied. Doorway states containing low-lying surface vibrations are found to play a central role in this process. The coupling to these states lead to damping widths consistent with the empirical systematics. It is however not possible to directly relate these two quantities, because of the central role played by the correlation between the particle and the hole in the vibration. (4 refs.)

112043 Search for the two-phonon 0^+ strength in ^{64}Zn . A.Passoja, J.Kantele, M.Luontama, J.Kumpulainen, R.Julin (Dept. of Phys., Univ. of Jyväskylä, Jyväskylä, Finland).

Phys. Scr. (Sweden), vol.T5, p.145-6 (1983). (Proceedings of the 4th Nordic Meeting on Nuclear Physics, Fuglso, Denmark, 16-20 Aug. 1982). The two-phonon 0^+ strength in ^{64}Zn has been searched for by obtaining experimental results for the E0 and E2 transitions depopulating the excited 0_2^+ and 0_3^+ states. The previous identification of the 0_2^+ state in ^{64}Zn at 1910.3 keV as a two-phonon state is completely washed out through the present experimental results: $B(E2; 0_2^+ \rightarrow 2_1^+) = 0.058(3) \text{ W.u.}$, $B(E2; 0_2^+ \rightarrow 2_2^+) = 62(8) \text{ W.u.}$ and $\rho(E0; 0_2^+ \rightarrow 0_1^+) = 3.9(4) \times 10^{-3}$. (9 refs.)

112044 Multi-step shell-model description of Sn isotopes. L.Rydström, J.Blomqvist, R.J.Liotta (Res. Inst. of Phys., Stockholm, Sweden), C.Pomar.

Phys. Scr. (Sweden), vol.T5, p.149-52 (1983). (Proceedings of the 4th Nordic Meeting on Nuclear Physics, Fuglso, Denmark, 16-20 Aug. 1982). A multi-step shell-model method is applied to calculate up to four neutron holes in the core ^{132}Sn . It is found that most low-lying states in the three- and four-hole nuclei are members of multiplets arising from the coupling of one- and two-hole states. (15 refs.)

112045 Microscopic calculations of nuclear wobbling rotation. P.Arve (NORDITA, Copenhagen, Denmark), Y.S.Chen, G.A.Leander.

Phys. Scr. (Sweden), vol.T5, p.157-61 (1983). (Proceedings of the 4th Nordic Meeting on Nuclear Physics, Fuglso, Denmark, 16-20 Aug. 1982). High- K rotational bands may correspond to classical wobbling, which is a more complex motion than rotation around an intrinsic axis and therefore can in general not be described by the cranking model. Two microscopic models of wobbling are developed and found to give compatible results. One diagonalizes the response of a valence shell to a wobbling rotational core. The other is RPA with the field $F \sim [H_N, J_+]$, which turns out to be a major improvement over $F \sim r^2 Y_{21}$ employed in previous calculations. General features seem to be $\mathcal{I} < \mathcal{I}_{\text{rigid}}$ under many circumstances a fragmentation of the collective mode. The highest- K data available, from a recent experiment on ^{179}W , are reproduced without parameter fitting. Recent quasicontinuum data on ^{158}Yb are discussed. (28 refs.)

112046 Intrinsic excitations as yrast structures in ^{179}W above $I \sim 35/2\hbar$. Pedersen, S.Bjornholm, J.Borggreen, J.Kownacki, G.Sletten (Niels Bohr Inst., Roskilde, Denmark).

Phys. Scr. (Sweden), vol.T5, p.162-4 (1983). (Proceedings of the 4th Nordic Meeting on Nuclear Physics, Fuglso, Denmark, 16-20 Aug. 1982).

Gamma cascades through high-spin configurations with high seniority are found to feed the $t_{1/2} = 710$ ns isomer in ^{179}W . The abnormally short half life of the isomeric state itself, which decays into the $K=7/2$ ground-state rotational $31/2$ member, violating the K -selection rule twelve times, is explained as a result of an accidental degeneracy in energy between the $K^\pi = 35/2^-$ isomeric state and the $35/2^-$ ground-band rotational state. Above the isomer, the yrast structure is dominated by deformation aligned states. (8 refs.)

112047 Shape changes, band crossings and band terminations in the very high spin region of $A=150-160$ nuclei. T.Bengtsson, I.Ragnarsson (Dept. of Math. Phys., Lund Inst. of Technol., Lund, Sweden).

Phys. Scr. (Sweden), vol.T5, p.165-70 (1983). (Proceedings of the 4th Nordic Meeting on Nuclear Physics, Fuglso, Denmark, 16-20 Aug. 1982).

The very high spin behaviour of nuclei with ~ 10 particles outside the ^{146}Gd core are studied. The method of calculation, which is based on the cranked Nilsson-Strutinsky formalism, makes possible to follow individual configurations as functions of spin. The authors concentrate on ^{158}Er and ^{154}Dy which nuclei become oblate with rotation around the symmetry axes for $I=40-50$. It is found that most such oblate states can be described as band termination, i.e. they correspond to the maximum spin which can be formed if the distribution of nucleons over the f -shells is kept fixed. A strong argument which supports this conclusion is the M1-bump which has recently been observed for ^{158}Yb . Such an M1-bump seems to be a natural consequence of the terminating bands. A further consequence is that these bands appear to prohibit the formation of yrast isomers for spins much larger than $I=40$. (19 refs.)

112048 Kinematical and dynamical moments of inertia and the Mottelson-Valatin effect at high spin excitations. J.Dudek (SERC, Daresbury Lab., Daresbury, Warrington, England), W.Nazarewicz, Z.Szymanski.

Phys. Scr. (Sweden), vol.T5, p.171-4 (1983). (Proceedings of the 4th Nordic Meeting on Nuclear Physics, Fuglso, Denmark, 16-20 Aug. 1982).

Theoretical arguments, based on the pairing-selfconsistent independent quasi-particle model, are presented to support the idea of a collective transition from the superfluid to the normal phase (Mottelson-Valatin effect) in selected actinide nuclei. Detailed calculation results are in good agreement with existing experimental data. The strong relationship between the nucleonic angular momentum alignment and the disappearance of pairing correlations in nuclei is also discussed. It is suggested that a Mottelson-Valatin type mechanism dominates in the excitation pattern of $^{232-238}\text{U}$, while in the neighbouring thorium and plutonium nuclei the influence of nucleonic alignment and of a band crossing on the high spin properties seems more pronounced. (16 refs.)

112049 High spin phenomena in the mass 100-200 region seen through the Crystall Ball. J.J.Gaardhoje, J.D.Garrett, G.B.Hagemann, B.Herskind, A.Holm, P.Nolan, G.Sletten (Niels Bohr Inst., Univ. of Copenhagen, Copenhagen, Denmark), J.R.Beene, M.L.Halbert, D.C.Hensley, I.Y.Lee, F.Plasil, F.A.Dilmanian, M.Jaaskelainen, H.Puchta, D.G.Sarantites, R.Woodward, T.Lindblad.

Phys. Scr. (Sweden), vol.T5, p.178-82 (1983). (Proceedings of the 4th Nordic Meeting on Nuclear Physics, Fuglso, Denmark, 16-20 Aug. 1982).

The average properties of the gamma ray entry region and the decay from it are studied systematically, for 49 nuclear systems, in the spin spectrometer. Preliminary results are given for the mass the neutron number of dependence of the gamma ray fold distribution and of unresolved γ spectra. The possibility of gating simultaneously on narrow regions of fold and excitation energy is exploited. (8 refs.)

112050 Coupling of two quasiparticles to coherent cores in the Pt isotopes. A.A.Raduta, C.Lima (Inst. fur Theoretische Phys., Univ. Tubingen, Tubingen, Germany), A.Faessler.

Z. Phys. A (Germany), vol.313, no.1-2, p.69-82 (1983).

A model for coupling the motion of particles to that of a quadrupole-collective core is proposed. The quadrupole vibrations and rotations of the core are described by angular momentum projected coherent states. The spherical shell model particles interact among themselves by pairing and surface delta interactions. The particles are coupled to the core through a multipole-multipole interaction. The method is applied to several even mass isotopes of Pt. The agreement with experimental data of the excitation energies, gyromagnetic factors and $E2$ probabilities is very good. (30 refs.)

112051 (p,p') scattering at 65 MeV on ^{12}C , ^{24}Mg , ^{28}Si and ^{32}S . S.Kato, K.Okada (Lab. of Nuclear Studies, Faculty of Sci., Osaka Univ., Toyonaka, Osaka, Japan), M.Kondo, K.Hosono, T.Saito, N.Matsuoka, K.Hatanaka, T.Noro, S.Nagamachi, H.Shimizu, K.Ogino, Y.Kadota, S.Matsuki, M.Wakai. Proceedings of the 1983 RCNP International Symposium on Light Ion Reaction Mechanism, Osaka, Japan, 16-20 May 1983 (Osaka, Japan: Osaka University 1983), p.241-5

Angular distributions of the cross sections and analyzing powers for the elastic and inelastic scatterings of 65 MeV polarised protons from ^{12}C , ^{24}Mg , ^{28}S and ^{32}S were measured. Coupled channels analyses of the scattering data to 0^+ , 2^+ , 4^+ states in the ground rotational bands, the 0^+ state in the β -band, 2^+ , 3^+ , 4^+ members in the γ -band, 3^- , 4^- members in the $K^\pi = 3^-$ octupole band and 1^- , 3^- members of the $K^\pi = 0^-$ octupole band were performed. A good agreement between data and the coupled channels calculation were obtained in analysing power for β -vibrational states and 3^- states. (9 refs.)

112052 Microscopic study of the resonant states with light-heavy di-nucleus configurations. A.Tohsaki-Suzuki (Faculty of Textile Sci. & Technol., Shinshu Univ., Nagano, Japan), K.Ikeda.

Proceedings of the 1983 RCNP International Symposium on Light Ion Reaction Mechanism, Osaka, Japan, 16-20 May 1983 (Osaka, Japan: Osaka University 1983), p.845-9

The energy quantities characterizing the molecular bands are considered on the basis of microscopic studies of $^{16}\text{O}+^{16}\text{O}$, $^{16}\text{O}+^{40}\text{Ca}$ and $^{40}\text{Ca}+^{40}\text{Ca}$ systems. The conditions are discussed on the formation of the resonant states with di-nucleus configurations. An obtained simple expression is applied to the other typical di-nucleus systems. (5 refs.)

112053 Energy of a nucleon in a nucleus. C.Mahaux (Inst. de Phys., Univ. de Liege au Sart Tilman, Liege, Belgium).

Symmetries in Nuclear Structure. Proceedings of a NATO Advanced Study Institute on Symmetries in Nuclear Structure, Dronter, Netherlands, 16-28 Aug. 1982 (New York, USA: Plenum Press 1983), p.151-76

In the independent particle model (IPM), the nuclear ground state wave function ϕ_A is a Slater determinant built with A single-particle wave functions $\phi_{\alpha}(r)$, where α generically denotes the orbit quantum numbers n,l,j,m . For simplicity, the author restricts the discussion to spherical nuclei. A consequence of the IPM is that the configurations $\phi_{A-1} = a_{\alpha}|\phi_A\rangle$, $\phi_{A+1} = a_{\alpha}^{\dagger}|\phi_A\rangle$ are eigenstates of the Hamiltonian H for $A-1$ and $A+1$ nucleons, respectively. Equations imply a symmetry property of H . The main purpose of these lectures is to discuss to what extent this symmetry holds in

nature. The amount of symmetry breaking depends upon the choice of the basis $\{\phi_{\alpha}\}$ and upon the particular nuclei which are considered. The author introduces some concepts in the idealized case of infinite nuclear matter. He then turns to actual nuclei. He considers single-particle states which are at positive energy, or are weakly, deeply or semi-deeply bound. Recent theoretical progress on the improvement of the independent particle model is discussed. (81 refs.)

Proceedings of the 4th Nordic Meeting on Nuclear Physics . See Entry 111306

Nuclear data sheets for $A=79$ See Entry 111327

Nuclear data sheets for $A=153$ See Entry 111328

Recent References, January through April 1983 [nuclear data sheets] See Entry 111329

Effect of the fourth-order Casimir invariants on $U_{6/4}$ and $U_{6/2}$ dynamical supersymmetries in nuclei and baryons See Entry 111912

Spherical, oblate, and prolate nuclear shapes near ^{146}Gd See Entry 112056

Nuclear shape transitions and some properties of aligned-particle configurations at high spin See Entry 112058

Transition from prolate to oblate to triaxial shapes in ^{158}Yb See Entry 112059

Shape coexistence and other aspects of nuclear structure in ^{40}Ar See Entry 112060

On the parity dependence of nuclear level densities See Entry 112068

Deformation aligned states See Entry 112074

Symmetry aspects of the shell model See Entry 112090

Rotational motion at finite temperature See Entry 112093

Coupling of surface and bulk vibrations in the nuclear breathing mode See Entry 112094

High excited α cluster state calculation of nuclei See Entry 112099

Multipole pair fields at finite temperature See Entry 112101

Band crossing in ^{130}Ba See Entry 112109

Electromagnetic transitions in ^{130}Ce See Entry 112112

First results on γ -ray spectroscopy in the second minimum of ^{238}U and ^{240}Pu See Entry 112113

^{17}O - ^{17}N analog states via the $^{14}\text{C}(^6\text{Li},t)$ and $^{14}\text{C}(^6\text{Li},^3\text{He})$ reactions See Entry 112148

Landau damping in the degenerate Fermi liquid See Entry 112150

Giant resonance splitting in deformed nuclei See Entry 112152

Test of vibrational current distributions in transverse electron scattering See Entry 112173

Low-lying levels, γ -ray transitions, and vibrational structure in ^{198}Pt from $(n,n'\gamma)$ reaction spectroscopy See Entry 112190

Search for two-phonon vibrations in ^{168}Er See Entry 112194

Characteristic 7^- and 5^- states observed in the (p,t) reactions on even-even rare earth nuclei See Entry 112211

High-spin states in ^{222}Th See Entry 112244

Coulomb excitation of ^{189}Os See Entry 112247

Penetration of the centrifugal barrier in the fusion of ^{16}O with heavy targets ... See Entry 112255

Fission and pairing degrees of freedom in collective transport theory See Entry 112290

Reassessment of fission fragment angular distributions from continuum states in the context of transition-state theory See Entry 112291

21.10D Binding energy and masses

112054 Nuclear binding energies from moment methods: realistic effective no-core Hamiltonian. F.J.Margetan (Dept. of Energy, Iowa State Univ., Ames, IA, USA), J.P.Vary.

Phys. Rev. C (USA), vol.28, no.2, p.907-15 (Aug. 1983).

Total binding energies for nuclei with $14 \leq A \leq 18$ are obtained from a realistic effective no-core Hamiltonian, H_{eff} , using moment methods. The lowest few moments of H_{eff} are evaluated in an oscillator model space of four major shells. These moments are then used to determine a number of continuous and discrete density of states functions, each of which yields an estimate for the H_{eff} ground state energy. The adjustable discrete density of states functions which we introduce are based upon realistic single-particle Hamiltonians. With a reasonable selection of moment method ingredients the authors obtain good agreement between theory and experiment for relative binding energies within each A chain. The most stable isobar is correctly predicted in all cases and Coulomb energy differences are in close agreement with experiment. Thus, the valley of β stability is well reproduced in this approach with a simple overall shift in absolute binding energies for each A chain. (16 refs.)

112055 Atomic mass of ^{145}Eu derived from relative P_K -ratios. U.J.Schrewe, W.-D.Schmidt-Ott (II. Phys. Inst., Univ. Gottingen, Gottingen, Germany).

Z. Phys. A (Germany), vol.313, no.1-2, p.137-8 (1983).

Using γ -ray spectroscopic methods relative P_K ratios were determined for individual β -transitions in the ^{145}Eu decay. Using the energy dependence of the P_K values the decay energy Q_{EC} was derived to be $Q_{\text{EC}} = 2647_{-10}^{+14}$ keV. The corresponding mass excess for ^{145}Eu of $-78008(15)$ keV is in good agreement with recent reaction studies. (14 refs.)

Tensor forces in the three-body problem See Entry 112077

Analysis of the evaporation-corrected mass and charge distributions in the $\text{Ar}+\text{Mo}$ reactions See Entry 112270

Formation and decay of the compound nucleus studied in the reaction $^{20}\text{Ne}+^{27}\text{Al}$ See Entry 112272

21.10F Shape, charge, radius and form factors

112056 Spherical, oblate, and prolate nuclear shapes near ^{146}Gd .

R.R.Chasman (Chem. Div., Argonne Nat. Lab., Argonne, IL, USA).

Phys. Rev. C (USA), vol.28, no.3, p.1374-8 (Sept. 1983).

Proton and neutron single particle level spacings are determined for the $A=146$ mass region, using a rotationally invariant interaction and recent experimental data. Excitation energies of spherical and deformed high spin states in ^{146}Gd , the transition probability $B(E2; 10^+ \rightarrow 8^+)$ for several $N=82$ isotones, and the 0^+ excited state spectra of, and neutron pair transfer probabilities for, levels in ^{146}Gd and ^{144}Sm are calculated. Comparisons with experimental data are made. (25 refs.)

112057 Effect of core polarization on the charge distribution in ^{208}Pb . P.Mukherjee, R.Bhattacharya, C.Samanta (Saha Inst. of Nuclear Phys., Calcutta, India).

Phys. Rev. C (USA), vol.28, no.3, p.1396-7 (Sept. 1983).

The coefficients of Fourier-Bessel expansion of charge distribution in ^{208}Pb are determined from the single proton wave functions derived from two sets of optimized Woods-Saxon potentials. The set of potentials optimized with respect to the observed single particle states in ^{208}Pb give excellent agreement with the model independent analysis of the charge distribution. But the potentials obtained from core-polarization corrected single particle states give very poor charge distribution. (8 refs.)

112058 Nuclear shape transitions and some properties of aligned-particle configurations at high spin. T.L.Khoo, P.Chowdhury, H.Emling, D.Frekers, R.V.F.Janssens, W.Kuhn (Argonne Nat. Lab., Argonne, IL, USA), A.Pakkanen, Y.H.Chung, P.J.Daly, Z.W.Grabowski, H.Helppi, M.Kortelahti, S.Bjornholm, J.Borggreen, J.Pedersen, G.Sletten.

Phys. Scr. (Sweden), vol.T5, p.16-20 (1983). (Proceedings of the 4th Nordic Meeting on Nuclear Physics, Fuglso, Denmark, 16-20 Aug. 1982).

The authors discuss the variation of shapes with spin and neutron number for nuclei in the $N \approx 88$ transitional region. They then present comments on the feeding times of very high spin single-particle yrast states. (18 refs.)

112059 Transition from prolate to oblate to triaxial shapes in ^{158}Yb . M.Jaaskelainen, D.G.Sarantites, F.A.Dilmanian, R.Woodward, H.Puchta (Dept. of Chem., Washington Univ., St. Louis, MO, USA), J.R.Beene, J.Hattula, M.L.Halbert, D.C.Hensley.

Phys. Scr. (Sweden), vol.T5, p.175-7 (1983). (Proceedings of the 4th Nordic Meeting on Nuclear Physics, Fuglso, Denmark, 16-20 Aug. 1982).

The decay of the entry states in ^{158}Yb populated in the reactions of 149 MeV ^{20}Ne with ^{144}Nd and ^{146}Nd has been investigated with a 4π multidetector system gated by a Ge counter. The average excitation energy, the γ -ray spectra and the angular distributions as a function of multiplicity show several changes in the γ -ray decay. These changes suggest a transition from prolate to particle aligned oblate configuration at low spin. At $I \approx 38-48$ collective transitions with dipole and quadrupole component possibly built on high K single particle states are observed. Furthermore, above $I \approx 48$ the dipole component disappears suggesting a further change toward more triaxial shape. (16 refs.)

112060 Shape coexistence and other aspects of nuclear structure in ^{40}Ar . E.Bitterwolf, A.Burkard, P.Betz, F.Glatz, F.Heidinger, Th.Kern, R.Lehmann, S.Norbert, H.Ropke, C.Schneider, J.Siefert (Fakultat fur Phys., Univ. Freiburg, Freiburg, Germany).

Z. Phys. A (Germany), vol.313, no.1-2, p.123-32 (1983).

The γ -decay of ^{40}Ar has been studied by particle- γ coincidence measurements in the $^{37}\text{Cl}(\alpha, p\gamma)$ reaction at 12 and 13 MeV bombarding energy. Particle- γ angular correlations and linear polarizations of γ -rays were measured at 12 MeV. A lifetime measurement using the Doppler-shift attenuation method was performed at 11 MeV. The coexistence of spherical and deformed states in ^{40}Ar could be concluded from the observation of a $K^\pi = 0^+$ rotational band which has its $I^\pi = 0^+$ through 6^+ members at 2121, 2524, 3515 and 4959 KeV excitation energy. The intrinsic quadrupole moment derived from $B(E2)$ values is $|Q_0| = 1320_{-120}^{+60}$ mb. Negative-parity states with high spin were observed at $4.858(5^-)$, $4.494(5^-)$, $4.226(4^-)$ and 4991 KeV (4^-) excitation energy. A complete account of all levels below 5 MeV excitation energy is obtained by a model in which two $d_{3/2}$ proton holes couple weakly to the ^{42}Ca levels below 4.75 MeV excitation energy. (21 refs.)

Proceedings of the 4th Nordic Meeting on Nuclear Physics. See Entry 111306

Energy dependence of the rotational enhancement factor in the level density See Entry 112032

Recent developments in the interpretation of the discrete line spectroscopy of deformed rare-earth nuclei See Entry 112039

Aligned bands and nuclear shapes in the $N=90$ region See Entry 112040

'Non-rotating' yrast states See Entry 112041

Shape changes, band crossings and band terminations in the very high spin region of $A=150-160$ nuclei See Entry 112047

Spin-isospin ordered shell model states in nuclei See Entry 112062

Deformation aligned states See Entry 112074

Dependence of the Fermi form factor on the dominant pole in the density See Entry 112086

Influence of shell structure on deep inelastic collisions See Entry 112089

Coupling of surface and bulk vibrations in the nuclear breathing mode See Entry 112094

Role of finite boson number in the interacting boson approximation description of γ -g transitions in deformed nuclei See Entry 112100

Nucleon currents between highly excited nuclei See Entry 112103

Parametrization of the short-range correlation and exchange matrix elements by the Landau-Migdal parameters See Entry 112108

The photoneutron cross section of ^{151}Eu , ^{153}Eu and ^{156}Gd in the giant resonance region See Entry 112170

Pion photoproduction off nuclei: a sensitive test of the nuclear transition densities See Entry 112171

Test of vibrational current distributions in transverse electron scattering See Entry 112173

Reaction $\mu^- + {}^6\text{Li} \rightarrow {}^3\text{H} + {}^3\text{H} + \nu_\mu$ and the axial current form factor in the time-like region See Entry 112178

Electron scattering See Entry 112180

Unified description of statistical excitations, deformations and charge transfer in a dynamical theory of deep-inelastic heavy-ion collisions See Entry 112242

Analysis of the evaporation-corrected mass and charge distributions in the $\text{Ar} + \text{Mo}$ reactions See Entry 112270

21.10H Spin, parity, and isobaric spin

112061 On the use of isomer ratios in ^{44}Sc for predicting spin populations in high energy heavy-ion nuclear reactions. H.Groening, K.J.Moody, G.T.Seaborg (Lawrence Berkeley Lab., Univ. of California, Berkeley, CA, USA).

Nucl. Instrum. & Methods Phys. Res. (Netherlands), vol.214, no.2-3, p.317-20 (1 Sept. 1983).

From fits of isomer ratio as a function of projectile kinetic energy the authors have calculated the centroids in the E - J plane for the $^{44}\text{Sc}^*$ population generated in the reactions $^{29}\text{Si}(^{18}\text{O}, p2n)^{44m}\text{Sc}$ and $^{41}\text{K}(\alpha, n)^{44m}\text{Sc}$. It is shown that ^{44}Sc isomer ratios can be used to predict average spins in $^{44}\text{Sc}^*$,

particularly if such ratios are low. As isomer ratios increase, unique identification of average spin populations becomes more difficult because average excitation energy becomes important in determining the isomer ratio. (15 refs.)

112062 Spin-isospin ordered shell model states in nuclei. G.Giberti, N.Lo Iudice, G.Varaccio (Istituto di Fisica Teorica, Univ. di Napoli, Sezione di Napoli, Napoli, Italy).

Phys. Rev. C (USA), vol.28, no.2, p.888-93 (Aug. 1983).

Several shell model configurations entitled to describe a spin-isospin phase in nuclei are analyzed at different nuclear densities and deformations in the region $A=12-36$. Shell effects are found to be dominant. As a result, the spin-isospin alignment ($\sigma_3\tau_3 = +1$ or $\sigma_3\tau_3 = -1$) is most favored in nuclei around $A=28$ because of their distinctive shell model structure. Moreover, in a given nucleus an energy gain over the normal and other possible phases can be obtained at reasonably low densities, if a fraction rather than the totality of nucleons have the same spin-isospin alignment. The analysis of the results strongly suggests that the ordered phase should be described by a correlated shell model state composed of a suitable number of these partially ordered configurations. The relevance of the results to possible collective properties of properly chosen nuclei at ordinary density is pointed out. (10 refs.)

112063 Spin and isospin characteristics of the excited states of ^{36}Ar through the reaction $^{32}\text{S}(\alpha, \gamma)^{36}\text{Ar}$ in the bombarding energy range $E_\alpha = 4$ to 5 MeV. D.R.Chakrabarty, M.A.Eswaran, N.L.Ragoowansi (Nuclear Phys. Div., Bhabha Atomic Res. Centre, Bombay, India).

Phys. Rev. C (USA), vol.28, no.3, p.1012-24 (Sept. 1983).

The α capture reaction $^{32}\text{S}(\alpha, \gamma)^{36}\text{Ar}$ was studied in the bombarding energy range of $E_\alpha = 4.13$ to 5.00 MeV corresponding to the excitation energy range of $E_x = 10.31$ to 11.08 MeV in ^{36}Ar . Seven resonances have been located and their resonance strengths determined. Two of the resonances decay predominantly to the ground state while the other five decay predominantly to the first excited state of ^{36}Ar . Angular distribution measurements of the predominant decay gamma ray have been performed and the spin and parity of all the resonances assigned. The isospin of two of the resonances have been assigned as $T=0$ while $T=1$ has been assigned for three others. Evidence has been obtained for the operation of the isospin selection rule for the dipole ($E1$ and $M1$) and quadrupole ($E2$) gamma decay. (16 refs.)

112064 Simple isospin relations for transitions in $A=13$. R.J.Peterson (Nuclear Phys. Lab., Univ. of Colorado, Boulder, CO, USA).

Phys. Scr. (Sweden), vol.T5, p.190-2 (1983). (Proceedings of the 4th Nordic Meeting on Nuclear Physics, Fuglso, Denmark, 16-20 Aug. 1982).

The isospin symmetry breaking noted in pion inelastic scattering on ^{13}C has been shown previously to be consistent with helium-ion scattering and charge exchange data. Here, proton scattering and charge exchange data at a beam energy of 26.1 MeV are shown to exhibit rather different features. Since the great isospin asymmetries are found for stretched-spin states very near the proper nucleon decay thresholds, it is suggested that external mixing is responsible for the consistent observations for strongly absorbed projectiles, but that nucleon beams are sensitive to different radial locations and so the proton-induced data may not be related simply to more surface dominated data. (26 refs.)

112065 Breaking of fundamental symmetries in nuclei. E.G.Adelberger (Max-Planck-Inst. fur Kernphys., Heidelberg, Germany).

Symmetries in Nuclear Structure. Proceedings of a NATO Advanced Study Institute on Symmetries in Nuclear Structure, Dronten, Netherlands, 16-28 Aug. 1982 (New York, USA: Plenum Press 1983), p.55-91

Nuclei are interesting systems in which to study symmetry breakdowns because of the rich variety of phenomena one can observe. The nucleus 'feels' the strong, electromagnetic (EM) and weak interaction which respect differing sets of fundamental symmetries so that one expects a hierarchy of symmetry breaking effects. The author discusses the breaking of 2 symmetries-isospin (I) which is respected by the strong interaction but broken by electromagnetism, and parity (P) which is violated only by the weak interaction. These two examples in some sense span the space of symmetry-breaking effects. The ratio of the EM to the strong force felt by a pair of nucleons is roughly $Z\alpha$ so that isospin is quite obviously broken in nuclei. Nevertheless in many cases the symmetry is better than one would expect from elementary considerations. Because I-breaking effects are so obvious and easily measurable it provides a nice understandable example of a broken symmetry and the author discusses it in some detail. (32 refs.)

Nuclear data sheets for $A=79$ See Entry 111327

Nuclear data sheets for $A=153$ See Entry 111328

Recent References, January through April 1983 [nuclear data sheets] See Entry 111329

High-spin states in $^{201,203}\text{At}$ and the systematic behavior of $Z=85$ isotopes See Entry 112035

Rotation-aligned bands in ^{196}Hg See Entry 112036

Properties of nuclei at high spins See Entry 112037

Single-particle and collective aspects of rotating nuclei See Entry 112038

Nuclear shape transitions and some properties of aligned-particle configurations at high spin See Entry 112058

On the parity dependence of nuclear level densities See Entry 112068

Shell-model calculations of high-spin isomers in neutron-deficient $1g_{9/2}$ -shell nuclei See Entry 112069

1p-2h and 2p-3h states in ^{15}C See Entry 112070

Implications of the recently discovered $^{208}\text{Pb}(1^+, E_x = 5.845 \text{ MeV})$ state for the spin-dependent nuclear interaction See Entry 112073

Determination of the multipolarity of prompt electromagnetic transitions from angular distributions of conversion electrons. I. Method See Entry 112106

Band crossing in ^{130}Ba See Entry 112109

Gamow-Teller strength function for ^{90}Zr : effects of spin and isospin exchange forces, and ground-state correlations See Entry 112128

Charged pion electroproduction, a selective probe of nuclear spin-isospin responses See Entry 112151

Gamow-Teller resonances See Entry 112154

Excitation of M1 resonances by medium energy protons See Entry 112158

$(e, e' \pi)$ reaction on light nuclei and spin-isospin strength distribution effects See Entry 112177

Elastic and inelastic scattering of polarized protons from ^{206}Pb near isobaric analog resonances See Entry 112199

Unnatural parity states studied in high resolution (p,p') experiments at 65 MeV and the effective nucleon-nucleon interaction See Entry 112207

Magnetic states observed in high-resolution (p,n) experiments See Entry 112208

The $^{52}\text{Cr}(t,p)^{54}\text{Cr}$ reaction at $E_t=15\text{ MeV}$ See Entry 112219
 High-spin states in ^{222}Th See Entry 112244

21.10J Spectroscopic factors

^{17}O - ^{17}N analog states via the $^{14}\text{C}(^6\text{Li},t)$ and $^{14}\text{C}(^6\text{Li},^3\text{He})$ reactions See Entry 112148
 Elastic and inelastic scattering of polarized protons from ^{206}Pb near isobaric analog resonances See Entry 112199
 Elastic and rearrangement scattering between two interacting deuterons as a four-body problem See Entry 112222
 Measurement of vector analyzing power in the reaction $^{12}\text{C}(d,^6\text{Li})^8\text{Be}$ See Entry 112227

21.10K Electromagnetic moments

112066 Electromagnetic properties of isomers in ^{210}Pb . D.J.Decman, J.A.Becker, J.B.Carlson, R.G.Lanier, L.G.Mann, G.L.Struble (Lawrence Livermore Nat. Lab., Livermore, CA, USA), K.H.Maier, W.Stoffl, R.K.Sheline. *Phys. Rev. C (USA)*, vol.28, no.3, p.1060-4 (Sept. 1983).
 The lifetimes and magnetic moments of the $J^\pi=8^+$ and 6^+ isomers in ^{210}Pb have been measured using the gamma-ray perturbed angular distribution technique. The levels were populated with the $^{208}\text{Pb}(t,p)^{210}\text{Pb}$ reaction. The g factors of the 8^+ and 6^+ states are found to be $-0.312(8)$ and $-0.312(15)$, respectively. The magnetic moment, $\mu=-1.42(7)\mu_N$, is deduced for the $2g_{7/2}^+$ neutron orbital. Mean lifetimes are $290(25)$ ns for the 8^+ state and $71(9)$ ns for the 6^+ state. The authors find $\langle g_{7/2}^2 \rangle / M(E2) \parallel \langle g_{7/2}^2 \rangle = -39(2) e\text{ fm}^2$ and an effective charge of $0.88(5) e$ for the $2g_{7/2}^+$ neutron orbital. (17 refs.)
 112067 Neutron versus proton moments of collective excitations from polarized deuteron scattering. G.Graw, H.Clement, H.Kader, F.Merz, P.Schiemenz, N.Seichert (Sektion Physik, Univ. Munchen, Garching, Germany).
 Proceedings of the 1983 RCNP International Symposium on Light Ion Reaction Mechanism, Osaka, Japan, 16-20 May 1983 (Osaka, Japan: Osaka University 1983), p.914
 The authors investigate the moments of neutron distribution for nuclei with $18 \leq A \leq 232$, by determining their mass transition moments with inelastic scattering of polarised deuterons. The results of a CC analysis are presented. (3 refs.)
 Large transient magnetic fields for rare-earth ions recoiling in gadolinium and g -factors of high-spin states in $^{156,158,160}\text{Gd}$ See Entry 112033
 Coupling of two quasiparticles to coherent cores in the Pt isotopes See Entry 112050
 Nuclear binding energies from moment methods: realistic effective no-core Hamiltonian See Entry 112054
 Shape coexistence and other aspects of nuclear structure in ^{40}Ar See Entry 112060
 Gamow-Teller and magnetic dipole transitions in nuclei See Entry 112116
 Elastic scattering and inelastic scattering of 65 MeV polarised protons See Entry 112204
 Nuclear g -factor of the $17/2^+$ isomeric state in ^{63}Cu See Entry 112235

21.10M Level density and structure

112068 On the parity dependence of nuclear level densities. G.Maino, A.Ventura (Div. Fisica e Calcolo Sci., ENEA, Bologna, Italy). *Lett. Nuovo Cimento (Italy)*, vol.37, ser.2, no.16, p.561-8 (20 Aug. 1983).
 The parity distribution of nuclear excited states is investigated in the frame of a statistical formalism based on realistic single-particle and collective configurations, and particularly suitable to the study of odd-mass, or odd-odd nuclei. Numerical results are presented for spherical nuclei in the mass range $A=48-65$. (8 refs.)
 112069 Shell-model calculations of high-spin isomers in neutron-deficient $1g_{7/2}$ -shell nuclei. K.Ogawa (Inst. for Nuclear Study, Univ. of Tokyo, Tokyo, Japan). *Phys. Rev. C (USA)*, vol.28, no.2, p.958-60 (Aug. 1983).
 The neutron-deficient $1g_{7/2}$ -shell nuclei are studied in the framework of the shell model with the $(1g_{7/2}, 2p_{1/2})^{-n}$ configuration. Several 'spin-gap' isomers with a half-life of an order of a second are predicted in ^{95}Pd , ^{95}Ag , ^{96}Cd , and ^{97}Cd . Among them, the $J=21/2^+$ state in ^{95}Pd is predicted to be an isomer which corresponds to $^{95}\text{Pd}^m$ recently observed by Nolte and Hick. It is also shown that the high-spin isomers above the proton threshold are rather stable against the proton emission. (15 refs.)
 112070 1p-2h and 2p-3h states in ^{15}C . S.Truong, H.T.Fortune (Dept. of Phys., Univ. of Pennsylvania, Philadelphia, PA, USA). *Phys. Rev. C (USA)*, vol.28, no.3, p.977-9 (Sept. 1983).
 The reaction $^{13}\text{C}(t,p)$ has been used to locate 1p-2h and 2p-3h states in ^{15}C . The results for the negative-parity levels are in good agreement with expectations for $(sd)^2 L=0, 2$, and 4 transfers as given by $^{14}\text{C}(t,p)^{16}\text{C}$. (11 refs.)
 112071 Level structure of ^{67}Ge and its implications for the general structure of nuclei in the 1f-2p shell. M.J.Murphy, C.N.Davids (Phys. Div., Argonne Nat. Lab., Argonne, IL, USA). *Phys. Rev. C (USA)*, vol.28, no.3, p.1069-79 (Sept. 1983).
 From the results of prompt and β -delayed γ -ray singles and γ - γ coincidence measurements, twenty-four excited states and forty-six gamma transitions are identified in the level scheme of ^{67}Ge . Angular distributions and directional correlations of prompt ^{67}Ge gamma rays have been measured to obtain the spins of the ^{67}Ge ground state and excited states at 18.2, 122.7, 243.6, 711.3, and 1019.9 keV. Parities are assigned to the first five states on the basis of fp shell systematics and observed ^{67}Ge gamma-ray branching ratios. The 752-keV excitation energy of the first $9/2^+$ level in ^{67}Ge is determined from an excitation function for the $^{64}\text{Zn}(\alpha,n\gamma)^{67}\text{Ge}$ reaction. The angular distribution and correlation measurements also provide $E2/M1$ mixing ratios for the 104.4, 120.8, 122.7, 243.6, 589.0, and 897.5 keV ^{67}Ge gamma rays. The level scheme of ^{67}Ge and the corresponding schemes for $^{63,65}\text{Ni}$, $^{65,67}\text{Zn}$, and ^{69}Ge are observed to have strong similarities at low excitation. Systematic trends in $E2$ transition rates are interpreted in the context of shell and collective features of the nuclei. It is found that models based on a single particle coupled to a vibrational or deformed core do not explain the observed systematics, and are an inaccurate representation of these nuclei. The systematics do agree with a many-nucleon shell model emphasizing the short-range pairing interaction and configuration mixing for the valence neutrons. (18 refs.)

112072 ^{234}U levels fed in the ^{234}Np electron capture decay. C.Ardisson-Marsol, G.Ardisson (Lab. de Chimie Phys. et Radiochimie, Univ. de Nice, Nice, France). *Phys. Rev. C (USA)*, vol.28, no.3, p.1334-42 (Sept. 1983).
 The decay of ^{234}Np has been investigated using a coaxial Ge(Li) detector. The source prepared by the $^{235}\text{U}(d,3n)$ reaction was purified from fission products by radiochemical separation. The analysis of the γ ray spectra revealed the presence of 59 photon lines, 29 of which were found for the first time. The absolute values of γ , EC, and β^+ intensities were deduced from Ux-K ray intensity. A ^{234}U decay scheme is suggested on the basis of the good sum relationships. Accurate values of 17 low-spin-energy levels are given, 6 of which were previously unreported in the ^{234}Np decay: 849.36(03 $^-$), 926.33(22 $^+$), 989.41(22 $^-$), 1457.1(12 $^-$), 1500.88(1), and 1510.22(2) keV. (35 refs.)
 112073 Implications of the recently discovered $^{208}\text{Pb}(1^+, E_x=5.845\text{ MeV})$ state for the spin-dependent nuclear interaction. H.Toki, G.F.Bertsch, D.Cha (Dept. of Phys., Michigan State Univ., East Lansing, MI, USA). *Phys. Rev. C (USA)*, vol.28, no.3, p.1398-401 (Sept. 1983).
 Measurements on the newly discovered 1^+ state at $E_x=5.845\text{ MeV}$ in ^{208}Pb provide an opportunity to examine the spin dependence in the nuclear effective Hamiltonian. The data require a somewhat weaker spin-orbit splitting than given by conventional Hamiltonians. The isoscalar spin-dependent residual interaction, which was poorly determined by previous data, is found to be much weaker than the isovector spin-dependent interaction, as predicted by Brueckner theory. (21 refs.)
 112074 Deformation aligned states. P.M.Walker (Daresbury Lab., SERC, Warrington, England). *Phys. Scr. (Sweden)*, vol.T5, p.29-35 (1983). (Proceedings of the 4th Nordic Meeting on Nuclear Physics, Fuglso, Denmark, 16-20 Aug. 1982).
 Experimental information on multi-quasiparticle isomers is compared, with special emphasis on the hafnium isotopes. New results for ^{174}Hf are presented. The co-existence of deformation-aligning and rotation-aligning influences is considered. Residual interactions are studied as a function of the number of quasiparticles, with large effects being evident for large numbers of quasiparticles. (21 refs.)
 112075 A study of the nuclear structure at high energy and low spin. J.Rekstad, A.Henriquez, F.Ingebretsen, G.Midditt, B.Skaali, R.Oyan, J.Wikne, T.Engeland (Inst. of Phys., Univ. of Oslo, Oslo, Norway), T.F.Thorsteinen, E.Hammaren, E.Liukkonen. *Phys. Scr. (Sweden)*, vol.T5, p.45-50 (1983). (Proceedings of the 4th Nordic Meeting on Nuclear Physics, Fuglso, Denmark, 16-20 Aug. 1982).
 A novel method to study nuclear structure at low spin as a function of temperature is developed and used on $^{146,148}\text{Sm}$, $^{154,156}\text{Gd}$ and $^{160,162}\text{Dy}$, by means of the $(^3\text{He}, \alpha)$ reaction. The nuclear level density for a wide energy range is also studied. The γ -multiplicities and the first generation γ -ray spectra indicate a structure change in deformed nuclei at about 6 MeV. (6 refs.)
 112076 Isoscalar character of the 1^+ state at 5.844 MeV in ^{208}Pb . G.P.A.Berg, W.Hurlimann, I.Katayama, S.A.Martin, J.Meissburger, J.G.M.Romer, B.Styczen, J.L.Tain (Inst. fur Kernphys., Kernforschungsanlage Julich, Julich, Germany).
 Proceedings of the 1983 RCNP International Symposium on Light Ion Reaction Mechanism, Osaka, Japan, 16-20 May 1983 (Osaka, Japan: Osaka University 1983), p.214-22
 High resolution proton and deuteron inelastic scattering angular distributions leading to the lowlying 1^+ spin-flip state at $E_x=5.844\text{ MeV}$ will be presented and discussed in the context of recent studies of this state by several different reactions. From the equally strong excitation in proton and deuteron scattering the predicted isoscalar character of this state is supported. For the proton scattering microscopic DWBA calculations will be shown and discussed. (23 refs.)
 Nuclear data sheets for $A=79$ See Entry 111327
 Nuclear data sheets for $A=153$ See Entry 111328
 Recent References, January through April 1983 [nuclear data sheets] See Entry 111329
 Spin and isospin characteristics of the excited states of ^{36}Ar through the reaction $^{32}\text{S}(\alpha,\gamma)^{36}\text{Ar}$ in the bombarding energy range $E_\alpha=4$ to 5 MeV See Entry 112063
 General principles of statistical spectroscopy See Entry 112091
 The application of lineshape analysis in plunger measurements See Entry 112118
 Lifetimes in ^{18}F See Entry 112120
 $(e,e'\pi)$ reaction on light nuclei and spin-isospin strength distribution effects See Entry 112177
 Investigation of the level scheme of ^{145}Nd in the $(n,n'\gamma)$ reaction See Entry 112189
 Gamma-ray transitions among levels of ^{206}Pb See Entry 112192
 Search for two-phonon vibrations in ^{168}Er See Entry 112194
 (p,t) and $(p,^3\text{He})$ reactions on ^{52}Cr and ^{54}Fe populating analog final states with $T_f=T_i$ See Entry 112212
 Direct contribution to the $^{19}\text{F}(p,\alpha)^{16}\text{O}$ reaction See Entry 112214
 The $^{52}\text{Cr}(t,p)^{54}\text{Cr}$ reaction at $E_t=15\text{ MeV}$ See Entry 112219
 Nuclear g -factor of the $17/2^+$ isomeric state in ^{63}Cu See Entry 112235

21.30 NUCLEAR FORCES

(see also 13.75C Nucleon-nucleon interactions)

112077 Tensor forces in the three-body problem. A.Osman (Internat. Centre for Theoretical Phys., Trieste, Italy). *Atomkernenerg. Kerntech. (Germany)*, vol.42, no.1, p.57-60 (1983).
 The three-body problem is considered using separable two-body interactions. The two-body potentials used contain both attraction and repulsion. Each of the attractive and repulsive parts of the two-body potentials also include tensor forces. The effect of the tensor forces is investigated by making use of the separable approximation. By introducing the separable expansion in the three-body problem, the Faddeev equations are reduced to a well-behaved set of coupled integral equations. The integral equations obtained are solved numerically using separable two-body interactions with potential functions of the Yamaguchi, Gaussian, Tabakin, Mongan and Reid forms. The calculated values of the binding energies for the nuclei ^3H , ^3He and ^6Li are in good agreement with the experimental values. The effect of the tensor forces is found to improve the binding energy by about 4.491% to 8.327%. (37 refs.)

112078 Configuration space Faddeev continuum calculations: p-d s-wave scattering length. J.L.Friar, B.F.Gibson (Theoretical Div., Los Alamos Nat. Lab., Los Alamos, NM, USA), G.L.Payne.

Phys. Rev. C (USA), vol.28, no.3, p.983-94 (Sept. 1983).

Formulation of s-wave zero-energy Faddeev-type scattering equations including a Coulomb interaction is discussed. Numerical solutions of these equations for the s-wave NN potential models of Malfliet and Tjon (1969) are obtained using spline techniques. Kohn variational estimates are presented and comparison is made to previously published results. The quartet pd scattering lengths are larger than others previously obtained, and the pd doublet results are smaller than the corresponding nd results, and thus in contrast to the experimental values. An explication of this feature is presented in terms of a model two-body problem. Perturbation theory for the Coulomb corrections to the scattering length is developed and confirms the Kohn estimates. (33 refs.)

112079 Spurious bound states in relativistic three-body equations. H.Garcilazo (Dept. of Phys., Texas A&M Univ., College Station, TX, USA), L.Mathelitsch.

Phys. Rev. C (USA), vol.28, no.3, p.1272-6 (Sept. 1983).

The authors point out that the most commonly used version of the relativistic Faddeev equations has spurious bound-state solutions and therefore it is unsuitable for calculations in the bound-state region. They propose a way to modify these equations which would correct the problem, but which leads to the loss of the clustering property. They present numerical examples for the case of the π^-nn system. (10 refs.)

112080 Theory for a hybrid quark-baryon model for the nucleon-nucleon system. E.M.Henley, L.S.Kisslinger, G.A.Miller (Dept. of Phys., Univ. of Washington, Seattle, WA, USA).

Phys. Rev. C (USA), vol.28, no.3, p.1277-85 (Sept. 1983).

A hybrid quark model for two baryons is developed. The short distance part is represented by six-quark wave functions, while the long distance part is described by conventional wave functions representing the relative motion of three-quark baryons. Formulae which give the probabilities of the six-quark configurations as a function of energy, in terms of the exterior NN interactions and experimental phase shifts, are derived and applied. (16 refs.)

112081 Coulomb plus separable potential in coupled channels. W.Schweiger, W.Plessas (Inst. for Theoretical Phys., Univ. of Graz, Graz, Austria), L.P.Kok, H.van Haeringen.

Phys. Rev. C (USA), vol.28, no.3, p.1414-16 (Sept. 1983).

The two-potential formalism for long-range forces is generalized to coupled channels. Assuming the short-range potential to be separable the authors treat the proton-proton interaction in the coupled partial waves 3P_2 - 3F_2 . They derive the corresponding Coulomb-modified nuclear transition matrices in closed analytic form and calculate the Coulomb distortion of the phase shifts and of the mixing parameter. The separable parametrization proposed for the p-p interaction in 3P_2 - 3F_2 yields an accurate fit to the experimental data available for these channels. The potential completes the description of the N-N interaction by the Graz-II separable model. (12 refs.)

112082 On parity- and angular-momentum-dependence of inter-nucleon potential. K.Aoki, H.Horiuchi (Dept. of Phys., Kyoto Univ., Kyoto, Japan). Proceedings of the 1983 RCNP International Symposium on Light Ion Reaction Mechanism, Osaka, Japan, 16-20 May 1983 (Osaka, Japan: Osaka University 1983), p.826-30.

The parity-dependence and the angular-momentum-dependence of the inter-nucleon potential are investigated by analyzing the equivalent local potential of $Z+^4\text{He}$, $Z+^{16}\text{O}$, $Z+^{40}\text{Ca}$ systems. A parameter is proposed to judge the importance of the parity-dependence among systems. The parity-dependence in all the Z -core systems is found to be governed by the same mechanism. The behaviour of the l -dependence is understood in connection with the parity-dependence. (4 refs.)

112083 Δ dynamics. E.J.Moniz (Center for Theoretical Phys., MIT, Cambridge, MA, USA).

Symmetries in Nuclear Structure. Proceedings of a NATO Advanced Study Institute on Symmetries in Nuclear Structure, Dronten, Netherlands, 16-28 Aug. 1982 (New York, USA: Plenum Press 1983), p.251-83.

The author discusses the properties and interactions with nuclei of Δ s. An isobar model is developed which allows one to discuss precisely the propagation and dynamics of the Δ as an 'unstable particle'. The need for the discussion is grounded in the apparently very different descriptions of the Δ offered by conventional meson-nucleon scattering theory and by the quark model. The phenomenological isobar model is compatible with both languages. The model provides a dynamically consistent approach to the many-body problem, and leads to dynamical modifications of quark model predictions of Δ properties. The author discusses the extraction of Δ -nucleus interaction parameters from an analysis of intermediate energy pion- and photon-initiated nuclear reactions. The central result is the strength of the Δ -nucleus optical potential, which is found to have a large imaginary part associated with intermediate coupling to purely nuclear states. The role of Δ s in low energy nuclear properties is discussed briefly. (25 refs.)

Comment on 'Monte Carlo evaluation of functional integrals using coherent-state Slater determinants' [and reply] See Entry 111550

Effect of core polarization on the charge distribution in ^{208}Pb See Entry 112057

Breaking of fundamental symmetries in nuclei See Entry 112065

Non-locality of the deuteron optical model potential due to coupling to inelastic channels See Entry 112084

Microscopic basis of collective symmetries See Entry 112098

High excited α cluster state calculation of nuclei See Entry 112099

Parametrization of the short-range correlation and exchange matrix elements by the Landau-Migdal parameters See Entry 112108

Gamow-Teller strength function for ^{90}Zr : effects of spin and isospin exchange forces, and ground-state correlations See Entry 112128

Charged pion electroproduction, a selective probe of nuclear spin-isospin responses See Entry 112151

Two body residual interaction in the statistical multistep compound and direct theories See Entry 112164

Effective interactions in (p,p') and (p,n) excitations See Entry 112206

Elastic scattering of ^7Li projectiles in the energy range of 20 to 34 MeV See Entry 112238

Calculation of the imaginary part of the heavy ion potential See Entry 112240

Nucleus-nucleus potential at close contact from fusion at 'high' energies See Entry 112248

$^{16}\text{O}+^{28}\text{Si}$ elastic scattering near the barrier See Entry 112259

Higher-order field effects in pion absorption on two nucleons See Entry 112284

21.40 FEW-NUCLEON SYSTEMS

112084 Non-locality of the deuteron optical model potential due to coupling to inelastic channels. G.H.Rawitscher (Phys. Dept., Univ. of Connecticut, Storrs, CT, USA), G.Delic.

Proceedings of the 1983 RCNP International Symposium on Light Ion Reaction Mechanism, Osaka, Japan, 16-20 May 1983 (Osaka, Japan: Osaka University 1983), p.590-9.

A new formulation is being developed for investigating the non-local part of the elastic optical potential, as well as that for the inelastic DWBA transition potential, which is due to coupling to a set N of inelastic channels. The method consists in using a basis set of Sturmian functions, one for each channel. The dimension of the set is truncated to a finite number M , and the elements of a $(N \times M)^2$ dimensional matrix are calculated. The truncation error can subsequently be removed by a sequence of iterations which converge. Applications to the case of 21.6 MeV deuterons incident on the nucleus of nickel is described, in which coupling to a discretized breakup space is taken into account. The non-local elastic optical potential is characterized in terms of the spectrum of its Sturmian eigenvalues. (10 refs.)

Tensor forces in the three-body problem See Entry 112077

21.60 NUCLEAR-STRUCTURE MODELS AND METHODS

(for hadronic atoms and molecules, see 36.10)

112085 A closed irreversible equation of motion for the one-body density. P.Buck (Inst. für Kernphys., Tech. Hochschule Darmstadt, Darmstadt, Germany), H.Feldmeier.

Phys. Lett. B (Netherlands), vol.129B, no.3-4, p.172-6 (22 Sept. 1983).

A closed irreversible equation of motion for the one-particle density is derived in a weak coupling limit. The only statistical assumption entering is the maximum entropy concept with the one-body density as constraints. The derivation provides general equations which for special cases reduce to known results. (19 refs.)

112086 Dependence of the Fermi form factor on the dominant pole in the density. J.S.Chalmers (Dept. of Phys., Univ. of Louisville, Louisville, KY, USA).

Phys. Rev. C (USA), vol.28, no.2, p.941-2 (Aug. 1983).

The nuclear form factor arising from the Fermi density function is shown to be completely determined by the pole of the density function closest to the real axis. (7 refs.)

Comment on 'Monte Carlo evaluation of functional integrals using coherent-state Slater determinants' [and reply] See Entry 111550

Effect of the fourth-order Casimir invariants on $U_{6/4}$ and $U_{6/2}$ dynamical supersymmetries in nuclei and baryons See Entry 111912

Energy of a nucleon in a nucleus See Entry 112053

Breaking of fundamental symmetries in nuclei See Entry 112065

A study of the nuclear structure at high energy and low spin See Entry 112075

Theory for a hybrid quark-baryon model for the nucleon-nucleon system See Entry 112080

Nucleon currents between highly excited nuclei See Entry 112103

A note on the Gamow-Teller sum rule with non-nucleonic degrees of freedom .. See Entry 112132

Calibration of histograms in nuclear structure physics See Entry 112600

21.60C Shell model

112087 Boson mapping in the deformed Nilsson scheme. H.T.Chen, S.Y.Lee, L.Lin, S.F.Tsai.

Annu. Rep. Inst. Phys. Acad. Sin. (Taiwan), vol.12, p.254 (Dec. 1982).

[received: Sept. 1983]

The authors analyze the importance of S and D bosons in the Dyson boson mapping of the deformed Nilsson scheme, i.e. $a^\alpha a^\beta \dots R^{\alpha\beta} = B^{\alpha\beta} - B^{\alpha\gamma} B^{\beta\gamma} B_{\gamma\delta}$, $a_\alpha a_\beta \dots R_{\alpha\beta} = B^{\alpha\gamma} B_{\gamma\beta}$, where α, β, γ and δ are the appropriate quantum numbers for the Fermion states in the Nilsson orbit, they have used the convention that a^α and a_β are fermion creation and annihilation operators for state α and β respectively. Double indices in the above equations are summed implicitly. Based on the Dyson mapping, the authors can obtain the analytic solution for the Nilsson Hamiltonian with pairing interaction. (no refs.)

112088 Dynamical content of the shell model. C.Mahaux (Inst. de Phys., Univ. de Liege, Liege, Belgium), H.Ngo.

Phys. Scr. (Sweden), vol.T5, p.74-9 (1983). (Proceedings of the 4th Nordic Meeting on Nuclear Physics, Fuglo, Denmark, 16-20 Aug. 1982).

A critical discussion is given of several recent attempts to introduce dynamical content in the shell model by means of adding corrections to the Hartree-Fock approximation. Numerical results are given for single-particle neutron energies in ^{208}Pb . (43 refs.)

112089 Influence of shell structure on deep inelastic collisions. Wu En-chiu (Inst. of Modern Phys., Acad. Sinica, Peking, China), K.D.Hildenbrand, A.Gobbi, A.Olmi, H.Sann, H.Friesleben, U.Lyden.

Phys. Energ. Forts & Phys. Nucl. (China), vol.7, no.3, p.379-94 (May 1983). In Chinese.

A kinematically complete study of the symmetric systems $^{154}\text{Sm}+^{154}\text{Sm}$ and $^{144}\text{Sm}+^{144}\text{Sm}$ has been performed at energies 30% in excess of the interaction barrier. They have been chosen because of their different internal structure: ^{144}Sm has a closed $N=82$ neutron shell and hence a spherical ground state configuration; ^{154}Sm with ten neutrons outside this shell is strongly deformed. Over the whole range of kinetic energy loss the variances of the measured mass distributions were found to be similar in both reactions, whereas the variances of the element distributions are considerably larger at small energy losses in the ^{144}Sm system. Based on the shell-corrected potential energy surface these observations are attributed to the closed $N=82$ neutron shell which, for ^{144}Sm , hinders the neutron exchange and leads to a preferential transfer of protons. (11 refs.)

112090 Symmetry aspects of the shell model. P.W.M.Glaudemans (Fysisch Lab., Rijksuniv. Utrecht, Utrecht, Netherlands).

Symmetries in Nuclear Structure. Proceedings of a NATO Advanced Study Institute on Symmetries in Nuclear Structure, Dronten, Netherlands, 16-28 Aug. 1982 (New York, USA: Plenum Press 1983), p.119-49.

The author has shown that the shell model can produce states which exhibit pure collective properties. It turns out that the nuclei in the middle of the fp shell are very good candidates for an investigation of the relation between the

microscopic and the collective interpretation. In the present phenomenological approach the shell model and the axially symmetric rotor are related to each other by a comparison of the numerical values of their observables. It would be very interesting to further study this relation by investigating whether collective states are related to possible cluster structures of the corresponding shell-model wave functions. Shell-model wave functions always contain an unphysical part, which corresponds to the center-of-mass motion of the nucleus. This may lead to spurious effects when calculating various observables. It is shown that under certain conditions the spurious effects can be isolated exactly from the nonspurious ones. The method has been applied to calculate various observables in p-shell nuclei. The translationally-invariant effective interaction has been obtained from a least-squares fit to the data. Because of the requirement of translational invariance the Hamiltonian can be expressed in a rather small number of parameters. (19 refs.)

112091 General principles of statistical spectroscopy. J.B.French (Dept. of Phys. & Astron., Univ. of Rochester, Rochester, NY, USA). *Symmetries in Nuclear Structure. Proceedings of a NATO Advanced Study Institute on Symmetries in Nuclear Structure*, Dronten, Netherlands, 16-28 Aug. 1982 (New York, USA: Plenum Press 1983), p.177-202. In the shell-model there is an implicit argument that, while the high states are not well treated, their effects on the low-lying states are, especially when one takes account of renormalizations of the Hamiltonian. In the author's case the high-lying states cannot be hidden, their centroid and width being basic parameters of the theory; but if the model spaces are not too large we can rely on a central limit theorem (CLT) to 'propagate' downwards from the centroid, and on a theorem of 'spectral rigidity' to keep the local fluctuations in check. For larger spaces a method of partitioning, when combined with these theorems, will do the same things. The author stresses that, whereas ordinary shell-model methods produce numerical values for quantities of interest, it is the author's aim to produce them as functions of the parameters of the system. In particular one should think of the spectrum as an immensely complicated structure which may display regularities both in its secular behavior and its fluctuations. Its levels move around as one varies the Hamiltonian matrix elements, these motions, under small variations of the elements, then informing about quantities of interest, expectation values, transition strengths and so forth, in a manner quite analogous to the way in which parametric derivatives on a partition function yield corresponding information. (28 refs.)

Symmetries in Nuclear Structure. Proceedings of a NATO Advanced Study Institute on Symmetries in Nuclear Structure See Entry 111295
Single-particle Glauber matrix elements See Entry 111324
Energy dependence of the rotational enhancement factor in the level density See Entry 112032
Rotation-aligned bands in ^{16}Hg See Entry 112036
Properties of nuclei at high spins See Entry 112037
Multi-step shell-model description of Sn isotopes See Entry 112044
Microscopic calculations of nuclear wobbling rotation See Entry 112045
Coupling of two quasiparticles to coherent cores in the Pt isotopes See Entry 112050
Spin-isospin ordered shell model states in nuclei See Entry 112062
Shell-model calculations of high-spin isomers in neutron-deficient $1g_{9/2}$ -shell nuclei See Entry 112069
Microscopic basis of collective symmetries See Entry 112098
Predicted features of the beta decay of neutron-rich sd -shell nuclei See Entry 112127
Gamow-Teller strength function for ^{90}Zr : effects of spin and isospin exchange forces, and ground-state correlations See Entry 112128
Charge symmetry breaking in ^4He See Entry 112172
Test of vibrational current distributions in transverse electron scattering See Entry 112173
High-resolution (e,e') study of isovector M1 and M2 transitions in the oxygen isotopes. I. ^{16}O See Entry 112174
High-resolution (e,e') study of isovector M1 and M2 transitions in the oxygen isotopes. II. ^{17}O See Entry 112175
High-resolution (e,e') study of isovector M1 and M2 transitions in the oxygen isotopes. III. ^{18}O See Entry 112176
The $^{52}\text{Cr}(t,p)^{54}\text{Cr}$ reaction at $E_t=15$ MeV See Entry 112219
(d, α) reaction and the α particle D state See Entry 112221
Transition probabilities between two-quasiparticle configurations in $^{170,172}\text{Yb}$ and ^{182}W See Entry 112236

21.60E Collective models

112092 Systematic analysis of medium heavy spectroscopy in the interacting-boson model. H.C.Chiang, S.T.Hsieh, M.M.King, S.Y.Lee. *Annu. Rep. Inst. Phys. Acad. Sin. (Taiwan)*, vol.12, p.255-6 (Dec. 1982). [received: Sept. 1983]
The interacting boson model (IBM) is a very useful theoretical tool in the spectroscopy of the medium heavy deformed nuclei. IBM assumes that the nucleon pairs can be considered as a boson where the bosons with angular momentum 0 and 2 dictate the low-lying spectrum of the nucleus. Several attempts in fitting the Hamiltonian to a series of nuclear spectra have been performed. Yet these efforts are limited by the limited number of parameters used. A much more general χ^2 -fitting is still lacking. The authors calculate the spectra and the transition rate of the rare earth nuclei systematically to understand the physical meaning of the parameters in equation. (no refs.)

112093 Rotational motion at finite temperature. J.Kunz (Theoretical Div., Los Alamos Nat. Lab., Los Alamos, NM, USA), U.Mosel. *Nucl. Phys. A (Netherlands)*, vol.A406, no.2, p.269-84 (19 Sept. 1983). Moments of inertia and rotational velocity fields are calculated in the cranking model for the harmonic oscillator and the Nilsson potential for even-even rare earth nuclei. By means of a temperature-averaging procedure these quantities are decomposed into a smooth and a shell-structure-dominated part. The results are in good agreement with the corresponding Strutinsky-averaged results. The velocity fields are analyzed in terms of vector spherical harmonics and compared to rigid flow. The smooth velocity fields reveal rigid flow in the nuclear interior; in the surface region a deviation from rigid flow occurs, giving rise to a backflow in the inner system. The temperature dependence of the smooth moment of inertia is approximated by a quadratic function. (37 refs.)

112094 Coupling of surface and bulk vibrations in the nuclear breathing mode. M.Brack (Inst. fur Theoretische Phys., Univ. Regensburg, Regensburg, Germany), W.Stocker.

Nucl. Phys. A (Netherlands), vol.A406, no.3, p.413-34 (26 Sept. 1983). The authors treat a general class of dynamical couplings of the surface to the bulk of a spherical nucleus during isoscalar breathing vibrations. Compressibilities are evaluated in the extended Thomas-Fermi approximation using a realistic Skyrme force (SkM*). Inertial parameters are obtained in a hydrodynamical framework. The lower of the two eigenmodes is found to be close in energy to the pure bulk vibration (and to the scaling mode), and to be in excellent agreement with the experimental giant monopole resonance energies. The coupling of surface and bulk vibrations shifts the pure surface mode to appreciably higher energies (~ 25 MeV in ^{208}Pb). This upper mode, which has a pronounced anti-scaling behaviour, might be identified through the analysis of its transition density. (31 refs.)

112095 Potential energy surfaces in the classical limit of the IBM-2. A.B.Balantekin, B.R.Barrett, S.Levit (Inst. for Theoretical Phys., Univ. of California, Santa Barbara, CA, USA). *Phys. Lett. B (Netherlands)*, vol.129B, no.3-4, p.153-6 (22 Sept. 1983). The classical limit of the Interacting Boson Model for both neutrons and protons (the IBM-2) is investigated. In particular, general expressions of the potential energy for the proton and neutron distributions aligned along the same axis are obtained and plotted for the even-even isotopes of tungsten. (10 refs.)

112096 Dynamical groups of liquid drop models. R.Gilmore, Da Hsuan Feng, M.Vallieres (Dept. of Phys. & Atmospheric Sci., Drexel Univ., Philadelphia, PA, USA), J.L.Wood. *Phys. Rev. C (USA)*, vol.28, no.2, p.903-6 (Aug. 1983). Two inequivalent quantum mechanical versions of the liquid drop model can be obtained, depending on whether the classical volume conservation condition is imposed to first or second order. These two models have dynamical groups $\text{IU}(5)$ and $\text{U}(6)$, respectively. The two models are related to each other through standard group contraction and group expansion procedures. (7 refs.)

112097 Deformed bosons in the Nilsson scheme. S.Y.Lee, S.F.Tsai (Inst. of Phys., Acad. Sinica, Taiwan), H.T.Chen, L.Lin. *Phys. Rev. C (USA)*, vol.28, no.2, p.955-7 (Aug. 1983). Dyson boson mapping is used to derive the deformed boson from the Nilsson Hamiltonian. Single j -shell Nilsson model with pairing interaction is treated as an example. A general method of reconstructing bosons with definite angular momentum is outlined. (7 refs.)

112098 Microscopic basis of collective symmetries. A.Arima (Dept. of Phys., Faculty of Sci., Univ. of Tokyo, Tokyo, Japan). *Symmetries in Nuclear Structure. Proceedings of a NATO Advanced Study Institute on Symmetries in Nuclear Structure*, Dronten, Netherlands, 16-28 Aug. 1982 (New York, USA: Plenum Press 1983), p.93-117. The author discusses mainly the seniority scheme, i.e. $\text{SU}(2)$ symmetry, in single closed shell nuclei. Conditions are shown for an effective interaction to conserve seniority. Then an approach to a microscopic basis of the interacting boson model is very briefly sketched. (17 refs.)

Symmetries in Nuclear Structure. Proceedings of a NATO Advanced Study Institute on Symmetries in Nuclear Structure See Entry 111295
Odd Ni isotopes in the Lipkin-Nogami approach See Entry 112034
Rotation-aligned bands in ^{16}Hg See Entry 112036
Microscopic calculations of nuclear wobbling rotation See Entry 112045
Shape changes, band crossings and band terminations in the very high spin region of $A=150$ -160 nuclei See Entry 112047
Kinematical and dynamical moments of inertia and the Mottelson-Valatin effect at high spin excitations See Entry 112048
Coupling of two quasiparticles to coherent cores in the Pt isotopes See Entry 112050
Symmetry aspects of the shell model See Entry 112090
High excited α cluster state calculation of nuclei See Entry 112099
Multipole pair fields at finite temperature See Entry 112101
Band crossing in ^{130}Ba See Entry 112109
Giant resonance splitting in deformed nuclei See Entry 112152
A constrained approximation for nuclear barrier penetration and fission See Entry 112167
The photoneutron cross section of ^{151}Eu , ^{153}Eu and ^{156}Gd in the giant resonance region See Entry 112170
Test of vibrational current distributions in transverse electron scattering See Entry 112173
Search for two-phonon vibrations in ^{168}Er See Entry 112194
Microscopic study of heavy-particle transfer reactions: the ($^{16}\text{O},\alpha$) reactions on ^{16}O and ^{28}Si See Entry 112243
Analysis of elastic and inelastic scattering of 162 MeV pions from ^{13}C by an optical potential and a collective model See Entry 112283
Fission and pairing degrees of freedom in collective transport theory See Entry 112290
Reassessment of fission fragment angular distributions from continuum states in the context of transition-state theory See Entry 112291

21.60F Models based on group theory

Symmetries in Nuclear Structure. Proceedings of a NATO Advanced Study Institute on Symmetries in Nuclear Structure See Entry 111295
Energy dependence of the rotational enhancement factor in the level density See Entry 112032
Systematic analysis of medium heavy spectroscopy in the interacting-boson model See Entry 112092
Potential energy surfaces in the classical limit of the IBM-2 See Entry 112095
Dynamical groups of liquid drop models See Entry 112096
Deformed bosons in the Nilsson scheme See Entry 112097
Microscopic basis of collective symmetries See Entry 112098
Role of finite boson number in the interacting boson approximation description of γ -g transitions in deformed nuclei See Entry 112100

21.60G Cluster models

112099 High excited α cluster state calculation of nuclei. S.Y.Lee, E.K.Lin, C.W.Wang. *Annu. Rep. Inst. Phys. Acad. Sin. (Taiwan)*, vol.12, p.238 (Dec. 1982). [received: Sept. 1983]
Recent studies on the intermediate structure of the light heavy ion reaction indicate that the cluster configuration may be the origin of the intermediate structure ($\Delta E \approx 600$ keV, $\Gamma \approx 400$ keV) (Lee, Wilschut, and Ledoux, 1982). The authors perform a cluster model calculation based on the method developed by Bloch and Brink. The single particle wave functions of nucleons are assumed to be the Gaussian. The Slater-determinant $|\phi\rangle$ of the trial wave function for 4 N nucleons is used to calculate the energy from the variational principle. Based on the Brink-Boeker force, or the N-N interaction derived from the shell model calculation by Hsieh et al., they calculate the high excited states of ^{24}Mg with ^{12}C - ^{12}C configuration, α - ^{20}Ne configuration and α - ^{16}O - α configuration to investigate the relevance of these cluster states in the heavy ion reaction of $^{12}\text{C} + ^{12}\text{C}$ system. (no refs.)

112100 Role of finite boson number in the interacting boson approximation description of $\gamma \rightarrow g$ transitions in deformed nuclei. R.F.Casten, D.D.Warner (Brookhaven Nat. Lab., Upton, NY, USA), A.Abrahamian. *Phys. Rev. C (USA)*, vol.28, no.2, p.894-902 (Aug. 1983).
The effect of finite boson number in the interacting boson approximation is one of its most distinguishing features. These effects are investigated in terms of the deviations of $\gamma \rightarrow g$ band $E2$ transitions from the rotational (Alaga) values which provide one of the most crucial tests of collective models of deformed nuclei. It is shown that the empirical systematics of these deviations displays a strong mass dependence, that the interacting boson approximation successfully reproduces these systematic trends, and does so primarily by virtue of the variations in boson number and not because of parameter variations. Moreover, the origin of the N dependence lies in the characteristic way in which the $\text{SU}(3)$ symmetry is broken in calculations for realistic deformed nuclei and involves, in an essential way, the N dependence of the $\text{SU}(3)$ $\gamma \rightarrow \beta$ transitions. (45 refs.)

On clustering effects and phase instabilities in high energy nuclear collisions See Entry 112104

A microscopic study on the particle-decay widths of excited states in light Δ -hypernuclei See Entry 112105

Clustering effects on neutron elastic scattering from boron isotopes See Entry 112183

21.60J Hartree-Fock and random-phase approximations

112101 Multipole pair fields at finite temperature. K.Muhlans, E.M.Muller, U.Mosel (Inst. fur Theoretische Phys., Univ. Giessen, Giessen, Germany), A.L.Goodman. *Z. Phys. A (Germany)*, vol.313, no.1-2, p.133-5 (1983).
Finite temperature HFB calculations have been performed in a model using the Surface Delta Interaction as the generating two body force. The $T=0$ as well as the $T=1$ multipole pair fields are studied at various temperatures and different angular momenta. Higher multipole modes appear not only to be more resistant against increasing angular frequency but also against increasing temperature in comparison with the standard monopole pairing mode. (10 refs.)

Microscopic calculations of nuclear wobbling rotation See Entry 112045

Dynamical content of the shell model See Entry 112088

^{17}O - ^{17}N analog states via the $^{14}\text{C}(^6\text{Li}, t)$ and $^{14}\text{C}(^6\text{Li}, ^3\text{He})$ reactions See Entry 112148

Landau damping in the degenerate Fermi liquid See Entry 112150

Giant resonance splitting in deformed nuclei See Entry 112152

A constrained approximation for nuclear barrier penetration and fission See Entry 112167

High-resolution (e, e') study of isovector M1 and M2 transitions in the oxygen isotopes. I. ^{16}O See Entry 112174

High-resolution (e, e') study of isovector M1 and M2 transitions in the oxygen isotopes. II. ^{17}O See Entry 112175

High-resolution (e, e') study of isovector M1 and M2 transitions in the oxygen isotopes. III. ^{18}O See Entry 112176

Electron scattering See Entry 112180

21.65 NUCLEAR MATTER

112102 New elements at the limit of stability of nuclear matter. The path to elements 107 and 109. G.zu Putlitz, G.Siegert (Gesellschaft fur Schwerionenforschung mbH, Darmstadt, Germany). *Naturwissenschaften (Germany)*, vol.70, no.8, p.383-7 (Aug. 1983). In German.

Man-made heavy-element production, previously accessible by successive neutron capture, has entered a new age by the invention of powerful heavy-ion accelerators. New insight in the fusion process and new experimental techniques have led to the discovery of two new elements with charge numbers 107 and 109 at GSI, the German Heavy Ion Research Laboratory. The production of very neutron-deficient Lu and Tm isotopes resulted in the discovery of a new mode of radioactive decay, proton radioactivity. Slow fusion of systems with nearly 500 nucleons as well as the dynamics of very fast fission processes have been studied. The future development investigating the properties of nuclear matter aims at high energy compression phenomena onsets of which have been discovered recently by a joint group from GSI Darmstadt and the Lawrence Berkeley Laboratory. (no refs.)

112103 Nucleon currents between highly excited nuclei. M.P.M.Barranco, X.Vinas (Facultad de Fisica, Univ. de Barcelona, Barcelona, Spain), C.Ngo, E.Tomasi.

Nucl. Phys. A (Netherlands), vol.A406, no.2, p.325-38 (19 Sept. 1983).
A finite temperature Thomas-Fermi method has been used to study the nucleon transfer between two hot slabs of symmetric nuclear matter. Special attention has been paid to temperature effects neglected in earlier calculations. As a result, closed and ready-to-use formulas for the exchange and transfer nucleon flux at zero relative momentum are given as a function of the temperature. (21 refs.)

112104 On clustering effects and phase instabilities in high energy nuclear collisions. O.Civitarese, A.Plastino (Inst. fur Theoretische Phys., Univ. Tubingen, Tubingen, Germany). *Z. Phys. A (Germany)*, vol.313, no.1-2, p.139-40 (1983).
Recent evidences concerning cluster formation in high energy nuclear collisions are analyzed within a 'lattice' approach for nuclear matter at finite temperature. (10 refs.)

Energy of a nucleon in a nucleus See Entry 112053

Study of non-static behavior of τ -modes by (p, n) reactions See Entry 112115

Relativistic nuclear optical models See Entry 112141

Microscopic optical potentials derived from free NN potentials See Entry 112147

Landau damping in the degenerate Fermi liquid See Entry 112150

Energy dependence of light particle emission from intermediate energy heavy ion collisions See Entry 112262

Dynamics of medium energy nuclear collisions See Entry 112263

Quarkochemistry of the heavy ion reactions See Entry 112266

21.80 HYPERNUCLEI

112105 A microscopic study on the particle-decay widths of excited states in light Δ -hypernuclei. T.Yamada, K.Ikeda (Dept. of Phys., Niigata Univ., Niigata, Japan), T.Motoba, H.Bando. Proceedings of the 1983 RCNP International Symposium on Light Ion Reaction Mechanism, Osaka, Japan, 16-20 May 1983 (Osaka, Japan: Osaka University 1983), p.901-5.
A systematic study of $A=6-9$ p-shell Δ -hypernuclei as well as $^{21}_{\Delta}\text{Ne}$ is carried out within the framework of the microscopic $\alpha + x + A$ three-cluster model dynamics ($x=n, p, d, t, \alpha$ or ^{16}O). The energy spectra can be classified into several characteristic 'bands' according to the underlying structures. The properties of resonance states, e.g. 'narrow' peak widths in the (K^-, π^-) reaction, are shown to be successfully explained by solving the coupled channel scattering equation. (5 refs.)

23.00 RADIOACTIVITY AND ELECTROMAGNETIC TRANSITIONS

(see also 82.55 Radiochemistry)

23.20 ELECTROMAGNETIC TRANSITIONS

112106 Determination of the multipolarity of prompt electromagnetic transitions from angular distributions of conversion electrons. I. Method. H.R.Faust (Inst. Laue-Langevin, Grenoble, France). *Nucl. Instrum. & Methods Phys. Res. (Netherlands)*, vol.213, no.2-3, p.271-5 (1 Aug. 1983).
The formalism for the angular distribution of conversion electrons from aligned states is described for transitions with multipole order ≤ 2 . It is shown that the determination of the leading term in both the e^- and γ angular distribution function provides an excellent method for assigning multipolarities $E1, M1, E2$ and $(M1+E2)$ to prompt decay lines. The applicability of the method is investigated for different spins, electron energies and Z -values. The influence of attenuation factors in angular distribution measurement is discussed and the effect on the multipole assignment is examined. (8 refs.)

112107 Determination of the final nucleus density matrix by measuring the angular correlation of charged particles and γ -quanta in various planes. N.S.Zelenskaya, I.B.Teplov (Inst. of Nuclear Phys., Moscow State Univ., Moscow, USSR). *Nucl. Phys. A (Netherlands)*, vol.A406, no.2, p.306-24 (19 Sept. 1983).
The measurements of the angular correlation function of charged particles and γ -quanta emitted by a final even-even nucleus in state J_f in different planes of γ -quantum ejection with respect to the reaction plane have been shown to offer the unique possibility of restoring all the even-rank components of the model-less density matrix in the transitions with $J_f=L$ (L is the multipolarity of the γ -transition). The minimum number of planes in which the angular correlation function should be measured to restore the density matrix has been found. The formulas relating the components of the model-less density matrix to the polarization characteristics of an even-even nucleus in a given state have been obtained. (15 refs.)

112108 Parametrization of the short-range correlation and exchange matrix elements by the Landau-Migdal parameters. T.Suzuki (Dept. of Phys., Nihon Univ., Tokyo, Japan). *Phys. Lett. B (Netherlands)*, vol.129B, no.3-4, p.157-61 (22 Sept. 1983).
The effects of the short-range correlation and the exchange part of two-body matrix elements in the particle-hole and Δ -hole excitation contributions in M1 form factors are parameterized by the Landau-Migdal parameters g'_N and g'_Δ . The momentum transfer (q) dependences of the parameterized values of g'_N and g'_Δ are investigated. (11 refs.)

112109 Band crossing in ^{130}Ba . Sun Xiangfu (Inst. of Modern Phys., Acad. Sinica, Lanzhou, China), D.Bazzacco, W.Gast, A.Gelberg, U.Kaup, A.Dewald, K.O.Zell, P.von Brentano. *Phys. Rev. C (USA)*, vol.28, no.3, p.1167-70 (Sept. 1983).
A complex band crossing of the yrast band has been observed at spin $I=10$ in ^{130}Ba by the reaction $^{120}\text{Sn}(^{13}\text{C}, 3n\gamma)$. Two of the three positive parity bands show backbending and may be the rotation aligned bands built upon $(\nu_{11/2})^{-2}$ and $(\pi_{11/2})^2$ configurations, respectively. The nature of the bands was deduced from a comparison with a cranking model calculation. A negative parity band and the quasi-gamma band were identified. (14 refs.)

112110 Comment on 'determination of gamma-ray energies and abundances of ^{229}Th '. J.K.Dickens (Oak Ridge Nat. Lab., Oak Ridge, TN, USA). *Phys. Rev. C (USA)*, vol.28, no.3, p.1404-6 (Sept. 1983).
It is shown that the absolute normalization of γ -ray yields (I_γ) for transitions among levels in ^{229}Ra following α decay of ^{229}Th reported by Rattan et al. (see *ibid.*, vol.27, p.327, 1983) should be increased by at least 22%. Disagreements of reported values of I_γ with those in a recent report are discussed but not resolved. (8 refs.)

112111 Electric monopole strengths in even-mass Ge and Se isotopes. A.Passoja, M.Vergnes, J.Kantele, M.Luontama (Dept. of Phys., Univ. of Jyväskylä, Jyväskylä, Finland). *Phys. Scr. (Sweden)*, vol.T5, p.147-8 (1983). (Proceedings of the 4th Nordic Meeting on Nuclear Physics, Fuglso, Denmark, 16-20 Aug. 1982). Branching ratios of E0 and E2 transitions depopulating excited O_2^+ states in $^{70,74}Ge$ and $^{74,76}Se$ have been measured using conversion-electron and gamma-ray spectroscopy, and new half-life measurement techniques. The E0/E2 branching ratios and the life-times of the O_2^+ states are used to extract the $B(E2;O_2^+ \rightarrow 2_1^+)$ and $\rho^2(O_2^+ \rightarrow 0_1^+)$ values. (9 refs.)

112112 Electromagnetic transitions in ^{130}Ce . P.J.Nolan, R.Aryaeinejad, D.J.G.Love, A.H.Nelson, P.J.Smith, D.M.Todd, P.J.Twin (Oliver Lodge Lab., Univ. of Liverpool, Liverpool, England), J.D.Garrett, G.B.Hagemann, B.Herskind. *Phys. Scr. (Sweden)*, vol.T5, p.153-6 (1983). (Proceedings of the 4th Nordic Meeting on Nuclear Physics, Fuglso, Denmark, 16-20 Aug. 1982). States in ^{130}Ce have been studied using ^{16}O induced reactions on ^{117}Sn and ^{118}Sn targets. Mean lifetimes have been measured for the yrast states up to $J^\pi=22^+$ using both the Doppler shift attenuation and recoil distance methods. Magnetic dipole transition rates have been deduced from branching ratio measurements within a band based on an isomeric state at 2454 keV. Electric quadrupole transition rates have been determined from mean lifetime measurements for states in the yrast band up to $J^\pi=22^+$. Both sets of results show an unexpected behaviour. (7 refs.)

112113 First results on γ -ray spectroscopy in the second minimum of ^{238}U and ^{240}Pu . D.Habs, U.v.Helmolt, H.W.Heyng, R.Kroth, B.Kolb, D.Pelte, D.Schwalb, H.J.Specht (Physik. Inst., Univ. Heidelberg, Heidelberg, Germany), W.Hennerici, H.J.Hennrich, G.Himmele, R.Repnow, W.Wahl, R.S.Simon, R.Albrecht, V.Metag. *Phys. Scr. (Sweden)*, vol.T5, p.183-5 (1983). (Proceedings of the 4th Nordic Meeting on Nuclear Physics, Fuglso, Denmark, 16-20 Aug. 1982). γ -transitions preceding the fission decay of the shape isomers in ^{238}U and ^{240}Pu have been measured with the Crystal Ball. Lines at 616 keV and 808 keV are observed in ^{238}U and ^{240}Pu , respectively, which are tentatively interpreted as deexcitations of the β -vibrational band in the second minimum. (6 refs.)

112114 Optical potentials and isoscalar transition rates from 104 MeV alpha-particle scattering by the $N=28$ isotopes ^{48}Ca , ^{50}Ti and ^{52}Cr . R.Pesl, H.J.Gils, H.Rebel, E.Friedman, J.Buschmann, H.Klewe-Nebenius, S.Zagorski (Inst. für Radiochem., Karlsruhe, Germany). *Z. Phys. A (Germany)*, vol.313, no.1-2, p.111-22 (1983). Precisely measured differential cross sections for elastic and inelastic scattering from 104 MeV alpha-particles by ^{48}Ca , ^{50}Ti and ^{52}Cr are reported. The analyses aim primarily at the determination of strength, radial shapes and deformation of the scattering potentials, looking for isotonic differences of $N=28$ isotones. The mean square radii of the (real) potentials are discussed in terms of mean square radius differences of the matter distributions. The isoscalar transition rates derived by coupled channel analyses of the measured cross sections are compared with electromagnetic rates. In addition to the analyses on the basis of a slightly generalized extended optical model a semi-microscopic deformed folding model has been applied, using a density-dependent effective alpha-bound nucleon interaction. Though an excellent description of the data over the full angular range is obtained the resulting values of the deformation parameters appear to be not consistent with results from various different methods. (33 refs.)

112115 Study of non-static behavior of $\tau\sigma$ -modes by (p,n) reactions. M.Ichimura (Inst. of Phys., Univ. of Tokyo, Tokyo, Japan), T.Izumoto, C.M.Ko, P.J.Siemens. Proceedings of the 1983 RCNP International Symposium on Light Ion Reaction Mechanism, Osaka, Japan, 16-20 May 1983 (Osaka, Japan: Osaka University 1983), p.196-205. The nuclear response function of $\tau\sigma$ -modes are investigated in the wide range of the energy-momentum plane (ω, q). The opalescence phenomena associated with the pion condensation is clearly seen at $q \approx 2.2 \mu$ (μ being the pion mass) and rather low ω in the response function of the normal nuclear matter if the Migdal parameter $g \leq 0.5$. To investigate such behavior of the nuclear response to the $\tau\sigma$ -modes, the $^{90}Zr(p,n)$ reaction to the continuum states is analyzed by DWBA. The response functions of the finite nucleus are constructed by the local density approximation from those of the nuclear matter. It is found that the finiteness and the distorted wave effects smear the enhancement (the opalescence phenomena) considerably, but it would still be seen if $q \leq 0.4$. (17 refs.)

112116 Gamow-Teller and magnetic dipole transitions in nuclei. A.Arima (Dept. of Phys., Faculty of Sci., Univ. of Tokyo, Tokyo, Japan). Proceedings of the 1983 RCNP International Symposium on Light Ion Reaction Mechanism, Osaka, Japan, 16-20 May 1983 (Osaka, Japan: Osaka University 1983), p.223-40. Several mechanisms for the quenching of Gamow-Teller and magnetic dipole transitions are discussed. It is pointed out that, contrary to common belief, the tensor correlation is much more important than the effect of Δ -hole states. The best evidence for this fact is the quenching of the expectation value of spin for which the Δ -hole states do not have any first order corrections at all. (16 refs.)

112117 Proton-carbon bremsstrahlung cross sections and nuclear time-delays near the $^{12}C(p,p)$ resonances. T.Suzuki, M.Adachi, T.Kohno, A.Makishima, N.Yamada, H.Taketani (Dept. of Appl. Phys., Tokyo Inst. of Technol., Tokyo, Japan). Proceedings of the 1983 RCNP International Symposium on Light Ion Reaction Mechanism, Osaka, Japan, 16-20 May 1983 (Osaka, Japan: Osaka University 1983), p.888-95. Bremsstrahlung spectra in coincidence with scattered protons have been measured at four incident proton energies near the $^{12}C(p,p)$ resonances at $E_{p,lab}=1.734$ MeV($5/2^+$), 1.686 MeV($3/2^-$) and 0.461 MeV($1/2^+$). By simultaneously measuring the bremsstrahlung spectra for protons scattered at $\theta_{cm}=90^\circ$ and at the desired angle ($\theta_{cm}=159^\circ$ or 146°), the authors have obtained reliable values for the phase difference and the time delay as well as for the absolute bremsstrahlung cross section. In particular, data of good quality have been obtained at an incident proton energy of 1.783 MeV for which a quantitative comparison with the Feshbach-Yennie theory has become possible for the first time. (12 refs.)

Proceedings of the 4th Nordic Meeting on Nuclear Physics . See Entry 111306

Nuclear data sheets for A=79 See Entry 111327

Nuclear data sheets for A=153 See Entry 111328

Recent References, January through April 1983 [nuclear data sheets] See Entry 111329

High-spin states in $^{201,203}At$ and the systematic behavior of $Z=85$ isotopes See Entry 112035

Recent developments in the interpretation of the discrete line spectroscopy of deformed rare-earth nuclei See Entry 112039

Aligned bands and nuclear shapes in the $N=90$ region See Entry 112040

Search for the two-phonon 0^+ strength in ^{64}Zn See Entry 112043

Intrinsic excitations as yrast structures in ^{179}W above $I \sim 35/2\hbar$ See Entry 112046

High spin phenomena in the mass 100-200 region seen through the Crystal Ball See Entry 112049

Coupling of two quasiparticles to coherent cores in the Pt isotopes See Entry 112050

Transition from prolate to oblate to triaxial shapes in ^{158}Yb See Entry 112059

Shape coexistence and other aspects of nuclear structure in ^{40}Ar See Entry 112060

Spin and isospin characteristics of the excited states of ^{36}Ar through the reaction $^{32}S(\alpha,\gamma)^{36}Ar$ in the bombarding energy range $E_\alpha=4$ to 5 MeV See Entry 112063

Level structure of ^{67}Ge and its implications for the general structure of nuclei in the $1f-2p$ shell See Entry 112071

A study of the nuclear structure at high energy and low spin See Entry 112075

General principles of statistical spectroscopy See Entry 112091

Role of finite boson number in the interacting boson approximation description of γ -g transitions in deformed nuclei See Entry 112100

A program for calculation of the E1, E2 and M1 transition probabilities in odd-odd nuclei taking the Coriolis mixing into account See Entry 112119

The decay of ^{75}Se See Entry 112122

Branching ratio in the decay of 7Be See Entry 112125

Branching ratio in the electron-capture decay of 7Be See Entry 112126

Charged pion electroproduction, a selective probe of nuclear spin-isospin responses See Entry 112151

Statistical properties of $3/2^-$ resonances in ^{45}Sc and ^{51}Mn See Entry 112157

Nonequilibrium decay process of giant resonances studied by gamma transitions See Entry 112160

Pion photoproduction off nuclei: a sensitive test of the nuclear transition densities See Entry 112171

High-resolution (e,e') study of isovector M1 and M2 transitions in the oxygen isotopes. I. ^{16}O See Entry 112174

High-resolution (e,e') study of isovector M1 and M2 transitions in the oxygen isotopes. II. ^{17}O See Entry 112175

High-resolution (e,e') study of isovector M1 and M2 transitions in the oxygen isotopes. III. ^{18}O See Entry 112176

Investigation of the level scheme of ^{145}Nd in the (n,n') reaction See Entry 112189

Low-lying levels, γ -ray transitions, and vibrational structure in ^{198}Pt from (n,n') reaction spectroscopy See Entry 112190

Gamma-ray transitions among levels of ^{206}Pb See Entry 112192

Proton capture by ^{15}N above the giant dipole resonance See Entry 112198

Polarizations, analysing powers and spin-current couplings in inelastic proton scattering See Entry 112205

Energy dependence of analyzing powers for the isoscalar and isovector transitions in (\bar{p},p') reaction See Entry 112210

High-spin states in ^{222}Th See Entry 112244

Penetration of the centrifugal barrier in the fusion of ^{16}O with heavy targets See Entry 112255

Analysis of elastic and inelastic scattering of 162 MeV pions from ^{13}C by an optical potential and a collective model See Entry 112283

Determination of the multipolarity of prompt electromagnetic transitions from angular distributions of conversion electrons. II. Spectrometer and measurements See Entry 112524

23.20C Lifetimes and transition probabilities

112118 The application of lineshape analysis in plunger measurements. G.Winter (Zentralinst. für Kernforschung Rossendorf, Dresden, Germany). *Nucl. Instrum. & Methods Phys. Res. (Netherlands)*, vol.214, no.2-3, p.537-9 (1 Sept. 1983). The evaluation of lifetimes of nuclear states from plunger measurements by means of lineshape analysis is described. The role of detailed stopping calculations (Monte Carlo method) is illustrated. (9 refs.)

112119 A program for calculation of the E1, E2 and M1 transition probabilities in odd-odd nuclei taking the Coriolis mixing into account. Z.Hons (Lab. of Nuclear Problems, JINR, Dubna, USSR), J.Kvasil. *Comput. Phys. Commun. (Netherlands)*, vol.30, no.1, p.59-69 (July-Aug. 1983). It is well known that comparison of experimental reduced transition probabilities with their model-dependent predictions is of great importance for studying nuclear structure. Namely, the influence of the Coriolis particle-rotational coupling on electromagnetic transitions between excited states in odd-A deformed nuclei has been the subject of interest in many papers and has been reliably demonstrated. The analogous situations in odd-odd nuclei has also been established. The program makes it possible to calculate the E1, E2 and M1 reduced transition probabilities in odd-odd deformed nuclei. The mixed wave functions used result from a least-squares fit of energy levels (taking the Coriolis effect into account) to the experimental ones, performed with the modified ODDODDCORI subprogram [2]. (4 refs.)

112120 Lifetimes in ^{18}F . R.Moro, A.Brondi, A.D'Onofrio, V.Roca, M.Romano, F.Terrasi (Istituto di Fisica Sperimentale, Univ. di Napoli, Napoli, Italy), B.Delaunay, H.Dumont. *Lett. Nuovo Cimento (Italy)*, vol.38, ser.2, no.1, p.7-10 (3 Sept. 1983). The lifetimes of nine levels in ^{18}F have been measured by using the DSAM and the $^3He(^{16}O,p)^{18}F$ inverse reaction at 21 MeV incident energy on Al backings. Particle-gamma coincidence was employed. Levels (MeV) and corresponding lifetime (ps) deduced by a line shape analysis are as follows: 1.70 (0.897 ± 0.057), 2.10 (4.93 ± 0.78), 2.52 (0.554 ± 0.045), 3.06 (< 0.004), 3.13 (0.343 ± 0.022), 3.36 (0.451 ± 0.034), 3.72 (< 0.007), 3.79 (1.90 ± 0.20) and 3.84 (0.021 ± 0.004). (5 refs.)

- High-spin states in $^{201,203}\text{At}$ and the systematic behavior of $Z=85$ isotopes See Entry 112035
- Intrinsic excitations as yrast structures in ^{178}W above $I\sim 35/2\hbar$ See Entry 112046
- Spherical, oblate, and prolate nuclear shapes near ^{146}Gd See Entry 112056
- Shape coexistence and other aspects of nuclear structure in ^{40}Ar See Entry 112060
- Electromagnetic properties of isomers in ^{210}Pb See Entry 112066
- Electric monopole strengths in even-mass Ge and Se isotopes See Entry 112111
- Electromagnetic transitions in ^{130}Ce See Entry 112112
- Transition probabilities between two-quasiparticle configurations in $^{170,172}\text{Yb}$ and ^{182}W See Entry 112236
- Analysis of elastic and inelastic scattering of 162 MeV pions from ^{13}C by an optical potential and a collective model See Entry 112283

23.20N Internal conversion and extranuclear effects

- Determination of the multipolarity of prompt electromagnetic transitions from angular distributions of conversion electrons. I. Method See Entry 112106
- The decay of ^{75}Se See Entry 112122
- Determination of the multipolarity of prompt electromagnetic transitions from angular distributions of conversion electrons. II. Spectrometer and measurements See Entry 112524

23.40 BETA DECAY; ELECTRON AND MUON CAPTURE

- 112121 The internal bremsstrahlung (IB) from the allowed beta-emitters. S.El-Konsol, A.M.Basha, S.A.Gaafar, A.A.El-Sayed, A.S.Yousef (Reactor & Neutron Phys. Dept., Atomic Energy Establ., Cairo, Egypt). *Atomkernenergie, Kerntechnik*, (Germany), vol.42, no.2, p.120-3 (1983). The IB spectrum of a complex source consisting of ^{35}S , ^{32}P and ^{32}P was measured in the energy range 80-1700 keV. A NaI(Tl) crystal spectrometer was used. A new approach was tried to decompose the IB spectrum into its three components. The resulting IB spectra were analyzed adopting the variable width peeling off method. The experimental IB probability is compared with the KUB, Nilsson and Lewis-Ford theories. A quite good agreement has been obtained. (27 refs.)
- 112122 The decay of ^{75}Se . K.Singh, R.Mittal, M.L.Hasiza, H.S.Sahota (Dept. of Phys., Punjabi Univ., Patiala, India). *Indian J. Phys. Part A*, vol.57A, no.3, p.127-34 (May 1983). Energy and intensity measurements for X-ray and gamma transitions in the decay of ^{75}Se have been made using Si (Li) and intrinsic Ge detectors below 300 keV. The measurements confirm the presence of 14.9, 24.4 and 80.8 keV transitions. Internal conversion analysis for the 66 keV transition yields $\delta_{66} = 0.0070 \pm 0.0005$ and $\lambda = 11.25 \pm 0.25$. From directional correlation measurements on the 136-66 keV cascade, the 136 keV transition is assigned as $E_1 + (0.15 \pm 0.10)\%$ M2. The influence of after-effects due to electron capture on the 121-279 keV cascade has been studied with different concentrations of the liquid surroundings of the active nuclei. Attenuation of the directional correlation coefficient has been observed. (13 refs.)
- 112123 Atomic effects on the tritium ft value. B.Budick (Phys. Dept., New York Univ., New York, NY, USA). *Phys. Rev. Lett. (USA)*, vol.51, no.12, p.1034-7 (19 Sept. 1983). Atomic effects on the tritium ft value including bound-state decay, imperfect wave-function overlap, screening, and electron exchange are considered for each of the species T^+ , T , T_2 , and T^- . Corrections to the f value are tabulated and can be combined to extract an improved estimate for the axial-vector matrix element in tritium β decay. (21 refs.)
- 112124 Search for mixing of heavy neutrinos in the β^+ and β^- spectra of the ^{64}Cu decay. K.Schreckenbach, G.Colvin (Inst. Laue-Langevin, Grenoble, France), F.von Feilitzsch. *Phys. Lett. B (Netherlands)*, vol.129B, no.3-4, p.265-8 (22 Sept. 1983). The β^+ and β^- spectral shape of the ^{64}Cu decay were analysed for admixtures of heavy neutrinos in the mass range 30 keV 460 keV. The resulting upper limits for the mixing angle $\sin^2\theta$ were determined, achieving a minimum limit of 3.5×10^{-3} at a neutrino mass of 350 keV. (9 refs.)
- 112125 Branching ratio in the decay of ^7Be . G.J.Mathews, R.C.Haight, R.G.Lanier, R.M.White (Lawrence Livermore Nat. Lab., Univ. of California, Livermore, CA, USA). *Phys. Rev. C (USA)*, vol.28, no.2, p.879-84 (Aug. 1983). The branching ratio for ^7Be electron-capture decay to the first excited state in ^7Li has been measured by implanting a 20-MeV ^7Be beam into a silicon detector telescope and counting the subsequent γ decays with well calibrated Ge(Li) detectors. A branching ratio of $10.7 \pm 0.2\%$ was obtained. This value is in agreement with past measurements but does not agree with a recently suggested higher value. Sources of uncertainties and implications for nuclear physics and astrophysics are discussed. (26 refs.)
- 112126 Branching ratio in the electron-capture decay of ^7Be . C.N.Davids, A.J.Elwyn, B.W.Filippone, S.B.Kaufman, K.E.Rehm, J.P.Schiffer (Argonne Nat. Lab., Argonne, IL, USA). *Phys. Rev. C (USA)*, vol.28, no.2, p.885-7 (Aug. 1983). The branching ratio for the electron-capture decay of ^7Be to the 478 keV state in ^7Li has been measured. ^7Be nuclei recoiling near zero degrees from the $^1\text{H}(^7\text{Li}, ^7\text{Be})n$ reaction were counted by and implanted into a Si detector placed in the focal plane of an Enge split-pole spectrograph. After determining the total number of implanted ^7Be nuclei from the pulse height spectrum, the absolute number of 478 keV γ rays was measured with a Ge(Li) detector. The resulting branching ratio of $10.61 \pm 0.23\%$ agrees well with previous measurements. (6 refs.)
- 112127 Predicted features of the beta decay of neutron-rich sd -shell nuclei. B.H.Wildenthal, M.S.Curtin, B.A.Brown (Dept. of Phys. & Astron., Michigan State Univ., East Lansing, MI, USA). *Phys. Rev. C (USA)*, vol.28, no.3, p.1343-66 (Sept. 1983). The Gamow-Teller beta-decay transitions of sd -shell nuclei with five or more excess neutrons are calculated from complete $(0d_{5/2}, 1s_{1/2}, 0d_{3/2})$ -space shell-model wave functions. These wave functions are obtained from diagonalizations of a model Hamiltonian formulation which reproduces observed energy-level structures throughout the sd shell. The calculations are carried out with both the 'free-nucleon' normalization for the Gamow-Teller single-nucleon matrix elements and one based on the empirical values obtained for these quantities from a comparison of corresponding theoretical and experimental Gamow-Teller magnitudes near the line of stability. The

phase-space factors f which connect the reduced Gamow-Teller strength to the total half-lives and the individual decay probabilities are calculated both from the energies obtained in the shell-model calculations and, alternatively, from hybrid energy spectra in which available experimental energies are substituted for the corresponding calculated values wherever possible. Comparisons of the beta-decay predictions to existing experimental results are presented and discussed. (41 refs.)

112128 Gamow-Teller strength function for ^{90}Zr : effects of spin and isospin exchange forces, and ground-state correlations. G.J.Mathews, S.D.Bloom (Lawrence Livermore Nat. Lab., Univ. of California, Livermore, CA, USA), R.F.Hausman, Jr. *Phys. Rev. C (USA)*, vol.28, no.3, p.1367-73 (Sept. 1983). Shell-model calculations of the Gamow-Teller strength function for ^{90}Zr have been performed utilizing a realistic finite-range two-body interaction in a model space consisting of the $2p$ and $1g$ shells. The effects of admixtures of two-particle two-hole excitations in ^{90}Nb , mostly due to the spin and isospin exchange components of the nucleon-nucleon force, are discussed. Ground state correlations in ^{90}Zr are also added via seniority-zero two-proton excitations from the $2p$ shell into the $1g_{9/2}$ shell. With the correlations the Gamow-Teller strength function is in good agreement with the experimental results and accounts for essentially all of the observed dispersion of strength. The inclusion of these correlations does not, however, produce either a displacement of Gamow-Teller strength to higher excitation energies, or a significant change in the total strength. Thus, they cannot account for the observed Gamow-Teller quenching. The quenching factor derived by a comparison of the calculated results with experiment is 0.52. (18 refs.)

112129 Identification of ^{233}Ac . Y.Y.Chu, M.L.Zhou (Dept. of Chem., Brookhaven Nat. Lab., Upton, NY, USA). *Phys. Rev. C (USA)*, vol.28, no.3, p.1379-81 (Sept. 1983). The authors report in this paper identification of the new isotope ^{233}Ac . Uranium targets were irradiated with 28 GeV protons; after rapid retrieval of the target and separation of actinium from thorium, ^{233}Ac was allowed to decay into the known ^{233}Th daughter. Exhaustive chemical purification was employed to permit the identification of ^{233}Th via its characteristic γ radiations. The half-life derived for ^{233}Ac from several experiments is 2.3 ± 0.3 min. The production cross section for ^{233}Ac is 100 μb . (12 refs.)

112130 Extensions of the theory of electromagnetically induced nuclear beta decay. H.R.Reiss (Arizona Res. Labs., Univ. of Arizona, Tucson, AZ, USA). *Phys. Rev. C (USA)*, vol.28, no.3, p.1402-3 (Sept. 1983). The theory of nuclear beta decays induced by intense electromagnetic fields as previously presented is applied to a much broader range of physical variables. The most important intensity domain is found to occur at lower values than had previously been estimated. Furthermore, electromagnetic field 'retardation terms', previously pointed out as potentially important but unevaluated, are found to be significant contributors to the overall transition probability. A treatment of the entire problem in 'electric field' gauge, instead of the original Coulomb gauge, gives identical results. (5 refs.)

112131 Studies of weak beta-delayed protons emitted in the decay of odd- Z , $T_z = -3/2$ nuclei. J.Aysto, P.Taskinen (Dept. of Phys., Univ. of Jyväskylä, Jyväskylä, Finland), K.Eskola, K.Vierinen, S.Messelt. *Phys. Scr. (Sweden)*, vol.T5, p.193-5 (1983). (Proceedings of the 4th Nordic Meeting on Nuclear Physics, Fuglso, Denmark, 16-20 Aug. 1982). Radioactive decay of $T_z = -3/2$ nuclides, ^{27}P and ^{31}Cl , predicted to be weak β -delayed proton precursors, have been looked for. Two proton groups having energies of 989 ± 15 and 1528 ± 20 keV and a half-life of 150 ± 25 ms were associated with the decay of ^{31}Cl . The search for ^{27}P is still under way, but the first qualitative results are briefly discussed.

112132 A note on the Gamow-Teller sum rule with non-nucleonic degrees of freedom. J.A.Niskanen (Res. Inst. for Theoretical Phys., Univ. of Helsinki, Helsinki, Finland). *Phys. Scr. (Sweden)*, vol.T5, p.196-8 (1983). (Proceedings of the 4th Nordic Meeting on Nuclear Physics, Fuglso, Denmark, 16-20 Aug. 1982). Derives a sum rule for the Gamow-Teller transition strength allowing for internal excitations of nucleons. The effect of the $\Delta(1236)$ isobar in the final state is to reduce the total strength to 36% of the purely nucleonic value. However, separately the strengths for opposite charge changes are both enhanced. The author also discusses the effect of Δ admixtures in the initial state and find the change in the sum rule to be very small. (6 refs.)

Unification of weak and electromagnetic forces See Entry 111939

Atomic mass of ^{145}Eu derived from relative P_K -ratios See Entry 112055

^{234}U levels fed in the ^{234}Np electron capture decay See Entry 112072

Determination of stellar neutron-capture rates for radioactive nuclei with the aid of β -delayed neutron emission See Entry 116445

23.60 ALPHA DECAY

112133 Identification of ^{222}U and ^{221}Pa by α -correlation chains. R.Hingmann, H.-G.Clerc, C.-C.Sahm, D.Vermeulen (Inst. für Kernphys., Tech. Hochschule Darmstadt, Darmstadt, Germany), K.-H.Schmidt, J.G.Keller. *Z. Phys. A (Germany)*, vol.313, no.1-2, p.141-2 (1983). In the course of fusion studies it was possible to identify the new isotopes ^{222}U ($T_{1/2} = 1 \mu\text{s}$) and ^{221}Pa ($T_{1/2} = 6.1 \mu\text{s}$) via α -decay chains. The measurement may serve as an example for the possibility of observing extremely shortlived evaporation residues with the help of the velocity filter SHIP. (7 refs.)

Comment on 'determination of gamma-ray energies and abundances of ^{229}Th ' See Entry 112110

24.00 NUCLEAR REACTIONS AND SCATTERING: GENERAL

24.10 NUCLEAR REACTION AND SCATTERING MODELS AND METHODS

112134 On direct mechanism of light-particle emission in incomplete-fusion reactions. C.V.Christov, I.I.Delchev, I.J.Petkov (Inst. of Nuclear Res. & Nuclear Energy, Bulgarian Acad. of Sci., Sofia, Bulgaria). *Bulg. J. Phys. (Bulgaria)*, vol.10, no.3, p.284-9 (1983). The light-particle emission in incomplete-fusion reactions is analyzed within the framework of a theoretical model based on a direct-reaction mechanism. In the model a more sophisticated version of complete-fusion theory is

employed. The theoretical results are in good agreement with experimental data. (16 refs.)

112135 Counting the peaks in the excitation function for precompound processes. R.Bonetti (Inst. de Fisica Generale Applicata, Univ. di Milano, Milano, Italy), M.S.Hussein, P.A.Mello. *Phys. Rev. C (USA)*, vol.28, no.2, p.923-5 (Aug. 1983).

The 'counting of maxima' method of Brink and Stephen, conventionally used for the extraction of the correlation width of statistical (compound nucleus) reactions, is generalized to include precompound processes as well. It is found that this method supplies an important independent check of the results obtained from autocorrelation studies. An application is made to the reaction $^{25}\text{Mg}(^3\text{He}, p)$. (11 refs.)

112136 Dynamics of damped nuclear reactions. J.Randrup (Lawrence Berkeley Lab., Univ. of California, Berkeley, CA, USA). *Phys. Scr. (Sweden)*, vol.T5, p.98-102 (1983). (Proceedings of the 4th Nordic Meeting on Nuclear Physics, Fuglso, Denmark, 16-20 Aug. 1982). The nucleon-exchange model for damped nuclear reactions is briefly reviewed in the framework of macroscopic transport theory. Recent developments are discussed and some future directions indicated. (9 refs.)

112137 Generalized Ramsauer effect in multistep reaction process. M.Nomura (Inst. of Phys., Univ. of Tokyo, Tokyo, Japan). Proceedings of the 1983 RCNP International Symposium on Light Ion Reaction Mechanism, Osaka, Japan, 16-20 May 1983 (Osaka, Japan: Osaka University 1983), p.517-21

Comparative study of a set of one-step-allowed reactions is discussed as a means to observation, with less ambiguity, of nonresonant interference inherent to multistep process. The discussion relies closely on nuclear structure of final states. Intuitive image of Ramsauer effect is utilized. (9 refs.)

112138 Reaction mechanism models embedded in the exact scattering theory. V.Vanzani (Istituto di Fisica, Univ. di Padova, Padova, Italy). Proceedings of the 1983 RCNP International Symposium on Light Ion Reaction Mechanism, Osaka, Japan, 16-20 May 1983 (Osaka, Japan: Osaka University 1983), p.522-6

Proves that, when the reaction dynamics is dominated by a limited number of cluster and/or channels, the exact multiparticle scattering theory, even in its most sophisticated chain-of-partitions labelled form, can be reduced to much more manageable proportions. The author considers the reductions which take place when a set of two-cluster partitions is physically important and when three clusters play a dominant role. (3 refs.)

112139 Molecular states for the transfer reactions (a new three-body equation). A.V.Matveenko (JINR, Dubna, USSR).

Proceedings of the 1983 RCNP International Symposium on Light Ion Reaction Mechanism, Osaka, Japan, 16-20 May 1983 (Osaka, Japan: Osaka University 1983), p.906-13

The author considers the transfer reaction $(a+c)+b \rightarrow (b+c)+a$. A molecular representation of the asymptotic states is derived, and a new molecular Hamiltonian presented. (5 refs.)

(p,p') scattering at 65 MeV on ^{12}C , ^{24}Mg , ^{28}Si and ^{32}S See Entry 112051

Neutron versus proton moments of collective excitations from polarized deuteron scattering See Entry 112067

Isoscalar character of the 1^+ state at 5.844 MeV in ^{208}Pb .. See Entry 112076

Configuration space Faddeev continuum calculations: p-d s-wave scattering length See Entry 112078

Coulomb plus separable potential in coupled channels See Entry 112081

High excited α cluster state calculation of nuclei See Entry 112099

A microscopic study on the particle-decay widths of excited states in light Δ -hypernuclei See Entry 112105

Determination of the final nucleus density matrix by measuring the angular correlation of charged particles and γ -quanta in various planes See Entry 112107

Study of non-static behavior of $\tau\sigma$ -modes by (p,n) reactions .. See Entry 112115

The nucleon optical potential at intermediate energies: new phenomenology and its microscopic basis See Entry 112144

^{17}O - ^{17}N analog states via the $^{14}\text{C}(^6\text{Li}, t)$ and $^{14}\text{C}(^6\text{Li}, ^3\text{He})$ reactions See Entry 112148

Fragmentation of light ions at relativistic energies See Entry 112162

Post-form DWBA description of coincidence spectra in light ion induced break-up reactions See Entry 112163

A constrained approximation for nuclear barrier penetration and fission See Entry 112167

The photoneutron cross section of ^{151}Eu , ^{153}Eu and ^{156}Gd in the giant resonance region See Entry 112170

Test of vibrational current distributions in transverse electron scattering See Entry 112173

Electron scattering See Entry 112180

On two-nucleon absorption of antiprotons by complex nuclei See Entry 112186

Parity violation in neutron elastic scattering around compound nucleus resonances See Entry 112191

Strong absorption limit of the Blankenbecler-Goldberger amplitude See Entry 112193

$^{14}\text{N}(\bar{p}, p)^{14}\text{N}$ (2.31 MeV) reaction at 159.4 MeV See Entry 112196

Elastic and inelastic scattering of polarized protons from ^{206}Pb near isobaric analog resonances See Entry 112199

Energy dependence of the relativistic impulse approximation for proton-nucleus elastic scattering See Entry 112203

Polarizations, analysing powers and spin-current couplings in inelastic proton scattering See Entry 112205

Unnatural parity states studied in high resolution (p,p') experiments at 65 MeV and the effective nucleon-nucleon interaction See Entry 112207

Magnetic states observed in high-resolution (p,n) experiments See Entry 112208

Lane model analysis of 80 MeV (p,n) IAS reactions See Entry 112209

Characteristic 7^- and 5^- states observed in the (p,t) reactions on even-even rare earth nuclei See Entry 112211

Effects of indirect knockout process in quasifree scattering .. See Entry 112215

Analyzing power of neutron continuum spectra for the $^{93}\text{Nb}(\bar{p}, nX)$ reaction at 65 MeV See Entry 112216

The $^{52}\text{Cr}(t, p)^{54}\text{Cr}$ reaction a $E_t=15$ MeV See Entry 112219

Calculation of proton-neutron coincidence cross sections in 56 MeV deuteron-induced breakup reactions by post form distorted-wave Born approximation See Entry 112220

(d, α) reaction and the α particle D state See Entry 112221

Elastic and rearrangement scattering between two interacting deuterons as a four-body problem See Entry 112222

Evidence for an imaginary spin-orbit term in deuteron optical potential from analysing power measurements of inelastic scattering See Entry 112223

DWBA with 'unrestricted' distorting potentials for (d,p) reactions with strongly coupled d- and p-channels See Entry 112226

Measurement of vector analyzing power in the reaction $^{12}\text{C}(\bar{d}, ^6\text{Li})^8\text{Be}$ See Entry 112227

Vector and tensor analyzing powers for (d, ^6Li) on ^{12}C See Entry 112228

Proton-neutron correlation in the deuteron breakup at 56 MeV and prior-form DWBA analysis See Entry 112229

Three-body coupled-channel study of projectile breakup effects in deuteron, ^6Li and ^{12}C induced reactions See Entry 112230

Investigation of adiabatic approximation of projectile-breakup effect on the elastic scattering and the projectile-breakup reactions See Entry 112231

The α - ^7Li and α - ^{12}C elastic scattering at $E_\alpha=5$, and 6, MeV See Entry 112234

Contributions of various particle-particle coincidences to the inclusive ($^3\text{He}, p$) spectra at $\theta_p=10^\circ$ on ^{12}C , ^{28}Si and ^{58}Ni at $E=52$ MeV See Entry 112237

Microscopic study of heavy-particle transfer reactions: the ($^{16}\text{O}, \alpha$) reactions on ^{16}O and ^{28}Si See Entry 112243

Gross structure resonance at 24.3 MeV in $^{12}\text{C}+^{12}\text{C}(2^+)$ See Entry 112245

Pauli forbidden states and nucleus-nucleus potentials See Entry 112258

The physics of heavy ion collisions at 100 MeV per nucleon See Entry 112264

Quarkochemistry of the heavy ion reactions See Entry 112266

Compression effects in relativistic nucleus-nucleus collisions .. See Entry 112267

On the fusion dynamics of $^{40}\text{Ar}+^{40}\text{Ca}$ -fusion-fission and fusion-evaporation See Entry 112273

Probing phase transitions via energetic nuclear collisions See Entry 112274

Projectile excitation and structure effects in polarized ^6Li scattering See Entry 112276

Semiquantal analysis of heavy-ion transfer reactions See Entry 112279

Parametrization of the total cross section for $\pi d \rightarrow pp$ below 330 MeV See Entry 112280

24.10H Optical and diffraction models

112140 The inverse mean field method and the energy dependence of the nuclear potential. E.F.Hefter, K.A.Gridnev (Inst. de Fisica, Univ. Nacional Autonoma de Mexico, Mexico City, Mexico).

Z. Naturforsch. Teil A (Germany), vol.38A, no.8, p.813-20 (Aug. 1983).

The foundations of the inverse mean field method (Imefim) and its relation to traditional approaches are discussed. Imefim predicts the energy dependence of the real central (nuclear) part of the optical model potential to have the functional form $(1+eE_p)^{-3}$. Treating for the time being the constant e as an adjustable parameter, this prediction is shown to compare nicely with well-established formal and heuristic results. (25 refs.)

112141 Relativistic nuclear optical models. L.S.Celenza, C.M.Shakin (Dept. of Phys., Brooklyn Coll., City Univ. of New York, New York, NY, USA).

Phys. Rev. C (USA), vol.28, no.3, p.1256-63 (Sept. 1983).

Recently it has been shown that the use of a relativistic impulse approximation allows one to calculate a nucleon optical potential for use in the Dirac equation. Excellent fits have been obtained for differential cross sections and spin-dependent observables for energies greater than 400 MeV. In this work the authors provide a general description of the form of the momentum-space optical potential for use in the Dirac equation. It is shown that there are eight invariant functions that determine the potential. Procedures for calculating these functions are given. (In the case of nuclear matter only three of these functions are required to specify the nucleon self-energy). (21 refs.)

112142 Radiative capture in the inelastic channel of the compound nucleus. Liu Jian-feng, Ho Yu-kun (Phys. Dept., Zhengzhou Univ., China). *Phys. Energ. Fortis & Phys. Nucl. (China)*, vol.7, no.3, p.355-60 (May 1983). In Chinese.

The radiative capture in the inelastic channel of the compound nucleus is discussed. Starting from the S-matrix theory, the calculation formula for this situation is derived. Then connected with the optical model and Hauser-Feshbach's statistical theory with the width fluctuation correction, a formula convenient for calculations is given. (9 refs.)

112143 The imaginary part of the nucleon-nucleus optical potential. S.Bhattacharya (Nuclear Phys. Div., Bhabha Atomic Res. Centre, Calcutta, India), S.Kailas.

Z. Phys. A (Germany), vol.313, no.1-2, p.99-103 (1983).

Volume integrals of the imaginary part of the proton and the neutron optical potentials obtained from the existing phenomenological analyses for the mass number range of 12-209 and for a range of nucleon energies ($E_p=10$ -180 MeV, $E_n=8$ -150 MeV) have been fitted with an empirical expression. The isoscalar, the isovector and the Coulomb components determined empirically have been compared with those obtained from the microscopic approach. Though there is qualitative agreement between the two predictions, there are differences when compared quantitatively. (19 refs.)

112144 The nucleon optical potential at intermediate energies: new phenomenology and its microscopic basis. P.Schwandt (Cyclotron Facility, Indiana Univ., Bloomington, IN, USA).

Proceedings of the 1983 RCNP International Symposium on Light Ion Reaction Mechanism, Osaka, Japan, 16-20 May 1983 (Osaka, Japan: Osaka University 1983), p.3-33

The validity and failure of conventional optical model phenomenology for the description of proton elastic scattering at intermediate energies is reviewed. The question of unorthodox (non-Woods-Saxon) shapes for the real central potential is discussed from phenomenological as well as microscopic points of view. Results of alternative, microscopically-based optical-model phenomenologies are presented, and the consequences of employing unorthodox optical potentials in distorted-wave calculations of reactions are explored. (37 refs.)

112145 Microscopic relativistic treatment of nucleon-nucleus scattering. J.R.Shepard (Nuclear Phys. Lab., Univ. of Colorado, Boulder, CO, USA). Proceedings of the 1983 RCNP International Symposium on Light Ion Reaction Mechanism, Osaka, Japan, 16-20 May 1983 (Osaka, Japan: Osaka University 1983), p.34-46.
The form of the Dirac impulse approximation optical potential is presented. This potential is used to calculate proton-nucleus elastic scattering and, at energies above ~ 500 MeV, the results are in excellent agreement with data and vastly superior to the Schroedinger-based impulse approximation, especially for the spin observables. Since the inputs for the Dirac and Schroedinger approaches are nearly identical, the differences between the two methods can be explored in detail. The extension of this approach to a microscopic treatment of proton-nucleus inelastic scattering is also discussed. (22 refs.)

112146 Volume integrals of optical potentials for composite projectiles. M.Matoba (Graduate School of Engng. Sci., Kyushu Univ., Kasuga, Japan), M.Hyakutake, I.Kumabe.
Proceedings of the 1983 RCNP International Symposium on Light Ion Reaction Mechanism, Osaka, Japan, 16-20 May 1983 (Osaka, Japan: Osaka University 1983), p.47-52.
Volume integrals of central optical potentials for scatterings of deuterons, ^3He and α -particles from nuclei are discussed. The correction factors of volume integrals of ^3He real central optical potentials to those estimated from nucleon-nucleus folded potentials are about 30% at the incident energy of 10–30 MeV/nucleon and approach to negligibly small values at 70–100 MeV/nucleon region. Volume integrals of imaginary central potentials are also discussed. (19 refs.)

112147 Microscopic optical potentials derived from free NN potentials. H.V.von Geramb, L.Rikus, K.Nakano (Theoretische Kernphys., Univ. Hamburg, Hamburg, Germany).
Proceedings of the 1983 RCNP International Symposium on Light Ion Reaction Mechanism, Osaka, Japan, 16-20 May 1983 (Osaka, Japan: Osaka University 1983), p.78-109.
First principle optical potentials are studied with the nuclear matter approach, which is based on Brueckner's development of the many-body problem (1955) and the hole-line expansion of Hufner and Mahaux (1972). This contribution concentrates on the most recent developments in calculations of the Bethe-Goldstone reaction matrix with free NN potentials as input. As an important intermediate result the authors give a comprehensive discussion of the effective energy and density dependent interaction with an outline of the limitations so far detected. The nonrelativistic nucleon-nucleus optical potential for energies below 400 MeV is formulated as a lowest order folding model result including proper treatment of knock-on exchange effects. A status report on the microscopic optical potential is given via its application to various case studies. (22 refs.)

Proceedings of the 1983 RCNP International Symposium on Light Ion Reaction Mechanism See Entry 111309
 Δ dynamics See Entry 112083

Optical potentials and isoscalar transition rates from 104 MeV alpha-particle scattering by the N=28 isotopes ^{48}Ca , ^{50}Ti and ^{52}Cr See Entry 112114
Clustering effects on neutron elastic scattering from boron isotopes See Entry 112183

Complex spin-orbit potential for $^{208}\text{Pb}(n,n)^{208}\text{Pb}$ at 10 MeV See Entry 112202

Elastic scattering and inelastic scattering of 65 MeV polarised protons See Entry 112204

Lane model analysis of 80 MeV (p,n) IAS reactions See Entry 112209

Evidence for an imaginary spin-orbit term in deuteron optical potential from analysing power measurements of inelastic scattering See Entry 112223

The difference in d- ^{12}C total cross section for $P_{zz}=+1$ and -1 tensor polarised beam See Entry 112224

Measurement of vector analyzing power in the reaction $^{12}\text{C}(\bar{d}, ^6\text{Li})^6\text{Be}$ See Entry 112227

Elastic scattering of ^7Li projectiles in the energy range of 20 to 34 MeV See Entry 112238

Calculation of the imaginary part of the heavy ion potential See Entry 112240

The role of particle transfer in large-angle scattering of 1p-shell nuclei See Entry 112241

Sensitivity of phase shifts to the optical potentials in heavy ion scattering See Entry 112250

^6Li - ^6Li and ^7Li - ^7Li elastic scattering from 2.0 to 5.5 MeV ... See Entry 112253

Systematics of pion-nucleus optical potentials from analysis of elastic scattering See Entry 112281

Nuclear medium effects in pion elastic scattering and charge exchange See Entry 112282

Analysis of elastic and inelastic scattering of 162 MeV pions from ^{13}C by an optical potential and a collective model See Entry 112283

24.30 RESONANCE REACTIONS AND SCATTERING

112148 ^{17}O - ^{17}N analog states via the $^{14}\text{C}(^6\text{Li},t)$ and $^{14}\text{C}(^6\text{Li}, ^3\text{He})$ reactions. A.Cunsolo, A.Foti, G.Imme, G.Pappalardo, G.Raciti (Istituto Nazionale di Fisica Nucleare, Catania, Italy), N.Saunier.
Lett. Nuovo Cimento (Italy), vol.38, ser.2, no.3, p.87-92 (17 Sept. 1983).
The reactions $^{14}\text{C}(^6\text{Li},t)^{17}\text{O}$ and $^{14}\text{C}(^6\text{Li},^3\text{He})^{17}\text{N}$ are investigated at $E(^6\text{Li})=34$ MeV. Energy spectra and angular distributions of tritons and ^3He -particles are measured and spectroscopic factors are obtained through a HF and EFR-DWBA analysis of the data. The $T=3/2$ analog pairs in the ^{17}O - ^{17}N nuclei are identified from the comparison of these data. (8 refs.)

112149 Excitation of the isoscalar giant quadrupole resonance in $^{118}\text{Sn}(\pi^{\pm}, \pi^{\pm})$. J.L.Ullmann, J.J.Kraushaar, T.G.Masterson, R.J.Peterson, R.S.Raymond, R.A.Ristinen (Univ. of Colorado, Boulder, CO, USA), N.S.P.King, R.L.Boudrie, C.L.Morris, W.W.True, R.E.Anderson, E.R.Siciliano.
Phys. Rev. Lett. (USA), vol.51, no.12, p.1038-41 (19 Sept. 1983).
The isoscalar giant quadrupole resonance is studied in $^{118}\text{Sn}(\pi^{\pm}, \pi^{\pm})$ at 130 MeV. It is found that the ratio of π^{-} to π^{+} cross sections at their maximum is 1.9 and that 57% of the energy-weighted sum rule is exhausted in π^{-} scattering. This large ratio of π^{-} to π^{+} cross sections is not anticipated by conventional models, and may be interpreted as evidence for substantial isovector strength. (17 refs.)

112150 Landau damping in the degenerate Fermi liquid. T.Yukawa, H.Kurasawa (KEK, Ibaraki, Japan).
Phys. Lett. B (Netherlands), vol.129B, no.3-4, p.162-6 (22 Sept. 1983).
The authors study the dispersion law of sound propagation in the degenerate Fermi liquid. In contrast with the Landau theory at zero temperature they find the damped oscillation mode (Landau damping) due to quantum effects. The relation between the frequency and the width of this mode has a similar character as found in giant resonances. (8 refs.)

112151 Charged pion electroproduction, a selective probe of nuclear spin-isospin responses. G.Chanfray, J.Delorme (Inst. de Phys. Nucleaire de Lyon, Univ. Claude Bernard, Villeurbanne, France).
Phys. Lett. B (Netherlands), vol.129B, no.3-4, p.167-71 (22 Sept. 1983).
The authors study the reaction of pion electroproduction on nuclei in the quasi-elastic region. They show that detection of the pion in the direction of the virtual photon permits the separation of the longitudinal and transverse spin responses through a Rosenbluth plot. Emphasis is also put on consistency between medium effects and gauge invariance. (10 refs.)

112152 Giant resonance splitting in deformed nuclei. M.Di Nardo, M.Di Toro, G.Giansiracusa, U.Lombardo, G.Russo (Istituto di Fisica, Univ. di Catania, Sezione di Catania, Catania, Italy).
Phys. Rev. C (USA), vol.28, no.2, p.929-32 (Aug. 1983).
The authors describe the giant resonances as simple scaling solutions of a linearized Vlasov equation obtained from a time-dependent Hartree-Fock theory in phase space. For ellipsoidal deformed nuclei they get a splitting of the isoscalar giant quadrupole resonance proportional to the ground state charge quadrupole moment. The lower energy state ($\hbar\omega_{\parallel}$ for prolate nuclei, $\hbar\omega_{\perp}$ for oblate) always gets the larger electromagnetic strength. (18 refs.)

112153 Observation of $2\hbar\omega$ hexadecapole strength in lead nuclei from 200 MeV inelastic proton scattering. J.R.Tinsley, D.K.McDaniels, J.Lisanti, L.W.Swensen, R.Liljestrang, D.M.Drake (Univ. of Oregon, Eugene, OR, USA), F.E.Bertrand, E.E.Gross, D.J.Horen, T.P.Sjoreen.
Phys. Rev. C (USA), vol.28, no.3, p.1417-20 (Sept. 1983).
Excitation of strength packed at 12.0 MeV is observed in ^{208}Pb and ^{206}Pb via the inelastic scattering of 200 MeV protons. Based upon angular distribution measurements in ^{208}Pb the authors interpret the strength as an isoscalar $2\hbar\omega$, $L=4$, excitation. (16 refs.)

112154 Gamow-Teller resonances. C.Gaarde (Niels Bohr Inst., Roskilde, Denmark).
Phys. Scr. (Sweden), vol.T5, p.55-62 (1983). (Proceedings of the 4th Nordic Meeting on Nuclear Physics, Fuglso, Denmark, 16-20 Aug. 1982).
Data from recent (p,n) and ($^3\text{H},t$) experiments at intermediate energies are presented. The reactions show a spectacular selectivity for excitation of isospin-spin models in nuclei. From the zero degree (p, n) spectra Gamow-Teller strength can be deduced, and only half the sum rule strength is observed. The very general nature of the sum rule for charge exchange modes suggests that internal degrees of freedom of the nucleon could be involved. The ($^3\text{He}, t$) reaction at 2 GeV shows a strong excitation of the Δ -resonance, indicating that this resonance could be important for the isospin-spin excitations in nuclei. (21 refs.)

112155 Inelastic electron scattering, fine structure of M1 giant resonances and Gamow-Teller states. A.Richter (Inst. fur Kernphys., Tech. Hochschule Darmstadt, Darmstadt, Germany).
Phys. Scr. (Sweden), vol.T5, p.63-73 (1983). (Proceedings of the 4th Nordic Meeting on Nuclear Physics, Fuglso, Denmark, 16-20 Aug. 1982).
Recent progress in obtaining detailed fine structure distributions of magnetic giant resonances in nuclei using high resolution inelastic electron scattering at low energy is discussed. The author considers $^{40,42,44,48}\text{Ca}$ in which M1 excitations are due to neutron spin-flip transitions, and the N-28 isotones ^{50}Ti , ^{52}Cr and ^{54}Fe where in addition proton excitations contribute to the measured M1 strength. It is found that the M1 strength is very fragmented and considerably quenched in comparison to predictions of shell model calculations. It is shown for two specific examples of M1 transitions in ^{48}Ca and ^{88}Sr that the $\Delta(1232)$ -hole model accounts for part of this quenching. The virtual Δ -isobar admixture in 1^{+} spin-isospin excitations in complex nuclei is estimated. Furthermore, the results from inelastic electron scattering are compared to (p,n) charge exchange reactions exciting Gamow-Teller states and to recent high resolution (p,p') results. Finally, the M1 strength in ^{208}Pb is studied and the results of a form factor measurement of a recently discovered low lying $J^{\pi}=1^{+}$ state are presented. (40 refs.)

112156 High spin resonances in heavy ion collisions. R.R.Betts, S.Saini (Argonne Nat. Lab., Argonne, IL, USA).
Phys. Scr. (Sweden), vol.T5, p.204-6 (1983). (Proceedings of the 4th Nordic Meeting on Nuclear Physics, Fuglso, Denmark, 16-20 Aug. 1982).
Excitation functions for elastic scattering and reactions of $^{28}\text{Si}+^{28}\text{Si}$ show evidence for the existence of narrow ($\Gamma=100$ -200 keV) high-spin ($J\approx 40$ \hbar) resonances. The interpretation of these resonances as high-spin fissioning shape isomers is discussed with reference to data for the $^{28}\text{Si}+^{30}\text{Si}$ and $^{30}\text{Si}+^{30}\text{Si}$ systems. (10 refs.)

112157 Statistical properties of $3/2^{-}$ resonances in ^{45}Sc and ^{51}Mn . J.F.Shirner, Jr., K.M.Whatley, E.G.Bilpuch, C.R.Westerfeldt (Duke Univ., Durham, NC, USA), G.E.Mitchell.
Z. Phys. A (Germany), vol.313, no.1-2, p.51-6 (1983).
Magnitudes and relative signs of reduced width amplitudes for two inelastic decay channels were obtained for $3/2^{-}$ resonances in ^{45}Sc and ^{51}Mn . Width and amplitude correlations were determined, and the first large amplitude correlation has been observed for $l=1$ resonances over a broad range. These results are consistent with the large amplitude correlations previously observed for $3/2^{+}$ and $5/2^{+}$ resonances. (24 refs.)

112158 Excitation of M1 resonances by medium energy protons. G.M.Crawley (Inst. de Phys. Nucleaire, Orsay, France), C.Djalali, N.Marty, M.Morlet, A.Willis, J.C.Jourdain, N.Anantaraman, A.Galonsky, J.Duffy.
Proceedings of the 1983 RCNP International Symposium on Light Ion Reaction Mechanism, Osaka, Japan, 16-20 May 1983 (Osaka, Japan: Osaka University 1983), p.153-75.
The results of 201 MeV (p,p') studies of $\Delta L=0$ spin-flip transitions at very forward angles are discussed. The reasons for making comparisons between (p,p'), (p,n) and electromagnetic measurements of M1 transitions are outlined. After presenting some of the experimental and theoretical uncertainties, a summary of the results on the Zr isotopes plus other nuclei to mass 140 is given. Results from ^{48}Ca , the N=28 nuclei ^{50}Ti , ^{51}V , ^{52}Cr and ^{54}Fe are discussed and compared with (p,n) and electromagnetic measurements. In the Ni isotopes, the T_0 and T_0+1 components of the 1^{+} spin-flip transition were observed both in (p,p') and in (p,n) reactions. (48 refs.)

112159 The giant isovector E2 resonance in calcium observed in radiative neutron capture. I. Bergqvist, A. Hakansson, A. Lika, A. Lindholm, L. Nilsson, N. Olsson, R. Zorro (Tandem Accelerator Lab., Univ. of Uppsala, Uppsala, Sweden).

Proceedings of the 1983 RCNP International Symposium on Light Ion Reaction Mechanism, Osaka, Japan, 16-20 May 1983 (Osaka, Japan: Osaka University 1983), p.861-9

The reaction $^{40}\text{Ca}(n,\gamma)^{41}\text{Ca}$ has been studied in the neutron energy range 20-28 MeV, where the isovector giant quadrupole resonance may be localized. It is expected that interference between E1 and E2 radiation will give rise to a fore-aft asymmetry of the emitted γ rays. This is also observed. The results are compared with calculations based on the direct-semidirect capture model. Good agreement with the experimental data is obtained assuming an isovector E2 resonance located at 32 MeV with a strength exhausting about 35% of the isovector E2 sum rule. This corresponds to the full strength of the T_{-} component. (18 refs.)

112160 Nonequilibrium decay process of giant resonances studied by gamma transitions. M. Tanaka (Kobe Tokiwa Jr. Coll., Kobe, Japan), K. Iwamoto, T. Yamagata, K. Yuasa, S. Nakayama, T. Fukuda, T. Shimoda, K. Okada, M. Wakai, M. Inoue, H. Ogata.

Proceedings of the 1983 RCNP International Symposium on Light Ion Reaction Mechanism, Osaka, Japan, 16-20 May 1983 (Osaka, Japan: Osaka University 1983), p.877-87

Gamma-decay of the low-energy octupole resonance (LEOR) in ^{90}Zr and ^{58}Ni was studied by inelastic α scattering at 99.3 MeV and 110 MeV, respectively. Correlation functions measured for the ground state transition support a sign 3 assignment for the LEOR. Observed branching ratios to the ground and the low-lying states around $E_x \sim 2.2$ MeV for ^{90}Zr are respectively $(7.9 \pm 1.0)\%$ and $(32 \pm 10)\%$, which are significantly larger than those predicted by the statistical-decay model and the latter enhanced branching ratio suggests the coupling of the giant resonances to the nuclear surface vibration. Observed branching ratios to the ground and the 2_1^+ state for ^{58}Ni , on the other hand, were $\sim 1\%$ and $\sim 7\%$, respectively, which were roughly in agreement with the statistical decay model. (27 refs.)

Proceedings of the 4th Nordic Meeting on Nuclear Physics. See Entry 111306

Collective vibrations as doorway states in the damping of nuclear motion See Entry 112042

Coupling of surface and bulk vibrations in the nuclear breathing mode See Entry 112094

Proton-carbon bremsstrahlung cross sections and nuclear time-delays near the $^{12}\text{C}(\text{p,p})$ resonances See Entry 112117

A note on the Gamow-Teller sum rule with non-nucleonic degrees of freedom .. See Entry 112132

The photoneutron cross section of ^{151}Eu , ^{153}Eu and ^{156}Gd in the giant resonance region See Entry 112170

Measurements of the ^3He and ^4He total neutron cross sections up to 40 MeV See Entry 112197

Elastic and inelastic scattering of polarized protons from ^{206}Pb near isobaric analog resonances See Entry 112199

(p,t) and (^3He) reactions on ^{52}Cr and ^{54}Fe populating analog final states with $T_f = T_i$ See Entry 112212

Gross structure resonance at 24.3 MeV in $^{12}\text{C} + ^{12}\text{C}(2^+)$ See Entry 112245

24.50 DIRECT REACTIONS

112161 Assessment of the Feshbach-Kerman-Koonin approximations in multistep direct reaction theories. T. Udagawa, K.S. Low, T. Tamura (Dept. of Phys., Univ. of Texas, Austin, TX, USA).

Phys. Rev. C (USA), vol.28, no.3, p.1033-9 (Sept. 1983).

The approximations made in the statistical multistep direct reaction theory of Feshbach, Kerman, and Koonin (1980) are examined. It is shown that these approximations individually produce rather large errors and that, although they sometimes cancel out partially, a significant amount of net error remains in general. (6 refs.)

112162 Fragmentation of light ions at relativistic energies. S. Garpman, G. Claesson, I. Lund, I. Otterlund (Div. of Cosmic & Subatomic Phys., Univ. of Lund, Lund, Sweden).

Phys. Scr. (Sweden), vol.T5, p.217-21 (1983). (Proceedings of the 4th Nordic Meeting on Nuclear Physics, Fuglo, Denmark, 16-20 Aug. 1982).

Some simple reaction mechanisms for fragmentation of nuclei at relativistic energies are discussed. The inclusive spectra of fragments in longitudinal and transverse momenta give valuable information about the momentum distribution of a nucleon inside the fragmenting nuclei as well as effects of the nuclear mean field. The authors also report on preliminary results from the experiment R418 at the CERN ISR, where $p\alpha$ and $\alpha\alpha$ reactions were studied at CM energies: $\sqrt{s} \approx 88$ and 125 GeV respectively. By examining two-particle correlations they can study the process of simple fragmentation and the so called hard-scattering process. (18 refs.)

112163 Post-form DWBA description of coincidence spectra in light ion induced break-up reactions. R. Shyam (GSI, Darmstadt, Germany), G. Baur, F. Rosel, D. Trautmann.

Proceedings of the 1983 RCNP International Symposium on Light Ion Reaction Mechanism, Osaka, Japan, 16-20 May 1983 (Osaka, Japan: Osaka University 1983), p.541-57

Some of the recently measured angular correlations between outgoing fragments on the break-up reactions induced by the light projectiles (like deuteron, ^3He and α -particle) have been analysed in terms of a break-up theory developed in the framework of the post-form DWBA. It is shown that this theory provides a good description of the experimental data over a wide range of the bombarding energies and the target nuclei. In some cases the results of the present calculations have been compared with those performed with a different theoretical model, and the results are discussed. (29 refs.)

Proceedings of the 1983 RCNP International Symposium on Light Ion Reaction Mechanism. See Entry 111309

On direct mechanism of light-particle emission in incomplete-fusion reactions .. See Entry 112134

Two body residual interaction in the statistical multistep compound and direct theories See Entry 112164

Angular distributions in pre-equilibrium reactions See Entry 112166

Parity violation in neutron elastic scattering around compound nucleus resonances See Entry 112191

Highly excited hole strength observed in the $^{90}\text{Zr}(\bar{p},d)^{89}\text{Zr}$ reaction See Entry 112200

Characteristic 7^- and 5^- states observed in the (p,t) reactions on even-even rare earth nuclei See Entry 112211

Direct contribution to the $^{19}\text{F}(\text{p},\alpha)^{16}\text{O}$ reaction See Entry 112214

Calculation of proton-neutron coincidence cross sections in 56 MeV deuteron-induced breakup reactions by post form distorted-wave Born approximation See Entry 112220

Proton-neutron correlation in the deuteron breakup at 56 MeV and prior-form DWBA analysis See Entry 112229

Three-body coupled-channel study of projectile breakup effects in deuteron, ^6Li and ^{12}C induced reactions See Entry 112230

Deuteron projectile breakup on ^{28}Si at $E_d = 17.85$ MeV See Entry 112232

Contributions of various particle-particle coincidences to the inclusive ($^3\text{He},\text{p}$) spectra at $\theta_p = 10^\circ$ on ^{12}C , ^{28}Si and ^{58}Ni at $E = 52$ MeV See Entry 112237

Multifragmentation of big nuclei See Entry 112269

The mechanism of the ($^6\text{Li},\text{p}$) reaction on light nuclei at $E_{Li} = 28$ MeV See Entry 112275

Characteristics of the $^{19}\text{F}(\text{p},\alpha)^{16}\text{O}$ reaction See Entry 112214

Calculation of proton-neutron coincidence cross sections in 56 MeV deuteron-induced breakup reactions by post form distorted-wave Born approximation See Entry 112220

Proton-neutron correlation in the deuteron breakup at 56 MeV and prior-form DWBA analysis See Entry 112229

Three-body coupled-channel study of projectile breakup effects in deuteron, ^6Li and ^{12}C induced reactions See Entry 112230

Deuteron projectile breakup on ^{28}Si at $E_d = 17.85$ MeV See Entry 112232

Contributions of various particle-particle coincidences to the inclusive ($^3\text{He},\text{p}$) spectra at $\theta_p = 10^\circ$ on ^{12}C , ^{28}Si and ^{58}Ni at $E = 52$ MeV See Entry 112237

Multifragmentation of big nuclei See Entry 112269

The mechanism of the ($^6\text{Li},\text{p}$) reaction on light nuclei at $E_{Li} = 28$ MeV See Entry 112275

24.60 STATISTICAL THEORY AND FLUCTUATIONS

112164 Two body residual interaction in the statistical multistep compound and direct theories. R. Bonetti, L. Colombo (Istituto di Fisica Generale Appl., Univ. di Milano, Milano, Italy).

Phys. Rev. C (USA), vol.28, no.3, p.980-2 (Sept. 1983).

It is shown that within the multistep compound theory the use of matrix elements calculated with a density dependent two-body residual interaction of the Yukawa form makes possible reproduction of the experimental data of multistep compound reactions with an interaction strength V_0 which turns out to be consistent with the one used in the analysis of multistep direct processes. (19 refs.)

112165 Random-walk model of precompound decay. II. Stochastic uncertainties in the lifetimes and cross-sections. J.M. Akkermans (Netherlands Energy Res. Foundation ECN, Petten, Netherlands).

Z. Phys. A (Germany), vol.313, no.1-2, p.83-92 (1983).

For pt.I see *ibid.*, vol.300, p.345 (1981). The uncertainties arising from the stochastic nature of precompound decay nuclear reactions are analyzed in the framework of the preequilibrium exciton and random-walk models. It is demonstrated that the standard deviations and the mean values of the exciton-state lifetimes are of the same order of magnitude. Their correlations are weakly positive, except for exciton states near the equilibrium number, where the correlations are significant. The usefulness and the limitations of the never-come-back approximation are discussed. A general proof is presented of the conditions under which the master-equation and random-walk approaches to Markov processes are equivalent. Connections between different preequilibrium models, e.g. the multi-step compound model and the microscopic statistical theory of precompound decay, are pointed out. It is shown that the waiting time between subsequent collisions is governed by a Poisson process, suggesting that the variance associated with the nucleon mean free path in nuclear matter, as estimated from preequilibrium models, is considerable. The stochastic uncertainties in the emission cross-sections correspond to those of a Bernoulli process. (14 refs.)

112166 Angular distributions in pre-equilibrium reactions. A. Chatterjee (Nuclear Phys. Div., Bhabha Atomic Res. Centre, Bombay, India), S.K. Gupta.

Z. Phys. A (Germany), vol.313, no.1-2, p.93-8 (1983).

A new model is proposed for calculating angular distributions in preequilibrium reactions. In this model, as in the model of Feshbach et al. (1979) the system consisting of target plus projectile initially branches into two sets of states with either no particle in the continuum (multistep compound states) or with at least one particle in the continuum (multistep direct states). The multistep compound emission is assumed to be isotropic while the angular distribution of the multistep direct emission is described using the fast particle model of Mantzouranis et al. (1975). A similar master equation is used for both chains of states differing only in the angular dependence of the emission rates. The two chains of states are treated independently neglecting inter-branch transitions. The angular distributions for 14.6 MeV neutrons calculated using this model are found to be in better agreement with the data than the fast particle model. (18 refs.)

Bose-Einstein correlations in $\alpha\alpha$, pp and pp interactions See Entry 112024

A closed irreversible equation of motion for the one-body density See Entry 112085

On clustering effects and phase instabilities in high energy nuclear collisions See Entry 112104

Dynamics of damped nuclear reactions See Entry 112136

Radiative capture in the inelastic channel of the compound nucleus See Entry 112142

Statistical properties of $3/2^-$ resonances in ^{45}Sc and ^{51}Mn See Entry 112157

Nonequilibrium decay process of giant resonances studied by gamma transitions See Entry 112160

Assessment of the Feshbach-Kerman-Koonin approximations in multistep direct reaction theories See Entry 112161

Absolute cross sections of proton induced reactions on ^{65}Cu , ^{64}Ni and ^{63}Cu See Entry 112181

Yields of medium mass nuclear fragments: statistical emission See Entry 112195

Direct contribution to the $^{19}\text{F}(\text{p},\alpha)^{16}\text{O}$ reaction See Entry 112214

Polarization transfer in $\text{A}(\text{d},\text{pX})$ reactions See Entry 112225

Two-steps analysis of alpha emission in $^{25}\text{Mg}(\text{He},\alpha)$ reaction See Entry 112233

Contributions of various particle-particle coincidences to the inclusive ($^3\text{He},\text{p}$) spectra at $\theta_p = 10^\circ$ on ^{12}C , ^{28}Si and ^{58}Ni at $E = 52$ MeV See Entry 112237

Unified description of statistical excitations, deformations and charge transfer in a dynamical theory of deep-inelastic heavy-ion collisions See Entry 112242

Viscous fluid dynamical calculation of the reaction $^{12}\text{C}(85 \text{ MeV/nucleon}) + ^{197}\text{Au}$ See Entry 112251

Heavy-ion reaction mechanisms studied with the spin spectrometer See Entry 112261

Dynamics of medium energy nuclear collisions See Entry 112263

Multifragmentation of big nuclei See Entry 112269

Analysis of the evaporation-corrected mass and charge distributions in the $\text{Ar} + \text{Mo}$ reactions See Entry 112270

- Formation and decay of the compound nucleus studied in the reaction $^{20}\text{Ne} + ^{27}\text{Al}$ See Entry 112272
- On the fusion dynamics of $^{40}\text{Ar} + ^{40}\text{Ca}$ -fusion-fission and fusion-evaporation See Entry 112273
- The mechanism of the $(^6\text{Li},p)$ reaction on light nuclei at $E_{\text{Li}} = 28$ MeV See Entry 112275
- ^3He -induced fission of nuclei $159 < A < 232$ See Entry 112289

24.70 POLARIZATION IN REACTIONS AND SCATTERING

- Proceedings of the 1983 RCNP International Symposium on Light Ion Reaction Mechanism See Entry 111309
- (p,p') scattering at 65 MeV on ^{12}C , ^{24}Mg , ^{28}Si and ^{32}S See Entry 112051
- Neutron versus proton moments of collective excitations from polarized deuteron scattering See Entry 112067
- Determination of the final nucleus density matrix by measuring the angular correlation of charged particles and γ -quanta in various planes See Entry 112107
- Parity violation in neutron elastic scattering around compound nucleus resonances See Entry 112191
- $^{14}\text{N}(\bar{p},p)^{14}\text{N}(2.31 \text{ MeV})$ reaction at 159.4 MeV See Entry 112196
- Elastic and inelastic scattering of polarized protons from ^{206}Pb near isobaric analog resonances See Entry 112199
- Highly excited hole strength observed in the $^{90}\text{Zr}(\bar{p},d)^{89}\text{Zr}$ reaction See Entry 112200
- Complex spin-orbit potential for $^{208}\text{Pb}(n,n)^{208}\text{Pb}$ at 10 MeV See Entry 112202
- Elastic scattering and inelastic scattering of 65 MeV polarised protons See Entry 112204
- Polarizations, analysing powers and spin-current couplings in inelastic proton scattering See Entry 112205
- Lane model analysis of 80 MeV (p,n) IAS reactions See Entry 112209
- Energy dependence of analyzing powers for the isoscalar and isovector transitions in (\bar{p},p') reaction See Entry 112210
- Study of one- and two-step processes in $^{208}\text{Pb}(p,t)^{206}\text{Pb}(0_+^+, 0_2^+)$ reactions by using analyzing powers at $E_p = 22$ and 50 MeV See Entry 112213
- Analyzing power of neutron continuum spectra for the $^{93}\text{Nb}(\bar{p},nX)$ reaction at 65 MeV See Entry 112216
- Evidence for a secondary doorway state in $A=13$ nuclei from unpolarized and polarized capture measurements See Entry 112217
- Medium energy gamma rays following radiative capture of 40 and 50 MeV polarized protons on ^{11}B and ^{12}C See Entry 112218
- (d,α) reaction and the α particle D state See Entry 112221
- Evidence for an imaginary spin-orbit term in deuteron optical potential from analysing power measurements of inelastic scattering See Entry 112223
- The difference in $d^{12}\text{C}$ total cross section for $P_{zz} = +1$ and -1 tensor polarised beam See Entry 112224
- Polarization transfer in $A(d,pX)$ reactions See Entry 112225
- Measurement of vector analyzing power in the reaction $^{12}\text{C}(\bar{d}, ^6\text{Li})^8\text{Be}$ See Entry 112227
- Vector and tensor analyzing powers for $(d,^6\text{Li})$ on ^{12}C See Entry 112228
- Three-body coupled-channel study of projectile breakup effects in deuteron, ^6Li and ^{12}C induced reactions See Entry 112230
- Projectile excitation and structure effects in polarized ^6Li scattering See Entry 112276
- Polarization in single-nucleon transfer reactions with ^{13}C and ^{11}B ions See Entry 112277
- Polarization of products ^{12}B in ^{14}N -induced reactions See Entry 112278
- Production of a very high intensity polarized ion beam and experiments of spin transfer reactions See Entry 112522

24.75 GENERAL PROPERTIES OF FISSION

- 112167 A constrained approximation for nuclear barrier penetration and fission. H.H.K.Tang, J.W.Negele (Dept. of Phys., MIT, Cambridge, MA, USA). *Nucl. Phys. A (Netherlands)*, vol.A406, no.2, p.205-35 (19 Sept. 1983). An approximation to the time-dependent mean-field theory for barrier penetration by a nucleus is obtained in terms of constrained Hartree-Fock wave functions and a coherent velocity field. A discrete approximation to the continuum theory suitable for practical numerical calculations is presented and applied to three illustrative models. Potential application of the theory to the study of nuclear fission is discussed. (12 refs.)
- 112168 Quantal dynamics of dissipation in heavy ion nuclear fission. S.N.Mukherjee, L.N.Pandey (Dept. of Phys., Banaras Hindu Univ., Varanasi, India). *Phys. Rev. C (USA)*, vol.28, no.3, p.1104-8 (Sept. 1983). Energy dissipation during heavy ion nuclear fission has been calculated by employing the one-dimensional time dependent frictional Schrodinger equation. The variation of loss of energy with respect to the shape of the fissioning system follows the same trend as the classical frictional matrix. The dissipative loss of kinetic energy with respect to time is also shown. (14 refs.)
- 112169 Effect of dissipation on the eigensolutions near the fission saddle point. K.Thomas, R.Davies (Phys. Dept., Oak Ridge Nat. Lab., Oak Ridge, TN, USA), J.Rayford Nix, A.J.Sierk. *Phys. Rev. C (USA)*, vol.28, no.3, p.1181-7 (Sept. 1983). Two equivalent methods are developed for solving the problem of small oscillations near equilibrium when dissipative forces are included in the dynamical equations of motion. One method relies on the Lagrangian formulation of the equations of motion, and the other method relies on the Hamiltonian formulation. The eigenvalues are in general complex, but for unstable or overdamped motion they are purely real. The authors use the Lagrangian formulation to calculate the two lowest symmetric eigensolutions at the fission saddle point for nuclei with Z^2/A ranging from 18.0 to 44.6 for ordinary two-body viscosity, one-body wall-formula dissipation, and one-body wall-and-window dissipation. (20 refs.)
- An extension to the Feynman method of detecting fission neutrons See Entry 112598

25.00 NUCLEAR REACTIONS AND SCATTERING: SPECIFIC REACTIONS

25.10 NUCLEAR REACTIONS AND SCATTERING INVOLVING FEW-NUCLEON SYSTEMS

- Bose-Einstein correlations in $\alpha\alpha$, pp and pp interactions See Entry 112024
- Configuration space Faddeev continuum calculations: p - d s -wave scattering length See Entry 112078
- On parity- and angular-momentum-dependence of inter-nucleus potential See Entry 112082
- Fragmentation of light ions at relativistic energies See Entry 112162
- Charge symmetry breaking in ^4He See Entry 112172
- Differential cross sections and analyzing powers for pd elastic scattering below 1.0 MeV See Entry 112187
- Phase-shift analysis of pd elastic scattering below break-up threshold See Entry 112188
- Measurements of the ^3He and ^4He total neutron cross sections up to 40 MeV See Entry 112197
- Elastic and rearrangement scattering between two interacting deuterons as a four-body problem See Entry 112222
- Inclusive particle production at forward angles from collisions of light relativistic nuclei: nuclear fragments See Entry 112256
- Inclusive particle production at forward angles from collisions of light relativistic nuclei: negative pions See Entry 112257

25.20 PHOTONUCLEAR REACTIONS AND PHOTON SCATTERING

- 112170 The photoneutron cross section of ^{151}Eu , ^{153}Eu and ^{156}Gd in the giant resonance region. T.J.Boal, E.G.Muirhead (School of Phys., Univ. of Melbourne, Parkville, Victoria, Australia), D.J.S.Findley. *Nucl. Phys. A (Netherlands)*, vol.A406, no.2, p.257-68 (19 Sept. 1983). The ^{151}Eu , ^{153}Eu and ^{156}Gd photoneutron cross sections in the giant dipole resonance region have been measured using bremsstrahlung from the University of Melbourne betatron. Absolute cross-section values, lorentzian parameters, intrinsic quadrupole moments, deformation parameters and integrated cross-section values are derived. For ^{151}Eu and ^{153}Eu the measured cross sections are in good agreement with the predictions of the extended dynamic collective model. (36 refs.)
- 112171 Pion photoproduction off nuclei: a sensitive test of the nuclear transition densities. R.A.Eramzhyan (Inst. of Nuclear Res., Acad. of Sci., Moscow, USSR), M.Gmitro, S.S.Kamalov. *Phys. Lett. B (Netherlands)*, vol.128B, no.6, p.371-4 (8 Sept. 1983). The available (e,e') data in most cases constrain just weakly the nuclear transition densities. As an example the authors have analysed the $^{16}\text{O}(\gamma, \pi^+)^{16}\text{N}$ (bound) reaction using two sets of nuclear matrix elements both consistent with the electromagnetic constraint. In spite of that fact they produce dramatically different photoproduction cross sections. New precise electron scattering data are needed to elucidate the situation. (13 refs.)
- 112172 Charge symmetry breaking in ^4He . D.Halderson, R.J.Philpott (Dept. of Phys., Florida State Univ., Tallahassee, FL, USA). *Phys. Rev. C (USA)*, vol.28, no.3, p.1000-4 (Sept. 1983). Calculations for $^4\text{He}(\gamma,p)^3\text{H}$ and $^4\text{He}(\gamma,n)^3\text{He}$ have been performed with the recoil-corrected continuum shell model. A charge-symmetry breaking interaction has been introduced in an effort to explain the large value (~ 2) observed in recent experiments for the cross section ratio $R = \sigma(\gamma,p)/\sigma(\gamma,n)$. The calculations indicate that it is highly unlikely that such a large value of the cross section ratio can be obtained within standard theoretical assumptions. (37 refs.)
- Measurement, parametrization and fast simulation of hadronic showers in lead See Entry 112008
- A modification to the Penfold-Leiss method of cross-section unfolding See Entry 112596

25.30 LEPTON-INDUCED REACTIONS AND SCATTERING

- 112173 Test of vibrational current distributions in transverse electron scattering. E.Wust, U.Mosel (Inst. fur Theoretische Phys., Univ. Giessen, Giessen, Germany), J.Kunz, A.Schuh. *Nucl. Phys. A (Netherlands)*, vol.A406, no.2, p.285-90 (19 Sept. 1983). The transition current distribution for the low-lying 2^+ state a 4.085 MeV in ^{208}Pb obtained in a realistic cranked shell-model calculation is used to calculate the transverse PWBA form factor for inelastic electron scattering to this state. By keeping the same density but changing the velocity field to that of irrotational, incompressible flow the sensitivity of the form factor to the dynamics of nuclear vibrational motion is explored. It is found that the two flow patterns lead to significant, observable differences in the form factors. (14 refs.)
- 112174 High-resolution (e,e') study of isovector M1 and M2 transitions in the oxygen isotopes. I. ^{16}O . G.Kuchler, A.Richter, E.Spamer, W.Steffen (Inst. fur Kernphys., Tech. Hochschule Darmstadt, Darmstadt, Germany), W.Knupfer. *Nucl. Phys. A (Netherlands)*, vol.A406, no.3, p.473-9 (26 Sept. 1983). The M1 and M2 transition strength distribution for ^{16}O in the excitation energy range from 16 to 20 MeV has been measured in a high-resolution electron scattering experiment. The M1 strength is concentrated in three sharp states at $E_x = 16.22$, 17.14 and 18.79 MeV (± 0.01 MeV) with $B(M1,k) = 0.20 \pm 0.02$, 0.32 ± 0.03 and $0.13 \pm 0.03 \mu_N^2$, respectively. An additional strength of $0.35 \pm 0.09 \mu_N^2$, distributed over eight weakly excited states with excitation energies $E_x = 17.4$ to 18.0 MeV, brings the total measured M1 strength to $B(M1,k) = 1.0 \pm 0.1 \mu_N^2$. The experimental M2 strength distributed over states at $E_x = 16.82$, 17.78, 18.50 and 19.0 MeV (± 0.01 MeV) with $B(M2,k) = 19 \pm 2$, 13 ± 2 , 59 ± 7 and $341 \pm 51 \mu_N^2 \cdot \text{fm}^2$, respectively. Electric transitions were also measured to states at $E_x = 16.45$ MeV (2^+ , E2), 17.30 MeV (1^+ , E1) and 18.20 MeV (2^+ , E2). Calculations were performed using the modified surface delta interaction in a 2p-2h shell model for the M1 transitions and the random phase approximation for the M2 transitions. The results show the sensitivity of the M1 strength as a measure of ground-

state correlations and compare well with results from the $^{15}\text{N}(\bar{p},\gamma)$ reaction. (21 refs.)

112175 High-resolution (e,e') study of isovector M1 and M2 transitions in the oxygen isotopes. II. ^{17}O . C.Rangacharyulu, E.J.Ansaldo (Dept. of Phys., Univ. of Saskatchewan, Saskatoon, Canada). *Nucl. Phys. A (Netherlands)*, vol.A406, no.3, p.493-503 (26 Sept. 1983). For pt.I see *ibid.*, vol.406, p.473-492 (1983). In a high-resolution electron scattering experiment, six isospin $T=3/2$ levels in the excitation energy region of 11-15.3 MeV were populated in ^{17}O . Five transitions at $E_x=11.08, 12.47, 12.99, 14.23$ and 14.75 MeV are predominantly of M2 nature with transition strengths $B(\text{M}2,k)=6.1\pm 1.9, 6\pm 3, 6\pm 3, 46\pm 7$ and $27\pm 9 \mu\text{N}^2\text{fm}^2$, respectively. The transition to the 15.10 MeV level is mainly M1 with $B(\text{M}1,k)=0.14\pm 0.04 \mu\text{N}^2$. For this level, a tentative spin-parity assignment of $J^\pi=3/2^+$ is possible. Also, a spin assignment of $J^\pi=9/2^+$ is preferred for the 14.75 MeV level. The comparison of the transition strength to the level at 11.08 MeV with the prediction from the analogous unique first-forbidden β^- decay of the ^{17}N ground state indicates that it may be important to include $p_{3/2}$ -hole configurations in the ground-state wave function of ^{17}O . A comparison made with the corresponding E1 transitions in ^{17}Fe , by estimating the possible longitudinal component for the 14.23 MeV transition and assuming that the 12.99 MeV transition is pure E1, shows that mirror asymmetries in the mass 17 pair may be of non-zero magnitudes. (17 refs.)

112176 High-resolution (e,e') study of isovector M1 and M2 transitions in the oxygen isotopes. III. ^{18}O . D.Bender, A.Richter, E.Spamer (Inst. für Kernphys., Tech. Hochschule Darmstadt, Darmstadt, Germany), E.J.Ansaldo, C.Rangacharyulu, W.Knupfer. *Nucl. Phys. A (Netherlands)*, vol.A406, no.3, p.504-18 (26 Sept. 1983). For pt.II, see *ibid.*, vol.406, p.493-503 (1983). The excitation energy region in ^{18}O from about $E_x=11-27$ MeV has been studied with low-momentum transfer, but high-resolution inelastic electron scattering. Two sharp lines are prominent in the spectra, corresponding to the excitation of $T=2$ levels at 16.399 ± 0.005 MeV and 18.871 ± 0.005 MeV of $J^\pi=2^-$ and 1^+ , respectively. In contradiction to theoretical predictions no more strong M2 transitions could be found. Broad peaks were observed at 18.5, 19.7, 20.2, 22.5 and 23.8 MeV, that latter two are due to the giant dipole resonance as known from photonuclear reactions. The spectra show in addition considerable fine structure and the application of a cross correlation function technique for its analysis resulted in the location of twelve more low multipolarity weak transitions in the excitation energy range between 16 and 19 MeV. Tentative J^π assignments are given for these levels. The spectra of isospin $T=2$ states of $A=18$ nuclei are discussed in view of the existing experimental and theoretical work. Finally, the pattern of the isovector M1 and M2 strength distributions of all the three oxygen isotopes $^{16,17,18}\text{O}$ is discussed. (24 refs.)

112177 (e,e'\pi) reaction on light nuclei and spin-isospin strength distribution effects. J.Cohen, J.M.Eisenberg (Dept. of Phys. & Astron., Tel Aviv Univ., Tel Aviv, Israel). *Phys. Rev. C (USA)*, vol.28, no.3, p.1309-17 (Sept. 1983). The authors study threshold pion electroproduction on light $T=0$ nuclei. The probe is essentially interesting because it mixes longitudinal (spin component parallel to momentum transfer, $\vec{\sigma}\cdot\vec{k}$ coupling) and transverse ($\vec{\sigma}\times\vec{k}$ coupling) channels. Using the local density approximation for the treatment of possible nuclear spin-isospin mode enhancements, they calculate cross sections for both exclusive and inclusive measurements. For discrete nuclear levels they study differential cross sections of various pionlike levels, and these are compared with a nonpionlike excitation. The cross sections for exclusive excitations are extremely small except for forward angles. The inclusive cross sections, achieved by summing over all nuclear states, are considerably larger since these include the quasifree excitation. All cases are studied as a function of q' , the Migdal spin-isospin parameter. The authors find a strong influence of kinematical conditions (especially the energy transfer) and of nuclear density on enhancement phenomena. (12 refs.)

112178 Reaction $\mu^- + {}^6\text{Li} \rightarrow {}^3\text{H} + {}^3\text{H} + \nu_\mu$ and the axial current form factor in the timelike region. S.L.Mintz (Florida Internat. Univ., Miami, FL, USA). *Phys. Rev. C (USA)*, vol.28, no.3, p.1389-92 (Sept. 1983). The differential muon-capture rate $d\Gamma/dE_T$ is obtained for the reaction $\mu^- + {}^6\text{Li} \rightarrow {}^3\text{H} + {}^3\text{H} + \nu_\mu$ over the allowed range of E_T , the tritium energy, for two assumptions concerning the behaviour of F_A , the axial current form factor, in the timelike region; analytic continuation from the spacelike region and mirror behaviour, $F_A(q^2, \text{timelike}) = F_A(q^2, \text{spacelike})$. The values of $d\Gamma/dE_T$ under these two assumptions are found to vary substantially in the timelike region as a function of the mass M_A in the dipole fit to F_A . Values of $d\Gamma/dE_T$ are given for $M_A^2 = 2m_\pi^2, 4.95 m_\pi^2$, and $8 m_\pi^2$. (10 refs.)

112179 Electromagnetic and weak currents in nuclei. T.W.Donnely (Center for Theoretical Phys., MIT, Cambridge, MA, USA). *Symmetries in Nuclear Structure. Proceedings of a NATO Advanced Study Institute on Symmetries in Nuclear Structure*, Dronen, Netherlands, 16-28 Aug. 1982 (New York, USA: Plenum Press 1983), p.1-33. The basic formalism used in descriptions of electromagnetic and weak interactions with nuclei is discussed. The author begins by considering the simple problem of electron scattering from a point Dirac proton. This description is improved by allowing the nucleon to have internal structure. Inclusive electron scattering from a nucleus is discussed. A general treatment of the (e,e') reaction is given. In this latter situation, a multipole analysis of the electromagnetic current is dictated. The author concludes the discussion of the electromagnetic interaction with the general formalism involved in treating exclusive electron scattering, (e,e'). The point Dirac nucleon and dressed nucleon weak currents are discussed, followed by consideration of general inclusive reactions and their nuclear response functions. The author concludes by displaying specific forms for a variety of charge-changing and neutral-current weak interaction cross sections. (11 refs.)

112180 Electron scattering. I.Sick (Dept. of Phys., Univ. of Basel, Basel, Switzerland). *Symmetries in Nuclear Structure. Proceedings of a NATO Advanced Study Institute on Symmetries in Nuclear Structure*, Dronen, Netherlands, 16-28 Aug. 1982 (New York, USA: Plenum Press 1983), p.223-50. The experimental equipment used for electron scattering experiments obviously is of great diversity. The author describes a 'typical' set by discussing some of the apparatus used at the three highest-energy facilities (Amsterdam, Bates and Saclay). The author discusses some of the development in the determination of ground state charge densities from the electron-nucleus scattering. He also deals with plastic scattering from nuclear magnetisation densities of high multipole order. (42 refs.)

Symmetries in Nuclear Structure. Proceedings of a NATO Advanced Study Institute on Symmetries in Nuclear Structure See Entry 111295

Differential bremsstrahlung cross sections for collisions of electrons with unscreened nuclei of low atomic numbers See Entry 111321

Inelastic electron scattering, fine structure of M1 giant resonances and Gamow-Teller states See Entry 112155

25.40 NUCLEON-INDUCED REACTIONS AND SCATTERING

(see also 28.20 Neutron physics)

112181 Absolute cross sections of proton induced reactions on ^{65}Cu , ^{64}Ni and ^{63}Cu . M.E.Sevior, L.W.Mitchell, M.R.Anderson, C.I.W.Tingwell, D.G.Sargood (School of Phys., Univ. of Melbourne, Parkville, Victoria, Australia). *Aust. J. Phys. (Australia)*, vol.36, no.4, p.463-71 (1983). Absolute cross sections have been measured for (p,\gamma) reactions on ^{65}Cu , ^{64}Ni and ^{63}Cu over proton energy ranges of 1.05-3.25, 1.00-3.45 and 1.05-4.70 MeV respectively, for (p,n) reactions over proton energy ranges from threshold to 3.25, 3.80 and 4.86 MeV respectively, and for $^{63}\text{Cu}(p,p)^{63}\text{Cu}$ over a proton energy range of 1.05-4.00 MeV. All the data are compared with global statistical model calculations. The agreement, to within a factor of 2, between theory and experiment is regarded as satisfactory for a global code, but the ^{64}Ni data are suggestive of a closed shell effect at $Z=28$. (15 refs.)

112182 (n,2n) cross-section measurement of ^{93}Nb , ^{197}Au and ^{238}U with fission-neutron spectrum and its dependence on the asymmetry term. G.Shani (Ben-Gurion Univ. of the Negev, Beer-Sheva, Israel). *Ann. Nucl. Energy (GB)*, vol.10, no.9, p.473-6 (1983). The (n,2n) reaction cross section was measured for ^{93}Nb , ^{197}Au and ^{238}U with fission-neutron spectrum from ^{252}Cf sources. The cross-section dependence on the asymmetry term $N-Z/A$ (where N , Z and A are the nucleus neutron, proton and mass numbers) was investigated and found to be an exponential growth. The mathematical function describing $\sigma_{n,2n}=f(N-Z/A)$ is dependent on the incoming neutron energy. The function at fission spectrum is of the shape e^{-x} while at 14-15 MeV it has the shape of $1-e^{-x}$ (where x stands for $N-Z/A$). Looking for an analogy between the asymmetry term dependence and energy dependence, a similar change occurs in the energy-dependent cross section near threshold. (24 refs.)

112183 Clustering effects on neutron elastic scattering from boron isotopes. S.Komoda, T.Sekiya (Dept. of Nuclear Engng., Osaka Univ., Osaka, Japan). *Atomkernenergie. Kerntechnik. (Germany)*, vol.42, no.2, p.101-4 (1983). The phenomenological optical model is applied to boron isotopes and the differential cross section data for neutron elastic scattering from ^{10}B and ^{11}B are reproduced at forward scattering angles at bombarding energies between 7 and 14 MeV. The magnitude of the discrepancy between the theoretical and experimental angular distributions at backward scattering angles decreases smoothly with the bombarding energy. (22 refs.)

112184 Measurement of the total neutron cross-section of germanium at energies below 2 eV. M.Salama (Reactor & Neutron Phys. Dept., Nuclear Res. Center, Atomic Energy Establish., Cairo, Egypt). *Atomkernenergie. Kerntechnik. (Germany)*, vol.42, no.2, p.105-6 (1983). The total neutron cross-section of germanium has been measured at room temperature as a function of neutron energy in the range between 2.2 eV and 7 meV for randomly distributed crystals of germanium by transmission method using a chopper time-of-flight spectrometer at ET-RR-1 research reactor. The measured cross-section showed an evidence of $1/v$ thermal slope in the energy range 1.20 eV to 0.20 eV. Crystal structure effects were also observed. Calculations were performed giving values for the coherent scattering amplitude as well as the coherent scattering cross-section. The results obtained showed also the absence of scattering nuclear spin dependence in case of germanium. (14 refs.)

112185 The activation cross-sections for (n,\gamma) reactions using ^{241}Am -Be neutron source. K.Kaminishi, S.Nureki (Dept. of Appl. Phys., Miyazaki Univ., Miyazaki, Japan). *Jpn. J. Appl. Phys. Part 1 (Japan)*, vol.22, no.6, p.1070 (June 1983). Reports the values of the activation cross-sections for more than twenty samples. The reported values were determined from the value of the thermal neutron cross-section of ^{197}Au , while previous results were obtained from that of aluminium. (2 refs.)

112186 On two-nucleon absorption of antiprotons by complex nuclei. A.S.Iljiov, V.L.Matushko (Inst. for Nuclear Res., Acad. of Sci., Moscow, USSR), G.Piragino. *Lett. Nuovo Cimento (Italy)*, vol.38, ser.2, no.3, p.83-6 (17 Sept. 1983). It is shown that the antiprotons can be absorbed by correlated pairs of intranuclear nucleons, with subsequent emission of a high-energy pion and nucleon pair. The estimation of the cross-section values of this process, performed on the framework of the quasi-deuteron model, shows the possibility of experimental detection of the \bar{p} two-nucleon absorption process. (11 refs.)

112187 Differential cross sections and analyzing powers for \bar{p} elastic scattering below 1.0 MeV. E.Hüttel, W.Arnold, H.Berg, H.H.Krause, J.Ulbricht, G.Clausnitzer (Inst. für Kernphys., Justus-Liebig-Universität Giessen, Giessen, Germany). *Nucl. Phys. A (Netherlands)*, vol.A406, no.3, p.435-42 (26 Sept. 1983). Differential cross sections for the elastic \bar{p} scattering were measured at seven energies between 0.4 and 1.0 MeV for scattering angles from $\theta_{\text{c.m.}}=44.5^\circ$ to 149.2° . A mixture of D_2 and Kr was used as target gas and the \bar{p} differential cross sections were determined relative to those of pKr scattering with a statistical error of $\Delta\sigma/\sigma \sim 5 \times 10^{-3}$. Analyzing power for \bar{p} scattering were measured at 0.8, 0.9 and 1.0 MeV with a statistical error of $\Delta A_y \sim 5 \times 10^{-4}$. (27 refs.)

112188 Phase-shift analysis of \bar{p} elastic scattering below break-up threshold. E.Hüttel, W.Arnold, H.Baumgart, H.Berg, G.Clausnitzer (Inst. für Kernphys., Justus-Liebig-Universität Giessen, Giessen, Germany). *Nucl. Phys. A (Netherlands)*, vol.A406, no.3, p.443-55 (26 Sept. 1983). A phase-shift analysis was performed for \bar{p} elastic scattering based on measurements of differential cross sections and proton and deuteron analyzing powers for energies below the break-up threshold. The angular momenta were restricted to $l \leq 3$; j -splitting and channel-spin mixing of the P-phases and the tensor coupling between the S- and D-phases were taken into account. The phase shifts were parameterized by the effective-range formalism and the corresponding parameters were directly deduced from the data. The results are compared with Faddeev calculations in which the Coulomb interaction is treated exactly or as a two-body approximation. (27 refs.)

112189 Investigation of the level scheme of ^{145}Nd in the $(n,n'\gamma)$ reaction. L.I.Govor, A.M.Demidov (Kurchatov Atomic Energy Inst., Moscow, USSR), M.A.Al-Amili, T.J.Al-Janabi, V.D.Avchukhov, K.A.Baskova, A.B.Vovk. *Nucl. Phys. A (Netherlands)*, vol.A406, no.3, p.456-72 (26 Sept. 1983). The spectrum of γ -rays from the inelastic scattering of reactor fast neutrons on ^{145}Nd is measured. The authors observed 169 γ -lines in the γ -ray spectrum and, among them, 94 γ -lines for the first time. The γ -transition scheme for ^{145}Nd is constructed. New levels are introduced for the most intense transitions. Multipole mixtures are determined from the measured angular distributions of γ -rays. The angular momenta for some of the levels are determined and the low-lying levels in ^{145}Nd are discussed. (13 refs.)

112190 Low-lying levels, γ -ray transitions, and vibrational structure in ^{198}Pt from $(n,n'\gamma)$ reaction spectroscopy. S.W.Yates, A.Khan, A.J.Filo (Dept. of Chem., Univ. of Kentucky, Lexington, KY, USA), M.c.Mirzaa, J.L.Weil, M.T.McEllistrem. *Nucl. Phys. A (Netherlands)*, vol.A406, no.3, p.519-32 (26 Sept. 1983).

Low-lying states in ^{198}Pt have been studied by $(n,n'\gamma)$ reaction spectroscopy at incident neutron energies below 2.5 MeV. Using detailed γ -ray excitation functions and angular distribution measurements, the authors have established a level scheme which includes 16 excited levels and is believed to include all levels below an excitation energy of 1.5 MeV. The positive-parity structure is believed to include all levels below an excitation energy of 1.5 MeV. The positive-parity structure is similar to the expected of an anharmonic vibrator; however, difficulties in asserting that the first 0^+ excited level is a collective excitation are encountered. Only two negative-parity states are observed, and they are adequately described in the semi-decoupled model. (22 refs.)

112191 Parity violation in neutron elastic scattering around compound nucleus resonances. S.Noguera, J.Bernabeu (Dept. de Física Teórica, Univ. de Valencia, Valencia, Spain).

Phys. Lett. B (Netherlands), vol.129B, no.1-2, p.125-9 (15 Sept. 1983). The parity-conserving asymmetry for elastic scattering of polarized neutrons in the energy region around compound nucleus resonances is considered. The mechanism of virtual excitation of the parity admixed compound nucleus state is used. The parity conserving elastic amplitudes are dominated by s wave, but the simultaneous presence of the p wave resonant state is crucial for the parity violating amplitudes. Effects for n - ^{117}Sn scattering are at the level of 10^{-5} - 10^{-6} , with a very peculiar energy dependence around the s wave resonance. (17 refs.)

112192 Gamma-ray transitions among levels of ^{206}Pb . J.K.Dickens (Oak Ridge Nat. Lab., Oak Ridge, TN, USA).

Phys. Rev. C (USA), vol.28, no.2, p.916-18 (Aug. 1983). A study of γ -ray data produced by neutron inelastic scattering from a lead sample enriched in the isotope ^{206}Pb has resulted in placements of 106 γ rays as transitions among 88 known or postulated levels of the ^{206}Pb level structure. (16 refs.)

112193 Strong absorption limit of the Blankenbecler-Goldberger amplitude. R.J.Lombard (Div. de Phys. Théorique, CNRS, Inst. de Phys. Nucleaire, Orsay, France).

Phys. Rev. C (USA), vol.28, no.2, p.938-40 (Aug. 1983). The strong absorption limit of the Blankenbecler-Goldberger amplitude for hadron-nucleus elastic scattering is studied by calculating the total cross section using the optical theorem, and comparing the results to values obtained in the Glauber model. It is shown that in spite of many defects, the Blankenbecler-Goldberger amplitude yields results not too far from those of Glauber. This is due to the fact that most of the elastic scattering is concentrated in the nuclear surface, and that the two multiple scattering expansions agree in low density regions. (5 refs.)

112194 Search for two-phonon vibrations in ^{168}Er . E.W.Kleppinger, S.W.Yates (Dept. of Chem., Univ. of Kentucky, Lexington, KY, USA).

Phys. Rev. C (USA), vol.28, no.2, p.943-5 (Aug. 1983). The low-lying level structure of ^{168}Er has been examined by the $(n,n'\gamma)$ reaction and all known levels with $J < 7$ and $E \leq 2.0$ MeV are observed. The discovery of a level at 1893 keV calls for a reexamination of the completeness of the level scheme assumed previously for this nucleus. No new low-lying candidates for two-phonon γ vibrations are observed. (13 refs.)

112195 Yields of medium mass nuclear fragments: statistical emission. W.A.Friedman (Phys. Dept., Univ. of Wisconsin, Madison, WI, USA), W.G.Lynch.

Phys. Rev. C (USA), vol.28, no.2, p.950-2 (Aug. 1983). The results of a calculation using a newly developed statistical emission formalism are compared with the recently published data of Finn et al. for nuclear fragment yields from high energy proton-nucleus interactions on ^{132}Xe . Good agreement is noted. (3 refs.)

112196 $^{14}\text{N}(\bar{p},p)^{14}\text{N}(2.31 \text{ MeV})$ reaction at 159.4 MeV. T.N.Taddeucci, J.Rapaport (Dept. of Phys., Ohio Univ., Athens, OH, USA), C.C.Foster, J.R.Comfort.

Phys. Rev. C (USA), vol.28, no.3, p.969-76 (Sept. 1983). Differential cross-section and analyzing-power angular distributions have been measured for the elastic scattering of 159.4 MeV protons on ^{14}N and for the inelastic transitions to the 2.31-MeV and 3.95-MeV states. Elastic-scattering data for \bar{p} - ^{12}C and inelastic data for the $^{12}\text{C}(\bar{p},p)^{12}\text{C}(4.44 \text{ MeV})$ reaction have also been obtained at the same energy as a normalization check. The $^{14}\text{N}(\bar{p},p)^{14}\text{N}(2.31 \text{ MeV})$ transition has been analyzed in the distorted-wave impulse approximation. This transition has long been regarded as a favorable test for the tensor component of the effective nucleon-nucleon interaction. Calculations employing wave functions that provide the necessary cancellation of the $L=0$ central-interaction transition strength do not provide a good description of the differential cross-section angular distribution. It is suggested that more complicated reaction mechanisms, e.g. (p,d)/(d,p') contributions, may be needed to describe this transition. (25 refs.)

112197 Measurements of the ^3He and ^4He total neutron cross sections up to 40 MeV. B.Haesner, W.Heeringa, H.O.Klages, H.Dobiasch, G.Schmalz, P.Schwarz, J.Wilczynski, B.Zeitnitz (Kernforschungszentrum Karlsruhe, Karlsruhe, Germany).

Phys. Rev. C (USA), vol.28, no.3, p.995-9 (Sept. 1983). The total neutron cross sections of the helium isotopes were measured in the energy range from 1.5 to 40 MeV. A continuous energy neutron source was used in connection with a 190 m long flight path and high resolution time-of-flight techniques. The energy resolution achieved enabled the authors to improve considerably the parameters of the narrow $^3/2^+$ resonance in the n - ^4He system. The position of the resonance was found to be 22133 ± 10 keV, with a total width of 76 ± 12 keV and a neutron width of 37 ± 5 keV. This agrees well with previous analyses, which yield $\Gamma_n \sim 1/2$. Absolute values for the cross sections were determined with an overall error smaller than 3%. Comparison with older data shows agreement within the total errors. The data are 4% to 5% higher than the most recent data set; however, in the case of ^3He , the data are still below the predictions from an R-matrix analysis. It was pointed out recently that a slight disagreement exists between the

total neutron cross section of ^3He and the sum of the partial n - ^3He cross sections. This discrepancy is removed by the new data. (16 refs.)

112198 Proton capture by ^{15}N above the giant dipole resonance. M.Ang-hinolfi, P.Corvisiero, G.Ricco, M.Sanzone, M.Taiuti, A.Zucchiatti (Istituto di Sci. Fisiche, Univ. di Genova, Genova, Italy).

Phys. Rev. C (USA), vol.28, no.3, p.1005-11 (Sept. 1983). The proton capture cross sections to the ground and excited states of ^{16}O have been measured at several angles in the proton energy interval between 18 and 40 MeV. The ground state angular distribution, which shows a significant $E1$ - $E2$ interference effect above 40 MeV, results in reasonable agreement with semidirect capture calculations. Transitions to final bound and unbound $1p$ - $1h$ states in ^{16}O having a dominant $1p_{1/2}^{-1}$ hole have also been measured. Resonances built on these residual states have been systematically observed above $E_p = 20$ MeV; the possible interpretation of these states as giant dipole resonances built on excited states is discussed. (27 refs.)

112199 Elastic and inelastic scattering of polarized protons from ^{206}Pb near isobaric analog resonances. N.L.Back, J.G.Cramer (Nuclear Phys. Lab., Univ. of Washington, Seattle, WA, USA).

Phys. Rev. C (USA), vol.28, no.3, p.1040-59 (Sept. 1983). Excitation functions have been measured for the elastic and inelastic scattering of polarized protons from ^{206}Pb at $\theta_{\text{lab}} = 120^\circ$, 135° , 150° , and 165° in the energy range $E_p = 14.25$ - 18.00 MeV. Excellent fits to the elastic scattering data were obtained using a parametrized background and the isobaric analog resonances of 35 states in ^{207}Pb (the 'parent states') with $E_x = 2.3$ - 5.7 MeV; spin-parity assignments and resonance parameters were determined for all of these isobaric analog resonances. The data for inelastic scattering to the first excited state (2^+ , 0.803 MeV) were described using a distorted-wave Born approximation background and the same isobaric analog resonances; good fits to the data were obtained by varying only the inelastic partial width amplitudes. A set of spectroscopic amplitudes was then found, for both the single-particle and the particle-core components of the parent states, by comparing the best-fit resonance parameters with those given by model calculations. The internal consistency of this set was verified by using sum rules. The spectroscopic amplitudes are compared with those given by simple weak-coupling model predictions; there is considerable disagreement, probably because too few configurations were used in the theoretical calculations. (42 refs.)

112200 Highly excited hole strength observed in the $^{90}\text{Zr}(\bar{p},d)^{89}\text{Zr}$ reaction. J.Kasagi, G.M.Crawley, E.Kashy, J.Duffy (Nat. Superconducting Cyclotron Lab., Michigan State Univ., East Lansing, MI, USA), S.Gales, E.Gerlic, D.Friesel.

Phys. Rev. C (USA), vol.28, no.3, p.1065-8 (Sept. 1983). The $^{90}\text{Zr}(\bar{p},d)^{89}\text{Zr}$ reaction has been studied at $E_p = 90$ MeV. Using analyzing power measurements, gross structures observed between $E_x \sim 3.4$ and $E_x \sim 7.0$ MeV are deduced to arise mainly from the pickup of $1f_{5/2}$ neutrons. Between 7.0 and 19 MeV, the main strength comes from the $1f_{7/2}$ transfer although $1d_{3/2}$ strength has also been observed between 16.0 and 20.0 MeV of excitation energy. (14 refs.)

112201 $^7\text{Be}(p,\gamma)^8\text{B}$ cross section at low energy. F.C.Barker (Dept. of Theoretical Phys., Australian Nat. Univ., Canberra, Australia).

Phys. Rev. C (USA), vol.28, no.3, p.1407-8 (Sept. 1983). The low-energy logarithmic derivative of the S factor for $^7\text{Be}(p,\gamma)^8\text{B}$ calculated by Williams and Koonin (1981) using only asymptotic wave functions differs from that obtained with a potential model. It is suggested that this is due at least in part to an inappropriate choice of nuclear phase shift in the former calculation. (9 refs.)

112202 Complex spin-orbit potential for $^{208}\text{Pb}(n,n)^{208}\text{Pb}$ at 10 MeV. J.P.Delaroche, C.E.Floyd, P.P.Guss, R.C.Byrd, K.Murphy, G.Tungate, R.L.Walter (Dept. of Phys., Duke Univ., Durham, NC, USA).

Phys. Rev. C (USA), vol.28, no.3, p.1410-13 (Sept. 1983). The analyzing power $A_y(\theta)$ and differential cross section $\sigma(\theta)$ have been measured for elastic scattering of 10-MeV neutrons from ^{208}Pb . These data were analyzed with a spherical optical model which has a real spin-orbit potential with either a three-parameter conventional form or a one-parameter semimicroscopic form. The predictions with both spin-orbit potentials reproduce the data equally well, suggesting that fewer free parameters can be used in spherical optical model calculations. Including an imaginary spin-orbit term $W_{\text{SO}}(r)$ in the optical potential greatly improves the fits to the $A_y(\theta)$ measurements and establishes the need for $W_{\text{SO}}(r) \neq 0$ in the n - ^{208}Pb potential. (9 refs.)

112203 Energy dependence of the relativistic impulse approximation for proton-nucleus elastic scattering. B.C.Clark, S.Hama (Dept. of Phys., Ohio State Univ., Columbus, OH, USA), R.L.Mercer, L.Ray, G.W.Hoffman, B.D.Serot.

Phys. Rev. C (USA), vol.28, no.3, p.1421-4 (Sept. 1983). Results of relativistic and nonrelativistic impulse approximation calculations are compared for p - ^{40}Ca elastic scattering observables between 181 and 1040 MeV. At 400 MeV and above, the relativistic approach is superior, especially with regard to spin observables. Below 400 MeV, neither calculation agrees well with experiment. (17 refs.)

112204 Elastic scattering and inelastic scattering of 65 MeV polarised protons. H.Sakaguchi (Dept. of Phys., Kyoto Univ., Kyoto, Japan).

Proceedings of the 1983 RCNP International Symposium on Light Ion Reaction Mechanism, Osaka, Japan, 16-20 May 1983 (Osaka, Japan: Osaka University 1983), p.58-77. Elastic scattering of 65 MeV polarised protons from 35 nuclei (^{16}O - ^{209}Bi) and inelastic scattering from rare earth nuclei have been measured. Based on the analysis of the systematic data, the following topics are discussed: (1) mass number dependence of the mean square radius of the optical potential; (2) energy and mass number dependence of the volume integral of the optical potential; (3) anomaly observed in J_g and J_p for rare earth nuclei; (4) quadrupole moments measured by proton scattering are larger than quadrupole moments measured by electron scattering. (27 refs.)

112205 Polarizations, analysing powers and spin-current couplings in inelastic proton scattering. W.G.Love (Dept. of Phys. & Astron., Univ. of Georgia, Athens, GA, USA).

Proceedings of the 1983 RCNP International Symposium on Light Ion Reaction Mechanism, Osaka, Japan, 16-20 May 1983 (Osaka, Japan: Osaka University 1983), p.110-23. Non-local spin-dependent couplings in the effective nucleon-nucleon interaction are shown to probe current-spin correlations in inelastic nuclear excitations. Together, these couplings and correlations provide an important dynamical source of polarisation-analyzing power differences observed in inelastic proton scattering. In most of the presently used models of inelastic scattering this type of coupling arises from knockon exchange effects. Plane wave impulse approximation (PWIA) results are given for $0^+ \rightarrow 1^+$ transitions to illustrate explicitly the role of these current-spin couplings in calculations of

P and A. The very selective $0^+ \rightarrow 0^-$ transitions are also briefly considered. (28 refs.)

112206 Effective interactions in (p,p') and (p,n) excitations. M.Yabe (Dept. of Phys., Faculty of Sci., Tokyo Metropolitan Univ., Setagaya-ku, Tokyo, Japan), A.Mori, K.Kubo. Proceedings of the 1983 RCNP International Symposium on Light Ion Reaction Mechanism, Osaka, Japan, 16-20 May 1983 (Osaka, Japan: Osaka University 1983), p.124-8
The authors analysed the proton inelastic scatterings and the charge exchange reactions to investigate the effective interactions and the reaction mechanisms. Firstly they report necessity of modification of the M3Y effective interaction in the framework of one-step and two-step processes. Secondly they compare this modified M3Y interaction with one constructed from the transition matrix based on Brueckner-Hartree-Fock treatment. The interaction is dependent on nuclear density with complex Gaussian form. Justification of the modification is then argued. (12 refs.)

112207 Unnatural parity states studied in high resolution (p,p') experiments at 65 MeV and the effective nucleon-nucleon interaction. M.Fujiwara, S.Imanishi, Y.Fujita, S.Morinobu, I.Katayama, T.Yamazaki, T.Itahashi, H.Ikegami (Res. Centre for Nuclear Phys., Osaka Univ., Ibaraki, Osaka, Japan), K.Katori, S.I.Hayakawa. Proceedings of the 1983 RCNP International Symposium on Light Ion Reaction Mechanism, Osaka, Japan, 16-20 May 1983 (Osaka, Japan: Osaka University 1983), p.134-52
The authors present experimental results and microscopic PWBA analyses of the (p,p') reactions at 65 MeV performed at RCNP. They focus mainly on the excitation of unnatural parity states in ^{40}Ca , ^{90}Zr , and ^{208}Pb . It was found that in order to fit the experimental data of the 1p-1h neutron excitations by the microscopic DWBA calculations using the M3Y interaction, a common renormalisation factor of about 0.3 was needed. (39 refs.)

112208 Magnetic states observed in high-resolution (p,n) experiments. H.Orihara, C.D.Zafiratos (Cyclotron & Radioisotope Center, Tohoku Univ., Sendai, Japan), S.Nishihara, K.Furukawa, M.Kabasawa, T.Nakagawa, K.Maeda, K.Miura, G.C.Kiang, H.Ohnuma. Proceedings of the 1983 RCNP International Symposium on Light Ion Reaction Mechanism, Osaka, Japan, 16-20 May 1983 (Osaka, Japan: Osaka University 1983), p.176-95
A study of magnetic (unnatural-parity) states observed in charge-exchange (p,n) experiments is presented. The (p,n) reactions on ^{12}C , ^{14}C , ^{16}O , ^{24}Mg and ^{28}Si have been investigated at $E_p=35$ MeV by means of the time-of-flight technique. Feasibility of analyses for the low-energy (p,n) data with use of the proposed realistic nucleon-nucleon interactions is discussed. Analyses for angular distributions of the differential cross section for the transitions of the spin-isospin type such as from 0^+ to 0^- , 2^- , 4^- and 6^- states are presented. (20 refs.)

112209 Lane model analysis of 80 MeV (p,n) IAS reactions. D.A.Lind, T.G.Masterson, R.S.Raymond, E.Sugarbaker, C.D.Zafiratos (Univ. of Colorado, Boulder, CO, USA), C.C.Foster. Proceedings of the 1983 RCNP International Symposium on Light Ion Reaction Mechanism, Osaka, Japan, 16-20 May 1983 (Osaka, Japan: Osaka University 1983), p.206-13
Angular distributions for the (p,n) IAS transition were measured for the targets $^{90,92,94}\text{Zr}$ and $^{112,116,124}\text{Sn}$ at $E_p=80$ MeV. These data were compared to a Lane model calculation using an existing global optical potential for protons. The real central isovector portion of that potential was a volume form and failed to fit the shape of the angular distribution, although the magnitude was reasonable. Changing the volume form to a surface-peaked form led to improved agreement with the data. Predictions of (p,n) IAS analyzing powers were made with this modified isovector potential and they differ considerably from those obtained with the global parameters. Measurement of those analyzing powers would help test the validity of the Lane model at 80 MeV. (8 refs.)

112210 Energy dependence of analyzing powers for the isoscalar and isovector transitions in (p,p') reaction. K.Hosono, N.Matsuoka, K.Hatanaka, M.Fujiwara, Y.Fujita, T.Saito, T.Noro, M.Kondo (Res. Centre for Nuclear Phys., Osaka Univ., Osaka, Japan), S.Kato, K.Okada, K.Ogino, Y.Kadota, S.Matsuki. Proceedings of the 1983 RCNP International Symposium on Light Ion Reaction Mechanism, Osaka, Japan, 16-20 May 1983 (Osaka, Japan: Osaka University 1983), p.246-9
Cross sections and analyzing powers in proton inelastic scattering leading to the 1^+ ($T=0$ and $T=1$) states in ^{12}C , the 6^- ($T=0$ and $T=1$) states in ^{28}Si and the 10.218 MeV, 1^+ state in ^{48}Ca were measured at 65 MeV. The data is compared with the results obtained at higher incident energies. In ^{12}C and ^{28}Si , the shapes of the analysing powers for the $T=0$ transitions vary drastically while those for the $T=1$ transitions do not vary with the incident energy. The authors briefly comment on the behaviour of the analysing power for the 10.218 MeV, 1^+ state in ^{48}Ca with the incident energy. (13 refs.)

112211 Characteristic 7^- and 5^- states observed in the (p,t) reactions on even-even rare earth nuclei. Y.Ishizaki, S.Kubono, Y.Iwasaki (Inst. for Nuclear Study, Univ. of Tokyo, Tokyo, Japan), T.Tohei, T.Nakagawa, J.Hirota, T.Suehiro, K.Miura, S.Kato, S.I.Hayakawa. Proceedings of the 1983 RCNP International Symposium on Light Ion Reaction Mechanism, Osaka, Japan, 16-20 May 1983 (Osaka, Japan: Osaka University 1983), p.468-72
The (p,t) reactions have been studied for the even-even rare earth nuclei with 40 MeV proton beam from the INS SF cyclotron. A pair of 7^- and 5^- states was observed with large cross sections in each of the nuclei with the neutron number (N) ranging from 86 to 100. For $^{140,142}\text{Nd}$ of $N=80$ and 82 the data were obtained at KVI in Groningen, and the data for ^{152}Sm of $N=90$ at MSU. Q value systematics of (p,t) reactions to these states seem to suggest that these are excited by the two neutron pick-up from the neutron core of $N=82$. The (p,t) cross sections leading to these states of N from 82 to 96 are nearly constant. (8 refs.)

112212 (p,t) and (p, ^3He) reactions on ^{52}Cr and ^{54}Fe populating analog final states with $T_1=T_2$. T.Yamazaki, Y.Fujita, M.Fujiwara, S.Morinobu (Res. Center for Nuclear Phys., Osaka Univ., Osaka, Japan), S.I.Hayakawa, K.Katori, S.Imanishi, M.Nomura, H.Ikegami. Proceedings of the 1983 RCNP International Symposium on Light Ion Reaction Mechanism, Osaka, Japan, 16-20 May 1983 (Osaka, Japan: Osaka University 1983), p.473-6
The angular distributions of the (p,t) and (p, ^3He) reactions on ^{52}Cr and ^{54}Fe to analog final states (isospin $T_1=T_2$) were studied. The contribution of the sequential p-d-t and p-d- ^3He processes is rather small. The difference of angular distributions to 4^+ states of $^{52}\text{Cr}(p,t)$ and $^{52}\text{Cr}(p,^3\text{He})$ reactions shows the possible presence of the sequential process. (6 refs.)

112213 Study of one- and two-step processes in $^{208}\text{Pb}(p,t)^{206}\text{Pb}(0^+, 0_2^+)$ reactions by using analyzing powers at $E_p=22$ and 50 MeV. H.Iida, Y.Aoki, K.Hashimoto, K.Nagano, H.Sakamoto, M.Takei, Y.Tagishi, K.Yagi (Inst. of Phys., Univ. of Tsukuba, Ibaraki, Japan). Proceedings of the 1983 RCNP International Symposium on Light Ion Reaction Mechanism, Osaka, Japan, 16-20 May 1983 (Osaka, Japan: Osaka University 1983), p.477-81
A marked difference between two $0^+ \rightarrow 0^+$ analyzing powers for $^{208}\text{Pb}(p,t)^{206}\text{Pb}$ (0_1^+ and 0_2^+) reactions is observed at $E_p=22$ and 50 MeV. The difference is explained successfully by taking into account sequential transfer processes as well as a one-step process at $E_p=22$ MeV. The difference of the interference between the one- and the two-step processes, which is due to the difference of nuclear-structure wave functions, is essential to explain the two $0^+ \rightarrow 0^+$ analyzing powers. The parameters employed in the (p,t) analyses reproduce the experimental data of the $^{208}\text{Pb}(p,d)^{207}\text{Pb}$ and $^{208}\text{Pb}(d,t)^{206}\text{Pb}$ reactions. The difference between the analyzing powers for the 0_1^+ and 0_2^+ transitions is not reproduced by taking into account only the one-step process. The two-step contributions play an important role at $E_p=50$ MeV. (5 refs.)

112214 Direct contribution to the $^{19}\text{F}(p,\alpha)^{16}\text{O}$ reaction. T.Inoue, A.Isoya (Faculty of Sci., Kyushu Univ., Fukuoka, Japan). Proceedings of the 1983 RCNP International Symposium on Light Ion Reaction Mechanism, Osaka, Japan, 16-20 May 1983 (Osaka, Japan: Osaka University 1983), p.482-6
The excitation functions have been measured for the reaction $^{19}\text{F}(p,\alpha)^{16}\text{O}$ leading to the first several states of ^{16}O in the incident proton energy range between 4.15 and 13.0 MeV in steps of 50 keV at $\theta_{\text{lab}}=30^\circ$, 70° , 120° and 160° . Ericson fluctuation analysis has been carried out and the fractions of direct reaction contributions in the differential cross sections have been deduced for the transitions to the ground state and to the first excited state of ^{16}O using a probability distribution formula of differential cross section. (13 refs.)

112215 Effects of indirect knockout process in quasifree scattering. Y.Ikebata, Y.Kudo (Dept. of Phys., Osaka City Univ., Osaka, Japan). Proceedings of the 1983 RCNP International Symposium on Light Ion Reaction Mechanism, Osaka, Japan, 16-20 May 1983 (Osaka, Japan: Osaka University 1983), p.512-16
Within the framework of the distorted wave impulse approximation (DWIA), the effects of the indirect proton-core nucleus knockout process (IK process) are investigated in the (p,2p) reactions for light target nuclei (^{14}N , ^{16}O and ^{19}F). (9 refs.)

112216 Analyzing power of neutron continuum spectra for the $^{93}\text{Nb}(\bar{p},nX)$ reaction at 65 MeV. H.Sakai, K.Hatanaka, N.Matusoka (Res. Center for Nuclear Phys., Osaka Univ., Osaka, Japan), T.Motobayashi, T.Saito, T.Shibata, A.Shimizu. Proceedings of the 1983 RCNP International Symposium on Light Ion Reaction Mechanism, Osaka, Japan, 16-20 May 1983 (Osaka, Japan: Osaka University 1983), p.610-16
Analyzing power of neutron continuum spectra for the $^{93}\text{Nb}(\bar{p},nX)$ reaction at 65 MeV has been measured for the wide angular range $\theta_n=20^\circ\text{--}130^\circ$. The analyzing powers are positive and large for the large angles $\theta_n>40^\circ$. The characteristic features in the analyzing power for the $^{93}\text{Nb}(\bar{p},nX)$ reaction are very similar to those for the $^{93}\text{Nb}(p,p'X)$ reaction indicating the importance of a common reaction mechanism for both reactions. A simple single step DWBA calculation was performed to compare with the data. (12 refs.)

112217 Evidence for a secondary doorway state in $A=13$ nuclei from unpolarized and polarized capture measurements. J.G.Woodworth (Lawrence Livermore Nat. Lab., Univ. of California, Livermore, CA, USA), R.A. August, N.R. Roberson, D.R. Tilley, H.R. Weller, J.W. Jury. Proceedings of the 1983 RCNP International Symposium on Light Ion Reaction Mechanism, Osaka, Japan, 16-20 May 1983 (Osaka, Japan: Osaka University 1983), p.855-60
Cross section, angular distribution and analyzing power measurements show structure and interference effects in neutron, proton and deuteron capture into the $A=13$ system at about 20 MeV excitation energy. By introducing a secondary doorway state at 20.6 MeV with a 0.5 MeV width it is possible to explain the shape of the $^{12}\text{C}(n,\gamma_0)^{13}\text{C}$ and $^{12}\text{C}(p,\gamma_0)^{13}\text{N}$ cross sections as well as the fluctuations observed in the experimental angular distributions and analyzing powers. (5 refs.)

112218 Medium energy gamma rays following radiative capture of 40 and 50 MeV polarized protons on ^{11}B and ^{12}C . M.Noumachi, T.Shibata, K.Okada, T.Motobayashi (Dept. of Phys., Osaka Univ., Osaka, Japan), T.Kishimoto, F.Ohtani, H.Ejiri. Proceedings of the 1983 RCNP International Symposium on Light Ion Reaction Mechanism, Osaka, Japan, 16-20 May 1983 (Osaka, Japan: Osaka University 1983), p.870-6
Medium energy (40~60 MeV) γ -rays following radiative capture of 40 and 50 MeV polarized protons on ^{11}B and ^{12}C were studied for the first time by using the NaI detector ensemble 'HERMES' with good energy resolution and good S/N ratio. Discrete γ -rays feeding the low-lying states in ^{12}C and ^{13}N , and prominent γ peaks feeding the 19 and 22 MeV excitation regions in ^{12}C were identified. All these gamma rays show uniformly a forward peak angular distributions, while the analyzing powers depend on the microscopic configurations of the final states. (11 refs.)

Proceedings of the 1983 RCNP International Symposium on Light Ion Reaction Mechanism See Entry 111309

Single-particle Glauber matrix elements See Entry 111324

The LEAR project and physics with low energy antiprotons at CERN. A summary See Entry 112026

Search for the two-phonon 0^+ strength in ^{64}Zn See Entry 112043

(p,p') scattering at 65 MeV on ^{12}C , ^{24}Mg , ^{28}Si and ^{32}S See Entry 112051

Simple isospin relations for transitions in $A=13$ See Entry 112064

Isoscalar character of the 1^+ state at 5.844 MeV in ^{208}Pb See Entry 112076

Configuration space Faddeev continuum calculations: p-d s-wave scattering length See Entry 112078

Electric monopole strengths in even-mass Ge and Se isotopes See Entry 112111

Study of non-static behavior of $\tau\sigma$ -modes by (p,n) reactions See Entry 112115

Proton-carbon bremsstrahlung cross sections and nuclear time-delays near the $^{12}\text{C}(p,p)$ resonances See Entry 112117

Identification of ^{233}Ac See Entry 112129

Radiative capture in the inelastic channel of the compound nucleus See Entry 112142

The imaginary part of the nucleon-nucleus optical potential See Entry 112143

- The nucleon optical potential at intermediate energies: new phenomenology and its microscopic basis See Entry 112144
- Microscopic relativistic treatment of nucleon-nucleus scattering See Entry 112145
- Microscopic optical potentials derived from free NN potentials See Entry 112147
- Observation of $2h\omega$ hexadecapole strength in lead nuclei from 200 MeV inelastic proton scattering See Entry 112153
- Gamow-Teller resonances See Entry 112154
- Statistical properties of $3/2^-$ resonances in ^{45}Sc and ^{51}Mn See Entry 112157
- Excitation of M1 resonances by medium energy protons See Entry 112158
- The giant isovector E2 resonance in calcium observed in radiative neutron capture See Entry 112159
- Fragmentation of light ions at relativistic energies See Entry 112162
- Inclusive particle production at forward angles from collisions of light relativistic nuclei: nuclear fragments See Entry 112256
- Inclusive particle production at forward angles from collisions of light relativistic nuclei: negative pions See Entry 112257
- Multifragmentation of big nuclei See Entry 112269
- Isotopic and neutron yields of products from the asymmetric and near-symmetric proton-induced fission of ^{235}U and ^{239}U See Entry 112286
- Neutron-induced fission of ^{232}Th near threshold See Entry 112288
- Determination of stellar neutron-capture rates for radioactive nuclei with the aid of β -delayed neutron emission See Entry 116445
- Effect of excited states on thermonuclear reaction rates See Entry 116631

25.50 ^2H - AND ^3H -INDUCED REACTIONS AND SCATTERING

- 112219 The $^{52}\text{Cr}(p)^{54}\text{Cr}$ reaction at $E_p=15$ MeV. D.L. Watson, M.A. Abouzeid (Postgraduate School of Studies in Phys., Univ. of Bradford, Bradford, England), H.T. Fortune, L.C. Bland, J.B. McGrory. *Nucl. Phys. A (Netherlands)*, vol. A406, no. 2, p.297-305 (19 Sept. 1983). Using the $^{52}\text{Cr}(p)^{54}\text{Cr}$ reaction at a bombarding energy of 15 MeV excitation energies have been measured for 30 levels up to $E_x=5.583$ MeV in ^{54}Cr . Angular distributions were obtained for all but one of these levels; these have been compared with distorted-wave Born approximation (DWBA) calculations to determine the L -transfer (and hence J^π). The measured cross sections have been compared to the predictions of DWBA calculations that use two-neutron transfer amplitudes from a shell-model calculation with the active neutrons restricted to the $(2p_{3/2}, 1f_{5/2}, 2p_{1/2})$ orbitals. (17 refs.)
- 112220 Calculation of proton-neutron coincidence cross sections in 56 MeV deuteron-induced breakup reactions by post form distorted-wave Born approximation. G. Baur, R. Shyam (Inst. fur Kernphys., KFA Julich, Julich, Germany), F. Rosel, D. Trautmann. *Phys. Rev. C (USA)*, vol. 28, no. 2, p.946-9 (Aug. 1983). Recently measured neutron-proton angular correlations in the deuteron-induced breakup reactions at 56 MeV incident energy have been analyzed in terms of the post form distorted-wave Born approximation theory of breakup reactions. Comparison of the present results is made with those of the prior form distorted-wave Born approximation calculations. It is found that the results of the post form distorted-wave Born approximation calculations are in better agreement with the experimental data than the prior form distorted-wave Born approximation results. (17 refs.)
- 112221 (d,α) reaction and the α particle D state. J.A. Tostevin (Dept. of Phys., Univ. of Surrey, Guildford, England). *Phys. Rev. C (USA)*, vol. 28, no. 2, p.94-4 (Aug. 1983). The recent suggestion that the effects of a D -state component of the α particle are being seen in (d,α) reaction tensor analyzing power data is reexamined using exact finite range distorted-wave Born approximation calculations. Results for $^{32}\text{S}(d,\alpha)^{30}\text{P(g.s.)}$, at $E=16$ MeV, are in considerable variance with two-nucleon-core relative motion amplitudes derived from shell model calculations. (15 refs.)
- 112222 Elastic and rearrangement scattering between two interacting deuterons as a four-body problem. A. Osman (Internat. Centre for Theoretical Phys., Trieste, Italy). *Phys. Rev. C (USA)*, vol. 28, no. 3, p.1025-32 (Sept. 1983). A four-body model is used in studying the four-nucleon system. This model is solvable and can be applied to nuclear reactions involving four nucleons. Intermediate quasiparticle states are used for the two- and three-body scattering leading to T matrices which are separable. The model leads to four-body equations which, by using partial wave decomposition, are reduced to single variable integral equations. Numerical calculations of the differential cross sections of the nuclear reactions $^2\text{H}(d,p)^3\text{H}$, $^2\text{H}(d,n)^3\text{He}$, and $^2\text{H}(d,d)^2\text{H}$ are carried out for different deuteron laboratory energies between 6.1 and 51.5 MeV. Inclusion of the p -wave three-body amplitudes is tested. Also, the simultaneous exchange of two nucleons between the incoming deuterons is investigated. The theoretically calculated angular distributions are in good agreement with the experimental measurements. The extracted values of the spectroscopic and normalization factors are reasonable. (18 refs.)
- 112223 Evidence for an imaginary spin-orbit term in deuteron optical potential from analysing power measurements of inelastic scattering. M. Takei, Y. Aoki, K. Hashimoto, H. Iida, K. Nagano, H. Sakamoto, H. Tanaka, Y. Tagishi, K. Yagi (Inst. of Phys. & Tandem Accelerator Centre, Univ. of Tsukuba, Ibaraki, Japan). Proceedings of the 1983 RCNP International Symposium on Light Ion Reaction Mechanism, Osaka, Japan, 16-20 May 1983 (Osaka, Japan: Osaka University 1983), p.53-7. Differential cross sections $\sigma(\theta)$, vector analysing powers $iT_{11}(\theta)$ and tensor analysing powers $T_{20}(\theta)$, $T_{21}(\theta)$ and $T_{22}(\theta)$ have been measured for elastic and inelastic scattering exciting the first 2^+ and 3^- states from $^{104,106}\text{Pd}$ by using a 21 MeV polarised deuteron beam. The analysis was made with the optical potential model and the first-order distorted-wave Born approximation calculations. It was found that an imaginary spin-orbit potential had a significant role in reproducing the iT_{11} data for the inelastic scattering. (4 refs.)
- 112224 The difference in $d\text{-}^{12}\text{C}$ total cross section for $P_{zz}=+1$ and -1 tensor polarised beam. K. Imai (Dept. of Phys., Kyoto Univ., Kyoto, Japan), K. Hatanaka, T. Ichihara, N. Matsuoka, K. Nisimura, T. Saito, H. Sakaguchi, T. Yoshida, M. Yosoi. Proceedings of the 1983 RCNP International Symposium on Light Ion Reaction Mechanism, Osaka, Japan, 16-20 May 1983 (Osaka, Japan: Osaka University 1983), p.129-33. The difference in $d\text{-}^{12}\text{C}$ total cross section for $P_{zz}=+1$ and -1 tensor polarised beam ($\Delta\sigma_{\text{tot}}$) has been measured for the first time. ($\Delta\sigma_{\text{tot}}$) is sensi-

tive to the tensor potential due to the D -state of the deuteron. The present result ($+2.4 \pm 2.0$ mb) is inconsistent with the value (-20 mb) predicted from folding model optical potential. (4 refs.)

112225 Polarization transfer in $A(d,pX)$ reactions. H. Sakamoto, M. Nakamura, H. Sakaguchi, H. Ogawa, S. Kobayashi (Dept. of Phys., Kyoto Univ., Kyoto, Japan), S. Kato, N. Matsuoka, K. Hatanaka, T. Noro. Proceedings of the 1983 RCNP International Symposium on Light Ion Reaction Mechanism, Osaka, Japan, 16-20 May 1983 (Osaka, Japan: Osaka University 1983), p.487-91. The transverse vector-to-vector polarization transfer coefficient K_y^y of inclusive protons emitted from deuteron induced reactions on targets on ^{12}C , ^{38}Ni and ^{209}Bi has been measured at 13.5° and 20.0° (lab) at $E_d=56$ MeV for the first time. The coefficient has been obtained for energy bins, center values of which are 22, 26, 31 and 36 MeV and width of which is ± 2 MeV. Though the K_y^y values obtained are roughly close to $2/3$ which is expected from a simple spectator model, a considerable decrease of K_y^y from $2/3$ is observed at the lower energy tail of the spectrum for all the targets studied. Another behavior of K_y^y lowered from $2/3$ can be seen at the higher tail. (6 refs.)

112226 DWBA with 'unrestricted' distorting potentials for (d,p) reactions with strongly coupled d - and p -channels. Y. Iseri, M. Kawai (Dept. of Phys., Kyushu Univ., Fukuoka, Japan). Proceedings of the 1983 RCNP International Symposium on Light Ion Reaction Mechanism, Osaka, Japan, 16-20 May 1983 (Osaka, Japan: Osaka University 1983), p.492-7. Attempts have been made to justify DWBA in terms of the coupled-channel (CC) method. It has been maintained (Ichimura and Kawai, 1983) that for inelastic scattering DWBA works, even when the coupling between the initial and final channels is strong, the distorting potentials are adjusted to fit the CC elastic cross sections. On the other hand, it was shown that for (d,p) reactions DWBA failed to reproduce CC results as long as distorting potentials were restricted to the standard Woods-Saxon type. The purpose of the work is to examine the same problem, relaxing, however, the restriction on the distorting potential by allowing the potential to have a wine-bottle shape, l -dependence or non-locality. (4 refs.)

112227 Measurement of vector analyzing power in the reaction $^{12}\text{C}(\bar{d},^6\text{Li})^8\text{Be}$. T. Yamaya, K. Takimoto, S. Shimoura, A. Sakaguchi, M. Fukada (Dept. of Phys., Tohoku Univ., Sendai, Japan), S. Kato, J. I. Hirota, S. Kubono, M. Sugitani, T. Suehiro. Proceedings of the 1983 RCNP International Symposium on Light Ion Reaction Mechanism, Osaka, Japan, 16-20 May 1983 (Osaka, Japan: Osaka University 1983), p.498-501. The vector analyzing power and the differential cross sections have been measured for the ground state and the excited states of ^8Be in the reaction $^{12}\text{C}(\bar{d},^6\text{Li})$ at $E_d=51.7$ MeV. The results of the DWBA calculation with a finite-range interaction are in agreement with the experimental cross section and analyzing power. In the DWBA analysis, the spin-orbit term of the deuteron optical potential is significant but this term of the lithium optical potential had the minor effect on the angular distributions and the vector analyzing power. The extracted absolute alpha-spectroscopic factor for the ground state of ^8Be is in agreement with the theoretical value. (6 refs.)

112228 Vector and tensor analyzing powers for $(d,^6\text{Li})$ on ^{12}C . Y. Tagishi, M. Ishikawa, H. Iida, T. Sugiyama, K. Hashimoto, M. Takei (Inst. of Phys., Univ. of Tsukuba, Ibaraki, Japan). Proceedings of the 1983 RCNP International Symposium on Light Ion Reaction Mechanism, Osaka, Japan, 16-20 May 1983 (Osaka, Japan: Osaka University 1983), p.502-6. Differential cross sections, vector analyzing power (iT_{11}) and tensor analyzing powers (T_{20} , T_{21} and T_{22}) are measured for the reaction $^{12}\text{C}(d,^6\text{Li})^8\text{Be(g.s.)}$ at deuteron energies 18 and 22 MeV. The zero-range distorted-wave Born approximation calculations have been performed on the present data. Angular distributions of cross section and vector analyzing power are fairly well reproduced by these simple calculations; however, the calculations predicted very small tensor analyzing powers T_{20} , T_{21} and T_{22} . (3 refs.)

112229 Proton-neutron correlation in the deuteron breakup at 56 MeV and prior-form DWBA analysis. N. Matsuoka, K. Hatanaka, T. Saito, T. Itahashi, K. Hosono, A. Shimizu, M. Kondo (Res. Center for Nuclear Phys., Osaka Univ., Osaka, Japan), F. Ohtani, O. Cynshi. Proceedings of the 1983 RCNP International Symposium on Light Ion Reaction Mechanism, Osaka, Japan, 16-20 May 1983 (Osaka, Japan: Osaka University 1983), p.527-40. Proton-neutron angular correlations in the ^{12}C , ^{51}V and $^{118}\text{Sn}(d,pn)$ reactions have been measured at 56 MeV to investigate the deuteron breakup process. The elastic breakup which leaves the target nucleus in its ground state dominates the coincident spectra. The experimental data have been analyzed using the prior-form DWBA. For both nuclear and Coulomb breakup, sufficient convergence of the calculations is obtained by including the pn angular momenta up to $l=2$. For the nuclear breakup calculations, the $l=0$ and 2 contributions dominate the cross sections. For the Coulomb breakup the $l=1$ contribution is predominant. The DWBA calculations reproduce the experimental data in the angular region where the protons are emitted on the side of the beam opposite to the neutrons. On the other hand the calculations overestimate the breakup cross sections by a factor of 2 to 10 in the angular region where the protons are emitted on the same side of the beam as the neutrons. The disagreement may be due to the insufficient treatment of the final-state distorted wave in the prior-form DWBA. (18 refs.)

112230 Three-body coupled-channel study of projectile breakup effects in deuteron, ^6Li and ^{12}C induced reactions. M. Kamimura (Dept. of Phys., Kyushu Univ., Fukuoka, Japan), M. Yahiro, Y. Iseri, Y. Sakuragi, M. Nakano, Y. Fukushima. Proceedings of the 1983 RCNP International Symposium on Light Ion Reaction Mechanism, Osaka, Japan, 16-20 May 1983 (Osaka, Japan: Osaka University 1983), p.558-80. Method of coupled discretized continuum channels is employed for taking into account the projectile-breakup continuum states in the framework of the three-body model. Analyses are performed of the multi-step breakup processes in the $^{58}\text{Ni}(d,d')^{58}\text{Ni}$ reaction at $E_i=80$ MeV and of the p -n angular correlations for the $^{12}\text{C}(d,pn)$ and $^{51}\text{V}(d,pn)$ reactions at $E_d=56$ MeV. The ^6Li projectile breakup effect on the elastic scattering from ^{28}Si at $E_{\text{lab}}=99$ MeV and from ^{40}Ca at $E_{\text{lab}}=156$ MeV are investigated. Breakup into the α -d resonant and non-resonant states are investigated. The ^{12}C excitation and breakup effect on the elastic and inelastic ^{12}C - ^{12}C scattering is studied for $E_{\text{lab}}=140\sim 300$ MeV. The dynamical polarization potentials due to the breakup (excitation) of the ^6Li and ^{12}C projectiles are discussed. (29 refs.)

- 112231 Investigation of adiabatic approximation of projectile-breakup effect on the elastic scattering and the projectile-breakup reactions.** M.Yahiro (Shimonoseki Univ. of Fisheries, Shimonoseki, Japan). Proceedings of the 1983 RCNP International Symposium on Light Ion Reaction Mechanism, Osaka, Japan, 16-20 May 1983 (Osaka, Japan: Osaka University 1983), p.617-20
Validity of adiabatic approximation is investigated in d- and ^6Li -induced reactions. The approximation is good for both the elastic scattering and the breakup reaction at the high incident energy. At the low incident energy the approximation is applicable only to the elastic scattering and poor for the breakup reaction. A modification of the approximation is discussed. (4 refs.)
- 112232 Deuteron projectile breakup on ^{28}Si at $E_d=17.85$ MeV.** C.A.Fields, R.J.Peterson, R.S.Raymond, J.L.Ullmann (Dept. of Phys., Univ. of Colorado, Boulder, CO, USA), R.J.DeMeijer, E.H.L.Aarts, M.B.Greenfield. Proceedings of the 1983 RCNP International Symposium on Light Ion Reaction Mechanism, Osaka, Japan, 16-20 May 1983 (Osaka, Japan: Osaka University 1983), p.621-5
Deuteron breakup on ^{28}Si has been studied at 17.85 MeV using both singles and p-n coincidence techniques. Angular correlation data were obtained between 144° and -144° for protons and between 120° and -120° for neutrons. These results allow the separation of the breakup reaction into elastic, inelastic, and absorptive parts, and the determination of the contribution of each part to the reaction cross-section. (6 refs.)
- Proceedings of the 1983 RCNP International Symposium on Light Ion Reaction Mechanism See Entry 111309
- Electromagnetic properties of isomers in ^{210}Pb See Entry 112066
- 1p-2h and 2p-3h states in ^{15}C See Entry 112070
- ^{234}U levels fed in the ^{234}Np electron capture decay See Entry 112072
- Isoscalar character of the 1^+ state at 5.844 MeV in ^{208}Pb See Entry 112076
- Non-locality of the deuteron optical model potential due to coupling to inelastic channels See Entry 112084
- Volume integrals of optical potentials for composite projectiles See Entry 112146
- Post-form DWBA description of coincidence spectra in light ion induced break-up reactions See Entry 112163
- Evidence for a secondary doorway state in $A=13$ nuclei from unpolarized and polarized capture measurements See Entry 112217
- Inclusive particle production at forward angles from collisions of light relativistic nuclei: nuclear fragments See Entry 112256
- Inclusive particle production at forward angles from collisions of light relativistic nuclei: negative pions See Entry 112257
- Production of a very high intensity polarized ion beam and experiments of spin transfer reactions See Entry 112522

25.60 ^3He - AND ^4He -INDUCED REACTIONS AND SCATTERING

- 112233 Two-steps analysis of alpha emission in $^{25}\text{Mg}(^3\text{He},\alpha)$ reaction.** F.Shahin, R.Bonetti (Phys. Dept., Mansoura Univ., Mansoura, Egypt). *Atomkernenerg. Kerntechnik. (Germany)*, vol.42, no.1, p.61-3 (1983).
Recent results on ^3He induced reactions have shown the importance of statistical multi-step compound emission. This process can explain the largely differing Γ -values extracted from the fluctuating excitation functions. Recently the Ericson's autocorrelation function $C(E)$ was generalized to cover the case in which many stages with different Γ -values contribute to the reaction. Analyses have been made by means of the generalized autocorrelation function on the $^{25}\text{Mg}(^3\text{He},\alpha)$ reaction in the ^3He energy range from 8.05 to 20.425 MeV. The spectral density method was also applied to the same data and gave consistent results. (9 refs.)
- 112234 The α - ^7Li and α - ^{12}C elastic scattering at $E_\alpha=5$, and 6, MeV.** C.W.Wang, G.C.Kiang, L.L.Kiang, G.C.Jon, E.K.Lin (Inst. of Phys., Acad. Sinica, Taipei, Taiwan). *Annu. Rep. Inst. Phys. Acad. Sin. (Taiwan)*, vol.12, p.239 (Dec. 1982). [received: Sept. 1983]
The differential cross section of α - ^7Li and α - ^{12}C elastic scattering have been measured at energies $E_\alpha=5$ and 6 MeV. The results are interpreted by using real phase-shift analysis. The real phase-shifts interpreted the α - ^{12}C scattering data very well at the energies investigated. The α - ^7Li scattering data are also fitted quite well by the real phase-shifts. The states at $E_\alpha=0.4776$ MeV in ^7Li and at $E_\alpha=4.439$ MeV in ^{12}C play little role in this experiment. For scattering angles $\theta_{\text{CM}} > 150^\circ$, the results show very prominent glory scattering and fit to the glory model very well. (no refs.)
- 112235 Nuclear g-factor of the $17/2^+$ isomeric state in ^{63}Cu .** N.Kawamura, K.Iura, Y.Kimura, K.Katsube, M.Kikuchi, S.Ali, S.Hayashibe, T.Ishimatsu (Dept. of Phys., Tohoku Univ., Sendai, Japan), M.Fujioka, K.Abe. *Nucl. Phys. A (Netherlands)*, vol.A406, no.3, p.533-40 (26 Sept. 1983).
The nuclear g-factor of the 4498 keV $17/2^+$ isomeric state in ^{63}Cu was measured with the in-beam perturbed angular distribution method, through the $^{62}\text{Ni}(\alpha,p2n\gamma)^{63}\text{Cu}$ reaction, to be $g_{\text{exp}}=0.184 \pm 0.012$. This value is in good agreement with a semiempirical g-factor for the three quasiparticle configuration $[\pi 2p_{3/2}(\nu 1f_{7/2}, 1g_{9/2})]17/2^+$ calculated using the experimental single-particle g-factors of neighbouring nuclei. At the same time the internal magnetic field at the Cu nuclei in Ni metal was obtained to be $B_{\text{int}} = -46.6 \pm 1.3$ kG. (13 refs.)
- 112236 Transition probabilities between two-quasiparticle configurations in $^{176,172}\text{Yb}$ and ^{182}W .** L.K.Kostov, W.Andrejschiff (Inst. of Nuclear Res. & Nuclear Energy, Bulgarian Acad. of Sci., Sofia, Bulgaria), H.Rotter, H.Prade, F.Stary. *Nucl. Phys. A (Netherlands)*, vol.A406, no.3, p.541-56 (26 Sept. 1983).
Applying the generalized centroid-shift method in (α,n) reactions, the following half-lives of 2 q.p. states have been measured: $T_{1/2}(1375.8 \text{ keV})=0.20 \pm 0.07 \text{ ns}$, $T_{1/2}(1640.8 \text{ keV})=0.5 \pm 0.2 \text{ ns}$, $T_{1/2}(2689.5 \text{ keV})=0.7 \pm 0.1 \text{ ns}$, $T_{1/2}(2189.9 \text{ keV})=2.2 \pm 0.3 \text{ ns}$, $T_{1/2}(1851.5 \text{ keV}) < 0.2 \text{ ns}$, $T_{1/2}(170 \text{ Yb})$; $T_{1/2}(100.1 \text{ keV})=1.4 \pm 0.2 \text{ ns}$, $T_{1/2}(1809.7 \text{ keV})=0.25 \pm 0.10 \text{ ns}$, $T_{1/2}(1829.5 \text{ keV})=0.25 \pm 0.10 \text{ ns}$, $T_{1/2}(1756.8 \text{ keV}) < 0.5 \text{ ns}$ (^{182}W). The experimental E1, M1 and E2 transition rates are compared to calculations within the Nilsson-plus-pairing model. The band-head $K^\pi=4^-$ of a semi-aligned band in ^{172}Yb appears as a deformation-aligned 2 q.p. configuration. The E2 transition rates indicate configuration mixing between the 2 q.p. $K^\pi=4^-$, 5^- and 6^- states in ^{182}W . (21 refs.)

- 112237 Contributions of various particle-particle coincidences to the inclusive $(^3\text{He},p)$ spectra at $\theta_p=10^\circ$ on ^{12}C , ^{28}Si and ^{58}Ni at $E=52$ MeV.** E.H.L.Aarts, R.A.R.L.Malfliet, R.J.de Meijer, S.Y.van der Werf (Kernfys. Versneller Inst., Rijksuniv. Groningen, Groningen, Netherlands). Proceedings of the 1983 RCNP International Symposium on Light Ion Reaction Mechanism, Osaka, Japan, 16-20 May 1983 (Osaka, Japan: Osaka University 1983), p.581-9
The authors present information on the inclusive spectra and identify the processes that contribute to the inclusive proton spectrum at $\theta_p=10^\circ$. In addition they present a simple model that relates the dominant coincidence yields to the total inclusive cross sections. (3 refs.)
- Proceedings of the 1983 RCNP International Symposium on Light Ion Reaction Mechanism See Entry 111309
- Bose-Einstein correlations in $\alpha\alpha$, pp and $p\bar{p}$ interactions See Entry 112024
- Rotation-aligned bands in ^{196}Hg See Entry 112036
- Shape coexistence and other aspects of nuclear structure in ^{40}Ar See Entry 112060
- On the use of isomer ratios in ^{44}Sc for predicting spin populations in high energy heavy-ion nuclear reactions See Entry 112061
- Spin and isospin characteristics of the excited states of ^{36}Ar through the reaction $^{32}\text{S}(\alpha,\gamma)^{36}\text{Ar}$ in the bombarding energy range $E_\alpha=4$ to 5 MeV See Entry 112063
- Neutron versus proton moments of collective excitations from polarized deuteron scattering See Entry 112067
- Level structure of ^{67}Ge and its implications for the general structure of nuclei in the 1f-2p shell See Entry 112071
- A study of the nuclear structure at high energy and low spin See Entry 112075
- Optical potentials and isoscalar transition rates from 104 MeV alpha-particle scattering by the N=28 isotopes ^{48}Ca , ^{50}Ti and ^{52}Cr See Entry 112114
- Counting the peaks in the excitation function for precompound processes See Entry 112135
- Volume integrals of optical potentials for composite projectiles See Entry 112146
- Gamow-Teller resonances See Entry 112154
- Nonequilibrium decay process of giant resonances studied by gamma transitions See Entry 112160
- Fragmentation of light ions at relativistic energies See Entry 112162
- Post-form DWBA description of coincidence spectra in light ion induced break-up reactions See Entry 112163
- Pauli forbidden states and nucleus-nucleus potentials See Entry 112258
- Dependence of fragment angular momentum on entrance channel in ^{236}U fission See Entry 112287
- ^3He -induced fission of nuclei $159 < A < 232$ See Entry 112289
- Complete and incomplete fusion-fission processes induced by light ions See Entry 112293
- Effect of excited states on thermonuclear reaction rates See Entry 116631

25.70 HEAVY ION INDUCED REACTIONS AND SCATTERING

- 112238 Elastic scattering of ^7Li projectiles in the energy range of 20 to 34 MeV.** S.A.E.Khallaf (Dept. of Phys., Faculty of Sci., Aswan, Egypt). *Atomkernenerg. Kerntechnik. (Germany)*, vol.42, no.2, p.126-8 (1983).
The author calculates the differential cross sections for ^7Li elastic scattering from ^{90}Zr , ^{48}Ca , ^{16}O and ^{12}C at incident energies of 20 to 34 MeV using the Watanabe folding model and studies the applicability of this model for ^7Li elastic scattering. The potentials of ^7Li ions are revealed by Taylor expansions of alpha and triton cluster potentials. The resulting differential cross sections are compared with the predicted cross sections using phenomenological potentials of ^7Li ions. (21 refs.)
- 112239 Strange encounters of the π kind.** D.W.Mingay. *Nucl. Active (S. Africa)*, no.29, p.5-9 (July 1983).
The Rutherford scattering cross section is the best established and tested of all theoretical predictions of nuclear reaction probabilities. An anomalously high yield, a factor greater than two larger than predicted, is seen when scattering is observed at an exact 180° angle for surface interactions. An investigation of this effect using a nitrogen ion beam together with a probable explanation of its cause are discussed. (10 refs.)
- 112240 Calculation of the imaginary part of the heavy ion potential.** G.Pollarolo, R.A.Brogia, A.Winther (The Niels Bohr Inst., Univ. of Copenhagen, Copenhagen, Denmark). *Nucl. Phys. A (Netherlands)*, vol.A406, no.2, p.369-89 (19 Sept. 1983).
The paper contains a numerical evaluation of the expressions for the absorptive potential in heavy ion reactions given earlier. With a standard folding expression for the real part of the ion-ion potential general good agreement is found with experimental data for the angular distributions of elastic and inelastic scattering. Special interest is attached to the case of $^{16}\text{O}+^{28}\text{Si}$ where the calculated imaginary potential is very small at low bombarding energies. (10 refs.)
- 112241 The role of particle transfer in large-angle scattering of 1p-shell nuclei.** J.Sromicki, M.Hugi, J.Lang, R.Muller, E.Ungriht (Lab. fur Kernphys., ETH, Zurich, Switzerland), L.Jarczyk, B.Kamys, A.Magiera, Z.Rudy, A.Strzalkowski, B.Zebik. *Nucl. Phys. A (Netherlands)*, vol.A406, no.2, p.390-412 (19 Sept. 1983).
The scattering of different 1p shell heavy ions on nuclei of the same species has been measured in the whole angular range up to 174° . Various pairs of interacting nuclei have been selected according to the different complexities of their properties which can influence the scattering through higher-order processes to different degrees. In general, the observed rise of the cross section in the backward region is satisfactorily described as a single-step transfer reaction. Second-order processes and compound-nucleus contributions are of no practical importance for the explanation of the elastic scattering data. The performed analysis, however, leaves some features in the experimental angular distributions not fully and satisfactorily understood. (51 refs.)
- 112242 Unified description of statistical excitations, deformations and charge transfer in a dynamical theory of deep-inelastic heavy-ion collisions.** P.Frobrich, B.Strack (Hahn-Meitner-Inst. fur Kernforschung, Berlin, Germany), M.Durand. *Nucl. Phys. A (Netherlands)*, vol.A406, no.3, p.557-73 (26 Sept. 1983).
In order to describe dissipative heavy-ion collisions a multi-dimensional Fokker-Planck equation including relative motion, quadrupole deformations and

charge transfer is solved within the quasilinear approximation (moment expansion up to second order). The authors aim at a unified description of Coulomb-like, focusing and orbiting systems by using a universal parametrization. Calculations for $^{136}\text{Xe} + ^{209}\text{Bi}$ at $E_{\text{lab}} = 940, 1130$ and 1422 MeV are compared with the experimental data. (30 refs.)

112243 Microscopic study of heavy-particle transfer reactions: the ($^{16}\text{O}, \alpha$) reactions on ^{16}O and ^{28}Si . K.Langanke, R.Stademann, A.Weiguny (Inst. für Theoretische Phys., Univ. Münster, Münster, Germany). *Nucl. Phys. A (Netherlands)*, vol. A406, no.3, p.574-90 (26 Sept. 1983). The transfer reactions $^{28}\text{Si}(^{16}\text{O}, \alpha)^{40}\text{Ca}$ and $^{16}\text{O}(^{16}\text{O}, \alpha)^{28}\text{Si}$ have been studied within the framework of the two-channel generator coordinate method. The geometry of the reactions has been discussed in terms of the cross-channel overlap kernels of the generating functions. A clear connection between maxima in the reaction rate and entrance channel resonances has been established. A two-step reaction mechanism involving quasimolecular resonances of inelastic ^{16}O - ^{16}O channels is discussed as a possible explanation for narrow structures seen in the $^{16}\text{O}(^{16}\text{O}, \alpha)^{28}\text{Si}$ reaction cross section. (24 refs.)

112244 High-spin states in ^{222}Th . D.Ward, G.D.Dracoulis, J.R.Leigh, R.J.Charity, D.J.Hinde, J.O.Newton (Dept. of Nuclear Phys., Australian Nat. Univ., Canberra, Australia). *Nucl. Phys. A (Netherlands)*, vol. A406, no.3, p.591-612 (26 Sept. 1983). Levels to spin 16^+ in the ground band and 17^- in the octupole band in ^{222}Th have been identified using the reaction $^{208}\text{Pb}(^{16}\text{O}, 4n)^{222}\text{Th}$ at 93 MeV. To suppress intense γ -ray background from fission a residue detector was built and operated in coincidence with the Ge(Li) and NaI(Tl) detectors. The apparent moment of inertia in the ground-state rotational band rises very rapidly with increasing spin, however, no indications of backbending were observed. The octupole band at low spin has an aligned angular momentum $J \approx 3\hbar$ relative to the ground-state band. Strong crossband E1 transitions competed with collective E2 transitions within each band. Analysis showed that the ratios $B(E1)/B(E2)$ were within experimental uncertainty independent of both the spin and parity of the parent state. The average γ -ray multiplicity per cascade was measured for ^{222}Th . The results were in reasonable agreement with the computer code ORNL-ALICE. (44 refs.)

112245 Gross structure resonance at 24.3 MeV in $^{12}\text{C} + ^{12}\text{C}(2^+)$. O.Tanimura, R.Wolf (Inst. für Theoretische Phys., Univ. Giessen, Giessen, Germany). *Phys. Lett. B (Netherlands)*, vol. 128B, no.6, p.375-80 (8 Sept. 1983). The 24.3 MeV peak observed in the integrated cross sections in the $^{12}\text{C} + ^{12}\text{C}(2^+)$ inelastic scattering is attributed to a $J^\pi = 16^+$ resonance; this assignment is based on a simultaneous coupled channel analysis of the angular distributions of the elastic and inelastic cross sections. (22 refs.)

112246 Atomic charge states of residual nuclei from compound nucleus reactions. W.S.Freeman, H.Ernst, D.F.Geesaman, W.Henning, T.J.Humanic, W.Kuhn, J.P.Schiffer, B.Zeidman (Argonne Nat. Lab., Argonne, IL, USA), F.W.Prosser. *Phys. Rev. C (USA)*, vol. 28, no.2, p.919-20 (Aug. 1983). The average energy-to-charge state ratios of evaporation residues from fusion of Ni+Sn are measured using an electrostatic deflector combined with ΔE - E particle identification. The deduced average atomic charge states are 5 to 13 units higher than the equilibrium values expected from stripping in the target, suggesting that nuclear decays outside the target foil play an important role. The importance of internal conversion in determining these anomalously high charge states is discussed. (8 refs.)

112247 Coulomb excitation of ^{189}Os . S.Jha (Inst. de Engenharia Nuclear, Rio de Janeiro, Brazil), W.A.Seale, R.V.Ribas, E.W.Cybulska, M.N.Rao, J.D.Rogers, G.M.Julian. *Phys. Rev. C (USA)*, vol. 28, no.2, p.921-2 (Aug. 1983). Coulomb excitation studies have been performed on an enriched ^{189}Os target with a 56 MeV ^{16}O beam. Gamma rays were measured in coincidence with the backscattered ^{16}O ions. Rotational bands built on $3/2^-$ [512], $1/2^-$ [510] up to spin $11/2$ have been identified. (5 refs.)

112248 Nucleus-nucleus potential at close contact from fusion at 'high' energies. J.Gomez del Campo, G.R.Satchler (Phys. Div., Oak Ridge Nat. Lab., Oak Ridge, TN, USA). *Phys. Rev. C (USA)*, vol. 28, no.2, p.952-4 (Aug. 1983). The authors compile the results of analyses, based upon the potential barrier penetration model, of fusion cross-section measurements at 'high' energies (those on the high-energy side of the bend in the σ_{fus} vs. $1/E_{\text{c.m.}}$ plot). A systematic correlation between the critical radius R_{cr} and the potential V_{cr} at that radius is demonstrated. These results provide information about the nucleus-nucleus potential at smaller distances than is usually available from scattering and 'low' energy fusion measurements. For some systems, nuclear potential depths of as much as -110 MeV are implied. (29 refs.)

112249 Charge and mass exchange in ^{56}Fe -induced reactions at 8.3 MeV/nucleon. H.Breuer, A.C.Mignerey (Univ. of Maryland, College Park, MD, USA), V.E.Viola, K.L.Wolf, J.R.Birkelund, D.Hilscher, J.R.Huizenga, W.U.Schroder, W.W.Wilcke. *Phys. Rev. C (USA)*, vol. 28, no.3, p.1080-103 (Sept. 1983). Projectilelike fragments from reactions of 465-MeV ^{56}Fe projectiles with targets of ^{56}Fe , ^{185}Ho , ^{209}Bi , and ^{238}U have been measured as a function of energy loss, and neutron and proton number. The mass and charge of each fragment were uniquely determined with discrete resolution. Data were analyzed as a function of energy loss by fitting a two-dimensional Gaussian function to the neutron-proton distributions. The fit parameters provide a convenient basis for comparison with theoretical predictions. In addition, centroids and variances derived from more detailed one-dimensional Gaussian fits to isobaric charge distributions are presented. Results are given for measured data as well as for the primary fragment distributions after correction for the dominant neutron evaporation. The centroid data show that in the asymmetric reactions proton transfer from projectile to target nucleus is preferred while the average fragment neutron number is largely preserved. This produces a charge equilibration process which is dependent on energy loss within the combined systems. The neutron and proton variances indicate an early dominant neutron flow followed by a constant relative neutron and proton exchange rate at energy losses above about 30 MeV. The degree of correlation of the neutron-proton distributions increases with energy loss and is found to be strongly related to the potential energy surface. Consistently observed negative correlation coefficients at low energy losses suggest the possible importance of processes other than particle exchange in the early stages of the interaction. Variances for constant N , Z , and A are found to saturate at energy losses and with magnitudes dependent on the target nucleus. (45 refs.)

112250 Sensitivity of phase shifts to the optical potentials in heavy ion scattering. C.S.Shastry, Y.K.Gambhir (Univ. Louis Pasteur de Strasbourg, Strasbourg, France). *Phys. Rev. C (USA)*, vol. 28, no.3, p.1109-18 (Sept. 1983). The authors formulate a procedure implicit in the Jost function formulation of the potential scattering in order to investigate the potential ambiguities occurring in two body scattering by a complex potential. The connection between this method and the distorted-wave Born approximation formalism is pointed out. They apply this method to study the potential ambiguities known to exist in heavy ion scattering by taking $^{18}\text{O} + ^{58}\text{Ni}$, $\alpha + ^{27}\text{Al}$, and $^6\text{Li} + ^{12}\text{C}$ for typical illustrative calculations. The calculations trace the origin of the potential ambiguities to the Coulomb potential and sizes and masses of the colliding nuclei. The regions of configuration space which contribute strongly to the partial wave S matrix are illustrated graphically. (17 refs.)

112251 Viscous fluid dynamical calculation of the reaction $^{12}\text{C}(85 \text{ MeV/nucleon}) + ^{197}\text{Au}$. G.Buchwald, G.Graebner, J.Theis, J.A.Maruhn, W.Greiner (Inst. für Theoretische Phys., J.W. Goethe Univ. Frankfurt, Frankfurt am Main, Germany), H.Stocker. *Phys. Rev. C (USA)*, vol. 28, no.3, p.1119-22 (Sept. 1983). Proton spectra have been calculated for the reaction $^{12}\text{C}(85 \text{ MeV/nucleon}) + ^{197}\text{Au}$ using a three-dimensional hydrodynamical model with viscosity and thermal conductivity and final thermal breakup. The theoretical results are compared to recent data. It is shown that the predicted flow effects are not observable as a result of the impact parameter averaging inherent in the inclusive proton spectra. In contrast, angular distributions of medium mass nuclei ($A > 3$) in nearly central collisions can provide signatures for flow effects. (20 refs.)

112252 Pion absorption versus compression effects in relativistic nucleus-nucleus collisions. R.Malfliet (Kernfys. Versneller Inst., Groningen, Netherlands), B.Schurmann. *Phys. Rev. C (USA)*, vol. 28, no.3, p.1136-9 (Sept. 1983). Inclusive particle spectra are calculated based on a multiple-collision model which fits the negative-pion multiplicity for central collisions using two different prescriptions. In one case pion absorption and in the other case compressional degrees of freedom are considered to effect this. From a comparison with measured proton, deuteron, triton, and negative pion inclusive spectra for the reaction Ar on KCl at 800 MeV/nucleon, no conclusive evidence for strong compression effects can be extracted. (15 refs.)

112253 ^6Li - ^6Li and ^7Li - ^7Li elastic scattering from 2.0 to 5.5 MeV. E.Norbeck, P.T.Wu, C.R.Chen, R.R.Carson (Dept. of Phys. & Astron., Univ. of Iowa, Iowa City, IA, USA). *Phys. Rev. C (USA)*, vol. 28, no.3, p.1140-7 (Sept. 1983). Elastic scattering of ^6Li from ^6Li and ^7Li from ^7Li has been studied for beam energies from 2.0 to 5.5 MeV using very thin films of isotopically separated LiF as targets. A double-folding model optical potential provided a good fit for $^7\text{Li} + ^7\text{Li}$ for the entire energy range, and for $^6\text{Li} + ^6\text{Li}$ for energies low enough that the breakup $^6\text{Li} \rightarrow \alpha + d$ could not occur. For higher energies, the real part of the $^6\text{Li} + ^6\text{Li}$ potential falls off rapidly with energy so that by 5.5 MeV the potential well required to fit the data is only about 40% as deep as is predicted by the folding model. (18 refs.)

112254 Fusion and peripheral processes in the collisions of $^{20}\text{Ne} + ^{20}\text{Ne}$ and $^{20}\text{Ne} + ^{16}\text{O}$. D.Shapira, D.DiGregorio, J.Gomez del Campo, R.A.Dayras, J.L.C.Ford, Jr., A.H.Snell, P.H.Stelson, R.G.Stokstad (Oak Ridge Nat. Lab., Oak Ridge, TN, USA), F.Pougeon. *Phys. Rev. C (USA)*, vol. 28, no.3, p.1148-60 (Sept. 1983). Reaction products from the bombardment of ^{20}Ne and ^{16}O gas targets with ^{20}Ne beams have been measured at five laboratory energies between 70 and 160 MeV. Fusion, deep inelastic, and quasielastic processes were studied. Large deep inelastic yields ($\sigma_{\text{DI}} \geq 600$ mb) with average Q values of -50 MeV are present at the highest energy. Analysis of the fusion cross sections for $^{20}\text{Ne} + ^{16}\text{O}$ suggests that the maximum angular momentum in ^{36}Ar populated via this entrance channel may be as low as $29 \pm 2\hbar$. (42 refs.)

112255 Penetration of the centrifugal barrier in the fusion of ^{16}O with heavy targets. R.Vandenbosch, B.B.Back, S.Gil, A.Lazzarini, A.Ray (Nuclear Phys. Lab., Univ. of Washington, Seattle, WA, USA). *Phys. Rev. C (USA)*, vol. 28, no.3, p.1161-6 (Sept. 1983). Gamma ray multiplicities and rotational band transition intensities have been measured for the $^{154}\text{Sm}(^{16}\text{O}, 4n)$ reaction for bombarding energies between 62.5 and 73.5 MeV. It is shown that centrifugal barrier penetration leads to a fairly broad spin distribution of the compound nucleus even at near-barrier energies. The results are discussed in terms of optical model absorption probabilities and parabolic barrier penetration probabilities. (20 refs.)

112256 Inclusive particle production at forward angles from collisions of light relativistic nuclei: nuclear fragments. L.Anderson, W.Bruckner, E.Moeller, S.Nagamiya, S.Nissen-Meyer, L.Schroeder, G.Shapiro, H.Steiner (Dept. of Phys., Univ. of California, Berkeley, CA, USA). *Phys. Rev. C (USA)*, vol. 28, no.3, p.1224-45 (Sept. 1983). The authors have measured the production of charged nuclear fragments in collisions of 1.05 GeV/nucleon and 2.1 GeV/nucleon proton, deuteron, alpha, and carbon projectiles as well as 0.4 GeV/nucleon alpha particles on targets of C, Cu, Pb, and H (from a CH_2 -C subtraction), using a double focusing spectrometer. They present single particle inclusive cross sections for the production of $Z=1$ and $Z=2$ fragments in the region $0.5 \leq (p/Z)_{\text{lab}} \leq 8.7$ GV/c and $0^\circ \leq \theta_{\text{lab}} \leq 12^\circ$. They discuss the relevance of the concept of limiting fragmentation to the data and point out possible uses of the data to study nuclear structure and particle production mechanisms. A detailed comparison is made with Glauber-type models and hard-scattering models as well as the coalescence model. (87 refs.)

112257 Inclusive particle production at forward angles from collisions of light relativistic nuclei: negative pions. E.Moeller, L.Anderson, W.Bruckner, S.Nagamiya, S.Nissen-Meyer, L.Schroeder, G.Shapiro, H.Steiner (Dept. of Phys., Univ. of California, Berkeley, CA, USA). *Phys. Rev. C (USA)*, vol. 28, no.3, p.1246-55 (Sept. 1983). The authors have measured single particle inclusive spectra of negative pions produced at angles from 0° to 12° (lab) in collision of 1.05 and 2.1 GeV/nucleon protons, deuterons, alpha particles, and carbon nuclei with targets of C, Cu, Pb, and H (from a CH_2 -C subtraction). Most of the pions are produced in the kinematical domains allowed in free nucleon-nucleon collisions but for alpha and carbon projectiles they have also observed pions whose energies range up to nearly twice the kinetic energy of a nucleon in the projectile. The results suggest that processes involving more than two colliding nucleons and/or high internal momentum components are involved in the production of these high energy pions. Comparison is made with several hypotheses of scaling including specific dynamical models, and some disagreement is observed. The authors present fits to the kinetic energy dependence of the data, and the target and projectile mass dependence. They also show transverse momentum distributions. (35 refs.)

- 112258 Pauli forbidden states and nucleus-nucleus potentials.** H.Friedrich, K.Langanke (W. K. Kellogg Radiation Lab., California Inst. of Technol., Pasadena, CA, USA). *Phys. Rev. C (USA)*, vol.28, no.3, p.1385-8 (Sept. 1983). The authors discuss the tangible consequences of the existence of Pauli forbidden states of relative motion of two nuclei for the nucleus-nucleus interaction. The ranges of the influence of the Pauli forbidden states are tabulated for the systems ^{12}C , $^{12,13,14}\text{C}$, ^{14}C , ^{14}C , $^{12,14}\text{C}$, ^{16}O , ^{16}O , α , ^{40}Ca , and α - ^{40}Ca . (16 refs.)
- 112259 $^{16}\text{O}+^{28}\text{Si}$ elastic scattering near the barrier.** S.Kahana, J.Barrette, B.Berthier, E.Chavez, A.Greiner, M.C.Mermaz (Dept. de Phys. Nucleaire/Basses Energies, CENS, Gif-sur-Yvette, France). *Phys. Rev. C (USA)*, vol.28, no.3, p.1393-5 (Sept. 1983). Elastic scattering angular distribution and 180° c.m. excitation function are rather well reproduced just above the Coulomb barrier by a heavy ion nuclear potential having a repulsive core at short distances and a very strong attractive behaviour at the nuclear surface. An important prediction of this potential, a precipitous drop in differential cross section at 180° , is verified experimentally. (15 refs.)
- 112260 Survey of low energy heavy ion reaction mechanisms.** A.Winther (Niels Bohr Inst., Univ. of Copenhagen, Copenhagen, Denmark). *Phys. Scr. (Sweden)*, vol.T5, p.84-90 (1983). (Proceedings of the 4th Nordic Meeting on Nuclear Physics, Fuglso, Denmark, 16-20 Aug. 1982). The author surveys the efforts that a group in Copenhagen has made in recent years in order to establish a firmer basis for the understanding of heavy ion reactions at low bombarding energies. The topics cover phenomena from the calculation of the absorptive potential and excitation of giant resonances to fusion and critical angular momentum for fission. (16 refs.)
- 112261 Heavy-ion reaction mechanisms studied with the spin spectrometer.** M.L.Halbert, J.H.Barker, J.R.Beene, R.L.Ferguson, D.C.Hensley, G.R.Young (Oak Ridge Nat. Lab., Oak Ridge, TN, USA), F.A.Dilmanian, M.Jaaskelainen, H.Puchta, D.G.Sarantidis, R.Woodward. *Phys. Scr. (Sweden)*, vol.T5, p.91-7 (1983). (Proceedings of the 4th Nordic Meeting on Nuclear Physics, Fuglso, Denmark, 16-20 Aug. 1982). Experimental data and statistical-model calculations for xn and axn products of the reaction $^{20}\text{Ne}+^{140}\text{Nd}$ at 136 MeV are shown to be in generally good agreement, indicating that equilibrium processes are dominant. Preliminary results on the heavy-ion ejectiles from $^{159}\text{F}+^{159}\text{Tb}$ are presented. (21 refs.)
- 112262 Energy dependence of light particle emission from intermediate energy heavy ion collisions.** G.D.Westfall (Nat. Superconducting Cyclotron Lab., Michigan State Univ., East Lansing, MI, USA). *Phys. Scr. (Sweden)*, vol.T5, p.103-7 (1983). (Proceedings of the 4th Nordic Meeting on Nuclear Physics, Fuglso, Denmark, 16-20 Aug. 1982). High energy nucleus-nucleus collisions can provide a unique method of studying nuclear matter at densities and excitations far from the normal ground state. In these collisions a source can be identified with a velocity intermediate between the projectile and target velocities as well as sources that can be associated with decay of excited projectile and target nuclei. The study of light particle spectra (p, d, t and alpha) associated with this intermediate source can provide information on the equation of state of nuclear matter. Results are presented for O and Ne induced reactions on heavy targets ranging in energy from 9 to 800 MeV/nucleon. Analysis of these light particle data in terms of a single moving source model leads to a consistent description of a system in thermodynamic and chemical equilibrium. Extracted d/p and t/p ratios are almost independent of incident energy while the alpha/proton ratio increases dramatically at low bombarding energies. (14 refs.)
- 112263 Dynamics of medium energy nuclear collisions.** H.Stocker (Dept. of Phys. & Astron., Michigan State Univ., East Lansing, MI, USA), G.Buchwald, L.P.Csernai, G.Graebner, P.R.Subramanian, J.Theis, J.A.Maruhn, W.Greiner. *Phys. Scr. (Sweden)*, vol.T5, p.108-13 (1983). (Proceedings of the 4th Nordic Meeting on Nuclear Physics, Fuglso, Denmark, 16-20 Aug. 1982). Recent theoretical attempts to study high energy heavy ion reactions are reviewed. Special emphasis is given to the description of the dynamical evolution and to the production of pions and light fragments in the collision. Evidence for a collective quasi-hydrodynamic flow behaviour of compressed nuclear matter is presented. The authors show that the pion yield is sensitive to the nuclear equation of state and to the viscosity in hot dense nuclear matter. A 4π exclusive flow analysis of intermediate energy nuclear collisions can be used to reveal the compressibility coefficient of nuclear matter. (31 refs.)
- 112264 The physics of heavy ion collisions at 100 MeV per nucleon.** H.Ryde (Dept. of Phys., Univ. of Lund, Lund, Sweden). *Phys. Scr. (Sweden)*, vol.T5, p.114-17 (1983). (Proceedings of the 4th Nordic Meeting on Nuclear Physics, Fuglso, Denmark, 16-20 Aug. 1982). Nuclear reactions induced by intermediate energy heavy ions are discussed. The observation of large nuclear surface transparency and of nuclear rainbow scattering in elastic scattering of ^{12}C ions is presented. The data obtained for projectile-like fragments are compared with corresponding results from collisions involving relativistic heavy ions. Finally, a model for the production of light particle spectra emitted in heavy ion reactions is suggested and compared with the experimental data. (9 refs.)
- 112265 The dynamics of heavy ion reactions at relativistic energies.** J.Knoll (Gesellschaft für Schwerionenforschung, Darmstadt, Germany). *Phys. Scr. (Sweden)*, vol.T5, p.118-23 (1983). (Proceedings of the 4th Nordic Meeting on Nuclear Physics, Fuglso, Denmark, 16-20 Aug. 1982). Some selected aspects of nuclear reactions at beam energies below a couple of GeV/nucleon are reviewed. The different dynamical regimes from the micro- and to the macro-dynamics and the late expansion stage are discussed and compared with respect to their implications on specific observable like inclusive data or global event observations. (17 refs.)
- 112266 Quarkochemistry of the heavy ion reactions.** T.S.Biro, J.Zimanyi (Central Res. Inst. for Phys., Budapest, Hungary). *Phys. Scr. (Sweden)*, vol.T5, p.124-9 (1983). (Proceedings of the 4th Nordic Meeting on Nuclear Physics, Fuglso, Denmark, 16-20 Aug. 1982). A review of a hadrochemical and quarkochemical model of relativistic heavy ion reactions is presented. It is pointed out that the minimal bombarding energy necessary to create baryonic gluon plasma is about 6 GeV/nucleon. The signature of the quark matter is also investigated in the strange meson production. (14 refs.)
- 112267 Compression effects in relativistic nucleus-nucleus collisions.** R.Stock, R.Bock, R.Brockmann (Gesellschaft für Schwerionenforschung, Darmstadt, Germany), A.Dacal, J.W.Harris, M.Maier, M.E.Ortiz, H.G.Pugh, R.E.Renfordt, A.Sandoval, L.S.Schroeder, H.Stroebele, K.L.Wolf. *Phys. Scr. (Sweden)*, vol.T5, p.130-5 (1983). (Proceedings of the 4th Nordic Meeting on Nuclear Physics, Fuglso, Denmark, 16-20 Aug. 1982). The negative pion multiplicity is measured for inelastic and central collisions of ^{40}Ar with KCl at eight energies from 0.36 to 1.8 GeV/nucleon and for ^{40}He and ^{40}Ar on BaF_2 at 977 and 772 MeV/nucleon, respectively. A systematic discrepancy in central collision data with a cascade model calculation which fits proton- and pion-nucleus cross sections but omits potential energy effects is used to derive the energy going into bulk compression of the system. A value of the compressibility constant of $K=240$ MeV is extracted in a parabolic form of the nuclear matter equation of state. (21 refs.)
- 112268 Pions produced in heavy reactions far below the free nucleon-nucleon scattering threshold.** B.Jakobsson (Dept. of Phys., Univ. of Lund, Lund, Sweden). *Phys. Scr. (Sweden)*, vol.T5, p.207-12 (1983). (Proceedings of the 4th Nordic Meeting on Nuclear Physics, Fuglso, Denmark, 16-20 Aug. 1982). Experimental data on pion production in heavy ion reactions at energies below 100 A MeV is presented. The inclusive spectra of π^+ and π^- from reactions at 50-100 A MeV are in general well reproduced by a first-nucleon-nucleon scattering mechanism when diffused internal momentum distributions, Pauli Blocking, and reabsorption is considered. (20 refs.)
- 112269 Multifragmentation of big nuclei.** D.H.E.Gross (Hahn-Meitner-Inst. für Kernforschung, Berlin, Germany). *Phys. Scr. (Sweden)*, vol.T5, p.213-16 (1983). (Proceedings of the 4th Nordic Meeting on Nuclear Physics, Fuglso, Denmark, 16-20 Aug. 1982). Heavy target nuclei split into many fragments when bombarded by protons or heavy ions at very high energies ($E_p > 10$ GeV). A statistical model is presented, which calculates the relative phase-space available for the various multifragment decay channels. It is shown that the Coulomb-interaction between the fragments is crucial. Including it by a self-consistent mean field method leads to a significant enhancement of the survival of the most heavy fragments and a strong suppression of the probability for splitting into many medium fragments. At a temperature of ~ 5 MeV an U-shaped mass-yield curve results from the model calculations for most of the heavy targets, whereas they show a clear fission peak for U-targets. Over the whole fragment-mass region the experimental mass-yield distributions for limiting fragmentation can thus be reproduced. Further investigations and refinements of the model are needed before a final judgement about the importance of the multifragment phase-space relative to dynamical effects is possible. (10 refs.)
- 112270 Analysis of the evaporation-corrected mass and charge distributions in the Ar+Mo reactions.** W.Bohne, P.Frobrich, K.Grabisch, K.Hartmann, H.Lehr, H.Morgenstern, W.Stoffler (Hahn-Meitner-Inst. für Kernforschung, Berlin, Germany). *Z. Phys. A (Germany)*, vol.313, no.1-2, p.19-29 (1983). Partly and strongly damped fragments from the reactions $^{36}\text{Ar}+^{92}\text{Mo}$ and $^{40}\text{Ar}+^{100}\text{Mo}$ are measured at $E_{\text{lab}}=270$ MeV. The extracted mass and charge distributions are carefully corrected for γ , n, p and α particle evaporation. The resulting primary distributions are analysed with theoretical models which assume statistical neutron and proton exchange on the potential energy surface of the projectile-target system. Dynamical deformation effects in the framework of the surface friction model are included. (26 refs.)
- 112271 Light charged particle emission and fission in $^{238}\text{U}+^{238}\text{U}$ collisions at 1740 MeV.** M.Kaplan, D.J.Moses, D.O.Eriksen, M.Kildir, D.R.G.Logan (Dept. of Chem., Carnegie-Mellon Univ., Pittsburgh, PA, USA), M.S.Zisman, R.J.McDonald. *Z. Phys. A (Germany)*, vol.313, no.1-2, p.31-7 (1983). Inclusive ^4He and ^3He energy spectra and heavy fragment coincidence correlations have been measured for reactions of 7.31 MeV/u ^{238}U with ^{238}U and ^{197}Au targets. The H/He production cross sections are in the range 15-26 mb, and their emission spectra are very similar for the two systems. The observed strong kinematic shifts with angle are reproduced in shape and magnitude by Monte Carlo simulations of particle evaporation from projectile-like and target-like fragments, indicating competition between charged particle emission and sequential fission. No evidence is found for high energy charged particle emission associated with ultra-high Z composite systems. Heavy fragment measurements indicate an abundance of quasielastic and deeply inelastic reaction fragments, as well as sequential fission of target and projectile nuclei. The surprisingly high survival probabilities of high-Z fragments imply a preponderance of very soft collisions in these very-heavy-ion reactions, at least at energies not very far over the Coulomb barrier. (23 refs.)
- 112272 Formation and decay of the compound nucleus studied in the reaction $^{20}\text{Ne}+^{27}\text{Al}$.** H.Morgenstern, W.Bohne, K.Grabisch, H.Lehr, W.Stoffler (Hahn-Meitner-Inst. für Kernforschung, Berlin, Germany). *Z. Phys. A (Germany)*, vol.313, no.1-2, p.39-49 (1983). Energy and velocity spectra, angular and mass distributions have been measured for evaporation residue products of the $^{20,22}\text{Ne}+^{27}\text{Al}$ system in the energy range of $E_L(^{20}\text{Ne})=51$ to 395 MeV and in the angular range $\theta=2^\circ$ and 30° . Calculations with simple assumptions of the velocity and angular distributions of the evaporation residues are presented and compared to the data. The structure seen in the mass distributions, a competition between α -particle and nucleon evaporation in the deexcitation of the compound nucleus, is described well by calculations with the computer code CASCADE. The evaporation residues exhibit mass distributions varying systematically as a function of the excitation energy. The excitation function of the evaporation residue cross section is compared with theoretical models. At higher incident energies contributions of incomplete momentum transfer (incomplete fusion) are observed. A limitation for complete compound nucleus formation with following light particle evaporation is found. (33 refs.)
- 112273 On the fusion dynamics of $^{40}\text{Ar}+^{40}\text{Ca}$ -fusion-fission and fusion-evaporation.** J.Carter, C.Brendel, A.Richter, G.Schrieder (Inst. für Kernphys., Tech. Hochschule, Darmstadt, Germany), H.Feldmeier, W.Bohne, K.Grabisch, H.Lehr, H.Morgenstern. *Z. Phys. A (Germany)*, vol.313, no.1-2, p.57-67 (1983). Evaporation residue measurements have been made for the $^{40}\text{Ar}+^{40}\text{Ca}$ system at high incident energies, $E_{\text{lab}}=161, 190, 236$ and 273 MeV. A dynamical description of the fusion process is presented, where in a trajectory model both rotational and neck degrees-of-freedom are included. Using this model maximum l-values for fusion are determined and at high incident energies are found to be significantly lower than those found when using the more usual one-dimensional effective nucleus-nucleus potential. The fusion cross sections minus the fission component yields evaporation residue cross sections that are in good agreement with the data. Also, mass distributions of the evaporation residues compare well with statistical-decay model predictions. A comparison is made with the similarly mass-symmetric $^{40}\text{Ca}+^{40}\text{Ca}$ system. (31 refs.)
- 112274 Probing phase transitions via energetic nuclear collisions.** B.Lukacs, L.P.Csernai. **Report KFKI-1983-76**, Hungarian Acad. Sci., Budapest (1983), 16 pp. The possible effects of the nucleon-quark phase transition on the dynamics of heavy ion collisions are discussed. It is shown that the formation of the quark phase can be expected at recent experiments. Nevertheless, the compressibility of the two-phase mixture remains relatively low, thus the quark phase remains limited in both space and time, and the observables are not strongly affected. (20 refs.)

112275 The mechanism of the ($^6\text{Li},p$) reaction on light nuclei at $E_L=28$ MeV. D.L.Watson, M.J.Smithson (Dept. of Phys., Univ. of Bradford, Bradford, England), H.T.Fortune.
Proceedings of the 1983 RCNP International Symposium on Light Ion Reaction Mechanism, Osaka, Japan, 16-20 May 1983 (Osaka, Japan: Osaka University 1983), p.507-11

Angular distributions for the ($^6\text{Li},p$) reaction on ^{12}C and ^{13}C are reported. Some of these distributions are forward peaked, indicative of a direct reaction; however, the magnitude of the backward angle cross section suggests that other processes such as compound nucleus and multistep reactions may be involved. The overall magnitude of the cross-section for many of the distributions can be reproduced by Hauser-Feshbach calculations and the gross features of the distribution for the ground state of ^{17}O have been reproduced by an incoherent sum of a compound nucleus contribution with a direct five nucleon cluster contribution, and also by a sequential transfer of $^{12}\text{C}(^6\text{Li},d)(d,p)^{17}\text{O}$. It is considered that at 28 MeV the ($^6\text{Li},p$) reaction mechanism is a complex mixture of several processes and that the reaction must be carried out at higher energies if it is to be useful as a spectroscopic tool. (6 refs.)

112276 Projectile excitation and structure effects in polarized ^6Li scattering. H.Nishioka (Dept. of Phys., Univ. of Surrey, Guildford, England).
Proceedings of the 1983 RCNP International Symposium on Light Ion Reaction Mechanism, Osaka, Japan, 16-20 May 1983 (Osaka, Japan: Osaka University 1983), p.600-9

The surprisingly large magnitude and opposite signs of the measured vector analysing powers of ^6Li and ^7Li elastic scattering from ^{58}Ni at $E_{\text{cm}}=20$ MeV are nicely reproduced by coupled-channel calculations including projectile excitation channels. The mechanism for producing an effective spin-orbit interaction between nuclei from projectile excitation is quite general and is applicable to other scatterings. The tensor analysing power of ^6Li scattering is found to be sensitive to the projectile surface structure. (20 refs.)

112277 Polarization in single-nucleon transfer reactions with ^{13}C and ^{11}B ions. N.Takahashi, R.Caplar, R.Wolski, H.Ho, E.Steffens, K.Busek, G.-Y.Fan, P.Wurm, N.Kato, A.Weller (Max-Planck-Inst. für Kernphys., Heidelberg, Germany).

Proceedings of the 1983 RCNP International Symposium on Light Ion Reaction Mechanism, Osaka, Japan, 16-20 May 1983 (Osaka, Japan: Osaka University 1983), p.831-5

Single nucleon transfer reactions (^{13}C , ^{12}B) on the ^{27}Al , ^{nat}Cu and ^{nat}Mo targets and (^{11}B , ^{12}B) on the ^{nat}Cu target were studied at 70 MeV and 60 MeV, respectively. Energy spectra and polarization of $^{12}\text{B}_{\text{gs}}$ were measured at laboratory angles of 20° and 30° . Large negative polarization is observed for the (^{13}C , ^{12}B) reactions on the ^{27}Al and ^{nat}Cu targets at the largest kinetic energy of ^{12}B . Polarization tends to zero toward the smaller kinetic energy corresponding to the Coulomb energy. Other reactions exhibit polarization vanishingly small at the largest kinetic energy and at the Coulomb energy. Polarization is negative in sign but small in the middle of the ^{12}B kinetic energy axes. The difference in the behaviour of polarization reflects contributions of different reaction regimes. (11 refs.)

112278 Polarization of products ^{12}B in ^{14}N -induced reactions. K.H.Tanaka, K.Asahi, Y.Nojiri, T.Minamisono, N.Takahashi (Coll. of General Education, Osaka Univ., Toyonaka, Japan).

Proceedings of the 1983 RCNP International Symposium on Light Ion Reaction Mechanism, Osaka, Japan, 16-20 May 1983 (Osaka, Japan: Osaka University 1983), p.836-40

Polarization of $^{12}\text{B}_{\text{gs}}$ ($I^\pi=1^+$, β^- decay to $^{12}\text{C}_{\text{gs}}$, $T_{1/2}=20.3$ ms) has been studied systematically at 120 MeV for two-nucleon transfer (^{14}N , ^{12}B) reactions on the ^{27}Al , ^{nat}Cu , ^{100}Mo and ^{232}Th targets. In the region near the largest kinetic energy of products, ^{12}B polarization is negative for the ^{nat}Cu , ^{100}Mo and ^{232}Th targets at angles around and forward of the grazing angle, but positive for ^{27}Al in the backward region of the grazing angle. As intermediates of these two cases, ^{nat}Fe and ^{45}Sc targets were used; polarization in the region of the largest kinetic energy is negative in sign for ^{nat}Fe and zero for ^{45}Sc intermediate of the lightest and the heavier targets. (8 refs.)

112279 Semiquantitative analysis of heavy-ion transfer reactions. Y.Miyama, T.Kammuri (Dept. of Phys., Osaka Univ., Osaka, Japan).

Proceedings of the 1983 RCNP International Symposium on Light Ion Reaction Mechanism, Osaka, Japan, 16-20 May 1983 (Osaka, Japan: Osaka University 1983), p.850-4

In their semiquantitative approximation to the DWBA transition matrix of the heavy-ion transfer reaction, Hasan and Brink (1978, 1979) used the Fourier expansion method and took the recoil effect into account. The authors reformulate it in a more conventional way by treating the coupling of angular momenta exactly. They apply the theory to the analysis of angular distributions and energy spectra of ejectiles. The calculated energy spectrum is composed of the cross sections to the bound, resonant and non-resonant states of the residual nucleus. (8 refs.)

Proceedings of the 4th Nordic Meeting on Nuclear Physics . See Entry 111306

Proceedings of the 1983 RCNP International Symposium on Light Ion Reaction Mechanism . See Entry 111309

Quantum tunneling in multidimensional systems . See Entry 111492

High-spin states in $^{201,203}\text{At}$ and the systematic behavior of $Z=85$ isotopes . See Entry 112035

Intrinsic excitations as yrast structures in ^{179}W above $I\sim 35/2\hbar$. See Entry 112046

Microscopic study of the resonant states with light-heavy di-nucleus configurations . See Entry 112052

Transition from prolate to oblate to triaxial shapes in ^{158}Yb . See Entry 112059

On the use of isomer ratios in ^{44}Sc for predicting spin populations in high energy heavy-ion nuclear reactions . See Entry 112061

Level structure of ^{67}Ge and its implications for the general structure of nuclei in the $1f-2p$ shell . See Entry 112071

High excited α cluster state calculation of nuclei . See Entry 112099

On clustering effects and phase instabilities in high energy nuclear collisions . See Entry 112104

Band crossing in ^{130}Ba . See Entry 112109

Electromagnetic transitions in ^{130}Ce . See Entry 112112

Lifetimes in ^{18}F . See Entry 112120

^{17}O - ^{17}N analog states via the $^{14}\text{C}(^6\text{Li},t)$ and $^{14}\text{C}(^6\text{Li}, ^3\text{He})$ reactions . See Entry 112148

High spin resonances in heavy ion collisions . See Entry 112156

Quantal dynamics of dissipation in heavy ion nuclear fission . See Entry 112168

Investigation of adiabatic approximation of projectile-breakup effect on the elastic scattering and the projectile-breakup reactions . See Entry 112231

Incomplete-fusion reactions in the $^{12}\text{C}+^{118}\text{Sn}$ system at $E(^{12}\text{C})=118$ MeV . See Entry 112292

Complete and incomplete fusion-fission processes induced by light ions . See Entry 112293

25.80 MESON- AND HYPERON-INDUCED REACTIONS AND SCATTERING

112280 Parametrization of the total cross section for $\pi d\rightarrow pp$ below 330 MeV. B.G.Ritchie (Dept. of Phys. & Astron., Univ. of South Carolina, Columbia, SC, USA).

Phys. Rev. C (USA), vol.28, no.2, p.926-8 (Aug. 1983).

The parametrizations developed by Spuller and Measday for the energy dependence of the total cross section for $\pi d\rightarrow pp$, which have been used to normalize some $\pi d\rightarrow pp$ angular distributions, are reviewed in light of high accuracy data taken since 1975. Slight modifications of the parameters of the earlier analysis yield significant improvement in the agreement with the newer data. A simpler parameterization which fits the data equally well is suggested for absolute normalizations of relative angular distributions for the process. (14 refs.)

112281 Systematics of pion-nucleus optical potentials from analysis of elastic scattering. E.Friedman (TRIUMF, Vancouver, BC, Canada).

Phys. Rev. C (USA), vol.28, no.3, p.1264-71 (Sept. 1983).

Most of the available data on the elastic scattering of pions by nuclei between 14 and 80 MeV are analyzed with a complex local optical potential which is parametrized by a bias-free Fourier-Bessel series, and is used as a means of extracting as much information from the data as possible without the explicit use of a model for the interaction. A typical shape of a negative real potential at large radii with a positive one at smaller radii is obtained and a systematic dependence on energy, charge of the pion, and isospin of the target is observed. The Kisslinger potential is shown to reproduce all these systematics, whereas the Laplacian potential fails to do so. Some results for energies of up to 230 MeV are also analyzed. The dependence of reaction cross sections on the real potential is discussed. (25 refs.)

112282 Nuclear medium effects in pion elastic scattering and charge exchange. W.B.Kaufmann, W.R.Gibbs (Dept. of Phys., Arizona State Univ., Tempe, AZ, USA).

Phys. Rev. C (USA), vol.28, no.3, p.1286-300 (Sept. 1983).

The three body approximation of the pion-nucleus optical model is used to calculate effective strengths to be used in conventional calculations. The resulting wave functions are used to calculate pion elastic scattering and single charge exchange. It is found that observed energy shifts in elastic scattering can be understood. Considerable change in the magnitude and shape (as a function of energy) of the charge exchange section is a direct result of these corrections. (29 refs.)

112283 Analysis of elastic and inelastic scattering of 162 MeV pions from ^{13}C by an optical potential and a collective model. S.J.Seestrom-Morris, D.Dehnhard, M.A.Francy (Univ. of Minnesota, Minneapolis, MN, USA), C.L.Morris, R.L.Boudrie, H.A.Thiessen.

Phys. Rev. C (USA), vol.28, no.3, p.1301-8 (Sept. 1983).

Data for elastic scattering of π^+ and π^- from ^{13}C at $T_\pi=162$ MeV between $\theta_{\text{lab}}=22^\circ$ and 105° were analyzed by an optical model. Good fits were obtained with neutron and proton ground state densities of three-parameter Fermi shape having the same RMS radius. Inelastic data for the quadrupole transitions to the $3/2^-$ (3.68 MeV) and $5/2^-$ (7.55 MeV) states and the octupole transition to a proposed $5/2^+$, $7/2^+$ doublet (11.82 MeV) were analyzed using a collective model. The extracted strengths for the neutron and proton parts of the transitions are compared to the results of electron scattering and γ -ray studies. (25 refs.)

112284 Higher-order field effects in pion absorption on two nucleons. G.Kalbermann, J.M.Eisenberg (Dept. of Phys. & Astron., Tel Aviv Univ., Tel Aviv, Israel).

Phys. Rev. C (USA), vol.28, no.3, p.1318-23 (Sept. 1983).

The authors estimate the rescattering diagrams involving intrinsically third-order effects in the pionic field for the process of pion absorption at rest on a pair of nucleons. The calculation is performed using a chiral bag model adapted for the correct description of higher-order pionic effects. The model provides the form factors needed in order to achieve a convergent result. The third-order diagrams cancel in part; nevertheless, the net result is as important as the conventional second-order s -wave rescattering mechanism for reasonable bag radii $R\sim 1$ fm and becomes dominant for bag radii $R\leq 0.7$ fm for internucleon distances less than about 2 fm. (12 refs.)

112285 Positive pion absorption on deuterium at energies above the 3,3 resonance. E.L.Mathie, G.R.Smith, E.Boschitz, J.Hoftiezer (Inst. für Experimentelle Kernphys., Univ. Karlsruhe, Karlsruhe, Germany), M.Meyer.

Z. Phys. A (Germany), vol.313, no.1-2, p.105-10 (1983).

Angular distributions of the differential cross section for positive pion absorption on the deuteron have been measured at 170, 208 and 285 MeV. The data have been fitted with Legendre polynomials. Along with other recent experiments, these data are compared with recent theoretical descriptions. (17 refs.)

Δ dynamics . See Entry 112083

Excitation of the isoscalar giant quadrupole resonance in $^{118}\text{Sn}(\pi^\pm, \pi^\pm\gamma)$. See Entry 112149

Strong absorption limit of the Blankenbecler-Goldberger amplitude . See Entry 112193

K^-p bound states with coupling to hyperon channels . See Entry 112881

25.85 FISSION REACTIONS

112286 Isotopic and neutron yields of products from the asymmetric and near-symmetric proton-induced fission of ^{233}U and ^{235}U . P.A.Beeley, L.Yaffe, M.Chatterjee, H.Dautet, J.K.P.Lee (Foster Radiation Lab., McGill Univ., Montreal, Quebec, Canada).

Phys. Rev. C (USA), vol.28, no.3, p.1188-205 (Sept. 1983).

The isotopic yields of Rb, In, and Cs from the 40-100 MeV proton-induced fission of ^{233}U and ^{235}U , and the isotopic yields of Ga from the 80 and 100 MeV proton-induced fission of ^{233}U have been measured by on-line mass spectrometry. The yields have been normalized to the independent formation cross sections of selected isotopes measured radiochemically. Total numbers of neutrons emitted per fission event have been deduced from the centroids of the isotopic distributions. The equal charge displacement, minimum potential energy, and unchanged charge distribution mechanisms have been investigated. It is found that the charge-division mechanism is fragment-mass depen-

dent, the minimum potential energy postulate being attributed to asymmetric fission events and the unchanged charge distribution postulate being attributed to near-symmetric fission events. (48 refs.)

112287 Dependence of fragment angular momentum on entrance channel in ^{236}U fission. T.Datta, S.M.Sahakundu, S.P.Dange, N.Chakravarty, R.Guin, S.Prakash (Radiochem. Div., Bhabha Atomic Res. Centre, Bombay, India). *Phys. Rev. C (USA)*, vol.28, no.3, p.1206-11 (Sept. 1983). In the present work the influence of initial excitation energy and angular momentum of the fissioning system on the angular momenta of fission fragments corresponding to ^{131}Te and ^{133}Te was studied in the $^{232}\text{Th}(\alpha_{30}\text{ MeV})$ system. The fragment angular momenta were estimated from the radiochemically determined independent isomeric yield ratios using a statistical model. The obtained data are discussed along with the literature data on the fragment angular momenta in the same fissioning nucleus ^{236}U formed in the $^{235}\text{U}(n_{\text{th}},f)$ and $^{232}\text{Th}(\alpha,f)$ systems. (21 refs.)

112288 Neutron-induced fission of ^{232}Th near threshold. S.T.Lam, L.L.Yu, H.W.Fielding, W.K.Dawson, G.C.Neilson (Nuclear Res. Centre, Univ. of Alberta, Edmonton, Alberta, Canada). *Phys. Rev. C (USA)*, vol.28, no.3, p.1212-16 (Sept. 1983). Fission of ^{232}Th was induced by a pulsed beam of monoenergetic fast neutrons. A heavy-ion surface barrier detector was used for the detection of fission fragments. Fragment mass was determined from measured fragment energy and fragment flight time. Fragment mass distribution and correlation of fragment kinetic energy with fragment mass were obtained for neutron incident energies of 1.6, 3.1, and 5.2 MeV. A strong dependence on shell energy is suggested from the increase of the most probable total kinetic energy of the fission fragments with increase in excitation energy of the compound nucleus. (10 refs.)

112289 ^3He -induced fission of nuclei $159 < A < 232$. F.D.Becchetti (Dept. of Phys., Univ. of Michigan, Ann Arbor, MI, USA), K.H.Hicks, C.A.Fields, R.J.Peterson, R.S.Raymond, R.A.Ristinen, J.L.Ullmann, C.S.Zaidins. *Phys. Rev. C (USA)*, vol.28, no.3, p.1217-23 (Sept. 1983). The fission of nuclei with $159 \leq A \leq 232$ induced by the bombardment of 19.1 to 44.5 MeV ^3He ions has been measured using solid-state detectors with time-of-flight measurements. Analysis with statistical fission theory, including precompound nucleon emission, indicates fission barriers which decrease not only slightly relative to the liquid-drop model values with decreasing Z, approaching about 90% of the liquid-drop model barrier for $A \approx 160$. These results are in contrast with measurements at higher angular momenta which indicate much lower fission barriers (60 to 70% of the liquid-drop model) for this mass region. (39 refs.)

112290 Fission and pairing degrees of freedom in collective transport theory. A.S.Jensen, J.Leffers (Inst. of Phys., Univ. of Aarhus, Aarhus, Denmark), H.Hofmann, P.J.Siemens. *Phys. Scr. (Sweden)*, vol.T5, p.186-9 (1983). (Proceedings of the 4th Nordic Meeting on Nuclear Physics, Fuglso, Denmark, 16-20 Aug. 1982). The relevant pieces of the collective transport theory is briefly sketched. Then numerical results for the fission and pairing degrees of freedom of the nucleus ^{238}U are presented. Quadrupole and hexadecapole vibrations around the equilibrium deformation are extracted. The β - and giant quadrupole vibrations are identified. One hexadecapole and two new quadrupole vibrations are predicted. Pairing vibrations are obtained and the number of broken pairs during descent from saddle to scission is estimated. (10 refs.)

112291 Reassessment of fission fragment angular distributions from continuum states in the context of transition-state theory. L.C.Vaz, J.M.Alexander (Dept. of Chem., State Univ. of New York, Stony Brook, NY, USA). *Phys. Rep. (Netherlands)*, vol.97, no.1, p.1-30 (July 1983). Fission angular distributions have been studied for years and have been treated as classic examples of transition-state theory. Early work involving composite nuclei of relatively low excitation energy E^* (≤ 35 MeV) and spin I ($\leq 25\hbar$) gave support to theory and delimited interesting properties of the transition-state nuclei. More recent research on fusion fission and sequential fission after deeply inelastic reactions involves composite nuclei of much higher energies (≤ 200 MeV) and spins ($\leq 100\hbar$). Extension of the basic ideas developed for low-spin nuclei requires detailed consideration of the role of these high spins and, in particular, the 'spin window' for fission. The authors have made empirical correlations of cross sections for evaporation residues and fission in order to get a description of this spin window. A systematic reanalysis has been made for fusion fission induced by H, He and heavier ions. Empirical correlations of K_0^2 ($K_0^2 = J_{\text{eff}}/h^2$) are presented along with comparisons of J_{eff} to moments of inertia for saddle-point nuclei from the rotating liquid drop model. This model gives an excellent guide for the intermediate spin zone ($30 \leq I \leq 65$), while strong shell and/or pairing effects are evident for excitations less than ≤ 35 MeV. Observations of strong anisotropies for very high-spin systems signal the demise of certain approximations commonly made in the theory, and suggestions are made toward this end. (120 refs.)

High spin resonances in heavy ion collisionsSee Entry 112156

A constrained approximation for nuclear barrier penetration and fissionSee Entry 112467

Quantal dynamics of dissipation in heavy ion nuclear fissionSee Entry 112168

Effect of dissipation on the eigensolutions near the fission saddle pointSee Entry 112169

Light charged particle emission and fission in $^{238}\text{U} + ^{238}\text{U}$ collisions at 1740 MeVSee Entry 112271

On the fusion dynamics of $^{40}\text{Ar} + ^{40}\text{Ca}$ -fusion-fission and fusion-evaporationSee Entry 112273

The implication of sensitivity analysis on the safety and delayed-neutron parameters for fast breeder reactorsSee Entry 112294

25.88 FUSION REACTIONS

112292 Incomplete-fusion reactions in the $^{12}\text{C} + ^{118}\text{Sn}$ system at $E(^{12}\text{C}) = 118$ MeV. S.E.Arnell, S.Mattsson, H.A.Roth, O.Skeppstedt (Chalmers Univ. of Technol., Goteborg, Sweden), S.A.Hjorth, A.Johnson, T.Lindblad, J.Nyberg, L.Westerberg. *Phys. Scr. (Sweden)*, vol.T5, p.199-203 (1983). (Proceedings of the 4th Nordic Meeting on Nuclear Physics, Fuglso, Denmark, 16-20 Aug. 1982). The emission of charged particles in coincidence with γ -rays from the $^{12}\text{C} + ^{118}\text{Sn}$ system at $E(^{12}\text{C}) = 118$ MeV has been studied. Energy spectra and relative cross sections for He, Li, Be and B ejectiles have been measured. The results are compared to the sum-rule model of Wilczynski et al., (1980). (27 refs.)

112293 Complete and incomplete fusion-fission processes induced by light ions. T.Matsuse (CRN, Univ. Louis Pasteur, Strasbourg, France), S.M.Lee, A.Arima. Proceedings of the 1983 RCNP International Symposium on Light Ion Reaction Mechanism, Osaka, Japan, 16-20 May 1983 (Osaka, Japan: Osaka University 1983), p.841-4. The authors discuss their model (1980, 1982) for understanding the heavy-ion fusion cross section quantitatively using a schematic diagram. The method for finding the fully equilibrated compound nucleus using the model is presented. In order to test the validity of the prediction for incomplete fusion, the model is applied to the $^{232}\text{U}(\alpha,X)$ system, whereas the complete fusion cross section is tested with $^{26}\text{Mg}(^{20}\text{Ne},X)$. (4 refs.)

Quantum tunneling in multidimensional systemsSee Entry 111492

On direct mechanism of light-particle emission in incomplete-fusion reactions ..See Entry 112134

Atomic charge states of residual nuclei from compound nucleus reactionsSee Entry 112246

Nucleus-nucleus potential at close contact from fusion at 'high' energiesSee Entry 112248

Fusion and peripheral processes in the collisions of $^{20}\text{Ne} + ^{20}\text{Ne}$ and $^{20}\text{Ne} + ^{16}\text{O}$ See Entry 112254

Penetration of the centrifugal barrier in the fusion of ^{16}O with heavy targets ...See Entry 112255

On the fusion dynamics of $^{40}\text{Ar} + ^{40}\text{Ca}$ -fusion-fission and fusion-evaporationSee Entry 112273

27.00 PROPERTIES OF SPECIFIC NUCLEI LISTED BY MASS RANGES

27.10 $A \leq 5$

Bose-Einstein correlations in α,α , pp and pp interactionsSee Entry 112024

Tensor forces in the three-body problemSee Entry 112077

Configuration space Faddeev continuum calculations: p-d s-wave scattering lengthSee Entry 112078

On parity- and angular-momentum-dependence of inter-nucleus potentialSee Entry 112082

Atomic effects on the tritium ft valueSee Entry 112123

Fragmentation of light ions at relativistic energiesSee Entry 112162

Charge symmetry breaking in ^4He See Entry 112172

Electromagnetic and weak currents in nucleiSee Entry 112179

Differential cross sections and analyzing powers for pd elastic scattering below 1.0 MeVSee Entry 112187

Phase-shift analysis of pd elastic scattering below break-up thresholdSee Entry 112188

Measurements of the ^3He and ^4He total neutron cross sections up to 40 MeVSee Entry 112197

Inclusive particle production at forward angles from collisions of light relativistic nuclei: nuclear fragmentsSee Entry 112256

Inclusive particle production at forward angles from collisions of light relativistic nuclei: negative pionsSee Entry 112257

Parametrization of the total cross section for $\pi d \rightarrow pp$ below 330 MeVSee Entry 112280

Positive pion absorption on deuterium at energies above the 3,3 resonanceSee Entry 112285

K^-p bound states with coupling to hyperon channelsSee Entry 112881

27.20 $6 \leq A \leq 19$

(p,p') scattering at 65 MeV on ^{12}C , ^{24}Mg , ^{28}Si and ^{32}S See Entry 112051

Microscopic study of the resonant states with light-heavy di-nucleus configurationsSee Entry 112052

Simple isospin relations for transitions in $A=13$ See Entry 112064

1p-2h and 2p-3h states in ^{15}C See Entry 112070

Tensor forces in the three-body problemSee Entry 112077

On parity- and angular-momentum-dependence of inter-nucleus potentialSee Entry 112082

High excited α cluster state calculation of nucleiSee Entry 112099

A microscopic study on the particle-decay widths of excited states in light Λ -hypernucleiSee Entry 112105

Proton-carbon bremsstrahlung cross sections and nuclear time-delays near the $^{12}\text{C}(p,p)$ resonancesSee Entry 112117

Lifetimes in ^{18}F See Entry 112120

Branching ratio in the decay of ^7Be See Entry 112125

Branching ratio in the electron-capture decay of ^7Be See Entry 112126

^{17}O - ^{17}N analog states via the $^{14}\text{C}(^6\text{Li},t)$ and $^{14}\text{C}(^6\text{Li},^3\text{He})$ reactionsSee Entry 112148

Pion photoproduction off nuclei: a sensitive test of the nuclear transition densitiesSee Entry 112171

High-resolution (e,e') study of isovector M1 and M2 transitions in the oxygen isotopes. I. ^{16}O See Entry 112174

High-resolution (e,e') study of isovector M1 and M2 transitions in the oxygen isotopes. II. ^{17}O See Entry 112175

High-resolution (e,e') study of isovector M1 and M2 transitions in the oxygen isotopes. III. ^{18}O See Entry 112176

(e,e' π) reaction on light nuclei and spin-isospin strength distribution effectsSee Entry 112177

Reaction $\mu^- + ^6\text{Li} \rightarrow ^3\text{H} + ^3\text{H} + \nu_\mu$ and the axial current form factor in the time-like regionSee Entry 112178

Clustering effects on neutron elastic scattering from boron isotopesSee Entry 112183

$^{14}\text{N}(p,p')^{14}\text{N}(2.31\text{ MeV})$ reaction at 159.4 MeVSee Entry 112196

Proton capture by ^{15}N above the giant dipole resonanceSee Entry 112198

- $^7\text{Be}(p,\gamma)^8\text{B}$ cross section at low energy See Entry 112201
- Magnetic states observed in high-resolution (p,n) experiments See Entry 112208
- Energy dependence of analyzing powers for the isoscalar and isovector transitions in the (\bar{p},p') reaction See Entry 112210
- Direct contribution to the $^{19}\text{F}(p,\alpha)^{16}\text{O}$ reaction See Entry 112214
- Effects of indirect knockout process in quasifree scattering See Entry 112215
- Evidence for a secondary doorway state in $A=13$ nuclei from unpolarized and polarized capture measurements See Entry 112217
- Medium energy gamma rays following radiative capture of 40 and 50 MeV polarized protons on ^{11}B and ^{12}C See Entry 112218
- Elastic and rearrangement scattering between two interacting deuterons as a four-body problem See Entry 112222
- The difference in $d\text{-}^{12}\text{C}$ total cross section for $P_{zz}=+1$ and -1 tensor polarised beam See Entry 112224
- Polarization transfer in $A(d,pX)$ reactions See Entry 112225
- DWBA with 'unrestricted' distorting potentials for (d,p) reactions with strongly coupled d - and p -channels See Entry 112226
- Measurement of vector analyzing power in the reaction $^{12}\text{C}(d,^6\text{Li})^8\text{Be}$ See Entry 112227
- Vector and tensor analyzing powers for $(d,^6\text{Li})$ on ^{12}C See Entry 112228
- Proton-neutron correlation in the deuteron breakup at 56 MeV and prior-form DWBA analysis See Entry 112229
- Three-body coupled-channel study of projectile breakup effects in deuteron, ^6Li and ^{12}C induced reactions See Entry 112230
- The $\alpha\text{-}^7\text{Li}$ and $\alpha\text{-}^{12}\text{C}$ elastic scattering at $E_\alpha=5$, and 6, MeV See Entry 112234
- Contributions of various particle-particle coincidences to the inclusive $(^3\text{He},p)$ spectra at $\theta_p=10^\circ$ on ^{12}C , ^{28}Si and ^{58}Ni at $E=52$ MeV See Entry 112237
- Elastic scattering of ^7Li projectiles in the energy range of 20 to 34 MeV See Entry 112238
- Strange encounters of the π kind See Entry 112239
- Microscopic study of heavy-particle transfer reactions: the $(^{16}\text{O},\alpha)$ reactions on ^{16}O and ^{28}Si See Entry 112243
- Gross structure resonance at 24.3 MeV in $^{12}\text{C}+^{12}\text{C}(2^+)$ See Entry 112245
- Sensitivity of phase shifts to the optical potentials in heavy ion scattering See Entry 112250
- ^6Li - ^6Li and ^7Li - ^7Li elastic scattering from 2.0 to 5.5 MeV See Entry 112253
- Fusion and peripheral processes in the collisions of $^{20}\text{Ne}+^{20}\text{Ne}$ and $^{20}\text{Ne}+^{16}\text{O}$ See Entry 112254
- Inclusive particle production at forward angles from collisions of light relativistic nuclei: nuclear fragments See Entry 112256
- Inclusive particle production at forward angles from collisions of light relativistic nuclei: negative pions See Entry 112257
- Pauli forbidden states and nucleus-nucleus potentials See Entry 112258
- Pions produced in heavy reactions far below the free nucleon-nucleon scattering threshold See Entry 112268
- The mechanism of the $(^6\text{Li},p)$ reaction on light nuclei at $E_{\text{Li}}=28$ MeV See Entry 112275
- Nuclear medium effects in pion elastic scattering and charge exchange See Entry 112282
- Analysis of elastic and inelastic scattering of 162 MeV pions from ^{13}C by an optical potential and a collective model See Entry 112283

27.30 $20 \leq A \leq 38$

- (p,p') scattering at 65 MeV on ^{12}C , ^{24}Mg , ^{28}Si and ^{32}S See Entry 112051
- Spin and isospin characteristics of the excited states of ^{36}Ar through the reaction $^{32}\text{S}(\alpha,\gamma)^{36}\text{Ar}$ in the bombarding energy range $E_\alpha=4$ to 5 MeV See Entry 112063
- A microscopic study on the particle-decay widths of excited states in light Λ -hypernuclei See Entry 112105
- The internal bremsstrahlung (IB) from the allowed beta-emitters See Entry 112121
- Studies of weak beta-delayed protons emitted in the decay of odd- Z , $T_1=-3/2$ nuclei See Entry 112131
- Counting the peaks in the excitation function for precompound processes See Entry 112135
- Magnetic states observed in high-resolution (p,n) experiments See Entry 112208
- Energy dependence of analyzing powers for the isoscalar and isovector transitions in the (\bar{p},p') reaction See Entry 112210
- (d,α) reaction and the α particle D state See Entry 112221
- Three-body coupled-channel study of projectile breakup effects in deuteron, ^6Li and ^{12}C induced reactions See Entry 112230
- Deuteron projectile breakup on ^{28}Si at $E_d=17.85$ MeV See Entry 112232
- Two-steps analysis of alpha emission in $^{25}\text{Mg}(^3\text{He},\alpha)$ reaction See Entry 112233
- Contributions of various particle-particle coincidences to the inclusive $(^3\text{He},p)$ spectra at $\theta_p=10^\circ$ on ^{12}C , ^{28}Si and ^{58}Ni at $E=52$ MeV See Entry 112237
- Calculation of the imaginary part of the heavy ion potential See Entry 112240
- Microscopic study of heavy-particle transfer reactions: the $(^{16}\text{O},\alpha)$ reactions on ^{16}O and ^{28}Si See Entry 112243
- Sensitivity of phase shifts to the optical potentials in heavy ion scattering See Entry 112250
- Pion absorption versus compression effects in relativistic nucleus-nucleus collisions See Entry 112252
- Fusion and peripheral processes in the collisions of $^{20}\text{Ne}+^{20}\text{Ne}$ and $^{20}\text{Ne}+^{16}\text{O}$ See Entry 112254
- Pauli forbidden states and nucleus-nucleus potentials See Entry 112258
- $^{16}\text{O}+^{28}\text{Si}$ elastic scattering near the barrier See Entry 112259
- Compression effects in relativistic nucleus-nucleus collisions See Entry 112267
- Formation and decay of the compound nucleus studied in the reaction $^{20}\text{Ne}+^{27}\text{Al}$ See Entry 112272

- Polarization in single-nucleon transfer reactions with ^{13}C and ^{11}B ions See Entry 112277
- Polarization of products ^{12}B in ^{14}N -induced reactions See Entry 112278
- Complete and incomplete fusion-fission processes induced by light ions See Entry 112293
- Effect of excited states on thermonuclear reaction rates See Entry 116631

27.40 $39 \leq A \leq 58$

- Microscopic study of the resonant states with light-heavy di-nucleus configurations See Entry 112052
- Shape coexistence and other aspects of nuclear structure in ^{40}Ar See Entry 112060
- On the use of isomer ratios in ^{44}Sc for predicting spin populations in high energy heavy-ion nuclear reactions See Entry 112061
- Level structure of ^{67}Ge and its implications for the general structure of nuclei in the $1f\text{-}2p$ shell See Entry 112071
- On parity- and angular-momentum-dependence of inter-nucleus potential See Entry 112082
- Non-locality of the deuteron optical model potential due to coupling to inelastic channels See Entry 112084
- Optical potentials and isoscalar transition rates from 104 MeV alpha-particle scattering by the $N=28$ isotopes ^{48}Ca , ^{50}Ti and ^{52}Cr See Entry 112114
- Statistical properties of $3/2^-$ resonances in ^{45}Se and ^{51}Mn See Entry 112157
- The giant isovector E2 resonance in calcium observed in radiative neutron capture See Entry 112159
- Nonequilibrium decay process of giant resonances studied by gamma transitions See Entry 112160
- Energy dependence of the relativistic impulse approximation for proton-nucleus elastic scattering See Entry 112203
- Unnatural parity states studied in high resolution (p,p') experiments at 65 MeV and the effective nucleon-nucleon interaction See Entry 112207
- Energy dependence of analyzing powers for the isoscalar and isovector transitions in the (\bar{p},p') reaction See Entry 112210
- (p,t) and $(p,^3\text{He})$ reactions on ^{52}Cr and ^{54}Fe populating analog final states with $T_1=T_2$ See Entry 112212
- The $^{52}\text{Cr}(t,p)^{54}\text{Cr}$ reaction at $E_t=15$ MeV See Entry 112219
- Polarization transfer in $A(d,pX)$ reactions See Entry 112225
- Proton-neutron correlation in the deuteron breakup at 56 MeV and prior-form DWBA analysis See Entry 112229
- Three-body coupled-channel study of projectile breakup effects in deuteron, ^6Li and ^{12}C induced reactions See Entry 112230
- Investigation of adiabatic approximation of projectile-breakup effect on the elastic scattering and the projectile-breakup reactions See Entry 112231
- Contributions of various particle-particle coincidences to the inclusive $(^3\text{He},p)$ spectra at $\theta_p=10^\circ$ on ^{12}C , ^{28}Si and ^{58}Ni at $E=52$ MeV See Entry 112237
- Elastic scattering of ^7Li projectiles in the energy range of 20 to 34 MeV See Entry 112238
- Calculation of the imaginary part of the heavy ion potential See Entry 112240
- Charge and mass exchange in ^{56}Fe -induced reactions at 8.3 MeV/nucleon See Entry 112249
- Sensitivity of phase shifts to the optical potentials in heavy ion scattering See Entry 112250
- Pion absorption versus compression effects in relativistic nucleus-nucleus collisions See Entry 112252
- Pauli forbidden states and nucleus-nucleus potentials See Entry 112258
- Compression effects in relativistic nucleus-nucleus collisions See Entry 112267
- On the fusion dynamics of $^{40}\text{Ar}+^{40}\text{Ca}$ -fusion-fission and fusion-evaporation See Entry 112273
- Projectile excitation and structure effects in polarized ^6Li scattering See Entry 112276
- Polarization of products ^{12}B in ^{14}N -induced reactions See Entry 112278
- Effect of excited states on thermonuclear reaction rates See Entry 116631

27.50 $59 \leq A \leq 89$

- Nuclear data sheets for $A=79$ See Entry 111327
- Odd Ni isotopes in the Lipkin-Nogami approach See Entry 112034
- Search for the two-phonon 0^+ strength in ^{64}Zn See Entry 112043
- Level structure of ^{67}Ge and its implications for the general structure of nuclei in the $1f\text{-}2p$ shell See Entry 112071
- Electric monopole strengths in even-mass Ge and Se isotopes See Entry 112111
- The decay of ^{75}Se See Entry 112122
- Search for mixing of heavy neutrinos in the β^+ and β^- spectra of the ^{64}Cu decay See Entry 112124
- Absolute cross sections of proton induced reactions on ^{65}Cu , ^{64}Ni and ^{63}Cu See Entry 112181
- Measurement of the total neutron cross-section of germanium at energies below 2 eV See Entry 112184
- Nuclear g -factor of the $^{17/2}^+$ isomeric state in ^{63}Cu See Entry 112235
- Calculation of the imaginary part of the heavy ion potential See Entry 112240
- Inclusive particle production at forward angles from collisions of light relativistic nuclei: nuclear fragments See Entry 112256
- Inclusive particle production at forward angles from collisions of light relativistic nuclei: negative pions See Entry 112257
- Polarization in single-nucleon transfer reactions with ^{13}C and ^{11}B ions See Entry 112277
- Polarization of products ^{12}B in ^{14}N -induced reactions See Entry 112278
- Effect of excited states on thermonuclear reaction rates See Entry 116631

27.60 90 ≤ A ≤ 149

'Non-rotating' yrast states See Entry 112041
Multi-step shell-model description of Sn isotopes See Entry 112044
High spin phenomena in the mass 100-200 region seen through the Crystal Ball See Entry 112049
Atomic mass of ¹⁴⁵Eu derived from relative P_K-ratios See Entry 112055
Spherical, oblate, and prolate nuclear shapes near ¹⁴⁶Gd See Entry 112056
Shell-model calculations of high-spin isomers in neutron-deficient 1g_{9/2}-shell nuclei See Entry 112069
A study of the nuclear structure at high energy and low spin See Entry 112075
Influence of shell structure on deep inelastic collisions See Entry 112089
Band crossing in ¹³⁶Ba See Entry 112109
Electromagnetic transitions in ¹³⁰Ce See Entry 112112
Study of non-static behavior of τ₀-modes by (p,n) reactions See Entry 112115
Gamow-Teller strength function for ⁹⁰Zr: effects of spin and isospin exchange forces, and ground-state correlations See Entry 112128
Excitation of the isoscalar giant quadrupole resonance in ¹¹⁸Sn(π[±],π[±]) See Entry 112149
Nonequilibrium decay process of giant resonances studied by gamma transitions See Entry 112160
(n,2n) cross-section measurement of ⁹³Nb, ¹⁹⁷Au and ²³⁸U with fission-neutron spectrum and its dependence on the asymmetry term See Entry 112182
Investigation of the level scheme of ¹⁴⁵Nd in the (n,n'γ) reaction See Entry 112189
Parity violation in neutron elastic scattering around compound nucleus resonances See Entry 112191
Yields of medium mass nuclear fragments: statistical emission See Entry 112195
Highly excited hole strength observed in the ⁹⁰Zr(̢,d)⁸⁹Zr reaction See Entry 112200
Unnatural parity states studied in high resolution (p,p') experiments at 65 MeV and the effective nucleon-nucleon interaction See Entry 112207
Lane model analysis of 80 MeV (p,n) IAS reactions See Entry 112209
Analyzing power of neutron continuum spectra for the ⁹³Nb(̢,nX) reaction at 65 MeV See Entry 112216
Evidence for an imaginary spin-orbit term in deuteron optical potential from analysing power measurements of inelastic scattering See Entry 112223
Proton-neutron correlation in the deuteron breakup at 56 MeV and prior-form DWBA analysis See Entry 112229
Elastic scattering of ⁷Li projectiles in the energy range of 20 to 34 MeV See Entry 112238
Atomic charge states of residual nuclei from compound nucleus reactions See Entry 112246
Heavy-ion reaction mechanisms studied with the spin spectrometer See Entry 112261
Compression effects in relativistic nucleus-nucleus collisions See Entry 112267
Analysis of the evaporation-corrected mass and charge distributions in the Ar+Mo reactions See Entry 112270
Polarization in single-nucleon transfer reactions with ¹³C and ¹¹B ions See Entry 112277
Polarization of products ¹²B in ¹⁴N-induced reactions See Entry 112278
Incomplete-fusion reactions in the ¹²C+¹¹⁸Sn system at E(¹²C)=118 MeV See Entry 112292

27.70 150 ≤ A ≤ 189

Nuclear data sheets for A=153 See Entry 111328
Large transient magnetic fields for rare-earth ions recoiling in gadolinium and g-factors of high-spin states in ^{156,158,160}Gd See Entry 112033
Microscopic calculations of nuclear wobbling rotation See Entry 112045
Intrinsic excitations as yrast structures in ¹⁷⁹W above I~35/2ħ See Entry 112046
Shape changes, band crossings and band terminations in the very high spin region of A=150-160 nuclei See Entry 112047
High spin phenomena in the mass 100-200 region seen through the Crystal Ball See Entry 112049
Spherical, oblate, and prolate nuclear shapes near ¹⁴⁶Gd See Entry 112056
Transition from prolate to oblate to triaxial shapes in ¹⁵⁸Yb See Entry 112059
Deformation aligned states See Entry 112074
A study of the nuclear structure at high energy and low spin See Entry 112075
Influence of shell structure on deep inelastic collisions See Entry 112089
Potential energy surfaces in the classical limit of the IBM-2 See Entry 112095
The photoneutron cross section of ¹⁵¹Eu, ¹⁵³Eu and ¹⁵⁶Gd in the giant resonance region See Entry 112170
Search for two-phonon vibrations in ¹⁶⁸Er See Entry 112194
Characteristic 7⁻ and 5⁻ states observed in the (p,t) reactions on even-even rare earth nuclei See Entry 112211
Transition probabilities between two-quasiparticle configurations in ^{170,172}Yb and ¹⁸²W See Entry 112236
Coulomb excitation of ¹⁸⁹Os See Entry 112247
Charge and mass exchange in ⁵⁶Fe-induced reactions at 8.3 MeV/nucleon See Entry 112249
Penetration of the centrifugal barrier in the fusion of ¹⁶O with heavy targets See Entry 112255
Heavy-ion reaction mechanisms studied with the spin spectrometer See Entry 112261
Energy dependence of light particle emission from intermediate energy heavy ion collisions See Entry 112262
³He-induced fission of nuclei 159<A<232 See Entry 112289

27.80 190 ≤ A ≤ 219

Effect of the fourth-order Casimir invariants on U_{6/4} and U_{6/2} dynamical supersymmetries in nuclei and baryons See Entry 111912
High-spin states in ^{201,203}At and the systematic behavior of Z=85 isotopes See Entry 112035
Rotation-aligned bands in ¹⁹⁶Hg See Entry 112036
High spin phenomena in the mass 100-200 region seen through the Crystal Ball See Entry 112049
Coupling of two quasiparticles to coherent cores in the Pt isotopes See Entry 112050
Effect of core polarization on the charge distribution in ²⁰⁸Pb See Entry 112057
Electromagnetic properties of isomers in ²¹⁰Pb See Entry 112066
Implications of the recently discovered ²⁰⁸Pb(1⁺,E_x=5.845 MeV) state for the spin-dependent nuclear interaction See Entry 112073
Isoscalar character of the 1⁺ state at 5.844 MeV in ²⁰⁸Pb See Entry 112076
Dynamical content of the shell model See Entry 112088
Potential energy surfaces in the classical limit of the IBM-2 See Entry 112095
Observation of 2ħω hexadecapole strength in lead nuclei from 200 MeV inelastic proton scattering See Entry 112153
Inelastic electron scattering, fine structure of M1 giant resonances and Gamow-Teller states See Entry 112155
Test of vibrational current distributions in transverse electron scattering See Entry 112173
Electron scattering See Entry 112180
(n,2n) cross-section measurement of ⁹³Nb, ¹⁹⁷Au and ²³⁸U with fission-neutron spectrum and its dependence on the asymmetry term See Entry 112182
Low-lying levels, γ-ray transitions, and vibrational structure in ¹⁹⁸Pt from (n,n'γ) reaction spectroscopy See Entry 112190
Gamma-ray transitions among levels of ²⁰⁶Pb See Entry 112192
Elastic and inelastic scattering of polarized protons from ²⁰⁶Pb near isobaric analog resonances See Entry 112199
Complex spin-orbit potential for ²⁰⁸Pb(n,n)²⁰⁸Pb at 10 MeV See Entry 112202
Unnatural parity states studied in high resolution (p,p') experiments at 65 MeV and the effective nucleon-nucleon interaction See Entry 112207
Study of one- and two-step processes in ²⁰⁸Pb(p,t)²⁰⁶Pb(0_g⁺,0₂⁺) reactions by using analyzing powers at E_p=22 and 50 MeV See Entry 112213
Polarization transfer in A(d,pX) reactions See Entry 112225
Calculation of the imaginary part of the heavy ion potential See Entry 112240
Unified description of statistical excitations, deformations and charge transfer in a dynamical theory of deep-inelastic heavy-ion collisions See Entry 112242
Charge and mass exchange in ⁵⁶Fe-induced reactions at 8.3 MeV/nucleon See Entry 112249
Viscous fluid dynamical calculation of the reaction ¹²C(85 MeV/nucleon)+¹⁹⁷Au See Entry 112251
Inclusive particle production at forward angles from collisions of light relativistic nuclei: nuclear fragments See Entry 112256
Inclusive particle production at forward angles from collisions of light relativistic nuclei: negative pions See Entry 112257
Energy dependence of light particle emission from intermediate energy heavy ion collisions See Entry 112262
Light charged particle emission and fission in ²³⁸U+²³⁸U collisions at 1740 MeV See Entry 112271
³He-induced fission of nuclei 159<A<232 See Entry 112289

27.90 220 ≤ A

Kinematical and dynamical moments of inertia and the Mottelson-Valatin effect at high spin excitations See Entry 112048
²³⁴U levels fed in the ²³⁴Np electron capture decay See Entry 112072
New elements at the limit of stability of nuclear matter. The path to elements 107 and 109 See Entry 112102
Comment on 'determination of gamma-ray energies and abundances of ²²⁹Th' See Entry 112110
First results on γ-ray spectroscopy in the second minimum of ²³⁸U and ²⁴⁰Pu See Entry 112113
Identification of ²³³Ac See Entry 112129
Identification of ²²²U and ²²¹Pa by α-correlation chains See Entry 112133
Quantal dynamics of dissipation in heavy ion nuclear fission See Entry 112168
(n,2n) cross-section measurement of ⁹³Nb, ¹⁹⁷Au and ²³⁸U with fission-neutron spectrum and its dependence on the asymmetry term See Entry 112182
High-spin states in ²²²Th See Entry 112244
Charge and mass exchange in ⁵⁶Fe-induced reactions at 8.3 MeV/nucleon See Entry 112249
Energy dependence of light particle emission from intermediate energy heavy ion collisions See Entry 112262
Light charged particle emission and fission in ²³⁸U+²³⁸U collisions at 1740 MeV See Entry 112271
Polarization of products ¹²B in ¹⁴N-induced reactions See Entry 112278
Isotopic and neutron yields of products from the asymmetric and near-symmetric proton-induced fission of ²³³U and ²³⁵U See Entry 112286
Dependence of fragment angular momentum on entrance channel in ²³⁶U fission See Entry 112287
Neutron-induced fission of ²³²Th near threshold See Entry 112288
³He-induced fission of nuclei 159<A<232 See Entry 112289
Fission and pairing degrees of freedom in collective transport theory See Entry 112290
Complete and incomplete fusion-fission processes induced by light ions See Entry 112293

28.00 NUCLEAR ENGINEERING AND NUCLEAR POWER STUDIES

(see also 86.10 Energy resources and their utilisation)

28.20 NEUTRON PHYSICS

(see also 25.40 Nucleon-induced reactions and scattering)

112294 The implication of sensitivity analysis on the safety and delayed-neutron parameters for fast breeder reactors. R.J. Onega, R.J. Florian (Dept. of Mech. Engng., Virginia Polytech. Inst. & State Univ., Blacksburg, VA, USA).

Ann. Nucl. Energy (GB), vol.10, no.9, p.477-90 (1983).

The delayed-neutron energy spectra for LMFBRs are not as well known as those for LWRs. These spectra are necessary for kinetics calculations which play an important role in safety and accident analyses. A sensitivity analysis was performed to study the response of the reactor power and power density to uncertainties in the delayed-neutron spectra during a rod-ejection accident. The accidents studied were central control-rod ejections with ejection times of 2, 10 and 30 s. A two-energy group and two-precursor group model was formulated for the International Nuclear Fuel Cycle Evaluation (INFCE) reference design MOX-fueled LMFBR. The power and power-density responses were found to be most sensitive to uncertainties in the spectrum of the second delayed-neutron precursor group, resulting from the fission of ^{238}U , producing neutrons in the first energy group. It was found, for example, that for a rod-ejection time of 30 s, an uncertainty of 7.2% in the fast components of the spectra resulted in a 24% uncertainty in the predicted power and power density. These responses were recalculated by repeatedly solving the kinetics equations. The maximum discrepancy between the recalculated and the sensitivity analysis response was only 1.6%. The results of the sensitivity analysis indicate the need for improved delayed-neutron spectral data in order to reduce the uncertainties in accident analyses. (12 refs.)

112295 Reproduction of transport calculation results by diffusion theory employing albedo boundary conditions. W. Waschull (Forschungszentrum Geesthacht GmbH, Geesthacht, Germany).

Atomkernenerg. Kerntechnik (Germany), vol.42, no.1, p.39-49 (1983).

The results of a transport calculation in 45 energy groups for the PWR Obrigheim should be reproduced by diffusion calculations. Indicators taken into account are the multiplication factor, the maximal shape factor and the flux ratio between fast and thermal neutron flux. It is shown, that a reproduction with normal core and reflector group constants is not possible, because of the insufficient description of the reflector by diffusion theory. The correction of reflection diffusion constants, is proved to be useless. Assessing the influence of all theoretically possible values for the albedo on the indicators mentioned above a simple method was found to determine 2-group-albedos. These albedos reproduce the results of the 45-group-transport-calculation. (6 refs.)

112296 Numerical performance of the A_n method and comparisons with S_N calculations. G. Coppa, P. Ravetto, M. Sumini (Dipartimento de Energetica, Politecnico di Torino, Torino, Italy).

Atomkernenerg. Kerntechnik (Germany), vol.42, no.2, p.107-10 (1983).

The numerical S_N code ANISN is employed to perform A_n calculations using its multigroup diffusion feature, in order to test the applicability of the A_n method to neutron reactor calculations. Different geometrical configurations are analysed. It is found that the A_n approximate method, which reduces to a system of second order differential equations, might well be used to yield reliable results in all sorts of neutron transport calculations. (10 refs.)

112297 Limitation of the Mellin transform for small angle scattering by nearly spherical particles. S. Melone, P. Puliti (Dipartimento di Sci. dei Materiali e della Terra, Facoltà di Ingegneria, Univ. di Ancona, Ancona, Italy), F. Rustichelli.

Nucl. Instrum. & Methods Phys. Res. (Netherlands), vol.214, no.2-3, p.459-62 (1 Sept. 1983).

An analysis of the limit of validity of the Mellin transform when applied to small angle scattering curves produced by nearly spherical particles, i.e. by ellipsoids of semi-axes a , a , va , was performed. The width of the assumed Gaussian distribution for the v values was used as a parameter. When this width tends to zero the inaccuracy of the Mellin transform vanishes as expected. However the inaccuracy becomes appreciable for large values of the width. In spite of this, the total volume fraction and the average radius of the scattering particles is also obtained by the Mellin transform with very high accuracy for large values of the width of the Gaussian distribution. (4 refs.)

112298 Neutron spectra unfolding from measured detector activations. The computer programme SAND-MX2. L. Weise.

Report JUL-1837, Kernforschungsanlage, Jülich, Germany (March 1983), 137 pp. In German.

Our knowledge of the neutron spectrum in irradiation facilities essentially rests on the calculation of the unfolding adjustment based on measured activations. In this situation the neutronic calculation by no means renders superfluous the unfolding because the measurements can confirm or possibly improve the calculational results. The FORTRAN code SAND-MX2 is a contribution of the KFA to the international repertoire of unfolding codes. With regard to its contents it is one of the newer versions of the original code SAND-II. This report may serve as an instruction manual for routinely neutron spectrum unfolding by means of the code SAND-MX2. (49 refs.)

Two-group criticality models for safety analysis considerations

..... See Entry 112423

Comments on 'Guidelines for the neutron scalar flux shaping of advanced nuclear energy device blankets' [and reply] See Entry 112431

28.41 FISSION REACTOR THEORY AND DESIGN

112299 On the non-linear dynamical power-reactor model with temperature feedback. H. Konno (Inst. of Materials Sci., Univ. of Tsukuba, Ibaraki, Japan).

Ann. Nucl. Energy (GB), vol.10, no.9, p.451-6 (1983).

The author studies the non-linear dynamical power-reactor model which has a simple feedback loop from temperature and three external noise sources. By contracting the temperature, the reduced non-linear stochastic differential equation for neutrons is derived. Then, the influence of the inherent and external noises upon the stationary distribution of the neutrons is clarified. It is shown that: (1) the contraction method developed in non-equilibrium statistical physics is available for power-reactor modelling; and (2) the correlations among the external noise sources not only characterize the existence of multiple feedback loops in power reactors but also play a role in suppressing the deterministic transition by external noises. (17 refs.)

112300 Integration of the time-dependent heat equation in the fuel rod performance program IAMBUS. G. West.

Atomkernenerg. Kerntechnik (Germany), vol.41, no.4, p.281-4 (1982). In German. [received: Sept. 1983]

An iterative numerical method for integration of the time-dependent heat equation is described. No presuppositions are made for the dependency of the thermal conductivity and heat capacity on space, time and temperature. (5 refs.)

112301 SUPERC, a one-dimensional code system for the analysis of the seed-blanket core with movable fuel control. A. Galperin (Dept. of Nuclear Engng., Ben-Gurion Univ. of the Negev, Beer Sheva, Israel).

Atomkernenerg. Kerntechnik (Germany), vol.42, no.1, p.16-18 (1983).

SUPERC, a code system for the analysis of the seed-blanket cores with movable fuel control is presented. Two main modules of this system are the WIMS-D and ANISN codes. SUPERC is 'easy-to-operate' and a relatively fast tool, thus suitable for the initial feasibility studies and parametric optimization of the new concept involving seed-blanket geometry. It is shown that the effect of the seed-blanket interaction is not negligible, in some cases, and should be taken into account in the depletion calculations. (10 refs.)

112302 Some remarks on modeling uncertainties. Y. Ronen (Dept. of Nuclear Engng., Ben-Gurion Univ. of the Negev, Beer Sheva, Israel).

Atomkernenerg. Kerntechnik (Germany), vol.42, no.1, p.29-32 (1983).

Several topics related to the question of modeling uncertainties are considered. The first topic is related to the use of the generalized bias operator method for modeling uncertainties. The method is expanded to a more general form of operators. The generalized bias operator is also used in the inverse problem and applied to determine the anisotropic scattering law. The last topic discussed is related to the question of the limit to accuracy and how to establish its value. (33 refs.)

112303 A simulator of the nuclear power plant and its functions.

R. Szczerski (Zakład Energetyczny, Bielsko-Biala, Poland).

Energetyka (Poland), vol.37, no.4, p.145-8 (April 1983). In Polish. [received: Sept. 1983] (no refs.)

112304 Neutron design study of BN 600 type reactor with plutonium fuel.

J. Kujal (Ústav Jaderneho Vyzkumu, Rez, Czechoslovakia).

Jad. Energ. (Czechoslovakia), vol.29, no.8-9, p.297-301 (Aug.-Sept. 1983). In Czech.

This paper contains a brief description of neutron design study of the BN 600 type reactor with plutonium fuel. Reactor parameters for both fundamental states of an equilibrium fuel cycle after and before charge-discharge are presented as well as some parameters of fuel cycles. (5 refs.)

112305 Comparison of measured fission gas releases for Windscale AGR fuel irradiated above 18 GwD/tU with those predicted using the computer code MINIPAT D. N. Beatham, R. Hargreaves, R. D. Walker, R. Kirkbride.

Report ND-R-803(W), UKAEA, Risley, Lancs., England (Aug. 1982), 26 pp.

Available from HMSO, London, England.

MINIPAT D is a computer code for predicting fission product gas release into the voidage of thermal reactor fuel pins. It also calculates the variation of internal pressure within a pin during irradiation. This paper examines how well the code predicts fission gas release from high burn-up AGR fuel. All the data are provided from the Windscale prototype AGR. Fuel pins included in the investigation came from elements where the mean burn-up exceeded 18 GwD/tU. (1 ref.)

112306 CANSWEL-2: A computer model of the creep deformation of Zircaloy cladding under loss-of-coolant accident conditions. Part II. User notes. T. J. Hastie.

Report ND-R-814 (S) Part 2, UKAEA, Risley, Lancs., England (March 1983), 49 pp.

Available from HMSO, London, England.

For pt. I see UKAEA Report ND-R-814 (S) 1, (1982). Notes are provided on the use of CANSWEL-2 in its stand-alone form. They include descriptions of the input data format, job control language for IBM and ICL computers, and examples of the different output options.

112307 SIMULATE-E: A nodal core analysis program for light water reactors. Computer code user's manual. W. R. Cobb, R. S. Borland, P. L. Versteegen.

Report EPRI-NP-2792-CCM, Electr. Power Res. Inst., Palo Alto, CA, USA (March 1983), 416 pp.

Available from Res. Rep. Center (RRC), Box 50490, Palo Alto, CA 94303, USA.

Contains the method descriptions and user's manual for the LWR nodal core analysis computer program SIMULATE-E. A description of the coding, several sample problems, one benchmark problem, and code installation instructions are provided.

112308 Assessment of SPEAR-FCODE-BETA for fuel licensing.

I. B. Fiero, H. R. Freeburn, A. M. Garde, M. A. Krammen, P. L. Rotondo.

Report EPRI-NP-2939, Electr. Power Res. Inst., Palo Alto, CA, USA (March 1983), 74 pp.

Available from Res. Rep. Center, Box 50490, Palo Alto, CA 94303, USA.

The SPEAR-FCODE-BETA fuel performance code is assessed for adequacy in simulating fuel performance in fuel licensing proceedings. A detailed review of the thermal and mechanical performance models of greatest import and to fuel licensing—including fission gas release, fuel temperatures, and cladding uniform strain—is presented. The report recommends modelling and usability improvements.

112309 Berechnungsmethoden und Analysen zum dynamischen Verhalten von Kraftwerksanlagen mit Hochtemperaturreaktor (Computation methods and analyses on the dynamic behaviour of power plants with high temperature gas cooled reactors). J. Banaschek.

Report JUL-1841, Kernforschungsanlage, Jülich, Germany (April 1983), 107 pp. In German.

The author describes the computation models and methods used in a new developed computer code for the analysis of the dynamic behaviour of nuclear power plants with High Temperature Gas Cooled Reactor. The subprograms which have been united to an integrated code are described in detail. The field of application of this code reaches from investigations on transients under normal operation to the thorough description of the load laid on the plant under extreme accidental conditions. The application of the code is shown in two sample cases. The investigations are done for a controlled variation in load of the THTR-300 MW_e power station and the behaviour of a 200 MJ/s process-steam-plant in case of a failure of active after-heat-removal. (42 refs.)

112310 First investigations on a wrapped fibre blanket insulation with massive spacers consisting of carbon fibre composite. P.Brockhoff, D.Stausebach.

Report JUL-1840, Kernforschungsanlage, Julich, Germany (April 1983), 62 pp. In German.

The insulation for the secondary hot gas duct system of a High Temperature Reactor is described. This insulation has been designed by INTERATOM. It consists of inner tubes made of graphite on which fibre blankets are wrapped. Massive spacers consisting of Carbon Fibre Composite (CFC) bear the inner tubes. Experiments have been carried out in the high pressure wind tunnel with the media air and helium. Because of corrosion the temperature was restricted to 300°C when using air. The maximum helium temperature was about 400°C. The influence of temperature, pressure and velocity was studied. (15 refs.)

112311 New HTR conception for a modular system with block-fuel elements and its comparison with an HTR with ball-shaped fuel shaped elements. K.Yamashita.

Report JUL-1842, Kernforschungsanlage, Julich, Germany (April 1983), 87 pp. In German.

The concept of the modular High Temperature Reactor with block-fuel elements is developed and a comparison with the modular Pebble Bed High Temperature Reactor is performed. The fitting of a graphite column into the mean core zone serves to limit the maximum fuel element temperature to less than 1600°C in the case of a loss-of-coolant-accident. The 'Push through'-loading can decrease the fuel element temperature under normal operation. Under normal operation the Pebble Bed High Temperature Reactor is characterized by a low fuel element temperature. The loss of pressure in the core has a low value of 0.2 bar at a system pressure of 40 bar. In the primary cycle therefore the system pressure can be decreased with respect to the endothermal reaction by the nuclear process heat application. (27 refs.)

112312 VIPRE-01: A thermal-hydraulic analysis code for reactor cores. Vol.I: Mathematical modeling. C.W.Stewart, J.M.Cuta, A.S.Koontz, J.M.Kelly, K.L.Basehore, T.L.George, D.S.Rowe.

Report EPRI-NP-2511-CCM, Electr. Power Res. Inst., Palo Alto, CA, USA (April 1983), 274 pp.

Available from Research Report Center, Box 50390, Palo Alto, CA 94303, USA.

Details the mathematical modeling of the VIPRE code, which was developed for nuclear power utility thermal-hydraulic analysis applications. The theoretical development of the general questions, constitutive relationships, correlations, and numerical solution techniques are summarized.

112313 VIPRE-01: A thermal-hydraulic analysis code for reactor cores. Vol.II: User's manual. J.M.Cuta, A.S.Koontz, C.W.Stewart, S.D.Montgomery.

Report EPRI-NP-2511-CCM, Electr. Power Res. Inst., Palo Alto, CA, USA (April 1983), 668 pp.

Available from Research Report Center, Box 50490, Palo Alto, CA 94303, USA.

For pt.I see EPRI Report EPRI-NP-2511-CCM (1983). Contains the user's manual for VIPRE, an EPRI computer code developed for nuclear power utility thermal-hydraulic analysis applications. Input requirements of VIPRE and its auxiliary programs—ASP, SPECSET, and DECCON—are described, and the input instructions for each code are provided.

112314 SPEAR-FCODE-GAMMA functional specifications. I.B.Fiero.

Report EPRI-NP-2941, Electr. Power Res. Inst., Palo Alto, CA, USA (March 1983), 44 pp.

Available from Research Report Center, Box 50490, Palo Alto, CA 94303, USA.

Documents SPEAR-FCODE-GAMMA (SFG), a conceptual fuel performance code for use in licensing analyses, which has been defined and characterized as a set of functional specifications. The potential licensing-related applications of SFG are established and discussed. General code specifications, including regulatory, interface, hardware application, code model and software, and operational specifications, are discussed as well as input and output data requirements, formatting aspects, and accuracy guidelines.

The implication of sensitivity analysis on the safety and delayed-neutron parameters for fast breeder reactorsSee Entry 112294

An advanced modular scheme for reactor and in-core fuel management calculationsSee Entry 112316

Licensing applications and requirements of an ideal steady-state fuel performance codeSee Entry 112340

Verification of the GFLOW computer code using experimental data from the Maine Yankee spent-fuel storage poolSee Entry 112345

A fuzzy-logic approach to HTR nuclear power plant model controlSee Entry 112361

A simple teaching model for transient fuel-cycle analysisSee Entry 112362

Simulation of THTR-steam generator control using artificial intelligence methodsSee Entry 112364

Measurement and evaluation of neutron spectra above 0.1 MeV in the JMTRSee Entry 112366

The prediction of critical mass flux by the use of Fanno linesSee Entry 112374

Reactor physics and economic aspects of the CANDU reactor systemSee Entry 112376

Numerische Untersuchung der 3-dimensionalen stationären Temperatur-und Stromungsverteilung im Core eines Kugelhaufen-Hochtemperaturreaktors (Numerical investigation of the 3-dimensional steady-state temperature - and flow-distribution in a pebble bed high temperature reactor core)See Entry 112382

Experimental investigation for the thermohydraulics of packed beds in the comparison with the computer code THERMIX-2D: The investigation of the dispersive heat transfer examined by a cold gasstreamSee Entry 112383

Concerning the Rayleigh-Ritz treatment of Flugge's equationsSee Entry 112405

A study using the MABEL-2C code of the effects of pellet and cladding asymmetries on PWR fuel rod deformation under conditions relevant to the NRU MT-3 ballooning experimentSee Entry 112417

Technical basis of 'spectral source terms' for assessing uncertainties in fission product release during accidents in PWRs with special reference to Sizewell-BSee Entry 112419

Two-group criticality models for safety analysis considerationsSee Entry 112423

Estimate of primary-system temperatures in severe reactor accidentsSee Entry 112429

Hitachi's large-scale FBR plant development programsSee Entry 112430

Comments on 'neutron spectral unfolding using the Monte Carlo method'See Entry 112610

Reply to Chambless and BroadwaySee Entry 112611

Relaxation of a rectangular beam and circular shaftSee Entry 113318

Elasto-plastic behaviour of a thin cylinder under thermal stress cyclingSee Entry 113319

28.42 FISSION REACTOR MATERIALS

112315 Calculation of carburization profiles in stainless steel components in a liquid sodium environment. S.R.Srinivasan (Res. & Dev. Dept., Rourkela Steel Plant, Rourkela, India).

Atomkernenerg. Kerntechnik. (Germany), vol.41, no.4, p.285-9 (1982). [received: Sept. 1983]

A method has been developed to calculate the carbon concentration profiles in stainless steel clad and intermediate heat exchanger tubes in a sodium cooled LMFBFR (liquid metal cooled fast breeder reactor). The method is based on solving the differential equation for coupled diffusion cum precipitation kinetics using the implicit finite difference technique. In this method the 'ad-hoc' manner, adopted by Snyder et al. (1974), of treating the precipitation reaction is avoided. The present method has several advantages including a significant saving in computation time. (7 refs.)

112316 An advanced modular scheme for reactor and in-core fuel management calculations. Y.Abushady (Nuclear Engng. Dept., Alexandria Univ., Alexandria, Egypt).

Atomkernenerg. Kerntechnik. (Germany), vol.42, no.1, p.50-4 (1983).

ALUN, in its present version, is a modular system for reactor and in-core fuel management calculations, specially recommended for installations having limited computational capabilities. The module is capable for the calculation of the power distribution, power peaking factor, reactivity, operating cycle length, criticality searches, thermal constraints, material temperatures, density distribution, pressure drop, pumping power, isotopic concentrations of the spent fuel and other requirements. The module can propose suggestions for different nuclear fuel management decisions involving; the enrichment of the fuel, the number of fuel assemblies, the placement of the assemblies within the core and the operating history of the reactor. New aspects in the application of different mathematical models are included in different stages of the module. (16 refs.)

112317 Analysis of radioactive waste solutions by atomic absorption spectrometry with electrothermal atomization. G.Rossi, N.Omenetto, G.Pigozzi, R.Vivian (Chem. Div., Joint Res. Centre Establ., Ispra, Italy), U.Mattiaz, F.Mousty, G.Crabi.

At. Spectrosc. (USA), vol.4, no.4, p.113-17 (July-Aug. 1983).

The application of electrothermal atomic absorption spectrometry to the analysis of nuclear high- and medium-activity waste solutions is presented. An apparatus based on that analytical technique has been devised and used for remote operation under safe conditions. For this purpose, the graphite furnace and the associated auto-sampler are enclosed in a specially devised glove box. The assembly, which required marginal modifications of the commercial components, was shown to be successfully applicable to routine determination of Ba, Cr, Fe, Mn, Mo, Pd, Rh, and Sr. (2 refs.)

112318 Primary coolant treatment by ion exchangers—experience from the operation of nuclear power stations with pressurized water reactors. K.-H.Walter (Gemeinschaftskernkraftwerk Neckar GmbH, Neckarwestheim, Germany).

VGB Kraftwerkstechnik. (German Ed.) (Germany), vol.63, no.8, p.706-12 (Aug. 1983). In German.

A working party of the VGB Specialist Committee on Chemistry in Nuclear Power Stations has collated and evaluated experience with ion exchangers for primary coolant treatment in pressurized water reactors. In spite of difficulties from time to time, a generally favourable picture of the effectiveness of this method of treatment emerged. Radioactive waste can be minimized by good operational planning. (5 refs.)

112319 Investigation of material movement within steel test sections by means of high speed X-ray photography. H.Will, P.Menzenhauer, W.Peppler (Inst. für Reaktorentwicklung, Kernforschungszentrum Karlsruhe, Karlsruhe, Germany).

Proc. SPIE Int. Soc. Opt. Eng. (USA), vol.312, p.16-21 (1983). (1st European Conference on Cineradiography with Photons or Particles, Paris, France, 18-21 May 1981).

In simulation experiments the consequences of hypothetical reactor accidents are investigated. The materials involved in the tests, as well as the temperatures, require test sections of steel. To follow the material movement and relocation X-ray cine equipment was developed. The test section is radiated from three axially positioned X-ray sources, electro-optical image amplifiers transform the material density distribution into a visible picture, which is picked up by high speed cameras with, typically, 1000 pictures per second. The resolution of the system is about 1 mm³ of steel with a small dependence on the total thickness of the test section. The technique, its main features and limitations are described and some experimental results are presented. The computer aided analysis of the X-ray high speed films is also explained. (2 refs.)

112320 The Synroc solution. A.E.Ringwood (Res School of Earth Sci., Australian Nat. Univ., Canberra, Australia).

Nucl. Active (S. Africa), no.29, p.16-20 (July 1983).

High-level radioactive wastes from nuclear reactors may be incorporated in synthetic rock (Synroc), claimed to be far more resistant to groundwater leaching than borosilicate glass. Australia's synthetic rock strategy simulates nature's method of immobilising radioactive elements. (11 refs.)

112321 More light on the U clan. S.A.de Waal (Potchefstroom Univ., Potchefstroom, S Africa).

Nucl. Active (S. Africa), no.29, p.21-3 (July 1983).

Uranium mineralogy has proved of vital importance in geological exploration and extraction engineering. As the demand for uranium as a fuel for nuclear power reactors escalates, research on the behaviour of uranium minerals in complex ores can be expected to intensify. (4 refs.)

112322 A risk count for nuclear waste. A.Jacobi,Jr. (Electrowatt Engng. Services Ltd., Zurich, Switzerland).

Nucl. Active (S. Africa), no.29, p.28-32 (July 1983).

Probabilistic risk assessment used increasingly to assess nuclear power plant safety could be applied equally well to nuclear waste repositories according to the author. He claims that the technique offers greater advantages than the classical, e.g. deterministic, safety analyses. (no refs.)

- 112323 Thermodynamic properties of $\text{Th}_{0.80}\text{U}_{0.20}\text{O}_{2+x}$ solid solution.** M.Ugajin, T.Shiratori, K.Shiba (Thorium Fuel Lab., JAERI, Tokai-mura, Ibaraki-ken, Japan). *J. Nucl. Mater. (Netherlands)*, vol.116, no.2-3, p.172-7 (June 1983). Oxygen-potential (ΔG_{O_2}) measurements employing a thermogravimetric method have been performed for $\text{Th}_{0.80}\text{U}_{0.20}\text{O}_{2+x}$. A complete set of data is presented at 1273-1473K in the ranges $2.000 \leq \text{O}/\text{M} \leq 2.024$ and $-95 \leq \Delta G_{\text{O}_2} \leq -32$ kcal/mol. Partial molar entropies and enthalpies of solution of oxygen in the mixed oxide were derived from the temperature variation of ΔG_{O_2} . Vapour pressures over $\text{Th}_{0.80}\text{U}_{0.20}\text{O}_{2+x}$ at 2000-2300K were calculated from experimental ΔG_{O_2} data and the known free energies of formation for gaseous and condensed oxides. It is predicted that with an increase in O/M ratio the vapour pressure of $\text{UO}_3(\text{g})$ increases rapidly while maintaining an extremely lower pressure of $\text{ThO}_2(\text{g})$. (22 refs.)
- 112324 Oxygen potential and lattice parameter measurements in (U, Ce) O_{2-x} .** D.I.R.Norris, P.Kay (Berkeley Nuclear Labs., CEGB, Berkeley, England). *J. Nucl. Mater. (Netherlands)*, vol.116, no.2-3, p.184-94 (June 1983). Studies have been carried out on (U, Ce) O_{2-x} to assist the understanding of oxygen behaviour in the fast reactor fuel (U, Pu) O_{2-x} . Oxygen potentials at 1123K and lattice parameters after rapid cooling to room temperature have been determined as functions of O/M ratio for Ce/(U+Ce) ratios of 0.148 and 0.282. The results show some similarities between the two mixed oxides, but also important differences. The Markin-McIver rule, that oxygen potential at a given temperature is a function only of the supposed plutonium valence, does not apply with cerium. Simple cluster models are basically inconsistent with experimental data and a complex cluster model requires further development before it can account for the oxygen potential behaviour of (U, Ce) O_{2-x} . The ratio of lattice parameter change to O/M ratio change in $\text{U}_{1-x}\text{Ce}_x\text{O}_{2-x}$ is not strongly dependent on y and averages 0.30 \AA , slightly greater than the corresponding value for $\text{U}_{1-y}\text{Pu}_y\text{O}_{2-x}$. A transition to a room-temperature two-phase structure occurs at an O/M ratio of about 1.985 for $y=0.282$. (20 refs.)
- 112325 Distribution of fission and activation products in the graphite sleeves of HTGR fuel rods: first and second OGL-1 fuels.** K.Hayashi, T.Kikuchi, F.Kobayashi, K.Minato, K.Fukuda, K.Ikawa (JAERI, Ibaraki-ken, Japan). *J. Nucl. Mater. (Netherlands)*, vol.116, no.2-3, p.233-43 (June 1983). In order to develop the fuel of a high temperature gas-cooled reactor, axial and radial profiles of fission and activation products in the graphite sleeves of the first and second fuel assemblies irradiated in the in-pile gas loop OGL-1 were measured by means of lathe sectioning, gamma spectrometry, and ion-exchange separation. Several sharp axial profile peaks of ^{90}Sr , ^{134}Cs , and ^{137}Cs were observed for the second fuel sleeves. The peaks are assigned to the failed coated fuel particles; the rest of the profiles to the contamination uranium contained in the fuel compact matrix. Fission products with lower diffusivity such as ^{90}Sr , ^{106}Ru , and ^{144}Ce were completely retained in the second fuel sleeve, whereas similar effectiveness in retention was not observed for ^{134}Cs and ^{137}Cs . Diffusion coefficients of cesium and strontium have been roughly estimated through the comparison between the measured and the simply calculated profiles in the sleeve. (15 refs.)
- 112326 Investigation of the oxygen activity of oxide fuels and fuel-fission product systems by solid electrolyte techniques. I. Qualification and limitations of the method.** K.Teske, H.Ullmann, D.Rettig (Central Inst. for Nuclear Res. Rossendorf, Dresden, Germany). *J. Nucl. Mater. (Netherlands)*, vol.116, no.2-3, p.260-6 (June 1983). The possibilities and limitations of the application of solid electrolyte techniques to the investigation of oxide nuclear fuel materials have been discussed. The solid electrolyte coulometry has been developed for the investigation of oxygen potentials and O/M-ratios of oxide samples. Example measurements on non-irradiated nuclear fuel oxide samples demonstrated the various possibilities of investigations such as O/M-determination, oxygen potential versus O/M-relations and simultaneous titration of impurities in oxide materials. The experimental arrangement and the small sample weights required are preferable conditions for the application of the method to alpha- or gamma-active materials. Solid electrolyte coulometry is recommended as a precise investigation method which works without calibration. (18 refs.)
- 112327 Thermal conductivity of near-stoichiometric (U, Pu, Nd) O_2 and (U, Pu, Eu) O_2 solid solutions.** S.Fukushima, T.Ohmichi, A.Maeda, M.Handa (JAERI, Tokai-mura, Naka-gun, Ibaraki-ken, Japan). *J. Nucl. Mater. (Netherlands)*, vol.116, no.2-3, p.287-96 (June 1983). The thermal conductivities of near-stoichiometric $(\text{U}_{0.8}\text{Pu}_{0.2})_2\text{R}_2\text{O}_2$ solid solutions containing $\text{RO}_{1.5}$ ($\text{R}=\text{Nd}$ or Eu) up to 10 mol.% were determined by the laser flash method in the temperature range 700-1900K. The thermal conductivities for the solid solutions up to about 1550K satisfied the phonon conduction equation, $K=(A+BT)^{-1}$. The thermal conductivity decreased gradually with the increase of the rare earth content. This decrease was mainly caused by the lattice defect thermal resistance. The measured defect thermal resistivities ($=A$) were in good agreement with the calculated results based on the lattice defect model in which U^{4+} , U^{5+} , Pu^{4+} and R^{3+} ions were considered as phonon scattering centers. The lattice strain parameter $e=97$ and 103 were obtained for (U, Pu, Nd) O_2 and (U, Pu, Eu) O_2 solid solutions, respectively. The lattice strain effects on the thermal resistivity was about 15 times larger than the mass difference one. (24 refs.)
- 112328 UO_2 fuel pellet microstructure modification through impurity additions.** K.C.Radford, J.M.Pope (Nuclear Materials Dept., Westinghouse Res. Labs., Pittsburgh, PA, USA). *J. Nucl. Mater. (Netherlands)*, vol.116, no.2-3, p.305-13 (June 1983). The thermal densification of UO_2 pellets containing small amounts of the sintering aids Ti, V, Nb and Ca+Ti has been studied to determine the changes in grain size and pore size distribution. Additive levels above 0.5 mol.% greatly increased the grain size and increased the size of the fine porosity, but also reduced the sintered density. A comparison was made between the microstructure of fuel whose density had been reduced by this means and that produced by the addition of small amounts of the known density suppressants, Ba and Sr. (30 refs.)
- 112329 Phase transitions, creep, and fission gas behaviour in actinide oxides.** L.Leibowitz, J.K.Fink (Argonne Nat. Lab., Chem. Technol. Div., Argonne, IL, USA), O.D.Slagle. *J. Nucl. Mater. (Netherlands)*, vol.116, no.2-3, p.324-5 (June 1983). Summarises the data available on phase transitions in the actinide oxides and discusses and possible connection with fission-gas release. (14 refs.)
- 112330 On the role of strain and graphite interlayer in clad failure.** S.Mehedinteanu, F.Glodeanu (Inst. for Nuclear Power Reactors, Pitesti, Rumania). *J. Nucl. Mater. (Netherlands)*, vol.116, no.2-3, p.332-5 (June 1983). The role of a plane-stress state in the clad failure during power transients is examined. Comments are made on the role of graphite interlayer in pellet-clad interaction (PCI) mechanisms. (9 refs.)
- 112331 Flow in a mixed UO_2 -Pu O_2 pile.** C.Milet (CEA, Fontenay-aux-Roses, France), C.Picini. *J. Nucl. Mater. (Netherlands)*, vol.116, no.2-3, p.195-9 (June 1983). In French. The flow under compression, of a mixed UO_2 -Pu O_2 file has been studied for stress values equal to or less than 26.5 MPa and temperatures from 500-1100°C. The results show that the rate of flow is proportional to the stress and to the fission rate in the region examined and up to a combustion rate of 4%. On the other hand the existence of a zone of transition from athermal to thermally active at 900°C has been established, and rates of flow have been measured of the same order of magnitude for a stoichiometric fuel (U,Pu) $\text{O}_{2.00}$ and a hypostoichiometric fuel (U,Pu) $\text{O}_{1.97}$ at a temperature around 800°C. (9 refs.) J.S.
- 112332 A new fission-gas release model.** R.J.White, M.O.Tucker (Berkeley Nuclear Labs., Central Electricity Generating Board, Berkeley, England). *J. Nucl. Mater. (Netherlands)*, vol.118, no.1, p.1-38 (Aug. 1983). The release of unstable fission products from irradiated UO_2 fuel is shown to be a sensitive function of many inter-related factors. The poly-granular-aggregate model for unstable gas release assumes that the release of fission products from the interior regions of UO_2 fuel occurs, first by direct diffusion to grain boundaries and, secondly by gaseous diffusive transfer through an intermittently open grain-edge tunnel network. During the early stages of irradiation a saturated network of grain-face lenticular porosity is established by the precipitation of stable fission-gas atoms. Lenticular bubbles which nucleate near to the grain edges—junctions of the three grains—will move to a lower free energy configuration on those edges and take up a triangulated cigar shape. Continued stable gas collection inflates these bubbles to a point of interlinkage beyond which point the fission gases are vented and tunnel collapse, by means of surface diffusion away from regions of high curvature, into a string of cigar-shaped bubbles occurs. A model incorporating the Speight-Turnbull stable gas release model (1969, 1974), the grain edge-corner swelling model and the Tucker-White percolation diffusion model from a polygranular aggregate is shown to account well for the experimental findings of Turnbull and Friskney (1978) on release rates of ^{131}I , ^{133}I , ^{135}Xe , ^{136}Xe , ^{88}Kr from 1.46% enriched stoichiometric UO_2 . (55 refs.)
- 112333 Modelling of fission-gas release from fuel undergoing isothermal heating.** I.R.Brearley, D.A.Macinnis (Safety & Reliability Directorate, UKAEA, Warrington, England). *J. Nucl. Mater. (Netherlands)*, vol.118, no.1, p.68-72 (Aug. 1983). Currently there is controversy surrounding the mechanism of fission-gas release from fuel subjected to transient heating. A recent model (SINGAR) suggests that the release mechanism is principally single-atom migration coupled with thermal resolution of atoms from intragranular bubbles. This contrasts markedly with the previous interpretation of the release in terms of biased gas bubble migration in the presence of a temperature gradient. The extensive release observed during isothermal annealing of irradiated fuel samples is modelled. This is major evidence in favour of the SINGAR model since, in the absence of a temperature gradient, the bubble migration model will predict no release, contrary to observation. (15 refs.)
- 112334 Stress analysis of core support post in a very high-temperature reactor.** K.Kikuchi (JAERI, Ibaraki-ken, Japan), T.Yokobori, K.Sanokawa, Y.Okamoto, T.Yokobori. *Nucl. Eng. & Des. (Netherlands)*, vol.75, no.1, p.23-31 (1982). [received: Sept. 1983] A very high-temperature gas-cooled reactor (VHTR) has been developed by Japan Atomic Energy Research Institute and its core consists of so-called fuel blocks, removable reflector blocks and so on. These graphite blocks are supported by thin cylindrical graphite bars called support posts. These posts are in contact with the blocks through hemispherical seats to absorb the relative displacement of blocks by small inclination or rotation of the posts. Stress distributions and stress concentration coefficients of the support post under the reactor core weight are analysed by means of photoelastic experiment and compared with two-dimensional calculation by using the finite element method. The following are the conclusions the authors have derived: (1) Stress concentration coefficients of the post are expressed uniquely as function of $Ed(1/r_p - 1/r_s)/\sigma_e$ regardless of the shapes of model and material properties. (2) Inclination of the post caused by small rotation has little effect on the stress concentration coefficients. (12 refs.)
- 112335 Thermoplastic analysis of a sphere-PAC fuel pin.** T.C.Kennedy (Dept. of Mech. Engng., Oregon State Univ., Corvallis, OR, USA), T.L.George, K.L.Peddicord. *Nucl. Eng. & Des. (Netherlands)*, vol.75, no.1, p.57-65 (1982). [received: Sept. 1983] This analysis is concerned with the thermomechanical response of a sphere-pac fuel pin. The fuel is modeled as an elastic-plastic continuum governed by the Mohr-Coulomb yield criterion and associated flow rule under plane strain conditions. Yielding is found to initiate at the outer edge of the fuel, and a plastic zone progresses inward. When the fuel has completely yielded, there exist three distinct plastic zones corresponding to stress states on different facets of the yield surface. Closed form expressions for the displacement and stresses in each of the plastic zones are presented. Numerical results illustrating the variation of displacement and stress with radial position are given. (11 refs.)
- 112336 Prepare for on-site storage of nuclear radwaste.** R.Beaudry (Detroit Edison Co., Detroit, MI, USA). *Power (USA)*, vol.127, no.8, p.51-4 (Aug. 1983). Faced with the steady disappearance of commercial disposal sites for radioactive waste material, Detroit Edison took matters into its own hands to make provision for the future at Fermi 2. (no refs.)
- 112337 Organisation of inspection of radioactive waste by the public health services.** P.Pellerin, M.-E.Gahinet. *Rev. Gen. Nucl. (France)*, no.3, p.194-203 (May-June 1983). In French. The liquid radioactive waste produced by nuclear plants is subjected to stringent regulations and strict controls by the administration for Public Health. The authors describe the principles underlying these regulations and the procedures and arrangements which they prescribe. They go on to examine the main aspects of the role played by the Central service for protection against ionic radiation (SCPRI) and how inspection of radioactive waste for which it is nationally responsible as part of its official public health vocation in the radioactive protection sector is organised. (9 refs.)
- 112338 Protection and control of nuclear materials: a pressing obligation.** Y.Duvaux. *Rev. Gen. Nucl. (France)*, no.3, p.219-21 (May-June 1983). In French. The author calls to mind the responsibilities of a country with an extensive nuclear programme and the associated increase in quantity of nuclear materials and those who stock them together with the necessity of taking stringent protective and control measures both within its own national territory and on an internal scale. The nature of the threat, the French laws and

regulations and the measures which have been taken are themes which are subsequently examined. (no refs.)

112339 Weld residual stress redistribution near growing cracks. D.F.Quinones, J.E.Reaugh.
Report EPRI-NP-2964, Electr. Power Res. Inst., Palo Alto, CA, USA (March 1983), 86 pp.
Available from Res. Rep. Center, Box 50490, Palo Alto, CA 94303, USA.
A numerical analysis is presented of intergranular stress corrosion cracking in a residual stress field of the heat-affected zone of a girth-butt weld. A complete preexisting circumferential crack, growing radially outward in a 10-cm schedule 80 recirculation line, is modelled using the elastic properties of BWR type-304 stainless steel. Results from these elastic calculations show that the axial extent of the initial residual stress field has little influence on the stress intensification and crack arrest for extents greater than three pipe wall thicknesses.

112340 Licensing applications and requirements of an ideal steady-state fuel performance code. I.B.Fiero.
Report EPRI-NP-2940, Electr. Power Res. Inst., Palo Alto, CA, USA (March 1983), 38 pp.
Available from Res. Rep. Center, Box 50490, Palo Alto, CA 94303, USA.
The author identifies and characterizes the licensing applications and requirements for an ideal steady-state fuel performance code. Fifteen licensing applications are examined with respect to specific requirements as set forth in the Code of Federal Regulations, the Nuclear Regulatory Guidelines and the NRC Standard Review Plans. Code input data needs and output requirements for each application as well as necessary models to represent the pertinent fuel behavior phenomena are identified.

112341 Constitutive equations for the creep behaviour of nickel-base alloys for HTR components in the temperature range 1023 - 1273 K. W.Osthoff, H.Schuster, P.J.Ennis, H.Nickel.
Report JUL-1843, Kernforschungsanlage, Julich, Germany (April 1983), 160 pp. In German.
The applicability and modification of constitutive equations for describing the creep and relaxation behaviour of the nickel-base alloys INCONEL 617, NIMONIC 86 and HASTELLOY S have been investigated. Creep tests at stresses in the range 10-150 MPa and temperatures in the range 1023-1273K were carried out for the three alloys and in addition for INCONEL 617 and HASTELLOY S relaxation and stress dip tests in the stress range 10-170 MPa and temperature range 1073-1223K were performed. The fitting of various creep equations to the measured creep curves showed that the best description of the primary and secondary creep regions was given by the equation formulated by Li (1963). (80 refs.)

112342 Experimental investigations of actinide release from coated fuel particles for high-temperature reactors. A.T.e Silva.
Report JUL-1833, Kernforschungsanlage, Julich, Germany (March 1983), 164 pp. In German.
The migrational behaviour of actinides in the coated fuel particles proposed for high-temperature reactors is investigated experimentally. Data are described in the framework of the diffusion model. The experimental procedures are presented and the necessary computer codes are discussed. The diffusion coefficients of the actinides—plutonium, americium and curium—as well as of the fission product cesium are derived from the experimental data by a nonlinear least squares fit procedure and are presented in the form of Arrhenius lines $D = D_0 e^{-Q/RT}$ for U(TH)-O₂, HTI-PyC and SiC. (37 refs.)

112343 Oxidation of Ni-Cr experimental alloys and the effectiveness of the oxide as a barrier against carburization in high-temperature reactor primary circuit helium. U.Thiele, H.Schuster, H.Nickel.
Report JUL-1790, Kernforschungsanlage, Julich, Germany (July 1982), 141 pp.
To study the corrosion mechanisms in the complex gas-metal systems of high temperature reactor (HTR) primary coolant circuits, 26 nickel-chromium experimental alloys have been exposed in different gas compositions. The alloys contained systematically varied Cr, Al, Ti and Si levels. For the first exposure of the specimens (oxidising conditions), the composition of the test gas was selected to give the same oxidation potential as the primary coolant of an HTR by adding to the helium controlled amounts of hydrogen and water. For the second exposure (carburising conditions) methane was added to the test gas to investigate the effectiveness of the oxide in preventing carburisation. The concentrations of the impurities in the test gases were a factor of 100 higher than in the PNP Standard helium, in order to accelerate the reactions, and so shorten the test durations. The results of these experiments were compared with those obtained for the same alloys exposed in PNP Standard helium. (73 refs.)

112344 Management and disposal of alpha-contaminated wastes. A survey of current practices, strategies and R & D activities in some EC countries and the USA. F.Mannone.
Report EUR 8574 EN, Comm. European Communities, Luxembourg (1983), 136 pp.
In view of the rationalization of radwaste pre-treatment, conditioning and storage procedures so far applied at the Ispra Establishment, a survey of alpha-waste management practices and strategies currently in use of under development in some EC countries and US has been carried out. In considering radwastes arising at nuclear research centres, and nuclear plants, the most importance has been here attached to their alpha- rather than to their beta, gamma-contamination degree. Various process technologies currently practised for pre-treatment, conditioning, storage and/or disposal of alpha-waste at several European nuclear centres and plants, as well as at some USDOE laboratories, have been surveyed, including also process operations aimed at recovering Pu, both for economical and ecological reasons. The present alpha-waste management and disposal scenario has been completed by the survey of research, development and demonstration work underway in Europe and USA in this field. Finally, national organizations, policies and strategies for radwaste management and disposal have been briefly outlined. (138 refs.)

112345 Verification of the GFLOW computer code using experimental data from the Maine Yankee spent-fuel storage pool. R.R.Gay, D.M.Gloski.
Report EPRI-NP-3097, Electr. Power Res. Inst., Palo Alto, CA, USA (May 1983), 94 pp.
Available from Research Report Center, Box 50490, Palo Alto, CA 94303, USA.
Presents the findings of a study to validate the GFLOW analytic model as an improved method for performing a thermal-hydraulic analysis of spent-fuel storage pools. In addition, a comparison of calculated results with experimental data taken at the Maine Yankee spent-fuel storage pool is discussed.

112346 Studsvik over-ramp project. S.Djurle.
Report EPRI-NP-3007, Electr. Power Res. Inst., Palo Alto, CA, USA (April 1983), 184 pp.
Available from Research Report Center, Box 50490, Palo Alto, CA 94303, USA.
Documents the results of ramp testing of 39 PWR design fuel rods under fast power increase. Failure thresholds were established within particular groups of rods having nearly identical design and base irradiation history, and the findings are presented. A useful data set on well-characterized rods is provided for nondestructive and destructive examinations. The data include both steady state and transient performance characteristics over a significant range of design and operating conditions.

112347 In-plant low-level radwaste technology needs. R.Baker, F.Feizollahi.
Report EPRI-NP-3117, Electr. Power Res. Inst., Palo Alto, CA, USA (May 1983), 116 pp.
Available from Research Report Center, Box 50490, Palo Alto, CA 94303, USA.
An industry-wide survey of current low-level radwaste technology, focusing on waste processing and packaging in nuclear power plants, is outlined. A three-part technology improvement program, involving existing waste generation and treatment systems, alternative technologies, and alternative operation and maintenance practice, is proposed, and alternatives for each subprogram are described.

112348 Low-level waste disposal site performance assessment with the RQ/PQ computer program. V.C.Rogers, M.W.Grant, G.B.Merrell, P.J.Macbeth.
Report EPRI-NP-2664, Electr. Power Res. Inst., Palo Alto, CA, USA (June 1983), 76 pp.
Available from Research Report Center, Box 50490, CA 94303, USA.
Presents the RQ/PQ computer program and a pathway analysis for use in screening and selecting shallow-land burial sites for low-level waste (LLW). The code's ability to calculate potential radioactive LLW hazards is discussed as well as the characteristics of natural and man-made barriers caused by the disposal facility. The bases for modelling nuclide releases from nine potential pathways are described and compared with NUREG-0782 methods, and a summary of the equations solved, a FORTRAN listing, and a sample problem's input and output are given.

112349 Summary of methods for conditioning and immobilizing ion-exchange resins. R.A.Speranzini, L.P.Buckley.
Report AECL-7976, Atomic Energy Canada Ltd., Chalk River, Ont. (Feb. 1983), 36 pp.
Ion-exchange resins are used in CANDU-PHW nuclear power stations to purify heavy water in the primary heat transport and moderator systems. Two promising techniques for conditioning spent ion-exchange resins for disposal have been evaluated: direct immobilization and incineration combined with immobilization of the ash and scrubbed off-gases. When ion-exchange resins were immobilized directly, volumes of bitumen products were about 0.75 times the volumes of untreated resin, while the volumes of cement and polyester products were 2 to 3 times larger. While incinerating the resin is an extra processing step, much smaller volumes result from the latter option. Bitumen and glass product volumes were six and ten times smaller, respectively, than the volumes of untreated resin, while cement and polyester product volumes were about one-half the volume of untreated resin. (17 refs.)

112350 Nuclear fuel waste disposal: Long-term stability analysis. G.J.Merrett, P.A.Gillespie.
Report AECL-6820, Atomic Energy Canada Ltd., Chalk River, Ont. (July 1983), 41 pp.
Discusses events and processes that could adversely affect the long-term stability of a nuclear fuel waste disposal vault or the regions of the geosphere and the biosphere to which radionuclides might migrate from such a vault. (45 refs.)

112351 Development of a CVD silica coating for UK advanced gas-cooled nuclear reactor fuel pins. M.J.Bennett, M.R.Houlton (UKAEA, AERE Harwell, Didcot, England), D.A.Moore, A.I.Foster, M.A.M.Swidzinski.
Proceedings of the 4th European Conference on Chemical Vapour Deposition, Eindhoven, Netherlands, 31 May-2 June 1983 (Eindhoven, Netherlands: Philips Centre Manuf. Technol. 1983), p.395-400
Vapour deposited silica coatings could extend the life of the 20% Cr/25% Ni niobium stabilised (20/25/Nb) stainless steel fuel cladding of the UK advanced gas cooled reactors. A CVD coating process developed originally to be undertaken at atmospheric pressure has now been adapted for operation at reduced pressure. Trials on the LP CVD process have been pursued to the production scale using commercial equipment. The effectiveness of the LP CVD silica coatings in providing protection to 20/25/Nb steel surfaces against oxidation and carbonaceous deposition has been evaluated. (6 refs.)

Recent bibliography on analytical and sampling problems of a PWR primary coolant. Supplement IISee Entry 112336
(n,2n) cross-section measurement of ⁹³Nb, ¹⁹⁷Au and ²³⁸U with fission-neutron spectrum and its dependence on the asymmetry termSee Entry 112182
Clustering effects on neutron elastic scattering from boron isotopesSee Entry 112183
Measurement of the total neutron cross-section of germanium at energies below 2 eVSee Entry 112184
Integration of the time-dependent heat equation in the fuel rod performance program IAMBUSSee Entry 112300
Neutron design study of BN 600 type reactor with plutonium fuelSee Entry 112304
Comparison of measured fission gas releases for Windscale AGR fuel irradiated above 18 GwD/tU with those predicted using the computer code MINIPAT DSee Entry 112305
CANSWEL-2: A computer model of the creep deformation of Zircaloy cladding under loss-of-coolant accident conditions. Part II. User notesSee Entry 112306
Assessment of SPEAR-FCODE-BETA for fuel licensingSee Entry 112308
New HTR conception for a modular system with block-fuel elements and its comparison with an HTR with ball-shaped fuel shaped elementsSee Entry 112311
SPEAR-FCODE-GAMMA functional specificationsSee Entry 112314
Investigation of the behaviour of TRISO coated UO₂-kernels in the head-end burning and experimental determination of the radioactive contents of irradiated particlesSee Entry 112359
A simple teaching model for transient fuel-cycle analysisSee Entry 112362
Hodoscope cineradiography of nuclear fuel destruction experimentsSee Entry 112368

- Survey of cineradiographic techniques applied to nuclear reactor safety experiments See Entry 112369
- Time-resolved neutron radiography of reactor fuel See Entry 112391
- Underwater neutron radiography facility utilizing small neutron generator See Entry 112392
- How good is nitrocellulose film for neutron radiography? See Entry 112393
- Variation of evaporation rate for a dynamic flow of water on stainless steel and aluminium rods See Entry 112397
- A study using the MABEL-2C code of the effects of pellet and cladding asymmetries on PWR fuel rod deformation under conditions relevant to the NRU MT-3 ballooning experiment See Entry 112417
- Two-group criticality models for safety analysis considerations See Entry 112423
- Proposal for decommissioning of contaminated steel parts from shut down nuclear power plants See Entry 112462
- The calculated defect structure of thorium See Entry 113862
- Direct evidence for stress-enhanced swelling in type 316 stainless steel See Entry 114041
- A study of defect states in neutron-irradiated zirconium using positron annihilation spectroscopy See Entry 114042
- Saturation exposure in ferritic stainless steels See Entry 114043
- Critical radius for bias-driven swelling—a further analysis and its application to bimodal cavity size distributions See Entry 114045
- Stability of the radiation-induced γ phase in 316 stainless steel See Entry 114182
- Some high-temperature properties of Zircaloy-oxygen alloys See Entry 114213
- Characterization of the oxide-metal interface at the surface of a stainless steel See Entry 114373
- Revision of the eutectoid isotherms of the uranium-chromium system See Entry 115166
- Composition of $Zr(Cr, Fe)_2$ -type precipitates in Zircaloy-2 and Zircaloy-4 See Entry 115196
- On the measurement of Young's modulus of tubes by propagation of longitudinal waves See Entry 115236
- Elongation minimum and strain rate sensitivity minimum of zircaloy-4 See Entry 115259
- Fractographic study of cracks produced by thermal shocks in 20MnMoNi55 and comparable weld material in water environment See Entry 115356
- Effecting the corrosion relationship of corroding element-cladding material of ZrNb1 by mechanical surface treatment See Entry 115416
- A new gas equilibration method for the measurement of carbon potential: carbon potential in austenitic 316 stainless steel at 1000°C See Entry 115417
- Inhomogeneous plastic deformation and its relevance to iodine stress corrosion cracking susceptibility in irradiated Zircaloy-2 tubing See Entry 115418
- Intergranular stress corrosion cracking of Ni-Cr-Fe Alloy 600 tubes in PWR primary water - Review and assessment for model development See Entry 115447
- Automated time-of-flight studies of the defect detection trial plates 1 and 2 See Entry 115454
- CEGB inspection of plates 1 and 2 in UKAEA defect detection trials See Entry 115455
- An in-service inspection method: the use of focused probes for the detection and sizing in DDT plates 1 and 2 See Entry 115456
- Operation of the EPRI nondestructive evaluation center. Annual report - 1982 See Entry 115495
- Biological elimination rates of radioisotopes by mallards contaminated at a liquid radioactive waste disposal area See Entry 115937

28.42H Fuel preparation and reprocessing (inc. isotope separation and enrichment)

- 112352 Thorium fuel reprocessing with pulse columns. II. H.Fumoto, E.Zimmer, R.Kiyose, E.Merz (Inst. für Chem. Technol., KFA Jülich, Jülich, Germany). *Atomkernenerg. Kerntech. (Germany)*, vol.41, no.4, p.273-8 (1982). [received: Sept. 1983]
- For pt.1 see Technol., vol.58, p.447 (1982). The acid deficient Thorex process has been investigated in view of concentration profiles along the pulse columns in the co-extraction and the co-stripping procedure. Because of the lower acidity, the acid deficient feed is more suitable for zirconium and less suitable for ruthenium decontamination. In the co-stripping of thorium and uranium, unexpected high uranium concentrations have been observed in the lower part of the column. During the acid deficient feed adjustment, a violent reaction of entrained organic phase with the nitrates has taken place. (14 refs.)
- 112353 Depletion functions and their use in the calculation of isotope transmutations. A.I.Shlyakhter (Leningrad Nuclear Phys. Inst., Leningrad, USSR). *Atomkernenerg. Kerntech. (Germany)*, vol.42, no.1, p.33-8 (1983).
- The basic points in the calculation of transmutations of isotopes are analyzed using the so-called 'deletion functions'. It is shown that conventional criteria used for selecting the most important nuclide chains and for eliminating the short-lived isotopes from them are sometimes misleading. In particular, the usual neglect of the short-lived nuclides may appear to be incorrect. At small irradiation time t the error introduced by this approximation is about $\epsilon \approx (n-2)\lambda_k t$, where n is the number of nuclides in the chain and λ_k is the destruction rate of the neglected isotope. At large t is $\epsilon \approx \lambda_m/\lambda_k$ where λ_m is the lowest destruction rate in the chain. As a result, the error does not tend to zero when t goes to infinity unless at least one nuclide is not depleted at all. Simple formulae for the sensitivity of the calculated nuclide concentrations to the adopted value of nuclear constants are obtained. To illustrate the result the author considers production of actinides. (23 refs.)
- 112354 Reaction of lithium and sodium nitrates and carbonates with uranium oxides. T.Fujino, K.Ouchi, T.Yamashita, H.Natsume (Div. of Chem., JAERI, Tokai-mura, Ibaraki-ken, Japan). *J. Nucl. Mater. (Netherlands)*, vol.116, no.2-3, p.157-65 (June 1983).
- The reactivity and reaction conditions to form lithium and sodium uranates were studied in an attempt to group some useful head-end processes in nuclear fuel reprocessing. In the reactions between alkali metal carbonates and U_3O_8 in air at 800°C, the products with Na/U ratios 0.8 and 0.857 gave

the same X-ray diffraction patterns in which the peaks of $\alpha-U_3O_8$ were almost not detected. The observed peaks for uranates with Li/U=1.205, 2, 4 and Na/U=1 are well consistent with the values reported previously. No indication of formation of $Li_2U_6O_{19}$, Li_6UO_6 and Na_4UO_6 was observed. Thermogravimetric observations on the reactions between the carbonates and U_3O_8 revealed that they consisted of two processes, i.e. (1) the formation of uranates and (2) the oxidation of the uranates formed. The rate of reaction (1) was higher than that of reaction (2) when the M/U (M=Li, Na) ratio was 0.5. When the ratio was 1, the rate of reaction (1) lowered and became rate determining. The reactions between alkali metal nitrates and UO_2 showed that the minimum M/U ratios for obtaining the uranates without U_3O_8 were 0.667 and 0.8 for lithium and sodium uranates, respectively. They were formed by heating at 600°C for 3 h in oxygen or air. Mixing process of initial materials is not required for these reactions. The uranates formed were found to be dissolved in 1 M HNO_3 within 1 min. (27 refs.)

112355 Leaching uranylhydrogel as one of the technological operations of the sol-gel process. I. F.Melichar (Ústav Jaderneho Vyzkumu, Rez, Czechoslovakia). *Jad. Energ. (Czechoslovakia)*, vol.29, no.8-9, p.302-5 (Aug.-Sept. 1983). In Czech.

The paper describes process leaching of gel particles of solid uranyl compounds prepared by the sol-gel method. The possibility of access to the description and interpretation of leaching kinetics of the ballast components containing carbon and nitrogen compounds in the form NO_3^- and NH_4^+ is discussed. The ballast components influence the following consequential operation processes of uranyl xerogel and negatively influence the quality of the resulting uranium dioxide. (7 refs.)

112356 A kinetic model of UO_2 dissolution in acid, H_2O_2 solutions that includes uranium peroxide hydrate precipitation. L.E.Eary (Dept. of Geosci., Pennsylvania State Univ., University Park, PA, USA), L.M.Cathles. *Mettall. Trans. B (USA)*, vol.14B, no.3, p.325-34 (Sept. 1983).

Laboratory experiments have been carried out to determine the dissolution kinetics of UO_2 in the UO_2 - H_2O_2 - SO_4 - H_2O system under conditions similar to those which occur during acid in situ leaching of sandstone uranium deposits. UO_2 dissolution proceeds by an electrochemical reaction at the UO_2 surface. Sulfate ions adsorb onto the UO_2 surface and reduce the rate of UO_2 dissolution by blocking sites of potential oxidation. UO_2^{2+} precipitates as insoluble uranium peroxide hydrate ($UO_4 \cdot xH_2O$), and under even moderate pH conditions can greatly reduce the UO_2 dissolution rate. The overall UO_2 dissolution (including $UO_4 \cdot xH_2O$ precipitation) can be usefully described by a simple kinetic model that considers dissolution and precipitation to be independent processes. The model has the advantage that the dissolution rate at a given temperature is a function only of solution composition and UO_2 surface area. The chemical model can thus be easily combined with fluid flow models to obtain a full chemical-physical model of the leaching of uranium ore in a column experiment or in situ. (20 refs.)

112357 Heavy species of enrichment by pulsed gas diffusion. S.Tanisho, Y.Honjo, N.Wakao (Dept. of Chem. Engng., Yokohama Nat. Univ., Yokohama, Japan). *Nucl. Eng. & Des. (Netherlands)*, vol.75, no.1, p.43-8 (1982). [received: Sept. 1983]

Heavy species enrichment based on pulsed gas diffusion was tested with a constant volume concentration. The separation factors measured were in good agreement with theory. Enrichment/recovery of heavy species in a constant pressure concentrator is also discussed. (3 refs.)

112358 Neutron physical and thermohydraulic investigations on the fissile fuel production with spallation neutrons. T.Schilling. *Report JUL-1835*, Kernforschungsanlage, Jülich, Germany (March 1983), 67 pp. In German.

In case of an enhanced utilisation of nuclear energy from fission reactors it is necessary to preserve the natural deposits of fissile material. One possibility for this preservation could be the breeding of synthetic fuel by the means of spallation neutrons. The configuration discussed here consists of an integral spallation target/breeding blanket pebble bed of hollow Thorium spheres, which is cooled alternatively with helium gas or liquid sodium or lithium. (25 refs.)

112359 Investigation of the behaviour of TRISO coated UO_2 kernels in the head-end burning and experimental determination of the radioactive contents of irradiated particles. H.-G.Aschhoff. *Report JUL-1857*, Kernforschungsanlage, Jülich, Germany (June 1983), 109 pp.

Because of the introduction of the HTR Low Enriched Uranium fuel cycle, the behaviour of UO_2 TRISO-coated fuel particles was investigated in the various HEAD-END unit operations. The potential impact of this particle design on the HEAD-END unit operations was evaluated. The oxidation behaviour of uncoated UO_2 kernels was characterised in both static and fluidised bed combustion tests. Using unirradiated TRISO-coated UO_2 particles, the radioactive inventory of the SiC coating fragments, which are a waste stream from fluid-bed burning, were determined. The measurements showed that the SiC fragments must be classified as 'long-lived, highly radioactive, alpha-containing' waste, and thus its heat generation rate must be considered. A possible conditioning might be hot-pressing and sintering using a vitreous or ceramic powder matrix. The use of a jet mill to crush the SiC coating after burning of the matrix graphite was investigated. Crushing experiments with unirradiated particles demonstrated excellent efficiency in both coating breakage and kernel-coating separation. Because of this, it is proposed to utilise a jet mill to replace both the roll crushing and secondary burning steps in the reference HEAD-END process. (52 refs.)

Reactor physics and economic aspects of the CANDU reactor system See Entry 112376

Möglichkeiten der Spaltstoffherzeugung für Hochtemperatur-Reaktoren im Verbundsystem von Hochtemperatur-Reaktor und Fusionsreaktor (Facilities for producing fissile fuel for high temperature gas-cooled reactors in a symbiotic fission-fusion system) See Entry 112444

Release of gaseous tritium during reprocessing See Entry 112455

28.43 FISSION REACTOR OPERATION

- 112360 Rationale for nuclear reactor control room data displays. R.W.Carson, J.L.Russell, Jr. (School of Nuclear Engng. & Health Phys., Georgia Inst. of Technol., Atlanta, GA, USA). *Ann. Nucl. Energy (GB)*, vol.10, no.9, p.457-65 (1983).
- One of the 'lessons learned' from the Three Mile Island accident focuses upon the need for a validated source of plant-status information in the control room. The utilization of computer-generated graphics to display the reduced readings of the plant instrumentation has introduced the need for a set of guidelines that focuses upon the mental image of plant conditions that the operators receive from viewing the computer monitors. The principles that

govern the design of displays are similar to those employed in the education process because the objective is the same, namely, to transfer information. The philosophy for the development of displays to portray the status of major plant systems bases the level of detail upon the needs of the user. Graphic displays that relate the plant system parameter to the plant systems are recommended along with bar-chart type representations of the relationship between plant parameters and allowable limits. (18 refs.)

112361 A fuzzy-logic approach to HTR nuclear power plant model control. M.Bubak, J.Moscinski (Inst. of Computer Sci. AGH, Cracow, Poland), J.Jewulski.

Ann. Nucl. Energy (GB), vol.10, no.9, p.467-71 (1983). The fuzzy-set theory is used to incorporate linguistic 'rules of thumb' of a human operator in the HTR nuclear power plant controller. The results of the extensive computer simulations are encouraging and confirm the usefulness of this approach in nuclear power plant control. In the Appendix a short introduction to fuzzy logic is given. (11 refs.)

112362 A simple teaching model for transient fuel-cycle analysis. J.D.Lewins (Dept. of Engng., Univ. of Cambridge, Cambridge, England). *Ann. Nucl. Energy (GB)*, vol.10, no.9, p.491-6 (1983). The author presents a 'lumped' model of batch loading fuel in a fission reactor. A linear representation of the increase in fuel utilisation is also made. (3 refs.)

112363 Power oscillations in a reactor with two temperature coefficients. R.S.Poddar, M.S.Trasi, V.Balaraman (Bhabha Atomic Res. Centre, Bombay, India).

Atomkernenerg. Kerntech. (Germany), vol.42, no.2, p.95-100 (1983). Oscillatory behaviour in a nuclear reactor with two temperature feedback is investigated using a perturbation technique. Necessary and sufficient conditions are established for the occurrence of oscillations, for the asymptotic damping, sustenance and divergence of oscillations, as well as for asymptotic stability under oscillatory conditions. Numerical methods are used for verifying the theoretical results and also to investigate the effect of large perturbations on an oscillatory system. (21 refs.)

112364 Simulation of THTR-steam generator control using artificial intelligence methods. J.Kitowski (Inst. of Computer Science, Univ. of Mining & Metall., Cracow, Poland).

Atomkernenerg. Kerntech. (Germany), vol.42, no.2, p.124-5 (1983). The author describes briefly and discusses the enlarged concept of the multi-dimensional heuristic learning controller with dynamic memory organization and linear reinforcement, equipped into multicriterial control ability. This was used for simulation of control of a THTR-steam generator. (8 refs.)

112365 Effect of pre-exposure of films on radiographic sensitivity. J.K.Ghosh, J.P.Panakkal, P.R.Roy (Radiometallurgy Div., Bhabha Atomic Res. Centre, Bombay, India).

Br. J. Non-Destr. Test. (GB), vol.25, no.5, p.238-9 (Sept. 1983). Fogging of films prior to actual radiography in nuclear fuel fabrication facilities using high burn-up recycled plutonium, affects the image quality. An investigation is presented on the effect of the pre-exposure on the radiographic sensitivity of industrial radiographic films evaluated by the use of conventional image quality indicators and micro-densitometry. (1 ref.)

112366 Measurement and evaluation of neutron spectra above 0.1 MeV in the JMTR. K.Sakurai (Div. of Japan Materials Testing Reactor, JAERI, Ibaraki-ken, Japan).

Nucl. Instrum. & Methods Phys. Res. (Netherlands), vol.213, no.2-3, p.359-71 (1 Aug. 1983).

The evaluation of fast neutron spectra from the Japan Materials Testing Reactor (JMTR) have been performed by using the critical facility of the JMTR and by a combination of the multi-foil activation method and the adjustment codes (SAND II and NEUPAC). In order to measure and evaluate the neutron spectra above 0.1 MeV, resonance detectors such as manganese, gold and copper have been used to determine the neutron flux level in the 1/E region and threshold detectors such as silver, rhodium, indium, uranium, aluminum, magnesium and titanium have been used to determine the neutron flux level above 0.1 MeV. The guess spectra for the neutron spectrum adjustment were calculated by using the one-dimensional discrete-ordinates code ANISN with the slab model for the JMTR core. Some important points were concluded through the adjustment procedure of the neutron spectrum: the adjusted spectrum from 0.1 to 1 MeV depends on the accuracy of the neutron cross section data for the threshold detectors such as silver and rhodium, and also on the accuracy of these reaction rates. The ratios of neutron flux above 0.183 MeV to neutron flux above 1 MeV were calculated from the guess spectra and the adjusted spectra, and the ratios were in good agreement with each other. (12 refs.)

112367 Post-critical heat flux heat transfer: a survey of current correlations and their applicability. S.W.Wang (Sargent & Lundy Engrs., Chicago, IL, USA), J.Weisman.

Prog. Nucl. Energy (GB), vol.12, no.2, p.149-68 (1983). Post-critical heat flux (CHF) heat transfer is of interest to nuclear engineers because of (a) the need to compute the consequences which immediately follow power in excess of the CHF and (b) the need to be able to determine when adequate cooling has been re-established once CHF has been exceeded. The information reported in this area has often seemed confusing because of the wide variety of conditions which have been considered. What appears as the poor performance of a given correlation is often due to inadvertent use of the correlation outside of the range of its derivation. The various regimes of post-CHF heat transfer pertaining to pool boiling and flow boiling are delineated. The correlations appropriate to each regime are indicated and an attempt is made to assess their utility. (71 refs.)

112368 Hodoscope cineradiography of nuclear fuel destruction experiments. A.De Volpi (Argonne Nat. Lab., Argonne, IL, USA).

Proc. SPIE Int. Soc. Opt. Eng. (USA), vol.312, p.22-9 (1983). (1st European Conference on Cineradiography with Photons or Particles, Paris, France, 18-21 May 1981).

Nuclear reactor safety studies have applied cineradiographic techniques to achieve key information regarding the durability of fuel elements that are subjected to destructive transients in test reactors. Beginning with its development in 1963, the fast-neutron hodoscope has recorded data at the TREAT reactor in the United States of America. Consisting of a collimator instrumented with several hundred parallel channels of detectors and associated instrumentation, the hodoscope measures fuel motion that takes place within thick-walled steel test containers. Fuel movement is determined by detecting the emission of fast neutrons induced in the test capsule by bursts of the test reactor that last from 0.3 to 30 s. The system has been designed so as to achieve under certain typical conditions (horizontal) spatial resolution less than 1 mm, time resolution close to 1 ms, mass resolution below 0.1 g, with adequate dynamic range and recording duration. A variety of imaging forms have been developed to display the results of processing and analyzing recorded data. (6 refs.)

112369 Survey of cineradiographic techniques applied to nuclear reactor safety experiments. A.De Volpi (Argonne Nat. Lab., Argonne, IL, USA).

Proc. SPIE Int. Soc. Opt. Eng. (USA), vol.312, p.30-9 (1983). (1st European Conference on Cineradiography with Photons or Particles, Paris, France, 18-21 May 1981).

After reviewing the role of in-pile and out-of-pile experiments in the United States fast-reactor safety testing program, The history of fuel-motion measurements is sketched. The fast neutron hodoscope is described, with particular emphasis on capabilities and principles of operation. Alternative devices for fuel-motion measurement are examined with a discussion of future improvements in material-motion diagnostics. Relationships of fuel-motion diagnostic techniques to other types of cineradiography are also covered. (22 refs.)

112370 MIRENE, a mini-nuclear reactor for neutronography—data and applications. M.Houelle, J.M.Gerberon (CEA, Tille, France).

Proc. SPIE Int. Soc. Opt. Eng. (USA), vol.312, p.262-9 (1983). In French. (1st European Conference on Cineradiography with Photons or Particles, Paris, France, 18-21 May 1981).

MIRENE is described and its characteristics are given. The core uses only 1 kg of enriched uranium in solution state. It works in a self-limited pulse mode. The neutron pulses are collimated in two beams which cross the concrete protection walls surrounding the reactor. Many applications of MIRENE in different fields are indicated. In nuclear engineering: testing of first neutron reactor fuel-pins; control of 'neutrophage screens' used in transport and storage of nuclear-fuel materials to secure the criticality-safety; observation of irradiated-oxide samples in order to determine the equation of state of the fuel used in fast-neutron reactors; observation of $\text{UO}_2\text{-H}_2\text{O}$ mixing conditions in the field of criticality experiments. In engineering, MIRENE has a large field of applications, two examples are given: the control of the sealing of an electric isolator; the visualization of the bonding layer between two high density metals. Finally an original application in agronomy is shown which has given very good results: the observation of the in-situ growth of a corn-root. (2 refs.)

112371 Development of key components for the heat transport system of prototype fast breeder reactor 'MONJU'. H.Ogasawara (Hitachi Works, Hitachi Ltd., Tokyo, Japan), A.Suzuoki.

Hitachi Rev. (Japan), vol.32, no.2, p.105-10 (April 1983). [received: Aug. 1983]

The heat transport system for the prototype fast breeder reactor 'MONJU' comprises a reactor vessel, intermediate heat exchangers for heat exchange between primary and intermediate sodium, steam generators for heat exchange between intermediate sodium and water/steam, main pumps for sodium circulation and pipings, etc. These components are required to absorb severe thermal shocks and expansions in high-temperature sodium environments. In order to improve the reliability of these components, extensive research and development programs are under way in the field of heat transfers and flow characteristics, materials, structures, strength evaluations, manufacturing and inspections. The paper describes the status in development of the intermediate heat exchanger, the primary main sodium pump and the steam generator, all of which are now under development by Hitachi Ltd, for 'MONJU'. (6 refs.)

112372 The development of high-temperature fission-counter chambers for nuclear-reactor control and protection. T.Tomoda, S.Fukakusa, S.Yamashita, N.Wakayama, H.Yamagishi.

Mitsubishi Denki Giho (Japan), vol.57, no.4, p.21-5 (1983). In Japanese.

The instrumentation for fast-breeder reactors, high-temperature gas reactors, and similar n-w reactors requires neutron detectors capable of operating at high temperatures. The authors have succeeded in developing fission-counter chambers possessing both improved operating characteristics and high heat resistance. The measurement range of these chambers is wide enough to cover all reactor conditions from start-up to full power. Measurements using them show no temperature dependence, and the chambers can withstand long-term operation at temperatures up to 600°C. In addition, the narrow, 100 ns pulse width enables neutron measurement to be performed under gamma-ray dosages of up to 10⁶R/h. (8 refs.)

112373 An investigation into the nature and significance of a new critical heat flux correlation. W.J.Green, D.R.H.Beattie (AAEC Res. Establ., Lucas Heights Res. Labs., Sutherland, Australia).

Nucl. Eng. & Des. (Netherlands), vol.75, no.1, p.33-41 (1982). [received: Sept. 1983]

An empirical critical heat flux correlation, which is based upon dimensionless groups, and which was developed from a wide range of experimental data for vertical upflow in uniformly heated tubes, has been further examined to determine if, because of its accuracy and generality, it might provide an insight into the mechanisms of boiling crisis. A parameter survey using the correlation showed that it was well able to predict the so-called 'crisis of the second kind' without needing to define any separate or distinct flow regimes. Comparison of the empirical correlation with a general form of theoretical correlation, developed from a combination of several simple physical models which occur during the crisis phenomenon, shows a strong similarity in the form of the dimensionless groups. It also indicates that a further dimensionless group may need to be incorporated in the empirical correlation to achieve complete generality. Rearrangement of the dimensionless groups, and the form of the empirical correlation, together with some minor approximations, indicate that boiling crisis is influenced by local hydrodynamic and thermal phenomena and can be related to pre- and post-crisis coolant conditions. (13 refs.)

112374 The prediction of critical mass flux by the use of Fanno lines. E.E.Michaelides, S.Parikh (Mech. & Aerospace Engrg., Univ. of Delaware, Newark, DE, USA).

Nucl. Eng. & Des. (Netherlands), vol.75, no.1, p.117-24 (1982). [received: Sept. 1983]

Fanno lines have been used extensively for the prediction of the critical flow in homogeneous single phase fluids. The authors attempt to apply this method for the prediction of critical flow in a two-phase evaporative fluid. Homogeneous and slip conditions are examined for water-steam flow. The criterion of critical flow is set as the turning point of the constant mass flow rate line in the entropy-enthalpy diagram. The proposed criterion gives very good agreement of the critical mass flux with experimental data, and with previous models on critical flows. (16 refs.)

112375 FBR wide-range neutron monitoring system. I.Tai, E.Seki, M.Sakamoto, T.Sakuma (Toshiba Corp., Kawasaki, Japan).

Toshiba Rev. (Int. Ed.) (Japan), no.143, p.11-13 (Spring 1983).

A new and practical wide-range neutron monitoring system for the fast breeder reactor was developed. The system can monitor all neutron flux levels from the startup to power range operation with only one neutron detector. This system was experimentally applied to the experimental RBR, JOYO. Its characteristics have been proved to be satisfactory and practical for reactor power monitoring based on application tests at JOYO. The realization of this

system is due to a new high performance preamplifier which was developed and manufactured by Toshiba. (2 refs.)

112376 Reactor physics and economic aspects of the CANDU reactor system.

Report AECL-7615, Atomic Energy Canada Ltd., Chalk River, Ont. (Feb. 1983), 269 pp.

Contains the material presented in nine lectures at the National School of Physics at Yogyakarta, Indonesia, 1981 November 9 to November 13. A history of the development of the CANDU system is given along with a fairly detailed description of the 600 MW(e) CANDU reactor. Reactor physics calculation methods are described as well as comparisons between calculated reactor physics parameters and those measured in research and power reactors. An examination of the economics of CANDU in the Ontario Hydro system and a comparison between fossil fuelled and light water reactors is presented. Some physics, economics and resource aspects are given for both low enriched uranium and thorium fuelled CANDU reactors. Finally the R&D program in Advanced Fuel Cycles is briefly described. (14 refs.)

112377 Evaluation of techniques to predict flow-induced tube vibration in a preheat steam generator. J.H.Stuhmiller, R.E.Ferguson, J.H.-Y.Yu, P.J.Masiello, C.J.Chuong.

Report EPRI-NP-2986, Electr. Power Res. Inst., Palo Alto, CA, USA (March 1983), 120 pp.

Available from Res. Rep. Center (RRC), Box 50490, Palo Alto, CA 94303, USA.

A mathematical modeling methodology is presented for combining steam generator geometry and operating conditions with structural and fluid dynamics in order to predict the location and severity of flow-induced tube vibration damage in a preheat generator. A description of the successful three-step mathematical technique is provided, and predictions are compared with the trends of laboratory data on separate effects and with field observations of damage.

112378 Thermal mixing in a model cold leg and downcomer at low flow rates. P.H.Rothe, M.W.Fanning.

Report EPRI-NP-2935, Electr. Power Res. Inst., Palo Alto, CA, USA (March 1983), 490 pp.

Available from Res. Rep. Center, Box 50490, Palo Alto, CA 94303, USA.

An experimental program of fluid mixing experiments performed in a 1/5-scale mixing facility to evaluate the effects of low flow rate and the thermal shield on the fluid and thermal mixing phenomena in the cold leg and downcomer of certain specified PWRs is described. Simulated steady-state conditions thought to be extreme for small-break loss-of-coolant accidents are analyzed, and details of the analysis of transient and steady-state temperature records documenting the mixing of the cold high-pressure injection coolant water and the hot primary coolant water are provided.

112379 Hydrazine usage for corrosion control in PWR plants with powdered resin condensate polishers. J.L.Barkich, P.J.Battaglia.

Report EPRI-NP-2969, Electr. Power Res. Inst., Palo Alto, CA, USA (March 1983), 44 pp.

Available from Res. Rep. Center, Box 50490, Palo Alto, CA 94303, USA.

The authors document the testing performed at North Anna Unit 2 to obtain the data necessary to determine the optimum injection point and amount of hydrazine to be used for oxygen control in PWR units with condensate polishing demineralizers. Conclusions and recommendations are presented.

112380 Diffusion and hideout in crevices. J.G.Cleary, G.E.Von Nieda, W.T.Lindsay, Jr..

Report EPRI-NP-2979, Electr. Power Res. Inst., Palo Alto, CA, USA (March 1983), 194 pp.

Available from Res. Rep. Center, Box 50490, Palo Alto, CA 94303, USA.

An investigation to identify and formulate the important variables that control contaminant hideout in and return from severely dented support plate crevices in steam generators is summarized. The results of the investigation are presented in four specific areas: (1) a literature review and estimation of diffusion coefficients for electrolytes in hot water, (2) an experimental study of diffusion rates through simulated crevice packing, (3) a study of contaminant hideout rates as a function of applied heat flux, and (4) the development of a mathematical model.

112381 Primary-side deposits on PWR steam generator tubes. C.A.Bergmann, J.Roesmer, D.W.Perone.

Report EPRI-NP-2968, Electr. Power Res. Inst., Palo Alto, CA, USA (March 1983), 82 pp.

Available from Res. Rep. Center, Box 50490, Palo Alto, CA 94303, USA.

Analyses conducted to determine the chemical nature of the oxide deposits on the primary side of steam generator tubing samples taken from eight nuclear plants and the radioisotopes incorporated in those deposits are described. Results of the analyses, which included radiochemical, chemical, scanning electron microscope, and energy dispersive X-ray techniques, are presented, and an evaluation of the data obtained and a comparison with in-core crud data and with values calculated by a mathematical activity transport model are provided.

112382 Numerische Untersuchung der 3-dimensionalen stationären Temperatur- und Stromungsverteilung im Core eines Kugelhaufen-Hochtemperaturreaktors (Numerical investigation of the 3-dimensional steady-state temperature - and flow-distribution in a pebble bed high temperature reactor core). K.Verfondern.

Report JUL-1826, Kernforschungsanlage, Jülich, Germany (Jan. 1983), 130 pp. In German.

This work presents a computer model determining the steady-state temperature- and flow field in 3 dimensions in the core of a pebble bed high temperature reactor. The numerical sprinkler method, basing on the THERMIX-model, allows to describe the thermo-hydraulics of a nonrotational-symmetric core-geometry. The AVR-reactor in Jülich, in operation since 1967, represents a suitable investigation-object for the computer model of THERMIX-3D. It is in a 3D-mesh-structure to reproduce very precisely the so called 'graphite noses', in which the shut-down rods are conducted as well as the filling cones in the inner and outer area. The results of the final calculation of the normal operation condition for the AVR-reactor unambiguously show, that within the core reproduced in 3 dimensions there are evident deviations in the flow profile and in the temperatures of the cooling gas in contrast to a 2D-handling. (19 refs.)

112383 Experimental investigation for the thermohydraulics of packed beds in the comparison with the computer code THERMIX-2D: The investigation of the dispersive heat transfer examined by a cold gasstream. M.Schurenkramer, H.Barthels.

Report JUL-1839, Kernforschungsanlage, Jülich, Germany (April 1983), 34 pp. In German.

The computer code THERMIX-2D is tested with regard to the formalism for the effective heat conductivity by experimental data. Especially the part of dispersion is investigated. In addition to the heated main stream a cooler gas

stream is injected into the center of the packed bed. The thermal compensation is measured and calculated. (12 refs.)

112384 Assessment of control rooms of nuclear power plants. L.Norros, J.Ranta, B.Wahlstrom.

Report 184, Tech. Res. Centre Finland, Electr. Eng. Lab., Espoo (May 1983), 29 pp.

To identify and correct the lacks in control rooms of operating nuclear power plants and plants under construction an extensive program has been started in the USA. In Finland as in other countries using nuclear power, the development in the USA particularly with regard to the requirements imposed on nuclear power plants is carefully followed. The changes in these requirements are sooner or later also reflected in the guidelines given by the Finnish authorities. It is therefore important to be able to form a notation of how the new requirements apply to Finnish conditions. Especially it is important to review the latest assessment guidelines for control room implementation (NUREG-0700). Thus one can avoid possible overhasty conclusions. (10 refs.)

112385 NBS reactor: Summary of activities July 1981 through June 1982.

Report NBS-TN-1178, Nat. Bur. Stand., Washington, DC, USA (June 1983), viii+222 pp.

This report summarizes all those programs which depend on the NBS reactor. It covers the period from July 1981 through June 1982. The programs range from the use of neutron beams to study the structure and dynamics of materials through nuclear physics and neutron standards to sample irradiations for activation analysis, isotope production, radiation effects studies, neutron radiography, and nondestructive evaluation.

112386 Secondary water chemistry at Millstone 2. T.A.Putkey, W.L.Pearl, S.G.Sawochka.

Report EPRI-NP-2974, Electr. Power Res. Inst., Palo Alto, CA, USA (April 1983), 112 pp.

Available from Research Reports Center, Box 50490, Palo Alto, CA 94303, USA.

Summarizes secondary-system chemistry and steam generator corrosion observations at the Millstone 2 PWR. A review of plant design characteristics, construction materials, and historical water chemistry performance is presented.

112387 On-line use of chelants in nuclear steam generators - Feasibility study. C.R.Wolfe, M.Ambrosino, Jr., W.M.Connor.

Report EPRI-NP-2973, Electr. Power Res. Inst., Palo Alto, CA, USA (April 1983), 190 pp.

Available from Research Report Center, Box 50490, Palo Alto, CA 94303, USA.

A test program designed to determine the feasibility of using an on-line application of chelants in nuclear steam generators is detailed. The report includes (1) the results of tests involving a recommended chelant formulation with selected pH control additives and (2) the applicability of these tests to the field situation.

112388 Evaluation of steam generator fluid mixing during layup.

A.D.MacArthur.

Report EPRI-NP-2993, Electr. Power Res. Inst., Palo Alto, CA, USA (May 1983), 324 pp.

Available from Research Report Center, Box 50490, Palo Alto, CA 94303, USA.

A project to develop practical methods of achieving an adequately mixed chemical environment on the secondary side of PWR steam generators during periods of shutdown, cold shutdown (layup), and startup is summarized. Systems for chemical feed, mixing, sampling, and removal of contaminant chemicals in the steam generator secondary side are evaluated, and recommendations are made. Test results from a Plexiglas model indicate that forced circulation and turbulent mixing are the most effective methods of achieving a rapid, homogeneous chemical environment.

112389 Condensate polisher resin leakage quantification and resin transport studies. C.C.Stauffer, P.L.Doss.

Report EPRI-NP-2981, Electr. Power Res. Inst., Palo Alto, CA, USA (April 1983), 240 pp.

Available from Research Report Center, Box 50490, Palo Alto, CA 94303, USA.

The results are presented of a study conducted at nine operating PWR power plants to quantify the resin released to the secondary cycle from the condensate polisher systems and to determine resin transport throughout the secondary cycle. The results indicate that polisher systems, of both the powdered resin and deep-bed cycle, release some resin, the quantity being largely a function of flow transients on an individual polisher vessel.

112390 Implementation of boric acid in the field - Indian Point Unit 3 plant. B.J.Jusino.

Report EPRI-NP-3066, Electr. Power Res. Inst., Palo Alto, CA, USA (May 1983), 496 pp.

Available from Research Report Center, Box 50490, Palo Alto, CA 94303, USA.

Details the results of a field test of the use of boric acid to arrest steam generator denting. The results indicate that although denting had continued, it had progressed at a significantly slower rate than the immediate period before the boric acid treatment. An on-line hydrogen monitoring technique and steam generator inspections were used to determine the baseline condition of the steam generators and to provide an indication of the rate of denting progression. The effect of boric acid on corrosion products transported through the secondary system was also monitored.

112391 Time-resolved neutron radiography of reactor fuel. A.DeVolpi (Reactor Analysis & Safety Div., Argonne Nat. Lab., Argonne, IL, USA).

Neutron Radiography. Proceedings of the First World Conference, San Diego, CA, USA, 7-10 Dec. 1981 (Dordrecht, Netherlands: Reidel 1983), p.661-9.

Under the US DOE fast-reactor safety program, fuel pins placed in a test container are irradiated to destruction at the TREAT reactor in Idaho. A diagnostic device called the fast-neutron hodoscope has been developed to generate time-resolved neutron radiographs of the fuel-destruction. The hodoscope records cineradiographic digital-data images of fuel motion during a transient experiment, which could be as brief as a few-hundred milliseconds or as long as a few minutes. Fission induced in the fuel produces fast neutrons that are collimated and detected by a multichannel array. Time resolution in the order of a millisecond is required during much of the power range of the transient. Vertical fuel-motion resolution of about half a centimeter and horizontal resolution of a millimeter or less can be achieved over an area of 6.6×121 cm. A very important and unusual feature of the hodoscope diagnostic system is the capability for data to be quantitatively analyzed in terms of mass of redistributed fuel. (6 refs.)

112392 Underwater neutron radiography facility utilizing small neutron generator. G.Matsumoto, K.Okubo, S.Doi (Nagoya Univ., Nagoya, Japan). Neutron Radiography. Proceedings of the First World Conference, San Diego, CA, USA, 7-10 Dec. 1981 (Dordrecht, Netherlands: Reidel 1983), p.699-706. To investigate the feasibility of applying portable neutron generator for neutron radiography (NRG), an underwater NRG facility was designed and fabricated. This is the preliminary stage of a facility which will be designed for non-destructive test of spent reactor fuels in a spent-fuel pond. Using the scintillation converter at the NRG facility, it took about ten min. to take a NRG image. (no refs.)

112393 How good is nitrocellulose film for neutron radiography? J.C.Domanus (Nuclear Dept., Elsinore Shipbuilding & Engng. Co. Ltd., Helsingør, Denmark).

Neutron Radiography. Proceedings of the First World Conference, San Diego, CA, USA, 7-10 Dec. 1981 (Dordrecht, Netherlands: Reidel 1983), p.729-36. A comparison was made of radiographic quality and sensitivity of neutron radiographs taken on silver halide and nitrocellulose film. For the quality comparison a special calibration fuel pin was used, containing calibrated fuel-to-clad gaps between the UO_2 pellets and zircaloy cladding tube. The neutron radiographs of this pin were assessed by three observers for radiographic image quality referred to X-ray radiographs of the pin. The radiographic sensitivity was investigated with ASTM E 545 sensitivity indicators and assessed in the same way as the calibration fuel pin. Results of the quality and sensitivity assessment done for the nitrocellulose film were compared with those for the silver halide film used in the direct and transfer neutron radiography of the same objects. (8 refs.)

112394 Time delay estimation: application to flow rate measurement of cooling fluid in nuclear power plants. J.-M.Favennec, B.Gergel (Electricite de France, Chatou, France), J.Masson.

Proceedings of ICASSP 82. IEEE International Conference on Acoustics, Speech and Signal Processing, Paris, France, 3-5 May 1982 (New York, USA: IEEE 1982), p.379-82 vol.1

Precise measurement of the coolant flow rate is of utmost importance for the control and safety of PWR nuclear power plants. In this paper several methods based on generalized cross-correlation of γ -radioactivity signals are tested. The authors examine the influence of hydrodynamical parameters such as velocity profile and turbulence on the measurement. It is shown that recently proposed sophisticated estimates (PHAT-SCOT) are not efficient for the purpose and that the Hannan-Thomson (HT) estimate is just slightly better than classical cross correlation (CC). (8 refs.)

Recent bibliography on analytical and sampling problems of a PWR primary coolant. Supplement IISee Entry 111336

Integration of the time-dependent heat equation in the fuel rod performance program IAMBUSSee Entry 112300

SUPERC, a one-dimensional code system for the analysis of the seed-blanket core with movable fuel controlSee Entry 112301

Neutron design study of BN 600 type reactor with plutonium fuelSee Entry 112304

SIMULATE-E: A nodal core analysis program for light water reactors. Computer code user's manualSee Entry 112307

First investigations on a wrapped fibre blanket insulation with massive spacers consisting of carbon fibre compositeSee Entry 112310

New HTR conception for a modular system with block-fuel elements and its comparison with an HTR with ball-shaped fuel shaped elementsSee Entry 112311

VIPRE-01: A thermal-hydraulic analysis code for reactor cores. Vol.I: Mathematical modelingSee Entry 112312

VIPRE-01: A thermal-hydraulic analysis code for reactor cores. Vol.II: User's manualSee Entry 112313

Calculation of carburization profiles in stainless steel components in a liquid sodium environmentSee Entry 112315

An advanced modular scheme for reactor and in-core fuel management calculationsSee Entry 112316

Primary coolant treatment by ion exchangers—experience from the operation of nuclear power stations with pressurized water reactorsSee Entry 112318

Models for calculating the mass flow of a two-phase system on the basis of measured density and momentum flux valuesSee Entry 112395

Investigations of the system behaviour of a pressurized-water reactor during loss-of-coolant accidents. The PKL experimentSee Entry 112396

Variation of evaporation rate for a dynamic flow of water on stainless steel and aluminium rodsSee Entry 112397

Investigations of the reflood-phase after a loss-of-coolant-accident of an advanced pressurized water reactor (APWR)See Entry 112398

Simple analysis of very long term processes without operational and emergency energy supply in the PWR power plantSee Entry 112399

The ignition and burning behaviour of sodium metal in airSee Entry 112401

Measurement of vibrations caused by leakages between pressurized circuits during the 30 MW Czech, modular steam generator operation at BOR 60See Entry 112404

Liquid solidification in laminar tube flow with internal heat sourcesSee Entry 112409

Void fraction under high pressure, low flow conditions in rod bundle geometrySee Entry 112411

Theoretical analysis of hydrogen concentration distribution and acoustic field in Na-water steam generator in presence of micro-leakSee Entry 112422

Two-group criticality models for safety analysis considerationsSee Entry 112423

Bubble growth in variable pressure fieldsSee Entry 112424

Evaluation of critical flow for supercritical steam-waterSee Entry 112425

Testing and evaluation of on-line leak sealing methodsSee Entry 112426

Transient cooldown in a model cold leg and downcomerSee Entry 112427

BWR spray nozzle performance in steam environmentSee Entry 112428

Estimate of primary-system temperatures in severe reactor accidentsSee Entry 112429

Experimental investigations on the rewetting of hot horizontal annular channelsSee Entry 113503

Intergranular stress corrosion cracking of Ni-Cr-Fe Alloy 600 tubes in PWR primary water - Review and assessment for model developmentSee Entry 115447

Steam generator U-bend eddy-current NDESee Entry 115496

28.44 FISSION REACTOR PROTECTION SYSTEMS, SAFETY AND ACCIDENTS

112395 Models for calculating the mass flow of a two-phase system on the basis of measured density and momentum flux values. H.Frohlich, E.Siefert (Battelle-Inst. e.V., Frankfurt, Germany).

Atomkernenerg. Kerntechnik. (Germany), vol.42, no.1, p.11-15 (1983). Several analytical functions have been developed which allow the closed form determination of the two-phase mass flow across a pipe cross-section by using an integral measurement of the density with a 3-beam- γ densitometer and a quasi-pointwise measurement of the momentum flux with dragbodies. Quadratic, cosine and arctangfunctions have been examined for their applicability as profile functions. The suitability of the proposed has been tested against measured blowdown data at the HDR facility and it is demonstrated that the proposed method consistently reproduces the profiles for annular and stratified flow regimes within the experimental limits of error. (10 refs.)

112396 Investigations of the system behaviour of a pressurized-water reactor during loss-of-coolant accidents. The PKL experiment. D.Hein, K.Riedle (Kraftwerk Union AG, Erlangen, Germany).

Atomkernenerg. Kerntechnik. (Germany), vol.42, no.1, p.19-27 (1983). In German.

The authors describe tests on pressurized-water-reactor system behaviour during a loss-of-coolant accident with the PKL test facility. These tests, carried out in a scaled-down model (1:134) of a 1300-MW reactor, have yielded a large amount of experimental data and supporting evidence for the efficiency of emergency core-cooling systems in the case of a large break. Tests dealing with loss of coolant following a small break concentrated on energy transport mechanisms from the core to the steam generators at different water inventories. (9 refs.)

112397 Variation of evaporation rate for a dynamic flow of water on stainless steel and aluminium rods. M.A.Bayoumi, M.E.Nagy, M.E.Sawan, G.A.Abu-Zaid (Arab Maritime Transport Acad. Engng. Dept., Alexandria, Egypt).

Atomkernenerg. Kerntechnik. (Germany), vol.42, no.1, p.55-7 (1983).

The experimental study has been carried out for investigating the parameters affecting the evaporation during an emergency cooling by bottom flooding in a loss of coolant accident (LOCA). The experiments have been done at different values of inlet subcooling, and initial surface temperatures for aluminium and stainless steel 304. For the same initial surface temperature and below the sputtering-Leidenfrost region, increasing of the coolant temperature increases the evaporation rate. Above the sputtering-Leidenfrost region, this relation is reversed. (5 refs.)

112398 Investigations of the reflood-phase after a loss-of-coolant-accident of an advanced pressurized water reactor (APWR). S.Schumann, W.Oldekop (Inst. für Raumflugtech. und Reaktortech., Tech. Univ. Braunschweig, Braunschweig, Germany).

Atomkernenerg. Kerntechnik. (Germany), vol.42, no.2, p.80-91 (1983). In German.

Differences between a high converting advanced pressurized-water reactor (APWR) and a conventional PWR, which are relevant to the reflood-phase after LOCA are presented. The used code and its verification by PWR-reflood experiments is explained. Comparative calculations for APWR and PWR with several conservative assumptions for example cold-leg-injection only, yield nearly the same maximum midplane-temperatures for the average-channel. For the APWR, however, the upper half of the rod shows higher temperatures. Quenchfront and core-water-level increase more slowly. The differences in the reflood-thermohydraulics are analysed in detail. A conservative hot-channel calculation shows maximum temperatures of about 920°C. Finally the influence of conservative assumptions is described and the necessity of experiments pointed out. (39 refs.)

112399 Simple analysis of very long term processes without operational and emergency energy supply in the PWR power plant. S.Benedek (Inst. for Electrical Power Res., Budapest, Hungary).

Atomkernenerg. Kerntechnik. (Germany), vol.42, no.2, p.91-4 (1983). Published calculational methods are cited and used for examination of PWR transients after a loss-of-coolant accident. For different sizes of breaks and breakdown of the pumps the long term transients—without operational and emergency power supply—were calculated. The results show the critical time interval until the operational or emergency/safety water pump/supply should be made into operation to avoid the core heat-up, melt down and the large radioactive issue. (27 refs.)

112400 Loss-of-coolant accident in the fluidized bed nuclear power reactor. F.Sefidvash (Dept. de Engenharia Nuclear, Rio Grande do Sul Univ., Porto Alegre, Brazil).

Atomkernenerg. Kerntechnik. (Germany), vol.42, no.2, p.125-6 (1983).

For the purpose of developing an independent national nuclear technology and an effective manner of transferring such a technology, as well as developing a simple and safe nuclear power reactor, a reactor system based on fluidized bed concept is under study. A preliminary analysis of the loss-of-coolant accident (LOCA) for this reactor is presented. (5 refs.)

112401 The ignition and burning behaviour of sodium metal in air. R.N.Newman (Berkeley Nuclear Labs., CEBG, Berkeley, England).

Prog. Nucl. Energy (GB), vol.12, no.2, p.119-47 (1983).

A review has been made of the ignition and combustion of sodium, both in terms of the fundamental chemistry and also with reference to its use as the heat transfer fluid of a fast breeder reactor. In the discussions of both the combustion chemistry and the scientific mechanisms of possible fire extinguishants comparisons are made with the burning of hydrocarbon fluids. A large part of the review is devoted to the considerable amount of quantitative data produced by various agencies in the world in their pursuit of commercial fast reactor technology. Both practical and theoretical studies have been carried out, some on a large scale, mainly in the field of spray fires and pool fires. Vapour combustion is briefly discussed as is the subject of passive and active fire extinction and possible corrosion damage to structures. Some suggestions are made as to which areas are adequately understood and which areas need significant further work in the context of sodium cooled fast reactors. (87 refs.)

112402 Analysis of parameter changes in the medium of the protective shield of a nuclear reactor after introducing a heat carrier to it. V.V.Fisenko, A.V.Alferov, V.V.Tosheva.

Izv. VUZ Energ. (USSR), no.6, p.59-63 (June 1983). In Russian.

A method is developed for calculating the rate of change of parameters of a water-air mixture in the protective shield of a reactor, for an arbitrary phase state of the water component. By introducing into the design formulae a thermodynamically balanced sound velocity and the Gruneisen factor, it is possible to evaluate directly the rate of change of the pressure, which is an important parameter in the estimation of the strength of the shield. The design formulae have an explicit significance, permitting a relatively straight

forward qualification and quantitative assessment of the process. (3 refs.)
Z.F.V.

112403 The Qualification Testing Evaluation (QTE) Program: NRC-sponsored research on safety-related equipment qualification methodologies. L.L.Bonzon (Sandia Nat. Lab., Albuquerque, NM, USA). *ISA Trans. (USA)*, vol.21, no.3, p.37-43 (1982).
The nuclear power industry is required to demonstrate that certain safety-related equipment is 'qualified' and will function even in the event of a severe reactor accident. Qualification testing of safety-related equipment must be demonstrated to be both realistic and conservative. The Nuclear Regulatory Commission is sponsoring the Qualification Testing Evaluation Program with the goal of obtaining data that will confirm or improve the technical bases for equipment qualification programs. This paper presents selected examples of results to illustrate the broad scope of research. (21 refs.)

112404 Measurement of vibrations caused by leakages between pressurized circuits during the 30 MW Czech, modular steam generator operation at BOR 60. O.Matal, J.Kunovsky, F.Varvarovsky, J.Rybnycek (Vyzkumny Ustav Energetických Zarizení, Brno, Czechoslovakia). *Jad. Energ. (Czechoslovakia)*, vol.29, no.8-9, p.311-15 (Aug.-Sept. 1983). In Slovenian.
The authors summarize and comment on chosen results of vibration measurements of accelerometers located in three places of a branch of the Czechoslovak modular 30 MW steam generator operating at the BOR 60 facility. (9 refs.)

112405 Concerning the Rayleigh-Ritz treatment of Flugge's equations. J.Bremer (Phys. Chem., Univ. of Sydney, New South Wales, Australia). *Nucl. Eng. & Des. (Netherlands)*, vol.75, no.1, p.1-3 (1982). [received: Sept. 1983]
Formulae for cross product integrals of Euler-Bernoulli functions are presented. It is established that cross products between derivatives are not orthogonal, and the implications are discussed in terms of an earlier Rayleigh-Ritz treatment of Flugge's equations (1973). (7 refs.)

112406 Analytical method for solving fluid-structure interactions in BWR pressure suppression pool. I.Namata, Y.Kukita, I.Takeshita (JAERI, Ibaraki-ken, Japan), Y.Shimoda. *Nucl. Eng. & Des. (Netherlands)*, vol.75, no.1, p.5-11 (1982). [received: Sept. 1983]
An analytical method is developed for solving the fluid-structure interactions (FSI) associated with hydraulic transients in the BWR pressure suppression pool during a hypothetical loss-of-coolant accident. The present method assumes inviscid and infinitesimal motion of pool water for which the governing fluid-dynamic equation reduces to a linear wave equation with inhomogeneous boundary conditions of flexible pool boundaries. The present method is applied to quantitative evaluation of the FSI effect on test data obtained from a large scale pressure suppression test which was performed to investigate the pressure oscillations in the pool induced by unstationary steam condensation. (8 refs.)

112407 A study of risk reduction for some mitigation features for PWRs. M.Gonzales-Cuesta, D.Okrent, W.E.Kastenbergh (Dept. of Mech. & Structures, Univ. of California, Los Angeles, CA, USA). *Nucl. Eng. & Des. (Netherlands)*, vol.75, no.1, p.13-22 (1982). [received: Sept. 1983]
The risk reduction attainable with mitigation features in a large-dry pressurized water nuclear reactor (PWR) is evaluated. The calculations are made in a probabilistic risk analysis framework, and they are based on Zion Probabilistic Safety Study. Some of the modifications made to this study are also taken into account. The mitigation designs considered consist of features for simultaneously controlling late containment overpressure, containment basement penetration, and hydrogen burning. The individual mitigation features include: a passive containment heat removal system (PCHRS), a filtered-vented containment system (FVCS), a core ladle, and controlled hydrogen burning. Emphasis is placed on comparison of PCHRS and FVCS design options. The results include calculations of the sensitivity to several failure mode probabilities and to the probability of core meltdowns with containment bypass. (9 refs.)

112408 A study on sodium spray combustion. R.Kawabe, A.Suzuoki, A.Minato (Energy Res. Lab., Hitachi Ltd., Hitachi-shi, Japan), N.Sagawa, S.Sakaguchi. *Nucl. Eng. & Des. (Netherlands)*, vol.75, no.1, p.49-56 (1982). [received: Sept. 1983]
Sodium spray combustion was studied through experiments and analysis, in order to clarify the burning rate, pressure and temperature transients in a sodium spray fire. In the experiments, about 400 g sodium was sprayed in a closed vessel of 2 m³, containing nitrogen and 0.21 vol.% oxygen. Pressure, temperature and oxygen concentration were measured during and after sodium injection. The experimental results revealed that the temperature in the spray outer region was higher than that of inner region and observed oxygen consumption was not more than 80% of that expected for complete combustion of sodium. Two analyze the experiments, a computer program SOFIA-II was developed based on an analytical single droplet combustion model and a two-dimensional temperature and oxygen concentration distribution model in the vessel. The calculated pressure agreed with the experimental pressure on the whole and the peak pressure difference was within 10% error. (no refs.)

112409 Liquid solidification in laminar tube flow with internal heat sources. Y.Kikuchi, Y.Shigemasa (Dept. of Nuclear Engng., Kyoto Univ., Kyoto, Japan). *Nucl. Eng. & Des. (Netherlands)*, vol.75, no.1, p.73-80 (1982). [received: Sept. 1983]
The effect of liquid solidification (freezing) on the heat transfer characteristics for laminar flow of a heat-generating fluid in a cooled circular tube is investigated analytically. Steady-state conditions and a uniform wall temperature, which is lower than the liquid freezing temperature, are assumed. The radius of the liquid-solid interface and local Nusselt number are determined as a function of position along the tube for several different values of the wall temperature and internal heat-generating rate. The thickness of the solid-phase shell increases with distance down the tube and approaches to its fully developed value depending upon a single dimensionless freezing parameter which measures the relative rate of external cooling and internal heating. The local Nusselt number, however, first decreases rapidly, attains a minimum and then increases towards its fully developed value, which is identical with 6. (11 refs.)

112410 Film boiling from a vertical jet of fuel entering a water pool. S.H.Han, S.G.Bankoff (Chem. Engng. Dept., Northwestern Univ., Evanston, IL, USA). *Nucl. Eng. & Des. (Netherlands)*, vol.75, no.1, p.81-6 (1982). [received: Sept. 1983]
The rate of removal of coolant is examined by means of quasi-steady film boiling from a jet of fuel falling into a water pool during a core meltdown accident in a light water reactor. A two-layer turbulence model in the vapor film is used. Entrainment of droplets due to the high vapor velocity is taken into account, which, for a jet of diameter 0.5 m, increases the removal rate by factor of 5 at 0.7 m behind the leading edge. However, the water removal rate is only of the order of kilograms/second, and the total amount of coolant removed is still small compared to the coolant inventory in the lower plenum. (14 refs.)

112411 Void fraction under high pressure, low flow conditions in rod bundle geometry. T.M.Anklaam (Engng. Technol. Div., Oak Ridge Nat. Lab., Oak Ridge, TN, USA), R.F.Miller. *Nucl. Eng. & Des. (Netherlands)*, vol.75, no.1, p.99-108 (1982). [received: Sept. 1983]
Void-fraction data are reported from a series of high pressure, low heat and mass flux experiments. Testing was performed in a heated vertical rod bundle with internal dimensions similar to a PWR fuel bundle. The results are of interest in analyses of small break loss of coolant accidents. The experiments showed that, at a given pressure, void-fraction data could be fitted to a drift-flux equation with a constant drift-velocity. The drift-velocity was observed to decrease with increasing pressure and was independent of void fraction; a characteristic normally associated with churn-turbulent flow. However, relevant drift-flux correlations found in the literature gave relatively poor predictions of void fraction. The best predictions were obtained from an empirical correlation based on dimensional analysis. (11 refs.)

112412 Component failure model dependent on time and causes. T.Matsuo (Ship Res. Inst., Nuclear Ship Div., Min. of Transport, Tokyo, Japan). *Nucl. Eng. & Des. (Netherlands)*, vol.75, no.1, p.109-16 (1982). [received: Sept. 1983]
Presents a failure model in which the failure rate is a function of cause, of severity of cause, of cause acting duration, and of failure mode. This model was constructed in order to treat the effects of an extreme environmental condition and the common mode failure on system reliability. Causes were classified into two types and failure modes in three types. The expressions of failure probabilities were obtained for combinations of these cause and failure mode types. This model was compared with failure data. The time dependence was well expressed by the α th power of time. The values of α were obtained in the range from 0 to 8. (12 refs.)

112413 The probability of a tornado missile hitting a target. J.Goodman, J.E.Koch (Bechtel Power Corp., Norwalk, CA, USA). *Nucl. Eng. & Des. (Netherlands)*, vol.75, no.1, p.125-55 (1982). [received: Sept. 1983]
It is shown that tornado missile transportation is a diffusion Markovian process. Therefore, the Green's function method is applied for the estimation of the probability of hitting a unit target area. This probability is expressed through a joint density of tornado intensity and path area, a probability of tornado missile injection and a tornado missile height distribution. (10 refs.)

112414 Transient analysis of glowdown thrust force under PWR LOCA. T.Yano, N.Miyazaki, T.Isozaki (Tokai Res. Establ., JAERI, Ibaraki-ken, Japan). *Nucl. Eng. & Des. (Netherlands)*, vol.75, no.1, p.157-68 (1982). [received: Sept. 1983]
The analytical results of blowdown characteristics and thrust forces were compared with the experiments, which were performed as pipe whip and jet discharge tests under the PWR LOCA conditions. The blowdown thrust forces were obtained by Navier-Stokes momentum equation for a single-phase, homogeneous and separated two-phase flow, assuming critical pressure at the exist if a critical flow condition was satisfied. The following results are obtained: (1) The node-junction method is useful for both the analyses of the blowdown thrust force and of the water hammer phenomena. (2) The Henry-Fauske model (1971) for subcooled critical flow is effective for the analysis of the maximum thrust force under the PWR LOCA conditions. The jet thrust parameter of the analysis and experiment is equal to 1.08. (3) The thrust parameter of saturated blowdown has the same one with the value under pressurized condition when the stagnant pressure is chosen as the saturated one. (4) The dominant terms of the blowdown thrust force in the momentum equation are the pressure and momentum terms except that the acceleration term has large contribution only just after the break. (15 refs.)

112415 Ten years of nuclear safety in France: administrative action. C.de Torquat (Min. de l'Industrie et de la Recherche, Paris, France). *Rev. Gen. Nucl. (France)*, no.3, p.187-93 (May-June 1983). In French.
Having recalled the general principles on which administrative action concerning nuclear safety has been based the author goes on to describe the three-principal and complementary aspects of this action: technical regulations; administrative procedure; inspection of plant being constructed or already in operation. Regarding nuclear safety, administrative action over the last ten years in France has focused on examining these three aspects in great depth. (no refs.)

112416 The importance of research for progress in nuclear safety. P.Tanguy, J.Pelce (Inst. de Protection et de Surete Nucleaire, Paris, France). *Rev. Gen. Nucl. (France)*, no.3, p.215-18 (May-June 1983). In French.
The authors describe the research programmes conducted in France with a view to laying down necessary safety arrangements which can be applied to nuclear reactors. They examine the case of light water reactors and then that of rapid neutron reactors. Results of studies up to the present show that the safety margins adopted are basically always valid. Although certain weaknesses have been highlighted (the accident at Three Mile Island is an example) this does not mean that the basic rules for reactor design need be questioned, say the authors. (no refs.)

112417 A study using the MABEL-2C code of the effects of pellet and cladding asymmetries on PWR fuel rod deformation under conditions relevant to the NRU MT-3 ballooning experiment. T.J.Haste. *Report ND-R-876 (S)*, UKAEA, Risley, Lancs., England (April 1983), 76 pp. Available from HMSO, London, England.
The presence of asymmetries in the positions of the fuel pellet stack with respect to the cladding, and of the rods with respect to each other, in PWR fuel bundles has a dominant effect in reducing the amount of strain and hence channel blockage under loss-of-coolant accident conditions. Multi-rod experiments in- and out-of-reactor show wide distributions in burst strain amongst the rods, indicating marked variations in heat source/cladding and rod-to-rod asymmetries. This phenomenon has been studied in detail using the MABEL-2C code, with the aim of assessing the relative importance of heat source asymmetry and thermal hydraulic effects. The transient studied was based on the thermal conditions experienced in the NRU MT-3 ballooning

experiment, where extensive deformation occurred in the high α -phase region. (22 refs.)

112418 Use of base isolation and energy-absorbing restrainers for the seismic protection of a large power plant component. J.M.Kelly.
Report EPRI-NP-2918, Electr. Power Res. Inst., Palo Alto, CA, USA (March 1983), 94 pp.
Available from Res. Rep. Center (RRC), Box 50490, Palo Alto, CA 94303, USA.

An assessment of the significance of the interaction between large power plant components and the plant structure of the seismic response of large components is reviewed. The feasibility of using rubber bearing isolation as a retrofit strategy to improve the structural integrity of the component and the use of various energy-absorbing restrainers for connecting the component to the primary structure are reported. Four test model configurations are described, and results of seismic shake table tests with a comparison of the results between the various configurations are presented.

112419 Technical basis of 'spectral source terms' for assessing uncertainties in fission product release during accidents in PWRs with special reference to Sizewell-B. M.R.Hayns, F.Abbey, P.N.Clough, I.H.Dunbar, D.H.Walker.
Report SRD R 256, UKAEA, Culcheth, Lancs., England (Nov. 1982), 105 pp.
A probabilistic approach is described by which the conservatism inherent in the traditional approach to determine PWR accident release source terms, exemplified by the Reactor Safety Study (WASH-1400), may be assessed, and spectral source terms generated. The method is developed by analysing the mechanisms of fission product retention in the reactor primary circuit and the conservatisms built into the conventional treatment of transport through the containment and leak path to the release point. Detailed probability distributions are derived for the reduction factors applicable to the point value source term at successive transport stages in a number of accident sequences, and the general value and validity of the approach is discussed. (18 refs.)

112420 Seismic response analysis with liquid-structure interaction. R.G.Thomas, L.P.Harrop.
Report SRD R 259, UKAEA, Culcheth, Lancs., England (June 1983), 98 pp.
A linear transient finite element stress analysis of a water filled tank has been carried out using the proprietary computer code ANSYS. The containment structure was represented as rigidly fixed to ground. The flexibility of the tank wall was modelled together with the hydrostatic and hydrodynamic effects of the water contents and attached concentrated masses. The foundations were considered to be laid in solid rock, and no soil-structure interaction effects were included. The seismic input was a ground response spectrum conservatively representing both the Temblor and Parkfield modified time history records. It was found that the response of the structure was greatest at the front end (furthest from the point at which the tank is connected to a rigid internal structure), and that this was dominated by the fundamental mode. Higher modes are important at the back end. Buckling at the front end of the tank has been identified as a potential failure mechanism, and attention has also been called to the tensile capacity of the wall to base junction in this region. The requirement for a proper criterion against which to assess the margin against plastic collapse in a safe shutdown analysis has been noted. In certain regions the structure does not shake-down under the repeated reversed cyclic loading, and the need for an assessment of the implications of this for fatigue resistance has been indicated. (44 refs.)

112421 Hydrogen phenomena in PWR degraded core accidents. S.F.Hall, J.MacKenzie.
Report SRD R 271, UKAEA, Culcheth, Lancs., England (May 1983), 56 pp.
Reviews and discusses recent data concerning hydrogen in PWR severe accidents. The mechanisms whereby hydrogen is distributed and mixed with the containment atmosphere are discussed in relation to experimental data. Experimental data on both hydrogen deflagration and detonation has significantly increased understanding of the physics of such phenomena, and given considerable predictive capability. A discussion of these is followed by its application to the analysis of likely plant damage, which includes recent data from entries into the damaged Three Mile Island Unit 2 containment building. (25 refs.)

112422 Theoretical analysis of hydrogen concentration distribution and acoustic field in Na-water steam generator in presence of micro-leak. R.Kozma, T.Katona.
Report KFKI-1983-60, Hungarian Acad. Sci., Budapest (1983), 25 pp.
The theoretical foundations of hydrogen concentration distribution and the acoustic field in a Na-water steam generator in the presence of a micro-leak are considered. It is shown that both problems lead to the solution of the same boundary value problem for the two-dimensional Helmholtz equation. For the solution of the Helmholtz equation the multiple scattering method is applied. The application of the presented theory in practice is discussed too. (6 refs.)

112423 Two-group criticality models for safety analysis considerations. O.Schaffer.
Report JUL-1856, Kernforschungsanlage, Jülich, Germany (June 1983), 60 pp.
Mathematical models based on the P_1 -approximation of the Boltzmann neutron transport equation (diffusion approximation) in two energy groups are presented in closed form in order to solve many criticality safety problems in handling fissionable material accurately. With regard to the complex subject of criticality a high degree of flexibility is emphasised in dealing with fuel moderator mixing ratios, reflector conditions, fuel interactions, geometry effects and component arrangements. Selected applications are directed in the investigation of the reflector effectiveness on critical and safe masses of highly enriched uranium mixed with graphite and hydrogenous moderators, considering different reflector materials, their positions and effects produced by material shifting and fuel condensation as well as the safe under-water storage of special MTR fuel elements and the safe storage of fuel-graphite specimens in a strongly concrete-shielded rectangular parallelepiped under water-flooding accident conditions. (15 refs.)

112424 Bubble growth in variable pressure fields. G.Egely.
Report KFKI-1983-72, Hungarian Acad. Sci., Budapest (1983), 24 pp.
Presents a study for the bubble behaviour in variable pressure fields. The presentation is started with the deduction of mass momentum and energy conservation equations in spherical form, and continued until the solution is presented in a closed integral form. The author outlines the numerical solution, too. The main object is to present a useful numerical tool for the study of growing or collapsing bubbles, in order to study the interface mass and energy transform terms, and the interface area. This is useful in reactor safety analyses.

112425 Evaluation of critical flow for supercritical steam-water. D.H.Lee, D.Swinnerton.

Report EPRI-NP-3086, Electr. Power Res. Inst., Palo Alto, CA, USA (May 1983), 172 pp.
Available from Research Report Center, Box 50490, Palo Alto, CA 94303, USA.
Subcooled water critical flow data from four simple geometries over the pressure range of 500 to 4500 psia, obtained on the UKAEA Winfrith high-pressure rig, are presented. A comparison of the results of these critical flow data to predictions of three critical flow models and the Bernoulli equation in order to demonstrate the degree of applicability of existing models to these data is reviewed. Comparison of high-pressure heat transfer data to previously reported work is also included.

112426 Testing and evaluation of on-line leak sealing methods. G.A.Smith.
Report EPRI-NP-3111, Electr. Power Res. Inst., Palo Alto, CA, USA (May 1983), 88 pp.
Available from Research Report Center, Box 50490, Palo Alto, CA 94303, USA.

A test program, conducted to evaluate the effectiveness of commercial leak repair services (with respect to the requirements of nuclear power plants), is summarized. Sealants, fixtures, and techniques of three companies that are commercially engaged in on-line leak sealing are demonstrated. Test results and observations show that the effectiveness of an injected-sealant repair is determined by the quality of the initial repair and by its performance within the first 48 hours following repair.

112427 Transient cooldown in a model cold leg and downcomer. M.W.Fanning, P.H.Rothe.
Report EPRI-NP-3118, Electr. Power Res. Inst., Palo Alto, CA, USA (May 1983), 146 pp.
Available from Research Report Center, Box 50490, Palo Alto, CA 94303, USA.

Generation and evaluation of data obtained from an investigation of the cool-down transient of water in the cold leg and downcomer due to high-pressure injection in a stagnant loop are reviewed. Details are provided on fluid-mixing experiments, which were conducted in a 1/5-scale transparent PWR model, experimental results, which focus on the phenomena of buoyant-dominant fluid flow and mixing under stagnant loop flow; temperature data analysis; supportive flow visualization, and full data traces and tables.

112428 BWR spray nozzle performance in steam environment. H.J.Richter, G.G.C.Durkee.
Report EPRI-NP-3119, Electr. Power Res. Inst., Palo Alto, CA, USA (May 1983), 172 pp.
Available from Research Report Center, Box 50490, Palo Alto, CA 94303, USA.

Presents measurements of the water distribution below single full-scale BWR spray nozzles under different environmental conditions. Droplet velocities and size distribution were measured as well, and the findings are presented. The critical flow, bubbly flow, countercurrent flow, deentrainment, distribution, and condensation of droplet flow are discussed.

112429 Estimate of primary-system temperatures in severe reactor accidents. M.S.Hoseyni, A.T.Wassel, R.L.Ritzman.
Report EPRI-NP-3120, Electr. Power Res. Inst., Palo Alto, CA, USA (May 1983), 132 pp.
Available from Research Report Center, Box 50490, Palo Alto, CA 94303, USA.

Engineering calculations performed to provide estimates of primary coolant system conditions for several risk dominant LWR severe accident sequences are described. The specific time span and core locations under consideration are identified; predictions of the MARCH code for time-histories of temperature, flow rate, pressure, and composition of the gas stream exiting the core are provided; and results for the accident sequences of TMLB, S₂D, and AD for PWRs and TW and TC for BWRs are presented.

1st European Conference on Cineradiography with Photons or Particles	See Entry 113300
The implication of sensitivity analysis on the safety and delayed-neutron parameters for fast breeder reactors	See Entry 112294
Comparison of measured fission gas releases for Windscale AGR fuel irradiated above 18 GWd/tU with those predicted using the computer code MINIPAT D	See Entry 112305
CANSWEL-2: A computer model of the creep deformation of Zircaloy cladding under loss-of-coolant accident conditions. Part II. User notes	See Entry 112306
Berechnungsmethoden und Analysen zum dynamischen Verhalten von Kraftwerksanlagen mit Hochtemperaturreaktor (Computation methods and analyses on the dynamic behaviour of power plants with high temperature gas cooled reactors)	See Entry 112309
VIPRE-01: A thermal-hydraulic analysis code for reactor cores. Vol.I: Mathematical modeling	See Entry 112312
VIPRE-01: A thermal-hydraulic analysis code for reactor cores. Vol.II: User's manual	See Entry 112313
Calculation of carburization profiles in stainless steel components in a liquid sodium environment	See Entry 112315
Investigation of material movement within steel test sections by means of high speed X-ray photography	See Entry 112319
Studs vik over-ramp project	See Entry 112346
Rationale for nuclear reactor control room data displays	See Entry 112360
Post-critical heat flux heat transfer: a survey of current correlations and their applicability	See Entry 112367
Hodoscope cineradiography of nuclear fuel destruction experiments	See Entry 112368
Survey of cineradiographic techniques applied to nuclear reactor safety experiments	See Entry 112369
An investigation into the nature and significance of a new critical heat flux correlation	See Entry 112373
The prediction of critical mass flux by the use of Fanno lines	See Entry 112374
Evaluation of techniques to predict flow-induced tube vibration in a preheat steam generator	See Entry 112377
Thermal mixing in a model cold leg and downcomer at low flow rates	See Entry 112378
Time-resolved neutron radiography of reactor fuel	See Entry 112391
Summary report on development of an integral model of a radioactive jet [from a reactor accident]	See Entry 112448

- Experimental investigations on the rewetting of hot horizontal annular channels See Entry 113503
- Some high-temperature properties of Zircaloy-oxygen alloys See Entry 114213
- Intergranular stress corrosion cracking of Ni-Cr-Fe Alloy 600 tubes in PWR primary water - Review and assessment for model development See Entry 115447
- Automated time-of-flight studies of the defect detection trial plates 1 and 2 See Entry 115454
- CEGB inspection of plates 1 and 2 in UKAEA defect detection trials See Entry 115455
- An in-service inspection method: the use of focused probes for the detection and sizing in DDT plates 1 and 2 See Entry 115456
- Dose-effect relationships for early response to total body irradiation See Entry 115863

28.50 FISSION REACTOR TYPES AND APPLICATIONS

- 112430 Hitachi's large-scale FBR plant development programs. H.Yamaki (Hitachi Works, Hitachi Ltd., Tokyo, Japan), H.Yamamoto. *Hitachi Rev. (Japan)*, vol.32, no.2, p.100-4 (April 1983). [received: Aug. 1983]
- Hitachi is involved in the development of a large-scale fast breeder reactor (FBR) plant (1000 MWe) as part of its contribution to Japanese FBR development programs sponsored by various organizations. These programs follow the experimental reactor JOYO, now in stretched power level operation (MK-II), and the prototype reactor MONJU, which is in the final stage of the licensing process. In addition to these projects, Hitachi is proceeding with its own development programs. To meet large-scale FBR plant core design requirements, an axially heterogeneous core concept has been evaluated and applied to a 1000 MWe tank-type plant design study program. The plant design is supported by newly developed thermal-hydraulic or plant-dynamics evaluation codes. The paper summarizes recent progress made in Hitachi's large-scale FBR programs. (7 refs.)
- Recent bibliography on analytical and sampling problems of a PWR primary coolant. Supplement II See Entry 111336
- The implication of sensitivity analysis on the safety and delayed-neutron parameters for fast breeder reactors See Entry 112294
- Reproduction of transport calculation results by diffusion theory employing albedo boundary conditions See Entry 112295
- Neutron design study of BN 600 type reactor with plutonium fuel See Entry 112304
- Comparison of measured fission gas releases for Windscale AGR fuel irradiated above 18 GWd/tU with those predicted using the computer code MINIPAT D See Entry 112305
- SIMULATE-E: A nodal core analysis program for light water reactors. Computer code user's manual See Entry 112307
- Berechnungsmethoden und Analysen zum dynamischen Verhalten von Kraftwerksanlagen mit Hochtemperaturreaktor (Computation methods and analyses on the dynamic behaviour of power plants with high temperature gas cooled reactors) See Entry 112309
- First investigations on a wrapped fibre blanket insulation with massive spacers consisting of carbon fibre composite See Entry 112310
- New HTR conception for a modular system with block-fuel elements and its comparison with an HTR with ball-shaped fuel shaped elements See Entry 112311
- VIPRE-01: A thermal-hydraulic analysis code for reactor cores. Vol.I: Mathematical modeling See Entry 112312
- VIPRE-01: A thermal-hydraulic analysis code for reactor cores. Vol.II: User's manual See Entry 112313
- Calculation of carburization profiles in stainless steel components in a liquid sodium environment See Entry 112315
- Primary coolant treatment by ion exchangers—experience from the operation of nuclear power stations with pressurized water reactors See Entry 112318
- Investigation of material movement within steel test sections by means of high speed X-ray photography See Entry 112319
- Oxygen potential and lattice parameter measurements in (U, Ce)O_{2-x} See Entry 112324
- Distribution of fission and activation products in the graphite sleeves of HTGR fuel rods: first and second OGL-1 fuels See Entry 112325
- Stress analysis of core support post in a very high-temperature reactor See Entry 112334
- Weld residual stress redistribution near growing cracks See Entry 112339
- Oxidation of Ni-Cr experimental alloys and the effectiveness of the oxide as a barrier against carburization in high-temperature reactor primary circuit helium See Entry 112343
- Studsvik over-ramp project See Entry 112346
- Reaction of lithium and sodium nitrates and carbonates with uranium oxides See Entry 112354
- A fuzzy-logic approach to HTR nuclear power plant model control See Entry 112361
- Hodoscope cineradiography of nuclear fuel destruction experiments See Entry 112368
- Survey of cineradiographic techniques applied to nuclear reactor safety experiments See Entry 112369
- MIRENE, a mini-nuclear reactor for neutronography—data and applications See Entry 112370
- Development of key components for the heat transport system of prototype fast breeder reactor 'MONJU' See Entry 112371
- FBR wide-range neutron monitoring system See Entry 112375
- Reactor physics and economic aspects of the CANDU reactor system See Entry 112376
- Evaluation of techniques to predict flow-induced tube vibration in a preheat steam generator See Entry 112377
- Thermal mixing in a model cold leg and downcomer at low flow rates See Entry 112378
- Hydrazine usage for corrosion control in PWR plants with powdered resin condensate polishers See Entry 112379

- Primary-side deposits on PWR steam generator tubes See Entry 112381
- Numerische Untersuchung der 3-dimensionalen stationären Temperatur- und Stromungsverteilung im Core eines Kugelhaufen-Hochtemperaturreaktors (Numerical investigation of the 3-dimensional steady-state temperature - and flow-distribution in a pebble bed high temperature reactor core) See Entry 112382
- Experimental investigation for the thermohydraulics of packed beds in the comparison with the computer code THERMIX-2D: The investigation of the dispersive heat transfer examined by a cold gasstream See Entry 112383
- NBS reactor: Summary of activities July 1981 through June 1982 See Entry 112385
- Secondary water chemistry at Millstone 2 See Entry 112386
- On-line use of chelants in nuclear steam generators - Feasibility study See Entry 112387
- Evaluation of steam generator fluid mixing during layup See Entry 112388
- Condensate polisher resin leakage quantification and resin transport studies See Entry 112389
- Implementation of boric acid in the field - Indian Point Unit 3 plant See Entry 112390
- Time delay estimation: application to flow rate measurement of cooling fluid in nuclear power plants See Entry 112394
- Models for calculating the mass flow of a two-phase system on the basis of measured density and momentum flux values See Entry 112395
- Investigations of the system behaviour of a pressurized-water reactor during loss-of-coolant accidents. The PKL experiment See Entry 112396
- Investigations of the reflow-phase after a loss-of-coolant-accident of an advanced pressurized water reactor (APWR) See Entry 112398
- Simple analysis of very long term processes without operational and emergency energy supply in the PWR power plant See Entry 112399
- Loss-of-coolant accident in the fluidized bed nuclear power reactor See Entry 112400
- The ignition and burning behaviour of sodium metal in air See Entry 112401
- Measurement of vibrations caused by leakages between pressurized circuits during the 30 MW Czech, modular steam generator operation at BOR 60 See Entry 112404
- Analytical method for solving fluid-structure interactions in BWR pressure suppression pool See Entry 112406
- A study of risk reduction for some mitigation features for PWRs See Entry 112407
- A study on sodium spray combustion See Entry 112408
- Liquid solidification in laminar tube flow with internal heat sources See Entry 112409
- Film boiling from a vertical jet of fuel entering a water pool See Entry 112410
- Void fraction under high pressure, low flow conditions in rod bundle geometry See Entry 112411
- Transient analysis of glowdown thrust force under PWR LOCA See Entry 112414
- Use of base isolation and energy-absorbing restrainers for the seismic protection of a large power plant component See Entry 112418
- Technical basis of 'spectral source terms' for assessing uncertainties in fission product release during accidents in PWRs with special reference to Sizewell-B See Entry 112419
- Hydrogen phenomena in PWR degraded core accidents See Entry 112421
- Theoretical analysis of hydrogen concentration distribution and acoustic field in Na-water steam generator in presence of micro-leak See Entry 112422
- Evaluation of critical flow for supercritical steam-water See Entry 112425
- Transient cooldown in a model cold leg and downcomer See Entry 112427
- BWR spray nozzle performance in steam environment See Entry 112428
- Estimate of primary-system temperatures in severe reactor accidents See Entry 112429
- Characterization of the oxide-metal interface at the surface of a stainless steel See Entry 112437
- Intergranular stress corrosion cracking of Ni-Cr-Fe Alloy 600 tubes in PWR primary water - Review and assessment for model development See Entry 115447
- Operation of the EPRI nondestructive evaluation center. Annual report - 1982 See Entry 115495
- Steam generator U-bend eddy-current NDE See Entry 115496

28.52 FUSION REACTORS

(for confinement, see 52.55)

- 112431 Comments on 'Guidelines for the neutron scalar flux shaping of advanced nuclear energy device blankets' [and reply]. E.Greenspan (Dept. of Phys., Nuclear Res. Centre-Negev, Beer Sheva, Israel), S.Taczanowski. *Ann. Nucl. Energy (GB)*, vol.10, no.9, p.497, 499 (1983).
- Greenspan discusses the use of neutron scalar flux shaping for breeding in fusion reactor blankets. Taczanowski replies to his comments. (7 refs.)
- 112432 The basis mapping method for solving plasma equilibrium. Luo Zhengming (Southwestern Univ. of Phys., China). *Acta Mech. Sin. (China)*, no.3, p.233-40 (1983). In Chinese.
- By using the basis napping method, the solution of an improperly posed Cauchy problem of the magnetic flux equation is expressed by a series in which every term is a solution of a well-posed Dirichlet problem. Then this problem is further reduced to an overdetermined linear system. Using the Moore-Penrose theory of generalized inverses optimal least square solutions can be obtained. The numerical solutions of several plasma configurations and the corresponding current distribution of the maintaining coils have been obtained. Comparison with analytical solution shows that the precision of the method presented is good. (15 refs.)
- 112433 Various kinds of radiation implosion targets. F.Winterberg (Desert Res. Inst., Univ. of Nevada System, Reno, NV, USA). *Atomkernenergie. Kerntechnik. (Germany)*, vol.41, no.4, p.291-2 (1982). [received: Sept. 1983]
- In 'Hohlraum' or cavity targets for beam induced thermonuclear microexplosions, the beam energy is trapped and converted into black body radiation within a cavity. It is in turn the black body radiation which ablatively implodes the thermonuclear target placed inside the cavity. If one desires

smaller cavities one may implode the cavity by which one can amplify the black body radiation entrapped in it, provided the implosion velocity is sufficiently large. The author reports another possibility to reduce the overall target dimension drastically. In this concept the cavity is filled with, or rather replaced by, a dense plasma of a low atomic weight substance, for example beryllium. The density can be less than solid state density, in which case the plasma is produced from a dense vapor or gas, but it can even have solid state density, in which case the cavity is filled with a solid, for example beryllium. (5 refs.)

112434 Interpenetration burn for controlled inertial confinement fusion driven by nonlinear laser forces. H.Hora (Dept. of Theoretical Phys., Univ. of New South Wales, Kensington, Australia). *Atomkernenerg. Kerntechnik. (Germany)*, vol.42, no.1, p.7-10 (1983). Contrary to the usual calculations of self-sustained fusion combustion fronts on the basis of shock waves, an interpenetration model is developed, where the α -reheat of a hot DT fusion layer compensates the heating up of a cold fuel layer into which the hot layer is penetrating. The basis of this process is that the propagation of the hot layer is not faster than its thermal expansion against vacuum what is justified due to recent results of space charge effects preventing very fast electron heat waves into the cold fuel. The needed energy densities of 2×10^{17} Joules/cm² are about 10 times less than in the shock wave model, but the penetration burn needs a very fast energy transfer for initiation (200 psec). For the powder densities of 10^{17} W/cm² and >300 kJ energy input, the CO₂ laser systems are preferable. The initiation heating is then possible by a radiation pressure transfer of the optical energy to 50 MeV, 10^{10} Amp/cm² space charge neutral 'ion beams'. (31 refs.)

112435 Net energy balance of Tokamak fusion power plants. R.Bunde (Max-Planck-Institut für Plasmaphysik, Garching, Germany). *Atomkernenerg. Kerntechnik. (Germany)*, vol.42, no.2, p.73-9 (1983). The net energy balance for a Tokamak fusion power plant of present day design is determined by using a PWR power plant as reference system, replacing the fission-specific components by fusion-specific components and adjusting the non-reactor-specific components to altered conditions. For determining the energy input to the fusion plant a method was developed that combines the advantages of the energy input-output method with those of process chain analysis. A comparison with PWR, HTR, FBR, and coal-fired power plants is made. As a result the energy expenditures of the fusion power plant turn out to be lower than that of the LWR, HTR, or coal-fired power plant of equal net electric power output and nearly in the same range as FBR power plants. (28 refs.)

112436 Neutron multiplier thermal stresses in pure fusion and fusion-fission reactor blankets. R.N.Kostoff (Office of Energy Res., US Dept. of Energy, Washington, DC, USA). *Res. Mech. (GB)*, vol.9, no.1, p.1-34 (1983). An algorithm was derived for computing cyclic thermal stresses in the cladding of flat plate (slab) neutron multipliers heated by fusion-produced neutrons and located in the blanket of a fusion reactor whose core operates at an arbitrary pulsing frequency. When the thermal time constant of the slab is large relative to the cycle length, the cladding thermal stresses are approximately the same for all of the five fusion core concepts examined and equal to the steady state value. As the slab thermal time constant is decreased by decreasing the thickness of the slab, the absolute values of the cladding thermal stresses decrease, but at substantially different rates for long- and short-pulse concepts. For small slab thermal time constants, the cladding thermal stresses of the long-pulse concepts are substantially smaller than those of the short-pulse concepts. (23 refs.)

112437 Multijoint inspection robot. K.Asano, M.Obama, Y.Arimura, M.Kondo, Y.Hitomi (Energy Sci. & Technol. Lab., Toshiba Corp., Kanagawa, Japan). *IEEE Trans. Ind. Electron. (USA)*, vol.IE-30, no.3, p.277-81 (Aug. 1983). Describes a newly developed multijoint inspection robot for use in a fusion reactor. The design philosophy of the CCTV inspection robot and its control system are discussed. Then, details of the robot's hardware and control system are presented. Several experiments were made with an inspection facility model, and it was verified that this robot can easily get to an inspection target by weaving through obstacles. It is believed that this robot will be used as a key component in a remote inspection system in physically difficult to reach or dangerous environments. (4 refs.)

112438 A class of similarity solutions for the nonlinear thermal conduction problem. F.J.Mayer, J.F.McGrath, J.W.Steele (KMS Fusion Inc., Ann Arbor, MI, USA). *J. Phys. A (GB)*, vol.16, no.14, p.3393-400 (1 Oct. 1983). A class of self-similar solutions are rederived for the nonlinear thermal conduction problem. Variational methods applied to the heat flux provide an expression valid over a broad range of physical parameters. The results are particularly useful for the understanding of heat flux in the plasmas of internal confinement fusion. They describe both rapid laser and radiant heating of matter. The developments are shown to correspond well to several classical examples. (6 refs.)

112439 Effect of ³He on a permeation membrane. M.Nishikawa (Dept. of Nuclear Engng., Kyushu Univ., Fukuoka, Japan). *J. Nucl. Mater. (Netherlands)*, vol.116, no.2-3, p.343-4 (June 1983). Discusses the behaviour of ³He, the decay product of tritium, in permeation membranes for extracting and purifying tritium in the fuelling and blanket cycles of conceptual fusion reactors. (4 refs.)

112440 The role of the jet projection in global fusion research. V.O.Jensen (Riso Nat. Lab., Riso Nat. Lab., Roskilde, Denmark). *Phys. Scr. (Sweden)*, vol.T5, p.136-9 (1983). (Proceedings of the 4th Nordic Meeting on Nuclear Physics, Fuglso, Denmark, 16-20 Aug. 1982). JET (Joint European Torus) is a major fusion experiment now under construction near Abingdon in the UK. It is aimed at producing conditions approximating those necessary in a fusion reactor. The results expected from JET should permit a realistic evaluation on the prospects for fusion power and serve as a basis for the design of the next major fusion experiment. (no refs.)

112441 Predicted behaviour of the single-null divertor of INTOR. M.F.A.Harrison, E.S.Holston. *Report CLM-R 226*, UKAEA, Culham, Abingdon, Oxon., England (1982), 24 pp. Available from HMSO, London, England.

The performance of the single-null divertor is modelled over a range of scrape-off plasma parameters appropriate to the concepts envisaged in the INTOR Phase I and Phase IIA and particular attention is given to a comparison of the behaviour of beryllium and tungsten targets. The models predict for INTOR conditions that the DT plasma within the divertor chamber is cooled by localised recycling and that most of the energy which flows into the chamber is eventually deposited upon the target by convective transport through the sheath. Catastrophic sputtering of a tungsten target is in principle

possible because the self-sputter yield of tungsten can exceed unity. However, the present analyses show that such conditions are unlikely when there is substantial recycling of DT within the divertor chamber; indeed the self-sputter rates predicted here for tungsten are less than those for beryllium. Moreover, the temperature of the plasma at the sheath edge and also the effective sputtering of impurity atoms are sensitive to the plasma density in the scrape-off region. Increasing the scrape-off density to about 8×10^{19} m⁻³ ensures that the effective sputter yield of tungsten does not exceed $\sim 10^{-4}$. (4 refs.)

112442 CVD coatings in fusion reactor technology. F.Brossa (Materials Sci. Div., Joint Res. Centre, Comm. of the European Communities, Ispra, Italy). Proceedings of the 4th European Conference on Chemical Vapour Deposition, Eindhoven, Netherlands, 31 May-2 June 1983 (Eindhoven, Netherlands: Philips Centre Manuf. Technol. 1983), p.340-9. A large number of coatings have been evaluated as a protective low Z layer for the first wall of a magnetically confined fusion reactor: B, Si, Al₂O₃, TiC, TiN, SiC and B₄C. High Z coatings Mo, Ta and W, have also been proposed for in-vessel component protection against heavy heat loads. CVD is the technique most commonly employed for coating first wall candidate materials (AISI 316, 310, 304, Inconel 600, Mo, Al and Cu). The coatings produced by this technique have a high adherence, are homogeneous and pore-free. The sputtering behaviour of these coatings has been tested under H⁺, D⁺ and He⁺ irradiation in the 100 eV-8 KeV energy regime. Other properties, such as arc erosion, evaporation rate, thermal fatigue resistance, compatibility and adherence to base material, have also been tested in laboratory scale equipment. (21 refs.)

Proceedings of the International Workshop on Cross Sections for Fusion and Other Applications See Entry 111298

Möglichkeiten der Spaltstoffherzeugung für Hochtemperatur-Reaktoren im Verbundsystem von Hochtemperatur-Reaktor und Fusionsreaktor (Facilities for producing fissile fuel for high temperature gas-cooled reactors in a symbiotic fission-fusion system) See Entry 112444

Converting thermal neutrons into 14 MeV DT neutrons using the suprathermal fusion principle See Entry 112496

Measurements of charge change in atomic collisions at MeV energies See Entry 112845

Properties of the corona generated by the incidence of intense CO₂ laser pulses on spherical targets See Entry 113638

Status of the US effort in atomic physics research relevant to the magnetically confined fusion program See Entry 113639

A comparison between laser induced fluorescence at Balmer-alpha and at Lyman-alpha for the measurement of neutral hydrogen densities in magnetically contained fusion plasmas See Entry 113648

Transport models of particle and energy balance in Tokamak devices See Entry 113670

Lattice expansion and broadening of the Bragg reflexion in thermal-neutron-irradiated Li₂O pellets See Entry 114044

Surface composition change of TiC under 0.15-3 keV hydrogen ion bombardment See Entry 114050

Solubility and diffusivity of hydrogen in Li₂O See Entry 114180

Diffusivity of tritium in Li-Al alloys See Entry 114260

Diffusion of tritium in single crystal Li₂O See Entry 114261

On the influence of incident energy of protons on chemical erosion of graphite See Entry 114990

On the reaction of graphite with atomic hydrogen See Entry 114991

Investigation of phase equilibria related to fusion reactor materials. I. The ternary system Zr-Al-N See Entry 115165

Frequency dependence of the high temperature fatigue properties of He-implanted stainless steel See Entry 115312

28.58 INTEGRATED REACTOR SYSTEMS

112443 A fusion-fusion reactor driven by plasma-liner impact. J.G.Linhart. *Atomkernenerg. Kerntechnik. (Germany)*, vol.42, no.1, p.1-6 (1983). It is shown that the impact of a quasi-spherical plasma liner on a spherical solid liner can produce a highly luminous source of soft X-rays. This radiation can be used for the ablation of an inner spherical liner, which can be thus accelerated to speeds above 10^7 cm/sec. Such a liner should be able to compress a core of fissionable material, surrounded by a D-T mantle to fission-criticality. The burst of the fission energy then ignites the D-T mantle which produces a larger burst of fusion energy. The energy liberated in such a microexplosion is estimated to be of the order of 1 GJ. An apparatus based on a symmetrical plasma-focus geometry should be able to produce the plasma liner. A reactor combining these concepts is described. (12 refs.)

112444 Möglichkeiten der Spaltstoffherzeugung für Hochtemperatur-Reaktoren im Verbundsystem von Hochtemperatur-Reaktor und Fusionsreaktor (Facilities for producing fissile fuel for high temperature gas-cooled reactors in a symbiotic fission-fusion system). S.Meuresch. *Report JUL-1827*, Kernforschungsanlage, Jülich, Germany (Jan. 1983), 75 pp. In German. In the blanket of a hybrid reactor the 14.1-MeV neutrons of the DT-fusion are used for breeding tritium and the fissile fuel U-233. Some different fertile materials are investigated. Best breeding results are achieved by using a Li-Pb-eutectic in conjunction with ThO₂ containing coated particles. The blanket region is subdivided in a 40-cm-thick breeding zone and a 59.2-cm-thick zone for fissile fuel production. A 60-cm-thick stainless-steel-boron carbide shield prevents radiation damage to the components of the superconducting magnet. The neutron and gamma-ray fluxes were calculated by solving the discrete ordinates form of the transport equation using the ANISN program in the P₃S₈ approximation in one-dimensional cylindrical geometry. The calculations for the isotope generation and depletion were performed using the ORIGEN code. Resonance calculations for Th-232 were done with the modul NITAWL of the AMPX code system. The nuclear cross sections were mainly taken from the ENDF/B-IV-Library. (28 refs.)

Neutron multiplier thermal stresses in pure fusion and fusion-fission reactor blankets See Entry 112436

Converting thermal neutrons into 14 MeV DT neutrons using the suprathermal fusion principle See Entry 112496

28.70 NUCLEAR EXPLOSIONS

(see also 47.40 Shock and detonation phenomena)

112445 Hot particles from nuclear atmospheric test of October 1980. S.Sonoc, C.Dovlete (Inst. de Meteorologie si Hidrologie, Bucuresti, Rumania). *Stud. & Cercet. Fiz. (Rumania)*, vol.35, no.8, p.744-7 (1983). In Rumanian. The first identification in Rumania of a hot particle from an atmospheric thermonuclear explosion is reported. The sample was collected by air filtration using a cellulose filter. Gamma spectroscopy with Ge(Li) detector measurement of the sample enabled one to identify Zr-95 and Nb-95. The presence of these radionuclides in quantities comparable to those reported by other authors in hot particles, as well as the absence of other radionuclides, agrees well with the models of hot particles generation and atmospheric transport. (7 refs.)

28.80 RADIATION TECHNOLOGY, INCLUDING SHIELDING

(see also 87.60 Medical and biomedical uses of fields, radiations and radioactivity)

112446 Gamma dosimetry using lyoluminescence of tris (hydroxymethyl) aminomethane. S.K.Mehta, I.K.Oommen, S.Sengupta, S.D.Soman (Health Phys. Div., Bhabha Atomic Res. Centre, Bombay, India). *Nucl. Instrum. & Methods Phys. Res. (Netherlands)*, vol.213, no.2-3, p.393-6 (1 Aug. 1983).

Lyoluminescence (LL) of tris (hydroxymethyl) aminomethane has been studied and compared with the LL of glucose, mannose, valine and glutamine. Among these materials, tris (hydroxymethyl) aminomethane on dissolution in luminol shows the highest LL sensitivity and stability. The linear dosimetric range of this system is $0.1-2 \times 10^2$ Gy which makes it useful in the fields of radiotherapy and radiation processing of food. (8 refs.)

112447 Experience in the use of lapel air samplers at AWRE. E.W.Jones, R.G.Hopkins, D.L.E.Smith, D.M.Wallace (Atomic Weapons Res. Estab., Min. of Defence Procurement Executive, Aldermaston, England). *J. Soc. Radiol. Prot. (GB)*, vol.3, no.3, p.11-17 (Autumn 1983).

The authors outline the experience at AWRE in making intensive use of small air samplers, commonly described as personal air samplers or lapel air samplers and for convenience referred to hereafter as 'PAS'. It indicates the general pattern of results obtained, the interpretation which has been placed upon them, the difficulties which have been encountered in conducting a routine sampling programme and in maintaining the instruments and summarises the expenditure of resources which has been required. It is hoped that the information may be of value to others who are contemplating large scale use of PAS or endeavouring to assess the value of this technique for operational control or dosimetry purposes. (1 ref.)

112448 Summary report on development of an integral model of a radioactive jet (from a reactor accident). A.Badre, D.Grand. *Eur. Appl. Res. Rep. Nucl. Sci. Technol. Sect. (USA)*, vol.5, no.1, p.1-119 (1983).

In the present survey of studies on radioactive jets, the main point of view considered has been the prediction of concentration and trajectory. Although it may be more important for practical purposes to determine the direct risks to the environment viewed as a whole (human, agricultural, economic, etc.), this aspect of the problem remains underlying since its determination depends mainly on the results of the calculations of trajectory and concentration. The present study is concerned with the near-field of jets (the near-field being the relation of the jet close to its source where the dynamic of the jet is still relevant compared to that of the ambient atmosphere). The authors consider the rise of a moist plume that contains radioactive products, by means of an integral method. (61 refs.)

112449 Study of shielding characteristics of certain materials. II. Change of dosimetric characteristics during irradiation on a ^{252}Cf -source depending on the type of shielding and geometric arrangement. Z.Prouza, J.Hermanska (Inst. of Biophysics & Nuclear Medicine, Charles Univ., Prague, Czechoslovakia), O.Neruda, J.Cerny, F.Spurney. *Jad. Energ. (Czechoslovakia)*, vol.29, no.8-9, p.319-23 (Aug.-Sept. 1983). For pt.1 see *ibid.*, vol.29, p.267, (1983). For a set of 18 spectra measured on a ^{252}Cf -source after the passage of radiation through different types of shielding dosimetric quantities are presented. Relations between these quantities are studied. (12 refs.)

112450 Electret dosimeter. M.Ikeya (Tech. Coll., Yamaguchi Univ., Ube, Japan).

Oyo Buturi (Japan), vol.52, no.4, p.305-9 (April 1983). In Japanese. Describes the principles and development history of dosimeters using electrets, whose surface charge quantity is lost by radiant-ray irradiation. The materials applicable to this service include fluorine polymers such as PVDF. These materials are characterized by their high stopping power compared to glasses, which permits a small-volume detector for high-energy particles. The author's developed neutron dosimeter using a fluorine polymer electret is measurable up to 10^{-2} mGy. (24 refs.) K.B.

112451 Computer-based system enhances radiation data management. J.H.G.Zdzieborski, D.Kahn (United Engrs. & Constructors Inc., Philadelphia, PA, USA), G.L.Waldkoetter.

Power (USA), vol.127, no.8, p.81-5 (Aug. 1983). Safety of plant personnel and the public dictates effective radiation control at nuclear powerplants. A state-of-the-art digital system will simplify this demanding task at a plant nearing completion. (no refs.)

112452 Plans for safeguarding the population with respect to nuclear power stations. H.Rouanet (Min. de l'Interieur et de la Decentralisation, Paris, France).

Rev. Gen. Nucl. (France), no.3, p.206-8 (May-June 1983). In French.

The Directorate of Civil Safety has drawn up its measures for safeguarding the population in the event of accidents in nuclear plans as part of the 'ORSEC' plans. These general safety measures, which are completed by the specialised, so-called 'ORSEC-RAD' appendices, are being put into effect at the individual nuclear power plant level by the creation of Special Safety Measures (PPI) which form an integral part of the ORSECRAD plans. The author describes the organisation of these ORSECRAD-PPI plans and the allocation of the responsibilities involved. The author then sets out their contents together with the specialised methods which exist for the different types of safety measures to be implemented. (no refs.)

112453 Inter-ministerial nuclear security exercises. P.O.Halpern (Comite Interministeriel de la Securite Nucleaire, Paris, France).

Rev. Gen. Nucl. (France), no.3, p.209-14 (May-June 1983). In French.

If a nuclear incident or accident occurs, a series of measures are planned which are aimed at protecting both workers at the plant and the general

public. This 'emergency programme', the arrangements of which are described by the author, involves coordinated action on the part of the plant operators, the safety authorities and, in a more general way, the public authorities. The efficiency of this emergency system has been tested several times up to now when inter-ministerial exercises based on simulated accidents affecting various nuclear power stations have been carried out. The author describes the objectives sought, the practical details of these exercises and the lessons which have been learnt from them. (no refs.)

112454 Quantifizierende Bemerkungen zur Frage der Konservativitat der 'Allgemeinen Berechnungsgrundlagen' (Quantified remarks on the question of the conservation of general calculation inputs). H.D.Brenk, K.J.Vogt.

Report JUL-1821, Kernforschungsanlage, Julich, Germany (Dec. 1982), 147 pp. In German.

Dose prediction models are always subject to uncertainties due to a number of factors including deficiencies in the model structure and uncertainties of the model input parameter values. In lieu of validation experiments the evaluation of these uncertainties is restricted to scientific judgement. Several attempts have been made in the literature to evaluate the uncertainties of the current dose assessment models resulting from uncertainties of the model input parameter values using stochastic approaches. Less attention, however, has been paid to potential sources of systematic over- and underestimations of the predicted doses due to deficiencies in the model structure. The present study addresses this aspect with regard to dose assessment models currently used for regulatory purposes. The influence of a number of basic simplifications and conservative assumptions has been investigated. (82 refs.)

112455 Release of gaseous tritium during reprocessing. H.Brucher, K.Hartmann.

Report JUL-1838, Kernforschungsanlage, Julich, Germany (Jan. 1983), 132 pp.

About 50% of the tritium put through an LWR reprocessing plant is obtained as tritium-bearing water, HTO. Gaseous tritium, HT, has a radiotoxicity which is by 4 orders of magnitude lower than that of HTO. A possibility for the removal of HTO could therefore be its conversion into the gas phase with subsequent emission of the HT into the atmosphere. However, model computations which are, in part, supported by experimental data reveal that the radiation exposure caused by HT release is only by about one order of magnitude below that caused by HTO. This is being attributed to the relatively quick reoxidation of HT by soil bacteria. Two alternatives for producing HT from HTO (electrolysis; voloxidation with subsequent electrolysis) are presented and compared with the reference process of deep-well injection of HTO. The authors come to the conclusion that tritium removal by HT release into the atmosphere cannot be recommended at present under either radiological or economic aspects. (30 refs.)

112456 SARTEMP2 - A computer program to calculate power and temperatures in a transport flask during a criticality accident. P.M.Shaw.

Report SRD R 266, UKAEA, Culcheth, Lancs., England (April 1983), 31 pp.

The program SARTEMP calculates the fission release and temperatures obtained in a transport flask following a hypothetical criticality incident. This extended version of the program has been developed, in association with a collaborative study between staff of the Commissariat a l'Energie Atomique (CEA) and UKAEA, to study the effects of an accident during water filling of a particular design of transport flask carrying a particular arrangement of fuel pins. Two cases are considered. The first case assumes a slow rate of filling corresponding to the flask being lowered into a pond. It has been determined that the flask will reach delayed critical when the water height is 1 m. For the second case, a faster rate of filling is assumed and delayed critical occurs at a water height of 3.5 m. These values are specific to this particular design. The program can, however, be used to analyse more general designs of flask.

112457 Neutron response of several fission track detectors worn on the body. J.Palfalvi.

Report KFKI-65, Hungarian Acad. Sci., Budapest (1983), 11 pp.

The combined effect of incident and albedo neutrons on the response of several fission track detectors was investigated by calculations for monoenergetic neutrons and for neutrons from different energetic sources. The response functions are presented in tables and plots. (9 refs.)

112458 Results of environmental radioactivity measurements in the Member States of the European Community for air - deposition - water - milk 1981.

Report EUR 8308 DA/DE/EN/FR/IT/NL, Comm. European Communities, Luxembourg (1983), 287 pp.

This is the 21st report on environmental radioactivity published by the Health and Safety Directorate of the Commission of the European Communities. It has been prepared from data gathered at the stations which monitor environmental radioactivity in the Member States. The results are taken from the data communicated to the Commission of the European Communities in accordance with Article 36 of the Treaty of Rome establishing the European Atomic Energy Community. The results contained in the report refer to radioactivity measurements for air, deposition, surface water and milk during 1981 in the ten Member States of the European Community (Belgium, Denmark, Federal Republic of Germany, Greece, France, Ireland, Italy, Luxembourg, The Netherlands and United Kingdom).

112459 Progress report programme. Radiation protection 1982.

Report EUR 8486 DE/EN/FR, Comm. European Communities, Luxembourg (1983), viii + 1225 pp.

The progress report of the radiation protection programme outlines the research work carried out in 1982 under contracts between the Commission of the European Communities and research groups in the Member States. Results of about 320 individual projects are reported. They are grouped into 6 sectors: radiation dosimetry and its interpretation, behaviour and control of radionuclides in the environment, short-term somatic effects, late somatic effects as well as genetic effects of ionizing radiation and evaluation of radiation risks. More than 900 scientific publications are referred to in this report. The role of this scientific programme is: (i) to study methods of reducing radiation exposure and minimizing the radiation hazards in all circumstances, (ii) to study ways and means of acting rapidly and effectively in the event of an accident, (iii) to acquire the research results necessary to update the basic principles of radiation protection, and (iv) to supply sufficient information to contribute to a framework for making informed decisions on issues on which public opinion has become very sensitive.

112460 Instrumentation developed by the Bureau of Mines for continuously monitoring radon and radon daughters. J.C.Franklin (Bur. of Mines, US Dept. of Interior, Spokane Res. Center, Spokane, WA, USA), R.F.Drouillard. Instrumentation in the Mining and Metallurgy Industries. Vol.9. Proceedings of the 10th Annual Mining and Metallurgy Industries Symposium and Exhibit, Denver, CO, USA, 5-7 May 1982 (Research Triangle Park, NC, USA: ISA 1982), p.103-15.

The US Bureau of Mines has developed instrumentation to continuously monitor radon and radon daughters in underground uranium mines. These

monitors have been used for several years by the Bureau and Bureau contractors to collect data in both active and experimental mines. The working level monitors are used with an alarm system to alert surface personnel when the underground working level is excessive. Other sensors have been developed for the alarm system that will notify surface personnel on loss of power to fans or air doors left open. Also developed was a personal radon daughter dosimeter using a thermoluminescent detector. The dosimeters can be worn on the miners' belts to measure their actual exposures. Both laboratory and field testing of these dosimeters were satisfactory. (13 refs.)

Organisation of inspection of radioactive waste by the public health services See Entry 112337

Technical basis of 'spectral source terms' for assessing uncertainties in fission product release during accidents in PWRs with special reference to Sizewell-B See Entry 112419

Proposal for decommissioning of contaminated steel parts from shut down nuclear power plants See Entry 112462

Plastic detector technique in fast neutron radiography See Entry 112570

The neutron sensitivity of a Geiger-Muller counter between 0.5 and 8 MeV See Entry 112571

Backscattering observation of radiation damage in optical fibers See Entry 113983

Kornyezi doziszintenzitas helyszini meghatarozasa Ge(Li)-spektrometriaval. A modszér (Environmental dose rate in situ determination by Ge(Li)-spectrometry See Entry 115715

Statistical procedures for assignments of upper bounds for radiation doses to an unbadged individual in a group for which some individuals are badged See Entry 115929

28.90 OTHER TOPICS IN NUCLEAR ENGINEERING AND NUCLEAR POWER STUDIES

112461 The significance of inertial confinement fusion for fundamental research. F.Winterberg (Desert Res. Inst., Univ. of Nevada System, Reno, NV, USA). *Atomkernenerg. Kerntech. (Germany)*, vol.41, no.4, p.267-72 (1982). [received: Sept. 1983]

Thermonuclear microexplosions have besides commercial energy production other very exciting applications. Rockets driven by thermonuclear microexplosions can lead to interstellar missions to neighboring solar systems. Particle accelerators capable of reaching ultrahigh energies, approaching the grand unification energy scale, are another exciting possibility. (no refs.)

112462 Proposal for decommissioning of contaminated steel parts from shut down nuclear power plants. W.M.Francioli (Eidgenössisches Inst. für Reaktorforschung, Würenlingen, Switzerland). *Atomkernenerg. Kerntech. (Germany)*, vol.41, no.4, p.279-80 (1982). In German. [received: Sept. 1983]

During the dismantling of a shut-down nuclear power plant a number of relatively strongly radioactive components (reactor internals, part of the pressure vessel) have to be removed from the reactor core region. These components need heavy shielding for the transport to their final disposal. Further, large amounts of contaminated steel parts have to be disposed of. It is suggested to melt down the contaminated steel and to use it as shielding material in the disposal of the highly radioactive components. On the basis of assumed contamination the dose rates for melt-down material are estimated. In addition, problems of melting are presented. (1 ref.)

Protection and control of nuclear materials: a pressing obligation See Entry 112338

29.00 EXPERIMENTAL METHODS AND INSTRUMENTATION FOR ELEMENTARY-PARTICLE AND NUCLEAR PHYSICS

29.10 PREACCELERATION (INJECTION)

112463 An injector for RFQ1. M.R.Shubaly, M.S.de Jong (AECL, Res. Co., Chalk River Nuclear Labs., Chalk River, Ontario, Canada). *IEEE Trans. Nucl. Sci. (USA)*, vol.ns-30, no.4, pt.2, p.3001-3 (Aug. 1983). (1983 Particle Accelerator Conference. Accelerator Engineering and Technology, Santa Fe, NM, USA, 21-23 March 1983).

RFQ1 has been designed as a 600 keV, 75 mA CW radiofrequency quadrupole (RFQ) accelerator with a 50 kV injector that will be used to study the operation and current limits of an RFQ structure. Its injector must operate over a wide current range at a fixed energy and must match the acceptance of the RFQ structure over the entire range. This paper discusses the requirements and the final design of the injector. Experiments performed on existing test facilities to study some aspects of the design are also presented. (7 refs.)

Update on the high-current injector for the Stanford linear collider See Entry 112471

Design and fabrication of the BNL radio frequency quadrupole See Entry 112473

Conversion of the AGS linac to H⁻ acceleration See Entry 112476

NBS-LANL RTM injector installation See Entry 112480

Injection and extraction at MAX See Entry 112505

A nanosecond pulsed electron gun system for BEPC See Entry 112511

29.15 ELECTROSTATIC AND LINEAR PARTICLE ACCELERATORS

112464 The FMIT accelerator. D.D.Armstrong (Los Alamos Nat. Lab., Los Alamos, NM, USA). *IEEE Trans. Nucl. Sci. (USA)*, vol.ns-30, no.4, pt.2, p.2965-9 (Aug. 1983). (1983 Particle Accelerator Conference. Accelerator Engineering and Technology, Santa Fe, NM, USA, 21-23 March 1983).

A 35-MeV 100-mA CW linear accelerator is being designed by Los Alamos for use in the Fusion Materials Irradiation Test Facility. Essential to this

program is the design, construction, and evaluation of performance of the accelerator's injector, low-energy beam transport, and radio-frequency quadrupole sections before they are shipped to the facility site. The installation and testing of some of these sections have begun as well as the testing of the RF, noninterceptive beam diagnostics, computer control, DC power, and vacuum systems. An overview of the accelerator systems and the performance to date is given. (30 refs.)

112465 The advanced test accelerator (ATA), a 50-MeV, 10-kA induction linac. L.Reginato (Lawrence Livermore Nat. Lab., Livermore, CA, USA). *IEEE Trans. Nucl. Sci. (USA)*, vol.ns-30, no.4, pt.2, p.2970-4 (Aug. 1983). (1983 Particle Accelerator Conference. Accelerator Engineering and Technology, Santa Fe, NM, USA, 21-23 March 1983).

The ATA is an induction accelerator designed to produce 70 ns pulses of electrons at currents of 10 kA and energies in excess of 50 MeV. The accelerator is capable of operating at an average rate of 5 Hz or at 1 kHz for ten pulses. The parameters were chosen primarily to provide the experimental basis for advancing the understanding of electron beam propagation physics. The 85 m accelerator has been under construction for the past four years and has adopted mainly an improved version of the ETA technology to satisfy the required parameters. Initial operation of the facility and the energy conversion system from primary power to axial electric field is described; recent advances in magnetic switching which have been incorporated in the injector are also discussed.

112466 Design, construction and performance of the INS RFQ linac 'LITL'. N.Ueda, T.Nakanishi, S.Arai, T.Hattori, T.Fukushima, Y.Sakurada, T.Honma, N.Tokuda, S.Yamada, M.Takanaka (Inst. for Nuclear Study, Univ. of Tokyo, Tokyo, Japan), A.Itano, A.Mizobuchi, Y.Hirao. *IEEE Trans. Nucl. Sci. (USA)*, vol.ns-30, no.4, pt.2, p.2975-9 (Aug. 1983). (1983 Particle Accelerator Conference. Accelerator Engineering and Technology, Santa Fe, NM, USA, 21-23 March 1983).

An RFQ linac 'LITL' (Lithium Ion Test Linac) was constructed and accelerated ion beams of H⁺, H₂⁺, H₃⁺, He⁺, Li⁺ and ⁷Li⁺. The machine was designed to accelerate particles with charge to mass ratio (q/A) of 1-1/7 injected at 5 keV/u up to 138 keV/u. The acceleration cavity of four vane structure is 56 cm in diameter and 138 cm in length. Transmission exceeding 90% has been obtained for proton beam of 80 μA. The acceleration characteristics agree well with the computer simulation with PARMTEQ. For the acceleration of ⁷Li⁺, an RF power of 22 kW is fed with a loop coupler. In CW operation, an electric field of 205 kV/cm has been applied, which is required for ⁷Li⁺ acceleration and corresponds to 1.8 times the Kilpatrick's criterion. A maximum field of 2.0 times the criterion has been achieved, in pulse operation, with a duration width of 5 ms and repetition period of 25 ms. Operation of the machine is easy and stable. (8 refs.)

112467 Status report on the upgraded Unilac. N.Angert (Gesellschaft für Schwerionenforschung mbH, Darmstadt, Germany).

IEEE Trans. Nucl. Sci. (USA), vol.ns-30, no.4, pt.2, p.2980-2 (Aug. 1983). (1983 Particle Accelerator Conference. Accelerator Engineering and Technology, Santa Fe, NM, USA, 21-23 March 1983).

By adding two Alvarez tanks to the Unilac post-stripper maximum energies can be achieved of 19 MeV/u for uranium, and more than 20 MeV/u for ions of medium mass (A<150) using a second stripper in front of the single-gap cavity resonators. The injector beam transport system was modified, too, resulting, together with ion source developments, in an increase of beam intensities of about one order of magnitude. Operating experience of the first year after the upgrading is reported. (9 refs.)

112468 Improved performance of the Munich heavy ion postaccelerator. E.Nolte, R.Geier, U.Ratzinger, W.Schollmeier, S.Gustavsson, N.Gartner, H.Moringa (Fachbereich Phys., Tech. Univ. München, München, Germany). *IEEE Trans. Nucl. Sci. (USA)*, vol.ns-30, no.4, pt.2, p.2983-5 (Aug. 1983). (1983 Particle Accelerator Conference. Accelerator Engineering and Technology, Santa Fe, NM, USA, 21-23 March 1983).

Improvement of the shunt impedance and of the phase acceptance of the Munich heavy ion postaccelerator is described. The shunt impedance has been increased by using slimmer drift tubes, by mounting more drift tubes and by installing a drift tube configuration with flat gap voltage distribution along the resonator axis. The phase acceptance has been increased by means of a three-harmonics double-drift buncher on the high-energy side of the tandem. The phase acceptance of the system buncher-booster is about 70%. (4 refs.)

112469 Radio-frequency accelerators for multi-kiloampere electron beams. S.Humphries, Jr., Chang-Sing Hwang. *IEEE Trans. Nucl. Sci. (USA)*, vol.ns-30, no.4, pt.2, p.2986-8 (Aug. 1983).

(1983 Particle Accelerator Conference. Accelerator Engineering and Technology, Santa Fe, NM, USA, 21-23 March 1983).

Most present work on intense pulsed electron beam accelerators is directed toward linear induction accelerators. The authors consider the application of resonant accelerators to the generation of pulsed, multi-kiloampere electron beams. The main relative advantages are: (1) low cost and high voltage gradient can be achieved by eliminating ferromagnetic isolation cores; (2) cavity designs are simpler (with optimum utilization of vacuum insulators); and (3) there are no high voltage shorting switches. The latter feature implies that RF (radio-frequency) accelerators may operate at higher repetition rate and duty cycle. (6 refs.)

112470 High charge picosecond pulses with a double gap subharmonic buncher. G.Mavrogenes (Argonne Nat. Lab., Argonne, IL, USA), W.Gallagher, T.Kohe, D.Ficht. *IEEE Trans. Nucl. Sci. (USA)*, vol.ns-30, no.4, pt.2, p.2989-91 (Aug. 1983).

(1983 Particle Accelerator Conference. Accelerator Engineering and Technology, Santa Fe, NM, USA, 21-23 March 1983).

A new improved bunching system was designed in 1976 and installed in 1981 in the Argonne Electron Linac to replace the one installed in 1972. In the new bunching system a spiral loaded double gap 12th subharmonic buncher is replacing the previous single gap 6th subharmonic buncher and a one wavelength fundamental frequency traveling wave prebuncher has replaced the previous two wavelength prebuncher. Individual pulses of picosecond (25 to 36) duration and up to 40 nC Coulomb in charge, with ΔE/E<±0.5% at FWHM over the energy range of 4 to 22 MeV, and a repetition rate from one to 1000 psec are available to the experimenter on a routine basis. The design and the microwave properties of the cavity are discussed along with the general design of the injector and the results achieved. (5 refs.)

112471 Update on the high-current injector for the Stanford linear collider. M.B.James, J.E.Cledenin, S.D.Ecklund, R.H.Miller, J.C.Sheppard, C.K.Sinclair, J.Sodja (Stanford Linear Accelerator Center, Stanford Univ., Stanford, CA, USA).

IEEE Trans. Nucl. Sci. (USA), vol.ns-30, no.4, pt.2, p.2992-4 (Aug. 1983). (1983 Particle Accelerator Conference. Accelerator Engineering and Technology, Santa Fe, NM, USA, 21-23 March 1983).

The high current injector has become operational. There are two crucial areas where improvements must be made to meet collider specifications. While the injector can produce up to 10¹¹ e⁻ in a single S-band bucket, initially much

of this charge was captured in a low energy tail and was thus not suitable for transport through the accelerator and injection into the damping ring. Pulse to pulse position jitter has been observed, resulting in transverse wake fields which increase beam emittance. The problems described above contribute to substantial current loss during transport from the injector (40 MeV) to the SLC damping ring (1.2 GeV). Experimental studies are continuing with the aim of understanding and improving beam characteristics including bunch length, pulse to pulse stability and emittance. The present status of these studies is reported. (5 refs.)

112472 Transient beam loading calculations and experiment at the Saclay electron linac. B.Aune, J.Leroy, A.Mosnier (DPH-N/AL, CENS, Gif-sur-Yvette, France).

IEEE Trans. Nucl. Sci. (USA), vol.ns-30, no.4, pt.2, p.2995-7 (Aug. 1983). (1983 Particle Accelerator Conference. Accelerator Engineering and Technology, Santa Fe, NM, USA, 21-23 March 1983).

The transformation of the Saclay electron linac (ALS) into an injector for a 2 GeV stretcher ring is under study. One of the problems associated with this transformation is the use of the existing sections in a new mode of operation. The sections were optimized for low current operation (high attenuation, high internal resistance), they will be used in a high current, short pulse (1 μ s) mode resulting in a prohibitive transient beam loading energy spectrum broadening. The compensation method used at SLAC, which consists in delaying the turn-on of some klystrons, has been studied theoretically and an experiment has been performed with a 1 μ s pulse, at the same beam loading level as for the future plans. (5 refs.)

112473 Design and fabrication of the BNL radio frequency quadrupole. R.B.McKenzie-Wilson (Brookhaven Nat. Lab., Upton, NY, USA).

IEEE Trans. Nucl. Sci. (USA), vol.ns-30, no.4, pt.2, p.2998-3000 (Aug. 1983). (1983 Particle Accelerator Conference. Accelerator Engineering and Technology, Santa Fe, NM, USA, 21-23 March 1983).

The Brookhaven National Laboratory polarized H^- injection program for the AGS will utilize a Radio Frequency Quadrupole for acceleration between the polarized source and the Alvarez Linac. Although operation will commence with a few μ amperes of H^- current, it is anticipated that future polarized H^- sources will have a considerably improved output. The RFQ will operate at 201.25 MHz and will be capable of handling a beam current of 0.02 amperes with a duty cycle of 0.25%. The resulting low average power has allowed novel solutions to the problems of vane alignment, RF current contacts, and removal of heat from the vanes. The cavity design philosophy is discussed together with the thermodynamics of heat removal from the vane. Details of the fabrication are presented with a status report. (no refs.)

112474 Mechanical design of a heavy ion RFQ. S.Abbott, R.MacGill, R.Yourd (Lawrence Berkeley Lab., Univ. of California, Berkeley, CA, USA).

IEEE Trans. Nucl. Sci. (USA), vol.ns-30, no.4, pt.2, p.3004-6 (Aug. 1983). (1983 Particle Accelerator Conference. Accelerator Engineering and Technology, Santa Fe, NM, USA, 21-23 March 1983).

The mechanical design and construction of a 199.3 MHz heavy ion RFQ for charge states q/A as low as 0.14 is described. The vane supports and positioning adjustments are significant features of this design. They provide the capability of achieving the precision vane alignment required. The maximum difference between calculated and measured apertures between the vanes is 0.0035 inches, and the average difference is 0.0010 inches. Various important aspects of the design and construction including material selection and plating, RF joints, thermal loading and vacuum system are described. Assembly techniques, methods of mechanical measurement, alignment and structure stability are discussed in detail. (6 refs.)

112475 Improved field stability in RFQ structures with vane coupling rings. H.R.Schneider, H.Lancaster (Lawrence Berkeley Lab., Univ. of California, Berkeley, CA, USA).

IEEE Trans. Nucl. Sci. (USA), vol.ns-30, no.4, pt.2, p.3007-9 (Aug. 1983). (1983 Particle Accelerator Conference. Accelerator Engineering and Technology, Santa Fe, NM, USA, 21-23 March 1983).

The small aperture common in many RFQ linac designs lead to tuning difficulties, primarily because asymmetries in the quadrant fields can arise as a result of small non-uniformities in the vane to vane capacitances. Sensitivity to such capacitance or other tuning variation in the quadrants is greatly reduced by the introduction of pairs of vane coupling rings that provide periodic electrical connections between diametrically opposite vanes. Results of measurements on a cold model RFQ structure with and without vane coupling rings are presented. The number of rings required for field stabilization and the effect of rings on mode frequencies are discussed. (4 refs.)

112476 Conversion of the AGS linac to H^- acceleration. R.L.Witkov, D.S.Barton, R.K.Reece (Brookhaven Nat. Lab., Upton, NY, USA).

IEEE Trans. Nucl. Sci. (USA), vol.ns-30, no.4, pt.2, p.3010-12 (Aug. 1983). (1983 Particle Accelerator Conference. Accelerator Engineering and Technology, Santa Fe, NM, USA, 21-23 March 1983).

The AGS 200 MeV linac was converted to an H^- accelerator during the summer of 1982 using a magnetron-type source in the column of the second pre-injector pit. Because of the re-entrant electrode design, a 20 keV transport line was required to carry the beam to the first electrode. Several changes were made to the source which enhanced its performance over previous designs. The same H^- beam current is available at 2.75 times the duty factor with reduced deterioration of its output over several months of operation. The source, 750 keV transport, and linac modifications and performance will be presented. (8 refs.)

112477 Post-coupler and stem current measurements for high current CW drift-tube linacs. J.Unguin, S.O.Schriber, R.A.Vokes (AECL, Res. Co., Chalk River Nuclear Labs., Chalk River, Ontario, Canada).

IEEE Trans. Nucl. Sci. (USA), vol.ns-30, no.4, pt.2, p.3013-15 (Aug. 1983). (1983 Particle Accelerator Conference. Accelerator Engineering and Technology, Santa Fe, NM, USA, 21-23 March 1983).

Post-coupler characteristics have been measured on a model Alvarez tank for drift-tube-to-outer tank diameter ratios from 0.10 to 0.25. A maximum ratio beyond which field stabilization is not possible and a minimum ratio where stabilization is difficult have been determined. Field stabilization has been studied using two to twenty-one post couplers in a 22 cell tank. A sensitive dependence of the drift-tube stem currents near the tank end walls on the end cell geometry has been found. (6 refs.)

112478 First operation of proton induction linac. S.Kawasaki (Faculty of Sci., Kanazawa Univ., Kanazawa, Japan), Y.Kubota, A.Miyahara, K.Yamamoto.

IEEE Trans. Nucl. Sci. (USA), vol.ns-30, no.4, pt.2, p.3016-18 (Aug. 1983). (1983 Particle Accelerator Conference. Accelerator Engineering and Technology, Santa Fe, NM, USA, 21-23 March 1983).

A prototype of proton induction linac was developed to study the beam dynamics and the operational characteristics in this type of the accelerator specifically in the case of the intense ion beam acceleration. The driver system is composed of three identical unit modules, each of which consists of three toroidal cores made of laminated silicon-iron foil of 0.1 mm thickness

and the driving circuit linked with the cores. The accelerating field of 28 kV/module is obtained typically during a period of 2-3 μ sec. A proton beam of about 200 mA is extracted directly with the field driven inductively by the first module and then accelerated with succeeding two units to give the particles of about 60 keV at the output of the modules. Preliminary results of the measurements of the beam characters are given with the design of the device. (3 refs.)

112479 Subharmonic beam-loading in electron linear accelerators. W.J.Gallagher (Boeing Aerospace Co., Seattle, WA, USA).

IEEE Trans. Nucl. Sci. (USA), vol.ns-30, no.4, pt.2, p.3019-20 (Aug. 1983). (1983 Particle Accelerator Conference. Accelerator Engineering and Technology, Santa Fe, NM, USA, 21-23 March 1983).

The intention of operating an electron linear accelerator subharmonically beam loaded for free electron laser (FEL) application requires justification of the beam-loaded energy gain equation. The mode of operation typically planned is 5-10 nanoCoulombs single RF cycle pulses at 25-50 nanosecond intervals. This inquiry investigates details of that sort of beam loading and the performance achievable. (6 refs.)

112480 NBS-LANL RTM injector installation. M.A.Wilson, R.I.Cutler, E.R.Lindstrom, S.Penner, N.R.Yoder, R.L.Ayres, D.L.Mohr (NBS, Washington, DC, USA), L.M.Young, E.R.Martin.

IEEE Trans. Nucl. Sci. (USA), vol.ns-30, no.4, pt.2, p.3021-3 (Aug. 1983). (1983 Particle Accelerator Conference. Accelerator Engineering and Technology, Santa Fe, NM, USA, 21-23 March 1983).

The injector for the NBS-LANL CW racetrack microtron (RTM) consists of a 100 keV electron gun and beam transport line followed by a 5 MeV linac. The function of the gun and transport line, which have been installed at NBS, is to provide a chopped and bunched, 100 keV, and up to 0.67 mA DC or pulsed beam of very low transverse emittance ($<5\pi$ mm-mrad) for matched insertion into the linac. The authors present both design and construction details of the 100 keV system and the results of preliminary beam tests. The tests conducted thus far show the gun and transport system to be performing well within design specifications. (3 refs.)

112481 Research on electron linear accelerators with traveling wave resonators. II. Wang Yuan-ling (Dept. of Phys., Univ. of Nanjing, Nanjing, China).

IEEE Trans. Nucl. Sci. (USA), vol.ns-30, no.4, pt.2, p.3024-6 (Aug. 1983). (1983 Particle Accelerator Conference. Accelerator Engineering and Technology, Santa Fe, NM, USA, 21-23 March 1983).

For pt.1 see *ibid.*, vol.NS28, p.3526 (1981). In the first part, under beam loading conditions, the formula of the energy gain of the electron linac with the traveling wave resonator was given by: $V_0 = M_0 E_0 L (1 - e^{-\tau}) / \tau - i r L (1 - (1 - e^{-\tau}) / \tau)$. In this paper, under beam loading conditions the field multiplication factor M_0 is derived. It makes this type of accelerator (including accelerators with feedback) design according to the same way as general electron traveling wave linacs. Under test of the electron linac with the traveling wave resonator, unstable phenomena are described. Their causes are discussed. They have been overcome. (3 refs.)

112482 A multidimensional study of a 50-MeV, 1500-rad/pulse radiographic linac, using the stagger-tuning concept. R.K.Owen, M.V.Fazio, T.J.Boyd (Los Alamos Nat. Lab., Los Alamos, NM, USA).

IEEE Trans. Nucl. Sci. (USA), vol.ns-30, no.4, pt.2, p.3027-9 (Aug. 1983). (1983 Particle Accelerator Conference. Accelerator Engineering and Technology, Santa Fe, NM, USA, 21-23 March 1983).

Stagger tuning of accelerator cavities, or blocks of cavities, can significantly enhance the achievable charge transfer through an electron linac operating in the stored-energy mode. The output bremsstrahlung flux can be increased over a conventional approach by an order of magnitude without any significant degradation in emittance growth or energy spread. Given a suitable injector, a 1500-rad/pulse, 50-MeV radiographic linac appears to be practical at a 400-MHz operating frequency; a 150-rad/pulse, 50-MeV radiographic linac will operate at 1300 MHz. A multidimensional study was made using the PARMELA code where several parameters, including beam current, synchronous phase angle, and beam radius were varied while observing the effects on emittance and transmission efficiency. (no refs.)

112483 Recent performance improvements on FXR. B.Kulke, R.Kihara (Lawrence Livermore Nat. Lab., Livermore, CA, USA).

IEEE Trans. Nucl. Sci. (USA), vol.ns-30, no.4, pt.2, p.3030-2 (Aug. 1983). (1983 Particle Accelerator Conference. Accelerator Engineering and Technology, Santa Fe, NM, USA, 21-23 March 1983).

The FXR machine is a nominal 4 kA, 20 MeV, linear induction, electron accelerator for flash radiography at LLNL. The machine met its baseline requirements in March 1982. Since then, the performance has been greatly improved. Stable and repeatable beam acceleration and transport have been achieved, with over 80% transmission to the tungsten bremsstrahlung target located some 35 m downstream. For best stability, external beam steering has been eliminated almost entirely. Over 500 Roentgen at 1 m from the target (TLD measurement) are regularly produced, with a radiographic spot size of 3-5 mm. Present efforts are directed towards the development of a 4 kA tune, working interactively with particle-field and beam transport code models. A remaining uncertainty is the possible onset of RF instabilities at the higher current levels. (3 refs.)

112484 Operation experience of the Riken variable-frequency heavy-ion linac, RILAC. M.Kase, M.Odera (Linac Lab., Inst. Phys. & Chem. Res., Saitama, Japan), Y.Chiba, Y.Miyazawa, M.Hemmi, T.Tonuma, T.Inoue, T.Kambara, M.Yanokura, T.Kubo, E.Ikezawa.

IEEE Trans. Nucl. Sci. (USA), vol.ns-30, no.4, pt.2, p.3033-5 (Aug. 1983). (1983 Particle Accelerator Conference. Accelerator Engineering and Technology, Santa Fe, NM, USA, 21-23 March 1983).

The RILAC, the variable-frequency heavy-ion linac, which will be used as an injector to the separated sector cyclotron, has provided useful beams to experimental groups. The frequency range available now is 18-30 MHz. The upper limit is determined by the parasitics mode at 35 MHz in the RF system. The beam energy can be varied in a wide range by changing the beam phase without degrading the beam quality so much. (5 refs.)

112485 4 π -mode acceleration in KEK 20-MeV proton linac. E.Takasaki, T.Kato, Z.Igarashi, K.Ikegami, C.Kubota, Y.Mori, A.Takagi, T.Takenaka, S.Fukumoto (Nat. Lab. for High Energy Phys., Ibaraki, Japan).

IEEE Trans. Nucl. Sci. (USA), vol.ns-30, no.4, pt.2, p.3036-8 (Aug. 1983). (1983 Particle Accelerator Conference. Accelerator Engineering and Technology, Santa Fe, NM, USA, 21-23 March 1983).

Ions of H_2^+ and He^{2+} were accelerated by 4 π -mode operation in the KEK 20 MeV proton linear accelerator. In this mode the same accelerating field distribution and the same focusing magnetic field strength as those for protons were used. This paper gives the experimental results of the relation between the injection energy and the accelerating field strength and of the beam intensity as a function of the field strength. (6 refs.)

112486 Collective acceleration of ions in straight relativistic electron beams. V.M.Bystritskii, A.N.Didenko (Inst. of Nuclear Phys., Tomsk, USSR).

Sov. J. Part. & Nucl. (USA), vol.14, no.1, p.76-97 (Jan.-Feb. 1983). Translation of: *Fiz. Elem. Chastits & At. Yadra (USSR)*, vol.14, no.1, p.181-226 (Jan.-Feb. 1983). [received: Sept. 1983]

A review is given of experimental and theoretical investigations on collective acceleration of ions in straight relativistic electron beams, an area which was first studied by V.I. Veksler (1956), G.I. Budker (1956) and B.Ya. Fainberg (1956). The acceleration methods considered are compared in relation to their promise of resulting in viable accelerators in the range up to several hundred MeV per nucleon. (115 refs.)

PHERMEX—pulsed high energy radiographic machine emitting X-rays See Entry 111843

Facility for cineradiography at high energy: the ARTEMIS project See Entry 111844

An injector for RFQ1 See Entry 112463

Envelope equation for a beam accelerated by a rotationally symmetric electrostatic field See Entry 112500

Neutralizer for Hall-current accelerator See Entry 112512

Evolution of control systems for accelerators See Entry 112523

29.20 CYCLIC ACCELERATORS AND STORAGE FACILITIES

(for plasma accelerators, see 52.75)

112487 Infrared synchrotron radiation from electron storage rings. W.D.Duncan (Royal Obs., Edinburgh, Scotland), G.P.Williams.

Appl. Opt. (USA), vol.22, no.18, p.2914-23 (15 Sept. 1983). Simple and useful approximations, valid at infrared wavelengths, to the equations for synchrotron radiation are presented and used to quantify the brightness and power advantage of current synchrotron radiation light sources over conventional infrared broadband laboratory sources. The Daresbury Synchrotron Radiation Source (SRS) and the Brookhaven National Synchrotron Light Source (vacuum ultraviolet) [NSLS(VUV)] storage rings are used as examples in the calculation of the properties of infrared synchrotron radiation. The pulsed nature of the emission is also discussed, and potential areas of application for the brightness, power, and time structure advantages are presented. The use of infrared free electron lasers and undulators on the next generation of storage ring light sources is briefly considered. (35 refs.)

112488 Betatron energy stabilization system. Yu.V.Kuznetsov, E.V.Lazutin, Yu.A.Novikov, V.M.Sorvin (Nuclear Phys. Res. Inst., Moscow State Univ., Moscow, USSR).

Instrum. & Exp. Tech. (USA), vol.25, no.6, pt.1, p.1333-7 (Nov.-Dec. 1982). Translation of: *Prib. & Tekh. Eksp. (USSR)*, vol.25, no.6, p.21-4 (Nov.-Dec. 1982). [received: Sept. 1983]

A system is described for the stabilization and control of the energy of a betatron. The system can operate both autonomously and in conjunction with a computer. Schematic diagrams are presented for the system control block, for the digital-analog converter, and for the comparison circuit. The stabilization system is made up mainly of integrated circuits of the series K155 and K140. (11 refs.)

112489 Study of the magnetic forces acting on the trim coils, for the Milan superconducting cyclotron. G.Bellomo, L.Serfini.

Report INFN/TC-83/7, Ist. Naz. Fis. Nucl., Milan, Italy (7 March 1983), 19 pp.

A three sector superconducting cyclotron, with a $K=800$ and a $K_{FOC}=200$, is under construction at the University of Milan. The machine will operate with average magnetic fields between 22 and 48 kGauss; the trimming of the field is obtained by the independent excitation of the two main coil sections (each one carrying up to 3500 A/cm²) and by 20 trim coils wound around the hills (with a max excitation of 4000 ampereturns each). The aim is to evaluate the forces acting on the trim coils because of the cyclotron magnetic field. Four trim coils, out of twenty, have been selected as representative of the entire set and the corresponding distribution of the forces has been computed. The results obtained are presented in some detail and their implications for the design of the mechanical structure of the trim coils are discussed. (4 refs.)

112490 Triggering and filtering in collider experiments. D.Notz (DESY, Hamburg, Germany).

Proceedings of the 1982 CERN School of Computing, Zinal, Valais, Switzerland, 29 Aug.-11 Sept. 1982 (Geneva, Switzerland: CERN 1983), p.229-36. Discusses rates for events and background in $p\bar{p}$ and e^+e^- storage rings. Electronic systems recognizing tracks within a few microseconds are presented. These systems work either in parallel or sequentially. (1 ref.)

The LEAR project and physics with low energy antiprotons at CERN. A summary See Entry 112026

The new high intensity polarized proton and deuteron source for the Bonn isochronous cyclotron See Entry 112497

Fast kicker magnet system See Entry 112504

Injection and extraction at MAX See Entry 112505

A superconducting accelerating cavity in PETRA See Entry 112506

Electron beam focusing effects and matching conditions in plane periodic magnets See Entry 112508

Optimization of a permanent magnet undulator for free electron laser studies on the ACO storage ring See Entry 112516

Evolution of control systems for accelerators See Entry 112523

29.25 PARTICLE SOURCES AND TARGETS, PREPARATION AND TECHNOLOGY

(see also 07.77 Particle production and handling: targets)

112491 The general concept for a spallation neutron source in the Federal Republic of Germany. G.S.Bauer (KFA Julich, Julich, Germany).

Atomkernenerg. Kerntechnik. (Germany), vol.41, no.4, p.234-42 (1982). [received: Sept. 1983]

In a collaborative effort between the two German nuclear research centres at Karlsruhe and at Julich, a reference concept for a spallation neutron source has been studied which would be suitable to satisfy the medium term needs in neutrons for fundamental research and to service a large number of other scientific disciplines as well. The reference facility, consisting of a high power proton linac for 5 mA time average current of 1.1 GeV protons and a rotating lead target with hybrid H₂O-D₂O moderators can deliver a thermal neutron

flux equivalent to 7×10^{14} cm⁻² s⁻¹ at the beam tube noses. Pulsed operation of the accelerator results in an intensity modulation of this flux at a repetition rate of 100 Hz with a peak flux of 1.3×10^{16} cm⁻² s⁻¹ and a pulse width of 510 μ s. Further possible improvements were considered, consisting in the use of uranium as target material and in the addition of a proton pulse compressor to increase the neutron peak flux especially in the epithermal energy range and to provide a time structure suitable for neutrino and muon research. To realize this concept in a fashion compatible with existing constraints while still serving a maximum number of users at the earliest possible date, a staged concept is being considered by KFA Julich. (17 refs.)

112492 Nuclear assessment of the DIANE target station. P.Cloth, D.Filges, R.Hecker (Inst. fur Reaktorenentwicklung, KFA Julich GmbH, Julich, Germany).

Atomkernenerg. Kerntechnik. (Germany), vol.41, no.4, p.243-52 (1982). [received: Sept. 1983]

Presents results of calculations that have been made for a spallation neutron source. The emphasis of this theoretical work has been directed toward assessing physics feasibility. Most of the calculations are related to predicting the neutronics output for a realistic target configuration with 'slow' and 'fast' moderators. The calculational approach has been to use the latest state-of-the-art radiation transport computer codes. The codes used allow three-dimensional target descriptions and employ Monte Carlo techniques, so it is possible to treat in detail the spallation reactions, the transport on the high-energy particles, low-energy neutrons and gammas created. An overview of the computer codes used is given. The main conclusion of the calculations is that, for the beam parameters of the proton accelerator (1100 MeV protons, average current of 5 milliamperes) and target parameters (target material of lead, clad with aluminium and cooled with water) considered, the peak and average thermal neutron flux goals of $\Phi_{th}=1.2 \times 10^{16}$, $\Phi_{th}=6.0 \times 10^{14}$ n cm⁻² s⁻¹ can be attained. Furthermore, results of the calculations for other important design questions, such as heating at the target and target station components, radiation environments for material damage and induced radioactivity are also described. (21 refs.)

112493 Behaviour of the spallation neutron source target wheel under thermal and mechanical loads. J.F.Stelzer (KFA Julich, Julich, Germany).

Atomkernenerg. Kerntechnik. (Germany), vol.41, no.4, p.253-8 (1982). [received: Sept. 1983]

Calculations dealing with the temperatures and stresses in the maximally loaded parts of the target wheel are described. They were carried out using the finite element method. There are three highly loaded areas: the outer housing, the beam window and the lead-filled target rods. The construction of the mathematical models is shown. The results are introduced and discussed. The design satisfies the mechanical demands. (11 refs.)

112494 Mechanical design of the target station DIANE of the German spallation neutron source project and its rotating target. H.Stechemesser (Zentralabteilung fur Allgemeine Technol., KFA Julich, Julich, Germany).

Atomkernenerg. Kerntechnik. (Germany), vol.41, no.4, p.259-63 (1982). [received: Sept. 1983]

The spallation neutron source is designed to substitute the beamhole reactors currently in use. Owing to the method of neutron production there are typical design features, which are described special for the spallation target, the surrounding shielding block and handling aspects. The design of the rotating wheel shaped target is lined out to give a good view to the detail design. (3 refs.)

112495 Dependence of the experimentally obtained age of the Am-Be neutrons ($\tau_{1.46}$) in water on the source-foil geometry. S.E.Simopoulos, D.J.Leonidou, M.G.Angelopoulos (Lab. of Nuclear Engng., Nat. Tech. Univ., Athens, Greece).

Atomkernenerg. Kerntechnik. (Germany), vol.41, no.4, p.293-4 (1982). [received: Sept. 1983]

In a previous publication by Simopoulos and Leonidou (1981) the measured age to indium resonance ($\tau_{1.46}$), in natural water, of neutrons from a 5 Curie Am-Be cylindrical source (diameter 1", length 1.5") was reported. This age was evaluated by the usual technique, i.e. from the saturation activity of pure indium foils (0.5" in diameter, 0.005" thick, 92.8 mg/cm²) enclosed in 0.020" thick cadmium boxes, positioned along the axis of the cylindrical source and facing one of its bases. The final average value of $\tau_{1.46}$ reported was: $\tau_{1.46}=65.2 \pm 1.5$ cm². This value was obtained without considering the possible combined effects of the finite size of the source and of the cubic water tank (1 m \times 1 m \times 1 m) used for the experiments. The possible effects of the above factors were investigated and a more representative value of the age $\tau_{1.46}$ was obtained when an arrangement of a finite Am-Be source and water tank was used and detailed measurements were performed. A short reference to the basic experimental procedure and the data reduction and pressing followed by a detailed description of the experiments and the results obtained are given. (3 refs.)

112496 Converting thermal neutrons into 14 MeV DT neutrons using the suprathermal fusion principle. W.Seifritz (Swiss Federal Inst. for Reactor Res., Wurenlingen, Switzerland).

Atomkernenerg. Kerntechnik. (Germany), vol.41, no.4, p.295-6 (1982). [received: Sept. 1983]

A severe problem to the experimental study of the neutronics of pure or hybrid fusion reactor blankets is the lack of a 14 MeV neutron source being strong enough to allow foil activation measurements up to a blanket thickness of at least 50 cm. It would be therefore preferable if thermal neutrons being abundantly available in fission reactors could be used for this task. (5 refs.)

112497 The new high intensity polarized proton and deuteron source for the Bonn isochronous cyclotron. H.-G.Mathews (Inst. fur Angewandte Phys., Univ. Bonn, Bonn, Germany), A.Kruger, S.Penselin, A.Weinig.

Nucl. Instrum. & Methods Phys. Res. (Netherlands), vol.213, no.2-3, p.155-64 (1 Aug. 1983).

An atomic-beam polarized ion source for the production of polarized protons and deuterons is described. Beam intensities of 160 μ A for polarized protons and deuterons are obtained at an emittance of 9π cm.rad./eV. Within the phase space accepted by the Bonn isochronous cyclotron 50 μ A of deuterons and 35 μ A of protons were measured. The atomic beam emerging from a liquid nitrogen cooled dissociator nozzle is polarized and focused by two tapered sextupole magnets. Two radiofrequency transitions can be mounted either before or behind the second sextupole, leading to theoretical values for deuterium vector and tensor polarizations of $P_z=\pm 1$ and $P_{zz}=-2$, respectively. The polarized atoms are ionized by electron impact inside a cold-cathode Penning ionizer working at a magnetic field of 4 T produced by a superconducting solenoid. The efficiency for this ionizer is estimated to be $\eta=6.2 \times 10^{-2}$. (11 refs.)

112498 Study of the production of metallic ions in the multiply charged ion source MINIMAFIOS. M.Delaunay, S.Dousson, R.Geller, B.Jacquot (CENG, Grenoble, France).

Nucl. Instrum. & Methods Phys. Res. (Netherlands), vol.213, no.2-3, p.165-9 (1 Aug. 1983). In French.

The authors show that multiply charged metallic ions can be produced inside an electron cyclotron resonance plasma (ECR) by utilizing directly the energy contained inside the plasma. The results corroborate the feasibility of the method. Experimental charge state distributions for ions of Al, Ni, Mo, W, Ta, Au etc. are shown. (4 refs.)

112499 Charged particle beam envelopes. E.V.Shpak (Ioffe Physicotech. Inst., Acad. of Sci., Leningrad, USSR).

Nucl. Instrum. & Methods Phys. Res. (Netherlands), vol.213, no.2-3, p.171-8 (1 Aug. 1983).

A method for the calculation of charged particle beam envelopes of various shapes is proposed. Expressions for the envelopes are obtained both in the paraxial approximation and taking into account some kinds of aberration. The two-dimensional quadrupole lens is used to illustrate the possibility of finding the envelopes for cases where exact equations of the particle trajectories are known. (3 refs.)

112500 Envelope equation for a beam accelerated by a rotationally symmetric electrostatic field. Jiang Bin-Yao (Shanghai Inst. of Metall., Acad. of Sci. of China, Shanghai, China), P.Tangy, Xia Jin-Zhi.

Nucl. Instrum. & Methods Phys. Res. (Netherlands), vol.213, no.2-3, p.179-85 (1 Aug. 1983). In French.

The envelope equation for heavy ion beams accelerated in a rotationally symmetric electric field is set up. Two cases are considered: beams with uniform distribution in cross section and beams with non-uniform distribution for which the RMS envelopes equation is obtained. An example of application is presented and possible improvements of calculations are discussed. (9 refs.)

112501 Design of a passive magnetic shunt for the extraction of electron beams from a photon tagging spectrometer. R.M.Laszewski (Dept. of Phys., Univ. of Illinois, Urbana, IL, USA).

Nucl. Instrum. & Methods Phys. Res. (Netherlands), vol.213, no.2-3, p.195-200 (1 Aug. 1983).

A method is described in which a passive magnetic shunt is used to provide clean extraction of primary electron beams from a photon tagging spectrometer. For a wide range of magnetic fields and incident electron energies, the point at which the primary beam leaves the system can be very well localized. The design, fabrication and testing of the magnetic shunt are described. (10 refs.)

112502 Absolute beam intensity measurements with a 200 watt calorimeter. A.E.Vlieks, M.Hilgemeier, C.Rolfs (Inst. fur Kernphys., Univ. Munster, Munster, Germany).

Nucl. Instrum. & Methods Phys. Res. (Netherlands), vol.213, no.2-3, p.291-9 (1 Aug. 1983).

A calorimeter has been constructed for absolute intensity measurements of ion beams with up to 200 W power. The technical aspects and features of the calorimeter are described. (7 refs.)

112503 A versatile high intensity negative ion source. R.Middleton (Phys. Dept., Univ. of Pennsylvania, Philadelphia, PA, USA).

Nucl. Instrum. & Methods Phys. Res. (Netherlands), vol.214, no.2-3, p.139-50 (1 Sept. 1983).

A new type of sputter negative ion source has been developed in which the sputter target and the surface ionizer are enclosed in a common chamber containing cesium vapor. Optimal neutral cesium coverage of the sputter target can be achieved resulting in efficient ionization and high intensities. Some typical negative ion currents are: 30 μA of $^{11}\text{B}^-$, 300 μA of $^{12}\text{C}^-$, 250 μA of $^{16}\text{O}^-$, 4 μA of $^{27}\text{Al}^-$, 200 μA of $^{28}\text{Si}^-$, 150 μA of $^{58}\text{Ni}^-$, 150 μA of $^{63}\text{Cu}^-$ and 200 μA of $^{197}\text{Au}^-$. Emission is relatively low, $\sim 2 \pi \text{ mm.mrad(MeV)}^{1/2}$ for 70% of the total current, and sputter targets can be changed in 5-10 min. Since the source operates efficiently with samples of a few milligrams and yields 5-10 μA of BeO^- ions from beryllium oxide and about 1 μA of $^{27}\text{Al}^-$ from aluminium oxide, it is likely to find application in accelerator mass spectrometry. (15 refs.)

112504 Fast kicker magnet system. L.J.Lindgren, A.Sandell, M.Eriksson (MAX Lab., Inst. of Phys., Lund, Sweden).

Nucl. Instrum. & Methods Phys. Res. (Netherlands), vol.214, no.2-3, p.175-8 (1 Sept. 1983).

A fast kicker magnet system has been developed to be used as a fast extraction device for electrons in a synchrotron. Measurements on pulse characteristics are presented. (6 refs.)

112505 Injection and extraction at MAX. L.J.Lindgren, M.Eriksson (MAX Lab., Inst. of Phys., Lund, Sweden).

Nucl. Instrum. & Methods Phys. Res. (Netherlands), vol.214, no.2-3, p.179-87 (1 Sept. 1983).

The MAX accelerator system will consist of a 100 MeV injector and a 550 MeV pulse-stretcher/storage ring. The authors describe the injection and extraction process. The third resonance extraction theory is outlined and discussed. (6 refs.)

112506 A superconducting accelerating cavity in PETRA. W.Bauer, A.Brandelik, A.Citron, F.Graf, L.Szecs (Kernforschungszentrum Karlsruhe, Univ. of Karlsruhe, Karlsruhe, Germany), D.Proch.

Nucl. Instrum. & Methods Phys. Res. (Netherlands), vol.214, no.2-3, p.189-99 (1 Sept. 1983).

To investigate the feasibility of superconducting accelerating cavities in electron-positron storage rings a single cell niobium cavity was constructed and tested in PETRA at DESY, Hamburg. The authors describe the experimental setup and summarize the results obtained. Accelerating field gradients of the order of 3 MV/m and Q -values of 10^9 can be obtained in an operating storage ring and maintained over many weeks. Synchrotron radiation impinging on the cavity surface does not affect the performance. Higher order mode excited by the beam were coupled out, their amplitudes were measured and agree with theory. PETRA could be operated at 5 GeV and 2 mA with the superconducting cavity alone. (21 refs.)

112507 Total neutron yields from 100 MeV protons on Pb and ^7Li targets. M.A.Lone, R.T.Jones, A.Okazaki, B.M.Townes, D.C.Santry, E.D.Earle (AECL, Chalk River Nuclear Labs., Chalk River, Ontario, Canada), J.K.P.Lee, J.M.Robson, R.B.Moore, L.Nikkinen, V.Raut.

Nucl. Instrum. & Methods Phys. Res. (Netherlands), vol.214, no.2-3, p.333-9 (1 Sept. 1983).

The neutron yield per proton from thick targets of Pb and ^7Li irradiated with 100 MeV protons has been measured and calculated. The water bath method was used to measure the neutron production and a Faraday cup was used to measure the proton beam current. Measured yields are 0.343 ± 0.021 for Pb and 0.123 ± 0.007 for ^7Li . Corresponding yields calculated with the nucleon-meson transport code NMTC are 0.363 ± 0.002 and 0.160 ± 0.001 .

Measured and calculated thermal neutron distributions in the water bath are also compared. (21 refs.)

112508 Electron beam focusing effects and matching conditions in plane periodic magnets. R.P.Walker (Sci. & Engng. Res. Council, Daresbury Lab., Warrington, England).

Nucl. Instrum. & Methods Phys. Res. (Netherlands), vol.214, no.2-3, p.497-504 (1 Sept. 1983).

Plane periodic magnets, undulators and wigglers, produce a focusing force in the nonbending plane which can be related simply to the RMS field strength. The effects that this can introduce in an electron storage ring are discussed and an optimum focusing condition for the electron beam is described. The role of the focusing in determining the performance of a free electron laser is also considered, leading to a different optimum matching condition in this case. (30 refs.)

112509 Production of circularly polarized light from synchrotron radiation in the vacuum ultraviolet region. P.D.Johnson, N.V.Smith (Bell Labs., Murray Hill, NJ, USA).

Nucl. Instrum. & Methods Phys. Res. (Netherlands), vol.214, no.2-3, p.505-8 (1 Sept. 1983).

The well-known three-reflection polarizer can be used to convert linearly polarized synchrotron radiation to circular polarization. Geometrical parameters are presented for the production of circularly polarized light in the photon energy range 5-30 eV using Au or Pt mirrors. (14 refs.)

112510 PHOCCA: a Monte Carlo program to calculate the characteristics of a beam of photons produced by annihilation and bremsstrahlung of relativistic positrons. E.De Sanctis, V.Lucherini (INFN, Lab. Nazionali di Frascati, Frascati, Italy), V.Bellini.

Comput. Phys. Commun. (Netherlands), vol.30, no.1, p.71-85 (July-Aug. 1983).

The program PHOCCA calculates the absolute energy spectra, the radial and vertical profiles and the angular distributions of annihilation and bremsstrahlung photons from intermediate energy positrons. The energy spread, the energy loss and the multiple scattering of the positrons in the annihilation target are taken into account. Moreover the positron emittance, the positron incidence angle and the finite angular acceptance of the photon collimation channel are explicitly considered. (3 refs.)

112511 A nanosecond pulsed electron gun system for BEPC. Gu Meng-Ping, Zhu Guo-Hui, Qian Zhu-Ming, Mi Jian-Lin (Inst. of High Energy Phys., Acad. Sinica, Beijing, China).

IEEE Trans. Nucl. Sci. (USA), vol.ns-30, no.4, pt.2, p.2962-4 (Aug. 1983).

(1983 Particle Accelerator Conference. Accelerator Engineering and Technology, Santa Fe, NM, USA, 21-23 March 1983).

A nanosecond pulsed electron gun has been installed at IHEP in Beijing. Two types of pulser have been tested for the fast pulsed gun. Instead of the hybrid fast pulser, a new transistor avalanche pulser was developed. 1.1 amp beam pulse current from the gun has already been obtained. Preliminary test and details of the gun system are presented. (3 refs.)

112512 Neutralizer for Hall-current accelerator. J.J.Cuomo, H.R.Kaufman (IBM Corp., Armonk, NY, USA).

IBM Tech. Disclosure Bull. (USA), vol.26, no.1, p.19-21 (June 1983).

An improved neutralizer is described which is located at the center of the Hall accelerator, and is preferably a hollow cathode electron source. (no refs.)

112513 Electron gun with plasma emitter made up of vacuum arcs. S.P.Bugaev, A.I.Klimov, S.M.Chesnokov (Inst. of High-Current Electronics, Acad. of Sci., Tomsk, USSR).

Instrum. & Exp. Tech. (USA), vol.25, no.6, pt.2, p.1436-8 (Nov.-Dec. 1982).

Translation of: *Prib. & Tekh. Eksp. (USSR)*, vol.25, no.6, p.110-12 (Nov.-Dec. 1982).

An electron gun with a plasma emitter made up of several hot vacuum arcs was experimentally investigated. The electron-beam current pulse duration is $\sim 200 \mu\text{s}$. The current density at the plasma cathode reached A/cm^2 at 24 kV. (4 refs.)

112514 A 500-kV vacuum lead for a high-current quasistationary electron accelerator with a heated cathode. G.N.Antipov, S.V.Rybalov, V.D.Sarbee.

Instrum. & Exp. Tech. (USA), vol.25, no.6, pt.2, p.1438-40 (Nov.-Dec. 1982).

Translation of: *Prib. & Tekh. Eksp. (USSR)*, vol.25, no.6, p.112-14 (Nov.-Dec. 1982).

The design of a high-voltage vacuum lead is described for an electron accelerator with a heated cathode. Results from tests on the electrical strength are given which show that the lead can be used up to 500 kV and a stationary cathode heating power of about 20 kW. (3 refs.)

112515 Resistance thermometer for ion-beam calorimetry. S.N.Dolya, V.A.Sviridov, V.P.Tokarskii (Joint Nuclear Res. Inst., Dubna, USSR).

Instrum. & Exp. Tech. (USA), vol.25, no.6, pt.2, p.1443-5 (Nov.-Dec. 1982).

Translation of: *Prib. & Tekh. Eksp. (USSR)*, vol.25, no.6, p.117-18 (Nov.-Dec. 1982).

A new type of calorimeter is described for measuring the parameters of low-energy ion beams. The sensitive material is a wire of diameter 10-15 μm . Test results with ion beams are described. The sensitivity is up to 200°C/J . (3 refs.)

112516 Optimization of a permanent magnet undulator for free electron laser studies on the ACO storage ring. J.M.Ortega, C.Bazin, D.A.G.Deacon (Lab. LURE, Univ. de Paris-Sud, Orsay, France).

J. Appl. Phys. (USA), vol.54, no.9, p.4776-83 (Sept. 1983).

Describes the magnetic design problems involved in the realization of the permanent magnetic undulator 'Nouvel Onduleur pour l'Etude du Laser (NOEL)' currently being used for the free electron laser experiments on the storage ring ACO. The undulator has been compensated for the magnetic imperfections of the magnet elements used for its construction. Each pole piece was made from two elements so that the authors could cancel out the transverse field errors. Each undulator pole was selected from a two-dimensional magnet distribution graph which was drawn with the results of a set of Hall-probe measurements. Magnetic measurements of the assembled undulator as well as the first experiments on the ACO storage ring indicate that the method has been successful. (16 refs.)

112517 Possible application of nuclear resonance fluorescence to study surface effects. L.Wielopolski, D.Vartsky, S.H.Cohn (Medical Res. Center, Brookhaven Nat. Lab., Upton, NY, USA).

J. Appl. Phys. (USA), vol.54, no.9, p.5449-50 (Sept. 1983).

Observations were made of the differences between the iron nuclear resonance fluorescence yield from a gaseous $^{59}\text{MnCl}_2$ source in a clear fused quartz vial and a source in a clear fused silica (Suprasil) vial. The nuclear resonance fluorescence may be applied to study surface effects in materials undergoing radiation damage. (6 refs.)

112518 **Resistive wall flute stability of magnetically guided relativistic electron beams.** R.G.Kleva (Lab. for Plasma & Fusion Energy Studies, Univ. of Maryland, College Park, MD, USA), E.Ott, P.Sprangle. *Phys. Fluids (USA)*, vol.26, no.9, p.2689-97 (Sept. 1983). The resistive wall stability of an electron beam is studied, and application of the theory to the modified betatron accelerator is considered. Only flute-like perturbations are analyzed ($n=0$, $l\geq 1$, where n and l are the toroidal and poloidal mode numbers, respectively). Included in the analysis are the effects of relativistic velocities, equilibrium and perturbed self-electromagnetic fields, and resonant particle effects due to density and velocity profiles. The principal results are (1) $l\geq 2$ modes are much more difficult to stabilize than is the $l=1$ mode; (2) the velocity gradient along the beam can provide an important stabilizing mechanism; (3) the stabilizing effect of the density gradient is reduced by relativistic effects; and (4) magnetic perturbations can be important even for nonrelativistic beams. (11 refs.)

112519 **The time response of the ferrite loaded cavity and stability of bias autotuning system.** Yan Tai-xuan, Sun Li-bo (Inst. of High Energy Phys., Acad. Sinica, Peking, China). *Phys. Energ. Fortis & Phys. Nucl. (China)*, vol.7, no.3, p.346-54 (May 1983). In Chinese. A state space model is described, the time response of ferrite loaded cavity is proposed and a new digital measuring method devised. Results of actual measurement on the model cavity are given. On these bases the stability of stationary state of bias autotuning system to fast external perturbation is discussed. (10 refs.)

112520 **Data processor for the magnet with curvature.** Du Wen-fu (Inst. of High Energy Phys., Acad. Sinica, Peking, China). *Phys. Energ. Fortis & Phys. Nucl. (China)*, vol.7, no.3, p.395-400 (May 1983). In Chinese. The data processor of the magnetic field in the bending magnet with curvature is described using a normal measurement device, moving along straight line. A formula for data transformation is introduced. The results show that it would have approximately no influence to the fitting coefficients in the longitudinal direction. (1 ref.)

112521 **Californium-252 as a source of subthermal neutrons.** J.J.Antal (Army Materials & Mech. Res. Center, Watertown, MA, USA). Neutron Radiography, Proceedings of the First World Conference, San Diego, CA, USA, 7-10 Dec. 1981 (Dordrecht, Netherlands: Reidel 1983), p.689-93. Radiography with subthermal (cold) neutrons is becoming increasingly interesting to those concerned with the evaluation of new composite structural materials. A subthermal neutron beam of sufficiently high intensity for radiography is difficult to obtain from common neutron sources. Californium-252 as a source of subthermal neutrons was explored and found to be an extremely efficient source, but one of still marginal applicability without further novel source development. (2 refs.)

112522 **Production of a very high intensity polarized ion beam and experiments of spin transfer reactions.** A.Isoya, T.Nakashima, K.Sagara, K.Kobayashi, H.Nakamura, K.Aita, O.Masutomi, K.Takada (Dept. of Phys., Kyushu Univ., Fukuoka, Japan). Proceedings of the 1983 RCNP International Symposium on Light Ion Reaction Mechanism, Osaka, Japan, 16-20 May 1983 (Osaka, Japan: Osaka University 1983), p.896-900. At the tandem laboratory of Kyushu University experimental studies of the spin transfer reactions, particularly induced by the polarized deuteron beam, are being planned and most of the facilities for these experiments have been completed. The authors describe several new features of the equipment. (no refs.)

112523 **Evolution of control systems for accelerators.** M.C.Crowley-Milling (CERN, Geneva, Switzerland). Proceedings of the 1982 CERN School of Computing, Zinal, Valais, Switzerland, 29 Aug.-11 Sept. 1982 (Geneva, Switzerland: CERN 1983), p.271-304. Discusses the historical development of the accelerators. The author details the requirements for the control system. The various aspects of CAMAC and process control are examined. Software aspects are explored. (no refs.)

Comment on 'Direct measurement of the longitudinal coherence length of a thermal neutron beam' [and reply]See Entry 111491

An energy/mass analyzer with two flat capacitorsSee Entry 111807

A pulsed surface muon beam/pion beam for the Rutherford Appleton Laboratory Spallation Neutron SourceSee Entry 111808

A novel design for a fast intense neutron beamSee Entry 111809

Compact metal-ion beam source using thermal contact ionizerSee Entry 111810

Study of beam divergence of a low-energy (1-3 keV) ion sourceSee Entry 111811

Ion sources (recent topics)See Entry 111812

Negative ion sourcesSee Entry 111813

Effect of magnetic field on the characteristics of a hollow cathode ion sourceSee Entry 111815

High-current pulsed proton sourceSee Entry 111816

High-voltage long-focus electron gunSee Entry 111821

Instrument for examining the polarization of low-energy electrons interacting with a solidSee Entry 111822

Charge-density measurement for single nanosecond electron-beam pulsesSee Entry 111824

Underwater neutron radiography facility utilizing small neutron generatorSee Entry 112392

An injector for RFQ1See Entry 112463

The FMIT acceleratorSee Entry 112464

Design, construction and performance of the INS RFQ linac 'LITL'See Entry 112466

Status report on the upgraded UnilacSee Entry 112467

Improved performance of the Munich heavy ion postacceleratorSee Entry 112468

Radio-frequency accelerators for multi-kiloampere electron beamsSee Entry 112469

High charge picosecond pulses with a double gap subharmonic buncherSee Entry 112470

Update on the high-current injector for the Stanford linear colliderSee Entry 112471

Transient beam loading calculations and experiment at the Saclay electron linacSee Entry 112472

Design and fabrication of the BNL radio frequency quadrupole	See Entry 112473
Mechanical design of a heavy ion RFQ	See Entry 112474
Improved field stability in RFQ structures with vane coupling rings	See Entry 112475
Conversion of the AGS linac to H ⁻ acceleration	See Entry 112476
Post-coupler and stem current measurements for high current CW drift-tube linacs	See Entry 112477
First operation of proton induction linac	See Entry 112478
Subharmonic beam-loading in electron linear accelerators	See Entry 112479
NBS-LANL RTM injector installation	See Entry 112480
Research on electron linear accelerators with traveling wave resonators. II	See Entry 112481
A multidimensional study of a 50-MeV, 1500-rad/pulse radiographic linac, using the stagger-tuning concept	See Entry 112482
Recent performance improvements on FXR	See Entry 112483
Operation experience of the Riken variable-frequency heavy-ion linac, RILAC	See Entry 112484
4 π -mode acceleration in KEK 20-MeV proton linac	See Entry 112485
Betatron energy stabilization system	See Entry 112488
Precise angular distribution measurements for high energetic ions	See Entry 112539
Ion neutralization in helical electron beams	See Entry 112973
Neutron radiography facility using ²⁵² Cf neutron source	See Entry 115498
Improvement of efficiency of n, α converters to realize NR with relatively low n flux sources	See Entry 115501
Three-dimensional beam scanning for proton therapy	See Entry 115924

29.30 RADIATION SPECTROMETERS AND SPECTROSCOPIC TECHNIQUES

112524 **Determination of the multipolarity of prompt electromagnetic transitions from angular distributions of conversion electrons. II. Spectrometer and measurements.** H.R.Faust (Inst. Laue-Langevin, Grenoble, France), H.Klewe-Nebenius, H.Rebel, K.Wisslak. *Nucl. Instrum. & Methods Phys. Res. (Netherlands)*, vol.213, no.2-3, p.277-83 (1 Aug. 1983). For pt.1 see *ibid.*, vol.213, no.2-3, p.271-5 (1983). A spectrometer to measure the angular distribution of conversion electrons in charged particle induced reactions is described. The spectrometer consists of a magnetic filter built with small permanent magnets and a Si(Li) detector. The parameters of the instrument are discussed and attenuation factors due to the finite solid angles are evaluated. Spectra of conversion electrons following the reaction ¹⁶⁹Tm(d,xn) and ¹⁸²Os(d,xn) at an incident deuteron energy of $E_d=52$ MeV taken at different angles are shown. Angular distribution coefficients are calculated and the evaluation of the data in the framework of the formalism developed in part I is demonstrated. (10 refs.)

112525 **Time focusing and resolution in resonance detector neutron spectrometers.** J.M.Carpenter, N.Watanabe (Nat. Lab. for High Energy Phys., Ibaraki, Japan). *Nucl. Instrum. & Methods Phys. Res. (Netherlands)*, vol.213, no.2-3, p.311-16 (1 Aug. 1983). Nuclear recoil produces a variation in the time of arrival of neutrons scattered through different angles in pulsed-source resonance detector neutron spectrometers. The coupled variation of recoil energy shifts, scattering angles and lengths of different paths from source to sample to detector leads to conditions on the orientation of source, sample and detector which minimize the resolution of these spectrometers. The conditions depend upon the mass of the scatterer, the excitation energy of the recoiling unit, the mean scattering angle and relative incident and scattered neutron flight paths, and apply strictly only for a single value of the excitation energy. The authors develop general expressions for the geometric contributions to the resolution, from which the focusing conditions emerge. The focusing effect on the resolution is significant and is similar to that in time of flight diffractometers. (10 refs.)

112526 **A multi-microprocessor neutron spectrometer computer interface system.** R.Berliner, J.Sudol, G.Moum (Univ. of Missouri, Columbia, MO, USA). *Nucl. Instrum. & Methods Phys. Res. (Netherlands)*, vol.213, no.2-3, p.333-42 (1 Aug. 1983). A novel computer interface system for neutron or X-ray diffraction instrumentation is described. Consisting of a set of microprocessor controllers, it provides a simple and flexible means of instrument control. (5 refs.)

112527 **An automatic gamma spectrometer for activation analysis.** L.Vanska, R.J.Rosenberg, V.Pitkanen (Reactor Lab., Tech. Res. Centre of Finland, Espoo, Finland). *Nucl. Instrum. & Methods Phys. Res. (Netherlands)*, vol.213, no.2-3, p.343-7 (1 Aug. 1983). An automatic gamma spectrometer for activation analysis has been developed at the Technical Research Centre of Finland. The online system comprises a sample changer for up to 120 samples, detector, multichannel analyser, microcomputer programmed with BASIC language and input/output devices. (2 refs.)

112528 **The QDDQ magnet spectrometer 'BIG KARL'.** S.A.Martin, A.Hardt, J.Meissburger, G.P.A.Berg, U.Hacker, W.Hurlimann, J.G.M.Romer, T.Sagefka, A.Retz, O.W.B.Schult (Inst. fur Kernphys., Kernforschungsanlage Julich, Julich, Germany), K.L.Brown, K.Halbach. *Nucl. Instrum. & Methods Phys. Res. (Netherlands)*, vol.214, no.2-3, p.281-303 (1 Sept. 1983). A magnet spectrometer consisting of two quadrupoles, two dipole magnets and another larger quadrupole in front of the detector was designed and installed at the nuclear research institute of the KFA Julich. It has been used for charged-particle spectroscopy as the isochronous cyclotron since early 1979. Special features of the spectrometer are variable and high dispersion, coils for higher order field corrections in the dipole magnets and a focal plane perpendicular to the optical axis. A large mass-energy product of $mE/q^2 < 540$ u.MeV, an angular acceptance of $d\Omega < 12.5$ msr, a high resolving power of $p/\Delta p$ up to 3×10^4 and the possibility of kinematical corrections up to $K=0.8$ make the instrument a very versatile tool for many experiments in the fields of nuclear and atomic physics. (51 refs.)

112529 A microprocessor controlled spectrometer for frequency modulation Mossbauer measurements. T.Obenhuber, A.Forster, W.Potzel, G.M.Kalvius (Phys. Dept., Tech. Univ. Munchen, Garching, Germany). *Nucl. Instrum. & Methods Phys. Res. (Netherlands)*, vol.214, no.2-3, p.361-79 (1 Sept. 1983).

A Mossbauer spectrometer for the frequency modulation technique using piezo-quartzes is described. All its subsystems like the wave form synthesizer, the voltage divider and the data storage system are centrally controlled by a microprocessor. The system has been used for precision determination of hyperfine splittings of the very high resolution 93.3 keV Mossbauer resonance in ^{67}Zn . (22 refs.)

112530 Simultaneous determination of exponential background and Gaussian peak functions in gamma ray scintillation spectrometers by maximum likelihood technique. P.Eisler, T.Lwin, G.Nelson, S.Youl (CSIRO, Port Melbourne, Australia).

Nucl. Instrum. & Methods Phys. Res. (Netherlands), vol.214, no.2-3, p.421-9 (1 Sept. 1983).

Simultaneous fitting of peaks and background functions from gamma-ray spectrometry using multichannel pulse height analysis is considered. The specific case of Gaussian peak and exponential background is treated in detail with respect to simultaneous estimation of both functions by using a technique which incorporates maximum likelihood method as well as a graphical method. Theoretical expressions for the standard errors of the estimates are also obtained. The technique is demonstrated for two experimental data sets. (5 refs.)

112531 Background estimation for gamma-ray spectrometry.

D.D.Burgess, R.J.Tervo (McMaster Univ., Hamilton, Ontario, Canada).

Nucl. Instrum. & Methods Phys. Res. (Netherlands), vol.214, no.2-3, p.431-4 (1 Sept. 1983).

An algorithm has been developed and implemented for estimation of the spectral background of high-resolution gamma-ray spectra. A digital filter is used to identify peak-free regions of spectra. (9 refs.)

112532 A pseudorandom pulser technique for the correction of dead-time and pile-up losses in γ -ray spectrometry. G.Dorfel, W.Kluge, M.Kubisch (Zentralinst. fur Festkorperphys. und Werkstofforschung, Acad. der Wissenschaften, Dresden, Germany).

Nucl. Instrum. & Methods Phys. Res. (Netherlands), vol.214, no.2-3, p.435-40 (1 Sept. 1983).

A pseudorandom pulser and its application in high precision gamma-ray spectrometry is described. A pulse train suitable for modelling dead-time and pile-up effects is obtained by an AND-connection of delayed pulse sequences delivered by a maximum length shift register generator. The heart of the problem consists in finding the appropriate delay indices and in implementing these indices by 'add and shift'. The related conditions and rules are described. These conditions ensure the occurrence of multiple pulses according to the binomial and Poisson distributions, respectively, within a predetermined range of multiplicity as well as ensuring other statistical properties. Results are given in a form comparable with the description of the results of a well-known international test. (18 refs.)

112533 Derivative method unfolding of gamma-ray spectra from NE-213 spectrometers. J.K.Korsah (Phys. Dept., Univ. of Maine, Orono, ME, UA), W.H.Miller.

Nucl. Instrum. & Methods Phys. Res. (Netherlands), vol.214, no.2-3, p.441-3 (1 Sept. 1983).

Derivative method unfolding used in MATXUF for on-line analysis of fast neutron spectra has been applied to the analysis of gamma-ray spectra measured by an NE-213 liquid scintillation spectrometer. To eliminate the negative fluxes in the unfolded spectrum created by the Compton scatter behaviour in the plateau portion of the knee response correcting equations using a linearized approximation to the electron recoil spectrum has been developed and incorporated in the MATXUF unfolding code. (11 refs.)

112534 The determination of X-ray spectra from attenuation data. II. Experimental results. H.M.Kramer (Phys.-Tech. Bundesanstalt, Braunschweig, Germany).

Nucl. Instrum. & Methods Phys. Res. (Netherlands), vol.214, no.2-3, p.445-50 (1 Sept. 1983).

For pt.I see *ibid.*, vol.213, p.373 (1983). After the principal limitations of any attenuation analysis in a previous publication have been sounded, experimental data are presented and analyzed critically in the paper work. The histogram spectra determined approximate the (known) input spectra quite well and are useful for the calculation of other spectral-dependent information such as, for example, attenuation curves for a different material. Various experimentally relevant errors and their relative importance are discussed. The tolerances of the absorber thickness and those values of the mass attenuation coefficients associated with the high energy end of a spectrum must be subject to the most stringent requirements. (5 refs.)

112535 A wire-chamber spectrometer for muon spin rotation. R.Tedeschi (CERN, Geneva, Switzerland), P.Podini, R.De Renzi, A.P.Jeavons, R.Magnanini, L.O.Norlin.

Nucl. Instrum. & Methods Phys. Res. (Netherlands), vol.214, no.2-3, p.509-16 (1 Sept. 1983).

The authors report on the development of a spectrometer for muon spin rotation based on multiwire proportional chambers. The coordinates provided by telescopes each composed of two chambers are used to reconstruct the muon and the positron trajectories in $\mu^+ \rightarrow e^+ + \nu_e + \bar{\nu}_\mu$ decay. A real-time analysis program verifies that the two tracks intersect within the target: this constitutes a very stringent test to veto events which do not correspond to a muon decay. The results of some experiments are given in order to illustrate the field of application of this spectrometer. (12 refs.)

112536 Combined spectrometer for small-angle and diffuse scattering of cold neutrons. V.S.Bedbenov, G.A.Oganezov (Phys. Inst., Acad. of Sci., Georgian SSR).

Instrum. & Exp. Tech. (USA), vol.25, no.6, pt.1, p.1340-4 (Nov.-Dec. 1982). Translation of: *Prib. & Tekh. Eksp. (USSR)*, vol.25, no.6, p.28-31 (Nov.-Dec. 1982). [received: Sept. 1983]

Describes a fully automated combined spectrometer for small-angle and diffuse scattering of cold neutrons, built for one of the horizontal channels of the IRT-M nuclear reactor of the Physics Institute of the Georgian Academy of Sciences. It is based on a new methodological approach that permits qualitative improvements in the spectral purity of the incident long-wave neutron beam, in the resolving power of the spectrometer, and in its transmission when used in experiments on the transmission and small-angle and diffuse scattering of neutrons. A distinguishing feature of the developed facility is the possibility of measuring the dependence of the cold-neutron scattering intensity on the momentum transfer both in time-of-flight measurements and when the usual stationary method is used. (10 refs.)

112537 Stabilized scintillation spectrometer for scattered low-energy gamma radiation. O.M.Anshakov, V.A.Chudakov, A.L.Kholmet'skii, V.I.Gurinovich (State Univ., Minsk, Belorussian SSR).

Instrum. & Exp. Tech. (USA), vol.25, no.6, pt.1, p.1345-8 (Nov.-Dec. 1982). Translation of: *Prib. & Tekh. Eksp. (USSR)*, vol.25, no.6, p.31-4 (Nov.-Dec. 1982). [received: Sept. 1983]

A spectrometer for scattered gamma radiation with differential stabilization against an X-ray fluorescence reference peak is described. The reference signal is produced in a special target made of barium titanate. The results of temperature tests of the spectrometer are presented. (16 refs.)

112538 A method of data analysis of the magnetic spectrometer. Shen Wen-qing (Inst. of Modern Phys., Acad. Sinica, Peking, China).

Phys. Energ. Fortis & Phys. Nucl. (China), vol.7, no.3, p.361-69 (May 1983). In Chinese.

A method of data analysis of the magnetic spectrometer with heavy ion is discussed. The determination of the charge state, the atomic number, the atomic mass and the energy of reaction products are described. The paper also deals with the software correction of $B\rho$ non-linear dispersion, kinematics and the difference of flight paths. (6 refs.)

A note on the interpretation of activation measurements on the Princeton large torus See Entry 111626

High-voltage long-focus electron gun See Entry 111821

Design of a passive magnetic shunt for the extraction of electron beams from a photon tagging spectrometer See Entry 112501

Alpha-spectrometric ionization chamber with an active area of 2m^2 See Entry 112577

A trigger system using wire chamber information See Entry 112589

Identification of heavy charged particles by using a fast amplifier to obtain E- and t-signals See Entry 112591

Universal coincidence circuit See Entry 112592

Radon daughter carousel: an automated instrument for measuring indoor concentrations of ^{218}Po , ^{214}Pb , and ^{214}Bi See Entry 112607

A photoelectron spectrometer for measurement of electron plasma temperature See Entry 113654

29.40 RADIATION DETECTORS

(for mass spectrometers, see 07.75)

112539 Precise angular distribution measurements for high energetic ions. H.Lettau, H.G.Bohlen, H.Rossner, W.von Oertzen, M.Martin (Hahn-Meitner-Inst., KFA Berlin GmbH, Berlin, Germany).

Nucl. Instrum. & Methods Phys. Res. (Netherlands), vol.213, no.2-3, p.187-94 (1 Aug. 1983).

The reliability of a position sensitive parallel plate avalanche counter as a start detector at the entrance of a magnetic spectrometer is demonstrated. Implications for experiments with high energy, heavy ions are discussed from the results. (18 refs.)

112540 First measurement of efficiency and precision of CCD detectors for high energy physics. R.Bailey, C.J.S.Damerell, R.L.English, A.R.Gillman, A.L.Lintern, S.J.Watts, F.J.Wickens (Rutherford Appleton Lab., Chilton, Didcot, England).

Nucl. Instrum. & Methods Phys. Res. (Netherlands), vol.213, no.2-3, p.201-15 (1 Aug. 1983).

It has been known for some time that a 2-dimensional charge-coupled device (CCD) might be used for detecting high energy particles with high precision and excellent 2-track resolution. Such detectors could be used to distinguish between prompt tracks and decay products in events producing short-lived particles (heavy leptons, charm, beauty, etc.). The authors present results in which a telescope of CCD detectors has been operated in a beam of high energy particles. The main results are that even these early detectors have excellent performance characteristics, namely efficiency for track detection of $98 \pm 2\%$ per plane, spatial resolution of $4.3 \mu\text{m}$ and $6.1 \mu\text{m}$ in two orthogonal directions and 2-track resolution of $40 \mu\text{m}$ in space. (9 refs.)

112541 Development of a small high-pressure streamer chamber for charm-lifetime measurements. V.Eckardt, S.Wenig (Max-Planck-Inst. fur Phys. und Astrophys., Munchen, Germany).

Nucl. Instrum. & Methods Phys. Res. (Netherlands), vol.213, no.2-3, p.217-21 (1 Aug. 1983).

The spatial resolution in a streamer chamber is investigated as a function of gas pressure in the chamber. For this purpose a small streamer chamber with a track sensitive volume of 50 mm diameter and 23 mm gap has been constructed and operated between 5 and 20 atm pressure. In this pressure range streamer densities from 43 to 67 streamers per centimeter were found. The track width 2σ is mainly determined by the diffusion of the electrons and shrinks proportionally to $1/\sqrt{p}$. In addition, the influence of a magnetic field of 1.8 T on the diffusion was studied. At 20 atm one reaches a σ of $70 \mu\text{m}$ in space, which allows a measurement of charmed particle lifetimes as short as 10^{-13} s. (7 refs.)

112542 Tests of gas sampling electromagnet shower calorimeter. A.Barbaro-Galtieri, W.Carithers, C.Day, K.J.Johnson, W.A.Wenzel, H.Videau (Lawrence Berkeley Lab., Univ. of California, Berkeley, CA, USA).

Nucl. Instrum. & Methods Phys. Res. (Netherlands), vol.213, no.2-3, p.223-41 (1 Aug. 1983).

An electromagnet shower gas-sampling calorimeter has been tested in both Geiger and proportional discharge modes for incident electron energies in the range 0.125-16 GeV. The 0.2 radiation length-thick layers were lead-fiberglass laminates with cathode strips normal to the sense wires. The $5 \times 10 \text{ mm}^2$ Geiger cells were formed with uniformly spaced nylon fibers perpendicular to the wires. Proportional mode measurements were carried out in the pressure range 1-10 atm. A Monte Carlo simulation is in good agreement with measured shower characteristics and has been used to predict the behavior for oblique angles of incidence and for various Geiger cell dimensions. (8 refs.)

112543 Effects of space charge, leakage currents and diffusion in large planar electrodeless drift chambers. C.Becker, W.Weihns, G.Zech (Dept. of Phys., Siegen Univ., Siegen, Germany).

Nucl. Instrum. & Methods Phys. Res. (Netherlands), vol.213, no.2-3, p.243-9 (1 Aug. 1983).

The authors calculate the effects of space charges, leakage currents and positive ion diffusion in large planar electrodeless drift chambers. Results are in qualitative agreement with measurements of the gas amplification and leakage currents at different rates of irradiation. Consequences on the construction of chambers and on their applications are discussed. (7 refs.)

112544 A modular NaI(Tl) detector for 20-1000 MeV photons. P.Blum, R.Guigas, H.Koch, M.Meyer, H.Poth, U.Raich, B.Richter (Inst. für Experimentelle Kernphys., Univ. Karlsruhe, Karlsruhe, Germany), G.Backenstoss, M.Hasinoff, P.Pavlopoulos, J.Repond, L.Tauscher, D.Troster, L.Adiels, I.Bergstrom, K.Fransson, A.Kerek, M.Suffert, K.Zioutas. *Nucl. Instrum. & Methods Phys. Res. (Netherlands)*, vol.213, no.2-3, p.251-9 (1 Aug. 1983).
A detector consisting of 54 NaI (Ti) modules is described. The detector has been optimized for the detection of 20-1000 MeV photons. An energy resolution (FWHM) of 5.5% at 130 MeV could be attained and the stability has been better than 1% over several months. (5 refs.)

112545 A new scintillator and wavelength shifter. T.Kamon, K.Kondo, A.Yamashita (Inst. of Phys., Univ. of Tsukuba, Ibaraki, Japan), T.Shimizu, L.Nodulman. *Nucl. Instrum. & Methods Phys. Res. (Netherlands)*, vol.213, no.2-3, p.261-9 (1 Aug. 1983).
The authors have developed a new type of scintillator and a wavelength shifter to be used for high energy particle calorimeters. To obtain a long attenuation length, two kinds of fluors are mixed in a polystyrene base. The wavelength shifter has a new material matching its absorption spectrum to the wavelength of the scintillation light. Their common characteristics are a relatively high light output and a long attenuation length with a reasonable cost. (7 refs.)

112546 A threshold Cherenkov counter for isotopic identification of high-energy heavy ions. J.D.Stevenson, J.A.Musser (Dept. of Phys., Univ. of California, Berkeley, CA, USA). *Nucl. Instrum. & Methods Phys. Res. (Netherlands)*, vol.213, no.2-3, p.285-9 (1 Aug. 1983).
The authors have developed an apparatus for isotope identification of heavy-ion projectile fragments with energies from ~330 to 600 MeV/nucleon. The detector uses a Cherenkov intensity measurement in conjunction with a measurement of magnetic rigidity to determine mass. An advantage of this technique is that it allows isotope identification of projectile fragments with higher energies than are possible for 'stopping type' detectors. Higher fragment energies allow the use of much thicker targets and, therefore, provide higher sensitivity to rare isotopes. In a recent test of the apparatus using a 670 MeV/nucleon ^{20}Ne beam and a 30 g/cm² aluminum target a mass resolution of $\sigma_A = 0.2$ amu was obtained for projectile fragments with charges $5 \leq Z \leq 9$. (6 refs.)

112547 The prompt response of bismuth germanate and NaI(Tl) scintillation detectors to fast neutrons. O.Hausser, M.A.Lone, T.K.Alexander, S.A.Kushneriuk (Chalk River Nuclear Labs., AECL, Chalk River, Ontario, Canada), J.Gascon. *Nucl. Instrum. & Methods Phys. Res. (Netherlands)*, vol.213, no.2-3, p.301-9 (1 Aug. 1983).
Spectral distributions and yields of scintillation pulses from the prompt interaction of neutrons with 7.6 cm diameter \times 7.6 cm long bismuth germanate (BGO) and NaI(Tl) detectors have been measured. Neutrons at energies between 0.4 and 10 MeV were produced by the $^7\text{Li}(p,n)$ and the $^{197}\text{Au}(p,n)$ reactions, respectively, and identified by their time-of-flight relative to the pulsed proton beam. For both scintillators the neutron response is dominated by $(n,n'\gamma)$ reactions, and the efficiencies are in qualitative agreement with simple estimates that depend on the non-elastic and elastic cross sections and on two geometrical factors. Compared to NaI(Tl), BGO exhibits a much superior gamma-ray-to-neutron detection ratio. (25 refs.)

112548 An arsenic-activation detector for bursts of 2.5 and 14 MeV neutrons. E.L.Jacobs, S.D.Bonaparte, P.D.Thacher (Sandia Nat. Lab., Albuquerque, NM, USA). *Nucl. Instrum. & Methods Phys. Res. (Netherlands)*, vol.213, no.2-3, p.387-92 (1 Aug. 1983).
An activation detector has been developed for measuring the output of pulsed neutron generators. This detector utilises the $^{75}\text{As}(n, n')^{75m}\text{As}$ reaction and detection of the 0.3 MeV gamma rays from $^{75m}\text{As}(\tau_{1/2} = 17 \text{ ms})$ by a plastic scintillator. The efficiency in counts per incident neutron is about 0.25% at 2.5 MeV and 0.35% at 14 MeV. (29 refs.)

112549 The design and calibration of precision drift chambers for use in a gluonium search experiment at the CERN ISR. M.G.Albrow (Rutherford Appleton Lab., Didcot, England), N.J.Beadle, A.A.Carter, J.R.Carter, P.C.Cecil, S.-U.Chung, D.J.A.Cockerill, W.M.Evans, M.D.Gibson, M.J.Goodrick, J.Hiddleston, N.A.McCubbin, T.W.Pritchard, D.P.Weygand. *Nucl. Instrum. & Methods Phys. Res. (Netherlands)*, vol.214, no.2-3, p.201-8 (1 Sept. 1983).
Describes the design, construction and calibration of a set of high precision drift chambers. The precise coordinate ($\sigma \sim 120 \mu\text{m}$) is determined by drift time measurement, with the orthogonal coordinate given by the charge division method ($\sigma \sim 1.2 \text{ mm}$). The chambers have been calibrated using a well-defined laser beam. Their use within a gluonium search experiment at the CERN ISR is also described. (3 refs.)

112550 Particle identification in the relativistic rise region using a longitudinal drift chamber. R.Arai, J.Bensinger, H.Boerner, Y.Fukushima, K.Hayashi, N.Ishihara, S.Inaba, T.Kohriki, S.Nakamura, K.Ogawa, F.Takasaka, Y.Unno, Y.Watase (KEK, Nat. Lab. for High Energy Phys., Ibaraki-Ken, Japan). *Nucl. Instrum. & Methods Phys. Res. (Netherlands)*, vol.214, no.2-3, p.209-16 (1 Sept. 1983).
Particle identification by energy loss measurement was tested using a longitudinal drift chamber equipped with a 25 MHz flash ADC. For 3 GeV/c pions the resolution σ_E/E was about 5%. The separation between pions and protons at this momentum was about 4 standard deviations. The influence of a magnetic field was examined. The deterioration of the separation was less than 15% up to a field strength of 5.2 kG. (7 refs.)

112551 MARS a fine grain aluminium-liquid argon calorimeter. C.Cerri (INFN, Pisa, Italy), S.P.Denisov, N.Krasnokutsky, S.A.Medved, V.S.Mikhailov, N.I.Naumov, S.A.Polovikov, E.A.Rasuvayev, F.Sergiampietri, R.S.Shulvalov, D.A.Stoyanova. *Nucl. Instrum. & Methods Phys. Res. (Netherlands)*, vol.214, no.2-3, p.271-35 (1 Sept. 1983).
The performance of a fine grain liquid argon calorimeter with aluminium electrodes has been studied. Measurements have been performed with 13.3-35 GeV/c electrons, muons and pions. The fine sampling structure and the large fraction of active absorber in this detector allowed an energy resolution for electrons of $\sigma(E)/E = \sqrt{(0.08/E)^2 + (0.036/\sqrt{E})^2}$ to be reached. The space and angular resolutions for electromagnetic showers can be represented as $\sigma(x) = \sqrt{(38.5/E)^2 + (12.8/\sqrt{E})^2} \text{ mm}$ and $\sigma(\theta) = \sqrt{(87.3/E)^2 + (33.8/\sqrt{E})^2} \text{ mrad}$. Due to the detailed measurements of the shower development a good electron/hadron discrimination is achieved. The low noise allows also the detection and identification of muons. (12 refs.)

112552 A prototype sampling calorimeter with photodiode readout (SPED). W.Kononenko, W.Selove, G.E.Theodosiou, R.Van Berg (Dept. of Phys., Univ. of Pennsylvania, Philadelphia, PA, USA). *Nucl. Instrum. & Methods Phys. Res. (Netherlands)*, vol.214, no.2-3, p.237-43 (1 Sept. 1983).
The authors have built and tested a new type of sampling calorimeter using scintillator as the material, and thin vacuum photodiodes for signal readout, the new feature. They measure an energy resolution of about $22\%/\sqrt{E}$ for electrons of 10-37.5 GeV. For muons the signal to noise ratio is about 2.4 corresponding to about 1000 pe/cm of scintillator. Important merits of such a design such as the excellent gain stability (photodetector gain=1), absence of the need for high voltages, and system simplicity in construction and operation, have been demonstrated. (2 refs.)

112553 A study of bubble chamber operating conditions for holographic image recording. J.L.Benichou, A.Herve, K.E.Johansson, P.Lecoq, P.Olivier, J.Pothier, G.Waurick, E.Wiatrowski (CERN, Geneva, Switzerland), R.Roosen, S.P.K.Tavernier, G.van Beek, O.R.Williams. *Nucl. Instrum. & Methods Phys. Res. (Netherlands)*, vol.214, no.2-3, p.245-51 (1 Sept. 1983).
Results of a systematic study of operating conditions for holographic image recording in a heavy liquid rapid cycling bubble chamber are presented. The authors find that the limiting phenomenon is the turbulence generated by the growth and recompression of the bubbles. To minimize this effect it is necessary to operate the chamber at high temperature where the bubble growth is slow. A total of 40000 useful holograms were recorded in the NA25 experiment at CERN. Typical running conditions were 10 Hz cycling rate, 80 beam tracks per expansion and a bubble density of 95 bubbles per cm. The bubble diameter was 12 μm . (7 refs.)

112554 Charge collection in silicon strip detectors. E.Belau, R.Klanner, G.Lutz, E.Neugebauer, H.J.Seebrunner, A.Wylie (Max-Planck Inst. für Phys. und Astrophys., Werner-Heisenberg-Inst., Munich, Germany), T.Bohringer, L.Hubbeling, P.Weilhammer, J.Kemmer, U.Kotz, M.Riebsell. *Nucl. Instrum. & Methods Phys. Res. (Netherlands)*, vol.214, no.2-3, p.253-60 (1 Sept. 1983).
The charge collection in silicon detectors has been studied by measuring the response to high-energy particles of a 20 μm pitch strip detector as a function of applied voltage and magnetic field. The results are well described by a simple model. The model is used to predict the spatial resolution of silicon strip detector and to propose a detectors and to propose a detector with optimized spatial resolution. (8 refs.)

112555 Electron identification beyond 1 GeV by means of transition radiation. A.Bungener, B.Koppitz, R.van Staa, P.Stahelin (II Inst. für Experimentalphys., Univ. Hamburg, Hamburg, Germany), M.Holder. *Nucl. Instrum. & Methods Phys. Res. (Netherlands)*, vol.214, no.2-3, p.261-8 (1 Sept. 1983).
The authors report on measurements with different configurations of transition radiation detectors, performed with electrons in the energy range between 0.75 GeV and 6 GeV. The radiator materials were foils of polyethylene or fibres of polypropylene or carbon. The multiwire proportional chambers for photon detection were operated with krypton, xenon or a mixture of xenon and argon. The transition radiation yield is compared to theory, and the pion rejection power is reported. It is shown that a very effective particle discrimination can be obtained from a rather simple detector configuration of moderate thickness, low weight and low cost. (22 refs.)

112556 Photomultiplier gain tuning system. F.Binon, S.V.Donskov, P.Duteil, M.Gouanere, V.A.Kachanov, A.V.Kulik, D.Michotte, Yu.V.Mikhailov, J.P.Peigneux, Yu.D.Prokoshkin, A.V.Singovsky, J.P.Stroot (Joint Experiment of IHEP, Serpukhov, USSR). *Nucl. Instrum. & Methods Phys. Res. (Netherlands)*, vol.214, no.2-3, p.269-72 (1 Sept. 1983).
Most high energy physics experiments today make use of a large number of photomultipliers (PM). The setting and the tuning of the high voltage on the photomultiplier dividers need automatic devices. A few of these have been developed and work satisfactorily. Nevertheless the authors describe a highly reliable system which is definitely cheaper to build and to maintain in most cases and which is particularly suited for large calorimeters with thousands of PM. (4 refs.)

112557 A simple method for direct compensation for kinematic energy spread using a silicon PSD. J.B.A.England, S.D.Hoath (Dept. of Phys., Univ. of Birmingham, Birmingham, England), T.R.Ophel, B.R.Fulton. *Nucl. Instrum. & Methods Phys. Res. (Netherlands)*, vol.214, no.2-3, p.305-9 (1 Sept. 1983).
A simple method of compensating for the kinematic energy spread of the particles from a nuclear reaction detected in a silicon PSD is described. The technique relies on a suitable choice of the series resistor for the reaction of interest and the degree of compensation is shown to be equivalent to the first order correction for the acceptance of a magnetic spectrometer. Experimental results using recoil protons, elastically scattered alpha-particles and carbon ions from a heavy ion induced reaction illustrate the practical application and success of the technique. The limit of the compensation for light ions is set by the resistive noise in the 'energy \times position' signal while for heavy ions the nuclear scattering spread sets the lower limit. (3 refs.)

112558 A multi-purpose NaI(Tl) detector system. S.Elfstrom, L.Hildingson, D.Jerrestam, T.Lindblad (Res. Inst. of Phys., Stockholm, Sweden). *Nucl. Instrum. & Methods Phys. Res. (Netherlands)*, vol.214, no.2-3, p.311-16 (1 Sept. 1983).
A multi-purpose detector system consisting of six hexagonal NaI(Tl) detectors is described. The detectors can be arranged as a total energy spectrometer or together with a Ge(Li) detector as a Compton suppression device. The detectors can also be used individually for detection of γ -ray energies in for example, E_γ - E_γ correlation measurements. (15 refs.)

112559 An interactive system for emulsion data acquisition. G.Baroni, S.Di Liberto, P.Ginobbi, F.Meddi, S.Petrera, G.Romano, C.Sgarbi (Istituto di Fisica, Univ. di Roma, Rome, Italy). *Nucl. Instrum. & Methods Phys. Res. (Netherlands)*, vol.214, no.2-3, p.381-4 (1 Sept. 1983).
The authors describe an interactive system, based on a micro-processor, for the acquisition and elaboration of nuclear emulsion measurements. The device consists of a Koritska R_4 microscope coupled with a telecamera and with a motor driven stage for automatic displacement in the three directions. Both the pair of internal coordinates and the three external coordinates are digitized. The interactive management of the system is carried out with a PDP11/34. (3 refs.)

112560 A laser system for monitoring photomultiplier tubes in counter arrays. P.Smith (Dept. of Phys., Indiana Univ., Bloomington, IN, USA). *Nucl. Instrum. & Methods Phys. Res. (Netherlands)*, vol.214, no.2-3, p.385-90 (1 Sept. 1983).

The design of two computer-controlled, pulsed laser systems used for monitoring gains and timing stability of photomultipliers in high energy physics experiments is described. Typical data obtained with these systems are presented. (9 refs.)

112561 Automatic scanning of solid state nuclear track detectors at low track density. H.X.Zhang, T.R.Yeh, H.Lancman (Phys. Dept., Brooklyn Coll., City Univ. of New York, New York, NY, USA). *Nucl. Instrum. & Methods Phys. Res. (Netherlands)*, vol.214, no.2-3, p.391-4 (1 Sept. 1983).

A device for scanning large areas of Kimfol fission track detectors is described. It is being used in photofission experiments where $\sim 10^4$ cm² of film per run have to be handled. The tracks are first enlarged by etching and sparking. The film is then scanned by a high resolution Vidicon camera and the x and y coordinates of each track are stored in a computer. A typical scanning speed is 10 cm²/s. The counting efficiency is close to 100%. (10 refs.)

112562 Large volume neutron detectors with subnanosecond time dispersions. R.Madey, J.W.Watson, M.Ahmad, B.D.Anderson, A.R.Baldwin, A.L.Casson, W.Casson, R.A.Cecil, A.Fazely, J.M.Knudson, C.Lebo, W.Pair-suwan, P.J.Pella, J.C.Varga, T.R.Witten (Dept. of Phys., Kent State Univ., Kent, OH, USA). *Nucl. Instrum. & Methods Phys. Res. (Netherlands)*, vol.214, no.2-3, p.401-13 (1 Sept. 1983).

Design criteria and performance characteristics are described for large-volume (13.1 l to 118 l) mean-timed plastic-scintillator detectors for neutrons from ~ 2 MeV to 2 GeV. Detectors were constructed in six sizes (all 0.102 m thick) from 0.126 m \times 1.016 m \times 0.102 m to 0.762 m \times 1.524 m \times 0.102 m. Overall energy resolutions of 230 keV for 80 MeV neutrons, 320 keV for 133 MeV neutrons, and 440 keV for 157 MeV neutrons were achieved in time-of-flight experiments with flight paths of 76, 68, and 91 m, respectively. The detectors have pulse-height responses uniform to $\pm 5\%$ except close to the ends, position resolutions less than 5 cm, and intrinsic time dispersions less than 400 ps. Typical neutron detection efficiencies are 20% for 20 MeV neutrons at a pulse-height threshold of 2 MeV equivalent-electron energy (MeV ee) and 3.5% for 200 MeV neutrons at a pulse-height threshold of 50 MeV ee. (23 refs.)

112563 Instrumental limit and number of effective granules in superheated superconducting detectors. A.Hrisoho (Lab. de l'Accelérateur Lineaire, Univ. Paris Sud, Orsay, France), G.Waysand. *Nucl. Instrum. & Methods Phys. Res. (Netherlands)*, vol.214, no.2-3, p.415-18 (1 Sept. 1983).

A relation has been established between the number of effective granules in a superheated superconducting detector and the noise factor of the electronic channel which is expressed in terms of the magnetic flux involved. Consequences for detector design are discussed. (7 refs.)

112564 A precision beta gauge using a plastic scintillator and photomultiplier detector. J.M.Jaklevic, N.W.Madden, C.E.Wiegand (Lawrence Berkeley Lab., Univ. of California, Berkeley, CA, USA). *Nucl. Instrum. & Methods Phys. Res. (Netherlands)*, vol.214, no.2-3, p.517-18 (1 Sept. 1983).

The authors describe the use of a plastic scintillator photomultiplier detector combination in applications involving the precision beta-gauge measurement of small mass deposits of thin substrates. The requisite precision (± 2 μ g/cm²) places stringent requirements on the beta-particle counter and associated electronics. The scintillator based system is shown to be equivalent if not superior to previously employed semiconductor detectors with respect to long-term counting stability. (3 refs.)

112565 Effect of electric field on cellulose nitrate track detector. S.K.Chakravarti (Dept. of Appl. Phys., Regional Engng. Coll., Kurukshetra, India), K.K.Nagpaul. *Nucl. Instrum. & Methods Phys. Res. (Netherlands)*, vol.214, no.2-3, p.519-24 (1 Sept. 1983).

The influence of DC electric fields ($0.3\text{--}5 \times 10^7$ V.m⁻¹) applied for different durations (0-2 h) on the track recording characteristics of CA80-15 Kodak Pathe' cellulose nitrate is reported. It is observed that at a lower etch time of 30 min (2.5 N NaOH, 55°C, without stirring), etched track diameters of normally incident 4 MeV α -particles remain unchanged almost up to the applied electric fields 0.3×10^7 V.m⁻¹ irrespective of the time duration of application of field. Track diameter increases on increasing the field further. At higher etching times (interrupted etching with 30 min step) track diameter and bulk etch velocity V_g go on decreasing in general at first, attain a minimum and then show an upward trend at fields $\sim 3 \times 10^7$ V.m⁻¹. However, for field values $> 3 \times 10^7$ V.m⁻¹ and longer field times (1.5-2 h), downward trend is indicated. Average bulk etch velocity calculated for a total etch time of 180 min for the samples treated with different electric fields for a maximum time of 2 h, increases first, acquires a maximum and then exhibits a falling trend with increasing fields. Average track etch velocity, V_t , however, decreases initially and then increases with the field followed by an abrupt rise at higher field values. The etch velocity ratio, V_t/V_g , shows peaking at 3.5×10^7 V.m⁻¹ in the upward direction. The etching efficiency, η , changes from 82% to 97% for the field values changing from 1×10^7 V.m⁻¹ to 3.5×10^7 V.m⁻¹ for a field duration of 2 h and total etch time of 180 min. An attempt has been made to correlate the observed results with the possible increased crystallinity with the application of electric field leading to the electret phenomenon involving molecular orientations and the ozone effects. (32 refs.)

112566 Special gas mixtures with very small drift angles at low drift velocities. U.Becker, M.Capell, M.Chen, M.White, C.H.Ye, K.Yee (Lab. for Nuclear Sci., MIT, Cambridge, MA, USA), J.Fehlmann, P.G.Seiler. *Nucl. Instrum. & Methods Phys. Res. (Netherlands)*, vol.214, no.2-3, p.525-30 (1 Sept. 1983).

Using the novel technique of UV laser-induced ionization, drift angles and drift velocities have been measured for various gas mixtures. In the region where the drift velocity is linearly dependent on the drift field and up to 10 kG, the measured values agree well with predictions by computations also described. Two gas mixtures were found which give small drift angles at low drift velocities. This is important for the operation of a time expansion chamber (TEC). (12 refs.)

112567 The absolute efficiency of a 7.6- by 7.6-cm bismuth germanate scintillator for 15-MeV gamma rays. N.R.Roberson, S.A.Wender, D.M.Drake (Los Alamos Nat. Lab., Univ. of California, Los Alamos, NM, USA).

Nucl. Instrum. & Methods Phys. Res. (Netherlands), vol.214, no.2-3, p.541-2 (1 Sept. 1983).

The absolute efficiency of an uncollimated 7.6- by 7.6-cm cylindrical bismuth germanate detector was measured at a gamma-ray energy of 15.1 MeV. The measured photopeak efficiency is 0.51 ± 0.04 . (4 refs.)

112568 A simple detector for locating radiography and radiotherapy gamma emitting radiation sources. P.H.Burgess (Nat. Radiological Protection Board, Chilton, Didcot, England). *J. Soc. Radiol. Prot. (GB)*, vol.3, no.3, p.21-2 (Autumn 1983).

The author provides a simple design of collimated Geiger-Muller tube detector which is simple to construct and would be useful in the recovery of lost gamma radiation sources. The detector is compatible with the majority of ratemeters in present use. (1 ref.)

112569 Radiography with fast neutrons by a plastic detector. E.Duhmke (Radiologische Univ., Kiel, Germany), L.Greim.

Proc. SPIE Int. Soc. Opt. Eng. (USA), vol.312, p.276-80 (1983). (1st European Conference on Cineradiography with Photons or Particles, Paris, France, 18-21 May 1981).

The image recording of fast neutron radiographs can be achieved sufficiently by means of plastic foils and the track etching technique. The optimal etching conditions for cellulose nitrate foils were studied. A mathematical model for the dependence of the optical density on the area and number of the etch pits is given and compared to measurements. Finally, two examples of radiographic applications may underline the possible importance of this method. (4 refs.)

112570 Plastic detector technique in fast neutron radiography. W.Hunger, R.Scherzer, W.Engel, G.Sermund (Inst. für Reine und Angewandte Kernphys., Univ. of Kiel, Kiel, Germany), U.Roose.

Proc. SPIE Int. Soc. Opt. Eng. (USA), vol.312, p.281-5 (1983). (1st European Conference on Cineradiography with Photons or Particles, Paris, France, 18-21 May 1981).

In order to detect fast neutrons, the Kodak CA 80-15 plastic detector can be used either as a screen in neutron radiography or as a neutron dosimeter. Especially for 14.9 MeV neutron dosimetry, the authors describe a helium converter test unit which increases the detection efficiency of cellulose nitrate plastic detectors by a factor of 3. (14 refs.)

112571 The neutron sensitivity of a Geiger-Muller counter between 0.5 and 8 MeV. D.T.L.Jones (Medical Component, Nat. Accelerator Centre, Faure, S Africa), W.R.McMurray.

Health Phys. (GB), vol.45, no.3, p.659-63 (Sept. 1983).

Geiger-Muller counters are often used in mixed-field dosimetry to determine the photon dose fraction. For accurate dose specification, their neutron sensitivities must be known. The pulsed beam time-of-flight method was used to determine the neutron sensitivities of an energy-compensated type ZP1320/PTFE Geiger-Muller counter in the 0.5-8-MeV region. The flux of monoenergetic neutrons from the T(p,n)³He and D(d,n)³He reactions, which were used in these measurements, were determined from time-of-flight spectra with an NE213 scintillation counter of known efficiency. (12 refs.)

112572 Performance of silicon surface barrier detectors (p- and n-type) under identical quenchant, postetch ambients and encapsulation. A.K.Batra (Dept. of Phys., Haryana Agricultural Univ., Kaul, India).

Indian J. Pure & Appl. Phys., vol.21, no.7, p.383-7 (July 1983).

p- and n-type silicon surface barrier detectors (p-SSBD and n-SSBD) have been fabricated by varying the three significant parameters, viz. quenchant, postetch ambients and encapsulations. Postetch exposures of two days' duration to deionized water for n-type and that to dust-free air for p-type have been found essential for SSBD technology. Quenchant experiments lead to their ranking in decreasing order of superiority as HNO₃, H₂O, HF in n-SSBD and HNO₃, HF, H₂O in p-SSBD. Stain film left as a result of quenching appears to have excess of chemisorbed fluoride group. Encapsulation of edges and free rear surface both in p- and n-SSBD reduces the leakage current. It has been applied prior to ambient exposure in p-SSBD and after this exposure in n-SSBD. Leakage currents of less than 1×10^{-8} A (n-SSBD) and 2×10^{-8} A (p-SSBD) have been obtained for reverse biases up to 100 V. The sample detectors yield energy resolutions of 30 keV FWHM (n-SSBD) and 50 keV FWHM (p-SSBD) for 5.47 MeV α -particles. Results indicate dominant dependence of SSBD technology on chemisorbed water and oxygen coverages at different stages of fabrication. (14 refs.)

112573 Thermal degradation of plastic scintillators. E.A.Andreeshchev, S.F.Kilin, Yu.P.Kushakevich, I.M.Rozman, V.M.Shoniya.

Instrum. & Exp. Tech. (USA), vol.25, no.6, pt.1, p.1348-52 (Nov.-Dec. 1982). Translation of: *Prib. & Tekh. Eksp. (USSR)*, vol.25, no.6, p.35-7 (Nov.-Dec. 1982). [received: Sept. 1983]

The thermal degradation of plastic scintillators (polymers of styrene and 2,4-dimethylstyrene and copolymers of these with polyfunctional monomers) has been examined. There is a reduction in light yield and shortening of the scintillation length when the temperature is raised in air. Molecular excited states are quenched in the surface layer and the luminescence is absorbed. (4 refs.)

112574 Scintillation pulse shape provided by polyvinylxylene plastic scintillators. N.Z.Galunov, O.A.Gunder, I.V.Kopina, Yu.A.Tsirlin.

Instrum. & Exp. Tech. (USA), vol.25, no.6, pt.1, p.1352-5 (Nov.-Dec. 1982). Translation of: *Prib. & Tekh. Eksp. (USSR)*, vol.25, no.6, p.38-40 (Nov.-Dec. 1982). [received: Sept. 1983]

Measurements have been made on the shape, size, and spectrum of the scintillations from plastic detectors based on polyvinylxylene containing 2-phenyl-5-(4-biphenyl)1,3,4-oxadiazole as additive and exposed to the β particles of ⁹⁰Sr+⁹⁰Y; these are in no way inferior in speed to NE111 detectors. A scintillator with a decay time of 0.9 nsec is obtained on increasing the concentration of the additive to 7% by mass. (7 refs.)

112575 Method of determining the thickness of nuclear photoemulsions in autoradiography. V.D.Rusov, M.Yu.Semenov, V.A.Barsuk (Odessa State Univ., Odessa, USSR).

Instrum. & Exp. Tech. (USA), vol.25, no.6, pt.1, p.1357-9 (Nov.-Dec. 1982). Translation of: *Prib. & Tekh. Eksp. (USSR)*, vol.25, no.6, p.42-4 (Nov.-Dec. 1982). [received: Sept. 1983]

A method is proposed for determining and monitoring the thicknesses of nuclear photoemulsions used in optical and electron-microscopy autoradiography. The method is based on measuring the rate of drawing out the samples from the emulsion melt. (10 refs.)

112576 Use of BPS-75+'Elektronika-1001' scanning-measuring system for analysis of photographs from wide-gap chambers. S.A.Averin, G.V.Veselova, G.V.Navasardyan (Inst. of Space Res., Acad. of Sci., Moscow, USSR). *Instrum. & Exp. Tech. (USA)*, vol.25, no.6, pt.1, p.1368-72 (Nov.-Dec. 1982). Translation of: *Prib. & Tekh. Eksp. (USSR)*, vol.25, no.6, p.52-5 (Nov.-Dec. 1982). [received: Sept. 1983]

A semiautomatic system based on the BPS-75 scanning and measuring projector, operating on line with an Elektronika-1001 minicomputer, has been built for processing data from films taken of wide-gap spark chambers of a γ -ray telescope. The system has been tested in processing data from the calibration of wide-gap spark chambers on the DESY accelerator (Hamburg). The angular resolution of the spark chambers is $\pm 1^\circ$ for 2-GeV positrons and 1.8° for 100-MeV γ -rays. On the basis of measurements made on the BPS-75 projector the extraction of information by other discrete devices has been simulated. (9 refs.)

112577 Alpha-spectrometric ionization chamber with an active area of 2m². S.Saro, M.Pikna (Matematicko-Fyzikálna Fakulta, Univ. Komenského, Bratislava, Czechoslovakia).

Jad. Energ. (Czechoslovakia), vol.29, no.8-9, p.306-8 (Aug.-Sept. 1983). In Slovenian.

A large area gridded cylindrical chamber was developed. Sources up to the area of 2 m² can be measured with an efficiency of 37%. The resolution of the detector system is 85 keV at 5.5 MeV. The background at 5.5 MeV is 10 cph/200 keV, the minimum measurable activity is 1 mBq (24 hour measuring time, 2 sigma statistics) and the minimum measurable specific activity at the source thickness 0.1 mg/cm² is as low as 0.5 mBq/g. The application of this spectrometer to the alpha spectrometry of environmental samples permits the direct measurement of very low alpha activities. (3 refs.)

112578 Test of a superconducting magnetic-monopole detector for spurious events due to sea-level cosmic rays. J.F.Ziegler, C.C.Tsuei, C.C.Chi, C.D.Tesche, P.Chaudhari (IBM-Res., Yorktown, NY, USA), K.W.Jones. *Phys. Rev. D (USA)*, vol.28, no.7, p.1793-5 (1 Oct. 1983).

An experimental superconducting magnetic-monopole detector has been constructed similar to that used by Cabrera (1982). It has been tested for spurious signals by immersing it in a high-radiation environment. No spurious events which could be mistaken for a monopole event occurred. The radiation dose of the experiment was equivalent to 1500X the total neutron dose experienced by the Cabrera experiment due to sea-level cosmic rays during its 151-day lifetime. (10 refs.)

112579 Research on some characteristics and improvements of a 70 cm streamer chamber. (The Second Experimental Div., Inst. of High Energy Phys., Acad. Sinica, Peking, China).

Phys. Energ. Fortis & Phys. Nucl. (China), vol.7, no.3, p.273-84 (May 1983). In Chinese.

The influence of the various proportions of Ne-He gases and the time delay on the quality of streamer tracks has been studied. The diameter and density of streamers under these mixed-gas conditions have been measured. (13 refs.)

112580 Performance of the parallel multilayer avalanche calorimeter. K.T.McDonald (Princeton Univ., Princeton, NJ, USA), A.H.Walenta, Lu Chang-guo.

Phys. Energ. Fortis & Phys. Nucl. (China), vol.7, no.3, p.285-93 (May 1983). In Chinese.

This is the first attempt to use the PPAC as a sampling calorimeter. The possible fluctuations in this type of calorimeter and the results of simulating measurements performed on a single gap PPAC and actual measurements for a multilayer PPAC calorimeter are presented. (10 refs.)

112581 A scintillation counter hodoscope and on-line experiments with computer. Wang Man, Li Jin, Li Pei-qin, Chen Xian-neng, Chen Le-jun, Jiang Chuen-hua, Xia Xiao-mi, Lu Wei-da, Que You-ken, Lai Yuan-fen, Lu Chang-guo, Cui Xiang-zong (Inst. of High Energy Phys., Acad. Sinica, Peking, China).

Phys. Energ. Fortis & Phys. Nucl. (China), vol.7, no.3, p.294-300 (May 1983). In Chinese.

A multi-strip scintillation counter hodoscope and a small on-line system are described. The hodoscope is a 4X4 array of scintillation strip counters, each of which consists of a plastic scintillation strip of type NE104 and a photomultiplier of type GDB-50L. An on-line program to test the hodoscope properties has been compiled. (6 refs.)

112582 Monte Carlo calculation of the efficiencies of the lead glass detectors for high-energy gamma rays. Zhang Gui-shan, Zhang Huan-qiao (Inst. of Atomic Energy, Acad. Sinica, Peking, China).

Phys. Energ. Fortis & Phys. Nucl. (China), vol.7, no.3, p.370-8 (May 1983). In Chinese.

The electromagnetic shower processes occurred in the lead glass detector are simulated by the Monte Carlo method, the light collection effects being taken into account. The primary energy of the gamma ray is from 8 to 300 MeV. The detected efficiency function, the energy resolution curve and photoelectron number distribution (the pulse-height spectra) are presented for the lead glass detector. The calculated results are satisfactory. (18 refs.)

112583 Vavilov-Cerenkov radiation as a source of photoradiation processes in electron tracks. I.G.Kaplan, N.V.Polyanskii (L.Ya. Karpov Physicochem. Sci. Res. Inst., Obninsk, USSR).

Sov. Phys.-Dokl. (USA), vol.27, no.12, p.1041-4 (Dec. 1982). Translation of: *Dokl. Akad. Nauk SSSR*, vol.267, no.4-6, p.1110-13 (Dec. 1982). [received: Sept. 1983]

It follows from the classic work of Tamm and Frank (1937) that when an electron travels with a velocity exceeding the phase velocity of light in the medium ($v > c/n$, where n is the index of refraction of the medium) the electromagnetic field of the electron lags behind the electron and excites in the medium radiated light, which has been given the name Vavilov-Cerenkov radiation after its discoverers. Cerenkov radiation has found wide application in high-energy physics. However, since the fraction of the energy going into Cerenkov radiation is very small, it is not, as a rule, taken into consideration in the physics of shielding or in radiation chemistry. None the less, as is shown the number of Cerenkov quanta radiated along the track of the electron is far from small, and can serve as a means of photoradiation conversion. (10 refs.)

112584 Optimierung sphärischer Ionisationskammern für die Neutronen-diagnostik an Tokamakanlagen (Optimisation of spherical ionisation chambers for neutron diagnostics in Tokamaks). F.Hoenen.

Report JUL-1848, Kernforschungsanlage, Jülich, Germany (March 1983), 32 pp. In German.

For the investigation of neutron emission from fusion plasmas, pulse-ion-chambers are favoured because of their high temporal resolution, the availability of results immediately after the discharge and their insensitivity to hard X-rays. However, to measure ion temperatures below 2 keV with the aid of neutron spectroscopy the detectors have to be improved. Difficulties arise from the fact that in pulse-ion-chambers the pulse height is a function of the

position in the chamber where the ion pairs are produced. It will be shown that this induction effect is smaller in spherical ionisation chambers than in cylindrical ones. This means an increase in energy resolution so that neutrons from the $D(D,n)^3\text{He}$ reaction can be analysed with an energy resolution of better than 3 percent in spherical chambers. (14 refs.)

112585 SCAMPI - A FORTRAN program simulating charge and mass particle identification. M.Annunziata, E.Binaghi, M.G.Fontaneto, P.Guazzoni, P.Mantica, P.Michelato, A.Pasquincucci, G.Sechi, A.Simonetto, L.Zetta. Report INFN/BE-83/1, Ist. Naz. Fis. Nucl., Milan, Italy (1 March 1983), 16 pp.

This paper describes a FORTRAN program simulating mass and charge ion discrimination, using a SSD telescope, the time of flight technique and different algorithms for MZ^2 identification. (9 refs.)

112586 Reconstruction of data for an experiment using multi-gap spark chambers with six-camera optics. R.Maybury, H.M.Daley. Report RL-82-085, Rutherford Appleton Lab., Chilton, Oxon., England (June 1983), 31 pp.

A program has been developed to reconstruct spark positions in a pair of multi-gap optical spark chambers viewed by six cameras, which were used by a Rutherford Laboratory experiment. The procedure for correlating camera views to calculate spark positions is described. Calibration of the apparatus, and the application of time- and intensity-dependent corrections are discussed. (5 refs.)

A note on the interpretation of activation measurements on the Princeton large torus See Entry 111626

Optimisation of etching conditions and shortening of the etching time of cellulose nitrate films See Entry 111861

The development of high-temperature fission-counter chambers for nuclear-reactor control and protection See Entry 112372

FBR wide-range neutron monitoring system See Entry 112375

Neutron response of several fission track detectors worn on the body See Entry 112457

Simultaneous determination of exponential background and Gaussian peak functions in gamma ray scintillation spectrometers by maximum likelihood technique See Entry 112530

A wire-chamber spectrometer for muon spin rotation See Entry 112535

Stabilized scintillation spectrometer for scattered low-energy gamma radiation See Entry 112537

A trigger system using wire chamber information See Entry 112589

A fast one-electron pulse discriminator See Entry 112594

Two-stage integrator for an X-ray tomograph See Entry 112605

Results of a quality assurance exercise for radon and radon decay product measurements See Entry 112608

Electrostatic fields in an ionization chamber electret See Entry 112895

Kornyezi doziszintenzitas helyszini meghatározása Ge(Li)-spektrometriával. A módszer (Environmental dose rate in situ determination by Ge(Li)-spectrometry) See Entry 115715

An imaging gas scintillation proportional counter for use in X-ray astronomy See Entry 116472

A proportional counter with one dimensional position sensitivity for image scanning in the soft X-ray region See Entry 116473

Design and performance of a one square meter proportional counter system for hard X-ray astronomy See Entry 116474

29.60 COUNTING CIRCUITS AND NUCLEAR ELECTRONICS

112587 A fast arithmetical unit used with microprogrammable processors. J.Lecoq, J.D.Berst, J.P.Froberger, J.M.Meyer, M.Perrin (Univ. Louis Pasteur, Strasbourg, France).

Nucl. Instrum. & Methods Phys. Res. (Netherlands), vol.213, no.2-3, p.329-32 (1 Aug. 1983).

Describes the 24-bit 200 ns combinatorial arithmetical unit for online dimuon mass computing. The arithmetical unit has been developed to boost the microprocessor GESPRO in the calculations performed for the second level trigger of the NA10 experiment at CERN. It performs one of five arithmetic operations in 200 ns, with 24-bit accuracy. (6 refs.)

112588 A channel profile analyser. S.G.Gobbur (Electronics Div., Bhabha Atomic Res. Centre, Bombay, India).

Nucl. Instrum. & Methods Phys. Res. (Netherlands), vol.213, no.2-3, p.349-51 (1 Aug. 1983).

It is well understood that due to the wide band noise present in a nuclear analog-to-digital converter, events at the boundaries of adjacent channels are shared. It is a difficult and laborious process to exactly find out the shape of the channels at the boundaries. A simple scheme has been developed for the direct display of channel shape of any type of ADC on a cathode ray oscilloscope display. This has been accomplished by sequentially incrementing the reference voltage of a precision pulse generator by a fraction of a channel and storing ADC data in alternative memory locations of a multichannel pulse height analyser. Alternative channels are needed due to the sharing at the boundaries of channels. In the flat region of the profile alternate memory locations are channels with zero counts and channels with the full scale counts. At the boundaries all memory locations will have counts. The shape of this is a direct display of the channel boundaries. (1 ref.)

112589 A trigger system using wire chamber information. G.Kernel, P.Krizan, M.Mikuz, A.Stanovnik, D.Zavrtanik (J. Stefan Inst., E. Kardelj Univ. of Ljubljana, Ljubljana, Yugoslavia), C.Engster, E.G.Michaelis, A.G.Zephat, J.Harvey, K.O.H.Ziock.

Nucl. Instrum. & Methods Phys. Res. (Netherlands), vol.214, no.2-3, p.273-9 (1 Sept. 1983).

A second level trigger system using conventional wire chamber readout and NIM modules is described. The events to be processed by the on-line computer are selected in a time interval of one microsecond on the basis of number of hits in the wire chambers. Some applications and performances of the system are described in detail. (8 refs.)

112590 Self adapting ratemeter. I.D.Vankov, G.S.Ganev, R.M.Ivanov, M.Muller (Inst. of Nuclear Res. & Nuclear Engng., Sofia, Bulgaria).

Nucl. Instrum. & Methods Phys. Res. (Netherlands), vol.214, no.2-3, p.395-400 (1 Sept. 1983).

A ratemeter with a self adapting duration of the averaging time interval is proposed. The conditions for choosing optimum values for its basic parameters are analysed and an equipment version with microprocessor control is

described. This ratemeter features improved statistical accuracy and shorter response time. (2 refs.)

112591 Identification of heavy charged particles by using a fast amplifier to obtain E- and t-signals. A.S.Gass, V.N.Dobrikov, O.F.Nemets, P.N.Svetlichnyi, V.A.Stepanenko, A.A.Shvedov (Nuclear Res. Inst., Acad. of Sci., Kiev, Ukrainian SSR). *Instrum. & Exp. Tech. (USA)*, vol.25, no.6, pt.1, p.1355-7 (Nov.-Dec. 1982). Translation of: *Prib. & Tekh. Eksp. (USSR)*, vol.25, no.6, p.41-2 (Nov.-Dec. 1982). [received: Sept. 1983]

An amplifier with summation of the signals at the output is used for the identification of heavy particles by determining the time of flight. The number of summation stages is three, so that the signal/noise is increased 1.6 times. (6 refs.)

112592 Universal coincidence circuit. Yu.A.Novikov. *Instrum. & Exp. Tech. (USA)*, vol.25, no.6, pt.1, p.1386-9 (Nov.-Dec. 1982). Translation of: *Prib. & Tekh. Eksp. (USSR)*, vol.25, no.6, p.69-72 (Nov.-Dec. 1982). [received: Sept. 1983]

A universal coincidence circuit (UCC) is described consisting of four coincidence circuits and memory. It is realized using series K137 integrate circuits. The UCC operates with input signals of positive and negative polarity with an amplitude of 0.5-10.0 V. The resolving time is adjustable (20 nsec minimum). A variant of the use of the UCC is introduced for the simultaneous measurement of gamma spectra with and without coincidence. (7 refs.)

112593 Units and devices enhancing the reliability and simplifying the operation of apparatus for studying double β -decay. Yu.G.Zdesenko, V.N.Kuts, I.A.Mysyk, A.S.Nikolaiko (Inst. of Nuclear Res., Acad. of Sci., Kiev, Ukrainian SSR). *Instrum. & Exp. Tech. (USA)*, vol.25, no.5, pt.1, p.1124-8 (Sept.-Oct. 1982). Translation of: *Prib. & Tekh. Eksp. (USSR)*, vol.25, no.5, p.77-80 (Sept.-Oct. 1982). [received: Sept. 1983]

Describes a monitor unit, a digital frequency discriminator for anticoincidence signals, a device for measuring the 'dead' time, a spectrometer stabilization system, and a signaling system, which have been developed to enhance the reliability and stability and to simplify the operation of a low-background apparatus for studying double β -decay. (3 refs.)

112594 A fast one-electron pulse discriminator. K.D.Shelevoi, V.V.Burkov, A.A.Venikov (Inst. of Atmospheric Optics, Acad. of Sci., Ukrainian SSR). *Instrum. & Exp. Tech. (USA)*, vol.25, no.5, pt.1, p.1150-1 (Sept.-Oct. 1982). Translation of: *Prib. & Tekh. Eksp. (USSR)*, vol.25, no.5, p.99-100 (Sept.-Oct. 1982). [received: Sept. 1983]

A description is given of a discriminator for one-electron photomultiplier pulses that consist of a preamplifier with $K_{om} \geq 110$ and a K597SA1 comparator. The discriminator detects single-electron pulses of duration ≥ 3 nsec. (3 refs.)

112595 Fast and low-cost discriminator and shaper. M.Ambrosio, G.C.Barbarino, M.Castellano, F.Cevenini, G.Paternoster, S.Patricelli. *Report INFN/TC-83/8*, Ist. Naz. Fis. Nucl., Naples, Italy (11 April 1983), 4 pp.

A simple and low-cost discriminator has been realized with emitter-coupled logic IC; input threshold and output width can be varied continuously; the maximum repetition rate is 55 MHz and the typical double pulse resolution is 18 nsec. (2 refs.)

FBR wide-range neutron monitoring systemSee Entry 112375

Betatron energy stabilization systemSee Entry 112488

Photomultiplier gain tuning systemSee Entry 112556

Two-stage integrator for an X-ray tomographSee Entry 112605

Electron temperature monitor for laser-produced plasmasSee Entry 113666

29.70 RADIATION MEASUREMENT, DETECTION AND COUNTING

(see also 29.30 Radiation spectrometers and spectroscopy, 29.40 Radiation detectors; for dosimetry, see 87.60M)

112596 A modification to the Penfold-Leiss method of cross-section unfolding. D.J.S.Findlay (Nuclear Phys. Div., AERE, Harwell, England). *Nucl. Instrum. & Methods Phys. Res. (Netherlands)*, vol.213, no.2-3, p.353-8 (1 Aug. 1983).

The standard Penfold-Leiss method of unfolding a photonuclear cross-section from a measured bremsstrahlung yield curve is shown to fail if the cross-section is unfolded in photon energy bins whose width is comparable with the range of any smearing of the bremsstrahlung spectrum near the endpoint. In the case decided in the text the smearing is due to the energy spread of electrons striking the bremsstrahlung radiator. A simple modification to the Penfold-Leiss prescription is described which overcomes this failure. (9 refs.)

112597 Some remarks concerning triple angular correlations. K.S.Krane (Dept. of Phys., Oregon State Univ., Corvallis, OR, USA). *Nucl. Instrum. & Methods Phys. Res. (Netherlands)*, vol.214, no.2-3, p.321-32 (1 Sept. 1983).

The theory and reported experiments involving triple angular correlations are reviewed. The sensitivity of these experiments to nuclear spectroscopic parameters is discussed. (20 refs.)

112598 An extension to the Feynman method of detecting fission neutrons. G.S.Brunson (Los Alamos Nat. Lab., Los Alamos, NM, USA). *Nucl. Instrum. & Methods Phys. Res. (Netherlands)*, vol.214, no.2-3, p.341-8 (1 Sept. 1983).

The Feynman method of analyzing a neutron flux has been widely used to characterize systems in which fission neutrons are present. John T. Caldwell (1980) of the Advanced Nuclear Technology group of the Los Alamos National Laboratory proposes a variation of this technique in which each sample gate is initiated by a neutron count. The author compared the two methods for a few specific cases and find the second method markedly superior. Moreover, it is possible to combine the two methods and obtain information about single chains that is not available when either method is used alone. For example, the combined methods permit us, without knowing the counter efficiency, to estimate the fraction of fission neutrons in an unknown neutron flux. (5 refs.)

112599 Measurement of bremsstrahlung spectra from 25 MeV electrons on Ta as a function of radiator thickness and emission angle. R.P.Lambert, J.W.Jury (Dept. of Phys., Trent Univ., Peterborough, Ontario, Canada), N.K.Sherman. *Nucl. Instrum. & Methods Phys. Res. (Netherlands)*, vol.214, no.2-3, p.349-60 (1 Sept. 1983).

The effects of radiator thickness and angle of emission in the energy spectra of photons produced by 25 MeV electrons were studied. Bremsstrahlung

energy spectra at four different angles relative to a beam of electrons incident on Ta radiators of three different thicknesses were measured by observing time of flight spectra of photoneutrons from a moveable liquid deuterium target. The radiators were 1/8, 1/2 and 1 radiation length thick. Observations were made at 0°, 1.7°, 3.4° and 5.1°. The photon flux at 5.1° was about 10% of the flux in the forward direction, where the maximum flux occurred. The angular distribution of mean intensity of photons is nearly the same for all the radiators, and is a consequence of multiple scattering of the incident electrons combined with the intrinsic angular distribution of bremsstrahlung. (29 refs.)

112600 Calibration of histograms in nuclear structure physics. C.Wooff (Dept. of Phys., Univ. of Liverpool, Liverpool, England). *Nucl. Instrum. & Methods Phys. Res. (Netherlands)*, vol.214, no.2-3, p.419-20 (1 Sept. 1983).

A procedure for the calibration of one dimensional histograms in nuclear structure physics experiments is presented. A cubic polynomial is used for this purpose. Scaling of the input data is used to improve the accuracy of the calibration. (2 refs.)

112601 The analysis of radioactive decay with a small number of counts by the method of maximum likelihood. B.T.Cleveland (Dept. of Chem., Brookhaven Nat. Lab., Upton, NY, USA).

Nucl. Instrum. & Methods Phys. Res. (Netherlands), vol.214, no.2-3, p.451-8 (1 Sept. 1983).

A general procedure is presented for the analysis of ultra low-level counting data for which the time of occurrence of each event is measured. The basic formalism is developed, methods of analysis are described, and an example of the application of the technique to simulated data, similar to that obtained in a solar neutrino experiment, is given. (11 refs.)

112602 Physics breakthrough to shape instrumentation of tomorrow. V.Buchstab. *Can. Controls & Instrum. (Canada)*, vol.22, no.4, p.7-8 (July 1983).

Describes a recent experiment which uncovered a link between electromagnetism and radioactivity. It is hoped that this experiment will result in new technologies. It also used measurement techniques which pave the way for future industrial instrumentation. (no refs.)

112603 The development of radioactive gas standards at LMRI. G.Dhilly, R.Rouxel, M.Despres (Lab. de Metrologie des Rayonnements Ionisants, Gif Sur Yvette, France).

Int. J. Appl. Radiat. & Isot. (GB), vol.34, no.8, p.1145-9 (1983). (Applied Radionuclide Metrology, Geel, Belgium, 16-17 May 1983).

The automation of a production line and of a measuring device for radioactive gas standards is described. These standards are supplied in metal containers of 7-dm³ volume in water at a 100-bar pressure with specific NTP (0°C and 1 atm.) activities ranging from 5.10⁻⁵ to 5.10⁻³ μ Ci.cm⁻³. (1 ref.)

112604 Electrostatic analyzer with variable field geometry. M.M.Dubrov, V.A.Belyaev. *Instrum. & Exp. Tech. (USA)*, vol.25, no.6, pt.1, p.1337-40 (Nov.-Dec. 1982).

Translation of: *Prib. & Tekh. Eksp. (USSR)*, vol.25, no.6, p.25-7 (Nov.-Dec. 1982). [received: Sept. 1983]

An energy analyzer (axisymmetric capacitor) is described, tunable from cylindrical to spatial focusing by changing the distribution of the potentials on its electrodes. The electrodes that bound the analyzer chamber admit the working-region dimensions not less than half the width and height of the interelectrode space at only six different electrode potentials. (3 refs.)

112605 Two-stage integrator for an X-ray tomograph. E.A.Andreev, S.A.Pshenichnyi, S.P.Sit'ko, M.I.Skopyuk, V.A.Shevchekno (Kiev State Univ., Kiev, Ukrainian SSR).

Instrum. & Exp. Tech. (USA), vol.25, no.6, pt.1, p.1412-14 (Nov.-Dec. 1982). Translation of: *Prib. & Tekh. Eksp. (USSR)*, vol.25, no.6, p.98-91 (Nov.-Dec. 1982). [received: Sept. 1983]

The instrument described is designed to measure the average current which arises in the sensitive layer of a semiconductor detector under the action of X-rays and is intended for use in scanning X-ray tomographs. In the range 10⁻⁸-10⁻⁶ A the integral and differential nonlinearity were 0.05 and 0.25%, respectively. At a noise current of 3 \times 10⁻¹¹ A the accuracy of measurement reaches 0.1%. (4 refs.)

112606 Stopping power for heavy ions in low energy region. M.Kitagawa (Dept. of Electron., North Shore Coll., Arsugi, Japan).

Oyo Buturi (Japan), vol.52, no.4, p.282-9 (April 1983). In Japanese.

Increase in analysis accuracy of light-ion stopping-power data, the need for establishing definite heavy-ion stopping-power data in the development and research of nuclear fusion, and the advance in heavy-ion accelerator experiments have resulted in progress in the study of the stopping power of heavy ions passing through a substance. The systematic tabulation and theoretical analysis of effective charges, which are inseparably related to heavy-ion stopping powers, have allowed stopping-power data to be analyzed within an error from ± 10 to $\pm 20\%$. The author describes the scaling law between heavy-ion stopping powers and effective charges, and reviews typical methods for analyzing heavy-ion stopping powers. (53 refs.) K.B.

112607 Radon daughter carousel: an automated instrument for measuring indoor concentrations of ²¹⁸Po, ²¹⁴Pb, and ²¹⁴Bi. W.W.Nazaroff (Lawrence Berkeley Lab., Univ. of California, Berkeley, CA, USA).

Rev. Sci. Instrum. (USA), vol.54, no.9, p.1227-33 (Sept. 1983).

A microprocessor-controlled instrument for measuring the concentrations of radon progeny in indoor air is described. The measurement technique is based on alpha spectroscopy and uses two counting intervals following a sampling period during which radon progeny are collected on a filter. The counting intervals are selected to provide optimal precision for measuring ²²²Rn progeny for fixed total measurement times ranging from 30 to 60 min: concentrations as low as 0.5 pCi/l can be measured with less than 20% uncertainty in 45 min. The instrument can also be used to estimate the potential alpha energy concentration of ²²²Rn decay products. The device operates under the control of a computer or a data terminal and functions for week-long periods between filter changes. The user can specify the sampling- and counting-interval timing over a wide range and select from among several operating modes. A number of performance tests are also described indicating that for typical indoor concentrations the measurement uncertainty is dominated by counting statistics. (20 refs.)

112608 Results of a quality assurance exercise for radon and radon decay product measurements. J.C.H.Miles, E.J.Stares, K.D.Cliff, J.Sinnaeve. *Report EUR 8629 EN*, Comm. European Communities, Luxembourg (1983), vi+55 pp.

Intercomparisons of both passive and active techniques of measuring radon and radon decay products have been carried out. Ten centres using fourteen types of dosimeters participated in the intercomparison of passive dosimeters, and eleven centres using eighteen sets of equipment participated in the intercomparison of active measurement techniques. Most of the exposures were carried out in a 43 m³ steel room at NRPB Chilton. (10 refs.)

- The determination of X-ray spectra from attenuation data. I. The potentials of various methods See Entry 111654
- Charge-density measurement for single nanosecond electron-beam pulses See Entry 111824
- Limitation of the Mellin transform for small angle scattering by nearly spherical particles See Entry 112297
- Measurement and evaluation of neutron spectra above 0.1 MeV in the JMTR .. See Entry 112366
- The development of high-temperature fission-counter chambers for nuclear-reactor control and protection See Entry 112372
- Gamma dosimetry using lyoluminescence of tris (hydroxymethyl) aminomethane See Entry 112446
- Triggering and filtering in collider experiments See Entry 112490
- Absolute beam intensity measurements with a 200 watt calorimeter See Entry 112502
- Resistance thermometer for ion-beam calorimetry See Entry 112515
- Derivative method unfolding of gamma-ray spectra from NE-213 spectrometers See Entry 112533
- First measurement of efficiency and precision of CCD detectors for high energy physics See Entry 112540
- Tests of gas sampling electromagnetic shower calorimeter See Entry 112542
- A modular NaI(Tl) detector for 20-1000 MeV photons See Entry 112544
- The prompt response of bismuth germanate and NaI(Tl) scintillation detectors to fast neutrons See Entry 112547
- An arsenic-activation detector for bursts of 2.5 and 14 MeV neutrons See Entry 112548
- Particle identification in the relativistic rise region using a longitudinal drift chamber See Entry 112550
- MARS a fine grain aluminium-liquid argon calorimeter See Entry 112551
- A prototype sampling calorimeter with photodiode readout (SPED) See Entry 112552
- A simple method for direct compensation for kinematic energy spread using a silicon PSD See Entry 112557
- A multi-purpose NaI(T) detector system See Entry 112558
- Performance of silicon surface barrier detectors (p- and n-type) under identical quenchants, postetch ambients and encapsulation See Entry 112572
- SCAMPI - A FORTRAN program simulating charge and mass particle identification See Entry 112585
- Universal coincidence circuit See Entry 112592
- Units and devices enhancing the reliability and simplifying the operation of apparatus for studying double β -decay See Entry 112593
- Recent muon fluence measurements at Fermilab See Entry 115927

29.80 NUCLEAR INFORMATION PROCESSING

- 112609 INS real-time data processing composite system using large scale general purpose computers. J.Kokame, M.Takano, T.Oshikubo, K.Chiba, K.Ukai, A.Imanishi, M.Yasue, K.Omata, S.-I.Watanabe (Inst. for Nuclear Study, Univ. of Tokyo, Tokyo, Japan), H.Hirai, M.Ogawa, N.Ishida, K.Kamakura, M.Fujita, K.Koba. *Nucl. Instrum. & Methods Phys. Res. (Netherlands)*, vol.213, no.2-3, p.317-27 (1 Aug. 1983). Quick response real-time facilities, with an overhead time of 18.3 ms, using a general purpose large scale computer, FACOM M-1801AD (2.5 MIPS), and channel coupled terminal minicomputers, PANAFACOM U-400, have been developed and are in operation at INS Tokyo. The system is useful for computer aided real-time data acquisition and for processing experimental nuclear and elementary particle physics data. Another batch processing system for the same type of large scale computer is connected with a real-time machine. Sophisticated analysis of experimental data as well as pure theoretical problems and design studies can be performed by this system. The system is also capable of backing up minicomputer terminals through a modem for the computer control of accelerators and beam diagnostics. (8 refs.)
- 112610 Comments on 'neutron spectral unfolding using the Monte Carlo method'. D.A.Chambless (Dept. of Maths., Auburn Univ., Montgomery, AL, USA), J.A.Broadway. *Nucl. Instrum. & Methods Phys. Res. (Netherlands)*, vol.214, no.2-3, p.543-5 (1 Sept. 1983). In this note a number of flaws in the article Neutron Spectral Unfolding Using the Monte Carlo Method are identified and discussed. The questions raised by the development of the proposed methodology are shown to be too fundamental to allow serious use of the technique presented. (3 refs.)
- 112611 Reply to Chambless and Broadway. K.O'Brien, R.Sanna (Environmental Measurements Lab., US DOE, New York, NY, USA). *Nucl. Instrum. & Methods Phys. Res. (Netherlands)*, vol.214, no.2-3, p.547-9 (1 Sept. 1983). The authors reply to Chambless and Broadway's comments on their previous paper (1981) on neutron spectral unfolding using Monte Carlo methods. They discuss the nonuniqueness of the deconvolution, the positivity of trial solutions and the underdeterminedness of the system. (5 refs.)
- 112612 Early experience with the programming language P+. R.Cailliau, B.Carpenter, I.Killner (CERN, Geneva, Switzerland). Proceedings of the International Computing Symposium 1983 on Application Systems Development, Nurnberg, Germany, 22-24 March 1983 (Stuttgart, Germany: B.G. Teubner 1983), p.286-300. Until the introduction of the high-level language P+ in September 1981, application programs for a large process control system at CERN were developed using classical methods and the high level languages Nodal, Pascal and machine language. The authors discuss how the changeover to P+ has fared so far, and compares actual experience with current academic and industrial trends. It tends to show that simplicity and orthogonality of design are incompatible with the needs of programmers in large projects. It is shown how P+ tries to resolve this dilemma by being able to adapt to project requirements while at the same time remaining a general purpose language. (15 refs.)
- 112613 Computers and data processing in high energy physics. R.K.Bock (CERN, Geneva, Switzerland). Proceedings of the International Computing Symposium 1983 on Application Systems Development, Nurnberg, Germany, 22-24 March 1983 (Stuttgart, Germany: B.G. Teubner 1983), p.506-28. Computer applications in high energy physics are described. The author shows that this area of physics offers some challenge to software technology.

Advances are needed in techniques and tools enhancing, adaptability to ending problems, exchange of code and data between different computers, and module definition at specifications and implementation levels. (10 refs.)

- Data processor for the magnet with curvature See Entry 112520
- A multi-microprocessor neutron spectrometer computer interface system See Entry 112526
- A method of data analysis of the magnetic spectrometer See Entry 112538
- A fast arithmetical unit used with microprogrammable processors See Entry 112587

29.90 OTHER TOPICS IN HIGH-ENERGY AND NUCLEAR EXPERIMENTAL METHODS AND INSTRUMENTATION

- The significance of inertial confinement fusion for fundamental research See Entry 112461

30.00 ATOMIC AND MOLECULAR PHYSICS

(for physical chemistry, see 82.)

31.00 THEORY OF ATOMS AND MOLECULES

(see also 71. Electron states in condensed matter)

31.10 GENERAL THEORY OF STRUCTURE, TRANSITIONS AND CHEMICAL BINDING

- 112614 Localizability of dynamic electron correlation. P.Pulay (Dept. of Chem., Univ. of Arkansas, Fayetteville, AZ, USA). *Chem. Phys. Lett. (Netherlands)*, vol.100, no.2, p.151-4 (2 Sept. 1983). The convergence of the intrapair correlation energy for a localized internal orbital is investigated as the virtual subspace is enlarged. At variance with previous investigations of this kind, the virtual subspace is presented in atomic orbitals. This allows to define spatial relations between the orbitals involved. Typically, over 98% of the pair correlation energy is recovered by a small local basis set, consisting of the valence orbitals of the atoms with which the electron pair is associated. This opens the possibility of an efficient CI procedure based on localized pairs. (13 refs.)
- 112615 Density functional calculations for atoms in the first transition series. J.G.Harrison (Dept. of Phys., North Dakota State Univ., Fargo, ND, USA). *J. Chem. Phys. (USA)*, vol.79, no.5, p.2265-9 (1 Sept. 1983). s-d interconfigurational energies and spin-flip energies for atoms in the first transition series are examined in the self-interaction-correlated local spin density approximation (SIC-LSDA). The results are substantially improved over previous LSDA calculations and SIC-LSDA calculations employing spherical-orbital densities. The implications for accurate cohesive energy calculations and molecular bonding in iron-series dimers are discussed. (35 refs.)
- 112616 Some remarks on the density functional theory of few-electron systems. R.G.Parr, L.J.Bartolotti (Dept. of Chem., Univ. of North Carolina, Chapel Hill, NC, USA). *J. Phys. Chem. (USA)*, vol.87, no.15, p.2810-15 (21 July 1983). The density functional theory for the ground state of an electronic system is re-formulated by replacing the electron density ρ by the product of the number of electrons N and a shape factor σ , and several features of the theory are elaborated in this formulation. Clarification is thereby provided for a number of subtle points in the theory for a finite number of electrons, especially aspects of the chemical potential μ . Among the questions considered are definition of the energy curve $E(N)$ and possible discontinuities in its slope μ , ambiguities in various functional derivatives and long-range behavior of them, and similar questions in Kohn-Sham theory. It is shown that without knowledge of an appropriate general functional $E[\rho]$, including its dependence on N , it is impossible to determine its chemical potential, from either the actual electron density of a system or a calculation of any kind on that system holding N constant. Nevertheless the chemical potential is well defined and physically meaningful for any specific system of interest. (20 refs.)
- 112617 Period doubling in the $n+1$ filling rule and dynamical symmetry of the Demkov-Ostrovsky atomic model. Y.Kitagawara, A.O.Barut (Dept. of Phys., Univ. of Colorado, Boulder, CO, USA). *J. Phys. B (GB)*, vol.16, no.18, p.3305-27 (28 Sept. 1983). The invariance properties of the Demkov-Ostrovsky (DO) equation are analysed. This equation models the $n+1$ filling rule of the atomic Aufbau principle. Contrary to a claim by Ostrovsky and contrary to generally known quantum problems, the degeneracy structure of the quantum number $n+1$ in this model is not associated with the representation of a finite-dimensional Lie algebra. It is found, however, that the degeneracy algebra does not close under the usual commutation relations, but under a generalised set of commutation rules. The properties of the new algebra are closely examined. It is shown that the characteristic 'period doubling' in the DO model follows from the structure of this algebra. It is also shown that the two-dimensional analogue of the DO equation admits an $SO(3,2)$ dynamical group which, however, allows more states than the physically required ones. Nevertheless, by a redefinition of the quantum labellings, one obtains a mapping to the appropriate state diagram corresponding to the Aufbau chart. (24 refs.)
- 112618 Historical survey and recent progress in the theory of non-rigid molecules. J.Serre (Lab. de Chimie, ENSJF, Montrouge, France). Symmetries and Properties of Non-Rigid Molecules. A Comprehensive Survey. Proceedings of an International Symposium, Paris, France, 1-7 July 1983 (Amsterdam, Netherlands: Elsevier 1983), p.1-12. After experimental considerations on the notion of non-rigid molecules, the main ideas of the applications of group theory in this field are given: semi-direct product, induced representations and wreath products. The structure of the groups in this last case is outlined and the generating of the character

tables is explained from precise examples. Different applications of non-rigid molecule theory to several kinds of spectroscopy are illustrated. (39 refs.)

112619 Classical molecular structure and the puzzle of 'classical limit' in quantum theory. P.Claverie (Lab. de Chimie Quantique, Inst. de Biologie Phys.-Chimique, Paris, France). Symmetries and Properties of Non-Rigid Molecules. A Comprehensive Survey. Proceedings of an International Symposium, Paris, France, 1-7 July 1983 (Amsterdam, Netherlands: Elsevier 1983), p.13-22
The classical concept of molecular structure plays a fundamental role in Chemical Physics. This concept appeared long before the advent of Quantum Theory, and, contrary to widespread views, these two conceptual frames (Classical Molecular Structure and Quantum Theory) cannot be easily reconciled. The author argues that the problem of the relationship between these two conceptual frameworks may be embedded in the wider problem of the 'classical limit' of Quantum Theory. He further argues that this latter problem has not yet received a genuinely satisfactory solution, by considering three examples: the behaviour of wave-packets in free translational and free rotational motion, and the non-positive character of the Wigner distribution function. The non-classical results obtained in these examples show, in the author's opinion, that the general problem of the classical limit, and more specifically the problem of the classical molecular structure, must be considered as essentially unsolved at the present time. (37 refs.)

112620 A molecular vision of the world. R.Daudel (Sorbonne & Centre de Mecanique Ondulatoire Appl., CNRS, Paris, France). Symmetries and Properties of Non-Rigid Molecules. A Comprehensive Survey. Proceedings of an International Symposium, Paris, France, 1-7 July 1983 (Amsterdam, Netherlands: Elsevier 1983), p.23-8
After having recalled the methods which give the most concrete images of the electronic organization of molecules, the author delineates the numerous applications of the concept of molecule in neurology, pathology, pharmacology, biology and social science. He concludes by mentioning the existence of a molecular art. (6 refs.)

112621 Moving and fixed reference frames for symmetry operations. Ph.R.Bunker, B.J.Howard (Herzberg Inst. of Astrophys., Nat. Res. Council of Canada, Ottawa, Ontario, Canada). Symmetries and Properties of Non-Rigid Molecules. A Comprehensive Survey. Proceedings of an International Symposium, Paris, France, 1-7 July 1983 (Amsterdam, Netherlands: Elsevier 1983), p.29-37
The approaches used in the books of Bunker and Wigner to generate matrix representations of groups are different, as can be seen by comparing Eq. (5-49) of Bunker's with Eq. (11.23) of Wigner's. The matrices generated in the one approach are the transpose of those generated in the other approach. The two approaches are compared by using the rotation group D_2 and the permutation group S_3 . For rotation groups the approach to be used depends on whether one is concerned with rotations about space fixed or molecular fixed axis systems. (2 refs.)

112622 Classification of mobile molecules by category theory. A.Dress (Fakultät für Math., Univ. Bielefeld, Bielefeld, Germany), A.Dreiding, H.Haegi. Symmetries and Properties of Non-Rigid Molecules. A Comprehensive Survey. Proceedings of an International Symposium, Paris, France, 1-7 July 1983 (Amsterdam, Netherlands: Elsevier 1983), p.39-58
Some geometric problems relating to the description of the spatial structures of mobile (non-rigid) molecules and the definition of their symmetry group are being discussed. (23 refs.)

112623 From mobile molecules to their symmetry groups: a computer-implemented method. P.Floersheim, K.Wirth, M.K.Huber, D.Pazis, F.Siegerist, H.R.Haegi, A.S.Dreiding (Organisch-Chem. Inst., Univ. Zurich, Zurich, Switzerland). Symmetries and Properties of Non-Rigid Molecules. A Comprehensive Survey. Proceedings of an International Symposium, Paris, France, 1-7 July 1983 (Amsterdam, Netherlands: Elsevier 1983), p.59-80
The authors present a symmetry perception method, applicable to mobile (non-rigid, quasi-rigid or rigid) molecular structures. It is based on symmetry consistent descriptions in the form of finite relational systems. The automorphisms and enantiomorphisms associated with such a relational system constitute the H-group which the authors take to be the symmetry group of the molecule. The M-group is obtained by a canonization algorithm applied to the relational system. The symmetry perception method has been implemented as a computer program, called ONOMA. ONOMA guides the user interactively to an adequate description of a given molecule, canonizes this description and computes the M-group in form of permutations of atom labels. This group correctly characterizes the chemically relevant equivalences of atoms or parts of the described molecule. (8 refs.)

112624 The semi-direct product structure of nonrigid molecule groups. G.S.Ezra (Chem. Dept., Univ. of Chicago, Chicago, IL, USA). Symmetries and Properties of Non-Rigid Molecules. A Comprehensive Survey. Proceedings of an International Symposium, Paris, France, 1-7 July 1983 (Amsterdam, Netherlands: Elsevier 1983), p.81-93
The properties of the semi-rigid molecular model and the definition of its symmetry group are reviewed. The semi-direct product structure of the symmetry group of the molecular model is considered. Previous treatments are discussed, and several examples of semi-direct product factorization given. Construction of the group character table is facilitated through use of induced representation theory. The associated nomenclature for irreducible representations is useful in obtaining rigid/nonrigid correlation diagrams. The author concludes with some remarks on selection rules and nuclear vibrations in nonrigid molecules. (24 refs.)

112625 The use of induced representations in nonrigid molecules. S.L.Altmann (Dept. of Metall. & Sci. of Materials, Univ. of Oxford, Oxford, England). Symmetries and Properties of Non-Rigid Molecules. A Comprehensive Survey. Proceedings of an International Symposium, Paris, France, 1-7 July 1983 (Amsterdam, Netherlands: Elsevier 1983), p.95-112
Concerned with molecules for which a semidirect product form obtains, in which case the methods of induced representation theory can readily be used. The main purpose of this work is to stress that the use of such methods must not be thought of as merely providing a convenient short cut. On the contrary, these methods provide a valuable and intuitive insight into the nature of the energy levels of the molecules. A brief review of induced representation theory, as supplied to these molecules, is given and an example is treated. Formal similarity with the Bouckaert, Smoluchowski and Wigner method in solids, which revolutionized the understanding of space-group representations, is pointed out. (25 refs.)

112626 Classification of nonrigid-molecule energy levels. B.J.Dalton (Phys. Dept., Univ. of Queensland, St. Lucia, Queensland, Australia). Symmetries and Properties of Non-Rigid Molecules. A Comprehensive Survey. Proceedings of an International Symposium, Paris, France, 1-7 July 1983 (Amsterdam, Netherlands: Elsevier 1983), p.169-200
The effective symmetry group used in classifying the energy levels, specifying the selection rules and calculating statistical weights is determined for nonrigid molecules where nonrigid effects are a small deviation from rigid molecule behaviour. The situation in which nuclear spin dependent (hyperfine) interactions are important is examined, and it is found that although the previous effective symmetry group species are no longer exact symmetry labels, they would still be useful in the case where hyperfine effects are not too large, leading to weak selection rules enabling predictions of which hyperfine spectral lines are weak or strong to be made. Illustrative applications of the theory are given throughout. (19 refs.)

112627 Symmetry analysis and conformational dependence of molecular properties in non-rigid systems. J.Marunani, A.Toro Labbe (CMOLA, CNRS, Paris, France). Symmetries and Properties of Non-Rigid Molecules. A Comprehensive Survey. Proceedings of an International Symposium, Paris, France, 1-7 July 1983 (Amsterdam, Netherlands: Elsevier 1983), p.291-314
In non-rigid molecules or molecular aggregates, the dependence of any property on the conformation of the system can be expressed in the form of a limited expansion in terms of appropriate harmonics. Use of the symmetry properties of the molecular groups to reduce such an expansion affords a double advantage: i) it helps reduce, sometimes drastically, the time required to compute the conformational dependence of the investigated property; ii) it provides a parameterized functional form which can be used by experimentalists to rationalize their results. The selection rules which define the non-zero harmonics are determined by a set of symmetry indices which depend on both the form of the property (scalar, vectorial, or tensorial; aggregate, mononuclear, or binuclear) and the nature of the isodynamic operations which characterize the system. (29 refs.)

Symmetries and Properties of Non-Rigid Molecules. A Comprehensive Survey. Proceedings of an International Symposium See Entry 111310
Site symmetry, interchange symmetry, and projection operators in non-rigid symmetry groups See Entry 111395
Remote quantum mechanical detection of gravitational radiation See Entry 111522

31.15 GENERAL MATHEMATICAL AND COMPUTATIONAL DEVELOPMENTS

Density functional calculations for atoms in the first transition series See Entry 112615
Some remarks on the density functional theory of few-electron systems See Entry 112616
From mobile molecules to their symmetry groups: a computer-implemented method See Entry 112623

31.20 SPECIFIC CALCULATIONS AND RESULTS

112628 Semiempirical studies of core electron binding energies. X. The SCC-MO calculations on some purines. Z.B.Maksic, K.Rupnik (Theoretical Chem. Group, 'Rudjer Boskovic' Inst., Zagreb, Yugoslavia), A.Veseli. *Z. Naturforsch. Teil A (Germany)*, vol.38A, no.8, p.866-73 (Aug. 1983).
The solid state binding energies of 8-azaguanine, 8-azaxanthine, hypoxanthine and xanthine were calculated by using semiempirical self-consistent charge intramolecular electrostatic potentials expressed in the point-charge approximation. The results are essentially in good agreement with the experimental data giving in the same time a very simple and transparent interpretation of ESCA spectra which is close to the chemical intuition. Splitting of some unresolved N(1s) peaks is proposed to separate binding energies are attributed to particular nitrogen atoms. Since the point-charge model describes a number of molecular properties, it is concluded that formal atomic charges are meaningful within the adopted theoretical framework despite the fact that they can not be defined in a unique fashion. The relaxation energy and work functions of the studied molecular crystals are briefly discussed. (26 refs.)

112629 Ab initio studies of hydrogen bond formation in methyl cyanide or methyl isocyanide and methanol systems. T.-H.Tang (Dept. of Chem., McMaster Univ., Hamilton, Ontario, Canada), X.-Y.Fu. *Int. J. Quantum Chem. (USA)*, vol.24, no.3, p.317-25 (Sept. 1983).
 $\text{CH}_3\text{CN} \cdots \text{HOCH}_3$ and $\text{CH}_3\text{NC} \cdots \text{HOCH}_3$ hydrogen-bonded systems have been studied theoretically by ab initio MO methods using a 4-31G basis set at their equilibrium geometries. The stabilization energies of these hydrogen bonds are 5.4 and 5.9 kcal/mol, respectively. The nature of these hydrogen bonds is discussed in the light of frontier orbital theory and the topological properties of the charge density of the chemical bond. (17 refs.)

112630 The properties of ferrocenyl-stabilised carbocations. W.E.Watts (Dept. of Chem. New Univ. of Ulster, Coleraine, N Ireland). *Indian J. Phys. Part B*, vol.57B, no.3, p.1-3 (June 1983).
Ferrocene (dicyclopentadienyl) is a stable covalent molecule which possess a 'Sandwich' structure. In the crystal, the C_5H_5 rings are staggered (antiprismatic structure) but in the vapour phase they are eclipsed (prismatic structure). The barrier to ring rotation is very low (ca. 0.9 Kcal mol⁻¹). The electronic structure of ferrocene has been calculated by the MO method. (no refs.)

112631 A new formulation of scaled atoms-in-molecules theory. F.O.Ellison (Dept. of Chem., Univ. of Pittsburgh, Pittsburgh, PA, USA). *J. Chem. Phys. (USA)*, vol.79, no.5, p.2278-83 (1 Sept. 1983).
In scaled atoms-in-molecules theory, variational scaling parameters are introduced into the A- and B-atom eigenfunctions from which molecular basis functions are constructed. All intraatomic contributions to matrix elements are determined rigorously in terms of scaling parameters and experimental atomic state energies. Approximate atomic state eigenfunctions are used to compute interatomic contributions. Ground and excited state energy roots of the resulting molecular eigenvalue problem can be independently minimized with respect to the scaling parameters. The original formulation of theory (SAIM.V) employed atomic potential energy operators as part of the intraatomic correction due to scaling. A new formulation (SAIM.T) using atomic kinetic energy operators in this role is tested in calculations on H_2 , HeH^+ , He_2^+ , and HeH . The simpler SAIM.T formulation is found to give results of the same quality as the original SAIM.V version. (9 refs.)

- 112632 Basis set effects in Hartree-Fock studies on aromatic molecules: Hartree-Fock calculations of properties in benzene and hexafluorobenzene.** J. Almlöf, K. Faegri, Jr. (Dept. of Chem., Univ. of Oslo, Oslo, Norway). *J. Chem. Phys. (USA)*, vol.79, no.5, p.2284-94 (1 Sept. 1983). A number of selected properties have been evaluated for the benzene and hexafluorobenzene molecules, using more than 20 different Gaussian basis sets. The effects of polarization functions have been studied and scaling of the orbital exponents in energy-optimized basis sets is commented on. The effects of extending the primitive basis sets are also discussed and the particular problems associated with LCAO studies on polar molecules are investigated. (33 refs.)
- 112633 The use of modified virtual orbitals in perturbative polarization propagator calculations.** J. Oddershede, J.R. Sabin (Dept. of Chem., Odense Univ., Odense, Denmark). *J. Chem. Phys. (USA)*, vol.79, no.5, p.2295-301 (1 Sept. 1983). The use of modified virtual orbital potentials in perturbative polarization propagator approaches has been investigated. The authors find that the random-phase approximation (RPA), which is identical to a first order polarization propagator approach, is invariant to modifications in the virtual orbital potential, provided that the authors include all possible excitations within a given basis set. Even in a moderately truncated excitation space the authors find only a small change in RPA. However, the second order polarization propagator approximation is not invariant to unitary transformations of the virtual orbitals. Certain dominator shifts in the correlation coefficients and in the two-particle, two-hole terms will reduce this dependence on the virtual orbital potential. Numerical applications to Be and CO show that the authors may have simple V^{N-1} potentials which do not give a convergent scheme. This happens when the virtual orbital energies are too close to the orbital energies of the occupied orbitals. (35 refs.)
- 112634 Perturbation theory of the electron correlation effects for atomic and molecular properties. VII. Complete fourth-order MBPT study of the dipole moment and dipole polarizability of H_2O .** G.H.F. Diercksen, V. Kello (Max-Planck-Institut für Physik und Astrophys., Garching bei München, Germany), A.J. Sadlej. *J. Chem. Phys. (USA)*, vol.79, no.6, p.2918-23 (15 Sept. 1983). The dipole moment and dipole polarizability tensor of the water molecule are calculated by using a complete fourth-order many-body perturbation theory (MBPT) approach based on the coupled Hartree-Fock (CHF) solution for the one-electron perturbation problem. The CHF-based MBPT calculations reveal that the fourth-order correlation corrections involving triple and single substitutions in the reference HF determinant are by no means negligible. On the contrary they represent the two largest in magnitude fourth-order terms. The present study reveals that good results obtained with several approximate fourth-order MBPT schemes follow from some mutual cancellations between the neglected lower and higher-order contributions. Among these approximate MBPT approaches particular attention is given to the CHF-based treatment which involves only singly and doubly substituted states (SD-MBPT) and which provides a reasonable agreement with both the experimental data and more accurate theoretical values. (39 refs.)
- 112635 A theoretical study of the properties of BH_3NH_3 .** J.S. Binkley, L.R. Thorne (Sandia Nat. Labs., Livermore, CA, USA). *J. Chem. Phys. (USA)*, vol.79, no.6, p.2932-40 (15 Sept. 1983). Borane monoammoniate (BH_3NH_3) has been studied using several ab initio electronic structure methods and Gaussian basis sets. Equilibrium geometries have been computed at the Hartree-Fock level and, using the electron-correlated Moller-Plesset perturbation method, carried out to third order (MP3) with double-zeta polarized quality basis sets. The computed MP3 geometry is in close agreement with recent microwave data; electron correlation is found to be necessary for a proper description of the B-N distance. Hartree-Fock dipole moments and harmonic vibrational frequencies are presented and discussed. Moller-Plesset perturbation theory carried out to fourth order with triple-zeta plus polarization basis sets is used to compute a B-N dissociation energy of $34.7 \text{ kcal mol}^{-1}$ and a (Hartree-Fock zero-point corrected) rotational barrier of $2.065 \text{ kcal mol}^{-1}$, which is in excellent agreement with the experimental value. Analysis of the dissociation energy as a function of perturbation order indicates that terms involving triple and quadruple substitutions are required in the dissociation energy. (46 refs.)
- 112636 Use of dimer potentials to calculate the energy levels of alkali atoms in rare-gas matrices.** L.C. Balling, J.J. Wright (Dept. of Phys., Univ. of New Hampshire, Durham, NH, USA). *J. Chem. Phys. (USA)*, vol.79, no.6, p.2941-4 (15 Sept. 1983). A simple procedure is described for calculating the energy levels of an alkali atom perturbed by rare-gas neighbors in a solid rare-gas matrix, using alkali-rare-gas dimer potentials available in the literature. Straightforward analysis leads to an expression for the perturbation due to an arbitrary number of rare-gas neighbors in terms of alkali-rare-gas dimer potentials. The results of calculations for Na trapped in Ar are presented and compared with experiment and with earlier pseudopotential calculations. (11 refs.)
- 112637 Hartree-Fock and Hartree-Fock-Slater electric field gradients (H_2 , CH_4) and their symmetry mode derivatives (CH_4).** J.G. Snijders, W. van der Meer, E.J. Baerends, C.A. de Lange (Scheikundig Lab., Vrije Univ., Amsterdam, Netherlands). *J. Chem. Phys. (USA)*, vol.79, no.6, p.2970-4 (15 Sept. 1983). Electric field gradients in the molecules H_2 and CH_4 are calculated by the Hartree-Fock and Hartree-Fock-Slater methods. In CH_4 , the derivatives of the electric field gradient with respect to the vibrational symmetry modes are determined. It is shown that one C-H stretch symmetry mode derivative is completely dominant. This derivative has recently been used to explain the quadrupole splittings found in the NMR spectra of the deuterated methanes dissolved in liquid crystals. (15 refs.)
- 112638 Theoretical studies of van der Waals molecules: general formulation.** G. Danby (Phys. Dept., Univ. of Durham, Durham, England). *J. Phys. B (GB)*, vol.16, no.18, p.3393-410 (28 Sept. 1983). The problem of calculating the bound-state energies of a molecular dimer, consisting of any two diatomics, treated as rigid rotors, is formulated. Full use is made of relevant symmetry properties. The R -matrix propagator and de Vogelaere methods are used to integrate the resulting coupled equations, and their convergence properties are compared. Results obtained for the Ar-HCl dimer are found to be in excellent agreement with previous calculations. (31 refs.)
- 112639 Theoretical studies of van der Waals molecules: the H_2-H_2 dimer.** G. Danby, D.R. Flower (Phys. Dept., Univ. of Durham, Durham, England). *J. Phys. B (GB)*, vol.16, no.18, p.3411-22 (28 Sept. 1983). The authors report calculations of the energy level structure of the H_2-H_2 dimer in which the coupled equations have been numerically integrated. The R -matrix propagator and de Vogelaere algorithms have been used, and their respective convergence properties are briefly discussed. The convergence of the eigenvalues with respect to the size of the rotational basis set is also illustrated. Satisfactory numerical agreement is found with calculations based

upon the secular equation method. Three independent ab initio potentials are studied. The recent CI potential of Meyer and Schaefer (1983) and Schaefer and Liu (1983) is found to give the best agreement with spectroscopic measurements, although a small shift of the position of the isotropic potential minimum is indicated. (18 refs.)

- 112640 Ab initio investigation of intramolecular rearrangements and nature of barriers in SH_6 and SF_6 molecules.** A.I. Boldyrev, V.G. Zakhevskii, O.P. Charkin (Inst. of Chem. Problems, Acad. of Sci., USSR). *J. Struct. Chem. (USA)*, vol.23, no.6, p.844-7 (Nov.-Dec. 1982). Translation of: *Zh. Strukt. Khim. (USSR)*, vol.23, no.6, p.30-4 (Nov.-Dec. 1982). [received: Sept. 1983] Within the framework of the ab initio Hartree-Fock-Roothaan method with a double-zeta Huzinaga-Dunning basis, calculations have been performed with complete optimization of the geometry of the basic octahedral configuration and the trigonal prism configuration corresponding to the apex of the barrier in the path of intramolecular rearrangement of SH_6 and SF_6 molecules. The barriers for the SH_6 and SF_6 are 68.6 and 61.7 kcal/mole, and the intramolecular rearrangements of both molecules are forbidden. The nature of the barrier has been analyzed in the language of correlation diagrams and populations according to Mulliken. The barrier in SH_6 and SF_6 is due mainly to nonbonding ligand-ligand interactions, whereas the central atom-ligand bonding interactions exhibit smaller changes. (10 refs.)

- 112641 Structure of protonated forms of coumarin and its hydroxy derivatives.** I.V. Sokolova, L.I. Loboda (Siberian Phys. Engng. Inst., V.D. Kuznetsov Tomsk State Univ., Tomsk, USSR). *J. Struct. Chem. (USA)*, vol.23, no.6, p.848-54 (Nov.-Dec. 1982). Translation of: *Zh. Strukt. Khim. (USSR)*, vol.23, no.6, p.35-41 (Nov.-Dec. 1982). [received: Sept. 1983] The molecular electrostatic potential method, together with experimental investigations of the main properties, was applied to the study of the proton acceptor capacity of coumarin, 7-OH-coumarin, and 7-OH-4CH₃-coumarin in various excited states. The influence of protonation of coumarins on their special properties is examined. A zone of negative potential with minimum around the C=O group in the plane of the molecule, common to the pyrone and carbonyl oxygens, was obtained for the coumarins studied. It was shown that forms protonated on the carbonyl and pyrone oxygens will have a flat structure, while those protonated on the substituents studied will have a non-planar structure. It was found that excitation to the $S_{n\pi^*}$ state increases the proton acceptor capacity of hydroxycoumarins, while excitation to $S_{n\pi^*}$ sharply decreases it. (17 refs.)

- 112642 Nonempirical calculations of molecular characteristics.** A.I. Dement'ev (All-Union Sci.-Res. Center for the Study of Surface & Vacuum Properties, USSR). *J. Struct. Chem. (USA)*, vol.23, no.6, p.947-55 (Nov.-Dec. 1982). Translation of: *Zh. Strukt. Khim. (USSR)*, vol.23, no.6, p.148-57 (Nov.-Dec. 1982). [received: Sept. 1983] A review is given of current directions for investigations in the fields of optimization of basis sets, the SCF method, configuration interaction, the multiconfiguration SCF method. Examples are given for calculations of molecular characteristics. (62 refs.)

- 112643 Improved bond-orbital calculations of rotation barriers in molecules containing lone pairs of electrons.** G.F. Musso, G. Figari, V. Magnasco (Istituto di Chimica Industriale, Genova Univ., Genova, Italy). *J. Chem. Soc. Faraday Trans. II (GB)*, vol.79, no.8, p.1283-98 (Aug. 1983). Improved bond-orbital calculations at the ab initio level using a STO-3G basis and assuming rigid rotation and experimental geometries have been performed for the eclipsed and staggered forms of CH_3NH_2 and CH_3OH , for 11 conformations of N_2H_4 and 12 of NH_2OH . The one-configuration wavefunction of strictly localized nonorthogonal bond-orbitals is improved in second-order perturbation theory by admitting CI with nonorthogonal configurations arising from single excitations to antibonding orbitals. The results obtained using bond orbitals variationally optimized with respect to hybridization and polarity parameters show that in the cases of lower local symmetry (N_2H_4 and NH_2OH) second-order delocalization is essential for a correct description of the dependence of molecular energy on the dihedral angle. All conformational parameters obtained in second order are in good agreement with the corresponding MO-SCF quantities in the same basis. (54 refs.)

- 112644 Energetics and structure of the hydrated gaseous halide anions.** B.T. Gowda, S.W. Benson (Dept. of Chem., Univ. of Southern California, Los Angeles, CA, USA). *J. Comput. Chem. (USA)*, vol.4, no.3, p.283-93 (Fall 1983). Energetics and geometries for the hydrated gaseous halide anions have been computed from a simple model in which the molecular dipole of water was composed of two parts, one due to a lone pair on oxygen (60%) and the rest to formal charges on the nuclei. The calculations were made for both symmetric and nonsymmetric structures. A variety of structures were used to compute potential energies and distances with up to six water molecules. The total energy consisted of a sum of electrostatic, polarization, dispersion, and repulsion terms. Various sets of repulsive potential parameters, ranging from those determined from molecular beam experiments to those determined using experimental ion-water distances or energies, have been employed to compute repulsive interaction energies. The range parameters play a significant role in deciding the magnitudes of the distances and energies, as the latter are most sensitive to them. It was also shown that with a simple correlation scheme the consistency of the experimental energies and distances can be tested separately without using repulsive potential parameters from other sources. It also suggests that a range of parameters can be used to compute repulsion energies. (44 refs.)

- 112645 Efficient diffuse function-augmented basis sets for anion calculations. III. The 3-21+G basis set for first-row elements.** Li-F. T. Clark, J. Chandrasekhar, G.W. Spitznagel, P. von Rague Schleyer (Inst. für Organische Chem., Friedrich-Alexander-Universität Erlangen-Nürnberg, Erlangen, Germany). *J. Comput. Chem. (USA)*, vol.4, no.3, p.294-301 (Fall 1983). For pt. II see *ibid.*, vol.3, p.363 (1982). The relatively small diffuse function-augmented basis set, 3-21+G, is shown to describe anion geometries and proton affinities adequately. The diffuse sp orbital exponents are recommended for general use to augment larger basis sets. (25 refs.)

- 112646 Computer generation of the symmetry elements of nonrigid molecules.** K. Balasubramanian (Dept. of Chem., Univ. of California, Berkeley, CA, USA). *J. Comput. Chem. (USA)*, vol.4, no.3, p.302-7 (Fall 1983). Algorithms and computer programs are developed for generating the symmetry elements of nonrigid molecules. These programs are based on the wreath product formalism for the symmetry groups of nonrigid molecules developed by the author. Several examples are given to illustrate the procedures. Applications to weakly bound van der Waal complexes synthesized by supersonic beam expansion are also presented. (29 refs.)

112647 Molecular mechanics with an array processor. P.H.Berens, K.R.Wilson (Dept. of Chem., Univ. of California, San Diego, La Jolla, CA, USA).

J. Comput. Chem. (USA), vol.4, no.3, p.313-32 (Fall 1983).

Computer simulation of the mechanics of molecular systems is a popular and powerful method for understanding chemical processes. The complexity of modeled chemical systems have advanced from hard spheres and rare gases to liquid solutions and biomolecules. Such simulations are computationally intensive and thus are limited by the speed of available computers. The article describes the use of specialized hardware, a high-speed floating-point array processor (AP), to dramatically speed up molecular mechanics, in other words molecular dynamics, Monte Carlo, and energy-minimization calculations. Since the architecture of the machine is dramatically different from conventional computers and utilizing its fast speed necessitates using this architecture on the assembly language level, the proper design and implementation of algorithms is critical. The molecular mechanics software design, consisting of 12000 lines of C and 7000 lines of AP assembly language code, is quite general and has been used to study systems ranging from rare gases to biomolecules. This implementation yields effective speeds approximately 35 times faster than a dedicated DEC VAX 11/780 computer with floating-point accelerator and optimized VMS FORTRAN, thus allowing simulations to be run in one and a half weeks on the AP which would require a year of dedicated VAX time. (66 refs.)

112648 Intramolecular interaction effects and the structure of N_2O_5 and N_2O_3 : an ab initio study. C.Bock, M.Trachtman (Chem. Dept., Philadelphia Coll. of Textiles & Sci., Philadelphia, PA, USA), A.Schmiedekamp, P.George, T.S.Chin.

J. Comput. Chem. (USA), vol.4, no.3, p.379-89 (Fall 1983).

An ab initio study of $O=N-N=S$ with full geometry optimization has been carried out to corroborate the presence of an interaction between the terminal atoms in this type of structure, which, in $O=N-N=O$, apparently stabilizes the cis conformer. Using the unscaled 4-31G basis set with a full set of d functions on the sulfur, there is a potential minimum at the trans but not the cis geometry. A gauche conformer with a torsional angle of 77.2° is the most stable. With N_2O_3 this basis set gives potential minima at both the cis and trans geometries, but the trans conformer is slightly more stable, contrary to experiment and the results of (7,3) basis-set calculations reported in the literature in which Gaussian lobe functions were employed. Using a (9,5) basis set there is no longer a potential minimum at the cis geometry, and a gauche structure is more stable than the cis conformer as in the case of N_2O_5 with the less-extended basis set. Force constants (harmonic and anharmonic), compliance constants, relaxed force constants, and interaction-displacement coordinates for both molecules are compared for key structural elements. (31 refs.)

112649 Three-electron bonds. III. Phosphorus and chlorine σ^* radical cations. T.Clark (Inst. für Organische Chem., Friedrich-Alexander-Univ. Erlangen-Nürnberg, Erlangen, Germany).

J. Comput. Chem. (USA), vol.4, no.3, p.404-9 (Fall 1983).

For pt.II see *ibid.*, vol.3, p.112 (1982). The radical cations $H_3PPH_3^+$, $H_3PSH_2^+$, H_3PCIH^+ , and $HCICIH^+$ have been studied by ab initio molecular-orbital theory. An increasing tendency to adopt trigonal bipyramidal (TBP) geometries is observed for the phosphorus radicals with sulfur and chlorine ligands. The three-electron bond dissociation energies are calculated to be between 7 and 31 kcal mol $^{-1}$. The dependence of these bond energies on the ionization potentials for the neutral hydrides is illustrated, and the deformation of phosphorus σ^* radicals towards TBP structures is discussed. (22 refs.)

112650 'Frozen' transition states: pentavalent carbon et al. J.C.Martin.

Science (USA), vol.221, no.4610, p.509-14 (5 Aug. 1983).

Organic ligands have been designed for the stabilization of specific geometries of compounds of nonmetallic elements. These ligands have made possible the isolation, or direct observation, of large numbers of trigonal bipyramidal organo-nonmetallic species. Many of these species are analogs of transition states for nucleophilic displacement reactions and have been stabilized by the ligands to such a degree that they have become ground-state energy minima. Ideas derived from research on these species have been applied to carbon species to generate a molecule that is an analog of the transition state for the associative nucleophilic displacement reaction. The molecule is a pentavalent carbon species that has been observed by nuclear magnetic resonance spectroscopy. (29 refs.)

112651 Refinement of Ruedenberg-Mulliken MO LCAO method and calculation of SF_6 molecule. V.V.Kirsanov, V.A.Tskhai (Inst. of Chem., Acad. of Sci., Sverdlovsk, USSR).

Theor. & Exp. Chem. (USA), vol.18, no.6, p.601-11 (Nov.-Dec. 1982). Translation of: *Teor. & Eksp. Khim. (USSR)*, vol.18, no.6, p.654-65 (Nov.-Dec. 1982). [received: Sept. 1983]

An analysis of the approximations used in the RM method showed that its main shortcoming is the neglect of certain many-center two-electron integrals that arise in calculating the energy of energy interaction of the electrons. The authors have obtained more nearly exact expressions for the matrix elements of the secular equation, based on Mulliken's approximation and the approximation of the two-center two-electron Coulomb integrals by one-electron. They also present results from a calculation of the SF_6 molecule by the modified RM method. (25 refs.)

Hartree-Fock momentum expectation values for atoms and ions See Entry 111322

Calculated oscillator strengths and wavelengths for allowed transitions within the third shell for ions in the Mg-like isoelectronic sequence between S V and Ni XVII See Entry 111326

Selected tables of atomic spectra. Atomic energy levels and multiplet table. O IV. Data derived from the analyses of optical spectra See Entry 111331

Conversion of bound states to resonances with changing internuclear distance in molecular anions See Entry 112675

Vibrational frequencies from anharmonic ab initio/empirical potential energy functions: stretching vibrations of hydroisocyanic acid, phosphacetylene, isocyanacetylene, and phosphabutadiyne See Entry 112705

Theoretical calculation of the absorption and magnetic circular dichroism spectrum of a Jahn-Teller distorted excited state: the $1E'$ excited state of cyclopropane See Entry 112766

A theoretical study of the radiative lifetime of the $CH A^2\Delta$ state See Entry 112788

Walking on potential energy surfaces See Entry 112807

Interaction of hydrogen atoms with polyatomic molecules studied by means of scattering experiments and hybrid Hartree-Fock plus damped dispersion calculations See Entry 112815

Accurate calculation of inner-shell ionization See Entry 112827

Optimized basis states for inner-shell ionization See Entry 112829

Theory of L-shell ion-impact ionization: inclusive cross sections and multiple-vacancy (K-satellite) distributions See Entry 112831

Screening effects for excitation probabilities in ion-atom collisions See Entry 112834

A simple classical model for the impact parameter dependence of electron capture See Entry 112847

Treatment of long-range couplings in collisional charge transfer from H(1s) to fully-stripped ions See Entry 112848

Molecular structure from the viewpoint of the experimenter—the evolution of the concept and the problems arising See Entry 112866

Calculation of molecular polarizabilities using a semiclassical Slater-type orbital-point dipole interaction (STOPDI) model See Entry 112876

Rare earth atom-to-solid core level shifts: sensitivity to valence changes See Entry 113797

Proton affinity See Entry 115518

Ionization potentials, electron affinities, and molecular orbitals of 2-substituted norbornadienes. Theory of 1,2 and homo-1,4 carbene cycloaddition selectivities See Entry 115529

Theoretical investigation of the cyclodimerization of acetylene and the stability of Hartree-Fock solutions See Entry 115547

31.20G Other accurate, or nearly ab initio calculations (DIM method, SAMO method, etc.)

112652 $X\alpha$ calculations of the EPR parameters of pseudotetrahedral copper(II) complexes. A.Bencini, D.Gatteschi (Istituto di Chimica Generale, Univ. di Firenze, Florence, Italy).

J. Am. Chem. Soc. (USA), vol.105, no.17, p.5535-41 (24 Aug. 1983).

The self-consistent-field multiple-scattering $X\alpha$ method has been used to calculate the electronic structure of pseudotetrahedral and square-planar $CuCl_4^{2-}$ ions, with the aim of checking the reliability of the method in the calculation of the spectral (electronic and EPR) properties of transition metal complexes. Several different calculation schemes were used in order to improve the fit to the experimental spectral transitions. Overlapping spheres were found to give the best agreement. The values of g and of the ^{63}Cu hyperfine constant were satisfactorily reproduced, showing that the low value of the latter in the pseudotetrahedral ion is due to covalency effects and not to 4p metal orbital mixing into the ground state. (53 refs.)

112653 $X\alpha$ multiple scattering calculations on iron (ii) porphine. S.F.Sonnum, D.A.Case (Dept. of Chem., Univ. of California, Davis, CA, USA), M.Karplus.

J. Chem. Phys. (USA), vol.79, no.6, p.2881-92 (15 Sept. 1983).

Spin-restricted and spin-unrestricted $X\alpha$ multiple scattering calculations are reported for iron porphine with D_{4h} symmetry in the absence of axial ligands. A $^3A_{2g}$ ground state is predicted when the radius of the porphyrin 'hole' is less than 2.0 Å, whereas a quintet ground state is expected for larger Fe-N distances. A large asymmetry is found in the occupations of the three Fe4p orbitals. This has important implications for the interpretation of Mossbauer quadrupole coupling constants. Magnetic susceptibility and NMR results can be understood in terms of a model that involves spin-orbit mixing of an excited 3E_g state with the ground $^3A_{2g}$ state; an essential element in explaining the NMR data is that the proton hyperfine constants are not the same in these two states. Tentative assignments are given for observed absorptions in the optical and near-infrared regions. It is shown that spin-unrestricted wave functions are particularly suited for the qualitative interpretation of electronic structure of metalloporphyrins. (51 refs.)

31.20L Statistical model calculations (Thomas-Fermi and Thomas-Fermi-Dirac models)

112654 The Aufbau principle revisited. L.Bosi (Istituto di Fisica del Politecnico, Milano, Italy).

Nuovo Cimento B (Italy), vol.76B, ser.2, no.2, p.89-96 (11 Aug. 1983).

A critical review of the Thomas-Fermi model applications in the literature concerning the Aufbau principle and its explanation is presented. The main conclusion is the following: a precise solution of the problem implies a new concept, that is the successive filling of $(n+l)$ groups. Furthermore, empirical rules introduced in the past in connection with the Aufbau principle are here presented in a simpler geometrical form and then explained. (11 refs.)

31.20N Semi-empirical NDO calculations (CNDO, INDO, MINDO, PCIO methods, etc.)

112655 Application of INDO method to calculation of electronic structure and electronic spectra of transition-metal complexes. N.V.Ivanova, O.V.Sizova, V.I.Baranovskii (A.A. Zhdanov Leningrad State Univ., Leningrad, USSR).

J. Struct. Chem. (USA), vol.23, no.6, p.838-44 (Nov.-Dec. 1982). Translation of: *Zh. Strukt. Khim. (USSR)*, vol.23, no.6, p.22-9 (Nov.-Dec. 1982). [received: Sept. 1983]

In the example of $Co(NH_3)_6^{3+}$ and $Co(CN)_6^{3-}$, an analysis has been made of the applicability of a new variant of the INDO method to the calculation of electronic structure and electronic spectra of complex compounds. The proposed parametrization is based on a system of parameters U_{ii} and γ_{AA} that was developed previously for the CNDO method, differing from the latter in the introduction of Slater-Condon parameters in accordance with the INDO approximation. It is shown that the scheme of MO levels and the distribution of electron density in the complexes that are obtained from these calculations are close to the analogous results obtained in CNDO calculation. At the same time, in comparison with the CNDO method, the INDO method gave a better reproduction of the splitting between the excited terms $^1T_{1g}$ and $^1T_{2g}$ that arise as a result of d-d transitions and between singlets and triplets $^1T_{1g}$ and $^3T_{1g}$. Consideration is given to the influence of breakdown of rotational invariance in the INDO method on the results from calculations of the electronic spectra of complex compounds. (24 refs.)

112656 Electronic structure and absorption spectra of phenol and the corresponding phenoxy radical and the cation and anion. L.S.Degtyarev, L.F.Protopenova, V.D.Pokhodenko (Acad. of Sci., L.V. Pisarzhevskii Inst. of Phys. Chem., Ukrainian SSR).

J. Struct. Chem. (USA), vol.23, no.6, p.860-4 (Nov.-Dec. 1982). Translation of: *Zh. Strukt. Khim. (USSR)*, vol.23, no.6, p.48-52 (Nov.-Dec. 1982). [received: Sept. 1983]

The equilibrium geometry of phenol, the phenolate anion, and the phenoxylium cation has been calculated in the INDO approximation, and the energies

of the transitions in their electronic absorption spectra have been calculated by the CNDO/S method. The difference in the g-factors of the phenoxyl radical and the benzyl radical, which is iso- π -electronic with it, has been used to find the energy of the $n \rightarrow \pi^*$ electronic transition of PhO \cdot . The data obtained have been compared with the experimental results. (32 refs.)

112657 Molecular mechanics studies of enthalpies of formation and strain energies of azoalkanes. K.Bystrom (Thermochem. Lab., Univ. of Lund, Lund, Sweden).

J. Comput. Chem. (USA), vol.4, no.3, p.308-12 (Fall 1983).

A force field has been developed, on the basis of available experimental and partial retention of diatomic differential overlap (PRDDO) data, to permit molecular mechanics calculations on azoalkanes. The calculated structures and enthalpies of formation are in fair agreement with experimental results. The calculated enthalpies of formation and strain energies are compared with the corresponding quantities for analogous azoalkanes. (13 refs.)

112658 Properties of excited states of aromatic rings containing nitrogen.

K.Jug, G.Hahn (Dept. of Theoretische Chem., Univ. Hannover, Hannover, Germany).

J. Comput. Chem. (USA), vol.4, no.3, p.410-18 (Fall 1983).

Quantum chemical calculations with the semiempirical molecular orbital (MO) method SINDO1 were performed on excited states of the following five- and six-membered heterocycles containing nitrogen: imidazole, pyrazole, pyridine, pyridazine, pyrimidine, pyrazine, and s-triazine. The geometries and adiabatic excitation energies of T_1 , S_1 , S_2 were calculated. The authors also present charges, bond orders, and dipole moments. Consequences of these results for UV spectroscopic data are discussed. (22 refs.)

112659 Quantum-chemical study of the electronic structure of unsaturated tetraazamacrocycles by the CNDO/2 method. I.P.Beletskii, Yu.I.Gorlov, V.I.Furman, K.B.Yatsimirskii (L.V. Pisarzhevskii Inst. of Phys. Chem., Acad. of Sci., Kiev, Ukrainian SSR).

Theor. & Exp. Chem. (USA), vol.18, no.6, p.673-7 (Nov.-Dec. 1982). Translation of: *Teor. & Eksp. Khim. (USSR)*, vol.18, no.6, p.730-4 (Nov.-Dec. 1982). [received: Sept. 1983]

The authors present the results of quantum-chemical calculations of the electronic structure of a number of 14-membered macrocycles which differ in the degree of unsaturation of the ring. The aim of the work was to study the possible effect of the degree of unsaturation of the macrocyclic ligands on their complex-forming properties and on the change in the charge distribution in the molecules under consideration. The calculations were carried out by the LCAO MO SCF method in the CNDO/2 approximation. (21 refs.)

112660 Theoretical interpretation of results from spectroscopic investigation of some derivatives of phenoxa- and phenazasilenes. S.G.Semenov, V.O.Reikhsfeld, I.E.Saratov (Lensovet Leningrad Technol. Inst., Leningrad, USSR).

Theor. & Exp. Chem. (USA), vol.18, no.6, p.677-80 (Nov.-Dec. 1982). Translation of: *Teor. & Eksp. Khim. (USSR)*, vol.18, no.6, p.734-7 (Nov.-Dec. 1982). [received: Sept. 1983]

The interest in the dihydroanthracene-type heterocyclic heteroorganic derivatives of phenoxa- and phenazasilenes is due to their antioxidant characteristics and biological activity. Such compounds have been investigated by many experimental methods. Valuable information on their electronic structure is provided, in particular, by photoelectron and ultraviolet spectroscopy and also by the study of charge-transfer complexes (CTC). The present work was devoted to interpretation of the spectroscopic data on the basis of LCAO-MO SCF calculations in the CNDO approximation for the $O(C_6H_4)_2SiHCH_3$ and $C_2H_5N(C_6H_4)_2SiHCH_3$ molecules. (14 refs.)

Through-space effects on vicinal proton spin-spin coupling constants mediated by hetero atoms: nonequivalence of cis couplings in five-membered rings See Entry 112751

Bound-water in biomolecules: a Monte Carlo simulation of the bifurcated hydrogen bond in violuric acid monohydrate See Entry 112803

Energy of a hydrogen bond between s trans molecules of N-methyl-formamide. Calculations by the CNDO/2 method See Entry 112871

Electronic structure and chemical conversions of peroxides. II. MINDO/3 calculations of reaction mechanism in noncatalytic epoxidation of olefins by hydroperoxides See Entry 115542

31.20P Other semi-empirical calculations (Hückel, generalized Hückel, PPP methods, etc.)

Vibrational spectra and structure of triazaphosphorines See Entry 112714

31.20R Valence bond calculations (ab initio or not)

Bond angles and hybridization indices in AX₂YZ and AX₂Y systems See Entry 111369

31.20T Electron correlation and CI calculations

112661 Topological effect on MO energies. III. Heterocyclic systems with non-isomorphic partial structures. W.Fabian, I.Motoc, O.E.Polansky (Max-Planck-Inst. für Strahlenchem., Mülheim, Germany).

Z. Naturforsch. Teil A (Germany), vol.38A, no.8, p.916-27 (Aug. 1983). For pt.II see ibid., vol.889, p.196 (1983). The approach of the S and T isomers is applied to eight pairs of topologically related heterocyclic molecules with non-isomorphic partial structures. The CNDO/2 calculations as well as the experimental data clearly support the TEMO predictions. (9 refs.)

112662 The electronic structure of the octa-sulphur molecule: an ab initio configuration interaction study. M.H.Palmer, R.H.Findlay (Dept. of Chem., Univ. of Edinburgh, Edinburgh, Scotland).

Z. Naturforsch. Teil A (Germany), vol.38A, no.9, p.1032-4 (Sept. 1983). An ab initio SCF calculation of better than double zeta quality (192 basic functions) acted as a starting point for a configuration interaction (CI) study. The final CI with 3408 configurations showed that the 3d orbital density was reduced further than the initial value of 0.1 e; the SCF configuration was dominant, but an element of in-out correlation occurred, with incorporation of the orbital 1 a₂ in replacement for 1 b₁ being notable in many configurations. (14 refs.)

112663 MRD-CI potential surfaces using balanced basis sets. I. First-row diatomic hydrides. J.S.Wright, R.J.Williams (Ottawa-Carleton Inst. for Res. & Graduate Studies in Chem., Carleton Univ., Ottawa, Ontario, Canada).

J. Chem. Phys. (USA), vol.79, no.6, p.2893-902 (15 Sept. 1983). Multireference configuration-interaction (MRD-CI) methods are used to calculate binding energies, potential curves, and vibrational energy levels for the diatomic hydrides H₂, BH, CH, NH, OH, and FH. The curves are calculated

out to the dissociation limit. It is shown how the use of bond functions (located midway between the nuclei) play an essential role in augmenting the standard double-zeta plus polarization basis set. This provides a relatively small but balanced basis set which describes equally well both atomic and molecular regions. The potential curves are accurately fitted by generalized Morse functions over a range of distance which spans 90% of the well depth. Computed binding energies are within 0.1 eV of experimental values, except for the experimentally uncertain NH, which is within 0.2 eV of an estimated value. Potential curves and vibrational levels for H₂, OH, and FH agree well with spectroscopic (and RKR) values. vibrational levels and potential curves for the other hydrides are compared to theoretical values since few experimental data are known, with less good but still reasonable agreement. The selection/extrapolation and multireference features of the MRD-CI method provide good energy continuity at modest computational expense over the whole range of internuclear distances. (51 refs.)

112664 A comparative study of the molecules Cu₂ and Ag₂ by all electron ab initio HF-CI methods. I.Shim, K.A.Gingerich (Dept. of Chem., Texas A&M Univ., College Station, TX, USA).

J. Chem. Phys. (USA), vol.79, no.6, p.2903-12 (15 Sept. 1983).

In the present work the molecules Cu₂ and Ag₂ have been investigated using all electron ab initio Hartree-Fock (HF) and configuration interaction (CI) calculations. The basis sets used were of double zeta quality in general, but the 3d orbital for Cu and the 4d orbital for Ag were represented by triple zeta functions. The wave functions for the Cu₂ and the Ag₂ molecules have been analyzed in detail. Calculated spectroscopic constants have been derived and compared to experimental data, where available. Both for the Cu₂ and the Ag₂ molecules the calculated spectroscopic data vary considerably as the CI calculations exclude or include excitations from the valence d orbitals. The chemical bonds for both molecules are single bonds almost entirely due to s_g molecular orbitals. (28 refs.)

112665 Dissociation curves for nine low lying states of Ti₂ from REP CI calculations. P.A.Christiansen (Dept. of Chem., Clarkson Coll. of Technol., Potsdam, NY, USA).

J. Chem. Phys. (USA), vol.79, no.6, p.2928-31 (15 Sept. 1983).

Dissociation curves for nine low lying states of Ti₂ have been computed using relativistic effective potential and configuration interaction techniques. The authors can identify the molecular ground state as 0_g⁺ with a dissociation energy of 0.16 eV. 0_g⁺ and 1_g states are about 0.1 eV higher in energy. The computed vibrational frequencies for these states are well below values from the Ti₂ thermal emission spectrum. The discrepancy between the author's bond energy and the value (0.63 eV) given in recent mass spectrometric work is due, in part, to the use of inappropriate molecular parameters in the mass spectrometric analysis. (8 refs.)

112666 On the low-lying states of CuO. P.S.Bagus (IBM Res. Lab., San Jose, CA, USA), C.J.Nelin, C.W.Bauschlicher, Jr.

J. Chem. Phys. (USA), vol.79, no.6, p.2975-81 (15 Sept. 1983).

Self-consistent field and correlated wave functions have been computed for the ground and for several low-lying states of CuO. The ground state is X²Π and the lowest excited state, at ~8000 cm⁻¹ above X²Π, is a previously unidentified ²Σ⁺ state. The separation of these states is compared to that for the similar states of KO and is analyzed in terms of integrals between orbitals of the separated free ions. The authors consider a classification of the states of the molecule based on states of Cu⁺ and O⁻ which leads to a division into manifolds of states arising from Cu⁺ 3d¹⁰ and Cu⁺ 3d⁹ 4s¹. They predict that the states of the 3d⁹ 4s¹ manifold are 10000-30000 cm⁻¹ above the ground state and assign the observed A²Σ⁺ state at 16500 cm⁻¹ to this manifold. (18 refs.)

112667 Model-potential calculations of wavelengths, transition probabilities and lifetimes for core-excited quartet levels of Be II. C.Laughlin (Math. Dept., Univ. of Nottingham, Nottingham, England).

J. Phys. B (GB), vol.16, no.18, p.3329-38 (28 Sept. 1983).

A non-local model potential v_M , which approximates the interaction of the 1s and nl electrons in 1s nl ³L levels of Be III to high accuracy, is used to construct an effective two-electron Schrödinger equation for 1s2s nl ⁴L and 1s2p nl ⁴L core-excited levels of Be II. Wavefunctions for quartet levels of Be II are found by a configuration-interaction expansion in terms of antisymmetrised products of eigenfunctions of v_M and wavelengths, transition probabilities and radiative lifetimes are calculated. Some outstanding lines in the beam-foil spectrum of beryllium are discussed. (27 refs.)

112668 The importance of continuum d states for the interaction $nsnp^6 - ns^4d$ in the rare gases. H.Smid, J.E.Hansen (Zeeman Lab., Univ. of Amsterdam, Amsterdam, Netherlands).

J. Phys. B (GB), vol.16, no.18, p.3339-70 (28 Sept. 1983).

Calculations are described of the interaction between the $nsnp^6$ ²S term and the ns^2np^4md/ed^2S series in atoms isoelectronic with the halogens, particularly the rare gases. For the halogens, it has been found earlier that the interaction with the continuum d series is crucial for a correct description of the term structure. A similar, although weaker, effect of the continuum is established for the rare gases. Detailed results for the admixture of $nsnp^6$ ²S in bound and continuum d states are reported for Cl I, Ar II, K III and Kr II. Only in K III is the effect of the continuum found to be negligible. The present results are important for the interpretation of satellite structures connected with the ejection of an ns electron from the rare gases. It is shown that there is good agreement between the present calculations and the satellite intensities in photoelectron experiments. The experimental uncertainties in photoelectron experiments are at present the limiting factors in the comparison and the need for better experimental values in order to test the calculations is stressed. Disagreements are found between the calculations and the results of (e, 2e) experiments. These disagreements are attributed to difficulties in the interpretation of the (e, 2e) experiments. (40 refs.)

112669 Configuration differentiation and localized properties of orbitals in multiconfiguration SCF theory. V.A.Kuprievich (Inst. of Theoretical Phys., Acad. of Sci., Kiev, Ukrainian SSR).

Theor. & Exp. Chem. (USA), vol.18, no.6, p.595-600 (Nov.-Dec. 1982). Translation of: *Teor. & Eksp. Khim. (USSR)*, vol.18, no.6, p.648-54 (Nov.-Dec. 1982). [received: Sept. 1983]

In the Veillard and Clementi modification of the MC SCF theory (1967), which is also known as the MC SCF theory with pair excitations (PE MC SCF), use is made of a set of configurations including, along with the ground configurations, all doubly excited configurations with closed shells. Calculations of specific systems performed by this method show that the optimized MOs are localized; and the resultant wave function proves to be similar to a wave function in the form of the antisymmetrized product of strongly orthogonal geminals (APSG). In the APSG approximation, the localization of the orbitals predetermines the requirement of a minimum in the energy of the individual electron pairs; with the PE MC SCF, such a result is not obvious, since in the set of configurations, each of the occupied orbitals is formally linked in an identical manner to all of the unoccupied orbitals. The premises leading to localization of orbitals in the PE MC SCF theory are examined,

and the question of the most significant configurations responsible for intrapair electron correlation in the molecules is discussed. (11 refs.)

112670 Simple estimation of correlation effects in molecular systems with an open shell. G.E. Whyman, M.M. Mestechkin (Inst. of Phys. Organic Chem. & Coal Chem., Acad. of Sci., Donetsk, Ukrainian SSR).

Theor. & Exp. Chem. (USA), vol.18, no.6, p.666-9 (Nov.-Dec. 1982). Translation of: *Teor. & Eksp. Khim. (USSR)*, vol.18, no.6, p.723-6 (Nov.-Dec. 1982). [received: Sept. 1983]

The use of different orbitals for different spins, which was subsequently transformed into the formalism of the spin-extended Hartree-Fock (EHF) method, was one of the very first techniques employed to take account of electron correlation in the multiparticle problem. The EHF technique involves two operations: spin projection and the subsequent minimization of the energy functional. The use of a single step in the gradient method with semiempirical determination of the scale factor for its approximate solution turned out to be fairly successful both in the PPP and the INDO computational schemes. Hence it is advisable that the above-mentioned procedure should be developed more consistently in order that it may also be used in nonempirical calculations. First of all, one should abandon the empirical determination of the step size which is insensitive to the difference between the unrestricted Hartree-Fock (UHF) and EHF wavefunctions. A solution to this problem is proposed, together with a simple technique for the estimation of the EHF energy which makes use of the energies obtained in the UHF method and the spin-projected version of this technique (SPUHF) without the enormous procedure of variation after projection. (8 refs.)

Calculated oscillator strengths and wavelengths for allowed transitions within the third shell for ions in the Al-like isoelectronic sequence between Cl V and Ni XVI See Entry 111325

Nonempirical calculations of molecular characteristics See Entry 112642

Vibrational spectra and structure of triazaphosphorines See Entry 112714

A new two-body water-water potential See Entry 112808

Ab initio CI study of chemical reactions of singlet and triplet NH radicals See Entry 115528

31.30 CORRECTIONS TO ELECTRONIC STRUCTURE

112671 Pseudo-Jahn-Teller effect as a source of tetragonal distortions in hexafluoride complexes. S.A. Borsch, I.Ya. Ogurtsov, I.B. Bersuker (Inst. of Chem., Acad. of Sci., Moldavian SSR).

J. Struct. Chem. (USA), vol.23, no.6, p.825-9 (Nov.-Dec. 1982). Translation of: *Zh. Strukt. Khim. (USSR)*, vol.23, no.6, p.7-12 (Nov.-Dec. 1982). [received: Sept. 1983]

An analysis has been made of possible modes of realization of the pseudo-Jahn-Teller effect in e_g vibrations in octahedral hexafluoride d^0 , d^4 , and d^6 molecules. The extrema of the adiabatic potentials have been determined, and the corresponding equilibrium configurations have been found. It is shown that under certain additional conditions, the pseudo-Jahn-Teller effect may lead to observable tetragonal distortions of the d^0 and d^4 -hexafluoride complexes. (9 refs.)

112672 Isotope effects in molecular mechanics (MM2). Calculations on deuterium compounds. N.L. Allinger, H.L. Flanagan (Dept. of Chem., Univ. of Georgia, Athens, GA, USA).

J. Comput. Chem. (USA), vol.4, no.3, p.399-403 (Fall 1983). Parameters have been derived so as to enable the inclusion of deuterium in the MM2 molecular mechanics force field. Several compounds were studied and the results are compared with experiment. The results are never qualitatively wrong, but the accuracy ranges from excellent to only fair. They are quite good for hydrocarbons, but less so for ketones. (17 refs.)

112673 Isomeric groups and hyperfine structure of nonrigid molecules. H.H. Günthard (Phys. Chem. Lab., Eidgenössische Tech. Hochschule, Zurich, Switzerland).

Symmetries and Properties of Non-Rigid Molecules. A Comprehensive Survey. Proceedings of an International Symposium, Paris, France, 1-7 July 1983 (Amsterdam, Netherlands: Elsevier 1983), p.133-47

Hyperfine structure of energy levels and transitions of semirigid molecules will be discussed within the framework of the isometric group of such systems. Starting from transformation properties of electronic and rotation-internal motion energy eigenfunctions, transformation properties and Wigner-Eckart theorems for a number of typical hyperfine interactions of the Breit-Bethe-Salpeter molecular Hamiltonian will be presented. Applications to some semirigid molecules within the adiabatic Born-Oppenheimer approach will be made and attention paid to particular effects on hyperfine structure related to nonrigidity, in particular for internal rotation involving quadrupole and magnetic nuclei. (22 refs.)

112674 The Jahn-Teller effect as a case of electronic non-rigidity. Application to the ground state of the symmetric $C_6F_5H_3^+$ ion. C. Cossart-Magos (Lab. de Photophys. Moléculaire, Univ. de Paris-Sud, Orsay, France).

Symmetries and Properties of Non-Rigid Molecules. A Comprehensive Survey. Proceedings of an International Symposium, Paris, France, 1-7 July 1983 (Amsterdam, Netherlands: Elsevier 1983), p.265-72

The Jahn-Teller effect, considered as a case of 'electronic non-rigidity', is compared to the effect of stereochemical non-rigidity. The principal features of the potential surfaces and vibronic level displacements and splittings are recalled in the case of linear and linear plus quadratic Jahn-Teller effect induced by a single vibrational mode. Recent studies on the Jahn-Teller effect in the electronic degenerate ground state X^2E'' of the symmetrical-trifluorobenzene cation in the gas phase are reviewed. The latest developments due to vibronic analysis of high-resolution emission and laser induced fluorescence excitation spectra of both the hydrogenated and fully deuterated species are briefly presented. (15 refs.)

Bound-state energies for the superposed screened Coulomb potential See Entry 111477

Classification of nonrigid-molecule energy levels See Entry 112626

The Aufbau principle revisited See Entry 112654

Nonrelativistic and quasirelativistic model potential calculations on AgH and Ag₂ See Entry 112678

State dependent volume isotope shift analysis of the low lying states of Ba I and Ba II See Entry 112686

Absolute strength of cooperative vibronic pair lines for Yb^{3+} -OH⁻ See Entry 112723

The infrared bands ν_2 and ν_3 of CH_3Br with Coriolis interaction See Entry 112724

Diode laser spectrum of HCCI near 5 μ m: the ν_2 fundamental and accompanying hot bands See Entry 112726

Spectral measurements of high temperature isotopic carbon dioxide in the 4.3- μ m region See Entry 112729

The 404.5-nm system of the ReO molecule See Entry 112745

Theoretical calculation of the absorption and magnetic circular dichroism spectrum of a Jahn-Teller distorted excited state: the $1E'$ excited state of cyclopropane See Entry 112766

The A—X transition in Cr_2 : predissociation, isotope effects, and the 1-1 sequence band See Entry 112798

Ultraviolet two-photon spectroscopy of benzene: a new gerade Rydberg series and evidence for the 1^1E_{2g} valence state See Entry 112802

L-shell Coulomb ionization See Entry 112830

31.50 EXCITED STATES

112675 Conversion of bound states to resonances with changing internuclear distance in molecular anions. J.G. Lauderdale, C.W. McCurdy (Dept. of Chem., Ohio State Univ., Columbus, OH, USA), A.U. Hazi.

J. Chem. Phys. (USA), vol.79, no.5, p.2200-5 (1 Sept. 1983).

The complex self-consistent field (CSCF) method has been used to compute the complex potential-energy curves of the lowest $2\pi_g^+$ autodetaching resonance state of F_2^- and the $2\Pi_g$ resonance state of N_2^- . The calculated width of the $2\Pi_g$ resonance of N_2^- as a function of internuclear distance is in excellent agreement with the results of previous calculations by other methods. The SCF energies of the anion and the neutral molecule in these examples cross at an internuclear distance different from that at which the SCF energy of the anion becomes complex. The authors find this to be a general feature of the SCF description of shape resonance states. Correlation effects appear to be of critical importance in determining the behavior of the resonance states in the crossing region. (21 refs.)

112676 Identification of the X state in Ca and a new Rydberg series. E.S. Chang (Dept. of Phys. & Astron., Univ. of Massachusetts, Amherst, MA, USA).

J. Phys. B (GB), vol.16, no.18, p.L539-41 (28 Sept. 1983).

The X state in Ca is identified as $4s5g^1G_4$ at $44874.5 \pm 0.2 \text{ cm}^{-1}$, and the upper states in the observed transitions are reassigned to the $4snh^1H_5$ series. The simple polarisation theory gives surprisingly good agreement with experiment for all the observed transitions. The extracted polarisability of $75.3 \pm 0.4 a_0^3$ is in excellent agreement with values calculated from oscillator strengths. (12 refs.)

112677 Synchrotron spectroscopy of the giant resonances in the lanthanides and actinides and its relevance to valence changes. J.P. Connerade (Blackett Lab., Imperial Coll., London, England).

J. Less-Common Met. (Switzerland), vol.93, no.1, p.171-81 (1983). (Proceedings of the Sixteenth Rare Earth Research Conference, Tallahassee, FL, USA, 18-21 April 1983).

The 'giant resonances' in the photoabsorption spectra of barium, lanthanum, the lanthanides and some actinides are discussed. They are quasi-atomic spectral features even when observed in related molecules and solids. Their study has led to a far greater understanding of the double-valley radial potential for f electrons and can indeed be viewed as a direct probe of its properties. The lanthanide contraction itself, which is responsible for the deep filling of the 4f and 5f subshells, is due to the quantum mechanics of the inner well. Dramatic changes in the atomic spectra for small changes in the potential have been observed. The atomic physics of this situation is described: it provides a simple model for a number of unusual atomic effects. It could also provide a driving mechanism for pressure-induced phase transitions in compounds such as SmS, and this suggestion is supported by an order-of-magnitude calculation. (26 refs.)

Electron impact excitation and UV emission in the Franck-Hertz experiment See Entry 111350

Model-potential calculations of wavelengths, transition probabilities and lifetimes for core-excited quartet levels of Be II See Entry 112667

High- n_l Stark-state production by sudden electric-field reversal in Rydberg sodium See Entry 112683

State dependent volume isotope shift analysis of the low lying states of Ba I and Ba II See Entry 112686

Characteristic features in photoionisation of excited atomic states See Entry 112690

Structure and dynamics of the non-rigid CONH unit in fundamental and excited states of its stretching mode. Influence of environment effects, side-chain substitutions and secondary structures See Entry 112744

Raman characteristics of the excited electronic state in the fluorescent band of molecules See Entry 112768

On the vibronic treatment of two photon absorption in polyatomic molecules See Entry 112801

Ultraviolet two-photon spectroscopy of benzene: a new gerade Rydberg series and evidence for the 1^1E_{2g} valence state See Entry 112802

Spectra of np -1s transitions excited during the passage of 48 MeV Mg ions through thin and thick carbon targets See Entry 112837

Electronic excitation in alkali-rare-gas collisions See Entry 112842

Treatment of long-range couplings in collisional charge transfer from H(1s) to fully-stripped ions See Entry 112848

Electron-ion collisions of fusion interest See Entry 112855

Resonances in the collision strength for electron excitation of the 1^1S - 2^3S and 1^1S - 2^3P^0 transitions in O VII See Entry 112858

Calculation of the effective rotational transition probabilities for excitation by electron impact from the ground state $N_2X^1\Sigma_g^+$ ($v=0, k$) to the excited state $N_2^+B^2\Sigma_u^+$ (v', k') of nitrogen See Entry 112863

A multiconfigurational self-consistent field study of the D_{2h} dissociation of excited-state ethylene See Entry 115540

Dissociation of Cn^+ into atomic excited states after acceleration in a tandem accelerator See Entry 115545

Resonant electron scattering by metastable nitrogen See Entry 115559

31.70 EFFECTS OF MOLECULAR INTERACTIONS ON ELECTRONIC STRUCTURE

(see also 34. Atomic and molecular collision processes and interactions)

31.70D Environmental and solvent effects

- Structure and dynamics of the non-rigid CONH unit in fundamental and excited states of its stretching mode. Influence of environment effects, side-chain substitutions and secondary structures See Entry 112744
- Radical cations of aldehydes and ketones See Entry 112757
- Applications of fluorescence from the second excited electronic level of rhodamine 6G See Entry 112783
- Theory of electron transfer in polar solvents See Entry 112849
- Electrochemical and spectral characterization of iron mono- and dinitrosyl porphyrins See Entry 115530
- Cage effect in recoil studies See Entry 115572

31.70F Potential-energy surfaces for collisions

(see also 82.20K in chemical kinetics, 34.20 Intermolecular forces, 34.50L in beam studies)

- Theoretical studies of van der Waals dimer depletion mechanisms in free jet expansions: the $\text{Ar}_2 + \text{X}$ ($\text{X} = \text{CO}_2, \text{CO}, \text{N}_2$) systems See Entry 112813
- Ab initio CI study of chemical reactions of singlet and triplet NH radicals See Entry 115528
- Correlation diagrams of states for certain 'forbidden' reactions See Entry 115548

31.90 OTHER TOPICS IN THE THEORY OF ATOMS AND MOLECULES

(inc. properties other than energy)

- 112678 Nonrelativistic and quasirelativistic model potential calculations on AgH and Ag_2 . M.Klobukowski (Dept. of Chem., Univ. of Alberta, Edmonton, Alberta, Canada). *J. Comput. Chem. (USA)*, vol.4, no.3, p.350-61 (Fall 1983). The major relativistic effects are included into the model potential (MP) method of Bonifacic and Huzinaga (1974). The effects are incorporated on the level of Cowan and Griffin's relativistic Hartree-Fock (RHF) method (1976). The model potential parameters are determined using the results of nonrelativistic Hartree-Fock (NHF) and RHF calculations. A new scheme of selection of the basis functions for use in atomic and molecular MP calculations is proposed. To obtain agreement with the Hartree-Fock calculations on AgH and Ag_2 , the $4p$ shell has to be included explicitly in the MP calculations. The explicit treatment of the $4p$ electrons and the resulting reduction of the core size are necessary in order to overcome difficulties with approximate representation of the large $4p$ - $4d$ core-valence interactions on the MP level. (41 refs.)
- Efficient diffuse function-augmented basis sets for anion calculations. III. The 3-21+G basis set for first-row elements, Li-F See Entry 112645
- The Jahn-Teller effect as a case of electronic non-rigidity. Application to the ground state of the symmetric $\text{C}_6\text{F}_3\text{H}_3^+$ ion See Entry 112674
- The properties of LiH in its ground and first excited electronic state See Entry 112704
- Symmetry classification of normal vibrations in molecules with internal rotation See Entry 112709
- Study of the 1750 Å mercury absorption band. Determination of the excited interaction potential and of the oscillator strength related to this band See Entry 112789

32.00 ATOMIC SPECTRA AND INTERACTIONS WITH PHOTONS

32.20 ATOMIC SPECTRA GROUPED BY WAVELENGTH RANGES

- 112679 Saturation spectroscopy of hydrogen H_α lines with a multi-mode CW dye laser. M.Schilling, R.Frankenberger, A.Bengtson, E.W.Weber (Phys. Inst., Univ. Heidelberg, Heidelberg, Germany). *Z. Phys. A (Germany)*, vol.313, no.1-2, p.1-7 (1983). With an intense, broadband multi-mode CW dye laser collisional studies of H_α fine-structure resonances with saturated absorption are extended to He buffer gas pressures larger than 30 mbar (0°C). The broadening and shift of the two prominent $\text{H}_\alpha(2P-3D)$ transitions are measured in a (He+4% H) gas discharge. The absolute magnitude and the differences in the width of the lines are explained theoretically by different inelastic fine-structure transfer cross sections which can also be deduced from the pressure effect data. Nuclear polarization of hydrogen atoms by H_α optical pumping and polarization transfer to the $\text{H}(1S)$ ground state via Ly- α decay and further applications of the multimode laser are discussed. (19 refs.)
- Selected tables of atomic spectra. Atomic energy levels and multiplet table. O IV. Data derived from the analyses of optical spectra See Entry 111331
- High resolution spectroscopy using picosecond pulse trains See Entry 111775
- Synchrotron spectroscopy of the giant resonances in the lanthanides and actinides and its relevance to valence changes See Entry 112677
- Revised $3p^63d^1$ 1S_0 level of Sr XIII, Y XIV, Zr XV, Nb XVI, and Mo XVII See Entry 112685

32.20B Radiofrequency, microwave, and infrared spectra

(inc. magnetic resonance spectra)

- Nonlinear optical indication in frequency stabilization systems See Entry 113046

32.20J Visible and ultraviolet spectra

(for fluorescence and phosphorescence spectra, see 32.50)

- 112680 Hyperfine structure measurements for lines of astrophysical interest in Mn I. A.J.Booth (Dept. of Astrophys., Oxford Univ., Oxford, England), M.J.Shallis, M.Wells. *Mon. Not. R. Astron. Soc. (GB)*, vol.205, no.1, p.191-205 (Oct. 1983). Reports an experiment to measure hyperfine structures for a wide variety of elements and spectral lines. The experiment has been designed to give an accuracy suitable for astrophysical applications and the Oxford total absorption oscillator strength measurements. A first application to 53 lines of Mn I is presented. (33 refs.)
- Electron impact excitation and UV emission in the Franck-Hertz experiment See Entry 111350
- Spectroscopy of laser-induced dielectric breakdown in gas mixtures See Entry 113555
- Experimental investigation of absorption coefficient of cesium resonance doublets in a plasma of combustion products See Entry 113660
- Magnesium II line formation: the contribution of high atomic levels to the resonance lines See Entry 116442
- Ca XVII line ratios in solar flares See Entry 116468
- Calculation or coronal line intensities for boron-like ions See Entry 116612

32.20R X-ray spectra

- Spectra of np -1s transitions excited during the passage of 48 MeV Mg ions through thin and thick carbon targets See Entry 112837
- Ca XVII line ratios in solar flares See Entry 116468
- Calculation or coronal line intensities for boron-like ions See Entry 116612

32.50 FLUORESCENCE, PHOSPHORESCENCE

(inc. quenching)

- 112681 Kinetic study of $\text{Ca}(4^3\text{P}_1)$ by time-resolved emission, $4^3\text{P}_1 \rightarrow 4^1\text{S}_0 + h\nu$ ($\lambda = 657.3$ nm), following dye-laser excitation: spontaneous emission, diffusion and collisional quenching. D.Husain, J.Schifino (Dept. of Phys. Chem., Univ. of Cambridge, Cambridge, England). *J. Chem. Soc. Faraday Trans. II (GB)*, vol.79, pt.8, p.1265-81 (Aug. 1983). The authors present a kinetic study of the low-lying electronically excited state of atomic calcium, $\text{Ca}[4s4p(^3\text{P})_1]$, 1.885 eV above the $4s^2(^1\text{S}_0)$ ground state. $\text{Ca}(4^3\text{P}_1)$ was generated by dye-laser pulsed excitation at $\lambda = 657.3$ nm of calcium vapour [$\text{Ca}(4^3\text{P}_1) \leftarrow \text{Ca}(4^1\text{S}_0)$] at elevated temperatures (1000K), in equilibrium with solid calcium, in a slow-flow system, kinetically equivalent to a static system. Following rapid Boltzmann equilibration within $\text{Ca}(4^3\text{P}_1)$ through collisions, the forbidden time-resolved atomic resonance fluorescence at the same wavelength was monitored using boxcar integration. The decay of $\text{Ca}(4^3\text{P}_1)$ in the presence of all the noble gases, He, Ne, Ar, Kr and Xe, was studied, yielding measurements of relative diffusion coefficients. Extrapolation of the diffusional component of the decay in each noble gas to infinite pressure yields an independent value of the mean radiative lifetime for $\text{Ca}(4^3\text{P}_1) \rightarrow \text{Ca}(4^1\text{S}_0) + h\nu$ ($\lambda = 657.3$ nm), the average of which from the measurements in all the noble gases yields $\tau_0 = 0.34 \pm 0.02$ ms (error 2σ). This result is compared with values reported from previous measurements, particularly atomic beams and time-resolved measurements. The kinetic analysis also gives rise to data for the collisional quenching of $\text{Ca}(4^3\text{P}_1)$, which is insignificant for most of the noble gases [$k_{\text{He,Ne,Ar,Kr}} \leq 4 \times 10^{-15}$ cm³ molecule⁻¹s⁻¹ (1000K)], in contrast to measurements from earlier work using phase-shift techniques. Xenon, however, exhibited measurable rates of collisional quenching of $\text{Ca}(4^3\text{P}_1)$ characterised by $k_{\text{Xe}} = 2.4 \pm 0.3 \times 10^{-14}$ cm³ molecule⁻¹s⁻¹ (1000K). The time-resolved emission technique is further applied to the study of the removal of $\text{Ca}(4^3\text{P}_1)$ by added gases. (47 refs.)
- Influence of SF_6 on the broadening and shift of the 535.0 nm thallium line See Entry 112684
- Electronic excitation in alkali-rare-gas collisions See Entry 112842
- Molecular velocity distribution functions in an argon normal shock wave at Mach number 7 See Entry 113476
- Resonant electron scattering by metastable nitrogen See Entry 115559

32.60 ZEEMAN AND STARK EFFECTS

- 112682 Zeeman effect in the forbidden lines of antimony Sb I. J.Heldt, M.Hults (Dept. of Phys. & Astron., Ball State Univ., Muncie, IN, USA). *J. Opt. Soc. Am. (USA)*, vol.73, no.9, p.1189-96 (Sept. 1983). The Zeeman effect was studied experimentally and theoretically for two mixed forbidden lines of Sb I. The experimental studies were performed on two separated isotopes (121 and 123) for two directions of observation, i.e. longitudinal (L) and transverse (π and σ) using a silver-coated Fabry-Perot etalon and a three-prism Steinheil spectrograph. The interference effect between M1 and E2 radiation in the $\Delta M = \pm 1$ Zeeman components has been observed in the 609.8-nm line. By using the percentage admixture of electric-quadrupole radiation predicted by Garstang (see J. Res. Nat. Bur. Stand., Sect.A, vol.68, p.61, 1964), the relative intensities of the $\Delta M = \pm 1$ and $\Delta M = 0$, ± 2 transitions of the hyperfine structure components were calculated as a function of the external magnetic field for both directions of observation. The agreement of the computed and experimentally determined relative intensities shows that the 609.8-nm line contains (1.43 \pm 0.45)% of electric-quadrupole radiation. In the Zeeman pattern of the 541.5-nm line of antimony, no interference effect is seen. Thus this line is of a predominantly magnetic-dipole type, which is in agreement with theoretical predictions. (16 refs.)
- 112683 High- n_1 Stark-state production by sudden electric-field reversal in Rydberg sodium. R.G.Rolfes, D.B.Smith, K.B.MacAdam (Dept. of Phys. & Astron., Univ. of Kentucky, Lexington, KY, USA). *J. Phys. B (GB)*, vol.16, no.18, p.L533-8 (28 Sept. 1983). By applying bipolar electric-field pulses of about 10 V cm⁻¹, $dE/dt \approx 10^9$ V cm⁻¹s⁻¹, the authors have demonstrated the conversion of laser-excited Na(nd) Rydberg states ($n = 30$ -38) to high- n_1 Stark states that lie at the top of the n manifold. These states correspond in zero field to orbits of the highest allowed angular momentum l . This transition phenomenon is believed to play an important role in the microwave electric-field ionisation of non-hydrogenic atoms. (18 refs.)

- Nonlinear Zeeman spectroscopy of ultrahigh resolution See Entry 111780
 Broadband linear polarization from magnetized stellar atmospheres. II. The influence of damping on net spectral line polarization See Entry 116640

32.70 SPECTRAL LINE SHAPES AND INTENSITIES

- 112684** Influence of SF_6 on the broadening and shift of the 535.0 nm thallium line. E.Lisicki, R.Bobkowski, J.Szudy, J.Wolnikowski (Inst. of Phys., Nicholas Copernicus Univ., Torun, Poland). *Z. Naturforsch. Teil A (Germany)*, vol.38A, no.8, p.838-40 (Aug. 1983). The pressure broadening and shift of the 535.0 nm Tl line resulting from the photodissociation of thallium iodide mixed with sulfur hexafluoride were studied at low densities using a Fabry-Perot interferometer. A linear variation of both the width and shift of the line with the SF_6 density was found and the cross sections for the broadening and shift were determined. (8 refs.)
- 112685** Revised $3p^63d^8\ ^1S_0$ level of Sr XIII, Y XIV, Zr XV, Nb XVI, and Mo XVII. J.Reader, A.Ryabtsev (NBS, Washington, DC, USA). *J. Opt. Soc. Am. (USA)*, vol.73, no.9, p.1207-8 (Sept. 1983). Following an observation by Wyart et al. (see Phys. Sci., vol.26, p.141, 1982), the authors have revised the position of the $3p^63d^8\ ^1S_0$ level in Sr XIII, Y XIV, Zr XV, Nb XVI, and Mo XVII and have redetermined the $3p^63d^8$ energy parameters in these ions. (4 refs.)
- 112686** State dependent volume isotope shift analysis of the low lying states of Ba I and Ba II. B.Fricke, P.Grundevik, I.Lindgren, G.Olsson, T.Olsson, A.Rosen, G.Torbohm (Dept. of Phys., Chalmers Univ. of Technol., Goteberg, Sweden). *Phys. Lett. A (Netherlands)*, vol.97A, no.5, p.183-6 (29 Aug. 1983). Relativistic multi-configuration Dirac-Fock wavefunctions, coupled to good angular momentum J , have been calculated for low lying states of Ba I and Ba II. The resulting electronic factors show good agreement with data derived from recent high-resolution laser spectroscopy experiments and results from a comparison of muonic and optical data. (14 refs.)
- Calculated oscillator strengths and wavelengths for allowed transitions within the third shell for ions in the Al-like isoelectronic sequence between Cl V and Ni XVI See Entry 111325
- Calculated oscillator strengths and wavelengths for allowed transitions within the third shell for ions in the Mg-like isoelectronic sequence between S V and Ni XVII See Entry 111326
- The use of modified virtual orbitals in perturbative polarization propagator calculations See Entry 112633
- Model-potential calculations of wavelengths, transition probabilities and lifetimes for core-excited quartet levels of Be II See Entry 112667
- Saturation spectroscopy of hydrogen H_α lines with a multi-mode CW dye laser See Entry 112679
- Relativistic long-range interactions between H, He and Li atoms See Entry 112810
- Screening effects for excitation probabilities in ion-atom collisions See Entry 112834
- Resonances in the collision strength for electron excitation of the 1^1S - 2^3S and 1^1S - 2^1P transitions in O VII See Entry 112858
- Isotope shift measurements of muonic X-rays in $^{134,136,138}\text{barium}$ See Entry 112884
- Magnesium II line formation: the contribution of high atomic levels to the resonance lines See Entry 116442

32.80 PHOTON INTERACTIONS WITH ATOMS

- 112687** Compton profiles for polarised targets. D.A.Owen (Dept. of Phys., Ben Gurion Univ. of the Negev, Beer-Sheva, Israel), H.Grotch. *J. Phys. B (GB)*, vol.16, no.18, p.3371-81 (28 Sept. 1983). It is shown that the Compton profile functions which describe Compton scattering from polarised atomic electrons are independent of the scattering angle when the direction of polarisation is perpendicular to the incident photon direction. Explicit calculations of these functions for hydrogen-like atoms are given as well as the angular integrals for $J(P_z, \theta)$ (through $j=3/2$) when the radial wavefunctions are not known. Since for other directions of electron polarisations the profile functions are dependent on the scattering angle, the importance of the profile functions being independent of the scattering angle is discussed. (4 refs.)

32.80B Level crossing and optical pumping

- 112688** Interaction of a two-level atom with a quantized field. B.B.Lall, S.N.Guha (Dept. of Phys., Sci. Coll., Patna, India). *Indian J. Phys. Part B*, vol.57B, no.3, p.229-33 (June 1983). Presents a model calculation for the physical quantities of interest for the problem where a single two-level atom interacts with a quantized field by representing the Hamiltonian for the system (atom plus radiation) in terms of Pauli spin operators and thereby obtaining the T -operator of interaction. (4 refs.)
- Saturation spectroscopy of hydrogen H_α lines with a multi-mode CW dye laser See Entry 112679

32.80F Photoionization and photodetachment

- 112689** Fano factors of krypton-xenon mixtures. M.M.F.Ribeirete, A.J.P.L.Policarpo, M.Saete, S.C.P.Leite, M.A.F.Alves, E.P.De Lima (Dept. de Fisica, Univ. de Coimbra, Coimbra, Portugal). *Nucl. Instrum. & Methods Phys. Res. (Netherlands)*, vol.214, no.2-3, p.561-3 (1 Sept. 1983). Measurements of FW (product of the Fano factor and the mean energy to make an ion pair) for several mixtures of krypton and xenon were made using the proportional scintillation method. The following results were obtained. (8 refs.)
- 112690** Characteristic features in photoionisation of excited atomic states. N.B.Avdonina, M.Ya.Amusia (A.F. Ioffe Phys.-Tech. Inst., Acad. of Sci., Leningrad, USSR). *J. Phys. B (GB)*, vol.16, no.18, p.L534-5 (28 Sept. 1983). Strong variation of excited levels ionisation cross sections with photon energy is demonstrated for $nd\ ^2D$ levels of Rb and Cs. The results of calculations proved to be sensitive to the choice of used approximation. (6 refs.)

32.90 OTHER TOPICS IN ATOMIC SPECTRA AND INTERACTIONS WITH PHOTONS

- 112691** Incoherent scattering of gamma rays by bound electrons of some intermediate Z elements. S.V.S.Ramana Reddy (Dept. of Phys., Regional Engng. Coll., Warangal, India), A.Raghava Rao, K.Parthasaradhi, V.Lakshminarayana. *Indian J. Phys. Part A*, vol.57A, no.3, p.135-42 (May 1983). A vast amount of experimental data are available in very low and very large momentum transfers; work in the intermediate range is limited. Two intermediate-Z elements, Ag and Zr, are selected and the binding effects are studied by using a primary photon source of 662 keV with a slow-fast coincidence. (9 refs.)
- Magnetic-field effects on the polarization correlation of photon couples emitted in an atomic cascade See Entry 111483
- Model-potential calculations of wavelengths, transition probabilities and lifetimes for core-excited quartet levels of Be II See Entry 112667

33.00 MOLECULAR SPECTRA AND INTERACTIONS WITH PHOTONS

33.10 CALCULATION OF MOLECULAR SPECTRA

- 112692** Vibrational band intensities of hydrocarbons. L.Dixit, P.Kumar, R.B.Gupta, P.L.Gupta (Analytical Phys. Section, Indian Inst. of Petroleum, Dehradun, India). *Appl. Spectrosc. Rev. (USA)*, vol.18, no.3, p.373-443 (1982-1983). [received: Sept. 1983] The major goal of the article is to review recent chemical literature concerning theoretical predictions and experimental measurements of infrared and Raman intensities of hydrocarbons suited to the needs of physicists, chemists, and industrial vibrational spectroscopists. It is a formidable task to give all the references; thus only pertinent ones have been incorporated. The review begins with information on the principles and methods. The article includes a compilation of the intensity data of hydrocarbons and the minimum material required to understand and generate them. The infrared and Raman intensities are discussed side by side. (275 refs.)
- 112693** Spectroscopic energy coefficients for vibration-rotational states of dinuclear molecules. J.F.Ogilvie (Res. School of Chem., Australian Nat. Univ., Canberra, Australia). *Comput. Phys. Commun. (Netherlands)*, vol.30, no.1, p.101-5 (July-Aug. 1983). The spectroscopic energy coefficients Y_{kl} and their derivatives with respect to the parameters are calculated from a known set of the parameters: coefficients c_i ($1 \leq i \leq 10$) in the potential-energy function, and harmonic vibrational, ω_e , and rotational, B_e , quantities. (12 refs.)
- 112694** Effect of phase choices in rovibrational wavefunctions on the labeling of K- and I-type doubling in molecular energy levels. K.Yamada (Erses Phys. Inst., Univ. zu Koln, Koln, Germany). *Z. Naturforsch. Teil A (Germany)*, vol.38A, no.8, p.821-34 (Aug. 1983). The change in phase factor of the wavefunction does not affect the absolute value of the matrix element, but does change the phase factor of the off-diagonal matrix element. This phase dependence causes a serious confusion in the sign of some parameters in the molecular Hamiltonian, which appear only in the off-diagonal matrix element; for example, the sign of the I-type doubling constant q of a linear or a symmetric-top molecule. The energy eigenvalues, symmetry species, and labeling of the eigenfunctions are discussed for the K-type doubling of asymmetric-top molecules and for the I-type doubling of linear or symmetric-top molecules in relation to the choices of phases in the basis wavefunctions. (24 refs.)
- 112695** Molecular vibration analysis of the cage-like molecules β - P_4S_6 , As_4S_6 , P_4S_7 , and $As_2P_2S_7$. S.J.Cyvin, B.N.Cyvin (Inst. for Teoretisk Kjemi, Univ. i Trondheim, Trondheim, Norway), H.Motz, C.Wibbelmann. *Z. Naturforsch. Teil A (Germany)*, vol.38A, no.9, p.987-94 (Sept. 1983). The cage-like molecules β - P_4S_6 , As_4S_6 , P_4S_7 and $As_2P_2S_7$ are all supposed to have C_{2v} -symmetry. A normal coordinate analysis was performed for those molecules, based on a very simple initial force field with three numerical parameters and valence coordinates including redundancies. A complete set of symmetry coordinates is given. The force field was refined by adjusting the symmetry force constants to fit exactly a set of observed frequencies. This was used to calculate the mean amplitudes of vibration and perpendicular amplitude correction coefficients. The standard thermodynamical values derived from spectroscopic data are also given. A set of frequencies was calculated for the so far unknown compound P_4S_6 . (20 refs.)
- 112696** On the determination of moment of inertia of prolate luminescent molecules. A.Kawski (Inst. of Experimental Phys., Univ. of Gdansk, Gdansk, Poland). *Z. Naturforsch. Teil A (Germany)*, vol.38A, no.9, p.1040-1 (Sept. 1983). The possibility to determine simultaneously the effective volume and the molecular moment of inertia on the basis of the generalized equation of the rotational motion of prolate luminescent molecules in solutions is discussed. (15 refs.)
- 112697** Vibronic coupling of electronic states. III. The definitive breakdown of the CBO potential picture within the framework of our model. K.Gustav, R.Colditz (Sektion Chem., Friedrich-Schiller-Univ. Jena, Jena, Germany). *Int. J. Quantum Chem. (USA)*, vol.24, no.3, p.327-32 (Sept. 1983). For pt.II see ibid., vol.22, p.31 (1982). The definitive breakdown of the CBO potential picture in consequence of the vibronic coupling of two electronic states is discussed on the basis of the authors' model. The present treatment differs from that given in the literature. (6 refs.)
- 112698** The vibronic analysis of the vapour-phase ultraviolet absorption frequencies of 2,3-dichloropyridine. K.C.Medhi (Dept. of Phys., Gauhati Univ., Gauhati, India). *Indian J. Phys. Part B*, vol.57B, no.3, p.262-3 (June 1983). In a previous paper (Medhi 1982) the frequencies of ultraviolet absorption of 2,3-dichloropyridine in the vapour state in the region 2850-2500 Å due to the $\pi \rightarrow \pi^*$ transition were reported. The 0,0 band and the four ground state and six excited state fundamental frequencies were identified. The present notes give a detailed vibronic analysis of the observed frequencies of the molecule in the gaseous state. (1 ref.)

112699 Nitric oxide vibrational excitation from the $N(^4S)+O_2$ reaction. R.R.Herm, B.J.Sullivan, M.E.Whitson, Jr. (Chem. & Phys. Lab., Aerospace Corp., Los Angeles, CA, USA).

J. Chem. Phys. (USA), vol.79, no.5, p.2221-30 (1 Sept. 1983). Measurements of the vibrational distribution of NO produced in a room temperature flowtube study of $N(^4S)+O_2 \rightarrow NO(0 \leq v \leq 7)+O$ are reported. Ultraviolet laser induced fluorescence detection of NO(v) in levels $v=0-7$ was employed to study NO production under conditions where O_2 vibrational quenching was insignificant. The results indicate that 42% of the NO molecules are produced in infrared-active states, 38% of them in levels ≥ 2 . This is considerably more NO vibrational excitation than had been inferred from infrared chemiluminescence studies. Moreover, production of infrared active states of NO by the $N(^4S)+O_2$ reaction may be even more efficient than these numbers indicate owing to possible vibrational relaxation of the nascent NO(v) distribution by nitrogen atoms in the flowtube. (42 refs.)

112700 Nascent NO vibrational distribution from 2485 Å NO_2 photodissociation. T.G.Slanger, W.K.Bischel, M.J.Dyer (Molecular Phys. Lab., SRI Internat., Menlo Park, CA, USA).

J. Chem. Phys. (USA), vol.79, no.5, p.2231-40 (1 Sept. 1983). The initial NO vibrational level distribution has been determined for NO_2 photodissociation at 2485 Å. Excitation spectra of the NO vibrational levels were measured by using both the $NO A^2\Sigma^+ \leftarrow X^2\Pi$ and $B^2\Pi \leftarrow X^2\Pi$ transitions, the latter being somewhat stronger due to saturation effects. It was determined that the NO population was strongly inverted, with most of the nascent NO being in $v=6-8$; the thermodynamic limits is $v=8$. Injection locking of the KrF laser output permitted study of the 2491 Å NO_2 band, and it was evident that the increased absorption in this region gave greatly enhanced signal levels in the excitation spectra, at those wavelengths where NO_2 and NO absorption lines coincide. It was demonstrated that in the 2640-2850 Å wavelength region, NO_2 can be detected by use of a single dye laser, simultaneously dissociating NO_2 and electronically exciting the resultant vibrationally hot NO. Deactivation of $NO(v=8)$ by NO_2 was found to proceed with a rate coefficient of $1.1 \times 10^{-11} \text{ cm}^3 \text{ molecule}^{-1} \text{ s}^{-1}$, whereas the coefficient for quenching by N_2 and He was $\leq 2 \times 10^{-13} \text{ cm}^3 \text{ molecule}^{-1} \text{ s}^{-1}$. The peculiar NO rotational distributions noted by Zacharias et al. (1981) in their study of NO_2 dissociation at 3371 Å were also observed in the present work. (19 refs.)

112701 A unified molecular force field via a model theory of isoelectronic diatomic molecules. B.J.Laurenzi (Dept. of Chem., State Univ. of New York, Albany, NY, USA).

J. Chem. Phys. (USA), vol.79, no.5, p.2246-55 (1 Sept. 1983). Electronic energy curves for diatomic molecules come in a wide variety of shapes. More categorically, these correspond to stable, metastable or repulsive states. The authors propose that a great deal of this apparently diverse behavior might in fact be contained in a single isoelectronic energy surface $E(R,Z,Z')$. That is, each kind of curve can be thought of as a particular cross section of the surface corresponding to some range of the nuclear charges Z and Z' . Analytic representations for these surfaces have been given and their properties examined. The authors have found that they are folded and contain critical points. These features put limits on the number of isoelectronic species that can exist in a sequence and interconnect their properties. By this the authors understand that data gathered on even the repulsive states of one molecule of an isoelectronic sequence contains information about the stable and metastable members of that sequence. (13 refs.)

112702 Algebraic approach to molecular rotation-vibration spectra. II. Triatomic molecules. O.S.van Roosmalen (Kernfysisch Versneller Inst., Rijksunivers. Groningen, Groningen, Netherlands), F.Iachello, R.D.Levine, A.E.L.Dieperink.

J. Chem. Phys. (USA), vol.79, no.6, p.2515-36 (15 Sept. 1983). For pt.I see ibid., vol.77, no.6, p.3046-55 (1982). The algebraic approach to molecular rotation-vibration spectra introduced in a previous article is extended from di- to tri- and polyatomic molecules. The spectrum generating algebra appropriate to triatomic molecules $U(4) \otimes U(4)$ is explicitly constructed. Its dynamical symmetries and their relation to rigid, nonrigid, linear, and nonlinear structures are discussed. Applications to the spectra of HCN, CO_2 , and H_3^+ are considered. In particular, it is shown that the algebraic description can account for the Fermi resonances occurring in CO_2 . Some remarks are made on the spectrum generating algebras appropriate to polyatomic molecules. (37 refs.)

112703 Nonadiabatic representations of the $^1\Sigma_u^+$ and $^1\Pi_u$ states of the N_2 molecule. D.Stahel, M.Leoni, K.Dressler (Phys. Chem. Lab., ETH-Zentrum, Zurich, Switzerland).

J. Chem. Phys. (USA), vol.79, no.6, p.2541-58 (15 Sept. 1983). The vibronic bands in the dipole-allowed absorption spectrum of N_2 associated with the lowest three electronic $^1\Sigma_u^+$ and the lowest three electronic $^1\Pi_u$ states are represented in a basis of electronically coupled diabatic states as well as in the basis of nuclear-momentum coupled adiabatic states. Parameters defining the diabatic states and their electronic coupling energies are first evaluated by fitting the eigenvalues of a vibronic interaction matrix to the observations. The coupled-oscillator equations are then solved directly by Johnson's numerical integration method and the diabatic representation is redetermined via the matrix method and coupled equations iteratively. The fit of the experimental vibronic terms, B values, and absorption intensities achieved with R-independent electronic coupling energies in a diabatic basis of valence and Rydberg-type states ($b'+c'+e'$) Σ_u^+ and ($b+c+o$) Π_u is satisfactory. Comparison with the corresponding adiabatic representation shows that the nonadiabatic perturbations are larger in that basis than in the diabatic one. The vibronic intensity distributions observed in the absorption spectrum show numerous interesting examples of intensity envelopes over discrete vibronic progressions with Fano-type resonance profiles as well as with distinctly non-Fano-type profiles which can be attributed to variations of the relevant coupling terms over the widths of the vibronic resonances. (36 refs.)

112704 The properties of LiH in its ground and first excited electronic state. D.M.Bishop, L.M.Cheung (Dept. of Chem., Univ. of Ottawa, Ottawa, Ontario, Canada).

J. Chem. Phys. (USA), vol.79, no.6, p.2945-50 (15 Sept. 1983). With the aid of recently produced potential curves for the $X^1\Sigma^+$ and $A^1\Sigma^+$ states of lithium hydride, the rovibronic energies of LiH have been calculated. From these energies the standard spectroscopic constants, have been evaluated. The effect on these constants of inclusion of adiabatic corrections (for diagonal nuclear motion) in the potential curves is discussed. The expectation values of certain powers of the electronic coordinates are also tabulated. (13 refs.)

112705 Vibrational frequencies from anharmonic ab initio/empirical potential energy functions: stretching vibrations of hydroisocyanic acid, phosphacetylene, isocyanocetylene, and phosphabutyne. P.Botschwin, P.Seibald (Fachbereich Chem., Univ. Kaiserslautern, Kaiserslautern, Germany).

J. Mol. Spectrosc. (USA), vol.100, no.1, p.1-23 (July 1983).

Anharmonic potential energy functions for the stretching vibrations of HNC, HCP, HCP⁺, HC₂NC, and HC₂P have been constructed from ab initio calculations and little experimental information. Stretching vibrational frequencies are calculated by a variational method employing an approximate vibrational Hamiltonian which neglects the anharmonic coupling between stretching and bending modes. Equilibrium geometries are estimated for HC₂NC and HC₂P and quartic and sextic centrifugal distortion constants have been calculated. (46 refs.)

112706 Rotational energies of polar symmetric-top molecules in high electric fields. S.A.Maluendes, F.M.Fernandez, E.A.Castro (Seccion Química Teórica, INIFTA, La Plata, Argentina).

J. Mol. Spectrosc. (USA), vol.100, no.1, p.24-35 (July 1983).

A method based on hypervirial theorems and perturbation theory is developed for calculating rotational energies of polar symmetric-top molecules in uniform electric fields. This procedure also provides expectation values of other physical observables such as the effective dipole moment. (20 refs.)

112707 Normal-coordinate analysis of retinal isomers and assignments of Raman and infrared bands. S.Saito, M.Tasumi (Dept. of Chem., Univ. of Tokyo, Tokyo, Japan).

J. Raman Spectrosc. (GB), vol.14, no.4, p.236-45 (Aug. 1983).

Normal-coordinate calculations have been performed for the all-trans, 9-cis, 11-cis and 13-cis isomers of retinal using a model structure in which the β -ionone ring was replaced with a simplified structure. Most of the Raman and infrared bands observed from these isomers in the solid state are assigned on the basis of the results of calculation. The vibrational characteristics of each isomer are discussed. (25 refs.)

112708 Vibronic activation of the CO molecule in transition-metal clusters in the one-parameter approximation. A.P.Svitin, S.S.Budnikov, I.B.Bersuker, D.V.Korol'kov (Inst. of Chem., Acad. of Sci., Kishinev, Moldavia SSR).

Theor. & Exp. Chem. (USA), vol.18, no.6, p.637-42 (Nov.-Dec. 1982). Translation of: *Theor. & Eksp. Khim. (USSR)*, vol.18, no.6, p.694-9 (Nov.-Dec. 1982). [received: Sept. 1983]

In order to study the high catalytic activity of transition-metal clusters in reactions involving carbon monoxide, the authors have investigated the vibronic activation of CO molecules in mononuclear $[Mo(CO)_6]$, binuclear $[Co_2(CO)_8]$, $Mn_2(CO)_{10}$, trinuclear $[Os_3(CO)_{12}]$, and hexanuclear $[Rh_6(CO)_{16}]$ complexes. In doing this, use was made of the vibronic theory of the elementary act of catalytic action. The greatest amount of attention has been paid to a consideration of the nature of the changes in the activation energies of reactions involving the participation of CO (regardless of the actual nature of the reaction) as a function of the mode of coordination of the CO groups in the clusters. Therefore, first of all, the authors considered the vibronic destabilization of a CO molecule upon its coordination to one or several (two-three) M atoms in mono- and polynuclear carbonyl complexes. (23 refs.)

112709 Symmetry classification of normal vibrations in molecules with internal rotation. G.A.Natanson (Chem. Dept., Univ. of Chicago, Chicago, IL, USA).

Symmetries and Properties of Non-Rigid Molecules. A Comprehensive Survey. Proceedings of an International Symposium, Paris, France, 1-7 July 1983 (Amsterdam, Netherlands: Elsevier 1983), p.201-18.

An important feature of the symmetry classification of normal vibrations in molecules with internal rotations is the fact that this classification may depend on nuclear masses and electronic structure of atoms. General rules limiting this ambiguity are formulated for the most common kinds of molecules. The most important property for the problem in question is the behavior of potential surfaces. Three kinds of behavior can be distinguished: noncrossing potential surfaces, surfaces having intersections in some configurations and pairs of surfaces coincident when all vibrational coordinates take zero values. All those cases are discussed in detail. (43 refs.)

Spectroscopically silent fundamental vibrations See Entry 111367

A theoretical study of the properties of BH_3NH_3 See Entry 112635

Hartree-Fock and Hartree-Fock-Slater electric field gradients (H_2 , CH_4) and their symmetry mode derivatives (CH_4) See Entry 112637

Theoretical interpretation of results from spectroscopic investigation of some derivatives of phenoxy- and phenazasilenes See Entry 112660

Dissociation curves for nine low lying states of Tl_2 from REP CI calculations See Entry 112665

Pseudo-Jahn-Teller effect as a source of tetragonal distortions in hexafluoride complexes See Entry 112671

The Duschinsky effect and optical spectra See Entry 112710

Reexamination of the I_2 spectrum near the $B^3\Pi_{0u^+}$ state dissociation limit See Entry 112711

Possibility of constructing a general semiempirical theory of the vibrational and electronic-vibrational spectra of multiatomic molecules .. See Entry 112713

Vibrational spectra and structure of triazaphosphorines See Entry 112714

The rotational spectra of fluorinated acetonitriles; ^{14}N -nuclear quadrupole hyperfine structures measured with a microwave Fourier transform spectrometer See Entry 112715

Microwave spectroscopic study of the SiF radical See Entry 112718

Vibrational spectra of 6-azauracil and 5-fluorouracil See Entry 112721

Absolute strength of cooperative vibronic pair lines for $Yb^{3+}-OH^-$ See Entry 112723

The infrared bands ν_2 and ν_3 of CH_3Br with Coriolis interaction See Entry 112724

Light-induced isomerization and photochemical transformation of methylformate in an Argon matrix. Vibrational frequencies, force field, and normal coordinate analysis of trans-methylformate See Entry 112725

Diode laser spectrum of HCl near 5 μm : the ν_2 fundamental and accompanying hot bands See Entry 112726

Gas phase vibrational fundamentals and vib-rotational parameters of $AsCl_3$ See Entry 112727

Effective Pade Hamiltonian operator and its application for treatment of $H_2^{16}O$ rotational spectrum in the ground state See Entry 112728

Spectral measurements of high temperature isotopic carbon dioxide in the 4.3- μm region See Entry 112729

High-resolution stimulated Raman spectroscopy of O_2 See Entry 112740

- Raman spectra and vibrational dephasing of methylacetylene See Entry 112742
- Structure and dynamics of the non-rigid CONH unit in fundamental and excited states of its stretching mode. Influence of environment effects, side-chain substitutions and secondary structures See Entry 112744
- The 404.5-nm system of the ReO molecule See Entry 112745
- $C^2\Pi_u-X^2\Sigma^+$ transition of AlO See Entry 112747
- A four-level double resonance experiment on HCCC¹⁵N with a bridge type superheterodyne microwave spectrometer See Entry 112761
- Vibration-rotation coupling in anisotropic environments. II. Quadrupolar couplings of methanes in liquid crystals See Entry 112763
- Magnetic susceptibility anisotropy, molecular *g* values, and other molecular properties of cyclopropane as determined from rotational Zeeman studies of the cyclopropane-H³⁵Cl and cyclopropane-HC¹⁵N complexes See Entry 112764
- Theoretical calculation of the absorption and magnetic circular dichroism spectrum of a Jahn-Teller distorted excited state: the $1E'$ excited state of cyclopropane See Entry 112766
- A molecular beam study of the trapping-desorption of I₂ from a LiF (001) surface See Entry 112769
- Observation of X ¹A₁ vinylidene by photoelectron spectroscopy of the C₂H₂⁺ ion See Entry 112785
- Vibrational predissociation of H₂, D₂, and HD-Ar van der Waals molecules See Entry 112800
- Ultraviolet two-photon spectroscopy of benzene: a new gerade Rydberg series and evidence for the 1^1E_{2g} valence state See Entry 112802
- Molecular constants of vanadium oxytrihalides See Entry 112805
- Group theory of non-rigid molecules and its applications See Entry 112809
- Application of scaling theory to vibrational relaxation in linear anharmonic triatomic molecules See Entry 112818
- Formation of NH (A³Π, c¹Π) by electron-impact dissociation of HN₃ See Entry 112861
- Electronic polarizabilities and molecular properties of diatomic alkali hydrides See Entry 112875
- Solution of the inverse spectral problem by variable metric methods See Entry 112879
- Vibrational kinetics in liquid nitrogen cooled 5% CO-He radio-frequency discharges See Entry 113686
- Infrared dephasing and libration motion in liquid methyl iodide See Entry 114850
- Temperature dependence of the Raman active B_{3g} torsional mode of sulphamic acid See Entry 114855
- Vibrational spectra and force constants for trans-sodium hyponitrite See Entry 114859
- Raman spectral studies of bleomycin A₂ and related structural fragments: a probe for bleomycin-DNA interactions See Entry 115749
- 3K cosmic microwave background radiation and the rotational levels of the atmospheric H₂O molecule See Entry 116248
- ¹²CH₃D rovibrational intensities and the Jovian D/H ratio See Entry 116460

33.20 MOLECULAR SPECTRA GROUPED BY WAVELENGTH RANGES

(for magneto-optical and electro-optical spectra, see 33.45; for fluorescence and phosphorescence spectra, see 33.50; for photoelectron spectra, see 33.65)

- 112710** The Duschinsky effect and optical spectra. G.Olbrich, H.Kupka (Max-Planck-Inst. für Strahlenchem., Mulheim, Germany). *Z. Naturforsch. Teil A (Germany)*, vol.38A, no.8, p.937-46 (Aug. 1983). The influence of the normal mode rotation (i.e. the Duschinsky mixing) on the molecular electronic spectra in polyatomic molecules is treated by means of multidimensional intramolecular distributions (MID). It is shown that symmetry properties of the two-dimensional MID which relate emission and absorption spectra or pertain to the exchange of modes do not exist if the number of non-separable modes exceeds 2. Specific examples of emission band shapes are calculated for weakly (linear) coupled electronic states for both, zero and finite temperatures. The strength of the mixed quadratic interaction parameter is shown to influence the shape considerably. (7 refs.)
- 112711** Reexamination of the I₂ spectrum near the B(³Π_{0u}⁺) state dissociation limit. J.W.Tromp, R.J.Le Roy (Guelph-Waterloo Center, Univ. of Waterloo, Waterloo, Ontario, Canada), S.Gerstenkorn, P.Luc. *J. Mol. Spectrosc. (USA)*, vol.100, no.1, p.82-94 (July 1983). The disagreement of Danyluk and King's (Chem. Phys., vol.25, p.343 (1977)) rotational constants for levels lying near the dissociation limit of B-state I₂ and the mechanical behaviour predicted by near-dissociation theory is investigated. The discrepancies are shown to be much too large to be explained by either the neglect of centrifugal distortion effects in the original analysis or by rotational or spin-rotation coupling to a nearby repulsive I_u state. These differences are therefore attributed to experimental error, a conclusion which is confirmed by more recent experimental results. A reanalysis of the best available data for levels near the dissociation limit of B-state I₂ then yields improved values for the B-state dissociation limit $D_0=20043.16(\pm 0.02)$ cm⁻¹ of the vibrational index at dissociation $\nu_D=87.32(\pm 0.04)$ and of the long-range potential constant $C_5=2.88(\pm 0.003)\times 10^3$ cm⁻¹ Å⁵. This in turn implies a slightly improved groundstate dissociation energy of $D_0=12440.18(\pm 0.02)$ cm⁻¹. (25 refs.)
- 112712** Polarization spectroscopy of the E₀⁺-B₀⁺ band system of Br₂. J.C.D.Brand, U.D.Deshpande, A.R.Hoy, S.M.Jaywant (Dept. of Chem., Univ. of Western Ontario, London, Ontario, Canada). *J. Mol. Spectrosc. (USA)*, vol.100, no.1, p.143-50 (July 1983). The E-B(O₀⁺-O₀⁺) band system of Br₂ has been investigated at Doppler-limited resolution using polarization labeling spectroscopy. Merged E state data for the three naturally occurring isotopes in the range $\nu_E=0-16$, expressed in terms of the constants for ⁷⁹Br₂, are (in cm⁻¹) $Y_{0,0}=48777.962(54)$, $Y_{1,0}=150.834(22)$, $Y_{2,0}=-0.4182(28)$, $Y_{3,0}=6.6(11)\times 10^{-4}$, $Y_{0,1}=4.1876(28)\times 10^{-2}$, $Y_{1,1}=-1.607(16)\times 10^{-4}$, and $Y_{0,2}=1.39(39)\times 10^{-8}$. The bond distance is $r_e=3.194$ Å, and the diabatic dissociation energy to Br^{(3)P₂}+Br^{(1)S₀} is 34700 cm⁻¹. (11 refs.)

112713 Possibility of constructing a general semiempirical theory of the vibrational and electronic-vibrational spectra of multiautomic molecules.

L.A.Gribov, V.I.Baranov.

J. Appl. Spectrosc. (USA), vol.37, no.6, p.1445-50 (Dec. 1982). Translation of: *Zh. Prikl. Spektrosk. (USSR)*, vol.37, no.6, p.1016-22 (Dec. 1982). [received: Sept. 1983]

The possibility of constructing a semiempirical scheme for the solution of the complete nonadiabatic electronic-vibrational problem on the basis of a system of semiempirical parameters adequately reflecting the electronic-vibrational interactions in the molecule, and thereby the same for the description of all possible electronic-vibrational spectra of multiautomic molecules, is considered. (8 refs.)

112714 Vibrational spectra and structure of triazaphosphorines. E.A.Romanenko, S.V.Iksanova, Yu.P.Egorov, P.P.Kornuta, T.N.Kasheva (Inst. of Organic Chem., Acad. of Sci., Kiev, Ukrainian SSR).

Theor. & Exp. Chem. (USA), vol.18, no.6, p.654-60 (Nov.-Dec. 1982). Translation of: *Teor. & Eksp. Khim. (USSR)*, vol.18, no.6, p.710-17 (Nov.-Dec. 1982). [received: Sept. 1983]

The π-electronic system of the triazaphosphorine heterocyclic ring has a decisive influence on the spectral-structural properties of the series of 1,3,5,2λ²-triazaphosphorines. The results of the calculation of frequencies and forms of in-plane normal vibrations of tetrachloro-1,3,5,2λ²-triazaphosphorines (TTP) are presented, the stretching and in-plane deformational vibrations of the heterocyclic ring in the series of substituted triazaphosphorines are assigned, and force fields and matrix elements, the charge-bond order (in the PPP/CI approximation) are calculated and compared for the molecules of TTP and pentachloro-1,3,2λ⁵-diazaphosphorine (PDP). (19 refs.)

Symmetries and Properties of Non-Rigid Molecules. A Comprehensive Survey. Proceedings of an International Symposium See Entry 111310

Electronic structure and absorption spectra of phenol and the corresponding phenoxyl radical and the cation and anion See Entry 112656

Nonadiabatic representations of the $^1\Sigma_u^+$ and $^1\Pi_u$ states of the N₂ molecule See Entry 112703

Electrochemical and spectral characterization of iron mono- and dinitrosyl porphyrins See Entry 115530

33.20B Radiofrequency and microwave spectra

(for NMR spectra, see 33.25; for EPR spectra, see 33.30)

112715 The rotational spectra of fluorinated acetonitriles; ¹⁴N-nuclear quadrupole hyperfine structures measured with a microwave Fourier transform spectrometer. W.Kasten, H.Dreizler (Inst. für Phys. Chem., Univ. Kiel, Kiel, Germany), B.E.Job, J.Sheridan.

Z. Naturforsch. Teil A (Germany), vol.38A, no.9, p.1015-21 (Sept. 1983). The microwave spectra of CF₃CN, CH₂FCN, CHDFCN, CD₂FCN and CHF₂CN have been measured and analysed. The nuclear quadrupole hyperfine splittings due to ¹⁴N have been measured by Microwave Fourier Transform spectroscopy. The nuclear quadrupole coupling constants, transformed to the bonding axis systems of the C≡N groups, are shown to be in accord with structural predictions of the p-electron populations at the nitrogen atom. (29 refs.)

112716 Nitrogen hyperfine structure in allyl cyanide synperiplanar—an application of microwave Fourier transform spectroscopy. G.Bestmann, H.Dreizler (Inst. für Phys. Chem., Christian-Albrechts-Univ. Kiel, Kiel, Germany).

Z. Naturforsch. Teil A (Germany), vol.38A, no.9, p.1044-5 (Sept. 1983). With the help of microwave Fourier transform spectroscopy the authors were able to resolve the nitrogen hyperfine structure of allyl cyanide (synperiplanar) (cis). As the rotational relaxation is relatively rapid this molecule is even for this technique at the limit of the present possibilities. (6 refs.)

112717 Microwave spectra of cyclohexyl bromide and cyclohexyl iodide. D.Damiani, F.Scappini, W.Caminati, G.Corbelli (Istituto di Spettroscopia Molecolare, CNR, Bologna, Italy).

J. Mol. Spectrosc. (USA), vol.100, no.1, p.36-53 (July 1983). The microwave spectra of cyclohexyl bromide and cyclohexyl iodide have been investigated in the gas phase between 8 and 40 GHz. While the cyclohexyl bromide only low resolution spectra have been recorded, for cyclohexyl iodide high resolution spectra of both the equatorial and the axial isomer have been analyzed. The energy difference between the axial and the equatorial form is $\Delta G^0=0.8\pm 0.4$ kcal/mol and $\Delta E_{0,0}=0.54\pm 0.15$ kcal/mole in C₆H₁₁Br and C₆H₁₁I, respectively, the equatorial forms being more stable. Iodine nuclear quadrupole coupling constants for equatorial and axial C₆H₁₁I have been obtained. The present analysis contributes to the microwave investigation of the cyclohexyl halides. (24 refs.)

112718 Microwave spectroscopic study of the SiF radical. M.Tanimoto (Sagami Chem. Res. Center, Nishi-Ohnuma, Kanagawa, Japan), S.Saito, Y.Endo, E.Hirota.

J. Mol. Spectrosc. (USA), vol.100, no.1, p.205-11 (July 1983). The microwave spectrum of the SiF radical was observed in both ²Π_{1/2} and ²Π_{3/2} of the ground vibronic state. The SiF radical was produced by a DC discharge either in a SiF₄/SiH₄ mixture or in a transient molecule SiF₂ generated by the reaction of SiF₄ with heated solid silicon. The latter gave twice as intense a spectrum. A least-squares fit to the observed spectrum showed the rotational constant and the centrifugal distortion constant to be 17350.2752(63) and 0.03188(13) MHz, respectively, with three standard errors in parentheses applying to the last digits of the constants. The lambda-doubling parameter *p*₀ was found to be negative, -87.67 MHz, indicating that the $^2\Sigma^+$ excited state contributions dominate over those of $^2\Sigma^-$. All four hyperfine coupling constants *a*, *b*, *c*, and *d* were determined and were employed to discuss the unpaired-electron spin and orbital distributions in the SiF radical. (20 refs.)

112719 Symmetry and microwave spectrum of nitromethane. G.O.Sorensen, T.Pedersen (Dept. of Chem. Phys., Univ. of Copenhagen, Copenhagen, Denmark).

Symmetries and Properties of Non-Rigid Molecules. A Comprehensive Survey. Proceedings of an International Symposium, Paris, France, 1-7 July 1983 (Amsterdam, Netherlands: Elsevier 1983), p.219-36. Concerned with the problems of symmetry and dynamics of nitromethane-like molecules which are representatives of the class of molecules with a C_{3v} top and a C_{2v} frame. These molecules invariably have low barriers to internal rotation, and the internal rotation angular momentum quantum number, *m*, is therefore a reasonably good quantum number. Previously the spectra of molecules belonging to this class have been analyzed on the basis of the rigid top/rigid frame (RTRF) model assuming an invariance group isomorphic with D_{6h}. It is demonstrated that the Longuet-Higgins approach to symmetry of nonrigid molecules implies an invariance group isomorphic with D_{3h} and it appears that the 'symmetry breaking' terms are crucial for the analysis of the

112734 Nitrite and nitrate ions as infrared pressure gauges for diamond anvils. D.D.Klug, E.Whalley (Div. of Chem., Nat. Res. Council, Ottawa, Canada). *Rev. Sci. Instrum. (USA)*, vol.54, no.9, p.1205-8 (Sept. 1983). The infrared spectra of the antisymmetric stretching bands of dilute solutions of nitrite and nitrate ions in sodium bromide are proposed as pressure gauges for use with anvils and other apparatuses. Their frequencies, which are at 1279.0 and 1401.3 cm^{-1} respectively at zero pressure, were measured up to 186 kbar relative to the R_1 fluorescence line of ruby. The pressure is related to the shift $\Delta\nu$ of the frequency of the nitrite ion at 22°C from the zero-pressure value by the equation $\rho/\text{kbar} = 2.356(\Delta\nu/\text{cm}^{-1}) - 1.334(\Delta\nu/\text{cm}^{-1})\exp(-\Delta\nu/92 \text{ cm}^{-1})$, and to the shift $\Delta\nu$ of the frequency of the nitrate ion by the equation

$\rho/\text{kbar} = 1.775(\Delta\nu/\text{cm}^{-1}) - 0.7495(\Delta\nu/\text{cm}^{-1}) \times \exp(-\Delta\nu/78 \text{ cm}^{-1})$. Both equations were fitted by least squares, assuming that the error is in the pressure only, and the standard deviation of the pressure is 1.1 and 1.4 kbar, respectively. (14 refs.)

112735 Infrared and Raman study of the fast internal motions of non-rigid molecules in condensed state: method of selective deuteration. J.Lascombe, D.Cavagnat, J.C.Lassegues, C.Rafilipomanana (Lab. de Spectroscopie Infrarouge, Univ. de Bordeaux I, Talence, France). Symmetries and Properties of Non-Rigid Molecules. A Comprehensive Survey. Proceedings of an International Symposium, Paris, France, 1-7 July 1983 (Amsterdam, Netherlands: Elsevier 1983), p.237-46

The dynamical behaviour of non-rigid molecules in the gas state is now well known but very little information is available on these molecules in condensed state. The authors present a method of study based on the analysis of the infrared and Raman spectra of selectively deuterated molecules. It is applied to the nitromethane and cyclopentene molecules which provide respectively characteristic examples of methyl internal rotation and ring-puckering motion. In each case, an isolated CH or CD oscillator is modulated by the internal motion and several $\nu(\text{CH})$ or $\nu(\text{CD})$ bands are observed as a result of the dependence of the vibrational frequency of the oscillator on its conformational situation. Moreover, in the case of crystalline nitromethane a detailed study of the temperature dependence of the band profiles allows the main mechanism of relaxation of the CH oscillator to be deduced. (16 refs.)

Vibrational band intensities of hydrocarbons See Entry 112692

Normal-coordinate analysis of retinal isomers and assignments of Raman and infrared bands See Entry 112707

Raman and infrared excitation of local mode states in neopentane See Entry 112738

Structure and dynamics of the non-rigid CONH unit in fundamental and excited states of its stretching mode. Influence of environment effects, side-chain substitutions and secondary structures See Entry 112744

^{35}Cl nuclear quadrupole resonance and infrared spectroscopic studies of 2,6-dichloro-4-nitrophenol-amine hydrogen-bonded adducts See Entry 112749

The collision half-width for the R(0) line of the ν_3 band of methane See Entry 112787

Study of the 1750 Å mercury absorption band. Determination of the excited interaction potential and of the oscillator strength related to this band See Entry 112789

Vibrational spectra and force constants for trans-sodium hyponitrite See Entry 114859

An infra-red reflection absorption study of the adsorption of NO on Pt(111) See Entry 114867

Relative quantum yield of $\text{I}^*(^2\text{P}_{1/2})$ in the tunable laser UV photodissociation of $\text{i-C}_3\text{F}_7\text{I}$ and $\text{n-C}_3\text{F}_7\text{I}$: effect of temperature and exciplex emission See Entry 115567

Monodeuterated methane in the outer solar system. I. Spectroscopic analysis of the bands at 1.55 and 1.95 microns See Entry 116439

$^{13}\text{CH}_3\text{D}$ rovibrational intensities and the Jovian D/H ratio See Entry 116460

33.20F Raman and Rayleigh spectra

(inc. scattering)

112736 The lineshape of motion-averaged isotropic Raman spectra. A.I.Burshtein, S.G.Fedorenko, A.Yu.Pusep (Inst. of Chem. Kinetics & Combustion, Novosibirsk, USSR).

Chem. Phys. Lett. (Netherlands), vol.100, no.2, p.155-8 (2 Sept. 1983).

The conventional Kubo model can be used to describe the spectrum modulation by slow to fast motion, i.e. even in the range of applicability of perturbation theory. However, the Kubo model assumes the gaussian shape of static spectra. A model free of this assumption has been to show that experimental data can be interpreted provided the initial static spectrum has non-gaussian wings. (23 refs.)

112737 The Raman spectra and conformational change of simple sodium alkylsulfates and sodium alkylsulfonates in aqueous solution. T.Ikeda, T.Yoshida, H.Okabayashi (Dept. of Industrial Chem., Nagoya Inst. of Technol., Nagoya, Japan).

Z. Naturforsch. Teil A (Germany), vol.38A, no.9, p.1046-7 (Sept. 1983).

In order to study the polar group effect upon conformations about $\text{CH}_2\text{-CH}_2$ single bonds, the Raman spectra of simple sodium alkylsulfates and sodium alkylsulfonates were measured. The ethylsulfate ion ($\text{CH}_3\text{-CH}_2\text{-O-SO}_3^-$) in aqueous solution was found to take the trans form about the $\text{CH}_2\text{-O}$ bond in 0.67-5.41 mol/l. For the n-propylsulfonate ion the Raman line due to the gauche form about the $\text{CH}_2\text{-CH}_2$ bond was also observed, the trans form becoming predominant at higher concentrations. For the sulfate and sulfonate ions having butyl and hexyl chains, the concentration dependence of their molecular conformations was also investigated. (13 refs.)

112738 Raman and infrared excitation of local mode states in neopentane. B.R.Henry, A.W.Tarr (Dept. of Chem., Univ. of Manitoba, Winnipeg, Manitoba, Canada), O.S.Mortensen, W.F.Murphy, D.A.C.Compton.

J. Chem. Phys. (USA), vol.79, no.6, p.2583-9 (15 Sept. 1983).

The Raman spectrum of neopentane is measured in the regions of $\Delta\nu_{\text{CH}}=1$ and 2. The results are compared to the absorption spectrum of neopentane in the region from $\Delta\nu_{\text{CH}}=2$ to 5. The peak positions are calculated within the local mode model. The intensity patterns observed in both types of spectra are explained. In particular, electrical anharmonicity is found to make a significant contribution to the observed peak intensities. (16 refs.)

112739 Optical anisotropies of aromatic esters and of oligomers of poly(p-oxybenzoate). P.A.Irvine, B.Erman, P.J.Flory (IBM Res. Lab., San Jose, CA, USA).

J. Phys. Chem. (USA), vol.87, no.15, p.2929-35 (21 July 1983).

Optical anisotropies γ^2 of phenyl acetate (PA), methyl benzoate (MB), phenyl benzoate (PB), and of the trimer ($n=3$) and tetramer ($n=4$) of the p-oxybenzoate series $\text{C}_6\text{H}_4\text{CO}(\text{OC}_6\text{H}_4\text{CO})_{n-2}\text{OC}_6\text{H}_5$ have been determined from the depolarized Rayleigh scattering of their solutions in CCl_4 or, in the case of the trimer and tetramer, in dioxane. Molar Kerr constants ${}_mK$ of PA and of the trimer have been evaluated from the electric birefringences of their solutions in CCl_4 and dioxane, respectively; the ${}_mK$ for MB and PB have been taken from the work of Le Fevre and Sundaram (1962). The observed values of γ^2 and ${}_mK$ are well reproduced by calculations based on anisotropy tensors $\hat{\alpha}$ for the optical polarizabilities of the homologous aromatic esters formulated from a plausible set of mutually consistent polarizability parameters for the ester group and for the phenyl and phenylene groups, with allowance for inductive effects of substitution. The validity of a constitutive scheme for constructing the polarizability tensors, and for treating properties related thereto, is thus demonstrated. The molar Kerr constant ${}_mK$ is very sensitive to

the direction of the dipole moment in the plane of the ester group. From the values found for ${}_mK$ for the aromatic esters, the authors obtain $\tau_E=123\pm3^\circ$ for the angle between the dipole moment and the C-CO axis, in excellent agreement with previous determinations by other means. (20 refs.)

112740 High-resolution stimulated Raman spectroscopy of O_2 . R.A.Hill, P.Esherick, A.Owyoung (Sandia Nat. Lab., Albuquerque, NM, USA).

J. Mol. Spectrosc. (USA), vol.100, no.1, p.119-33 (July 1983).

High-resolution (0.002 cm^{-1}) stimulated Raman spectroscopy has been applied to the study of both normal and satellite Q branches of the fundamental vibrational band of molecular oxygen. Using a pulsed molecular free-expansion jet to adiabatically cool the oxygen sample, satellite Q branches at 1554 and 1558 cm^{-1} that arise due to the splitting of the $^3\Sigma_g$ ground state by spin-spin and spin-rotation interactions were completely resolved for the first time. Measured intensity ratios for the $^{\Delta N}\Delta J(J,N)=Q(2,1)$ and $^{\Delta N}\Delta J(J,N)=Q(1,1)$ lines, and for the $^{\Delta N}\Delta J(J,N)=Q(2,1)$ and $^{\Delta N}\Delta J(J,N)=Q(1,1)$ lines compare favorably with that for a coupling case intermediate between Hund's cases (a) and (b). Depolarization ratios, measured for a series of Q-branch (unresolved) triplets, give a value of 0.164 \pm 0.004 for the depolarization ratio of the fundamental vibrational band. (21 refs.)

112741 Raman spectra of Cl_3^+ and Br_3^+ at 12K produced from the reaction of HCl or HBr with NO_2 . L.-H.Chen, E.M.Nour, J.Laane (Dept. of Chem., Texas A&M Univ., College Station, TX, USA).

J. Raman Spectrosc. (GB), vol.14, no.4, p.232-5 (Aug. 1983).

The products of the reactions of HCl or HBr with nitrogen dioxide at 12K have been examined using Raman spectroscopy. For the NO_2+HCl reaction spectroscopic evidence for Cl_3^+ , asym- N_2O_2 , N_2O_3 , N_2O_4 , ClNO_2 , ClNO_3 , NO_2^+ , NO_2^- , and sym- N_2O_2 was found. For the reaction with HBr only Br_3^+ was detected due to resonance Raman enhancement effects. These results are consistent with the previously proposed gas-phase reaction scheme for $\text{HCl}+\text{NO}_2$. However, the reaction proceeds further at low temperatures to produce Cl_3^+ (or Br_3^+). The Raman frequencies for Cl_3^+ were observed at 515(ν_3), 462(ν_1), and 236 cm^{-1} (ν_2). The Br_3^+ resonance Raman spectra, which represent the first well documented spectra for this species, show strong fundamental bands at 281(ν_1) and 227 and 238 cm^{-1} (doublet for ν_2) as well as an overtone doublet at 471 and 487 cm^{-1} . (10 refs.)

112742 Raman spectra and vibrational dephasing of methylacetylene. V.F.Kalasinsky, T.S.Little (Dept. of Chem., Mississippi State Univ., Mississippi State, MS, USA).

J. Raman Spectrosc. (GB), vol.14, no.4, p.253-8 (Aug. 1983).

The Raman spectra of gaseous and liquid methylacetylene have been recorded. The spectrum of the gas provides new data for verifying the vibrational assignments of certain A_1 and E fundamentals. Some of the vibrations exhibit hot bands whose origins have been determined on the basis of their Raman intensities. The isotropic scattering for the three fundamentals in the liquid state was studied as a function of temperature. The hot band structure in the liquid state was modeled by using curve-fitting procedures and the assignments made for the gas phase. The isotropic bandwidths for the fundamentals were observed to increase with decreasing temperature, and the broadening is consistent with the existence of a weak hydrogen bond in pure methylacetylene. (24 refs.)

112743 Properties, formation, and interpretation of stimulated resonance Raman scattering spectra of dyes. Ya.S.Bobovich, V.I.Petrov.

J. Appl. Spectrosc. (USA), vol.37, no.6, p.1405-13 (Dec. 1982). Translation of: *Zh. Prikl. Spektrosk. (USSR)*, vol.37, no.6, p.971-81 (Dec. 1982).

[received: Sept. 1983] (20 refs.)

112744 Structure and dynamics of the non-rigid CONH unit in fundamental and excited states of its stretching mode. Influence of environment effects, side-chain substitutions and secondary structures. F.Fillaux (LASIR, CNRS, Thiais, France), M.Jaber, M.H.Baron.

Symmetries and Properties of Non-Rigid Molecules. A Comprehensive Survey. Proceedings of an International Symposium, Paris, France, 1-7 July 1983 (Amsterdam, Netherlands: Elsevier 1983), p.247-56

Vibrational spectra (infrared, Raman and neutron inelastic scattering) or N-methyl acetamide ($\text{CH}_3\text{CONHCH}_3$) and its deuterated derivatives in various physical states show large amplitude motions for the torsional mode around the C-N bond and for the out-of-plane bending of NH(ND) groups. Potential functions with double minimum have been calculated which are consistent with the nonrigidity of this molecule. Infrared and Raman bands in the NH(ND) stretching region show rather complicated profiles which are ascribed to a strong coupling with bending modes and corresponding potential functions are estimated in the ν NH(ND) excited state. A general method for structure and dynamics studies of amides and peptides is presented and is used to discuss the influence of solvent or salt interactions, aliphatic side-chains and secondary structure of homopolypeptides. (25 refs.)

Vibrational band intensities of hydrocarbons See Entry 112692

Normal-coordinate analysis of retinal isomers and assignments of Raman and infrared bands See Entry 112707

Infrared and Raman study of the fast internal motions of non-rigid molecules in condensed state: method of selective deuteration See Entry 112735

Raman characteristics of the excited electronic state in the fluorescent band of molecules See Entry 112768

Hybrid four-wave mixing in liquid pyridine See Entry 113054

Infrared dephasing and libration motion in liquid methyl iodide See Entry 114850

The hyper Raman spectra of some chloro- and bromo-methanes and some Group IV tetrachlorides See Entry 114854

Temperature dependence of the Raman active B_{3g} torsional mode of sulphamic acid See Entry 114855

Vibrational spectra and force constants for trans-sodium hyponitrite See Entry 114859

Theory of charge transfer excitation in surface enhanced Raman scattering See Entry 114865

Surface enhanced Raman scattering from pyridine on copper in UHV See Entry 114866

Brillouin scattering in liquid benzene under high pressure See Entry 114872

Raman spectral studies of bleomycin A_2 and related structural fragments: a probe for bleomycin-DNA interactions See Entry 115749

33.20K Visible spectra

112745 The 404.5-nm system of the ReO molecule. W.J.Balfour, R.S.Ram (Dept. of Chem., Univ. of Victoria, Victoria, BC, Canada).

J. Mol. Spectrosc. (USA), vol.100, no.1, p.164-73 (July 1983).

Observations on the emission spectrum of ReO in the region 375-870 nm are reported. Five bands of a $\Delta\Omega=0$ system with (0,0) band at 404.5 nm have

been rotationally analyzed and the principal results for ^{187}ReO are (in cm^{-1}) $\nu_0 = 24\,709.90$, $B'_e = 0.3819$, $B''_e = 0.4252$, $\omega'_e = 874.8_2$, and $\Delta G^\circ(1/2) = 979.1_2$. Data on the minor isotopic species ^{185}ReO are also reported. It is suggested that broad rotational profiles found in bands near 842 nm may be due to nuclear hyperfine structure. (2 refs.)

112746 Ion-cluster formation and its effect on the electronic spectrum of radical-ion pairs. B.J.McClelland (Dept. of Chem., Univ. of Salford, Salford, England).

J. Chem. Soc. Faraday Trans. II (GB), vol.79, pt.8, p.1233-41 (Aug. 1983). The visible-region band in the spectrum of the lithium-benzophenone radical-ion pair is shifted towards the blue by added lithium bromide, and the effect has been interpreted in terms of the formation of multi-ion-pair clusters. A more consistent interpretation of the data can be given in terms of the formation of a well defined 1:1 (or possibly 1:2) electrostatically bound complex. A general theory is given for interpreting the effect of such complex formation on the band position, and it is deduced that the equilibrium constant for the formation reaction is 580 at room temperature. This value, and the observed magnitude of the spectral shift, agrees with predictions derived from a simple electrostatic treatment of the complex. (9 refs.)

The A—X transition in Cr_2 : predissociation, isotope effects, and the 1-1 sequence band See Entry 112798

Formation of NH ($A^3\Pi$, $e^1\Pi$) by electron-impact dissociation of HN_3 See Entry 112861

Determination of the dissociation energies of molecules from absolute intensity measurements of their electronic transitions in SrCl flame spectra See Entry 112878

Dissociation of Cn^+ into atomic excited states after acceleration in a tandem accelerator See Entry 115545

Fourier spectroscopy of the $^{12}\text{C}_2$, $^{13}\text{C}_2$, and $^{12}\text{C}^{13}\text{C}$ (0-0) Swann bands See Entry 116462

33.20L Ultraviolet spectra

112747 $\text{C}^2\Pi_u - X^2\Sigma^+$ transition of AlO . M.Singh, M.D.Saksena (Spectroscopy Div., Bhabha Atomic Res. Centre, Bombay, India). *Can. J. Phys. (Canada)*, vol.61, no.9, p.1347-58 (Sept. 1983). Several bands of the $\text{C}^2\Pi_u - X^2\Sigma^+$ transition of AlO in the region 2800-3400 Å have been photographed at high resolution. A unique and unambiguous analysis of the rotational structure has been done for the first time for the 2-0, 1-0, 2-1, 0-0, 1-1, 0-1, 1-2, and 0-2 bands of this system. Fairly accurate rotational constants B_{eff} and D_{eff} have been determined for the $v=2$, 1, and 0 levels of the $\text{C}^2\Pi_u$ state. Severe rotational perturbations have been observed in the $\text{C}^2\Pi_u$ state. Equilibrium rotational constants (in cm^{-1}) of the $\text{C}^2\Pi_u$ state are $B_e \approx 0.6049$ and $\alpha_e \approx 0.0046$. (15 refs.)

The vibronic analysis of the vapour-phase ultraviolet absorption frequencies of 2,3-dichloropyridine See Entry 112698

Nascent NO vibrational distribution from 2485 Å NO_2 photodissociation See Entry 112700

Ultraviolet two-photon spectroscopy of benzene: a new gerade Rydberg series and evidence for the 1^1E_g valence state See Entry 112802

Formation of NH ($A^3\Pi$, $e^1\Pi$) by electron-impact dissociation of HN_3 See Entry 112861

33.25 NUCLEAR MAGNETIC RESONANCE AND RELAXATION; NUCLEAR QUADRUPOLE RESONANCE (NQR)

112748 Carbon-13 NMR study on liquid crystal solutions. Chemical shift tensors in benzonitrile. B.M.Fung (Dept. of Chem., Univ. of Oklahoma, Norman, OK, USA).

J. Am. Chem. Soc. (USA), vol.105, no.17, p.5713-14 (24 Aug. 1983). Carbon-13 chemical shifts have been widely used in the study of molecular structure, motion, and properties. The components of the chemical shift tensor are a more sensitive probe into molecular structure than the trace alone. The most straightforward way of determining the chemical shift tensor is to perform a line-shape analysis of the proton-decoupled carbon-13 NMR spectrum of a polycrystalline solid. When there are overlapping signals, they can be resolved by using magic angle spinning, and the anisotropic patterns of individual signals can be reconstructed from the spinning sidebands or by using pulses synchronized with the rotation of the spinner. Another approach to measuring the chemical shift tensor is to study the NMR spectra of molecules in liquid crystal solutions. In the past, this has been limited to the investigation of very simple molecules, and compounds with carbon-13 enrichment were often used for carbon-13 NMR study. This is mainly due to problems in solvent interference and insufficient decoupling power in spectrometers designed for studying liquid samples. The first problem can be solved by using a simple spin-echo sequence of $90^\circ - \tau - 180^\circ - 2\tau - 180^\circ - \tau$ acquisition, and the second problem can be solved or at least reduced by using phase-alternated broad-band decoupling. The author reports the determination of carbon-13 chemical shift tensors of all carbon atoms in benzonitrile by this approach. (31 refs.)

112749 ^{35}Cl nuclear quadrupole resonance and infrared spectroscopic studies of 2,6-dichloro-4-nitrophenol-amine hydrogen-bonded adducts. E.Grech, J.Kalenki, Z.Malarski, L.Sobczyk (Inst. of Chem., Univ. of Wrocław, Wrocław, Poland).

J. Chem. Soc. Faraday Trans. I (GB), vol.79, pt.9, p.2005-12 (Sept. 1983). The charge distribution in hydrogen bridges of varying strengths in solid 2,6-dichloro-4-nitrophenol complexes has been studied using the n.q.r. technique. The dependence of the average ^{35}Cl n.q.r. frequencies, $\bar{\nu}_{\text{n.q.r.}}$, on the pK_a can be analyzed in terms of the proton-transfer equilibrium $\bar{\nu}_{\text{n.q.r.}}$ provides evidence for the existence of either a double-minimum potential function or one broad minimum. Infrared spectra of such complexes show very broad absorptions extending to the far-infrared, with numerous so-called 'Evans holes' and a weakening or complete disappearance of the protonic stretching vibration band in the usual range above 1800 cm^{-1} . (18 refs.)

112750 Computer-assisted pseudorotation analysis of five-membered rings by means of proton spin-spin coupling constants: program PSEUROT. F.A.A.M.de Leeuw, C.Altona (Gorlaeus Labs, Univ. of Leiden, Leiden, Netherlands).

J. Comput. Chem. (USA), vol.4, no.3, p.428-37 (Fall 1983). A computer method for the calculation of the pseudorotational parameters in five-membered rings from vicinal proton spin-spin coupling constants is described. Some typical problems met in practice are discussed. Applications of the program in the conformational analysis of some substituted cyclopentanes are presented. (28 refs.)

112751 Through-space effects on vicinal proton spin-spin coupling constants mediated via hetero atoms: nonequivalence of cis couplings in five-membered rings. F.A.A.M.de Leeuw, A.A.van Beuzekom, C.Altona (Dept. of Organic Chem., Univ. of Leiden, Leiden, Netherlands). *J. Comput. Chem. (USA)*, vol.4, no.3, p.438-48 (Fall 1983). Theoretical studies are presented, aimed at the elucidation of through-space effects exerted by bridge-head oxygen and nitrogen atoms on cisoidal proton spin-spin coupling constants in 7-hetero-substituted norbornanes. The finite perturbation theory intermediate neglect of differential overlap (INDO) self-consistent field (SCF) molecular orbital (MO) method, modified according to the description given by Barfield (1980), was employed. It is predicted that the known nonequivalence between $J_{\text{endo-endo}}$ and $J_{\text{exo-exo}}$ in norbornanes, which is in part mediated by the bridgehead methylene group (Barfield transmission effect), also occurs in 7-heteronorbornanes. A trend is recognized in which the nonequivalence induced by oxygen is rather smaller than that induced by the rear lobe of the N-H bond or by the nitrogen lone pair. The Barfield effect also explains the observed nonequivalence between cisoidal H-C^β-C^γ-H and H-C^γ-C^β-H couplings in prolines. The calculations also predict similar, though smaller, effects on cisoidal couplings in the tetrahydrofuran ring system. (27 refs.)

112752 Possible mechanism of extraspheric shifts of PWR signals in aqueous solutions of paramagnetic ions. V.V.Matveev (State Univ., Saransk, USSR).

Theor. & Exp. Chem. (USA), vol.18, no.6, p.685-7 (Nov.-Dec. 1982). Translation of: *Teor. & Eksp. Khim. (USSR)*, vol.18, no.6, p.742-5 (Nov.-Dec. 1982). [received: Sept. 1983]

Paramagnetic shifts (PS) of PMR signals of acetone and certain other compounds were discovered in aqueous solutions in the presence of Co^{2+} , Fe^{2+} , and also of REE ions. These shifts are dipolar (pseudocontact) and occur during extraspheric interactions of metal ions with the above compounds. However, the reasons for these shifts remain far from clear, and no satisfactory explanation of the mechanism of their appearance is available in the literature. The author attempts to analyze the conditions required for the occurrence and experimental appearance of the dipole PS of the extraspheric ligands in aqueous solutions. (10 refs.)

112753 ^{19}F NMR spectra and structure of α,ω -diarylperfluoropolyenes. V.M.Yurchenko, M.M.Kremlev, Yu.A.Fialkov, V.P.Sass, V.A.Khranovskii, Yu.P.Egorov, L.M.Yagupol'skii (Inst. of Organic Chem., Acad. of Sci., Kiev, Ukrainian SSR).

Theor. & Exp. Chem. (USA), vol.18, no.6, p.687-92 (Nov.-Dec. 1982). Translation of: *Teor. & Eksp. Khim. (USSR)*, vol.18, no.6, p.745-50 (Nov.-Dec. 1982). [received: Sept. 1983]

The work is concerned with interpretation of the ^{19}F NMR spectra of a series of α,ω -diarylperfluoropolyenes of type $\text{p-XC}_6\text{H}_4\text{-(CF=CF)}_n\text{-C}_6\text{H}_4\text{X-p}$, where $\text{X}=\text{H}$, CH_3 , CH_3O , $(\text{CH}_3)_2\text{N}$; $n=2-4$, to obtain more information on the relationship between spectral parameters and the structure of the fluorinated polyenes. The ^{19}F NMR spectra of α,β -difluorostilbenes ($n=1$) were studied previously. From the dependence of the NMR chemical shifts of ^{19}F nuclei on the electronic nature of the substituents on the benzene rings, it was concluded that the planarity of the α,β -difluorostilbene molecule is distorted. In the spectra of 1,4-diphenylperfluoro-1,3-butadiene ($\text{X}=\text{H}$, $n=2$), two doublets were observed with splitting at 130 Hz, from which a conclusion was made on the trans configuration of the fluorine atoms with respect to the double bonds. According to UV spectroscopy data, these double bonds form a nonplanar cisoid conformation. (21 refs.)

112754 Recent progresses in the applications of nuclear magnetic resonance to the conformations and dynamics of flexible molecules in solution. C.Chachaty, B.Perly, T.Zemb (Dept. de Phys. Chimie, CENS, Gif-sur-Yvette, France).

Symmetries and Properties of Non-Rigid Molecules. A Comprehensive Survey. Proceedings of an International Symposium, Paris, France, 1-7 July 1983 (Amsterdam, Netherlands: Elsevier 1983), p.273-90

Some recent applications of nuclear magnetic resonance to studies of small flexible molecules, micellar aggregates and macromolecules are reported. In several cases these investigations are performed by means of the relaxation of ^{13}C induced by a paramagnetic ion bound to the molecule. Comparing the data obtained with paramagnetic probes with very different electron spin relaxation times T_{1e} allows the determination of the conformer probabilities and of the rates of internal motions. (20 refs.)

'Frozen' transition states: pentavalent carbon et al See Entry 112650

χ_α calculations of the EPR parameters of pseudotetrahedral copper(II) complexes See Entry 112652

Microwave spectra of cyclohexyl bromide and cyclohexyl iodide See Entry 112717

Intramolecular $\text{NH}\cdots\text{N}\cdots\text{HN}$ hydrogen bonds with large proton polarizability in monosalts of diamines See Entry 112730

Group theory of non-rigid molecules and its applications See Entry 112809

Orientation and molecular structure of 1,5 and 1,8 dichloroanthraquinones by PMR in a nematic solution See Entry 114742

Spin-lattice relaxation times of ^1H in aqueous gadolinium chloride solutions See Entry 114746

Second order rate constants for intramolecular conversions: application to gas-phase NMR relaxation times See Entry 115537

Different nature of outer-sphere complex formation between chloroform and bis-(N-phenyl-salicylaldiminate)Cu(II) and its adduct with pyridine See Entry 115543

Carbon-13 nuclear magnetic resonance spectroscopy of some biologically active imidazoles See Entry 115752

33.30 ELECTRON PARAMAGNETIC RESONANCE AND RELAXATION

112755 The configuration of the tin-centered radical $\text{R}_3\text{Sn(R=2,4,6-tri-}i\text{-propylphenyl)}$ as studied by ESR. M.Lehnig, Th.Apoussidis, W.P.Neumann (Lehrstuhl für Organische Chem., Univ. Dortmund, Dortmund, Germany).

Chem. Phys. Lett. (Netherlands), vol.100, no.2, p.189-92 (2 Sept. 1983). ESR data of the stannyl radical ($i\text{-Pr}_3\text{Ph}$)Sn. At temperatures between -140 and $+200^\circ\text{C}$ are presented. In solution, the isotropic ^{119}Sn hyperfine coupling decreases with increasing temperature ($20^\circ\text{C} < T < 200^\circ\text{C}$) indicating that the radical is non-planar and configurationally stable. At -140°C in a toluene matrix, anisotropic features have been observed ($A_{\parallel}(A_{\perp}(^{119}\text{Sn}))=211\text{ mT}$, $A_{\parallel}(^{119}\text{Sn})=139\text{ mT}$; $g_{\parallel}=1.995$, $g_{\perp}=2.016$) leading to an out-of-plane angle of 12.7° . (25 refs.)

112756 ESR evidence for the formation of the ring-opened cation $\text{CH}_2\text{OCH}_2^+$ from ethylene oxide. L.D.Snow, J.T.Wang, F.Williams (Dept. of Chem., Univ. of Tennessee, Knoxville, TN, USA). *Chem. Phys. Lett. (Netherlands)*, vol.100, no.2, p.193-7 (2 Sept. 1983). ESR results show that the radical cation formed from ethylene oxide in the solid state is the ring-opened 2-oxa-trimethylene cation with a symmetrical (C_2) planar structure similar to that of the isoelectronic allyl radical. In contrast, the trimethylene oxide radical cation retains the ring structure of the parent molecule and its ESR parameters are characteristic of an oxygen-centred species. (17 refs.)

112757 Radical cations of aldehydes and ketones. M.C.R.Symons, P.J.Boon (Dept. of Chem., Leicester Univ., Leicester, England). *Chem. Phys. Lett. (Netherlands)*, vol.100, no.2, p.203-4 (2 Sept. 1983). The authors confirm the observation made by Snow and Williams (1983) in the previous letter that the quartet substructure observed in the ESR spectrum of acetaldehyde is due to hyperfine coupling to a single chlorine nucleus of the solvent, fluorotrichloromethane. Reasons for this reversible interaction, and its absence for other similar cations are discussed. (8 refs.)

112758 ESR spectra and structures of radical cations of some branched alkanes: β -proton couplings in C-C σ cations. K.Nunome, K.Toriyama, M.Iwasaki (Government Industrial Res. Inst., Nagoya, Japan). *J. Chem. Phys. (USA)*, vol.79, no.6, p.2499-503 (15 Sept. 1983).

The systematic ESR studies of radical cations of five kinds of methyl substituted butanes show that the unpaired electron is rather confined to one of the C-C σ bonds in contrast to the linear alkane cations, in which the unpaired electron delocalizes over the entire σ molecular chain. Analyses of the origin of the trans C-H β proton couplings indicate that spin transfer due to hyperconjugation plays an important role in these branched alkane cations. It is also shown that the hyperconjugative effect in these branched alkane cations is two times higher than that in the neutral alkyl π radicals. The large difference of the front and back lobe interactions in the β -proton couplings in these C-C σ radicals is attributable to the bent structure of the radical carbon atom. The front lobe interaction is about one-half of that of the back lobe interaction as is the case of vinyl radicals. (16 refs.)

112759 Influence of the N-oxide group in biradicals of the imidazole series in the intramolecular spin exchange over systems of conjugated bonds. I.A.Grigor'ev, S.A.Dikanov, G.I.Shekunin, L.B.Volodarskii, Yu.D.Tsvetkov (Inst. of Chem. Kinetics & Combustion, Acad. of Sci., USSR). *J. Struct. Chem. (USA)*, vol.23, no.6, p.870-5 (Nov.-Dec. 1982). Translation of: *Zh. Strukt. Khim. (USSR)*, vol.23, no.6, p.59-65 (Nov.-Dec. 1982). [received: Sept. 1983]

Nitroxyl radicals were synthesized with a rigid system of conjugated bonds, containing both imidazole and imidazole oxide, as well as imidazole and imidazole oxide radical fragments. The EPR method was used to study the characteristic features of intramolecular electronic spin exchange in nitroxyl biradicals of the imidazole series with a rigid system of conjugated multiple bonds. It was shown that the introduction of the N-oxide group into the imidazole radical fragment leads to considerable increase (tens of times) in the value of the exchange integral, characterizing the electronic spin exchange over the system of conjugated bonds. (16 refs.)

112760 Electron spin resonance investigation of cation-radical salts of N,N,N',N' -tetramethyl- p -phenylenediaminium (TMPD) hexafluorophosphate, hexafluoroarsenate and hexafluoroantimonate. H.Fujita (Coll. of Liberal Arts & Sci., Kyoto Univ., Kyoto, Japan). *J. Chem. Soc. Faraday Trans. I (GB)*, vol.79, pt.9, p.2077-83 (Sept. 1983). The cation-radical salts of N,N,N',N' -tetramethyl- p -phenylenediaminium (TMPD) hexafluorophosphate, hexafluoroarsenate and hexafluoroantimonate have been isolated. The temperature dependences of the hyperfine splitting constants of these salts have been investigated in solution. Also, it was found by means of e.s.r. spectroscopy that these salts follow the Curie-Weiss law in the solid state. (19 refs.)

Rotational correlation times of a nitroxide spin probe in low temperature matrices determined by saturation transfer ESR: their correlation to dynamic behavior of radiation products See Entry 114736

Spectroscopic and structural properties of metallo-proteins ... See Entry 115739

33.35 DOUBLE RESONANCES AND OTHER MULTIPLE RESONANCES

112761 A four-level double resonance experiment on HCCC^{15}N with a bridge type superheterodyne microwave spectrometer. H.Bomsdorf, H.Dreizler (Inst. für Phys. Chem., Univ. Kiel, Kiel, Germany). *Z. Naturforsch. Teil A (Germany)*, vol.38A, no.9, p.1003-9 (Sept. 1983).

A four-level double resonance method has been developed allowing the determination of the relative collision induced change in signal intensity η without application of the Stark modulation technique. The method is based on certain properties of the bridge type superheterodyne spectrometer and may be applied to molecular transitions showing strong microwave absorption. η -values have been determined for various four-level systems consisting of $|M|$ -resolved rotational levels of the linear molecule HCCC^{15}N . In addition to the measurements on the pure substance the influence of foreign gas admixtures with H_2 , He, Ne and Ar on the results has been investigated. (14 refs.)

33.35H MODR and PMDR (microwave optical double resonance and phosphorescence microwave double resonance)

112762 Phosphorescence and triplet-state optically detected magnetic resonance studies of acetylacetonates of the ammonium and some group 2 metal ions. J.J.Sabbari, K.D.Bomben, D.S.Tinti (Dept. of Chem., Univ. of California, Davis, CA, USA).

J. Am. Chem. Soc. (USA), vol.105, no.17, p.5577-83 (24 Aug. 1983). The phosphorescence and triplet-state optically detected magnetic resonance (ODMR) spectra of NH_4^+ , Be^{2+} , Mg^{2+} , Zn^{2+} , Ca^{2+} , and Ba^{2+} complexes of acetylacetonate are reported in EPA glass and for the group 2 complexes as neat crystals. The phosphorescence origins, phosphorescence lifetimes, and fine structure splittings of the $\pi\pi^*$ triplet state localized on the acetylacetonate anion are dependent on the cation. The results are compared to earlier studies of group 1 metal acetylacetonates and show a correlation to the cation radius that extends over the ammonium and group 1 and 2 metal complexes. An electrostatic perturbation of the acetylacetonate anion by the cation seems able to explain the observed variations in the triplet-state properties. (21 refs.)

33.40 MÖSSBAUER SPECTRA

Spectroscopic and structural properties of metallo-proteins ... See Entry 115739

33.45 MAGNETO-OPTICAL AND ELECTRO-OPTICAL SPECTRA; DICHOISM

112763 Vibration-rotation coupling in anisotropic environments. II. Quadrupolar couplings of methanes in liquid crystals. J.G.Snijders, C.A.de Lange (Dept. of Theoretical & Phys. Chem., Free Univ., Amsterdam, Netherlands), E.E.Burnell.

J. Chem. Phys. (USA), vol.79, no.6, p.2964-9 (15 Sept. 1983). For pt.1 see *ibid.*, vol.76, p.3474 (1982). It is shown that deuterium quadrupolar couplings observed when the deuterated methanes are dissolved in liquid crystals can be understood on the basis of the same vibration-rotation coupling mechanism which can explain the measured dipolar couplings. Two quantities are obtained from the analysis: (i) the electric field gradient at the site of the deuterium nucleus when the deuterated methane possesses its equilibrium geometry; and (ii) the derivative of this field gradient with respect to the F_2 stretch symmetry mode, taken at the equilibrium geometry. In order to obtain consistency, the presence of an external electric field gradient in the liquid-crystal solvent is required and its magnitude is estimated. (12 refs.)

Recording linear dichroism spectra with the Spectropol-1 spectropolarimeter See Entry 111740

Picosecond photoinduced dichroism detected by photothermal deflection See Entry 111776

Optical anisotropies of aromatic esters and of oligomers of poly(p -oxybenzoate) See Entry 112739

Permanent dipole moment and polarizability of a class of merocyanine dyes in their ground and first excited singlet state See Entry 112873

Asymmetries in Stokes profiles of magnetic lines: a linear analysis in terms of velocity gradients See Entry 116611

33.45B Zeeman and Stark effects

112764 Magnetic susceptibility anisotropy, molecular g values, and other molecular properties of cyclopropane as determined from rotational Zeeman studies of the cyclopropane- H^{35}Cl and cyclopropane- H^{15}N complexes. P.D.Aldrich, S.G.Kukolich, E.J.Campbell, W.G.Read (Noyes Chem. Lab., Univ. of Illinois, Urbana, IL, USA).

J. Am. Chem. Soc. (USA), vol.105, no.17, p.5569-76 (24 Aug. 1983). A pulses, Fourier-transform microwave spectrometer has been used to observe the rotational Zeeman effect with the cyclopropane-HCl and cyclopropane-HCN complexes. The molecular g values and magnetic susceptibility anisotropies have been determined for the cyclopropane-HCl complex and have been used to obtain the molecular quadrupole moment, magnetic susceptibility tensor elements as well as the paramagnetic and diamagnetic contributions, and the second moment of the electronic charge distribution. Certain Zeeman parameters along with zero-field rotational constants have been obtained for cyclopropane- H^{15}N . The Zeeman constants for both complexes have then been used to extract various magnetic properties of cyclopropane. (59 refs.)

112765 The rotational Zeeman effect in the ArOCS van der Waals complex. J.A.Shea, W.G.Read, E.J.Campbell (Noyes Chem. Lab., Univ. of Illinois, Urbana, IL, USA).

J. Chem. Phys. (USA), vol.79, no.6, p.2559-68 (15 Sept. 1983). The rotational Zeeman effect has been measured in the weakly bound complex ArOCS. The study was carried out on a pulsed Fourier-transform microwave spectrometer employing a supersonic nozzle and a Fabry-Perot cavity. The following spectroscopic constants were obtained: $g_{aa} = -0.024\ 83$ (21), $2\chi_{aa} - \chi_{bb} - \chi_{cc} = 1.313(32) \times 10^{-9}$ MHz/G 2 , $g_{bb} = -0.00086(23)$, $2\chi_{bb} - \chi_{cc} - \chi_{aa} = -3.762(26) \times 10^{-9}$ MHz/G 2 , $g_{cc} = -0.00558(11)$. Projection equations are used to relate the magnetic properties of free OCS to those of the complex. An analysis of the force field as obtained from centrifugal distortion is used to determine an average structure for ArOCS and mean square amplitudes of the van der Waals motions. These are used to augment the projection analysis. The molecular quadrupole moment of ArOCS is calculated from the Zeeman parameters. With an estimated bulk magnetic susceptibility, diamagnetic susceptibilities and the second moments of electronic charge distribution are also calculated. (30 refs.)

112766 Theoretical calculation of the absorption and magnetic circular dichroism spectrum of a Jahn-Teller distorted excited state: the $1E'$ excited state of cyclopropane. W.Duch, G.A.Segal (Dept. of Chem., Univ. of Southern California, Los Angeles, CA, USA).

J. Chem. Phys. (USA), vol.79, no.6, p.2951-63 (15 Sept. 1983). This paper reports the ab initio calculation of the absorption and magnetic circular dichroism spectrum of a Jahn-Teller distorted system, the $1E'$ (s) excited state of cyclopropane, interacting with the doubly degenerate ring stretching mode. The vibronic problem is treated in the adiabatic approximation. Good agreement is found with the observed vibronic spectrum and a distinctive behaviour is predicted for the MCD. (19 refs.)

Nonlinear Zeeman spectroscopy of ultrahigh resolution See Entry 111780

Rotational energies of polar symmetric-top molecules in high electric fields See Entry 112706

33.45C Magnetic circular dichroism

112767 Theory of multiphoton magnetic circular dichroism: two identical photon case. S.H.Lin (Dept. of Chem., Arizona State Univ., Tempe, AZ, USA), Y.Fujimura, M.Saito, T.Nakajima.

J. Phys. Chem. (USA), vol.87, no.15, p.2895-900 (21 July 1983). A theory of multiphoton magnetic circular dichroism (MCD) is developed for the two identical photon case. It is shown that, in the nonresonant intermediate state case, the transition probability of the two-photon MCD consists of A , B , and C terms as is well-known in the one-photon MCD. In the resonant case, another term which vanishes if both the initial and resonant electronic states are nondegenerate makes a contribution to the transition probability in addition to the A , B , and C terms. Expressions for those terms for the two-photon MCD of molecules are derived in the adiabatic approximation. Band shapes appearing in the two-photon MCD are discussed. Analytical expressions for the band shapes including the temperature effect have been derived in the displaced harmonic oscillator model. The expressions can be applied for both the weak and strong coupling cases. Model calculations of the band shapes are performed to demonstrate the effects of the potential displacement on the band shapes of the two-photon MCD. (12 refs.)

Spectroscopic and structural properties of metallo-proteins ... See Entry 115739

33.50 FLUORESCENCE, PHOSPHORESCENCE; RADIATIONLESS TRANSITIONS (INTERSYSTEM CROSSING, INTERNAL CONVERSION)

112768 Raman characteristics of the excited electronic state in the fluorescent band of molecules. P.P.Kircheva (Inst. of Solid State Phys., Bulgarian Acad. of Sci., Sofia, Bulgaria).

Bulg. J. Phys. (Bulgaria), vol.10, no.3, p.309-22 (1983). Stimulated emission of molecules driven to the first excited electronic state and interacting with monochromatic light is discussed. An energy level diagram with 'up' and 'down' intermediate levels is used. The cases of weak and strong pumping waves are considered. The calculated amplification spectra are presented and qualitatively compared with the existing in the literature experimental data for stimulated emission of dye molecules. (16 refs.)

112769 A molecular beam study of the trapping-desorption of I_2 from a LiF (001) surface. J.B.Cross, J.B.Lurie (Chem. Div., Los Alamos Nat. Lab., Los Alamos, NM, USA).

Chem. Phys. Lett. (Netherlands), vol.100, no.2, p.174-7 (2 Sept. 1983). Rotational, vibrational and translational Boltzmann distributions of I_2 desorbing from LiF (001) were measured using laser-induced fluorescence. The I_2 rotational temperature is lower than the surface temperature (T_S) at $T_S > 300K$ while the vibrational and translational temperatures are $\approx T_S$. An upper limit on the I_2 -LiF(001) potential well depth was found to be 0.45 ± 0.03 eV. (17 refs.)

112770 Dynamical study of twisted intramolecular charge transfer in *p*-dimethylaminobenzonitrile solutions. F.Heisel, J.A.Miche (Lab. de Phys. des Rayonnements et Electronique Nucleaire, Strasbourg, France).

Chem. Phys. Lett. (Netherlands), vol.100, no.2, p.183-8 (2 Sept. 1983). To characterize the intramolecular charge-transfer process of DMABN, pico- and nano-second measurements in different polar solutions and at various temperatures were undertaken. Evidence of (i) time-dependent interconversion rates describing the formation of the charge-transfer state and (ii) fluorescence solvachromic effects is presented. (4 refs.)

112771 Argon ion laser excitation of supersonic seeded molecular beams of I_2 . F.J.Aoiz, M.M.Oprysko, R.B.Bernstein (Dept. of Chem., Columbia Univ., New York, NY, USA).

Chem. Phys. (Netherlands), vol.79, no.3, p.321-39 (15 Sept. 1983). Experiments on the laser excitation ($B \leftarrow X$) of seeded supersonic beams of I_2 by a CW argon-ion laser at 514.5 nm are reported. Measurements consisted of laser-induced fluorescence and I_2 beam attenuations and I_2 time-of-flight distributions as a function of carrier-gas pressure and nozzle temperature. From the laser-induced beam loss, the direct photodissociation cross section is found to be $(2.4 \pm 0.5) \times 10^{-19}$ cm². A simple model has been formulated to determine the fraction of molecules that are excited by the laser, utilizing the above data base and available spectroscopic data. From the laser power dependence of the fluorescence, the model also yields the magnitude of the hyperfine-averaged Einstein B coefficient, found to be $(4.9 \pm 1.0) \times 10^{16}$ erg⁻¹ cm² s⁻². The fractional excitation of fast, cold beams of I_2 is much greater than for slow or Maxwellian beams, and dependent (via the Doppler effect) upon the angle of intersection of the laser and molecular beams. (43 refs.)

112772 Fluorescence lifetime and collisional quenching of the predissociative NO $B^2\Pi$ ($v'=7$) state. K.Shibuya, F.Stühl (Phys. Chem. I, Ruhr Univ., Bochum, Germany).

Chem. Phys. (Netherlands), vol.79, no.3, p.367-81 (15 Sept. 1983). Fluorescence lifetimes of NO $B^2\Pi$ ($v'=7$) were measured in pure NO and in mixtures of NO and M ($M=O_2, N_2, H_2, Ar$, and He) using single vibronic level excitation by an ArF excimer laser ($\lambda=193$ nm). The zero-pressure lifetime was determined to be 0.33 ± 0.03 μ s. This value of the lifetime is about six times shorter than the radiative lifetime of the $B^2\Pi$ ($v'=7$) state (≈ 2 μ s). The quantum yield of the fluorescence is hence estimated to be ≈ 0.15 . Irradiation of NO by the ArF laser prepares highly excited rotational levels ($J'=22.5-33.5$) in the B ($v'=7$) state. These levels are evidently predissociated in accordance with the energetical dissociation limit which corresponds to $J' \approx 6.5$ for $B^2\Pi_{1/2}$ ($v'=7$) and to $J' \approx 3.5$ for $B^2\Pi_{3/2}$ ($v'=7$). (42 refs.)

112773 Theory of fluorescence depolarization by anisotropic Brownian rotations. R.Alicki, M.Alicka (Sektion Phys., Univ. Munchen, Munchen, Germany).

Z. Naturforsch. Teil A (Germany), vol.38A, no.8, p.835-7 (Aug. 1983). On the basis of a generalized diffusion equation for the rotational motion of an asymmetric rigid rotor a general expression for steady-state fluorescence depolarization has been obtained. (5 refs.)

112774 Fluorescence of trans-4-cyano-4'-dimethylaminostilbene; no evidence for a TICT state. H.Gruen, H.Gorner (Max-Planck-Inst. fur Strahlenchem., Mulheim, Germany).

Z. Naturforsch. Teil A (Germany), vol.38A, no.8, p.928-36 (Aug. 1983). The fluorescence properties of trans-4-cyano-4'-dimethylaminostilbene (trans-1) and a rigid analogue, in which the dimethylaminophenyl group is replaced by an indoline ring, trans-1-(4-cyanophenyl)-2-(5-[2,3-dihydro]N-methylindolyl)ethylene (trans-2) were studied in 20 solvents. The quantum yields of fluorescence (Φ_f) and of trans-cis photoisomerization (Φ_{isc}) as well as the fluorescence maximum ($\bar{\nu}_f$) and the bandwidth ($\Delta\bar{\nu}_f$) were examined. The activation energies (range: 3.5-7.8 kcal/mol) obtained from Φ_f and Φ_{isc} measurements are nearly the same for 1 and 2 in a given solvent Φ_f , $\bar{\nu}_f$ and $\Delta\bar{\nu}_f$ as a function of solvent polarity and temperature show similar trends for 1 and 2. No dual emission was observed for either of the cyanostilbenes. These findings indicate that a twisted intramolecular charge transfer (TICT) state is not involved in the relaxation process of the first excited trans single state (t^*). The main deactivation pathway of t^* competing with fluorescence in trans-cis photoisomerization by twisting about the C=C double bond in the first excited singlet state for both. (41 refs.)

112775 Radiationless transitions in linear polyenes. U.Dinur, B.Scharf (Dept. of Chem., Ben-Gurion Univ. of the Negev, Beer-Sheva, Israel).

J. Chem. Phys. (USA), vol.79, no.6, p.2600-8 (15 Sept. 1983). Electronic radiationless transitions in linear polyenes are discussed from a theoretical point of view. Only inplane relaxation is considered. It is concluded that for a given energy gap, the nonradiative decay rate is a decreasing function of the chain length. Model calculations of the nonradiative lifetime as a function of the polyene chain length are presented. For those cases where comparison with the experiment is possible (8 to 12 membered polyenes) agreement with the calculations is reasonable. The decrease in the rate of radiationless transitions with the increase in the molecular system is shown to have implications for biological systems, such as rhodopsin, that undergo a fast photochemical change. (28 refs.)

112776 Laser-induced fluorescence of PuF_6 in the $3^1G_4 \rightarrow 1^1G_4$ electronic band at room temperature. J.E.Barefield, II., W.W.Rice, J.J.Tice, R.T.Walters (Los Alamos Nat. Lab., Univ. of California, Los Alamos, NM, USA). *J. Chem. Phys. (USA)*, vol.79, no.6, p.2621-5 (15 Sept. 1983). When PuF_6 is photoexcited at 797.3 nm, fluorescence is observed from the 1^1G_4 electronic energy level. The lifetime τ of the fluorescence signal varies with pressure. The lifetimes cover a range of 655 to 243 ns for a pressure range of 0.5 to 72 Torr. A linear Stern-Volmer relationship was obtained over the complete pressure range considered. An extrapolation to zero pressure yields an intercept of $\tau_0 = 663$ ns and a slope of 3.62×10^4 Torr⁻¹ s⁻¹. Fluorescence and excitation spectra are reported and are in good agreement with the previously reported absorption spectrum of PuF_6 . (9 refs.)

112777 Roles of the Rydberg transitions in fast excitation transfer studied in cyclohexane and *n*-heptane using synchrotron radiation. K.Kimura (Inst. of Phys. & Chem. Res., Wako Saitama, Japan), J.Hormes.

J. Chem. Phys. (USA), vol.79, no.6, p.2756-62 (15 Sept. 1983). Excitation spectra of PPO (2,5-diphenyl oxazole) in cyclohexane solution show peaks at 63000 and 78000 cm⁻¹, while those in *n*-heptane solution show a single peak near 66000 cm⁻¹. The 63000 cm⁻¹ peak for cyclohexane and 66000 cm⁻¹ peak for *n*-heptane are ascribed to excitation transfer at respective valence-band absorption peaks. An extra peak at 78000 cm⁻¹ for cyclohexane solution is tentatively ascribable to the Rydberg transitions and it is situated near the eighth peak of the Rydberg series. The expanded reaction radius is, therefore, estimated to be about 30 Å. Taking account of the Rydberg series can explain the known fact that excitation transfer in cyclohexane is extraordinarily fast compared with that in *n*-heptane. Kinetic analysis shows that these upper excited states at 63000 and 78000 cm⁻¹ of cyclohexane make direct excitation transfer, competing with relaxation to the lowest excited state at 49750 cm⁻¹. It is briefly discussed that the Rydberg series, which can be observed only in cyclic (or round) alkanes, may also be one of the key processes that explain molecular structural dependence observed in the excitation transfer and electron mobilities in alkanes. (24 refs.)

112778 Fluorescence quenching interactions of L(-)-tryptophan in dimethyl sulfoxide with trivalent lanthanides. V.Anantharaman, J.Chrysoschoos (Dept. of Chem., Univ. of Toledo, Toledo, OH, USA).

J. Less-Common Met. (Switzerland), vol.93, no.1, p.59-66 (1983). (Proceedings of the Sixteenth Rare Earth Research Conference, Tallahassee, FL, USA, 18-21 April 1983).

Excited singlet-triplet crossing of tryptophan in dimethyl sulfoxide is enhanced in the presence of trivalent lanthanide ions, leading to fluorescence quenching and subsequent initial phosphorescence enhancement. The induced system crossing rate constant k_{isc}^{ind} ranges from 1.9×10^7 to 1.5×10^8 s⁻¹ at room temperature for the seven lanthanide ions used. A gradual fluorescence quenching accompanies the initial induced system crossing with a rate constant k_S^{ind} ranging from 3×10^8 to 1.4×10^{10} M⁻¹ s⁻¹. The value of k_S^{ind} is proportional to the spectral overlap between the fluorescence of tryptophan and the absorption of the lanthanides. Values of k_{isc}^{ind} and k_S^{ind} are correlated with several parameters of the lanthanides employed. (14 refs.)

112779 Phosphorescence quenching of L(-)-tryptophan in dimethyl sulfoxide at 77K by trivalent lanthanide ions. V.Anantharaman, J.Chrysoschoos (Dept. of Chem., Univ. of Toledo, Toledo, OH, USA).

J. Less-Common Met. (Switzerland), vol.93, no.1, p.67-72 (1983). (Proceedings of the Sixteenth Rare Earth Research Conference, Tallahassee, FL, USA, 18-21 April 1983).

Quenching of the corrected phosphorescence emission of tryptophan in dimethyl sulfoxide by trivalent lanthanide ions Ln^{3+} can be interpreted in terms of a static model leading to triplet quenching constants k_Q^T ranging from 1.3×10^7 to 9.1×10^7 M⁻¹. The values of k_Q^T increase with increasing spectral overlap and J values of the ground state of the appropriate lanthanide ions. The phosphorescence lifetime of tryptophan is virtually independent of $[Ln^{3+}]$ and has a value of 6.15 ± 0.25 s, in agreement with the static model of triplet quenching. (10 refs.)

112780 Luminescence of divalent europium complexes with crown ethers, cryptands and polyethylene glycols. G.-Y.Adachi, K.Sorita, K.Kawata, K.Tomokiyo, J.Shiohara (Dept. of Appl. Chem., Osaka Univ., Osaka, Japan).

J. Less-Common Met. (Switzerland), vol.93, no.1, p.81-7 (1983). (Proceedings of the Sixteenth Rare Earth Research Conference, Tallahassee, FL, USA, 18-21 April 1983).

The luminescence properties of the divalent europium complexes with crown ethers, cryptands and polyethylene glycols were studied. The observed intensity of luminescence is generally reported. The most intense luminescence is produced by a methanolic solution of the 15-crown-5 complex with europium(II), the intensity of which is 600 times greater than that of a solution of $EuCl_2$ in methanol with the same europium(II) concentration. The enhancement of the emission intensity as a result of the formation of complexes with crown ethers can be attributed to 'insulation' of the europium(II) ion from close approach of the solvent molecules which would produce radiationless energy losses. (7 refs.)

112781 Laser-induced fluorescence of Pb_2 . H.Sontag, R.Weber (Fakultat fur Phys., Univ. Konstanz, Konstanz, Germany).

J. Mol. Spectrosc. (USA), vol.100, no.1, p.75-81 (July 1983). Pb_2 , which occurs in lead vapor, was studied by the technique of laser-induced fluorescence using single-mode Ar-laser excitation. The fluorescence observed could be classified into the $F-X$ system. Ten progressions involving vibrational quantum numbers $v'=0..9$ and $v''=0..22$ were analyzed. Including collision-induced lines, rotational quantum numbers from $J=25$ to $J=300$ were observed. The vibrational constants and the numbering of the states had to be reassigned. For the first time rotational constants were determined for the Pb_2 molecule. The internuclear distances of $^{208}Pb_2$ in the F and X state are $r=3.079$ Å and $r_e=2.930$ Å, respectively. Using the constants derived RKR potentials and Franck-Condon factors were calculated, which confirmed the vibrational assignments and constants. (10 refs.)

112782 A well-resolved carbazole excimer emission from a conformationally pure polymer. L.L.Chapoy (Tech. Univ. of Denmark, Lyngby, Denmark), D.Biddle.

J. Polym. Sci. Polym. Lett. Ed. (USA), vol.21, no.8, p.621-5 (Aug. 1983). The authors present novel spectral evidence for an energetically well-resolved carbazole excimer emission spectrum for a polymer in solution. The polymer in question is an α -helical-forming poly(amino acid), (9-carbazolyl)-carboxyl-L-lysine (PKL), containing pendant carbazole groups and is both stereoisomerically and conformationally pure. The spectrum for PKL under consideration probably results from a few well-defined excimer states as dictated by nearest-neighbour carbazole interactions under the constant of the α -helix. The authors believe that this could have profound photobiological implications. (12 refs.)

112783 Applications of fluorescence from the second excited electronic level of rhodamine 6G. M.D.Galanin, Z.A.Chizhikova. *J. Appl. Spectrosc. (USA)*, vol.37, no.6, p.1440-4 (Dec. 1982). Translation of: *Zh. Prikl. Spektrosk. (USSR)*, vol.37, no.6, p.1010-15 (Dec. 1982). [received: Sept. 1983]

The authors discuss fluorescence from high-lying electronic states of organic compounds, and in particular the S_0-S_1 and S_2-S_0 transitions of rhodamine 6G and various other compounds. The use of S_2-S_0 fluorescence in picosecond measurements is discussed, along with nonlinearity in S_2-S_0 fluorescence and thermalisation-time estimation for a liquid solvent. Thermal quenching and S_2-S_0 fluorescence saturation in various solvents are also reviewed. (18 refs.)

112784 Spectroluminescence study of the behavior of organic molecules in a finely porous glass matrix. V.I.Zemskii, I.K.Meshkovskii, A.V.Sechkarev (Inst. of Precision Mech. & Optics, Leningrad, USSR).

Sov. Phys.-Dokl. (USA), vol.27, no.12, p.1047-9 (Dec. 1982). Translation of: *Dokl. Akad. Nauk SSSR*, vol.267, no.4-6, p.1357-60 (Dec. 1982). [received: Sept. 1983]

The behavior of molecules introduced into a solid glass matrix is of great interest in connection with the wide-ranging possibilities for technical applications of the microcomposition materials obtained in this way. Important information can be obtained from a study of the luminescence spectra. The authors report the results of a study of the fluorescence spectra of molecules of 3-amino-N'-methyl-phthalimide (3-AMP) and rhodamine-6G in a finely porous glass matrix. (8 refs.)

Excitation pulse-shape mimic technique for improving picosecond-laser-excited time-correlated single-photon counting deconvolutions See Entry 111771

The Jahn-Teller effect as a case of electronic non-rigidity. Application to the ground state of the symmetric $C_6F_5H_3^+$ ion See Entry 112674

On the determination of moment of inertia of prolate luminescent molecules See Entry 112696

Nitric oxide vibrational excitation from the $N(^4S)+O_2$ reaction See Entry 112699

Phosphorescence and triplet-state optically detected magnetic resonance studies of acetylacetonates of the ammonium and some group 2 metal ions See Entry 112762

State-to-state dissociation dynamics in CF_3NO See Entry 112799

Temperature dependence of near-resonant vibrational energy transfer between CO_2 and deuterated methanes See Entry 112819

Collisional coupling and relaxation of $N_2(B^3\Pi_g)$ and $N_2(W^3\Delta_u)$ vibrational levels in Ar and Ne See Entry 112820

Vibrational relaxation and vibrational predissociation in DCl gas See Entry 112821

Translational temperature dependence of mode-to-mode vibrational energy flow in B_{3u} naphthalene induced by low energy collisions with Ar See Entry 112822

Site selective rare earth spectroscopy in proteins See Entry 112886

Study of elementary photophysical and photochemical processes in organic molecules using the optocatalytic effect See Entry 113251

Fluorescence spectra, hypersensitivity and lifetimes of the carbonate and related ligand complexes of the lanthanides in aqueous media See Entry 114911

On the trail of bastnasite: a study of the ternary complex $(MFCO_3)$ of europium(III) using a fluorescence lifetime criterion See Entry 114912

Site selective excitation of 1-hydronaphthyl radical in irradiated naphthalene crystal See Entry 114918

Kinetics and detection of $F(^2P)$ atoms in a discharge flow system See Entry 115520

Laser flash photolysis of benzene. VIII. Formation of hot benzene from the S_2 state and its collisional deactivation See Entry 115568

Time-resolved studies of fluorescence quenching in a water-in-oil microemulsion See Entry 115590

33.65 PHOTOELECTRON SPECTRA

112785 Observation of X^1A_1 vinylidene by photoelectron spectroscopy of the $C_2H_2^-$ ion. S.M.Burnett, A.E.Stevens, C.S.Feigerle, W.C.Lineberger (Dept. of Chem., Univ. of Colorado, Boulder, CO, USA).

Chem. Phys. Lett. (Netherlands), vol.100, no.2, p.124-8 (2 Sept. 1983). Photoelectron spectra of the vinylidene anion ($C_2H_2^-$) show vibrational structure in X^1A_1 vinylidene up to 12 kcal/mol above the vibrational ground state. Analysis yields an EA ($C_2H_2 X^1A_1$) of 0.47 ± 0.02 eV, and frequencies for the CC stretch and HCH bend. Absence of the 3B_2 state in the photoelectron spectra indicates the $^1A_1-^3B_2$ splitting in vinylidene is ≥ 1.7 eV. (34 refs.)

112786 Vibrational broadening in F 1s hole states and the $8a_{1g}$ valence orbital of XeF_6 structure of XeF_6 and heats of formation of unusual cations. D.J.Bristow, G.M.Bancroft (Dept. of Chem., Univ. of Western Ontario, London, Ontario, Canada).

J. Am. Chem. Soc. (USA), vol.105, no.17, p.5634-8 (24 Aug. 1983). The authors have recorded the F 1s X-ray photoelectron spectra of the rare gas fluorides (KrF_2 , XeF_2 , XeF_4 , and XeF_6), the fluoromethanes (CH_3F , CF_3H , and CF_4), and HF. The large range of F 1s line widths for these and other fluorinated compounds (1.2 to 2.6 eV) is due to vibrational broadening. Using the equivalent cores approximation to quantify this broadening, they show that there is a rather good correlation between the dissociation energy for the reaction: $XNe^+ \rightarrow X^+ + Ne$ ($X^+ = KrF^+$, XeF^+ , etc.) and the F 1s line width. Relative Lewis acidities toward Ne have been obtained from the dissociation energies or line widths, and heats of formation of the unusual cations (i.e. linear ClF_2^+ and T-shaped SF_3^+) are derived. The vibrational structure on the $8a_{1g}$ valence orbital of XeF_6 shows an average vibrational splitting of ~ 530 cm $^{-1}$. This splitting is considerably smaller than the ground-state value and suggests that the $8a_{1g}$ orbital is bonding rather than antibonding as previously suggested. This vibrational analysis, the authors' X α calculations, and the F 1s line width treatment all indicate that the very broad F 1s line width in XeF_6 is caused by vibrational broadening rather than inequivalent fluorines. (39 refs.)

Study of electron distributions of molecular orbitals by Penning ionization electron spectroscopy See Entry 112839

A multiphoton spectroscopic investigation of the electronic structure of luminescent, tetrahedrally coordinated vanadium-oxygen compounds: case of YVO_4 See Entry 115012

33.70 INTENSITIES AND SHAPES OF MOLECULAR SPECTRAL LINES AND BANDS

112787 The collision half-width for the $R(0)$ line of the ν_3 band of methane. H.C.Walker, Jr., W.J.Phillips (Sverdrup Technol., Arnold Air Force Station, TN, USA).

J. Appl. Phys. (USA), vol.54, no.9, p.4729-33 (Sept. 1983). The collision half-width for the $R(0)$ absorption line of the ν_3 band of methane has been determined as a function of temperature with nitrogen and carbon dioxide as the broadening gases. The measurements were made in the temperature range from 300 to 1000K with broadening gas pressures in the range from 5 to 15 psi (absolute). Methane partial pressures sufficient to produce approximately 60% absorption at line center for each condition were used. The line spectrum was produced with a Laser Analytic LS-3 tunable diode laser spectrometer. A best-fit Voigt profile to the experimental line shape was used to determine the broadening which is characterized by the collisional or Lorentz half-width. (10 refs.)

112788 A theoretical study of the radiative lifetime of the $CH A^2\Delta$ state. M.Larsson (Res. Inst. of Phys., Stockholm, Sweden), E.M.Siegbahn.

J. Chem. Phys. (USA), vol.79, no.5, p.2270-7 (1 Sept. 1983). The complete active space (CASSCF) method has been used to generate wave functions for calculations of the $A^2\Delta-X^2\Pi$ transition moment. This transition provides an interesting test case for different ab initio methods since the experimental data for the A state radiative lifetime should be very accurate. The two most accurate recent experiments agree to within 1% of each other, with a value of 536 ns. The best earlier theoretical value is 397 ns. The authors calculations show an extremely slow convergence with basis sets and active spaces. A calculation with a basis set of more than quadruple zeta quality with two d and one f function on carbon and three p and one d function of hydrogen gave an error of 20% (446 ns compared to 536 ns) for the lifetime, even when a large active space of 5σ , 3π , and 1δ orbital was used. The authors best calculated value 525 ns finally agreed very well with the experimental value, and is consequently larger compared to the earlier theoretical value by more than 30%. (36 refs.)

112789 Study of the 1750 Å mercury absorption band. Determination of the excited interaction potential and of the oscillator strength related to this band. N.Bras, C.Bousquet (Dept. de Recherches Phys., Univ. Pierre et Marie Curie, Paris, France).

J. Phys. B (GB), vol.16, no.18, p.3383-92 (28 Sept. 1983). The 1750 Å mercury absorption band is analysed. The temperature dependence of the profile is studied and interpreted in the framework of the quasi-static theory. The energy curve of the ground state of Hg_2 being available, the upper-state potential curve as well as the oscillator strength of the transition are derived between about 3.2 and 3.6 Å. Additional information about the upper-state energy curve is drawn from the analysis of the vibrational structure of the band. In view of the results obtained it seems reasonable to attribute this 1750 Å absorption band to transitions ending at the $^3\Sigma_u^+$ Rydberg state arising from $Hg(^7S_1) + Hg(6^1S_0)$. (12 refs.)

112790 The measurement of pressure-induced shifts and widths of the $(J,K)=(3,3)$ inversion line of NH_3 at various temperatures. I.R.Dagg, P.S.Atherton, R.W.Parsons (Dept. of Phys., Univ. of Queensland, Brisbane, Queensland, Australia).

J. Mol. Spectrosc. (USA), vol.100, no.1, p.134-42 (July 1983). Line-shift and line-width parameters for the $(J,K)=(3,3)$ inversion line of NH_3 have been measured at various temperatures in the range 213 to 373K, and the results are compared with those predicted theoretically. The line-width parameter decreases with increasing temperature, in qualitative agreement with the theory, but the predicted widths are between 10 and 20% too large. The line-shift parameter is positive, so that the center frequency of the spectral line increases with increasing pressure, and the parameter decreases with increasing temperature. This is also in qualitative agreement with the theory but the predicted results are too large by factors of between 3.8 and 7.2. In addition to the experimental results, details are also given of a number of improvements which have been made to the spectrometer which had been used for earlier shift measurements. (14 refs.)

112791 Zero-phonon lines in spectra of large molecules. K.K.Rebane. *J. Appl. Spectrosc. (USA)*, vol.37, no.6, p.1346-61 (Dec. 1982). Translation of: *Zh. Prikl. Spektrosk. (USSR)*, vol.37, no.6, p.906-22 (Dec. 1982). [received: Sept. 1983]

The article is devoted to a basic aspect of the problem of inhomogeneous broadening of a zero-phonon line, namely, the role of the specific structure of a homogeneous low-temperature spectrum of an impurity molecule. The author considers why and precisely how the simultaneous presence in a homogeneous spectrum of narrow intense zero-phonon lines and wide phonon wings causes the peculiar and clear manifestations of the inhomogeneous structure of the impurity-molecules-matrix system in the overall spectrum of a large number of impurities. (46 refs.)

112792 Theory of the radiative lifetime of the 3B_1 state of SO_2 . P.Phillips, E.R.Davidson (Dept. of Chem., Univ. of Washington, Seattle, WA, USA).

J. Comput. Chem. (USA), vol.4, no.3, p.337-44 (Fall 1983). Interchange and many-body perturbation theory are applied to the calculation of the radiative lifetime of the 3B_1 state of SO_2 . The radiative lifetime of 3B_1 SO_2 is predicted to be 7.6 msec, in excellent agreement with the experimental collision-free phosphorescence lifetime. As a separate calculation, interchange perturbation theory is used to determine the radiative lifetime of the 1A_1 state of CH_2 . (24 refs.)

112793 Parameters of a stochastic oscillator describing a hydrogen-bonded system in a cryosolution. A.V.Bobrov, N.N.Gadzhieva, Ya.M.Kimel'fel'd (Inst. of Spectroscopy, Acad. of Sci., Moscow, USSR).

Theor. & Exp. Chem. (USA), vol.18, no.6, p.620-6 (Nov.-Dec. 1982). Translation of: *Teor. & Eksp. Khim. (USSR)*, vol.18, no.6, p.675-81 (Nov.-Dec. 1982). [received: Sept. 1983]

The Pimentel-Huggins empirical linear relationship (1956) between the shift $\Delta\nu$ and the half-width $\nu_{1/2}$ ($\nu_{1/2} \approx 0.7\Delta\nu$) is isolated to varying extents for all complexes that have been examined in cryosolutions: The authors have examined the shapes of the $\nu_s(X-H)$ bands in cryosolutions within the framework of the Robertson-Yarwood model (1978). (17 refs.)

112794 Permutational analysis and tunnelling effects in XeF_6 . J.Brocas, C.Rusu (Univ. Libre de Bruxelles, Bruxelles, Belgium).

Symmetries and Properties of Non-Rigid Molecules. A Comprehensive Survey. Proceedings of an International Symposium, Paris, France, 1-7 July 1983 (Amsterdam, Netherlands: Elsevier 1983), p.257-63. The modes of rearrangements and the possible Longuet-Higgins groups of XeF_6 have been derived assuming a D_{3d} static or averaged symmetry. Within the same model, it is shown that the nonrigid multiplet line-shape of BPR-3, 6 mechanism is distinct from the line-shape of the other mechanisms generating the same Longuet-Higgins group. It has not been possible to obtain this

pe of discrimination between BPR-6, transverse diagonal or Bailar twists, id turnstile pseudorotation; they all generate the same Longuet-Higgins group and give rise to identical splitting scheme and statistical weights. (17 fs.)

excitation pulse-shape mimic technique for improving picosecond-laser-excited me-correlated single-photon counting deconvolutions See Entry 111771

he use of modified virtual orbitals in perturbative polarization propagator calculations See Entry 112633

onadiabatic representations of the $^1\Sigma_u^+$ and $^1\Pi_u$ states of the N_2 molecule See Entry 112703

as phase vibrational fundamentals and vib-rotational parameters of $AsCl_3$ See Entry 112727

itrite and nitrate ions as infrared pressure gauges for diamond anvils See Entry 112734

he lineshape of motion-averaged isotropic Raman spectra See Entry 112736

he 404.5-nm system of the ReO molecule See Entry 112745

on-cluster formation and its effect on the electronic spectrum of radical-ion pairs See Entry 112746

hosphorescence and triplet-state optically detected magnetic resonance studies of acetylacetonates of the ammonium and some group 2 metal ions See Entry 112762

heory of multiphoton magnetic circular dichroism: two identical photon case See Entry 112767

luorescence lifetime and collisional quenching of the predissociative $NO\ B^2\Pi$ ($v=7$) state See Entry 112772

luorescence of trans-4-cyano-4'-dimethylaminostilbene; no evidence for a ICT state See Entry 112774

hosphorescence quenching of $L(-)$ -tryptophan in dimethyl sulfoxide at 77K y trivalent lanthanide ions See Entry 112779

aser-induced fluorescence of Pb_2 See Entry 112781

vibrational broadening in $F\ 1s$ hole states and the $8a_{1g}$ valence orbital of eF_6 : structure of XeF_6 and heats of formation of unusual cations See Entry 112786

ate-to-state dissociation dynamics in CF_3NO See Entry 112799

Ultraviolet two-photon spectroscopy of benzene: a new gerade Rydberg series and evidence for the 1^1E_{2g} valence state See Entry 112802

Collisional coupling and relaxation of $N_2\ (B^3\Pi_g)$ and $N_2(W^3\Delta_u)$ vibrational levels in Ar and Ne See Entry 112820

Study of electron distributions of molecular orbitals by Penning ionization electron spectroscopy See Entry 112839

Calculation of the effective rotational transition probabilities for excitation by electron impact from the ground state $N_2X^1\Sigma_g^+$ ($v=0, k$) to the excited state $V_2+B^2\Sigma_u^+$ (v', k) of nitrogen See Entry 112863

Determination of the dissociation energies of molecules from absolute intensity measurements of their electronic transitions in SrCl flame spectra See Entry 112878

Hybrid four-wave mixing in liquid pyridine See Entry 113054

Vibrational spectra and force constants for trans-sodium hyponitrite See Entry 114859

An infra-red reflection absorption study of the adsorption of NO on Pt(111) See Entry 114867

2CH_3D rovibrational intensities and the Jovian D/H ratio See Entry 116460

Fourier spectroscopy of the $^{12}C_2$, $^{13}C_2$, and $^{12}C^{13}C$ (0-0) Swann bands See Entry 116462

33.80 PHOTON INTERACTIONS WITH MOLECULES

112795 Theoretical Compton profile anisotropies in molecules and solids. IX. Chemical bonding and 0-90 anisotropies in the first-row diatomic hydrides AH. B.M.Pettitt, R.L.Matcha (Dept. of Chem., Univ. of Houston, Houston, TX, USA), B.I.Ramirez. *J. Chem. Phys. (USA)*, vol.79, no.6, p.2913-17 (15 Sept. 1983).

An analysis of the parallel-perpendicular Compton profile anisotropies in the first-row diatomic hydrides is presented. Both the total and molecular orbital anisotropies present trends that may be related to the nature of the chemical bonding in the molecules. (11 refs.)

Scattering of circularly polarized radiation See Entry 112931

33.80B Level crossing and optical pumping

Secondary-emission spectra of rhodamine 6G solutions with various levels of population inversion See Entry 113056

33.80E Autoionization, photoionization, and photodetachment

112796 Improved calculations on the outer-valence Auger spectrum of F_2 . C.-M.Liegender (Inst. fur Theoretische Phys., Tech. Univ. Berlin, Berlin, Germany). *J. Chem. Phys. (USA)*, vol.79, no.6, p.2924-7 (15 Sept. 1983).

The outer-valence Auger spectrum of F_2 has been calculated by methods of many-body perturbation theory. The results have been compared with the recently recorded experimental spectrum and some partially new assignments have been proposed. (14 refs.)

112797 Photoionisation and molecular structure. A.Palma (Investigacion Basica de Procesos, Inst. Mexicano del Petroleo, Mexico City, Mexico). *Rev. Mex. Fis. (Mexico)*, vol.29, no.3, p.387-99 (May 1983). In Spanish. [received: Sept. 1983]

A presentation is given of the theoretical work on photoionization and molecular structure carried out by the author and coworkers. The implications of the photoionization process on the molecular geometry are emphasized. In particular, the ionization effect on deep orbitals is considered and it is shown that, contrary to traditional thinking, these orbitals have relevant effects on the molecular geometry. The problem of calculating photoionization relative intensities for the full spectrum is also considered, and the results of the present model are compared with experimental and other theoretical results. (16 refs.)

Ultraviolet two-photon spectroscopy of benzene: a new gerade Rydberg series and evidence for the 1^1E_{2g} valence state See Entry 112802

33.80G Diffuse spectra; predissociation, photodissociation

112798 The A-X transition in Cr_2 : predissociation, isotope effects, and the 1-1 sequence band. S.J.Riley, E.K.Parks, L.G.Pobo, S.Wexler (Chem. Div., Argonne Nat. Lab., Argonne, IL, USA). *J. Chem. Phys. (USA)*, vol.79, no.6, p.2577-82 (15 Sept. 1983).

Two-color resonance-enhanced ionization spectroscopy with mass analysis is performed on beams of Cr_2 produced by laser vaporization and isentropic expansion cooling. For the A-X 0-0 band near 459.6 nm an extensive rotational spectrum is observed and its intensity profile is found to have a systematic modulation with J. This modulation, and its surprisingly strong dependence on isotopic composition, are interpreted in terms of a two-step predissociation of the A state and suggest a potentially important new procedure for isotope enrichment in metal systems. An additional resonant feature is found ~ 1 nm to the red of the origin band and is assigned to the 1-1 sequence band. (20 refs.)

112799 State-to-state dissociation dynamics in CF_3NO . R.D.Bower, R.W.Jones, P.L.Houston (Dept. of Chem., Cornell Univ., Ithaca, NY, USA). *J. Chem. Phys. (USA)*, vol.79, no.6, p.2799-807 (15 Sept. 1983).

The state-to-state dissociation dynamics of CF_3NO have been investigated by exciting the parent compound in a supersonic jet expansion with one tunable laser and monitoring the state distribution of the NO fragment by one- or two-photon laser-induced fluorescence using a second tunable laser. At the lowest levels of excitation, CF_3NO dissociates to give an NO distribution which is consistent with a statistical distribution of energy in the products. As more highly excited vibronic states of S_1 are selected, the product distribution begins to show signs of nonstatistical behavior, although the deviations are small. The appearance time of the NO decreases nearly monotonically with increasing energy above the S_1 origin and is equal to the fluorescence lifetime of the CF_3NO^* to within experimental error. It is likely that both the appearance time of the NO and the fluorescence lifetime of the CF_3NO^* measure the rate of internal conversion from S_1 to highly excited vibrational levels of S_0 , which then dissociate in a nearly statistical fashion on the S_0 surface. The barrier to dissociation of the CF_3-NO bond is 39.6 ± 0.23 kcal/mol. (26 refs.)

112800 Vibrational predissociation of H_2 , D_2 , and HD-Ar van der Waals molecules. J.M.Hutson, C.J.Ashton, R.J.Le Roy (Guelph-Waterloo Centre, Univ. of Waterloo, Waterloo, Ontario, Canada). *J. Phys. Chem. (USA)*, vol.87, no.15, p.2713-20 (21 July 1983).

Accurate close-coupling calculations are performed for vibrationally predissociating states of H_2 -Ar, D_2 -Ar, and HD-Ar, using the best potential energy surface available. All the states examined have very small widths ($\Gamma \ll 10^{-6}$ cm $^{-1}$, corresponding to lifetimes > 20 μ s). There is a pronounced tendency for predissociation to yield rotationally hot diatomic molecules, even for the H_2 -Ar and D_2 -Ar complexes where the present potential has no anisotropic terms of higher order than $P_2(\cos \theta)$. This near-resonant effect is particularly strong for HD-Ar, where all Legendre terms are present in the potential; in this case, about 50% of the HD products are formed in the highest two accessible rotational levels. There is some evidence for a rotational rainbow effect in the product rotational state distributions. Perturbation theory calculations which attempt to reproduce the accurate calculations are also reported. They successfully model the qualitative features of the close-coupling results, but are not quantitatively accurate even for these weakly coupled systems. It appears that this inadequacy is due to the need for a very accurate representation of the bound state wave function and to the neglect of important couplings between the different open channels. This conclusion is supported by the observation that very large basis sets are required to obtain convergence of the close-coupling calculations. (22 refs.)

Dissociation curves for nine low lying states of Tl_2 from REP CI calculations See Entry 112665

Nascent NO vibrational distribution from 2485 Å NO_2 photodissociation See Entry 112700

Argon ion laser excitation of supersonic seeded molecular beams of I_2 See Entry 112771

Fluorescence lifetime and collisional quenching of the predissociative $NO\ B^2\Pi$ ($v'=7$) state See Entry 112772

Vibrational relaxation and vibrational predissociation in DCI gas See Entry 112821

Relative quantum yield of $I(^2P_{1/2})$ in the tunable laser UV photodissociation of $i-C_3F_7I$ and $n-C_3F_7I$: effect of temperature and exciplex emission See Entry 115567

33.80K Multiphoton processes

112801 On the vibronic treatment of two photon absorption in polyatomic molecules. P.P.Kiricheva, S.D.Simeonov (Inst. of Solid State Phys., Bulgarian Acad. of Sci., Sofia, Bulgaria). *Bulg. J. Phys. (Bulgaria)*, vol.10, no.3, p.297-309 (1983).

A general expression for nonlinear susceptibility of two-photon absorption by a multilevel system is applied in the case of polyatomic molecules in conditions of one-photon resonance. On the basis of a known model for the vibronic states, it is shown what kind of information can be given by the calculated spectra when they fit with the experimental data. (20 refs.)

112802 Ultraviolet two-photon spectroscopy of benzene: a new gerade Rydberg series and evidence for the 1^1E_{2g} valence state. R.L.Whetten, Ke-Jian Fu, E.R.Grant (Dept. of Chem., Cornell Univ., Ithaca, NY, USA). *J. Chem. Phys. (USA)*, vol.79, no.6, p.2626-40 (15 Sept. 1983).

In the first application of continuously tunable ultraviolet two-photon absorption spectroscopy to a study of the higher excited states of a polyatomic molecule, the authors obtained the two-photon absorption spectrum of jet-cooled benzene in the energy region from 55000 to 75000 cm $^{-1}$. The strongest features of this spectrum, seen as two-photon resonance structure in three-photon ionization, are assigned to members of a new Rydberg series. Vibronic elements of these Rydberg states show evidence of dynamical effects associated with a Jahn-Teller instability in the $^2E_{1g}$ ionic core toward which the series converges. Notably, the magnitude of vibronic coupling terms in these states appears quite comparable to that present in $C_6H_6^+$ and the sym-halobenzene cation ground states, while differing significantly from theoretical calculations predicting ν_8 (ring stretch) as the major distorting mode. In addition, we observe two other new band systems: the first, with an origin at 60800 cm $^{-1}$, has vibronic structure, isotope shifts, and dramatically increased diffuseness upon deuteration, which taken together suggest its

assignment as a highly valenized 3d Rydberg state or a degenerate valence state, most likely the lower of the two 1E_g states predicted by molecular orbital theory. The second, lying in the 55000-58000 cm^{-1} region, can be at least partially assigned to the two-photon forbidden $3p_{xy}$ Rydberg states. (65 refs.)

Theory of multiphoton magnetic circular dichroism: two identical photon case See Entry 112767

34.00 ATOMIC AND MOLECULAR COLLISION PROCESSES AND INTERACTIONS

34.10 GENERAL THEORIES AND MODELS

(inc. statistical theories, transition state, stochastic and trajectory models, etc; see also 82.20)

Molecular mechanics with an array processor See Entry 112647
Dielectronic recombination at low temperatures See Entry 116447

34.20 INTERATOMIC AND INTERMOLECULAR POTENTIALS AND FORCES

(for molecular solids, see 31.70K)

112803 Bound-water in biomolecules: a Monte Carlo simulation of the bifurcated hydrogen bond in violic acid monohydrate. S.Mascarenhas, J.N.Onuchic (Inst. de Fisica e Quimica de Sao Carlos, Univ. de Sao Paulo, Sao Carlos, Brazil).

An. Acad. Bras. Cienc. (Brazil), vol.55, no.2, p.165-72 (June 1983).

A Monte Carlo simulation is obtained for the well established case of the bifurcated hydrogen bond of the water molecule in violic acid monohydrate. This is done by the use of a multipole interaction potential for water in the field of the charges of the violic acid as given by a CNDO calculation. To these were added Lennard Jones potentials for all centers involved. All four crystallographic equivalent waters in the unit cell are allowed to move and rotate their dipole and quadrupole moments allowed to change in response to changes in local field during the interactive procedure for energy minimization. The final average position of the waters and their RMS motion agrees well with X-ray and neutron results indicating that the bifurcated hydrogen bond proposed for this structure is an energetically stable configuration. (15 refs.)

112804 On the use of a MO polarized basis for the analysis of the interaction energy in molecular interactions: application to amine complexes. R.Bonaccorsi, P.Palla (Istituto di Chimica Quantistica ed Energetica Molecolare CNR, Pisa, Italy), R.Cimiraglia, J.Tomasi.

Int. J. Quantum Chem. (USA), vol.24, no.3, p.307-16 (Sept. 1983).

A variant of the interaction energy decomposition scheme proposed by Morokuma (1977) which gives more emphasis to polarized MOs is presented and tested on complexes of amines with Li^+ , BH_3 , and SO_2 . A more systematic utilization of polarized MOs (i.e. of orbitals of the interacting molecules computed with the SCF formalism in the Coulombic field of the other molecular components of the system) is adopted, and the connection of this decomposition of the supermolecule interaction energy with perturbation approaches utilizing such polarized MOs is discussed. (21 refs.)

112805 Molecular constants of vanadium oxytrihalides. A.Natarajan, S.Somasundaram (Dept. of Phys., Madras Univ. Autonomous P.G. Centre, Tiruchirappalli, India).

Indian J. Phys. Part B, vol.57B, no.3, p.234-40 (June 1983).

The potential energy constants of vanadium oxytrihalides VOX_3 ($\text{X}=\text{F}$, Cl , Br) in general valence force field have been evaluated using the new procedure involving kinetic constants. Using this force field, the other molecular constants viz. mean square amplitudes of vibration, generalised mean square amplitudes, shrinkage constants, Coriolis coupling coefficients and centrifugal distortion constants have also been estimated. (16 refs.)

112806 Expectation values for Morse oscillators. R.H.Tipping (Air Force Geophys. Lab., Hanscom AFB, MA, USA), J.F.Ogilvie.

J. Chem. Phys. (USA), vol.79, no.6, p.2537-40 (15 Sept. 1983).

Several exact recursion relations for expectation values of different operators are derived for the Morse potential using the hypervirial and Hellmann-Feynman theorems. These results enable one to express the expectation values of other useful operators as series expansions in terms of the dimensionless anharmonicity parameter $\omega_e X_e/\omega_e$. The present results, obtained without explicit use of the eigenfunctions, are compared with similar results derived by other techniques, and it is illustrated how accurate values can be obtained with very little computational effort. (26 refs.)

112807 Walking on potential energy surfaces. J.Simons, P.Jorgensen, H.Taylor, J.Ozment (Chem. Dept., Univ. of Utah, Salt Lake City, UT, USA).

J. Phys. Chem. (USA), vol.87, no.15, p.2745-53 (21 July 1983).

By combining a local quadratic approximation to the potential energy surface with the concept of a trust radius within which this quadratic approximation is accurate, and a scaling of one active coordinate, the authors have developed an automated surface walking algorithm. This algorithm allows one to walk from geometries characteristic of equilibrium molecular structures, uphill along stream beds, through transition-state geometries, and onward to product-molecule equilibrium geometries. The method has been applied to model and ab initio test cases with encouraging results. The success of using the algorithm in connection with approximate Hessian matrices formed via so-called update techniques, which require only local force information, is especially encouraging in light of the high cost of ab initio analytical evaluation of the Hessian. (17 refs.)

112808 A new two-body water-water potential. E.Clementi, P.Habitz (IBM Corp., Poughkeepsie, NY, USA).

J. Phys. Chem. (USA), vol.87, no.15, p.2815-20 (21 July 1983).

The potential energies for the water dimer in various geometrical configurations have been calculated with the direct configuration interaction method, including all single and double excitations out of the Hartree-Fock reference. The basis set includes two d sets on the oxygen atom and describes the experimental dipole moment within 0.5%. The authors selected 169 geometries to scan the minimum and repulsive area of the potential surface. The results match the experimental minimum geometry and energy for the dimer. Comparison with previous work, Matsuoka et al. (1976), show appreciable deriva-

tions in the repulsive area. The authors have fitted the quantum mechanical result and calculated the second virial coefficient, which is, unfortunately, a factor of 2 off the experimental values. (31 refs.)

112809 Group theory of non-rigid molecules and its applications. K.Balasubramanian (Dept. of Chem. & Lawrence Berkeley Lab., Univ. of California, Berkeley, CA, USA).

Symmetries and Properties of Non-Rigid Molecules. A Comprehensive Survey. Proceedings of an International Symposium, Paris, France, 1-7 July 1983 (Amsterdam, Netherlands: Elsevier 1983), p.149-68. The use of generalized wreath product groups as representations of symmetry groups of non-rigid molecules is considered. Generating function techniques are outlined for nuclear spin statistics and character tables of the symmetry groups of non-rigid molecules. Several applications of non-rigid molecular group theory to NMR spectroscopy, rovibronic splitting and nuclear spin statistics of non-rigid molecules, molecular beam deflection and electric resonance experiments weakly-bound van-der Waals complexes, isomerization processes, configuration interaction calculations and the symmetry of crystals with structural distortions are described. (81 refs.)

Mass dependence of the Kolmogorov-Arnold-Moser stability and low-order resonances in the kinetically coupled two-degree-of-freedom Morse system See Entry 111553

A new formulation of scaled atoms-in-molecules theory See Entry 112631

Theoretical studies of van der Waals molecules: the $\text{H}_2\text{-H}_2$ dimer See Entry 112639

Energetics and structure of the hydrated gaseous halide anions See Entry 112644

Computer generation of the symmetry elements of nonrigid molecules See Entry 112646

Conversion of bound states to resonances with changing internuclear distance in molecular anions See Entry 112675

Synchrotron spectroscopy of the giant resonances in the lanthanides and actinides and its relevance to valence changes See Entry 112677

Nonrelativistic and quasirelativistic model potential calculations on AgH and Ag_2 See Entry 112678

Vibronic coupling of electronic states. III. The definitive breakdown of the CBO potential picture within the framework of our model See Entry 112697

Nonadiabatic representations of the $^1\Sigma_u^+$ and $^1\Pi_u$ states of the N_2 molecule See Entry 112703

Vibrational frequencies from anharmonic ab initio/empirical potential energy functions: stretching vibrations of hydroisocyanic acid, phosphacetylene, isocyanacetylene, and phosphabutadiene See Entry 112705

Reexamination of the I_2 spectrum near the $B(\Pi_{O_u}^+)$ state dissociation limit See Entry 112711

Gas phase vibrational fundamentals and vib-rotational parameters of AsCl_3 See Entry 112727

Ion-cluster formation and its effect on the electronic spectrum of radical-ion pairs See Entry 112746

Laser-induced fluorescence of Pb_2 See Entry 112781

Study of the 1750 Å mercury absorption band. Determination of the excited interaction potential and of the oscillator strength related to this band See Entry 112789

Vibrational predissociation of H_2 , D_2 , and HD-Ar van der Waals molecules See Entry 112800

Anharmonic model for intensity of scattering of electrons by polyatomic molecules in the gas phase See Entry 112854

Electronic polarizabilities and molecular properties of diatomic alkali hydrides See Entry 112875

A multiconfigurational self-consistent field study of the D_{2h} dissociation of excited-state ethylene See Entry 115540

34.50 INELASTIC SCATTERING OF ATOMS AND MOLECULES

112810 Relativistic long-range interactions between H, He and Li atoms. S.I.Easa (Dept. of Phys., Coll. of Education, Basrah Univ., Basrah, Iraq), G.C.Shukla.

Indian J. Phys. Part B, vol.57B, no.3, p.225-8 (June 1983).

Relativistic long-range interactions between H, He and Li atoms have been worked out by using variational calculations of dipole polarizabilities of these atoms. The results are in harmony with earlier works. (7 refs.)

112811 Total scattering cross sections for the helium-argon system at low relative velocities. R.W.York, W.L.Taylor, P.T.Pickett (Monsanto Res. Corp., Miamisburg, OH, USA).

J. Chem. Phys. (USA), vol.79, no.6, p.2831-8 (15 Sept. 1983).

Absolute total cross sections for He-Ar were measured in the relative velocity range of $\sim 800\text{-}2000$ m/s by passing a supersonic nozzle beam through a cell containing the target gas. The beam attenuation was determined by passing the unscattered beam particles into a quadrupole detector. The absolute number density of target gas particles in the target cell was obtained by a calibrated-flow method of introducing gas into the cell during an experiment. A correction was applied for the angular resolution of the apparatus. The average experimental uncertainty was estimated to be $\sim 3\%$ to 3.5% . The present results, as well as other available data, were deconvoluted in a two-step process to yield Q^0 and Q^1 , the first and second approximations to the total cross section, as a function of the relative velocity. The composite results of all experimental data were compared to seven interatomic potentials and the Hartree-Fock-dispersion (HFD) potential represented the data best. (31 refs.)

112812 Influence of the rotational energy of the molecular perturber on the $\text{Rb}(5P)\text{-H}_2, \text{D}_2$ fine structure changing collisions. J.Cuvellier, J.M.Mestdagh, M.Ferray, P.de Pujol (Service de Phys. des Atomes et des Surfaces, CENS, Gif-sur-Yvette, France).

J. Chem. Phys. (USA), vol.79, no.6, p.2848-53 (15 Sept. 1983).

A crossed beam apparatus has been used to study the $\text{Rb}(5P_{1/2} \rightarrow 5P_{3/2})$ fine-structure-changing (FSC) transitions induced by D_2 and H_2 molecules. The rotational temperature of the molecular perturber and the relative energy E_R of the colliding atom-molecule pair were varied independently. The observed FSC cross section for H_2 remains almost unchanged as the rotational temperature is varied. On the contrary, the rotational temperature of D_2 results, in some cases, in a rather distinct variation of the FSC cross section; this is most pronounced of $E_R \sim 0.08$ eV and $T_{\text{rot}}(\text{D}_2) < 200\text{K}$. Reference is made to the theoretical model of Hickman (1982); it accounts well for the general trend in the cross section measured with H_2 . The results

for D_2 -Rb collisions imply that the various rotational levels of D_2 do not seem to contribute equally to the observed FSC cross sections. This work supports the assumption that for D_2 molecules in the rotational level $J=2$ (and probably also $J=3$), the FSC cross section is larger than for D_2 in its other rotational levels. (13 refs.)

112813 Theoretical studies of van der Waals dimer depletion mechanisms in free jet expansions: the Ar_2+X ($X=CO_2$, CO , N_2) systems. R. Viswanathan, L.M. Raff, D.L. Thompson (Dept. of Chem., Oklahoma State Univ., Stillwater, OK, USA). *J. Chem. Phys. (USA)*, vol.79, no.6, p.2857-68 (15 Sept. 1983).

Collisional energy transfer, exchange, and complex formation mechanisms for Ar_2 dimer depletion in free jet expansions have been investigated using quasi-classical trajectory methods on several different potential-energy surfaces. Computed Ar_2 dissociation cross sections show that $V \rightarrow V$ energy transfer is an unimportant mechanistic pathway for Ar_2 dissociation in collisions with CO_2 , N_2 , and CO . An $R \rightarrow V$ energy transfer pathway is found to be important at translational energies of 0.03 eV. However, there is very little difference among the results obtained for CO_2 , N_2 , and CO . At higher translational energies, around 0.10 eV, the importance of an $R \rightarrow V$ energy transfer mechanism in Ar_2 dissociation decreases. The results are found to be insensitive to moderate variations in the pairwise LJ(12,6) potential parameters. Three-body potential terms are shown to be of negligible importance. Rate coefficients for collisional dissociation, exchange, and complex formation have been computed for (CO_2, Ar_2) and (N_2, Ar_2) systems under conditions that approximate those existing in the experiments reported by Yamahita et al. [*J. Chem. Phys.* 75, 5355 (1981)]. For the CO_2 system, collisional dissociation is the major mechanistic pathway for Ar_2 depletion. Exchange plays only a minor role. Complex formation does not occur. For the N_2 system, collisional dissociation predominates for a rotational temperature equal to 298K. At lower rotational temperatures, exchange becomes the major process. Complex formation does not occur. Yield computed from a simple pseudo-first-order rate model are found to be in good accord with the experimental data for most systems. The exceptions are (C_2H_4, Ar_2) when the mole fraction of C_2H_4 is 0.10 or greater, and the $[C_4H_6, (CO_2)_2]$ system. (18 refs.)

112814 Inelastic differential and integral cross sections for $^{2S+1}\Sigma$ linear molecule- 1S atom scattering: the use of Hund's case (b) representation. G.C. Corey, F.R. McCourt (Dept. of Chem., Univ. of Waterloo, Waterloo, Ontario, Canada).

J. Phys. Chem. (USA), vol.87, no.15, p.2723-30 (21 July 1983). Exact close-coupled scattering equations are established for multiplet- Σ molecule-structureless atom collisions by using a Hund's case (b) coupling scheme for the description of the paramagnetic molecule. Coupled-states and infinite-order sudden approximation expressions are presented for T matrices and for differential and integral cross sections. The importance of transforming to a spin-free total- J basis is emphasized, especially its eventual usefulness in reducing the computing time that will be required for the solution of paramagnetic scattering problems. The result of a lack of J -state resolution in beam-scattering experiments is discussed and it is shown that, in such a case, formulas originally obtained for diamagnetic molecule-atom scattering apply. (29 refs.)

112815 Interaction of hydrogen atoms with polyatomic molecules studied by means of scattering experiments and hybrid Hartree-Fock plus damped dispersion calculations. G.O. Este, D.G. Knight, G. Scoles, U. Valbusa (Centre for Molecular Beams & Laser Chem., Univ. of Waterloo, Waterloo, Ontario, Canada), F. Grein.

J. Phys. Chem. (USA), vol.87, no.15, p.2772-80 (21 July 1983). Total differential collision cross sections for the scattering of H atoms from C_2H_6 , C_3H_8 , C_2H_2 , CO_2 , and O_2 have been measured and information on the spherical and nonspherical parts of the interaction potential extracted by means of scattering calculations which make use of the infinite-order sudden (IOS) approximation. The interactions of three other systems, $H+Ar$, $H+CH_4$, and $H+CO$, previously measured in the authors' laboratory have been calculated by means of hybrid Hartree-Fock plus damped dispersion (HFD) energy calculation and found to be in good agreement with the 'experimental' potentials. A model is then constructed to derive the main features of the interaction of H atoms with the higher hydrocarbons from the knowledge of the $H+CH_4$ interaction. The predictions of this model are found to be in excellent agreement with the experimental parameters for both the spherical and nonspherical parts of the potentials. (26 refs.)

Kinetic study of $Ca(4^3P_1)$ by time-resolved emission, $4^3P_1 \rightarrow 4^1S_0 + h\nu$ ($\lambda = 657.3$ nm), following dye-laser excitation: spontaneous emission, diffusion and collisional quenching See Entry 112681

Dissociation of Cn^+ into atomic excited states after acceleration in a tandem accelerator See Entry 115545

34.50E Rotational and vibrational energy transfer

112816 Vibrational energy relaxation of highly compressed gaseous H_2 and N_2 . M. Chatelet, J. Kieffer, B. Oksengorn (Lab. des Interactions Moléculaires et des Hautes Pressions, Univ. Paris-Nord, Villetaneuse, France).

Chem. Phys. (Netherlands), vol.79, no.3, p.413-29 (15 Sept. 1983). The authors have measured the vibrational energy relaxation time of dense gaseous hydrogen at 400K up to 250 MPa and of nitrogen at 293K up to 290 MPa. Following a short theoretical overview, the experimental results are analysed in terms of two different isolated binary collision (IBC) models. Qualitative agreement is found with the Gale and Delalande (1978) model, but the hard-sphere diameters deduced from the fit show a large discrepancy from theoretical predictions. This deviation seems to question the IBC assumption in the high-density domain. The comparison of the vibrational energy relaxation time with the self-diffusion coefficient, as suggested by Zwanzig (1961), gives further support to this view. (57 refs.)

112817 Optogalvanic effect study of vibrational relaxation in CO_2 laser process. F.O. Shimizu, K. Sasaki, K. Ueda (Dept. of Phys., Sophia Univ., Tokyo, Japan).

Jpn. J. Appl. Phys. Part 1 (Japan), vol.22, no.7, p.1144-51 (July 1983). The amplitude and phase retardation of the optogalvanic signal in a CO_2 - N_2 -He laser plasma irradiated by a 10.6 μm CO_2 laser were measured under various experimental conditions. It is shown that the mechanism of the optogalvanic effect is related to the vibrational relaxation processes of the laser levels. The collisional rate constant relevant to the upper laser level (001) is determined as $(2.6 \pm 0.5) \times 10^2 / \text{Torr.s}$ at 300K. Good agreement is obtained between the present value and the value previously obtained by the infrared pulse gain method. A new model for the optogalvanic effect is proposed, taking three relaxation processes into consideration. The dependence of the optogalvanic effect on the pressure and modulation frequency is calculated using this method and a reasonable set of parameters, and shows good agreement with the observations. (30 refs.)

112818 Application of scaling theory to vibrational relaxation in linear anharmonic triatomic molecules. D.C. Clary (Dept. of Chem., Univ. of Manchester Inst. of Sci. & Technol., Manchester, England), A.E. DePristo.

J. Chem. Phys. (USA), vol.79, no.5, p.2206-11 (1 Sept. 1983). The energy-corrected-sudden (ECS) scaling theory is extended to vibrational relaxation in the collisions of anharmonic linear triatomic molecules with atoms. Application is made to the collisions of He atoms with $^{12}C^{16}O_2$, $^{14}C^{16}O_2$, and $^{12}C^{18}O_2$. By combining the rate constants for the (01^0-00^0) transitions, calculated using the vibrational close-coupling rotational infinite-order-sudden (VCC-IOS) method, with the ECS scaling theory, the authors predict rate constants for the transitions (10^0-01^0) , (02^0-01^0) , and (02^0-01^0) . These agree very well with the rate constants computed directly using the VCC-IOS technique. This comparison presents a particularly severe test of the accuracy of the ECS scaling theory for anharmonic polyatomics since Fermi resonance effects are large for the 10^0 and 02^0 levels in CO_2 . (26 refs.)

112819 Temperature dependence of near-resonant vibrational energy transfer between CO_2 and deuterated methanes. C. Manzanarez, J. Carrazza (Dept. de Quimica, Univ. Simon Bolivar, Caracas, Venezuela).

J. Chem. Phys. (USA), vol.79, no.5, p.2212-20 (1 Sept. 1983). Vibrational deactivation of $CO_2(00^1)$ by CD_4 , CHD_3 , CH_2D_2 and CH_3D has been studied using the laser fluorescence method. Rates are determined as a function of temperature in the range 220-300K. The rate constants increase as the temperature decreases for all the systems studied. The deactivation of $CO_2(00^1)$ correlates linearly with the number of stretching modes between the 2109 and 2263 cm^{-1} region of CH_nD_{4-n} ($n=0-4$) molecules which, in turn, correlates with the number of deuterium atoms in the collision partner. The linear correlation occurs at all the temperatures studied. This result is interpreted as a near-resonant vibrational-rotational energy transfer process in which two vibrational quantum numbers change as the energy is shared between the collision partners. The rotational distribution of population of each CH_nD_{4-n} molecule is calculated and compared with the rotational distribution of the initially excited CO_2 molecule. Sharma-Brau probabilities are calculated and compared with experimental probabilities. These calculated probabilities include average over the distribution of velocities, impact parameter, and rotational distributions. Experimental and calculated results indicate the effect of attractive forces in the energy transfer process and the importance of the rotational transitions decreasing the ΔE released to translational motion of the collision pair. (29 refs.)

112820 Collisional coupling and relaxation of $N_2(B^3\Pi_g)$ and $N_2(W^3\Delta_u)$ vibrational levels in Ar and Ne. N. Sadeghi (Lab. de Spectrometric Phys., Univ. de Grenoble, Saint-Martin d'Heres, France), D.W. Setser.

J. Chem. Phys. (USA), vol.79, no.6, p.2710-26 (15 Sept. 1983). Laser excitation from $N_2(A^3\Sigma_u^+, v=0-6)$ in Ne and Ar carrier gas in a flowing afterglow apparatus has been used to prepare $N_2(B^3\Pi_g)$ molecules in individual levels from $v=3-10$. The subsequent $N_2(B-A)$ fluorescence intensity was observed to study the coupling and relaxation kinetics of $N_2(B^3\Pi_g, v=2-10)$. The decay curves from each level show double (or higher) exponential relaxation. The first component is assigned as primarily the rapid coupling of the $N_2(B^3\Pi_g, v)$ and $N_2(W^3\Delta_u, v$ or $v+1)$ levels, however, the $N_2(B^3\Sigma_u^-, v-4)$ levels also may be involved for $N_2(B, v \geq 5)$. The slowest decay component represents the subsequent relaxation of the coupled levels. The combination of the two steps is equivalent to apparent stepwise vibrational relaxation of $N_2(B^3\Pi_g, v)$, such relaxation occurs even at low Ar pressures because of the large rate constants and long radiative lifetimes of $N_2(B)$ and $N_2(W)$. The coupling pattern between $N_2(B)$ and $N_2(W)$ is analyzed, and rate constants are assigned to elementary steps in the relaxation sequence and the scheme is evaluated. From the analysis of the slow decay components in argon, estimates (20-90 μs) are obtained for the radiative lifetimes for the reservoir levels, which are assigned as $N_2(W^3\Delta_u, v)$ for $N_2(B, v \leq 4)$ and $N_2(W^3\Delta_u, v$ or $v+1)$ levels plus $N_2(B^3\Sigma_u^-, v-4)$ levels, for some cases, for $N_2(B, v \geq 5)$. (28 refs.)

112821 Vibrational relaxation and vibrational predissociation in DCI gas.

J. Chesnoy (Lab. d'Optique Quantique, Ecole Polytech., Palaiseau, France).

J. Chem. Phys. (USA), vol.79, no.6, p.2793-8 (15 Sept. 1983). The vibrational relaxation lifetime of compressed deuterium chloride is measured at room temperature as a function of density using time resolved laser induced fluorescence. The results, showing a deviation from the simple gas behavior, are interpreted as giving evidence of the role played by vibrational predissociation of dimers in vibrational relaxation, according to recent theories of vibrational predissociation. The lifetime measurement of low density deuterium chloride, obtained between -95 and $+55^\circ C$ is first described and the results are quantitatively interpreted and compared to HCl gas. (32 refs.)

112822 Translational temperature dependence of mode-to-mode vibrational energy flow in $^{13}B_{30}$ naphthalene induced by low energy collisions with Ar. D.B. Moss, S.H. Kable, A.E.W. Knight (School of Sci., Griffith Univ., Brisbane, Queensland, Australia).

J. Chem. Phys. (USA), vol.79, no.6, p.2869-80 (15 Sept. 1983). Mode-to-mode vibrational energy flow from the $8^1(b_{1g})$ level in the $^{13}B_{30}$ state of naphthalene ($C_{10}H_8$) has been mapped in the energy regime $\epsilon_{vib} \leq 800$ cm^{-1} . Vibrational state changes are induced by low energy collisions with the carrier gas Ar in the warm to cool regions of a supersonic expansion. The pattern of energy transfer is estimated from time-resolved dispersed fluorescence spectra obtained following laser excitation of the absorption transition 8_0^1 . Propensities for particular transfer channels are found to be in qualitative accord with expectations based on studies of single-ring aromatics such as benzene and aniline. One-quantum changes are preferred over two-quantum changes and an energy gap law is evident. The competition between certain vibrational energy transfer channels is examined as a function of the translational temperature T_{trans} at specific distances X/D from the nozzle aperture. At $X/D \leq 1.5$, evidence is found for both endoergic and exoergic transfer channels. T_{trans} at $X/D = 1.5$ is determined from the authors' data to be 80 ± 10 K. It is established that the collision energy here is sufficient to support vibrational relaxation out of the 8^1 level via some endoergic transfers. The most efficient endoergic channel involves the addition of a single quantum of a low frequency out-of-plane mode with $\epsilon_{vib} = 127$ cm^{-1} . At $X/D \geq 2$, endoergic channels appear to close and only exoergic transfer is observed. The dominant exoergic channel from 8^1 is found to be transfer to the $^{13}B_{30}$ zero point level, reached through the loss of the v_8 quantum ($\Delta E = 435$ cm^{-1}). The collision energies at which endoergic transfer ceases to occur are found to agree with expectations based on an assumption of Maxwell-Boltzmann statistics and the estimation of T_{trans} for particular values of X/D using their spectroscopic data. (38 refs.)

112823 Self-correlation functions of rotational and translational motion in simple fluids. O.P.Revokatov, N.V.Brilliantov (Dept. of Molecular Phys., Moscow Univ., Moscow, USSR).

Moscow Univ. Phys. Bull. (USA), vol.38, no.1, p.90-3 (1983). Translation of: *Vestn. Mosk. Univ. Ser. 3 (USSR)*, vol.38, no.1, p.76-9 (1983).

A model in which the motion of a molecule is regarded as a sequence of free paths and strong multiparticle collisions is proposed. The result of collision is characterized by conditional probability functions. The analytical expressions obtained for the self-correlation functions are in good agreement with machine experiments. (4 refs.)

112824 Vibrational relaxation of Ne_2^+ molecular ions during collisions with neon atoms. V.A.Ivanov, V.S.Sukhomlinov (A.A. Zhdanov State Univ., Leningrad, USSR).

Sov. Phys.-Tech. Phys. (USA), vol.28, no.2, p.213-14 (Feb. 1983). Translation of: *Zh. Tekh. Fiz. (USSR)*, vol.53, no.2, p.348-50 (Feb. 1983). [received: Sept. 1983]

The authors demonstrate that the vibrational relaxation rates of molecular ions can be found by analyzing the time behavior of the spectral line intensities in a decaying plasma. They studied the decay of the intensities of the 3593 Å ($3s'J[1/2]_0 - 4p'[1/2]_1$) and 5852 Å ($3s'J[1/2]_0 - 3p'[1/2]_1$) lines in a neon plasma. In the experiments the pressure ranged from 40-80 torr, the electron density was $n_e \approx 10^{10} \text{ cm}^{-3}$, the electron temperature in the afterglow was $T_e \approx 300\text{K}$, and the radius of the discharge tube was $R=2 \text{ cm}$. (8 refs.)

112825 Description of rotational energy exchange in collisions of diatomics. R.E.Mukhametzyanov.

Vestn. Leningr. Univ. Ser. Mat. Mekh. & Astron. (USSR), no.3, p.92-4 (July 1983). In Russian.

Analytical expressions for RT - and R - R -cross-sections of diatomics based on a generalized quasiclassical theory are proposed. All the considerations have been carried out for the N_2 - N_2 system. Results of calculations of rate constants and cross-sections are compared with other calculations and experimental data. (6 refs.)

Relaxation processes in polyatomic molecular vapors using infrared absorption bands See Entry 112733

Vibrational broadening in F 1s hole states and the $8a_{1g}$ valence orbital of XeF_6 : structure of XeF_6 and heats of formation of unusual cations See Entry 112786

The collision half-width for the $R(0)$ line of the ν_3 band of methane See Entry 112787

Growth and decay of acceleration waves in relaxing gases See Entry 113475

Laser flash photolysis of benzene. VIII. Formation of hot benzene from the S_2 state and its collisional deactivation See Entry 115568

34.50H Electronic excitation and ionization (inc. beam-foil excitation and ionization)

112826 Reference cross sections for K-shell ionization by light ions. H.Paul, W.Obermann (Inst. für Experimentalphys., Johannes-Kepler-Univ. Linz, Linz, Austria).

Nucl. Instrum. & Methods Phys. Res. (Netherlands), vol.214, no.1, p.15-19 (1983). (Proceedings of the International Workshop on Cross Sections for Fusion and Other Applications, College Station, TX, USA, 4-6 Nov. 1982).

Reference cross sections, i.e. accurate cross sections obtained by averaging all the relevant published data points, are useful for practical applications and for comparison with theories. It is shown how such cross sections can be calculated for one type of projectile by using the data from a large range of target atomic numbers after normalizing the data by the Brandt-Lapicki (1981) theory. For protons, an analytical curve is given that describes the empirical deviation from that theory. This deviation is found to be small except at low scaled velocities. As an example, $\sigma = (95.2 \pm 1) \text{ b}$ is suggested as reference ionization cross section for 2 MeV protons on Cu; this is compared to recent theoretical values. For heavier projectiles up to chlorine, the deviation between the Brandt-Lapicki theory and experiment is found to be slightly larger, but qualitatively similar. (13 refs.)

112827 Accurate calculation of inner-shell ionization. D.Trautmann, F.Rosel (Inst. für Phys., Univ. Basel, Basel, Switzerland), G.Baur.

Nucl. Instrum. & Methods Phys. Res. (Netherlands), vol.214, no.1, p.21-7 (1983). (Proceedings of the International Workshop on Cross Sections for Fusion and Other Applications, College Station, TX, USA, 4-6 Nov. 1982).

Inner-shell ionization is formulated in the semiclassical approximation, starting from a fully quantal approach. Classical trajectories in a screened Coulomb potential are used and the electron in the initial and final states are described by relativistic Hartree-Fock-Slater wave functions. Binding energy corrections due to the projectile field are applied. The agreement of the theoretical calculations with the rather detailed experiments (total cross sections, electron spectra, alignment) is generally very good. (22 refs.)

112828 The binding effect in alpha- and deuteron-induced L-shell X-ray production in the $Z=32$ -47 region. A.P.Jesus (Centro de Física Nuclear, Univ. de Lisboa, Lisboa, Portugal), I.R.Pimental, J.S.Lopes.

Nucl. Instrum. & Methods Phys. Res. (Netherlands), vol.214, no.1, p.29-34 (1983). (Proceedings of the International Workshop on Cross Sections for Fusion and Other Applications, College Station, TX, USA, 4-6 Nov. 1982).

Experimental alpha- and deuteron-induced total L-shell X-ray production cross section ratios, $R = \sigma_{\alpha}/\sigma_{d\alpha}$, in the incident energy range 0.20 to 0.45 MeV/u are presented for elements Ge, Br, Zr, Mo and Ag; absolute cross section values are presented for Zr, Mo and Ag. The experimental ratios are always larger than the theoretical ones; further, the ratios of the higher-Z elements are quite independent of the reduced velocity. This is analogous to the situation found in the K-shell for elements ranging from Ca to Cu in a similar projectile reduced velocity range. The experimental absolute deuteron cross section values are lower than the theoretical ones by 10-30%; there is agreement with theory within the estimated errors. The alpha results show that, in the present incident energy range, the theoretical values decrease faster with energy decrease than the experimental ones. (18 refs.)

112829 Optimized basis states for inner-shell ionization. D.J.Land, D.G.Simons, M.D.Brown (Naval Surface Weapons Center, Silver Spring, MD, USA).

Nucl. Instrum. & Methods Phys. Res. (Netherlands), vol.214, no.1, p.35-41 (1983). (Proceedings of the International Workshop on Cross Sections for Fusion and Other Applications, College Station, TX, USA, 4-6 Nov. 1982).

A theoretical study is described in which the region of validity of perturbed-stationary-state theory, the application of the adiabatic limit in the semiclassical approximation, is investigated for inner-shell ionization processes. The authors' particular interest is the proton-induced ionization probability of the K-shell. Time-dependent, perturbed basis states are constructed by means of a variational principle which minimizes the strength of excitation for an individual state as a function of projectile velocity. By using copper as a target,

they estimate that the adiabatic limit is appropriate for values of ξ , the ratio of the K-shell adiabatic radius to the K-shell radius itself, less than 0.8 to 1.0. Comparisons of calculations performed using perturbed-stationary-state theory are made with recent experimental data for the proton-induced total K-shell ionization cross section at energies between 0.5 and 2.4 MeV in targets from Sc ($Z=21$) to Zn ($Z=30$). Overall the agreement is quite good. However, a systematic trend for perturbed-stationary-state theory to overpredict the experimental values at the lower values of ξ is found. (14 refs.)

112830 L-shell Coulomb ionization. L.Sarkadi (Inst. of Nuclear Res., Hungarian Acad. of Sci., Debrecen, Hungary).

Nucl. Instrum. & Methods Phys. Res. (Netherlands), vol.214, no.1, p.43-8 (1983). (Proceedings of the International Workshop on Cross Sections for Fusion and Other Applications, College Station, TX, USA, 4-6 Nov. 1982).

A brief review of the most important features of the L-shell ionization of atoms by charged particle impact is given. It is shown that the direct Coulomb theories successfully describe the ionization processes as long as the perturbing effect of the projectile is small. For stronger perturbations induced by low velocity heavy ions, however, serious disagreement has been observed between the experimental cross section data and the theoretical predictions which indicates the failure of the hypothesis of the independent ionization of the individual atomic L sublevels. (15 refs.)

112831 Theory of L-shell ion-impact ionization: inclusive cross sections and multiple-vacancy (K-satellite) distributions. R.L.Becker (Oak Ridge Nat. Lab., Oak Ridge, TN, USA), A.L.Ford, J.F.Reading.

Nucl. Instrum. & Methods Phys. Res. (Netherlands), vol.214, no.1, p.49-55 (1983). (Proceedings of the International Workshop on Cross Sections for Fusion and Other Applications, College Station, TX, USA, 4-6 Nov. 1982).

The authors' recent contributions to the theory of collisions of ions with target L-shell electrons are reviewed. They consider in particular KL' and KL'' multiple vacancy distributions. They have generalized from the traditional single-particle model to the independent Fermi particle model, thereby providing the first quantal derivation of the nearly binomial distribution which characterizes the K satellites and hypersatellites. The hole-hole Pauli correlation terms tend to average out because of 'random' phases, leaving a nearly classical distribution. Coupled-channels calculations of the mean L-shell vacancy probability per electron, \bar{p}_L , are described. The inclusion of shakeoff contributions to \bar{p}_L , particularly important for hypersatellites, is outlined. New questions raised by the present work are discussed. (17 refs.)

112832 Direct ionization and capture in inner-shell processes. F.D.McDaniel (Dept. of Phys., North Texas State Univ., Denton, TX, USA).

Nucl. Instrum. & Methods Phys. Res. (Netherlands), vol.214, no.1, p.57-63 (1983). (Proceedings of the International Workshop on Cross Sections for Fusion and Other Applications, College Station, TX, USA, 4-6 Nov. 1982).

Direct ionization (DI) and electron capture (EC) contributions have been inferred from target X-ray cross sections. Measurements have been made for the K-, L-, and M-shells for a range of selected projectile-target systems and ion-target electron velocity ratios. The inferred DI and EC results have been compared to Coulomb ionization theories consisting of the first Born and the perturbed stationary state (PSS) approaches. The comparison provides evidence of the validity of the PSS theory for the range of projectile-target systems and velocity ratios studied. (30 refs.)

112833 Probabilities for K-shell ionization and capture by light ions: scaling properties. E.Horsdal-Pedersen (Inst. of Phys., Univ. of Aarhus, Aarhus, Denmark).

Nucl. Instrum. & Methods Phys. Res. (Netherlands), vol.214, no.1, p.65-71 (1983). (Proceedings of the International Workshop on Cross Sections for Fusion and Other Applications, College Station, TX, USA, 4-6 Nov. 1982).

Theoretical approximate scaling relations for the probability of K-shell ionization and K-shell capture in collisions between moderately heavy target atoms (C, Ne and Ar) and light bare ions (H^+ , He^{2+} and Li^{3+}) have been tested experimentally. The scaling with respect to the projectile charge was studied only at one intermediate scaled velocity whereas the scaling with respect to the target atomic number has been tested at several intermediate or high velocities. The scaling laws are obeyed fairly well by the present set of experimental data. (18 refs.)

112834 Screening effects for excitation probabilities in ion-atom collisions. T.L.McAbee (Univ. of North Carolina, Chapel Hill, NC, USA).

Nucl. Instrum. & Methods Phys. Res. (Netherlands), vol.214, no.1, p.89-92 (1983). (Proceedings of the International Workshop on Cross Sections for Fusion and Other Applications, College Station, TX, USA, 4-6 Nov. 1982).

Transition probabilities for 1s-2s, 1s-2p and 2s-2p excitations due to the Coulomb interaction of a structureless projectile with a target atom or ion are derived in the first-order semi-classical approximation. Screened hydrogenic wave functions are used for the target electron, with the screening parameters determined through a self-consistent minimization of the total binding energy of the target atom. A straight line trajectory is assumed for the projectile. Analytic expressions are derived for the transition probabilities and compared with previous work by other authors. (6 refs.)

112835 Angular scattering in ion-atom collisions at intermediate energies. R.E.Olson (Phys. Dept., Univ. of Missouri-Rolla, Rolla, MO, USA).

Nucl. Instrum. & Methods Phys. Res. (Netherlands), vol.214, no.1, p.103-7 (1983). (Proceedings of the International Workshop on Cross Sections for Fusion and Other Applications, College Station, TX, USA, 4-6 Nov. 1982).

The classical trajectory Monte Carlo method has been used to calculate $\text{H}^+ + \text{H}(1s)$ electron capture and ionization differential cross sections at energies of 25-200 keV. Angular scattering of the electron removed by the ionization process has been studied as a function of ejected electron velocity v_e . The classical calculations are in reasonable agreement with coupled-channel results for the 'electron capture to the continuum' (ECC) component of the ionization process where this term is defined as the ejected electron being more closely centered to the projectile than the target nucleus after the collision. The ECC cross section σ_{ECC} was studied as a function of collision energy (50-500 keV/amu) and projectile charge state ($q=1$ to 10). At high energies, σ_{ECC} scaled as $q^{2.3}/E^{2.5}$. The maximum value for σ_{ECC} was found at an energy $E_{\text{max}} \approx (56 \text{ keV/amu})q^{0.4}$. (17 refs.)

112836 Collisions involving hydrogen atoms. H.B.Gilbody (Dept. of Pure & Appl. Phys., Queen's Univ. of Belfast, Belfast, N Ireland).

Nucl. Instrum. & Methods Phys. Res. (Netherlands), vol.214, no.1, p.109-15 (1983). (Proceedings of the International Workshop on Cross Sections for Fusion and Other Applications, College Station, TX, USA, 4-6 Nov. 1982).

Experimental data on charge transfer and ionization obtained in this laboratory for collisions involving multiply charged ions are discussed and considered in relation to current theoretical models. (37 refs.)

12837 Spectra of np -1s transitions excited during the passage of 48 MeV lg ions through thin and thick carbon targets. R.J.Maurer, R.L.Watson, J.Pedrazzini (Dept. of Chem., Texas A&M Univ., College Station, TX, USA).

Nucl. Instrum. & Methods Phys. Res. (Netherlands), vol.214, no.1, p.117-22 (1983). (Proceedings of the International Workshop on Cross Sections for Fusion and Other Applications, College Station, TX, USA, 4-6 Nov. 1982). The spectra of Mg K X-rays produced during the passage of 48 MeV Mg ions through $8 \mu g/cm^2$, $800 \mu g/cm^2$, and thick carbon targets were measured using a curved crystal spectrometer. Transitions of the type np -1s in Li-, He-, and H-like Mg ions were identified for $n=1$ to 6. Detailed analyses of the peaks arising from the initial state configurations 1s2p, 2p, and 1s3p were performed to determine the energies and relative intensities of associated satellite components. (21 refs.)

12838 Excitation of hydrogen atom to the $n=2$ state by helium-ion impact. S.Datta, K.Roy, S.C.Mukherjee (Dept. of Theoretical Phys., Indian Assoc. for the Cultivation of Sci., Calcutta, India).

Indian J. Pure & Appl. Phys., vol.21, no.7, p.401-3 (July 1983). The two-state distortion approximation in the impact parameter formulation is employed to calculate the cross-sections for $He^+(1s)+H(1s)\rightarrow He^+(1s)+H(n=2)$ collision process for the incident energy ranging from 16 to 2500 keV. The present results are in reasonably good agreement with those of the existing four-state calculation and the experimental findings. (10 refs.)

12839 Study of electron distributions of molecular orbitals by Penning ionization electron spectroscopy. K.Ohno, H.Mutoh, Y.Harada (Dept. of Chem., Univ. of Tokyo, Tokyo, Japan).

J. Am. Chem. Soc. (USA), vol.105, no.14, p.4555-61 (13 July 1983). Penning ionization electron spectroscopy (PIES) has been used to study spatial electron distributions of individual molecular orbitals. On the basis of comparison of observed band intensities with electron densities of ab initio molecular orbitals, a simple principle for orbital activities in Penning ionization has been established; the outer orbital which is exposed outside the van der Waals surface is active and the inner orbital which is localized inside the van der Waals surface is inactive. Penning ionization can be considered as an electrophilic reaction of rare gas atoms in metastable states with sample molecules. It is concluded that PIES is a sensitive method for probing orbital electron densities at the very frontier of the molecule where the molecule is attacked by the reagent. (39 refs.)

12840 On the origin of the dynamical differences between the Tang and Dalgarno-Henry-Roberts potentials for rigid rotor H_2 -H collisions. S.Margolis, B.A.Garetz (Dept. of Chem., Polytech. Inst. of New York, New York, NY, USA), N.Sathyamurthy.

J. Chem. Phys. (USA), vol.79, no.6, p.2736-41 (15 Sept. 1983). The authors compare their quasiclassical trajectory results for the $J=0\rightarrow 2$ rotational excitation in rigid rotor H_2 -H collisions with the close-coupling results of Choi and Tang (1975) on two different potentials. The authors trace the dynamical differences between the two potentials to the differences in the ellipticity of the repulsive potential-energy contours. They also discuss the application of their results to rotational excitation on the most accurate Siegbahn-Liu-Truhlar-Horowitz surface for the collision. (14 refs.)

12841 Collisional ionization as a nonlocalized process and the breakdown of the Franck-Condon approximation. K.-S.Lam, T.F.George (Dept. of Chem., Univ. of Rochester, Rochester, NY, USA).

J. Phys. Chem. (USA), vol.87, no.15, p.2799-803 (21 July 1983). It is demonstrated by a model computation based on a semiclassical theory that in collisional ionization the Franck-Condon approximation, equivalent to the assumption that the ionization event takes place locally, does not always apply. (13 refs.)

12842 Electronic excitation in alkali-rare-gas collisions. P.Andresen, R.Duren, H.Joswig (Max-Planck-Inst. fur Stromungsforschung, Gottingen, Germany).

J. Phys. B (GB), vol.16, no.18, p.3423-42 (28 Sept. 1983). The electronic excitation in collisions of potassium with rare gases (Ne, Kr and Xe) has been studied by measuring the dispersed fluorescence between 1300 and 9000 Å and the energy dependence of the fluorescence for some of the excited states. From these measurements for several collision energies the calibrated spectra, and the absolute emission cross sections for the K(4p) excitation and the Xe(6s) excitation have been deduced. A new theoretical model based on the interaction of the valence electron with the rare-gas atom is described. The properties of this interaction are found to be responsible for the qualitative features and with reasonable accuracy for the quantitative behaviour of the cross sections measured in collisional excitation experiments. (25 refs.)

Proceedings of the International Workshop on Cross Sections for Fusion and Other Applications See Entry 112198

Roles of the Rydberg transitions in fast excitation transfer studied in cyclohexane and n -heptane using synchrotron radiation See Entry 112777

Near-thermal multi-charged ion interactions with hydrogen .. See Entry 112844

Measurements of charge change in atomic collisions at MeV energies See Entry 112845

Additivity failure in charge transfer from molecules to bound and continuum states of $\sim MeV/uH^+$, He^{+2+} projectiles See Entry 112846

A simple classical model for the impact parameter dependence of electron capture See Entry 112847

Treatment of long-range couplings in collisional charge transfer from H(1s) to fully-stripped ions See Entry 112848

Status of the US effort in atomic physics research relevant to the magnetically confined fusion program See Entry 113639

34.50L Chemical reactions, energy disposal, and angular distribution, as studied by atomic and molecular beams

(see also 31.70F and 82.20K Potential-energy surfaces, 82.40D Beam reactions)

112843 Collisions of hydrogen ions in a focused hollow beam. V.A.Belyaev, M.M.Dubrov, A.N.Khlopkin (I.V. Kurchatov Inst. of Atomic Energy, Moscow, USSR).

Sov. Tech. Phys. Lett. (USA), vol.8, no.11, p.601-2 (Nov. 1982). Translation of: *Pis'ma v Zh. Tekh. Fiz. (USSR)*, vol.8, no.21-22, p.1399-401 (Nov. 1982). [received: Sept. 1983]

The dissociation of molecular hydrogen ions in collision with each of ($H_2^+ + H_2^+$), has recently attracted interest in connection with research on controlled fusion. For an experimental study of the collisions of two ions at

low energies, the method of overtaking coincident beams would be quite useful. This method can be used to study ion-ion collisions at low energies, where experiments by other methods are extremely difficult (and have not been carried out). (5 refs.)

34.70 CHARGE TRANSFER

(see also 82.30 Charge transfer reactions)

112844 Near-thermal multi-charged ion interactions with hydrogen. D.A.Church (Phys. Dept., Texas A&M Univ., College Station, TX, USA).

Nucl. Instrum. & Methods Phys. Res. (Netherlands), vol.214, no.1, p.9-13 (1983). (Proceedings of the International Workshop on Cross Sections for Fusion and Other Applications, College Station, TX, USA, 4-6 Nov. 1982). Extensions of a method are discussed for studying charge transfer from hydrogen atoms to multi-charged ions stored at energies near 1 eV in a Penning ion trap. These extensions include spin-dependent charge transfer, electron spin-exchange between polarized hydrogen atoms and multi-charged ions, and laser excitation of the 2^3S-2^3P transitions of low Z helium-like ions for the purpose of ion detection. (24 refs.)

112845 Measurements of charge change in atomic collisions at MeV energies. B.M.Johnson (Brookhaven Nat. Lab., Upton, NY, USA).

Nucl. Instrum. & Methods Phys. Res. (Netherlands), vol.214, no.1, p.73-9 (1983). (Proceedings of the International Workshop on Cross Sections for Fusion and Other Applications, College Station, TX, USA, 4-6 Nov. 1982). Studies of the capture and loss of electrons to and from a fast moving ion as it interacts with atoms or electrons can reveal aspects of atomic-collision phenomena which have important implications for controlled fusion research. Several examples and the fusion relevance of such charge-change measurements for negative and high stripped positive ions at MeV energies are discussed. (28 refs.)

112846 Additivity failure in charge transfer from molecules to bound and continuum states of $\sim MeV/uH^+$, He^{+2+} projectiles. G.Bissinger (East Carolina Univ., Greenville, NC, USA).

Nucl. Instrum. & Methods Phys. Res. (Netherlands), vol.214, no.1, p.81-7 (1983). (Proceedings of the International Workshop on Cross Sections for Fusion and Other Applications, College Station, TX, USA, 4-6 Nov. 1982). Additivity of 'atomic' cross sections has been observed to fail in electron capture from hydrocarbon molecules to bound and continuum states of 0.6-3.2 MeV H^+ , He^{+2+} projectiles. This failure has been attributed to, and interpreted as, intramolecular secondary collisions that 'outscatter' the electrons from their original projectile-centered states. Estimates of the magnitude of this 'outscattering' effect from capture-loss calculations or a geometrical scattering model agree quite well with experimental results. These calculations have been used to estimate 'atomic' capture cross sections for the oxides and fluorides of C. In the case of bound state capture, these loss processes inject electrons into the continuum; evidence is presented for the observation of these electrons in the continuum cusp, but only in the case of the larger hydrocarbon molecules. (16 refs.)

112847 A simple classical model for the impact parameter dependence of electron capture. D.Brandt (Dept. of Phys. & Astron., Univ. of North Carolina, Chapel Hill, NC, USA).

Nucl. Instrum. & Methods Phys. Res. (Netherlands), vol.214, no.1, p.93-6 (1983). (Proceedings of the International Workshop on Cross Sections for Fusion and Other Applications, College Station, TX, USA, 4-6 Nov. 1982). A simple expression for the one electron capture probability in collisions of intermediate velocity, highly charged ions with atoms been derived in accordance with the Bohr-Lindhard capture model. Calculated total cross sections for capture from a helium target agree well with experimental data. The model has been applied to estimate nonresonant capture and excitation in $S^{13+} + He$ collisions. (13 refs.)

112848 Treatment of long-range couplings in collisional charge transfer from H(1s) to fully-stripped ions. W.R.Thorson (Dept. of Chem., Univ. of Alberta, Edmonton, Canada).

Nucl. Instrum. & Methods Phys. Res. (Netherlands), vol.214, no.1, p.97-101 (1983). (Proceedings of the International Workshop on Cross Sections for Fusion and Other Applications, College Station, TX, USA, 4-6 Nov. 1982). Electron transfer from H(1s) to a fully-stripped ion of charge $+Z_A$ occurs dominantly to excited levels (nSZ_A), for low to intermediate collision energies ($E \leq 20$ keV/amu). To compute cross sections for capture into individual states (e.g. for predicting radiative emission in a plasma) it is necessary not only to solve the molecular-state close-coupling problem entailed in the primary charge-transfer event, but also to treat the effects of long-range dipole and quadrupole couplings produced by the receding proton among the n^2 quasi-degenerate levels with a given principal quantum number n . A simple, computationally efficient solution to the long-range coupling problem can be given, based on an application of the exact solution for the dipole coupling problem given previously by Demkov et al. (1974). If the quadrupole couplings are treated by the first Magnus approximation, the entire long-range coupling problem is reduced to calculation of the $n \times n$ matrix representation of a finite rotation for angular momentum $j=1/2(n-1)$, and the evaluation of simple numerical quadratures. (13 refs.)

112849 Theory of electron transfer in polar solvents. L.D.Zusman (Inst. of Inorganic Chem., Acad. of Sci., Novosibirsk, USSR).

Theor. & Exp. Chem. (USA), vol.18, no.6, p.611-20 (Nov.-Dec. 1982). Translation of: *Teor. & Eksp. Khim. (USSR)*, vol.18, no.6, p.665-75 (Nov.-Dec. 1982). [received: Sept. 1983]

Electron-transfer reactions represent one of the most important classes of reactions occurring in polar solvents. The rate constant of such a reaction is dependent on how close the reactants come together and what are the interactions of the reactants with one another and with the polar solvent, and also on how fast the reactants pass through the reaction zone. The sphere model is familiar in formal chemical kinetics in describing reactions. In this model, the rate constant is specified at the boundary of the reaction zone, which is taken as independent of the diffusion coefficient. That value is considered as the phenomenological parameter of the model. Logical calculation on the rate constant should first provide a basis for the model from the microscopic theory of the elementary act; it is then possible to relate the phenomenological parameter to the probability of electron transfer in unit time $W_{12}(r)$, which is dependent on the distance between the reactants. Second, such a calculation indicates the applicability of the sphere model and gives a solution outside the limits of applicability. The author considers the construction of this theory in the approximation of pair encounters between reactants. (14 refs.)

Proceedings of the International Workshop on Cross Sections for Fusion and Other Applications See Entry 112198

Dynamical study of twisted intramolecular charge transfer in p -dimethylaminobenzonitrile solutions See Entry 112770

- Direct ionization and capture in inner-shell processes See Entry 112832
- Probabilities for K-shell ionization and capture by light ions: scaling properties See Entry 112833
- Angular scattering in ion-atom collisions at intermediate energies See Entry 112835
- Collisions involving hydrogen atoms See Entry 112836
- Status of the US effort in atomic physics research relevant to the magnetically confined fusion program See Entry 113639

34.80 ELECTRON SCATTERING

112850 Nonlinear absorption of electromagnetic radiation during collisions of particles in a strong magnetic field. S.A.Uryupin (V.I. Lenin All-Union Electrotech. Inst., Moscow, USSR). *Sov. Phys.-Tech. Phys. (USA)*, vol.28, no.2, p.131-6 (Feb. 1983). Translation of: *Zh. Tekh. Fiz. (USSR)*, vol.53, no.2, p.209-18 (Feb. 1983). [received: Sept. 1983]

The energy evolved per second per unit volume resulting from electron collisions in an intense RF electromagnetic field and in a strong magnetic field is calculated. It is shown that in the absence of a magnetic field, the effective electron-atom collision frequency ν_{e-n} determining the rate of absorption is directly proportional to the intensity of the varying electric field. An investigation of the effects of an external magnetic field on ν_{e-n} revealed that a nonquantizing magnetic field reduces the absorption of high-power radiation if the electron gyration frequency Ω is greater than the frequency of the absorbed radiation ω . If on the other hand $\omega \gg \Omega$, an external magnetic field has no effect on the electron-atom collision frequency. New nonlinear features of the collisional absorption of radiation are also discovered for quantizing magnetic fields when electron transitions to the zeroth Landau level are the main factor determining the absorption coefficient. It is found that ν_{e-n} is decreased in a quantizing magnetic field or in an intense RF field. Numerical estimates indicate that many of these effects should be experimentally observable. (26 refs.)

34.80B Elastic scattering of electrons by atoms and molecules

112851 Elastic scattering of electrons by hydrogen atoms in a laser field. M.A.Prasad (Div. of Radiological Protection, Bhabha Atomic Res. Center, Bombay, India), K.Unnikrishnan. *J. Phys. B (GB)*, vol.16, no.18, p.3443-51 (28 Sept. 1983). Cross sections for the elastic scattering of electrons by hydrogen atoms in a laser field have been calculated. Both direct and exchange amplitudes have been computed in the Born and Glauber approximations. The Franco-Halpern modification of the Ochkur approximation has been used to evaluate the exchange amplitudes. Differential cross sections are presented and discussed for electron energies of 100 eV and 54.4 eV, and for laser field orientations parallel and perpendicular to the direction of incidence of the electrons. (12 refs.)

112852 Measurement of differential cross sections of low-energy electrons elastically scattered by gaseous molecules. IV. Effect of intramolecular double scattering as observed in the scattering of 100 and 500 eV electrons by As_4 . H.Daimon, T.Kondow, K.Kuchitsu (Dept. of Chem., Univ. of Tokyo, Tokyo, Japan). *J. Phys. B (GB)*, vol.16, no.18, p.3453-64 (28 Sept. 1983). For pt.III see *J.Phys. Soc. Japan*, vol.52, no.1, p.84 (1983). The relative differential cross sections of electrons scattered by gaseous As_4 at 300°C were measured by a cross-beam method at incident energies of 100 and 500 eV and at scattering angles between 2 and 135°. Calculations based on the independent-atom model including intramolecular double scattering and polarisation accounted for the measured cross sections; they were used to normalise the measured relative cross sections. (26 refs.)

112853 Future prospects in the development of gaseous electron diffraction. V.P.Spiridonov (M.V. Lomonosov Moscow State Univ., Moscow, USSR). *J. Struct. Chem. (USA)*, vol.23, no.6, p.939-42 (Nov.-Dec. 1982). Translation of: *Zh. Strukt. Khim. (USSR)*, vol.23, no.6, p.138-42 (Nov.-Dec. 1982). [received: Sept. 1983]

The present review analyses unresolved problems, trends, and future prospects in the development of electron diffraction studies. (25 refs.)

112854 Anharmonic model for intensity of scattering of electrons by polyatomic molecules in the gas phase. A.G.Gershikov (Inst. of Phys. Organic Chem. & Coal Chem., Acad. of Sci., Ukrainian SSR). *J. Struct. Chem. (USA)*, vol.23, no.6, p.943-7 (Nov.-Dec. 1982). Translation of: *Zh. Strukt. Khim. (USSR)*, vol.23, no.6, p.143-7 (Nov.-Dec. 1982). [received: Sept. 1983]

Equations are obtained for the intensity of scattering of fast electrons by an ensemble of polyatomic molecules and for the radial distribution function in the anharmonic approximation for the vibrational potential function. The physical meaning of the anharmonic parameters of the intensity equation is analyzed; these quantities are calculated for linear triatomic molecules; and the results are compared with those of other approaches. (21 refs.)

High energy elastic and inelastic electron scattering by the Ne and Ar atoms: electron correlation effects See Entry 112857

34.80D Atomic excitation and ionization by electron impact

112855 Electron-ion collisions of fusion interest. D.H.Crandall (Phys. Div., Oak Ridge Nat. Lab., Oak Ridge, TN, USA). *Nucl. Instrum. & Methods Phys. Res. (Netherlands)*, vol.214, no.1, p.129-37 (1983). (Proceedings of the International Workshop on Cross Sections for Fusion and Other Applications, College Station, TX, USA, 4-6 Nov. 1982). A brief review of current activities in research on collision of electrons and multicharged ions is presented. The relative importance of intermediate excited states, i.e. recombination resonances and directly excited autoionizing levels, is greater for multicharged ions than for singly charge ions. A few examples of fusion interest are presented to illustrate the effects of intermediate states and our developing understanding of their importance in all inelastic electron-ion collisions. (34 refs.)

112856 Ionization of the hydrogen atom by electron impact using adiabatic method. P.S.Mazumdar, M.Basu, A.S.Ghosh (Dept. of Theoretical Phys., Indian Assoc. for the Cultivation of Sci., Calcutta, India). *Indian J. Phys. Part B*, vol.57B, no.3, p.215-24 (June 1983). A distorted wave method in which the incident channel wavefunction is represented by an adiabatic one, is employed to calculate the triple differential cross section of the electron-impact ionization of the hydrogen atom at the incident energies 100 and 250 eV. The effect of exchange is neglected in the present calculations. The agreement between the present result with those of experiment and the corresponding theoretical prediction of Smith et al. (1979) is fair. (6 refs.)

112857 High energy elastic and inelastic electron scattering by the Ne and Ar atoms: electron correlation effects. A.Duguet, A.Lahmam Bennani, M.Rouault (Lab. des Collisions Atomiques et Moléculaires, Univ. de Paris-Sud, Orsay, France). *J. Chem. Phys. (USA)*, vol.79, no.6, p.2786-92 (15 Sept. 1983). Elastic and inelastic differential cross sections (DCS) of high energy electrons (25 keV) scattered by neon and argon have been separately measured by totally independent methods. The effect of electronic correlations on the DCS and on the radial distribution functions $D(R)$ and $P(R)$ are deduced from experiment by comparison with theoretical Hartree-Fock values. An estimate of the correlation energy is also given. In the case of neon, the differences, with respect to Hartree-Fock, of the various contributions to atomic potential energy ΔV_{ne} , ΔV_{ee}^{Coul} , and ΔV_{ee}^{exch} are calculated from experiment and compared to theoretical results. (23 refs.)

112858 Resonances in the collision strength for electron excitation of the $1'S-2'S$ and $1'S-2^3P^0$ transitions in O VII. A.E.Kingston, S.S.Tayal (Dept. of Appl. Math. & Theoretical Phys., Queens' Univ. of Belfast, Belfast, N Ireland). *J. Phys. B (GB)*, vol.16, no.18, p.3465-78 (28 Sept. 1983). The R -matrix method is used to calculate the collision strengths for the electron excitation of the ground state of O VII to the $2'S$ and 2^3P^0 states. Results are presented for calculations in which the five lowest states (all $n=1$ and $n=2$ states) were included as target states and also for calculations in which the eleven lowest states (all $n=1$, $n=2$ and $n=3$ states) were included. The five-state calculations for the $1'S-2'S$ transition give many series of large resonances of the form $1s2ln'l'$ converging to the other $n=2$ thresholds. For the eleven-state calculations but for the eleven-state calculations there are also significant resonances of the form $1s3ln'l'$ converging to the $n=3$ thresholds. Resonance effects are quite small for the $1'S-2^3P^0$ transition. (23 refs.)

112859 Excitation of the 1P and 3P levels of a magnesium atom by electron impact. N.B.Avdonina, M.Ya.Amus'ya (Inst. of Refrigeration Technol., Leningrad, USSR). *Sov. Phys.-Tech. Phys. (USA)*, vol.28, no.2, p.209-13 (Feb. 1983). Translation of: *Zh. Tekh. Fiz. (USSR)*, vol.53, no.2, p.341-7 (Feb. 1983). [received: Sept. 1983]

Expressions for the differential and total cross sections for the $3s \rightarrow 3p$ 1P and $3s \rightarrow 3p$ 3P excitations in magnesium are derived to first order in perturbation theory using Feynman diagrams. The results are compared with experiment and with values derived in the close-coupling approximation. Good agreement with experimental cross sections is found for a wide range of scattering angles. It is concluded from the comparison with experiment that higher-order graphs must be included for small-angle scattering. (15 refs.)

Proceedings of the International Workshop on Cross Sections for Fusion and Other Applications See Entry 111298

Shape functions for atomic-field bremsstrahlung from electrons of kinetic energy 1-500 keV on selected neutral atoms $1 \leq Z \leq 92$ See Entry 111320

Electron impact excitation and UV emission in the Franck-Hertz experiment See Entry 111350

L-shell Coulomb ionization See Entry 112830

Status of the US effort in atomic physics research relevant to the magnetically confined fusion program See Entry 113639

Ca XVII line ratios in solar flares See Entry 116468

34.80G Molecular excitation, ionization, and dissociation by electron impact

112860 Cross sections for electron-carbon monoxide collisions in the range 1-4 eV. G.N.Haddad, H.B.Milloy (Electron & Ion Diffusion Unit, Res. School of Phys. Sci., Australian Nat. Univ., Canberra, Australia). *Aust. J. Phys. (Australia)*, vol.36, no.4, p.473-84 (1983). The scattering of electrons from CO molecules has been studied over the energy range from 1 to 4 eV by analysing drift velocity data for pure CO and CO-inert gas mixtures at 294K. The validity of using the so-called 'two term approximation' for the velocity distribution function in the solution of the Boltzmann equation to analyse drift velocity data for the pure gas (and thus also for the gas mixtures) has been established. The momentum transfer cross section for CO has been determined in the energy range 1-4 eV, and the measurements of the vibrational cross sections by Ehrhardt et al. (1968) have been renormalized. By using a solution of the Boltzmann equation which avoids the two term approximation, these cross sections have been shown to be consistent with previous measurements of the transport parameter D_{\perp}/u in pure CO. (22 refs.)

112861 Formation of NH ($A^3\Pi$, $c^1\Pi$) by electron-impact dissociation of HN_3 . I.Tokue, Y.Ito (Dept. of Chem., Niigata Univ., Niigata, Japan). *Chem. Phys. (Netherlands)*, vol.79, no.3, p.383-9 (15 Sept. 1983). Emission spectra of the NH ($A^3\Pi-X^2\Sigma$) and NH ($c^1\Pi-a^1\Delta$) systems were observed by electron impact on HN_3 from threshold energies up to 70 eV. A new threshold for the formation of NH(A) is found near 16 eV. The relative vibrational population, $P(\nu=1)/P(\nu=0)$, for MH(A) depends on the impact energy. The rotational energy distribution of the $\nu=0$ level of the $c^1\Pi$ state can be approximated by an effective temperature of $2000 \pm 200K$, which is independent of the impact energy. The rotational temperature of the $\nu=0$ level of the $A^3\Pi$ state is $4500 \pm 400K$ at impact energy higher than 15 eV but is lower near the onset. The observed NH rotational temperatures are compared with those predicted by a simple statistical model. (23 refs.)

112862 Angular intensity distribution of Balmer- α emission excited by electron impact on H_2 . N.Takahashi, S.Arai, N.Kouchi (Dept. of Chem., Tokyo Inst. Of Technol., Meguro-ku, Tokyo, Japan), N.Oda, Y.Hatano. *J. Phys. B (GB)*, vol.16, no.18, p.L547-52 (28 Sept. 1983). The angular distribution of Balmer- α emission excited by electron impact on H_2 has been measured and compared with the results of polarisation measurements. A new factor, r , instead of a polarisation degree, has been presented to describe the anisotropy of emission of atomic radiation following dissociative excitation of molecules. (14 refs.)

112863 Calculation of the effective rotational transition probabilities for excitation by electron impact from the ground state $N_2 X^1\Sigma_u^+$ ($v=0$, k) to the excited state $N_2^+ B^2\Sigma_u^+$ (v', k') of nitrogen. G.I.Sukhinin, R.G.Sharafutdinov (Inst. of Heat Phys., Acad. of Sci., Novosibirsk, USSR). *Sov. Phys.-Tech. Phys. (USA)*, vol.28, no.2, p.204-9 (Feb. 1983). Translation of: *Zh. Tekh. Fiz. (USSR)*, vol.53, no.2, p.333-40 (Feb. 1983). [received: Sept. 1983]

Results are reported from a calculation of the effective probabilities of electron-vibrational-rotational transitions when the state $N_2^+ B^2\Sigma_u^+$ ($v'=0$) is excited by secondary electrons produced by ionization of nitrogen by a 10 eV primary electron beam. Use is made of the fact that the relative contribution from secondary electrons to emission from the first negative system of N_2^+ increases with distance from the center of the primary beam. The adiabatic approximation is used to calculate the transition probabilities from experimental data. It is shown that for secondary electrons, the probabilities of transitions with $\Delta k=3, 4, 5, \dots$ are comparable in magnitude to the probabilities of transitions with $\Delta k=\pm 1$. (14 refs.)

Resonant electron scattering by metastable nitrogen See Entry 115559

34.90 OTHER TOPICS IN ATOMIC AND MOLECULAR COLLISION PROCESSES AND INTERACTIONS

Incoherent scattering of gamma rays by bound electrons of some intermediate Z elements See Entry 112691

Structure and dynamics of the non-rigid CONH unit in fundamental and excited states of its stretching mode. Influence of environment effects, side-chain substitutions and secondary structures See Entry 112744

35.00 PROPERTIES OF ATOMS AND MOLECULES; INSTRUMENTS AND TECHNIQUES

35.10 ATOMS

35.10B Atomic masses, mass spectra, abundances, and isotopes

(inc. isotope separation; for mass spectrometry, see also 07.75; for radioisotope separation see 28.42H or 82.55)

A threshold Cherenkov counter for isotopic identification of high-energy heavy ions See Entry 112546

On the analysis of MHD flow of a two-component gas and its application See Entry 113514

Centrifugal isotope separation in zirconium plasmas See Entry 113613

Reactions of energetic tritium atoms with ethyl fluoride over an extensive pressure range See Entry 115531

35.10D Electric and magnetic moments, polarizability

Identification of the X state in Ca and a new Rydberg series See Entry 112676

Relativistic long-range interactions between H, He and Li atoms See Entry 112810

35.10F Relativistic corrections, fine- and hyperfine-structure constants

Saturation spectroscopy of hydrogen H_α lines with a multi-mode CW dye laser See Entry 112679

Zeeman effect in the forbidden lines of antimony Sb I See Entry 112682

35.10H Ionization potentials, electron affinities

112864 Nonperturbative solutions for screened Coulomb potentials. A.P.Kajwadkar, L.K.Sharma (Dept. of Appl. Phys., Government Engng. Coll., Jabalpur, India). *Indian J. Pure & Appl. Phys.*, vol.21, no.7, p.404-7 (July 1983). Using nonperturbative solutions, the binding energies for different atoms have been evaluated for screened Coulomb potentials. The variation of the wavefunction with r has also been studied. The results obtained are in excellent agreement with earlier calculations. (19 refs.)

Density functional calculations for atoms in the first transition series See Entry 112615

Incoherent scattering of gamma rays by bound electrons of some intermediate Z elements See Entry 112691

35.10W Weak Interactions

Parity non-conservation in muonic helium atoms See Entry 112885

35.20 MOLECULES

(see also 61.55, 61.60, and 61.65 Specific structures of metals and alloys, of other inorganic materials, and of organic materials, respectively)

35.20B General molecular conformation and symmetry; stereochemistry

112865 Three-dimensional structure of the methyl ester of N-(1-carbomethoxy-2-phenylethyl)azyl-phenylalanine, $C_{23}H_{26}N_2O_5$. A.F.Mishnev, Ya.Ya.Bleidelis, A.V.Eremeev, F.D.Polyak, B.S.Kataev (Inst. of Organic Synthesis, Acad. of Sci., Latvian SSR). *J. Struct. Chem. (USA)*, vol.23, no.6, p.984-8 (Nov.-Dec. 1982). Translation of: *Zh. Strukt. Khim. (USSR)*, vol.23, no.6, p.86-90 (Nov.-Dec. 1982). [received: Sept. 1983]

The molecular and crystal structure was found for the methyl ester of N-(1-carbomethoxy-2-phenylethyl)-azyl-phenylalanine by the direct method and anisotropic refinement: All the hydrogen atoms were located. $R=0.056$. The azyl-phenylalanine dipeptide fragment showed shortening of the C=O bond (1.21 Å) and extension of the C-N bond (1.35 Å) relative to standard values. The substituents on the aziridine ring have trans orientation. The L-configuration of the azyl-phenyl residue was established using the known absolute configuration of the phenylalanine residues. Circular dichroism indicated L-configuration of the phenylalanine fragments of this molecule in solution. (29 refs.)

112866 Molecular structure from the viewpoint of the experimenter—the evolution of the concept and the problems arising. N.G.Rambidi (All-Union Sci.-Res. Center for the Study of Surface & Vacuum Properties, USSR). *J. Struct. Chem. (USA)*, vol.23, no.6, p.918-35 (Nov.-Dec. 1982). Translation of: *Zh. Strukt. Khim. (USSR)*, vol.23, no.6, p.113-33 (Nov.-Dec. 1982). [received: Sept. 1983]

The problems and achievements in the study of the structure of molecules have been reviewed. Present-day ideas on the actual concept of the 'structure of a molecule' have been examined. Molecular structure has been defined as the set of functional characteristics and constants describing the relative positions and the relative motion of the electrons and nuclei in a molecule. The relationship between the molecular constants and models of the molecular structure has been examined, and the geometric structure and electronic structure of many interesting molecules have been analyzed. Considerable attention has been paid to the examination of 'nonrigid molecules'. (42 refs.)

112867 Standard reference data on the structure of inorganic molecules in the gaseous phase. S.M.Tolmachev (All-Union Sci.-Res. Center for the Study of Surface & Vacuum Properties, USSR). *J. Struct. Chem. (USA)*, vol.23, no.6, p.936-8 (Nov.-Dec. 1982). Translation of: *Zh. Strukt. Khim. (USSR)*, vol.23, no.6, p.134-7 (Nov.-Dec. 1982). [received: Sept. 1983]

The basic principles of the preparation of tables of standard reference data on the structure of molecules, and the information content of tables of internuclear distances in diatomic molecules and of structures of tri- and tetraatomic molecules have been examined. (8 refs.)

112868 Molecular and crystal structure of 2,2',4,4'-tetraaminodiphenyl at -120°C . G.V.Gridunova, V.E.Shklover, Yu.T.Struchkov, B.A.Chayanov (Sci.-Res. Inst. of Organic Intermediate Products & Dyes, Acad. of Sci., USSR). *Sov. Phys.-Crystallogr. (USA)*, vol.28, no.2, p.166-9 (March-April 1983). Translation of: *Kristallografiya (USSR)*, vol.28, no.2, p.286-90 (March-April 1983). [received: Sept. 1983]

An X-ray structural investigation of 2,2',4,4'-tetraaminodiphenyl (TADP) is made at -120°C . The angle of rotation of the Ph rings is 72° , and the conformation of the molecule is closer to the syn than the anti form. The packing of molecules in the crystal is governed by a branched system of intermolecular hydrogen bonds N-H...N. (23 refs.)

112869 Conformation of the four independent molecules in the structure of cyclo[-L-Val-L-Hyi-] and symmetry relations between them. N.E.Zhukhlis-tova, G.N.Tishchenko (Inst. of Crystallography, Acad. of Sci., USSR). *Sov. Phys.-Crystallogr. (USA)*, vol.28, no.2, p.177-8 (March-April 1983). Translation of: *Kristallografiya (USSR)*, vol.28, no.2, p.303-5 (March-April 1983). [received: Sept. 1983]

The authors give the results of a quantitative comparison of the geometries of the four independent molecules in cyclo[-L-Val-L-Hyi-]. The conformation of one molecule differs from that of the other three, which closely resemble one another. The 'odd-man-out' molecule forms the greatest number of relatively short contacts with the other molecules. The loosest binding is observed in the peripheral C γ atoms, and the values of S—the criterion of geometrical likeness of the molecules—enable them to regard the molecules as identical or alike; the crystal structure is therefore considered from the viewpoint of the phenomenon of supersymmetry, and a system of local closed supersymmetry elements is found. (5 refs.)

112870 Effect of nonvalence interactions on the orientation of the phenyl ring at the tricoordinated phosphorus atom. O.A.Raevskii, I.O.Umarova, E.N.Tsvetkov (Inst. of Physiologically Active Substances, Acad. of Sci., Moscow, USSR). *Theor. & Exp. Chem. (USA)*, vol.18, no.6, p.643-8 (Nov.-Dec. 1982). Translation of: *Teor. & Eksp. Khim. (USSR)*, vol.18, no.6, p.700-4 (Nov.-Dec. 1982). [received: Sept. 1983]

The authors have carried out a theoretical conformational analysis of derivatives of phenyl phosphine in the atom-atom approximation with the aim of studying the nonvalence interactions on the orientation of the phenyl ring attached to a tricoordinated phosphorus atom. Compounds of the general formula R_2PPh , where $R=H, F, Cl, Br, I, CH_3, C_2H_5, i-C_3H_7, t-C_4H_9$, as well as unsymmetric derivatives of the type $CH_3R(P)Ph$, where $R=H, F, Cl, Br, I$, were considered. (23 refs.)

Symmetries and Properties of Non-Rigid Molecules. A Comprehensive Survey. Proceedings of an International Symposium See Entry 111310

Site symmetry, interchange symmetry, and projection operators in non-rigid symmetry groups See Entry 111395

Classical molecular structure and the puzzle of 'classical limit' in quantum theory See Entry 112619

A molecular vision of the world See Entry 112620

Moving and fixed reference frames for symmetry operations See Entry 112621

Classification of mobile molecules by category theory See Entry 112622

From mobile molecules to their symmetry groups: a computer-implemented method See Entry 112623

- The semi-direct product structure of nonrigid molecule groups See Entry 112624
- The use of induced representations in nonrigid molecules See Entry 112625
- Symmetry analysis and conformational dependence of molecular properties in non-rigid systems See Entry 112627
- The properties of ferrocenyl-stabilised carbocations See Entry 112630
- A theoretical study of the properties of BH_3NH_3 See Entry 112635
- Structure of protonated forms of coumarin and its hydroxy derivatives See Entry 112641
- Energetics and structure of the hydrated gaseous halide anions See Entry 112644
- Computer generation of the symmetry elements of nonrigid molecules See Entry 112646
- Intramolecular interaction effects and the structure of N_2OS and N_2O_2 : an ab initio study See Entry 112648
- Three-electron bonds. III. Phosphorus and chlorine σ^* radical cations See Entry 112649
- 'Frozen' transition states: pentavalent carbon et al See Entry 112650
- X α calculations of the EPR parameters of pseudotetrahedral copper(II) complexes See Entry 112652
- Electronic structure and absorption spectra of phenol and the corresponding phenoxyl radical and the cation and anion See Entry 112656
- Molecular mechanics studies of enthalpies of formation and strain energies of azoxyalkanes See Entry 112657
- A comparative study of the molecules Cu_2 and Ag_2 by all electron ab initio HF-CI methods See Entry 112664
- Isometric groups and hyperfine structure of nonrigid molecules See Entry 112673
- Vibrational frequencies from anharmonic ab initio/empirical potential energy functions: stretching vibrations of hydroisocyanic acid, phosphathyne, isocyanacetylene, and phosphabutadiene See Entry 112705
- Vibrational spectra and structure of triazaphosphorines See Entry 112714
- Microwave spectra of cyclohexyl bromide and cyclohexyl iodide See Entry 112717
- Symmetry and microwave spectrum of nitromethane See Entry 112719
- Relation between the orientation of OH groups in stereoisomers of derivatives of 3,4-dioxy-1-methylpiperidine and their IR absorption See Entry 112732
- The Raman spectra and conformational change of simple sodium alkylsulfates and sodium alkylsulfonates in aqueous solution See Entry 112737
- Structure and dynamics of the non-rigid CONH unit in fundamental and excited states of its stretching mode. Influence of environment effects, side-chain substitutions and secondary structures See Entry 112744
- Computer-assisted pseudorotation analysis of five-membered rings by means of proton spin-spin coupling constants: program PSEUROT See Entry 112750
- ^{19}F NMR spectra and structure of α,ω -diarylperfluoropolyenes See Entry 112753
- Recent progresses in the applications of nuclear magnetic resonance to the conformations and dynamics of flexible molecules in solution See Entry 112754
- The configuration of the tin-centered radical R_3Sn ($\text{R} = 2,4,6$ -tri-*i*-propylphenyl) as studied by ESR See Entry 112755
- ESR spectra and structures of radical cations of some branched alkanes: β -proton couplings in C- σ cations See Entry 112758
- Permutational analysis and tunnelling effects in XeF_6 See Entry 112794
- Photoionisation and molecular structure See Entry 112797
- Bound-water in biomolecules: a Monte Carlo simulation of the bifurcated hydrogen bond in violuric acid monohydrate See Entry 112803
- Group theory of non-rigid molecules and its applications See Entry 112809
- Anharmonic model for intensity of scattering of electrons by polyatomic molecules in the gas phase See Entry 112854
- Scattering of circularly polarized radiation See Entry 112931
- The crystal and molecular structure of $\text{N,N}'$ -bis[(S)-1-phenylethyl]benzamidine See Entry 113835
- Crystal and molecular structure of betulin diacetate, $\text{C}_{34}\text{H}_{54}\text{O}_4$ See Entry 113836
- Crystal and molecular structure and IR spectra of 1-hydroxy-4-dibromomethyl-2,2,5,5-tetramethyl- and 4-dibromomethyl-1,2,2,5,5-pentamethyl-3-imidazoline-3-oxide See Entry 113837
- Crystal and molecular structures of *p*-nitrophenyl vinyl ether See Entry 113846
- Crystal and molecular structures of 2,2'-dimethoxy-1,1'-dinaphthyl See Entry 113847
- Crystal and molecular structure of the 1:1 complex of 7,7,8,8-tetracyanoquinodimethane and 9,9'-trans-bis-telluraxanthenyl ($\text{C}_{12}\text{H}_4\text{N}_4/\text{C}_{26}\text{H}_{18}\text{Te}_2$) See Entry 113851
- X-ray structural investigation of perfluoro-3,3,6,6,4',4'',4'''-octamethyl-1,2,4,5-dicyclobutenocyclohexa-1,4-diene, $\text{C}_{18}\text{F}_{28}$ See Entry 113852
- Crystal and molecular structure of tetracyclic nitroxyl biradical with three bridging bonds between the piperidine and dehydropiperidineoxyl fragments, $\text{C}_{22}\text{H}_{36}\text{N}_2\text{O}_4$ See Entry 113853
- Orientation and molecular structure of 1,5 and 1,8 dichloroanthraquinones by PMR in a nematic solution See Entry 114742

35.20D Interatomic distances and angles

- Bond angles and hybridization indices in AX_2YZ and AX_2Y systems See Entry 111369
- Mass dependence of the Kolmogorov-Arnold-Moser stability and low-order resonances in the kinetically coupled two-degree-of-freedom Morse system See Entry 111553
- Electronic structure and absorption spectra of phenol and the corresponding phenoxyl radical and the cation and anion See Entry 112656
- Conversion of bound states to resonances with changing internuclear distance in molecular anions See Entry 112675
- Polarization spectroscopy of the $\text{E0}_g^+ - \text{B0}_u^+$ band system of Br_2 See Entry 112712

Standard reference data on the structure of inorganic molecules in the gaseous phase See Entry 112867

Crystal and molecular structure of the 1:1 complex of 7,7,8,8-tetracyanoquinodimethane and 9,9'-trans-bis-telluraxanthenyl ($\text{C}_{12}\text{H}_4\text{N}_4/\text{C}_{26}\text{H}_{18}\text{Te}_2$) See Entry 113851

Crystal and molecular structure of tetracyclic nitroxyl biradical with three bridging bonds between the piperidine and dehydropiperidineoxyl fragments, $\text{C}_{22}\text{H}_{36}\text{N}_2\text{O}_4$ See Entry 113853

35.20G Bond strengths, dissociation energies, hydrogen bonding, etc

- 112871 Energy of a hydrogen bond between *s trans* molecules of N-methyl-formamide. Calculations by the CNDO/2 method. O.A.C. Antunes, R.B. Faria, R.B. Alencastro, M.L.A. von Holleben, I. Sartor, P.R.R. Costa, A.C. Pinto (Univ. Federal do Rio de Janeiro, Rio de Janeiro, Brazil). *An. Acad. Bras. Cienc. (Brazil)*, vol.55, no.2, p.183-8 (June 1983). In Portuguese.
- Hydrogen bridges from amide groups have important properties as connections between peptides, proteins and/or nucleic acids. The authors investigate some of the properties of such bridges. It uses N-methyl formamide as a basic model. The method used has been described by Pople et al. and is based on the approximate solutions of Hartree-Fock for the problem of many electrons and atoms with connections. The geometry used is that of Del Bene (1978), with modifications. (no refs.) G.V.D.
- Ab initio studies of hydrogen bond formation in methyl cyanide or methyl isocyanide and methanol systems See Entry 112629
- Three-electron bonds. III. Phosphorus and chlorine σ^* radical cations See Entry 112649
- 'Frozen' transition states: pentavalent carbon et al See Entry 112650
- MRD-CI potential surfaces using balanced basis sets. I. First-row diatomic hydrides See Entry 112663
- A comparative study of the molecules Cu_2 and Ag_2 by all electron ab initio HF-CI methods See Entry 112664
- Dissociation curves for nine low lying states of Ti_2 from REP CI calculations See Entry 112665
- Reexamination of the I_2 spectrum near the $B(^3\Pi_{ou}^+)$ state dissociation limit See Entry 112711
- Polarization spectroscopy of the $\text{E0}_g^+ - \text{B0}_u^+$ band system of Br_2 See Entry 112712
- The acetylene-water complex. A matrix isolation study See Entry 112720
- Intramolecular $\text{NH}\cdots\text{N}=\text{N}\cdots\text{HN}$ hydrogen bonds with large proton polarizability in monosalts of diamines See Entry 112730
- ^{35}Cl nuclear quadrupole resonance and infrared spectroscopic studies of 2,6-dichloro-4-nitrophenol-amine hydrogen-bonded adducts See Entry 112749
- Influence of the N-oxide group in biradicals of the imidazoline series in the intramolecular spin exchange over systems of conjugated bonds See Entry 112759
- Vibrational broadening in F 1s hole states and the $8a_{1g}$ valence orbital of XeF_6 : structure of XeF_6 and heats of formation of unusual cations See Entry 112786
- Parameters of a stochastic oscillator describing a hydrogen-bonded system in a cryosolution See Entry 112793
- Theoretical Compton profile anisotropies in molecules and solids. IX. Chemical bonding and 0-90 anisotropies in the first-row diatomic hydrides AH See Entry 112795
- Bound-water in biomolecules: a Monte Carlo simulation of the bifurcated hydrogen bond in violuric acid monohydrate See Entry 112803
- Standard reference data on the structure of inorganic molecules in the gaseous phase See Entry 112867
- Molecular and crystal structure of 2,2',4,4'-tetraaminodiphenyl at -120°C See Entry 112868
- Determination of the dissociation energies of molecules from absolute intensity measurements of their electronic transitions in SrCl flame spectra See Entry 112878
- Crystal and molecular structure and IR spectra of 1-hydroxy-4-dibromomethyl-2,2,5,5-tetramethyl- and 4-dibromomethyl-1,2,2,5,5-pentamethyl-3-imidazoline-3-oxide See Entry 113837
- Structure of salts of arylthioniacycloalkanes with a hydroxy group in the benzene ring. VIII. The crystal structure of 1-(2,5-dihydroxyphenyl)-thianium chloride monohydrate See Entry 113845
- Different nature of outer-sphere complex formation between chloroform and bis-(N-phenyl-salicylaldimine) $\text{Cu}(\text{II})$ and its adduct with pyridine See Entry 115543

35.20J Barrier heights (internal rotation, inversion); rotational isomerism, conformational dynamics

- 112872 Determination of a high potential barrier hindering internal rotation from the ground state spectrum—the methyl barrier of ethylchloride. W. Stahl, H. Dreizler (Inst. für Phys. Chem., Univ. Kiel, Kiel, Germany), M. Hayashi.
- Z. Naturforsch. Teil A (Germany)*, vol.38A, no.9, p.1010-14 (Sept. 1983).
- The authors present an analysis of the rotational spectrum of ethylchloride- ^{35}Cl in the ground state. The ^{35}Cl -HFS analysis was extended and the barrier to internal rotation determined from narrow splittings of high *J*-transitions. (15 refs.)
- Moving and fixed reference frames for symmetry operations See Entry 112621
- The properties of ferrocenyl-stabilised carbocations See Entry 112630
- A theoretical study of the properties of BH_3NH_3 See Entry 112635
- Improved bond-orbital calculations of rotation barriers in molecules containing lone pairs of electrons See Entry 112643
- Intramolecular interaction effects and the structure of N_2OS and N_2O_2 : an ab initio study See Entry 112648
- Isometric groups and hyperfine structure of nonrigid molecules See Entry 112673
- Symmetry classification of normal vibrations in molecules with internal rotation See Entry 112709

Microwave spectra of cyclohexyl bromide and cyclohexyl iodide	See Entry 112717
Symmetry and microwave spectrum of nitromethane	See Entry 112719
Relation between the orientation of OH groups in stereoisomers of derivatives of 3,4-dioxy-1-methylpiperidine and their IR absorption	See Entry 112732
Infrared and Raman study of the fast internal motions of non-rigid molecules in condensed state: method of selective deuteration	See Entry 112735
Molecular and crystal structure of 2,2',4,4'-tetraaminodiphenyl at -120°C	See Entry 112868
Evidence for stereoselectivity in the copper (2^{+})-valine system	See Entry 115516

35.20M Electric and magnetic moments (and derivatives), polarizability, and magnetic susceptibility

112873 Permanent dipole moment and polarizability of a class of merocyanine dyes in their ground and first excited singlet state. W.Baumann (Inst. fur Phys. Chem., Univ. Mainz, Mainz, Germany). *Z. Naturforsch. Teil A (Germany)*, vol.38A, no.9, p.995-1002 (Sept. 1983). The permanent dipole moment of a class of merocyanine dyes in their ground and first excited singlet state has been determined studying the influence of an external electric field on the absorption of the compounds in various solvents. Evaluation of the experimental results on the basis of the Onsager reaction field model also gives values for the polarizability in the ground and excited state, the latter approaches the value of a respective conducting ellipsoid with the longer chainlength molecules. (19 refs.)

112874 An experimental and theoretical dipole moment study of 2-chloropyridine-5-sulphonyl chloride. H.Lumproso (Lab. de Chimie Generale, Univ. Pierre et Marie Curie, Paris, France), E.Montoneri, G.C.Pappalardo. *Z. Naturforsch. Teil A (Germany)*, vol.38A, no.9, p.1042-5 (Sept. 1983). Analysis of the dipole moment of 2-chloropyridine-5-sulphonyl chloride in benzene at 30°C (2.00 D) supports a model in which the C(5)-S-Cl group is rotated by 40° from the 2-chloro-1-pyridyl group. Such a model, with the S-Cl chlorine atom close to the 1-azanitrogen atom, may be explained by interplay of two conflicting factors, namely sulphony chloride-arene conjugation and lesser repulsion between one of the oxygen atoms and the azanitrogen atom. (24 refs.)

112875 Electronic polarizabilities and molecular properties of diatomic alkali hydrides. J.Shanker, H.B.Agrawal, A.K.Rajauria (Phys. Dept., Agra Coll., Agra, India). *Indian J. Phys. Part A*, vol.57A, no.3, p.155-63 (May 1983). Values of the binding energy, rotational-vibrational constants, dipole moments and their dependence on internuclear separation, and other higher order molecular spectroscopic constants are calculated for LiH, NaH, KH, RbH and CsH molecules using three different potential forms for the repulsion energy, and new values of molecular state polarizabilities calculated from the Seitz-Ruffa energy level analysis. The results obtained have been discussed and compared with experimental data. (20 refs.)

112876 Calculation of molecular polarizabilities using a semiclassical Slater-type orbital-point dipole interaction (STOPDI) model. R.R.Birge, G.A.Schick, D.F.Bocian (Dept. of Chem., Univ. of California, Riverside, CA, USA). *J. Chem. Phys. (USA)*, vol.79, no.5, p.2256-64 (1 Sept. 1983). The point dipole interaction model for molecular polarizability proposed by Applequist, Carl, and Fung [J. Am. Chem. Soc., 94, 295, 1972] is modified by replacing the point dipole interaction tensor with a descaled distributed charge interaction tensor. The authors procedure is based on the descaled tensor algorithm proposed by Thole [Chem. Phys., 59, 341, 1981] and uses a Slater-type orbital (STO) function to represent the charge distribution. The resulting STOPDI formalism calculates mean molecular polarizabilities and the components of the molecular polarizabilities with errors comparable to experimental uncertainty. Furthermore, these procedures require only one optimized parameter per atom, the average atomic polarizability. The formalism is invariant to coordinate transformations and avoids the discontinuities and/or false resonances that are characteristic of previous classical and semiclassical formalisms. The STOPDI algorithm requires less parameterization and computation time than the anisotropic atom point dipole interaction (AAPDI) model of Birge [J. Chem. Phys., 72, 5312, 1980] and is more reliable for the calculation of polarizability derivatives and Raman cross sections. The authors demonstrate, however, that none of the above significant bond stretching components. This is an inherent limitation of any formalism which does not explicitly account for electron density redistribution accompanying changes in the internuclear distances of covalently bonded atoms. (26 refs.)

Density functional calculations for atoms in the first transition series

Perturbation theory of the electron correlation effects for atomic and molecular properties. VII. Complete fourth-order BMPT study of the dipole moment and dipole polarizability of H_2O

A theoretical study of the properties of BH_3NH_3

X α multiple scattering calculations on iron (ii) porphine

Electronic structure and absorption spectra of phenol and the corresponding phenoxyl radical and the cation and anion

Rotational energies of polar symmetric-top molecules in high electric fields

Diode laser spectrum of HCCI near $5\text{ }\mu\text{m}$: the ν_2 fundamental and accompanying hot bands

Intramolecular $\text{NH}\cdots\text{N}\equiv\text{N}\cdots\text{HN}$ hydrogen bonds with large proton polarizability in monosalts of diamines

Optical anisotropies of aromatic esters and of oligomers of poly(p-oxybenzoate)

Magnetic susceptibility anisotropy, molecular g values, and other molecular properties of cyclopropane as determined from rotational Zeeman studies of the cyclopropane- H^{35}Cl and cyclopropane- HC^{15}N complexes

The rotational Zeeman effect in the ArOCS van der Waals complex

A new two-body water-water potential

35.20P Rotation, vibration, and vibration-rotation constants

Spectroscopically silent fundamental vibrations

Molecular vibration analysis of the cage-like molecules $\beta\text{-P}_4\text{S}_6$, As_4S_6 , P_4S_7 , and $\text{As}_2\text{P}_2\text{S}_7$

Nitric oxide vibrational excitation from the $\text{N}(^4\text{S})+\text{O}_2$ reaction

Nascent NO vibrational distribution from $2485\text{ }\text{\AA}$ NO_2 photodissociation

Rotational energies of polar symmetric-top molecules in high electric fields

Reexamination of the I_2 spectrum near the $B(^3\Pi_{\text{ou}}^+)$ state dissociation limit

Vibrational spectra of 6-azauracil and 5-fluorouracil

Light-induced isomerization and photochemical transformation of methylformate in an Argon matrix. Vibrational frequencies, force field, and normal coordinate analysis of trans-methylformate

Gas phase vibrational fundamentals and vib-rotational parameters of AsCl_3

Analysis of the absorption spectrum of heavy water vapor near $1.06\text{ }\mu\text{m}$

Raman and infrared excitation of local mode states in neopentane

$\text{C}^2\Pi_r-X^2\Sigma^+$ transition of AlO

The rotational Zeeman effect in the ArOCS van der Waals complex

Laser-induced fluorescence of Pb_2

Molecular constants of vanadium oxytrihalides

Anharmonic model for intensity of scattering of electrons by polyatomic molecules in the gas phase

Cross sections for electron-carbon monoxide collisions in the range 1-4 eV

Solution of the inverse spectral problem by variable metric methods

Coherent pulse propagation in the infrared on the picosecond time scale

Monodeuterated methane in the outer solar system. I. Spectroscopic analysis of the bands at 1.55 and 1.95 microns

35.20S Hyperfine and fine-structure constants

Hyperfine structure measurements for lines of astrophysical interest in Mn I

The rotational spectra of fluorinated acetonitriles; ^{14}N -nuclear quadrupole hyperfine structures measured with a microwave Fourier transform spectrometer

Nitrogen hyperfine structure in allylcyanide synperiplanar—an application of microwave Fourier transform spectroscopy

Microwave spectroscopic study of the SiF radical

The configuration of the tin-centered radical $\text{R}_3\text{Sn}(\text{R}=2,4,6\text{-tri-}i\text{-propylphenyl})$ as studied by ESR

Radical cations of aldehydes and ketones

Influence of the rotational energy of the molecular perturber on the $\text{Rb}(5\text{P})\text{-H}_2\text{D}_2$ fine structure changing collisions

Determination of a high potential barrier hindering internal rotation from the ground state spectrum—the methylbarrier of ethylchloride

35.20V Ionization potentials, electron affinities, molecular core binding energy

Density functional calculations for atoms in the first transition series

Semiempirical studies of core electron binding energies. X. The SCC-MO calculations on some purines

MRD-CI potential surfaces using balanced basis sets. I. First-row diatomic hydrides

Electronic polarizabilities and molecular properties of diatomic alkali hydrides

Ionization potentials, electron affinities, and molecular orbitals of 2-substituted norbornadienes. Theory of 1,2 and homo-1,4 carbene cycloaddition selectivities

Heats of formation and ionization potentials of some α -aminoalkyl radicals

..... See Entry 115574

35.20X Mass spectra

The A—X transition in Cr_2 : predissociation, isotope effects, and the 1-1 sequence band

Three-body association reactions of NO^+ and O_2^+ with N_2

35.80 ATOMIC AND MOLECULAR MEASUREMENTS AND TECHNIQUES

112877 Photoacoustic-spectroscopic investigation on solutions of dyes in polymer matrices. W.Gortz, H.-H.Perkampus (Inst. fur Phys. Chem., Univ. Dusseldorf, Dusseldorf, Germany). *Z. Naturforsch. Teil A (Germany)*, vol.38A, no.9, p.1022-31 (Sept. 1983). In German. Dyes dissolved in polymer matrices are ideal systems to examine the RG theory. PVA and PVP were used as matrices. In these polymer matrices the thermal properties are given by the matrix molecules being present in excess. The dye molecule serves as an indicator. Thus the thermal properties, specific heat, temperature and heat conductivity of the matrix can be measured for thermally thick layers. Further investigations to examine the RG theory show that this theory can be used for the quantitative evaluation of photoacoustic measurements of thermally thick, non scattering samples. (14 refs.)

112878 Determination of the dissociation energies of molecules from absolute intensity measurements of their electronic transitions in SrCl flame spectra. V.N.Belyaev, N.L.Lebedeva, K.S.Krasnov, L.V.Gurvich (Inst. for High Temperatures, Acad. of Sci., USSR).

High Temp. (USA), vol.20, no.6, p.844-8 (Nov.-Dec. 1982). Translation of: *Teplofiz. Vys. Temp. (USSR)*, vol.20, no.6, p.1072-5 (Nov.-Dec. 1982). [received: Sept. 1983]

A procedure is presented for determining dissociation energies from measurements of absolute intensities of optical transitions of molecules in flame spectra. For a test of the method SrCl was chosen, for which the value $D_0(\text{SrCl}) = 417 \pm 8$ kJ/mole was obtained, in good agreement with data in the literature. The possibility is investigated of determining optical transition probabilities of molecules from spectroscopic measurements in flames on compounds with known dissociation energies. (14 refs.)

112879 Solution of the inverse spectral problem by variable metric methods. L.L.Gladkov.

J. Appl. Spectrosc. (USA), vol.37, no.5, p.1309-12 (Nov. 1982). Translation of: *Zh. Prikl. Spektrosk. (USSR)*, vol.37, no.5, p.827-32 (Nov. 1982). [received: Sept. 1983]

The problem of the application of a number of methods of nonlinear programming to the solution of inverse spectral problems is discussed, and an algorithm is developed for the computer solution of this problem. The methods under consideration proceed from a quadratic approximation of the function f to be minimized, which is dependent on the force constant vector U : $f(U) = f(U_0) + \nabla^2 f(U_0) \Delta U + 1/2 \Delta U^T \nabla^2 f(U_0) \Delta U$, where ΔU is the vector of corrections to the force constants, ∇f is the gradient of the function, the superscript 'T' denotes transposition, and $\nabla^2 f$ is the matrix of the second derivatives, which is usually called the Hesse matrix. (6 refs.)

112880 Semiconductor detector for the selective detection of atomic hydrogen. K.C.Harvey, C.Fehrenbach, Jr. (Harrison M. Randall Lab., Univ. of Michigan, Ann Arbor, MI, USA).

Rev. Sci. Instrum. (USA), vol.54, no.9, p.1117-20 (Sept. 1983).

A semiconductor detector is described which responds to the atomic hydrogen in an atomic beam but is insensitive to molecular hydrogen. The hydrogen flux is measured through the change in conductivity of the semiconductor material which occurs when the hydrogen is chemisorbed. The atomic flux from a RF hydrogen discharge is used to determine the sensitivity of the detector. The minimum detectable signal is $\sim 10^9$ hydrogen atoms $\text{mm}^{-2} \text{s}^{-1}$. The detector has a response time of less than 2 ms. (10 refs.)

Reactive scattering cell for atomic hydrogen and deuterium ..See Entry 111689

Recording linear dichroism spectra with the Spectropol-1 spectropolarimeterSee Entry 111740

A simple optical electron polarimeterSee Entry 111741

High resolution spectroscopy using picosecond pulse trainsSee Entry 111775

Performance characteristics of a small side-window photomultiplier in laser single-photon fluorescence decay measurementsSee Entry 111783

Nitrite and nitrate ions as infrared pressure gauges for diamond anvilsSee Entry 112734

The A—X transition in Cr_2 : predissociation, isotope effects, and the 1-1 sequence bandSee Entry 112798

Optogalvanic effect study of vibrational relaxation in CO_2 laser processSee Entry 112817

36.00 STUDIES OF SPECIAL ATOMS AND MOLECULES

36.10 EXOTIC ATOMS AND MOLECULES (CONTAINING MESONS, MUONS, AND OTHER ABNORMAL PARTICLES)

112881 K^-p bound states with coupling to hyperon channels. R.H.Landau (Dept. of Phys., Oregon State Univ., Corvallis, OR, USA).

Phys. Rev. C (USA), vol.28, no.3, p.1324-33 (Sept. 1983).

The states of kaonic hydrogen bound by the combined Coulomb plus nuclear potentials are determined exactly in momentum space and a study is made of the dominant physics. Couplings to the Σ , K^0 , and Λ channels are included with different models for the strong potentials and different wave equations. The existence of both open and closed channels demands an extension of the Kwon, Tabakin, Lande treatment of the Coulomb singularity. Model studies indicate a high sensitivity to channel coupling and relativistic kinematics. The calculated K^-p atomic shift and width agree in magnitude with recent experiments, but the theoretical shift is towards the less bound whereas the experimental shifts appear more bound. (24 refs.)

112882 Mechanism of positronium ortho-para conversion in noble liquids. V.M.Byakov, V.R.Petuchov (Inst. of Theoretical & Experimental Phys., Moscow, USSR).

Radiochem. & Radioanal. Lett. (Switzerland), vol.58, no.2, p.75-89 (19 Aug. 1983).

It is suggested that for noble liquids the violation of the well known relation $I_N = I_2/3$ between the intensity I_N of the narrow component in the angular correlation curve of annihilation γ -quanta and the intensity I_2 of long lived components in their lifetime spectrum is caused by positronium orthopara conversion on the electrons knocked out by a positron at the terminal part of its track (where the motion of e^+ is diffusive). The expression is derived relating I_N/I_2 with the electron solvation time and parameters of the diffusive part of the e^+ track. (14 refs.)

112883 On the bubble model of positronium atom in liquids. V.M.Byakov, V.R.Petuchov (Inst. of Theoretical & Experimental Phys., Moscow, USSR).

Radiochem. & Radioanal. Lett. (Switzerland), vol.58, no.2, p.91-102 (19 Aug. 1983).

A bubble model of positronium atom in liquids is suggested, taking into account the surface tension dependence on bubble radius. This dependence is substantial since the bubble radius and diameter of the surrounding molecules are of the same order of magnitude. The conditions for positronium bubble formation are fulfilled also in liquids with high (up to 100 erg/cm^2) surface tensions. At the same time contradictions in theoretical conclusions and experimental results are explained. (7 refs.)

112884 Isotope shift measurements of muonic X-rays in $^{134,136,138}\text{Ba}$. W.Kunold, M.Schneider, L.M.Simons (Inst. fur Kernphys., Univ. Karlsruhe, Karlsruhe, Germany), J.Wust, R.Abel.

Z. Phys. A (Germany), vol.313, no.1-2, p.11-17 (1983).

The isotope shifts of muonic X-rays for the three stable Ba-isotopes $^{134,136,138}\text{Ba}$ have been measured with high accuracy. Especially the differences in the RMS radii $\Delta\langle r^2 \rangle$ have been determined in a model independent way and have been used to calibrate optical isotope shift data. (11 refs.)

112885 Parity non-conservation in muonic helium atoms. J.Bailey (NIK-HEF-K, Amsterdam, Netherlands).

Symmetries in Nuclear Structure. Proceedings of a NATO Advanced Study Institute on Symmetries in Nuclear Structure, Dronen, Netherlands, 16-28 Aug. 1982 (New York, USA: Plenum Press 1983), p.285-8

The author describes a difficult experiment, which may succeed if several unknown factors are favourable. The reason for doing the experiment is as follows. The electroweak interaction Hamiltonian H between a lepton (electron or muon) and a nucleus is $H = NC_1 H_1 + ZC_2 H_2 + S_0 C_3 H_3 + S_0 C_4 H_4$, where $C_2 = -C_3 = 1.2$, $C_1 = \epsilon = 1/2(1 - 4 \sin^2 \theta_w) \approx 0$; $C_4 = -1/2$; θ_w is the Glashow angle, so C_1 is much bigger than the other C s. This Hamiltonian contains 4 constants C , and different experiments test different combinations of these 4 constants, most measurements until now having been confined to electrons. In the standard model, the same 4 constants are also valid for muons, but this should be tested. The present experiment attempts to do this by making two measurements, on the muonic atoms of the two He isotopes. It is based on a suggestion by Bernabeu et al. (1974). Muonic atoms are smaller than normal atoms by a factor $m_\mu/m_e = 200$, so the muon is very close to the nucleus, thus enhancing weak-interaction effects (which are short-range). (no refs.)

Symmetries in Nuclear Structure. Proceedings of a NATO Advanced Study Institute on Symmetries in Nuclear StructureSee Entry 111295

An exotic decay of orthopositronium?See Entry 111943

36.20 MACROMOLECULES AND POLYMER MOLECULES

(for biological macromolecules, see also 87.15; for polymer reactions and polymerization, see 82.35)

112886 Site selective rare earth spectroscopy in proteins. M.A.Valentini, J.C.Wright (Dept. of Chem., Univ. of Wisconsin, Madison, WI, USA).

Chem. Phys. Lett. (Netherlands), vol.100, no.2, p.133-7 (2 Sept. 1983).

High-resolution laser techniques are shown to spectrally resolve europium substituted calcium ion binding sites of the protein thermolysin. Fluorescence line narrowing techniques are shown to reduce the linewidths by 30% for non-resonant transitions indicating that accidental degeneracies limit the spectral resolution attainable. (20 refs.)

112887 Time-correlation functions from computer simulations of polymers. T.A.Weber, E.Helfand (Bell Labs., Murray Hill, NJ, USA).

J. Phys. Chem. (USA), vol.87, no.15, p.2881-9 (21 July 1983).

Many of the rapid relaxation processes in polymers are related to conformational transitions of bonds from one state to another. Earlier research, based on Brownian motion computer simulation and kinetic theory, revealed that conformational transitions occur as single events and also as cooperative pairs. That research focused on kinetic rate parameters, but the experiments generally measure time-correlation functions of the system's properties. This paper is a report on the results of computer simulations of polymer time-correlation functions. The decay with time of both initial conformational states and initial vector orientations has been studied. The correlation functions fit well to a two-factor functional form, suggested by recent theoretical research. The first factor is an exponential decay arising from single transitions. The second is a diffusional term related to the correlated pair transitions. The total transition rate when compared with the earlier kinetic studies is in reasonable agreement. Since the functional form has been shown here to fit the simulations, it is suggested that it will be of value in interpreting relaxation experiments. (11 refs.)

112888 Conformational properties of perfluoroalkane chains. VII. Carbon-13, fluorine, and proton spin-lattice relaxation of poly(decamethylene perfluorosebacate) in solution and the local mobility of the fluorocarbon chain. K.Matsuo, W.H.Stockmayer (Dept. of Chem., Dartmouth Coll., Hanover, NH, USA).

J. Phys. Chem. (USA), vol.87, no.15, p.2911-14 (21 July 1983).

Chloroform- d solutions of poly(decamethylene perfluorosebacate) were studied by ^{13}C , ^{19}F , and ^1H NMR. Proton-decoupled or fluorine-decoupled ^{13}C spin-lattice relaxation times were measured over the temperature range $5-75^\circ\text{C}$. Mean orientational correlation times for C-F and C-H bonds are found to differ by a factor of only about 2.3 (e.g., 104 and 45 ps at 25°C), and have equal activation energies of about 3 kcal mol^{-1} . The ^{19}F relaxation data are consistent with the ^{13}C results. (30 refs.)

112889 Conformational aspects of a 'very simple' chain: polyacetylene. E.Cernia, L.D'Illario (Assoreni, Monterotondo, Rome, Italy).

J. Polym. Sci. Polym. Chem. Ed. (USA), vol.21, no.8, p.163-76 (Aug. 1983).

Potential energy calculations of the isolated chains of trans- and cis-polyacetylene (PA) were made to obtain information on the most probable conformations. Different sets of van der Waals potential functions, different values for the barrier height to the bond rotation, and different geometries for the repeating unit were used. Calculations were also made of the seven-atom chains of PA for which independent rotations were allowed around three consecutive 'quasi-single' bonds. The deepest minima on the potential energy map of the trans three-atom chain were consistent with an all-trans conformation (the most stable one) and with a 'distorted cis' conformation, which deviated from the planarity because of the repulsion between hydrogen atoms 1 and 4. The energy maps of the cis polymer showed two minima, both of which corresponded to nonplanar conformations. From the seven-atom chain analysis of trans- and cis-PA, in addition to the stable conformations obtained for the three-atom chains, other minima correspond to triplets formed from both conformers. (34 refs.)

112890 Network structure description and analysis of amine-cured epoxy matrices. H.S.Chu, J.C.Seferis (Dept. of Chem. Engng., Univ. of Washington, Seattle, WA, USA).

Role of the Polymeric Matrix in the Processing and Structural Properties of Composite Materials. Proceedings of a Joint US-Italy Symposium, Capri, Italy, 15-19 June 1981 (New York, USA: Plenum 1983), p.53-126

A network description and analysis for relatively complex epoxy-diamine systems of commercial significance as matrix materials for high performance composites is presented. The method of analysis was based on the probability of the epoxide groups reacting with an amino hydrogen as a function of reactant composition and extent of secondary amine reaction. Application of this analysis was focused on epoxy-diamine systems approximating commercial

compositions with stoichiometric or excess amounts of epoxies reacting with a multifunctional diamine. Systems made up with a single epoxy or two distinct epoxies with functionalities of two or larger were described. (30 refs.)

Optical anisotropies of aromatic esters and of oligomers of poly(p-oxybenzoate) See Entry 112739

Recent progresses in the applications of nuclear magnetic resonance to the conformations and dynamics of flexible molecules in solution See Entry 112754

Supermolecular structure of liquid crystalline polymer with mesogenic side groups and brominated main chain See Entry 113761

Characterization of high performance composite matrices See Entry 115361

Computer simulation of the dynamics of hydrated protein crystals and its comparison with X-ray data See Entry 115727

Computer representation of molecular surfaces See Entry 115730

Structure of polylysine-DNA complexes See Entry 115731

Heterogeneity of the structure of histone dimers (H2A-H2B) See Entry 115732

The theory and practice of distance geometry See Entry 115735

Energetic approach to the packing of α -helices. I. Equivalent helices See Entry 115736

Interior turns in globular proteins See Entry 115737

36.40 ATOMIC AND MOLECULAR CLUSTERS

12891 An ab initio SCF study on the stability and structure of $\text{H}_2\text{CN}^+ \cdot n\text{N}_2$ clusters. T.-K.Ha (Lab. of Phys. Chem., Swiss Federal Inst. of Technology, Zurich, Switzerland), M.T.Nguyen. *Z. Naturforsch. Teil A (Germany)*, vol.38A, no.8, p.855-8 (Aug. 1983).

The clustering energies and geometries of the $\text{H}_2\text{CN}^+ \cdot n\text{N}_2$ ($n=1, 2$ and 3) species have been determined by ab initio SCF calculations with the 4-31G basis set. The calculated clustering energies are in good agreement with the experimentally estimated heats of formation of the corresponding clusters. The stability of various conformers has been studied in terms of localized orbitals and charge distributions. (11 refs.)

12892 A digital processing method for structural analysis of atom clusters from high resolution electron micrographs. K.Kanaya, K.Takamiya, M.Shino, C.Shinohara (Dept. of Electrical Engng., Kogakuin Univ., Tokyo, Japan). *Micron (GB)*, vol.14, no.2, p.119-34 (1983).

The electron image contrast of tungsten atom clusters changes remarkably depending on the spatial frequency, scattering factor phase, lens aberration and defocusing, but it is confirmed that the image appears in negative contrast and satisfies an anastigmatic condition when recorded under optimum focus. When based on a cluster model, the spatial frequencies can be divided into individual atom clusters by successive band pass filters. An electron micrograph taken at the optimum focus condition is selected from a defocus series of micrographs and is used for digital processing. In order to measure the exact size of the clusters, the enhancement of filtered images by their gradient images to extract edge information and the subsequent superimposition of both images are derived. Based on Fourier analysis, it is proposed that tungsten films consist of double cluster layers which correspond to a thickness consisting of 3-5 single atoms. In addition, their three-dimensional localization can be determined more precisely than by earlier computer-aided reconstruction methods. The cluster models are in good agreement with the processed data suggesting that the amorphous phase is a distinct phase and not microcrystalline. (39 refs.)

40.00 CLASSICAL AREAS OF PHENOMENOLOGY

(inc. applications)

41.00 ELECTRICITY AND MAGNETISM; FIELDS AND CHARGED PARTICLES

(see also 03.50 Maxwell theory: general mathematical aspects)

41.10 CLASSICAL ELECTROMAGNETISM

41.10D Electrostatics, magnetostatics

12893 Zonal harmonic functions from two dimensional analogs of Jacobi polynomials. J.N.Boyd, P.N.Raychowdhury (Virginia Commonwealth Univ., Richmond, VA, USA).

Appl. Anal. (GB), vol.16, no.3, p.243-59 (1983).

The class I orthogonal polynomials in the complex variables z and \bar{z} are reviewed. These polynomials are two dimensional analogs of the Jacobi polynomials and are orthogonal on the unit disk with respect to the weight function $w(z, \bar{z})$. The polynomials are then shown to be eigenfunctions of a certain partial differential operator. Using these polynomials, a class of zonal, harmonic, homogeneous polynomials is defined in \mathbb{C}^n . In the case that $n=2$, applications to electrostatic potentials are given. (9 refs.)

12894 A Fourier series approach to magnetostatic field calculations involving magnetic material. J.Caldwell (School of Math., Statistics & Computing, Newcastle upon Tyne Polytech., Newcastle upon Tyne, England), A.Zisserman.

J. Appl. Phys. (USA), vol.54, no.9, p.4734-8 (Sept. 1983).

The effect of iron on the uniformity of the field produced by an axisymmetric thick solenoid is considered. Using a Fourier series approach, an exact solution for the vector potential A is found and from this the magnetic induction B is derived. The results are compared with those obtained from previous approximate methods. (3 refs.)

112895 Electrostatic fields in an ionization chamber electret. B.G.Fallone, E.B.Podgorsak (Dept. of Radiation Oncology, McGill Univ., Montreal, Quebec, Canada).

J. Appl. Phys. (USA), vol.54, no.9, p.4739-48 (Sept. 1983).

The theory of linear systems is used to derive the potential and electric field in distance space in a cylindrical polarization/depolarization electret chamber. General solutions for the near, intermediate, and far regions are given and their domains of convergence discussed. On the axis of the chamber the solutions for the electret surface are equal to those obtained from Gauss's and Kirchhoff's laws, and at large distances from the surface to those obtained from the introduction of a dipole layer model. (30 refs.)

Electrostatic acceleration of a modulated electron beam See Entry 112917

41.10F Steady-state electromagnetic fields; electromagnetic induction

112896 On the convergence of numerical results in modal analysis.

M.Leroy (Sedacip Sarl, Tour Alpha, Les Ulis, France).

IEEE Trans. Antennas & Propag. (USA), vol.AP-31, no.4, p.655-9 (July 1983).

Previous studies of the relative convergence (RC) phenomenon in modal analysis showed the need to introduce the edge condition by using an explicit asymptotic behavior of modal coefficients. The author does not agree that the edge condition is the only means of uniquely defining a solution. It is demonstrated that the RC can be avoided by including only the bounded feature of modal coefficients. The analytical computations are given in solving the bifurcated parallel plate waveguide. To solve the general problem of convergence of numerical results, a proof is given of this convergence in modal analysis. The required condition is the use of a 'well-conditioned' linear system. With this demonstration, the use of the condition number as purely numerical criterion is justified to ensure the convergence of results. (9 refs.)

112897 First indication of ampere tension in solid electric conductors.

P.Graneau (Francis Bitter Nat. Magnet Lab., MIT, Cambridge, MA, USA).

Phys. Lett. A (Netherlands), vol.97A, no.6, p.253-5 (5 Sept. 1983).

An empirical law for the mechanical force between two current-elements, originally deduced by Ampere from a series of classical experiments, asserts that an electric current flowing along a straight wire should place the wire in tension. The existence of longitudinal Ampere forces at solid-liquid conductor interfaces has been demonstrated by various investigators during the past 160 years. This letter contains the first report of pulse currents creating sufficient tension to cause fracture in hot copper and aluminium wires. (6 refs.)

112898 Fourth moments of thermal fluctuations in the electromagnetic field in a homogeneous and isotropic medium. R.L.Stratonovich, A.V.Tolstopyatenko.

Radio Eng. & Electron. Phys. (USA), vol.27, no.11, p.107-12 (Nov. 1982).

Translation of: *Radiotekh. & Elektron. (USSR)*, vol.27, no.11, p.2185-90 (Nov. 1982). [received: Sept. 1983]

Using the cubic relationships of nonlinear fluctuation-dissipation thermodynamics, four-point correlators are obtained and, as a result, also the moments of the thermal fluctuations in an electromagnetic field. The nonlinear medium is assumed to be unbounded. The result is given in spectral form. In the absence of spatial dispersion, the obtained expression contains two numerical parameters that are not determined by dissipation. (7 refs.)

112899 Constant boundary element solution for steady-state convective diffusion equation in three dimensions. M.Ikeuchi, M.Sakakihara (Graduate School of Sci., Okayama Univ. of Sci., Okayama, Japan), K.Onishi.

Trans. Inst. Electron. & Commun. Eng. Jpn. Sect. E (Japan), vol.E66, no.6, p.373-6 (June 1983).

A boundary element solution is formulated for steady-state convective diffusion equation with the Dirichlet's boundary condition. A simple example is considered in three dimensions. It is shown that the boundary element solution is unconditionally stable. In order to demonstrate the usefulness of the boundary element solution, the comparison with finite element solutions is given. (12 refs.)

Direct observation of microscopic electromagnetic fields by means of electron holography See Entry 111828

Influence of magnetization on eddy current inspection of ferromagnetic tubes See Entry 115493

41.10H Electromagnetic waves: theory

112900 Diffraction of an EM wave by an absorbing circular cylinder.

P.Langlois (Dept. de Radioelectricite, Univ. de Provence, Marseille, France).

Opt. Acta (GB), vol.30, no.10, p.1373-96 (Oct. 1983).

Some expressions for the EM field diffracted by an absorbing circular cylinder of large radius in the Fresnel region are developed. Until recently results were available only for the far field of 'good conductors'. The derived equations agree with Young's theory of diffraction since the diffracted field may be expressed as two cylindrical waves which seem to arise from the two 'edges' of the cylinder. Numerical calculations are also presented and compared with previous experimental results. (20 refs.)

112901 Ray model for attenuated total reflection from a weakly absorbing dielectric. S.S.Gupta, D.P.Tewari (Dept. of Phys., Indian Inst. of Technol., New Delhi, India).

Opt. Acta (GB), vol.30, no.10, p.1397-403 (Oct. 1983).

An approximate ray picture has been presented for attenuated total reflection of a plane electromagnetic wave from a weakly absorbing dielectric. An analytical expression for the reflection coefficient has been obtained for an angle of incidence larger than the critical angle. The method of limiting absorption is seen to establish the Carter-Hora conjecture regarding the validity of Renard's formula for lateral shift on account of total reflection. Potential applications of the work are discussed. (22 refs.)

112902 Propagation of waves in a medium with large-scale random inhomogeneities. M.V.Tinin (Irkutsk State Univ., Irkutsk, USSR).

Radiophys. & Quantum Electron. (USA), vol.26, no.1, p.29-36 (Jan. 1983).

Translation of: *Izv. VUZ Radiofiz. (USSR)*, vol.26, no.1, p.36-43 (Jan. 1983).

[received: Sept. 1983]

Describes an integral representation for the field in a randomly inhomogeneous medium. This integral representation takes care of the problem summing the fields of geometric-optic waves in a region where multiple rays occur. Asymptotic analysis of the integral representations for the second and fourth moments are in good agreement with results obtained previously by the phase-screen method. The behavior of the mean intensity in the vicinity of a simple caustic of the unperturbed field is analysed. In the presence of large phase fluctuations, the scale on which the intensity falls off exponentially in the region of the caustic shadow does not depend obviously on the frequency

(unlike the case of no fluctuations), but is determined by the dispersion of the ray deviations. (15 refs.)

112903 Electromagnetic wave diffraction on a two-dimensionally periodic lattice of semiinfinite dielectric rods. V.M.Krekhtunov, V.A.Tyulin (N.E. Bauman Higher Tech. School, Moscow, USSR). *Radiophys. & Quantum Electron. (USA)*, vol.26, no.1, p.63-9 (Jan. 1983). Translation of: *Izv. VUZ Radiofiz. (USSR)*, vol.26, no.1, p.74-81 (Jan. 1983). [received: Sept. 1983]

The field projection matching method is used to solve the problem of electromagnetic wave diffraction on a 'free space-two-dimensionally periodic dielectric structure' boundary. In certain regions, orthonormalized systems of the transverse vector functions of homogeneous and transverse-inhomogeneous Floke channels are used. The problem is reduced to solution of an inhomogeneous system of linear algebraic equations in elements of the scattering matrix of the system considered. The convergence of the solution is studied numerically for increasing number of base functions in the representation of the unknown field, and the behavior of the lattice reflection coefficient as a function of the incident wave and structure parameters is analyzed. (15 refs.)

112904 Simulation model of ray propagation in a three-dimensional turbulent medium. P.I.Akimov, S.I.Baskakov (Moscow Power Inst., Moscow, USSR).

Radiophys. & Quantum Electron. (USA), vol.26, no.1, p.70-8 (Jan. 1983). Translation of: *Izv. VUZ Radiofiz. (USSR)*, vol.26, no.1, p.82-90 (Jan. 1983). [received: Sept. 1983]

The principle of modeling a three-dimensional turbulent medium by a set of spherically symmetrical inhomogeneities of various space scales is described. A relationship is established between the parameters of the model and the parameters of the spatial spectrum of the permittivity fluctuations of the modeled medium. An algorithm is described for plotting the ray paths in the modeled medium, along with a method for determining the eikonal and electromagnetic wave intensity in Lagrangian coordinates. The results of numerical experiments to calculate the ray-path characteristics and fluctuations of the eikonal are given for a medium in which the permittivity fluctuations have a Karman spectral function. The modeling results are compared with the existing analytical solutions for a continuous medium. (15 refs.)

112905 Reflectivity of spherical shield. S.S.Vinogradov (Inst. of Radiophys. & Electronics, Acad. of Sci., Ukrainian SSR).

Radiophys. & Quantum Electron. (USA), vol.26, no.1, p.78-88 (Jan. 1983). Translation of: *Izv. VUZ Radiofiz. (USSR)*, vol.26, no.1, p.91-102 (Jan. 1983). [received: Sept. 1983]

A rigorous solution to the vector problem of diffraction by an ideally conducting sphere with a hole is obtained by a numerical method. The boundary conditions for Debye potentials are formulated correctly and found to be intervalled. Both total cross section for scattering and cross section from backscattering are calculated. (12 refs.)

112906 Scattering of a planar wave from solids of revolution, covered by absorptive materials. I.Ye.Arsayev.

Radio Eng. & Electron. Phys. (USA), vol.27, no.11, p.33-41 (Nov. 1982). Translation of: *Radiotekh. & Elektron. (USSR)*, vol.27, no.11, p.2101-9 (Nov. 1982). [received: Sept. 1983]

The method of geometric optics is used to solve the problem of scattering of electromagnetic waves from an impedance solid of revolution, covered by a homogeneous absorptive material when the wave is incident along the body axis. The solution is obtained in the form of a series whose terms are determined from recursive formulae. The terms of the series are derived in an explicit form for backscattering. The accuracy of the obtained solution is estimated. The effect of the curvature of the body surface and of the cover on the scattering characteristics is investigated. Conditions are determined under which the backscattering can be substantially decreased. (9 refs.)

112907 The method of variation of constants for the solution of the Helmholtz equation, illustrated by the problem of diffraction on a nonhomogeneous sphere. Ya.N.Fel'd.

Radio Eng. & Electron. Phys. (USA), vol.27, no.12, p.42-52 (Dec. 1982). Translation of: *Radiotekh. & Elektron. (USSR)*, vol.27, no.12, p.2323-32 (Dec. 1982). [received: Sept. 1983]

A method of variation of constants is developed for solution of nonhomogeneous problems of mathematical physics. The presentation is based on the example of the Helmholtz equation. The excitation of a radially nonhomogeneous sphere by an arbitrary system of sources is considered. The solution is constructed in the form of partial-wave expansions of discrete and continuous spectra, with coefficients which depend on a single variable. Different forms of solution are obtained, depending on the choice of that variable. These solutions are suitable for computations when the radius of the sphere is large or comparable to a wavelength. The method is illustrated by the example of a homogeneous Lunenburg lens. (6 refs.)

112908 Anomalous wave scattering by a finite number of longitudinally slit cylinders of small wave dimensions. E.I.Veliev, V.V.Veremei, V.P.Shestopalov (Inst. of Radiophys. & Electronics, Acad. of Sci., Kharkov, Ukrainian SSR). *Sov. Tech. Phys. Lett. (USA)*, vol.8, no.11, p.580-1 (Nov. 1982). Translation of: *Pis'ma v Zh. Tekh. Fiz. (USSR)*, vol.8, no.21-22, p.1349-53 (Nov. 1982). [received: Sept. 1983]

Considers the excitation by a magnetic-current filament of a reflector formed by a finite number (N) of circular cylinders with a longitudinal slit (the angular size of the slit is θ) distributed uniformly over a circular arc of angle α and radius R_1 . The authors assume that the cylindrical screens are infinitesimally thin and ideally conducting. This problem has been solved rigorously for an arbitrary arrangement of screens. (5 refs.)

112909 Diffraction of electromagnetic waves by a periodic screen with holes of arbitrary shape. V.A.Kaplun, I.T.Kravchenko, D.A.Tsaryuk.

Telecommun. & Radio Eng. Part 2 (USA), vol.37, no.9, p.72-6 (Sept. 1982). Translation of: *Radiotekhnika, Moskva (USSR)*, vol.37, no.9, p.32-7 (Sept. 1982).

The transverse section method is used to solve the problem of the diffraction of a plane wave by an infinite perforated metal screen, taking into account its finite thickness and assuming the holes to be filled with a dielectric. The working relations obtained are in a good agreement with experimental data. The screens considered can be used as radomes for protecting antenna systems. (7 refs.)

112910 Analysis of scattering problems by means of charge simulation method. A.Komiyama (Faculty of Engng., Meiji Univ., Kawasaki, Japan).

Trans. Inst. Electron. & Commun. Eng. Jpn. Part B (Japan), vol.166B, no.6, p.790-7 (June 1983). In Japanese.

The charge simulation method is a numerical technique which is used in electrostatics, especially for calculation of the electric field in high voltage apparatus. It has recently been used in fields other than electrostatics. The author applies the charge simulation method to the problem of electromagnetic scattering by a perfectly conducting cylinder with arbitrary cross section and demonstrates the effectiveness of the technique in this field. Firstly,

theory and formulae for the method of source simulation are given. The scattering by a circular cylinder with known exact solution is treated, and characteristics of its errors are discussed. Finally, to show the effectiveness of this technique, scattering problem by two circular cylinders having different radii is treated. Total electric field distribution in the vicinity of cylinders, forward scattering cross section and scattering pattern are given. (13 refs.)

Nonionizing radiation: appropriate topic in a physics curriculum See Entry 111349

Resonant transitional scattering in vacuum in the presence of an external electromagnetic field See Entry 112968

An iterative extended boundary condition method for solving the absorption characteristics of lossy dielectric objects of large aspect ratios See Entry 115829

Intensity fluctuations due to a deeply modulated phase screen. I. Theory See Entry 116235

Intensity fluctuations due to a deeply modulated phase screen. II. Results See Entry 116236

41.70 PARTICLES IN ELECTROMAGNETIC FIELDS: CLASSICAL ASPECTS

(inc. synchrotron radiation)

112911 An explicit Lagrangian for a system of charged particles to higher-order terms: quadrupole radiation. D.Dionysiou (Dept. of Math., Hellenic Air-Force Acad., Dekelia-Attica, Greece).

Astrophys. & Space Sci. (Netherlands), vol.94, no.2, p.413-18 (Aug. 1983). Gives an explicit formula for the Lagrangian for any number of charged particles interacting with each other up to the fifth-order terms, assuming that this system does not emit dipole radiation. The quadrupole radiation, in exact agreement with the classical electromagnetic theory. (8 refs.)

112912 Microdischarge characteristics in air gap between spherical particle and plane. M.Hara (Dept. of Electrical Engng., Kyushu Univ., Fukuoka, Japan), T.Yamashita, M.Akazaki.

IEE Proc. A (GB), vol.130, no.6, p.329-35 (Sept. 1983).

Microdischarge behaviours in a gap between the plane electrode and a charged conducting spherical particle moving in the presence of external electric field have been investigated. The microgap studied has distinctive features: the field strength in the microgap changes very rapidly with the motion of the sphere even if the applied external electric field is static, the boundary of the microgap changes with time, and the potential difference across the microgap is influenced from the occurrence of discharge due to the neutralisation of charge on the sphere by the charge carrier in the discharge itself. The random appearance of an initiating electron required for the development of an avalanche and the rapid changes of electric field, gap boundary and potential difference result in the statistical behaviours of microdischarge. The statistical characteristics at the microdischarge threshold and on the microdischarge length have been measured, and the microdischarge mechanism has been discussed to explain the characteristics. (21 refs.)

112913 Synchrotron radiation of wiggled electron beam in rectangular waveguide. H.A.Haus, M.N.Islam (Dept. of Electrical Engng. & Computer Sci., MIT, Cambridge, MA, USA).

J. Appl. Phys. (USA), vol.54, no.9, p.4784-93 (Sept. 1983).

An analysis is presented of the spectrum radiated by an electron beam passing through a magnetic wiggler in a rectangular waveguide using a coupled-mode approach. The noise power radiated into each mode of the waveguide is calculated. In the limit of a highly overmoded waveguide and large relativistic parameter, the total emitted spectrum approaches that of a beam in free space. The radiation formulas are greatly simplified for a weak magnetic field. (8 refs.)

112914 Analysis of the propagation of electron waves inside and outside the passband of periodic structures. A.V.Osin, V.A.Solntsev.

Radio Eng. & Electron. Phys. (USA), vol.27, no.11, p.127-33 (Nov. 1982). Translation of: *Radiotekh. & Elektron. (USSR)*, vol.27, no.11, p.2207-14 (Nov. 1982). [received: Sept. 1983]

On the basis of the theory of excitation, the propagation and attenuation constants of electron waves are analyzed as a function of the parameters of the interaction between the electron stream and the periodic slow-waves structure field at frequencies close to a positive and negative dispersion are discussed. A comparison is made with the well-known theory of three electron waves within the passband, as well as with the known results obtained on the basis of the method of equivalent circuits within and outside the passband. The limits of applicability of the three-electron-wave theory are determined. (6 refs.)

112915 Coherent scattering of surface waves from an electron stream whose velocity is modulated in space. N.B.Lerner, B.G.Tsikin.

Radio Eng. & Electron. Phys. (USA), vol.27, no.12, p.147-53 (Dec. 1982). Translation of: *Radiotekh. & Elektron. (USSR)*, vol.27, no.12, p.2442-7 (Dec. 1982). [received: Sept. 1983]

An approximate nonlinear theory is developed of the interaction between a surface electromagnetic wave and electron beam whose velocity is modulated in space. Conditions are determined for conversion of the surface wave into a volume wave without changing frequency, as well as conditions for generation of volume waves in such interaction systems. The intensities of volume waves for the fundamental frequency and second harmonic are analytically estimated. (3 refs.)

Lagrangian dynamics of a classical spinning particle with dipole moments See Entry 111467

Random electrodynamics of nonlinear system. I. Quartic anharmonic oscillator See Entry 111941

Infrared synchrotron radiation from electron storage rings See Entry 112487

Optimization of a permanent magnet undulator for free electron laser studies on the ACO storage ring See Entry 112516

Theory of radiation in media with changing anisotropy See Entry 112933

Sources of stimulated radiation using resonance electron accelerators See Entry 113004

41.80 PARTICLE BEAMS AND PARTICLE OPTICS

(see also 07.80 Electron and ion microscopy, 07.77 Beam handling equipment)

112916 Charged particle ray simulator and monitor. E.Kisker (Inst. für Festkörperforschung, KFA Jülich, Jülich, Germany). *Rev. Sci. Instrum. (USA)*, vol.54, no.9, p.1113-16 (Sept. 1983). A new method is described for simulating charged particle rays in arbitrary electrostatic lens system of cylindrical symmetry. The method is so efficient (>4 ms/step) that even for complex lens systems the trajectories can be computed and displayed during the lens voltage adjustment, using the same laboratory microcomputer which controls the lens voltages. The time lag between a change of a lens element voltage and the trajectory display is of the order of a few seconds for long, multielement lens systems. This also allows one to optimize the voltage combinations by performing trajectory calculations for many lens voltage settings. The performance is demonstrated by comparing with recent experimental data of Heddle and co-workers on imaging properties of a three-element tube lens. As an application of the fast computation time feature, trajectories and voltages are shown for a lens system providing an electron optically adjustable angle resolution as used in a spin polarized photoemission experiment with synchrotron radiation. (9 refs.)

Charged particle beam envelopes See Entry 112499

41.80D Electron beams and electron optics

112917 Electrostatic acceleration of a modulated electron beam. Yu.K.Alekseev, A.I.Kostienko (Dept. of VHF Radiophys., Moscow Univ., Moscow, USSR). *Moscow Univ. Phys. Bull. (USA)*, vol.38, no.1, p.28-31 (1983). Translation of: *Vestn. Mosk. Univ. Ser. 3 (USSR)*, vol.38, no.1, p.25-9 (1983). The problem of pumping power into a modulated electron flux is considered. With dynamic modulation of the flux, power pumping leads to slowing of the grouping process and reduction in beam efficiency. In the case of electrostatic control of the current's form however, its spectral composition and electron efficiency are retained. (4 refs.)

112918 Interferometrical processing of electron microscopic holograms. III. Investigation of special features of the differential interferometry including noise problems. K.-J.Hanssen (Phys.-Tech. Bundesanstalt, Braunschweig, Germany). *Optik (Germany)*, vol.65, no.2, p.153-77 (1983). In German. For pt.II see ibid., vol.63, p.285 (1983). The graininess in reconstructions of electron off-axis-holograms is essentially caused by the unscreened part of the noise spectrum which is introduced by the granularity of the photographic plate. It is a linear function of the scattering amplitude within the aperture. Expressions for the noise in simultaneous reconstructions are given. In the case of reconstructions with differential contrast employing two holograms with identical grain, the interference patterns in the noise spectra offer great help for adjustment purposes. Additional experimental results and some advantages and disadvantages of two different interferometrical reconstruction arrangements are discussed. (11 refs.)

112919 Investigation of a double-beam linear high-voltage electron-optic system with centrifugal electrostatic shaping and recovery of electron energy. L.I.Andrikanis, N.S.Bunina, M.Z.Melikov. *Radio Eng. & Electron. Phys. (USA)*, vol.27, no.11, p.140-3 (Nov. 1982). Translation of: *Radiotekh. & Elektron. (USSR)*, vol.27, no.11, p.2222-5 (Nov. 1982). [received: Sept. 1983] Results were presented of an experimental investigation and calculation of a linear double-beam electron-optic system with centrifugal electrostatic shaping (the length of the high-voltage gap was 6 cm). Recovery of the energy of the electron streams after striking the open surface type collector was ensured. (4 refs.)

Magnetic-field-free objective lens around a specimen for observing fine structure of ferromagnetic materials in a transmission electron microscope See Entry 111820

Direct observation of microscopic electromagnetic fields by means of electron holography See Entry 111828

Analysis of the propagation of electron waves inside and outside the passband of periodic structures See Entry 112914

Ion neutralization in helical electron beams See Entry 112973

41.80G Ion beams and ion optics

Refraction of an ion beam by the fringe electric field in a mass spectrometer with a laser ion source See Entry 111805

Use of the 'large particle' method to calculate parameters of ion sources which employ electron impact ionization See Entry 111806

Fine-focus ion beam technology for microfabrication See Entry 111814

Effect of magnetic field on the characteristics of a hollow cathode ion source See Entry 111815

42.00 OPTICS

(for properties of gases and of liquids and solids, see 51.70 and 78. respectively; for atmospheric optics, see 92.65; for physiology of the eye, see 87.32)

42.10 PROPAGATION AND TRANSMISSION IN HOMOGENEOUS MEDIA

112920 Sellmeier fits with linear regression; multiple data sets; dispersion formulas for helium. E.R.Peck (Phys. Dept., Univ. of Idaho, Moscow, ID, USA). *Appl. Opt. (USA)*, vol.22, no.18, p.2906-13 (15 Sept. 1983).

Linear regression, combined with search over nonlinear parameters is useful in fitting Sellmeier formulas to dispersion data. A special advantage accrues in fitting several sets of data to one formula: linear regression permits systematic normalization to a common absolute value. Rational procedures are discussed also for weighting of data set of unequal precision. The fitting of

common formulas to six sets of data on helium, for wavelengths from 0.09 to 2 μ m, illustrates the various procedures. (13 refs.)

112921 Tracing finite rays through a Fresnel lens. I.Powell (Nat. Res. Council of Canada, Ottawa, Ontario, Canada). *Appl. Opt. (USA)*, vol.22, no.18, p.2924-6 (15 Sept. 1983). In this study the author shows that with minor modifications it is possible to adapt an existing optical design program to trace finite rays through a system containing Fresnel surfaces. Practical examples are given to illustrate the validity of the author's rather simple approach to this problem. (2 refs.)

112922 Complex amplitude propagation through a quadratic-index medium: characteristic point function. C.Gomez-Reino, E.Larrea, M.V.Perez (Dept. de Optica, Santiago de Compostela, Spain). *Appl. Opt. (USA)*, vol.22, no.18, p.2927-9 (15 Sept. 1983). The propagation of a complex amplitude distribution in quadratic-index material is studied by the characteristic point function, and the authors determine the maximum distance for which an optical image and transform can be transmitted without estimable loss of information due to modal dispersion. (7 refs.)

112923 The spot of Arago and its role in wavefront analysis. J.E.Harvey (Inst. for Modern Optics, Univ. of New Mexico, Albuquerque, NM, USA), J.L.Forgham, K.Von Bieren. *Proc. SPIE Int. Soc. Opt. Eng. (USA)*, vol.351, p.2-9 (1983). [received: Sept. 1983] (SPIE Proceedings on Wavefront Sensing, San Diego, CA, USA, 24-25 Aug. 1982).

The 'spot of Arago' has been a controversial topic since its inception in 1818 when Poisson predicted its existence, which violated common sense, in an attempt to discredit Fresnel's wave theory of light. Arago performed the experiment and found the surprising prediction was true, thus putting Fresnel's theory on a firm technical foundation. In recent years, the spot of Arago, which exists as a bright spot at the center of the geometrical shadow of a circular obstruction, has caused substantial grief in various high energy laser applications and has come to be considered more of a nuisance than a curiosity. The authors suggest that the size and shape of the spot of Arago is characteristic of the wavefront aberrations of the incident beam and can therefore be used to advantage as a beam sample for wavefront analysis of annular beams. The implementation of this wavefront sampling scheme would eliminate the requirement for a special beam sampling optical component and thus reduce to a minimum the deleterious effects upon the beam frequently accompanying the use of such components. Both experimental and numerical results are presented along with a discussion of the capabilities and limitations of this particular beam sample for performing various wavefront sensing functions. (2 refs.)

112924 Study of spatial filtering using LOTS-MCI. C.A.Boye (Air Force Weapons Lab., Kirtland Air Force Base, NM, USA), W.Swantner, G.Lawrence. *Proc. SPIE Int. Soc. Opt. Eng. (USA)*, vol.351, p.15-18 (1983). [received: Sept. 1983] (SPIE Proceedings on Wavefront Sensing, San Diego, CA, USA, 24-25 Aug. 1982).

The Laser Optical Train Simulation (LOTS) computer program was developed for the Los Alamos National Laboratory laser fusion program and was built to do end-to-end physical optics analysis of the laser train. The wavefront analysis program MCI was originally written as an interferogram reduction program. Given a data set of triplets (fringe number, x-coordinate, y-coordinate), the coefficients for Zernike polynomials are computed. The program has also been linked with the optical design and analysis program ACCOS V for the purpose of wavefront analysis. The authors have recently attached MCI to LOTS, so that the wavefront analysis would consider the effects of diffraction through a small aperture. As an application of LOTS-MCI, the authors performed the present study of beam clean-up. LOTS's input language allows the user to impose third order aberrations on a beam at any location in the beam path. The aberrations may be given arbitrary orientation. LOTS then propagates the beam to a focus in these examples, where the user may place an aperture of arbitrary diameter. The light passing through the aperture is propagated to the far field, and the wavefront data is passed to MCI for the calculation of wavefront information. (5 refs.)

112925 Bases and applications of the induced resonance absorption. I. H.Pohlack (VEB Carl Zeiss Jena, Jena, Germany). *Feingeraetetechnik (Germany)*, vol.32, no.7, p.321-6 (1983). In German. The induced resonance absorption—an optical interference effect in thin absorbing films—is presented. The parameter conditions for the fundamental modes are developed. Applications of the effect in photothermal and photovoltaic energy conversion processes are explained. (31 refs.)

112926 Encircled energy of diffracted covering spherical waves. Yajun Li (Inst. für Nachrichtentech., Tech. Univ. München, München, Germany). *J. Opt. Soc. Am. (USA)*, vol.73, no.9, p.1101-4 (Sept. 1983). The author studied the diffraction phenomenon of a circular aperture that was illuminated by a monochromatic converging spherical wave. The theoretical part of this study was based on the scalar Huygens-Fresnel integral. In the experiments the author used a circular detector centered on-axis to measure the encircled energy. The author varied both the radius and the longitudinal position of the detector. The principal maximum of the encircled energy received by the detector was usually not in the geometrical focal plane, and its position changed abruptly when the radius of the detector was varied. These abrupt changes look like sawtooth variations, which are superimposed upon a slowly changing curve. The author's experiments were in a good agreement with calculations. (12 refs.)

112927 Three-dimensional vector coupled-wave analysis of planar-grating diffraction. M.G.Moharam, T.K.Gaylord (School of Electrical Engng., Georgia Inst. of Technol., Atlanta, GA, USA). *J. Opt. Soc. Am. (USA)*, vol.73, no.9, p.1105-12 (Sept. 1983). Diffraction by an arbitrarily oriented planar grating with slanted fringes is analyzed using rigorous three-dimensional vector coupled-wave analysis. The method applies to any sinusoidal or nonsinusoidal amplitude and/or phase grating, any plane-wave angle of incidence, and any linear polarization. In the resulting (conical) diffraction, it is shown that coupling exists between all space-harmonic vector fields inside the grating (corresponding to diffracted orders outside the grating). Therefore the TE and TM components of an incident wave are each coupled to all the TE and TM components of all the forward- and backward-diffracted waves. For a general Bragg angle of incidence it is shown that the diffraction efficiency can approach 100% for a lossless grating if either the incident electric field or the magnetic field is perpendicular to the grating vector. Maximum coupling between incident and diffracted waves is shown to occur when the incident electric field is perpendicular to the grating vector. In general, the diffracted waves are shown to be elliptically polarized. The three-dimensional vector coupled-wave analysis presented is shown to reduce to ordinary rigorous coupled-wave theory when the grating vector lies in the plane of incidence. (31 refs.)

- 112928 Paraxial ray paths in spherical gradient-index media.** T.Sakamoto (Industrial Lab. of Hyogo Prefecture, Suma, Kobe, Japan). *J. Opt. Soc. Am. (USA)*, vol.73, no.9, p.1209-10 (Sept. 1983). Paraxial ray paths are derived for spherical gradient-index media whose index distributions are expressed as infinite even-power series of the distance from the center. (3 refs.)
- 112929 Explicit equations for the second Brewster angle of an interface between a transparent and an absorbing medium.** R.M.A.Azzam (Dept. of Electrical Engng., Univ. of New Orleans, Lakefront, New Orleans, LA, USA). *J. Opt. Soc. Am. (USA)*, vol.73, no.9, p.1211-12 (Sept. 1983). The second Brewster angle ϕ_{B2} , at which the ratio R_p/R_s of intensity reflectances R_p and R_s for the parallel (p) and the perpendicular (s) polarizations of a dielectric-conductor interface reaches a minimum, is determined by $\text{Im}[(u-\epsilon)(u-\bar{\epsilon})^2/(u-2\bar{\epsilon})^2]=0$, where ϵ is the complex ratio of dielectric constants of the media of refraction and incidence, $\bar{\epsilon}=\epsilon/(\epsilon+1)$, and $u=\sin^2\phi_{B2}$. An equivalent quartic equation in u is also derived that can be solved exactly and explicitly to determine ϕ_{B2} in terms of ϵ . (7 refs.)
- 112930 Reflection of a linearly polarized plane wave from a lossless stratified mirror in the presence of a phase-conjugate mirror.** A.T.Friberg, P.D.Drummond (Dept. of Phys. & Astron., Univ. of Rochester, Rochester, NY, USA). *J. Opt. Soc. Am. (USA)*, vol.73, no.9, p.1216-19 (Sept. 1983). Reflection of a linearly polarized electromagnetic plane wave from an ordinary lossless stratified plane mirror is analyzed in the presence of a phase-conjugate mirror. It is shown that, if the conjugated waves are generated without losses or gains and also without a change in the state of polarization, the specularly reflected wave will be extinguished completely and a phase-conjugated replica of the incident wave will be formed. This result, which clearly illustrates a recently derived general theorem on phase conjugation, is independent of the reflectivity of the ordinary mirror and the separation between the two mirrors. New results for arbitrary reflectivities are also obtained. (10 refs.)
- 112931 Scattering of circularly polarized radiation.** I.Tinoco, Jr., D.Keller (Dept. of Chem., Univ. of California, Berkeley, CA, USA). *J. Phys. Chem. (USA)*, vol.87, no.15, p.2915-17 (21 July 1983). The differential refraction and absorption of circularly polarized light was applied by Henry Eyring and co-workers to study the configuration and conformation of small molecules. The differential scattering as a function of angle of circularly polarized light can provide structural information about large scattering systems. The authors present the general equations relating circular differential scattering to the eigenfunctions of a scatterer which is of arbitrary size relative to the wavelength of light. An equivalent experiment is to measure the ellipticity of the scattered light when linearly polarized light is incident. (17 refs.)
- 112932 Validity conditions of the thickness function method for determining the transmittance function.** C.Gomez-Reino (Dept. de Fisica Fundamental (Optica), Santiago, Univ. de Santiago de Compostela, Spain), E.Larrea. *Lett. Nuovo Cimento (Italy)*, vol.38, ser.2, no.1, p.11-15 (3 Sept. 1983). Validity conditions of the thickness function method for determining the transmittance function are obtained by a general method developed by the authors (1982). (5 refs.)
- 112933 Theory of radiation in media with changing anisotropy.** V.A.Davydov (Dept. of Quantum Theory, Moscow Univ., Moscow, USSR). *Moscow Univ. Phys. Bull. (USA)*, vol.38, no.1, p.94-7 (1983). Translation of: *Vestn. Mosk. Univ. Ser. 3 (USSR)*, vol.38, no.1, p.79-82 (1983). The radiation of a charge moving in a crystal with periodic change in direction of the optical axis over time is considered. Polarizational, angular, and spectral characteristics of the radiation are obtained and investigated. (4 refs.)
- 112934 Determination of small double refractions of plane-parallel glass plates.** H.Melle (Phys.-Tech. Bundesanstalt, Braunschweig, Germany). *Optik (Germany)*, vol.65, no.2, p.115-22 (1983). In German. The modification of the vibration azimuth of a linearly polarized coherent light wave passing through plane-parallel glass plates is treated experimentally and theoretically. Due to insignificant residual double refractions, real glass plates show a marked influence on the vibration azimuth of the transmitted wave. This results in a new method of measuring double refractions in a simple and exact way. (2 refs.)
- 112935 Reciprocity relations with partially coherent sources.** A.T.Friberg (Dept. of Tech. Phys., Helsinki Univ. of Technol., Espoo, Finland), E.Wolf. *Opt. Acta (GB)*, vol.30, no.10, p.1417-35 (Oct. 1983). Two general reciprocity relations are formulated, relating to planar sources of any state of spatial coherence and the radiation fields they generate. One of them expresses a reciprocity between the effective coherence area of the source and the effective angular spread of the radiation. The other expresses a reciprocity between the effective intensity spread across the source and the effective angular domain subtended at the source by the coherence area of the far field. Two well-known reciprocity relations associated with coherent and incoherent sources are obtained as special cases. The general reciprocity relations take a particularly simple form when the source is quasi-homogeneous. (32 refs.)
- 112936 Reciprocity principles for focused wavefields and the modified Debye integral.** H.M.Pedersen, J.J.Stamnes (Central Inst. for Industrial Res., Oslo, Norway). *Opt. Acta (GB)*, vol.30, no.10, p.1437-54 (Oct. 1983). It is shown that focused wavefields satisfy a reciprocity principle concerning the roles of the focal point and the observation point. According to this principle, the diffracted field at a point P_2 of a converging spherical wave centred on the focal point P_1 is the complex conjugate of the diffracted field observed at P_1 if the focal point is at P_2 . The commonly used Debye integral representation of focused wavefields violates the reciprocity principle. Therefore the authors derive a new diffraction formula for focused wavefields which the authors call the modified Debye integral (MDI). It is constructed so as to satisfy the reciprocity principle, and may be considered as a generalization of the Debye integral and also as a refinement on a diffraction integral derived by Hopkins. For focusing of a two-dimensional perfect wave the authors show that the MDI gives the same f -number dependent parabolic phase factor on the geometrical focal line as is obtained numerically in the Kirchhoff approximation. For focusing of three-dimensional waves the MDI and the Kirchhoff theory are shown to predict the same focal shift in the paraxial approximation, as long as the shift is small compared with the focal distance. (31 refs.)
- 112937 Absorption of conical load with diffuse reflection of internal surface.** V.M.Kuz'michev, E.Ya.Govorun. *Radiotekhnika, Kharkov (USSR)*, no.61, p.82-8 (1982). In Russian. [received: Aug. 1983] A multiple reflection method, which takes into account the distribution of the energy after each reflection, is proposed for calculating the absorption of the

optical emission in conical loads with diffuse reflection of the internal surface. Expressions are derived for the absorptive power of the loads as a function of the coefficient of reflection and the semiflare angle of the cone, of the derived radius of the homogeneous axial beam and of the point of impact of the narrow beam onto the flare of the cone. The results of the numerical calculations are compared with the data obtained by other writers. (5 refs.) L.M.H.

- SPIE Proceedings on Wavefront Sensing** See Entry 111301
- A spherical viewing screen for diffraction patterns** See Entry 111353
- More on two-dimensional scattering** See Entry 111364
- Homemade rainbows: a backyard experiment** See Entry 111377
- Self-study manual on optical radiation measurements: Part I -Concepts, chapter 10. Introduction to coherence in radiometry** See Entry 111382
- The introduction of wave optics: the Fresnel explanation of diffraction** See Entry 111388
- Determination of the film thickness in localized epitaxial structures** See Entry 111642
- Optimal post detection phase estimation for wavefront sensing** See Entry 111722
- Comparison of wavefront sensor configurations using optimal reconstruction and correction** See Entry 111723
- Fundamentals of wavefront sensing by phase retrieval** See Entry 111724
- Fundamental performance limitations for the phase retrieval problem** See Entry 111725
- Phase retrieval by optical phase differentiation** See Entry 111726
- Role of diffraction in phase retrieval from intensity measurements** See Entry 111727
- Linear methods in phase retrieval** See Entry 111728
- Linear and circular polarisation modulation for measuring complex magneto-optical rotation. I. Principles and performance** See Entry 111742
- Analysis of two-beam interferometry for bulk wave measurements** See Entry 111748
- Contribution to the automatic fringe analysis using Zernike polynomials** See Entry 111757
- Subcoded information carriers: hybrid moire system** See Entry 112950
- Self-imaging through a Fabry-Perot interferometer** See Entry 112954
- Reflex diffraction grating—an effective transducer of infrared radiation polarization** See Entry 113081
- Anisotropic gratings recorded from two circularly polarized coherent waves** See Entry 113083
- Asymmetric extinction in anisotropic diffraction gratings** See Entry 113084
- Optical wave propagation in form-birefringent media and waveguides** See Entry 113092
- Calculation of stress birefringence in fibers by an infinitesimal element method** See Entry 113116
- Origins and control of polarization effects in single-mode fibers** See Entry 113118
- Analytic solution for the birefringence produced by thermal stress in polarization-maintaining optical fibers** See Entry 113119
- A single-polarization fiber** See Entry 113123
- Single-mode, single-polarization fibers made of birefringent material** See Entry 113127
- Rayleigh backscattering theory for single-mode optical fibers** See Entry 113128

42.20 PROPAGATION AND TRANSMISSION IN INHOMOGENEOUS MEDIA

- 112938 Coherent detection of scattered light from submicron aerosols.** D.R.Petit, T.W.Peterson (Dept. of Chem. Engng., Univ. of Arizona, Tucson, AZ, USA). *Aerosol Sci. & Technol. (USA)*, vol.2, no.3, p.351-68 (1983). The van Cittert-Zenike theorem states that light scattered from small particles can be made coherent if gathered at the focal point of a lens. Coherent-detection techniques can then be used to measure the extent of the phase shift due to the particles. Scattering mechanisms can relate the phase shift to the particle diameter, so particle size can be determined. Theoretical estimates of the ideal minimum detectable particle diameters are of the order of $5 \times 10^{-3} \mu\text{m}$; estimates of the minimum detectable diameters for a practical system are of the order of $5 \times 10^{-2} \mu\text{m}$. Particles are counted one at a time as they travel through an optically defined view to volume. Electronic signal processing allows particle size distributions to be deduced from the individual signals. The sampling of particle concentrations up to $10^9/\text{cm}^3$ is possible with this technique. The coherent optical particle spectrometer can be used to measure aerosol dynamics in high-temperature environments and to determine the properties of single submicron particles. (42 refs.)
- 112939 Onefold photoelectron-counting statistics for non-Gaussian light: scattering from an arbitrary number of weak scatterers.** R.Barakat (Div. of Appl. Sci., Harvard Univ., Cambridge, MA, USA). *J. Opt. Soc. Am. (USA)*, vol.73, no.9, p.1138-42 (Sept. 1983). The onefold photoelectron-counting statistics (e.g. probability distribution and moments) are obtained when the physical system under study contains an arbitrary number of independent weak (i.e. nonuniform phase) scatterers. The results are generalized by letting the number of scatterers be random and be governed by a Poisson distribution. (11 refs.)
- 112940 Stationarity of speckle in laser refraction.** R.D.Bahuguna, D.Malacara (Centro de Investigaciones en Optica, AC, Leon, Mexico). *J. Opt. Soc. Am. (USA)*, vol.73, no.9, p.1213-15 (Sept. 1983). The equation that describes the tangential focal conditions for a curved grating is found to be a natural solution for the position of the plane of stationarity in laser refraction. It is found that the imaging equation of the macroscopic surface treated as a mirror is a particular solution when (1) the observation is in the specular direction or (2) the incidence and observation directions are close to the normal to the surface. When speckle is viewed in this way, some errors in previous research on speckle motion are brought to light. (17 refs.)
- More on two-dimensional scattering** See Entry 111364
- Enhanced-displacement measurement using a generalized formulation for double-aperture specklegrams** See Entry 111636
- Advances in optical metrology of complex objects** See Entry 111754

- Number fluctuation spectroscopy in standing-wave fringes See Entry 111782
- Reflection of light by an inhomogeneous inversion medium with dispersion See Entry 112967
- Strehl's ratio for a two-wavelength continuously deformable optical adaptive transmitter See Entry 113074
- Application of fiber optics to speckle metrology—a feasibility study See Entry 113115
- Effects of photon noise on speckle image reconstruction with the Knox-Thompson algorithm See Entry 116489

42.30 OPTICAL INFORMATION, IMAGE FORMATION AND ANALYSIS

- 112941 Image restoration for a defocused optical system.** L.R.Berriel, J.Bescos (Inst. de Optica, Madrid, Spain), A.Santesteban. *Appl. Opt. (USA)*, vol.22, no.18, p.2772-80 (15 Sept. 1983). Images obtained by an aberration-free system are digitally defocused with progressive values of defocusing. Wiener filtering restoration is applied to the defocused images, and the defocusing range for effective restoration is shown. The stability of the filters for restoring images with spatially variant defocusing is also discussed. (4 refs.)
- 112942 Image restoration by convex projections in the presence of noise.** M.I.Sezan, H.Stark (Dept. of Electrical, Computer & Systems Engng., Rensselaer Polytech. Inst., Troy, NY, USA). *Appl. Opt. (USA)*, vol.22, no.18, p.2781-9 (15 Sept. 1983). In this paper the authors investigate how the method of convex projections for image restoration behaves in the presence of noise. The authors also introduce and test a new noise-smoothing procedure in which the restored image is forced to lie within a certain L_2 distance of the noisy data. The authors show that, in the presence of noise, restoration by convex projections is superior to the Gerchberg-Papoulis method. (15 refs.)
- 112943 Simplified calculation of the effects of jitter on clutter leakage.** N.G.Kulgein (Electro-Optics Lab., Lockheed Palo Alto Labs., Palo Alto, CA, USA). *Appl. Opt. (USA)*, vol.22, no.18, p.2794-7 (15 Sept. 1983). A simple analytical solution has been found that enables prediction of the effects of line-of-sight motion of a sensor on clutter leakage after first differencing. The effect of finite footprint size is included, and the crucial importance of the ratio of this quantity to the background correlation length is given. For small motions the clutter leakage as a fraction of the value of background standard deviation is given by the very simple formula $\sqrt{2[1 - \exp(-L/D)]}$, where L is the footprint size, and d is the background correlation length. (5 refs.)
- 112944 Statistical performance of the circular harmonic filter for rotation-invariant pattern recognition.** Yuan-Neng Hsu, H.H.Arsenault (Dept. de Phys., Lab. de Recherches en Optique et Laser, Univ. Laval, Quebec, Canada). *Appl. Opt. (USA)*, vol.22, no.18, p.2804-9 (15 Sept. 1983). Circular harmonic filters of different orders are compared using a criterion of separability between the target and object output probability densities. A holographic computer-generated circular harmonic filter was used to recognize aircraft from an air photograph. (9 refs.)
- 112945 Image-based focusing.** T.Selker (Computer Sci. Dept., Stanford Univ., Stanford, CA, USA). *Proc. SPIE Int. Soc. Opt. Eng. (USA)*, vol.360, p.96-9 (1982). [received: July 1983] (Robotics and Industrial Inspection, San Diego, CA, USA, 24-27 Aug. 1982). Lens focusing using a hardware model of a retina (Reticon RL256 light sensitive array) with a low cost processor (8085 with 512 bytes of ROM and 512 bytes of RAM) was built. This system was developed and tested on a variety of visual stimuli to demonstrate that: a) an algorithm which moves a lens to maximize the sum of the difference of light level on adjacent light sensors will converge to best focus in all but contrived situations. This is a simpler algorithm than any previously suggested; b) it is feasible to use unmodified video sensor arrays with inexpensive processors to aid video camera use. In the future, software could be developed to extend the processor's usefulness, possibly to track an actor by panning and zooming to give a camera operator increased ease of framing; c) lateral inhibition is an adequate basis for determining best focus. This supports a simple anatomically motivated model of how the brain focuses the eyes. (5 refs.)
- 112946 Minimum variance estimation of wavefront aberration.** G.S.Um (Rockwell Internat., Seal Beach, CA, USA), B.F.Smithgall, C.L.O'Bryan. *Proc. SPIE Int. Soc. Opt. Eng. (USA)*, vol.351, p.96-102 (1983). [received: Sept. 1983] (SPIE Proceedings on Wavefront Sensing, San Diego, CA, USA, 24-25 Aug. 1982). Presents an image-based indirect wavefront aberration estimation which is noise optimal. The minimum variance estimation is obtained by linearising the focal plane intensity distribution in terms of the aberration parameters and a known set of derivatives of the point spread function. The technique was also made to work successfully for unknown extended sources by Fourier transforming the image to the frequency space. The results obtained from a computer simulation show excellent noise rejection. With a signal-to-noise ratio of 5, the wavefront correction is achieved down to 0.1 λ . In some cases, this method worked when the initial signal-to-noise ratio was less than one. Since the estimation is performed with a linear approximation, the dynamic range of operation was found to be limited to 0.35 RMS λ . (8 refs.)
- 112947 Optical image processing in coherent and incoherent light: a short comparative review.** P.Chavel (Inst. d'Optique, Univ. de Paris-Sud, Orsay, France). *Proc. SPIE Int. Soc. Opt. Eng. (USA)*, vol.369, p.442-9 (1983). (SPIE Proceedings of the Max Born Centenary Conference OPTICS 82, ECOSA 82, Edinburgh, Scotland, 7-10 Sept. 1982). In recent years, a number of methods have been developed to overcome the limitations of the classical coherent and incoherent image processing methods. A review of the main trends in this area is presented, indicating the principles of low-noise coherent processing, of incoherent processing of complex quantities and of white light processing; it is seen that optical processing can now in a number of cases perform nonlinear operations, or shift invariant operations while still keeping the advantage of parallelism. (52 refs.)
- 112948 Thermal aspects of magneto-optical recording.** M.Mansuripur, G.A.N.Connell (Xerox Palo Alto Res. Center, Palo Alto, CA, USA). *J. Appl. Phys. (USA)*, vol.54, no.9, p.4794-8 (Sept. 1983). Discusses the influence of thermal response on the magneto-optic readout performance of optically similar but thermally different quadrilayer media, using newly developed computational techniques for examining laser-induced heat flow in moving multilayer media. They first emphasize the importance of

- time scale for differentiating the write and read processes. They then show that the optimum design is a function of the medium velocity and available laser power for writing and is not normally one that provides maximum signal-to-noise ratio in the limit that laser heating during readout can be ignored. Finally, the authors describe a systematic approach to the selection of the best quadrilayer design for a given set of system conditions. (10 refs.)
- 112949 Ablative optical recording using organic dye-in-polymer thin films: some mechanistic aspects.** Kock-Yee Law, G.E.Johnson (Xerox Webster Res. Center, Webster, NY, USA). *J. Appl. Phys. (USA)*, vol.54, no.9, p.4799-805 (Sept. 1983). The influence of a number of materials properties and device structure variations on the energy threshold for laser marking of organic dye-in-polymer films has been investigated. The author's results indicate that the write-sensitivity of these organic dye-in-polymer optical recording media is strongly dependent on the absorption efficiency of the recording film, the quantum efficiency of generation of thermal energy by the dye and the recording film thickness for films > 100 nm. The write-sensitivity is however, not dependent on the glass transition temperature, the surface tension or the melt viscosity of the polymer binder. This independence is attributed to the very rapid nature of the mark formation process. The technological implications of the present work are discussed. (20 refs.)
- 112950 Subcoded information carriers: hybrid moire system.** R.Eschbach, O.Bryndahl (Dept. of Phys., Univ. of Essen, Essen, Germany). *J. Opt. Soc. Am. (USA)*, vol.73, no.9, p.1123-9 (Sept. 1983). Investigation and application of subcoded information carriers are discussed. Sequences of orthogonal states introduce basic systems that allow for parallel processing in the spatial domain. Moire simulation experiments illustrate some peculiarities of the coding and decoding procedures. Characteristic features achievable by using subcoded carriers are sign determination of displayed variations, phase multiplication, and improved signal-to-noise ratio. A hybrid version of a moire test method is described to show the flexibility and filtering possibilities when orthogonal subcodes are used under realistic conditions. (11 refs.)
- 112951 Fast algorithm for the computation of the zero-order Hankel transform.** P.K.Murphy, N.C.Gallagher (Purdue Univ., West Lafayette, IN, USA). *J. Opt. Soc. Am. (USA)*, vol.73, no.9, p.1130-7 (Sept. 1983). The Hankel transform may be defined as the two-dimensional Fourier transform of a circularly symmetric function. A new Hankel-transform algorithm based on this definition is described. The proposed algorithm efficiently generates a rectangularly sampled two-dimensional output array by using the circular symmetry properties of the input array and two-dimensional vector radix fast-Fourier transform techniques. It accomplishes this by partitioning the input matrix into smaller and smaller processing blocks while removing redundant blocks from data manipulations. For applications that require the output data to be sampled on a two-dimensional rectangular raster, the convenience and the computational speed of the resulting algorithm offer advantages over the one-dimensional Hankel-transform algorithms currently available. (9 refs.)
- 112952 Fifth-order aberration theory of gradient-index optics.** S.D.Fantone (Inst. of Optics, Univ. of Rochester, Rochester, NY, USA). *J. Opt. Soc. Am. (USA)*, vol.73, no.9, p.1149-61 (Sept. 1983). The fifth-order aberration coefficients for gradient-index lenses are presented. A procedure for calculation is outlined. (5 refs.)
- 112953 Fifth-order aberration theory of gradient-index optics—examples.** S.D.Fantone (Inst. of Optics, Univ. of Rochester, Rochester, NY, USA). *J. Opt. Soc. Am. (USA)*, vol.73, no.9, p.1162-4 (Sept. 1983). Four examples are presented as verification of the validity and the usefulness of the equations derived earlier (see *ibid.*, vol.73, p.1149, 1983). In each example, the aberration coefficients derived by algebraic methods are compared with those obtained from ray-trace data to a seventh-order aberration polynomial including ninth-order spherical aberration and distortion. In all cases good agreement is obtained between the two methods. (3 refs.)
- 112954 Self-imaging through a Fabry-Perot interferometer.** G.Indebetouw (Phys. Dept., Virginia Polytech. Inst. & State Univ., Blacksburg, VA, USA). *Opt. Acta (GB)*, vol.30, no.10, p.1463-71 (Oct. 1983). The spatial filtering property of a Fabry-Perot interferometer is shown to transform the spatial spectrum of an arbitrary image into a form which satisfies, approximately, the conditions for self-imaging. The limitations of the technique are studied and checked experimentally. (4 refs.)
- SPIE Proceedings on Wavefront Sensing** See Entry 111301
- A simple demonstration of spherical aberration See Entry 111363
- Edge scan wave-front analyzer for low order aberrations See Entry 111721
- Optimal post detection phase estimation for wavefront sensing See Entry 111722
- Fundamentals of wavefront sensing by phase retrieval See Entry 111724
- Phase retrieval by optical phase differentiation See Entry 111726
- Wavefront sensors for turbulence correction See Entry 111729
- Experimental verification of an image-based alignment technique for optical systems in space See Entry 111731
- Point image focus sensing using an automated Foucault test See Entry 111733
- Fringe pattern recognition and interpolation using nonlinear regression analysis See Entry 111747
- Contribution to the automatic fringe analysis using Zernike polynomials See Entry 111757
- Complex amplitude propagation through a quadratic-index medium: characteristic point function See Entry 112922
- The spot of Arago and its role in wavefront analysis See Entry 112923
- Study of spatial filtering using LOTS-MCI See Entry 112924
- Paraxial ray paths in spherical gradient-index media See Entry 112928
- Low-noise multicolor archival storage with broad source interferometric imaging See Entry 112955
- Volume-type multiple hologram memory using PMMA thick films See Entry 112963
- Quasi-one-dimensional volume-type hologram memory See Entry 112964
- Optical recording media with thermal coloration See Entry 113071
- Wavefront analysis of objectives using ACCOS-MCI See Entry 113072
- Full aperture testing with subaperture test optics See Entry 113073
- Application of the theory of image formation to calculations on optical resonators See Entry 113076

- The effects of manufacturing inaccuracies on the imaging properties of Fresnel zone plates See Entry 113078
- Simple synchronous video image combiner See Entry 113143
- Hybrid processing for phase measurement in metrology and flow diagnostics See Entry 113522
- Intensity fluctuations due to a deeply modulated phase screen. I. Theory See Entry 116235
- Intensity fluctuations due to a deeply modulated phase screen. II. Results See Entry 116236
- Finite exposure time, astronomical speckle transfer function See Entry 116274
- The Couder telescope-better than the Schmidt? See Entry 116476
- Effects of photon noise on speckle image reconstruction with the Knox-Thompson algorithm See Entry 116489

42.40 HOLOGRAPHY

(for acoustic holography, see 43.63)

- 112955 Low-noise multicolor archival storage with broad source interferometric imaging.** Hsuan Chen, Y.S.Cheng (Univ. of Michigan, Ann Arbor, MI, USA). *Appl. Opt. (USA)*, vol.22, no.18, p.2790-3 (15 Sept. 1983).
A low-noise true color image plane rainbow hologram is formed with a modified Mach-Zehnder interferometer using an extended source. Experiments show excellent results in the noise suppression and resolution preservation capabilities of this system. (5 refs.)
- 112956 Image formation by multifacet holograms.** P.R.Haugen, H.Bartelt, S.K.Case (Electrical Engng. Dept., Univ. of Minnesota, Minneapolis, MN, USA). *Appl. Opt. (USA)*, vol.22, no.18, p.2822-9 (15 Sept. 1983).
A method is described in which arbitrary images are formed via Fresnel diffraction. In this method, a multifacet hologram is used to deflect small square areas of light from a given spatial location in the input plane to an arbitrarily prescribed location in the output plane, producing an image composed of small square patches of light. Five different variations of multifaceted holography are presented. Volume phase holograms are used in the deflection process resulting in nearly 100% efficiency. (11 refs.)
- 112957 Gaussian beam effects in far-field in-line holography.** C.S.Vikram (Pennsylvania State Univ., University Park, PA, USA), M.L.Billet. *Appl. Opt. (USA)*, vol.22, no.18, p.2830-5 (15 Sept. 1983).
Far-field in-line holography has been studied in detail when one or both of the beams used for recording and reconstruction are Gaussian. The contrast of the high frequency interference fringes and hence their recordability have been investigated with a specific example of the object having circular cross section. For reconstruction the effects of uniform as well as Gaussian beams are studied and compared. (15 refs.)
- 112958 Computer-generated holograms in biology and medicine.** R.J.Perlmutter (Stanford Univ., Stanford, CA, USA), S.S.Friedland. *IEEE Comput. Graphics & Appl. (USA)*, vol.3, no.5, p.47-51 (Aug. 1983).
Shows how holographic images of diagnostic scan data can be invaluable in many medical procedures. A method is described, which makes possible the efficient computer generation of holograms. (9 refs.)
- 112959 Coherent image amplification and optical phase conjugation with photorefractive materials.** P.Gunter (Lab. of Solid State Phys., Swiss Federal Inst. of Technol., Zurich, Switzerland). *Proc. SPIE Int. Soc. Opt. Eng. (USA)*, vol.369, p.230-6 (1983). (SPIE Proceedings of the Max Born Centenary Conference OPTICS 82, ECOSA 82, Edinburgh, Scotland, 7-10 Sept. 1982).
The electric field and fringe spacing dependence of the stationary energy transfer between two writing beams in volume phase-hologram formation with photoconductive electro-optic materials ($\text{KNbO}_3\text{:Fe}^{2+}$, $\text{Bi}_{12}(\text{Si,Ge})\text{O}_{20}$,...) has been studied. Experimental results are compared with the theoretical expressions describing the influence of the different photoinduced spacecharge fields in photorefractive media. A peak exponential gain of $\Gamma=15\text{ cm}^{-1}$ has been reached in $\text{KNbO}_3\text{:Fe}^{2+}$ for the proper choice of experimental parameters such as recording wavelength fringe spacing, applied electric field, etc. Results of the electric field dependence of the wavefront reflectivity ρ in degenerate four-wave mixing experiments are reported and discussed in terms of a similar theoretical treatment as the two-wave mixing experiments. It is shown, that peak reflectivities of $\rho=25$ percent have been reached for $\text{KNbO}_3\text{:Fe}^{2+}$, that conjugate complex wavefronts can be generated and that distorted optical wave-fronts can be effectively corrected by four-wave mixing experiments in $\text{KNbO}_3\text{:Fe}^{2+}$. (12 refs.)

112960 High-frequency holographic transmission gratings in photoresist. R.C.Enger, S.K.Case (Dept. of Electrical Engng., Univ. of Minnesota, Minneapolis, MN, USA). *J. Opt. Soc. Am. (USA)*, vol.73, no.9, p.1113-18 (Sept. 1983).
This paper describes an experimental study of the diffraction properties of high-spatial-frequency gratings recorded in relatively thin photoresist layers. Angular selectivity, wavelength selectivity and peak efficiencies are investigated. Details on grating fabrication are given. The study shows that optical elements with efficiencies greater than 88% can be recorded in media less than one wavelength thick ($\sim 0.5\text{ }\mu\text{m}$ for our visible-light experiments). The results are important in that such diffractive structures could be replicated by embossing, chemical-vapor deposition, or other means. (15 refs.)

112961 Recording a binary computer-generated hologram on a thermoplastic film. T.Minemoto, T.Nonami (Dept. of Instrumentation Engng., Kobe Univ., Kobe, Japan). *Opt. Commun. (Netherlands)*, vol.47, no.2, p.97-100 (15 Aug. 1983).
A computer-generated hologram was recorded on a thermoplastic film using an electron-beam recording device. The hologram was a binary one of detour phase type and of surface relief type. A bright image was reconstructed from the recorded hologram. (4 refs.)

112962 High-sensitivity material with reversible photo-induced anisotropy [holographic recording]. T.Todorov, N.Tomova, L.Nikolova (Central Lab. of Optical Storage & Processing of Information, Bulgarian Acad. of Sci., Sofia, Bulgaria). *Opt. Commun. (Netherlands)*, vol.47, no.2, p.123-6 (15 Aug. 1983).
A new high-sensitivity material with reversible photo-induced anisotropy, suitable for real-time recording, is investigated. The material (methyl-red dye introduced in a polymer layer) requires low recording intensities (tens of mW cm^{-2}) and possesses excellent reusability. (10 refs.)

112963 Volume-type multiple hologram memory using PMMA thick films. Jon-Chi Chang, T.Okoshi (Faculty of Engng., Univ. of Tokyo, Tokyo, Japan). *Trans. Inst. Electron. & Commun. Eng. Jpn. Part C (Japan)*, vol.J66C, no.7, p.505-12 (July 1983). In Japanese.
The characteristics of polymethyl methacrylate (PMMA) sensitized by *p*-benzoquinone at $\lambda=488\text{ nm}$ as a volume-type phase hologram memory material are investigated. Dynamic coupled-wave theory considering the saturation behavior of the PMMA material is used to describe the measured exposure characteristics of PMMA hologram gratings. A particle model is assumed to construct an optimum design theory of the hologram using PMMA thick films, and the optimum design parameters and maximum storage density of such hologram memories have been calculated. Experiments on a multiple-exposure hologram memory have been performed using the design parameters obtained, achieving a storage density of $(0.2\sim 1.5)\times 10^6\text{ bit/mm}^2$. (14 refs.)

112964 Quasi-one-dimensional volume-type hologram memory. Jon-Chi Chang, T.Okoshi (Faculty of Engng., Univ. of Tokyo, Tokyo, Japan). *Trans. Inst. Electron. & Commun. Eng. Jpn. Part C (Japan)*, vol.J66C, no.7, p.513-20 (July 1983). In Japanese.
A volume-type hologram memory featuring a strip-shaped information composer (quasi-one-dimensional hologram memory) is proposed. The advantage is that the spatial modulator and the photodiode array can easily be constructed even when the writing and reading wavelengths are different. The design criteria are discussed. Experimental results are shown. A storage density of $(0.3\sim 1.0)\times 10^5\text{ bit/mm}^2$ has been realized by using a PMMA (polymethyl methacrylate) thick film with $400\text{ }\mu\text{m}$ thickness. (7 refs.)

112965 The optical target. A new five dimensional transducer using laser holography. Ye Sheng-Hua, Xu Ring-Ting, Wei Shang-Chen (Dept. of Precision Instruments Engng., Tianjin Univ., Tianjin, China).
Technological and Methodological Advances in Measurement. Acta IMEKO 1982. Proceedings of the 9th IMEKO Congress of the International Measurement Confederation, Berlin, Germany, 24-28 May 1982 (Amsterdam, Netherlands: North-Holland 1983), p.219-27 vol.1.
The fundamental principle of a five dimensional transducer of laser holographic light splitting is presented including a brief mathematical analysis. This kind of multi-dimensional transducer can be used both in production and in scientific research, especially for calibration of balance for sensing the force and movement of force from various directions in aerodynamics. (no refs.)

Holography applied to stereomicroscopy See Entry 111762

Direct observation of microscopic electromagnetic fields by means of electron holography See Entry 111828

Interferometrical processing of electron microscopic holograms. III. Investigation of special features of the differential interferometry including noise problems See Entry 112918

Statistical performance of the circular harmonic filter for rotation-invariant pattern recognition See Entry 112944

Stigmatic systems with concave spherical holographic diffraction gratings See Entry 113082

Anisotropic gratings recorded from two circularly polarized coherent waves See Entry 113083

Design of an experiment to determine deformations using holographic interferometry See Entry 113390

Converging shock on laser plasma: density profiles by holographic interferometry See Entry 113663

Holographic plasma interferometry in the infrared spectrum. II. Using nonlinear effects to increase the sensitivity See Entry 113667

Thermal conductivity measurements on fluids under microgravity using holographic interferometry See Entry 114291

42.50 QUANTUM OPTICS

112966 Propagation, transverse and diffraction effects and coherent pump dynamics in three-level superfluorescence and light control by light. F.P.Mattar (Aerodynamics Lab., Polytech. Inst. of New York, NY, USA), C.M.Bowden. *Proc. SPIE Int. Soc. Opt. Eng. (USA)*, vol.369, p.245-52 (1983). (SPIE Proceedings of the Max Born Centenary Conference OPTICS 82, ECOSA 82, Edinburgh, Scotland, 7-10 Sept. 1982).
Calculational results and analysis are presented and discussed for the effects of coherent pump dynamics, propagation, transverse and diffraction effects on superfluorescent (SR) emission from an optically-pumped three-level system. The full, copropagational aspects of the injected pump pulse together with the SF which evolves are explicitly treated in the calculation. It is shown that the injection pulse initial characteristics can have a strong effect on the SF emission. (20 refs.)

112967 Reflection of light by an inhomogeneous inversion medium with dispersion. A.B.Zimin, N.S.Petrov. *J. Appl. Spectrosc. (USA)*, vol.37, no.5, p.1322-7 (Nov. 1982). Translation of: *Zh. Prikl. Spektrosk. (USSR)*, vol.37, no.5, p.843-9 (Nov. 1982). [received: Sept. 1983] (14 refs.)

112968 Resonant transitional scattering in vacuum in the presence of an external electromagnetic field. V.R.Khalilov (Dept. of Theoretical Phys., Moscow Univ., Moscow, USSR). *Moscow Univ. Phys. Bull. (USA)*, vol.38, no.1, p.105-7 (1983). Translation of: *Vestn. Mosk. Univ. Ser. 3 (USSR)*, vol.38, no.1, p.88-90 (1983).
The probability of scattering (in time τ) of a strong, circularly polarized, electromagnetic wave with frequency doubling, propagating in vacuum in a periodic (in space) external electroamgnetic field under definite conditions, is proportional to τ^2 . (5 refs.)

112969 Collisionless cyclotron absorption of photons by electrons in a laser beam. M.B.S.Lima, C.A.S.Lima (Inst. de Fisica, Univ. Estadual de Campinas, Sao Paulo, Brazil), L.C.M.Miranda. *Opt. Acta (GB)*, vol.30, no.10, p.1359-62 (Oct. 1983).
Charged particle acceleration in a laser beam with a superimposed cyclotron motion is considered. The energy absorption process is analysed using an exact quantum mechanical description of the particle motion. The results permit a simple quantum mechanical interpretation of energy absorption under a cyclotron resonance regime. (8 refs.)

112970 Classical statistical mechanics of a lattice model of superradiance. V.Benza, E.Montaldi (Dipartimento di Fisica, Univ. di Milano, Milan, Italy).

Phys. Lett. A (Netherlands), vol.97A, no.6, p.231-4 (5 Sept. 1983).

A classical model of the interaction of N two-level atoms with the radiation field discretized on a lattice, having particular relevance for superradiance, is discussed. By evaluating the corresponding partition function the threshold condition for the occurrence of a second-order phase transition is derived. A comparison with previous work, where a finite number of field modes was considered, is also given. (7 refs.)

Coherent light scattering from ruby dressed with RF photons

See Entry 113044

42.52 MASERS

112971 Comment on 'Stimulated bremsstrahlung masers'. Y.Ben-Aryeh, J.Felsteiner, J.Politch, A.Rosenberg (Dept. of Phys., Technion-Israel Inst. of Technol., Haifa, Israel), A.J.Palmer.

Appl. Phys. Lett. (USA), vol.43, no.6, p.614-15 (15 Sept. 1983). For original paper see A.J. Palmer, *ibid.*, vol.42, p.1011 (1983). Presents a proper interpretation of Palmer's experiments in which he tried to get evidence of amplification or oscillation produced by stimulated bremsstrahlung in an open resonator which encloses a glow discharge plasma. The authors maintain that Palmer disregarded important differences in the experimental conditions. A reply by Palmer is included. (11 refs.)

112972 Analysis of the Majorana transition and beam optics for the state selection of a hydrogen maser. S.Urabe, Y.Ohta (Radio Res. Labs., Ministry of Posts & Telecommunications, Tokyo, Japan).

Jpn. J. Appl. Phys. Part 1 (Japan), vol.22, no.6, p.1009-16 (June 1983). The Majorana transition and the beam optics configuration are analysed for the purpose of designing the hydrogen maser state selector which selects only desired atoms for oscillation. In this state selection, the double focalization method and the Majorana transitions which reverse the atomic polarization are used in order to eliminate undesirable atoms. The polarization reversal is obtained by calculating the transition probabilities of the atomic spin in the reverse magnetic field. The beam optics configuration is also analysed for the purpose of effective elimination. Based on these analyses, the state selection is successfully attained, and about 90% of the undesirable atoms are eliminated. (11 refs.)

112973 Ion neutralization in helical electron beams. V.A.Varentsov, Sh.E.Tsimring (Inst. of Appl. Phys., Acad. of Sci., Gor'kii, USSR).

Sov. Phys.-Tech. Phys. (USA), vol.28, no.2, p.163-6 (Feb. 1983). Translation of: *Zh. Tekh. Fiz. (USSR)*, vol.53, no.2, p.264-9 (Feb. 1983). [received: Sept. 1983]

Space-charge neutralization is studied in intense helical beams produced by cyclotron resonance masers. The beams are produced by magnetron injection guns together with particles formed by ionization of residual gases. The experimental findings indicate the ion neutralization causes the average gyration velocity and velocity spread to become almost identical to the values observed at small currents. An analysis of pulse measurements indicates that the space charge field causes the regions of velocity spreading to be localized. The consequences of ion neutralization can be exploited in intense helical beam diagnostics. (10 refs.)

112974 Cyclotron-autoresonance maser with a wavelength of 2.4 mm. I.E.Botvinnik, V.L.Bratman, A.B.Volkov, G.G.Denisov, B.D.Kol'chugin, M.M.Ofitserov (Inst. of Appl. Phys., Acad. of Sci., Gorki, USSR).

Sov. Tech. Phys. Lett. (USA), vol.8, no.11, p.596-7 (Nov. 1982). Translation of: *Pisma v Zh. Tekh. Fiz. (USSR)*, vol.8, no.21-22, p.1386-9 (Nov. 1982). [received: Sept. 1983]

The cyclotron-autoresonance maser (CARM) is predicted to be one of the most promising relativistic millimeter and submillimeter-wave sources. The authors report a 2-mm source which uses $H_{1,1}$ as the working mode. The experiments were carried out with the Neptun-2 high-current accelerator, which produces an electron beam with a pulse length of 100 ns, an energy adjustable over the range 500-600 keV, and a current adjustable over the range 0.3-1.5 kA. (9 refs.)

Four-centimeter traveling-wave maser with high amplitude and phase stability [radioastronomy application]

See Entry 116482

42.55 LASING PROCESSES

42.55B General theory of lasing action

112975 Nonequilibrium kinetics of coupled photons and electrons in two-level systems of the laser type. E.Scholl (Inst. für Theoretische Phys. B, RWTH Aachen, Aachen, Germany), P.T.Landsberg.

J. Opt. Soc. Am. (USA), vol.73, no.9, p.1197-206 (Sept. 1983). Rate equations for photons and for electrons in systems of two groups of energy levels (energy separation kT_0) are set up allowing for absorption, stimulated and spontaneous emission, nonradiative transitions, photon loss or dissipation as well as photon gain from the ambient, and an externally applied pumping rate. The rate equations are discussed qualitatively, and the stability of the solutions is obtained by the use of phase portraits. The quantitative discussion includes steady-state photon distributions. Earlier work showing that these distributions can obey the Bose-Einstein law with a nonzero chemical potential kT is taken into the laser regime, which was not covered by recent relevant work. The second-order phase transition that occurs at threshold is established explicitly, and it is shown that the transition requires one to neglect certain generation terms in the rate equations. Some time-dependent solutions of the rate equations are also discussed, using the slaving principle of adiabatic elimination for the electrons. The application of this work to semiconductors is discussed. (28 refs.)

112976 Generation of short laser pulses during coherent amplification. A.V.Nazarkin, I.A.Poluektov, I.I.Sobel'man (P.N. Lebedev Phys. Inst., Acad. of Sci., Moscow, USSR).

JETP Lett. (USA), vol.37, no.7, p.371-5 (5 April 1983). Translation of: *Pisma v Zh. Eksp. & Teor. Fiz. (USSR)*, vol.37, no.7, p.313-16 (5 April 1983). [received: Oct. 1983]

Laser pulses can be frequency-converted by an π -pulse technique with a high energy efficiency and with a substantial reduction in length. (3 refs.)

112977 Bifurcation of solutions of the laser equations. M.Renardy (Math. Res. Center, Univ. of Wisconsin, Madison, WI, USA), H.Haken.

Physica D (Netherlands), vol.8D, no.1-2, p.57-89 (July 1983). The authors prove the existence and stability of bifurcating periodic and quasiperiodic solutions of the equations describing a ring laser. (29 refs.)

112978 Use of the method of ordered operators in the theory of laser systems. Derivation asymptotically exact equations for radiation. I. G.O.Balabanyan (Moscow Inst. of Electronic Engng., Moscow, USSR).

Theor. & Math. Phys. (USA), vol.54, no.1, p.82-92 (Jan. 1983). Translation of: *Teor. & Mat. Fiz. (USSR)*, vol.54, no.1, p.130-46 (Jan. 1983). [received: Sept. 1983]

In the framework of Dicke type models, a theory of laser radiation of two-level systems is constructed. The theory uses the method of ordered operators, which makes it possible to eliminate the atomic variables and obtain an asymptotically exact (in the sense of the thermodynamic limit) hierarchy of equations for the mean values, which depend only on the variables of the radiation. The author also considers the derivation of kinetic equations describing the radiation. (17 refs.)

Stability of a detuned single mode homogeneously broadened ring laser

See Entry 113021

42.55D CO₂ lasers

112979 Operating characteristics of a fixed alignment CO₂ waveguide laser. Z.Kucеровsky, E.Brannen (Dept. of Phys., Univ. of Western Ontario, London, Canada).

Rev. Sci. Instrum. (USA), vol.54, no.9, p.1135-7 (Sept. 1983).

A simple CO₂ waveguide laser with fixed alignment is described and the operating characteristics for various gas mixtures given. Maximum power obtained was 3 W at a working pressure of 120 Torr. Alignment was still maintained after three years of operation. With a fresh filling of gas, power at the 1-W level was routinely obtained over a day's running time. (5 refs.)

Optogalvanic effect study of vibrational relaxation in CO₂ laser process

See Entry 112817

High-speed, low-cost laser-triggered plasma shutter

See Entry 113017

Line selection in carbon dioxide waveguide lasers using diffraction gratings

See Entry 113020

Acoustic wave calibration for CO₂ laser scattering experiments

See Entry 113034

The thermal self-excitation of the beam of a continuous CO₂ laser which interacts with water aerosol

See Entry 113035

42.55F Inert gas lasers

112980 The investigation on low noise discharge tubes in short single-mode He-Ne/CH₄ lasers. K.M.Abramski (Inst. of Telecommunication & Acoustics, Tech. Univ. of Wrocław, Wrocław, Poland).

Jpn. J. Appl. Phys. Part 1 (Japan), vol.22, no.6, p.1068 (June 1983).

The frequency-stabilized He-Ne/CH₄ laser requires a stable radiation to be interacted with the absorber. One of the problems of frequency instability minimalization is to suppress the laser tube noise. The author investigated the noise properties in three types of laser tubes: an ordinary tube, a tube with spacing between capillary elements, as proposed by Suzuki (1970) and a tube with spherical spacing as proposed by Koshelyaevskii et al. (1972). The construction by Suzuki exhibited the best properties for the low noise region close to 2.1 Tr pressure. The tube with the spherical spacing, however, shows a higher threshold of random noise. Both constructions prove to be much better than the ordinary tube. (4 refs.)

112981 Estimated lifetime of an H microwave-pumped laser using a spectroscopic method. A.P.Golovitskii, V.A.Kruzhvalov, T.M.Perchanok (M.I. Kalinin Polytech. Inst., Leningrad, USSR).

Sov. Phys.-Tech. Phys. (USA), vol.28, no.2, p.171-3 (Feb. 1983). Translation of: *Zh. Tekh. Fiz. (USSR)*, vol.53, no.2, p.278-81 (Feb. 1983). [received: Sept. 1983]

He-Ne laser efficiencies can be increased by using microwave excitation, as opposed to pumping by a constant-current discharge. To estimate the lifetime of the microwave-pumped laser the gas composition and pressure were monitored spectroscopically. Calibration curves were obtained by studying how the intensity of a series of spectral lines depended on the pressure and composition of the mixture. While recording the calibration curves the authors also determined the range of pressures and mixture compositions at which lasing is observed at $\lambda=632.8$ nm with power comparable to that needed for lasing using a constant-current discharge. It was noted that the efficiency of the microwave-pumped laser was 3-5 times higher than for a constant-current discharge laser at comparable laser powers. (11 refs.)

Measurements on the He-Ne laser lines near 633 nm

See Entry 111354

Intense proton beam excitation of the high pressure Ar/N₂ laser

See Entry 113014

Generation of continuous-wave 243-nm radiation by sum-frequency mixing

See Entry 113057

42.55H Lasing action in other gas lasers

112982 Gain on the green (504 nm) excimer band of I₂. K.P.Killeen, J.G.Eden (Dept. of Electrical Engng., Univ. of Illinois, Urbana, IL, USA).

Appl. Phys. Lett. (USA), vol.43, no.6, p.539-41 (15 Sept. 1983).

Gain on the green excimer band ($\lambda \sim 504$ nm) of the iodine dimer has been observed in electron-beam-pumped mixture of Ar (or Ne), and hydrogen iodide. A peak gain coefficient of $\gamma > 1.1\%$ cm⁻¹ is measured at 506 nm with a tunable dye laser and the full width at half-maximum (FWHM) of the gain spectrum in Ar diluent is 13 nm. Temporally resolved gain and fluorescence measurements show that the green emission originates from an I₂ ion pair state other than D'. However, strong collisional coupling between the upper states of the UV ($\lambda=342$ nm) and green bands and superfluorescence on the UV band ($1_{3/2} \sim 2$ MW cm⁻²) appear to limit the green gain coefficient to <20% of its small-signal value. Consequently, suppression of superfluorescence on the UV D' \rightarrow A' bands of the homonuclear halogens should lead to a new family of excimer lasers with wavelengths extending from the green in the ultraviolet. (16 refs.)

112983 Relative efficiency of ²⁰⁰Hg ⁷⁹Br, Hg ⁷⁹Br, and HgBr electric discharge lasers. F.E.Hanson, H.Rieger, D.B.Cavanaugh (Naval Ocean Systems Center, San Diego, CA, USA).

Appl. Phys. Lett. (USA), vol.43, no.7, p.622-3 (1 Oct. 1983).

The spectra and relative efficiency of ²⁰⁰Hg ⁷⁹Br, Hg ⁷⁹Br, and HgBr in a small UV preionized electric discharge laser have been measured. There is a similar improvement in laser energy for both isotopic samples compared to the natural abundance mixture which can be attributed to a narrower gain spectrum and consequent higher peak gain. At the highest output measured, the increase in laser energy was about 25%. The authors estimate this is due to roughly 15% increase in small-signal gain. (10 refs.)

112984 Analysis of temporal-length limitations in XeCl lasers. R.Bruzese, D.C.Hogan (Clarendon Lab., Univ. of Oxford, Oxford, England). *Nuovo Cimento B (Italy)*, vol.76B, ser.2, no.1, p.54-61 (11 July 1983). Experimental observations of the development of constrictions in rare-gas halide laser discharges are reported. The onset of constriction is related to the premature termination of both spontaneous emission and laser pulses in a discharge-excited XeCl laser. A mechanism is proposed to account for the onset of constriction in this laser which may be more generally applicable to other discharge-excited devices. (5 refs.)

112985 A 1.5 W CW optically pumped 12.08 μm NH_3 laser. P.Wazen, J.-M.Lourtioz (Inst. d'Electronique Fondamentale, Univ. Paris XI, Orsay, France). *Opt. Commun. (Netherlands)*, vol.47, no.2, p.137-40 (15 Aug. 1983). Order-of-magnitude increase in output power and efficiency has been obtained from the new CW 12.08 μm NH_3 Raman laser optically pumped by a low-pressure CO_2 laser. The 12.08 μm output power is analyzed as a function of the main operational parameters. (6 refs.)

Discharge-pumped high pulse rate excimer laserSee Entry 113018

Passive mode locking of a long pulse XeCl laserSee Entry 113025

Generation of coherent far-infrared radiation using lasersSee Entry 113059

Vibrational kinetics in liquid nitrogen cooled 5% CO-He radio-frequency dischargesSee Entry 113686

42.55K Chemical lasers

(see also 82.40T Chemiluminescence and chemical laser kinetics)

112986 Temperature requirements and corrosion rates in combustion driven hydrogen fluoride supersonic diffusion lasers. P.C.Nordine (Yale Univ., New Haven, CT, USA).

AIAA J. (USA), vol.21, no.8, p.1089-92 (Aug. 1983).

A maximum F-atom yield from F_2 occurs in a combustion driven hydrogen fluoride supersonic diffusion laser (HFSDL) because the amount of fluorine reacted with hydrogen (or deuterium) continues to increase with temperature after most of the unreacted fluorine has been thermally dissociated. A small decrease from the maximum combustor F-atom yield allows a significant decrease in the required temperature and in the corrosion rates that uncooled laser nozzles would display. The temperatures that give F-atom yields equal to 95% of the maximum values were calculated for typical HFSDL combustor pressures and F-atom mole fractions and the corrosion rates of uncooled nozzles were evaluated at these temperatures. The corrosion rates of materials resistant to fluorine attack at the highest temperatures would allow HFSDL applications or test experiments up to several hours duration. (33 refs.)

112987 Simple model for base pressure effects in source flow chemical lasers. K.E.Patterson, J.H.Batteh, S.S.Howie (Sci. Applications Inc., Maritta, GA, USA).

AIAA J. (USA), vol.21, no.8, p.1093-9 (Aug. 1983).

A simple model is developed to investigate the effects of base on the performance of source flow chemical lasers. The laser flowfield is divided into two coupled, one-dimensional regions representing the pure source flow region and a region influenced by the base pressure. The differential equations describing the gasdynamics, mixing, reaction and lasing in the two regions are formulated. The model indicates that lasing performance decreases as the base pressure increases. However, performance can approach and even exceed that of a pure source flow laser if the base pressure is controlled. (11 refs.)

42.55M Lasing action in liquids and organic dyes

112988 Generation of tunable CW radiation near 875 nm. K.W.Giberson, T.H.Jeys, F.B.Dunning (Phys. Dept., Rice Univ., Houston, TX, USA).

Appl. Opt. (USA), vol.22, no.18, p.2768-9 (15 Sept. 1983).

In an attempt to obtain more efficient pumping of the color-center laser, the authors undertook a detailed comparative study of the performance characteristics of Styryl 9 and HITEC using a Spectra-Physics model 375 dye laser equipped with HITEC optics and a high pressure (120-psi) dye circulator. The results of this study are reported. (8 refs.)

Picosecond continuum generation and spectroscopySee Entry 111785

Some ring-dye-laser designs incorporating a low-concentration double dye cell for 20-nsec pump pulsesSee Entry 113006

Preventing beam shifting in a nitrogen-dye laserSee Entry 113012

Generation of continuous-wave 243-nm radiation by sum-frequency mixingSee Entry 113057

Evaluation of spectroscopic parameters for the Pr^{3+} ion in a laser liquidSee Entry 114900

42.55P Lasing action in semiconductors with junctions

112989 Electronic wavelength tuning with semiconductor integrated etalon interference lasers. A.Antreasyan, S.Wang (Dept. of Electrical Engng. & Computer Sci., Univ. of California, Berkeley, CA, USA).

Appl. Phys. Lett. (USA), vol.43, no.6, p.530-2 (15 Sept. 1983).

A novel method for broadband quasicontinuous wavelength tuning in GaAs-GaAlAs semiconductor lasers is reported. The wavelength tuning experiment is performed with an interferometric laser consisting of a resonator with curved and straight segments. By separately pumping different segments of the laser the output wavelength can be tuned over a wide range. The outstanding features of the device are (1) very stable single longitudinal mode and stable transverse mode operation, and (2) a wavelength tuning range of as much as 90 Å. (9 refs.)

112990 Longitudinal mode spectrum of GaAs injection lasers under high-frequency microwave modulation. K.Y.Lau (Ortel Corp., Alhambra, CA, USA), Ch.Harder, A.Yariv.

Appl. Phys. Lett. (USA), vol.43, no.7, p.619-21 (1 Oct. 1983).

Experimental observations of the lasing spectrum of a single mode semiconductor laser under continuous microwave modulation reveal that the lasing spectrum is apparently locked to a single longitudinal mode for optical modulation depths up to ~80%, beyond which the lasing spectrum becomes multimoded, whose envelope width increases very rapidly with further increase in modulation depth. These results are satisfactorily explained by a theoretical treatment which enables one to predict the dynamic lasing spectrum of a laser from its CW lasing spectra at various output powers. (15 refs.)

112991 Fundamental linewidth in solitary, ultranarrow output $\text{PbS}_{1-x}\text{Se}_x$ diode lasers. C.Freed, J.W.Bielinski (Lincoln Lab., MIT, Lexington, MA, USA), W.Lo.

Appl. Phys. Lett. (USA), vol.43, no.7, p.629-31 (1 Oct. 1983).

The fundamental, quantum phase noise limited Lorentzian linewidth was directly measured from the beat-note spectra generated by heterodyning $\text{PbS}_{1-x}\text{Se}_x$ diode lasers with a stable CO gas laser. The experimental results were matched by calculated theoretical line profiles. Linewidths as narrow as 22 kHz full width at half-maximum power were observed. (16 refs.)

112992 Low ohmic multilayer contacts in lead-tin-telluride diode lasers. Ka.Herrmann, B.Sumpf, D.Bohme, M.Hannemann (Sektion Phys., Humboldt-Univ., Berlin, Germany).

Cryst. Res. & Technol. (Germany), vol.18, no.8, p.1083-9 (1983).

The preparation and the influence of low ohmic multilayer thin film contacts of lead-salt homo- and heterolasers on the degradation of lasing parameters during recycling processes between low working temperatures and room temperatures storage are described and discussed in detail. (14 refs.)

112993 Linewidth of a single mode in a multimode injection laser. M.J.Adams (British Telecom Res. Labs., Ipswich, England).

Electron. Lett. (GB), vol.19, no.17, p.652-3 (18 Aug. 1983).

An expression is derived for the quantum noise-limited linewidth of each individual mode in a multimode laser. Numerical calculations show that the mode linewidth of a two-mode 1.55 μm laser is only about 10% larger than that in a single-mode device. (6 refs.)

112994 Quantum mechanical explanation of spontaneous emission K-factor [comment]. J.Arnaud (Univ. des Sci. et Techniques du Languedoc, Bataillon, France).

Electron. Lett. (GB), vol.19, no.17, p.688-9 (18 Aug. 1983).

For original article see *ibid.*, vol.18, p.920-22 (1982). Marcuse has described gain-guided semiconductor lasers as 'inherently lossy'. The author feels that it is misleading to call the gain-guided configuration with net gain 'inherently lossy'. His conclusion is that, whenever there is a net gain, gain-guided modes and index-guided modes do not differ in nature but only in degree. Both are inherently lossless. (2 refs.)

112995 Automatic frequency control in a semiconductor laser and an optical amplifier. S.Koabayashi, T.Kimura (Musashino Electrical Communication Lab., Nippon Telegraph & Telephone Public Corp., Tokyo, Japan).

J. Lightwave Technol. (USA), vol.LT-1, no.2, p.394-402 (June 1983).

Automatic frequency control (AFC) in an injection locked or resonant type amplifier in a AlGaAs semiconductor laser was achieved through using the terminal voltage change induced by light injection. Signal-to-noise in the control signal of 10 dB was obtained when the input optical power was -47 dBm and the optical gain was 51 dB. The AFC was maintained for 3 h with an 0.3 per cent output power fluctuation for 2°C ambient temperature change and 65-MHz frequency stability. Step response showed that the system response time was 1.5 s. Sensitivity to input optical power deteriorates at -49 dBm, with a 53-dB locking gain, because of frequency deviation caused by temperature modulation. The second derivative of the induced voltage and its relation to the optical frequency is constant at 5×10^{-10} [V/(MHz)²] for all input power levels in a buried-heterostructure (BH)-AlGaAs laser. Terminal voltage change induced by light injection is calculated by simple rate equations with a Gaussian-Halperin-Lax (GHL) bandtail model. Good agreement with experimental results was seen. (26 refs.)

112996 Influence of the luminescence saturation effect on the lasing threshold of InGaAsP/InP double heterostructure lasers ($\lambda=1.3 \mu\text{m}$) at $T \geq 300\text{K}$. D.Z.Garbuzov, V.P.Chalyi, V.V.Trukan, Agaev, M.K. (A.F. Ioffe Physicotech. Inst., Acad. of Sci., Leningrad, USSR).

Sov. Phys.-Semicond. (USA), vol.17, no.3, p.338-9 (March 1983). Translation of: *Fiz. & Tekh. Poluprovodn. (USSR)*, vol.17, no.3, p.538-40 (March 1983). [received: Sept. 1983]

Investigates for the first time the influence of the luminescence saturation effect on the nature of the temperature dependence of the threshold of InGaAsP/InP double heterostructures. The results obtained were compared with the data of corresponding investigations carried out in the case of electric current excitation of InGaAsP/InP double heterostructure lasers. (6 refs.)

112997 Degradation behavior of optoelectronic devices. J.Matsui (Fundamental Res. Labs., Nippon Electric Co. Ltd., Kawasaki, Japan).

Defects in Semiconductors II, Symposium Proceedings, Boston, MA, USA, Nov. 1982 (New York, USA: North-Holland 1983), p.477-90

Various degradation modes and features of crystalline defects associated with the degradation observed both in GaAlAs/GaAs and InGaAsP/InP double heterostructure light emitting sources (LEDs and Lasers) are reviewed, noticing similarities and differences between those two material systems. Non-existence of rapid degradation in the quaternary caused by DLD formation (dislocation motion) will be discussed in terms of atomic rearrangements around the dislocation core. (23 refs.)

Generation of single-longitudinal-mode gigabit-rate optical pulses from semiconductor lasers through harmonic-frequency sinusoidal modulationSee Entry 113005

Phase-locked semiconductor laser array with separate contactsSee Entry 113007

Wavelength tuning of GaInAsP/InP integrated laser with butt-jointed built-in distributed Bragg reflectorSee Entry 113008

Far-field distributions of semiconductor phase-locked arrays with multiple contactsSee Entry 113009

Emission frequency stability in single-mode-fibre optical feedback controlled semiconductor lasersSee Entry 113010

1.3 μm InGaAsP/InP multiquantum-well lasers grown by vapour-phase epitaxySee Entry 113011

Facet-coated graded-index separate-confinement-heterostructure single-quantum-well lasers having low degradation rates (<1 percent/kh) at 70°CSee Entry 113013

Recent progress on semiconductor lasersSee Entry 113019

Enhanced frequency modulation in cleaved-coupled-cavity semiconductor lasers with reduced spurious intensity modulationSee Entry 113024

Bandwidth-limited picosecond pulse generation in a synchronously pumped GaAs laser containing a variable absorber diodeSee Entry 113026

Relation between frequency and intensity stabilities in AlGaAs semiconductor laserSee Entry 113027

Estimation of the ultimate frequency stability of semiconductor lasersSee Entry 113028

Direct observation of visibility curve of semiconductor lasersSee Entry 113030

Optical coupling between single-mode semiconductor lasers and strip waveguidesSee Entry 113095

Double-barrel III-V compound vapor-phase epitaxy systems .See Entry 115072

Enhanced InP substrate protection for LPE growth of InGaAsP DH lasersSee Entry 115115

42.55R Lasing action in other solids

(inc. solid Raman lasers)

112998 Rare-earth converters of neodymium laser radiation. A.A.Mak, B.M.Antipenko.

J. Appl. Spectrosc. (USA), vol.37, no.6, p.1458-71 (Dec. 1982). Translation of: *Zh. Prikl. Spektrosk. (USSR)*, vol.37, no.6, p.1029-45 (Dec. 1982). [received: Sept. 1983]

The paper is concerned with an analysis of the status of the authors' research on broadening the spectrum of lasing frequencies of solid-state rare-earth lasers using the method of optical pumping of their media by neodymium laser radiation. In this method, spectral transformation of the radiation of the pumping laser is achieved by processes occurring in optically excited crystals, such as radiative and nonradiative transitions, intercenter transfer of excitation energy, and interaction of excited states, in particular, leading to the summation of the electronic excitation energy. (46 refs.)

112999 The slab geometry laser. W.B.Jones (General Electric Corporate Res. & Dev. Center, Schenectady, NY, USA).

Laser Focus (USA), vol.19, no.9, p.106-14 (Sept. 1983). Solid-state laser material, especially Nd^{3+} -glass, has been used for many years in a slab geometry for high-peak-power laser amplifiers. During the past 10 years, however, a slab geometry has been developed that is useful for high-average-power Q-switched oscillator and amplifier applications. With the near-diffraction-limited beam quality that can be obtained from a solid-state slab laser, nonlinear mixing techniques can be used for efficient conversion of the Nd^{3+} laser wavelength to shorter wavelengths. Efficient down-conversion of a beam wavelength to longer wavelengths can be carried out, for example, by stimulated Raman scattering in high-pressure gases. Thus, the slab geometry development has significantly expanded the utility of the solid-state laser. Nd^{3+} , which lases efficiently at a single wavelength, is the active ion that has been used in most of the slab laser development. In addition, the recent development of Cr^{3+} -doped solid-state materials offers the potential for a high-average-power tunable laser. (8 refs.)

113000 Emerald—a new gem laser material. J.Buchert (Inst. of Ultrafast Spectroscopy & Lasers, City Coll. of New York, New York, NY, USA), R.R.Alfano.

Laser Focus (USA), vol.19, no.9, p.117-23 (Sept. 1983). Describes the physics, current status, and potential of emerald ($\text{Be}_3\text{Al}_2(\text{SiO}_3)_6\text{-Cr}^{3+}$) as a new laser source. Emerald, a wideband tunable laser, has ideal characteristics for fast Q-switching and ultrafast pulse generation by mode-locking. This material improves its performance at elevated temperatures instead of stopping laser action as in many others. (21 refs.)

113001 Chaotic and periodic emission of high power solid state lasers. R.Hauck, F.Hollinger, H.Weber (Dept. of Phys., Univ. of Kaiserslautern, Kaiserslautern, Germany).

Comm. Commun. (Netherlands), vol.47, no.2, p.141-5 (15 Aug. 1983). Nonlinear, dynamical systems even with a few degrees of freedom may show chaotic or periodic behaviour, depending on the parameters of the system. Recently it was demonstrated, both experimentally and theoretically, that the temporal emission of a laser can become chaotic, if several longitudinal modes oscillate [Brunner and Paul (1983), and Abraham et al. (1982)]. The chaotic emission is caused by the nonlinear interaction of the modes and the longitudinal gain structure [Komtomseva et al. (1982)]. In this paper it is pointed out that the transverse mode structure and the radial gain profile produced by the transversal modes, may give rise to temporal instabilities of the laser emission. If the relevant parameters of the laser oscillator—Fresnel number, resonator losses, pump rate—exceed certain critical values, the output intensity becomes unstable. The damped relaxation oscillation changes into undamped periodic oscillation or, with increasing values of the above parameters, into chaotic emission. The theory, using the nonlinear Kirchhoff-Fresnel integral equation and the rate equation approach, is confirmed by experimental results. (14 refs.)

113002 Cascade laser generation by Er^{3+} ions in YAlO_3 crystals by the scheme $^4\text{S}_{3/2} \rightarrow ^4\text{I}_{13/2} \rightarrow ^4\text{I}_{11/2} \rightarrow ^4\text{I}_{13/2}$. A.A.Kaminskii (A.V. Shubnikov Inst. of Crystallography, Acad. of Sci., Moscow, USSR).

Sov. Phys.-Dokl. (USA), vol.27, no.12, p.1039-41 (Dec. 1982). Translation of: *Dokl. Akad. Nauk SSSR*, vol.267, no.4-6, p.1106-9 (Dec. 1982). [received: Sept. 1983] New data are presented on the spectral composition of cascade stimulated emission of Er^{3+} ions in a YAlO_3 crystal (space group $\text{D}_{2h}^{16}\text{-Pbnm}$) at ~ 110 and 300K in the two sequential losing channels $^4\text{S}_{3/2} \rightarrow ^4\text{I}_{9/2}$ and $^4\text{I}_{11/2} \rightarrow ^4\text{I}_{13/2}$ with an intermediate $^4\text{I}_{9/2} \rightarrow ^4\text{I}_{11/2}$ ($\Delta E \approx 1990 \text{ cm}^{-1}$). From the data on the kinetics of cascade generation it was concluded that there occurs stimulated emission of extremely-high-frequency phonons between the states $^4\text{I}_{9/2}$ and $^4\text{I}_{11/2}$ in $\text{YAlO}_3\text{-Er}^{3+}$. (13 refs.)

Fading properties of a NaF:F_2^{++} color center laserSee Entry 113015

A novel distributed feedback colour centre laserSee Entry 113016

Dewar design for optically pumped semiconductor ring laserSee Entry 113022

Large crystal sapphire opticsSee Entry 113069

42.55T Free electron lasers

113003 Study of gain, bandwidth, and tunability of a millimeter-wave free-electron laser operating in the collective regime. S.H.Gold, W.M.Black, H.P.Freund, V.L.Granatstein, R.H.Jackson, P.C.Efthimion, A.K.Kincaid (Naval Res. Lab., Washington, DC, USA).

Phys. Fluids (USA), vol.26, no.9, p.2683-8 (Sept. 1983). Frequency-resolved measurements of the emission of a collective free-electron laser operating at millimeter wavelengths have shown emission spectra that agree well with theoretical predictions for the collective free-electron laser instability. Broad tunability, moderate emission linewidths, and high single-frequency gain have been observed. In addition, adjusting the axial field in the end region of the interaction has been found in some cases to cause a large increase in measured power and efficiency. (16 refs.)

113004 Sources of stimulated radiation using resonance electron accelerators. D.F.Alferov, Yu.A.Bashmakov, K.A.Belovintsev, E.G.Bessonov, A.V.Serov, P.A.Cherenkov (P.N. Lebedev Phys. Inst., Acad. of Sci., Moscow, USSR).

Sov. Phys.-Tech. Phys. (USA), vol.28, no.2, p.167-71 (Feb. 1983). Translation of: *Zh. Tekh. Fiz. (USSR)*, vol.53, no.2, p.270-7 (Feb. 1983). [received: Sept. 1983]

The main properties of spontaneous incoherent and coherent emission from relativistic particles in undulators are briefly discussed. Basic aspects of the classical theory of stimulated electron emission in undulators are considered, and an assessment is made of the possible use of standard electron accelerators in designing undulator lasers with a broad electromagnetic emission spectrum. (44 refs.)

Electron beam focusing effects and matching conditions in plane periodic magnetsSee Entry 112508

Optimization of a permanent magnet undulator for free electron laser studies on the ACO storage ringSee Entry 112516

42.60 LASER SYSTEMS AND LASER BEAM APPLICATIONS

113005 Generation of single-longitudinal-mode gigabit-rate optical pulses from semiconductor lasers through harmonic-frequency sinusoidal modulation. H.Kawaguchi, K.Otsuka (Nippon Telegraph & Telephone Public Corp., Tokyo, Japan).

Electron. Lett. (GB), vol.19, no.17, p.668-9 (18 Aug. 1983). Generation of optical pulses at gigabit rates from semiconductor lasers by means of harmonic-frequency sinusoidal injection current modulation has been demonstrated for the first time. It was confirmed that these optical pulses consisted of one longitudinal oscillating mode because of the presence of a 'self-optical injection-locking effect'. (6 refs.)

Collisionless cyclotron absorption of photons by electrons in a laser beamSee Entry 112969

42.60B Design of specific laser systems

113006 Some ring-dye-laser designs incorporating a low-concentration double dye cell for 20-nsec pump pulses. J.Nildebrandt.

Appl. Opt. (USA), vol.22, no.18, p.2930-2 (15 Sept. 1983). Using a special cell design for low dye concentrations that limits the thickness of the transversely pumped dye solution by an exit window for the pump beam (1) sharp longitudinal modes with steep spectral line shapes develop because of the low small signal gain, and (2) the beam profile follows a Gaussian over 3 decades because both pump windows act as a mode selective aperture. The rest of the pump beam excites a second dye solution, separated from the first by a 1-cm thick window, so that a variety of different ring designs can easily be tested. The tendency of the linear resonator to form a double peaked output cross section was not observed with the running wave. (9 refs.)

113007 Phase-locked semiconductor laser array with separate contacts. J.Katz (Jet Propulsion Lab., California Inst. of Technol., Pasadena, CA, USA), E.Kapon, C.Lindsey, S.Margalit, U.Shreter, A.Yariv.

Appl. Phys. Lett. (USA), vol.43, no.6, p.521-3 (15 Sept. 1983). A new monolithic phase-locked semiconductor laser array has been fabricated. Employing two-level metallization, each of the eight elements in the array has a separate contact, thus making it possible to compensate for device nonuniformities and control the near-field and far-field patterns. Threshold currents are approximately 60 mA for each 5- μm -wide laser in the array. Phase locking has been observed via the narrowing of the far-field pattern. Experimental results are compared to those obtained from the same arrays operated with all the lasers connected in parallel. (13 refs.)

113008 Wavelength tuning of GaInAsP/InP integrated laser with butt-jointed built-in distributed Bragg reflector. Y.Tohmori, Y.Suematsu, H.Tsushima, S.Arai (Dept. of Phys. Electronics, Tokyo Inst. of Technol., Tokyo, Japan).

Electron. Lett. (GB), vol.19, no.17, p.656-7 (18 Aug. 1983). Fine tuning of lasing wavelength was achieved with a butt-jointed built-in DBR laser integrated with an additional tuning waveguide. The plasma effect of the injected carrier was utilised. The wavelength shift of 4.0 Å was demonstrated by an injected tuning current of 4.1 mA. (5 refs.)

113009 Far-field distributions of semiconductor phase-locked arrays with multiple contacts. J.Katz (Jet Propulsion Lab., Pasadena, CA, USA), E.Kapon, C.Lindsey, S.Margalit, A.Yariv.

Electron. Lett. (GB), vol.19, no.17, p.660-2 (18 Aug. 1983). Experimental results of far-field patterns of semiconductor laser arrays with multiple contacts are reported. It is found that, by tailoring the distribution of the currents through the array elements, narrow single-lobe patterns—which are more useful in most applications—can be obtained from arrays that usually operate in a double-lobe mode. A diffraction-limited 1.8°-wide far-field pattern was obtained from a three-element array. (10 refs.)

113010 Emission frequency stability in single-mode-fibre optical feedback controlled semiconductor lasers. F.Favre, D.Le Guen (CNET, Lannion, France).

Electron. Lett. (GB), vol.19, no.17, p.663-5 (18 Aug. 1983). A newly designed semiconductor laser emitter with adjustable linewidth by controlling the coupling to a single-mode fibre is described with emphasis on thermal requirements to obtain a high-frequency stability. A stable operation has been achieved during more than 1 h using an AlGaAs laser diode with optical feedback from a 50 cm-long single-mode fibre resulting in a 50-fold reduction of the spectral linewidth. (5 refs.)

113011 1.3 μm InGaAsP/InP multiquantum-well lasers grown by vapour-phase epitaxy. T.Yanase, Y.Kato, I.Mito, M.Yamaguchi, K.Nishi, K.Kobayashi, R.Lang (Opto-Electronics Res. Labs., NEC Corp., Kawasaki, Japan).

Electron. Lett. (GB), vol.19, no.17, p.700-1 (18 Aug. 1983). Low-threshold InGaAsP/InP multiquantum-well lasers emitting at 1.3 μm have been successfully fabricated. The multilayer structure has been grown by hydride transport vapour-phase epitaxy with a double-growth chamber reactor. Broad-area structure threshold current density as low as 1.2 kA/cm^2 has been obtained. (10 refs.)

113012 Preventing beam shifting in a nitrogen-dye laser. R.C.Arnold (IBM Corp., Armonk, NY, USA).

IBM Tech. Disclosure Bull. (USA), vol.26, no.1, p.9-10 (June 1983). A shim was created to hold the dye cell rigid, which solved the beam shifting problem. (no refs.)

113013 Facet-coated graded-index separate-confinement-heterostructure single-quantum-well lasers having low degradation rates (<1 percent/kh) at 70°C. R.D.Dupuis, R.L.Hartman, F.R.Nash (Bell Labs., Murray Hill, NJ, USA).

IEEE Electron Device Lett. (USA), vol.EDL-4, no.8, p.286-8 (Aug. 1983). The results of accelerated life testing of $\text{Al}_x\text{Ga}_{1-x}\text{As-GaAs}$ single-quantum-well (QW) lasers having graded-index (GRIN) separate-confinement heterostructure (SCH) active regions are reported. These results are the first to show that lasers grown by MOCVD can have low degradation rates (<1 percent/kh) at 70°C and are also the first light-emitting lifetime data for GRIN-SCH quantum-well lasers. The laser structures were grown by metal-organic chemical vapor deposition (MOCVD) at atmospheric pressure using an uninterrupted growth sequence. Shallow proton-bombarded $5\text{-}\mu\text{m}\times 250\text{-}\mu\text{m}$ stripe-geometry lasers were fabricated from these wafers and lasers with and without Al_2O_3 facet coatings were life tested at 70°C and 5 mW per mirrors facet. Facet-coated lasers have lived longer than 1100 h with degradation rates as low as 0.5 percent/kh. (18 refs.)

113014 Intense proton beam excitation of the high pressure Ar/N₂ laser. L.G.Wiley, D.A.Hammer (Lab. of Plasma Studies, Cornell Univ., Ithaca, NY, USA).

J. Appl. Phys. (USA), vol.54, no.9, p.4806-20 (Sept. 1983). In this paper, parametric studies are presented of a high pressure Ar/N₂ gas laser excited by an intense proton beam from a magnetically insulated diode. Using power deposition of up to a 140 MW/cm², gas pressure up to 3040 Torr, variable N₂ fraction (5%-90%), and several mirror reflectivities and gain lengths, laser power (up to 500 kW), efficiency ($\leq 0.4\%$), gain, threshold conditions, and spectral characteristics have been studied. Laser action was achieved at three wavelengths in the second positive band of N₂: 337.1, 357.1, and 380.5 nm. Comparison of the observations with predictions of a model showed that emission at all three wavelengths was expected, and initiation times and pulse durations of the three lines were accurately predicted. Observed similarities and differences between proton beam and electron beam excitation of the Ar/N₂ laser are discussed. (36 refs.)

113015 Fading properties of a NaF:F₂⁺⁺ color center laser. H.Eisele, H.J.Paus, J.Wagner (Phys. Inst., Univ. Stuttgart, Stuttgart, Germany), M.Leduc.

J. Appl. Phys. (USA), vol.54, no.9, p.4821-5 (Sept. 1983). An investigation of the temporal stability of a color center laser based on F₂⁺⁺ centers in NaF is presented. It is found that the fading of the output power strongly depends on pump power, intracavity power, pump wavelength, and temperature. Optimum conditions for operation were thus derived to improve the temporal stability of this tunable laser. (22 refs.)

113016 A novel distributed feedback colour centre laser. T.Kurobiri, N.Takeuchi (Faculty of Technol., Kanazawa Univ., Kanazawa, Japan).

Opt. Acta (GB), vol.30, no.10, p.1363-6 (Oct. 1983). A novel distributed feedback (DFB) colour centre laser is proposed. The feedback mechanism is provided by the periodic spatial modulation of the refractive index which is induced by applying an acoustic wave to the crystal coloured by X-ray irradiation. Numerical estimates for this method are also presented. (19 refs.)

113017 High-speed, low-cost laser-triggered plasma shutter. M.Hasselbeck, L.Huang, S.C.Hsu, H.S.Kwok (Dept. of Electrical & Computer Engng., State Univ. of New York, Buffalo, NY, USA).

Rev. Sci. Instrum. (USA), vol.54, no.9, p.1131-4 (Sept. 1983). Design and construction of a CO₂ laser-triggered plasma shutter is described. An inexpensive pyroelectric detector and a novel needle-resistor spark gap, requiring an applied voltage of less than 500 V, are employed. The total electronic delay can be made to be less than 15 ns with subnanosecond jitter. This plasma shutter finds applications in producing picosecond CO₂ laser pulses and in optical isolation. (10 refs.)

113018 Discharge-pumped high pulse rate excimer laser. A.Vill, T.Klementi, V.Mikhel'son, V.Altukhov.

Toim. Eesti NSV Tead. Akad. Fuus. Mat. (USSR), vol.32, no.1, p.109-13 (1983). In Russian. The authors developed and investigated a compact excimer pulse-periodic XeF laser with comparatively high efficiency and with high pulse energy. They show how it is possible to choose optimal parameters for the pumping system and the laser radiation by way of a model calculation of the discharge current and voltage circuit oscillograms. (6 refs.) V.G.P.

113019 Recent progress on semiconductor lasers. S.Wang (Dept. of EECS, Univ. of California, Berkeley, CA, USA).

Wescon/82 Conference Record, Anaheim, CA, USA, 14-16 Sept. 1982 (El Segundo, CA, USA: Electron. Conventions 1982), p.26-1/1. Semiconductor lasers for signal processing and optical fiber communication require a stable radiation pattern and single longitudinal mode operation. Two-dimensional guiding structures for lateral mode stability are reviewed. Current research on improving longitudinal mode behavior is discussed for laser operation over an extended temperature range and at a high data rate. (no refs.)

Operating characteristics of a fixed alignment CO₂ waveguide laser See Entry 112979

Line selection in carbon dioxide waveguide lasers using diffraction gratings See Entry 113020

Dewar design for optically pumped semiconductor ring laser See Entry 113022

42.60D Laser resonators and cavities

113020 Line selection in carbon dioxide waveguide lasers using diffraction gratings. A.M.Holohan, S.L.Pruntz (Dept. of Electrical Engng., Univ. Coll., Cork, Ireland).

Infrared Phys. (GB), vol.23, no.3, p.149-56 (May 1983). Treats theoretically the coupling losses which arise in square dielectric waveguide CO₂ lasers when one element of the optical resonator is a diffraction grating. These losses are due to imperfect coupling of the radiation which is launched from the end of the guide to the grating and returned from the grating back to the guide. The results of the calculations show that the coupling efficiency is a sensitive function of radiation wavelength. This result is then used to investigate the ability of a 150 lines/mm diffraction grating to resolve adjacent rotational-vibrational transitions in the CO₂ emission. It is shown that 'line-hopping' places a limitation on the maximum tunability which can be obtained and is a result of the poor discrimination at the grating surface especially in the case of waveguide lasers having much reduced apertures. Computations based on the scaling laws are employed to maximise the tunability as a function of waveguide aperture taking into account limitations imposed by 'line-hopping', cut-off and the optical resonator frequency offset conditions of $c/4L$. Comparisons are made between

theory and experiment, and design guidelines for the construction of widely tunable CO₂ waveguide lasers are presented graphically. (19 refs.)

113021 Stability of a detuned single mode homogeneously broadened ring laser. P.Mandel, H.Zeghlache (Service de Chimie-Physique II, Univ. Libre de Bruxelles, Bruxelles, Belgium).

Opt. Commun. (Netherlands), vol.47, no.2, p.146-50 (15 Aug. 1983). Studies analytically the influence of detuning on the properties of a homogeneously broadened single mode ring laser. In the good cavity domain the stationary output is stable. In the bad cavity domain the stationary output becomes unstable via a Hopf bifurcation. Near linear center this Hopf bifurcation is subcritical, leading to unstable small amplitude oscillations. Far from line center this Hopf bifurcation is supercritical and leads to stable small amplitude output. (15 refs.)

113022 Dewar design for optically pumped semiconductor ring laser. A.Fuchs, M.M.Salour (Dept. of Electrical Engng. & Computer Sci., MIT, Cambridge, MA, USA).

Rev. Sci. Instrum. (USA), vol.54, no.9, p.1143-4 (Sept. 1983). A simple liquid-nitrogen Dewar has been constructed to hold semiconductor platelets for use in a ring laser assembly. Laser action in an external ring cavity is observed when the platelets are longitudinally pumped by an Ar⁺ laser. Microscope objectives mounted outside the Dewar are used to focus the pump beam as well as the lasing beam into the crystal. Positioning of the platelets in horizontal and vertical directions is accomplished by attaching the Dewar to an xyz stage. (8 refs.)

113023 High-Q open resonant structures with a sparse spectrum. A.A.Kuraev, E.I.Nefedov, A.Ya.Slepian, G.Ya.Slepian (Inst. of Radio Engng. & Electronics, Acad. of Sci., USSR).

Sov. Tech. Phys. Lett. (USA), vol.8, no.11, p.603 (Nov. 1982). Translation of: *Pisma v Zh. Tekh. Fiz. (USSR)*, vol.8, no.21-22, p.1402-3 (Nov. 1982). [received: Sept. 1983]

Calls attention here to the possibility of developing high-Q (in particular, coaxial) open resonant structures using surface magnetic modes with a nonunit radial index. Coaxial H_{m1q} open resonant structures can be constructed because the 'dispersion' characteristics of H_{m1} waves have a descending region as the ratio of radii of the coaxial structure, $\Delta = a/b$, decreases from 0 to 1 (a and b are the radii of the inner and outer parts of the coaxial structure): $\tilde{\kappa} = \tilde{\kappa}(\Delta)$, where $\tilde{\kappa}$ is the transverse eigenvalue for H_{m1} magnetic waves. Knowing the dependence $\tilde{\kappa} = \tilde{\kappa}(\Delta)$ for magnetic modes one can tailor the profile of the structure to produce the required configuration of an open resonant structure with 'nonfocusing' mirrors operating in H_{m1q}, $n \geq 2$ modes. The remarkable property of open resonant structures with nonfocusing mirrors—one mode per octave—is preserved, and the Q turns out to be considerably higher because of the larger working volume (in comparisons with an H_{m1q} open resonant structure). (3 refs.)

Bifurcation of solutions of the laser equations See Entry 112977

The investigation on low noise discharge tubes in short single-mode He-Ne/CH₄ lasers See Entry 112980

Electronic wavelength tuning with semiconductor integrated etalon interference lasers See Entry 112989

Some ring-dye-laser designs incorporating a low-concentration double dye cell for 20-nsec pump pulses See Entry 113006

Enhanced frequency modulation in cleaved-coupled-cavity semiconductor lasers with reduced spurious intensity modulation See Entry 113024

Generation of continuous-wave 243-nm radiation by sum-frequency mixing See Entry 113057

Application of the theory of image formation to calculations on optical resonators See Entry 113076

42.60F Laser beam modulation

113024 Enhanced frequency modulation in cleaved-coupled-cavity semiconductor lasers with reduced spurious intensity modulation. W.T.Tsang, N.A.Olsson (Bell Labs., Murray Hill, NJ, USA).

Appl. Phys. Lett. (USA), vol.43, no.6, p.527-9 (15 Sept. 1983). The authors have observed enhanced analog frequency modulation in a cleaved-coupled-cavity (C³) laser. One diode is DC biased above threshold to produce the desired output power and the other diode, the modulator, is biased below threshold with a DC current and a small modulating current superimposed to achieve analog frequency modulation of the output beam. Comparing with direct analog frequency modulation of a conventional semiconductor laser, the C³ laser has allowed the authors to obtain significantly larger frequency deviation with negligible spurious intensity modulation. Further, the present frequency modulation response is also much more uniform with respect to modulation frequency. In addition, this scheme is applicable to C³ lasers formed from all laser structures. (18 refs.)

113025 Passive mode locking of a long pulse XeCl laser. S.Watanabe, M.Watanabe, A.Endoh (Inst. for Solid State Phys., Univ. of Tokyo, Tokyo, Japan).

Appl. Phys. Lett. (USA), vol.43, no.6, p.533-5 (15 Sept. 1983). Passive mode locking has been achieved in a XeCl laser with the gain duration over 150 ns. The saturation characteristics of absorber dyes including BBQ, BPBD, and PTP were measured, resulting in the lowest saturation intensity of BBQ. The almost 100% modulated train of 12 pulses was achieved with the rapid pulse sharpening to the duration of ~ 2 ns, when BBQ was used as a saturable absorber. (17 refs.)

113026 Bandwidth-limited picosecond pulse generation in a synchronously pumped GaAs laser containing a variable absorber diode. W.A.Stallard, D.J.Bradley (Phys. Dept., Trinity Coll., Dublin, Ireland).

Appl. Phys. Lett. (USA), vol.43, no.7, p.626-8 (1 Oct. 1983). The authors report combined active and passive mode locking of an external cavity semiconductor laser containing one absorbing and one gain diode. Compared with active mode locking alone this method requires less critical tuning of the RF modulation frequency and is not limited to operation close to threshold. Colliding pulse mode locking is achieved by placing the absorber diode at one end of the cavity so as to increase the effective absorber cross section. Streak camera measurements show that the pulse trains are free from background noise and that the 30-ps pulses are bandwidth limited with sech² profiles. (23 refs.)

Generation of short laser pulses during coherent amplification See Entry 112976

Longitudinal mode spectrum of GaAs injection lasers under high-frequency microwave modulation See Entry 112990

Automatic frequency control in a semiconductor laser and an optical amplifier See Entry 112995

Emerald—a new gem laser material See Entry 113000

- Laser-beam attenuation measurement using acousto-optic modulator** See Entry 113029
- Beam-splitter mount for efficient monitoring of mode-locked and synchronously pumped CW lasers** See Entry 113033
- Transient stimulated Raman scattering of femtosecond laser pulses** See Entry 113052

42.60H Optical problems related to properties and interactions of laser beams

113027 Relation between frequency and intensity stabilities in AlGaAs semiconductor laser. H.Tsuchida, T.Tako (Res. Lab. of Precision Machinery & Electronics, Tokyo Inst. of Technol., Yokohama, Japan). *Jpn. J. Appl. Phys. Part 1 (Japan)*, vol.22, no.7, p.1152-6 (July 1983). The frequency and intensity stabilities of an AlGaAs semiconductor laser are measured during free-running, frequency-stabilized and intensity-stabilized operations. Each stabilization mode is achieved by controlling the injection current. The experimental results are discussed and the causes for the frequency and intensity fluctuations considered. The feasibility of simultaneously stabilizing both the frequency and the intensity is also discussed. It is concluded that simultaneous stabilization cannot be achieved by controlling the injection current alone. (25 refs.)

113028 Estimation of the ultimate frequency stability of semiconductor lasers. M.Ohtsu (Internat. Cooperation Center for Sci. & Technol., Tokyo Inst. of Technol., Tokyo, Japan), H.Fukuda, T.Tako, H.Tsuchida. *Jpn. J. Appl. Phys. Part 1 (Japan)*, vol.22, no.7, p.1157-66 (July 1983). The frequency stabilities of 0.8 μm AlGaAs lasers were estimated by using the Allan variance as a measure of the stability. The contributions of the quantum noise (the spontaneous emission, carrier, and current noise) and additional noise (current source noise and temperature noise) are given. The highest frequency stability of the free-running laser was estimated to be 6.3×10^{-11} at an integration time of 0.1 s. It is shown that the frequency stability of the stabilized laser is limited by the quantum noise. The estimated results were compared with the experimental results and with the estimated stability of 3.39 μm He-²²Ne lasers. The derivations of the spectral width from the frequency stability are also given. The narrowest limit of the spectral width was estimated to be 5.5 MHz (HWHM) for $I/I_0 = 1.3$, while the corresponding experimental result was 6.2 MHz for a channeled-substrate planar (CSP)-type laser. (33 refs.)

113029 Laser-beam attenuation measurement using acousto-optic modulator. T.Kawakami, I.Yokoshima (Electrotech. Lab., Ibaraki, Japan). *Electron. Lett. (GB)*, vol.19, no.17, p.653-4 (18 Aug. 1983). A laser-beam attenuation-measurement method using the first-order diffraction from an acousto-optic modulator is developed. The attenuation is determined from the voltage of the 30 MHz driving signal of the modulator. A value of attenuation of more than 50 dB can be measured at 633 nm. (3 refs.)

113030 Direct observation of visibility curve of semiconductor lasers. W.Eickhoff, E.Brinkmeyer, H.Barfuss (Tech. Univ. Hamburg-Harburg, Hamburg, Germany). *Electron. Lett. (GB)*, vol.19, no.18, p.739-40 (1 Sept. 1983).

A method for the determination of the linewidth of semiconductor lasers is demonstrated. It employs tuning of the laser frequency, observation of the backscattered light from a single-mode fibre and Fourier-transform evaluation. (3 refs.)

113031 Thermoelastic stresses produced in an absorbing layer by the action of a laser pulse. A.A.Bakeev, A.P.Sobolev, V.I.Yakovlev. *J. Appl. Mech. & Tech. Phys. (USA)*, vol.23, no.6, p.821-6 (Nov.-Dec. 1982). Translation of: *Zh. Prikl. Mekh. & Tekh. Fiz. (USSR)*, vol.23, no.6, p.92-8 (Nov.-Dec. 1982). [received: Sept. 1983]

By solving the thermoelasticity problem for a semispace, the dimensionless parameter range characteristic of the material and laser action are determined, in which exfoliation of the irradiated surface is possible. It is obvious that with other conditions being equal the thermoelastic stress is highest if cooling of the absorbing layer of material over the duration of energy liberation can be neglected. (12 refs.)

113032 Vernier fringe-counting device for laser wavelength measurements. A.Kahane, M.S.O'Sullivan, N.M.Sanford, B.P.Stoicheff (Dept. of Phys., Univ. of Toronto, Toronto, Ontario, Canada). *Rev. Sci. Instrum. (USA)*, vol.54, no.9, p.1138-42 (Sept. 1983).

A vernier fringe-counting circuit designed for use with a Kowalski-type wavemeter is described. Wavelength measurements made with this device have a high reproducibility of 5×10^{-9} (or 1/50 of a fringe) and measured accuracy of 4×10^{-9} . The results of accuracy tests are presented along with systematic errors incurred when the wavelengths of two He-Ne lasers (632.9 nm) are compared by the vernier method. (14 refs.)

113033 Beam-splitter mount for efficient monitoring of mode-locked and synchronously pumped CW lasers. A.van Hoek (Dept. of Molecular Phys., Agricultural Univ., Wageningen, Netherlands), A.J.W.G.Visser. *Rev. Sci. Instrum. (USA)*, vol.54, no.9, p.1145-7 (Sept. 1983).

Monitoring the optical pulses from mode-locked and synchronously pumped continuous wave (CW) lasers, reference beams are taken from the main beams with beam splitters. Depending on the angle with respect to the incident beam and the direction of the rotation axis of the beam splitter, light fractions of different polarizations can be selected. Based on practical and theoretical considerations an alternative beam-splitter mount has been designed which efficiently utilizes the available optical power. (14 refs.)

113034 Acoustic wave calibration for CO₂ laser scattering experiments. J.F.Valley, R.E.Slusher (Bell Labs., Murray Hill, NJ, USA). *Rev. Sci. Instrum. (USA)*, vol.54, no.9, p.1157-62 (Sept. 1983).

An acoustic wave technique is described which provides an absolute calibration of the amplitude of the light scattered from a CO₂ laser light scattering. Using simple vibrating membranes, acoustic waves with wavelengths from a few millimeters to several centimeters can be generated with accurately measured amplitudes. Laser scattering from these waves verifies that wavelengths as long as 2 cm can be resolved with small-angle CO₂ laser scattering. For the case of heterodyne detection, calibration of the scattered wave amplitudes is obtained to within $\pm 20\%$. (11 refs.)

113035 The thermal self-excitation of the beam of a continuous CO₂ laser which interacts with water aerosol. S.A.Armand, V.P.Bisyrin, V.V.Yefremenko, M.A.Kolosov, L.N.Kornilov. *Radio Eng. & Electron. Phys. (USA)*, vol.27, no.11, p.86-90 (Nov. 1982). Translation of: *Radiotekh. & Elektron. (USSR)*, vol.27, no.11, p.2162-6 (Nov. 1982). [received: Sept. 1983]

The results of measurement of divergence of the beam of a continuous CO₂ laser are given when such a beam propagates through an evaporating water aerosol. The measurements are taken by using transit bolometers for measure-

ment of distribution of intensity in the transverse cross-section of the beam. Experimental results are compared with computations of thermal self-defocusing by using the thin-lens approximation. (12 refs.)

Flow field testing with a 64 parallel channel heterodyne interferometer See Entry 111751

The spot of Arago and its role in wavefront analysis See Entry 112923

Study of spatial filtering using LOTS-MCI See Entry 112924

Stationarity of speckle in laser refraction See Entry 112940

Emission frequency stability in single-mode-fibre optical feedback controlled semiconductor lasers See Entry 113010

Emission of melt during laser vaporization of metallic films See Entry 113999

42.60K Optical problems related to applications of laser beams

Surface coordinate measurement using high resolution TV cameras See Entry 111635

Comparison of optical depth-measurement methods on real metal surfaces with sine-phase-gratings See Entry 111638

Uncertainty of measurements made by laser interferometer See Entry 111647

Performance characteristics of a small side-window photomultiplier in laser single-photon fluorescence decay measurements See Entry 111783

Optimization of a permanent magnet undulator for free electron laser studies on the ACO storage ring See Entry 112516

Thermal aspects of magneto-optical recording See Entry 112948

Ablative optical recording using organic dye-in-polymer thin films: some mechanistic aspects See Entry 112949

Thermoelastic stresses produced in an absorbing layer by the action of a laser pulse See Entry 113031

Methods for the investigation of laser mirrors for laser gyros See Entry 113075

Laser alignment of parallel mechanical axes 10 metres apart See Entry 113153

Comparison of photon correlation laser Doppler anemometry data processing techniques See Entry 113526

Thermal stress limitations to laser fire polishing of glasses See Entry 115376

Stress activated Raman scattering and microcrack detection See Entry 115461

Laser instrumentation: analytical uses are growing See Entry 115598

42.65 NONLINEAR OPTICS

113036 Nonlinear magneto-optics in semiconductors. R.B.Dennis, H.A.MacKenzie (Dept. of Phys., Heriot-Watt Univ., Edinburgh, Scotland). *Proc. SPIE Int. Soc. Opt. Eng. (USA)*, vol.369, p.237-44 (1983). (SPIE Proceedings of the Max Born Centenary Conference OPTICS 82, ECOSA 82, Edinburgh, Scotland, 7-10 Sept. 1982).

Extends to finite magnetic fields the study of the exceptionally large value of $\chi^{(3)}$ found for moderate radiation intensities close to resonance with interband transitions in Indium Antimonide (InSb). The intensity dependence of both interband magneto-absorption and dispersion for transitions between individual identifiable Landau levels, was examined experimentally. The intensity dependence of the magnetic field dependent oscillations, in non-resonant interband Faraday rotation, provided a sensitive technique for the study of changes in magneto-dispersion. An intensity induced rotation corresponding to a maximum nonlinear refractive index of $-9 \times 10^{-5} \text{ W}^{-1} \text{ cm}^2$ ($\chi^{(3)}$ can 10^{-1} esu , or $ca 10^{-9} \text{ m}^2 \text{ V}^{-2}$) was observed. This effect exhibited resonant enhancement as the pump photon energy approached that of both the fundamental bandgap and an acceptor transition and showed saturation at increased incident intensity. The effect was determined to be primarily the result of the blocking of the interband transition by photoexcited carriers. The results are compared with two new microscopic models, the direct saturation model, which assumes a non-thermal distribution of the photoexcited carriers, and the dynamic Burstein-Moss model, which assumes a thermalised distribution. Comparison with experimental results yields values for the electron-hole dephasing time of T_2 of the order of 3 ps and an interband relaxation time of T_1 of the order of 100 ns. (13 refs.)

113037 Resonant modes in a dispersive cavity. K.Gardner, J.M.Vaughan (Royal Signals & Radar Establ., Gt. Malvern, England). *Proc. SPIE Int. Soc. Opt. Eng. (USA)*, vol.369, p.253-56 (1983). (SPIE Proceedings of the Max Born Centenary Conference OPTICS 82, ECOSA 82, Edinburgh, Scotland, 7-10 Sept. 1982). During some initial investigations of bistability, in an optical cavity containing calcium vapour, a hitherto unrecorded modification of the resonant mode separation was found. This unusual phenomenon occurs symmetrically on either side of the absorption line and is shown to result from the dispersive character of the cavity. (3 refs.)

113038 Low intensity nonlinear refraction in cadmium mercury telluride at 10.6 μm . G.Parry, J.R.Hill, A.Miller (Royal Signals & Radar Establ., Gt. Malvern, England).

Proc. SPIE Int. Soc. Opt. Eng. (USA), vol.369, p.266-8 (1983). (SPIE Proceedings of the Max Born Centenary Conference OPTICS 82, ECOSA 82, Edinburgh, Scotland, 7-10 Sept. 1982). The authors report the observation of large intensity dependent refractive index changes in cadmium mercury telluride at 175K and at 10.6 μm wavelength. The effects are observed by measuring changes in the half power width of a Gaussian laser beam focused through a thin sample of the material. (8 refs.)

113039 Solitons in single mode optical fibres. A.D.Boardman, G.S.Brown, G.S.Cooper (Dept. of Phys., Univ. of Salford, Salford, England). *Proc. SPIE Int. Soc. Opt. Eng. (USA)*, vol.369, p.422-8 (1983). (SPIE Proceedings of the Max Born Centenary Conference OPTICS 82, ECOSA 82, Edinburgh, Scotland, 7-10 Sept. 1982).

A first principles derivation is given of the evolution equation for nonlinear pulse propagation in an optical fibre. It avoids many of the difficulties encountered in some other theories and emphasises that waveguide effects can be included in a natural and logical manner. It is preceded by a brief review of the principal features of solitons in optical guides, and a critical discussion is given of previous theoretical descriptive roles of waveguide and material dispersion and some examples of the behaviour of solitary wave solutions of the nonlinear Schrödinger equation. (19 refs.)

113040 Hysteresis in the reflection of light at the boundary with a nonlinear medium in the presence of a transition layer. B.B.Boiko, N.S.Petrov. *J. Appl. Spectrosc. (USA)*, vol.37, no.6, p.1386-90 (Dec. 1982). Translation of: *Zh. Prikl. Spektrosk. (USSR)*, vol.37, no.6, p.949-55 (Dec. 1982). [received: Sept. 1983]

Hysteresis properties in the reflection (transmission) of light in the optical system containing a transparent plane-parallel transition layer at the boundary with the nonlinear medium are investigated. In particular, the possibility of realizing conditions of total transmission in this optical system at the hysteresis jump close to the limiting angle, and also the possibility of reducing the threshold intensities at which hysteresis occurs is elucidated. (6 refs.)

113041 Nonlinear optical activity. M.P.Lisitsa.

J. Appl. Spectrosc. (USA), vol.37, no.6, p.1391-9 (Dec. 1982). Translation of: *Zh. Prikl. Spektrosk. (USSR)*, vol.37, no.6, p.955-65 (Dec. 1982). [received: Sept. 1983]

The natural rotation of the plane of polarization in the case of solids may be caused by the presence of gyrotropy associated with spatial dispersion and pleochroism due to the dependence of the absorption spectra on the orientation of the light vector with respect to the crystallographic axes. Pleochroism is characteristic of crystals of low symmetry, but may also occur in the case of centrosymmetric cubic lattices with impurity centers of nonspherical symmetry. Nonlinear optical activity was observed at large light-beam intensities in gyrotropic crystals and also at very small intensities in cubic lattices with F_A centers. (22 refs.)

113042 Light reflection from the interface of media with thermal nonlinearity. S.P.Chernov, A.V.Shepelev (Dept. of Quantum Theory, Moscow Univ., Moscow, USSR).

Moscow Univ. Phys. Bull. (USA), vol.38, no.1, p.47-53 (1983). Translation of: *Vestn. Mosk. Univ. Ser. 3 (USSR)*, vol.38, no.1, p.41-7 (1983).

Consideration is given to nonlinear thermal reflection, which consists in change in the Fresnel reflection coefficient with heating of the interface by radiation. A theory of this effect is proposed, and results are given of its experimental investigation and application for resonator Q-factor modulation. The possibility of using the effect for the anodization of radiation is discussed. (8 refs.)

113043 Subharmonic and chaotic bifurcation structure in optical bistability. P.Mandel, R.Kapral (Service de Chimie-Phys. II, Univ. Libre de Bruxelles, Bruxelles, Belgium).

Opt. Commun. (Netherlands), vol.47, no.2, p.151-6 (15 Aug. 1983). Provides a global view of optical bistability in the domain described by the Ikeda finite difference equation through a study of the boundary structure for marginally stable period N solutions in the parameter space. (13 refs.)

113044 Coherent light scattering from ruby dressed with RF photons.

T.Endo, T.Muramoto (Dept. of Phys., Kyoto Univ., Kyoto, Japan). *Opt. Commun. (Netherlands)*, vol.47, no.2, p.165-9 (15 Aug. 1983).

The authors observed a new kind of coherent light scattering from ruby subjected to an RF Stark field and explained it in terms of RF photon dressing. The theory is also applied to explain the sublevel coherence generation by an RF Stark field in coherent Raman beat spectroscopy. (6 refs.)

113045 Quantitative investigation of critical slowing down in all-optical bistability. S.Cribier, F.Giacobino, G.Grynberg (Lab. de Spectroscopie Hertzienne, ENS, Univ. Pierre et Marie Curie, Paris, France).

Opt. Commun. (Netherlands), vol.47, no.2, p.170-2 (15 Aug. 1983). Optical bistability has been observed in rubidium vapor enclosed in a Fabry-Perot cavity for $\lambda \sim 7779 \text{ \AA}$ (two-photon transition) and $\lambda \sim 7800 \text{ \AA}$ (one-photon transition). The switching time τ_S has been measured as a function of $(I - I_c)$ where I_c is the last value of the length of the cavity for which switching occurs. All the experimental situations, the authors have found a similar law $\tau_S \sim (I - I_c)^{-\alpha}$ with $\alpha \sim 0.5$. This result is in agreement with theoretical predictions. (12 refs.)

113046 Nonlinear optical indication in frequency stabilization systems.

L.A.Budkin, V.V.Mityugov, A.I.Pikhtev, A.N.Yashina. *Radiophys. & Quantum Electron. (USA)*, vol.26, no.1, p.23-9 (Jan. 1983). Translation of: *Izv. VUZ Radiofiz. (USSR)*, vol.26, no.1, p.29-35 (Jan. 1983). [received: Sept. 1983]

Double resonance in a cell with alkali-metal vapor placed inside a laser resonator is investigated. The equations for the density matrix of the atomic vapor subjected to the combined action of a radio-frequency field and a standing light wave are solved. The parameters of the nonlinear optical indication signal under double-resonance conditions are calculated taking into account various physical factors. (12 refs.)

113047 Effects of the Abraham ponderomotive force induced by RF and laser light pulses. N.E.Galich (M.I. Kalinin Polytech. Inst., Leningrad, USSR).

Sov. Phys.-Tech. Phys. (USA), vol.28, no.2, p.136-9 (Feb. 1983). Translation of: *Zh. Tekh. Fiz. (USSR)*, vol.53, no.2, p.219-23 (Feb. 1983). [received: Sept. 1983]

The interaction of short RF and laser light pulses with transparent dispersive and nondispersive media is considered. As the pulse duration decreases, there is an increase in the Abraham ponderomotive force acting along the light beam. On the leading edge of a pulse the Abraham force is parallel to the wave vector, whereas it is opposite to the wave vector on the trailing edge. Dilating stresses are therefore produced in the medium. The strictional pressure along the beam has the opposite effect, but the Abraham force is greater than the strictional pressure and does not reach equilibrium with it. The dilating stresses may be large enough to pull a liquid apart and form cavities. The leading or trailing pulse fronts separately induce compressing forces in the medium. It is possible by changing the time dependence of the radiation pulse to regulate constriction and dilation of the medium parallel to the beam. In the region of frequency dispersion of the dielectric permittivity, the Abraham force increased when the medium is polarized at resonance and decreases due to relaxation processes as compared with the Abraham force for a nondispersive medium. Various nonlinear effects induced by the Abraham force are discussed (cavitation, liquid breakdown, self-focusing of backscattered light, phase transitions) when laser light pulses interact with liquids, gases, and solids. (12 refs.)

Phase-polarization laser spectroscopy See Entry 111779

Nonlinear Zeeman spectroscopy of ultrahigh resolution See Entry 111780

A bistable hybrid optical device using an integrated modulator with an induced dielectric channel See Entry 113085

Soliton analysis with the propagating beam method See Entry 113134

42.65B General theory

113048 Optical extinction theorem in the nonlinear theory of optical multistability. R.K.Bullough, S.S.Hassan (Dept. of Math., Univ. Manchester Inst. of Sci. & Technol., Manchester, England).

Proc. SPIE Int. Soc. Opt. Eng. (USA), vol.369, p.257-63 (1983). (SPIE Proceedings of the Max Born Centenary Conference OPTICS 82, ECOSA 82, Edinburgh, Scotland, 7-10 Sept. 1982).

The optical extinction theorem due to P.P. Ewald, C.W. Oseen and C.G. Darwin is used completely to describe the action of a dielectric slab as a Fabry-Perot interferometer. The analysis is very comparable to that given by Born and Wolf. It is then shown that by generalising the optical extinction theorem to the nonlinear regime essentially the same Fabry-Perot cavity action is regained but in this case the refractive index and hence the cavity tuning depends on the input intensity. This way a multistable output/input relation is derived. It is shown further how the extinction theorem will also handle the problem of 'standing waves' in the cavity. The possibility of optical turbulence in a Fabry-Perot cavity is briefly mentioned. (24 refs.)

113049 Self-pulsing and transients of a Fabry-Perot interferometer with quadratic nonlinear medium. B.Wedding, A.Gasch, D.Jager (Inst. fur Angewandte Phys., Univ. Munster, Munster, Germany).

J. Appl. Phys. (USA), vol.54, no.9, p.4826-31 (Sept. 1983).

The dynamic properties of a Fabry-Perot interferometer filled with a material exhibiting second-order dispersive nonlinearity are studied both theoretically and experimentally. The response of the medium is described by an intensity dependent phase constant as derived from self-action effects. Considering two relaxation times, that of the material and that of the cavity, the basic relations for the stability analysis and for the numerical calculations are obtained. Bistability and self-pulsing effects are predicted. Moreover, the transient behavior is characterized by anomalous switching properties like overshoot and alternate switching. The corresponding experiments performed on a nonlinear transmission line resonator confirm the theoretical results. In a final discussion, the relations to the field of nonlinear optics are outlined. (23 refs.)

113050 Theory of the interaction of waves traveling in opposite directions in a nonlinear cubic medium. S.N.Vlasov, E.V.Sheinina (Inst. of Appl. Phys., Acad. of Sci., USSR).

Radiophys. & Quantum Electron. (USA), vol.26, no.1, p.15-22 (Jan. 1983). Translation of: *Izv. VUZ Radiofiz. (USSR)*, vol.26, no.1, p.20-8 (Jan. 1983). [received: Sept. 1983]

A theoretical study is made of the interaction of waves traveling in opposite directions in a finite nonlinear cubic medium. It is shown that the system is unstable. The authors determine the self-excitation thresholds of various modes of the system, and show that the frequency spectrum of the generated modes broadens rapidly (exponentially) with increasing pumping. The discussion is carried out by using parabolic equations. (13 refs.)

Optical amplitude and polarization multistability in a nonlinear interferometer See Entry 111759

42.65C Stimulated Raman, Brillouin and Rayleigh scattering; parametric oscillations and harmonic generation

113051 Wideband frequency conversion in the UV by nine orders of stimulated Raman scattering in a XeCl laser pumped multimode silica fiber. R.Pini, R.Salimbeni (Istituto di Elettronica Quantistica, CNR, Firenze, Italy), M.Matera, C.Lin.

Appl. Phys. Lett. (USA), vol.43, no.6, p.517-18 (15 Sept. 1983). Efficient wideband frequency conversion of the UV XeCl excimer laser wavelength has been accomplished by stimulated Raman scattering in a multimode UV silica fiber. Nine Stokes orders have been generated in the 308-350-nm spectral region at 650-kW input power. (9 refs.)

113052 Transient stimulated Raman scattering of femtosecond laser pulses. P.G.May, W.Sibbett (Optics Section, Blackett Lab., Imperial Coll., London, England).

Appl. Phys. Lett. (USA), vol.43, no.7, p.624-6 (1 Oct. 1983). Transient stimulated Raman scattering of amplified pulses from a passively mode-locked ring CW dye laser has been demonstrated to be a useful method for the production of coherent near infrared femtosecond light pulses. Hyper-short Stokes radiation is generated in capillary waveguides containing high pressure hydrogen (830 nm, 1265 nm) and methane (752 nm, 964 nm, 1340 nm) and pulse shortening factors as large as 2.9 have been observed. (13 refs.)

113053 Sum-frequency wave generation in optical fibers. Y.Sasaki, Y.Ohmori (Ibaraki Electrical Communication Lab., Nippon Telegraph & Telephone Public Corp., Ibaraki-Ken, Japan).

J. Opt. Commun. (Germany), vol.4, no.3, p.83-90 (Sept. 1983). The generation of two-wave sum-frequency waves in optical fibers is presented. A mode-locked and/or Q-switched Nd:YAG laser operating at 1.064 μm wavelength is used as a pump laser. The sum-frequency waves are regenerated from the pump and the Raman Stokes lines. Phase matching is achieved by using the dispersion of the waveguide modes or the cladding modes in the optical fibers. When utilizing waveguide modes, 10^{-3} conversion efficiency from the pump into the sum-frequency wave, whose peak wavelength is 0.54 μm , is obtained with a 0.8 kW peak pump power. The observed coherence length for the sum-frequency wave generation is found to be about 200 meters. The experimental results indicate that the origin for the sum-frequency wave generation in the optical fibers is quadrupole nonlinearity. (29 refs.)

113054 Hybrid four-wave mixing in liquid pyridine. Guo Chu, Gao Zheng, Hua Luan, Chang Ai-Zhen, J.R.Lombardi (Inst. of Chem., Acad. Sinica, Beijing, China).

Chem. Phys. Lett. (Netherlands), vol.100, no.2, p.159-62 (2 Sept. 1983). Four-wave mixing spectra for liquid pyridine are obtained with broadband laser beam. A comparison of Stokes and anti-Stokes spectra allows the assignment of several lines (951, 991, 1030 cm^{-1}) to CARS and CSRS processes. Two additional moderately intense lines on the Stokes side between 951 and 991 cm^{-1} as well as 991 and 1030 cm^{-1} , which do not appear on the anti-Stokes side, are assigned to a 'hybrid four-wave mixing' process, in which two active Raman modes of pyridine are involved. This process previously unrevealed in experiment seems to be important for correct assignment of the spectral lines in four-wave mixing experiments with a broadband laser beam. (12 refs.)

113055 Optical second harmonic generation in LiNbO_3 crystals induced by a photovoltaic grating. S.K.Esayan, V.V.Lemanov, A.M.Arutunyan (A.F. Ioffe Physico. Tech. Inst., Leningrad, USSR). *Ferroelectr. Lett. Sect. (GB)*, vol.1, no.1, p.13-18 (1983).
Optical second harmonic induced by a photovoltaic grating written in LiNbO_3 :Fe was observed. Harmonic generation was due to the third-order nonlinear coefficient f_{333} linearized in the electric field of the grating. The phase matching condition was achieved by a suitable choice of the grating period. (5 refs.)

113056 Secondary-emission spectra of rhodamine 6G solutions with various levels of population inversion. B.S.Neporent, A.G.Spiro, V.B.Shilov. *J. Appl. Spectrosc. (USA)*, vol.37, no.6, p.1471-7 (Dec. 1982). Translation of: *Zh. Prikl. Spektrosk. (USSR)*, vol.37, no.6, p.1045-53 (Dec. 1982). [received: Sept. 1983]
The authors present an experimental study of the secondary-emission spectra of rhodamine 6G solutions occurring in ranges with different population inversions in order to check the conclusions of Neporent et al. (1981) on shapes of stimulated secondary emission spectra of dye solutions and Spiro et al. (1981) on interpretation of the superluminescence and stimulated Raman scattering of solutions of complex organic compounds. (23 refs.)

113057 Generation of continuous-wave 243-nm radiation by sum-frequency mixing. H.Hemmati, J.C.Bergquist (NBS, Time & Frequency Div., Boulder, CO, USA). *Opt. Commun. (Netherlands)*, vol.47, no.2, p.157-60 (15 Aug. 1983).
Tunable CW radiation near 243 nm with a linewidth of less than 4 MHz has been generated by sum-frequency mixing the 351-nm radiation from an argon-ion laser with the 789 nm radiation from a ring dye laser in a crystal of ammonium dihydrogen phosphate held at moderate temperature. An external ring cavity, resonant with the dye laser, gives a power enhancement of about 12 in the sum-frequency generated radiation. Thermal lensing due to laser heating of the nonlinear crystal, distorted the 351 nm mode structure. This effect could limit the efficiency of the sum frequency mixing process. (11 refs.)

113058 Stimulated Brillouin scattering in optical fibers, and wavefront reversal. M.P.Petrov, E.A.Kuzin (A.F. Ioffe Physicotech. Inst., Acad. of Sci., Leningrad, USSR). *Sov. Phys.-Solid State (USA)*, vol.25, no.2, p.188-90 (Feb. 1983). Translation of: *Fiz. Tverd. Tela (USSR)*, vol.25, no.2, p.334-8 (Feb. 1983). [received: Sept. 1983]
Stimulated Brillouin scattering was investigated in a multimode optical fiber with core diameter 30 μ . The threshold pump power for a pulse length 30 nsec was found to be 4 kW and 1 kW for $\lambda=1.06$ and 0.53 μ respectively, in good agreement with the theory of STBS in a transient regime. It is shown that wavefront reversal accompanies STBS in a multimode optical fiber. The efficiency of pump radiation conversion into the reversed wave reached 50% or more. (8 refs.)

113059 Generation of coherent far-infrared radiation using lasers. A.A.Vedenov, G.D.Myl'nikov, D.N.Sobolenko (I.V. Kurchatov Inst. of Atomic Energy, Acad. of Sci., Moscow, USSR). *Sov. Phys.-Usp. (USA)*, vol.25, no.11, p.833-53 (Nov. 1982). Translation of: *Usp. Fiz. Nauk (USSR)*, vol.138, no.3, p.477-515 (Nov. 1982). [received: Sept. 1983]
A review is given of methods used for generating coherent far-infrared radiation. They include the isolation of the frequency difference between two lasers, SRS by polaritons, optical pumping of gases, and the development of the electrical-discharge laser. Basic principles underlying the realization of the phenomena on which the above methods of generating far-infrared radiation are based are discussed. The properties of the working media, i.e. nonlinear properties of crystal converters (exploited in isolating the difference frequency and in SRS by polaritons), are described. Methods of producing inversion of level populations in gases used in lasers (pumped optically or by an electrical discharge) are analyzed. Specific schemes and device designs for the far infrared are described, and the possibilities and likely performance of these schemes are discussed. The review does not cover electron-beam generators (backward-wave tube, gyrotrons, etc.). (234 refs.)

113060 Phase matching during harmonic generation in high-pressure gas mixtures. S.A.Batishche, V.S.Burakov, V.I.Gladushchak, V.A.Mostovnikov, S.A.Moshkalev, G.T.Razdobarin, V.V.Semenov, N.V.Tarasenko, E.Ya.Shreider (A.F. Ioffe Physicotech. Inst., Acad. of Sci., Leningrad, USSR). *Sov. Tech. Phys. Lett. (USA)*, vol.8, no.11, p.591-2 (Nov. 1982). Translation of: *Pis'ma v Zh. Tekh. Fiz. (USSR)*, vol.8, no.21-22, p.1375-7 (Nov. 1982). [received: Sept. 1983]
Odd harmonics are generated in gas mixtures under phase-matching conditions. Increasing the generation efficiency requires increasing the pressure of the gas, whose nonlinear susceptibility determines the properties of the nonlinear medium. This phase-matching method has been used for third-harmonic generation at the wavelength of the hydrogen L_α line in mixtures of krypton with argon at the high pressures. (6 refs.)

113061 Effects of interference on output in a proustite upconverter. K.Koyanagi, H.Hirayama, T.Mishima, I.Sakuraba (Faculty of Engng., Hokkaido Univ., Sapporo, Japan). *Trans. Inst. Electron. & Commun. Eng. Jpn. Sect. E (Japan)*, vol.E66, no.6, p.401-2 (June 1983).
Periodic variations of sum-frequency output are observed in upconversion of 10.6 μ m radiation from a CO_2 laser in a proustite crystal pumped by a Nd:YAG laser beam and concluded to be caused by multiple reflection of infrared waves which occurs inside the nonlinear crystal. (5 refs.)

Frequency modulation coherent anti-Stokes Raman spectroscopy (FM-CARS): a novel sensitive nonlinear optical method See Entry 111778

Properties, formation, and interpretation of stimulated resonance Raman scattering spectra of dyes See Entry 112743

A 1.5 W CW optically pumped 12.08 μ m NH_3 laser See Entry 112985

The slab geometry laser See Entry 112999

Theory of prism coupling with a nonlinear optical waveguide: second harmonic generation See Entry 113096

Stimulated Raman emission of coherent phonons by impurities in a crystal See Entry 114883

42.65F Phase conjugation

113062 Degenerate forward four-wave mixing in LiNbO_3 . V.Kondilenko, S.Odoulou, M.Soskin (Inst. of Phys., Acad. of Sci., Kiev, Ukrainian SSR). *Ferroelectr. Lett. Sect. (GB)*, vol.1, no.1, p.19-26 (1983).
Forward four-wave mixing in LiNbO_3 :Fe is used for generation of a phase-conjugate replica of unfocused beams of a CW He-Cd laser. The possibility

of partial self-compensation for static and light-induced optical inhomogeneities of a nonlinear sample is demonstrated. (15 refs.)

113063 Deflection of a phase-conjugate wave in nondegenerate four-wave mixing. A.I.Erokhin (Lebedev Inst. of Phys., Acad. of Sci., Moscow, USSR), V.R.Mironenko, V.I.Yudson. *Opt. Commun. (Netherlands)*, vol.47, no.2, p.161-4 (15 Aug. 1983).
The boundary problem for signal phase conjugation at nondegenerated four-wave mixing (FWM) is considered. In contrast to the statements of some authors it is shown that noncollinearity of the incident and the phase-conjugate waves occur. Expressions have been obtained for the deflection angle for a number of configurations of practical importance. Useful analogy between linear and nonlinear reflection at the FWM is noted. (9 refs.)

113064 Strong four-wave mixing with phase conjugation in a nematic liquid crystal. S.M.Arakelyan, S.D.Darbin, I.R.Shen (State Univ., Erevan, USSR). *Sov. Tech. Phys. Lett. (USA)*, vol.8, no.11, p.581-3 (Nov. 1982). Translation of: *Pis'ma v Zh. Tekh. Fiz. (USSR)*, vol.8, no.21-22, p.1353-7 (Nov. 1982). [received: Sept. 1983]
The parametric four-wave interaction with oppositely propagating waves (in the frequency-degenerate case) appears to be one of the most interesting laser effects associated with wave propagation in nematic liquid crystals having a large optical orientational nonlinearity. The authors report an experiment for a purely optical nonlinearity of a standard nematic-liquid-crystal cell. The authors have taken some measurements, which they interpret at a qualitative level. (11 refs.)

Reflection of a linearly polarized plane wave from a lossless stratified mirror in the presence of a phase-conjugate mirror See Entry 112930

Coherent image amplification and optical phase conjugation with photorefractive materials See Entry 112959

Stimulated Brillouin scattering in optical fibers, and wavefront reversal See Entry 113058

Submillisecond grating diffractions in nematic liquid crystal films See Entry 113733

42.65G Photon echoes, self-induced transparency, optical saturation and related effects

113065 Coherent pulse propagation in the infrared on the picosecond time scale. H.-J.Hartmann, A.Lauberau (Phys. Inst., Univ. Bayreuth, Bayreuth, Germany). *Opt. Commun. (Netherlands)*, vol.47, no.2, p.117-22 (15 Aug. 1983).
Coherent propagation of resonant ultrashort pulses in gases is investigated theoretically and experimentally at medium pressure values. Drastic changes of the pulse wings extending over several ten picoseconds are predicted and experimentally observed using tunable pulses of 4 ps produced by a parametric generator device and picosecond IR light gates. The dephasing time T_2 of the R(3) vibration-rotation transition of HCl is measured to be $T_2 \times p = 21.5$ ps \times bar in the pressure range $p=1$ to 3 bar. Quantitative agreement between theory and experiment demonstrates that a novel transient spectroscopy in the infrared can be accomplished by coherent pulse reshaping. (27 refs.)

Passive mode locking of a long pulse XeCl laser See Entry 113025

42.65J Beam trapping, self focusing, thermal blooming, and related effects

113066 Distortions of a CW light beam propagating through gas: self-lensing and spatial ringings. M.Le Berre (Lab. des Signaux et Systemes, Gif-sur-Yvette, France), F.Mattar, E.Ressayre, A.Tallet. *Proc. SPIE Int. Soc. Opt. Eng. (USA)*, vol.369, p.269-75 (1983). (SPIE Proceedings of the Max Born Centenary Conference OPTICS 82, ECOSA 82, Edinburgh, Scotland, 7-10 Sept. 1982).
Transverse effects on the profile of an intense off-resonant CW light beam, propagating through a gaseous cell of length l , are numerically displayed in both cases of the very small absorption length ($\alpha^{-1} \ll l$) and the intermediate case ($\alpha^{-1} \sim l$). As predicted by the theory, self-focusing and spatial ringings are obtained. Moreover for $\alpha l \sim 1$, these distortions generally appear as a recurrent process. (5 refs.)

113067 Reflection of wave beams from a screen in a nonlinear medium. A.P.Sukhorukov, V.A.Trofimov (Moscow State Univ., Moscow, USSR). *RadioPhys. & Quantum Electron. (USA)*, vol.26, no.1, p.8-14 (Jan. 1983). Translation of: *Izv. VUZ Radiofiz. (USSR)*, vol.26, no.1, p.12-19 (Jan. 1983). [received: Sept. 1983]
A theoretical study is made of the interaction of optical beams, one of which is reflected from a screen positioned in a nonlinear medium. The authors numerically model the Kerr and thermal self-interaction of Gaussian and annular beams and also optimize the entrance aperture of the beam to achieve the maximum energy concentration on the reflecting mirror. (5 refs.)

The thermal self-excitation of the beam of a continuous CO_2 laser which interacts with water aerosol See Entry 113035

Self-focusing in laser produced spark See Entry 113621

42.70 OPTICAL MATERIALS

113068 Thermal emissivities of films on substrates. A.Thakur, R.Raman (Centre of Energy Studies, Indian Inst. of Technol., New Delhi, India). *Appl. Energy (GB)*, vol.15, no.1, p.1-13 (1983).
An explicit expression for thermal emissivity of thin films has been derived in terms of optical constants of the substrate and film. At millimicron film thicknesses, the substrate plays a vital role in governing the emissivities of the films. For low values of the coefficient of absorption, the emissivity has a value of $\epsilon_1(\lambda)$ for zero film thickness, reaches a minimum at an optimum value of thickness and then increases monotonically to $\epsilon_2(\lambda)$ for very large values of thickness. $\epsilon_1(\lambda)$ and $\epsilon_2(\lambda)$ are, respectively, the emissivities of the bulk substrate and the film material. For large values of the coefficient of absorption, the emissivity passes through a minimum and then a maximum before monotonically decreasing to $\epsilon_2(\lambda)$ (for large values of the thickness), as the thickness is increased. (15 refs.)

Single-crystal fiber [of CsBr] See Entry 113131

Polycrystalline infrared optical fibers See Entry 113132

Selective solar absorption of chemically etched aluminum-silicon films See Entry 115698

42.70C Glass

113069 Large crystal sapphire optics. F.Schmid, C.P.Khattak (Crystal Systems, Salem, MA, USA).

Laser Focus (USA), vol.19, no.9, p.147-52 (Sept. 1983).

Large sapphire boules are grown free of light scatter by the heat exchanger method (HEM) for varied electro-optic and laser applications. Sapphire optical components of various sizes, shapes, and orientations can be fabricated out of this material to produce scatter-free optics with good transmission from the UV to IR. (18 refs.)

113070 Study of the OH content of CVD silica glass for optical fibres. A.Sartre, J.Dazord, J.Bouix (Lab. de Phys. Minerale I, Univ. Claude Bernard Lyon I, Villeurbanne, France), M.C.Schouler, C.Bernard. Proceedings of the 4th European Conference on Chemical Vapour Deposition, Eindhoven, Netherlands, 31 May-2 June 1983 (Eindhoven, Netherlands: Philips Centre Manuf. Technol. 1983), p.459-64.

Water impurity in CVD SiO₂ dissociates after dissolution in glasses to form OH groups. A thermodynamic study is undertaken to investigate the influence of experimental parameters on the partial pressure of water vapour in contact with the deposition surface. The diffusion of atmospheric water vapour through the lateral surface of the preform during formation is also studied. It is shown that, when the initial pressure of SiCl₄ is constant, an increase in the O₂ partial pressure is a favourable factor to the presence of water vapour in the flame and thus to OH groups in the glass. (15 refs.)

Quantitative shadow method for measuring a one-dimensional refractive index distribution See Entry 111744

Fluoride glass fiber See Entry 113133

42.70G Light-sensitive materials

113071 Optical recording media with thermal coloration. A.Morinaka, S.Oikawa, H.Yamazaki (Ibaraki Electrical Communication Lab., Nippon Telegraph & Telephone Public Corp., Ibaraki, Japan).

Appl. Phys. Lett. (USA), vol.43, no.6, p.524-6 (15 Sept. 1983).

Laser recording on novel optical recording media with thermal coloration is reported. The basic recording mechanism is thermally induced chemical reaction between a coloring reagent and a coupling reagent that are deposited in vacuum, separated by a light absorbing layer. Transmittance changes on a 1- μ m size recording pit have been observed by writing with a laser diode at 830 nm. This medium is colored blue, red, or black by selecting a coloring reagent layer. It is applied to multicolor recording by accumulating units of media. (5 refs.)

Improved Eastman Colour print films See Entry 111792

Coherent image amplification and optical phase conjugation with photorefractive materials See Entry 112959

High-sensitivity material with reversible photo-induced anisotropy [holographic recording] See Entry 112962

42.72 OPTICAL SOURCES AND STANDARDS

(for spectroscopic light sources, see also 07.65)

Picosecond continuum generation and spectroscopy See Entry 111785

Infrared synchrotron radiation from electron storage rings See Entry 112487

Reciprocity relations with partially coherent sources See Entry 112935

Generation of coherent far-infrared radiation using lasers See Entry 113059

Rayleigh backscattering in a fiber gyroscope with limited coherence sources See Entry 113124

Light sources for fluorescein fluorophotometry See Entry 115893

42.78 OPTICAL LENS AND MIRROR SYSTEMS

(for microscopes, see 07.60P; for photographic instruments, see 07.68; for astronomical telescopes, see 95.55)

113072 Wavefront analysis of objectives using ACCOS-MCI. W.Swantner, G.Lawrence (Inst. for Modern Optics, Univ. of New Mexico, Albuquerque, NM, USA).

Proc. SPIE Int. Soc. Opt. Eng. (USA), vol.351, p.10-14 (1983). [received: Sept. 1983] (SPIE Proceedings on Wavefront Sensing, San Diego, CA, USA, 24-25 Aug. 1982).

ACCOS V is an optical design and analysis program copyrighted by SC, Inc., of Fishers, NY. MCI is a wavefront and interferogram analysis program developed by UNM personnel. These programs have been linked on the Cray and CDC computers at Kirtland AFB. The authors present information on the use and capabilities of this arrangement, showing examples of ACCOS input and optical path difference (OPD) calculations, and what features MCI adds to ACCOS analysis. Included are Zernike wavefront coefficients, contour plots, OPD maps, and some new developments in the capabilities of MCI. (4 refs.)

113073 Full aperture testing with subaperture test optics. J.G.Thunen, O.Y.Kwon (Electro-Optics Lab., Lockheed Palo Alto Res. Lab., Palo Alto, CA, USA).

Proc. SPIE Int. Soc. Opt. Eng. (USA), vol.351, p.19-27 (1983). [received: Sept. 1983] (SPIE Proceedings on Wavefront Sensing, San Diego, CA, USA, 24-25 Aug. 1982).

Presents an overview of recent work of the Lockheed Palo Alto Research Laboratory on the use of subaperture test optics to evaluate the performance of large optical systems. Supported by selected subscale experiments, a theory has been developed that addresses two test conditions, each based on the use of a known test flat in a double-pass configuration with a collimated optical system of unknown quality. The two test conditions, in order of increasing theoretical complexity, are: (1) a single test flat covering only a portion of the full system aperture, and (2) multiple (not necessarily coherent) test flats. Analyses predict limited utility of a single test subaperture as a function of a subaperture size and location, and aberration content. Multiple subapertures viewing the full system are shown to give good results for higher order aberrations even when the individual test flats are unphased and contain large relative tilt errors. The test techniques described are fully scalable to future optical systems of arbitrary size. The authors summarise the theoretical basis for subaperture testing, give quantitative performance predictions for some selected cases, and present the results of supporting experimental work. (10 refs.)

113074 Strehl's ratio for a two-wavelength continuously deformable optical adaptive transmitter. J.F.Holmes, V.S.R.Gudimetta (Dept. of Appl. Phys. & Electrical Engng., Oregon Graduate Center, Beaverton, OR, USA).

J. Opt. Soc. Am. (USA), vol.73, no.9, p.1119-22 (Sept. 1983).

Polychromatic adaptive optical systems differ from monochromatic systems in that the required phase compensation is measured at a wavelength (or wavelengths) different from that at which compensation is required. Unfortunately, the effect of turbulence is dispersive, and consequently, because of the wavelength difference, the compensation will not be exact. In effort to determine the magnitude of the effect, a formulation of Strehl's ratio for the polychromatic case has been developed and numerical data generated for both horizontal and vertical paths. (7 refs.)

113075 Methods for the investigation of laser mirrors for laser gyros. B.Grosser (Inst. fur Optik und Halbleiterphys., Tech. Univ. Braunschweig, Braunschweig, Germany).

Optik (Germany), vol.65, no.2, p.143-51 (1983). In German.

Laser mirror specimens were investigated using several methods: integral and differential backscattering and dark field microscopy. All the methods yielded comparable results, therefore each method is qualified for examination. The kind of pretreatment used was found to be crucial for the quality of the coating and the authors also estimated values of mean roughness for the samples. (10 refs.)

113076 Application of the theory of image formation to calculations on optical resonators. V.K.Ablekov, Yu.N.Babaev, M.F.Dmitriev, S.A.Kolyadin, A.V.Frolov.

Sov. Phys.-Dokl. (USA), vol.27, no.12, p.1058-60 (Dec. 1982). Translation of: *Dokl. Akad. Nauk SSSR*, vol.267, no.4-6, p.1114-17 (Dec. 1982). [received: Sept. 1983]

By treating the mode structure of an optical resonator as an optical image, one can describe the resonator in terms of the theory of image formation. The simplest description of an optical resonator can be given if the reflection coefficient of the resonator mirrors is a periodic function. In this case one can make use of the effect that images of grids are reproduced when the grids are illuminated by coherent light. The authors consider the condition for the formation of a field inside a resonator having infinite mirrors in the form of periodic structures. (4 refs.)

A simple demonstration of spherical aberration See Entry 111363

Experimental verification of an image-based alignment technique for optical systems in space See Entry 111731

Point image focus sensing using an automated Foucault test See Entry 111733

Resonator technique for absolute reflection and transmission measurements See Entry 111734

Polynomial fit of subaperture interferograms See Entry 111749

Interferometer detection system for optical testing See Entry 111753

Tracing finite rays through a Fresnel lens See Entry 112921

Paraxial ray paths in spherical gradient-index media See Entry 112928

Reflection of a linearly polarized plane wave from a lossless stratified mirror in the presence of a phase-conjugate mirror See Entry 112930

Fifth-order aberration theory of gradient-index optics See Entry 112952

Fifth-order aberration theory of gradient-index optics—examples See Entry 112953

High-Q open resonant structures with a sparse spectrum See Entry 113023

Low-loss wavelength division multiplexing (WDMK) devices for single-mode systems See Entry 113148

Diamond flycut multifaceted mirror See Entry 113155

The Couder telescope-better than the Schmidt? See Entry 116476

42.80 OPTICAL DEVICES, TECHNIQUES AND APPLICATIONS

(for optical instruments and techniques, see 07.60; for optical spectroscopy, see 07.65; for photography, see 07.68; for holography, see 42.40; for lasers, see 42.55 and 42.60; for masers, see 42.52)

113077 Structured target light valve. C.Altman (IBM Corp., Armonk, NY, USA).

IBM Tech. Disclosure Bull. (USA), vol.26, no.2, p.701-2 (July 1983).

A light valve, which for practicable electron-beam diameters will have a greater resolution capability than the conventional light valve, is described. (no refs.)

Evaluation and optimization by colorimetry of polarizers for liquid crystal display See Entry 111735

Beam-splitter mount for efficient monitoring of mode-locked and synchronously pumped CW lasers See Entry 113033

Strehl's ratio for a two-wavelength continuously deformable optical adaptive transmitter See Entry 113074

Prism excitation of highly multimode deep planar waveguides See Entry 113087

Theory of prism coupling with a nonlinear optical waveguide: second harmonic generation See Entry 113096

Schlieren optical imaging of weak objects See Entry 115992

42.80B Spatial filters, zone plates

113078 The effects of manufacturing inaccuracies on the imaging properties of Fresnel zone plates. M.J.Simpson, A.G.Michette (Phys. Dept., Queen Elizabeth Coll., London, England).

Opt. Acta (GB), vol.30, no.10, p.1455-62 (Oct. 1983).

The imaging properties of Fresnel zone plates are discussed in terms of possible manufacturing inaccuracies such as noncircularity and displacement of zones. The degradation on the on-axis intensity is used to establish manufacturing tolerances. (6 refs.)

Image restoration for a defocused optical system See Entry 112941

Statistical performance of the circular harmonic filter for rotation-invariant pattern recognition See Entry 112944

Self-imaging through a Fabry-Perot interferometer See Entry 112954

Spatial filtering of backscattering signal in optical fibers See Entry 113135

42.80C Spectral and other filters

- 113079 Properties of multilayer interference absorber with oblique incidence of radiation.** A.N.Baskakov, A.V.Tikhonravov (Dept. of Math., Moscow Univ., Moscow, USSR). *Moscow Univ. Phys. Bull. (USA)*, vol.38, no.1, p.7-10 (1983). Translation of: *Vestn. Mosk. Univ. Ser. 3 (USSR)*, vol.38, no.1, p.8-11 (1983). The angular properties of a multilayer interference absorber (MIA) are theoretically investigated. With inclination of the MIA, its resonant curve is shifted into the short-wave region, and the magnitude of the shift is proportion to the square of the angle of incidence of the radiation. A simple expression is obtained, describing the form of the central lobe of the MIA directionality diagram. The laws for the suppression of external noise in receivers with MIA at the inlet are discussed, together with the possibilities of tuning these receivers with respect to the resonant frequency following from the MIA angular properties. (6 refs.)
- Phase retrieval by optical phase differentiation** See Entry 111726
- Measurement Assurance Program transmittance standards for spectrophotometric linearity testing: preparation and calibration** See Entry 111781
- Low-loss wavelength division multiplexing (WDMK) devices for single-mode systems** See Entry 113148
- Linear absorption coefficient of beryllium in the 50-300-Å wavelength range** See Entry 114943

42.80D Monochromators

- Self-study manual on optical radiation measurements: Part I -Concepts, chapter 10. Introduction to coherence in radiometry** See Entry 111382

42.80E Shutters, windows, diaphragms, deflectors, choppers

- High-speed, low-cost laser-triggered plasma shutter** See Entry 113017

42.80F Gratings, echelles

- 113080 Blaze angle of the Bausch & Lomb R4 echelle grating.** S.Engman, P.Lindblom (Phys. Dept., Abo Akademi, Turku, Finland). *Appl. Opt. (USA)*, vol.22, no.17, p.2512-13 (1983). In a recent paper by R.A. Brown et al. (see *ibid.*, vol.21, p.167, 1982) the blaze angle of the extremely high-blazed R4 echelle grating manufactured by Bausch & Lomb was measured. The measurements gave a blaze angle $\theta = 72.5^\circ$, i.e. 3.5° less than that specified by Bausch & Lomb. Based on a recently published new model for the blaze of echelle gratings (see *ibid.*, vol.21, p.4356, 1982) the present authors present a new determination of the blaze angle that deviates from that obtained by Brown et al. It is concluded that the blaze angle of the R4 grating as specified by Bausch & Lomb can be too high by at most 1° . There is at present no model that described the blaze characteristics of high-blazed echelle gratings in the Littrow or near Littrow mounting. However, the maximum intensity of the blaze in this mounting is shifted from the blaze angle toward smaller α values. This shift seems to be proportional to λ^2 . (2 refs.)
- 113081 Reflex diffraction grating—an effective transducer of infrared radiation polarization.** A.N.Bobrovskii, G.D.Myl'nikov. *Instrum. & Exp. Tech. (USA)*, vol.25, no.6, pt.2, p.1466-7 (Nov.-Dec. 1982). Translation of: *Prib. & Tekh. Eksp. (USSR)*, vol.25, no.6, p.136-7 (Nov.-Dec. 1982). A reflex diffraction grating is used as an IR radiation polarization transducer. A method of setting up the grating is described that permits obtaining elliptically and circularly polarized radiation from linearly polarized radiation. The radiation energy losses during conversion are $\leq 7\%$. (4 refs.)
- 113082 Stigmatic systems with concave spherical holographic diffraction gratings.** V.K.Prokof'ev. *J. Appl. Spectrosc. (USA)*, vol.37, no.6, p.1478-82 (Dec. 1982). Translation of: *Zh. Prikl. Spektrosk. (USSR)*, vol.37, no.6, p.1053-9 (Dec. 1982). [received: Sept. 1983] In recent years there has been a considerable increase in the interest in concave holographic gratings, mainly on account of their specific focusing properties. With a concave diffraction grating, an important part is played in a modern spectral instrument by the astigmatism and consequent increase in the height of the spectral lines. In photographic recording, this reduces the intensity of illumination, while in photoelectric recording there is a considerable loss of energy because of the small size of the entrance window in the photomultiplier (for example, the window of a photomultiplier for the vacuum ultraviolet region has a size of only 10 mm). The author examines the disposition of the meridional and sagittal focal curves for a concave holographic diffraction grating made on a spherical substrate. The main attention is given to schemes that reduce the astigmatism considerably and that enable one to use existing vacuum-ultraviolet photomultipliers without energy loss. (2 refs.)
- 113083 Anisotropic gratings recorded from two circularly polarized coherent waves.** M.Attia, J.M.C.Jonathan (Inst. d'Optique, Univ. Pierre et Marie Curie, Paris, France). *Opt. Commun. (Netherlands)*, vol.47, no.2, p.85-90 (15 Aug. 1983). A constant intensity, rectilinear light vibration, with spatially varying orientation, is obtained from superposition of two orthogonal circularly polarized waves propagating in slightly different directions. Such an exposure on a photoanisotropic medium prints a grating characterized only by spatial variations in the orientation of the induced optic axis. The diffraction properties of such a grating are investigated. It behaves as a uniformly transparent isotropic medium when illuminated by the same waves as during the recording process. Illumination by a circular wave generates a transmitted and a single diffracted beam, while an incident elliptically polarized one would produce, apart from the central order, two diffracted beams with orthogonal circular polarizations. (10 refs.)
- 113084 Asymmetric extinction in anisotropic diffraction gratings.** L.K.Vistin', A.Yu.Kabaenkov, S.S.Yakovenko (A.V. Shubnikov Inst. of Crystallography, Acad. of Sci., Moscow, USSR). *Sov. Phys.-Dokl. (USA)*, vol.27, no.12, p.1044-6 (Dec. 1982). Translation of: *Dokl. Akad. Nauk SSSR*, vol.267, no.4-6, p.1353-7 (Dec. 1982). [received: Sept. 1983] The subject of the present paper is an experimental study of the diffraction of a beam at oblique incidence on modulated liquid crystal structures forming various types of diffraction gratings. Some new experimental results have been obtained, and analytical expressions have been found for some of the data.

- Asymmetric extinction of the odd diffraction orders was detected for certain angles of incidence of the light beam on the liquid crystal layer. (11 refs.)
- Comparison of optical depth-measurement methods on real metal surfaces with sine-phase-gratings** See Entry 111638
- Three-dimensional vector coupled-wave analysis of planar-grating diffraction** See Entry 112927
- High-frequency holographic transmission gratings in photoresist** See Entry 112960
- Line selection in carbon dioxide waveguide lasers using diffraction gratings** See Entry 113020
- Optical second harmonic generation in LiNbO₃ crystals induced by a photovoltaic grating** See Entry 113055
- Low-loss wavelength division multiplexing (WDMK) devices for single-mode systems** See Entry 113148
- Submillisecond grating diffractions in nematic liquid crystal films** See Entry 113733

42.80K Optical beam modulators

- 113085 A bistable hybrid optical device using an integrated modulator with an induced dielectric channel.** E.T.Aksenov, A.V.Kukharev, A.A.Lipovskii, A.V.Pavlenko (M.I. Kalinin Polytech. Inst., Leningrad, USSR). *Sov. Phys.-Tech. Phys. (USA)*, vol.28, no.2, p.185-7 (Feb. 1983). Translation of: *Zh. Tekh. Fiz. (USSR)*, vol.53, no.2, p.301-5 (Feb. 1983). [received: Sept. 1983] Experimental results are reported for a hybrid bistable optical device based on an integrated-optics modulator with an induced dielectric channel. Hysteresis is produced in the dependence of the light intensity at the modulator output on the input intensity by adding an external circuit providing positive intensity feedback (with respect to the intensity of the reflected light beam). Test results of the bistable optical device are reported for operation in the optical memory and 'optical transistor' modes. A light pulse amplification of 6 dB was achieved. (19 refs.)
- Linear and circular polarisation modulation for measuring complex magneto-optical rotation. I. Principles and performance** See Entry 111742
- Laser-beam attenuation measurement using acousto-optic modulator** See Entry 113029

42.80L Optical waveguides

(for fibre optical waveguides, see 42.80M)

- 113086 Low-loss integrated optical waveguides fabricated by nitrogen ion implantation.** I.K.Naik (Northrop Res. & Technol. Center, Palos Verdes Peninsula, CA, USA). *Appl. Phys. Lett. (USA)*, vol.43, no.6, p.519-20 (15 Sept. 1983). A technique for fabricating low-loss (on the order of 0.1 dB/cm) integrated optical waveguides in amorphous SiO₂-based material by nitrogen ion implantation is reported. By comparing the results of nitrogen implantation and oxygen implantation in SiO₂, the mechanism of waveguide formation in the nitrogen-implanted waveguides is shown to be chemical doping effect of the nitrogen dissolved in amorphous SiO₂. (8 refs.)
- 113087 Prism excitation of highly multimode deep planar waveguides.** J.Ctyroky, J.Janta (Inst. of Radio Engng. & Electronics, Czechoslovak Acad. of Sci., Prague, Czechoslovakia), J.Schrofel. *J. Opt. Commun. (Germany)*, vol.4, no.3, p.104-9 (Sept. 1983). The period-of-propagation length concept for guided modes in planar waveguides is used to derive a simple expression for the coupling length of prism coupler. It is shown that the prism coupling strength for deep multimode waveguides strongly depends on the shape of the refractive index profile as well as—except for the linear profile—on the mode order. Further it is shown that for multimode waveguides simultaneous excitation of several guided modes is typical. Arising interference effects at the waveguide surface are explained and illustrated by experimental results obtained with ion-exchanged waveguides in glass. (13 refs.)
- 113088 Coupling of dielectric waveguides.** M.L.Calvo, R.F.Alvarez-Estrada (Dept. de Optica, Facultad de Ciencias Fisicas, Univ. Complutense, Madrid, Spain). *Proc. SPIE Int. Soc. Opt. Eng. (USA)*, vol.369, p.401-6 (1983). (SPIE Proceedings of the Max Born Centenary Conference OPTICS 82, ECOSA 82, Edinburgh, Scotland, 7-10 Sept. 1982). A general integral equation for the total scattered magnetic field is presented. Thus, the coupling phenomena between N identical dielectric waveguides can be interpreted as a multiple scattering process. Application to the case of two identical dielectric waveguides allows a numerical behaviour to be obtained where the control of the degree of coupling is also known. (9 refs.)
- 113089 Optical losses in metal/SiO₂-clad Ti:LiNbO₃ waveguides.** L.L.Buhl (Bell Labs., Holmdel, NJ, USA). *Electron. Lett. (GB)*, vol.19, no.17, p.659-60 (18 Aug. 1983). Presents measured excess loss resulting from electrode overlays for both TE and TM polarisations as a function of SiO₂ buffer layer thickness for Ti:LiNbO₃ strip waveguides at $\lambda = 1.32 \mu\text{m}$. There is negligible excess loss to the TE mode with no buffer layer and the excess loss to the TM mode can be essentially eliminated with a SiO₂ layer only 700 Å thick. A passive polariser with ~ 1.5 dB fibre-waveguide-fibre insertion loss and >13 dB extinction ratio is also demonstrated. (6 refs.)
- 113090 Wavelength-discriminating photodetector for lightwave systems.** J.C.Campbell, C.A.Burrus, J.A.Copeland, A.G.Dentai (Bell Labs., Holmdel, NJ, USA). *Electron. Lett. (GB)*, vol.19, no.17, p.672-4 (18 Aug. 1983). Demonstrates that a dual-wavelength photodetector can be used to determine simultaneously the wavelength and the power level of a lightwave signal. The signal wavelength is determined by monitoring the ratio of the two outputs from this photodetector at the crossover of its responsivity curves; the signal level is determined from the sum of the two outputs. Possible applications for this type of photodetector include mode-control of single-frequency injection lasers, direct demodulation for lightwave systems utilising frequency-shift-keyed transmission, wavelength-division multiplexing and optical logic. (7 refs.)
- 113091 Scattering and mode conversion of guided modes by an arbitrary cross-sectional cylindrical object in an optical slab waveguide.** T.Nobuyoshi, N.Morita, N.Kumagai (Dept. of Communication Engng., Osaka Univ., Osaka, Japan). *J. Lightwave Technol. (USA)*, vol.LT-1, no.2, p.374-80 (June 1983). The scattering and mode conversion of guided modes caused by a cylindrical scatterer of arbitrary cross section embedded in, or placed on, a dielectric slab

waveguide are investigated theoretically. The method employed for the analysis is the surface current integral equation technique. The total scattered power, mode-conversion coefficients, and scattering patterns for the typical numerical examples are shown. (21 refs.)

113092 Optical wave propagation in form-birefringent media and waveguides. M.Tateda, T.Kimura (Musashino Electrical Communication Lab., Nippon Telegraph & Telephone Public Corp., Tokyo, Japan). *J. Lightwave Technol. (USA)*, vol.LT-1, no.2, p.402-7 (June 1983). Characteristics of a periodic structure waveguide with a finite width are studied theoretically and numerically. Propagation constants of two orthogonally polarized fundamental modes converge to values which are different from each other, when the total periodic structure width exceeds twice the wavelength. The asymptotic characteristic equation is derived analytically. The normalized frequency V of the high-index layers must be less than unity in order that the optical energy does not localize in the high-index layers. Both the magnitude of the birefringence and the effective refractive index in the form-birefringent media can be controlled by varying the thickness of the high-index layer and the thickness ratio of the high- and low-index materials. (7 refs.)

113093 Numerical field solution for an arbitrary asymmetrical graded-index planar waveguide. V.Ramaswamy, R.K.Lagu (Dept. of Electrical Engng., Univ. of Florida, Gainesville, FL, USA). *J. Lightwave Technol. (USA)*, vol.LT-1, no.2, p.408-17 (June 1983). Presents a numerical solution for the field amplitudes in an asymmetrical graded-index planar waveguide with an arbitrary index profile. For small index differences between the surface and bulk indexes and for large differences between the cover and surface indexes, the modes of the diffused waveguides can be described entirely in terms of normalized mode index, diffusion depth, effective modal width, and the V number. The results show a high degree of accuracy when checked against exact published results for the parabolic and exponential index profiles. Universal charts for the modal fields in terms of the normalized quantities are presented for profiles of practical interest, namely, Gaussian and complimentary error function index profiles. It is shown that the modal width, while somewhat sensitive to the V number, is surprisingly insensitive to the index profile. Tailoring of the index profile, therefore, does not seem important for the efficient fibre-waveguide endfire coupling. Error involved in the estimation of the phase shift at the cover-surface boundary as function of the asymmetry parameter is shown to be rather small for practical cases. (29 refs.)

113094 Three-guide optical couplers in GaAs. J.P.Donnelly, N.L.DeMeo, Jr., G.A.Ferrante (Lincoln Lab., MIT, Lexington, MA, USA). *J. Lightwave Technol. (USA)*, vol.LT-1, no.2, p.417-24 (June 1983). Three-guide optical couplers consisting of three 4.75- μ m-wide slab-coupled rib guides separated by 4.25 μ m have been fabricated in GaAs. The performance of these couplers at 1.28 μ m is in close agreement with that predicted using a modified effective-index method to obtain an approximate analytical solution for this type of coupler. The coupling length needed to symmetrically transfer power from the center guide to the two outside guides was 3.2 mm. At this length, less than 1 percent of the power remained in the center guide. The length needed to transfer power from one outside guide to the other outside guide was ≈ 6.4 mm, which is $\approx \sqrt{2}$ times that of a similar two-guide coupler and twice that required to couple power from the center guide to the two outside guides. The power transfer efficiency in this case is not as good as when power was inputted into the center guide. Three-guide couplers of this type should prove useful as power dividers and combiners, especially in cases where waveguide bend losses preclude the use of 'Y'-junctions. They may also prove useful as replacements for two-guide couplers where either sharper transfer characteristics are desired or where losses due to waveguide bends are again unacceptable. (20 refs.)

113095 Optical coupling between single-mode semiconductor lasers and strip waveguides. W.L.Emkey (Bell Labs., Allentown, PA, USA). *J. Lightwave Technol. (USA)*, vol.LT-1, no.2, p.436-43 (June 1983). This analysis describes the optimum conditions for coupling a single-mode semiconductor laser to a single-mode strip waveguide, when both the laser and the waveguide have asymmetric optical beam profiles. The outputs are approximated by two Gaussian fields. Two waveguide cases are treated: (1) the case where the two orthogonal waveguide waists are independent and (2) where the ratio of these waists is fixed. The effect on the coupling efficiency of a spherical surface on the waveguide input face is discussed. The results demonstrate the importance of coupling in the laser far-field and indicate the advantage of having relatively large waveguide modes. An intrinsic minimum in the optimum coupling efficiency was found to exist in the near-field for asymmetric laser/waveguide systems. Expressions describing the optimum waveguide waists and the focal length of the lensed waveguide are given for the waveguide parameters that yield the best coupling conditions. (43 refs.)

113096 Theory of prism coupling with a nonlinear optical waveguide: second harmonic generation. V.V.Malov, A.V.Turovtssev, L.V.Iogansen (All-Union Correspondence Inst. of the Textile & Consumer Industry, Moscow, USSR). *Sov. Phys.-Tech. Phys. (USA)*, vol.28, no.2, p.174-9 (Feb. 1983). Translation of: *Zh. Tekh. Fiz. (USSR)*, vol.53, no.2, p.282-91 (Feb. 1983). [received: Sept. 1983]

A theory of resonant tunnel prism coupling with a nonlinear optical waveguide is derived. Approximate analytic solutions are obtained for the amplitudes of the fundamental and second-harmonic waves, and the equations are also solved numerically. It is found that there are two pumping efficiency maxima depending on the width of the beam. It is shown that under optical conditions, when the nonlinear interaction length is comparable to the characteristic coupling length of the waveguide with the prism, the pumping and the conversion efficiencies may exceed 90% and remain high when the beam width varies by a factor $\sim 2-4$. (6 refs.)

113097 Determining the characteristics of Ag:LiTaO₃ diffused optical waveguides. A.K.Angelov, E.M.Zolotov, A.M.Prokhorov, V.A.Chernykh (P.N. Lebedev Phys. Inst., Acad. of Sci., Moscow, USSR). *Sov. Tech. Phys. Lett. (USA)*, vol.8, no.11, p.578-9 (Nov. 1982). Translation of: *Pis'ma v Zh. Tekh. Fiz. (USSR)*, vol.8, no.21-22, p.1345-9 (Nov. 1982). [received: Sept. 1983]

Studies the changes in the profile of the refractive index caused by changes in the annealing time. The authors have also calculated the optical field distributions for diffused Ag:LiTaO₃ waveguides. (4 refs.)

Line selection in carbon dioxide waveguide lasers using diffraction gratings See Entry 113020

High-Q open resonant structures with a sparse spectrum See Entry 113023

Plug connectors for fiber-optic waveguide systems and components See Entry 113136

A guided-wave optical arbiter circuit See Entry 113149

Optical switching characteristics in slightly nondegenerated multilayered couplers using acousto-optic interaction by surface acoustic waves See Entry 113152

A two-component optomechanical speed transducer for use with turbulent flows of liquid metal See Entry 113529

Permeability at optical frequencies See Entry 114947

42.80M Fibre optics

113098 Characterization of a microlens-ended optical fiber. V.Russo, G.C.Righini, S.Sottini, S.Trigari (Istituto di Ricerca Sulle Onde Elettromagnetiche, CNR, Firenze, Italy).

Alta Freq. (Italy), vol.52, no.3, p.197-9 (May-June 1983). (4th Italian National Meeting on Applied Electromagnetics, Florence, Italy, 4-6 Oct. 1982).

Lens-ended optical fibers are suitable devices in optical communications and in laser medical applications. The theoretical analysis and the experimental results carried out on two types of microlenses, arc- and bulb-shaped, are reported for multimode step-index fibers. The output characteristics (intensity distribution, focal length, loss) of these fiber ends are described and suggestions for their proper use are given. (7 refs.)

113099 Analysis of differential-mode-delay measurements in optical fibres. G.Coppa, P.di Vita (CSELT, Torino, Italy).

Alta Freq. (Italy), vol.52, no.3, p.203-5 (May-June 1983). (4th Italian National Meeting on Applied Electromagnetics, Florence, Italy, 4-6 Oct. 1982).

The use of the measurements of differential mode delay (DMD) for the derivation of the index profile dispersion is discussed. The method of processing of DMD measurements, in the case of fibre with non-monotonic index profiles, is described. Finally means to take into account mode conversion are provided. (3 refs.)

113100 Propagating beam analysis of bent optical waveguides. P.Danielson (Electromagnetics Inst., Tech. Univ. of Denmark, Lyngby, Denmark), D.Yevick.

J. Opt. Commun. (Germany), vol.4, no.3, p.94-8 (Sept. 1983).

The propagating beam method is employed to analyze mode coupling in both bent waveguides with a periodic structure and circularly bent waveguides. The results illustrate the physical origin of and provide error estimates for the often-employed method of transforming a circular fiber in an equivalent straight fiber with a modified refractive index profile. (7 refs.)

113101 Review of fiber optic gyroscopes. H.C.Lefevre, Y.Bourbin, P.Graindorge, H.J.Arditty (Central Res. Lab., Thomson-CSF, France).

Proc. SPIE Int. Soc. Opt. Eng. (USA), vol.369, p.386-94 (1983). (SPIE Proceedings of the Max Born Centenary Conference OPTICS 82, ECOSA 82, Edinburgh, Scotland, 7-10 Sept. 1982).

The fiber optic gyroscope is now within the high sensitivity predicted by theoretical studies. The authors review the different steps involved in the progress realized over the last five years by the various research teams working on this subject around the world. Measurement of rotation rates of 10^{-2} deg/h have been demonstrated. This corresponds to measurements of phase shift of 10^{-7} rad in this interferometric system, five orders of magnitude better than the earliest results. The first major breakthrough was the detailed analysis of the effects of fiber birefringence and of mechanical stability of the system, using the fundamental principle of reciprocity of model propagation. The need for single mode filtering has led to a so-called minimum reciprocal configuration which improves dramatically the sensitivity of the system when it is used in addition to biasing detection techniques. The authors present the various technological approaches which have been used (bulk optics, all-fiber optics and integrated optics) and analyse the residual parasitic phenomena which had to be reduced (thermal and acoustic noise, Faraday and optical Kerr effects). Experimental data of an all-fiber system and of a brass board using a single multifunction integrated optic circuit are reported. Finally the current problems and the future directions of research which should lead to an actual navigation instrument are discussed. (34 refs.)

113102 Feasibility of fiber optical hydrophone. E.Giese, K.Schatzel, E.O.Schulz-DuBois (Inst. fur Angewandte Phys., Christian-Albrechts-Univ. Kiel, Kiel, Germany).

Proc. SPIE Int. Soc. Opt. Eng. (USA), vol.369, p.408-11 (1983). (SPIE Proceedings of the Max Born Centenary Conference OPTICS 82, ECOSA 82, Edinburgh, Scotland, 7-10 Sept. 1982).

Pressure induced changes in optical pathlength are being utilized to realize a hydrophone consisting of glass fibers in a Mach-Zehnder interferometric arrangement. In the experimental setup the authors use single-mode fiber optical power dividers and a simple control system that maintains the polarization of both light signals so that interference with constant contrast is obtained after superposition. A modified phase-tracking detection system is used to maintain maximum interferometer sensitivity and a design shown for a sensor-body with high acoustical sensitivity. (2 refs.)

113103 Fiber optic scattering monitor for application on bulk biological tissue, paper, and plastic. P.C.F.Borsboom, J.J.ten Bosch (Materia Tech., Dental School, State Univ. Groningen, Groningen, Netherlands).

Proc. SPIE Int. Soc. Opt. Eng. (USA), vol.369, p.417-21 (1983). (SPIE Proceedings of the Max Born Centenary Conference OPTICS 82, ECOSA 82, Edinburgh, Scotland, 7-10 Sept. 1982).

A method and apparatus is described to monitor non-destructively the turbidity of near white materials based on edge-losses from a small illuminated area. Measurements are shown on paper and plastic; on teeth during carious demineralization; on the whiteness of the human eyeball and on milk, changing the fat concentration. (2 refs.)

113104 Optical fibre sensors: principles and applications. J.P.Dakin (Plessey Electronic Systems Res. Ltd., Havant, England).

Proc. SPIE Int. Soc. Opt. Eng. (USA), vol.369, p.429-40 (1983). (SPIE Proceedings of the Max Born Centenary Conference OPTICS 82, ECOSA 82, Edinburgh, Scotland, 7-10 Sept. 1982).

Presents a review of the basic principles of a number of optical fibre sensors with discussion on the advantages and disadvantages of various types. In order to give an overview of what is rapidly becoming a very broad subject, the author has concentrated on the major classes of sensor of practical interest. (32 refs.)

113105 Fitting of a weighted Gaussian lowpass filter to the transfer function of graded-index fibres to reduce bandwidth ambiguities. D.Schickeltanz (Res. Labs., Siemens AG, Muenchen, Germany).

Electron. Lett. (GB), vol.19, no.17, p.650-2 (18 Aug. 1983).

To reduce the ambiguity in the bandwidth value, it is proposed to fit a weighted Gaussian lowpass filter response to the measured transfer function, and to take the bandwidth of this filter as the bandwidth of the fibre. At the same time a correlation value is obtained which may be used to characterise

the difference between the fit and the original transfer function, and to indicate the suitability of the fibre use in concatenated links. (5 refs.)

113106 Joint-loss dependence on mismatch parameters in graded-index optical fibres. G.Coppa, P.Di Vita, U.Rossi (CELT, Torino, Italy). *Electron. Lett. (GB)*, vol.19, no.17, p.654-6 (18 Aug. 1983). The dependence of the mean value and the RMS joint-loss distribution on geometrical and optical parameters is deduced in practical cases by simple and compact formulas. The different sensitivities of the various parameters can suggest different, more advantageous choices of the tolerance set. (4 refs.)

113107 New method for equivalent-step-index fibre for determination. C.Pask, F.Ruhl (Res. School. of Phys. Sci., Australian Nat. Univ., Canberra, Australia). *Electron. Lett. (GB)*, vol.19, no.17, p.658-9 (18 Aug. 1983). Proposes a new method for determining equivalent-step-index fibres; the far-field intensity halfangle is measured for a range of wavelengths and the data fitted by the step-fibre formula. A simple analytical formula aids the analysis. Proven experimental techniques can be used and no Gaussian or other theoretical approximations are involved. (6 refs.)

113108 Optical fibre jacketed with high-modulus low-linear-expansion-coefficient polymer. F.Yamamoto, K.Nakagawa, Y.Shuto, S.Yamakawa (Nippon Telegraph & Telephone Public Corp., Ibaraki, Japan). *Electron. Lett. (GB)*, vol.19, no.17, p.674-5 (18 Aug. 1983). A high Young's modulus, low-linear-expansion-coefficient-polymer loose-jacket optical fibre has been developed using oriented polyoxymethylene (POM), which exhibits Young's moduli 20 to 40 GPa and linear expansion coefficients $\leq 10^{-6}/^{\circ}\text{C}^{-1}$. The highly orientated POM loose-jacket fibre has no microbending losses in a temperature range -60 to 80°C . (3 refs.)

113109 Bend behaviour of polarising optical fibres. M.P.Varnham, D.N.Payne, R.D.Birch, E.J.Tarbox (Dept. of Electronics, Univ. of Southampton, Southampton, England). *Electron. Lett. (GB)*, vol.19, no.17, p.679-80 (18 Aug. 1983). Experimental results are presented which show how both bend radius and the orientation of the fibre in the bend considerably affect the single-polarisation operation of bow-tie fibres. (7 refs.)

113110 Practical single-polarisation anisotropic fibres. A.W.Snyder, F.Ruhl (Inst. of Advanced Studies, Australian Nat. Univ., Canberra, Australia). *Electron. Lett. (GB)*, vol.19, no.17, p.687-8 (18 Aug. 1983). Explains why single-mode single-polarisation operation is possible in practical fibres using less stress-induced birefringence than predicted for ideal anisotropic fibres. Furthermore, the 'leaky-mode' design is shown to be superior to more conventional strategies for single-polarisation operation. (6 refs.)

113111 Comparing the chromatic dispersions of two single-mode silica fibres with pure F and pure GeO_2 doping, respectively. T.Muller, W.E.Heinlein (Univ. Kaiserslautern, Kaiserslautern, Germany). *Electron. Lett. (GB)*, vol.19, no.17, p.692-4 (18 Aug. 1983). The refractive-index profile and the group-delay spectrum of a purely F-doped silica fibre were measured. This fibre's chromatic dispersion behaves considerably differently from that of a purely GeO_2 -doped fibre having the same profile function and V-parameter at $\lambda=0.633 \mu\text{m}$. (5 refs.)

113112 New and simple method for selective mode group excitation in graded-index optical fibres. A.K.Agarwal, G.Evers, U.Unrau (Inst. für Hochfrequenztech., Tech. Univ. Braunschweig, Braunschweig, Germany). *Electron. Lett. (GB)*, vol.19, no.17, p.694-5 (18 Aug. 1983). A modified monomode-fibre offset technique as well as a new and very simple method for selective mode excitation in multimode graded-index fibres is presented. It is shown that an inclined plane wave launch followed by a mandrel-wrap mode filter is a powerful way to excite a definite number of mode groups in graded-index fibres. Besides its extreme simplicity this method yields improved selectivity. Experimental results are presented. (7 refs.)

113113 Constraints for fundamental-mode spot size for broadband dispersion-compensated single-mode fibres. K.Petermann (Forschungsinst., AEG-Telefunken, Ulm, Germany). *Electron. Lett. (GB)*, vol.19, no.18, p.712-14 (1 Sept. 1983). Constraints exist for the fundamental-mode spot size for broadband dispersion-compensated fibres because of the relationship between dispersion and spot size. Dispersion compensation between 1.3 and $1.55 \mu\text{m}$ is still possible with the usual spot radius of about $5 \mu\text{m}$ at $\lambda=1.3 \mu\text{m}$, while dispersion compensation between 1.3 and $1.8 \mu\text{m}$ would require a spot radius of less than $4 \mu\text{m}$. (9 refs.)

113114 Near-field measurements in monomode fibres: determination of chromatic dispersion. G.Coppa, P.Di Vita, M.Potenza, U.Rossi (CELT, Torino, Italy). *Electron. Lett. (GB)*, vol.19, no.18, p.731-3 (1 Sept. 1983). A new dispersion measurement for monomode fibres is proposed. It is based on an elaboration of the near-field intensities at different wavelengths. The measurement is considerably simplified and the results are highly accurate. (5 refs.)

113115 Application of fiber optics to speckle metrology—a feasibility study. T.D.Dudderar (Bell Labs., Murray Hill, NJ, USA), J.A.Gilbert, A.J.Boehnlein, M.E.Schultz. *Exp. Mech. (USA)*, vol.23, no.3, p.289-97 (Sept. 1983). The development of fiber optics provides a potential means of simplifying coherent-light-metrology techniques and, simultaneously, increasing their realms of applicability by suppressing the negative effects of hostile mechanical and thermal environments. Describes a series of experiments which explore some of the possibilities for applying fiber optics to speckle metrology, and, at the same time, demonstrates the use of both photoelectronic-numerical and conventional optical systems for recording and correlating the resulting speckle fields. (20 refs.)

113116 Calculation of stress birefringence in fibers by an infinitesimal element method. R.H.Stolen (Bell Labs., Holmdel, NJ, USA). *J. Lightwave Technol. (USA)*, vol.LT-1, no.2, p.297-301 (June 1983). It is shown that stress birefringence in polarization-preserving fibers can be calculated by the simple addition of contributions from infinitesimal elements of the highly doped stress regions. This method provides insight into the properties of stress-birefringent fibers and shows the equivalence between the various types of such fibers. In particular, it is seen that a circular barrier layer around the core does not reduce the birefringence and that high birefringence does not require a large stress cladding. (16 refs.)

113117 Measurement of the core diameter of multimode graded-index fibers: a comparison of transmitted near-field and index profiling techniques. A.H.Chern, P.J.Rich, S.C.Mettler (Bell Labs., Norcross, GA, USA). *J. Lightwave Technol. (USA)*, vol.LT-1, no.2, p.302-11 (June 1983). The core diameters of six graded-index fibers from four different fiber manufacturers were compared using the transmitted near-field (TNF), the refracted near-field (RNF), and the transverse-interferometric (TI) measurement methods. This study was part of an effort to develop a standardized, industry-wide definition of core diameter and to determine the precision of interlaboratory core-diameter measurements using different measurement techniques. For fibers with smooth index-of-refraction profiles, all three methods were in good agreement ($<1.0\text{-}\mu\text{m}$ difference). Substantial differences between the transmitted near field and the two profiling methods (RNF and TI) were observed for fibers having step structure near the core-cladding boundary. In an attempt to resolve these differences, splice-loss measurements were used as an indicator of diameter differences. These experiments suggested that curve-fitting routines should be applied to the two profiling methods. A comparison of the curve-fitted profile data with measured transmitted near-field data at points 2 percent above the baseline produced values for the diameters which agreed to within $1 \mu\text{m}$ for all of the fibers measured. (5 refs.)

113118 Origins and control of polarization effects in single-mode fibers. S.C.Rashleigh (Naval Res. Lab., Washington, DC, USA). *J. Lightwave Technol. (USA)*, vol.LT-1, no.2, p.312-31 (June 1983). The polarization state of light in single-mode fibers is very sensitive to any perturbation which is not symmetric about the fiber axis. While this is a source of noise, drift, or signal fading in some applications, it can also be exploited in novel guided-wave devices. The basic birefringences that couple the two modes and change the polarization state along the fiber are reviewed. The three cases of uniform, phase-matched, and random coupling are considered. Polarization preservation in both low- and high-birefringence fibers is achieved by reducing this coupling. In addition to polarization-state changes, birefringent fibers can quickly reduce the polarization degree of nonmonochromatic light if both modes are excited, a characteristic that greatly simplifies evaluation of the degree of polarization preservation in these fibers. Current evaluations of the birefringence and the polarization-holding ability of state-of-the-art fibers are discussed, and it is concluded that fibers with good polarization-holding properties are becoming available. (81 refs.)

113119 Analytic solution for the birefringence produced by thermal stress in polarization-maintaining optical fibers. M.P.Varnham, D.N.Payne, A.J.Barlow, R.D.Birch (Dept. of Electronics, Univ. of Southampton, Southampton, England). *J. Lightwave Technol. (USA)*, vol.LT-1, no.2, p.332-9 (June 1983). Polarization-maintaining optical fibers are usually made by inducing a large anisotropic thermal stress in the core so that it appears highly birefringent. A simple analytic solution has been found for the birefringence in terms of the cross-sectional distribution of the high-expansion material used to create the thermal stress. The analysis is able to predict optimal structures which efficiently utilize the available stress and thus maximize the birefringence. It is shown that the optimum structure has a cross-sectional geometry resembling a bow-tie. Design rules are given whereby the dimensions may be chosen and these are verified in a simple experiment. (19 refs.)

113120 Studies on high-tensile proof tests of optical fibers. Y.Miyajima (Ibaraki Electrical Communication Lab., Nippon Telegraph & Telephone Public Corp., Ibaraki, Japan). *J. Lightwave Technol. (USA)*, vol.LT-1, no.2, p.340-6 (June 1983). By conducting high-tensile proof tests on optical fibers in order to eliminate weak points such as cracks or flaws, fiber strength is improved, but fiber length becomes shorter because of fiber breakage during proof tests. When the application is for submarine optical-fiber cables, the upper limit of proof-test strain is determined based on theoretical and experimental studies on fiber strength and fiber length after proof tests. (10 refs.)

113121 Length dependence of bandwidth for fibers with random-axial profile fluctuations. M.Miyamoto, R.Yamauchi, K.Inada (Fujikura Ltd., Chiba, Japan). *J. Lightwave Technol. (USA)*, vol.LT-1, no.2, p.354-9 (June 1983). Length dependence of bandwidth for graded-index optical fibers with random-axial profile fluctuations is investigated theoretically in connection with optical equalization in long spliced fibers. Based on the statistical approach, a simple analytical formula is derived on the assumption that the profile fluctuation does not cause mode coupling. At a short distance, the bandwidth has been found to be inversely proportional to square root of distance due to the profile fluctuation. The length dependence presents a remarkable contrast to that of the mode-coupling case showing the same dependence at a long distance. (16 refs.)

113122 Design considerations for the structural optimization of a single-mode fiber. K.Kitayama (Electronics Res. Lab., Univ. of California, Berkeley, CA, USA), Y.Kato, M.Ohashi, Y.Ishida, N.Uchida. *J. Lightwave Technol. (USA)*, vol.LT-1, no.2, p.363-9 (June 1983). Design considerations are made for the structural optimization of single-mode fibers used in high-bit-rate and long-haul transmission systems in the long-wavelength region. As the basic fiber parameters, a combination of the spot size W_0 and the effective cutoff wavelength λ_{ce} is newly chosen, because the combination is found to suitably describe various actual index profiles which deviate from an ideal step-index profile. A procedure to specify the usable range of W_0 and λ_{ce} is established, whereby the overall transmission-line loss in one repeater section is calculated using simple expressions for fiber intrinsic loss, excess loss in the cabling process, and splice loss, etc. The optimum values for a 400 Mbit/s transmission system operating at $1.3 \mu\text{m}$ with a repeater spacing of 20 km are obtained as $W_0=5.0 \pm 0.5 \mu\text{m}$ and $1.1 \mu\text{m} \leq \lambda_{ce} \leq 1.28 \mu\text{m}$, taking into consideration the additional requirement for the possible use at $\lambda=1.55 \mu\text{m}$. (18 refs.)

113123 A single-polarization fiber. J.R.Simpson (Bell Labs., Murray Hill, NJ, USA), R.H.Stolen, F.M.Sears, W.Pleibel, J.B.Macchesney, R.E.Howard. *J. Lightwave Technol. (USA)*, vol.LT-1, no.2, p.370-4 (June 1983). Reports an optical fiber which guides only one polarization. This fiber polarizes utilizes high modal birefringence (4.7×10^{-4}) to split the two polarizations of the fundamental mode and an elliptical depressed-index cladding to provide a steep wavelength-dependent tunneling loss to the fast axis mode. The stress-induced birefringence is created by an elliptical $\text{SiO}_2\text{-B}_2\text{O}_3$ inner cladding. A 4.7 m length of polarizer fiber exhibits an extinction ratio of 34 dB at a wavelength of 633 nm, with polarizing behavior over a bandwidth of 50 nm. Insertion loss of less than 1 dB has been observed for the guided linear-polarization mode. The polarizing band may be shifted from 620 to 525 nm by bending the fiber to a radius of 0.67 cm. Such fiber polarizers should find a variety of applications in fiber sensors, attenuators, isolators, wavelength filters, and tuners. (12 refs.)

113124 Rayleigh backscattering in a fiber gyroscope with limited coherence sources. W.K.Burns, R.P.Moeller (Naval Res. Lab., Washington, DC, USA).

J. Lightwave Technol. (USA), vol.LT-1, no.2, p.381-16 (June 1983).

Noise due to temporal fluctuations of Rayleigh backscattering light in fiber-optical gyroscopes is studied experimentally with various sources whose coherence length is less than the fiber length. The reduction of the coherent fraction of backscattered light and its fluctuation frequencies with reduced source coherence is demonstrated and fit to an analytical model. Measured backscatter parameters for the fiber and sources used are presented. (11 refs.)

113125 Broad-band ultrasonic sensor based on induced optical phase shifts in single-mode fibers. R.P.De Paula, J.H.Cole, J.A.Bucaro (Naval Res. Lab., Washington, DC, USA).

J. Lightwave Technol. (USA), vol.LT-1, no.2, p.390-3 (June 1983).

A broad-band ultrasonic sensor based on induced optical phase shifts in single-mode fibers (fiber-optic interferometer) is demonstrated over a frequency regime of 0.5-50 MHz. In addition, a recently developed theory used to predict the magnitudes of acoustically induced strains in optical fibers is verified. (9 refs.)

113126 An all fiber-optic sensor for surface acoustic wave measurements. J.E.Bowers (Bell Labs., Holmdel, NJ USA), R.L.Jungerman, B.T.Khuri-Yakub, G.S.Kino.

J. Lightwave Technol. (USA), vol.LT-1, no.2, p.429-36 (June 1983).

A surface acoustic wave (SAW) sensor constructed from single-mode fiber-optical components is described. An analysis of reciprocal and nonreciprocal modes of operation of the sensor is presented. Results from measurements on a variety of SAW devices illustrate the use of the sensor. The amplitude sensitivity is 0.0003 Å for an integration time of 0.1 s. (27 refs.)

113127 Single-mode, single-polarization fibers made of birefringent material. A.W.Snyder, F.Ruhl (Inst. of Advanced Studies, Australian Nat. Univ., Canberra, Australia).

J. Opt. Soc. Am. (USA), vol.73, no.9, p.1165-74 (Sept. 1983).

Optical fibers composed of highly birefringent material are studied. One of the two fundamental modes can be made leaky when the birefringence is sufficiently large. This suggests a novel single-mode, single-polarization fiber design that can be realized by stress-induced birefringence. The leakage rate is calculated by a perturbation method, which accounts for degeneracy between a bound mode and a packet of radiation modes. (27 refs.)

113128 Rayleigh backscattering theory for single-mode optical fibers. M.Nakazawa (Ibaraki Electrical Communication Lab., Nippon Telegraph & Telephone Public Corp., Tokai, Ibaraki-ken, Japan).

J. Opt. Soc. Am. (USA), vol.73, no.9, p.1175-80 (Sept. 1983).

The theory of backscattering in single-mode optical fibers is described through use of a correlation function for the refractive-index fluctuation in the fiber. A simple formula for the backscattered power is derived using two correlation functions for the Booker-Gordon and Gaussian models. The zeroth-order approximation of the formula, in which the correlation length is much smaller than the spot size of the waveguide mode, coincides with Brinkmeyer's model. The backscattered power at the input end of single-mode fiber is compared with that for multimode fiber. It is also shown that the backscattered power level at the input end is lower by approximately 55 dB than the input power level. (17 refs.)

113129 Information transmission with light. A new transmission medium for a wide range of applications. W.S.Ludolf, E.Gauger.

Mikrowellen Mag. (Germany), vol.8, no.5, p.580-90 (Oct. 1982). In German. [received: Aug. 1983]

This is a tutorial article which discusses the basic principles of light transmission over optical fibres. It discusses such topics as fibre profile-alignment and connectors as well as light loss and optimizing link lengths. (7 refs.) J.R.B.

113130 Fiber-optic temperature sensor. T.Taniuchi, Y.Tsujimoto (Central Res. Lab., Matsushita Electrical Industrial Co. Ltd., Osaka, Japan).

Natl. Tech. Rep. (Japan), vol.29, no.3, p.387-92 (June 1983). In Japanese.

A new optical sensor utilizing temperature variations of birefringence has been developed. A LiTaO₃ single crystal is used as the sensing material, a rutile plate as the polarizer, and an optical fiber as the signal transmission line. The nonmetallic optical sensor components offer electrical noise immunity and high electric insulation. Because a light emitting diode is applied as the light source, this sensor is highly stable and less expensive to manufacture. (9 refs.)

113131 Single-crystal fiber [of CsBr]. Y.Mimura.

Oyo Buturi (Japan), vol.52, no.4, p.311-12 (April 1983). In Japanese.

A fabrication method and characteristics of CsBr single-crystal fibers are described. The minimum loss of the fabricated CsBr fiber was less than 0.1 dB/m at 5.7 μm wavelength. The CsBr fiber shows relatively low loss at 10.6 μm. Therefore, the fiber can be used as a power light guide for CO₂ laser beams. A CsBr fiber with 1 mm diameter is capable of transmitting approximately 50 watts of CO₂ laser beams and has the total power loss of 25 to 30% per meter. (4 refs.) K.B.

113132 Polycrystalline infrared optical fibers. M.Kimura, S.Kachi, K.Shioyama.

Oyo Buturi (Japan), vol.52, no.4, p.313-14 (April 1983). In Japanese.

A fabrication method and transmission characteristics of polycrystalline optical fibers are presented. The materials applicable to these fibers include KCl, AgCl, AgBr and KRS-5. These materials are characterized by their low melting point. The fabrication method is capable of preventing the transmission loss of fibers from being increased by fabrication conditions. The transmission loss for 10.6-μm CO₂ laser beams was 0.25 dB/m for a KRS-5 fiber with 1.0 mm diameter. The numerical aperture of laser beam incidence to the fiber was as small as 0.01. The loss measurement using a CO₂ laser source showed 1.2 dB/m loss at 10.6 μm. This large loss resulted from scattering loss due to bad fiber-surface condition. (6 refs.) K.B.

113133 Fluoride glass fiber. T.Miyashita.

Oyo Buturi (Japan), vol.52, no.4, p.315-6 (April 1983). In Japanese.

The possible transmission loss of fluoride glass optical fibers may be about 10⁻³ dB per kilometer. The suitable material for implementing low-loss fibers is ZrF₄-BaF₂-GdF₃ glass. At the present time the lowest loss is 12 dB/km at 2.55 μm. A transmission loss of less than 3 dB/m is at wavelengths from 0.5 to 4.6 μm. For low-loss fiber-fabrication to be implemented, the impurity contents should be reduced from the present ppm level (10⁻⁶) to a ppb level (10⁻⁹). (6 refs.) K.B.

113134 Soliton analysis with the propagating beam method. D.Yevick, B.Hermansson (Inst. of Optical Res., Stockholm, Sweden).

Opt. Commun. (Netherlands), vol.47, no.2, p.101-6 (15 Aug. 1983).

It is demonstrated that the propagating beam method can be employed to determine the behavior of optical fiber solitons in the presence of optical loss, third order dispersion and fifth order nonlinearity. Using the method, the authors analyze and extend analytical and numerical results of other authors,

concentrating principally on calculations involving $N=3$ solitons. The results demonstrate that in fibers with large third order dispersion, only the lowest-order solitons should be excited in communication applications. (8 refs.)

113135 Spatial filtering of backscattering signal in optical fibers. M.Biet (Thomas-CSF, Lab. de Recherches, Orsay, France).

Rev. Sci. Instrum. (USA), vol.54, no.9, p.1163-4 (Sept. 1983).

Reducing the front face echo is one of the major problems encountered in backscattering measurements of optical fibers. A simple method is proposed in order to eliminate completely this unwanted signal for both multimode and single-mode fibers. The setup is very simple and no special preparation of the fiber is needed. The insertion losses of the filtering device are very low and the detector is protected against direct reflections. In the case of multimode fibers a selective analysis of the backscattered signal can be performed. (10 refs.)

113136 Plug connectors for fiber-optic waveguide systems and components. G.Knoblauch (Siemens AG, Munchen, Germany), H.-N.Toussaint.

Siemens Components (Engl. Ed.) (Germany), vol.18, no.3, p.81-6 (June 1983).

Discusses plug connections on optical transmission paths that serve to interlink two fiber-optic waveguide components in a simple and reproducible manner with low loss and, if necessary, in such a way that the components can be disconnected easily. Components covered by this definition include lines, filters, and junction boxes in addition to optoelectronic converters at the transmission and reception side. Various requirements are made of the mechanical tolerances of the plug connectors dependent upon the core diameter of the fibers used and the required insertion loss of the plug connection. However, the resultant insertion loss of a plug connection is highly dependent upon the fiber tolerances. (no refs.)

113137 Strength assurance of optical fiber based on screening test. Y.Mitsunaga, Y.Katsuyama, H.Kobayashi, Y.Ishida (Ibaraki Electrical Communication Lab., NTT, Ibaraki, Japan).

Trans. Inst. Electron. & Commun. Eng. Jpn. Part B (Japan), vol.J66B, no.7, p.829-36 (July 1983). In Japanese.

The author describes a long-term assurance method of optical fiber strength based on the screening test. General equations for assurance, which are applicable for various environmental and strain conditions are derived theoretically. Fatigue and strength distribution parameters of fibers contained in the equations are quantitatively evaluated from test data, and an allowable failure ratio is determined considering the transmission system reliability. Using the derived equations and the determined parameter values, the required screening test condition for reliability assurance of the optical fiber is clarified in relation to the strain applied to the fiber for long period. (8 refs.)

113138 Fényvezető uvegcsalak a tavkozlesben (Light propagation in optical fibres). I.Kosa Somogyi.

Report KFKI-1983-75, Hungarian Acad. Sci., Budapest (1983), 16 pp. In Hungarian.

A short survey is given of the light propagation in optical fibres and the different technologies for their production. (15 refs.)

113139 A fibre optic displacement sensor. H.Sohlstrom, U.Holm (Instrumentation Lab., Royal Inst. of Technol., Stockholm, Sweden).

Technological and Methodological Advances in Measurement. Acta IMEKO 1982. Proceedings of the 9th IMEKO Congress of the International Measurement Confederation, Berlin, Germany, 24-28 May 1982 (Amsterdam, Netherlands: North-Holland 1983), p.183-92 vol.1

Different sensor principles are first outlined. A displacement sensor using multimode, step index fibres is described. Measurement data showing a resolution of 0.05 nm/√Hz in a 150 μm linear range is given. In this sensor, the light coupling between two fibre ends varies with the position of a movable mirror. A mathematical model of the sensor is presented. Application to pressure sensing is also discussed. (9 refs.)

Optical fiber systems: Technology, design, and applications ..See Entry 111330

Sensor for non-optical measuring quantities using optical principles and outputs. ISee Entry 111663

Multimode optical fiber sensorsSee Entry 111674

Polarimetric strain gauges using high birefringence fibreSee Entry 111738

The resolving power of a reflectometer with compensation of background reflectionsSee Entry 111745

Refractive index measurement using an optical fiberSee Entry 111746

Emission frequency stability in single-mode-fibre optical feedback controlled semiconductor lasersSee Entry 113010

Solitons in single mode optical fibresSee Entry 113039

Wideband frequency conversion in the UV by nine orders of stimulated Raman scattering in a XeCl laser pumped multimode silica fiberSee Entry 113051

Sum-frequency wave generation in optical fibersSee Entry 113053

Stimulated Brillouin scattering in optical fibers, and wavefront reversalSee Entry 113058

Study of the OH content of CVD silica glass for optical fibresSee Entry 113070

Low-loss wavelength division multiplexing (WDMK) devices for single-mode systemsSee Entry 113148

ALPD (axial lateral plasma deposition): a new process for the production of high quality optical fibersSee Entry 113154

Optical waveguide manufacturing techniquesSee Entry 113156

The production of optical fibers and optical fiber cablesSee Entry 113157

Optical probe for narrow sound fieldSee Entry 113223

Backscattering observation of radiation damage in optical fibersSee Entry 113983

Optical remote monitoring of CH₄ gas using low-loss optical fiber link and InGaAsP light-emitting diode in 1.33-μm regionSee Entry 115714

42.80Q Image detectors, convertors, and intensifiers

113140 Portable real-time coherent optical correlator. J.Upatnieks (Infrared & Optics Div., Environmental Res. Inst. of Michigan, Ann Arbor, MI, USA).

Appl. Opt. (USA), vol.22, no.18, p.2798-803 (15 Sept. 1983).

A real-time coherent optical correlator is mounted inside a 15-×23-×38-cm enclosure and features laser diode light sources and a liquid crystal incoherent-to-coherent image converter. Each of four reference filters is illuminated by a separate laser diode, real-time operation is achieved by the image converter, and a zoom lens forming the incoherent image allows a scale search. The correlator can be mounted on a tripod and performs correlations indoors or outdoors. (11 refs.)

113141 AGA infrared techniques. H.Schachinger (AGA-IRS Internat. GmbH, Wien, Austria). *Finomtech.-Mikrotech. (Hungary)*, vol.22, no.5, p.129-34 (May 1983). In Hungarian.

Grounds of measurements based on the perception of infrared radiation and alternatives of its application are reported. This paper is addressed to experts who intend to get acquainted with the physical and technical bases of the method (called also thermography) in order to pick up subjects for which this method provide for technical-scientific or economical advantages. (no refs.)

113142 Infra-red image sensing and conversion into visible light. N.R.Mantena (Electronic Watch Div., Hindustan Machine Tools Ltd., Bangalore, India). *J. Inst. Electron. & Telecommun. Eng. (India)*, vol.29, no.2, p.71-6 (Feb. 1983).

An integrated circuit configuration consisting of an operational amplifier with metal insulator semiconductor transistors coupled to a *pn* junction photovoltaic detector and a feedback diode is proposed for fabricating integrated arrays which will form the image-sensor mosaic. The output of this array can be used to drive the mosaic panel of electroluminescent diodes, either directly or through scanning type of system in order to obtain a visible output which is a replica of the infra-red signal at the input. Using the present-day IC technology, it should be possible to fabricate compact all-solid-state infra-red sensors and converters for use in binocular type of viewing by the nightglow. Experimental data on the devices required for integration of a unit-cell detector-amplifier system are presented. For the system proposed for infra-red image sensing and conversion into visible light, an analysis of the system time constant is presented, and, it is shown that a system time constant of 0.1 sec or less can be obtained by the integrated system proposed here. On the basis of this analysis, an integrated format was selected and preliminary integrated circuits were fabricated which were close to meeting parameters of the system design. This system has a good application in the nightviewing of slow to medium-speed objects with the help of nightlight reflections. (8 refs.)

113143 Simple synchronous video image combiner. A.L.V.S.Lage, A.O.S.Gomes, O.D.D.Souares (Centro de Fisica, Univ. do Porto, Porto, Portugal). *Rev. Sci. Instrum. (USA)*, vol.54, no.9, p.1248-50 (Sept. 1983).

A simple and inexpensive TV camera image combiner for several purposes in current video dual image acquisition is described. (3 refs.)

113144 Adaptive randomized detector of optical signals. R.G.Tolparyev, E.V.Borisov. *Telecommun. & Radio Eng. Part 2 (USA)*, vol.37, no.9, p.113-15 (Sept. 1982). Translation of: *Radiotekhnika, Moskva (USSR)*, vol.37, no.9, p.77-9 (Sept. 1982).

A practical circuit and operating algorithm of an optical signal detector with randomized decision rule are described. (1 ref.)

Magnetic focus/deflection image converter camera for cineradiography See Entry 111846

Image converter tubes for radiology and neutronography used in nondestructive testing See Entry 11847

42.80S Optical communications devices

113145 Optical comms: system elements reviewed. J.Williamson. *Commun. Eng. Int. (GB)*, vol.5, no.2, p.15-22 (April 1983).

Surveys recent developments in fibre optic systems. In addition to main system components, some aspects of manufacturing, installation and testing are included. The basic elements of an optical fibre communication system are the dielectric waveguide, optical sources and optical detectors. Signal processing devices like wavelength division multiplexers also find application in optical systems. (no refs.)

113146 Physical obstacles to optical communications. J.Williamson. *Commun. Eng. Int. (GB)*, vol.5, no.2, p.23-9 (April 1983).

Optical fibre manufacture using vapour phase processes is briefly discussed. To maintain comprehensive quality control a measuring system from Vickers Instruments is available. In the majority of commercially available systems, the demountable coupling of fibres is accomplished by precisely aligning the two prepared fibre ends in a mechanical connector. Some of the most popular mechanical connector systems are reviewed. (no refs.)

113147 Light fantastic and light fact [fibre optic communication]. J.Williamson. *Commun. Eng. Int. (GB)*, vol.5, no.2, p.30-5 (April 1983).

Presents an account of the main application areas for optical fibre communication systems. The most obvious candidate for the early deployment of optical transmission systems is the public switched telephone network. Contention channel type local area networks (LAN) are difficult to implement with optical fibre since the signal losses which occur at each tap exert an inhibiting effect on system length and tap number. A number of other market areas exist such as the military and television. (no refs.)

113148 Low-loss wavelength division multiplexing (WDMK) devices for single-mode systems. J.Lipson (Bell Telephone Labs. Inc., Allentown, PA, USA), G.T.Harvey. *J. Lightwave Technol. (USA)*, vol.LT-1, no.2, p.387-90 (June 1983).

Reports on single-mode microoptic wavelength division multiplexing (WDM) devices with two channels located at 1275 and 1345 nm, respectively. Data are presented for four multiplexers and four demultiplexers. The average insertion loss for the multiplexers was 0.5 ± 0.2 and 1.0 ± 0.3 dB for the short and long wavelength channels, respectively. For the demultiplexers, the average losses were 0.8 ± 0.2 dB and 1.0 ± 0.1 dB, respectively. The full channel widths of the demultiplexers for 0.5 dB of additional loss were about 22 nm. All measurements included the presence of prototype precision single-mode connectors. The multiplexers were based on interference filters and GRIN lenses with identical single-mode fibers used for inputs and output. The demultiplexers employed diffraction gratings and GRIN lenses with 50- μ m core graded-index fibers. In addition three of the demultiplexers included a third output channel centered at 1521 nm. The 28-dB dynamic range of the monochromatic-based test apparatus was insufficient to evaluate the crosstalk performance. Measurements on two demultiplexers, using a 1295-nm laser, yielded values of -33 and -38 dB, respectively for the crosstalk in the 1345-nm channel. (7 refs.)

113149 A guided-wave optical arbiter circuit. N.Shimizu, M.Ikeda, M.Imase, K.Okada, T.Kimura (Musashino Electrical Communication Lab., Nippon Telegraph & Telephone Public Corp., Tokyo, Japan). *J. Lightwave Technol. (USA)*, vol.LT-1, no.2, p.424-9 (June 1983).

An optical waveguide circuit which can be used as an arbiter for priority allocation in data communication system is proposed. The waveguide circuit was fabricated by silica deposition and its basic performance as an arbiter was measured. The average insertion loss and the crosstalk level for a 10-port

circuit was measured to be 9.8 and -26.8 dB, respectively. In obtaining a large number of fan-out on a compact substrate, it is important to provide a large refractive-index difference between the core and cladding to allow for a sharp bend and to decrease the excess branching loss. The number of fan-out of about 250 is expected on a 50-mm-square substrate. (5 refs.)

113150 A high resolution bar code reader. H.Burkett (Consumer Products Group, Texas Instruments Inc., Lubbock, TX, USA), G.Frazier. *IEEE Trans. Consum. Electron. (USA)*, vol.CE-29, no.3, p.443-9 (1983). (1983 IEEE International Conference on Consumer Electronics. ICCE, Des Plaines, IL, USA, 8-10 June 1983).

Discusses the development of an optical 'wand' which is capable of very dense bar code reading. This wand was initially used in conjunction with a speaking learning aid. The simple interface can provide for an analog or digital output. The electronic components used in the readhead are an IR LED and a phototransistor. (no refs.)

Optical fiber systems: Technology, design, and applications .. See Entry 111330

Recent progress on semiconductor lasers See Entry 113019

Information transmission with light. A new transmission medium for a wide range of applications See Entry 113129

42.82 INTEGRATED OPTICS
(for optical waveguides see also 42.80L)

113151 Some results and problems in integrated-optics developments. A.M.Goncharenko. *J. Appl. Spectrosc. (USA)*, vol.37, no.6, p.1400-5 (Dec. 1982). Translation of: *Zh. Prikl. Spektrosk. (USSR)*, vol.37, no.6, p.965-71 (Dec. 1982). [received: Sept. 1983]

Integrated optics is concerned with the generation, propagation, and different types of conversion and detection of light waves in thin-film waveguide devices. The practical purpose of integrated optics is to design optical arrangements similar in their functional possibilities to existing electronic integrated circuits based on semiconductors. The information carrier in integrated optics is light (photons). This ensures a high speed of response and a considerable bandwidth, noise immunity, and certain other advantages compared with electronic devices. The author presents some results and points out the problems that still need to be solved in this new area of science. (33 refs.)

113152 Optical switching characteristics in slightly nondegenerated multilayered couplers using acousto-optic interaction by surface acoustic waves. N.Goto (Faculty of Engng., Nagoya Univ., Nagoya, Japan), Y.Miyazaki, Y.Akao. *Trans. Inst. Electron. & Commun. Eng. Jpn. Sect. E (Japan)*, vol.E66, no.7, p.442-9 (July 1983).

Experiments of acousto-optic interaction in integrated optics slightly non-degenerated couplers are firstly demonstrated with comparison to the theoretical results. The switching mechanism is based on the even-odd mode conversion by acousto-optic effects and on the probe splitting in the separating branch. The device consists of ZnS/Ta₂O₃/Nb₂O₅ thin films on Y-cut LiNbO₃ substrates with propagation in the X direction. Surface acoustic waves of approximately 0.5 W, 71.2 MHz switch optical power about 90 percent. The frequency characteristics agree well with the theoretical results. These experiment characteristics may give the design base of useful tunable optical filters and multiwavelength separators. (15 refs.)

Electronic wavelength tuning with semiconductor integrated etalon interference lasers See Entry 112989

Phase-locked semiconductor laser array with separate contacts See Entry 113007

A bistable hybrid optical device using an integrated modulator with an induced dielectric channel See Entry 113085

Low-loss integrated optical waveguides fabricated by nitrogen ion implantation See Entry 113086

Prism excitation of highly multimode deep planar waveguides See Entry 113087

Optical losses in metal/SiO₂-clad Ti:LiNbO₃ waveguides See Entry 113089

Optical wave propagation in form-birefringent media and waveguides See Entry 113092

Numerical field solution for an arbitrary asymmetrical graded-index planar waveguide See Entry 113093

Three-guide optical couplers in GaAs See Entry 113094

Optical coupling between single-mode semiconductor lasers and strip waveguides See Entry 113095

Theory of prism coupling with a nonlinear optical waveguide: second harmonic generation See Entry 113096

Review of fiber optic gyroscopes See Entry 113101

A guided-wave optical arbiter circuit See Entry 113149

42.85 OPTICAL TESTING AND WORKSHOP TECHNIQUES

113153 Laser alignment of parallel mechanical axes 10 metres apart. G.F.Marshall, C.L.Taylor (Dept. of Optics, Energy Conversion Devices Inc., Troy, MI, USA). *Proc. SPIE Int. Soc. Opt. Eng. (USA)*, vol.369, p.207-10 (1983). (SPIE Proceedings of the Max Born Centenary Conference OPTICS 82, ECOSA 82, Edinburgh, Scotland, 7-10 Sept. 1982).

A technique using a laser to align the parallelism of a nest of rotational axes or surfaces 10 metres apart to within one-half arc minute is described. (no refs.)

113154 ALPD (axial lateral plasma deposition): a new process for the production of high quality optical fibers. D.Boucher, B.Wurrier, P.Aldebert, V.Neuman, P.Ripoche (Fibres Optiques Industries, Pithiviers, France). *Proc. SPIE Int. Soc. Opt. Eng. (USA)*, vol.369, p.395-400 (1983). (SPIE Proceedings of the Max Born Centenary Conference OPTICS 82, ECOSA 82, Edinburgh, Scotland, 7-10 Sept. 1982).

A quasi-continuous process for production of large core low-loss step index all-silica fibers has been developed by combining axial plasma deposition and lateral plasma deposition. Named ALPD (axial lateral plasma deposition), this process allows industrial production of 2 db/km fibers (0.85 micron) which is almost equivalent to the loss limit of silica fibers estimated from the characteristics of intrinsic infrared absorption and Rayleigh scattering losses. Furthermore thanks to the pure fused silica core these fibers show an excellent radiation hardness and high power throughput capability. (15 refs.)

113155 Diamond flycut multifaceted mirror. S.M.Allen, M.J.Stanich (IBM Corp., Armonk, NY, USA). *IBM Tech. Disclosure Bull. (USA)*, vol.26, no.2, p.559-60 (July 1983).

Describes a manufacturing technique for machining optical surfaces on a multifaceted mirror by offsetting the flycutter from the center of the facet to angle any resulting tool marks. (no refs.)

113156 Optical waveguide manufacturing techniques. M.G.Blankenship (Optical Waveguide Technol., Corning Glass Works, Corning, NY, USA). Southcon/81 Conference Record, Atlanta, GA, USA, 13-15 Jan. 1981 (El Segundo, CA, USA: Electron. Conventions 1981), p.16-2/1-5

Several manufacturing techniques are currently in use for fabricating high quality glass optical waveguide fibers. The total process can be divided into four major process areas as follows: materials preparation, glass (or preform) making, drawing/coating of fiber and testing/characterization. The author deals primarily with the glass making and drawing steps. The glass making tends to be the controlling process step and the leading technologies for this are the vapor deposition processes and the direct melt process. The vapor and deposition processes include outside vapor deposition, axial vapor deposition and inside vapor deposition. Fiber drawing/coating for high silica vapor deposited preforms utilizes high temperature radiant sources whereas fibers are directly drawn from the lower temperature double crucible processes. Polymer coatings are typically applied during fiber drawing to protect the glass fiber from abrasion and loss inducing microbending. (28 refs.)

113157 The production of optical fibers and optical fiber cables. B.K.Tariyal, J.G.Wright, R.Iyengar (Western Electric Co., Norcross, GA, USA).

Southcon/81 Conference Record, Atlanta, GA, USA, 13-15 Jan. 1981 (El Segundo, CA, USA: Electron. Conventions 1981), p.16-3/1-12

Optical fibers and cables constitute the transmission media through which light travels in an optical communication system. Low loss and high strength optical fibers with a high bandwidth are essential to the economic viability of a system. The authors describe the production methods for optical fiber and optical fiber cables. Special emphasis is given to the factors which affect the performance of the fibers and the cables, in particular, their mechanical reliability. The processes described are the Western Electric processes as currently practiced. However, development work continues on all aspects of fiber and cable production and will result in continuing changes. (17 refs.)

Point image focus sensing using an automated Foucault test See Entry 111733

Polynomial fit of subaperture interferograms See Entry 111749

Interferometer detection system for optical testing See Entry 111753

Advances in optical metrology of complex objects See Entry 111754

Large crystal sapphire optics See Entry 113069

Full aperture testing with subaperture test optics See Entry 113073

Methods for the investigation of laser mirrors for laser gyro See Entry 113075

Low-loss integrated optical waveguides fabricated by nitrogen ion implantation See Entry 113086

Studies on high-tensile proof tests of optical fibers See Entry 113120

Fényvezető uvegcsalak a tavkozlesben (Light propagation in optical fibres) See Entry 113138

Thermal stress limitations to laser fire polishing of glasses ... See Entry 115376

43.00 ACOUSTICS

(for audition, see 87.34; for speech, see 87.36; for sound effects on living matter, see 87.50C)

43.20 GENERAL LINEAR ACOUSTICS

(see also 03.40K Mathematical problems in waves and wave propagation)

113158 On the determination of the acoustical characteristics of absorbent materials. V.Legeay, R.Seznec (Lab. Central des Ponts et Chaussées, Paris, France).

Acustica (Germany), vol.53, no.4, p.171-92 (Aug. 1983). In French.

This article presents a method for determining a reflection coefficient of sound waves incident normally or obliquely at a plane interface. Only the modulus of the reflection coefficients is evaluated through the spectra of the incident and reflected waves; its phase is determined as a result of the splitting-up of the modulus by the calculation of natural logarithm of its Hilbert transformation. The reason for this procedure depends on the properties of linear systems at minimal dephasing. The various steps of the calculations are presented: the discrete Hilbert transformation of the amplitudes, extrapolation of the modulus and final verification of the hypothesis of minimal dephasing. The principle interest of this method is the avoidance of defining a phase reference plane, a hazardous definition notably in the case of the surface of a ground with vegetation. An application of this method of characterising the acoustic properties of industrial absorbing materials is described, as well as the application to the determination of the specific impedance of sandy ground or of closely cut grass. (14 refs.)

113159 'Bimorph' ultrasonic wave guides. M.Touratier (ENSAM, Paris, France).

Int. J. Eng. Sci. (GB), vol.21, no.12, p.1411-36 (1983). In French.

An analysis of the dispersion of elastic waves is presented for two types of long ultrasonic wave-guides that are termed 'bimorph': (i) a 'three-layer' guide made of two different materials and (ii) a 'clad core' guide built up of a rectangular core surrounded by a cladding, the materials of the rod and cladding having different properties. An analytical model is proposed to describe the extensional, flexural and torsional motions in 'bimorph' wave guides having two geometrical and material symmetry axes. The asymptotic behaviour of the model allows one to select the material properties which lead to modes guided essentially either in the central layer or in the core of the bimorph guide. Moreover, the dispersive properties of a 'bimorph' can be controlled through the choice of geometrical and material parameters. (14 refs.)

113160 Supersaturation of complex-amplitude fluctuations of waves propagating in a random medium. A.R.Wenzel (Naval Ocean Res. & Dev. Activity, NSTL Station, MS, USA).

J. Acoust. Soc. Am. (USA), vol.74, no.3, p.1021-4 (Sept. 1983).

A theoretical analysis of the wave field radiated by a point source in a one-dimensional random medium is presented. The analysis is based on the

quasi-Rytov method, and includes both multiple forward scatter and multiple backscatter effects. An approximate expression for the mean square of the modulus of the fluctuating part of the complex wave amplitude is derived under conditions of a weakly dissipative medium. For the high-frequency case, this expression shows that the complex-amplitude fluctuations increase relatively rapidly with propagation range until a maximum value (the supersaturation value) is reached, after which they decrease relatively slowly with further increase in range. These results are in qualitative agreement with observations of intensity fluctuations of optical waves propagating in the lower atmosphere. (11 refs.)

113161 Reflection from a boundary with periodic roughness: theory and experiment. A.Jungman, L.Adler (Dept. of Welding Engng., Ohio State Univ., Columbus, OH, USA), J.D.Achenbach, R.Roberts.

J. Acoust. Soc. Am. (USA), vol.74, no.3, p.1025-32 (Sept. 1983).

Reflection of elastic waves from a traction-free solid-air boundary of periodic sawtooth profile is investigated experimentally and analytically. For an incident plane wave the surface displacements on the profile are computed as the solution of a singular integral equation. The reflected field is subsequently obtained by using an integral representation for the reflected field. Experimental results are presented for the relative amplitude spectrum for reflection from brass-air, perspex-air, and steel-air boundaries. Both the theoretical and the experimental results show that surface resonances of the profile significantly affect the frequency spectrum of the reflected waves. It is shown that the existence of sharp dips in the amplitude spectra of reflected waves can be attributed to destructive interference between direct reflections and reradiation from surface resonance motions. Good agreement is obtained between calculated results and experimental data. (16 refs.)

113162 Single and multiple scattering of elastic waves in two dimensions.

A.H.Shah, K.C.Wong (Dept. of Civil Engng., Univ. of Manitoba, Winnipeg, Manitoba, Canada), S.K.Datta.

J. Acoust. Soc. Am. (USA), vol.74, no.3, p.1033-43 (Sept. 1983).

In this paper a combined analytical and finite element method is presented for studying diffraction of elastic waves by cylindrical cavities in two dimensions. The method consists of dividing the infinite space into two regions: an interior bounded region containing the cavities and an exterior unbounded region. The interior region is represented by finite elements and wavefunction expansions are used to represent the field in the exterior homogeneous isotropic medium. Numerical results obtained by this method for scattering of plane longitudinal (P) and shear (SV) waves by a circular cylindrical cavity are shown to be in agreement with the exact solution. The method is then applied to problems of single scattering by triangular and square shaped cavities. Finally, multiple scattering by two circular, and one circular and one square shaped cavity are solved. (14 refs.)

113163 A new rigorous expansion for the velocity potential of a circular piston source. T.Hasegawa, N.Inoue, K.Matsuzawa (Dept. of Phys., Faculty of Sci., Ehime Univ., Ehime, Japan).

J. Acoust. Soc. Am. (USA), vol.74, no.3, p.1044-7 (Sept. 1983).

In the case of boundary value problems such as the sound scattering from a sphere placed in the nearfield of a plane piston source, it is sometimes essential to express the velocity potentials in terms of the orthogonal expansion. It is demonstrated in the present work that the Rayleigh surface integral, giving the velocity potential for a plane piston source surrounded by an infinite rigid flange, reduces to a rigorous expansion of the simplest form for a circular piston as series of spherical surface harmonics. The resulting equation is valid for any field points even on the piston surface. Sample calculations made with a microcomputer are presented with three-dimensional and contour plots. (13 refs.)

113164 Acoustic coupling between a pulsating and an oscillating sphere.

W.Thompson, Jr., J.M.Reese (Appl. Res. Lab., Pennsylvania State Univ., State College, PA, USA).

J. Acoust. Soc. Am. (USA), vol.74, no.3, p.1048-50 (Sept. 1983).

The modification of the radiation impedance load on each of two equal-sized spherical-shaped sources, one vibrating in the pulsating or $n=0$ mode and the other in the oscillating or $n=1$ mode has been calculated. Plots of the normalized resistive and reactive components of the modified radiation impedance are presented as a function of the wavelength size and separation of the two spheres. (5 refs.)

113165 T-matrix approach to study the vibration frequencies of elastic bodies in fluids. B.A.Peterson, V.V.Varadan, V.K.Varadan (Dept. of Engng. Mech., Ohio State Univ., Columbus, OH, USA).

J. Acoust. Soc. Am. (USA), vol.74, no.3, p.1051-6 (Sept. 1983).

The T matrix or null field method is used as a computational scheme for analyzing the scattering frequencies of a homogeneous elastic body in a fluid. These frequencies have a unique distribution, in the complex plane, for each body. The authors solve a scalar transcendental equation to find the scattering frequencies for a sphere. These frequencies are used as starting points in a matrix approach to find the scattering frequencies for a prolate spheroid. Lists and figures of the most important scattering frequencies for a sphere and a prolate spheroid are given. (34 refs.)

113166 Compact sound scatterers with constraints. I.Tolstoy.

J. Acoust. Soc. Am. (USA), vol.74, no.3, p.1068-70 (Sept. 1983).

Lighthill's method of formulating acoustic scatter allows the explicit introduction of constraints upon the motion of the (small) scatterer. Such constraints can be important in the modeling of rough surfaces by extensions of the Biot technique. (8 refs.)

113167 Comments on 'Kramers-Kronig relationships and wave propagation in composites' by A.I. Beltzer [J. Acoust. Soc. Am. 73, 355 (1983)]. C.M.Sayers (Materials Phys. Div., AERE Harwell, England).

J. Acoust. Soc. Am. (USA), vol.74, no.3, p.1070-1 (Sept. 1983).

It will be shown that local approximations to the Kramers-Kronig relations are not applicable to scattering systems. (6 refs.)

113168 Comments on 'Dynamics of composites and the K-K relations', a reply to C.M. Sayers. A.I.Beltzer (Holon Technol. Inst., Holon, Israel).

J. Acoust. Soc. Am. (USA), vol.74, no.3, p.1071-2 (Sept. 1983).

For C.M. Sayers paper see *ibid.*, vol.74, p.1070 (1983). It is shown that the original formulas [J. Acoust. Soc. Am. 73, p.355-6 (1983)] are correct. (12 refs.)

113169 Multiple sound reflections between plane panels covered with reflection coefficients. Y.Sakurai, K.Ishida (Faculty of Engng., Kansai Univ., Osaka, Japan).

J. Acoust. Soc. Jpn. (E) (Japan), vol.4, no.3, p.121-6 (July 1983).

The sound reflection coefficient of a given material, which is measured from a sufficiently large plane of it for spherical wave incidence, has been used previously to predict the first reflection for plane, convex or concave, finite size panels covered with that material. The first reflection of such a panel can be treated as two separate waves. One is the wave from the specular reflection point and the other is a boundary wave comprised of components from the lined point sources at each edge. Here, multiple reflections between two

plane panels covered with materials having reflection coefficients that may be different are approximately calculated from such separate waves as in the same treatment of rigid plane panels. (5 refs.)

113170 The effect of incident pulse width on transient waveform from a circular plate. I.Nakayama, A.Nakamura (Inst. of Sci. & Industrial Res., Osaka Univ., Osaka, Japan). *J. Acoust. Soc. Jpn. (E) (Japan)*, vol.4, no.3, p.165-7 (July 1983). The effect of the pulse width on the transient waveform radiated from a clamped circular plate has been examined in the time domain when a plane triangular sound pulse impinges normally on the plate. It has been noted that with increasing the pulse width the initial peak level becomes small and the successive part becomes a simple oscillating waveform with large amplitude. It may be valid that in impulsive sound insulation problems one should direct one's attention to the properties of the incident wave. (3 refs.)

113171 Interior and exterior resonances in acoustic scattering. I. Spherical targets. G.C.Gaunaurd, E.Tanglis, H.Uberall (Naval Surface Weapons Center, White Oak, Silver Spring, MD, USA), D.Brill. *Nuovo Cimento B (Italy)*, vol.76B, ser.2, no.2, p.153-75 (11 Aug. 1983). In acoustic scattering from elastic objects, resonance features appear in the returned echo at frequencies at which the object's eigenfrequencies are located, which are explained by the excitation of interior creeping waves. Corresponding resonance terms may be split off from the total scattering amplitude, leaving behind an apparently nonresonant background amplitude. This is demonstrated for scatterers of spherical geometry and in a companion paper also for scatterers of arbitrary geometry, by using the *T*-matrix approach. For the case of near-impenetrable spheres, it is subsequently shown that the background amplitude can be split further into specularly reflected contributions, plus highly attenuated resonance terms which are explained by the excitation of exterior (Franz-type) creeping waves. The singularity structure of the scattering function is shown mathematically, by using the *R*-matrix approach of the nuclear-scattering theory, as that of a meromorphic function without any additional 'entire function' (as had been postulated by the singularity expansion method). (21 refs.)

113172 Analysis of the elastic field of ultrasonic waves scattered by a cylindrical cavity. N.P.Aleshin, L.Yu.Mogil'ner (N.E. Bauman Moscow Advanced Tech. School, Moscow, USSR). *Sov. J. Nondestr. Test. (USA)*, vol.18, no.12, p.939-49 (Dec. 1982). Translation of: *Defektoskopiya (USSR)*, vol.18, no.12, p.18-30 (Dec. 1982). [received: Sept. 1983] The scattering of a transverse wave by a lateral cylindrical reflector is investigated. The resultant field is represented by the sum of a specularly reflected field and diffraction fields, where the last are due to the reradiation into the volume of surface waves that are produced at the cylinder. The surface waves may propagate with velocities close to those of longitudinal and transverse waves in the volume. Expressions are derived for the velocities of the surface waves. (17 refs.)

113173 Calculated reflection and transmission of a plane wave at the interface between two liquids with viscosity and thermal conductivity. F.F.Legusha. *Sov. Tech. Phys. Lett. (USA)*, vol.8, no.11, p.597-8 (Nov. 1982). Translation of: *Pis'ma v Zh. Tekh. Fiz. (USSR)*, vol.8, no.21-22, p.1390-2 (Nov. 1982). [received: Sept. 1983] Examines the problem of the transmission of a plane acoustic wave across a plane interface between two immiscible liquids with an arbitrary set of physical parameters. The problem is solved by the Kirchhoff-Konstantinov method. Expressions for the reflection and transmission coefficients are derived. (3 refs.)

113174 A few remarks on the calculation of sound field by the contour-integral method. M.Hirone (Faculty of Engng., Tohoku Univ., Sendai, Japan), Y.Kagawa. *Trans. Inst. Electron. & Commun. Eng. Jpn. Part A (Japan)*, vol.J66A, no.7, p.617-24 (July 1983). In Japanese. Attempts to expand the contour-integral method to three-dimensional problems and to deal with the relation between the division or the integration of the elemental area and the accuracy of the calculation. This report also provided a comparative study of the present method and FEM. In the case of FEM, the accuracy is rapidly lost when the dimension of element/wavelength exceeds settled ratio but its condition is slow in the present method. It is made clear that FEM is not always profitable as compared with CPU time of the present method at higher frequency. (8 refs.)

113175 On the uniqueness of the acoustic boundary-contact problems solution. B.P.Belinsky. *Vestn. Leningr. Univ. Ser. Mat. Mekh. & Astron. (USSR)*, no.3, p.5-10 (July 1983). In Russian. The construction of plates placed in an acoustic medium is considered. The uniqueness of the solution of a stationary acoustic problem for this system is proved. The connection of the uniqueness problem with the simple solvability of a linear system, originating from the problem, is discussed. (12 refs.)

Experimental observations of magneto-acoustic fieldsSee Entry 113187
Acoustic wave diffraction for array processingSee Entry 113204
Side-lobe reduction in the ring array pattern for synthetic aperture imaging of coherent sourcesSee Entry 113206
Optimum SNR enhancement of narrow-band signals in surface reverberationSee Entry 113208
Dynamic focusing of an ultrasonic beam by means of a phased annular array using a pulse techniqueSee Entry 113232
Transmission and reflection of a surface wave at a corner of two planes on an isotropic bodySee Entry 114324
On the propagation of acoustic waves in a radiating fluidSee Entry 116438

43.25 NONLINEAR ACOUSTICS AND MACROSONICS

(see also 43.60 Acoustic signal processing; 43.88 Transduction; devices for generation and production of sound)

113176 High-frequency acoustic properties of a fluid/porous solid interface. I. New surface mode. S.Feng, D.L.Johnson (Schlumberger-Doll Res., Ridgefield, CT, USA). *J. Acoust. Soc. Am. (USA)*, vol.74, no.3, p.906-14 (Sept. 1983). The authors use Biot's theory to search numerically for the velocities of the various surface waves, both the true slow surface wave and the pseudosurface waves, at an interface between a fluid half-space and a half-space of a fluid-saturated porous medium. They focus on the high-frequency range where the Biot-Plona slow wave is propagatory. They find that for an open-pore surface situation, the true surface mode exists for a limited range of material

parameters and changes continuously into a slightly leaky pseudo-Stonley mode as the mode speed increases past the slowest bulk wave speed; for the sealed pore situation there exist simultaneously a true surface mode (for all values of material parameters) and a pseudo-Stonley mode. The pseudo-Rayleigh mode has features similar to those of the pseudo-Rayleigh mode for a fluid/nonporous solid case. (23 refs.)

113177 High-frequency acoustic properties of a fluid/porous solid interface. II. The 2D reflection Green's function. S.Feng, D.L.Johnson (Schlumberger-Doll Res., Ridgefield, CT, USA). *J. Acoust. Soc. Am. (USA)*, vol.74, no.3, p.915-24 (Sept. 1983). For pt.1 see *ibid.*, vol.74, p.906 (1983). A 2-D space-time reflection Green's function is developed using the Cagniard-de Hoop technique for a fluid/lossless porous media planar interface configuration. It is then used to study the effects of the various surface waves whose velocities were calculated in the previous article. The time-dependent pressure response to a modeling source signal (Blackman-Harris pulse) for certain simulated experimental configurations is also presented. It is concluded that the amplitude with which the new surface modes are generated are large enough to enable their detection. (12 refs.)

113178 A method for generation of finite amplitude pulse of sinusoidal sound in free space. T.Nakamura, A.Nakamura (Inst. of Sci. & Industrial Res., Osaka Univ., Osaka, Japan). *J. Acoust. Soc. Jpn. (E) (Japan)*, vol.4, no.3, p.149-55 (July 1983). Nonlinear response of acoustic materials to a large amplitude sound depends upon the incident waveform itself. For this reason, the authors attempt to control the radiated waveform of finite amplitude in free space. In order to control the radiated waveform, the waveform control in a pipe was performed by the use of a loudspeaker driven by the computed waveform, and the generated wave was radiated from an exponential horn connected to the end of the pipe. However, the observed waveform in free space was different slightly from expected one. As the result of the simulation for the sound transmission through the exponential horn, it became clear that the reflection of the mouth of the horn affected the radiated waveform in free space. Therefore, the waveform control in the pipe was performed by taking account of the effect of the horn and then the result obtained agreed approximately with the waveform expected. (9 refs.)

113179 A method for radiation of a large-amplitude single shock pulse with sharp width into free space. T.Nakamura, A.Nakamura (Inst. of Sci. & Industrial Res., Osaka Univ., Osaka, Japan). *J. Acoust. Soc. Jpn. (E) (Japan)*, vol.4, no.3, p.161-3 (July 1983). The authors describe a sound source utilizing actively the waveform distortion due to the nonlinearity in air in order to radiate a sound pulse of sharp width with large amplitude into free space. (4 refs.)

113180 Phase relations for nonlinear acoustic phenomena in media with relaxation. A.D.Nosenko (Dept. of Acoustics, Moscow Univ., Moscow, USSR). *Moscow Univ. Phys. Bull. (USA)*, vol.37, no.5, p.118 (1982). Translation of: *Vestn. Mosk. Univ. Ser. 3 (USSR)*, vol.37, no.5, p.100 (1982). The phase relations in nonlinear acoustic interactions are experimentally investigated. (no refs.)

113181 Self-induced acoustic transparency of dilute paramagnetic crystals. G.T.Adamashvili, L.L.Buishvili, M.D.Zviadadze (State Univ., Tbilisi, USSR). *Sov. Phys.-Solid State (USA)*, vol.25, no.2, p.317-18 (Feb. 1983). Translation of: *Fiz. Tverd. Tela (USSR)*, vol.25, no.2, p.562-3 (Feb. 1983). [received: Sept. 1983] Describes the interaction of a coherent acoustic pulse with an electron-nuclear spin system of a dilute paramagnetic crystal of cubic symmetry by adopting the following simple model. The authors consider a system of equivalent pairs consisting of an impurity electron spin *S* and a nuclear spin *I* of the host matrix (*S*=1=1/2) subjected to a static magnetic field *H*₀||*z*. Since the impurity concentration is low, the mutual interaction of such pairs can be neglected. (3 refs.)

113182 Note on the axisymmetric sonic jet. J.D.Cole (Dept. of Math. Sci., Rensselaer Polytech. Inst., Troy, NY, USA). *SIAM J. Appl. Math. (USA)*, vol.43, no.4, p.944-8 (Aug. 1983). The axisymmetric sonic jet is considered in transonic small disturbance theory. A new hodograph equation is derived from which it can be deduced that there is a local similarity solution describing the final state. From this similarity solution it follows that the uniform sonic state is reached at a finite distance from the orifice. (1 ref.)

Nonlinear electroacoustic equations for piezoelectric powdersSee Entry 114786
Continuum approach to electroacoustic echoes in piezoelectric powdersSee Entry 114787

43.30 UNDERWATER SOUND (see also 92.10 Physics of the ocean)

113183 The group velocity of normal modes. D.M.F.Chapman, D.D.Ellis (Defence Res. Establ. Atlantic, Dartmouth, Nova Scotia, Canada). *J. Acoust. Soc. Am. (USA)*, vol.74, no.3, p.973-9 (Sept. 1983). A simple, general formula for normal mode group velocities provides an intuitive grasp of the factors influencing group velocity, especially for shallow water environments associated with strong seabed interaction. This is demonstrated using some hypothetical shallow water environments, and by comparing mode shapes at different frequencies. The formula is especially convenient to implement in normal mode computer codes which already perform similar calculations for mode normalization and attenuation coefficients. Using the WKB approximation to the normal mode functions, the formula is identified with the average horizontal speed of the ray equivalent to the mode. For a shallow water environment with bottom interaction, the group velocity formula is shown to include the beam and the time displacement effects of modified ray theory. This result strengthens the ray/mode analogy which is used in analyzing ocean acoustics problems. (20 refs.)

113184 Inverse scattering in a stratified medium. D.C.Stickler (Courant Inst. of Math. Sci., New York Univ., New York, NY, USA). *J. Acoust. Soc. Am. (USA)*, vol.74, no.3, p.994-1005 (Sept. 1983). In this analysis the following problem is considered: A point harmonic source at frequencies ω_1 and ω_2 is located in the region $z < 0$, where the assumption is made that both the sound speed and density profiles are known. For $z > 0$ the sound speed and density profiles are unknown. These two profiles are recovered from a measurement of the pressure field for all *r* at some fixed depth $z < 0$ at the two frequencies. Trace formula methods are used. The following assumptions are needed: First, $c(z)$ and $\rho(z)$ approach c_1, ρ_1 as $z \rightarrow -\infty$, and c_2, ρ_2 as $z \rightarrow +\infty$, and although c_2, ρ_2 are not known, it must be known that $c_2 < c_1$. Second, the angular frequency of the source must be such

that no trapped modes are excited. While the sound speed $c(z)$ can be complex, the limiting values c_1 and c_2 must be real. If $c(z)$ also depends on frequency and the form of the dependence is known, say, $c(z) = c_R(z) + i\omega^{\lambda(z)}c_I(z)$, then $c_R(z)$, $c_I(z)$, and $\lambda(z)$ can be recovered. Explicit expressions are obtained in the realistic case when $c_I(z)$ is not large. If a density is known and $c_I(z) = 0$, then only a measurement at one frequency is required. Two numerical examples are given; in both examples $\rho(z) \equiv 1$ and $c(z)$ is real. The first example is for a monotonically increasing profile and the second has a low velocity zone. Typical sediment parameters are used. (12 refs.)

113185 Scattering of focused ultrasound by spherical microparticles. P.L. Edwards (Univ. of West Florida, Pensacola, FL, USA), J. Jarzynski. *J. Acoust. Soc. Am. (USA)*, vol.74, no.3, p.1006-12 (Sept. 1983).

The scattering of focused ultrasound in water by three different types of microspheres (25-55 μ m diameter), with $ka < 1$, was studied. The three scatterers were a spherical glass bubble, solid polystyrene spheres and hydrogen bubbles. The measurement arrangement consisted of two transducers (transmitter and receiver) of 1.27-cm diameter with focusing lenses mounted on their faces. They were positioned so that their focal regions overlapped and their axes were 60° apart. A swept frequency ultrasonic signal was used, of 30 μ s duration, in which the frequency increased linearly from 3.5-6.8 MHz. The glass bubble was mounted on a nylon filament and positioned in the overlapping focal regions. The polystyrene spheres were in solution, and reflections were obtained as they drifted through the focal regions. The hydrogen bubbles were generated by electrolysis and reflections obtained as they rose through the focal regions. From the shape of the echo envelope the frequency dependence of the scattered-pressure amplitude was determined for each scatterer, and significant differences were observed between the echoes from the solid scatterers and the gas bubbles. The experiment results are compared with theoretical predictions. (13 refs.)

113186 Nearfield of a large acoustic transducer. II. Parametric radiation. G.S. Garrett (Appl. Res. Labs., Univ. of Texas, Austin, TX, USA), J.N. Tjotta, S. Tjotta.

J. Acoust. Soc. Am. (USA), vol.74, no.3, p.1013-20 (Sept. 1983). For part I see *ibid.*, vol.72, p.1056 (1982). The transducer is the same as the one considered in an accompanying paper by the same authors [Part I, *J. Acoust. Soc. Am.*, vol.72, 1056-1061 (1982)]. It has a diameter of 182 cm, and is composed of 364 elements, 4.8×6.4 cm each, which are distributed in 13 equally spaced rings. It is used to generate difference frequency sound at 0.5-5 kHz in water. Amplitude and phase of the generated sound are measured at various distances in the nearfield of the transducer. The results are compared with calculations based on the quasilinear approximation of the governing equations. Simplifications are obtained by utilizing the parabolic approximations [J. Naze Tjotta and S. Tjotta, *J. Acoust. Soc. Am.*, 67, 484-490 (1980)]. This also makes it possible to use a realistic model for the primaries (see the accompanying paper) when evaluating the nonlinear source term, such that all effects of the nearfield oscillations in amplitude and phase are fully accounted for. The analytical results obtained also apply to the case of an amplitude and/or phase shaded source. (16 refs.)

113187 Experimental observations of magneto-acoustic fields. P.H. Moose (Dept. of Electrical Engng., Naval Postgraduate School, Monterey, CA, USA), R.F. Klaus.

J. Acoust. Soc. Am. (USA), vol.74, no.3, p.1066-8 (Sept. 1983). Experimental observations of electric fields induced in salt water by acoustic waves in a resonant cavity interacting with a strong constant magnetic field are described. The fields are found to behave linearly with the constant magnetic field strength as well as with the acoustic field strength as predicted theoretically. However, the measured electric fields are an order of magnitude greater than predicted by the theory. A similar result has been obtained recently by independent investigators in an open ocean experiment. The discrepancy may be related to the similarity between electromagnetic and acoustic phase velocities in salt water at low frequencies. (5 refs.)

Calculated reflection and transmission of a plane wave at the interface between two liquids with viscosity and thermal conductivity See Entry 113173

Recursive techniques for passive source location See Entry 113210

Range ambiguity and pulse interval jitter in the bottlenose dolphin See Entry 115811

Wind dependence of underwater ambient noise See Entry 116090

Experimental studies of low-frequency waterborne and sediment-borne acoustic wave propagation on a continental shelf See Entry 116101

Investigation of chemical sound absorption in seawater. IV See Entry 116102

43.35 ULTRASONICS, QUANTUM ACOUSTICS, AND PHYSICAL EFFECTS OF SOUND

(for phonons in crystal lattices, see 63.; for plasma acoustics, see 52.35; for low-temperature acoustics and sound in liquid helium, see 67.; for acoustic properties of liquids, see 62.60; for acoustical properties of solids, see 62.65; for ultrasonic relaxation, see 62.80; for acoustic properties of thin films, see 68.60; for surface waves in solids, see 68.25; for acoustoelectric effects and acoustic wave amplification, see 72.50; for magnetoacoustic effects, oscillations and resonance, see 72.55; for acousto-optical effects and acoustic holography, see 78.20H and 43.63; for sound effects on living matter, see 87.50)

Improved feed network for group-type unidirectional transducers See Entry 113247

Influence of losses on the characteristics of a distributed-feedback surface-acoustic wave resonator See Entry 113253

43.40 MECHANICAL VIBRATIONS AND SHOCK

(see also 46.30M Vibrations, aeroelasticity, hydroelasticity, mechanical waves and shocks)

113188 Vibration isolation from irregularity in a nearly periodic structure: theory and measurements. C.H. Hodges, J. Woodhouse (Topexpross Ltd., Cambridge, England).

J. Acoust. Soc. Am. (USA), vol.74, no.3, p.894-905 (Sept. 1983). This article describes the theory and a simple experiment carried out to demonstrate the phenomenon of Anderson localization in an acoustical context. This is an effect whereby the propagation of vibration in a structure which is not entirely regular is impeded by the irregularities, giving rise on

the average to an exponential decay of vibration level away from the driving point, even in the absence of any dissipation. The structure used in the experiment was a stretched string with masses attached to it. This string was studied with regular spacings of the masses and after the masses had been moved in a controlled way to provide a small degree of irregularity. In both cases, the transmission of energy from end to end of the string was measured as a function of frequency, and also the mode shapes in the second and fourth passbands were measured so as to demonstrate the underlying physics of the localization phenomenon, in which the individual modes making up each passband change from being extended throughout the structure in the regular case to being localized in specific areas of the structure in the presence of irregularity. All measurements yielded satisfactory agreement with the theoretical predictions. (13 refs.)

113189 Complexity of string vibration estimated from a concept of entropy. K. Imai, K. Kuno, K. Ikegaya (Dept. of Electrical Engng., Nagoya Univ., Nagoya, Japan).

J. Acoust. Soc. Jpn. (E) (Japan), vol.4, no.3, p.127-37 (July 1983). Describes the complexity of the forced vibration of a flexible string, on the basis of the concept analogous to entropy, popular in thermodynamics and communication theory, which the authors have introduced for evaluating the complexity of a reverberant field in a recent paper (see *ibid.*, vol.38, p.461, 1982). The entropy of string vibration is defined in terms of the energy contribution of each normal mode in which the vibration is formulated, and is discussed in connection with the frequency components and location of a driving force and with transient characteristics by a unit impulsive force. As a result, it is found that the entropy increases with an increase in frequency band width of the force and approaches infinity, and that although the driving point varies the entropy according to the band width, it tends to be raised under random excitation. Moreover, in the transient response of the string, the entropy is shown to decrease with time after the excitation. Thus, the entropy employed here represents well the degree of energy distribution in each mode, and within this meaning, seems to be fit for a measure of the complexity of the string vibration. (8 refs.)

113190 Noncontact measurement of vibrating membrane and plate parameters. R.A. Dudnik, A.E. Ekimov (Appl. Phys. Inst., Acad. of Sci., USSR).

Radiophys. & Quantum Electron. (USA), vol.26, no.1, p.94-7 (Jan. 1983). Translation of: *Izv. VUZ Radiofiz. (USSR)*, vol.26, no.1, p.110-13 (Jan. 1983). [received: Sept. 1983]

An algorithm is proposed for determining the parameters of vibrating membranes and plates from the characteristics of the radiation field in the Fraunhofer zone. The algorithm is based on use of the similarity criterion for the problem of oscillating plates and membranes in an elastic medium. The parameters to be determined are: for membranes; the length and stress/density per unit surface ratio; for plates; length, thickness, cylindrical stiffness/density per unit surface ratio, and form of boundary conditions at the plate perimeter. (4 refs.)

The effect of incident pulse width on transient waveform from a circular plate See Entry 113170

A method for radiation of a large-amplitude single shock pulse with sharp width into free space See Entry 113179

Control of noise and vibration with damping materials See Entry 113198

43.50 NOISE, ITS EFFECTS AND CONTROL

(see also 86.70J Environmental science)

113191 Focus on absorbing materials intended for acoustic screens for transformers. J.-G. Migneron (Univ. Laval, Quebec, Canada).

Can. Acoust./Acoust. Can. (Canada), vol.11, no.4, p.28-36 (Oct. 1983). In French.

The research work presented in this article was originally subsidized by Hydro-Quebec; it constitutes the second part of a project dealing with transformer noise and means of controlling it. The present article is thus a continuation of that published in the preceding issue (see *ibid.*, vol.11, no.3, p.16, 1983) in which a model of the noise impact of transformer stations was described. The materials tested fall into three broad categories: masonry units with resonators, steel resonators with common cavities and tuned membranes. In all three cases these devices were optimized for special use in controlling transformer noise. In addition, the devices were treated to protect them against mechanical failure and climate so as to ensure their effectiveness under real conditions. (8 refs.)

113192 Subjective rating of party walls. J.S. Bradley (Nat. Res. Council Canada, Ottawa, Ontario, Canada).

Can. Acoust./Acoust. Can. (Canada), vol.11, no.4, p.37-45 (Oct. 1983). Results of a field survey of 98 subjects have been analysed and sound isolation measures have been compared to establish the influence of residential noise levels and nonacoustical factors on subjective judgements. A procedure is considered for estimating the properties of an ideal wall. (13 refs.)

113193 Nonstationarity in acoustic fields. Y.H. Tsao, J.K. Hammond (Inst. of Sound & Vibration Res., Univ. of Southampton, Southampton, England).

J. Acoust. Soc. Am. (USA), vol.74, no.3, p.827-39 (Sept. 1983). Acoustic pressure fields measured by an observer when the source or observer or both are moving is a nonstationary random process even if the source generates a random process which is stationary in the reference frame of the source. The causes of nonstationarity are classified as being due to wave expansion, directivity, and Doppler shift. This paper is concerned with developing two-dimensional (frequency-time) spectral descriptions for the processes by constraining the processes to fit within the framework of the 'evolutionary spectral density'. Earlier literature has described how evolutionary spectra may be estimated from single sample realizations. Spectral representation forms for free-field acoustic processes produced by moving monopole and dipole excitations are derived from the fundamental wave equations. (29 refs.)

113194 On the application of coherence techniques for source identification in a multiple noise source environment. M.E. Wang, M.J. Crocker (Ray W. Herrick Lab., School of Mech. Engng., Purdue Univ., West Lafayette, IN, USA).

J. Acoust. Soc. Am. (USA), vol.74, no.3, p.861-72 (Sept. 1983). Two approaches for noise source identification based on theory for multiple-input systems have been investigated. The concepts of the frequency response function and the coherent residual spectral density function were used to estimate the spectra of the noise sources that were accounted for in the multiple-input model. The key factors which determine the applicability of the techniques for noise source identification are found to be the degrees of coherence between the measured inputs. The experimental results showed that, for a noise system with multiple sources which were slightly coherent to

each other, the techniques presented might be able to estimate the spectra of the noise sources, provided there was only modest measurement contamination. (17 refs.)

113195 Community response to blasting. S.Fidell, R.Horoneff, T.Schultz, S.Teffteller (Bolt Beranek & Newman Inc., Canoga Park, CA, USA). *J. Acoust. Soc. Am. (USA)*, vol.74, no.3, p.888-93 (Sept. 1983). Annoyance due to chronic exposure to blast noise and vibration was assessed in residential areas near two surface mines and a quarry. It was found possible to base useful prediction of the prevalence of high annoyance on a metric of outdoor ground vibration related to high centiles of the long term distribution of exposure levels. (6 refs.)

113196 Single-number quantity for airborne sound insulation. G.Thurzo. *Kep- & Hangtech. (Hungary)*, vol.29, no.4, p.105-8 (Aug. 1983). A characteristic for airborne sound insulation is its frequency dependence. A standardized number of airborne sound insulation is a quantity, characteristic for the one-third octave band which, from the point of view of the number of the one-third octave bands, is to be considered as a data set. As a result of simplification efforts, airborne sound insulation can be described by frequency-independent single-number quantities. Although the single-numbers prevailing in practice for airborne sound insulation have a physical meaning, they cannot form a narrow relationship with the definition, i.e. with the physical content of airborne sound insulation. This paper studies the relationship between current single-number quantities of airborne sound insulation and this latter definition. (no refs.)

113197 Acoustical design and evaluation of silencers. L.J.Eriksson, P.T.Thawani, R.H.Hoops (Nelson Industries Inc., Stoughton, WI, USA). *Sound & Vib. (USA)*, vol.17, no.7, p.20-7 (July 1983). Considerable advances have been made in the last decade in the development of silencer design and evaluation techniques. More accurate computer-based procedures evolved from analytical models have become available. Evaluation techniques utilizing two-channel digital signal analyzers have added a new dimension in the efficient measurement of silencer performance. This article describes various design and evaluation approaches that have significantly improved the capabilities of the modern silencer designer. (42 refs.)

113198 Control of noise and vibration with damping materials. A.D.Nashif (Anatrol Corp., Cincinnati, OH, USA). *Sound & Vib. (USA)*, vol.17, no.7, p.28-36 (July 1983). Damping materials are being used to control noise and vibration in a wide variety of structures. Commercial damping materials that can be used effectively over broader temperature and frequency ranges have become available. Several analytical tools and methods have also been developed to design damping treatments to solve specific noise and/or vibration control problems. The properties of typical commercially-available damping materials are discussed in this article along with application techniques. Criteria for rating the effectiveness of damping treatments are also provided. The article concludes with an example of how damping technology was used to solve a noise and vibration control problem. (7 refs.)

113199 Effect on the measurement of aircraft noise of reflections from the ground. R.C.Payne. *Report Ac 102*, Nat. Phys. Lab., Teddington, England (Dec. 1982), 33 pp. Published data relating to the acoustic impedance of various ground surfaces have been used to estimate the influence of ground reflection on levels of aircraft noise measured at the conventional height of 1.2 m. It is shown that the effect on the perceived noise level can be determined by means of the pressure reflection coefficient at a frequency of 2 kHz, hence removing the requirement for information on acoustic impedance as a function of frequency. A number of techniques for determining the reflection coefficient of ground surfaces at a single frequency have been evaluated and a practical procedure for in-situ measurements has been developed. Using this the reflection coefficients of a variety of ground surfaces have been measured and data are reported. (22 refs.)

Determination and statistical evaluation of the sound power level of machines and their qualification according to the noise emission See Entry 113239
An identification system for traveling sound sources See Entry 113241
Acoustic characteristics of porous bronze See Entry 114096
6-kHz notch in noise-induced hearing loss See Entry 115799
The effect of loud sound and traffic noise on the vestibular system See Entry 115832

43.55 ARCHITECTURAL ACOUSTICS

113200 Sound reinforcement—equalization in sound reinforcement systems: control room monitors. J.Eargle. *DB Control Eng. Mag. (USA)*, vol.17, no.6, p.18-20 (June 1983). Two methods of equalizing a room are shown. One method uses pink noise generator inserted ahead of the equalizer, and the room response monitored on a real time analyzer. In the other method, one-third octave bands of noise are individually measured and plotted. The individual noise bands enable the user to check the balance between the stereo speakers by noting the position of center phantom images one band at a time. For equalizing a monitor system a high-quality 0.5 inch microphone should be used. (no refs.)

113201 Acoustics+electroacoustics—but how? H.-H.Gruhn. *Funk-Tech. (Germany)*, vol.38, no.7, p.291-2 (July 1983). In German. Based on the theoretical laws of acoustics and electroacoustics the author explains and defines the principles for correct acoustic irradiation of large rooms and in the open air. While stressing the importance of the wavelength and the nature of acoustic absorption, the author explains the possibilities for the adjustment of acoustic power and acoustic scattering by electroacoustic means. Several practical examples, including definition of proper acoustic source arrangements, are presented for better understanding. (no refs.) K.A.K.

113202 Acoustics+electroacoustics—but how? H.-H.Gruhn. *Funk-Tech. (Germany)*, vol.38, no.8, p.335-7 (Aug. 1983). In German. A guide to the placement, powers and directions of loudspeakers, with illustrative examples of a supermarket, church, sports hall and open grounds. (no refs.) F.Q.

113203 Calculation of subjective preference at each seat in a concert hall. Y.Ando (Faculty of Engng., Kobe Univ., Kobe, Japan). *J. Acoust. Soc. Am. (USA)*, vol.74, no.3, p.873-87 (Sept. 1983). This paper represents a method of calculating the subjective preference of sound fields in concert halls before construction. Subjective preference judgements (paired comparison tests) were systematically performed using fully independent objective parameters of acoustic information which describe the signals to the two ears. The sound fields with various combinations of listening level, delay of early multiple reflections, subsequent reverberation time, and magnitude of the interaural cross correlation were simulated with the aid

of a digital computer. The optimal conditions maximizing the subjective preference could be found for each objective parameter, because the parameters had an almost independent effect on the subjective preference judgements. Based on the linear scale value, which is obtained by applying the law of comparative judgement, we can calculate a total preference value according to the 'principle of superposition.' Examples of calculating the preference values by use of the plan and the cross section of a concert hall are described. (18 refs.)

Subjective rating of party walls See Entry 113192

43.60 ACOUSTIC SIGNAL PROCESSING

113204 Acoustic wave diffraction for array processing. R.E.Brooks (TRW Defense & Electronics, Redondo Beach, CA, USA). *Appl. Opt. (USA)*, vol.22, no.18, p.2810-16 (15 Sept. 1983).

Many coherent optical processing techniques that are based on wave diffraction can be carried out using acoustic waves. An array of acoustic transducers serves as a coherent radiation source, spatial modulator, and lens. Complex input data are entered by amplitude and phase modulation of the RF transducer drives. The output is retrieved from a second transducer array. This paper discusses the surface acoustic wave (SAW) implementation of space and time Fourier transforms the effect of material anisotropy and the results of an experimental SAW RF spectrum analyzer fabricated on LiNbO₃. (12 refs.)

113205 Equivalent bandwidth of a general class of polynomial smoothers. L.C.Ng, R.A.LaTourette (Naval Underwater Systems Center, New London, CT, USA).

J. Acoust. Soc. Am. (USA), vol.74, no.3, p.814-26 (Sept. 1983). This paper presents a detailed investigation of the properties of a general class of least-mean-square-fit (LMSF) smoothers in the presence of a white or colored input sequence. The results of the investigation show that the LMSF can be described as a low-pass filter whose frequency response characteristics can be calculated exactly. A particularly useful result derived from the frequency response characteristics is the LMSF equivalent bandwidth. It was shown that knowledge of LMSF bandwidth, plus knowledge of the input bandwidth, provides the second-order statistical description of the LMSF output noise process. Results of the analysis are verified by extensive computer simulation. (9 refs.)

113206 Side-lobe reduction in the ring array pattern for synthetic aperture imaging of coherent sources. A.K.Luthra (Interspec Inc., Philadelphia, PA, USA), S.A.Kassam.

J. Acoust. Soc. Am. (USA), vol.74, no.3, p.840-6 (Sept. 1983). A new technique is described for image formation using a circular array of transducer elements in which each element acts as both a transmitter and receiver. By processing the amplitude and phase measurements acquired in such a system in a particular way, it is shown that it is possible to approach the performance of a transmit-receive filled circular aperture of the same dimension. The technique combines a synthetic aperture scheme with an earlier approach for array pattern synthesis (J^2 synthesis). The proposed technique does not require spatial incoherence of reflections from the object plane, which was a severe limitation in earlier use of J^2 synthesis. The effect of array sampling with a finite number of transducer elements is also examined. (8 refs.)

113207 Some simple expressions for the beamforming properties of focused high-resolution circular arrays, with applications to refocusing systems. J.F.Lynch (Woods Hole Oceanographic Inst., Woods Hole, MA, USA).

J. Acoust. Soc. Am. (USA), vol.74, no.3, p.847-50 (Sept. 1983). Some simple analytical expressions for two important optical characteristics of focused high-resolution circular arrays are derived, specifically those for beam patterns and depths of field. The expressions generated, in addition to providing simple estimational tools for array design purposes, also lend themselves to straightforward interpretation in terms of the Fourier (farfield) and Fresnel (nearfield) kernels. Applications to refocusing arrays are discussed, as well as similarities and differences between such (sonar oriented) systems and radar and optical systems. (8 refs.)

113208 Optimum SNR enhancement of narrow-band signals in surface reverberation. F.W.Symons (Appl. Res. Lab., Pennsylvania State Univ., State College, PA, USA).

J. Acoust. Soc. Am. (USA), vol.74, no.3, p.851-60 (Sept. 1983). Theoretical performance capabilities of the optimum filter for maximization of signal-to-noise ratio (SNR) and a suboptimum approximation, easy to realize in practice, are compared to the conventional matched filter (designed for white noise only) in the case of low Doppler signals masked by surface reverberation. Spectrum models for surface backscattering as a function of local environmental parameters are based on recent results describing scattering from a subsurface bubble layer. Significant improvements in SNR in the low Doppler region as well as a dramatic dependence of performance on windspeed and direction, and the ratio of reverberation to uncorrelated noise power are predicted. Results serve as average performance limits to be compared to those obtained by algorithmic implementations of optimum and adaptive filters. (19 refs.)

113209 A post-processing on linear predictors equivalent to differencing for pre-emphasis. M.Yanagida, H.Takeyama, O.Kakusho (Inst. of Sci. & Industrial Res., Osaka Univ., Osaka, Japan).

J. Acoust. Soc. Jpn. (E) (Japan), vol.4, no.3, p.157-9 (July 1983). The effects of differencing on linear predictors have been studied theoretically and were confirmed on natural speech data. After weighing the relative advantages between degradation in S/N ratios, improvement in condition number by differencing, and efficiency of computation, a fast processing scheme for an adaptive flattening filter is developed. (3 refs.)

113210 Recursive techniques for passive source location. J.M.F.Moura (Inst. Superior Tecnico Lisboa, Lisbon, Portugal). *Proceedings of ICASSP 82. IEEE International Conference on Acoustics, Speech and Signal Processing, Paris, France, 3-5 May 1982 (New York, USA: IEEE 1982), p.403-6 vol.1*

The paper is concerned with the location of passive sources. Conceptually, this is viewed as a time delay estimation followed by a geometry determination. Signal, noise, and channel modeling questions affect the first block of the processor, i.e. the delay estimator. The second block is sensitive to the geometry description, namely the hypotheses on the dynamics, the array shape, and the relative observer/source configuration. Commonly used assumptions lead to decoupled effects which simplify the receiver structure. For deterministic array and source dynamics, a finite parameter description results. The receiver is designed via maximum-likelihood techniques. These do not encompass more general situations. To treat the problem of uncertain sensor location, or of stochastic dynamics, a different geometry description is considered. This description represents line arrays and motions as curves in space. Recalling simple facts from differential geometry, one is naturally led

to describe the array geometry and/or the motion dynamics by a set of differential equations. This casts the passive positioning problem in the context of recursive Kalman-Bucy filtering. The problem of sensor uncertainty location and stochastic dynamics can then be dealt with, without having to consider Taylor series type arguments or other unnatural approximations. (5 refs.)

43.63 ACOUSTIC HOLOGRAPHY

113211 Imaging property of acoustical holography for identifying spread sound sources. H.Houjou, K.Umezawa (Res. Lab. of Precision Machinery and Electronics, Tokyo Inst. of Technol., Yokohama, Japan). *Acoust. Lett. (GB)*, vol.6, no.11, p.158-63 (May 1983).

Acoustical holography is one of the most useful methods to reveal sound radiation from a machine of acoustic interest. It is able to show an intensity distribution of the sound sources. In the case when the source is like a point source, the system recognizes the source as it is. However, when the source spreads to some extent in any direction, it is not known how holography displays the source shape. This paper concerns this property of acoustical holography systems, simulating the radiation from line sources. A limited length straight line source placed in a 3-dimensional space and a circular ring source are dealt with. (4 refs.)

43.70 SPEECH COMMUNICATION

(inc. speech perception, speech intelligibility, and speech synthesis; see also 87.36 Speech)

113212 Comparative performance evaluation of different pitch estimation methods for noisy speech. K.K.Pailwal (Div. of Telecommunication, Univ. of Trondheim, Trondheim, Norway).

Acoust. Lett. (GB), vol.6, no.11, p.164-6 (May 1983).

Four different pitch estimation methods are compared as to their performance on noisy voiced speech. These are: 1. the modified autocorrelation method (AUTOC), 2. the cepstral method (CEP), 3. the simplified inverse filtering technique (SIFT), and 4. the average magnitude difference function method (AMDF). Noisy speech is generated by adding white (Gaussian) noise to the natural speech signal. Two types of errors, gross error and fine errors, are measured for each method under different noise conditions. The AMDF method is found to give the best pitch estimation results for noisy speech. (6 refs.)

113213 Residually excited LPC processor for enhancing helium speech intelligibility. G.Duncan (Wolfson Microelectronics Inst., Univ. of Edinburgh, Edinburgh, Scotland), M.A.Jack.

Electron. Lett. (GB), vol.19, no.18, p.710-11 (1 Sept. 1983).

A new approach to restoring the intelligibility of divers' speech uttered in a high-pressure atmosphere containing high percentages of helium gas is presented. The system processing architecture consists of a residually excited linear predictive coder (RELPC) with a novel implementation of time/frequency-domain relationships to simplify processing. (3 refs.)

113214 Characteristics of the glottal turbulent noise source. R.E.Hillman (Dept. of Communication Disorders, Boston Univ., Boston, MA, USA), E.Oesterle, L.L.Feth.

J. Acoust. Soc. Am. (USA), vol.74, no.3, p.691-4 (Sept. 1983).

This investigation utilized a reflectionless tube technique to obtain direct estimates of turbulent noise produced at the glottis during whispered vowels. In the past, the glottal turbulent noise source has been described theoretically as a series pressure source having a spectrum that is relatively flat for 2 or 3 oct around a center frequency [K.N. Stevens, *J. Acoust. Soc. Am.* 50, 1180-1192 (1971)]. Center frequency is determined primarily by the area of the constriction at which turbulence is produced with the volume velocity of air flowing through the constriction. The present results were shown to substantiate this theoretically based description of the glottal turbulent noise source. In addition, there was no significant difference between the glottal turbulent noise spectra of male and female speakers. The application of these findings to the synthesis of whispered vowels is discussed. (8 refs.)

113215 Dynamic specification of coarticulated vowels. W.Strange, J.J.Jenkins, T.L.Johnson (Center for Res. in Human Learning, Univ. of Minnesota, Minneapolis, MN, USA).

J. Acoust. Soc. Am. (USA), vol.74, no.3, p.695-705 (Sept. 1983).

An adequate theory of vowel perception must account for perceptual constancy over variations in the acoustic structure of coarticulated vowels contributed by speakers, speaking rate, and consonantal context. The authors modified recorded consonant-vowel-consonant syllables electronically to investigate the perceptual efficacy of three types of acoustic information for vowel identification: (1) static spectral 'targets', (2) duration of syllabic nuclei, and (3) formant transitions into and out of the vowel nucleus. Vowels in /b/-vowel-/b/ syllables spoken by one adult male (experiment 1) and by two females and two males (experiment 2) served as the corpus, and seven modified syllable conditions were generated in which different parts of the digitized waveforms of the syllables were deleted and the temporal relationships of the remaining parts were manipulated. Results of identification tests by untrained listeners indicated that dynamic spectral information, contained in initial and final transitions taken together, was sufficient for accurate identification of vowels even when vowel nuclei were attenuated to silence. Furthermore, the dynamic spectral information appeared to be efficacious even when durational parameters specifying intrinsic vowel length were eliminated. (25 refs.)

113216 Effect of burst amplitude on the perception of stop consonant place of articulation. R.N.Ohde (Bill Wilkerson Hearing & Speech Center, Vanderbilt Univ. School of Medicine, Nashville, TN, USA), K.N.Stevens.

J. Acoust. Soc. Am. (USA), vol.74, no.3, p.706-14 (Sept. 1983).

The author has examined the effects of the relative amplitude of the release burst on perception of the place of articulation of utterance-initial voiceless and voiced stop consonants. The amplitude of the burst, which occurs within the first 10-15 ms following consonant release, was systematically varied in 5-dB steps from -10 to +10 dB relative to a 'normal' burst amplitude for two labial-to-alveolar synthetic speech continua—one comprising voiceless stops and the other, voiced stops. The distribution of spectral energy in the bursts for the labial and alveolar stops at the ends of the continuum was consistent with the spectrum shapes observed in natural utterances, and intermediate shapes were used for intermediate stimuli on the continuum. The results of identification tests with these stimuli showed that the relative amplitude of the burst significantly affected the perception of the place of articulation of both voiceless and voiced stops, but the effect was greater for the former than the latter. The results are consistent with a view that two basic properties contribute to the labial-alveolar distinction in English. One of these is determined by the time course of the change in amplitude in the high-frequency range (above 2500 Hz) in the few tens of ms following consonantal

release, and the other is determined by the frequencies of spectral peaks associated with the second and third formants in relation to the first formant. (36 refs.)

113217 Perception of intervocalic stop consonants: the contributions of closure duration and formant transitions. V.C.Tartter (Rutgers Univ., Camden, NJ, USA), D.Kat, A.G.Samuel, B.H.Repp.

J. Acoust. Soc. Am. (USA), vol.74, no.3, p.715-25 (Sept. 1983).

Acoustic analyses of vowel-consonant-vowel (VCV) utterances indicate that they generally include formant transitions from the first vowel into a period of closure (VC transitions), and transitions out of the closure into the second vowel (CV transitions). Three experiments investigated the perceptual importance of the VC transitions, the CV transitions, and the closure period in identification of medial stop consonants varying in place of articulation. Experiment 1 compared identification of members of synthetic VC and CV continua with those from VCV series made by concatenating corresponding VC and CV stimuli using various closure durations. Experiment 2 examined identification of VCV stimuli constructed with only VC, only CV, or both VC and CV transitions; again closure duration was systematically varied. Experiment 3 correlated CV and VC identification with identification of VCV stimuli. Neither closure duration nor formant transition structure (i.e. only VC, only CV, or both) had an independent effect on identification. Instead, the formant structure and closure duration together strongly affected stop identification. When both VC and CV transitions were present, the CV transitions contributed somewhat more to identification of medial stops with short closures, than the VC transitions did. With longer closure durations, neither set of transitions appeared to determine perceived place of articulation in any simple way. Overall, the data indicate that the perception of a medial consonant is more than simply a (weighted) sum of its parts. (17 refs.)

113218 Intelligibility of VCV segments excised from connected speech.

A.Schmidt-Nielsen (Naval Res. Lab., Washington, DC, USA).

J. Acoust. Soc. Am. (USA), vol.74, no.3, p.726-38 (Sept. 1983).

Confusions between pairs of intervocalic consonants excised from connected speech were investigated under several conditions of speech degradation: digital voice processing, noise, and bandpass limiting. The distribution of the types of errors that were made, e.g., voicing, nasality, place of articulation, differed from those made on citation form syllable-initial consonants. Intervocalic consonants that were taken from word-initial position scored higher with no degradations than those taken from word-medial or word-final position, but the medial and final segments suffered less under mild degradations than did the initial ones. (22 refs.)

113219 Effect of a single interfering noise or speech source upon the binaural sentence intelligibility of aged persons. A.J.Duquesnoy (Faculty of Medicine, Free Univ., Amsterdam, Netherlands).

J. Acoust. Soc. Am. (USA), vol.74, no.3, p.739-43 (Sept. 1983).

The free-field speech-reception threshold (SRT) for sentences was investigated in quiet and under nine conditions involving noise or competing speech for a group of 20 elderly subjects (ten male, age 75-85; ten female, age 76-88) and a reference group of ten young normal-hearing subjects. The noise source had the same long-term average spectrum as the competing speech. The interfering signals were presented at a constant level of 55 dBA. All elderly subjects had moderate, nearly symmetrical pure-tone hearing losses with an average loss at 500, 1000, and 2000 Hz of between 9 and 40 dB re: ISO-389. The main results are (1) the SRT values in noise and competing speech are about equal, whereas the normal-hearing subjects showed a lower SRT (7 dB lower for the condition that both sound sources are in front) in competing speech than in noise; apparently, the elderly subjects do not benefit from the relatively silent periods in competing speech; (2) the gain obtained by moving the interfering noise source from the front to the lateral position is only 2.5 dB, in contrast to a gain of 9.6 dB for the young subjects; apparently, the elderly are unable to make full use of the spatial divergence between primary speaker and noise source. (16 refs.)

113220 Experimental manipulation of speaking rate for studying temporal variability in children's speech. B.L.Smith, M.D.Sugarman (Speech & Language Pathology, Northwestern Univ., Evanston, IL, USA), S.H.Long.

J. Acoust. Soc. Am. (USA), vol.74, no.3, p.744-9 (Sept. 1983).

Children's speech timing is often more variable than adults'. In the present study, two hypotheses that have been proposed to account for this observation are considered. One claims that children do not have neuromotor control capabilities comparable to adults. The other suggests that the greater variability is a statistical consequence of children's longer segment durations. These two hypotheses were examined by having children and adults speak at both faster and slower rates than normal. Within-group comparisons across different rates and between-group comparisons for similar durational values were made from spectrographic measurements. Results indicate that both statistical and neuromotor factors seem to contribute to the greater variability commonly observed in children's speech. (29 refs.)

113221 Speaker recognition by statistical features and dynamic features.

S.Furui (Res. Div., NTT, Tokyo, Japan).

Rev. Electr. Commun. Lab. (Japan), vol.30, no.3, p.467-82 (May 1982).

[received: Aug. 1983]

Performance of four text-dependent speaker recognition methods using statistical or dynamic features of speech spectrum extracted from spoken words or a short sentence were compared with each other. It has been clarified that almost the same recognition accuracies can be obtained by either statistical or dynamic features, and that the statistical features have advantages of a small amount of calculation and memory size for feature extraction and recognition. The combination effect of these two kinds of features and effectiveness of a spectral equalization technique have been ascertained. Very high speaker recognition performance can be obtained by a new method using statistical features. (25 refs.)

113222 Acoustic characteristics of professional male announcers' speech.

H.Kuwabara, K.Ohgushi (NHK Broadcasting Sci. Res. Labs., Tokyo, Japan).

Trans. Inst. Electron. & Commun. Eng. Jpn. Part A (Japan), vol.J66A, no.6, p.545-52 (June 1983). In Japanese.

Acoustic analyses were performed to investigate voice-qualities and acoustic characteristics of professional male announcers' speech by making a contrast with laymen's speech. Ten professional announcers and five laymen pronounced a short Japanese sentence [a o i so ra] which was used as the speech material. Four acoustic features, pitch pattern and mean pitch frequency as the vocal cord parameters and formant pattern and average spectral envelope as the vocal tract parameters, were extracted. Dynamic aspect of such acoustic features as pitch and formant patterns was found to be specific to the announcer's voice and the formant pattern, in particular, was the one which contributed the most to the announcer's voice-quality. Characteristics of the announcer's voice were also found in the average spectral envelope in that their voices showed a relatively high spectral level in the range from 3 to 4 kHz. This seems to be a primary acoustic correlate which makes the announcer's voice rather 'brilliant'. (17 refs.)

113223 Optical probe for narrow sound field. R.Ohba (Dept. of Appl. Phys., Hokkaido Univ., Sapporo, Japan).
Technological and Methodological Advances in Measurement, Acta IMEKO 1982. Proceedings of the 9th IMEKO Congress of the International Measurement Confederation, Berlin, Germany, 24-28 May 1982 (Amsterdam, Netherlands: North-Holland 1983), p.453-62 vol.2
An optical probe microphone is proposed which detects the movement of a sound receiving micro diaphragm located at a distant point using a graded-index optical fiber. The sensitivity, frequency response and relations between the SNR performance and structure of the microphone system are investigated theoretically. It is confirmed that experimentally constructed microphones are as sensitive as the standard half inch condenser microphone and that the results of the theoretical investigation are valid. Applications of the microphone to a probe for narrow sound fields in an acoustic tube and in local tracts are described. (5 refs.)

113224 An introduction to speech recognition. T.A.Williams (Motorola Inc., Austin, TX, USA).
Electro/82 Conference Record, Boston, MA, USA, 25-27 May 1982 (El Segundo, CA, USA: Electron. Conventions 1982), p.11-1/1-3
A brief description of the two major classifications of speech recognition systems is given, followed by considerations involved in the real world application of these systems. (3 refs.)

113225 A high-quality real-time text-to-speech converter. D.L.Gilblom (Telesensory Speech Systems, Palo Alto, CA, USA).
Electro/82 Conference Record, Boston, MA, USA, 25-27 May 1982 (El Segundo, CA, USA: Electron. Conventions 1982), p.11-2/1-6
Recent advances in digital signal processing devices have made it possible to produce a compact unit capable of converting unrestricted English text (in serial ASCII form) into readily intelligible spoken English. The PROSE 2000(tm) text-to-speech converter described in the paper was developed by Telesensory Speech Systems to perform this function. In addition to producing clear spoken English, the PROSE 2000 board can accept a variety of user commands which control aspects of text interpretation and speech style. Independent tests demonstrate that listeners will understand paragraph-length passages spoken by the PROSE 2000 board about as well as they would understand human speech. (3 refs.)

113226 DIGITALKER™ vocabulary selection system. J.Costello (Nat. Semiconductor Corp., Santa Clara, CA, USA), G.B.Smith.
Electro/82 Conference Record, Boston, MA, USA, 25-27 May 1982 (El Segundo, CA, USA: Electron. Conventions 1982), p.11-3/1-6
For the past two years, National Semiconductor has been selling the low cost, high quality DIGITALKER speech synthesis system. The DIGITALKER speech synthesis system is actually a speech processor which produces a speech output when coupled with input from a standard semiconductor memory that contains speech data pre-encoded in a highly compressed format. Since the original introduction of the DIGITALKER speech synthesis system, NSC has provided users with two kinds of synthetic speech data: standard vocabulary ROMs and custom vocabularies encoded to customer specification. In looking for a more flexible way to provide users with standard vocabularies for the DIGITALKER SPC, NSC developed the DVSS which is a tool for creating user-selected vocabularies from a large data base of standard words. (no refs.)

113227 Low cost voice recognition systems. S.S.Viglione (Interstate Electronics Corp., Anaheim, CA, USA).
Electro/82 Conference Record, Boston, MA, USA, 25-27 May 1982 (El Segundo, CA, USA: Electron. Conventions 1982), p.11-4/1-10
A low cost, high performance discrete word, speaker dependent word recognition module, capable of recognizing 100 word vocabularies is discussed. A switched capacitor filter chip, implementing the front end processor of the word recognition system, is presented. The filter chip, with a companion microprocessor with on board ROM, forms the basis for a speech recognition chip set. This chip set reduces the original board component count by 60-70% permitting dramatic economies in the use of speech recognition systems. (no refs.)

A post-processing on linear predictors equivalent to differencing for pre-emphasis See Entry 113209
Performance of hearing-impaired listeners under various types of amplitude compression See Entry 115804
Equivalency of lossless n -tubes See Entry 115808
Changing the shape of lossless n -tubes See Entry 115809
Multidimensional analysis of alaryngeal voice quality See Entry 115810

43.75 MUSIC AND MUSICAL INSTRUMENTS

113228 Considerations on physical characteristics of samisen tones. S.Ando, K.Yamaguchi (Nippon Gakki Co. Ltd., Hamamatsu, Japan).
J. Acoust. Soc. Jpn. (Japan), vol.39, no.7, p.433-43 (July 1983). In Japanese.
'Nagauta' samisen tones are analyzed and several physical values are extracted using digital signal processing techniques. The synthesized tones based on these data are produced and studied with regard to the features of physical parameters contributing to the tone quality of samisens. Physical parameters of samisen tones are classified according to the following, (1) attack noise, (2) spectrum, (3) overall amplitude envelope, (4) amplitude envelopes of each harmonic, and (5) time variance of pitch after attack transient, and they are analyzed for several notes and for several playing styles. The results show that in the spectrum, amplitude levels of lower harmonics are very small, and in the amplitude envelope, they have very rapid raises and rather rapid exponential decays compared with other musical instrument tones. Using these data, the synthesized tones are made by means of additive synthesis and compared to the original tones of samisens. As a result, it is verified that the synthesized tones with the amplitude of each harmonic being time-variant have a rather good similarity to original samisen tones, and that the synthesized tones with attack noise in the attack transient part are distinguishably improved. (24 refs.)

43.85 ACOUSTICAL MEASUREMENTS AND INSTRUMENTATION

(for acoustic noise measurement, see also 43.50; for photoacoustic spectroscopy, see 07.65)

113229 Numerical ultrasonic interferometry for the determination of the stiffness matrix of compound materials. B.Hosten, A.Barrot, J.Roux (Univ. de Bordeaux I, Talence, France).
Acustica (Germany), vol.53, no.4, p.211-17 (Aug. 1983). In French.
Ultrasonic interferometry based on a numerical method for the measurement of elastic constants in anisotropic materials (wood, CFR, fiber glass, etc...) has lead to an apparatus, which is described. The device and the metrology procedure have also been developed in order to achieve complete automatization. The large amount of experimental data allows one to use an optimization method for more reliable results. (6 refs.)

113230 On the float method of measuring ultrasonic output. V.N.Bindal, A.Kumar, R.C.Chivers (Nat. Phys. Lab., New Delhi, India).
Acustica (Germany), vol.53, no.4, p.219-23 (Aug. 1983).
Two new systems have been reported which were developed in order to try and improve the float method of ultrasonic power measurement, to achieve better sensitivity and higher accuracy. In both these methods the distance between the float and the transducer remains fixed, and thus the methods have the advantage over the null method. The lift method maintains the distance between float and transducer (within the nearfield region) but does not improve the sensitivity or accuracy. The side tube method improves both the sensitivity and accuracy and, at the same time, keeps the float at a fixed distance from the transducer. The sensitivity of a float system can be increased by suitably changing the liquids. Use of a mixture of benzene and carbon tetrachloride (50:50) in place of pure carbon tetrachloride has been shown to increase the sensitivity of the float system by a factor of 2.56. This makes the system more useful for the measurement of low powers, including the average power of pulsed systems. (12 refs.)

113231 The effect of the modulation transfer function on the image in an acoustic microscope. J.Litniewski (Inst. of Fundamental Technol. Res., Polish Acad. of Sci., Warsaw, Poland).
Arch. Acoust. (Poland), vol.8, no.1, p.31-40 (1983).
Considers the effect of the diffraction phenomenon and of errors in the geometry of the system on the quality of images obtained using a scanning acoustic microscope working in a transmission. An analysis of image formation is presented, permitting the derivation of the formula for the modulation transfer function (MTF). The effect of nonaxial and out-of-parallel elements of the system on the symmetry of this function with respect to zero frequency is determined. The paper also shows microscopic images obtained from numerical simulation for two selected objects with different magnitude of deviation from the symmetry of the function MTF. The shape of the function MTF for a system working at a relatively low frequency of 3 MHz was also determined experimentally and compared with the shape expected according to the theoretical formula derived in this paper. Satisfactory agreement was observed. (5 refs.)

113232 Dynamic focusing of an ultrasonic beam by means of a phased annular array using a pulse technique. T.Kujawska (Inst. of Fundamental Technol. Res., Polish Acad. of Sci., Warsaw, Poland).
Arch. Acoust. (Poland), vol.8, no.1, p.69-82 (1983).
An approach to compute the transient radiation resulting from an impulse velocity motion of an array of annular pistons in a rigid planar infinite baffle is presented. The approach is based on developing the expression for an impulse response function, which is the time-dependent velocity potential at a spatial point resulting from an impulse velocity of a piston. The time-dependent pressure for any piston velocity motion may then be computed by a convolution of the piston velocity with the appropriate impulse response. Numerical results of near field time-dependent radiation from annular phased array are discussed for pulsed velocity conditions. The lateral acoustical pressure distribution at different field depths is shown. The ultrasonic beamwidth as a function of the depth for every focal zone is also presented. Obtained results were compared with corresponding dependences for steady states. (14 refs.)

113233 Scanning acoustic microscopy: review of recent developments. H.K.Wickramasinghe (Univ. Coll., Univ. of London, London, England).
Proc. SPIE Int. Soc. Opt. Eng. (USA), vol.368, p.52 (1983). [received: Sept. 1983] (SPIE Proceedings on Microscopy Techniques and Capabilities, London, England, 21-22 Sept. 1982).
Summary form only given. Scanning acoustic microscopy has advanced to the point where the resolution in water is comparable to that of a high quality optical microscope. The resolving power of the acoustic microscope can be further improved by resorting to a fluid which has a lower sound velocity than water. The two practical possibilities are cryogenic liquids, and higher pressure gases. Progress on both these fronts is discussed. Improving the resolving power is only one aspect of the author's research effort; it is equally important to obtain quantitative information from the recorded images. Several schemes are being investigated whereby it is possible to record the spatial frequency transmittance or reflectance of the object and hence deduce the sound velocity and density on a microscopic scale. In order to make accurate predictions on the elastic parameters in certain experiments it is necessary to measure the phase of the acoustic beam with great accuracy. For this purpose, a differential interference contrast acoustic microscope has been developed. Finally, two new forms of microscopy are described—photodisplacement and photothermal microscopy—which are based on the microscopic measurement of some thermometric property. (no refs.)

113234 Applications of acoustic microscopy in the semiconductor industry. A.J.Miller (GEC plc, Hirst Res. Centre, Wembley, England).
Proc. SPIE Int. Soc. Opt. Eng. (USA), vol.368, p.53-7 (1983). [received: Sept. 1983] (SPIE Proceedings on Microscopy Techniques and Capabilities, London, England, 21-22 Sept. 1982).
The Quate scanning acoustic microscope has now become established in university research groups, and interest is being shown from industry. The author has constructed a 1 GHz reflection instrument with lateral resolution better than 2 μ m, and has been evaluating a number of possible applications. Some of these are discussed in detail and include: (i) The examination of integrated circuit chips processed in MOS technologies, using the subsurface capability of the instrument. (ii) Metallurgical studies. (iii) Thin-film studies, including organic thin films. Emphasis is placed on the merits of acoustic microscopy as opposed to other methods, and further developments of the technique likely to be of use are discussed. (9 refs.)

113235 Scanning electron acoustic microscopy. G.Davies, A.Howie, L.Staveley-Smith (Cavendish Lab., Univ. of Cambridge, Cambridge, England).
Proc. SPIE Int. Soc. Opt. Eng. (USA), vol.368, p.58-65 (1983). [received: Sept. 1983] (SPIE Proceedings on Microscopy Techniques and Capabilities, London, England, 21-22 Sept. 1982).
The principles and basic imaging theory of electron acoustic microscopy are outlined and illustrated with images of semiconductor devices. Image contrast arises from local variations in stopping power and thermal properties of the specimen, but variations in elastic properties are also important. In elastically anisotropic materials the contrast depends on crystallographic grain orientation. Examples of such grain contrast are discussed as well as of grain boundary contrast which is interesting but less well understood. (16 refs.)

113236 Helium acoustic microscopy. A.F.G.Wyatt (Dept. of Phys., Univ. of Exeter, Exeter, England). *Proc. SPIE Int. Soc. Opt. Eng. (USA)*, vol.368, p.66-73 (1983). [received: Sept. 1983] (SPIE Proceedings on Microscopy Techniques and Capabilities, London, England, 21-22 Sept. 1982). Acoustic microscopy using liquid ^4He offers the possibility of considerably higher resolution than microscopes at room temperature which use water as the coupling medium. At the same frequency the wavelength of sound in liquid helium is a sixth of that in water and because there is no attenuation in liquid ^4He there is the possibility of using much higher frequencies than is presently used (3 GHz) with water. The properties of liquid ^4He relevant to this application are reviewed together with the equipment necessary to work to 0.1K. The information likely to be obtained from helium microscopy is considered and compared to room temperature acoustic microscopy. Although helium acoustic microscopy is still in its infancy recent results indicate that it is likely to be a valuable new tool. (12 refs.)

113237 Acoustic microscopy in materials science. G.A.D.Briggs, M.G.Somekh, C.Ilett (Dept. of Metall. & Sci. of Materials, Univ. of Oxford, Oxford, England). *Proc. SPIE Int. Soc. Opt. Eng. (USA)*, vol.368, p.74-80 (1983). [received: Sept. 1983] (SPIE Proceedings on Microscopy Techniques and Capabilities, London, England, 21-22 Sept. 1982). Images are presented which illustrate applications of the scanning acoustic microscope to problems in studies of materials. In transmission the structure of a diffusion bond is revealed; in reflection images of grains, cracks and oxides are shown. A theoretical outline is given indicating how the microscope may be used as a quantitative elastic microprobe. (14 refs.)

113238 Temporal peak intensity. E.L.Carstensen, K.J.Parker, D.B.Barbee (Dept. of Electrical Engng., Univ. of Rochester, Rochester, NY, USA). *J. Acoust. Soc. Am. (USA)*, vol.74, no.3, p.1057-8 (Sept. 1983). Two methods for measurement of the maximum intensity I_m as defined by the National Council for Radiation Protection are compared. One uses a calibrated broadband hydrophone; the other uses a spherical radiometer. A suggestion is made for measurement of a spatial average, temporal maximum intensity to be used in the nearfield of a transducer. (5 refs.)

113239 Determination and statistical evaluation of the sound power level of machines and their qualification according to the noise emission. F.Augusztnovicz, L.Czabaly. *KeP- & Hangtech. (Hungary)*, vol.29, no.4, p.97-104 (Aug. 1983). The sound power level is the most suitable quantity for the characterization of the noise production of machines because it is determined by the noise emission of the machine only. There is an international standard for determining the sound level which is spreading more and more in Hungary. The paper gives a brief survey of the system of standards and discusses the method of statistical evaluation of sound power levels determined by statistical methods. It gives a summary of the theoretical basis of the statistical evaluation and presents the results of a measurement series accomplished on a machine-type as well as the conclusions drawn from them. (11 refs.)

113240 Measuring the energy characteristics of a sound field in an interferometer. A.N.Ivannikov, F.V.Rozhin, O.S.Tonakanov (Dept. of Acoustics, Moscow Univ., Moscow, USSR). *Moscow Univ. Phys. Bull. (USA)*, vol.38, no.1, p.54-9 (1983). Translation of: *Vestn. Mosk. Univ. Ser. 3 (USSR)*, vol.38, no.1, p.47-52 (1983). The basic relations characterizing the parameters of a sound field in an interferometer are considered. An experimental apparatus and procedure is described, allowing the characteristics of the reflective surface to be described on the basis of measurements of the power flux density. (2 refs.)

113241 An identification system for traveling sound sources. F.Suzuki, F.Sasaki, S.Furukawa (Acoustics & Audio Engng. Res. Div., NHK, Tokyo, Japan). *NHK Lab. Note (Japan)*, no.286, p.1-11 (March 1983). [received: Aug. 1983] For the measurement of sound from a traveling source, such as aircraft noise, it is necessary to collect the source noise alone. Identification and the automatic measurement of noise from such sources are needed to save work and to offer the advantages of continuous measurement under bad conditions, or for long periods. The authors propose a method for the identification of noise sources by using spatial information from a traveling noise source. This they do by finding a cross-correlation function for the outputs of two microphones located separately, and by identifying the pattern of this function. Furthermore, they propose a good circuit-design for a correlator, and have succeeded in building a simple identifier, using a microcomputer, for the pattern-identification process. Theoretical identification using this method produced good results in field tests. (1 ref.)

113242 Measurement of the velocity of acoustic surface waves using the pulse superposition method. A.L.Bolotyuk, S.N.Naumov, V.K.Razgonyayev, I.B.Yakovkin. *Radio Eng. & Electron. Phys. (USA)*, vol.27, no.12, p.163-7 (Dec. 1982). Translation of: *Radiotekh. & Elektron. (USSR)*, vol.27, no.12, p.2464 et seq. (Dec. 1982). [received: Sept. 1983] A lowpass filter is used to enhance the accuracy of measuring the velocity of acoustic waves using the pulse superposition method. The obtained experimental data are presented and the measurement method is described in detail. (8 refs.)

113243 Smooth separate adjustment of the group delay and phase of the carrier frequency of a signal in an acoustic delay line. A.F.Bessonov, L.N.Deryugin, V.A.Komotskiy, M.V.Kotyukov. *Telecommun. & Radio Eng. Part 2 (USA)*, vol.37, no.9, p.96-8 (Sept. 1982). Translation of: *Radiotekhnika, Moskva (USSR)*, vol.37, no.9, p.58-60 (Sept. 1982). A delay line using surface acoustic waves with optical readout of the signal in the presence of a stationary reference grating whose lines are inclined to the waveguide is discussed. (5 refs.)

113244 New electrostatic method for absolute pressure calibration of pressure sensors. Z.Skvor (Electrotech. Faculty, Tech. Univ., Prague, Czechoslovakia). *Technological and Methodological Advances in Measurement. Acta IMEKO 1982. Proceedings of the 9th IMEKO Congress of the International Measurement Confederation, Berlin, Germany, 24-28 May 1982 (Amsterdam, Netherlands: North-Holland 1983), p.533-40 vol.2* Describes an electrostatic method for pressure calibration of acoustic sensors, especially the condenser microphones, at middle and low sonic and infrasonic frequencies. The fundamental arrangement forms an electrostatic transducer with a thin air gap acting as a calibration cavity. Another arrangement is an electrostatic transducer whose diaphragm is loaded on both sides by cavities of adjustable volume. This method is based on the measurement of electrical quantities, i.e., the capacitance and voltage, and geometrical dimensions and eliminates application of correction at infrasonic frequencies. (3 refs.)

SPIE Proceedings on Microscopy Techniques and Capabilities	See Entry 111302
Anomalous enhancement of photoacoustic signal in metal-film/metal-foil system	See Entry 111777
Acoustic wave calibration for CO₂ laser scattering experiments	See Entry 113034
Feasibility of fiber optical hydrophone	See Entry 113102
An all fiber-optic sensor for surface acoustic wave measurements	See Entry 113126
Analysis of the elastic field of ultrasonic waves scattered by a cylindrical cavity	See Entry 113172
Acoustic wave diffraction for array processing	See Entry 113204
Optical probe for narrow sound field	See Entry 113223
A Lamb wave voltage sensor	See Entry 113249
Ultrasonic flow metering based on transit time differentials which are insensitive to flow profile	See Entry 113531
Photoacoustic determination of thermal diffusivity of solids: Application to CdS	See Entry 114292
The coefficient of reflection of ultrasonic waves from an adhesive bond interface	See Entry 115452
Automated time-of-flight studies of the defect detection trial plates 1 and 2	See Entry 115454
CEGB inspection of plates 1 and 2 in UKAEA defect detection trials	See Entry 115455
An in-service inspection method: the use of focused probes for the detection and sizing in DDT plates 1 and 2	See Entry 115456
Beam spread variations with change of angle	See Entry 115457
Non-destructive measurement of plastic anisotropy of sheets by ultrasonics	See Entry 115463
Influence of magnetomechanical damping on resonance electromagnetic-acoustic conversion in ferromagnets	See Entry 115483
Conversion of zero-order Lamb-wave modes into an electromagnetic field in ferromagnetic metals	See Entry 115484
Ultrasonic inspection of the structure of G13FL steel parts	See Entry 115485
Simple apparatus for concentration determinations in binary-gas mixtures	See Entry 115604
Effect of half-wavelength membranes on the axial resolution of real-time ultrasonic scanners	See Entry 115890

43.88 TRANSDUCTION; DEVICES FOR THE GENERATION AND REPRODUCTION OF SOUND

- 113245 The creation of a new studio microphone.** J.C.Hansen (Bruel & Kjaer, Naerum, Denmark), P.S.White. *DB Sound Eng. Mag. (USA)*, vol.17, no.6, p.27-31 (June 1983). The design goals to be met by an acoustically transparent microphone are summarized. To meet these requirements Bruel & Kjaer developed two basic condenser microphone constructions utilizing the pre-polarized technique. In addition to swept-sine methods of measurement, time delay spectrometry was used for evaluating the microphones at various stages of development. Amplitude and phase responses of the microphones are also given. (6 refs.)
- 113246 You can't just listen to a microphone.** G.M.Hockman. *DB Sound Eng. Mag. (USA)*, vol.17, no.6, p.32-4 (June 1983). The use of a FFT system to evaluate microphone responses is discussed. FFT-based tests are proving valuable in designing vocal microphones. In using FFT to address the problems of handling noise, the analyzer displays specific amplitude and spectral content of the handling noise. The result of an FFT analysis of typical handling noise response compared to a shock-mount system employing acoustic feedback is given. Also the result of the hand-held response of a vocal microphone with and without an external windscreen is included. (no refs.)
- 113247 Improved feed network for group-type unidirectional transducers.** G.Macchiarella, G.Viola (Politecnico di Milano, Milano, Italy). *Electron. Lett. (GB)*, vol.19, no.17, p.680-1 (18 Aug. 1983). Proposes a phasing and matching network for group-type unidirectional transducers (GT-UDTs) which takes into account the electroacoustic interactions between the two phases of the GT-UDT. In comparison with analogous feed circuits from the literature, this network represents an improvement as far as the reduction of the residual fluctuations in the passband frequency response of a GT-UDT device is concerned. (6 refs.)
- 113248 Experimental method for determination of the vibrations distribution of the diaphragms of electroacoustic transducers.** E.Hojan, M.Niewiarowicz, J.Florkowski (Inst. fur Akustik, Adam Mickiewicz Univ., Poznan, Poland). *Frequenz (Germany)*, vol.37, no.1, p.12-15 (Jan. 1983). In German. [received: Aug. 1983] The elaborated contactless measuring method of the diaphragm vibrations of electroacoustic transducers by applying an optical 'transmission' permits the recording of vibrations of diaphragms in the whole range of acoustic frequencies. This method may also be utilized for investigating diaphragms made of semi-transparent materials. (6 refs.)
- 113249 A Lamb wave voltage sensor.** K.Toda, K.Mizutani (Dept. of Electrical Engng., Nat. Defense Acad., Yokosuka, Japan). *J. Acoust. Soc. Am. (USA)*, vol.74, no.3, p.677-9 (Sept. 1983). A voltage sensor using a Lamb wave delay line oscillator is described. The device consists of two pairs of interdigital transducers and one plate electrode at the central part of the device. All of these transducers have the counter electrodes on the bottom surface of the substrate. The oscillation frequency of the device changes significantly with the voltage applied to the central plate electrode. Performances of the voltage sensor are given, including sensitivity and its frequency dependence. (3 refs.)
- 113250 Analysis and reduction techniques of the driving force distortion of loudspeakers.** T.Ueno, K.I.Takahashi, S.I.Ishii, T.Fukuyama (Matsushita Electric Industrial Co. Ltd., Moriguchi, Japan). *J. Acoust. Soc. Jpn. (Japan)*, vol.39, no.7, p.444-51 (July 1983). In Japanese. The conventional distortion reduction methods such as copper cap, laminate, core can not satisfy the recently developed low distortion reproduction systems like PCM. Corresponding to this situation, the author tried to analyse the force distortion of a loudspeaker and develop new low distortion techniques. The driving force of a loudspeaker is expressed as Bli , whereby B is called the force factor and i is the voice coil current. To reduce the driving force distortion, the force factor must be constant and the voice coil current has to

be linear. From their analysis, the condition for the constant force factor is that the magnetic flux variation across the voice coil must be zero. For this purpose, two techniques are proposed by the authors: one is the magnetic flux feedback (MFFB) and another is the pushpull construction. MFFB is a feedback system which cancels the flux variation across the voice coil. 2nd HD is reduced to 0.03% at 90 dB/m. The pushpull construction has a symmetrical magnetic circuit with a voice coil pair, so the 2nd HD is reduced. To reduce the voice coil current distortion, the constant current drive amplifier is used. By this amplifier, 3rd HD is reduced to 0.01% at 1 W. (8 refs.)

113251 Study of elementary photophysical and photochemical processes in organic molecules using the optoacoustical effect. A.M.Bonch-Bruevich, T.K.Razumova, I.O.Starobogatov. *J. Appl. Spectrosc. (USA)*, vol.37, no.6, p.1413-27 (Dec. 1982). Translation of: *Zh. Prikl. Spektrosk. (USSR)*, vol.37, no.6, p.981-96 (Dec. 1982). [received: Sept. 1983]

Photophysical and photochemical processes in organic molecules have been studied intensively for many years. New possibilities for studying them are opened up by optoacoustical (OA) methods which permit recording nonradiative transitions in molecules. Such transitions lead to liberation of part of the absorbed energy in the form of heat and then to excitation of the acoustical signal. Under certain conditions when a liquid is excited by a nanosecond pulse of radiation, the amplitude of a signal on a piezosensor, recording the acoustic wave, is proportional to the absorbed energy liberated as heat and does not depend on the cross section of the beam of exciting radiation. With single-photon absorption, the signal amplitude is likewise independent of the intensity distribution of the exciting radiation over the beam cross section. This permits using the pulsed OA effect for measuring the fraction of absorbed energy of the exciting optical pulse liberated as heat and thus obtaining data necessary to determine the relative probability of a nonradiative transition out of the excited states of the molecules being studied. Application of the OA technique in itself, as well as together with luminescence measurements, greatly enlarges the possibilities for obtaining information on elementary processes occurring in molecules with optical excitation, simplifies the procedure for a number of measurements, and also permits observing processes that are inaccessible to other techniques. These possibilities are illustrated for photophysical and photochemical processes in solutions of complex molecules. (36 refs.)

113252 A flat piezoelectric polymer film loudspeaker as a multi-resonance system. J.Ohga (Musashino Electrical Communication Lab., NTT, Tokyo, Japan).

J. Acoust. Soc. Jpn. (E) (Japan), vol.4, no.3, p.113-20 (July 1983). A flat diaphragm full-range loudspeaker utilizing a piezoelectric polymer is described. This loudspeaker is characterized by an excellently simple constitution and multiresonance response characteristics. Since the fundamental resonant frequency of a loudspeaker should be as low as possible, it is convenient to utilize the flexural vibration of a bimorph diaphragm. The input-output relation of a bimorph diaphragm radiator in a multi-resonance frequency region is studied theoretically, and the formula for estimating output and sound pressure level for the resonant peak is given. This is also examined experimentally. (15 refs.)

113253 Influence of losses on the characteristics of a distributed-feedback surface-acoustic wave resonator. V.M.Pashkin, M.S.Sandler, B.V.Sveshnikov. *Radiophys. & Quantum Electron. (USA)*, vol.26, no.1, p.89-94 (Jan. 1983). Translation of: *Izv. VUZ Radiofiz. (USSR)*, vol.26, no.1, p.103-9 (Jan. 1983). [received: Sept. 1983]

The characteristics of a distributed-feedback resonator in the form of a long interdigital SAW transducer are investigated. The dependence of the resonator Q on the typical scales of the system—the diffraction length and the attenuation length—is analyzed. (11 refs.)

Application of surface acoustic waves for measuring linear and angular displacementSee Entry 111644

Broad-band ultrasonic sensor based on induced optical phase shifts in single-mode fibersSee Entry 113125

Optical switching characteristics in slightly nondegenerated multilayered couplers using acousto-optic interaction by surface acoustic wavesSee Entry 113152

A method for generation of finite amplitude pulse of sinusoidal sound in free spaceSee Entry 113178

A method for radiation of a large-amplitude single shock pulse with sharp width into free spaceSee Entry 113179

Nearfield of a large acoustic transducer. II. Parametric radiationSee Entry 113186

New electrostatic method for absolute pressure calibration of pressure sensorsSee Entry 113244

Sound generation by an electric current in a fluidSee Entry 114570

Foil electret transducer for blood pressure monitoringSee Entry 115955

44.00 HEAT FLOW, THERMAL AND THERMODYNAMIC PROCESSES

44.10 HEAT CONDUCTION (MODELS, PHENOMENOLOGICAL DESCRIPTION)

113254 'Transient heat conduction in composite plates, cylinders or spheres'. P.C.Wankhede (Dept. of Education, Nagpur Univ., Nagpur, India), B.R.Bhonsle.

Proc. Natl. Acad. Sci. India Sect. A, vol.52, pt.2, p.245-56 (1982). [received: Aug. 1983]

The solution of the problem of transient heat conduction in composite plates, cylinders or spheres, consisting of k-layers of different materials with different thermal properties is studied. These are subjected to the generation of heat in the body as well as at the interfaces with imperfect thermal contact under arbitrary initial temperature distribution. The authors employ the integral transformation technique, in the form of an infinite series for which two alternative suitable forms for detailed numerical commutation under different boundary and interfacial conditions are given by introducing the so-called pseudosteady temperature distribution function. (11 refs.)

A class of similarity solutions for the nonlinear thermal conduction problemSee Entry 112438

The micropolar thermoelastic problem of uniform heat-flow interrupted by an insulated penny-shaped crackSee Entry 113301

Elastic-plastic state of bodies of revolution under variable nonisothermal loading, taking account of creepSee Entry 113323

Stability of flexible sloping shells in a temperature fieldSee Entry 113333

44.25 CONVECTIVE AND CONSTRAINED HEAT TRANSFER

(see also 47.25Q Convection and heat transfer)

Conjugate mixed convection heat transfer from a vertical rectangular finSee Entry 113433

Phase space analysis of convection in a ³He-superfluid ⁴He solutionSee Entry 114299

Effect of a thermal trap on the performance of a solar sand collectorSee Entry 115694

Conductive heat transfer in salt gradient stabilized solar pondsSee Entry 115695

44.30 HEAT TRANSFER IN INHOMOGENEOUS MEDIA AND THROUGH INTERFACES

113255 A note on the heat balance integral method applied to the resolution of a one-phase Stefan problem with an increasing prescribed flux on the fixed face. G.G.Garguichevich (Univ. of Nacional de Rosario, Rosario, Argentina).

Int. Commun. Heat & Mass Transfer (GB), vol.10, no.4, p.349-55 (July-Aug. 1983).

The author applies the heat balance integral method to solve the problem of melting in a semiinfinite slab with a prescribed flux on the fixed face. The author obtains a satisfactory approximate solution considering the results of Tarzia (1982), in opposition to the fact stated by Goodman (1958) for generally increasing fluxes on the fixed face. (3 refs.)

113256 Optimization of work regimes and geometrical parameters of spirally corrugated tubes in heat exchanges. Yu.S.Voskresenskii, P.A.Savel'ev. *Latv. PSR Zinat. Akad. Vestis Fiz. Teh. Zinat. Ser. (USSR)*, no.4, p.86-93 (1983). In Russian.

The paper presents a generalization of experimental data of various authors on convective heat transfers in spirally corrugated tubes (SCT). For the cases considered the optimum SCT geometry in the Reynolds range 1×10⁴ to 5×10⁴ are derived. (13 refs.)

113257 Heat transfer to refrigerant in horizontal tubes of evaporator. S.Yoshida, K.Nishikawa, T.Matsunaga, H.Nakata. *Refrigeration (Japan)*, vol.58, no.666, p.331-8 (April 1983). In Japanese.

Experimental investigations were made of heat transfer to Refrigerant-22 inside horizontal, smooth evaporator-tubes. Data of the local heat transfer coefficients as well as circumferentially averaged heat transfer coefficients were obtained for pressures of 0.29 to 0.59 MPa, mass velocities of 100 to 500 kg/m²s, heat fluxes of 5 to 35 kW/m², and inside diameters of 7.0 and 10.2 mm. The flow patterns were observed through a sight glass at the tube exit. The effects of the various parameters on the heat transfer were clarified, and a dimensionless correlation of the heat transfer coefficients was obtained, which agreed with the present experimental data within the limit of ±30 percent. (18 refs.)

113258 Study of the operation of heat pipes with gas-liquid solutions. R.Muller (Tech. Univ. Dresden, Dresden, Germany). *Wiss. Z. Tech. Univ. Dresden (Germany)*, vol.32, no.2, p.175-9 (1983). In German.

Analyses heat pipes with two-component filling, such as water and ammonia. The heat pipes operate in three regimes: single component, transition and two-component zones. Equations for the static performance are presented, and theoretical and experimental results of dynamic studies are plotted for various solubilities. (6 refs.) G.M.E.

Stress state of a heated flattened spherical shell caused by thermal diffusionSee Entry 113304

Effect of a thermal trap on the performance of a solar sand collectorSee Entry 115694

44.40 RADIATIVE HEAT TRANSFER

113259 P-N approximation for radiative heat transfer in a nongray medium. A.Yucel, Y.Bayazitoglu (Rice Univ., Houston, TX, USA). *AIAA J. (USA)*, vol.21, no.8, p.1196-203 (Aug. 1983).

Using the rectangular model to characterize the spectral dependence of the absorption coefficient, the P-N approximation is extended to treat nongray radiative transfer problems in planar media. Specifically, the P-1 and P-3 approximation formulations are developed for a medium with any number of bands. Analytical solutions are derived for the special case of a single-level absorption coefficient. Numerical solutions are obtained for a medium with a two-level absorption coefficient. Comparisons with the available exact solutions for radiative equilibrium show that the P-1 and P-3 approximations generate accurate results. Solutions for internal heat generation are also discussed. (29 refs.)

113260 Effectiveness of the model of volume backscattering in the theory of radiation transfer in media with axisymmetric scattering indices. G.Ya.Belov.

High Temp. (USA), vol.20, no.6, p.871-8 (Nov.-Dec. 1982). Translation of: *Teplotiz. Vys. Temp. (USSR)*, vol.20, no.6, p.1102-9 (Nov.-Dec. 1982). [received: Sept. 1983]

The effectiveness of the backscattering model is verified by analytical (backscattering) and numerical (the real index) solution of the problem of diffuse-radiation transfer in a layer of a medium with nonreflecting boundaries in the case of an isotropic-isotropic 'forward-backward' scattering index, and by comparison with known accurate solutions for media with isotropic and linearly anisotropic scattering. A simple arithmetical relation is established between the parameter taking the form of the axisymmetric index into account and the quantity characterizing the fraction of the radiation scattered in backward directions. Calculations of the characteristics of the radiation field in a light-scattering layer lead to close results over a broad range of variation of the independent parameters. (32 refs.)

Dynamics of self-sustaining processes in solid matrices when heat evolution is triggered by stressSee Entry 114218

A useful integral function and its application in thermal radiation calculationsSee Entry 114219

Effect of a thermal trap on the performance of a solar sand collectorSee Entry 115694

44.50 THERMAL PROPERTIES OF MATTER (PHENOMENOLOGY, EXPERIMENTAL TECHNIQUES)

(see also 07.20 Thermal instruments and techniques)

113261 Theoretical model on the temperature profile within the cylindrical conductor heated by induction current. Dae Soo Kim. *J. Korean Inst. Met.*, vol.21, no.2, p.117-32 (Feb. 1983). In Korean. [received: Sept. 1983]

A theoretical model was proposed to predict the temperature profile within the solid cylindrical conductor subject to induction heating. The model takes into account of heat conduction inside the conductor with the volumetric heat source supplied by induced current, incorporated with heat transfer between the cylindrical conductor and surrounding fluid. It is found that the geometrical shape and the frequency can affect the temperature distribution within the conductor. (25 refs.)

Surface undulations in explosive crystallization: a thermal instability See Entry 113740

44.60 THERMODYNAMIC PROCESSES (PHENOMENOLOGY, EXPERIMENTAL TECHNIQUES)

(see also 05.70 Thermodynamics, 07.20 Thermal instruments and techniques)

113262 The second law as a selection principle: the microscopic theory of dissipative processes in quantum systems. I.Prigogine, C.George (Faculte des Sci., Univ. Libre de Bruxelles, Brussels, Belgium). *Proc. Natl. Acad. Sci. USA*, vol.80, no.14, p.4590-4 (July 1983).

The second law of thermodynamics, for quantum systems, is formulated, on the microscopic level. As for classical systems, such a formulation is only possible when specific conditions are satisfied (continuous spectrum, nonvanishing of the collision operator, etc.). The unitary dynamical group can then be mapped into two contractive semigroups, reaching equilibrium either for $t \rightarrow +\infty$ or for $t \rightarrow -\infty$. The second law appears as a symmetry-breaking selection principle, limiting the observables and density functions to the class that tends to thermodynamic equilibrium in the future (for $t \rightarrow +\infty$). The physical content of the dynamical structure is now displayed in terms of the appropriate semigroup, which is realized through a nonunitary transformation. The superposition principle of quantum mechanics has to be considered as irreversible processes transform pure states into mixtures and unitary transformations are limited by the requirement that entropy remains invariant. In the semigroup representation, interacting fields lead to units that behave incoherently at equilibrium. Inversely, nonequilibrium constraints introduce correlations between these units. (21 refs.)

Newton's law of cooling with finite reservoirs See Entry 111365

High-temperature calorimeter for the measurement of vapor pressure and enthalpy of vaporization See Entry 111684

Fourth moments of thermal fluctuations in the electromagnetic field in a homogeneous and isotropic medium See Entry 112898

44.90 OTHER TOPICS IN HEAT FLOW, THERMAL AND THERMODYNAMIC PROCESSES

113263 Experimental study of heat-transfer burnout in horizontal steam-generating channels with a porous inner lining and circumferentially nonuniform heating. A.I.Leont'ev, I.L.Mostinskii, V.S.Polonskii, M.A.Strykovich, I.M.Chernika (Inst. of High Temperatures, Acad. of Sci., USSR). *High Temp. (USA)*, vol.20, no.6, p.897-901 (Nov.-Dec. 1982). Translation of: *Teplofiz. Vys. Temp. (USSR)*, vol.20, no.6, p.1131-5 (Nov.-Dec. 1982). [received: Sept. 1983]

Heat-tran horizontal steam-generating channels with a capillary-porous inner lining in the form of filter gauze for various circumferential-heating laws. The experiments are performed on stainless steel tubes. The heat transfer medium is chemically desalinated water. A comparison of the data under conditions of identical circumferential heat-release laws shows that for large flow velocities, the porous structure raises the critical steam content considerably and broadens the burnout-safe operating range of steam-generating channels. Nonuniform heating helps to raise the local burnout heat fluxes. On the other hand, at lower mass-flow rate the critical steam content and pressure are observed to have a complicated influence on q_{cr} . (12 refs.)

46.00 MECHANICS, ELASTICITY, RHEOLOGY

113264 Analogies of 6 classic properties of materials. B.Melz. *Bull. Assoc. Suisse Electr. (Switzerland)*, vol.74, no.15, p.861-3 (6 Aug. 1983). In German.

Discusses relations between mechanical elasticity, hydromechanical permeability, thermal conductivity, magnetic permeability, dielectric displacement and electric conductivity. They can all be represented by identical mathematical equations of the general type $E = (x/A) dF/dx$, where dF/dx is the spring constant, hydromechanical conductivity, thermal conductivity, magnetic inductivity, capacitance, or electric conductivity, A a cross-section, F a force, flux or current, E a modulus, x a length. (5 refs.) J.S.

46.10 MECHANICS OF DISCRETE SYSTEMS

(see also 03.20 General mathematical aspects)

113265 Stability of steady motions of a rigid body with an elastic shell partially filled with fluid. V.N.Rubanovskii.

Appl. Math. & Mech. (USA), vol.46, no.4, p.430-7 (1982). Translation of: *Prikl. Mat. & Mekh. (USSR)*, vol.46, no.4, p.543-52 (1982). [received: Sept. 1983]

A problem of stability of steady motions of a rigid body with a cavity in the form of a closed thin elastic shell partially filled with fluid, in a conservative force field, is considered. It is assumed that stationary holonomic constraints are imposed on the body allowing its rotation about some spatially fixed axis, and the forces acting on the body have zero moment about this axis. The

conditions of stability are obtained from the solution of the problem dealing with the minimum of the changed potential energy W of the system obtained by studying its second variation. Sufficient conditions of the positive definiteness of $\delta^2 W$ are obtained in the form of the Silvester condition of positive definiteness of some quadratic form of a finite number of variables. A method for constructing this quadratic form is given. (7 refs.)

113266 On the motion of a heavy homogeneous ellipsoid on a fixed horizontal plane. A.P.Markeev. *Appl. Math. & Mech. (USA)*, vol.46, no.4, p.438-49 (1982). Translation of: *Prikl. Mat. & Mekh. (USSR)*, vol.46, no.4, p.553-67 (1982). [received: Sept. 1983]

Periodic motions without sliding of a heavy homogeneous ellipsoid of nearly spherical shape on a horizontal plane is investigated. The existence of periodic motions of the ellipsoid relative to its center of mass is established on the basis of known solutions to the problem of the homogeneous sphere steady motions on a plane. Periodic motions are determined, their stability is investigated, the reaction of the plane is calculated and traces of the ellipsoid-plane contact point on the plane and ellipsoid surface and the ellipsoid orientation in absolute space are determined. The motion of such an ellipsoid on an absolutely smooth plane is analyzed, and is shown to be perpetual (for all times) and close to regular precession about the moment of the momentum vector of constant length and precessing at constant angular velocity about the vertical to which it is inclined at a constant angle. (21 refs.)

113267 On the regular precession of a body of revolution on a horizontal plane with friction. A.V.Karapetian. *Appl. Math. & Mech. (USA)*, vol.46, no.4, p.450-3 (1982). Translation of: *Prikl. Mat. & Mekh. (USSR)*, vol.46, no.4, p.568-72 (1982). [received: Sept. 1983]

Conditions of existence and stability of regular precession of a heavy body of revolution on a horizontal plane with friction are determined. The results are compared with those of similar investigations for the regular precession of bodies of revolution on smooth and rough surfaces. (8 refs.)

113268 On the stability of steady rotation of a cylinder partly filled with a viscous incompressible fluid. N.V.Derendiaev, V.M.Sandalov.

Appl. Math. & Mech. (USA), vol.46, no.4, p.458-64 (1982). Translation of: *Prikl. Mat. & Mekh. (USSR)*, vol.46, no.4, p.578-86 (1982). [received: Sept. 1983]

The problem of stability in the case of steady rotation at constant angular velocity of a cylinder partly filled with viscous incompressible fluid with its axis held in viscoelastic supports is considered within the limits of a plane model. Taking into account the problem symmetry the authors reduce the conditions that define parameters for which a change of the system degree of instability occurs to conditions of existence of solutions of the equations in variations that define the circular precession of a cylinder containing a fluid. The exact solution of the hydrodynamic problem defines the forces exerted by the viscous incompressible fluid that partly fills the rotating cylinder under conditions of circular precession. Expressions for components of that force are used for dividing the parameter plane of the cylinder axis supports into regions of different degrees of instability. (6 refs.)

113269 On controlled rotation of an elastic rod. L.D.Akulenko, N.N.Bolotnik.

Appl. Math. & Mech. (USA), vol.46, no.4, p.465-71 (1982). Translation of: *Prikl. Mat. & Mekh. (USSR)*, vol.46, no.4, p.587-95 (1982). [received: Sept. 1983]

Plane rotational motions of an elastic rod loaded by a perfectly rigid body and acted upon by a controlling force moment, are considered. A system of integro-differential equations with initial and boundary conditions is obtained. The problems of control are studied, which carried the system from some initial state to a given angular state with damping of elastic oscillations or to a state in which the system rotates as a whole with fixed angular velocity. These formulations appear in the course of considering a whole series of practical problems of controlling the systems with elastic constraints such as robots and manipulators, weight lifting machines, etc. The asymptotic methods are used to obtain the solution of the control problems stated, close to the two limiting cases: 1) the case of a weightless rod (quasistatic approximation) and 2) the case of high flexural rigidity. (11 refs.)

113270 Finite amplitude oscillations of a simple rubber support system. M.F.Beatty (Dept. of Engng. Mechanics, Univ. of Kentucky, Lexington, KY, USA).

Arch. Ration. Mech. & Anal. (Germany), vol.83, no.3, p.195-219 (1983). Exact solution of the nonlinear problem of undamped, finite amplitude, free vertical oscillations of a mass supported by a rubber spring made of a neo-Hookean material is presented for both suspension and compression supports. The motion in the special case of free fall of the mass from rest at the unstretched state is characterized in terms of elliptic integrals, and it is shown that the periodic time may be expressed universally in terms of the tabulated Heuman lambda-function. The finite amplitude, free vibrational frequency and the dynamic deflection of a neo-Hookean oscillator are compared with those for a linear spring oscillator having the same constant stiffness; and both upper and lower bounds on the ratio of these frequencies are presented. Numerical values for several cases are illustrated, and the physical results are described graphically. General solutions for the free vibrations with arbitrary initial data are obtained in terms of certain generalized lambda and beta-functions, and some transformation identities relating these functions are derived. (7 refs.)

113271 Solution of the axisymmetric problem of the torsion of an inhomogeneous layer. A.E.Puro (Kaliningrad Tech. Inst. of Fishing Industry & Economy, Kaliningrad, USSR).

Sov. Appl. Mech. (USA), vol.18, no.12, p.1071-5 (Dec. 1982). Translation of: *Prikl. Mekh. (USSR)*, vol.18, no.12, p.31-5 (Dec. 1982). [received: Sept. 1983]

The solution of the axisymmetric problem of the torsion of a layer, inhomogeneous with respect to the axial coordinate, reduces to the solution of an ordinary second-order equation in Hankel space. The boundary-value problem was solved by finding the matrix of the corresponding first-order system. It is complicated to obtain a numerical solution as the parameter approaches infinity because the ratio of the elements of the matrix increases exponentially with increasing size. (5 refs.)

113272 Instability of gyrocompass with variable torques acting on wheel under resonance conditions. V.M.Vorob'ev.

Sov. Appl. Mech. (USA), vol.18, no.12, p.1138-44 (Dec. 1982). Translation of: *Prikl. Mekh. (USSR)*, vol.18, no.12, p.102-7 (Dec. 1982). [received: Sept. 1983]

The author establishes the conditions under which nonlinear resonance vibrations of a gyrocompass are excited by variable perturbation torques acting on the wheel. The author also determines qualitatively the dependence of the system stability on the main gyrocompass parameters. (12 refs.)

- 113273 Finite-dimensional representation of model of solid body with attached elastic elements.** A.E.Zakrzhevskii (Inst. of Mech., Acad. of Sci., Kiev, Ukrainian SSR). *Sov. Appl. Mech. (USA)*, vol.19, no.1, p.80-4 (Jan. 1983). Translation of: *Prikl. Mekh. (USSR)*, vol.19, no.1, p.95-100 (Jan. 1983). [received: Sept. 1983]
Considers an object consisting of a solid carrier and elastic elements attached to it. The carrier is assumed to be in motion in such a way that the relative displacements of the elastic elements remain sufficiently small, so that only the terms which are linear with respect to elastic displacements need to be retained in the equations of this motion. (4 refs.)
Nonlinear oscillations of weakly asymmetric elastic systems with several degrees of freedom See Entry 113347

46.20 CONTINUUM MECHANICS

(see also 03.40 General mathematical aspects)

- 113274 Two problems with mixed boundary conditions for an incompressible isotropic hyperelastic material.** V.M.Aleksandrov, S.R.Brudnyi. *Appl. Math. & Mech. (USA)*, vol.46, no.4, p.559-63 (1982). Translation of: *Prikl. Mat. & Mekh. (USSR)*, vol.46, no.4, p.700-4 (1982). [received: Sept. 1983]
Within the framework of nonlinear elasticity theory there is considered the equilibrium of the layer of incompressible isotropic hyperelastic material under plane strain under the effect of gravity and forces P applied at infinity. The linearized equations generated by this state of stress and strain are investigated. It is shown that for relationships between the material parameters, layer thickness and the force P , the equilibrium position can become unstable. Two problems are considered: the contact problem for a strip and the problem of a vertical crack of finite length emerging on the half-plane boundary. The action of the stamp and the crack is considered as a small perturbation of the state of stress and strain caused by the action of the intrinsic weight and the force P . (7 refs.)
113275 A theory of shells with small strain accompanied by moderate rotation. P.M.Naghdi, L.Vongsarnpigoon (Dept. of Mech. Engng., Univ. of California, Berkeley, CA, USA). *Arch. Ration. Mech. & Anal. (Germany)*, vol.83, no.3, p.245-83 (1983).
Concerned with a constrained theory of shells in the presence of small strain accompanied by moderate rotation. The constrained theory accounts for the effect of transverse normal strain and includes, of course, the special case (corresponding to the Kirchhoff-Love theory of shells) in which the effect of transverse normal strain is absent. After precise estimates for (local) moderate rotation and relative displacement gradients in terms of infinitesimal strain have been effected, a complete theory is formulated with the use of linear constitutive equations. The nature of the complete theory is further examined when initially the shell-like body is a plate; and it is shown that the kinematical formulae (strain-displacement relations), as well as the relevant differential equations of the theory in the absence of the effect of transverse normal strain, systematically reduce to those used in the von Karman plate equations. Also, in the light of the present results, an assessment of kinematical aspects of previously developed theories of shells undergoing small strain and moderate rotation is indicated. (16 refs.)
113276 Axial symmetrical problems for conical thin shells with linearly varying wall thickness. Chen Guodong (Tientsin General Paint Factory, China). *Acta Mech. Sin. (China)*, no.3, p.249-58 (1983). In Chinese.
Using the theory of thin shells, a basic equation in complex form is derived for conical thin shells with linearly varying wall thickness under symmetric load. Exact solutions are given. (5 refs.)
113277 On plane Prager-structures. I. G.I.N.Rozvany (Dept. of Civil Engng., Monash Univ., Clayton, Victoria, Australia), C.-M.Wang. *Int. J. Mech. Sci. (GB)*, vol.25, no.7, p.519-27 (1983).
Prager-structures differ from classical least-weight trusses (or Michell continua) in two respects: the sign of all member forces must be the same and the vertical location of all external loads is to be optimized. A systematic method for constructing plane Prager-structures for any system of vertical loads is outlined and illustrated with examples. It is established at plane Prager-structures (a) always consist of a single funicular and (b) the optimal elevation of the loads also provides an influence line for the minimum weight. (15 refs.)
113278 On plane Prager-structures. II. Non-parallel external loads and allowances for selfweight. C.-M.Wang (Dept. of Civil Engng., Nat. Univ. of Singapore, Kent Ridge, Singapore), G.I.N.Rozvany. *Int. J. Mech. Sci. (GB)*, vol.25, no.7, p.529-41 (1983).
For pt.I see *ibid.*, vol.25, no.7, p.519-27 (1983). In part I of this study, the construction of plane Prager-structures for any parallel load system was outlined. In this paper, the same method is extended to non-parallel forces and a procedure for determining plane Prager-structures for any vertical load system plus selfweight is presented. (10 refs.)
113279 End stress calculations on elastic cylinders. P.J.D.Mayes (Dept. of Engng. Sci., Univ. of Oxford, Oxford, England). *Int. J. Solids & Struct. (GB)*, vol.19, no.10, p.895-906 (1983).
For a semi-infinite circular elastic cylinder $z \geq 0$, $r \leq 1$ deformed solely by a distribution of stress and displacements on its flat end $z=0$, the Love stress function can be expanded in a series of eigenfunctions of known form. For problems in which suitable mixed stress and displacements boundary conditions are prescribed on $z=0$ the coefficients appearing in the expansion can be determined in an explicit form via sets of biorthogonal functions. When normal and shear stresses are prescribed on $z=0$ no such closed expressions for the coefficients exist and approximate methods usually lead to infinite systems of linear equations which are solved by truncation. Stability of solution as the order of truncation is increased can only be guaranteed theoretically when the infinite matrix is diagonally dominated, and this is not the case for existing methods. A Galerkin method has been developed using weighting functions chosen so as to optimise the diagonal dominance of the infinite matrix, and numerical results show that, although the resulting matrix is not completely diagonally dominated, the resulting coefficients show an improvement in stability in the sense that they do not change significantly as the order of truncation is increased. (11 refs.)
113280 Elastic response to a time-harmonic torsion-force acting on a bore surface. R.Parnes (Dept. of Solid Mech., Materials & Structures, School of Engng., Tel-Aviv Univ., Tel-Aviv, Israel). *Int. J. Solids & Struct. (GB)*, vol.19, no.10, p.925-34 (1983).
The response of an elastic medium to torsional line loads applied on the surface of a cylindrical cavity, and having a harmonic time-dependence, is studied. Integral representations of the stress and displacement fields are obtained and numerical results along a radial line emanating from the point of load applications and along the bore surface are presented. The dynamic

effect is represented by dynamic amplification factors and it is shown that, compared to the static case, the resulting outward radiating waves increase the effective radial penetration of the response. (8 refs.)

- 113281 Energy-consistent large rotating shell theories in Lagrangian description.** L.-P.Nolte, H.Stumpf (Lehrstuhl für Mech. II, Ruhr-Univ. Bochum, Bochum, Germany). *Mech. Res. Commun. (GB)*, vol.10, no.4, p.213-21 (July-Aug. 1983).
Presents two fairly simple versions of the geometrically nonlinear shell theories for large rotations, where the governing shell equations are the weak solution of the principle of stationary total potential energy. For these theories powerful approximating procedures such as finite element methods can be constructed. (6 refs.)
113282 An updated Lagrangian formulation for Timoshenko beams including non-conservative loads for divergence-type systems. K.-D.Klee, P.Wriggers (Inst. für Baumech. und Numerische Mech., Univ. Hannover, Hannover, Germany). *Mech. Res. Commun. (GB)*, vol.10, no.4, p.239-44 (July-Aug. 1983).
Attention is focused on non-conservative forces of the circulatory type for divergence-type systems, and their influence on a finite element formulation for beam structures. Forces of the circulatory type are velocity-independent, i.e. purely displacement-dependent, and belong to the class of polygenic forces. The finite element method presented, based on an updated Lagrangian (UL) formulation, has been proved to be a powerful tool for the solution of large displacement and rotation problems of beams. Circulatory forces lead i.g. to a non-symmetric load correction stiffness matrix. Since this work is limited to a large displacement-small strain analysis, a consistent linearization is carried out in order to obtain a simple and symmetric matrix formulation. Within this concept, no iteration process is necessary during a load step if the chosen load increment is sufficiently small. (3 refs.)
113283 Axisymmetric stress state of thick-walled elastic near-spherical shells. Yu.N.Nemish, D.F.Lyaluk, D.I.Chernopiskii (Inst. of Mech., Acad. of Sci., Kiev, Ukrainian SSR). *Sov. Appl. Mech. (USA)*, vol.18, no.12, p.1059-65 (Dec. 1982). Translation of: *Prikl. Mekh. (USSR)*, vol.18, no.12, p.18-24 (Dec. 1982). [received: Sept. 1983]
Investigates the stress state of thick-walled shells (of constant and variable thickness), nearly spherical, under the influence of internal pressure or centrifugal forces. The variant of the boundary form perturbation method is used to solve the boundary-value problems. (7 refs.)
113284 Calculation of the stress-strain state of a composite pressure cylinder with an elastic interlayer between the shell and flange. V.A.Nikituk. *Sov. Appl. Mech. (USA)*, vol.18, no.12, p.1075-9 (Dec. 1982). Translation of: *Prikl. Mekh. (USSR)*, vol.18, no.12, p.36-40 (Dec. 1982). [received: Sept. 1983]
Looks into the problem of the effect of shear forces on the stress-strain state from the direction of an elastic interlayer, attached to the shell by means of a flange. (5 refs.)
113285 Optimizing reinforced cylindrical shells with local loads from strength conditions. V.P.Maksimenco (Inst. of Mech., Acad. of Sci., Kiev, Ukrainian SSR). *Sov. Appl. Mech. (USA)*, vol.18, no.12, p.1080-6 (Dec. 1982). Translation of: *Prikl. Mekh. (USSR)*, vol.18, no.12, p.41-7 (Dec. 1982). [received: Sept. 1983]
Examines the problem of determining the minimum weight of a discretely reinforced cylindrical shell under the influence of local loads applied to a curvilinear contour. In the case considered, the number of ribs in both directions and their stiffness may differ, and their arrangement may be regular or irregular. The load can be assigned in accordance with almost any law. The problem is solved by the method of finite differences. (14 refs.)
113286 Phenomenon of internal instability in mixtures. Ya.Ya.Rushchitskii (Inst. of Mech., Acad. of Sci., Kiev, Ukrainian SSR). *Sov. Appl. Mech. (USA)*, vol.18, no.12, p.1087-92 (Dec. 1982). Translation of: *Prikl. Mekh. (USSR)*, vol.18, no.12, p.48-53 (Dec. 1982). [received: Sept. 1983]
Examines the internal instability of a mixture. By a mixture, the author means an idealized continuum consisting of two interpenetrating and interacting elastic continua. The author uses a linearized theory of mixtures for small strains and angles of rotation and also assumes that the main state is determined from linear mixture theory. (5 refs.)
113287 Linear theory of thin shells on the basis of the concept of added vectors. Ya.F.Kayuk, A.P.Zhukovskii (Inst. of Mech., Acad. of Sci., Kiev, Ukrainian SSR). *Sov. Appl. Mech. (USA)*, vol.19, no.1, p.7-11 (Jan. 1983). Translation of: *Prikl. Mekh. (USSR)*, vol.19, no.1, p.10-15 (Jan. 1983). [received: Sept. 1983]
The correspondence between the basic quantities of the linear variants of shell theory constructed taking the added-vector concept (AVC) into account and the well-known classical hypotheses is investigated. At the same time, it is shown how more general relations of thin-shell theory may be obtained on the basis of AVC by the uniform method than the traditional method (for example, according to the Timoshenko method). (5 refs.)
113288 Calculating shells of revolution with axisymmetric deformation. V.V.Pikul' (Inst. of Automation & Control Processes, DVNTs, Acad. of Sci., Vladivostok, Ukrainian SSR). *Sov. Appl. Mech. (USA)*, vol.19, no.1, p.19-24 (Jan. 1983). Translation of: *Prikl. Mekh. (USSR)*, vol.19, no.1, p.24-30 (Jan. 1983). [received: Sept. 1983]
Using the familiar property of sloping-shell equations of describing the stress-strain state associated with the edge effect in nonsloping shells, along with features of the coordinate system in the simplest variant of the theory of sloping shells of Vlasov (1949), the author was able to find a single method of calculating nonsloping shells of revolution that does not involve their differentiation into separate regions. The formulas of this method turn out to be simpler than the well-known formulas, and they have the same degree of accuracy. (10 refs.)
113289 Numerical solution of axisymmetric problems of the dynamics of thin orthotropic shells of revolution. A.Kh.Valiullin (Kazan' Chem. Engng. Inst., Kazan, USSR). *Sov. Appl. Mech. (USA)*, vol.19, no.1, p.24-8 (Jan. 1983). Translation of: *Prikl. Mekh. (USSR)*, vol.19, no.1, p.31-5 (Jan. 1983). [received: Sept. 1983]
Based on the equations of the nonlinear theory of shells, the author obtained equations to describe the axisymmetric motion of a thin shell of revolution. Having expressed the derivatives in finite differences and having combined the boundary-condition equations in their most general form a system of algebraic equations is derived. The system is linear for both linear and nonlinear problems. (6 refs.)

Limiting point load applied to an arbitrary point of a shell .. See Entry 113327
Stability of thin-walled ribbed conical shells See Entry 113334

46.30 MECHANICS OF SOLIDS AND RHEOLOGY

(see also 62.20 Mechanical properties of solids, as related to microscopic structure)

113290 Hybrid experimental-numerical stress analysis. A.S.Kobayashi (Dept. of Mech. Engng., Seattle, WA, USA). *Exp. Mech. (USA)*, vol.23, no.3, p.338-47 (Sept. 1983).

The hybrid experimental-numerical stress-analysis technique, which saw limited applications during the 1950s, has been resurrected with the vastly improved numerical techniques of the 1970s. By inputting the experimental results as initial and boundary conditions, modern computer codes are executed in its generation and application modes to yield results which are unobtainable when only one of the two techniques is used. The hybrid technique thus exemplifies the complementary role of the experimental and numerical techniques. (46 refs.)

113291 Design of continuous fiber composite structures. Crivelli Visconti (Istituto di Tecnol., Univ. di Napoli, Napoli, Italy).

Role of the Polymeric Matrix in the Processing and Structural Properties of Composite Materials. Proceedings of a Joint US-Italy Symposium, Capri, Italy, 15-19 June 1981 (New York, USA: Plenum 1983), p.545-86

Discusses the most peculiar aspects of designing a composite structure, considering the properties of the material from a more general point of view and taking into account the influence of technology on the design. It is shown that a design must consider element mission, technological aspects, and material properties at the same time. (70 refs.)

113292 Unresolved stress analysis problems in Kevlar composite pressure vessels. J.E.Fitzgerald (School of Civil Engng., Georgia Inst. of Technol., Atlanta, GA, USA).

Role of the Polymeric Matrix in the Processing and Structural Properties of Composite Materials. Proceedings of a Joint US-Italy Symposium, Capri, Italy, 15-19 June 1981 (New York, USA: Plenum 1983), p.625-7

The deflections, strains, and stresses in helically wound Kevlar/epoxy composite solid rocket motor cases using a two step analysis. (no refs.)

Elastic media with microstructure II. Three-dimensional models See Entry 111318

46.30C Static elasticity

113293 Dynamic response of orthotropic curved bridge decks due to moving loads. S.S.Dey (Dept. of Civil Engng., Indian Inst. of Technol., Kharagpur, India), N.Balasubramanian.

Comput. & Struct. (GB), vol.18, no.1, p.27-32 (1984).

The dynamic response of horizontally curved bridge decks simply supported along the radial edges under the action of the moving vehicle is investigated. The bridge deck is idealised as a number of finite strips with orthotropic elastic properties. The stiffness and mass matrix of an individual element were derived using a homogeneous differential equation of an orthotropic plate in polar co-ordinates. The vehicle is idealised as a sprung mass moving at a constant speed in a circular path parallel to the central line of the bridge. The unsprung mass of the vehicle is assumed to be always in contact with the bridge surface during its motion. Viscous damping is taken into account for both bridge and vehicle. Dynamic deflections and moments are presented for the mid-point of the bridge deck and the values have been compared with the available analytical solution. (16 refs.)

113294 Alternate stress and conjugate strain measures, and mixed variational formulations involving rigid rotations, for computational analyses of finitely deformed solids, with application to plates and shells. I. Theory. S.N.Atluri (Center for the Advancement of Computational Mech., Georgia Inst. of Technol., Atlanta, GA, USA).

Comput. & Struct. (GB), vol.18, no.1, p.93-116 (1984).

Attention is focused on: (i) definitions of alternate measures of 'stress-resultants' and 'stress-couples' in a finitely deformed shell (finite mid-plane stretches as well as finite rotations); (ii) mixed variational principles for shells, undergoing large mid-plane stretches and large rotations, in terms of a stress function vector and the rotation tensor. In doing so, both types of polar decomposition, namely rotation followed by stretch, as well as stretch followed by rotation, of the shell midsurface, are considered; (iii) two alternate bending strain measures which depend on rotation alone for a finitely deformed shell; (iv) objectivity of constitutive relations, in terms of these alternate strain/stress-resultants, and 'stress-couple' measures, for finitely deformed shells. To motivate these topics, and for added clarity, a discussion of relevant alternate stress measures, work-conjugate strain measures, and mixed variational principles with rotations as variables, is presented first in the context of three-dimensional continuum mechanics. Comments are also made on the use of the presently developed theories in conjunction with mixed-hybrid finite element methods. (34 refs.)

113295 Variation of stress resultants in concrete structures due to time-dependent creep and shrinkage strains of concrete. G.D.Stefanou (Univ. of Patras, Patras, Greece).

Comput. & Struct. (GB), vol.18, no.1, p.117-26 (1984).

A general procedure for calculating the variation with time of the internal stress resultants, and hence the stresses, in concrete structures is discussed. In particular, a study is made of the changes in the stress resultants due to time-dependent creep and shrinkage strains of concrete. A general procedure of calculating the variation in the stress resultants due to differential creep strains in concrete structures has been proposed by the author (1981). A similar procedure is followed in this paper to study these variations when creep and shrinkage strains take place simultaneously. The method leads to a system of n -linear differential equations of the form: $\dot{X} = AX + B$ the solution of which is performed by a computer using Runge-Kutta numerical procedures. A reinforced concrete portal frame exhibiting creep and shrinkage strains is solved by the proposed method and the results are given in tabular and graphical form. (6 refs.)

113296 Nonlinear viscoelastic stress analysis—a finite element approach. M.Henriksen (Dept. of Mech. Engng., Texas A&M Univ., College Station, TX, USA).

Comput. & Struct. (GB), vol.18, no.1, p.133-9 (1984).

This paper describes a finite element algorithm developed for analysis of nonlinear viscoelastic materials. A single integral constitutive law proposed by Schapery (1969) is used to describe viscoelastic material behavior. Work leading to this paper focused on adhesives, but the FE formulation is general and readily extended to structural systems other than plane strain, plane stress and axisymmetric analysis as described. Cartesian strain components are written in terms of current and past stress states. Thus strains are conveniently

defined by a stress operator that includes instantaneous compliance and hereditary strain which is updated by recursive computation. Equilibrium at each time step is insured with a modified Newton Raphson technique, incorporating convergence acceleration. Verification analyses show excellent agreement with experimental data for FM-73 adhesive systems. A plane strain analysis of a butt joint is included. (18 refs.)

113297 Minimum mass design of elastic frames subjected to multiple load cases. P.Pedersen, L.Jorgensen (Dept. of Solid Mech., Tech. Univ. of Denmark, Lyngby, Denmark).

Comput. & Struct. (GB), vol.18, no.1, p.147-57 (1984).

For frames with stress- and displacement constraints subjected to multiple load cases the formulation is given that enables use of the unified optimization approach which combines finite element and linear programming. Sensitivity analysis is shown analytically for Timoshenko beam models with transformations for eccentricities. For a specific case of a portal frame for a crane a study is made of the influence of the given portal columns (boundary conditions), the relations to fully stressed designs, and the influence of slenderness, when displacement constraints are involved. (9 refs.)

113298 A direct solution of the equivalent frame for two-way slabs. F.Arbabi (Michigan Technol. Univ., Houghton, MI, USA).

Comput. & Struct. (GB), vol.18, no.1, p.159-64 (1984).

A common procedure for the analysis of concrete buildings with two-way slabs is to reduce the slab along with other components of the building to a series of equivalent frames representing portions of the building between center-lines of spans. This paper presents a direct solution of the equivalent frame. Variations of slab geometry, flexural and torsional beams as well as columns are included in the model considered. The equations derived are cast into a short computer program which can be used for the design of concrete buildings with flat plate, flat slab, and two-way slabs with beams. (7 refs.)

113299 A convergence theorem for a periodic media with thermoelastic properties. G.I.Pasa (Dept. of Math., INCREST, Bucharest, Rumania).

Int. J. Eng. Sci. (GB), vol.21, no.11, p.1313-19 (1983).

The equations of the linear thermoelasticity for the media with periodic structure have been obtained by Ene (see *ibid.*, vol.21, no.5, p.443, 1983). The author proves that the asymptotic process $\epsilon \rightarrow 0$ is convergent and that in the limit the equations are those of Ene. (5 refs.)

113300 On the role of the strong ellipticity condition in nonlinear elasticity. M.Aron (Dept. of Math., Plymouth Polytech., Plymouth, England).

Int. J. Eng. Sci. (GB), vol.21, no.11, p.1359-67 (1983).

The author shows that if an elastic material is strongly elliptic on certain subdomains of the domain of the strain energy function then, provided that a mild boundedness condition (which may be regarded as restricting the class of considered materials) is satisfied, the nominal work of the deformation and the strain energy must satisfy certain growth conditions on these subdomains. The author uses the growth conditions to find upper and lower bounds for solutions to the boundary value problem of place (with dead loading) which belong to the considered subdomains. If the ellipticity condition is not satisfied at all points of the considered subdomains the author shows that the strain energy may satisfy certain inequalities which are shown to imply the Liapunov instability of equilibrium solutions to the boundary value problem of place and the fact that solutions to the dynamical problem cannot exist globally in time for arbitrary initial data. (35 refs.)

113301 The micropolar thermoelastic problem of uniform heat-flow interrupted by an insulated penny-shaped crack. K.Sridharan (Dept. of Math., Pachaiyappa's Coll., Madras, India).

Int. J. Eng. Sci. (GB), vol.21, no.12, p.1459-69 (1983).

The classical problem of uniform heat-flow disturbed by an insulated penny-shaped crack is solved in the context of micropolar elasticity. The mode II stress intensity factor, K_{II} is found to depend on two new non-dimensional parameters N and τ . N is a measure of the coupling of the displacement field with the microstructure of the medium ($0 \leq N \leq \sqrt{2}$) and τ is the ratio of a material characteristics length to the crack radius. K_{II} remains higher than its classical value when $N > 0, \tau > 0$ and attains the classical value as N and τ vanish. A closed-form expression to K_{II} is obtained in the physically important limiting case of $\tau \rightarrow 0$ with N fixed. In this limit the relative increment in K_{II} , over its classical value, is found to be $(1-\nu')N^2$ where ν' is the micropolar Poisson's ratio. (16 refs.)

113302 Integrated photoelasticity of cylindrical bodies with measurement of the deviation of light beams. Kh.K.Aben (Inst. of Cybernetics, Acad. of Sci., Tallinn, Estonian SSR).

Sov. Phys.-Dokl. (USA), vol.27, no.12, p.1068-9 (Dec. 1982). Translation of: *Dokl. Akad. Nauk SSSR*, vol.267, no.4-6, p.812-14 (Dec. 1982). [received: Sept. 1983]

In the method of photoelasticity it is usually assumed that light passes rectilinearly through the sample. However, because of the nonuniform distribution of the dielectric tensor in photoelastic materials, the light rays will deviate somewhat from straight lines. This deviation can amount to several mrad and can sometimes affect the experimental data. The author considers the transillumination of a transverse cross section of a cylinder in an axisymmetric stress state with no stress gradient in the axial direction. (10 refs.)

113303 Torsion of a rectangular beam with circular cavities. O.P.Orzhikhovskaya (Zhdanov Evening & Extramural Faculty of OIIMF, Zhdanov, USSR).

Strength Mater. (USA), vol.14, no.11, p.1494-7 (Nov. 1982). Translation of: *Probl. Prochn. (USSR)*, vol.14, no.11, p.61-3 (Nov. 1982). [received: Sept. 1983]

A homogeneous isotropic beam weakened by a number of equal longitudinal cylindrical cavities is examined. The cross section of the beam is a rectangle with a number of circular holes whose centers lie on the axis of symmetry of the rectangle and at the distance l from each other. The beam is twisted by the moment M . The problem of determined the state of stress of such a beam is investigated. (3 refs.)

113304 Stress state of a heated flattened spherical shell caused by thermal diffusion. R.N.Shvets, M.S.Ravrik, A.L.Bichuya (Inst. of Appl. Problems of Mech. & Math., Acad. of Sci., Ukrainian SSR).

Strength Mater. (USA), vol.14, no.11, p.1509-15 (Nov. 1982). Translation of: *Probl. Prochn. (USSR)*, vol.14, no.11, p.72-6 (Nov. 1982). [received: Sept. 1983]

It is concluded that there is a specific range of oscillation frequency for temperature of the environment at which the steady force amplitude takes on the maximum value, and this should be considered in the design of thin-walled structural elements for thermal fatigue. Consideration of diffusion processes and diffusion reactions at the test body with the working medium has a marked effect on the magnitude and nature of stress state distribution with time. (8 refs.)

113305 Effect of shear modulus on the elastic behavior of strongly anisotropic plates. Yu.A.Bogan (Inst. of Hydrodynamics, Acad. of Sci., Novosibirsk, USSR). *Strength Mater. (USA)*, vol.14, no.11, p.1518-23 (Nov. 1982). Translation of: *Probl. Prochn. (USSR)*, vol.14, no.11, p.79-83 (Nov. 1982). [received: Sept. 1983]
Investigates the strongly anisotropic elastic properties of modern fiber-composite materials. (6 refs.)

113306 Computation of imperfection-sensitivity at two-fold branching points. Z.Gaspar (Dept. of Civil Engng., Tech. Univ. of Budapest, Budapest, Hungary). *Z. Angew. Math. & Mech. (Germany)*, vol.63, no.8, p.359-70 (1983).
There is a degenerate critical point (usually illoptic or hyperbolic umbilic) of the potential function of semisymmetric conservative systems in the case of a two-fold branching point. The bifurcation set of a standard form is known in both cases in a parametrized form. In an imperfection-sensitivity examination the relevant critical point is regarded as the first one reached by a continuously changing load, starting from a stable equilibrium state. The coordinate system of the imperfection-sensitivity surface is transformed so that it coincides with a part of the bifurcation set of the standard form. Analysis of this reveals imperfections which decrease the critical load. Algorithms are given to compute these decreases. Finally the different possible forms of the equilibrium paths are sketched. (16 refs.)

An improved treatment of transverse shear in the Mindlin-type four-node quadrilateral element See Entry 111444

On differential equations of nonlocal elasticity and solutions of screw dislocation and surface waves See Entry 111445

Analysis of two-beam interferometry for bulk wave measurements See Entry 111748

Calculating shells of revolution with axisymmetric deformation See Entry 113288

Note on the applications of the Frechet derivative See Entry 113309

Torsion of rods of hardening material with almost-circular cross section See Entry 113322

Stability of flexible sloping shells in a temperature field See Entry 113333

The elastostatic axisymmetric problem of a sphere containing a penny-shaped crack in a nonequatorial plane See Entry 113356

Longitudinal shear of an anisotropic body with a sharp-ended anisotropic inclusion See Entry 113358

Partially contacting crack in a plate with an elliptic hole See Entry 113368

Definition of interphase in composites See Entry 113372

Analysis of contact problems with friction under oscillating loads See Entry 113373

The interaction between a system of circular punches on a nonhomogeneous elastic half space See Entry 113376

Prevention of 'mottle' in an epoxy resin as a photoelasticity material See Entry 113379

Thermoelectric method for studying stresses in plates weakened by holes See Entry 113391

Elastic modulus of syntactic foams See Entry 115239

Analysis of process stresses in two-layer SiC-Si disks See Entry 115246

46.30J Viscoelasticity, plasticity, viscoplasticity, creep, and stress relaxation
(inc. rheology of solids)

113307 Contact problem for a two-layer aging viscoelastic foundation. E.V.Kovalenko, A.V.Manzhirov. *Appl. Math. & Mech. (USA)*, vol.46, no.4, p.536-42 (1982). Translation of: *Prikl. Mat. & Mekh. (USSR)*, vol.46, no.4, p.674-82 (1982). [received: Sept. 1983]
A solution is given for the problem of the frictionless impression of a stamp into a two-layered aging viscoelastic strip in the case of plane strain. The upper layer is thin. The lower layer is hinge-fixed along the foundation. It is assumed that the layers are in contact without friction, that the forces acting on the stamp and the domain of contact do not change with time, that the rheological properties of the layers are described by the equations of the linear creep theory of aging materials and that the layers are fabricated at different times. (10 refs.)

113308 Strength optimization of the shape of a viscoelastic inhomogeneously-aged reinforced rod. L.V.Genkin, V.B.Kolmanovskii. *Appl. Math. & Mech. (USA)*, vol.46, no.4, p.543-9 (1982). Translation of: *Prikl. Mat. & Mekh. (USSR)*, vol.46, no.4, p.683-90 (1982). [received: Sept. 1983]
Examines the problem of selecting the shape of a minimal volume rod for which normal stresses in the reinforcements and the main material do not exceed given values. Relationships are established that govern the optimal shape. The dependence of the optimal shape on the magnitude of the bending moment and functions characterizing the inhomogeneity of the aging is studied. Results are presented of numerical computations. (5 refs.)

113309 Note on the applications of the Frechet derivative. J.L.Nowinski (Dept. Mech. & Aerospace Engng., Univ. of Delaware, Newark, DE, USA). *Int. J. Non-Linear Mech. (GB)*, vol.18, no.4, p.297-306 (1983).
A brief review of the main concepts underlying the operation of differentiation of non-linear mappings is followed by examples of the application of the operation; two of the five examples given concern the theory of the non-linear viscoelasticity and the theory of the non-linear non-local elasticity. (29 refs.)

113310 On the characteristic equations of elasto-plastic flow. R.M.Guo, J.L.Swedlow (Dept. of Mech. Engng., Carnegie-Mellon Univ., Pittsburgh, PA, USA). *Int. J. Non-Linear Mech. (GB)*, vol.18, no.4, p.321-34 (1983).
Three dimensional characteristic surfaces (slip surfaces) of elasto-plastic Navier's equations and the criteria for their existence are discussed, and the solutions are also applied to two dimensional cases. By making use of isotropic yield function, the following results proved. If, and only if the plastic/elastic moduli ratio is zero and $\text{Det}(\phi_{ij})=0$, ($\phi_{ij}=\partial\phi/\partial\sigma_{ij}$; yield function, σ_{ij} : stress tensor), characteristic surfaces exist. There are two and only two characteristic surface elements at each point, and they are identical with the surfaces of maximum shearing stress. (10 refs.)

113311 A plasticity theory for fluid-saturated porous solids. R.de Boer (Fachgebiet Mech., Univ.-GH-Essen, Essen, Germany), S.J.Kowalski. *Int. J. Eng. Sci. (GB)*, vol.21, no.11, p.1343-57 (1983).
A theory of plastic flow is developed for an elastic-perfectly plastic porous solid with its intercommunicating void spaces filled with a viscous fluid. The constitutive equations are established where full use is made of the thermodynamical equations. The final result is the complete set of equations of the theory and the boundary conditions for the medium in question. (18 refs.)

113312 Isotropic stochastic visco-elastic strain modelled as a second moment white noise field. O.Ditlevsen (Danmarks Ingeniorakademi, Lyngby, Denmark). *Int. J. Solids & Struct. (GB)*, vol.19, no.10, p.873-83 (1983).
Constitutive equations for statistically isotropic triaxial visco-elastic stochastic creep are formulated by generalized from a previous formulated theory of uniaxial stochastic creep. The constitutive equations define a random strain tensor as a function of a given deterministic stress tensor history. Compatibility constraints imply that stresses become random even for a deterministic external load history. In order to reach solutions in terms of means and covariances it turns out to be necessary to linearize the constitutive equations with respect to the stress tensor increments. This Part 1 of the paper terminates by discussing some solutions of relevance for comparisons with the uniaxial theory of combined elongation and bending of slender prismatic bodies. Part 2 discusses solutions for biaxial stress histories that are homogeneous in the mean. (5 refs.)

113313 Conservation laws for material exhibiting power-law creep. T.J.Delph (Lehigh Univ., Bethlehem, PA, USA). *Int. J. Solids & Struct. (GB)*, vol.19, no.10, p.907-13 (1983).
Conservation laws are derived for materials whose constitutive behavior is characterized by power-law creep with elastic strains. This is accomplished by formulating an adjoint variational principle which has as its Euler-Lagrange equations the governing equations as well as a set of adjoint equations involving adjoint variables. Conservation laws are then derived by an application of Noether's theorem to the variational principle. The results are analogous to those obtained in linear elasticity, in that conservation laws are shown to arise from translations of spatial and temporal coordinates, rigid-body rotations, and self-similar scalings. A path-independent integral formulation of one of the conservation laws, valid under special circumstances, is derived. (24 refs.)

113314 'Frictional slip between a layer and a substrate due to a periodic force' by M. Comninou and J.R. Barber, *Int. J. Solids Structures* 19(6), 533-539 (1983). K.L.Johnson (Engng. Lab., Cambridge Univ., Cambridge, England). *Int. J. Solids & Struct. (GB)*, vol.19, no.10, p.935-6 (1983).
Looks further at the question of shakedown in frictional systems raised in the paper by Comninou and Barber. To the author's knowledge the equivalent of Molan's theorem in slipping systems has not been proved and so the author puts it to an empirical test in the case outlined by Comninou and Barber. (3 refs.)

113315 Biaxial unsteady strain of a rectilinear strip in the scheme of a compressible viscoplastic medium. S.V.Serikov. *J. Appl. Mech. & Tech. Phys. (USA)*, vol.23, no.6, p.850-5 (Nov.-Dec. 1982). Translation of: *Zh. Prikl. Mekh. & Tekh. Fiz. (USSR)*, vol.23, no.6, p.123-9 (Nov.-Dec. 1982). [received: Sept. 1983]
The exact solution of a mathematical model for unsteady strain of a rectilinear strip under tension is determined with a linear velocity field and with zero tangential stress in the scheme of a compressible viscoplastic medium. Analytical dependences are deduced to estimate the strip rupture time. The existence of a plasticity peak is noted. (11 refs.)

113316 Approximate calculation of binding forces for plastic flows. M.Abouaf, J.L.Chenot, J.J.Perouze (CEMEF, Ecole des Mines de Paris, Valbonne, France). *Mech. Res. Commun. (GB)*, vol.10, no.4, p.187-92 (July-Aug. 1983).
The kinematic method of limit loads theory (or upper bound method) has always been used for the determination of active loads. The authors propose its utilization for the calculation of reactions by introducing the (virtual) displacements prohibited by these constraints. As an example the authors calculate the reaction exerted on rolling mill rolls. (5 refs.)

113317 Bending of plates based on improved theory. K.Shirakawa (Dept. of Mech. Engng., Univ. of Osaka Prefecture, Sakai, Japan). *Mech. Res. Commun. (GB)*, vol.10, no.4, p.205-11 (July-Aug. 1983).
The plate theory which is not based on the Kirchhoff assumptions has been developed by Reissner (1945, 1975) and Ambartsumyan (1970) by taking into account the effects of shear deformation and normal stress. This so-called improved theory is the one to complement the classical plate theory and the extend its range of application. The author uses the Ambartsumyan theory, and finds that the resulting equation is quite the same as that in Reissner theory. The statical equation including both effects is presented in terms of a single deflection which seem useful to the analysis of practically important problems. In the improved theory, even for a simply supported edge, there are methods of support, that is in addition to the classical boundary condition (a) rotation angle=0 or (b) twisting moment=0. It is in general not easy to obtain solutions in the case of (b). The author presents the analytical method for the basic problem for a rectangular plate with any boundary condition and the effects of shear deformation and normal stress on the deflection are examined and compared with the classical values. (5 refs.)

113318 Relaxation of a rectangular beam and circular shaft. N.S.Ottosen (Engng. Dept., Riso Nat. Lab., Roskilde, Denmark). *Nucl. Eng. & Des. (Netherlands)*, vol.75, no.1, p.67-72 (1982). [received: Sept. 1983]
Provides exact and approximate solutions to the title problems. Time-hardening creep is adopted and the stress dependence is assumed to follow the exponential expression proposed by Soderberg (1936). Even though the exact solutions are easy to work with, some approximate solutions are discussed. These approximate solutions are obtained from the exact ones by simply ignoring certain terms; errors bounds are then directly available. The exact and approximate solutions are applied to specific problems and compared with the predictions following the exact, numerical or approximate solution of Norton's power law. (13 refs.)

113319 Elasto-plastic behaviour of a thin cylinder under thermal stress cycling. S.Govindarajan (Reactor Design Section, Reactor Res. Center, Kalpakkam, India), V.Sundararajan. *Nucl. Eng. & Des. (Netherlands)*, vol.75, no.1, p.87-98 (1982). [received: Sept. 1983]
A simple biaxial model is chosen to represent the stress state of a thin cylinder and the elasto-plastic behaviour under thermal stress cycling is studied to determine: shakedown limits, plastic cycling limits, magnitude of cyclic strains and ratchet strains, and strain ratios in various regimes. The studies have been carried out for two material models: elastic-perfectly plastic

and Prager-hardening. Results are given in the form of graphs and compared with the results of uniaxial models. (7 refs.)

113320 Generalized solutions of the dynamical theory of plasticity and thermoplasticity. B.A.Druyanov (All-Union Correspondence Inst. of Mech. Engng., Moscow, USSR). *Sov. Phys.-Dokl. (USA)*, vol.27, no.12, p.1026-7 (Dec. 1982). Translation of: *Dokl. Akad. Nauk SSSR*, vol.267, no.4-6, p.1073-5 (Dec. 1982). [received: Sept. 1983]

The author considers the dynamic flow of a hardening rigid-plastic medium, taking account of heat release and its effect on the plastic and thermodynamic potentials. (3 refs.)

113321 Inelastic torsion of plane rods. M.Ya.Leonov, V.D.Perederi (Automation Inst., Acad. of Sci., Frunze, Kirghiz SSR). *Strength Mater. (USA)*, vol.14, no.11, p.1490-3 (Nov. 1982). Translation of: *Probl. Prochn. (USSR)*, vol.14, no.11, p.58-60 (Nov. 1982). [received: Sept. 1983]

Investigates rods which, in pure torsion, have tangential-stress trajectories within the elastic limit that are close to the stress trajectories of the limiting state with ideal plasticity in every direction, in addition to fields with relatively small deformations, can be called plane. This condition is not satisfied only in the vicinity of an acute center of stress concentration; these cases are excluded from the investigation. (1 ref.)

113322 Torsion of rods of hardening material with almost-circular cross section. S.B.Maksimov, V.A.Lupin, A.A.Ost-semin, L.V.Maksimova (Ural Res. Inst. of Pipe Industry, Chelyabinsk, USSR). *Strength Mater. (USA)*, vol.14, no.11, p.1498-501 (Nov. 1982). Translation of: *Probl. Prochn. (USSR)*, vol.14, no.11, p.63-6 (Nov. 1982). [received: Sept. 1983]

The problem of torsion of hardening rods whose section is close to being circular or annular is solved by the perturbation method. Analytical dependencies for evaluating the state of stress and strain of hardening rods are suggested. (7 refs.)

113323 Elastic-plastic state of bodies of revolution under variable nonisothermal loading, taking account of creep. V.G.Savchenko (Inst. of Mech., Acad. of Sci., Kiev, Ukrainian SSR).

Sov. Appl. Mech. (USA), vol.18, no.12, p.1053-8 (Dec. 1982). Translation of: *Prikl. Mekh. (USSR)*, vol.18, no.12, p.12-17 (Dec. 1982). [received: Sept. 1983]

Considers the axisymmetric stressed state of a body of compound meridional cross section which is subjected to unsteady heating and surface t_n and body K forces. In general the temperature of the medium T_{med} , the surface t_n and the body K forces, and the heat-transfer coefficient α may be known functions of the coordinates z, r, ϕ and the time t . Their time dependence is such that the temperature distribution generated in the body satisfies the heat-conduction equation and boundary conditions of the third kind, and the thermoplasticity problem can be treated in the quasistatic formulation. The thermophysical and mechanical characteristics of the material of the body are assumed to be temperature dependent. Under the action of the loads mentioned, loading processes may occur in the body along rectilinear trajectories or strain trajectories of small curvature. Finding the stress-strain state of a body of revolution during the heating process reduces to the problem of solving the heat-conduction equation to determine the temperature T of points of the body at given times, and the thermoplasticity problem to determine the stresses $\sigma_{zz}, \sigma_{rr}, \sigma_{\phi\phi}$ and σ_{zr} , the strains $\epsilon_{zz}, \epsilon_{rr}, \epsilon_{\phi\phi}, \epsilon_{zr}$, and the displacements w and u at specified times. (4 refs.)

113324 Approximate representation of the equations of viscoelasticity for vibrations with variable amplitude. I.K.Senchenkov (Inst. of Mech., Acad. of Sci., Kiev, Ukrainian SSR).

Sov. Appl. Mech. (USA), vol.18, no.12, p.1065-70 (Dec. 1982). Translation of: *Prikl. Mekh. (USSR)*, vol.18, no.12, p.25-30 (Dec. 1982). [received: Sept. 1983]

The application of physical and kinematic models for the simplification of the viscoelastic equations for a medium with memory was carried out. It was shown that for slow enough motion and also for a medium with fast (in some sense) relaxation, the very general viscoelastic equations can be approximated by differential equations. The author uses these two models in a somewhat different form to construct approximate viscoelastic equations in the linear and nonlinear cases, for vibrations with variable amplitude. (7 refs.)

113325 Study of the bending of a multilaminate plate on the basis of finite-shear theory. A.G.Bondar, A.O.Rasskazov (Kiev Automobile Road Inst., Kiev, Ukrainian SSR).

Sov. Appl. Mech. (USA), vol.18, no.12, p.1097-101 (Dec. 1982). Translation of: *Prikl. Mekh. (USSR)*, vol.18, no.12, p.59-63 (Dec. 1982). [received: Sept. 1983]

In designing multilaminate orthotropic plates and sloping shells in which the layers differ significantly in their physical characteristics, it is necessary to consider the phenomenon of transverse shear and normal compression. The use of classical hypotheses in designing this class of structures leads to intolerable errors. Accounting for transverse shear strains considerably complicates the equilibrium equations of multilaminate structures. In accordance with finite-shear theory, which makes it possible to take into account anisotropy and significant physical inhomogeneity among the layers of a packet, the bending of multilaminate plates is described by a system of three differential equations in partial derivatives with respect to the deflection of the reduction surface and the shear functions. (6 refs.)

113326 Elastic-plastic state of a coiled cylindrical shell loaded with internal pressure. L.A.Ilin, N.A.Lobkova (Inst. of Mech., Acad. of Sci., Kiev, Ukrainian SSR).

Sov. Appl. Mech. (USA), vol.19, no.1, p.32-7 (Jan. 1983). Translation of: *Prikl. Mekh. (USSR)*, vol.19, no.1, p.41-6 (Jan. 1983). [received: Sept. 1983]

A study was previously made of the character of slip and the stress-strain state of the layers of an infinite thin multilayer coiled shell under internal pressure during the elastic stage of its work. The shell was schematized as a multisheeted circular cylindrical surface with a finite stiffness in tension and zero stiffness in bending. The investigators studied different cases of slip in the coil in relation to the value of the coefficient of friction f between the layers. The present authors use the previous design method to study the elastic-plastic stress-strain state of a coiled shell made of an ideally elastic-plastic material. The study was conducted for large values of $f \geq \ln 2/2\pi \approx 0.110$. The statement by A.E. Babenko (1978) that the stress distribution is the same in the elastic and plastic states is untrue, and it stemmed from the fact that the strain compatibility conditions of the turns were not taken into account. (5 refs.)

113327 Limiting point load applied to an arbitrary point of a shell. A.S.Dekhtyar', L.B.Kotova (Kiev State Art Inst., Kiev, Ukrainian SSR). *Sov. Appl. Mech. (USA)*, vol.19, no.1, p.37-41 (Jan. 1983). Translation of: *Prikl. Mekh. (USSR)*, vol.19, no.1, p.47-51 (Jan. 1983). [received: Sept. 1983]

Considers a hollow, constant-thickness shell, rectangular in plan, which has arbitrarily fixed edges. Its mean surface has positive, negative, or alternating Gaussian curvature. The shell material follows the generalized logansen plasticity condition, proposing complete independence of the internal force factors in the limiting state. In the particular case under the action of a vertical load and momentless fixing of the edges, it is usually assumed that the displacement $U=V=0$, and then all that is required for minimization of K is the selection of the field of flexure rates. Essentially, it is the choice of the configuration of the field $W(x,y)$ which is the distinctive feature of the problems considered, distinguishing them from problems of the limiting analysis of rigid-plastic shells with large—for example, distributed—loads. (9 refs.)

Analyses of large quasistatic deformations of inelastic bodies by a new hybrid-stress finite element algorithm See Entry 111443

Torsion of a rectangular beam with circular cavities See Entry 113303

Buckling of beam under compression and torsion beyond elastic limit See Entry 113335

Propagation of elastic-plastic compression-shear waves in materials having delayed yield See Entry 113346

Geometrically non-linear eccentrically compressed columns of uniform creep strength vs optimal columns See Entry 113355

Contour J-integral in the plastic region See Entry 113362

Plastic bands at the tip of a linear rigid inclusion See Entry 113363

Examination of the stress state of a helically reinforced composite in shearing See Entry 113364

Continuum theory of fracture in the compression of composite materials with a metallic matrix See Entry 113365

Finite element model simulation of creep crack growth in low-ductility material See Entry 113371

Nonlinear photoviscoelasticity: theory and measurement See Entry 113384

A noncontacting system for measuring effective stress-strain curves of ultra-thin X-ray-mask materials See Entry 113385

A technique for cyclic-plastic notch-strain measurements See Entry 113386

Modification of the theory of plastic flow based on a shear-strain mechanism See Entry 114073

Deformation of semibrittle solids See Entry 114075

Deformation and fracture of a material in plane stress under complex loading See Entry 114088

Densification and change in shape of porous materials during hot pressing under conditions of nonuniform triaxial compression See Entry 115128

Plastic deformation of spherical steel shells under internal blast loading See Entry 115260

Variational functional for a rigid-plastic porous material See Entry 115279

Strength of porous net materials in the uniaxial strain state See Entry 115287

A stress transfer model for the deformation and failure of polymeric matrices under swelling conditions See Entry 115292

Stress and strength analysis in and around composite inclusions in polymer matrices See Entry 115297

46.30L Static buckling and instability

113328 Generic buckling curves for specially orthotropic rectangular plates. E.J.Brunelle, G.A.Oyibo (Rensselaer Polytech. Inst., Troy, NY, USA).

AIAA J. (USA), vol.21, no.8, p.1150-6 (Aug. 1983).

Using a double affine transformation, the classical buckling equation for specially orthotropic plates and the corresponding virtual work theorem are presented in a particularly simple fashion. These dual representations are characterized by a single material constant, called the generalized rigidity ratio D^* , whose range is predicted to be the closed interval from 0 to 1 (if this prediction is correct then the numerical results using $D^* > 1$ in the specially orthotropic plate literature are incorrect); when natural boundary conditions are considered a generalized Poisson's ratio ϵ is introduced. Thus the buckling results are valid for any specially orthotropic material; hence the curves presented in the text are generic rather than specific. The solution trends are twofold: the buckling coefficients decrease with decreasing D^* and, when applicable, they decrease with increasing ϵ . Since the isotropic plate is one limiting case of the above analysis, it is also true that isotropic buckling coefficients decrease with increasing Poisson's ratio. (21 refs.)

113329 Postbuckling behavior of a thick plate. Lien-Wen Chen, Ji-Liang Doong (Nat. Cheng Kung Univ., Tainan, Taiwan).

AIAA J. (USA), vol.21, no.8, p.1157-61 (Aug. 1983).

The postbuckling behavior of a simply supported rectangular thick plate subjected to arbitrary loading conditions is investigated. The applied stress is taken to be a combination of a pure bending stress plus an extensional stress in the plane of the plate. Governing equations based on von Karman assumptions are used to solve the postbuckling problems by the Galerkin method. Buckling loads are obtained to compare with the results of Brunelle and Robertson (1974). Postbuckled deflection is shown to increase with the transverse isotropic coefficient S , and the effects of the in-plane bending stress are found to be quite significant for a thick plate. (14 refs.)

113330 Buckling of sinusoidally corrugated plates under axial compression. S.Toda (Nat. Aerospace Lab., Tokyo, Japan).

AIAA J. (USA), vol.21, no.8, p.1211-13 (Aug. 1983).

The author presents an analytical explanation of the buckling characteristics of sinusoidally corrugated plates under axial compression. Assuming that the buckling deflection components are in the form of a Fourier series, the second increment of the potential energy is evaluated with the aid of linear shell theory. Then the eigenvalue equations for neutral equilibrium are obtained by variations in the potential energy. An approximate but closed-form solution is presented for the critical axial compressive stress. (4 refs.)

113331 Method of averaging in the problems of stability of elastic plates possessing fine periodic structure. S.I.Boiarchenko, L.M.Zubov.

Appl. Math. & Mech. (USA), vol.46, no.4, p.513-19 (1982). Translation of: *Prikl. Mat. & Mekh. (USSR)*, vol.46, no.4, p.647-54 (1982). [received: Sept. 1983]

Studies the buckling of an elastic plate with mechanical properties inhomogeneous across its thickness. The character of the inhomogeneity is

described by periodic rapidly oscillating functions of the transverse coordinate. The method of averaging is used to construct an asymptotic to the solution of the problem of stability in the case when the period of the inhomogeneity oscillations tends to zero. An averaged system of differential equations is obtained in the case of a homogeneous (affine) subcritical deformation, separately, for the case of a compressible and an incompressible materials. The system is used for determining, in the given approximation, the bifurcation values of the load parameters. The general theory is illustrated by an example of computing the stability of a rectangular plate uniformly compressed in its plane, with the plate made of a resin-like incompressible one-constant material, the modulus of elasticity of which is a rapidly oscillating function of the transverse coordinate. The results obtained using the method of averaging are compared, for a thin plate, with those of the buckling theory based on the Kirchhoff hypothesis. (10 refs.)

113332 On the transition from a diamond mode to an axisymmetric mode of collapse in cylindrical shells. V.Tvergaard (Dept. of Solid Mech., Tech. Univ. of Denmark, Lyngby, Denmark).

Int. J. Solids & Struct. (GB), vol.19, no.10, p.845-56 (1983).

The influence of buckling pattern localization on the collapse mode of axially compressed elastic-plastic circular cylindrical shells is investigated. Initial imperfections are assumed to be axisymmetric and the possibility of bifurcation into a non-axisymmetric shape is analysed. For sufficiently thin-walled shells bifurcation occurs before the load maximum: but in more thick-walled shells the axisymmetric deformations are stable beyond the maximum load, at which localization into a single outward buckle takes place. It is found that the localization delays bifurcation considerably, such that sufficiently thick-walled shells will collapse in an axisymmetric mode. The theoretical predictions are compared with a number of published experimental results. (16 refs.)

113333 Stability of flexible sloping shells in a temperature field. L.F.Vakhaeva, V.A.Krys'ko (Saratov Polytech. Inst., Saratov, USSR). *Sov. Appl. Mech. (USA)*, vol.19, no.1, p.12-18 (Jan. 1983). Translation of: *Prikl. Mekh. (USSR)*, vol.19, no.1, p.16-23 (Jan. 1983). [received: Sept. 1983]

Investigates the stability of flexible sloping shells, rectangular in plan, under the influence of different loads and temperatures. The initial equations of thermoelasticity for sloping shells were obtained using the following assumptions: the material of the structure obeys Hooke's law, the Kirchhoff-Love hypothesis is valid, and E , ν , and α are independent of temperature. The method developed makes it possible to study the stability of shells under the influence of any possible temperature field without making assumptions on the law of temperature distribution. Instead, the distribution is obtained from a three-dimensional heat conduction equation with assigned boundary conditions and an assigned heat-flux distribution. (5 refs.)

113334 Stability of thin-walled ribbed conical shells. G.D.Gavrilenko (Inst. of Mech., Acad. of Sci., Kiev, Ukrainian SSR).

Sov. Appl. Mech. (USA), vol.19, no.1, p.28-32 (Jan. 1983). Translation of: *Prikl. Mekh. (USSR)*, vol.19, no.1, p.36-40 (Jan. 1983). [received: Sept. 1983]

Examples of calculating the stability of specific thin-walled ribbed conical shells with consideration of the discreteness of the rib placement are provided. The calculations are based on the assumptions of momentlessness and uniformity of the subcritical stress state. (5 refs.)

113335 Buckling of beam under compression and torsion beyond elastic limit. V.S.Davydov (Sci.-Res. Correspondence Inst. of Economics & Planning, Kiev, Ukrainian SSR).

Sov. Appl. Mech. (USA), vol.19, no.1, p.68-74 (Jan. 1983). Translation of: *Prikl. Mekh. (USSR)*, vol.19, no.1, p.82-8 (Jan. 1983). [received: Sept. 1983]

The need to account for complexity of loading conditions during loss of stability beyond the elastic limit was for the first time pointed out by Il'yushin (1963). Subsequent studies have revealed that different theories of plasticity yield different solutions to the problem of buckling of a beam under compression and torsion. In this study the problem is solved on the basis of the relations, in general form, between stresses and strains during loss of stability after prior simple loading. (13 refs.)

Stability of steady motions of a rigid body with an elastic shell partially filled with fluid See Entry 113265

On the motion of a heavy homogeneous ellipsoid on a fixed horizontal plane See Entry 113266

On the stability of steady rotation of a cylinder partly filled with a viscous incompressible fluid See Entry 113268

Instability of gyrocompass with variable torques acting on wheel under resonance conditions See Entry 113272

Volume, surface and interface fracture statistics of brittle materials under flexure See Entry 113349

Observation of damage growth in compressively loaded laminates See Entry 113375

46.30M Vibrations, aeroelasticity, hydroelasticity, mechanical waves, and shocks

(see also 43.40 Mechanical vibrations and shock)

113336 Simple waves in nonlinearly elastic media. E.I.Sveshnikova. *Appl. Math. & Mech. (USA)*, vol.46, no.4, p.509-12 (1982). Translation of: *Prikl. Mat. & Mekh. (USSR)*, vol.46, no.4, p.642-6 (1982). [received: Sept. 1983]

Plane isentropic waves (simple waves) are studied in the prestressed medium. The author determines the variation in the parameters of simple waves in a prestressed medium together with the characteristic velocities, and their dependence on the current state of the medium and on the prior deformation. It is shown that all three waves (one quasilongitudinal and two quasitransverse) can break, and conditions under which this can happen are given. (3 refs.)

113337 Effects of uni-directional geometric imperfections on vibrations of pressurized shallow spherical shells. D.Hui, A.W.Leissa (Dept. of Engng. Mech., Ohio State Univ., Columbus, OH, USA).

Int. J. Non-Linear Mech. (GB), vol.18, no.4, p.279-85 (1983).

Deals with the effects of initial geometric uni-directional imperfections on vibrations of a pressurized spherical shell or spherical cap. The analysis is based upon shallow shell theory. Frequency vs. applied pressure interaction curves are plotted for various values of the imperfection amplitude. Imperfections are shown to have a severe effect in reducing the natural frequencies similar to that demonstrated in the buckling behavior of spherical shells. (13 refs.)

113338 Note on the propagation of Love waves in a half-space with an elastic triple superficial layer subject to a high two-dimensional stress. H.Ohnabe (Ishikawajima-Harima Heavy Industries Co. Ltd., Tokyo, Japan), F.Mizuguchi.

Int. J. Non-Linear Mech. (GB), vol.18, no.4, p.307-12 (1983).

The propagation of Love waves is investigated involving a triple superficial layer on a half-space, the entire system being elastic and highly stressed in two horizontal directions. The non-linear problem is illustrated numerically. A graph displays the phase velocity dependence on the wavelength. (4 refs.)

113339 Love type waves in a porous layer with irregular interface. A.Chattopadhyay, R.K.De (Dept. of Phys. & Math., Indian School of Mines, Dhanbad, India).

Int. J. Eng. Sci. (GB), vol.21, no.11, p.1295-303 (1983).

The dispersion equation is derived relating to the frequency and the phase velocity of propagation of Love waves in a nondissipative liquid filled porous solid underlain by an isotropic and homogeneous half space. The rectangular irregularity in the interface between the upper porous layer and the lower semi-infinite medium with a source in it is studied herein. The modified dispersion equation of Mal (1962) and the standard dispersion equation of Love waves are deduced as particular cases. The frequency equation is obtained by applying the method of perturbation and the phase velocity curves have been drawn for different irregularities by using the numerical parametric values as suggested by Biot (1956). (14 refs.)

113340 Nonlinear surface waves on an elastic solid. R.W.Lardner (Dept. of Math. Sci., Univ. of Petroleum & Minerals, Dhahran, Saudi Arabia).

Int. J. Eng. Sci. (GB), vol.21, no.11, p.1331-42 (1983).

The effect of quadratic elastic nonlinearity on the propagation of surface Rayleigh waves on an isotropic elastic solid is examined. Using the method of multiple scales an approximate solution is obtained which is uniformly valid in both spatial directions as well as in time. An arbitrary wave profile is considered and an integro-differential equation is derived for the Fourier transform of the displacement on the boundary. In the case of a quasi-monochromatic wave explicit expressions are derived for the variations of the amplitudes of the fundamental and second and third harmonics along the boundary. (11 refs.)

113341 Elastic waves generated by loading applied to surface of spherical cavity. T.B.Moodie, A.Mioduchowski, J.B.Haddow, R.J.Tait (Univ. of Alberta, Edmonton, Alberta, Canada).

Int. J. Eng. Sci. (GB), vol.21, no.11, p.1369-78 (1983).

The elastodynamic problem of an unbounded body, subjected to a rotationally symmetric application of tractions at the surface of a spherical cavity, is studied. In general this problem involves three independent variables, which are the radius, colatitude and time but it is shown how the method of characteristics for one spatial variable and time can be applied when the dependent variables are expanded as series of Legendre polynomials. The procedure is different to those employed previously in that it does not involve integral transforms or asymptotic approximations and the field variables can be obtained for small and large times. (6 refs.)

113342 Crack transient torsional wave interaction in an elastic bi-material. O.D.George (Dept. of Math., Univ. of Calabar, Calabar, Nigeria).

Int. J. Eng. Sci. (GB), vol.21, no.11, p.1379-95 (1983).

An infinitely long cylindrical elastic solid of finite radius is imbedded in another infinite elastic cylindrical solid to form an elastic bi-material composite perfectly bonded at their bi-material interface. The early-time response of the composite to a sudden twist applied axisymmetrically over a stationary penny-shaped crack which appears over a cross-section of the fibre and terminates orthogonally at the bi-material interface, is investigated. The magnitude of the applied twist is assumed to be less than that for which debonding or crack propagation can take place. For a bi-material composite the square of whose matrix shear-wave speed is less than twice the square of the fibre shear-wave speed, uniform asymptotic analytic results, whose accuracy can be improved by taking higher order terms in the solution, are obtained for the time-dependent surface displacement gradient normal to the plane of the crack and outside the crack region, the dynamic stress intensity factor, and also the stress singularity strength eigenvalue—all as functions of the fibre-matrix material disparities. (16 refs.)

113343 Torsional oscillations of a finite inhomogeneous piezoelectric cylindrical shell. K.Venkateswara Sarma (Dept. of Math., PSG Coll. of Arts & Sci., Coimbatore, India).

Int. J. Eng. Sci. (GB), vol.21, no.12, p.1483-91 (1983).

Torsional wave motion of a finite right circular cylindrical shell of inhomogeneous piezoelectric material of (622) crystal class under time independent electric potential on the boundary is investigated. The inhomogeneity is restricted to the variations of density and other physical constants of the medium as $\exp(f(r))$ where f is a suitable function of the radial distance. (5 refs.)

113344 Diffraction of Rayleigh waves in a quarter-space. V.K.Kinra, B.Q.Vu (Aerospace Engng. Dept., Texas A&M Univ., College Station, TX, USA).

Mech. Res. Commun. (GB), vol.10, no.4, p.193-8 (July-Aug. 1983).

The authors consider a plane Rayleigh wave incident at the corner of a quarter-space. Upon diffraction, it is partly reflected and partly transmitted; the remainder of the energy is propagated into the interior in the form of body waves. Let u_0 , u_i , u_r , u_t be, respectively, the amplitudes of the vertical motion associated with the incident, the transmitted, and the reflected Rayleigh waves. The authors define the transmission coefficient $A_t = u_t/u_0$ and the reflection coefficient $A_r = u_r/u_0$. Calculation of A_t and A_r is a classical problem in elastodynamics and has been studied extensively. Yet this canonical problem has, to date, defied an exact solution. A partial compendium of the results available in the literature is presented. Evidently there is substantial disagreement amongst the theoretically, the numerically, and the experimentally produced results. This provided the motivation for carrying out the present experiments. The authors have measured A_t and A_r accurate to about 3%. These are found to be in very good agreement with some of the most recent numerical and analytical results. (13 refs.)

113345 Energy balance equations describing point sources of elastic waves in a continuously varying medium. A.P.Kiselev (Rudgeofizika Sci. & Industrial Union, Leningrad, USSR).

Sov. Phys.-Tech. Phys. (USA), vol.28, no.2, p.139-42 (Feb. 1983). Translation of: *Zh. Tekh. Fiz. (USSR)*, vol.53, no.2, p.224-9 (Feb. 1983). [received: Sept. 1983]

The energy distribution of longitudinal and transverse high-frequency modulated oscillations is studied. The oscillations are excited by various types of fixed point sources, and problems involving a localized force, a center of expansion and a center of rotation are examined. Transverse wave excitation when an expansion center is present and longitudinal wave excitation when a rotation center is present are second-order effects. (7 refs.)

113346 Propagation of elastic-plastic compression-shear waves in materials having delayed yield. N.Zh.Zhubaev, A.Ya.Sinyayev, N.P.Stepanenko (Inst. of Seismology, Acad. of Sci., Alma-Ata, Kazakh SSR).

Sov. Appl. Mech. (USA), vol.19, no.1, p.63-8 (Jan. 1983). Translation of: *Prikl. Mekh. (USSR)*, vol.19, no.1, p.76-81 (Jan. 1983). [received: Sept. 1983]

The effect of yield delay refers to phenomena of hereditary type. The true dynamic yield stress, corresponding to an infinitely large strain rate, and the lower yield stress, attained after elastic unloading, are determined from theory. In the present study, where biaxial dynamic loading is considered, the instantaneous and lower yield surfaces are determined from experimental data obtained from uniaxial dynamic extension of thin rods. (5 refs.)

113347 Nonlinear oscillations of weakly asymmetric elastic systems with several degrees of freedom. L.N.Pokrovskii (Moscow Evening Metall. Inst., Moscow, USSR).

Sov. Appl. Mech. (USA), vol.19, no.1, p.85-91 (Jan. 1983). Translation of: *Prikl. Mekh. (USSR)*, vol.19, no.1, p.101-8 (Jan. 1983). [received: Sept. 1983]

By asymmetric elastic systems the author means constructions of the type of sloping shells and membranes, sloping arches and flexible filaments, sloping guying systems, etc. The nonlinear oscillations of these systems is described by a system of coupled differential equations. A solution to the differential equation (under certain conditions) is obtained without restricting the number of the generalized coordinates considered. A definite relation is established between the oscillations of the asymmetric and the corresponding symmetric systems and an estimate given of the connectedness of the generalized coordinates on the frequencies and the amplitudes of the oscillations. The results obtained are based on asymptotic methods of the theory of nonlinear oscillations. (10 refs.)

113348 Rayleigh wave excitation by pulses of penetrating radiation at the free surface of a homogeneous and isotropic solid half-space. L.M.Lyamshev, B.I.Chelnokov.

Sov. Tech. Phys. Lett. (USA), vol.8, no.11, p.585-6 (Nov. 1982). Translation of: *Pis'ma v Zh. Tekh. Fiz. (USSR)*, vol.8, no.21-22, p.1361-5 (Nov. 1982). [received: Sept. 1983]

The absorption of various types of penetrating radiation (laser pulses or particle beams from accelerators, for example) in a solid gives rise to acoustic waves. At moderate levels of the energy deposited in the medium, a thermal mechanism plays a dominant role: the sound waves are excited by the thermal expansion of the solid. In addition to the longitudinal and transverse sound waves in a solid, a Rayleigh wave is excited at the free boundary of the solid. It decays more slowly with distance than do waves in the volume. (4 refs.)

On differential equations of nonlocal elasticity and solutions of screw dislocation and surface waves See Entry 111445

Propagation reflection and transmission of waves under initial shear stresses See Entry 111452

RF-transducer for mechanical vibration See Entry 111661

Analysis of the elastic field of ultrasonic waves scattered by a cylindrical cavity See Entry 113172

Complexity of string vibration estimated from a concept of entropy See Entry 113189

Noncontact measurement of vibrating membrane and plate parameters See Entry 113190

Elastic response to a time-harmonic torsion-force acting on a bore surface See Entry 113280

Dynamic response of orthotropic curved bridge decks due to moving loads See Entry 113293

Approximate representation of the equations of viscoelasticity for vibrations with variable amplitude See Entry 113324

Shear crack extension through an incident influence See Entry 113370

A new method for the direct measurement of EOS—the improvement of an EMV gauge See Entry 113380

Dynamic analysis of dislocation generation due to sudden indentation See Entry 113912

On the measurement of Young's modulus of tubes by propagation of longitudinal waves See Entry 115236

46.30N Fracture mechanics, fatigue, and cracks

113349 Volume, surface and interface fracture statistics of brittle materials under flexure. P.Kittel (Inst. de Investigaciones y Ensayos de Materiales, Univ. de Chile, Santiago, Chile).

Res Mech. (GB), vol.9, no.2, p.73-86 (1983).

Fracture of brittle materials under flexure with isolated volume, surface and interface flaws is analyzed in order to obtain the specific Weibull risk function for any of these defects. A special composite, corresponding to a reinforced concrete beam, is theoretically studied in order to predict the local and cumulative fracture probability. (6 refs.)

113350 Green's function solution and applications for cracks emanating from a circular hole in an infinite sheet. V.Shivakumar (Lockheed-EMSCO, Houston, TX, USA), R.G.Forman, R.Rosenclanz, Jr..

Res Mech. (GB), vol.9, no.2, p.87-104 (1983).

Stress-intensity factors are obtained for point loaded equal length cracks emanating from a circular hole in an infinite plate. A series approach and the Muskhelishvili formulation in the two-dimensional theory of elasticity are used to derive the solution. The applicability of the solution is demonstrated by using it as a Green's function to obtain stress-intensity factors in the case of (1) biaxial tension and pure shear of an infinite plate and (2) tension and pin loading of a plate with cracks emanating from one hole in a row of holes. (16 refs.)

113351 Determination of stress-intensity factors for cracks in tubes under torsion. L.S.Srinath, N.Srinivasa Murthy, T.V.Hareesh (Dept. of Mech. Engng., Indian Inst. of Sci., Bangalore, India).

Exp. Mech. (USA), vol.23, no.3, p.262-7 (Sept. 1983).

An experimental investigation by two-dimensional photoelastic technique is carried out to study the stress distribution and to determine the stress-intensity factors for arbitrarily oriented cracks in thin cylindrical shells subjected to torsion. A new method is employed to evaluate the pure and mixed-mode SIFs. (7 refs.)

113352 Influence of late-breaking ligaments on crack propagation in compact specimens—a photoelastic study. A.Shukla (Dept. of Mech. Engng. & Appl. Mech., Univ. of Rhode Island, Kingston, RI, USA), J.W.Dally.

Exp. Mech. (USA), vol.23, no.3, p.298-303 (Sept. 1983).

Dynamic photoelasticity and high-speed photography were utilized to study the influence of tough ligaments on crack propagation in compact specimens.

The data obtained during the fracture experiments were analyzed to obtain crack velocity, instantaneous stress-intensity factor and the energy losses away from the crack tip. The results showed that the ligaments can behave as crack arrestors or decelerators. The crack if not arrested at the ligament slowly tunnels in between the ligaments without immediately rupturing them. The ligaments also tend to increase damping losses in the specimens. (8 refs.)

113353 A finite element analysis of a crack growing under cyclic loading. S.Wastberg (Dept. of Strength of Materials & Solid Mech., Royal Inst. of Technol., Stockholm, Sweden).

Fatigue Eng. Mater. & Struct. (GB), vol.6, no.2, p.149-58 (1983).

Crack growth under cyclic loading has been studied by the finite element method. The calculation was made for plane stress conditions. The crack tip zone was modelled as a cohesive zone. The displacement of the free crack surface during unloading was found to be governed by the surrounding continuum and was independent of the details in the fracture zone. This means that crack closure upon unloading is directly related to the ultimate separation, of the cohesive zone, which in turn controls the residual plastic deformation left in the wake of the growing crack. If the distance over which closure takes place is rather small, closure may be very difficult to detect by the compliance technique. (23 refs.)

113354 A crack-tip-zone interaction model for creep-fatigue crack growth. C.E.Jaske (Phys. Metall. Section, Battelle Columbus Labs., Columbus, OH, USA).

Fatigue Eng. Mater. & Struct. (GB), vol.6, no.2, p.159-66 (1983).

A crack-tip-zone interaction model for creep-fatigue crack growth is proposed. The basic details of the model are described. Experimental evidence in support of this model is presented. Existing data on creep-fatigue crack growth interaction agree qualitatively with the model. Some quantitative evidence for the model is presented. (10 refs.)

113355 Geometrically non-linear eccentrically compressed columns of uniform creep strength vs optimal columns. W.Swisterski, A.Wroblewski, M.Zyczkowski (Inst. of Mech. & Machine Design, Tech. Univ. of Cracow, Cracow, Poland).

Int. J. Non-Linear Mech. (GB), vol.18, no.4, p.287-96 (1983).

Optimality of geometrically non-linear eccentrically compressed columns of uniform strength in creep conditions is investigated. A third-order theory with stretchability of axis taken into account is employed. Norton's non-linear creep law and Kachanov's hypothesis (1958) of brittle creep rupture is used and an I -column of uniform strength for a given life-time is numerically evaluated. Then this column is found to be non-optimal and a further parametrical optimization is performed under the constraint of constant volume of the column. The life-time of the optimal column is considerably increased. (26 refs.)

113356 The elastostatic axisymmetric problem of a sphere containing a penny-shaped crack in a nonequatorial plane. R.Kant (Magnetic Recording Inst., IBM Corp., San Jose, CA, USA).

Int. J. Eng. Sci. (GB), vol.21, no.11, p.1321-6 (1983).

The axisymmetric problem of a sphere containing a penny-shaped crack in a nonequatorial plane is solved with the use of Boussinesq stress functions. Two coordinate systems—oblate spheroidal for representing the crack surface and spherical polars for the spherical surface, translated along the z -axis with respect to each other—are used to satisfy boundary conditions. Integral representations and transformations of harmonic functions are used to relate stress functions in the two coordinate systems. This procedure leads to a system of algebraic equations which is solved, for axisymmetric tractions on both the surfaces. Graphical results are presented for a specific loading case. (4 refs.)

113357 A path-independent integral for 2-dimensional cracks in homogeneous isotropic conductive plate. M.Saka, H.Abe (Dept. of Mech. Engng., Tohoku Univ., Sendai, Japan).

Int. J. Eng. Sci. (GB), vol.21, no.12, p.1451-7 (1983).

A path-independent integral which is denoted by J_e is introduced for the 2-dimensional crack problems in the homogeneous isotropic conductor in which the steady current flows. By utilizing the J_e -integral the distributions of the electric potential, current density and the Joule heating rate near the crack tip are derived. It is shown that the J_e -integral provides a parameter which dominates the distributions of the electric potential and current density near the crack tip as the square of the amplitude. (9 refs.)

113358 Longitudinal shear of an anisotropic body with a sharp-ended anisotropic inclusion. L.T.Berezhnitskii, I.T.Denisyuk (G.V. Karpenko Physicochem. Inst., Acad. of Sci., Lvov, Ukrainian SSR).

Sov. Mater. Sci. (USA), vol.18, no.6, p.508-14 (Nov.-Dec. 1982). Translation of: *Fiz.-Khim. Mekh. Mater. (USSR)*, vol.18, no.6, p.58-66 (Nov.-Dec. 1982).

Considers an anisotropic body containing a sealed-in anisotropic elastic foreign inclusion and subjected to antiplane deformation. The contour of the defect has cusps and the dimensions of the inclusion are small in comparison with the external dimensions of the cylindrical body. It is assumed that such a composite has at each point a plane of elastic symmetry normal to the generatrix of the cylinder. (7 refs.)

113359 Fracture criteria under creep conditions. R.A.Arutyunyan.

Strength Mater. (USA), vol.14, no.9, p.1205-9 (Sept. 1982). Translation of: *Probl. Prochn. (USSR)*, vol.14, no.9, p.42-5 (Sept. 1982).

The author uses well known empirical data to concretise the functions and parameters which enter into the proposed fracture criterion. It is shown that this criterion effectively describes experimental fracture curves, embracing both the ductile and brittle fracture sections. The case of a cylindrical rod subjected to tension is used to develop the criterion. (18 refs.)

113360 Calculation of the static crack propagation trajectory. M.P.Savruk, P.N.Osiv (Physicochem. Inst., Acad. of Sci., Lvov, Ukrainian SSR).

Strength Mater. (USA), vol.14, no.11, p.1443-7 (Nov. 1982). Translation of: *Probl. Prochn. (USSR)*, vol.14, no.11, p.19-23 (Nov. 1982). [received: Sept. 1983]

The problems linked with the determination of trajectories of quasistatic crack growth in brittle plates are solved by a method of singular integral equations, which is extensively used in determining the stress-strain crack-bearing bodies. (13 refs.)

113361 Fracture toughness of high-strength layered plates containing plastic interlayers with a high elastic modulus. E.N.Rudnitskii, P.G.Miklyayev, D.A.Andreev.

Strength Mater. (USA), vol.14, no.11, p.1448-50 (Nov. 1982). Translation of: *Probl. Prochn. (USSR)*, vol.14, no.11, p.23-5 (Nov. 1982). [received: Sept. 1983]

General postulates of linear fracture mechanics are used to examine the laws governing the increase in fracture toughness under plane-stress conditions during the propagation of a through crack in relation to the content of the high-modulus plastic component. This component is introduced in the form of a single intermediate layer located in the center of the cross section of the composite. The increase in fracture toughness realized by increasing the elas-

tic modulus of the interlayer was found to be quite insubstantial. The major increases in fracture toughness were realized as a result of the high fracture toughness of the material of the plastic interlayer during its joint work with other layers in the composite. (4 refs.)

113362 Contour J-integral in the plastic region. Yu.G.Matvienko, V.Yu.Gol'tsev (Moscow Engng. Phys. Inst., Moscow, USSR). *Strength Mater. (USA)*, vol.14, no.11, p.1451-5 (Nov. 1982). Translation of: *Probl. Prochn. (USSR)*, vol.14, no.11, p.25-9 (Nov. 1982). [received: Sept. 1983]

The method of dividing grids was used to study the contour invariance of the J-integral and the possibility of using it as a fracture-resistance characteristic in the case of developed plastic flow at a crack tip under plane-stress conditions. Flat specimens 300×700 mm with a central notch, made of aluminum alloy AMtsM and stainless steel 1Kh18N9T, were tested in tension. It is concluded that the contour J-integral is roughly invariant in the small region of plastic strain at the crack tip outside the strain localization zone and that the integration contour affects the value of J with increasing distance of the contour from this zone. To apply the results obtained on specimens to the condition of general plastic yielding in structural elements, it is best to take as the J-integral mean values of same calculated over contours which pass along the boundaries of the localized zone. (14 refs.)

113363 Plastic bands at the tip of a linear rigid inclusion. L.T.Berezhnitskii, N.M.Kundrat (Physicomech. Inst., Acad. of Sci., Lvov, Ukrainian SSR). *Strength Mater. (USA)*, vol.14, no.11, p.1502-5 (Nov. 1982). Translation of: *Probl. Prochn. (USSR)*, vol.14, no.11, p.66-9 (Nov. 1982). [received: Sept. 1983]

Examines an infinite isotropic body under conditions of plane strain in the system of polar coordinates r, θ , and containing a semi-infinite rigid laminar inclusion which is considered infinitesimally thin. The material of the body (matrix) is ideally elastoplastic and satisfies the Tresca-St. Venant yield condition. It assumed that the plastic deformations are concentrated along narrow straight slip bands emerging from the end of the inclusion. These bands are simulated by transverse shear cracks. The external load is assumed to be symmetrical about the line along which the inclusion extends. It is taken that there are two slip bands; arranged symmetrically about the plane of the inclusion and make with its prolongation the angle α . (9 refs.)

113364 Examination of the stress state of a helically reinforced composite in shearing. G.E.Freger (Voroshilovgrad Engng. Inst., Voroshilovgrad, USSR).

Strength Mater. (USA), vol.14, no.11, p.1564-8 (Nov. 1982). Translation of: *Probl. Prochn. (USSR)*, vol.14, no.11, p.116-19 (Nov. 1982). [received: Sept. 1983]

Attention is given to the stress state of a helically reinforced composite with an auxiliary layer consisting of two sections with different physicomechanical properties. The model of a unidirectional reinforced material with a small amount of filling subjected to transverse shearing is examined. It is assumed that the cross section of the main reinforcement is circular, the properties of the main reinforcement in the examined section are isotropic in the transverse direction, and the main reinforcement is encircled by the auxiliary layer consisting of two parts whose material is assumed to be homogeneous and isotropic. When a shear load is applied to the matrix, a plane strain state will form in the system. The problem is solved using Kolosol-Muskhelishvili complex potentials. (5 refs.)

113365 Continuum theory of fracture in the compression of composite materials with a metallic matrix. A.N.Guz' (Inst. of Mech., Acad. of Sci., Kiev, Ukrainian SSR).

Sov. Appl. Mech. (USA), vol.18, no.12, p.1045-53 (Dec. 1982). Translation of: *Prikl. Mekh. (USSR)*, vol.18, no.12, p.3-11 (Dec. 1982). [received: Sept. 1983]

Examines within the framework of the continuum theory of fracture, the following questions relating to the compression of composite materials with a metallic matrix: formulation of the basic relations with a more rigorous evaluation of the corrected transverse-shear modulus, corresponding to the two-sided estimate of Hashin-Shtrikman; determination of theoretical values of the limiting contraction (fracture strain) and ultimate strength with allowance for the elastic-plastic stage of deformation of the filler and binder, with the derivation of approximate expressions for these quantities with allowance for the zeroth and first approximations; analysis of numerical results obtained with allowance for the zeroth and first approximations and their comparison with experimental results. (8 refs.)

113366 Problem of a crack in an orthotropic strip. B.Rogovskii (Polytech. Inst., Lodz, Poland).

Sov. Appl. Mech. (USA), vol.18, no.12, p.1101-8 (Dec. 1982). Translation of: *Prikl. Mekh. (USSR)*, vol.18, no.12, p.64-71 (Dec. 1982). [received: Sept. 1983]

Solves the problem of a crack in an orthotropic strip with elastically supported edges. The results are used to analyze the effect of reinforcement anisotropy and boundary conditions on characteristic physical quantities for two types of composite materials. (7 refs.)

113367 Energy criteria for the brittle fracture of composite materials with initial stresses. A.N.Guz' (Mech. Inst., Acad. of Sci., Kiev, Ukrainian SSR).

Sov. Appl. Mech. (USA), vol.19, no.1, p.1-6 (Jan. 1983). Translation of: *Prikl. Mekh. (USSR)*, vol.19, no.1, p.3-9 (Jan. 1983). [received: Sept. 1983]

Considers the case in which the minimum dimensions of the crack are substantially larger than the dimensions of the structural elements of the composite materials, not investigating fracture processes in which the properties of the piecewise-homogeneous-medium model appear (for example, fracture at the interface between two media, etc.). For the indicated assumptions, the composite material can be simulated (for problems in the mechanics of brittle fracture) by an orthotropic linearly elastic body with reduced constants; for numerical investigations one can take account of one of the main features of composite materials: their low shear rigidity. The investigation is carried out in Cartesian coordinates of the initial deformed state; a variant of a previous theory, when the initial state is determined by the geometrically linear theory and the initial deformations are small, is used. (25 refs.)

113368 Partially contacting crack in a plate with an elliptic hole. M.G.Krivtsov (Inst. for Appl. Problems of Mech. & Math., Acad. of Sci., Lvov, Ukrainian SSR).

Sov. Appl. Mech. (USA), vol.19, no.1, p.48-55 (Jan. 1983). Translation of: *Prikl. Mekh. (USSR)*, vol.19, no.1, p.59-66 (Jan. 1983). [received: Sept. 1983]

A method for solving stationary problems of thermoelasticity for a plane with curvilinear holes and cracks, under the assumption that the edges of the crack are not in contact in the process of the deformation, is well known. However, when solving problems in this formation, it is possible that the discontinuity of the normal displacements has a negative value on certain parts of the crack. Consequently, on these parts it is possible to have contact between the edges of the crack, whose presence may affect essentially the magnitude of the intensity of the stresses in the noncontacting vertices of the crack. On the

example of the plane with an elliptic hole, the author shows the method of solving thermoelasticity problems, considering a smooth contact of the edges of a rectilinear crack. (5 refs.)

113369 The state of stress and strain at the point of accumulation of collinear cracks. S.A.Nazarov.

Vestn. Leningr. Univ. Ser. Mat. Mekh. & Astron. (USSR), no.3, p.63-8 (July 1983). In Russian.

The state of stress and strain caused by an infinite system of cracks on a beam which accumulate towards one point is investigated. On a logarithmic scale the cracks are supposed to be arranged periodically. (10 refs.)

113370 Shear crack extension through an incident influence. Lim Chee-seng (Nat. Univ. of Singapore, Singapore).

Z. Angew. Math. & Mech. (Germany), vol.63, no.8, p.349-58 (1983).

SH motion is triggered by the nonuniform extension of a crack under an applied, general body force. The net incident force-field along the fault plane converts into an incident influence which plays an important role in the source mechanism. With subsonic extension, fault plane perturbations ahead of a foremost crack-emitted wavefront, naturally originate entirely at the applied force. Nonetheless, they contribute to the incident influence everywhere behind such a wavefront. For a trailing mode of reception preceding the crack, repeated inversion of a governing inhomogeneous integral equation yields a displacement gradient that behaves singularly near the advancing crack edge. On invoking a Barenblatt type criterion, this singularity gets eliminated, essentially, because of the incident influence. A nonlinear integral equation governing that particular crack edge results. Another nonlinear integral equation can be formulated for an arrested advance. Besides the desingularized displacement gradient derived outside the crack, the displacement difference across the crack faces is also determined. A vital question throughout concerns the availability of bounded quantities. (31 refs.)

113371 Finite element model simulation of creep crack growth in low-ductility material. A.Nitta, K.Kuwabara, T.Kitamura.

Report E281005, Central Res. Inst. Electr. Power Ind., Tokyo, Japan (Jan. 1982), 48 pp.

The finite element method was applied to the simulation of creep crack growth (CCG) in a center cracked plate, and single and double edge cracked specimens for the purpose of discussion on a fracture mechanics parameter controlling the rate of CCG under small scale yielding (where a creep zone ahead of a crack tip is much smaller than the surrounding elastic region) and extensive creep conditions. As a result, it was recognized that the small scale yielding condition in creep was satisfied in case of fracture strain of the order of 0.001. The correlation of CCG rate with the elastic stress intensity factor, K, was found to depend on the specimen geometry, although K could be a good parameter individually for each specimen geometry under the small scale yielding condition. On the other hand it was found that the so-called C* parameter based on the concept of nonlinear fracture mechanics was a CCG controlling parameter for the small scale yielding condition as well as under the extensive creep condition. (56 refs.)

113372 Definition of interphase in composites. P.S.Theocaris (Dept. of Mech., Nat. Tech. Univ., Athens, Greece).

Role of the Polymeric Matrix in the Processing and Structural Properties of Composite Materials. Proceedings of a Joint US-Italy Symposium, Capri, Italy, 15-19 June 1981 (New York, USA: Plenum 1983), p.481-502. The role of the boundary interphase on the determination of crack propagation, as well as the thermomechanical behaviour of composite materials, was investigated. Theoretical models taking into account the presence of a third phase, surrounding each one of the inclusions are presented, and the influence of a large number of parameters on the modes of fracture of composite materials was studied. It is shown that the method of caustics is an experimental method suitable in determining the crack-propagation behavior of composites. (19 refs.)

Singular problems in the theory of stress-assisted diffusion ...See Entry 111616

Two problems with mixed boundary conditions for an incompressible isotropic hyperelastic materialSee Entry 113274

Variation of stress resultants in concrete structures due to time-dependent creep and shrinkage strains of concreteSee Entry 113295

The micropolar thermoelastic problem of uniform heat-flow interrupted by an insulated penny-shaped crackSee Entry 113301

Crack transient torsional wave interaction in an elastic bi-materialSee Entry 113342

An edge-cracked mode II fracture specimenSee Entry 113381

Effect of side-grooves on fatigue crack retardationSee Entry 113387

The transition from an emitting to a cleaving crackSee Entry 114084

Dislocation emission from cracks in the presence of liquids ..See Entry 114085

Evaluating the durability of materials on the basis of thermal fluctuation theorySee Entry 114087

Deformation and fracture of a material in plane stress under complex loadingSee Entry 114088

Analysis of process stresses in two-layer SiC-Si disksSee Entry 115246

A stress transfer model for the deformation and failure of polymeric matrices under swelling conditionsSee Entry 115292

Stress and strength analysis in and around composite inclusions in polymer matricesSee Entry 115297

Mixed-mode fracture mechanisms near the fatigue threshold of AISI 316 stainless steelSee Entry 115310

Mixed-mode crack opening in fatigueSee Entry 115320

Crack propagation in titanium alloys in a hydrogen atmosphere under constant loadSee Entry 115336

Subcritical crack growth in brittle materials in microcracking conditionsSee Entry 115343

Fracture mechanics of syntactic foam compositesSee Entry 115350

The K_{Ic} values of silicon nitride and zirconia obtained by micro-crack indentation method and single-edge notched beam methodSee Entry 115355

46.30P Friction, wear, adherence, hardness, mechanical contacts

113373 Analysis of contact problems with friction under oscillating loads. E.B.Pires (Techn. Univ. of Lisbon, Lisbon, Portugal), J.T.Oden.

Comput. Methods Appl. Mech. & Eng. (Netherlands), vol.39, no.3, p.337-62 (Sept. 1983).

The numerical analysis of a class of contact problems with friction is considered. The problems considered involve the contact of linearly elastic bodies on material surfaces on which nonclassical friction laws are assumed to hold.

The problems are two-dimensional (plane stress, plane strain, or axisymmetric deformations of bodies of revolution) and finite element methods are developed to study these problems. Two general types of problems are studied. First, the equilibrium problem of the contact of a linearly elastic body with a foundation is considered. The foundation can be rigid (i.e. the Signorini problem) or of a Winkler-type characterized by a distributed system of linear springs, and dry static friction forces are assumed to be developed on the contact surface. Second, a class of quasi-static contact problems is considered in which particular attention is given to modelling the evolution of stresses and deformations on the contact surface for various load histories, including slowly oscillating loads applied tangent to the contact surface. (18 refs.)

113374 The photoelastic-coating technique for plastic-elastic contact. H.Fessler (Dept. of Mech. Engng., Univ. of Nottingham, University Park, Nottingham, England), M.Eissa.

Exp. Mech. (USA), vol.23, no.3, p.282-8 (Sept. 1983).

Steel models coated with thin birefringent layers representing transverse sections through British-Standard-inch keyed shafts and hubs have been loaded in torsion. Models with two different steel shafts and clearance fits between key and keyways and between shaft and hub have been analyzed over a large range of torques. Large plastic strains occurred at six contact positions where there are discontinuities of profile and surface contact of the chamfered key or the shaft. Contact strains have been measured, corrected for shear lag and normalized. Plastic-elastic SCFs are lower than corresponding elastic values. (7 refs.)

113375 Observation of damage growth in compressively loaded laminates. H.Chai, W.G.Knauss, C.D.Babcock (California Inst. of Technol., Pasadena, CA, USA).

Exp. Mech. (USA), vol.23, no.3, p.329-37 (Sept. 1983).

An experimental program to determine the phenomenological aspects of composite-panel failure under simultaneous compressive in-plane loading and low-velocity transverse impact [0.75 m/s (0.250 ft/s)] is described. High-speed photography coupled with the shadow-moire technique is used to record the phenomenon of failure propagation. The information gained from these records, supplemented by plate sectioning and observation for interior damage, has provided information regarding the failure-propagation mechanism. The results show that the failure process can be divided roughly into two phases. In the first phase the plate is inspected, and the resulting response causes interlaminar separation. In the second phase the local damage spreads to the undamaged portion of the plate through a combination of laminae buckling and further delamination. (10 refs.)

113376 The interaction between a system of circular punches on a nonhomogeneous elastic half space. V.I.Fabrikant (Dept. of Mech. Engng., Concordia Univ., Montreal, Quebec, Canada), L.M.Keer.

Int. J. Mech. Sci. (GB), vol.25, no.7, p.513-18 (1983).

The present analysis considers an integral equation formulation for the problem of the indentation of a nonhomogeneous elastic half space by an arbitrary number of punches. The elastic half space is represented by a material whose deformation modulus varies with the depth according to a power law. An analytical solution is obtained subject to the approximation that the separation of the punches is large when compared with dimensions of the punches. (8 refs.)

113377 Torsional impact of a layer or a cylinder bonded to an elastic half-space. R.S.Dhaliwal, B.M.Singh, J.Vrbik (Dept. of Math. & Statistics, Univ. of Calgary, Alberta, Canada).

Int. J. Eng. Sci. (GB), vol.21, no.11, p.1397-408 (1983).

Considers two torsional impact problems. The first problem deals with the solution of a layer bonded to an elastic half-space when the layer is driven by the torsional impact over a bonded rigid circular disc. In the second problem sudden torsion by a rigid disc attached over the plane face of a circular cylinder is considered and the rest of the plane surface of the cylinder is stress free. The cylinder is bonded to the half-space, making use of Laplace and Hankel transforms the solution of each problem is reduced into Fredholm integral equations of the second kind. A numerical Laplace inversion technique is then used to recover the time dependence of the solution. The numerical values for the applied torque at the surface of the rigid disc are calculated for each problem and then are displayed graphically. (10 refs.)

113378 Movement of spheres on rotating discs—a new method to measure coefficients of rolling friction by the central drift. K.Weltner (Inst. für Didaktik der Phys., Univ. Frankfurt/Main, Frankfurt am Main, Germany).

Mech. Res. Commun. (GB), vol.10, no.4, p.223-32 (July-Aug. 1983).

A sphere freely rolling without slipping on a rotating platform moves on stable circular orbits with regard to the laboratory system. The center of the sphere may even rest at a given place while the sphere spins around. If a force parallel to the plane of the rotating disc acts on the sphere a drift movement results perpendicular to the force. In the case of rolling resistance a drift of the sphere to the center of rotation can be observed. This effect is used to measure coefficients of rolling friction. Furthermore with rotating cones and funnels there exist stable modes of movement on orbits around the cone or funnel. (5 refs.)

On the motion of a heavy homogeneous ellipsoid on a fixed horizontal plane See Entry 113266

On the regular precession of a body of revolution on a horizontal plane with friction See Entry 113267

Two problems with mixed boundary conditions for an incompressible isotropic hyperelastic material See Entry 113274

Contact problem for a two-layer aging viscoelastic foundation See Entry 113307

Elastic-plastic state of a coiled cylindrical shell loaded with internal pressure See Entry 113326

Mechanical and electromechanical behaviour of fibre brushes See Entry 115372

46.30R Measurement methods and techniques

(see also 07.10 Mechanical instruments and techniques, 81.70 Materials testing)

113379 Prevention of 'mottle' in an epoxy resin as a photoelasticity material. Feng Zhensheng (Inst. of Engng. Mech., Acad. Sinica, Peking, China).

Acta Mech. Sin. (China), no.3, p.278-85 (1983). In Chinese.

The cause of 'mottle' in an epoxy resin material for photoelasticity is investigated. Several effective methods are presented to avoiding it. These methods amount eventually to the introduction of complex groups in the molecular-chain to break its systematic nature, an increase in internal friction and the prevention of the occurrence of microliths or conglomerate microliths in the casting caused by molecular-chain disposal due to stress. (18 refs.)

113380 A new method for the direct measurement of EOS—the improvement of an EMV gauge. Liang Yunmin (Peking Inst. of Technol., Peking, China).

Acta Mech. Sin. (China), no.3, p.298-300 (1983). In Chinese.

The author has developed an in-situ electro-magnetic velocity gauge system for measuring both the velocity of a shock wave and the velocity of particles at the same place insulate material, directly. Two normal velocity gauges were welded in series, each sensitive arm was inserted in a different plane perpendicular to the direction of shock wave. It simplified the method for measuring the shock relations. Data was obtained from a PMMA plate. (3 refs.)

113381 An edge-cracked mode II fracture specimen. L.Banks-Sills, M.Arcan (Dept. of Solid Mech., Materials & Structures, Tel-Aviv Univ., Ramat-Aviv, Israel).

Exp. Mech. (USA), vol.23, no.3, p.257-61 (Sept. 1983).

A proposed edge-cracked Mode II fracture specimen is analyzed using an extended photoelastic-numerical procedure. It is shown that the Mode II stress-intensity factor is significantly higher for the longest edge-crack considered and the Mode I deformation is negligible, demonstrating the merits of this specimen for Mode II fracture-toughness testing. (12 refs.)

113382 Another method to separate principal strains in photoelastic coatings. P.J.Sevenhuijsen (Nat. Aerospace Lab., Amsterdam, Netherlands).

Exp. Mech. (USA), vol.23, no.3, p.268-9 (Sept. 1983).

It is shown that the combination of a prism and a reflection polariscope provided with a Babinet-Soleil compensator offers a simple practical solution to the problem of separation of the principal strains in photoelastic coatings. (2 refs.)

113383 Half-fringe photoelasticity: a new approach to whole-field stress analysis. A.S.Voloshin, C.P.Burger (Dept. of Engng. Sci. & Mech., Iowa State Univ., Ames, IA, USA).

Exp. Mech. (USA), vol.23, no.3, p.304-13 (Sept. 1983).

Presents a new method for whole-field stress analysis based on a symbiosis of two techniques—classical photoelasticity and modern digital image analysis. The resulting method is called 'half-fringe photoelasticity (HFP)'. Classical photoelasticity demands materials with high birefringence which leads to extensive use of plastics as model materials. Since the behavior of these materials is often different from that of the prototype materials, their use distorts the similitude relationships. In many contemporary problems this distortion is untenable. HFP offers a way of this dilemma. It permits materials and loads to be chosen so that no more than one half of a fringe order appears in the area of interest. Thus, for example, glass, which behaves linearly up to high stress levels and over a wide range of temperatures, could be used as model material. Alternatively, models from polymeric materials could be used under very low load in order to stay within the linear part of the stress strain diagram and to prevent large deformations. The half-fringe-photoelasticity system, which is described here, utilizes the resulting low levels of birefringence for effective stress analysis. (8 refs.)

113384 Nonlinear photoviscoelasticity: theory and measurement. A.Tougui (Univ. Cadi-Ayyad, Marrakech, Morocco), D.Gamby, A.Lagarde, H.F.Brinson.

Exp. Mech. (USA), vol.23, no.3, p.314-21 (Sept. 1983).

Photoviscoelasticity and photoplasticity concepts are reviewed and differences and similarities are discussed. The suggestion is made that a better understanding of nonlinear-time-varying birefringence enhances the utilization of polymeric materials for photoplasticity studies. A mathematical model for nonlinear photoviscoelasticity is presented. Measurements of optical creep and creep recovery are given and comparisons between theory and experiments are made and discussed. (29 refs.)

113385 A noncontacting system for measuring effective stress-strain curves of ultra-thin X-ray-mask materials. T.D.Dudderar, L.R.Thibault (Bell Labs., Murray Hill, NJ, USA).

Exp. Mech. (USA), vol.23, no.3, p.322-8 (Sept. 1983).

A noncontacting test system has been developed for making measurements of the deformation characteristics of the ultra-thin (~10 μm) membrane structures of X-ray masks using a pneumatic bulge test. These measurements, which include the bulge height and radius-of-curvature at the pole, are then analyzed to provide composite estimates of the effective stress and effective strain of the mask membrane materials. (5 refs.)

113386 A technique for cyclic-plastic notch-strain measurements. M.W.Guillot (Engng. Dept., Ethyl Corp., Baton Rouge, LA, USA), W.N.Sharpe, Jr.

Exp. Mech. (USA), vol.23, no.3, p.354-60 (Sept. 1983).

The interferometric strain/displacement gage was used to measure local strains of approximately ± 1 percent strain near a central notch in specimens undergoing completely reversed loading. Two notch geometries were tested: a circular hole and a keyhole slot with theoretical stress-concentration factors of 3.1 and 5.9 respectively. Measurements were made at both room and elevated temperatures (149° and 260°C) on three materials having different cyclic properties. The authors describe the experimental techniques for making the notch-strain measurements. The results of this series of tests are used in evaluating Neuber's cyclic rule. (15 refs.)

113387 Effect of side-grooves on fatigue crack retardation. J.P.Hess, A.F.Grandt, Jr., A.Dumanis (School of Aeronaut., Purdue Univ., West Lafayette, IN, USA).

Fatigue Eng. Mater. & Struct. (GB), vol.6, no.2, p.189-99 (1983).

Describes results of an experimental program conducted to determine the influence of deep side-grooves on fatigue crack retardation. The results indicate that side-grooves significantly reduce the delay in fatigue crack growth caused by single peak overloads. It is suggested that the decreased retardation is due to simulation of plane strain conditions in the 'thin' test sections by the stress field at the root of the side-groove. (24 refs.)

113388 Influence of thickness and temperature on stretched zone size in J_{IC} tests. C.M.Gilmore (Dept. of Civil, Mech. & Environmental Engng., George Washington Univ., Washington, DC, USA), V.Provenzano, F.A.Smidt, Jr., J.R.Hawthorne.

Met. Sci. (GB), vol.17, no.4, p.177-85 (April 1983). [received: Sept. 1983]

The nature of the microscopic processes occurring at the crack tip during crack initiation and the early stages of propagation were investigated by detailed characterisation of the stretched zone in J integral specimens of two thicknesses tested at two different temperatures. The J integral tests were conducted on HT-9, a martensitic stainless steel, using the single specimen compliance method. The topography of the crack tip region was mapped by detailed stereographic measurements on scanning electron micrographs of the region containing the stretched zone. The measured J_{IC} values and the stretched zone dimensions for each test condition were then compared using the relationship of Knott: $J_{IC} = m\sigma_0\delta_c$, where m is a constraint factor, σ_0 is the flow stress, and δ_c is the crack opening displacement taken as twice the stretched zone height. Theory predicts values of m of about 2 for specimens

under plane strain conditions and lower values of m for thin specimens under plane stress conditions. The current experiments showed good agreement with theory for the thicker specimens but larger values of m , near 6.0, for the thin specimens. A rationale for this lack of agreement and an analysis of the crack tip deformation processes are presented. (17 refs.)

113389 Device for measuring the loss factor of insulating materials. D.Schmitz. *Plaste & Kautsch. (Germany)*, vol.30, no.7, p.408-12 (July 1983). In German. The electromagnetically induced vibrations of metal strips of 1 mm thickness were examined when they had been coated with an insulating lacquer. The strips were clamped at one end. They had been cut from sheet along the direction of rolling. Care was taken to grind the edges of the strips and to make them of uniform width. The loss factor was determined by the resonance method. (10 refs.) R.S.

113390 Design of an experiment to determine deformations using holographic interferometry. V.S.Pisarev, V.V.Yakovlev, V.O.Indisov, V.P.Shechepinov (Engng.-Phys. Inst., Moscow, USSR). *Sov. Phys.-Tech. Phys. (USA)*, vol.28, no.2, p.179-84 (Feb. 1983). Translation of: *Zh. Tekh. Fiz. (USSR)*, vol.53, no.2, p.292-300 (Feb. 1983). [received: Sept. 1983]

The design of an experiment is considered in which holographic interferometry is used to determine displacements produced by deformation. The technique uses the C -optimality criterion and is suitable for all types of holographic interference patterns whose analysis involves solving a system of linear algebraic equations. It is shown that C -optimal designs can be obtained by estimating the magnitude of the error vector for the solution of the system of equations for the scaled sensitivity matrix if the absolute fringe orders are known. The practical use of optimally designed interferometers is illustrated by calculating the surface deformation of a cylindrical shell containing a round hole when the shell is loaded by an internal pressure. (31 refs.)

113391 Thermoelectric method for studying stresses in plates weakened by holes. V.Ya.Bash (Inst. of Mech., Acad. of Sci., Kiev, Ukrainian SSR). *Strength Mater. (USA)*, vol.14, no.11, p.1506-8 (Nov. 1982). Translation of: *Probl. Prochn. (USSR)*, vol.14, no.11, p.69-72 (Nov. 1982). [received: Sept. 1983]

Results are presented of using a thermoelectric method, which is based on the mechanism of change in solid body temperature during its active deformation, for studying stresses in the area of an active concentrator in the form of a hole in thin plates. The results obtained are compared with elasticity theory data. (6 refs.)

RF-transducer for mechanical vibration See Entry 111661

Sensors using strain gages See Entry 111669

Noncontact measurement of vibrating membrane and plate parameters See Entry 113190

Determination of stress-intensity factors for cracks in tubes under torsion See Entry 113351

Influence of late-breaking ligaments on crack propagation in compact specimens—a photoelastic study See Entry 113352

The photoelastic-coating technique for plastic-elastic contact See Entry 113374

Strain modulation measurements of stiffening effects in carbon fibers See Entry 115242

Prediction of stress relaxation and stress relief cracking in SEN testpieces See Entry 115327

The K_{Ic} values of silicon nitride and zirconia obtained by micro-crack indentation method and single-edge notched beam method See Entry 115355

Specimen size dependence of low frequency fatigue tests in high-pressure hydrogen See Entry 115460

Stress activated Raman scattering and microcrack detection See Entry 115461

An analytical description of fatigue failure curves by portions See Entry 115466

Plotting stress-strain diagrams by recalculation of the computer diagram See Entry 115477

Determination of certain elastic characteristics of materials with the use of parabolic interpolation of strain curves See Entry 115478

Changes in the strain energy and the surface structure generated during the rotatory bending fatigue test for smooth and notched carbon steel specimens See Entry 115491

A high accuracy micro hardness tester See Entry 115497

An analytical description of fatigue failure curves by portions See Entry 115466

Plotting stress-strain diagrams by recalculation of the computer diagram See Entry 115477

Determination of certain elastic characteristics of materials with the use of parabolic interpolation of strain curves See Entry 115478

Changes in the strain energy and the surface structure generated during the rotatory bending fatigue test for smooth and notched carbon steel specimens See Entry 115491

A high accuracy micro hardness tester See Entry 115497

46.60 RHEOLOGY OF FLUIDS AND PASTES

113392 Relation between the deformation of macromolecules and a polymer melt under uniaxial tension. V.E.Dreval, G.V.Vinogradov. *Vysokomol. Soedin. Ser. B (USSR)*, vol.25, no.6, p.448-50 (1983). In Russian.

The opinion expressed by the present authors and others in 1981 (G.V. Vinogradov et al., *Vysokomol. Soedin.*, vol.21, no.12, p.2627), according to which the maximum values of the high elastic deformation of polymer melts should approach the value of the deformation for the most straightened macromolecules is substantiated by a consideration of additional data. It is noted that the strength of materials obtained from amorphous or weakly crystalline polymers under conditions where $(l_e/l_0) = (l_e/l_0)_{max}$, where l is the final length of a specimen at the moment of rupture and l_0 is the length of the specimen rupture and deformational relaxation is much lower than that of materials from oriented easily crystallizing polymers. (9 refs.) N.S.

113393 Anomalous rheological behaviour of poly(vinyl alcohol) gels. M.Watake (Chem. Res. Lab., Faculty of Liberal Arts, Shizuoka Univ., Shizuoka, Japan), K.Nishinari. *Polym. Commun. (GB)*, vol.24, no.9, p.270-3 (Sept. 1983).

The rheological properties of poly(vinyl alcohol) gels, which were evacuated in a frozen state and then immersed in distilled water, have been investigated as a function of temperature, concentration and evacuation time. Dynamic Young's modules E' increased with an increase in concentration and evacuation time. The modulus increased up to a certain temperature and then began to decrease with any further increase in temperature. These behavioural characteristics were compared with those of agar-agar gels. (22 refs.)

113394 Oscillations generated in the compression of a viscoelastic body. G.I.Burde, T.M.Burde.

J. Appl. Mech. & Tech. Phys. (USA), vol.23, no.6, p.841-9 (Nov.-Dec. 1982). Translation of: *Zh. Prikl. Mekh. & Tekh. Fiz. (USSR)*, vol.23, no.6, p.114-23 (Nov.-Dec. 1982). [received: Sept. 1983]

It is shown that in deformations of compressible viscoelastic bodies another type of instability is possible, namely oscillations induced by the bulk elasticity of the material and driven up in hydrostatic compression of the sample as a result of inertial interaction of the disturbances with the main flow. The conditions for growth of the oscillations are determined from the linearized small-perturbation equations; on the basis of a nonlinear analysis, the nature of the excitation is investigated, and the amplitude of the oscillations is determined. Calculations are carried out for the case of uniform planar deformation and ideally smooth and rigid bounding surfaces. (9 refs.)

113395 Nonlinear viscoelasticity and the Cox-Merz relations for polymeric fluids. H.C.Booij, P.Lebians, J.Palmen, G.Tiemersma-Thoone (DSM, Central Res., Geleen, Netherlands).

J. Polym. Sci. Polym. Phys. Ed. (USA), vol.21, no.9, p.1703-11 (Sept. 1983). An investigation is made of the important class of fluids whose rheological properties are described by a quasilinear viscoelastic constitutive equation of the Boltzmann superposition type. The first Cox-Merz relation is closely approximated by such a fluid if its nonlinearity in shear can be described by the strain measure $S_{12}(\gamma) = \int_0^\gamma J_0(v)dv$, irrespective of the distribution of its relaxation times and, hence, its linear viscoelastic properties. Here γ equals the shear strain and J_0 the zeroth-order Bessel function. The second Cox-Merz relation is met by materials with a different nonlinearity, namely $S_{12}(\gamma) = Si(\gamma)$, where Si is the sine integral. Experimental data on melts of a polystyrene and a low-density polyethylene sample were utilized to demonstrate that both Cox-Merz relations cannot hold simultaneously. (18 refs.)

113396 Viscoelastic fluid flow exhibiting hysteretic phase changes. J.K.Hunter (Dept. of Maths., Colorado State Univ., Fort Collins, CO, USA), M.Slemrod.

Phys. Fluids (USA), vol.26, no.9, p.2345-51 (Sept. 1983).

In the present paper a mathematical theory is given for a viscoelastic fluid exhibiting a hysteresis loop in the shear stress versus shear rate plane. The main rheological idea is to introduce a constitutive equation of rate type whose steady shear stress versus shear rate locus is nonmonotone. The main mathematical idea is to use a local shock structure theory to pick out the admissible solutions in loading and unloading of the applied driving force. (21 refs.)

Polymer Alloys III Blends, Blocks, Grafts and Interpenetrating Networks.

Proceedings of a Symposium See Entry 111311

Contact problem for a two-layer aging viscoelastic foundation See Entry 113307

Domain stability during capillary flow of well dispersed two phase polymer blends. Polystyrene/polymethylmethacrylate blends See Entry 113727

Melt rheology of blends of semi-crystalline polymers. II. Dynamic properties of poly(ethylene terephthalate)-poly(amide-6,6) molten blends See Entry 114069

Viscoelastic properties of linear low density polyethylene melts See Entry 114234

Elongation rheology of polyolefins and its relation to processability See Entry 114237

Stationary configuration of fibers formed under nonisothermal conditions See Entry 115121

Melt compounding of PVC with ethylene copolymer resins ... See Entry 115159

47.00 FLUID DYNAMICS

(for fluid dynamics of quantum fluids, see 67.; for geophysical fluid dynamics, see 92.10; for astrophysical gas dynamics, see 95.30; for biological fluid dynamics, see 87.45)

47.10 GENERAL THEORY

(see also 03.40G Mathematical aspects)

113397 Applications of exponential splines in computational fluid dynamics. B.J.McCartin (Pratt & Whitney Aircraft, East Hartford, CT, USA).

AIAA J. (USA), vol.21, no.8, p.1059-65 (Aug. 1983).

Recurrent problems in the use of cubic spline interpolation are investigated. It is shown how to automatically resolve any difficulties that do arise, by the alternative use of exponential spline interpolation. Numerical examples of a general nature are presented first illustrating the inherent superiority of the exponential spline to the cubic spline. Attention is then focused on a variety of problems from computational fluid dynamics. The discussion culminates in the detailed exposition of a typical boundary-layer calculation. (17 refs.)

113398 Pseudospectral approximation in a three-dimensional Navier-Stokes code. K.C.Reddy (Arnold Engng., Dev. Center, Arnold Air Force Station, TN, USA).

AIAA J. (USA), vol.21, no.8, p.1208-10 (Aug. 1983).

Pseudospectral methods have the potential of yielding high accuracy for a given number of spatial nodes or collocation points in solving certain classes of partial-differential equations. Spectral and pseudospectral methods are formally infinite-order accurate, according to Gottlieb and Orszag (1977). For problems with periodic boundary conditions, Fourier spectral methods can be efficiently implemented to obtain highly accurate solutions. The author describes a solution scheme for three-dimensional Navier-Stokes equations using a pseudospectral approximation in one of the spatial directions. He considers the flow over a hemisphere cylinder at an angle of attack. The flow is three dimensional but has a plane of symmetry. (4 refs.)

113399 Estimates near the boundary of solutions in H_{loc}^1 of the Dirichlet problem. M.I.Hassan (Dept. of Math., King Abdulaziz Univ., Jeddah, Saudi Arabia).

Appl. Anal. (GB), vol.16, no.3, p.195-203 (1983).

Solutions in H_{loc}^1 of Dirichlet's problem for a linear second-order elliptic equation are considered. The nature of singularities which higher derivatives of such solutions may have near the boundary is investigated. (3 refs.)

113400 A geometric property of level sets of solutions to semilinear elliptic Dirichlet problems. B.Kawohl (Div. of Appl. Math., Brown Univ., Providence, RI, USA).

Appl. Anal. (GB), vol.16, no.3, p.229-33 (1983).

It is shown that under certain geometrical assumptions on a domain $D \subset \mathbb{R}^n$ any positive solution of $\Delta u + f(u) = 0$ in D , $u = 0$ on ∂D has level sets

$D_c = \{x \in D | u(x) \geq c\}$ with the same geometrical properties as D . This implies that u has only one critical point and extends results of Payne (1973) and Sperb (1975). (13 refs.)

113401 Local regularity, boundary values and maximum principles for pseudoparabolic equations. R.E.Showalter (Div. of Appl. Math., Brown Univ., Providence, RI, USA).

Appl. Anal. (GB), vol.16, no.3, p.235-41 (1983).

The regularity or singularity of data at a point is shown to be preserved for all time at that point along the solution of a pseudoparabolic equation. This significantly strengthens earlier results on the perseverance of global regularity of data and furthermore shows that any local singularities in initial data are stationary. These results yield a precise description of the boundary values of a solution and explain certain non-standard maximum principles for pseudoparabolic equations. (9 refs.)

113402 Eigenvalues of the Orr-Sommerfeld equation in an unbounded domain. M.Miklavic (Dept. of Math. Sci., Rensselaer Polytech. Inst., Troy, NY, USA).

Arch. Ration. Mech. & Anal. (Germany), vol.83, no.3, p.221-8 (1983).

The author proves that in the space $(L^2(0, \infty))^4$ the generalized Orr-Sommerfeld equation has only finitely many eigenvalues when the mean flow exponentially approaches a constant. This surprising fact was discovered by numerical studies of eigenvalues for Blasius mean flow. (12 refs.)

113403 Domain decomposition methods for nonlinear problems in fluid dynamics. R.Glowinski (Univ. Paris VI, Paris, France), Q.V.Dinh, J.Periaux. *Comput. Methods Appl. Mech. & Eng. (Netherlands)*, vol.40, no.1, p.27-109 (Sept. 1983).

The numerical solution of finite element approximations of complicated two- and three-dimensional nonlinear problems can be a most formidable task. In order to overcome this difficulty related to dimensionality, domain-splitting methods can be very effective, particularly in view of obtaining a fast and economical conjugate gradient solver, which can be used to precondition the solution of nonlinear problems by optimization methods via nonlinear least squares or weighted residual formulations. A new technique of this type is introduced and analysed and its efficiency discussed from numerical experiments concerning the numerical simulation of transonic flows for compressible inviscid fluids and incompressible viscous flows modelled by the Navier-Stokes equations. (33 refs.)

113404 A nonexistence result for axially symmetric flows with constant angular velocities at infinity. A.R.Elcrat (Wichita State Univ., Wichita, KS, USA), D.Siegel.

Proc. R. Soc. Edinburgh Sect. A (GB), vol.93, pt.3-4, p.229-31 (1983).

If von Karman's substitution is made in the Navier-Stokes equations, and boundary conditions corresponding to a flow in all of space with constant angular velocities at infinity are imposed, a boundary value problem analogous to those for flow above a rotating disk and between rotating disks is obtained. It is shown here that this problem has no solution. (4 refs.)

113405 The real and complex Lorenz equations and their relevance to physical systems. A.C.Fowler (Dept. of Math., MIT, Cambridge, MA, USA), J.D.Gibbon, M.J.McGinness.

Physica D (Netherlands), vol.7D, no.1-3, p.126-34 (May 1983). (Proceedings of the International Conference on Order in Chaos, Los Alamos, NM, USA, 24-28 May 1982).

Summarizes some recently obtained results on real and complex Lorenz equations and discusses their possible significance in relation to real fluid dynamical processes. (70 refs.)

113406 Stokes equations approximation: a spectral method for error estimation. Y.Maday, B.Metivet (Onera, Chatillon, France).

Rech. Aerosp. (France), no.4, p.237-44 (July-Aug. 1983). In French.

For solving partial differential equations, the authors propose using Chebyshev polynomial expansions. Such expansions allow them to obtain errors of the same order as in the Fourier series in the periodic case. They also make it possible to use the fast Fourier transform for computing. Functional frame—which makes it possible to estimate the approximation error for different spectral methods—is introduced on a monodimensional problem (Poisson equation) with nonperiodic boundary conditions. The study is then extended to the 2-D current function Stokes equations. (13 refs.)

113407 Fundamental solutions of the linearized equations of the hydrodynamics of a viscous fluid. L.S.Pal'ko (Inst. of Mech., Acad. of Sci., Kiev, Ukrainian SSR).

Sov. Appl. Mech. (USA), vol.18, no.12, p.1118-25 (Dec. 1982). Translation of: *Prikl. Mekh. (USSR)*, vol.18, no.12, p.83-90 (Dec. 1982). [received: Sept. 1983] (4 refs.)

113408 Streamlining of a sphere when the Mach and Knudsen numbers are small. D.A.Shapiro.

Vestn. Leningr. Univ. Ser. Mat. Mekh. & Astron. (USSR), no.3, p.108-12 (July 1983). In Russian.

The problem of a stationary flow with sliding on the surface of a streamlined sphere is considered. Assuming the Mach and Knudsen numbers to be small and of the same order, an even asymptotic expansion of the solution of a corresponding stationary border problem for a nonlinear Boltzmann equation is built. Navier-Stokes equations with asymptotic precise border conditions are obtained for values which define macroparameters. (2 refs.)

A rigorous study of periodic orbits by means of a computer. See Entry 111449

New splitting-up schemes for solving hyperbolic and parabolic non linear problems: applications to Euler and Navier-Stokes equationsSee Entry 111450

Logarithmic self-similar solutionsSee Entry 111451

The boundary perturbation solution of the fluid flow between two co-axial cones, which are in relative rotation, with axial flowSee Entry 113448

The streamline behaviour near the separation point and separation criterion for viscous flowSee Entry 113483

Continuous coating with gravity and jet strippingSee Entry 115052

47.15 LAMINAR FLOWS

Liquid solidification in laminar tube flow with internal heat sourcesSee Entry 112409

Streamlining of a sphere when the Mach and Knudsen numbers are smallSee Entry 113408

Effects of viscous dissipation on temperature field in flows through ducts of nonuniform cross-sectionSee Entry 113438

Flow in an open channel bend with permeable bedSee Entry 113506

Effects of axial conduction in laminar tube flow with convective boundariesSee Entry 113507

47.15C Laminar boundary layers

113409 Compressible laminar boundary layers on a yawed infinite cylinder. R.Krishnaswamy, G.Nath (Dept. of Appl. Maths., Indian Inst. of Sci., Bangalore, India).

Indian J. Technol., vol.21, no.2, p.43-8 (Feb. 1983). [received: Sept. 1983]

The solution of the steady compressible laminar boundary-layer equations for a yawed infinite circular cylinder is presented which is valid from the origin of the coordinates to the point of separation. The nonlinear partial differential equations governing the nonsimilar flow have been solved numerically using the implicit finite-difference scheme in combination with the quasilinearization technique. It is found that the injection, hot wall and Mach number cause separation to occur earlier, whereas cold wall and suction delay separation. The yaw angle has very little effect on the location of the point of separation. (34 refs.)

113410 Unsteady attachment line flow on a flat plate with attached cylinder. M.Kumari, G.Nath (Dept. of Appl. Math., Indian Inst. of Sci., Bangalore, India).

Int. J. Eng. Sci. (GB), vol.21, no.12, p.1493-503 (1983).

The unsteady laminar incompressible boundary-layer attachment-line flow on a flat plate with attached cylinder with heat and mass transfer has been studied when the free stream velocity, mass transfer and surface wall temperature vary arbitrarily with time. The governing partial differential equations with three independent variables have been solved numerically using an implicit finite-difference scheme. The heat transfer was found to be strongly dependent on the Prandtl number, variation of wall temperature with time and dissipation parameter (for large times). However, the free stream velocity distribution and mass transfer affect both the heat transfer and skin friction. (12 refs.)

113411 A note on expansions for the two-dimensional, compressible, laminar boundary layer equations near a point of zero skin friction. G.Wilks (Dept. of Math., Univ. of Strathclyde, Glasgow, Scotland).

Proc. R. Soc. Edinburgh Sect. A (GB), vol.94, pt.1-2, p.93-6 (1983).

The first non-arbitrary coefficient, α_2 , of the Buckmaster expansions is evaluated in the context of the extended Goldstein-Stewartson theory. Leading terms of the next order contributions to the skin friction and heat transfer coefficients are also obtained. (4 refs.)

113412 A view of the triple deck. R.E.Meyer (Dept. of Math., Univ. of Wisconsin, Madison, WI, USA).

SIAM J. Appl. Math. (USA), vol.43, no.4, p.639-63 (Aug. 1983).

An introduction to triple-deck theory for steady, two-dimensional boundary layers in low-speed flow is presented. It aims to clarify how the rational structure of the theory can rest on few premises and to make its new ideas and challenges more widely accessible. (19 refs.)

113413 Laminar flow in a meandering channel. M.Van Dyke (Dept. of Mech. Engng., Stanford Univ., Stanford, CA, USA).

SIAM J. Appl. Math. (USA), vol.43, no.4, p.696-702 (Aug. 1983).

Plane laminar flow through a meandering channel of constant width is approximated on the basis that the curvature of the centerline is both small and slowly varying. The fourth approximation is calculated for a general shape of centerline. It is used to discuss whether the flow can separate from the walls of such a channel. An alternative scheme of successive approximations is outlined, based on fitting at each station the flow through a tangent annulus. (13 refs.)

113414 Axial flow past a cylinder with uniform injection. L.J.Crane (School of Math., Trinity Coll., Univ. of Dublin, Dublin, Ireland).

Z. Angew. Math. & Mech. (Germany), vol.63, no.8, p.391-3 (1983).

In view of its practical importance the effect of injection on boundary layers has attracted the attention of many authors. An approximate similarity solution of the boundary layer equations is derived; this solution is valid at sufficiently large axial distances from the nose of the cylinder. The basic properties of the flow depend on m , the Reynolds number of the injection velocity based on the radius a of the cylinder. When m is of order unity a continuous boundary layer is formed between the cylinder and the outer stream; when $m \gg 1$ this boundary layer separates from the wall to form a thin axially symmetric shear layer. (6 refs.)

Stagnation point heat transfer for Jet impingement to a plane surfaceSee Entry 113431

Heat transfer in laminar free convection near a vertical plate for fluids in the supercritical regions of state variablesSee Entry 113437

The boundary perturbation solution of the fluid flow between two co-axial cones, which are in relative rotation, with axial flowSee Entry 113448

A note on the Falkner-Skan flows of a non-Newtonian fluidSee Entry 113480

Calculation of transient heat transfer in channels with Neumann boundary conditionsSee Entry 113505

47.15F Stability of laminar flows

113415 Limits of regions of strict hyperbolic and composite type for nonlinear equations of two-layer shallow water. G.G.Elenin.

Moscow Univ. Comput. Math. & Cybern. (USA), no.4, p.69-72 (1982). Translation of: *Vestn. Mosk. Univ. Ser. 15 (USSR)*, no.4, p.57-9 (1982). [received: Sept. 1983]

The properties of the stability limits of strictly hyperbolic and composite type for the system of equations of two-layer shallow water are analytically and numerically investigated. (4 refs.)

47.20 HYDRODYNAMIC STABILITY

113416 Supersonic stabilization of a tangential shear in a thin atmosphere. S.V.Bazdenkov, O.P.Pogutse (I.V. Kurchatov Inst. of Atomic Energy, Moscow, USSR).

JETP Lett. (USA), vol.37, no.7, p.375-7 (5 April 1983). Translation of: *Pis'ma v Zh. Eksp. & Teor. Fiz. (USSR)*, vol.37, no.7, p.317-19 (5 April 1983). [received: Oct. 1983]

A tangential shear in a thin atmosphere is stable if the amplitude of the velocity jump $V > 2\sqrt{2c_g}$, where c_g is the velocity of surface gravity waves. The Coriolis force and the finite width of the flow region are destabilizing factors. (5 refs.)

113417 Stabilization of tangential shear instability in shallow water with 'supersonic' fluid flow. S.V.Antipov, M.V.Nezlin, V.K.Rodionov, E.N.Snezhkin, A.S.Trubnikov (I.V. Kurchatov Inst. of Atomic Energy, Moscow, USSR). *JETP Lett. (USA)*, vol.37, no.7, p.378-81 (5 April 1983). Translation of: *Pis'ma v Zh. Eksp. & Teor. Fiz. (USSR)*, vol.37, no.7, p.319-22 (5 April 1983). [received: Oct. 1983]

It is demonstrated experimentally that under conditions of (two-dimensional) 'shallow water' Landau's conclusion (1953) that the instability of the super-sonic tangential shear is stabilized for $u > (2g^*H_0)^{1/2}$, where $2u$ is the relative velocity of countermoving flows, H_0 is the depth of the fluid, and g^* is the effective acceleration of gravity, is correct. The result obtained corresponds to the theory of S.V. Bazdenkov and O.P. Pogutse [*Pis'ma Zh. Eksp. Teor. Fiz.* 37, 317 (1983)]. (5 refs.)

113418 Stability of rotating liquids drops. I. Uncharged drops. P.Luyten, D.K.Callebaut (Phys. Dept., Univ. Instelling Antwerpen, Anwerp, Belgium). *Phys. Fluids (USA)*, vol.26, no.9, p.2359-67 (Sept. 1983).

The oscillations and the instability of a uniformly rotating liquid drop endowed with surface tension are investigated. The linearized equations of motion are solved using 'modified' spheroidal coordinates. A general energy integral technique which is more adequate than the virial method is developed to yield the dispersion relations. The equilibrium figure is first approximated by a spheroid. The dynamical and secular instabilities are calculated in general. In the latter case bifurcation occurs towards nonrotationally symmetric equilibria. Then the exact equilibrium figure is studied by the same energy integral technique. The results are compared with those of the spheroidal approximation and with the numerical calculations of Brown and Scriven (1980). (16 refs.)

113419 Transitions to chaos in the Ginzburg-Landau equation. H.T.Moon, P.Huerre, L.G.Redekopp (Dept. of Aerospace Engng., Univ. of Southern California, Los Angeles, CA, USA).

Physica D (Netherlands), vol.7D, no.1-3, p.135-50 (May 1983). (Proceedings of the International Conference on Order in Chaos, Los Alamos, NM, USA, 24-28 May 1982).

The amplitude evolution of instability waves in many dissipative systems is described close to criticality, by the Ginzburg-Landau partial differential equation. A numerical study of the long-time behavior of amplitude-modulated waves governed by this equation allows the identification of two distinct routes of the Ruelle-Takens-Newhouse type (1978) as the modulation wavenumber is decreased. The first route involves a sequence of bifurcations from a limit cycle to a two-torus to a three-torus and to a turbulent regime, the last stage being preceded by frequency locking. The turbulent regime is itself followed by a new two-torus. In the second route, this two-torus exhibits a single subharmonic bifurcation which immediately results in transition to chaos. A description of the various possible dynamical states is tentatively given in the plane of the two control parameters c_4 and c_6 . (43 refs.)

113420 Behavior of a local cluster of gas bubbles in a vibrating fluid. V.D.Lakiza, A.S.Tsypenko (Inst. of Mech., Acad. of Sci., Kiev, Ukrainian SSR).

Sov. Appl. Mech. (USA), vol.19, no.1, p.92-6 (Jan. 1983). Translation of: *Prikl. Mekh. (USSR)*, vol.19, no.1, p.109-14 (Jan. 1983). [received: Sept. 1983]

The dynamical behavior and questions of the vibrational stability of a local gas bubble cluster in a vibrating fluid are treated theoretically and experimentally. The cluster interaction with the solid vessel surface is taken into account. (6 refs.)

Limits of regions of strict hyperbolic and composite type for nonlinear equations of two-layer shallow water See Entry 113415

Reynolds stresses for unsteady turbulent flows See Entry 113424

A pair of semicircle theorems in rotatory thermohaline convection See Entry 113442

Vortex motion in the early stages of unsteady flow around a circular cylinder See Entry 113447

The stability of internal solitary waves See Entry 113459

Destabilization of an initially stable shear flow by internal waves See Entry 113460

The streamline behaviour near the separation point and separation criterion for viscous flow See Entry 113483

Axial coherence functions of circular turbulent jets based on an inviscid calculation of damped modes See Entry 113488

Unsteady magnetohydrodynamic Couette flow See Entry 113519

Barotropic instability of weakly non-parallel zonal flows See Entry 116095

Radiating barotropic instability See Entry 116107

Bounds on the growth of perturbations to non-parallel steady flow on the barotropic beta plane See Entry 116222

On the effect of oblique disturbances on Kelvin-Helmholtz instability at magnetospheric boundary layers and in solar wind See Entry 116411

47.25 TURBULENT FLOWS, CONVECTION, AND HEAT TRANSFER

113421 Mixing and diffusion of heated water discharge for power plants. R.R.Hwang, Shian-Woei Jeng, B.S.Shiau (Inst. of Phys., Acad. Sinica, Taipei, Taiwan).

Annu. Rep. Inst. Phys. Acad. Sin. (Taiwan), vol.12, p.250 (Dec. 1982). [received: Sept. 1983]

The study treats a buoyant surface discharge into a large body of water and integrates the near-field and the far-field analysis in predictions of water temperatures resulting from the surface discharge of heated water in ambient flow configurations. The main objectives are to develop a framework for integrating the near-field and the far-field models. The near-field model includes buoyant jet interaction with a shallow bottom while the far-field model is capable of predicting temperatures in a large body of water which is subject to a range of transient current conditions. Therefore, the authors investigate the basic behavior of buoyant surface discharge and attempt to improve their ability to predict water temperatures resulting from these discharges. (no refs.)

113422 The turbulence problem: a survey. R.Narasimha (Dept. of Aerospace Engng., Indian Inst. of Sci., Bangalore, India).

J. Indian Inst. Sci., vol.64, no.1, p.1-59 (Jan. 1983). [received: Sept. 1983]

The paper is a survey of the present state of understanding, prediction and control of turbulent flows, intended to be intelligible also to workers not directly involved in research in turbulence. 'Complex' turbulent flows, as affected by such factors as rotation, additional rates of strain, compressibility, etc., are not covered by the survey, but an attempt has been made to include all aspects of simpler flows in an incompressible fluid. Inevitably, the survey

is strongly influenced by the work done by the author himself and his colleagues. A major conclusion of the survey is that there are still wide gaps between the experimental discoveries being made on the structure of turbulent flows, the mathematical tools necessary for describing such structure, the numerical models invented for predicting turbulent shear flow behaviour, and the devices being tried for turbulence management. A great deal of work is necessary in all areas before these gaps can be bridged. (131 refs.)

113423 A method for turbulent flow calculations. H.-J.Maschek (Sektion Energieumwandlung, Tech. Univ. Dresden, Dresden, Germany). *Wiss. Z. Tech. Univ. Dresden (Germany)*, vol.32, no.2, p.167-70 (1983). In German.

Multi-parameter approaches to the analysis of turbulent flow are discussed, starting with a historical review from Taylor's (1938) turbulence spectrum. Turbulent flow is separated into micro-turbulence and macro-turbulence regions, and an attempt is made to explain numerical modelling. The consequences of empirical coefficient selection are considered and uncertainties are mentioned. (15 refs.) G.M.E.

Proceedings of the International Conference on Order in Chaos See Entry 111307

Five turbulent problems See Entry 111566

Transitions to chaos in the Ginzburg-Landau equation See Entry 113419

Drag coefficients of a sphere and a bed of spherical elements See Entry 113504

A Eulerian-Lagrangian model for turbulent combustion See Entry 113521

A two-component optomechanical speed transducer for use with turbulent flows of liquid metal See Entry 113529

Dependence of MHD turbulence spectra on the velocity field-magnetic field correlation See Entry 116446

A second-order correlation approximation for thermal conductivity and Prandtl number of free turbulence See Entry 116461

47.25C Isotropic turbulence

113424 Reynolds stresses for unsteady turbulent flows. W.L.Hankey, W.Calarese (Air Force Wright Aeronautical Labs., WPAFB, OH, USA). *AIAA J. (USA)*, vol.21, no.8, p.1210-11 (Aug. 1983).

Reynolds averaged equations are currently employed in the numerical analysis of turbulent flows. In these equations an 'apparent stress' that requires empirical data (e.g. eddy viscosity) is introduced to close the system and permit calculation of the flowfield. A predicament arises when calculating unsteady turbulent flows in which the empirical apparent stress level is of concern. For example, if all of the apparent stress obtained experimentally over the whole frequency spectrum were used in the calculation, this value would be added to the stress generated by the numerical algorithm, causing overestimation of the turbulence. This error would produce excessive dissipation of the unsteady phenomenon with potential attendant disappearance of the unsteady solution. The authors address the procedure required to evaluate the frequency range of the Reynolds stress to be used for unsteady turbulent flows. To demonstrate the procedure, the Reynolds-averaged equations are examined for two-dimensional, incompressible flow. (4 refs.)

113425 Velocity statistics in premixed turbulent flames. R.K.Cheng, T.T.Ng (Lawrence Berkeley Lab., Univ. of California, Berkeley, CA, USA). *Combust. & Flame (USA)*, vol.52, no.2, p.185-202 (Sept. 1983).

Laser Doppler velocimetry was used to measure velocity statistics in six unconfined v-shaped premixed ethylene/air turbulent flames with incident turbulence generated by grid or perforated plate. Also obtained were high speed schlieren movies of the turbulent flames. The results discussed include two components of mean and RMS velocities, probability density functions, macroscales, and Reynolds stress. In most cases, turbulent intensities increase within the flame zone. This increase is attributed to the intermittent measurement of the flow velocities in the burned and unburned states as the thin flame sheet fluctuates about the stationary measurement point. Reynolds stress also increases in the flame zone, but its sign suggests removal of turbulent kinetic energy. Therefore, conventional gradient transport modeling would break down for these flames. The sign of the Reynolds stress is in qualitative agreement with contributions due to intermittent measurement of the turbulent components in the burned and unburned states. These results show that the intermittency effect is a major influence on turbulent statistics in premixed flames and should require careful consideration in numerical models. (28 refs.)

113426 Experimental investigation of turbulent characteristics in the axisymmetric swirling flow. Yu.B.Kolesnikov, E.P.Sukhovich.

Lav. PSR Zinat. Akad. Vestis Fiz. Teh. Zinat. Ser. (USSR), no.4, p.72-8 (1983). In Russian.

An experimental investigation of an averaged velocity component field and static pressure field is carried out, and six components of tensor stresses are measured in the finite swirling flow in a cylindrical channel. Near the channel axis unusual turbulent energy transfer to the mean flow is detected. In this case turbulent coefficients are essentially anisotropic over all the flow range, however near the axis they are negative. The results of this investigation are of interest for explanation of the effects associated with the influence of swirling on turbulent flow hydrodynamics. (12 refs.)

113427 Has a small-scale structure in turbulence been experimentally verified? F.D.Johnson, H.Eckelmann (Max-Planck-Inst. fur Stromungsforschung, Gottingen, Germany).

Phys. Fluids (USA), vol.26, no.9, p.2408-14 (Sept. 1983).

Various investigators have found considerable experimental evidence for small-scale flow structures in wall-bounded turbulent flow within the last 15 years. Experiments by Willmarth and Bogar in 1977 (*Phys. Fluids* 20, S9, October, part II, 1977) provided the high point to date in efforts to measure small-scale phenomena associated with turbulence; the unexpected results of these investigations were ascribed to extremely small flow structures of a scale which previously had remained undetected. Since publication of the work of Willmarth and Bogar, neither verifications nor contradictory results have been published by other investigators. The present experimental studies seem to contradict the thesis of Willmarth and Bogar, making small-scale phenomena responsible for the unusual results of their experiments. (9 refs.)

113428 Turbulent time scales and the dissipation rate of temperature variance in the thermal mixing layer. S.E.Elghobashi (Mech. Engng. Dept., Univ. of California, Irvine, CA, USA), B.E.Laund.

Phys. Fluids (USA), vol.26, no.9, p.2415-19 (Sept. 1983).

In a turbulent flow where the mechanisms and/or the importance of the generation processes of turbulent kinetic energy k and mean square scalar variance $\bar{\epsilon}^2$ are dissimilar, no simple connection exists between the turnover time scale of the fluctuating velocity and fluctuating scalar fields. To allow the computation of the turbulent scalar field in these situations a means of

calculating the scalar time is required. Here, in an extension of work by Newman, Launder, and Lumley (J. Fluid Mech. 111, 217, 1981), the time scale is obtained via a proposed transport equation for the dissipation rate of mean square scalar variance. The modeled equation has been applied successfully to the calculation of the spread of a thermal mixing layer in grid-generated turbulence and the decay of temperature variance in a homogeneous field. (12 refs.)

113429 Indirect measurement of the thermal-acoustic efficiency spectrum of a long turbulent burner. J.R.Mahan (Virginia Polytech. Inst. & State Univ., Blacksburg, VA, USA), J.D.Jones, L.R.Blevins, J.G.Cline. *Rech. Aerosp. (France)*, no.4, p.311-21 (July-Aug. 1983). In French.

A new method is described for deducing the thermal-acoustic efficiency spectrum (defined as the fraction of combustion heat release converted to acoustic energy at a given frequency) of a long turbulent burner from the sound spectrum measured in the far field. The method, which is based on a one-dimensional model of the unsteady flow in the burner, is applied to a tubular diffusion-flame hydrogen burner whose length is large compared to its diameter. The results for thermal powers ranging from 4.5 to 22.3 kW show that the thermal-acoustic efficiency is relatively insensitive to the burner power level, decreasing from a value of around 10^{-4} at 150 Hz with a slope of about 20 dB per decade. Evidence is presented indicating that acoustic agitation of the flame below 500 Hz, especially in the neighborhood of the resonant frequencies of the burner, is a significant acoustic source. (19 refs.)

Turbulent natural convection in a rectangular enclosure See Entry 113440

First order numerical solution of the statistical vorticity structure theory of homogeneous isotropic turbulence See Entry 113449

Acoustic interaction with a turbulent plane jet—some effects on turbulent structure See Entry 113486

Axial coherence functions of circular turbulent jets based on an inviscid calculation of damped modes See Entry 113488

Momentum implications for buoyant diffusion flames See Entry 113548

Fluorescence measurements of OH in a turbulent flame See Entry 115550

Acoustic signature from flames as a combustion diagnostic tool See Entry 115551

Diagnostic possibilities on the basis of premixed flame noise levels See Entry 115554

47.25F Boundary layer and shear turbulence

113430 Experimental and numerical investigation of a turbulent boundary layer subjected to a sudden transverse strain. J.Cousteix, B.Aupoix (Office Nat. d'Etudes et de Recherches Aérospatiales, CERT, Toulouse, France), E.Arzuomanian, L.Fulachier. *Phys. Fluids (USA)*, vol.26, no.9, p.2399-407 (Sept. 1983).

A fully developed two-dimensional boundary layer on a cylinder is subjected to a sudden transverse strain by rotating the downstream part of the cylinder with a peripheral wall velocity approximately equal to the external velocity. This distorted boundary layer has a 'complex-flow structure'. The present paper deals with both experimental and numerical investigations of this complex flow. The experiments have been carried out in the near-wall region (buffer layer and viscous sublayer). Calculations have been made with a model of the $k-\epsilon$ type which takes into account the anisotropy of turbulent viscosity. Although the general agreement between experiment and calculations is good, some discrepancy, especially with respect to the behavior of the mean flow, is observed in the near-wall region and experiments do not support the linear evolution of the hodograph as predicted by calculations. The results suggest that the collaterality of the flow is first obtained in a very thin wall layer and extends progressively into the outer boundary layer. (23 refs.)

Observations of order and chaos in nonlinear systems See Entry 111564

A view of the triple deck See Entry 113412

Axial flow past a cylinder with uniform injection See Entry 113414

Free-stream turbulence effects on the heat transfer through the turbulent boundary layer behind a fence See Entry 113434

Ergodic stream-lines in steady convection See Entry 113441

Flow and heat transfer on a disk rotating beneath a forced vortex See Entry 113445

Vortex motion in the early stages of unsteady flow around a circular cylinder See Entry 113447

The boundary perturbation solution of the fluid flow between two co-axial cones, which are in relative rotation, with axial flow See Entry 113448

47.25J Turbulent diffusion

The visible shape and size of a turbulent hydrocarbon jet diffusion flame in a cross-wind See Entry 115553

47.25Q Convection and heat transfer

(see also 44.25 Convective and constrained heat transfer)

113431 Stagnation point heat transfer for Jet impingement to a plane surface. P.S.Shadlesky (Morton Thiokol Corp., Brigham City, UT, USA). *AIAA J. (USA)*, vol.21, no.8, p.1214-15 (Aug. 1983).

The author considers a finite jet impinging against an infinite plane, about which in comparison to the conventional convective flow and heat-transfer fields relatively little is known. A theoretical heat-transfer correlation has been derived that is an extension of the analyses presented by Square and Sibulkin incorporating a modification of the potential flow for a two-dimensional jet normal to a flat plate as given by Milne-Thomson (1960). In the neighbourhood of a stagnation point the flow can be considered incompressible and laminar regardless of the mainstream flowfield. This leads to a marked simplification of both the momentum and energy equations that becomes amenable to closed-form solutions. Although the flow is considered incompressible, the analysis should be applicable to supersonic conditions, provided the properties just downstream of the normal shock are selected as freestream conditions. (9 refs.)

113432 Heat transfer from an impulsively started circular cylinder. Lai-chen Chien, In-shieh Kung (Inst. of Phys., Acad. Sinica, Taipei, Taiwan). *Annu. Rep. Inst. Phys. Acad. Sin. (Taiwan)*, vol.12, p.248 (Dec. 1982). [received: Sept. 1983]

The analytic solution for forced convection heat transfer from an impulsively started heated circular cylinder is studied. The nonlinear energy equation is solved by the method of matched asymptotic expansion to the third order. A solution for the temperature field in term of exponential and error functions is

found. The time development of the temperature field is plotted. The local Nusselt number over the cylinder surface and progress of minimum Nusselt number point with time obtained are compared with the existing solutions with satisfactory results. (no refs.)

113433 Conjugate mixed convection heat transfer from a vertical rectangular fin. B.Sunden (Dept. of Appl. Thermo & Fluid Dynamics, Chalmers Univ. of Technol., Goteborg, Sweden). *Int. Commun. Heat & Mass Transfer (GB)*, vol.10, no.4, p.267-76 (July-Aug. 1983).

A numerical investigation of the heat transfer from a rectangular fin by combined forced and natural convection is presented. Results are given for buoyancy parameters in the range of $0 \leq Gr/Re^2 \leq 2$ and convection-conduction parameters in the range of $0 \leq \sqrt{Re} k_f/k_b \leq 10$. The results are compared with the convection fin theory and it is found that concerning the fin efficiency, the latter produces acceptable results although it is not strictly correct. (5 refs.)

113434 Free-stream turbulence effects on the heat transfer through the turbulent boundary layer behind a fence. A.Zukauskas (Acad. of Sci., Vilnius, Lithuanian SSR).

Int. Commun. Heat & Mass Transfer (GB), vol.10, no.4, p.277-86 (July-Aug. 1983).

Experimental results on the reattachment length and heat transfer behind the fence under a variable free-stream turbulence on air are presented. The study covered Re_{θ} from 2×10^5 to 2×10^6 , turbulence from 0.1 to 7%, and fence heights from 0.002 to 0.0135 m. Shorter reattachment lengths and augmented heat transfer at the reattachment were observed under higher turbulences. (10 refs.)

113435 The effect of Prandtl number on heat transfer from an isothermal rotating disk with blowing at the wall. P.H.Muir (Dept. of Computer Sci., Univ. of Toronto, Toronto, Canada), G.Fairweather, M.Vedha-Nayagam. *Int. Commun. Heat & Mass Transfer (GB)*, vol.10, no.4, p.287-97 (July-Aug. 1983).

Numerical results for heat transfer from an isothermal rotating disk with moderate to massive blowing at the wall are presented for a wide range of Prandtl numbers. Results show that for a given finite rate of blowing at the wall, the heat transfer rate first increases, reaching a maximum value before falling sharply, as the Prandtl number is increased. The maximum value of heat transfer rate decreases as the blowing rate increases. The phenomenon of boundary layer blow-off is also investigated. (23 refs.)

113436 Free convection flow through a porous medium bounded by two horizontal walls. C.Perdikis (Dept. of Mech., Univ. of Ioannina, Ioannina, Greece).

Int. Commun. Heat & Mass Transfer (GB), vol.10, no.4, p.357-9 (July-Aug. 1983).

Steady free convection flow through a porous medium bounded by two horizontal walls with a uniform axial temperature variation along the walls is considered. The author gives an analytical solution of the velocity field and discusses the effects of the permeability parameter K and Grashof number G on the velocity. (2 refs.)

113437 Heat transfer in laminar free convection near a vertical plate for fluids in the supercritical regions of state variables. V.N.Popov, G.C.Yan'kov (Moscow Power Inst., Moscow, USSR).

High Temp. (USA), vol.20, no.6, p.878-86 (Nov.-Dec. 1982). Translation of: *Teplofiz. Vys. Temp. (USSR)*, vol.20, no.6, p.1110-18 (Nov.-Dec. 1982). [received: Sept. 1983]

Heat transfer in laminar free convection near a vertical plate for water, carbon dioxide, and nitrogen in the supercritical region for boundary conditions $T_w = \text{const}$ and $q_w = \text{const}$ is calculated. It is shown that a consideration of the thermal conductivity peak has a significant effect on the results of heat-transfer calculations. An interpolation formula that gives the results of calculations of the Nusselt numbers for the considered substances for both types of boundary conditions and previously obtained data for helium is selected. The results of calculated are compared with experimental data and some empirical formulas. (27 refs.)

113438 Effects of viscous dissipation on temperature field in flows through ducts of nonuniform cross-section. C.V.Mahalakshmi (Dept. of Appl. Maths., Indian Inst. of Sci., Bangalore, India).

Indian J. Technol., vol.21, no.2, p.53-6 (Feb. 1983). [received: Sept. 1983]

An analytical expression for the temperature distribution for forced convective heat transfer in a flow through a tube of slowly varying cross-section is obtained taking into account the viscous dissipative effects. The Nusselt number is calculated. (12 refs.)

113439 Marangoni convection in cholesteric liquid crystals of low thermal sensitivity. I.I.Gorina, N.L.Sizova, I.G.Chistyakov (Inst. of Crystallography, Acad. of Sci., Leningrad, USSR).

Mol. Cryst. & Liq. Cryst. (GB), vol.95, no.3-4, p.271-8 (1983).

The Marangoni convection in a layer of nonthermosensitive cholesteric has been obtained. To induce the first stage of the convection (streaming the substance away from the 'hot' area), a local heating of the layer is necessary which is from 3 to 4 times as much as that required for thermosensitive cholesterics. The CLC convection motion structures of 'roll' type appeared when the layer was locally heated in a thermostat at temperatures close to the clearing point (T_a) of the cholesteric. The results obtained are discussed in terms of thermal stability of the original cholesteric texture. (5 refs.)

113440 Turbulent natural convection in a rectangular enclosure. C.Renault, Doan-Kim-Son (Lab. de Thermique, ENSMA, Poitiers, France). *Mech. Res. Commun. (GB)*, vol.10, no.4, p.245-51 (July-Aug. 1983).

As very little information is available about the structure of the natural convection flow in a rectangular cavity at high Grashof numbers, and with an aim at the further development of a numerical model, the authors have planned an experimental program in which the effects of the governing parameters, boundary conditions (insulation of walls), and inclination of the cavity are studied for Grashof numbers higher than 10^7 . The aim is to provide the first experimental contribution to the knowledge of the flow structure at $Gr_p = 8.3 \times 10^7$. (10 refs.)

113441 Ergodic stream-lines in steady convection. W.Arter (Culham Lab., UKAEA, Abingdon, England). *Phys. Lett. A (Netherlands)*, vol.97A, no.5, p.171-4 (29 Aug. 1983).

Stream-lines of steady Rayleigh-Benard convection with square planform are displayed using Poincaré maps. As the second order mode becomes more important the flow becomes ergodic from the boundaries inward, like a perturbed, integrable Hamiltonian system. (9 refs.)

113442 A pair of semicircle theorems in rotatory thermohaline convection. M.B.Banerjee, D.C.Katoch (Dept. of Math., Himachal Pradesh Univ., Simla, India), G.S.Dube, K.Banerjee. *Proc. Natl. Acad. Sci. India Sect. A*, vol.52, pt.2, p.150-8 (1982). [received: Aug. 1983]
The present investigation is concerned with the problem of obtaining bounds for the complex growth rate of an arbitrary oscillatory perturbation, neutral or unstable in the domain of infinitesimal amplitude instability in rotatory thermohaline convection. A pair of semicircle theorems, one each for both Stern's and Veronis' configurations, under the influence of a uniform rotation transverse to the fluid layer, are established in this connection. These results are new and are uniformly valid for all combinations of dynamically free and rigid boundaries. (4 refs.)

113443 Two-parameter study of the routes to chaos. A.Libchaber, S.Eauve, C.Laroche (Ecole Normale Supérieure, Paris, France). *Physica D (Netherlands)*, vol.7D, no.1-3, p.73-84 (May 1983). (Proceedings of the International Conference on Order in Chaos, Los Alamos, NM, USA, 24-28 May 1982).
The authors study the routes to chaos for a Rayleigh-Benard experiment in mercury, as a function of two parameters, the Rayleigh number (R) and the Chandrasekhar number (Q). For low Q the main route is a period-doubling cascade of bifurcations occurring at low R . For higher values of Q , two routes are observed, one related to a soft mode instability for moderate R , and a second one related to a three oscillators state, occurring at higher Rayleigh number values. (25 refs.)

113444 Oscillatory convection in a spherical cavity due to G-jitter. D.Langbein (Battelle-Inst. eV, Frankfurt-am-Main, Germany). Proceedings of the 4th European Symposium on Materials Sciences under Microgravity (ESA SP-191), Madrid, Spain, 5-8 April 1983 (Paris, France: ESA 1983), p.359-63
The convection caused by residual acceleration in an axial direction in a spherical cavity heated at the equator and cooled at the poles is investigated. The spherical cavity is intended to model in first order the melting zone in a typical crystal growth experiment under microgravity. The spherical symmetry is a concession to mathematical simplicity. The resulting shift of the isotherms is calculated. If in order to avoid striations of the growing crystal a shift of the solidification isotherm by less than $1\text{ }\mu\text{m}$ is required, the amplitude of residual accelerations of 1 Hz and 10 Hz must be smaller than 10^{-5} g and 10^{-3} g , respectively ($g=9.81\text{ m/s}^2$). (3 refs.)

Liquid solidification in laminar tube flow with internal heat sourcesSee Entry 112409

Experimental study of heat-transfer burnout in horizontal steam-generating channels with a porous inner lining and circumferentially nonuniform heatingSee Entry 113263

Unsteady attachment line flow on a flat plate with attached cylinderSee Entry 113410

A note on expansions for the two-dimensional, compressible, laminar boundary layer equations near a point of zero skin frictionSee Entry 113411

Axial flow past a cylinder with uniform injectionSee Entry 113414

Flow and heat transfer on a disk rotating beneath a forced vortexSee Entry 113445

A stability model for steam generatorsSee Entry 113498

Flow of a viscous fluid through a porous medium bounded by a vertical surfaceSee Entry 113501

Calculation of transient heat transfer in channels with Neumann boundary conditionsSee Entry 113505

Effects of axial conduction in laminar tube flow with convective boundariesSee Entry 113507

Magnetohydrodynamic free convective effect for an incompressible viscous fluid past an infinite limiting surfaceSee Entry 113510

Finite difference analysis of MHD free-convection flow past an accelerated vertical porous plateSee Entry 113513

MHD free convection flow past an accelerated vertical plateSee Entry 113515

Procedure for measuring the thickness and wave characteristics of the surface of the liquid film in annular-mist flows of steam and waterSee Entry 113528

Simulation studies of the hydrodynamics in high-temperature solutions for crystal growth. V. Shape of the crystal/liquid interface in the presence of simultaneous free and forced convectionsSee Entry 113785

Acoustic signature from flames as a combustion diagnostic toolSee Entry 115551

Structure and extinction of convective diffusion flames with general Lewis numbersSee Entry 115552

Radiative heat exchange in the vicinity of the critical point of a blunt body with an intensely vaporizing surface in a three-dimensional hypersonic stream of a hydrogen-helium mixture [planetary atmosphere entry]See Entry 116423

47.25R Wakes

A vortex sheet method for calculating separated two-dimensional flowsSee Entry 113446

Vortex motion in the early stages of unsteady flow around a circular cylinderSee Entry 113447

47.30 ROTATIONAL FLOW AND VORTICITY

113445 Flow and heat transfer on a disk rotating beneath a forced vortex. B.G.Newman (McGill Univ., Montreal, Quebec, Canada). *AIAA J. (USA)*, vol.21, no.8, p.1066-70 (Aug. 1983).
The integral method of von Karman for calculating the turbulent boundary layer on a rotating disk has been extended to cases for which the outer flow is rotating at a constant angular velocity. The method predicts the nondimensional radial mass flux, the windage, and, by analogy, the Nusselt number. It enables quick estimates to be made for the flow over the rear of compressor and turbine disks. (8 refs.)

113446 A vortex sheet method for calculating separated two-dimensional flows. M.Ribaut (Brown Boveri Ltd., Baden, Switzerland). *AIAA J. (USA)*, vol.21, no.8, p.1079-84 (Aug. 1983).
A mixed boundary condition problem for the time-average separated flow of a compressible and viscous fluid at high Reynolds number is formulated and solved by means of vortex and source integral equations involving vorticity diffusion. Application of the method to the flow past a flat plate and a blunt trailing-edge section has shown that the extension and underpressure of the

calculated wakes directly depend on the amount of vorticity diffusion and dissipation occurring in the flow. Computed velocity distributions and wake underpressures are compared with the experiment. (14 refs.)

113447 Vortex motion in the early stages of unsteady flow around a circular cylinder. Ling Guocan (Inst. of Mech., Acad. Sinica, Peking, China). *Acta Mech. Sin. (China)*, no.3, p.209-16 (1983). In Chinese.
The early stages of vortex motion in the near wake of unsteady flow around a circular cylinder at high Reynold's number is investigated, by combining the discrete vortex model with boundary layer theory and by taking into consideration the separation of boundary layer and rear shear layer in the recirculating flow region. The development of flow structures and vortex motion, particularly the formation and growth of secondary vortices and their effect on the flow field are calculated. The calculated results clearly show that the flow structures and vortex motion go through a series of complicated processes before the symmetric main vortices become asymmetric: development of main vortices induces secondary vortices; growth of the secondary vortices causes the symmetric main vortex sheets to break off and the symmetric main vortices to become free vortices, while a pair of secondary vortices is formed; then the vortex sheet, after breaking off, gradually extends downstream and a pair of secondary vortices become loose. Positions of separation point, pressure and velocity distributions on the surface and drag coefficients are also given. (26 refs.)

113448 The boundary perturbation solution of the fluid flow between two co-axial cones, which are in relative rotation, with axial flow. Chu Yuenrei (Dept. of Engng. Mech., Jiaotong Univ., Shanghai, China). *Acta Mech. Sin. (China)*, no.3, p.217-26 (1983). In Chinese.
The fluid flow between two relatively rotating co-axial cones with axial flow is investigated. The flow is governed by the Navier-Stokes equations. It is extremely difficult to obtain an accurate solution, but if the cone angle is assumed to be small then a boundary perturbation scheme can be developed. The asymptotic analytical solution of this flow is given. (3 refs.)

113449 First order numerical solution of the statistical vorticity structure theory of homogeneous isotropic turbulence. Wei Zhonglei, Li Wenxuan (Peking Univ., Peking, China). *Acta Mech. Sin. (China)*, no.3, p.241-8 (1983). In Chinese.
This is a further development of the vorticity structure theory of homogeneous isotropic turbulence by P.Y. Chou and Y.N. Huang (1975). (4 refs.)

113450 Impulsively started viscous flow over a rotating circular cylinder. Lai-Chen Chien, Ching-Shang Chen (Inst. of Phys., Acad. Sinica, Taipei, Taiwan). *Annu. Rep. Inst. Phys. Acad. Sin. (Taiwan)*, vol.12, p.77-86 (Dec. 1982). [received: Sept. 1983]
The impulsively started flow of an incompressible viscous fluid over a circular cylinder with circulation is studied. Because of the impulsive start, there is a singularity at time zero plus. The accurate solution in the neighborhood of the singularity by the matched asymptotic expansion to the second order is extended to the third order. Then the analytic solutions considered for the viscous layer are employed as initial conditions for numerical integration to obtain the solutions for larger time. The finite difference scheme adapted for the vorticity equation is the hopscotch method and that for the Poisson equation is the direct method. The time development of the flow properties, lift and moment coefficients are obtained and plotted. (8 refs.)

113451 A steady rotational plane gas flow problem by hodograph method. O.P.Chandna, A.Murgai, G.W.Rankin (Univ. of Windsor, Windsor, Ontario, Canada). *Int. J. Eng. Sci. (GB)*, vol.21, no.12, p.1443-9 (1983).
The geometry and the solutions are investigated for steady rotational plane gas flows with arbitrary equation of state when the velocity magnitude is constant along each individual streamline by using the hodographic technique. (5 refs.)

113452 Vortex structure of circular jets in crossflow. N.Rajaratnam (Univ. of Alberta, Edmonton, Alberta, Canada), T.Gangadharaiah. *J. Wind Eng. & Ind. Aerodyn. (Netherlands)*, vol.12, no.2, p.155-64 (July 1983).
Presents the results of an experimental study of the properties of the bound vortex system housed in a circular jet issuing perpendicularly into a crossflow for three values of the ratio of the jet to crossflow velocity equal to 2.73, 4.52 and 7.05. (10 refs.)

113453 On the geometry of vortex-line in rotating viscous incompressible hydromagnetic fluid flows. G.Purushotham (Nagrunasagar Engng. Coll., JNT Univ., Hyderabad, India), M.A.Rasheed. *Proc. Natl. Acad. Sci. India Sect. A*, vol.52, pt.2, p.194-206 (1982). [received: Aug. 1983]
Following Bjorgum (1951), Bjorgum and Godal (1952) description of the geometries of vortex-line triad O^3 in an anholonomic space is completed and is utilised to study the kinetic and the kinematic properties of steady, rotating, viscous, incompressible hydromagnetic fluid flows, which generalise the studies of Gopalkrishna and Ramchandra Rao (1975). The role of Beltrami and complex-lamellar characters of the vortex-lines are examined to study the kinematic properties of the flows described. (15 refs.)

113454 Growth of localized disturbances on a vortex sheet. A.D.D.Craik (Dept. of Appl. Math., Univ. of St. Andrews, St. Andrews, Scotland). *Proc. R. Soc. Edinburgh Sect. A (GB)*, vol.94, pt.1-2, p.85-8 (1983).
Linearized local disturbances on a vortex sheet are known to develop singularities after a finite term in some cases but not in others. A simple test for the appearance of such singularities is given in terms of the Fourier transform of the initial disturbance. Such singularities are a consequence of the artificiality of the vortex sheet model and should not be regarded as physically meaningful. (11 refs.)

113455 Coadjoint orbits, vortices, and Clebsch variables for incompressible fluids. J.Marsden, A.Weinstein (Dept. of Maths., Univ. of California, Berkeley, CA, USA). *Physica D (Netherlands)*, vol.7D, no.1-3, p.305-23 (May 1983). (Proceedings of the International Conference on Order in Chaos, Los Alamos, NM, USA, 24-28 May 1982).
This is a study of incompressible fluids, especially their Clebsch variables and vortices, using symplectic geometry and the Lie-Poisson structure on the dual of a Lie algebra. Following ideas of Arnold (1978) and others it is shown that Euler's equations are Lie-Poisson equations associated to the group of volume-preserving diffeomorphisms. The dual of the Lie algebra is seen to be the space of vorticities, and Kelvin's circulation theorem is interpreted as preservation of coadjoint orbits. In this context, Clebsch variables can be understood as momentum maps. The motion of N point vortices is shown to be identifiable with the dynamics on a special coadjoint orbit, and the standard canonical variables for them are a special kind of Clebsch variables. Point vortices with cores, vortex patches, and vortex filaments can be under-

stood in a similar way. This leads to an explanation of the geometry behind the Hald-Beale-Majda convergence theorems for vorticity algorithms. Symplectic structures on the coadjoint orbits of a vortex patch and filament are computed and shown to be closely related to those commonly used for the KdV and the Schrödinger equations respectively. (64 refs.)

113456 Bifurcation of stationary vortex configurations. II. Topology and integrability. J.J.Palmore (Univ. of Illinois, Urbana, IL, USA). *Physica D (Netherlands)*, vol.7D, no.1-3, p.324-9 (May 1983). (Proceedings of the International Conference on Order in Chaos, Los Alamos, NM, USA, 24-28 May 1982).

For pt.I see Nonlinear Problems: Present and Future, p.127, (1982). Studies the dynamics of finitely many vortices in a circular disk and compare the integrability of this problem with that of Kirchhoff's problem of vortices in the plane. The effect of the topology of the phase space on the two Hamiltonian systems is compared. The goal is to apply topological methods uniformly to investigate the flow of these dynamical systems. (4 refs.)

- Proceedings of the International Conference on Order in Chaos See Entry 111307
- Bernoulli on a large scale See Entry 111374
- Observations of order and chaos in nonlinear systems See Entry 111564
- Stability of rotating liquids drops. I. Uncharged drops See Entry 113418
- Experimental investigation of turbulent characteristics in the axisymmetric swirling flow See Entry 113426
- A pair of semicircle theorems in rotatory thermohaline convection See Entry 113442
- Interaction of rotating waves in an active chemical medium .. See Entry 113466
- Viscous flows of stably stratified fluids over semi-circular obstacles See Entry 113490
- Magnetic tornadoes: three-dimensional affine motions in ideal magnetohydrodynamics See Entry 113518
- An experimental and analytical investigation of the particle loss mechanism in a circular flow for laser anemometry See Entry 113523
- Vortex flowmetering See Entry 113534
- Bifurcation and the universal sequence for first-sound subharmonic generation in superfluid helium-4 See Entry 114297
- Bounds on the growth of perturbations to non-parallel steady flow on the barotropic beta plane See Entry 116222

47.35 WAVES

113457 Second order wave diffraction by large cylinders. M.Rahman (Dept. of Appl. Math., Tech. Univ. of Nova Scotia, Halifax, Nova Scotia, Canada).

Int. J. Eng. Sci. (GB), vol.21, no.12, p.1471-82 (1983). A non-linear mathematical model of diffraction theory is formulated to evaluate the wave forces on large cylinders. An attempt is made to amend the coefficient of mass C_M arising in the Morison equation on the linear theory by introducing second-order effects on the irrotational flow part of the wave loading. Analytical solutions are obtained and compared with the experimental data collected by the Hydraulics Laboratory of the National Research Council of Canada, Ottawa. The comparison shows favourable agreement. (9 refs.)

113458 Cyclic gravity waves in deep water. P.J.Bryant (Maths. Dept., Univ. of Canterbury, Christchurch, New Zealand).

J. Aust. Math. Soc. Ser. B (Australia), vol.25, pt.1, p.2-15 (July 1983). Numerical evidence is presented for the existence of unsteady periodic gravity waves of large height in deep water whose shape changes cyclically as they propagate. It is found that, for a given wavelength and maximum wave height, cyclic waves with a range of cyclic periods exist, with a steady wave of permanent shape being an extreme member of the range. The method of solution, using Fourier transforms of the nonlinear surface boundary conditions, determines the irrotational velocity field in the water and the water surface displacement as functions of space and time, from which properties of the waves are demonstrated. In particular, it is shown that cyclic waves are closer to the point of wave breaking than are steady permanent waves of the same wave height and wavelength. (4 refs.)

113459 The stability of internal solitary waves. D.P.Bennett, R.W.Brown, S.E.Stansfield, J.D.Stoughair (Phys. Dept., Case Western Reserve Univ., Cleveland, OH, USA), J.L.Bona.

Math. Proc. Cambridge Philos. Soc. (GB), vol.94, pt.2, p.351-79 (Sept. 1983). A theory is developed relating to the stability of solitary-wave solutions of the Benjamin-Ono equation. This equation is a model for the propagation of internal waves in an incompressible nondiffusive heterogeneous fluid for which the density is nonconstant only within a layer whose thickness is much smaller than the total depth. The authors deal with the full nonlinear problem, and so allowance is made for small but finite perturbations of the solitary-wave solutions of the Benjamin-Ono equation. A result about stability which is practically satisfactory, in that it bears upon the size and shape of the wave in question is presented. (39 refs.)

113460 Destabilization of an initially stable shear flow by internal waves. L.Sh.Tsimring (Inst. of Appl. Phys., Acad. of Sci., Gorkii, USSR).

Oceanology (USA), vol.22, no.4, p.396-9 (1982). Translation of: *Okeanologiya (USSR)*, vol.22, no.4 (1982). [received: Aug. 1983] The effect of a train of internal waves of finite spectral width on shear flow in the neighborhood of the critical layer is analyzed in the quasilinear approximation. The resulting equation describes the deformation of the mean velocity profile. The simple Riemann wave solution for this equation shows that the interaction of the internal waves with the critical layer accelerates the flow and increases the shear velocity in the lower part of this layer. Characteristic times, at which instabilities are generated in the flow by the internal waves, are estimated. (13 refs.)

113461 Nonlinear waves: from hydrodynamics to plasma theory. E.Infeld (Inst. Badan Jadrowych, Warszawa, Poland).

Postepy Fiz. (Poland), vol.34, no.3, p.215-36 (1983). In Polish. Nonlinear hydrodynamic and plasma wave phenomena are considered jointly. A survey of recent theoretical, numerical, and experimental results is given. The bias, if any, is towards plasma physics, but analogies are stressed. (80 refs.)

113462 Surface waves induced by an impinging jet. M.J.Miksis, Lu Ting (Courant Inst. of Math. Sci., New York Univ., New York, NY, USA).

Phys. Fluids (USA), vol.26, no.9, p.2378-84 (Sept. 1983). The oblique impact of a thin or slender jet on the free surface of a semi-infinite stream is studied. Based on the thickness or radius of the jet the Froude number is assumed to be large and the fluid is assumed to be viscous.

By the method of matched asymptotics, the leading term of the solution behind the impact area is constructed. The perturbation solution for the stream away from the impact region and its wake is shown to be equivalent by the linear theory of surface waves with a concentrated load at the impact point and a distributed line load along the wake. The equivalent loads are consistent with considerations of mass and momentum balances and other judicial arguments. (8 refs.)

113463 Some new gravity waves in water of finite depth. J.-M.Vanden-Broeck (Dept. of Math., Univ. of Wisconsin, Madison, WI, USA).

Phys. Fluids (USA), vol.26, no.9, p.2385-7 (Sept. 1983). The results of Chen and Saffman (1980) showing that periodic gravity waves in water of infinite depth are not unique, are generalized for waves in water of finite depth. Some new types of waves are discovered and discussed. (6 refs.)

113464 The calculation of nonlinear short-crested gravity waves. A.J.Roberts (Dept. of Appl. Maths. & Theoretical Phys., Univ. of Cambridge, Cambridge, England).

Phys. Fluids (USA), vol.26, no.9, p.2388-92 (Sept. 1983). A numerical method involving truncated Fourier series is presented for the calculation of properties of short-crested water waves. The method produces accurate results over much of the nonlinear regime. In the case of infinite water depth, calculated results include a representative wave profile and the variation in frequency and energy densities with wave steepness and planform skewness. (12 refs.)

113465 Self-refraction of nonlinear capillary-gravity waves. P.P.Banerjee, A.Korpe, K.E.Lonngrén (Dept. of Electrical & Computer Engng., Univ. of Iowa, Iowa City, IA, USA).

Phys. Fluids (USA), vol.26, no.9, p.2393-8 (Sept. 1983). Self-refraction effects have been observed during the propagation of deep-water capillary-gravity waves. The observations are shown to be in qualitative agreement with the theory of self-focusing and defocusing in a cubically nonlinear medium in the presence of diffraction. (8 refs.)

113466 Interaction of rotating waves in an active chemical medium. V.I.Krinsky, K.I.Agladze (Inst. of Biological Phys., Acad. of Sci., Pushchino, USSR).

Physica D (Netherlands), vol.8D, no.1-2, p.50-6 (July 1983). The interaction of autowave sources is experimentally studied in an active chemical medium with excitable kinetics. Three types of vortices are considered: (1) A spiral wave (S) rotating in a simply-connected medium; (2) a spiral wave rotating around a hole (SH); and (3) a spiral wave (S_N) with topological charge N . It is found that S synchronizes SH (except for very small holes), and spiral waves with lower topological charge synchronize those with higher topological charge. It is also found that the interaction of autowave sources displays some unique properties because of their ability to appear on inhomogeneities, to vanish and to move in the medium. A new phenomenon of induced drift of spiral waves is demonstrated. The drift was induced by high-frequency concentration waves propagating in the medium. A similar drift is observed upon interaction of vortices. The mechanism of the induced drift is explained in terms of wave-break translocation from one wave to another. Using this effect, one can control the location of wave sources in an active medium. (15 refs.)

Singular filaments organize chemical waves in three dimensions. I. Geometrically simple waves See Entry 111460

Transitions to chaos in the Ginzburg-Landau equation See Entry 113419

Thermal waves in a supersonic boundary layer with self-induced pressure See Entry 113472

Radiating barotropic instability See Entry 116107

Water waves, nonlinear Schrödinger equations and their solutions See Entry 116114

Scattering analysis and synthesis of wave trains See Entry 116115

Surface-wave interaction with a deeply submerged circular duct See Entry 116117

Bounds on the growth of perturbations to non-parallel steady flow on the barotropic beta plane See Entry 116222

On the propagation of acoustic waves in a radiating fluid See Entry 116438

47.40 COMPRESSIBLE FLOWS; SHOCK AND DETONATION PHENOMENA

(see also 28.70 Nuclear explosions, 52.35T Plasma shock waves)

113467 On intrinsic properties of viscous, compressible steady plane flows. P.A.Reddy (Evening Coll., Secunderabad, India).

Proc. Natl. Acad. Sci. India Sect. A, vol.52, pt.1, p.99-103 (1982). [received: Aug. 1983] Defining an orthogonal plane geometric net related to the stream-lines and their orthogonal trajectories in an anholonomic space, intrinsic properties of viscous, compressible steady plane flows are studied and enquired as how far the geometry describes the physical laws of the flows under study. (6 refs.)

113468 Effect of the number density of heterogeneities on the critical diameter of condensed explosives. R.Engelke (Los Alamos Nat. Lab., Univ. of California, Los Alamos, NM, USA).

Phys. Fluids (USA), vol.26, no.9, p.2420-4 (Sept. 1983). Experiments are reported which examine the dependence of the critical diameter of a condensed explosive on the number density of heterogeneities present within the material. The form and quantity of heterogeneities present were closely controlled by constructing the heterogeneous materials from a homogeneous one. Reductions in critical diameter of over 40% were produced in some cases, even though a chemically inert material was being introduced into the explosive. The experiments indicate that the distance between heterogeneities is an important parameter in the production of a critical-diameter reduction. (13 refs.)

113469 Ray method for flow of a compressible viscous fluid. M.C.Shen (Dept. of Math., Univ. of Wisconsin, Madison, WI, USA).

SIAM J. Appl. Math. (USA), vol.43, no.4, p.822-33 (Aug. 1983). An asymptotic method is developed for the solution of linear equations governing compressible viscous flow with free surface. The approach used is based upon the ray expansion originally developed by Keller (1978). A general uniform asymptotic expansion is also constructed to remove anomalies where an amplitude function in the ray method expansion becomes infinite. (12 refs.)

113470 Effect of thermal relaxation of attenuation of shock waves in two-phase medium. V.A.Vakhnenko, V.M.Kudinov, B.I.Palamarchuk (Inst. of Electric Welding, Acad. of Sci., Kiev, Ukrainian SSR). *Sov. Appl. Mech. (USA)*, vol.18, no.12, p.1126-33 (Dec. 1982). Translation of: *Prikl. Mekh. (USSR)*, vol.18, no.12, p.91-7 (Dec. 1982). [received: Sept. 1983]

For the purpose of analyzing the effect of relaxation processes on the attenuation of strong shock waves, the authors consider a homogeneous two-phase medium consisting of a gaseous phase and a condensate phase. An explosion occurs in this medium and, as a result, an energy E producing a shock wave be released instantaneously within an infinitesimally small volume. A number of assumptions are made. (11 refs.)

Pulsed high-energy radiographic machine emitting X-rays (PHERMEX): applications to study high-pressure flow and detonation waves See Entry 111838

Compressible laminar boundary layers on a yawed infinite cylinder See Entry 113409

A vortex sheet method for calculating separated two-dimensional flows See Entry 113446

Use of a generalized Stokes model to determine the aerodynamic capture efficiency of non-Stokesian particles from a compressible gas flow See Entry 113492

The discrete Boltzmann equation for gas mixtures. A regular space model and a shock wave problem See Entry 113544

47.40H Transonic flows

113471 Finite element methods for transonic flow analysis. K.E.Tatum (McDonnell Douglas Corp., St. Louis, MO, USA). *AIAA J. (USA)*, vol.21, no.8, p.1071-8 (Aug. 1983).

A finite element method (FEM) for solution of the conservative full potential flow equation is presented as a means for improving the computation of transonic flows about complex geometries. The method does not require and orthogonal mesh, thus removing a major constraint in grid generation. A standard Galerkin finite element formulation is used in conjunction with the artificial compressibility method which stabilizes the algorithm in transonic flow and allows the capture of embedded shock waves. Solution comparisons, including one test case which stresses the capabilities of state-of-the-art finite difference methods, verify the FEM accuracy and geometric capability. (16 refs.)

New splitting-up schemes for solving hyperbolic and parabolic non linear problems: applications to Euler and Navier-Stokes equations See Entry 111450

Domain decomposition methods for nonlinear problems in fluid dynamics See Entry 113403

47.40K Supersonic and hypersonic flows

113472 Thermal waves in a supersonic boundary layer with self-induced pressure. A.I.Derzhavina.

Appl. Math. & Mech. (USA), vol.46, no.4, p.503-8 (1982). Translation of: *Prikl. Mat. & Mekh. (USSR)*, vol.46, no.4, p.635-41 (1982). [received: Sept. 1983]

The linear problem of temperature perturbation on a flat plate in a supersonic stream of gas is considered using the asymptotic theory of plane flow in a boundary layer with free interaction. The problem is solved by applying the Fourier transform in the longitudinal coordinate. The effect of wall temperature variations on the physical characteristics of the gas flow in the boundary layer is investigated. Numerical application of the inverse Fourier transform is used for determining the effect of a given temperature variation on the pressure distribution. (9 refs.)

Temperature requirements and corrosion rates in combustion driven hydrogen fluoride supersonic diffusion lasers See Entry 112986

Simple model for base pressure effects in source flow chemical lasers See Entry 112987

Stabilization of tangential shear instability in shallow water with 'supersonic' fluid flow See Entry 113417

Radiative heat exchange in the vicinity of the critical point of a blunt body with an intensely vaporizing surface in a three-dimensional hypersonic stream of a hydrogen-helium mixture [planetary atmosphere entry] .. See Entry 116423

47.40N Shock-wave interactions

113473 Flame velocity for the onset of detonation. T.Inomata, S.Okazaki, T.Moriwaki, M.Suzuki (Sophia Univ., Tokyo, Japan).

AIAA J. (USA), vol.21, no.8, p.115-18 (Aug. 1983).

Of interest in this study was the collision of a flame with a shock wave emitted from the flame itself and propagated in the opposite direction to the flame after reflection at the end of a combustion tube. The transition to detonate occurred at a critical initial pressure for various tube lengths. It did not begin below a certain limit of the flame velocity. Relations between the detonation induction distance and the minimum flame velocity leading to the detonation and relations between the flame velocity at the collision point and the distance from the collision point and the detonation point are presented. (15 refs.)

113474 The regular case of shock wave diffraction on a wedge partly submerged in fluid. K.A.Bezhanov.

Appl. Math. & Mech. (USA), vol.46, no.4, p.497-502 (1982). Translation of: *Prikl. Mat. & Mekh. (USSR)*, vol.46, no.4, p.628-34 (1982). [received: Sept. 1983]

The pattern of diffraction at the gas-liquid interface, induced by a system of oncoming shock waves of regular interaction in gas impinging on a wedge submerged in the liquid is considered. The wedge of arbitrary angle has its apex at the unperturbed interface with one of its sides at a nearly straight angle to the liquid unperturbed surface. The liquid is assumed only slightly compressible, which makes it possible to consider the problem in linear formulation by the methods proposed. (12 refs.)

113475 Growth and decay of acceleration waves in relaxing gases. A.Rai, K.S.Pandey (School of Appl. Sci., Banaras Hindu Univ., Varanasi, India).

Indian J. Technol., vol.21, no.1, p.5-7 (Jan. 1983). [received: Sept. 1983]

The propagation of acceleration waves has been studied along the characteristic path using the characteristics of the governing quasi-linear system with vibrational relaxation. The law of propagation is determined and the problem of growth and decay of waves has been solved. The critical time t_c is determined when the breakdown of the wave occurs. It is concluded that there exists a critical value of the initial amplitude of the acceleration wave such

that all compressive waves with initial amplitude greater than the critical one will terminate into a shock wave. An initial amplitude less than the critical one will result in a continuous decay. It is also concluded that vibrational relaxation has a stabilizing effect on the wave propagation. (8 refs.)

113476 Molecular velocity distribution functions in an argon normal shock wave at Mach number 7. T.Holtz, E.P.Muntz (Univ. of Southern California, Los Angeles, CA, USA).

Phys. Fluids (USA), vol.26, no.9, p.2425-36 (Sept. 1983).

The streamwise and normal moments of molecular velocity distribution functions throughout an argon normal shock wave have been measured in a Mach number 7.18 wind tunnel flow, and the experimental data have been compared with several analytical and numerical solutions. In the experiments, the molecular population distributions parallel and perpendicular to the direction of flow were derived using a Fabry-Perot etalon to resolve the Doppler shifts in electron-beam-stimulated fluorescence of the gas atoms. Predictions from Monte Carlo techniques give close agreement with the details of the experimental nonequilibrium distribution function contours. Bimodal Maxwellian and ellipsoidal functional forms show only general agreement with overall profile breadth. (37 refs.)

113477 Propagation of strong detonation waves in a dispersed mixture. I.S.Men'shov (V.A. Steklov Math. Inst., Acad. of Sci., Moscow, USSR).

Sov. Phys.-Dokl. (USA), vol.27, no.12, p.1009-11 (Dec. 1982). Translation of:

Dokl. Akad. Nauk SSSR, vol.267, no.4-6, p.808-11 (Dec. 1982). [received: Sept. 1983]

The author examines the problem of propagation of a strong detonation wave in a two-phase medium consisting of gas and solid particles. A difference in the velocities and temperatures of the phases can have a large effect on the structure of the flow of the mixture. (6 refs.)

113478 Structure of detonation waves with unsteady wave fronts in condensed media. V.A.Danilenko, V.M.Kudinov (E.O. Paton Inst. of Electric Welding, Acad. of Sci., Kiev, Ukrainian SSR).

Sov. Phys.-Dokl. (USA), vol.27, no.12, p.1052-3 (Dec. 1982). Translation of: *Dokl. Akad. Nauk SSSR*, vol.267, no.4-6, p.841-3 (Dec. 1982). [received: Sept. 1983]

The authors present results of a physical and a numerical experiment on the structure of the detonation front in liquid-saturated porous explosives and explosive suspensions arranged in cylindrical charges. (11 refs.)

Detonic research infrared radiometer with nanosecond response See Entry 111772

Finite element methods for transonic flow analysis See Entry 113471

Experimental investigation of shock waves produced in water when a cavitation bubble collapses See Entry 113485

Equilibrium parameters behind a shock wave in wet vapor See Entry 113493

Relaxation processes in aerosol streams with polydisperse particle phase See Entry 113496

Growth and decay of sonic discontinuities in nonequilibrium magnetogasdynamics See Entry 113511

47.50 NON-NEWTONIAN DYNAMICS

113479 Local existence theorems for the first and second initial-boundary value problems for a weakly non-Newtonian fluid. M.Renardy (Math. Res. Center, Univ. of Wisconsin, Madison, WI, USA).

Arch. Ration. Mech. & Anal. (Germany), vol.83, no.3, p.229-44 (1983).

The author proves an existence and uniqueness theorem for three-dimensional motions of a certain class of simple, incompressible materials. The constitutive equation is assumed to have, in addition to a Newtonian part, a viscoelastic part given by a smooth, bounded functional of the history of the displacement gradient. Both displacement and traction boundary conditions are considered. (19 refs.)

113480 A note on the Falkner-Skan flows of a non-Newtonian fluid. K.R.Rajagopal (Dept. of Mech. Engng., Univ. of Pittsburgh, Pittsburgh, PA, USA), A.S.Gupta, T.Y.Na.

Int. J. Non-Linear Mech. (GB), vol.18, no.4, p.313-20 (1983).

Non-similar solutions are established for the boundary layer flow of a homogeneous incompressible fluid of second grade past a wedge place symmetrically with respect to the flow direction. The variation of the skin-friction with respect to the non-Newtonian parameters is discussed. (11 refs.)

113481 Shear rate dependence of non-Newtonian viscosity of fluids. Byung Chan Eu (Dept. of Chem., McGill Univ., Montreal, Quebec, Canada). *J. Chem. Phys. (USA)*, vol.79, no.5, p.2315-24 (1 Sept. 1983).

A pair of analytic formulas for the shear viscosity of simple fluids are derived from kinetic equations as functions of shear rate ($\dot{\gamma}$), temperature, and density. One of the formulas is of the form $\eta = \eta_0 \ln[\tau\dot{\gamma} + (1 + \tau^2\dot{\gamma}^2)^{1/2}]/(\tau\dot{\gamma})$, where $\chi = \sqrt{2}\gamma$ and τ is a function of Newtonian shear viscosity η_0 , temperature, and density. The shear viscosities calculated with the formulas compare well with the molecular dynamics shear viscosities of argon. (11 refs.)

113482 Fundamental matrices in micropolar fluids. L.Dragos (Faculty of Math., Bucharest, Rumania), D.Homentcovschi.

Z. Angew. Math. & Mech. (Germany), vol.63, no.8, p.389-91 (1983).

A direct derivation of the two- and three-dimensional fundamental matrices and solutions for the equations of incompressible micropolar fluids which have a steady motion is presented and the integral representation of the solutions of the equations of motion by means of these matrices, is given. (5 refs.)

Oscillations generated in the compression of a viscoelastic body See Entry 113394

Viscoelastic fluid flow exhibiting hysteretic phase changes See Entry 113396

Ray method for flow of a compressible viscous fluid See Entry 113469

47.55 NONHOMOGENEOUS FLOWS

113483 The streamline behaviour near the separation point and separation criterion for viscous flow. Zhang Hanxin, Lu Linsheng, Yu Zechu (Chinese Aerodynamic Res. & Dev. Center, China).

Acta Mech. Sin. (China), no.3, p.227-32 (1983). In Chinese.

The streamline behaviour near the separation point of steady and unsteady viscous flow is studied, and the separation criteria are discussed. It is pointed out that the MRS criterion is necessary when there are two lines with $u=0$, passing through the separation point. For flow described by boundary layer equations, the separation point is a Goldstein singularity, and the MRS criterion is equivalent to the singularity criterion. However, for flow described by Navier-Stokes equations, the separation point is not a singularity, so the singularity criterion is not valid. (8 refs.)

- Axial flow past a cylinder with uniform injectionSee Entry 113414
 Stability of rotating liquids drops. I. Uncharged dropsSee Entry 113418
 Vortex motion in the early stages of unsteady flow around a circular cylinder
See Entry 113447
 Theory of the Leidenfrost phenomenonSee Entry 114301

47.55B Cavitation

- 113484 Comparison of some tubular and Kaplan turbine properties.** J.Kirejczyk (Inst. Maszyn Przepływowych PAN, Gdansk, Poland). *Energetyka (Poland)*, vol.37, no.4, p.148-52 (April 1983). In Polish. [received: Sept. 1983]
 Describes flow, cavitation, dynamic and operating properties of tubular turbines and explains the advantages of their use. Some of the properties are compared with those of Kaplan turbines. (18 refs.)
- 113485 Experimental investigation of shock waves produced in water when a cavitation bubble collapses.** G.V.Dreiden, A.P.Dmitriev, Yu.I.Ostrovskii, M.I.Etinberg (A.F. Ioffe Physicotech. Inst., Acad. of Sci., Leningrad, USSR). *Sov. Phys.-Tech. Phys. (USA)*, vol.28, no.2, p.191-3 (Feb. 1983). Translation of: *Zh. Tekh. Fiz. (USSR)*, vol.53, no.2, p.311-14 (Feb. 1983). [received: Sept. 1983]
 The velocity of shock waves has been measured for shock waves produced by collapsing bubbles in water. The bubbles were produced by focusing light from a pulsed ruby laser to a point in water. The velocity of the shock waves was determined from dark-field Schlieren photographs using double laser pulses produced by an optical delay line. The shock wave velocities were used to calculate the shock wave pressure. The formation of radially irregular regions surrounding a collapsing bubble is explained, and it is found that they form when the gas-liquid interface moves toward the center of collapse of the 'crinkled' boundary of the bubble. (8 refs.)

47.55C Jets

- 113486 Acoustic interaction with a turbulent plane jet—some effects on turbulent structure.** F.W.Chambers (Lockheed-Georgia Co., Marietta, GA, USA), V.W.Goldschmidt. *AIAA J. (USA)*, vol.21, no.8, p.1057-8 (Aug. 1983).
 Results of a study to determine the nature of the interaction mechanism linking an applied sound field and an incompressible turbulent plane jet are reported. Measurements of the effects of applied sound on the jet mean flow behaviour and measurements of turbulence intensities, Reynolds shear stresses, and turbulent energy spectra were performed and reported by Chambers and Goldschmidt (1982). The results of some of the turbulence measurements and the conclusions that may be drawn about the interaction mechanism are presented. (8 refs.)
- 113487 Numerical study on flow developments for the rise of buoyant plumes in a stratified environment.** R.R.Hwang, Chyi-Jang Shiau (Inst. of Phys., Acad. Sinica, Taipei, Taiwan). *Annu. Rep. Inst. Phys. Acad. Sin. (Taiwan)*, vol.12, p.251 (Dec. 1982). [received: Sept. 1983]
 A numerical technique for integrating the full Navier-Stokes and diffusion equations through an initial value problem has been used to investigate the time development of a line buoyant source issuing in a density-stratified environment. The basic physical features and some structures of the interactions of the motion at the intermediate mixing region are obtained. The stratification tends to inhibit the flow development of the buoyant source and to encourage the formation of a recirculatory vortex on the lower region near the source and the upper region. (no refs.)
- 113488 Axial coherence functions of circular turbulent jets based on an inviscid calculation of damped modes.** P.Plaschko (Hermann-Fottinger-Inst. für Thermo- und Fluidodynamik, Tech. Univ. Berlin, Berlin, Germany). *Phys. Fluids (USA)*, vol.26, no.9, p.2368-72 (Sept. 1983).
 It is often assumed that damped instability modes may exist even in the absence of viscosity, if during the downstream evolution of the waves, velocity gradients become so small to support amplified disturbances. A modified inviscid calculation of damped modes is done, and the corresponding eigenvalues are compared with those given by the Orr-Sommerfeld theory. It is shown that the use of inviscid results in a slow-flow divergence stability and in a linear turbulence model yields theoretical predictions for amplitudes, phases, and coherence functions that are in reasonable agreement with experimental trends. (16 refs.)

- Mixing and diffusion of heated water discharge for power plantsSee Entry 113421
 Stagnation point heat transfer for Jet impingement to a plane surfaceSee Entry 113431
 Vortex structure of circular jets in crossflowSee Entry 113452
 Surface waves induced by an impinging jetSee Entry 113462
 The visible shape and size of a turbulent hydrocarbon jet diffusion flame in a cross-windSee Entry 115553

47.55H Stratified flows

- 113489 Laboratory study on the two-dimensional flows of stratified fluids over barriers.** R.R.Hwang, Shain-Way Jang (Inst. of Phys., Acad. Sinica, Taipei, Taiwan). *Annu. Rep. Inst. Phys. Acad. Sin. (Taiwan)*, vol.12, p.249 (Dec. 1982). [received: Sept. 1983]
 Describes an experimental study of a stratified fluid of finite depth flowing over obstacles which induce flow separation and turbulence on the lee side, in which the inviscid model is no longer useful. Various properties of the flow field, such as the development of lee waves behind the obstacle, the blocking effect upstream, the effect of viscosity, and in particular the criterion for the onset of gravitational instability in the lee-wave field are observed and analysed. Lee waves produced by obstacles in stratified flow depend on the internal Froude number, the ratio of the height of obstacles to the channel depth, the ratio of the height to the half width of obstacles and the Reynolds number of the flow. Therefore, the existence of upstream influence and the flow separation induced by the obstacle have great effect in some flow conditions on the development of the lee-wave field. (no refs.)

- 113490 Viscous flows of stably stratified fluids over semi-circular obstacles.** R.R.Hwang, Shain-Way Jang (Inst. of Phys., Acad. Sinica, Taipei, Taiwan). *Annu. Rep. Inst. Phys. Acad. Sin. (Taiwan)*, vol.12, p.252 (Dec. 1982). [received: Sept. 1983]
 Numerical techniques of the ADI method for integrating the time-dependent Navier-Stokes equations, which have proven useful in the study of homogeneous viscous flows, have been extended to handle the flow of a stably stratified viscous fluid over a ridge of semi-circular cylinders of infinite length. Various properties of the flow field and the characteristics of the lee waves formulated are investigated. The stratification tends to encourage the development of overturning flow regions (rotors) on the lee slope of the ridge and the formation of such region on the upstream slope and down-stream from the ridge. For stratified flows over obstacles, the fluid below the top of the obstacle becomes partially blocked for flows with slow motion or small values of internal Froude number. (no refs.)
- Models for calculating the mass flow of a two-phase system on the basis of measured density and momentum flux valuesSee Entry 112395**
Numerical study on flow developments for the rise of buoyant plumes in a stratified environmentSee Entry 113487

47.55K Multiphase flows

- 113491 Diffusional transport of nonspherical aerosol particles.** J.Heyder, G.Scheuch (Gesellschaft für Strahlen- und Umweltforschung mbH, Frankfurt am Main, Germany). *Aerosol Sci. & Technol. (USA)*, vol.2, no.1, p.41-4 (1983).
 The diffusional losses of spheres and particles consisting of two equal spheres in contact (dumbbells) from laminar aerosol-flows on surfaces of cylindrical tubes were measured with a laser aerosol size spectrometer. From losses of the nonspherical particles in the tubes a diameter could be calculated for a fictitious sphere that would have been lost in the tubes with the same average probability as the nonspherical particle. This diameter is termed the thermodynamic diameter of the nonspherical particle. It was larger than the volume equivalent diameter of the nonspherical particles. The shape factors were 1.052 for dumbbells consisting of two 82 nm spheres and 1.069 for dumbbells consisting of two 102 nm spheres. (6 refs.)
- 113492 Use of a generalized Stokes number to determine the aerodynamic capture efficiency of non-Stokesian particles from a compressible gas flow.** R.Israel, D.E.Rosner (Chem. Engng. Dept., Yale Univ., New Haven, CT, USA). *Aerosol Sci. & Technol. (USA)*, vol.2, no.1, p.45-51 (1983).
 The aerodynamic capture efficiency of small but non-diffusing particles suspended in a high-speed stream flowing past a target is known to be influenced by parameters governing (a) small particle inertia, (b) departures from the Stokes drag law (associated with local particle Reynolds numbers greater than unity), and (c) carrier fluid compressibility (at nonnegligible free-stream Mach numbers). By defining an effective Stokes number in terms of the actual (prevailing) particle stopping distance, local fluid viscosity, and inviscid fluid velocity gradient at the target nose. The authors show that these effects are well correlated in terms of a 'standard' (cylindrical collector, Stokes drag, incompressible flow $Re^{1/2} \gg 1$) capture efficiency curve. They are thus led to a correlation that (a) simplifies aerosol capture calculations in the parameter range already included in previous numerical solutions, (b) allows rational engineering predictions of deposition in situations not previously specifically calculated, (c) should facilitate the presentation of performance data for gas cleaning equipment and aerosol instruments. (15 refs.)
- 113493 Equilibrium parameters behind a shock wave in wet vapor.** N.M.Kuznetsov, E.I.Timofeev, B.E.Gelfand (Inst. of Chem. Phys., Acad. of Sci., USSR). *High Temp. (USA)*, vol.20, no.6, p.917-21 (Nov.-Dec. 1982). Translation of: *Teplofiz. Vys. Temp. (USSR)*, vol.20, no.6, p.1153-7 (Nov.-Dec. 1982). [received: Sept. 1983]
 Relations are presented for the shock wave speed and the specific volume. The authors have investigated regions of condensation or evaporation behind the shock front as a function of the state of the water vapor mixture ahead of the wave. They have determined conditions for which there is transition from condensation to evaporation. It is shown that for low values of the specific volume, close to that of the liquid, there is always condensation of vapor behind the shock. For large initial values of specific volume there is partial vapor condensation behind the shock wave, and this is replaced by evaporation as the pressure in the wave increases. (9 refs.)
- 113494 Motion and precipitation of a cloud of hot particles.** G.M.Makhviladze, O.I.Melikhov (Inst. of Problems in Mech., Acad. of Sci., Moscow, USSR). *Sov. Phys.-Dokl. (USA)*, vol.27, no.12, p.1054-6 (Dec. 1982). Translation of: *Dokl. Akad. Nauk SSSR*, vol.267, no.4-6, p.844-7 (Dec. 1982). [received: Sept. 1983]
 The authors consider the case of gas suspensions having a small volume fraction of particles, $\alpha_2 \ll 1$, and a small ratio of the true densities of the phases, $\epsilon = \rho_{10}/\rho_2 \ll 1$. It is assumed that the temperature is constant over the volume of a particle, that the collisions, fractionation, and evaporation of the particles are not important, that the viscous dissipation of energy does not come into play, and that the viscosity η and thermal conductivity λ are constant. (6 refs.)
- 113495 Vibration effects in bodies with a gas-liquid medium.** V.D.Kubenko, V.D.Lakiza, V.S.Pavlovskii, N.A.Pelykh (Inst. of Mech., Acad. of Sci., Kiev, Ukrainian SSR). *Sov. Appl. Mech. (USA)*, vol.18, no.12, p.1109-18 (Dec. 1982). Translation of: *Prikl. Mekh. (USSR)*, vol.18, no.12, p.72-82 (Dec. 1982). [received: Sept. 1983]
 Investigates the dynamic behavior and the stability of gas bubbles and their local accumulations in homogeneous and two-layer liquids with allowance for such factors as vibrations of the free surface of the liquids and their interface, the elastic properties of the carrying body, and the interaction of the gas-liquid system with the carrying body and the vibration source, which have a significant effect on the realization of various modes in such systems. (9 refs.)
- 113496 Relaxation processes in aerosol streams with polydisperse particle phase.** P.Roth (Univ. Gesamthochschule, Duisburg, Germany), K.Thielen. *Z. Angew. Math. & Mech. (Germany)*, vol.63, no.8, p.341-8 (1983). In German.
 Starting from the principles of two-phase-flow theory the relaxation process of an aerosol with very small polydisperse solid particles behind shock waves has been studied. Different size distributions of the particles in the initial state have been assumed. The overall volume concentration of the particles should be small. Therefore the exchange processes between the phases have a weak influence on the gas phase, only. For the momentum and heat transfer proc-

esses, molecular effects have been taken into account by simple Knudsen number corrections. Different computations show the time-dependent deformation of the particle size distribution function during the aerosol relaxation behind shock waves. (15 refs.)

113497 Study of momentum transfer in two-fluid formulation of two-phase flow. G.Egely, P.Saha.

Report KFKI-1983-84, Hungarian Acad. Sci., Budapest (1983), 22 pp.

The following topics were dealt with: Advanced nuclear safety codes such as TRAC and RELAP5 use two-fluid hydraulic models. However, there are uncertainties for the application of different correlations. This paper intends to show the effects and importance of a number of correlations for wall friction, interphase drag, and virtual mass. It has been shown that the homogeneous wall shear model yields good results up to the annular flow regime, the single-bubble drag correlation is acceptable, and the inclusion of virtual mass coefficient is helpful. It has been found that the critical Weber number is not appropriate for bubble radius calculation; it predicts an opposing tendency when compared with the test data. Also, a two-phase diffuser efficiency is required for diverging ducts and a correlation for the same has been proposed. (24 refs.)

Bernoulli on a large scale See Entry 111374

High frame-rate neutron radiography of dynamic events See Entry 111858

Models for calculating the mass flow of a two-phase system on the basis of measured density and momentum flux values See Entry 112395

Bubble growth in variable pressure fields See Entry 112424

Behavior of a local cluster of gas bubbles in a vibrating fluid See Entry 113420

Propagation of strong detonation waves in a dispersed mixture See Entry 113477

An experimental and analytical investigation of the particle loss mechanism in a circular flow for laser anemometry See Entry 113523

Procedure for measuring the thickness and wave characteristics of the surface of the liquid film in annular-mist flows of steam and water See Entry 113528

High speed motion neutron radiography of two-phase flow See Entry 113541

Critical point phenomena in fluids See Entry 114130

47.55M Flow through porous media

113498 A stability model for steam generators. A.Duyar (Dept. of Mech. Engrg., Florida Atlantic Univ., Boca Raton, FL, USA), R.J.Gross.

Math. Modelling (USA), vol.4, no.1, p.41-59 (1983).

A mathematical model to analyze the stability of the two-phase flow in a generalized steam generator is developed. A counter flow heat exchanger in which a high temperature primary fluid heats and vaporizes a lower temperature secondary fluid is considered as the system. The governing equations of this system is obtained by using the transient field equations, constitutive relations, boundary conditions and the initial conditions of both the primary and the secondary fluids. The governing equations of the secondary fluid are decoupled from the equations of the primary fluid by determining a heat flux profile and superimposing it on the wall of the channel of the secondary fluid. With this superimposed heat flux profile an equivalent system is obtained which utilizes the fundamental equations of the secondary fluid to analyze the stability of the flow. To investigate the stability of the system, a relation between the variation of the inlet velocity and the variation of the total channel pressure drop is needed. The Laplace transform of this relation is called the transfer function of this system and is obtained by using a small perturbation technique and linearization. Liapunov's theorem is used to investigate the stability of the nonlinear system from linearized system. The theoretical predictions of this model are observed to be in agreement with experimental results. (10 refs.)

113499 Solid particle mixing in a continuously operated fluidized bed reactor. K.Wittmann, D.Wipperm (Inst. fur Tech. Chem., Univ. Hannover, Hannover, Germany), H.Schlingmann, H.Helmrich, K.Schugerl.

Chem. Eng. Sci. (GB), vol.38, no.9, p.1391-7 (1983).

In a bench-scale fluidized bed reactor, 20 cm in dia., residence time distribution of solid particles ($d_p = 137 \mu\text{m}$) were measured by the radionuclide technique ($^{24}\text{Na}_2\text{CO}_3$) in the absence and in the presence of the chemical reaction $2\text{NaHCO}_3 \rightarrow \text{Na}_2\text{CO}_3 + \text{CO}_2 + \text{H}_2\text{O}$. The residence time distributions were evaluated by a backflow cascade model by nonlinear optimization. The radial and longitudinal concentration profiles of NaHCO_3 in the emulsion phase of the reactor were measured during steady-state operation. The solid is well-mixed. The connection of the measured bubble properties with the longitudinal solid dispersion coefficient and the use of the Haines-King-Woodburn model (1972) allows one to calculate the solid dispersion coefficient in the bubble-free emulsion phase. (19 refs.)

113500 Effect of shape factor and solid concentration on electrical conductivities of fluidized beds. P.Dakshinamurthy, C.V.Ramachandramurthy, V.Subrahmanyam, K.S.Rajanandam (Dept. of Chem. Engrg., Andhra Univ., Waltair, India).

Indian J. Technol., vol.21, no.1, p.37-8 (Jan. 1983). [received: Sept. 1983]

The dependence of electrical conductivities of two-phase fluidized beds on solid concentration and particle shape factor is established. The electrical conductivities of liquid fluidized beds with salt water as the continuous medium and particles of different sizes and shapes covering a range of shape factor 0.54-1.0 and solid concentration 0.05 to that of packed bed were measured. The data are correlated by the equation: $\epsilon_s = (0.59 + 0.41\psi_s)(1 - \alpha)$. (11 refs.)

113501 Flow of a viscous fluid through a porous medium bounded by a vertical surface. A.Raptis, C.Perdikis (Dept. of Mech., Univ. of Ioannina, Ioannina, Greece).

Int. J. Eng. Sci. (GB), vol.21, no.11, p.1327-30 (1983).

Unsteady free convection flow of a viscous fluid through a porous medium bounded by a vertical porous infinite surface is presented. Analytical expressions for the velocity and temperature fields are obtained when the temperature of the fluid and the temperature away from the surface have a difference which varies as some power of time. Also the velocity profiles are shown graphically for different values of the permeability parameter. (6 refs.)

Free convection flow through a porous medium bounded by two horizontal walls See Entry 113436

Drag coefficients of a sphere and a bed of spherical elements See Entry 113504

Flow in an open channel bend with permeable bed See Entry 113506

47.60 FLOWS IN DUCTS, CHANNELS, AND CONDUITS

(for biological fluid dynamics, see 87.45)

113502 Unsteady flow in branched pipeline systems. B.F.Glikman.

Power Eng. (J. Acad. Sci. USSR) (USA), vol.21, no.1, p.83-92 (1983). Translation of: **Izv. Akad. Nauk SSSR Energ. & Transp.,** vol.21, no.1, p.88-99 (1983).

The problem of formation of a linear mathematical model for a branched pipeline system with distributed parameters is considered. The matrix topology of circuit theory is used to develop a technique for formalized construction of the transfer functions of pipeline systems made up of passive and active elements and containing elements with both distributed and lumped parameters. An example is given of the formation of a mathematical model for a branched (ramified) pipeline system containing elements with distributed parameters. (4 refs.)

113503 Experimental investigations on the rewetting of hot horizontal annular channels. V.V.Raj (Reactor Engng. Div., Bhabha Atomic Res. Centre, Bombay, India).

Int. Commun. Heat & Mass Transfer (GB), vol.10, no.4, p.299-311 (July-Aug. 1983).

Deals with experimental investigations on the rewetting of hot horizontal annular channels. Experiments have been carried out, at atmospheric pressure, on a stainless steel test section. The temperature of the inner surface of the annular channel was varied from 200 to 500°C and the flow rate from about 0.7 kg/min. to 9.5f kg/min. These experiments indicate that stratification effects are significant, more so at lower flows. The rewetting front is included. The rewetting velocity increases as the flow rate is increased and decreases as the initial wall temperature is increased. (3 refs.)

113504 Drag coefficients of a sphere and a bed of spherical elements. A.R.Khenven, D.M.Lyakhov.

High Temp. (USA), vol.20, no.6, p.886-90 (Nov.-Dec. 1982). Translation of: **Teplofiz. Vys. Temp. (USSR),** vol.20, no.6, p.1119-23 (Nov.-Dec. 1982). [received: Sept. 1983]

A nonlinear model of the relation between the drag coefficient and the Reynolds number is used to obtain expressions connecting the drag coefficients of a sphere and a bed of spherical elements with the Reynolds number in a wide range of the latter. (7 refs.)

113505 Calculation of transient heat transfer in channels with Neumann boundary conditions. A.A.Ryadno (Dnepropetrovsk State Univ., Ukrainian SSR).

High Temp. (USA), vol.20, no.6, p.890-6 (Nov.-Dec. 1982). Translation of: **Teplofiz. Vys. Temp. (USSR),** vol.20, no.6, p.1124-30 (Nov.-Dec. 1982). [received: Sept. 1983]

An algorithm is developed for the solution of transient boundary-value problems in convective heat transfer with specific application to the case of longitudinal laminar flow of an incompressible fluid past a bundle of rods. (7 refs.)

113506 Flow in an open channel bend with permeable bed. M.N.Channabasappa, K.G.Umapathy, I.V.Nayak (Dept. of Maths., Karnataka Regional Engng. Coll., Srinivasnagar, India).

Indian J. Technol., vol.21, no.2, p.49-52 (Feb. 1983). [received: Sept. 1983]

The flow of viscous fluid in an open channel bend with a non-erodible permeable bed is considered. Using the slip boundary condition at the nominal surface proposed by Beavers and Joseph (1967), the authors obtain expressions for velocity components and the free surface profile. It is seen that the effect of the permeability of the bed is to increase the velocity components and the super-elevation. (4 refs.)

113507 Effects of axial conduction in laminar tube flow with convective boundaries. B.Vick (Mech. Engrg. Dept., Virginia Polytech. Inst. & State Univ., Blacksburg, VA, USA), M.N.Ozisik, D.F.Ullrich.

J. Franklin Inst. (USA), vol.316, no.2, p.159-73 (Aug. 1983).

Heat transfer in laminar tube flow with convective boundary conditions and axial heat conduction in the fluid is solved exactly. The effects of the external Biot numbers and the axial conduction in fluid on the temperature distribution and the local Nusselt number are determined for both the upstream and the downstream regions. In order to illustrate the effects of velocity profile, the results for the slug flow and the parabolic velocity profiles are plotted simultaneously. The heat transfer characteristics of the flow are found to be rather sensitive to the Peclet number, the external Biot numbers and the velocity profile in the thermal entrance region. (37 refs.)

113508 Generalization of experimental data of hydraulic friction, inside helically corrugated tubes. P.A.Savel'ev, Yu.S.Voskresenskii.

Latv. PSR Zinat. Akad. Vestis Fiz. Teh. Zinat. Ser. (USSR), no.4, p.79-85 (1983). In Russian.

The authors have made an analysis of geometrical ratios of helically corrugated tubes on hydraulic friction. A new generally geometric parameter h/D_e has been proposed with resulting formulae for calculating hydraulic friction. Here h is the height of the spiral projections, D_e diameter of the helical curve lying on the face of the supposed cylinder with the diameter d_e . The offered formulae approximate experimental results of various investigators, error maximum being 10.8%. In the region of Reynold's number from 1×10^4 to 5×10^4 for tubes with the height of helical projections $0.1 < h/d < 0.3$, where d is diameter of the smooth portion within the tube. (20 refs.)

113509 Current structure of channel flows according to the mean velocity distribution in the channel cross section. O.N.Me'n'nikova, Yu.G.Pyrkin (Dept. of Phys. of Sea & Inland Water, Moscow Univ., Moscow, USSR).

Moscow Univ. Phys. Bull. (USA), vol.37, no.5, p.114-17 (1982). Translation of: **Vestn. Mosk. Univ. Ser. 3 (USSR),** vol.37, no.5, p.97-9 (1982).

Riparian autonomous currents are investigated in channel flow, and the force field is determined from the isotach distribution in the flow cross section. The criteria determining the flow parameters at which riparian autonomous currents arise are discussed. (3 refs.)

Liquid solidification in laminar tube flow with internal heat sources See Entry 112409

Laminar flow in a meandering channel See Entry 113413

Has a small-scale structure in turbulence been experimentally verified? See Entry 113427

Effects of viscous dissipation on temperature field in flows through ducts of nonuniform cross-section See Entry 113438

Diffusional transport of nonspherical aerosol particles See Entry 113491

An approximate solution for diffusion and reaction in a non-ideal tubular reactor See Entry 113520

Procedure for measuring the thickness and wave characteristics of the surface of the liquid film in annular-mist flows of steam and water ..See Entry 113528
 Flowmetering in a long-distance pipeline grid for ethylene under high pressureSee Entry 113539

47.65 MAGNETOHYDRODYNAMICS AND ELECTROHYDRODYNAMICS

(for MHD in plasma, see 52.30)

113510 Magnetohydrodynamic free convective effect for an incompressible viscous fluid past an infinite limiting surface. A.Raptis, G.Tzivanidis (Dept. of Mech., Univ. of Ioannina, Ioannina, Greece).

Astrophys. & Space Sci. (Netherlands), vol.94, no.2, p.311-17 (Aug. 1983).
 An analysis of the effect of a magnetic field on the free convective flow of an incompressible, electrically conducting and viscous fluid past at infinite vertical limiting surface, has been carried out. The limiting surface does not move, there is a constant heat flux at the limiting surface, the free velocity is constant and the magnetic Reynolds number is not small. The effects of the magnetic parameter and the Grashoff number on the flow are discussed. (6 refs.)

113511 Growth and decay of sonic discontinuities in nonequilibrium magnetogasdynamics. B.G.Verma, R.C.Srivastava, A.H.Khan (Dept. of Math., Gorakhpur Univ., Gorakhpur, India).

Astrophys. & Space Sci. (Netherlands), vol.94, no.2, p.361-9 (Aug. 1983).
 The phenomenon associated with sonic discontinuities in nonequilibrium magnetogasdynamics is studied by the use of singular surface theory. The fundamental differential equations for growth and decay of sonic discontinuities are formulated. This class of equations is solved completely and for plane case in particular. The critical time at which a sonic wave terminates in the shock waves is also obtained. (8 refs.)

113512 Heat and mass transfer of an oscillatory flow with Hall current. H.L.Agrawal, P.C.Ram, V.Singh (Dept. of Appl. Math., Banaras Hindu Univ., Varanasi, India).

Astrophys. & Space Sci. (Netherlands), vol.94, no.2, p.383-93 (Aug. 1983).
 Analyzes the effect of a Hall current on the thermal and mass diffusion of an electrically conducting liquid past an infinite vertical porous plate. Analytical expressions for the transient velocity, the transient temperature in the boundary layer and the skin-friction on the plate are derived. The defects of various parameters on the velocity, temperature, shearing stresses and rate of heat transfer are shown. (5 refs.)

113513 Finite difference analysis of MHD free-convection flow past an accelerated vertical porous plate. A.K.Singh (Dept. of Math., Banaras Hindu Univ., Varanasi, India).

Astrophys. & Space Sci. (Netherlands), vol.94, no.2, p.395-400 (Aug. 1983).
 The effect of a uniform transverse magnetic field on the free-convection flow of an electrically conducting fluid past a uniformly accelerated infinite vertical porous plate is discussed. A finite-difference method is used to obtain the solution of the governing equations when the Prandtl number is not equal to unity. The velocity profiles are shown graphically for both cooling and heating of the porous plate. The numerical values of the skin-friction are entered in table and the effects of the various parameter on the flow field are discussed. (5 refs.)

113514 On the analysis of MHD flow of a two-component gas and its application. Rong Sheng (Inst. of Mech., Acad. Sinica, Peking, China).

Acta Mech. Sin. (China), no.3, p.293-7 (1983). In Chinese.
 The MHD flow of a two-component gas under the action of an axial magnetic and radial electric field is studied. The distributions of rotational velocity, temperature, concentration and separation coefficient of isotopes Ne^{20} and Ne^{22} in an electromagnetic separator are given. (3 refs.)

113515 MHD free convection flow past an accelerated vertical plate. A.Raptis (Dept. of Mech., Univ. Ioannina, Ioannina, Greece), A.K.Singh.

Int. Commun. Heat & Mass Transfer (GB), vol.10, no.4, p.313-21 (July-Aug. 1983).
 The effect of a uniform transverse magnetic field on the free convection flow of an electrically conducting fluid past an infinite vertical plate for both the classes of impulsive as well as uniformly accelerated motion of the plate is discussed. In this analysis, the magnetic lines of force are assumed to be fixed relative to the plate. Laplace transform technique has been used to obtain the expressions for the velocity field and skin-friction for both cases. It is found that the effect of the magnetic field is to increase the velocity field in both cases. (4 refs.)

113516 On kinematic properties of hydromagnetic fluid flows. G.Purushotham (Dept. of Math., Jawaharlal Nehru Technol. Univ., Nagarjunasagar Engng. Coll., Hyderabad, India).

Proc. Natl. Acad. Sci. India Sect. A, vol.52, pt.2, p.131-40 (1982). [received: Aug. 1983]

The nonlinear character of the differential equations governing fluid-dynamic problems has presented enormous mathematical difficulties to find out exact possible flows. Consequently many interesting methods (inverse and semi-inverse) have been introduced, to study the kinematic and the kinetic properties of the flows. The introduction of the geometric theory of curves and surfaces in fluid flow theory is also one such method, which received considerable attention of the investigators in recent years, and presents the possible flows. Extending this concept to the hydromagnetic fluid flows, in which the field is assigned unidirectional and introducing triply orthogonal spatial curves of congruences C^3 in Euclidean space E^3 , related to the streamline, various kinematic properties of the flows are examined. (9 refs.)

113517 Noncanonical Hamiltonian formulation of ideal magnetohydrodynamics. D.D.Holm, B.A.Kupershmidt (Center for Nonlinear Studies, Los Alamos Nat. Lab., Los Alamos, NM, USA).

Physica D (Netherlands), vol.7D, no.1-3, p.330-3 (May 1983). (Proceedings of the International Conference on Order in Chaos, Los Alamos, NM, USA, 24-28 May 1982).

A noncanonical Poisson structure for ideal magnetohydrodynamics is presented and identified with a differential Lie algebra. (10 refs.)

113518 Magnetic tornadoes: three-dimensional affine motions in ideal magnetohydrodynamics. D.D.Holm (Center for Nonlinear Studies, Los Alamos Nat. Lab., Los Alamos, NM, USA).

Physica D (Netherlands), vol.8D, no.1-2, p.170-82 (July 1983).

From Hamilton's principle and a factorization Ansatz the author derives a class of exact solutions for three-dimensional motion in ideal, compressible MHD. These exact nonlinear solutions are motions generated by time-dependent affine transformations, under which the fluid rotates, circulates and deforms. They reduce to three-dimensional self-similar solutions when rotation is absent. Continuous symmetries of Hamilton's principle for the affine MHD motions generate various constants of motion. Discrete symmetries establish duality relations among classes of solutions. In a special case, rotational and

circulatory MHD motion is expressed as classical mechanical motion upon its own symmetry group, the Lie group $O(4)$, in the well-known Arnold-Lax-Euler commutator form, $M = [\omega, M]$. (20 refs.)

113519 Unsteady magnetohydrodynamic Couette flow. A.K.Singh, N.Kumar (Dept. of Math., Banaras Hindu Univ., Varanasi, India).

Wear (Switzerland), vol.89, no.2, p.125-9 (15 Aug. 1983).
 The effect of a uniform transverse magnetic field on the Couette flow of an electrically conducting fluid between two parallel plates for impulsive and uniformly accelerated motion of one of the plates is discussed. The magnetic lines of force are assumed to be fixed relative to the moving plate. The Laplace transform technique has been used to obtain the expressions for the velocity field and skin friction. The effect of the magnetic field is to increase the velocity field in both cases. (3 refs.)

On the geometry of vortex-line in rotating viscous incompressible hydromagnetic fluid flowsSee Entry 113453

Czochralski crystal growth in an axial magnetic field: effects of Joule heatingSee Entry 115044

Dependence of MHD turbulence spectra on the velocity field-magnetic field correlationSee Entry 116446

47.70 REACTIVE, RADIATIVE, OR NONEQUILIBRIUM FLOWS

113520 An approximate solution for diffusion and reaction in a non-ideal tubular reactor. K.M.Nigam, K.D.P.Nigam, V.K.Srivastava (Dept. of Chem. Engng., Indian Inst. of Technol., New Delhi, India).

Int. Commun. Heat & Mass Transfer (GB), vol.10, no.4, p.341-8 (July-Aug. 1983).

An analytical solution for diffusion with homogeneous first order chemical reaction in laminar flow of a Newtonian fluid through tubular reactor is presented within the framework of Taylor's dispersion theory. The novelty about the work is the Galerkin's technique has been used for the first time to obtain the expression for the effective dispersion coefficient. (18 refs.)

113521 A Eulerian-Lagrangian model for turbulent combustion. R.Borghi, E.Pourbaix (ONERA, Chatillon, France).

Rech. Aerosp. (France), no.4, p.245-55 (July-Aug. 1983). In French.
 For predicting reactive flows in turbomachine combustion chambers, both turbulence and combustion (usually represented by a set of chemical reactions involving several species) must be taken into account simultaneously. When this is done, the classical Eulerian models, using the probability density function (PDF) of mass fractions and temperature become doubtful or impossible to solve numerically. However, the use of 'Lagrangian models in the phase space', makes it possible to define a sort of sketch on the PDF, even in the case of a multidimensional PDF. A simple integration along this sketch then provides all the mean characteristic values, at each point of the flow field. (18 refs.)

Singular filaments organize chemical waves in three dimensions. I. Geometrically simple wavesSee Entry 111460

Temperature requirements and corrosion rates in combustion driven hydrogen fluoride supersonic diffusion lasersSee Entry 112986

Simple model for base pressure effects in source flow chemical lasersSee Entry 112987

Velocity statistics in premixed turbulent flamesSee Entry 113425

Indirect measurement of the thermal-acoustic efficiency spectrum of a long turbulent burnerSee Entry 113429

Interaction of rotating waves in an active chemical medium ..See Entry 113466

Solid particle mixing in a continuously operated fluidized bed reactorSee Entry 113499

Growth and decay of sonic discontinuities in nonequilibrium magnetogasdynamicsSee Entry 113511

47.80 INSTRUMENTATION FOR FLUID DYNAMICS

113522 Hybrid processing for phase measurement in metrology and flow diagnostics. I.Prikryl, C.M.Vest (Dept. of Mech. Engng. & Appl. Mech., Univ. of Michigan, Ann Arbor, MI, USA).

Appl. Opt. (USA), vol.22, no.18, p.2844-9 (15 Sept. 1983).
 A hybrid optical/digital processing scheme for measuring phase distributions is described and demonstrated. It is intended to be an alternative to interferometric methods of measuring optical path length changes in flow diagnostics and can also be used as a flow visualization technique. The processing scheme enables one to make accurate measurements of phase at arbitrary points in the image plane. The system is based on a simple coherent optical Fourier processor but incorporates three separate measurements and postdetection digital processing to eliminate extraneous parts of the signal. The addition of a holographic filter to the system enables one to measure deformation or displacement of diffusely reflecting opaque objects. The technique is demonstrated by using it to visualize the flow of an expanding compressible gas jet and to measure the optical path length through a heated plume of air. (11 refs.)

113523 An experimental and analytical investigation of the particle loss mechanism in a circular flow for laser anemometry. H.Bessling (Inst. fur Entwurfsaerodynamik, DFVLR, Braunschweig, Germany).

Atomkernenerg. Kerntechnik (Germany), vol.42, no.2, p.111-16 (1983). In German.
 Investigations by laser anemometry in wind tunnels concerning the construction of airfoils or blades of turbines require light scattering particles of definite particle number concentration and particle size distribution in the test volume. Particle analysis was performed by addition of aerosol in order to reach the standard values. A simplified model conception also applicable for other devices with circular flow was developed for the particle loss mechanism. The comparison of calculated and experimentally estimated data are satisfactory in considering the magnitude of errors by aerosol measurement. (16 refs.)

113524 Fluid flow control for the intermittent extended aeration process. R.Olavarria, V.H.Pham, G.Malvicini.

Process Eng. (Australia), vol.11, no.3, p.27, 29 (March 1983).
 Intermittent extended aeration processes are being more and more frequently used by the relevant authorities to treat both municipal and industrial waste water. Inherent in this process is the fact that while the inflow of waste water can occur throughout the entire cycle, the withdrawal of the effluent is on an intermittent basis. The process is characterized by low F/M ratio in a normal operation and a very slow rate of sludge formation. (3 refs.)

113525 X-ray visualisation of high speed phenomena: application to the behavior of materials under high explosives loading. A.Hauducoeur, J.Fischer, R.Guix (CEA-Vaujours, Sevran, France).

Proc. SPIE Int. Soc. Opt. Eng. (USA), vol.312, p.60-5 (1983). In French. 1st European Conference on Cineradiography with Photons or Particles, Paris, France, 18-21 May 1981).

Flash Radiography and Cineradiography allow the visualisation of high speed phenomena and the stop-motion effect with recording on film of qualitative and quantitative data on the dynamic state of the matter under very intense shock waves. The authors present a set of experimental devices and results obtained with a large range of flash X-ray generators, i.e. small generators made with Marx discharge circuits coupled to void X-ray tubes, working up to 2.5 MV and a big flash machine, GREC used with very absorbing materials. The applications illustrate a large field of experiments in the field of shock waves, interaction of 2 shock or detonation waves, flow visualisation of detonation, Taylor instabilities, metal jetting, spalling in iron, etc. (1 ref.)

113526 Comparison of photon correlation laser Doppler anemometry data processing techniques. R.G.Brown (Royal Signals & Radar Estab., Malvern, England), M.E.Gill.

Proc. SPIE Int. Soc. Opt. Eng. (USA), vol.369, p.220-8 (1983). (SPIE Proceedings of the Max Born Centenary Conference OPTICS 82, ECOSA 82, Edinburgh, Scotland, 7-10 Sept. 1982).

The truncated and statistical nature of photon correlation functions obtained from laser Doppler anemometry experiments and the ill-conditioned problem of their inversion, has led to a wide variety of approaches to the extraction of reliable information from the data. The authors have performed direct experimental comparisons (using identical data) of the four widely used methods of data reduction, ranging from simple to highly sophisticated. The authors comparisons covered most forms of correlogram likely to be encountered experimentally and the authors draw conclusions on the practicability, limitations and error magnitudes of current techniques. (12 refs.)

113527 A method for liquid velocity measurement by using two interdigital transducers. H.Urabe, K.Toda (Dept. of Electrical Engng., Nat. Defense Acad., Yokosuka, Japan).

Ferroelectr. Lett. Sect. (GB), vol.1, no.1, p.1-5 (1983).

A technique using a liquid delay line oscillator is presented for measuring the liquid velocity. The key element of the delay line oscillator is two interdigital transducers operating at a liquid-solid interface, which are used for the radiation or the detection of the longitudinal wave in the liquid. The oscillation frequency of the device changes with the liquid velocity. The validity of the operation principle is verified experimentally for the water velocity change. (2 refs.)

113528 Procedure for measuring the thickness and wave characteristics of the surface of the liquid film in annular-mist flows of steam and water. B.I.Nigmatulin, A.A.Vinogradov, V.A.Vinogradov, Sh.E.Kurbanov.

High Temp. (USA), vol.20, no.6, p.910-17 (Nov.-Dec. 1982). Translation of: *Teplofiz. Vys. Temp. (USSR)*, vol.20, no.6, p.1145-52 (Nov.-Dec. 1982). [received: Sept. 1983]

A procedure and equipment have been developed for measuring in real time the thickness of the liquid wall film in annular steam-water flow at pressures up to 12 MPa. The construction of the film-thickness sensor unit and schematic diagrams of the arrangement for measuring the liquid film thickness and the experimental section are given, along with their principles of operation. The results of measurements of the liquid film thickness and the velocities of the wave crests and troughs of the disturbed phase interface are given, and the variation of the interface profile as a function of the regime parameters of the steam-water flow is described. (11 refs.)

113529 A two-component optomechanical speed transducer for use with turbulent flows of liquid metal. V.G.Zhilin, Yu.P.Ivochkin, V.P.Ogorodnikov, V.V.Osipov (High-Temperature Inst., Acad. of Sci., USSR).

High Temp. (USA), vol.20, no.6, p.926-9 (Nov.-Dec. 1982). Translation of: *Teplofiz. Vys. Temp. (USSR)*, vol.20, no.6, p.1164-8 (Nov.-Dec. 1982). [received: Sept. 1983]

An optomechanical speed transducer is described for use with turbulent flows of liquid metal. The structural scheme is examined and calibration results obtained with mercury are given for a unit in which the sensitive element has a diameter of about 50 μm and an effective length of about 1.5 μm . The dynamic characteristics are evaluated. (9 refs.)

113530 Characteristics of a film-type heat-flux transducer. Yu.A.Polyakov, S.A.Degtyarev, A.V.Klygin (Higher Fire Service Engng. School, Min. of Higher Education, USSR).

High Temp. (USA), vol.20, no.6, p.930-6 (Nov.-Dec. 1982). Translation of: *Teplofiz. Vys. Temp. (USSR)*, vol.20, no.6, p.1169-75 (Nov.-Dec. 1982). [received: Sept. 1983]

A theoretical study is presented of the dynamic characteristics of a film-type transducer with a thin protective layer. Studies have been made of the insulation heating time and the temperature delay. The effects of the coating and substrate materials on the time characteristics are examined. Estimates have been made of the coating heating time and temperature delay for a particular transducer. It is found to be desirable to choose a substrate of low thermal conductivity for a threshold transducer. The conclusions are illustrated from experiments with pulsed radiation. (3 refs.)

113531 Adjustable isokinetic sampling horn. S.E.Spedden (IBM Corp., Armonk, NY, USA).

IBM Tech. Disclosure Bull. (USA), vol.26, no.2, p.853-5 (July 1983).

The author describes the design of an adjustable sampling horn for use with optical particle counters to allow for isokinetic sampling of aerosols in laminar gas flow environments of differing velocities. (no refs.)

113532 Ultrasonic flow metering based on transit time differentials which are insensitive to flow profile. H.Lechner (LGZ Landis & Gyr Zug AG, Zug, Switzerland).

J. Acoust. Soc. Am. (USA), vol.74, no.3, p.955-9 (Sept. 1983).

This paper describes a theoretical study of the performance of a transit time ultrasonic flowmeter which uses a flow tube to contain the interaction between the flow and the ultrasonic wave field. The flow tube is treated as an acoustic waveguide and it is seen that the transit time differentials of the higher order acoustic modes are affected by the type of flow profile encountered, resulting in errors in the volume throughput measurement. Nevertheless these errors can be minimized by an appropriate choice of transducer separation. (4 refs.)

113533 A simple, cost-effective automatic capillary viscometer system. M.Breton, D.Gustafson (Xerox Res. Centre of Canada, Mississauga, Ontario, Canada).

J. Polym. Sci. Polym. Phys. Ed. (USA), vol.21, no.8, p.1559-62 (Aug. 1983).

The interfacing of an Ubbelohde-type capillary viscometer to a microprocessor controller such as the AIM-65 gives the polymer chemist a convenient, precise and reliable way to measure the viscosity of solvent and polymer solutions. One of the first applications of a low-cost microprocessor to the measurement

of viscosity is reported here. Reproducible, high-precision data, the statistical nature of the results generated by the instrument, and the flexibility of the software strategy are important characteristics of the system. (4 refs.)

113534 Vortex flowmetering. C.Floria, T.K.Matsuura (Yokogawa Corp. of America, Shenandoah, GA, USA).

J. A (Belgium), vol.24, no.3, p.149-53 (July 1983).

This article describes the characteristics of vortex flowmeters and explains the advantages to be gained from their use. The problems encountered in the design of flowmeters are examined with particular emphasis on the stress sensing system. (no refs.)

113535 A new rheometer with autoranging function, controlled by a micro-computer. K.Takahashi, S.Yokoyama (Dept. of Electronic Engng., Shibaura Inst. of Technol., Tokyo, Japan), H.Fujihira, N.Hirose.

Oyo Buturi (Japan), vol.52, no.7, p.607-13 (July 1983). In Japanese.

A new rheometer, which can measure a wide range of viscosity by automatically adjusting the arm length and balancing force in detecting the torque by the rotary cylinder method was developed with the use of a micro-computer. The measurement can be conveniently made by interaction with the micro-computer through a console. (3 refs.)

113536 Movable channel flowmeter. K.Shiba, T.Ichinose, J.Kitamura, R.Kobayashi (Faculty of Engng., Tokyo Univ., Kawagoe, Japan).

Oyo Buturi (Japan), vol.52, no.7, p.614-18 (July 1983). In Japanese.

The movable channel flowmeter reported is a device of a very simple construction for measuring flow rate in an open channel. The measuring principle of this flowmeter is based on the law of conservation of momentum or angular momentum similarly to the movable tube flowmeter. It has been found from the results of experiments that the L bend flowmeter of two measured quantities type is better than the straight flowmeter. (no refs.)

113537 Present developmental trends in flow measurement technology.

H.Umbach (BASF AG, Ludwigshafen am Rhein, Germany).

Regelungstech. Prax. (Germany), vol.25, no.6, p.225-8 (June 1983). In German.

Surveys the latest techniques and the potentialities of microelectronics in flow measurement and discusses the application of materials and physical effects which have not up to the present time been effectively exploited. In particular, the magnetic-inductive flowmeter using a switched unidirectional field is discussed in detail and some examples of compact instruments based on this principle are described and illustrated by photos. This includes an illustration of a flowmeter using a measuring tube of sintered corundum. Some examples of meters, using the Karmans wake effect, which have overcome the difficulties of recognizing the turbulence under all operating conditions by the use of two independent sensors and computerized evaluation are given. Finally, an example of a meter which utilizes the Coriolis force by passing the fluid through a U-tube and measuring the angle of torsion which is proportional to the mass flow, is described. (1 ref.) L.M.W.

113538 The practical calibration of water flowmeters under realistic temperature conditions. C.Meisser (LGZ Landis & Gyr AG, Zug, Switzerland).

Technological and Methodological Advances in Measurement. Acta IMEKO 1982. Proceedings of the 9th IMEKO Congress of the International Measurement Confederation, Berlin, Germany, 24-28 May 1982 (Amsterdam, Netherlands: North-Holland 1983), p.299-307 vol.2

With the displacement prover, flowmeters can be tested automatically within the entire temperature range without a comparison standard. The WPV 2-180 was designed for a T_{max} of 120°C and a P_{max} of 16 bar. The flow extends from 10 l/h to 18000 l/h. For flow rates over 100 l/h the errors remain smaller than $\pm 0.2\%$. For lower flow rates and temperatures above 60°C the cooling within the meters to be calibrated must be taken into consideration. (4 refs.)

113539 Flowmetering in a long-distance pipeline grid for ethylene under high pressure. P.J.Orbons, F.A.Van Laak (DSM Transportmaatschappij, Beek, Netherlands).

Technological and Methodological Advances in Measurement. Acta IMEKO 1982. Proceedings of the 9th IMEKO Congress of the International Measurement Confederation, Berlin, Germany, 24-28 May 1982 (Amsterdam, Netherlands: North-Holland 1983), p.541-50 vol.2

Deals with a new metering system which has become necessary by the change-over of an ethylene pipeline to supercritical operation, with measures for maintaining and improving the accuracy, with the recording of the measuring data and with the new leak detection facilities. (no refs.)

113540 A new primary rig for accurate flowmeter calibration. C.Cignolo, F.Alasia, R.Goria, G.Martini, A.Rivetti (Istituto di Metrologia 'G. Colonetti', Torino, Italy).

Technological and Methodological Advances in Measurement. Acta IMEKO 1982. Proceedings of the 9th IMEKO Congress of the International Measurement Confederation, Berlin, Germany, 24-28 May 1982 (Amsterdam, Netherlands: North-Holland 1983), p.551-62 vol.2

Describes a primary calibration rig built at the IMGC flow measurement laboratory, in which flow rates of several types of liquids can be measured from about 0.05 up to 200 l/min over wide temperature and pressure ranges. The aim was to obtain maximum uniformity in flow conditions, as well as the highest accuracy and versatility. In the description of the apparatus emphasis is given to a rectangular variable-area nozzle and to a new ballistic diverter, with which flow diversion can take place in an extremely short time (approx. 2 ms), so that substantial reduction in timing uncertainty can be obtained. (4 refs.)

113541 High speed motion neutron radiography of two-phase flow.

A.H.Robinson, S.L.Wang (Oregon State Univ., Corvallis, OR, USA).

Neutron Radiography. Proceedings of the First World Conference, San Diego, CA, USA, 7-10 Dec. 1981 (Dordrecht, Netherlands: Reidel 1983), p.653-9

A system to perform neutron radiographic analysis of dynamic events which occur on the order of several milliseconds has been developed. Two different methods have been used to radiograph the simulated two-phase flow. These are pulsed, or 'flash' radiography, and high speed movie neutron radiography. The pulsed method serves as a 'snapshot' with an exposure time ranging from 10 to 20 milliseconds. In high speed movie radiography, a scintillator is used to convert neutrons into light which is enhanced by an optical intensifier and then photographed by a high speed camera. The results obtained demonstrate the feasibility of using neutron radiography to obtain data in two-phase flow situations. Both movies and flash radiographs have been obtained of air bubbles in water and boiling from a heater element. The neutron radiographs of the boiling element show both nucleate boiling and film boiling. (no refs.)

Bernoulli on a large scale See Entry 111374

Flow field testing with a 64 parallel channel heterodyne interferometer See Entry 111751

Some applications of cineradiography to gas turbines See Entry 111836

- Pulsed high-energy radiographic machine emitting X-rays (PHERMEX): applications to study high-pressure flow and detonation waves See Entry 111838
- High frame-rate neutron radiography of dynamic events See Entry 111858
- Time delay estimation: application to flow rate measurement of cooling fluid in nuclear power plants See Entry 112394
- Velocity statistics in premixed turbulent flames See Entry 113425
- Radar-acoustic probing of randomly oriented air flows See Entry 116306

50.00 FLUIDS, PLASMAS AND ELECTRIC DISCHARGES

(for fluid dynamics, see 47.; for the physics of condensed matter, see 60. and 70.)

51.00 KINETIC AND TRANSPORT THEORY OF FLUIDS; PHYSICAL PROPERTIES OF GASES

51.10 KINETIC AND TRANSPORT THEORY

113542 Kinetic perturbation theory. Structure of collision integrals for the square-well gas. J.Karkheck (Dept. of Sci. & Math., GMI Engng. & Management Inst., Flint, MI, USA), G.Stell. *J. Phys. Chem. (USA)*, vol.87, no.15, p.2858-66 (21 July 1983). The authors seek a better understanding of the structure of kinetic perturbation theory, in inverse temperature T^{-1} , for fluids. For a prototypic pair potential (hard core of unit diameter plus square well of width R and depth ϵ) they obtain exact results on the Boltzmann-equation level of description. The authors find the following: (i) For the self-diffusion collision integral $\Omega^{(1,1)}$, the nonanalytic terms in $w = \epsilon/kT$ are all of the form $w^n \ln w$ and $w^{n+1} \ln^2 w$, $n=2, 3, 4, \dots$ (ii) $\Omega^{(1,1)}$ also has an essential singularity in R at $R=1$. (iii) First-order perturbation theory in w is unreasonably accurate. It yields a good approximation for $\Omega^{(1,1)}$ (and hence for the coefficient of self-diffusion) over a considerable region of parameter space (R^{-1}, w), including domains over which individual higher order terms in w are larger than the first-order terms. (iv) Partial sums through $O(w^3 \ln w)$ yield approximations of decreasing accuracy as more terms are included. (v) A result similar to iii is found for the thermal conductivity and its collision integral, though over a more limited region of parameter space. (vi) The linear term in w and the leading nonanalytic terms are traced to different collision types. The significance of the above findings for perturbative treatments of the dense fluid is discussed. Results are presented also for the simpler cases of coreless square-well and repulsive (square) mound pair potentials. (36 refs.)

113543 An improved reduced Van der Waals equation of state for helium at high pressures. J.I.Benneth, W.A.Jesser (Materials Sci. Dept., Univ. of Virginia, Charlottesville, VA, USA). *J. Nucl. Mater. (Netherlands)*, vol.116, no.2-3, p.339-42 (June 1983). Equations of state (EOS) for helium are examined. Of all the EOS investigated, the hard sphere EOS reproduced the experimental data the best, followed by the virial EOS and the 'improved' reduced van der Waals EOS. The ease of computation of these three EOS follows a reverse order, with the 'improved' reduced van der Waals EOS being the easiest by far and the hard sphere EOS the most difficult to calculate. At 600°C the virial EOS converged very rapidly to the most accurate hard sphere EOS, even at high pressures. The ratio of the number of helium atoms/vacancy for very small equilibrium bubbles as predicted by these three EOS is almost temperature independent. (16 refs.)

113544 The discrete Boltzmann equation for gas mixtures. A regular space model and a shock wave problem. N.Bellomo (Dept. of Math., Polytech. of Turin, Turin, Italy), L.M.de Socio. *Mech. Res. Commun. (GB)*, vol.10, no.4, p.233-8 (July-Aug. 1983). Reports on the construction of a discrete velocity model (DVM) for a multiple species gas mixture, a subject that has so far not been investigated. The general methodology is indicated and a regular 6.R velocity model is proposed for a R species gas, from which a system of 6.R partial differential equations is obtained for the fluid flow, as the velocity distribution function for each species is replaced by constant velocities. An application and a final discussion follow. (8 refs.)

113545 Kinetic equation for a spontaneously dissociating gas. V.K.Ablekov, Yu.N.Babaev, A.M.Frolov. *Sov. Phys.-Dokl. (USA)*, vol.27, no.12, p.1013-15 (Dec. 1982). Translation of: *Dokl. Akad. Nauk SSSR*, vol.267, no.4-6, p.1089-93 (Dec. 1982). [received: Sept. 1983] The dissociation process has been examined in gases of dissociating particles in the case when collisions of gas particles cause the disintegration of one of the particles as a result of breaking of the bonds among its constituent particles by the incident particle. A bound state of two particles comprising the gas particle is the most widely used model for analyzing the inelastic processes of dissociation or synthesis of the gas particles, such as ionization in weakly-ionized plasmas or in chemically reacting gases. The authors attempt to construct kinetic equations describing the kinetic properties of gases consisting of spontaneously dissociating particles by including terms for this type of decay in the equations. (14 refs.)

113546 The hard-sphere model in plasma and gas physics. B.M.Smirnov (L.V. Kurchatov Inst. of Atomic Energy, Moscow, USSR). *Sov. Phys.-Usp. (USA)*, vol.25, no.11, p.854-62 (Nov. 1982). Translation of: *Usp. Fiz. Nauk (USSR)*, vol.138, no.3, p.517-33 (Nov. 1982). [received: Sept. 1983] Expressions are derived for the scattering cross sections and the macroscopic properties of gases and plasmas in a hard-sphere model in which the first two terms are retained in the expansion in the small parameter of the theory. These expressions are analyzed and compared with the results of the Maxwell model and also with numerical calculations for model interaction potentials. (20 refs.)

- 113547 Some remarks on the theory of local interaction in a rarefied gas.** R.N.Moroshin. *Vestn. Leningr. Univ. Ser. Mat. Mekh. & Astron. (USSR)*, no.3, p.51-7 (July 1983). In Russian. A new version of the theory of local interactions is presented. The form functions being determined by means of a recurrent system of differential equations. (15 refs.)
- Kinetic models for adiabatic reversible expansion of a monatomic ideal gas** See Entry 111371
- Expansions of the kinetic hierarchy for a massive particle: the repeated ring and Fokker-Planck equations** See Entry 111540
- Vibrational energy relaxation of highly compressed gaseous H₂ and N₂** See Entry 112816
- Self-correlation functions of rotational and translational motion in simple fluids** See Entry 112823
- Thermally induced nucleation. I. A new way to obtain activation energies for unimolecular reactions** See Entry 115535

51.20 VISCOSITY AND DIFFUSION: EXPERIMENTAL

113548 Momentum implications for buoyant diffusion flames. B.J.McCaffrey (Center for Fire Res., NBS, Washington, DC, USA). *Combust. & Flame (USA)*, vol.52, no.2, p.149-67 (Sept. 1983). Using assumed Gaussian forms for the transverse variation of mean quantities and well-established centerline variations, the integrated form of the momentum equation is solved for the vertical variation of the radial extent of buoyant diffusion flames. Closure is obtained by assuming that the convective heat flux at the flame tip is equal to the total heat release rate minus the radiative fraction. Solutions are obtained in terms of λ , which is the ratio of the $1/e$ transverse widths of the thermal energy profile to that of the velocity profile, and a local, centerline Froude numberlike parameter, $C_B = U/\sqrt{2gz} \Delta T/T_0$. The parameters differentiate between initial buoyancy-dominated (necking-in) behaviour associated with solid or liquid pool flames versus momentum-dominated gas jet flame behavior. Recent data from porous refractory gas burners at flame conditions near the transition are compared to the simple analysis. Calculated transverse components of velocity compare favourably to Thomas's thistledown tracer experiments and provide the basis for an evaluation of the use of the boundary layer equations in pool fire modeling. Estimates of the effects of turbulence in the upper portion of the flame are presented. (21 refs.)

Vibrational energy relaxation of highly compressed gaseous H₂ and N₂ See Entry 112816

51.30 THERMAL PROPERTIES OF GASES

113549 The PVT properties of nitrogen from -20 to +35°C and 200 to 570 MPa, and some comparisons with argon and the Lennard-Jones (6-12) fluid. E.C.Morris, R.G.Wylie (CSIRO Div. of Appl. Phys., Sydney, Australia). *J. Chem. Phys. (USA)*, vol.79, no.6, p.2982-8 (15 Sept. 1983). The density $\rho(T,p)$ of nitrogen has been measured for $T = -20$ to $+35^\circ\text{C}$ and p in the range 200 to 570 MPa, using a method already described in a paper which included results for argon. An improvement in the accuracy with which the quantities of gas are measured has reduced the overall uncertainty in $\rho(T,p)$ to 0.03% at the 95% confidence level. The results are presented graphically and in the form of a fitted equation, and are compared with those of other workers. A comparison is made with the results of the argon study and a hypothetical Lennard-Jones fluid, in terms of the density, the internal energy and the entropy, and the internal kinetic energy of the molecules as calculated by Schottky's method. (17 refs.)

113550 Low-density isochoric (p, V, T) measurements on (nitrogen+methane). W.M.Haynes, R.D.McCarty (Nat. Engng. Lab., NBS, Boulder, CO, USA). *J. Chem. Thermodyn. (GB)*, vol.15, no.9, p.815-19 (Sept. 1983). Isochoric (p, V, T) measurements have been made on three mixtures of nitrogen and methane (0.29N₂+0.71CH₄), (0.50N₂+0.50CH₄), and (0.68N₂+0.32CH₄) at densities of 1 to 6 mol.dm⁻³. The three isochores for each mixture cover a temperature range from approximately 150 to 320K up to a maximum pressure of 16 MPa. Comparisons with other experimental results and with values calculated from an extended corresponding-states model are discussed. (10 refs.)

113551 Diamond-anvil system for the investigation of phase equilibria in mixtures at high pressures. J.A.Schouten, N.J.Trappeniers, L.C.van den Bergh (Van der Waals Lab., Univ. of Amsterdam, Amsterdam, Netherlands). *Rev. Sci. Instrum. (USA)*, vol.54, no.9, p.1209-12 (Sept. 1983). In order to investigate the phase behavior of mixtures at high pressures the authors have developed a system consisting of a diamond-anvil cell with a high-pressure vessel to match. The diamond cell can be filled at room temperature and pressures up to 10 kbar with a gaseous mixture of known composition. The cell is constructed such that a constant volume method can be used to measure the dew- and bubble-point curves of a mixture. (8 refs.)

113552 Substance compressibility and 'gravitation effect' near the critical point. A.D.Alekhin. *Ukr. Fiz. Zh. (USSR)*, vol.28, no.8, p.1261-3 (Aug. 1983). In Russian. Investigates substance compressibility using two methods simultaneously—light scattering and measuring the refractive index gradient. The substances studied were n-heptane and freon-113, C₂F₃Cl₃. (16 refs.) V.G.P.

High-temperature calorimeter for the measurement of vapor pressure and enthalpy of vaporization See Entry 111684

Unsteady method of measuring the thermal conductivity of gases at high temperatures See Entry 111688

Kinetic perturbation theory. Structure of collision integrals for the square-well gas See Entry 113542

51.50 ELECTRICAL PHENOMENA IN GASES

(see also 52. Plasma and electric discharges)

113553 The local field inside a dielectric gas. F.Hynne (Chem. Lab. III, H.C. Orsted Inst., Copenhagen, Denmark). *Am. J. Phys. (USA)*, vol.51, no.9, p.837-42 (Sept. 1983). The Clausius-Mossotti relation is systematically in error for molecular gases. The dielectric constant is more adequately described in terms of an effective polarizability, which accounts for the interaction of a molecular dipole with

self through the surrounding molecules. These aspects of the local field problem of dielectric theory are discussed on the basis of a simple macroscopic model due to Onsager and Bottcher. The conclusions drawn from the model have been established by strictly microscopic arguments, however, and the authors briefly discuss the microscopic representations of the concepts used. (13 refs.)

13554 On the computation of ionization levels in rocket exhaust flames. M.Cousins, D.E.Jensen (Propellants, Explosives & Rocket Motor Establ., Min. of Defence, Aylesbury, England).

Combust. & Flame (USA), vol.52, no.2, p.111-25 (Sept. 1983). An up-to-date account of chemical processes determining electron concentrations in rocket exhaust flames is offered. Nonequilibrium charge production/removal reactions play important parts. So do electron attachment processes, formation of Cl^- and of OH^- being particularly significant in exhausts of motors with composite and double-base propellants, respectively. Uncertainties in various rate coefficients are among the sources of substantial possible errors in calculations of noise levels imposed on microwave guidance signals passing through the flames. (29 refs.)

13555 Spectroscopy of laser-induced dielectric breakdown in gas mixtures. A.H.Schwebel, A.M.Ronn (Dept. of Chem., City Univ. of New York, New York, NY, USA).

Chem. Phys. Lett. (Netherlands), vol.100, no.2, p.178-82 (2 Sept. 1983). Laser-induced dielectric breakdown has been used to initiate fragmentation in molecular gases and gas mixtures. The emission spectra of the atoms, ions, and molecular fragments has been assigned and used to identify specific components of given mixtures. While this study only reports on mixtures of hydrocarbons and halogenated hydrocarbons, the technique is general and does not rely on laser absorption in any component of the mixtures. (9 refs.)

13556 Electrical conductivity of alkali metal vapors in the neighborhood of the critical point. A.A.Likal'ter (Inst. of High Temperatures, Acad. of Sci., USSR).

High Temp. (USA), vol.20, no.6, p.848-52 (Nov.-Dec. 1982). Translation of: *Teplofiz. Vys. Temp. (USSR)*, vol.20, no.6, p.1076-80 (Nov.-Dec. 1982). [received: Sept. 1983]

A strongly interacting alkali metal plasma in the neighborhood of the critical point is described in terms of quasiatoms with a continuous excitation spectrum. A phenomenological theory of the conductivity is constructed which agrees well with experimental data. (7 refs.)

13557 Dielectric constant of water at very high temperature and pressure. K.S.Pitzer (Dept. of Chem., Univ. of California, Berkeley, CA, USA).

Proc. Natl. Acad. Sci. USA, vol.80, no.14, p.4575-6 (July 1983). Pertinent statistical mechanical theory is combined with the available measurements of the dielectric constant of water at high temperature and pressure to predict that property at still higher temperature. The dielectric constant is needed in connection with studies of electrolytes such as $\text{NaCl}/\text{H}_2\text{O}$ at very high temperature. (10 refs.)

13558 On the energy losses of slow ions in an interacting degenerate electron gas. Yu.S.Sayasov (Inst. fur Kernphysik II, Kernforschungszentrum Karlsruhe GmbH, Karlsruhe, Germany).

Z. Phys. A (Germany), vol.313, no.1-2, p.9-10 (1983). Energy losses of slow ions with velocities $v \ll v_F$ (v_F is the Fermi velocity) in an interacting degenerate electron gas are calculated on the basis of the dielectric theory of Singwi (1968). It is shown that the local field effects taken into account in this theory lead to an increase of the energy losses as compared with the Lindhard stopping power by a factor which can reach a few tens of percent for some compressed ICF plasmas. Corresponding factors for simple metals are as much as 2-3 and are in agreement with experiment. (10 refs.)

Microdischarge characteristics in air gap between spherical particle and plane See Entry 112912

A far-infrared interferometer for the measurement of electron concentration in flames and plasmas with high spatial resolution See Entry 113562

51.70 OPTICAL PHENOMENA IN GASES

(for liquids, see 78.)

13559 Fire flame radiation. P.Vervisch, A.Coppalle (Lab. de Thermodynamique, Faculte des Sci. et des Tech. de Rouen, Mont-Saint-Aignan, France).

Combust. & Flame (USA), vol.52, no.2, p.127-35 (Sept. 1983). Measurements of intensity and transmittance in the spectral range 0.5-6 μm are reported for polypropylene in flaming or smoldering combustion. The influence of air velocity, radiant heat flux, and O_2 concentration is examined. A comparison between experimental results and band models is present. (10 refs.)

13560 Multilevel description of flow birefringence in binary mixtures of linear molecules with noble gases. W.-K.Liu, F.R.McCourt (Guelph-Waterloo Centre, Univ. of Waterloo, Waterloo, Ontario, Canada).

J. Phys. Chem. (USA), vol.87, no.15, p.2923-8 (21 July 1983). A multilevel description is given of the flow birefringence in a binary mixture of linear molecules and noble gases. The moment method is used in the derivation, and spherical tensors are used throughout. Exact expressions of the effective cross sections determining the flow birefringence coefficients are given explicitly. (31 refs.)

Sellmeier fits with linear regression; multiple data sets; dispersion formulas for helium See Entry 112920

Effects of the Abraham ponderomotive force induced by RF and laser light pulses See Entry 113047

Phase matching during harmonic generation in high-pressure gas mixtures See Entry 113060

Coherent pulse propagation in the infrared on the picosecond time scale See Entry 113065

Substance compressibility and 'gravitation effect' near the critical point See Entry 113552

Optical investigation of critical behaviour in simple fluids at reduced gravity See Entry 114131

Calculation of optical anisotropy of hydrocarbon chains by the Monte Carlo method See Entry 114820

51.90 OTHER TOPICS IN THE PHYSICS OF FLUIDS

Simple apparatus for concentration determinations in binary-gas mixtures See Entry 115604

52.00 THE PHYSICS OF PLASMAS AND ELECTRIC DISCHARGES

(for solid-state plasma, see 72.30)

52.20 ELEMENTARY PROCESSES IN PLASMA

113561 Relativistic corrections for the conventional, classical Nyquist theorem. O.Theimer (Arts & Sci. Res. Center, New Mexico State Univ., Las Cruces, NM, USA), E.H.Dirk.

Nuovo Cimento B (Italy), vol.76B, ser.2, no.1, p.73-86 (11 July 1983). New expressions for the Nyquist theorem are derived under the condition in which the random thermal speed of electrons, in a system of charged and neutral particles, can approach the speed of light. Both the case in which the electrons have not net drift velocity relative to the ions or neutral particles and the case in which drift occurs are investigated. In both instances, the new expressions for the Nyquist theorem are found to contain relativistic correction terms; however, for electron temperatures $T \approx 10^4 \text{ K}$ and drift velocity magnitudes $|w| \approx 0.5 c$, where c is the speed of light, the effects of these correction terms are generally small. The derivation of these relativistic corrections is carried out by means of procedures developed in an earlier work (1982). A relativistic distribution function, which incorporates a constant drift velocity with a random thermal velocity for a given particle species, is developed. (11 refs.)

The hard-sphere model in plasma and gas physics See Entry 113546

Unified kinetic theory in toroidal systems See Entry 113566

Effect of collisionless detrapping on nonaxisymmetric transport in a stellarator with radial electric field See Entry 113572

Electromagnetic two-stream and filamentation instabilities for a relativistic beam-plasma system See Entry 113626

Numerical fits to important rates in high temperature astrophysical plasmas See Entry 116467

52.20H Atomic, molecular, heavy-particle collisions

Collisions of hydrogen ions in a focused hollow beam See Entry 112843

On the energy losses of slow ions in an interacting degenerate electron gas See Entry 113558

52.25 PLASMA BASIC PROPERTIES

113562 A far-infrared interferometer for the measurement of electron concentration in flames and plasmas with high spatial resolution. A.K.F.Chan, A.R.Jones (Dept. of Chem. Engng. & Chem. Technol., Imperial Coll. London, London, England).

Combust. & Flame (USA), vol.52, no.2, p.203-10 (Sept. 1983). A far-infrared interferometer employing an HCN laser has been designed which uses only simple, inexpensive optical components. It can operate either as a lateral shearing or Mach-Zehnder-type interferometer. Spatial resolution down to 0.5 mm is the test space was achieved. Good agreement was found with the theoretical resolution limit calculated from diffraction theory. The interferometer was used to measure electron densities in premixed flames with and without cesium seeding. The results confirmed the high electron concentration in the reaction zone of an unseeded methane-air flame. (16 refs.)

113563 Thermodynamic properties of ion clusters and their effect on the mechanism of homogeneous nucleation in an ion plasma. Calculation by the Monte Carlo method in an NpT ensemble. S.V.Shevkinov, P.N.Vorontsov-Vel'yaminov (A.A. Zhdanov Leningrad State Univ., Leningrad, USSR).

High Temp. (USA), vol.20, no.6, p.803-9 (Nov.-Dec. 1982). Translation of: *Teplofiz. Vys. Temp. (USSR)*, vol.20, no.6, p.1025-31 (Nov.-Dec. 1982). [received: Sept. 1983]

The Monte Carlo method in an isothermal-isobaric ensemble is used to simulate the equilibrium thermodynamic properties of ion clusters. A region of thermodynamic stability of the ion chainlike nuclei toward folding up into a compact structure is discovered. It is shown that in this region of parameters the mechanism of homogeneous nucleation of the plasma differs qualitatively from the ordinary mechanism of nucleation through a critical nucleus, and the ion plasma cannot be supersaturated in this region. Previously discovered structural changes in a small ion system are discussed and a qualitative picture of the phase diagram is proposed. (23 refs.)

113564 Two-dimensional electron fluid at high temperature. C.Deutsch (Lab. de Phys. des Plasmas, Universite Paris XI, Orsay, France).

J. Stat. Phys. (USA), vol.32, no.1, p.115-22 (July 1983). The two-dimensional and one-component plasma (OCP) model with r^{-1} interactions is investigated in the high-temperature limit, where the thermal wavelength gets larger than the classical distance of closest approach. Non-negligible diffraction effects are rigorously taken care of (up to e^2) through a temperature-dependent effective interaction, Debye thermodynamics, analyzed in terms of a classical plasma parameter Λ , is shown to diverge as $\Lambda \ln \Lambda$, when $\hbar \rightarrow 0$. There is no classical limit. A result at variance with the corresponding one in three dimensions. (7 refs.)

113565 The self-consistent mean spherical approximation for the one-component plasma. D.MacGowan (Dept. of Math., Rutgers Univ., New Brunswick, NJ, USA).

J. Stat. Phys. (USA), vol.32, no.1, p.123-39 (July 1983).

The consequences of choosing the adjustable hard-core diameter in the mean spherical approximation for the one-component plasma so as to achieve thermodynamic consistency between the energy and compressibility equations are investigated. Such a choice is found to be possible only for $\Gamma \geq 8.5$ and, although the resulting correlation functions are discontinuous, the height of the main peak in the static structure factor is remarkably accurate. Two especially noteworthy aspects of the thermodynamic results are that the compressibility equation is much more accurate than in any previous approximation free of input from computer simulations and that the nonstatic part of the internal energy has a $\Gamma^{1/4}$ dependence in the strong coupling limit in agreement with Monte Carlo data. (33 refs.)

113566 Unified kinetic theory in toroidal systems. D.A.Hitchcock, R.D.Hazeltine, S.M.Mahajan (Inst. for Fusion Studies, Univ. of Texas, Austin, TX, USA).

Phys. Fluids (USA), vol.26, no.9, p.2603-8 (Sept. 1983). A kinetic theory for toroidal systems which includes the effects of collisions as well as instabilities is constructed. This yields a pair of evolution equations; one for the spectrum and one for the distribution function. In addition, this theory yields a toroidal generalization of the usual collision operator which is

shown to have many similar properties, conservation laws, and H theorem, to the usual collision operator. (7 refs.)

113567 Plasma electron density measurements by the laser- and collision-induced fluorescence method. K.Tsuchida, S.Miyake, K.Kadota, J.Fujita (Inst. of Plasma Phys., Nagoya Univ., Chikusa-ku, Nagoya, Japan). *Plasma Phys. (GB)*, vol.25, no.9, p.991-9 (Sept. 1983).

A new method based on the laser-induced fluorescence method has been developed to measure the spatial electron density distribution in plasmas. The local electron density can be determined by observing the intensity ratio of the laser- to the collision-induced fluorescence. A spatial electron density distribution of a helium plasma ($T_e \sim 6$ eV, $n_e \cdot 10^{11-12}$ cm $^{-3}$) has been determined by observing the He($3^1P_{-2}^1S$) laser-induced fluorescence and the He($3^1D_{-2}^1P$) collision-induced fluorescence resulting from the He($3^1P_{-3}^1D$) process due to collisions with electrons. The comparison of the result with that of a conventional method proves this new method is of practical use in the space-resolved measurements of plasma electron density. (12 refs.)

113568 Existence of Debye screening in classical ion-dipole systems. A.L.Rebenko (Inst. of Theoretical Phys., Acad. of Sci., Kiev, Ukrainian SSR).

Sov. Phys.-Dokl. (USA), vol.27, no.12, p.1024-5 (Dec. 1982). Translation of: *Dokl. Akad. Nauk SSSR*, vol.267, no.4-6, p.1350-2 (Dec. 1982). [received: Sept. 1983]

The author generalizes the results of Brydges and Federbush (1980) to the case of ion-dipole systems. It is rigorously proved that if the density of ions is not zero then there is screening not only of the ion-dipole interactions but of the dipole-dipole interactions as well. (12 refs.)

113569 Thermodynamics of a highly compressed plasma in the megabar range. V.K.Gryaznov, I.L.Iosilevskii, V.E.Fortov (Inst. of Chem. Phys., Acad. of Sci., USSR).

Sov. Tech. Phys. Lett. (USA), vol.8, no.11, p.592-3 (Nov. 1982). Translation of: *Pis'ma v Zh. Tekh. Fiz. (USSR)*, vol.8, no.21-22, p.1378-81 (Nov. 1982). [received: Sept. 1983]

Works from experiments on the compression and irreversible heating of copper by intense shock waves to draw conclusions regarding the applicability of the ionizational ('gas') model of a plasma under rather unusual conditions for plasma physics: extremely high pressures, in the range of tens of millions of atmospheres, and densities n_e up to 10^{23} cm $^{-3}$. (11 refs.)

113570 Local determination of the ion temperature from the Doppler broadening of hydrogen lines through the use of a fast atomic beam. E.L.Berezovskii, M.M.Berezovskaya, A.B.Izvozhnikov, V.A.Kurpin.

Sov. Tech. Phys. Lett. (USA), vol.8, no.11, p.594-5 (Nov. 1982). Translation of: *Pis'ma v Zh. Tekh. Fiz. (USSR)*, vol.8, no.21-22, p.1382-6 (Nov. 1982). [received: Sept. 1983]

It is worth while to develop methods which can measure the temperature of the bulk of the plasma ions even if the distribution functions of certain groups of ions are non-Maxwellian. One such method is to measure the Doppler broadening of the emission lines of atoms of the working gas, which are excited during charge exchange between an injected beam of fast neutrals and ions of the working gas. The DINA-3 injector has been used as a diagnostic injector in the T-10 tokamak. In these measurements, this injector produced a beam of hydrogen atoms with an energy $E_0 = 20$ keV. For the spectral measurements, an MDR-2 monochromator was combined with a FEU-51 photomultiplier. (4 refs.)

A class of similarity solutions for the nonlinear thermal conduction problem See Entry 112438

The hard-sphere model in plasma and gas physics See Entry 113546

On the energy losses of slow ions in an interacting degenerate electron gas See Entry 113558

Relativistic corrections for the conventional, classical Nyquist theorem See Entry 113561

Forward CW CO $_2$ -laser scattering on a high density plasma column See Entry 113576

Nonlinear electron oscillation driven by an external wave in a plasma See Entry 113586

Scattering of lower-hybrid waves by drift-wave density fluctuations: solutions of the radiative transfer equation See Entry 113592

Spectral broadening of lower-hybrid waves by time-dependent density fluctuations See Entry 113593

On tearing modes in a resistive medium See Entry 113595

Surface ionic-sonic oscillations in inhomogeneous plasma See Entry 113606

Observation of self-binding turbulent fluctuations in simulation plasma and their relevance to plasma kinetic theories See Entry 113610

A new interpretation of the alpha effect See Entry 113612

Potential double layer formed by a laminar shock wave in a collisionless plasma See Entry 113615

Nonlinearly induced radiation from an overdense plasma region See Entry 113617

CO $_2$ collective laser scattering on moving density perturbations in a plasma See Entry 113618

Wall material characteristics in reacting plasma modelling See Entry 113622

Measurements of electron and ion heating by Alfvén waves in the TCA Tokamak See Entry 113630

Dynamic methods in plasma physics See Entry 113633

A comparison between laser induced fluorescence at Balmer-alpha and at Lyman-alpha for the measurement of neutral hydrogen densities in magnetically contained fusion plasmas See Entry 113648

Simultaneous measurement of magnetic field direction and ion temperature in a plasma by collective scattering with a CO $_2$ laser See Entry 113652

Approximation of the Langmuir-Blodgett function See Entry 113653

A photoelectron spectrometer for measurement of electron plasma temperature See Entry 113654

Converging shock on laser plasma: density profiles by holographic interferometry See Entry 113663

Ten-channel grating chromator for electron cyclotron emission plasma diagnostics See Entry 113665

Construction of a high density plasma device for microwave-plasma interaction experiment See Entry 113671

Electron temperature in HF discharge plasma columns See Entry 113676

Measurement of electron temperature in a glow discharge with a double probe method See Entry 113677

Anode-plasma parameters of a high-voltage glow discharge ≈ 150 kV See Entry 113683

Observation of a significant density of negative ions in a currentless discharge in air; the possibility of an attachment instability See Entry 113694

52.25F Transport properties

113571 Nonresonant electron transport on the ELMO bumpy torus (EBT) for multitemperature Maxwellians. D.E.Hastings (Oak Ridge Nat. Lab., Oak Ridge, TN, USA).

Phys. Fluids (USA), vol.26, no.9, p.2338-41 (Sept. 1983). For the experimental conditions in the ELMO Bumpy Torus (EBT), it appears that the electron distribution function may not be a single-temperature Maxwellian. Neoclassical transport coefficients have been developed for the nonresonant electron species in a bumpy torus with the assumption that the lowest-order distribution function is the sum of l different Maxwellians. These show that there can be significant coupling between the different electron species. For comparison the diffusion coefficients are contrasted to single-temperature diffusion coefficients. (6 refs.)

113572 Effect of collisionless detrapping on nonaxisymmetric transport in a stellarator with radial electric field. H.E.Mynick (Torsatron/Stellarator Lab., Univ. of Wisconsin, Madison, WI, USA).

Phys. Fluids (USA), vol.26, no.9, p.2609-15 (Sept. 1983). A derivation is given for expressions describing transport rates in a stellarator operating at low collisionality ν , in the presence of a radial electric field. It is shown that collisionless detrapping (and retrapping) of particles in superbanana orbits can substantially modify this transport. The detrapping provides a collisionless lower bound on the width of the collisional boundary layer which, in previous work, gave rise to transport coefficients scaling as $\nu^{1/2}$. With this lower bound, these coefficients will instead scale as ν , implying more favorable confinement than indicated by the $\nu^{1/2}$ result commonly employed. (7 refs.)

113573 Measurements of fluctuations in the flux of runaway electrons to the PLT Tokamak limiter. C.W.Barnes, J.D.Strachan (Plasma Phys. Lab., Princeton Univ., Princeton, NJ, USA).

Phys. Fluids (USA), vol.26, no.9, p.2668-75 (Sept. 1983). Fluctuations in the flux of runaway electrons to the limiter are measured during many PLT (Princeton Large torus) discharges. Oscillations at 60, 120 and 720 Hz are driven by variations in the vertical magnetic field which moves the plasma major radius. Fluctuations are seen with frequencies in the range of 2-20 kHz because of magnetohydrodynamic (MHD) magnetic islands which extend to the plasma surface. A continuous spectrum of fluctuations is observed up to 200 kHz which correlates with drift-wave turbulence. The magnitude of the driven fluctuations can be used to measure transport properties of the runaway electrons. The amplitude of electron motion due to the MHD and drift-wave oscillations, and hence a measure of the radial size of the instability, can be determined as a function of frequency. The slope of the frequency power spectrum of the drift-wave-induced fluctuations steepens with increasing runaway-electron drift orbit displacement during the current drop at the end of the discharge, and as the power in the MHD oscillations increases. A magnetic probe is used to confirm the presence of oscillating magnetic fields capable of perturbing the electron orbits. (18 refs.)

113574 Transport properties of drift waves. A.Rogister, G.Hasselberg, F.Waelbroeck.

Report JUL-1829, Kernforschungsanlage, Jülich, Germany (Feb. 1983), 10 pp.

The authors present the results and discuss the prospects of a study of plasma transport which is based on a recent theory of drift wave turbulence. The specific questions addressed are the turbulence spectrum, the electron heat conduction, the impurity transport, the evacuation of the power released during sawtooth relaxations, the cleaning action of these sawteeth, the cause of the high density limit and of the gross plasma disruptions. (9 refs.)

113575 Anomalous impurity transport in plasmas. A.Rogister, G.Hasselberg.

Report JUL-1846, Kernforschungsanlage, Jülich, Germany (March 1983), 30 pp.

The transport of high Z impurities resulting from Compton and induced scattering by drift waves is found to be comparable in magnitude with base ion and electron transport when the fluctuation spectrum is obtained from a recent theory of drift turbulence. The anomalous frictional flux is marginally subdominant whilst the diffusion flux is enhanced over the neoclassical value by a numerical factor which (i) agrees quantitatively with the results of impurity injection experiments, (ii) decreases with increasing base ion atomic mass, and (iii) is independent from the impurity charge to mass ratio. The theory further predicts a dramatic increase of the anomaly, also in agreement with experimental results, when the growth rate is enhanced within the heat pulse released by the sawtooth relaxations of the core. (32 refs.)

Stochastic behavior in presence of an electrostatic wave due to the crossing of multiple cyclotron resonances in an inhomogeneous magnetic field See Entry 113587

Spectral broadening of lower-hybrid waves by time-dependent density fluctuations See Entry 113593

Spectrum of compressional Alfvén waves See Entry 113594

Formation of electrodynamic boundary layers during the propagation of sound in a confined low-temperature plasma See Entry 113607

Effects of ion-acoustic instability on light ion beam transport in deuterium channels See Entry 113625

Numerical simulations for intense light-ion beam propagation in channel under influence of plasma inertia See Entry 113628

Properties of the corona generated by the incidence of intense CO $_2$ laser pulses on spherical targets See Entry 113638

Waves and turbulence in a Tokamak fusion plasma See Entry 113649

Plasma equilibrium and field diffusion during current rise phase of STP-2 screw pinch tokamak See Entry 113651

Transport models of particle and energy balance in Tokamak devices See Entry 113670

2.25P Emission, absorption, and scattering of radiation

- 13576 Forward CW CO₂-laser scattering on a high density plasma column. J.L.Lachambre, R.Decoste, A.Robert, P.Noel (Inst. de Recherche Hydro-Quebec, Varennes, Quebec, Canada). *Appl. Phys. (USA)*, vol.54, no.9, p.4722-8 (Sept. 1983). Wave-number and frequency spectra $S(k, \omega)$ associated with spontaneous electrostatic fluctuations in a high-density ($5 \times 10^{21} \text{ m}^{-3}$) current-driven plasma are measured using forward CO₂-laser scattering with homodyne detection. Scattering measurements during the quiescent plateau phase of the discharge show fluctuation levels several orders of magnitude above the thermal level with k^{-4} and ω^{-2} spectral amplitude dependences. The fluctuations are found to be isotropic in a plane transverse to the magnetic axis with $\langle k_{\perp} \rangle \propto S(k_{\perp}, \omega)$. The scattering apparatus is also shown to be a valuable diagnostic tool for basic studies of plasma current transport across magnetic field lines. In fact, a clear correlation is observed between the appearance of strong fluctuations and the rapid current penetration during fast plasma current reversal experiments. Finally, CW scattering results are used to find a set of experimental conditions suitable for the measurement of the ion temperature using a CO₂ pulsed scattering system. (28 refs.)
- 13577 Vibrational relaxation of Ne₂⁺ molecular ions during collisions with neon ions. See Entry 112824
- 13578 Acoustic wave calibration for CO₂ laser scattering experiments. See Entry 113034
- 13579 Local determination of the ion temperature from the Doppler broadening of hydrogen lines through the use of a fast atomic beam. See Entry 113570
- 13580 O₂ collective laser scattering on moving density perturbations in a plasma. See Entry 113618
- 13581 On the theory of induced electromagnetic wave scattering in heterogeneous plasma. See Entry 113620
- 13582 Generation of higher harmonics of an intense laser beam in a plasma. See Entry 113623
- 13583 Simultaneous measurement of magnetic field direction and ion temperature in a plasma by collective scattering with a CO₂ laser. See Entry 113652
- 13584 Experimental investigation of absorption coefficient of cesium resonance doublets in a plasma of combustion products. See Entry 113660
- 13585 Holographic plasma interferometry in the infrared spectrum. II. Using non-linear effects to increase the sensitivity. See Entry 113667
- 13586 Calculation of spectrum line emission from plasmas. See Entry 113668
- 13587 Brillouin scattering of multiline laser light in a flowing plasma corona. See Entry 113688

52.30 PLASMA FLOW; MAGNETOHYDRODYNAMICS

(see also 47.65 Fluid dynamics)

- 13577 On the geometry of vortex lines in magnetofluid flows. S.N.Singh, R.Babu (Dept. of Maths., Banaras Hindu Univ., Varanasi, India). *Nuovo Cimento B (Italy)*, vol.76B, ser.2, no.1, p.47-53 (11 July 1983). By employing the anholonomic description of basic equations governing MFD flows, certain geometrical results of physical importance are obtained. By assuming Beltrami flow, the conditions are derived for which the Maxwellian surfaces can be developed. The variation of the total energy along the vortex lines is also discussed. (7 refs.)
- 13578 A comparison of the full and reduced sets of magnetohydrodynamic equations for resistive tearing modes in cylindrical geometry. J.A.Holmes, B.A.Carreras, T.C.Hender, H.R.Hicks, V.E.Lynch, B.F.Masden (Oak Ridge Nat. Lab., Oak Ridge, TN, USA). *Phys. Fluids (USA)*, vol.26, no.9, p.2569-77 (Sept. 1983). The results of numerical calculations using a full set of resistive magnetohydrodynamic equations are compared with the results of similar calculations using a reduced set of equations derived for Tokamaks in the limits of low beta and large aspect ratio ($\beta \sim \epsilon \ll 1$). The calculations, which are carried out in three-dimensional cylindrical geometry using initial value techniques, allow the comparison of linear stability properties as well as detailed nonlinear studies. The results of these calculations (including linear growth rates and eigenfunctions, the nonlinear evolution of single-helicity magnetic islands, and the nonlinear evolution of multihelicity cases) confirm the validity of the reduced set of equations at low beta in cylindrical geometry. (18 refs.)
- 13579 Axisymmetric toroidal equilibria with plasma flow. C.Copenhaver (Dept. de Recherches sur la Fusion Controlée, Centre d'Etudes Nucleaires, Fontenay-aux-Roses, France). *Phys. Fluids (USA)*, vol.26, no.9, p.2635-41 (Sept. 1983). A general equilibrium equation for an axisymmetric toroidal plasma having both toroidal and poloidal components of the magnetic field and plasma flow is derived. The possibility of a numerical treatment is discussed and polynomial solutions are obtained for several limiting cases. These solutions show that with flow rotation, the pressure and magnetic surfaces are no longer concentric, and that there is a significant displacement between these surfaces. A new result of hydrodynamic interest is the equilibrium equation for a compressible fluid. (19 refs.)
- 13580 Comment on 'Steady-state planar ablative flow' [Phys. Fluids 25, 1644 (1982)] [and reply]. J.R.Sanmartin, J.L.Montanes (Escuela Tecnica Superior de Ingenieros Aeronauticos, Univ. Politecnica de Madrid, Madrid, Spain), A.Barrero, W.Manheimer, D.G.Colombant, J.H.Gardner. *Phys. Fluids (USA)*, vol.26, no.9, p.2754-6 (Sept. 1983). For original paper see W. Manheimer et al., *ibid.*, vol.25, p.1644 (1982). Manheimer et al. used a steady-state model to calculate planar ablative flow under both uniform and nonuniform illumination. The model assumed an underdense isothermal rarefaction linking up to a steady-state overdense plasma. Sanmartin et al. comment that the underdense plasma cannot be in steady state if the rarefaction is isothermal. They calculate similarity solutions for the case where the absorbed irradiance increases linearly in time. Manheimer et al. reply to these comments. (6 refs.)
- 13581 The gravitational instability of a rotating plasma in the presence of finite Larmor radius, Hall currents and suspended particles. See Entry 113582
- 13582 Hydromagnetic stability of a self-gravitating rotating viscous plasma in the presence of gyroviscosity. See Entry 113585
- 13583 Energetics and the resistive tearing mode: effects of Joule heating and radiation. See Entry 113596
- 13584 Ballooning mode calculations in stellarators. See Entry 113597

- Asymptotic theory of the internal kink mode in current-carrying toroidal plasmas. See Entry 113598
- Nonlinear periodic solutions for the isothermal magnetostatic atmosphere. See Entry 113601
- Formation of electrodynamic boundary layers during the propagation of sound in a confined low-temperature plasma. See Entry 113607
- Effects of ion-acoustic instability on light ion beam transport in deuterium channels. See Entry 113625
- Numerical studies of toroidal coupling on low- m resistive modes. See Entry 113647
- Formation of an anode spot in a vacuum arc. See Entry 113692
- Causes of cathode spot motion in a vacuum arc and an estimate of retrograde velocity in a magnetic field. See Entry 113693
- Propagation characteristics of hydromagnetic waves in a cold plasma mixed with a hot plasma and right-hand polarized Pc 1 and Pc 5. See Entry 116410
- Dependence of MHD turbulence spectra on the velocity field-magnetic field correlation. See Entry 116446
- The expansion of a plasma into a vacuum: basic phenomena and processes and applications to space plasma physics. See Entry 116470

52.35 WAVES, OSCILLATIONS, AND INSTABILITIES IN PLASMA

- 113581 Solenoidal excitation of eigenmodes in cylindrical magnetized plasma with two ion species. T.D.Kieu, W.N.-C.Sy (Dept. of Theoretical Phys., Res. School of Phys. Sci., Australian Nat. Univ., Canberra, Australia). *Aust. J. Phys. (Australia)*, vol.36, no.4, p.491-9 (1983). The conditions for the experimental observation of new types of eigenmodes in a typical laboratory magnetized plasma with two ion species are discussed. It is shown that the most favourable condition occurs during the current carrying phase of the discharge, with an appropriately chosen mixture of ions. (13 refs.)
- 113582 The gravitational instability of a rotating plasma in the presence of finite Larmor radius, Hall currents and suspended particles. K.C.Sharma (Dept. of Math., Himachal Pradesh Univ., Simla, India). *Astrophys. & Space Sci. (Netherlands)*, vol.94, no.2, p.419-24 (Aug. 1983). The gravitational instability of an infinite homogeneous self-gravitating and finitely conducting, rotating gas-particle medium, in the presence of finite Larmor radius, Hall currents and suspended particles effects is considered. Particular cases of the effects of rotation, finite conductivity, finite Larmor radius, Hall currents, and suspended particles on waves propagating along and perpendicular to magnetic fields are discussed. It is found that the Jeans's criterion remains unchanged in the presence of rotation, finite conductivity, finite Larmor radius, Hall currents, and suspended particles. (9 refs.)
- 113583 To a nonlinear theory of interaction of radiation with plasma surface vibrations. I.H.Peneva, G.I.Zaginailov, A.N.Kondratenko, V.M.Kuklin. *Bulg. J. Phys. (Bulgaria)*, vol.10, no.3, p.3531-67 (1983). In Russian. The nonlinear mechanism of saturation and the consequences of instability development under the action of external radiation with the plasma surface is considered in this work in the case of excitation of surface vibrations. The phase shift and amplitude of the surface vibrations as well as the condition for the instability development have been found. Nonlinear damping of the surface vibration, defined by the process of scattering of the external radiation has been determined as a function of the surface wave amplitude. (13 refs.)
- 113584 Two-dimensional problem of the formation of a disturbed zone in the vicinity of a plate when a supersonic rarefied plasma flows over it. V.A.Semenov. *Cosmic Res. (USA)*, vol.20, no.6, p.597-606 (Nov.-Dec. 1982). Translation of: *Kosm. Issled. (USSR)*, vol.20, no.6, p.848-58 (Nov.-Dec. 1982). [received: Sept. 1983]. The planar problem of the formation of a disturbed zone in the vicinity of a long strip moving with a high supersonic velocity in a Maxwellian collisionless plasma is analyzed allowing for the effect of electric fields on the structure of the disturbed zone. A statement of the problem is given and a critical analysis is made of the existing approaches to its investigation. (7 refs.)
- 113585 Hydromagnetic stability of a self-gravitating rotating viscous plasma in the presence of gyroviscosity. V.D.Sankhla, J.L.Bansal (Dept. of Maths., Univ. of Jodhpur, Jodhpur, India). *Indian J. Phys. Part B*, vol.57B, no.3, p.246-54 (June 1983). The hydromagnetic stability of a self-gravitating, incompressible, infinitely conducting, rotating viscous plasma of variable density is studied to include the effects of finiteness of the ion Larmor radius (FLR). The ambient magnetic field is assumed to be uniform and horizontal. The FLR effects have been included through stress tensor. Making use of existence of the variational principle which is shown to characterize the problem, proper solutions have been obtained for a semi-infinite plasma having density stratification along the vertical direction, according to the exponential law of density. The dispersion relation has been solved numerically for different values of the parameters involved. It is found that effect of FLR is destabilizing whereas character of viscosity and that of coriolis forces is stabilizing. (10 refs.)
- 113586 Nonlinear electron oscillation driven by an external wave in a plasma. M.Mengoli, V.G.Molinari (Lab. di Ingegneria Nucleare di Montecucolino, Univ. di Bologna, Bologna, Italy), F.Pizzio. *Nuovo Cimento B (Italy)*, vol.76B, ser.2, no.2, p.130-8 (11 Aug. 1983). The authors deal with electron oscillations in the field of a monochromatic wave having large phase velocity. The aim of this work is to extend to the hot-plasma case, by taking into account also the collision effects, the results obtained in the framework of the cold-plasma approximation. The expressions of the electron densities, as functions of space and time, are given for the two cases of a progressive and a stationary excited longitudinal wave. (4 refs.)
- 113587 Stochastic behavior in presence of an electrostatic wave due to the crossing of multiple cyclotron resonances in an inhomogeneous magnetic field. N.A.Ryabova, D.R.Shklyar. *Phys. Lett. A (Netherlands)*, vol.97A, no.5, p.194-8 (29 Aug. 1983). The criterion for the occurrence of stochastic behavior of particle trajectories in the field of an electrostatic wave is obtained taking into account the longitudinal inhomogeneity of the ambient magnetic field. The origin of the stochasticity is explained. The optimum conditions for particle heating are obtained at a wave amplitude below the threshold of stochasticity in a homogeneous plasma. (5 refs.)

- 113588 Nonlinear evolution of an obliquely propagating Langmuir wave: boundary-value problem.** C.R.Menyuk (Lab. for Plasma & Fusion Energy Studies, Univ. of Maryland, College Park, MD, USA). *Phys. Fluids (USA)*, vol.26, no.9, p.2482-7 (Sept. 1983). The nonlinear evolution of an obliquely propagating Langmuir wave is explored given boundary-value conditions, with emphasis on determining the effect of a transition between regular and stochastic electron motion. It is shown that when the angle of propagation is increased, the usual amplitude oscillations disappear because of destructive interference between the different, isolated resonances. It is also shown that the final ($z \rightarrow \infty$) wave amplitude decreases when there is a parameter transition from the trapping to the stochastic regime because electrons become free to travel large distances in velocity space, taking large amounts of energy from the wave. (16 refs.)
- 113589 Stabilization of the lower-hybrid drift instability by resonant electrons.** Yu-Juan Chen (Electronics Res. Lab., Univ. of California, Berkeley, CA, USA), W.M.Nevins, C.K.Birdsall. *Phys. Fluids (USA)*, vol.26, no.9, p.2501-8 (Sept. 1983). The lower-hybrid drift instability is studied with a two-dimensional electrostatic simulation code. Simulations show good agreement of the measured local growth rates and frequencies with the results of local theory during the early stage of wave growth. At later times nonlocal effects become important, and a coherent mode structure develops. This normal mode is observed to propagate up the density gradient. At zero plasma beta and zero electron temperature, it is found that the lower-hybrid drift instability is stabilized by the local current relaxation due to both ion quasilinear diffusion and electron $\mathbf{E} \times \mathbf{B}$ trapping which causes electron heating to occur. (10 refs.)
- 113590 Stabilization of the tearing mode in high-temperature plasma.** J.F.Drake, T.M.Antonsen, Jr., A.B.Hassam, N.T.Gladd (Lab. for Plasma & Fusion Energy Studies, Univ. of Maryland, College Park, MD, USA). *Phys. Fluids (USA)*, vol.26, no.9, p.2509-28 (Sept. 1983). An analytical and numerical study of the stability of tearing modes is carried out using the Braginskii fluid equations. An electron temperature gradient coupled with finite (nonzero) parallel thermal conductivity causes large parallel currents to flow in the vicinity of the singular layer (where $\mathbf{k} \cdot \mathbf{B} = 0$). The pressure-driven currents are stabilizing and in the limit $\beta L_e^2 / L_n^2 > 1$, where β is the ratio of the thermal to magnetic pressure and L_e and L_n are the magnetic shear and density scale lengths, the linear tearing mode no longer exists. In this high- β limit, the magnetic perturbation of the tearing mode is completely shielded from the singular layer so that no reconnection of the magnetic field can take place. The relationship between the tearing mode and previously investigated temperature-gradient-driven modes and the implications of the results for resistive modes in present and future Tokamak discharges is discussed. (28 refs.)
- 113591 Filamentation instability in magneto plasmas.** S.P.Kuo (Polytech. Inst. of New York, Farmingdale, NY, USA), G.Schmidt. *Phys. Fluids (USA)*, vol.26, no.9, p.2529-36 (Sept. 1983). It is shown that the filamentation of ordinary-mode pumps propagating at an arbitrary angle with respect to the magnetic field has to be magnetic field-aligned, but not for extraordinary-mode pumps. A general dispersion relation is derived including the effects of magnetic field and collisions, and the nonlinear effects of ponderomotive force, thermal focusing force, and the beating currents. Threshold field and growth rates are obtained and compared to the results of the unmagnetized and collisionless case. Applications of these results to ionospheric modifications are discussed. (14 refs.)
- 113592 Scattering of lower-hybrid waves by drift-wave density fluctuations: solutions of the radiative transfer equation.** P.L.Andrews, F.W.Perkins (Plasma Phys. Lab., Princeton Univ., Princeton, NJ, USA). *Phys. Fluids (USA)*, vol.26, no.9, p.2537-45 (Sept. 1983). The investigation of the scattering of lower-hybrid waves by density fluctuations arising from drift waves in Tokamaks is distinguished by the presence in the wave equation of a large, random, derivative-coupling term. The propagation of the lower-hybrid waves is well represented by a radiative transfer equation when the scale size of the density fluctuations is small compared to the overall plasma size. The radiative transfer equation is solved in two limits: first, the forward scattering limit, where the scale size of density fluctuations is large compared to the lower-hybrid perpendicular wavelength, and second, the large-angle scattering limit, where this inequality is reversed. The most important features of these solutions are well represented by analytical formulas derived by simple arguments. Based on conventional estimates for density fluctuations arising from drift waves and a parabolic density profile, the optical depth τ for scattering through a significant angle, is given by $\tau \approx 2(N_e / n_e) (\omega_{pe} / \omega)^2 (m_e c^2 / 2T_i)^{1/2} [c / \alpha (R_i \Omega_e)^{1/2}]$, where ω_{pe} is the central ion plasma frequency and T_i denotes the ion temperature near the edge of the plasma. Most of the scattering occurs near the surface. The transmission through the scattering region scales as τ^{-1} and the emerging intensity has an angular spectrum proportional to $\cos \theta$, where $\sin \theta = \mathbf{k}_\perp \cdot \mathbf{B}_p / (k_\perp B_p)$, and \mathbf{B}_p is the poloidal field. (21 refs.)
- 113593 Spectral broadening of lower-hybrid waves by time-dependent density fluctuations.** P.L.Andrews, F.W.Perkins (Plasma Phys. Lab., Princeton Univ., Princeton, NJ, USA). *Phys. Fluids (USA)*, vol.26, no.9, p.2546-57 (Sept. 1983). Lower-hybrid waves injected into Tokamaks are scattered by turbulent time-dependent drift-wave density fluctuations. This scattering process gives rise to frequency shifts as well as angular deviations. In Tokamaks, most of the frequency spreading occurs in a regime where the angular scattering results from multiple scattering events, each event having a small mean-square scattering angle. A radiative transport equation governing diffusion in both angle and frequency is derived. The solution is obtained in slab geometry via separation of variables and leads to a Mathieu equation. In the limit where the slab thickness l exceeds the typical distance for diffusion through a large angle l_0 , an explicit generalization of the diffusion solution to the radiative transfer equation is formed. This solution gives the combined angular and frequency spectrum in the scattering layer. In the thick slab limit, the RMS frequency width of lower-hybrid waves emerging from the layer is given by $\Delta\omega = (\omega_{pe} / \omega) N_e (M_i / m_e) \beta_i^{1/2} (1/l_0)$, where ω_{pe} and β_i^{-1} are the characteristic angular frequency correlation length of the drift-wave turbulence. (20 refs.)
- 113594 Spectrum of compressional Alfvén waves.** S.M.Mahajan, D.W.Ross (Fusion Res. Center, Univ. of Texas, Austin, TX, USA). *Phys. Fluids (USA)*, vol.26, no.9, p.2561-4 (Sept. 1983). The spectrum of compressional Alfvén eigenmodes localized in the potential well created by a combination of the variation in plasma density and the wavenumber $k_\perp = m/r$ is obtained, and its importance for radio frequency current drive is discussed. It is found that modes with small parallel wavenumbers and frequencies below the ion cyclotron frequency are attractive for current drive. (11 refs.)
- 113595 On tearing modes in a resistive medium.** P.Rosenau (Dept. of Nuclear Engng., MIT, Cambridge, MA, USA). *Phys. Fluids (USA)*, vol.26, no.9, p.2578-89 (Sept. 1983). The theory of tearing modes in cylindrical symmetry is reexamined. The resistive medium is characterized by the simplest Ohm's law. By considering β , the ratio of thermal to magnetic pressure, as a parameter with respect to which the sought-after eigenvalues were scaled, a very simple description was obtained. Many of the classical results were obtained in a more simple way. Among the new results are: (1) the possibility of the existence of a tearing mode on a resistive time scale, which is hardly affected by drift effects; and (2) for modes of an almost marginal growth rate inertia does not play an important role, slab and cylindrical modes are fundamentally different, and finite- β effects play a crucial role. (18 refs.)
- 113596 Energetics and the resistive tearing mode: effects of Joule heating and radiation.** R.S.Steinolfson (Dept. of Phys., Univ. of California, Irvine, CA, USA). *Phys. Fluids (USA)*, vol.26, no.9, p.2590-602 (Sept. 1983). Hydromagnetic theory is used to investigate the influence of Joule heating and temperature-dependent radiation on the linear development of the incompressible, resistive tearing instability in both force-free and neutral-sheet magnetic fields in a slab geometry. A temperature-dependent resistivity couples the energetics and the dynamics of the instability. Analytical expressions are derived for the growth rates utilizing, in separate analyses, the constant- Ψ and the long-wavelength (nonconstant- Ψ) approximations. The solutions indicate the occurrence of several modes in addition to the usual tearing mode. A number of the modes have relatively slow, complex growth rates. However, at large values of the magnetic Reynolds number S ($S \geq 10^7$), the actual value depending on the relevant parametric values, there are at least two modes with purely exponential growth (real, positive growth rates) when the radiative loss decreases with increasing temperature. One is the resistive tearing mode, and the other is a more rapidly growing mode with a growth rate resembling that of a thermal instability. If the radiation is neglected, the Joule heating alone also results in two modes with real, positive growth at large S . One mode is again the tearing mode, but, in this case, the second mode is a more slowly growing Joule-heating mode. Another point of departure from previous theoretical results is that, below a particular value of S ($S \leq 10^6$, the value once again being determined by the parameters), all the modes are generally stabilized. (31 refs.)
- 113597 Ballooning mode calculations in stellarators.** H.L.Berk, M.N.Rosenbluth (Inst. for Fusion Studies, Univ. of Texas, Austin, TX, USA), J.L.Shohet. *Phys. Fluids (USA)*, vol.26, no.9, p.2616-20 (Sept. 1983). A magnetohydrodynamic (MHD) ballooning mode formalism and calculation is used to show how a field-line-following code can be used to study MHD stability. The asymptotic analysis of the ballooning equation yields the Mercier condition. It is shown that first-order equilibrium effects on the vacuum fields from finite pressure cancel the intrinsically destabilizing term of the Mercier condition. A ballooning unstable solution is found in a Helic configuration that has a magnetic well at zero beta and a rotational transform that increases radially outward. (12 refs.)
- 113598 Asymptotic theory of the internal kink mode in current-carrying toroidal plasmas.** G.B.Crew, J.J.Ramos (MIT, Cambridge, MA, USA). *Phys. Fluids (USA)*, vol.26, no.9, p.2621-34 (Sept. 1983). An asymptotic approach to the linear stability of the ideal magnetohydrodynamic internal kink mode in large-aspect-ratio Tokamak plasmas is presented. This analysis spans arbitrary values of the plasma pressure gradient, and in particular demonstrates the stabilization of the mode at sufficiently high beta. (17 refs.)
- 113599 Anisotropy effects on curvature-driven flute instabilities in a hot-electron plasma.** D.A.Spong (Oak Ridge Nat. Lab., Oak Ridge, TN, USA), H.L.Berk, J.W.Van Dam, M.N.Rosenbluth. *Phys. Fluids (USA)*, vol.26, no.9, p.2652-6 (Sept. 1983). The effects of finite parallel temperature are investigated for a hot-electron plasma with sufficiently large beta that the magnetic field scale length (Δ_B) is small compared with the vacuum field radius of curvature (R). Numerical and analytical estimates of stability boundaries are obtained for the four possible modes that can be treated in this limit: the conventional hot-electron interchange, the high-frequency hot-electron interchange ($\omega > \omega_{ce}$), the compressional Alfvén mode, and the interacting pressure-driven interchange. (9 refs.)
- 113600 Backscattering cascade of beam modes off ambient density fluctuations.** D.A.Russell, M.V.Goldman (Dept. of Astro-Geophys., Univ. of Colorado, Boulder, CO, USA). *Phys. Fluids (USA)*, vol.26, no.9, p.2717-30 (Sept. 1983). The effects of a given nonthermal low-frequency density-fluctuation spectrum on the amplification of Langmuir waves by a 'bump-on-tail' beam of electrons are studied. The density-fluctuation spectrum is assumed to contain a uniform distribution of wavelengths ranging from much shorter than the beam mode wavelength to of the same order. This permits multiple large-angle (back) scattering to occur. One-dimensional numerical solutions of the kinetic equations are found which yield criteria for linear saturation of the beam instability by a cascade of backscattering to high wavenumber. The relevant time scales and spectral shapes are also determined in both the stable and unstable regions. Linear damping and Cerenkov emission by a possible nonthermal tail of electrons is taken into account. An application is made to the beam modes observed simultaneously with density fluctuations off the Jovian bow shock. It is shown that the observed level of density fluctuations is sufficient to saturate the unstable Langmuir waves, although nonthermal Landau damping may prevent a cascade to very high wavenumbers. (6 refs.)
- 113601 Nonlinear periodic solutions for the isothermal magnetostatic atmosphere.** B.C.Low, A.J.Hundhausen (High Altitude Obs., Nat. Center for Atmospheric Res., Boulder, CO, USA), E.G.Zweibel. *Phys. Fluids (USA)*, vol.26, no.9, p.2731-41 (Sept. 1983). A set of analytical, periodic magnetostatic solutions is presented describing parallel filaments of diffuse, magnetized plasma suspended horizontally in equilibrium in a uniform gravitational field. The magnetic field has no component along the filament, and the temperature is uniform in space. The problem is two dimensional and reduces to solving the magnetostatic equation of Dungey in a nonlinear form. Different field topologies are associated with the same basic plasma structure, depending on the sign and strength of the field far above and below the array of parallel filaments. These equilibria are shown to be locally unstable against ideal magnetohydrodynamic perturbations having large wavenumbers along the plasma filaments. It is suggested that the system may be stabilized if there is a component of the magnetic field parallel to the plasma filaments. (23 refs.)

- 3602 Soliton experiments in plasmas.** K.E.Lonngrén (Dept. of Electrical & Computer Engng., Univ. of Iowa, Iowa City, IA, USA). *Plasma Phys. (GB)*, vol.25, no.9, p.943-82 (Sept. 1983). The experiments on solitons in plasmas performed during the period 1970 to 1982 are reviewed. Suggestions for future experiments are presented. (309 refs.)
- 3603 Effect of nonlinear Landau damping on long time behaviour of modulational instability of Langmuir wave.** J.C.Bhaktia (Dept. of Appl. Math., Calcutta Univ., Calcutta, India), D.Majumder, M.R.Gupta. *Plasma Phys. (GB)*, vol.25, no.9, p.983-90 (Sept. 1983). The effect of nonlinear Landau damping on the long term behaviour of the modulational instability of a monochromatic Langmuir wave has been investigated. The growth or decay of the perturbation amplitude is oscillatory in character. Most of the time the amplitude changes approximately linearly with time. Growth occurs for negative nonlinear frequency shift while it decays when the frequency shift is positive. (8 refs.)
- 3604 Selective destabilization of ion cyclotron modes.** M.J.Alpert, J.Barrett, M.A.Behrens (Plasma Phys. Res. Inst., Univ. of Natal, Durban, S Africa). *Plasma Phys. (GB)*, vol.25, no.9, p.1059-64 (Sept. 1983). Observations of the current-driven electrostatic ion cyclotron instability, both $T_e/T_i=1$ and $T_e/T_i \gg 1$, show that as the normalized wave number, $k_{\perp}\rho_i$ is varied, different modes ($m=1, 2, 3, \dots$) become successively the most unstable mode. The calculated values of $k_{\perp}\rho_i$ at which the cross-over from one mode to the next occurs are in reasonable agreement with the observed values provided that the local density gradient is taken into account. (18 refs.)
- 3605 Recurrence of electron cyclotron harmonic wave instability in a beam-plasma system.** V.K.Jain, P.J.Christiansen (School of Math. & Phys. Sci., Univ. of Sussex, Brighton, England). *Plasma Phys. (GB)*, vol.25, no.10, p.1169-72 (Oct. 1983). The recurrence phenomenon characterised by spatial amplitude modulation is observed on the first harmonic of electron cyclotron harmonic wave instability excited in a beam-plasma system. It is found that it results from an interference between a forced and a natural mode of oscillation at the harmonic frequency. (11 refs.)
- 3606 Surface ionic-sonic oscillations in inhomogeneous plasma.** M.Vorob'ev, A.N.Kondratenko, V.M.Kuklin. *Radio Eng. & Electron. Phys. (USA)*, vol.27, no.11, p.124-6 (Nov. 1982). Translation of: *Radiotekh. & Elektron. (USSR)*, vol.27, no.11, p.2203-6 (Nov. 1982). [received: Sept. 1983] Dispersion characteristics of surface ionic-sonic waves are obtained and the effectiveness of exciting them by charged particle streams is discussed. It is shown that inhomogeneity in the density of plasma, with a subsequent frequency of the wave, leads to a qualitative change in the nature of its dispersion. The increments in the excitation of these waves by streams of charged particles depend weakly on the degree of plasma density inhomogeneity. (6 refs.)
- 3607 Formation of electrodynamic boundary layers during the propagation of sound in a confined low-temperature plasma.** I.M.Rutkevich (Inst. of High Temperatures, Acad. of Sci., Moscow, USSR). *Sov. Phys.-Dokl. (USA)*, vol.27, no.12, p.1035-6 (Dec. 1982). Translation of: *Dokl. Akad. Nauk SSSR*, vol.267, no.4-6, p.837-40 (Dec. 1982). [received: Sept. 1983] The problems of sound propagation in a low-temperature plasma occupy an important place in research on wave processes and instabilities in magnetogas-dynamic flows and gas discharges. The one-dimensional description of short-wave disturbances has been applied not only to an unbounded plasma but also to the investigation of the longitudinal propagation of disturbances in channels. In this connection the author focuses attention on the formation of a distinctly multidimensional structure of electric-current disturbances in a sound wave propagating in a magnetic field along a channel of finite width. (8 refs.)
- 3608 Dissipative trapped ion instability in PLT and INTOR.** A.Wakamatsu, K.Shimizu, M.Ogasawara. *Report IPPJ-635*, Nagoya Univ., Japan (June 1983), 20 pp. The generation conditions of the dissipative trapped ion instability (DTII) are investigated for the parameters of PLT and INTOR. The finite banana width effect is taken into account in the dispersion relation. The conditions are greatly influenced by the impurities. Though the plasmas are well in the banana regime in both PLT and INTOR, DTII is not excited for $Z_{\text{eff}}=3.5$, and excited but it has negative growth rate for $Z_{\text{eff}}=1.5$, where Z_{eff} is the effective charge number. Only for the pure case ($Z_{\text{eff}}=1.0$), the growth rate has small positive value in INTOR. (6 refs.)
- American Geophysical Union Chapman Conference on Waves in Magnetospheric Plasma** See Entry 111303
- Nonlinear waves: from hydrodynamics to plasma theory** See Entry 113461
- Unified kinetic theory in toroidal systems** See Entry 113566
- Effect of collisionless detrappping on nonaxisymmetric transport in a stellarator with radial electric field** See Entry 113572
- Measurements of fluctuations in the flux of runaway electrons to the PLT Tokamak limiter** See Entry 113573
- Transport properties of drift waves** See Entry 113574
- Anomalous impurity transport in plasmas** See Entry 113575
- A comparison of the full and reduced sets of magnetohydrodynamic equations for resistive tearing modes in cylindrical geometry** See Entry 113578
- Growth of phase-space density holes** See Entry 113611
- On the theory of induced electromagnetic wave scattering in heterogeneous plasma** See Entry 113620
- Ion heating due to explosive instability in an ion beam-plasma system** See Entry 113624
- Effects of ion-acoustic instability on light ion beam transport in deuterium channels** See Entry 113625
- Electromagnetic two-stream and filamentation instabilities for a relativistic beam-plasma system** See Entry 113626
- Measurements of electron and ion heating by Alfvén waves in the TCA Tokamak** See Entry 113630
- Energy deposition profile of shear Alfvén wave heating** See Entry 113631
- Growth rate reduction of the curvature-driven flute instability by plasma blanket line tying** See Entry 113642
- Finite Larmor radius stability theory of ELMO Bumpy Torus plasmas** See Entry 113643
- Rotational stability of tandem mirrors** See Entry 113644

- Quadrupole stabilization of the $n=2$ rotational instability of a field-reversed theta-pinch plasma** See Entry 113645
- Numerical studies of toroidal coupling on low- m resistive modes** See Entry 113647
- Waves and turbulence in a Tokamak fusion plasma** See Entry 113649
- Applications of the Fraunhofer-diffraction method for plasma-wave measurements** See Entry 113664
- Relativistic plasma microwave generator** See Entry 113672
- Observation of a significant density of negative ions in a currentless discharge in air; the possibility of an attachment instability** See Entry 113694
- Propagation characteristics of hydromagnetic waves in a cold plasma mixed with a hot plasma and right-hand polarized Pc 1 and Pc 5** See Entry 116410
- On the effect of oblique disturbances on Kelvin-Helmholtz instability at magnetospheric boundary layers and in solar wind** See Entry 116411
- Effect of rotation on magnetogravitational instability of finite conducting gas in presence of suspended particles** See Entry 116441
- The expansion of a plasma into a vacuum: basic phenomena and processes and applications to space plasma physics** See Entry 116470

52.35R Plasma turbulence

- 113609 Magnetically induced plasma rotation and the dense plasma focus.** E.A.Witalis (Nat. Defence Res. Inst., Stockholm, Sweden). *Z. Naturforsch. Teil A (Germany)*, vol.38A, no.9, p.949-58 (Sept. 1983). Fusion for fission fuel breeding and other incentives for unconventional magnetic fusion research are introductorily mentioned. The design, operation and peculiar characteristics of dense plasma foci are briefly described with attention to their remarkable ion acceleration and plasma heating capabilities. Attempts for interpretations are reviewed, and a brief account is given for an explanation based on the concept of magnetically induced plasma rotation, recently derived in detail in this journal. Basically an ion acceleration mechanism of betatron character, it describes (in combination with a dynamic, generalized Bennett relation focus plasma) characteristics like the polarity dependence, the current channel disruption, the axial ion beam formation and the pre-requisites for the ensuing turbulent plasma dissipative stage. Fundamental differences with respect to mainline fusion research are emphasized, and some conjectures and proposals are presented as to the further development of plasma focus nuclear fusion or fission energy production. (46 refs.)
- 113610 Observation of self-binding turbulent fluctuations in simulation plasma and their relevance to plasma kinetic theories.** R.H.Berman, D.J.Tetreault, T.H.Dupree (MIT, Cambridge, MA, USA). *Phys. Fluids (USA)*, vol.26, no.9, p.2437-59 (Sept. 1983). Non-wave-like fluctuations of the phase-space density are observed in simulations of turbulent plasma. During decay from an initial state, the mean square fluctuation level decays at a much slower rate than that of an individual fluctuation. The distribution function of the fluctuation amplitudes becomes non-Gaussian (skewed) in favor of negative fluctuations. An enhancement in the aggregate fluctuation lifetime is also observed when the turbulence is driven by an external source. A model based on a collection of self-binding negative fluctuations, called phase-space density holes, can explain the observations. Collisions between holes produce hole fragments and lead to fluctuation decay. However, the hole fragments are self-binding and tend to recombine into new holes. The implications of these results for kinetic theories of plasma turbulence are discussed. In particular, it is shown that the theory of clumps, when suitably modified to include fluctuation self-binding, can explain many features of the nonlinear instability recently observed in computer simulations. (14 refs.)
- 113611 Growth of phase-space density holes.** T.H.Dupree (MIT, Cambridge, MA, USA). *Phys. Fluids (USA)*, vol.26, no.9, p.2460-81 (Sept. 1983). Phase-space density holes are shown to grow in a plasma for any nonzero electron-ion drift velocity. As a hole grows, its depth, velocity width, and electrostatic potential increase. For a hole with velocity u , the growth rate is of order $-v_{Te}^2 f_{0e}(u) v_{Te}^2 f_{0e}(u)$ times the bounce frequency of a particle trapped in the hole. The theoretical predictions agree reasonably well with a recent computer simulation. The results call into question the role of linear stability theory. Energy and momentum conservation are analyzed in detail, and the relationship to the clump instability is discussed. (8 refs.)
- 113612 A new interpretation of the alpha effect.** R.K.Keinigs (Los Alamos Nat. Lab., Los Alamos, NM, USA). *Phys. Fluids (USA)*, vol.26, no.9, p.2558-60 (Sept. 1983). In a magnetized plasma the alpha effect represents a turbulently generated EMF directed along the mean magnetic field. This EMF is central to the understanding of turbulent generation of large-scale magnetic fields. The alpha effect is reevaluated in terms of ensemble-averaged properties of the magnetic fluctuation spectrum. The results indicate that it is current helicity as opposed to kinetic helicity that is required to produce an alpha effect. (9 refs.)
- 113613 Centrifugal isotope separation in zirconium plasmas.** M.Krishnan (Appl. Phys. Section, Yale Univ., New Haven, CT, USA). *Phys. Fluids (USA)*, vol.26, no.9, p.2676-82 (Sept. 1983). Centrifugal isotopic enrichment in a zirconium vacuum arc centrifuge is described. Peak, single-pass enrichments up to 1700% for $^{96}\text{Zr}^{2+}$, 330% for $^{94}\text{Zr}^{2+}$, 280% for $^{92}\text{Zr}^{2+}$, and 50% for $^{91}\text{Zr}^{2+}$ were measured, for a discharge current of 3.7 kA and magnetic field strength of 0.17 T. Such high enrichments are compared with predictions of a simple, two-fluid centrifuge model. (23 refs.)
- Transport properties of drift waves** See Entry 113574
- Anomalous impurity transport in plasmas** See Entry 113575
- Axisymmetric toroidal equilibria with plasma flow** See Entry 113579
- The gravitational instability of a rotating plasma in the presence of finite Larmor radius, Hall currents and suspended particles** See Entry 113582
- Rotational stability of tandem mirrors** See Entry 113644
- Waves and turbulence in a Tokamak fusion plasma** See Entry 113649
- Applications of the Fraunhofer-diffraction method for plasma-wave measurements** See Entry 113664
- Effect of rotation on magnetogravitational instability of finite conducting gas in presence of suspended particles** See Entry 116441
- Dependence of MHD turbulence spectra on the velocity field-magnetic field correlation** See Entry 116446

52.35T Shock waves

113614 Structure of perpendicular shocks in collisionless plasma. M.M.Leroy (Univ. of Maryland, College Park, MD, USA). *Phys. Fluids (USA)*, vol.26, no.9, p.2742-53 (Sept. 1983). The macrostructure of perpendicular shocks in the supercritical regime is investigated theoretically. The coupling between the shock precursor (foot region) associated with reflected ions and the magnetic ramp associated with electron Ohmic heating is analyzed using a model in which the ions are treated as a multifluid and the electrons as a massless fluid. The results are found to be in good agreement with a number of features exhibited by recent numerical simulations of perpendicular shocks, including the morphology of the reflected-gyrating ion stream, the presence of potential and magnetic field overshoots, and the Mach number dependence of the shock structure. (36 refs.)

113615 Potential double layer formed by a laminar shock wave in a collisionless plasma. S.Yagura, H.Fujita (Dept. of Electrical Engng., Saga Univ., Saga, Japan). *Plasma Phys. (GB)*, vol.25, no.10, p.1087-95 (Oct. 1983). A potential double layer is formed by exciting a laminar shock wave with a step injection of ion beam in a triple plasma device. A potential jump of the double layer moving with a velocity of laminar shock wave is $(1-1.4)kT_e/e$ and the density fluctuation is 15-40%. Time resolved measurements of energy distribution function of both ions and electrons reveal that electrons are trapped and ions are reflected due to the formation of the potential double layer. (20 refs.)

Shock wave pressure enhancement using short wavelength (0.35 μ m) laser irradiation See Entry 113635

Converging shock on laser plasma: density profiles by holographic interferometry See Entry 113663

52.40 PLASMA INTERACTIONS

52.40D Electromagnetic wave propagation in plasma

113616 Localization of circularly polarized intense electromagnetic waves in relativistic plasmas. N.Nagesha Rao, R.K.Varma (Phys. Res. Lab., Navrangpura, Ahmedabad, India), P.K.Shukla, M.Y.Yu. *Phys. Fluids (USA)*, vol.26, no.9, p.2488-500 (Sept. 1983).

Localization of a circularly polarized, high-intensity electromagnetic field in a relativistic, unmagnetized plasma is considered. A new class of double-hump electromagnetic soliton solutions having nonzero high-frequency field intensity at the center is found for subsonic as well as supersonic velocities. For subsonic velocities, these solitons are found to be accompanied by density dips whereas supersonic solitons are associated with density humps. Parameter regions for the existence of different types of electromagnetic solitons are obtained explicitly. A few limiting cases of the general solutions obtained in the present theory are also discussed. (20 refs.)

113617 Nonlinearly induced radiation from an overdense plasma region. O.M.Gradov (Lebedev Phys. Inst., Acad. of Sci., Moscow, USSR), L.Stenflo. *Plasma Phys. (GB)*, vol.25, no.9, p.1051-8 (Sept. 1983). A new mechanism for the nonlinear transparency of a bounded plasma is considered. The incident electromagnetic wave is supposed to decay into quasi-static eigenmodes which can propagate around the overdense region. Most of the transformed energy can be reradiated in specific directions from the particular plasma surface regions where the plasma parameters have proper values. The stationary state, that is established when the power of the induced radiation is equal to that of the incident, is also studied. (4 refs.)

113618 CO₂ collective laser scattering on moving density perturbations in a plasma. D.C.Schram, H.W.H.van Andel, G.le Clair, P.Brøderup (Dept. de Phys., Univ. de Montreal, Montreal, Quebec, Canada). *Plasma Phys. (GB)*, vol.25, no.10, p.1133-48 (Oct. 1983). CO₂ laser scattering from plasma density perturbations which are not wave-like in nature moving through the beam is calculated for various geometries and scale-lengths. Exact expressions are found for the heterodyne detector currents as a function of time, and for the corresponding frequency spectra. In particular, the cases of small-scale rotating density perturbations in cylindrical plasmas and off-axis rotation of the entire plasma column are analyzed in detail. By way of illustration, the theoretical results are compared with some measured scattering spectra from a magnetized arc. (16 refs.)

113619 Reflection, transmission and absorption of electromagnetic waves by an inhomogeneous random plasma slab. S.Yamaguchi, K.Mori, T.Hosono (Coll. of Sci. & Technol., Nihon Univ., Tokyo, Japan). *Trans. Inst. Electron. & Commun. Eng. Jpn. Part B (Japan)*, vol.166B, no.6, p.751-8 (June 1983). In Japanese.

The authors analyze interactions of electromagnetic waves with an inhomogeneous random plasma slab. Reflection phenomena of the electromagnetic waves in the case of oblique incidence are analyzed numerically. It is concluded that the obliquely incident TM wave is collisionlessly absorbed if plasma density becomes critical at some places, and then the usual homogeneous multilayer method is no longer applicable. Improvement of the physical model for random plasma and application of a modified homogeneous multilayer method are proposed to allow correct analysis under the previously mentioned conditions. (10 refs.)

113620 On the theory of induced electromagnetic wave scattering in heterogeneous plasma. V.N.Radzievskii. *Ukr. Fiz. Zh. (USSR)*, vol.28, no.8, p.1259-61 (Aug. 1983). In Russian. Investigates the induced Raman backscattering of one of the pumping waves by a high-frequency component of plasma waves (superposed Langmuir and ion-acoustic waves). (2 refs.) V.G.P.

113621 Self-focusing in laser produced spark. J.S.Bakos, I.B.Foldes. *Report KFKI-1983-50*, Hungarian Acad. Sci., Budapest (1983), 14 pp. The self-focusing effect appearing in different phases of development of the laser produced breakdown plasma in air is investigated. Self-focusing during the ionization process is demonstrated. Thermal self-focusing was observed in the later stage of the plasma development at moderate light intensities. Plasma development was investigated by forward and side scattering of the laser light in the plasma. A crossed beam experiment gave evidence of the thermal mechanism of self-focusing. (17 refs.)

Acoustic wave calibration for CO₂ laser scattering experiments See Entry 113034

Forward CW CO₂-laser scattering on a high density plasma column See Entry 113576

Construction of a high density plasma device for microwave-plasma interaction experiment See Entry 113671

52.40F Antennas in plasma; plasma-filled wave guides

Solenoidal excitation of eigenmodes in cylindrical magnetized plasma with two ion species See Entry 113581

52.40H Solid-plasma interactions

113622 Wall material characteristics in reacting plasma modelling. T.Kawamura, K.Akaiishi, A.Miyahara. *Report IPPJ-592*, Nagoya Univ., Japan (June 1982), 15 pp. Using the one-dimensional diffusion equation for impurities and energy balance equation for ions and electrons in the steady state Tokamak plasma, the self-consistent solutions of the impurity density profile and the temperature profile for a reacting DT plasma are analyzed, by taking into account of the plasma-surface interaction. On the basis of these results the influences of the impurities originated from the wall on the central plasma conditions and the Q-value of a reacting plasma are discussed. (8 refs.)

A fusion-fusion reactor driven by plasma-liner impact See Entry 112443

Resonant-fluorescence plasma diagnostics near the chamber wall in the TUMAN-3 tokamak See Entry 113661

52.40K Sheaths

Potential double layer formed by a laminar shock wave in a collisionless plasma See Entry 113615

Growth rate reduction of the curvature-driven flute instability by plasma blanket line tying See Entry 113642

52.40M Beam interactions in plasma

113623 Generation of higher harmonics of an intense laser beam in a plasma. M.B.Isichenko, V.V.Yan'kov (I.V. Kurchatov Inst. of Atomic Energy, Moscow, USSR). *JETP Lett. (USA)*, vol.37, no.7, p.351-3 (5 April 1983). Translation of: *Pis'ma v Zh. Eksp. & Teor. Fiz. (USSR)*, vol.37, no.7, p.297-8 (5 April 1983). [received: Oct. 1983]

The generation of higher harmonics of a pump beam by a mechanism involving a breaking of an electron wave is analyzed. The emission intensity is found to depend on the harmonic index in a power-law fashion, in agreement with experiment. (8 refs.)

113624 Ion heating due to explosive instability in an ion beam-plasma system. R.Sugaya (Dept. of Phys., Ehime Univ., Matsuyama, Japan). *Phys. Fluids (USA)*, vol.26, no.9, p.2698-703 (Sept. 1983).

Ion heating by the explosive instability in an ion beam-plasma system is studied theoretically. Two electrostatic waves with negative and positive energies become simultaneously unstable by nonlinear wave-particle interaction (nonlinear Landau damping) with plasma ions accompanying ion heating. The relaxation of the ion beam makes the explosion time of the waves much larger and causes saturation of the ion heating. It is shown quantitatively that the decrement of beam energy is transferred into thermal energies of plasma and beam ions by this explosive instability. (22 refs.)

113625 Effects of ion-acoustic instability on light ion beam transport in deuterium channels. D.G.Colombant, W.M.Manheimer (Plasma Phys. Div., Naval Res. Lab., Washington, DC, USA). *Phys. Fluids (USA)*, vol.26, no.9, p.2704-6 (Sept. 1983).

Moderate density deuterium channels can be ion-acoustic unstable when bunched high-intensity light ion beams are propagated into them. The magnetohydrodynamic response of these channels is investigated under these conditions. Anomalous effects like enhanced energy deposition, anomalous electron and ion heating, and anomalous resistivity are included in the model. Only at low channel densities does the instability cause an additional slowing down of the beam. However, the hydrodynamic motion of the channel remains unaffected. (5 refs.)

113626 Electromagnetic two-stream and filamentation instabilities for a relativistic beam-plasma system. Huan Lee, L.E.Thode (Los Alamos Nat. Lab., Univ. of California, Los Alamos, NM, USA). *Phys. Fluids (USA)*, vol.26, no.9, p.2707-16 (Sept. 1983).

Previous investigations on the two-stream and filamentation instabilities are based on either the electrostatic or the ordinary-mode approximation. A general relativistic dispersion formulation is presented to study these two instabilities for a scattered electron beam propagating a collisional, bi-Maxwellian plasma. New analytical results that apply to a general beam distribution are obtained for the stability boundary of the filamentation instability. The general dispersion relation uncovers the inadequacy in applying the ordinary-mode approximation in a frame other than the rest frame of the plasma. Analytical expressions for the growth rates of the filamentation modes in various parameter regimes are obtained. Finally, numerical comparisons are made between the general dispersion results and the earlier results based on the electrostatic and ordinary-mode approximations. (17 refs.)

113627 Nonlinear interaction of high-current H⁺ and H⁻ ion beams. P.N.Ostroumov, O.V.Serdyuk (Inst. of Nuclear Res., Acad. of Sci., Moscow, USSR). *Sov. Phys.-Tech. Phys. (USA)*, vol.28, no.2, p.143-5 (Feb. 1983). Translation of: *Zh. Tekh. Fiz. (USSR)*, vol.53, no.2, p.230-4 (Feb. 1983). [received: Sept. 1983]

Results of a numerical simulation of nonlinear interaction of two high-current H⁺ and H⁻ beams are reported. A qualitative explanation is given for the interaction processes which occur when the relaxation time to the steady-state distribution is $\sim 20 T_0$, where T_0 is the period of the plasma oscillations. (4 refs.)

113628 Numerical simulations for intense light-ion beam propagation in channel under influence of plasma inertia. S.Kawata, K.Niu. *Report IPPJ-627*, Nagoya Univ., Japan (March 1983), 12 pp.

The intense light-ion beam (LIB) propagation through a plasma channel is numerically investigated by using a two-dimensional simulation code. Analyses are given for the LIB propagation which couples with the motion of channel plasma. Although the electron back current neutralizes the LIB current under a typical beam and channel plasma condition, the Lorentz force by the electron back current expands the LIB radially. The expansion of the LIB depends strongly on the density of the channel plasma. A strong current of the order of 1 MA is shown to propagate stably in the argon plasma channel. (11 refs.)

- cal determination of the ion temperature from the Doppler broadening of hydrogen lines through the use of a fast atomic beam See Entry 113570
- Utilization of the lower-hybrid drift instability by resonant electrons See Entry 113589
- Backscattering cascade of beam modes off ambient density fluctuations See Entry 113600
- Current of electron cyclotron harmonic wave instability in a beam-plasma system See Entry 113605
- Potential double layer formed by a laminar shock wave in a collisionless plasma See Entry 113615
- Measurement of sloshing-ion spatial profiles in end cell of tandem mirror experiment-upgrade (TMX-U) See Entry 113641
- Relativistic plasma microwave generator See Entry 113672
- Characteristics of two types of beam plasma discharge in a laboratory experiment See Entry 116357

52.50 PLASMA PRODUCTION AND HEATING

- 3629 Motional impedance and heating of perfectly diamagnetic plasmas. B.N.Marihal, B.G.Jyoti (Dept. of Studies in Phys., Karnatak Univ., Dharwad, India). *Indian J. Phys. Part B*, vol.57B, no.3, p.255-61 (June 1983).
- Acceleration of solid diamagnetic spheres by a uniformly varying magnetic field is considered. Motional impedance which absorbs considerable amounts of energy even when its ohmic resistance becomes negligible is obtained for a perfectly diamagnetic plasma. Using equations of motion and circuit, the energy of the system is shown to be conserved. It is also shown that the mutual impact of two diamagnetic spheres gives rise to a temperature thermodynamic interest. Physical significance of the results is discussed with typical examples. A few important applications have also been discussed. (7 refs.)
- 3630 Measurements of electron and ion heating by Alfvén waves in the TCA Tokamak. A.De Chambrier, A.Heym, F.Hofmann, B.Joye, R.Keller, L.Lietti, J.B.Lister, P.D.Morgan (Centre de Recherches en Phys. des Plasmas, Ecole Polytech. Federale de Lausanne, Lausanne, Switzerland), J.I.Peacock, A.Pochelon, M.F.Stamp. *Plasma Phys. (GB)*, vol.25, no.9, p.1021-35 (Sept. 1983).
- Alfvén wave heating experiments have been carried out in the TCA Tokamak. RF power up to 75% of the value of the ohmic heating power has been delivered to the plasma. Increases in axial electron temperature of up to 80% ($T_e \sim 400$ eV) and in axial ion temperature of up to 50% ($\Delta T_i \sim 75$ eV) have been measured. The RF pulse is accompanied by an increase in the radiated power loss, which becomes peaked on axis, and which is due to line emission from impurities predominantly iron. (36 refs.)
- 3631 Energy deposition profile of shear Alfvén wave heating. K.Itoh, Div. of Thermonuclear Fusion Res., JAERI, Tokai Ibaraki, Japan), S.-I.Itoh. *Plasma Phys. (GB)*, vol.25, no.9, p.1037-49 (Sept. 1983).
- The energy deposition profile of the shear Alfvén wave in a cylindrical tokamak is obtained. The radial propagation and the absorption are solved by use of the kinetic equations for collisionless inhomogeneous plasmas. The absorption is mainly by the resonance Landau damping, and occurs not only at the resonance surface, $k_{\parallel}(r)v_A(r) = \omega$, but also in the propagation region, $k_{\parallel}(r)|V_A(r)| \geq \omega \leq k_{\parallel}(r)|v_e(r)|$ (V_A : Alfvén velocity, v_e : electron thermal velocity, k_{\parallel} : parallel wave number and ω : frequency). The parameter dependence is studied and the magnetic shear and plasma profiles have important roles for the deposition profile. Efficient heating is possible if the condition $k_{\parallel}V_A \approx \omega$ is widely satisfied in the propagation region. The bulk heating does not always correspond to good antenna coupling, which often causes an unfavourable edge heating. For some typical parameters the energy input $W \sim 1$ W cm $^{-3}$ is expected when the wave amplitude B_{\parallel} is several gauss. (12 refs.)
- 3632 Multiple filament plug-in module for use on the Tara neutral beam source. J.W.Coleman, R.S.Post, R.P.Torti, J.E.Tracey (Plasma Fusion Center, MIT, Cambridge, MA, USA). *Rev. Sci. Instrum. (USA)*, vol.54, no.9, p.1100-3 (Sept. 1983).
- A plug-in module bearing 14-20 tungsten filament emitters has been developed for use with the field-free neutral beam sources to be employed in the Tara tandem mirror experiments. Eight such modules constitute the total distributed cathode for one source. Each module has its own plug-in power connector, and may be removed from the source assembly as a unit, independently of the outer modules. The plug-in approach to construction results in a reduction both in the cost to build the source and in the time required for routine servicing and filament replacement. Plasma profiles are the same as in conventionally engineered sources of the same geometry. (4 refs.)
- 3633 Dynamic methods in plasma physics. V.E.Fortov (Inst. of Chem. Phys., Acad. of Sci. USSR). *Sov. Phys.-Usp. (USA)*, vol.25, no.11, p.781-809 (Nov. 1982). Translation of: *Sov. Fiz. Nauk (USSR)*, vol.138, no.3, p.361-412 (Nov. 1982). [received: Sept. 1983]
- Hydrodynamic methods of generating and diagnosing dense plasmas with strong interparticle interaction are reviewed. Experiments in shock and isentropic compression of matter to produce Boltzmann and degenerate plasma with maximum pressures in the tens of megabars are discussed. A method for isentropic expansion of metals that have been compressed by strong shock waves, which makes it possible to investigate a broad range of the phase diagram, including the high-temperature boiling curve and the neighborhood of the critical point, is described. The experimental schemes and designs of compressed-air and explosion-type nonideal-plasma generators and the diagnostic tools used are discussed. The results of experiments with nonideal plasmas are reported, and the influence of the interparticle interaction on the thermodynamic, electrophysical and optical properties of the strongly compressed plasma is analyzed on the basis of theoretical models. The properties of ultrahigh-pressure plasmas and prospects for laser electrodynamic and electroexplosive methods of generating strong shock waves in condensed media are discussed. (240 refs.)
- 3634 Simple method of sheet plasma production in lower pressure. U.Uramoto. *Report IPPJ-628*, Nagoya Univ., Japan (March 1983), 12 pp.
- A method of sheet plasma production in a lower pressure ($\sim 2 \times 10^{-4}$ Torr of H_2) is described. A primary sheet plasma produced between a discharge anode and cathode by the previous method due to two rectangular permanent magnets, diffuses into the low pressure region through a rectangular slit of the anode while electrons are reflected along magnetic field by a floating metal plate at the end of the plasma. (4 refs.)
- High-current pulsed proton source See Entry 111816
- Scattering of lower-hybrid waves by drift-wave density fluctuations: solutions of the radiative transfer equation See Entry 113592
- Spectrum of compressional Alfvén waves See Entry 113594

- Energetics and the resistive tearing mode: effects of Joule heating and radiation See Entry 113596
- Magnetically induced plasma rotation and the dense plasma focus See Entry 113609
- Ion heating due to explosive instability in an ion beam-plasma system See Entry 113624
- Waves and turbulence in a Tokamak fusion plasma See Entry 113649

52.50J Plasma production and heating by laser beams

- 113635 Shock wave pressure enhancement using short wavelength (0.35 μ m) laser irradiation. R.J.Trainor, N.C.Holmes, R.A.Anderson, E.M.Campbell, W.C.Mead, R.J.Olness, R.E.Turner, F.Ze (Univ. of California, Lawrence Livermore Nat. Lab., Livermore, CA, USA). *Appl. Phys. Lett. (USA)*, vol.43, no.6, p.542-4 (15 Sept. 1983).
- Shock velocities in planar aluminum targets irradiated at 0.35- and 1.06- μ m laser wavelengths have been measured. Absorbed intensities of $\sim 1.0 \times 10^{14}$ W/cm 2 , produced by 700-ps full width at half-maximum Gaussian pulses, generated shock pressures of 1.0 ± 0.2 and 0.6 ± 0.2 TPa, respectively, demonstrating an enhancement of shock pressure at decreased laser wavelength. (10 refs.)
- 113636 X-ray images and collapse time of gas-filled glass microspheres with an aspect ratio of 100-200 at a specific energy deposition 0.2 J/ng. V.V.Volenko, A.F.Ivanov, L.A.Myalitsin, L.A.Osadchuk, A.I.Saukov. *JETP Lett. (USA)*, vol.37, no.7, p.389-92 (5 April 1983). Translation of: *Pis'ma v Zh. Eksp. & Teor. Fiz. (USSR)*, vol.37, no.7, p.328-31 (5 April 1983). [received: Oct. 1983]
- Experiments on the laser bombardment of gas-filled glass microspheres with an aspect ratio $R/\Delta R = 100-200$ are reported. The SOKOL laser installation was used. The laser power density at the target was $q \approx (2-4) \times 10^{14}$ W/cm 2 ; the laser pulse length was $\tau_p \approx 1.0$ ns or $\tau_p \approx 0.3$ ns; and the specific energy deposition was $C_0 \approx 0.2$ J/ng. (9 refs.)
- 113637 Time-delayed filaments of prolonged durability on laser irradiated microspheres. S.Denus, H.Fiedorowicz, S.Nagraba, W.Pawlowicz, L.Sulwinski, A.Wilczynski, J.Wolowski (Inst. of Plasma Phys. & Laser Microfusion, Warsaw, Poland). *Opt. Commun. (Netherlands)*, vol.47, no.2, p.127-30 (15 Aug. 1983).
- The results of investigations of a plasma generated by irradiation of glass microspheres with high power laser pulses, and carried out with optical and X-ray diagnostics, are presented. Plasma jets appearing in the expanding laser plasma region were observed and hypotheses concerning their interpretation are suggested. Presented results were obtained in the course of experimental investigations within the range of laser microfusion carried out at the IPPLM. (10 refs.)
- 113638 Properties of the corona generated by the incidence of intense CO $_2$ laser pulses on spherical targets. R.Gratton, A.R.Piriz (Univ. Nacional del Centro de la Provincia de Buenos Aires, Tandil, Argentina). *Plasma Phys. (GB)*, vol.25, no.9, p.1009-20 (Sept. 1983).
- An analytic steady state model is described for the corona generated when a microsphere is isotropically irradiated by an intense CO $_2$ laser pulse. The main hypothesis of the model is that the energy transport from the absorption region to the pellet surface is due to a cloud of relatively high energy electrons (suprathermal electrons) whose mean free path is large with respect to the dimension of the corona, except in a thin layer close to the pellet surface. (23 refs.)
- Interpenetration burn for controlled inertial confinement fusion driven by non-linear laser forces See Entry 112434
- Comment on 'Steady-state planar ablative flow' [Phys. Fluids 25, 1644 (1982)] [and reply] See Entry 113580
- Self-focusing in laser produced spark See Entry 113621
- Very high speed cinematography in the X-ray spectra applied to experiments of laser-matter interaction See Entry 113655
- Imagery of laser imploded targets in the X-ray domain See Entry 113656
- Converging shock on laser plasma: density profiles by holographic interferometry See Entry 113663
- Electron temperature monitor for laser-produced plasmas See Entry 113666

52.50L Plasma production and heating by shock wave and wire explosion

- Thermodynamics of a highly compressed plasma in the megabar range See Entry 113569

52.55 PLASMA EQUILIBRIUM AND CONFINEMENT

- 113639 Status of the US effort in atomic physics research relevant to the magnetically confined fusion program. C.F.Barnett (Oak Ridge Nat. Lab., Oak Ridge, TN, USA). *Nucl. Instrum. & Methods Phys. Res. (Netherlands)*, vol.214, no.1, p.1-7 (1983). (Proceedings of the International Workshop on Cross Sections for Fusion and Other Applications, College Station, TX, USA, 4-6 Nov. 1982).
- The status of atomic physics research in the United States relevant to magnetically confined fusion plasmas is briefly reviewed. Program support is concentrated on performing benchmark experiments to confirm theory which will be used for a large fraction of the required data base. Recent advances and present needs in electron-ion collisions, ion-atom collisions, low energy collisions in ion sources, and atomic structure are emphasized. (31 refs.)
- 113640 Control of plasma in Tokamak equipment. V.F.Gubarev, M.M.Dargeiko, Yu.G.Krivosos, Yu.I.Samoilenko. *Cybernetics (USA)*, vol.18, no.5, p.687-93 (Sept.-Oct. 1982). Translation of: *Kibernetika (USSR)*, vol.18, no.5, p.127-31 (Sept.-Oct. 1982).
- Great attention has been and is being given to plasma research from which results of practical importance have been obtained. Most of these relate to Tokamak equipment that is currently regarded as the most promising solution for the problem of controlled thermonuclear fusion. The authors describe how at the Cybernetics Institute, Academy of Sciences of the Ukrainian SSR, there have been proposed and developed for such equipments certain fast-acting automatic magnetic-field regulators having spatially distributed members that interact with the plasma. Their operation is based on an essentially new impedance principle of regulation. This, first of all, has made it possible to create an automatic-control system for the position of a plasma column on the axis of the vacuum chamber with an effectiveness that was demonstrated for the first time in world practice on the type TO-1 equipment at the I.V.

Kurchatov Institute of Atomic Energy. The importance of this result can be judged by the fact that there are practically no modern Tokamak designs without an automatic control for the plasma column. (10 refs.)

113641 Measurement of sloshing-ion spatial profiles in end cell of tandem mirror experiment-upgrade (TMX-U). T.J.Orzechowski, S.L.Allen, J.H.Foote, R.K.Goodman, A.W.Molvik, T.C.Simonen (Lawrence Livermore Nat. Lab., Univ. of California, Livermore, CA, USA). *Phys. Fluids (USA)*, vol.26, no.9, p.2335-8 (Sept. 1983). Neutral-beam injection is used to establish an energetic sloshing-ion distribution in the end cells of the Tandem Mirror Experiment-Upgrade (TMX-U). The angular and radial distributions of these ions are measured with arrays of secondary-emission detectors. Unfolding the angular distribution gives the axial extent of the sloshing ions. Sloshing-ion density measurements from the charge-exchange flux indicate a high-density ($n_{\text{e}} \approx 3$ to $6 \times 10^{12} \text{ cm}^{-3}$) but narrow (FWHM $\sim 16 \text{ cm}$) sloshing-ion plasma. (15 refs.)

113642 Growth rate reduction of the curvature-driven flute instability by plasma blanket line tying. D.Segal (Dept. of Phys., Univ. of California, Irvine, CA, USA). *Phys. Fluids (USA)*, vol.26, no.9, p.2565-8 (Sept. 1983). The effect of an annular, line-tied blanket, on the curvature-driven flute in a magnetic mirror is considered. The blanket is assumed to be line tied to a thermoionically emitting annular end plate. Reduction of the flute growth rate is computed as function of Larmor radius, blanket radius and axial plasma conductance through either an external plasma or mirror sheath. It is found that significant reduction in growth rate can be achieved. (16 refs.)

113643 Finite Larmor radius stability theory of ELMO Bumpy Torus plasmas. H.L.Berk, C.Z.Cheng, M.N.Rosenbluth, J.W.Van Dam (Inst. for Fusion Studies, Univ. of Texas, Austin, TX, USA). *Phys. Fluids (USA)*, vol.26, no.9, p.2642-51 (Sept. 1983). An eikonal ballooning mode formalism is developed to describe curvature-driven modes of hot electron plasmas in bumpy tori. The formalism treats frequencies comparable to the ion cyclotron frequency, as well as arbitrary finite Larmor radius and field polarization, although the detailed analysis is restricted to $E_{\parallel}=0$. Moderate hot electron finite Larmor radius effects are found to lower the background beta core limit, whereas strong finite Larmor radius effects produce stabilization. The critical finite Larmor radius parameter with weak curvature is $FR = k_{\perp}^2 \rho_{\text{h}}^2 R / \Delta_{\text{b}} (1 + P_{\perp} / P_{\parallel})$ where k_{\perp} is the perpendicular wavenumber, ρ_{h} the hot electron Larmor radius, R the magnetic field radius of curvature at the hot-electron layer, Δ_{b} the magnetic field scale length in the diamagnetic well, and $P_{\perp, \parallel}$ are the parallel and perpendicular pressure gradients. The interchange instability arises if $1 > FR > -\beta_{\text{e}} R / [2\Delta (1 + P_{\perp} / P_{\parallel})]$, whereas all modes are stable if $FR > 1$, where β_{e} is the core plasma beta and Δ is the core plasma pressure gradient length. (19 refs.)

113644 Rotational stability of tandem mirrors. J.P.Freidberg, D.A.D'Ippolito (Plasma Res. Inst., Sci. Applications Inc., Boulder, CO, USA). *Phys. Fluids (USA)*, vol.26, no.9, p.2657-67 (Sept. 1983). The general stability equation for low- m rotational-ballooning instabilities in axisymmetric mirror geometry is derived for an isotropic pressure plasma, including a boundary term which represents the stabilizing effect of an unspecified anchor. The corresponding variational principle, together with a particular quadrupole anchor model, is used to compute the low- β rotational-interchange marginal stability condition for a conventional tandem mirror. The stability criterion is applied to show that low- m rotational modes are stable in the TMX experiment. Also, a mechanism for enhanced stabilization of curvature-driven modes when $E_{\parallel} < 0$ is discussed. (16 refs.)

113645 Quadrupole stabilization of the $n=2$ rotational instability of a field-reversed theta-pinch plasma. S.Ohi, T.Minato, Y.Kawakami, M.Tanjo, S.Okada, Y.Ito, M.Kako, S.Goto, T.Ishimura, H.Ito (Plasma Phys. Lab., Osaka Univ., Osaka, Japan). *Phys. Rev. Lett. (USA)*, vol.51, no.12, p.1042-5 (19 Sept. 1983). The $n=2$ rotational instability is the most dangerous gross instability in a field-reversed theta pinch. It is demonstrated for the first time that the instability is completely suppressed by superposing a quadrupole field which is much smaller than the axial confinement field at the separatrix. The experimental threshold intensity of the field for stabilization is about 2.5 times less than that predicted by theoretical stability analysis. (16 refs.)

113646 Confinement in a double-cusp electromagnetic trap. P.Couture, B.L.Stansfield (INRS-Energie, Univ. du Quebec, Varennes, Quebec, Canada). *Plasma Phys. (GB)*, vol.25, no.9, p.1001-8 (Sept. 1983). Measurements in an electrostatically stoppered double-cusp machine have verified the formation of an ion-confining potential well. However, a significant ion-confining barrier is not formed in the electrode region, and ions penetrate freely out to the grounded, interior electrode. It is only in the space between the interior electrode and the outer, negatively-biased, electrode that a large current drop is found to occur. (18 refs.)

113647 Numerical studies of toroidal coupling on low- m resistive modes. G.Kurita, M.Azumi, T.Tsunematsu, T.Takeda (JAERI, Ibaraki, Japan). *Plasma Phys. (GB)*, vol.25, no.10, p.1097-112 (Oct. 1983). Effects of the toroidicity and finite pressure on low- m ideal and resistive modes are studied numerically on the basis of the reduced set of the MHD equations. Both the linear and nonlinear analyses show that the $m=2$ mode is strongly destabilized by the above effects. The destabilization of the $m=2$ mode, however, is not directly related to the major disruptions. It is conjectured that the destabilized $m=2$ mode may change the equilibrium to the one unstable against the major disruption. (14 refs.)

113648 A comparison between laser induced fluorescence at Balmer-alpha and at Lyman-alpha for the measurement of neutral hydrogen densities in magnetically contained fusion plasmas. P.Gohil, D.D.Burgess (Blackett Lab., Imperial Coll. of Sci. & Technol., London, England). *Plasma Phys. (GB)*, vol.25, no.10, p.1149-67 (Oct. 1983). The authors examine the relative merits of laser induced fluorescence scattering at the Lyman-alpha and Balmer-alpha wavelengths for the measurement of both the spatial distribution and absolute magnitude of neutral hydrogen densities in fusion plasmas. The enhancements of the fluorescence signals for present and for saturation laser intensities are determined and signal to noise ratios are presented for a range of fusion plasma conditions. Details of the interpretation of the fluorescence signals, and the limitations, at the two wavelengths are discussed. In the hotter regions of the plasma, Balmer-alpha fluorescence scattering allows the measurement of neutral densities as low as 10^7 cm^{-3} , whereas present intensities from Lyman-alpha sources permit fluorescence measurements only for neutral hydrogen densities approaching 10^{10} cm^{-3} . Also presented is a technique for the spatial measurement of the electron number density based upon fluorescence scattering on the Balmer transitions, this process not being possible at Lyman-alpha for the range of electron densities in magnetically contained fusion plasmas. This may have applica-

tions in regions of the plasma otherwise difficult to diagnose, for example, near divertors and limiters. (42 refs.)

113649 Waves and turbulence in a Tokamak fusion plasma. C.M.Surko (Semiconductor & Chem. Phys. Res. Dept., Bell Labs., Murray Hill, NJ, USA), R.E.Slusher. *Science (USA)*, vol.221, no.4613, p.817-22 (26 Aug. 1983). The Tokamak is a prototype fusion device in which a toroidal magnetic field is used to confine a hot plasma. Coherent waves, excited near the plasma edge, can be used to transport energy into the plasma in order to heat it to the temperatures required for thermonuclear fusion. In addition, Tokamak plasmas are known to exhibit high levels of turbulent density fluctuations, which can transport particles and energy out of the plasma. Recently, experiments have been conducted to elucidate the nature of both the coherent waves and the turbulence. The experiments provide insight into a broad range of interesting linear and nonlinear plasma phenomena and into many of the processes that determine such practical things as plasma heating and confinement. (42 refs.)

113650 Feedback control experiment for plasma equilibrium in ASPERA-TOR-TM. S.Kitajima (Dept. of Nuclear Engng., Tohoku Univ., Sendai, Japan), Y.Funato, H.Watanabe. *Technol. Rep. Tohoku Univ. (Japan)*, vol.48, no.1, p.93-106 (1983). A simple method for a feedback control of the position of the plasma column in a small Tokamak discharge is presented. The analysis of this control system by means of the simple model is described. Applying this system to the shell-less small Tokamak, the authors clarify experimentally this system useful for the positional control. (11 refs.)

113651 Plasma equilibrium and field diffusion during current rise phase of STP-2 screw pinch tokamak. A.Nagata. *Report IPPJ-594*, Nagoya Univ., Japan (June 1982), 33 pp. Plasma equilibrium and field diffusion during the current rise phase of the discharge have been investigated in STP-2 screw pinch tokamak. The plasma with maximum poloidal beta value β_{p} of 3.0 has been obtained by compression and joule heating. However the maximum β_{p} value without strong wall contacts was about 1.3. The authors observed that force-free current is formed in the periphery of the plasma and the penetration rate of the poloidal magnetic field is much faster than the penetration rate calculated from the classical resistivity. To understand the high-beta plasma equilibrium and the mechanism of fast penetration rate observed in STP-2 plasmas the authors have performed a numerical simulation using a 2-D MHD pinch code 'TOPICS'. (15 refs.)

Proceedings of the International Workshop on Cross Sections for Fusion and Other Applications	See Entry 111298
Interpenetration burn for controlled inertial confinement fusion driven by nonlinear laser forces	See Entry 112434
Predicted behaviour of the single-null divertor of INTOR	See Entry 112441
Optimierung sphärischer Ionisationskammern für die Neutronendiagnostik an Tokamakanlagen (Optimisation of spherical ionisation chambers for neutron diagnostics in Tokamaks)	See Entry 112584
Measurements of charge change in atomic collisions at MeV energies	See Entry 112845
Unified kinetic theory in toroidal systems	See Entry 113566
Nonresonant electron transport on the ELMO bumpy torus (EBT) for multitemperature Maxwellians	See Entry 113571
Effect of collisionless detrapping on nonaxisymmetric transport in a stellarator with radial electric field	See Entry 113572
Measurements of fluctuations in the flux of runaway electrons to the PLT Tokamak limiter	See Entry 113573
Anomalous impurity transport in plasmas	See Entry 113575
A comparison of the full and reduced sets of magnetohydrodynamic equations for resistive tearing modes in cylindrical geometry	See Entry 113578
Axisymmetric toroidal equilibria with plasma flow	See Entry 113579
Scattering of lower-hybrid waves by drift-wave density fluctuations: solutions of the radiative transfer equation	See Entry 113592
Spectral broadening of lower-hybrid waves by time-dependent density fluctuations	See Entry 113593
Spectrum of compressional Alfvén waves	See Entry 113594
Ballooning mode calculations in stellarators	See Entry 113597
Asymptotic theory of the internal kink mode in current-carrying toroidal plasmas	See Entry 113598
Dissipative trapped ion instability in PLT and INTOR	See Entry 113608
Wall material characteristics in reacting plasma modelling	See Entry 113622
Multiple filament plug-in module for use on the Tara neutral beam source	See Entry 113632
Resonant-fluorescence plasma diagnostics near the chamber wall in the TUMAN-3 tokamak	See Entry 113661
Ten-channel grating chromator for electron cyclotron emission plasma diagnostics	See Entry 113665
Holographic plasma interferometry in the infrared spectrum. II. Using nonlinear effects to increase the sensitivity	See Entry 113667
Resonant helical magnetic limiter	See Entry 113673
The behaviour of impurities out of coronal equilibrium	See Entry 113689
Formation of an anode spot in a vacuum arc	See Entry 113692

52.60 RELATIVISTIC PLASMA

Relativistic corrections for the conventional, classical Nyquist theorem	See Entry 113561
Localization of circularly polarized intense electromagnetic waves in relativistic plasmas	See Entry 113616
Numerical fits to important rates in high temperature astrophysical plasmas	See Entry 116467

52.65 PLASMA SIMULATION

Thermodynamic properties of ion clusters and their effect on the mechanism of homogeneous nucleation in an ion plasma. Calculation by the Monte Carlo method in an NpT ensemble	See Entry 113563
The self-consistent mean spherical approximation for the one-component plasma	See Entry 113565

- utilization of the lower-hybrid drift instability by resonant electrons See Entry 113589
- ervation of self-binding turbulent fluctuations in simulation plasma and relevance to plasma kinetic theories See Entry 113610
- linear interaction of high-current H^+ and H^- ion beams See Entry 113627
- merical simulations for intense light-ion beam propagation in channel under influence of plasma inertia See Entry 113628
- ma equilibrium and field diffusion during current rise phase of STP-2 pinch tokamak See Entry 113651
- ulation of spectrum line emission from plasmas See Entry 113668

70 PLASMA DIAGNOSTIC TECHNIQUES AND INSTRUMENTATION

- 652 Simultaneous measurement of magnetic field direction and ion temperature in a plasma by collective scattering with a CO_2 laser. W.Kasperek, H. J. Phys. (Bulgaria), vol.10, no.3, p.268-9 (1983).
- Approximations of the inverse functions $(-\alpha^2)$ and $(-\beta^2)$ suitable for computer treatment have been found from the two-thirds law for the vacuum diode. The accuracy of approximation and the region of validity satisfy completely the requirements of the probe diagnostics. (5 refs.)
- 653 A photoelectron spectrometer for measurement of electron plasma temperature. Yu.V.Gott, A.N.Silaev, R.R.Chistyakov, V.A.Shurygin (I.V. Kurchatov Inst. of Atomic Energy, Moscow, USSR).
- J. Instrum. & Methods Phys. Res. (Netherlands), vol.214, no.2-3, p.463-7 (Sept. 1983).
- Results of work on a photoelectron spectrometer intended for the measurement of plasma electron temperature are described. The principle of its operation is based on the fact that the energy of a photoelectron knocked out of a target by an X-ray quantum unambiguously depends on the energy of this quantum. Thus, if one measures the energy spectrum of photoelectrons, one can find the energy distribution in a flux of radiation from a plasma. Resolution of the spectrometer and the efficiency of registration dependent on the radiation energy, thickness and material of the target are given. It is shown that the energy resolution varies from 15% to 45% with a change in the Ge target-thickness from 100 Å to 5100 Å. The calculated radiation registration efficiency with an energy of 8 keV for a Ge target 5100 Å thick is 1.3×10^{-4} electrons/quantum. Plasma electron temperature measurement with a photoelectron spectrometer has been simulated on a computer. (6 refs.)
- 655 Very high speed cinematography in the X-ray spectra applied to experiments of laser-matter interaction. C.Cavailler, N.Fleurot, M.Rostaing, Sauneuf (Centre d'Etudes de Limeil, CEA, Villeneuve-Saint-Georges, France).
- Proc. SPIE Int. Soc. Opt. Eng. (USA), vol.312, p.93-100 (1983). In French. 1st European Conference on Cineradiography with Photons or Particles, Paris, France, 18-21 May 1981).
- The interpretation of experiments in pulsed laser-matter interaction requires the dynamic recording of phenomena involved in the plasma created by the high energy density concentrated in the target. For a number of years observations and measurements in the X spectral region, and particularly in the 1-10 keV range, have gained importance both in studies of the radiation emitted by the plasmas and in plasma diagnostics an external X-ray source. With these applications in view the authors have developed space and time resolved X-ray detectors with time resolution in the picosecond range. The authors present a survey of the design and operation of streak cameras their performance measured in terms of spatial and temporal resolution (3 to 10 ps at 15 lmm⁻¹). A large family of image tubes and cameras are described which have been studied and made in collaboration with Thomson-CSF and Laboratoire d'Electronique et de Physique Appliquées (LEP). The authors also present the range of cameras which are now under development at Limeil, with a spectral response in the soft X-ray region (2 to 20 V). Finally the authors present the results of two dimensional (framing) image studies with the 300 ps planar shutter tube from LEP. (7 refs.)
- 656 Imagery of laser imploded targets in the X-ray domain. J.Launach, C.Bayer, D.Billon, M.Decroisette, D.Juraszek, D.Maynial (Centre d'Etudes de Limeil, CEA, Villeneuve-Saint-Georges, France).
- Proc. SPIE Int. Soc. Opt. Eng. (USA), vol.312, p.101-9 (1983). In French. 1st European Conference on Cineradiography with Photons or Particles, Paris, France, 18-21 May 1981).
- The authors present detail of an experimental device currently used at Limeil and outline the main phenomena and mechanisms involved in the implosion of a spherical target by intense lasers. With some results obtained in typical experiments the authors discuss the different possibilities for imagery in the X-ray domain. Namely: imagery by target emission and radiography of the target with an external X-ray source obtained using a laser beam (backlighting). A device is described which combines these two possibilities used simultaneously in the same experiment. Imagery by self-emission or backlighting with time resolution. Some results are given which are in agreement with numerical models. (8 refs.)
- 657 Two-frame flash X-radiography system for the study of particle beam fusion target implosions. J.Chang, D.L.Fehl (Sandia Nat. Labs., Albuquerque, NM, USA).
- Proc. SPIE Int. Soc. Opt. Eng. (USA), vol.312, p.110-15 (1983). (1st European Conference on Cineradiography with Photons or Particles, Paris, France, 18-21 May 1981).
- A two-frame flash X-radiographic system has been developed for studying the plasma hydrodynamics of particle beam driven inertial confinement fusion targets. This system consists of two micro-point flash X-ray (FXR) sources, a micro-channel plate (MCP) X-ray sensitive cameras, and a space frame. The sources and cameras are arranged in pairs on the space frame to secure registration of the sources with the cameras and to provide ease of alignment with the target. The micro-point FXR sources have an output spectrum characteristic of a tungsten bremsstrahlung source with an end point energy of 600 keV, a source intensity of 8 mRad at 46 cm, and a spot size of approximately 100 μ m. A direct 4X magnification of a 3 mm gold target was

achieved by using this source in a backlighting arrangement with an overall system resolution of 4 lp/mm. This system has been used successfully to observe relativistic electron beam driven ablative pusher target implosions. (6 refs.)

- 113658 X-ray backlighting sources of 4 to 10 keV for laser fusion targets. V.C.Rupert, D.L.Matthews, L.N.Koppel (Lawrence Livermore Nat. Lab., Livermore, CA, USA).
- Proc. SPIE Int. Soc. Opt. Eng. (USA), vol.312, p.116-22 (1983). (1st European Conference on Cineradiography with Photons or Particles, Paris, France, 18-21 May 1981).
- High-density, short-duration X-ray pulses are necessary to diagnose the compression of laser fusion targets. Present target designs are such that backlighting sources range from a few thousand electron volts to 100 keV will be necessary. The desired source durations range from a few tens of picoseconds for flash radiography to several nanoseconds for streak irradiation laser pulse. For the latter reason, a laser-induced X-ray pulse is preferred. An initial study of the K lines of Ti, Ni and Zn as possible backlighting sources was conducted. The conversion efficiency of laser light into line radiation was obtained as a function of laser intensity, pulse length, and wavelength. A threshold laser intensity for X-ray line production was identified. Information was obtained on the size and duration of the X-ray emission source, in relation to laser parameters. The experimental results, and their impact on backlighting capability for high-density laser fusion targets, are discussed. (12 refs.)
- 113659 Ray tracing of a concave-curved-crystal spectrometer and its detailed characteristics for X-ray spectroscopic diagnostics of high-temperature plasmas. S.Morita (Inst. of Plasma Phys., Nagoya Univ., Nagoya, Japan).
- Jpn. J. Appl. Phys. Part 1 (Japan), vol.22, no.6, p.1030-40 (June 1983).
- A method of ray tracing is presented for a spectrometer with a concave-curved crystal to be used for X-ray spectroscopic diagnostics of high-temperature plasmas. Calculations have been carried out for a LiF(200) crystal with a Rowland circle of radius 50 cm and a Gaussian rocking curve. With a linear X-ray source, the most suitable parameters of the spectrometer were accurately determined by use of the ray tracing, and the characteristics were investigated in detail. The ray tracing was also applied to a point source of X-rays, and the best conditions for geometric relations between the point source and the spectrometer were found. The spectral distortion is also described here analytically. The calculated line profile including the natural broadening of the X-ray source is compared with the experimental result of $FeK\alpha$. Good agreement is obtained. (15 refs.)
- 113660 Experimental investigation of absorption coefficient of cesium resonance doublets in a plasma of combustion products. I.A.Vasil'eva, L.V.Deputatova, A.P.Nefedov (Inst. of High Temperatures, Acad. of Sci., USSR).
- High Temp. (USA), vol.20, no.6, p.809-14 (Nov-Dec. 1982). Translation of: Teplofiz. Vys. Temp. (USSR), vol.20, no.6, p.1032-7 (Nov-Dec. 1982). [received: Sept. 1983]
- The authors give the results of an experimental investigation of the relation between the absorption coefficient and the emission frequency $\kappa(\Delta\nu)$ for the cesium resonance doublets 4555/4593 Å and 8521/8943 Å in a plasma of combustion products ($p=1$ atm, $T=2050$ K) with an alkali seed. The relative variation of the absorption coefficient at distances of 5-400 cm⁻¹ from the line centers is obtained. Individual regions of $\kappa(\Delta\nu)$ are approximated by an expression of the form $\kappa(\Delta\nu) \sim (\Delta\nu)^{-x}$. Near the line centers (up to 10-30 cm⁻¹) $x=2$, and on the line wings $x=1.2-0.7$. (11 refs.)
- 113661 Resonant-fluorescence plasma diagnostics near the chamber wall in the TUMAN-3 tokamak. V.S.Burakov, S.A.Moshkalev, P.A.Naumenkov, G.T.Razdobarin, V.V.Semenov, V.M.Talybov, N.V.Tarasenko (A.F. Ioffe Physicotech. Inst., Acad. of Sci., Leningrad, USSR).
- JETP Lett. (USA), vol.37, no.7, p.365-7 (5 April 1983). Translation of: Pis'ma v Zh. Eksp. & Teor. Fiz. (USSR), vol.37, no.7, p.308-10 (5 April 1983). [received: Oct. 1983]
- Experiments have been carried out on plasma diagnostics near the chamber wall in a tokamak. The spatial and temporal distributions of impurity metal atoms have been found during ohmic heating and during adiabatic compression. (3 refs.)
- 113662 Determining the plasma potential from the ionic part of the volt-ampere characteristic of an electrical probe. V.S.Nikolaev (Dept. of Electronics, Moscow Univ., Moscow, USSR).
- Moscow Univ. Phys. Bull. (USA), vol.38, no.1, p.32-7 (1983). Translation of: Vestn. Mosk. Univ. Ser. 3 (USSR), vol.38, no.1, p.29-33 (1983).
- A method of determining the plasma potential is proposed, on the basis of the ionic part of the volt-ampere characteristics of an electric probe. (5 refs.)
- 113663 Converging shock on laser plasma: density profiles by holographic interferometry. A.Giulietti, D.Giulietti, M.Lucchesi, M.Vaselli (Istituto di Fisica Atomica e Molecolare, CNR, Pisa, Italy).
- Opt. Commun. (Netherlands), vol.47, no.2, p.131-6 (15 Aug. 1983).
- A double pulse ruby laser was used to obtain interference patterns from a laser produced plasma in helium. From patterns obtained at different times the electron density evolution was inferred by Abel inversion, with suitable approximations. There was a net evidence for electron density increase due to the action of a converging shock wave produced by reflection. (7 refs.)
- 113664 Applications of the Fraunhofer-diffraction method for plasma-wave measurements. Y.Sonoda, Y.Suetsugu, K.Muraoka, M.Akazaki (Dept. of Energy Conversion, Interdisciplinary Graduate School of Engng. Sci., Kyushu Univ., Fukuoka, Japan).
- Plasma Phys. (GB), vol.25, no.10, p.1113-32 (Oct. 1983).
- The improved theoretical analysis of Fraunhofer-diffraction method as a new means to measure the frequency, wavenumber, intensity and even spatial position and propagating direction of plasma waves is presented. It is further, experimentally verified and the measuring accuracies are ascertained by measurements in a microwave region, of ion-acoustic waves in a DC discharge. Successes of introducing the practically important conditions into theoretical analysis have made it possible to establish this method as a standard and powerful diagnostic technique for measurements of plasma waves and turbulences in various plasmas such as in Tokamaks. (17 refs.)
- 113665 Ten-channel grating chormator for electron cyclotron emission plasma diagnostics. J.Fischer, D.A.Boyd, J.Cavallo, J.Benson (Lab. for Plasma & Fusion Energy Studies, Univ. of Maryland, College Park, MD, USA).
- Rev. Sci. Instrum. (USA), vol.54, no.9, p.1085-90 (Sept. 1983).
- A grating polychromator for electron cyclotron temperature diagnostic experiments is described. Two aluminum gratings are used to allow the instrument to operate for Tokamak magnetic fields between 16-25 kG, i.e. for second harmonic electron cyclotron emission frequencies ranging between 90-140 GHz. The instrument utilizes an array of ten cryogenically cooled InSb hot electron bolometers to collect radiation at the focal surface of the spectrometer covering a fractional plasma radial distance of $\Delta R/R_0 \sim 0.3-0.4$, where R_0 is the major radius of the plasma. The resolving power of the

spectrometer has been measured to be $R = \nu/\delta\nu \approx 50$. This instrument thus provides high spatial (3 cm) and temporal resolution ($\sim 1 \mu\text{s}$) and large spatial coverage. The detector cryostat has measured cryogen hold times of $\geq 24 \text{ h}$ (liquid nitrogen) and $\approx 9 \text{ days}$ (liquid helium) providing ease of operation during long plasma runs. (14 refs.)

113666 Electron temperature monitor for laser-produced plasmas. A.Ng, K.Fong, A.J.Barnard, J.Kwan, D.Pasini (Phys. Dept., Univ. of British Columbia, Vancouver, British Columbia, Canada). *Rev. Sci. Instrum. (USA)*, vol.54, no.9, p.1091-4 (Sept. 1983).

The authors have developed a multichannel X-ray analyzer for monitoring electron temperatures in plasmas. The device consists of a step-wedge X-ray filter and a Reticon sensor array. By measuring the X-ray continuum emission from a laser-produced plasma with the device, the electron temperature can be determined to within 10%. (10 refs.)

113667 Holographic plasma interferometry in the infrared spectrum. II. Using nonlinear effects to increase the sensitivity. I.I.Komissarova, G.V.Ostrovskaya, V.N.Filippov, E.N.Shedova (A.F. Ioffe Physicotech. Inst., Acad. of Sci., Leningrad, USSR).

Sov. Phys.-Tech. Phys. (USA), vol.28, no.2, p.156-9 (Feb. 1983). Translation of: *Zh. Tekh. Fiz. (USSR)*, vol.53, no.2, p.251-7 (Feb. 1983). [received: Sept. 1983]

Experiments are described in which wave interference patterns reconstructed in high diffraction orders from holograms recorded in CO_2 laser light are exploited to increase the sensitivity of the interference/holographic technique. The factors determining the fringe quality in the interference patterns and the accuracy in measuring the shifts are examined, methods are given for eliminating fringe distortion, and optimal conditions are found for recording interference patterns. An accuracy of $\sim 2 \times 10^{14} \text{ cm}^{-2}$ in measuring $N_e l$ has been achieved, where N_e is the electron density and l is the transverse diameter of the probed plasma region. It is thus demonstrated that the interference/holographic method can be used to study plasma in Tokamaks. (4 refs.)

113668 Calculation of spectrum line emission from plasmas. H.Gordon, H.P.Summers, J.A.Tully.

Report CLM-R 229, UKAEA, Culham, Abingdon, Oxon., England (1982), 42 pp.

Available from HMSO, London, England.

The authors describe a number of Fortran computer programs and their associated data sets which will predict spectrum line emission from important species in fusion plasmas. The present work is concerned with the emission of line radiation by low lying excited states of ions. Three sets of plasma conditions are investigated, namely, the ionisation equilibrium plasma, the plasma developing in time and the plasma in a spatially inhomogeneous state. (24 refs.)

1st European Conference on Cineradiography with Photons or Particles See Entry 111300

Compact metal-ion beam source using thermal contact ionizer See Entry 111810

Acoustic wave calibration for CO_2 laser scattering experiments See Entry 113034

A far-infrared interferometer for the measurement of electron concentration in flames and plasmas with high spatial resolution See Entry 113562

Plasma electron density measurements by the laser- and collision-induced fluorescence method See Entry 113567

Local determination of the ion temperature from the Doppler broadening of hydrogen lines through the use of a fast atomic beam See Entry 113570

Measurements of fluctuations in the flux of runaway electrons to the PLT Tokamak limiter See Entry 113573

Forward CW CO_2 -laser scattering on a high density plasma column See Entry 113576

X-ray images and collapse time of gas-filled glass microspheres with an aspect ratio of 100-200 at a specific energy deposition 0.2 J/ng See Entry 113636

Time-delayed filaments of prolonged durability on laser irradiated microspheres See Entry 113637

A comparison between laser induced fluorescence at Balmer-alpha and at Lyman-alpha for the measurement of neutral hydrogen densities in magnetically contained fusion plasmas See Entry 113648

Electron temperature in HF discharge plasma columns See Entry 113676

Measurement of electron temperature in a glow discharge with a double probe method See Entry 113677

Anode-plasma parameters of a high-voltage glow discharge $\approx 150 \text{ kV}$ See Entry 113683

Relationship of the laser-induced population perturbation of excited levels with the dynamical optogalvanic signal in a discharge plasma See Entry 113687

Observation of a significant density of negative ions in a currentless discharge in air; the possibility of an attachment instability See Entry 113694

52.75 PLASMA DEVICES AND APPLICATIONS

(see also 28.52 Fusion reactors, 86.30L Electrogasdynamics and magnetohydrodynamic conversion; for ion sources, see 29.25 Particle sources and targets)

113669 Cathode spots and erosion of metal electrodes in channel of an open-cycle MHD generator. V.I.Zalkind, V.V.Kirillov, A.I.Markina.

High Temp. (USA), vol.20, no.6, p.941-6 (Nov.-Dec. 1982). Translation of: *Teplofiz. Vys. Temp. (USSR)*, vol.20, no.6, p.1182-7 (Nov.-Dec. 1982). [received: Sept. 1983]

Correlation of the experimental data obtained on several MHD devices reveals the main features of the behaviour of cathode spots in open-cycle MHD channels. The parameters of the cathode spots in MHD channels operating in different conditions were measured. The characteristics of the discharge and erosion of the electrodes were greatly affected by the film of seed compounds deposited on the electrode surface by the plasma stream in the channel of an open-cycle MHD generator. Data were obtained for the erosion of electrodes of different materials. (9 refs.)

113670 Transport models of particle and energy balance in Tokamak devices. D.P.Kostomarov.

Moscow Univ. Comput. Math. & Cybern. (USA), no.4, p.1-9 (1982). Translation of: *Vestn. Mosk. Univ. Ser. 15 (USSR)*, no.4, p.6-12 (1982). [received: Sept. 1983]

A brief characterisation of the part played by mathematical modelling in research into plasma physics and controlled thermonuclear synthesis is provided. Transport models of particle and energy balance in Tokamak devices are described. Issues related to the incorporation of neutral residual-gas

particles into the transport model are considered. The use of the neutral-particle model for solving direct and inverse problems of corpuscular plasma diagnostics is described. (8 refs.)

113671 Construction of a high density plasma device for microwave-plasma interaction experiment. H.Mori, I.Iwamoto, E.Sagawa, T.Suiz, S.Yoshikado.

Rev. Radio Res. Lab. (Japan), vol.28, no.147, p.607-14 (Sept. 1982). In Japanese. [received: Sept. 1983]

A multi-dipole type plasma device was constructed for simulation experiments concerning the propagation of electromagnetic waves in the ionosphere. The device has the shape of a rectangular parallelepiped, the size of which is 60 cm in height, 60 cm in width, and 120 cm in length. In its early experiments, it was confirmed that very homogeneous and quiescent plasmas could be generated. A typical value of the electron density of the plasma is $3 \times 10^{10} \text{ cm}^{-3}$ under the condition that the emission current from the tungsten filaments is 2 A and the argon gas pressure is $4 \times 10^{-2} \text{ Pa}$. As a next step, the authors are going to construct a powerful microwave beam transmitter and receiving system to observe the interaction between the microwave beam and the high density plasma. (1 ref.)

113672 Relativistic plasma microwave generator. M.V.Kuzelev, F.Kh.Mukhametzyanov, M.S.Rabinovich, A.A.Rukhadze, P.S.Strelkov, A.G.Shkvarunets (P.N. Lebedev Phys. Inst., Acad. of Sci., Moscow, USSR).

Sov. Phys.-Dokl. (USA), vol.27, no.12, p.1030-2 (Dec. 1982). Translation of: *Dokl. Akad. Nauk SSSR*, vol.267, no.4-6, p.829-32 (Dec. 1982). [received: Sept. 1983]

The possibility of generating electromagnetic waves in a plasma was essentially predicted when the beam-plasma instability was discovered. However, it became possible to build a plasma microwave generator only after theoretical and experimental studies had been made of the beam-plasma instability in finite magnetized plasmas using relativistic electron beams and after a general theory of plasma microwave generators had been developed. The authors describe an experimental realization of a relativistic plasma microwave generator and give a theoretical analysis of the experimental results. The excitation mechanism and basic parameters of this plasma generator are described well by the general theory of these devices. (8 refs.)

113673 Resonant helical magnetic limiter. G.Fuchs, A.Nicolai, G.H.Wolf, B.Steffen.

Report JUL-1820, Kernforschungsanlage, Jülich, Germany (Dec. 1982), 54 pp.

The physical goals and principles of helical magnetic limiters are described. They are used to develop design criteria for modular structures of helical conductors, which are then applied to a special case (TEXTOR). A 1-dimensional transport code is used to predict the plasma-parameters for the helical magnetic limiter case. These calculations show a substantial reduction (as compared to a normal limiter case) of the temperatures in the plasma boundary, while the plasma density stays high. (31 refs.)

Net energy balance of Tokamak fusion power plants See Entry 112435

The role of the jet projection in global fusion research See Entry 112440

A fusion-fusion reactor driven by plasma-liner impact See Entry 112443

High-speed, low-cost laser-triggered plasma shutter See Entry 113017

Potential double layer formed by a laminar shock wave in a collisionless plasma See Entry 113615

52.80 ELECTRIC DISCHARGES

(see also 51.50 Electrical phenomena in gases)

113674 Light emission of spark discharges in liquids. R.Germer (Inst. Tech. Akustik, Tech. Univ. Berlin, Berlin, Germany).

Proc. SPIE Int. Soc. Opt. Eng. (USA), vol.312, p.123-8 (1983). (1st European Conference on Cineradiography with Photons or Particles, Paris, France, 18-21 May 1981).

When a condensor is discharged between two electrodes in a thin layer of liquid, a light flash is produced. The light emission is detected with a fast silicon detector filtered for red, green and blue light. The spark discharge and the shock waves in the liquid layer are photographed with X-ray flashes. The energy transfer to the gas plasma is much higher for a second or third discharge which follows the first discharge after some microseconds, if it is a discharge into the spark induced gas plasma and not in the liquid. The expansion of the gas plasma has therefore been studied in detail. A simple arrangement of two condensers and a coil makes it possible to produce flash sequences. The spark was produced in different organic liquids and H_2O . (6 refs.)

113675 Residual gas adsorption on electrode surfaces in vacuum. K.Tsuruta, M.Yano (Dept. of Electrical Engng., Ibaraki Univ., Hitachi, Japan).

Jpn. J. Appl. Phys. Part 1 (Japan), vol.22, no.6, p.1017-19 (June 1983).

The pre-breakdown currents of a vacuum gap both just after spark conditioning of the electrodes and after exposure to a vacuum were measured in a vacuum of $3 \times 10^{-5} \text{ Pa}$ using a switching impulse voltage. It was found that the exposure reduced the field emission current and that this reduction became greater with the exposure time. The reduction in the field emission current is considered to be the result of an increase in the work function due to adsorption of residual gases on the electrode surfaces. Current pulses were also observed to appear on the pre-breakdown currents measured after exposures of longer than 5 minutes. (5 refs.)

113676 Electron temperature in HF discharge plasma columns. G.Cicconi (Istituto di Elettrotecnica, Univ. of Genoa, Genoa, Italy).

Jpn. J. Appl. Phys. Part 1 (Japan), vol.22, no.6, p.1063-5 (June 1983).

Assuming the validity of Schottky's theory for the positive column, the electron temperature of plasma columns in HF stationary discharges is estimated by measuring their length. The discharges are produced in narrow quartz tubes. At particularly low pressure for a quasi capillary column, the estimation is made by a microwave reflectometric diagnostic using various equilibrium models to describe the column. (16 refs.)

113677 Measurement of electron temperature in a glow discharge with a double probe method. Dock-Chool Lee, Young-Il Kim, Dong-Ha Kim, Sang-Hyun Park.

Trans. Korean Inst. Electr. Eng., vol.32, no.4, p.128-35 (1983). In Korean.

As preliminary experiments for the formation of thin polymer films, electron temperature T_e in glow discharge of various gases has been studied with a double probe method. In a glow discharge at pure gases (Ar , N_2 , O_2), electron temperature decreases as gas flow rate, gas pressure in reactor and discharge power (Input) increase. The value of T_e in O_2 gas is greater than those of Ar , N_2 gases and T_e of Ar gas is almost the same as the value of T_e in N_2 gas. Electron temperature of glow discharge in gas mixtures ($\text{Ar}+\text{N}_2$, $\text{Ar}+\text{O}_2$, and $\text{Ar}+\text{H}_2$) indicates the same tendency as those in the pure gases but generally, the value of T_e is lower than those of pure gases. The value of

Te in case of $\text{Ar}+\text{O}_2$ is especially when lower compared with *Te* of other gases, i.e. Ar , O_2 , $\text{Ar}+\text{H}_2$ or $\text{Ar}+\text{N}_2$. (10 refs.)

113678 On trajectories of positive pulse charge streamers. A.V.Ivanov, V.P.Larionov.

Elektrichestvo (USSR), no.5, p.64-6 (May 1982). In Russian.

Studies the effect of electric field configuration on trajectories of streamer development. Reports on experiments with gaps of type bar-plane and bar-plane with a cylindrical projection. It is found that the trajectory of development of a positive discharge streamer zone can be influenced by very weak disturbances of the field of the order 1 kV/cm. An external field and the space-charge field have about equally the same influence on discharge development. (6 refs.)

113679 Endurance of electrically stressed epoxy resins determination by internal partial discharge amplitude distribution analysis. C.Mangiavacchi, G.Rabach (Istituto di Elettrotecnica e di Elettronica, Univ. di Trieste, Trieste, Italy).

Energ. Elett. (Italy), vol.60, no.6, p.211-20 (June 1983). In Italian.

An experimental study concerning epoxy resin endurance to partial discharge activity by means of partial discharge amplitude distribution (PDAD) analysis is presented. After discussing the preliminary choice of the samples to test and the possibility of fitting the experimental results with suitable multimodal distributions, some experimental histograms obtained during the test are analyzed. The possibility of detecting the beginning of new degradation processes during the test, by which, in a relatively short time, sample breakdown occurs is pointed out. (13 refs.)

113680 Electrical characteristics of a high-voltage electropulse discharge in a small enclosed volume of fluid. V.S.Goldaev.

Elektron. Obrab. Mater. (USSR), no.3, p.43-6 (1983). In Russian. English translation in: *Electrochem. Ind. Process. & Biol. (GB)*

A method is given of calculating the electrical efficiency of a pulse discharge in a small volume of fluid with the use of pulse-voltage and pulse-current generators, with a combined switching device and oscillograms of current and voltage. (5 refs.) *A.J.B.*

113681 Effect of water vapor on an externally maintained gas discharge.

Y.Yu.Baranov, R.K.Bevo, F.I.Vyskailo, A.P.Napartovich, S.V.Khomenko.

High Temp. (USA), vol.20, no.6, p.815-19 (Nov.-Dec. 1982). Translation of: *Teplofiz. Vys. Temp. (USSR)*, vol.20, no.6, p.1038-43 (Nov.-Dec. 1982). [received: Sept. 1983]

An investigation of the characteristics of an externally maintained discharge and the decay of its plasma in an electric field when the electron beam was cut off led to the measurement of a number of constants characterizing attachment and recombination in the discharge. In particular, the constant for three-body attachment of an electron to oxygen in air in the presence of water molecules is $K=3.5\cdot10^{-30}\text{ cm}^6\text{ sec}^{-1}$ for $E/N=1.5\cdot10^{-16}\text{ V cm}^{-1}$ and $K=3\cdot10^{-30}\text{ cm}^6\text{ sec}^{-1}$ for $E/N=3\cdot10^{-16}\text{ V cm}^{-1}$. The dependences of the effective recombination constant in nitrogen, air, and air-helium mixtures on the water vapor concentration, reduced electric field E/N , and energy input to the discharge were investigated. (11 refs.)

113682 Integral characteristics of electrode layers in capacitive medium-pressure HF discharge. N.A.Yatsenko (Inst. of Problems of Mech., Acad. of Sci., USSR).

High Temp. (USA), vol.20, no.6, p.820-6 (Nov.-Dec. 1982). Translation of: *Teplofiz. Vys. Temp. (USSR)*, vol.20, no.6, p.1044-51 (Nov.-Dec. 1982). [received: Sept. 1983]

The integral characteristics of the electrode layers of a spatial discharge and the discharge current density were experimentally investigated in relation to pressure up to tens of kilopascals in the unconstricted type of capacitive HF discharge burning steadily in air, helium, or CO_2 in normal current density conditions between plane cooled electrodes and the distant walls of the discharge chamber. The parameters of the spatially homogeneous plasma of the positive column of this type of discharge depend very strongly on the structure of the electrode regions, which may be qualitatively different. The role of a dielectric coating on the electrodes in a capacitive HF discharge is analysed. (20 refs.)

113683 Anode-plasma parameters of a high-voltage glow discharge ≈ 150 kV. L.N.Pustynskii, S.R.Kholev, G.V.Yakushin.

High Temp. (USA), vol.20, no.6, p.831-7 (Nov.-Dec. 1982). Translation of: *Teplofiz. Vys. Temp. (USSR)*, vol.20, no.6, p.1057-63 (Nov.-Dec. 1982). [received: Sept. 1983]

A single Langmuir probe has been used to examine the spatial distribution of the electron concentration in the anode plasma of a high-voltage glow discharge in deuterium at a maximum voltage of 150 kV. The electron temperature and the plasma potential have been determined. It is found that the length of the cathode-potential region is independent of the voltage but is determined by the pressure in the discharge tube. The pressure dependence of this length at the axis of the discharge $d_{\sim}p^{-1.4}$. The plasma propagates along the glass wall of the discharge tube, which causes curvature of the plasma boundary. The plasma-density relaxation time is not less than 10 μsec . (22 refs.)

113684 Gas breakdown in a dielectric cell with external electrodes.

Yu.I.Chutov, O.V.Korolyuk (Shevchenko Univ., Kiev, Ukrainian SSR).

High Temp. (USA), vol.20, no.6, p.837-44 (Nov.-Dec. 1982). Translation of: *Teplofiz. Vys. Temp. (USSR)*, vol.20, no.6, p.1064-71 (Nov.-Dec. 1982). [received: Sept. 1983]

A numerical solution has been obtained to the equations describing ionization in a dielectric cell with external electrodes filled with neon at $p_d=0.2\text{--}24\text{ mm Hg cm}$. The two-liquid hydrodynamic approximation is used with a self-consistent electric field and a Townsend ionization model. Allowance is made for the effects of the charges deposited on the inner walls of the cell. The distributions of the electrons and ions in space and time are derived along with the electric field strength, the ionization intensity, and the current pulses in the external circuit. Three phases in the ionization are observed, which differ in the mode of variation in the field in the gap. (17 refs.)

113685 Excitation of striations in the positive column of a glow discharge. D.Sengupta, S.N.Sengupta (Saha Inst. of Nuclear Phys., Calcutta, India).

J. Appl. Phys. (USA), vol.54, no.9, p.5451-2 (Sept. 1983).

A new method of exciting striations in the positive column of a glow discharge, by introducing a stream of electrons in the Faraday dark space, is presented. The method is capable of exciting striations at the natural frequencies of self-excited striations under similar discharge conditions. (5 refs.)

113686 Vibrational kinetics in liquid nitrogen cooled 5% CO-He radio-frequency discharges. S.De Benedictis, M.Capitelli, F.Cramarossa, R.d'Agostino, C.Gorse (Dipartimento di Chimica, Univ. di Bari, Bari, Italy), P.Brechignac.

Opt. Commun. (Netherlands), vol.47, no.2, p.107-10 (15 Aug. 1983).

5% CO-He radiofrequency discharges have been theoretically and experimentally studied in a liquid N_2 -cooled reactor operated at 6 torr as a function of

the residence time. The discharges are characterized by CO dissociation rates higher than those observed in uncooled discharges and by time-dependent non-Boltzmann vibrational distributions. A purely vibrational mechanism can reasonably be considered the main CO dissociation channel. The importance of O atoms as the main deactivating species, when CO_2 and C are at low density because they are trapped by the cooled walls, is stressed. (6 refs.)

113687 Relationship of the laser-induced population perturbation of excited levels with the dynamical optogalvanic signal in a discharge plasma. T.Fujimoto, Y.Uetani, Y.Sato, C.Goto, K.Fukuda (Dept. of Engng. Sci., Kyoto Univ., Kyoto, Japan).

Opt. Commun. (Netherlands), vol.47, no.2, p.111-16 (15 Aug. 1983).

For a pulsed-laser excitation of various neon transitions ($1s_2\text{--}2p_6$) in a glow discharge the population perturbations in the upper and lower levels are measured by emission and absorption spectroscopy, and the dynamical optogalvanic signals are observed. It is proposed that the population perturbation in the lower levels ($1s_2\text{--}1s_5$) as a whole is responsible for the optogalvanic signal, and that metastable-level populations determine its decay characteristics. The sign reversal of the optogalvanic signal that depends on the excitation condition is interpreted in this context. (6 refs.)

113688 Brillouin scattering of multiline laser light in a flowing plasma corona. R.W.Short, E.A.Williams (Lab. for Laser Energetics, Univ. of Rochester, Rochester, NY, USA).

Phys. Fluids (USA), vol.26, no.9, p.2342-4 (Sept. 1983).

Multiline lasers have been suggested as a means of reducing stimulated Brillouin scattering (SBS) from laser fusion target plasmas. It is shown that because of interaction between incident and reflected laser lines, Brillouin scattering may still occur even if each line individually is below SBS threshold. The resultant scattering tends to be beneficial, however, as it is primarily the outgoing light which is scattered back into the plasma by the interaction. (4 refs.)

113689 The behaviour of impurities out of coronal equilibrium.

P.G.Carolan (UKAEA, Culham Lab., Abingdon, England), V.A.Piotrowicz.

Plasma Phys. (GB), vol.25, no.10, p.1065-86 (Oct. 1983).

The behaviour of a range of impurities, in the presence of neutral thermal hydrogen atoms, is examined analytically for non-equilibrium coronal conditions. The time, τ_{eq} , required for an impurity species to establish equilibrium is found to be sensitively dependent on the plasma electron temperature and is strongly correlated with the ionisation state distribution at equilibrium. Peak values of $n_{\text{eq}}\tau_{\text{eq}}\approx 2\times 10^{18}\text{ m}^{-3}\text{ s}$ are found. The temporal and ensemble averaged calculations of the impurity charge states and radiation power which are presented here allow for the treatment of impurities without recourse to lengthy computation. The impurities (carbon, oxygen, iron and molybdenum) are considered in terms of the electron temperature, the fractional neutral hydrogen concentration, and the time spent by the impurities in the plasma. (18 refs.)

113690 Nonlinear theory of standing striations in a high-frequency gaseous discharge. B.S.Kerner, V.V.Osipov.

Radio Eng. & Electron. Phys. (USA), vol.27, no.12, p.122-32 (Dec. 1982).

Translation of: *Radiotekh. & Elektron. (USSR)*, vol.27, no.12, p.2415-25 (Dec. 1982). [received: Sept. 1983]

The hydrodynamic theory of high-amplitude standing striations in a high-frequency discharge is developed: the shape and stability of striations as well as their evolution with changes of current are investigated. It is shown that the shape of striations is determined by the form of the dependence of ionization rate ν_i on electron concentration n and the effective temperature of the electrons T as well as on the ratio $\epsilon=|L|/L$ (L , L are lengths of bipolar diffusion and of cooling of hot electrons). The distributions $n(x)$ and $T(x)$ in striations for $\epsilon\ll 1$ are close to quasi-harmonic distributions. For $\epsilon\ll 1$ the distribution $n(x)$ represents a contrast pattern, i.e. in some regions of size $\sim l$ (in walls of striations) electron concentration sharply changes and in other regions it changes smoothly; $T(x)$ changes everywhere smoothly with length of about L that characterizes the period of striations. In addition to periodic striations, by external excitation for $\epsilon\ll 1$ one can excite more complex distributions including a distribution in the form of one striation in the region of stability of the uniform state. It was established from analysis of stability that for a given current several stable states are realized. (21 refs.)

113691 Streamer discharges in semiconductors in the temperature range 4.2-530K.

V.V.Zubritskii, G.P.Yablonskii, V.P.Gribkovskii (Inst. of Phys., Acad. of Sci., Minsk, Belorussian SSR).

Sov. Phys.-Semicond. (USA), vol.17, no.3, p.250-3 (March 1983). Translation of: *Fiz. & Tekh. Poluprovodn. (USSR)*, vol.17, no.3, p.402-8 (March 1983). [received: Sept. 1983]

Streamer discharges were excited and investigated in cadmium sulfide and zinc selenide single crystals at temperatures 4.2-530K. It was established that on increase in temperature the streamer orientation became more definite and there was a change in the preferred crystallographic directions of discharge propagation. Surface streamers were observed in layers less than 5 μ thick. The streamer and photoluminescence spectra were determined at temperatures 4.2, 12, 300, 373, and 473K. It was found that the main mechanism of radiative transitions was recombination in an electron-hole plasma in the discharge channel. (13 refs.)

113692 Formation of an anode spot in a vacuum arc. V.A.Nemchinskii (All-Union Sci. & Tech. Res. Inst. for Current Source Design & Engng., Leningrad, USSR).

Sov. Phys.-Tech. Phys. (USA), vol.28, no.2, p.146-9 (Feb. 1983). Translation of: *Zh. Tekh. Fiz. (USSR)*, vol.53, no.2, p.235-40 (Feb. 1983). [received: Sept. 1983]

Processes preceding anode spot formation in a high-current vacuum arc are examined. It is shown that at currents above a threshold value I_{cr} the magnetic field induced by the current in the arc affects the arc current and the plasma flow and results in pinching of the plasma column and a region of critical plasma flow near the anode. The critical current I_{cr} agrees closely with the experimentally observed current at which the voltage across the arc rises abruptly and anode spot formation commences. This agreement is observed for copper electrodes and for electrodes consisting of other metals. The sequence of events leading to anode spot formation is discussed. (17 refs.)

113693 Causes of cathode spot motion in a vacuum arc and an estimate of retrograde velocity in a magnetic field. V.A.Nemchinskii (All-Union Sci. Res. Inst. of Current Source Design & Engng., Leningrad, USSR).

Sov. Phys.-Tech. Phys. (USA), vol.28, no.2, p.150-5 (Feb. 1983). Translation of: *Zh. Tekh. Fiz. (USSR)*, vol.53, no.2, p.241-50 (Feb. 1983). [received: Sept. 1983]

Cathode spots in a vacuum arc mode randomly—a spot remains stationary during its 'lifetime', after which it jumps a distance $\sim R$, where R is the spot radius, in a random direction. It is suggested that the factor responsible for spot movement is the additional voltage drop across the plasma which is required for current transmission from the eroded crater, which becomes steadily deeper while the spot remains fixed. When the voltage inside the

crater exceeds a certain value, it becomes more 'advantageous' for the arc to move onto the cooler rim of the crater. Spot jumping occurs when the arc voltage is maximal. The amplitude of the voltage oscillations ΔV_c caused by spot jumping is estimated in terms of R and τ and it is found that V_c is a few volts, in agreement with experimental findings. Retrograde spot motion in a magnetic field is analyzed and attributed to the Hall field E_H in the plasma near the cathode, which makes the cathode voltage drop symmetric. On the boundary toward which the Lorentz force $\mathbf{I} \times \mathbf{B}$ is directed, the cathode drop is $\delta V_c \approx 2E_H R$ less than on the opposite boundary. The character of the spot motion (jumps over distances $\sim R$) remains the same, but the field now gives rise to a preferred direction and the spots move backward at a velocity determined by the ratio $\delta V_c / \Delta V_c$. Experimental data on the amplitude and frequency of the arc voltage fluctuations (or else values determined from R and τ) are used to estimate the retrograde velocity in a weak field, B_{sat} (the magnetic field at which the velocity 'saturates'), and the absolute value v_{sat} of the saturated velocity. The findings are compared with experimental data for arcs with copper, molybdenum, or stainless steel electrodes, and a satisfactory agreement is obtained. (36 refs.)

113694 Observation of a significant density of negative ions in a currentless discharge in air; the possibility of an attachment instability. A.S.Zarin, V.N.Kulikov, V.E.Mitsuk (M.V. Lomonosov State Univ., Moscow, USSR). *Sov. Tech. Phys. Lett. (USA)*, vol.8, no.11, p.590 (Nov. 1982). Translation of: *Pisma v Zh. Tekh. Fiz. (USSR)*, vol.8, no.21-22, p.1373-4 (Nov. 1982). [received: Sept. 1983]

Reports direct measurements of the electron density n_e , the negative-ion density n_n , and the ratio $\eta = n_n/n_e$ for pressures in the range 10^{-2} -20 torr in an RF discharge in air. (8 refs.)

113695 Observations of the development processes of the discharges in the air gaps with insulating barrier arrangements. T.Hirano (Dept. of Electrical Engng., Nat. Defense Acad., Yokosuka, Japan). *Sci. & Eng. Rep. Natl. Def. Acad. (Jpn.) (Japan)*, vol.20, no.2, p.125-44 (June 1982). In Japanese. [received: Aug. 1983]

The development processes of discharges in air gaps between rod-to-rod and rod-to-plane electrodes with acrylic insulating plate barriers arranged at right angles to the rod electrode have been observed using a still camera and a lightning impulse voltage-chopping method. The development of the positive streamers and leaders is suppressed with the positive electric charges accumulated on the surface of one barrier of 400 mm in width. A solid angle of the positive discharges at the tip of the rod electrode with the barrier is larger than that without any barrier. The flashover paths with the barrier have gas discharge and surface discharge types. In the case of two barriers joined (probably with a small crack), it is found that the streamer and leader strokes can easily pass through the crack. (13 refs.)

Effect of magnetic field on the characteristics of a hollow cathode ion source See Entry 111815

High-current pulsed proton source See Entry 111816

Microdischarge characteristics in air gap between spherical particle and plane See Entry 112912

Analysis of temporal-length limitations in XeCl lasers See Entry 112984

High-speed, low-cost laser-triggered plasma shutter See Entry 113017

Centrifugal isotope separation in zirconium plasmas See Entry 113613

Self-focusing in laser produced spark See Entry 113621

Properties of the corona generated by the incidence of intense CO₂ laser pulses on spherical targets See Entry 113638

Plasmastructural transformations in amorphous chalcogenide semiconductors See Entry 114423

Tunneling afterglow and anomalous fading in dosimetry with CaSO₄:Dy See Entry 115925

Characteristics of two types of beam plasma discharge in a laboratory experiment See Entry 116357

60.00 CONDENSED MATTER: STRUCTURE, THERMAL AND MECHANICAL PROPERTIES

Proceedings of the Sixteenth Rare Earth Research Conference See Entry 111304

61.00 STRUCTURE OF LIQUIDS AND SOLIDS; CRYSTALLOGRAPHY

(see also 68.20 Solid surface structure, 71. Electron states)

113696 Stereographic representation of three-dimensional density distributions. M.Van Heel (Fritz-Haber-Inst., Max-Planck-Gesellschaft, Berlin, Germany). *Ultramicroscopy (Netherlands)*, vol.11, no.4, p.307-13 (1983). The representation of three-dimensional density data in a manner that is transparent to the human observer is a problem that has a number of solutions. All solutions rely on the definition of one or more 'surfaces' ('contours') in the 3D data set which are presented to the observer in one way or another. The algorithm promoted by the author allows the calculation of 'photographs of the model' without building a model. The technique allows rapid visual evaluation of results of 3D reconstructions at various density levels. Apart from being time-saving, this procedure has the advantage that the models need not be buildable, that is, the object may consist of subunits that do not touch each other at all; connectivity is not needed as nothing has to be glued together. (10 refs.)

61.10 X-RAY DETERMINATION OF STRUCTURES

(see also 61.80 Radiation damage and other irradiation effects; for specific determinations, see 61.55 to 61.80)

61.10D Theories of diffraction and scattering

113697 Remarks on the nature of the X-ray diffraction line profiles due to small crystallite size. G.B.Mitra, P.S.Mukherjee (Dept. of Phys., Indian Inst. of Technol., Kharagpur, India).

Indian J. Phys. Part A, vol.57A, no.3, p.143-54 (May 1983). Gaussian and Cauchy approximation for X-ray diffraction line profiles due to small crystallite size have been critically discussed. The effects of these approximations on the profile parameters, viz. integral width, Fourier coefficients, variance and fourth moment have been discussed. Expression for variance and fourth moment of X-ray diffraction line profile derived for the general case by Wilson (1963) and Mitra (1964) have been examined. It has been found that a Cauchy approximation is more realistic than Gaussian approximation for a X-ray diffraction line profile due to small crystallite size. (20 refs.)

113698 Dynamic diffraction of X-rays in a harmonic superlattice. Yu.P.Khapachev, G.F.Kuznetsov (Inst. of Radio Engng. & Electronics, Acad. of Sci., USSR).

Sov. Phys.-Crystallogr. (USA), vol.28, no.1, p.12-14 (Jan.-Feb. 1983). Translation of: *Kristallografiya (USSR)*, vol.28, no.1, p.27-31 (Jan.-Feb. 1983). [received: Sept. 1983] The authors discuss the dynamic diffraction of X-rays in a harmonic superlattice. They show that in general the widths of the satellites are unequal to one another and to the width of the main diffraction maximum. They give experimental results which support the theory. (4 refs.)

113699 A completely probabilistic approach to the determination of centrosymmetric structures. A.N.Chekhlov (Inst. of Physiologically Active Substances, Acad. of Sci., USSR).

Sov. Phys.-Crystallogr. (USA), vol.28, no.1, p.19-21 (Jan.-Feb. 1983). Translation of: *Kristallografiya (USSR)*, vol.28, no.1, p.42-6 (Jan.-Feb. 1983). [received: Sept. 1983] For centrosymmetric crystals, new probabilistic expressions are derived, permitting iterative calculation not only of the signs of the reflections but also of their probabilities, making the multivariant procedure of solving the phase problem more reliable and objective. This completely probabilistic approach is realized in the crystallographic program complex LUCH-77, compiled by the author, and is used to determine several fairly complex structure. (6 refs.)

113700 The difference interatomic function $D(u)$. I. Definition and characteristics of peaks. E.V.Slavyanov, V.N.Biyushkin (Inst. of Appl. Phys., Acad. of Sci., Moldavian SSR).

Sov. Phys.-Crystallogr. (USA), vol.28, no.1, p.22-4 (Jan.-Feb. 1983). Translation of: *Kristallografiya (USSR)*, vol.28, no.1, p.47-50 (Jan.-Feb. 1983). [received: Sept. 1983] The function $D(u)$ is defined as the difference between the modified and ordinary Patterson functions, reduced to a definite relative scale. The function enables the authors to distinguish or eliminate the interatomic vectors corresponding to a given species of atoms. The peak weightings of the function depend on the relative scales or the functions in the subtraction and may be either positive, zero, or negative. (3 refs.)

Symmetry of phase space and direct methods of X-ray structural analysis of crystals See Entry 113703

61.10F Experimental techniques

(inc. apparatus, techniques and calculation methods for analyzing experimental results; see also 07.85 X-ray, gamma-ray instruments and techniques)

113701 A note on the reproducibility of experimental radial distribution functions. G.Hermes, M.Derno, H.Steil (Sektion Phys., Wilhelm-Pieck-Univ. Rostock, Rostock, Germany).

Chem. Scr. (Sweden), vol.22, no.3, p.155-6 (1983). An example is given showing the good reproducibility in modern X-ray diffraction studies on amorphous materials even if specimens of different form (powder and bulk materials) are used. (9 refs.)

113702 On the evaluations of Fourier coefficients in X-ray line profile analysis of crystalline materials. E.Chatterjee, S.P.Sen Gupta (Dept. of General Phys. & X-rays, Indian Assoc. for the Cultivation of Sci., Calcutta, India).

Indian J. Phys. Part A, vol.57A, no.3, p.200-4 (May 1983). X-ray diffraction line profile analysis (XRDLPA) using Warren-Averbach's Fourier method (1969) is well known for its wide application in the evaluations of microstructural parameters in polycrystalline materials in terms of lattice imperfections, namely small coherently diffracting domains or crystallites, root-mean-square strains in these crystallites, stacking fault concentrations, etc. In this analysis, the true diffraction profile originating from imperfections in the materials is unfolded from the experimentally recorded profile of the sample and the instrumental profile of the standard through Stokes' method of deconvolution (1948). (3 refs.)

113703 Symmetry of phase space and direct methods of X-ray structural analysis of crystals. V.A.Koptsik, E.N.Ovchinnikova, A.Yu.Papaev (M.V. Lomonosov State Univ., Moscow, USSR).

Sov. Phys.-Crystallogr. (USA), vol.28, no.1, p.14-19 (Jan.-Feb. 1983). Translation of: *Kristallografiya (USSR)*, vol.28, no.1, p.32-41 (Jan.-Feb. 1983). [received: Sept. 1983] The authors discuss the problem of mapping the symmetry of physical space into the space of structure amplitudes (Fourier space). The symmetry of phase space, for which the geometrical basis is the reciprocal lattice consisting of points (hkl) while the weightings are the assigned structure amplitudes $a(hkl)$, is a positional $G^{(w)}$ color symmetry. The authors derive the 156 point groups of $G^{(w)}$ symmetry into which tetragonal, hexagonal, and cubic Fedorov groups Φ are mapped. It is shown that reciprocal space also has translational color symmetry, so that the Fedorov groups Φ can be mapped into the spatial color groups $\Phi|_{\alpha}^{w(F),w(\alpha)}$. (24 refs.)

113704 Programs for indexing powder patterns. V.A.Zabolotnyi, V.E.Ovchinnikov, L.P.Solov'eva, B.M.Shchedrin (Inst. of Tectonics & Geophys. of the Far-Eastern Sci. Center, Acad. of Sci., USSR). *Sov. Phys.-Crystallogr. (USA)*, vol.28, no.1, p.24-6 (Jan.-Feb. 1983). Translation of: *Kristallografiya (USSR)*, vol.28, no.1, p.51-5 (Jan.-Feb. 1983). [received: Sept. 1983]

An algorithm is developed for finding lattice parameters from powder data; it is suitable for realization on small and medium-sized computers. The algorithm is based on representing the indexing problem as a problem of minimization of the sum of the discrepancies of the ratios of the interplanar distances. (10 refs.)

113705 Two approaches to the interpretation of X-ray investigations of liquids. T.V.Gorbulova, G.I.Batalin (State Univ., Kiev, Ukrainian SSR). *Sov. Phys.-Crystallogr. (USA)*, vol.28, no.1, p.27-30 (Jan.-Feb. 1983). Translation of: *Kristallografiya (USSR)*, vol.28, no.1, p.56-61 (Jan.-Feb. 1983). [received: Sept. 1983]

The authors discuss two approaches to the interpretation of X-ray diffraction experiments on liquids: calculation of theoretical intensity curves, and of atomic radial distribution curves (RDC) for short-range order models. They show that comparison between the experimental and theoretical RDC in the region of short-range order enables the authors to select the most probable model for the structure of the ordered regions. Comparison of the intensity (structure factor) curves is less suitable for this purpose, because it is not possible to distinguish the contributions made to these curves by the individual interatomic distances. (4 refs.)

113706 A new method for calculating the intensity of the diffuse X-ray scattering by point defects in cubic crystals. W.Kienle, A.Seiger, W.Frank (Max-Planck-Inst. für Metall., Stuttgart, Germany). Point Defects and Defect Interactions in Metals. Proceedings of the Yamada Conference V, Kyoto, Japan, 16-20 Nov. 1981 (Amsterdam, Netherlands: North-Holland 1982), p.228-31

Homogeneously distributed point defects in a cubic crystal give rise to diffuse X-ray scattering with cubic symmetry in k space. This allows one to expand the single-defect approximation of the diffuse X-ray intensity in an alternating series of cubic harmonics. In contrast to the usual approximations valid in the regimes of small-angle and Huang scattering, this series is a good approximation in the entire k space. The method is illustrated for monovacancies in a face-centred cubic crystal. (7 refs.)

The difference interatomic function $D(u)$. I. Definition and characteristics of peaks See Entry 113700

Temperature dependence of the X-ray diffuse scattering intensity in V_2Si in the temperature range from 8 to 300K See Entry 114964

61.12 NEUTRON DETERMINATION OF STRUCTURES

(for specific determinations, see 61.55 to 61.80)

The Australian high resolution neutron powder diffractometer See Entry 111854

Combined spectrometer for small-angle and diffuse scattering of cold neutrons See Entry 112536

61.14 ELECTRON DETERMINATION OF STRUCTURES

(for specific determinations, see 61.55 to 61.80)

61.14H Low-energy electron diffraction (LEED) and reflection High-energy electron diffraction (RHEED)

Quantitative analysis of LEED measurements See Entry 114309

61.16 OTHER DETERMINATION OF STRUCTURES

(for specific determinations, see 61.55 to 61.80)

Advances in the infrared microscopy of electronic materials .. See Entry 111761

61.16D Electron microscopy determinations

113707 The importance of beam alignment and crystal tilt in high resolution electron microscopy. D.J.Smith, W.O.Saxton, M.A.O'Keefe, G.J.Wood, W.M.Stobbs (High Resolution Electron Microscope, Univ. of Cambridge, Cambridge, England).

Ultramicroscopy (Netherlands), vol.11, no.4, p.263-81 (1983).

The relative influences of crystal tilt and beam alignment on high-resolution electron-microscopic imaging have been investigated. With the use of contrast transfer theory in generalised dimensionless form, the major effect of slight beam misalignment has been shown to be the introduction of an antisymmetric phase shift in the diffracted beams so that the presence of any such misalignment cannot be detected by the standard diagnostic tool of high-resolution electron microscopy, namely the optical diffractogram. Specific image simulations, at 100 and 500 keV, for materials of both small and large unit cells (SnO_2 and $Ti_2Nb_{10}O_{29}$ respectively) show, however, that even slight beam tilt can have a marked effect on the images of crystalline materials, causing considerable spurious detail and a loss of expected symmetry. The various options for ensuring accurate beam and crystal alignment are briefly reviewed, and some aspects of the alignment problems are demonstrated using some recent experimental images recorded at 500 kV. (30 refs.)

113708 Real space image simulation in high resolution electron microscopy. R.Kilaas, R.Gronsky (Lawrence Berkeley Lab., Univ. of California, Berkeley, CA, USA).

Ultramicroscopy (Netherlands), vol.11, no.4, p.289-98 (1983).

The validity of a new method for simulating high resolution electron microscope images has been critically examined. This method, which has been termed the real space method since the entire calculation is performed without any Fourier transforms, offers a considerable reduction in computing time over the conventional multislice approach when identical sampling conditions are employed. However, for the same level of accuracy the real space method requires more sampling points and more computing time than the conventional multislice method. These characteristics are illustrated with calculated results using both methods to identify practical limitations. (9 refs.)

113709 Microstructure and topography [laser annealing of semiconductors]. A.G.Cullis (Royal Signals & Radar Establ., Great Malvern, England). In book: *Laser annealing of semiconductors*, J.M.Poate, J.W.Mayer [Ed.], p.147-201. London, England: Academic Press (1982), xi+564 pp. [0 12 558820 8]

A wide variety of physical analytical techniques have been employed in the study of annealed layer structures, and perhaps the most widely used method is Rutherford backscattering and channeling of megaelectron volt ions. However, this does not give direct information about individual crystallographic defects that may be present, and, for this purpose, electron microscopy is unrivalled. The author reviews mainly the results of transmission electron microscope (TEM) investigations in revealing the microstructural properties of annealed layers. In many cases conventional plan view specimens have been adequate to show details of interest. However, the layers often exhibit a defect depth stratification that can be revealed satisfactorily only by use of cross-sectional specimens. Such work has the additional advantage that the final micrographs can be compared directly with the results of ion-backscattering studies. (126 refs.)

A novel sample preparation technique for cross-sectional TEM investigation of integrated circuits See Entry 111659

A fast-response EBIC system See Entry 111817

Applications of high voltage electron microscopy in materials science See Entry 111819

Observation of surface atomic structure in real space scanning tunneling microscopy—Si (111) 7×7 super-structure See Entry 114316

61.16F Field-ion microscopy determinations

Statistics of the atom-by-atom dissection of planes in an atom-probe field-ion microscope: the number of atoms detected per plane See Entry 111826

61.16N EPR and NMR determinations

113710 The use of ^{29}Si Fourier transform nuclear magnetic resonance spectroscopy for the characterisation of polymers and paints. G.L.Marshall (Materials Quality Assurance Directorate, London, England). *Br. Polym. J. (GB)*, vol.14, no.1, p.19-22 (March 1982).

A range of commercial paint binders and two-pack elastomers containing silicone materials have been investigated by ^{29}Si Fourier transform nuclear magnetic resonance spectroscopy at 17.76 MHz. In order to obtain good quality spectra within a minimum of time period, a relaxation agent was used to suppress nuclear Overhauser effects, and to improve the relaxation times of the silicon nuclei. (12 refs.)

61.20 CLASSICAL, SEMICLASSICAL, AND QUANTUM THEORIES OF LIQUID STRUCTURE

(for kinetic and transport theory, see 51.10; for electronic states, see 71.; for liquid helium, see 67.)

113711 Lattice theory of binary fluid mixtures: phase diagrams with upper and lower critical solution points from a renormalization-group calculation. J.S.Walker (Dept. of Phys., MIT, Cambridge, MA, USA), C.A.Vause. *J. Chem. Phys. (USA)*, vol.79, no.6, p.2660-76 (15 Sept. 1983).

A generalized lattice model representing the interaction between two molecular species in a binary liquid mixture is introduced. The model interaction potential consists of a highly directionally dependent orientational part, due to hydrogen bonding, coupled to the configurational van der Waals interaction. Closed-loop temperature vs. concentration solubility phase diagrams are produced in good agreement with experimental systems. These diagrams are obtained using renormalization-group methods. The possible types of phase diagrams predicted by the phenomenological Landau theory are also discussed. (39 refs.)

113712 The density profile of a fluid bounded by a soft wall. J.K.Percus (Phys. Dept., New York Univ., New York, NY, USA), G.O.Williams. *J. Chem. Phys. (USA)*, vol.79, no.6, p.3009-17 (15 Sept. 1983).

An approximate relationship is developed between the density profile of a simple classical fluid bounded by a soft wall and that bounded by an idealized hard wall. This relationship is exact for a class of one-dimensional fluids, and also constitutes a simplification of the 'shielding approximation'. It accurately reproduces several Monte Carlo calculations. (16 refs.)

113713 Equilibrium properties of the Gaussian overlap fluid. Monte Carlo simulation and thermodynamic perturbation theory. P.A.Monson, K.E.Gubbins (School of Chem. Engng., Cornell Univ., Ithaca, NY, USA). *J. Phys. Chem. (USA)*, vol.87, no.15, p.2852-8 (21 July 1983).

The structure and thermodynamic properties of fluids of molecules interacting with a Gaussian overlap potential are calculated by Monte Carlo (MC) simulation and thermodynamic perturbation theory. Both prolate and oblate molecules are considered. The perturbation theory is based on an extension of the Weeks-Chandler-Andersen (WCA) theory to orientation-dependent potentials and uses a Mayer-function expansion about a spherically averaged reference potential to compute the structure of the hard-core reference system. The theory predicts the structural features of the fluid quite accurately except for the most anisotropic system at high density. The thermodynamic properties are given quite accurately by the theory for mildly anisotropic molecules, but the agreement is only qualitative for the most anisotropic case. The molecular shape dependence of the orientational correlation parameter G_2 has been studied for the hard-core Gaussian overlap potential, using the computer simulation results. Large positive values of G_2 are reported for an oblate system at high density. (23 refs.)

Self-correlation functions of rotational and translational motion in simple fluids See Entry 112823

Structure of water solutions. I. Viscosities of aqueous substituted ammonium chlorides See Entry 114235

On the dielectric theory and computer simulation of water ... See Entry 114769

61.25 STUDIES OF SPECIFIC LIQUID STRUCTURES

(see also 61.40 Amorphous and polymeric materials)

113714 Evidence of compatibility in the melt for poly(ethylene oxide)/poly(methyl methacrylate) blends by ^{13}C n.m.r. investigations. E.Martuscelli, G.Demma (Istituto di Ricerche su Tecnologia dei Polimeri e Reologia, Napoli, Italy), E.Rossi, A.L.Segre. *Polym. Commun. (GB)*, vol.24, no.9, p.266-7 (Sept. 1983).

Evidence of compatibility in the melt for poly(ethylene oxide) PEO and poly(methyl methacrylate) PMMA was obtained in Martuscelli et al. (1980) while studying the crystallization and thermal behaviour and the wide- and small-angle X-ray scattering of corresponding binary blends. The present authors report preliminary results concerning a ^{13}C n.m.r. study of PEO/PMMA blends in the melt state with particular attention to the dynamic parameters. In the case of mixability, the ^{13}C dynamic parameters are composition dependent due to molecular entangling effects and to variations of chain mobility. In fact, both in the melt (90°C) and in the supercooled melt (60°C), T_g is strongly composition dependent, i.e. 840 to 240 ms at 90°C and 283 to 168 ms at 60°C, going from pure PEO to the 1:1 blend. This result is interpreted as being due to complete mixability in the melt of PEO and PMMA. (7 refs.)

113715 Inherent structure in water. F.H.Stillinger, T.A.Weber (Bell Labs., Murray Hill, NJ, USA).

J. Phys. Chem. (USA), vol.87, no.15, p.2833-40 (21 July 1983). The statistical thermodynamics of water has been recast in a form which distinguishes two basic contributions, one of purely structural origin, and one due to anharmonic vibrations. The former involves the collection of potential energy minima ('inherent structures') while the latter concerns thermal motions away from these minima. Information about the inherent structures has been adduced from crystallography and from molecular dynamics simulation for a 250-molecule cluster with free surfaces. The authors concluded that near 0°C the mean molar volume of relevant inherent structures contributing to the liquid phase increases as temperature decreases, and that this increase probably has a singularity at the supercooling limit due to cooperative aggregation of hydrogen-bond polyhedra. Approximately 85-90% of the latent heat of melting ice can be attributed to upward shift in potential energy of the inherent structures across the transition, the remainder to changing anharmonicity. (35 refs.)

113716 The role of attractive force on the behavior of a polymer chain in solution. Seung Ho Jeon, In Joon Oh, Talkyue Ree (Dept. of Chem., Korea Advanced Inst. of Sci. & Technol., Seoul, Korea).

J. Phys. Chem. (USA), vol.87, no.15, p.2890-4 (21 July 1983). The authors investigated the behavior of a polymer chain in solution by the molecular dynamics (MD) technique. For this purpose, the polymer was represented by a semirigid chain having a fixed bond length and bond angle with allowance for a hindered internal rotation. The interaction potentials for solvent-solvent (SS), chain-solvent (CS), and chain-chain (CC) particles were chosen to be an exp-6 potential form, with a provision that the CC potential acts only between nonnearest-neighbor particle pairs. The effect of the attractive interactions on the physical properties of the polymer was investigated by comparing the results based on the exp-6 potentials with those based on a 'shifted' exp-6 potential which includes only the repulsive part of the exp-6 potential. The present work includes the calculations on the equilibrium quantities such as the SS, CS, and CC pair correlation functions, the mean square end-to-end distance, the mean square radius of gyration, and the eigenvalues of the moment of inertia tensor as well as the dynamic properties such as the autocorrelation functions for the mean square end-to-end distance and the mean square radius of gyration. The calculations show that the polymer configuration depends sensitively not only on the repulsive interaction but also on the attractive interaction. Namely, omitting the attractive term makes the polymer more compact, making the gauche conformations more favorable than trans conformations. The attractive interaction also produces autocorrelation functions which decay slower than those for the pure repulsive potential. (29 refs.)

113717 Raman scattering from molten alkali iodides. C.Raptis, R.A.J.Bunten, E.W.J.Mitchell (Clarendon Lab., Univ. of Oxford, Oxford, England).

J. Phys. C (GB), vol.16, no.27, p.5351-62 (30 Sept. 1983). Polarised and depolarised light scattering spectra of molten Na, K, Rb and Cs iodides have been measured at about 35° above the melting point in the range of frequency shifts (ν) of 4-350 cm^{-1} (0.5-45 meV). All polarised spectra show a broad shoulder centred about the mid-point of each frequency spectrum, a feature that is not observed in the depolarised spectra. The resulting depolarisation ratio (ρ_d) spectra show values of ρ_d increasing in the sequence NaI, KI, RbI to CsI, while the frequencies at peak positions in the reduced-intensity spectra decrease in the same sequence and are in close agreement with the Debye temperatures of the solids. Comparisons of the results are made with those from alkali chlorides and bromides reported previously. (19 refs.)

113718 X-ray diffraction investigation of the structure of liquid and supercritical water at high temperatures and pressures. I. Molecular functions of structurally sensitive scattering components at a pressure of 1000 bars and temperatures from 298 to 773K. Yu.E.Gorbatyi, Yu.N.Dem'yanets (Inst. of Experimental Mineralogy, Acad. of Sci., Chernogolovka, USSR).

J. Struct. Chem. (USA), vol.23, no.6, p.882-94 (Nov.-Dec. 1982). Translation of: *Zh. Strukt. Khim. (USSR)*, vol.23, no.6, p.73-85 (Nov.-Dec. 1982). [received: Sept. 1983] Using an experimental technique based on energy-dispersive X-ray diffraction, the authors have determined the molecular functions for structurally-sensitive components of the scattering of X-ray beams in liquid and supercritical phases of water at a constant pressure of 1000 bars and temperatures from 298 to 773K. The authors describe the experimental technique and the basic procedures for treatment of the experimental data. The final results are given in the form of tables which may be used to calculate correlation functions. (16 refs.)

113719 Studies on dilute solutions of rodlike macroions. I. Light scattering, densitometry, and cryoscopy. C.C.Lee, S.-G.Chu, G.C.Berry (Dept. of Chem., Carnegie-Mellon Univ., Pittsburgh, PA, USA).

J. Polym. Sci. Polym. Phys. Ed. (USA), vol.21, no.9, p.1573-97 (Sept. 1983). Total integrated and photon correlation light scattering have been used to study two samples of poly(1,4-phenylene-2,6-benzobisthiazole) (PBT) representing two methods of precipitation to recover the polymer from the polymerization solvent. Some details of the light-scattering instrument are given. It is found that the PBT sample is rodlike, with persistence length of at least 50 nm, but that the postpolymerization processing method influences the state of interchain aggregation. The data are augmented by measurements of freezing-point depression to estimate the degree of protonation of PBT in

sulfuric acid, and by measurements of partial specific volume to provide an estimate for the geometric diameter of the chain in solution. The results show a degree of protonation of 2-4 protons per repeating unit, and partial specific volumes that are appreciably smaller than the specific volume determined for the polymers. Similar data and results are reported for poly(1,4-phenylene-2,6-benzobisoxazole) and poly(1,4-phenylene terephthalamide). (25 refs.)

113720 The application of neutron scattering methods to aqueous electrolyte solutions. G.W.Neilson (H.H. Wills Phys. Lab., Univ. of Bristol, Bristol, England).

Physica B & C (Netherlands), vol.120B+C, no.1-3, p.325-34 (May 1983). (Yamada Conference VI on Neutron Scattering in Condensed Matter, Hakone, Japan, 1-4 Sept. 1982).

The author reviews recent developments in the application of neutron diffraction and quasi-elastic neutron scattering (QNS) to aqueous electrolyte solutions. The diffraction studies are based on the method isotopic differences which facilitates the extraction of detailed information regarding ionic hydration and ion-ion correlations respectively. The QNS results are derived from data obtained from the IN10 back scattering spectrometer of the ILL. IN10 provides a range of energy and momentum transfer ideal for studies of aqueous systems. The structural and dynamical information obtained from these investigations provide a series of crucial tests of liquid state theories and theoretical models currently used in solution science. Two models are discussed: the Frank-Wen dynamical model of ionic solution and the primitive model of ion-ion structure. (29 refs.)

113721 Many-body effects in the structure of water. P.A.Egelstaff (Tohoku Univ., Sendai, Japan).

Physica B & C (Netherlands), vol.120B+C, no.1-3, p.335-41 (May 1983). (Yamada Conference VI on Neutron Scattering in Condensed Matter, Hakone, Japan, 1-4 Sept. 1982).

Non-additive forces are believed to be important in the case of water because they are involved in the formation of 'hydrogen bonds'. The influence this has on the microscopic structure of the liquid is shown to lead to unusual effects in the isochoric temperature derivative of the neutron and X-ray structure factors. A new method of measuring these derivatives is described and recent published work using this method will be interpreted in terms of non-additive many-body effects. (11 refs.)

113722 Melt flow of polymer blends. L.A.Utracki (Nat. Res. Council of Canada, Industrial Materials Res. Inst., Montreal, Quebec, Canada).

Polym. Eng. & Sci. (USA), vol.23, no.11, p.602-9 (mid-Aug. 1983).

The results published during the last five years are reviewed. The data for polymer blends are compared with those obtained for simpler model systems: liquid mixtures, emulsions, and polymer blends. From the rheological point of view, the blends are divided into three groups: those where viscosity shows positive deviation from the log-additivity rule, PDB, those where the opposite effect is observed, NDB, and the remaining mixed-behavior systems, PNDB. To PDB belong the miscible blends and those with strong inter-domain interactions. To NDB belong those where the interactions are weak. To PNDB belong the blends in which there is a concentration-dependent transition of structure. The shear dependent properties of blends are also discussed. (87 refs.)

113723 A phenomenological master curve for viscosity-structure data for two phase polymer systems in simple shear flow. J.Lyngaae-Jorgensen (Inst. for Kemindustri, Tech. Univ. of Denmark, Lyngby, Denmark).

Polym. Eng. & Sci. (USA), vol.23, no.11, p.610-13 (mid-Aug. 1983).

A master curve hypothesis is established based on a mass balance and an assumption of continuous stress through interfaces for well dispersed two phase systems with 'defined' zero shear viscosity. The master curve, which is in reasonable accordance with experimental data is represented in a double logarithmic plot. M_c is the molecular weight between entanglements, $H = M_w/M_n$, ρ is the density, c is the polymer concentration, all defined for the continuous phase. η_r and $G_{H,0}$ are the viscosity and zero shear viscosity of the blend, $\dot{\gamma}_r$ is the apparent shear rate, R is the gas constant, and T is the absolute temperature. (18 refs.)

113724 Competitive equilibria in miscible polymer blends and low molecular weight analogues: a Fourier transform infrared study. A.Garton (Div. of Chem., Nat. Res. Council of Canada, Ottawa, Canada).

Polym. Eng. & Sci. (USA), vol.23, no.12, p.663-8 (Aug. 1983).

The relative magnitudes of specific interactions are compared by setting up competitive equilibria in mixed solvent systems. The positions of the equilibria are determined spectroscopically by resolving the overlapping absorptions of the two solvation states. This technique is applied to the study of interactions between polyesters (or model compounds) and a variety of solvents which mimic possible interacting centers in halogenated polymers. Using the same technique of resolving overlapping bands, it is also demonstrated that in a miscible blend of polycaprolactone and Phenoxy (a polyhydroxyether of bisphenol A) only a relatively small proportion of carbonyl groups of polycaprolactone are involved in specific interactions with the Phenoxy. (15 refs.)

113725 Fourier transform infrared studies of poly(vinyl chloride) blends with ethylene co- and terpolymers. M.Iskandar, C.Tran, L.M.Robeson, J.E.McGrath (Dept. of Chem. & Polymer Materials & Interfaces Lab., Virginia Polytech. Inst. & State Univ., Blacksburg, VA, USA).

Polym. Eng. & Sci. (USA), vol.23, no.12, p.682-8 (Aug. 1983).

The miscibility of poly(vinyl chloride) (PVC) with various ethylene copolymers and terpolymers were investigated using FT-IR spectroscopy. All blends reported were 50/50 by weight. In blends of PVC with ethylene/dimethyl acrylamide copolymer (E/DMA), frequency shifts were observed in the amide carbonyl (proton acceptor) and the α -hydrogen of PVC (proton donor) characteristic bands. In blends of PVC with ethylene/ethyl acrylate/carbon monoxide terpolymer (E/EA/CO), both the ester carbonyl and the ketone carbonyl characteristic frequencies showed mutual shifts and appeared as if they merged together. Small frequency shifts were also observed in the α -hydrogen of PVC characteristic bands. In blends of PVC with ethylene/vinyl acetate/carbon monoxide terpolymer (E/VA/CO), the ester carbonyl frequency showed a shift while that of the ketone carbonyl was essentially unchanged. On the other hand, in PVC blends with ethylene/vinyl acetate copolymer (E/VA), the ester CO frequency did not show any shift, which is consistent with their observed immiscibility. Thus, it is clear that incorporating a ketone -C=O in ethylene/ester copolymers to form the corresponding terpolymers enhances their miscibility with PVC as earlier proposed on the basis of dynamic mechanical studies. Similar results were shown for blends of PVC with ethylene/2 ethyl hexyl acrylate/carbon monoxide terpolymer (E/2EHA/CO). Frequency shifts imply specific interactions which suggest polymer-polymer miscibility on a molecular scale. (15 refs.)

113726 Fluorescence study of polymer chain interpenetration and of the rate of phase separation in incompatible polymer blends. H.Morawetz (Polymer Res. Inst., Polytech. Inst. of New York, New York, NY, USA).

Polym. Eng. & Sci. (USA), vol.23, no.12, p.689-92 (Aug. 1983).

The application of fluorescence techniques has been demonstrated for the study of four polymer problems: (a) If two different polymers are labeled

with donor and acceptor fluorophores, respectively, which exhibit nonradiative energy transfer, the emission spectrum of their blends will depend on whether the two polymeric species are miscible or segregated into separate phases. Thus, the emission spectrum may be used as a measure of polymer compatibility. (b) Since rapid freeze-drying preserves the extent of chain interpenetration which existed in solution, the energy transfer between labeled polymers may be used to study the extent of such interpenetration on solution concentration. (c) Phase separation when heating blends of poly(methyl methacrylate) and poly(benzyl methacrylate) may be followed by the change in the emission spectrum of the latter. (d) The interdiffusion of separated poly(ethyl methacrylate) molecules labeled with donor and acceptor fluorophores may be monitored by the increase in the nonradiative energy transfer. (16 refs.)

113727 Domain stability during capillary flow of well dispersed two phase polymer blends. Polystyrene/polymethylmethacrylate blends. J.Lyngaae-Jorgensen, F.E.Andersen, N.Alle (Inst. for Kemiindustri, Tech. Univ. of Denmark, Lyngby, Denmark).

Polymer Alloys III Blends, Blocks, Grafts and Interpenetrating Networks. Proceedings of a Symposium, New York, USA, 23-28 Aug. 1981 (New York, USA: Plenum 1983), p.105-47

A hypothesis for domain stability, i.e. the conditions where each domain of a dispersed phase remains as a coherent domain during capillary flow, is tested with data for polystyrene-polymethylmethacrylate melts. It is found that stable domains exist when the ratio between the (Trouton) zero shear viscosity of the discrete phase to the continuous phase is larger than approximately one. Blends of two thermodynamically incompatible polymers, polystyrene (PS) and poly(methylmethacrylate) (PMMA), were melt blended in a Brabender Plasticorder over the compositions: 100% PS, 75%, 50%, 25% and 0% PS. Viscous and die swell behaviour of pure polymers and the blends at different temperature were obtained using an Instron capillary rheometer and the microstructure of the melt blends was studied by transmission electron-microscopy. (47 refs.)

Polymer Alloys III Blends, Blocks, Grafts and Interpenetrating Networks. Proceedings of a Symposium See Entry 113131

Two approaches to the interpretation of X-ray investigations of liquids See Entry 113705

Thermotropic homopolymers. III. Preparation and properties of polymers based on 4'-hydroxyphenyl-4-hydroxycinnamate See Entry 113735

Melt rheology of polymer blends: the morphology feedback ... See Entry 114068

Ultrasonic and hypersonic investigations of structural relaxation in aqueous solutions of hexamethylphosphoramide See Entry 114097

Formation of a liquid crystal phase in the conversion of isotropic solutions of cellulose acetates into the solid state See Entry 114171

Observations upon the dynamic structure factor of interacting spherical polyelectrolytes See Entry 114228

A ^{13}C NMR study of mesomorphic solutions of poly(p-phenylene terephthalamide) See Entry 114750

On the dielectric theory and computer simulation of water ... See Entry 114769

Properties of semidilute polymer solutions: investigation of an optically labeled three-component system See Entry 114804

Raman spectroscopic study on molten polyethylene under high pressure See Entry 114843

61.25M Liquid metals

113728 Shape control of non-metallic inclusions in Al-deoxidized steel by calcium treatment. K.S.Kim, J.D.Shim (Korean Advanced Inst. of Sci. Technol., Seoul, Korea), W.J.Lee, J.K.Yoon.

J. Korean Inst. Met., vol.21, no.6, p.548-57 (June 1983). In Korean.

In order to clarify the shape control mechanism of nonmetallic inclusions in molten steel, the morphology changes of oxide and sulfide inclusions were investigated by Ca treatment in Al-deoxidized steel at 1600°C. The Ca addition of a suitable amount into Al-deoxidized steel considerably improved the degree of steel cleanliness because the alumina cluster formed after Al-deoxidization changed to liquid phase calcium-aluminates which float out rapidly from steel bath. Also, when the total oxygen content in molten steel was less than about 20 ppm, MnS sulfide and Al_2O_3 oxide were modified to C type inclusions such as $(\text{Ca},\text{Al},\text{Mn})\text{O}-(\text{Ca},\text{Mn})\text{S}$ or $\text{CaO}-\text{Al}_2\text{O}_3-\text{CaS}$. (12 refs.)

113729 Modeling the radial distribution function of liquid gallium based on the quasicrystalline model. N.N.Medvedev, Yu.I.Naberukhin, I.Yu.Semenova (Inst. of Chem. Kinetics & Combustion, Acad. of Sci., USSR).

J. Struct. Chem. (USA), vol.23, no.6, p.876-82 (Nov.-Dec. 1982). Translation of: *Zh. Strukt. Khim. (USSR)*, vol.23, no.6, p.66-72 (Nov.-Dec. 1982). [received: Sept. 1983]

The authors attempt to describe the radial distribution function of liquid gallium within the framework of the quasicrystalline model. They show that the structures of the α and β crystalline forms of gallium do not describe the radial distribution function of the liquid. A better description of the function over the entire available experimental range of separations (beyond the first peak) is obtained if the model is based on a modified bcc lattice in which the central atom is displaced along the diagonal. The authors conclude that the structure of liquid gallium involves irregular close packing in which separate pairs of atoms are closer than the average separation between particles. (25 refs.)

The study of thermal equilibrium defects and melting in indium by two-parameter correlation measurement of positron annihilation ..See Entry 114956

61.30 LIQUID CRYSTALS

(see also 64.70M Transitions in liquid crystals)

113730 New liquid crystalline tetrazine derivatives for guest-host displays. A.Isenberg, B.Krucke, G.Pelzl, H.Zaschke, D.Demus (Sektion Chem., Martin-Luther-Univ., Halle-Wittenberg, Germany).

Cry. Res. & Technol. (Germany), vol.18, no.8, p.1059-68 (1983). A number of new liquid crystalline tetrazine derivatives was synthesized. The electro-optical studies showed that the 3-n-alkyl-6-[4-(4-n-alkyl-cyclohexanoyloxy)phenyl]-1,2,4,5-tetrazines are excellent dyes for guest-host displays with positive colour contrast. (17 refs.)

113731 Cause of coherent oscillation of domains of nematic liquid crystals in DC electric field. S.Hirata, T.Tako (Res. Lab. of Precision Machinery & Electronics, Tokyo Inst. of Technol., Yokohama, Japan).

Jpn. J. Appl. Phys. Part 1 (Japan), vol.22, no.7, p.1073-9 (July 1983). The domains of nematic liquid crystals begin to oscillate coherently at a certain threshold voltage in a DC electric field. The structures of the hydrodynamic motion and the molecular alignment of this oscillation are investi-

gated and its mechanism is explained. The oscillation is attributed to the time-dependent competition between the hydrodynamic instability and the elastic stability in a nonequilibrium system. Some features of the oscillation are discussed on the basis of this mechanism. (10 refs.)

113732 Ferroelectric liquid crystals and their applications. L.K.Vistin', I.I.Sakharova, S.S.Yakovenko (A.V. Shubnikov Inst. of Crystallography, Acad. of Sci., Moscow, USSR).

Inorg. Mater. (USA), vol.18, no.10, p.1420-5 (Oct. 1982). Translation of: *Izv. Akad. Nauk SSSR Neorg. Mater.*, vol.18, no.10, p.1656-61 (Oct. 1982). [received: Sept. 1983]

The problem of ferroelectricity in liquid crystals is briefly analyzed. Electrostructural transitions in chiral smectics and electrooptical effects accompanying these transitions are studied. It was shown that the electrooptical effects can be used to modulate light over a wide range of frequencies. (14 refs.)

113733 Submillisecond grating diffractions in nematic liquid crystal films. I.C.Khoo, S.Shepard (Dept. of Phys. & Astron., Wayne State Univ., Detroit, MI, USA).

J. Appl. Phys. (USA), vol.54, no.9, p.5491-3 (Sept. 1983).

The authors have quantitatively observed a large fast component in the laser induced thermal grating in nematic liquid crystal films. This effect can be successfully utilized in submillisecond and high spatial frequency four wave mixing processes with low power lasers. (10 refs.)

113734 Liquid-crystalline copolyesters based on poly(p-oxybenzoate) and poly(p,p-biphenylene terephthalate). W.Volksen, J.R.Lyerla, Jr., J.Economy, B.Dawson (IBM Res., San Jose, CA, USA).

J. Polym. Sci. Polym. Chem. Ed. (USA), vol.21, no.8, p.2249-59 (Aug. 1983).

Two copolymers composed of p-hydroxybenzoate (PHB) and biphenylene terephthalate (BPT) with PHB/BPT ratios of 1/2 and 2/1 were characterized with respect to their tendency to exhibit liquid-crystalline behaviour in the melt phase. The BPT-rich copolyester, PHB/BPT=1/2, displayed a birefringent melt phase of very high viscosity and no tendency to crystallize on cooling. The resulting fused material exhibited what appeared to be a second-order transition at 170°C. The PHB-rich composition, PHB/BPT=2/1, also exhibited a highly birefringent melt phase of high viscosity which was quite shear sensitive. This polymer melt has little tendency to crystallize on cooling; however, on reheating no apparent second-order transition could be detected. The observed phase changes were characterized by differential scanning calorimetry, hot-stage microscopy, and wide-angle X-ray diffraction techniques. Additional data, pertaining to the compositional nature and apparent sequence distribution, were obtained by ^{13}C -NMR spectroscopy of the solid materials through magic-angle spinning, dipolar decoupling, and cross-polarization techniques. (15 refs.)

113735 Thermotropic homopolymers. III. Preparation and properties of polymers based on 4'-hydroxyphenyl-4-hydroxycinnamate. W.R.Krigbaum, T.Ishikawa, J.Watanabe, H.Toriumi, K.Kubota (Gross Chem. Lab., Duke Univ., Durham, NC, USA), J.Preston.

J. Polym. Sci. Polym. Phys. Ed. (USA), vol.21, no.9, p.1851-72 (Sept. 1983).

Low-molecular-weight 4'-acetoxyphenyl-4-acetoxycinnamate, as well as several polyesters synthesized from this monomer and aliphatic dibasic acids, exhibit thermotropic nematic phases. DSC heating curves for all the polymers exhibit multiple transitions. The amount of crystallinity of the polymers at room temperature is small and the degree of order along the chain axis in the crystalline phase is poor. For the lower homologues the nematic phase exists over a broad temperature range of approximately 100°C. The polyester from chiral (+)-3-methyl adipate forms a thermotropic cholesteric phase. Both the diacetoxy monomer and azelate polymers of low molecular weight adopt the homeotropic texture on glass slides, but with increasing molecular weight the planar texture becomes preferred. Investigation of the effects of electric fields in the conduction regime upon the nematic phase of the diacetoxy monomer revealed that Williams domains are formed only with difficulty. In most cases, a stationary pattern appeared instead. At higher voltage the dynamic mode (DSM) was obtained, and above this a field-induced transition to the isotropic phase. (19 refs.)

113736 Microscopy and deuterium NMR studies on induced cholesteric lyotropic mesophases of potassium laurate. M.R.Alcantara, M.V.M.C.De Melo, V.R.Paoli, J.A.Vanin (Inst. de Quimica, Univ. de Sao Paulo, Sao Paulo, Brazil).

Mol. Cryst. & Liq. Cryst. (GB), vol.95, no.3-4, p.299-307 (1983).

Induced cholesteric lyotropic mesophases can be formed by the addition of cholesterol to 'nematic' phases of potassium laurate/n-decanol/water and electrolyte. The resulting mesophases are oriented by magnetic fields, the helical axes being collinear with the field (type II) or perpendicular to it (type I). The associated patterns depended on the mesophase type and on the applied field direction. The usual chevron and focal-conic textures were seen in type II cholesteric mesophases. More complex disclinations were exhibited by type I cholesteric phases. The comparison between the relative order profiles for type I and type II mesophases, nematic and cholesteric, obtained by deuterium NMR, shows that great distortions are not present in the micelles of the cholesteric systems. The overall picture suggests that mainly electrostatic interactions are responsible for the cholesteric properties in induced mesophases. (35 refs.)

113737 Dependence of the tilt angle on external forces for smectic-C and chiral smectic-C liquid crystals—measurement of the heat capacity of DOBAMBC. T.Carlssohn (Inst. of Theoretical Phys., Chalmers Univ. of Technol., Goteborg, Sweden), I.Dahl.

Mol. Cryst. & Liq. Cryst. (GB), vol.95, no.3-4, p.373-400 (1983).

A measurement of the specific heat of DOBAMBC is presented, and it is shown that a Landau expansion of the free-energy density with a sixth-order term is adequate to describe the measurement. The coefficients in the Landau expansion are estimated from this measurement. The dependence of the tilt angle on applied electric and magnetic fields is discussed for both smectic-C and chiral (ferroelectric) smectic-C liquid crystals. Numerical estimates of the Landau coefficients are used to show that the effect of external forces on the tilt angle is negligible except when being less than approximately 0.2K from the transition to the smectic-A-phase. The effect on the smectic-C-smectic-A phase-transition temperature is also discussed. Boundary effects can also affect the tilt angle, and an expression for the penetration depth of a boundary-induced disturbance is calculated. For thin, planar samples, a coupling between the two boundaries can induce a transition to the smectic-A phase. It is demonstrated that this transition is analogous to the ordinary Freederickz transition in nematic liquid crystals. (20 refs.)

Strong four-wave mixing with phase conjugation in a nematic liquid crystal See Entry 113064

Marangoni convection in cholesteric liquid crystals of low thermal sensitivity See Entry 113439

Supermolecular structure of liquid crystalline polymer with mesogenic side groups and brominated main chain See Entry 113761

- Elastic constants of some nematic liquid crystals with banana-shaped molecules See Entry 114067
- Formation of a liquid crystal phase in the conversion of isotropic solutions of cellulose acetates into the solid state See Entry 114171
- Mesomorphic salts of pyrylium and thiopyrylium See Entry 114172
- Translational diffusion in CH_4 and CH_2Cl_2 dissolved in cholesteric liquid crystals See Entry 114229
- Self-diffusion coefficients of cholesteric/nematic systems with dynamic mass transport method See Entry 114230
- Orientation and molecular structure of 1,5 and 1,8 dichloroanthraquinones by PMR in a nematic solution See Entry 114742
- A ^{13}C NMR study of mesomorphic solutions of poly(*p*-phenylene terephthalamide) See Entry 114750
- A Sn-119 and Fe-57 Mossbauer effect study of the crystalline phase of 7S5 ... See Entry 114760
- Anisotropy of electric properties in binary cholesteric mixtures See Entry 114771
- Influence of solid support sorptive properties on the colour of cholesteric liquid crystals. II. Quantitative results See Entry 114805
- Pretranslational anomalies in the rotation of the plane of polarization of light in ferroelectric liquid crystals See Entry 114821
- Propagation of light in cholesteric liquid crystals with frequency dispersion See Entry 114822
- Experimental studies on reflection spectra in monodomain cholesteric liquid crystal cells: total reflection, subsidiary oscillation and its beat or swell structure See Entry 114876
- Syntheses and thermal properties of new liquid crystalline materials involving tropolone See Entry 115122

61.40 AMORPHOUS AND POLYMERIC MATERIALS

(see also 64.70P Glass transitions 81.20P to 81.20T, and 81.60 Materials science)

- 113738 Non-crystalline semiconductors.** H.Fritzsche (Dept. of Phys., Univ. of Chicago, Chicago, IL, USA). *Acta Polytech. Scand. Electr. Eng. Ser. (Finland)*, no.EL50, p.3-46 (1983). (Proceedings of Helsinki International Summer School on Semiconductors 1982, Espoo, Finland, 14-18 June 1982). Discusses some important concepts which clarify the fundamental difference between the two main classes of noncrystalline semiconductors, the glasses and the amorphous films. A glass is considered to be a material, which can be quenched from the supercooled melt and usually exhibits a glass transition. The term amorphous is restricted to noncrystalline materials which can normally be prepared only in the form of thin films by deposition on substrates which are kept sufficiently cool to prevent crystallization. A simple band model for non-crystalline semiconductors are described. Finally, the author deals with the understanding of electronic transport, the determination of the density of electronic states, and the relation of gap states with certain bonding or structural defects in the materials. (59 refs.)
- 113739 Electron-diffraction investigation of amorphous titanium dioxide films.** S.S.Olevskii, M.S.Sergeev, A.L.Tolstikhina, A.V.Koshchenko, B.S.Khavin, I.G.Tonoyan. *Inorg. Mater. (USA)*, vol.18, no.9, p.1313-16 (Sept. 1982). Translation of: *Izv. Akad. Nauk SSSR Neorg. Mater.*, vol.18, no.9, p.1534-7 (Sept. 1982). [received: Sept. 1983] A new algorithm for the machine calculation of the short-range atomic order, which provides for complete automation of the determination of the electron-density radial distribution function, has been described. The method has been used to study the structure of amorphous TiO_2 films obtained by pyrolysis. It has been found that the short-range order characteristic of crystalline modifications of TiO_2 is maintained in these films. (8 refs.)
- 113740 Surface undulations in explosive crystallization: a thermal instability.** W.van Saarloos, J.D.Weeks (Bell Labs., Murray Hill, NJ, USA). *Phys. Rev. Lett. (USA)*, vol.51, no.12, p.1046-9 (19 Sept. 1983). It is argued that surface undulations observed after self-sustained rapid crystallization of amorphous films result from a thermal instability that induces a periodically varying crystallization rate. Its physical origin is discussed for a simple nonlinear heat-conduction model which yields good agreement with experimental observations. A numerical analysis of the nonlinear oscillations shows that these may, in turn, bifurcate via a series of period-doubling bifurcations. (17 refs.)
- 113741 Study of crystallisation on non-crystalline V_2O_5 by electrical resistivity measurements.** J.C.Rifflet, A.M.Anthony (Centre de Recherches sur la Phys. des Hautes Températures, CNRS, Orleans, France). *Rev. Int. Hautes Temp. & Refract. (France)*, vol.20, no.1, p.37-44 (1983). In French. Electrical resistivity of non-crystalline vanadium pentoxide obtained by rapid quenching has been studied. The current-voltage characteristics show that the behavior of the conductivity cell is not ohmic and that the current is limited by space charge effects. Important instabilities in measurements appear in the vicinity of 190°C while water is eliminated before crystallisation. The activation energy of the process is high and the electrical conductivity varies according to the sample. Many factors seem to contribute to the mechanism of conducting, including microstructure, water content, surface conduction, and quenching rate. (20 refs.)
- 113742 Defects in amorphous silicon.** D.K.Biegelsen (Xerox Palo Alto Res. Centers, Palo Alto, CA, USA). Defects in Semiconductors II, Symposium Proceedings, Boston, MA, USA, Nov. 1982 (New York, USA: North-Holland 1983), p.75-86 It is argued that amorphous silicon can be treated as a relaxed continuous random network. The optical and electronic properties are controlled by localized gap states which arise from characteristic features of a disordered tetrahedrally-bonded covalent network. Experimental results are reviewed which indicate that the dominant (perhaps only) electrically-active defect in hydrogenated amorphous silicon is the topologically distinct, silicon dangling bond. Finally, the author suggests that the same, disorder-related characteristics might also typify the electronic properties of some macroscopic crystalline silicon defects. (36 refs.)
- Proceedings of Helsinki International Summer School on Semiconductors 1982 See Entry 111297
- Crystallization of amorphous silicon films by pulsed ion beam annealing See Entry 114054

- Computer simulation of high speed melting of amorphous silicon See Entry 114133
- Indirect and direct formation of polycrystalline silicon during CVD See Entry 114415
- Effect of TiCl_4 addition on the structure of chemically vapor-deposited Si_3N_4 .. See Entry 114422

61.40D Glasses

- 113743 On the crystallization of $\text{Fe}_{67}\text{Co}_{18}\text{Si}_{14}$ metallic glass.** F.L.Cumbrera, C.F.Conde, M.Millan, A.Conde, R.Marquez (Dept. de Optica, Facultad de Fisica, Univ. de Sevilla, Sevilla, Spain). *J. Mater. Sci. Lett. (GB)*, vol.2, no.9, p.499-502 (Sept. 1983). The authors present a short report about microstructural changes during crystallization of $\text{Fe}_{67}\text{Co}_{18}\text{Si}_{14}$ alloy from transmission electron microscopy studies. (14 refs.)
- 113744 Molecular dynamics studies on the structure of binary metallic glasses based on Lennard-Jones (12-6) potentials.** I. $\text{Ni}_{81}\text{B}_{19}$ and $\text{Cu}_{57}\text{Zr}_{43}$. O.Beyer, C.Hoheisel (Lehrstuhl für Theoretische Chem., Ruhr-Univ. Bochum, Bochum, Germany). *Z. Naturforsch. Teil A (Germany)*, vol.38A, no.8, p.859-65 (Aug. 1983). For the metallic glass $\text{Ni}_{81}\text{B}_{19}$ the partial pair-distribution functions are determined up to 14 \AA by a molecular dynamics simulation using effective Lennard-Jones potentials. The obtained pair-distribution functions are in good agreement with the measured ones. As the simulation was carried out at the thermodynamic conditions for a liquid, the authors conclude that the characteristic features of the structure of the metallic glass are essentially not different from those of the fluid system $\text{Ni}_{81}\text{B}_{19}$ at high temperature and pressure. both the high reduced density of the system and the large differences in the atomic radii of the two species dominantly determine the form of the partial structure factors of the glass. These findings have been confirmed by the molecular dynamics simulation of a further metallic glass, the $\text{Cu}_{57}\text{Zr}_{43}$ system. (33 refs.)
- 113745 Interaction of transition metals with metalloids and thermodynamic stability of amorphous alloys.** A.Ya.Belen'kii (Inst. of Metall. & Phys. of Metals, Moscow, USSR). *Fiz. Met. & Metalloved. (USSR)*, vol.56, no.2, p.290-7 (Aug. 1983). In Russian. English translation in: *Phys. Met. & Metallogr. (GB)* A new concept of the thermodynamic stability of amorphous alloys between transition metals and metalloids is proposed. It is based on the hypothesis that the amorphous structure minimizes the heat of solution of the metalloid impurity. The experimental data on solid solutions and interstitial phases, and also on chemisorption heats are analysed and presented in a systematic manner. The results account for the observed tendency for the formation of glasses by alloys of transition metals characterized by almost filled d bands with metalloids of sufficiently large atomic size. (22 refs.) A.T.
- 113746 Microscopic inhomogeneities in silicate glass.** N.P.Novikov, L.Ya.Denisova, N.N.Novikova (S. Ordzhonikidze Moscow Geological Prospecting Inst., Moscow, USSR). *Inorg. Mater. (USA)*, vol.18, no.9, p.1368-9 (Sept. 1982). Translation of: *Izv. Akad. Nauk SSSR Neorg. Mater.*, vol.18, no.9, p.1592-4 (Sept. 1982). [received: Sept. 1983] The authors propose a new method for revealing silicon dioxide crystal inclusions. This method for observing silicon dioxide crystals is based on their local heating under the influence of high intensity monochromatic radiation. The most common crystallization form for silicon dioxide is cristobalite, therefore the work was directed at detection of cristobalite crystals in samples of K-8 glass. (5 refs.)
- 113747 Effect of CaO and MgO on crystallization in lead borosilicate glasses.** S.Sachdev, R.C.Buchanan (Dept. of Ceramic Engng., Univ. of Illinois, Urbana, IL, USA). *J. Electrochem. Soc. (USA)*, vol.130, no.9, p.1884-8 (Sept. 1983). The effects of crystallization of CaO and MgO additions to high lead borosilicate glasses were investigated. Both oxides were found to promote crystallization when added in amounts $> 10 \text{ mol.}\%$ (m/o), with CaO being the more effective additive. Crystal phases $4\text{PbO} \cdot 3\text{CaO} \cdot \text{SiO}_2$ and $8\text{PbO} \cdot \text{MgO} \cdot 6\text{SiO}_2$ were identified in the crystallized CaO and MgO containing glasses, respectively. Morphology of the crystals was hexagonal. (11 refs.)
- 113748 Transition metal ions in glasses: network modifiers or quasi-molecular complexes?.** C.Nelson (Sandia Nat. Labs., Albuquerque, NM, USA), T.Furukawa, W.B.White. *Mater. Res. Bull. (USA)*, vol.18, no.8, p.959-66 (Aug. 1983). Transition metal ions dissolve in silicate, phosphate, and borate glasses as molecular units, quasi-molecular complexes, and occupants of large, framework structure-controlled sites depending on size and ionic charge. Raman spectra and optical absorption spectra support this hypothesis and offer a new interpretation for the assignment of certain transition metal ions to tetrahedral sites in the glass structure. (19 refs.)
- 113749 The local environment around hydrogen atoms in hydrogenated NiTi_2 alloy glass.** K.Kai (Res. Inst. for Iron, Steel & Other Metals, Tohoku Univ., Sendai, Japan), S.Ikeda, T.Fukunaga, N.Watanabe, K.Suzuki. *Physica B & C (Netherlands)*, vol.120B+C, no.1-3, p.342-6 (May 1983). (Yamada Conference VI on Neutron Scattering in Condensed Matter, Hakone, Japan, 1-4 Sept. 1982). The local environments around H and D atoms absorbed into NiTi_2 alloy glass have been studied by neutron inelastic and total scattering using the KENS spallation neutron source. The local hydrogen atom vibration spectrum of NiTi_2 glass shows much broader peaks, the positions of which are nearly identical with those of the corresponding crystal. Higher harmonics of the local hydrogen atom vibration are clearly observed up to the fourth order for $\text{NiTi}_2\text{H}_{1.5}$ glass. The frequency shifts relative to the harmonic value indicate an anharmonic potential of hydrogen atoms in the glass hydride. The RDFs for $\text{Ni}_{0.33}\text{Ti}_{0.67}\text{D}_x$ ($x=0, 0.08, 0.26$ and 0.60) have a negative peak at 1.95 \AA originating mostly from D-Ti pairs in the glass hydrides. The greater fraction of D atoms occupies the tetrahedral site mainly consisting of Ti atoms even in the glass hydrides. From the D-D correlations in the RDF and a low energy shoulder in the hydrogen atom vibration spectrum, a small part of the hydrogen atoms is found to be trapped in the octahedral site surrounded by six metal atoms. (11 refs.)
- 113750 On the change in coordination of Ge atoms in $\text{Na}_2\text{O-GeO}_2$ glasses.** M.Ueno, M.Misawa, K.Suzuki (Res. Inst. for Iron, Steel & Other Metals, Tohoku Univ., Sendai, Japan). *Physica B & C (Netherlands)*, vol.120B+C, no.1-3, p.347-51 (May 1983). (Yamada Conference VI on Neutron Scattering in Condensed Matter, Hakone, Japan, 1-4 Sept. 1982). High resolution observations of the short-range structure in $\text{Na}_2\text{O-GeO}_2$ glasses were carried out by TOF pulsed neutron total scattering using an

electron LINAC neutron source. With increasing Na_2O content, the average coordination number of O atoms around a Ge atom increases from 4.0 and reaches a maximum of about 4.5 at the composition of 20 mol% Na_2O , beyond which the coordination number decreases to approach 4.0 at the composition of 40 mol% Na_2O . The nearest neighbouring Ge-O correlation in a GeO_6 -octahedron structural unit is evidently separated from that in a GeO_4 -tetrahedron structural unit in the first peak profile of the radial distribution function in the cases of GeO_2 -8, 16 and 21 mol% Na_2O glasses. When one molecule of Na_2O is added to the glasses, one GeO_4 -tetrahedron structural unit is modified into one GeO_6 -octahedron structural unit without forming non-bridging O atoms up to the composition of 20 mol% Na_2O . (19 refs.)

113751 Chemical short-range structure of $\text{Ni}_x\text{Ti}_{1-x}$ ($x=0.26-0.40$) alloy glasses. T.Fukunaga, N.Hayashi, K.Kai, N.Watanabe, K.Suzuki (Res. Inst. for Iron, Steel & Other Metals, Tohoku Univ., Sendai, Japan). *Physica B & C (Netherlands)*, vol.120B+C, no.1-3, p.352-6 (May 1983). (Yamada Conference VI on Neutron Scattering in Condensed Matter, Hakone, Japan, 1-4 Sept. 1982).

The Bhatia-Thornton (1970) neutron total structure factors of Ni-Ti alloy glasses containing 74, 67 and 60 at% Ti were measured by a pulsed neutron scattering technique using a spallation neutron source. All the Ni-Ti alloy glasses were prepared by rapid quenching from the molten state and their average coherent neutron scattering lengths were artificially adjusted to zero by ^{60}Ni -isotope substitution. Therefore, experimental Bhatia-Thornton neutron total structure factors of the alloy glasses provide exclusively the concentration-concentration structure factor $S_{CC}(Q)$. The reduced concentration correlation function $G_{CC}(r)$ obtained as the Fourier transform of $S_{CC}(Q)$ shows a sharp and negative minimum at about $r \sim 2.54$ Å. This implies that there are predominantly Ni-Ti unlike atom neighbours at the nearest distance in Ni-Ti alloy glasses. The generalised Warren chemical short-range order parameters calculated from the $G_{CC}(r)$ have negative values in all the Ni-Ti alloy glasses. Based on these experimental observations, the authors conclude that the chemical short-range structure of Ni-Ti alloy glasses over the composition range from 60 to 74 at% Ti is quite close to that found in the crystalline NiTi_2 compound. (11 refs.)

113752 The very-small angle neutron scattering from SiO_2 -PbO glasses. T.Takahashi (Faculty of Engng., Univ. of Tokyo, Tokyo, Japan), H.Tominitsu, Y.Ushigami, S.Kikuta, K.Doi, S.Hoshino. *Physica B & C (Netherlands)*, vol.120B+C, no.1-3, p.362-6 (May 1983). (Yamada Conference VI on Neutron Scattering in Condensed Matter, Hakone, Japan, 1-4 Sept. 1982).

The very-small angle scattering (VSAS) of neutrons, an angular range of a few seconds, has been measured by means of a double-crystal diffractometer of Bonse-Hart type. With a plate of silica glass, no evidence for the VSAS was observed. After it was irradiated with thermal neutrons at a fluence of $3 \times 10^{19}/\text{cm}^2$ at 48°C , a VSAS central peak with a FWHM of 2.2 s was observed. A radius of gyration of 3×10^5 Å was obtained when the effects of multiple scatterings were corrected for. The lead glass $(1-x)\text{SiO}_2 \cdot x\text{PbO}$ was examined by the neutron VSAS. For $x < 60\%$ no VSAS were observed, while at $x = 65\%$ a VSAS central peak with a FWHM of 0.24 s appeared, for which a radius of gyration of 10^5 Å was derived. An argument is advanced to verify that the observed VSASs are really produced by the scattering and not by the refraction of neutrons. (9 refs.)

113753 Polarised neutron scattering from the amorphous ferromagnet, $\text{Fe}_{83}\text{B}_{17}$. R.A.Cowley, D.McK.Paul (Dept. of Phys., Univ. of Edinburgh, Edinburgh, Scotland), W.G.Stirling, N.Cowlam. *Physica B & C (Netherlands)*, vol.120B+C, no.1-3, p.373-5 (May 1983). (Yamada Conference VI on Neutron Scattering in Condensed Matter, Hakone, Japan, 1-4 Sept. 1982).

A polarised neutron triple axis crystal spectrometer at the Institut Laue Langevin has been used to measure the inelastic nuclear and magnetic scattering from the amorphous ferromagnet, $\text{Fe}_{83}\text{B}_{17}$. The theory of the experiment in which a polarised beam is scattered by the sample and analysed by an unpolarised analyser is developed. The difference in the scattering when the polarisation of the incident beam is reversed is not simply related to the magnetic susceptibility. The experimental results for wavevector transfers close to the peak of the magnetic structure factor show magnetic scattering which is very similar to that which would be expected from a Heisenberg-like powdered ferromagnet, although the specimen is truly amorphous. (6 refs.)

113754 Molecular dynamics simulation of the structure of soda silica. S.K.Mitra, R.W.Hockney (Dept. of Computer Sci., Univ. of Reading, Reading, England). *Philos. Mag. B (GB)*, vol.48, no.2, p.151-67 (Aug. 1983).

In this work five soda silica glasses containing 5, 10, 15, 20 and 33 mole per cent of soda are simulated by using the molecular dynamics method. The calculated structures of these systems are compared with recent neutron diffraction and EXAFS results. As in pure silica glass, a network of silicon-oxygen tetrahedra exists in these systems. The sodium ions are connected to this network through non-bridging oxygen 'bonds'. The ratio of bridging to non-bridging oxygen ions depends on the composition of the system. In low soda containing systems, microclusters rich in soda are formed. From the hole analysis in these systems, it appears that the sodium ions tend to occupy holes in the silica network. (20 refs.)

113755 Vitrification kinetics of ternary silica-alumina-lime glass powders. A.Lerich, P.Pilate, M.R.Anseau, C.Lebud, F.Cambier (Centre de Recherches de l'Industrie Belge de la Ceramique, Mons, Belgium). *Rev. Int. Hautes Temp. & Refract. (France)*, vol.20, no.1, p.25-36 (1983). In French.

Vitrification kinetics of glass powders was first studied by Frenkel (see J. Tech. Phys., vol.9, p.385, 1945) who proposed an idealised model describing the beginning of the phenomenon. Since his work a lot of empirical or phenomenological equations or geometrical models based relations have been proposed in order to describe the vitrification kinetic. The authors have investigated the applicability of these different equations on the sintering of ternary silica-alumina-lime glass powders. (14 refs.)

113756 Influence of preparation techniques on the structure of amorphous metallic alloy $(\text{Mo}_{0.6}\text{Ru}_{0.4})_{25}\text{B}_{18}$. M.Mehra, W.L.Johnson (W.M. Keck Lab. for Engng. Materials, California Inst. of Technol., Pasadena, CA, USA), A.P.Thakoor, S.K.Khanna. *Solid State Commun. (USA)*, vol.47, no.11, p.859-62 (Sept. 1983).

The authors report X-ray diffraction studies and density measurements on liquid quenched foils and sputter deposited films of the amorphous metallic alloy $(\text{Mo}_{0.6}\text{Ru}_{0.4})_{25}\text{B}_{18}$. The crystallization temperature (T_c) for both the films and the foils is $\sim 800 \pm 10^\circ\text{C}$. The density of the as-sputtered films is $\sim 4\%$ less than that of the foils. The annealing of these films at $\sim T_c/2$ increases the density to within $\sim 1.7\%$ of the value for the foils. The X-ray diffraction patterns for both the foils and films are similar and show the amorphous nature of the samples. The reduced radial distribution functions suggest that as-sputtered films have noticeably larger second and third nearest

neighbor distances, probably due to excess residual stresses and voids in them. (11 refs.)

113757 Variation of the glass-forming regions in the B_2O_3 - Li_2O system with cooling rate. R.Ota, N.Soga (Dept. of Industrial Chem., Kyoto Univ., Kyoto, Japan).

Yogyo-Kyokai-Shi (Japan), vol.91, no.6, p.265-71 (1983). In Japanese. By cooling a number of B_2O_3 - Li_2O melts containing 96~20 mol% B_2O_3 from the liquidus to room temperature, glass-forming regions have been determined under various cooling rates; $Q_1 = 1.2 \times 10^{-3}$, $Q_2 = 9.1 \times 10^{-3}$, $Q_3 = 7.9 \times 10^{-2}$, $Q_4 \approx 3 \times 10^{-1}$, $Q_5 \approx 2$, $Q_6 \approx 7$, $Q_7 \approx 50$, $Q_8 \approx 2 \times 10^3$ and $Q_9 \approx 10^5$ K/s. The glass-forming region, which is restricted in a narrow range of high content of $\text{B}_2\text{O}_3 \geq 86$ mol% at Q_1 , extends continuously with increasing rate of cooling, and glass can be obtained in a range of $\text{B}_2\text{O}_3 \geq 25$ mol% at the cooling rate of Q_9 . An examination of the liquid viscosities in and out of the glass-forming regions in the system revealed that (1) increasing rate of cooling Q decreases the critical liquidus viscosity η_L^* of the melt and accordingly (2) the critical cooling rate Q^* for glass formation is dependent on the liquidus viscosity η_L of the melt. In order to understand the slope of the $\log Q^* - \log \eta_L$ or $\log Q - \log \eta_L^*$ diagram in the system, the composition dependence of the fusion entropy ΔS_f was computed from the equation proposed for glass formation. It was found that η_L and $1/Q^*$ change monotonously with composition while E_a/T_L or ΔS_f goes through a maximum or a minimum. (17 refs.)

Low temperature irradiation of FeB amorphous alloys See Entry 114035

Pattern formation in metallic glasses induced by helium ion implantation See Entry 114053

Radiation damage in glassy $\text{Pd}_{80}\text{Si}_{20}$ and $\text{Cu}_{50}\text{Zr}_{50}$ See Entry 114058

Inelastic scattering of polarised neutrons by amorphous $\text{Fe}_{47}\text{Co}_{70.3}\text{Si}_{15}\text{B}_{10}$ See Entry 114114

Glass formation region and electrical conductivity in the system B_2O_3 - Li_2O - Li_3PO_4 See Entry 114173

Plasmastructural transformations in amorphous chalcogenide semiconductors See Entry 114423

Metallic glass—a new material for electrical engineering and electronics See Entry 114703

Influence of structural relaxation on the magnetic permeability aftereffect of amorphous ferromagnetic alloys See Entry 114712

NMR in quadrupole glasses and the spectral density of orientation fluctuations See Entry 114752

Local boron environment in $\text{Ni}_{100-x}\text{B}_x$ metallic glasses: A NMR study See Entry 114754

Mossbauer investigation on SiO_2 - Fe_2O_3 glasses obtained from gel See Entry 114759

Polar glass ceramics—a new family of electroceramic materials: tailoring the piezoelectric and pyroelectric properties See Entry 114789

Al-induced enhancement colouration by gamma irradiation in some borate glasses See Entry 114884

Internal friction study on structural relaxation of a glassy metal $\text{Fe}_{32}\text{Ni}_{36}\text{Cr}_{14}\text{P}_{12}\text{B}_6$ See Entry 115241

61.40K Polymers, elastomers, and plastics

113758 Self-diffusion of macromolecules in the crystallization of a polymer from solution. A.I.Maklakov, N.K.Dvoyashkin. *Vysokomol. Soedin. Ser. B (USSR)*, vol.25, no.6, p.397-400 (1983). In Russian.

The selfdiffusion of polyethyleneglycol molecules in crystallization from concentrated solution in deuterated benzene, acetone, and chemically pure CCl_4 is studied by a pulsed magnetic field NMR method, using a dimensionless parameter D^* for determining the degree of change in the rate of translational motion of the macromolecules, where D^* is related to the coefficients of selfdiffusion of polyethyleneglycol initially and at a time t_k of phase transformation, and on the assumption that the crystals of polyethyleneglycol formed in solution do not significantly affect the selfdiffusion process. It is noted that the process of selfdiffusion of polyethyleneglycol macromolecules in crystallization of the polymer from solution can be disturbed by the appearance of a concentration gradient close to the surfaces of the crystalline structures formed. However, because of the high viscosity of the solution, the high concentration of nuclei, and the marked localization of the gradient this disturbance is small, so that conventional selfdiffusion laws can be applied. (5 refs.) N.S.

113759 Structural changes in a cross-linked and plasticized amorphous polymer. O.V.Startsev, I.I.Perepechko, L.T.Startseva, G.P.Mashinskaya. *Vysokomol. Soedin. Ser. B (USSR)*, vol.25, no.6, p.457-61 (1983). In Russian.

Previous work on epoxide polymers is discussed in detail and curves are reproduced showing $\log T_c$ is versus plasticizer concentration w , the density of the epoxide polymer as a function of plasticizer concentration, and $\tan \delta$ for the epoxide polymer as a function of temperature, where T_c is the glass transition temperature and δ is the mechanical loss angle. On graphical resolution of the whole of the wide unsymmetrical peak for the mechanical losses into three Gaussian curves it is found that each of these peaks can be assigned to a corresponding level of supermolecular organization of the plasticized polymer. (3 refs.) N.S.

113760 X-ray diffraction study of the drawn poly(aryletherketone) (PEEK). D.R.Rueda, F.Ania, A.Richardson, I.M.Ward (Dept. of Phys., Univ. of Leeds, Leeds, England), F.J.Balta Calleja. *Polym. Commun. (GB)*, vol.24, no.9, p.258-60 (Sept. 1983).

Oriented PEEK rods obtained by die drawing have been analysed by wide-angle X-ray diffraction. Fibre patterns reveal that orientation mainly improves with draw ratio. An orthorhombic unit cell with $a = 7.75 \pm 0.01$, $b = 5.89 \pm 0.01$ and c (fibre axis) $= 9.883 \pm 0.005$ Å has been found. The unit cell parameters for isotropic and oriented PEEK are similar, remaining constant through the investigated die drawing conditions. The fibre periodicity differs from that reported previously for PEEK. The similarity between the structure of PEEK and that reported for poly(p -phenylene oxide) is confirmed. (9 refs.)

113761 Supermolecular structure of liquid crystalline polymer with mesogenic side groups and brominated main chain. V.V.Tsukruk, V.V.Shilov, Yu.S.Lipatov (Inst. of Macromolecular Chem., Acad. of Sci., Kiev, Ukrainian SSR).

Polym. Commun. (GB), vol.24, no.9, p.260-2 (Sept. 1983). Structural studies on the supermolecular organization in a polymer with mesogenic side groups and a brominated main chain have been conducted. A smectic structure is shown to be realized in this polymer. Planar smectic

layers are aggregated into layered packs 20 to 25 nm in size. The number of closely packed layers in such a pack is 4 or 6. (10 refs.)

113762 Effect of moisture on physical properties of nylon. B.L.Deopura, A.K.Sengupta, A.Verma (Fibre Sci. Lab., Indian Inst. of Technol., New Delhi, India).

Polym. Commun. (GB), vol.24, no.9, p.287-8 (Sept. 1983).

The physical properties (glass transition temperature and mechanical behaviour) of nylon are highly sensitive to moisture content in the polymer. Several independent studies by a number of authors have shown that variation in properties with increasing moisture regain is non-linear. Most of the observations can be explained on the basis of the differences in mobility and free volume of the nylon structure due to the different methods of bonding of water molecules within the polyamide chains, at different regains. (12 refs.)

113763 Small-angle X-ray scattering studies of microdomain structure in segmented polyurethane elastomers. J.T.Koberstein (Polymer Materials Program, Dept. of Chem. Engng., Princeton Univ., Princeton, NJ, USA), R.S.Stein.

J. Polym. Sci. Polym. Phys. Ed. (USA), vol.21, no.8, p.1439-72 (Aug. 1983).

The small-angle X-ray scattering (SAXS) technique has been used to characterize the detailed microphase structure of two crosslinked segmented polyurethane elastomers. Both copolymers contain trifunctional polypropylene ether triols in the rubbery elastomeric block, but are synthesized with different hard segments: a symmetric 4,4'-diphenylmethane diisocyanate (MDI) chain extended with butanediol (BD); and an 80/20 mixture of asymmetric 2,4-toluene diisocyanate (TDI) and symmetric 2,6-toluene diisocyanate (TDI) chain extended with ethylene glycol (EG). Calculations of SAXS invariants and determinations of deviations from Porod's law are used to examine the degree of phase segregation of the hard- and soft-segment domains. Results show that the overall degree of phase separation is poorer in the asymmetric TDI/EG-based copolymer than in the symmetric MDI/BD-based copolymer. Determination of diffuse phase boundary thicknesses, however, reveals that the domain boundaries are sharper in the asymmetric TDI/EG system. The contrasting morphologies found in the two systems are interpreted in terms of differences in hard-soft segment compatibility, diisocyanate symmetry, and diisocyanate length. Coupled with conformational considerations, this information is used to construct a new model for polyurethane hard-segment microdomain structure. (47 refs.)

113764 Spectroscopic characterization of solvent-induced crystallization of PET. S.-B.Lin, J.L.Koenig (Dept. of Macromolecular Sci., Case Western Reserve Univ., Cleveland, OH, USA).

J. Polym. Sci. Polym. Phys. Ed. (USA), vol.21, no.8, p.1539-58 (Aug. 1983).

Using recently developed quantitative FTIR methods, the gauche and trans conformer compositions have been measured for polyethylene terephthalate (PET) samples exposed to benzene and acetone. The kinetics of the primary and secondary isomerization stages of the solvent-induced crystallization process have been studied and compared with the thermally crystallized system. The Arrhenius activation energies of isomerization in the primary stage in which Fickian diffusion behavior is followed for the benzene- and acetone-induced PET systems are 8.2 ± 0.4 and 7.7 ± 0.4 kcal/mol., respectively. (31 refs.)

113765 Polymer single crystals of poly(4-hydroxybenzoate). I. Morphology. G.Leiser, G.Schwarz, H.R.Kricheldorf (Inst. für Makromolekulare Chem. der Univ., Freiburg, Freiburg, Germany).

J. Polym. Sci. Polym. Phys. Ed. (USA), vol.21, no.9, p.1599-609 (Sept. 1983).

Poly(4-hydroxybenzoate) was prepared from 4-acetoxybenzoic acid, 4-pivaloxybenzoic acid, and 4-trimethylsiloxy benzoyl chloride by condensation without the addition of a catalyst. Although various reaction conditions were used the products were always crystalline. The morphology of the as-polymerized crystals has been studied by transmission electron microscopy as a function of molecular weight and end-group type. It was possible to detect morphological features during the course of reaction from oligomers to polymer which enable us to determine the mechanisms that are likely to control chain growth for different regimes of polymerization kinetics. (11 refs.)

113766 Polymer single crystals of poly(4-hydroxybenzoate). II. A contribution to crystal structure and polymorphism. G.Lieser (Inst. für Makromolekulare Chem., Univ. Freiburg, Freiburg, Germany).

J. Polym. Sci. Polym. Phys. Ed. (USA), vol.21, no.9, p.1611-33 (Sept. 1983).

For pt.I see *ibid.*, vol.21, no.9, p.1599-609 (1983). Electron diffraction has been used to investigate the structure of a wide range of as-polymerized crystals of poly(4-hydroxybenzoate) [systematic name: poly(1,4-oxycarbonyl)]. The chemical composition and the degree of polymerization (DP) have been varied and some samples have been thermally treated. At room temperature two crystalline modifications with orthorhombic unit cells coexist. The chains adopt a 2_1 helical conformation in both forms, but there are differences for oligomer and polymer crystals. Oligomers of low DP have an extended chain-conformation, whereas in polymers a shortening of the repeat distance along the chain is observed as a function of both the DP and the crystallization conditions. From the most extensive data sets the lattice parameters $a=7.52$, $b=5.70$, and $c=12.49$ Å were derived for polymer crystals of phase I, and the subcell parameters for oligomer crystals of phase II $a=3.77$, $b=11.06$, and $c=12.89$ Å. Both phases contain two chains per unit cell. In addition to modifications I and II several defect structures exist the unit cells of which contain more than two chains. At temperatures which depend on the degree of polymerization, a phase transition to a third modification takes place. (12 refs.)

113767 Small-angle X-ray scattering study of density fluctuation in pressure-densified polystyrene glasses. J.J.Curro, R.J.Roe (Dept. of Materials Sci. & Metallurgical Engng., Univ. of Cincinnati, Cincinnati, OH, USA).

J. Polym. Sci. Polym. Phys. Ed. (USA), vol.21, no.9, p.1785-96 (Sept. 1983).

Densified polystyrene glasses, prepared by cooling from the liquid state under elevated pressure, were studied by small-angle X-ray scattering at ambient pressure. The density fluctuation, determined from the X-ray data, showed a decrease with increasing pressure up to about 1.5 kbar, and then leveled off to a fairly constant value. The reduction in the density fluctuation produced by the pressure is much greater than the associated decrease in the specific volume. The observed change in density fluctuation is consistent with the view that the density fluctuation in glassy polymers consists of dynamic and quasistatic components and that the first of these can be correlated with the compressibility of the glass. The present data on the density fluctuation, in conjunction with the available data on volume and enthalpy, can be interpreted to mean that in pressure-densified glasses unfavorable chain configurations are trapped in local energy minima, and the strain energy thus stored can promote segmental motion leading to volume expansion at temperatures far below T_g . (25 refs.)

113768 Characterization of lattice disorder in the low-temperature phase of irradiated PTFE by vibrational spectroscopy. J.F.Rabolt (IBM Res. Lab., San Jose, CA, USA).

J. Polym. Sci. Polym. Phys. Ed. (USA), vol.21, no.9, p.1797-805 (Sept. 1983).

In an effort to elucidate the structure of the low-temperature phase of PTFE, a spectroscopic study of the effect of progressive irradiation on the low-frequency infrared spectrum was undertaken. Previous infrared and Raman measurements indicated that irradiation of PTFE decreases its crystalline content, resulting in a lowering of the 19°C phase transition temperature due to the introduction of disorder and defect structures into the lattice by chain scission. Far-infrared studies of virgin and irradiated PTFE at liquid nitrogen temperatures show that the medium to strong bands at 45, 54, 58 and 71 cm^{-1} , attributed to lattice vibrations, decrease in intensity as the crystalline content decreases. These findings support the assignment of these bands to intermolecular vibrations of the crystalline lattice and are an indication of the presence of more than one molecule in the crystallographic unit cell. (24 refs.)

113769 Chain orientation in polystyrene/poly(2,6-dimethyl-1,4-phenylene oxide) blends. L.H.Wang, R.S.Porter (Polymer Sci. & Engng. Dept., Univ. of Massachusetts, Amherst, MA, USA).

J. Polym. Sci. Polym. Phys. Ed. (USA), vol.21, no.9, p.1815-23 (Sept. 1983).

The differential orientation of polymer chains has been measured in polystyrene (PS)/poly(2,6-dimethyl-1,4-phenylene oxide) (PPO) compatible blends. Density measurements are reported as a function of primary blend compositions at 23°C. Drawing was performed by solid-state coextrusion. PS/PPO blend compositions of 90/10 and 75/25 were drawn within sandwiches of polyethylene at 145°C and isotactic polypropylene at 155°C, i.e. at ca. 25°C above the glass transition temperatures of the two blends. The change in Fourier-transform infrared dichroisms on drawing these blends was measured at 906 and 1190 cm^{-1} , corresponding to predominantly PS and PPO, respectively. The orientation of PS and PPO was observed as a function of draw ratio λ in the range 1-5; orientations increased with λ for both PS and PPO in both blends but to different degrees. Both polymers decreased in orientation with increasing PPO content. Annealing with fixed ends showed that the PPO chains disorient more slowly than those of PS. All binary systems were found to be amorphous and compatible. (22 refs.)

113770 Polyvinylidene fluoride (PVDF). K.-I.Nakamura, Y.Teramoto, N.Murayama.

Solid State Phys. (Japan), vol.18, no.6, p.344-51 (June 1983). In Japanese.

PVDF is a semicrystalline polymer which may exist in four crystalline forms α , β , γ and polar α -form. Polarized films of PVDF exhibit large piezo and pyro-electricity. (27 refs.)

113771 A critical assessment of the application of FT-IR spectroscopy to the study of crystalline/compatible polymer blends. M.M.Coleman, D.F.Varnell, J.P.Runt (Dept. of Materials Sci. & Engng., Pennsylvania State Univ., Univ. Park, PA, USA).

Polymer Alloys III Blends, Blocks, Grafts and Interpenetrating Networks. Proceedings of a Symposium, New York, USA, 23-28 Aug. 1981 (New York, USA: Plenum 1983), p.59-70.

The application of Fourier transform infrared spectroscopy to the study of polymer blends is discussed. Its use in determining compatibility of blends and their degree of crystallinity is critically examined. The technique is used to determine the state of order of both components in a crystalline/compatible polymer blend. (15 refs.)

113772 Phase domain size and continuity in sequential IPNs: a review. L.H.Sperling, J.M.Widmaier, J.K.Yeo, J.Michel (Materials Res. Center, Lehigh Univ., Bethlehem, PA, USA).

Polymer Alloys III Blends, Blocks, Grafts and Interpenetrating Networks. Proceedings of a Symposium, New York, USA, 23-28 Aug. 1981 (New York, USA: Plenum 1983), p.191-218.

Two theories of phase domain size in sequential interpenetrating polymer networks were developed and compared, using results based on poly(n-butylacrylate)/polystyrene. While the earlier theory of Donatelli (1967) yielded good results as far as it went, the newer theory of Yeo is much more comprehensive. Both theories assume the existence of isolated spheres, a major drawback. Scanning electron microscopy and density measurements on decrosslinked and extracted materials indicate that midrange compositions have dual phase continuity. However, assuming equivalent spheres for the domains, both transmission and scanning electron microscopy yield good comparisons with theory. (25 refs.)

Polymer Alloys III Blends, Blocks, Grafts and Interpenetrating Networks. Proceedings of a Symposium See Entry 113111

Network structure description and analysis of amine-cured epoxy matrices See Entry 112890

Competitive equilibria in miscible polymer blends and low molecular weight analogues: a Fourier transform infrared study See Entry 113724

Fourier transform infrared studies of poly(vinyl chloride) blends with ethylene co- and terpolymers See Entry 113725

Fluorescence study of polymer chain interpenetration and of the rate of phase separation in incompatible polymer blends See Entry 113726

Retardation of spherulitic growth rate in the crystallization of isotactic polystyrene due to the presence of nucleant See Entry 114139

The effect of micro-structure on the diffusion of n-hexadecane and DDT in poly(1,4-butadienes) See Entry 114264

Diffusion and solution of methanol vapor in poly(2-vinylpyridine)-block-polyisoprene and poly(2-vinyl-pyridine)-block-polystyrene See Entry 114268

Electrically conductive thermoplastic elastomer/polyacetylene blends See Entry 114513

^{13}C high resolution solid state NMR studies on cellulose samples of different physical structure See Entry 114743

How electric strength of polyethylene and polystyrene is influenced by residual phenomena caused by ionising radiation and pressure See Entry 114781

Polymer deformation studies by time resolved Fourier transform infrared spectroscopy See Entry 114862

Vibrational spectroscopic characterization of rigid rod polymers. IV. Crystalline modifications of poly(p-phenylene terephthalamide) See Entry 114863

In-plane orientation of polyimide See Entry 114944

Melt compounding of PVC with ethylene copolymer resins See Entry 115159

An analysis of local flow effects in flow-induced orientation and crystallization See Entry 115184

Microphase segregation in segmented amine-cured polyurethanes See Entry 115203

Polymer-performance on the dimensional stability and the mechanical properties of wood-polymer composites prepared by an electron beam accelerator See Entry 115248

Study of molecular deformation mechanisms in the glassy state. I. Temperature effect on stress-birefringence and strain-birefringence responses of poly(methyl methacrylate) See Entry 115261

Rheo-optical studies on the deformation mechanism of semicrystalline polymers. XIV. Alpha and beta mechanical dispersions of spherulitic high-density polyethylene and the dynamic orientation distribution function of crystallites See Entry 115262

On the correlation of mechanical properties of high impact polystyrene with its morphology, molecular-weight characteristics and extrusion conditions See Entry 115289

Correlation of morphology, mechanical properties and processing conditions of modified high impact polystyrene See Entry 115290

The relationship between the physical structure and the microscopic deformation and failure processes of poly(*p*-phenylene terephthalamide) fibers See Entry 115318

Characterization of high performance composite matrices See Entry 115361

Phase separation of phosphonated polystyrenes in the solid state. IV. Influence of this phenomenon on their flame retardancy properties [ESCA observations] See Entry 115602

61.50 CRYSTALLINE STATE

(inc. molecular motions in solids; for magnetic structure and spin systems, see 75.25)

113773 A new method of site occupancy analysis in substitutional mixed crystals by means of X-ray crystal structure analysis. I. Pseudo lattice and superposition structure of a substitutional mixed crystal. A.Zedler (Zentralinst. fur Phys. Chem., Akad. der Wissenschaften, Berlin, Germany). *Cryst. Res. & Technol. (Germany)*, vol.18, no.8, p.985-95 (1983).

In pt.I the nature of disorder in mixed crystal structures will be discussed on the basis of a pseudo lattice concept. A mixed crystal pseudo lattice applicable to all atomic positions of these mixed crystal structures will be defined, and the concept of a statistically global-disordered ideal structure will be introduced. The structure factor for mixed crystal structures will be derived in consideration of the statistic disorder of position and sort of the atoms. The interpretation of the mixed crystal structure as a superposition structure requires the replacement of Vegard's rule by a new one having a wider range of validity. (14 refs.)

113774 Hindered rotational energy levels of a tetrahedron in a tetragonal crystalline field. D.Smith (Dept. of Chem., Pennsylvania State Univ., Hazleton, PA, USA). *J. Chem. Phys. (USA)*, vol.79, no.6, p.2989-94 (15 Sept. 1983).

The hindered rotational energy levels of a tetrahedron in a tetragonal crystalline field have been computed. The symmetry group of the Hamiltonian is $T \times D_2$, where T is the tetrahedral group of rotations about body-fixed axes and D_2 represents the tetragonal group of rotations about space-fixed axes. The parameters in the potential function are determined for the tetragonal phases of NH_4Br and NH_4I assuming an electrostatic model. (13 refs.)

Infrared and Raman study of the fast internal motions of non-rigid molecules in condensed state: method of selective deuteration See Entry 112735

Structure refinements of some thermally disordered dolomites See Entry 113803

Inelastic neutron scattering study of the structural glass transition in a $\text{K}(\text{Br}, \text{CN})$ mixed crystal See Entry 114174

Negative thermal expansion due to the hindered rotation of the ammonium ion or the methyl group in solids with low barriers to rotation and the anisotropic thermal expansion in solids having polyatomic groups See Entry 114212

Low-energy excitations in $(\text{KBr})_{1-x}(\text{KCN})_x$ in the orientational glass state See Entry 114294

A general NMR spectral density and its experimental verification See Entry 114749

Ammonium ion rotation in ammonium perchlorate as studied by infrared spectroscopy See Entry 114849

Spontaneous site reorientation in a mixed molecular crystal: tetracene in benzoic acid See Entry 114903

61.50C Physics of crystal growth

(for techniques of crystal growth and film deposition, see 81.10 and 81.15; for epitaxy, thin films, see 68.55; for whiskers, see 68.70)

113775 Crystallization of quartz from fluoride solutions. G.M.Safronov, V.V.Popov, A.F.Kuznetsov, A.A.Lepkov (N.S. Kurnakov Inst. of General & Inorganic Chem., Acad. of Sci., USSR). *Inorg. Mater. (USA)*, vol.18, no.9, p.1310-12 (Sept. 1982). Translation of: *Izv. Akad. Nauk SSSR Neorg. Mater.*, vol.18, no.9, p.1531-3 (Sept. 1982). [received: Sept. 1983]

The possibility of growing quartz crystals from aqueous solutions of ammonium fluoride has been demonstrated. It has been found that the dependence of the rate of growth of the crystals on the crystallographic orientation of the seed during the growth of quartz from fluoride solutions is the same as in the case of alkaline solutions. The use of fluoride solutions makes it possible to grow quartz crystals at rates more than twice as great as those for crystals grown from alkaline solutions without worsening of their quality. In the quartz crystals grown from fluoride solutions there is practically no sodium impurity, and the content of aluminum and several other impurities is reduced considerably. (6 refs.)

113776 Production and properties of crystals of complex refractory oxides with perovskite structure. B.T.Melek, A.A.Andreev, N.F.Kartenko, A.B.Pevtsov, V.A.Trepakov, Yu.N.Filin (A.F. Ioffe Physicotech. Inst., Acad. of Sci., USSR). *Inorg. Mater. (USA)*, vol.18, no.10, p.1388-92 (Oct. 1982). Translation of: *Izv. Akad. Nauk SSSR Neorg. Mater.*, vol.18, no.10, p.1620-4 (Oct. 1982). [received: Sept. 1983]

The authors have studied the characteristic features of direct high-frequency melting and growth of crystals of a number of complex refractory oxides with perovskite structure, and carried out X-ray diffraction studies of the materials obtained. They have studied the spectroscopic properties of crystals of BaZrO_3 , BaHfO_3 , $\text{Pr}_2\text{Ti}_2\text{O}_7$. (17 refs.)

113777 Correlation between growth hillocks and dislocations on the {110} faces of flux grown yttrium aluminium garnet. K.J.Roberts (Inst. fur Kristallographie, RWTH, Aachen, Aachen, Germany), D.Elwell. *J. Cryst. Growth (Netherlands)*, vol.62, no.3, p.449-57 (Aug. 1983).

A direct correlation between the growth hillocks observed on the {110} habit faces of flux grown yttrium aluminium garnet and dislocations in the crystal bulk is demonstrated. The dislocations were analyzed by X-ray topography using diffraction contrast experiments and by utilizing theoretical deductions of the preferred dislocation line directions. The dislocations were found to be of mixed character with a substantial screw component along the growth normal. Possible crystal growth mechanisms are discussed. (30 refs.)

113778 Growth of $\text{Cd}_2\text{Hg}_{1-x}\text{Te}$: comparison of some properties with the predictions of two melt growth models. P.Capper, C.L.Jones, E.J.Pearce, M.J.T.Quelch (Mullard Ltd., Millbrook Industrial Estate, Southampton, England). *J. Cryst. Growth (Netherlands)*, vol.62, no.3, p.487-97 (Aug. 1983).

The theoretical predictions of the two normal freeze growth models involving no convective mixing and complete mixing are described. Crystals have been grown using a range of growth speeds and initial compositions in two temperature profiles designed to affect these conditions in the $\text{Cd}_2\text{Hg}_{1-x}\text{Te}$ (CMT) system. The axial and radial compositional uniformity found in these crystals is compared with the predictions of the two models. The relative effects on radial compositional uniformity of isotherm shape, radial segregation, density-driven convective flow and convection imposed by the temperature profiles are also discussed. It is found that radial variations in composition decrease as the growth rate decreases and that these variations must be taken into account when interpreting axial composition profiles. It is considered that density-driven convective flow is the most significant force in determining radial variations in composition. Convective flow induced by the temperature profile is also seen to influence these variations while isotherm effects and radial segregation are thought to be much less significant. (13 refs.)

113779 Some formulae describing spherical and hemispherical diffusion to small crystals in unstirred solutions. S.Fletcher (CSIRO Inst. of Energy & Earth Resources, Div. of Mineral Chem., Port Melbourne, Victoria, Australia). *J. Cryst. Growth (Netherlands)*, vol.62, no.3, p.505-12 (Aug. 1983).

Formulae for the growth rates of spherical and hemispherical crystals are derived taking into account interfacial kinetics and bulk diffusion. Also included are the effects of preceding chemical reactions, time-varying nucleation rates, and reactant depletion. The results are written in two ways depending on whether the driving force for crystallization is an overpotential (electrochemical kinetics) or a supersaturation (solution kinetics). (15 refs.)

113780 Finite analysis of the control of interface shape in Bridgman crystal growth. L.-Y.Chin (Phillips Petroleum Co., Bartlesville, OK, USA), F.M.Carson. *J. Cryst. Growth (Netherlands)*, vol.62, no.3, p.561-7 (Aug. 1983).

Numerical experiments were performed on a vertical Bridgman crystal growth system. The thermal field was studied in the absence of fluid motion by solving the steady state energy equation using a finite element method. Key parameters were isolated and their influence on the interface curvature was assessed. These included insulation zone thickness, system temperatures, Biot numbers, solid-liquid thermal conductivity ratio, and ampoule location in the furnace. It was concluded that interface curvature could be controlled by the crystal grower to achieve any desired shape. (3 refs.)

113781 The influence of glycine, according to pH, upon the growth habit of NaCl and KI, in aqueous solution. A.Julg, B.Deprick (Lab. de Chimie Théorique, Univ. de Provence, Marseille, France). *J. Cryst. Growth (Netherlands)*, vol.62, no.3, p.587-94 (Aug. 1983).

The authors have studied the effect of glycine molecules upon the growth habit of NaCl and KI structures, in aqueous solution. The electronic adsorption energy is evaluated by means of an 'ab-initio' SCF method and the dispersion energy, arising from the fact that the structure ions are not point charges, by means of a semiempirical Lennard-Jones pair potential. Solvation of the substrate and of the glycine molecules, as well as the association between glycine molecules are taken into account. The total energy balance is positive (8.9 kcal/mole) only for the adsorption of zwitterion chains close to a {110}₂ double step of NaCl. This result allows one to explain the modifications of the growth habit of NaCl $\{100\} \rightarrow \{110\}$. (21 refs.)

113782 In situ observations of the growth behaviour of the {010} face of potassium hydrogen phthalate. L.A.M.J.Jetten, B.Van Der Hoek, W.J.P.Van Enckevort (RIM Lab. of Solid State Chem., Univ. of Nijmegen, Nijmegen, Netherlands). *J. Cryst. Growth (Netherlands)*, vol.62, no.3, p.603-11 (Aug. 1983).

The surface morphologies of the {010} face of potassium hydrogen phthalate crystals, growing in an aqueous solution, have been studied in situ by means of optical reflection microscopy. The observations have been recorded by means of a video system. Several phenomena have been investigated by this method, namely: spiral growth via high (10-250 nm) and low steps (2.8-10 nm), step acceleration near reentrant corners in step patterns, inclusion formation via step overhangs, the formation of etch pits and the reactivation of the centre of a blocked spiral. (6 refs.)

113783 Comments on the role of the cubic structure in ice nucleation. C.A.Knight (Nat. Center for Atmospheric Res., Boulder, CO, USA). *J. Cryst. Growth (Netherlands)*, vol.62, no.3, p.633-4 (Aug. 1983).

Takahashi's calculation (ibid., vol.59, p.441, 1982) that hexagonal ice may nucleate as cubic ice applies for homogeneous nucleation. The special bicrystal orientations that he discusses have only been observed from heterogeneous nucleation, and may be explainable in another way. (7 refs.)

113784 An effect of roughened layer clustering on crystal growth rates. D.Nason (Capricornia Inst., Rockhampton, Australia). *J. Cryst. Growth (Netherlands)*, vol.62, no.3, p.645-7 (Aug. 1983).

The growth rates of solid/liquid interfaces as predicted by Monte Carlo and by analytical methods are modified to account for co-operative effects in the roughened layers by the requirement of a minimum cluster size. The results predict a decrease in growth rate in all cases, but the reduction is only significant for higher melting entropy materials. (10 refs.)

113785 Simulation studies of the hydrodynamics in high-temperature solutions for crystal growth. V. Shape of the crystal/liquid interface in the presence of simultaneous free and forced convections. V.Nikolov, K.Iliev, P.Peshev (Inst. of General & Inorganic Chem., Bulgarian Acad. of Sci., Sofia, Bulgaria). *Mater. Res. Bull. (USA)*, vol.18, no.8, p.1037-44 (Aug. 1983).

The formation conditions of a concave, convex or flat crystal/liquid interface in the presence of simultaneous free forced convections have been investigated using model liquids. Simultaneous free and forced convections with both the same and opposite flow directions have been considered. The interface shape was found to depend on the direction and rate of the resultant convection flow under the crystal. The formation conditions of a flat interface for liquids

having kinematic viscosities of 0.001×10^{-3} – 0.5×10^{-3} m²/s and for crystal diameters of 10, 15 and 20 mm, respectively, have been established. These conditions have been compared with the optimum conditions found experimentally by other authors for the growth of several kinds of crystals from high-temperature solutions by the TSSG method and from melts by the Czochralski method. The comparison has shown that the model proposed describes well the real processes. (12 refs.)

113786 Formation of crystal structures in microgravitational conditions. N.B.Brandt, A.G.Belov, L.I.Devyatkov, G.S.Zhdanov, V.V.Zubenko, V.G.Karavaev, V.V.Moshchalkov, N.R.Nurtdinov, G.N.Ronami, I.V.Telegina, M.V.Chukichev, T.D.Sherbatova, A.B.Yunovich (Dept. of Solid State Phys., Moscow Univ., Moscow, USSR).

Moscow Univ. Phys. Bull. (USA), vol.38, no.1, p.1-6 (1983). Translation of: *Vestn. Mosk. Univ. Ser. 3 (USSR)*, vol.38, no.1, p.3-8 (1983).

The structure and some physical properties of a series of solid structures, eutectic compositions, and epitaxial layers are investigated. The study is performed on samples grown under conditions of microgravitation, in comparison with samples obtained under terrestrial conditions. Methods of optical and electron-raster spectroscopy, X-ray structural, and X-ray spectral analysis, photoluminescence, and cathode luminescence are used; quantum oscillational and optical effects are investigated. Certain peculiarities in the formation of the crystal and electronic structure of the material are observed. (5 refs.)

113787 Kinetics of normal growth of an ordering crystal. E.A.Brener, D.E.Temkin (Inst. of Solid State Phys., Acad. of Sci., USSR). *Sov. Phys.-Crystallogr. (USA)*, vol.28, no.1, p.7-11 (Jan.-Feb. 1983). Translation of: *Kristallografiya (USSR)*, vol.28, no.1, p.18-26 (Jan.-Feb. 1983). [received: Sept. 1983]

In the framework of the phenomenological theory equations are derived for the growth kinetics of an ordering crystal. The authors investigate the case in which crystallization occurs without change of composition and ordering is a second-order transition. By solving the resulting equations they are able to determine how the growth rate depends on the temperature at the crystallization front and to find the distribution of the long-range order parameter relative to the moving interface. In all the cases the theory predicts the existence of a critical transition point from growth of an ordered crystal to growth of a disordered one. The authors investigate the behavior of the growth rate as a function of temperature in the neighborhood of the transition point. For various cases they give an estimate of the critical rate corresponding to the transition point. (9 refs.)

113788 Kinetic transition during growth of a crystal undergoing ordering. E.A.Brener, D.E.Temkin (Inst. of Solid State Phys., Acad. of Sci., USSR). *Sov. Phys.-Crystallogr. (USA)*, vol.28, no.2, p.142-6 (March-April 1983). Translation of: *Kristallografiya (USSR)*, vol.28, no.2, p.244-51 (March-April 1983). [received: Sept. 1983]

The authors consider normal growth of a crystal undergoing ordering, and take account of relaxation of the order parameter in the crystal. A previously formulated phenomenological equation is qualitatively investigated for the case in which ordering is a first-order phase transition. If, during fall of temperature, the velocity of the ordering front v_f becomes less than the rate of growth of the disordered crystal v_0 , then as the supercooling increases, at the crystallization front there may be a kinetic phase transition from growth of an ordered crystal to growth of a disordered one. This transition can be continuous or discontinuous. In the former case, the graphs of the order parameter and growth rate vs. the supercooling have breaks at the transition point, and the transition point is determined by the equation $v_f = v_0$. In the second case, which is analogous to a thermodynamic first-order transition, the order parameter and the growth rate have discontinuities at the transition point. During growth in nonisothermal conditions, a situation can arise in which the ordering front, located at a certain distance from the crystallization front, moves at the same rate as the latter. The fronts interact via the thermal field. The authors investigate the stability of stationary solutions and formulate a general criterion determining the limit of stability for growth in either isothermal or nonisothermal conditions. (8 refs.)

113789 Experiments on crystallization of semiconductors aboard Salyut 6-Soyuz orbital complex. V.S.Zemskov, M.R.Raukhan, I.N.Belokurova (Baikov Inst. of Metall., Acad. of Sci., Moscow, USSR). Proceedings of the 4th European Symposium on Materials Sciences under Microgravity (ESA SP-191), Madrid, Spain, 5-8 April 1983 (Paris, France: ESA 1983), p.325-9

Experimental data on space crystallization of Ge-Si solid solution from the gaseous phase by chemical transport reaction method have shown the pure diffusive mechanism of mass transport in microgravity environment. It has been found that on-seed growth of Te doped InSb single crystals in space could occur without contact between the melt and the ampoule walls, which provided high structural perfection of the neck region. The dominating mechanism of mass transfer in the melt was diffusion, with Marangoni convection induced in the neck region. The crystallization features of InSb-InBi alloys are indicative of a specific segregation behavior of the alloy constituents depending on microacceleration. (12 refs.)

113790 In situ observations of crystal growth processes. L.A.M.J.Jetten, W.J.P.van Enckevort (RIM Lab. of Solid State Chem., Faculty of Sci., Univ. of Nijmegen, Nijmegen, Netherlands). Proceedings of the 4th European Conference on Chemical Vapour Deposition, Eindhoven, Netherlands, 31 May-2 June 1983 (Eindhoven, Netherlands: Philips Centre Manuf. Technol. 1983), p.97-102

The authors present a study of fundamental crystal growth processes for crystallization from solution and from the vapour phase. Generally in such studies the crystal growth process has been investigated by measuring growth kinetics or by a posteriori characterization of the crystal surface or the internal defect structure. Interpretation however is often hindered, because of limitations of these experimental methods. By in situ observation both growth kinetics and surface morphology can be studied simultaneously. Video recording permits high resolution and analog contrast amplification. With a diode array camera the image can be digitized and by subtracting two subsequent pictures even more information can be derived for a dynamic process. (4 refs.)

Electron diffraction studies of supersonic jets. V. Low temperature crystalline forms of SF₆, SeF₆, and TeF₆ See Entry 113824

Growth structure and optical properties of single crystals of rubrene See Entry 113841

Twin growth of sucrose crystals See Entry 113928

Doping of indium phosphide with germanium See Entry 113938

Evaluation of kinetic parameters from non-isothermal experiments: Application to crystallization kinetics See Entry 114146

The characteristics of salt fingers in a variety of fluid systems, including stellar interiors, liquid metals, oceans, and magmas See Entry 114232

Interfacial stability of migrating brine inclusions in alkali halide single crystals supporting a temperature gradient See Entry 114280

Surface structure change of a crystal in solution See Entry 114307

Effect of additives and dopants on the growth of KDP crystals See Entry 115035

Effects of ultrasonic waves on crystal growth See Entry 115036

Growth of KH₂PO₄ crystals at constant temperature and supersaturation See Entry 115037

Crystal growth of NbC by flux method See Entry 115038

Flow-induced crystallization by surface growth of polyethylene fibers See Entry 115041

Spreading resistance of InSb crystals pulled under ultrasonic vibrations See Entry 115042

Preparation of Li₃N single crystal by floating zone technique See Entry 115046

Magnetic field effects on float-zone Si crystal growth See Entry 115047

An analysis of local flow effects in flow-induced orientation and crystallization See Entry 115184

61.50E Crystal symmetry; models and space groups, and crystalline systems and classes

113791 Determinantal representations for the crystallographic point groups. K.J.Duff, E.H.Salib (Dept. of Phys., Univ. of Wollongong, Wollongong, New South Wales, Australia).

Aust. J. Phys. (Australia), vol.36, no.4, p.485-9 (1983).

A table of the values of the determinants of the representation matrices for the crystallographic point groups is given to facilitate the application of some recent theorems concerning determinantal wavefunctions. (3 refs.)

113792 Determination of phases from linear relations between structure amplitudes. E.A.Soldatov, E.A.Kuz'min, V.V.Ilyukhin, N.V.Belov (Physicochem. Inst. & N.I. Lobachevski State Univ., Gorki, USSR).

Sov. Phys.-Dokl. (USA), vol.27, no.12, p.993-4 (Dec. 1982). Translation of: *Dokl. Akad. Nauk SSSR*, vol.267, no.4-6, p.853-5 (Dec. 1982). [received: Sept. 1983]

In an earlier paper (see *ibid.*, vol.27, p.908, 1982) the authors presented a method of determining the phases of structure amplitudes on the basis of the linear relation between structure amplitudes. The system of linear equations for the phase parts of the structure amplitudes (exp *iφ*) corresponds to the case when one of the atoms of the structure is at the origin (image of the structure at an atom). It must be assumed that it would be advantageous to have the coordinates of the heavy atom. With the standard crystallographical method of choosing the origin (on the basis of the symmetry group of the crystal) this condition cannot always be satisfied (except in the case of the symmetry group P1). In the general case, this makes it difficult to take the symmetry into account. It is thus worth endeavoring to find relations of the above type such that their phase part would be invariant with respect to the choice of origin. (5 refs.)

113793 A theorem on rotations in the space of quaternions. V.I.Burdina (A.V. Shubnikov Inst. of Crystallography, Acad. of Sci., Moscow, USSR).

Sov. Phys.-Dokl. (USA), vol.27, no.12, p.994-6 (Dec. 1982). Translation of: *Dokl. Akad. Nauk SSSR*, vol.267, no.4-6, p.1122-4 (Dec. 1982). [received: Sept. 1983]

In the study of the proper subdivisions of a three-dimensional sphere of rotations in the process of reducing the individual subunits—rotation stereohedra—to a central gnomonic projection use is made of the smallest-angle rotation in four-dimensional Euclidean space R⁴ that takes the center of the stereohedron (generally speaking, any point of the sphere S³) into a pole P. In computer calculations these rotations may be required in order to effect the rotation of a polyhedron located in the three-dimensional tangential subspace so as to obtain the most appropriate image on the plotting board of a graph plotter connected to the computer. (4 refs.)

Crystal chemistry, phase transitions, and physical properties of halide crystals with perovskite-like structure See Entry 113822

Crystal structure of the semihydrate of the sodium salt of 5-sulfo-8-methylthioquinoline See Entry 113838

61.50J Crystal morphology and orientation

Surface structure change of a crystal in solution See Entry 114307

Orientation of (100) InGaAsP/InP wafers by HCl chemical etching See Entry 115381

On the formation of planar-etched facets in GaInAsP/InP double heterostructures See Entry 115387

61.50K Crystallographic aspects of polymorphic and order-disorder transformations

113794 Phase transitions in Na₃Sc₂(PO₄)₃ and in related compounds with [M₂(EO₄)₃]³⁻ frameworks. V.B.Kalinin, B.I.Lazoryak, S.Yu.Stefanovich (L.Ya. Karpov Sci.-Res. Physicochem. Inst., USSR).

Sov. Phys.-Crystallogr. (USA), vol.28, no.2, p.154-8 (March-April 1983). Translation of: *Kristallografiya (USSR)*, vol.28, no.2, p.264-70 (March-April 1983). [received: Sept. 1983]

The authors discuss the mechanism of the phase transitions in the ferroelectric ionic conductor Na₃Sc₂(PO₄)₃. They elucidate the crystal-chemical causes of the polymorphism of this compound and of Na₃M₂(PO₄)₃ (M=Cr,Fe) and Na₃Zr₂Si₂PO₁₂. They analyze the composition-structure-property relationships for Me_nM₂(EO₄)₃, where E is a Group IV, V, or VI element, M is a divalent, trivalent, or quadrivalent cation, Me is a small cation compensator and n=0-4. (23 refs.)

Room-temperature structure of carbon monoxide at 2.7 and 3.6 GPa See Entry 113809

Ammonium trifluoroberyllate(II), (NH₄)₂[BeF₃], at room temperature See Entry 113815

Structure of orthopyroxene-type and clinopyroxene-type magnesium germanium oxide MgGeO₃ See Entry 113816

Structural modifications of silicon nitride as a function of temperature See Entry 113826

Kinetics of the order-disorder reaction under irradiation See Entry 113992

Pressure-induced phase transition of HgS See Entry 114157

61.50L Crystal binding

113795 X-ray spectroscopic investigation of the nature of chemical binding in metal-like titanium carboaluminides of variable composition. I.A.Brytov, V.S.Neshpor, Yu.N.Romashchenko, E.A.Obolenskii, V.I.Ivchenko (Sci.-Production Combine "Burevestnik", Leningrad, USSR). *Fiz. Met. & Metalloved. (USSR)*, vol.56, no.2, p.253-60 (Aug. 1983). In Russian. English translation in: *Phys. Met. & Metallogr. (GB)*

The X-ray spectroscopy method was used to study the nature of chemical binding in metal-like carboaluminides Ti_2AlC_x and Ti_3AlC_x ($0.2 \leq x \leq 1.2$). Information was obtained on the relative contribution of the valence electrons of the atoms of the components to the valence bands of these carboaluminides. The special features of the electron structure of these compounds compared with the binary carbides $TiC_{0.96}$ and Al_4C_3 were identified and the nature of the interaction of the atoms of the components with one another was determined. (23 refs.) *A.T.*

113796 Calculation of the unit-cell parameter for solid solutions with the spinel structure. V.M.Talanov (Novocherkassk Polytech. Inst., USSR). *Inorg. Mater. (USA)*, vol.18, no.9, p.1316-21 (Sept. 1982). Translation of: *Izv. Akad. Nauk SSSR Neorg. Mater.*, vol.18, no.9, p.1538-43 (Sept. 1982). [received: Sept. 1983]

A new method is proposed for calculating the unit-cell parameter of solid solutions with the spinel structure; results of the method agree well with available experimental data. (12 refs.)

113797 Rare earth atom-to-solid core level shifts: sensitivity to valence changes. J.F.Herbst (Phys. Dept., General Motors Res. Labs., Warren, MI, USA).

J. Less-Common Met. (Switzerland), vol.93, no.1, p.227-34 (1983). (Proceedings of the Sixteenth Rare Earth Research Conference, Tallahassee, FL, USA, 18-21 April 1983).

Free-atom-to-metal shifts of several lanthanide core electron binding energies were calculated. The shifts were obtained directly from relativistic Hartree-Fock calculations of the individual atomic and solid state binding energies. Results for the 2p, 3d, 4f, 5s and 5p levels are reported. A marked dependence on the core state quantum numbers is apparent in the shifts derived for the elements praseodymium to samarium and terbium to thulium which undergo a valence change on formation of the metal. A single shift characterizing all core levels of a given element cannot be assumed therefore when a configuration change involving the 4f states occurs on solid formation. (8 refs.)

113798 Photoabsorption study of bonding in some 3d-4f intermetallics and other compounds. K.B.Garg, H.S.Chauhan, S.G.Saxena, S.Chandra (Dept. of Phys., Univ. of Rajasthan, Jaipur, India).

J. Less-Common Met. (Switzerland), vol.93, no.1, p.242 (1983). (Proceedings of the Sixteenth Rare Earth Research Conference, Tallahassee, FL, USA, 18-21 April 1983).

Summary form only given. 3d-4f intermetallics of the type R_2T_3 (where R is a 4f metal and T is a 3d metal) are industrially important magnetic materials. The bonding in these compounds is expected to involve a decrease in the size of the R atoms and an increase in the size of the T atoms. The authors studied this question by making measurements on the X-ray absorption near the edge structure, particularly on the energy position of the edge and the so-called white lines, for both types of constituent atoms in these compounds. The energy shifts observed for the L_{III} edges of the R constituent and for the K edge of the T constituent appear to lend support to the idea of change in the relative sizes of the two types of atoms. No changes have been observed in the intensities of the white lines at the L_{II} and the L_{III} edges and in the areas under them. These are interpreted in terms of non-participation of d states in bonding. Similar photoabsorption measurements were carried out on a number of organic complexes of some rare earth metals. The measurements were made using a 400 mm bent crystal spectrograph. The intermetallic compounds were prepared by arc melting the constituents in an argon atmosphere followed by annealing and characterization using X-ray diffraction. (no refs.)

113799 Calculation of lattice sums for polarization energy of an NaCl-type crystal. B.M.Bulakh (Inst. of Semiconductors, Acad. of Sci., Ukrainian SSR).

Sov. Phys.-Crystallogr. (USA), vol.28, no.1, p.1-5 (Jan.-Feb. 1983). Translation of: *Kristallografiya (USSR)*, vol.28, no.1, p.5-13 (Jan.-Feb. 1983). [received: Sept. 1983]

Representation of lattice sums by finite algebraic functions permits their direct summation over an infinite lattice. This method is used to calculate the lattice sums of the component of the band energy due to polarization of crystal by a charged particle at any lattice point in the crystal or above its surface. (7 refs.)

Molecular and crystal structure of 2,2',4,4'-tetraaminodiphenyl at -120°C See Entry 112868

New structure determination of murchicht, Cu_6PbO_8 See Entry 113808

Synthesis and structure of a nonstoichiometric caesium niobate, $Cs_3Nb_{5.96}O_{16.4}$ See Entry 113810

Ammonium trifluoroberyllate(II), $(NH_4)[BeF_3]$, at room temperature See Entry 113815

Structural modifications of silicon nitride as a function of temperature See Entry 113826

Crystal structure of $GaSc_2O_4$; its relation with perovskite See Entry 113828

Crystal and molecular structure and IR spectra of 1-hydroxy-4-dibromomethyl-2,2,5,5-tetramethyl- and 4-dibromomethyl-1,2,2,5,5-pentamethyl-3-imidazoline-3-oxide See Entry 113837

An X-ray diffraction structural study of nonbonded interactions in heteroorganic compounds. XXII. Crystal structure of triphenyltin 2dimethylaminothiophenolate See Entry 113840

Crystal and molecular structure of the 1:1 complex of 7,7,8,8-tetracyanoquinodimethane and 9,9'-trans-bis-telluraxanthylene ($C_{12}H_4N_4(C_6H_4)_2Te_2$) See Entry 113851

Crystal and molecular structure of tetracyclic nitroxyl biradical with three bridging bonds between the piperidine and dehydropiperidineoxy fragments, $C_{27}H_{36}N_2O_4$ See Entry 113853

Structure of electrically conducting complexes based on cation radicals. X. Cation-radical salts of tetrathiotetracene and tetrasetenotetracene with hexabromodimercurate dianion, $(TTT)_3^{2+}(Hg_2Br_6)^{2-}$ and $(TSeT)_3^{2+}(Hg_2Br_6)^{2-}$ See Entry 113854

Study of vacancy-solute interactions in dilute Al based alloys by thermal equilibrium measurements of positron annihilation See Entry 113969

Interaction and charge transfer between vacancy and solute in dilute aluminium alloys See Entry 113970

Mossbauer study on Fe-vacancy interaction in aluminum See Entry 113971

Formation of vacancies in thermal equilibrium in α -range alloys See Entry 113972

Mossbauer analysis on the annealing process of a quenched Al-Sn dilute alloy See Entry 113973

Electronic interaction between impurity and grain boundary in iron See Entry 113978

Lattice dynamics of solid I_2 under high pressure See Entry 114102

Electronic structure of zintl compounds (NaTi) and alkali pnictides See Entry 114439

Electronic structures of sulfide minerals—theory and experiment See Entry 114444

Study of the ferroelectric phase transition in rubidium hydrogen selenate by high-resolution NMR of ^{77}Se See Entry 114793

61.55 SPECIFIC STRUCTURE OF ELEMENTS AND ALLOYS

61.55D Nonmetallic elements

113800 Structure of N_2 at 2.94 GPa and 300K. D.Schiferl, D.T.Cromer, R.R.Ryan, A.C.Larson, R.LeSar, R.L.Mills (Los Alamos Nat. Lab., Univ. of California, Los Alamos, NM, USA).

Acta Crystallogr. Sect. C (Denmark), vol.C39, pt.9, p.1151-3 (15 Sept. 1983). A single crystal of β - N_2 was grown in a Merrill-Bassett diamond-anvil cell and examined by X-ray diffraction at 2.94 (6) GPa and 300 (2) K. As observed in an earlier high-pressure study, the structure is hexagonal, space group $P6_3/mmc$, with two molecules per unit cell. The lattice constants are $a=3.595$ (1) and $c=5.845$ (1) Å, giving a molar volume of 19.71 (1) cm^3 . The value of R_w , refined from 9 observed reflections, is 0.041, for a model with statistically disordered molecules tilted 54° from the c axis, and 0.040 for a spherically disordered model. Calculations using a Gordon-Kim electron-gas model show that the $P6_3/mmc$ structure has a minimum energy when the N_2 molecules are tilted at an angle of 51° . (20 refs.)

Graphite produced by extrusion of pitch mesophase See Entry 115116

61.55H Alloys

113801 High temperature X-ray study of some iron-nickel alloys. A.Sen Gupta, B.K.Banerjee (Phys. Res. Wing, Projects & Dev. India Ltd., Sindi, India).

Indian J. Phys. Part A, vol.57A, no.3, p.196-9 (May 1983). High temperature X-ray diffraction studies were carried out on Fe-Ni samples at a temperature from 400 to 700°C to know more about the nature of lattice parameter changes. (10 refs.)

113802 Structure formation in lightly-doped chromium alloys during plastic deformation in the 1400-1450K region. V.I.Trefilov, N.A.Storchak, V.N.Minakov, V.A.Manilov, L.S.Igolkina, Yu.E.Zubets (Inst. of Problems in Materials Sci., Acad. of Sci., Kiev, Ukrainian SSR).

Sov. Phys.-Dokl. (USA), vol.27, no.12, p.1060-2 (Dec. 1982). Translation of: *Dokl. Akad. Nauk SSSR*, vol.267, no.4-6, p.1117-21 (Dec. 1982). [received: Sept. 1983]

Despite the large number of studies that have been done on the structure of deformed single-crystal and polycrystalline materials with the BCC lattice, there is still no agreement on the features of the structure formation at high degrees of deformation in polycrystalline alloys, and no universally acknowledged model for a highly deformed polycrystalline material has yet been proposed. The goal of the present study was to investigate the structural changes in lightly doped polycrystalline alloys of chromium ($\text{Cr}+0.5\text{La}+0.5\text{V}+0.5\text{Ta}$) following plastic deformation produced by rolling at temperatures of 1400-1450K with various degrees of plastic deformation (reductions) per pass. The total quantity of introduced impurities ($\text{C}+\text{N}+\text{O}$) was not more than 0.015% by mass. (7 refs.)

Recovery of radiation-induced defects in dilute Al-Ge alloys after fast neutron irradiation at 5K See Entry 114047

Superconducting equiatomic ternary transition metal arsenides See Entry 114635

61.60 SPECIFIC STRUCTURE OF INORGANIC COMPOUNDS

113803 Structure refinements of some thermally disordered dolomites. R.J.Reeder (Dept. of Earth & Space Sci., State Univ. of New York, Stony Brook, NY, USA), H.R.Wenk.

Am. Mineral. (USA), vol.68, no.7-8, p.769-76 (July-Aug. 1983). Single crystal X-ray structure refinements of one ideally ordered and two partially disordered dolomites provide structural data about the thermally induced, cation disordering process. Most refined parameters show progressive and gradual changes as disorder increases. It was found that completely disordered crystals could not be recovered using piston-cylinder methods owing to reordering during the quench. This factor limited the range over which disorder in quenched specimens could be studied, although some parameters are extrapolated to complete disorder. New experiments confirm that disorder is complete by 1150°C. Electron density maps based on intensity data from specimens which exceeded the critical disordering temperature suggest CO_3 group disorder of a rotational kind. (23 refs.)

113804 Surinamite, $\text{Ca}_2\text{Mg}_2\text{Al}_2\text{Si}_2\text{BeO}_{16}$; its crystal structure and relation to sapphirine, $\text{Ca}_2\text{Mg}_2\text{Al}_2\text{Si}_2\text{O}_{16}$. P.B.Moore, T.Araki (Dept. of the Geophys. Sci., Univ. of Chicago, Chicago, IL, USA).

Am. Mineral. (USA), vol.68, no.7-8, p.804-10 (July-Aug. 1983). Surinamite is monoclinic, space group $P2_1/n$, with $a=9.916$ (1), $b=11.384$ (1), $c=9.631$ (1) Å, $\beta=109.30$ (1)°. The asymmetric unit contains $\text{Ca}_2\text{Mg}_2\text{Al}_2\text{Si}_2\text{BeO}_{16}$ comprised of nine octahedral cations and five tetrahedral cations incorporated in a cubic close-packed array of sixteen independent oxygen atoms. $R=0.047$ for 2998 independent reflections. The structure consists of octahedral walls running parallel to x which are connected along y by an open branched chain $[\text{TeO}_5]$ where one of the tetrahedra, $\text{T}(1)$, is principally occupied by Be^{2+} . This tetrahedron is unique in the asymmetric unit in that three of its vertices are shared by other tetrahedra. (12 refs.)

113805 A refinement of the crystal structure of ohmilitite, $\text{Sr}_3(\text{Ti,Fe}^{3+})(\text{O,OH})(\text{Si}_2\text{O}_6)_2 \cdot 2\text{-}3\text{H}_2\text{O}$. T.Mizota (Dept. of Mining & Mineral Engng., Yamaguchi Univ., Ube, Yamaguchi, Japan), M.Komatsu, K.Chihara. *Am. Mineral.* (USA), vol.68, no.7-8, p.811-17 (July-Aug. 1983).

The monoclinic unit cell of ohmilitite, $\text{Sr}_3(\text{Ti,Fe}^{3+})(\text{O,OH})(\text{Si}_2\text{O}_6)_2 \cdot 2\text{-}3\text{H}_2\text{O}$, has dimensions $a=10.979(6)$, $b=7.799(5)$, $c=7.818(4)$ Å, $\beta=100.90(3)^\circ$, and space group $P2_1/m$; $Z=2$, $V=657.4(6)$ Å³. The crystal structure has been refined to an R-value of 5.9% for 2121 independent reflections. Vertex-sharing Ti-O octahedra form chains parallel to b . Each of the octahedral chains is flanked by a pair of $[\text{Si}_2\text{O}_6]^{2-}$ chains, which are similar to those found in batistite and haradaite, thus forming a composite chain of composition $[\text{Si}_4\text{O}_{12}(\text{Ti}_2\text{O}_7)\text{Si}_4\text{O}_{12}]^{12-}$. These composite chains are joined together by Sr atoms and water molecules to form the structure. Of the three independent Sr atoms, $\text{Sr}(1)$ and $\text{Sr}(3)$ are 9-coordinated, with average Sr-O distances of 2.675 Å. $\text{Sr}(2)$ is 8-coordinated, with average bond length of 2.586 Å. The average Ti(Fe)-O bond length is 1.992 Å. Average Si-O distances are 1.643 and 1.606 Å for bridging and nonbridging bonds, respectively. As consistent with the IR data, hydrogen is present as both H_2O and OH. The former forms hydrogen bonds with the oxygen atoms of the composite chains, with O-O distances from 2.69 to 2.83 Å. The latter is associated with the octahedral cations in accordance with the substitution scheme, $\text{Ti}^{4+}\text{O}^{2-} \rightarrow \text{Fe}^{3+}\text{OH}^-$. (13 refs.)

113806 Crystal structure and Mossbauer spectrum of vonsenite, $2\text{FeO} \cdot \text{FeBO}_3$. J.S.Winnear, H.Steinink (Dept. of Chem. Engng., Univ. of Texas, Austin, TX, USA). *Am. Mineral.* (USA), vol.68, no.7-8, p.827-32 (July-Aug. 1983).

The crystal structure of the mineral vonsenite has been redetermined from a synthesized specimen of composition $2\text{FeO} \cdot \text{FeBO}_3$. The unit cell dimensions are $a=9.463(1)$ Å, $b=12.305(1)$ Å, $c=3.0727(6)$ Å, $Z=4$, space group $Pbam$. The final coordinates gave $R=0.054$ and $\omega R=0.029$ for 614 structure amplitudes and $R=0.030$, $\omega R=0.027$ for 461 amplitudes greater than $2\sigma(F)$. The crystal structure is essentially unchanged from the structure reported in 1950 but the precision of the parameters is at least an order of magnitude better. Values of valence sums, Mossbauer spectra, and the distortions present in the four crystallographically independent octahedra containing Fe1, Fe2, Fe3 and Fe4 are consistent with the presence of two pairs of physically distinct iron ions. Fe1 and Fe3 are divalent; the bond distance between Fe2 and Fe4 is 2.787 Å and direct exchange occurs so that an intermediate oxidation state of +2.5 is observed. The Mossbauer spectra are complex and indicate the presence in the structure of Fe^{2+} , Fe^{3+} and $\text{Fe}^{2.5+}$. As the temperature is lowered from room temperature the Mossbauer spectra show the migration of a low velocity peak due to Fe^{3+} towards the high velocity peak due to the dinuclear complex Fe2-Fe4 in which Fe has an intermediate valence state. (21 refs.)

113807 X-ray and electron diffraction analysis of GaSe crystals. M.K.Anis, F.M.Nazar (Thin Films Res. Lab., Punjab Univ., Lahore, Pakistan).

J. Mater. Sci. Lett. (GB), vol.2, no.9, p.471-4 (Sept. 1983).

Both X-ray and electron diffraction techniques have been used to study single crystals grown by the Bridgman-Stockbarger method. It has been found that these crystals are hexagonal ζ -GaSe. (14 refs.)

113808 New structure determination of murchichtite, Cu_2PbO_8 . E.Dubler, A.Vedani, H.R.Oswald (Inst. of Inorganic Chem., Univ. of Zurich, Zurich, Switzerland).

Acta Crystallogr. Sect. C (Denmark), vol.C39, pt.9, p.1143-6 (15 Sept. 1983). $M_r=716.4$, cubic, space group $Fm\bar{3}m$, $a=9.224(2)$ Å, $V=784.8(3)$ Å³, $Z=4$, $D_x=6.06$ Mg m⁻³, $5.9 \leq D_m \leq 6.7$ Mg m⁻³, $\lambda(\text{Mo K}\alpha)=0.71069$ Å, $\mu=37.55$ mm⁻¹, $T=295$ K. Final $R=0.027$ for 255 unique observed reflections. The structure consists of $[\text{PbO}_8]$ cubes with Cu^{2+} ions spanning the 12 edges of the O_8 cubes building up a three-dimensional network to give a square-planar $[\text{CuO}_4]$ coordination. Halogen ions which occupy the interstices complete a (4+2) elongated $[\text{CuO}_4\text{X}_2]$ octahedron. The four Cu-O separations are 1.921 (1) Å and the Cu-X separations 3.261 (2) Å. Therefore, murchichtite is not a representative of a compound with an undistorted octahedral copper coordination (dynamic Jahn-Teller effect) as proposed by Christ & Clark (1955). This fact is consistent with thermoanalytical measurements. In view of the varying content of chloride and bromide in natural samples of murchichtite its general formula may best be described as $\text{Cu}_2\text{PbO}_{8-x}(\text{Cl,Br})_{2x}$, with $x \leq 0.5$. (11 refs.)

113809 Room-temperature structure of carbon monoxide at 2.7 and 3.6 GPa. D.T.Cromer, D.Schiffel, R.LeSar, R.L.Mills (Los Alamos Nat. Lab., Univ. of California, Los Alamos, NM, USA).

Acta Crystallogr. Sect. C (Denmark), vol.C39, pt.9, p.1146-50 (15 Sept. 1983).

A single crystal of CO was grown at room temperature in a high-pressure Merrill-Bassett diamond cell and examined by X-ray diffraction at 2.7 and 3.6 GPa. At 4.2 GPa the sample appeared to undergo a photochemical change induced by the weak laser light used to make ruby fluorescence pressure measurements. The unit cell is hexagonal, space group $P6_3/mmc$, with two molecules per unit cell, which is the same as that of β -CO near the triple point. At $P=2.7$ GPa the lattice constants are $a=3.615(1)$ and $c=5.880(1)$ Å, and at 3.6 GPa they are $a=3.532(1)$ and $c=5.744(2)$ Å, giving molar volumes very near to those for β -N₂ under similar conditions. The final R_w refined from ten observations, is 0.103 for a model with molecules tilted 40° from the c axis, statistically disordered, and randomly polarized. Calculations using a Gordon-Kim electron-gas model show that the $P6_3/mmc$ structure with randomly polarized CO molecules should have a minimum energy at a tilt angle of 50°, while polarized molecules give 48°. The melting pressure of CO at room temperature is about 2.6 GPa and is considerably lower than published measurements would indicate. (54 refs.)

113810 Synthesis and structure of a nonstoichiometric caesium niobate, $\text{Cs}_3\text{Nb}_{5.9}\text{O}_{16.4}$. M.-C.Saine, M.Gasperin (Lab. de Mineralogie-Cristallographie, Univ. Pierre et Marie Curie, Paris, France).

Acta Crystallogr. Sect. C (Denmark), vol.C39, pt.9, p.1153-6 (15 Sept. 1983). In French.

$M_r=1214.86$, orthorhombic, *Amam*, $a=18.315(3)$, $b=24.506(4)$, $c=7.296(2)$ Å, $V=3274.6$ Å³, $Z=8$, $D_x=4.93$ Mg m⁻³, $\lambda=0.7107$ Å, $\mu(\text{Mo K}\alpha)=10.9$ mm⁻¹, $F(000)=4324.48$, room temperature, $R=0.040$ for 3034 reflections. The crystal composition is very close to $\text{Cs}_2\text{O} \cdot 2\text{Nb}_2\text{O}_5$ but the deficiency of Nb_2O_5 results in a new structural type derived from $\text{Cs}_3\text{Nb}_6\text{O}_{11}$ and pyrochlore by the breaking of octahedral chains. Moreover, the structure contains $(\text{NbO}_4)^{3-}$ tetrahedra linked by one corner to form $(\text{Nb}_2\text{O}_7)^{4-}$ groups. The Nb-O distances range from 1.71 (1) to 2.3 (1) Å in the octahedra and from 1.55 (1) to 2.76 (1) Å in the tetrahedra. Cs-O ranges from 2.78 (1) to 3.52 (1) Å. (3 refs.)

113811 Tricobalt hexasodium hexakis(hexahydroxohexaborate) hexacosahydrate, $\text{Na}_6\text{Co}_3[\text{B}_6\text{O}_7(\text{OH})_6]_6 \cdot 26\text{H}_2\text{O}$. H.Behm (Inst. fur Kristallographie, Univ. Karlsruhe, Karlsruhe, Germany).

Acta Crystallogr. Sect. C (Denmark), vol.C39, pt.9, p.1156-9 (15 Sept. 1983). $M_r=2456.5$, triclinic, *P1*, $a=9.572(4)$, $b=13.560(6)$, $c=18.034(6)$ Å, $\alpha=109.04(3)^\circ$, $\beta=96.46(3)^\circ$, $\gamma=102.37(3)^\circ$, $Z=1$, $V=2119(1)$ Å³, $D_x=1.92$, $D_m(\text{floatation})=1.88$ Mg m⁻³, $\lambda(\text{Mo K}\alpha)=0.71069$ Å, $\mu(\text{Mo K}\alpha)=7.63$ cm⁻¹, $F(000)=1246.8$, room temperature, $R=0.042$ for 6670 reflections. The structure belongs to the class of soroborates and consists of hexaborate groups between which the Co atoms are octahedrally coordinated. These Co hexaborate units are surrounded by hydrated Na atoms and water molecules. (12 refs.)

113812 Structures of 20 new polytypes of cadmium iodide. B.Palosz (Inst. of Phys., Warsaw Tech. Univ., Warszawa, Poland).

Acta Crystallogr. Sect. C (Denmark), vol.C39, pt.9, p.1160-3 (15 Sept. 1983). The structures of 20 new polytypes of CdI₂ obtained from solution are presented: $18H_2$: $(1/5)f(1/2)(o)3f1$; $20H_{13}$: $(1/3)f(1/2)f(1/2)f1$; $28H_6$: $(1/3)f(1/2)(1/2)f1$; $28H_7$: $(1/3)f(1/2)(1/2)f(1/2)(1/2)f1$; $30H_6$: $(1/5)f(1/2)(1/2)f(1/2)f1$; $34H_4$: $(1/5)f(1/2)f1$; $34H_5$: $(1/3)f(1/2)f(1/2)f(1/2)f(1/2)f1$; $(1/3)f(1/2)(1/2)f(1/2)f1$; $(1/3)f(1/2)(1/2)f(1/2)f1$; $60R_3$: $(1/3)f(1/2)(1/2)f(1/2)f1$; $66R_3$: $(1/4)f(1/2)(1/2)f(1/2)f1$; $72R_3$: $(1/4)f(1/2)(1/2)f(1/2)f1$; $78R_3$: $(1/4)f(1/2)(1/2)f(1/2)f1$; $84R_3$: $(1/4)f(1/2)(1/2)f(1/2)f1$; $90R_3$: $(1/4)f(1/2)(1/2)f(1/2)f1$; $96R_3$: $(1/4)f(1/2)(1/2)f(1/2)f1$; $102R_3$: $(1/4)f(1/2)(1/2)f(1/2)f1$; $108R_3$: $(1/4)f(1/2)(1/2)f(1/2)f1$; $120R_3$: $(1/4)f(1/2)(1/2)f(1/2)f1$. Similarities and differences between hexagonal and rhombohedral polytypes are discussed. (18 refs.)

113813 Orthorhombic uranium(IV) molybdenum(VI) oxide, UMo_2O_8 . T.L.Cremers, P.G.Eller, R.A.Penneman, C.C.Herrick (Los Alamos Nat. Lab., Univ. of California, Los Alamos, NM, USA).

Acta Crystallogr. Sect. C (Denmark), vol.C39, pt.9, p.1163-5 (15 Sept. 1983). $M_r=557.8$, orthorhombic, *Pbam*, $a=20.076(4)$, $b=7.323(1)$, $c=4.1164(6)$ Å, $V=605.2$ Å³, $Z=4$, $D_m=6.08(6)$, $D_x=6.12$ Mg m⁻³, $\text{Mo K}\alpha$, $\lambda=0.70930$ Å, $\mu=367$ cm⁻¹, $F(000)=960$, $T=298$ K, $R=0.049$ for 1347 reflections. The structure consists of layers of oxide-bridged uranium and molybdenum atoms connected by infinite interlayer U-O-U and Mo-O-Mo chains. The uranium atoms have pentagonal bipyramidal coordination [U-O equatorial=2.202 (6)=2.394 (8) Å, U-O axial=2.0584 (3) Å]; the molybdenum atoms are in a highly distorted octahedral [Mo-O=1.684 (7)-2.432 (7) Å] arrangement. The presence of oxide ions not connected to molybdenum suggests that this structure is better formulated as a double oxide-molybdate than as a true molybdate. (20 refs.)

113814 Orthorhombic thorium(IV) molybdate, $\text{Th}(\text{MoO}_4)_2$. T.L.Cremers, P.G.Eller, R.A.Penneman (Los Alamos Nat. Lab., Univ. of California, Los Alamos, NM, USA).

Acta Crystallogr. Sect. C (Denmark), vol.C39, pt.9, p.1165-7 (15 Sept. 1983). $M_r=551.9$, orthorhombic, *Pbca*, $a=10.318(5)$, $b=9.737(4)$, $c=14.475(6)$ Å, $V=1454$ Å³, $Z=8$, $D_x=5.04$ Mg m⁻³, $\text{Mo K}\alpha$, $\lambda=0.70930$ Å, $\mu=244$ cm⁻¹, $F(000)=1904$, $T=298$ K, $R=0.038$ for 3167 unique reflections. The structure is that of a true molybdate, with nearly regular molybdate tetrahedra bridging to thorium coordinated in a nearly regular square antiprismatic environment. (9 refs.)

113815 Ammonium trifluoroberyllate(II), $(\text{NH}_4)_3[\text{BeF}_6]$, at room temperature. A.Waskowska (Inst. for Low Temperature & Structure Res., Polish Acad. of Sci., Wrocław, Poland).

Acta Crystallogr. Sect. C (Denmark), vol.C39, pt.9, p.1167-9 (15 Sept. 1983). $M_r=84$, monoclinic, *Pn*, $a=5.770(2)$, $b=4.619(3)$, $c=12.819(1)$ Å, $\beta=90.12(2)^\circ$, $V=341.6(4)$ Å³, $Z=4$, $D_m=1.63(2)$, $D_x=1.632(3)$ Mg m⁻³, $\lambda(\text{Cu K}\alpha)=1.54051$ Å, $\mu=2.04$ mm⁻¹, $F(000)=168$. Final $R=0.049$ for 536 observed reflections. At room temperature the crystal is ferroelastic. Hydrogen-bonded chains of BeF_4 tetrahedra run along the b axis and undergo a pronounced thermal motion around this axis. Diffuse streaks observed at room temperature on Weissenberg photographs are probably connected with the phase transition to the orthorhombic phase at 334.3K. (11 refs.)

113816 Structure of orthopyroxene-type and clinopyroxene-type magnesium germanium oxide MgGeO_3 . M.Ozima (Inst. for Solid State Phys., Univ. of Tokyo, Tokyo, Japan).

Acta Crystallogr. Sect. C (Denmark), vol.C39, pt.9, p.1169-72 (15 Sept. 1983).

Orthopyroxene-type: $M_r=144.92$, orthorhombic, *Pbca*, $a=18.809(12)$, $b=8.9484(8)$, $c=5.3451(4)$ Å, $V=899.69(12)$ Å³, $Z=16$, $D_x=4.28$ gcm⁻³, $\lambda(\text{Ag K}\alpha)=0.56087$ Å, $\mu(\text{Ag K}\alpha)=75.64$ cm⁻¹, $T=300$ K, $F(000)=1088$, $R=0.025$ for 975 independent reflections. Clinopyroxene-type: $M_r=144.92$, monoclinic, *C2/c*, $a=9.6010(8)$, $b=8.9323(6)$, $c=5.1592(5)$ Å, $\beta=101.034(9)^\circ$, $V=434.27(6)$ Å³, $Z=8$, $D_x=4.43$ gcm⁻³, $\lambda(\text{Ag K}\alpha)=0.56087$ Å, $\mu(\text{Ag K}\alpha)=78.35$ cm⁻¹, $T=300$ K, $F(000)=544$, $R=0.021$ for 1025 independent reflections. Orthorhombic MgGeO_3 (the high-temperature and low-pressure phase) is isostructural with orthoenstatite, MgSiO_3 . The structure of monoclinic MgGeO_3 (the low-temperature and high-pressure phase) is different from that of clinoenstatite which crystallizes in $P2_1/c$. The orthorhombic (*Pbca*) to monoclinic (*C2/c*) transformation in MgGeO_3 is accompanied by a fairly large volume decrease (3.5%). A smaller distortion of the $\text{Mg}(2)$ octahedron in the structure of monoclinic MgGeO_3 causes the higher density. (11 refs.)

113817 Disilver(I) decachlorodioxotetraaluminate(III), $\text{Ag}_2[\text{Al}_4\text{Cl}_{10}\text{O}_2]$. D.Jentsch, P.G.Jones, E.Schwarzmann, G.M.Sheldrick (Inst. fur Anorganische Chem., Univ. Göttingen, Göttingen, Germany).

Acta Crystallogr. Sect. C (Denmark), vol.C39, pt.9, p.1173-4 (15 Sept. 1983). $M_r=710.20$, orthorhombic, *Pbca*, $a=11.240(2)$, $b=12.278(4)$, $c=12.955(3)$ Å, $V=1788$ Å³, $Z=4$, $D_x=2.64$ g cm⁻³, $\text{Mo K}\alpha$ radiation ($\lambda=0.71069$ Å, $\mu=39$ cm⁻¹), $F(000)=1328$, $R=0.045$ for 1802 unique observed reflections. The compound is formed in the system $\text{AgCl}/\text{AlCl}_3$ when traces of water are present; the deliberate use of the theoretical amount of $\text{AlCl}_3 \cdot 6\text{H}_2\text{O}$ gives a quantitative yield of polycrystalline material. The structure contains $[\text{Al}_4\text{Cl}_{10}\text{O}_2]^{2-}$ ions with crystallographic 1 symmetry. The Ag^+ ions are coordinated by five chlorines in a distorted trigonal-bipyramidal arrangement (the first observation of such coordination of Ag⁺). The extended structure is a three-dimensional polymer. (5 refs.)

113818 Single-crystal refinement of the structure of LaOCl . L.H.Brixner, E.P.Moore (Central Res. & Dev. Dept., E.I. du Pont de Nemours & Co., Wilmington, DE, USA).

Acta Crystallogr. Sect. C (Denmark), vol.C39, pt.9, p.1316 (15 Sept. 1983). LaOCl crystallizes in the tetragonal $P4/nmm$ structure of PbFCl with $a=4.1209(2)$ and $c=6.8840(7)$ Å; $Z=2$. Single crystals of LaOCl were grown from a BaCl_2 flux. Least-squares single-crystal refinement based on 81 independent reflections led to an R value of 0.011. Powder data based on Guinier refinements are also reported. No significant differences over the previous powder work [Sillen & Nylander (1941)] are found. (4 refs.)

113819 Crystal structure and vibrational spectra of $\text{Pb}_2\text{P}_2\text{S}_6$. R.Becker, W.Brockner (Inst. für Anorganische Chem., Tech. Univ. Clausthal, Clausthal, Germany), H.Schafer. *Z. Naturforsch. Teil A (Germany)*, vol.38A, no.8, p.874-9 (Aug. 1983). In German.

$\text{Pb}_2\text{P}_2\text{S}_6$ crystallizes in the monoclinic systems, space group Pn with the lattice constants $a=940.2(4)$ pm, $b=746.6(3)$ pm, $c=661.2(3)$ pm, $\beta=91.53(5)^\circ$. The compound is isotypic to the monoclinic dimorphous II of $\text{Sn}_2\text{P}_2\text{S}_6$. In the structure there are discrete $\text{P}_2\text{S}_6^{4-}$ anions. Far infrared, infrared and Raman spectra of this compound have been recorded. The observed frequencies are assigned on the basis of $\text{P}_2\text{S}_6^{4-}$ units with C_{2h} symmetry in the crystal. DTA-data have been determined and interpreted. (20 refs.)

113820 Crystal-chemical principles of prediction of ferroelectrics and related materials in the case of compounds with $\{[\text{M}_2(\text{EO}_4)_3]^\text{P}\}_{3\infty}$ frameworks. V.B.Kalinin, S.Yu.Stefanovich (L.Ya. Karpov Sci.-Res. Physicochem. Inst., USSR).

Inorg. Mater. (USA), vol.18, no.9, p.1342-6 (Sept. 1982). Translation of: *Izv. Akad. Nauk SSSR Neorg. Mater.*, vol.18, no.9, p.1567-71 (Sept. 1982). [received: Sept. 1983]

A genetic scheme has been presented for the coordination of structures of compounds with frameworks of the composition $\{[\text{M}_2(\text{EO}_4)_3]^\text{P}\}_{3\infty}$. The structures and properties of compounds of the rhombohedral type $[\text{Fe}_2(\text{SO}_4)_3]$ type and langbeinite have been established. With the example of some double phosphates the authors have found an interrelationship between ferroelectricity and ionic conduction, arising because of the existence of large cavities of two types which link up into channels in their structures. (26 refs.)

113821 Crystal chemistry of piezoelectric with a sillenite structure. Yu.F.Kargin, A.A.Mar'in, V.M.Skorikov (N.S. Kurnakov Inst. of General & Inorganic Chem., Acad. of Sci., USSR).

Inorg. Mater. (USA), vol.18, no.10, p.1375-84 (Oct. 1982). Translation of: *Izv. Akad. Nauk SSSR Neorg. Mater.*, vol.18, no.10, p.1605-14 (Oct. 1982). [received: Sept. 1983]

The authors have synthesized 23 sillenite-structure compounds and carried out physicochemical investigations on them. It was found that Bi^{3+} and Bi^{5+} occupy the tetrahedral sites of the sillenite lattice formed by elements of groups II, III, V, and VI. With the aid of the IR spectra of the respective crystals they showed that ions of different charge are randomly distributed over the tetrahedral sites of the sillenite lattice. These investigations of sillenites allow them to be classified as follows: (a) constant composition compounds in which the tetrahedral positions of the BCC structure are occupied only by tetravalent ions of group-IV elements—Si, Ge, Ti; (b) variable-composition compounds in which the tetrahedral sites are occupied by randomly distributed ions of two or more elements, on the basis of phases in which the average charge of the tetrahedral cations is four. Sillenite-structure compounds in many cases do not form continuous solid solutions with each other. (51 refs.)

113822 Crystal chemistry, phase transitions, and physical properties of halide crystals with perovskite-like structure. B.V.Beznosikov, A.T.Anistratov, K.S.Aleksandrov (A.V. Kirenskiy Inst. of Phys., Acad. of Sci., USSR).

Inorg. Mater. (USA), vol.18, no.10, p.1406-11 (Oct. 1982). Translation of: *Izv. Akad. Nauk SSSR Neorg. Mater.*, vol.18, no.10, p.1640-4 (Oct. 1982). [received: Sept. 1983]

Complex investigations of perovskite-like crystals show that, with the aid of structure prognosis and clarification of the structural elements determining the specified properties, one may synthesize new materials on the basis of halide compounds in a directed manner. (13 refs.)

113823 Crystal data for $\text{C}_{24}\text{N}_6\text{CuClO}_4\text{H}_{18}$, $\text{C}_6\text{N}_6\text{PdS}_2\text{Cl}_2\text{O}_7\text{H}_{16}$. K.Chakrabarty, S.P.Sen Gupta (Dept. of General Phys. & X-rays, Indian Assoc. for the Cultivation of Sci., Calcutta, India).

Indian J. Phys. Part A, vol.57A, no.3, p.205-7 (May 1983). Reports preliminary information on the crystallographic data of the two compounds $\text{C}_{24}\text{N}_6\text{CuClO}_4\text{H}_{18}$ (I) and $\text{C}_6\text{N}_6\text{PdS}_2\text{Cl}_2\text{O}_7\text{H}_{16}$ (II) of considerable chemical and structural interest. The first compound, bis[2-(phenylazo)pyridine] copper (I) perchlorate gives dark purple crystals. The second one, palladium bis-1-amidino-2-thiourea, is light yellow in colour and quite hard. The unit cell dimensions and space groups were determined from standard oscillation, rotation and Weissenberg (zero- and upper-layer) photographs taken along two crystallographic axes with copper-radiation. (no refs.)

113824 Electron diffraction studies of supersonic jets. V. Low temperature crystalline forms of SF_6 , SeF_6 , and TeF_6 . E.J.Valente, L.S.Bartell (Dept. of Chem., Univ. of Michigan, Ann Arbor, MI, USA).

J. Chem. Phys. (USA), vol.79, no.6, p.2683-6 (15 Sept. 1983).

Condensation of SF_6 , SeF_6 , and TeF_6 in nozzle flows with inert carrier gases produces microcrystals of these materials. All form the higher temperature body-centered cubic structure at higher partial pressures of hexafluoride. At lower partial pressures and colder nucleation conditions a lower symmetry form of each has been produced. Electron diffraction powder patterns are consistent with the space group Pnma to which metal hexafluorides of UF_6 type belong. Low temperature phases of the present materials differ from those of the metal compounds, however, in being less dense than the cubic forms. Aspects of the gas dynamics affording a control over nucleated species are briefly discussed. (14 refs.)

113825 Site symmetry of the metal ion in rare earth oxynitrates doped with europium(III). J.-C.G.Bunzli, B.Klein, V.Kasperek (Inst. de Chimie Minérale et Analytique, Univ. de Lausanne, Lausanne, Switzerland).

J. Less-Common Met. (Switzerland), vol.93, no.1, p.157-8 (1983). (Proceedings of the Sixteenth Rare Earth Research Conference, Tallahassee, FL, USA, 18-21 April 1983).

The high resolution laser-excited emission spectra at 273 and 77K of europium-doped lanthanum and gadolinium oxynitrates ($\text{LnONO}_3\text{:Eu}$) are analysed in terms of the site symmetry of the metal ion. To be consistent with X-ray diffraction powder diagrams the data have to be interpreted as reflecting the presence of at least two metal ion sites, one with T symmetry and the other with S_4 symmetry. (4 refs.)

113826 Structural modifications of silicon nitride as a function of temperature. M.Billy, J.C.Labbe, A.Selvaraj (Centre de Recherches et d'Etudes Ceramiques, Univ. de Limoges, Limoges, France), G.Roult.

Mater. Res. Bull. (USA), vol.18, no.8, p.921-34 (Aug. 1983). In French.

The structural evolution of α and β - Si_3N_4 has been studied up to 900°C by means of the time of flight neutron diffraction method. It has been shown that the relative evolution of lattice parameters is the same for both phases; the modifications versus temperature are isotropic along the crystallographic axes a and c. However, the atomic positions, bond angles and bond lengths at different temperatures, as well as the volume evolution of SiN_4 tetrahedra compared to that of the unit cell volume, suggest a lower stability of α - Si_3N_4 with regard to the β phase which explains the α - β transformation at higher temperatures. (23 refs.)

113827 Properties of Cu^{2+} ion in the γ - AgCuPO_4 structure. M.Quarton, M.T.Oumba (Lab. de Chimie Minérale, Univ. Pierre et Marie Curie, Paris, France).

Mater. Res. Bull. (USA), vol.18, no.8, p.967-74 (Aug. 1983). In French. AgCuPO_4 - β (high temp.) crystallizes with orthorhombic symmetry, space group: Pbc₂, Z=8 and unit-cell parameters: $a=7.500$ (1), $b=15.751$ (2), $c=5.702$ (1) Å. Its structure has been solved and refined to $R=0.046$ for 664 independent reflexions. The framework is built up with PO_4 tetrahedra, AgO_4 pyramids and CuO_5 bipyramids. The Jahn-Teller effect of Cu^{2+} and magnetic properties are discussed. (21 refs.)

113828 Crystal structure of GaSc_2O_4 ; its relation with perovskite. V.Agafonov, A.Khan, D.Michael (Lab. de Chimie Appliquée de l'Etat Solide, Urbain, Vitry, France), M.Guymont.

Mater. Res. Bull. (USA), vol.18, no.8, p.975-81 (Aug. 1983). The crystal structure of BaSc_2O_4 has been determined on single crystals. The crystal symmetry is monoclinic (C_2/c , Z=12) with a pseudorhombic unit cell. The relationship with parent perovskite structure is discussed in terms of coordination polyhedra and bond lengths. (16 refs.)

113829 New island tetrahedral $[\text{Ge}_2\text{O}_5]^\text{P}$ radical in the structure of $\text{Na}_2\text{Sn}_2[\text{Ge}_2\text{O}_5]_4\text{H}_2\text{O}$. A.N.Safronov, N.N.Nevskii, V.V.Ilyukhin, N.V.Belov (A.V. Shubnikov Inst. of Crystallography, Acad. of Sci., Moscow, USSR).

Sov. Phys.-Dokl. (USA), vol.27, no.12, p.991-3 (Dec. 1982). Translation of: *Dokl. Akad. Nauk SSSR*, vol.267, no.4-6, p.850-3 (Dec. 1982). [received: Sept. 1983]

Colorless transparent single crystals of unknown composition were found during the study of hydrothermal reactions in the system SnO_2 - GeO_2 - Na_2O - H_2O (450°C, 1000 atm). The initial X-ray analysis revealed a monoclinic P unit cell $a=6.951$ (1), $b=20.062$ (2), $c=5.370$ (1) Å; $\gamma=93.25^\circ$ (1); $V=748$ Å³. The three-dimensional set of intensities, consisting of 1780 independent reflections with $I(\text{hkl}) \geq 3\sigma(I)$, was obtained from an isometric specimen on an Enraf-Nonius automatic diffractometer (MoK α radiation, $\sin\theta/\lambda \leq 0.7$ Å⁻¹, graphite monochromator). Analysis of the location of the maxima of the Patterson function in the absence of systematic extinctions pointed to P2 as the most probable space group. (5 refs.)

113830 Crystal structure of barium chlorosilicate. A.M.Ilinets, V.V.Ilyukhin, N.V.Belov, N.N.Nevskii (A.V. Shubnikov Inst. of Crystallography, Acad. of Sci., Moscow, USSR).

Sov. Phys.-Dokl. (USA), vol.27, no.12, p.996-7 (Dec. 1982). Translation of: *Dokl. Akad. Nauk SSSR*, vol.267, no.4-6, p.1125-7 (Dec. 1982). [received: Sept. 1983]

Colorless transparent single crystals of unknown composition in the form of flat hexagonal plates have been isolated from products of hydrothermal crystallization during the study of the system BaO - SiO_2 - LiCl - H_2O ($T=450^\circ\text{C}$, $P=1000$ atm). The ratio of the components in the initial mixture was $\text{BaO}:\text{SiO}_2=4:1$ with a 40% concentration of the solvent LiCl. It was not possible to make a chemical analysis of the compound because the quantity of the given crystallization product was too small and the crystal structure was interpreted without knowledge of the chemical formula of the compound. (2 refs.)

113831 The crystal structure of the A phase of KLiSO_4 . P.A.Sandomirskii, S.S.Meshalkin, I.V.Rozhdestvenskaya (Inst. of Geochem. & Analytical Chem., Acad. of Sci., USSR).

Sov. Phys.-Crystallogr. (USA), vol.28, no.1, p.33-5 (Jan.-Feb. 1983). Translation of: *Kristallografiya (USSR)*, vol.28, no.1, p.67-71 (Jan.-Feb. 1983). [received: Sept. 1983]

The authors have refined the crystal structure of the A phase of KLiSO_4 , which is stable at room temperature. They discuss the nature of the strong anisotropy of the thermal vibrations of the oxygen atoms. (9 refs.)

113832 The crystal structure of Na-X zeolite in hydrated and dehydrated forms. Yu.I.Smolín, Yu.F.Shepelev, I.K.Butikova, V.P.Petranskii (Inst. of Chem. of Silicates, Acad. of Sci., USSR).

Sov. Phys.-Crystallogr. (USA), vol.28, no.1, p.36-9 (Jan.-Feb. 1983). Translation of: *Kristallografiya (USSR)*, vol.28, no.1, p.72-8 (Jan.-Feb. 1983). [received: Sept. 1983]

The crystal structure of Na₉₂-X zeolite ($a=25.01$ Å, $Fd\bar{3}$) is refined by the method of least squares in the hydrated, dehydrated, and rehydrated forms. It is shown that when water is evaporated some of the sodium atoms in the large cavities occupy crystallographic positions. It is demonstrated that some of the S1 positions at the centers of hexagonal prisms are occupied by water molecules. It is also demonstrated that when the crystal is rehydrated there is an increase in the number of water molecules occupying crystallographic positions. (9 refs.)

113833 The crystal structure of Y_3Ge_5 ($\text{YGe}_{1.7}$). V.A.Bruskov, O.I.Bodak, V.K.Pecharskii, E.I.Gladyshevskii, L.A.Muratova (State Univ., L'vov, Ukrainian SSR).

Sov. Phys.-Crystallogr. (USA), vol.28, no.2, p.151-3 (March-April 1983). Translation of: *Kristallografiya (USSR)*, vol.28, no.2, p.260-3 (March-April 1983). [received: Sept. 1983]

The authors determine the crystal structure of the compound Y_3Ge_5 , which belongs to a new type: space group Fdd_2 , $a=5.746$ (2), $b=17.284$ (5), $c=13.696$ (3) Å, $V=1360.1$ (6) Å³. In the calculations use is made of the intensities of 318 independent observed reflections ($I > 2\sigma(I)$) measured on a Syntex P2₁ automatic diffractometer in Mo K α radiation (parallel graphite monochromator); $R=0.068$ in the isotropic approximation and $R=0.061$ in the anisotropic approximation. The structure of Y_3Ge_5 is a deformed derivative of the α - ThSi_2 type and is related to the Eu_3As_4 type. The coordination numbers of the atoms are: Y, 18; Ge, 9 and 8. (5 refs.)

113834 Observed atomic charges in β - NaN_3 crystals. A.N.Chekhlov, S.P.Ionov (Inst. of Physiologically Active Substances, Acad. of Sci., Moscow, USSR).

Theor. & Exp. Chem. (USA), vol.18, no.6, p.626-31 (Nov.-Dec. 1982). Translation of: *Teor. & Eksp. Khim. (USSR)*, vol.18, no.6, p.682-8 (Nov.-Dec. 1982). [received: Sept. 1983] (14 refs.)

Oxygen potential and lattice parameter measurements in (U, Ce) O_{2-x} See Entry 112324

Phase transitions in $\text{Na}_3\text{Sc}_2(\text{PO}_4)_3$ and in related compounds with $\{[\text{M}_2(\text{EO}_4)_3]^\text{P}\}_{3\infty}$ frameworks See Entry 113794

Lattice expansion and broadening of the Bragg reflexion in thermal-neutron-irradiated Li_2O pellets See Entry 114044

Phase equilibria in $\text{Ln}_2\text{V}_2\text{O}_7$ - $\text{Ln}_2\text{Ti}_2\text{O}_7$ systems ($\text{Ln}=\text{Er, Lu}$) See Entry 114127

Pressure-induced phase transition of HgS See Entry 114157

The phase transitions and crystal structures of a new compound— Sr_2CaWO_6 See Entry 114170

Effect of the structural properties of compounds in the system Bi_2O_3 - EO_2 ($\text{E}=\text{Ge, Si}$) on their dissolution See Entry 114177

- Thermal expansion and electrical conductivity in the $\text{HfO}_2\text{-TiO}_2$ system See Entry 114216
- Preparation and investigations of polycrystalline samples of copper sulphides Cu_{2-x}S ($0 \leq x \leq 0.2$) See Entry 114521
- Behaviour of large-grain polycrystalline $n\text{-InP}$ grown by SSD technique See Entry 114551
- Synthesis and physical properties of new superconducting Chevrel phases $\text{Hg}_x\text{Mo}_6\text{S}_8$ See Entry 114639
- Free parameter of spinel structure and Mossbauer lineshift ... See Entry 114761
- The flux growth of some transition metal phosphates See Entry 115033
- Preparation of MnCo_2O_4 by a wet method and its metal ion distribution See Entry 115034
- Synthesis of acid polyphosphates of rare-earth metals and the structure of $\text{ErH}(\text{PO}_3)_4$ See Entry 115120
- Physicochemical aspects of production of ferroelectric ceramics See Entry 115148
- Properties of hot-pressed zirconium pyrovanadate ceramics ... See Entry 115149

61.65 SPECIFIC STRUCTURE OF ORGANIC COMPOUNDS

- 113835** The crystal and molecular structure of $\text{N,N}'\text{-bis}[(\text{S})\text{-1-phenylethyl}]benzamide$. J.D.Korp, I.Bernal (Dept. of Chem., Univ. of Houston, Houston, TX, USA). *Chem. Scr. (Sweden)*, vol.22, no.2, p.60-3 (1983).
The structure of $\text{N,N}'\text{-bis}[(\text{S})\text{-1-phenylethyl}]benzamide$ has been determined by single crystal X-ray diffraction. Crystals are orthorhombic, space group $P2_12_12_1$, with four molecules in a unit cell of dimensions $a=8.273(4)$, $b=12.433(3)$, and $c=19.042(5)$ Å. The structure was solved by direct methods and refined to a final R value of 6.4%. The bond distances and angles are similar to those found in metal complexes with the deprotonated molecule. There is conjugation of the double bond with the adjacent C-N bond, as evidenced by the bond lengths and the tendency towards planarity of the amine nitrogen. There is no hydrogen bonding, due to the bulk of the phenyl substituents. (17 refs.)
- 113836** Crystal and molecular structure of betulin diacetate, $\text{C}_{44}\text{H}_{54}\text{O}_4$. P.K.Das (Dept. of Phys., Surendranath Coll., Calcutta, India), M.Mukherjee, S.Ray. *Indian J. Phys. Part A*, vol.57A, no.3, p.182-9 (May 1983).
The crystal structure of betulin diacetate, $\text{C}_{44}\text{H}_{54}\text{O}_4$, has been determined using 1314 data observed by diffractometry. The space group is $P2_12_12_1$ with $a=15.788(1)$, $b=12.566(2)$, $c=15.673(1)$ Å; $Z=4$. The structure was solved by direct methods and was refined to $R=0.055$. (3 refs.)
- 113837** Crystal and molecular structure and IR spectra of 1-hydroxy-4-dibromomethyl-2,2,5,5-tetramethyl- and 4-dibromomethyl-1,2,2,5,5-pentamethyl-3-imidazoline-3-oxide. Yu.V.Gatilov, M.M.Mitasov, I.A.Grigor'ev, L.B.Volodarskii (Novosibirsk Inst. of Organic Chem., Acad. of Sci., Novosibirsk, USSR). *J. Struct. Chem. (USA)*, vol.23, no.6, p.899-904 (Nov.-Dec. 1982). Translation of: *Zh. Strukt. Khim. (USSR)*, vol.23, no.6, p.91-7 (Nov.-Dec. 1982). [received: Sept. 1983]
The crystal and molecular structures of 1-hydroxy-4-dibromomethyl-2,2,5,5-tetramethyl- (I) and 4-dibromomethyl-1,2,2,5,5-pentamethyl-3-imidazoline-3-oxide (II) were established. In crystal (I), the α -dibromomethylnitron group is found in conformation A, where the dibromomethyl group is turned in such a way that the torsion angle between its C-H bond and the plane of the double bond is 29.5° . In molecule (II), the α -dibromomethylnitron group is characterized by a restrained conformation B, in which the H atom of the dibromomethyl group is found in an antiposition relative to the double bond. The IR spectra of (I) and (II) were investigated, and a correlation between the conformation of the α -dibromomethylnitron group and its characteristic frequencies was established. (13 refs.)
- 113838** Crystal structure of the semihydrate of the sodium salt of 5-sulfo-8-methylthioquinoline. A.D.Ozola, Ya.K.Ozols, A.A.Kemme, Ya.Ya.Bleidelis, Ya.V.Ashaks (Inst. of Inorganic Chem., Acad. of Sci., Latvian SSR). *J. Struct. Chem. (USA)*, vol.23, no.6, p.905-8 (Nov.-Dec. 1982). Translation of: *Zh. Strukt. Khim. (USSR)*, vol.23, no.6, p.98-102 (Nov.-Dec. 1982). [received: Sept. 1983]
X-ray analysis was used to investigate the semihydrate of the sodium salt of 5-sulfo-8-methylthioquinoline $\text{C}_{10}\text{H}_8\text{O}_3\text{NS}_2\text{Na} \cdot 0.5\text{H}_2\text{O}$ ($a=10.889(1)$, $b=5.510(1)$, $c=39.752(4)$ Å, $\beta=105.10(3)^\circ$, space group Aa, $Z=8$, diffractometer, $\lambda\text{CuK}\alpha$, 1815 reflections, direct method, $R=0.046$). The structure consists of alternating Na^+ cations, anions of 8-S-methylquinoline-5-sulfoacid, and H_2O molecules. (11 refs.)
- 113839** Structure of macrocyclic diamides of phthalic acid. Yu.G.Ganin, E.V.Ganin, Yu.A.Simonov, V.F.Anikin, G.L.Kamalov (Inst. of Appl. Phys., Acad. of Sci., Moldavian SSR). *J. Struct. Chem. (USA)*, vol.23, no.6, p.909-13 (Nov.-Dec. 1982). Translation of: *Zh. Strukt. Khim. (USSR)*, vol.23, no.6, p.103-7 (Nov.-Dec. 1982). [received: Sept. 1983]
The effect of ring size on the conformation of individual fragments and of the macrocycle as a whole was considered on the basis of an X-ray diffraction structural study of macrocyclic diamides of phthalic acid. 9,10-benz-1,7-diaza-4-oxacycloundecane-8,11-dione (I) and 12,13-benz-1,10-diaza-4,7-dioxacyclotetra-decane-11,14-dione (II). The phthalic acid fragments in the 11-membered ring in I and in the 14-membered ring in II have different structures. Features of the non-bonded 1,4-interactions involving the carbonyl groups were noted. (5 refs.)
- 113840** An X-ray diffraction structural study of nonbonded interactions in heteroorganic compounds. XXII. Crystal structure of triphenyltin 2dimethylamino-thiophenolate. L.G.Kuz'mina, Yu.T.Struchkov, E.M.Rokhlina, A.S.Peregudov, D.N.Kravtsov (A.N. Nesmeyanov Inst. of Heteroorganic Compounds, Acad. of Sci., USSR). *J. Struct. Chem. (USA)*, vol.23, no.6, p.914-18 (Nov.-Dec. 1982). Translation of: *Zh. Strukt. Khim. (USSR)*, vol.23, no.6, p.108-12 (Nov.-Dec. 1982). [received: Sept. 1983]
For pt.XXI see ibid., vol.23, no.1, p.102 (1982). The structure of triphenyltin 2-dimethylaminothiophenolate was determined by X-ray diffraction ($R=0.0271$ for 5365 reflections). The tin atom has trigonal-bipyramidal coordination with the sulfur atom in the equatorial position (Sn-S 2.429 (1) Å) and the nitrogen atom in the axial position (Sn-N 2.893 Å). Some lengthening of the axial Sn-C bond (2.172(3) Å) is noted relative to the equatorial Sn-C bonds (2.142(5) and 2.127(6) Å). The dimethylamino group has pyram-

idal structure. The nitrogen unshared electron pair is oriented toward the tin atom. (16 refs.)

- 113841** Growth structure and optical properties of single crystals of rubrene. I.V.Bulgarovskaya, V.M.Vozzhennikov, S.B.Aleksandrov, V.K.Bel'skii. *Latv. PSR Zinat. Akad. Vestis Fiz. Teh. Zinat. Ser. (USSR)*, no.4, p.53-9 (1983). In Russian.
The single crystals of rubrene $\text{C}_{42}\text{H}_{28}$ are grown by sublimation in the atmosphere of an inert gas, and an X-ray diffraction study is reported (diffractometer λMo , 669 reflections, by LSM in the anisotropic approximation to $R=0.032$). These are rhombic crystals, $a=7.184$, $b=14.433$, $c=26.897$ Å, $Z=4$, space group B, b, a, m . The inherent rubrene molecular symmetry in a crystal is $2/m$. The naphthalene nucleus on the whole is plane, the phenyl cycles are turned at an angle of 80.5° with respect to the midplane nucleus. The longwave absorption band of the rubrene crystal (max. 500, 472 and 439 nm) is in a good agreement with the analogue absorption band of the naphthalene crystal (max. 503, 472 and 439 nm). The dipole transition moments in the crystal of the translation non-equivalent molecules are parallel, being a cause of the absence of Davydov splitting in the absorption spectrum. The photoconduction and absorption spectra of the single crystal are negatively correlated. The photoconduction threshold has the value of 2.0 eV. (13 refs.)
- 113842** Structural analysis of the complex compound $[\text{Cr}(\text{OCN}_2\text{H}_4)_6][\text{Co}(\text{DH})_2(\text{NO}_2)_4]_2 \cdot 0.5\text{I}^- \cdot 0.5\text{X}^- \cdot n\text{H}_2\text{O}$. V.G.Rau, V.I.Bondar', V.V.Ilyukhin, Yu.T.Struchkov, N.V.Belov (P.I. Lebedev-Polyanski State Pedagogical Inst., Vladimir, USSR). *Sov. Phys.-Dokl. (USA)*, vol.27, no.12, p.998-1000 (Dec. 1982). Translation of: *Dokl. Akad. Nauk SSSR*, vol.267, no.4-6, p.1128-31 (Dec. 1982). [received: Sept. 1983]
The incompleteness of the Patterson function with respect to the 'light' fragment of a structure often requires that during the interpretation uses special Fourier syntheses whose structure is based on knowledge of the 'heavy' fragment of the basic system. In this case the choice of method for finding the solution is determined by probabilistic characteristics calculated within the framework of a generalized probabilistic approach, and the better one knows the chemical composition of the compound and the distinctive features of its structure, the more exact the recommendations that this approach gives. In the structure of the compound $[\text{Cr}(\text{OCN}_2\text{H}_4)_6][\text{Co}(\text{DH})_2(\text{NO}_2)_4]_2 \cdot 0.5\text{I}^- \cdot 0.5\text{X}^- \cdot n\text{H}_2\text{O}$ of incompletely known chemical composition, notwithstanding the likelihood of the appearance of maxima corresponding to the 'heavy' (I, Co, Cr) part of the basic system, the interpretation was complicated considerably by the formation of a 'grid' Cochran fragment in the vector system (VS) of the compound. The authors consider stages in the interpretation of the VS of the given structure with allowance for the homometric properties which manifested themselves. (4 refs.)
- 113843** Crystal structure of $[\text{Cr}(\text{OCN}_2\text{H}_4)_6][\text{Co}(\text{NH}_3)_2(\text{NO}_2)_4]_3 \cdot 0.5\text{CCl}_4 \cdot 1.5\text{H}_2\text{O}$. V.G.Rau, V.I.Bondar', T.F.Rau, V.V.Ilyukhin, Yu.T.Struchkov, N.V.Belov (P.I. Lebedev-Polyanski State Pedagogical Inst., Vladimir, USSR). *Sov. Phys.-Dokl. (USA)*, vol.27, no.12, p.1000-2 (Dec. 1982). Translation of: *Dokl. Akad. Nauk SSSR*, vol.267, no.4-6, p.1371-3 (Dec. 1982). [received: Sept. 1983]
This compound was obtained by adding carbon tetrachloride to an aqueous solution of $[\text{Cr}(\text{OCN}_2\text{H}_4)_6][\text{Co}(\text{NH}_3)_2(\text{NO}_2)_4]_3 \cdot 3\text{H}_2\text{O}$. The authors carried out an X-ray analysis of the resulting product $[\text{Cr}(\text{OCN}_2\text{H}_4)_6][\text{Co}(\text{NH}_3)_2(\text{NO}_2)_4]_3 \cdot 0.5\text{CCl}_4 \cdot 1.5\text{H}_2\text{O}$ with a view to making a further analysis of the structure of the chromium-urea complex in complicated hetero-complex compounds. From the methodological point of view they continued their study of the incomplete Patterson function with a heavy fragment, the degree of incompleteness and the search for methods of interpretation of which were determined by means of the generalized probabilistic approach. (3 refs.)
- 113844** The crystal structure of ytterbium formate dihydrate, and morphotropy in the series $\text{Ln}(\text{HCOO})_3 \cdot 2\text{H}_2\text{O}$. N.G.Furmanova, L.V.Soboleva, L.I.Khapaeva, N.V.Belov (Inst. of Crystallography, Acad. of Sci., USSR). *Sov. Phys.-Crystallogr. (USA)*, vol.28, no.1, p.30-3 (Jan.-Feb. 1983). Translation of: *Kristallografiya (USSR)*, vol.28, no.1, p.62-6 (Jan.-Feb. 1983). [received: Sept. 1983]
From formic-acid solutions of anhydrous formates, one obtains crystals of $\text{Yb}(\text{HCOO})_3 \cdot 2\text{H}_2\text{O}$ and two modifications of $\text{Tm}(\text{HCOO})_3 \cdot 2\text{H}_2\text{O}$; Tm_I , which belongs to a previously investigated isostructural series, and Tm_{II} . The authors have made an X-ray structural analysis of $\text{Yb}(\text{HCOO})_3 \cdot 2\text{H}_2\text{O}$ (method of least squares in anisotropic approximation, $R=0.081$ for 1920 reflections). Of the three formate groups, two are bidentately cyclic, and one is bidentately bridging. In the crystal the bridging formate groups form chains along [001], linked into layers by H bonds. It is found that the dihydrates Tm_{II} and Yb formate are isostructural, and the morphotropic transition Tm in the series $\text{Ln}(\text{HCOO})_3 \cdot 2\text{H}_2\text{O}$ with $\text{Ln}=\text{Tb-Yb}$ is thus fixed. (9 refs.)
- 113845** Structure of salts of arylthioniacycloalkanes with a hydroxy group in the benzene ring. VIII. The crystal structure of 1-(2,5-dihydroxyphenyl)-thianium chloride monohydrate. D.S.Yufit, A.I.Yanovskii, A.E.Kalinin, Yu.T.Struchkov, L.R.Barykina, I.N.Degtyareva (Inst. of Heteroorganic Compounds, Acad. of Sci., USSR). *Sov. Phys.-Crystallogr. (USA)*, vol.28, no.1, p.40-2 (Jan.-Feb. 1983). Translation of: *Kristallografiya (USSR)*, vol.28, no.1, p.79-83 (Jan.-Feb. 1983). [received: Sept. 1983]
For pt.VII see *Kristallografiya*, vol.27, p.258 or *Sov. Phys. Crystallogr.*, vol.27, p.158 (1982). The authors have made X-ray structural and IR spectroscopic investigations of 1-(2,5-dihydroxyphenyl)-thianium chloride monohydrate, $[\text{C}_6\text{H}_4\text{SO}^+\text{C}_6\text{H}_3(\text{OH})_2]\text{Cl}^- \cdot \text{H}_2\text{O}$, which has four symmetrically independent H bonds. The OH group in the ortho position is associated with the chlorine atom, the OH group in the meta position is associated with the oxygen atom of the water molecule, and the hydrogen atoms of the water form H bonds with chlorine atoms. Thus each chlorine atom is a proton acceptor for three hydrogen bonds simultaneously. The energies of the H bonds involving the hydroxyl groups are 7.4 ± 0.9 kcal/mole; the energies of the H bonds between the chloride anions and the water molecules are 5.0 ± 0.1 kcal/mole and 5.60 ± 0.04 kcal/mole. The conformation of the thianium ring is of the chair type; the sulfur atom has pyramidal bond configuration. (13 refs.)
- 113846** Crystal and molecular structures of *p*-nitrophenyl vinyl ether. D.S.Yufit, A.I.Yanovskii, Yu.L.Frolov, Yu.T.Struchkov (Inst. of Heteroorganic Compounds, Acad. of Sci., USSR). *Sov. Phys.-Crystallogr. (USA)*, vol.28, no.1, p.43-4 (Jan.-Feb. 1983). Translation of: *Kristallografiya (USSR)*, vol.28, no.1, p.84-6 (Jan.-Feb. 1983). [received: Sept. 1983]
The authors have made an X-ray structural analysis of *p*-nitrophenyl vinyl ether. They have determined the angles corresponding to the rotations of the benzene ring (27.4°) and vinyl group (36.6°) relative to the C-O-C plane. On

the basis of a comparison of the results with the IR and UV spectra, they advance the hypothesis that there are no appreciable changes in the molecular structure when the substance is dissolved in neutral solvents. (12 refs.)

113847 Crystal and molecular structures of 2,2'-dimethoxy-1,1'-dinaphthyl. G.V.Gridunova, V.E.Shklover, Yu.T.Struchkov, B.A.Chayonov (Sci.-Res. Inst. of Organic Intermediate Products & Dyes, USSR). *Sov. Phys.-Crystallogr. (USA)*, vol.28, no.1, p.45-7 (Jan.-Feb. 1983). Translation of: *Kristallografiya (USSR)*, vol.28, no.1, p.87-91 (Jan.-Feb. 1983). [received: Sept. 1983]

The authors have made an X-ray structural investigation of 2,2'-dimethoxy-1,1'-dinaphthyl. The molecule lies on the dyad axis. The slight increase in the length of the exocyclic C-O bond to 1.396(6) Å and the increase in the opposite endocyclic angle to 124.1(5)° apparently indicate that the methoxy substituent is an electron acceptor. The dihedral angle between the planes of the naphthyl groups within the molecule is 111°. (15 refs.)

113848 Structure of electrically conducting complexes based on cation radicals. IX. The cation-radical salt of tetraselenotetracene with the dibromocuprate anion (TSeT)⁺(CuBr₂)⁻. R.P.Shibaeva, V.F.Kaminskii, E.B.Yagubskii, L.A.Kushch (Inst. of Chem. Phys., Acad. of Sci., USSR). *Sov. Phys.-Crystallogr. (USA)*, vol.28, no.1, p.48-50 (Jan.-Feb. 1983). Translation of: *Kristallografiya (USSR)*, vol.28, no.1, p.92-5 (Jan.-Feb. 1983). [received: Sept. 1983]

For pt.VIII see *Kristallografiya*, vol.16, p.1224 or *Sov. Phys. Crystallogr.*, vol.26, p.695 (1981). The authors have made an X-ray structural investigation of the cation radical salt TSeT⁺(CuBr₂)⁻ (*a*=12.478 Å, *b*=9.997 Å, *c*=3.859 Å, α =96.70°, β =86.28°, γ =111.35°, space group P1). The structure was refined by the method of least squares to *R*=0.056. It contains infinite (along *c*) regular stacks of cation radicals TSeT⁺ with an interplanar distance TSeT⁺...TSeT⁺ of 3.55 Å. The CuBr₂⁻ anions have a very distorted linear configuration with the BrCuBr angle equal to 154°, and form zigzag chains, in which one of the Br atoms is bridging, extending along the direction of the cation-radical stacks. (12 refs.)

113849 Chelate-forming derivatives of 8-hydroxyquinoline. V. A complex dimer cation involving a protonized molecule in the crystal structure of bis-(8-hydroxy-2-quinolyl)amine. I.N.Polyakova, Z.A.Starikova, B.V.Parusnikov, I.A.Krasavin (All-Union Sci.-Res. Inst. of Chem. Reagents & Very Pure Chem. Substances, USSR). *Sov. Phys.-Crystallogr. (USA)*, vol.28, no.1, p.50-3 (Jan.-Feb. 1983). Translation of: *Kristallografiya (USSR)*, vol.28, no.1, p.96-101 (Jan.-Feb. 1983). [received: Sept. 1983]

The crystal structure of bis-(8-hydroxy-2-quinolyl)amine (AMIN-4) (diffractometer, method of least squares in anisotropic approximation to *R*=0.037) consists of complex dimer cations and OH⁻ anions. The cation is formed on account of a short H bond O...H...O (O...O=2.437 Å) between two AMIN-4 molecules, one of them being the hydroxy form protonized at N_{ox}, the other a bipolar ion, the independent part of the cation (its intrinsic symmetry is C₂) contains hydroxyquinoline and hydroxyquinolinium fragments; their combination in one molecule enables the authors to make a correct comparison of their geometries. Within the cation there are intramolecular H bonds N-H...N (N...N=2.606 Å), N-H...O (N...O=2.644 Å), and O-H...O (O...O=2.741 Å). (11 refs.)

113850 The crystal structure of [(CH₃)₂SiCH₂]₂SnF. L.N.Zakharov, Yu.T.Struchkov, E.A.Kuz'min, B.I.Petrov (Physicotech. Res. Inst., Acad. of Sci., USSR). *Sov. Phys.-Crystallogr. (USA)*, vol.28, no.2, p.158-61 (March-April 1983). Translation of: *Kristallografiya (USSR)*, vol.28, no.2, p.271-5 (March-April 1983). [received: Sept. 1983]

An X-ray structural investigation of [(CH₃)₂SiCH₂]₂SnF is made with the aim of elucidating the cause of the fact that organometallic compounds containing the substituent R=(CH₃)₂SiCH₂ are more thermostable than their alkyl analogs with less complex (unbranched) R. The crystal structure consists of one-dimensional chains of molecules in which the plane-trigonal [(CH₃)₂SiCH₂]₂Sn groups are linked by symmetrical bridges of F atoms, making up the coordination of the Sn atom to trigonal-bipyramidal. The Sn-F bonds in the chain are ionic-covalent. The crystal structure of [(CH₃)₂SiCH₂]₂SnF differs from the structures of [(CH₃)₂SiCH₂]₂SnI and (CH₃)₂SiSnF, which have been described previously. (24 refs.)

113851 Crystal and molecular structure of the 1:1 complex of 7,7,8,8-tetracyanoquinodimethane and 9,9'-trans-bis-telluraxanthenyl (C₁₂H₄N₄)(C₂₆H₁₈Te₂). R.M.Lobkovskaya, R.P.Shibaeva, O.N.Ermenko (Inst. of Chem. Phys., Acad. of Sci., USSR). *Sov. Phys.-Crystallogr. (USA)*, vol.28, no.2, p.161-3 (March-April 1983). Translation of: *Kristallografiya (USSR)*, vol.28, no.2, p.276-9 (March-April 1983). [received: Sept. 1983]

The authors have made an X-ray structural investigation of crystals of the complex (C₁₂H₄N₄)(C₂₆H₁₈Te₂) (*a*=8.878 Å, *b*=10.602 Å, *c*=10.275 Å, β =80.25°, γ =116.03°, space group P1, Z=1). The structure contains stacks of alternate donor (D) and acceptor (TCNQ) molecules with a mean interplanar distance of 3.37 Å. The D molecule lies at the center of symmetry and consists of two parts joined by a single bond C(sp²)-C(sp²)=1.586 Å, with the 'butterfly' conformation. The mean length of the Te-C(sp²) bond is 2.112 Å. The angle of bending of the three-ring system about the Te...C(sp²) line is 141°. (7 refs.)

113852 X-ray structural investigation of perfluoro-3,3,6,6,4',4'',4'''-octamethyl-1,2,4,5-dicyclobutenocyclohexa-1,4-diene, C₁₈F₂₈. M.Yu.Antipin, Yu.T.Struchkov, N.I.Delyagina, I.L.Knunyants (Inst. of Heteroorganic Compounds, Acad. of Sci., USSR). *Sov. Phys.-Crystallogr. (USA)*, vol.28, no.2, p.163-6 (March-April 1983). Translation of: *Kristallografiya (USSR)*, vol.28, no.2, p.280-5 (March-April 1983). [received: Sept. 1983]

The authors have made an X-ray structural investigation (diffractometer, direct method, method of least squares to *R*=0.095 from 1462 reflections) of the compound C₁₈F₂₈—the product of the reaction of chloroform with perfluoroisobutylene in the presence of cesium fluoride. They have found that the compound is an unsaturated perfluorooctamethyl-1,2,4,5-dicyclobutenocyclohexa-1,4-diene in which all the carbon atoms in the three-ring framework are practically collinear. The values of the geometric parameters of the molecule indicate that there are marked steric stresses due to the large number of bulky, electronegative CF₃ groups. (13 refs.)

113853 Crystal and molecular structure of tetracyclic nitroxyl biradical with three bridging bonds between the piperidine and dehydropiperidineoxyl fragments, C₂₂H₃₆N₂O₄. R.M.Lobkovskaya, R.P.Shibaeva, M.V.Sudnik, A.B.Shapiro (Inst. of Chem. Phys., Acad. of Sci., USSR). *Sov. Phys.-Crystallogr. (USA)*, vol.28, no.2, p.170-2 (March-April 1983). Translation of: *Kristallografiya (USSR)*, vol.28, no.2, p.291-5 (March-April 1983). [received: Sept. 1983]

The authors have made an X-ray structural investigation of the stable nitroxyl biradical C₂₂H₃₆N₂O₄ (*a*=11.340 Å, *b*=12.425 Å, *c*=8.360 Å, α =110.28°, β =100.77°, γ =93.98°, space group P1, Z=2). They show that

two of the six-membered hetero rings in the nitroxyl have chair conformation and one has half-boat conformation, while the five-membered hetero ring has envelope conformation. The mean length of the N-O bonds is 1.277(2) Å. For the paramagnetic centers in the crystal, the intermolecular distances are shorter than the intramolecular distances. (7 refs.)

113854 Structure of electrically conducting complexes based on cation radicals. X. Cation-radical salts of tetrathiotetracene and tetraselenotetracene with hexabromodimercure dication, (TTT)₂²⁺(Hg₂Br₆)²⁻ and (TSeT)₂²⁺(Hg₂Br₆)²⁻. R.P.Shibaeva, V.F.Kaminskii (Inst. of Chem. Phys., Acad. of Sci., USSR).

Sov. Phys.-Crystallogr. (USA), vol.28, no.2, p.173-6 (March-April 1983). Translation of: *Kristallografiya (USSR)*, vol.28, no.2, p.296-302 (March-April 1983). [received: Sept. 1983]

For pt.IX see *Kristallografiya*, vol.28, p.92 (1983) or *Sov. Phys. Crystallogr.*, vol.28, p.48 (1983). The authors have made an X-ray structural investigation of the cation-radical salts (TTT)₂(Hg₂Br₆) (*a*=14.155 Å, *b*=17.776 Å, *c*=10.752 Å, α =94.06°, β =100.33°, γ =96.87°, space group I1, Z=2) and (TSeT)₂(Hg₂Br₆) (*a*=10.617 Å, *b*=13.471 Å, *c*=10.582 Å, α =111.73°, β =100.92°, γ =81.77°, space group P1, Z=1). The structures are refined by the method of least squares to *R*=0.062 and *R*=0.049, respectively. The structures contain stacks of cation radicals parallel to the *c* direction with interplanar distances of TTT-TTT=3.44 Å and TSeT-TSeT=3.49 Å. The anionic part of the structure consists of centrosymmetric dimers (Hg₂Br₆)²⁻. (13 refs.)

Three-dimensional structure of the methyl ester of N-(1-carbomethoxy-2-phenylethyl)azyllyl phenylalanine, C₂₃H₂₆N₂O₅ See Entry 112865

Molecular and crystal structure of 2,2',4,4'-tetraaminodiphenyl at -120°C See Entry 112868

Conformation of the four independent molecules in the structure of cyclo[*L*-Val-*L*-His-] and symmetry relations between them See Entry 112869

Structure factors and elementary excitations of condensed matter See Entry 114459

Emission spectrum and crystal field parameters of pentanitratoeuropiate (III) ions See Entry 114501

Role of monovalent anions in organic superconductors See Entry 114637

61.70 DEFECTS IN CRYSTALS

(see also 61.80 Radiation damage, 62. Mechanical and acoustic properties, 71.55 Impurity and defect levels, 76.30M EPR of colour centres and other defects, 78.50 Impurity and defect absorption in solids, 81.40 Treatment of materials)

113855 A new method of the calculation of the hydrogen trap activation energy in metals. K.Y.Lee, J.-Y.Lee (Dept. of Materials Sci. & Engng., Korea Advanced Inst. of Sci. & Technol., Seoul, Korea). *J. Mater. Sci. Lett. (GB)*, vol.2, no.9, p.538-40 (Sept. 1983).

When several types of trapping site exist in one specimen several corresponding thermal analysis peaks will appear from the low temperature to the high temperature region at a heating rate. The trap activation energy, *E*_{tr}, for low temperature peaks can be calculated from the existing experimental data. The authors show how it is possible to calculate *E*_{tr} for the high temperature peaks without further experiments using an equation. (3 refs.)

113856 High resolution electron microscopy study of phosphate tungsten bronzes KP₂O₈(WO₃)_{2m}. I. Investigation of non-integral and high *m* values: defects resulting from intergrowths and interruption of 'P₂O₇' rows. M.Hervieu, B.Raveau (Lab. de Cristallographie, Univ. de Caen, Caen, France). *Chem. Scr. (Sweden)*, vol.22, no.3, p.117-22 (1983).

Previous investigations have reported the existence of a series of phosphate tungsten bronzes A₂P₂O₈(WO₃)_{2m} for integral *m* values ranging from 5 to 10. The authors' work deals with the high resolution electron microscopy study of the non integral *m* compositions and high *m* values (*m*>10). Crystals corresponding to these nominal compositions were frequently imperfect, contrary to the intermediate *m* values (5≤*m*≤10). However microcrystals corresponding to integral values higher than 10 have been isolated and characterized. This first part concerns phenomena related to intergrowths and defects resulting from the interruption of P₂O₇ rows. Two coherent intergrown phases have been observed for the lowest *m* values. The specific defects corresponding to the interruption of P₂O₇ rows in the ReO₃-type matrix confirms the great adaptability of the P₂O₇ groups to the ReO₃ type framework. (13 refs.)

113857 Planar defect in A15 structure observed in Cr-Si fine particles. T.Ishimasa, Y.Fukano (Coll. of General Education, Nagoya Univ., Nagoya, Japan).

Jpn. J. Appl. Phys. Part 1 (Japan), vol.22, no.7, p.1092-7 (July 1983). A new planar defect in the A15 structure was found in fine particles formed by the evaporation of Cr-Si alloy in Xe gas. Electron microscopic analysis showed that the planar defect lies on the {100} plane and the displacement vector due to the defect is <±1/8, 1/2, 0>*a*. A probable model of the defect is proposed. (9 refs.)

113858 A representation of the defect structure of pure barium titanate. J.F.Baumard, P.Abelard (Centre de Recherches sur la Phys. des Hautes Températures, CNRS, Orleans, France), D.M.Smyth.

Rev. Int. Hautes Temp. & Refract. (France), vol.20, no.1, p.3-16 (1983). In ternary oxides such as barium titanate, BaTiO₃, the concentration of point defects responsible for a departure from stoichiometry at constant total pressure depends on three thermodynamic variables, generally chosen as the temperature and two activities. As a consequence, the thermodynamic state of the compound may be represented by a point in a three-dimensional space, the coordinates of which are the temperature and two activities. Isothermal sections of this space are developed, in which domains of existence of majority defect pairs are established once a suitable intrinsic disorder has been selected. Such representations appear to be complementary to Kroger and Vink diagrams, as they allow a systematic study of point defects in ternary oxides. (23 refs.)

113859 Creation of point defects in superconductors. A short review. Y.Quere, F.Rullier-Albenque (SESI, CEN, Fontenay-aux-Roses, France). *Point Defects and Defect Interactions in Metals. Proceedings of the Yamada Conference V, Kyoto, Japan, 16-20 Nov. 1981 (Amsterdam, Netherlands: North-Holland 1982)*, p.609-13

Many experiments have been published concerning the radiation damage in superconductors, but relatively few about the mechanisms of defect creation. A short review is presented of what is known on point defect creation in superconductors either by coldwork or by irradiation. (21 refs.)

- 113860 Free energy calculation of small clusters.** G.Martin (Section de Recherches de Metall. Phys., CENS, Gif-sur-Yvette, France), A.Perini, G.Jacucci.
Point Defects and Defect Interactions in Metals. Proceedings of the Yamada Conference V, Kyoto, Japan, 16-20 Nov. 1981 (Amsterdam, Netherlands: North-Holland 1982), p.718-21.
A new Monte Carlo technique is proposed to compute directly the free energy difference of two clusters of $N+1$ and N particles. The algorithm has been checked on the 2-dimensional lattice gas model with nearest neighbour interactions and produced high accuracy data. The results match very well the predictions of capillarity approximation down to $N \approx 10$ provided that the logarithmic correction $\tau \ln N$ is included; $\tau = 1.25$ in agreement with most recent theoretical predictions. (10 refs.)
- Defects in Semiconductors II, Symposium Proceedings** See Entry 11315
- Elastic media with microstructure II. Three-dimensional models** See Entry 11318
- Radiation effects computer experiments** See Entry 11332
- Advances in the infrared microscopy of electronic materials** See Entry 11761
- Microstructure and topography [laser annealing of semiconductors]** See Entry 113709
- Shape control of non-metallic inclusions in Al-deoxidized steel by calcium treatment** See Entry 113728
- Identification of small point defect clusters by high resolution electron microscopy** See Entry 113893
- Studies of point defect clusters with an electron microscope** See Entry 113895
- Effect of impurity atoms on the formation of secondary defects in quenched aluminium** See Entry 113921
- Appearance of an impurity ionization mechanism of defect formation in indium antimonide as a result of 'suprathreshold' irradiation** See Entry 113986
- Monte-Carlo simulation of void nucleation during irradiation** See Entry 113993
- Mechanism of void formation of iron and iron-alloys irradiated by electrons** See Entry 114039
- Voids and bubbles in argon irradiated nickel** See Entry 114061
- Structure and dynamics of disordered solids: a neutron scattering study of $Ba_{1-x}La_xF_{2+x}$** See Entry 114250
- The effects of defect character on hydrogen diffusion in metals** See Entry 114257
- Interfacial stability of migrating brine inclusions in alkali halide single crystals supporting a temperature gradient** See Entry 114280
- RF plasma annealing of as-grown defects in the Si/SiO₂ system** See Entry 114374
- Energy spectrum of defects in silicon irradiated with hydrogen and helium ions** See Entry 114474
- Muon spin relaxation analysis by trapping model with detrapping** See Entry 114768
- Two-dimensional angular correlation positron studies of defect and defect related problems in metals** See Entry 114955
- The study of thermal equilibrium defects and melting in indium by two-parameter correlation measurement of positron annihilation** See Entry 114956
- Improved hetroback procedures for liquid-phase-epitaxial growth of planar and buried heterostructures** See Entry 115114
- Physicochemical aspects of production of ferroelectric ceramics** See Entry 115148
- Formation of defects during the solidification of alloys in a two-dimensional region with a short-life internal heat sink** See Entry 115187

61.70B Interstitials and vacancies

(exc. colour centres)

- 113861 Defects in quenched and annealed Al-Ge alloys.** H.Murakami, I.Kanazawa, Y.Tsumigi (Dept. of Phys., Tokyo Gakugei Univ., Tokyo, Japan).
Jpn. J. Appl. Phys. Part 1 (Japan), vol.22, no.6, p.1066 (June 1983).
In a study carried out using transmission electron microscopy, it was found that the small clusters formed in the quenched alloys annihilate through vacancy emission during annealing at 423K; and dislocation loops, formed together with the clusters, grow by the absorption of vacancies emitted by the clusters. (6 refs.)
- 113862 The calculated defect structure of thorium.** E.A.Colbourn, W.C.Mackrodt (New Sci. Group, ICI plc, Runcorn, England).
J. Nucl. Mater. (Netherlands), vol.118, no.1, p.50-9 (Aug. 1983).
The calculated energies of lattice and electronic disorder in thorium are outlined. From these the fundamental defect structure, electronic energy levels and oxidation-reduction potentials are deduced. This enables the reported diffusion and electrical conductivity data to be reassessed and alternative defect mechanisms for these processes to be suggested. (41 refs.)
- 113863 A quantitative study of vacancy defects in quenched tungsten by combined field-ion microscopy and electrical resistometry.** J.Y.Park (Materials Sci. & Technol. Div., Argonne Nat. Lab., Argonne, IL, USA), H.-C.W.Huang, R.W.Siegel, R.W.Balluffi.
Philos. Mag. A (GB), vol.48, no.3, p.397-419 (Sept. 1983).
A study of quenched, high-purity tungsten has been carried out with a combination of field-ion microscopy (FIM) and electrical resistivity measurements. It is concluded that the quenched-in vacancy defects observed by FIM are monovacancies and nearest-neighbour divacancies. From the partitioning during quenching between these two species, a divacancy binding enthalpy $H_{2v}^b \approx 0.7$ eV is deduced. A monovacancy resistivity of $7 \times 10^{-4} \Omega$ cm is obtained from the combined measurements. The quenched-in vacancy concentrations measured directly by FIM are consistent with previous results, if the total vacancy concentration at the melting temperature of tungsten (3695K) is about 3×10^{-4} and the monovacancy formation enthalpy and entropy are 3.6 eV and 3.2k, respectively. The results are discussed in terms of the atom-defect mechanisms for self-diffusion in tungsten. (28 refs.)
- 113864 Mobilities of quenched-in defects in NiAl.** Tian-Min Wang, M.Shimotomai, M.Doyama (Dept. of Materials Sci., Univ. of Tokyo, Tokyo, Japan).
Philos. Mag. A (GB), vol.48, no.3, p.L5-7 (Sept. 1983).
Samples of the intermetallic compound NiAl have been quenched from 800-1400°C and their recovery behaviour studied by positron annihilation techniques. Two distinct recovery stages were found by Doppler broadening measurements, one at around 280°C and the other at around 500°C. It is

shown that vacancies anneal out at the latter stage. The former stage is ascribed to the migration of divacancies to form voids. (7 refs.)

- 113865 Estimation of the vacancy formation enthalpy of metals.** A.R.Patete, J.P.Neumann (Dept. of Metall. Engng., Univ. of Alabama, University, AL, USA).
Ser. Metall. (USA), vol.17, no.8, p.1047-8 (Aug. 1983).
Examines the work of Neumann (see *Acta Metall.*, vol.28, p.1165, 1980) and Tiwari and Patil (see *Scripta Metall.*, vol.9, p.833, 1975) both concerning the vacancy formation enthalpy (ΔH_v) of metals. The present authors attempt to explain the considerable discrepancy that exists between the ΔH_v values predicted by the two different correlations. (12 refs.)
- 113866 New exciton mechanism for the formation of Frenkel defects in ionic crystals.** P.K.Khabibullaev, S.Dzhumanov (Inst. of Nuclear Phys., Acad. of Sci., Ulugbek, Uzbek SSR).
Sov. Phys.-Dokl. (USA), vol.27, no.12, p.1050-1 (Dec. 1982). Translation of: *Dokl. Akad. Nauk SSSR*, vol.267, no.4-6, p.1361-3 (Dec. 1982). [received: Sept. 1983].
The excitation of excitons in alkali-halide and fluorite crystals leads to the formation of Frenkel pairs of effects (F-H pairs). However, the mechanism for this effect is not completely understood. The mechanisms which have been proposed earlier first of all do not consider all the stages of the exciton-defect transformation and, secondly, predict that the defect production is temperature dependent in all alkali-halide crystals, a prediction which is not borne out by experiment. The authors develop a theory of the exciton mechanism for the formation of defects in ionic crystals. (10 refs.)
- 113867 Distribution of the internal distances in Frenkel pairs in irradiated silicon and germanium.** A.N.Kraichinskii, L.V.Mizrukhn, V.I.Shakhovtsov (Inst. of Phys., Acad. of Sci., Kiev, Ukrainian SSR).
Sov. Phys.-Semicond. (USA), vol.17, no.3, p.269-72 (March 1983). Translation of: *Fiz. & Tekh. Poluprovodn. (USSR)*, vol.17, no.3, p.437-40 (March 1983). [received: Sept. 1983].
A model is proposed for the process of formation of defects in semiconductors in which the components of Frenkel pairs are mobile during irradiation. The model is based on the screening of these components by equilibrium or nonequilibrium carriers. A study is made of the possibility of deriving the distribution function of the internal distances in genetic Frenkel pairs using the experimental dependences of the defect formation efficiency on the rate of electron irradiation or on the concentration of dopant impurities. A calculation is made of the distribution function of the internal distances in Frenkel pairs formed in silicon and in germanium. (8 refs.)
- 113868 Effects of relaxation round point defects in the alkali metals on formation energies.** F.Flores (Dept. del Estado Solido, Univ. Autonoma, Madrid, Spain), N.H.March.
Point Defects and Defect Interactions in Metals. Proceedings of the Yamada Conference V, Kyoto, Japan, 16-20 Nov. 1981 (Amsterdam, Netherlands: North-Holland 1982), p.85-92.
Vacancy and interstitial formation energies in the nearly-free electron alkali metals Na and K are studied using a model of complete relaxation. It is argued then that the interstitial with the lowest formation energy is that in which the relaxed near-neighbour configuration most closely resembles the local relaxation round the vacancy. For this configuration, the ratio of interstitial to vacancy formation energy is calculated. Reasonable estimates show that the formation energy of the interstitial in Na is only some hundredths of an electron volt higher than that for the vacancy. The interest for diffusion mechanisms in Na and K is emphasized. (6 refs.)
- 113869 Point defects and radiation effects in BCC metals.** W.Frank (Max-Planck-Inst. fur Metall., Stuttgart, Germany).
Point Defects and Defect Interactions in Metals. Proceedings of the Yamada Conference V, Kyoto, Japan, 16-20 Nov. 1981 (Amsterdam, Netherlands: North-Holland 1982), p.203-8.
Gives an overview of scientific knowledge on intrinsic point defects in α -Fe and Ta deduced from equilibrium experiments (self-diffusion, positron annihilation) and steady-state experiments (growth of dislocation loops under irradiation in a transmission electron microscope) at elevated temperatures as well as from non-equilibrium studies (electrical resistivity, internal friction, magnetic after-effect, positron annihilation) performed at low temperatures after particle irradiation, cold-work, or quenching. It is shown that the one-interstitial model fails to explain the observations. By contrast, in the two-interstitial model a natural and internally consistent interpretation is possible, which may be extended to the other BCC refractory metals. (41 refs.)
- 113870 On the validity of the one- and two-interstitial models.** W.Schule (Materials Sci. Div., Joint Res. Centre, Ispra, Italy).
Point Defects and Defect Interactions in Metals. Proceedings of the Yamada Conference V, Kyoto, Japan, 16-20 Nov. 1981 (Amsterdam, Netherlands: North-Holland 1982), p.209-12.
Attention is focused on inconsistencies of results of experiments with predictions of the one-interstitial model, e.g. the stage III dilemma. It is then shown that results of measurements of radiation enhanced self-diffusion in nickel and of the radiation damage rate performed in many different laboratories are not consistent with the predictions of the two existing radiation damage models. It is found from the above-mentioned experimental results that the recombination volume between self-interstitials and vacancies, and between defects and defect clusters, must be of the order of $2 \cdot 10^3$ and 10^5 atomic volumes, respectively, and that the migration activation energies of defects decreases with increasing irradiation flux because of an interaction between the high energy particles with the lattice atoms. A modified two-interstitial model is presented which contains these new features. (15 refs.)
- 113871 Defects in copper studied by PAC between 10K and 800K.** M.Deicher, G.Grubel, R.Minde, E.Reckagel, Th.Wichert (Fakultat fur Phys., Univ. Konstanz, Konstanz, Germany).
Point Defects and Defect Interactions in Metals. Proceedings of the Yamada Conference V, Kyoto, Japan, 16-20 Nov. 1981 (Amsterdam, Netherlands: North-Holland 1982), p.220-3.
The perturbed angular correlation technique (PAC) is used to clarify the defect situation in copper between stages I and V. The experimental results obtained for self-interstitials, vacancies and defect clusters under different damaging conditions are shown. Their microscopic interpretation within the scope of the results of complementary experimental methods is discussed. (10 refs.)
- 113872 Intrinsic thermal expansion of point defects in metals.** J.P.Ganne, Y.Quere (Section d'Etudes des Solides Irradies, CEN, Fontenay aux Roses, France).
Point Defects and Defect Interactions in Metals. Proceedings of the Yamada Conference V, Kyoto, Japan, 16-20 Nov. 1981 (Amsterdam, Netherlands: North-Holland 1982), p.232-5.
The intrinsic thermal expansion coefficient of various intrinsic or extrinsic point defects has been measured. For radiation defects in aluminium, the authors have found a high value of its ratio to the matrix coefficient

($\beta_D/\beta_0=12$). This result confirms the idea that a point defect may be strongly anharmonic. Many data on dilute copper alloys are given. Comparison with theoretical calculations is made when possible. (12 refs.)

113873 Thermal generation of vacancies in aluminum. T.Kino, K.Ono (Lab. of Crystal Phys., Hiroshima Univ., Hiroshima, Japan). Point Defects and Defect Interactions in Metals. Proceedings of the Yamada Conference V, Kyoto, Japan, 16-20 Nov. 1981 (Amsterdam, Netherlands: North-Holland 1982), p.247-52.
Thermal generation of vacancies from dislocations, faulted loops and octahedral voids in zone refined aluminum were investigated by means of the pulse heating technique. These sources were examined by an electron microscope to determine their densities and sizes. The concentration of vacancies generated from the faulted loops and small voids attained to over-saturation within 10 m sec, but the ones from dislocations and large voids did not exceed the equilibrium concentration. Especially in the case generation from dislocations, it took a long time to attain the equilibrium level. These differences in the generation profile are explained by the characteristic energy to promote or suppress the generation of a vacancy from various sources. (13 refs.)

113874 Vacancy clustering during oxidation of nickel, magnesium, and zinc. C.G.Deacon, M.H.Loretto, R.E.Smallman (Dept. of Metall. & Materials, Univ. of Birmingham, Birmingham, England). Point Defects and Defect Interactions in Metals. Proceedings of the Yamada Conference V, Kyoto, Japan, 16-20 Nov. 1981 (Amsterdam, Netherlands: North-Holland 1982), p.253-6.
Specimens of nickel have been oxidised at 1000°C and measurements of weight gain, density change, length change and void density have been made together with measurements of the stress exerted by the oxide on the metal in an attempt to understand the origin of vacancy clusters found during the oxidation of nickel. Observations have also been carried out of the oxide-metal interface of oxidised Mg and Zn single crystals of (1120) and [0001] orientations. The observations are discussed in terms of the role of vacancy injection, stress and gas in void formation. (4 refs.)

113875 Properties of point defects in FCC metals. W.Schule, R.Scholz (Materials Sci. Div., Joint Res. Centre, Ispra, Italy). Point Defects and Defect Interactions in Metals. Proceedings of the Yamada Conference V, Kyoto, Japan, 16-20 Nov. 1981 (Amsterdam, Netherlands: North-Holland 1982), p.257-60.
The resistivity changes due to vacancies in copper, silver and gold were determined by: (i) quenching from temperatures between 300 and 600°C and by (ii) making measurements of the electrical resistivity as a function of the temperature between ambient temperature and the melting temperature. The resulting resistivity changes due to vacancies were much larger than those reported so far in the literature which were mainly obtained by quenching from high temperatures. The authors analysed their data together with results obtained in other laboratories by Simmons and Balluffi by quenching, by measurements of self-diffusion coefficients and of the isotope effect, and by positron annihilation. The metals nickel, aluminium and platinum were also included in this analysis and information was obtained on E_{IV}^F , E_{IV}^M , E_{2V}^M , E_{2V}^F , S_{IV}^F and S_{2V}^F . (11 refs.)

113876 Vacancies in silver: a resistivity and positron annihilation study. J.Hillairet, C.Mairy (Dept. de Recherche Fondamentale, CENG Grenoble, Grenoble, France), C.Minier, P.Hautajarvi, A.Vehanen. Point Defects and Defect Interactions in Metals. Proceedings of the Yamada Conference V, Kyoto, Japan, 16-20 Nov. 1981 (Amsterdam, Netherlands: North-Holland 1982), p.284-7.
Resistivity and positron lifetime measurements were performed to follow the annealing of the vacancy defects in quenched or irradiated high purity silver. For quench temperatures in the range 400°C to 500°C, the quenched-in resistivity is restored in one single stage centered at 40°C. An activation energy of 0.64±0.06 eV is inferred for the migration of the single vacancies. This result together with information derived from the evolution of positron lifetime spectra leads to the conclusion that stage III is to be assigned to monovacancy migration. Further results obtained in α -AgZn solid solutions support this view. (20 refs.)

113877 Vacancy-thermal expansion in aluminium. Ph.Audit (Lab. PMTM, Univ. Paris-Nord, Villetaneuse, France). Point Defects and Defect Interactions in Metals. Proceedings of the Yamada Conference V, Kyoto, Japan, 16-20 Nov. 1981 (Amsterdam, Netherlands: North-Holland 1982), p.291-3.
Using thermodynamics the author has derived a temperature-differential equation for the vacancy formation volume in terms of the bulk modulus and the static ion displacements. Combining the DRT interionic potentials with a lattice statics calculations of the displacements one is able to solve the equation for the vacancy formation volume as a function of temperature. The author obtains values of the vacancy thermal expansion coefficient ranging between 4.4 β_0 at T=250K and 12.6 β_0 at 800K where β_0 is the perfect crystal coefficient. (7 refs.)

113878 Configurations of point defects in neutron-irradiated iron. M.Weller, J.Diehl (Max-Planck-Inst. fur Metallforschung, Inst. fur Werkstoffwissenschaften, Stuttgart, Germany). Point Defects and Defect Interactions in Metals. Proceedings of the Yamada Conference V, Kyoto, Japan, 16-20 Nov. 1981 (Amsterdam, Netherlands: North-Holland 1982), p.417-20.
High purity iron part of it doped with 150 at.ppm carbon, was irradiated with 3.10^{17} n/cm² at 20K. The internal friction (1 Hz) of poly and monocrystals with (110) or (100) oriented torsion axes was measured (starting at 4K) after irradiation and after annealing treatments between 170K and 385K. From the anisotropy of the relaxation strength conclusions are drawn on the configurations of reorientating (anisotropic) point defects such as SIAs (self interstitial atoms), SIA-clusters, SIA-carbon and vacancy-carbon complexes. (7 refs.)

113879 Submicroscopic vacancy defects in pure and doped gold. C.Corbelle (CEN, Fontenay-aux-Roses, France), P.Moser. Point Defects and Defect Interactions in Metals. Proceedings of the Yamada Conference V, Kyoto, Japan, 16-20 Nov. 1981 (Amsterdam, Netherlands: North-Holland 1982), p.445-8.
A positron lifetime investigation of the annealing behaviour of irradiated pure Au and doped Au with the solute Sb, Ge and Fe atoms shows that submicroscopic vacancy clusters are formed during the stage III. In doped Au, they are heterogeneously formed which enhances their density in Au-Ge, enhances their average size in Au-Sb and delays their formation in Au-Fe. Mobile vacancy-solute Sb or Ge complexes are involved in the clustering process in Au-Sb and Au-Ge. (7 refs.)

113880 Vacancy formation in Ni and Ni(Ge). L.C.Smedskjaer, M.J.Flus, D.G.Legnini, M.K.Chason, R.W.Siegel (Materials Sci. Div., Argonne Nat Lab., Argonne, IL, USA). Point Defects and Defect Interactions in Metals. Proceedings of the Yamada Conference V, Kyoto, Japan, 16-20 Nov. 1981 (Amsterdam, Netherlands: North-Holland 1982), p.449-52.
Vacancy formation in Ni and Ni(1 at.% Ge) was studied under thermal equilibrium conditions using positron annihilation Doppler-broadening. A monovacancy formation enthalpy of 1.8 ± 0.1 eV was determined for pure Ni; combining this result with those from previous tracer self-diffusion measurements, a monovacancy migration enthalpy of 1.1 ± 0.1 eV was also deduced. An effective vacancy formation enthalpy of 1.4 eV was found for Ni(1 at.% Ge). Using a model to simulate the free and bound-vacancy ensemble in the alloy, a value of 0.7 eV was obtained for the formation enthalpy of Ge-bound vacancies. The results are compared with previous theoretical and experimental results. (14 refs.)

113881 Behavior of point defects in ice crystals revealed by X-ray topography. T.Hondoh, T.Itoh, A.Higashi (Dept. of Appl. Phys., Hokkaido Univ., Sapporo, Japan). Point Defects and Defect Interactions in Metals. Proceedings of the Yamada Conference V, Kyoto, Japan, 16-20 Nov. 1981 (Amsterdam, Netherlands: North-Holland 1982), p.599-601.
Formation process and behavior of various features of dislocation loops and minute defects found in ice crystals subjected to heat treatment were investigated by X-ray diffraction topographic method. It was found that dominant point defects in ice are interstitials at temperatures above -50°C, while they are vacancies below -50°C. Formation energies of both interstitials and vacancies are discussed in the light of new data of equilibrium concentrations of both defects in the authors' studies. (7 refs.)

113882 Defects and diffusion in intermetallic compounds. G.Frohberg, H.Weber (Inst. fur Metallforschung, Tech. Univ. Berlin, Berlin, Germany). Point Defects and Defect Interactions in Metals. Proceedings of the Yamada Conference V, Kyoto, Japan, 16-20 Nov. 1981 (Amsterdam, Netherlands: North-Holland 1982), p.614-18.
In the intermetallic compounds γ -Cu₃Sn and β -CoGa the formation enthalpy of vacancies strongly depends on vacancy concentration. Theoretical investigations yield the same result. Thus it is possible to explain the existence of structural vacancies in terms of usual thermodynamic relations. The diffusion mechanism in these compounds is discussed on the basis of recent experimental results. (10 refs.)

113883 Point defects in BCC Fe-Al, Fe-Co, and Fe-Co-V ordered alloys. J.P.Riviere, J.F.Dinhut (Lab. de Metall. Phys., Univ. de Poitiers, Poitiers, France). Point Defects and Defect Interactions in Metals. Proceedings of the Yamada Conference V, Kyoto, Japan, 16-20 Nov. 1981 (Amsterdam, Netherlands: North-Holland 1982), p.619-26.
Radiation damage produced at 20K by 2.5 MeV electrons is studied in three B₂ type Fe-40 at.% Al, Fe-Co, Fe-Co-V ordered alloys. The resistivity damage in Fe-40 at.% Al ordered single crystals is found less effective in the (111) directions. The results suggest that replacement collision chains are difficult to propagate along the (111) direction. Frenkel pair creation superimposed with disordering can account for the resistivity damage in the initially ordered Fe-Co alloy. Information concerning replacement collision sequences in (111) direction is derived. During the recovery of all the alloys, three main stages are observed and an ordering enhancement occurs. (30 refs.)

113884 Vacancies in B₂(CsCl) type ordered alloys. F.Nakamura, J.Takamura (Dept. of Metal Sci. & Technol., Kyoto Univ., Kyoto, Japan). Point Defects and Defect Interactions in Metals. Proceedings of the Yamada Conference V, Kyoto, Japan, 16-20 Nov. 1981 (Amsterdam, Netherlands: North-Holland 1982), p.627-30.
The formation of vacancies (structural and thermal vacancies) in the B₂ type ordered alloy is discussed with a model based upon the Bragg-Williams approximation assuming the nearest neighbor interaction, where A-, B-atoms and vacancies are allowed to be located on both α - and β -sublattices. Calculations were made of the composition dependence of the effective formation energy of thermal vacancies in NiAl alloys and also the temperature dependence of the positron annihilation parameter in a CuZn alloy, and the results successfully describe the experimental results in the literature. (13 refs.)

113885 Defect structures in β -NiAl and their response to electron irradiation. H.C.Liu, T.Mukai, T.E.Mitchell (Dept. of Metall., Case Western Reserve Univ., Cleveland, OH, USA). Point Defects and Defect Interactions in Metals. Proceedings of the Yamada Conference V, Kyoto, Japan, 16-20 Nov. 1981 (Amsterdam, Netherlands: North-Holland 1982), p.635-8.
Defect structures in β -NiAl alloys were studied by TEM. Diffuse rings of intensity maxima have been observed in diffraction patterns of both Ni-poor and Ni-rich NiAl, providing evidence for short-range ordering of structural point defects in β -Ni_{1-x}Al. Furthermore, diffuse streaks along (110) and (112) directions are also observed in diffraction patterns of 50, 55, 58 and 60 at.% Ni alloys. These diffuse streaks are related to pre-martensitic instabilities of Ni-rich NiAl. Electron irradiation by HVEM was found to destroy the short-range order. Irradiation of 50, 55 and 58 at.% Ni specimens at 700K created high densities of {001}{001} interstitial loops, but only created a low density of small defect clusters in 46 at.% Ni specimen. This is interpreted in terms of recombination of radiation-induced interstitials with the high concentration of structural Ni vacancies in Ni-poor NiAl. (10 refs.)

113886 Frenkel defects in Ni and Ni-base alloys. O.Bender, P.Ehrhart (Inst. fur Festkörperforschung, KFA, Jülich, Germany). Point Defects and Defect Interactions in Metals. Proceedings of the Yamada Conference V, Kyoto, Japan, 16-20 Nov. 1981 (Amsterdam, Netherlands: North-Holland 1982), p.639-42.
The defect structure produced by low temperature (4K) electron irradiation in single crystals of Ni, Ni₆₂Cu₃₈ and Ni₃Fe was investigated by measurements of the diffuse scattering of X-rays (Huang Diffuse Scattering), the change of the lattice parameter and the change of the electrical resistivity. The volume relaxation and the structure of the selfinterstitial atom (SIA) are very similar for the alloys and the pure FCC metals. The interstitial clustering processes during stage I and II proceed progressively more slowly in Cu, Ni, NiCu and Ni₃Fe respectively. In Ni₃Fe even the di-interstitial seems immobile up to stage III. The formation of large vacancy agglomerates during stage III annealing is only observed with the pure metals Ni and Cu. Interstitial mobility during annealing in stage II contributes to the decomposition of NiCu but not to the ordering of Ni₃Fe. There is an increase of order for highly ordered Ni₃Fe (S=0.7) during annealing in stage III and, within the errors, no change for samples with S=0. (8 refs.)

113887 Vacancies in concentrated alloys. M.Doyama (Dept. of Metall., Univ. of Tokyo, Tokyo, Japan), J.S.Koehler.

Point Defects and Defect Interactions in Metals. Proceedings of the Yamada Conference V, Kyoto, Japan, 16-20 Nov. 1981 (Amsterdam, Netherlands: North-Holland 1982), p.643-6

The quasi-chemical approach has been applied to calculate the formation energies of a vacancy in pure metals and random concentrated binary alloys. The relation between the observed formation energies and the melting point (solidus temperature), and electron per atom ratio, and the ratio of the fractional concentration of alloying element to the solubility limit of the alloying element, and the Fermi energy are discussed. (4 refs.)

113888 A method for determining the vacancy concentration in concentrated alloys by resistivity measurements utilizing the rate of short range order formation. K.Lucke (RWTH Aachen, Aachen, Germany), H.Heidsiek, W.Kohl, R.Scheffel.

Point Defects and Defect Interactions in Metals. Proceedings of the Yamada Conference V, Kyoto, Japan, 16-20 Nov. 1981 (Amsterdam, Netherlands: North-Holland 1982), p.647-52

A method is presented to determine the vacancy concentration in concentrated alloys by electrical resistivity measurements in cases in which the direct vacancy induced resistivity is negligibly small compared to the contributions due to changes in short range order. By assuming that the ordering rate as diffusion controlled is proportional to the vacancy concentration, the vacancy concentration can be determined, if the relationship between short range order and resistivity and the kinetics of ordering are known. For two different examples, Au15 at.% Ag and Ni11.4 at.% Cr, it is shown how to derive these relationships and the activation energies for formation and migration of vacancies and independently that for selfdiffusion. Also the annihilation kinetics of quenched-in vacancies can be derived in this way. (12 refs.)

113889 Formation and migration energies of a vacancy and kinetics of short range ordering in α -Cu-Al alloys. C.Kinoshita, M.Kutsuwada, T.Kamino (Dept. of Nuclear Engng., Kyushu Univ., Fukuoka, Japan).

Point Defects and Defect Interactions in Metals. Proceedings of the Yamada Conference V, Kyoto, Japan, 16-20 Nov. 1981 (Amsterdam, Netherlands: North-Holland 1982), p.653-5

A general equation is derived which describes the time dependence of the vacancy concentration as well as the short-range ordering in binary substitutional alloys. The general equation is applied for an analysis of observed variation in electrical resistivity of α -Cu-Al alloys during isothermal annealing after quenching. It is shown that those data fit on a single master curve for each alloy by a suitable choice of the values for the formation and migration energies of a vacancy. (8 refs.)

113890 Self-interstitial mobility in a neutron-irradiated austenitic $\text{Fe}_{90}\text{Cr}_{16}\text{Ni}_{25}$ alloy. C.Dimitrov, M.Da Cunha Belo, O.Dimitrov (Centre d'Etudes de Chimie Metall., CNRS, Vitry, France).

Point Defects and Defect Interactions in Metals. Proceedings of the Yamada Conference V, Kyoto, Japan, 16-20 Nov. 1981 (Amsterdam, Netherlands: North-Holland 1982), p.660-3

The annealing of the electrical resistivity of a $\text{Fe}_{90}\text{Cr}_{16}\text{Ni}_{25}$ austenitic alloy has been investigated after neutron irradiation at 23K to doses of 2.1×10^{17} to $2.7 \times 10^{18} \text{ n.cm}^{-2}$. The influence of defect concentration on recovery processes and determinations of activation energy were used for obtaining information on the point defect mobility. It is concluded that, in this alloy, the more mobile defects (probably self-interstitials) perform long range migration at a relatively high temperature ($\geq 190\text{K}$) with a migration energy of $86 \pm 6 \text{ kJ.mol}^{-1}$. Slower defects, probably vacancies, migrate with an energy of $128 \pm 7 \text{ kJ.mol}^{-1}$. (6 refs.)

113891 Detection of point defects and dynamic observation of defect interaction by atom resolution electron microscopy. H.Hashimoto, Y.Takai, N.Ajika, Y.Yokota, H.Endoh (Dept. of Appl. Phys., Osaka Univ., Osaka, Japan).

Point Defects and Defect Interactions in Metals. Proceedings of the Yamada Conference V, Kyoto, Japan, 16-20 Nov. 1981 (Amsterdam, Netherlands: North-Holland 1982), p.698-701

Gold films containing a few percent silver are exposed to 2 MeV electrons to introduce the vacancy and stacking fault tetrahedra and are studied by an atom resolution electron microscope which can obtain the images of atoms at atom positions and TV system. Atom images with less bright contrast are attributed to the images of single vacancies by comparing the theoretical calculation. Stacking fault tetrahedra (SFT) with black and white contrast are studied. The contrast change of atom images in the region of SFT is attributed to the movement of vacancies. Contrast anomalies of the images of the twins and their intermittent growth are attributed to the included silver atoms. (5 refs.)

113892 Image contrast of single vacancies and small stacking fault tetrahedra in gold crystals studied by an atom resolution electron microscope. Y.Takai, N.Ajika, H.Hashimoto (Dept. of Appl. Phys., Osaka Univ., Osaka, Japan).

Point Defects and Defect Interactions in Metals. Proceedings of the Yamada Conference V, Kyoto, Japan, 16-20 Nov. 1981 (Amsterdam, Netherlands: North-Holland 1982), p.702-4

Small stacking fault tetrahedra in gold crystals produced by the irradiation of 2 MeV electrons were observed in atomic scale by using a 100 kV high resolution electron microscope. By comparison with theoretical calculations, the smallest one observed with good contrast seems to be formed by several vacancies. Contrast anomalies which seem to be due to single vacancies were also observed and discussed by comparing with the calculated results by using a proposed model of a single vacancy. (5 refs.)

113893 Identification of small point defect clusters by high resolution electron microscopy. T.Nishida, K.Izui (JAERI, Ibaraki, Japan).

Point Defects and Defect Interactions in Metals. Proceedings of the Yamada Conference V, Kyoto, Japan, 16-20 Nov. 1981 (Amsterdam, Netherlands: North-Holland 1982), p.705-7

Many beam lattice images of small point defect clusters such as interstitial loops, vacancy loops and voids in an aluminium crystal are calculated by using the multislice theory under various imaging conditions. High voltage Scherzer focus images are found to be useful for the identification of these point defect clusters. (5 refs.)

113894 High resolution electron microscopic observations of small point defect clusters and their thermal stability. Y.Shimomura, K.Kitagawa, Y.Takai, H.Hashimoto (Appl. Phys. & Chem. Dept., Hiroshima Univ., Hiroshima, Japan).

Point Defects and Defect Interactions in Metals. Proceedings of the Yamada Conference V, Kyoto, Japan, 16-20 Nov. 1981 (Amsterdam, Netherlands: North-Holland 1982), p.708-11

Pure aluminium foils were irradiated at 130K with 200 keV electrons in an electron microscope and radiation induced point defect clusters were observed by the weak beam method. Vacancy clusters are formed only near the bottom surface. The number density of small vacancy clusters decreases at about

-50°C during warming up of irradiated specimens. In order to study the atomic structure of small point defect clusters in metals, high resolution structure image method have been carried out for small voids and dislocation loops in quenched pure aluminium. Details of structure of these small clusters were revealed clearly on the pictures. (no refs.)

113895 Studies of point defect clusters with an electron microscope. Y.Shimomura, K.Yamakawa, K.Kitagawa, H.Oda (Appl. Phys. & Chem. Dept., Hiroshima Univ., Hiroshima, Japan).

Point Defects and Defect Interactions in Metals. Proceedings of the Yamada Conference V, Kyoto, Japan, 16-20 Nov. 1981 (Amsterdam, Netherlands: North-Holland 1982), p.712-17

Two related topics are reported briefly. One of the formation of voids in quenched pure aluminium and aluminium dilute alloys. In quenched pure aluminium, a void is formed at a small vacancy cluster which contains a single hydrogen atom. Moreover voids are nucleated at small solute atom clusters in quenched aluminium dilute alloys. Another is the formation of vacancy clusters in pure copper and silver which are quenched in ultra-high vacuum. Vacancy clusters are observed only in the specimen outgassed elaborately. These suggest that a vacancy interacts strongly with gas atoms in these metals. (4 refs.)

113896 Structure of small vacancy clusters in FCC solids and influence of the interatomic potentials. N.V.Doan (Section de Recherches de Metall. Phys., CENS, Gif-sur-Yvette, France).

Point Defects and Defect Interactions in Metals. Proceedings of the Yamada Conference V, Kyoto, Japan, 16-20 Nov. 1981 (Amsterdam, Netherlands: North-Holland 1982), p.722-5

The structure of small vacancy clusters in copper and argon solids were investigated using the molecular-dynamics technique. It was pointed out that the clusters have a different behaviour in these solids. The role of the interatomic potentials is discussed. (1 ref.)

113897 Vacancy clustering in dilute aluminum alloys. N.Kamigaki, E.Hashimoto, Y.Deguchi, T.Kino (Dept. of Phys., Ehime Univ., Matsuyama, Japan).

Point Defects and Defect Interactions in Metals. Proceedings of the Yamada Conference V, Kyoto, Japan, 16-20 Nov. 1981 (Amsterdam, Netherlands: North-Holland 1982), p.730-2

Pure Al and dilute Al-Mg alloys were quenched from 600°C at various quenching rates $5 \times 10^3 \sim 5 \times 10^4^\circ\text{C/s}$ and aged at $3^\circ\text{C} \sim 80^\circ\text{C}$, and observed with an electron microscope. The density of faulted loops largely depends on the quenching rate in pure Al and this tendency decreases with the increase of Mg content. Furthermore, the density of loops depends on the aging temperature and it becomes higher with the increase of Mg content at the same aging temperature. On the other hand, vacancy clustering process is simulated by a clustering model taking into account a role of Mg atoms on the process. From these results, it is concluded that the vacancy clusters and complexes composed of around ten vacancies are the origin of faulted loops, and that the binding energy between a mono-vacancy and a Mg atom is less than 0.08 eV. (10 refs.)

113898 The study of vacancy clustering in deformed metals by positron annihilation. S.Tanigawa, I.Shinta, H.Iriyama (Inst. of Materials Sci., Univ. of Tsukuba, Ibaraki, Japan).

Point Defects and Defect Interactions in Metals. Proceedings of the Yamada Conference V, Kyoto, Japan, 16-20 Nov. 1981 (Amsterdam, Netherlands: North-Holland 1982), p.736-9

High counting rate measurements of positron lifetimes were applied to the isochronal annealing study of deformed metals. In iron and vanadium, mean lifetimes initially increased and then decreased and showed a shoulder at high temperatures. On the other hand, in nickel, tantalum and niobium, mean lifetimes initially decreased and made a hump at temperatures characteristic for metals. Application of three state trapping model clearly predicts that vacancies migrate below room temperature in iron and vanadium, at about 570K in nickel, at about 620K in niobium and 570K in tantalum. (6 refs.)

113899 Influence of vacancies and interstitials on the Bordoni peaks in copper and silver. C.Minier, J.Lauzier (Univ. Sci. et Medicale de Grenoble, Grenoble, France).

Point Defects and Defect Interactions in Metals. Proceedings of the Yamada Conference V, Kyoto, Japan, 16-20 Nov. 1981 (Amsterdam, Netherlands: North-Holland 1982), p.749-52

The variation of the Bordoni peaks is studied during electron bombardments of copper and silver and their subsequent annealings. The temperature range of diffusion of selfinterstitials along different kinds of dislocations is inferred. (4 refs.)

113900 Softening and hardening induced by point defects and defect clusters in BCC metals. K.Kitajima, E.Kuramoto, H.Abe, Y.Aono (Res. Inst. for Appl. Mech., Kyushu Univ., Fukuoka, Japan).

Point Defects and Defect Interactions in Metals. Proceedings of the Yamada Conference V, Kyoto, Japan, 16-20 Nov. 1981 (Amsterdam, Netherlands: North-Holland 1982), p.762-5

Softening and hardening characteristics induced by point defects and defect clusters in BCC metals were compared among pure iron single crystals irradiated at a low temperature by 2.5 MeV and 28 MeV electrons and those doped with solute nitrogen, and also among Mo single crystals to which similar irradiations were given. It was concluded that the controlling factors were misfit strain and migration energy of point defects or stability under stress field of a dislocation in case of clusters. Explanations were presented on the mechanism due to these factors. (10 refs.)

113901 The temperature dependence of the displacement threshold energy in FCC and BCC metals. K.Urban, B.Saile (Inst. für Phys., Max-Planck-Inst. für Metallforschung, Stuttgart, Germany), N.Yoshida, W.Zag.

Point Defects and Defect Interactions in Metals. Proceedings of the Yamada Conference V, Kyoto, Japan, 16-20 Nov. 1981 (Amsterdam, Netherlands: North-Holland 1982), p.783-8

Experimental results on the temperature dependence of the displacement threshold energy in Cu, Mo, and Nb are reported which were obtained by high-voltage electron microscopy. In Cu the minimum threshold energy decreases continuously from 17.5 eV at 70K to 10.5 eV at 550K. In Mo it decreases from 34.5 eV at 70K to 26.5 eV at 800K and in Nb from 28.5 eV at 50K to 25 eV at 300K. This pronounced temperature dependence is explained by the existence of Frenkel pair configurations which can be created at low energies but whose stability decreases from higher to lower temperatures. (19 refs.)

113902 Kinetic behavior of point defects in electron irradiated FeAl alloy. C.Kinoshita (Dept. of Nuclear Engng., Kyushu Univ., Fukuoka, Japan), T.Mukai, S.Kitajima.

Point Defects and Defect Interactions in Metals. Proceedings of the Yamada Conference V, Kyoto, Japan, 16-20 Nov. 1981 (Amsterdam, Netherlands: North-Holland 1982), p.857-60

The disordering process and the nucleation-growth process of dislocation loops in FeAl have been examined during irradiation in a HVEM. Experimental

results are successfully analyzed by a theory based on uncorrelated recombination of interstitials and structural vacancies as well as induced vacancies. (6 refs.)

113903 Interstitials and interstitial clusters in fast-neutron irradiated molybdenum by X-ray Huang scattering. H.Maeta (Div. of Phys., JAERI, Ibaraki, Japan). Point Defects and Defect Interactions in Metals. Proceedings of the Yamada Conference V, Kyoto, Japan, 16-20 Nov. 1981 (Amsterdam, Netherlands: North-Holland 1982), p.873-5. Measurements of X-ray Huang scattering and the change in the lattice parameter were made for molybdenum during an isochronal annealing program after fast neutron irradiation at 5K. Above 30K, interstitials form clusters and then grow up to large clusters. Between 100 and 200K, interstitial clusters take the form of a dislocation loop which then grow to large dislocation loops. The origin and final orientation of the interstitial loops is discussed. (8 refs.)

113904 Vacancy dipole loops observed in low temperature neutron irradiated pure gold and pure aluminum. Y.Shimomura (Dept. of Appl. Phys. & Chem., Hiroshima Univ., Hiroshima, Japan), E.Naya, H.Yoshida. Point Defects and Defect Interactions in Metals. Proceedings of the Yamada Conference V, Kyoto, Japan, 16-20 Nov. 1981 (Amsterdam, Netherlands: North-Holland 1982), p.884-6. Thin foils of pure gold and pure aluminum were quenched from high temperature. Without exposing the specimens to the temperatures at which vacancies can migrate by thermal motion, specimens were irradiated with fission neutrons at about 20K. After the specimens were annealed at room temperature, it was observed by electron microscopy. Long straight rod shaped defects were observed together with small dotted defects. In pure gold, rod shaped defects were along (110) directions and found to be narrow faulted dipoles. In pure aluminum they were perfect dipole and did not align to any low index direction. Possible mechanism for the formation of vacancy dipole loops are discussed. (no refs.)

113905 Microdefects and impurities in dislocation-free silicon crystals. T.Abe, H.Harada (Shin-Etsu Handotai Co., Gunma-ken, Japan), J.Chikawa. Defects in Semiconductors II, Symposium Proceedings, Boston, MA, USA, Nov. 1982 (New York, USA: North-Holland 1983), p.1-17. Microdefects in striated (swirl defects) and non-striated distribution (D-defects) have been observed in float-zoned crystals doped with various impurities by X-ray topography following copper decoration. A new type of defect was found to be present in swirl-free and D-defect-free regions and to become invisible by doping gallium. This gallium effect led to the conclusion that they are microprecipitates produced from residual oxygen impurity in FZ crystals. Effects of various impurities on defect formation indicate that D-defects are of vacancy agglomerates. It was observed that swirl defects are formed when the temperature gradient near the interface is high, and that their formation is suppressed by doping nitrogen. Formation processes of microprecipitates, swirls, and D-defects are discussed on the basis of observation of their mutual interaction and the impurity effects. (26 refs.)

113906 The nature of point defects and their influence on diffusion processes in silicon at high temperatures. U.Gosele (Max-Planck-Inst. für Metallforschung, Stuttgart, Germany), T.Y.Tan. Defects in Semiconductors II, Symposium Proceedings, Boston, MA, USA, Nov. 1982 (New York, USA: North-Holland 1983), p.45-59. Highlights recent progress in understanding the role of vacancies and self-interstitials in self- and impurity diffusion in silicon above about 700°C. How surface oxidation of silicon leads to a perturbation of the point-defect population is described. An analysis of the resulting oxidation-enhanced or -retarded diffusion of group III and group V dopants shows that under thermal equilibrium as well as under oxidation conditions both vacancies and self-interstitials are present. For sufficiently long times vacancies and self-interstitials attain dynamical equilibrium which involves their recombination and spontaneous thermal creation in the bulk of silicon crystals. The existence and the nature of a recombination barrier slowing down the recombination process are discussed in this context. Recent experimental and theoretical results on the diffusion of gold in silicon enable the authors to determine the self-interstitial component of silicon self-diffusion and to obtain an estimate of the respective vacancy contribution. The two components turn out to be of the same order of magnitude from 700°C up to the melting point. (72 refs.)

113907 Point defect thermodynamics of compound semiconductors and their alloys. F.A.Kroger (Dept. of Materials Sci., Univ. of Southern California, Los Angeles, CA, USA). Defects in Semiconductors II, Symposium Proceedings, Boston, MA, USA, Nov. 1982 (New York, USA: North-Holland 1983), p.207-24. The physical properties of crystalline solids depend on the presence of point defects. The concentrations of these defects in turn depend on the conditions of preparation and the presence of dopants. Quantitative relations between these condition (partial pressures of components, concentrations of dopants, temperature) and the defect concentrations is arrived at on the basis of defect chemistry. Examples of pure and doped binary compounds, alloys of binary compounds, and ternary compounds, are given. Whereas binary compounds have one composition variable, the alloy systems and the ternary compounds have two. The role of phase diagrams in preparing systems of required composition and properties is stressed. (196 refs.)

Fading properties of a NaF:F₂⁺ color center laser See Entry 113015
A new method for calculating the intensity of the diffuse X-ray scattering by point defects in cubic crystals See Entry 113706

Defects, dislocations and degradation of compound semiconductors See Entry 113915

Vacancy and interstitial loops in irradiated copper See Entry 113919

Agglomerates of interstitial-atoms and vacancies in e⁻-irradiated copper See Entry 113920

Effect of impurity atoms on the formation of secondary defects in quenched aluminum See Entry 113921

HVEM in-situ observation of formation of helical dislocations in Ag-10 at.% Al See Entry 113922

Localized formation of stacking fault tetrahedra by electron irradiation in FCC metals See Entry 113934

Transition metal impurities in silicon See Entry 113936

Simulation of the interaction of a vacancy with special tilt boundaries in a body-centred cubic lattice See Entry 113956

Modification of defects during irradiation of Si with high electron doses See Entry 113958

Mossbauer study of defect trapping at ⁵⁷Co in cold worked aluminium See Entry 113959

PAC study of defect trapping at ¹¹¹In in cold worked aluminium See Entry 113960

A new doping technique for the PAC probes ¹⁰⁰Pd and ¹¹¹In and its application to the study of point defects in BCC metals See Entry 113961

Interstitial trapping by zinc atoms in electron-irradiated silver See Entry 113962

Trapping of interstitials at ¹⁰⁰Pd-, ¹¹¹In-, and ¹⁸¹Hf-impurities in irradiated cubic metals See Entry 113963

Dose dependence of interstitial trapping at ¹¹¹In impurities in e⁻-irradiated aluminium See Entry 113964

Interactions of defects with Co implanted into Al at 4.2K See Entry 113965

Interaction of vacancies and self-interstitials with interstitial solute atoms in α -iron See Entry 113966

Strong interaction between vacancy and solute in gold See Entry 113967

A positron lifetime study of vacancy-solute complexes in dilute gold alloys See Entry 113968

Study of vacancy-solute interactions in dilute Al based alloys by thermal equilibrium measurements of positron annihilation See Entry 113969

Interaction and charge transfer between vacancy and solute in dilute aluminium alloys See Entry 113970

Mossbauer study on Fe-vacancy interaction in aluminium See Entry 113971

Formation of vacancies in thermal equilibrium in α -range alloys See Entry 113972

Mossbauer analysis on the annealing process of a quenched Al-Sn dilute alloy See Entry 113973

Recovery in electron irradiated aluminium observed by Mossbauer spectroscopy See Entry 113974

Calculation of interaction energies between point defects and (1/2) (111) dislocation in BCC transition metals (self-interstitial and interstitial solute atom) See Entry 113977

Effect of the interaction between solute atoms and defects on formation of defect clusters See Entry 113979

A role of helium and hydrogen atoms in the formation of interstitial loops See Entry 113980

Vacancy-interstitial recombination coefficients in radiation-induced growth models See Entry 113985

Low-temperature exciton decay with production of defects in KBr and KBr-Cl See Entry 113987

Molecular dynamics simulation of displacement cascades in Cu: analysis of replacement sequences See Entry 113990

The damage function based on the focusing collision model See Entry 113991

Kinetics of the order-disorder reaction under irradiation See Entry 113992

Monte-Carlo simulation of void nucleation during irradiation See Entry 113993

Shrinkage of voids in electron irradiation of thin foils See Entry 114024

Influence of alloy composition on defect production and recovery, in austenitic Fe-Cr-Ni solid solutions electron-irradiated at low temperature See Entry 114032

Re-examination of the threshold energy surface in copper See Entry 114033

Differences in saturation of defects between electrons and reactor neutron irradiations at low temperature See Entry 114034

On the evolution of microstructure during irradiation See Entry 114036

Radiation damage in Zr and Ti See Entry 114037

A study of irradiation damage in β Nb-3.1wt.% Zr alloy using a high voltage electron microscope See Entry 114038

Mechanism of void formation of iron and iron-alloys irradiated by electrons See Entry 114039

A study of defect states in neutron-irradiated zirconium using positron annihilation spectroscopy See Entry 114042

Recovery of Cu, Ag, and Ni dilute alloys after low temperature irradiation See Entry 114046

Recovery of radiation-induced defects in dilute Al-Ge alloys after fast neutron irradiation at 5K See Entry 114047

Direct determination of a radiation damage profile with atomic resolution in ion-irradiated platinum See Entry 114048

Radiation damage in tantalum observed by PAC See Entry 114055

Displacement cascade damage in irradiated metals See Entry 114056

Direct observation of heavy radiation damage process by field ion microscopy See Entry 114057

Statistical theory of the evolution of damage structure under irradiation with cascades See Entry 114059

The kinetics of the interaction between helium and displacement damage in irradiated materials See Entry 114060

Void and bubbles in argon irradiated nickel See Entry 114061

Investigation of radiation induced impurity complexes in aluminium alloys by channeling. A critical analysis by computer simulation See Entry 114062

Local optical oscillations near point and extended defects in ionic crystals See Entry 114112

Dimensional shifts in phonon spectra See Entry 114116

A HVEM study of radiation-induced segregation in dilute Ni-Be alloys See Entry 114188

Radiation-induced segregation at internal defect sinks in electron irradiated FCC alloys See Entry 114189

Oxygen precipitation in silicon—its effects on minority carrier recombination and generation lifetime See Entry 114194

Microstructure induced ordering effects in solids See Entry 114200

Investigation of vacancy diffusion in niobium, molybdenum, and tantalum by means of high-voltage electron microscopy See Entry 114246

Vacancies in zinc and cadmium produced by proton- and electron-irradiation See Entry 114247

Direct evidence of diffusion of self-interstitials in silicon See Entry 114251

Vibrational state and jump frequency of Mossbauer impurity associated with a vacancy in metals See Entry 114273

Modeling of dopant diffusion and associated effects in silicon See Entry 114275

- Formation of interstitial defects in high concentration shallow phosphorus diffusions in Si See Entry 114276
- Observation of oxidation-enhanced and -retarded diffusion of antimony in silicon: the behavior of (111) wafers See Entry 114277
- Effect of oxygen on radiation-enhanced diffusion in silicon See Entry 114278
- Migration of interstitial dumbbell in concentrated solid solutions See Entry 114281
- Radiation enhanced diffusion in FCC alloys See Entry 114282
- A diffusion-reaction model for solid solutions under irradiation See Entry 114283
- Radiation induced interdiffusion and phase transformation in electron irradiated Cu-Ni alloys See Entry 114287
- Thermal conductivity of irradiated graphite See Entry 114296
- Electronic structure and interparticle interaction in defect cubic oxides of vanadium and titanium See Entry 114443
- Thermal donor formation by the agglomeration of oxygen in silicon See Entry 114478
- Complex defects in GaAs and GaP See Entry 114479
- Quenched-in defects in CW laser irradiated virgin silicon See Entry 114483
- Isothermal recovery of electrical resistivity in aluminum immediately after deformation See Entry 114511
- Ultraviolet A-band absorption in NaCl:Pb²⁺ and clustering of lattice defects See Entry 114887
- Deep radiative transitions in InP See Entry 114927
- Positron study of a vacancy in graphite See Entry 114957
- Positron studies of recovery processes in aluminium and aluminium alloys See Entry 114958
- Positron lifetimes in Pb-Ag dilute alloys See Entry 114959
- Threshold temperature of positron capture in Cu-Zn vacancies See Entry 114960
- A positron annihilation study of neutron irradiated titanium See Entry 114962
- Positron annihilation in molybdenum single crystals irradiated with electrons, neutrons, and α -particles See Entry 114963
- Sputter-induced surface modification in Cu-Ni alloys at elevated temperatures See Entry 115005
- Excess energy stored in the fine powder system See Entry 115130
- Quenching investigations on BCC transition metals See Entry 115230
- Quenching secondary defects in austenitic steels containing phosphorus See Entry 115231

61.70D Colour centres

- 113908 Surface modification by ion implantation—effects on fatigue.** K.V.Jata, E.A.Starke, Jr., *J. Met. (USA)*, vol.35, no.8, p.23-7 (Aug. 1983). Recent work by the authors on ion implanted single and polycrystalline metals and alloys has shown that ion implantation can have beneficial effects on the fatigue life of materials. For an exact determination of the influence of a particular implanted species, they have shown that it is necessary to characterize the defect structure, deformation modes, and surface residual stresses produced. These studies have shown that the fatigue crack initiation and lifetime could be extended by choosing an ion species which leads to more homogeneous deformation near the surface region. On the other hand, implantation into some alloy systems extends the fatigue life by forming second phases or producing compressive residual stresses. This paper will give an overview of the various effects that ion implantation can have on microstructure, deformation behavior, and fatigue crack initiation resistance. The base materials that have been examined include aluminum, copper, 4140 steel, and two titanium alloys. (20 refs.)
- 113909 The role of the state of dispersion of impurity on Z₁-centres in NaCl:Ca²⁺ crystals.** K.N.Reddy, M.L.Rao, V.Haribabu (Dept. of Phys., Osmania Univ., Hyderabad, India). *Mater. Res. Bull. (USA)*, vol.18, no.8, p.1021-5 (Aug. 1983). Thermoluminescence and optical absorption studies were carried out to study the bleaching kinetics of F-centre and the formation of Z₁-centres in X-irradiated calcium doped NaCl crystals, both in as-received crystals and after quenching them from 555°C. An additional TL peak was observed in this system after F-bleaching of X-irradiated samples, which is attributed to thermal annealing of Z₁-centres. The various models proposed for Z₁-centres were reviewed in the light of these results, and it was concluded that the Z₁-centres are associated with impurity-vacancy dipoles. (7 refs.)
- 113910 Color centers in K₂S₂O₆ and Rb₂S₂O₆ crystals.** A.G.Badalyan, A.Yu.Klimova, Z.B.Perekalina, V.A.Khrantsov (A.F. Ioffe Physicotech. Inst., Acad. of Sci., Leningrad, USSR). *Sov. Phys.-Solid State (USA)*, vol.25, no.2, p.348-9 (Feb. 1983). Translation of: *Fiz. Tverd. Tela (USSR)*, vol.25, no.2, p.610-12 (Feb. 1983). [received: Sept. 1983] The authors study the color centers occurring in X-irradiated K₂S₂O₆ and Rb₂S₂O₆ crystals using ESR as well as optical spectroscopy. The EPR spectra were recorded on radiospectrometers (ranges of 3 cm and 8 mm). The optical absorption spectra were taken with a two-beam automatic ESR-3 Hitachi spectrophotometer. (6 refs.)
- Low-temperature exciton decay with production of defects in KBr and KBr-Cl** See Entry 113987
- Recombination-driven precipitate coarsening in alloys under irradiation** See Entry 113996
- Microstructure induced ordering effects in solids** See Entry 114200
- The influence of fusion temperature on the defect center concentration of GeO₂ glass** See Entry 114733
- Attenuation of optical irradiation by bismuth colloidal colour centres** See Entry 114891
- Two-photon absorption cross section at F₂⁺ centers of alkali-halide crystals** See Entry 114893

61.70E Other point defects

- Complex defects in GaAs and GaP See Entry 114479
- ESR of defects in III-V compounds See Entry 114734

61.70G Dislocations: theory

- 113911 Penetration depth of diffusion-induced dislocations.** N.Itoh, T.Nakau (Dept. of Electronics, Univ. of Osaka Prefecture, Osaka, Japan). *Jpn. J. Appl. Phys. Part 1 (Japan)*, vol.22, no.7, p.1106-11 (July 1983). To estimate the penetration depth of diffusion-induced dislocations, the depth of the neutral plane of internal stress is obtained quantitatively in values relative to the junction depth of the usual diffusion profiles. The following two cases are considered: (1) the stress distribution is due mainly to the distribution of impurity atoms and (2) the stress is relieved by the generation of a majority of dislocations. The shallow penetration of (1/3-2/3) X_j observed so far is explained by case (1). Deep penetration beyond the junction is shown to be generally possible only in case (2) and at this time, the change of the depth of the neutral plane depths on the moment of the dislocation distribution. It is also explained that the force on a dislocation due to the diffusion-induced stress causes the climbing motion. (28 refs.)
- 113912 Dynamic analysis of dislocation generation due to sudden indentation.** L.M.Brock (Dept. of Engng. Mech., Univ. of Kentucky, Lexington, KY, USA). *Int. J. Eng. Sci. (GB)*, vol.21, no.12, p.1437-42 (1983). The dynamic analysis of an edge dislocation generated under the edge of a rigid smooth indenter applied suddenly to an elastic half-plane is presented. The physical requirement that the indenter edge cannot induce a corner yields an equation relating the dislocation, indenter and half-plane parameter. Study of the equation allows several general observations on the dislocation motion. In particular, a given dislocation moving at a given speed can move along either of two paths below a certain indentation level. (11 refs.)
- 113913 Structure of triple dislocation points forming in the course of dislocational reactions in HCP crystals.** G.V.Bushueva, E.M.Yakhshaatova (Dept. of Molecular Phys., Moscow Univ., Moscow, USSR). *Moscow Univ. Phys. Bull. (USA)*, vol.38, no.1, p.21-7 (1983). Translation of: *Vestn. Mosk. Univ. Ser. 3 (USSR)*, vol.38, no.1, p.20-5 (1983). The moment method is used to investigate the structure and stability of triple spatial dislocational points in HCP crystals. The moment method offers the possibility of more rigorous estimation of the conditions of occurrence of dislocation reactions than the Frank criterion. The 'moment' criterion allows the region of guaranteed occurrence of dislocational reactions to be determined, i.e. the region of mutual orientations of the dislocations for which the occurrence of reactions between them is favorable. (17 refs.)
- 113914 Obstacle-dragging movement of dislocations.** S.I.Zaltsev (Inst. of Solid-State Phys., Acad. of Sci., Chernogolovka, USSR). *Sov. Phys.-Solid State (USA)*, vol.25, no.2, p.222-5 (Feb. 1983). Translation of: *Fiz. Tverd. Tela (USSR)*, vol.25, no.2, p.394-9 (Feb. 1983). [received: Sept. 1983] A model is formulated for the movement of dislocations, taking into account the dragging of obstacles and based on the idea of obstacle diffusion across a dislocation as a result of the interaction with the latter. A kinetic equation is obtained for the time variation of the mean length of a dislocation segment, the dislocation velocity and the obstacle transport characteristics being defined in terms of this length. A transient-state model is used to explain qualitatively some phenomena, such as the nonlinear variation of the dislocation travel with the load action time and the 'delay time'. (9 refs.)
- 113915 Defects, dislocations and degradation of compound semiconductors.** W.D.Johnston, Jr. (Bell Labs., Murray Hill, NJ, USA). Defects in Semiconductors II, Symposium Proceedings, Boston, MA, USA, Nov. 1982 (New York, USA: North-Holland 1983), p.453-60 Diode lasers and/or LEDs fabricated from the Ga_{1-x}Al_xAs/GaAs for In_{1-x}Ga_xAs₂P_{1-y} alloy system provide the basis for rapidly developing optical communications systems. These devices are operated at very high optical and electrical power densities, and the inevitable less-than-perfect efficiency results in intense local thermal and athermal lattice excitation. This in turn can lead to generation, motion and growth of extended defect structures including dislocation networks, precipitation of impurities, or phase separation. For the Al_{1-x}Ga_xAs material, a predominant degradation effect is the development of so-called (100) 'dark line defects' (DLDs). These have been shown to arise from recombination enhanced climb of threading dislocations giving rise to dipole loops of a primarily interstitial character. A less common form, the (100) DLD, is associated with slip and typically arises from the strain associated with mechanical damage or careless handling or device processing. The In_{1-x}Ga_xAs₂P_{1-y} device material affords less energy per recombination event by virtue of its smaller band-gaps, but is likely to have more lattice mismatch strain than Ga_{1-x}Al_xAs for typical compositions of device interest. Thus slip, (110) DLDs, and precipitates are the commonly observed features of In_{1-x}Ga_xAs₂P_{1-y} degradation. (28 refs.)
- Elastic media with microstructure II. Three-dimensional models** See Entry 111318
- Calculation of interaction energies between point defects and (1/2) (111) dislocation in BCC transition metals (self-interstitial and interstitial solute atom)** See Entry 113977
- Laser annealing of ion implanted semiconductors** See Entry 114020
- Characteristics of plastic flow of interstitial phases** See Entry 114072
- The transition from an emitting to a cleaving crack** See Entry 114084
- Dislocation mechanism of crystal melting** See Entry 114145
- 61.70J Etch pits, decoration, transmission electron-microscopy and other direct observations of dislocations**
- 113916 TEM studies of natural WS₂ crystals.** M.K.Agarwal, K.Nagi Reddy, J.D.Kshatriya (Dept. of Phys., Sardar Patel Univ., Vallabh Vidyanagar, India). *Indian J. Phys. Part A*, vol.57A, no.3, p.175-81 (May 1983). TEM studies of natural WS₂ single crystals have been investigated. Dissociated dislocation ribbons, isolated contracted and extended nodes, star-like pattern, etc. are observed and discussed using bright field and dark field microscopy. (3 refs.)
- 113917 Weak-beam study of glide dislocations in HCP cobalt.** A.Korner, H.P.Karntaler (Inst. fur Festkorperphys., Univ. Wien, Wien, Austria). *Philos. Mag. A (GB)*, vol.48, no.3, p.469-77 (Sept. 1983). The weak-beam method of electron microscopy has been used to analyse the Shockley partial dislocation in a pure HCP metal. Single crystals of cobalt were grown oriented for basal slip and deformed in compression. The dissociation of the basal glide dislocations into partials is resolved; the arrangement of the magnetic domains does not influence the splitting width of the partials. From a careful analysis of the observed image peak separations, a room-

temperature stacking-fault energy $\gamma=27\pm4$ mJ m⁻² is deduced. The basal glide dislocations contain many jogs. Frequently the sequence of the partials is reversed at a jog, which leads to the conclusion that the dislocation is jogging over an odd number of lattice planes and has a stacking fault of the same intrinsic type I₂ on both sides of the jog. It should be pointed out that in the FCC structure this behaviour has not been observed, since the reversed sequence of the partials would lead to a glide dislocation containing an extrinsic fault. (21 refs.)

113918 Investigation of defect structure of metal-semiconductor interface in SMS by the method of high-voltage electron microscopy. B.I.Smirnov, G.Kestner, A.V.Ryabov, I.A.Smirnov (A.F. Ioffe Physicotech. Inst., Acad. of Sci., Leningrad, USSR). *Sov. Phys.-Solid State (USA)*, vol.25, no.2, p.305-7 (Feb. 1983). Translation of: *Fiz. Tverd. Tela (USSR)*, vol.25, no.2, p.541-6 (Feb. 1983). [received: Sept. 1983]

Using the method of high-voltage electron microscopy (accelerating voltage 1000 kV), the authors have investigated the defect structure of the metal-semiconductor interface in samarium monosulfide crystals. It is shown that, with the semiconductor-metal phase transition that occurs in thin surface layers of specimens during mechanical polishing a characteristic net of misfit dislocations is formed in the interphasal surface. (6 refs.)

113919 Vacancy and interstitial loops in irradiated copper. B.C.Larson, F.W.Young,Jr. (Solid State Div., Oak Ridge Nat. Lab., Oak Ridge, TN, USA).

Point Defects and Defect Interactions in Metals. Proceedings of the Yamada Conference V, Kyoto, Japan, 16-20 Nov. 1981 (Amsterdam, Netherlands: North-Holland 1982), p.679-86

Significant advances have been made in diffuse scattering studies of irradiation induced dislocation loops in metals. Numerical calculational procedures have been developed that provide accurate diffuse scattering cross sections for vacancy and interstitial loops, and these cross sections have been used in conjunction with X-ray diffuse scattering studies of neutron and ion irradiated copper. Size distributions and concentrations have been obtained for both vacancy and interstitial loops and these results are compared with electron microscopy measurements. The size distributions obtained from diffuse scattering measurements show the vacancy loops to be smaller and more numerous than the interstitial loops, and indicate that equal numbers of vacancies and interstitials are in loops. The diffuse scattering and microscopy size distributions agree at the larger sizes, but the diffuse scattering method identifies more loops of the smaller sizes. (17 refs.)

113920 Agglomerates of interstitial-atoms and vacancies in e⁻-irradiated copper. P.Ehrhart, B.Schonfeld, K.Sonnenberg (Inst. fur Festkorperforschung, KFA Jülich, Jülich, Germany).

Point Defects and Defect Interactions in Metals. Proceedings of the Yamada Conference V, Kyoto, Japan, 16-20 Nov. 1981 (Amsterdam, Netherlands: North-Holland 1982), p.687-90

Diffuse X-ray scattering from dislocation loops has been treated by new calculational methods that allow the discrimination between vacancy and interstitial type loops and also a quantitative determination of loop sizes and concentrations. Based on these calculations the interaction of vacancies with interstitial loops and the formation of vacancy agglomerates during annealing stage III in Cu has been investigated after electron irradiation at different temperatures. Independent of the behaviour of the interstitial loops, which grew or shrank dependent on their size and concentration at the end of stage II, vacancy agglomerates were observed after annealing stage III. A decrease of ρ_F was always observed along with the vacancy clustering. The vacancy agglomeration processes seem to be more sensitive to impurities than the interstitial loop growth. (6 refs.)

113921 Effect of impurity atoms on the formation of secondary defects in quenched aluminium. K.Watanabe (Tokyo Metropolitan Tech. Coll., Tokyo, Japan), Y.Morishita, H.Yamaguchi, S.Yoshida.

Point Defects and Defect Interactions in Metals. Proceedings of the Yamada Conference V, Kyoto, Japan, 16-20 Nov. 1981 (Amsterdam, Netherlands: North-Holland 1982), p.726-9

The effect of impurity atoms on the formation of dislocation loops and voids is examined with an electron microscope. The result obtained is summarized as follows: (i) The formation of dislocation loops is promoted by small amount of substitutional impurity atoms and the order of the promotive effect is Ge>In>Si>Cu>Sb>Bi>Ni>Mg>Zn>Ag>Au>Sn. (ii) Helium atoms as well as hydrogen atoms promote the formation of voids and the effect of helium atoms is smaller than that of hydrogen atoms. These results are discussed briefly from the binding energy between a vacancy and a small vacancy cluster containing impurity atoms using the rate equations taking into account the diffusion motion of vacancies in a crystal. (7 refs.)

113922 HVEM in-situ observation of formation of helical dislocations in Ag-10 at.% Al. H.Saka, T.Kondo (Dept. of Metall., Nagoya Univ., Nagoya, Japan).

Point Defects and Defect Interactions in Metals. Proceedings of the Yamada Conference V, Kyoto, Japan, 16-20 Nov. 1981 (Amsterdam, Netherlands: North-Holland 1982), p.770-2

Dissociated near-screw dislocations in Ag-10 at.% Al were irradiated with 1 MeV electrons at 473K in a HVEM and the transformation of the dissociated screws into helices as a result of the interaction of point defects introduced was observed in situ using the 'weak-beam' electron microscopy. Results of observations have been analyzed in terms of the 'loop-jog' model of climb of dissociated dislocations proposed by Cherns, Hirsch and Saka. (6 refs.)

113923 Analysis of defects in heavily-doped MBE-GaAs. C.B.Carter, D.M.Desimone, H.T.Griem, C.E.C.Wood (Dept. of Materials Sci. & Engng., Cornell Univ., Ithaca, NY, USA).

Defects in Semiconductors II, Symposium Proceedings, Boston, MA, USA, Nov. 1982 (New York, USA: North-Holland 1983), p.271-5
GaAs has been grown by molecular-beam epitaxy (MBE) with large concentrations (~10¹⁸ cm⁻²) of Sn, Si, Ge, and Mn as dopants. The heavily-doped n-type material has been found to contain regions of a very high dislocation density. An analysis of the less complex defect areas shows that the dislocations originate in the MBE-grown layer. These observations and others on more complex defect clusters are compared with recent studies of defects in material grown by liquid phase epitaxy (LPE). The more heavily doped p-type material contains discs of Mn-rich material at the surface of the MBE-grown epilayer. Both the structure and composition of these regions have been examined. (8 refs.)

Correlation between growth hillocks and dislocations on the {110} faces of flux grown yttrium aluminium garnetSee Entry 113777

Defects in quenched and annealed Al-Ge alloysSee Entry 113861

Thermal generation of vacancies in aluminumSee Entry 113873

Behavior of point defects in ice crystals revealed by X-ray topographySee Entry 113881

Defect structures in β -NiAl and their response to electron irradiationSee Entry 113885

High resolution electron microscopic observations of small point defect clusters and their thermal stabilitySee Entry 113894

Vacancy clustering in dilute aluminum alloysSee Entry 113897

Influence of vacancies and interstitials on the Bordoni peaks in copper and silverSee Entry 113899

Softening and hardening induced by point defects and defect clusters in BCC metalsSee Entry 113900

Kinetic behavior of point defects in electron irradiated FeAl alloySee Entry 113902

Interstitials and interstitial clusters in fast-neutron irradiated molybdenum by X-ray Huang scatteringSee Entry 113903

The interface structure of grain boundaries in polysiliconSee Entry 113930

The structure of a near coincidence $\Sigma=5$, [001] twist boundary in siliconSee Entry 113931

Effect of the interaction between solute atoms and defects on formation of defect clustersSee Entry 113979

A role of helium and hydrogen atoms in the formation of interstitial loopsSee Entry 113980

Interaction of dislocations with impurities and its influence on the mechanical properties of silicon crystalsSee Entry 113981

Helium bubbles in palladium tritideSee Entry 113984

Void-swelling in cold-worked copper during HVEM irradiationSee Entry 114023

On the evolution of microstructure during irradiationSee Entry 114036

Voids and bubbles in argon irradiated nickelSee Entry 114061

Photoplastic effects in II-VI crystalsSee Entry 114077

Shock effects in MgAl₂O₄-spinelSee Entry 114094

A HVEM study of radiation-induced segregation in dilute Ni-Be alloysSee Entry 114188

Oxygen precipitation effects in degenerately-doped siliconSee Entry 114193

Electrically active defects in CID imaging arrays fabricated on Hg_{0.7}Cd_{0.3}Te ...See Entry 114201

Investigation of vacancy diffusion in niobium, molybdenum, and tantalum by means of high-voltage electron microscopySee Entry 114246

Formation of interstitial defects in high concentration shallow phosphorus diffusions in SiSee Entry 114276

Structural studies of metal-semiconductor interfaces with high-resolution electron microscopySee Entry 114322

Structure of two-layer epitaxial Ag-Al filmsSee Entry 114380

A TEM study of fibrous cuprite (chalcotrichite): microstructures and growth mechanismsSee Entry 114426

Electrical properties of dislocations and boundaries in semiconductorsSee Entry 114481

Kinetics and mechanism of cluster growth in mixtures of calcia and magnesiaSee Entry 115150

Electron microscopic investigation of the growth of martensite plateletsSee Entry 115190

The segregation of osmium to grain boundary dislocations in tungstenSee Entry 115201

Electron microscopic investigation of structural changes caused by annealing of tungsten wiresSee Entry 115220

Quenching secondary defects in austenitic steels containing phosphorusSee Entry 115231

Large strain plastic deformation of commercially pure nickelSee Entry 115267

Some aspects of improving abrasive resistanceSee Entry 115373

Application of DSL photoetching for defect revealing in epitaxially grown GaAs samplesSee Entry 115397

Inhomogeneous plastic deformation and its relevance to iodine stress corrosion cracking susceptibility in irradiated Zircaloy-2 tubingSee Entry 115418

61.70L Slip, creep, internal friction and other indirect evidence of dislocations

(see also 62.20H Creep, 62.40 Internal friction)

113924 Influence of temperature on the mobility of dislocations in iron and martensite during internal friction measurements. V.I.Sarrak, S.O.Suvorova (Inst. of Metall. & Phys. of Metals, Moscow, USSR).

Fiz. Met. & Metalloved. (USSR), vol.56, no.2, p.379-82 (Aug. 1983). In Russian. English translation in: *Phys. Met. & Metallogr. (GB)*

When iron was annealed to temperatures below 400°C there was no motion of dislocations pinned by impurity atoms when the stresses were of the kind used in the internal friction measurements. An increase in the dislocation mobility above 400°C was due to the breakup of the atmospheres of impurity atoms around dislocations. The motion of dislocations (pinned by impurity atoms in martensite) under the influence of stresses used to measure the internal friction was observed even at room temperature. At temperatures near 200°C the mobility of dislocations pinned by impurity atoms was maximal. (9 refs.) *A.T.*

113925 Dislocation structure of large-domain ordered Ni₃V alloy. G.I.Nosova, N.A.Polyakova (Inst. of Metall. & Phys. of Metals, Moscow, USSR).

Fiz. Met. & Metalloved. (USSR), vol.56, no.2, p.383-9 (Aug. 1983). In Russian. English translation in: *Phys. Met. & Metallogr. (GB)*

A dislocation structure with domains of about 5000 nm size was studied in the ordered Ni₃V alloy. Even at the earliest stages of the deformation the shear involved multiple glide of single dislocations. In some domains they split forming extending stacking faults. Accumulation of such defects in nearby parallel planes during the later stages of deformation of the alloy produced twin layers. The reasons responsible for the glide of single dislocations, generating antiphase boundaries, and formation of extended stacking faults in domains in specific orientation were considered. The nature of the barriers appearing in alloys because of the interaction with strongly split dislocations was determined. (11 refs.) *A.T.*

113926 Dislocation structure and amplitude-dependent internal friction of LiF crystals. B.I.Smirnov, V.A.Chelnokov, N.L.Kuz'min (M.I. Kalinin Polytech. Inst., Leningrad, USSR).

Sov. Phys.-Solid State (USA), vol.25, no.2, p.293-5 (Feb. 1983). Translation of: *Fiz. Tverd. Tela (USSR)*, vol.25, no.2, p.519-24 (Feb. 1983). [received: Sept. 1983]

A study was made of the changes in the dislocation structure during measurements of the amplitude-dependent internal friction of LiF crystals. The parameters of the dislocation structure were compared with the behavior of the amplitude dependence of the decrement. For vibration amplitudes corresponding to an amplitude dependence of the decrement, a multiplication of dislocations in the surface layers of the crystals occurs. The amplitude dependence of the decrement, measured for a progressive increase in vibration amplitude, corresponds to motion of a variable number of dislocations. For decreasing vibration amplitudes, the amplitude dependence characterizes the motion of a constant number of dislocations, while the parameters of this motion are independent of the number of induced dislocations. (8 refs.)

Defects, dislocations and degradation of compound semiconductors See Entry 113915

Solute atom-dislocation interactions studied by ultrasonic method See Entry 113975

Theoretical relationships between creep and swelling by point defect absorption during irradiation See Entry 113994

A study of defect states in neutron-irradiated zirconium using positron annihilation spectroscopy See Entry 114042

Characteristics of plastic flow of interstitial phases See Entry 114072

Photoplastic effects in II-VI crystals See Entry 114077

Creep of weakly strained LiF crystals in the temperature range 1.6-300K See Entry 114078

Experimental observation of decreased Hall mobility of conduction electrons in ZnSe with moving dislocations See Entry 114555

Magnetomechanical damping of nickel See Entry 114720

Dynamic dislocation-induced broadening of a homogeneous ferromagnetic resonance line See Entry 114740

Substructure hardening of polycrystalline niobium See Entry 115209

Influence of the degree of preliminary strain on the strain aging of pearlitic casing steel See Entry 115216

Elastic properties (the stiffness constants, the shear modulus and the dislocation line energy and tension) of Ni-Al solid solutions and of the Nimonic alloy Pe16 See Entry 115240

Fatigue and recovery processes in a multilayer iron-copper composite material See Entry 115243

Influence of stress cycling on creep behaviour of an Al-Mg alloys under strain ageing conditions See Entry 115253

Steady state and transient creep of Al at 400K—an analysis in terms of recovery controlled by thermally activated glide See Entry 115254

Temperature-time dependence of the cyclic-creep activation energy of heat-resistant alloys See Entry 115283

Study of the high-temperature creep of multilaminar iron/copper and nickel/copper condensates See Entry 115284

Effect of texture and grain size on the fracture behaviour of hot rolled Mg, Mg-12.5% Li and Mg-5% Ti alloys See Entry 115300

Mixed-mode fracture mechanisms near the fatigue threshold of AISI 316 stainless steel See Entry 115310

Effect of molybdenum on temper brittleness and internal friction behaviour of medium carbon alloy steels See Entry 115326

Shape effect of particles on high-temperature hardness of dispersion-hardened Ni-SiO₂ alloys See Entry 115352

An analytical method of evaluating angles in Brookes' formula for effective resolved shear stress on slip systems in crystals See Entry 115453

61.70N Grain and twin boundaries

113927 Morphology and polarity of twinned crystals in II-VI compounds. H.Iwanaga, T.Yoshiie, T.Yamaguchi, N.Shibata (Faculty of Liberal Arts, Nagasaki Univ., Nagasaki, Japan).

Jpn. J. Appl. Phys. Part 1 (Japan), vol.22, no.7, p.1098-100 (July 1983). ZnO twinned crystals with the composition plane (1011) or (1122) were grown by oxidizing ZnSe in the vapor phase. The twinned crystals consisted of two plate crystals grown in the $+c$ and $-c$ directions. CdS and CdSe twinned crystals with the composition plane (1011) were also grown by the sublimation method. Both of these consisted of branch crystals growing around an original (central) c -needle which grew in the $-c$ direction. These branch crystals made an angle of 56° with the original c -needle. They grew in the $+c$ direction in CdS and in the $-c$ direction in CdSe. (9 refs.)

113928 Twin growth of sucrose crystals. G.Mantovani, G.Vaccari, C.A.Accorsi (Scuola 'Serafino Cevasco', Univ. di Ferrara, Ferrara, Italy), D.Aquilano, M.rubbo.

J. Cryst. Growth (Netherlands), vol.62, no.3, p.595-602 (Aug. 1983). A crystallographic and kinetic approach is given to understand twinning of sucrose crystals. The twin law is redefined and original composition planes for twinning (OCP) are found consistent with experiments. The elongation parameter II is defined as a function of supersaturation and growth time. The calculated and measured II values compare favourably both in pure solution growth and in the presence of low concentrations of raffinose. Experiments stress that the polar character of sucrose is determining both the crystallographic properties and kinetic behaviour of twins. (15 refs.)

113929 Simple structural unit model for core-dependent properties of symmetrical tilt boundaries. R.W.Balluffi (Dept. of Materials Sci. & Engng., MIT, Cambridge, MA, USA), A.Brokman.

Ser. Metall. (USA), vol.17, no.8, p.1027-30 (Aug. 1983). It is demonstrated that the recently determined structural unit model for the core structure allows one to estimate any physical property, p , for any boundary in a series of symmetrical tilt boundaries possessing a range of tilt angles if values of p for a few particular boundaries in the series are known. More specifically, it is shown that p for all boundaries with misorientations between those of two so-called 'favored boundaries' can be estimated from a knowledge of the equal numbers of the structural units comprising the two favored boundaries. Applications of the results to measurements of boundary diffusivities and boundary energies are indicated briefly. (11 refs.)

113930 The interface structure of grain boundaries in polysilicon. S.M.Johnson (Solarex Corp., Rockville, MD, USA), K.C.Yoo, R.G.Rosemeier, P.Soltani, H.C.Lin.

Defects in Semiconductors II, Symposium Proceedings, Boston, MA, USA, Nov. 1982 (New York, USA: North-Holland 1983), p.357-61. Normal grain growth in polysilicon material proceeds by a twinning mechanism such that the individual grain orientations are related by single or multiple twinning steps. The twinning relationship between adjacent grains can result in the alignment of their boundary interfaces along certain planar segments which have a very low electrical activity. The varying degree of electrical activity of these boundaries, and boundary positions, is attributed to the smaller dislocation portion of the larger change in orientation across the grains. (11 refs.)

113931 The structure of a near coincidence $\Sigma=5$, [001] twist boundary in silicon. M.Vaudin, D.Ast (Dept. of Materials Sci. & Engng., Cornell Univ., Ithaca, NY, USA).

Defects in Semiconductors II, Symposium Proceedings, Boston, MA, USA, Nov. 1982 (New York, USA: North-Holland 1983), p.369-73. The dislocation structure of a near coincidence $\Sigma=5$ (001) twist boundary in silicon was studied using transmission electron microscopy. Secondary dislocations, with localized cores were observed in the boundary accommodating a small deviation ($<0.5^\circ$) from perfect coincidence. The O-lattice theory for general low angle boundaries was extended to calculate the expected dislocation content of near coincidence boundaries. Comparison between predictions and observations was used to deduce information on the primary dislocation structure of the boundary. (11 refs.)

Detection of point defects and dynamic observation of defect interaction by atom resolution electron microscopy See Entry 113891

Dislocation structure of large-domain ordered Ni₃V alloy See Entry 113925

Electronic interaction between impurity and grain boundary in iron See Entry 113978

A study of defect states in neutron-irradiated zirconium using positron annihilation spectroscopy See Entry 114042

Parameters of mechanical twins emitted by a crack See Entry 114080

Conditions for cavity growth during slow-fast fatigue See Entry 114083

Shock effects in MgAl₂O₄-spinel See Entry 114094

Phase transformation in a linear polycrystal with a rate law of n -th order See Entry 114122

Radiation-induced segregation at internal defect sinks in electron irradiated FCC alloys See Entry 114189

Electrically active defects in CID imaging arrays fabricated on Hg_{0.7}Cd_{0.3}Te See Entry 114201

Enhanced diffusion of phosphorus at grain boundaries in silicon See Entry 114279

Contribution to the theory of grain-boundary electromigration See Entry 114289

Thermal conductivity of irradiated graphite See Entry 114296

Orientation and structure of bismuth films on virgin surface of zinc See Entry 114382

Electrical properties of dislocations and boundaries in semiconductors See Entry 114481

Electronic states of grain boundaries in bicrystal silicon See Entry 114482

The electrical behavior of grain boundaries in silicon See Entry 114549

Metallurgically grown Schottky junction in directionally solidified eutectic Ag-Si alloys See Entry 114590

Electrical conductivity of semiconductors with grain boundaries and spectroscopy of boundary states in the presence of a tunnel current See Entry 114603

Electronic properties of grain boundaries in GaAs: a study of oriented bicrystals prepared by epitaxial lateral overgrowth See Entry 114629

Stress relaxation in ferroelectric materials See Entry 114799

Sputter-induced surface modification in Cu-Ni alloys at elevated temperatures See Entry 115005

Mechanism of formation of martensite single crystals as a result of plastic deformation of the alloys based on γ -Mn See Entry 115191

Reversion of BCC α' martensite in Fe-Cr-Ni austenitic stainless steels See Entry 115195

The segregation of osmium to grain boundary dislocations in tungsten See Entry 115201

Recrystallization mechanisms in commercial Al-2Mg alloy See Entry 115212

Relationship between grain boundary segregation and heat-treatment parameters in an aluminium alloy See Entry 115218

Large strain plastic deformation of commercially pure nickel See Entry 115267

Mixed-mode fracture mechanisms near the fatigue threshold of AISI 316 stainless steel See Entry 115310

Frequency dependence of the high temperature fatigue properties of He-implanted stainless steel See Entry 115312

On the modeling of the high-temperature embrittlement of metals containing helium See Entry 115313

Influence of slow strain rate tensile deformation on creep-fatigue endurance of 20Cr-25Ni-Nb stainless steel at 593°C See Entry 115328

Intergranular fracture of a high purity iron due to oxygen See Entry 115351

Some aspects of improving abrasive resistance See Entry 115373

61.70P Stacking faults, stacking fault tetrahedra and other planar or extended defects

113932 Crystallographic shear in the Nb₂O₅-Ta₂O₅-WO₃ quaternary system at 1623K. P.J.England, R.J.D.Tilley (School of Materials Sci., Univ. of Bradford, Bradford, England).

Chem. Scr. (Sweden), vol.22, no.3, p.108-16 (1983). The microstructures occurring in the quaternary system Nb₂O₅-Ta₂O₅-WO₃ at 1623K and in the composition range between WO₃ and (Nb, Ta)₂O_{2.86} have been determined. Samples were prepared by heating appropriate mixtures of the parent oxides in sealed Pt ampoules for 5 days, and structural information was obtained mainly by way of high resolution electron microscopy. A CS phase field was found between the composition limits of (Nb, W)O_{2.965} and (Nb, W)O_{2.875} on the Nb rich side of the phase interval and

between (Ta, W)O_{2.96} and (Ta, W)O_{2.943} on the Ta rich side of the phase interval. The CS microstructures consisted of intergrowths of {001}, {104} and {103} CS and varied in a consistent manner across the CS phase field. No ordered 'swinging CS' regions were found. (12 refs.)

113933 High resolution electron microscopy study of phosphate tungsten bronzes KP₂O₈(WO₃)_{2m}. II. Crystallographic shear planes observation. M.Hervieu, B.Raveau (Lab. de Cristallographie, Univ. de Caen, Caen, France). *Chem. Scr. (Sweden)*, vol.22, no.3, p.123-8 (1983). For pt.I see *ibid.*, vol.22, no.3, p.117-22 (1983). The high integral *m* compositions of the phosphate tungsten bronzes were studied by means of high resolution transmission electron microscopy. Non-stoichiometric defects by intergrowth or by P₂O₅ rows interruption have been previously reported in the first part of the study. Besides these specific defects, phosphate tungsten bronzes exhibit another type of nonstoichiometry related to the formation of crystallographic shear planes in the ReO₃-type slabs. Two types of CS planes {102} and mixed {103}/{001} CSP have been observed. Various arrangements of these defects are visualized: located defects as well as coherent intergrowths with the P₂O₇ planes. The CS structures were also seen to form during the observation in the electron microscope. The type of CS defects which occurred in the phosphate tungsten bronzes seems to be related with the width of the ReO₃-type slabs. (24 refs.)

113934 Localized formation of stacking fault tetrahedra by electron irradiation in FCC metals. M.Suehiro (Dept. of Material Phys., Osaka Univ., Osaka, Japan), N.Yoshida, M.Kiritani. *Point Defects and Defect Interactions in Metals. Proceedings of the Yamada Conference V, Kyoto, Japan, 16-20 Nov. 1981 (Amsterdam, Netherlands: North-Holland 1982)*, p.795-8
The distributions of stacking fault tetrahedra formed in copper, nickel and gold by electron irradiation in a high voltage electron microscope have been observed with stereo-electron-microscopy. Their distributions have the localized regions near the electron incident surface and/or near the bottom surface. These distributions are attributed to the two distinct damage processes which directly lead to local enrichment of vacancies. One is the replacement sequence collision damage and the other is the sputtering of atoms. Both processes are found to change remarkably with a slight change in the electron diffraction condition, and the oscillation of the current density of electrons at the atom row is proved to exist along the depth distance through the crystal. (2 refs.)

Detection of point defects and dynamic observation of defect interaction by atom resolution electron microscopySee Entry 113891
Image contrast of single vacancies and small stacking fault tetrahedra in gold crystals studied by an atom resolution electron microscope ...See Entry 113892
Weak-beam study of glide dislocations in HCP cobaltSee Entry 113917
Dislocation structure of large-domain ordered Ni₃V alloySee Entry 113925
Strong interaction between vacancy and solute in goldSee Entry 113967
Interaction of implanted impurities with extended defect configurations in tungsten single crystalSee Entry 113976
Local optical oscillations near point and extended defects in ionic crystalsSee Entry 114112
Precipitation of oxygen and mechanism of stacking fault formation in Czochralski silicon bulk crystalsSee Entry 114191
Modeling of dopant diffusion and associated effects in siliconSee Entry 114275
On a relationship between substrate perfection and stacking faults in homoepitaxial siliconSee Entry 114391
Leakage and breakdown in thin oxide capacitors correlation with decorated stacking faultsSee Entry 114783
Influence of substructure on the mechanical properties of austenitic alloys deformed by warm rollingSee Entry 115257
Application of DSL photoetching for defect revealing in epitaxially grown GaAs samplesSee Entry 115397

61.70R Crystal impurities: general
(see also 71.55 Impurity and defect levels; 81.10 Purification techniques)

113935 On the precrystallization phase formation. Yu.M.Gerasimov, G.I.Distler, V.P.Makarov, A.Sh.Shalpikov (Inst. of Crystallography, Acad. of Sci., Moscow, USSR). *Naturwissenschaften (Germany)*, vol.70, no.8, p.412 (Aug. 1983).
By means of the decoration method at an electronmicroscopic scale it was previously established that impurities in crystals are distributed unequally, forming micro- and macroassemblies. Based on the example of KCl crystals doped with 0.5 mass-% SrCl₂, the authors studied surface crystallization reactions of this impurity stimulated by thermal treatment at 350-550°C. On thermal treatment at 350°C for 20 min SrCl₂ impurity assemblies on cleavage surface begin to dissociate. On thermal treatment at 450°C for 20 min isolated anisometric impurity formations appear, oriented mainly along (110)_{KCl}. (5 refs.)

113936 Transition metal impurities in silicon. E.R.Weber (II. Phys. Inst., Univ. of Koln, Koln, Germany), N.Wiffl. *Defects in Semiconductors II, Symposium Proceedings, Boston, MA, USA, Nov. 1982 (New York, USA: North-Holland 1983)*, p.19-32
The properties of transition metals in silicon are reviewed, emphasizing those observations which allow conclusions to be drawn with respect to microscopic defect models. 3d metals diffuse interstitially into silicon and stay predominantly in these sites at high temperatures. 3d elements lighter than Co can be quenched into these interstitial sites, giving rise to well-established energy levels. First theoretic calculations for these ions yield promising results. Co, Ni and Cu vanish out of the interstitial solution during quenching; an appreciable fraction of Cu may form pairs. The understanding of 4d and 5d metals in silicon is much less advanced at present, even for the technologically important elements Au and Pt. Some observations indicate that for Au and Pt pair formation might as well be important. (55 refs.)

The calculated defect structure of thoriaSee Entry 113862
Microdefects and impurities in dislocation-free silicon crystalsSee Entry 113905
Defects, dislocations and degradation of compound semiconductorsSee Entry 113915

Silicon-oxygen complexes containing three oxygen atoms as the dominant thermal donor species in heat-treated oxygen-containing silicon ..See Entry 113957
Scanning electron beam annealing of oxygen donors in Czochralski siliconSee Entry 114027

61.70T Doping and implantation of impurities

113937 Ultraviolet (UV) photochemical doping of silicon. K.G.Ibbs, M.L.Lloyd, R.D.Chad (General Electric Co. plc, Hirst Res. Centre, Wembley, England). *Proc. SPIE Int. Soc. Opt. Eng. (USA)*, vol.369, p.361-4 (1983). (SPIE Proceedings of the Max Born Centenary Conference OPTICS 82, ECOSA 82, Edinburgh, Scotland, 7-10 Sept. 1982).
Describes a method of producing p-n junctions in silicon using an ArF laser to dissociate triethyl boron. Junction depths of 0-0.8 µm and peak electrically active dopant concentrations of 8×10¹⁸-2×10²⁰ have been measured. (3 refs.)

113938 Doping of indium phosphide with germanium. L.M.Pavlova, V.A.Antonov, N.V.Vanyukova, A.G.Karamov, L.I.Perederri, V.V.Selin (Moscow Inst. of Electronic Technol., Moscow, USSR). *Inorg. Mater. (USA)*, vol.18, no.9, p.1229-32 (Sept. 1982). Translation of: *Izv. Akad. Nauk SSSR Neorg. Mater.*, vol.18, no.9, p.1444-7 (Sept. 1982). [received: Sept. 1983]
Using microstructural analysis and by measuring the microhardness the authors have determined the limits of the solubility of germanium in indium phosphide at different temperatures. The maximum solubility at 900°C is ~7×10¹⁹ at/cm³. Using the Czochralski method and liquid hermetic sealing of the melt at an inert-gas pressure of 490×10⁴ Pa, single crystals of indium phosphide doped with germanium have been grown. The range of experimental values of the effective distribution coefficient of germanium in indium phosphide has been obtained. The authors have measured the electrical parameters of single crystals of indium phosphide for different degrees of germanium doping. Curves of the Hall density and electron mobility as a function of the germanium density have been drawn. By comparing these curves with the limit saturation at a given temperature the authors have been able to draw conclusions on the mechanism by which germanium enters into the indium phosphide lattice. By analyzing the theoretical and experimental curves of the Hall mobility of the electrons against their density they have shown that in single crystals of indium phosphide doped with germanium scattering by charged centers predominates. (9 refs.)

113939 Autodoping phenomena in epitaxial silicon. G.K.Ackermann (Tech. Fachhochschule, Berlin, Germany), E.Ebert. *J. Electrochem. Soc. (USA)*, vol.130, no.9, p.1910-15 (Sept. 1983).
Autodoping experiments were performed using a radiation-heated Applied Materials Corporation (AMC) 7600 epitaxial reactor, (100) n-doped silicon wafers, arsenic-doped buried layers (subcollector) of total implanted or diffused dose of 7×10¹⁵-3×10¹⁶ cm⁻², and buried layer areas between 10 and 100% wafer area. Intentionally undoped epitaxial layers of 1.4 µm thickness were grown. The lateral autodoping was found to be very uniform with no distinct flow pattern-induced spatial distribution. Autodoping follows a square root law with respect to buried layer area. Autodoping shows a linear relationship with respect to buried layer doping. An analysis of the buried layer doping profile identifies the out-diffusion source with electrically inactive arsenic, about 50% of total implanted or diffused dopant. Less than 1% of the out-diffusing arsenic is incorporated into the wafer surface and growing epitaxial layer. (18 refs.)

113940 Metallurgical surfaces produced by ion implantation. D.I.Potter, M.Ahmed, S.Lamond. *J. Met. (USA)*, vol.35, no.8, p.17-22 (Aug. 1983).
Ion implantation, the process of embedding ions accelerated through high voltages, is described as a metallurgical tool for altering surface microstructure and properties. Examples of applications to improve resistance to wear, oxidation, and corrosion are provided. The possibilities for producing surface 'superalloys' is explored using Al³⁺ ion implantation into nickel as a prototype alloy system. The micromechanisms which operate and determine implanted surface chemistry are presented, and a predictive capability is demonstrated. Factors determining the phases that are stable in implanted alloys are outlined and demonstrated using P³⁺ and Al³⁺ ion implantation of nickel. Future directions using ion implantation for metallurgical purposes are discussed. (33 refs.)

113941 Role of channeling in the implantation of low-energy ions. N.P.Stepina, G.A.Kachurin (Inst. of Semiconductor Phys., Acad. of Sci., Novosibirsk, USSR). *Sov. Phys.-Semicond. (USA)*, vol.17, no.3, p.278-80 (March 1983). Translation of: *Fiz. & Tekh. Poluprovodn. (USSR)*, vol.17, no.3, p.449-52 (March 1983). [received: Sept. 1983]
An investigation was made of the impurity profile of silicon doped by implantation of low-energy boron ions. The dependences on the ion energy, ion dose, target orientation, and implantation temperature were determined. The measurements were carried out by electrophysical methods after activation of the implanted impurity by annealing and also by the method of mass spectrometry of secondary ions. It was found that the observed deep penetration of boron was associated with channeling. The proportion of the channeled ions was fairly high up to a dose of 10¹⁵ cm⁻² even at a temperature of 20°C, indicating a low degree of disordering of the lattice by the low-energy boron ions. It was concluded that utilization of the channeling of low-energy ions is a promising method of doping of layers of very precise thickness and estimates were obtained of the channeling parameters of impurity ions of different masses in the energy range 1-10 keV. (8 refs.)

113942 Transient annealing of ion-implanted silicon using a scanning IR line source. Y.S.Liu, H.E.Cline, G.E.Possin, H.G.Parks, W.Katz (General Electric Res. & Dev. Center, Schenectady, NY, USA). *Laser-Solid Interactions and Transient Thermal Processing of Materials, Boston, MA, USA, 1-4 Nov. 1982 (New York, USA: Elsevier 1983)*, p.425-30
Recent interest in finding an efficient method for transient annealing of ion-implanted silicon has led to studies of various rapid annealing schemes such as graphite heaters and high intensity incoherent light sources as alternative methods to laser annealing. In this paper the authors describe a recent study of transient annealing of ion-implanted silicon using a scanning IR line source created by a single tungsten filament enclosed in a quartz envelope. Various dopants (B⁺, P⁺ and As⁺) with fluences of 10¹⁴ to 10¹⁶ ions/cm² were implanted and annealed under both transient and steady-state thermal conditions. Dopant depth distributions were analyzed using the SIMS technique. Sheet resistance measurements indicated that almost 100% activations of the implanted dopants were achieved. Sensitivities of dopant activation to transient annealing conditions were studied as a function of dopant concentrations, and high-dose As- and B-implanted samples were found to be sensitive to

transient thermal cycle, particularly to the peak temperature. Recrystallization was studied with Rutherford backscattering spectroscopy using 2 MeV He⁺ ions. (5 refs.)

113943 Measurements of ion-implantation damage in GaP. D.R. Myers, P.S. Percy, P.L. Gourley (Sandia Nat. Labs., Albuquerque, NM, USA). Defects in Semiconductors II, Symposium Proceedings, Boston, MA, USA, Nov. 1982 (New York, USA: North-Holland 1983), p.505-9. The authors have applied stress measurements using the cantilever beam technique and Raman spectroscopy to characterize the dose dependence of damage production for He⁺, C⁺, or Ar⁺ implants into GaP. Stress increases monotonically with dose until a species-dependent critical dose is reached. Above that dose, the material yields at an integrated lateral stress of $\sim 2 \times 10^5$ dynes/cm², corresponding to an expansion of $\sim 1\%$ in the implanted volume. The dose dependence of stress scales well with the volume density of ion energy deposited into atomic collisions. Raman measurements indicate that the material is still crystalline when the yield stress is reached. (10 refs.)

113944 Damage and in situ annealing during ion implantation. D.K. Sadana, J. Washburn (Dept. of Materials Sci. & Mineral Engng., Univ. of California, Berkeley, CA, USA), P.F. Byrne, N.W. Cheung. Defects in Semiconductors II, Symposium Proceedings, Boston, MA, USA, Nov. 1982 (New York, USA: North-Holland 1983), p.511-16. Formation of amorphous (α) layers in Si during ion implantation in the energy range 100 KeV-11 MeV and temperature range liquid nitrogen (LN)-100°C has been investigated. Cross-sectional transmission electron microscopy (XTEM) shows that buried amorphous layers can be created for both room temperature (RT) and LN temperature implants, with a wider 100 percent amorphous region for the LN cooled case. The relative narrowing of the α layer during RT implantation is attributed to in situ annealing. Implantation to the same fluence at temperatures above 100°C does not produce α layers. To further investigate in situ annealing effects, specimens already containing buried α layers were further irradiated with ion beams in the temperature range RT-400°C. It was found that isolated small α zones (≤ 50 Å diameter) embedded in the crystalline matrix near the two a/c interfaces dissolved into the crystal but the thickness of the 100 percent α layer was not appreciably affected by further implantation at 200°C. A model for in situ annealing during implantation is presented. (6 refs.)

113945 A comparison of ellipsometer and RBS analysis of implant damage in silicon. W.M. Paulson, S.R. Wilson (Semiconductor Res. & Dev. Lab., Motorola Inc., Phoenix, AZ, USA), C.W. White, B.R. Appleton. Defects in Semiconductors II, Symposium Proceedings, Boston, MA, USA, Nov. 1982 (New York, USA: North-Holland 1983), p.523-7. The purpose of this study is to analyze ion implant damage profile using RBS and ellipsometry. Silicon wafers were implanted with ⁷⁵As at 100, 200 or 300 keV; doses were chosen to generate constant peak impurity concentrations at each energy. The samples were then analyzed using RBS to obtain damage-depth profiles and ellipsometry to obtain Δ , Ψ parameters. At light doses decreasing Δ values correspond to increased scattering yield; at higher doses Ψ increases rapidly as the scattering yield approaches the random value. The higher energy implants shift the Δ - Ψ curves to larger Ψ values. Multilayer structures, that include lightly damaged silicon on either side of the project range as well as more damaged near the projected range, are required to model the ellipsometer parameters. (16 refs.)

113946 The study of damage profile of ion implanted layer on Si by spectroscopic ellipsometry. J. Luo, P.J. Mc Marr, K. Vedam (Materials Res. Lab., Pennsylvania State Univ., University Park, PA, USA). Defects in Semiconductors II, Symposium Proceedings, Boston, MA, USA, Nov. 1982 (New York, USA: North-Holland 1983), p.529-33. The authors have determined the dielectric function of silicon samples which were implanted with 100-150 keV P, As, Si ions to doses of 2×10^{14} - 1×10^{16} cm⁻², by a rotating analyser Automated ellipsometer in the spectral range 1.77-4.59 eV. These data have been analyzed using a simplified three layer model. (5 refs.)

113947 Si-on-sapphire and Si implanted with Zr ions: lattice location, solid phase epitaxial regrowth and electrical properties. I. Golecki (Rockwell Internat. Corp., Anaheim, CA, USA), I. Suni. Defects in Semiconductors II, Symposium Proceedings, Boston, MA, USA, Nov. 1982 (New York, USA: North-Holland 1983), p.541-5. Zr ions have been implanted at 300 keV ($R_p=1400$ Å) and doses of 3×10^{12} - 3×10^{15} Zr/cm² into Si-implanted, amorphous Si layers on (100) bulk Si and Si-on-sapphire. Rutherford backscattering and channeling spectroscopy was used to study the Zr distribution and lattice location during solid-phase regrowth of the Si layers. The regrowth at 500-550°C stops at 3.4×10^{20} Zr/cm³, and Zr exhibits interface trapping and surface segregation effects. In this temperature range, Zr is essentially non-substitutional, and inactive electrically. (10 refs.)

Low-loss integrated optical waveguides fabricated by nitrogen ion implantation. See Entry 113086

Correlation among secondary ion mass spectrometry, cross-section transmission electron microscopy, and Rutherford backscattering analyses for defect density and depth distribution determination. See Entry 113948

A new doping technique for the PAC probes ¹⁰⁰Pd and ¹¹¹In and its application to the study of point defects in BCC metals. See Entry 113961

Interactions of defects with Co implanted into Al at 4.2K. See Entry 113965

Interaction of implanted impurities with extended defect configurations in tungsten single crystal. See Entry 113976

Applications of a continuous wave incoherent light source (CWILS) to semiconductor processing. See Entry 113988

Subnanosecond pulsed laser annealing of Si-implanted InP. See Entry 113997

Compound semiconductors [laser and electron beam annealing]. See Entry 114007

Effect of pulse duration on the annealing of ion implanted silicon with a XeCl excimer laser and solar cells. See Entry 114010

Pulsed excimer laser (308 nm) annealing of ion implanted silicon and solar cell fabrication. See Entry 114011

Oxygen and nitrogen incorporation during CW laser recrystallization of polysilicon. See Entry 114014

CW laser annealing of ion implanted oxidized silicon layers on sapphire. See Entry 114015

Laser annealing of ion implanted semiconductors. See Entry 114020

Comparison between thermal and laser annealing in ion-implanted silicon. See Entry 114021

Arsenic implant activation and redistribution in p-type silicon induced by pulsed electron beam annealing. See Entry 114028

Processing of shallow ($R_p < 150$ Å) implanted layers with electron beams. See Entry 114029

Pattern formation in metallic glasses induced by helium ion implantation. See Entry 114053

Crystallization of amorphous silicon films by pulsed ion beam annealing. See Entry 114054

Radiation damage in tantalum observed by PAC. See Entry 114055

Incoherent light-induced diffusion of arsenic into silicon from a spin-on source. See Entry 114253

Double zinc diffusion fronts in InP—theory and experiment. See Entry 114254

Comparisons of the nuclear reactions ¹⁸O(p, α)¹⁵N and ¹⁶O(d, α)¹⁴N to study the oxygen effects in Pt silicide formation. See Entry 114285

Material surface modified by ion implantation and ion beam mixing. See Entry 114308

Role of electronic processes in epitaxial recrystallization of amorphous semiconductors. See Entry 114390

Modeling of doping during CVD growth of semiconductor films. See Entry 114409

Reduction in the localized band-gap states in amorphous silicon by annealing and hydrogen implantation. See Entry 114484

Effects of doping on transport and deep trapping in hydrogenated amorphous silicon. See Entry 114533

Effect of grain size on the resistivity of polycrystalline material. See Entry 114548

Electrical characteristics of Be-implanted GaAs diodes annealed with an ultrahigh power argon arc lamp. See Entry 114594

Der Einfluss von Wasserstoff auf die Supraleitung von Nichtbergangsmetallen (The influence of hydrogen on the superconductivity of non-transition metals). See Entry 114640

Mossbauer spectroscopy on ¹³³Cs as a method to study vacancy migration in metals. See Entry 114766

Non destructive optical analysis of implanted layers in GaAs by Raman scattering and spectroscopic ellipsometry. See Entry 114871

Molecular effect of Al K α -ray yields from aluminum oxide films for H⁺ and H₂⁺ ion bombardments. See Entry 114974

Enhancement of growth rate due to tin doping in GaAs epilayer grown by low pressure metal-organic chemical vapor deposition. See Entry 115064

Tin doping of gallium arsenide by metallic organic chemical vapor deposition (MOCVD). See Entry 115065

Use of diethylberyllium for metal organic chemical vapor deposition of beryllium-doped gallium arsenide. See Entry 115066

Friction and wear properties of nitrided and N⁺-implanted 17-4 PH stainless steel. See Entry 115370

The effects of arsenic doping in reactive ion etching of silicon in chlorinated plasmas. See Entry 115386

High-efficiency Si solar cells by beam processing. See Entry 115636

61.70W Impurity concentration, distribution, and gradients

(see also 66.30J Diffusion, migration and displacement of impurities)

113948 Correlation among secondary ion mass spectrometry, cross-section transmission electron microscopy, and Rutherford backscattering analyses for defect density and depth distribution determination. R.G. Wilson (Hughes Res. Labs., Malibu, CA, USA), D.K. Sadana, T.W. Sigmon, C.A. Evans, Jr., *Appl. Phys. Lett. (USA)*, vol.43, no.6, p.549-51 (15 Sept. 1983). Correlation is found between the relative densities and depth distributions of defect clusters/disorder/damage measured by cross-section transmission electron microscopy and Rutherford backscattering and silver atom depth distributions measured by secondary ion mass spectrometry for (100) and (111) silicon implanted with silver ions and annealed at 550°C. (4 refs.)

113949 Direct hydrogen profile determination in TiO₂ after electrochemical treatment. P. Clechet, C. Martelet, R. Olier (Ecole Centrale de Lyon, Ecully, France), J.P. Thomas, M. Fallavier, *J. Electrochem. Soc. (USA)*, vol.130, no.8, p.1795-6 (Aug. 1983). Electrochemical treatments of titanium oxide are well known as leading to important changes in physical (color, IR absorption), electrical (capacitance, conductivity) and photoelectrochemical properties either for single crystal material or RF reactively sputtered or thermally grown thin layers. Here the authors report observations on highly doped ($\sim 10^{19}$ cm⁻³) 200 nm thick layers obtained by anodic oxidation of bulk electropolished titanium, at 80 V in 1 M sulfuric acid. Nuclear analysis brings out direct evidence of the existence of at least two forms of incorporated hydrogen within TiO₂ layers as is often proposed in the literature. Incorporation mechanism seems to be intricate and the hydrogen profile in the authors samples cannot be explained by a simple diffusion law. Probably some hydrogen species are trapped on defects resulting from crystallization during film growth (11). (11 refs.)

113950 Chlorine redistribution in HCl oxides due to high temperature annealing. B.C. Beard (Center for Surface & Coatings Res., Lehigh Univ., Bethlehem, PA, USA), S. Titcomb, S.R. Butler, *J. Electrochem. Soc. (USA)*, vol.130, no.9, p.1959-61 (Sept. 1983). The incorporation of chlorine in the growing SiO₂ film during O₃/HCl oxidation of silicon has been studied. Under certain oxidation conditions a Cl-rich phase develops at the interface of the SiO₂ film and the Si substrate. The redistribution of the Cl from the SiO₂/Si interface region in response to high temperature annealing is discussed. Secondary ion mass spectrometry (SIMS) analysis was performed on a number of Cl containing specimens. The superior depth resolution of SIMS (< 18 nm) over RBS (35 nm) allowed for more detailed depth profiles of Cl. (5 refs.)

113951 Investigating the distribution of impurity iron atoms in the compounds Ni₃Al, NiAl and Ni₂Al₃. I.A. Zelenkov, S.N. Pastushenko, *Russ. Metall. (GB)*, no.3, p.165-6 (1982). Translation of: *Izv. Akad. Nauk. SSSR Met.*, no.3, p.189-90 (1982).

Iron-57 impurity atoms in nickel aluminides can be located in both the aluminum and the nickel sublattices. The iron atoms are mainly in the aluminum sublattice in Ni₃Al, and in the nickel in NiAl and Ni₂Al₃. One reason for the growth of the ⁵⁷Fe isomer shift in nickel aluminides is due to the increase in the number of aluminum atoms in the local environment of the Mossbauer atom. Another is the filling of the d-band of the alloys with increasing aluminum content in the compounds investigated. (5 refs.)

- 113952 Amounts and character of distribution of impurities in zone-melted single-crystal lanthanum hexaboride.** Yu.B.Paderno, V.I.Lazorenko, N.I.Buryak, A.V.Kovalev, A.A.Matvienko, A.P.Galasun (Inst. of Materials Sci., Acad. of Sci., Ukrainian SSR). *Sov. Powder Metall. & Met. Ceram. (USA)*, vol.22, no.1, p.50-3 (Jan. 1983). Translation of: *Poroshk. Metall. (USSR)*, vol.22, no.1, p.60-3 (Jan. 1983). [received: Aug. 1983]
Lanthanum hexaboride single crystals were grown and refined by the levitation zone melting technique with induction heating. The amounts and character of distribution of impurities in the starting and zone-melted materials were determined by quantitative spectral analysis. It is shown that zone melting effectively purifies a starting lanthanum hexaboride powder from many contaminants. The effectiveness of removal of some low-melting-point and volatile elements is increased by their evaporation and escape in the gaseous form from the molten zone. Estimated values of effective coefficients of distribution of many impurities are given. (7 refs.)
- 113953 Character of impurity distribution in comminuted β -boron crystals.** T.Sh.Badzagua, M.V.Vlasova, D.L.Gabuniya, N.G.Kakazei (Inst. of Materials Sci., Acad. of Sci., Ukrainian SSR). *Sov. Powder Metall. & Met. Ceram. (USA)*, vol.22, no.1, p.54-6 (Jan. 1983). Translation of: *Poroshk. Metall. (USSR)*, vol.22, no.1, p.60-3 (Jan. 1983). [received: Aug. 1983]
With the aid of EPR data, the character of distribution of impurities in fine β -boron crystals was studied as a function of crystal particle size. Specimens for investigation were prepared by melting, using graphite and boron nitride crucibles, a boron powder of $\sim 98\%$ purity was produced in a vacuum corresponding to 10^{-1} - 10^{-2} Pa. The specimens were comminuted by the application of sharp shock loads and by abrasion. Powders produced by both methods were carefully purified from magnetic inclusions. The particles were divided into 50- to 500- μ m fractions by standard sieve analysis methods and into finer fractions by liquid sedimentation. The mean particle size (less than 50 μ m) was determined by microscopical analysis. EPR spectra were measured in a 3-cm range at room temperature. (9 refs.)
- 113954 Correlation of oxygen and recombination centers on a microscale in as-grown Czochralski silicon crystals.** K.Nauka, H.C.Gatos, J.Lagowski (MIT, Cambridge, MA, USA). Defects in Semiconductors II, Symposium Proceedings, Boston, MA, USA, Nov. 1982 (New York, USA: North-Holland 1983), p.177-80
Quantitative microprofiles of the interstitial oxygen concentration and of the excess carrier lifetime, with a spatial resolution of about 20 μ m, were obtained in as-grown dislocation-free CZ-Si crystals employing a double laser absorption technique. It was found that maxima (minima) in oxygen concentration along the crystal growth direction coincide with minima (maxima) of the lifetime. It was further found that the relation between changes in oxygen concentration and in lifetime varies in the radial direction indicating that 'as-grown' oxygen precipitates are involved in lifetime limiting processes. (9 refs.)
- The role of the state of dispersion of impurity on Z_1 -centres in $\text{NaCl}:\text{Ca}^{2+}$ crystals** See Entry 113909
- Doping of indium phosphide with germanium** See Entry 113938
- Role of channeling in the implantation of low-energy ions** See Entry 113941
- Measurements of ion-implantation damage in GaP** See Entry 113943
- A comparison of ellipsometer and RBS analysis of implant damage in silicon** See Entry 113945
- The study of damage profile of ion implanted layer on Si by spectroscopic ellipsometry** See Entry 113946
- Si-on-sapphire and Si implanted with Zr ions: lattice location, solid phase epitaxial regrowth and electrical properties** See Entry 113947
- Supersaturated alloys, solute trapping, and zone refining [laser annealing of semiconductors]** See Entry 114005
- Irradiation-induced segregation in multi-component alloys** See Entry 114181
- Iron diffusion in indium phosphide and gallium arsenide** See Entry 114272
- Effect of oxygen on radiation-enhanced diffusion in silicon** See Entry 114278
- Comparisons of the nuclear reactions $^{18}\text{O}(\text{p}, \alpha)^{15}\text{N}$ and $^{16}\text{O}(\text{d}, \alpha)^{14}\text{N}$ to study the oxygen effects in Pt silicide formation** See Entry 114285
- Effect of grain size on the resistivity of polycrystalline material** See Entry 114548
- Hall effect and sheet resistivity measurements at low temperatures on silicon implanted with iron** See Entry 114552
- Investigation of the surface of gallium arsenide doped by aluminum recoil atoms** See Entry 114584
- Auger voltage contrast depth profiling of shallow p - n junctions** See Entry 114597
- Simulation and measurement of C/V doping profiles in multilayer structures $[\text{Ga}_{1-x}\text{Al}_x\text{As}]$** See Entry 114599
- Absence of hydrogen in superconducting molybdenum sulfide, MoS_4** See Entry 114744
- Non destructive optical analysis of implanted layers in GaAs by Raman scattering and spectroscopic ellipsometry** See Entry 114871
- Spreading resistance of InSb crystals pulled under ultrasonic vibrations** See Entry 115042
- On the modeling of the high-temperature embrittlement of metals containing helium** See Entry 115313
- Material analysis by means of high energy ion beams** See Entry 115600

61.70Y Interaction between different crystal structure defects

- 113955 Interaction of hydrogen with nonmetallic inclusions of the different shapes in ferrite-pearlite steels.** V.L.Mirochnik, A.P.Okenko, V.I.Sarrak, G.A.Filippov (Inst. of Metall. & Phys. of Metals, Moscow, USSR). *Fiz. Met. & Metalloved. (USSR)*, vol.56, no.2, p.308-14 (Aug. 1983). In Russian. English translation in: *Phys. Met. & Metallogr. (GB)*
The low permeability to hydrogen and the rate of evolution of hydrogen from ferrite-pearlite steel with elongated sulphide nonmetallic inclusions and its ability to absorb hydrogen were found to be due to the interaction of hydrogen with two types of defect: collectors and traps. Globularization of the inclusions increased the permeability to hydrogen and the rate of evolution of hydrogen, but it reduced the ability of steel to absorb hydrogen. The traps in the hydrogenated ferrite-pearlite steel in the absence of load were regions of bulk elongation in the metal matrix in the vicinity of the inclusions, which were formed as a result of the pressure of molecular hydrogen in the collectors located at the sulphide-matrix interfaces. (13 refs.) A.T.

- 113956 Simulation of the interaction of a vacancy with special tilt boundaries in a body-centred cubic lattice.** V.V.Pokropivnyi, V.V.Yagodkin (Inst. of Problems in Materials Sci., Acad. of Sci., Kiev, Ukrainian SSR). *Fiz. Met. & Metalloved. (USSR)*, vol.56, no.2, p.392-6 (Aug. 1983). In Russian. English translation in: *Phys. Met. & Metallogr. (GB)*
A detailed numerical study is made of the interaction between vacancies and various special tilt boundaries in body-centred chromium as a function of the position of a vacancy on a boundary. The results indicated a strong dependence of the energy formation of a vacancy on the point at which it is located on a boundary and this can be explained by local inhomogeneities of the boundary structure. (15 refs.) A.T.
- 113957 Silicon-oxygen complexes containing three oxygen atoms as the dominant thermal donor species in heat-treated oxygen-containing silicon.** G.S.Oehrlein (IBM Thomas J. Watson Res. Center, Yorktown Heights, NY, USA). *J. Appl. Phys. (USA)*, vol.54, no.9, p.5453-5 (Sept. 1983).
A kinetic study of thermal donor formation in 450°C heat-treated modern silicon crystals has been performed and it is concluded that SiO_3 complexes are the dominant thermal donor species (for heat-treatment times of up to about 100 h), rather than SiO_4 complexes. Clusters containing a number of oxygen atoms other than three or four seem to be also electrically active. (10 refs.)
- 113958 Modification of defects during irradiation of Si with high electron doses.** A.V.Dvurechenskii, B.P.Kashnikov, V.I.Panov (Inst. of Semiconductor Phys., Acad. of Sci., Novosibirsk, USSR). *Sov. Phys.-Semicond. (USA)*, vol.17, no.3, p.344-5 (March 1983). Translation of: *Fiz. & Tekh. Poluprovodn. (USSR)*, vol.17, no.3, p.546-8 (March 1983). [received: Sept. 1983]
Provides a quantitative description of the behavior of vacancy defects on the assumption that V_2P (H) complexes are formed in silicon containing oxygen (OX-Si) and that oxygen provides effective vacancy annihilation centers. The authors consider a defect formation model which allows for reactions of two types: (1) formation of vacancy complexes with oxygen (O) and phosphorus (P) and (2) annihilation at vacancy complexes. The reactions which represent the loss of interstices to impurity atoms (C) followed by annihilation are also allowed for. This model can be described by a system of nonlinear first-order differential equations. (6 refs.)
- 113959 Mossbauer study of defect trapping at ^{57}Co in cold worked aluminium.** K.Sassa, W.Petry, G.Vogl (Freie Univ. Berlin, Berlin, Germany). Point Defects and Defect Interactions in Metals. Proceedings of the Yamada Conference V, Kyoto, Japan, 16-20 Nov. 1981 (Amsterdam, Netherlands: North-Holland 1982), p.213-15
Point defects induced by cold work of Al at various temperatures between 4.2K and 80K were trapped at $^{57}\text{Co}/^{57}\text{Fe}$ atoms and studied by Mossbauer spectroscopy. No free migration of interstitials was observed, whereas enhanced and free diffusion of vacancies respectively, was found at 100K and 200K. (12 refs.)
- 113960 PAC study of defect trapping at ^{111}In in cold worked aluminium.** H.G.Muller (Hahn-Meitner-Inst. für Kernforschung, Berlin, Germany). Point Defects and Defect Interactions in Metals. Proceedings of the Yamada Conference V, Kyoto, Japan, 16-20 Nov. 1981 (Amsterdam, Netherlands: North-Holland 1982), p.216-19
The PAC technique was applied to study the interaction of lattice defects with indium impurities in cold worked Al. Several In doped Al specimens were extended by different amounts of strain at 77K. No trapping of interstitials is observed, whereas after annealing between 110K and 210K an increasing fraction of the In impurities traps a lattice defect of vacancy type. The symmetry axis of the resulting In-vacancy-complex points along $\langle 111 \rangle$ directions. It is concluded that the In atoms trap divacancies, which at least partly migrate along dislocation lines. (15 refs.)
- 113961 A new doping technique for the PAC probes ^{100}Pd and ^{111}In and its application to the study of point defects in BCC metals.** H.Metzner, R.Sielemann, S.Klaumunzer, R.Butt, W.Semmler (Freie Univ. Berlin, Berlin, Germany). Point Defects and Defect Interactions in Metals. Proceedings of the Yamada Conference V, Kyoto, Japan, 16-20 Nov. 1981 (Amsterdam, Netherlands: North-Holland 1982), p.224-7
The authors show that heavy ion induced nuclear reactions are particularly well suited to dope highly impurity-sensitive materials with radioactive nuclear probes. The application of various probes (^{111}In , ^{100}Pd , ^{99}Rh) allows comparative PAC studies which take advantage of the different trapping behaviour of the probes. Thus detailed information about the properties of intrinsic point defects in niobium and first results on defect trapping at ^{100}Pd atoms in molybdenum were obtained. (7 refs.)
- 113962 Interstitial trapping by zinc atoms in electron-irradiated silver.** F.Maury (CNRS, Univ. Paris XI, Orsay, France), A.Lucasson, P.Vajda, M.Halbwachs, P.Lucasson. Point Defects and Defect Interactions in Metals. Proceedings of the Yamada Conference V, Kyoto, Japan, 16-20 Nov. 1981 (Amsterdam, Netherlands: North-Holland 1982), p.392-5
The trapping radius of self-interstitials by zinc atoms in a silver matrix is determined by the damage rate method. It is found $r_t = (0.6 \pm 0.25)r_v$, where r_v is the capture radius of a self-interstitial by a vacancy, if one assumes that the resistivity of the complex impurity+single interstitial is not smaller than the resistivity of the self-interstitial. The isochronal recovery spectra of the specimens (two dilute alloys containing respectively 200 and 1100 at.ppm of zinc) have been measured together with that of pure silver from 12 to 290K. An interpretation is proposed for the major recovery peaks. (7 refs.)
- 113963 Trapping of interstitials at ^{100}Pd , ^{111}In , and ^{181}Hf -impurities in irradiated cubic metals.** R.Sielemann, H.G.Muller, W.Semmler, R.Butt, H.Metzner (Hahn-Meitner-Inst. für Kernforschung, Berlin, Germany). Point Defects and Defect Interactions in Metals. Proceedings of the Yamada Conference V, Kyoto, Japan, 16-20 Nov. 1981 (Amsterdam, Netherlands: North-Holland 1982), p.403-6
The authors have used three different PAC probes (^{100}Pd , ^{111}In , ^{181}Hf) to study the behaviour of self-interstitials produced by low temperature electron or heavy ion irradiation in Al, Nb, and Mo. Their results demonstrate that selective trapping of certain types of defects occurs at the different impurities. General trends for the trapping behaviour are shown up and results on symmetries of the impurity-interstitial-complexes as well as on their annealing behaviour are reported. The electric field gradients generated by these complexes are remarkably large in the b.c.c. metals as compared with f.c.c. metals. (10 refs.)

113964 Dose dependence of interstitial trapping at ^{111}In impurities in e^- -irradiated aluminum. R. Butt, W. Semmler, H.G. Muller (Freie Univ. Berlin, Berlin, Germany).

Point Defects and Defect Interactions in Metals. Proceedings of the Yamada Conference V, Kyoto, Japan, 16-20 Nov. 1981 (Amsterdam, Netherlands: North-Holland 1982), p.407-9

The perturbed angular correlation method (PAC) was applied to the investigation of defect trapping during electron irradiation above Stage I_g. The observed trapped defect can be attributed to a simple interstitial configuration. The dose dependence of the trapping behavior of the In-impurity atoms shows a saturation of the fraction of the trapped interstitial configuration at about 20%. There is no additional PAC component observed, which could account for the continuous increase of the residual resistivity. This requires the assumption that at least one configuration is not visible by PAC. (3 refs.)

113965 Interactions of defects with Co implanted into Al at 4.2K. E. Verbiest, H. Pattyn (Inst. voor Kern- en Stralingsfysika, Univ. of Leuven, Leuven, Belgium).

Point Defects and Defect Interactions in Metals. Proceedings of the Yamada Conference V, Kyoto, Japan, 16-20 Nov. 1981 (Amsterdam, Netherlands: North-Holland 1982), p.410-12

Presented are the results of a mathematical model to calculate the concentrations of mono- and di-interstitials, mono- and divacancies and the interstitial and vacancy clusters and the fractions of Co impurity atoms associated with these defects as a function of the irradiation dose and during a thermal annealing treatment. The Co-defect fractions have been measured using Mossbauer spectroscopy and these experimental results have been used to check the model calculations and to adjust certain parameters. (4 refs.)

113966 Interaction of vacancies and self-interstitials with interstitial solute atoms in α -iron. J. Diehl, M. Weller, W. Mensch (Max-Planck-Inst. fur Metallforschung, Inst. fur Werkstoffwissenschaften, Stuttgart, Germany).

Point Defects and Defect Interactions in Metals. Proceedings of the Yamada Conference V, Kyoto, Japan, 16-20 Nov. 1981 (Amsterdam, Netherlands: North-Holland 1982), p.413-16

An overview is given of the complexes generated in α -iron after low temperature irradiation by reactions between intrinsic defects and carbon atoms in solid solution, as they are revealed by internal-friction and magnetic aftereffect measurements. By correlation of both techniques precise values of the reorientation parameters are obtained. Formation, stability and configurations of the various complexes are discussed in the light of recent observations, including those on their symmetries. (17 refs.)

113967 Strong interaction between vacancy and solute in gold. J. Takamura (Dept. of Metal Sci. & Technol., Kyoto Univ., Kyoto, Japan).

Point Defects and Defect Interactions in Metals. Proceedings of the Yamada Conference V, Kyoto, Japan, 16-20 Nov. 1981 (Amsterdam, Netherlands: North-Holland 1982), p.431-6

On isochronal annealing of quenched-in resistivity in dilute gold alloys containing Ge, Sn and Sb, the consecutive motion of vacancy-solute pairs has been observed owing to the strong binding between a vacancy (V) and a solute atom (S). The anomalous annealing behaviours in these alloys are fully understood in terms of the motion of VS pairs, which leads to the successive formation and dissociation of multiple complexes V_nS_i ($i,j \geq 1$), eventually stacking fault tetrahedra and voids. The nature of vacancy-solute complexes and the nucleation kinetics of microvoids are discussed. (24 refs.)

113968 A positron lifetime study of vacancy-solute complexes in dilute gold alloys. Y. Shirai, T. Hamamoto, T. Takeshita, K. Furukawa, J. Takamura (Dept. of Metal Sci. & Technol., Kyoto Univ., Kyoto, Japan).

Point Defects and Defect Interactions in Metals. Proceedings of the Yamada Conference V, Kyoto, Japan, 16-20 Nov. 1981 (Amsterdam, Netherlands: North-Holland 1982), p.441-4

Positron lifetime measurements have been made for vacancy-solute complexes in quenched dilute gold alloys containing multi-valent solutes such as Ge, Sn and Sb. Based on the two-component analysis, the vacancy-solute binding energies in these alloys were estimated as 0.37 ± 0.05 eV in good agreement with the results of the resistivity study. The lifetime (τ) and the specific trapping rate (ν) for vacancy (V)-solute (S) complexes were also determined, which are in order of magnitude as $\tau_{V2S2} > \tau_V > \tau_{VS} \gg \tau_{VS2} > \tau_{VS3} > \tau_{VS4}$. In addition, a marked increase in the defect lifetime, indicative of the nucleation of microvoids, has been first observed on isochronal annealing of the quenched gold alloys. (6 refs.)

113969 Study of vacancy-solute interactions in dilute Al based alloys by thermal equilibrium measurements of positron annihilation. K. Ito, Y. Ohtsu, K. Shima, S. Tanigawa (Inst. of Materials Sci., Univ. of Tsukuba, Ibaraki, Japan).

Point Defects and Defect Interactions in Metals. Proceedings of the Yamada Conference V, Kyoto, Japan, 16-20 Nov. 1981 (Amsterdam, Netherlands: North-Holland 1982), p.453-6

Thermal equilibrium measurements of the Doppler broadened line shapes of annihilation radiations have been applied to a series of aluminum based dilute alloys (Al-0.5 at.% Li, Al-0.5 at.% Mg, Al-0.18 at.% Ca, Al-0.03 at.% Cu and Al-0.08 at.% Mg). The temperature dependence of line shape parameter in dilute alloys was found to be quite different from that in pure aluminum. In the intermediate temperature range, the formation of vacancy-solute pairs was found. The derived values for the vacancy-solute binding enthalpy were 0.08 ± 0.04 eV for lithium, 0.10 ± 0.04 eV for magnesium, 0.02 ± 0.04 eV for calcium, 0.09 ± 0.04 eV for copper and 0.09 ± 0.04 eV for silver, respectively. In the high temperature range, the line shape parameter in dilute alloys showed an abrupt increase toward the melting points. This effect was attributed to the formation of divacancy-solute pairs and suggests the existence of strong interactions with large binding enthalpy or large binding entropy between a divacancy and a solute atom. (9 refs.)

113970 Interaction and charge transfer between vacancy and solute in dilute aluminum alloys. M. Koike, K. Furukawa, J. Takamura, H. Hira, N. Yamamoto, F. Nakamura (Dept. of Metal Sci. & Technol., Kyoto Univ., Kyoto, Japan).

Point Defects and Defect Interactions in Metals. Proceedings of the Yamada Conference V, Kyoto, Japan, 16-20 Nov. 1981 (Amsterdam, Netherlands: North-Holland 1982), p.457-60

A summary report based on detailed analyses of quenched-in resistivities in dilute Al alloys is made on the vacancy-solute binding energy and entropy, and also on the resistivity contribution of vacancy-solute pairs. Particular attention is drawn to the binding entropy whose values are negative and large, indicating that the vibrational frequency is much reduced upon binding. The values of the binding entropy can be correlated to the rate of electron transfer which has been calculated by the Thomas-Fermi method. It is also shown that the rate of electron transfer becomes larger for larger core radii of solute atoms. (13 refs.)

113971 Mossbauer study on Fe-vacancy interaction in aluminum. S. Nasu, M. Kiritani (Dept. of Material Phys., Osaka Univ., Osaka, Japan).

Point Defects and Defect Interactions in Metals. Proceedings of the Yamada Conference V, Kyoto, Japan, 16-20 Nov. 1981 (Amsterdam, Netherlands: North-Holland 1982), p.461-4

^{57}Fe Mossbauer spectroscopy was used to discuss about Fe-vacancy interaction in aluminum. Satellite lines have been observed in low-temperature deformation experiment and suggested the satellites are due to the multiple complex reactions between Fe and vacancies. On the other hand, the satellite observed in quench-experiment suggested that binding energy between Fe and vacancy is rather small. Origin of the satellite seems to be different in both experiments, but isomer shift values are quite similar with each other. (2 refs.)

113972 Formation of vacancies in thermal equilibrium in α -range alloys. T. Hehenkamp (Inst. fur Metallphys., Univ. Gottingen, Gottingen/Clausthal, Germany).

Point Defects and Defect Interactions in Metals. Proceedings of the Yamada Conference V, Kyoto, Japan, 16-20 Nov. 1981 (Amsterdam, Netherlands: North-Holland 1982), p.465-8

A model for aggregates (complexes) between vacancies and one or more impurity atoms is described for nearest neighbor interactions. Binding enthalpies in the different complexes have been unambiguously derived therefrom employing a variety of experimental techniques for the determination of vacancy concentrations as function of composition and temperature, (resistivity, positron annihilation, calorimetry, dI/dA techniques), for some noble metals alloys. Solvent diffusion in these alloys has been found to be essentially governed by the increase of vacancy concentrations as function of these variables. Approximation for changes in the migration and correlation permits one to obtain the different binding enthalpies from measurements of solvent diffusion enhancement in an independent fashion and gives comparable results to the former techniques. (13 refs.)

113973 Mossbauer analysis on the annealing process of a quenched Al-Sn dilute alloy. M. Taniwaki (Div. of Electronic Engng., Hokkaido Univ., Sapporo, Japan), S. Uemeyama, Y. Ishida.

Point Defects and Defect Interactions in Metals. Proceedings of the Yamada Conference V, Kyoto, Japan, 16-20 Nov. 1981 (Amsterdam, Netherlands: North-Holland 1982), p.477-80

The interactions between Sn and vacancies during annealing process of a quenched Al-45 ppm Sn alloy are studied directly by Mossbauer effect. The binding energy between a Sn atom and a vacancy is 0.10-0.15 eV and this value is much smaller than those obtained by others. But stable Sn vacancies aggregates retard the recovery of Al alloys. (11 refs.)

113974 Recovery in electron irradiated aluminium observed by Mossbauer spectroscopy. S. Uemeyama, K. Sassa (Inst. of Industrial Sci., Univ. of Tokyo, Tokyo, Japan), M. Taniwaki, Y. Ishida, H. Yoshida.

Point Defects and Defect Interactions in Metals. Proceedings of the Yamada Conference V, Kyoto, Japan, 16-20 Nov. 1981 (Amsterdam, Netherlands: North-Holland 1982), p.481-4

Recovery of vacancies in prequenched and electron irradiated aluminium is studied using Mossbauer spectrum of ^{57}Co . The growth of Co-vacancy clusters occurs at 175K, showing that the vacancies migrate at the temperature. Above the stage, no interaction is detected between vacancies and Co atoms. The interaction between Co impurity and single vacancy appears to be weak. (12 refs.)

113975 Solute atom-dislocation interactions studied by ultrasonic method. Y. Hiki, T. Kosugi (Tokyo Inst. of Technol., Tokyo, Japan), K. Mizuno, T. Kino.

Point Defects and Defect Interactions in Metals. Proceedings of the Yamada Conference V, Kyoto, Japan, 16-20 Nov. 1981 (Amsterdam, Netherlands: North-Holland 1982), p.753-5

Frequency dependent decrement caused from dislocation damping in zone-refined and neutron-irradiated aluminum single crystals was measured, and changes of dislocation density and pinning length with aging time were studied. The solute atom (silicon)-dislocation binding energy and the diffusion constant of solute atom in the crystals were determined. (7 refs.)

113976 Interaction of implanted impurities with extended defect configurations in tungsten single crystal. J. Claes, M. Rots (Inst. voor Kern-en Stralingsfysika, Katholieke Univ. Leuven, Leuven, Belgium).

Point Defects and Defect Interactions in Metals. Proceedings of the Yamada Conference V, Kyoto, Japan, 16-20 Nov. 1981 (Amsterdam, Netherlands: North-Holland 1982), p.756-8

Using a special feature of the perturbed angular correlation technique, the authors have demonstrated that the energy of the heavy ion cascade is anisotropically distributed over close packed planes in the cubic lattice. Implanted impurity interaction with extended loop configurations was observed where the deposited energy density is high and the impurity insoluble in the host. In addition the effect of temperature on the impurity nearest neighbour geometry in such a defect cluster was measured in the 77-520K range. (2 refs.)

113977 Calculation of interaction energies between point defects and (1/2) (111) dislocation in BCC transition metals (self-interstitial and interstitial solute atom). A. Sato, K. Masuda (Dept. of Materials Sci. & Engng., Tokyo Inst. of Technol., Yokohama, Japan).

Point Defects and Defect Interactions in Metals. Proceedings of the Yamada Conference V, Kyoto, Japan, 16-20 Nov. 1981 (Amsterdam, Netherlands: North-Holland 1982), p.759-61

Selfenergies of various lattice imperfections, a straight screw dislocation, split selfinterstitials and an interstitial carbon, are calculated and their stabilities are examined by using a tight-binding type electronic theory coupled to the moments approach. Introducing the most stable type of a point defect into a screw dislocation core, the interaction energy is calculated as a function of the point defect orientation and the location with respect to the dislocation. (11 refs.)

113978 Electronic interaction between impurity and grain boundary in iron. M. Hashimoto, Y. Ishida (Inst. of Industrial Sci., Univ. of Tokyo, Tokyo, Japan), R. Yamamoto, M. Doyama, T. Fujiwara.

Point Defects and Defect Interactions in Metals. Proceedings of the Yamada Conference V, Kyoto, Japan, 16-20 Nov. 1981 (Amsterdam, Netherlands: North-Holland 1982), p.776-9

The electronic structures in both the pure and phosphorus segregated iron boundary were calculated by the recursion method using the model structure. The results showed that strong bonds are formed between the P-atom and Fe-atoms nearest to the P-atom, while the bonds between these Fe-atoms and their surrounding Fe-atoms are weakened. (6 refs.)

- 113979 Effect of the interaction between solute atoms and defects on formation of defect clusters.** H.Takahashi, T.Takeyama, S.Ohnuiki, T.Kato (Metals Res. Inst., Hokkaido Univ., Sapporo, Japan). Point Defects and Defect Interactions in Metals. Proceedings of the Yamada Conference V, Kyoto, Japan, 16-20 Nov. 1981 (Amsterdam, Netherlands: North-Holland 1982), p.861-4.
- The behavior of defect cluster formation has been studied in Fe-Ti, Fe-Mn, Fe-Mo alloys and Fe during electron irradiation in an electron microscope operated at 650 or 1000 kV in the temperature range between 525 and 725K. Interstitial type dislocation loops initially nucleated and grew during irradiation of all the specimens used. By prolonged irradiation voids were formed in Fe, Fe-Mo and Fe-Mn alloys, but in Fe-Ti alloy void nucleation was suppressed with increasing Ti content, and instead of it small dislocation loops which seemed to be of vacancy type were formed near the interstitial type loops formed initially. The activation energies for migration obtained from the temperature dependence of the growth speed of interstitial loops were 0.58 eV for Fe-0.1 at.% Ti alloy and 1.21-1.42 eV for Fe and the other alloys used, which suggest the interaction between solute and vacancy. (6 refs.)
- 113980 A role of helium and hydrogen atoms in the formation of interstitial loops.** N.Yoshida, E.Kuramoto, K.Kitajima (Res. Inst. for Appl. Mech., Kyushu Univ., Fukuoka, Japan). Point Defects and Defect Interactions in Metals. Proceedings of the Yamada Conference V, Kyoto, Japan, 16-20 Nov. 1981 (Amsterdam, Netherlands: North-Holland 1982), p.869-72.
- Formation processes of defect clusters in Mo and W due to the irradiation of He⁺ and H⁺ were investigated by means of TEM. Vacancy-He atom complexes are considered to act as nucleation sites of interstitial type dislocation loops. In the case of H⁺ irradiation it was found that platelike hydrogen clusters were formed. (9 refs.)
- 113981 Interaction of dislocations with impurities and its influence on the mechanical properties of silicon crystals.** K.Sumino (Res. Inst. for Iron, Steel & Other Metals, Tohoku Univ., Sendai, Japan). Defects in Semiconductors II, Symposium Proceedings, Boston, MA, USA, Nov. 1982 (New York, USA: North-Holland 1983), p.307-21.
- A review is presented of the work on the influence of impurities on the dynamic behavior of dislocations in silicon crystals and also on the resulting effects in the mechanical strength performed by the author's group. Special emphasis is laid on the effects of light element impurities such as oxygen, nitrogen and carbon. Although all of these impurities do not affect the velocities of dislocations moving under relatively high stresses, oxygen and nitrogen atoms are found to lock slowly moving dislocations and dislocations at rest very effectively. Such locking of dislocations results in the decreases in the activities of generation and multiplication centers for dislocations, leading to the strengthening of the crystals. The high strength of silicon crystals brought about by the impurities is lost when the crystals are subjected to the heat treatments which allow the precipitation of the impurities on a macroscopic scale. This softening is shown to be caused by dislocations punched out from precipitates and by the exhaustion of the impurities dissolved in the matrix crystal. (33 refs.)
- An improved reduced Van der Waals equation of state for helium at high pressures**See Entry 113543
- Defects in quenched and annealed Al-Ge alloys**See Entry 113861
- Thermal generation of vacancies in aluminum**See Entry 113873
- Configurations of point defects in neutron-irradiated iron**See Entry 113878
- Submicroscopic vacancy defects in pure and doped gold**See Entry 113879
- Microdefects and impurities in dislocation-free silicon crystals**See Entry 113905
- Effect of impurity atoms on the formation of secondary defects in quenched aluminium**See Entry 113921
- HVEM in-situ observation of formation of helical dislocations in Ag-10 at.% Al**See Entry 113922
- Vacancy-interstitial recombination coefficients in radiation-induced growth models**See Entry 113985
- Theoretical relationships between creep and swelling by point defect absorption during irradiation**See Entry 113994
- Recombination-driven precipitate coarsening in alloys under irradiation**See Entry 113996
- On the evolution of microstructure during irradiation**See Entry 114036
- Radiation damage in Zr and Ti**See Entry 114037
- Recovery of radiation-induced defects in dilute Al-Ge alloys after fast neutron irradiation at 5K**See Entry 114047
- The kinetics of the interaction between helium and displacement damage in irradiated materials**See Entry 114060
- Radiation-induced segregation at internal defect sinks in electron irradiated FCC alloys**See Entry 114189
- Effect of oxygen on radiation-enhanced diffusion in silicon** ..See Entry 114278
- Quenched-in defects in CW laser irradiated virgin silicon**See Entry 114483
- Correlated radiation damage induced by heavy ion recoil in cadmium and zinc**See Entry 114767
- Ultraviolet A-band absorption in NaCl:Pb²⁺ and clustering of lattice defects** ...See Entry 114887
- Positron studies of recovery processes in aluminium and aluminium alloys**See Entry 114958
- Influence of the degree of preliminary strain on the strain aging of pearlitic casing steel**See Entry 115216
- Quenching investigations on BCC transition metals**See Entry 115230
- Influence of impurity atoms on the mechanical properties of group Va metals and alloys based on them**See Entry 115277

61.80 RADIATION DAMAGE AND OTHER IRRADIATION EFFECTS

(for techniques of structure determination, see 61.10 to 61.16; for electron and ion impact phenomena, see 79.20)

- 113982 Life performance of an EPR-insulated power cable exposed in service beyond 3 MGy in a high-level radiation area.** R.Grub, B.Langeset, P.Maier, H.Schonbacher (CERN, Geneva, Switzerland). Nucl. Instrum. & Methods Phys. Res. (Netherlands), vol.214, no.2-3, p.469-80 (1 Sept. 1983).
- Mechanical and electrical test results are reported for a power cable that has been installed for three and a half years in a high-level radiation area at the

European Organization for Nuclear Research (CERN). The degradation of selected mechanical properties as a function of absorbed dose is compared with results of a short-term irradiation in a nuclear reactor. The tensile test specimens have been taken from the ethylene propylene rubber insulation and the polyvinyl chloride sheath material of the cable after exposure in service. For the measurement of breakdown voltage, short portions of insulated cable have been used. The aim of this work was to verify that the combined functional and environmental stress factors did not lead to more damage of the cable than was expected from the value of absorbed dose, and eventually to predict more precisely the service life of similar cables. The ratios of doses after service and short-term irradiation at 50% reduction of elongation at break were about 0.5 for the insulation and 1.0 for the sheath material at a dose of about 1 MGy. However, the breakdown voltage did not show any significant variation in the dose range covered up to 3.6 MGy. Therefore, a safe lower dose limit may readily be derived from accelerated tests, but the margin until failure in service remains to be determined. (11 refs.)

- 113983 Backscattering observation of radiation damage in optical fibers.** F.Menaglia, L.Piccarini (Fondazione U. Bordon, Roma, Italy), M.Bertolotti, A.Serra, A.M.Scheggi. Proc. SPIE Int. Soc. Opt. Eng. (USA), vol.369, p.4120-16 (1983). (SPIE Proceedings of the Max Born Centenary Conference OPTICS 82, ECOSA 82, Edinburgh, Scotland, 7-10 Sept. 1982).

The use of light backscattering in a fiber is suggested as a probe for hot radiation points in nuclear environments. Preliminary experiments show the feasibility of the method. (6 refs.)

- 113984 Helium bubbles in palladium tritide.** G.J.Thomas, J.M.Mintz (Sandai Nat. Labs., Livermore, CA, USA).

J. Nucl. Mater. (Netherlands), vol.116, no.2-3, p.336-8 (June 1983).

A study was carried out in order to determine the fate of He born in a metal tritide, PdT_{0.6}, without (a) irradiation damage, (b) other impurities or phases present, and (c) thermal cycling. Microscopic evidence is presented which clearly shows that He can spontaneously generate bubbles and dislocation loops at room temperature in a metal tritide. It is recognized that hydrogen (tritium) itself can produce dislocation structures upon hydriding and dehydriding effects which are separate and distinct from those described here. (5 refs.)

- 113985 Vacancy-interstitial recombination coefficients in radiation-induced growth models.** G.V.Kidson (Materials Sci. Branch, Whiteshell Nuclear Res. Establ., AECL, Pinawa, Manitoba, Canada).

J. Nucl. Mater. (Netherlands), vol.118, no.1, p.115-20 (Aug. 1983).

The jump method for the calculation of the intrinsic recombination coefficient α^* for vacancies and interstitials, as used in the analysis of radiation-induced growth in metals, is re-examined. A straightforward procedure is presented which can accommodate simple or complex defect configurations in isotropic or anisotropic lattices. The method is applied to two recent analyses (1980) of radiation growth in HCP zirconium. It is shown that differences in the values of α^* are not, as previously suggested, associated with the interstitial configuration, but with an inconsistent definition of the atomic jump frequencies. The removal of the inconsistency is such that it would improve the agreement between calculated and measured growth rates in one of the analyses. (15 refs.)

- 113986 Appearance of an impurity ionization mechanism of defect formation in indium antimonide as a result of 'suprathreshold' irradiation.** T.V.Mashovets, N.A.Vitovskii (A.F. Ioffe Physicotech. Inst., Acad. of Sci., Leningrad, USSR).

Sov. Phys.-Semicond. (USA), vol.17, no.3, p.326-7 (March 1983). Translation of: Fiz. & Tekh. Poluprovodn. (USSR), vol.17, no.3, p.521-3 (March 1983). [received: Sept. 1983]

It has been shown that the impurity ionization mechanism (IIM) is very effective when indium antimonide is subjected to 'suprathreshold' irradiation. In the case of germanium with a sufficiently high concentration of shallow donors the IIM may be more effective than the elastic displacement mechanism even in the case of 'suprathreshold' irradiation. The authors analyze some characteristic features of the IIM in the case of binary semiconductors that have not been understood clearly before and show that in the case of indium antimonide the IIM may be observed for 'suprathreshold' irradiation under conditions such that intrinsic defects are immobile. (7 refs.)

- 113987 Low-temperature exciton decay with production of defects in KBr and KBr-Cl.** M.M.Tairov (Inst. of Phys., Acad. of Sci., Tartu, Estonian SSR).

Sov. Phys.-Solid State (USA), vol.25, no.2, p.254-7 (Feb. 1983). Translation of: Fiz. Tverd. Tela (USSR), vol.25, no.2, p.450-5 (Feb. 1983). [received: Sept. 1983]

The spectra of anion Frenkel defects created by 6.5-7.5-eV photons in crystals of KBr and KBr-Cl at 4.2K are measured by highly sensitive luminescence techniques. Long-lived pairs of neutral defects (F-H pairs) and charged defects (α -I pairs) are created upon self-localization of optically created excitons. In crystals of KBr containing 1% KCl, F and H centers distorted by Cl⁻ ions (the H_{Cl} centers are stable up to 65K), and also anion vacancies and interstitial Cl₂⁻ ions (stable up to 95K), are formed on the decay of the excitons. Mechanisms of defect formation in KBr and KBr-Cl are discussed. (27 refs.)

- 113988 Applications of a continuous wave incoherent light source (CWILS) to semiconductor processing.** H.B.Harrison, S.T.Johnson, B.Cornish, F.M.Adams, K.T.Short, J.S.Williams (Faculty of Engng., Royal Melbourne Inst. of Technol., Melbourne, Australia).

Laser-Solid Interactions and Transient Thermal Processing of Materials, Boston, MA, USA, 1-4 Nov. 1982 (New York, USA: Elsevier 1983), p.393-9.

The authors present results which highlight applications of a continuous wave incoherent light source in the processing of semiconductor devices. In particular, damage removal and activation of ion implanted gallium arsenide is demonstrated for both capless and capped annealing of low dose implants at temperatures of >800°C for times <10 s. For gallium arsenide FET applications, they demonstrate that it is possible to simultaneously carry out activation, contacting and interconnection steps by utilizing thermomigration processes which are not available with conventional furnace processing. In silicon they demonstrate that shallow multi layer bipolar structures can be successfully fabricated with anneal cycles that lead to supersaturation effects and negligible diffusion. (14 refs.)

- 113989 Beam processing of silicon with a scanning CW Hg lamp.** T.Stultz, J.Sturm, J.Gibbons (Stanford Electronics Lab., Stanford, CA, USA).

Laser-Solid Interactions and Transient Thermal Processing of Materials, Boston, MA, USA, 1-4 Nov. 1982 (New York, USA: Elsevier 1983), p.463-76.

A scanning arc lamp annealing system has been built using a 3" long mercury arc lamp with an elliptical reflector. The reflector focuses the light into a high intensity narrow line source. Silicon wafers implanted with 100 keV ⁷⁵As⁺ to 1×10¹⁵ cm⁻² have been uniformly annealed with a single scan,

resulting in complete activation and negligible redistribution of the implanted species. Using a scan rate of 1 cm/s, entire 3" wafers have been annealed in less than 10 seconds with this system. The system has also been used to recrystallize thin films of polysilicon deposited on thermally grown silicon dioxide. The crystallized films contain grains that are typically 0.5-1 mm in width and several centimeters long. Surface texture measurements show the crystallites to be almost entirely (100) in the plane of the film with the orthogonal (100) direction closely paralleling the scan direction. MOSFETs were fabricated in these films with surface mobilities 66% of ones fabricated in single crystal silicon. An epitaxial layer with the same crystallographic features as the recrystallized film was grown on the film itself. (18 refs.)

113990 Molecular dynamics simulation of displacement cascades in Cu: analysis of replacement sequences. W.E.King, R.Benedek (Materials Sci. Div., Argonne Nat. Lab., Argonne, IL, USA).

Point Defects and Defect Interactions in Metals. Proceedings of the Yamada Conference V, Kyoto, Japan, 16-20 Nov. 1981 (Amsterdam, Netherlands: North-Holland 1982), p.807-10

Molecular dynamics computer simulations of displacement cascades in copper have been performed for recoil energies up to 450 eV. Statistical analyses of the atomic replacements are presented. Linear replacement sequence lengths are extremely short on the average. The effect of the cooling phase of the cascade is discussed. (12 refs.)

113991 The damage function based on the focusing collision model. H.Sakairi, E.Yagi, A.Koyama (Inst. of Phys. & Chem. Res., Wako, Japan), R.R.Hasiguti.

Point Defects and Defect Interactions in Metals. Proceedings of the Yamada Conference V, Kyoto, Japan, 16-20 Nov. 1981 (Amsterdam, Netherlands: North-Holland 1982), p.818-20

The Snyder-Neufeld integral equation of the damage function was numerically solved under a boundary condition which includes the effect of focused replacement. The result can be well approximated by the Kinchin-Pease like formula, $\nu(E_i) = E_i / (E_3 + E_i)$. A ratio of the number of Frenkel pairs in irradiated Cu and Au which was calculated with this formula is quite consistent with the experimental value. The absolute value of ν_{Fe} in Cu can be given with a constant factor $k (=0.6)$: $\nu(E_i) = 0.6 E_i / (E_3 + E_i)$. (12 refs.)

113992 Kinetics of the order-disorder reaction under irradiation. S.Banerjee, U.D.Kulkarni (Metall. Div., Bhabha Atomic Res. Centre, Bombay, India), K.Urban.

Point Defects and Defect Interactions in Metals. Proceedings of the Yamada Conference V, Kyoto, Japan, 16-20 Nov. 1981 (Amsterdam, Netherlands: North-Holland 1982), p.853-6

A model has been developed to study the kinetics of the order-disorder transition under irradiation. In this model vacancies at different sublattice sites are distinguished and their steady state concentrations are evaluated as a function of the order parameter, S. The rate of change of the order parameter, dS/dt , is expressed in terms of various radiation and sample parameters so that the influence of these factors can be assessed. This formulation has been applied to some specific systems such as Cu_3Au and Ni_3Mo in order to compare the theoretical results with the available experimental data. (7 refs.)

113993 Monte-Carlo simulation of void nucleation during irradiation. T.Muroga, S.Ishino (Dept. of Nuclear Engng., Univ. of Tokyo, Tokyo, Japan).

Point Defects and Defect Interactions in Metals. Proceedings of the Yamada Conference V, Kyoto, Japan, 16-20 Nov. 1981 (Amsterdam, Netherlands: North-Holland 1982), p.895-8

A Monte-Carlo calculation has been carried out to simulate void nucleation process in which defects are moved in random walks on BCC and FCC lattices. Optimum values of interstitial and helium concentrations as well as temperature are found to exist for cluster growth. (10 refs.)

113994 Theoretical relationships between creep and swelling by point defect absorption during irradiation. L.K.Mansur, W.A.Coghlan (Metals & Ceramics Div., Oak Ridge Nat. Lab., Oak Ridge, TN, USA).

Point Defects and Defect Interactions in Metals. Proceedings of the Yamada Conference V, Kyoto, Japan, 16-20 Nov. 1981 (Amsterdam, Netherlands: North-Holland 1982), p.907-12

Relationships between irradiation creep and swelling implicit in the theories of these processes are derived. Four mechanisms of irradiation creep are treated. These are the climb only process of preferred point defect absorption on dislocations; the climb and glide processes resulting from cumulative absorption of defects at dislocations, i.e. preferred absorption glide and swelling-driven creep; and the recently developed climb and glide process enabled by point defect concentration fluctuations resulting from cascades. The results are expressed both as differential equations for creep rate in terms of swelling rate and as integrated forms giving creep strain in terms of swelling for stabilized microstructures. (18 refs.)

113995 Irradiation induced solid solution instability. G.Martin, R.Cauvin, J.-L.Bocquet, A.Barbu (Section de Recherches de Metall. Phys., CENS, Gif-sur-Yvette, France).

Point Defects and Defect Interactions in Metals. Proceedings of the Yamada Conference V, Kyoto, Japan, 16-20 Nov. 1981 (Amsterdam, Netherlands: North-Holland 1982), p.923-30

The authors summarize the main experimental evidences and successful theories for irradiation induced precipitation in undersaturated solid solutions. The solubility limit under irradiation is shown to be flux dependent. Simple expressions thereof are given. Complicated coupling of the solubility limit to the microstructural evolution is anticipated but not yet properly modeled. (48 refs.)

113996 Recombination-driven precipitate coarsening in alloys under irradiation. K.Urban (Inst. fur Phys., Max-Planck-Institut fur Metallforschung, Stuttgart, Germany).

Point Defects and Defect Interactions in Metals. Proceedings of the Yamada Conference V, Kyoto, Japan, 16-20 Nov. 1981 (Amsterdam, Netherlands: North-Holland 1982), p.942-5

A new theory for the coarsening of precipitates in alloys under irradiation is described. It is shown that point-defect recombination on solute clusters leads to a reduction of the solute solubility limit and to a novel driving force for coarsening. Taking the classical coarsening theory as reference irradiation leads with increasing mean radius to a modification of coarsening in 3 phases: (1) Acceleration of coarsening accompanied by a widening of the size distribution; (2) retardation of coarsening and narrowing of the distribution; (3) approach to classical behaviour. (6 refs.)

Transactions of the 4th International Meeting on Radiation Processing See Entry 111308

Defects in Semiconductors II, Symposium Proceedings See Entry 111315

Radiation effects computer experiments See Entry 111332

Creation of point defects in superconductors. A short review See Entry 113859

Point defects and radiation effects in BCC metals See Entry 113869

On the validity of the one- and two-interstitial models See Entry 113870

Defects in copper studied by PAC between 10K and 800K See Entry 113871

Transient annealing of ion-implanted silicon using a scanning IR line source See Entry 113942

Interaction of vacancies and self-interstitials with interstitial solute atoms in α -iron See Entry 113966

Irradiation-induced segregation in multi-component alloys See Entry 114181

Microstructure induced ordering effects in solids See Entry 114200

Incoherent light-induced diffusion of arsenic into silicon from a spin-on source See Entry 114253

Radiation enhanced diffusion in FCC alloys See Entry 114282

A diffusion-reaction model for solid solutions under irradiation See Entry 114283

Stability of the plane wave front of fluid evaporation See Entry 114305

Correlated radiation damage induced by heavy ion recoil in cadmium and zinc See Entry 114767

Fundamental absorption edge of irradiated alkali halides See Entry 114892

61.80B Laser beams

113997 Subnanosecond pulsed laser annealing of Si-implanted InP. B.Tell, J.E.Bjorkholm, E.D.Beebe (Bell Labs., Holmdel, NJ, USA).

Appl. Phys. Lett. (USA), vol.43, no.7, p.655-7 (1 Oct. 1983). Indium phosphide implanted with Se^{+} has been laser annealed with 70 ps pulses at both $\lambda=0.53$ and $1.06 \mu m$. For doses of $1 \times 10^{15} cm^{-2}$ activations of $\sim 70\%$ with peak electron concentrations of $6 \times 10^{19} cm^{-3}$ have been achieved, while for doses of $3 \times 10^{15} cm^{-2}$, activations of 33% with peak electron concentrations of $1.2 \times 10^{20} cm^{-3}$ were measured. The carrier depth profiles for the laser annealed samples are shallow while those for thermal annealing are broad compared to the as-implanted profiles. The morphology of the laser annealed spots is briefly discussed. (19 refs.)

113998 Surface damage of transparent dielectrics and semiconductors by high-power laser pulses. Y.T.Vassilev (Faculty of Phys., Univ. of Sofia, Sofia, Bulgaria).

Bulg. J. Phys. (Bulgaria), vol.10, no.3, p.344-52 (1983). The surface damage by short and ultrashort laser pulses passing through solid state transparent media has been studied theoretically under the assumption that the pressure of the laser light is a real damage mechanism. Analytical expressions for the damage thresholds of the entrance and exit surfaces as well as for their ratio have been obtained. These expressions may be used to interpret more accurately and correctly the experimental findings on surface damage of solid transparent dielectrics and semiconductors. (17 refs.)

113999 Emission of melt during laser vaporization of metallic films. V.P.Veiko, A.I.Kaidanov, E.A.Tuchkova, E.B.Yakovlev.

Elektron. Obrab. Mater. (USSR), no.3, p.18-21 (1983). In Russian. English translation in: *Electrochem. Ind. Process. & Biol. (GB)*. A theoretical model of the emission of melt from the zone of vaporization during laser irradiation of metallic films is examined. It is shown that a molten metallic film can be regarded as a plane boundary layer, movement of which results from the action of an output pulse during vaporization. In this connection a study is made of the influence of surface tension forces, the adhesion of the film to the substrate, and viscous friction in the molten layer. The kinetics of emission and the phase composition of the products of the laser destruction of thin films are also investigated. (7 refs.) *A.J.B.*

114000 Direct observation of the melting of a semiconductor during pulsed laser annealing. V.N.Abakumov, O.V.Zelenova, Yu.V.Koval'chuk, E.L.Portnoi, V.B.Smirnitskii, I.A.Sokolov (A.F. Ioffe Physicotech. Inst., Acad. of Sci., Leningrad, USSR).

Sov. Tech. Phys. Lett. (USA), vol.8, no.11, p.586-7 (Nov. 1982). Translation of: *Pis'ma v Zh. Tekh. Fiz. (USSR)*, vol.8, no.21-22, p.1365-8 (Nov. 1982). [received: Sept. 1983]

Reports an attempt to directly observe melting of the surface of a semiconductor subjected to pulsed laser bombardment. In the experiments, a regular sawtooth profile with a period $\approx 2 \mu m$ is produced on the (100) surface of a single-crystal gallium arsenide wafer. After this preparation, the samples are subjected to pulsed bombardment by a ruby laser ($\lambda=0.69 \mu m$). (5 refs.)

114001 Introduction [laser annealing of semiconductors]. J.M.Poate (Bell Labs., Murray Hill, NJ, USA), J.W.Mayer.

In book: *Laser annealing of semiconductors*, J.M.Poate, J.W.Mayer [Ed.], p.1-14. London, England: Academic Press (1982), xi+564 pp. [0 12 558820 8]

The authors discuss direct energy processing of semiconductors using lasers. Energy deposition and heat flow are briefly reviewed. Studies of surfaces and interfaces are discussed. The use of lasers for epitaxial regrowth and alloying is outlined and a brief mention is made of surface crystallization. (no refs.)

114002 Crystallization processes [laser annealing of semiconductors]. F.Spaepen, D.Turnbull (Div. of Appl. Sci., Harvard Univ., Cambridge, MA, USA).

In book: *Laser annealing of semiconductors*, J.M.Poate, J.W.Mayer [Ed.], p.15-42. London, England: Academic Press (1982), xi+564 pp. [0 12 558820 8]

Discusses the melting and solidification that may occur during laser annealing. Although crystallization is the thermodynamically preferred mode of solidification, a melt may under certain conditions solidify to an amorphous solid. (48 refs.)

114003 Fundamentals of energy deposition [laser annealing of semiconductors]. M.F.von Allmen (Inst. of Appl. Phys., Univ. of Bern, Bern, Switzerland).

In book: *Laser annealing of semiconductors*, J.M.Poate, J.W.Mayer [Ed.], p.43-74. London, England: Academic Press (1982), xi+564 pp. [0 12 558820 8]

Reviews the main mechanisms of interaction of photon and electron beams with condensed matter from the point of view of energy deposition. The influence of coupling phenomena on the final sample temperature is discussed. Beam intensities of interest range up to about $10^8 W/cm^2$, sufficient to heat and even melt the surface region of the irradiated material. Even though the basic mechanisms of absorption are well known, coupling phenomena in this high-flux regime are not as well understood as they are at low intensities. (50 refs.)

114004 Heat flow calculations [laser annealing of semiconductors]. P.Baeri, S.U.Campisano (Istituto di Struttura della Materia, Univ. di Catania, Catania, Italy).

In book: *Laser annealing of semiconductors*, J.M.Poate, J.W.Mayer [Ed.], p.75-109. London, England: Academic Press (1982), xi+564 pp. [0 12 558820 8]

Heating in an irradiated sample is a consequence of the balance between the deposited energy, governed by optical parameters of the sample and characteristics of the laser pulse, and the heat diffusion, determined by thermal parameters and the pulse duration. In the two limiting cases in which the optical absorption depth is small compared with the thermal diffusion length during the pulse, and vice versa, simple estimates of the temperature rise have been outlined by Bloembergen (1979). However, in many practical cases, exact calculations are needed, and complex analytical or numerical evaluations must be used. In particular, for phase transitions occurring during the irradiation, only numerical solutions are available. The mathematical problem is stressed and a set of numerical solutions are given in order to cover a broad range of cases of practical interest. The calculations presented in these sections agree well with experimental data. However, if more exact knowledge of the optical and thermal parameters becomes available, their numerical values could change, but the trends will still be valid. Simple scaling rules are given for this purpose. Applications to Ge and GaAs are presented. The problem of diffusion and segregation of impurities during the liquid transient produced by the laser pulse is considered. The effect of a very long pulse duration is outlined. Appendixes report details of the numerical method used to solve the heat and mass transport equations. (33 refs.)

114005 Supersaturated alloys, solute trapping, and zone refining [laser annealing of semiconductors]. C.W.White, B.R.Appleton (Solid State Div., Oak Ridge Nat. Lab., Oak Ridge, TN, USA), S.R.Wilson.

In book: *Laser annealing of semiconductors*, J.M.Poate, J.W.Mayer [Ed.], p.111-46. London, England: Academic Press (1982), xi+564 pp. [0 12 558820 8]

The authors discuss studies of high-speed crystal growth achieved by laser annealing of ion-implanted silicon. These studies show that Group III and V impurities can be incorporated by solute trapping into substitutional lattice sites at concentrations that far exceed equilibrium solubility limits. Values for the interfacial distribution coefficient are much greater than equilibrium values because of the high velocity of the liquid-solid interface. Values for k' are functions of both growth velocity and crystal orientation. For each Group III and V dopant there is a maximum concentration C_s^{\max} that can be incorporated substitutionally into the lattice, and values for C_s^{\max} are functions of growth velocity. Mechanisms that limit substitutional solubilities are discussed. Values obtained for C_s^{\max} are compared with recent predictions of thermodynamic limits of solute trapping in silicon. Finally, the behavior exhibited by Group III and V species is contrasted with that exhibited by interstitial species (such as Cu, Fe) where, for low concentrations, complete zone refining to the surface can be achieved. (37 refs.)

114006 Solid phase regrowth. J.F.Gibbons, T.W.Sigmon (Stanford Electronics Labs., Stanford Univ., Stanford, CA, USA).

In book: *Laser annealing of semiconductors*, J.M.Poate, J.W.Mayer [Ed.], p.325-81. London, England: Academic Press (1982), xi+564 pp. [0 12 558820 8]

Reviews the areas of continuous-wave (CW) beam processing of semiconductors that can be adequately understood in terms of solid phase regrowth mechanisms. For this purpose the authors begin with a brief review of solid phase regrowth results obtained from low-temperature (400-600°C) furnace annealing experiments and then proceed to discuss parallel results obtained when a scanning CW laser or electron beam is used to promote the regrowth process. In most of this discussion they treat the scanning CW beam system as being equivalent to a high-temperature, short-time-duration annealing furnace with large heating and cooling rates. In most cases CW beam processing causes solid phase regrowth and diffusion to occur at rates that can be obtained from a straightforward extrapolation of the low-temperature furnace results. It is possible to calculate the spatial temperature profile by assuming steady state heat flow in a moving frame of reference. Such calculations provide the theoretical basis for the relationship between the beam processing parameters and solid phase regrowth mechanisms. (70 refs.)

114007 Compound semiconductors [laser and electron beam annealing]. J.S.Williams (Dept. of Communications & Electronic Engng., Royal Melbourne Inst. of Technol., Melbourne, Victoria, Australia).

In book: *Laser annealing of semiconductors*, J.M.Poate, J.W.Mayer [Ed.], p.383-438. London, England: Academic Press (1982), xi+564 pp. [0 12 558820 8]

Laser and electron beam applications in the processing of compound semiconductors are reviewed, with particular emphasis on GaAs. The author concentrates on the two particular applications of transient annealing that have received the most attention in the literature: (i) the removal of ion implant damage and dopant effects in GaAs, and (ii) the formation of ohmic contacts to compound semiconductors. An attempt has been made to correlate the available physical and electrical data and to present current understanding of the various transient annealing processes. Solid phase annealing of ion-implanted GaAs is discussed, and results of conventional furnace processing are compared with the sparse data available on transient annealing. The author discusses pulsed (liquid phase) annealing in implanted GaAs, a topic that has been of considerable recent interest. Transient annealing both in the formation of ohmic contacts to GaAs and in the mixing of deposited layers with GaAs is examined. Finally, the available data on compound semiconductors other than GaAs are reviewed. (80 refs.)

114008 Silicides and metastable phases [laser annealing]. M.F.von Allmen (Inst. of Appl. Phys., Univ. of Bern, Bern, Switzerland), S.S.Lau.

In book: *Laser annealing of semiconductors*, J.M.Poate, J.W.Mayer [Ed.], p.439-78. London, England: Academic Press (1982), xi+564 pp. [0 12 558820 8]

The authors discuss reactions in metal semiconductor systems subject to fast melting and solidification. In their discussion, a brief summary of solid state reactions is given first, followed by an introduction to general concepts of laser-induced melting, mixing and quenching. Experimental results of laser-induced interactions in metal-semiconductor systems are presented. The composition and phases in the reacted layers depend on the pulse energy via the melt depth. The structure of the mixed layers is often laterally nonuniform and cellular in nature as a result of constitutional supercooling. Because of the very rapid solidification from the melt, not all alloys and compounds formed are necessarily thermodynamically stable. Alternatively, amorphous phases over extended compositional ranges may be obtained under appropriate conditions. Pulsed irradiation, therefore, permits a systematic search for, and the investigation of, metastable phases inaccessible by other means. These results are in marked contrast to those obtained with furnace or continuous-wave scanning laser annealing, where simple and uniform reactions take place in the solid phase. (49 refs.)

114009 Factors influencing application [laser annealing of semiconductors]. C.Hill (Plessey Res. (Caswell), AllenClark Res.Centre.Ltd., Caswell, England).

In book: *Laser annealing of semiconductors*, J.M.Poate, J.W.Mayer [Ed.], p.479-557. London, England: Academic Press (1982), xi+564 pp. [0 12 558820 8]

In order to discuss the criteria for applications systematically, the techniques for beam processing have been classified into three basic modes, determined by pulse length, and the materials changes that can be effected have been grouped into six basic categories. The factors involved in control of the heat treatment process are covered. The occurrence of secondary effects and compatibility with other process steps and structures are dealt with. The problems of processing large areas of material rapidly and the economics of beam processing are also considered. (130 refs.)

114010 Effect of pulse duration on the annealing of ion implanted silicon with a XeCl excimer laser and solar cells. R.T.Young (Helionetics Inc., San Diego, CA, USA), J.Narayan, W.H.Christie, G.A.van der Leeden, D.E.Rothe, R.L.Sandstrom.

Laser-Solid Interactions and Transient Thermal Processing of Materials, Boston, MA, USA, 1-4 Nov. 1982 (New York, USA: Elsevier 1983), p.401-6. The advantages of pulsed excimer lasers for semiconductor processing are reviewed. Studies of XeCl excimer laser annealing with pulses of 25 and 70 nsec duration and energy densities in the range from 0.5-3.0 J/cm² are discussed. The annealing characteristics are described in terms of the results of melt depth, dopant profile spreading, and electrical properties (sheet resistivity, diode characteristics) measurements. Solar cells with efficiencies as high as 16.7% AM1 have been fabricated using glow discharge implantation and XeCl laser annealing. (8 refs.)

114011 Pulsed excimer laser (308 nm) annealing of ion implanted silicon and solar cell fabrication. D.H.Lowndes, J.W.Cleland, W.H.Christie, R.E.Eby, G.E.Jellison, Jr., J.Narayan, R.D.Westbrook, R.F.Wood (Solid State Div., Oak Ridge Nat. Lab., Oak Ridge, TN, USA), J.A.Nilson, S.C.Dass.

Laser-Solid Interactions and Transient Thermal Processing of Materials, Boston, MA, USA, 1-4 Nov. 1982 (New York, USA: Elsevier 1983), p.407-12

A pulsed ultraviolet excimer laser (XeCl, 308 nm wavelength, 40 nsec FWHM pulse duration) has been successfully used for laser annealing of both boron- and arsenic-implanted silicon. TEM, SIMS, and sheet electrical measurements are used to characterize specimens. C-V and I-V measurements demonstrate that near-ideal p-n junctions are formed (diode perfection factor A=1.2). Electrical activation of implanted ions by single laser pulses is essentially complete for energy densities $E_j \geq 1.4$ J/cm², far below the threshold for substantial surface damage ~ 4.5 J/cm². Melting model calculations are in good agreement with observed thresholds for dopant redistribution and for epitaxial regrowth. Changes in annealing behavior resulting from multiple (1,2,5) laser pulses are also reported. Finally, the authors demonstrate the use of scanned overlapping excimer laser pulses for fabrication of large area (2 cm²) solar cells with good performance characteristics. In contrast to pulsed ruby laser annealing, high open circuit voltages can be obtained without the use of substrate heating. (12 refs.)

114012 Selective laser annealing for device processing. I.D.Calder, A.A.Naem, H.H.Naguib (Bell-Northern Res., Ottawa, Ontario, Canada).

Laser-Solid Interactions and Transient Thermal Processing of Materials, Boston, MA, USA, 1-4 Nov. 1982 (New York, USA: Elsevier 1983), p.443-8. Selective laser crystallization of undoped polysilicon films has been achieved through the use of a patterned Si₃N₄ anti-reflection (AR) coating. The recrystallized poly-Si beneath the AR cap exhibits an etch rate 50-90% lower than the surrounding uncapped material, allowing anisotropic etching of poly-Si for the fabrication of MOSFET gates. Undercut is reduced by at least a factor of two from unannealed material. Annealed edge profiles are uniform within ± 0.03 μ m for plasma etching (± 0.05 for wet etching) compared to ± 0.1 μ m (± 0.25 μ m for wet etching) for unannealed regions. The sheet resistivity of 0.5 μ m films doped by phosphorus diffusion was reduced from an initial value of 82 ± 5 Ω/\square to 40 ± 8 Ω/\square when the dopant was diffused into recrystallized poly-Si and to a final value of 10.2 ± 0.2 Ω/\square after a further laser activation step. Potential applications in VLSIC processing are discussed. (10 refs.)

114013 Characterization and application of laser induced seeded-lateral epitaxial Si layers on SiO₂. M.Miyao, M.Ohkura, T.Warabisako, T.Tokuyama (Central Res. Lab., Hitachi Ltd., Tokyo, Japan).

Laser-Solid Interactions and Transient Thermal Processing of Materials, Boston, MA, USA, 1-4 Nov. 1982 (New York, USA: Elsevier 1983), p.499-510

Electrical and crystal properties of seeded lateral epitaxial Si are evaluated as a function of distance from seeding area with the aid of a micro-probe RHEED and MOSFET fabrication. The results indicate that the quality of a grown layer is as good as that of bulk Si crystal for most of the epitaxial layer. However, at the SiO₂ edge, electrical properties are somewhat poor due to the existence of dislocations and residual stresses. Element devices useful for SOI structures are fabricated. Electrical properties of MOSFETs with double active area indicate that surface and bottom regions of the epitaxial layer are all of device worthy quality. Insulated control gate bipolar type transistors are proposed and some preliminary results are shown. (32 refs.)

114014 Oxygen and nitrogen incorporation during CW laser recrystallization of polysilicon. C.I.Drowley, T.I.Kamins (Hewlett-Packard Labs., Palo Alto, CA, USA).

Laser-Solid Interactions and Transient Thermal Processing of Materials, Boston, MA, USA, 1-4 Nov. 1982 (New York, USA: Elsevier 1983), p.511-16

The incorporation of nitrogen and oxygen in polysilicon has been examined by SIMS. The analysis, combined with C-V measurements and ion implantation, has been used to correlate the incorporation of the two species with the fixed-charge density at the back polysilicon/SiO₂ interface. Laser recrystallization with a silicon-nitride encapsulation layer results in the inclusion of 2.4×10^{17} cm⁻³ nitrogen atoms in the polysilicon; if an oxide capping layer is used, the nitrogen level observed is at the background of the SIMS system ($\sim 10^{15}$ cm⁻³). Either type of capping layer results in 3.4×10^{18} cm⁻³ oxygen atoms being incorporated into the polysilicon. Implantation of nitrogen into the polysilicon before recrystallization increases the fixed-charge density (N_{fb}) at the back interface, while implanted oxygen decreases N_{fb} . The high N_{fb} found with a nitride capping layer is attributed to deposition of nitrogen of SiN_x at the back interface. (6 refs.)

114015 CW laser annealing of ion implanted oxidized silicon layers on sapphire. G.Alestig, G.Holmen, S.Peterstrom (Dept. of Phys., Chalmers Univ. of Technol., Goteborg, Sweden).

Laser-Solid Interactions and Transient Thermal Processing of Materials, Boston, MA, USA, 1-4 Nov. 1982 (New York, USA: Elsevier 1983), p.517-22.

CW laser annealing has been performed on silicon on sapphire (SOS) implanted with boron or phosphorus ions to a dose of 10^{15} ions/cm². The laser irradiation was done both with and without an oxide layer on top of the silicon and from both the silicon and the sapphire side. Sheet resistivity and hall effect measurements were used for the analysis of the samples. Good annealing and high activation of the dopants were obtained for both oxidized and unoxidized SOS. For samples irradiated from the silicon side, the needed laser power changed depending on the thickness of the oxide. For samples irradiated from the sapphire side, the needed laser power was independent of oxide thickness. (18 refs.)

114016 Beam shaping for CW laser recrystallization of polysilicon films. P.Zorabedian, C.I.Drowley, T.I.Kamins, T.R.Cass (Hewlett-Packard Labs., Palo Alto, CA, USA).

Laser-Solid Interactions and Transient Thermal Processing of Materials, Boston, MA, USA, 1-4 Nov. 1982 (New York, USA: Elsevier 1983), p.523-8. A shaped laser beam has been used for laterally seeded recrystallization of polysilicon films over oxide. Direct maps of the shaped-beam intensity distribution in the wafer plane are correlated with the grain structure of the recrystallized polysilicon. Using 60% overlapping of shaped-beams scans along (100) directions, the authors have obtained seeded areas one mm wide and 50 to 500 μ m long. These consist of 40 μ m-wide adjacent single-crystal strips regularly separated by low-angle grain boundaries extending laterally away from the seed openings. The spacing between grain boundaries is equal to the scan spacing, providing a means for controlling the location of grain boundaries in otherwise defect-free, single-crystal films. (5 refs.)

114017 A comparison of CW laser and electron-beam recrystallization of polysilicon in multilayer structures. C.I.Drowley (Hewlett-Packard Lab., Palo Alto, CA, USA), C.Hu.

Laser-Solid Interactions and Transient Thermal Processing of Materials, Boston, MA, USA, 1-4 Nov. 1982 (New York, USA: Elsevier 1983), p.529-34.

A thermal model for beam-induced melting of polysilicon in polysilicon/insulator/silicon structures has been used to compare CW Ar⁺ laser and electron-beam melting processes. The laser melting process exhibits a decreasing recrystallization threshold power and an increasing substrate melting threshold power with increasing insulator thickness. The decrease in recrystallization threshold with increasing insulator thickness is generally smaller for electron beams because of their deep penetration. The substrate melting threshold is approximately independent of insulator thickness for e-beams since no change in the power absorption occurs on melting of the polysilicon. As a result, the process window between the onset of recrystallization and melting of the substrate is narrower for e-beams than for laser beams. Also, essentially no window will exist between the onset of melting over a seed and substrate melting under an oxide if lateral epitaxy is performed with an electron beam. (8 refs.)

114018 Laser-induced crystallization of silicon on bulk amorphous substrates: an overview. D.K.Biegelsen, N.M.Johnson, W.G.Hawkins, L.E.Fennell, M.D.Moyer (Xerox Palo Alto Res. Centers, Palo Alto, CA, USA).

Laser-Solid Interactions and Transient Thermal Processing of Materials, Boston, MA, USA, 1-4 Nov. 1982 (New York, USA: Elsevier 1983), p.537-48.

The authors review the current understanding of laser-induced silicon thin film crystal growth on bulk amorphous substrates. They propose a model for oriented nucleation and show that the silicon reflectivity jump on melting coupled with radiant heating lead naturally to this autonucleation mechanism. They then survey various techniques for control of lateral epitaxial growth and conclude with the results of some recent electrical device characterization. (18 refs.)

114019 The effects of selectively absorbing dielectric layers and beam shaping on recrystallization and FET characteristics in laser recrystallized silicon on amorphous substrates. G.E.Possin, H.G.Parks, S.W.Chiang, Y.S.Liu (General Electric Res. & Dev. Center, Schenectady, NY, USA).

Laser-Solid Interactions and Transient Thermal Processing of Materials, Boston, MA, USA, 1-4 Nov. 1982 (New York, USA: Elsevier 1983), p.549-56.

Selective absorption, using patterned dielectric films, and beam shaping were used as means for improving the recrystallization of LPCVD polysilicon islands on fused quartz. IR imaging of the laser heated region was used to optimize and control the recrystallization. MOSFETs were fabricated in laser-recrystallized silicon islands on amorphous substrates using a standard n-channel poly-gate process. Devices with various channel lengths and widths were fabricated, and the dependence of threshold voltage, channel mobility, and leakage on recrystallization conditions and device dimensions was studied. (11 refs.)

114020 Laser anealing of ion implanted semiconductors. J.Narayan (Solid State Div., Oak Ridge Nat. Lab., Oak Ridge, TN, USA).

Defects in Semiconductors II, Symposium Proceedings, Boston, MA, USA, Nov. 1982 (New York, USA: North-Holland 1983), p.491-504.

Photon energy from laser beams can be used to rapidly heat and melt localized regions of semiconductors with a high degree of spatial and temporal selectivity. Pulsed lasers have been successfully used to anneal displacement damage and to remove other defects. However, the number density of trapped defects increases with velocity of solidification and finally thin layers turn directly amorphous after laser-melt quenching. Annealing characteristics are found to be a strong function of ion implantation variables, which determine optical properties of materials. By both solid- and liquid-phase crystallization, supersaturated solid solutions can be formed. Residual defects in SPE grown layers primarily consist of dislocation loops. Device applications utilizing these transient thermal processing techniques are reviewed briefly. (21 refs.)

114021 Comparison between thermal and laser annealing in ion-implanted silicon. A.Blosse (Lab. de Phys. des Solides, Lille, France), J.C.Bourgoin.

Defects in Semiconductors II, Symposium Proceedings, Boston, MA, USA, Nov. 1982 (New York, USA: North-Holland 1983), p.535-9.

N-type, 10^{15} - 10^{16} cm⁻³ doped, Fz, silicon has been implanted with 1 to 4×10^{12} cm⁻², 100 or 300 keV, As ions. The nature and concentration of the defects has been monitored using Deep Level transient Spectroscopy as a function of the thermal treatment (in the range 500-900°C) and of the energy of the pulse (15 ns) of a ruby (0.69 μ m) laser (in the range 0.3 to 0.6 J cm⁻²). The defects resulting from annealing by the two treatments are found to be the same. Only, for energies higher than 0.5 J cm⁻², the laser treatment introduced new defects (at $E_c - 0.32$ eV), presumably resulting from a quenching process. Thus a laser energy below the threshold for melting and epitaxial recrystallization is able to anneal the defects produced by

implantation, demonstrating that the annealing process induced by the laser pulse is not a purely thermal process but probably involves an ionization enhanced mechanism. (9 refs.)

Laser annealing of semiconductors See Entry 111333

Thermoelastic stresses produced in an absorbing layer by the action of a laser pulse See Entry 113031

Microstructure and topography [laser annealing of semiconductors] See Entry 113709

Computer simulation of high speed melting of amorphous silicon See Entry 114133

Surface properties of laser-annealed semiconductors See Entry 114321

Epitaxy by pulsed annealing of ion-implanted silicon See Entry 114398

Epitaxy of deposited Si See Entry 114399

Quenched-in defects in CW laser irradiated virgin silicon See Entry 114483

Conduction in polycrystalline silicon: generalized thermionic emission-diffusion theory and extended state mobility model See Entry 114530

Comment on 'Raman scattering with nanosecond resolution during pulsed laser annealing of silicon' See Entry 114837

Heterojunction formation in (CdZnS/CuInSe₂) ternary solar cells See Entry 115635

High-efficiency Si solar cells by beam processing See Entry 115636

61.80C X-rays

The role of the state of dispersion of impurity on Z₁-centres in NaCl:Ca²⁺ crystals See Entry 113909

Color centers in K₂S₂O₆ and Rb₂S₂O₆ crystals See Entry 113910

Effect of flux content on thermoluminescence yield of BaS phosphors See Entry 114937

61.80E Gamma rays

Characterization of lattice disorder in the low-temperature phase of irradiated PTFE by vibrational spectroscopy See Entry 113768

The influence of fusion temperature on the defect center concentration of GeO₂ glass See Entry 114733

How electric strength of polyethylene and polystyrene is influenced by residual phenomena caused by ionising radiation and pressure See Entry 114781

Al-induced enhancement colouration by gamma irradiation in some borate glasses See Entry 114884

Photoluminescence of germanium irradiated with ⁶⁰Co γ rays See Entry 114922

Thermoluminescence from extended-chain crystals of polyethylene See Entry 114938

Kinetics of a polymorphic transition in an Ag-Zn alloy under the action of γ rays See Entry 115188

The gamma ray-induced crosslinking of polyacrylamide in the solid state See Entry 115549

61.80F Electrons and positrons

114022 Mobilities of radiation-induced vacancies in Ni₃Al and NIAL studied by positron techniques. M.Shimotomai, T.-M.Wang, M.Doyama (Dept. of Materials Sci., Faculty of Engng., Univ. of Tokyo, Tokyo, Japan).

J. Nucl. Mater. (Netherlands), vol.116, no.2-3, p.347-8 (June 1983).

Discusses the mobilities of radiation-induced vacancies in Ni₃Al and NIAL probed by positrons. The positron lifetime spectrum for an annealed specimen was well fitted with a single component of $\tau_1 = 110 \pm 5$ ps. This value represents the lifetime of delocalized positrons in Ni₃Al. Upon irradiation the second lifetime component of considerable intensity with $\tau_2 = 180 \pm 5$ ps appeared. This manifests the production of vacancy-type defects in Ni₃Al since positrons preferentially probe defects which have low electron density. (6 refs.)

114023 Void-swelling in cold-worked copper during HVEM irradiation. T.Leffers, B.N.Singh (Metall. Dept., Riso Nat. Lab., Roskilde, Denmark), S.N.Buckley, S.A.Manthorpe.

J. Nucl. Mater. (Netherlands), vol.118, no.1, p.60-7 (Aug. 1983).

Void formation and growth in pure cold-worked copper and the parallel evolution in dislocation structure during HVEM irradiation have been investigated. Degrees of cold work in the range 10-90% rolling reduction and irradiation temperatures in the range 250-450°C have been covered. The cold-worked structure basically survives irradiation. Initially (for low degrees of cold work), void density and swelling rate increase with increasing degree of cold work; they then level off and eventually start decreasing with further cold work. The decrease in swelling rate cannot be explained in terms of a simple increase in dislocation density; one will have to consider the real, heterogeneous dislocation distribution. (2 refs.)

114024 Shrinkage of voids in electron irradiation of thin foils. S.M.Murphy, A.Scott, E.Diana (Theoretical Phys. Div., AERE Harwell, Didcot, England).

J. Nucl. Mater. (Netherlands), vol.118, no.1, p.121-4 (Aug. 1983).

In HVEM experiments, voids close to the surface of the irradiated foil are observed to shrink. Makin suggests (see *ibid.*, vol.71, p.300-8, 1978) that the shrinkage occurs because voids are preferential sinks for interstitials relative to the surface of the thin foil. This is supported by results of some rate theory calculations of the shrinkage of voids within a thin foil. (5 refs.)

114025 Influence of electron irradiation at various temperatures on the minority carrier lifetime in epitaxial silicon p-n structures. F.P.Korshunov, I.G.Marchenko (Inst. of Solid-State & Semiconductor Phys., Acad. of Sci., Minsk, Belorussian SSR).

Sov. Phys.-Semicond. (USA), vol.17, no.3, p.340-1 (March 1983). Translation of: *Fiz. & Tekh. Poluprovodn. (USSR)*, vol.17, no.3, p.540-2 (March 1983).

[received: Sept. 1983]

The authors investigated the influence of electron irradiation at temperatures T_{irr} in the range from -150°C to 330°C on the minority carrier lifetime in the bases of p-n structures made of epitaxial silicon. The measurements of τ were carried out by the Lax-Neustadter method using transient processes of recovery of the reverse resistance of p-n structures (the base material was an epitaxial film of the KEF-0.5 grade). Structures were irradiated using a linear accelerator generating electrons of $E_e = 4$ MeV energy and the density of the fast-electron current was $0.05 \mu\text{A}/\text{cm}^2$. The irradiated samples were annealed at temperatures up to 460°C . The experimental results on changes in τ in p-n

structures irradiated with electrons at T_{irr} ranging from -150°C to 330°C are plotted as a function of the radiation dose Φ . An increase in Φ reduced τ in samples irradiated at 150 – 180°C . At higher irradiation temperatures (270 and 330°C) there was a considerable increase in τ in the dose range 10^{12} – 10^{14} cm^{-2} , whereas at higher doses the value of τ fell. (8 refs.)

114026 Temperature dependence of the critical electron exposure for hydrocarbon monolayers. K.H.Downing (Lawrence Berkeley Lab., Univ. of California, Berkeley, CA, USA).

Ultramicroscopy (Netherlands), vol.11, no.4, p.229-37 (1983).

Effects of electron-beam-induced radiation damage in monolayers of several saturated fatty acids and related molecules have been measured by observation of the fading of electron diffraction patterns produced by the crystalline monolayers. Measurements were made with the specimens at temperatures in the range from about 6 to 310K . Near room temperature, exposures of approximately 50 and $200\text{ electrons/nm}^2$ are required to reduce the intensities of the diffraction patterns of stearic and benenic acids, respectively, to $1/e$ of their initial intensities. These critical exposures increase smoothly as the temperature decreases, to 1600 and 2200 e/nm^2 , respectively, at a specimen temperature of about 6K . A strong correlation was observed between the critical exposures and melting temperatures of the various specimens examined. These results can be interpreted in terms of radiolysis pathways that are highly specific to hydrocarbons. (28 refs.)

114027 Scanning electron beam annealing of oxygen donors in Czochralski silicon. C.J.Pollard, J.D.Speight (British Telecom Res. Labs., Martlesham Heath, England), K.G.Barracough.

Laser-Solid Interactions and Transient Thermal Processing of Materials, Boston, MA, USA, 1-4 Nov. 1982 (New York, USA: Elsevier 1983), p.413-18.

The destruction of the oxygen donor complex in Czochralski silicon has been studied using scanning electron beam annealing in the range 550°C to 1050°C for 5 s to 1000 s . A two stage annealing schedule ensured a rapid rise to the target temperature and overscanning provided a uniform, non-distorting heating field. Four point probe and spreading resistance measurements showed a very rapid donor destruction rate above 650°C ; between 550°C and 650°C the lower donor destruction rate allowed a study of the annealing behaviour. (11 refs.)

114028 Arsenic implant activation and redistribution in p-type silicon induced by pulsed electron beam annealing. D.Barbier (Lab. de Phys. de la Matière, Inst. Nat. des Sci. Appliquées de Lyon, Villeurbanne, France), M.Baghdadi, A.Laugier, A.Cachard.

Laser-Solid Interactions and Transient Thermal Processing of Materials, Boston, MA, USA, 1-4 Nov. 1982 (New York, USA: Elsevier 1983), p.419-24.

In this work Pulsed Electron Beam Annealing has been used to activate As implanted in (100) and (111) silicon ($140\text{ keV}\cdot 10^{15}\text{ cm}^{-2}$). With a selected electron beam energy deposition profile excellent regrowth layer quality and As activation has been obtained in the 1.2 – 1.4 J/cm^2 fluence range. As redistribution is consistent with the melting model assuming a diffusivity of $10^{-4}\text{ cm}^2/\text{s}$ in liquid silicon. As losses might slightly reduce the carrier concentration near the surface in the case of (100) silicon. However a shallow and highly active N^+ layer have been achieved with optimized PEBA conditions. (6 refs.)

114029 Processing of shallow ($\text{Rp}<150\text{\AA}$) implanted layers with electron beams. G.B.McMillan (Engng. Dept., Univ. of Cambridge, Cambridge, England), J.M.Shannon, H.Ahmed.

Laser-Solid Interactions and Transient Thermal Processing of Materials, Boston, MA, USA, 1-4 Nov. 1982 (New York, USA: Elsevier 1983), p.437-42.

The multiple-scan method of electron beam annealing has been used to activate shallow ($\text{Rp}<150\text{\AA}$), highly doped silicon layers produced by ion implantation of arsenic at 10 keV . Beam conditions have been optimised (600 W cm^{-2} for 100 ms) to produce essentially undiffused layers, as determined by high resolution SIMS, containing high concentrations of electrically active arsenic impurities. Computer modelling of diffusion effects in such layers has been used to identify optimum beam conditions and the calculations have been compared with experimental results. Hot electron device structures, which depend on negligible diffusion and high electrical activity, have been fabricated using the multiple-scan method with a peak annealing temperature of 900°C . (8 refs.)

114030 Pulsed electron beam annealing induced deep level defects in virgin silicon. D.Barbier (Lab. de Phys. de la Matière, INSA de Lyon, Villeurbanne, France), M.Kechouane, A.Chantre, A.Laugier.

Laser-Solid Interactions and Transient Thermal Processing of Materials, Boston, MA, USA, 1-4 Nov. 1982 (New York, USA: Elsevier 1983), p.449-54.

DLTS has been used to investigate deep level defects induced by Pulsed Electron Beam Annealing (PEBA) in virgin (100) boron doped silicon. Various PEBA conditions were selected resulting in different molten layer thicknesses, melt front velocities and thermal gradient distributions. Discrete hole traps distributed in the regrowth layer were observed in all the annealed samples. The activation energies and thermal signatures of these levels do not correspond to already known defects except for one level which has been assigned to the carbon interstitial substitutional pair. Carbon contamination during irradiation is the most probable explanation for the creation of this defect. Other discrete hole trap levels are likely to be generated by quenching of the molten layer as far as their profiles do not extend beyond the regrowth layer. Moreover, a broad band of levels, characteristic of extended defects, has been observed only on the samples which have suffered the highest thermal stresses. This band of levels might be related to the generation of dislocation networks as recently observed by means of TEM on the same PEBA processed samples. (8 refs.)

114031 Growth of silicon-on-insulator films using a line-source electron beam. J.A.Knapp, S.T.Picraux (Sandia Nat. Labs., Albuquerque, NM, USA).

Laser-Solid Interactions and Transient Thermal Processing of Materials, Boston, MA, USA, 1-4 Nov. 1982 (New York, USA: Elsevier 1983), p.557-62.

A swept line-source electron beam has been used to study unseeded Si-on-insulator crystallization at beam scan speeds of 150 – 1500 cm/s . For a particular sample configuration a maximum linear crystallization velocity of $\sim 350\text{ cm/s}$ was observed. At higher sweep speeds, competing nucleation occurred at intervals across the film. Both the limit in crystallization velocity and the intervals between nucleation are tentatively explained by a simple model. (9 refs.)

114032 Influence of alloy composition on defect production and recovery, in austenitic Fe-Cr-Ni solid solutions electron-irradiated at low temperature. O.Dimitrov, C.Dimitrov (Centre d'Etudes de Chimie Metall., CNRS, Vitry, France).

Point Defects and Defect Interactions in Metals. Proceedings of the Yamada Conference V, Kyoto, Japan, 16-20 Nov. 1981 (Amsterdam, Netherlands: North-Holland 1982), p.656-9.

Austenitic Fe-16 wt.% Cr-20 to 45 wt.% Ni alloys have been studied by electrical resistivity measurements during 21K electron irradiation and during subsequent anneals. The Frenkel pair resistivity and the activation enthalpy for interstitial and vacancy migration have been evaluated in the 16-45 alloy. An increase in nickel concentration results in a strongly increased interstitial mobility and a slightly reduced vacancy mobility. The low swelling of the 16-45 alloy could be due to a lower vacancy formation energy. (9 refs.)

114033 Re-examination of the threshold energy surface in copper. W.E.King, R.Benedek, K.L.Merkle (Materials Sci. Div., Argonne Nat. Lab., Argonne, IL, USA), M.Meshi.

Point Defects and Defect Interactions in Metals. Proceedings of the Yamada Conference V, Kyoto, Japan, 16-20 Nov. 1981 (Amsterdam, Netherlands: North-Holland 1982), p.789-94.

Radiation-induced defect production in copper has been studied using in-situ electrical resistivity damage-range measurements in the HVEM and molecular dynamics simulations. Analysis of the results yields a threshold energy surface characterized by two isolated pockets of low threshold energy centered at (100) and (110) surrounded by regions of much higher threshold energy; the corresponding damage function exhibits a plateau at 0.65 Frenkel pairs. A Frenkel pair resistivity of $(2.75\text{--}0.2^{+0.6})\times 10^{-4}\text{ }\Omega\cdot\text{cm}$ is proposed. A model damage function is constructed and compared to results from ion irradiation damage-rate measurements. (18 refs.)

114034 Differences in saturation of defects between electrons and reactor neutron irradiations at low temperature. M.Nakagawa (Res. Reactor Inst., Kyoto Univ., Osaka, Japan).

Point Defects and Defect Interactions in Metals. Proceedings of the Yamada Conference V, Kyoto, Japan, 16-20 Nov. 1981 (Amsterdam, Netherlands: North-Holland 1982), p.821-4.

The influence of the kind of irradiating particles on the defect saturation behavior in some FCC metals is surveyed by plotting the relative production rate versus the irradiation induced resistivity increment $\Delta\rho$. The largest spontaneous recombination volume was obtained for fission fragments, the next for neutron, and the smallest for electron irradiations, in the case of copper, and also similarly for aluminum and platinum. Comparative studies are made as well on the recovery characteristics after heavy irradiations by electrons or reactor neutrons at low temperature. (11 refs.)

114035 Low temperature irradiation of FeB amorphous alloys. A.Audouard (Lab. de Metall., CENS, Gif-sur-Yvette, France), J.C.Jousset.

Point Defects and Defect Interactions in Metals. Proceedings of the Yamada Conference V, Kyoto, Japan, 16-20 Nov. 1981 (Amsterdam, Netherlands: North-Holland 1982), p.825-8.

21K 2.5 MeV electron irradiations induce localized defects in the short range order of the amorphous structure of FeB alloys. The idea which led to the results reported is the following: as in the comparatively well-known pure crystalline metal irradiation case, is it possible to define the elementary processes of the damage for an amorphous metallic alloy? If so, is it possible to characterize the 'defects' so created? The answer is thought to be positive. (12 refs.)

114036 On the evolution of microstructure during irradiation. R.Bullough (Theoretical Phys. Div., AERE, Harwell, England), T.M.Quigley.

Point Defects and Defect Interactions in Metals. Proceedings of the Yamada Conference V, Kyoto, Japan, 16-20 Nov. 1981 (Amsterdam, Netherlands: North-Holland 1982), p.839-46.

The long range interaction fields between dislocations and point defects and between voids and point defects have been included, using the embedding procedure, to yield new sink strengths for these two sink types for use in the rate theory of radiation damage. These sink strengths have been used to interpret various electron irradiation observations of microstructural evolution. (25 refs.)

114037 Radiation damage in Zr and Ti. M.Griffiths, J.White, M.H.Loretto, R.E.Smallman (Dept. of Metall. & Materials, Univ. of Birmingham, Birmingham, England).

Point Defects and Defect Interactions in Metals. Proceedings of the Yamada Conference V, Kyoto, Japan, 16-20 Nov. 1981 (Amsterdam, Netherlands: North-Holland 1982), p.880-2.

The nature of damage has been assessed in electron and proton irradiated Zr and Ti. In Zr loops of $b=1/3(1120)$, $1/3(1123)$ and $1/6(2023)$ have been observed. The loops of $b=1/3(1120)$ are found to be vacancy and interstitial. In Ti complex loops are found after electron irradiation and after proton irradiation defects which are found to be Fe-rich and which show vacancy type displacement contrast are observed. These results are discussed in terms of stress induced loop growth and impurity-defect interactions. (2 refs.)

114038 A study of irradiation damage in $\beta\text{Nb-3.1wt.\% Zr}$ alloy using a high voltage electron microscope. K.Nakai, Y.Muroo, K.Kinoshita, S.Kitajima (Dept. of Nuclear Engng., Kyushu Univ., Fukuoka, Japan).

Point Defects and Defect Interactions in Metals. Proceedings of the Yamada Conference V, Kyoto, Japan, 16-20 Nov. 1981 (Amsterdam, Netherlands: North-Holland 1982), p.887-90.

The kinetic behavior of point defects in electron irradiated $\beta\text{Nb-3.1wt.\% Zr}$ has been examined at temperatures from 300 to 675K by use of a HVEM. Two kinds of impurities denoted with X and Y are concerned with the formation of complexes which act as nuclei of loops below 335K . Dissociation of X- and Y-complexes takes place in the regions 335 to 413K and 483 to 578K , respectively, resulting in a decrease in loop density with increasing temperature. Above 578K the impurities have no influence on the loop nucleation because of a high dissociation rate between interstitials and them. Migration energy of free interstitials and binding energies of X- and Y-impurities with interstitials are estimated to be $(3.36\pm 0.48)\times 10^{-20}\text{ J}$, $(7.24\pm 0.60)\times 10^{-20}\text{ J}$ and $(1.13\pm 0.10)\times 10^{-19}\text{ J}$, respectively. (12 refs.)

114039 Mechanism of void formation of iron and iron-alloys irradiated by electrons. E.Kuramoto, N.Yoshida, K.Kitajima (Res. Inst. for Appl. Mech., Kyushu Univ., Fukuoka, Japan).

Point Defects and Defect Interactions in Metals. Proceedings of the Yamada Conference V, Kyoto, Japan, 16-20 Nov. 1981 (Amsterdam, Netherlands: North-Holland 1982), p.899-902.

Analyses of void nucleation and growth in high-purity iron ($\text{RRR}_H 3500$) and iron alloys (Ti, Si and He) have been performed mainly for the results obtained from the electron irradiation in a high voltage electron microscope using a low vacancy migration energy (0.8 eV) in iron. (19 refs.)

- Distribution of the internal distances in Frenkel pairs in irradiated silicon and germanium See Entry 113867
- Vacancies in silver: a resistivity and positron annihilation study See Entry 113876
- Submicroscopic vacancy defects in pure and doped gold See Entry 113879
- Point defects in BCC Fe-Al, Fe-Co, and Fe-Co-V ordered alloys See Entry 113883
- Defect structures in β -NiAl and their response to electron irradiation See Entry 113885
- Frenkel defects in Ni and Ni-base alloys See Entry 113886
- Detection of point defects and dynamic observation of defect interaction by atom resolution electron microscopy See Entry 113891
- Image contrast of single vacancies and small stacking fault tetrahedra in gold crystals studied by an atom resolution electron microscope See Entry 113892
- Influence of vacancies and interstitials on the Bordoni peaks in copper and silver See Entry 113899
- Softening and hardening induced by point defects and defect clusters in BCC metals See Entry 113900
- Kinetic behavior of point defects in electron irradiated FeAl alloy See Entry 113902
- Agglomerates of interstitial-atoms and vacancies in e^- -irradiated copper See Entry 113920
- HVEM in-situ observation of formation of helical dislocations in Ag-10 at.% Al See Entry 113922
- Localized formation of stacking fault tetrahedra by electron irradiation in FCC metals See Entry 113934
- Modification of defects during irradiation of Si with high electron doses See Entry 113958
- Interstitial trapping by zinc atoms in electron-irradiated silver See Entry 113962
- Trapping of interstitials at ^{100}Pd , ^{111}In , and ^{181}Hf -impurities in irradiated cubic metals See Entry 113963
- Dose dependence of interstitial trapping at ^{111}In impurities in e^- -irradiated aluminium See Entry 113964
- Recovery in electron irradiated aluminium observed by Mossbauer spectroscopy See Entry 113974
- Effect of the interaction between solute atoms and defects on formation of defect clusters See Entry 113979
- Solid phase regrowth See Entry 114006
- Compound semiconductors [laser and electron beam annealing] See Entry 114007
- A comparison of CW laser and electron-beam recrystallization of polysilicon in multilayer structures See Entry 114017
- Radiation damage in glassy $\text{Pd}_{80}\text{Si}_{20}$ and $\text{Cu}_{50}\text{Zr}_{50}$ See Entry 114058
- A HVEM study of radiation-induced segregation in dilute Ni-Be alloys See Entry 114188
- Radiation-induced segregation at internal defect sinks in electron irradiated FCC alloys See Entry 114189
- Investigation of vacancy diffusion in niobium, molybdenum, and tantalum by means of high-voltage electron microscopy See Entry 114246
- Vacancies in zinc and cadmium produced by proton- and electron-irradiation See Entry 114247
- Radiation induced interdiffusion and phase transformation in electron irradiated Cu-Ni alloys See Entry 114287
- Thermal conductivity of irradiated graphite See Entry 114296
- Correlation of lifetime with recombination centers in electron-irradiated P-type silicon See Entry 114536
- Existence of a distribution of hole-trap activation energies in FEP-Teflon See Entry 114537
- Characteristics of the optical quenching of the photoconductivity of CdS single crystals irradiated with $E=10$ MeV electrons See Entry 114564
- Superconductivity in irradiated charge-density-wave compounds 2H-NbSe_2 , 2H-TaS_2 , and 2H-TaSe_2 See Entry 114636
- Temperature dependence of positron annihilation parameters in irradiated molybdenum See Entry 114961
- Positron annihilation in molybdenum single crystals irradiated with electrons, neutrons, and α -particles See Entry 114963
- Electronic excitation in electron bombardment enhancement of chemical reactions See Entry 115577
- Study of deep-level defects and annealing effects in undoped and Sn-doped GaAs solar cells irradiated by one-MeV electrons See Entry 115647

61.80H Neutrons

- 114040 Influence of mechanical stresses on the accumulation of radiation defects in Nb and NbTi. L.S.Tophchyan (Inst. of Phys., Acad. of Sci., Tbilisi, Georgian SSR). *Fiz. Met. & Metalloved. (USSR)*, vol.56, no.2, p.334-9 (Aug. 1983). In Russian. English translation in: *Phys. Met. & Metallogr. (GB)*
- The combined effects of reactor radiation and mechanical stresses at low temperatures on the radiation-induced increase in the electrical resistivity of Nb and NbTi were studied. In the case of pure Nb a mechanical stress slowed down the rate of accumulation of radiation defects, whereas in the case of NbTi alloys it enhanced the radiation-induced increase in the electrical resistance. The processes which could account for these experimental results were considered. (25 refs.) A.T.
- 114041 Direct evidence for stress-enhanced swelling in type 316 stainless steel. D.L.Porter, M.L.Takata, E.L.Wood (Argonne Nat. Lab., Idaho Falls, ID, USA). *J. Nucl. Mater. (Netherlands)*, vol.116, no.2-3, p.272-6 (June 1983).
- Immersion density analysis of sections of Type 316 stainless steel tubes from He-pressurised in-reactor creep experiments has unequivocally demonstrated an enhancement of void swelling by an applied stress. In addition, the study has shown that in most cases of irradiation temperature and applied stress level, the void sizes and number densities are unaffected by stress at a given magnitude of swelling. Swelling versus irradiation dose relationships and microscopic examinations imply that the stress effect is to initiate swelling at a lower dose, while not affecting the nature of the mechanisms causing swelling. (12 refs.)

- 114042 A study of defect states in neutron-irradiated zirconium using positron annihilation spectroscopy. Carpenter G.J.C. (AECL, Chalk River Nuclear Labs., Chalk River, Ontario, Canada), H.T.Easterday, B.T.A.McKee. *J. Nucl. Mater. (Netherlands)*, vol.116, no.2-3, p.277-86 (June 1983).
- Positron annihilation spectroscopy has been used to examine specimens of iodide-purity zirconium, irradiated with neutrons in the temperature range 355K to 725K. The mean positron lifetimes and Doppler broadening lineshape parameters from the irradiated specimens showed significant increases over values for annealed material. A two-component analysis of the lifetime spectra indicated saturation trapping at vacancies and dislocations for the lower irradiation temperatures. No evidence was found for the presence of trapped components with long lifetimes ($\tau \geq 300$ ps), indicative of three-dimensional vacancy clusters. Recovery of the 355K irradiation damage during annealing was interpreted in terms of the annihilation of vacancies at sinks (dislocations and grain boundaries) and recovery of the irradiation-induced dislocation structure. (39 refs.)
- 114043 Saturation exposure in ferritic stainless steels. K.Suganuma, H.Kayano (Inst. of Sci. & Industrial Res., Osaka Univ., Osaka, Japan). *J. Nucl. Mater. (Netherlands)*, vol.116, no.2-3, p.326-67 (June 1983).
- Briefly reports on the saturation phenomena of irradiation hardening in some ferritic stainless steels. The results indicate the possibility of a low-embrittlement alloy with a fine-grained microstructure. (11 refs.)
- 114044 Lattice expansion and broadening of the Bragg reflexion in thermal-neutron-irradiated Li_2O pellets. N.Masaki (JAERI, Tokai-mura, Ibaraki-ken, Japan), S.Nasu, T.Tanifuji, K.Uchida, K.Noda, H.Takeshita, T.Kurasawa, H.Watanabe. *J. Nucl. Mater. (Netherlands)*, vol.116, no.2-3, p.345-6 (June 1983).
- Presents data about lattice expansion and broadening of the Bragg reflexions in Li_2O induced by thermal neutron irradiation. For the specimen irradiated to 1.44×10^{22} neutrons m^{-2} , the diffraction lines of the 422, 511 and 333 and 440 showed no striking shift compared to those of nonirradiated specimens. For the specimen irradiated to 2×10^{23} neutrons m^{-2} , the diffraction lines showed a drastic broadening and a considerable shift which corresponds to the 0.15% lattice expansion. (14 refs.)
- 114045 Critical radius for bias-driven swelling—a further analysis and its application to bimodal cavity size distributions. A.Hishinuma, L.K.Mansur (Metals & Ceramics Div., Oak Ridge Nat. Lab., Oak Ridge, TN, USA). *J. Nucl. Mater. (Netherlands)*, vol.118, no.1, p.91-9 (Aug. 1983).
- Cavities grow during irradiation only when the net vacancy influx caused by the dislocation-cavity bias is greater than the thermally emitted vacancy outflux. The cavity radius at which the strongly radius-dependent outflux equals the net influx has been termed the critical radius. An analysis is given for critical radius based on a derived expression containing functional dependences on gas pressure, dislocation and cavity capture efficiencies, temperature, and the other material and irradiation variables. Based on the solution of this equation a cavity stability diagram is obtained. The necessity for the development of a bimodal cavity distribution during irradiation after helium preinjection arises naturally from this construction. The dependence of critical radius on number of gas atoms, temperature, dose rate, and bias is illustrated for ranges of interest in the important variables. These results are consistent with recent experimental data. (14 refs.)
- 114046 Recovery of Cu, Ag, and Ni dilute alloys after low temperature irradiation. S.Takamura, M.Kobiyama (JAERI, Ibaraki, Japan).
- Point Defects and Defect Interactions in Metals. Proceedings of the Yamada Conference V, Kyoto, Japan, 16-20 Nov. 1981 (Amsterdam, Netherlands: North-Holland 1982), p.396-9
- Effect of solute atoms on the recovery of Cu, Ag and Ni after fast neutron irradiation at low temperature has been studied using electrical resistivity measurements. By doping with solute atoms, recovery stage I is suppressed and the substages are observed during stage II which is due to release of interstitial from trapping solute atom. The binding energies between solute atom and interstitial are estimated from the temperature of substage in recovery curves. The relation between the binding energies and the size effect is discussed. (12 refs.)
- 114047 Recovery of radiation-induced defects in dilute Al-Ge alloys after fast neutron irradiation at 5K. T.Kittaka (Coll. of Liberal Arts & Sci., Okayama Univ., Okayama, Japan), H.Maeta, F.Ono, H.Murakami, Y.Mizoguchi.
- Point Defects and Defect Interactions in Metals. Proceedings of the Yamada Conference V, Kyoto, Japan, 16-20 Nov. 1981 (Amsterdam, Netherlands: North-Holland 1982), p.400-2
- By measuring the lattice parameters with X-ray techniques, the recovery process and the interaction between solute atoms and interstitials were investigated in fast neutron irradiated single crystals of Al and dilute Al-Ge alloys containing 0.2 and 1.1 at.% Ge. It was found that the change in the lattice parameter due to the neutron irradiation is proportional to the fluence. In the recovery curves of the Al-0.2 at.% Ge alloy obtained from (333) reflection, a remarkable suppression of recovery was found at stage I, and this suppression was released at the end of stage II. In the recovery curve obtained by the (400) reflection, a similar tendency was observed at stage I, while a small difference was found in a temperature range around 100K. These results were discussed in terms of the interaction between interstitials and impurities. (4 refs.)
- An improved reduced Van der Waals equation of state for helium at high pressures See Entry 113543
- The very-small angle neutron scattering from $\text{SiO}_2\text{-PbO}$ glasses See Entry 113752
- Configurations of point defects in neutron-irradiated iron See Entry 113878
- Self-interstitial mobility in a neutron-irradiated austenitic $\text{Fe}_{50}\text{Cr}_{16}\text{Ni}_{32}$ alloy See Entry 113890
- Interstitials and interstitial clusters in fast-neutron irradiated molybdenum by X-ray Huang scattering See Entry 113903
- Vacancy dipole loops observed in low temperature neutron irradiated pure gold and pure aluminum See Entry 113904
- Vacancy and interstitial loops in irradiated copper See Entry 113919
- Solute atom-dislocation interactions studied by ultrasonic method See Entry 113975
- Differences in saturation of defects between electrons and reactor neutron irradiations at low temperature See Entry 114034
- Flow behaviour of nickel irradiated with 15 MeV neutrons and 16 MeV protons See Entry 114049
- Displacement cascade damage in irradiated metals See Entry 114056
- Statistical theory of the evolution of damage structure under irradiation with cascades See Entry 114059

- Stability of the radiation-induced γ phase in 316 stainless steel** See Entry 114182
- Diffusion of tritium in single crystal Li_2O** See Entry 114261
- Thermal conductivity of irradiated graphite** See Entry 114296
- Increase of transition temperature T_c in A15 superconductors after neutron irradiation** See Entry 114634
- How electric strength of polyethylene and polystyrene is influenced by residual phenomena caused by ionising radiation and pressure** See Entry 114781
- Positron studies of recovery processes in aluminium and aluminium alloys** See Entry 114958
- A positron annihilation study of neutron irradiated titanium** . See Entry 114962
- Positron annihilation in molybdenum single crystals irradiated with electrons, neutrons, and α -particles** See Entry 114963
- The effect of fast neutron irradiation on the compressive stress-strain relationships of graphite** See Entry 115256
- Inhomogeneous plastic deformation and its relevance to iodine stress corrosion cracking susceptibility in irradiated Zircaloy-2 tubing** See Entry 115418

61.80J Ions

(for ion implantation, see 61.70T)

- 114048 Direct determination of a radiation damage profile with atomic resolution in ion-irradiated platinum.** D.Pramanik (AMI, Santa Clara, CA, USA), D.N.Seidman.
Appl. Phys. Lett. (USA), vol.43, no.7, p.639-41 (1 Oct. 1983).
The field-ion microscope technique has been employed to determine directly a radiation damage profile, with atomic resolution, in a platinum specimen which had been irradiated at 60K with 20 keV Kr^+ ions to a fluence of $5 \times 10^{12} \text{ cm}^{-2}$. It is shown that the microscopic spatial vacancy distribution (radiation damage profile) is directly related to the elastically deposited energy profile. The experimentally constructed radiation damage profile is compared with a theoretical damage profile—calculated employing the transport of ions in matter (TRIM) Monte Carlo code—and excellent agreement is obtained between the two. Thus, it is demonstrated that it is possible to go directly from a microscopic spatial distribution of vacancies to a continuous radiation damage profile. (17 refs.)
- 114049 Flow behaviour of nickel irradiated with 15 MeV neutrons and 16 MeV protons.** R.H.Jones, E.R.Bradley, D.L.Styris (Pacific Northwest Lab., Richland, WA, USA).
J. Nucl. Mater. (Netherlands), vol.116, no.2-3, p.297-304 (June 1983).
The yield strength of zone refined nickel that was irradiated at 300K with T(d,n) and Be(d,n) neutrons and 16 MeV protons was found to increase by a similar amount when compared at equal fluence levels. A factor of 2.5 increase in the yield strength was determined for a 15 MeV neutron fluence of $1 \times 10^{22} \text{ m}^{-2}$ and a 16 MeV proton fluence of $2 \times 10^{22} \text{ m}^{-2}$. The strength increase was associated with defect clusters or small prismatic loops and could be described by a strong barrier model for both neutron and proton irradiated nickel. Serrated plastic deformation was observed for samples irradiated with 15 MeV neutrons and 16 MeV protons to fluences higher than $3 \times 10^{21} \text{ m}^{-2}$. The similarity in the hardening process of 15 MeV neutron and 16 MeV proton irradiated nickel is consistent with their damage energy cross sections being equal at high primary knock-on energies ($>10 \text{ keV}$). (25 refs.)
- 114050 Surface composition change of TiC under 0.15-3 keV hydrogen ion bombardment.** H.Tanaka, K.Saiki, S.Otani, A.Koma, S.Tanaka (Dept. of Appl. Phys., Univ. of Tokyo, Tokyo, Japan).
J. Nucl. Mater. (Netherlands), vol.116, no.2-3, p.317-20 (June 1983).
Reports the surface composition change in single crystal TiC, which is one of the candidate compound materials, under bombardment of high-density, hydrogen-ion beam. The results show that carbon atoms are highly depleted from the surface of TiC under bombardment of hydrogen ions in the energy range of 0.15-1 keV, which is the most probable energy range of fuel particles impacting the first wall in a fusion reactor. Therefore the problem of surface composition change becomes important for the characterization of TiC as the first wall material. (7 refs.)
- 114051 The effect of primary recoil spectrum on radiation induced segregation in nickel-silicon alloys.** R.S.Averback, L.E.Rehn, W.Wagner (Argonne Nat. Lab., Argonne, IL, USA), P.Ehrhart.
J. Nucl. Mater. (Netherlands), vol.118, no.1, p.83-90 (Aug. 1983).
Segregation of silicon to the surface of Ni-12.7 at.% Si alloys during 2.0-MeV He and 3.25-MeV Kr irradiations was measured using Rutherford backscattering spectrometry. For equal calculated defect production rates the Kr irradiation was $<3\%$ as efficient as the He irradiation for promoting segregation in the temperature range, 450-580°C. It was further observed that Kr preirradiation of specimens dramatically reduced segregation during subsequent He irradiation. A model for cascade annealing in Ni-Si alloys is presented which qualitatively explains the segregation results. The model assumes that small interstitial-atom-clusters form in individual cascades and that these clusters become trapped at silicon solute atoms. The vacancy thereby becomes the more mobile defect. The model should also have relevance for the observation that void swelling in nickel is suppressed by the addition of silicon solute. (26 refs.)
- 114052 Radiation-induced segregation in titanium alloys.** Z.Wang, G.Ayrault, H.Wiedersich (Materials Sci. & Technol. Div., Argonne Nat. Lab., Argonne, IL, USA).
J. Nucl. Mater. (Netherlands), vol.118, no.1, p.109-14 (Aug. 1983).
Radiation-induced segregation (RIS) of V, Mo, Nb, Ta, Zr, and Sn in binary titanium alloys was investigated to test the solute size effect correlation in HCP alloys. Undersize Mo segregates weakly toward the sinks. Nb and Ta, which are slightly oversize in Ti, undergo little or no RIS. Oversize Zr solute in Ti segregates away from the sinks, whereas undersize Ti solute in Zr is enriched at sinks. All of these results are in accord with the solute size effect correlation. Surprisingly, Sn, which is significantly oversize in Ti, appears to segregate very little. The postirradiation annealing of Ti-3V and Ti-8Al-1V-1Mo confirmed that segregation of undersize V toward sinks is radiation-induced. Measurements of temperature and dose dependence in binary and complex alloys showed that the degree of V segregation has a maximum at $\sim 600^\circ\text{C}$ and obeys parabolic growth kinetics in its early stages but probably saturates at a rather low dose ($\sim 0.8 \text{ dpa}$). (8 refs.)
- 114053 Pattern formation in metallic glasses induced by helium ion implantation.** I.Lovas, T.Tel.
Report KFKI-1983-82, Hungarian Acad. Sci., Budapest (1983), 7 pp.
A model is constructed to explain the pattern formation. The migration of helium atoms is considered. The helium atoms are assumed to be in quasi free, in trapped, or in captured states. The density of the quasi free atoms and the energy density are governed by nonlinearly coupled diffusion type equations. The critical value of the control parameter and the critical wave-

number characterizing the soft-mode instability of the system are determined. Their orders of magnitude agree with that of the experimental data. Formally, the model can be reduced to the well-known Brusselator but the control parameter differs from that of the standard case. (11 refs.)

114054 Crystallization of amorphous silicon films by pulsed ion beam annealing. J.Gyulai, R.Fastow, K.Kavanagh, M.O.Thompson, C.J.Palmstrom, C.A.Hewett, J.W.Mayer (Dept. of Materials Sci., Cornell Univ., Ithaca, NY, USA).

Laser-Solid Interactions and Transient Thermal Processing of Materials, Boston, MA, USA, 1-4 Nov. 1982 (New York, USA: Elsevier 1983), p.455-60

Regrowth by pulsed proton beam was studied for evaporated amorphous Si layers, for layers converted to polycrystalline by annealing (both with and without Ge markers) and for implantation-amorphized SOS films. Silicon-on-sapphire showed the lowest threshold for regrowth. Amorphous silicon melted at about 0.2 J/cm^2 lower fluences of protons of 380 keV energy than crystalline Si. Implanted Sb into SOS occupies lattice positions exceeding the solid solubility. (4 refs.)

114055 Radiation damage in tantalum observed by PAC. A.Weidinger, M.Deicher, J.Busse (Fakultat fur Phys., Univ. Konstanz, Konstanz, Germany).

Point Defects and Defect Interactions in Metals. Proceedings of the Yamada Conference V, Kyoto, Japan, 16-20 Nov. 1981 (Amsterdam, Netherlands: North-Holland 1982), p.268-70

Stage III defects in Ta were investigated by the PAC method using ^{111}In as a radioactive probe. A unique defect configuration with $\nu_{Q1}=98(2) \text{ MHz}$, $\eta=0$ was found between 360K and 380K. In addition, unresolved signals from other defects with about twice the quadrupole interaction strength of ν_{Q1} were observed in the stage III region. If the sample was stored in air for a long period, a shift in the defect frequencies, probably due to interstitially dissolved impurities, was measured. (5 refs.)

114056 Displacement cascade damage in irradiated metals. B.L.Eyre, C.A.English (Metall. Div., AERE, Harwell, England).

Point Defects and Defect Interactions in Metals. Proceedings of the Yamada Conference V, Kyoto, Japan, 16-20 Nov. 1981 (Amsterdam, Netherlands: North-Holland 1982), p.799-806

Results from electron microscope studies of vacancy clusters formed by the collapse of displacement cascades in heavy ion and neutron irradiated Cu, Mo and Fe are discussed. It is shown that the three metals exhibit considerable differences in cascade collapse behaviour although in each metal good agreement exists between the results obtained using heavy ion and neutron irradiation. (23 refs.)

114057 Direct observation of heavy radiation damage process by field ion microscopy. N.Igata, S.Sato, T.Sawai (Dept. of Metall. & Materials Sci., Univ. of Tokyo, Tokyo, Japan).

Point Defects and Defect Interactions in Metals. Proceedings of the Yamada Conference V, Kyoto, Japan, 16-20 Nov. 1981 (Amsterdam, Netherlands: North-Holland 1982), p.811-14

Observed the point defects in heavily irradiated tungsten by field ion microscopy (FIM) and analysed surface radiation damage process from atomistic standpoints. The material used was a tungsten wire of 0.1 mm in diameter with a purity of 99.95%. The specimens were irradiated with various kinds of ions having energy 100~400 keV. The total dose was 0.01~10 dpa and the irradiation temperature was 20°C . The FIM observation was performed within (112), (121) and (211) planes for every atomic layer within the mean projected range. The calculated values from Lindhard's theory coincided with the observed damage depth profile within a factor of 2. The average size distribution was taken through the mean projected range. The maximum vacancy cluster size was 15 A, as caused by various kinds of ion irradiation. The total vacancy concentration was proportional to the square root of the total dose at 20°C irradiation. The total number of vacancies at the same level of average concentration of injected charged particles was proportional to the square root of the maximum primary knock-on energy. The annealing process was also investigated. (6 refs.)

114058 Radiation damage in glassy $\text{Pd}_{80}\text{Si}_{20}$ and $\text{Cu}_{50}\text{Zr}_{50}$. S.Klaumunzer, S.Rentzsch, G.Schumacher, G.Vogl (Hahn-Meitner-Inst. fur Kernforschung, Berlin, Germany).

Point Defects and Defect Interactions in Metals. Proceedings of the Yamada Conference V, Kyoto, Japan, 16-20 Nov. 1981 (Amsterdam, Netherlands: North-Holland 1982), p.829

Summary form only given. Different samples of the metallic glass $\text{Pd}_{80}\text{Si}_{20}$ were irradiated at 4.6K with 3 MeV-electrons and at 50K to 140K with high energy (25 MeV to 250 MeV) heavy ions (0, Ar, Kr). Care was taken to avoid implantation. Radiation-induced changes were monitored in situ by electrical resistance measurements and isochronal annealing treatments were performed up to 400K. The damage rate curves from electron irradiation of $\text{Pd}_{80}\text{Si}_{20}$ are very similar to those of pure metals. This similarity shows the existence of spontaneous recombination processes in metallic glasses. The saturation of the increase in resistivity is extrapolated to be about $2.45 \mu\Omega\text{cm}$. The authors conclude that the change in resistivity is proportional to the radiation-induced defect concentration. Similar effects are found after Ar- and Kr-irradiation of glassy $\text{Cu}_{50}\text{Zr}_{50}$ at about 60K to 120K. (2 refs.)

114059 Statistical theory of the evolution of damage structure under irradiation with cascades. K.Kitajima (Res. Inst. for Appl. Mech., Kyushu Univ., Fukuoka, Japan).

Point Defects and Defect Interactions in Metals. Proceedings of the Yamada Conference V, Kyoto, Japan, 16-20 Nov. 1981 (Amsterdam, Netherlands: North-Holland 1982), p.847-52

A general statistical theory was presented for processes of cascade damage. Fluctuations of collisional and diffusional processes having wide range of relaxation times are approximated by a hierarchy of Fokker-Planck type equations. Methods of calculations are presented for transfer terms and applied for explanations of simulation irradiation studies made on metals. (18 refs.)

114060 The kinetics of the interaction between helium and displacement damage in irradiated materials. N.M.Ghoniem, S.Sharafat (School of Engng. & Appl. Sci., Univ. of California, Los Angeles, CA, USA), L.K.Mansur.

Point Defects and Defect Interactions in Metals. Proceedings of the Yamada Conference V, Kyoto, Japan, 16-20 Nov. 1981 (Amsterdam, Netherlands: North-Holland 1982), p.865-8

Helium migration and clustering is affected by the presence of the primary damage components, vacancies and interstitials. A kinetic rate theory is developed to describe the migration, interaction and clustering of small helium-vacancy complexes. Numerical solutions of a set of rate equations are performed for transient as well as steady-state conditions. The study shows that helium migrates as an interstitial atom during early irradiation, turning gradually to a trapped helium mode by about a vacancy mean lifetime. At temperatures up to $\sim 550^\circ\text{C}$, helium migration in nickel irradiated in typical reactor conditions is primarily by a self interstitial replacement mechanism.

Self interstitials replace helium in substitutional sites and detrapp it into interstitial sites. The kinetics of cavity nucleation is investigated with particular emphasis on the kinetic stability of vacancy-helium complexes. (14 refs.)

114061 Voids and bubbles in argon irradiated nickel. S.Sasaki, M.Kiritani (Dept. of Material Phys., Osaka Univ., Osaka, Japan), A.Iwase, T.Iwata, F.E.Fujita.

Point Defects and Defect Interactions in Metals. Proceedings of the Yamada Conference V, Kyoto, Japan, 16-20 Nov. 1981 (Amsterdam, Netherlands: North-Holland 1982), p.903-6

At the very beginning of energetic argon ion irradiation, interstitial type dislocation loops finish their nucleation, and then grow linearly with time. By continued irradiation, voids nucleate and grow without increasing their number density. Stereoscopic TEM observations of interstitial loops and voids show the distributions deeper and shallower than the ion stopping range respectively. Post-irradiation annealing experiment shows each void contains gas atoms depending on the depth from the ion-incident surface. All the observed processes of formation and annihilation of different types of defect clusters by irradiation and annealing are explained by using the diffusion kinetics of point defects. The influence of gas atoms on the formation of these defects are discussed. (1 ref.)

Vacancy and interstitial loops in irradiated copper See Entry 113919

Measurements of ion-implantation damage in GaP See Entry 113943

Damage and in situ annealing during ion implantation See Entry 113944

A comparison of ellipsometer and RBS analysis of implant damage in silicon See Entry 113945

The study of damage profile of ion implanted layer on Si by spectroscopic ellipsometry See Entry 113946

Trapping of interstitials at ^{100}Pd -, ^{111}In -, and ^{181}Hf -impurities in irradiated cubic metals See Entry 113963

Interactions of defects with Co implanted into Al at 4.2K See Entry 113965

Interaction of implanted impurities with extended defect configurations in tungsten single crystal See Entry 113976

A role of helium and hydrogen atoms in the formation of interstitial loops See Entry 113980

Radiation damage in Zr and Ti See Entry 114037

Critical radius for bias-driven swelling—a further analysis and its application to bimodal cavity size distributions See Entry 114045

Investigation of radiation induced impurity complexes in aluminium alloys by channeling. A critical analysis by computer simulation See Entry 114062

Mechanism and kinetics of radiation-induced segregation in Ni-Si alloys See Entry 114187

Ion-induced diffusion and surface segregation See Entry 114239

Fast interstitial-solute complex diffusion under irradiation in Cu/Be See Entry 114244

Vacancies in zinc and cadmium produced by proton- and electron-irradiation .. See Entry 114247

Measurement of radiation induced impurity diffusion in copper See Entry 114274

Effect of oxygen on radiation-enhanced diffusion in silicon .. See Entry 114278

Energy spectrum of defects in silicon irradiated with hydrogen and helium ions See Entry 114474

Ion irradiation effects on Pt contacts to Si with and without interfacial chemical oxide See Entry 114611

Der Einfluss von Wasserstoff auf die Supraleitung von Nichtbergangsmetallen (The influence of hydrogen on the superconductivity of non-transition metals) .. See Entry 114640

Infrared absorption in proton-irradiated solid deuterium See Entry 114894

Positron annihilation in molybdenum single crystals irradiated with electrons, neutrons, and α -particles See Entry 114963

Molecular effect of Al K α -x-ray yields from aluminum oxide films for H^+ and H_2^+ ion bombardments See Entry 114974

61.80L Atoms and molecules

The kinetics of the interaction between helium and displacement damage in irradiated materials See Entry 114060

61.80M Channelling, blocking and energy loss of particles

(see also 29.70 Energy loss and range relations)

114062 Investigation of radiation induced impurity complexes in aluminium alloys by channeling. A critical analysis by computer simulation. M.Muller (Hahn-Meitner-Inst., KFA Berlin GmbH, Berlin, Germany).

Nucl. Instrum. & Methods Phys. Res. (Netherlands), vol.213, no.2-3, p.453-62 (1 Aug. 1983).

The flux distributions of channelled He^+ ions in Al and their development with penetration depth are calculated for the major axial and planar directions using Monte Carlo simulations. A strong depth oscillation of the flux in the channel centre is observed in the near surface region indicating the statistical nonequilibrium of the flux. The Monte Carlo program is applied to evaluate published yields measured in different directions ((100), (110), (111), [100], {111}) of He^+ irradiated Al alloys. It is shown that the solute atoms Mn, Cu, Zn, Ge and Ag which react with irradiation induced self-interstitials are displaced from their lattice site into the (100) or (111) direction. The distance of the displaced atoms to the octahedral interstitial site is found to be less than 0.1 nm. The displacement of the solute atom in the (100) direction agrees quite well with published analytically determined values. (35 refs.)

114063 A performance test of the recovery of single energy loss profiles via matrix analysis. P.Schattschneider (Inst. of Appl. & Tech. Phys., Tech. Univ. Vienna, Vienna, Austria).

Ultramicroscopy (Netherlands), vol.11, no.4, p.321-2 (1983).

From a hypothetical single scattering loss spectrum, revealing a broad plasmon and some unimportant structure, the multiple loss spectrum for a specimen thickness of three mean free path lengths was constructed. From the tests carried out up to now, it is concluded that the matrix approach is superior to the Fourier method with respect to the energy range afforded for the retrieval. Moreover, convergence of the procedure is guaranteed for any thickness parameter, contrary to the convolution approach which is the second well-established method. (3 refs.)

Role of channeling in the implantation of low-energy ions See Entry 113941

Si-on-sapphire and Si implanted with Zr ions: lattice location, solid phase epitaxial regrowth and electrical properties See Entry 113947

The scattering of hydrogen from a cesiated tungsten surface See Entry 115000

Sputter-induced surface modification in Cu-Ni alloys at elevated temperatures See Entry 115005

Material analysis by means of high energy ion beams See Entry 115600

62.00 MECHANICAL AND ACOUSTIC PROPERTIES OF CONDENSED MATTER

(see also 46.30 Mechanics of solids and rheology, 61.70 Defects in crystals, 68.25 Surfaces and interfaces, 81. Materials science; for thermomechanical effects, see 65.70; for magnetomechanical effects, see 75.80; for piezoelectric effects, see 77.60; for elasto-optical effects, see 78.20H)

62.10 MECHANICAL PROPERTIES OF LIQUIDS

(for viscosity of liquids, see 66.20)

114064 Molar volumes and molar excess volumes of molten alkali chloride+silver chloride mixtures. A.Krekberg, W.Merkens, J.Richter (Inst. fur Phys. Chemie, RWTH Aachen, Aachen, Germany).

Z. Naturforsch. Teil A (Germany), vol.38A, no.8, p.890-2 (Aug. 1983).

Measurements of the densities (and with these of the molar volumes and the excess volumes) of the molten salt systems $\text{LiCl}+\text{AgCl}$, $\text{NaCl}+\text{AgCl}$, $\text{KCl}+\text{AgCl}$, $\text{RbCl}+\text{AgCl}$, and $\text{CsCl}+\text{AgCl}$ as functions of composition and temperature from the liquidus curve up to 1200K are reported. It is shown that a linear relation with the volume fraction fits the measured densities of the alkali chloride+silver chloride mixtures better than one with the mole fraction. (5 refs.)

114065 Measurements of densities and dielectric constants of liquid normal butane from 140 to 300K at pressures to 35 MPa. W.M.Haynes (Nat. Engng. Lab., NBS, Boulder, CO, USA).

J. Chem. Thermodyn. (GB), vol.15, no.9, p.801-5 (Sept. 1983).

Results of density and dielectric-constant measurements on compressed liquid normal butane at temperatures from 140 to 300K and pressures to 36 MPa are reported. Simultaneous measurements of these properties were carried out using a magnetic-suspension densimeter and a concentric-cylinder capacitor. Also presented are computed values of the Clausius-Mossotti function. (11 refs.)

114066 Viscoelastic relaxation in the acetamide+sodium thiocyanate binary system. G.Berchiesi, C.Vitali, P.Passamonti (Dipartimento di Sci. Chimiche, Camerino Univ., Camerino, Italy), R.Plowiec.

J. Chem. Soc. Faraday Trans. II (GB), vol.79, pt.8, p.1257-63 (Aug. 1983).

The shear impedance, density and viscosity of the eutectic mixture $\text{NaCNS}+\text{CH}_3\text{CONH}_2$ have been measured in the temperature range 253-313K and at the frequencies 31 and 87 MHz. The real parts of the complex impedance and of the rigidity modulus have been obtained. The relaxation region is shifted in comparison with that of the Maxwell model and is interpreted using the modified BEL model. Irregularities in the real part of the mechanical impedance (around 283K) and in the Arrhenius plot of the viscosity (around 293K) may be attributed to changes in the liquid structure. (15 refs.)

114067 Elastic constants of some nematic liquid crystals with banana-shaped molecules. E.F.Gramsbergen, W.H.De Jeu (Solid State Phys. Lab., Groningen, Netherlands).

Phys. Lett. A (Netherlands), vol.97A, no.5, p.199-201 (29 Aug. 1983).

Results are given for the elastic constants in the nematic phase of some molecules with a curved (banana-like) molecular shape. In principle this could lead to a reduced bend elastic constant due to the possibility of adjusting to a bend deformation by a redistribution of the molecules. However, the elastic constants turn out to have quite normal values as compared with similar non-curved molecules. (10 refs.)

114068 Melt rheology of polymer blends: the morphology feedback. A.Plochocki (Polymer Engng. Dept., Univ. of Tennessee, Knoxville, TN, USA).

Polym. Eng. & Sci. (USA), vol.23, no.11, p.618-26 (mid-Aug. 1983).

Particular rheology compositions (PRC) so far observed for blends of polyolefins are confirmed with composition dependence of melt elasticity and viscosity functions for polypropylene/rubbers and blends of other commercial polymers. Particular morphology at PRC was indirectly ascertained from the composition dependence of specific volume, v_T -compositions for which the maximum v_T observed are those of minimum viscoelasticity. Direct evidence from scanning electron microscopy (SEM) indicates that the disperse morphology undergoes distinct change at PRC: from uniform into bimodal, with coarser core. Rubber rich mixtures display stratified texture confirming that the melt elasticity ratio (Van Oene's 1982) criterion for disperse/stratified morphology transition is valid in case of polypropylene/rubber blends. For a set of polymers of given melt elasticity ratios and at a composition ratio, static and rotational distributive mixers generate polyblends differing significantly in the melt rheology-morphology interaction. (43 refs.)

114069 Melt rheology of blends of semi-crystalline polymers. II. Dynamic properties of poly(ethylene terephthalate)-poly(amide-6,6) molten blends. L.A.Utracki, G.L.Bata (Industrial Materials Res. Inst., Nat. Res. Council of Canada, Montreal, Canada).

Polymer Alloys III Blends, Blocks, Grafts and Interpenetrating Networks. Proceedings of a Symposium, New York, USA, 23-28 Aug. 1981 (New York, USA: Plenum 1983), p.91-103

Melt rheology of poly(ethylene terephthalate), PET, poly(amide-6,6), PA, and their blends were investigated at 240, 260, 280 and 300°C on a Rheometrics Mechanical Spectrometer in a dynamic mode within the frequency range from 10^{-1} to 10^2 (rads/sec). Dynamic viscosity, storage and loss shear moduli were recorded. First, the isothermal rate of the overall thermal degradation process for each sample was determined, from which the activation energy of the process, E_p , as a function of the composition was computed. The rates of degradation as well as E_p s of the blends were found to be larger than those calculated from the properties of PET and PA by using an additivity rule. Next, subtracting the degradation effect from the recorded rheological signals, the true flowcurves result. The dynamic viscosity, η^* , and the dynamic measure of the primary normal stress difference coefficient, ψ^* , as functions

of the frequency, ω , were computed for each temperature, T , and composition, c . (23 refs.)

Anomalous rheological behaviour of poly(vinyl alcohol) gels ...See Entry 113393

Nonlinear viscoelasticity and the Cox-Merz relations for polymeric fluids See Entry 113395

Studies on dilute solutions of rodlike macroions. I. Light scattering, densitometry, and cryoscopy See Entry 113719

Elongation rheology of polyolefins and its relation to processability See Entry 114237

High-temperature solution properties in the flux systems $\text{RPO}_4\text{-Pb}_2\text{P}_2\text{O}_7$ ($\text{R}=\text{Dy}, \text{Y}$) See Entry 115040

Mechanical properties of injection molded blends of poly(ethylene-terephthalate) and poly(amide-6,6) See Entry 115332

62.20 MECHANICAL PROPERTIES OF SOLIDS (RELATED TO MICROSCOPIC STRUCTURE)

(see also 81.40 Treatment of materials and its effects on microstructures and properties, 81.70 Materials testing)

Effect of moisture on physical properties of nylon See Entry 113762

Vacancy clustering during oxidation of nickel, magnesium, and zinc See Entry 113874

Interaction of dislocations with impurities and its influence on the mechanical properties of silicon crystals See Entry 113981

How electric strength of polyethylene and polystyrene is influenced by residual phenomena caused by ionising radiation and pressure See Entry 114781

Effect of loading prehistory on mechanical properties of steel in single-axis extension See Entry 115204

62.20D Elastic constants

(see also 03.40D Mathematical theory of elasticity, 81.40J Elasticity and anelasticity)

114070 Shear elastic constant softening in $(\text{V}_{1-x}\text{Cr}_x)_2\text{O}_3$: second-order nature of the low temperature phase transition. H.Yang, R.J.Sladek (Dept. of Phys., Purdue Univ., West Lafayette, IN, USA), H.R.Harrison. *Solid State Commun. (USA)*, vol.47, no.12, p.955-7 (Sept. 1983). From ultrasonic wave velocities in semiconducting, corundum-structured $(\text{V}_{1-x}\text{Cr}_x)_2\text{O}_3$ with $x=0.015$ and 0.03 , the authors find that the C_{44} shear modulus softens drastically with decreasing temperature. Along with other elastic behavior this indicates a smooth change from rhombohedral to almost hexagonal elastic symmetry before a nearly second-order transition to the low T monoclinic phase. (17 refs.)

Effect of shear modulus on the elastic behavior of strongly anisotropic plates .. See Entry 113305

On the physics of state transition See Entry 114136

Structural transformations and their precursors See Entry 114154

Absence of pressure-induced valence change in CeAs See Entry 114162

Some high-temperature properties of Zircaloy-oxygen alloys See Entry 114213

Solid solutions based on lead barium metaniobate See Entry 114785

The effect of dye sorption on electromechanical properties in sodium poly(L-glutamate) See Entry 114788

Effect of strain rate on the resistance of metals to plastic deformation See Entry 115213

Elastic constants of fiber-reinforced boron-aluminum: observation and theory .. See Entry 115233

Dependence of the elastomechanical properties of granular corundum-zirconium refractory materials on their microstructure See Entry 115234

On the measurement of Young's modulus of tubes by propagation of longitudinal waves See Entry 115236

Poisson's ratio in zirconium single crystals See Entry 115237

Ab initio calculation of polyethylene deformation including electron correlation effects See Entry 115238

Elastic modulus of syndactic foams See Entry 115239

Elastic properties (the stiffness constants, the shear modulus and the dislocation line energy and tension) of Ni-Al solid solutions and of the Nimonic alloy Pe16 See Entry 115240

Strain modulation measurements of stiffening effects in carbon fibers See Entry 115242

Anisotropy of elastic properties of titanium base α -alloys See Entry 115245

Influence of the level of stresses on the static Young's modulus of a number of constructional materials See Entry 115247

Polymer-performance on the dimensional stability and the mechanical properties of wood-polymer composites prepared by an electron beam accelerator See Entry 115248

Reinforced polyester structural foam See Entry 115250

The effect of fast neutron irradiation on the compressive stress-strain relationships of graphite See Entry 115256

RIM systems from interpenetrating polymer networks See Entry 115291

Failure of rubber-modified plastic liners See Entry 115331

Some aspects of improving abrasive resistance See Entry 115373

Assessment of residual stresses in coatings applied to P/M parts See Entry 115441

62.20F Deformation and plasticity

(inc. yield, ductility and superplasticity; see also 81.40L Deformation, plasticity and creep)

114071 Interlayering and interlayer slip in biotite as seen by HRTEM. J.O.Banos, M.Amouric (Centre de Recherche sur les Mecanismes de la Croissance Cristalline, CNRS, Marseille, France), C.De Fouquet, A.Baronnet. *Am. Mineral. (USA)*, vol.68, no.7-8, p.754-8 (July-Aug. 1983). Interlayering, slip, and cleavage phenomena have been observed using high-resolution transmission electron microscopy in tectonically deformed biotite. The unit mica layers and the positions of the interlayer cations can be imaged

with this technique. From the observations, the authors conclude first that slip and cleavage occur in the interlayer level of the structure. The biotite shows partial interlayers of brucite-like sheets, which form, with the adjacent talc-like layers of the mica, single chlorite layers interstratified in the mica structure. From structural and physical considerations, brucite interlayering is interpreted here as a 'brucitization' of an interlayer level of the mica where partial slip or cleavage has previously occurred. It is an example of a chemical process at the atomic scale (local chloritization of the mica) favored by deformation microstructures. (19 refs.)

114072 Characteristics of plastic flow of interstitial phases. N.M.Vlasov, P.V.Zubarev. *Fiz. Met. & Metalloved. (USSR)*, vol.56, no.2, p.361-5 (Aug. 1983). In Russian. English translation in: *Phys. Met. & Metallogr. (GB)*

An analysis was made of the experimental data on the high-temperature creep of interstitial phases on the basis of dislocation theory. The cubic dependence of the rate of creep on the stress is accounted for by a mechanism of plastic flow of interstitial phases in which the glide of a dislocation in the lattice of a metal is accompanied by diffusion jumps of nonmetal atoms. The nonmetal atoms do not follow the dislocation, in contrast to impurity atmospheres in solid solutions, but remain close to 'their' metal atoms and together with the latter they produce disordered regions near dislocation lines. (9 refs.) A.T.

114073 Modification of the theory of plastic flow based on a shear-strain mechanism. A.M.Kovrizhnykh. *J. Appl. Mech. & Tech. Phys. (USA)*, vol.23, no.6, p.860-5 (Nov-Dec. 1982). Translation of: *Zh. Prikl. Mekh. & Tekh. Fiz. (USSR)*, vol.23, no.6, p.133-8 (Nov-Dec. 1982). [received: Sept. 1983]

An experimentally based modification of the theory of plastic flow is proposed, in which a macroscopic shear strain mechanism is taken as the basis for constructing the governing relationships. Such an approach does not use the concept of a loading surface to construct the governing relationships, but allows interpretation in this terminology. The loading surface is singular in the hardening stage, and comprised of piecewise-smooth sections of surfaces of constant principal tangential stresses. The appearance of plastic strain is associated with the Tresk-Saint-Venant plasticity condition, and hardening is developed as follows: the loading point in stress space displaces piecewise-smooth sections of the surfaces of constant principal tangential stresses parallel to themselves by withdrawing them from the origin. (9 refs.)

114074 The characteristic equation for superplastic flow. B.Burton (Technol. Planning & Res. Div., Berkeley Nuclear Labs., Berkeley, England). *Philos. Mag. A (GB)*, vol.48, no.3, p.L9-13 (Sept. 1983).

The characteristic-area concept of steady-state flow is applied to superplasticity. It is shown that the parametric dependence of flow rate upon stress and grain size is satisfied if it is assumed that an interface reaction controls the diffusion fluxes which lead to strain development. The characteristic area is shown to be equal to the produce of the grain diameter and the interfacial line-defect spacing. (9 refs.)

114075 Deformation of semibrittle solids. B.I.Koval'chuk (Inst. of Strength Problems, Acad. of Sci., Kiev, Ukrainian SSR). *Strength Mater. (USA)*, vol.14, no.9, p.1217-24 (Sept. 1982). Translation of: *Probl. Prochn. (USSR)*, vol.14, no.9, p.51-7 (Sept. 1982).

The author proposes a variant of the strain theory of plasticity of isotropic semibrittle solids for the case of simple loading. The effect of the first stress-tensor invariant on plastic flow and dilatation of the material is considered. (21 refs.)

114076 Laws of the limiting plasticity of metals. V.A.Skudnov (Gorky Polytech. Inst., Gorky, USSR). *Strength Mater. (USA)*, vol.14, no.9, p.1243-52 (Sept. 1982). Translation of: *Probl. Prochn. (USSR)*, vol.14, no.9, p.72-80 (Sept. 1982).

The author obtains a general phenomenological equation permitting theoretical analysis of the general and particular behaviour of the end point of the stress/strain curve and determination of the role of any parameter of interest, including defect parameters, in the kinetics of changes in the end point. (27 refs.)

114077 Photoplastic effects in II-VI crystals. S.Takeuchi, K.Maeda, K.Nakagawa (Inst. for Solid State Phys., Univ. of Tokyo, Tokyo, Japan). Defects in Semiconductors II, Symposium Proceedings, Boston, MA, USA, Nov. 1982 (New York, USA: North-Holland 1983), p.461-75

A reversible change in the flow stress with the illumination of a band gap light (photoplastic effect: PPE) is observed commonly in II-VI semiconducting compounds both with the zincblende and the wurtzite structures. After reviewing the experimental results accumulated so far concerning the usually observed PPE, detailed microscopic experiments on CdTe (partly on CdS) single crystals are described. In-situ TEM straining experiments with a laser illumination system clarified that the dislocation mobility, evidently controlled by the Peierls mechanism, is not affected by light illumination. The investigation of the dislocation glide behavior over a longer range using the etch pit method and the cathodoluminescence microscopy with a SEM revealed that the dislocations are apt to become immobilized after traveling a certain distance from the sources with a high velocity. The dislocation loops and cusps observed by TEM suggest that the immobilization is caused by jog formation along screw segments. (29 refs.)

Longitudinal shear of an anisotropic body with a sharp-ended anisotropic inclusion See Entry 113358

Contour J-integral in the plastic region See Entry 113362

Plastic bands at the tip of a linear rigid inclusion See Entry 113363

Examination of the stress state of a helically reinforced composite in shearing See Entry 113364

Small-angle X-ray scattering study of density fluctuation in pressure-densified polystyrene glasses See Entry 113767

Structure formation in lightly-doped chromium alloys during plastic deformation in the 1400-1450K region See Entry 113802

Ammonium trifluoroberyllate(II), $(\text{NH}_4)[\text{BeF}_3]$, at room temperature See Entry 113815

Dislocation structure of large-domain ordered Ni_3V alloy See Entry 113925

Influence of mechanical stresses on the accumulation of radiation defects in Nb and NbTi See Entry 114040

Direct evidence for stress-enhanced swelling in type 316 stainless steel See Entry 114041

Flow behaviour of nickel irradiated with 15 MeV neutrons and 16 MeV protons See Entry 114049

Creep of weakly strained LiF crystals in the temperature range 1.6-300K See Entry 114078

Parameters of mechanical twins emitted by a crack See Entry 114080

A method of creep damage summation based on accumulated strain for the assessment of creep-fatigue endurance See Entry 114081

The breaking of polycrystalline ice See Entry 114086

Deformation and fracture of a material in plane stress under complex loading See Entry 114088

Phase transitions in $\text{Pb}_3(\text{P}_{1-x}\text{As}_x\text{O}_4)_2$: influence of the central peak and flip mode on the Raman scattering of hard modes See Entry 114159

Proton dynamics at the ferroelastic phase transition in $\text{KH}_2(\text{SeO}_3)_2$ See Entry 114163

Statistical model of the phase transition in $\text{KH}_2(\text{SeO}_3)_2$ See Entry 114169

Isothermal recovery of electrical resistivity in aluminum immediately after deformation See Entry 114511

Curie-Weiss law for improper ferroelectric or ferroelastic phase transitions See Entry 114794

Stress relaxation in ferroelectric materials See Entry 114799

Polymer deformation studies by time resolved Fourier transform infrared spectroscopy See Entry 114862

Nature of the luminescence lines of heavily doped *p*-type gallium arsenide under uniaxial deformation See Entry 114923

Cold sintering under high pressure—mechanisms and application See Entry 115127

Densification and change in shape of porous materials during hot pressing under conditions of nonuniform triaxial compression See Entry 115128

Liquid phase sintering of tungsten [and optimum mechanical properties] See Entry 115134

Structure and mechanical and corrosion properties of P/M Kh23N18 stainless steel See Entry 115140

Preparation of superconducting lead-alloy long filaments by glass-coated melt spinning See Entry 115143

Mechanism of formation of martensite single crystals as a result of plastic deformation of the alloys based on γ -Mn See Entry 115191

Structural and phase transition of γ' martensite in binary Cu-Al alloy during deformation See Entry 115192

Influence of the quenching temperature on the onset of the α - γ transition and mechanical properties of maraging steel See Entry 115193

Shape memory effect in martensitic transformations in TiNi-TiCu alloys See Entry 115194

Precipitation processes in a β -phase Cu-15 at.% Sn shape memory alloy See Entry 115202

Investigation of the influence of thermomechanical treatment on the hardening of AlMgSiCu alloys See Entry 115208

Substructure hardening of polycrystalline niobium See Entry 115209

Effect of strain rate on the resistance of metals to plastic deformation See Entry 115213

Recovery behavior of hydrogen charged 7075-T6 aluminum See Entry 115215

The mechanical properties and structure of Ti-Al-Zr-Mo alloys See Entry 115227

Thermal stresses and viscoelastic relaxation in metallic glasses prepared by liquid quenching See Entry 115232

Local acoustoelasticity in poly(methyl methacrylate) by Brillouin scattering See Entry 115235

Process of α -relaxation in dense network epoxide polymers obtained under deformation conditions See Entry 115252

On the mixture rule for strength of fibre reinforced cements See Entry 115255

The effect of fast neutron irradiation on the compressive stress-strain relationships of graphite See Entry 115256

Influence of substructure on the mechanical properties of austenitic alloys deformed by warm rolling See Entry 115257

Finite plastic strain in annealed mild steel during proportional and non-proportional loading See Entry 115258

Elongation minimum and strain rate sensitivity minimum of zircaloy-4 See Entry 115259

Plastic deformation of spherical steel shells under internal blast loading See Entry 115260

Study of molecular deformation mechanisms in the glassy state. I. Temperature effect on stress-birefringence and strain-birefringence responses of poly(methyl methacrylate) See Entry 115261

Rheo-optical studies on the deformation mechanism of semicrystalline polymers. XIV. Alpha and beta mechanical dispersions of spherulitic high-density polyethylene and the dynamic orientation distribution function of crystallites See Entry 115262

Properties of two high strength, high temperature, high conductivity copper-base alloys See Entry 115264

Large strain plastic deformation of commercially pure nickel See Entry 115267

Luder's strain and ductility of ordered Fe-Co-2V and Fe-Co-V-Ni See Entry 115268

Effects of V and Nb additions on high temperature deformation properties of low alloy martensites See Entry 115269

Role of molybdenum in sintered steels [tensile properties] See Entry 115270

Work hardening and the stability of deformation in AlZnMg alloys See Entry 115271

The plastic compression of copper cones See Entry 115272

Deformation properties of refractory glass-fiber goods based on mullite-silicate fiber See Entry 115273

Rheological properties of ShKh15 steel under multistage loading See Entry 115274

Influence of silicon on the structure and properties of alloyed compound Ni_3Al See Entry 115275

Influence of impurity atoms on the mechanical properties of group Va metals and alloys based on them See Entry 115277

Creep of hardened steel in tempering See Entry 115278

Variational functional for a rigid-plastic porous material See Entry 115279

Effect of small amounts of tungsten carbide on the strength, creep, and brittle-to-ductile transition temperature of zirconium carbide See Entry 115280

Experimental investigation of laws governing the hardening of initially anisotropic materials See Entry 115281

Experimental study of the effect of scale and shape of a body on deformation and failure mechanisms of structurally inhomogeneous materials See Entry 115282

Influence of alloying on the strength of vanadium See Entry 115285

Experimental examination of the strength of a glass-fiber plastic with longitudinal-transverse reinforcement in the plane stress state See Entry 115286

Strength of porous net materials in the uniaxial strain state See Entry 115287

Model plastic-rubber composites from emulsion polymers See Entry 115288

On the correlation of mechanical properties of high impact polystyrene with its morphology, molecular-weight characteristics and extrusion conditions See Entry 115289

Correlation of morphology, mechanical properties and processing conditions of modified high impact polystyrene See Entry 115290

RIM systems from interpenetrating polymer networks See Entry 115291

A stress transfer model for the deformation and failure of polymeric matrices under swelling conditions See Entry 115292

Effect of fiber aspect ratio on ultimate properties of short-fiber composites See Entry 115293

Dimensional stability of reinforced matrices See Entry 115294

In situ analysis of the interface See Entry 115295

Internal stresses in fibre reinforced plastics See Entry 115296

Stress and strength analysis in and around composite inclusions in polymer matrices See Entry 115297

The mechanical properties and failure modes in reinforced polypropylene See Entry 115298

Embrittlement of construction steel with bainite structure during tempering See Entry 115308

The relationship between the physical structure and the microscopic deformation and failure processes of poly(*p*-phenylene terephthalamide) fibers See Entry 115318

Prediction of stress relaxation and stress relief cracking in SEN testpieces See Entry 115327

Influence of slow strain rate tensile deformation on creep-fatigue endurance of 20Cr-25Ni-Nb stainless steel at 593°C See Entry 115328

Failure of rubber-modified plastic liners See Entry 115331

Embrittlement of chrome-nickel-molybdenum steel after the high-temperature action of hydrogen See Entry 115335

Low-cycle deformation and failure of die steels at service temperatures See Entry 115338

Microstructure and mechanical strength of aluminum titanate ceramics prepared from synthesized powders See Entry 115353

Rubber modified matrices See Entry 115360

Characterization of high performance composite matrices See Entry 115361

Volume changes and the technical properties of composites in the spinel-manganese oxide system See Entry 115392

A study of the thermo-oxidative process and stability of graphite and glass/PMF polyimide composites See Entry 115394

Environmental aging of epoxy composites See Entry 115395

Effect of surface stresses on ductility and fatigue strength of wear resisting coatings See Entry 115396

Inhomogeneous plastic deformation and its relevance to iodine stress corrosion cracking susceptibility in irradiated Zircaloy-2 tubing See Entry 115418

Plotting stress-strain diagrams by recalculation of the computer diagram See Entry 115477

62.20H Creep

(see also 81.40L Deformation, plasticity and creep)

114078 Creep of weakly strained LiF crystals in the temperature range 1.6-300K. H.-J.Kaufmann, S.V.Lubenets, V.V.Abraimov (Physicotech. Inst. for Low Temperatures, Acad. of Sci., Kharkov, Ukrainian SSR). *Sov. Phys.-Solid State (USA)*, vol.25, no.2, p.181-4 (Feb. 1983). Translation of: *Fiz. Tverd. Tela (USSR)*, vol.25, no.2, p.321 (Feb. 1983). [received: Sept. 1983]

At the initial stage of plastic deformation the creep of LiF crystals was shown to be described by the logarithmic relation $y = a \ln(vt + 1)$. The coefficient *a* decreases with decreasing temperature in the neighbourhood of 300K and for $T < 10\text{K}$, but remains practically constant over the wide range from 150 to 10K. An analysis of the temperature dependence of the flow stress $\tau_0(T)$ and the activation volume $V(T)$ suggests that the creep is due to thermal activation determined by the interaction of dislocation with local lattice defects. At liquid-helium temperatures, the Peierls barriers may have an effect on the mobility of dislocations. The distinctive features of the dependences $\tau_0(T)$ and $V(T)$ in the range 100-200K can be related to the formation of an ordered atmosphere of impurity defects in the elastic field of mobile dislocations (induced Snoek effect). No influence of quantum properties of the dislocation on the creep of LiF crystals was observed. (33 refs.)

CANSWEL-2: A computer model of the creep deformation of Zircaloy cladding under loss-of-coolant accident conditions. Part II. User notes See Entry 112306

Phase transitions, creep, and fission gas behaviour in actinide oxides See Entry 112329

Constitutive equations for the creep behaviour of nickel-base alloys for HTR components in the temperature range 1023 - 1273 K See Entry 112341

Theoretical relationships between creep and swelling by point defect absorption during irradiation See Entry 113994

A method of creep damage summation based on accumulated strain for the assessment of creep-fatigue endurance See Entry 114081

Investigation of material damage under creep and creep strength See Entry 114082

Surface tension of some rare-earth metals in the solid state See Entry 114328

Effect of strain rate on the resistance of metals to plastic deformation See Entry 115213

Influence of stress cycling on creep behaviour of an Al-Mg alloys under strain ageing conditions See Entry 115253

Steady state and transient creep of Al at 400K—an analysis in terms of recovery controlled by thermally activated glide See Entry 115254

Coble and Harper-Dorn creep in iron at homologous temperatures T/T_m of 0.40-0.54 See Entry 115263

Work-hardening rates during the high temperature creep of aluminium determined from the instantaneous strain on sudden stress changes See Entry 115265

Role of eutectoid transformation and grain size on the creep behaviour of mild steel See Entry 115266

Effects of stabilization on the elastic to visco-plastic transition in metallic glasses See Entry 115276

Creep of hardened steel in tempering See Entry 115278

Temperature-time dependence of the cyclic-creep activation energy of heat-resistant alloys See Entry 115283

Study of the high-temperature creep of multilaminate iron/copper and nickel/copper condensates See Entry 115284

Prediction of stress relaxation and stress relief cracking in SEN testpieces See Entry 115327

Influence of slow strain rate tensile deformation on creep-fatigue endurance of 20Cr-25Ni-Nb stainless steel at 593°C See Entry 115328

Shape effect of particles on high-temperature hardness of dispersion-hardened Ni-SiO₂ alloys See Entry 115352

Creep and fracture initiation in fibre reinforced plastics See Entry 115363

Predicting the long-term creep of organic-fiber-reinforced plastics See Entry 115472

Relationship between parameters of elastic-wave propagation and rupture-strength characteristics of structural materials See Entry 115473

62.20M Fatigue, brittleness, fracture, and cracks

(inc. hardness; see also 81.40N Fatigue, embrittlement and fracture)

114079 Microhardness of rhombohedral crystals: Calcite and sodium nitrate. J.R.Pandya, L.J.Bhagia, A.J.Shah (Dept. of Appl. Phys., M.S. Univ. of Baroda, Baroda, India). *Bull. Mater. Sci. (India)*, vol.5, no.1, p.79-82 (March 1983). [received: Sept. 1983]

The variation of hardness of rhombohedral single crystals of calcite and sodium nitrate with quenching temperature is studied. Vickers and Knoop hardness numbers are determined from the indentations produced on freshly-cleaved crystal surfaces for various loads. The variation of hardness number with quenching temperature can be represented by $HT_k^k = \text{constant}$ where the exponent k is less than unity and its sign determines the nature of material. (6 refs.)

114080 Parameters of mechanical twins emitted by a crack. A.P.Korolev, V.A.Fedorov (Inst. of Chem. Machine Construction, Tambov, USSR). *Fiz. Met. & Metalloved. (USSR)*, vol.56, no.2, p.390-2 (Aug. 1983). In Russian. English translation in: *Phys. Met. & Metallogr. (GB)* Coarse-grained samples of Fe+3.25% Si were subjected to dynamic stretching along the [001] axis at temperatures in the range 77-273K. The density and dimensions of twins emitted by rapidly travelling cracks were determined after fracture for regions where the crack velocity was known. Changes in the test conditions, such as a preliminary deformation by slip, increased considerably the frequency of appearance of twins which accompanied the dynamic propagation of cracks. Such active control of the parameters of the concomitant twins altered considerably the mechanism and kinetics of fracture. (6 refs.) A.T.

114081 A method of creep damage summation based on accumulated strain for the assessment of creep-fatigue endurance. R.Hales (Berkeley Nuclear Labs., CEBG, Berkeley, England). *Fatigue Eng. Mater. & Struct. (GB)*, vol.6, no.2, p.121-35 (1983). A method of combining long term creep data with relatively short term mechanical behaviour to provide an estimate of creep-fatigue endurance is presented. It is proposed that the creep-fatigue effect in high temperature cyclic deformation is governed by a difference in strain rate around the cycle and the associated variation in ductility with strain rate. (21 refs.)

114082 Investigation of material damage under creep and creep strength. A.M.Lokoshchenko. *J. Appl. Mech. & Tech. Phys. (USA)*, vol.23, no.6, p.855-9 (Nov.-Dec. 1982). Translation of: *Zh. Prikl. Mekh. & Tekh. Fiz. (USSR)*, vol.23, no.6, p.129-33 (Nov.-Dec. 1982). [received: Sept. 1983] The author presents results of an experimental investigation of $\omega(t)$, the measure of material damage in creep. The rupture time $t=t^*$ is the time at which the damage reaches unit [$\omega^*=\omega(t^*)=1$]. It is shown that $\omega^*<1$, where the dependence of ω^* on stress is monotonically decreasing in nature; an analytic description of this effect is obtained. The specimens were various Cu rods. (4 refs.)

114083 Conditions for cavity growth during slow-fast fatigue. W.Beere (Berkeley Nuclear Labs., CEBG, Berkeley, England). *Met. Sci. (GB)*, vol.17, no.4, p.187-91 (April 1983). [received: Sept. 1983] The growth rates of grain boundary cavities during slow-fast fatigue are calculated by assessing the rates of four growth mechanisms. It is shown that cavity growth can take place providing the strain rate during tension is below a critical value. Also at sufficiently low strain rates cavities can grow to a large size before the life of a fast-fast test is achieved. The author suggests that a better understanding of cavity nucleation is desirable. (14 refs.)

114084 The transition from an emitting to a cleaving crack. I.-H.Lin (Fracture & Deformation Div., NBS, Boulder, CO, USA), R.Thomson. *Scr. Metall. (USA)*, vol.17, no.8, p.1031-4 (Aug. 1983). Proposes two mechanisms by which a crack, able to produce dislocations either from its own tip or from external sources, with increasing external stress intensity will undergo a transition to cleavage after a critical dislocation shielding charge has built up. (3 refs.)

114085 Dislocation emission from cracks in the presence of liquids. I.-H.Lin (Fracture & Deformation Div., NBS, Boulder, CO, USA), R.Thomson. *Scr. Metall. (USA)*, vol.17, no.8, p.1035-7 (Aug. 1983). Presents a mechanism by which a wetting liquid can modify the emission criterion at the tip, and discusses the requirements for embrittlement. There are three general prototype models for mode I fracture: (1) cleavage in which bonds are pulled apart in tension by the stress concentration at the tip; (2) crack growth by dislocation slide-off at the crack-tip; (3) fully ductile crack growth by hole nucleation ahead of the crack. It is shown that possibilities exist for mechanism transitions from type 3 to type 1 and from type 3 to type 2 when liquid metal is introduced. (10 refs.)

114086 The breaking of polycrystalline ice. V.P.Epifanov (Inst. of Problems in Mech., Acad. of Sci., Moscow, USSR).

Sov. Phys.-Dokl. (USA), vol.27, no.12, p.1063-5 (Dec. 1982). Translation of: *Dokl. Akad. Nauk SSSR*, vol.267, no.4-6, p.1364-7 (Dec. 1982). [received: Sept. 1983]

The breaking of ice during uniaxial compression was investigated by means of a procedure for the comprehensive determination of the mechanical characteristics of a deformable material. The longitudinal and transverse deformations, and the amplitude and time of the passage of an elastic disturbance through the specimen, were measured synchronously, and the amplitudes and spectra of acoustic-emission signals, the load, and the temperature were recorded. The frequency of transmission of the sounding pulse was varied from 0.6 MHz to 6 MHz. The attenuation coefficient α and the propagation speed v of an acoustic disturbance were determined by the pulse-phase method. (8 refs.)

114087 Evaluating the durability of materials on the basis of thermal fluctuation theory. E.S.Pereverzev (Inst. of Engng. Mech., Acad. of Sci., Dnepropetrovsk, USSR).

Strength Mater. (USA), vol.14, no.11, p.1477-82 (Nov. 1982). Translation of: *Probl. Prochn. (USSR)*, vol.14, no.11, p.48-51 (Nov. 1982). [received: Sept. 1983]

The kinetics of brittle fracture of a specimen are examined for the case when thermal fluctuation processes caused by the oscillatory motion of atoms play the deciding role in the fracture process. In the case of fracture, the rupture and restoration of interatomic bonds represent a thermal fluctuation process. Only the rupture of interatomic bonds is examined. (13 refs.)

114088 Deformation and fracture of a material in plane stress under complex loading. N.S.Mozharovskii, K.N.Rudakov, A.A.Zakhovai (Kiev Polytech. Inst., Kiev, Ukrainian SSR).

Sov. Appl. Mech. (USA), vol.18, no.12, p.1092-6 (Dec. 1982). Translation of: *Prikl. Mekh. (USSR)*, vol.18, no.12, p.54-8 (Dec. 1982). [received: Sept. 1983]

Cyclic loading according to complex paths may lower the load-carrying capacity of materials compared to simple (proportional) loading. In particular, in the cyclic loading of tubular specimens of steel there was an intensification of creep and fracture. The authors present the basic results of studies undertaken to explain the reasons for this intensification. In connection with the fact that the unloading is elastic, the authors compared results obtained with active loading. It was assumed that the effects of complex loading are the reasons for the intensification of creep and fracture, and that the effect of complex loading on strain and load-carrying capacity should also be manifest in one-time loading. (9 refs.)

Polymer Alloys III Blends, Blocks, Grafts and Interpenetrating Networks. Proceedings of a Symposium See Entry 111311

Volume, surface and interface fracture statistics of brittle materials under flexure See Entry 113349

A crack-tip-zone interaction model for creep-fatigue crack growth See Entry 113354

Longitudinal shear of an anisotropic body with a sharp-ended anisotropic inclusion See Entry 113358

Fracture criteria under creep conditions See Entry 113359

Fracture toughness of high-strength layered plates containing plastic interlayers with a high elastic modulus See Entry 113361

Contour J-integral in the plastic region See Entry 113362

Plastic bands at the tip of a linear rigid inclusion See Entry 113363

Examination of the stress state of a helically reinforced composite in shearing See Entry 113364

Energy criteria for the brittle fracture of composite materials with initial stresses See Entry 113367

Definition of interphase in composites See Entry 113372

Influence of thickness and temperature on stretched zone size in J_{IC} tests See Entry 113388

Surface modification by ion implantation—effects on fatigue See Entry 113908

Doping of indium phosphide with germanium See Entry 113938

Measurements of ion-implantation damage in GaP See Entry 113943

Tracer diffusion of P in iron and iron alloys See Entry 114271

Band-state interpretation of lattice thermal conductivity and microhardness of ternary chalcopyrite semiconductors See Entry 114293

Liquid phase sintering of tungsten [and optimum mechanical properties] See Entry 115134

Directionally solidified structure and mechanical properties in monovariant Al-Fe-Ni eutectic alloy See Entry 115183

The use of microscopic and hardness measurement methods in recrystallization studies See Entry 115211

Recovery behavior of hydrogen charged 7075-T6 aluminum .. See Entry 115215

Electron microscopic studies on the effect of Sn addition on the ageing characteristics of Al-0.7% Mg₂Si alloy See Entry 115217

The effect of hydrogen on reversible and irreversible softening of spheroidized steel See Entry 115223

Possibility of predicting hardening cracks See Entry 115229

Fatigue and recovery processes in a multilayer iron-copper composite material See Entry 115243

Analysis of process stresses in two-layer SiC-Si disks See Entry 115246

Polymer-performance on the dimensional stability and the mechanical properties of wood-polymer composites prepared by an electron beam accelerator See Entry 115248

The effect of fast neutron irradiation on the compressive stress-strain relationships of graphite See Entry 115256

Elongation minimum and strain rate sensitivity minimum of zircaloy-4 See Entry 115259

Properties of two high strength, high temperature, high conductivity copper-base alloys See Entry 115264

Effects of V and Nb additions on high temperature deformation properties of low alloy martensites See Entry 115269

Work hardening and the stability of deformation in AlZnMg alloys See Entry 115271

Influence of silicon on the structure and properties of alloyed compound Ni₃Al See Entry 115275

- Effect of small amounts of tungsten carbide on the strength, creep, and brittle-to-ductile transition temperature of zirconium carbide See Entry 115280
- Experimental study of the effect of scale and shape of a body on deformation and failure mechanisms of structurally inhomogeneous materials See Entry 115282
- On the correlation of mechanical properties of high impact polystyrene with its morphology, molecular-weight characteristics and extrusion conditions See Entry 115289
- Correlation of morphology, mechanical properties and processing conditions of modified high impact polystyrene See Entry 115290
- RIM systems from interpenetrating polymer networks See Entry 115291
- A stress transfer model for the deformation and failure of polymeric matrices under swelling conditions See Entry 115292
- Stress and strength analysis in and around composite inclusions in polymer matrices See Entry 115297
- The mechanical properties and failure modes in reinforced polypropylene See Entry 115298
- Discrete spectrum for the strength of Capron fibres See Entry 115299
- Effect of texture and grain size on the fracture behaviour of hot rolled Mg, Mg-12.5% Li and Mg-5% Ti alloys See Entry 115300
- The surface microhardness of nickel alloys cut with a low speed diamond saw See Entry 115301
- Fracture, strength and fatigue of filled thermoset composites See Entry 115302
- Microstructure and thickness effects on fracture in a glass thermoplastic PET injection moulding compound See Entry 115303
- Environmental influences of fatigue damage in glass fibre reinforced polyester See Entry 115304
- Design for toughness in polymers. IV. The effect of geometry on stable crack propagation in thermoplastics for pressure pipe duties See Entry 115305
- Cavitation in high purity aluminium during fatigue at elevated temperatures See Entry 115306
- The impact endurance of polycrystalline graphite See Entry 115307
- Embrittlement of construction steel with bainite structure during tempering See Entry 115308
- Fatigue strength of a rotor steel subjected to torsional loading simulating that occurring due to circuit breaker reclosing in an electric power plant See Entry 115309
- Mixed-mode fracture mechanisms near the fatigue threshold of AISI 316 stainless steel See Entry 115310
- Fatigue crack propagation in a cast magnesium alloy See Entry 115311
- Frequency dependence of the high temperature fatigue properties of He-implanted stainless steel See Entry 115312
- On the modeling of the high-temperature embrittlement of metals containing helium See Entry 115313
- Fatigue and overload fracture of carburized steels See Entry 115314
- Rupture and viscosity of lead during spall See Entry 115315
- Effect of cold working and annealing on stress corrosion cracking of AISI 304 stainless steel See Entry 115316
- Study on the strengthening mechanism by diffusion of temper carbon into ferritic matrix See Entry 115317
- The relationship between the physical structure and the microscopic deformation and failure processes of poly(*p*-phenylene terephthalamide) fibers See Entry 115318
- The incipient characteristic tearing energy for an elastomer crosslinked under strain See Entry 115319
- Mixed-mode crack opening in fatigue See Entry 115320
- Fractographic aspects of cyclic cleavage See Entry 115321
- Studies for the interpretation of fatigue behaviour of prime quality chrome nickel stainless steels—presented on wires which for example may be used for orthodontic purposes See Entry 115322
- A note on the correlation between sulfide inclusion level and fracture toughness of a 12 weight % chromium steel See Entry 115323
- Interfacial segregation and embrittlement in liquid phase sintered tungsten alloys See Entry 115324
- Relationships between microstructure and mechanical properties of microduplex $\alpha+(\gamma+\epsilon)$ 6 and 9% Mn steels for cryogenic applications See Entry 115325
- Effect of molybdenum on temper brittleness and internal friction behaviour of medium carbon alloy steels See Entry 115326
- Prediction of stress relaxation and stress relief cracking in SEN testpieces See Entry 115327
- Influence of slow strain rate tensile deformation on creep-fatigue endurance of 20Cr-25Ni-Nb stainless steel at 593°C See Entry 115328
- Mechanical parameters used for the propagation of creep cracks See Entry 115329
- Effect of structure modifying additives on wear resistance and fatigue strength of polyamide 6 See Entry 115330
- Failure of rubber-modified plastic liners See Entry 115331
- Effect of bluing on fatigue strength of cold drawn steel wire See Entry 115333
- A phenomenological model of embrittlement of metals under conditions of the adsorption action of liquid metal media See Entry 115334
- Embrittlement of chrome-nickel-molybdenum steel after the high-temperature action of hydrogen See Entry 115335
- Crack propagation in titanium alloys in a hydrogen atmosphere under constant load See Entry 115336
- Influence of internal microstresses in martensite on near-threshold fatigue crack growth See Entry 115337
- Low-cycle deformation and failure of die steels at service temperatures See Entry 115338
- Influence of melting method on the crack resistance of 42KhMFA steel See Entry 115339
- Fatigue failure in the grain boundaries in lead and lead alloys See Entry 115340
- Delayed fracture of structural alloy E1607A in plane stress See Entry 115341
- Critical size for structural fragments of thermal-shock-resistant refractories See Entry 115342
- Subcritical crack growth in brittle materials in microcracking conditions See Entry 115343
- Fractographic features of failure of tungsten cermet in the temperature range 20-2000°C See Entry 115344
- Calculation of fatigue and life of crack-bearing structural elements under cyclic load See Entry 115345
- Fracture toughness of aluminium alloys of the system Al-Mg-Si for cyclic and static loads See Entry 115346
- Effect of loading-cycle asymmetry on the crack resistance of structural alloys See Entry 115347
- Evaluating the limiting states of a steel under combined low-cycle loading and diffusion of sorbed hydrogen See Entry 115348
- Intergranular brittle fracture resistance of 18Kh2N4VA steel after hardening See Entry 115349
- Fracture mechanics of syntactic foam composites See Entry 115350
- Intergranular fracture of a high purity iron due to oxygen See Entry 115351
- Shape effect of particles on high-temperature hardness of dispersion-hardened Ni-SiO₂ alloys See Entry 115352
- Microstructure and mechanical strength of aluminum titanate ceramics prepared from synthesized powders See Entry 115353
- Tensile strength of pressureless-sintered silicon nitride at elevated temperature See Entry 115354
- The K_{Ic} values of silicon nitride and zirconia obtained by micro-crack indentation method and single-edge notched beam method See Entry 115355
- Fractographic study of cracks produced by thermal shocks in 20MnMoNi55 and comparable weld material in water environment See Entry 115356
- High strength sheet steel of medium thickness See Entry 115357
- Resistenza a fatica di acciai ad alto limite di snervamento laminati a caldo (Fatigue resistance of high strength hot rolled steels) See Entry 115358
- Fracture toughness of poly(methyl methacrylate) blends See Entry 115359
- Rubber modified matrices See Entry 115360
- Characterization of high performance composite matrices See Entry 115361
- Fatigue crack propagation in short-glass-fiber-reinforced nylon 66: effect of frequency See Entry 115362
- Creep and fracture initiation in fibre reinforced plastics See Entry 115363
- Compression fatigue behaviour of notched composite laminates See Entry 115364
- Delamination in graphite-epoxy See Entry 115365
- Electron-microscopical investigations of the structure of the surface layers of titanium carbide after friction at 20-1400°C See Entry 115366
- Effects of hardness on the solid particle erosion mechanisms in AISI 1060 steel See Entry 115374
- The use of transmission electron microscopy to study the effects of abrasive wear on the matrix structure of a high chromium cast iron See Entry 115375
- The long term durability of stressed GRP in acidic environments See Entry 115377
- Effect of surface stresses on ductility and fatigue strength of wear resisting coatings See Entry 115396
- SiC-coatings as protective layers for carbon fibers and adhesion promoters for superconducting niobium carbonitride See Entry 115398
- Stress corrosion cracking of aged Al-5Zn-4Mg alloy in 3.5% NaCl solution See Entry 115419
- Problems of the life of constructional materials in nitrogen- and hydrogen-containing media See Entry 115434
- Local corrosion of martensitic stainless steel in a medium containing chloride ions and hydrogen sulfide See Entry 115435
- Some problems of investigation of the cyclic crack resistance of materials in liquid media See Entry 115436
- An analytical method of evaluating angles in Brookes' formula for effective resolved shear stress on slip systems in crystals See Entry 115453
- Decomposition of austenitic phase in work hardened steel samples, using hardness measurements See Entry 115464
- Results of an investigation of the service life of heat-resistant materials under repeated static load See Entry 115469
- Representation of fatigue damage to a component in terms of reliability theory See Entry 115470
- Effect of step duration on the evaluation of the fatigue limit of welded steel structures See Entry 115471
- Relationship between parameters of elastic-wave propagation and rupture-strength characteristics of structural materials See Entry 115473
- Effect of stored elastic energy on breaking stress See Entry 115476
- The measure of fracture toughness of cemented carbide by means of CVD coated layers See Entry 115506

62.20P Tribology

(see also 81.40P Friction, lubrication and wear)

- Metallurgical surfaces produced by ion implantation See Entry 113940
- CVD of TiN at the tempering temperature of alloy-steels See Entry 115097
- Formation of thin refractory coatings, their properties and fields of application See Entry 115098
- Modern trends in creating sintered antifriction materials See Entry 115137
- Vibration-resistant composites intended for damping devices See Entry 115158
- Effect of structure modifying additives on wear resistance and fatigue strength of polyamide 6 See Entry 115330
- Electron-microscopical investigations of the structure of the surface layers of titanium carbide after friction at 20-1400°C See Entry 115366
- Dry wear studies on glass-fibre-reinforced epoxy composites See Entry 115367
- The effects of erodent composition and shape on the erosion of steel See Entry 115368
- Comparison of the wear resistance of various grades of cemented carbides that may find application in wood machining See Entry 115369

Friction and wear properties of nitrided and N⁺-implanted 17-4 PH stainless steelSee Entry 115370

The effect of surface hardness of carbon steels on scuffing resistance in rolling-sliding contactSee Entry 115371

Mechanical and electromechanical behaviour of fibre brushesSee Entry 115372

Some aspects of improving abrasive resistanceSee Entry 115373

Effects of hardness on the solid particle erosion mechanisms in AISI 1060 steelSee Entry 115374

The use of transmission electron microscopy to study the effects of abrasive wear on the matrix structure of a high chromium cast iron ...See Entry 115375

A study of friction and wear resistance of two-layer TiN+Mo vacuum-plasma coatingsSee Entry 115401

Effecting the corrosion relationship of corroding element-cladding material of ZrNb1 by mechanical surface treatmentSee Entry 115416

Role of CVD in providing wear resistant filmsSee Entry 115450

62.30 MECHANICAL AND ELASTIC WAVES
(see also 03.40K Mathematical aspects)

114089 Analysis of the elasticoelectric effect. V.A.Shkitin, N.V.Pereloma, L.E.Chirkov (Inst. of Steel & Alloys, Moscow, USSR). *Sov. Phys.-Crystallogr. (USA)*, vol.28, no.1, p.5-7 (Jan.-Feb. 1983). Translation of: *Kristallografiya (USSR)*, vol.28, no.1, p.14-17 (Jan.-Feb. 1983). [received: Sept. 1983]

General equations are derived representing the variation of the elastic-wave displacement and phase-velocity vectors in the case of the elasticoelectric effect in an anisotropic medium of arbitrary symmetry. Conditions formulated and expressions derived for determining the directions of maximum change of the elastic-wave phase velocities in the case of arbitrary orientation of the wave normal and electric field, and also of the transverse elasticoelectric effect. (7 refs.)

114090 Leaky elastic waves in hexagonal crystals. V.I.Al'shits, V.N.Lyubimov (Inst. of Crystallography, Acad. of Sci., USSR). *Sov. Phys.-Crystallogr. (USA)*, vol.28, no.2, p.130-5 (March-April 1983). Translation of: *Kristallografiya (USSR)*, vol.28, no.2, p.224-33 (March-April 1983). [received: Sept. 1983]

The authors investigate types of leaky elastic waves arising in the vicinity of a transversely isotropic direction in a semiinfinite hexagonal crystal with a surface parallel to the hexad symmetry axis. They show that in addition to the known class of leaky pseudosurface waves, which pass over to the usual Rayleigh surface wave for a transversely isotropic direction, there are two new types of leaky waves, which for symmetrical orientation correspond to Brewster reflections and to the transverse body wave. The authors indicate the ranges of values of the elastic constants of the crystal for which leaky waves of various types arise. (14 refs.)

114091 Method of obtaining dispersion equation for normal and surface waves in layered anisotropic systems. V.V.Filippov (Inst. of Phys., Acad. of Sci., Belorussian SSR). *Sov. Phys.-Crystallogr. (USA)*, vol.28, no.2, p.136-9 (March-April 1983). Translation of: *Kristallografiya (USSR)*, vol.28, no.2, p.234-9 (March-April 1983). [received: Sept. 1983]

Dispersion equations for normal and surface waves in plane-layer systems are obtained from the condition that the reflection coefficient of the system becomes infinite. General dispersion equations are derived for the cases in which the surface or normal waves are bipartial or tripartial. For systems containing intensifying layers, the conditions for the existence of surface or normal waves coincide with the condition of self-excitation of such a system. (8 refs.)

Elastic media with microstructure II. Three-dimensional modelsSee Entry 111318

Love type waves in a porous layer with irregular interfaceSee Entry 113339

Relationship between parameters of elastic-wave propagation and rupture-strength characteristics of structural materialsSee Entry 115473

62.40 ANELASTICITY, INTERNAL FRICTION, AND DAMPING
(see also 81.40J Elasticity and anelasticity)

114092 Zener relaxation in copper-indium-aluminium alloys. I.M.Sharshakov, V.V.Putilin (Polytech. Inst., Voronezh, USSR). *Fiz. Met. & Metalloved. (USSR)*, vol.56, no.2, p.406-8 (Aug. 1983). In Russian. English translation in: *Phys. Met. & Metallogr. (GB)*

The internal friction was determined for alloys with the same amounts of indium and aluminium (from 10 to 20 at.%) but different amounts of copper (from 80 to 60 at.%). The dependence of the amplitude of the Zener internal friction peak on the copper concentration indicated that the relaxation process was dominated by copper-aluminium pairs of atoms. (6 refs.) A.T.

Device for measuring the loss factor of insulating materials .See Entry 113389

Configurations of point defects in neutron-irradiated ironSee Entry 113878

Influence of vacancies and interstitials on the Bordoni peaks in copper and silverSee Entry 113899

Influence of temperature on the mobility of dislocations in iron and martensite during internal friction measurementsSee Entry 113924

Dislocation structure and amplitude-dependent internal friction of LiF crystalsSee Entry 113926

Interaction of vacancies and self-interstitials with interstitial solute atoms in α -ironSee Entry 113966

Creep of weakly strained LiF crystals in the temperature range 1.6-300KSee Entry 114078

Solubility of carbon and ageing of Kh15Yu5 type alloysSee Entry 114175

Internal friction study on diffusivity on the Cu-SiO₂ interfaceSee Entry 114286

Magnetomechanical damping of nickelSee Entry 114720

Internal friction study on structural relaxation of a glassy metal Fe₃₂Ni₃₆Cr₁₄P₁₂B₆See Entry 115241

Fatigue and recovery processes in a multilayer iron-copper composite materialSee Entry 115243

Effect of static tensile stresses on the dissipative properties of copper-aluminum-zinc alloysSee Entry 115244

Viscoelastic properties of particulate reinforced matricesSee Entry 115249

Study of molecular deformation mechanisms in the glassy state. I. Temperature effect on stress-birefringence and strain-birefringence responses of poly(methyl methacrylate)See Entry 115261

Effect of molybdenum on temper brittleness and internal friction behaviour of medium carbon alloy steelsSee Entry 115326

62.50 HIGH-PRESSURE AND SHOCK-WAVE EFFECTS IN SOLIDS

114093 Shock compression of zirconia ZrO₂ and zircon ZrSiO₄ in the pressure range up to 150 GPa. T.Mashimo (Faculty of Engng., Kumamoto Univ., Kumamoto, Japan), K.Nagayama, A.Sawaoka. *Phys. & Chem. Miner. (Germany)*, vol.9, no.6, p.237-47 (1983).

The shock compression state of zirconia ZrO₂ and zircon ZrSiO₄ in the pressure range up to 150 GPa (1.5 Mbar) are studied on the basis of the measurements of shock velocities, particle-velocity histories, free surface motions, and electrical conductivities. Zircon transforms, and zirconia probably does, to high pressure phases up to 90 GPa. The shock velocity (U_s)-particle velocity (U_p) Hugoniot can be described as $U_s=4.38+1.37 U_p$ km/s above 90 GPa for ZrO₂, and $U_s=6.50+0.49 U_p$ km/s (mixed phase region), and $U_s=1.54+2.30 U_p$ km/s (high pressure phase region) for ZrSiO₄. The corrected isothermal densities of the high pressure phase ZrSiO₄ are roughly consistent with the isothermal ones of mixtures of ZrO₂ and SiO₂. Bulk sound velocities in the high-pressure phase region of these oxides are discussed in comparison with other oxides. Electrical conductivities of these oxides increase from lower than 10⁻¹² S/m to greater than 10⁰ S/m in the shock-stress range up to 70 GPa, and remain as constant values up to higher than 100 GPa. (57 refs.)

114094 Shock effects in MgAl₂O₄-spinel. H.Schafer (Inst. fur Mineralogie, Tech. Hochschule Darmstadt, Darmstadt, Germany), W.F.Muller, U.Hornemann. *Phys. & Chem. Miner. (Germany)*, vol.9, no.6, p.248-52 (1983).

Shock recovery experiments on synthetic MgAl₂O₄-spinel samples in the pressure range 25.5 to 50.5 GPa have been performed in order to examine the effects of shock waves on this material. The shocked samples were subsequently studied in the transmission electron microscope. All samples showed shock-induced dislocations with the Burgers vector 1/2 {110} and twin lamellae of the twin-law {111}. In addition, samples, which had experienced the higher pressures, showed lamellar areas of a crystalline phase that the authors have not yet been able fully to characterize. It is probably not ϵ -MgAl₂O₄. (27 refs.)

Structure of N₂ at 2.94 GPa and 300KSee Entry 113800

Room-temperature structure of carbon monoxide at 2.7 and 3.6 GPaSee Entry 113809

Pressure-induced phase transition of HgSSee Entry 114157

How electric strength of polyethylene and polystyrene is influenced by residual phenomena caused by ionising radiation and pressureSee Entry 114781

Influence of uniaxial pressure on the impurity photoluminescence band of GaAs:Cu with a maximum near 1.02 eVSee Entry 114920

Plastic deformation of spherical steel shells under internal blast loadingSee Entry 115260

Rupture and viscosity of lead during spallSee Entry 115315

Dynamic compression of diopside and salite to 200 GPaSee Entry 116080

Influence of the type of thermodynamic approximation on the description of the dynamic compressibility of multicomponent mediaSee Entry 116082

62.60 ACOUSTIC PROPERTIES OF LIQUIDS

(see also 62.80 Ultrasonic relaxation; for sound propagation, see 43.; for second sound in quantum fluids, see 67.40, 67.50 and 67.60)

Calculated reflection and transmission of a plane wave at the interface between two liquids with viscosity and thermal conductivitySee Entry 113173

Ultrasonic and hypersonic investigations of structural relaxation in aqueous solutions of hexamethylphosphortriamideSee Entry 114097

62.65 ACOUSTIC PROPERTIES OF SOLIDS

(see also 62.80 Ultrasonic relaxation; for sound propagation, see 43.; for lattice dynamics and phonons, see 63.; for magnetoacoustic effects, see 72.55; for acoustoelectric effects, see 72.50; for acousto-optical effects, see 78.20H)

114095 Acoustic properties of cadmium pyroniobate single crystal. N.K.Yushin, A.N.Nasyrov, F.M.Salaev, E.S.Sher (A.F. Ioffe Physicotech. Inst., Acad. of Sci., Leningrad, USSR). *Sov. Phys.-Solid State (USA)*, vol.25, no.2, p.326-7 (Feb. 1983). Translation of: *Fiz. Tverd. Tela (USSR)*, vol.25, no.2, p.575-7 (Feb. 1983). [received: Sept. 1983]

The authors investigate the acoustic properties of a cadmium pyroniobate single crystal. Single crystals of Cd₂Nb₂O₇ were grown by the method of a solution in a melt. The geometry of the specimen allowed measurements to be made only for elastic waves propagating along the [110] direction (in the axes of the cubic phase at 300K). Elastic waves were excited by a lithium niobate piezoelectric transducer. The velocity of propagation V of the elastic waves was measured at a frequency of 30 MHz by the pulse interference method. (19 refs.)

114096 Acoustic characteristics of porous bronze. S.V.Belov, A.S.Terekhin, S.K.Balantsev, P.A.Vityaz', V.M.Kaptevich, V.K.Shelyag (N.E. Bauman Moscow High Tech. Coll., Moscow, USSR). *Sov. Powder Metall. & Met. Ceram. (USA)*, vol.22, no.1, p.20-3 (Jan. 1983). Translation of: *Poroshk. Metall. (USSR)*, vol.22, no.1, p.22-5 (Jan. 1983). [received: Aug. 1983]

It is shown that sound absorption by porous bronze is influenced by the specimen thickness and pore size and also by the size of the gap between the specimen and a rigid bottom. The highest values of coefficient of sound absorption α (0.9-0.95) in a wide sound frequency range were attained with 8- to 10-mm-thick specimens having pores of 100- to 200- μ m size. By varying the size of the gap between the specimen and a rigid bottom it is possible to vary the position of the sound absorption coefficient maximum on the frequency scale without affecting its absolute value. There was good agreement between values of specific resistance to blowing through obtained as a result

of acoustic and hydraulic tests. It is therefore possible to predict the acoustic properties of porous metals from data yielded by hydraulic tests and vice versa. (3 refs.)

- Self-induced acoustic transparency of dilute paramagnetic crystals** See Entry 113181
- Shear elastic constant softening in $(V_{1-x}Cr_x)_2O_3$: second-order nature of the low temperature phase transition** See Entry 114070
- The breaking of polycrystalline ice** See Entry 114086
- Thermodynamic and kinetic properties of amorphous dielectrics at low temperatures** See Entry 114295
- Resonant amplification of sound near the spontaneous oscillation threshold of semiconductors under impurity and interband breakdown conditions** See Entry 114571
- Effects of ultrasonic waves on crystal growth** See Entry 115036
- Local acoustoelasticity in poly(methyl methacrylate) by Brillouin scattering** See Entry 115235
- Relationship between parameters of elastic-wave propagation and rupture-strength characteristics of structural materials** See Entry 115473

62.80 ULTRASONIC RELAXATION

(see also 74.30G Ultrasonic attenuation in superconductors, 43.35 Ultrasonics)

114097 Ultrasonic and hypersonic investigations of structural relaxation in aqueous solutions of hexamethylphosphortriamide. P.Miecznik (Mickiewicz Univ., Poznan, Poland). *Arch. Acoust. (Poland)*, vol.8, no.1, p.55-68 (1983). Measurements of the absorption coefficient of ultrasonic waves in the frequency range 10-100 MHz and of the propagation velocity of ultra- and hypersonic waves in aqueous solutions of hexamethylphosphortriamide (HMPT) were carried out. In addition the density of the solutions and the coefficient of shear viscosity was measured. On the basis of the quantities measured, the coefficient of bulk viscosity, relaxation parameters of the process observed and, on the basis of the theory of compressibility relaxation, change in free energy and volume between two structural states were measured. The analysis of the results of measurements of the absorption coefficient of ultrasonic waves, depending on the frequency, temperature, and composition of solutions, shows the presence in aqueous solutions of HMPT of a relaxation process related to the formation and disintegration of clathrate structures with the composition HMPT.17 H₂O. On the basis of compressibility relaxation theory, it was shown that the process of structural relaxation is related to a change in volume ΔV and in free energy ΔF between two structural states. (15 refs.)

63.00 LATTICE DYNAMICS AND CRYSTAL STATISTICS

(see also 05.50 Lattice theory, 65. Thermal properties, 66.70 Thermal conduction, 68.30 Dynamics of surface and interface vibrations, 78.30 Infrared and Raman spectra)

63.10 GENERAL THEORY

- Group theoretical classification of two-dimensional lattice vibrations** See Entry 114327

63.20 PHONONS AND VIBRATIONS IN CRYSTAL LATTICES

114098 Force constant model of crystalline HI in its low temperature phase. Chia-Nan Chang (Dept. of Electronic Engng. & Technol., Nat. Taiwan Inst. of Technol., Taipei, Taiwan), Wan-Sun Tse. *Annu. Rep. Inst. Phys. Acad. Sin. (Taiwan)*, vol.12, p.54-8 (Dec. 1982). [received: Sept. 1983] Lattice dynamics of crystalline HI in phase III is studied by using the Born-Von Karman force constant model with five different kinds of interatomic force constants and the results are compared to observed zone centre ($k=0$) frequencies (Raman and IR). (9 refs.)

114099 Lattice vibrations of solid hydrofluoric acid. Wan-Sun Tse (Inst. of Phys., Acad. Sinica, Taipei, Taiwan), Chia-Nan Chang. *Annu. Rep. Inst. Phys. Acad. Sin. (Taiwan)*, vol.12, p.59-66 (Dec. 1982). [received: Sept. 1983] Lattice dynamics calculations on the solid hydrofluoric acid are presented. It is found that six interatomic force constants using the Born-Von Karman model are capable of giving acceptable values of the zone center frequencies. (10 refs.)

114100 Lattice dynamics of the hydrogen halide crystals. Chia-Nan Chang (Dept. of Electronic Engng. & Technol., Nat. Taiwan Inst. of Technol., Taipei, Taiwan), Wan-Sun Tse, Li Chang. *Annu. Rep. Inst. Phys. Acad. Sin. (Taiwan)*, vol.12, p.67-76 (Dec. 1982). [received: Sept. 1983] A lattice dynamical model for three of the four hydrogen halide molecular crystals in their low temperature phase III has been investigated by using the Born-Von Karman model with different interatomic force constants and the results are compared to observed zone centre ($k=0$) frequencies (Raman). This simple model is also used to estimate hydrogen bond strengths in different crystals. (9 refs.)

114101 Properties of solid potassium cyanide: is the physics of cyanide crystals really chemistry?. M.L.Klein (Div. of Chem., Nat. Res. Council of Canada, Ottawa, Ontario, Canada), I.R.McDonald. *J. Chem. Phys. (USA)*, vol.79, no.5, p.2333-42 (1 Sept. 1983). Molecular dynamics simulations are reported for the orientationally disordered phase I of solid potassium cyanide. The calculations are based on an ionic potential incorporating a charge distribution for the cyanide ion which gives realistic values for the electrostatic moments up to and including the hexadecapole. Semiquantitative agreement with experiment is obtained for a wide range of static and dynamic properties of the crystal. Comparison with results obtained earlier for simple electrostatic models shows that the high order moments are an essential ingredient of a satisfactory potential. (31 refs.)

114102 Lattice dynamics of solid I₂ under high pressure. K.Kobashi, R.D.Eiters (Phys. Dept., Colorado State Univ., Fort Collins, CO, USA). *J. Chem. Phys. (USA)*, vol.79, no.6, p.3018-25 (15 Sept. 1983).

A calculation of the lattice dynamics of solid I₂ is made on the basis of a semiphenomenological potential with terms describing the intramolecular interaction, orientation-dependent charge transfer interactions, and nonbonding interactions. In addition, two terms describing a coupling between intramolecular vibrations of different molecules and a vibrational coupling between charge transferred bonds are included. At normal pressure, calculated vibrational frequencies are in good agreement with Raman and neutron scattering data. Agreement with experiment at high pressures requires that some potential parameters be volume dependent, and the implication of this result to the pressure induced changes in the electronic states of solid I₂ is discussed. The merging of the intramolecular A_g and B_{3g} Raman bands upon compression is explained quantitatively. The pressure dependence of several lattice vibrational mode frequencies are predicted but the observed softening of the librational A_g mode is not reproduced. The crystal energy is also calculated and compared with experiment. (27 refs.)

114103 The parameterization of vibronic transitions for lanthanide and actinide ions in crystals. R.A.Satten (Dept. of Phys., Univ. of California, Los Angeles, CA, USA). *J. Less-Common Met. (Switzerland)*, vol.93, no.1, p.235 (1983). (Proceedings of the Sixteenth Rare Earth Research Conference, Tallahassee, FL, USA, 18-21 April 1983).

Summary form only given, as follows. Some of the problems associated with parameterizing vibronic transitions of lanthanide and actinide ions in crystals and interpreting the results are discussed. Much of the discussion is centered on the vibronic intensity parametrization of the UCl_6^{2-} complex in crystals. (no refs.)

114104 Low frequency lattice vibrations of LaF₃ by neutron scattering. G.S.Dixon (Dept. of Phys., Oklahoma State Univ., Stillwater, OK, USA), R.M.Nicklow. *Solid State Commun. (USA)*, vol.47, no.11, p.877-9 (Sept. 1983).

The phonon modes having frequencies less than 3 THz in the high symmetry directions of LaF₃ are reported. These are compared to the results of previous optical studies. A previously unobserved branch of low group velocity is found near 1.2 THz polarized both parallel and perpendicular to the basal plane. Its significance for the lifetimes of zone boundary acoustic phonons is discussed. (19 refs.)

- Crystal structure and vibrational spectra of Pb₂P₂S₆** See Entry 113819
- Influence of Jahn-Teller impurities on phase transitions** See Entry 114125
- Critical fluctuations at the phase transition in benzil** See Entry 114158
- Phase transitions in Pb₃(P_{1-x}As_xO₄)₂: influence of the central peak and flip mode on the Raman scattering of hard modes** See Entry 114159
- Inelastic neutron scattering study of the structural glass transition in a K(Br,CN) mixed crystal** See Entry 114174
- Negative thermal expansion due to the hindered rotation of the ammonium ion or the methyl group in solids with low barriers to rotation and the anisotropic thermal expansion in solids having polyatomic groups** See Entry 114212
- Vibrational state and jump frequency of Mossbauer impurity associated with a vacancy in metals** See Entry 114273
- Spin-phonon interaction in the Ni²⁺:Al₂O₃ system at low temperatures** See Entry 114726
- Dipole-phonon coupling and dielectric relaxation** See Entry 114778
- Comment on 'Raman scattering with nanosecond resolution during pulsed laser annealing of silicon'** See Entry 114837
- Fermi resonance effect and vibrational intensity in the weak charge-transfer complexes** See Entry 114841
- Low frequency infrared spectra of copper(II) pyridine N-oxide complexes** See Entry 114842
- Raman spectra of rhombohedral and α -monoclinic selenium under high hydrostatic pressure** See Entry 114844
- Raman spectra of ⁷Li₂SO₄ and ⁶Li₂SO₄** See Entry 114848
- Ammonium ion rotation in ammonium perchlorate as studied by infrared spectroscopy** See Entry 114849
- Vibrational spectra and force constants for trans-sodium hyponitrite** See Entry 114859
- Low temperature Raman spectra of dibenzyl; comparison with biphenyl and paraterphenyl** See Entry 114861
- Raman scattering in Bi₁₂TiO₂₀** See Entry 114869
- The lowest triplet state of tetramethyl-1,3-cyclobutanedithione. I. Single-crystal polarized absorption spectrum** See Entry 114875
- Emission from free and bound excitons in gallium selenide layered crystals** See Entry 114924

63.20D Phonon states and bands, normal modes, and phonon dispersion

114105 Harmonics of phonons in Al. Y.Nakai, Y.Tsunoda (Faculty of Sci., Osaka Univ., Osaka, Japan). *Physica B & C (Netherlands)*, vol.120B+C, no.1-3, p.286-90 (May 1983). (Yamada Conference VI on Neutron Scattering in Condensed Matter, Hakone, Japan, 1-4 Sept. 1982).

According to the Toda theory (1967) for a one-dimensional exponential lattice, the lattice vibrations have higher harmonics without damping in time. This is contrasted to phonons with a finite life-time obtained by the perturbation theory in the pseudoharmonic approximation. A search for the higher harmonics in the phonons of Al was carried out by means of inelastic scattering of neutrons. Neutron groups observed at elevated temperatures are explained as the second harmonic wave expected for the Toda lattice although other explanations cannot be excluded. (5 refs.)

114106 Coupling of longitudinal phonons with transverse Einstein mode in C₂₄Rb. S.Funahashi, T.Kondow, M.Iizumi (Div. of Phys., JAERI, Ibaraki-ken, Japan). *Physica B & C (Netherlands)*, vol.120B+C, no.1-3, p.305-9 (May 1983).

(Yamada Conference VI on Neutron Scattering in Condensed Matter, Hakone, Japan, 1-4 Sept. 1982). Phonon dispersion relations in C₂₄Rb made from HOPG were measured at 30, 80 and 120K. Three L mode phonon branches were observed for $q||c^*$ axis. A small gap was discovered at $\hbar\omega \approx 5$ meV on the acoustic branch. Except for this gap region, the dispersion curves were explained in terms of the one-dimensional Born-von Karman model. Three interlayer force constants were evaluated. The nearest neighbour (NN) carbon-carbon force is nearly

equal to that of pristine graphite. The NN carbon-rubidium force agrees with Dresselhaus's empirical law. The second neighbour carbon-carbon force across rubidium layer is 12% that of the first neighbour force but cannot be ignored. The small gap in the acoustic branch is satisfactorily explained as a result of coupling with transverse Einstein oscillations predicted by Suganuma et al. (1981) from low temperature specific heat measurements. An appreciable change in the results at the three temperatures was not observed. (7 refs.)

114107 Coupled quadrupole-phonon excitations: inelastic neutron scattering on Van Vleck paramagnet PrNi₂. V.L.Aksenov, E.A.Goremychkin, E.Muhle (Joint Inst. for Nuclear Res., Dubna, USSR), Th.Frauenheim, W.Buhrer. *Physica B & C (Netherlands)*, vol.120B+C, no.1-3, p.310-13 (May 1983). (Yamada Conference VI on Neutron Scattering in Condensed Matter, Hakone, Japan, 1-4 Sept. 1982). Inelastic neutron scattering experiments on a single crystal of PrNi₂ (0.4 cm³) were performed at the sample temperature T=8K. The dispersion relations of the acoustic transverse phonons and the low energy magnetic excitations were measured in the T and Δ-directions. An analysis of the intersection region of these excitations shows that an additional neutron intensity to the nuclear and magnetic dipolar scattering occurs due to magnetoelastic scattering. The hybridised spectra of phonons and quadrupole excitons are discussed. (5 refs.)

114108 Calculation of the phonon width and phonon shifts in naphthalene-d₈. V.K.Jindal, J.Kalus (Phys. Inst., Univ. Bayreuth, Bayreuth, Germany). *Physica B & C (Netherlands)*, vol.120B+C, no.1-3, p.314-16 (May 1983). (Yamada Conference VI on Neutron Scattering in Condensed Matter, Hakone, Japan, 1-4 Sept. 1982). The width Γ and the shift Δ of the q=(0, 0, 0) phonon at 2.52 THz were calculated with three different sets for the forces of a 6-exp-potential. The molecules were assumed to be rigid. The authors took into account cubic and quartic anharmonicity terms. The three models differ in magnitude for Γ and Δ by about 25%. A comparison is made with inelastic neutron scattering data. (10 refs.)

114109 Lattice dynamics of FePt alloys of AB₂ type ordered structure. Y.Noda, Y.Endoh (Dept. of Phys., Tohoku Univ., Sendai, Japan), S.Katano, M.Iizumi. *Physica B & C (Netherlands)*, vol.120B+C, no.1-3, p.317-22 (May 1983). (Yamada Conference VI on Neutron Scattering in Condensed Matter, Hakone, Japan, 1-4 Sept. 1982). The lattice dynamics of FePt alloys with the Cu₃Au type crystal structure, Fe₃Pt and FePt₃, have been studied by inelastic neutron scattering. The phonon dispersion curves along the [100], [110] and [111] directions have been observed over the whole Brillouin zone at room temperature. The observed phonon energies of acoustic modes of Fe₃Pt are almost the same as those of FePt₃ except the [110]TA₁ branch, although the average atomic mass is different by a factor of 1.8. The dispersion relations have been analysed by the Born-von Karman (BvK) force constant model where the first two neighbour forces were employed. It turns out that the nearest neighbour Fe-Fe force constant (1xx) is unusually small in the ferromagnetic Fe₃Pt Invar alloy. (10 refs.)

114110 Gitterdynamik von Imidazol (Lattice dynamics of Imidazol). K.H.Link. **Report JUL-1850**, Kernforschungsanlage, Julich, Germany (May 1983), 125 pp. In German. The lattice dynamics of imidazole have been investigated. To this end dispersion curves have been determined at 10K by inelastic coherent neutron scattering. Strictly speaking, of the 24 expected external curves 22 were measured along the symmetry directions (100) and (001) and ten branches along (010). Raman measurements have been done to investigate Γ-point modes. The combination of extinction rules for Raman and neutron scattering leads to the symmetry assignment of Γ-point modes. The experiment yields a force constant for the stretching vibration of the hydrogen bond of 0.33 mdyn/Å. A force model has been developed to describe the intermolecular atom-atom interactions in imidazole. In a minimisation routine the open parameters of the force model have been fitted to the observed dispersion branches. The force model contains the van der Waals, the exchange interaction and the interactions of static monopoles and dipoles. These static multipoles take into account the differences of the electronegativities within the molecule and its asymmetric shape. An essential part of the hydrogen bond is provided by the static multipole interaction. (47 refs.)

Dimensional shifts in phonon spectra	See Entry 114116
Neutron observations of phasons and amplitudons in incommensurate phases	See Entry 114119
Neutron spectroscopy of anilinium bromide	See Entry 114165
Group theoretical classification of two-dimensional lattice vibrations	See Entry 114327
Polaron model of the electronic spectrum and the superconductivity of compounds having the A-15 structure	See Entry 114456
The polarized Raman spectra of CsCdCl ₃ single crystals	See Entry 114858
Radiative recombination at Ir ³⁺ sites in doped AgBr. Visible luminescence	See Entry 114914

63.20H Phonon-phonon interactions

Pressure dependence of the electron capture cross section of the B hole trap in liquid phase epitaxial gallium arsenideSee Entry 114464

63.20K Phonon-electron interactions

Polaron model of the electronic spectrum and the superconductivity of compounds having the A-15 structure	See Entry 114456
Influence of the anisotropy of the elastic electron-phonon scattering on the carrier mobility in tellurium	See Entry 114544
Inverted population of light-hole band pumped at cyclotron resonance	See Entry 114739

63.20M Phonon-defect interactions

Thermal conductivity of irradiated graphite	See Entry 114296
Stimulated Raman emission of coherent phonons by impurities in a crystal	See Entry 114883

63.20P Localized modes

114111 Spectroscopic properties and relaxation processes of impurity molecules in solids. II. Vibrational relaxations. H.Kono, S.H.Lin (Dept. of Chem., Arizona State Univ., Tempe, AZ, USA). *J. Chem. Phys. (USA)*, vol.79, no.6, p.2748-55 (15 Sept. 1983). For pt.I see *ibid.*, vol.78, no.5, p.2607 (1983). The authors have calculated the vibrational relaxation rates for HCl (DCI)/Ar matrix systems. The quantitative agreement between their calculations and experimental data is fairly good. Their approach based on the adiabatic approximation can consistently treat the eigenvalue problems and vibrational relaxation processes for diatomic molecules embedded in monatomic crystals. The adiabatic approximation is used to separate high (intramolecular vibration) and low frequency modes (molecular rotation and lattice vibration). The nonadiabatic couplings (the kinetic energy operators for the low frequency modes) induce the vibrational relaxation processes. Their numerical calculations support the mechanism proposed by Bondybey and Brus (1980) that for small hydrides molecular rotation is the dominant accepting mode. The A_{1g} totally symmetric lattice modes in the classification by the irreducible representations of the substitutional site symmetry O_h are shown to be dominant to accept the energy mismatch between initial and final rotational levels. For the DCI/Ar system, they have found that the mixing of initial rotational levels due to the rotation-lattice vibration coupling is responsible for the vibrational relaxation. The calculated relaxation rate for DCI is smaller than that of HCl by one order of magnitude. (35 refs.)

114112 Local optical oscillations near point and extended defects in ionic crystals. A.M.Kosevich (Physicotech. Inst. for Low Temperatures, Acad. of Sci., Ukrainian SSR), V.A.Pogrebnyak. *Sov. Phys.-JETP (USA)*, vol.83, no.5, p.1090-4 (Nov. 1982). Translation of: *Zh. Eksp. & Teor. Fiz. (USSR)*, vol.83, no.5, p.1886-93 (Nov. 1982). [received: Sept. 1983] It is shown that the vector-like field of the relative displacements of the ions in the unit cell during optical oscillations of an ionic crystal leads to a nonexponential (power-law) decrease of the amplitude of the local optical oscillations at large distances from point and linear defects. In the case of a planar defect the amplitude decreases exponentially over a macroscopic distance equal to the wavelength. The dispersion laws of oscillations localized near linear and planar defects are obtained. (13 refs.)

Structural phase transitions and superconducting transition temperatures of hexagonal M_xWO₃ compounds See Entry 114633

63.50 VIBRATIONAL STATES IN DISORDERED SYSTEMS

114113 Effect of amorphous sequences on the longitudinal acoustic modes in partially crystalline polymers. I. Transfer matrix method. G.R.Strobl (Fachbereich Chem., Inst. for Phys. Chem., Johannes-Gutenberg-Univ., Mainz, Germany). *J. Polym. Sci. Polym. Phys. Ed. (USA)*, vol.21, no.8, p.1357-80 (Aug. 1983). A novel theoretical scheme is developed which enables the determination of the LAM-like vibrations of polymer chains made up of crystalline and amorphous parts as they occur in partially crystalline structures. The boundary conditions effective at the junction points are formulated in terms of the compliances of the associated amorphous sequences. These compliances can be derived from their eigenfrequencies and eigenvectors in a disconnected state. The treatment uses a matrix formalism which can be extended to include bending and torsional motions in a general state of vibration of the crystalline stem. A first numerical example demonstrates that the LA mode of a crystalline stem can be strongly perturbed by the coupling to the adjacent amorphous sequences. Interpretation of frequencies and line shapes of observed LA modes should always include these coupling effects; their neglect can lead to considerable errors. (14 refs.)

114114 Inelastic scattering of polarised neutrons by amorphous Fe₄C₇₀Si₁₅B₁₀. D.E.G.Williams, K.R.A.Ziebeck (Dept. of Phys., Loughborough Univ. of Technol., Loughborough, England). *Physica B & C (Netherlands)*, vol.120B+C, no.1-3, p.367-72 (May 1983). (Yamada Conference VI on Neutron Scattering in Condensed Matter, Hakone, Japan, 1-4 Sept. 1982). The inelastic scattering of polarised neutrons has been used to investigate the possible existence of magnetic excitations in the amorphous alloy Fe₄C₇₀Si₁₅B₁₀. The measurements were confined to wave vectors close to 3.18 Å⁻¹ which corresponded to the position of the first peak in the static structure factor. Extensive scans both in wave vector and in energy revealed several features but only one of these was found to be an intrinsic excitation of the system. This mode, which was extremely weak was non-magnetic and was found to disperse with a sound velocity of 1636 m s⁻¹. (9 refs.)

114115 Resonant photon scattering in metallic glasses. N.Thomas (Dept. of Phys., Univ. of Birmingham, Birmingham, England). *Philos. Mag. B (GB)*, vol.48, no.3, p.297-305 (Sept. 1983). The two-level systems (TLS) in metallic glasses at low temperatures are so heavily damped by inelastic electron scattering that one cannot realistically describe the resonant absorption of phonons by these systems using Fermi's Golden Rule. A simple idealized model is considered in which both the TLS-phonon and TLS-electron interactions are off-diagonal, and this is analysed to infinite-order perturbation theory using quantum-field techniques. The result for the total phonon scattering rate is almost identical to Fermi's Golden Rule, except that the density of final states is replaced by the spectral density of the TLS. This spectral density cannot be calculated exactly, but consideration of its low-frequency limiting behaviour shows that resonant scattering alone cannot explain the anomalous behaviour in the saturation of the ultrasonic attenuation observed by Araki, Park, Hikata and Elbaum (1979). (18 refs.)

The local environment around hydrogen atoms in hydrogenated NiTi₂ alloy glass See Entry 113749

Characterization of lattice disorder in the low-temperature phase of irradiated PTFE by vibrational spectroscopy See Entry 113768

Inelastic neutron scattering study of the structural glass transition in a K(Br,CN) mixed crystal See Entry 114174

Low-energy excitations in (KBr)_{1-x}(KCN)_x in the orientational glass state See Entry 114294

Thermodynamic and kinetic properties of amorphous dielectrics at low temperatures See Entry 114295

Infrared dephasing and libration motion in liquid methyl iodide See Entry 114850

Low-frequency Raman scattering from methylene-oxyethylene-methylene triblock oligomers See Entry 114852

63.70 STATISTICAL MECHANICS OF LATTICE VIBRATIONS

(see also 65. Thermal properties of condensed matter, 66.70 Thermal conduction)

114116 Dimensional shifts in phonon spectra. S.P.Chizhik, N.T.Gladikh, L.K.Grigor'yeva, R.N.Kuklin, R.G.Melkadze. *Russ. Metall. (GB)*, no.3, p.142-4 (1982). Translation of: *Izv. Akad. Nauk. SSSR Met.*, no.3, p.165-7 (1982). Examines the functional relationship of the Debye energy in relation to the magnitude of disperse particles. On the basis of the dimensional vacancy effect, which occurs in high-dispersion systems, the Debye temperature in a small particle is lower than in a large specimen. The change in Debye frequency was used to determine the ratio of the volumes corresponding to an atom and a vacancy. Estimates of the decrease of the melting point for small particles, based on the dimensional shift in the Debye temperature, is in agreement with experiment. (9 refs.)

114117 Instability of an atomic chain in a thermal force field. V.L.Gilyarov, V.A.Petrov (A.F. Ioffe Physicotech. Inst., Acad. of Sci., Lenin-grad, USSR). *Sov. Phys.-Solid State (USA)*, vol.25, no.2, p.267-9 (Feb. 1983). Translation of: *Fiz. Tverd. Tela (USSR)*, vol.25, no.2, p.472-7 (Feb. 1983). [received: Sept. 1983] Solutions of thermodynamic equilibrium equations for an atomic chain in a thermal force field are obtained. The solutions are used to study the simplest unstable configurations whose excitations due to thermal fluctuations can lead to the fracture of the chain. (5 refs.)

Low temperature heat capacities of SrF₂ and other fluoride compounds See Entry 114203
Thermal expansion of (Pd_xPt_{1-x})₃Fe alloys See Entry 114211

63.75 STATISTICAL MECHANICS OF DISPLACIVE PHASE-TRANSITIONS

(for order-disorder and statistical mechanics of model systems, see 64.60; for crystallographic aspects of polymorphic and order-disorder transformations, see 61.50K)

Critical fluctuations at the phase transition in benzil See Entry 114158
Phase transitions in Pb₃(P_{1-x}As_xO₄)₂: influence of the central peak and flip mode on the Raman scattering of hard modes See Entry 114159
On the relation between the dielectric anomalies and the isofrequency dependences of inelastic scattering of light in lithium tantalate crystals See Entry 114795

63.90 OTHER TOPICS IN LATTICE DYNAMICS AND CRYSTAL STATISTICS

114118 Hyper-Raman spectra and frequency dependence of soft mode damping in SrTiO₃. V.N.Denisov, B.N.Mavrin, V.B.Podobedov (Inst. for Spectroscopy, Acad. of Sci., Troitzk, USSR), J.F.Scott. *J. Raman Spectrosc. (GB)*, vol.14, no.4, p.276-83 (Aug. 1983). The hyper-Raman spectra of SrTiO₃ were studied in the range 85-710K. The temperature dependence of frequencies and damping of all the vibrations, including the soft F_{1u} and silent F_{2u} modes, was obtained. Using the hyper-Raman spectra and a Green's function analysis, the authors calculated the damping function Γ_s(ω,T) in the frequency region 20-200 cm⁻¹ for temperatures between 300 and 710K. It was shown that the behavior of the soft mode damping may be described by invoking soft mode decay into two acoustic phonons (ω_s→ω_{ac}+ω_{ac}) plus an additional channel via annihilation of one acoustic phonon (ω_s+ω_{ac}→ω₁₇₆). The temperature dependence of the phonon resonance between the soft mode and the nearest polar optical phonon (at 176 cm⁻¹) was studied. Quantitative analysis of this phonon resonance was carried out to obtain parameters characterizing both modes: signs and relative magnitude of the hyper-Raman matrix elements; the soft mode damping; and the resonance coupling constant, which yields interference effects. (28 refs.)

114119 Neutron observations of phasons and amplitudons in incommensurate phases. C.M.E.Zeyen (Inst. Laue-Langevin, Grenoble, France). *Physica B & C (Netherlands)*, vol.120B+C, no.1-3, p.283-5 (May 1983). (Yamada Conference VI on Neutron Scattering in Condensed Matter, Hakone, Japan, 1-4 Sept. 1982). The author presents the first observations of phase modes in low-temperature incommensurate phases. The experiments were performed using thermal and cold neutron triple-axis-spectrometers at ILL on biphenyl and thorium bromide. Biphenyl is a molecular crystal exhibiting two distinct low-temperature incommensurate phases but no lock-in transition. Despite its structural complexity two low-lying phonon branches corresponding to torsional motions of the biphenyl molecule can be well studied. In the high-temperature phase one of these modes becomes soft and condenses at an incommensurate lattice position near the zone boundary. Within the incommensurate phases this mode splits into a phason with a linear dispersion and a soft-mode-like amplitudon. The other mode also splits into two distinct branches in the incommensurate phase. Thorium bromide is a structurally much simpler system which displays an incommensurate phase below 95K. Here too a high-temperature soft mode is clearly observed, and below T_C it splits into a phason and an amplitudon branch. (3 refs.)

114120 Incommensurate lattice instability in [N(CD₃)₄]₂ZnCl₄. M.Iizumi, K.Gesi (Div. of Phys., JAERI, Ibaraki, Japan). *Physica B & C (Netherlands)*, vol.120B+C, no.1-3, p.291-5 (May 1983). (Yamada Conference VI on Neutron Scattering in Condensed Matter, Hakone, Japan, 1-4 Sept. 1982). Neutron scattering measurements carried out for the deuterated crystal of tetramethylammonium tetrachlorozincate at temperatures above the normal-to-incommensurate phase transition temperature (25.5°C) have shown that the A₁ transverse phonon indicates a slight softening at q~(0, 0, 0.35) and that the quasielastic critical scattering without energy broadening develops along the (0, 0, q_z) line with a peak increasing at q_z=0.41 with decreasing temperature. The existence of the two incommensurate phases is suggested from the measurements of the modulation wave vector in the incommensurate phase (1.8 to 25.5°C) (10 refs.)

114121 Mode softening and the temperature dependence of the atomic mean-square displacement. S.L.Mair (Div. of Chem. Phys., CSIRO, Clayton, Victoria, Australia). *Phys. Rev. B (USA)*, vol.28, no.5, p.2866-8 (1 Sept. 1983). The form of the temperature dependence of the mean-square displacement is derived for an atom vibrating in the presence of soft modes. The derivation, which is based on Ornstein-Zernike theory, results in a mean-square displacement with an anomalous temperature-independent positive component at temperatures greater than twice the critical temperature. (16 refs.)
Shear elastic constant softening in (V_{1-x}Cr_x)₂O₃: second-order nature of the low temperature phase transition See Entry 114070
Influence of Jahn-Teller impurities on phase transitions See Entry 114125
Phase transitions in Pb₃(P_{1-x}As_xO₄)₂: influence of the central peak and flip mode on the Raman scattering of hard modes See Entry 114159
Neutron diffraction and scattering study on M_xWO₃ (M=Rb and K) See Entry 114164
Structural phase transitions and superconducting transition temperatures of hexagonal M_xWO₃ compounds See Entry 114633

64.00 EQUATIONS OF STATE, PHASE EQUILIBRIA, AND PHASE TRANSITIONS

(see also 82.60 Chemical thermodynamics)

64.30 EQUATIONS OF STATE OF SPECIFIC SUBSTANCES

(see also 65.70 Thermal expansion)

Dynamic compression of diopside and salite to 200 GPa See Entry 116080

64.60 GENERAL STUDIES OF PHASE TRANSITIONS

(for critical phenomena in quantum fluids, superconductors, magnetic materials and ferroelectrics, see 67., 74.40, 75.40 and 77.80 respectively)

114122 Phase transformation in a linear polycrystal with a rate law of n-th order. G.E.W.Schulze (Phys. Inst., Univ. Dusseldorf, Dusseldorf, Germany). *Cryst. Res. & Technol. (Germany)*, vol.18, no.8, p.977-84 (1983). A phase transformation in a one component polycrystal starts to grow instantaneously and with a constant rate from the grain boundaries. After the time *t* there exist regions of the old and of the new phase. The derivation of the statistical quantities characterizing this state at *t* is unknown yet. Therefore the author reduces this complicated three-dimensional problem to a one-dimensional model analogously to the linear chain in lattice dynamics or to the one-dimensional energy band model. A closed analytical treatment of this model is practicable. It is derived in detail for those one-dimensional systems, which transform according to a rate law of n-th order (n≥0). (6 refs.)
114123 Hard-sphere fluid-to-solid transition and the virial expansion. V.C.Aguilera-Navarro (Instituto de Fisica, Univ. Nacional Autonoma de Mexico, Mexico City, Mexico), M.Fortes, M.de Llano, A.Plastino, J.del Rio, O.Rojo. *J. Stat. Phys. (USA)*, vol.32, no.1, p.95-104 (July 1983). An exhaustive Pade approximant study of the Mayer (1977) virial series expansion is carried out for the classical hard-sphere system. As one increases the order of the different approximants a clear tendency is seen to reproduce both the random close packing divergence of the fluid branch as well as its instability (towards the crystalline phase) at the spinodal point. (27 refs.)
114124 Effect of interplane coupling in quasi-two-dimensional systems. S.T.Chui (Franklin Inst., Univ. of Delaware, Newark, DE, USA). *Phys. Rev. B (USA)*, vol.28, no.5, p.2863-5 (1 Sept. 1983). There are many divergent susceptibilities in two-dimensional systems that are not associated with phase transitions. The authors propose that when stacks of planes of these two-dimensional systems are coupled together, these divergences indicate genuine phase transitions. Applications to melting, commensurate-incommensurate transitions, and superconductivity are pointed out. (14 refs.)
114125 Influence of Jahn-Teller impurities on phase transitions. V.S.Vikhnin (Inst. of Semiconductors, Acad. of Sci., Ukrainian SSR). *Sov. Phys.-Crystallogr. (USA)*, vol.28, no.2, p.127-9 (March-April 1983). Translation of: *Kristallografiya (USSR)*, vol.28, no.2, p.219-23 (March-April 1983). [received: Sept. 1983] The author investigates the influence of Jahn-Teller impurities on ferroelectric and nonferroelectric structural phase transitions. As mechanisms of interaction of Jahn-Teller impurities with soft modes, he considers quadratic vibron interaction with a soft mode, anharmonic third-order interaction quadratic with respect to a soft lattice mode and linear with respect to a quasilocal Jahn-Teller mode, and linear interaction with respect to soft lattice and quasilocal modes. He shows that Jahn-Teller impurities can lead to a shift of the phase transition (PT) temperature, and can induce PT in virtual ferroelectrics. He also shows that in low-symmetry phase, on account of interaction with the order parameter, acentricity of Jahn-Teller impurities is induced. Jahn-Teller impurities can lead to splitting of a PT into two PT and to reorientation of the distortion in a PT. Owing to indirect interaction between Jahn-Teller impurities via soft phonons, a quadruple pseudospin glass phase can be realized. (10 refs.)
New spontaneous symmetry breaking for the cubic XY model See Entry 111603
Renormalization-group study of the Hamiltonian version of the Potts model. III. Improved results for larger cells See Entry 111605
Kinetic transition during growth of a crystal undergoing ordering See Entry 113788
Critical point phenomena in fluids See Entry 114130
Dynamics of NH₄Cl particle nucleation and growth at 253-296K See Entry 114153
Thermodynamic theory of phase transitions in solid solutions based on lead metaniobate See Entry 114156

Statistical model of the phase transition in $\text{KH}_3(\text{SeO}_3)_2$ See Entry 114169

Theory of inhomogeneous states of a solid solution in the neighborhood of second-order phase transitionsSee Entry 114186

Curie-Weiss law for improper ferroelectric or ferroelastic phase transitionsSee Entry 114794

64.70 PHASE EQUILIBRIA, PHASE TRANSITIONS, AND CRITICAL POINTS

(see also 81.30 Phase diagrams and microstructures developed by solidification and solid-solid phase transformations)

114126 Alloys with the $\text{Ge}_{1-x}\text{Ni}_x\text{Te}$ composition. M.A.Alidzhanov, I.Sh.Dadashev, L.K.Vagabova, G.I.Safaraliev (V.I. Lenin Azerbaidzhan State Pedagogic Inst., Acad. of Sci., Azerbaidzhan SSR). *Inorg. Mater. (USA)*, vol.18, no.9, p.1361-2 (Sept. 1982). Translation of: *Izv. Akad. Nauk SSSR Neorg. Mater.*, vol.18, no.9, p.1587-9 (Sept. 1982). [received: Sept. 1983]

It has been supposed that solid solutions of the GeTe-NiTe system have high thermoelectric efficiency, and it was therefore expedient to investigate the properties of this system. The authors have studied part of the phase diagram on the GeTe side, constructed by thermal analysis, microhardness determination, and certain kinetic coefficients. It was established that in the region of solid solutions based on GeTe there is a slight increase in the microhardness from $12.1 \cdot 10^{-7}$ Pa for GeTe to $15.3 \cdot 10^{-7}$ Pa for the alloy containing 20 mole % NiTe . From measurements of the Hall effect and electrical conductivity they calculated the mobility of the current carriers, which decreases smoothly with increase in the NiTe content of the GeTe . The decrease in mobility is due to the appearance of additional scattering centers. Since the germanium and nickel in this case have identical valence, these additional centers can be regarded as neutral impurities. (4 refs.)

114127 Phase equilibria in $\text{Ln}_2\text{V}_2\text{O}_7\text{-Ln}_2\text{Ti}_2\text{O}_7$ systems ($\text{Ln}=\text{Er, Lu}$). A.K.Molodkin, Yu.E.Bogotov, V.I.Moskalenko, V.N.Belan, A.V.Ershov (Patrice Lumumba Harmony of the Nations Univ., Moscow, USSR). *Inorg. Mater. (USA)*, vol.18, no.10, p.1393-5 (Oct. 1982). Translation of: *Izv. Akad. Nauk SSSR Neorg. Mater.*, vol.18, no.10, p.1625-7 (Oct. 1982). [received: Sept. 1983]

The phase equilibria in $\text{Ln}_2\text{V}_2\text{O}_7\text{-Ln}_2\text{Ti}_2\text{O}_7$ systems ($\text{Ln}=\text{Er}$ or Lu) have been studied by the method of X-ray phase analysis. In the systems investigated, $\text{Er}_2\text{V}_2\text{Ti}_{2-x}\text{O}_7$ and $\text{Lu}_2\text{V}_2\text{Ti}_{2-x}\text{O}_7$ solid solutions are formed, which crystallize in structures of the pyrochlore type. The unit cell parameters and the values of the dielectric constants of the solid solutions vary linearly as a function of the composition. (7 refs.)

114128 Order parameter for tricritical phenomena. I.L.Pegg, C.M.Knobler, R.L.Scott (Dept. of Chem., Univ. of California, Los Angeles, CA, USA). *J. Phys. Chem. (USA)*, vol.87, no.15, p.2866-8 (21 July 1983).

Experimental three-phase coexistence curves in the tricritical region do not show the complete symmetry predicted by the simplest theories. Model calculations using the van der Waals equation yield the expected asymptotic behavior, but show that the magnitude of the departures from this behavior differs for different properties. In particular, the concentration differences at the upper and lower critical end points show the limiting form only very close to the tricritical point. (8 refs.)

114129 Model calculations for the thermodynamic equilibria in intermetallics in La-Ni under hydrogen. H.Oesterreicher (Dept. of Chem., Univ. of California, San Diego, La Jolla, CA, USA). *J. Less-Common Met. (Switzerland)*, vol.93, no.1, p.L1-3 (1983).

In previous communications the author has shown that equilibrium states of intermetallics in La-Ni under hydrogen involve complex ternary hydride phases. Examples are the transformation reactions under increasing hydrogen pressure around 500°C: $\text{LaNi}_5 \rightleftharpoons \text{LaH}_{3-x}$ and $\text{LaNi}_5 \rightleftharpoons \text{LaNiH}_{3.1}$. For LaNi_5 small changes in composition decide between the transformation reactions $\text{LaNi}_5 \rightleftharpoons \text{LaNiH}_{3.1}$, Ni and $\text{LaNi}_5 \rightleftharpoons \text{LaNi}_{3.1}$, $\text{LaNi}_{1.5}\text{H}_2$. The simple cleavage or lysis-type reaction $\text{LaNi}_5 \rightleftharpoons \text{LaH}_3$, Ni , for which evidence has been presented in the past, appears not to be an equilibrium reaction under these conditions. The author shows that simple enthalpy considerations are in accord with these findings. Furthermore they provide evidence that the energetics of a series of reactions are rather competitive and that the mode of decomposition of important hydrogen storage materials can therefore be influenced by modification of ΔH_F of the intermetallic in question through pseudobinary formation. The authors present the results of simplified model calculations for the thermodynamic drive of various possible reactions of LaNi_5 under hydrogen. (7 refs.)

114130 Critical point phenomena in fluids. D.Beyens (CENS, Gif-sur-Yvette, France).

Proceedings of the 4th European Symposium on Materials Sciences under Microgravity (ESA SP-191), Madrid, Spain, 5-8 April 1983 (Paris, France: ESA 1983), p.367-76

A review of critical phenomena in simple fluids and mixtures is presented, including: introduction to the universality of critical phenomena by means of the Landau theory, critical enhancement of the fluctuations, critical properties near T_c , corrections far from T_c , dynamics of fluctuations, kinetics of the phase separation process, shear flow phenomena, wetting problems. The influence of gravity is also discussed. (33 refs.)

114131 Optical investigation of critical behaviour in simple fluids at reduced gravity. P.H.Huisser, A.C.Michels, N.J.Trappeniers (Van der Waals Lab., Univ. of Amsterdam, Amsterdam, Netherlands). Proceedings of the 4th European Symposium on Materials Sciences under Microgravity (ESA SP-191), Madrid, Spain, 5-8 April 1983 (Paris, France: ESA 1983), p.377-84

The authors have devised an experiment to study critical behaviour in a simple fluid under strongly reduced gravitational conditions. The proposed optical techniques, elastic light scattering and interferometry are essentially noninvasive to the critical sample conditions, yield detailed quantitative information on well-defined physical quantities and, not in the last place, may allow an, albeit more qualitative, visual investigation of the underlying transient processes. In order to study the feasibility of performing such an experiment in Spacelab, the authors have been developing a full-scale engineering model, which meets the typical requirements regarding size, mass, power consumption and autonomy of operation. The authors describe this model and discuss some preliminary results. (17 refs.)

On the energy of interaction in the Si-B systemSee Entry 114210

Adsorption behaviour of pure fluids near the gas-liquid critical pointSee Entry 114371

Metallurgically grown Schottky junction in directionally solidified eutectic Ag-Si alloysSee Entry 114590

Concentration and temperature dependences of the magnetic susceptibility of binary alloys of indium with potassium and rubidiumSee Entry 114678

Physicochemical aspects of production of ferroelectric ceramicsSee Entry 115148

Investigation of phase equilibria related to fusion reactor materials. I. The ternary system Zr-Al-NSee Entry 115165

Revision of the eutectoid isotherms of the uranium-chromium systemSee Entry 115166

Phase equilibria in nickel rich Ni-Al-Mo and Ni-Al-W alloysSee Entry 115167

Robust numerical procedure for calculating equilibrium compositions in binary alloy systemsSee Entry 115168

Influence of alloying with germanium and copper on the conditions of formation of the superconducting compound Nb_3Si See Entry 115170

On the thermodynamic properties of Co-Cu meltsSee Entry 115171

Examination of alloys of the Pd-Ni-Th system in the palladium-rich regionSee Entry 115172

The Zn-Bi-Hg phase diagramSee Entry 115173

Thermodynamic study of oxidation of molybdenum sulfides ..See Entry 115174

Predominance area diagrams of the system Co-S-O between 583 and 1148K ...See Entry 115176

Influence of pressure on the equilibrium of the melt with graphite, diamond and carbide Mn_7C_3 in the Mn-C systemSee Entry 115177

Calculation of complex equilibria in ceramic systemsSee Entry 115178

A quantitative investigation of phase compositions in magnesia- R_2O_3 -silicate systems. IV. A study of commercial magnesia-chrome mixturesSee Entry 115179

The time-temperature-transformation (TTT) state diagram and cureSee Entry 115180

64.70D Solid-liquid transitions

(see also 81.30F Solidification)

114132 Dissipation-theory treatment of the transition from diffusion-controlled to diffusionless solidification. M.J.Aziz (Div. of Appl. Sci., Harvard Univ., Cambridge, MA, USA). *Appl. Phys. Lett. (USA)*, vol.43, no.6, p.552-4 (15 Sept. 1983).

The steady-state velocity of a planar liquid-solid interface is predicted by calculating the free energy dissipated by irreversible processes at the interface and equating it to the available driving free energy. A solute drag term and an intrinsic interfacial mobility term are included in the dissipation calculations for a binary alloy. The solute drag calculation employs a solute trapping model, which has been extended to concentrated alloys. The result is presented in terms of a single unknown parameter, the interfacial diffusivity D_i . A transition from diffusion-controlled to diffusionless solidification occurs over approximately an order of magnitude in growth velocity, as the interface speed surpasses the maximum speed with which solute atoms can diffuse across the interface to remain ahead of the growing crystal. (28 refs.)

114133 Computer simulation of high speed melting of amorphous silicon. H.C.Webber, A.G.Cullis, N.G.Chew (Royal Signals & Radar Establ., Malvern, England). *Appl. Phys. Lett. (USA)*, vol.43, no.7, p.669-71 (1 Oct. 1983).

The laser melting of amorphous Si is accurately modelled by computer calculations. It is found that the thermal conductivity of the amorphous phase must be set at approximately 10^{-2} W/cm K, a value much lower than that of crystalline material to obtain close agreement with experimental measurements. This low value is, however, consistent with the thermal conductivities of other amorphous materials. The results of the computations, when compared with experimental observations, confirm that the melting point of ion implanted amorphous Si is below that of crystalline Si, with a best estimate in the range 1185-1385K. (21 refs.)

114134 Construction of the liquidus surface in the In-InP-GaAs-InAs system using simplex-centroid design. A.A.Selin, V.N.Vigdorovich, V.P.Batura (Moscow Inst. of Electronic Engng., Moscow, USSR). *Inorg. Mater. (USA)*, vol.18, no.10, p.1454-7 (Oct. 1982). Translation of: *Izv. Akad. Nauk SSSR Neorg. Mater.*, vol.18, no.10, p.1693-6 (Oct. 1982). [received: Sept. 1983]

With the use of simplex-centroid design the liquidus surface of the In-InP-GaAs-InAs system has been constructed. Analysis of the results obtained establishes that in a quaternary section of this system at constant indium content an increase in the indium phosphide concentration increases the liquidus temperature, an increase in the indium arsenide concentration has the opposite effect, while a change in the gallium arsenide concentration has no significant effect on the liquidus temperature, at constant concentration ratio of the other two compounds. (6 refs.)

114135 Solidification processes in saline solutions. B.Rubinsky (Dept. of Mech. Engng., Univ. of California, Berkeley, CA, USA). *J. Cryst. Growth (Netherlands)*, vol.62, no.3, p.513-22 (Aug. 1983).

A numerical study using a 'front tracking' finite element method, has been performed to investigate, in conjunction with the Mullins-Sekerka stability criteria, the stability of a one-dimensional planar phase change interface (ice-water) during the solidification of a binary aqueous-saline solution, for various thermal initial and boundary conditions and various initial solute concentrations. Transient heat and mass transfer equations were solved in the solid and liquid regions. The forced convection caused by change in density between ice and water was considered. The results indicate that the proposed method can be employed to determine the morphology of a phase change interface as a function of exterior thermal boundary conditions and to determine the transition between a stable planar front and an unstable (perturbed) front. (21 refs.)

114136 On the physics of state transition. G.V.Abi-Ghanem, V.V.Nguyen (Dept. of Civil Engng., Princeton Univ., Princeton, NJ, USA). *J. Phys. A (GB)*, vol.16, no.14, p.3401-8 (1 Oct. 1983).

In the melting of a solid crystalline medium, the shear modulus changes abruptly to zero. This behaviour can be explained firstly by representing the stress tensor in terms of the correlation function and the potential of interaction of the system and secondly by using an extension of Ruelle's criterion (1977) for thermodynamic stability. (17 refs.)

114137 Localized volume deficiencies as an effect of spherulite growth. I. The two-dimensional case. A.Galeski, E.Piorkowska (Centre of Molecular & Macromolecular Studies, Polish Acad. of Sci., Lodz, Poland). *J. Polym. Sci. Polym. Phys. Ed. (USA)*, vol.21, no.8, p.1299-312 (Aug. 1983).

Two-dimensional spherulite growth leads to the encirclement of regions of molten polymer in a polymer film. On further crystallization localized volume defects arise, resulting in thin spots in the film. Since this effect lowers the mechanical strength of films, the authors call these volume defects 'weak spots'. A computer program is developed to evaluate the number, size, and shape of such volume defects for athermal, thermal, and mixed modes of primary nucleation of spherulites. It is shown that the total area of weak spots exceeds 10% of the sample area for all types of nucleation studied. The largest weak spots arise in samples crystallized via athermal and mixed nucleation; their size is of the same order as that of an average spherulite. Formation of weak spots is observed in thin films of poly(ethylene oxide) and poly(methylene oxide). The disadvantageous role of weak spots is confirmed by observation of electric breakdown occurring preferentially in weak spots in polypropylene films. (7 refs.)

114138 Localized volume deficiencies as an effect of spherulite growth. II. The three-dimensional case. A.Galeski, E.Piorkowska (Centre of Molecular & Macromolecular Studies, Polish Acad. of Sci., Lodz, Poland). *J. Polym. Sci. Polym. Phys. Ed. (USA)*, vol.21, no.8, p.1313-22 (Aug. 1983). For pt.1 see *ibid.*, vol.21, no.8, p.1299-312 (1983). As in the two-dimensional case, the density change due to crystallization leads to a buildup of internal strain in some regions of a polymer melt occluded by growing spherulites. The occluded parts of the sample are called 'weak spots.' Computer simulation of spherulite growth in bulk samples shows that the largest weak spots have the size of an average spherulite. The total volumes of weak spots are 0.47, 0.094, and 0.119% of the sample for athermal, thermal, and mixed primary nucleation, respectively. The weak spots in the bulk material exhibit distance correlation. Within weak spots, internal strain is released (Raman spectroscopy), and holes develop. Polypropylene bulk spherulite samples contain holes distinctly visible under a microscope with infrared optics and illumination. The number of visible holes is in agreement with the computer prediction. The increase of impact strength with decreasing spherulite size is explained in terms of changes in the number and size of weak spots. (23 refs.)

114139 Retardation of spherulitic growth rate in the crystallization of isotactic polystyrene due to the presence of nucleant. M.A.Kennedy, G.Turturro, G.R.Brown, L.E.St-Pierre (Dept. of Chem., McGill Univ., Montreal, Canada).

J. Polym. Sci. Polym. Phys. Ed. (USA), vol.21, no.8, p.1403-13 (Aug. 1983). Although the rate of heterogeneous nucleation of crystallization in isotactic polystyrene, as studied by photomicroscopy, is markedly increased by addition of fine-particle silica, the rate of subsequent radial growth of spherulites formed is diminished. The latter observation is rationalized on the basis of a modified Hoffman-Lauritzen treatment wherein the nucleant is depicted as a quasicrosslink which impedes the transport of polymer segments. (20 refs.)

114140 Calculation of phase equilibria of ternary additive molten salt systems with a common anion. I.J.Gal (Dept. of Chem., Univ. of Belgrade, Belgrade, Yugoslavia), I.J.Zsigrai, I.Paligoric, K.Szecsényi-Meszaros. *J. Chem. Soc. Faraday Trans. 1 (GB)*, vol.79, pt.9, p.2171-8 (Sept. 1983). Phase diagrams for ternary additive systems $\text{LiF}+\text{NaF}+\text{KF}$, $\text{LiF}+\text{NaF}+\text{CaF}_2$, $\text{LiF}+\text{NaF}+\text{SrF}_2$ and $\text{NaF}+\text{KF}+\text{SrF}_2$ have been calculated a priori using a set of readily available physical parameters for each component. The method of calculation is based on a simple ion-interaction model developed for binary molten salt systems and now extended to ternary additive salt mixtures. Calculated and experimentally derived phase diagrams are compared and discussed. (18 refs.)

114141 The precipitation and characterization of cobalt (II) oxalate tetrahydrate. E.Wisgerhof, J.W.Geus (Dept. of Inorganic Chem., Univ. of Utrecht, Utrecht, Netherlands).

Mater. Res. Bull. (USA), vol.18, no.8, p.993-1000 (Aug. 1983). Mixing of solutions of Co^{2+} and $\text{C}_2\text{O}_4^{2-}$ ions can lead to crystallization of cobalt (II) oxalate both as a tetrahydrate and a dihydrate. Up to about 60°C acicular crystallinities of a greyish pink tetrahydrate initially result. In a period depending mainly on the temperature and to a lesser extent on the degree of supersaturation and the $[\text{C}_2\text{O}_4^{2-}]/[\text{Co}^{2+}]$ ratio, the precipitated tetrahydrate recrystallizes to β -cobalt (II) oxalate, a bright pink dihydrate. The two cobalt (II) oxalates have been distinguished by means of X-ray diffraction (XRD), (electron)microscopy and thermal analysis. The d-values and relative peak heights of the most pronounced maxima of the XRD-pattern of the tetrahydrate are presented, as these are not available in standard reference works. (7 refs.)

114142 On cellular instability in the solidification of a dilute binary alloy. G.I.Sivashinsky (Lawrence Berkeley Lab., Univ. of California, Berkeley, CA, USA).

Physica D (Netherlands), vol.8D, no.1-2, p.243-8 (July 1983). In the solidification of a dilute binary alloy, a planar solid-liquid interface is often found to be unstable, spontaneously assuming a cellular structure. If the solute rejection coefficient is close to unity, then, near the stability threshold, the characteristic cell size may significantly exceed the diffusional width of the solidification zone. This situation enables one to derive an asymptotic nonlinear equation which directly describes the dynamics of the onset and stabilization of cellular structure: $f_t + \nabla^2 f + \nabla[(2-f)\nabla f] + af = 0$. (12 refs.)

114143 The supercooling of the water droplets. R.Shimomura, K.Ichimiya, T.Miyazawa, Y.Hanada, Y.Shintani. *Refrigeration (Japan)*, vol.58, no.666, p.339-45 (April 1983). In Japanese.

In order to study the freezing of supercooled water, measurements were made of the freezing point of water droplets, ranging from 1.2 mm to 4.00 mm in diameter, suspended at the interface of two insoluble liquids and cooled at rates of 0.13-0.75°C/min. The relation between the degree of supercooling, the cooling rate and the diameter of water droplets was arranged experimentally by using probability of freezing. Additionally, the relation was generally extended by three kinds of dimensionless parameters which were obtained by dimensional analysis. (14 refs.)

114144 Melting in a two-dimensional system with dipolar interactions. V.M.Bedanov, G.V.Gadiyak, Yu.E.Lozovik (Inst. of Theoretical & Appl. Mech., Acad. of Sci., Novosibirsk, USSR).

Sov. Phys.-Solid State (USA), vol.25, no.2, p.328-9 (Feb. 1983). Translation of: *Fiz. Tverd. Tela (USSR)*, vol.25, no.2, p.577-80 (Feb. 1983). [received: Sept. 1983]

The authors use molecular dynamic methods to study the phase transition in a system of classical dipoles and discuss qualitative and quantitative differences between such a system and a system of classical electrons moving in a homogeneous positively charged background. They assume that all the dipoles are oriented in the vertical direction and can move freely in the horizontal plane. (11 refs.)

114145 Dislocation mechanism of crystal melting. S.P.Obukhov (L.D. Landau Inst. of Theoretical Phys., Acad. of Sci., USSR).

Sov. Phys.-JETP (USA), vol.83, no.5, p.1144-7 (Nov. 1982). Translation of: *Zh. Eksp. & Teor. Fiz. (USSR)*, vol.83, no.5, p.1978-84 (Nov. 1982). [received: Sept. 1983]

A field model is constructed for the description of a system of interacting dislocation lines. In this model the liquid-crystal transition corresponds to the appearance of infinitely long (unclosed) dislocation lines. It is shown that this transition is of first order. (10 refs.)

114146 Evaluation of kinetic parameters from non-isothermal experiments: Application to crystallization kinetics. T.Kemeny, L.Granasy. *Report KFKI-1983-73*, Hungarian Acad. Sci., Budapest (1983), 10 pp.

Kinetic parameters are usually evaluated from nonisothermal experiments by supposing the same form of the rate equation in isothermal and dynamic investigations. The capabilities and limitations of this approach will be discussed. The applicability of the alternative hypothesis where the transformed fraction is a state function of its variables and the rate equation is different under isothermal and nonisothermal conditions is highly questionable for any processes. This approach is definitely invalid for crystallization kinetics as it contradicts the formal theory of solid state transformations. (27 refs.)

114147 Solidification front dynamics in model systems. A.Ecker, P.R.Sahm (Aachen Inst. of Technol., Aachen, Germany).

Proceedings of the 4th European Symposium on Materials Sciences under Microgravity (ESA SP-191), Madrid, Spain, 5-8 April 1983 (Paris, France: ESA 1983), p.331-6

Optical methods are particularly useful for the analysis of solidification phenomena in transparent model systems. The authors describe work carried out on thermo-solutal boundary layers which interact with 'macroscopic' convective melt movement. Both pure and alloyed succinonitrile probes are investigated. The measurement system ODES (optical diagnostic experiment system) has been mounted around a 'transparent mold' that is controllable with respect to temperature gradients, velocity of the melt and also growth velocities of the crystallization front. The particular research is being performed in preparation of the German D1-Mission by the experiment GETS (boundary layers in transparent solidifying melts). The results are to be checked against existing stability criteria of the solidification front. (7 refs.)

114148 Solidification of Pb-Sn alloys under microgravity conditions. L.L.Regel, I.V.Barmine, A.M.Durachenko (Space Res. Inst., Acad. of Sci., Moscow, USSR), L.Oyunbiling.

Proceedings of the 4th European Symposium on Materials Sciences under Microgravity (ESA SP-191), Madrid, Spain, 5-8 April 1983 (Paris, France: ESA 1983), p.417-20

Discusses the experimental results of studying the effect of microgravity conditions on a homogenization of metal melts and on a subsequent bulk crystallization using Pb-Sn alloys as an example. The experiment was carried out on board the Salyut-6 station following the ALTAI Soviet-Mongolian program. (4 refs.)

114149 Periodic crystallization of binary melts under diffusion-controlled mass transfer. L.L.Regel, Nguyen Thanh Nghi (Space Res. Inst., Acad. of Sci., Moscow, USSR).

Proceedings of the 4th European Symposium on Materials Sciences under Microgravity (ESA SP-191), Madrid, Spain, 5-8 April 1983 (Paris, France: ESA 1983), p.421-7

The peculiarities of the crystallization process from the liquid phase under purely diffusion mass transfer conditions leading to the macroperiodic variations of crystal composition and structural perfection are considered. The results of a number of the crystal growth experiments are given in which the periodic composition distribution with large period and amplitude of fluctuations were observed. The criteria for the choice of technological parameters of growth process with account for phase diagram and component diffusion coefficients of concrete systems for preventing the macroinhomogeneity in the crystals grown are discussed. (16 refs.)

114150 Directional crystallization of PbTe under microgravity conditions. L.L.Regel, Nguyen Thanh Nghi, O.I.Rachmatov (Inst. for Space Res., Acad. of Sci., Moscow, USSR).

Proceedings of the 4th European Symposium on Materials Sciences under Microgravity (ESA SP-191), Madrid, Spain, 5-8 April 1983 (Paris, France: ESA 1983), p.429-33

The PbTe undoped single crystals were grown by directional crystallization from partially remelted cylindrical ingots in the [100] direction in the Splay furnace under microgravity conditions and on Earth. The surface morphology, structural perfection and electrical physical parameters of the space- and earth-grown crystals were comparatively investigated. The differences in morphological characteristics of space- and earth-grown PbTe crystal were found. Significant inhomogeneities were observed both in space- and earth-grown ingots which indicate a nonsteady-state of the growth process. (2 refs.)

Oscillatory convection in a spherical cavity due to G-jitterSee Entry 113444

Inherent structure in waterSee Entry 113715

Studies on dilute solutions of rodlike macroions. I. Light scattering, densitometry, and cryoscopySee Entry 113719

Self-diffusion of macromolecules in the crystallization of a polymer from solutionSee Entry 113758

Spectroscopic characterization of solvent-induced crystallization of PETSee Entry 113764

Crystallization of quartz from fluoride solutionsSee Entry 113775

Production and properties of crystals of complex refractory oxides with perovskite structureSee Entry 113776

Experiments on crystallization of semiconductors aboard Salyut 6-Soyuz orbital complexSee Entry 113789

Vacancies in concentrated alloysSee Entry 113887

Study of vacancy-solute interactions in dilute Al based alloys by thermal equilibrium measurements of positron annihilationSee Entry 113969

Direct observation of the melting of a semiconductor during pulsed laser annealingSee Entry 114000

Crystallization processes [laser annealing of semiconductors]See Entry 114002

A comparison of CW laser and electron-beam recrystallization of polysilicon in multilayer structuresSee Entry 114017

Laser annealing of ion implanted semiconductorsSee Entry 114020

Hard-sphere fluid-to-solid transition and the virial expansionSee Entry 114123

Effect of interplane coupling in quasi-two-dimensional systemsSee Entry 114124

- Determination of the phase ranges during cooling and heating of Al-40 wt.-% (0-3) wt. % Mg alloys See Entry 114155
- Interpretation of the enthalpy in a discretised multidimensional region undergoing a melting/freezing phase change See Entry 114208
- The influence of fusion temperature on the defect center concentration of GeO₂ glass See Entry 114733
- A new interpretation of spectral data on SbCl₅OSeCl₂ See Entry 114836
- The study of thermal equilibrium defects and melting in indium by two-parameter correlation measurement of positron annihilation See Entry 114956
- Flow-induced crystallization by surface growth of polyethylene fibers See Entry 115041
- Possibility of melting of silica particles in a plasma jet See Entry 115053
- Skin technology—fundamentals and applications See Entry 115123
- A thermodynamic analysis of the Cu-O system with an associated solution model See Entry 115175
- Strontium as a modifier for aluminium-silicon-copper alloys See Entry 115181
- Unidirectional growth of dilute Bi-Sb alloys See Entry 115182
- Directionally solidified structure and mechanical properties in monovariant Al-Fe-Ni eutectic alloy See Entry 115183
- An analysis of local flow effects in flow-induced orientation and crystallization See Entry 115184
- The formation of coarse intermetallics in rapidly solidified Al-Co alloys See Entry 115185
- Analysis of the effect of the comparative number of primary crystals on the kinetics of peritectic transformation See Entry 115186
- Formation of defects during the solidification of alloys in a two-dimensional region with a short-life internal heat sink See Entry 115187
- Non-equilibrium phases in laser-processed Fe-0.2 wt. % C-20 wt. % Cr alloys See Entry 115425

64.70F Liquid-vapour transitions

- 114151 Vaporisation of tungsten bronzes. II. Sodium and potassium tungsten bronzes. N.J.Clark, P.L.Mart (School of Phys. Sci., Flinders Univ. of South Australia, Bedford Park, Australia). *Mater. Res. Bull. (USA)*, vol.18, no.8, p.951-8 (Aug. 1983). Thermodynamic calculations indicate that the disproportionation of sodium tungsten bronze is expected to occur at a lower temperature than that required for direct decomposition via congruent vaporisation. This expectation has been tested for cubic sodium bronzes and also for cubic europium and cerium bronzes, a tetragonal II potassium bronze and hexagonal bronzes of potassium, indium and thallium. Knudsen weight loss and Knudsen mass spectrometry results confirm that disproportionation is the dominant reaction for cubic and tetragonal bronzes. The hexagonal bronzes are resistant to disproportionation and vaporisation of K_{0.22}WO₃ occurs by the following K_{0.22}WO₃(s)→0.22K(g)+0.14 O₂(g)+0.056 W₁₈O₄₉(s) with an enthalpy of vaporisation of 405 kJ mol.⁻¹. (15 refs.)
- 114152 Computation of the steam-liquid equilibrium of ternary systems. G.S.Gottschling, H.-J.Wohner (Krupp-Koppers GmbH, Essen, Germany). *Tech. Mitt. Krupp Forschungsber. (Germany)*, vol.41, no.1, p.49-57 (July 1983). In German. An outline is given of a process in which actual mixing behaviour is described by the activity coefficients of liquids. From it is developed a program for programmable pocket calculators (TI-59/PC 100 C) with which phase equilibrium computations for ternary systems can be easily carried out. (17 refs.)
- High-temperature calorimeter for the measurement of vapor pressure and enthalpy of vaporization See Entry 111684
- Electrical conductivity of alkali metal vapors in the neighborhood of the critical point See Entry 113556
- Electron diffraction studies of supersonic jets. V. Low temperature crystalline forms of SF₆, SeF₆, and TeF₆ See Entry 113824
- Emission of melt during laser vaporization of metallic films See Entry 113999
- Formation of a liquid crystal phase in the conversion of isotropic solutions of cellulose acetates into the solid state See Entry 114171
- Enthalpy-concentration data for the system ethanol-toluene See Entry 114209
- Theory of the Leidenfrost phenomenon See Entry 114301
- Electron phase transitions in highly anisotropic two-dimensional systems See Entry 114460
- Experimental investigation of positron self-trapping near the vapour-liquid critical point of helium-4 See Entry 114954
- The role of metal-zeolite interactions in indirect liquefaction catalysis See Entry 115579

64.70H Solid-vapour transitions

- 114153 Dynamics of NH₄Cl particle nucleation and growth at 253-296K. J.F.Henry, A.Gonzalez, L.K.Peters (Dept. of Chem. Engng., Univ. of Kentucky, Lexington, KY, USA). *Aerosol Sci. & Technol. (USA)*, vol.2, no.3, p.321-39 (1983). Particle dynamics in the NH₃-HCl-NH₄Cl particle system are modeled for particle growth times exceeding the induction time for the initial appearance of particles. The model results of Dhalin et al. (1981) at 296K are confirmed, and the appropriate microscopic surface free energy is practically independent of reactant concentrations over small concentration ranges at 296K. Over larger concentration ranges, the value of the surface free energy required to explain the data varies appreciably, increasing as initial reactant concentration increases. At relatively long particle growth times, diffusional growth together with coagulation adequately describes the experimental data, although the coagulation coefficient must be increased over the Brownian value to account for other effects. Possible mechanisms such as cluster scavenging, charge-induced coagulation, particle evaporation and NH₄Cl vapor formation on reactor walls apparently do not affect the model predictions even at small particle growth times. (52 refs.)
- Experiments on crystallization of semiconductors aboard Salyut 6-Soyuz orbital complex See Entry 113789
- Vapor pressure of dysprosium in the Dy-Pt system See Entry 115164

64.70J Liquid-liquid transitions

- Lattice theory of binary fluid mixtures: phase diagrams with upper and lower critical solution points from a renormalization-group calculation See Entry 113711
- Diffusion coefficient of a binary stratifying system along the coexistence curve See Entry 114231

64.70K Solid-solid transitions

(see also 61.50K Crystallographic aspects of polymorphic and order-disorder transformations, 81.30H, 81.30K, 81.30M Microstructures developed by solid-solid phase transformations)

- 114154 Structural transformations and their precursors. T.R.Finlayson (Phys. Dept., Monash Univ., Clayton, Victoria, Australia). *Aust. J. Phys. (Australia)*, vol.36, no.4, p.553-63 (1983). For a number of materials which exhibit a change of structure on being cooled below a certain temperature T_m , some physical properties display anomalous behaviour at temperatures above T_m . The particular structural transformations in mind have been broadly classified as 'martensitic' and the anomalous physical properties as 'precursive phenomena'. Some debate exists regarding the role of the precursive phenomenon in the kinetics of the structural transformation. The most direct evidence for 'martensite precursors' is obtained from electron diffraction, although various indirect evidence is contained in X-ray, neutron and γ -ray diffraction and various physical properties, for example, elastic constants and thermal expansion. In the paper current understanding of 'martensite precursors' is reviewed and examples of data from the Al₅ structure compounds V₃Si and Nb₃Sn, In-Tl and Ti-Ni alloys are discussed. (33 refs.)
- 114155 Determination of the phase ranges during cooling and heating of Al-40 wt.-% (0-3) wt. % Mg alloys. B.Major, R.Ciach, G.Wendrock, H.Löffler (Inst. für Metallforschung, Polnischen Akad. der Wissenschaften, Krakow, Poland). *Cryst. Res. & Technol. (Germany)*, vol.18, no.8, p.1021-8 (1983). The various phases and the respective ranges of their existence were determined during continuous cooling from temperatures close below the solidus line to RT with a rate of 2K min.⁻¹ as well as during the subsequent heating in few Al-Zn(40 wt.%)Mg(X) alloys (X=0; 0.5; 1.0; and 3.0 wt.%) by means of X-ray phase-analysis, small angle X-ray scattering, differential thermo-analysis, optical microscopy, and X-ray micro-analysis. The most striking features are that even addition of only 0.5 wt. % Mg cause the formation of precursors of the MgZn₂ equilibrium phase few degrees below the solidus line. (7 refs.)
- 114156 Thermodynamic theory of phase transitions in solid solutions based on lead metaniobate. I.L.Kraizman, V.P.Sakhnenko (Rostov State Univ., Rostov, USSR). *Inorg. Mater. (USA)*, vol.18, no.10, p.1395-8 (Oct. 1982). Translation of: *Izv. Akad. Nauk SSSR Neorg. Mater.*, vol.18, no.10, p.1628-31 (Oct. 1982). [received: Sept. 1983] It is shown that phase transitions in lead niobate, lead tantalate, and their solid solutions can be described by a single thermodynamic potential with second-order parameters. The x, T phase diagram for the solid solutions Pb(Nb_{1-x}Ta_x)₂O₆ should contain two closely situated triple points and a critical point. An assumption is expressed that the paraelectric phase of lead tantalate is crystallized into the space group D_{2h}¹⁷ or D_{2h}¹⁸. The ferroelectric transition in lead tantalate is a transition close to the critical point. (9 refs.)
- 114157 Pressure-induced phase transition of HgS. T.Huang, A.L.Ruoff (Dept. of Materials Sci. & Engng., Cornell Univ., Ithaca, NY, USA). *J. Appl. Phys. (USA)*, vol.54, no.9, p.5459-61 (Sept. 1983). The high pressure phase transition of cinnabar (α -HgS) was studied by energy dispersive X-ray diffraction using a synchrotron X-ray source. The cinnabar crystal structure was found to transform to the sodium-chloride structure at about 130 kbar. The lattice parameter of the new phase was determined to be 5.070±0.005 Å at 300 kbar. No further phase transition was observed up to 400 kbar. (18 refs.)
- 114158 Critical fluctuations at the phase transition in benzil. A.Yoshihara, E.R.Bernstein, J.C.Raich (Depts. of Chem. & Phys., Colorado State Univ., Fort Collins, CO, USA). *J. Chem. Phys. (USA)*, vol.79, no.6, p.2504-14 (15 Sept. 1983). New Brillouin scattering data are presented for benzil single crystals near the phase transition at 83.5K. These data demonstrate that for the c₁₁ governed longitudinal acoustic (LA) mode at ~15 GHz, critical fluctuations are quite large near the phase transition and dominate the behaviour of this mode within +40K of the transition. These observations are analyzed in terms of four contributing soft modes: an optical soft mode and two transverse acoustic (TA) soft modes at the zone center and a zone boundary M-point soft mode. It is argued that the zone boundary mode is the major contributor to the width and elastic constant anomalies of the LA mode. Calculations of these properties support these conclusions. Critical exponents are evaluated for Δc_{11} and $\Delta \Gamma_{\text{ac}}$, the critical contributions to the elastic constant and width of the c₁₁ governed LA mode, based on the experimental data. (22 refs.)
- 114159 Phase transitions in Pb₃(P_{1-x}As_xO₄)₂: influence of the central peak and flip mode on the Raman scattering of hard modes. E.Salje, V.Devarajan, U.Bismayer, D.M.C.Guimaraes (Inst. für Kristallographie und Petrographie, Univ. Hannover, Hannover, Germany). *J. Phys. C (GB)*, vol.16, no.27, p.5233-43 (30 Sept. 1983). The integrated intensities and full width at half maximum (FWHM) of the 80 cm⁻¹ Raman bands (hard modes) of ferroelastic Pb₃(PO₄)₂ and Pb₃(P_{0.77}As_{0.23}O₄)₂ were investigated in both the ferro and 'intermediate' phases for different polarisations as functions of temperature. The observed behaviour of these quantities has been interpreted in terms of interactions of hard modes with the central peak, flip mode and soft mode. The consequences of the three-component order parameter interpretation of the phase transition are also discussed. The integrated intensity curves in the 'intermediate' phase revealed a 'precursor order parameter' type of dependence. The numerical value of this 'precursor order parameter' at T_c is also estimated for Pb₃(PO₄)₂. From the FWHM versus temperature curves in the 'intermediate' phase, the flip mode frequency is estimated to be 3×10¹⁰ Hz. (21 refs.)
- 114160 Mossbauer and X-ray structure studies on the phase transition in the Fe(III) dimethylsulfoxide complex. I.G.Gusakovskaya, T.I.Larkina, V.I.Ponomarev, L.O.Atomyan (Inst. of Chem. Phys., Acad. of Sci., USSR). *J. Struct. Chem. (USA)*, vol.23, no.6, p.864-9 (Nov.-Dec. 1982). Translation of: *Zh. Strukt. Khim. (USSR)*, vol.23, no.6, p.53-8 (Nov.-Dec. 1982). [received: Sept. 1983] Spectrometry, calorimetry, and X-ray structure analysis have been used to examine the structure of the [Fe(DMSO)₅Cl]²⁺ cation in the [Fe(DMSO)₅Cl][Fe₂Cl₆O] complex over a wide temperature range. There is a

first-order phase transition in the cation associated with position change in one of the five DMSO addends from the octahedral environment of the Fe ion. (12 refs.)

114161 Physics of diffused phase transitions in silver chalcogenides. B.N.Rolov. *Lav. PSR Zinat. Akad. Vestis Fiz. Teh. Zinat. Ser. (USSR)*, no.4, p.33-6 (1983). In Russian.

The thermodynamic theory of diffused phase transitions in silver chalcogenides is considered. The correspondence of the observed substance phase transitions in this group to the general theory of diffused phase transitions in condensed matter is treated. In correspondence to experimental data the main characteristics of the switching function are evaluated. The minimum volume of the sharp phase transition is calculated. The proposed mechanism of phase transitions in chalcogenides is considered. (6 refs.)

114162 Absence of pressure-induced valence change in CeAs. A.Werner, H.D.Hochheimer (Max-Planck-Inst. fur Festkörperforschung, Stuttgart, Germany), R.L.Meng, E.Bucher.

Phys. Lett. A (Netherlands), vol.97A, no.5, p.207-9 (29 Aug. 1983). The pressure-volume relationship for cerium monoarsenide has been determined up to a pressure of 32 GPa using energy dispersive X-ray diffraction. Contrary to expectations based on the behaviour of CeP, cerium arsenide does not show a pressure-induced valence change in this pressure range. Instead the authors find a structural transition from the NaCl-type to the CsCl-type structure, which exhibits a large hysteresis. Contrary to other results the value of the bulk modulus ($B_0 = 69 \pm 1$ GPa) agrees well with the value expected from an Anderson-Nafe plot for CeAs with the Ce ion in the trivalent state. (11 refs.)

114163 Proton dynamics at the ferroelastic phase transition in $\text{KH}_2(\text{SeO}_3)_2$. Y.Yamada, Y.Noda, Y.Endoh (Faculty of Engng. Sci., Osaka Univ., Osaka, Japan).

Physica B & C (Netherlands), vol.120B+C, no.1-3, p.270-4 (May 1983). (Yamada Conference VI on Neutron Scattering in Condensed Matter, Hakone, Japan, 1-4 Sept. 1982).

The authors observed the neutron inelastic scattering at the ferroelastic phase transition point of $\text{KH}_2(\text{SeO}_3)_2$ in order to investigate the dynamical properties of proton tunneling and its role in triggering the phase transition. The parameters ω_p (tunneling frequency), γ_p (damping constant of proton motion), and G (effective coupling constant between phonons and protons) have been determined by fitting the obtained profiles of neutron spectra in the (k - ω) space at various temperatures. It has been shown that $\hbar\omega_p \ll kT_c$, which excludes the possibility that the dynamical property of protons is the essential origin of the large isotope effect in this substance. (10 refs.)

114164 Neutron diffraction and scattering study on M_xWO_3 ($\text{M}=\text{Rb}$ and K). M.Sato, H.Fujishita, A.R.Moodenbaugh, S.Hoshino, B.H.Grier (Inst. for Solid State Phys., Univ. of Tokyo, Tokyo, Japan).

Physica B & C (Netherlands), vol.120B+C, no.1-3, p.275-9 (May 1983). (Yamada Conference VI on Neutron Scattering in Condensed Matter, Hakone, Japan, 1-4 Sept. 1982).

To study the relationship between the lattice instability and the superconductivity of nonstoichiometric hexagonal tungsten bronze, M_xWO_3 , neutron diffraction and scattering studies were made. Two types of the structural phase transitions were observed. One is associated with the distortion of the corner linked WO_6 octahedra. The other is associated with the ordering of the M atoms which partially fill the sites in the WO_3 cage. A long period modulation of the structure appears for some values of x at low temperature. A discussion on the x dependence of the superconducting transition temperature is presented. (10 refs.)

114165 Neutron spectroscopy of anilinium bromide. B.P.Schweiss, H.Fuess, G.Flecher, A.Weiss (Inst. fur Kristallographie und Mineralogie, Univ. Frankfurt am Main, Frankfurt am Main, Germany).

Physica B & C (Netherlands), vol.120B+C, no.1-3, p.300-4 (May 1983). (Yamada Conference VI on Neutron Scattering in Condensed Matter, Hakone, Japan, 1-4 Sept. 1982).

The phase transition from the orthorhombic high temperature phase (I) to the monoclinic low temperature phase (II) in anilinium bromide which occurs at $T_c = 296.9\text{K}$ was studied by incoherent inelastic neutron scattering. Time-of-flight data were obtained from a hydrogenated $\text{C}_6\text{H}_5\text{NH}_2\text{Br}$ and partially deuterated samples ($\text{C}_6\text{D}_5\text{NH}_2\text{Br}$ and $\text{C}_6\text{H}_5\text{ND}_2\text{Br}$) below and above the transition temperature. Phonon frequency distributions in the range of the intermolecular vibrations were derived from the spectra. The analysis of the quasielastic line revealed substantial broadening. The interpretation lead to reorientational jump processes in the orthorhombic phase (I) and—with a markedly diminished rate—in the monoclinic phase (II). The activation energies were estimated for both phases. (12 refs.)

114166 Phase transitions between incommensurate phases in systems with a four-component order parameter illustrated for BaMnF_4 . V.A.Golovko (Evening Inst. of Metall., Moscow, USSR).

Sov. Phys.-Solid State (USA), vol.25, no.2, p.314-15 (Feb. 1983). Translation of: *Fiz. Tverd. Tela (USSR)*, vol.25, no.2, p.557-9 (Feb. 1983). [received: Sept. 1983]

In contrast to systems described by a two-component order parameter, which have been studied extensively, incommensurate phases of different symmetries can occur for systems described by a many-component order parameter (depending on crystal parameters). Changes in external parameters may lead to phase transitions between various incommensurate phases as in the case of commensurate phases. The author studies phase transitions between incommensurate phases of BaMnF_4 crystals for which an incommensurate phase is described by a four-component order parameter. (8 refs.)

114167 Effect of pressure on the phase transitions in the elpasolites $\text{Cs}_2\text{NaB}^{3+}\text{Cl}_6$. M.V.Gorev (L.V. Kirenskii Phys. Inst., Acad. of Sci., Krasnoyarsk, USSR).

Sov. Phys.-Solid State (USA), vol.25, no.2, p.320-1 (Feb. 1983). Translation of: *Fiz. Tverd. Tela (USSR)*, vol.25, no.2, p.566-8 (Feb. 1983). [received: Sept. 1983]

The author reports a study of the influence of pressure up to 5 kbar on the phase transitions in three crystals of the family $\text{Cs}_2\text{NaB}^{3+}\text{Cl}_6$ ($\text{B}^{3+}=\text{Bi}$, Nd , or Pr). Differential thermal analysis (DTA) with a copper-germanium thermocouple was used to detect the transition. (8 refs.)

114168 Influence of the degree of purity on high-temperature phase transitions in samarium. A.T.Burkov, M.V.Vedernikov, T.V.Nikiforova, N.N.Rytus (A.F. Ioffe Physicotech. Inst., Acad. of Sci., Leningrad, USSR).

Sov. Phys.-Solid State (USA), vol.25, no.2, p.323-4 (Feb. 1983). Translation of: *Fiz. Tverd. Tela (USSR)*, vol.25, no.2, p.570-2 (Feb. 1983). [received: Sept. 1983]

On the whole, investigations conducted to date do not enable one to say whether one or two phase transformations exist in samarium between 500 and 1000K, whether they exist in perfectly pure samarium, and how the degree of purity of the metal affects the transformation temperature. To clarify these

questions the authors have made a detailed investigation of the thermoelectromotive force and the electrical resistivity of samarium of two different degrees of purity at temperatures ranging from 300 to 1300K. (11 refs.)

114169 Statistical model of the phase transition in $\text{KH}_2(\text{SeO}_3)_2$. R.Kh.Sol'tsas, V.E.Shneider (Inst. of Semiconductor of Phys., Acad. of Sci., Lithuanian SSR).

Sov. Phys.-Crystallogr. (USA), vol.28, no.2, p.123-6 (March-April 1983). Translation of: *Kristallografiya (USSR)*, vol.28, no.2, p.213-18 (March-April 1983). [received: Sept. 1983]

A statistical model of the phase transition in $\text{KH}_2(\text{SeO}_3)_2$ is constructed on the assumption that the transition causes ordering of one of the three nonequivalent hydrogen ions in the molecule. Tunneling of this proton under the potential barrier is neglected. The thermodynamic properties of the model are studied in the cluster approximation. A comparison is made with the available experimental data for $\text{KH}_2(\text{SeO}_3)_2$ and $\text{KD}_2(\text{SeO}_3)_2$. The correspondence between the micromechanisms of the phase transition in $\text{KH}_2(\text{SeO}_3)_2$ and $\text{NaH}_2(\text{SeO}_3)_2$ crystals is discussed. (18 refs.)

114170 The phase transitions and crystal structures of a new compound— Sr_2CaWO_6 . Fu Zhengmin, Li Wenxiu (Inst. of Phys., Acad. Sinica, Beijing, China), Liang Dongcai.

Sci. Sin. (China), vol.26, no.8, p.835-47 (Aug. 1983).

The phase transitions of the new compound Sr_2CaWO_6 have been investigated by means of DTA, X-ray powder diffraction, precise measurement of lattice parameters and other methods. It has been discovered that the compound has a displacive phase transition of the first order. The low temperature phase, $\alpha\text{-Sr}_2\text{CaWO}_6$, belongs to orthorhombic crystal system, with space group $\text{Pmm}2$, lattice parameters at room temperature are: $a=8.2033\text{Å}$, $b=5.7676\text{Å}$ and $c=5.8489\text{Å}$, the measured density is $D_m=5.981\text{g/cm}^3$, and each unit cell contains two formula weight. The high temperature phase, $\beta\text{-Sr}_2\text{CaWO}_6$, belongs to the cubic system, with space group $\text{Fm}3m$ and the lattice parameter is $a=8.308\text{Å}$ at 900°C ; $z=4$. The crystal structures of $\alpha\text{-Sr}_2\text{CaWO}_6$ and $\beta\text{-Sr}_2\text{CaWO}_6$ have been determined by means of the X-ray polycrystal diffraction method. The character of the structures and the possibilities of phase transition are discussed. (4 refs.)

Phase transitions, creep, and fission gas behaviour in actinide oxides See Entry 112329

Phase transitions in $\text{Na}_2\text{Sc}_2(\text{PO}_4)_3$ and in related compounds with $\{[\text{M}_2(\text{EO}_4)_3]^{p-}\}_{300}$ frameworks See Entry 113794

Room-temperature structure of carbon monoxide at 2.7 and 3.6 GPa See Entry 113809

Ammonium trifluoroberyllate(II), $(\text{NH}_4)[\text{BeF}_3]$, at room temperature See Entry 113815

Structure of orthopyroxene-type and clinopyroxene-type magnesium germanium oxide MgGeO_3 See Entry 113816

Crystal chemistry, phase transitions, and physical properties of halide crystals with perovskite-like structure See Entry 113822

Kinetics of the order-disorder reaction under irradiation See Entry 113992

Shear elastic constant softening in $(\text{V}_{1-x}\text{Cr}_x)_2\text{O}_3$: second-order nature of the low temperature phase transition See Entry 114070

Shock compression of zirconia ZrO_2 and zircon ZrSiO_4 in the pressure range up to 150 GPa See Entry 114093

Neutron observations of phasons and amplitudons in incommensurate phases See Entry 114119

Incommensurate lattice instability in $[\text{N}(\text{CD}_3)_4]_2\text{ZnCl}_4$ See Entry 114120

Phase transformation in a linear polycrystal with a rate law of n -th order See Entry 114122

Solid-solution decomposition in CdS-CdTe films See Entry 114176

Heat capacity of zinc oxysulfate from 7.5 to 309.4K with a transition from 270 to 306K See Entry 114206

Thermodynamic properties and phase transitions of salt hydrates between 270 and 400K. II. $\text{Na}_2\text{CO}_3\cdot\text{H}_2\text{O}$ and $\text{Na}_2\text{CO}_3\cdot 10\text{H}_2\text{O}$ See Entry 114207

Neutron and calorimetric observation of a modulated structure in quartz just above the α - β phase transition See Entry 114215

Clean and adsorbate-induced surface phase transitions on $\text{W}\{100\}$ See Entry 114310

Phase formation and kinetics of the phase transition in Ag_2Se thin films See Entry 114396

Plasmastructural transformations in amorphous chalcogenide semiconductors See Entry 114423

Structural phase transitions and superconducting transition temperatures of hexagonal M_xWO_3 compounds See Entry 114633

Observations of crystalline and amorphous Sb films by Raman scattering See Entry 114839

Influence of repeated phase transitions on the annihilation of positrons in brass See Entry 114952

Short-range atomic order in the Fe-Ni system See Entry 115169

Kinetics of a polymorphic transition in an Ag-Zn alloy under the action of γ rays See Entry 115188

The cooling behavior of deep penetration welds undergoing austenite-ferrite transformation See Entry 115189

Electron microscopic investigation of the growth of martensite platelets See Entry 115190

Mechanism of formation of martensite single crystals as a result of plastic deformation of the alloys based on γ -Mn See Entry 115191

Structural and phase transition of γ' martensite in binary Cu-Al alloy during deformation See Entry 115192

Influence of the quenching temperature on the onset of the α - γ transition and mechanical properties of maraging steel See Entry 115193

Shape memory effect in martensitic transformations in TiNi-TiCu alloys See Entry 115194

Reversion of BCC α' martensite in Fe-Cr-Ni austenitic stainless steels See Entry 115195

Microstructural stability of γ' strengthened Co-Cr-Ti alloys See Entry 115224

Role of eutectoid transformation and grain size on the creep behaviour of mild steel See Entry 115266

Non-equilibrium phases in laser-processed Fe-0.2 wt.% C-20 wt.% Cr alloys See Entry 115425

- Decomposition of austenitic phase in work hardened steel samples, using hardness measurements See Entry 115464
- Dynamic compression of diopside and salite to 200 GPa See Entry 116080

64.70M Transitions in liquid crystals

- 114171** Formation of a liquid crystal phase in the conversion of isotropic solutions of cellulose acetates into the solid state. V.Yu.Yunusov, O.A.Khanchich, A.T.Serkov, M.T.Primkulov. *Vysokomol. Soedin. Ser. B (USSR)*, vol.25, no.6, p.395-6 (1983). In Russian. The conditions for the conversion of an isotropic solution into the mesomorphic state on evaporation of the solvent are studied, using solutions of cellulose diacetate and cellulose triacetate in mixtures of N-methylpyrrolidone with methylene chloride and butan-2-one as test materials. The structural changes occurring during evaporation are followed by means of low angle scattering of polarized light, polarization microscopy, and measurement of the light transmission intensity. The results show that after the evaporation of low boiling point solvents a liquid crystal phase is produced in solutions of cellulose diacetate and triacetate and anisometric structures characteristic of liquid crystal systems are formed. (5 refs.) *N.S.*
- 114172** Mesomorphic salts of pyrylium and thiopyrylium. V.Gionis, R.Fugnitto, H.Strzelecka (CNRS, Thiais, France), P.Le Barny. *Mol. Cryst. & Liq. Cryst. (GB)*, vol.95, no.3-4, p.351-8 (1983). In French. Some of the synthesis intermediate perchlorate salts of 2,6- λ diaryl pyrylium and thiopyrylium shown a mesomorphic behaviour. So the introduction of long alkyl or alkoxy chain substituents, in para position of the phenyls leads to liquid-crystals for both pyrylium and thiopyrylium perchlorates, but the mesomorphic phase is larger for the thiopyrylium ones. The systematic study of the position of the substituent in the phenyl cycle of pyrylium salts demonstrates that the meta-substituted compounds have a lower transition temperature (Cr-M) than the para. Finally the ortho ones do not exhibit a liquid-crystal behaviour. Between the dialcoxy-substituted pyrylium salts, only the ortho, meta ones show mesomorphic phase, and the effect of the introduction of the second alkoxy-chain is the decrease of the transition temperature (Cr-M). The latter leads to liquid crystals at room temperature. (15 refs.)
- New liquid crystalline tetrazine derivatives for guest-host displays See Entry 113730
- Thermotropic homopolylesters. III. Preparation and properties of polymers based on 4'-hydroxyphenyl-4-hydroxycinnamate See Entry 113735
- Dependence of the tilt angle on external forces for smectic-C and chiral smectic-C liquid crystals—measurement of the heat capacity of DOBAMBC See Entry 113737
- Anisotropy of electric properties in binary cholesteric mixtures See Entry 114771
- Pretransitional anomalies in the rotation of the plane of polarization of light in ferroelectric liquid crystals See Entry 114821

64.70P Glass transitions

- 114173** Glass formation region and electrical conductivity in the system $B_2O_3-Li_2O-Li_3PO_4$. B.Basu, H.S.Maiti, A.Paul (Materials Sci. Centre, Indian Inst. of Technol., Kharagpur, India). *Bull. Mater. Sci. (India)*, vol.5, no.1, p.21-8 (March 1983). [received: Sept. 1983]
- The glass formation region was determined for the $B_2O_3-Li_2O-Li_3PO_4$ system. Under the present experimental conditions, binary lithium borate glasses could be formed containing a maximum of 27 mol.% Li_2O . However, this could be increased to 36 mol.% in the ternary system. Electrical conductivity was measured at temperatures ranging from room temperature to 350°C. The temperature dependence of the electrical conductivity of these glasses follows an Arrhenius equation. The conductivity increased with increasing alkali content. Maximum conductivity of the order of $10^{-4} \text{ ohm}^{-1} \text{ cm}^{-1}$ was obtained with the glass containing about 36 mol.% Li_2O at 250°C. Activation energy for conduction also varied with the total Li_2O content. (12 refs.)
- 114174** Inelastic neutron scattering study of the structural glass transition in a K(Br,CN) mixed crystal. A.Loidl, K.Knorr (Inst. für Phys., Johannes Gutenberg Univ., Mainz, Germany), R.Feile, J.K.Kjems. *Phys. Rev. Lett. (USA)*, vol.51, no.12, p.1054-7 (19 Sept. 1983). The coupled rotational-translational excitations in $(KBr)_{0.992}(KCN)_{0.008}$ were studied by inelastic neutron scattering. For the first time the $A_{1g}-T_{2g}$ tunneling transition and the $A_{1g}-E_g$ librational excitation were followed at the transition from the paraelastic to the structural glass state. The drastic reduction of the T_{2g} rotation-translation coupling suggests that the number of free-ion tunneling states is reduced in favor of cluster reorientation modes which are effectively decoupled from the lattice. (13 refs.)
- On the crystallization of $Fe_{67}Co_{18}Si_1B_{14}$ metallic glass See Entry 113743
- Variation of the glass-forming regions in the $B_2O_3-Li_2O$ system with cooling rate See Entry 113757
- Structural changes in a cross-linked and plasticized amorphous polymer See Entry 113759
- Effect of moisture on physical properties of nylon See Entry 113762
- The time-temperature-transformation (TTT) state diagram and cure See Entry 115180
- Viscoelastic properties of particulate reinforced matrices See Entry 115249
- Characterization of the matrix glass transition in carbon-epoxy laminates using the CSD test geometry See Entry 115502

64.75 SOLUBILITY, SEGREGATION, AND MIXING

- 114175** Solubility of carbon and ageing of Kh15Yu5 type alloys. N.A.Gorokhova, S.O.Suvorova, V.I.Sarrak, L.L.Zhukov (Inst. of Metall. & Phys. of Metals, Moscow, USSR). *Fiz. Met. & Metalloved. (USSR)*, vol.56, no.2, p.280-5 (Aug. 1983). In Russian. English translation in: *Phys. Met. & Metallogr. (GB)*
- Changes in the mechanical properties of iron-chromium-aluminium alloys with the ageing temperature was compared with the solubility curves of carbon obtained by the internal friction method. The changes in the strength of iron-chromium-aluminium alloys were correlated with changes in the carbon content in the solid solution. (14 refs.) *A.T.*

- 114176** Solid-solution decomposition in CdS-CdTe films. V.Ya.Vityuk, V.A.Sanitarov, N.N.Zavleshko, I.P.Kalinkin (Lensovet Technol. Inst., Leningrad, USSR). *Inorg. Mater. (USA)*, vol.18, no.9, p.1294-8 (Sept. 1982). Translation of: *Izv. Akad. Nauk SSSR Neorg. Mater.*, vol.18, no.9, p.1514-17 (Sept. 1982). [received: Sept. 1983]
- It has been found that thermodynamically unstable films of $CdS_{1-x}Te_x$ ($0.1 < x < 0.9$) solid solutions decompose above 573K with the formation of α_1 and α_2 solid solutions. The degree of phase transformation is determined by the dispersion of the structure and the nonequilibrium state of the initial film. The decomposition occurs most completely and with a high rate in films produced under maximally nonequilibrium conditions. (10 refs.)
- 114177** Effect of the structural properties of compounds in the system $Bi_2O_3-EO_2$ (E=Ge, Si) on their dissolution. L.S.Tarasova, A.V.Kosov (Krasnoyarsk State Univ., Krasnoyarsk, USSR). *Inorg. Mater. (USA)*, vol.18, no.10, p.1384-8 (Oct. 1982). Translation of: *Izv. Akad. Nauk SSSR Neorg. Mater.*, vol.18, no.10, p.1615-19 (Oct. 1982). [received: Sept. 1983]
- The effect of the structural characteristics on the dissolution of compounds in the systems $Bi_2O_3-EO_2$ (E=Ge, Si) was investigated. It was found that the dissolution of the compound $6Bi_2O_3 \cdot EO_2$ with the sillenite structure is a two-stage process, which is explained with the help of a model in which bismuth atoms can occupy two crystallochemical positions. The single-stage nature of dissolution of compounds $2Bi_2O_3 \cdot 3EO_2$ with the evlinitic structure is due to the fact that bismuth atoms occupy single positions in them, which agrees with the generally accepted structural model of these compounds. The two-position distribution of bismuth atoms in the structure of sillenites is confirmed by NMR and IR spectroscopy. (7 refs.)
- 114178** Effect of composition on the properties of five-component solid solutions. V.N.Vigdorovich, A.A.Selin, V.A.Khanin (Moscow Inst. of Electronic Engng., Moscow, USSR). *Inorg. Mater. (USA)*, vol.18, no.10, p.1457-60 (Oct. 1982). Translation of: *Izv. Akad. Nauk SSSR Neorg. Mater.*, vol.18, no.10, p.1697-9 (Oct. 1982). [received: Sept. 1983]
- The authors have analyzed five-component systems formed by III-V elements and determined spectral ranges over which ideal heterostructures, i.e. two-component substrate/five-component solid solutions, can function. Analytical expressions were obtained for calculating the properties of five-component solid solutions. (6 refs.)
- 114179** Solubility of H_2 -He mixtures in fluid phases to 1 GPa. F.H.Ree (Lawrence Livermore Nat. Lab., Univ. of California, Livermore, CA, USA). *J. Phys. Chem. (USA)*, vol.87, no.15, p.2846-52 (21 July 1983).
- Statistical mechanical variational theory and an improved van der Waals one-fluid model have been used to compute the solubility lines of hydrogen-helium mixtures in fluid phases at several temperatures. Quantum corrections to $O(h^2)$ are included. This is done by developing a new formula for the effective one-component mass for the mixtures. Monte Carlo simulations were performed to show the reliability of the new theoretical model. The solubility lines of the H_2 -He mixtures predicted with the new theory give satisfactory agreement with the experimental data of Streett at 7261.5K and to 1 GPa in pressure. At lower temperatures higher order quantum corrections to thermodynamic data become increasingly important. (56 refs.)
- 114180** Solubility and diffusivity of hydrogen in Li_2O . H.Katsuta, S.Konishi, H.Yoshida (JAERI, Ibaraki-ken, Japan). *J. Nucl. Mater. (Netherlands)*, vol.116, no.2-3, p.244-8 (June 1983).
- The solubility and the diffusivity of hydrogen and deuterium in sintered Li_2O pellets were measured by a thermodynamical technique such as equilibrium-quenching and the hot-extraction method. The hydrogen solubility was found to obey Sieverts' law. The diffusion coefficient and its activation energy for hydrogen (deuterium) in Li_2O at the temperature region from 500 to 800°C were similar to those for tritium in neutron irradiated Li_2O . These hydrogen behaviours seem to be different from those in the lower temperature region where $LiOH$ can stably exist. (18 refs.)
- 114181** Irradiation-induced segregation in multi-component alloys. I.-W.Chen (MIT, Cambridge, MA, USA). *J. Nucl. Mater. (Netherlands)*, vol.116, no.2-3, p.249-59 (June 1983).
- A unified analysis of irradiation-induced segregation in multi-component alloys is developed using the formulation of irreversible thermodynamics. Three distinct mechanisms for segregation, namely the inverse Kirkendall effect, the vacancy-wind effect, and the solute drag of interstitials, are identified. In particular, the inverse Kirkendall effect due to interstitials arises only if a solute-interstitial interaction or a mutual conversion among interstitials via lattice atom intermediaries operates simultaneously. In the limit of fast conversion a paraequilibrium state may be reached between interstitials and lattice atoms, and the interstitial mechanism becomes formally analogous to the vacancy mechanism. Although the past treatment of rate phenomena in this field was apparently limited to the latter case, the importance of the consideration of separate chemical potentials for interstitials of different species, in segregation and other irradiation effects, is emphasized. (35 refs.)
- 114182** Stability of the radiation-induced γ' phase in 316 stainless steel. H.R.Brager, F.A.Garner (Hanford Engng. Dev. Lab., Richland, WA, USA). *J. Nucl. Mater. (Netherlands)*, vol.116, no.2-3, p.267-71 (June 1983).
- The γ' phase observed in AISI 316 is only stable during irradiation. It dissolves during annealing at the temperature of its formation in a manner which suggests that the dissolution rate is sensitive to the precipitate radius. The instability of this precipitate in the absence of irradiation confirms the expectation that this precipitate will exhibit a sensitivity to displacement rate. (13 refs.)
- 114183** Enthalpies of solution of some uni-univalent electrolytes in hexamethylphosphotriamide at 298.15K. M.Castagnolo, G.Petrella, A.Inglese, A.Sacco, M.Della Monica (Dept. of Chem., Univ. of Bari, Bari, Italy). *J. Chem. Soc. Faraday Trans. I (GB)*, vol.79, pt.9, p.2211-17 (Sept. 1983).
- Enthalpies of solution of various uni-univalent electrolytes in hexamethylphosphotriamide (HMPT) have been measured at 298.15K. Ionic enthalpies of transfer from water to HMPT and from HMPT to propylene carbonate (PC) were calculated on the basis of the assumption that the transfer enthalpy of the tetraphenylborate ion is the same as that of the tetraphenylarsonium ion. The results are compared with those of the same ions in other solvent pairs and discussed in terms of specific ion-solvent interactions. (24 refs.)
- 114184** Metastable phase separation in Au-Fe alloys. C.E.Violet, R.J.Borg (Lawrence Livermore Nat. Lab., Livermore, CA, USA). *Phys. Rev. Lett. (USA)*, vol.51, no.12, p.1073-6 (19 Sept. 1983).
- ^{57}Fe Mossbauer spectra at 4.2K of Au-Fe alloys with Fe concentration between 10.5 and 33 at.% are well described by two superposed six-line spectra. Presumably, these derive from two different chemical environments which are identified with the (420)-platelet and solid-solution phases. (22 refs.)

114185 On the gas absorption properties of rare-earth metals and their compounds. V.A.Latysheva, V.S.Mordyuk, A.T.Tokarev. *Svetotekhnika (USSR)*, no.8, p.5-6 (1983). In Russian.

A sorption capacity of a number of rare-earth metals and alloys has been found. They are compared with the commercially available getters. A zirconium-aluminum-samarium alloy and pure samarium are shown to possess a high sorption capacity. (3 refs.)

114186 Theory of inhomogeneous states of a solid solution in the neighborhood of second-order phase transitions. I.E.Dikhshtein, V.V.Tarasenko (Inst. of Radio Engng. & Electronics, Acad. of Sci., Moscow, USSR). *Sov. Phys.-Solid State (USA)*, vol.25, no.2, p.272-6 (Feb. 1983). Translation of: *Fiz. Tverd. Tela (USSR)*, vol.25, no.2, p.482-9 (Feb. 1983). [received: Sept. 1983]

The precipitation of a single-phase two-component solid solution in finite samples is studied. The situation when a spatially periodic distribution of the concentrations of its components (modulated structure) occurs is considered. The case when the phase transition from a single-phase state of a solid solution to an inhomogeneous state is either a second-order phase transition or a first-order phase transition resembling a second-order transition is investigated. A rigorous thermodynamic theory free of any model assumptions on the nucleation of a structure with one-dimensional modulation is developed. The proposed theory is valid in the vicinity of phase transitions. All the quantities characterizing an inhomogeneous distribution of the concentrations and of elastic strains in a crystal are evaluated. The phase diagram of a solid solution in the coordinates of the temperature T and the average concentration \bar{c} of one of the components is constructed. It is shown that a phase transition from a homogeneous state to an inhomogeneous state is of second order in an interval of average concentrations bounded by \bar{c}_{1k} and \bar{c}_{2k} . Outside this interval, this phase transition is first order resembling a second-order transition. (16 refs.)

114187 Mechanism and kinetics of radiation-induced segregation in Ni-Si alloys. P.R.Okamoto, L.E.Rehn, R.S.Averback (Materials Sci. Div., Argonne Nat. Lab., Argonne, IL, USA), K.-H.Robrock.

Point Defects and Defect Interactions in Metals. Proceedings of the Yamada Conference V, Kyoto, Japan, 16-20 Nov. 1981 (Amsterdam, Netherlands: North-Holland 1982), p.946-9

Rutherford backscattering and Auger chemical depth profiling measurements show that films of the γ -Ni₃Si phase produced on the ion bombarded surfaces of Ni-Si alloys obey simple parabolic growth kinetics. At low temperatures the film growth-rate constant exhibits Arrhenius behavior and varies with the fourth root of the dose-rate. The apparent activation energy in this low temperature region is ~ 0.3 eV. At high temperatures the growth constant is independent of the dose-rate. The results are consistent with a diffusion-controlled growth model, which assumes Si atoms migrate in the form of a fast diffusing Si-interstitial complex. (7 refs.)

114188 A HVEM study of radiation-induced segregation in dilute Ni-Be alloys. T.Mukai, T.E.Mitchell (Dept. of Metall. & Materials Sci., Case Western Reserve Univ., Cleveland, OH, USA).

Point Defects and Defect Interactions in Metals. Proceedings of the Yamada Conference V, Kyoto, Japan, 16-20 Nov. 1981 (Amsterdam, Netherlands: North-Holland 1982), p.950-3

High voltage electron microscopy has been used for in-situ observations of precipitation in undersaturated solid solutions of Ni-1 at.% Be alloys under electron irradiation. The results show that the precipitation follows the normal ageing sequence of saturated solid solutions without irradiation: G.P. zones $\rightarrow \gamma'' \rightarrow \gamma'$. At the beginning of irradiation, the precipitation is homogeneously induced. Later on dislocation loops on {100} planes, having a (100) Burgers vector. Longer irradiations produce dislocation tangles containing precipitates. In thin specimen regions, however, faulted Frank loops form after {100}/{100} loops disappear. (5 refs.)

114189 Radiation-induced segregation at internal defect sinks in electron irradiated FCC alloys. S.Ohnuki, T.Takeyama, H.Takahashi (Metals Res. Inst., Hokkaido Univ., Sapporo, Japan).

Point Defects and Defect Interactions in Metals. Proceedings of the Yamada Conference V, Kyoto, Japan, 16-20 Nov. 1981 (Amsterdam, Netherlands: North-Holland 1982), p.954-7

Radiation-induced segregation near internal defect sinks was investigated through the interaction between point defects and solute atoms in copper and nickel base alloys. Electron irradiation was performed in HVEM and solute concentration profile near grain boundaries and voids was measured by EDX. Oversize solute atoms depleted and undersize ones enriched at the sinks. The vacancy migration energy from loop growth rate was slightly higher in alloys containing oversize solute atoms than pure metals. The temperature dependence of the segregation showed a maximum value at $0.3-0.4 T_m$. These results indicate the evidence of two types of the interaction between defects and solute atoms, which is predominant in these temperatures. (12 refs.)

114190 Early stages of oxygen clustering and its influence on electrical behavior of silicon. G.S.Oehrlein (IBM Thomas J. Watson Res. Center, Yorktown Heights, NY, USA), J.W.Corbett.

Defects in Semiconductors II, Symposium Proceedings, Boston, MA, USA, Nov. 1982 (New York, USA: North-Holland 1983), p.107-23

Knowledge of phenomena connected to the early stages of oxygen clusters, especially their electrical activity is reviewed. In addition to the well-known 450°C thermal donors, 'new oxygen donors', which occur in ca. 650°C annealing have emerged in conjunction with low temperature processing for VLSI and are discussed. The existing models of thermal donors are viewed as metastable oxygen clusters which lower the compressive strain of the surrounding silicon matrix via bonding of 2p oxygen lone pair orbitals. It is shown how this bonding can result in shallow double donor states. (102 refs.)

114191 Precipitation of oxygen and mechanism of stacking fault formation in Czochralski silicon bulk crystals. K.Wada, N.Inoue, J.Osaka (Musashino Electrical Communication Lab., NTT, Tokyo, Japan).

Defects in Semiconductors II, Symposium Proceedings, Boston, MA, USA, Nov. 1982 (New York, USA: North-Holland 1983), p.125-39

Describes recent progress on nucleation and growth of oxide precipitates and stacking faults in Czochralski silicon. Conclusions on the growth kinetics of oxide precipitates are drawn from the experiments and analysis of growth kinetics of two-dimensional precipitates. The experimentally obtained growth kinetics, three-quarter power law is theoretically derived and the precipitate growth is demonstrated to be diffusion-limited by oxygen interstitials. The formation mechanism of stacking faults is the Bardeen-Herring mechanism. Based on the diffusional growth model, the growth kinetics of stacking faults are analyzed, assuming a coexistence of self-interstitial supersaturation and vacancy undersaturation. It is found that the growth is driven by vacancies in undersaturation. Vacancy component of self-diffusion has been determined and found to be predominant at low temperature. The possibility of the growth model proposed for increase of oxide precipitate density during annealing has been excluded. Both processes, homogeneous and heterogeneous nucleation, take place during annealing. (45 refs.)

114192 Carbon and the kinetics of oxygen precipitation in silicon. R.F.Pinizzotto, S.Marks (Central Res. Labs., Texas Instruments Inc., Dallas, TX, USA).

Defects in Semiconductors II, Symposium Proceedings, Boston, MA, USA, Nov. 1982 (New York, USA: North-Holland 1983), p.147-52

Oxygen precipitation in Czochralski silicon has been studied as a function of anneal time, oxygen concentration and carbon concentration using FTIR. It was found that the oxygen supersaturation controls the precipitation kinetics in high oxygen content samples, whereas the carbon concentration is of prime importance in low oxygen content samples. The decrease in substitutional carbon concentration after nucleation and its subsequent increase with extended growth anneals supports the view that carbon affects precipitate nucleation, but not precipitate growth. The measured oxygen solubility at 1000°C was found to depend on both the initial oxygen concentration and the initial carbon concentration. (17 refs.)

114193 Oxygen precipitation effects in degenerately-doped silicon. G.A.Rozgonyi (North Carolina State Univ., Raleigh, NC, USA), R.J.Jacodine, C.W.Pearce.

Defects in Semiconductors II, Symposium Proceedings, Boston, MA, USA, Nov. 1982 (New York, USA: North-Holland 1983), p.181-5

Reports preliminary observations of oxygen precipitation in degenerately-doped silicon using etching, optical microscopy and transmission electron microscopy. It was found that n+ material was resistant to precipitation, but p+ material precipitated readily. A multistep heat treatment starting with a low temperature step to achieve a high supersaturation ratio was successfully used to induce precipitation in n+ material. (5 refs.)

114194 Oxygen precipitation in silicon—its effects on minority carrier recombination and generation lifetime. C.J.Varker, J.D.Whitfield, P.L.Fejes (Semiconductor Res. & Dev. Lab., Motorola Inc., Phoenix, AZ, USA).

Defects in Semiconductors II, Symposium Proceedings, Boston, MA, USA, Nov. 1982 (New York, USA: North-Holland 1983), p.187-93

The effects of oxygen precipitation on the minority carrier recombination lifetime (τ_R) and the carrier generation lifetime (τ_G) have been characterized for a 'typical' silicon crystal grown with the Czochralski method. Infrared (IR) absorption measurements were obtained on polished wafers, before and after 2 step thermal anneals at 800°C and 1050°C to characterize the axial distribution of interstitial and precipitated oxygen in the ingot. Computerized measurements on NMOS diode and capacitor arrays were used to characterize the axial and radial distributions of carrier lifetime. The results indicate that oxygen precipitation is the dominant mechanism contributing to the degradation of both minority carrier recombination and generation lifetime. (19 refs.)

114195 Structural and chemical microanalysis of oxygen-bearing precipitates in silicon. R.W.Carpenter, I.Chan, H.L.Tsai (Center for Solid State Sci., Arizona State Univ., Tempe, AZ, USA), C.Varker, L.J.Demer.

Defects in Semiconductors II, Symposium Proceedings, Boston, MA, USA, Nov. 1982 (New York, USA: North-Holland 1983), p.195-9

Precipitation in CZ-silicon during post-growth two-stage heat treatment has been examined using the methods of high resolution analytical electron microscopy. Electron transparent specimens prepared from these specimens, exhibited a low density of plate type precipitates on {100} planes. Microdiffraction experiments showed the precipitates to be consistently non-crystalline. Electron energy loss spectra showed that the precipitates contained oxygen, but carbon was not detected. It was found that carbon artifact absorption edges could be induced in spectra by specimen contamination in the microscope. The use of a low temperature stage eliminated this problem. Complementary characteristic X-ray microanalysis showed that metallic impurities had not segregated to these precipitates in this particular case, although this has been observed elsewhere. (10 refs.)

114196 Crystalline particles in thermally grown silicon dioxide. F.A.Ponce, T.Yamashita (Materials Res. Labs., Hewlett-Packard Labs., Palo Alto, CA, USA).

Defects in Semiconductors II, Symposium Proceedings, Boston, MA, USA, Nov. 1982 (New York, USA: North-Holland 1983), p.201-5

Small crystalline particles in the vicinity of the Si/SiO₂ interface have been directly observed by high resolution transmission electron microscopy. These crystallites have typical diameters between 20 and 120 Å. Based on the observed interplanar spacings and angles in lattice images, the structure of these particles has been found to match those of cristobalite. Some orientation relationships also appear to exist between these particles and the silicon layer. (9 refs.)

Polymer Alloys III Blends, Blocks, Grafts and Interpenetrating Networks. Proceedings of a Symposium See Entry 113111

Thermodynamic properties of Th_{0.80}O_{0.20}2+x solid solution See Entry 112323

Lattice theory of binary fluid mixtures: phase diagrams with upper and lower critical solution points from a renormalization-group calculation See Entry 113711

Evidence of compatibility in the melt for poly(ethylene oxide)/poly(methyl methacrylate) blends by ¹³C n.m.r. investigations See Entry 113714

Competitive equilibria in miscible polymer blends and low molecular weight analogues: a Fourier transform infrared study See Entry 113724

Fourier transform infrared studies of poly(vinyl chloride) blends with ethylene co- and terpolymers See Entry 113725

Interaction of transition metals with metalloids and thermodynamic stability of amorphous alloys See Entry 113745

The local environment around hydrogen atoms in hydrogenated NiTi₂ alloy glass See Entry 113749

Experiments on crystallization of semiconductors aboard Salyut 6-Soyuz orbital complex See Entry 113789

Microdefects and impurities in dislocation-free silicon crystals See Entry 113905

Defects, dislocations and degradation of compound semiconductors See Entry 113915

Analysis of defects in heavily-doped MBE-GaAs See Entry 113923

Correlation of oxygen and recombination centers on a microscale in as-grown Czochralski silicon crystals See Entry 113954

Interaction of hydrogen with nonmetallic inclusions of the different shapes in ferrite-pearlite steels See Entry 113955

Interaction of dislocations with impurities and its influence on the mechanical properties of silicon crystals See Entry 113981

Irradiation induced solid solution instability See Entry 113995

Recombination-driven precipitate coarsening in alloys under irradiation See Entry 113996

The effect of primary recoil spectrum on radiation induced segregation in nickel-silicon alloys See Entry 114051

Radiation-induced segregation in titanium alloys See Entry 114052

Computation of the steam-liquid equilibrium of ternary systems See Entry 114152

Tweed microstructures. II. In several phases of the Ni-Al system See Entry 114199

Ion-induced diffusion and surface segregation See Entry 114239

Structure and dynamics of disordered solids: a neutron scattering study of $Ba_{1-x}La_xF_{2+x}$ See Entry 114250

Diffusion and solution of methanol vapor in poly(2-vinylpyridine)-block-polyisoprene and poly(2-vinyl-pyridine)-block-polystyrene See Entry 114268

Tracer diffusion of P in iron and iron alloys See Entry 114271

Modeling of dopant diffusion and associated effects in silicon See Entry 114275

Interfacial stability of migrating brine inclusions in alkali halide single crystals supporting a temperature gradient See Entry 114280

A diffusion-reaction model for solid solutions under irradiation See Entry 114283

Radiation induced interdiffusion and phase transformation in electron irradiated Cu-Ni alloys See Entry 114287

Non-equilibrium surface segregation of silicon in Fe-6.3 at.% Si (110) See Entry 114315

Line width of exciton absorption in solid solutions See Entry 114450

Thermal donor formation by the agglomeration of oxygen in silicon See Entry 114478

Phase components and electrical conduction in the Sm_2O_3 -SrO system See Entry 114573

Metallurgically grown Schottky junction in directionally solidified eutectic Ag-Si alloys See Entry 114590

A Raman study of solubilization of aromatics by non-ionic surfactants See Entry 114856

Vibrational spectra of coadsorbed CO and H on Ni(100) and Ni(111) See Entry 114984

Formation of $ZnAl_2O_4$ in ZnO - Al_2O_3 system accompanied by uneven mixing and composition change See Entry 115154

Melt compounding of PVC with ethylene copolymer resins See Entry 115159

Investigation of phase equilibria related to fusion reactor materials. I. The ternary system Zr-Al-N See Entry 115165

Phase equilibria in nickel rich Ni-Al-Mo and Ni-Al-W alloys See Entry 115167

The formation of coarse intermetallics in rapidly solidified Al-Co alloys See Entry 115185

Composition of $Zr(Cr, Fe)_2$ -type precipitates in Zircaloy-2 and Zircaloy-4 See Entry 115196

The influence of molybdenum on the solubility of phosphorus in α -Fe See Entry 115197

Aging behaviour of 18Mn-18Cr high nitrogen austenitic steel for end rings See Entry 115198

Chemical composition of σ phase precipitated in chromium-nickel austenitic steels See Entry 115199

Crystalline defects in M_7C_3 carbides See Entry 115200

The segregation of osmium to grain boundary dislocations in tungsten See Entry 115201

Precipitation processes in a β -phase Cu-15 at.% Sn shape memory alloy See Entry 115202

Microphase segregation in segmented amine-cured polyurethanes See Entry 115203

Electron microscopic studies on the effect of Sn addition on the ageing characteristics of Al-0.7% Mg_2Si alloy See Entry 115217

Relationship between grain boundary segregation and heat-treatment parameters in an aluminium alloy See Entry 115218

Microstructural stability of γ' strengthened Co-Cr-Ti alloys See Entry 115224

Tempering of cast nickel-aluminium bronze See Entry 115225

Role of eutectoid transformation and grain size on the creep behaviour of mild steel See Entry 115266

Effects of V and Nb additions on high temperature deformation properties of low alloy martensites See Entry 115269

Interfacial segregation and embrittlement in liquid phase sintered tungsten alloys See Entry 115324

Relationships between microstructure and mechanical properties of microduplex $\alpha + (\gamma + \epsilon)$ 6 and 9% Mn steels for cryogenic applications See Entry 115325

Intergranular brittle fracture resistance of 18Kh2N4VA steel after hardening See Entry 115349

Intergranular fracture of a high purity iron due to oxygen See Entry 115351

Diffusion-coupled active dissolution in the localized corrosion of stainless steels See Entry 115409

Gas permeation through composite two-layer systems and the graphical solution See Entry 115583

64.80 OTHER PHASE PROPERTIES OF SYSTEMS

114197 Microstructural changes in vanadium pentoxide in controlled environments. P.L.Gai (Dept. of Metall. & Sci. of Materials, Univ. of Oxford, Oxford, England). *Philos. Mag. A (GB)*, vol.48, no.3, p.359-71 (Sept. 1983). Direct observations have been made of the reduction of V_2O_5 between room temperature and $\sim 600^\circ\text{C}$ in reducing gases such as H_2 , balanced by He, CO and C_2H_4 , using a gas-reaction cell in a high-voltage electron microscope. The systematic study has revealed microstructural changes relevant to structural and catalytic properties of the system. The reduction of the surface begins at low temperatures of ~ 80 - 100°C . The defect structures formed are analysed, and it is shown that these are important in understanding redox reactions. The results could also perhaps explain chemical studies of oxygen desorption from V_2O_5 . (13 refs.)

114198 Tweed microstructures. I. Characterization in β -NiAl. I.M.Robertson, C.M.Wayman (Dept. of Metall., Univ. of Illinois, Urbana, IL, USA). *Philos. Mag. A (GB)*, vol.48, no.3, p.421-42 (Sept. 1983). The authors describe an electron microscopy investigation of an as-quenched 63 at.% Ni-Al alloy. This material exhibits strong tweed contrast and associated diffraction effects commonly called 'premartensitic effects'. Anomalous diffraction effects in martensite-forming β Hume-Rothery phases have been studied extensively, but the mottled microstructures have received little attention. This paper describes an attempt to characterize the microstructure systematically. In addition to some well-known characteristics, the authors have discovered that in many ways tweed contrast resembles the fringe contrast observed on stacking faults. This includes the variation of fringe spacing with foil orientation, with the extinction distance of the diffraction vector and with the deviation from the Bragg condition. Such behaviour provides a basis for understanding the origin of premartensitic effects in Hume-Rothery phases, and tweed microstructures in general. (30 refs.)

114199 Tweed microstructures. II. In several phases of the Ni-Al system. I.M.Robertson, C.M.Wayman (Dept. of Metall., Univ. of Illinois, Urbana, IL, USA). *Philos. Mag. A (GB)*, vol.48, no.3, p.443-67 (Sept. 1983). For pt.I see *ibid.*, vol.48, no.3, p.421 (1983). In this second in a series of papers on tweed microstructures in phases of the Ni-Al system, the authors describe the electron microstructure of the 3R and 7R martensites, the γ phase and the newly discovered Ni_3Al_3 phase in an alloy of average composition 63 at.% Ni-Al. The alloy was subjected to ageing treatments at temperatures ranging from 300 to 850°C for periods of up to 15 days, which resulted in the precipitation of the γ and Ni_3Al_3 phases from the supersaturated β phase. The metastable Ni_2Al phase has also been found to occur, and its effect on the tweed microstructure in the β phase is examined. The authors conclude that Ni_2Al precipitation is not the cause of tweed in β -Ni-Al. The cubic γ phase exhibits a tweed microstructure almost identical to that of the β phase. The tweed microstructures of the tetragonal 3R martensite and orthorhombic Ni_5Al_3 differ from those of the cubic phases in ways which reflect their different symmetries. These differences provide further clues to the origin of tweed microstructures. (29 refs.)

114200 Microstructure induced ordering effects in solids. K.Krishnan (Reactor Res. Centre, Tamil Nadu, India). Point Defects and Defect Interactions in Metals. Proceedings of the Yamada Conference V, Kyoto, Japan, 16-20 Nov. 1981 (Amsterdam, Netherlands: North-Holland 1982), p.891-4. It is shown that spatial and temporal ordering can arise due to point defect reactions with microstructure when a material is subjected to non-equilibrium conditions during radiation, quenching of strain rates. In particular the bias effect which causes random void growth is also responsible for void ordering in the presence of vacancy loops. Applications to other systems are also mentioned. (13 refs.)

114201 Electrically active defects in CID imaging arrays fabricated on $Hg_{0.7}Cd_{0.3}Te$. H.F.Schaaake, A.J.Lewis (Central Res. Labs., Texas Instruments Inc., Dallas, TX, USA). Defects in Semiconductors II, Symposium Proceedings, Boston, MA, USA, Nov. 1982 (New York, USA: North-Holland 1983), p.301-5. CID imaging arrays were fabricated on $Hg_{0.7}Cd_{0.3}Te$ produced by the solid state recrystallization technique. It was found that the most serious source of dark current was sub-grain boundaries. SEM studies of the microstructure revealed by etching showed that boundaries with a high density of dislocations were detectable sources of dark current, while those boundaries with a low density of dislocations, as well as individual dislocations were not. TEM showed that all dislocations were free of precipitates, and most were not dissociated. The sub-grain boundaries were found to arise from misorientation between dendrites which form during the solidification from the melt. (10 refs.)

Microstructure and topography [laser annealing of semiconductors] See Entry 113709

A representation of the defect structure of pure barium titanate See Entry 113858

Surface modification by ion implantation—effects on fatigue See Entry 113908

Crystallographic shear in the Nb_2O_5 - Ta_2O_5 - WO_3 quaternary system at 1623K See Entry 113932

Metallurgical surfaces produced by ion implantation See Entry 113940

Theoretical relationships between creep and swelling by point defect absorption during irradiation See Entry 113994

On the evolution of microstructure during irradiation See Entry 114036

Crystalline particles in thermally grown silicon dioxide See Entry 114196

Microstructural study of alumina/TiC coated cemented carbide See Entry 114375

Study of the uniformity and stoichiometry of $CoSi_2$ films using Rutherford backscattering spectroscopy and scanning electron microscopy See Entry 114376

A TEM study of fibrous cuprite (chalcotrichite): microstructures and growth mechanisms See Entry 114426

Change in samarium valence in SmB_6 - NdB_6 solid solutions See Entry 114487

Investigation of gallium arsenide subjected to an intensive plasma treatment See Entry 115003

Hydrodynamic pressing of β -alumina components See Entry 115124

The use of microscopic and hardness measurement methods in recrystallization studies See Entry 115211

Recrystallization mechanisms in commercial Al-2Mg alloy See Entry 115212

Dependence of the elastomechanical properties of granular corundum-zirconium refractory materials on their microstructure See Entry 115234

65.00 THERMAL PROPERTIES OF CONDENSED MATTER

(see also 05.70 Thermodynamics, 63. Lattice dynamics; for thermal conduction in nonmetallic liquids, see 66.60; for thermal conduction in nonmetallic solids, see 66.70; for electronic thermal conduction, see 72.15, 72.20 and 74.30E; for thermodynamic properties of quantum fluids, see 67.40, 67.50, and 67.60; for thermal properties of solid helium, see 67.80)

Syntheses and thermal properties of new liquid crystalline materials involving tropolone See Entry 115122

65.20 HEAT CAPACITIES OF LIQUIDS

114202 Electrostatic contribution to heat capacity of polyelectrolyte solutions. H.Daoust, P.Ferland, D.St.-Cyr (Dept. of Chem., Univ. de Montreal, Montreal, Quebec, Canada).

J. Polym. Sci. Polym. Phys. Ed. (USA), vol.21, no.8, p.1563-6 (Aug. 1983).

An expression is derived for the electrostatic contribution to the heat capacity of a polyelectrolyte solution, with the help of the Lifson-Katchalsky cell model (1954) and Manning's infinite-line-charge theory (1969). The calculated values are compared with experimental values obtained for aqueous solutions of sodium-polyacrylate and sodium poly-L-glutamate. (17 refs.)

AC calorimeter for liquid including suspension of biological materials See Entry 111685

Dependence of the tilt angle on external forces for smectic-C and chiral smectic-C liquid crystals—measurement of the heat capacity of DOBAMBC See Entry 113737

Brillouin scattering in liquid benzene under high pressure See Entry 114872

65.40 HEAT CAPACITIES OF SOLIDS

(for specific heat of superconductors, see 74.30E; for specific heat of magnetic systems, see 75.40)

114203 Low temperature heat capacities of SrF_2 and other fluoride compounds. L.T.Ho (Inst. of Phys., Acad. Sinica, Taipei, Taiwan), D.P.Dandekar, J.C.Ho.

Annu. Rep. Inst. Phys. Acad. Sin. (Taiwan), vol.12, p.10-17 (Dec. 1982). [received: Sept. 1983]

Heat capacity measurements between 2 and 22K have been made on SrF_2 , yielding a limiting value of Debye temperature $\Theta_D(0)=385\text{K}$. A brief review is then given, for various fluoride compounds XF_2 ($\text{X}=\text{Ba}$, Ca , Cd , Mn , Pb and Sr), on the general agreement between their $\Theta_D(0)$ values as determined from calorimetric measurements and those from elastic constant measurements, as well as on the general trend of deviations of their lattice heat capacity from a simple Debye behavior. (18 refs.)

114204 Specific heat of $\text{Li}_{0.27}\text{V}_2\text{O}_5$ bronze in the range 295-650K. S.E.Filippova, G.K.Demenskii, O.A.Teplov, L.A.Reznitskii (M.V. Lomonosov State Univ., Moscow, USSR).

Inorg. Mater. (USA), vol.18, no.9, p.1373-4 (Sept. 1982). Translation of: *Izv. Akad. Nauk SSSR Mater. Mater.*, vol.18, no.9, p.1597-8 (Sept. 1982). [received: Sept. 1983]

The authors have used DTA and true specific-heat methods to examine $\text{Li}_{0.27}\text{V}_2\text{O}_5$; the specimens were made by coulometric titration in electrochemical circuits with a lithium-bearing solid electrolyte: Pt , $\text{Li}_{0.26}\text{V}_2\text{O}_5\text{--yLi}^+|\text{Li}_{0.26}\text{V}_2\text{O}_5\text{--y}$, Pt ; $p(\text{O}_2)=10^{-1}\text{Pa}$, $T=830\text{K}$. The electrolyte was β -spodumene $\text{Li-AlSi}_3\text{O}_6$. The high mobility of Li^+ in $\beta\text{-Li}_x\text{V}_2\text{O}_5$ provided uniform distribution in the specimen. (3 refs.)

114205 Study of low temperature specific heat and DC electrical conductivity of NH_4Cl in pure powder form and in crystalline form grown from urea solution. S.S.Mitra, S.K.Ghorai, S.K.Dutta Roy (Cryogenic Engng. Centre, Indian Inst. of Technol., Kharagpur, India).

Indian J. Cryog., vol.8, no.1, p.52-6 (1983).

A continuous heating cryostat developed for the precision measurement of specific heats over the range 4K to 300K is described. The calibration data up to 77K with powdered NH_4Cl are presented and compared with previous measurements. Further measurements were carried on polycrystalline NH_4Cl , crystallised from 25% urea solution. The results were compared around the phase transition temperature (242K). DC electrical conductivity of single crystal NH_4Cl grown from urea was also studied. A large anomalous fluctuation in conductivity has been observed around the said transition temperature. The activation energy up to the transition temperature was found to be comparable to the data of Herrington and Staveland but differs considerably from the data on pure crystal grown by vapour deposition method. The role of incipient dissociation of urea in the single crystal of NH_4Cl has been discussed in the light of specific heat and electrical conductivity measurements. (9 refs.)

114206 Heat capacity of zinc oxysulfate from 7.5 to 309.4K with a transition from 270 to 306K. R.P.Beyer (Albany Res. Center, Bur. of Mines, US Dept. of the Interior, Albany, OR, USA).

J. Chem. Thermodyn. (GB), vol.15, no.9, p.835-40 (Sept. 1983).

The heat capacity of zinc oxysulfate ($\text{ZnO} \cdot 2\text{ZnSO}_4$) was measured from 7.5 to 309.4K by adiabatic calorimetry. A second-order transition was observed in the temperature range 270 to 306K with a peak at 279.2K. The values at 298.15K for $C_{p,m}$, $\{S_m^\circ(T) - S_m^\circ(0)\}$, $-\{G_m^\circ(T) - H_m^\circ(0)\}/T$, and $\{H_m^\circ(T) - H_m^\circ(0)\}$ are 246.86, 290.58, and 164.72 $\text{J.K}^{-1}\text{mol}^{-1}$, and 37.53 kJ.mol^{-1} , respectively. These properties are also reported from 5 to 1200K at convenient temperature intervals. (13 refs.)

114207 Thermodynamic properties and phase transitions of salt hydrates between 270 and 400K. II. $\text{Na}_2\text{CO}_3 \cdot \text{H}_2\text{O}$ and $\text{Na}_2\text{CO}_3 \cdot 10\text{H}_2\text{O}$. F.Gronvold, K.K.Meisingset (Dept. of Chem., Univ. of Oslo, Oslo, Norway).

J. Chem. Thermodyn. (GB), vol.15, no.9, p.881-9 (Sept. 1983).

For pt.I see *ibid.*, vol.14, p.1083 (1982). Heat capacities and phase-transition enthalpies between 270 and 400K have been measured for commercial samples of sodium carbonate monohydrate and decahydrate by adiabatic-shield calorimetry. Enthalpies and entropies at selected temperatures have been derived for the exact stoichiometries. The molar enthalpy of transition of $\text{Na}_2\text{CO}_3 \cdot \text{H}_2\text{O}$ to $(\text{Na}_2\text{CO}_3 + \text{aqueous solution})$ at 380.8K was found to be $(15.00 \pm 0.20) \text{kJ.mol}^{-1}$. The molar enthalpy of transition of $\text{Na}_2\text{CO}_3 \cdot 10\text{H}_2\text{O}$ to $(\text{Na}_2\text{CO}_3 \cdot 7\text{H}_2\text{O} + \text{aqueous solution})$ at 305.167 is $(48.2 \pm 0.6) \text{kJ.mol}^{-1}$. The molar enthalpy of transition of $\text{Na}_2\text{CO}_3 \cdot 10\text{H}_2\text{O}$ to $(\text{Na}_2\text{CO}_3 \cdot \text{H}_2\text{O} + \text{aqueous solution})$ at 306.11K is $(67.1 \pm 0.5) \text{kJ.mol}^{-1}$. Lattice constants determined from Guinier photographs for $\text{Na}_2\text{CO}_3 \cdot \text{H}_2\text{O}$ are $a=646.5$, $b=1072.0$,

and $c=525.0 \text{ pm}$ at 300K; for $\text{Na}_2\text{CO}_3 \cdot 10\text{H}_2\text{O}$: $a=1275.6$, $b=898.0$, and $c=1346.2 \text{ pm}$, and $\beta=122.66^\circ$ at 285K. Segregation of less-hydrated solid phases might be a problem for the use of $\text{Na}_2\text{CO}_3 \cdot 10\text{H}_2\text{O}$ as an energy-storage material. (24 refs.)

A simple microcomputer-controlled calorimeter: the heat capacity of copper, Invar and RbNiCl_3 in the range 2-20K See Entry 111681

An automated calorimeter for heat-capacity measurements from 5 to 300K. The heat capacity of cadmium sulfide from 5.37 to 301.8K and the relative enthalpy to 1103.4K See Entry 111682

Neutron and calorimetric observation of a modulated structure in quartz just above the α - β phase transition See Entry 114215

Low-energy excitations in $(\text{KBr})_{1-x}(\text{KCN})_x$ in the orientational glass state See Entry 114294

Density-of-state effects in the low temperature properties of TiBe_2 See Entry 114431

Polaron model of the electronic spectrum and the superconductivity of compounds having the A-15 structure See Entry 114456

65.50 THERMODYNAMIC PROPERTIES AND ENTROPY

114208 Interpretation of the enthalpy in a discretised multidimensional region undergoing a melting/freezing phase change. V.R.Voller (School of Math., Thames Polytech., London, England).

Int. Commun. Heat & Mass Transfer (GB), vol.10, no.4, p.323-8 (July-Aug. 1983).

Theoretical justification is presented for relating the values of nodal enthalpy in a discretised region undergoing a melting/freezing phase change to the rate at which the change of state occurs. (7 refs.)

114209 Enthalpy-concentration data for the system ethanol-toluene. J.Wisniak (Dept. of Chem. Engng., Ben-Gurion Univ. of the Negev, Beer-Sheva, Israel).

Indian J. Technol., vol.21, no.2, p.86-7 (Feb. 1983). [received: Sept. 1983]

Enthalpy-concentration data and boiling-composition correlations have been determined for the binary system ethanol-toluene at 760 mm Hg. This information should be useful for distillation studies and other processes in which the analytical relations between boiling (condensation) point and phase composition are required. (10 refs.)

114210 On the energy of interaction in the Si-B system. T.A.Chubnidze, A.L.Okley, M.A.Zhuruli.

Russ. Metall. (GB), no.3, p.175-8 (1982). Translation of: *Izv. Akad. Nauk. SSSR Met.*, no.3, p.199-201 (1982).

On the basis of the given values of the melting temperature, density and structure of boride SiB_4 , its thermodynamic functions and energy of interaction in the Si-B system as an approximation to regular solutions were calculated. The data obtained can be used in the theory of production and application for the deoxidation of metallic silicon alloys with boron. (5 refs.)

Thermodynamic properties of $\text{Th}_{0.80}\text{U}_{0.20}\text{O}_{2+x}$ solid solution See Entry 112323

Oxygen potential and lattice parameter measurements in $(\text{U}, \text{Ce})\text{O}_{2-x}$ See Entry 112324

Investigation of the oxygen activity of oxide fuels and fuel-fission product systems by solid electrolyte techniques. I. Qualification and limitations of the method See Entry 112326

Molecular vibration analysis of the cage-like molecules $\beta\text{-P}_2\text{S}_5$, As_2S_5 , P_4S_7 , and $\text{As}_2\text{P}_2\text{S}_7$ See Entry 112695

Equilibrium properties of the Gaussian overlap fluid. Monte Carlo simulation and thermodynamic perturbation theory See Entry 113713

Interaction of transition metals with metalloids and thermodynamic stability of amorphous alloys See Entry 113745

A representation of the defect structure of pure barium titanate See Entry 113858

Free energy calculation of small clusters See Entry 113860

Estimation of the vacancy formation enthalpy of metals See Entry 113865

Vacancy formation in Ni and Ni(Ge) See Entry 113880

Point defect thermodynamics of compound semiconductors and their alloys See Entry 113907

Study of vacancy-solute interactions in dilute Al based alloys by thermal equilibrium measurements of positron annihilation See Entry 113969

Interaction and charge transfer between vacancy and solute in dilute aluminium alloys See Entry 113970

Formation of vacancies in thermal equilibrium in α -range alloys See Entry 113972

Thermodynamic theory of phase transitions in solid solutions based on lead metaniobate See Entry 114156

Statistical model of the phase transition in $\text{KH}_3(\text{SeO}_3)_2$ See Entry 114169

Thermodynamic properties and phase transitions of salt hydrates between 270 and 400K. II. $\text{Na}_2\text{CO}_3 \cdot \text{H}_2\text{O}$ and $\text{Na}_2\text{CO}_3 \cdot 10\text{H}_2\text{O}$ See Entry 114207

Concentration and temperature dependences of the magnetic susceptibility of binary alloys of indium with potassium and rubidium See Entry 114678

Free energy of a tetragonal ferroelectric in the region of strong critical fluctuations See Entry 114797

Robust numerical procedure for calculating equilibrium compositions in binary alloy systems See Entry 115168

On the thermodynamic properties of Co-Cu melts See Entry 115171

A thermodynamic analysis of the Cu-O system with an associated solution model See Entry 115175

Predominance area diagrams of the system Co-S-O between 583 and 1148K See Entry 115176

Influence of pressure on the equilibrium of the melt with graphite, diamond and carbide Mn_7C_3 in the Mn-C system See Entry 115177

Evaluating the limiting states of a steel under combined low-cycle loading and diffusion of sorbed hydrogen See Entry 115348

A new gas equilibration method for the measurement of carbon potential: carbon potential in austenitic 316 stainless steel at 1000°C See Entry 115417

Thermodynamic stability of complex oxides in alkali metals See Entry 115573

65.70 THERMAL EXPANSION AND THERMOMECHANICAL EFFECTS

(see also 64.30 Equations of state; for electronic thermal conduction, see 72.15 and 72.20; for thermal conductivity of superconductors, see 74.30E; for pyroelectric and electrocaloric effects, see 77.70)

114211 Thermal expansion of (Pd,Pt_{1-x})Fe alloys. S.M.Podgornykh, Yu.N.Tsiovin, N.I.Kourov, N.V.Volkenshtein (Inst. of Metal Phys., Ural Sci. Centre, Acad. of Sci., Sverdlovsk, USSR). *Fiz. Met. & Metalloved. (USSR)*, vol.56, no.2, p.403-6 (Aug. 1983). In Russian. English translation in: *Phys. Met. & Metallogr. (GB)* Measurements of the thermal expansion coefficient were carried out on polycrystalline samples of ordered alloys with compositions in the range x=0-0.62. The magnetic component of the thermal expansion coefficient, defined as the difference between the experimental values and the Gruneisen function, was also found. The results indicated that the magnetic contribution to the thermal expansion was always positive and this was true of antiferromagnetic alloys of the system, ferromagnetic alloys, and those with intermediate compositions. (8 refs.) *A.T.*

114212 Negative thermal expansion due to the hindered rotation of the ammonium ion or the methyl group in solids with low barriers to rotation and the anisotropic thermal expansion in solids having polyatomic groups. D.Smith (Dept. of Chem., Pennsylvania State Univ., Hazleton, PA, USA). *J. Chem. Phys. (USA)*, vol.79, no.6, p.2995-3001 (15 Sept. 1983). The thermal expansion due to the hindered rotation of the ammonium ion or the methyl group is negative at liquid helium temperatures, if the tunneling frequencies of these polyatomic groups are greater than 0.3 cm⁻¹. Since the thermal expansion due to the hindered rotation of polyatomic groups with large tunneling frequencies is much greater than that due to the lattice vibrations at very low temperatures, the observed thermal expansion should also be negative. For barriers to rotation less than 500 cal/mol, the tunneling frequencies of NH₄⁺ and CH₃ are large enough to cause a negative thermal expansion. The thermal expansion due to hindered rotation of NH₄⁺ has been computed for NH₄⁺ in crystalline fields of trigonal, tetrahedral, and octahedral symmetry. Some noncubic ammonium compounds with relatively high barriers to rotation have been found to have a negative thermal expansion along one of their crystallographic axes. Expressions for the contribution to the thermal expansion from the hindered rotation of polyatomic groups are derived for tetragonal, hexagonal, and orthorhombic crystals. From these expressions, the probable source of the negative thermal expansion in one of the crystallographic directions in compounds such as NH₄ReO₄ and NH₄ClO₄ is deduced. (22 refs.)

114213 Some high-temperature properties of Zircaloy-oxygen alloys. L.R.Bunnell, J.L.Bates, G.B.Mellinger (Pacific Northwest Labs., Richland, WA, USA). *J. Nucl. Mater. (Netherlands)*, vol.116, no.2-3, p.219-32 (June 1983). The effect of oxygen on thermal expansion, elastic moduli, and thermal diffusivity of Zircaloy-4 nuclear reactor fuel cladding was determined for the main purpose of providing baseline data for LOCA evaluation codes. Measurements were made over the temperature range 298 to 1473K and 0.7 to 28 at.% oxygen. Expansion and moduli were measured in the two relevant directions, while diffusivity was measured in the principal heat transfer direction (through the clad). Thermal expansion and elastic moduli both increased with oxygen, while diffusivity decreased. Similar measurements were made on Zircaloy-2, but only to 5 at.% oxygen. Differences between the two alloys were within experimental error of the measurements made. (24 refs.)

114214 Thermal expansivity of oriented poly(ethylene terephthalate). C.L.Choy (Dept. of Phys., Chinese Univ. of Hong Kong, Hong Kong), M.Ito, R.S.Porter. *J. Polym. Sci. Polym. Phys. Ed. (USA)*, vol.21, no.8, p.1427-38 (Aug. 1983). The linear thermal expansivity of poly(ethylene terephthalate) extruded at 50 and 90°C to extrusion ratios λ of 1-4.8 has been measured between 120 and 300K. With increasing λ, the expansivity along the extrusion direction (α_{||}) decreases sharply, while that in the transverse direction (α_⊥) shows a slight increase. For λ<3, the large drop in α_{||} and the accompanying increase in the axial Young's modulus E_{||} can be ascribed to chain alignment in the crystalline regions and to an increase in number and tautness of intercrystalline tie chains. At higher λ, however, the crystalline orientation apparently becomes saturated, so that taut tie molecules are solely responsible for further changes in both α_{||} and E_{||}. On the other hand, α_⊥ is mainly determined by crystalline orientation for all λ, thus showing very little increase at large λ. For the highly oriented samples (λ≥3), the Takayanagi model provides a reasonable description of the behavior of α_{||} and α_⊥. (22 refs.)

114215 Neutron and calorimetric observation of a modulated structure in quartz just above the α-β phase transition. C.M.E.Zeyen (Inst. Laue-Langevin, Grenoble, France), G.Dolino, J.P.Bachheimer. *Physica B & C (Netherlands)*, vol.120B+C, no.1-3, p.280-2 (May 1983). (Yamada Conference VI on Neutron Scattering in Condensed Matter, Hakone, Japan, 1-4 Sept. 1982). At 573°C quartz undergoes a first order phase transition with symmetry breaking, around which many physical properties show important variations. Recently a new anomaly has been observed in the thermal dilatation just above T_{β-α}. As the possibility of an incommensurate phase has been predicted theoretically by Aslanyan and Levanyuk (1979), it was interesting to test whether the anomaly of thermal dilation corresponds indeed to such a phase. This experiment has been made by neutron diffraction at the ILL. Scans along the [001] direction revealed the existence, in a temperature interval of 1.3K above T_{β-α}, of incommensurate satellite peaks. Recently the authors have also repeated calorimetric measurements near T_{β-α} using the DSC technique and an anomalous behaviour of C_p well correlated with the thermal expansion data, is clearly observed. (13 refs.)

114216 Thermal expansion and electrical conductivity in the HfO₂-TiO₂ system. P.Odier, B.Cales, P.Etcheug, Vu Tien Loc (Centre de Recherche sur la Phys. des Hautes Températures, CNRS, Orleans, France). *Rev. Int. Hautes Temp. & Refract. (France)*, vol.20, no.1, p.45-54 (1983). Presents and comments on some of the data obtained for the thermal expansion of compounds in the system HfO₂-TiO₂. Results of X-ray crystallography are reviewed and macroscopic measurements of the thermal expansion are presented and explained using X-ray data and microstructural aspects of these compounds. Finally some results of electrical conductivity are analysed in terms of nonstoichiometry. (24 refs.)

114217 Nature of residual stresses in carbon fibre reinforced 12% silicon aluminium alloy. A.S.Viskov, V.K.Ivanov, B.E.Popov, E.V.Ufimtsev, V.I.Shulepov. *Russ. Metall. (GB)*, no.3, p.133-6 (1982). Translation of: *Izv. Akad. Nauk. SSSR Met.*, no.3, p.155-9 (1982). Carbon-reinforced aluminium obtained by soaking carbon fibres with molten 'Silumin', followed by subsequent cooling in water, contains residual stresses. The magnitude of these stresses is determined basically by thermal stresses which result from the different values of the coefficients of thermal expansion in the basic phases of the composite material. Phase stresses, which may arise in preparing carbon-fibre reinforced aluminium as a result of the formation of aluminium carbide and the dissociation of a supersaturated solid solution of silicon in aluminium, must play a secondary role because, under conditions of short-term dwell of the material at high temperatures followed by accelerated cooling, they have no time for significant development. (11 refs.)

114218 Dynamics of self-sustaining processes in solid matrices when heat evolution is triggered by stress. N.M.Biturin, V.N.Genkin, M.Yu.Myl'nikov (Inst. of Appl. Phys., Acad. of Sci., Gorki, USSR). *Sov. Tech. Phys. Lett. (USA)*, vol.8, no.11, p.600-1 (Nov. 1982). Translation of: *Pis'ma v Zh. Tekh. Fiz. (USSR)*, vol.8, no.21-22, p.1395-8 (Nov. 1982). [received: Sept. 1983] The self-sustaining process involving heat evolution triggered by stresses due to nonuniform heating is analyzed in the small-strain approximation. The process initially propagates at an exponentially increasing velocity, and later at the speed of sound. (6 refs.)

Interferometric determination of slow movements	See Entry 111634
An automated calorimeter for heat-capacity measurements from 5 to 300K. The heat capacity of cadmium sulfide from 5.37 to 301.8K and the relative enthalpy to 1103.4K	See Entry 111682
A semi-micro rotating-bomb combustion calorimeter	See Entry 111683
Intrinsic thermal expansion of point defects in metals	See Entry 113872
Vacancy-thermal expansion in aluminium	See Entry 113877
Structural transformations and their precursors	See Entry 114154
Thermodynamic properties and phase transitions of salt hydrates between 270 and 400K. II. Na ₂ CO ₃ ·H ₂ O and Na ₂ CO ₃ ·10H ₂ O	See Entry 114207
Effect of magnetic transformation on the nonmagnetic properties of Ce ₂ Ge ₃	See Entry 114690
Thermal expansion and compressibility of magnetic materials under hydrostatic pressure conditions	See Entry 114719
Graphite produced by extrusion of pitch mesophase	See Entry 115116
Properties of hot-pressed zirconium pyrovanadate ceramics ...	See Entry 115149
Microstructure and mechanical strength of aluminium titanate ceramics prepared from synthesized powders	See Entry 115353

65.90 OTHER TOPICS IN THERMAL PROPERTIES OF CONDENSED MATTER

114219 A useful integral function and its application in thermal radiation calculations. S.L.Chang, K.T.Rhee (Dept. of Mech. & Aerospace Engng., Rutgers Univ., New Brunswick, NJ, USA). *Int. Commun. Heat & Mass Transfer (GB)*, vol.10, no.4, p.329-33 (July-Aug. 1983).

A new integral function has been discovered. The present function is found to be useful in computing the spectral emissivity of an isothermal volume containing either soot or gaseous species, or both. Examples of its application are discussed herein. (11 refs.)

114220 Peculiarities of spectral emission of titanium during high-temperature oxidation. V.E.Liepinia, V.K.Mel'nikov. *Latv. PSR Zinat. Akad. Vestis Fiz. Teh. Zinat. Ser. (USSR)*, no.4, p.66-71 (1983). In Russian. The paper presents experimental results of a study of spectral emissivity of a titanium surface during chemical interactions with a low temperature plasma. The emissivity of surface changes according to the oxide film thickness in the temperature region up to 1400K. At temperatures of 1420-1600K during the process of chemical interactions of the metal surface with the plasma within the region of λ<2μ the metal emissivity exceeds that of the thermal emissivity which could be explained by chemiluminescence of titanium dioxide. (8 refs.)

Thermal emissivities of films on substrates	See Entry 113068
---	------------------

66.00 TRANSPORT PROPERTIES OF CONDENSED MATTER (NONELECTRONIC)

66.10 DIFFUSION AND IONIC CONDUCTION IN LIQUIDS

114221 Self-diffusion of polyethyleneglycol molecules in concentrated solutions and melts. A.I.Maklakov, N.K.Dvoyashkin. *Vysokomol. Soedin. Ser. B (USSR)*, vol.25, no.6, p.424-7 (1983). In Russian. The selfdiffusion of polyethyleneglycol molecules in the aprotic solvents benzene, acetone, chloroform, and water and in melts is studied, and the coefficient of selfdiffusion D is measured by an NMR method with a pulsed magnetic field gradient. The relation between D and temperature in solutions of these solvents can be expressed by an Arrhenius type equation, D=D₀exp(-E_D/RT), where E_D is the activation energy for diffusion. The values of D and E_D depend on the solvent. No direct relation obtains between the selfdiffusion characteristics of polyethyleneglycol in solutions and the viscosity and selfdiffusion parameters of the solvents. For example, the values of D for pure benzene and water are close, and the coefficients of selfdiffusion for polyethyleneglycol in these solvents differ markedly. Also, the value of D for polyethyleneglycol in chloroform is less than for benzene although D for pure chloroform is higher than for benzene. (12 refs.) *N.S.*

114222 A conductance study of magnesium, manganese II and barium malonates in dioxane-water mixtures at 25°C. A.A.Al Najar, A.M.Ibrahim (Dept. of Chem., Coll. of Education, Univ. of Basrah, Basrah, Iraq). *Iraqi J. Sci.*, vol.22, no.4, p.466-90 (1981). [received: Aug. 1983] Conductances of solutions of magnesium, manganese II and barium malonates have been measured in dioxane-water mixture at 25°C. The experimental

data have been analyzed by the complete and expanded form of Fuoss-Hsia (F/H) as well as by Lee-Wheaton (L/W) equations. The conductance parameters derived from the analysis with these theories indicated that the equation of L/W reproduces the data more satisfactorily than the others. The low distance parameter values obtained show clearly the non-existence of solvent-separated ion-pairs. The plot of $\log K_A$ vs. $1/D$ show a concave downward curvature for all malonate salts. This association behaviour was discussed in terms of the interaction of the chelate salts with dioxane-water mixture systems. (16 refs.)

114223 Effect of concentration and ionic strength on the translational diffusion coefficient of Lysozyme. B.Nystrom, R.M.Johnsen (Inst. of Phys. Chem., Univ. of Uppsala, Uppsala, Sweden). *Chem. Scr. (Sweden)*, vol.22, no.2, p.82-4 (1983).

Photon correlation spectroscopy has been used to measure the translational diffusion coefficient (D) of lysozyme at pH 4.0 as a function of concentration and ionic strength. The lysozyme concentrations ranged from 5 to 80 kg m⁻³. At low ionic strengths D increases with concentration, whereas at high ionic strength (0.2M) D decreases with concentration. These features are discussed in terms of electrostatic interactions. (17 refs.)

114224 Comments on the diffusion behaviour in semidilute solutions of polystyrene at marginal solvent conditions. J.Carlfors, R.Rymden (Inst. of Phys. Chem., Univ. of Uppsala, Uppsala, Sweden), B.Nystrom. *Polym. Commun. (GB)*, vol.24, no.9, p.263-5 (Sept. 1983).

The concentration dependence of the diffusion coefficient in semidilute solutions of both low and high molecular weight samples of polystyrene ($1.1 \times 10^5 \leq M \leq 2.06 \times 10^6$) has been studied in a marginal solvent (2-butanone) by means of the classical diffusion technique. By comparing the results with those reported from quasi-elastic light scattering measurements on the same polymer/solvent system it is found that the diffusion coefficient in the semidilute regime depends on the time scale over which the measurement is made. Interpreting the results in terms of the pseudogel model, the indication is that the isothermal and adiabatic moduli are not equal. (23 refs.)

114225 Fused salt concentration cells with transference. Transport numbers of molten (Li,Ag)Cl and molten alkali iodide and silver iodide mixtures. J.Richter, E.Kirschbaum, H.Valenta (Inst. für Phys. Chem., RWTH, Aachen, Germany).

Z. Naturforsch. Teil A (Germany), vol.38A, no.8, p.880-4 (Aug. 1983). The transport numbers of the molten systems (Li,Ag)Cl, (Na,Ag)I, (K,Ag)I, and (Rb,Ag)I have been determined by e.m.f. measurements on concentration cells with transference. With the exception of (Na,Ag)I, for these systems the existence of inversion points (the mobility ratio reverses at a certain mixing ratio) is proven within experimental accuracy. For (Na,Ag)I an inversion point might exist at the high AgI concentration side. (5 refs.)

114226 Concentration dependence of the interdiffusion coefficients in molten alkali nitrate-silver nitrate mixtures. A.Hahne, J.Richter (Inst. für Phys. Chem., RWTH Aachen, Aachen, Germany).

Z. Naturforsch. Teil A (Germany), vol.38A, no.8, p.885-9 (Aug. 1983). To measure the composition dependence of the interdiffusion coefficients in molten mixtures of alkali nitrates and silver nitrate, a wave-front-shearing interferometer, together with an initial 'planes source' was used. With this technique, the diffusion coefficients were measured in nearly differential steps in the three mixtures (Na,Ag)NO₃, (K,Ag)NO₃, and (Rb,Ag)NO₃ at 300°C. The composition dependence of the diffusion coefficients D of all three systems could be described by parabolas of the form $D = a + bx_2 + cx_2^2$, where x_2 denotes the mole fraction of the silver nitrate. The three coefficients a , b , and c all show a clear proportionality to the radii of the alkali ions. Thus an extrapolation to the not measured systems (Li,Ag)NO₃ and (Cs,Ag)NO₃ was possible. (20 refs.)

114227 Conductivity of magnesium valerate solutions in binary liquid mixtures. S.N.Gour, U.Kumar (Dept. of Phys., DAV Coll., Muzaffarnagar, India), R.P.Varma.

Indian J. Pure & Appl. Phys., vol.21, no.7, p.398-400 (July 1983). Specific conductivity of magnesium valerate (soap) solutions in binary liquid mixtures has been studied. It is found that the soap aggregates into micelle and the CMC is independent of benzene, chlorobenzene and *p*-xylene concentrations in methanol and the temperature. The conductivity data fit well in the equation: $\log \lambda = A + B \log C$ where A and B are constants and C is the concentration of soap in mol. dm⁻³. Constant A increases with increase in temperature and methanol concentration in the mixture but the values of $-B$ are found independent. The soap is a weak electrolyte which dissociates below the CMC. Molecular conductivity at infinite dilution, λ_{∞} , dissociation constant (K), activation parameters of dissociation, ΔH° , ΔG° and ΔS° have been evaluated and the effect of composition of binary liquid mixtures has been discussed. (13 refs.)

114228 Observations upon the dynamic structure factor of interacting spherical polyelectrolytes. G.D.J.Phillips (Dept. of Chem., Univ. of Michigan, Ann Arbor, MI, USA).

J. Chem. Phys. (USA), vol.79, no.5, p.2325-32 (1 Sept. 1983). Experimental studies are reported on the light-scattering spectrum of 0.038 μ carboxylate-modified polystyrene latex spheres in deionized water. In concentrated suspensions, the long-time decay of the two-particle dynamic structure factor is given by a power law ($t^{-\alpha}$) form, not by a slow exponential. Non-linear least squares fits found $\alpha \approx 1.2$ -1.5, smaller values of α corresponding to higher sphere concentrations. The reduction of the mutual diffusion coefficient of 0.15 μ spheres in mixtures of 0.15 and 0.38 μ spheres was examined, and is interpreted in terms of the dynamic friction modification to the drag coefficients. Multiple scattering artifacts were shown to be absent with homodyne coincidence spectroscopy. (30 refs.)

114229 Translational diffusion in CH₄ and CH₂Cl₂ dissolved in cholesteric liquid crystals. M.E.Moseley, R.Poupko, Z.Luz (Weizmann Inst. of Sci., Rehovot, Israel).

Mol. Cryst. & Liq. Cryst. (GB), vol.95, no.3-4, p.279-85 (1983). Translational diffusion coefficients of CH₄ and CH₂Cl₂ dissolved in five cholesteric mixtures of alkylcyanobiphenylhexane-cholesterylchloride were measured in the temperature range 25°C to 75°C, using the NMR pulse gradient spin echo method. The pitch of the solvents studied depends on the cholesterylchloride concentration and ranged between ∞ and 2.2 μ . The results indicate a slight difference in the diffusion constant parallel (D_{\parallel}) and perpendicular (D_{\perp}) to the cholesteric pitch axis, with $D_{\parallel}/D_{\perp} \approx 1.1$. The Arrhenius activation energies for the diffusion constants are about 6 to 7 kcal/mole for both probes. No dependence of the diffusion coefficients on the cholesterylchloride concentration and thus on the pitch was observed. (11 refs.)

114230 Self-diffusion coefficients of cholesteric/nematic systems with dynamic mass transport method. H.Hakemi (Dept. of Chem., Duke Univ., Durham, NC, USA).

Mol. Cryst. & Liq. Cryst. (GB), vol.95, no.3-4, p.309-22 (1983). Dynamic approach to mass transport study in cholesteric/nematic systems by the optical method provides the evaluation of the self-diffusion coefficients of

both solute and solvent. These values are obtained by extrapolating to the $C=0$ and $C=1$ limits from the scaling law found between the diffusion coefficient and the concentration gradient. The numerical values of the local concentrations are obtained from the pitch values in both homogeneous and homeotropic boundary conditions. (17 refs.)

114231 Diffusion coefficient of a binary stratifying system along the coexistence curve. N.I.Chernova, S.V.Kazakov, F.El Mekawey (Dept. of Molecular Phys., Moscow Univ., Moscow, USSR).

Moscow Univ. Phys. Bull. (USA), vol.37, no.5, p.110-13 (1982). Translation of: *Vestn. Mosk. Univ. Ser. 3 (USSR)*, vol.37, no.5, p.94-6 (1982). The results of investigating the diffusion coefficient in the nitrobenzene-heptane system along the coexistence curve are presented. The parameters of the temperature and concentration dependences of diffusion are measured. It is shown that the character of the singularity in the diffusion coefficient as a function of the concentration is due to the properties of the coexistence curve. (9 refs.)

114232 The characteristics of salt fingers in a variety of fluid systems, including stellar interiors, liquid metals, oceans, and magmas. R.W.Schmitt (Woods Hole Oceanographic Instn., Woods Hole, MA, USA).

Phys. Fluids (USA), vol.26, no.9, p.2373-7 (Sept. 1983). The growth rates, flux ratios, wavenumbers, and bandwidths of salt fingers are computed for Prandtl numbers from 10^{-7} to 10^4 and diffusivity ratios from 1 to 10^8 using the exact similarity solutions of Schmitt [Deep-Sea Res. 26A, 23 (1979)]. This model successfully explains the variation in flux ratio in the heat/salt and salt/sugar systems and produces salt-finger spectra in agreement with ocean observations. The calculations presented should be useful in the study of double diffusion in astrophysics, chemistry, geology, metallurgy, meteorology, and oceanography, and may be applicable to problems in the growth of semiconductor crystals. (19 refs.)

114233 Electrolyte solutions near the critical point of water: a review and proposal for studies under microgravity conditions. D.J.Turner (Central Electricity Res. Labs., Leatherhead, England).

Proceedings of the 4th European Symposium on Materials Sciences under Microgravity (ESA SP-191), Madrid, Spain, 5-8 April 1983 (Paris, France: ESA 1983), p.393-400

All ions in a solution exert a compressional influence on the solvent molecules in their vicinity. When a solvent has a high compressibility, as it will near its critical point, the effect is expected to be very large, especially at low concentrations. These expectations are born out in practice in measurements of apparent molal volumes, molal compressibilities and heat capacities of ions in water. Reported data on these properties and on conductance are reviewed for NaCl solutions along the SVP curve and in a supercritical fluid just above the critical point. They are rationalized using a simple two state model which treats the solvent as either fully compressed by the ions or as free solvent. A proposal is outlined for a conductance study on aqueous NaCl solutions at a temperature just below critical. A description is given of the conductance equipment being developed for use in a Texus flight and of the objectives of the first experiment planned. (27 refs.)

Self-diffusion of macromolecules in the crystallization of a polymer from solution See Entry 113758

Some formulae describing spherical and hemispherical diffusion to small crystals in unstirred solutions See Entry 113779

Periodic crystallization of binary melts under diffusion-controlled mass transfer See Entry 114149

High voltage electric field and space-charge distributions in highly purified water See Entry 114782

On the dissociation conductivity of fluid dielectrics See Entry 114801

66.20 DIFFUSIVE MOMENTUM TRANSPORT

(inc. viscosity of liquids)

114234 Viscoelastic properties of linear low density polyethylene melts.

D.R.Saini, A.V.Shenoy (Chem. Engng. Div., Nat. Chem. Lab., Pune, India). *Eur. Polym. J. (GB)*, vol.19, no.9, p.811-16 (1983).

The importance of linear low density polyethylene (LLDPE) is being rapidly felt. The combination of favourable production economics and excellent product performance characteristics has enabled this new plastic to gain acceptance for a wide variety of applications. No studies on the rheological properties of LLDPE exist to date. The viscous and elastic properties of this new polymer has now been investigated and unified curves for viscosity and normal stress differences are given. The temperature dependence of the rheological properties of LLDPE has also been studied. (22 refs.)

114235 Structure of water solutions. I. Viscosities of aqueous substituted ammonium chlorides. R.Bhanumathi, S.K.Vijayalakshamma (Dept. of Inorganic & Phys. Chem., Indian Inst. of Sci., Bangalore, India).

J. Electrochem. Soc. India, vol.32, no.1, p.11-15 (Jan. 1983). [received: Sept. 1983]

Relative viscosities of methyl, ethyl and benzyl ammonium chlorides are measured at three temperatures 35°C, 45°C, 60°C. The data at low concentration is analysed using the Jones-Dole equation. B_+ coefficients are obtained using the method of Sacco (1981) ($B(BPh_4^-) = B(PPh_4^+)$). The temperature dependence of B_+ coefficients indicates structure forming tendency in all three cases and no ion-ion association. The viscosity data is also analysed using Vand's treatment (1948) and Breslau and Miller's treatment (1970) at higher concentration. Breslau-Miller's V_e values show a linear negative dependence on concentration thus agreeing with the conclusion that no ion-ion associate is present till 1 M. The volume obtained from the various treatments are compared with van der Waals volume calculated from X-ray data. The interaction constant K of Vand's treatment decrease with temperature in all cases probably indicating structure-forming tendency. (18 refs.)

114236 Pressure dependence of the viscosity of dilute polystyrene solutions in toluene. S.Claesson, J.L.McAtee, Jr., S.Ali (Dept. of Chem., Baylor Univ., Waco, TX, USA).

J. Polym. Sci. Polym. Phys. Ed. (USA), vol.21, no.9, p.1873-81 (Sept. 1983). The effect of pressure on the viscosity of dilute solutions of anionically polymerized polystyrene ($M_w = 209000$; $M_w/M_n = 1.12$) in toluene has been studied at different temperatures and concentrations using a falling-body viscometer. Measurements were performed in the concentration range from 0.0025 to 0.2 g/mL and at temperatures from 25 to 45°C under pressure up to 1057 bars. The viscosity coefficient η increases exponentially with pressure at a given temperature and concentration, while the apparent volume of activation V^\ddagger decreases with increasing temperature. The hypothesis that the pressure dependence of η is given by the pressure dependence of the activation energy holds true under the prevailing thermodynamic conditions. Log η increases linearly with increasing concentration at a given pressure. Intrinsic viscosity increases with increasing pressure, whereas the Huggins constant decreases. (40 refs.)

114237 Elongation rheology of polyolefins and its relation to processability. D.H.Sebastian (Dept. of Chem. & Chem. Engng., Stevens Inst. of Technol., Hoboken, NJ, USA), J.R.Dearborn. *Polym. Eng. & Sci. (USA)*, vol.23, no.10, p.572-5 (July 1983). The rheology of a variety of polyolefin resins, and resin blends, has been examined under conditions of constant strain rate elongation. These include high, low, and linear low density polyethylene, as well as polypropylene, commercially modified polypropylene, and elastomer blends with polypropylene. Two distinctly different classes of behavior are apparent in the viscosity growth patterns during uniaxial extension. Some resins display unbounded stress growth even at low strain rates. Others quickly attain a time independent value of extensional viscosity even at increased strain rates. The former behavior is identified with favorable blow molding behavior, while the latter was characteristic of resins unsuitable for such processing. The class of elongation behavior depends not only on resin type, but may be influenced by molecular weight distribution or blend morphology. (5 refs.)

Anomalous rheological behaviour of poly(vinyl alcohol) gels ...See Entry 113393

Nonlinear viscoelasticity and the Cox-Merz relations for polymeric fluidsSee Entry 113395

A phenomenological master curve for viscosity—structure data for two phase polymer systems in simple shear flowSee Entry 113723

Domain stability during capillary flow of well dispersed two phase polymer blends. Polystyrene/polymethylmethacrylate blendsSee Entry 113727

Liquid-crystalline copolyesters based on poly(*p*-oxybenzoate) and poly(*p*,*p*-biphenylene terephthalate)See Entry 113734

Viscoelastic relaxation in the acetamide+sodium thiocyanate binary systemSee Entry 114066

Melt rheology of polymer blends: the morphology feedback ..See Entry 114068

Melt rheology of blends of semi-crystalline polymers. II. Dynamic properties of poly(ethylene terephthalate)-poly(amide-6,6) molten blendsSee Entry 114069

Ultrasonic and hypersonic investigations of structural relaxation in aqueous solutions of hexamethylphosphortriamideSee Entry 114097

A ¹³C NMR study of mesomorphic solutions of poly(*p*-phenylene terephthalamide)See Entry 114750

66.30 DIFFUSION IN SOLIDS

114238 Gaseous diffusion in glassy polymers. D.S.Cohen, E.A.Stanley (Dept. of Appl. Math., California Inst. of Technol., Pasadena, CA, USA). *SIAM J. Appl. Math. (USA)*, vol.43, no.4, p.949-70 (Aug. 1983). A model for gaseous diffusion in glassy polymers is developed with a view to accounting for the observations made in dual sorption and certain other phenomena in polymers below their glass transition temperature. In this paper a preliminary study of the effects of both the immobilizing mechanism and the generalized diffusion mechanism on travelling waves and the diffusive wave-fronts is made. (21 refs.)

The kinetics of the interaction between helium and displacement damage in irradiated materialsSee Entry 114060

¹H NMR study of hydrogen motion in the β phase of the Mg₂NiH_x systemSee Entry 114747

66.30D Theory of diffusion and ionic conduction in solids

114239 Ion-induced diffusion and surface segregation. K.Morita (Dept. of Crystalline Materials Sci., Nagoya Univ., Nagoya, Japan), H.Shimizu. *J. Vac. Soc. Jpn. (Japan)*, vol.26, no.2, p.88-98 (1983). In Japanese. Discusses the effect of ion irradiation on compound material from the standpoint of surface thermodynamics, surface segregation and ion-induced diffusion. The topical areas include: (1) segregation models—Fowler-Guggenheim model and Langmuir-McLean model, (2) two-dimensional phase diagram, (3) irradiation-induced diffusion and grain-boundary diffusion, and (4) ion-induced diffusion and surface segregation in ion beam processing for semiconductor-device fabrication. (47 refs.) *K.B.*

114240 Phenomenological coefficients for atom transport in dilute interstitial solid solutions. Y.Ökamura, A.R.Allnatt (Dept. of Chem., Univ. of Western Ontario, London, Ontario, Canada). *Philos. Mag. A (GB)*, vol.48, no.3, p.387-96 (Sept. 1983). The phenomenological coefficients, in the form of flux equations suggested by the thermodynamics of irreversible processes, are calculated for two dilute interstitial species for models in which binding between nearest-neighbour interstitials occurs. Linear-response formulae for the coefficients are analysed by an extension of the matrix method of random-walk theory familiar in the calculation of impurity correlation factors. The terms correct to first order in the concentrations of paired and unpaired species are calculated exactly. The origin of the close relationship in structure between results for this model and results for a model of a dilute binary alloy with the vacancy mechanism is traced through the steps of the calculation. (11 refs.)

114241 The role of vacancies in grain boundary motion. Y.Estrin (Tech. Univ. Hamburg-Harburg, Hamburg, Germany), K.Lucke, G.Gottstein. Point Defects and Defect Interactions in Metals. Proceedings of the Yamada Conference V, Kyoto, Japan, 16-20 Nov. 1981 (Amsterdam, Netherlands: North-Holland 1982), p.773-5. Grain boundary motion (GMB) by transfer of individual atoms across the grain boundary (GB) is considered. Competing models of GBM, different as to the role of vacancies in the elementary effect of boundary displacement, are analyzed. Qualitative differences in the predictions of these models provide a basis for experimental identification of the operating mechanism of GBM. (7 refs.)

Solute-enhanced self-diffusion. On the validity of the Howard-Manning theorySee Entry 114245

A stress transfer model for the deformation and failure of polymeric matrices under swelling conditionsSee Entry 115292

66.30F Self-diffusion in metals, semimetals, and alloys

114242 Self-diffusion of carbon in Ti-C alloys. V.S.Zotov, V.I.Sukharev. *Fiz. Met. & Metalloved. (USSR)*, vol.56, no.2, p.410-13 (Aug. 1983). In Russian. English translation in: *Phys. Met. & Metallogr. (GB)* Alloys of titanium containing up to 2.0 at.% were investigated using radioactive carbon (¹⁴C). At low carbon concentrations an increase in the amount of carbon reduced the diffusion coefficient, but at higher concentrations the carbon content had no effect. (17 refs.) *A.T.*

114243 Lateral self-diffusion in indium thin films. J.J.B.Prasad, K.V.Reddy (Dept. of Phys., Indian Inst. of Technol., Madras, India). *Indian J. Pure & Appl. Phys.*, vol.21, no.7, p.391-4 (July 1983). Lateral self-diffusion has been studied in indium thin films. A thin-film sample with a well defined radioactive region in the middle was prepared by neutron activation technique. An experimental set-up was fabricated to scan the concentration of the radioactive indium in the sample. A non-linear fitting procedure was employed to determine the self-diffusion coefficient from the experimental data. The diffusion data obtained in the temperature range 93-145°C could be fitted to the equation $D=0.22 \exp (-0.60/kT)$. The thin-film data were compared with the available data on bulk indium. A grain boundary diffusion mechanism has been concluded for the lateral self-diffusion in indium thin films in the temperature range studied. (13 refs.)

114244 Fast interstitial-solute complex diffusion under irradiation in Cu/Be. H.-J.Gudlart, V.Naundorf, M.-P.Macht, H.Wollenberger (Hahn-Meitner-Inst. fur Kernforschung Berlin GmbH, Berlin, Germany). *J. Nucl. Mater. (Netherlands)*, vol.118, no.1, p.73-7 (Aug. 1983). Diffusion of beryllium in copper has been investigated under self-ion irradiation at temperatures between 295K and 700K. After irradiation Be was found in the initially Be free zone far outside the region damaged by irradiation. This observation is interpreted by long range diffusion of highly mobile interstitial Be complexes. (10 refs.)

114245 Solute-enhanced self-diffusion. On the validity of the Howard-Manning theory. S.Ishioka, M.Koiwa, H.Nakajima (Res. Inst. for Iron, Steel & Other Metals, Tohoku Univ., Sendai, Japan). *Philos. Mag. A (GB)*, vol.48, no.3, p.341-58 (Sept. 1983). The Howard-Manning theory of the effect of solutes on solvent self-diffusion is examined critically. A model problem (the diffusion of a random walker on an imperfect lattice with a regular array of blocked sites), which can be solved rigorously, is solved by the Howard-Manning approach. A comparison of the results obtained by both rigorous and approximate methods throws light on the validity of the approximations. It is concluded that a more extensive calculation is required when the vacancy jump frequencies in the vicinity of an impurity are very much different from that at normal sites. (5 refs.)

114246 Investigation of vacancy diffusion in niobium, molybdenum, and tantalum by means of high-voltage electron microscopy. F.Phillipp, B.Saile, K.Urban (Max-Planck-Inst. fur Metall., Stuttgart, Germany). Point Defects and Defect Interactions in Metals. Proceedings of the Yamada Conference V, Kyoto, Japan, 16-20 Nov. 1981 (Amsterdam, Netherlands: North-Holland 1982), p.261-4. The growth of interstitial dislocation loops during high-temperature irradiation was investigated in Nb, Mo and Ta by means of high-voltage electron microscopy. The growth rate is at temperatures higher than 420K (Nb), 600K (Mo) and 550K (Ta) independent of irradiation time. This provides direct evidence for the onset of long-range vacancy migration at the indicated temperatures. The loop growth rate is found to be proportional to P^n where P is the defect production rate and $0.7 \leq n \leq 0.8$. This indicates that the rate of mutual recombination and that of the annihilation of point defects at sinks are of comparable order of magnitude. Employing an extended rate equation description of damage formation in which the formation of submicroscopic vacancy clusters is taken into account, a good fit to the quantitative results can be achieved. The activation enthalpies for vacancy migration thus obtained are (0.95±0.15)eV for Nb, (1.3±0.2)eV for Mo and (1.1±0.2)eV for Ta. (9 refs.)

114247 Vacancies in zinc and cadmium produced by proton- and electron-irradiation. R.Seeboeck, W.Engel, S.Hoth, R.Keitel, W.Witthuhn (Phys. Inst., Univ. Erlangen-Nurnberg, Erlangen, Germany). Point Defects and Defect Interactions in Metals. Proceedings of the Yamada Conference V, Kyoto, Japan, 16-20 Nov. 1981 (Amsterdam, Netherlands: North-Holland 1982), p.271-3. The annealing behaviour of lattice defects in Zn and Cd was investigated by the PAC-method. The defects were produced by proton- and electron-irradiation and by quenching. The experiments clearly show that in annealing stage III in Zn and Cd, vacancies are migrating freely. (21 refs.)

A quantitative study of vacancy defects in quenched tungsten by combined field-ion microscopy and electrical resistometrySee Entry 113863

Vacancies in silver: a resistivity and positron annihilation studySee Entry 113876

Vacancy formation in Ni and Ni(Ge)See Entry 113880

Defects and diffusion in intermetallic compoundsSee Entry 113882

Mossbauer study of defect trapping at ⁵⁷Co in cold worked aluminiumSee Entry 113959

Kinetics of structural multiplets during diffusion homogenization of polycrystalline filmsSee Entry 114381

66.30H Self-diffusion and ionic conduction in nonmetals

114248 Electrical conductivity measurements of some layered magnetic structures. C.P.Tigges, J.E.Drumheller, L.O.Snively (Dept. of Phys., Montana State Univ., Bozeman, MT, USA). *J. Appl. Phys. (USA)*, vol.54, no.9, p.5473-5 (Sept. 1983). The electrical conductivity for temperatures up to 416K has been measured in several of the alkylammonium tetrahalidemetallates and the alkanediammonium tetrahalidemetallates where the halides were bromine and chlorine and the metal was copper or, in one case, cadmium. These salts are all good magnetic insulators at low temperature but behave as ionic, probably protonic, semiconductors as the temperature is increased. Room temperature conductivity for these samples is of order $10^{-12} \Omega^{-1} \text{ cm}^{-1}$ and varies as much as ten orders of magnitude over the measured temperature range. The possibility that the changes in activation energy are related to known structural phase transitions is discussed. (12 refs.)

114249 Diffusion of long chain n-alkylammonium cations in layer compounds (*n*-C_nH_{2n+1}NH₃)₂MCl₄. V.Busico, M.Vacatello (Istituto Chimico, Univ. di Naples, Naples, Italy). *Mol. Cryst. & Liq. Cryst. (GB)*, vol.95, no.3-4, p.251-69 (1983). Evidence for long range, anisotropic diffusion of the long chain *n*-alkylammonium cations in layer compounds (*n*-C_nH_{2n+1}NH₃)₂MCl₄ is presented. Annealing mechanical mixtures of such compounds with $M=\text{Mn}$, Zn; $n=12$, 18 results in the formation of mixed crystals of composition (*n*-C₁₂H₂₅NH₃)_{2x(12)} (*n*-C₁₈H₃₇NH₃)_{2-2x(12)}MCl₄ in which bilayers of *n*-alkylammonium groups with differing chain lengths, positionally and conformationally disordered, alternate with crystalline metal halide layers (modification β'). When the ionic layers are polymeric ($M=\text{Mn}$), solid solutions are obtained on cooling from modification β' in which the polymethylenic chains

of the alkylammonium groups, while maintaining positional disorder, are partly cocrystallised in spite of the high difference in chain length (modification α'). Demixing into the pure components, on the other hand, is observed on cooling for nonmacroanionic systems ($M=Zn$). Possible structural models of the mixed compounds in modifications α' , β' are described, and the stability of such modifications relative to the unmixed components evaluated on the basis of a simple thermodynamical treatment. (26 refs.)

114250 Structure and dynamics of disordered solids: a neutron scattering study of $Ba_{1-x}La_xF_{2+x}$. J.K.Kjems, N.H.Andersen, J.Schoonman (Riso Nat. Lab., Roskilde, Denmark), K.Clausen. *Physica B & C (Netherlands)*, vol.120B+C, no.1-3, p.357-61 (May 1983). (Yamada Conference VI on Neutron Scattering in Condensed Matter, Hakone, Japan, 1-4 Sept. 1982).

Single crystals of the fluorite-type solid solutions $Ba_{1-x}La_xF_{2+x}$, $x=0.209$ and $x=0.492$, show strong anisotropic diffuse neutron scattering which is quantitatively explained in terms of simple models involving defect clusters of the 222 type. The concentrated sample shows additional evidence for short range correlations between such clusters which tend to form larger, roughly linear aggregates. The aggregates dissociate at temperatures above 500°C. The implications for the conduction mechanism are discussed. (7 refs.)

114251 Direct evidence of diffusion of self-interstitials in silicon. G.Das (IBM General Technol. Div., East Fishkill, NY, USA). Defects in Semiconductors II, Symposium Proceedings, Boston, MA, USA, Nov. 1982 (New York, USA: North-Holland 1983), p.87-93.

High temperature (1200°C) HCl oxidation treatment has been employed to float-zone (FZ) silicon wafers (625 μ m thick) containing swirl defects in order to study their diffusion characteristics. In treated wafers, swirl defects can be eliminated from both surfaces up to a depth of ~ 30 μ m. In the bulk of the wafers, however, large swirl defects (A-swirls) rearrange themselves into many small defects. The untreated portions of wafers contain large swirl defects (A-swirls) that extend up to both surfaces. Since swirl defects are primarily clusters of silicon self-interstitials, their rearrangement in the bulk and elimination from the surfaces demonstrate that migration of interstitials takes place on a large scale and is not confined to SiO_2 /silicon interface only. The above observations appear to provide direct evidence for the dominant role of self interstitials for diffusion mechanism in silicon at high temperature and can be rationalized in terms of an interstitially mechanism. Alternatively, however, dominance of interstitials can be related to a higher migration energy of vacancies proposed in a model where both species coexist at high temperature. The preference of one model over another must await theoretical calculations of diffusion energetics derived from both models. (22 refs.)

114252 Self-diffusion in compound semiconductors. A.F.W. Willoughby (Engng. Materials Labs., Univ. of Southampton, Southampton, England). Defects in Semiconductors II, Symposium Proceedings, Boston, MA, USA, Nov. 1982 (New York, USA: North-Holland 1983), p.237-52.

Self-diffusion studies are vital in the elucidation of atomic mechanisms of diffusion, as well as in the better understanding of device fabrication processes, such as the annealing of ion-implanted layers. This review outlines first the major reasons for interest in self-diffusion in III-V and III-VI compounds. It discusses the main differences with elemental semiconductors, including the wide variety of possible defects in the compounds, the role of departures from stoichiometry, and the value of tracer and interdiffusion studies. Self-diffusion studies in III-V compounds are reviewed, including recent measurements in GaAs, where more information on diffusion mechanisms is becoming available. Interdiffusion between different III-V compounds is also discussed in the light of self-diffusion studies. Recent progress on self-diffusion in certain II-VI compounds is discussed, where interdiffusion studies have also provided a significant contribution. The review concludes by suggesting areas where research is urgently needed to clarify diffusion mechanisms. (40 refs.)

Phase transitions in $Na_3Sc_2(PO_4)_3$ and in related compounds with $\{[M_2(EO_4)_3]^{P-}\}_{3\infty}$ frameworks See Entry 113794

Crystal-chemical principles of prediction of ferroelectrics and related materials in the case of compounds with $\{[M_2(EO_4)_3]^{P-}\}_{3\infty}$ frameworks See Entry 113820

The calculated defect structure of thorium See Entry 113862

The study of vacancy clustering in deformed metals by positron annihilation See Entry 113898

Influence of vacancies and interstitials on the Bordoni peaks in copper and silver See Entry 113899

The nature of point defects and their influence on diffusion processes in silicon at high temperatures See Entry 113906

Solute atom-dislocation interactions studied by ultrasonic method See Entry 113975

Study of low temperature specific heat and DC electrical conductivity of NH_4Cl in pure powder form and in crystalline form grown from urea solution See Entry 114205

Dynamic observation of atomic-level events in cadmium telluride by high resolution TEM See Entry 114284

Nuclear magnetic resonance investigations of lithium diffusion in Li_2O , Li_2SiO_3 and $LiAlO_2$ See Entry 114751

NMR study of both ^{19}F and ^{205}Tl motions in $TlZrF_5$ See Entry 114753

Dielectric properties of Ag_3AsS_3 in the region of high ionic conductivity See Entry 114772

Preparation of Li_3N single crystal by floating zone technique See Entry 115046

Cation and anion transport numbers in anodic GaAs oxides .. See Entry 115384

66.30J Diffusion, migration, and displacement of impurities

114253 Incoherent light-induced diffusion of arsenic into silicon from a spin-on source. V.E.Borisenko, A.Nylandsted Larsen (Inst. of Phys., Univ. of Aarhus, Aarhus, Denmark).

Appl. Phys. Lett. (USA), vol.43, no.6, p.582-4 (15 Sept. 1983). A new approach to impurity diffusion in semiconductors based on the use of a spin-on source and short-time incoherent light exposure has been developed and experimentally investigated for arsenic diffusion into silicon. Arsenic-doped oxide films, ~ 0.19 μ m thick, were spin-on deposited onto (100) oriented silicon crystals and heated with radiation from a xenon lamp to temperatures between 950 and 1200°C for times of 10 and 25 s. Arsenic diffused layers tested with resistivity measurements and Rutherford backscattering analysis were characterized by a maximum surface concentration $\sim 1 \times 10^{20}$ atom/cm³ and a maximum depth ~ 0.40 μ m. (19 refs.)

114254 Double zinc diffusion fronts in InP—theory and experiment. M.Yamada, P.K.Tien, R.J.Martin, R.E.Nahory, A.A.Ballman (Bell Telephone Labs., Holmdel, NJ, USA).

Appl. Phys. Lett. (USA), vol.43, no.6, p.594-6 (15 Sept. 1983). Diffusion of Zn or Cd in *n*-type III-V material has been extensively used for forming *p-n* junctions in lasers and detectors. However, if the substrate material used for diffusion has an electron concentration less than 5×10^{16} cm⁻³, two separate diffusion fronts will appear which alter completely the electrical property of the junction. The authors have investigated this phenomenon by electron beam induced current (EBIC) and secondary ion mass spectroscopy (SIMS). A theory is proposed, for the first time, in good agreement with experiment. (7 refs.)

114255 Effect of thermal nitridation processes on boron and phosphorus diffusion in (100) silicon. P.Fahey, R.W.Dutton, M.Moslehi (Stanford Electronics Labs., Stanford Univ., Stanford, CA, USA).

Appl. Phys. Lett. (USA), vol.43, no.7, p.683-5 (1 Oct. 1983). The effect of the silicon thermal nitridation processes, nitridation of SiO_2 (oxynitridation), and direct nitridation of the silicon surface on boron and phosphorus diffusion is examined. It is found that oxynitridation results in enhanced diffusion of both impurities while direct nitridation of the silicon surface causes retarded diffusion for both. These phenomena are explained by the mechanisms of silicon self-interstitial injection in the case of oxynitridation and self-interstitial depletion in the case of direct nitridation. (13 refs.)

114256 Asymmetry of the permeability of multilayer films. F.A.Makhmutov, V.G.Nazarov, V.K.Belyakov, V.N.Manin. *Vysokomol. Soedin. Ser. B (USSR)*, vol.25, no.6, p.387-91 (1983). In Russian.

The conditions for the attainment of high values of the permeability asymmetry of multilayer polymer films are studied with the aid of a model for explaining and predicting the values of the permeability asymmetry for multilayer polymer films on the basis of an analysis of the concentration relations for the permeability of individual layers, and with special reference to the permeability of various homopolymers and copolymers, e.g. of the vinyl chloride-vinyl acetate and ethylene-vinyl chloride systems with various ratios of the monomer linkages, and also of polyvinyl alcohol and hydrated cellulose systems with various degrees of cyanethylation and acetylation, with respect to *n*-heptane and methanol. (8 refs.) N.S.

114257 The effects of defect character on hydrogen diffusion in metals. C.N.Park, J.-Y.Lee, G.W.Hong (Dept. of Materials Sci. & Engng., Korea Advanced Inst. of Sci. & Technol., Seoul, Korea).

J. Mater. Sci. Lett. (GB), vol.2, no.9, p.475-9 (Sept. 1983). The hydrogen diffusion flux equations are established considering trap characteristics and their effects on apparent diffusivity is analysed; the effect of shape—spherical (vacancy, substitutional atom and microvoid), cylindrical (dislocation) and spherical skin (grain boundary)—density, size of defects and temperature are examined. (9 refs.)

114258 Marker experiments for diffusion in the silicide during oxidation of $PdSi$, Pd_2Si , $CoSi_2$, and $NiSi_2$ films on (Si). M.Bartur, M.-A.Nicolet (California Inst. of Technol., Pasadena, CA, USA).

J. Appl. Phys. (USA), vol.54, no.9, p.5404-15 (Sept. 1983). Inert markers (evaporated tungsten and ion implanted xenon) were used to investigate the mass transport through a silicide layer on a (Si) substrate during thermal oxidation at 700-900°C. The SiO_2 growth from $PdSi$, Pd_2Si , $CoSi_2$, and $NiSi_2$ films on (Si) is a process limited by the diffusion of the oxidant from the ambient gas to the silicide/oxide interface. Possible diffusion processes through the silicide that supply Si to the growing SiO_2 layer, but keep the silicide stoichiometry intact, are discussed. Backscattering spectrometry is used to monitor the marker position in the silicide layer. The authors find that the diffusing species during oxidation correlate with the moving species during silicide formation. (18 refs.)

114259 Effects of back-side oxidation of Si substrates on Sb diffusion at front side. S.Mizuo, H.Higuchi (Hitachi Ltd., Central Res. Lab., Kokubunji, Tokyo, Japan).

J. Electrochem. Soc. (USA), vol.130, no.9, p.1942-7 (Sept. 1983). The effect of back-side oxidation of Si wafers on the diffusion of Sb in the front of wafers is investigated with back-side selective oxidation (BSO) at 1100°C in dry O_2 ambients. It is found that the diffusion of Sb in the front of the wafers is retarded by BSO only for FZ Si substrates under directly formed Si_3N_4 films, and that Sb diffusion in CZ Si substrates and under double-layered SiO_2 - Si_3N_4 films in both FZ and CZ substrates is not affected by BSO. The effective range over which BSO affects Sb diffusion is found to increase with oxidation time. The range and extent of oxidation retarded diffusion (ORD) for Sb are shown to agree with those of oxidation enhanced diffusion (OED) for B and P. These results are explained with a proposed model: (i) there is a thermal equilibrium between vacancies and interstitials, and (ii) the Si- SiO_2 interface provides sinks and generation centers for point defects in Si, though the Si- Si_3N_4 interface does not react with point defects. (25 refs.)

114260 Diffusivity of tritium in Li-Al alloys. M.Nakashima, M.Saeki, Y.Arakono, E.Tachikawa (Div. of Chem., JAERI, Tokai, Ibaraki, Japan).

J. Nucl. Mater. (Netherlands), vol.116, no.2-3, p.141-6 (June 1983). The diffusion coefficients of tritium in Li-Al alloys were measured. The observed diffusion coefficients were expressed by the following equations: $D = 8.5 \times 10^{-5} \exp[-43.9 \pm 14.8 (kJ/mol)/RT]$ (cm²/s), $D = 9.3 \times 10^{-5} \exp[-48.5 \pm 15.0 (kJ/mol)/RT]$ (cm²/s), and $D = 5.3 \times 10^{-5} \exp[-62.7 \pm 13.8 (kJ/mol)/RT]$ (cm²/s) for 0.02, 0.26 and 1.12% Li-Al alloys, respectively. Results showed that the diffusion coefficients as well as the apparent activation energy for diffusion depend upon the lithium concentration in the alloy. (13 refs.)

114261 Diffusion of tritium in single crystal Li_2O . D.Guggi, H.R.Ihle, D.Bruning, U.Kurz (Inst. für Chem., Kernforschungsanlage Jülich GmbH, Jülich, Germany), S.Nasu, K.Noda, T.Tanifuji.

J. Nucl. Mater. (Netherlands), vol.118, no.1, p.100-8 (Aug. 1983). The release of tritium from neutron irradiated spherical samples of single crystal Li_2O was measured by isothermal annealing experiments. The release is shown to be controlled by diffusion of tritium in the solid under appropriate experimental conditions. Deviations from solely diffusion controlled release were observed when traces of water were present in the He-purge gas used in the experiments. The diffusivity of tritium in single crystal Li_2O is given by $\ln(D/cm^2 s^{-1}) = -(5.93 \pm 0.48) - (81.73 \pm 4.24) 10^3/RT$ for $850K < T < 1200K$ ($R = 8.314 J K^{-1} mol^{-1}$). (20 refs.)

114262 Tests of a free-volume model for the permeation of gas mixtures through polymer membranes. CO_2 - C_2H_4 , CO_2 - C_3H_8 , and C_2H_4 - C_3H_8 mixtures in polyethylene. S.A.Stern, G.R.Mauze (Dept. of Chem. Engng. & Materials Sci., Syracuse Univ., Syracuse, NY, USA), H.L.Frisch. *J. Polym. Sci. Polym. Phys. Ed. (USA)*, vol.21, no.8, p.1275-98 (Aug. 1983). Steady-state permeability coefficients have been measured for equimolar mixtures of CO_2 - C_2H_4 , CO_2 - C_3H_8 , and C_2H_4 - C_3H_8 , as well as for a mixture of

74.9 mol.% CO₂ and 25.1 mol.% C₂H₄ in polyethylene membranes. The measurements were made at 20, 35, and 50°C and at pressures of up to 28 atm. Each component of the permeating mixtures studied had the effect of increasing the permeability coefficient for the other component. Furthermore, at equal partial pressures and at the same temperature, the component exhibiting the highest solubility in the polymer had the largest effect in increasing the permeability coefficient of the other component. This behaviour is in agreement with the predictions of a free-volume model for the permeation of gas mixtures proposed by Fang, Stern, and Frisch (see J. Polym. Sci. A-2, vol.10, p.201, 1972). From a quantitative viewpoint, the permeability coefficients for the components of the mixtures agreed, on the average, to better than 25% with the predicted values. The theoretical permeability coefficients can be estimated from the model by using parameters determined with the pure components only. (21 refs.)

114263 Diffusion of iodine into PE and PET. L.F.Pender, H.-B.Mak, H.J.Wintle (Dept. of Phys., Queen's Univ., Kingston, Canada). *J. Polym. Sci. Polym. Phys. Ed. (USA)*, vol.21, no.9, p.1635-46 (Sept. 1983). The Rutherford backscattering technique is very useful for studying the kinetics of diffusion processes in polymers. The diffusion of iodine into low-density polyethylene (LDPE) was measured by optical absorbance and by Rutherford backscattering. The optical results appear to be normal, and show no electric field dependence, but the backscattering results reveal that this is misleading, because there is fast diffusion in the bulk accompanied by large surface concentrations of iodine. PET was studied by the backscattering technique, and in this case the behavior corresponds to a weakly concentration-dependent diffusion coefficient with no observable surface effects. Neither set of results gives support of the domain theories of low-frequency electrical oscillation in these materials. (51 refs.)

114264 The effect of micro-structure on the diffusion of n-hexadecane and DDT in poly(1,4-butadienes). R.B.Jenkins, G.S.Park (Dept. of Appl. Chem., Univ. of Wales Inst. of Sci. & Technol., Cardiff, Wales). *J. Membrane Sci. (Netherlands)*, vol.15, no.2, p.127-40 (Sept. 1983). Diffusion coefficients of the large inflexible DDT molecule [1,1-bis(4-chlorophenyl)-2,2,2-trichloroethane] and of the long flexible n-hexadecane molecule have been obtained in various polybutadienes using ¹⁴C labelled molecules and the thin smear surface activity method at temperatures of 25, 35 and 45°C. In all cases, the diffusion coefficients decrease slowly as the trans content of the polymer increases from zero to 75%. This can be attributed to a decrease of free volume with decreasing cis content. There is a much more rapid fall in the diffusion coefficient at higher trans contents due to the presence of crystallites and the fall is greater for DDT than for n-hexadecane. At trans contents above 90%, the diffusion coefficient, *D*, in polymer having a volume fraction, *V_a*, of amorphous material, fits the relationship *D_a*=*D_a*(*V_a*)^x with *x* between 0.85 and 1.28 for n-hexadecane and between 1.42 and 1.67 for DDT. The activation energies, *E_D*, for both the diffusants are similar and in the case of the amorphous polybutadienes they are quite close to the activation energies for viscous flow of the polymers. There is only a slow increase of *E_D* with trans content of the polymer until the highly crystalline 100% trans material is reached. A much more marked increase in *E_D* is then obtained indicating a change in the remaining amorphous polymer as a diffusion medium. (15 refs.)

114265 Diffusion of water vapour in polymethyl methacrylate. P.P.Rousis (Chem. Dept., Nuclear Res. Center 'Demokritos', Aghia Paraskevi Attikis, Athens, Greece). *J. Membrane Sci. (Netherlands)*, vol.15, no.2, p.141-55 (Sept. 1983). Certain aspects of the concentration dependence of the diffusion coefficient and on the mechanism of sorption of water vapour in PMMA are investigated. Early time integral sorption kinetics follow the Fickian pattern of initial linearity. Diffusion coefficients deduced from the slopes of these lines are independent of concentration and satisfactorily agree with those obtained from late-time analysis; however, desorption values are higher throughout the whole range of activities than the corresponding absorption ones. On the contrary, typical 'non-Fickian' features are discerned in differential absorption kinetics on membranes of different thickness. These anomalies are attributed to rate-determining relaxation processes concurrent with diffusion, whereas other sorption models are incompatible with the general behaviour of this system. General trends of the equilibrium and kinetic data are compared with those of other polymer-water systems and the observed differences are interpreted in terms of the molecular relaxation model. (27 refs.)

114266 Dye diffusion in anisotropic polyamide fibres. I.D.Rattee, S.S.O (Dept. of Colour Chem., Leeds Univ., Leeds, England). *J. Membrane Sci. (Netherlands)*, vol.15, no.2, p.171-80 (Sept. 1983). Radioactive tracer techniques have been used to study the diffusion of three dyes in polyamide fibres produced under different conditions. Drawn nylon fibres have a surface barrier layer which limits diffusion. The permeability of the layer is reduced by drawing, and varies with drawing conditions. The dependence of dye diffusion on concentration, ionic size and draw ratio is less in the surface than in the bulk of the fibre, but variations in dyeing behaviour have been shown to follow surface rather than bulk diffusion characteristics. (12 refs.)

114267 Diffusion of alcohols and relaxation in poly(methyl methacrylate): effect of thermal history. G.C.Sarti, C.Gostoli, S.Masoni (Inst. di Impianti Chimici, Facoltà di Ingegneria, Univ. di Bologna, Bologna, Italy). *J. Membrane Sci. (Netherlands)*, vol.15, no.2, p.181-92 (Sept. 1983). The sorption behavior of alkyl alcohols in poly(methyl methacrylate) is analyzed after predetermined annealing treatments of the polymer matrix. Weight uptake, penetration depth and sample dimensions are reported versus time. Dimensionless parameters are used, through which master curves are obtained for both weight uptake and the area perpendicular to the main penetration direction. Contrary to what is observed in polystyrene-*n*-alkane systems, in the present case either the specific plasticization of the penetrant must be accounted for, or a non-localized swelling model must be used to explain the behavior. (22 refs.)

114268 Diffusion and solution of methanol vapor in poly(2-vinylpyridine)-block-polyisoprene and poly(2-vinylpyridine)-block-polystyrene. H.Odani, M.Uchikura, Y.Ogino, M.Kurata (Inst. for Chem. Res., Kyoto Univ., Kyoto-fu, Japan). *J. Membrane Sci. (Netherlands)*, vol.15, no.2, p.193-208 (Sept. 1983). Diffusion and solution behavior of methanol vapor in two diblock copolymers, poly(2-vinylpyridine)-block-polyisoprene [P(2VP-b-I)] and poly(2-vinylpyridine)-block-polystyrene [P(2VP-b-S)], was studied by the weighing method at 25°C. The domain structure of films of both copolymers showed an alternating lamellar arrangement. Methanol is a good solvent for P2VP, but a nonsolvent for PI and PS. Methanol dissolved exclusively in the P2VP phase of the copolymers. For both copolymer systems, absorption and desorption processes of non-Fickian type were observed as characterized by a thickness anomaly. However, the magnitude of the deviations from purely Fickian behavior was small, and the integral diffusion coefficient, *D*, was obtainable with reasonable accuracy. At low and medium concentrations, *D* for P(2VP-

b-I) was greater, by about one order of magnitude, than that for P2VP, while *D* for P(2VP-b-S) was lower than that for P2VP. A similar trend was observed in plots of the permeability coefficient against the vapor pressure of methanol. The results indicate that the rubbery PI phase may facilitate the transport of penetrant molecules in the P(2VP-b-I) film. On the other hand, the glassy PS phase in the P(2VP-b-S) film merely interferes with the transport of methanol molecules. (14 refs.)

114269 Determination of hydrogen diffusion in palladium by chemichromic effect. Ya.Ya.Kleperis, S.Ya.Takeris, A.P.Lusis. *Lav. PSR Zinat. Akad. Vestis Fiz. Teh. Zinat. Ser. (USSR)*, no.4, p.122-4 (1983). In Russian.

Hydrogen diffusion in a palladium membrane is determined by optical density measurements of the chemichromic layer—tungsten trioxide. In the pulse method the time dependence of optical density changes repeats the time dependence of potential changes on a clean palladium membrane surface. The coefficients of diffusion and initial concentration of hydrogen in palladium are determined by optical density change measurements. (5 refs.)

114270 Lattice diffusion of substitutional elements in iron and iron-base solid solutions. A critical review. H.Oikawa (Dept. of Materials Sci., Tohoku Univ., Sendai, Japan). *Technol. Rep. Tohoku Univ. (Japan)*, vol.48, no.1, p.7-77 (1983). Lattice diffusion has been reviewed in 33 Fe-X Systems: X=Ag, Al, As, Au, Be, Bi, Ce, Co, Cr, Cu, Ge, Hf, K, Mg, Mn, Mo, Na, Nb, Ni, P, Pb, Pd, Pt, S, Sb, Se, Si, Sn, Ti, U, V, W, Zn. Individual datum points of impurity diffusion of most elements in pure iron were plotted on the log*D*/*T* diagrams and representative diffusion parameters, *D₀* and *Q*, were calculated. Tracer diffusion of constituent elements and interdiffusion in Fe-base binary solid solutions were also reviewed. The enhancement parameters, *b* and *B*, were calculated in many systems. (248 refs.)

114271 Tracer diffusion of P in iron and iron alloys. T.Matsuyama (Faculty of Engng., Tohoku Univ., Sendai, Japan), H.Hosokawa, H.Suto. *Trans. Jpn. Inst. Met. (Japan)*, vol.24, no.8, p.589-94 (Aug. 1983). The lattice and grain boundary tracer diffusion coefficients *D_{PL}* and *P_P* of P in BCC iron, Fe-P binary alloys and Fe-0.1 at.% P-M (M: Cr, Si, Mn, Mo and Ni) alloys were measured. There was a break in each of the *D_{PL}*-1/*T* and *P_P*-1/*T* lines at temperatures near and below the Curie temperature, respectively. It is considered that the anomalous breaks were caused by magnetic transformation in the bulk and grain boundary. The effects of Cr, Si and Ni on *D_{PL}* and *P_P* were small. Alloying with Mn increased *D_{PL}* and *P_P*, but alloying with Mo decreased them. (14 refs.)

114272 Iron diffusion in indium phosphide and gallium arsenide. E.J.Foulkes. Univ. Nottingham, England thesis, 1983. Using radiotracer techniques, the diffusion of Fe⁵⁹ in indium phosphide and gallium arsenide was studied for a range of experimental conditions. Iron diffusion in InP was observed for the temperature range 700-900°C. Although problems were encountered with the formation of Fe₂P phases, the tracer profiles were found to consist of two sections, one close to the surface with steep gradient and the other extending throughout the entire thickness of the sample. Such a rapid iron diffusion has not previously been reported and is indicative of an interstitial motion of atoms. The redistribution of iron in diffused substrates was investigated during annealing at 700 and 900°C. Surface pile-ups were observed and were found to be influenced by a phosphorus overpressure. The out diffusion of iron from diffused substrates was investigated during PCl₃ vapour epitaxy. Substantial amounts of out diffused Fe were measured in the epilayer. Iron diffusion into GaAs was studied for the temperature range 700-1000°C. At 1000°C the diffusion profile shapes were similar to those observed for diffusion into InP. For lower temperatures a rapid cut-off in the GaAs bulk indicated a much smaller effective diffusivity. The EPR technique was successfully applied to substrates diffused with iron at 1000°C enabling quantitative measurements of the density of FeGa₃⁺ centres to be undertaken.

114273 Vibrational state and jump frequency of Mossbauer impurity associated with a vacancy in metals. M.Hashimoto, Y.Ishida (Inst. of Industrial Sci., Univ. of Tokyo, Tokyo, Japan), R.Yamamoto, M.Doyama. Point Defects and Defect Interactions in Metals. Proceedings of the Yamada Conference V, Kyoto, Japan, 16-20 Nov. 1981 (Amsterdam, Netherlands: North-Holland 1982), p.437-40. Vibrational local densities of states for the equilibrium configuration and the saddle-point configuration of a vacancy.¹⁹⁷Au complex in copper were calculated by the recursion method using the Morse potential. The jump frequencies of the impurity diffusion were estimated. A correlation was found between the pre-exponential factor of the jump frequency and the activation energy for migration. (9 refs.)

114274 Measurement of radiation induced impurity diffusion in copper. V.Naundorf, M.-P.Macht, H.-J.Gudlart, H.Wollenberger (Hahn-Meitner-Inst., KFA, Berlin GmbH, Berlin, Germany). Point Defects and Defect Interactions in Metals. Proceedings of the Yamada Conference V, Kyoto, Japan, 16-20 Nov. 1981 (Amsterdam, Netherlands: North-Holland 1982), p.934-7. Partial diffusion coefficients of nickel and beryllium in copper have been measured after irradiation with 300 keV Cu⁺ ions between 300 and 600K. For both solutes the diffusion coefficients exhibit a rather small temperature dependence. At room temperature and for a defect production rate of 8×10⁻⁴ sec⁻¹ the partial diffusion coefficients of Ni and Be in Cu are 9×10⁻¹⁷ cm²/sec and 8×10⁻⁶ cm²/sec, respectively under stationary conditions. The results are discussed within the framework of well-known defect reaction schemes. In particular, the possibility of slowing down of long range transport by solute trapping at internal defect sinks is considered. (22 refs.)

114275 Modeling of dopant diffusion and associated effects in silicon. R.B.Fair (Microelectronics Center of North Carolina, Research Triangle Park, NC, USA). Defects in Semiconductors II, Symposium Proceedings, Boston, MA, USA, Nov. 1982 (New York, USA: North-Holland 1983), p.61-74. Research in the area of dopant diffusion in Si has focused on identifying the specific mechanisms and point defects involved. Recent approaches include observing the effects of diffusion and doping on oxygen precipitation, stacking fault growth or shrinkage, enhanced/retarded diffusion of one dopant in the presence of another. Very few of these studies have yielded unambiguous interpretations as a result of the indirect nature of the experiments. However, taken together one can infer the relative importance of vacancies versus Si self-interstitials in the diffusion of each dopant species. (45 refs.)

114276 Formation of interstitial defects in high concentration shallow phosphorus diffusions in Si. R.Jaccodine (Sherman Fairchild Lab., Lehigh Univ., Bethlehem, PA, USA).

Defects in Semiconductors II, Symposium Proceedings, Boston, MA, USA, Nov. 1982 (New York, USA: North-Holland 1983), p.101-6.
An experimental study of high concentration (10^{19} - $10^{21}/\text{cm}^3$) shallow diffusion was undertaken using TEM to investigate the nature of these diffusion-related defects. Phosphorus from a wide variety of sources (PBr_3 , POCl_3 , etc.) other than ion implantation was used in temperature range from 950° - 1100°C and for times of 15 minutes to 1 hour. Care was taken in surface preparation and material selection to avoid extraneous defects from sources other than diffusions. A high concentration of small dislocation loops ($10^{12}/\text{cm}^2$) was present in the top few microns of the wafers. Diffraction contrast on the loops revealed that they are of edge character with Burger's vector $\mathbf{b} = \frac{1}{2}(110)$. Identification of the nature of these loops by tilting method [(g.b).s] and anomalous dark-faced black-white lobes show they are of the interstitial type, i.e. the observed defects place the surrounding matrix in a compressive state. (14 refs.)

114277 Observation of oxidation-enhanced and -retarded diffusion of antimony in silicon: the behavior of (111) wafers. T.Y.Tan, B.J.Ginsberg (IBM Thomas J. Watson Res. Center, Yorktown Heights, NY, USA).

Defects in Semiconductors II, Symposium Proceedings, Boston, MA, USA, Nov. 1982 (New York, USA: North-Holland 1983), p.141-5.
An experiment was performed to study the oxidation-enhanced and -retarded diffusion (OED and ORD) of Sb in silicon wafers oxidized in dry O_2 at 1160°C . The ORD data of (100) wafers agree well with the prediction of a model assuming that Si self-interstitials (I) and vacancies (V) coexist in thermal equilibrium at high temperatures. An adjustment of the I supersaturation values is needed to bring the ORD/OED data of (111) wafers to fit with the model satisfactorily. This indicates the existence of a mechanism which injects V into (111) wafers in addition to the normal mechanism of I injection due to SiO_2 growth. (18 refs.)

114278 Effect of oxygen on radiation-enhanced diffusion in silicon. V.E.Borisenko (Minsk Radioengng. Inst., Minsk, Belorussian SSR).

Defects in Semiconductors II, Symposium Proceedings, Boston, MA, USA, Nov. 1982 (New York, USA: North-Holland 1983), p.159-64.
Low-energy ion bombardment has been used to enhance diffusion of phosphorus and antimony atoms in silicon. Oxygen free silicon crystals both containing phosphorus and antimony doped surface layers and original crystals were bombarded at 400 - 700°C with 400 eV oxygen or argon ions. Impurity and electrical carrier profiles were measured to analyse the role of oxygen in the radiation-enhanced diffusion. The results obtained are explained by assuming complexes such as vacancy-oxygen and vacancy substitutional impurity to be involved in the process. (16 refs.)

114279 Enhanced diffusion of phosphorus at grain boundaries in silicon. L.J.Cheng, C.M.Shyu, K.M.Stika (Jet Propulsion Lab., California Inst. of Technol., Pasadena, CA, USA).

Defects in Semiconductors II, Symposium Proceedings, Boston, MA, USA, Nov. 1982 (New York, USA: North-Holland 1983), p.383-7.
It is found that the grain boundaries in cast polycrystalline silicon material capable of enhancing diffusion always have strong recombination activities. Both phenomena could be related to the existence of dangling bonds at boundaries. Because the enhanced diffusion is an atomic transport phenomenon and the recombination is an electronic process, the relationship between the two phenomena is still not clear at this moment. The present study gives the first evidence that incoherent second order twins of $\{111/115\}$ type are phosphorus diffusion-active. (6 refs.)

A new fission-gas release model See Entry 112332

Study of the OH content of CVD silica glass for optical fibres See Entry 113070

The nature of point defects and their influence on diffusion processes in silicon at high temperatures See Entry 113906

Interaction of hydrogen with nonmetallic inclusions of the different shapes in ferrite-pearlite steels See Entry 113955

Formation of vacancies in thermal equilibrium in α -range alloys See Entry 113972

Pattern formation in metallic glasses induced by helium ion implantation See Entry 114053

Solubility and diffusivity of hydrogen in Li_2O See Entry 114180

Irradiation-induced segregation in multi-component alloys See Entry 114181

Mechanism and kinetics of radiation-induced segregation in Ni-Si alloys See Entry 114187

Dynamics and mechanism of iodine sorption by polyacetylene See Entry 114334

Heat treatments of CVD-coatings on hardmetals See Entry 114425

Thermal donor formation by the agglomeration of oxygen in silicon See Entry 114478

Study on the strengthening mechanism by diffusion of temper carbon into ferritic matrix See Entry 115317

Gas permeation through composite two-layer systems and the graphical solution See Entry 115583

66.30L Diffusion, migration, and displacement of other defects

114280 Interfacial stability of migrating brine inclusions in alkali halide single crystals supporting a temperature gradient. S.K.Yagnik (Dept. of Nuclear Engng., Iowa State Univ., IA, USA).

J. Cryst. Growth (Netherlands), vol.62, no.3, p.612-26 (Aug. 1983).
Application of a temperature gradient to a solid containing inclusions exerts a driving force which sets the inclusions in motion towards higher temperatures. Since the inclusions are essentially negative crystals, they retain definite shape with the inclusion walls being low index crystallographic planes of the host solid matrix. The migration speed of these inclusions is known to depend on the kinetics of interfacial crystallization/dissolution, which favors layer-by-layer growth/dissolution. Despite these effects, which tend to keep the inclusion walls stable and straight, interfacial instabilities are occasionally observed in the migrating inclusions. A perturbation method is used to analyze such instabilities at a planar interface growing from solution. The model is applied to the interfaces of the temperature gradient driven brine inclusions in alkali halide single crystals, and the resulting stability criteria are checked against limited available experimental data. (16 refs.)

114281 Migration of interstitial dumbbell in concentrated solid solutions. J.-L.Bocquet (CENS, Gif-sur-Yvette, France).

Point Defects and Defect Interactions in Metals. Proceedings of the Yamada Conference V, Kyoto, Japan, 16-20 Nov. 1981 (Amsterdam, Netherlands: North-Holland 1982), p.664-6.
It is shown that a mean-field formulation provides a convenient frame to evaluate the diffusivity of interstitial dumbbell-like defects. Monte Carlo simulation runs yield results in good agreement with the mean field approximation. (5 refs.)

114282 Radiation enhanced diffusion in FCC alloys. W.Schule (Joint Res. Centre, Ispra, Italy).

Point Defects and Defect Interactions in Metals. Proceedings of the Yamada Conference V, Kyoto, Japan, 16-20 Nov. 1981 (Amsterdam, Netherlands: North-Holland 1982), p.667-9.
In many alloys vacancies and interstitials can be identified in a straightforward way by measurements of radiation enhanced diffusion. In some alloys, however, quenching experiments are also necessary for the identification of these defects. Results for two characteristic alloys in which the transformation rate during high energy particle irradiation is determined by an interstitially and by a vacancy diffusion mechanism only are discussed. It is also shown that a decrease of the migration energy of defects due to an interaction of the high energy particles with the lattice atoms must be taken into account in the interpretation of the results. (16 refs.)

114283 A diffusion-reaction model for solid solutions under irradiation. R.Cauvin, G.Martin (Section de Recherches de Metall. Phys., CENS, Gif-sur-Yvette, France).

Point Defects and Defect Interactions in Metals. Proceedings of the Yamada Conference V, Kyoto, Japan, 16-20 Nov. 1981 (Amsterdam, Netherlands: North-Holland 1982), p.931-3.
The diffusion matrix for the four component system (solvent, solute, vacancy, interstitial) is derived as a function of the various defects jump frequencies. The state of the solid solution under irradiation is shown to be described by a system of three coupled balance equations for the total concentrations of vacancies, interstitials and solute atoms. The relevance of this model to the theory of homogeneous and heterogeneous irradiation induced precipitation, as well as to other high temperature irradiation effects is discussed. (15 refs.)

114284 Dynamic observation of atomic-level events in cadmium telluride by high resolution TEM. T.Yamashita, R.Sinclair (Dept. of Materials Sci. & Engng., Stanford Univ., Stanford, CA, USA).

Defects in Semiconductors II, Symposium Proceedings, Boston, MA, USA, Nov. 1982 (New York, USA: North-Holland 1983), p.295-9.
A conventional 120 keV high resolution TEM equipped with a TV camera has been used to make lattice resolution video recordings of cadmium telluride in the $\langle 110 \rangle$ orientation. The motion of dislocations and the migration of atomic species at the edge of the crystal have been studied. These processes are thought to be induced in the crystal by localized heating of the specimen by the electron beam. The observations are made on a TV monitor at a total magnification of 15 million times. (8 refs.)

Mobilities of quenched-in defects in NiAl See Entry 113864

Formation and migration energies of a vacancy and kinetics of short range ordering in $\alpha\text{Cu-Al}$ alloys See Entry 113889

Self-interstitial mobility in a neutron-irradiated austenitic $\text{Fe}_{50}\text{Cr}_{16}\text{Ni}_{25}$ alloy See Entry 113890

Recovery in electron irradiated aluminium observed by Mossbauer spectroscopy See Entry 113974

Interaction of dislocations with impurities and its influence on the mechanical properties of silicon crystals See Entry 113981

Mossbauer spectroscopy on ^{133}Cs as a method to study vacancy migration in metals See Entry 114766

66.30N Chemical interdiffusion

114285 Comparisons of the nuclear reactions $^{18}\text{O}(p, \alpha)^{15}\text{N}$ and $^{16}\text{O}(d, \alpha)^{14}\text{N}$ to study the oxygen effects in Pt silicide formation. C.-D.Lien, L.Wielunski, M.-A.Nicolet (California Inst. of Technol., Pasadena, CA, USA).

Nucl. Instrum. & Methods Phys. Res. (Netherlands), vol.213, no.2-3, p.463-7 (1 Aug. 1983).
2 MeV backscattering spectrometry (BS) and nuclear reactions (NRs) $^{18}\text{O}(p, \alpha)^{15}\text{N}$ induced by 1.5 MeV H_2^+ and $^{16}\text{O}(d, \alpha)^{14}\text{N}$ induced by 900 keV D^+ have been used to study the effect of implanted oxygen on Pt silicide formation. The location of oxygen before and after silicide formation was deduced from NR spectra. Advantages and disadvantages of these two NRs in this application are discussed. (21 refs.)

114286 Internal friction study on diffusivity on the Cu-SiO₂ interface. N.Shigenaka, M.Koda, T.Mori (Dept. of Materials Sci. & Engng., Tokyo Inst. of Technol., Yokohama, Japan).

Scr. Metall. (USA), vol.17, no.8, p.1021-2 (Aug. 1983).
Describes two indirect but convenient methods, both of which utilise internal friction measurements, for studying matrix-particle interface diffusion. The authors supplement the work of Mori et al. (see Acta Metall. vol.31, p.275, 1983) on Cu-SiO₂ by repeating the experiment using method 2. (10 refs.)

114287 Radiation induced interdiffusion and phase transformation in electron irradiated Cu-Ni alloys. R.Poerschke, W.Wagner, H.Wollenberger (Hahn-Meitner-Inst., KFA Berlin GmbH, Berlin, Germany).

Point Defects and Defect Interactions in Metals. Proceedings of the Yamada Conference V, Kyoto, Japan, 16-20 Nov. 1981 (Amsterdam, Netherlands: North-Holland 1982), p.938-41.

The Cu-Ni alloys in the composition range around 50:50 have shown considerable interdiffusion by an interstitial mechanism. The present paper collects all available experimental data which yield quantitative information on this diffusion mechanism. Also treated is the question of irradiation induced phase transformation as origin of the observed periodic decomposition structure in these alloys. (24 refs.)

Self-diffusion in compound semiconductors See Entry 114252

Observation of rapid field aided diffusion of silver in metal-oxide-semiconductor structures See Entry 114288

Structure of two-layer epitaxial Ag-Al films See Entry 114380

Sputter-induced surface modification in Cu-Ni alloys at elevated temperatures See Entry 115005

Evaluating the limiting states of a steel under combined low-cycle loading and diffusion of sorbed hydrogen See Entry 115348

Optimization of the parameters of obtaining noncarbide-forming coatings See Entry 115439

Production of bimetallic contact elements by a diffusion impregnation method See Entry 115440

Metallurgy of interfaces in hardmetal/metal diffusion bonds See Entry 115508

66.30Q Electromigration

114288 Observation of rapid field aided diffusion of silver in metal-oxide-semiconductor structures. J.D.McBrayer, R.M.Swanson, T.W.Sigmon (Stanford Electronics Labs., Stanford Univ., Stanford, CA, USA), J.Bravman. *Appl. Phys. Lett. (USA)*, vol.43, no.7, p.653-4 (1 Oct. 1983). Fast electric field aided diffusion of silver in SiO₂ has been observed for fields of 10⁴ V/cm and temperatures as low as 275°C. The diffusion coefficient of silver in SiO₂ is estimated to be 10⁻¹³ cm²/s at 300°C, with an activation energy of 1.24 eV. The consequences of Ag contamination in very large scale integrated metallization systems are discussed. (4 refs.)

114289 Contribution to the theory of grain-boundary electromigration. M.Kedro. *Elektrotech. Cas. (Czechoslovakia)*, vol.34, no.5, p.313-17 (1983). In Slovak. The system of electromigration equations for a model of two grains with an interface is solved considering nonsteady electron-wind force. Results involve time dependence of the migrating atoms concentration. (7 refs.)

114290 Electromigration of fast diffusers in lead, lead solders, and tin. H.B.Huntington (Dept. of Phys., Rensselaer Polytech. Inst., Troy, NY, USA). Point Defects and Defect Interactions in Metals. Proceedings of the Yamada Conference V, Kyoto, Japan, 16-20 Nov. 1981 (Amsterdam, Netherlands: North-Holland 1982), p.589-95. Electromigration by the steady state technique has been applied to several fast diffusers in lead. The resulting Z*’s are mostly small and may be of either sign, although Z_{Ni}* turned out to be -6 at dilute concentration. When tin is added to lead up to the solubility limit Z_{Ag}* decreases in magnitude and changes sign, although the diffusivity is only moderately increased. Nickel, gold and copper show rapidly decreasing diffusivity since they apparently bind to the tin atoms. No marked changes in Z* for these impurities have yet been noted. Down the c-axis of single crystal tin the authors find Z_{Ag}* of -4.5 and Z_{Au}* of -1.2. (16 refs.)

66.60 THERMAL CONDUCTION IN NONMETALLIC LIQUIDS
(for thermal conduction in liquid metals, see 72.15C)

114291 Thermal conductivity measurements on fluids under microgravity using holographic interferometry. K.Wanders (DFVLR, Advanced Programme Div., Koln, Germany), G.P.Gorler, H.Steinbichler. Proceedings of the 4th European Symposium on Materials Sciences under Microgravity (ESA SP-191), Madrid, Spain, 5-8 April 1983 (Paris, France: ESA 1983), p.403-8. Measurement of the thermal conductivity of a fluid medium under normal gravitational conditions basically is affected by the additional heat transfer caused by thermal convection in the medium. The condition prevailing on board of SPACELAB now offers the possibility of carrying out precise measurements under reduced gravity and under essential elimination of convection. The objective of the proposed measurements is to investigate and measure the various phenomena occurring in connection with heat transfer in in the vicinity of a filament extended in a fluid. Measurement is performed by means of holographic interferometry which allows high-resolution observation of temperature distribution and heat transfer processes in transparent media as a function of location and time. The advantage of this laser measuring method is its special feature of three-dimensional resolution and the rather simple equipment requirements. (14 refs.)

66.70 NONELECTRONIC THERMAL CONDUCTION AND HEAT-PULSE PROPAGATION IN NONMETALLIC SOLIDS
(for thermal conduction in solid metals, see 72.15C and 72.15E; for statistical mechanics of lattice vibrations, see 63.70)

114292 Photoacoustic determination of thermal diffusivity of solids: Application to CdS. C.L.Cesar, H.Vargas, J.Mendes Filho (Inst. de Fisica, Univ. Estadual de Campinas, Campinas, Sao Paulo, Brazil), L.C.M.Miranda. *Appl. Phys. Lett. (USA)*, vol.43, no.6, p.555-7 (15 Sept. 1983). A novel and simple approach, which uses a lateral heating source for the sample, is proposed as an alternative method for the photoacoustic determination of the thermal diffusivity of solids. The method is experimentally tested using a CdS sample. (9 refs.)

114293 Band-state interpretation of lattice thermal conductivity and microhardness of ternary chalcopyrite semiconductors. L.K.Samanta, D.K.Ghosh, G.C.Bhar (Dept. of Phys., Burdwan Univ., Burdwan, India). *Chem. Phys. (Netherlands)*, vol.79, no.3, p.361-5 (15 Sept. 1983). A new approach utilising the concept of band states and periodicity has been used to explain the lattice thermal conductivity and microhardness of ternary chalcopyrite crystals. The experimental values agree quite well with the calculated values using the authors’ model. A single fitting parameter used in each case explains the uniqueness of the model. (19 refs.)

114294 Low-energy excitations in (KBr)_{1-x}(KCN)_x in the orientational glass state. J.J.De Yoreo, M.Meissner, R.O.Pohl (Lab. of Atomic & Solid State Phys., Cornell Univ., Ithaca, NY, USA), J.M.Rowe, J.J.Rush, S.S.Susman. *Phys. Rev. Lett. (USA)*, vol.51, no.12, p.1050-3 (19 Sept. 1983). The thermal conductivity of single-crystal (KBr)_{1-x}(KCN)_x, 0.05 ≤ x ≤ 0.5, in the temperature range 0.08-100K shows behavior characteristic of amorphous solids. The low-temperature specific heats (T < 2.5K), measured on long (~50 s) and on short (<0.2 ms) time scales, also are identical to those found in amorphous solids. It is proposed that the KBr-KCN system provides a connecting link between the low-energy excitations in amorphous solids and in spin-glasses. (17 refs.)

114295 Thermodynamic and kinetic properties of amorphous dielectrics at low temperatures. L.I.Trakhtenberg, V.N.Flerov (Inst. of Chem. Phys., Acad. of Sci., Moscow, USSR). *Sov. Phys.-JETP (USA)*, vol.83, no.5, p.1103-11 (Nov. 1982). Translation of: *Zh. Eksp. & Teor. Fiz. (USSR)*, vol.83, no.5, p.1908-23 (Nov. 1982). [received: Sept. 1983]. It is shown that it is important to take account of the influence of vibrations of the medium on the tunneling of heavy particles in a two-level system when studying relaxation processes in glasses. Zero-point vibrations increase the

probability of tunneling by several orders of magnitude. As the temperature is raised, single-phonon processes first give a contribution and then multiphonon processes. The periodic reduction in the potential barrier by vibrations of the medium play an appreciable role. With this mechanism the double-peaked temperature dependence of the inverse ultrasonic attenuation length can be explained and also the temperature dependence of the thermal conductivity and of the luminescence intensity (the so-called ‘inverse Arrhenius law’). (32 refs.)

114296 Thermal conductivity of irradiated graphite. T.Nihura (Faculty of Engng., Ibaraki Univ., Ibaraki, Japan), T.Iwata. Point Defects and Defect Interactions in Metals. Proceedings of the Yamada Conference V, Kyoto, Japan, 16-20 Nov. 1981 (Amsterdam, Netherlands: North-Holland 1982), p.236-8. Phonon scattering by lattice defects in graphite has been studied by measuring the a-axis thermal conductivity of electron-irradiated and neutron-irradiated pyrolytic graphite crystals. Phonon scattering by interstitial atoms, interstitial clusters, vacancies and grain boundaries, and a resonance-like scattering are distinguished. (3 refs.)

Thermal conductivity of near-stoichiometric (U, Pu, Nd)O₂ and (U, Pu, Eu)O₂ solid solutions See Entry 112327

Kinetic properties of chromium-doped lead telluride See Entry 114550

67.00 QUANTUM FLUIDS AND SOLIDS; LIQUID AND SOLID HELIUM
(see also 05.30 Quantum statistical mechanics)

67.40 BOSON DEGENERACY AND SUPERFLUIDITY OF HELIUM-4

114297 Bifurcation and the universal sequence for first-sound subharmonic generation in superfluid helium-4. C.W.Smith, M.J.Teiwani (Dept. of Phys. & Astron., Univ. of Maine, Orono, ME, USA). *Physica D (Netherlands)*, vol.7D, no.1-3, p.85-8 (May 1983). (Proceedings of the International Conference on Order in Chaos, Los Alamos, NM, USA, 24-28 May 1982). Measurements show that below the superfluid transition, the generation of first-sound subharmonics in the low-megahertz range quantitatively follows the Feigenbaum universal convergence for period doubling and qualitatively includes frequencies which correspond to the universal sequence. In addition, by using ion-trapping techniques the physical nature of the onset of the first bifurcation is identified as the threshold for the generation of quantum vortex line, not the threshold for the production of macroscopic classical turbulence, i.e. acoustic cavitation. (12 refs.)

Proceedings of the International Conference on Order in Chaos See Entry 111307

Apparatus for the measurement of the magnetic susceptibility of liquids in high magnetic fields See Entry 111711

Structure factors and elementary excitations of condensed matter See Entry 114459

Experimental investigation of positron self-trapping near the vapour-liquid critical point of helium-4 See Entry 114954

67.50 FERMI FLUIDS; LIQUID HELIUM-3

114298 Soliton propagation of zero sound in superfluid ³He-B. M.Rouff, E.Varoquaux (Lab. de Phys. des Solides, Univ. Paris-Sud, Orsay, France). *Phys. Rev. Lett. (USA)*, vol.51, no.12, p.1107 (19 Sept. 1983). A remarkable transparency effect in the propagation of zero sound in superfluid ³He B-phase has been observed by Polturak et al. (1981) in the vicinity of a weekly excited pair vibration mode called the real squashing mode. It is shown that such nonlinear propagation phenomena can be attributed to sine-Gordon solitons. (6 refs.)

Apparatus for the measurement of the magnetic susceptibility of liquids in high magnetic fields See Entry 111711

67.60 MIXED SYSTEMS; LIQUID HELIUM 3-4 MIXTURES

114299 Phase space analysis of convection in a ³He-superfluid ⁴He solution. H.Haucke, Y.Maeno (Los Alamos Nat. Lab., Los Alamos, NM, USA). *Physica D (Netherlands)*, vol.7D, no.1-3, p.69-72 (May 1983). (Proceedings of the International Conference on Order in Chaos, Los Alamos, NM, USA, 24-28 May 1982). Observations have been made on thermal convection below 1K in a dilute solution of ³He in superfluid ⁴He contained in a cylindrical cell of aspect ratio Γ=1.20. Complicated oscillatory phenomena were observed with a high degree of reproducibility using two temperature sensors. Phase space analysis suggests a description in terms of strange attractor dynamics. (6 refs.)

67.80 SOLID HELIUM AND RELATED QUANTUM CRYSTALS

114300 Vacancies in the core of a dislocation in solid helium. H.Suzuki (Dept. of Phys., Univ. of Tokyo, Tokyo, Japan). Point Defects and Defect Interactions in Metals. Proceedings of the Yamada Conference V, Kyoto, Japan, 16-20 Nov. 1981 (Amsterdam, Netherlands: North-Holland 1982), p.766-9. Diffusion of vacancies in the core of a dislocation in solid helium is discussed. The vacancies have a negative formation energy and behave as free particles in a one dimensional space. The vacancies are scattered by vibrations of the dislocation and the diffusion constant of vacancies is given by D=hv_s²/4kT, where v_s is the shear wave velocity of solid helium. Nodes of a dislocation network in solid helium are not pinning points in low-frequency measurements of mechanical properties. It is concluded that climb of dislocation networks is the most important cause of internal friction at low frequencies. (8 refs.)

68.00 SURFACES AND INTERFACES; THIN FILMS AND WHISKERS

(for impact phenomena, see 79.; for physics of crystal growth, see 61.50C; for corrosion, oxidation, and surface treatments, see 81.60)

68.10 FLUID SURFACES AND INTERFACES WITH FLUIDS

(inc. surface tension, capillarity, wetting and related phenomena)

114301 Theory of the Leidenfrost phenomenon. Yu.A.Buevich, V.N.Man-kevich (Ural State Univ., Sverdlovsk, USSR).

High Temp. (USA), vol.20, no.6, p.902-9 (Nov.-Dec. 1982). Translation of: *Teplofiz. Vys. Temp. (USSR)*, vol.20, no.6, p.1136-44 (Nov.-Dec. 1982). [received: Sept. 1983]

The spheroidal state of a drop evaporating on a heated horizontal surface is examined, allowing for the dependence of the equilibrium temperature at the evaporation surface (the lower surface of the drop) on the excess pressure below it, the effects of molecular slip at the boundaries of the vapor layer, and of molecular forces of surface interaction. For drops heated to saturation temperature this state is possible in the case where the surface temperature exceeds some critical value, the Leidenfrost temperature. The authors evaluate a critical surface temperature above which an underheated drop does not come in direct contact with the surface, i.e. the spheroidal state is set up. (14 refs.)

114302 Effects of adsorbed films on gas bubble radial oscillations. R.E.Glazman (Dept. of Ocean Engng., Univ. of Rhode Island, Kingston, RI, USA).

J. Acoust. Soc. Am. (USA), vol.74, no.3, p.980-6 (Sept. 1983).

Adsorption films' mechanical properties are discussed. With regard to a problem of bubble oscillations in a surfactant solution, dynamical boundary conditions at the bubble wall are modified by including a new term to account for a normal force component caused by dilational elasticity of an adsorbed film. Consequently, the Rayleigh-Plesset equation acquires a term which affects the restoring force of bubble oscillations. A linearized theory (for small-magnitude oscillations) is developed which shows that the film dilational elasticity induces a change in the mean radius and a shift in the natural frequency of bubble oscillations. These effects become extremely important when a capillary component $2\sigma/R_0$ accounts for at least 20% of the total pressure inside the bubble. (33 refs.)

114303 Computer-controlled apparatus for interfacial tension measurements. M.Carla, G.Aloisi, G.Papeschi, S.Bordi (Istituto di Chimica Fisica, Univ. di Firenze, Firenze, Italy).

J. Electrochem. Soc. (USA), vol.130, no.9, p.1859-62 (Sept. 1983).

A fully computer-controlled apparatus for interfacial tension measurements at the mercury/solution interface is described. The apparatus is based on the drop time method, whose reproducibility and accuracy have been improved by a new calibration technique and the use of a glass polyethylene dropping electrode. (15 refs.)

114304 Surface tension variation in multiphase fluid systems. D.J.Klinger, M.E.Fisher, B.Widom (Baker Lab., Cornell Univ., Ithaca, NY, USA).

J. Phys. Chem. (USA), vol.87, no.15, p.2841-5 (21 July 1983).

The isothermal variation of surface tension with composition is computed through contiguous two- and three-phase regions within the van der Waals theory of interfaces using the Griffiths thermodynamic model of multicomponent fluids. The surface tension is continuous on crossing from the two- to three-phase region but, in general, its derivative with respect to composition is discontinuous. Recent surface tension measurements on oil-brine-surfactant systems agree qualitatively with the theory but are inadequate to check the finer points. (13 refs.)

114305 Stability of the plane wave front of fluid evaporation. E.B.Levchenko, A.L.Chernyakov.

J. Appl. Mech. & Tech. Phys. (USA), vol.23, no.6, p.870-6 (Nov.-Dec. 1982). Translation of: *Zh. Prikl. Mekh. & Tekh. Fiz. (USSR)*, vol.23, no.6, p.144-50 (Nov.-Dec. 1982). [received: Sept. 1983]

An evaporation wave is propagated in the bulk of a substance subjected to a powerful radiation flux in a condensed medium. The stability of the plane fluid evaporation wave front considered as the surface of discontinuity of the thermodynamic functions of the substance is investigated. An instability mechanism turns out to be decisive for the development of fluctuations of a front with wavelengths commensurate to the diameter of the radiation focusing spot. A substantial feature of the evaporation process is the high velocity of vapor escape, which is commensurate with the speed of sound in a gas. Taking account of the vapor compressibility results in a change in both the conditions of origination and the nature of the development of the instability of the plane fluid evaporation wavefront. (7 refs.)

114306 Spreading of Ni-Fe-W melts on polycrystalline tungsten. V.L.Yupko, R.V.Minakova, O.P.Kolchin, L.S.Vodopyanova, N.I.Monastayeva, V.L.Voitenko (Inst. of Materials Sci., Acad. of Sci., Ukrainian SSR).

Sov. Powder Metall. & Met. Ceram. (USA), vol.22, no.1, p.44-7 (Jan. 1983). Translation of: *Poroshk. Metall. (USSR)*, vol.22, no.1, p.49-53 (Jan. 1983). [received: Aug. 1983]

A study was made of the wetting of polycrystalline tungsten by Ni-Fe-W alloys with a nickel-to-iron ratio of 7:3 and tungsten contents ranging from 0 to 40%. Similar experiments were conducted on porous tungsten. In addition, an investigation was carried out into the wetting of polycrystalline tungsten by alloys of constant tungsten content (24%) and different nickel-to-iron ratios (3:7, 5:5, 7:3, and 8:2). Experiments were carried out in a vacuum corresponding to $(5-10) \cdot 10^{-3}$ Pa at a temperature of 1763 ± 10 K. (9 refs.)

Calculated reflection and transmission of a plane wave at the interface between two liquids with viscosity and thermal conductivity See Entry 113173

Domain stability during capillary flow of well dispersed two phase polymer blends. Polystyrene/polymethylmethacrylate blends See Entry 113727

Critical point phenomena in fluids See Entry 114130

High-temperature solution properties in the flux systems $\text{RPO}_4\text{-Pb}_2\text{P}_2\text{O}_7$ ($\text{R} = \text{Dy, Y}$) See Entry 115040

The influence of axial microgravity on the breakage of axisymmetric slender liquid bridges See Entry 115048

An analysis of the driving forces in liquid-phase sintering See Entry 115131

68.15 LIQUID THIN FILMS

Procedure for measuring the thickness and wave characteristics of the surface of the liquid film in annular-mist flows of steam and water .. See Entry 113528

68.20 SOLID SURFACE STRUCTURE

114307 Surface structure change of a crystal in solution. V.V.Podolinsky, V.G.Drykin (Dept. of Phys., Inst. of Construction Engng., Dnepropetrovsk, USSR).

J. Cryst. Growth (Netherlands), vol.62, no.3, p.532-8 (Aug. 1983).

A given substance can crystallize from various solvents with different morphology. In the case of organic systems the solvent has a larger influence on the solid-liquid interface than the temperature. The degree of molecule roughness of the solid-liquid interface can be increased or decreased by selection of the solvent. As a result faceted to nonfaceted or nonfaceted to faceted transitions can occur by increasing the concentration of the solvent. (28 refs.)

114308 Material surface modified by ion implantation and ion beam mixing. M.Iwaki (Inst. of Phys. & Chem. Res., Saitama, Japan).

J. Vac. Soc. Jpn. (Japan), vol.26, no.2, p.189-95 (1983). In Japanese.

The ion injection technique that modifies properties of the surface layer of a solid material by injection of an accelerated ion into the layer is indispensable as an impurity doping method in semiconductor element fabrication. The author describes: (1) the distribution of injected ions, (2) mechanical properties of ion-injected iron, (3) chemical and electrical properties of ion-injected iron, and (4) surface quality improvement by ion beam mixing. (26 refs.) K.B.

114309 Quantitative analysis of LEED measurements. D.L.Adams, H.B.Nielsen, J.N.Andersen (Inst. of Phys., Univ. of Aarhus, Aarhus, Denmark).

Phys. Scr. (Sweden), vol.T4, p.22-8 (1983). (Nordic Conference on Surface Science, Tampere, Finland, 18-20 Aug. 1982).

Experimental LEED intensity-energy spectra measured for the Al(111), Al(110), V(110), V(100), and Cu(110) surfaces are analyzed by means of r -factor comparisons with calculated spectra. The surfaces of Al(111) and V(110) are shown to correspond to nearly perfect terminations of the corresponding bulk structures. These systems are used to investigate the influence of the nonstructural variables of the calculations on the structure determination. The r -factor procedures are then applied to the determination of the surface structures of Al(110), V(100), and Cu(110). For these systems, it is found that the surface interlayer spacings exhibit a damped, oscillatory deviation from the bulk value, in qualitative agreement with the recent predictions of Landman et al. (1980). (31 refs.)

114310 Clean and adsorbate-induced surface phase transitions on W{100}. D.A.King (Donnan Labs., Univ. of Liverpool, Liverpool, England).

Phys. Scr. (Sweden), vol.T4, p.34-43 (1983). (Nordic Conference on Surface Science, Tampere, Finland, 18-20 Aug. 1982).

The clean surface of W{100} undergoes a reversible phase transition from (1×1) to $(\sqrt{2} \times \sqrt{2})R45^\circ$ on cooling below room temperature, attributable to inherent instabilities of top layer W atoms. These instabilities are also revealed in studies of adsorbate-induced structures and phase transitions on this surface. A review is presented of the now numerous experimental studies of these phase transitions on W{100}, particularly LEED and angle-resolved photoelectron spectroscopy but also including high and low energy ion scattering, field ion microscopy, thermal desorption, vibrational spectroscopy, electron stimulated desorption, surface core level spectroscopy, and spin-polarized LEED, with a view to consolidating the present status of both the surface crystallography and the surface electronic structures of the various phases. The substantial input from theoretical groups concerning the driving force for the phase transitions is briefly reviewed in the light of experimental results. (73 refs.)

114311 Analysis of magnetic and nonmagnetic surfaces by spin-polarized low-energy electron diffraction. R.Feder (Theoretische Festkörperphys., Univ. Duisburg, Duisburg, Germany).

Phys. Scr. (Sweden), vol.T4, p.47-51 (1983). (Nordic Conference on Surface Science, Tampere, Finland, 18-20 Aug. 1982).

A survey is given of most recent progress in harnessing electron spin polarization for the study of crystalline surfaces by low-energy electron diffraction (LEED). Spin-polarized LEED from nonmagnetic surfaces has been extended both experimentally and theoretically to low-Z surfaces, for which spin-orbit coupling is weak, to adsorbate systems, and to very low energies, where fine structure effects associated with the surface potential barrier are prominent. For ferromagnetic transition metal surfaces, measurement of the exchange-induced scattering asymmetry has revealed the surface Curie temperature and the critical exponent of the surface magnetization. At lower temperature, comparison with corresponding calculated exchange asymmetry profiles has successfully been employed for the determination of the layer dependence of the magnetization in the surface region. (35 refs.)

114312 (111) facets as the origin of reconstructed Au(110) surfaces.

G.Binnig, H.Rohrer, Ch.Gerber, E.Weibel (IBM Zurich Res. Lab., Ruschlikon, Switzerland).

Surf. Sci. (Netherlands), vol.131, no.1, p.L379-84 (Aug. 1983).

The Au(110) surface has been investigated by scanning tunneling microscopy. The reconstructed surface consists of long ribbons of narrow (111) facets along the [110] direction with maximum three free rows. Two-row facets give rise to the 1×2 reconstruction of the missing-row type while three-row facets account for the 1×3 reconstruction. Disorder arises from locally random sequences of the two facets. (18 refs.)

114313 Surface structure of the Si (111)- 5×1 -Au studied by low-energy ion scattering spectroscopy. Y.Yabuuchi, F.Shoji, K.Oura, T.Hanawa (Electron Beam Lab., Osaka Univ., Osaka, Japan).

Surf. Sci. (Netherlands), vol.131, no.2-3, p.L412-18 (Sept. 1983).

The Au/Si (111) system has been studied by low-energy ion scattering spectroscopy combined with LEED-AES. It has been found that the Au atoms causing the 5×1 structure are slightly embedded below the outermost Si layer. A new model of the 5×1 -Au structure is presented. (10 refs.)

114314 Helium diffraction from Ni (100). A study of the clean surface and of hydrogen and carbon adsorption phases. K.H.Rieder, H.Wilsch (IBM Zurich Res. Lab., Ruschlikon, Switzerland).

Surf. Sci. (Netherlands), vol.131, no.2-3, p.245-57 (Sept. 1983).

He scattering from the clean Ni (100) surface gives extremely weak diffraction beams, corresponding to a very small corrugation amplitude of ≈ 0.01 Å. Hydrogen adsorption at temperatures between 100 and 200K leads to the formation of an ordered (1×1) phase with a corrugation amplitude only three times larger than that of the clean surface. Surface charge-density calculations using overlapping atomic charge densities indicate a normal distance of the hydrogens from the topmost Ni layer $d_h \approx 0.9-1.0$ Å. He diffraction from the $c(2 \times 2)$ structure of carbon on Ni (100) confirms the $p4g$ symmetry of this phase, and the best-fit corrugation function reflects the different local distortions of the substrate atoms around the corner and centre carbon atoms. Charge-density calculations yield for the carbon atoms in fourfold hollows $d_h \approx 0.1-0.2$ Å, in good agreement with earlier LEED results. (30 refs.)

114315 Non-equilibrium surface segregation of silicon in Fe-6.3 at.% Si (110). J.du Plessis, P.E.Viljoen (Dept. of Phys., Univ. of the Orange Free State, Bloemfontein, S Africa). *Surf. Sci. (Netherlands)*, vol.131, no.2-3, p.321-7 (Sept. 1983).

The non-equilibrium segregation of silicon from the bulk to the (110) surface of a Fe-6.3 at.% Si single crystal was monitored in the temperature range 484 to 536°C by means of AES. Two distinct processes were observed. Initially a diffusion process controlling the initial surface enrichment of Si up to a temporary equilibrium value of about 15% was observed. This value corresponds to a 7×1 LEED pattern observed in similar crystals. Subsequently a two-dimensional nucleation process starts allowing more atoms onto the surface. Activation energies for both mechanisms were determined and are respectively 170±20 and 480±60 kJ/mol. (19 refs.)

114316 Observation of surface atomic structure in real space scanning tunneling microscopy—Si (111) 7×7 super-structure. H.Iwasaki, S.Nakamura. *Solid State Phys. (Japan)*, vol.18, no.6, p.351-6 (June 1983). In Japanese. A novel type of microscope developed by G. Binnig et al. (1982, 1983) is introduced with its successful application to the Si 7×7 structure. Its atomic resolution is discussed by analogy to the field ion microscope. (13 refs.)

114317 Analysis of surfaces and thin films. M.Hayes (Hirst Res. Centre, GEC plc, Wembley, England). *Surf. Technol. (Switzerland)*, vol.20, no.1, p.3-27 (Sept. 1983).

The aim of this review is to provide a guide for the occasional user or would-be user to the readily available and best-documented techniques that have been used or may be used to supplement the data from other experimental methods. The following types of technique are described: techniques utilizing an incident beam of electrons; techniques utilizing an incident beam of ions; techniques utilizing an incident beam of photons. Acoustic microscopy and spark source mass spectrometry are also mentioned. (353 refs.)

114318 Surface relief of crystalline quartz etched in a planar plasma reactor. B.G.Pantchev, M.G.Mikhailov, P.Danesh (Inst. of Solid State Phys., Bulgarian Acad. of Sci., Sofia, Bulgaria). *Thin Solid Films (Switzerland)*, vol.106, no.3, p.137-44 (19 Aug. 1983).

The surface morphology of dry etched crystalline quartz was studied by transmission electron microscopy (replica technique). The experiments were carried out by reactive ion etching (RIE), plasma etching and argon sputter etching. Argon sputter etching does not alter the sample surface. RIE and plasma etching lead to surface roughness when an aluminium electrode is used. The cone-like asperities produced, typical of the beginning of etching, develop into island-like relief during a longer experiment. It is concluded that the surface roughness is caused by the combined action of backscattering of aluminium particles and their protecting effect in a CF₄ plasma. (11 refs.)

114319 ESCA studies of the incorporation of oxygen into nickel surfaces.

H.Matsueda, B.L.Averbach (MIT, Cambridge, MA, USA). *Trans. Jpn. Inst. Met. (Japan)*, vol.24, no.8, p.574-80 (Aug. 1983).

ESCA data have been obtained on the incorporation of oxygen into nickel surfaces at room temperature. The surfaces were cleaned by argon ion bombardment, and the Ni 2p 3/2 line was observed as a function of the exposure to oxygen. The development of NiO-like components indicated that oxygen was being incorporated into the surface lattice. At low oxygen exposures a linear kinetic law was observed, with $W=1.65 \times 10^{-3} L+0.226$, where W is the thickness of the incorporated layer in nm and the exposure, L , is $tp^{1/2}$, t being the exposure time in seconds and p the oxygen pressure in Pa. At high exposures, which were defined approximately as $L>250$, the thickness followed the logarithmic tarnishing law, with $W=1.44 \times 10^{-2}$ in $L+0.533$. The authors have postulated that the initial stage involves the incorporation of oxygen into the surface lattice via a cooperative displacement of the surface nickel atoms by a process of thermal activation assisted by a surface electric field induced by a charge transfer from a chemisorbed layer. The second stage appears to require the diffusion of oxygen into the bulk by means of thermal activation assisted by a strong electric field across the oxidized layer maintained by electron tunneling from the valence band of the bulk nickel. (24 refs.)

114320 Reflection electron microscopy (REM) of FCC metals. T.Hsu, J.M.Cowley (Dept. of Phys., Arizona State Univ., Tempe, AZ, USA).

Ultramicroscopy (Netherlands), vol.11, no.4, p.239-50 (1983). Reflection electron microscopy (REM) using diffracted beams from bulk specimens is shown to be possible with commercial electron microscopes. Surface images have been recorded from single crystal Au and Pt (111) surfaces. These images reveal growth steps, dislocations, slip traces, and other features. Geometrical restoration has been made of foreshortened images, and analysis of image contrast shows the importance of out-of-focus phase contrast and the diffraction contrast from strain fields. (13 refs.)

114321 Surface properties of laser-annealed semiconductors. D.M.Zehner, C.W.White (Solid State Div., Oak Ridge Nat. Lab., Oak Ridge, TN, USA). In book: *Laser annealing of semiconductors*, J.M.Poate, J.W.Mayer [Ed.], p.281-324. London, England: Academic Press (1982), xi+564 pp. [0 12 558820 8]

The authors show that pulsed laser irradiation can be used to produce atomically clean surfaces, metastable surface structures, and surfaces with electronic properties that cannot be achieved by conventional methods. Details concerned with processing of the surface in order to achieve these conditions and the measurement of surface properties are discussed. They show that levels of unwanted impurities on semiconductors (O, C, etc.) can be reduced to near the practical detection limits [using Auger electron spectroscopy (AES)]. This is accompanied by the observation of well-defined low-energy electron diffraction (LEED) patterns and evidence of ordered surface structures is discussed. The authors also show that, for (111)-oriented crystals of Si and Ge, laser irradiation leads to a metastable (1×1) surface structure and that a dynamical LEED analysis of the Si surface suggests that the first and second outermost interlayer spacings exhibit substantial relaxation (in the absence of ordered lateral reconstruction). However, the proposed surface structure is not in agreement with results of photoemission experiments when interpreted using one-electron-band structure calculations. Possible reasons for this discrepancy are cited. Finally, they show that the combination of ion implantation and laser annealing can be used to produce surfaces with electronic properties that cannot be achieved by conventional methods. (49 refs.)

114322 Structural studies of metal-semiconductor interfaces with high-resolution electron microscopy. J.M.Gibson, R.T.Tung, J.M.Poate (Bell Labs., Murray Hill, NJ, USA).

Defects in Semiconductors II, Symposium Proceedings, Boston, MA, USA, Nov. 1982 (New York, USA: North-Holland 1983), p.395-409

The authors have studied interface atomic structure in epitaxial cobalt and nickel disilicides on silicon using high-resolution transmission electron microscopy. By employing UHV techniques during deposition and reaction they have grown truly single-crystalline NiSi₂ and CoSi₂ films on (111) Si and in the former case on (100) Si. These films are shown to be continuous to below 10 Å thickness. By close control over preparation conditions, afforded by UHV, they can greatly influence the nucleation and growth of these films to

the extent, for example with NiSi₂ on (111) Si, of yielding continuous single-crystal films with either of two orientations as desired. Whilst in the (111) NiSi₂ on Si system the interfacial structure invariably appears to well-fit a model in which metal atoms nearest to the interface are 7-fold co-ordinated, for (111) CoSi₂ on Si agreement is generally better with a model involving 5-fold co-ordination of these atoms. A misfit dislocation core is also imaged. Results are discussed in the light of silicide nucleation and growth. The structure and stability of the (100) NiSi₂ on Si interface is also considered. (19 refs.)

114323 Investigations of metal-silicon interfaces by time-of-flight atom probe. C.Grovenor, G.Smith (Dept. of Metall. & Sci. of Materials, Oxford, England).

Defects in Semiconductors II, Symposium Proceedings, Boston, MA, USA, Nov. 1982 (New York, USA: North-Holland 1983), p.429-33

The use of a Time-of-Flight Atom Probe in the analysis of silicon surfaces, and the interfaces between metals and silicon, promises to provide very accurate chemical analysis allied with structural information from Field Ion Microscopy images. This paper presents results on the analysis of silicon surfaces by this technique, showing that good spectra can be obtained without difficulty. Some preliminary experiments on the structure of such specimens after the deposition of thin layers of Pd and Ni will be described, concentrating on the analysis of the stoichiometry of the reacted layers. (12 refs.)

Nordic Conference on Surface Science See Entry 111305

Surface physics. Second edition See Entry 113335

In situ observations of the growth behaviour of the {010} face of potassium hydrogen phthalate See Entry 113782

Subnanosecond pulsed laser annealing of Si-implanted InP See Entry 113997

Surface composition change of TiC under 0.15-3 keV hydrogen ion bombardment See Entry 114050

Direct observation of heavy radiation damage process by field ion microscopy See Entry 114057

Ion-induced diffusion and surface segregation See Entry 114239

Correlation between pair interactions of adsorbed atoms and adsorption layer superstructure formation See Entry 114338

Chemisorption properties of thin Pd overlayers on Nb (110) and Ag (111) See Entry 114362

Characterization of the oxide-metal interface at the surface of a stainless steel See Entry 114373

Crystallographic orientation and surface morphology of chemical vapor deposited Al₂O₃ See Entry 114385

EELS and AES study of epitaxially grown Pd(111) thin films See Entry 114392

Process of formation of porous silicon and autoepitaxy on its surface See Entry 114394

The effect of reaction condition on the crystallographic orientation and surface morphology of chemical vapor deposited Al₂O₃ See Entry 114419

The effect of the microscopic structure of metal surfaces on their optical properties See Entry 114807

Surface physics with slow positrons See Entry 114953

Angle-resolved Auger electron emission from LaB₆(001) with and without chemisorbed oxygen See Entry 114979

Angular dependence of the electron energy loss spectra of the reconstructed Si(001) clean surfaces See Entry 114985

Electron-microscopical investigations of the structure of the surface layers of titanium carbide after friction at 20-1400°C See Entry 115366

On the preferential etching of GaAs by H₂SO₄-H₂O₂-H₂O See Entry 115388

Decomposition of HCOOH on gold studied by XPS and TDS spectroscopies and its behaviour under very low energy electron excitation See Entry 115581

Techniques in surface microscopy and analysis See Entry 115596

Material analysis by means of high energy ion beams See Entry 115600

68.25 MECHANICAL AND ACOUSTICAL PROPERTIES OF SOLID SURFACES AND INTERFACES

(for tribology, see 62.20P and 81.40P)

114324 Transmission and reflection of a surface wave at a corner of two planes on an isotropic body. W.Pajewski, M.Szalewski (Inst. of Fundamental Technol. Res., Polish Acad. of Sci., Warsaw, Poland).

Arch. Acoust. (Poland), vol.8, no.1, p.3-10 (1983).

Reports an experimental investigation of the diffraction of a Rayleigh wave at a corner of an isotropic solid bounded by two planes forming a dihedral angle with respect to each other. Application of piezoelectric transducers and their appropriate setting on samples permitted the determination of the coefficient of reflection and transmission of Rayleigh waves at a corner and the directional characteristics of transverse waves, with polarisation in a plane perpendicular to the surface of R propagation, radiated at that time by the corner. The results were compared with the results of papers published in the world literature. (5 refs.)

114325 Surface friction constant and range of dynamical interaction between adatoms on metal surfaces. J.S.McCaskill, N.H.March (Theoretical Chem. Dept., Univ. of Oxford, Oxford, England). *Surf. Sci. (Netherlands)*, vol.131, no.1, p.34-48 (Aug. 1983).

The electronic contribution to the surface friction constant of an adatom on a metal surface is calculated using: (i) the Dirac density matrix for an infinite barrier model of an inhomogeneous electron gas, and (ii) two simple models of screened potentials at the surface based on reliable asymptotes in and outside the surface respectively. Though the results are clearly approximate attention is drawn especially to the predictions of the models concerning long-range dynamic interactions between adatoms on metal surfaces. (26 refs.)

114326 Propagation of high-intensity surface acoustic waves in lithium niobate. M.K.Balakirev, A.L.Belostotskii, L.A.Fedyukhin (Inst. of Semiconductor Phys., Acad. of Sci., Novosibirsk, USSR).

Sov. Phys.-Solid State (USA), vol.25, no.2, p.191-3 (Feb. 1983). Translation of: *Fiz. Tverd. Tela (USSR)*, vol.25, no.2, p.339-42 (Feb. 1983). [received: Sept. 1983]

The results of an experimental investigation of the nonlinear propagation of surface acoustic waves along the free surface of lithium niobate are presented. For large initial surface acoustic wave amplitudes a surface shock wave is formed and propagates. The amplitude and phase relations between the spec-

tral components of this wave are determined, the wave profile on the surface is established, and the nature of the decline in intensity with distance is established. (7 refs.)

- Reflection from a boundary with periodic roughness: theory and experiment See Entry 113161
- High-frequency acoustic properties of a fluid/porous solid interface. I. New surface mode See Entry 113176
- High-frequency acoustic properties of a fluid/porous solid interface. II. The 2D reflection Green's function See Entry 113177
- Rayleigh wave excitation by pulses of penetrating radiation at the free surface of a homogeneous and isotropic solid half-space See Entry 113348
- Definition of interphase in composites See Entry 113372
- Leaky elastic waves in hexagonal crystals See Entry 114090
- Method of obtaining dispersion equation for normal and surface waves in layered anisotropic systems See Entry 114091
- In situ analysis of the interface See Entry 115295

68.30 DYNAMICS OF SOLID SURFACES AND INTERFACE VIBRATIONS

- 114327 Group theoretical classification of two-dimensional lattice vibrations. D.B.Litvin (Dept. of Phys., Pennsylvania State Univ., Reading, PA, USA). *Thin Solid Films (Switzerland)*, vol.106, no.3, p.203-17 (19 Aug. 1983). Tables of the group theoretical classification of all possible two-dimensional lattice vibrations are presented, using the labeling of the irreducible representations of the two-dimensional space groups. As an example of their use, the group theoretical labeling of the phonon dispersion curves of methane physisorbed on graphite is given. (1 ref.)
- Quantum motion of chemisorbed hydrogen on Ni surfaces See Entry 114336
- Semi-empirical calculation of H atom interaction with a 12 atom iron cluster .. See Entry 114364
- Surface effects of Raman scattering from semi-metal Sb deposited on island Ag films See Entry 114838
- An infra-red reflection absorption study of the adsorption of NO on Pt(111) ... See Entry 114867
- Vibrational spectra of coadsorbed CO and H on Ni(100) and Ni(111) See Entry 114984

68.40 SURFACE ENERGY OF SOLIDS; THERMODYNAMIC PROPERTIES

- 114328 Surface tension of some rare-earth metals in the solid state. V.K.Kumykov, Kh.M.Guketlov (Kabardino-Balkarian State Univ., Nalchik, USSR). *Fiz. Met. & Metalloved. (USSR)*, vol.56, no.2, p.408-9 (Aug. 1983). In Russian. English translation in: *Phys. Met. & Metallogr. (GB)*
- The zero-creep method was used to determine the surface tension of polycrystalline samples of solid iridium, hafnium, palladium, rhodium, strontium, and zirconium. The measurements were carried out in vacuum in the range of temperatures corresponding to the diffuse creep of samples. The values (with the exception of those for strontium) was approximately 10-30% higher than the surface tension in the liquid state. (8 refs.) A.T.
- 114329 The measurement of the surface tension of some pure metals in the solid state. V.K.Kumykov (Dept. of Phys., Univ. of Houston, Houston, TX, USA). *Mater. Sci. & Eng. (Switzerland)*, vol.60, no.3, p.L23-4 (Sept. 1983). Measurements of the surface tension of pure solid aluminum, beryllium, iron, titanium and rhenium are reported and are compared with previous work. The values obtained using the compensated zero-creep method are shown to be consistent with those in previous work but are of a higher accuracy than the previous values. (15 refs.)
- Excess energy stored in the fine powder system See Entry 115130

68.45 SOLID-FLUID INTERFACE PROCESSES

(see also 82.65 Sorption and accommodation coefficients)

- 114330 A topological approach to studies of ordered structures of adsorbed gases in host lattices. I. The structure of γ -PdD_{0.5}. H.-G.Fritsche (Sektion Chem., Friedrich-Schiller-Univ., Jena, Germany), D.Bonchev, O.Mekenyan. *Cryst. Res. & Technol. (Germany)*, vol.18, no.8, p.1075-81 (1983). A graph-theoretical method is proposed which describes the deformation caused in the host lattice by adsorbed gas atoms, as well as their ordering. The method predicts correctly the ordered γ -phase of PdD_{0.5}. (20 refs.)
- 114331 Studies of the temperature dependence of gas adsorption data on graphite and boron nitride in terms of the partially mobile adsorption model. A.Patrykiewicz, M.Jaronec, A.W.Marczewski (Inst. of Chem., Marie-Curie-Sklodowskiej Univ., Lublin, Poland). *Chem. Scr. (Sweden)*, vol.22, no.3, p.136-45 (1983). A simple theory of partially mobile monolayer adsorption is presented. It is demonstrated that this theory properly predicts the critical parameters of monolayers of simple gases adsorbed on homogeneous surfaces. The comparison of theory with experimentally obtained adsorption isotherms for krypton, xenon, methane, and oxygen adsorbed on graphite, and for krypton, xenon, and methane adsorbed on boron nitride is presented. The model can be satisfactorily used for prediction of temperature dependence of adsorption isotherms. The molecular parameters characterizing adsorption systems can also be estimated, and in many cases they agree quite well with other estimations. (61 refs.)
- 114332 Adsorption of phosphoric acid solutions on the surface of solid oxides. O.S.Sirotkin, I.A.Zhenzhurist, R.S.Saifullin (S.M. Kirov Kazan' Chem.-Engng. Inst., USSR). *Inorg. Mater. (USA)*, vol.18, no.9, p.1365-7 (Sept. 1982). Translation of: *Izv. Akad. Nauk SSSR Neorg. Mater.*, vol.18, no.9, p.1590-2 (Sept. 1982). [received: Sept. 1983]
- The authors present an investigation into the adsorption on model systems of the phosphoric acid-solid oxide support type. The initial solutions were 87, 60, and 40% aqueous solutions of phosphoric acid most often used for the production of phosphate binders. The supporting materials were the oxides MgO, Al₂O₃, SiO₂, and Cr₂O₃ of analytical grade. In order to increase the water resistance a small amount of phosphoric acid was added to the samples at a rate corresponding to R=0.2 (where R=P₂O₅/M₂O_n). The samples were

dried and the percentage of uncombined oxide in the adsorbants was calculated. (1 ref.)

- 114333 Pore size distribution in porous silicon studied by adsorption isotherms. G.Bomchil, R.Herino, K.Barla, J.C.Pfister (Centre Nat. d'Etudes des Telecommunications, Grenoble, France). *J. Electrochem. Soc. (USA)*, vol.130, no.7, p.1611-14 (July 1983). Porous silicon was obtained by anodic attack of single crystal silicon substrates in 25% hydrofluoric acid solutions. Specific surface area, total porous volume, and pore size distribution of porous silicon have been determined. The experimental technique used is based on the measurement of the volume of gas adsorbed at low constant temperature by the porous silicon. The adsorption isotherms show the general behavior found for porous materials, but at the same time, they show clear differences following different preparation conditions of porous layers. Quantitative analysis using models extensively used in the catalysis field lead to large values for the porous silicon specific surface area and sharp pore size distribution. Mean pore radii are found to vary in the range 20-100 Å when forming current density varies from 10 to 240 mA/cm². (12 refs.)
- 114334 Dynamics and mechanism of iodine sorption by polyacetylene. T.Danno, K.Miyasaka, K.Ishikawa (Dept. of Textile & Polymeric Materials, Tokyo Inst. of Technol., Ookayama, Meguro-ku, Tokyo). *J. Polym. Sci. Polym. Phys. Ed. (USA)*, vol.21, no.8, p.1527-37 (Aug. 1983). Sorption of iodine by bulk polyacetylene was studied under various I₂ gas pressures at 25°C. The sorption dynamics show that the penetration of iodine into PA is not Fickian and the diffusion coefficient increases with time of sorption. A discontinuous increase in the sorption isotherm is observed at P/P₀=0.25 (P is the pressure of the I₂ gas and P₀ is the saturation value at 25°C). It is due to iodine penetration into PA crystals, as evidenced by X-ray analysis. The distribution of iodine within crystals is apparently inhomogeneous: some unit cells are changed into 'iodine-PA' cells, while others remain unchanged. The electrical conductivity depends not only on the amount of iodine but also on the I₂ gas pressure under which sorption is carried out. At given iodine content, the conductivity of a sample doped under higher I₂ pressure is greater than that of a sample doped under lower pressure. (17 refs.)
- 114335 'Second component' effects in sorption and permeation of gases in glassy polymers. R.T.Chern, W.J.Koros, E.S.Sanders, R.Yui (Dept. of Chem. Engng., North Carolina State Univ., Raleigh, NC, USA). *J. Membrane Sci. (Netherlands)*, vol.15, no.2, p.157-69 (Sept. 1983). Data for CO₂ permeability through Kapton polyimide at 60°C are reported for upstream pressures up to 240 psia (16.33 atm) in the presence and absence of water vapor in the feed. The carbon dioxide flux was depressed by the presence of the water vapor. This phenomenon is analyzed in terms of the dual mode sorption and transport models. Together with other recent sorption and permeation data, the study suggests that competition of mixed penetrants for sorption sites and transport pathways associated with unrelaxed volume in glassy polymers is a general feature of gas/glassy polymer systems. The permselectivity of a membrane to a mixture of penetrants is strongly related to its ability to maintain a size and shape differentiating matrix, that is, to remain essentially unplasticized under operating conditions. Under such conditions, competition among penetrants for excess volume will be a generally important consideration for modeling gas permeation in permselective membranes. (21 refs.)
- 114336 Quantum motion of chemisorbed hydrogen on Ni surfaces. R.M.Puska (Lab. of Phys., Helsinki Univ. of Technol., Espoo, Finland), M.J.Nieminen, M.Manninen, B.Chakraborty, S.Holloway, J.K.Norskov. *Phys. Rev. Lett. (USA)*, vol.51, no.12, p.1081-4 (19 Sept. 1983). Quantum mechanical energy levels and wave functions have been calculated for the motion of chemisorbed hydrogen atoms on Ni surfaces. The results show considerable quantum effects for the adatom in both the ground and the excited states. The description of the adparticles as being delocalized along the surface offers a novel interpretation of several phenomena, in particular the vibrational excitations. (9 refs.)
- 114337 On the physisorption interaction of H₂ with Cu-metal. J.Harris, A.Liebsch (IFF, KFA, Jülich, Germany). *Phys. Scr. (Sweden)*, vol.T4, p.14-16 (1983). (Nordic Conference on Surface Science, Tampere, Finland, 18-20 Aug. 1982). The physisorption of H₂ on copper is discussed in the light of a recent theory of the helium-metal interaction. The theory relates the repulsive branch of the physisorption well to the scattering of individual evanescent band electrons by the ad-particle potential. Metal electrons are expelled from the region near the ad-particle and the band energy is driven up. The H₂-Cu physisorption well is found to be 23 meV deep, and only very weakly dependent on the orientation of the molecular axis. (16 refs.)
- 114338 Correlation between pair interactions of adsorbed atoms and adsorption layer superstructure formation. T.T.Tsong (Phys. Dept., Pennsylvania State Univ., University Park, PA, USA). *Phys. Scr. (Sweden)*, vol.T4, p.17-21 (1983). (Nordic Conference on Surface Science, Tampere, Finland, 18-20 Aug. 1982). When atoms adsorb on an atomically perfect surface, they often form a superstructured adsorption layer at sub-monolayer coverages. Although it is generally agreed that the lateral interactions between adatoms are responsible for the formation of adlayer superstructures, no direct experimental evidence exists. Using the field ion microscope, the author measured pair energies as function of distances for a few atomic pairs on the W (110) plane. In general, the interactions are nonmonotonic in distance dependence, and are about 100 meV in strength. The Si-Si interaction is most interesting. Using this data the relative two dimensional binding energy per adatom in an adsorption layer can be calculated. The author finds the (2√2/√3×4/√3) R35.26° superstructure, or in a conventional unit cell the p(2×1), has the lowest energy. The author's Monte Carlo simulation, which generates an adlayer of minimum free energy and maximum entropy consistent with the measured pair energies, also shows the same superstructure. Thus the lateral interaction of adatoms is indeed responsible for the adlayer superstructure formation, and the pair potential between two adatoms can now be measured from the FIM experiment with sufficient accuracy to correlate well with the formation of adlayer superstructure. No covalent bonds are formed between Si adatoms. (16 refs.)
- 114339 On the surface reaction of hydrogen with FeTi. A.S.Pedersen, P.J.Moller (Chem. Lab. IV, HC Ørsted Inst., Univ. of Copenhagen, Copenhagen, Denmark). *Phys. Scr. (Sweden)*, vol.T4, p.83-5 (1983). (Nordic Conference on Surface Science, Tampere, Finland, 18-20 Aug. 1982). The surface reaction of hydrogen (and of deuterium) with activated FeTi was studied by UHV volumetric vapour pressure measurements in the 3×10⁻⁸ Pa to 1.3×10⁻⁵ Pa range at 78K and 88K. At the low temperatures a dissociative nonactivated Temkin chemisorption process was found. An isosteric heat of adsorption, q, was described by the expression q=24(1-θ)kJ/(mole H₂) for a broad range of coverages. It was demonstrated that the dissociation

occurred on a nonoxidized Ti-surface and not—as has been suggested—on a segregated subsurface Fe-layer. (14 refs.)

114340 Coadsorption systems with electrochemical relevance: coadsorption of water with oxygen, bromine and sodium on Cu(110). D.E.Grider, K.Bange, J.K.Sass, G.Paolucci (Fritz-Haber-Inst., Max-Planck-Gesellschaft, Berlin, Germany).

Phys. Scr. (Sweden), vol.T4, p.92-5 (1983). (Nordic Conference on Surface Science, Tampere, Finland, 18-20 Aug. 1982).

A unique approach of synthesizing the electric double layer at a metal-electrolyte interface under ultra-high vacuum conditions is briefly outlined. Results are presented of a study of water adsorption on clean Cu(110) using ultra-violet photoelectron spectroscopy (UPS), low energy electron diffraction (LEED), thermal desorption spectroscopy (TDS), as well as changes in the work function ($\Delta\phi$) as determined by the Kelvin method. In addition, changes in the nature of water adsorption due to the presence of coadsorbed oxygen, bromine, and sodium are also discussed. (24 refs.)

114341 Oxygen adsorption on a cylindrical GaAs single crystal prepared by molecular beam epitaxy. W.Ranke (Fritz-Haber-Inst., Max-Planck-Gesellschaft, Berlin, Germany).

Phys. Scr. (Sweden), vol.T4, p.100-2 (1983). (Nordic Conference on Surface Science, Tampere, Finland, 18-20 Aug. 1982).

The orientation dependence of oxygen adsorption was studied by AES and LEED using a cylindrical GaAs sample which exposes the low index orientations (001), (111), (110), (111), and (001) as well as all intermediate orientations on its surface. For the sample prepared by ion bombardment (IB) only, the adsorption is strong and nearly orientation independent. After ion bombardment and annealing (IBA), the oxygen adsorption on (001), (001) and (111) still is comparatively strong due to the influence of residual defects. In the range (331)-(110)-(111)-(113), a strong orientation dependence is observed which can be understood in terms of enhanced adsorption on edge adjacent sites. When the surface is prepared by molecular beam epitaxy (MBE), the overall amount of adsorbed oxygen is reduced indicating smaller defect concentrations. Also the orientation dependence becomes weaker. LEED observations show that in this case the regions between most of the low index orientations show only weak indications for steps but strong faceting which greatly reduces the edge site concentration. Obviously MBE promotes the formation of low index facets representing the state of lowest surface energy. However, in the range (110)-(111)-(112), also after MBE stable steps are formed which near (110) are two (110)-layers high. (13 refs.)

114342 Oxidation of Pb monolayers on Cu(100). D.Chadwick, M.A.Karolewski (Dept. of Chem. Engng. & Chem. Technol., Imperial Coll., London, England).

Phys. Scr. (Sweden), vol.T4, p.103-5 (1983). (Nordic Conference on Surface Science, Tampere, Finland, 18-20 Aug. 1982).

The interaction of oxygen with Pb-covered Cu(100) surfaces in the range 0-1.2 monolayers has been studied by X-ray photoelectron spectroscopy. Oxygen reacts with the Pb overlayers to form lead monoxide. The oxidation rate of the overlayers decreases with increasing Pb coverage below 1 monolayer. Definite changes in reactivity can be observed at coverages where submonolayer structural changes have been reported. No evidence was found for the spill-over promotion of overlayer oxidation rate reported on other Cu surfaces. (22 refs.)

114343 Bromine and iodine adsorption on an Fe(100) surface. P.A.Dowben, M.Grunze (Fritz-Haber-Inst., Max-Planck-Gesellschaft, Berlin, Germany), D.Tomanek.

Phys. Scr. (Sweden), vol.T4, p.106-9 (1983). (Nordic Conference on Surface Science, Tampere, Finland, 18-20 Aug. 1982).

The authors studied bromine and iodine adsorption on an Fe(100) surface in the temperature range of 110K to 700K. The authors compare core-level binding energies of dissociatively and molecularly adsorbed halogen species as a function of coverage. The valence band photoemission data suggest that bromine and iodine adsorption at 300K is always dissociative. At 110K, initial dissociative adsorption is followed by condensation of molecular halogens. At 300K the core-level binding energies E_B^F of bromine and iodine decrease as a function of coverage by 0.2 eV and 0.7 eV, respectively. The E_B^F values found for the condensed molecular species are identical to or even lower by 0.3 eV than for the room temperature saturated bromine and iodine overlayers, respectively. (15 refs.)

114344 Electron spectroscopy on adsorption of Cs on transition metals. P.Soukiasian, R.Riwan, C.Guillot, J.Lecante, Y.Borensztein (Service de Phys. des Atomes et des Surfaces, CENS, Gif-sur-Yvette, France).

Phys. Scr. (Sweden), vol.T4, p.110-12 (1983). (Nordic Conference on Surface Science, Tampere, Finland, 18-20 Aug. 1982).

The electronic properties of Cs adsorbed on W(100) and Mo(100) are studied by ELS and UPS. For W(100), the main loss observed in ELS has a constant value of 1.5 eV for coverage θ between 0.6 and 1 monolayer while a small increase from 1.58 to 1.65 eV is observed for Cs on Mo(100). These results are in opposition to the energy loss increase on Cs adsorbed on Cu(111) which is found equal to $n^{1/2}$ (n being the surface atom density) and attributed to the excitation of a surface plasmon. An interband transition involving the Cs6s-6p resonances is postulated for Cs on Mo(100) and W(100). Preliminary UPS results indicate that the tungsten surface state observed at normal emission remains sharp and intense and suffers a 1 eV shift to higher binding energy but disappears on Mo(100). (23 refs.)

114345 Characterisation of a low temperature surface phase of CO on Pt {110}. P.Hofmann, S.R.Bare, D.A.King (Donnan Labs., Univ. of Liverpool, Liverpool, England).

Phys. Scr. (Sweden), vol.T4, p.118-21 (1983). (Nordic Conference on Surface Science, Tampere, Finland, 18-20 Aug. 1982).

Adsorption of CO on a Pt{110}(1 \times 2) surface precooled to 160K is found to proceed without loss of the (1 \times 2) reconstruction, in contrast to adsorption at higher temperatures. Using high resolution electron energy loss spectroscopy, the authors find that adsorption occurs initially into a linear species, with the additional occupation of bridged sites at fractional coverages above 0.2. At saturation, the ratio of bridged to linear species is 1:3. The absorption intensity from the linear species is shown to be 2.5 times that of the bridged species. Heating the saturated surface to temperatures between 280 and 340K results in an irreversible transformation of the bridged species to linear, and a lifting of the (1 \times 2) reconstruction to (1 \times 1). The orientation of CO molecules in the low temperature metastable phase on the (1 \times 2) surface was determined using angle-resolved photoemission, with electron collection in the plane orthogonal to the incidence plane. The CO molecules are found to be tilted away from the macroscopic surface normal, along the [100] azimuth, by $15\pm 5^\circ$. This contrasts with previous findings for the stable phase of CO on the annealed (1 \times 1) surface, where the tilt angle was found to be $26\pm 2^\circ$ along the [211] azimuth. (12 refs.)

114346 Ion scattering spectroscopy of β -N and β -Co ($\sqrt{2}\times\sqrt{2}$) R45° structures on W{100}. N.R.Palmer, D.A.King (Donnan Labs., Univ. of Liverpool, Liverpool, England).

Phys. Scr. (Sweden), vol.T4, p.122-5 (1983). (Nordic Conference on Surface Science, Tampere, Finland, 18-20 Aug. 1982).

Ion scattering spectroscopy has been applied in the present work in an attempt to determine the positions of N, C and O adatoms in the selvage of W{100}. LEED, AES, thermal desorption, and UPS were used to characterise the adsorbate structures. With the instrument, the incidence angle of the ion beam (He^+ , 1 keV) at the surface, the scattering angle, and the azimuthal angle, could be independently varied. For β -N, the results clearly favour the four-fold hollow site over the two-fold bridge or the on-top site at half monolayer coverage, with the adatoms shadowed by neighbouring surface W atoms at grazing incidence. For β -CO, the C and O adatoms again occupy the four-fold hollow sites; in this case, C (as with N) sits well into the hollow, being shadowed at grazing incidence by surrounding W atoms, while the O adatom sits slightly proud of the surface as shown by its shadowing neighbouring W atoms at grazing incidence. It is concluded that while C and N atoms are covalently bonded, the large radius of oxygen indicates ionic bonding. This study independently confirms and extends the previous LEED structural analysis of this system. (18 refs.)

114347 Photon stimulated desorption of ions from water and methanol adsorbed on a Ti(0001) surface. R.Stockbauer, D.M.Hanson, S.A.Flodstrom, E.Bertel, T.E.Madey (Surface Sci. Div., NBS, Washington, DC, USA).

Phys. Scr. (Sweden), vol.T4, p.126-8 (1983). (Nordic Conference on Surface Science, Tampere, Finland, 18-20 Aug. 1982).

Synchrotron radiation ($15\leq h\nu\leq 75$ eV) has been used to study ion desorption from water and methanol adsorbed on a Ti(0001) surface, in an effort to understand ion desorption from covalently bonded systems. Both water and methanol dissociate at all coverages upon adsorption on Ti at 300K. Using variable wavelength UPS, the adsorbed fragments OH, O and H are identified for water and CH_3O , C, O and H for methanol. At 90K, dissociation occurs initially to yield the same products, while at higher exposures, condensed overlayers are formed. PSD of ions from the two adsorbates show very different behaviour. In the water experiment, ion desorption originates from the dissociated species at both 300 and 90K. H^+ emission from dissociated water is correlated with the presence of OH on the surface while ion desorption from the ice multilayer is almost an order of magnitude less. In contrast, ion emission from the dissociated methanol is immeasurably low in the authors' instrument while a large H^+ signal is observed from the condensed layer. It is obvious that different molecular states are involved in the ion desorption in these cases. The H^+ emission from OH appears to be correlated with the O 2s level near 25 eV and the Ti 3p core level near 33 eV. However, ion desorption could arise strictly from different localized two hole states in OH. The H^+ observed from methanol appears to be initiated by ionization of the $4a'$ orbital with an onset near 18 eV. Using isotopic labelling experiments, it is shown that H^+ originates from the methyl group rather than the OH. (19 refs.)

114348 ESD spectra during adsorption at 300K and thermal desorption of $\text{H}_2/\text{W}(\text{poly})$. F.Gonzalez, J.L.de Segovia (Surface Phys. Lab., Inst. de Fisica de Materiales, CSIC, Madrid, Spain).

Phys. Scr. (Sweden), vol.T4, p.129-32 (1983). (Nordic Conference on Surface Science, Tampere, Finland, 18-20 Aug. 1982).

The present work is related with the EDS spectra of the $\text{H}_2/\text{W}(\text{poly})$ system during the adsorption at 300K and thermal desorption processes. Significant differences with the usual spectra already described in the literature are found. They are characterized by a decrease of the maximum of the surface ion current of H^+ ($I^+(\text{H}^+)$), and a broadening of the peak with increasing pressure. Nevertheless, the ESD spectra during thermal desorption show that $I^+(\text{H}^+)$ reaches the same maximum value, irrespectively of the value obtained during the adsorption cycle. From the simultaneous ESD and thermal desorption spectra it is possible to establish a good correlation between $I^+(\text{H}^+)$ and p - t curves and, subsequently, with the desorbed entities (H_2). This relationship shows that there are four clearly different regions which can be assigned, at least in part, to the desorption states labelled β_1 , β_2 , β_3 and β_4 of polycrystalline samples. Using the $I^+(\text{H}^+)$ signal, the desorption energies and ion cross-sections have been determined for those states which are excitable electronically. (8 refs.)

114349 Floating phase in the chiral Potts model. A Monte Carlo renormalization-group analysis. J.M.Houlik, S.J.K.Jensen (Dept. of Phys. Chem., Aarhus Univ., Aarhus, Denmark), P.Bak.

Phys. Rev. B (USA), vol.28, no.5, p.2883-5 (1 Sept. 1983).

Layers of atoms or molecules adsorbed on surfaces may exhibit floating critical phases. To investigate this phenomenon the authors have developed a Monte Carlo renormalization-group scheme and performed calculations on the three-state chiral Potts model. The results indicate a continuous transition from a floating phase to a liquid phase at a temperature much higher than that found by series-expansion methods. (18 refs.)

114350 Phase diagrams of multilayer films and the Potts lattice-gas model of adsorption. C.Ebner (Dept. of Phys., Ohio State Univ., Columbus, OH, USA).

Phys. Rev. B (USA), vol.28, no.5, p.2890-2 (1 Sept. 1983).

The Potts lattice-gas model is examined via Monte Carlo simulations and a mean-field approximation to obtain phase diagrams for multilayer adsorbed films. The advantage of the model is that it has three bulk phases, interpreted here as solid, liquid, and gas, allowing one to study the relationships between the phase transitions of the film and the bulk triple point. For the author's choices of coupling parameters, we find a solid film that wets the substrate and that melts, forming a liquid film, below the bulk triple-point temperature and either above or below the bulk roughening temperature. The liquid film wets the substrate above the bulk triple point but not below. (12 refs.)

114351 Negligible adsorbent cooling in thermal desorption. Z.W.Gortel, H.J.Kreuzer (Dept. of Phys., Dalhousie Univ., Halifax, Nova Scotia, Canada).

Surf. Sci. (Netherlands), vol.131, no.1, p.L359-66 (Aug. 1983).

A simple argument and a detailed calculation, the latter based on the master equation and the heat conduction equation, show that adsorbent cooling in thermal desorption is at best at the percent level. The time dependent temperature field in the surface region is calculated and discussed. (14 refs.)

114352 Absolute coverage measurements of deuterium on Ni(110). I.Stensgaard, R.Feidenhans'l (Inst. of Phys., Univ. of Aarhus, Aarhus, Denmark).

Surf. Sci. (Netherlands), vol.131, no.1, p.L373-8 (Aug. 1983).

The absolute coverage of deuterium adsorbed on Ni(110) at temperatures below 170K to the formation of a (1 \times 2) LEED pattern has been determined by nuclear microanalysis (NMA). The result, $\theta_D = 0.96\pm 0.08$, is consistent with a saturation coverage of one full monolayer. Heating the crystal above $\sim 190\text{K}$ is shown to result in a gradual loss of deuterium from the system, accompanied by streaking of the LEED pattern, with complete desorption above $\sim 340\text{K}$. The low-temperature (2 \times 1)-D phase was found to correspond

to $\theta_D = 0.64 \pm 0.05$ monolayers. The results are expected to be valid also for the equivalent phases obtained by hydrogen adsorption. (17 refs.)

114353 An XPS study of carbon monoxide and nitric oxide adsorption on platinum (410): unusual dissociation activity. Y.O.Park, R.I.Masel (Dept. of Chem. Engng., Univ. of Illinois, Urbana, IL, USA), K.Stolt. *Surf. Sci. (Netherlands)*, vol.131, no.1, p.L385-9 (Aug. 1983). The adsorption of NO and CO on platinum (410) is studied by X-ray photoemission spectroscopy (XPS). It is found that the (410) surface shows unusual activity for NO and CO bond breaking. CO is found to adsorb molecularly on Pt(410) at 300K, but it partially dissociates upon heating to 500K. NO is found to adsorb dissociatively under all conditions studied. By comparison, the low index faces of platinum and stepped surfaces considered previously give negligible dissociation of CO and negligible dissociation of NO up to 450K. The (410) surface is also unusual from an orbital symmetry standpoint; in fact, it was predicted to be unusually active for NO and CO bond breaking based on Woodward-Hoffman ideas. The present results show, then, that Woodward-Hoffman (i.e. orbital symmetry conservation) methods could yield valuable insights into the nature of active sites on single crystal catalysts. (17 refs.)

114354 Theoretical study of oxygen chemisorption on zinc surface by cluster models. E.Miyazaki (Dept. of Chem., Tokyo Inst. of Technol., Tokyo, Japan), M.Tsukada, H.Adachi. *Surf. Sci. (Netherlands)*, vol.131, no.1, p.L390-8 (Aug. 1983). Theoretical calculations by DV-X α -MO have been performed for clusters representing a Zn(0001) surface with oxygen. The calculated DOS is in good agreement with the experimental UPS spectra found by Briggs (1975) or by Abbati et al. (1977). A large amount of electron flow from Zn atoms into the oxygen atom occurs and this causes (1) a remarkable upward shift of the oxygen 2p level and (2) formation of an unoccupied level near the highest occupied level. The bonds between the oxygen 2p and the zinc 4s or 4p orbitals have a strong bonding character, and the contribution of the zinc 3d orbital to the Zn-O bond is not important. (12 refs.)

114355 Adsorption and decomposition of ammonia on W(100): XPS and UPS studies. C.Egawa, S.Naito, K.Tamaru (Dept. of Chem., Univ. of Tokyo, Tokyo, Japan). *Surf. Sci. (Netherlands)*, vol.131, no.1, p.49-60 (Aug. 1983). The adsorption and decomposition of ammonia on a clean and c(2 \times 2)-N ordered W(100) surface has been studied by photoemission spectroscopy (XPS and UPS). At 120K molecularly adsorbed ammonia was identified by N(1s) core level emission at 400.9 eV and the valence emissions at 7.6 and 11.7 eV. By heating the sample stepwise the N(1s) core level shifted to lower binding energy. In the valence region, the corresponding spectral changes were obtained, where the dependence of the peak intensity on photon energy was observed. These observations were interpreted to demonstrate that adsorbed ammonia dissociates its hydrogen successively to form NH₃(a) and finally to atomic nitrogen. On the other hand, ammonia was molecularly adsorbed on a c(2 \times 2)-N ordered surface even at temperatures as high as 300K, although the spectra at 400K or above were very similar to those under a steady state flow condition, where the tungsten surface was mostly covered by atomic nitrogen. At higher ammonia pressure up to about 100 Pa thicker nitride layers were formed at 700K, which were characterized by the N(1s) core level at 397.3 eV and a broad emission around 6 eV in the valence level. (16 refs.)

114356 Thermodynamics of xenon adsorption on Pd(s)[8(100) \times (110)]: from steps to multilayers. R.Miranda, S.Daiser, K.Wandelt, G.Ertl (Inst. fur Phys. Chem., Univ. Munchen, Munchen, Germany). *Surf. Sci. (Netherlands)*, vol.131, no.1, p.61-91 (Aug. 1983). The thermodynamic properties of the adsorption of xenon on the stepped Pd(s)[8(100) \times (110)] surface have been studied over a wide range of pressure (5×10^{-11} to 1×10^{-4} Torr) and temperature (40-140K). The authors have measured adsorption isobars using AES in order to evaluate the surface coverage. By choosing pressure and temperature they have studied under equilibrium conditions the successive adsorption of xenon on the steps and on the terraces until the first layer is formed, the condensation of the second layer as well as the formation of xenon multilayers. For a small range of pressure and temperature, adsorption takes place only on the atomic steps. The LEED pattern shows that only every other site along the steps is occupied. The extrapolated initial heat of adsorption for steps is $E_{ad}^S = 10.2$ kcal/mol, decreasing monotonically by about 2 kcal/mol as the relative coverage of the sites increases. The dipole moment of the Xe atoms adsorbed on steps is 1.12 D. During adsorption on the terraces the LEED observations suggest that the xenon adlayer is non-localized up to completion of the hexagonally close packed monolayer. The initial heat of adsorption on the terraces, E_{ad}^T is 8.2 kcal/mol and decreases continuously to a value of 6.9 kcal/mol for a complete monolayer due to lateral repulsive interactions between the adsorbed xenon atoms. (65 refs.)

114357 On the role of image forces in chemisorption theory. O.M.Braun (Inst. of Phys., Acad. of Sci., Kiev, Ukrainian SSR), A.I.Volokitin. *Surf. Sci. (Netherlands)*, vol.131, no.1, p.148-58 (Aug. 1983). The Extended Anderson Hamiltonian is used to study the effect of fluctuations of an adatom charge Q on the ionic part of the chemisorption energy. It is shown that dynamical effects essentially modify the classical expression $E = -\phi Q^2$ for the energy of interaction between a static charge Q and a metal (ϕ is the interaction energy for a unit charge). The exact solution for the one-electron two-level model as well as a variational solution for the Extended Anderson Hamiltonian model are given. Validity conditions for a variety of approximate schemes are studied. The results are presented for the Extended Anderson Hamiltonian model parameterized so as to describe some aspects of the Li/W and Li/Mo chemisorption systems. (15 refs.)

114358 Site-specific interaction of H₂O with ZnO single-crystal surfaces studied by thermal desorption and UV photoelectron spectroscopy. G.Zwicker, K.Jacobi (Fritz-Haber-Inst., Max-Planck-Gesellschaft, Berlin, Germany). *Surf. Sci. (Netherlands)*, vol.131, no.1, p.179-94 (Aug. 1983). The adsorption and condensation of H₂O (D₂O) on ZnO(10 $\bar{1}$ 0), (0001)Zn and (0001)O surfaces was investigated by means of thermal desorption (TDS) and UV photoelectron spectroscopy (UPS). The clean ZnO single-crystal surfaces were prepared by Ar-ion sputtering and annealing and characterised by Auger electron spectroscopy, LEED, UPS and work-function measurements. On all three surfaces six different adsorption states were found. In the monolayer regime there is a stronger bonding to Zn sites (desorption temperature 340K) than to O sites (190K). The bonding to the Zn sites seems to be accompanied by some clustering. Before the chemisorption layer is completed a first ice state is found whose desorption temperature shifts from 162 to 168K with increasing exposures. At higher exposures the multilayer ice state is found at 152K. On the (0001)O face defect-induced features were identified. The water lone-pair orbital 1b₁, whose energy falls between the O p and Zn 3d emission of the substrate and which is known to show bonding shifts, was analysed using angle-resolved UPS. In the monolayer, the main chemisorption states are found at $E_B^V(1b_1) = -9.6$ eV for the (0001)Zn face

and at -10.6 eV for the (0001)O face and are compared with the multilayer ice emission at -11.1 eV. The difference in binding energies shows the same trend at the TDS data. For the (1010) face the 1b₁ emission is very broad, indicating some overlap between different states. (18 refs.)

114359 Classical stochastic diffusion theory for desorption from solid surfaces. Y.Zeiri, A.Redondo, W.A.Goddard, III (Arthur Amos Noyes Lab. of Chem. Phys., California Inst. of Technol., Pasadena, CA, USA). *Surf. Sci. (Netherlands)*, vol.131, no.1, p.221-38 (Aug. 1983). The authors present a theory of desorption of atoms and molecules from solid surfaces based on a classical stochastic diffusion formulation. They obtain a simple rate expression which has the form $R = (\Omega_0/2\pi) f(T) \exp(-D_c/kT)$, where T is the temperature, k is Boltzmann's constant, D_c is the bond enthalpy and Ω_0 is the surface-adsorbate vibrational frequency. For atoms $f(T) = 1$, while for molecules $f(T)$ depends on the parameters for the frustrated rotations at the surface. Application of this theory is reported for the desorption of atoms and molecules. They find that molecules lead to a greatly increased (factor of 100) Arrhenius preexponential factor in excellent agreement with experiment. (18 refs.)

114360 The adsorption of methane on polycrystalline iron films. G.Wedler, M.Mengel (Inst. fur Phys. und Theoretische Chemie., Univ. Erlangen-Nurnberg, Erlangen, Germany). *Surf. Sci. (Netherlands)*, vol.131, no.2-3, p.L423-8 (Sept. 1983). The adsorption of methane on evaporation iron films at 77K is discussed by means of adsorption isotherms, changes in resistance and work function. The thermal desorption spectrum shows only one peak at about 130K. There is no adsorption of methane at 273K. The results are compared with those found for methane adsorption on nickel films. (15 refs.)

114361 Kinetics of nitrogen adsorption on iron. J.Boheim, W.Brenig (Dept. of Phys., Tech. Univ. Munchen, Munchen, Germany). *Surf. Sci. (Netherlands)*, vol.131, no.2-3, p.258-72 (Sept. 1983). A model for the dissociative adsorption of N₂ on Fe single crystals is investigated, in which the sticking of N₂ proceeds via a precursor. In particular, a situation is discussed where the translational energy of incident N₂ is of the order of the activation barrier between the molecular precursor and the chemisorbed state. It turns out that in this case the energy transfer to phonons is greatly reduced. The rotational degrees of freedom are taken into account only in a very rough way in a kinetic equation: The detailed balance relations for the kinetic coefficients i in this equation contain rotational partition functions, describing free rotations in the gas phase and assuming totally frozen rotations in the precursor. A consequence of the reduced energy transfer and the freezing of rotations is an anomalously low overall sticking coefficient in agreement with the experimental results of Ertl, Lee and Weiss (1982). The angular distribution of inelastically scattered N₂/Fe was measured and found to be unusually narrow, again consistent with the prediction of an unusually low energy transfer. (11 refs.)

114362 Chemisorption properties of thin Pd overlayers on Nb (110) and Ag (111). J.P.Muscat (Dept. of Appl. Math., Univ. of Waterloo, Waterloo, Ontario, Canada). *Surf. Sci. (Netherlands)*, vol.131, no.2-3, p.299-308 (Sept. 1983). A simple model of hydrogen adsorption on a Pd covered Nb (110) substrate is presented. In agreement with recent experiments, it is found that for the commensurate BCC (110) phase, dissociation H₂ adsorption is not favoured in contrast to the incommensurate FCC (111) phase. The major reason for the dramatic reduction in surface reactivity for the BCC (110) phase, is due to the increase in Pd-Pd distances which results in a narrowing of the d band and also a lowering of the antibonding resonance made up of the H 1s orbital and the substrate d states, to an energy position where it is now occupied. A similar behaviour is expected for H adsorbed on a Pd/Ag (111) composite substrate, where at low Pd coverages (less than one monolayer) the expanded Pd layer is expected to act against the H₂ dissociation. Calculations of the one-electron energies due to the metal d states for H and Pd and Nb surfaces, indicate a larger chemisorption energy for Nb than Pd. The H-surface bond is thus more easily broken for a Pd covered Nb surface, than for a clean Nb surface, thereby resulting in a faster H penetration into the bulk of the composite substrate. (23 refs.)

114363 Effects of oxygen adsorption on the LEED fine structure features of Cu (001), Cu (110), Cu (111) and Ni (001). S.M.Thurgate, P.J.Jennings (School of Math. & Phys. Sci., Murdoch Univ., Murdoch, Australia). *Surf. Sci. (Netherlands)*, vol.131, no.2-3, p.309-20 (Sept. 1983). The effect of adsorbed oxygen on the LEED fine structure features of Cu (001), Cu (110) and Cu (111) is investigated. The adsorption process is followed by AES and CPD measurements. Changes in the relative intensity of the fine structure features are related to changes in the surface order and smoothness. It is empirically established that a rough surface produces relatively weak fine structure features compared with a similar smooth surface. This is attributed to a reduction in reflectivity of the surface potential barrier. It is also shown empirically that increasing disorder on the crystal surface leads to a preferential damping of the fine structure close to the emergence. This effect is seen in the change of the relative intensity of the fine structure features during the adsorption of oxygen. Observations of these features are used to test several models proposed for the oxygen adsorption sites on these surfaces. (18 refs.)

114364 Semi-empirical calculation of H atom interaction with a 12 atom iron cluster. G.Blyholder, J.Head, F.Ruette (Dept. of Chem., Univ. of Arkansas, Fayetteville, AR, USA). *Surf. Sci. (Netherlands)*, vol.131, no.2-3, p.403-18 (Sept. 1983). Calculations have been made using the MINDO/SR procedure for Fe₂, Fe₁₂, FeH and Fe₁₂H. The order of stability for H on Fe (100) symmetric sites is bridge > 4-fold > linear. Adsorption on edges is favored over center sites. The most stable plane site was a displaced bridge site. The H atom charges in the 4-fold, bridge and linear sites are +0.16, +0.03, and -0.17e respectively. The vibrational frequencies are 1150, 1340 and 1950 cm⁻¹, respectively. No simple correlation of H binding energies with coordination numbers was found to exist. The calculations correlate the binding energy, vibrational frequency, work function change, photoelectron spectra and LEED data into a consistent view. (31 refs.)

114365 Interactions of sulfur with nickel surfaces: adsorption, diffusion and desorption. M.Blaszczyszyn, R.Blaszczyszyn, R.McClews (Inst. of Experimental Phys., Univ. of Wroclaw, Wroclaw, Poland), A.J.Melmed, T.E.Madey. *Surf. Sci. (Netherlands)*, vol.131, no.2-3, p.433-47 (Sept. 1983). The kinetics of adsorption, surface diffusion and thermal desorption of sulfur on Ni surfaces have been studied using field electron emission microscopy methods. The sticking probability for elemental sulfur sublimed onto a Ni specimen is approximately unity for Ni substrate temperatures from 77 to 530K. The maximum average work function for ~monolayer coverage of S ranged from 4.7 to 5.05 eV in different experiments; for fractional monolayer doses of S, surface diffusion was rapid at $T > 400$ K, with activation energies ranging from 15 to 28 kcal/mol. For multilayer adsorption of sulfur, diffusion

occurs without motion of a sharp boundary, and there is evidence of extensive surface reaction between S and Ni (emission from small 'crystallites' is evident in the field emission patterns). Sulfur desorbes for Ni at temperatures above 1500K. (17 refs.)

114366 Electron-enhanced CO₂ adsorption and stabilization on aluminum films. J.L.Falconer, S.D.Bischke, G.J.Hanna (Dept. of Chem. Engng., Univ. of Colorado, Boulder, CO, USA).

Surf. Sci. (Netherlands), vol.131, no.2-3, p.455-62 (Sept. 1983).
The rate of carbon dioxide adsorption and surface oxidation on aluminum films is significantly enhanced by an electron beam. Though oxygen accumulates in the beam-exposed area, carbon does not significantly accumulate on the surface; apparently the electron beam dissociates CO₂ to oxygen and carbon monoxide, which desorbs. The surface concentrations of oxygen and aluminum oxide are measured by Auger spectroscopy at locations that were exposed and not exposed to the electron beam during adsorption. These measurements show that an oxide can be formed with a sharp concentration gradient on the surface. The oxide formed by electron beam enhancement is not stable and can apparently diffuse into the bulk. However, this oxide can be stabilized by additional electron beam exposure in the absence of gas-phase carbon dioxide. (21 refs.)

114367 A model for non-adiabatic coupling on metals: the sticking problem. G.P.Brivio (Istituto di Fisica, Univ. di Milan, Milan, Italy), T.B.Grimley.

Surf. Sci. (Netherlands), vol.131, no.2-3, p.475-90 (Sept. 1983).
A simple quantum model is introduced to deal with the continuum of electron-hole pair excitations produced by a reactive gas atom moving near a metal surface. The sticking coefficient due to the electron-hole pair mechanism is defined for both box- and δ -function-normalization of the gas atom's nuclear wavefunctions, and the equivalence of the two definitions is proved for a large box. The sticking coefficient is calculated in the distorted wave Born approximation for hydrogen atoms with kinetic energies in the range 0-80 meV. It shows a maximum at about 21 meV due to a quantum mechanical resonance in the transmission of the hydrogen atom into the chemisorption potential well. The maximum value of the sticking coefficient is 0.4. The role in electron-hole pair sticking of the spectral density at the Fermi level of the surface bond order is emphasized, and discussed. (11 refs.)

114368 Numerical simulations of adatom pair distribution functions. H.K.McDowell, S.M.Valone, J.D.Doll (Los Alamos Nat. Lab., Univ. of California, Los Alamos, NM, USA).

Surf. Sci. (Netherlands), vol.131, no.2-3, p.511-16 (Sept. 1983).
Numerical simulations of the pair correlation for two adatoms on a solid surface with smooth (Lennard-Jones) pair potentials as input exhibit long range oscillations in spite of the low adatom density. Other simulations of a pair distribution with only the adatom-adatom interaction switched off show that this distribution may be combined with the experimental pair distribution to provide an estimate of the adatom interaction. (6 refs.)

114369 Adsorption of mixtures of methane and krypton on CaA zeolite. II. Analysis of the experimental data using Freundlich- and D dubinin-Radushkevich-type equations derived by assuming similar heterogeneity parameters for single-gas adsorption. M.Jaroniec, J.Piotrowska (Dept. of Theoretical Chem., Inst. of Chem., Maria Curie-Sklodowska Univ., Lublin, Poland), M.Bulow.

Thin Solid Films (Switzerland), vol.106, no.3, p.219-24 (19 Aug. 1983).
Equations for mixed-gas adsorption isotherms were derived on the basis of the integral equation of the adsorption isotherm by assuming constant differences in the adsorption energies for all types of adsorption sites. The application of Freundlich- and Dubinin-Radushkevich-type isotherms to the interpretation of experimental data for methane-krypton mixtures is also presented. (12 refs.)

114370 Construction of an Eisenman series for an ion-exchange material containing phosphate groups. E.D.Lavrinenko-Ometinskaya, V.V.Strelko (Inst. of General & Inorganic Chem., Acad. of Sci., Kiev, Ukrainian SSR). *Theor. & Exp. Chem. (USA)*, vol.18, no.6, p.680-2 (Nov-Dec. 1982). Translation of: *Teor. & Eksp. Khim. (USSR)*, vol.18, no.6, p.737-40 (Nov-Dec. 1982). [received: Sept. 1983]

A major problem is to develop scientifically sound methods of synthesizing sorbents of specific performance, in particular in relation to given substances. Particular interest attaches to inorganic ion-exchange materials, which sometimes show unique selectivity in the sorption of ions from solutions of complicated composition. The authors use a model discussion of alkali metal sorption by inorganic sorbents with phosphate groups to show that it is possible to construct selectivity series by quantum-chemical calculation. The basis is Eisenman's simple scheme for selective absorption (1972), which is represented as competition between the cation and the solvent molecules in the interaction with the counterion in the sorbent matrix. (11 refs.)

114371 Adsorption behaviour of pure fluids near the gas-liquid critical point. G.H.Findenegg (Phys. Chem. II, Ruhr-Univ. Bochum, Bochum, Germany).

Proceedings of the 4th European Symposium on Materials Sciences under Microgravity (ESA SP-191), Madrid, Spain, 5-8 April 1983 (Paris, France: ESA 1983), p.385-91

The interface between a nonreactive solid and a fluid near its critical point is investigated. Whereas the interface between near-critical fluid phases disappears as the critical point is approached through the range of two-phase states, the interface between a near-critical phase and a noncritical phase exhibits pronounced adsorption phenomena, due to the long range of the coherence length of density (or concentration) fluctuations in the critical region. The theoretical background of these phenomena is discussed on the basis of Widom's theory. Experimental measurements for the adsorption of fluids (ethylene, SF₆) on the basal plane of graphite are reviewed. Finally, a new apparatus for extending these measurements to the near-critical region of pure fluids in a low-gravity environment is described. (19 refs.)

Nordic Conference on Surface ScienceSee Entry 111305

Surface physics. Second editionSee Entry 111335

A molecular beam study of the trapping-desorption of I₂ from a LiF (001) surfaceSee Entry 112769

The influence of glycine, according to pH, upon the growth habit of NaCl and KI, in aqueous solutionSee Entry 113781

Interaction of hydrogen with nonmetallic inclusions of the different shapes in ferrite-pearlite steelsSee Entry 113955

Temperature dependence of the critical electron exposure for hydrocarbon monolayersSee Entry 114026

On the gas absorption properties of rare-earth metals and their compoundsSee Entry 114185

Diffusion of water vapour in polymethyl methacrylateSee Entry 114265

Clean and adsorbate-induced surface phase transitions on W{100}See Entry 114310

Helium diffraction from Ni (100). A study of the clean surface and of hydrogen and carbon adsorption phasesSee Entry 114314

Surface friction constant and range of dynamical interaction between adatoms on metal surfacesSee Entry 114325

Photon-stimulated desorption from rare earth oxidesSee Entry 114489

NMR studies of pyridine on silica-aluminaSee Entry 114741

Influence of solid support sorptive properties on the colour of cholesteric liquid crystals. II. Quantitative resultsSee Entry 114805

The effect of the microscopic structure of metal surfaces on their optical propertiesSee Entry 114807

Theory of Raman scattering from molecules adsorbed at semiconductor surfacesSee Entry 114864

Theory of charge transfer excitation in surface enhanced Raman scatteringSee Entry 114865

Surface enhanced Raman scattering from pyridine on copper in UHVSee Entry 114866

An infra-red reflection absorption study of the adsorption of NO on Pt(111)See Entry 114867

Angle-resolved Auger electron emission from LaB₆(001) with and without chemisorbed oxygenSee Entry 114979

Vibrational spectra of coadsorbed CO and H on Ni(100) and Ni(111)See Entry 114984

An EELS study of N₂O adsorption of Pt(111)See Entry 114986

Rotational state populations of NO molecules scattered from clean and adsorbate-covered Pt (111) surfacesSee Entry 115006

Diffraction of UV excited photoelectrons by an ordered overlayerSee Entry 115013

Rydberg screening in core level photoemission of ammonia adsorbed on nickel surfacesSee Entry 115015

UV photoemission from sulphur saturated (111), [6(111)×(100)] and (100) platinum surfacesSee Entry 115016

Chlorine adsorption on copper. II. Photoemission from Cu(001)c(2×2)-Cl and Cu(1110)√3×√3/R30°-ClSee Entry 115020

Adsorbate band structure of bromine on Pd(111) studied by angle resolved ultraviolet photoemissionSee Entry 115021

Reduced evaporation field by the field induced dipoles of physisorbed He Ne and H₂See Entry 115028

Internal stresses in fibre reinforced plasticsSee Entry 115296

Environmental aging of epoxy compositesSee Entry 115395

Irreversible loss of adatoms on Ag electrodes during potential cycling determined from surface enhanced Raman intensitiesSee Entry 115564

Langevin analysis of the diffusion model for surface chemical reactionsSee Entry 115578

Decomposition of HCOOH on gold studied by XPS and TDS spectroscopies and its behaviour under very low energy electron excitation ..See Entry 115581

Time-resolved photoelectron spectroscopy for the study of dynamic surface speciesSee Entry 115603

Surface physics and biological phenomenaSee Entry 115729

68.48 SOLID-SOLID INTERFACES (inc. bicrystals; for grain boundaries, see 61.70N)

114372 Studies of chemistry at the Ta/Si interface as a function of thermal processing. P.W.Lew, C.R.Helms (Dept. of Electrical Engng., Stanford Univ., Stanford, CA, USA), T.M.Reith.

J. Electrochem. Soc. (USA), vol.130, no.8, p.1730-5 (Aug. 1983).
Ta and Ta-oxide Schottky barrier diodes structures on n-type (100) Si substrates were prepared under various standard processing conditions using either sputter deposition or electron beam (E-beam) evaporation, and these samples were analyzed for their oxygen and carbon content using high resolution Auger sputter profiling. The authors found that the bulk Ta of the sputter-deposited and E-beam-deposited Ta films contain 3 atomic percent (a/o) oxygen. In addition, E-beam-deposited Ta films contain approximately 0.3 a/o carbon in the bulk and 1-3 a/o carbon at the interface. Photoresist use prior to deposition left residual carbon at the Ta-Si interface, and this carbon remained intact after an anneal of 400°C for 1 hr in vacuum. Oxygen present in Ta-oxides at the Ta-Si interface diffused away from the interface and tended to redistribute itself uniformly throughout the Ta layer for anneals of 400°C for 1 hr. Greater redistribution occurred for annealing at 450°C for 3 hr. (9 refs.)

114373 Characterization of the oxide-metal interface at the surface of a stainless steel. G.C.Allen, R.K.Wild (Berkeley Labs., CEBG, Berkeley, England), M.Weiss.

Philos. Mag. A (GB), vol.48, no.3, p.373-86 (Sept. 1983).
The alloy-oxide interface from 20 at.% Cr-25 at.% Ni-1 at.% Nb stabilized steel oxidized at 850°C in CO₂/1% CO has been examined on both sides using scanning Auger electron spectroscopy. The interface which was exposed using a sputter ion-plating technique consists of a silicon-rich chromium sesquioxide. When the oxide separates it does so at this interface within the silicon-rich layer. (8 refs.)

114374 RF plasma annealing of as-grown defects in the Si/SiO₂ system. A.Szekeress, S.Alexandrova (Inst. of Solid State Phys., Bulgarian Acad. of Sci., Sofia, Bulgaria).

Thin Solid Films (Switzerland), vol.106, no.3, p.153-8 (19 Aug. 1983).
The annealing effect of an RF hydrogen plasma on the interface properties in Si/SiO₂ systems was investigated. The fixed oxide charge is found to be sensitive to the low temperature plasma annealing. Annealing is more effective at higher temperatures and when applied to metallized structures. With bare oxides the generation of slow states is observed whose concentration depends on the substrate temperature. A final 450°C hydrogen anneal gives very low fixed charge densities. Comments on the annealing mechanism are also given. (14 refs.)

114375 Microstructural study of alumina/TiC coated cemented carbide. S.Vuorinen (Lab. of Appl. Phys. I, Tech. Univ. of Denmark, Lyngby, Denmark).

Proceedings of the 4th European Conference on Chemical Vapour Deposition, Eindhoven, Netherlands, 31 May-2 June 1983 (Eindhoven, Netherlands: Philips Centre Manuf. Technol. 1983), p.357-62
The aim of the author's transmission electron microscope (TEM) study of the alumina/TiC double coating deposited on cemented carbide substrate has been to characterize the microstructures present at different levels in the

double coating. The microstructures of the alpha-alumina ($\alpha\text{-Al}_2\text{O}_3$) layer, the intermediate titanium carbide (TiC) layer and the microstructure of the TiC/cemented carbide interface are reported. The results are compared with previous related studies of the single TiC coated cemented carbide microstructure. The Al_2O_3 /TiC interface, which seems initially to be less complicated than the TiC cemented carbide interface is not dealt with in this connection. (4 refs.)

Effect of composition on the properties of five-component solid solutions See Entry 114178

Electronic states of grain boundaries in bicrystal silicon See Entry 114482

Small device technology, dielectric semiconductor systems ... See Entry 114614

On the formation of planar-etched facets in GaInAsP/InP double heterostructures See Entry 115387

68.55 THIN FILM GROWTH, STRUCTURE, AND EPITAXY

(for techniques of crystal growth and film deposition, see 81.10 and 81.15)

114376 Study of the uniformity and stoichiometry of CoSi_2 films using Rutherford backscattering spectroscopy and scanning electron microscopy. K.Ishibashi, S.Furukawa (Dept. of Appl. Electronics, Graduate School of Sci. & Engng., Tokyo Inst. of Technol., Yokohama, Japan). *Appl. Phys. Lett. (USA)*, vol.43, no.7, p.660-2 (1 Oct. 1983).

Uniformity and stoichiometry of solid phase epitaxial CoSi_2 films were investigated by Rutherford backscattering spectroscopy (RBS) and scanning electron microscopy (SEM). In a series of samples, small deviations of the composition ratio from the silicide stoichiometry were always observed in the RBS spectra for the films. Furthermore, it was found from SEM observation that these films were not uniform and the surfaces of the samples consisted of two kinds of materials. From these results and the spectra of micro Auger electron spectroscopy, it was concluded that the surfaces of the samples consisted of a stoichiometric CoSi_2 region and exposed Si regions. (8 refs.)

114377 Thermal nitridation of silicon in nitrogen plasma. H.Nakamura, M.Kaneko, S.Matsumoto (Dept. of Electrical Engng., Keio Univ., Yokohama, Japan), S.Fujita, A.Sasaki. *Appl. Phys. Lett. (USA)*, vol.43, no.7, p.691-3 (1 Oct. 1983).

Direct thermal nitridation of silicon in a nitrogen plasma has been performed above 1000°C . From an Auger electron spectroscopy analysis, the formed films contain some oxygen and are identified as oxynitride films. The refractive indices of these films varied from 1.5 to 1.9 with nitridation time. The film thickness is about 40 \AA after nitridation of 10 h at 1145°C and the film growth is saturated at this value. Capacitance-voltage characteristics of Al gate metal-nitride-semiconductor capacitors show a stable behavior. The fixed charge density Q_{ss} is estimated to be on the order of 10^{12} cm^{-2} . (8 refs.)

114378 On the substructure of epitaxial (Pb,Sn)Te films grown on KCl cleavage faces. M.Schenk, Ngo Dien Tap (Sektion Phys., Humboldt-Univ., Berlin, Germany).

Cryst. Res. & Technol. (Germany), vol.18, no.8, p.997-1001 (1983). The X-ray diffraction rocking curve analysis has been employed for the measurement of crystallite sizes of (Pb,Sn)Te films for different thickness, epitaxially grown on KCl cleavage faces by the hot-wall technique. The size of the coherently scattering regions parallel to the reflecting planes did not depend on film thickness and agreed with the mean distance of nuclei just before coalescence investigated by means of replica electron microscopy. The results are consistent with a model of stalk-like growth of crystallites in film growth direction. (11 refs.)

114379 TEM-electron energy loss spectroscopy study of the diamond particles prepared by the chemical vapour deposition from methane. Y.Matsui, S.Matsumoto, N.Setaka (Nat. Inst. for Res. in Inorganic Materials, Ibaraki, Japan).

J. Mater. Sci. Lett. (GB), vol.2, no.9, p.532-4 (Sept. 1983). The authors report the results of their TEM-EELS characterisations of particles grown by S. Matsumoto et al.'s CVD method (1982). The Debye-Scherrer rings in the diffraction pattern of the particles were reasonably indexed based on the diamond structure. It was experimentally confirmed, through the EELS and EDX microanalyses that the particles were composed only of C atoms. The profiles of both the plasmon loss spectra and the near edge fine structures in the EELS were very similar to those of previous data on diamond. (12 refs.)

114380 Structure of two-layer epitaxial Ag-Al films. V.M.Ievlev, E.K.Belonogov (Polytech. Inst., Voronezh, USSR).

Fiz. Met. & Metalloved. (USSR), vol.56, no.2, p.322-6 (Aug. 1983). In Russian. English translation in: *Phys. Met. & Metallogr. (GB)*. A clear noncoherent Ag-Al interface formed only when an Al film was grown on a (111) Ag film at substrate temperatures $T_s \geq 300\text{K}$. At high values of T_s the structure was characterized by the presence of hexagonal networks of misfit dislocations with the Burgers vector $1/2\text{ [110]}$ lying in the plane of the interface. The structure was then determined by the ratio of the thicknesses of the two metal layers and its formation was accompanied by the appearance of an intermetallic phase. The irregularity of the network period was attributed to the nonuniform nature of the process of mutual diffusion within the film. (6 refs.) A.T.

114381 Kinetics of structural multiplets during diffusion homogenization of polycrystalline films. L.A.Yudina, E.L.Fedorova, G.P.Timakova, L.M.Antonova, V.A.Gulenko, V.V.Yudin (Far-East State Univ., Vladivostok, USSR). *Fiz. Met. & Metalloved. (USSR)*, vol.56, no.2, p.351-7 (Aug. 1983). In Russian. English translation in: *Phys. Met. & Metallogr. (GB)*. Thin polycrystalline Permalloy films were prepared by vacuum evaporation. The processes of diffusion homogenization during high-temperature annealing, resulting in macrodiscontinuities, were studied. Electron microscopy and coherent optics were used to identify the structural multiplets and to study their kinetics during high-temperature isothermal annealing. Ways of increasing the stability of the magnetic structure of planar memory materials were suggested. (25 refs.) A.T.

114382 Orientation and structure of bismuth films on virgin surface of zinc. N.V.Barmina, V.M.Ievlev (Polytech. Inst., Voronezh, USSR). *Fiz. Met. & Metalloved. (USSR)*, vol.56, no.2, p.413-16 (Aug. 1983). In Russian. English translation in: *Phys. Met. & Metallogr. (GB)*. A study was made of the orientation and substructure of bismuth films condensed on virgin (00.1) surfaces of Zn. The study was carried out by electron diffraction and electron microscopy methods. The films had three equivalent orientations so that their structure was polycrystalline. Twinning was also observed. (12 refs.) A.T.

114383 Properties of films of GaP on Si obtained by ion-liquid epitaxy. N.N.Gerasimenko, L.V.Lezheiko, E.V.Lyubopytova, S.M.Pintus, A.G.Sharshunov (Inst. of Phys. of Semiconductors, Acad. of Sci., Novosibirsk, USSR). *Inorg. Mater. (USA)*, vol.18, no.10, p.1451-4 (Oct. 1982). Translation of: *Izv. Akad. Nauk SSSR Neorg. Mater.*, vol.18, no.10, p.1689-92 (Oct. 1982). [received: Sept. 1983]

By injecting phosphorus ions into a gallium melt on the surface of silicon at $300\text{--}500^\circ\text{C}$ it is possible to obtain epitaxial temperature-stable low-defect GaP films with n-type conductivity. By changing the synthesis temperature it is possible to control the concentration of charge carriers in the films over a wide interval. (10 refs.)

114384 Properties of molybdenum silicide film deposited by chemical vapor deposition. S.Inoue, N.Toyokura, T.Nakamura (Fujitsu Labs. Ltd., Kawasaki, Japan), M.Maeda, M.Takagi. *J. Electrochem. Soc. (USA)*, vol.130, no.7, p.1603-7 (July 1983).

MoSi_2 films used as gate electrodes and interconnects were deposited on oxidized Si substrates via reactions between MoCl_5 and SiH_4 . At high temperatures, HCl generated by reactions involving MoCl_5 , H_2 , and SiH_4 reacts with Si to form volatile SiH_3Cl , SiH_2Cl , SiHCl_3 , and SiCl_4 ; thus Si is etched away and is not available to form MoSi_2 , resulting in deposited film consisting of only metallic Mo. At low temperatures, the deposited film consists of MoSi_2 , which is thermodynamically stable. The deposited films show characteristics (resistivity, crystal structure, and so forth) similar to those of MoSi_2 films deposited by sputtering. Chlorine in the deposited films has a gettering effect for mobile ions such as Na^+ . (10 refs.)

114385 Crystallographic orientation and surface morphology of chemical vapor deposited Al_2O_3 . C.-S.Park, J.-G.Kim, J.S.Chun (Dept. of Materials Sci. & Engng., Korea Advanced Inst. of Sci. & Technol., Seoul, Korea).

J. Electrochem. Soc. (USA), vol.130, no.7, p.1607-11 (July 1983). Deposits of aluminum oxides (Al_2O_3) have been formed by a chemical vapor deposition technique involving the application of gaseous mixtures of AlCl_3 , CO_2 onto TiN-coated cemented carbide substrates. Reaction parameters (deposition temperature, system pressure, and composition of reactant gases) and their effects on the crystalline structure, crystallographic orientation, and surface morphology of the Al_2O_3 deposit have been studied. Al_2O_3 crystals maintain a corundum structure throughout the entire range of deposition conditions. Crystals of Al_2O_3 appear to nucleate in random orientations on the TiN layer, and further growth proceeds with (1014) and (1126) preferred orientations. The effects of reaction parameters on the final surface morphology of the Al_2O_3 deposit can be described by considering the supersaturations of the reactants and the growth rate. The crystals of the Al_2O_3 deposit become finer and more uniform as the supersaturation of the reactant controlling the Al_2O_3 nucleation increases. (10 refs.)

114386 A new electrodeposited oxide film containing lead and thallium with the cubic fluorite-type structure. M.Sakai, T.Sekine, Y.Yamazaki (Dept. of Electronic Chem., Tokyo Inst. of Technol., Yokohama, Japan).

J. Electrochem. Soc. (USA), vol.130, no.7, p.1631-3 (July 1983). A new compound having the cubic fluorite-type structure was obtained by means of the anodic oxidation of the mixture of Pb (II) and Tl (I) under a certain electrolytic condition. The obtained electrodeposited oxide on the platinum substrate was black with metallic luster and had a good electric conductivity. The composition of the electro-deposited oxide was determined as $\text{Pb}_3\text{Tl}_2\text{O}_{24}$. (6 refs.)

114387 Mathematical modeling of high-current chromium plating with application of a rotating disk electrode. I.Drela, W.Popytak, J.Kubicki (Politech. Wroclawskiej, Wroclaw, Poland).

J. Electrochem. Soc. (USA), vol.130, no.8, p.1671-6 (Aug. 1983). Based on a mathematical design of experiments, the effect of temperature, current density, H_2SO_4 , and K_2SiF_6 concentrations, and hydrodynamic conditions on the current efficiency, electrical energy consumption, speed of deposition, gloss, and the microhardness of chromium coatings obtained at current densities of $200\text{--}400\text{ A/dm}^2$ was investigated. The results are presented by means of regression equations in the form of quadratic polynomials. (17 refs.)

114388 Si on cubic zirconia. H.M.Manasevit, I.Golecki, L.A.Moudy, J.J.Yang, J.E.Mee (Microelectronics Res. & Dev. Center, Rockwell Internat., Anaheim, CA, USA).

J. Electrochem. Soc. (USA), vol.130, no.8, p.1752-8 (Aug. 1983). Epitaxial growth of single-crystal Si films has been realized on the (100), (110), and (111) crystallographic planes of yttria-stabilized, cubic zirconia single crystals. The Si films were grown by chemical vapor deposition, using the pyrolysis of SiH_4 at temperatures in the range $950\text{--}1075^\circ\text{C}$ and at deposition rates of $0.08\text{--}1.2\text{ }\mu\text{m/min}$. A predeposition annealing procedure has been developed, resulting in a quasi-stable, oxygen-deficient zirconia surface. A model is presented to explain the dependence of oxygen kinetics in cubic zirconia on temperature and yttria content. The heteroepitaxial Si films have been characterized by optical and scanning electron microscopies, reflection electron diffraction, X-ray diffraction, Rutherford backscattering and channeling, and surface electrical conductivity and Hall effect measurements. Several $0.4\text{--}0.5\text{ }\mu\text{m}$ thick (100)- and (110)-oriented Si films on cubic zirconia were found to be of higher crystal quality than commercial (100) Si on sapphire films of similar thickness. (32 refs.)

114389 Liquid phase epitaxial growth of $\text{In}_{1-x}\text{Ga}_x\text{P}_{1-y}\text{As}_y$ on GaAs substrates. S.Kaneishi, T.Takenaka, S.Yano, T.Hijikata (Central Res. Labs., Sharp Corp., Tenri, Japan).

J. Cryst. Growth (Netherlands), vol.62, no.3, p.498-504 (Aug. 1983). $\text{In}_{1-x}\text{Ga}_x\text{P}_{1-y}\text{As}_y$ layers were grown on GaAs substrates by LPE at 700°C . A great difference was found between the growth on (100) and (111)B substrates. On (100) substrates, mirror-like $\text{In}_{1-x}\text{Ga}_x\text{P}_{1-y}\text{As}_y$ ($y < 0.01$) layers were obtained with a lattice mismatch ranging from 0 to 0.32%. $\text{In}_{1-x}\text{Ga}_x\text{P}_{1-y}\text{As}_y$ ($y \geq 0.01$) layers had flat interfaces but their surfaces were rough. On the other hand, mirror-like $\text{In}_{1-x}\text{Ga}_x\text{P}_{1-y}\text{As}_y$ ($0 \leq y \leq 0.5$) layers were obtained on (111)B substrates with a smallest mismatch of about 0.5%. The composition range of mirror-like layers was dependent on the substrate orientation. The results indicate that the immiscible region of the epitaxial layer on the (100) face is wider than that on the (111)B face. (16 refs.)

114390 Role of electronic processes in epitaxial recrystallization of amorphous semiconductors. J.S.Williams (Microelectronics Technol. Centre, Royal Melbourne Inst. of Technol., Melbourne, Australia), R.G.Elliman. *Phys. Rev. Lett. (USA)*, vol.51, no.12, p.1069-72 (19 Sept. 1983).

A phenomenological model of the solid-phase epitaxial growth process is proposed to account for the influence of substrate orientation and doping on growth kinetics. The model combines structural features of the amorphous-crystalline interface with electronic processes related to changes in the Fermi level. The basic premise is that the concentration of kinklike growth sites at the interface, and hence the growth velocity, can be influenced by doping in a manner analogous to the enhancement of dislocation velocities by doping. (18 refs.)

114391 On a relationship between substrate perfection and stacking faults in homoepitaxial silicon. A.Dreeben, A.Schujko (RCA Labs., Princeton, NJ, USA).

RCA Rev. (USA), vol.44, no.2, p.217-30 (June 1983).

Imperfections and defects in silicon substrates used for homoepitaxial devices can be sources for the nucleation of stacking faults at the epi layer-substrate interface. These faults can be electrically active and degrade device performance. In addition to dislocations and impurity atoms, damaged layers on the substrate are also possible sources. Such damage can arise from the mechanical polishing processes for preparing the substrate and from ion implantation. An evaluation of residual substrate damage resulting from ion implantation and its effect on epitaxial layers has been made. Chemical etching has been used to reveal the damage in patterned device wafers prior to vapour phase epitaxy. Using Nomarski microscopy, the authors have compared these samples with similarly etched epitaxial layers on companion wafers. Stacking faults in the epilayers have been correlated with etch pit formation in the buried layer pockets. The results show that residual damage and stacking fault formation are related. (17 refs.)

114392 EELS and AES study of epitaxially grown Pd(111) thin films. V.D.Vankar, R.W.Vook (Dept. of Chem. Engng. & Materials Sci., Syracuse Univ., Syracuse, NY, USA).

Surf. Sci. (Netherlands), vol.131, no.2-3, p.463-74 (Sept. 1983).

Electron energy loss spectroscopy and Auger electron spectroscopy have been used to study epitaxially grown Pd(111) thin films on mica. Four loss lines at 7, 18, 24 and 33 eV have been observed and are interpreted as due to combinations of surface and bulk plasmon excitations. The effect of trace amounts of surface impurities, as detected by AES, was correlated with ELS spectra. The plasmon loss line at 7 eV was found to decrease in intensity in varying amounts due to the presence of surface impurities. The other lines, being in rich in bulk character, were not affected significantly. (21 refs.)

114393 UHV-SEM study of the nucleation and growth of Ag/W(110). G.D.T.Spiller, P.Akhter, J.A.Venables (School of Math. & Phys. Sci., Univ. of Sussex, Brighton, England).

Surf. Sci. (Netherlands), vol.131, no.2-3, p.517-33 (Sept. 1983).

The nucleation and growth of Ag on W(110) single crystals has been studied by ultra-high vacuum SEM, AES and electron backscattering techniques. The system is confirmed to grow in the Stranski-Krastanov growth mode with 2 stable monolayers (ML) in the intermediate layer. Island density measurements are reported in the temperature range $473 < T < 823$ K at a deposition rate $R = 0.3 \text{ ML min}^{-1}$, and at $T = 573$ and 773 K for $0.03 < R < 0.8 \text{ ML min}^{-1}$. These results are interpreted in terms of nucleation theory. They are consistent with critical nucleus sizes in the range 7-10 atoms, and binding energies of small, two-dimensional Ag clusters which are less than expected on the simplest pair-bonding arguments. More qualitative observations on defect-induced nucleation and the shape of the growing islands are also reported. (24 refs.)

114394 Process of formation of porous silicon and autoepitaxy on its surface. V.A.Labunov, V.P.Bondarenko, L.K.Glinenko, I.N.Basmanov (Minsk Radiotech. Inst., Minsk, Belorussian SSR).

Sov. Microelectron. (USA), vol.12, no.1, p.8-13 (Jan.-Feb. 1983). Translation of: *Mikroelektronika (USSR)*, vol.12, no.1, p.11-16 (Jan.-Feb. 1983). [received: Sept. 1983]

During anodic electrochemical treatments in electrolytes based on hydrofluoric acid it is possible to form a layer of porous silicon (PS) at the surface of single-crystal silicon. A distinguishing feature of PS is that it can preserve the crystalline structure of the initial material. The authors established the presence of a stable correlation between the anodization conditions, the density of the PS, and the structure of its surface. It has been shown that the structure of an epitaxial film on porous silicon is determined by its density. With a density $\approx 1.90 \text{ g/cm}^3$ the hydride method forms single-crystal epitaxial films on porous silicon with a defect density less than $10^5 \text{ defects/cm}^2$; with density $\leq 1.5 \text{ g/cm}^3$ an amorphous phase is seen in the structure of the epitaxial film. The authors have found the anodization regime for $\text{N}^+ \text{Si}$ which will provide growth of high-quality single-crystal epitaxial films on the porous silicon produced. (4 refs.)

114395 Process study of chemically vapour-deposited SnO_x ($x \approx 2$) films. J.C.Lou, M.S.Lin, J.I.Chi, J.H.Shieh (Dept. of Electrical Engng., Nat. Tsing Hua Univ., Hsinchu, Taiwan).

Thin Solid Films (Switzerland), vol.106, no.3, p.163-73 (19 Aug. 1983).

The physical characteristics of SnO_x ($x \approx 2$) films deposited onto Pyrex glass substrates by chemical vapour deposition are studied. The temperature dependence indicates that films deposited at 600°C have good polycrystallinity. The electrical conductivity of the 600°C films is mainly controlled by the variation in the SnCl_4 vapour flow rate. A subsequent thermal annealing process can even reduce the sheet resistance to $400 \Omega/\square$. In addition, the visible absorption shows that the 600°C films tend to lose their transparency in the short wavelength range of the visible spectrum. (14 refs.)

114396 Phase formation and kinetics of the phase transition in Ag_2Se thin films. A.G.Abdullayev, R.B.Shafizade, E.S.Krupnikov, K.V.Kiriluk (Inst. of Phys. of the Acad. of Sci., Baku, Azerbaijan SSR).

Thin Solid Films (Switzerland), vol.106, no.3, p.175-84 (19 Aug. 1983).

The results of an investigation of phase formation and the kinetics of the phase transition in Ag_2Se thin films by kinematic electron diffraction are reported. Information on the phase transition $\text{Ag}_2\text{Se}(\text{orthorhombic}) \rightarrow \text{Ag}_2\text{Se}(\text{tetragonal})$ was obtained from measurements of the ion current. The band gap, the Fermi level and the effective mass of the carriers for both the orthorhombic and the tetragonal phase of Ag_2Se were obtained from tunnel spectroscopy. (33 refs.)

114397 Properties and structure of carbon excess $\text{Ti}_x\text{C}_{1-x}$ deposited onto molybdenum by magnetron sputtering. T.Shikama, H.Araki, M.Fujitsuka, M.Fukutomi, H.Shinno, M.Okada (Nat. Res. Inst. for Metals, Tsukuba Labs., Ibaraki, Japan).

Thin Solid Films (Switzerland), vol.106, no.3, p.185-94 (19 Aug. 1983).

There has been little concern about the properties and structure of the carbon excess $\text{Ti}_x\text{C}_{1-x}$ ($x < 0.5$) deposits, although many investigations have been conducted on the single-phase $\text{Ti}_x\text{C}_{1-x}$ ($x > 0.5$) deposits. It is found that carbon excess $\text{Ti}_x\text{C}_{1-x}$ deposits prepared by magnetron sputter coating have a higher microhardness than the stoichiometric deposits and show a strongly (111)-preferred orientation. The results of C K α X-ray spectroscopy of these films strongly suggest that carbon excess $\text{Ti}_x\text{C}_{1-x}$ exists as a single phase of titanium carbide without the formation of a secondary graphite phase. The abnormal diffusion of substrate molybdenum atoms into the carbon excess $\text{Ti}_x\text{C}_{1-x}$ deposits suggests that they contain a high population of the titanium vacancies. (21 refs.)

114398 Epitaxy by pulsed annealing of ion-implanted silicon. G.Foti, E.Rimini (Istituto di Struttura della Materia, Univ. di Catania, Catania, Italy).

In book: *Laser annealing of semiconductors*, J.M.Poate, J.W.Mayer [Ed.], p.203-45. London, England: Academic Press (1982), xi+564 pp. [0 12 558820 8]

The authors consider in some detail the experiments performed on ion-implanted silicon samples irradiated with a laser or electron beam single pulse. Structural changes from amorphous to crystalline material are reviewed and described in terms of a liquid transient formation. The energy of the incident beam is absorbed by the matrix and subsequently converted to heat. The surface layer of the irradiated material can be melted, and a defect-free crystalline layer results from liquid epitaxial growth on a single-crystal substrate. Residual defects resulting from irradiation are also described. The melting of amorphous material should require less energy than that required to melt the corresponding amount of crystalline material. In addition the melting of the amorphous layer should occur at a temperature lower than that of a crystalline layer. These phenomena can give rise, under suitable experimental conditions, to regions of considerable undercooling. (69 refs.)

114399 Epitaxy of deposited Si. J.M.Poate, J.C.Bean (Bell Labs., Murray Hill, NJ, USA).

In book: *Laser annealing of semiconductors*, J.M.Poate, J.W.Mayer [Ed.], p.247-80. London, England: Academic Press (1982), xi+564 pp. [0 12 558820 8]

Laser processing of deposited layers has been intensively investigated over the past few years. In most experiments, laser epitaxy begins with a CVD- or MBE-like deposition done at so low a temperature that amorphous or polycrystalline growth occurs. The low temperature eliminates diffusion, and one can either exploit the thick, rapid, low-cost deposition of CVD or the good control of MBE. The role of the laser is then to produce the one factor that has been sacrificed, crystallinity. The laser accomplishes this by heating the deposited layer to a temperature where it will crystallize either by solid phase epitaxial growth or by melting and crystalline resolidification. The authors show that the spatial and temporal localization of the laser irradiation permits crystallization with little or no disturbance of the underlying structure. This has the obvious potential advantage of permitting epitaxy over processed semiconductor structures. The most active and exciting area of laser epitaxy at present is not the conventional vertical epitaxy but rather lateral epitaxy over amorphous and insulating substrates. The ability to controllably melt and recrystallize Si on SiO_2 , Si_3N_4 , and fused quartz has opened new dimensions of epitaxy and devices. This field is progressing extremely rapidly, and the authors summarize the methods by which nucleation and growth are controlled. (81 refs.)

114400 Formation of titanium silicide at atmospheric pressure. P.Revesz, J.Gyimesi, J.Gyulai (Central Res. Inst. for Phys., Budapest, Hungary).

Defects in Semiconductors II, Symposium Proceedings, Boston, MA, USA, Nov. 1982 (New York, USA: North-Holland 1983), p.417-21.

Two problems connected with the growth of Ti-silicide have been investigated. It is shown if a silicon dioxide step on a single crystal of silicon covered with titanium is annealed then, following vertical growth on the silicon part, lateral growth of Ti-silicide takes place over the oxide layer. The authors also studied the problems of Ti-silicide growth on samples implanted with high doses of Sb, As, P, Ar and O prior to Ti evaporation. (7 refs.)

114401 The effect of oxygen in cosputtered (titanium+silicon) films. R.Beyers, R.Sinclair (Dept. of Materials Sci. & Engng., Stanford Univ., Stanford, CA, USA), M.E.Thomas.

Defects in Semiconductors II, Symposium Proceedings, Boston, MA, USA, Nov. 1982 (New York, USA: North-Holland 1983), p.423-7.

The effect of oxygen incorporation on the growth and microstructure of TiSi₂ has been investigated. Cosputtered films, with Si/Ti ratios between one and three, were deposited on (100) Si substrates and reacted at temperatures from 650° to 1050°C . Both Auger electron spectroscopy, in conjunction with sputter profiling, and Rutherford backscattering spectrometry indicate that oxygen in the as-deposited films redistributes to the silicide-silicon interface upon heating. Cross sectional transmission electron microscope images show that the oxygen is present as an amorphous oxide. (4 refs.)

114402 Simulation of CVD-processes. G.Wahl (Brown Boveri & Cie AG, Res. Center, Heidelberg, Germany).

Proceedings of the 4th European Conference on Chemical Vapour Deposition, Eindhoven, Netherlands, 31 May-2 June 1983 (Eindhoven, Netherlands: Philips Centre Manuf. Technol. 1983), p.19-29.

CVD-processes are determined by gas flow phenomena: by convection, by diffusion, and by chemical reactions in the gas phase and/or on the surface. A computer program is described which calculated the gas flow and which takes into account both homogeneous and heterogeneous reactions. The program is applied to a deposition process. $A + B \rightarrow C + D$, whereby this reaction can occur in the surface or in the gas phase. In both cases the molecule C is deposited. The mass fractions of A, B, C and D are assumed to be small in comparison to the inert diluent gas. The influence of the deposition parameters on the deposition profile on the deposition surface is discussed. It is demonstrated under which deposition conditions a surface layer with constant thickness can be produced. (8 refs.)

114403 Potentials of X-ray diffraction and electron microscopy for the characterization of thin polycrystalline CVD layers. R.Delhez, M.Hendriks, T.H.de Keijser, S.Radelaar (Lab. of Metall., Delft, Netherlands).

Proceedings of the 4th European Conference on Chemical Vapour Deposition, Eindhoven, Netherlands, 31 May-2 June 1983 (Eindhoven, Netherlands: Philips Centre Manuf. Technol. 1983), p.30-5.

Although polycrystalline layers produced by chemical vapour deposition (CVD) have found widespread application, comparatively little work has been done on the characterization of the structure and morphology of these layers by X-ray diffraction and transmission electron microscopy. The authors give a brief survey of the kind of information that can be obtained by these techniques. The emphasis is on X-ray diffraction since this technique is nondestructive and averages over an area of $\sim 1 \text{ cm}^2$ and provides information which cannot easily (or as in the case of internal stresses) be obtained by electron microscopy. Information that can be obtained from X-ray diffraction concerns composition, preferred orientation (texture), long-range mechanical stresses, crystallite size and microstrain (due to short-range stresses). As examples the authors present results obtained on polycrystalline silicon layers. (11 refs.)

114404 Theoretical influence of the deposition conditions on the uniformity of boron carbide coatings. L.Vandenbulcke (Univ. of Orleans, Orleans, France).

Proceedings of the 4th European Conference on Chemical Vapour Deposition, Eindhoven, Netherlands, 31 May-2 June 1983 (Eindhoven, Netherlands: Philips Centre Manuf. Technol. 1983), p.44-50.

Calculations are presented for the CVD deposition of boron carbide from $\text{BCl}_3\text{-CH}_4\text{-H}_2$ where the process determines in addition the composition uni-

formity. The theoretical treatment is based on a model coupling surface kinetics and diffusion through the boundary layer. It is applied to a deposition system where the direction of gas flow is parallel to a flat surface. This simple system exhibits the double influence of the depletion of the reactants and the variation of the boundary layer thickness along the surface. The results can be qualitatively extended to other geometries where these problems are encountered such as deposition inside tubes, and also the deposition on complex-shaped substrates or in a large-scale deposition chamber. (7 refs.)

114405 Atom-probe microanalysis and field-ion microscopy of TiC-coatings on cemented carbides. A.Henjered, H.Norden, L.Kjellsson, J.Skogsmo (Dept. of Phys., Chalmers Univ. of Technol., Goteborg, Sweden). Proceedings of the 4th European Conference on Chemical Vapour Deposition, Eindhoven, Netherlands, 31 May-2 June 1983 (Eindhoven, Netherlands: Philips Centre Manuf. Technol. 1983), p.91-6

One way to improve the wear resistance of cemented carbides is to coat them with a 5-10 μm thick layer of titanium carbide, using CVD. In spite of the importance of the coated cutting tools very little is known about the nucleation and growth of the coating. Methods to coat needle-formed specimens of WC-Co-type cemented carbides with TiC were previously developed (Henjered et al. 1981). Such specimens were studied with both transmission electron microscopy (TEM) and atom-probe field-ion microscopy. A combination of these two techniques offers a possibility to determine the structure and the elemental composition of the titanium carbide layer as well as the composition of the coating substrate interfacial region. (4 refs.)

114406 Modeling of GaAs growth in the MOCVD system. N.Putz, J.Korec, M.Heyen, P.Balk (Inst. of Semiconductor Electronics, Tech. Univ. Aachen, Aachen, Germany).

Proceedings of the 4th European Conference on Chemical Vapour Deposition, Eindhoven, Netherlands, 31 May-2 June 1983 (Eindhoven, Netherlands: Philips Centre Manuf. Technol. 1983), p.103-9

Presents a first attempt to give a simple but comprehensive description of MOCVD growth of GaAs. As is always the case in growth experiments, the data are to some extent determined by the geometry of the apparatus and by the shapes of the steep temperature gradient in the cold wall reactor, which complicates the analysis. The present study is based on a set of data for MOCVD growth of GaAs in the pressure range 10^4Pa and temperatures between 743 and 1023K. Growth was only obtained for $p(\text{AsH}_3) > p_{\text{TMG}}$. Since the precise course of the deposition reaction is not known the authors consider two simple possibilities: (a) breakdown of TMG and AsH_3 in the gas phase followed by adsorption of some of the reaction products (including Ga and As) at the surface and (b) formation of TMG- AsH_3 complexes in the gas phase with subsequent adsorption and breakdown of the complex to form GaAs. (5 refs.)

114407 CVD-deposition of aluminium on nickel-based alloys from AlCl_3/H_2 -gas-mixtures. A.Reich, L.Singheiser, G.Wahl (Brown, Boveri & Cie AG, Res. Centre, Heidelberg, Germany).

Proceedings of the 4th European Conference on Chemical Vapour Deposition, Eindhoven, Netherlands, 31 May-2 June 1983 (Eindhoven, Netherlands: Philips Centre Manuf. Technol. 1983), p.122-9

The oxidation behaviour of nickel-based alloys at high temperature can be raised by using Al-enriched layers on these alloys. Deposition of Al on nickel-based alloys results in the formation of Ni-Al intermetallic compounds, depending on the Al-activity during the deposition process. Deposition of Al on nickel and nickel-based alloys is possible by CVD from AlCl_3/H_2 -gas mixture in contact with pure aluminium. Deposition of Al results in the formation of NiAl-layers on nickel and the nickel-based alloys investigated. The growth-rate of the NiAl-layer is followed by a parabolic rate law with rate limiting diffusion processes occurring in the alloy. The parabolic rate constant linearly decreases with increasing content of alloying additions. (6 refs.)

114408 Chemical vapour deposition of boron on silicon. M.Boman, J.-O.Carlsson (Dept. of Chem., Univ. of Uppsala, Uppsala, Sweden).

Proceedings of the 4th European Conference on Chemical Vapour Deposition, Eindhoven, Netherlands, 31 May-2 June 1983 (Eindhoven, Netherlands: Philips Centre Manuf. Technol. 1983), p.134-40

The chemical reactions occurring during the initial stages of growth in a CVD process, i.e. as long as the substrate is present in the reaction gas mixture, are mostly quite different from those taking place later, when a completely intact coating has been grown. These initial reactions may influence the adherence of the coating as well as the grain size of the coating near the coating/substrate interface. The results are summarized of a study of the initial interfacial reactions occurring during CVD of amorphous boron on a silicon substrate from a reaction gas mixture containing boron trichloride and hydrogen. (7 refs.)

114409 Modeling of doping during CVD growth of semiconductor films. J.Korec, M.Heyen (Inst. of Semiconductor Electronics, Tech. Univ. Aachen, Aachen, Germany).

Proceedings of the 4th European Conference on Chemical Vapour Deposition, Eindhoven, Netherlands, 31 May-2 June 1983 (Eindhoven, Netherlands: Philips Centre Manuf. Technol. 1983), p.176-83

Modeling of the epitaxial deposition of undoped semiconductor material has been discussed in detail in an earlier study (see J. Cryst. Growth, vol.60, p.286, 1982). This paper shows a possibility to complete the above model to include intentional doping. The molar fraction of dopant atoms in the deposited material is given by the ratio of the flux of the incorporated dopant and the condensation flux of the host material. These fluxes are calculated from a dynamic balance of the rates of the mass transport in the gas phase and of the following sequence of surface processes: adsorption, chemical reaction, surface diffusion and binding to the substrate. The deposited film is described in terms of a regular solution model. The possibility of redistribution of dopant atoms between the interface and the volume of the semiconductor is also taken into consideration. The author's model is valid for the CVD of elemental and compound semiconductors. The applicability of the model is demonstrated for the case of sulfur doped GaAs films, which is considered as a regular solution $\text{GaAs}_{1-x}\text{S}_x$. It is shown that the experimentally observed dependences of the sulfur concentration in the film on the H_2S , GaCl and hydrogen pressures are reproduced in the authors' calculations. (15 refs.)

114410 The incorporation of dopants during growth of GaAs by CVD. L.J.Giling, H.H.C.de Moor (Dept. of Solid State III, Catholic Univ., Nijmegen, Netherlands).

Proceedings of the 4th European Conference on Chemical Vapour Deposition, Eindhoven, Netherlands, 31 May-2 June 1983 (Eindhoven, Netherlands: Philips Centre Manuf. Technol. 1983), p.184-93

The slope which is observed in the log-log plot of incorporated dopant versus the partial pressure of the dopant gas is explained by assuming that the growth rate is faster than the exchange rate of dopant atoms between bulk and surface. This trapping mechanism is shown to be valid for the incorporation of S in GaAs and Te in GaP for growth rates larger than $10\text{ }\mu\text{m/h}$. For the doping of GaAs with S at growth rates of $5\text{ }\mu\text{m/h}$ or smaller theoretically

an S-shaped curve is predicted. All curves saturate at a level of $3 \times 10^{18}\text{ cm}^{-3}$. (12 refs.)

114411 CVD a-Ge and a-Ge:X films: preparation and properties. D.D.Allred, J.A.Pionkowski (Energy Conversion Devices, Troy, MI, USA).

Proceedings of the 4th European Conference on Chemical Vapour Deposition, Eindhoven, Netherlands, 31 May-2 June 1983 (Eindhoven, Netherlands: Philips Centre Manuf. Technol. 1983), p.197

Summary form only given. Germanium films were deposited by the low pressure (approximately 20-55 Torr) pyrolytic decomposition of germane on substrates held at various temperatures, Ts, in the range of 635 to 700K. Optical properties: absorption coefficient and the refractive index; electronic properties: conductivity and activation energy, and the X-ray diffraction pattern on these films were determined. The films deposited at or below approximately 660K are amorphous with an optical gap of 1.0 eV. This is the first report of the preparation of a-Ge via CVD. The absorption profile of the films resembles that reported for sputtered or evaporated films deposited at elevated temperatures or exposed to a long-term anneal. Amorphous Ge:X (X=B, C, etc.) alloys have also been prepared and characterized. These materials may find utility in solar spectrally selective absorbers. The authors' results show that the superior absorbance of amorphous germanium may be employed in producing selective surfaces with the advantage of CVD fabrication. (no refs.)

114412 The mechanism of the growth of InP by MOCVD. J.Haigh, S.O'Brien (British Telecom Res. Labs., Ipswich, England).

Proceedings of the 4th European Conference on Chemical Vapour Deposition, Eindhoven, Netherlands, 31 May-2 June 1983 (Eindhoven, Netherlands: Philips Centre Manuf. Technol. 1983), p.198

Summary form only given. The authors present two spectroscopic investigations of the pyrolytic decomposition of group III metallo-organics relevant to the MOCVD process. Firstly, using atomic absorption spectrometry they show that the pyrolysis of GaEt_3 and InMe_3 do not generate measurable quantities of gallium and indium atoms in the vapour phase, under MOCVD conditions. This implies that the MOCVD process goes via surface-adsorbed species containing metal-carbon bonds. Secondly, using ultra-violet spectroscopy to monitor the metallo-organic content of a vapour stream passing over InP, GaAs and glass surfaces, as a function of the temperature of the stream, the authors show that there is no appreciable acceleration of the decomposition of the metallo-organic by the semiconductor surface, as opposed to the glass. This implies that heterogeneous decomposition reactions of the type described previously do not show surface specificity. (3 refs.)

114413 Characterization of thin plasma silicon-nitride layers. W.A.P.Claassen, W.G.J.N.Valkenburg, A.E.T.Kuiper, Y.Tamminga (Philips Res. Labs., Eindhoven, Netherlands).

Proceedings of the 4th European Conference on Chemical Vapour Deposition, Eindhoven, Netherlands, 31 May-2 June 1983 (Eindhoven, Netherlands: Philips Centre Manuf. Technol. 1983), p.199-205

The composition is studied of silicon-nitride layers, grown by plasma CVD from $\text{SiH}_4\text{-NH}_3\text{-N}_2$ mixtures at temperatures of about 300°C and an operating frequency of 50 kHz. The layers as deposited on silicon substrates, were characterized with Auger electron spectroscopy (AES) and Rutherford back-scattering spectroscopy (RBS). AES in-depth profiles and RBS measurements at glancing angles reveal that oxygen is present at the interface between silicon and silicon nitride and at the surface. It is demonstrated that the interfacial oxygen can be removed by in-situ plasma etching with SF_6 or NF_3 , prior to deposition. However, a sulphur pile-up is found in the case of an SF_6 etch. With both etchants some fluorine is also detected in the nitride layer, especially when SF_6 is used. (7 refs.)

114414 Electrical versus structural properties of polycrystalline silicon deposited by plasma enhanced LPCVD below 550°C . N.Ababou, C.Chaussat, A.Deneuville (Groupe des Transitions de Phases, CNRS, Grenoble, France), L.Brunel, M.Toulemonde.

Proceedings of the 4th European Conference on Chemical Vapour Deposition, Eindhoven, Netherlands, 31 May-2 June 1983 (Eindhoven, Netherlands: Philips Centre Manuf. Technol. 1983), p.206-10

As the channel lengths of MOS transistors decreases, 'cold' technologies are sought to avoid impurities or doping atoms diffusion in the Si under the gate during the various processes. Moreover, for three dimensional microelectronic thin films the goal is to attain a deposition temperature T_D below 550°C on glass. Besides classical LPCVD which needs $T_D > 630^\circ\text{C}$ to get poly Si, such films can be obtained at lower temperature by chemical transport by a hydrogen plasma or glow discharge decomposition of SiH_4 . The authors delineate an easier preparation range to obtain poly Si, at low T_D , whose physicochemical as well as electrical properties are described. (14 refs.)

114415 Indirect and direct formation of polycrystalline silicon during CVD. A.M.Beers, J.Bloem (RIM Dept. of Solid State Chem., Univ. of Nijmegen, Nijmegen, Netherlands).

Proceedings of the 4th European Conference on Chemical Vapour Deposition, Eindhoven, Netherlands, 31 May-2 June 1983 (Eindhoven, Netherlands: Philips Centre Manuf. Technol. 1983), p.211-16

Amorphous growth and subsequent crystallization in the grown layer is investigated and compared with crystalline growth from the gas phase. Based on time-resolved optical reflectivity measurements, a non-destructive in situ method is developed for the determination of the crystallization rate in addition to the growth rate of amorphous silicon during CVD. The results of optical measurements are related to the crystallization process and the resulting film structure. Good correspondence is found for the crystallization rates of CVD a-Si as compared to the (111) crystallization rates of a-Si prepared by other methods. (7 refs.)

114416 Properties of thin polycrystalline silicon films deposited by plasma-assisted CVD. W.R.Burger, T.J.Donahue, R.Reif (Dept. of Electrical Engng. & Computer Sci., MIT, Cambridge, MA, USA).

Proceedings of the 4th European Conference on Chemical Vapour Deposition, Eindhoven, Netherlands, 31 May-2 June 1983 (Eindhoven, Netherlands: Philips Centre Manuf. Technol. 1983), p.265-72

The electrical and structural properties of thin polysilicon films deposited by plasma-assisted CVD (PACVD) are being investigated and compared to those of films deposited without plasma by low-pressure CVD (LPCVD). The intrinsic resistivity of the PACVD films was found to be lower than the LPCVD films deposited under the same conditions over the temperature range examined, with the difference becoming greater the lower the deposition temperature. The X-ray texture of the films was also examined. The PACVD films exhibited a texture versus deposition temperature trend similar to the LPCVD films, though a given structure tended to appear at a lower temperature in the PACVD films. Upon annealing, the intrinsic resistivity of the LPCVD films decreased from their as-deposited values, while the intrinsic resistivity of the PACVD films increased upon annealing. The texture of both the PACVD films and the LPCVD films remained unaffected by the anneal; however, the lowest deposition temperature PACVD film showed a substantial enhancement in the perfection of the alignment of the grains upon annealing. (4 refs.)

114417 Adsorption phenomena in CVD systems. L.J.Giling, A.A.Saaman (Dept. of Solid State III, Faculty of Sci., Catholic Univ., Nijmegen, Netherlands).
Proceedings of the 4th European Conference on Chemical Vapour Deposition, Eindhoven, Netherlands, 31 May-2 June 1983 (Eindhoven, Netherlands: Philips Centre Manuf. Technol. 1983), p.280-2
Calculations have made it clear that as long as accurate numerical data for the adsorption process are unknown, no reliable opinion can be expressed whether a surface is fully covered with adsorbed species or not. This means that—contrary to earlier calculations—during the CVD of silicon and gallium arsenide at the high temperature side, the surface may be clean and adsorption is only of minor importance. Only at lower temperatures will adsorption indeed become important for what may be responsible for hillock formation and finally polycrystalline growth. (no refs.)

114418 Al₂O₃ deposition by CVD. B.Lux (Tech. Univ. Wien, Vienna, Austria).
Proceedings of the 4th European Conference on Chemical Vapour Deposition, Eindhoven, Netherlands, 31 May-2 June 1983 (Eindhoven, Netherlands: Philips Centre Manuf. Technol. 1983), p.379-84
About one decade ago a major breakthrough in the development of chip forming steel cutting tools was brought about by the coating of cemented carbides with Al₂O₃ layers. Compared with the various other layers (TiC, TiN, HfN, etc.) known before the introduction of Al₂O₃ for this purpose, the Al₂O₃ coating gives the most outstanding results and can be found today—frequently in combination with other layers—in many industrial products. The reasons for the spectacular increase in the wear resistance of a cutting tool with a CVD coating are manifold. Today the industrial production of Al₂O₃ layers by CVD is done worldwide and has a yearly business volume exceeding several 100 millions of dollars and there are today in the open literature still more patent applications available than scientific and technical publications. The author discusses further the applications of CVD deposited Al₂O₃ layers. (13 refs.)

114419 The effect of reaction condition on the crystallographic orientation and surface morphology of chemical vapor deposited Al₂O₃. C.Park, J.Kim, J.S.Chun (Dept. of Materials Sci. & Engng., Korea Advanced Inst. of Sci. & Technol., Seoul, Korea).
Proceedings of the 4th European Conference on Chemical Vapour Deposition, Eindhoven, Netherlands, 31 May-2 June 1983 (Eindhoven, Netherlands: Philips Centre Manuf. Technol. 1983), p.410-20
Deposits of aluminium oxides (Al₂O₃) have been formed by a chemical vapor deposition technique involving the application of gaseous mixtures of AlCl₃, CO₂, and H₂ onto TiN-coated cemented carbide substrates. Reaction parameters (deposition temperature, system pressure, and composition of reactant gases) and their effects on the crystalline structure, crystallographic orientation, and surface morphology of the Al₂O₃ deposit have been studied. Al₂O₃ crystals maintain a corundum structure throughout the entire range of deposition conditions. Crystals of Al₂O₃ appear to nucleate in random orientations on the TiN layer, and further growth proceeds with (1014) and (1126) preferred orientations. The effects of reaction parameters on the final surface morphology of the Al₂O₃ deposit can be described by considering the supersaturations of the reactants and the growth rate. The crystals of the Al₂O₃ deposit become finer and more uniform as the supersaturation of the reactant controlling the Al₂O₃ nucleation increases. (10 refs.)

114420 Growth of α -Al₂O₃ on single- and polycrystalline alumina substrates by CVD. H.Altena, C.Colombier, B.Lux (Tech. Univ. Wien, Vienna, Austria).
Proceedings of the 4th European Conference on Chemical Vapour Deposition, Eindhoven, Netherlands, 31 May-2 June 1983 (Eindhoven, Netherlands: Philips Centre Manuf. Technol. 1983), p.435-43
The crystal orientation of Al₂O₃ substrates has a definite influence on the growth rate of the Al₂O₃-layer during CVD growth. Epitaxial growth generally takes place on highly polished polycrystalline surfaces, while on unpolished, rough surfaces nucleation occurred which led to non-epitaxial relationships. Nucleation and growth of epitaxially linked individual crystals were observed on single crystalline substrates, too. In this case, a coin-shaped crystal habitus grew on locations where presumably lattice defects existed in the single crystalline substrate. (15 refs.)

114421 Influence of trace impurities on the formation of α -Al₂O₃ layers by CVD. H.Altena, C.Colombier, B.Lux (Tech. Univ. Wien, Vienna, Austria).
Proceedings of the 4th European Conference on Chemical Vapour Deposition, Eindhoven, Netherlands, 31 May-2 June 1983 (Eindhoven, Netherlands: Philips Centre Manuf. Technol. 1983), p.451-8
During the industrial CVD process, the presence of trace impurities can disturb the formation of Al₂O₃ coatings on cemented carbides. Such impurities could originate from the raw materials by reaction on the construction materials (Cr, Ni, Fe) with the gases used or could diffuse from the substrate (Co, Ti) to the solid/gas interface. The action of Cr, Ni, Fe, Ti and Au on Al₂O₃ CVD deposits is discussed. (13 refs.)

114422 Effect of TiCl₄ addition on the structure of chemically vapor-deposited Si₃N₄. T.Hirai, S.Hayashi, A.Tanaka (Res. Inst. for Iron, Steel & Other Metals, Tohoku Univ., Sendai, Japan).
Proceedings of the 4th European Conference on Chemical Vapour Deposition, Eindhoven, Netherlands, 31 May-2 June 1983 (Eindhoven, Netherlands: Philips Centre Manuf. Technol. 1983), p.503-8
The increase in TiCl₄ flow rate caused a variation in the structure of Si₃N₄ matrix in the Si₃N₄-TiN composite from amorphous to α - and β -phases. The abrupt increase in the β -Si₃N₄ content was observed in a narrow flow rate range at T_{dep} of 1350 and 1450°C. The density of the crystalline Si₃N₄ matrix was close to the theoretical density, while the composites including the amorphous Si₃N₄ exhibited a lower density than the theoretical density. The surface morphology of the composites reflected well the structures of CVD-Si₃N₄. (4 refs.)

Proceedings of the 4th European Conference on Chemical Vapour Deposition .. See Entry 111316

CVD coatings in fusion reactor technology .. See Entry 112442

Study of the OH content of CVD silica glass for optical fibres .. See Entry 113070

Electron-diffraction investigation of amorphous titanium dioxide films .. See Entry 113739

Formation of crystal structures in microgravitational conditions .. See Entry 113786

In situ observations of crystal growth processes .. See Entry 113790

Introduction [laser annealing of semiconductors] .. See Entry 114001

Pulsed excimer laser (308 nm) annealing of ion implanted silicon and solar cell fabrication .. See Entry 114011

Characterization and application of laser induced seeded-lateral epitaxial Si layers on SiO₂ .. See Entry 114013

Beam shaping for CW laser recrystallization of polysilicon films .. See Entry 114016

A comparison of CW laser and electron-beam recrystallization of polysilicon in multilayer structures .. See Entry 114017

Laser-induced crystallization of silicon on bulk amorphous substrates: an overview .. See Entry 114018

Growth of silicon-on-insulator films using a line-source electron beam .. See Entry 114031

Analysis of surfaces and thin films .. See Entry 114317

Structural studies of metal-semiconductor interfaces with high-resolution electron microscopy .. See Entry 114322

Investigations of metal-silicon interfaces by time-of-flight atom probe .. See Entry 114323

Oxygen adsorption on a cylindrical GaAs single crystal prepared by molecular beam epitaxy .. See Entry 114341

Studies of chemistry at the Ta/Si interface as a function of thermal processing .. See Entry 114372

Microstructural study of alumina/TiC coated cemented carbide .. See Entry 114375

The mode of detachment of HfN coatings .. See Entry 114424

Heat treatments of CVD-coatings on hardmetals .. See Entry 114425

Epitaxial InP/fluoride/InP(001) double heterostructures grown by molecular beam epitaxy .. See Entry 114593

Electronic properties of grain boundaries in GaAs: a study of oriented bicrystals prepared by epitaxial lateral overgrowth .. See Entry 114629

Improvement of photoluminescence of molecular beam epitaxially grown Ga_xAl_{1-x}In_{1-x-y}As by using an As₂ molecular beam .. See Entry 114901

Some characteristics of the electroluminescence emitted by epitaxial Al-Ga-Sb heterostructures .. See Entry 114934

Abnormal optical absorption of quenched Ag films due to surface roughness .. See Entry 114946

Influence of film structure on the electron energy loss spectra of GaAs thin films .. See Entry 114982

Investigation of gallium arsenide subjected to an intensive plasma treatment .. See Entry 115003

Zone-melting recrystallization of semiconductor films .. See Entry 115050

Plasma-sprayed silicon as a possible base material for the production of low cost solar cells .. See Entry 115051

Control of DC diode sputtering by control electrodes .. See Entry 115054

Some physicochemical problems of vacuum epitaxial growth of ferroelectrics .. See Entry 115056

Computer-aided study of hot wall epitaxy system using a Monte Carlo technique .. See Entry 115057

The heteroepitaxy of Ge on Si(100) by vacuum evaporation .. See Entry 115058

Silicon molecular beam epitaxy .. See Entry 115059

The growth of epitaxial NiSi₂ single crystals on silicon by the use of template layers .. See Entry 115060

Growth of Ga_{0.47}In_{0.53}As-InP quantum wells by low pressure metalorganic chemical vapor deposition .. See Entry 115061

In_xGa_{1-x}As-epitaxy with metalorganic adducts .. See Entry 115062

Plasma enhanced metal-organic chemical vapor deposition of aluminum oxide dielectric film for device applications .. See Entry 115063

Enhancement of growth rate due to tin doping in GaAs epilayer grown by low pressure metal-organic chemical vapor deposition .. See Entry 115064

Tin doping of gallium arsenide by metallic organic chemical vapor deposition (MOCVD) .. See Entry 115065

Use of diethylberyllium for metal organic chemical vapor deposition of beryllium-doped gallium arsenide .. See Entry 115066

A theoretical study of the low-temperature chemical vapor deposition of SiO₂ films .. See Entry 115067

Epitaxial growth of GaAs_{1-x}P_x (0<x<0.6) by OM-CVD from ClEt₂Ga.AsEt₃ complex and diethyl phosphine: HPET₂ as original source of phosphorus .. See Entry 115068

An investigation of the factors that influence the deposit/etch balance in a radiant-heated silicon epitaxial reactor .. See Entry 115071

LPCVD polycrystalline silicon: growth and physical properties of in-situ phosphorus doped and undoped films .. See Entry 115073

LPCVD polycrystalline silicon: growth and physical properties of diffusion-doped, ion-implanted, and undoped films .. See Entry 115074

A physicomathematical model for the polycrystalline silicon thin film deposition process in a reduced-pressure horizontal reactor .. See Entry 115075

A systematic approach of the low temperature CVD with organometallic compounds .. See Entry 115077

Chemical vapor deposition of Si in stagnation point flow .. See Entry 115078

Low pressure aluminium CVD .. See Entry 115079

CVD-NbC_{1-y}N_y-carbon fiber superconductors .. See Entry 115080

Chemical vapor deposition of Nb₂Sn in a fluidized bed .. See Entry 115081

Kinetics and transport in the CVD of epitaxial silicon .. See Entry 115082

Laser induced chemical vapor deposition of hydrogenated amorphous silicon .. See Entry 115083

Deposit of germanium monocrystalline thin films by chemical vapour transport in a diffusional flow system .. See Entry 115084

Analysis of low pressure CVD processes .. See Entry 115085

Low pressure photosensitized chemical vapour deposition. Equipment and application for SiO₂ depositions below 100°C .. See Entry 115086

Crystal growth mechanisms of semiconductor A^{III}B^{VI} and A^{III}B^V compounds by metalorganic chemical vapor deposition .. See Entry 115087

LPCVD at quasi high flow .. See Entry 115088

GaP and InP films elaborated with the covalent molecules (Et₂M^{III}-PEt₂)₃ (M^{III}=Ga, In): a possible step in III-V MO-CVD process .. See Entry 115089

Epitaxial growth of silicon by CVD in a furnace .. See Entry 115090

Chemical vapor infiltration technique .. See Entry 115091

Low pressure CVD of pyrolytic carbon .. See Entry 115093

Influence of temperature and substrate on Al₂O₃ CVD from AlCl₃/H₂/CO₂ gas mixtures .. See Entry 115095

- Deposition and characterization of MO-CVD ZrO_2 See Entry 115096
- On the theoretical conditions of deposition of refractory solid solutions: titanium carbonitride See Entry 115099
- Effects of the experimental conditions of chemical vapor deposition on TiC/TiN double layer coating See Entry 115101
- The growth of TiC on iron-carbon substrates by CVD See Entry 115102
- Homoeptitaxial growth of ZnTe by horizontal open-tube method See Entry 115105
- Low-temperature epitaxial growth of (100) silicon See Entry 115106
- Control of the uniformity of thin films formed by an RF plasma [Josephson technology application] See Entry 115107
- Deposition rate and structural properties of microcrystalline glow discharge Si:H,Cl films See Entry 115108
- Liquid phase epitaxial growth on $\{111\}_{\text{In}}$ planes of InP See Entry 115109
- Electroepitaxial growth of HgCdTe from Te-rich solution See Entry 115110
- Liquid phase epitaxial growth conditions of lattice-matched $\text{Al}_{0.48}\text{In}_{0.52}\text{As}$ and $\text{Al}_x\text{Ga}_{1-x-y}\text{As}$ layers without surface defects See Entry 115112
- In situ electrochemical monitoring and control of oxygen in liquid phase epitaxial growth of GaAs See Entry 115113
- Properties of thermal oxides grown on phosphorus in situ doped polysilicon See Entry 115383
- Application of DSL photoetching for defect revealing in epitaxially grown GaAs samples See Entry 115397
- Electrodeposition of zinc on glassy carbon from ZnCl_2 and ZnBr_2 electrolytes [batteries] See Entry 115629
- $\text{pAlGa}_{1-x}\text{As-pGaAs-nGaAs}$ heterostructure concentrator photocells synthesized by liquid-gas-phase epitaxy See Entry 115652

68.60 PHYSICAL PROPERTIES OF THIN FILMS, NONELECTRONIC

- 114423 Plasmastructural transformations in amorphous chalcogenide semiconductors. P.N.Dashuk, V.M.Lyubin (A.F. Ioffe Physicotech. Inst., Acad. of Sci., Leningrad, USSR). *Sov. Tech. Phys. Lett. (USA)*, vol.8, no.11, p.583-4 (Nov. 1982). Translation of: *Pis'ma v Zh. Tekh. Fiz. (USSR)*, vol.8, no.21-22, p.1357-61 (Nov. 1982). [received: Sept. 1983]
- Reports a study of the effect of the plasma of an electric discharge on amorphous chalcogenide semiconductors. Changes occur in several properties of the semiconductors. The experiments were carried out with amorphous chalcogenide semiconductor films of the As-Se and As-S systems, in particular with As_2Se_3 , AsSe, As_3Se_2 , and As_2S_3 films, in which the photostructural transformations are most obvious. The films were synthesized by vacuum deposition on a 2-mm oxide glass substrate. (5 refs.)
- 114424 The mode of detachment of HfN coatings. A.J.Perry, B.Hammer, M.Groessl (Balzers AG, Balzers, Liechtenstein). Proceedings of the 4th European Conference on Chemical Vapour Deposition, Eindhoven, Netherlands, 31 May-2 June 1983 (Eindhoven, Netherlands: Philips Centre Manuf. Technol. 1983), p.70-5
- Hafnium nitride coatings deposited on to cemented carbides by chemical vapour deposition have been subjected to the scratch test for adhesion. The critical loads recorded (5-12 kg) are the highest so far observed for any system. Many of the samples showed a mode of loss which had not been observed before: a wave-like pattern where cracking appears to be confined to the scratch channel and to run parallel to the interface. Some preliminary studies of the acoustic signal in the range centered around 200 kHz are reported. (7 refs.)
- 114425 Heat treatments of CVD-coatings on hardmetals. O.Pacher, J.Stamberger, J.Kiefer (Res. & Dev. Div., VEW Ltd., Kapfenberg, Austria). Proceedings of the 4th European Conference on Chemical Vapour Deposition, Eindhoven, Netherlands, 31 May-2 June 1983 (Eindhoven, Netherlands: Philips Centre Manuf. Technol. 1983), p.491-502
- The change in lattice parameter of TiC, $\text{Ti}(\text{C}_x\text{N}_y)$ and TiN coatings on P 20 hardmetal after a heat treatment is reported. Metallographical examinations and microprobe analyses show that W, Ta, Nb and Co diffuse into the coating. This changes the hardness and may lead to precipitations. (4 refs.)
- Formation of crystal structures in microgravitational conditions See Entry 113786
- Autodoping phenomena in epitaxial silicon See Entry 113939
- Emission of melt during laser vaporization of metallic films See Entry 113999
- Lateral self-diffusion in indium thin films See Entry 114243
- Phase formation and kinetics of the phase transition in Ag_2Se thin films See Entry 114396
- Properties and structure of carbon excess $\text{Ti}_2\text{C}_{1-x}$ deposited onto molybdenum by magnetron sputtering See Entry 114397
- Potentials of X-ray diffraction and electron microscopy for the characterization of thin polycrystalline CVD layers See Entry 114403
- CVD of TiN at the tempering temperature of alloy-steels See Entry 115097
- Role of CVD in providing wear resistant films See Entry 115450

68.70 WHISKERS AND DENDRITES: GROWTH, STRUCTURE, AND NONELECTRONIC PROPERTIES

- 114426 A TEM study of fibrous cuprite (chalcotrichite): microstructures and growth mechanisms. D.R.Veblen (Dept. of Earth & Planetary Sci., Johns Hopkins Univ., Baltimore, MD, USA), J.E.Post. *Am. Mineral. (USA)*, vol.68, no.7-8, p.790-803 (July-Aug. 1983).
- A specimen of the fibrous, or whisker variety of cuprite ('chalcotrichite') was examined with transmission electron microscopy (TEM). Of several morphologically distinct whisker types, only those with square cross sections were observed to contain screw dislocations. The dislocations generally are straight and close to the whisker axis, although in some cases the dislocations approach the crystal surface, and in one case a helical dislocation was observed. In addition, one whisker with a very large Burgers vector contained a hollow axial tube in accordance with Frank's (1951) theory. The presence of axial screw dislocations in almost all of the chalcotrichite whiskers of square cross section indicates that they formed by a spiral growth mechanism, thus accounting for their extreme elongation. The growth mechanisms of the chalcotrichite ribbons cannot be determined from the available observations,

but it is likely that several complex mechanisms operated, since there are a variety of different whisker types present. This variety also suggests that it is the growth conditions (temperature, pressure, vapor composition, degree of supersaturation) that determine whether whiskers or equidimensional crystals will grow, rather than the specific mechanisms of whisker growth. (58 refs.)

- 114427 The formation of filamentous carbon from decomposition of acetylene over vanadium and molybdenum. R.T.K.Baker, J.J.Chludzinski, N.S.Dudash, A.J.Simoens (Exxon Res. & Engng. Co., Linden, NJ, USA). *Carbon (GB)*, vol.21, no.5, p.463-8 (1983).
- Controlled atmosphere electron microscopy has been used to investigate the deposition of carbon on vanadium and molybdenum surfaces during the thermal decomposition of acetylene. Both metals were found to be active catalysts for carbon filament formation, whereas the carbides, VC and Mo_2C were found to be inactive. The filament growth kinetics indicates that these structures are produced via the same mechanism as that proposed for the production of filaments from the interaction of hydrocarbons with Fe, Ni and Co. It was also shown that the strength of the metal-support interaction can have a profound effect on the mode by which carbon filaments grow. (14 refs.)
- 114428 Formation of whiskers on Al_2O_3 CVD layers. H.Altena, C.Colombier, A.Lebbl, J.Lindstrom, B.Lux (Tech. Univ. Wien, Vienna, Austria). Proceedings of the 4th European Conference on Chemical Vapour Deposition, Eindhoven, Netherlands, 31 May-2 June 1983 (Eindhoven, Netherlands: Philips Centre Manuf. Technol. 1983), p.428-34
- So-called A- and C-whiskers of $\alpha\text{-Al}_2\text{O}_3$, which differ in their main growth direction, are described in the literature. C-type whiskers are quite frequently observed during the coating of cemented carbides with Al_2O_3 by CVD. Small impurities of Co and Si can lead to the whisker formation by a VLS (vapor-liquid-solid) mechanism. A cobalt silicide acts as the liquid phase. The VLS mechanism is, however, not the only possibility for whisker formation. (13 refs.)
- The formation of coarse intermetallics in rapidly solidified Al-Co alloys See Entry 115185

70.00 CONDENSED MATTER: ELECTRONIC STRUCTURE, ELECTRICAL, MAGNETIC, AND OPTICAL PROPERTIES

(see also 81.40R Electrical and magnetic properties related to materials treatment, 81.40T Optical properties related to materials treatment)

- Proceedings of the Sixteenth Rare Earth Research Conference See Entry 111304

71.00 ELECTRON STATES

(see also 63. Lattice dynamics, 73. Surfaces, interfaces, and thin films)

71.10 GENERAL THEORIES AND COMPUTATIONAL TECHNIQUES

- 114429 Spin excitations in a Hubbard chain. F.Woynarovich (Central Res. Inst. for Phys., Budapest, Hungary). *J. Phys. C (GB)*, vol.16, no.27, p.5293-304 (30 Sept. 1983).
- The spin excitations of a Hubbard chain are calculated on the basis of the Lieb-Wu equations (1968). A system of equations, which contains the parameters of the excitation only, is derived. It is found that both the energy and the momentum of the spin excitations depend only on the positions of the holes in the real γ distribution. The energy-momentum dispersion for a half-filled band is given. The structure and degeneracy of the lowest energy excitations are also discussed. (8 refs.)

71.20 ELECTRONIC DENSITY OF STATES DETERMINATIONS

(inc. energy states of liquid semiconductors; see also 65.40 Lattice and electronic heat capacity)

- 114430 Analytic-quadratic method of calculating the density of states. M.S.Methfessel, M.H.Boon, F.M.Mueller (Res. Inst. for Materials, Nijmegen, Netherlands). *J. Phys. C (GB)*, vol.16, no.27, p.1949-54 (30 Sept. 1983).
- A new analytic method of calculating the density of states based on local quadratic expansions is given. Results are presented for the tight binding s band and for the valence bands of silicon. These show that the new technique properly treats van Hove singularities, where the commonly applied method using local linear expansions fails. (5 refs.)
- 114431 Density-of-state effects in the low temperature properties of TiBe_2 . T.Jarlborg (Dept. de Phys. de la Matière Condensée, Univ. de Genève, Genève, Switzerland), P.Monod, M.Peter. *Solid State Commun. (USA)*, vol.47, no.11, p.889-93 (Sept. 1983).
- The importance of exact theoretical and experimental determination of the band structure near E_F for an understanding of the properties of TiBe_2 is pointed out. Precise density-of-state data, obtained from ab initio self-consistent band calculations, are used to determine low temperature variations in the susceptibility χ and specified heat γ . The influence on the field and temperature variations on χ is striking and qualitative agreement with experiment is possible without invoking spin-fluctuations. The field and temperature variations of γ are important enough to be considered, but are smaller than for χ and considerably smaller than observed experimentally by Stewart et al. (1982). Thus evidence of spin-fluctuations are more convincing when extracted from γ -data than from χ -data. (20 refs.)

Non-crystalline semiconductors See Entry 113738

Ab initio mixed basis method of band structure calculation: γ -Fe and cubic ZnS electronic structures See Entry 114435

Polaron model of the electronic spectrum and the superconductivity of compounds having the A-15 structure See Entry 114456

Electronic states of grain boundaries in bicrystal silicon See Entry 114482

71.25 NONLOCALIZED SINGLE-PARTICLE ELECTRONIC STATES

114432 The controllable variband structures in a ferroelectric semiconductor. V.B.Sandomirskii, Sh.S.Khalilov, E.V.Chensky (Azerbaijan State Univ., Baku, USSR). *Ferroelectr. Lett. Sect. (GB)*, vol.1, no.1, p.7-12 (1983). The possibility of formation of the variband structure in a ferroelectric semiconductor is pointed out. The energy scheme of such variband structure depends on temperature, electric bias, light intensity and possesses hysteresis. (6 refs.)

114433 Surface and bulk electronic structure of disordered metallic alloys. A.Bansil (Dept. of Phys., Northeastern Univ., Boston, MA, USA), M.Pessa. *Phys. Scr. (Sweden)*, vol.T4, p.52-60 (1983). (Nordic Conference on Surface Science, Tampere, Finland, 18-20 Aug. 1982). The understanding of electronic structure of disordered alloys has advanced rapidly during the last decade, and the basic elements of a band theory of the bulk electronic structure of random alloys have emerged clearly during this period. In providing an overview of this theory, the authors focus on the question of how the concept of a Bloch energy band generalizes to the disordered case; illustrative examples of Cu-based solid solutions are presented. On the experimental side, the application of angle-resolved photoemission spectroscopy (ARPES) to the alloy problem is discussed. The use of ARPES in this context is quite recent, although extensive studies of alloys, using a variety of solid state techniques, have been carried out. The existing ARPES work aimed at delineating the surface and bulk electronic structure in metallic alloys is reviewed. The authors also allude to some of the relevant theoretical and experimental issues that arise in connection with developing this application of the ARPES. (69 refs.)

114434 Band theory of some polymers derived from polyparaphenylene. M.Dugay, C.Fabre (Lab. d'Electronique et Resonance Magnetique, Univ. de Clermont II, Aubiere, France). *Solid State Commun. (USA)*, vol.47, no.12, p.965-8 (Sept. 1983). Reports the results of calculations dealing with a series of polymers related to polyparaphenylene. In order to investigate the possible effects of linking aromatic rings with segments having conjugated bonds and/or heteroatoms, semi-empirical calculations have been performed from a Pariser-Parr-Pople Hamiltonian. It is shown that, within this simple methodology, reliable information can be obtained concerning the ability of a polymer to form a conducting system upon doping. (28 refs.)

Electron phase transitions in highly anisotropic two-dimensional systems See Entry 114460

71.25C Techniques of band-structure calculation (general theory, applications of group theory, analytic continuation, etc)

114435 Ab initio mixed basis method of band structure calculation: γ -Fe and cubic ZnS electronic structures. M.T.Czyzyk (Inst. of Phys., Jagellonian Univ., Krakow, Poland), F.M.Mueller. *J. Phys. C (GB)*, vol.16, no.27, p.5255-66 (30 Sept. 1983). A new approach has been developed for electronic band structure calculation. The method consists of two consecutive steps. In the first step the combined tight-binding-plane-wave (TB-PW) Hamiltonian is solved at the centre of the Brillouin zone (BZ). In the second step the k . p method is used in order to extend the solution at $k=0$ to the band structure throughout the entire BZ. The method developed has been used to calculate the band structure of FCC γ -Fe and cubic ZnS. The density of states, effective masses, the dielectric function and the reflectivity coefficient have been calculated as well. The results are compared with those obtained by other methods and with experimental data. (36 refs.)

114436 On the electronic structure of CeN and CeAl₂. W.E.Pickett, B.M.Klein (Condensed Matter Phys. Branch, Naval Res. Lab., Washington, DC, USA). *J. Less-Common Met. (Switzerland)*, vol.93, no.1, p.219-25 (1983). (Proceedings of the Sixteenth Rare Earth Research Conference, Tallahassee, FL, USA, 18-21 April 1983). The electronic band structures of CeAl₂ are studied using the self-consistent augmented plane wave method. By artificially shifting logarithmic derivatives of the self-consistent potential, the authors are able to demonstrate that (N p)-(Ce f) hybridization is substantial in CeN. The calculated valence band densities of states are in good agreement with X-ray photoelectron spectroscopy data on CeN and UV photoelectron spectroscopy data on CeAl₂. The effects of interatomic f-f overlap interactions in these compounds (mixed valent and Kondo lattice respectively) are identified. (16 refs.)

Analytic-quadratic method of calculating the density of states See Entry 114430

Electronic spectrum of a magnetic semiconductor in the s - f exchange model approximation See Entry 114442

71.25H Measurement of Fermi surface parameters (inc. $dH\nu A$, magnetoacoustic, position annihilation, and cyclotron resonance studies, etc.)

Electronic structure of the alloy Fe₈₀P₁₃C₇ in the liquid, crystalline, and solid amorphous states See Entry 114440

On the symmetry of the electronic states in silicon carbide crystals See Entry 114446

71.25J Effective mass and g-factors

Phase formation and kinetics of the phase transition in Ag₂Se thin films See Entry 114396

Ab initio mixed basis method of band structure calculation: γ -Fe and cubic ZnS electronic structures See Entry 114435

Polar, intervalley and acoustic scatterings in III-V group semiconductors. Application to GaAs and InSb See Entry 114519

71.25L Electron energy states in liquid metals

Electronic structure of the alloy Fe₈₀P₁₃C₇ in the liquid, crystalline, and solid amorphous states See Entry 114440

71.25M Electron energy states in amorphous and glassy solids

114437 On the band structure of Mobius polymers. O.E.Polansky (Max-Planck-Inst. fur Strahlenchem., Mulheim, Germany). *Z. Naturforsch. Teil A (Germany)*, vol.38A, no.8, p.909-15 (Aug. 1983). The π -band structure of Mobius polymers (M) is compared with that of the open strip (F) and the cylindrical form (R) of the polymer considered. Under certain conditions, the bands of all these forms coincide. This is to be expected also for the σ -bands within the framework of extended Huckel theory. (13 refs.)

114438 Effect of random doping on the electronic spectrum in trans-polyacetylene. W.P.Su (Dept. of Phys., Univ. of Illinois, Urbana, IL, USA). *Solid State Commun. (USA)*, vol.47, no.11, p.947-9 (Sept. 1983). Random dopants in trans (CH)_x introduce a broad band of gap states which merge with the conduction and valence band edges at a doping concentration n_c of a few percent. This overlap of band and gap states leads to an onset of Pauli susceptibility, since the density of states at the Fermi energy E_F is nonzero for $n > n_c$. However, E_F lies in a region of localized states until n is considerably greater than n_c and the system remains a semiconductor. (8 refs.)

Non-crystalline semiconductors See Entry 113738

Role of electronic processes in epitaxial recrystallization of amorphous semiconductors See Entry 114390

Electronic structure of the alloy Fe₈₀P₁₃C₇ in the liquid, crystalline, and solid amorphous states See Entry 114440

Comment on the optical absorption edge in α -Si:H See Entry 114817

The optical absorption edge of amorphous thin films of borosilicate glass See Entry 114939

71.25P Band structure of crystalline metals

114439 Electronic structure of zintl compounds (NaTi) and alkali pnictides. J.Robertson (Central Electricity Res. Labs., Leatherhead, England). *Solid State Commun. (USA)*, vol.47, no.11, p.899-902 (Sept. 1983). The presence of both like and unlike atom nearest neighbours in the NaTi lattice is used to test the dependence of tight-binding interactions on bond type. The atoms are found to be almost neutral, and little evidence of the classic Na⁺Ti⁻ bonding models is found. The bands of alkali pnictides such as Li₃Sb are calculated by scaling interactions from LiAl. The Li salts are found to have almost neutral sites whereas the Cs salts are strongly ionic. The author classifies the bonding generally as charge transfer, not covalent. (19 refs.)

114440 Electronic structure of the alloy Fe₈₀P₁₃C₇ in the liquid, crystalline, and solid amorphous states. I.N.Shabanova, S.S.Samolovich, V.A.Zhuravlev, V.T.Borisov (State Univ., Udmurt, Izhevsk, USSR). *Sov. Phys.-Dokl. (USA)*, vol.27, no.12, p.1057-8 (Dec. 1982). Translation of: *Dokl. Akad. Nauk SSSR*, vol.267, no.4-6, p.848-9 (Dec. 1982). [received: Sept. 1983] The authors report the results of an investigation of the electronic spectra of the carbon core 1S levels and the valence band (0-35 eV, as measured from the Fermi level) of the surface layers (~ 20 Å) of the amorphous alloy Fe₈₀P₁₃C₇ over a wide temperature range (from 293K to the melting temperature 1120K). The samples were made in the shape of ribbons 0.4-0.5 cm wide and 10 μ m thick by quenching the alloy from the liquid state on a rapidly rotating copper cylinder. The spectra were measured with a magnetic electron spectrometer having a resolution of 1.0 eV with the use of the Al K α line for excitation of the electrons. The samples were heated directly in the vacuum chamber of the electron spectrometer. (2 refs.)

Ab initio mixed basis method of band structure calculation: γ -Fe and cubic ZnS electronic structures See Entry 114435

On the electronic structure of CeN and CeAl₂ See Entry 114436

X-ray and photoelectron spectroscopy of light rare earths See Entry 115010

Chlorine adsorption on copper. I. Photoemission from clean Cu(001) and Cu(111) substrates See Entry 115019

Core-level XPS studies of Ce and La intermetallic compounds and their implications for the 4f levels of Ce compounds See Entry 115023

71.25R Band structure of crystalline elemental semiconductors

114441 Mapping bulk Ge electronic energy bands along Δ using ARPES spectra of the (001) 2 \times 1 surface. J.G.Nelson, W.J.Gignac, R.S.Williams (Dept. of Chem. & Biochem., Univ. of California, Los Angeles, CA, USA), S.W.Robey, J.G.Tobin, D.A.Shirley. *Surf. Sci. (Netherlands)*, vol.131, no.2-3, p.290-8 (Sept. 1983). The E versus k dispersion relations of the second and third bulk valence bands as well as one conduction band of Ge along the Δ line of the Brillouin Zone have been experimentally determined from angle-resolved photoelectron spectra collected at the Stanford Synchrotron Radiation Laboratory. The experimentally observed bands show good agreement with those calculated using the empirical pseudopotential parameter of Chelikowsky and Cohen (1976) for bulk Ge, even though the Ge (001) surface is reconstructed and ARPES is generally considered to be a surface sensitive technique. (20 refs.)

Analytic-quadratic method of calculating the density of states See Entry 114430

71.25T Band structure of crystalline semiconductor compounds and insulators

114442 Electronic spectrum of a magnetic semiconductor in the s - f exchange model approximation. A.L.Kuzemsky (Lab. of Theoretical Phys., JINR, Dubna, USSR), D.I.Marvakov, J.P.Vlahov. *Bulg. J. Phys. (Bulgaria)*, vol.10, no.3, p.290-6 (1983).

The electronic spectrum of a magnetic semiconductor has been analysed in the s - f exchange model approximation using the irreducible green function method. An analytic expression of the electronic self-energy operator has been obtained and it may be used to find a self-consistent procedure in separate specific cases. The electronic spectrum of a wide-band magnetic semiconductor has been studied in detail. (16 refs.)

114443 Electronic structure and interparticle interaction in defect cubic oxides of vanadium and titanium. A.L.Ivanovskii, V.A.Gubanov, Yu.G.Zainulin, E.Z.Kurmaev, M.P.Butsman, B.I.Zborovskii (Inst. of Chem., Acad. of Sci., USSR).

J. Struct. Chem. (USA), vol.23, no.6, p.854-60 (Nov.-Dec. 1982). Translation of: *Zh. Strukt. Khim. (USSR)*, vol.23, no.6, p.42-7 (Nov.-Dec. 1982). [received: Sept. 1983]

The X-ray ultrafast emission (V, Ti) L_{α} -spectra have been obtained, and cluster quantum-chemical calculations of the electronic structure carried out, for a number of nonstoichiometric oxides of V and Ti, containing a variable concentration of vacancies in the metal and nonmetal sublattices, with allowance for their possible ordering. The role of interstitial V atoms in the energetic stabilization of the ordered phase $VO_{1.3}$ has been studied. (25 refs.)

114444 Electronic structures of sulfide minerals—theory and experiment. D.J.Vaughan (Dept. of Geological Sci., Univ. of Aston, Birmingham, England), J.A.Tossell.

Phys. & Chem. Miner. (Germany), vol.9, no.6, p.253-62 (1983).

The sulfide minerals exhibit a rich diversity in structural chemistry and in electrical, magnetic and other physical properties. Models based on molecular orbital theory and incorporating some elements of band theory can be developed to describe the diverse valence electron behavior in these minerals. Qualitative models can be proposed on the basis of observed properties, and the models can be tested and refined using experimental data from X-ray emission and X-ray photoelectron spectroscopy and quantum mechanical calculations performed on cluster units which form the basic building blocks of the crystals. This approach to chemical bonding in sulfide minerals is illustrated for binary nontransition metal sulfides (ZnS, CdS, HgS, PbS), binary transition metal sulfides (FeS₂, CoS₂, NiS₂, CuS₂, ZnS₂) and more complex sulfides (CuFeS₂, Cu₂S, Ag₂S, CuS, Co₃S₄, CuCo₂S₄, Fe₃S₄). The relationship between qualitative and quantitative theories is reviewed with reference to the pyrite-marcasite-arsenopyrite-loellingite series of minerals. Application of the models to understanding structure-determining principles, relative stabilities, solid solution limits and properties such as color, reflectance and hardness are discussed. (42 refs.)

114445 Anomalous temperature dependence of the band gap of intrinsic semiconductors. N.V.Fomin (M.I. Kalinin Polytech. Inst., Leningrad, USSR).

Sov. Phys.-Semicond. (USA), vol.17, no.3, p.349-50 (March 1983). Translation of: *Fiz. & Tekh. Poluprovodn. (USSR)*, vol.17, no.3, p.553-5 (March 1983). [received: Sept. 1983]

It is known that in the case of IV-VI and II-VI semiconductors the temperature coefficient of the band gap E_g is anomalous (positive). The author considers possible reasons for this anomaly. (4 refs.)

114446 On the symmetry of the electronic states in silicon carbide crystals. G.B.Dubrovskii (A.F. Ioffe Physicotech. Inst., Acad. of Sci., USSR).

Sov. Phys.-Solid State (USA), vol.25, no.2, p.288-92 (Feb. 1983). Translation of: *Fiz. Tverd. Tela (USSR)*, vol.25, no.2, p.512-18 (Feb. 1983). [received: Sept. 1983]

The reflection of electrons by the various Bragg planes in SiC crystals is considered and it is shown that the principal reflecting planes in all the SiC modifications, except the 2H modification, coincide with the planes bounding the Brillouin zone of the cubic β -SiC crystal if it is assumed that the electronic states of the conduction band are formed by only the sublattice made up of the Si atoms. It is also shown that the superlattice in SiC can be described by superposing a screw axis on the cubic lattice. A primary-reflection zone is constructed in the reciprocal space of the superlattice on the basis of the Brillouin zone of β -SiC, and its symmetry is considered. (7 refs.)

X-ray spectroscopic investigation of the nature of chemical binding in metal-like titanium carboaluminides of variable composition See Entry 113795

Band-state interpretation of lattice thermal conductivity and microhardness of ternary chalcopyrite semiconductors See Entry 114293

Density-of-state effects in the low temperature properties of TiBe₂ See Entry 114431

Ab initio mixed basis method of band structure calculation: γ -Fe and cubic ZnS electronic structures See Entry 114435

On the electronic structure of CeN and CeAl₂ See Entry 114436

First-principles calculation of the insulator-to-metal transition pressure in CsI See Entry 114447

Complex band structure and deep impurities. II. Γ_{15} and Γ_{12} states See Entry 114468

Polar, intervalley and acoustic scatterings in III-V group semiconductors. Application to GaAs and InSb See Entry 114519

The electronic structure of f element compounds elucidated by less common spectroscopic methods See Entry 114851

The diffuse reflectance spectra of mono-cadmium and di-cadmium stannates See Entry 114874

Edge absorption and band gap of CuAl_xGa_{1-x}Se₂ solid solutions See Entry 114881

Optical properties of ferroelectrics with tetragonal potassium-tungsten-bronze in the fundamental absorption region See Entry 114882

Nature of the luminescence lines of heavily doped p-type gallium arsenide under uniaxial deformation See Entry 114923

The 4f spectral weight in cerium materials—facts and issues See Entry 115011

Systematics of optical energy gaps and XPS core level satellites in CuO and copper dihalides See Entry 115018

71.30 METAL-INSULATOR TRANSITIONS

114447 First-principles calculation of the insulator-to-metal transition pressure in CsI. J.Aidun, M.S.T.Bukowski (Dept. of Geology & Geophys., Univ. of California, Berkeley, CA, USA).

Solid State Commun. (USA), vol.47, no.11, p.855-7 (Sept. 1983).

The room temperature compression isotherm and electronic band structure of CsI have been computed with the nonrelativistic self-consistent augmented-plane-wave method. The isotherm is in excellent agreement with available static and ultrasonic measurements, and hence allows an improved extrapolation of Asaumi and Kondo's measurements (1981) of the absorption edge to gap closure in the range 38-46 Å⁻¹ and 65-105 GPa when uncertainties in the experimental determination of the band gap are accounted for. The calculated band structure suggests that the band gap is direct and it is in close agreement with the corresponding experimentally determined band gap when the Slater exchange potential is used. These consistencies between the measurements and calculations suggest that the insulator-to-metal transition occurs in the 100±10 GPa range, somewhat higher than Asaumi and Kondo's estimate of 70 GPa, but in good agreement with the prediction from Herzfield's theory. (23 refs.)

Investigation of defect structure of metal-semiconductor interface in SmS by the method of high-voltage electron microscopy See Entry 113918

Localization and interactions See Entry 114463

Macroscopic coherence length of charge-density waves in orthorhombic TaS₃ See Entry 114516

71.35 EXCITONS AND RELATED PHENOMENA

(inc. electron-hole drops)

114448 Detection of exciton luminescence of indium antimonide crystals. V.I.Ivanov-Omskii, S.I.Kokhanovskii, R.P.Seisyan, V.A.Smirnov, Sh.U.Yuldashev (A.F. Ioffe Physicotech. Inst., Acad. of Sci., Leningrad, USSR).

Sov. Phys.-Semicond. (USA), vol.17, no.3, p.334-5 (March 1983). Translation of: *Fiz. & Tekh. Poluprovodn. (USSR)*, vol.17, no.3, p.532-4 (March 1983). [received: Sept. 1983]

Kanskaya et al. (1979) reported a discovery of a discrete structure of Wannier-Mott excitons in the absorption edge spectra of InSb crystals ($n_{77} \approx 6 \times 10^{13} \text{ cm}^{-3}$) at 2K when special measures were taken to eliminate the influence of bound states. It seemed natural to investigate also the low temperature edge luminescence of the same samples in order to detect radiative recombination channels involving these bound exciton states. The experiments were carried out at temperatures 2-25K and the source of excitation was a GaAs heterojunction laser emitting at $\lambda_{\text{max}} = 0.9 \mu$. (10 refs.)

114449 Polarized luminescence due to localized excitons in CdS_{1-x}Se_x solid solutions. S.Yu.Verbin, S.A.Permogorov, A.N.Reznitskii (A.F. Ioffe Physicotech. Inst., Acad. of Sci., Leningrad, USSR).

Sov. Phys.-Solid State (USA), vol.25, no.2, p.195-8 (Feb. 1983). Translation of: *Fiz. Tverd. Tela (USSR)*, vol.25, no.2, p.346-52 (Feb. 1983). [received: Sept. 1983]

The polarization of luminescence due to excitons localized by composition fluctuations at 2K was investigated in single crystals of CdS_{1-x}Se_x semiconducting solid solutions. The measurements were made on cleaved or growth surfaces perpendicular to the optic axis of the samples. It was found that the luminescence excited by linearly polarized radiation has a large positive degree of polarization. For excitation by circularly polarized radiation, there is not circular polarization of the luminescence. The conclusion is drawn that the observed polarization reflects the latent anisotropy of localized excitons and is due to the splitting of the doubly degenerate exciton level Γ_2 in a random anisotropic field due to the anisotropy of the potential wells that localize the excitons. The wavelength and temperature dependence of the degree of polarization of the luminescence due to localized excitons are examined. (15 refs.)

114450 Line width of exciton absorption in solid solutions. N.N.Abyazov, M.E.Raikh, A.L.Efros (A.F. Ioffe Physicotech. Inst., Acad. of Sci., Leningrad, USSR).

Sov. Phys.-Solid State (USA), vol.25, no.2, p.199-202 (Feb. 1983). Translation of: *Fiz. Tverd. Tela (USSR)*, vol.25, no.2, p.353-8 (Feb. 1983). [received: Sept. 1983]

The line width of exciton absorption in solid solutions is estimated under the assumption that broadening is due to fluctuations of the composition. Exact expressions for the wings of the absorption line are obtained and an interpolation expression, which reduces to these exact expressions in the appropriate limits, is derived. (10 refs.)

114451 Absorption of light by bound electron-exciton states in two-dimensional molecular crystals. N.I.Grigorchuk (Inst. of Nuclear Res., Acad. of Sci., Kiev, Ukrainian SSR).

Sov. Phys.-Solid State (USA), vol.25, no.2, p.218-22 (Feb. 1983). Translation of: *Fiz. Tverd. Tela (USSR)*, vol.25, no.2, p.387-93 (Feb. 1983). [received: Sept. 1983]

The Green function method is used to study the spectrum of bound electron-exciton states in a two-dimensional molecular lattice and the absorption coefficient of light due to such states is obtained. Depending on the signs of the effective masses of an electron and of an exciton and on the interaction potential, the case when a bound pair of particles can travel in a crystal is discussed in detail. The effect of bound states on the absorption spectra is discussed. (9 refs.)

114452 Local excitons and effects of their mixing with electronic impurity states in naphthalene. I.V.Brovchenko, L.L.Valkuns, N.I.Ostapenko, S.G.Tret'yakov, M.T.Shpak (Inst. of Phys., Acad. of Sci., Kiev, Ukrainian SSR).

Sov. Phys.-Solid State (USA), vol.25, no.2, p.262-6 (Feb. 1983). Translation of: *Fiz. Tverd. Tela (USSR)*, vol.25, no.2, p.465-71 (Feb. 1983). [received: Sept. 1983]

Experimental and theoretical investigations of crystals of naphthalene with benzoselenophene impurities showed that the properties of local exciton states in this system are significantly different from those of similar states in crystals of naphthalene with benzofuran, indole and thionaphthene impurities. Three bands of local excitons are obtained (instead of one) at distances of 20, 46 and 72 cm⁻¹ from the exciton band; this is due to the perturbation of three molecules of the crystal simultaneously by the impurity molecule. An anomalous polarization is observed in the local exciton bands: all three are polarized predominantly along the a axis of the crystal, whereas, in cases previously investigated, these bands, situated at the same distances from the exciton band, are polarized predominantly along the b axis. As the local energy level approaches the exciton band their intensity falls, while the polarization ratios increase in favor of the b component. The anomalous

polarization is qualitatively explained by effects of mixing impurity and local states due to intermolecular interactions. (14 refs.)

114453 Emission spectra of electron-hole drops in gallium phosphide. N.R.Nurtdinov, A.E.Yunovich (Moscow State Univ., Moscow, USSR). *Sov. Phys.-JETP (USA)*, vol.83, no.5, p.1080-5 (Nov. 1982). Translation of: *Zh. Eksp. & Teor. Fiz. (USSR)*, vol.83, no.5, p.1870-8 (Nov. 1982). [received: Sept. 1983]
The photoluminescence spectra of epitaxial GaP layers with impurity density $\lesssim 10^{16}$ cm⁻³ are investigated at $T=8-60$ K. Emission due to electron-hole drops (EHD) is observed at excitation levels $W=3\times 10^{-2}\text{--}2\times 10^2$ W/cm². The shape of the EHD spectral band with a maximum at $\hbar\omega_m=2.268$ eV is independent of W and T at $T\leq 40$ K, and the band has characteristic recombination times 30 ± 3 nsec and a critical temperature $T_c=50_{-3}^{+3}$ K. The shape of the EHD spectrum is analyzed with account taken of the two-hump structure of the conduction band and of the different ratios of the probabilities of emission of TO , LA , and TA phonons in indirect transitions. The obtained values of the Fermi levels, of the carrier-pair densities in the EHD, and of the binding energy require corrections necessitated by allowance for the phonon dispersion and carrier heating in the EHD. The recombination band assumed to be due to a low-density electron-hole plasma is found to be significant in the quantum-energy region ~ 2.29 eV near the short-wave edge of the EHD band at high T . (22 refs.)

114454 Radiative recombination of localized Mott excitons in a strong magnetic field. V.A.Kharchenko (Leningrad Polytech. Inst., Leningrad, USSR). *Sov. Phys.-JETP (USA)*, vol.83, no.5, p.1140-3 (Nov. 1982). Translation of: *Zh. Eksp. & Teor. Fiz. (USSR)*, vol.83, no.5, p.1971-7 (Nov. 1982). [received: Sept. 1983]
The effect is considered of a strong magnetic field on the formation and recombination of Mott excitons localized at defects and impurities in semiconducting crystals. It is shown that the motion of the exciton mass center across the magnetic field plays a decisive role in the formation of localized excitons. It is found that by varying the magnetic-field intensity one can control the relative brightness (radiative recombination probability) of the spectral lines of optical recombination and or absorption of bound excitons. This possibility is due here to the dependence of the effective mass of the transverse motion of the exciton mass center on the magnetic field intensity. (5 refs.)

Streamer discharges in semiconductors in the temperature range 4.2-530K	See Entry 113691
Low-temperature exciton decay with production of defects in KBr and KBr-Cl	See Entry 113987
Coupled quadrupole-phonon excitations: inelastic neutron scattering on Van Vleck paramagnet PrNi ₅	See Entry 114107
The lowest triplet state of tetramethyl-1,3-cyclobutanedithione. II. Calculation of spin-orbit coupling	See Entry 114503
Optical detection of EPR of self-trapped excitons using photostimulated luminescence of crystals	See Entry 114755
Inhomogeneous and 'lost' optical waves in a bounded anisotropic crystal and supplementary boundary conditions in the theory of additional optical waves	See Entry 114806
Fundamental absorption of test radiation in a semiconductor subjected to the field of a strong electromagnetic wave	See Entry 114818
Influence of compositional variations in thin solid PbI _{2-2x} Br _{2x} films on their excitonic spectra	See Entry 114832
Theory of Raman scattering from molecules adsorbed at semiconductor surfaces	See Entry 114864
Photoabsorption effect in diamagnetic exciton spectra of InSb crystals	See Entry 114868
The lowest triplet state of tetramethyl-1,3-cyclobutanedithione. I. Single-crystal polarized absorption spectrum	See Entry 114875
Electronic absorption and emission spectra of binuclear platinum(II) complexes. Characterization of the lowest singlet and triplet excited states of Pt ₂ (H ₂ P ₂ O ₅) ₄ ⁴⁻	See Entry 114877
Picosecond dynamics of hot carrier relaxation in highly excited multi-quantum well structures	See Entry 114879
Fundamental absorption edge of irradiated alkali halides	See Entry 114892
Optical studies of In _x Ga _{1-x} As-GaAs strained multiquantum well structures	See Entry 114898
Characterization of polycrystalline electrodeposited CdSe photoelectrodes using photoluminescence spectroscopy	See Entry 114902
Emission from free and bound excitons in gallium selenide layered crystals	See Entry 114924
Kinetics of exciton radiation in fluorite type crystals	See Entry 114925
Production and release of light sums in thin films of activated alkali halides with different crystal structure	See Entry 114945
Surface core-level shifts for Ge(100)-(2x1)	See Entry 115017

71.36 POLARITONS

(inc. photon-phonon and photon-magnon interactions)

114455 Self-focusing of polaritons on a metal surface covered by a nonlinear film. V.Ya.Chernyak (Inst. of Spectroscopy, Acad. of Sci., Troitsk, USSR). *Sov. Phys.-Solid State (USA)*, vol.25, no.2, p.351-2 (Feb. 1983). Translation of: *Fiz. Tverd. Tela (USSR)*, vol.25, no.2, p.614-16 (Feb. 1983). [received: Sept. 1983]
The problem of self-focusing of surface polaritons is of great interest in the spectroscopy of surfaces. However, the contribution of an electric field (normal to the surface) to the nonlinearity as a surface film was ignored, and this has led to highly overestimated values of the self-focusing length. The author considers a system consisting of two media: $z<0$ and $z>0$ with permittivities ϵ_1 and ϵ_2 at whose interface $z=0$ there is a thin optically nonlinear film with a permittivity $\tilde{\epsilon}(\mathbf{E})=\epsilon_0+a|\mathbf{E}|^2$ depending on an electric field and such that $a|\mathbf{E}|^2\ll\epsilon_0$. The thickness of this film satisfies $L\ll Q^{-1}$, where Q is the wave vector of carriers. (3 refs.)

71.38 POLARONS AND ELECTRON-PHONON INTERACTIONS

(for electron-phonon interactions in lattices, see also 63.20K)

114456 Polaron model of the electronic spectrum and the superconductivity of compounds having the A-15 structure. A.S.Aleksandrov, V.F.Elesin (Engng.-Phys. Inst., Moscow, USSR). *Sov. Phys.-Solid State (USA)*, vol.25, no.2, p.257-62 (Feb. 1983). Translation of: *Fiz. Tverd. Tela (USSR)*, vol.25, no.2, p.456-64 (Feb. 1983). [received: Sept. 1983]
The existence of a narrow peak in the electronic density of states in A-15 compounds is explained by a strong electron-phonon interaction that leads to the polaron narrowing of the band. An analytic expression relating the transition temperature T_c to the phonon spectrum is derived under the assumption of a weak and an intermediate-strength coupling. The model allows the explanation of the correlation of T_c with the number of electrons per atom, the temperature dependence of the resistance, the magnitude and temperature dependence of the magnetic susceptibility, and the electronic specific heat. (40 refs.)

Polyacetylene: A perspective in scientific and technological research of condensed matter physics See Entry 114515

Influence of the anisotropy of the elastic electron-phonon scattering on the carrier mobility in tellurium See Entry 114544

71.45 COLLECTIVE EFFECTS

114457 The effect of disorder on the quantised Hall conductivity. A.MacKinnon (Blackett Lab., Imperial Coll. London, London, England). <i>J. Phys. C (GB)</i> , vol.16, no.27, p.L945-8 (30 Sept. 1983). It is shown that the quantised value of the Hall conductivity of a two-dimensional electron gas is unaffected by an arbitrary potential through which the Hall current must pass. When the current passes through an insulating region radiation may be emitted at the cyclotron energy. (13 refs.)	
114458 Landau levels in the generalized Kildal-Bodnar model (with Cd₃P₂ and Cd₃As₂ as examples). G.P.Chuiko (Marshal of Engng. Forces V.K. Kharchenko Higher Military Engng. Command Coll., Kamenets-Podolski, Ukrainian SSR). <i>Sov. Phys.-Semicond. (USA)</i> , vol.17, no.3, p.301-3 (March 1983). Translation of: <i>Fiz. & Tekh. Poluprovodn. (USSR)</i> , vol.17, no.3, p.486-8 (March 1983). [received: Sept. 1983] The Bodnar model generalizing the Kildal model which itself is a generalization of the familiar Kane model, does not allow for the anisotropy of the spin-orbit splitting. Bodnar and Kildal assume that $\Delta=\Delta_{\perp}$. Here, Δ is the spin-orbit splitting parameter along a fourfold axis of a tetragonal crystal and Δ_{\perp} is the corresponding parameter in a plane perpendicular to this axis. The sensitivity of the Landau levels and of the spectroscopic splitting factor g to various types of anisotropy of the energy spectrum of carriers suggests that the anisotropy of Δ may be significant in studies of these levels and of g . (8 refs.)	
Nonlinear and frequency-dependent transport phenomena in low-dimensional conductors	See Entry 114514
Estimation of alloy scattering potential in ternaries from the study of two-dimensional electron transport	See Entry 114518
Calculation of the cyclotron resonance linewidth in GaAs-AlGaAs heterostructures	See Entry 114602

71.45G Exchange, correlation, dielectric and magnetic functions, plasmons

114459 Structure factors and elementary excitations of condensed matter. A.Isihara, Y.Nakane (Dept. of Phys., State Univ. of New York, Buffalo, NY, USA). <i>Physica B & C (Netherlands)</i> , vol.120B+C, no.1-3, p.296-9 (May 1983). (Yamada Conference VI on Neutron Scattering in Condensed Matter, Hakone, Japan, 1-4 Sept. 1982). An inelastic electron scattering experiment performed at Princeton on thin films of the quasi one-dimensional organic metal tetrathiafulvalene tetracyanoquinodimethane (TTF-TCNQ) reveals an anomalous negative plasmon dispersion. On the other hand, a recent neutron scattering experiment on liquid ⁴ He at Chalk River shows that the structure factor of this liquid varies with temperature and momentum in an interesting way. In particular, it is observed that at small momentum and above a certain temperature, the structure factor shows an anomalous dip before it starts increasing towards the first peak which is higher for higher temperatures. The structure factors in these completely different systems are related in an analogous way to their elementary excitations which determine the anomalous properties. (7 refs.)
114460 Electron phase transitions in highly anisotropic two-dimensional systems. P.A.Vorob'ev (M.V. Lomonosov State Univ., Moscow, USSR). <i>Sov. Phys.-Solid State (USA)</i> , vol.25, no.2, p.243-6 (Feb. 1983). Translation of: <i>Fiz. Tverd. Tela (USSR)</i> , vol.25, no.2, p.430-5 (Feb. 1983). [received: Sept. 1983] It is shown that correlation effects in strongly anisotropic two-dimensional systems lead to a liquid-gas phase transition. The parameters of the critical point are determined and asymptotic expressions for the densities of the liquid and gas phases are obtained. The width of the dielectric gap in the spectrum of carriers is calculated and it is shown that it is numerically small compared with the Fermi energy. (9 refs.)
114461 Spin splitting of spectrum of two-dimensional electrons in magnetic field parallel to layer. F.T.Vas'ko, N.A.Prima (Inst. of Semiconductors, Acad. of Sci., Kiev, Ukrainian SSR). <i>Sov. Phys.-Solid State (USA)</i> , vol.25, no.2, p.331-2 (Feb. 1983). Translation of: <i>Fiz. Tverd. Tela (USSR)</i> , vol.25, no.2, p.582-4 (Feb. 1983). [received: Sept. 1983] The Hamiltonian of a two-dimensional (2D) electron in an inversion layer or in a nonsymmetric field contains the invariant $V_0[\mathbf{n}\times\mathbf{p}]$ (\mathbf{n} is the normal to the surface, \mathbf{p} is the two-dimensional momentum, and σ is the spin matrix), leading to spin splitting of the spectrum. The authors find the spectrum of 2D electrons in a magnetic field, strictly parallel to the surface. The main result consists in a qualitative conclusion that it is possible for the spectrum to be a highly non-center-of-inversion spectrum for $V_{\text{PF}}\lesssim\mu_{\text{BH}}$. (16 refs.)

114462 Surface plasmon scattering on flat surfaces at grazing incidence. P.E.Batson (IBM Thomas J. Watson Res. Center, Yorktown Heights, NY, USA).

Ultramicroscopy (Netherlands), vol.11, no.4, p.299-302 (1983).

Reports a study of surface plasmon excitation on the flat, oxide-covered aluminum surface, using high energy electrons which pass the surface at a finite, and sometimes large, impact parameter. The scattering probability dependence on impact parameter agrees qualitatively with classical, quasi-static calculations, which assume that the materials are characterized by homogeneous dielectric constants. A broad intensity maximum near 16 eV is identified as a surface plasmon made possible by the frequency dependence of the aluminum oxide dielectric constant. (13 refs.)

A performance test of the recovery of single energy loss profiles via matrix analysis See Entry 114063

Electron spectroscopy on adsorption of Cs on transition metals See Entry 114344

On the role of image forces in chemisorption theory See Entry 114357

Ab initio mixed basis method of band structure calculation: γ -Fe and cubic ZnS electronic structures See Entry 114435

New type of local resonances in thin rough films See Entry 114582

Surface plasmon emission in metal-insulator-degenerate p -type semiconductor structures See Entry 114613

Optical properties of small metallic particles in a continuous dielectric medium See Entry 114803

The effect of the microscopic structure of metal surfaces on their optical properties See Entry 114807

Dynamical conductivity and dielectric function of general semiconductors and of magnetic semiconductors See Entry 114810

Optical determination of the electronic characteristics of Nb-Al alloys with the A15 lattice See Entry 114845

Incomplete relaxation and plasmon formation in the K emission band of copper See Entry 114975

Influence of film structure on the electron energy loss spectra of GaAs thin films See Entry 114982

Excitation of surface plasmons on He-filled cavities in Al See Entry 114983

71.45J Fermi-Thomas model

Interaction and charge transfer between vacancy and solute in dilute aluminium alloys See Entry 113970

71.50 LOCALIZED SINGLE-PARTICLE ELECTRONIC STATES

(*exc. impurities; for localisation in disordered structures, see 71.55J*)

114463 Localization and interactions. T.M.Rice (Theoretical Phys., ETH Zurich, Zurich, Switzerland).

Europhys. News (Switzerland), vol.14, no.7, p.6-7 (July 1983).

Progress made in the past few years in this field has been remarkable. Not only have spectacular new and unsuspected effects, such as the absence of true metallic conduction in two dimensions been discovered, but also a much better understanding of the metal-insulator transition has been obtained. The goal of a complete understanding, which has eluded us for more than 40 years, is in sight. The talks at the EPS meeting conveyed this progress but gave just a selection of the work underway in many groups in all parts of the world. (no refs.)

Rare earth atom-to-solid core level shifts: sensitivity to valence changes See Entry 113797

Effect of random doping on the electronic spectrum in trans-polyacetylene See Entry 114438

Electronic properties of a size-quantized film with uneven boundaries See Entry 114624

Soft X-ray appearance potential spectroscopy of the lanthanide rare earths See Entry 114972

Appearance potential study of the 4f levels of cerium, praseodymium and their oxides See Entry 114973

Core-level XPS studies of Ce and La intermetallic compounds and their implications for the 4f levels of Ce compounds See Entry 115023

71.55 IMPURITY AND DEFECT LEVELS

114464 Pressure dependence of the electron capture cross section of the B hole trap in liquid phase epitaxial gallium arsenide. C.E.Barnes, G.A.Samara (Sandia Nat. Lab., Albuquerque, NM, USA).

Appl. Phys. Lett. (USA), vol.43, no.7, p.677-9 (1 Oct. 1983).

A study of the hydrostatic pressure dependence of the electron capture cross section of the B hole trap in liquid phase epitaxial gallium arsenide has revealed that this cross section is strongly affected by pressure. The results are consistent with, and provide support for, the multiphonon emission model for the capture process at this trap. (12 refs.)

114465 Deep levels in semiconductors. P.J.Dean (Royal Signals & Radar Estab., Malvern, England).

Europhys. News (Switzerland), vol.14, no.7, p.9-10 (July 1983).

The amount of accurate experimental data on many deep level systems has grown rapidly in the past decade. We are still far from a thorough theoretical account of the complete set of properties for any one system, however. Current indications are that each system may require particular, special treatments. Excited states are hard to calculate on the self consistent basis used for ground states. However, useful generic trends have emerged within series of closely related defects or for a given defect in different binary hosts, or as a function of ternary alloy composition. An important joint outcome of the theoretical and experimental work is the recent recognition of the importance of antisite defects in the electronic properties of semiconductors. (no refs.)

114466 Spontaneous tunnel transitions induced by redistribution of trapped electrons over impurity centers. A.A.Berezin (Dept. of Engng. Phys., McMaster Univ., Hamilton, Ontario, Canada).

Z. Naturforsch. Teil A (Germany), vol.38A, no.9, p.959-62 (Sept. 1983).

A system of polyvalent impurity centers in a semiconductor (i.e. Au-centers in Si) is considered. The ground state of the impurity pair $Au^- + Au^0$ (b), where an extra electron is localized on the site a, may be turned into an

excited state due to a change of the charge state of a third nearby impurity site. This happens because of different shifts of the Au^- level at sites a and b due to their different distances from the third center. As a result, the original pair is able to reach a new ground state Au^0 (a) + Au^- (b) through a slow spontaneous tunnel transition. The probability of this transition, when it is accompanied by an emission of a low energy photon, is calculated explicitly. (10 refs.)

114467 Impurity-to-band tunneling in semiconductors. S.Chaudhuri (Univ. Res. Center, Wright State Univ., Dayton, OH, USA), D.D.Coon, R.P.G.Karunasiri.

J. Appl. Phys. (USA), vol.54, no.9, p.5476-8 (Sept. 1983).

Rate formulas for impurity-to-band tunneling from shallow and deep impurity levels are discussed. For the case of deep levels involving carriers bound to neutral impurity centers, it is shown that there is no substantial difference between the results of Anderson and Hoffman and those of Chaudhuri, Coon, Derkits, and Banavar. On the other hand, a different field dependence is found for the case of deep levels associated with carriers bound to charged impurity centers. (20 refs.)

114468 Complex band structure and deep impurities. II. Γ_{15} and Γ_{12} states. K.J.Blow, J.C.Inkson (Cavendish Lab., Univ. of Cambridge, Cambridge, England).

J. Phys. C (GB), vol.16, no.27, p.5267-75 (30 Sept. 1983).

For pt.1 see *ibid.*, vol.15, p.3711 (1982). The authors apply a model described in their paper I to Γ_{15} and Γ_{12} (p-and d-like) impurity states in zincblende structure semiconductors. The complex band structure for these symmetries is obtained and this is then related through the matching conditions, which are different for each irreducible representation, to the impurity wavefunction. These wave functions are then used to calculate the optical cross section and elucidate its dependence on the symmetry of the impurity. (15 refs.)

114469 Three holes bound to a double acceptor: Be^+ in germanium. E.E.Haller, R.E.McMurray, Jr., L.M.Falicov, N.M.Haegel, W.L.Hansen (Lawrence Berkeley Lab., Univ. of California, Berkeley, CA, USA).

Phys. Rev. Lett. (USA), vol.51, no.12, p.1089-91 (19 Sept. 1983).

A double acceptor binding three holes has been observed for the first time with photoconductive far-infrared spectroscopy in beryllium-doped germanium single crystals. This new center, Be^+ , has a hole binding energy of ~ 5 meV and is only present when free holes are generated by ionization of either neutral shallow acceptors or neutral Be double acceptors. The Be^+ center thermally ionizes above 4K. It disappears at a uniaxial stress $\geq 10^8$ dyn cm^{-2} parallel to [111] as a result of the lifting of the valence-band degeneracy. (11 refs.)

114470 The use of spatially-dependent carrier capture rates for deep-level-defect transient studies. G.P.Li, K.L.Wang (Electrical Engng. Dept., Univ. of California, Los Angeles, CA, USA).

Solid-State Electron. (GB), vol.26, no.9, p.825-33 (Sept. 1983).

The spatial dependence of the free carrier capture rate for the defect states located near the edge of the depletion layer is investigated. A theoretical treatment is presented here to illustrate the strong variation of the capture rate near the depletion edge with distance. If a transient capacitance technique is used to observe this capture transient, computer-calculated data confirm that the resulting signal comes only from the capture of electrons by those states located near the point at which the Fermi level and the deep level intersect. The capture of electrons by the states that are located in regions other than near the intersection point does not contribute to the detectable signal. Thus the transient signal measures the empty state concentration in a narrow region. Since the electric field in the narrow region can be accurately chosen by the use of different reverse pulse heights, the empty state concentration at that region can be controlled by the emission at different field strengths. The electric field dependence of the emission rate can be measured directly from the capture transient capacitance. Detailed comparisons of the calculated and experimentally measured data show good agreement. Possible applications using this technique in the study of deep-level defects are outlined. (8 refs.)

114471 Impurity states in undoped β -TiInS₂ crystals. A.E.Bakhyshov, S.R.Samedov, M.Ben'yamin, V.E.Bagiev, S.Bules, V.I.Tagirov (S.M. Kirov Azerbaidzhan State Univ., Baku, Azerbaidzhan SSR).

Sov. Phys.-Semicond. (USA), vol.17, no.3, p.307-8 (March 1983). Translation of: *Fiz. & Tekh. Poluprovodn. (USSR)*, vol.17, no.3, p.493-6 (March 1983).

[received: Sept. 1983]

The authors report the results of a study of impurity states in undoped β -TiInS₂ single crystals grown by the directional crystallization method. Measurements of the thermally stimulated current (TSC) were made as follows: a sample was cooled to 100K, a field of 100 V/cm intensity was then applied and at the same time the sample was illuminated with light of photon energy $h\nu \geq E_g$ for 15-20 min. After the end of illumination and establishment of a quasisteady state (at 100K), the sample was heated at a constant rate and the TSC curves were recorded. (11 refs.)

114472 Possibility of formation of an inverted distribution function of free carriers in semiconductors as a result of capture by shallow neutral impurities. E.M.Gershenzon, A.P.Mel'nikov, R.I.Rabinovich, V.B.Smirnova (V.I. Lenin State Pedagogical Inst., Moscow, USSR).

Sov. Phys.-Semicond. (USA), vol.17, no.3, p.311-12 (March 1983). Translation of: *Fiz. & Tekh. Poluprovodn. (USSR)*, vol.17, no.3, p.499-501 (March 1983).

[received: Sept. 1983]

The authors consider the formation of an inverted distribution function. When photoelectrons of energy $\epsilon \ll R_y$ are captured by shallow natural impurities, giving rise to negatively charged donors D^- (analogs of the negative hydrogen ion H^-), a one-phonon inelastic process becomes important and the lifetime τ may become shorter than τ_e . (6 refs.)

114473 Determination of the positions of iron impurities in gallium arsenide and phosphide by the ENDOR method. V.V.Teslenko (Inst. of Semiconductors, Acad. of Sci., Kiev, Ukrainian SSR).

Sov. Phys.-Semicond. (USA), vol.17, no.3, p.330-2 (March 1983). Translation of: *Fiz. & Tekh. Poluprovodn. (USSR)*, vol.17, no.3, p.526-8 (March 1983).

[received: Sept. 1983]

The author reviews the ENDOR data and obtains additional information on the interaction of iron impurities with ligand nuclei. Crystals used, were grown by the Czochralski method. They were doped with iron in the melt. Crystals grown by this method had seminsulating properties. The ENDOR spectra were determined using a superheterodyne spectrometer operating in the 3-cm range. The measurements were made at 4.2K. The ESR spectra included signals with the parameters $g=2.042$, $120B_0=330.10^{-4}$ cm⁻¹ and $g=2.025$, $120B_0=390.10^{-4}$ cm⁻¹ in the case of GaAs and GaP, respectively. These signals were due to an ion with the 3d⁵ configuration in the $^{65}S_{1/2}$ state. The concentrations of this ion were 10^{17} and 3.10^{17} cm⁻³ for GaAs and GaP, respectively. (9 refs.)

114474 Energy spectrum of defects in silicon irradiated with hydrogen and helium ions. A.I.Aeshin, L.S.Smirnov, V.F.Stas' (Inst. of Semiconductor Phys., Acad. of Sci., Novosibirsk, USSR).

Sov. Phys.-Semicond. (USA), vol.17, no.3, p.348-9 (March 1983). Translation of: *Fiz. & Tekh. Poluprovodn. (USSR)*, vol.17, no.3, p.551-3 (March 1983). [received: Sept. 1983]

Describes a study carried out by the deep level transient spectroscopy (DLTS) method which yielded the spectrum of defects generated by light hydrogen and helium ions, and gave information on the behavior of defects during annealing. The authors investigated oxygen-free silicon doped with phosphorus and gold (BKEFZ-3 grade). A p-n junction was formed by implantation of boron ions followed by 30-min annealing at 980°C. Diode structures were irradiated with hydrogen and helium ions in a Van de Graaff accelerator. After fabrication of mesa-diode structures, the irradiated and control (unirradiated) samples were annealed isochronously by 600°C. Unirradiated samples had deep centers with levels at $E_c-0.24$ and $E_c-0.54$ eV, typical of the gold atoms. The concentrations of these centers were not affected by the isochronous annealing. (5 refs.)

114475 Detection of electronic defects in strip-heater crystallized silicon thin films. N.M.Johnson, M.D.Moyer, L.E.Fennell (Xerox Palo Alto Res. Centers, Palo Alto, CA, USA), E.W.Maby, H.Atwater.

Laser-Solid Interactions and Transient Thermal Processing of Materials, Boston, MA, USA, 1-4 Nov. 1982 (New York, USA: Elsevier 1983), p.491-7. Electronic defects in strip-heater crystallized silicon thin films have been investigated with capacitance-voltage (C-V), deep-level spectroscopic, and scanning-electron microscopic techniques. For electrical characterization the crystallized silicon films were used to fabricate inverted metal-oxide-silicon capacitors in which degenerately doped bulk silicon substrates provided the gate electrode. High-frequency C-V characteristics yield effective fixed-charge densities in the oxide of $\leq 2 \times 10^{11} \text{ cm}^{-2}$. Trap-emission spectra, recorded with deep-level transient spectroscopy on both p-type and n-type capacitors, indicate a continuous distribution of deep levels throughout the silicon bandgap. The Si-SiO₂ interface is considered to be the principal source of this deep-level continuum, since the films are essentially single crystal with a low density of subgrain boundaries; the effective interface-state density is $\leq 2.5 \times 10^{10} \text{ eV}^{-1} \text{ cm}^{-2}$. A discrete energy level, detectable above the background continuum, appears in the upper half of the silicon bandgap; it may identify a point defect in the bulk of the silicon film with a spatially uniform density of approximately $1 \times 10^{13} \text{ cm}^{-3}$. On lateral p-n junction diodes, electron-beam-induced-current images reveal enhanced diffusion of arsenic along structural defects intersecting the junction. (18 refs.)

114476 Chalcogenides in silicon. H.G.Grimmeiss, E.Janzen (Dept. of Solid State Phys., Univ. of Lund, Lund, Sweden). Defects in Semiconductors II, Symposium Proceedings, Boston, MA, USA, Nov. 1982 (New York, USA: North-Holland 1983), p.33-44. If a host atom in Si is replaced by an atom from the sixth group in the periodic table, two extra electrons are available, which may give rise to double donors. In addition, the ground state of chalcogenide atoms in Si lies at much greater distance from the conduction band than impurity atoms from the fifth group and so chalcogenides create deep levels. The energy spectrum of a group VI impurity in Si is discussed and the spin-valley splitting of the $1s$ (T_2) state is examined. The optical absorption spectrum and Fano resonances are also described. (34 refs.)

114477 Metastable defect configurations in semiconductors. J.L.Benton, M.Levinson (Bell Labs., Murray Hill, NJ, USA). Defects in Semiconductors II, Symposium Proceedings, Boston, MA, USA, Nov. 1982 (New York, USA: North-Holland 1983), p.95-100.

Deep Level Transient Spectroscopy is used to examine the stability of defect configurations in Si and InP. A systematic approach has been developed to study alternate structures of metastable defects through their representative electronic states. Regulation of defect charge state prior to analysis reveals dramatic transformations in the resulting spectra. These defect states are metastable and can be controlled with thermal or electronic energy. Model studies in electron irradiated InP and Si are presented. The barriers to configurational change are determined from the reaction kinetics. The roles of electric field, minority carrier injection and charge state are explored through junction bias techniques. It is believed that the observed behavior represent a new class of defect reactions. The systematics of detecting and studying these reactions are presented. Model defect structures are discussed. (9 refs.)

114478 Thermal donor formation by the agglomeration of oxygen in silicon. U.Gosele (Max-Planck-Inst. für Metallforschung, Stuttgart, Germany), T.Y.Tan.

Defects in Semiconductors II, Symposium Proceedings, Boston, MA, USA, Nov. 1982 (New York, USA: North-Holland 1983), p.153-7. The authors suggest that thermal donor formation in silicon involves fast-diffusing, gas-like molecular oxygen in dynamical equilibrium with atomic oxygen in interstitial position. They discuss still remaining difficulties in understanding thermal donor formation in the light of recent experimental observations by Stavola et al. (1983), indicating that the diffusivity of interstitial oxygen apparently depends on the thermal history of the silicon sample. (18 refs.)

114479 Complex defects in GaAs and GaP. P.J.Lin-Chung (Naval Res. Lab., Washington, DC, USA).

Defects in Semiconductors II, Symposium Proceedings, Boston, MA, USA, Nov. 1982 (New York, USA: North-Holland 1983), p.267-70. A study of the electronic states associated with divacancy defects and with the defect complexes involving an anion antisite with a group IV atom (A_c-IV) in GaAs and GaP is reported. The local densities of states have been determined using the large cluster recursion approach. The properties as well as the position of the GaP states of the divacancy defect in GaAs are found to be consistent with the experimental results for the EL2 level. The change of the position of the defect levels of (A_c-IV) as a result of the change of bonding is analyzed. The effect of GaAs-AlAs interface on the (A_c-IV) defect level is also examined. (8 refs.)

114480 Process-induced defects in high-purity GaAs. P.M.Campbell, O.Aina, B.J.Baliga, R.Ehle (General Electric Res. & Dev. Center, Schenectady, NY, USA).

Defects in Semiconductors II, Symposium Proceedings, Boston, MA, USA, Nov. 1982 (New York, USA: North-Holland 1983), p.283-7. High temperature annealing of Si₃N₄ and SiO₂ capped high purity LPE GaAs is shown to result in a reduction in the surface carrier concentration by about an order of magnitude. Au Schottky contacts made on the annealed samples were found to have severely degraded breakdown characteristics. Using deep level transient spectroscopy, deep levels at E_c-58 eV, E_c-785 eV were detected in the SiO₂ capped samples and E_c-62 eV, E_c-728 eV in the Si₃N₄ capped samples while none was detected in the unannealed samples. The electrical degradations are explained in terms of compensation mechanisms and depletion layer recombination-generation currents due to the deep levels. (9 refs.)

114481 Electrical properties of dislocations and boundaries in semiconductors. H.J.Quisser (Max-Planck-Inst. für Festkörperforschung, Stuttgart, Germany).

Defects in Semiconductors II, Symposium Proceedings, Boston, MA, USA, Nov. 1982 (New York, USA: North-Holland 1983), p.323-41.

Simple models have been suggested to predict electronic properties of lattice defects in semiconductor crystals: dislocations ought to act via the acceptor character of dangling bonds, and small-angle grain boundaries ought to consist of regular arrays of dislocations. The actual situation in most semiconductors is, however, much more complicated. The observed electrical effects of dislocations do not confirm the dangling-bond concept, they are affected by dissociation and reconstruction. There appear to be differences between straight and kinked dislocations. Dislocations owe much of their electronic behavior to clouds and precipitates of impurities; oxygen in silicon plays a significant role. This review summarizes the present status of experimental methods and results, including luminescence and capacitance spectroscopy as well as mapping and imaging techniques using electron-microscopes. (95 refs.)

114482 Electronic states of grain boundaries in bicrystal silicon. C.M.Shyu, L.J.Cheng (Jet Propulsion Lab., California Inst. of Technol., Pasadena, CA, USA), K.L.Wang.

Defects in Semiconductors II, Symposium Proceedings, Boston, MA, USA, Nov. 1982 (New York, USA: North-Holland 1983), p.363-7.

Electronic states at a 20° symmetrical (100) tilt boundary in p-type silicon were studied using deep level transient spectroscopy (DLTS) and other electrical measurements. The data can be explained with a model in which the local barrier height at the grain boundary varies on a scale much smaller than the boundary plane ($\sim 1 \text{ nm}^2$) under study. Based on a relationship between the carrier capture cross section and energy level deduced from the experimental data, the authors have been able to calculate the distribution of the density of states in the energy bandgap at the boundary, which contains two groups of continuously distributed states; a major one whose density of states increases monotonically with the position of the state from the valence band, and a minor narrow one whose density of states is centered at $E_v+0.20$ eV. (9 refs.)

114483 Quenched-in defects in CW laser irradiated virgin silicon.

A.Chantre, M.Kechouane, D.Bois (CNET/CNS, Meylan, France). Defects in Semiconductors II, Symposium Proceedings, Boston, MA, USA, Nov. 1982 (New York, USA: North-Holland 1983), p.547-51.

Quenched-in defects in CW laser irradiated silicon have been identified using deep level transient spectroscopy. Four among the five dominant defect states arise from transition metal impurities (iron, chromium) present in precipitates in the as-grown material and dispersed into the crystal upon heat treatment. Native defects are involved in the form of phosphorous-vacancy complexes, which account for the remaining level. (18 refs.)

Defects in Semiconductors II, Symposium Proceedings See Entry 111315

Site symmetry of the metal ion in rare earth oxynitrates doped with europium(III) See Entry 113825

The calculated defect structure of thorium See Entry 113862

Transition metal impurities in silicon See Entry 113936

Appearance of an impurity ionization mechanism of defect formation in indium antimonide as a result of 'suprathreshold' irradiation See Entry 113986

Comparison between thermal and laser annealing in ion-implanted silicon See Entry 114021

Pulsed electron beam annealing induced deep level defects in virgin silicon See Entry 114030

Early stages of oxygen clustering and its influence on electrical behavior of silicon See Entry 114190

Detection of exciton luminescence of indium antimonide crystals See Entry 114448

Polarized luminescence due to localized excitons in CdS_{1-x}Se solid solutions See Entry 114449

Absorption of light by bound electron-exciton states in two-dimensional molecular crystals See Entry 114451

Local excitons and effects of their mixing with electronic impurity states in naphthalene See Entry 114452

Reduction in the localized band-gap states in amorphous silicon by annealing and hydrogen implantation See Entry 114484

Zeeman spectroscopy of crystal-field transitions of Co-doped InP See Entry 114492

Analysis of the Pr³⁺ spectrum in the incommensurate phase of ThCl₃ See Entry 114500

Effects of doping on transport and deep trapping in hydrogenated amorphous silicon See Entry 114533

Thermally stimulated current studies on cadmium selenide single crystals heat-treated in selenium vapour See Entry 114534

Correlation of lifetime with recombination centers in electron-irradiated P-type silicon See Entry 114536

Physical properties and functional possibilities for silicon structures compensated with zinc See Entry 114547

Influence of an electric field on the anomalous magnetoresistance of n-type Al_{0.5}Ga_{0.5}As See Entry 114554

Influence of external conditions on oscillations of the photocurrent in CdSe single crystals See Entry 114560

Photostimulated formation of shallow donors in 'pure' CdS crystals See Entry 114563

Mechanism of the photoconductivity of nickel-compensated gallium phosphide See Entry 114565

Photoconductivity of n-type germanium with 'repulsive' impurity centers at photon energies less than the thermal ionization energy See Entry 114566

Optical and thermal transitions in bismuth silicate See Entry 114567

Resonant amplification of sound near the spontaneous oscillation threshold of semiconductors under impurity and interband breakdown conditions See Entry 114571

Determination of the pressure of the semimetal-semiconductor transition in the presence of a resonant acceptor level See Entry 114574

Recombination processes in polycrystalline PbSe films See Entry 114627

Electronic properties of grain boundaries in GaAs: a study of oriented bicrystals prepared by epitaxial lateral overgrowth See Entry 114629

ESR of defects in III-V compounds See Entry 114734

Raman scattering of light in N activated CdS crystals See Entry 114870

- Ultraviolet A-band absorption in NaCl:Pb^{2+} and clustering of lattice defects ... See Entry 114887
- Color centers and electron spin resonance in chrysoberyl containing Mn and Ti guest ions ... See Entry 114890
- Spectrum of localized states near the fundamental absorption edge and likely mechanism of compensation of CdTe:Cl crystals ... See Entry 114896
- Infrared-absorption of thermal donors in silicon ... See Entry 114897
- The terbium-activated rare earth oxysulphide binary systems $(\text{Y}_{1-x}\text{La}_x)_2\text{O}_2\text{S}$, $(\text{Y}_{1-x}\text{Gd}_x)_2\text{O}_2\text{S}$ and $(\text{Gd}_{1-x}\text{La}_x)_2\text{O}_2\text{S}$ and their luminescence properties ... See Entry 114910
- Energy transfer processes between Eu^{3+} and Tb^{3+} in KY_3F_{10} ... See Entry 114913
- Influence of uniaxial pressure on the impurity photoluminescence band of GaAs:Cu with a maximum near 1.02 eV ... See Entry 114920
- Photoluminescence study of thermally treated silicon crystals ... See Entry 114926
- Deep radiative transitions in InP ... See Entry 114927
- Positron study of a vacancy in graphite ... See Entry 114957
- Enhancement of growth rate due to tin doping in GaAs epilayer grown by low pressure metal-organic chemical vapor deposition ... See Entry 115064
- Study of deep-level defects and annealing effects in undoped and Sn-doped GaAs solar cells irradiated by one-MeV electrons ... See Entry 115647

71.55J Localization in disordered structures

- 114484** Reduction in the localized band-gap states in amorphous silicon by annealing and hydrogen implantation. G.W.Neudeck, T.C.Lee (School of Electrical Engng., Purdue Univ., West Lafayette, IN, USA). *Appl. Phys. Lett. (USA)*, vol.43, no.7, p.680-2 (1 Oct. 1983). The effect of in situ thermal annealing prior to hydrogen implantation is reported on vacuum evaporated amorphous silicon. By performing a 400°C anneal for 4 h immediately following film deposition the film porosity is greatly reduced. The film is then implanted with hydrogen to a dose of $5 \times 10^{16}/\text{cm}^2$. A field-effect conductance change of six orders of magnitude was observed which yielded a density of localized states near the Fermi level of $4 \times 10^{17}/\text{cm}^3 \text{ eV}$. (16 refs.)
- 114485** Deep-level spectroscopy of reactively sputtered a-Si:H films. Ai-Lien Jung, Jin-Shen Luo, Xi Yao, Chen-Hsi Lin, Ya-Wen Yang, D.Adler (Center for Materials Sci. & Engng., MIT, Cambridge, MA, USA). *J. Non-Cryst. Solids (Netherlands)*, vol.57, no.2, p.241-50 (1 Sept. 1983). The authors have performed light-induced modulation of absorption spectroscopy, thermally stimulated current spectroscopy, capacitance measurements as a function of temperature and frequency, and electron spin resonance experiments on reactively sputtered a-Si:H films. They find evidence for seven different localized gap states in a range of $\pm 0.4 \text{ eV}$ around the midgap region. The possible origin of these states is discussed. (10 refs.)
- 114486** Determination of localized state distributions from anomalously-dispersive transport data. H.Michiel, J.M.Marshall, G.J.Adriaenssens (Lab. voor Vaste Stof en Hoge Druk-fysica, Katholieke Univ., Leuven, Belgium). *Philos. Mag. B (GB)*, vol.48, no.2, p.187-202 (Aug. 1983). A general relation is deduced between the density of localized states $N(E)$ and the transient photocurrent $I(t)$ for an amorphous semiconductor exhibiting trap-controlled electronic transport. It is demonstrated that the waiting-time distribution function $\psi(t)$ is related to $I(t)$ through a Volterra integral equation, which may be solved numerically. The relative density of states $N(S)$ may be deduced in a straightforward manner from $\psi(t)$, using an approximation which should not introduce more than a small degree of distortion. The computational method is applied to the case of an exponential tail of localized states, and to a system with three discrete sets of trapping centres. Finally, the consequences of an incomplete knowledge of some of the system parameters are considered. (23 refs.)
- Defects in amorphous silicon ... See Entry 113742
- Positron study of a vacancy in graphite ... See Entry 114957
- Angle-resolved photoemission study of some first-row transition-metal intercalates of NbS_2 and TaS_2 ... See Entry 115009

71.65 POSITRON STATES

(see also 78.70B Positron annihilation)

- Positronium velocity spectroscopy of the electronic density of states at a metal surface ... See Entry 114580
- Atomistic calculations of positron surface states ... See Entry 114581
- The study of thermal equilibrium defects and melting in indium by two-parameter correlation measurement of positron annihilation ... See Entry 114956

71.70 LEVEL SPLITTING AND INTERACTIONS

(see also 75.10 - in magnetic phenomena, 75.30E Exchange and superexchange interactions, 73.20 Electronic surface states)

- 114487** Change in samarium valence in $\text{SmB}_6\text{-NdB}_6$ solid solutions. M.I.Aivazov, S.V.Aleksandrovich, B.A.Evseev, V.S.Mkrtychyan, V.N.Sorokin, O.M.Tsarev. *Inorg. Mater. (USA)*, vol.18, no.9, p.1298-301 (Sept. 1982). Translation of: *Izv. Akad. Nauk SSSR Neorg. Mater.*, vol.18, no.9, p.1518-20 (Sept. 1982). [received: Sept. 1983]
- Two isostructural samarium hexaboride phases have been used in synthesizing $(\text{Sm}_{1-x}\text{Nd}_x)_2\text{B}_6$ solid solutions with the CaB_6 structure. When up to 30% of the samarium is replaced by neodymium, one gets solid solutions in the $\alpha\text{-SmB}_6\text{-NdB}_6$ ($y=1$) and $\beta\text{-SmB}_6\text{-NdB}_6$ ($y=0.8$) systems. For $x>0.3$ there is a region of homogeneity in the metal $0.8 \leq y \leq 1$. It is found that the average valence of the samarium ions decreases linearly as the samarium is replaced by neodymium. (6 refs.)
- 114488** Valence instabilities in rare earth systems as revealed by photoemission. R.A.Pollak (IBM Thomas J. Watson Res. Center, Yorktown Heights, NY, USA). *J. Less-Common Met. (Switzerland)*, vol.93, no.1, p.201-2 (1983). (Proceedings of the Sixteenth Rare Earth Research Conference, Tallahassee, FL, USA, 18-21 April 1983). The author used high resolution ($\delta E < 150 \text{ meV}$) photoemission with synchrotron radiation in the range 10 eV $< h\nu < 130 \text{ eV}$ to study archetypal mixed valent and related cerium-, samarium-, europium-, thulium- and ytterbium-based systems. Generally all mixed valent systems (except the cerium-based

system which is not yet fully characterized) exhibit an integer valent surface layer which has the lower value of the two bulk valence configurations. Temperature-dependent changes in bulk valence were observed in the europium and samarium compounds. Mixed valence was observed to persist down to at least 5 at.% dilution of thulium in $\text{Tm}_x\text{Y}_{1-x}\text{Se}$ while thulium appears to remain trivalent in all $\text{Tm}_x\text{Y}_{1-x}\text{S}$ compounds studied. (10 refs.)

114489 Photon-stimulated desorption from rare earth oxides. G.Loubriel (Sandia Nat. Labs., Albuquerque, NM, USA), C.C.Parks. *J. Less-Common Met. (Switzerland)*, vol.93, no.1, p.213-18 (1983). (Proceedings of the Sixteenth Rare Earth Research Conference, Tallahassee, FL, USA, 18-21 April 1983). Resonances in the photon-stimulated desorption (PSD) spectra of praseodymium, samarium, erbium, thulium and ytterbium oxides are reported at photon energies near their 4d edges. These resonances, which are also seen in soft X-ray absorption (SXA), arise from excitations of 4d electrons to the 4f shell. Comparisons of SXA and PSD show how PSD can be used to determine surface valency. (14 refs.)

114490 The role of the exchange interaction in the valence transition of Sm chalcogenides. N.Porrás-Montenegro (Dept. de Física, Univ. del Valle, Cali, Colombia). *Phys. Lett. A (Netherlands)*, vol.97A, no.5, p.202-6 (29 Aug. 1983). The indirect exchange interaction J between localized and conduction electrons has been included in the Hamiltonian of the hybridized RKK model. It was found that there are continuous and discontinuous transitions of $\langle \eta \rangle$ for different values of J . (13 refs.)

Crystal structure and Mossbauer spectrum of vonsenite, $2\text{FeO} \cdot \text{FeBO}_3$... See Entry 113806

Magnetic susceptibility of solid solutions based on two isostructural SmB_6 phases ... See Entry 114663

Fermi resonance effect and vibrational intensity in the weak charge-transfer complexes ... See Entry 114841

Theory of charge transfer excitation in surface enhanced Raman scattering ... See Entry 114865

X-ray spectroscopy contributions to the study of iron oxide mixed valence compounds. Analysis of K absorption fine structure ... See Entry 114967

Detailed absorption, reflectance, and UV photoelectron spectroscopic and theoretical studies of the charge-transfer transitions of CuCl_4^{2-} : correlation of the square-planar and the tetrahedral limits ... See Entry 115008

71.70C Crystal and ligand fields

114491 Two-dimensional dynamical Jahn-Teller effects in a mixed-valence benzotriazolato copper cluster, $\text{Cu}_5(\text{BTA})_6(\text{RNC})_4$. G.F.Kokoszka, J.Baranowski, C.Goldstein, J.Orsini, A.D.Mighell, V.L.Himes, A.R.Siedle (Dept. of Chem., State Univ. of New York, Plattsburg, NY, USA). *J. Am. Chem. Soc. (USA)*, vol.105, no.17, p.5627-33 (24 Aug. 1983). Clusters of composition $\text{Cu}_5(\text{BTA})_6(\text{RNC})_4$ [$\text{BTA} = \text{benzotriazolato}(1-)]$ were prepared from the reaction of copper(I) thiophenoxide, benzotriazole, and an organic isocyanide. $\text{Cu}_5(\text{BTA})_6(t\text{-C}_4\text{H}_9\text{NC})_4$ crystallizes in space group $P4_2/c$, $a = 13.836$ (4) Å, $c = 16.686$ (4) Å, $Z = 2$, $D_{\text{calc}} = 1.413$, $D_{\text{obsd}} = 1.41$ (2) Mg m^{-3} . The structure solution, based on 903 reflections, converged at $R = 0.063$ and $R_w = 0.047$. The molecular structure has 4 symmetry; compressed octahedral copper(II) is surrounded by four tetrahedrally coordinated copper(I) ions. η_5 -benzotriazolato(1-) ligands connect each Cu(I) ion with three symmetry-related Cu(I) sites and with the central Cu(II). Terminal $t\text{-C}_4\text{H}_9\text{NC}$ ligands are bonded to Cu(I). EPR data were obtained at various temperatures in the liquid nitrogen to room temperature range. Data were recorded at 9, 24, and 54 GHz. The large Cu(II)-Cu(II) distance of 12.858 Å in this cluster ensures that the effects of exchange interactions are virtually nonexistent and that electronic dipolar broadening would be small. The appearance of Cu(II) hyperfine structure in almost all of the spectra supports this expectation. Furthermore, the EPR data are not consistent with a d_{z^2} ground state in spite of the compressed octahedral molecular geometry. At low temperatures, the EPR spectra are quite normal: $g_{\parallel} = 2.271$ (4), $g_{\perp} = 2.069$ (4), $A_{\parallel} = (145 \pm 4) \times 10^{-4} \text{ cm}^{-1}$, and $A_{\perp} = 0$, consistent with a $d_{x^2-y^2}$ type ground state. Above 128K, a 'reversed spectrum' is observed and is interpreted in terms of a two-dimensional dynamical Jahn-Teller effect. The other three compounds also showed interesting temperature-dependent effects. (31 refs.)

114492 Zeeman spectroscopy of crystal-field transitions of Co-doped InP. M.J.Kane (Clarendon Lab., Univ. of Oxford, Oxford, England), C.Uihlein, M.S.Skolnick, P.J.Dean, W.Hayes, B.Cockayne. *J. Phys. C (GB)*, vol.16, no.27, p.5277-91 (30 Sept. 1983). The 474.0 meV and 785.8 meV crystal-field transitions of Co_2^{2+} in InP observed in photoluminescence (PL) and optical absorption respectively are studied in magnetic fields of up to 10 T. The 474.0 meV PL line is shown to arise from a $\Gamma_8\text{-}\Gamma_8$ transition in T_d symmetry between the lowest spin-orbit state (Γ_8) of the ${}^4T_2(\text{F})$ level of Co_2^{2+} and the spin-only $\Gamma_8({}^4A_2(\text{F}))$ ground state. The anisotropic g -values of the excited state, g_{\parallel} and g_{\perp} , are 5.48 ± 0.2 and -2.98 ± 0.15 respectively. An isotropic g -value of 2.14 ± 0.05 is obtained for the ground state, in agreement with the results of electron spin resonance on Co_2^{2+} . The Zeeman pattern of the 785.8 meV absorption line shows a marked trigonal (C_{3v}) symmetry due to Jahn-Teller (JT) coupling to T_2 distortion modes in the excited state. The Zeeman data are shown to be consistent with the behaviour expected from the ${}^4A_2(\text{F}) \rightarrow {}^4T_1(\text{F})$ transition of Co_2^{2+} , the ${}^4T_1(\text{F})$ state undergoing an almost static JT distortion. Anticrossings in the anisotropy plot of the Zeeman pattern are observed at the main symmetry directions. This cannot be explained on a model of static C_{3v} trigonal complexes, and is attributed to tunnelling between the magnetically equivalent distortion directions. Analysis of the Zeeman data gives $g_{\parallel} = 0.96 \pm 0.05$ and $g_{\perp} = 3.76 \pm 0.05$ for the ${}^4T_1(\text{F})$ excited state and $g = 2.10 \pm 0.10$ for the ${}^4A_2(\text{F})$ ground state. (15 refs.)

114493 Crystal field effects on 4f electrons: theories and reality. M.Faucher, D.Garcia (Lab. des Elements de Transition dans les Solides, CNRS, Meudon Bellevue, France). *J. Less-Common Met. (Switzerland)*, vol.93, no.1, p.31-44 (1983). (Proceedings of the Sixteenth Rare Earth Research Conference, Tallahassee, FL, USA, 18-21 April 1983). The present methods of calculating crystal field effects in a solid are examined. Several models intermediate between the entirely phenomenological model leading to the determination of the so-called 'experimental' crystal field parameters and a complete linear combination of atomic orbitals calculation have been constructed. In these models simplifying hypotheses lead to descriptions of crystal field effects which have some degree of parametricity, so that the term 'a priori determination' is sometimes misleading and should be redefined. The most sophisticated models are characterized by the smallest number of a priori assumptions. However, it is questionable whether an

increase in sophistication improves the agreement between theory and experiment. Practical methods of calculating crystal field parameters, i.e. in the framework of the electrostatic, angular overlap and weakly covalent models, are described. (48 refs.)

114494 Localized systems mechanisms for f-f transition probabilities in lanthanide coordination compounds. S.F.Mason (Chem. Dept., King's Coll., London, England).

J. Less-Common Met. (Switzerland), vol.93, no.1, p.45-58 (1983). (Proceedings of the Sixteenth Rare Earth Research Conference, Tallahassee, FL, USA, 18-21 April 1983).

The origins and development of the ligand polarization mechanism for f-f transition probabilities in lanthanide coordination compounds are briefly surveyed. Applied initially to lanthanide(III) complexes containing monoatomic ligands, which have an effectively isotropic polarizability, the mechanism is found to depend, on extension to the corresponding polyatomic ligand cases, on the anisotropy of the ligand polarizability tensor in complexes of the higher non-centric symmetries. The crystal field and the ligand polarization mechanisms make complementary intensity contributions to the f-f transitions of a given lanthanide(III) complex type which are dependent on the rank of the leading electric multipole transition moment. The latter mechanism contributes principally to the intensities of the ligand-hypersensitive 2^2 -pole f-f transitions, whereas the former mechanism is predominant for the 2^6 -pole transition intensities and makes the more important contribution in the 2^4 -pole cases. (72 refs.)

114495 Crystal field of europium doped in yttrium oxychloride: the covalent model. D.Garcia, M.Faucher (Lab. des Elements de Transition dans les Solides, CNRS, Meudon Bellevue, France).

J. Less-Common Met. (Switzerland), vol.93, no.1, p.119-25 (1983). (Proceedings of the Sixteenth Rare Earth Research Conference, Tallahassee, FL, USA, 18-21 April 1983).

A weakly covalent model is applied to calculate the crystal field splittings of the 4f energy levels of europium doped in yttrium oxychloride. The diagonal element of the hamiltonian matrix is approximated using a published orbital eigenvalue in the neutral atom ground state. The approximation proposed by Wolfsberg and Helmholz (1952) is utilized to evaluate the off-diagonal matrix elements for electron-electron interaction within a group of atoms including the rare earth and its nine first-nearest neighbours (four oxygen atoms and five chlorine atoms). The basis wavefunction of the interaction hamiltonian includes the 4f wavefunctions of the rare earth, the 2p and 2s wavefunctions of the four oxygen atoms, and the 3p and 3s wavefunctions of the five chlorine atoms. Ligand-ligand interactions are taken into account. The 4f electron energy levels lie well above the ns and np levels of the ligands so that the diagonalization of the interaction hamiltonian results in a small antibonding lifting of the degeneracy. The contribution to the splitting of the 4f orbitals from the remainder of the lattice (more distant ions) is calculated using the electrostatic model including consistent dipoles and is added to the first-neighbour contribution. (20 refs.)

114496 Further interpretation of the spectra of Pr^{3+} - LaF_3 and Tm^{3+} - LaF_3 . W.T.Carnall, H.Crosswhite (Chem. Div., Argonne Nat. Lab., Argonne, IL, USA).

J. Less-Common Met. (Switzerland), vol.93, no.1, p.127-35 (1983). (Proceedings of the Sixteenth Rare Earth Research Conference, Tallahassee, FL, USA, 18-21 April 1983).

The results of model crystal field calculations in C_{2v} symmetry for Pr^{3+} - LaF_3 and Tm^{3+} - LaF_3 are compared with experimental data for the nearly complete f^2 (f^2) configurations. It is shown that the method used results in computed levels that generally correlate closely with level energies deduced from experiment. However, a number of important new insights are gained and some previous assignments are questioned. (11 refs.)

114497 The experimental determination of second-rank crystal field parameters for rare earth compounds. E.Antic-Fidancev, M.Lemaitre-Blaise, P.Caro (Lab. des Elements de Transition dans les Solides, CNRS, Meudon Bellevue, France).

J. Less-Common Met. (Switzerland), vol.93, no.1, p.137-42 (1983). (Proceedings of the Sixteenth Rare Earth Research Conference, Tallahassee, FL, USA, 18-21 April 1983).

The second-rank crystal field parameters obtained for some Gd^{3+} and Eu^{2+} compounds with the $(4f)^7$ configuration using the experimental ${}^6\text{P}_{7/2}$ overall splitting and the intermediate Stark components can be tested by comparing the calculated ratios of the overall splitting of the three ${}^6\text{P}_i$ levels with the experimental values. The calculated value for ${}^6\text{P}_{7/2}/{}^6\text{P}_{5/2}$ is roughly 1.80, for ${}^6\text{P}_{7/2}/{}^6\text{P}_{3/2}$ it is 2.80 and for ${}^6\text{P}_{5/2}/{}^6\text{P}_{3/2}$ it is 1.55. The experimental values are usually in reasonable agreement with the theoretical values. Deviations may be due to a misidentification of the levels or to a very low symmetry such that the spacings cannot be adjusted using only two second-rank crystal field parameters. (14 refs.)

114498 Crystal field theory: past, present and future. D.J.Newman (Dept. of Phys., Univ. of Hong Kong, Hong Kong).

J. Less-Common Met. (Switzerland), vol.93, no.1, p.235 (1983). (Proceedings of the Sixteenth Rare Earth Research Conference, Tallahassee, FL, USA, 18-21 April 1983).

Summary form only given, as follows. Both the phenomenological and the ab initio approaches to interpreting crystal field splitting are described. The phenomenological approach is viewed as a hierarchy of parametrized models, each model being characterized by explicit hypotheses about the nature of the crystal field. Ab initio calculations can be made in relation to any level of this hierarchy, the hypotheses of the phenomenological model being included in the calculation. It is emphasized that the ab initio approach is necessary to bring the theory into contact with experimental data other than crystal field splitting. Several possible lines of future development are described, including extensions of the phenomenological approach to include new systems, such as metals, and ways of improving the description of the experimental data by including more parameters. Developments of the theory of transition intensities and dynamic crystal field interactions are also discussed. (no refs.)

114499 Spin-correlated crystal field effects in lanthanide ions. W.Y.P.Fung, D.J.Newman (Dept. of Phys., Univ. of Hong Kong, Hong Kong).

J. Less-Common Met. (Switzerland), vol.93, no.1, p.241 (1983). (Proceedings of the Sixteenth Rare Earth Research Conference, Tallahassee, FL, USA, 18-21 April 1983).

Summary form only given as follows. Ab initio calculations of overlap and covalency contributions to the spin-correlated crystal field (SCCF) in Pr^{3+} with a single ligand are described. It is shown that covalency provides a positive contribution to the c_2 parameters describing the SCCF, thus giving a possible explanation of some characteristic experimental results. Numerical results for various types of contribution to the SCCF are tabulated. (no refs.)

114500 Analysis of the Pr^{3+} spectrum in the incommensurate phase of ThCl_4 . C.Khan Malek, J.C.Krupa, M.Genet (Lab. de Radiochimie, Inst. de Phys. Nucleaire, Orsay, France).

J. Less-Common Met. (Switzerland), vol.93, no.1, p.241 (1983). (Proceedings of the Sixteenth Rare Earth Research Conference, Tallahassee, FL, USA, 18-21 April 1983).

Summary form only given. The crystal energy level structure problem in the Pr^{3+} ($4f^3$) configuration is formally equivalent to that for its isoelectronic actinide ion U^{4+} ($5f^3$). The modulated and incommensurate low temperature phase of the matrix in a U^{4+} doped single crystal of ThCl_4 produces characteristic lineshapes owing to the modulation of the crystal field. The modulation of the halide position reduces the site symmetry from D_{2d} to D_2 and, as has been shown from spectral singularities, some of the U^{4+} impurity ions pin the phase of the modulation and remain in D_{2d} sites. This behaviour is not obvious in the Pr^{3+} - ThCl_4 spectra where the lineshapes are more conventional and the transitions are less intense. This is due to the fact that the protected 4f electrons are less sensitive to the crystal field manifestation than are the 5f electrons which are characterized by a greater extension of the radial wavefunction. As a consequence the crystal Stark splitting is roughly half that in U^{4+} - ThCl_4 and the SLJ multiplets of Pr^{3+} can easily be labelled because there is no significant overlapping except, possibly, in the weak lines of the ${}^1\text{I}_6$ group. 34 crystal field states were identified as being associated with D_{2d} site symmetry and were fitted to the parameters with a deviation of 29 cm^{-1} . (no refs.)

114501 Emission spectrum and crystal field parameters of pentanitratouropate (III) ions. J.-C.G.Bunzli, B.Klein, G.-O.Pradervand (Inst. de Chimie Minerale et Analytique, Univ. de Lausanne, Lausanne, Switzerland), P.Porcher.

J. Less-Common Met. (Switzerland), vol.93, no.1, p.241-2 (1983). (Proceedings of the Sixteenth Rare Earth Research Conference, Tallahassee, FL, USA, 18-21 April 1983).

Summary form only given, as follows. A spectroscopic investigation at 77K of finely powdered samples of $\text{A}_2[\text{Eu}(\text{NO}_3)_5]$ with $\text{A} \equiv (\text{C}_6\text{H}_5)_4\text{As}^+$, $(\text{C}_6\text{H}_5)_3\text{P}^+$ and $(\text{CH}_3)_4\text{N}^+$ is reported. The crystal structure of $((\text{C}_6\text{H}_5)_4\text{As})_2[\text{Eu}(\text{NO}_3)_5]$ reveals a ten-coordinate polyhedron which can be approximately fitted to a bicapped dodecahedron; the site symmetry of the europium(III) ion is C_2 . However, if the nitrate ions are assumed to occupy one coordination site, the resulting polyhedron is almost a trigonal bipyramid and this pseudosymmetry is reflected in the pattern of the emission spectrum. The authors have attempted to reproduce the crystal field splitting by various sets of parameters using the method of descending symmetry. For $((\text{C}_6\text{H}_5)_3\text{P})_2[\text{Eu}(\text{NO}_3)_5]$ standard deviations of 18 cm^{-1} and 11 cm^{-1} are obtained with hamiltonians of D_{3h} and C_{2v} symmetry respectively. The influence of the counter-cation on the local pseudosymmetry is discussed. (2 refs.)

114502 Hyperfine fields of ${}^{61}\text{Ni}$ in an Ni-Fe alloy. V.S.Pokatilov (I.P. Bardin Central Sci.-Res. Inst. of Ferrous Metall., Moscow, USSR).

Sov. Phys.-Dokl. (USA), vol.27, no.12, p.1065-7 (Dec. 1982). Translation of: *Dokl. Akad. Nauk SSSR*, vol.267, no.4-6, p.1368-70 (Dec. 1982). [received: Sept. 1983]

The author studies the influence of the environment on the hyperfine fields of ${}^{61}\text{Ni}$ in an Ni-Fe alloy with the aim of separating the contributions to the hyperfine field from the nickel atom and from its nearest-neighbor environment. (8 refs.)

Self-induced acoustic transparency of dilute paramagnetic crystals See Entry 113181

Hindered rotational energy levels of a tetrahedron in a tetragonal crystalline field See Entry 113774

Properties of Cu^{2+} ion in the $\gamma\text{-AgCuPO}_4$ structure See Entry 113827

Radiation damage in tantalum observed by PAC See Entry 114055

Nonlinear static magnetic susceptibility of the Van Vleck paramagnet TmPO_4 See Entry 114666

Inelastic scattering of neutrons by paramagnetic ions under relaxation conditions See Entry 114668

Magnetic crystallographic anisotropy of the ferrimagnetic iron oxide $\gamma\text{-Fe}_2\text{O}_3$ See Entry 114683

The unusual EPR spectra in single crystals of $\text{CuSiF}_6 \cdot 6\text{H}_2\text{O}$ and $\text{CuSiF}_6 \cdot 6\text{D}_2\text{O}$ See Entry 114729

The influence of Cr and W contents of the isomer shift, hyperfine field distribution, and magnetic anisotropy of Fe-based amorphous alloys See Entry 114758

Comment on 'Mossbauer studies of the 6.2 keV γ -rays of ${}^{181}\text{Ta}$ in Ta-dichalcogenides' See Entry 114764

Magnetic circularly polarized luminescence as a probe of ligand fields in the solid state and in solution See Entry 114833

The electronic structure of f element compounds elucidated by less common spectroscopic methods See Entry 114851

Raman scattering of light in N activated CdS crystals See Entry 114870

Judd-Ofelt parameters and chemical bonding See Entry 114888

Rationalization of the f-f intensity parameters for transitions between crystal field levels of lanthanide ions See Entry 114889

Absorption spectrum of Cr^{3+} ion doped in lithium ammonium sulphate single crystal See Entry 114895

Has the $(\text{LnO})_n^{++}$ ($\text{Ln} \equiv$ lanthanide) complex cation a spectroscopic 'fingerprint'? See Entry 114909

71.70E Spin-orbit coupling, Zeeman, Stark and strain splitting

114503 The lowest triplet state of tetramethyl-1,3-cyclobutanedithione. II. Calculation of spin-orbit coupling. J.Baiardo, M.Vala (Dept. of Chem., Univ. of Florida, Gainesville, FL, USA).

Chem. Phys. (Netherlands), vol.79, no.3, p.403-12 (15 Sept. 1983). For pt.1 see ibid., vol.79, p.391 (1983). A calculation of the spin-orbit coupling in the lowest excited triplet state of tetramethyl-1,3-cyclobutanedithione (TMCBDT) has been performed. The results show the following. (1) In the TMCBDT crystal the ground single-to-lowest triplet transition moment is predicted to be exclusively \perp c polarized as observed. (2) The assignment of the lowest triplet state should be ${}^3\text{A}_{u_g}$, as found earlier for the oxygen analog, TMCBD. (3) The two largest contributors ($\approx 60\%$) to the isolated-molecule $\text{T}_{1u} \rightarrow \text{S}_0$ transition moment come from the two triplet-triplet transitions ${}^3\text{n}_+\pi^* \leftarrow {}^3\text{n}_+\pi^*$ and ${}^3\text{n}_-\pi^* \leftarrow {}^3\text{n}_+\pi^*$, both of which are polarized along the C=S bonds. (4) The total contribution to the transition moment parallel to the C=S bonds is 76% from the $\text{T}_{1u} \rightarrow \text{T}_1$ transitions and 24% from the $\text{S}_k \rightarrow \text{S}_0$ transitions. And, finally, (5) the calculated oscillator strength of

2×10^{-4} for the largest $T_1\leftarrow S_0$ component (along y) falls within the range of typical spin-allowed, singlet-singlet $n\pi^*$ transitions. (14 refs.)

114504 Suppression by a longitudinal magnetic field of spin relaxation of conduction electrons in semiconductor crystals lacking an inversion center. V.A.Marushchak, M.N.Stepanova, A.N.Titkov (A.F. Ioffe Physicotech. Inst., Acad. of Sci., Leningrad, USSR). *JETP Lett. (USA)*, vol.37, no.7, p.400-3 (5 April 1983). Translation of: *Pis'ma v Zh. Eksp. & Teor. Fiz. (USSR)*, vol.37, no.7, p.337-40 (5 April 1983). [received: Oct. 1983]
Experiments have shown that the orbital motion of conduction electrons in a magnetic field effectively suppresses the spin relaxation of electrons caused by the spin-orbit splitting of the conduction band in crystals lacking an inversion center. (11 refs.)

Landau levels in the generalized Kildal-Bodnar model (with Cd_3P_2 and Cd_3As_2 as examples)See Entry 114458

Zeeman spectroscopy of crystal-field transitions of Co-doped InPSee Entry 114492

The experimental determination of second-rank crystal field parameters for rare earth compoundsSee Entry 114497

Analysis of the Pr^{3+} spectrum in the incommensurate phase of $TbCl_4$ See Entry 114500

Laser-induced emission of $CaF_2\cdot Tb^{3+}$ at room and low temperaturesSee Entry 114905

Luminescence properties and two-photon absorption of Gd^{3+} -doped $LaCl_3$ See Entry 114906

71.70G Exchange interactions

The role of the exchange interaction in the valence transition of Sm chalcogenidesSee Entry 114490

Ni^{2+} pair spectra in the excited orbitally degenerate states ...See Entry 114880

Appearance potential study of the 4f levels of cerium, praseodymium and their oxidesSee Entry 114973

71.70J Nuclear states and interactions

114505 Interference of the sign of electric field gradient QS-IS correlation in iron compounds. N.D.Sharma, F.A.Kasir (Dept. of Phys., Coll. of Sci., Univ. of Mosul, Mosul, Iraq). *Iraqi J. Sci.*, vol.22, no.4, p.544-53 (1981). [received: Aug. 1983]
It is reported that from the correlation which exists between quadrupole splitting (QS) and isomer shift (IS) for a series of iron compounds; it is possible to infer the sign of the electric field gradient (EFG) for the whole series, provided the sign of EFG for one of the compounds is known by either the magnetic perturbation or the single crystal technique. (20 refs.)

Self-induced acoustic transparency of dilute paramagnetic crystalsSee Entry 113181

Radiation damage in tantalum observed by PACSee Entry 114055

Nonlinear static magnetic susceptibility of the Van Vleck paramagnet $TmPO_4$ See Entry 114666

Local boron environment in $Ni_{100-x}B_x$ metallic glasses: A NMR studySee Entry 114754

Comment on 'Mossbauer studies of the 6.2 keV γ -rays of ^{181}Ta in Ta-dichalcogenides'See Entry 114764

72.00 ELECTRONIC TRANSPORT IN CONDENSED MATTER

(for surfaces, interfaces, and thin films, see 73.)

Proceedings of Helsinki International Summer School on Semiconductors 1982See Entry 111297

72.15 ELECTRONIC CONDUCTION IN METALS AND ALLOYS

114506 Electrical conductivity and galvanomagnetic properties of $SbCl_5$ intercalated graphite. E.I.Khar'kov, L.L.Koletsnichenko, L.Yu.Matsui (T.G. Shevchenko State Univ., Kiev, Ukrainian SSR). *Sov. Phys.-Solid State (USA)*, vol.25, no.2, p.338-9 (Feb. 1983). Translation of: *Fiz. Tverd. Tela (USSR)*, vol.25, no.2, p.594-6 (Feb. 1983). [received: Sept. 1983]
The authors report an investigation of the electrical conductivity, magnetoresistance and Hall coefficient of $SbCl_5$ intercalated graphite based on fine grained highly oriented pyrolytic graphite. The measurements were carried out by the usual four probe method. (14 refs.)

Gas-phase insertion of fluorine anions (BF_4^- and PF_6^-) in graphite using nitril saltsSee Entry 115031

72.15C Electrical and thermal conduction in amorphous and liquid metals and alloys

114507 Electrical resistivity and magnetoresistivity of amorphous $Fe_{80}B_{20}$, $Fe_{80}B_{18}Si_2$, $Fe_{80}B_{13}Si_4C_3$ and $Cu_{60}Zr_{40}$ alloys. Y.D.Yao (Inst. of Phys., Acad. Sinica, Taipei, Taiwan), S.Arajs, S.T.Lin. *Annu. Rep. Inst. Phys. Acad. Sin. (Taiwan)*, vol.12, p.243 (Dec. 1982). [received: Sept. 1983]
The authors report measurements on the temperature dependent electrical resistivity and on the field dependence of magnetoresistivity on the amorphous nonmagnetic alloy $Cu_{60}Zr_{40}$ and the amorphous ferromagnetic alloys $Fe_{80}B_{20}$, $Fe_{80}B_{18}Si_2$ and $Fe_{80}B_{13}Si_4C_3$. (no refs.)

114508 Features of the electrical resistivity of liquid tungsten under conditions of restricted volume and of free expansion. V.V.Ivanov, S.V.Lebedev, A.I.Savvatimskii (Inst. of High Temperatures, Acad. of Sci., USSR). *High Temp. (USA)*, vol.20, no.6, p.862-7 (Nov.-Dec. 1982). Translation of: *Teplotiz. Vys. Temp. (USSR)*, vol.20, no.6, p.1093-7 (Nov.-Dec. 1982). [received: Sept. 1983]
It is found that on heating metals with a pulsed current of high density without restricting expansion, the quantity $K=m/\alpha T$ entering the expression for the resistivity (α is the number of conduction electrons per atom, τ and m are there relaxation time and effective electron mass) decreases for tungsten and increases for Cu, Au, Ni, Ir, and Rh at the initial stage of the liquid state. The observed decrease in K is related to the thermal expansion of the liquid tungsten: on heating in a restricted volume, the fall in K at the beginning of the liquid region is less pronounced. For liquid copper restricting the volume weakens the rise in K compared with the case of heating with free expansion. (9 refs.)

114509 Electrical resistance of Fe-Zr and Fe-Ni-Zr amorphous alloys under hydrostatic pressure. K.Shirakawa (Res. Inst. of Electric & Magnetic Alloys, Sendai, Japan), K.Fukamichi, T.Kaneko, T.Masumoto. *Phys. Lett. A (Netherlands)*, vol.97A, no.5, p.213-16 (29 Aug. 1983).
The effect of pressure on the electrical resistance of $Fe_{90}Zr_{10}$ and $(Fe_{0.96}Ni_{0.04})_{90}Zr_{10}$ amorphous alloys has been investigated. The minimum point in the electrical resistance versus temperature curve shifts toward lower temperature range with increasing hydrostatic pressure, corresponding to the shift of the Curie temperature. The decrement of the electrical resistance below the Curie temperature T_c is about twice that above T_c , suggesting a large compressibility in the ferromagnetic state of the amorphous Invar alloys. (28 refs.)

Radiation damage in glassy $Pd_{80}Si_{20}$ and $Cu_{50}Zr_{50}$ See Entry 114058

72.15E Electrical and thermal conduction in crystalline metals and alloys

114510 The electrical resistivity of GP zones. Temperature dependence. A.J.Hillel (Dept. of Theoretical Phys., Manchester Univ., Manchester, England). *Philos. Mag. B (GB)*, vol.48, no.3, p.237-43 (Sept. 1983).
The influence of the measuring temperature on the resistivity of GP zone-forming alloys is investigated theoretically in the light of recent measurements. The current theory explains the observations satisfactorily: for spherical clusters the measuring temperature has little influence on the resistivity, while for platelets, an increase in measuring temperature leads to a substantially higher peak resistivity occurring at a later ageing time. It remains slightly mysterious that the measuring temperature has absolutely no detectable influence in the case of Al-Zn. (17 refs.)

114511 Isothermal recovery of electrical resistivity in aluminum immediately after deformation. O.Haruyama, H.Yamaguchi, S.Yoshida (Dept. of Phys., Sci. Univ. of Tokyo, Tokyo, Japan).
Point Defects and Defect Interactions in Metals. Proceedings of the Yamada Conference V, Kyoto, Japan, 16-20 Nov. 1981 (Amsterdam, Netherlands: North-Holland 1982), p.740-2
Isothermal recovery curves of the electrical resistivity of deformed aluminum (99.995 at.% purity) were measured immediately after the elongation, 4, 7, 13%. Peaks indicating a reverse recovery of resistivity were observed at adequate aging temperatures except for the specimen elongated about 4%. These reverse recoveries were interpreted from the dissociation of small vacancy clusters formed during the elongation. (5 refs.)

A quantitative study of vacancy defects in quenched tungsten by combined field-ion microscopy and electrical resistometrySee Entry 113863

Properties of point defects in FCC metalsSee Entry 113875

Vacancies in silver: a resistivity and positron annihilation studySee Entry 113876

Point defects in BCC Fe-Al, Fe-Co, and Fe-Co-V ordered alloysSee Entry 113883

A method for determining the vacancy concentration in concentrated alloys by resistivity measurements utilizing the rate of short range order formationSee Entry 113888

Self-interstitial mobility in a neutron-irradiated austenitic $Fe_{50}Cr_{16}Ni_{25}$ alloySee Entry 113890

Strong interaction between vacancy and solute in goldSee Entry 113967

A positron lifetime study of vacancy-solute complexes in dilute gold alloysSee Entry 113968

Interaction and charge transfer between vacancy and solute in dilute aluminium alloysSee Entry 113970

Formation of vacancies in thermal equilibrium in α -range alloysSee Entry 113972

Influence of alloy composition on defect production and recovery, in austenitic Fe-Cr-Ni solid solutions electron-irradiated at low temperatureSee Entry 114032

Re-examination of the threshold energy surface in copperSee Entry 114033

Differences in saturation of defects between electrons and reactor neutron irradiations at low temperatureSee Entry 114034

Recovery of Cu, Ag, and Ni dilute alloys after low temperature irradiationSee Entry 114046

Influence of the degree of purity on high-temperature phase transitions in samariumSee Entry 114168

Some high-temperature properties of Zircaloy-oxygen alloysSee Entry 114213

Effect of magnetic transformation on the nonmagnetic properties of Ce_2Ge_3 See Entry 114690

Kinetics of a polymorphic transition in an Ag-Zn alloy under the action of γ raysSee Entry 115188

Quenching investigations on BCC transition metalsSee Entry 115230

Properties of two high strength, high temperature, high conductivity copper-base alloysSee Entry 115264

The preparation and properties of metallic optically transparent electrodesSee Entry 115565

72.15G Galvanomagnetic and other magnetotransport effects

Pulse technique for measuring magnetoresistance of metals in high magnetic fieldsSee Entry 111704

The effect of disorder on the quantised Hall conductivitySee Entry 114457

Electrical conductivity and galvanomagnetic properties of SbCl₅ intercalated graphiteSee Entry 114506

Electrical resistivity and magnetoresistivity of amorphous Fe₈₀B₂₀, Fe₈₀B₁₈Si₂, Fe₈₀B₁₃Si₄C₃ and Cu₆₀Zr₄₀ alloysSee Entry 114507

Oscillations of metal-plate impedance and character of electron reflectionSee Entry 114587

72.15J Thermoelectric effects

114512 Change in structure of chromel-alumel thermoelectric transducers used in a medium of natural gas. R.V.Druk, V.S.Frenchko, B.I.Gil', V.I.Lakh, I.E.Lopatinskii (Thermal Instrument Sci. & Production Union, Lvov, Ukrainian SSR). *Sov. Mater. Sci. (USA)*, vol.18, no.6, p.536-7 (Nov.-Dec. 1982). Translation of: *Fiz.-Khim. Mekh. Mater. (USSR)*, vol.18, no.6, p.85-6 (Nov.-Dec. 1982). Investigations were made of the structure of the thermoelectric properties of 1.2-mm-diameter thermoelectrodes of Chromel (9.8 Cr, 0.10 Si, 0.02 Mn, 0.63 Co, 0.15 Fe, 0.07 C, and 0.12 Mg) and Alumel (1.24 Si, 1.95 Al, 2.10 Mn, 0.80 Co, 0.05 Fe, 0.01 C, and 0.07 Mg) in service at 800°C for 10, 3000, 6500, and 10000 h in natural gas. The basic component of the gaseous medium was methane with small amounts of impurities of oxygen, nitrogen, and carbon dioxide. The thermoelectric transducers were used in sheaths of Kh25T steel but there was not full protection from penetration of the gaseous medium. The processes occurring close to the surface and in the depth of thermal electrodes were studied by X-ray, optical, and spectral methods and by metallographic analysis. (3 refs.)

Influence of the degree of purity on high-temperature phase transitions in samariumSee Entry 114168

72.15L Relaxation times and mean free paths

Oscillations of metal-plate impedance and character of electron reflectionSee Entry 114587

72.15N Collective modes, e.g. in one-dimensional conductors

114513 Electrically conductive thermoplastic elastomer/polyacetylene blends. K.I.Lee, H.Jopson (Fundamental Res. Lab., GTE Labs. Inc., Waltham, MA, USA). *Polym. Bull. (Germany)*, vol.10, no.1-2, p.105-8 (June 1983). Three different types of thermoplastic elastomers, styrene-butadiene-styrene, styrene-isoprene-styrene, and styrene-ethylenebutylene-styrene triblock copolymers have been blended with polyacetylene utilizing various blending techniques. In one method, acetylene gas was polymerized with the Ziegler-Natta catalyst in the presence of either the thermoplastic elastomer film or a hydrocarbon solution of the thermoplastic elastomer. The resulting polyacetylene/thermoplastic elastomer blend has been characterized with infrared spectroscopy, X-ray diffraction and electron microscopy. Upon doping with either iodine or ferric chloride, the ultimate conductivities of the blends were found to be 60-100 Ω⁻¹. (5 refs.)

114514 Nonlinear and frequency-dependent transport phenomena in low-dimensional conductors. G.Gruner (Dept. of Phys., Univ. of California, Los Angeles, CA, USA). *Physica D (Netherlands)*, vol.8D, no.1-2, p.1-34 (July 1983). Nonlinear and frequency-dependent electrical conductivity is more a rule than an exception in materials with highly anisotropic electronic structure. Disorder leads to localization of the electronic wave functions, and the temperature-(T), electric field-(E), and frequency (ω)-dependent transport are due to random transfer rates between localized single particle states, a process fundamentally different from band transport. Interactions lead to collective modes, represented by a periodic modulation of the charge or spin density. The charge density wave (CDW) mode is pinned by impurities, but for small pinning forces it can be depinned by moderate electric fields, leading to nonlinear conductivity due to a sliding CDW. Both classical and quantum models account for the field and frequency dependent response; they also describe current oscillation phenomena and effects which arise when both DC and AC excitations are applied. For strong pinning the collective mode cannot be depinned at small electric field strengths, but nonlinear (soliton) excitations of the collective modes may be responsible for the nonlinear conductivity observed. In all these cases field- and frequency-dependent transport is strongly related. This feature is reproduced by various models, and therefore a detailed study of σ(T,E,ω) is called for to distinguish between the various sources of novel transport phenomena in these new types of solids. (98 refs.)

114515 Polyacetylene: A perspective in scientific and technological research of condensed matter physics. M.Apostol (Sectia Fizica Fundamentala, Inst. de Fizica si Inginerie Nucleara, Bucuresti, Rumania). *Stud. & Cercet. Fiz. (Rumania)*, vol.35, no.8, p.681-9 (1983). In Rumanian. Physical and chemical properties of polyacetylene (trans isomer) are briefly reviewed. Soliton theory of the electron-phonon coupling in polyacetylene is discussed. The possible practical applications of this material are emphasized. (7 refs.)

114516 Macroscopic coherence length of charge-density waves in orthorhombic TaS₃. G.Mihaly, G.Hutiray, L.Mihaly. *Report KFKI-1983-52*, Hungarian Acad. Sci., Budapest (1983), 15 pp. Four probe continuous and pulsed DC current-voltage measurements on orthorhombic TaS₃ showed that the distance between potential contacts influences (i) the sharpness of the metal-semiconductor transition at 222K and (ii) the threshold potential at which, in the low temperature phase, nonlinearity sets in. The closeness of voltage contacts on the 100 μm scale smears out the phase transition and increases the threshold field indicating that the coherence of CDW states is destroyed by the perturbation of contacts. (11 refs.)

Band theory of some polymers derived from polyparaphenyleneSee Entry 114434

Structure factors and elementary excitations of condensed matterSee Entry 114459

Tunneling between conductors with a charge-density waveSee Entry 114595

72.15Q Scattering mechanisms and Kondo effect
(see also 75.20H Local moments in dilute alloys)

114517 Electron-deformation currents in metals. V.B.Fiks (A.F. Ioffe Physicotech. Inst., Acad. of Sci., USSR). *Sov. Phys.-JETP (USA)*, vol.83, no.5, p.1077-9 (Nov. 1982). Translation of: *Zh. Eksp. & Teor. Fiz. (USSR)*, vol.83, no.5, p.1864-9 (Nov. 1982). [received: Sept. 1983]

It is shown that a defect flux in a metal gives rise to an electron-deformation (ED) current. Since deformations give rise to dislocation fluxes, the metal deformations cause electron currents. The ED currents are proportional to the deformation rate $\dot{\epsilon}$ and increase with decreasing temperature like T⁻⁵ in the isotropic model of the metal. Below the superconducting-transition point the ED currents are proportional to the density of the normal electrons and are equal to zero in a superconducting metal. (9 refs.)

Oscillations of metal-plate impedance and character of electron reflectionSee Entry 114587

72.20 CONDUCTIVITY PHENOMENA IN SEMICONDUCTORS AND INSULATORS
(for nonelectronic thermal conduction, see 66.70)

Non-crystalline semiconductorsSee Entry 113738

72.20D General theory, scattering mechanisms

114518 Estimation of alloy scattering potential in ternaries from the study of two-dimensional electron transport. P.K.Basu, B.R.Nag (Inst. of Radio Phys. & Electronics, Calcutta, India). *Appl. Phys. Lett. (USA)*, vol.43, no.7, p.689-91 (1 Oct. 1983). A theory of alloy scattering of a two-dimensional electron gas in ternary semiconductors is developed by assuming a spherically symmetric square potential, randomly distributed between two kinds of alloy sites. The theory predicts a temperature independent mobility, in agreement with the experimental results for In_{0.53}Ga_{0.47}As. The calculated value at 4.2K comes close to the experimental value, in which the effect of impurity scattering has been reduced by using an undoped spacer layer. It is concluded that the study of two-dimensional transport in the devices may lead to a correct estimation of the alloy scattering potential. (16 refs.)

114519 Polar, intervalley and acoustic scatterings in III-V group semiconductors. Application to GaAs and InSb. N.A.Saleh, K.S.Dubey (Dept. of Phys., Coll. of Sci., Univ. of Basrah, Basrah, Iraq). *Iraqi J. Sci.*, vol.22, no.4, p.520-43 (1981). [received: Aug. 1983]

Polar, intervalley and acoustic scattering have been studied in III-V group semiconductors by studying the variation of the polar, intervalley and acoustic scattering relaxation rates with temperature in the entire temperature range 50-500K for GaAs and InSb. The variations of these scattering relaxation rates with the effective mass m* as well as with the energy E have also been studied at a constant temperature T=300K for both semiconductors GaAs and InSb. The percentage contributions due to absorption and emission towards the total scattering relaxation rates due to polar and intervalley scatterings have been studied. (16 refs.)

Hot carrier physics and higher order electron phonon dynamicsSee Entry 114531

Experimental observation of decreased Hall mobility of conduction electrons in ZnSe with moving dislocationsSee Entry 114555

Theory of magnetokinetic phenomena for small-radius scatterers in semiconductorsSee Entry 114556

Inhomogeneous magnetic state in the system of solid solutions (1-x)Cu_{0.5}Al_{0.5}Cr₂S₄-xCuCr₂S₄See Entry 114709

Dynamical conductivity and dielectric function of general semiconductors and of magnetic semiconductorsSee Entry 114810

72.20F Low-field transport and mobility; piezoresistance

114520 Electronic transport in tetrahedral amorphous semiconductors. P.Thomas (Fachbereich Phys., Univ. Marburg, Marburg, Germany). *Acta Polytech. Scand. Electr. Eng. Ser. (Finland)*, no.EL50, p.279-364 (1983). (Proceedings of Helsinki International Summer School on Semiconductors 1982, Espoo, Finland, 14-18 June 1982).

Present knowledge about the atomic structure of amorphous tetrahedrally-bonded semiconductors is briefly reviewed. A presentation of typical transport data is given, mainly for amorphous silicon. Current theoretical concepts are discussed and it is shown how they are used to formulate transport theories. The calculation of transport coefficients is demonstrated, and typical results are discussed in order to understand the transport properties of amorphous semiconductors. It is shown that a number of quite generally observed transport properties still remain unexplained. (92 refs.)

114521 Preparation and investigations of polycrystalline samples of copper sulphides Cu_{2-x}S (0≤x≤0.2). S.V.Pakeva, Z.S.Begova, V.P.Krusev, S.K.Plachkova (Faculty of Phys., Univ. of Sofia, Sofia, Bulgaria). *Bulg. J. Phys. (Bulgaria)*, vol.10, no.3, p.322-7 (1983). The structural and electrical properties of polycrystalline samples of copper sulphides Cu_{2-x}S (0≤x≤0.2) are studied. The samples have been prepared by direct synthesis of copper and sulphur taken in a ratio corresponding to the stoichiometric composition Cu₂S. Depending on the conditions of additional thermal treatment, two types of polycrystalline samples, with quite different physico-chemical properties, are obtained. One type of the samples consists mainly of orthorhombic Cu₂S; they are of low resistivity with specific conductivity σ of about 20 Ω⁻¹ cm⁻¹. The other type of samples consists mainly of tetragonal Cu_{1.96}S₁; they have three orders of magnitude lower conductivity σ~10⁻² Ω⁻¹ cm⁻¹. The last samples show photoconductivity at temperatures lower than 100K. (20 refs.)

114522 Electrical properties of ZnSe. S.Satoh, M.Isshiki, K.Igaki (Dept. of Materials Sci., Tohoku Univ., Sendai, Japan). *Jpn. J. Appl. Phys. Part 1 (Japan)*, vol.22, no.7, p.1167-9 (July 1983). The electrical conductivity and electron concentration were measured as a function of deviation from stoichiometry in high-purity undoped and Cl-doped ZnSe single crystals. The In and Cl concentrations in high-purity undoped ZnSe were estimated using activation analysis. It was determined that the shallow donors are due to native defects. (12 refs.)

114523 Thickness dependence of electrical resistivity of vacuum-deposited selenium films. A.K.Sharma, B.Singh (Vacuum Tubes Div., Central Electronics Engng. Res. Inst., Pilani, India).

Indian J. Pure & Appl. Phys., vol.21, no.7, p.420-1 (July 1983).

Thickness dependence of electrical resistivity of vacuum deposited selenium films (thickness, 500 to 4420 Å) has been reported in vacuum, after an annealing cycle (30 to 150°C and back) and in residual vacuum after 24 hr. Unusual increase of electrical resistivity from 500 to 3400 Å thickness has been explained in terms of localized surface states. (9 refs.)

114524 Effect of gallium selenide on some physical characteristics of germanium selenide. M.A.Aliidzhanov, G.B.Abdullaev, K.O.Dovletov (S. Agamaliogla Azerbaizhdan Agricultural Inst., Azerbaizhdan SSR).

Inorg. Mater. (USA), vol.18, no.9, p.1359-60 (Sept. 1982). Translation of: *Izv. Akad. Nauk SSSR Neorg. Mater.*, vol.18, no.9, p.1586-7 (Sept. 1982). [received: Sept. 1983]

Some physical characteristics of solid solutions based on GeSe were investigated. The limiting mole fraction of GaSe dissolved in GeSe corresponds to the formula $\text{Ge}_{1-x}\text{Ga}_x\text{Se}$ (where $x \leq 0.05$). It has been supposed that solid solutions based on germanium selenide, in which the germanium is directly substituted by gallium, are formed. From the curves for the dependence of the electrical conductivity σ on the composition at 300K it is seen that with increase in the GaSe content of the germanium selenide up to 1 mole % the σ value first increases and then decreases a little. On the basis of the results from measurement of the Hall effect the authors calculated the mobility and concentration of current carriers, which varies significantly with increase in the GaSe content of the GeSe. The variation of the concentration p and mobility μ of the current carriers and the electrical conductivity, which is directly related to p and μ , accordingly as a function of the composition may be due to the large difference of the current carrier concentrations in the initial components. (8 refs.)

114525 Calculation and measurement of the effect of pressure on charge carrier transport in naphthalene. M.El Hamamsy, A.C.Damask (Queens Coll. of the City, Univ. of New York, Flushing, NY, USA), S.A.Elnahwy.

Mol. Cryst. & Liq. Cryst. (GB), vol.95, no.3-4, p.209-35 (1983). Intermolecular transfer integrals, including exchange and vibrational effects, for an excess electron and an excess hole in a naphthalene crystal are calculated as functions of pressure using the linear compressibilities. These integrals are then used to calculate the pressure dependence of the band structure, the drift mobility components and the Hall mobility. A novel design of a nonmagnetic high pressure cell with optical windows is described. Hall mobility of an excess hole was measured at high pressure by a photoinjection technique. The results of the calculations give a good agreement with available drift mobility data and with the Hall mobility measured in this work. Comparison between the calculated and observed mobilities shows that the constant mean-free-path approximation is superior to the constant-relaxation-time approximation for naphthalene. (31 refs.)

114526 Influence of additions on the electrical insulation properties of fused periclase. V.A.Bron, I.S.Raeva, L.P.Kostromina, A.S.Kondrashova, V.G.Sivash, A.D.Khomutina, E.A.Egorov (Eastern Refractory Inst., USSR).

Refractories (USA), vol.23, no.11-12, p.621-4 (Nov.-Dec. 1982). Translation of: *Ogneupory (USSR)*, vol.23, no.12, p.45-9 (Dec. 1982). Investigations were carried out into the influence of additions containing primarily SiO_2 , Al_2O_3 , and MgO on the electrophysical properties of periclase. The additions in the form of dispersed powders were made to the periclase after melting and pulverizing, and the mixtures were carefully mixed. Determinations of the specific electrical resistance of the periclase with additions showed that their use significantly increased the electrical resistance of the material. The possibility of strengthening the action of additions by heat treatment of them was investigated. (3 refs.)

114527 Numerical analysis of the sheet resistance of ion-implanted phosphorus layers in silicon. R.F.Schmucker, L.M.Scarfone (Univ. of Vermont, Burlington, VT, USA).

Solid-State Electron. (GB), vol.26, no.9, p.923-5 (Sept. 1983).

The authors present improved values of the sheet resistance at 300K resulting from the use of a more accurate treatment of electron conductivity mobility at both nondegenerate and degenerate doping levels. A comparison between the present calculation of sheet resistance and that obtained from various empirical mobility formulas, the Smith and Stephen curves (1972), and experimental data is shown. (9 refs.)

114528 AC conductivity in AsF_5 doped polyphenylacetylene (PPA). A.P.Bhatt, W.A.Anderson, P.Ehrlich (State Univ. of New York, Amherst, NY, USA).

Solid State Commun. (USA), vol.47, no.12, p.997-9 (Sept. 1983).

The AC conductivity of semiconducting cis-cisoid polyphenylacetylene (PPA) pellets has been studied at temperatures between 230 and 290K and frequencies, f , from 37 to 10^5 Hz. The AC conductivity (σ_{ac}) is found to be strongly temperature dependent. σ_{ac} is proportional to f^s with s varying from 0.45 to 0.75 as the temperature is raised from 230 to 290K. Both frequency dispersion and strong temperature dependence of σ_{ac} are best explained by the mechanism of hopping conduction in the band-tails. (no refs.)

114529 Electrical conductivity of Cr_2O_3 doped with La_2O_3 , Y_2O_3 and NiO. H.Nagai (Dept. of Materials Sci. & Engng., Faculty of Engng., Osaka Univ., Yamada-oka, Suita, Osaka, Japan), T.Fujikawa, K.Shoji.

Trans. Jpn. Inst. Met. (Japan), vol.24, no.8, p.581-8 (Aug. 1983). In order to obtain a better fundamental understanding of factors responsible for an excellent improving effect of rare earths addition on the high temperature oxidation resistance of Ni-Cr alloys, the electrical conductivities of sintered Cr_2O_3 doped with various amounts of La_2O_3 , Y_2O_3 and NiO were measured in the temperature range from 773 to 1473K at near atmospheric oxygen pressures. The electrical conductivities of Cr_2O_3 doped with La_2O_3 and Y_2O_3 up to 0.5 mass% gradually increased. The increase in the electrical conductivity by the addition of La_2O_3 was larger than that caused by the addition of Y_2O_3 . The electrical conductivities of Cr_2O_3 undoped and doped with La_2O_3 and Y_2O_3 decreased with decreasing partial pressure of oxygen. This result showed that they were p-type semiconductors under the conditions investigated. The pressure dependence of the electrical conductivity of Cr_2O_3 slightly changed with the addition of La_2O_3 and Y_2O_3 . The electrical conductivity of Cr_2O_3 markedly increased with increasing NiO content up to 1 mass%. In contrast, the temperature and pressure dependence of the electrical conductivity of Cr_2O_3 doped with NiO abruptly changed with the addition of more than 0.2 mass%. The electrical conductivity of Cr_2O_3 doped with NiO more than 0.2% was independent of the partial pressure of oxygen at all temperatures investigated. Both the magnitude and the temperature and pressure dependence of the electrical conductivities of Cr_2O_3 -1%NiO-1% R_2O_3 (R:La and Y) were very close to those of Cr_2O_3 -1%NiO. This result suggested that there was little interaction between NiO and R_2O_3 in Cr_2O_3 . (11 refs.)

114530 Conduction in polycrystalline silicon: generalized thermionic emission-diffusion theory and extended state mobility model. A.N.Khondker (Electrical Engng. Dept., Rice Univ., Houston, TX, USA), D.M.Kim, R.R.Shah.

Laser-Solid Interactions and Transient Thermal Processing of Materials, Boston, MA, USA, 1-4 Nov. 1982 (New York, USA: Elsevier 1983), p.431-6. The authors present a general theory of conduction in polysilicon. The theoretical framework reconciles two apparently divergent approaches for modeling conduction processes in polysilicon and provides a physical basis to correctly interpret and to point out the deficiencies of previously reported thermionic and thermionic field emission theory. This model is based on an extended state mobility in the disordered grain boundary and the thermionic emission-diffusion theory for conduction of current. The attractive features of the theory are (a) it can explain the experimental data without the use of an artificial factor, f, (b) the conduction process is characterized explicitly by the inherent material properties of the grain and the grain boundary. The model is particularly suited for describing the electrical properties of laser restructured polysilicon, where, because of large grain size, the diffusion process is expected to be dominant. (7 refs.)

Study of crystallisation on non-crystalline V_2O_5 by electrical resistivity measurements See Entry 113741

The calculated defect structure of thorium See Entry 113862

Doping of indium phosphide with germanium See Entry 113938

Shock compression of zirconia ZrO_2 and zircon ZrSiO_4 in the pressure range up to 150 GPa See Entry 114093

Alloys with the $\text{Ge}_{1-x}\text{Ni}_x\text{Te}$ composition See Entry 114126

Glass formation region and electrical conductivity in the system $\text{B}_2\text{O}_3\text{-Li}_2\text{O-Li}_3\text{PO}_4$ See Entry 114173

Thermal expansion and electrical conductivity in the $\text{HfO}_2\text{-TiO}_2$ system See Entry 114216

Electrical conductivity measurements of some layered magnetic structures See Entry 114248

CVD a-Ge and a-Ge:X films: preparation and properties See Entry 114411

Reduction in the localized band-gap states in amorphous silicon by annealing and hydrogen implantation See Entry 114484

Effects of doping on transport and deep trapping in hydrogenated amorphous silicon See Entry 114533

Mechanism of carrier scattering in $\text{Ag}_3\text{In}_2\text{Se}_9$ See Entry 114546

Effect of grain size on the resistivity of polycrystalline material See Entry 114548

Hall effect and sheet resistivity measurements at low temperatures on silicon implanted with iron See Entry 114552

Magnetoresistance of germanium in the range of hopping conduction with a variable jump length See Entry 114553

Influence of an electric field on the anomalous magnetoresistance of n-type $\text{AlGa}_{1-x}\text{As}$ See Entry 114554

Electrical conductivity of semiconductors with grain boundaries and spectroscopy of boundary states in the presence of a tunnel current See Entry 114603

Dielectric relaxation and modulus of $\text{V}_2\text{O}_5\text{-TeO}_2$ glasses See Entry 114779

Electrolytic growth, electrical conductivity and magnetic susceptibility of stannous iodide See Entry 115032

Spreading resistance of InSb crystals pulled under ultrasonic vibrations See Entry 115042

Properties of hot-pressed zirconium pyrovanadate ceramics See Entry 115149

Sintering and electrical resistivity of $\text{ZnO-Nb}_2\text{O}_5$ ceramic See Entry 115155

72.20H High-field and nonlinear effects

114531 Hot carrier physics and higher order electron phonon dynamics.

P.Kocevar (Univ. Graz, Graz, Austria). *Acta Polytech. Scand. Electr. Eng. Ser. (Finland)*, no.EL50, p.102-38 (1983). (Proceedings of Helsinki International Summer School on Semiconductors 1982, Espoo, Finland, 14-18 June 1982).

The performance of most semiconductor devices is strongly influenced by nonohmic effects due to the high electric fields inside the individual device components. Such 'hot electron' phenomena limit the speed, power and lifetime of the device by determining ultimate drift- and diffusion-velocities, generation- and recombination rates of carriers, Joule heating and thermal as well as dielectric breakdown. The use of nonohmic transport as a spectroscopic tool has brought many new insights into the electronic structure of semiconductors. Finally, some recent results are presented on higher order electron-phonon dynamics obtained from high field research. (25 refs.)

114532 Linear coefficients of equation of motion of a drift electron. T.K.Ishii (Dept. of Electrical Engng. & Computer Sci., Marquette Univ., Milwaukee, WI, USA).

Proc. IEEE (USA), vol.71, no.8, p.1010-12 (Aug. 1983).

A simple method of calculating the friction coefficient and the restraining coefficient of a linear equation of motion of a drift electron in an isotropic medium is presented. This new method is applied for an electron in the high-field domain in a magnetically biased Gunn diode as an example. (6 refs.)

Broad and narrow band noise of monoclinic TaS_3 See Entry 114575

Field quenching of the surface conduction and two-dimensional hopping conduction of p-type InAs See Entry 114585

Inverted population of light-hole band pumped at cyclotron resonance See Entry 114739

72.20J Charge carriers: generation, recombination, lifetime, and trapping

114533 Effects of doping on transport and deep trapping in hydrogenated amorphous silicon. R.A.Street, J.Zesch, M.J.Thompson (Xerox Palo Alto Res. Center, Palo Alto, CA, USA).

Appl. Phys. Lett. (USA), vol.43, no.7, p.672-4 (1 Oct. 1983).

The authors report a quantitative comparison of the trapping rates of carriers at charged and neutral dangling bonds in hydrogenated amorphous silicon (a-Si:H). The data are obtained from time-of-flight photoconductivity studies of doped and undoped samples. The temperature dependence of the trapping rates, as well as the effect of boron doping on the hole drift mobility, is also reported. (11 refs.)

- 114534 Thermally stimulated current studies on cadmium selenide single crystals heat-treated in selenium vapour.** D.Raja Reddy, P.Chandrasekharam, B.Krishnamma (Dept. of Phys., SV Univ., Tirupati, India). *Indian J. Phys. Part A*, vol.57A, no.3, p.170-4 (May 1983). Thermally stimulated current (TSC) measurements were made on vapour phase-grown CdSe single crystals heat-treated in selenium vapour to make them photosensitive. Two TSC peaks were observed near 110K, and 180K. These peaks correspond to two electron trap levels at 0.14 eV and 0.28 eV, respectively, below the bottom of the conduction band. The cross-sections of the traps for electron capture, and the attempt-to-escape frequency for electrons in traps have been calculated. These crystals did not show any photochemical effects. (15 refs.)
- 114535 Detection of minority traps by simultaneous measurement of thermoluminescence and thermally stimulated conductivity.** V.K.Mathur, M.D.Brown (Naval Surface Weapons Center, Silver Spring, MD, USA). *J. Appl. Phys. (USA)*, vol.54, no.9, p.5485-7 (Sept. 1983). Generally, thermoluminescence (TL) and thermally stimulated conductivity (TSC) measurements are carried out to detect majority traps. It is pointed out in this communication that a careful analysis of the ratio $R(=\sigma_{TSC}/I_{TL})$ and I_{TL} , where σ_{TSC} is the thermally stimulated conductivity and I_{TL} is the intensity of thermoluminescence, has the potential of revealing information about the hole emission and hole traps. These two cases can be differentiated by comparing the initial rise of the temperature derivative of $1/R$, i.e. $(d/dT)(1/R)$ and I_{TL} . It is also possible to estimate the activation energy of shallow hole traps. (8 refs.)
- 114536 Correlation of lifetime with recombination centers in electron-irradiated P-type silicon.** B.J.Baliga, A.O.Ewvaraye (General Electric Co., Corporate Res. & Dev. Center, Schenectady, NY, USA). *J. Electrochem. Soc. (USA)*, vol.130, no.9, p.1916-18 (Sept. 1983). Four majority carrier trap levels have been observed in p-type (boron-doped) silicon after 1.5 MeV electron irradiation. By correlation of the annealing rate of the minority carrier recombination lifetime with the concentration of these levels, it has been found that the divacancy-induced level at $(E_v+0.23$ eV) controls the lifetime. Since this level begins to anneal out only at temperatures above 300°C, it can be concluded that electron irradiation of p-base silicon devices can be used to control their switching speed. (7 refs.)
- 114537 Existence of a distribution of hole-trap activation energies in FEP-Teflon.** J.Hagekyriakou, R.J.Fleming (Dept. of Phys., Monash Univ., Clayton, Victoria, Australia). *J. Polym. Sci. Polym. Phys. Ed. (USA)*, vol.21, no.9, p.1691-701 (Sept. 1983). When FEP-Teflon samples are electron irradiated at room temperature in open circuit and stored in that state for varying times following the end of irradiation, the temperature of the first current peak of the short-circuit TSC plot increases with increasing storage time. A new model is presented to explain this phenomenon, its main features being (i) a quasicontinuous distribution of hole-trap activation energies, the 'center of mass' of the trapped hole population moving toward the deeper end of the distribution during the storage time, and (ii) an electron/hole recombination coefficient much smaller than that implied in an earlier model. It is shown that the assumption of a single dominant type of hole trap implies an unrealistically large frequency factor. (27 refs.)
- 114538 Charge carrier trapping states in tetracene and pentacene crystals.** I.Ya.Muzikante, A.Yu.Rampans, E.A.Silin'sh, L.F.Taure. *Latv. PSR Zinat. Akad. Vestis Fiz. Teh. Zinat. Ser. (USSR)*, no.4, p.18-27 (1983). In Russian. Charge carrier trapping states have been studied in oriented vacuum evaporated layers of tetracene (Tc) and pentacene (Pc) by space-charge-limited currents (SCLC) and thermally stimulated current (TSC) techniques. Several sets of trapping states of Gaussian distribution have been observed in the energy gap of Tc and Pc layers: the shallow set of hole traps with distribution maximum at $E_t=0.08$ to 0.10 eV above the hole conductivity level and several sets of hole traps in the energy intervals from $E_t=0.2$ to $E_t=0.5$ eV both for Tc and Pc, as well as deep electron trapping states at $E_t=0.68$ eV for Pc and $E_t=0.72$ eV and 1.0 eV for Tc. The total trap density N_t and dispersion parameter σ have been determined for all the above mentioned sets of trapping states; trapping cross-sections for several sets of trapping states have also been estimated. (16 refs.)
- 114539 Thermally stimulated current transport peak in a system with spatially disordered hopping sites.** J.Plans, F.J.Balta Calleja (Instituto de Estructura de la Materia, CSIC, Madrid, Spain), M.Zielinski, M.Kryszewski. *Philos. Mag. B (GB)*, vol.48, no.3, p.289-96 (Sept. 1983). The continuous-time random-walk model used by Seher and Montroll (1975) to account for the dispersive transport phenomena observed in time-of-flight experiments on amorphous solids is extended to the non-isothermal case of thermally stimulated currents (TSCs). The basic implications of the theory of a TSC transport peak resulting from a system with random distribution of iso-energetic hopping sites are presented. (12 refs.)
- 114540 Silicon-wafer process evaluation using minority-carrier diffusion-length measurement by the SPV method.** A.M.Goodman, L.A.Goodman, H.F.Gossenberger (RCA Labs., Princeton, NJ, USA). *RCA Rev. (USA)*, vol.44, no.2, p.326-41 (June 1983). Measurement of the minority-carrier diffusion length L by the constant-magnitude steady-state surface photovoltage (SPV) method has become an important tool within RCA for evaluating the effect (on L) of silicon device fabrication steps. The authors present first a simplified description of the method and the practical information required for implementing this measurement technique. Substrate selection, sample preparation, data evaluation, and the limitations of the method are discussed in detail. Next, they describe the use of the SPV technique to monitor the unintentional introduction of heavy metal impurities at five different steps during wafer processing. The beneficial effect of adding 1-1-1 trichloroethane (TCA) to a furnace ambient is assessed by using the SPV technique and also by counting the number of crystalline defects delineated with Wright etch. (18 refs.)
- 114541 Surface recombination statistics at traps.** P.T.Landsberg, M.S.Abrahams (Dept. of Math., Univ. of Southampton, Southampton, England). *Solid-State Electron. (GB)*, vol.26, no.9, p.841-9 (Sept. 1983). The Shockley-Read-Hall recombination statistics were recently generalised by Dhariwal, Kothari and Jain (1981) to include the effect of a finite time of relaxation before the captured carrier settles into its ground state, and by Landsberg (1982) to allow for Auger effects and so-called 'extra' carriers supplied to the semiconductor from the outside. The combined result of these effects is studied here theoretically, together with the consideration of a simple distribution of trap states. It is found that the surface recombination velocity s has the usual minimum in the near intrinsic state and that s passes through a maximum as a function of excess electron concentration. Both extrema are enhanced if the trap states are distributed over an energy range. Experimental plots of s as a function of excess electron and hole concentra-

tions should yield insight concerning the numerical importance of (a) Auger effects with the participation of traps and (b) relaxation times. (18 refs.)

- 114542 Carrier drift time from pulsed photoconductivity in as-grown trans-polyacetylene.** Y.Yacoby, S.Roth, K.Menke, F.Keilmann, J.Kuhl (Max-Planck-Inst. fur Festkorperforschung, Stuttgart, Germany). *Solid State Commun. (USA)*, vol.47, no.11, p.869-71 (Sept. 1983). Nanosecond pulsed photoconductivity experiments in as-grown trans-polyacetylene at room temperature are reported. From the decay of the photoresponse the free drift time of photogenerated carriers is found to be $\tau_{fd}<10^{-9}$ sec. From the amount of collected charge the upper limit of τ_{fd} is reduced to picoseconds so that the relaxation of electrons and holes into mobile solitons and anti-solitons in questionable. (19 refs.)
- 114543 Auger recombination in a degenerate electron-hole plasma in InGaAsP solid solutions.** B.L.Gel'mont, Z.N.Sokolova, V.B.Khalfin (A.F. Ioffe Physicotech. Inst., Acad. of Sci., Leningrad, USSR). *Sov. Phys.-Semicond. (USA)*, vol.17, no.3, p.280-3 (March 1983). Translation of: *Fiz. & Tekh. Poluprovodn. (USSR)*, vol.17, no.3, p.453-8 (March 1983). [received: Sept. 1983] Calculations are made of the Auger recombination rate for an electron-hole plasma in a semiconductor with the zinc-blende structure in the case of nondegenerate holes and an arbitrary degree of degeneracy of electrons. Semiconductors in which the band gap is greater than the spin-orbit splitting are considered and it is found that the most probable process is the Auger recombination with a transition of a heavy hole to a spin-orbit split-off band. Calculated temperature and carrier-density dependences of the nonradiative recombination times are reported for InGaAsP solid solutions. The dependences of the internal quantum efficiency of the luminescence on the current are deduced allowing for the Auger process under consideration and also for the Auger recombination accompanied by the transfer of energy to an electron (the latter process is important at high nonequilibrium carrier densities). (14 refs.)
- 114544 Influence of the anisotropy of the elastic electron-phonon scattering on the carrier mobility in tellurium.** N.Ya.Kushnir, N.P.Gavaleshko, P.N.Gorlei (State Univ., Chernovtsy, Ukrainian SSR). *Sov. Phys.-Semicond. (USA)*, vol.17, no.3, p.321-2 (March 1983). Translation of: *Fiz. & Tekh. Poluprovodn. (USSR)*, vol.17, no.3, p.513-15 (March 1983). [received: Sept. 1983] In view of the considerable mathematical difficulties arising from the complex nature of the collision integrals, many theoreticians simplify the real phonon spectrum of low-symmetry crystals by averaging this spectrum in a certain manner. However, it has not yet been determined how such a simplification affects, for example, the electron-phonon coupling constants found by comparing the theory with experiment. The authors establish the effects of such simplification in the case of group D_3 crystals that do not include inversion as one of the symmetry elements. (7 refs.)
- 114545 Photon transfer of nonequilibrium carriers in a variable-gap semiconductor at right-angles to the band gap gradient.** A.S.Volkov, A.L.Lipko (A.F. Ioffe Physicotech. Inst., Acad. of Sci., Leningrad, USSR). *Sov. Phys.-Semicond. (USA)*, vol.17, no.3, p.322-2 (March 1983). Translation of: *Fiz. & Tekh. Poluprovodn. (USSR)*, vol.17, no.3, p.515-17 (March 1983). [received: Sept. 1983] The authors show that under the conditions of the photon drift of nonequilibrium carriers in a variable-gap semiconductor subjected to an inhomogeneous excitation of the wide-gap surface one can expect photon-transfer-induced diffusion fluxes of nonequilibrium carriers in a plane perpendicular to ∇E_g , and these fluxes transfer nonequilibrium carriers over distances much greater than the displacement length of these carriers in the direction of decreasing band gap. (8 refs.)
- 114546 Mechanism of carrier scattering in $Ag_3In_2Se_9$.** V.I.Tagirov, A.G.Guseinov, N.F.Gakhramanov, F.M.Aliev (S.M. Kirov Azerbaidzhan State Univ., Baku, Azerbaidzhan SSR). *Sov. Phys.-Semicond. (USA)*, vol.17, no.3, p.329 (March 1983). Translation of: *Fiz. & Tekh. Poluprovodn. (USSR)*, vol.17, no.3, p.524-5 (March 1983). [received: Sept. 1983] The authors report the results of an investigation of the current-voltage characteristics, Hall coefficient, and saturation of the current in $Ag_3In_2Se_9$, which is a member of a new class of materials with the general formula $A_3B_5C_9$. (7 refs.)
- 114547 Physical properties and functional possibilities for silicon structures compensated with zinc.** V.M.Arutyunyan (Erevan State Univ., Erevan, USSR). *Sov. Microelectron. (USA)*, vol.11, no.6, p.291-301 (Nov.-Dec. 1982). Translation of: *Mikroelektronika (USSR)*, vol.11, no.6, p.539-50 (Nov.-Dec. 1982). [received: Sept. 1983] It is known that the introduction of zinc into N type silicon substantially sensitizes it. The parameters of the centers (the energy position in the forbidden band, the charge state and type of the centers, and the electron and hole capture cross sections) have been thoroughly studied as well as the optical and photoelectric properties of Si<Zn>. The possibilities for creating functional microelectronic elements with Si<Zn> are based, in particular, on the comparatively high solid solubility and diffusivity (5×10^{16} cm $^{-3}$ at 1350°C and 10^{-6} - 10^{-7} cm 2 /s at 1000-1200°C, respectively) of electrically active zinc atoms in silicon, the stability of the energy arrangement of the zinc levels, the weak 'inclination' toward formation of a large number of complexes, the compatibility of the photosensitivity spectrum with the characteristics of semiconductor light-emitting diodes, and the large range of variation of the minority and majority carrier lifetimes (10^{-10} -0.01 s). (69 refs.)
- 114548 Effect of grain size on the resistivity of polycrystalline material.** D.P.Joshi, K.Sen (Dept. of Phys., Dayanand Brijendra Swaroop Coll., Dehra Dun, India). *Sol. Cells (Switzerland)*, vol.9, no.4, p.261-7 (Sept. 1983). The effects of grain size and doping concentration on the resistivity of polycrystalline silicon are investigated. A new relation is presented for the resistivity of large-grain polycrystalline material. Assuming localized states at the grain boundaries, the predicted variations in resistivity with grain size and doping concentration show reasonable agreement with the experimentally observed variations. Computations show that, as the grain size increases, the sensitivity of the resistivity of the polycrystalline material to the doping concentration decreases. For grain sizes less than 10 μ m, the resistivity is predominantly controlled by the average carrier concentration, while for grain sizes greater than 10 μ m the resistivity is mainly controlled by the effective mobility. (18 refs.)
- 114549 The electrical behavior of grain boundaries in silicon.** C.H.Seager (Sandia Nat. Labs., Albuquerque, NM, USA). Defects in Semiconductors II, Symposium Proceedings, Boston, MA, USA, Nov. 1982 (New York, USA: North-Holland 1983), p.343-55. Despite the fact that lattice imaging studies have shown that grain boundaries in group IV semiconductors often have structures which are complicated and

inhomogeneous on the scale of tens-to-hundreds of angstroms, simple theories assuming uniform double depletion layers have recently been shown to successfully predict many of the majority carrier transport properties of these defects. On the other hand the knowledge of the interaction of grain boundaries with minority carriers is in a considerably more primitive state. The author describes recent attempts to understand the effects of illumination on grain boundary potential barrier heights and the influence of these defects on the optically generated minority carrier population. Quantifying this latter interaction is particularly important in estimating the performance of polycrystalline solar cells. Simple but elegant scanned excitation measurements for measuring s , the minority carrier recombination velocity at grain boundaries, will be reviewed. The author discusses recent measurements of s as a function of temperature and illumination intensity and shows how these data can be correlated with zero-bias impedance measurements. (43 refs.)

Improved differential photocurrent method for measurement of optical-absorption coefficient and minority-carrier diffusion length in a semiconductor See Entry 111703

The interface structure of grain boundaries in polysilicon See Entry 113930

Correlation of oxygen and recombination centers on a microscale in as-grown Czochralski silicon crystals See Entry 113954

Subnanosecond pulsed laser annealing of Si-implanted InP See Entry 113997

Oxygen precipitation in silicon—its effects on minority carrier recombination and generation lifetime See Entry 114194

Properties of films of GaP on Si obtained by ion-liquid epitaxy See Entry 114383

Spontaneous tunnel transitions induced by redistribution of trapped electrons over impurity centers See Entry 114466

Impurity states in undoped β -TiInS₂ crystals See Entry 114471

Process-induced defects in high-purity GaAs See Entry 114480

Effect of gallium selenide on some physical characteristics of germanium selenide See Entry 114524

Calculation and measurement of the effect of pressure on charge carrier transport in naphthalene See Entry 114525

Hot carrier physics and higher order electron phonon dynamics See Entry 114531

Kinetic properties of chromium-doped lead telluride See Entry 114550

Theory of generation-recombination noise and responsivity in overlap structure photoconductors See Entry 114559

Photoconductivity and determination of the fundamental parameters of uniaxial crystals (with specific example of CdGeP₂:Cu) See Entry 114561

Mechanism of the photoconductivity of nickel-compensated gallium phosphide See Entry 114565

Optical and thermal transitions in bismuth silicate See Entry 114567

Photovoltaic effect, diffusion and drift of nonequilibrium electrons having finite mean free paths See Entry 114568

Two-dimensional surface electrons in semiconducting p -type $\text{Hg}_{1-x}\text{Cd}_x\text{Te}$ with an anodic oxide See Entry 114586

Investigation of the influence of the Auger recombination process on the current-voltage characteristics of multilayer silicon structures See Entry 114604

Recombination processes in polycrystalline PbSe films See Entry 114627

The influence of the hydrogen reduction process on the electrical properties of $\text{In}_2\text{O}_3/\text{Sn}$ thin films See Entry 114628

Electronic properties of grain boundaries in GaAs: a study of oriented bicrystals prepared by epitaxial lateral overgrowth See Entry 114629

Radiative lifetime in semiconductors for infrared detection See Entry 114899

Radiative recombination at Ir^{3+} sites in doped AgBr. Visible luminescence See Entry 114914

Calculation of Auger recombination times in p -type InGaAsP solid solutions See Entry 114980

Optimization of GaAs photocell properties using a thin $\text{Al}_x\text{Ga}_{1-x}\text{As}$ interlayer See Entry 115643

Study of deep-level defects and annealing effects in undoped and Sn-doped GaAs solar cells irradiated by one-MeV electrons See Entry 115647

Multiwavelength analyzer for the determination of diffusion lengths See Entry 115653

The effective lifetime in semicrystalline silicon See Entry 115660

The significance of interference effects in thin film $\text{Cu}_2\text{S}/\text{CdS}$ solar cells See Entry 115661

72.20M Galvanomagnetic and other magnetotransport effects

114550 Kinetic properties of chromium-doped lead telluride. L.D.Borisova, L.S.Parfenieva, L.V.Prokofeva, M.V.Romanova, I.A.Smirnov, T.T.Dedegkaev.

Bulg. J. Phys. (Bulgaria), vol.10, no.3, p.337-43 (1983). In Russian. The kinetic coefficients: electric conductivity (σ), thermoelectric power (α), thermal conductivity (κ) and Hall coefficient (R) of chromium-doped lead telluride samples have been studied. The samples have been prepared by powder metallurgy. Anomalous dependences of the kinetic coefficients (α , R) on the composition, current carrier concentration and temperature have been observed. The experimental results have been explained in terms of the presence of chromium impurity states in the PbTe conduction band. (4 refs.)

114551 Behaviour of large-grain polycrystalline n -InP grown by SSD technique. J.N.Roy, S.Basu, D.N.Bose (Materials Sci. Centre, Indian Inst. of Technol., Kharagpur, India), A.J.Singh.

Indian J. Pure & Appl. Phys., vol.21, no.7, p.395-7 (July 1983). Large-grain (2-3 mm) polycrystalline n -InP was prepared by synthesis solute diffusion (SSD) technique. The material thus prepared was fully characterized by X-ray, conductivity and Hall-effect measurements. Room temperature measurements showed carrier concentration $n_s = 3 \times 10^{23}/\text{m}^3$, resistivity $\rho = 3.46 \times 10^{-4}$ ohm-m and Hall mobility $= 6.91 \times 10^{-2}$ m²/V-sec. The grain-boundary scattering effect was determined taking compensation into account. Using electrochemical technique the band gap was measured as 1.28 eV. These results were compared with the standard sample obtained from Metals Research, UK. From the temperature variation of carrier concentration and conductivity the activation energies were determined. The conductivity activation energy (E_c) and the carrier activation energy (E_n) were 9.09×10^{-3} and 1.39×10^{-2} eV respectively. The temperature (T) dependence

of mobility (μ) was found to follow the relation $\mu \propto T^{-x}$ with $x=2.44$. The mobility at 160K was found to be 0.276 m²/V-sec. (9 refs.)

114552 Hall effect and sheet resistivity measurements at low temperatures on silicon implanted with iron. S.V.Joshi, M.C.Joshi (Dept. of Phys., Univ. of Bombay, Bombay, India).

Indian J. Cryog., vol.8, no.1, p.48-51 (1983). Iron ions were implanted in p -type silicon at room temperature at two different doses, 1×10^{17} ions/m² and 1×10^{19} ions/m², using an isotope separator. The implanted samples were annealed for $1/2$ hr at 400°C and 650°C. Hall effect and sheet resistivity measurements were made on these annealed samples in the temperature range 100K-300K. The sample implanted at dose 1×10^{19} ions/m² and annealed at 400°C for $1/2$ hr was p -type just after annealing and, after keeping it at room temperature for about one month, it became n -type. Sheet resistivity measurements were made on this sample after conversion and the plot of $\log \rho$ vs. $1/T$ was not linear. The sample implanted at dose 1×10^{17} ions/m² and annealed at 650°C for $1/2$ hr did not show any conversion. For this sample, the plot $\log \rho$ vs. $1/T$ was linear. The nonlinear plot for the first sample suggested that the radiation damage was not completely annealed and the linear plot for the second sample showed that the damage was almost removed. (11 refs.)

114553 Magnetoresistance of germanium in the range of hopping conduction with a variable jump length. I.S.Shlimak, A.N.Ionov, B.I.Shklovskii (A.F. Ioffe Physicotech. Inst., Acad. of Sci., Leningrad, USSR).

Sov. Phys.-Semicond. (USA), vol.17, no.3, p.314-15 (March 1983). Translation of: *Fiz. & Tekh. Poluprovodn. (USSR)*, vol.17, no.3, p.503-6 (March 1983). [received: Sept. 1983]

The authors measured the electrical conductivity and magnetoresistance of heavily doped and compensated Ge. The concentration of phosphorus, representing the main donor impurity, was $N_D = 5 \times 10^{18} \text{ cm}^{-3}$; the compensating acceptor impurity was gallium and the degree of compensation was $K=0.8$ to 0.9. (8 refs.)

114554 Influence of an electric field on the anomalous magnetoresistance of n -type $\text{Al}_x\text{Ga}_{1-x}\text{As}$. K.Durshimbetov, A.F.Kravchenko, A.M.Palkin (Inst. of Semiconductor Phys., Acad. of Sci., Novosibirsk, USSR).

Sov. Phys.-Semicond. (USA), vol.17, no.3, p.341-2 (March 1983). Translation of: *Fiz. & Tekh. Poluprovodn. (USSR)*, vol.17, no.3, p.542-4 (March 1983). [received: Sept. 1983]

An anomalous negative magnetoresistance of n -type $\text{Al}_x\text{Ga}_{1-x}\text{As}$ has been observed in a wide range of impurity concentrations, compositions, and temperatures. The authors found this anomalous magnetoresistance to be highly sensitive to an applied electric field. They investigated this sensitivity at 4.2K. The electron density in the samples was within the range 10^{16} - 10^{17} cm^{-3} at 300K. All samples exhibited quasimetallic impurity-band conduction at temperatures below 50K. A graph shows typical dependences of the anomalous negative magnetoresistance on a longitudinal electric field, determined at fixed values of T and H . This negative magnetoresistance decreases strongly at a rate which depends on the magnetic field. In high fields H the negative magnetoresistance decreases more rapidly on increase in the magnetic field and becomes positive at low values of E . An investigation of the Hall coefficient and electrical conductivity showed that the reduction in the negative magnetoresistance on increase in the electric field is due to a change in the electron mobility and not in the electron density. (6 refs.)

114555 Experimental observation of decreased Hall mobility of conduction electrons in ZnSe with moving dislocations. A.V.Zaretskii, V.F.Petrenko (Inst. of Solid-State Phys., Acad. of Sci., Chernogolovka, USSR).

Sov. Phys.-Solid State (USA), vol.25, no.2, p.300-4 (Feb. 1983). Translation of: *Fiz. Tverd. Tela (USSR)*, vol.25, no.2, p.532-40 (Feb. 1983). [received: Sept. 1983]

It has been experimentally observed that the motion of dislocations already existing in ZnSe crystals decreases the Hall mobility and increases the concentration of conduction electrons. The authors describe the results of an experimental study of these phenomena and discuss their possible mechanism. The decrease in the Hall mobility is evidently due to a significant amount of scattering of electrons by the Coulomb potential of strongly charged moving dislocations unscreened by point defects. The increase in concentration of conduction electrons is due to the emptying of electrons from point centers into the conduction band by strongly charged dislocations during the motion of the dislocations through the crystal. (27 refs.)

114556 Theory of magnetokinetic phenomena for small-radius scatterers in semiconductors. S.P.Andreev, S.V.Tkachenko (Moscow Engng. Phys. Inst., Moscow, USSR).

Sov. Phys.-JETP (USA), vol.83, no.5, p.1050-8 (Nov. 1982). Translation of: *Zh. Eksp. & Teor. Fiz. (USSR)*, vol.83, no.5, p.1816-30 (Nov. 1982). [received: Sept. 1983]

The Schrodinger equation for an electron in the field of an attraction center of arbitrary depth and in a uniform magnetic field is solved under the assumption that the attraction-center effective radius a is small compared with the magnetic length $l = (\hbar/|e|H)^{1/2}$. The spectra of the bound and quasibound states are obtained and their dependence on the depth of the potential center U is studied in detail. The width and the real part of the energy of the quasibound state in the higher Landau bands $N \neq 0$ is investigated at arbitrary values of U . A system of wave equations is constructed for the bound and quasibound states, as well as the wave functions of the continuous spectrum. On the basis of these functions it is possible to calculate any semiconductor kinetic coefficient due to interaction of the carriers with small-radius centers in a quantizing magnetic field. The transverse and longitudinal static conductivities of a carrier gas scattered by such centers in a quantizing magnetic field are calculated. Expressions for them are obtained in general form in terms of the operators for scattering by a center in an axisymmetric gauge at an arbitrary depth of the scatterer potential. Oscillations of the transverse and longitudinal conductivities with changing depth of the potential of the center are observed. It is shown that the dependences of the conductivity on the temperature and on the field are governed essentially by depth of the scatterer potential, i.e. by the type of impurity in the semiconductor. (19 refs.)

Doping of indium phosphide with germanium See Entry 113938

Alloys with the $\text{Ge}_{1-x}\text{Ni}_x\text{Te}$ composition See Entry 114126

Si on cubic zirconia See Entry 114388

The effect of disorder on the quantised Hall conductivity See Entry 114457

Electronic transport in tetrahedral amorphous semiconductors See Entry 114520

Effect of gallium selenide on some physical characteristics of germanium selenide See Entry 114524

Calculation and measurement of the effect of pressure on charge carrier transport in naphthalene See Entry 114525

Mechanism of carrier scattering in $\text{Ag}_3\text{In}_2\text{Se}_9$ See Entry 114546

- Two-dimensional surface electrons in semiconducting p -type $\text{Hg}_{1-x}\text{Cd}_x\text{Te}$ with an anodic oxide See Entry 114586
- Effect of thickness on the electrical properties of AISb thin films See Entry 114625

- The influence of the hydrogen reduction process on the electrical properties of $\text{In}_2\text{O}_3/\text{Sn}$ thin films See Entry 114628
- Resonance near the Fermi energy in a Kondo lattice See Entry 114669

72.30 HIGH-FREQUENCY EFFECTS; PLASMA EFFECTS

- 114557 Pinch effect in a narrow-gap semiconductor with advanced interband breakdown. A.V.Dmitriev, L.S.Fleishman (M.V. Lomonosov State Univ., Moscow, USSR).

Sov. Phys.-Solid State (USA), vol.25, no.2, p.234-8 (Feb. 1983). Translation of: *Fiz. Tverd. Tela (USSR)*, vol.25, no.2, p.416-22 (Feb. 1983). [received: Sept. 1983]

The pinch effect is considered in an electron-hole plasma formed in a narrow-gap semiconductor of the $\text{Bi}_{1-x}\text{Sb}_x$ alloy type by interband breakdown in a strong electric field. Electron and hole scattering by acoustic phonons, lattice defects, and one another is taken into account. The calculations are based on the Boltzmann transport equation and the effective temperature approximation. The carrier distribution in the sample is found as a function of the electric field, together with the current-voltage characteristics of the sample. (17 refs.)

- Streamer discharges in semiconductors in the temperature range 4.2-530K See Entry 113691

- Hot carrier physics and higher order electron phonon dynamics See Entry 114531

- Auger recombination in a degenerate electron-hole plasma in InGaAsP solid solutions See Entry 114543

- Picosecond dynamics of hot carrier relaxation in highly excited multi-quantum well structures See Entry 114879

72.40 PHOTOCONDUCTION AND PHOTOVOLTAIC EFFECTS; PHOTODIELECTRIC EFFECTS

- 114558 Generation and detection of millimeter waves by picosecond photoconductivity. D.H.Auston, P.R.Smith (Bell Labs., Murray Hill, NJ, USA).

Appl. Phys. Lett. (USA), vol.43, no.7, p.631-3 (1 Oct. 1983). Picosecond photoconductors in the form of dielectric resonators have been used to generate and detect extremely short bursts of millimeter wave radiation at 55 GHz with a repetition rate of 100 MHz. Both the generator and detector are tuned to a frequency which is determined by the length of the photoconducting dielectric resonators. The detector, which is phase coherent, has an estimated noise equivalent power of only 4×10^{-11} W for an integration bandwidth of 1 Hz, and is capable of resolving time intervals corresponding to a small fraction of one millimeter-wave cycle. (8 refs.)

- 114559 Theory of generation-recombination noise and responsivity in overlap structure photoconductors. D.L.Smith (Honeywell Systems & Res. Center, Minneapolis, MN, USA).

J. Appl. Phys. (USA), vol.54, no.9, p.5441-8 (Sept. 1983). A rigorous theory of both responsivity and generation-recombination noise in overlap structure photoconductors is presented. Because generation-recombination noise dominates under typical operating conditions, these results combine to give the detectivity D^* . It is found that both responsivity and D^* can be improved by use of the overlap structure. The dependence of the optimum device geometry on the operating conditions, such as bias conditions, and on the parameter to be maximized (e.g. responsivity or D^*), is derived. Symmetric and asymmetric overlap structure are compared, and it is found that, except at very small bias fields, an asymmetric structure gives the largest improvement in both the responsivity and D^* . Both responsivity and noise voltage are found to roll off at lower frequencies for the overlap structure than for the standard design, but become equal to the standard design values at high frequencies. Numerical results for $x \approx 0.1$ HgCdTe detectors are presented. Using an asymmetrical overlap structure the theory predicts that, under usual operating conditions, the responsivity can be more than doubled and simultaneously D^* increased by over 15%. Under optimum conditions D^* for the overlap structure photoconductor can equal the usually quoted value of D_{BLIP}^* for a photovoltaic device; that is it can exceed the usually quoted value of D_{BLIP}^* for a photoconductor by as much as a factor of $\sqrt{2}$. (7 refs.)

- 114560 Influence of external conditions on oscillations of the photocurrent in CdSe single crystals. B.S.Vakarov, V.V.Serdyuk, I.A.Starostin (Sci.-Res. Inst. of Phys., I.I. Mechnikov State Univ., Odessa, Ukrainian SSR).

Sov. Phys.-Semicond. (USA), vol.17, no.3, p.253-5 (March 1983). Translation of: *Fiz. & Tekh. Poluprovodn. (USSR)*, vol.17, no.3, p.409-12 (March 1983). [received: Sept. 1983]

An investigation is made of the influence of the intensity of the exciting light and of the voltage applied to the electrodes of a sample on the frequency of oscillations of the photocurrent in cadmium selenide single crystals. It is assumed that these oscillations are due to the trapping of free carriers dependent on the electric field intensity and a transformation procedure is applied to a system of equations describing such a model using the parameters of trapping centers deduced from the time dependence of the current during the oscillations. The initial system of equations is reduced to the van der Pol equation and analytic expressions are obtained for the photoconductivity oscillation frequency. The experimentally observed dependences of the oscillation frequency on the rate of photoexcitation and on the voltage applied to the sample are found to agree with the corresponding dependences deduced from the proposed model of the effect. (6 refs.)

- 114561 Photoconductivity and determination of the fundamental parameters of uniaxial crystals (with specific example of CdGeP_2/Cu). Yu.V.Rud', V.E.Skoryukin (A.F. Ioffe Physicotech. Inst., Acad. of Sci., Leningrad, USSR).

Sov. Phys.-Semicond. (USA), vol.17, no.3, p.263-5 (March 1983). Translation of: *Fiz. & Tekh. Poluprovodn. (USSR)*, vol.17, no.3, p.426-30 (March 1983). [received: Sept. 1983]

A method is proposed for the determination of the fundamental parameters of a semiconductor from the photoconductivity spectra. The method is tested by applying it to CdGeP_2/Cu crystals. An analysis of the photoconductivity spectra is used to find the spectral dependences of the absorption coefficient throughout the photosensitivity range, as well as the values of the diffusion length ($\approx 0.9 \mu$), surface recombination velocity, hole lifetime ($\approx 5 \times 10^{-8}$

sec), and optical and photoelectric anisotropy coefficients. Certain relationships are derived and an analysis is made of the influence of the surface recombination velocity and of the thickness of a photoresistor on its polarization sensitivity. (5 refs.)

- 114562 Photoresponse of germanium p^+-p junctions. I.Ya.Marmur, Ya.A.Oksman, E.Yu.Perlin, A.V.Fedorov.

Sov. Phys.-Semicond. (USA), vol.17, no.3, p.290-2 (March 1983). Translation of: *Fiz. & Tekh. Poluprovodn. (USSR)*, vol.17, no.3, p.469-73 (March 1983). [received: Sept. 1983]

A photo-emf was observed at alloyed p^+-p contacts illuminated with CO_2 laser radiation. The fast-response component of this emf due to the 'heating' of the hole subsystem by laser radiation rapidly decreased on increase in temperature from 77 to 120-150K. The temperature dependence of the photo-emf was explained allowing for the influence of temperature on the height of a barrier separating regions of heavy and light doping, and also allowing for the rate of relaxation of photoholes. (13 refs.)

- 114563 Photostimulated formation of shallow donors in 'pure' CdS crystals. E.Vateva, B.Embergenov, N.E.Korsunskaya, I.V.Markevich, D.Nesheva (Inst. of Semiconductors, Acad. of Sci., Kiev, Ukrainian SSR).

Sov. Phys.-Semicond. (USA), vol.17, no.3, p.300-1 (March 1983). Translation of: *Fiz. & Tekh. Poluprovodn. (USSR)*, vol.17, no.3, p.484-5 (March 1983). [received: Sept. 1983]

The authors find the reasons for the change in the photosensitivity by a comprehensive investigation of photo-electric properties and luminescence of platelet and bulk crystals in two states: before and after the occurrence of the photochemical reaction (states A and B, respectively). State A was produced by heating a sample to 450K and cooling it in darkness to 80 or 4.2K (measurement temperature). State B was obtained by heating to 400K and cooling during illumination to 300K. The subsequent cooling to 80 or 4.2K took place in darkness in order to avoid superposition of a low-temperature photochemical reaction which also occurred in these crystals. (3 refs.)

- 114564 Characteristics of the optical quenching of the photoconductivity of CdS single crystals irradiated with $E=10$ MeV electrons. G.E.Davidyuk, N.S.Bogdanyuk, A.P.Galushka (Lesia Ukrainka State Pedagogical Inst., Lutsk, Ukrainian SSR).

Sov. Phys.-Semicond. (USA), vol.17, no.3, p.316-17 (March 1983). Translation of: *Fiz. & Tekh. Poluprovodn. (USSR)*, vol.17, no.3, p.506-7 (March 1983). [received: Sept. 1983]

The author studied the characteristics of the optical quenching of the photoconductivity of undoped CdS single crystals irradiated with $E=10$ MeV electrons. The irradiation was carried out at room temperature. The radiation dose was $D \approx 4.10^{16}$ electrons/cm². (9 refs.)

- 114565 Mechanism of the photoconductivity of nickel-compensated gallium phosphide. M.S.Saidov, K.Abdirmov, A.S.Saidov, V.G.Makarenko (S.V. Starodubtsev Physicotech. Inst., Acad. of Sci., Tashkent, USSR).

Sov. Phys.-Semicond. (USA), vol.17, no.3, p.332 (March 1983). Translation of: *Fiz. & Tekh. Poluprovodn. (USSR)*, vol.17, no.3, p.529-30 (March 1983). [received: Sept. 1983]

Considers a likely mechanism of the photosensitivity of GaP:Ni crystals. It has been shown that nickel can have three charge states in GaP: neutral $\text{Ni}^0(3d^8)$, with one electron $\text{Ni}^-(3d^8)$, and with two electrons $\text{Ni}^{2-}(3d^9)$, acting as a trap. The ESR spectra of $\text{Ni}^0(3d^8)$ consist of hyperfine structure lines with $g=2.089$ and the ionization energy of the Ni^- state is 0.5 eV. The ionization energy of this second state Ni^{2-} has not been determined accurately. The authors found the Ni^{2-} level more accurately and accounted for the observed photosensitivity by considering measurements of the optical absorption exhibited at 300K by GaP crystals with different nickel concentrations. (4 refs.)

- 114566 Photoconductivity of n -type germanium with 'repulsive' impurity centers at photon energies less than the thermal ionization energy. I.A.Kurova, N.N.Ormont (M.V. Lomonosov State Univ., Moscow, USSR).

Sov. Phys.-Semicond. (USA), vol.17, no.3, p.346-7 (March 1983). Translation of: *Fiz. & Tekh. Poluprovodn. (USSR)*, vol.17, no.3, p.549-51 (March 1983). [received: Sept. 1983]

The authors have reported earlier (1981) that n -type Ge exhibits a low temperature photoconductivity when electrons are generated in the field of negatively charged impurity centers by photons of energies less than the thermal ionization energy of the impurity. It seemed desirable to carry out an investigation at higher temperatures in order to establish the nature of this photoconductivity. The authors report the results of a study carried out in the temperature range 40-150K on germanium samples with a partly compensated second acceptor level of gold ($E_1^+ = E_c - 0.2$ eV). (4 refs.)

- 114567 Optical and thermal transitions in bismuth silicate. V.I.Berezhkin (A.F. Ioffe Physicotech. Inst., Acad. of Sci., Leningrad, USSR).

Sov. Phys.-Solid State (USA), vol.25, no.2, p.276-9 (Feb. 1983). Translation of: *Fiz. Tverd. Tela (USSR)*, vol.25, no.2, p.490-4 (Feb. 1983). [received: Sept. 1983]

The paper reports the results of investigations of the optical and photoelectric properties of $\text{Bi}_{12}\text{SiO}_{20}$ in a broad range of temperatures. It is shown that the ratio of the energies of the optical and thermal transitions is equal to 3.1, so that the anomalies observed in the optical measurements in the 1-2 eV region and the set of peaks that appear on the curves of the thermally stimulated currents at negative temperatures pertain to the same localized centers, which were previously considered separately. It is assumed that these centers can be due to different states of one and the same impurity. Estimates for their concentration and the degree of occupancy at room temperature are given. The photon capture cross sections by electron traps of depth 1-2 eV are determined and the conditions for weak and strong repeated electron capture are estimated. A level diagram for the localized centers in the forbidden band of the crystal is presented. (9 refs.)

- 114568 Photovoltaic effect, diffusion and drift of nonequilibrium electrons having finite mean free paths. B.I.Sturman (Inst. of Automation & Electrometry, Acad. of Sci., USSR).

Sov. Phys.-JETP (USA), vol.83, no.5, p.1116-21 (Nov. 1982). Translation of: *Zh. Eksp. & Teor. Fiz. (USSR)*, vol.83, no.5, p.1939-40 (Nov. 1982). [received: Sept. 1983]

The photovoltaic effect, nonequilibrium diffusion, and nonequilibrium photoconductivity are investigated for an arbitrary relation between the period of the photoinduced grating and the diffusion length of energy-relaxing photoelectrons. It is shown that under rather lax conditions the nonequilibrium photoelectric phenomena prevail over effects connected with thermalized electrons. Manifestations of nonequilibrium effects in the optical properties of crystals are investigated. (17 refs.)

114569 In_2O_3 heterojunction photocells using compounds of type $\text{A}^{\text{II}}\text{B}^{\text{IV}}\text{C}_2\text{V}$. A.A.Abdurakhimov, Yu.V.Rud', K.V.Sanin, M.Serginov, V.E.Skoryukin (A.F. Ioffe Physicotech. Inst., Acad. of Sci., Leningrad, USSR).

Sov. Phys.-Tech. Phys. (USA), vol.28, no.2, p.199-201 (Feb. 1983). Translation of: *Zh. Tekh. Fiz. (USSR)*, vol.53, no.2, p.325-8 (Feb. 1983). [received: Sept. 1983]

Advances in optoelectronics have made it possible to design a large and diverse class of heterophotocells. Polarimetric effects can be achieved in heterophotocells with anisotropic semiconductors which can be exploited in photoanalyzers for analyzing linearly polarized light. Currently there is interest in using uniaxial crystals of the type $\text{A}^{\text{II}}\text{B}^{\text{IV}}\text{C}_2\text{V}$ to produce effective energy barriers. The authors examine the photoelectric properties of anisotropic n-p heterophotocells fabricated for the first time from semiconductors with a different crystal structure: a wide-gap ($E_g=3.6$ eV, $T=300\text{K}$) In_2O_3 oxide layer combined with crystals of ternary compounds of the form $\text{A}^{\text{II}}\text{B}^{\text{IV}}\text{C}_2\text{V}$. (9 refs.)

Improved differential photocurrent method for measurement of optical-absorption coefficient and minority-carrier diffusion length in a semiconductor See Entry 111703

Optical second harmonic generation in LiNbO_3 crystals induced by a photovoltaic grating See Entry 113055

Growth structure and optical properties of single crystals of rubrene See Entry 113841

Three holes bound to a double acceptor: Be^+ in germanium See Entry 114469

Determination of localized state distributions from anomalously-dispersive transport data See Entry 114486

Preparation and investigations of polycrystalline samples of copper sulphides Cu_{2-x}S ($0 \leq x \leq 0.2$) See Entry 114521

Effects of doping on transport and deep trapping in hydrogenated amorphous silicon See Entry 114533

Silicon-wafer process evaluation using minority-carrier diffusion-length measurement by the SPV method See Entry 114540

Carrier drift time from pulsed photoconductivity in as-grown transpolyacetylene See Entry 114542

Physical properties and functional possibilities for silicon structures compensated with zinc See Entry 114547

The recombination of photogenerated minority carriers in the depletion layer of semiconductor electrodes See Entry 114607

Generation of surface states in MOS structures based on indium antimonide See Entry 114619

Some peculiarities in the spectral characteristics of metal/insulator/metal structures at constant biases See Entry 114623

Recombination processes in polycrystalline PbSe films See Entry 114627

On magneto-photo-electret of sulphur and time-variation of its dielectric constant See Entry 114774

Comment on the optical absorption edge in $\alpha\text{-Si:H}$ See Entry 114817

Spectrum of localized states near the fundamental absorption edge and likely mechanism of compensation of CdTe:Cl crystals See Entry 114896

Radiative lifetime in semiconductors for infrared detection See Entry 114899

Plasma-sprayed silicon as a possible base material for the production of low cost solar cells See Entry 115051

Photoelectrochemical properties and optical quenching of photocurrent in $\text{Bi}_{12}\text{SiO}_{20}$ single crystals See Entry 115563

$\text{Al}_x\text{Ga}_{1-x}\text{As}/\text{GaAs}$ thin window concentrator solar cells by LPE plus vapour phase diffusion See Entry 115641

Optimization of GaAs photocell properties using a thin $\text{Al}_x\text{Ga}_{1-x}\text{As}$ interlayer See Entry 115643

Studies of electroluminescence in $p\text{AlGaAs}-p\text{GaAs}-n\text{GaAs}$ heterophotocells with distributed parameters See Entry 115651

Quality factors of solar cell arrays See Entry 115656

The significance of interference effects in thin film $\text{Cu}_2\text{S}/\text{CdS}$ solar cells See Entry 115661

Point-contact silicon solar cells See Entry 115662

72.50 ACOUSTOELECTRIC EFFECTS

114570 Sound generation by an electric current in a fluid. I.N.Didenkulov (Inst. of Appl. Phys., Acad. of Sci., Gorky, USSR).

Acoust. Lett. (GB), vol.6, no.11, p.168-71 (May 1983). Gives a calculation performed within the framework of a precise physical model. It is assumed that the region occupied by the current flowing in the fluid represents an infinite cylinder. The direction of the external homogeneous magnetic field is perpendicular to the cylinder axis. Three mechanisms of acoustic wave generation are considered. The first one is associated with the ponderomotive action of the external magnetic field on the region occupied by the current, as a result of which a dipole radiation occurs. Another mechanism of sound radiation consists in the following: The electric current flowing in the fluid induces a magnetic field, which in turn, as a result of interaction with the current, generates a force tending to reduce the size of the region occupied by the current. Finally, one more mechanism of sound excitation is possible, associated with the thermal expansion of the region occupied by the current due to its heating by the flowing electric current. Here also there is a monopole radiation. (5 refs.)

114571 Resonant amplification of sound near the spontaneous oscillation threshold of semiconductors under impurity and interband breakdown conditions. A.A.Zakharova, Yu.I.Balkarei, A.S.Bugaev, Yu.V.Gulyaev (Inst. of Radio Engng. & Electronics, Acad. of Sci., Moscow, USSR).

Sov. Phys.-Semicond. (USA), vol.17, no.3, p.256-8 (March 1983). Translation of: *Fiz. & Tekh. Poluprovodn. (USSR)*, vol.17, no.3, p.413-17 (March 1983). [received: Sept. 1983]

An analysis is made of the problem of using self-oscillatory or potentially self-oscillatory semiconductor systems for the amplification of sound. Attention is specifically given to the possibility of resonant amplification of sound in the case when a semiconductor is close to the point of instability resulting in generation of homogeneous spontaneous oscillations associated with impurity or interband electric breakdown. (10 refs.)

72.60 MIXED CONDUCTIVITY AND CONDUCTIVITY TRANSITIONS

114572 On the stability, switching voltage and transient on-characteristics of amorphous thin films. Chun Chiang (Inst. of Phys., Acad. Sinica, Taipei, Taiwan).

Annu. Rep. Inst. Phys. Acad. Sin. (Taiwan), vol.12, p.29-36 (Dec. 1982). [received: Sept. 1983]

By proposing that two types of reversible configurations co-existing in the film, that the ratio of two configurations is determined by current according to the law of mass action and the electronic energy transfer, that the difference of configurations may be due to phase, bonding state, filament formation, valence alternation pairs, etc., mathematical equations can be derived to explain the threshold switching, the time dependence of the threshold voltage, transient ON characteristics and the nonlinearity of the conductance. (21 refs.)

114573 Phase components and electrical conduction in the $\text{Sm}_2\text{O}_3\text{-SrO}$ system. V.B.Balakireva, A.D.Neuimin, S.F.Pal'guyev (Inst. of Electrochem., Acad. of Sci., USSR).

Inorg. Mater. (USA), vol.18, no.9, p.1305-10 (Sept. 1982). Translation of: *Izv. Akad. Nauk SSSR Neorg. Mater.*, vol.18, no.9, p.1525-30 (Sept. 1982). [received: Sept. 1983]

The regions for the existence of solid solutions based on the oxides of samarium and strontium in the $\text{Sm}_2\text{O}_3\text{-SrO}$ system have been determined. About 6 to 7 mol.% SrO dissolves in samarium oxide, and up to 2 mol.% SmO_x dissolves in strontium oxide during the heat treatment of the samples described. The samples containing 6-7 mol.% SrO (2 mol.% vacancies) have the greatest fraction and value for the ionic conductivity. A directly proportional dependence of the ionic and electronic components of the conductivity on the SrO concentration in the solid solution is observed at low concentrations of strontium oxide (up to 1 mol.%), the slope being equal to $1/2$ for the electronic component. The introduction of strontium oxide into samarium oxide displaces the range of $\text{P}(\text{O}_2)$ in which the ionic component of the conductivity is predominant to higher partial pressures of oxygen. (11 refs.)

114574 Determination of the pressure of the semimetal-semiconductor transition in the presence of a resonant acceptor level. M.M.G.de Carvalho (Inst. de Fisica, Univ. Catolica de Campinas, Sao Paulo, Brazil), C.Fau, M.Averous.

J. Appl. Phys. (USA), vol.54, no.9, p.5470-2 (Sept. 1983).

An expression relating the pressure dependences of the resistivity and the mobile electron concentration is derived and used along with Hall effect and resistivity data to determine the pressure at which the semimetal-semiconductor transition occurs in $\text{Hg}_{1-x}\text{Cd}_x\text{Te}$ for $x=0.124$, at low temperatures. The method is applicable in the presence of a resonant acceptor level. (9 refs.)

Electrical conductivity measurements of some layered magnetic structures See Entry 114248

72.70 NOISE PROCESSES AND PHENOMENA

114575 Broad and narrow band noise of monoclinic TaS_3 . A.Maeda, M.Naito, S.Tanaka (Dept. of Appl. Phys., Univ. of Tokyo, Tokyo, Japan).

Solid State Commun. (USA), vol.47, no.12, p.1001-5 (Sept. 1983).

Narrow band noise was detected in a linear-chain CDW semiconductor, monoclinic TaS_3 in the low temperature CDW region. Broad band noise with $1/f$ spectrum in the frequency range lower than 100 kHz was also observed. The noise power was decreased with increasing temperature. The number of the CDW segments in the sample was estimated from the analysis of the broad band noise measurements. The results indicate that about 10^4 segments exist in the sample at 116K, and this number decreases with decreasing temperature. The same analysis was applied to NbSe_3 , and it was found that CDW properties are very similar between metallic NbSe_3 and semiconducting monoclinic TaS_3 . (17 refs.)

114576 Contribution to the theory of flicker noise. L.A.Vainshtein (S.I. Vavilov Inst. of Phys. Problems, Acad. of Sci., Moscow, USSR).

Sov. Phys.-JETP (USA), vol.83, no.5, p.1064-9 (Nov. 1982). Translation of: *Zh. Eksp. & Teor. Fiz. (USSR)*, vol.83, no.5, p.1841-50 (Nov. 1982). [received: Sept. 1983]

An analysis is made of thermodynamic (equilibrium) fluctuations of the resistance due to fluctuations of the average (over the volume of a cylindrical sample) temperature because of heat exchange with an external circuit. The simplest models are used to investigate the problem of whether the spectral intensity of such fluctuations can be proportional to $1/\omega$, i.e. whether these fluctuations can be the cause of the flicker noise (known also as the excess or residual noise) and also of the $1/\omega$ or $1/f$ noise. (10 refs.)

114577 Three guises of generation-recombination noise. J.Cohen. Report NBS-TN-1173, Nat. Bur. Stand., Washington, DC, USA (April 1983), 9 pp.

It is shown that the noise in a zero-biased junction may be just a manifestation of the normally-occurring generation-recombination process, rather than shot noise, as is usually presumed. In addition, an attempt is made to clarify some noise mechanisms in semiconductors by addressing mathematical interpretation and terminology. In particular, for a biased homogeneous material at low frequencies, where the relevant transport mechanism is drift, a shot-like expression of the g-r noise equation is derived. For a zero-biased junction at low frequencies, where the relevant transport mechanism is diffusion, a pure shot-like expression of the g-r noise equation and an equivalent thermal (Nyquist) expression is derived. In both the homogeneous and the junction cases, however, the true noise remains generation-recombination noise, i.e., the origin of the noise is the fluctuations in the rates of generation and recombination of free carriers. (12 refs.)

Theory of generation-recombination noise and responsivity in overlap structure photoconductors See Entry 114559

72.80 CONDUCTIVITY OF SPECIFIC SEMICONDUCTORS AND INSULATORS

(see also 81.40R Electrical and magnetic properties related to materials treatment)

Glass formation region and electrical conductivity in the system $\text{B}_2\text{O}_3\text{-Li}_2\text{O-Li}_3\text{PO}_4$ See Entry 114173

Influence of additions on the electrical insulation properties of fused periclase See Entry 114526

72.80C Elemental semiconductors

Oxygen precipitation in silicon—its effects on minority carrier recombination and generation lifetimeSee Entry 114194

Si on cubic zirconiaSee Entry 114388

CVD a-Ge and a-Ge:X films: preparation and propertiesSee Entry 114411

Electrical versus structural properties of polycrystalline silicon deposited by plasma enhanced LPCVD below 550°CSee Entry 114414

Properties of thin polycrystalline silicon films deposited by plasma-assisted CVDSee Entry 114416

Electronic transport in tetrahedral amorphous semiconductorsSee Entry 114520

Thickness dependence of electrical resistivity of vacuum-deposited selenium filmsSee Entry 114523

Conduction in polycrystalline silicon: generalized thermionic emission-diffusion theory and extended state mobility modelSee Entry 114530

Effects of doping on transport and deep trapping in hydrogenated amorphous siliconSee Entry 114533

Correlation of lifetime with recombination centers in electron-irradiated P-type siliconSee Entry 114536

Silicon-wafer process evaluation using minority-carrier diffusion-length measurement by the SPV methodSee Entry 114540

Influence of the anisotropy of the elastic electron-phonon scattering on the carrier mobility in telluriumSee Entry 114544

Physical properties and functional possibilities for silicon structures compensated with zincSee Entry 114547

Effect of grain size on the resistivity of polycrystalline materialSee Entry 114548

The electrical behavior of grain boundaries in siliconSee Entry 114549

Hall effect and sheet resistivity measurements at low temperatures on silicon implanted with ironSee Entry 114552

Magnetoresistance of germanium in the range of hopping conduction with a variable jump lengthSee Entry 114553

Photoconductivity of n-type germanium with ‘repulsive’ impurity centers at photon energies less than the thermal ionization energySee Entry 114566

Investigation of the influence of the Auger recombination process on the current-voltage characteristics of multilayer silicon structuresSee Entry 114604

Plasma-sprayed silicon as a possible base material for the production of low cost solar cellsSee Entry 115051

The heteroepitaxy of Ge on Si(100) by vacuum evaporation ..See Entry 115058

LPCVD polycrystalline silicon: growth and physical properties of in-situ phosphorus doped and undoped filmsSee Entry 115073

LPCVD polycrystalline silicon: growth and physical properties of diffusion-doped, ion-implanted, and undoped filmsSee Entry 115074

Multiwavelength analyzer for the determination of diffusion lengthsSee Entry 115653

The effective lifetime in semicrystalline siliconSee Entry 115660

72.80E III-V and II-VI semiconductors

Doping of indium phosphide with germaniumSee Entry 113938

Subnanosecond pulsed laser annealing of Si-implanted InPSee Entry 113997

Properties of films of GaP on Si obtained by ion-liquid epitaxySee Entry 114383

Pressure dependence of the electron capture cross section of the B hole trap in liquid phase epitaxial gallium arsenideSee Entry 114464

Process-induced defects in high-purity GaAsSee Entry 114480

Polar, intervalley and acoustic scatterings in III-V group semiconductors. Application to GaAs and InSbSee Entry 114519

Electrical properties of ZnSeSee Entry 114522

Thermally stimulated current studies on cadmium selenide single crystals heat-treated in selenium vapourSee Entry 114534

Behaviour of large-grain polycrystalline n-InP grown by SSD techniqueSee Entry 114551

Influence of an electric field on the anomalous magnetoresistance of n-type Al_xGa_{1-x}AsSee Entry 114554

Experimental observation of decreased Hall mobility of conduction electrons in ZnSe with moving dislocationsSee Entry 114555

Influence of external conditions on oscillations of the photocurrent in CdSe single crystalsSee Entry 114560

Photostimulated formation of shallow donors in ‘pure’ CdS crystalsSee Entry 114563

Characteristics of the optical quenching of the photoconductivity of CdS single crystals irradiated with E=10 MeV electronsSee Entry 114564

Mechanism of the photoconductivity of nickel-compensated gallium phosphideSee Entry 114565

Determination of the pressure of the semimetal-semiconductor transition in the presence of a resonant acceptor levelSee Entry 114574

Two-dimensional surface electrons in semiconducting p-type Hg_{1-x}Cd_xTe with an anodic oxideSee Entry 114586

Effect of thickness on the electrical properties of AISb thin filmsSee Entry 114625

Electronic properties of grain boundaries in GaAs: a study of oriented bicrystals prepared by epitaxial lateral overgrowthSee Entry 114629

Calculation of Auger recombination times in p-type InGaAsP solid solutions ...See Entry 114980

Spreading resistance of InSb crystals pulled under ultrasonic vibrationsSee Entry 115042

Use of diethylberyllium for metal organic chemical vapor deposition of beryllium-doped gallium arsenideSee Entry 115066

Optimization of GaAs photocell properties using a thin Al_xGa_{1-x}As interlayerSee Entry 115643

Study of deep-level defects and annealing effects in undoped and Sn-doped GaAs solar cells irradiated by one-MeV electronsSee Entry 115647

The significance of interference effects in thin film Cu₂S/CdS solar cellsSee Entry 115661

72.80G Transition-metal compounds

Shock compression of zirconia ZrO₂ and zircon ZrSiO₄ in the pressure range up to 150 GPaSee Entry 114093

Thermal expansion and electrical conductivity in the HfO₂-TiO₂ systemSee Entry 114216

Preparation and investigations of polycrystalline samples of copper sulphides Cu_{2-x}S (0≤x≤0.2)See Entry 114521

Electrical conductivity of Cr₂O₃ doped with La₂O₃, Y₂O₃ and NiOSee Entry 114529

Broad and narrow band noise of monoclinic TaS₃See Entry 114575

Dielectric relaxation and modulus of V₂O₅-TeO₂ glassesSee Entry 114779

72.80J Other crystalline inorganic semiconductors

Effect of gallium selenide on some physical characteristics of germanium selenideSee Entry 114524

Mechanism of carrier scattering in Ag₃In₅Se₉See Entry 114546

Kinetic properties of chromium-doped lead tellurideSee Entry 114550

Pinch effect in a narrow-gap semiconductor with advanced interband breakdownSee Entry 114557

Photoconductivity and determination of the fundamental parameters of uniaxial crystals (with specific example of CdGeP₂:Cu)See Entry 114561

Recombination processes in polycrystalline PbSe filmsSee Entry 114627

The influence of the hydrogen reduction process on the electrical properties of In₂O₃:Sn thin filmsSee Entry 114628

Inhomogeneous magnetic state in the system of solid solutions (1-x)Cu_{0.5}Al_{0.5}Cr₂S₄-xCuCr₂S₄See Entry 114709

Electrolytic growth, electrical conductivity and magnetic susceptibility of stannous iodideSee Entry 115032

72.80L Organic semiconductors

Electrical conductivity measurements of some layered magnetic structuresSee Entry 114248

AC conductivity in AsF₅ doped polyphenylacetylene (PPA)See Entry 114528

Charge carrier trapping states in tetracene and pentacene crystalsSee Entry 114538

72.80N Amorphous and glassy semiconductors

Study of crystallisation on non-crystalline V₂O₅ by electrical resistivity measurementsSee Entry 113741

CVD a-Ge and a-Ge:X films: preparation and propertiesSee Entry 114411

Electronic transport in tetrahedral amorphous semiconductorsSee Entry 114520

Effects of doping on transport and deep trapping in hydrogenated amorphous siliconSee Entry 114533

Dark conductivity peak in p-type glow-discharged a-SiC:H filmsSee Entry 114626

72.90 OTHER TOPICS IN ELECTRONIC TRANSPORT IN CONDENSED MATTER

114578 Effects of axial stretching on the resistivity of carbon black filled silicone rubber. J.Kost, M.Narkis, A.Foux (Depts. of Biomedical & Chem. Engng., Technion-Israel Inst. Technol., Haifa, Israel). *Polym. Eng. & Sci. (USA)*, vol.23, no.10, p.567-71 (July 1983). The resistance and resistivity of Ketjenblack EC/silicone rubber compounds were studied as function of strain in constant strain rate experiments. Both strain and rate of strain affect the electrical resistivity of the compounds. Such effects are carbon black concentration dependent. Ketjenblack EC, a low structure black, is shown to behave differently than other blacks of high structure in the electrical resistivity-strain experiments. The resistivity in the straining experiments is determined by the transient distribution of the conductive particle array. (15 refs.)

114579 Anisotropic percolation in carbon black-polyvinylchloride composites. I.Balberg (Racah Inst. of Phys., Hebrew Univ., Jerusalem, Israel), N.Binenbaum, S.Bozowski. *Solid State Commun. (USA)*, vol.47, no.12, p.989-92 (Sept. 1983). New features of the resistivity dependence on the melt-flow-distance of carbon black-polyvinylchloride are presented. These features are compared with features obtained from the first computer study on the resistance of a two-dimensional system of conducting sticks and its dependence on the system's anisotropy. The qualitative resemblance between the two dependences and the effect of the conducting material content on these dependences, indicate clearly that the conduction in the composites is well described by an anisotropic percolation process. (16 refs.)

Anisotropy of electric properties in binary cholesteric mixturesSee Entry 114771

73.00 ELECTRONIC STRUCTURE AND ELECTRICAL PROPERTIES OF SURFACES, INTERFACES, AND THIN FILMS

73.20 ELECTRONIC SURFACE STATES

(for emission and impact phenomena, see 79.)

114580 Positronium velocity spectroscopy of the electronic density of states at a metal surface. A.P.Mills, Jr., L.Pfeiffer, P.M.Platzman (Bell Labs., Murray Hill, NJ, USA).

Phys. Rev. Lett. (USA), vol.51, no.12, p.1085-8 (19 Sept. 1983).

The velocity of positronium (Ps) formed when 1-2-keV positrons are implanted into an Al(111) target and diffuse to the clean surface has been measured. The time-of-flight distribution exhibits a sharp step at a Ps energy 2.62(4) eV in excellent agreement with the expected Ps work function $\phi_{\text{Ps}} = -2.60(3)$ eV obtained from the known electron and positron work functions of Al(111). The presence of less than a monolayer of oxygen reduces the step amplitude by a factor of 2. It is shown that this spectrum is a measure of the surface density of states. (12 refs.)

114581 Atomistic calculations of positron surface states. M.J.Puska, R.M.Nieminen (Lab. of Phys., Helsinki Univ. of Technol., Espoo, Finland). *Phys. Scr. (Sweden)*, vol.T4, p.79-82 (1983). (Nordic Conference on Surface Science, Tampere, Finland, 18-20 Aug. 1982).

The authors report on the results of an atomistic, discrete-lattice calculation of positron surface states on the three principal surfaces of Al and Cu. They are able to (i) accurately reproduce the observed values and anisotropy of the binding energies, and (ii) predict the surface state lifetimes. Furthermore, the authors calculate (iii) the positron lateral diffusion constant, and find it considerably enhanced over the bulk value. They also investigate (iv) the positron trapping at surface vacancies, and (v) the effect of ordered chemisorbed monolayers of oxygen. The authors find that the oxidation lowers the binding energy and makes the surface state unstable with respect to positronium emission on Al(100) and Al(111). Implications to surface studies are discussed. (21 refs.)

114582 New type of local resonances in thin rough films. V.M.Agranovich, V.E.Kravtsov, T.A.Leskova (Inst. of Spectroscopy, Acad. of Sci., Moscow, USSR).

Solid State Commun. (USA), vol.47, no.11, p.925-30 (Sept. 1983).

A new type of local resonance is predicted. Two different mechanisms of their formation are pointed out. The first one is connected with a peculiarity of the Coulomb interaction in thin films. The second type of resonance appears when spatial dispersion in films is taken into account. The considered local resonances can take place in metal as well as semiconductor and dielectric films. (4 refs.)

114583 Temperature effects on the highly correlated electron gas of a Si-111(1×1) surface. E.Louis (ENDASA, Alicante, Spain), C.Tejedor, F.Flores.

Solid State Commun. (USA), vol.47, no.11, p.939-41 (Sept. 1983).

The effects of the temperature on the highly correlated two-dimensional electron gas of a Si-111(1×1) surface have been analysed within a Hubbard Hamiltonian, going beyond the Hartree-Fock approximation. The authors' results show that a Kondo-like peak appearing at low T disappears around 700K; moreover, they find that the surface chemical potential shifts towards the valence band. All these results offer an explanation to recent experimental data of Yokotsuka et al. (1983). (14 refs.)

114584 Investigation of the surface of gallium arsenide doped by aluminum recoil atoms. Yu.Kamenetskii, G.Petrauskas, I.Prosychev, A.Sakalas, G.Skorobogatov (V. Kapsukas Lithuanian State Univ., Vilnius, Lithuanian SSR).

Sov. Phys.-Semicond. (USA), vol.17, no.3, p.239-41 (March 1983). Translation of: *Fiz. i Tekh. Poluprovodn. (USSR)*, vol.17, no.3, p.385-9 (March 1983). [received: Sept. 1983]

An investigation was made of the surface layer of gallium arsenide doped by aluminum recoil atoms. The investigation was carried out by the methods of secondary-ion mass spectrometry, ellipsometry, and infrared spectroscopy. Doping by recoil atoms involved bombardment with 75 keV P^+ ions in doses of 1×10^{14} – 1×10^{16} cm^{-2} . The aluminum and gallium distribution profiles were determined for undoped and doped samples, the dependences of the ellipsometric parameters ψ and Δ were obtained for a surface layer of GaAs, and a study was made of a shift of the free-electron plasma reflection band as a function of the phosphorus ion dose and of the annealing temperature. It was established that doping of gallium arsenide with aluminum recoil atoms generated defects of a different type than by conventional ion implantation. (17 refs.)

Surface physics. Second edition See Entry 111335

Surface friction constant and range of dynamical interaction between adatoms on metal surfaces See Entry 114325

Quantum motion of chemisorbed hydrogen on Ni surfaces See Entry 114336

Electron spectroscopy on adsorption of Cs on transition metals See Entry 114344

Theoretical study of oxygen chemisorption on zinc surface by cluster models See Entry 114354

On the role of image forces in chemisorption theory See Entry 114357

Semi-empirical calculation of H atom interaction with a 12 atom iron cluster .. See Entry 114364

A model for non-adiabatic coupling on metals: the sticking problem See Entry 114367

Surface and bulk electronic structure of disordered metallic alloys See Entry 114433

Surface plasmon scattering on flat surfaces at grazing incidence See Entry 114462

Photon-stimulated desorption from rare earth oxides See Entry 114489

Surface recombination statistics at traps See Entry 114541

Field quenching of the surface conduction and two-dimensional hopping conduction of p -type InAs See Entry 114585

Screening length in an extrinsic semiconductor See Entry 114592

Electrical conductivity of semiconductors with grain boundaries and spectroscopy of boundary states in the presence of a tunnel current See Entry 114603

Physics of two dimensional electron system in $\text{Al}_x\text{Ga}_{1-x}\text{As}/\text{GaAs}$ heterojunction interface See Entry 114605

Semiconductor electrodes. XLIX. Evidence for Fermi level pinning and surface-state distributions from impedance measurements in acetonitrile solutions with various redox couples See Entry 114606

Small device technology, dielectric semiconductor systems ... See Entry 114614

Problem of the relaxation spectroscopy of deep centers in semiconductors See Entry 114617

Generation of surface states in MOS structures based on indium antimonide See Entry 114619

The effect of the microscopic structure of metal surfaces on their optical properties See Entry 114807

Theory of charge transfer excitation in surface enhanced Raman scattering See Entry 114865

Excitation of surface plasmons on He-filled cavities in Al See Entry 114983

Angular dependence of the electron energy loss spectra of the reconstructed Si(001) clean surfaces See Entry 114985

Damping effects in angular-resolved ultraviolet photoemission spectroscopy on Cu(111) See Entry 115014

Rydberg screening in core level photoemission of ammonia adsorbed on nickel surfaces See Entry 115015

Surface core-level shifts for Ge(100)-(2×1) See Entry 115017

Chlorine adsorption on copper. I. Photoemission from clean Cu(001) and Cu(111) substrates See Entry 115019

Chlorine adsorption on copper. II. Photoemission from Cu(001)(2×2)-Cl and Cu(111)($\sqrt{3} \times \sqrt{3}$)R30°-Cl See Entry 115020

Adsorbate band structure of bromine on Pd(111) studied by angle resolved ultraviolet photoemission See Entry 115021

Comment on 'Temperature dependence of the silicon field evaporation voltage' by G.L. Kellogg See Entry 115026

73.25 SURFACE CONDUCTIVITY

114585 Field quenching of the surface conduction and two-dimensional hopping conduction of p -type InAs. I.N.Timchenko, N.N.Smironova, N.M.Stus' (A.F. Ioffe Physicotech. Inst., Acad. of Sci., Leningrad, USSR).

Sov. Phys.-Semicond. (USA), vol.17, no.3, p.261-3 (March 1983). Translation of: *Fiz. i Tekh. Poluprovodn. (USSR)*, vol.17, no.3, p.422-5 (March 1983). [received: Sept. 1983]

Surface conduction of p -type InAs was investigated at low temperatures using samples in the form of n - p - n structures. Under a certain voltage such a structure switched from a low-resistivity state to one with a much higher resistivity and this was attributed to the field quenching of the 'frozen-in' conductivity of an inversion channel. Hopping conduction was observed and it was attributed to jumps of electrons between localization centers in the inversion channel. Some parameters of the energy band of localized states were estimated. (10 refs.)

114586 Two-dimensional surface electrons in semiconducting p -type $\text{Hg}_{1-x}\text{Cd}_x\text{Te}$ with an anodic oxide. A.I.Elizarov, L.P.Zverev, V.V.Kruzhav, G.M.Min'kov, O.E.Rut (A.M. Gorki Ural State Univ., Sverdlovsk, USSR).

Sov. Phys.-Semicond. (USA), vol.17, no.3, p.284-6 (March 1983). Translation of: *Fiz. i Tekh. Poluprovodn. (USSR)*, vol.17, no.3, p.459-63 (March 1983). [received: Sept. 1983]

An investigation was made of the influence of anodic oxidation on galvanomagnetic effects in semiconducting p -type $\text{Hg}_{1-x}\text{Cd}_x\text{Te}$ with $x=0.19$ -0.20 and $N_A \approx 1 \times 10^{17} \text{ cm}^{-3}$. Anodic oxidation produced an n -type inversion layer on the semiconductor surface and the presence of this layer increased the conductivity at $T < 40\text{K}$ and resulted in double reversal of the sign of the temperature dependence of the Hall coefficient. Samples with an anodic oxide exhibited Shubnikov-de Haas oscillations of the transverse magnetoresistance, the period and position of which were governed by the magnetic field component normal to the anodized surface of the sample, demonstrating the two-dimensional nature of carriers in the inversion layer. Estimates were obtained of the density and mobility of these size-quantized surface electrons. (14 refs.)

114587 Oscillations of metal-plate impedance and character of electron reflection. I.F.Voloshin, N.A.Podlevskikh, V.G.Skobov, L.M.Fisher, A.S.Chernov (V.I. Lenin All-Union Electrotech. Inst., USSR).

Sov. Phys.-JETP (USA), vol.83, no.5, p.1130-9 (Nov. 1982). Translation of: *Zh. Eksp. i Teor. Fiz. (USSR)*, vol.83, no.5, p.1955-70 (Nov. 1982). [received: Sept. 1983]

The surface impedance of a metallic plate as a function of a magnetic field perpendicular to the plate is investigated theoretically and experimentally. The integro-differential equation for the RF field distribution in the plate is solved under the assumption that electron reflection from the surface can be described by an arbitrary Fuchs specular coefficient p . A solution is obtained for magnetic field values greatly exceeding the doppleron threshold field. The plate impedance is calculated on the basis of the obtained field distribution. The influence of specularly reflected electrons on the shape of the impedance oscillations is studied. It is shown that analysis of the shapes of the doppleron oscillations and of the Gantmakher-Kaner oscillations can yield the value of p for resonant carriers. A method is developed for the analysis of the shape of the experimentally recorded oscillations. Tungsten-plate-impedance measurements needed to determine the specularly coefficient of resonant electrons and their mean free paths are performed. The values of the specularly coefficients are found. The behavior of p when the magnetic field deviates from normal to the surface is studied experimentally. (16 refs.)

Si on cubic zirconia See Entry 114388

73.30 SURFACE DOUBLE LAYERS, SCHOTTKY BARRIERS, AND WORK FUNCTIONS

114588 Characteristics of Schottky diodes with microcluster interface. M.V.Schneider (Bell Labs., Crawford Hill Lab., Holmdel, NJ, USA), A.Y.Cho, E.Kollberg, H.Zirath.

Appl. Phys. Lett. (USA), vol.43, no.6, p.558-60 (15 Sept. 1983).

The author present experimental evidence that a single Schottky diode on GaAs is an agglomerate of paralleled microjunctions with different barrier heights and saturation currents. The current-voltage characteristic of the cluster breaks up into sections of exponentials with different slopes as one cools the diode from 300 to 10K. Noise measurements performed on cooled diodes at 4 GHz also confirm that a single device is a cluster of paralleled diodes. (8 refs.)

114589 Characterization of WSi_2/GaAs Schottky contacts. T.Ohnishi, N.Yokoyama, H.Onodera, S.Suzuki, A.Shibatomi (Fujitsu Labs. Ltd., Atsugi, Japan).

Appl. Phys. Lett. (USA), vol.43, no.6, p.600-2 (15 Sept. 1983).

The Schottky diode characteristics of WSi_2 contacts on n -type GaAs have been investigated and correlated to the film stress in WSi_2 and crystallographic properties of the film. Experimental results show that (1) the high-temperature stability of WSi_2/GaAs Schottky diode characteristics depends significantly on Si content; (2) WSi_2/GaAs contacts exhibit very high-temperature-stable Schottky diode characteristics at Si content around 0.60, and at this Si content no metallurgical interactions between WSi_2 and GaAs are observed by 2-MeV $^4\text{He}^+$ Rutherford backscattering (RBS) measurements; (3) the optimum Si content for Schottky diode characteristics coincides with that for stress minimum in WSi_2 ; (4) the Schottky diode characteristics are not affected by whether WSi_2 is crystallized or not, and a common feature of the regions where the Schottky diode characteristics are very high-temperature stable is that each consists of single-phase (W_5Si_3 secondary solid solution or amorphous). (7 refs.)

114590 Metallurgically grown Schottky junction in directionally solidified eutectic Ag-Si alloys. M.Arnold, J.Fruhauf, H.G.Schneider (Sektion Phys.-Elektronische Bauelemente, Tech. Hochschule Karl-Marx-Stadt, Karl-Marx-Stadt, Germany).

Cryst. Res. & Technol. (Germany), vol.18, no.8, p.1015-20 (1983).

Metallurgically grown M(metal)-S(semiconductor) phase boundaries in directionally solidified Ag-Si alloys were investigated relative to their behaviour as Schottky junctions. By the aid of point contacts I/V characteristics have been measured which correspond to these ones of Schottky diodes. The Si crystallites were proved to be n -doped. Reverse breakdown voltages of 8...24 V are not incompatible with the purity of the used materials. In forward direction the value of diode factor $n=1.1...5$ shows the existence of several current flow mechanisms. In order to be able to interpret the characteristics it is necessary to have exact information on the specific resistivity of the Si crystallites and on the content of grain boundaries and dislocation in silicon. Beyond that the complicated shape of Si crystallites prevents the necessary determination of the interface size. (11 refs.)

114591 A theory of the admittance of an amorphous silicon Schottky barrier. I.W.Archibald, R.A.Abram (Dept. of Appl. Phys. & Electronics, Univ. of Durham, Durham, England).

Philos. Mag. B (GB), vol.48, no.2, p.111-25 (Aug. 1983).

In a recent paper Abram and Doherty (1982) described a calculation of the frequency-dependent differential capacitance of an amorphous silicon Schottky barrier. In this paper the authors adopt the same model of the Schottky barrier but employ a rather different method of analysis to calculate both the capacitance and the conductance. These are given at explicit formulae in terms of the angular frequency, the d.c. bias and the density of electronic states of the amorphous silicon. The expression for the capacitance is identical to that obtained by Abram and Doherty. Numerical results for the admittance as a function of frequency and bias are presented for a density of states consisting of a single peak in a constant background, and for two forms of the density of states that have recently been proposed for amorphous silicon. The results suggest that the frequency dependence of the conductance is the most sensitive indicator of features in the density of states of amorphous silicon. (6 refs.)

114592 Screening length in an extrinsic semiconductor. N.A.Penin (P.N. Lebedev Phys. Inst., Acad. of Sci., Moscow, USSR).

Sov. Phys.-Semicond. (USA), vol.17, no.3, p.266-9 (March 1983). Translation of: *Fiz. & Tekh. Poluprovodn. (USSR)*, vol.17, no.3, p.431-6 (March 1983). [received: Sept. 1983]

A definition of the screening length of an extrinsic semiconductor is proposed. It represents a combination of two limiting cases of the Debye screening ($|e\phi| \ll kT$) and of the Schottky process ($|e\phi| \gg kT$). A derivation is given of a formula for the screening length of an extrinsic semiconductor containing one-level (or two-level) and compensating impurities in the absence of the minority carriers. The dependences of the screening length on the magnitude and sign of the screened potential are considered for different degrees of compensation and for temperatures corresponding to incomplete ionization of the impurities. (2 refs.)

The adsorption of methane on polycrystalline iron filmsSee Entry 114360

Interactions of sulfur with nickel surfaces: adsorption, diffusion and desorptionSee Entry 114365

Positronium velocity spectroscopy of the electronic density of states at a metal surfaceSee Entry 114580

Some peculiarities in the spectral characteristics of metal/insulator/metal structures at constant biasesSee Entry 114623

Work function of $\text{Mo}(110)$ in mixed cesium and cesium monoxide vaporsSee Entry 115007

Sputtered Schottky barrier solar cells on p -type GaAsSee Entry 115631

73.40 INTERFACES

114593 Epitaxial $\text{InP}/\text{fluoride}/\text{InP}(001)$ double heterostructures grown by molecular beam epitaxy. C.W.Tu, S.R.Forrest, W.D.Johnston, Jr. (Bell Labs., Murray Hill, NJ, USA).

Appl. Phys. Lett. (USA), vol.43, no.6, p.569-71 (15 Sept. 1983).

The authors report the first epitaxial semiconductor-dielectric-semiconductor (SDS) double heterostructures using the III-V compound semiconductor InP . The samples, $\text{InP}/\text{CaF}_2/\text{InP}(001)$ and $\text{InP}/\text{Ba}_2\text{Sr}_{1-x}\text{F}_2/\text{InP}(001)$, were grown by molecular beam epitaxy and have lattice mismatches of -6.9% and $+2.0\%$, respectively. In situ high-energy electron diffraction showed that the initial stage of epitaxy of the $\text{InP}/\text{fluoride}$ structure, unlike that of the $\text{fluoride}/\text{InP}$ structure, exhibits pseudomorphism. Analysis of the electrical properties of SDS devices with an insulator thickness of $\sim 100 \text{ \AA}$ indicates both Ohmic and trap-assisted tunneling conduction. (18 refs.)

114594 Electrical characteristics of Be-implanted GaAs diodes annealed with an ultrahigh power argon arc lamp. K.Tabatabaie-Alavi, A.N.M.M.Choudhury, H.Kanbe, C.G.Fonstad (Dept. of Electrical Engng. & Computer Sci., MIT, Cambridge, MA, USA), J.C.Gelpey.

Appl. Phys. Lett. (USA), vol.43, no.7, p.647-9 (1 Oct. 1983). The potential of arc lamp annealing techniques in GaAs device processing is demonstrated by the fabrication of Be-implanted mesa pin diodes. Implants were done at 50 and 120 keV with doses of 4.4×10^{14} and $5.1 \times 10^{14} \text{ cm}^{-2}$, respectively (total dose $= 9.5 \times 10^{14} \text{ cm}^{-2}$) into a $14\text{-}\mu\text{m}$ -thick undoped ($N_D \sim 7.5 \times 10^{14} \text{ cm}^{-3}$) GaAs epitaxial layer grown by vapor phase epitaxy. Ten second annealing cycles with peak temperatures of 950°C and 1050°C have been studied. The electrical characteristics of these diodes are superior to published furnace-annealed, Be-implanted GaAs diodes. (13 refs.)

Interface between a semiconductor and an ultrathin film of its oxideSee Entry 114616

Initial (nonintrinsic) breakdown and defects in the dielectrics of MOS structures based on siliconSee Entry 114618

73.40G Tunnelling: general (see also 74.50 in superconductors)

114595 Tunneling between conductors with a charge-density wave. S.N.Artemenko, A.F.Volkov (Inst. of Radio Engng. & Electronics, Acad. of Sci., USSR).

JETP Lett. (USA), vol.37, no.7, p.368-70 (5 April 1983). Translation of: *Pis'ma v Zh. Eksp. & Teor. Fiz. (USSR)*, vol.37, no.7, p.310-13 (5 April 1983). [received: Oct. 1983]

The current through a P_1 - I - P_2 tunnel junction [$P_{1,2}$ are conductors with a charge-density wave (CDW)] is calculated. It is shown that aside from a term proportional to the product of the densities of states, the current includes a term containing $\cos(\chi_1 - \chi_2)$, where $\chi_{1,2}$ are the phases of the CDW. (6 refs.)

73.40J Metal-to-metal contacts

Production of bimetallic contact elements by a diffusion impregnation methodSee Entry 115440

73.40L Semiconductor-to-semiconductor contacts, p - n junctions, and heterojunctions

114596 Energy levels and alloy scattering in InP-In(Ga)As heterojunctions. G.Bastard (Ecole Normale Supérieure, Paris, France).

Appl. Phys. Lett. (USA), vol.43, no.6, p.591-3 (15 Sept. 1983).

The author presents the results of self-consistent variational calculations for the energy levels and wave functions of modulation-doped InP-In(Ga)As heterojunctions. With the variational wave functions they calculate the electron scattering by alloy disorder. Retaining the bulk In(Ga)As value ($\sim 0.6 \text{ eV}$) for the alloy disorder potential the mobility limited by alloy disorder is only $\sim 2 \times 10^5 \text{ cm}^2/\text{Vs}$ for $n_c \sim 3 \times 10^{11} \text{ cm}^{-2}$. (9 refs.)

114597 Auger voltage contrast depth profiling of shallow p - n junctions. R.Pantel (CNET, Meylan, France).

Appl. Phys. Lett. (USA), vol.43, no.7, p.650-2 (1 Oct. 1983).

A contactless measurement technique for electrical depth profiling of very shallow p - n junctions using a scanning Auger microscope is presented. The physical principle is the detection of variations in internal potential via shifts in the Auger peaks. Depth profiling of shallow junctions is realized by ion milling. Deep junctions are more rapidly analyzed via bevelling. For a p - n junction of classical depth (3500 \AA), Auger voltage contrast depth profiling is compared with spreading resistance measurements and shown to be an accurate and sensitive means of detecting low concentrations of electrically active impurities (in the 10^{15} cm^{-3} range). The main advantage of the method is excellent depth resolution when using ion milling. This is demonstrated for a very shallow p - n junction (400 \AA). (24 refs.)

114598 Inequality of semiconductor heterojunction conduction-band-edge discontinuity and electron affinity difference. R.S.Bauer, P.Zurcher, H.W.Sang (Xerox Palo Alto Res. Center, Palo Alto, CA, USA).

Appl. Phys. Lett. (USA), vol.43, no.7, p.663-5 (1 Oct. 1983).

The commonly used Anderson electron affinity rule is shown not to provide the band-edge offsets at the interface between different semiconductors. Using synchrotron radiation excited photoelectron spectroscopy, the authors determine electron affinities χ of $4.14_{-0.09}^{+0.17} \text{ eV}$ for a $\text{Ge}(110)$ surface and of $4.15_{-0.09}^{+0.17} \text{ eV}$ for a $18\text{-}\text{\AA}$ $\text{GaAs}(110)$ epitaxial overlayer on $\text{Ge}(110)$. In the same experiment, for the same layers, a conduction-band discontinuity ΔE_c of $0.54 \pm 0.08 \text{ eV}$ is measured for the heterojunction of GaAs grown by molecular beam epitaxy on $\text{Ge}(110)$. Compilation of data on 14 recent photoemission studies confirms that $\Delta E_c \neq \Delta\chi$ for most heterojunction systems investigated to date. (25 refs.)

114599 Simulation and measurement of C/V doping profiles in multilayer structures $[\text{Ga}_{1-x}\text{Al}_x\text{As}]$. J.E.A.Whiteaway (Standard Telecommunication Labs. Ltd., Harlow, England).

IEEE Proc. I (GB), vol.130, no.4, p.165-70 (Aug. 1983).

C/V doping profiles are simulated through n -type multilayer structures containing heterojunctions. The perceived doping profile obtained from C/V measurements can differ markedly from the actual carrier profile in the vicinity of a hetero- or homojunction. The model is applied to conventional FET structures, high-electron-mobility transistors and superlattices. (12 refs.)

114600 Response to 'Critique of two recent theories of heterojunction lineups'. A.Nussbaum (Dept. of Electrical Engng., Univ. of Minnesota, Minneapolis, MN, USA).

IEEE Electron Device Lett. (USA), vol.EDL-4, no.8, p.267-8 (Aug. 1983).

The author clarifies some misunderstandings in a recent paper by Kroemer (see *ibid.*, vol.EDL-4, no.2, p.25-6, 1983). (12 refs.)

114601 A comparative study of the properties of single velocity and double velocity heterojunction IMPATT diodes. R.U.Khan (Dept. of Electronics Engng., Inst. of Technol., Banaras Hindu Univ., Varanasi, India), B.B.Pal.

J. Inst. Electron. & Telecommun. Eng. (India), vol.29, no.2, p.68-71 (Feb. 1983).

A comparative study has been made on the properties of Ge-GaAs single velocity and double velocity heterojunction (HJ) IMPATT diodes. It is observed that for high frequency operation double velocity HJ IMPATT will give more power than the single velocity HJ IMPATT and the homo junction IMPATT (i.e. SDR IMPATT). (7 refs.)

114602 Calculation of the cyclotron resonance linewidth in GaAs-AlGaAs heterostructures. R.Lassnig, E.Gornik (Inst. für Experimentalphys., Univ. Innsbruck, Innsbruck, Austria).

Solid State Commun. (USA), vol.47, no.12, p.959-63 (Sept. 1983).

The influence of various scattering center distributions on the Landau level width and the cyclotron resonance linewidth is calculated for GaAs-AlGaAs heterostructures in high magnetic fields. The filling factor dependent dielectric screening of long range potentials leads to an oscillating behavior of the linewidth. Good agreement with recent cyclotron resonance linewidth measurements is obtained. (9 refs.)

114603 Electrical conductivity of semiconductors with grain boundaries and spectroscopy of boundary states in the presence of a tunnel current. E.I.Gol'dman, A.G.Zhdan, Yu.V.Markin, P.S.Sul'zhenko (Inst. of Radio Engng. & Electronics, Acad. of Sci., Moscow, USSR). *Sov. Phys.-Semicond. (USA)*, vol.17, no.3, p.242-4 (March 1983). Translation of: *Fiz. & Tekh. Poluprovodn. (USSR)*, vol.17, no.3, p.390-3 (March 1983). [received: Sept. 1983]

The conditions for effective tunneling of carriers across a semiconductor-semiconductor grain-boundary barrier are determined and possible errors due to lack of allowance for the tunneling are estimated for the case when the parameters of semiconductors are deduced from the current-voltage characteristics of a grain boundary. It is shown that, depending on the characteristics of a material and the experimental conditions, the tunnel mechanism of electrical conduction may predominate. Families of characteristic curves are obtained and these can be used to estimate the contribution of the tunneling to the electrical conductivity of a boundary region in real materials. The conditions under which a theory developed without allowance for the tunneling of carriers can be used in spectroscopy of boundary states are determined for the case when the tunnel component of the current reduces the barrier effectively by $\approx kT$. This theory describes the conductivity of grain boundaries in a wide range of fields and temperatures that do not suppress the boundary barrier and it is in quantitative agreement with the results of similar earlier calculations carried out for the same range of conditions. (13 refs.)

114604 Investigation of the influence of the Auger recombination process on the current-voltage characteristics of multilayer silicon structures. A.S.Zubrilov, V.A.Kuz'min, T.T.Mnatsakanov, L.I.Pomortseva, V.B.Shuman (V.I. Lenin All-Union Electrical Engng. Inst., Moscow, USSR). *Sov. Phys.-Semicond. (USA)*, vol.17, no.3, p.293-6 (March 1983). Translation of: *Fiz. & Tekh. Poluprovodn. (USSR)*, vol.17, no.3, p.474-8 (March 1983). [received: Sept. 1983]

A study was made of the influence of the Auger recombination process on the current-voltage characteristics of multilayer silicon structures in the intermediate range of current densities, when several nonlinear effects such as the Auger recombination process, electron-hole scattering, etc. make considerable contributions to the current-voltage characteristics, but none of them predominates over the others. Analytic expressions for the current-voltage characteristics and for the injection efficiencies of abrupt p - n junctions are derived and analyzed. The results of calculations are found to be in agreement with the experimental data. (10 refs.)

114605 Physics of two dimensional electron system in $\text{Al}_x\text{Ga}_{1-x}\text{As}/\text{GaAs}$ heterojunction interface. S.-I.Narita. *Solid State Phys. (Japan)*, vol.18, no.6, p.315-32 (June 1983). In Japanese. Recent investigations on the two dimensional electron gas in $\text{Al}_x\text{Ga}_{1-x}\text{As}/\text{GaAs}$ heterostructures are introduced and discussed in comparison with those on the Si-MOS system. (43 refs.)

Ultraviolet (UV) photochemical doping of silicon See Entry 113937

Pulsed excimer laser (308 nm) annealing of ion implanted silicon and solar cell fabrication See Entry 114011

Influence of electron irradiation at various temperatures on the minority carrier lifetime in epitaxial silicon p - n structures See Entry 114025

Double zinc diffusion fronts in InP—theory and experiment See Entry 114254

Photoresponse of germanium p^+-p junctions See Entry 114562

In_2O_3 heterojunction photocells using compounds of type $A^{II}\text{B}^{\text{IV}}\text{C}_2^{\text{V}}$ See Entry 114569

Three guises of generation-recombination noise See Entry 114577

Modification of optical properties of $\text{GaAs-Ga}_{1-x}\text{Al}_x$ superlattices due to band mixing See Entry 114809

Picosecond dynamics of hot carrier relaxation in highly excited multi-quantum well structures See Entry 114879

Optical studies of $\text{In}_x\text{Ga}_{1-x}\text{As-GaAs}$ strained multiquantum well structures See Entry 114898

Investigation of the saturation of the intensity of the $\lambda=1.3 \mu$ luminescence emitted from InGaAsP/InP structures at high rates of excitation See Entry 114921

Some characteristics of the electroluminescence emitted by epitaxial Al-Ga-Sb heterostructures See Entry 114934

Growth of $\text{Ga}_{0.47}\text{In}_{0.53}\text{As-InP}$ quantum wells by low pressure metalorganic chemical vapor deposition See Entry 115061

Heterojunction formation in $(\text{CdZnS})/\text{CuInSe}_2$ ternary solar cells See Entry 115635

Solar converters based on degenerate semiconductor-semiconductor p - n heterojunctions See Entry 115637

Photoconverters based on InP-CdS heterostructure See Entry 115638

Solar elements based on polycrystalline cadmium telluride See Entry 115639

Production and some properties of photoelements based on layers of polycrystalline silicon See Entry 115640

Mutual influence of wide- and narrow-gap photocells in the operation of multistage n -GaAs- p -AlGaAs- n -AlGaAs heterojunction solar cells See Entry 115649

Studies of electroluminescence in $p\text{AlGaAs-}p\text{GaAs-}n\text{GaAs}$ heterophotocells with distributed parameters See Entry 115651

$p\text{Al}_x\text{Ga}_{1-x}\text{As-}p\text{GaAs-}n\text{GaAs}$ heterostructure concentrator photocells synthesized by liquid-gas-phase epitaxy See Entry 115652

The effective lifetime in semicrystalline silicon See Entry 115660

73.40M Semiconductor-electrolyte contacts

114606 Semiconductor electrodes. XLIX. Evidence for Fermi level pinning and surface-state distributions from impedance measurements in acetonitrile solutions with various redox couples. G.Nagasubramanian, B.L.Wheeler, A.J.Bard (Dept. of Chem., Univ. of Texas, Austin, TX, USA). *J. Electrochem. Soc. (USA)*, vol.130, no.8, p.1680-7 (Aug. 1983). Capacitance-voltage (C - V) measurements were made for the single crystal semiconductors $n\text{-TiO}_2$, n -CdS, n -InP, p -Si, p -GaAs, n - and p - WSe_2 , and n - MoSe_2 in acetonitrile containing a number of redox couples whose potentials (V_{redox}) spanned a potential regime much wider than the bandgaps. The flat-band potential (V_{FB}) evaluated from capacitance-potential (C - V) measurements (Mott-Schottky plots) exhibited three types of behavior with varying solution redox potentials: (i) V_{FB} varied monotonically with V_{redox} for p -Si, p -GaAs, and n -InP; (ii) for n - TiO_2 and n -CdS, V_{FB} did not shift for couples located negative of the midgap potential, but varied monotonically for couples positive of this value; (iii) for the layer-type, compounds (MoSe_2 , WSe_2), V_{FB}

was almost independent of V_{redox} . These differences were ascribed to differences in surface-state densities. For n - TiO_2 crystals, (001) face etched with molten KHSO_4 and reduced, evidence for surface states at two different potentials was obtained from the in-phase component of the total admittance. Tentative assignment of these states is to lattice defects. The states closer to the conduction band are assigned to oxygen vacancies and the deeper states to Ti(III) . The densities of surface state (N_s) evaluated from G_p/ω vs. ω plots for TiO_2 and p -Si are around 10^{10} and 10^{13} cm^{-2} , respectively. (34 refs.)

114607 The recombination of photogenerated minority carriers in the depletion layer of semiconductor electrodes. W.J.Albery, P.N.Bartlett (Dept. of Chem., Imperial Coll. London, London, England). *J. Electrochem. Soc. (USA)*, vol.130, no.8, p.1699-706 (Aug. 1983).

The problem of depletion layer recombination in illuminated semiconductor electrolyte systems, as used for solar energy conversion, is considered. It is shown that there can be four different kinetic cases. The conditions for the existence of these different cases as a function of the potential drop across the depletion layer, the irradiance, and the photocurrent are derived. Analytical solutions for current voltage curves for the different cases are derived and criteria for distinguishing between the different cases are given. The effects of concentration polarization of the majority carriers are considered and shown to be negligible for typical semiconductors. (7 refs.)

Interface between a semiconductor and an ultrathin film of its oxide See Entry 114616

Characterization of polycrystalline electrodeposited CdSe photoelectrodes using photoluminescence spectroscopy See Entry 114902

73.40N Metal-nonmetal contacts

114608 Surface compensation of p -InP as observed by capacitance dispersion. R.K.Ahrenkiel, P.Sheldon, D.Dunlavy, L.Roybal (Solar Energy Res. Inst., Golden, CO, USA), R.E.Hayes. *Appl. Phys. Lett. (USA)*, vol.43, no.7, p.675-6 (1 Oct. 1983).

Very strong capacitance-voltage dispersive effects are observed in mercury/indium phosphide Schottky diodes. These effects are related to a partially compensated region at the surface for which the Debye length is relatively large. The small-signal capacitance is indicative of a critical dielectric relaxation time exceeding the period of the AC probe. This effect may be used to characterize the majority-carrier profile in lightly doped or low mobility semiconductors. (7 refs.)

114609 Serial-layered-transmission line contact-resistance representation for partially overlaid Al-to-contacts to silicon. A.Sugerman (IBM General Technol. Div., Hopewell Junction, NY, USA). *Solid-State Electron. (GB)*, vol.26, no.9, p.917-22 (Sept. 1983).

The author has developed a contact resistance representation for metallurgical systems having two interfacial conductive and resistive layers to a semiconductor surface. This configuration results when an interconnect metal (e.g. Al), which only partially overlays a contact metal (e.g. silicide), reacts with it to form a less conductive interface. As a consequence, circuit designers can take advantage of the unreacted region's lower contact resistance to ease circuit layout constraints. Contact resistance minima are suggested by the degree of overlaid or reacted segment and specific contact resistance degradation trade-off. A coupling of two layered transmission lines is used to simulate these two segment contacts. The model is compared to measurements of hardware. (6 refs.)

114610 Properties of metal-chalcogenide glassy semiconductor structures in the case of occurrence of electrically stimulated chemical reactions at the interface. D.I.Tsiulyanu, E.P.Kolomeiko, N.G.Bazik (Inst. of Appl. Phys., Acad. of Sci., Kishinev, Moldavian SSR). *Sov. Phys.-Semicond. (USA)*, vol.17, no.3, p.305-6 (March 1983). Translation of: *Fiz. & Tekh. Poluprovodn. (USSR)*, vol.17, no.3, p.491-3 (March 1983). [received: Sept. 1983]

The authors report the results of an experimental investigation of the absorption spectra and of the temperature dependence of the electrical conductivity of Al-GCS structures in the case of occurrence of electrically stimulated chemical changes at the interface. (7 refs.)

114611 Ion irradiation effects on Pt contacts to Si with and without interfacial chemical oxide. T.Banwell, M.Finetti, I.Suni, M.-A.Nicolet (California Inst. of Technol., Pasadena, CA, USA), S.S.Lau, D.M.Scott. Defects in Semiconductors II, Symposium Proceedings, Boston, MA, USA, Nov. 1982 (New York, USA: North-Holland 1983), p.411-15.

The electrical properties of ion irradiated metal-semiconductor contacts are investigated. Silicide contacts are fabricated by depositing Pt on chemically clean or slightly oxidized ($\sim 14 \text{ \AA SiO}_2$) n^+ - and n -type (111) Si, followed by a Si ion irradiation ($10^{14.6} \times 10^{15} \text{ Si/cm}^2$) through the metal-Si interface at various substrate temperatures, and a final thermal annealing in vacuum to form the silicide. Forward I-V measurements are employed for electrical characterization. Metal-Si interaction and substrate damage are measured by MeV ion backscattering and channeling, and interfacial oxygen monitored by nuclear $^{16}\text{O}(d,\alpha)^{14}\text{N}$ reaction. (9 refs.)

Compound semiconductors [laser and electron beam annealing] See Entry 114007

Silicides and metastable phases [laser annealing] See Entry 114008

Studies of chemistry at the Ta/Si interface as a function of thermal processing See Entry 114372

Process-induced defects in high-purity GaAs See Entry 114480

Characteristics of Schottky diodes with microcluster interface See Entry 114588

Characterization of WSi_2/GaAs Schottky contacts See Entry 114589

Metallurgically grown Schottky junction in directionally solidified eutectic Ag-Si alloys See Entry 114590

73.40Q Metal-insulator-semiconductor structures

(inc. semiconductor-to-insulator)

114612 Characteristic electronic defects at the Si-SiO₂ interface. N.M.Johnson, D.K.Biegelsen, M.D.Moyer, S.T.Chang (Xerox Palo Alto Res. Center, Palo Alto, CA, USA), E.H.Poindexter, P.J.Caplan. *Appl. Phys. Lett. (USA)*, vol.43, no.6, p.563-5 (15 Sept. 1983).

On unannealed, thermally oxidized silicon, electron spin resonance reveals an oriented interface defect which is termed the P_b center and identified as the trivalent silicon defect. Deep level transient spectroscopy (DLTS) reveals two broad characteristic peaks in the interface-state distribution: one $\sim 0.3 \text{ eV}$ above the silicon valence-band maximum and a second $\sim 0.25 \text{ eV}$ below the conduction band. Isochronal anneals of oxidized silicon, coated with aluminum, show that the spin density and the densities of the two DLTS peaks

have the same annealing kinetics. On large-area, Al-gated capacitors the spin density can be modulated with an applied voltage; sweeping the silicon band gap at the interface through the Fermi level reveals that the spin density is approximately constant over the central region of the band gap but decreases near the band edges. The variation of the spin density with gate voltage identifies an amphoteric center with both electronic transitions in the band gap. Both the annealing behavior and the voltage dependence of the P_b center support the conclusion that these transitions correspond to the two characteristic peaks in the interface-state distribution. The ~ 0.6 eV separation of the peaks is the effective correlation energy of the dangling orbital on a trivalent silicon defect at the Si-SiO₂ interface. The similarity between the disordered interface and amorphous silicon is discussed. (16 refs.)

114613 Surface plasmon emission in metal-insulator-degenerate p-type semiconductor structures. S.R.Whiteley, L.Z.Xie, R.Hemphill, T.K.Gustafson (Dept. of Electrical Engng. & Computer Sci., Univ. of California, Berkeley, CA, USA).

Appl. Phys. Lett. (USA), vol.43, no.6, p.566-8 (15 Sept. 1983). The complex dispersion relation for the antisymmetric plasmon mode in the presence of the tunneling interaction in In-In₂O₃-SnTe tunnel junctions is solved numerically. Net amplification of the mode may be possible at submillimeter and far infrared wavelengths in cooled junctions. (13 refs.)

114614 Small device technology, dielectric semiconductor systems. T.Sugano (Dept. of Electronic Engng., Univ. of Tokyo, Tokyo, Japan). *Acta Polytech. Scand. Electr. Eng. Ser. (Finland)*, no.EL50, p.183-278 (1983). (Proceedings of Helsinki International Summer School on Semiconductors 1982, Espoo, Finland, 14-18 June 1982).

Rutherford backscattering spectrometry has been proved to be useful for detecting non-registered Si atom layers of the Si substrate in the vicinity of the interface with the SiO₂ film. Chemical structure of the Si-SiO₂ transition region has been revealed by X-ray photoelectron spectroscopy (XPS). Morphology of Si-SiO₂ interfaces has been examined with both cross-sectional and normal transmission electron microscopy in conjunction with surface roughness scattering of electrons in the surface inversion layer. Much effort has been expended into the electrical characterization of the trap states of Si-SiO₂ interfaces, and a physical model of interface trap states with U-shaped continuous distribution has been proposed. Current understanding of Si-SiO₂ systems is reviewed and properties of dielectric III-V semiconductors are discussed. (43 refs.)

114615 Electrical characteristics of an upper interface on a buried SiO₂ layer formed by oxygen implantation. S.Nakashima, K.Ohwada (Musashino Electrical Communication Lab., Nippon Telegraph & Telephone Public Corp., Tokyo, Japan).

Jpn. J. Appl. Phys. Part 1 (Japan), vol.22, no.7, p.1119-24 (July 1983). The electrical characteristics of an upper interface on a buried oxide layer formed by oxygen implantation in an Si wafer, and subsequent thermal annealing were studied using an MOS diode and capacitance-voltage (C-V) measurements. The measured C-V curves strongly depended on the ion dose. The C-V curve was independent of the gate voltage for a dose of 1.2×10^{18} cm⁻², voltage-dependent for doses above 1.8×10^{18} cm⁻², and similar to those for thermal oxide for a dose of 2.4×10^{18} cm⁻². This strong dependence on the ion dose is considered to result from a change in the interface structure with increase in dose. In this change, the transition layer existing between the buried oxide and the upper Si layer at low doses, which shields the upper Si layer from external electric fields, disappears with increase in dose. (26 refs.)

114616 Interface between a semiconductor and an ultrathin film of its oxide. O.V.Romanov (A.A. Zhdanov State Univ., Leningrad, USSR).

Sov. Phys.-Semicond. (USA), vol.17, no.3, p.247-9 (March 1983). Translation of: *Fiz. & Tekh. Poluprovodn. (USSR)*, vol.17, no.3, p.398-401 (March 1983). [received: Sept. 1983]

A systematic investigation was made of the laws governing the formation of a double electric layer at an interface between a semiconductor and an ultrathin film of its intrinsic oxide. This was done for a large number of semiconductor materials belonging to vertical series of analogs of group IV elements (Si, Ge) and of III-V compounds (InP, InAs, InSb, GaN, GaP, GaAs, GaSb). It was found that already at the stage of nucleation of an oxide of a given semiconductor ($d_{ox} < 10^2$ Å) a specific double electric layer appeared on the surface and the nature of this layer was governed by the structure as well as by the physical and chemical properties of the investigated system. The results obtained were used to develop a model of an insulator-semiconductor interface. (15 refs.)

114617 Problem of the relaxation spectroscopy of deep centers in semiconductors. P.T.Oreshkin, Yu.V.Garmash, A.I.Perelygin (Radio Engng. Inst., Ryazan, USSR).

Sov. Phys.-Semicond. (USA), vol.17, no.3, p.309-10 (March 1983). Translation of: *Fiz. & Tekh. Poluprovodn. (USSR)*, vol.17, no.3, p.496-8 (March 1983). [received: Sept. 1983]

The authors report experimental results obtained for Al-Si₃N₄-SiO₂-Si type MIS structures which confirm their previously reported relaxation mechanism (see *ibid.*, vol.15, p.105, 1981). They used the usual C-t method but determined the transient process time t_c instead of the relaxation time τ . (15 refs.)

114618 Initial (nonintrinsic) breakdown and defects in the dielectrics of MOS structures based on silicon. G.N.Demidova, N.I.Gavrilin, O.P.Gludkin, S.K.Korovin (Moscow Aviation Technol. Inst., Moscow, USSR).

Sov. Microelectron. (USA), vol.12, no.1, p.20-5 (Jan.-Feb. 1983). Translation of: *Mikroelektronika (USSR)*, vol.12, no.1, p.24-8 (Jan.-Feb. 1983). [received: Sept. 1983]

An investigation of the initial breakdown of silicon oxide in industrially prepared MOS structure is the subject of the present work. In n⁺ polysilicon-SiO₂-p-Si structures there was no correlation between the excess current (up to four orders of magnitude) and the field strength for initial breakdown. It is possible that the initial breakdown and the excess currents are due to a different type of defect for electron injection from the polysilicon gate. The authors obtained the dependence of the defect density on the field strength with which they appear. It is shown that in the oxide of a n⁺ polysilicon-SiO₂-n type single crystal Si structure with injection of electrons from the substrate there is a single type of defect density of about 330 cm⁻² whose spatial distribution obeys Boltzmann statistics. (11 refs.)

114619 Generation of surface states in MOS structures based on indium antimonide. V.N.Davydov, E.A.Loskutova (Siberian Physicotech. Inst., USSR).

Sov. Microelectron. (USA), vol.12, no.1, p.25-9 (Jan.-Feb. 1983). Translation of: *Mikroelektronika (USSR)*, vol.12, no.1, p.37-41 (Jan.-Feb. 1983). [received: Sept. 1983]

Discusses anodized InSb structures and investigates the effect of a voltage applied to the structure and of short-wavelength radiation with a wavelength 0.3-1.0 μm on the amount of fixed charge Q_g in the dielectric, the distribution N_{ss}(E) of the surface state density (SSD) over the band, and the dependence of the stationary photovoltage on the voltage U_c(V) on the field electrode in n type INSb structures. The authors used single crystals with a [211] orienta-

tion and a minority carrier concentration of 2.10¹⁴ cm⁻³ at 77K for preparing the structures. The electrochemical oxidation of the semiconductor surface was carried out in a solution of orthophosphoric acid in ethylene glycol under galvanostatic conditions with a current density of 1 mA/cm² for 10 min. The anodic oxide film produced had a thickness of ~ 0.1 μm and a leakage current density less than 10⁻¹² A/cm². (15 refs.)

Characterization and application of laser induced seeded-lateral epitaxial Si layers on SiO₂ See Entry 114013

Thermal nitridation of silicon in nitrogen plasma See Entry 114377

Detection of electronic defects in strip-heater crystallized silicon thin films See Entry 114475

Lowering of the breakdown voltage of silicon dioxide by asperities and at spherical electrodes See Entry 114630

Cyclotron resonance of inversion electrons on InSb in tilted magnetic fields See Entry 114738

Plasma enhanced metal-organic chemical vapor deposition of aluminum oxide dielectric film for device applications See Entry 115063

Deposition and characterization of MO-CVD ZrO₂ See Entry 115096

73.40R Metal-insulator-metal structures

114620 Inelastic electron tunneling spectroscopy on ultrahigh vacuum prepared tunnel junctions. M.Liehr, S.Ewert (2. Phys. Inst., Rheinisch-Westfälischen Tech. Hochschule Aachen, Aachen, Germany). *Z. Phys. B (Germany)*, vol.52, no.2, p.95-7 (1983).

Inelastic electron tunneling (IET) spectra of clean ultrahigh vacuum (UHV) prepared (Al/Al oxide/Pb) tunnel junctions are discussed. Microcrystalline Al oxide is shown to grow on these Al films. This is in contrast to the formation of amorphous Al oxide in the common high vacuum (HV) preparation process. The IET-spectra of UHV prepared tunnel junctions are free of peaks due to contaminations. Conclusions concerning the growth of oxides on Al films are drawn. (16 refs.)

114621 Tunnelling in aluminium/aluminium-oxide/palladium junctions: hydrogen-induced variations. A.Diligenti, M.Stagi (Istituto di Elettronica e Telecomunicazioni, Univ. de Pisa, Pisa, Italy).

Electron. Lett. (GB), vol.19, no.18, p.717-18 (1 Sept. 1983). The tunnel current of aluminium/aluminium-oxide/palladium (Al/Al₂O₃/Pd) junctions, obtained by means of sapphire sputtering has been measured in air and in hydrogen-nitrogen atmosphere at various H₂ concentrations ranging from 2 to 100% and at room temperature. It has been found that the tunnel current undergoes a significant change as a consequence of Pd work function lowering induced by the hydrogen. The ratio between the tunnel current in H₂ and in air has a value in the range 10⁻²-10⁰, depending on the oxide thickness. The increase of the current occurs in some hundreds of milliseconds if the hydrogen is emitted at atmospheric pressure. (12 refs.)

114622 Study of lead-lead-oxide-lead tunnel junctions down to liquid nitrogen temperature. M.Prasad, A.K.Gupta, N.D.Kataria, V.S.Tomar (Nat. Phys. Lab., New Delhi, India).

Indian J. Cryog., vol.8, no.1, p.39-42 (1983). A detailed study of lead-lead-oxide-lead junctions has been carried out to study temperature dependence of the junction resistance in the range 30° to -196°C. The oxide barriers in all cases are grown using the thermal oxidation technique. Junctions are classified in two categories: one with resistance of order of 0.5 ohm and more as high resistance (HR) and those below as low resistance junctions (LR). HR junctions show linear increase of resistivity as the temperatures are lowered from room temperature down to -196°C. However, LR junctions show an anomalous behaviour which is due to the temperature variation of the film resistance. (5 refs.)

114623 Some peculiarities in the spectral characteristics of metal/insulator/metal structures at constant biases. A.G.Abdullayev, A.M.Karnaukhov, K.I.Abdullayev, Sh.B.Azizov (Inst. of Space Res. for Natural Resources, Acad. of Sci., Baku, Azerbaijan SSR).

Thin Solid Films (Switzerland), vol.106, no.3, p.L89-L90 (19 Aug. 1983). Investigations of the mechanism of the current transition in thin film Al/Al₂O₃/M structures with an electrolytically anodized layer showed Schottky emission for Al₂O₃ thicknesses of 150-2000 Å, at temperatures of 300-600 K and at electric fields E of 5×10⁴ V cm⁻¹ or more. This allowed the authors to determine the average magnitude of the dielectric constant ε(Al₂O₃) to be 7.8, which agrees well with the data of other researchers. However, they observed no marked asymmetry in the current-voltage characteristics when copper, silver or gold, which have different work functions, were used for the upper (non-oxidized) electrode. Hence the spectral characteristics of the photocurrent through the structure with a semitransparent upper electrode were investigated. (3 refs.)

73.60 ELECTRONIC PROPERTIES OF THIN FILMS

114624 Electronic properties of a size-quantized film with uneven boundaries. S.Yu.Potapenko, A.M.Satanin (Physicotech. Res. Inst., Gorki, USSR).

Sov. Phys.-Solid State (USA), vol.25, no.2, p.334 (Feb. 1983). Translation of: *Fiz. Tverd. Tela (USSR)*, vol.25, no.2, p.587-8 (Feb. 1983). [received: Sept. 1983]

The authors present a new approach to the study of electronic states in a film with rough surfaces described by the functions $z_1 = \xi(\rho)$, $z_2 = a + \eta(\rho)$, $\rho = (x, y)$. By a transformation to a curvilinear coordinate system the problem reduces to an analysis of the Schrodinger equation with an effective Hamiltonian. (4 refs.)

On the stability, switching voltage and transient on-characteristics of amorphous thin films See Entry 114572

73.60D Metallic thin films

The adsorption of methane on polycrystalline iron films See Entry 114360

Properties of molybdenum silicide film deposited by chemical vapor deposition See Entry 114384

Control of DC diode sputtering by control electrodes See Entry 115054

The preparation and properties of metallic optically transparent electrodes See Entry 115565

73.60F Semiconductor films

114625 Effect of thickness on the electrical properties of AlSb thin films. S.M.Patel, A.M.Biradar (Dept. of Phys., Sardar Patel Univ., Vallabh Vidyanagar, India).

Indian J. Pure & Appl. Phys., vol.21, no.7, p.418-19 (July 1983). Aluminium antimonide thin films of different thicknesses were prepared using co-evaporation method. The variations, with film thickness, of the Hall coefficient R_H , Hall mobility μ_H , and carrier concentration n , have been determined. It is observed that with increase in the film thickness the mobility of the carriers increases whereas the carrier concentration decreases. The maximum carrier mobility observed in the present study is $15 \text{ cm}^2 \text{ V}^{-1} \text{ s}^{-1}$ on the thickest film ($t=8000 \text{ \AA}$) with lowest carrier concentration of $7 \times 10^{17} \text{ cm}^{-3}$. (5 refs.)

114626 Dark conductivity peak in p-type glow-discharged a-SiC:H films. O.Kuboi (Komatsu Electronic Metals Co., Kanagawa, Japan).

J. Electrochem. Soc. (USA), vol.130, no.8, p.1749-52 (Aug. 1983). The author reports the doping characteristics of a-SiC:H, specifically the dark conductivity peak of p-type a-SiC:H. When the CH_4 concentration in the gas mixture of SiH_4 , CH_4 and B_2H_6 was varied under constant B_2H_6 concentration, a clear dark-conductivity peak was observed for glow-discharged a-SiC:H film at nearly 20% of CH_4 . The peak becomes clearer below 0.5% of B_2H_6 in the gas mixture. The author has not yet seen this feature reported in the literature. No peak is observed for undoped and phosphorus-doped a-SiC:H. (6 refs.)

114627 Recombination processes in polycrystalline PbSe films. N.P.Anisimova, T.R.Globus, L.K.Diklov, Yu.V.Kalinin, T.G.Nikolaeva, A.O.Olesk. *Sov. Phys.-Semicond. (USA)*, vol.17, no.3, p.336-8 (March 1983). Translation of: *Fiz. & Tekh. Poluprovodn. (USSR)*, vol.17, no.3, p.534-7 (March 1983). [received: Sept. 1983]

The authors examined the carrier recombination mechanisms governing the photoconductivity of oxidized polycrystalline PbSe films by investigating the room-temperature dependence of the photoconductivity time constant τ_{ph} on the majority carrier (hole) density p in the range $3 \times 10^{16} - 10^{18} \text{ cm}^{-3}$. Measurements of τ_{ph} were made on samples with the Hall configuration so that the hole density was determined simultaneously. The time constant was deduced from the photoconductivity decay after a rectangular light pulse of 0.9μ wavelength supplied by a light-emitting diode. The dependences of the impurity photoconductivity on the energy of the incident radiation was investigated in order to detect the recombination level and to find its energy position in the band gap. (12 refs.)

114628 The influence of the hydrogen reduction process on the electrical properties of $\text{In}_2\text{O}_3/\text{Sn}$ thin films. T.Horodyski, K.Budzynska, A.Leja (Dept. of Solid State Phys., Acad. of Mining & Metal, Krakow, Poland).

Thin Solid Films (Switzerland), vol.106, no.3, p.195-202 (19 Aug. 1983). Highly degenerate thin $\text{In}_2\text{O}_3/\text{Sn}$ films were prepared by DC reactive sputtering of In-Sn alloy targets in Ar-O_2 mixtures with a wide range of oxygen concentrations. The influence of both the oxygen concentration in the reactive mixture and the tin content of the target on the structure and electrical properties was studied. Hall measurements indicate that ionized impurities and interphase boundaries play a dominant role as causes of carrier scattering. The effect of post-deposition heat treatment in vacuum and in hydrogen was also studied. The considerable increase in the carrier concentration during reduction in hydrogen is explained in terms of the reduction mechanism. (20 refs.)

114629 Electronic properties of grain boundaries in GaAs: a study of oriented bicrystals prepared by epitaxial lateral overgrowth. J.P.Salerno, R.W.McClelland, J.G.Mavroides, J.C.C.Fan (Lincoln Lab., MIT, Lexington, MA, USA), A.F.Witt. Defects in Semiconductors II, Symposium Proceedings, Boston, MA, USA, Nov. 1982 (New York, USA: North-Holland 1983), p.375-82

The electronic properties of tilt boundaries with misorientation angles ranging from 0 to 30° in n-type GaAs bicrystal layers have been investigated. The current-voltage and capacitance-voltage characteristics are consistent with a double-depletion-region model. The height of the grain boundary potential barrier remains constant while the density of grain boundary states varies with misorientation angle. Deep level transient spectroscopy has revealed the presence of two bands of grain boundary states at approximately 0.65 and 0.9 eV below the conduction band. These states are attributed to bond reconstruction at the grain boundary. (20 refs.)

Si on cubic zirconiaSee Entry 114388

Phase formation and kinetics of the phase transition in Ag_2Se thin filmsSee Entry 114396

Electrical versus structural properties of polycrystalline silicon deposited by plasma enhanced LPCVD below 550°C See Entry 114414

Properties of thin polycrystalline silicon films deposited by plasma-assisted CVDSee Entry 114416

Pressure dependence of the electron capture cross section of the B hole trap in liquid phase epitaxial gallium arsenideSee Entry 114464

Detection of electronic defects in strip-heater crystallized silicon thin filmsSee Entry 114475

Reduction in the localized band-gap states in amorphous silicon by annealing and hydrogen implantationSee Entry 114484

Thickness dependence of electrical resistivity of vacuum-deposited selenium filmsSee Entry 114523

The optical absorption edge of amorphous thin films of borosilicate glassSee Entry 114939

Plasma-sprayed silicon as a possible base material for the production of low cost solar cellsSee Entry 115051

The heteroepitaxy of Ge on Si(100) by vacuum evaporation ..See Entry 115058

Use of diethylberyllium for metal organic chemical vapor deposition of beryllium-doped gallium arsenideSee Entry 115066

LPCVD polycrystalline silicon: growth and physical properties of in-situ phosphorus doped and undoped filmsSee Entry 115073

LPCVD polycrystalline silicon: growth and physical properties of diffusion-doped, ion-implanted, and undoped filmsSee Entry 115074

73.60H Insulating thin films

114630 Lowering of the breakdown voltage of silicon dioxide by asperities and at spherical electrodes. N.Klein, O.Nevanlinna (IBM Thomas J. Watson Res. Lab., Yorktown Heights, NY, USA).

Solid-State Electron. (GB), vol.26, no.9, p.883-92 (Sept. 1983). Examines the assumption that asperities and corners in electrodes can be preferential sites for electrical breakdown of silicon dioxide capacitors. It was assumed for this purpose that asperities can be approximated by spherical surfaces, and the breakdown voltage was then calculated at such asperities. Calculations showed that the breakdown voltage of a planar silicon dioxide capacitor can be lowered by one half to two thirds by asperities, when their radius is less than about one half of the oxide thickness. Such a decrease in the breakdown voltage is widely observed in polysilicon oxide capacitors. The effect of asperities is alleviated by a trapped electron charge, which can increase the breakdown voltage significantly. The spherical asperity model accounted for the breakdown voltages observed on a wide range of polysilicon oxide capacitors with oxide thicknesses varying from 45 to 820 nm. The radius of asperities responsible for breakdown in these experiments was roughly estimated 25-35 nm. (26 refs.)

Process study of chemically vapour-deposited SnO_x ($x \approx 2$) filmsSee Entry 114395

Initial (nonintrinsic) breakdown and defects in the dielectrics of MOS structures based on siliconSee Entry 114618

Generation of surface states in MOS structures based on indium antimonideSee Entry 114619

Plasma enhanced metal-organic chemical vapor deposition of aluminum oxide dielectric film for device applicationsSee Entry 115063

Deposition and characterization of MO-CVD ZrO_2 See Entry 115096

Properties of thermal oxides grown on phosphorus in situ doped polysiliconSee Entry 115383

73.90 OTHER TOPICS IN ELECTRICAL PROPERTIES OF SURFACES, INTERFACES, AND THIN FILMS

Direct intersubband optical absorption of semiconducting thin wireSee Entry 114812

74.00 SUPERCONDUCTIVITY

74.10 OCCURRENCE, CRITICAL TEMPERATURE

114631 Superconducting materials. M.Jergel, P.Hutka. *Elektrotech. Cas. (Czechoslovakia)*, vol.34, no.7, p.528-36 (1983). In Slovak. After a brief description of the principle of superconductivity and its most frequent applications, the developments of superconducting materials are dealt with. In particular, the properties of NbTi, Nb₃Sn and V₃Ga are discussed. Problems encountered in the fabrication of superconducting materials are illustrated with an example of Nb₃Ge. Amongst the topics discussed are stabilisation of the A-15 structure by means of gas additions and the presence of other Nb-Ge phases, selection of suitable substrates, the effects of technological conditions and the influence of the amorphous Nb-Ge. Future development trends discussed include materials based on carbonitrides, substances with crystalline hexagonal phase C15 (MgCr_2), chalcogenides based on ternary molybden sulphides, Chevrel phase materials and various types of palladium hydrides and deuterides. (4 refs.) E.D.

114632 ATA and the electron phonon coupling constant in calculating T_c of superconducting alloys. P.Chatterjee, S.Chatterjee (Dept. of General Phys. & X-rays, Indian Assoc. for the Cultivation of Sci., Calcutta, India).

Indian J. Cryog., vol.8, no.1, p.13-16 (1983). The theoretical formula of McMillan (1968) has been very successful in explaining the superconducting transition temperature. In this theory the electron-phonon coupling constant was very difficult to calculate from a purely theoretical standpoint until Gyorffy and Gaspari (1972) gave a theoretical formulation from the multiple scattering point of view. This theory has been very successful in explaining T_c of many superconducting elements and compounds. For the disordered solid, such as substitution alloys, this theory fails because of the breakdown of the translational symmetry used in the multiple scattering theory of Gyorffy and Gaspari. This problem can however be solved if the Green's function is averaged in random phase approximation (ATA). In this work Gyorffy and Gaspari's expression of the electron phonon coupling constant in the random phase approximation has been reformulated. This theory has been applied to alloys of Nb and Mo with different concentrations. (6 refs.)

114633 Structural phase transitions and superconducting transition temperatures of hexagonal M_xWO_3 compounds. M.Sato, B.H.Grier, H.Fujishita, S.Hoshino, A.R.Moodenbaugh (Inst. for Solid State Phys., Univ. of Tokyo, Tokyo, Japan).

J. Phys. C (GB), vol.16, no.27, p.5217-32 (30 Sept. 1983). Neutron scattering experiments have been performed on non-stoichiometric compounds of the hexagonal tungsten bronzes M_xWO_3 ($\text{M}=\text{Rb}$ and K). A nearly dispersionless phonon branch has been observed in $\text{Rb}_{0.33}\text{WO}_3$ at an energy $\omega_M \approx 5.5 \text{ meV}$. This branch reflects the local-mode character of the Rb atoms, which are loosely trapped at their sites within the large channel along the c direction formed by the linkage of WO_6 octahedra. The x dependence of the energy ω_M of this low-lying phonon (LLP) has been determined by measurements of the peak position in the powder inelastic scattering spectra. Since ω_M depends only weakly on x , the variation in ω_M appears not to be related to the anomalous x dependences of the superconducting transition temperature T_c observed previously in Rb_xWO_3 and K_xWO_3 . Two kinds of structural phase transitions were observed using powder diffraction measurements. One transition, which takes place above room temperature at T_{c1} , is due to a distortion of the WO_3 host cage of M_xWO_3 . It is accompanied by an optical phonon softening at the Γ point. The second transition is an order-disorder transition of the M atoms. It produces for a certain value of x a long-wavelength incommensurate structure as the low-temperature phase. This is in contrast with the other incommensurate phases such as the CDW states of two-dimensional conductors, where the incommensurate structures generally appear at high temperatures. A local structural excitation model is adopted in the discussion of the superconductivity, and the x dependences of T_c in

Cs₈WO₃ and Rb₈WO₃ are consistently explained in relation to the ordering schemes of the M atoms. (34 refs.)

114634 Increase of transition temperature T_c in A15 superconductors after neutron irradiation. E.S.Plechkins, V.D.R.Radzhus, A.E.Petrov. *Latv. PSR Zinat. Akad. Vestis Fiz. Teh. Zinat. Ser. (USSR)*, no.4, p.41-5 (1983). In Russian.

The results of investigation of transition temperature T_c and transition widths T_c in A15 compounds Nb_{2.77}Ge_{1.23} and Nb₃Al_{0.7}Ge_{0.3} at the radiation temperature about 750K and fast neutron flow Φ up to 4×10¹⁸n/cm² are presented. The method of measuring T_c is described. The curve T_c(Φ) has a weak maximum for both the samples. The curve T_c(Φ) at radiation temperatures higher than 800K decreases monotonously with the fluence increase. The effect on T_c(Φ) is interpreted by the variations of the reduced density of electron states at the Fermi level due to structural defects. (8 refs.)

114635 Superconducting equiatomic ternary transition metal arsenides. G.P.Meisner, H.C.Ku (Inst. for Pure & Appl. Phys. Sci., Univ. of California, San Diego, La Jolla, CA, USA), H.Barz. *Mater. Res. Bull. (USA)*, vol.18, no.8, p.983-91 (Aug. 1983). The superconductivity and crystal structure of new transition metal arsenide compounds MM'As, where M=Zr or Hf and M'=Ru or Os, are reported. The ZrRuSi-type hexagonal structure of these compounds is metastable at low temperatures. The superconducting transition temperature of 12K for ZrRuAs is very high for an arsenide compound, and this is the first system of true ternary transition metal arsenides to exhibit superconductivity. (14 refs.)

114636 Superconductivity in irradiated charge-density-wave compounds 2H-NbSe₂, 2H-TaS₂, and 2H-TaSe₂. H.Mutka (Section d'Etude des Solides Irradies, CEN, Fontenay-aux-Roses, France). *Phys. Rev. B (USA)*, vol.28, no.5, p.2855-8 (1 Sept. 1983). Superconducting T_c can be increased by a low concentration, less than 1%, of irradiation-induced defects in the layered charge-density-wave (CDW) compounds 2H-NbSe₂, 2H-TaS₂, and 2H-TaSe₂. This is due to the pinning effect of the defects which perturbs the long-range coherence of the CDW. Resistive transitions show tails below a first drop, suggesting inhomogeneous superconductivity. Such effects are proposed to be related to CDW domains. (29 refs.)

114637 Role of monovalent anions in organic superconductors. J.M.Williams, M.A.Beno, J.C.Sullivan, L.M.Banovetz, J.M.Braam, G.S.Blackman, C.D.Carson, D.L.Greer, D.M.Loensing (Argonne Nat. Lab., Argonne, IL, USA), K.Carneiro. *Phys. Rev. B (USA)*, vol.28, no.5, p.2873-6 (1 Sept. 1983). From an analysis of the crystallographic structures of 13 (TMTSF)₂X salts (TMTSF, tetramethyl-tetraselenafulvalene and X, monovalent anion), at ambient temperature and 125K, the authors demonstrate that the interchain Se-Se contacts correlate well with the observed physical properties of the salts. This is in contrast with earlier and less complete analyses which have focused on unit-cell dimensions or intrachain contacts. (27 refs.)

114638 Appearance of localized superconductivity in magnetic field; possible percolation mechanism of conductivity. A.I.Buzdin (Phys. Dept., Moscow State Univ., Moscow, USSR), M.L.Kulic. *Solid State Commun. (USA)*, vol.47, no.11, p.913-16 (Sept. 1983). The case of a material with a small defect where the transition temperature is higher than in the bulk is studied. It is shown that localized superconductivity appears in magnetic field—in zero field it does not exist. The percolation mechanism as well as anisotropic character resistivity is studied. (9 refs.)

114639 Synthesis and physical properties of new superconducting Chevrel phases Hg₂Mo₆S₈. J.M.Tarascon, J.V.Waszcak, G.W.Hull,Jr., F.J.DiSalvo, L.D.Blitzer (Bell Labs., Murray Hill, NJ, USA). *Solid State Commun. (USA)*, vol.47, no.12, p.973-9 (Sept. 1983). New ternary molybdenum chalcogenides Hg₂Mo₆S₈ (0<x<1) have been synthesized and investigated for their structural, magnetic, and superconducting behavior. These new phases prepared at low temperature by reaction of mercury with Mo₆S₈ (obtained from oxidation of Cu₂Mo₆S₈ by iodine) have been characterized by X-ray diffraction, static Faraday susceptibility, and superconducting transition temperature studies. HgMo₆S₈ crystallizes in the rhombohedral space group R3 (a₀=6.51 Å, α₀=92.53°), has a paramagnetic, temperature dependent susceptibility, and superconducts at 8.1K. As the mercury content decreases, a continuous decrease in T_c from 8.1K to 1.7K for x=0 (Mo₆S₈) is observed. (17 refs.)

114640 Der Einfluss von Wasserstoff auf die Supraleitung von Nichtubergangsmetallen (The influence of hydrogen on the superconductivity of non-transition metals). F.Ochmann. *Report JUL-1849*, Kernforschungsanlage, Julich, Germany (May 1983), 47 pp. In German. The aim was to perform a systematic study of the hydrogen influence on the superconductivity of the non-transition elements Be, Zn, Cd, In, Sn, Tl and Pb. Since hydrogen is almost insoluble in these metals it was introduced into the host lattices by ion implantation at low temperatures. In all cases the critical temperature could be enhanced. In comparison the implantation of deuterium also lead to an improved superconductivity. The observed isotope effects are not understood. By implantation of He those effects on the critical temperature, which occur by radiation damage caused by H(D) implantation, were measured. The critical temperatures achieved in these experiments were always significantly smaller than those caused by H and D respectively. By an application of McMillan's theory (1968) it was possible to show that a phononic origin of the hydrogen effect can explain the experimental results. (44 refs.)

Effect of interplane coupling in quasi-two-dimensional systemsSee Entry 114124

Neutron diffraction and scattering study on M₈WO₃ (M=Rb and K)See Entry 114164

Polaron model of the electronic spectrum and the superconductivity of compounds having the A-15 structureSee Entry 114456

Superconducting behavior of amorphous Zr₇₀Cu₃₀See Entry 114642

The theory of the spin-spin relaxation of electron subsystem in antiferromagnets and polyenesSee Entry 114643

CVD-NbC₁₋₃N_y-carbon fiber superconductorsSee Entry 115080

Production of artificial channel insulating matrices and ultrathin metal filamentsSee Entry 115142

Preparation of superconducting lead-alloy long filaments by glass-coated melt spinningSee Entry 115143

Influence of alloying with germanium and copper on the conditions of formation of the superconducting compound Nb₃SiSee Entry 115170

74.30 GENERAL PROPERTIES

114641 Nonlinear dynamics of resistive domains in inhomogeneous superconductors. A.Vi.Gurevich, R.G.Mints (Inst. of High Temperatures, Acad. of Sci., Moscow, USSR). *Sov. Phys.-Dokl. (USA)*, vol.27, no.12, p.1037-8 (Dec. 1982). Translation of: *Dokl. Akad. Nauk SSSR*, vol.267, no.4-6, p.1103-5 (Dec. 1982). [received: Sept. 1983] The static properties, stability, motion, and localization of the resistive domains which arise as a result of Joule heating in superconductors with a transport current I have been investigated. However, the kinetics of the non-linear processes which accompany, for instance, the interaction between a moving domain and an inhomogeneity, the effect produced on a domain by perturbations of finite amplitude, the nucleation of a domain at an inhomogeneity, etc. have been practically unstudied. The purpose of this paper is to examine these problems. (9 refs.)

Electron-deformation currents in metalsSee Entry 114517

74.30C Magnetization curves, Meissner effect, penetration depth

114642 Superconducting behavior of amorphous Zr₇₀Cu₃₀. R.Arce, F.de la Cruz, J.Guimpel (Centro Atomico Bariloche, Bariloche, Argentina). *Solid State Commun. (USA)*, vol.47, no.11, p.885-7 (Sept. 1983). Measurement of the Meissner penetration depth, λ(T) were made in amorphous Zr₇₀Cu₃₀ samples. The results indicate that this amorphous alloy behaves as a BCS superconductor with 2Δ(0)/kT_c=3.8, where Δ(0) is the superconducting energy gap at T=0 and T_c the critical temperature. It is also concluded that the low energy excitation, TLS, characteristics of amorphous material does not contribute to T_c. (11 refs.)

74.30E Thermodynamic properties; thermal conductivity

Polaron model of the electronic spectrum and the superconductivity of compounds having the A-15 structureSee Entry 114456

74.40 FLUCTUATIONS AND CRITICAL EFFECTS

114643 The theory of the spin-spin relaxation of electron subsystem in antiferromagnets and polyenes. M.A.Savchenko, A.V.Stephanovitch (Inst. of Radioengng., Electronics & Automation, Moscow, USSR). *Solid State Commun. (USA)*, vol.47, no.11, p.863-8 (Sept. 1983). The theory of conductivity of rare earth compounds and polyenes is constructed on the basis of the fluctuational theory of magnetic superconductors. The criterion of the appearance of the high-temperature superconducting phase in rare earth antiferromagnetic compounds and of the superconductivity in polyene systems is found. (9 refs.)

74.50 PROXIMITY EFFECTS, TUNNELLING PHENOMENA, AND JOSEPHSON EFFECT

114644 Nb₃Al/oxide/Pb Josephson tunnel junctions fabricated using a CF₄ cleaning process. K.Tanabe, Y.Kato, O.Michikami (Ibaraki Electrical Communication Lab., Nippon Telegraph & Telephone Public Corp., Ibaraki, Japan). *Appl. Phys. Lett. (USA)*, vol.43, no.6, p.603-5 (15 Sept. 1983). Nb₃Al/oxide/Pb Josephson tunnel junctions have been fabricated using a new surface cleaning technique, the CF₄ cleaning process (CFCP), in which the base electrode is cleaned prior to oxide barrier formation in an Ar and CF₄ RF plasma mixture. Adopting lower cleaning voltages than for Nb/oxide/Pb junctions, makes it possible to obtain high-quality junctions with very low leakage (V_m=30 mV) and uniform Josephson current distribution. Such good junction characteristics indicate the formation of damage-free cleaned electrode surfaces and highly insulating mixed oxide barriers. (14 refs.)

114645 Nb₃Sn-Pb Josephson tunnel junctions using patterned RF sputtered material and RF oxidation. H.Tsuge, L.L.Houck, J.E.Nordman (Dept. of Electrical & Computer Engng., Univ. of Wisconsin, Madison, WI, USA). *Appl. Phys. Lett. (USA)*, vol.43, no.6, p.606-8 (15 Sept. 1983). Josephson tunnel junctions have been fabricated using standard photolithography and RF plasma oxidation on RF sputtered Nb₃Sn films. Good quality Nb₃Sn surfaces have been obtained by evaporating a Sn layer of 50-70 nm on the Nb₃Sn films and annealing at 800-850°C in a high vacuum. The measured energy gap values for the Nb₃Sn films are between 3.0 and 3.1 meV. The subgap resistance is more than six times the normal resistance. A significant improvement in tunnel characteristics can be achieved by using this surface treatment process on sputtered Nb₃Sn films. (8 refs.)

114646 Lead-lead oxide-lead tunnel junction fabrication technique and performance. M.Prasad, A.K.Gupta, V.S.Tomar, N.D.Kataria (Nat. Phys. Lab., New Delhi, India). *Indian J. Cryog.*, vol.6, no.4, p.192-5 (1981).

Preparation of thin film (tunnel) junctions suitable for Josephson voltage standard application needs several considerations. Such junctions should show large amplitude microwave induced steps up to a few millivolts. In other words, the junction should have better microwave coupling which is achieved by mounting the junction in a resonant field and by having the junction dimensions suitable for such resonance. Lead-lead oxide-lead tunnel junctions of dimensions 0.2×0.2 mm² and 0.2×0.8 mm² are prepared in cross type geometry. The evaporation of lead is done through a precise pattern mask prepared photolithographically. Oxidation of the film is done in situ. The oxide barrier thickness is very critical for Josephson behaviour and has aging effects at ambient temperatures. I-V characteristics of typical junctions are presented and discussed. (5 refs.)

114647 Fluxon reflection at loaded terminations of long Josephson junctions. O.H.Olsen (R&D System & Design Div., NIRO Atomizer, Soeborg, Denmark), M.Salerno, M.R.Samuelsen. *Physica D (Netherlands)*, vol.8D, no.1-2, p.267-72 (July 1983). The reflection process of fluxons at loaded terminations of long lossless Josephson junctions is examined numerically. The energy absorbed by the load, modelling an external circuit, is calculated and compared to an approximate analytical expression. Further an estimate of the energy of the radiation into the junction resulting from the reflection is calculated. The absorbed energy and the energy of the radiation increase linearly and quadratically with the reciprocal load, respectively. (6 refs.)

114648 Electric-field penetration into a superconductor in a Josephson microjunction. L.E.Amatuni, V.N.Gubankov, A.V.Zaitsev, G.A.Ovsyannikov (Inst. of Radio Engng. & Electronics, Acad. of Sci., USSR). *Sov. Phys.-JETP (USA)*, vol.83, no.5, p.1070-6 (Nov. 1982). Translation of: *Zh. Eksp. & Teor. Fiz. (USSR)*, vol.83, no.5, p.1851-63 (Nov. 1982). [received: Sept. 1983]

The influence of penetration of a constant and alternating field into the superconducting films of the electrodes (banks) on the properties of individual Josephson junctions and of their chains is investigated theoretically and experimentally. It is found that these phenomena are of substantial significance despite the considerable current density in the film junctions. It is shown that the interaction efficiency of series-connected junctions has a non-monotonic dependence on the distance between them, on the chain voltage, and on the temperature; this is due to the quasiwave character of the propagation of the alternating electric field in the film of the superconducting electrodes. (19 refs.)

Development of a cryostat for AC Josephson effect studies ...See Entry 111693

74.60 TYPE-II SUPERCONDUCTIVITY

74.60E Mixed state, H_{c2} , surface sheath

114649 Unusual critical-field behavior in $Y_{1-x}Er_xRh_4B_4$. H.B.Radousky, A.T.Aldred, G.S.Knapp, J.S.Kouvel (Materials Sci. & Technol. Div., Argonne Nat. Lab., Argonne, IL, USA).

Phys. Rev. B (USA), vol.28, no.5, p.2859-62 (1 Sept. 1983).

Measurements of the upper critical fields versus temperature in $Y_{1-x}Er_xRh_4B_4$ reveal that the system undergoes a nearly abrupt change from very weak to very strong pair breaking in an applied field with increasing Er concentration. This abrupt change in behavior occurs for $0.10 < x < 0.17$, and can be characterized by the relative variation of the magnetic correlation length ξ_{sc} , which are the relevant length scales for this problem. (19 refs.)

114650 Critical field measurements in superconductors using AC inductive techniques. S.A.Campbell, J.B.Ketterson (Argonne Nat. Lab., Argonne, IL, USA), G.W.Crabtree.

Rev. Sci. Instrum. (USA), vol.54, no.9, p.1191-8 (Sept. 1983).

The AC in-phase and out-of-phase response of type II superconductors is discussed in terms of DC magnetization curves. Hysteresis in the DC magnetization is shown to lead to a dependence of the AC response on the rate at which an external field is swept. This effect allows both H_{c1} and H_{c2} to be measured by AC techniques. A relatively simple mutual inductance bridge for making such measurements is described in the text, and factors affecting bridge sensitivity are discussed in the Appendix. Data for the magnetic superconductor $ErRh_4B_4$ obtained using this bridge are reported. (15 refs.)

74.60G Flux pinning; fluxon-defect interactions

Fluxon reflection at loaded terminations of long Josephson junctionsSee Entry 114647

74.60J Critical currents

114651 50-Hz AC losses in inductive coils with mixed matrix fine filament NbTi composites at fields up to 1 T. I.Hlasnik, E.W.Seibt (Inst. fur Tech. Phys., Kernforschungszentrum Karlsruhe, Karlsruhe, Germany).

J. Appl. Phys. (USA), vol.54, no.9, p.5479-81 (Sept. 1983).

Measurements of 50-Hz AC losses were performed using three characteristic NbTi coil samples with ultrafine filaments and a Cu-CuNi mixed matrix at fields up to 1 T and 4.2K. Critical current and quenching current densities were measured under DC and AC conditions as well as the losses with their hysteresis and eddy current loss proportions. To characterize the samples by their eddy current loss proportions the transverse resistivity of the matrix ρ_{trans} was determined. The results for losses show that under 50-Hz AC loads alternating fields up to approximately 1 T are attained without quenching. The fact that the associated eddy current losses of about 10^3 W/m³ remain comparatively low at 0.5 T and 4.2K opens up for such structured mixed matrix NbTi composites a novel field of application for superconducting generators and pulsed magnets with 50-60 Hz fed windings. (5 refs.)

CVD-NbC_{1-y}N_y-carbon fiber superconductorsSee Entry 115080

SiC-coatings as protective layers for carbon fibers and adhesion promoters for superconducting niobium carbonitrideSee Entry 115398

74.70 SUPERCONDUCTING MATERIALS

Point defect thermodynamics of compound semiconductors and their alloysSee Entry 113907

Production of artificial channel insulating matrices and ultrathin metal filamentsSee Entry 115142

74.70D Material effects on T_c , K, critical currents

(see also 81.40R Electrical properties related to materials treatment)

Increase of transition temperature T_c in A15 superconductors after neutron irradiationSee Entry 114634

Synthesis and physical properties of new superconducting Chevrel phases $Hg_xMo_6S_8$ See Entry 114639

Der Einfluss von Wasserstoff auf die Supraleitung von Nichtbergangsmetallen (The influence of hydrogen on the superconductivity of non-transition metals) ..See Entry 114640

74.70G Type-I superconductors (non transition metals)

Der Einfluss von Wasserstoff auf die Supraleitung von Nichtbergangsmetallen (The influence of hydrogen on the superconductivity of non-transition metals) ..See Entry 114640

Preparation of superconducting lead-alloy long filaments by glass-coated melt spinningSee Entry 115143

74.70L Type-II superconductors (transition metals, alloys and compounds)

Neutron diffraction and scattering study on M_xWO_3 ($M=Rb$ and K)See Entry 114164

Polaron model of the electronic spectrum and the superconductivity of compounds having the A-15 structureSee Entry 114456

Superconducting materialsSee Entry 114631

ATA and the electron phonon coupling constant in calculating T_c of superconducting alloysSee Entry 114632

Structural phase transitions and superconducting transition temperatures of hexagonal M_xWO_3 compoundsSee Entry 114633

Increase of transition temperature T_c in A15 superconductors after neutron irradiationSee Entry 114634

Superconducting equiatomic ternary transition metal arsenidesSee Entry 114635

Superconductivity in irradiated charge-density-wave compounds 2H-NbSe₂, 2H-TaS₂, and 2H-TaSe₂See Entry 114636

Role of monovalent anions in organic superconductorsSee Entry 114637

Synthesis and physical properties of new superconducting Chevrel phases $Hg_xMo_6S_8$ See Entry 114639

Unusual critical-field behavior in $Y_{1-x}Er_xRh_4B_4$ See Entry 114649

Critical field measurements in superconductors using AC inductive techniques ..See Entry 114650

Resonance near the Fermi energy in a Kondo latticeSee Entry 114669

Absence of hydrogen in superconducting molybdenum sulfide, Mo_3S_4 See Entry 114744

The float-zone growth of Ti_3Au and Ti_3Pt See Entry 115049

Chemical vapor deposition of Nb_3Sn in a fluidized bedSee Entry 115081

Influence of alloying with germanium and copper on the conditions of formation of the superconducting compound Nb_3Si See Entry 115170

74.70P Materials for high-field applications

50-Hz AC losses in inductive coils with mixed matrix fine filament NbTi composites at fields up to 1 TSee Entry 114651

CVD-NbC_{1-y}N_y-carbon fiber superconductorsSee Entry 115080

74.90 OTHER TOPICS IN SUPERCONDUCTIVITY

Creation of point defects in superconductors. A short reviewSee Entry 113859

75.00 MAGNETIC PROPERTIES AND MATERIALS

(see also 81.40R Magnetic properties related to materials treatment; for galvanomagnetic effects, see 72.15G and 72.20M; for magneto-optical effects, see 78.20L)

Proceedings of Helsinki International Summer School on Semiconductors 1982See Entry 111297

75.10 GENERAL THEORY AND MODELS OF MAGNETIC ORDERING

(see also 05.50 Ising problems, 71.25 Nonlocalized single-particle electronic states, 71.70 Level splitting and interactions)

114652 Some ideas related to magnetism in the rare earths. S.Legvold (Dept. of Phys., Iowa State Univ., Ames, IA, USA).

J. Less-Common Met. (Switzerland), vol.93, no.1, p.1-14 (1983). (Proceedings of the Sixteenth Rare Earth Research Conference, Tallahassee, FL, USA, 18-21 April 1983).

In 1962 it was found that rare earth metal single crystals could be grown by the strain anneal method. This breakthrough made it possible to obtain illuminating magnetic and transport data on these metals. The author gives a brief summary of some of the results obtained and then discusses some more recent findings about Lifshitz points, 'double' ferromagnetism and the suppression of superconductivity in lanthanum by the magnetic rare earths. (40 refs.)

75.10D Crystal-field theory and spin Hamiltonians

Spectrum of a one-dimensional ferromagnet in a transverse fieldSee Entry 114682

The influence of Cr and W contents of the isomer shift, hyperfine field distribution, and magnetic anisotropy of Fe-based amorphous alloysSee Entry 114758

75.10H Ising and other classical spin models

114653 Transport properties of nearly magnetic alloys and metals. A.B.Kaiser (Phys. Dept., Victoria Univ. of Wellington, Wellington, New Zealand).

Aust. J. Phys. (Australia), vol.36, no.4, p.537-51 (1983).

The author gives an elementary review of how simple spin fluctuation models can account for the distinctive transport properties of nearly magnetic alloys and metals. The principal systems considered are dilute alloys such as $PdNi$ in which host and impurity have somewhat similar electronic structure but with the impurity more nearly magnetic than the host. Similar effects occurring in pure metals or concentrated alloys are also mentioned. (44 refs.)

114654 Magnets with random anisotropies: the random cubic model and other models with p -fold spin interactions. Y.Y.Goldschmidt (Dept. of Phys. & Astron., Univ. of Pittsburgh, Pittsburgh, PA, USA). *Nucl. Phys. B, Field Theory & Stat. Syst. (Netherlands)*, vol.B220(FS8), no.4, p.351-65 (5 Sept. 1983).

The author investigates in detail models with random anisotropies and p -fold spin interactions. He constructs the random cubic model ($p=4$) and shows that when $N>2$ (N being the number of spin components) its properties are similar to the random uniaxial anisotropy model, since quartic interactions characteristic of the random uniaxial model, are generated through renormalization even if they vanish to start with. Similar conclusions apply to a random p -fold interaction model of the form $-\Delta\sum_i(\hat{n}_i\cdot\hat{S}_i)^p$, when p is even. In the case of odd p , a random field interaction is generated. Other models are also discussed. (13 refs.)

114655 Competing Ising interactions and chaotic glass-like behaviour on a Cayley tree. S.Inawashiro, C.J.Thompson (Dept. of Math., Univ. of Melbourne, Parkville, Australia). *Phys. Lett. A (Netherlands)*, vol.97A, no.6, p.245-8 (5 Sept. 1983). For the Ising model on a Cayley tree with competing nearest neighbour coupling J and next nearest neighbour coupling J' , the authors find in addition to the expected paramagnetic, ferromagnetic and antiferromagnetic phases, an intermediate range of $J'/J<0$ values where the local magnetization has chaotic oscillatory glass-like behaviour. (9 refs.)

The thermodynamic limit for long-range random systems See Entry 111600
Classical treatment of a Heisenberg linear chain with spin alternation; application to the $\text{MnNi(EDTA).6H}_2\text{O}$ complex See Entry 114699

75.10J Heisenberg and other quantized localized spin models

114656 Magnetic ordering phenomena in rare earth semiconductors. W.Zinn (Inst. fur Festkörperforschung KFA, Jülich, Germany). *Acta Polytech. Scand. Electr. Eng. Ser. (Finland)*, no.EL50, p.365-446 (1983). (Proceedings of Helsinki International Summer School on Semiconductors 1982, Espoo, Finland, 14-18 June 1982). The general features of 4f-magnetic semiconductors are introduced by outlining their most characteristic properties in comparison to those of the 5f-actinide and chalcogenide classes of binary compounds. An overview on the $\text{EuX(X=0, S, Se, Te)}$ model substances for the Heisenberg theory of exchange and ferromagnetism is given. In particular, recent systematic neutron scattering, NMR, and Mossbauer effect studies on correlations between the individual exchange interactions, $-2J\text{S}_i\text{S}_j$, and attributed transferred hyperfine interactions, $A_{ij}\text{I}_i\text{S}_j$, between an Eu^{2+} ion of 4f-spin S_0 and nuclear spin I_i and an Eu-ion of spin S_i in the i -th neighbour shell, respectively are discussed. These results are shown to provide a good quantitative basis for detailed further experimental and theoretical studies of frustration and spin glass phenomena observed generally on disordering or diluting spin systems, which are coupled by competing exchange interactions. These features are demonstrated by results of recent systematic neutron scattering experiments on the spin structures, correlation lengths, and magnetic excitation spectra of the magnetic phases observed in $\text{Eu}_x\text{Sr}_{1-x}\text{S}_y\text{Se}_{1-y}$ compounds, which are considered model systems for disordered and diluted Heisenberg ferromagnets and spin glasses. (71 refs.)

114657 Relaxation in linear ferromagnetic chain. II. Spin relaxation in the case of cubic anisotropy. V.N.Kasheev. *Latv. PSR Zinat. Akad. Vestis Fiz. Teh. Zinat. Ser. (USSR)*, no.4, p.3-9 (1983). In Russian. For pt.I see ibid., no.3, p.6 (1983). In the classical linear Heisenberg chain the asymptotics of correlator of the transverse spin component (traced back to the spin-phonon interaction of exchange origin) is calculated in the hydrodynamic limit. (26 refs.)

114658 Mean-field solution of a spherical model for Heisenberg spins with complicated coupling. K.G.Chakraborty (Dept. of Phys., Basirhat Coll., West Bengal, India). *Phys. Rev. B (USA)*, vol.28, no.5, p.2827-38 (1 Sept. 1983). Mean-field solution of a spherical model for complicated magnetic systems is presented. The magnetic systems include those which favor dipolar, quadrupolar, and biaxial ordering. The author employs a Lagrange multiplier method to calculate the partition functions of the systems and hence the expressions for the ordering parameters. The phase transitions of the model systems are studied and the results are compared with those obtained by earlier approximation methods. (21 refs.)

114659 Exact solution of the Bethe lattice with long-range interactions: Application to a Heisenberg ferromagnet. A.Trias, F.Yndurain (Dept. de Fisica, Univ. Autonoma de Madrid, Madrid, Spain). *Phys. Rev. B (USA)*, vol.28, no.5, p.2839-44 (1 Sept. 1983). The authors have found the exact solution for the density of states of a tight-binding Hamiltonian describing the interactions between orbitals (spins, atomic orbitals, atomic displacements, etc.) in atoms on a Bethe lattice. These interactions are not necessarily restricted only to near-neighbor atoms because long-range interactions between distant atoms are included. A dispersion relations characteristic of the Bethe lattice appears very naturally in the solution. As an example, the dispersion relation in the one-spin-wave approximation for a ferromagnetic Heisenberg Hamiltonian is calculated. A Ruderman-Kittel-Kasuya-Yosida-type interaction between all pairs of spins is considered. The authors find that when the interaction between spins decays with the distance at a slower rate than a critical value, the ferromagnetic ground state is unstable and a new helical spin array appears. (11 refs.)

The thermodynamic limit for long-range random systems See Entry 111600
Classical treatment of a Heisenberg linear chain with spin alternation; application to the $\text{MnNi(EDTA).6H}_2\text{O}$ complex See Entry 114699
Steepest descent approach to the domain-wall thermodynamics of a classical easy-plane ferromagnetic chain: application to CsNiF_3 See Entry 114702

75.10L Band and itinerant models

114660 Itinerant electron magnetism. E.P.Wohlfarth (Imperial Coll., London, England). *Europhys. News (Switzerland)*, vol.14, no.7, p.7-8 (July 1983). Itinerant electron magnetism as a subject had its birth in the 1930s and, after a lengthy period of relative neglect, it experienced a renaissance beginning about 20 years ago. At the present time it has reached an exciting stage of development to which there is no rapid end in sight. Contributing to the evolution of the subject, concerned as it is with the magnetic properties of metals and alloys are: theoretical sophistication, advanced computations and advances in experimental techniques. All three of these facets appeared in an

exciting way at a recent Workshop on 3d metallic magnetism, held in Grenoble on 25-26 March, 1983, and at the 3rd General Conference of the Condensed Matter Division in Lausanne. (no refs.)

114661 Strong electronic correlations in magnetic semiconductors: the functional integral approach to the Hubbard model. P.L.Hugon, D.Paquet (Univ. Paris VII, Paris, France). *Acta Polytech. Scand. Electr. Eng. Ser. (Finland)*, no.EL50, p.139-82 (1983). (Proceedings of Helsinki International Summer School on Semiconductors 1982, Espoo, Finland, 14-18 June 1982).

Discusses magnetic semiconductors in the intermediate-coupling situation within the framework of the Hubbard model. The experimental facts which motivate the recourse to the Hubbard model are recalled and the model itself is introduced. The standard treatment of the Hubbard model in terms of the functional integral is discussed with emphasis on the series of approximations which underlie it. The thermodynamics of the half-filled Hubbard system is discussed by introducing a functional order parameter which is the probability density of exchange field on a site. For large values of the intra-atomic interaction energy U , a cross-over temperature separates a low temperature regime, exhibiting quasi-local magnetic moments and non-conducting states at the Fermi level, from a high temperature regime characterized by spin-fluctuations in a poor metal. It is shown how the functional integral formalism lends itself to estimate the linear responses of the system. The magnetic susceptibility evolves continuously from a Curie-Weiss behaviour (large U , small T) to an enhanced Pauli one (small U , large T). Finally, results regarding the exchange field dynamics are given. (34 refs.)

114662 Band-model approach to magnetic excitations in a disordered ferromagnet: one-dimensional case. S.Krompiewski (Inst. of Molecular Phys., Polish Acad. of Sci., Poznan, Poland). *Phys. Rev. Lett. (USA)*, vol.51, no.12, p.1092-4 (19 Sept. 1983). A disordered ferromagnet is studied with use of the Hubbard model. A systematic method of finding the spin transverse susceptibility for any random configuration is developed. The computer results for a one-dimensional case reveal gapless magnetic excitations centered around a wave vector corresponding to the first maximum of the structure factor in qualitative accordance with recent experimental data. (10 refs.)

Transport properties of nearly magnetic alloys and metals See Entry 114653

75.20 DIAMAGNETISM AND PARAMAGNETISM

Apparatus for the measurement of the magnetic susceptibility of liquids in high magnetic fields See Entry 111711
Theory of saturation of magnetic resonance in solids at low temperatures See Entry 114725

75.20C Nonmetals

114663 Magnetic susceptibility of solid solutions based on two isostructural SmB_6 phases. M.I.Aivazov, S.V.Aleksandrovich, B.A.Evseev, O.M.Tsarev (Sci.-Production Combine 'Energiya', Moscow, USSR). *Fiz. Met. & Metalloved. (USSR)*, vol.56, no.2, p.249-52 (Aug. 1983). In Russian. English translation in: *Phys. Met. & Metallogr. (GB)*. The magnetic susceptibility of the $\text{Sm}_{1-x}\text{Pr}_x\text{B}_6$, $(\text{Sm}_{1-x}\text{Gd}_x)_{0.8}\text{B}_6$, and $(\text{Sm}_{1-x}\text{Eu}_x)_{0.8}\text{B}_6$ solid solution systems was determined in the temperature range 80-1100K. At low Sm concentrations the values of the Weiss constants were in agreement with the predictions of the RKKY theory of indirect exchange via the conduction electrons. The magnetic susceptibility and the lattice period data were used to determine the valence of ions in the isostructural SmB_6 and $\text{Sm}_{0.8}\text{B}_6$ phases. (12 refs.) *A.T.*

114664 Field dependence of the paramagnetic susceptibility of the antiferromagnets $\text{CoCl}_2\cdot 6\text{H}_2\text{O}$, $\text{NiCl}_2\cdot 4\text{H}_2\text{O}$, $\text{MnCl}_2\cdot 4\text{H}_2\text{O}$, and $\text{MnBr}_2\cdot 4\text{H}_2\text{O}$. S.S.Vianna (Dept. de Fisica, Univ. Federal de Pernambuco, Pernambuco, Brazil), C.C.Becerra. *Phys. Rev. B (USA)*, vol.28, no.5, p.2816-26 (1 Sept. 1983). Reports differential paramagnetic susceptibility (χ) measurements as a function of an applied magnetic field (H) for the antiferromagnets $\text{CoCl}_2\cdot 6\text{H}_2\text{O}$, $\text{NiCl}_2\cdot 4\text{H}_2\text{O}$, $\text{MnCl}_2\cdot 4\text{H}_2\text{O}$, and $\text{MnBr}_2\cdot 4\text{H}_2\text{O}$. Above the ordering temperature, the χ vs H curves exhibit a characteristic maximum which is attributed to short-range order. This effect is more pronounced in the cobalt compound (spin $1/2$) and less pronounced in the manganese compounds (spin $5/2$). Using simple models suitable to describe the above-mentioned systems, they discuss the dependence of this maximum with spin magnitude, anisotropy, and lattice dimensionality. The theoretical treatment is based on a variational method in which correlation effects between pairs of spins are considered. (23 refs.)

114665 Magnetism in Ti_6O_{11} . S.P.McAlister, A.D.Inglis (Solid State Chem., National Res. Council of Canada, Ottawa, Ontario, Canada). *Solid State Commun. (USA)*, vol.47, no.11, p.931-3 (Sept. 1983). Measurements of the magnetization of Ti_6O_{11} show transitions of $119\pm 1\text{K}$ and $147\pm 1\text{K}$. Above 147K the authors attribute the paramagnetism to d^1 electrons on Ti^{3+} ions. Below 147K there are contributions from both Ti_2^{7+} dimers and Ti^{3+} ions. The gradual increase in magnetic moment with increasing temperature to 119K the authors interpret as an increase in spins due to the break up of Ti_2^{6+} dimers to Ti^{3+} ions. (13 refs.)

114666 Nonlinear static magnetic susceptibility of the Van Vleck paramagnet TiMPo_4 . S.I.Andronenko, A.N.Bazhan, I.A.Bondar, V.A.Ioffe, B.Z.Malkin, L.P.Mezentseva (I.V. Grebenshchikov Inst. of Silicate Chem., Acad. of Sci., Leningrad, USSR). *Sov. Phys.-Solid State (USA)*, vol.25, no.2, p.239-42 (Feb. 1983). Translation of: *Fiz. Tverd. Tela (USSR)*, vol.25, no.2, p.423-9 (Feb. 1983). [received: Sept. 1983]

A theoretical and experimental study is made of the anisotropy, temperature dependence, and field dependence of the magnetic moment of Ti^{3+} ions having a singlet ground state in the TiMPo_4 lattice, at temperatures from 2 to 50K in fields up to 65 kOe. It is shown that the anomalously large nonlinear static magnetic susceptibility found in the [110] direction is due to the inverse magnetostriiction effect and cooperative quadrupole-quadrupole interaction in rare-earth ions via the field of deformations with B_2 symmetry. (11 refs.)

Apparatus for measuring the magnetic susceptibility of a diamagnetic or paramagnetic material in the solid or molten state See Entry 111710
Density-of-state effects in the low temperature properties of TiBe_2 See Entry 114431
Synthesis and physical properties of new superconducting Chevrel phases $\text{Hg}_x\text{Mo}_6\text{S}_8$ See Entry 114639
Electrolytic growth, electrical conductivity and magnetic susceptibility of stannous iodide See Entry 115032

75.20E Metals and alloys

114667 Magnetic properties of Fe-Ni-Zr and Fe-Ni-Nb alloys. L.V.Osipova, L.A.Panteleymonov. *Russ. Metall. (GB)*, no.3, p.183-5 (1982). Translation of: *Izv. Akad. Nauk. SSSR Met.*, no.3, p.205-7 (1982). Compounds FeZr_2 , NiZr_2 , Ni_2Zr , Fe_2Nb , FeNb , NiNb and Ni_2Nb are paramagnetic under normal conditions, while the intermetallics Fe_2Nb , FeNb , NiNb and Ni_2Zr are temperature-independent paramagnetics in the range 293-1073K. The Laves phase Fe_2Zr is ferromagnetic with the Curie point at 370K. Alloying of Fe_2Zr -base alloys with nickel causes a drop in transition temperature into the magnetically ordered state. The addition of 27 at.% Ni leads to complete loss of the ferromagnetic properties of alloys from the range of ternary solid solution $\text{Fe}_{2-x}\text{ZrNi}_x$. (8 refs.)

114668 Inelastic scattering of neutrons by paramagnetic ions under relaxation conditions. V.N.Peregudov, A.M.Afanasyev, V.D.Gorobchenko (I.V. Kurchatov Inst. of Atomic Energy, Moscow, USSR). *Sov. Phys.-JETP (USA)*, vol.83, no.5, p.1059-63 (Nov. 1982). Translation of: *Zh. Eksp. i Teor. Fiz. (USSR)*, vol.83, no.5, p.1831-40 (Nov. 1982). [received: Sept. 1983]

A general theoretical analysis is made of the inelastic scattering of neutrons by paramagnetic ions interacting with the environment. A situation is considered in which a paramagnetic ion interacts statically with a crystal field and the total angular momentum of a partly filled electron shell of the ion relaxes because of the contact interaction with conduction electrons. A detailed calculation is made of inelastic scattering of neutrons in an intermetallic compound PrAl_2 at low temperatures. Analytic expressions are obtained for the profiles of the inelastic scattering peaks and for the temperature dependences of the peak parameters. It is shown that the interaction of the f electrons of Pr with the conduction electrons broadens and shifts the peaks corresponding to transitions between the f -electron states in a crystal field, and also splits the peaks and makes them asymmetric. (19 refs.)

Coupled quadrupole-phonon excitations: inelastic neutron scattering on Van Vleck paramagnet PrNi_2 See Entry 114107

Lattice dynamics of FePt alloys of AB_3 type ordered structure See Entry 114109

Polaron model of the electronic spectrum and the superconductivity of compounds having the A-15 structure See Entry 114456

The magnetic structures of the rare earth metals—a historical survey See Entry 114673

75.20H Local moment in dilute alloys; Kondo effect

(see also 72.15Q Electronic conduction)

114669 Resonance near the Fermi energy in a Kondo lattice. F.G.Aliev, N.B.Brandt, V.V.Moshchalkov, N.E.Sluchanko, S.M.Chudinov, R.I.Yasnitskii (M.V. Lomonosov Moscow State Univ., Moscow, USSR). *JETP Lett. (USA)*, vol.37, no.7, p.353-7 (5 April 1983). Translation of: *Pis'ma v Zh. Eksp. i Teor. Fiz. (USSR)*, vol.37, no.7, p.299-302 (5 April 1983). [received: Oct. 1983]

An anomalous increase (by a factor of 40-60) in the Hall coefficient R_H has been observed in the CeCu_2Si_2 superconducting Kondo system as the temperature is lowered from 60 to 4K. This effect is evidence of the formation of a narrow resonance near the Fermi level in CeCu_2Si_2 . (9 refs.)

75.25 SPIN ARRANGEMENTS IN MAGNETICALLY ORDERED MATERIALS (NEUTRON STUDIES, ETC)

114670 Investigations on the magnetic structure of pseudobinary intermetallic compounds from the $\text{Tb}(\text{Co}_x\text{Ni}_{1-x})_2$ system. B.Sidzhimov (Inst. of Nuclear Res. & Nuclear Energy, Bulgarian Acad. of Sci., Sofia, Bulgaria), N.Stanev, L.Bozakov, S.Neov. *Bulg. J. Phys. (Bulgaria)*, vol.10, no.3, p.328-36 (1983).

Neutron diffraction and magnetic measurements by a vibrating magnetometer in the 78-293K range were used to study the magnetic structure of the intermetallic compounds $\text{Tb}(\text{Co}_x\text{Ni}_{1-x})_2$ prepared by arc melting. The studied compounds were found to crystallize in a MgCu_2 -type cubic lattice. The unit cell parameters and the atomic radii were calculated as a function of composition and nearest neighbour's distances in the structures of the investigated compounds. The Curie temperature were found from the temperature dependence of the bulk magnetization. The neutron diffraction patterns below T_C show antiparallel alignment of the magnetic moments in the two sublattices. The sublattice and molecular magnetic moments were found for each of the studied compounds in magnetically ordered state. (17 refs.)

114671 Magnetic structure of Tb_3Co . N.V.Baranov, A.P.Vokhmyanin, A.V.Deryagin, V.V.Kelarev, A.N.Pirogov, V.A.Reimer, V.N.Syromyatnikov (A.M. Gorki Ural State Univ., Sverdlovsk, USSR). *Fiz. Met. & Metalloved. (USSR)*, vol.56, no.2, p.261-5 (Aug. 1983). In Russian. English translation in: *Phys. Met. & Metallogr. (GB)*

A neutron-diffraction study was made of an intermetallic compound Tb_3Co at 4.2 and 300K. The parameters describing its magnetic structure were determined. It was found that the noncoplanar nature of the magnetic moments of the Tb ions was mainly due to the electrostatic interaction of their 4f shell with the crystal field of the lattice. (9 refs.) A.T.

114672 Magnetic ordering of the quasi-two-dimensional system VOCl . A.Wiedenmann (Inst. fur Phys. Chem., Univ. Hamburg, Hamburg, Germany), J.P.Venien, P.Palvadeau, J.Rossat-Mignod. *J. Phys. C (GB)*, vol.16, no.27, p.5339-50 (30 Sept. 1983).

The susceptibility of single crystals of VOCl is isotropic above $T_N=80.5\text{K}$ and well described by a quadratic two-dimensional (2D) Heisenberg system with a strong antiferromagnetic intra-layer coupling ($J/k=-34.5\text{K}$). Neutron diffraction revealed a collinear antiferromagnetic order with a wavevector $k=[1/2, 1/2, 1/2]$ and the moments along the a axis. Two structures, corresponding to both a ferromagnetic and an antiferromagnetic coupling between the two magnetic Bravais lattices, coexist as a result of the particular value of the wavevector. The order parameter follows a power law at the magnetic transition, with a critical exponent $\beta=0.143$, in agreement with the 2D character and anisotropy of Ising type. (12 refs.)

114673 The magnetic structures of the rare earth metals—a historical survey. W.C.Kochler (Oak Ridge Nat. Lab., Oak Ridge, TN, USA). *J. Less-Common Met. (Switzerland)*, vol.93, no.1, p.15-30 (1983). (Proceedings of the Sixteenth Rare Earth Research Conference, Tallahassee, FL, USA, 18-21 April 1983).

Presents a brief survey of the magnetic structure determination in rare earth metals using neutron diffraction. Studies of both paramagnets and magnetically ordered phases are included. (37 refs.)

114674 Modulated magnetic structure of the Kondo compound TmS . Y.Lassailly, C.Vettier (Inst. Laue-Langevin, Grenoble, France), F.Holtzberg, J.Flouquet, C.M.E.Zeyen, F.Lapierre. *Phys. Rev. B (USA)*, vol.28, no.5, p.2880-2 (1 Sept. 1983).

Single-crystal neutron-diffraction experiments have revealed a modulated antiferromagnetic structure in TmS below the Neel temperature $T_N=5.2\text{K}$. At 1.5K the propagation vector \vec{q} is $(1/2-\eta, 1/2+\eta, 1/2)$ with $\eta=0.075$ and the modulation amplitude $3.4 \mu_B$ along the $[112]$ direction. No lock-in transition is observed even when hydrostatic pressure up to 16 kbar is applied. While the magnetic-transition temperature increases under pressure, the modulation amplitude appears to be pressure independent. Comparison is made with CeAl_2 and other chalcogenide Tm compounds. (16 refs.)

114675 Ferrimagnetism in the MnCrG-MnFeG garnet solid solution system. S.A.Bogoslovskii, T.V.Valyanskaya, I.V.Golosovskii, V.P.Plakhtii, O.P.Smirnov, V.I.Sokolov. *Sov. Phys.-Solid State (USA)*, vol.25, no.2, p.185-7 (Feb. 1983). Translation of: *Fiz. Tverd. Tela (USSR)*, vol.25, no.2, p.328-33 (Feb. 1983). [received: Sept. 1983]

Magnetic, calorimetric, and neutron diffraction studies of the $\text{Mn}_3\text{Fe}_x\text{Cr}_{2-x}\text{Ge}_3\text{O}_{12}$ ($0 \leq x \leq 2$) garnets, which are solid solutions of the antiferromagnetic garnets $\text{Mn}_3\text{Fe}_2\text{Ge}_3\text{O}_{12}$ and $\text{Mn}_3\text{Cr}_2\text{Ge}_3\text{O}_{12}$, were carried out at liquid helium temperatures. It was found that samples with $0.25 \leq x \leq 1.5$ show a special kind of ferrimagnetic order. The experimental results indicate that the mixed-composition garnets contain states of the ferrimagnetic spin glass type. (12 refs.)

Kinetics of structural multiplets during diffusion homogenization of polycrystalline films See Entry 114381

Magnetic ordering phenomena in rare earth semiconductors See Entry 114656

Noncollinear magnetic phases in a strongly anisotropic antiferromagnet CoF_2 with large Dzyaloshinskii interaction See Entry 114679

75.30 MAGNETICALLY ORDERED MATERIALS, OTHER INTRINSIC PROPERTIES

(for critical point effects, see 75.40)

75.30C Saturation moments and magnetic susceptibility

114676 A reexamination of the magnetic susceptibility of the coordination complex $\mu_4\text{-oxohexa-}\mu\text{-chlorotetrakis-(triphenylphosphine oxide) copper (II), Cu}_4\text{OCl}_6(\text{TPO})_4$. R.D.Dickinson, W.A.Baker, Jr. (Dept. of Chem., Univ. of Texas, Arlington, TX, USA), T.D.Black, R.S.Rubins. *J. Chem. Phys. (USA)*, vol.79, no.6, p.2609-14 (15 Sept. 1983).

High purity samples of Cu_4OCl_6 (triphenylphosphine oxide), have been prepared for a reexamination of the χ vs. T behavior of this compound. EPR studies on single crystals of the compound have revealed the ground state to be $S'=0$ and an observed spectrum from an excited $S'=2$ manifold with a g factor of 2.10 ± 0.01 . The ordering of the energies of the spin manifolds is proposed to be $S'=0, S'=2, S'=1$. On this basis, experimentally determined χ vs. T data were fitted to a modified Heisenberg exchange model for $g=2.10, E(S'=1)-E(S'=0)=85 \pm 13 \text{ cm}^{-1}, E(S'=2)-E(S'=0)=10 \pm 1 \text{ cm}^{-1}$, and $z'J'=0 \pm 1 \text{ cm}^{-1}$. Magnetic susceptibility measurements were also made on samples prepared by 'doping' the tetramer into the pores of a cross-linked polymer. (35 refs.)

114677 Magnetochemical study of iron molybdates obtained from precursor precipitates with different Mo- and Fe-content. S.Angelov, St.Karagiozova, K.Petrov (Inst. of General & Inorganic Chem., Bulgarian Acad. of Sci., Sofia, Bulgaria). *Mater. Res. Bull. (USA)*, vol.18, no.8, p.909-14 (Aug. 1983).

The calcination, above 350°C , of precursor precipitates with well-defined stoichiometry and different fixed Mo-to-Fe ratios leads to the formation of undistinguishable, by X-ray diffractometry, crystal iron molybdates. At Mo-to-Fe ratios higher than 1.5 a phase of MoO_3 appears. The parameters describing the temperature dependence of the magnetic susceptibility and the EPR-lines belonging to the iron molybdates depend on the initial-precipitate composition. This is an evidence for the presence of some structural differences in iron molybdate phases. (10 refs.)

114678 Concentration and temperature dependences of the magnetic susceptibility of binary alloys of indium with potassium and rubidium. L.Z.Melekhov, S.P.Yatsenko, K.A.Chuntanov, Sh.R.Zhakupov. *Russ. Metall. (GB)*, no.3, p.179-82 (1982). Translation of: *Izv. Akad. Nauk. SSSR Met.*, no.3, p.202-4 (1982).

The concentration and temperature dependences have been obtained for the magnetic susceptibility of In-K and In-Rb alloys. The concentration characteristics are satisfactorily explained by a model in which the presence of quasimolecules is assumed. The composition dependence of the quasimolecule distribution has been plotted for In-K alloys. The susceptibility polytherms in the liquid homogeneous range are represented in the form $\chi=aT+b$. (9 refs.)

114679 Noncollinear magnetic phases in a strongly anisotropic antiferromagnet CoF_2 with large Dzyaloshinskii interaction. K.G.Gurtovoi, A.S.Lagutin, V.I.Ozhogin (I.V. Kurchatov Inst. of Atomic Energy, Moscow, USSR). *Sov. Phys.-JETP (USA)*, vol.83, no.5, p.1122-9 (Nov. 1982). Translation of: *Zh. Eksp. i Teor. Fiz. (USSR)*, vol.83, no.5, p.1941-54 (Nov. 1982). [received: Sept. 1983]

The magnetization and differential magnetic susceptibilities are measured in a field H up to 500 kOe directed along the U_2 and C_4 axes of the tetragonal crystal CoF_2 . Antiferromagnetic resonance in the wavelength range from 1 to 8 mm is also investigated at $H \parallel C_4$. Softening of one of the AFMR modes in a field $H_{c1}=210 \text{ kOe}$ is observed, as well as a jump of the magnetic moment in a field $H_{c2}=255 \text{ kOe}$ when the field deviates from the C_4 axis by an angle not more than 30° . The phenomena are interpreted on the basis of a model in which it is assumed that at field strengths between H_{c1} and H_{c2} there exists a canted phase in which the sublattice moments make various angles with the C_4 axis. The magnetization curves for CoF_2 , which has an exceptionally high single-ion magnetic anisotropy, are calculated on the basis of a semiphenomenological theory within the framework of the model in a longitudinal and a transverse field. Satisfactory agreement with the measured magnetization curves is obtained. (31 refs.)

Properties of Cu^{2+} ion in the $\gamma\text{-AgCuPO}_4$ structure See Entry 113827
Investigations on the magnetic structure of pseudobinary intermetallic compounds from the $\text{Tb}(\text{Co}_x\text{Ni}_{1-x})_2$ system See Entry 114670
Magnetic ordering of the quasi-two-dimensional system VOCl_2 See Entry 114672
Ferrimagnetism in the MnCrG-MnFeG garnet solid solution system See Entry 114675
Nonmagnetic state of cobalt ions in chromium alloys See Entry 114684
Labile magnetic state in the spin-reorientational transition in magnetite See Entry 114687
Magnetic properties and the magnetic phase diagram of the $\text{Cr}_{1-x}\text{Ni}_x\text{S}$ system See Entry 114688
Theory of ferromagnetism of metallic glasses See Entry 114689
Classical treatment of a Heisenberg linear chain with spin alternation; application to the $\text{MnNi}(\text{EDTA})_2\cdot 6\text{H}_2\text{O}$ complex See Entry 114699
Magnetic properties of HoPr alloys See Entry 114705
Inhomogeneous magnetic state in the system of solid solutions $(1-x)\text{Cu}_{0.5}\text{Al}_{0.5}\text{Cr}_2\text{S}_4-x\text{CuCr}_2\text{S}_4$ See Entry 114709

75.30D Spin waves
(see also 76.50 Spin wave resonance)

114680 Gap surface waves in magnetic materials. I.A.Gilinskii, I.M.Shecheglov (Inst. of Semiconductor Phys., Acad. of Sci., Novosibirsk, USSR). *Fiz. Met. & Metalloved. (USSR)*, vol.56, no.2, p.234-8 (Aug. 1983). In Russian. English translation in: *Phys. Met. & Metallogr. (GB)*
A theoretical study is made of surface magnetostatic waves in a system of two different magnetic materials separated by an insulating gap. An allowance is made for the exchange interaction. It is shown that two branches of surface oscillations are possible. The emission of bulk magnons does not occur in the case of the low-frequency branch at long wavelengths. (7 refs.) A.T.
114681 Influence of the domain structure on the magnetostatic-oscillation spectrum of a ferrite plate. S.A.Vyzulin, S.A.Kirov, N.E.Syr'ev (Dept. of VHF Radiophys., Moscow Univ., Moscow, USSR). *Moscow Univ. Phys. Bull. (USA)*, vol.38, no.1, p.111-14 (1983). Translation of: *Vestn. Mosk. Univ. Ser. 3 (USSR)*, vol.38, no.1, p.92-4 (1983).
The resonant frequencies of long-wave magnetostatic oscillations are calculated theoretically for a plate of a cubic magnet ($K_1 < 0$) with a two-phase domain structure in the case of magnetization along the axis [110]. In the range 0.4-1.85 GHz, the spectrum of a YIG plate was investigated experimentally. Good agreement of theory and experiment is obtained both in the saturation region and in the field range where there is two-phase plate domain structure. (6 refs.)
114682 Spectrum of a one-dimensional ferromagnet in a transverse field. I.G.Gochev. *Sov. Phys.-Solid State (USA)*, vol.25, no.2, p.246-8 (Feb. 1983). Translation of: *Fiz. Tverd. Tela (USSR)*, vol.25, no.2, p.436-40 (Feb. 1983). [received: Sept. 1983]
The spectrum of low-lying states of a one-dimensional uniaxial ferromagnet in a weak transverse field is determined. The possibility of observing spin complexes in quasione-dimensional magnetic materials is discussed. (16 refs.)
Magnetic ordering phenomena in rare earth semiconductors See Entry 114656
Exact solution of the Bethe lattice with long-range interactions: Application to a Heisenberg ferromagnet See Entry 114659
Band-model approach to magnetic excitations in a disordered ferromagnet: one-dimensional case See Entry 114662
Theory of ferromagnetism of metallic glasses See Entry 114689
Specific heat of compounds $\text{Ni}_x\text{Co}_{1-x}\text{Cl}_2$ See Entry 114694
Temperature dependence of the fluctuations of exchange interaction in amorphous Co-P alloys See Entry 114714
Free-carrier multiphoton laser absorption in magnetic semiconductors See Entry 114816

75.30E Exchange and superexchange interactions
(see also 71.70 Level splitting and interactions)

Magnetic ordering phenomena in rare earth semiconductors See Entry 114656
Ground state and the spectrum of spin excitations of a uniaxial ferromagnet with a planar defect See Entry 114692
Inhomogeneous magnetic state in the system of solid solutions $(1-x)\text{Cu}_{0.5}\text{Al}_{0.5}\text{Cr}_2\text{S}_4-x\text{CuCr}_2\text{S}_4$ See Entry 114709
Temperature dependence of the fluctuations of exchange interaction in amorphous Co-P alloys See Entry 114714
Variation of properties of multilayer films of bismuth-containing ferrite-garnets under high-temperature annealing See Entry 114718

75.30G Anisotropy

114683 Magnetic crystallographic anisotropy of the ferrimagnetic iron oxide $\gamma\text{-Fe}_2\text{O}_3$. E.V.Babkin, K.P.Koval', V.G.Pyn'ko (L.V. Kirenskii Inst. of Phys., Acad. of Sci., Krasnoyarsk, USSR). *Sov. Phys.-Solid State (USA)*, vol.25, no.2, p.3320-3 (Feb. 1983). Translation of: *Fiz. Tverd. Tela (USSR)*, vol.25, no.2, p.585-7 (Feb. 1983). [received: Sept. 1983]
In order to determine how a crystalline field of cubic and axial symmetry affects the magnetic crystallographic anisotropy of $\gamma\text{-Fe}_2\text{O}_3$ the authors have studied the temperature dependence of the first constant K_1 of magnetic crystallographic anisotropy of $\gamma\text{-Fe}_2\text{O}_3$ single-crystal films. To find the parameters of the crystalline field they employed a traditional device based on comparison of the experimental and theoretically calculated functions $K_1(T)$ for known values of the sublattice magnetizations. The latter were determined from the experimentally measured temperature dependence of the saturation magnetization of ferrite. (9 refs.)
Noncollinear magnetic phases in a strongly anisotropic antiferromagnet CoF_2 with large Dyzhaloshinskii interaction See Entry 114679
Orientational phase diagram of cubic magnetic materials derived allowing for eighth-order anisotropic interactions See Entry 114686
High remanence Fe-Co-W semihard magnetic alloys for relay or switch applications See Entry 114710

Variation of properties of multilayer films of bismuth-containing ferrite-garnets under high-temperature annealing See Entry 114718
The influence of Cr and W contents of the isomer shift, hyperfine field distribution, and magnetic anisotropy of Fe-based amorphous alloys See Entry 114758

75.30H Magnetic impurity interactions

114684 Nonmagnetic state of cobalt ions in chromium alloys. E.I.Kondorskii, K.I.Kostina, N.V.Trubitsina, I.V.L'vova (M.V. Lomonosov State Univ., Moscow, USSR). *Fiz. Met. & Metalloved. (USSR)*, vol.56, no.2, p.396-8 (Aug. 1983). In Russian. English translation in: *Phys. Met. & Metallogr. (GB)*
The magnetic properties of Cr-Co alloys with up to 10 at.% Co were investigated in fields up to 10^5 A/m at temperatures 4.2-450K. The magnetic susceptibility was determined in the range 77-450K by the Faraday method. The field dependences of the magnetization at 4.2K were found by the compensation ballistic method, whereas in weak fields a vibration magnetometer was employed. The results indicated that the cobalt ions had zero magnetic moment right up to 6 at.%; above this concentration the magnetic moment was two orders of magnitude less than the effective magnetic moment per iron ion in Cr-Fe alloys. (4 refs.) A.T.

75.30K Magnetic phase boundaries
(inc. magnetic transitions, metamagnetism, etc)

114685 Spin glasses in transition?. T.J.Hicks (Dept. of Phys., Monash Univ., Clayton, Victoria, Australia). *Aust. J. Phys. (Australia)*, vol.36, no.4, p.519-36 (1983).
Spin glasses have variously been described as apparently frozen but very slowly relaxing spin systems, and also as magnetic phases below a second order transition. The structural and dynamic properties of metallic spin glasses are surveyed with emphasis on neutron scattering and low field magnetic measurements. Spin glass regions in phases with magnetic long range order are included, and an attempt is made to assess spin glass theories with respect to the various transitions. (35 refs.)
114686 Orientational phase diagram of cubic magnetic materials derived allowing for eighth-order anisotropic interactions. V.A.Borodin, V.D.Doroshchikov, T.N.Tarasenko (Physicotech. Inst., Acad. of Sci., Donetsk, Ukrainian SSR). *Fiz. Met. & Metalloved. (USSR)*, vol.56, no.2, p.220-5 (Aug. 1983). In Russian. English translation in: *Phys. Met. & Metallogr. (GB)*
A calculation is made of the orientational phase diagram of a cubic magnetic material allowing for anisotropic interactions of the fourth, sixth, and eighth orders (using magnetocrystalline anisotropy constants K_1 , K_2 , and K_3). The ranges of stability of symmetric and canted magnetic phases and the nature of spontaneous spin-reorientation phase transitions are determined. (14 refs.) A.T.
114687 Labile magnetic state in the spin-reorientational transition in magnetite. K.P.Belov, A.N.Goryaga, L.A.Skipetrova, V.N.Pronin, R.V.Senina (Dept. of General Phys. for Natural Faculties, Moscow Univ., Moscow, USSR). *Moscow Univ. Phys. Bull. (USA)*, vol.37, no.5, p.119-21 (1982). Translation of: *Vestn. Mosk. Univ. Ser. 3 (USSR)*, vol.37, no.5, p.101-3 (1982).
It is established that in magnetite, in the vicinity of the spin-reorientational transition, the spin system is unstable not only with respect to strong, but also to weak, external perturbations. An analysis of the results on magnetization, magnetocaloric effect, magnetic permittivity, and specific heat leads to the conclusion that the spin-reorientational transition $\Phi(111) \rightleftharpoons \Phi(100)$ in magnetite at low temperatures occurs without spinodal decay. (8 refs.)
114688 Magnetic properties and the magnetic phase diagram of the $\text{Cr}_{1-x}\text{Ni}_x\text{S}$ system. G.I.Makovetskii, K.I.Yanushkevich, E.A.Vasil'ev, A.V.Shablovskii (Inst. of Solid-State & Semiconductor Phys., Acad. of Sci., Minsk, Belorussian SSR). *Sov. Phys.-Solid State (USA)*, vol.25, no.2, p.285-8 (Feb. 1983). Translation of: *Fiz. Tverd. Tela (USSR)*, vol.25, no.2, p.506-11 (Feb. 1983). [received: Sept. 1983]
The effect of cationic substitution on the properties of solid solutions in the $\text{Cr}_{1-x}\text{Ni}_x\text{S}$ system is discussed. Measurements of the magnetic susceptibility and Mossbauer spectra show that, for chromium sulfide, $T=460\text{K}$ is an intermediate phase transformation temperature of the spin reorientation type, the transition from antiferromagnet to paramagnet occurring at $T_N=860\text{K}$. It is also shown that the compositions with $0.2 \leq x \leq 0.7$ have an uncompensated magnetic moment. The effective magnetic fields at ^{57}Fe nuclei in cationic positions are determined, and are found to be zero for nuclei at anionic sites. The magnetic phase diagram of the system is plotted. (12 refs.)
114689 Theory of ferromagnetism of metallic glasses. I.A.Akhiezer (Physicotech. Inst., Acad. of Sci., Kiev, Ukrainian SSR). *Sov. Phys.-Solid State (USA)*, vol.25, no.2, p.308-10 (Feb. 1983). Translation of: *Fiz. Tverd. Tela (USSR)*, vol.25, no.2, p.547-51 (Feb. 1983). [received: Sept. 1983]
The Curie temperature, the spin-wave frequency, and the temperature dependence of the spontaneous magnetization are determined for ferromagnetic metal-metalloid glasses. The model of the structure of such glasses adopted in the present paper allows for the short-range order (formation of complexes with strong covalent bonds) and for the random nature of the distances between atoms of a 3d metal. Such a model can explain the apparent discrepancy between the observed relatively high Curie temperatures and the very large values of the coefficient B in the Bloch formula for the temperature dependence of the spontaneous magnetization $m(T)=m_0(1-BT^{3/2})$. The principal physical idea of the present theory is based on the fundamental difference between two characteristics of a random quantity: the average value (in the present case, it determines the exchange 'stiffness' of spin waves) and the percolation threshold (which determines the ordering temperature). (6 refs.)
114690 Effect of magnetic transformation on the nonmagnetic properties of Ce_2Ge_3 . A.A.Sevast'yanov, S.M.Barmin, S.V.Kortov, R.P.Krentsis, I.V.Gel'd (S.M. Kirov Ural Polytech. Inst., Sverdlovsk, USSR). *Sov. Phys.-Solid State (USA)*, vol.25, no.2, p.336-7 (Feb. 1983). Translation of: *Fiz. Tverd. Tela (USSR)*, vol.25, no.2, p.591-3 (Feb. 1983). [received: Sept. 1983]
The authors determine more accurately the phase transition temperature T_c in cerium germanate and study the behavior of its linear thermal expansion coefficient α and electrical resistivity ρ near T_c . (6 refs.)

114691 Diagram of corresponding states of easy-axis antiferromagnets. V.G.Bar'yakhtar, A.A.Galkin, A.N.Bogdanov, V.A.Galusko, V.T.Telepa (Donets Physicotech. Inst., Acad. of Sci., Donetsk, Ukrainian SSR). *Sov. Phys.-JETP (USA)*, vol.83, no.5, p.1086-9 (Nov. 1982). Translation of: *Zh. Eksp. & Teor. Fiz. (USSR)*, vol.83, no.5, p.1879-85 (Nov. 1982). [received: Sept. 1983]

Experimental investigations are made of the effect of high hydrostatic pressure (up to 15 kbar) on the spin-flop transition field (H_T), the Neel temperature (T_N), and the triple-point parameters (T_1, H_1) of the easy-axis antiferromagnets $\text{CuCl}_2 \cdot 2\text{H}_2\text{O}$ and $\text{CuCl}_2 \cdot 2\text{D}_2\text{O}$. The functional relations $H_T/H_1 = f(T/T_1)$ are the same for both the antiferromagnets studied and are independent of the value of the hydrostatic pressure; that is, a law of corresponding states holds. Analytical expressions are obtained for the dependence of H_T on pressure and temperature. The limits of applicability of the law of corresponding states are discussed. (19 refs.)

Properties of Cu^{2+} ion in the $\gamma\text{-AgCuPO}_4$ structure See Entry 113827

Analysis of magnetic and nonmagnetic surfaces by spin-polarized low-energy electron diffraction See Entry 114311

Electrical resistance of Fe-Zr and Fe-Ni-Zr amorphous alloys under hydrostatic pressure See Entry 114509

Some ideas related to magnetism in the rare earths See Entry 114652

Magnetism in TiO_{11} See Entry 114665

Magnetic properties of Fe-Ni-Zr and Fe-Ni-Nb alloys See Entry 114667

Investigations on the magnetic structure of pseudobinary intermetallic compounds from the $\text{Tb}(\text{Co}_x\text{Ni}_{1-x})_2$ system See Entry 114670

Magnetic ordering of the quasi-two-dimensional system VOCl See Entry 114672

Modulated magnetic structure of the Kondo compound TmS See Entry 114674

Inhomogeneous magnetic state in the system of solid solutions $(1-x)\text{Cu}_{0.5}\text{Al}_{0.5}\text{Cr}_7\text{S}_4-x\text{CuCr}_7\text{S}_4$ See Entry 114709

75.30S Magnetocaloric effect

Thermal aspects of magneto-optical recording See Entry 112948

Labile magnetic state in the spin-reorientational transition in magnetite See Entry 114687

75.40 CRITICAL-POINT EFFECTS, SPECIFIC HEATS, SHORT-RANGE ORDER

(inc. spin glasses)

114692 Ground state and the spectrum of spin excitations of a uniaxial ferromagnet with a planar defect. Yu.I.Gorobets, V.I.Finokhin (State Univ., Donetsk, Ukrainian SSR).

Fiz. Met. & Metalloved. (USSR), vol.56, no.2, p.226-33 (Aug. 1983). In Russian. English translation in: *Phys. Met. & Metallogr. (GB)*. A distribution of the magnetization is found for a ferromagnet with a planar defect which alters the exchange integrals. It is shown that defects of this kind can give rise to specific magnetic inhomogeneities. A discrete part of the spectrum of spin excitations is found theoretically and, in particular, it is shown that new discrete levels may appear in the presence of defects. (16 refs.) *A.T.*

114693 Spin glass, ferromagnetic and mixed phases in the disordered Potts model. D.Elderfield, D.Sherrington (Dept. of Phys., Imperial Coll. London, London, England).

J. Phys. C (GB), vol.16, no.27, p.L971-7 (30 Sept. 1983). For a Potts spin glass model with Sherrington-Kirkpatrick exchange disorder the full phase structure in (J_0, J, h, T) is indicated. The phases predicted are analogous to those of a Heisenberg spin glass but there are important differences of transition orders and regions of stability. (11 refs.)

114694 Specific heat of compounds $\text{Ni}_x\text{Co}_{1-x}\text{Cl}_2$. M.O.Kostruykova, T.G.Sokolovskaya (Dept. of Low Temperature Phys., Moscow Univ., Moscow, USSR).

Moscow Univ. Phys. Bull. (USA), vol.37, no.5, p.126-30 (1982). Translation of: *Vestn. Mosk. Univ. Ser. 3 (USSR)*, vol.37, no.5, p.107-10 (1982).

The specific heat of three compounds $\text{Ni}_x\text{Co}_{1-x}\text{Cl}_2$ with $x=0.10, 0.18$, and 0.90 in the temperature range 2-27K is measured. Together with previous measurements on NiCl_2 and CoCl_2 , the results are compared with the theory of spin waves of laminar antiferromagnets. (13 refs.)

114695 Nearest-neighbor Ising model with an incommensurate phase and a Lifshitz point. B.Schaub, E.Domany (Dept. of Electronics, Weizmann Inst. of Sci., Rehovot, Israel).

Phys. Rev. B (USA), vol.28, no.5, p.2897-900 (1 Sept. 1983). An anisotropic triangular nearest-neighbor Ising model, with antiferromagnetic interactions, was studied. The phase diagram as a function of temperature and magnetic field was determined with the use of symmetry analysis, free-fermion approximation, phenomenological renormalization group, and Monte Carlo simulation. A massless phase, a Lifshitz point, and transition lines to commensurate phases were identified. (21 refs.)

Quantum field theory models with a large number of colours and the statistical physics of disordered systems See Entry 111909

Some ideas related to magnetism in the rare earths See Entry 114652

Strong electronic correlations in magnetic semiconductors: the functional integral approach to the Hubbard model See Entry 114661

Labile magnetic state in the spin-reorientational transition in magnetite See Entry 114687

Theory of saturation of magnetic resonance in solids at low temperatures See Entry 114725

75.40D Ising and other classical spin models

114696 The critical isotherm of the mixed spin Ising model. B.Y.Yousif, R.G.Bowers (Dept. of Appl. Math. & Theoretical Phys., Univ. of Liverpool, Liverpool, England).

J. Phys. A (GB), vol.16, no.14, p.3361-4 (1 Oct. 1983). Series expansions are used to estimate the critical exponent δ for several two- and three-dimensional mixed spin Ising models. The evidence supports the conjecture of extended spin independence. This suggests that mixed models and the standard 'single spin' models share the same value of δ . (9 refs.)

114697 Phase diagram of the ANNNI model in a field using a low-temperature series technique. J.Smith, J.Yeomans (Dept. of Phys., Univ. Southampton, Southampton, England).

J. Phys. C (GB), vol.16, no.27, p.5305-20 (30 Sept. 1983). The authors study the behaviour of the axial next-nearest-neighbour Ising (ANNNI) model in a field using low-temperature series. The analysis is a generalisation of the inductive scheme introduced by Fisher and Selke (1980, 1981) for the zero-field case. An infinite sequence of commensurate phases of mean wavevectors $q_j = \pi/(2j+1)a$, $j=2, 4, 6, \dots$, is shown to exist in the vicinity of a multiphase line. These phases form a subset of the sequence occurring for zero field. At large fields, the long-wavelength commensurate phases become unstable to the ferromagnetic state and an infinite sequence of triple points is seen. (13 refs.)

114698 Statics and dynamics of the infinite-range Ising spin glass model. N.D.Mackenzie (Dept. of Phys., Univ. of Edinburgh, Edinburgh, Scotland), A.P.Young.

J. Phys. C (GB), vol.16, no.27, p.5321-37 (30 Sept. 1983). The Sherrington-Kirkpatrick (SK) spin glass model (1975) is studied by Monte Carlo simulation. Below T_c there is a spectrum of relaxation times which diverge like $\exp(cN^{1/4})$ as N , the number of spins, tends to infinity. In zero field, \hat{h} , there is one more timescale, $\hat{\tau}_{eg}$, which is the time to turn over all the spins. Averaging over samples $(\ln \hat{\tau}_{eg})/(\ln \tau_{eg}) \propto N^{1/2}$. However, $\ln \hat{\tau}_{eg}$ is not a self-averaging quantity and there are large sample-to-sample variations even for $N \rightarrow \infty$. For $h \gg h^* = T/N^{1/2}$, where T is the temperature, fluctuations on timescale τ_{eg} may not occur. Above the Almeida-Thouless line (1978) relaxation times are finite and the SK solution is correct. Below this line, the results agree well with Parisi's theory (1983) if the latter is correctly interpreted. (40 refs.)

Mathematical theory of phase transitions [Ising model] See Entry 111617

Spin glasses in transition? See Entry 114685

Classical treatment of a Heisenberg linear chain with spin alternation; application to the $\text{MnNi(EDTA).6H}_2\text{O}$ complex See Entry 114699

75.40F Heisenberg and other quantized spin models

114699 Classical treatment of a Heisenberg linear chain with spin alternation; application to the $\text{MnNi(EDTA).6H}_2\text{O}$ complex. M.Drillon, E.Coronado (Dept. Sci. des Matériaux, CNRS, Strasbourg, France), D.Beltran, R.Georges.

Chem. Phys. (Netherlands), vol.79, no.3, p.449-53 (15 Sept. 1983). The thermodynamic behaviour of an exchange-coupled linear system with two alternating spin sublattices is investigated from a classical point of view. A closed formula is derived for the magnetic susceptibility which is easily adapted to real spin systems, using appropriate scaling transformations. The proposed approach is shown to describe successfully the behaviour of a new bimetallic chain complex $\text{MnNi(EDTA).6H}_2\text{O}$. In particular, a minimum in the χT versus T plot is observed at very low temperature, in agreement with theory. (14 refs.)

114700 Self-consistent mean-field theory of the dynamics of a Heisenberg spin-glass. J.A.Hertz (Nordsk Inst. for Teoretisk Atomfysik, Copenhagen, Denmark), R.A.Klemm.

Phys. Rev. B (USA), vol.28, no.5, p.2877-9 (1 Sept. 1983). The dynamical properties of a Heisenberg spin-glass with mode coupling and a conserved spin are studied. The authors find critical slowing down and effectively relaxational dynamics in most of k space [$k \gg 1$, where $\xi \sim (T - T_g)^{-1/2}$]. At very long wavelengths ($k \xi \gg 1$) the effective transport coefficient is logarithmically divergent [$\sim (\ln \xi)^{1/2}$], and this correction induces similar logarithmic corrections to the power-law behavior at $k \xi \gg 1$. (10 refs.)

114701 Ground-state properties of the infinite-range vector spin-glasses. G.S.Grest, C.M.Soukoulis (Corporate Res. Sci. Labs., Exxon Res. & Engng. Co., Linden, NJ, USA).

Phys. Rev. B (USA), vol.28, no.5, p.2886-9 (1 Sept. 1983). The ground-state properties of the infinite-range vector spin-glasses are studied by a 'slow-cooling' iterative solution of the mean-field equations. Results are presented for the zero-temperature probability distribution $P(H)$ of internal fields with and without an external magnetic field present. The authors also find the ground-state energy for the XY and Heisenberg models. $P(H)$ has a hole; i.e., $P(H)=0$ for $H < H_0$, which persists in high magnetic fields and relatively high temperatures, $T/T_c \lesssim 1/2$. The author studies for the infinite-range Heisenberg spin-glass appear to show macroscopic irreversibility, in contrast to the short-range Heisenberg case which has no irreversibility. Therefore the range of interaction plays an important role in determining the irreversible behavior. (15 refs.)

114702 Steepest descent approach to the domain-wall thermodynamics of a classical easy-plane ferromagnetic chain: application to CsNiF_3 . H.C.Fogedby, P.Hedegard, A.Svane (Inst. of Phys., Univ. of Aarhus, Aarhus, Denmark).

Phys. Rev. B (USA), vol.28, no.5, p.2893-6 (1 Sept. 1983). The authors derive asymptotic low-temperature expressions for the free energy, the specific heat, and the magnetization of the classical easy-plane Heisenberg chain in a field. At low field the system forms a stable gas of spin waves and domain walls. In a temperature-broadened region about a characteristic field given by the anisotropy, the domain-wall gas becomes unstable and dissociates into spin waves. At higher fields the domain-wall gas is absent. Applying the authors results to CsNiF_3 they find qualitative agreement. (17 refs.)

Magnetic ordering phenomena in rare earth semiconductors . See Entry 114656

75.50 STUDIES OF SPECIFIC MAGNETIC MATERIALS

(see also 81.40R Magnetic properties related to materials treatment)

75.50B Ferromagnetism of Fe and its alloys

Polarised neutron scattering from the amorphous ferromagnet, $\text{Fe}_{83}\text{B}_{17}$ See Entry 113753

Low temperature irradiation of FeB amorphous alloys See Entry 114035

Lattice dynamics of FePt alloys of AB_3 type ordered structure See Entry 114109

Inelastic scattering of polarised neutrons by amorphous $\text{Fe}_{47}\text{Co}_{70.3}\text{Si}_{15}\text{B}_{10}$ See Entry 114114

Electrical resistance of Fe-Zr and Fe-Ni-Zr amorphous alloys under hydrostatic pressure See Entry 114509

Analytic separation of the factors contributing to the eddy current loss in magnetically nonlinear steel See Entry 114707
Single crystal magnets See Entry 114708
High remanence Fe-Co-W semihard magnetic alloys for relay or switch applications See Entry 114710
Influence of structural relaxation on the magnetic permeability aftereffect of amorphous ferromagnetic alloys See Entry 114712
Structure of charged domain boundaries in Permalloy films See Entry 114715
Thermal expansion and compressibility of magnetic materials under hydrostatic pressure conditions See Entry 114719
Ferromagnetic multifilamentary Fe and Ni wires with high coercive fields produced by powder metallurgy processing See Entry 115132
The effect of sintering in hydrogen-nitrogen atmospheres and subsequent aging on the magnetic properties of iron See Entry 115138
Effect of cold rolling on the magnetic properties of nonoriented silicon steel See Entry 115210
Internal friction study on structural relaxation of a glassy metal $\text{Fe}_{32}\text{Ni}_{36}\text{Cr}_{14}\text{P}_{12}\text{B}_6$ See Entry 115241

75.50C Ferromagnetism of other metals

Magnetic properties of Fe-Ni-Zr and Fe-Ni-Nb alloys See Entry 114667
Investigations on the magnetic structure of pseudobinary intermetallic compounds from the $\text{Tb}(\text{Co}_x\text{Ni}_{1-x})_2$ system See Entry 114670
Effect of magnetic transformation on the nonmagnetic properties of Ce_2Ge_3 See Entry 114690
Temperature dependence of the fluctuations of exchange interaction in amorphous Co-P alloys See Entry 114714
Ferromagnetic multifilamentary Fe and Ni wires with high coercive fields produced by powder metallurgy processing See Entry 115132

75.50D Ferromagnetism of nonmetals

Magnetic ordering phenomena in rare earth semiconductors See Entry 114656

75.50E Antiferromagnetics

Properties of Cu^{2+} ion in the $\gamma\text{-AgCuPO}_4$ structure See Entry 113827
Lattice dynamics of FePt alloys of AB_3 type ordered structure See Entry 114109
Electrical conductivity measurements of some layered magnetic structures See Entry 114248
Field dependence of the paramagnetic susceptibility of the antiferromagnets $\text{CoCl}_2\cdot 6\text{H}_2\text{O}$, $\text{NiCl}_2\cdot 4\text{H}_2\text{O}$, $\text{MnCl}_2\cdot 4\text{H}_2\text{O}$, and $\text{MnBr}_2\cdot 4\text{H}_2\text{O}$ See Entry 114664
Magnetic ordering of the quasi-two-dimensional system VOCl_2 See Entry 114672
Modulated magnetic structure of the Kondo compound TmS See Entry 114674
Ferrimagnetism in the MnCrG-MnFeG garnet solid solution system See Entry 114675
Noncollinear magnetic phases in a strongly anisotropic antiferromagnet CoF_2 with large Dzyaloshinskii interaction See Entry 114679
Magnetic properties and the magnetic phase diagram of the $\text{Cr}_{1-x}\text{Ni}_x\text{S}$ system See Entry 114688
Diagram of corresponding states of easy-axis antiferromagnets See Entry 114691
Specific heat of compounds $\text{Ni}_x\text{Co}_{1-x}\text{Cl}_2$ See Entry 114694
Classical treatment of a Heisenberg linear chain with spin alternation; application to the $\text{MnNi}(\text{EDTA})\cdot 6\text{H}_2\text{O}$ complex See Entry 114699
Magnetic properties of HoPr alloys See Entry 114705
Inhomogeneous magnetic state in the system of solid solutions $(1-x)\text{Cu}_{0.5}\text{Al}_{0.5}\text{Cr}_2\text{S}_4-x\text{CuCr}_2\text{S}_4$ See Entry 114709

75.50G Ferrimagnetics

Investigations on the magnetic structure of pseudobinary intermetallic compounds from the $\text{Tb}(\text{Co}_x\text{Ni}_{1-x})_2$ system See Entry 114670
Ferrimagnetism in the MnCrG-MnFeG garnet solid solution system See Entry 114675
Magnetochemical study of iron molybdates obtained from precursor precipitates with different Mo- and Fe-content See Entry 114677
Influence of the domain structure on the magnetostatic-oscillation spectrum of a ferrite plate See Entry 114681
Magnetic crystallographic anisotropy of the ferrimagnetic iron oxide $\gamma\text{-Fe}_2\text{O}_3$ See Entry 114683
Labile magnetic state in the spin-reorientational transition in magnetite See Entry 114687
Variation of properties of multilayer films of bismuth-containing ferrite-garnets under high-temperature annealing See Entry 114718
Preparation of MnCo_2O_4 by a wet method and its metal ion distribution See Entry 115034

75.50K Amorphous magnetic materials

114703 Metallic glass—a new material for electrical engineering and electronics. W.Dmowski (Instytut Inżynierii Materialowej, Politech. Warszawskiej, Warszawa, Poland). *Wiad. Elektrotech. (Poland)*, vol.51, no.7-8, p.193-200 (1-15 April 1983). In Polish. [received: Sept. 1983]
Theoretical foundations and methods of the production of metallic glass are presented. The paper also reviews the research and development work on this subject and comments on how the magnetic properties of this material can be made use of in practical applications. (16 refs.)
Polarised neutron scattering from the amorphous ferromagnet, $\text{Fe}_{83}\text{B}_{17}$ See Entry 113753
Inelastic scattering of polarised neutrons by amorphous $\text{Fe}_{47}\text{Co}_{70.3}\text{Si}_{15}\text{B}_{10}$ See Entry 114114

Electrical resistance of Fe-Zr and Fe-Ni-Zr amorphous alloys under hydrostatic pressure See Entry 114509
Theory of ferromagnetism of metallic glasses See Entry 114689
Theory of magnetic after-effects in ferromagnetic amorphous alloys See Entry 114711
Influence of structural relaxation on the magnetic permeability aftereffect of amorphous ferromagnetic alloys See Entry 114712
Temperature dependence of the fluctuations of exchange interaction in amorphous Co-P alloys See Entry 114714
Internal friction study on structural relaxation of a glassy metal $\text{Fe}_{32}\text{Ni}_{36}\text{Cr}_{14}\text{P}_{12}\text{B}_6$ See Entry 115241

75.60 DOMAIN EFFECTS, MAGNETIZATION CURVES, AND HYSTERESIS

75.60C Domain walls and domain structure (for magnetic bubbles, see 75.70K)

114704 Ferromagnetic domain wall pinning by a random array of inhomogeneities. P.Gaunt (Dept. of Phys., Univ. of Manitoba, Winnipeg, Canada). *Philos. Mag. B (GB)*, vol.48, no.3, p.261-76 (Sept. 1983).
The pinning site inhomogeneities interacting with a domain wall are characterized by the maximum restoring force, f , acting on an area A or domain wall. The critical field, H_0 , required to release this area from the pin is given by $f/2IA$ where I is the magnetic moment per unit volume. The area A is not independent of the applied field H and a statistical treatment is required to evaluate it. The Friedel 'steady state' model assumes that the volume swept out when a wall breaks away from a pin contains, on average, one replacement pin. This leads to the relation $A \propto 1/H^{1/2}$ and hence to the critical field $H_0 = 3\rho^2/(4\pi\gamma I)$ where ρ is the pin density and γ is the wall energy per unit area. If the parameter $\beta_0 = 3f/(8\pi\gamma b) > 1$, where $4b$ is the interaction range of the pin, then the Friedel model holds and the pinning is 'strong'. If $\beta < 1$ the Friedel model breaks down and the pinning is 'weak'. The unpinning process is then no longer connected with unit steps related to breakaway from single pins but with cooperative breakaway from many pinning sites. The effective pin density is expressed as $\rho' = \sqrt{\rho/v}$ where v is the volume swept out between minimum and maximum energy positions on the wall. The demagnetizing effects are considered in detail for both strong and weak pinning. (16 refs.)
Magnetic-field-free objective lens around a specimen for observing fine structure of ferromagnetic materials in a transmission electron microscope See Entry 111820
Steepest descent approach to the domain-wall thermodynamics of a classical easy-plane ferromagnetic chain: application to CsNiF_3 See Entry 114702
Structure of charged domain boundaries in Permalloy films See Entry 114715

75.60E Magnetization curves, hysteresis, Barkhausen and related effects

114705 Magnetic properties of HoPr alloys. O.S.Galkina, B.I.Urusova, V.F.Shalashov (M.V. Lomonosov State Univ., Moscow, USSR). *Fiz. Met. & Metalloved. (USSR)*, vol.56, no.2, p.398-401 (Aug. 1983). In Russian. English translation in: *Phys. Met. & Metallogr. (GB)*
The magnetic properties were determined for alloys belonging to the $\text{Ho}_{1-x}\text{Pr}_x$ system with praseodymium concentrations in the range 0.0-12.2 at.%. The field and temperature dependence of the magnetization were determined in the range 4.2-400K using magnetic fields up to 4×10^6 A/m. The magnetization depended on the praseodymium concentration and for $x=1.2$ at.% Pr the magnetization of the alloy was 4.5% higher than the magnetization of pure holmium subjected to a field of 4×10^6 A/m. Moreover, the magnetic moment had a maximum at 1.4 at.% Pr. (6 refs.) A.T.
114706 Magnetic properties of a nonlinear medium with ordered non-uniformities. S.T.Tolmachev. *Izv. VUZ Elektromekh. (USSR)*, no.6, p.31-7 (June 1983). In Russian.
Discusses a technique for identifying nonlinear isotropic properties of a two-dimensional heterogeneous medium, characterised by ordered non-uniformities. It is shown that the effective properties of such a medium, with arbitrary shape and concentration of the occlusions, can be determined by a solution of an integral equation for a constrained magnetisation region, corresponding to the main parallelogram of the periods. (10 refs.)
114707 Analytic separation of the factors contributing to the eddy current loss in magnetically nonlinear steel. A.L.Bowden, E.J.Davies (Dept. of Electrical & Electronic Engng., Univ. of Aston, Birmingham, England). *IEE Proc. B (GB)*, vol.130, no.5, p.364-72 (Sept. 1983).
Many approximate solutions for eddy-current loss in solid steel have been published, but little attention has been given to identifying the effects of magnetic nonlinearity on the loss and electromagnetic-field distribution. An analytic solution is described in which these effects are identified, and defined by simple factors which are determined from the B/H -curve for the steel; this curve is represented by the function $B=aH^b$. Saturation harmonics are accounted for approximately by the use of the single derived function $B_1=AH_1^b$; this is validated by a separate analytic investigation. Comparison with the limiting nonlinear theory, for which $B=\pm B_s$, leads to a definition of B_s which relates it to the shape of the B/H -curve. An experimental investigation to test the theory is also described. (17 refs.)
114708 Single crystal magnets. N.Ikuta (Miyagi Tech. Coll., Natori, Japan), M.Okada, M.Homma, T.Minowa. *J. Appl. Phys. (USA)*, vol.54, no.9, p.5400-3 (Sept. 1983).
Single crystals of the Fe-Cr-Co alloys without and with 3% Mo were prepared by a recrystallization process. The microstructures and the magnetic properties of (100), (110), and (111) single crystals were investigated after the heat treatment in the ridge region of the miscibility gap. The magnetic properties of the Fe-22 Cr-17 Co ridge single crystals were not affected very much by the crystal orientation. However, the Fe-23 Cr-20 Co-3 Mo alloys show the crystal orientation dependence of the magnetic properties. The single crystal alloys are aged in a magnetic field, the direction of which is varied around (100) axes. The magnetic properties are measured parallel to the applied field directions and are summarized in view of deviated angle from a (100) axis. The greater the deviation of the applied field direction from a (100) axis, the poorer are the magnetic properties of the Mo single crystal alloy. The best magnetic properties are achieved with Fe-22 Cr-18.5 Co-3 Mo (100) ridge single crystal as $B_r=1.58$ T (15.8 kG), $bH_c=72.8$ kA/m (910

Oe), and (BH) $\max=91.2$ kJ/m³ (11.4 MGOe), which is the highest energy product reported for the Fe-Cr-Co magnet family. (19 refs.)

114709 Inhomogeneous magnetic state in the system of solid solutions $(1-x)\text{Cu}_{0.5}\text{Al}_{0.5}\text{Cr}_2\text{S}_4-x\text{CuCr}_2\text{S}_4$. L.I.Koroleva, A.I.Kuz'minykh, I.V.Gordeev, Ya.A.Kesler (Dept. of General Phys. for Natural Faculties, Moscow Univ., Moscow, USSR).

Moscow Univ. Phys. Bull. (USA), vol.38, no.1, p.38-42 (1983). Translation of: *Vestn. Mosk. Univ. Ser. 3 (USSR)*, vol.38, no.1, p.34-8 (1983).

The magnetic and electrical properties of the system of solid solutions $(1-x)\text{Cu}_{0.5}\text{Al}_{0.5}\text{Cr}_2\text{S}_4-x\text{CuCr}_2\text{S}_4$ ($0\leq x\leq 0.2$) are studied. All the compositions studied have semiconductor conductivity of p type. The dependence of the magnetization on the field strength is a superposition of the magnetization characteristic for an antiferromagnet and the small spontaneous magnetization. The spontaneous moment corresponding to one impurity ion Cu^{2+} is close to the magnetization of the ferromagnetic cluster formed by Cr^{3+} ions, the nearest neighbors of Cu^{2+} . It is suggested that these clusters (ferrons) are created by localization of holes around the acceptor copper ion because of the energy gain of s-d exchange. The presence of ferrons in these materials is also confirmed by the sharp rise in paramagnetic susceptibility in the region of the Curie point. Estimates of the magnitude of s-d exchange in these materials are given. (11 refs.)

Analogies of 6 classic properties of materials See Entry 113264

Analysis of magnetic and nonmagnetic surfaces by spin-polarized low-energy electron diffraction See Entry 114311

Noncollinear magnetic phases in a strongly anisotropic antiferromagnet CoF_2 with large Dzyaloshinskii interaction See Entry 114679

Influence of the domain structure on the magnetostatic-oscillation spectrum of a ferrite plate See Entry 114681

Nonmagnetic state of cobalt ions in chromium alloys See Entry 114684

Labile magnetic state in the spin-reorientational transition in magnetite See Entry 114687

High remanence Fe-Co-W semihard magnetic alloys for relay or switch applications See Entry 114710

Slow fluctuations in the cyclical magnetic reversal of thin magnetic films See Entry 114713

Variation of properties of multilayer films of bismuth-containing ferrite-garnets under high-temperature annealing See Entry 114718

Energy dissipation due to macroeddy currents with mechanical vibrations See Entry 114721

The influence of Cr and W contents of the isomer shift, hyperfine field distribution, and magnetic anisotropy of Fe-based amorphous alloys See Entry 114758

Admissible values of permittivity and magnetic permeability of matter See Entry 114773

The effect of sintering in hydrogen-nitrogen atmospheres and subsequent aging on the magnetic properties of iron See Entry 115138

75.60G High coercivity materials

114710 High remanence Fe-Co-W semihard magnetic alloys for relay or switch applications. K.Kumasaka, K.Ono (Electrical Communication Labs., NTT, Tokyo, Japan).

Rev. Electr. Commun. Lab. (Japan), vol.30, no.4, p.712-23 (July 1982). [received: Aug. 1983]

Magnetic properties of Fe-Co-W alloys have been investigated. Remanence, squareness ratio and coercive force are enhanced by aging after cold working and obtained remanence; $18\sim 19.2$ kG, squareness ratio >0.9 , coercive force; $20\sim 100$ Oe. These magnetic properties are suitable for relay or switch applications. Especially, Fe-12%Co-10%W alloy shows remanence; 19.2 kG, coercive force; 26 Oe, and has a good sealability with glass. Therefore, it is adequate for remanent reed switch application. A fine precipitate structure enhances coercive force. Developing a uniaxial magnetic anisotropy with easy magnetizing in the working direction enhances the squareness ratio. (15 refs.)

Single crystal magnets See Entry 114708

75.60L Magnetic aftereffects

114711 Theory of magnetic after-effects in ferromagnetic amorphous alloys. H.Kronmüller (Inst. für Phys. am Max-Planck-Inst. für Metallforschung, Stuttgart, Germany).

Philos. Mag. B (GB), vol.48, no.2, p.127-50 (Aug. 1983).

The magnetic after-effect spectrum of amorphous alloys is attributed to rearrangements of defect structures which are described by two-level systems. Using first-order reaction kinetics, the so-called stabilization potential of domain walls is determined for both 'reversible' and 'irreversible' after-effects. It is shown that by an appropriate averaging over the energy gap parameters and the activation energies, the relaxation phenomena in amorphous alloys can be described explicitly. (42 refs.)

114712 Influence of structural relaxation on the magnetic permeability aftereffect of amorphous ferromagnetic alloys. P.Allia, R.Sato Turtelli, F.Vinai (Istituto Elettrotecnico Nazionale 'Galileo Ferraris', Torino, Italy).

Solid State Commun. (USA), vol.47, no.12, p.951-4 (Sept. 1983).

Room temperature measurements of the aftereffect of the magnetic permeability have been performed on amorphous Fe-(Cu-Cr)-B ribbons annealed at various temperatures. The results, in good agreement with the predictions of a new theory, give information on the effect of structural relaxation on the shear stress defects responsible for the magnetic aftereffect. (13 refs.)

Interaction of vacancies and self-interstitials with interstitial solute atoms in α -iron See Entry 113966

75.60N Magnetic annealing and temperature-hysteresis effects

Towards the analysis of magnetothermoelastic effects in metallic specimens during magnetic treatment See Entry 115219

75.70 MAGNETIC FILMS AND PLATES

114713 Slow fluctuations in the cyclical magnetic reversal of thin magnetic films. A.M.Buz'ko, V.V.Potemkin (Dept. of Oscillation of Phys., Moscow Univ., Moscow, USSR).

Moscow Univ. Phys. Bull. (USA), vol.38, no.1, p.60-5 (1983). Translation of: *Vestn. Mosk. Univ. Ser. 3 (USSR)*, vol.38, no.1, p.52-7 (1983).

A theoretical analysis is made of noise of type $1/f^\alpha$ arising in the cyclical magnetic reversal of ferromagnetic films. On the basis of the idea that, in the course of magnetic reversal without saturation of the sample, there is slow variation in the magnitude of the film volume undergoing magnetic reversal per cycle and also its 'switching' moments, an expression is found for the spectral density of the fluctuations of the magnetization, describing the rise in spectral density of the magnetic noise close to frequencies which are multiples of the pumping frequency. (7 refs.)

114714 Temperature dependence of the fluctuations of exchange interaction in amorphous Co-P alloys. R.S.Iskhakov, G.I.Fish, R.G.Khlebov (L.V. Kirenskiy Inst. of Phys., Acad. of Sci., Krasnoyarsk, USSR).

Sov. Phys.-Solid State (USA), vol.25, no.2, p.321-2 (Feb. 1983). Translation of: *Fiz. Tverd. Tela (USSR)*, vol.25, no.2, p.568-70 (Feb. 1983). [received: Sept. 1983]

The authors have performed systematic studies of the changes in the main characteristics of exchange fluctuations, such as the correlation radius and the mean-square deviation $\gamma_\alpha=\Delta\alpha/\alpha$ determined from a modification of the dispersion law for spin waves, in the course of crystallization of an amorphous alloy. The measurements were performed using the method of spin-wave resonance ($f=9.2$ GHz) on films of amorphous Co-P alloys having a thickness of 2000-3000 Å. (5 refs.)

Magnetic crystallographic anisotropy of the ferrimagnetic iron oxide $\gamma\text{-Fe}_2\text{O}_3$ See Entry 114683

Permeability at optical frequencies See Entry 114947

75.70K Domain structure (magnetic bubbles)

114715 Structure of charged domain boundaries in Permalloy films. S.V.Kudryatsev, V.I.Malyutin (Moldavian State Univ., Saransk, Moldavian SSR).

Fiz. Met. & Metalloved. (USSR), vol.56, no.2, p.213-19 (Aug. 1983). In Russian. English translation in: *Phys. Met. & Metallogr. (GB)*

Minimization of the total energy is used to calculate the structure of Neel branches in an isolated charged 180° domain boundary directed at an arbitrary angle to the easy magnetization axis. The equilibrium width of these branches is also determined. (12 refs.) A.T.

114716 Investigation of a magnetostatic model in the theory of bubble domains. V.V.Dyakin, Yu.G.Lebede, V.Ya.Raevskii (Inst. of Metal Phys., Ural Sci. Centre, Acad. of Sci., Sverdlovsk, USSR).

Fiz. Met. & Metalloved. (USSR), vol.56, no.2, p.245-8 (Aug. 1983). In Russian. English translation in: *Phys. Met. & Metallogr. (GB)*

The equations of the magnetostatic model employed in studies of the motion of bubble domains are analysed. It is shown that the problem of the distribution of the magnetization tackled within the framework of this model does not have a unique solution, but this does not affect the description of bubble domain motion. A functional class is found for which the solution is unique and this is very important in practical calculations. (6 refs.) A.T.

114717 Magnetic domain structure observation by electron holography. A.Tonomura (Hitachi Ltd., Tokyo, Japan).

Oyo Buturi (Japan), vol.52, no.4, p.290-7 (April 1983). In Japanese.

Electron-beam holography using an electron-operated field-emission microscope has reached practical stage, and its new application has been developed for the observation of magnetic-field distributions. This observation method has proved to be capable of providing as a magnetic-field pattern the direct observation not only of the magnetization distribution in ferromagnetic thin-films but also of spatial magnetic-field distributions. The author describes the theory of this observation technique and presents experimental results of magnetic-domain observation in ferromagnetic thin-films, of spatial magnetic-field observation and of the Aharonov-Bohm effect. (25 refs.) K.B.

114718 Variation of properties of multilayer films of bismuth-containing ferrite-garnets under high-temperature annealing. G.V.Arzamastseva, F.V.Lisovskii, E.G.Mansvetova (Inst. of Radio Engng. & Electronics, Acad. of Sci., Moscow, USSR).

Sov. Phys.-Solid State (USA), vol.25, no.2, p.343-4 (Feb. 1983). Translation of: *Fiz. Tverd. Tela (USSR)*, vol.25, no.2, p.602-4 (Feb. 1983). [received: Sept. 1983]

The authors ascertain the influence of high-temperature annealing on the layered structure of ferrite-garnet films. They investigated epitaxial films of ferrite-garnets of the composition $(\text{YGdYbBi})_3(\text{FeAl})_2\text{O}_{12}$ with a thickness of $5\text{-}20\ \mu$. The anneal was carried out isothermally (in several stages) in a muffle furnace in air at temperatures $T_a=800\text{-}1200^\circ\text{C}$. After each annealing operation (over several hours) they determined (at $R=290\text{K}$) the following film parameters: the period D of the labyrinth domain structure (from the diameter of the diffraction ring), the magnetization M_0 and the characteristic length l_w , the uniaxial, cubic, and rhombic anisotropy constants K_u , K_c , and K_r , as well as the angle ϑ_0 of the deviation of the axis of easy magnetization from the normal. (6 refs.)

Influence of the domain structure on the magnetostatic-oscillation spectrum of a ferrite plate See Entry 114681

75.80 MAGNETOMECHANICAL AND MAGNETOELECTRIC EFFECTS, MAGNETOSTRICTION

114719 Thermal expansion and compressibility of magnetic materials under hydrostatic pressure conditions. I.F.Mirsaev, G.G.Taluts (Inst. of Metal Phys., Ural Sci. Centre, Acad. of Sci., Sverdlovsk, USSR).

Fiz. Met. & Metalloved. (USSR), vol.56, no.2, p.239-44 (Aug. 1983). In Russian. English translation in: *Phys. Met. & Metallogr. (GB)*

The magnetic components of the thermal expansion coefficients and of the compressibility are calculated for uniaxial and cubic crystals subjected to hydrostatic pressures. The calculations are carried out using a nonlinear exchange-striction model. Nonlinear interactions are shown to make a considerable contribution to these components in the case of Invar FeNi alloys. An analysis is made of the relationship between the compressibilities determined by dynamic and static methods. (15 refs.) A.T.

114720 Magnetomechanical damping of nickel. S.A.Mahmoud, M.A.Semary (Phys. Dept., Cairo Univ., Cairo, Egypt). *Mater. Sci. & Eng. (Switzerland)*, vol.60, no.3, p.L9-11 (Sept. 1983). The magnetomechanical damping of nickel was measured in AC and DC magnetic fields. The position and magnitude of the peak value of the internal friction Q^{-1} were dependent on the amount of cold working, heat treatment and strain amplitude. A discussion of the results is given on the basis of dislocation-domain wall interactions. (11 refs.)

114721 Energy dissipation due to macroeddy currents with mechanical vibrations. V.V.Khil'chevskii, V.D.Deigraf (Kiev Polytech. Inst., Kiev, Ukrainian SSR). *Strength Mater. (USA)*, vol.14, no.9, p.1275-80 (Sept. 1982). Translation of: *Probl. Prochn. (USSR)*, vol.14, no.9, p.99-102 (Sept. 1982). Losses due to macroeddy currents occur when a magnetised specimen carries out mechanical vibrations. The authors demonstrate that the logarithmic vibration decrement due to macroeddy currents is amplitude-dependent in a large range of stresses. (9 refs.)

Coupled quadrupole-phonon excitations: inelastic neutron scattering on Van Vleck paramagnet PrNi₂See Entry 114107

Nonlinear static magnetic susceptibility of the Van Vleck paramagnet TmPO₄See Entry 114666

Modulated magnetic structure of the Kondo compound TmSSee Entry 114674

Towards the analysis of magnetothermoelastic effects in metallic specimens during magnetic treatmentSee Entry 115219

Influence of magnetomechanical damping on resonance electromagnetic-acoustic conversion in ferromagnetsSee Entry 115483

Conversion of zero-order Lamb-wave modes into an electromagnetic field in ferromagnetic metalsSee Entry 115484

75.90 OTHER TOPICS IN MAGNETIC PROPERTIES AND MATERIALS

114722 Localized retarded modes in a ferromagnetic slab. N.P.Lima, F.A.Oliveira (Inst. de Fisica, Univ. Federal Fluminense, Niteroi, Brazil). *Solid State Commun. (USA)*, vol.47, no.11, p.921-3 (Sept. 1983). General results are given for Green functions, mode frequencies and light scattering cross section for retarded modes in a ferromagnetic slab. These results hold for a more general geometry than the Voigt's one. The authors show that they fulfil very general symmetry requirements. (14 refs.)

Mossbauer spectroscopic studies of surface magnetismSee Entry 114763

76.00 MAGNETIC RESONANCES AND RELAXATION IN CONDENSED MATTER; MOSSBAUER EFFECT (for measurement techniques, see 07.58)

76.20 GENERAL THEORY OF RESONANCES AND RELAXATION

Theory of saturation of magnetic resonance in solids at low temperaturesSee Entry 114725

76.30 ELECTRON PARAMAGNETIC RESONANCE AND RELAXATION

114723 The effect of lattice discreteness on the linewidth of the electron spin resonance of local moments in metals. A.M.Stewart (W.M. Keck Lab. of Engng. Materials, California Inst. of Technol., Pasadena, CA, USA). *Aust. J. Phys. (Australia)*, vol.36, no.4, p.501-5 (1983). Solutions of the Hasegawa-Bloch equations for the electron spin resonance of local moments in metals are obtained which take account of the discrete nature of the lattice. The most notable result derived is that the resonance linewidth is proportional to $T-\theta$ for any degree of bottlenecking, where θ is the paramagnetic Curie temperature calculated with lattice discreteness. An alternative derivation of the appropriate Hasegawa-Bloch equations is also given. (12 refs.)

114724 Time-domain analysis of EPR measurements of polyacetylene and soliton diffusion. J.Tang, C.P.Lin, M.K.Bowman, J.R.Norris (Chem. Div., Argonne Nat. Lab., Argonne, IL, USA), J.Isoya, H.Shirakawa. *Phys. Rev. B (USA)*, vol.28, no.5, p.2845-7 (1 Sept. 1983). A novel analysis of EPR measurements on polyacetylene is demonstrated by the analysis of the conventional line shape in time domain. Quantitative results of the hyperfine-coupling constant, the on-chain diffusion rate, and the off-chain hopping rate were extracted by nonlinear curve fitting to the time-domain signals, and they are consistent with the soliton model of polyacetylene. (16 refs.)

114725 Theory of saturation of magnetic resonance in solids at low temperatures. L.L.Buishvili, N.P.Fokina (Inst. of Phys., Acad. of Sci., Tbilisi, Georgian SSR). *Sov. Phys.-Solid State (USA)*, vol.25, no.2, p.215-18 (Feb. 1983). Translation of: *Fiz. Tverd. Tela (USSR)*, vol.25, no.2, p.381-6 (Feb. 1983). [received: Sept. 1983] A study is made of the low-temperature dynamics of the spin system of a solid paramagnet saturated by an alternating magnetic field. The Zeeman and dipole-dipole subsystems are redefined to allow for the effect of a demagnetizing field. Equations for the reciprocal temperatures of the subsystems are derived. Approximate solutions are obtained for certain special cases. (10 refs.)

114726 Spin-phonon interaction in the Ni²⁺:Al₂O₃ system at low temperatures. E.M.Ganapol'skii, D.N.Makovetskii (Inst. of Radio Phys. & Electronics, Acad. of Sci., Kharkov, Ukrainian SSR). *Sov. Phys.-Solid State (USA)*, vol.25, no.2 (Feb. 1983). Translation of: *Fiz. Tverd. Tela (USSR)*, vol.25, no.2, p.607-10 346-8 (Feb. 1983). [received: Sept. 1983] The authors have used linear and nonlinear APR methods to investigate the spin-phonon interaction: in particular, to measure the spin-lattice relaxation time τ_1 in the system Ni²⁺:Al₂O₃ at a transition E₂-E₁ which is strictly forbidden for the electromagnetic field. This system is extremely interesting

from the standpoint of realizing phaser amplification and generation of hypersound, since here the conditions are such that the hypersonic wave to be amplified interacts efficiently with the paramagnetic centers. (12 refs.)

114727 Dipole broadening of the EPR line in case of non-Kramers ions. R.Kh.Sabirov. *Ukr. Fiz. Zh. (USSR)*, vol.28, no.8, p.1263-5 (Aug. 1983). In Russian. Non-Kramers ions have a large g-factor anisotropy. The splitting factor for the non-Kramers doublets along the axis and perpendicular to the crystal symmetry axis O_z, is equal to zero ($g_{\perp}=0$). The EPR spectrum of such ions is described by the Hamiltonian $H_0=g_{\parallel}\beta H_z S_z^2+\Delta S_z^2$, where g_{\parallel} -splitting factor along O_z axis, H_z-z component of the magnetic field, Δ -splitting at zero magnetic field. It is proposed that at large ion concentrations the EPR line shape is determined by the dipole-dipole interaction described by $H_d=\sum_{ij}A_{ij}S_i^zS_j^z$. (7 refs.) V.G.P.

76.30F Iron group (3d) ions and impurities (Ti-Cu)

114728 EPR of Cu²⁺ in MgSeO₄·6H₂O single crystals. V.K.Jain (Dept. of Phys., M.D. Univ., Rohtak, India). *Indian J. Pure & Appl. Phys.*, vol.21, no.7, p.430-1 (July 1983). The EPR spectrum of Cu²⁺ ($S=1/2$, $I=3/2$) in MgSeO₄·6H₂O consists of two overlapping angle-dependent four-line hyperfine patterns arising from two differently but magnetically equivalent Cu²⁺ complexes located at a specific site. The angular variation of the spectrum indicates that Cu²⁺ substitutes for Mg²⁺ at Y-ion sites only. (8 refs.)

114729 The unusual EPR spectra in single crystals of CuSiF₆·6H₂O and CuSiF₆·6D₂O. D.De Kumar (Dept. of Phys., Univ. of Texas, Arlington, TX, USA). *Indian J. Cryog.*, vol.8, no.1, p.17-23 (1983). EPR studies have been performed on single crystals of CuSiF₆·6D₂O in the range 35-16 GHz, and compared with EPR data of CuSiF₆·6H₂O in the range 4.2-400K. The inversion of the line shape of the highest resonant field has been observed for the first time in CuSiF₆·6H₂O in the neighborhood of its phase transition point around 294K as well as with orientation of the magnetic field at fixed temperature 298K. This is related to the cross relaxation between B-type complexes to the A-type complexes in CuSiF₆·6H₂O. Studies show that the structure of CuSiF₆·6D₂O should be identical to that of CuSiF₆·6H₂O. There may be a possibility of building a MASER with a single crystal of CuSiF₆·6H₂O. (17 refs.)

114730 Analysis of the spin-Hamiltonian parameters for Cr³⁺ in mirror and inversion symmetry sites of alexandrite (Al₂₋₃Cr₃BeO₄). Determination of the relative site occupancy by EPR. C.E.Forbes (Corporate Res. Center, Allied Corp., Morristown, NJ, USA). *J. Chem. Phys. (USA)*, vol.79, no.6, p.2590-9 (15 Sept. 1983). The EPR spectra of Cr³⁺ in single crystals of alexandrite (Al₂₋₃Cr₃BeO₄, x<0.01) have been obtained at temperatures between RT and 4.2K in the frequency range 9.5-9.1 GHz. The orthorhombic structure of Al₂BeO₄ has two distinct Al³⁺ sites in the unit cell corresponding to C_s and C_i symmetry. The EPR spectra at 35 GHz of Cr³⁺ in the C_s site have been previously analyzed by other investigators. This study reports the observation of Cr³⁺ in the C_i site and the refined spin-Hamiltonian parameters for both magnetic centers. The absolute sign of the fine structure tensor elements for the C_i site has been determined to be positive. The observed orientations of both the chromium mirror and inversion magnetic axes are consistent with the crystallographic symmetry relationships of pure Al₂BeO₄. A comparison of the measured Cr³⁺ EPR intensities for resonances from both sites indicates that for two magnetically dilute crystals, the mirror site is preferentially occupied with a relative site occupancy of 78%±3%. (33 refs.)

114731 Optical absorption and electron spin resonance in blue and green natural beryl: a comment [on paper by A. Blak et al., with their reply]. G.Lehmann (Inst. fur Phys. Chem., Westfälische Wilhelms-Univ., Munster, Germany), A.R.Blak, S.Isotani, S.Watanabe. *Phys. & Chem. Miner. (Germany)*, vol.9, no.6, p.278-80 (1983). For original paper see A.R. Blak et al., *ibid.*, vol.8, p.161 (1982). The angular variations of the central EPR signal in green beryl may result from superposition of unresolved components from crystallographically equivalent, but magnetically inequivalent, sites. Lehmann's analysis of the EPR spectra leads to the conclusion that the postulated position of the supposed Fe³⁺ in the structural channels is inconclusive. Rather, the signal may be due to a radiation defect not the Fe³⁺ species. Blak et al. reassert that the EPR spectrum can be attributed to Fe³⁺ located in the structural channels and that substitutional Fe³⁺ for Al, Be, and Si does not reduce to Fe²⁺ on heating. (7 refs.)

Determination of the positions of iron impurities in gallium arsenide and phosphide by the ENDOR methodSee Entry 114473

A reexamination of the magnetic susceptibility of the coordination complex μ_2 -oxohexa- μ -chlorotetrakis-(triphenylphosphine oxide) copper (II), Cu₂OCl₆(TPPO)₄See Entry 114676

Magnetochemical study of iron molybdates obtained from precursor precipitates with different Mo- and Fe-contentSee Entry 114677

Color centers and electron spin resonance in chrysoberyl containing Mn and Ti guest ionsSee Entry 114890

76.30K Rare-earth ions and impurities

114732 The influence of spin-coupling on the ESR-spectra of the orthochromites YCrO₃ and LuCrO₃. K.Drager (Inst. fur Phys. Chem., Univ. Hamburg, Hamburg, Germany). *Z. Naturforsch. Teil A (Germany)*, vol.38A, no.8, p.848-54 (Aug. 1983). In German. Polycrystalline samples of stoichiometric YCrO₃ and LuCrO₃ were investigated by ESR in the temperature range between 140 K and 520 K. Although the orthochromites have a complicated spin structure, the line width shows the temperature dependence of simple antiferromagnetic systems. Up to a high degree the spectra have a Lorentzian line shape. The ESR intensity confirms the predictions of a cluster model. The coupling energy describing the gap between the bounded and the resonance state was found to be $\Delta E=250$ cm⁻¹ for YCrO₃ and $\Delta E=210$ cm⁻¹ for LuCrO₃. There is a distinct relation between the excitation energy ΔE and the volume V of the elementary cell. Further calculations concerning the isotropic exchange interaction result in a coupling constant of $J=5.55$ cm⁻¹ for YCrO₃ and $J=4.67$ cm⁻¹ for LuCrO₃. (22 refs.)

Quantum-beat free-induction decay in Tm²⁺:SrF₂: Fourier-transform ESR spectroscopy by optical meansSee Entry 114757

76.30L Other ions and impurities

(for colour centres, see 76.30M)

- Character of impurity distribution in comminuted β -boron crystals See Entry 113953
Deep-level spectroscopy of reactively sputtered a-Si:H films . See Entry 114485

76.30M Colour centres and other defects

114733 The influence of fusion temperature on the defect center concentration of GeO_2 glass. G.Kordas, R.A.Weeks, D.L.Kinser (Vanderbilt Univ., Nashville, TN, USA).

J. Appl. Phys. (USA), vol.54, no.9, p.5394-9 (Sept. 1983).

Paramagnetic resonance spectra of virgin glasses and γ -ray irradiated GeO_2 glasses were studied with the electron spin resonance (ESR) method as a function of fusion temperatures. Fusions were made in air at temperatures between 1200 and 1650°C and cooled at constant rate. In virgin glasses, only the E' center was detected at concentrations of about $10^{15}/\text{g}$. After a γ -ray irradiation, a new resonance at the low-field side (LFS) of the E' center and a symmetric line with $g=1.91$ were observed. Measurements at various temperatures, power levels, and frequencies provide a basis for resolving the overlapping resonances. The authors labeled the paramagnetic center which produces the LFS signal, the H_0 center. The g values of the H_0 center are the basis for attributing this center to a hole located on a nonbridging oxygen. The $g=1.91$ resonance is attributed to Cr^{3+} or Mn^{2+} impurities in the GeO_2 glasses. At constant γ -ray dose, the H_0 center concentration decreased and the E' -center concentrations increased with increase of fusion temperature. (22 refs.)

114734 ESR of defects in III-V compounds. J.Schneider (Fraunhofer-Inst. fur Angewandte Festkorperphys., Freiburg, Germany).

Defects in Semiconductors II, Symposium Proceedings, Boston, MA, USA, Nov. 1982 (New York, USA: North-Holland Pressing), p.225-35

A survey is given on deep defects in GaP, GaAs and InP identified by electron spin resonance (ESR). Defect structures to be discussed are (i) 3d transition metals, (ii) antisite defects and (iii) radiation induced centers. The relevance of such defects for the III-V materials technology will be illustrated by representative examples. (25 refs.)

Color centers in $\text{K}_2\text{S}_2\text{O}_6$ and $\text{Rb}_2\text{S}_2\text{O}_6$ crystals See Entry 113910

Characteristic electronic defects at the Si-SiO₂ interface See Entry 114612

Color centers and electron spin resonance in chrysoberyl containing Mn and Ti guest ions See Entry 114890

76.30R Free radicals

114735 ESR study on radical existing in plasma-polymerized styrene thin film. K.Ohno, N.Ishii, J.Sohma (Faculty of Engng., Hokkaido Univ., Sapporo, Japan).

Jpn. J. Appl. Phys. Part 1 (Japan), vol.22, no.6, p.996-1000 (June 1983).

The residual radicals formed in plasma-polymerized styrene (PPS) thin films are investigated by ESR measurement. An asymmetric singlet line characteristic of oxide radicals with an-isotropic g -values ($g_1=2.008$, $g_2=2.006$, and $g_3=1.993$) is observed in PPS produced under oxygen carrier gas, whereas a symmetric line is observed in PPS produced under nitrogen carrier gas, as previously reported. Castner's and Korb and Marauni's methods are used to extract the unresolved inhomogeneous and homogeneous broadenings ΔH_G and ΔH_L , from which the spin-relaxation times T_1 and T_2 are obtained. In the case of the PPS with nitrogen carriers, the introduction of air accelerates the decrease in the concentration of radical ions and ΔH_G , while it keeps ΔH_L constant. The opposite variations in T_1 and T_2 mean that no annealing effect appear explicitly up to 100°C. At temperatures higher than 100°C, the increase in T_2 due to the decrease in the concentration of radicals makes the experimentally-recorded linewidth ΔH_{msl} narrower. (8 refs.)

114736 Rotational correlation times of a nitroxide spin probe in low temperature matrices determined by saturation transfer ESR: their correlation to dynamic behavior of radiation products. Y.Ito (Res. Reactor Inst., Kyoto Univ., Osaka, Japan).

J. Chem. Phys. (USA), vol.79, no.6, p.2650-9 (15 Sept. 1983).

Rotational correlation times τ_c of the spin probe, di-tert-butyl nitroxide, in several organic solvents cooled to temperatures lower than their melting points have been measured using a saturation transfer (ST) ESR technique. Since the ST spectra changed markedly depending on microwave power, the authors introduced a scaled ST parameter to eliminate this effect. The temperature dependence of τ_c in a noncrystalline phase can be described by the Arrhenius relation. The activation energies are 17.6 kJ mol⁻¹ for methanol containing 5% water, 20.8 kJ mol⁻¹ for ethanol, and 18.9 kJ mol⁻¹ for n-propanol. The values are close to the activation energies reported for the solvation and decay rates of electrons in the solvents. The rotational correlation time can be expressed in terms of a viscosity using the Stokes-Einstein equation. However, a macroscopic viscosity fails to reproduce the observed τ_c , especially at low temperatures. On the other hand, the authors have evaluated the solvation rate of an electron in n-propanol and the diffusion coefficients of radicals in methanol and 3-methylpentane on the basis of the tentative viscosity derived from τ_c using the same expression. The results are in good agreement with the experimental data. The temperature and phase dependences of τ_c will also be discussed. (27 refs.)

114737 Electron spin resonance study of spin exchange in a nematic solvent. N.M.Atherton, M.C.B.Shohoji (Dept. of Chem., Sheffield Univ., Sheffield, England).

J. Chem. Soc. Faraday Trans. II (GB), vol.79, pt.8, p.1243-7 (Aug. 1983).

Spin-exchange rate constants have been measured from the concentration dependence of the ESR linewidths of two nitroxide radicals, TANONE (4-oxo-2,2,6,6-tetramethylpiperidino-oxy) and M-DOXYL (2-hexyl-2-(10-methoxycarbonyldecyl)-4,4-dimethylazolidinyl-3-oxy), in the isotropic and nematic phases of MBBA. Strong exchange is observed for TANONE in both phases and for M-DOXYL in the isotropic phase but the latter radical exhibits weak exchange in the nematic phase. A qualitative discussion of the nature of the radical-radical encounters affords an explanation of the observations. (3 refs.)

Electron spin resonance investigation of cation-radical salts of N,N,N',N' -tetramethyl- p -phenylenediaminium (TMPD) hexafluorophosphate, hexafluoroarsenate and hexafluoroantimonate See Entry 112760

76.40 DIAMAGNETIC AND CYCLOTRON RESONANCES

114738 Cyclotron resonance of inversion electrons on InSb in tilted magnetic fields. J.H.Crasemann, U.Merkt (Inst. fur Angewandte Phys., Univ. Hamburg, Hamburg, Germany).

Solid State Commun. (USA), vol.47, no.11, p.917-20 (Sept. 1983).

Cyclotron resonance (CR) of inversion electrons on InSb is studied in magnetic fields tilted away from the surface normal. Particularly, a pronounced splitting of the CR signals into two distinct resonances is observed. When the magnetic field is parallel to the inversion layer one of the two resonances vanishes and the other evolves into a bulk like CR at sufficiently low electron densities and in sufficiently high resonance magnetic fields. The different absorption modes are explained by a strong coupling of the electric and magnetic quantization on InSb in tilted magnetic fields. (16 refs.)

114739 Inverted population of light-hole band pumped at cyclotron resonance. V.A.Kozlov, L.S.Mazov, I.M.Nefedov (Inst. of Appl. Phys., Acad. of Sci., USSR).

Sov. Phys.-JETP (USA), vol.83, no.5, p.1037-42 (Nov. 1982). Translation of: *Zh. Eksp. & Teor. Fiz. (USSR)*, vol.83, no.5, p.1794-803 (Nov. 1982). [received: Sept. 1983]

The authors investigate the behavior of a system of hot carriers inelastically scattered by optical phonons in a semiconductor in a strong microwave field and a magnetic field. A mechanism is proposed for the redistribution of the holes among the heavy and light subbands of the valence band; this mechanism is capable of controlling the relative hole densities. At cyclotron resonance of the heavy holes it is possible to produce inverted population of the light-hole subband with a relative density higher than in constant fields $E \perp B$. Cyclotron resonance of the light holes causes strong depletion of the light-carrier subband. (42 refs.)

Calculation of the cyclotron resonance linewidth in GaAs-AlGaAs heterostructures See Entry 114602

76.50 FERROMAGNETIC, ANTIFERROMAGNETIC, AND FERRIMAGNETIC RESONANCES; SPIN WAVE RESONANCE

(see also 75.30D Spin waves)

114740 Dynamic dislocation-induced broadening of a homogeneous ferromagnetic resonance line. E.I.Druinskii, A.I.Spol'nik (Physicotech. Inst., Acad. of Sci., Kharkov, Ukrainian SSR).

Sov. Phys.-Solid State (USA), vol.25, no.2, p.283-5 (Feb. 1983). Translation of: *Fiz. Tverd. Tela (USSR)*, vol.25, no.2, p.501-5 (Feb. 1983). [received: Sept. 1983]

The effect of mobile dislocations of the width of a homogeneous ferromagnetic resonance line is investigated. The line width is analyzed as a function of the velocity of the dislocations, of the relative density of mobile dislocations, and of the orientation of the glide plane in the crystal. The results are compared with those for sessile dislocations. (9 refs.)

Noncollinear magnetic phases in a strongly anisotropic antiferromagnet CoF₂ with large Dzyaloshinskii interaction See Entry 114679

Temperature dependence of the fluctuations of exchange interaction in amorphous Co-P alloys See Entry 114714

76.60 NUCLEAR MAGNETIC RESONANCE AND RELAXATION

114741 NMR studies of pyridine on silica-alumina. G.E.Maciel, J.F.Haw, I-Suer Chuang, B.L.Hawkins, T.A.Early, D.R.McKay, L.Petrakis (Colorado State Univ., Fort Collins, CO, USA).

J. Am. Chem. Soc. (USA), vol.105, no.17, p.5529-35 (24 Aug. 1983).

¹³C and ¹⁵N NMR spectroscopy with cross-polarization and magic-angle spinning have been used to study the structure and dynamics of pyridine adsorbed on silica-alumina. Hydrogen bonding is the dominant interaction at high loadings levels (0.5 to 1 monolayer). At lower coverages, a Lewis acid-base complex dominates and the pyridine is significantly less mobile. Brønsted complexes are found if the surface has been pretreated with HCl gas; ¹⁵N NMR provides evidence for two distinct protonated forms of adsorbed pyridine. Experiments with variable contact time or with the decoupler off provide evidence for rotational diffusion about the C₂ axis of adsorbed pyridine. (32 refs.)

114742 Orientation and molecular structure of 1,5 and 1,8 dichloroanthraquinones by PMR in a nematic solution. B.B.Sharma, A.Saupe (Dept. of Phys., Kent State Univ., Kent, OH, USA), C.L.Khetrapal, A.C.Kunwar.

Mol. Cryst. & Liq. Cryst. (GB), vol.95, no.3-4, p.359-66 (1983).

The structures and the order parameters of 1,5 and 1,8 dichloroanthraquinones have been determined from the dipolar couplings between the protons in the nematic solutions. The results show the effect of steric interactions on the molecular structure. The aromatic rings of 1,8 dichloroanthraquinone are in different planes making an angle of 15° while 1,5 dichloroanthraquinone appears to be flat. The two molecules show peculiar differences in orientation. The 'in-plane' order parameters of the 1,8 derivative are about equal while the 1,5 derivative has a strongly preferred alignment axis close to the Cl-Cl internuclear axis. (9 refs.)

114743 ¹³C high resolution solid state NMR studies on cellulose samples of different physical structure. J.Kunze (Inst. fur Polymerchem. Erich Correns, Akad. der Wissenschaften, Teltow-Seehof, Germany), G.Scheler, B.Schroter, B.Philipp.

Polym. Bull. (Germany), vol.10, no.1-2, p.56-62 (June 1983).

¹³C high resolution solid state NMR spectra of cellulose samples differing in lattice type, crystallinity and gross morphology (pulp, filament, film, bead) are presented and discussed with regard to the above mentioned parameters of physical structure. (13 refs.)

114744 Absence of hydrogen in superconducting molybdenum sulfide, MoS₄. R.Baillif (Dept. de Phys. de la Matière Condensée, Univ. de Genève, Genève, Switzerland), K.Yvon, P.Fischer.

Solid State Commun. (USA), vol.47, no.11, p.895-8 (Sept. 1983).

Superconducting MoS₄ (T_c=1.8K) was prepared from the ternary sulfides MMo₂S₄ (M=Cu,Ni) by the acid extraction method, and was studied by neutron diffraction and NMR spectroscopy. In contrast to earlier reports no significant amounts of hydrogen could be found in the rhombohedral structure. However, large proton concentrations were found in samples which had been exposed to moist air. (15 refs.)

- Spin-pattern recognition in high-resolution proton NMR spectroscopy** See Entry 111715
- The use of ^{29}Si Fourier transform nuclear magnetic resonance spectroscopy for the characterisation of polymers and paints** See Entry 113710
- Evidence of compatibility in the melt for poly(ethylene oxide)/poly(methyl methacrylate) blends by ^{13}C n.m.r. investigations** See Entry 113714
- Liquid-crystalline copolyesters based on poly(*p*-oxybenzoate) and poly(*p*-biphenylene terephthalate)** See Entry 113734
- Microscopy and deuterium NMR studies on induced cholesteric lyotropic mesophases of potassium laurate** See Entry 113736
- Self-diffusion of macromolecules in the crystallization of a polymer from solution** See Entry 113758
- Effect of the structural properties of compounds in the system $\text{Bi}_2\text{O}_3\text{-EO}_2$ ($\text{E}=\text{Ge}, \text{Si}$) on their dissolution** See Entry 114177
- Self-diffusion of polyethyleneglycol molecules in concentrated solutions and melts** See Entry 114221
- Hyperfine fields of ^{61}Ni in an Ni-Fe alloy** See Entry 114502
- Study of the ferroelectric phase transition in rubidium hydrogen selenate by high-resolution NMR of ^{77}Se** See Entry 114793

76.60C Chemical and Knight shifts

- 114745 NMR studies of Ge atoms in quenched f.c.c.-Ge alloys.** H.Murakami, I.Kanazawa, T.Shimizu (Dept. of Phys., Tokyo Gakuji Univ., Tokyo, Japan), K.Matsushita. Point Defects and Defect Interactions in Metals. Proceedings of the Yamada Conference V, Kyoto, Japan, 16-20 Nov. 1981 (Amsterdam, Netherlands: North-Holland 1982), p.489-92. The values of Knight shift of Ge in Cu-Ge and in Al-Ge dilute alloys were estimated to be about 480 ± 160 ppm. The effect of quenching on the Knight shift was studied on the Cu-Ge alloys. The ratio of Knight shift in quenched alloy to that in annealed one was about 1.4. The brief discussion on this ratio was reported. (5 refs.)

76.60E Relaxation effects

- 114746 Spin-lattice relaxation times of ^1H in aqueous gadolinium chloride solutions.** D.Kohnlein, O.Lutz, R.Ulmer (Phys. Inst., Univ. Tübingen, Tübingen, Germany). *Z. Naturforsch. Teil A (Germany)*, vol.38A, no.8, p.947-8 (Aug. 1983). Spin-lattice relaxation times T_1 of protons in aqueous solutions of gadolinium chloride have been measured at 2.11 T for a larger range of concentrations down to 0.035 millimolar. Very small amounts of GdCl_3 decrease strongly T_1 of the water protons. (17 refs.)
- 114747 ^1H NMR study of hydrogen motion in the β phase of the Mg_2NiH_x system.** S.Hayashi, K.Hayamizu, O.Yamamoto (Nat. Chem. Lab. for Industry, Ibaraki, Japan). *J. Chem. Phys. (USA)*, vol.79, no.5, p.2308-14 (1 Sept. 1983). The motion of hydrogen atoms in the β -phase of Mg_2NiH_x was studied by the ^1H pulsed NMR spectroscopy. Fourier-transformed spectra and spin-lattice relaxation times in the laboratory frame (T_1) and in the rotating frame ($T_{1\rho}$) for $\text{Mg}_2\text{NiH}_{0.85}$ were measured in the temperature range between 170 and 460K. The ^1H magnetization in the hydride relaxes by the dipolar modulation caused by the hydrogen motion and paramagnetic impurities. It was confirmed that all hydrogen atoms in the hydride are equivalent with respect to their motion. The correlation frequencies were determined by the temperature dependences of the linewidth and the two relaxation times T_1 and $T_{1\rho}$, and they are in good agreement among them, giving a single activation energy 12 kcal/mol in the temperature range between 210 and 460K. The ^1H - ^1H dipole-dipole interaction exists in the motional narrowing region, which supports that the hydrogen motion is not a diffusion but a kind of rotation. (32 refs.)
- 114748 Carbon-13 line shape study of two-site exchange in solid dimethyl sulfone.** M.S.Solum, K.W.Zilm, J.Michl, D.M.Grant (Dept. of Chem., Univ. of Utah, Salt Lake City, UT, USA). *J. Phys. Chem. (USA)*, vol.87, no.15, p.2940-4 (21 July 1983). The two-site exchange in dimethyl sulfone of methyl carbons having axially symmetric chemical shift tensors is studied by ^{13}C solid-state NMR. The rate constants for this motion as a function of temperature are determined by a comparison of experimental spectra from 297 to 337K with theoretically calculated ones. Fitting this kinetic data to the Eyring equation gave an enthalpy of activation of 13.3 ± 0.5 kcal/mol and entropy of activation of -1.4 ± 1.7 cal/(molK). The geometrical relationship between the principal axes of the shift tensors of the two methyl groups was also determined. (20 refs.)
- 114749 A general NMR spectral density and its experimental verification.** A.M.Albano, P.A.Beckmann, M.E.Carrington, F.A.Fusco, A.E.O'Neill, M.E.Scott (Dept. of Phys., Bryn Mawr College, Bryn Mawr, PA, USA). *J. Phys. C (GB)*, vol.16, no.27, p.L979-83 (30 Sept. 1983). The authors develop a new general spectral density for use in interpreting nuclear spin-lattice relaxation measurements in molecular solids where molecular and/or intramolecular reorientation is responsible for the relaxation. They show that the simplest case of the general theory fits both the temperature and Lamor frequency dependence of some very complicated relaxation measurements which could not be previously fitted using several standard spectral densities. The relationship of the spectral density to a distribution of molecular potentials is briefly outlined. (6 refs.)
- 114750 A ^{13}C NMR study of mesomorphic solutions of poly(*p*-phenylene terephthalamide).** L.G.Close Jr., R.E.Fornes, R.D.Gilbert (Fiber & Polymer Sci. Program, North Carolina State Univ., Raleigh, NC, USA). *J. Polym. Sci. Polym. Phys. Ed. (USA)*, vol.21, no.9, p.1825-37 (Sept. 1983). Solutions of poly(*p*-phenylene terephthalamide) in fuming sulfuric acid were characterized by ^{13}C NMR spectroscopy and solution viscosity measurements over the 2-28% w/w concentration range. The spectra showed the presence of two distinct amide carbonyl resonances at low concentration, tentatively assigned to cis and trans conformations. As the concentration increased, additional carbonyl lines were observed along with significant broadening. Peak area measurements showed that only the polymer molecules in the isotropic environments contributed to the ^{13}C NMR spectra and a considerable amount of the polymer remained in the isotropic phase at concentrations previously considered to consist of polymer in highly anisotropic regions. Spin-lattice relaxation times were measured at six concentrations using the inversion recovery method. The aromatic carbons relaxed at a much faster rate (ca. 0.10 s) than the carbonyls (ca. 0.45 s), but the relaxation rates for both carbons were essentially constant over the concentration range, indicating that

the observed isotropic phase is not affected by changes in the macroscopic solution behavior so as to alter spin-lattice relaxation mechanisms. (9 refs.)

- 114751 Nuclear magnetic resonance investigations of lithium diffusion in Li_2O , Li_2SiO_3 and LiAlO_2 .** T.Matsuo (Dept. of Phys., Toyo Univ., Saitama, Japan), H.Ohno, K.Noda, S.Konishi, H.Yoshida, H.Watanabe. *J. Chem. Soc. Faraday Trans. II (GB)*, vol.79, pt.8, p.1205-16 (Aug. 1983). Spin-lattice relaxation rates of ^7Li have been measured for Li_2O , Li_2SiO_3 and LiAlO_2 with pulsed nuclear magnetic resonance. Relaxation due to cation diffusion is observed with quadrupole and dipole interactions. Cation jump frequencies in the extrinsic region with apparent activation energies of ca. 0.4 eV for Li_2O , 0.81 eV for Li_2SiO_3 and 0.77 eV for LiAlO_2 are obtained. These activation energies are in good agreement with those of ionic conductivities in the extrinsic region. (7 refs.)
- 114752 NMR in quadrupole glasses and the spectral density of orientation fluctuations.** M.S.Conradi (Dept. of Phys., Coll. of William & Mary, Williamsburg, VA, USA). *Phys. Rev. B (USA)*, vol.28, no.5, p.2848-51 (1 Sept. 1983). Previous NMR experiments on H_2 at low temperatures ($T \leq 0.3\text{K}$) and intermediate orthohydrogen concentrations ($0.1 < x < 0.55$) indicate that H_2 forms a quadrupole glass state. The interpretation of the NMR data in terms of molecular orientations and/or reorientations has not been clear. The authors propose a unified explanation of the many NMR measurements (T_1 , line shape, spin echoes, and stimulated echoes) in terms of the spectral density of the molecular orientations. All the data are compatible with the development of a DC component in the spectral density as the temperature is decreased while the AC parts are not greatly changed. Strictly dynamic theories are shown not to agree with the experiments. The NMR behaviors of ordinary glasses and quadrupole glasses are compared and found to reflect fundamental symmetry differences between the two states. The spin-lattice relaxation data in H_2 appear to indicate a broad distribution of fluctuation frequencies. Interpretation of the observed minimum in T_1 as a motional minimum may be incorrect. Finally, an experimental test of the ergodicity of quadrupole glasses is proposed. (23 refs.)
- 114753 NMR study of both ^{19}F and ^{205}Tl motions in TlZrF_6 .** J.Alizon, J.P.Battut, J.Dupuis, H.Robert, I.Mansouri, D.Avignat (Univ. de Clermont-Ferrand II, Aubiere, France). *Solid State Commun. (USA)*, vol.47, no.12, p.969-72 (Sept. 1983). Spin-lattice relaxation times in the laboratory T_1 and rotating frames $T_{1\rho}$ for both ^{19}F and ^{205}Tl nuclei were measured as a function of temperature. Comparison of the temperature dependence of longitudinal NMR relaxation rates of both ^{19}F and ^{205}Tl suggests that Ti^+ ions are more mobile than F^- ones at high temperatures. Furthermore Fourier transform experiments show that two kinds of Ti^+ ion can be distinguished at high temperatures, one of them being more mobile than the other one and probably responsible for the ionic conductivity of this material. (13 refs.)
- 114754 Local boron environment in $\text{Ni}_{100-x}\text{B}_x$ metallic glasses: A NMR study.** P.Panissod, I.Bakonyi, R.Hasegawa. *Report KFKI-1983-57*, Hungarian Acad. Sci., Budapest (1983), 15 pp. From the analysis of the ^{11}B NMR spectra in a $a\text{-Ni}_{100-x}\text{B}_x$ ($18.5 \leq x \leq 40$) the electric field gradient (EFG) components on the B sites and their distributions are deduced, giving an insight into the local atomic arrangements. For $x=18.5$ and $x=40$, one finds relatively narrow distributions of the EFG components indicating weak fluctuations of the bonding angles, distances and nature of the atoms in the B coordination shell. The comparison with the compositionally closest nickel borides (Ni_3B and Ni_4B_3) immediately suggests that the local structure around B is similar in these glasses and in the related crystals, i.e. nickel trigonal prisms (6 Ni) whose rectangular faces are capped by 3 Ni (Ni_3B) or 3 Ni (Ni_4B_3). For intermediate concentrations the EFG components distributions are found significantly broader and comparable with those expected from random packing of spheres. However, the continuous evolution of the NMR spectra shape with increasing B content rather suggests an admixture of $c\text{-Ni}_3\text{B}$ like and $c\text{-Ni}_4\text{B}_3$ like B local environment, i.e. when B concentration increases more prisms share rectangular faces allowing boron-boron contact as in $c\text{-Ni}_4\text{B}_3$. No sign of a B coordination shell similar to that in $c\text{-Ni}_3\text{B}$ (8 Ni anticubes $+ 2\text{B}$) is found in the glasses. Measurements of transverse relaxation times T_2 , which reflect essentially the B-B bondings, qualitatively support these conclusions. (11 refs.)
- Conformational properties of perfluoroalkane chains. VII. Carbon-13, fluorine, and proton spin-lattice relaxation of poly(decamethylene perfluorosebacate) in solution and the local mobility of the fluorocarbon chain** See Entry 112888

76.60L Spin echoes

- Translational diffusion in CH_4 and CH_2Cl_2 dissolved in cholesteric liquid crystals** See Entry 114229
- NMR in quadrupole glasses and the spectral density of orientation fluctuations** See Entry 114752

76.70 MAGNETIC DOUBLE RESONANCES AND CROSS EFFECTS

76.70D Electron-nuclear double resonance (ENDOR)

- Determination of the positions of iron impurities in gallium arsenide and phosphide by the ENDOR method** See Entry 114473

76.70H Optical double magnetic resonance (ODMR)

- 114755 Optical detection of EPR of self-trapped excitons using photostimulated luminescence of crystals.** N.G.Romanov, V.A.Vetrov, P.G.Baranov (A.F. Ioffe Physicotech. Inst., Acad. of Sci., USSR). *JETP Lett. (USA)*, vol.37, no.7, p.386-8 (5 April 1983). Translation of: *Pis'ma v Zh. Eksp. & Teor. Fiz. (USSR)*, vol.37, no.7, p.325-8 (5 April 1983). [received: Oct. 1983] Optically detected EPR spectra are recorded for the first time using photostimulated luminescence of crystals. The mechanism of the formation of self-trapped excitons in fluorite crystals is clarified. (6 refs.)
- 114756 Determination of the g values of the ODMR signals in a-Si:H.** B.C.Cavenett, S.P.Depinna (Dept. of Phys., Univ. of Hull, Hull, England), I.G.Austin, T.M.Searle. *Philos. Mag. B (GB)*, vol.48, no.2, p.169-85 (Aug. 1983). Recent studies of optically detected magnetic resonance (ODMR) in a-Si:H have provided conflicting interpretations of the principal recombination processes in this material. In all cases the identification of the ODMR signals has rested on a comparison of the ODMR signal g values and those from the reported ESR and light-induced ESR (LESER) measurements in the literature.

The present controversy arises because of the diverse g values reported for the ODMR signals. The problem of measuring the g values associated with the ODMR signals in α -Si:H is discussed, and it is shown how most of the present discrepancies among the various reports can be resolved by experimental consideration. Finally, the implications of this study for the various recombination models deduced from the ODMR results are mentioned. (21 refs.)

114757 Quantum-beat free-induction decay in $\text{Tm}^{2+}:\text{SrF}_2$. Fourier-transform ESR spectroscopy by optical means. T.Kohmoto, Y.Fukuda, M.Tanigawa, T.Mishina, T.Hashi (Dept. of Phys., Kyoto Univ., Kyoto, Japan).

Phys. Rev. B (USA), vol.28, no.5, p.2869-72 (1-Sept. 1983).

The authors demonstrate, for the first time, a nanosecond Fourier-transform ESR experiment in solids achieved by optical means. ESR free-induction-decay signals in 0-100 Oe have been observed in the ground state of $\text{Tm}^{2+}:\text{SrF}_2$ as a new type of quantum beat generated by an optical excitation to the absorption band with a circularly polarized light pulse. The Fourier transform of the observed signals gives the ESR spectrum, and the origin of the decay is attributed to the superhyperfine interaction between the Tm^{2+} ion and neighboring fluorine nuclei. (15 refs.)

76.80 MÖSSBAUER EFFECT; OTHER GAMMA-RAY SPECTROSCOPY

114758 The influence of Cr and W contents of the isomer shift, hyperfine field distribution, and magnetic anisotropy of Fe-based amorphous alloys. S.T.Lin, L.Y.Jang, W.T.Ku, L.S.Chou (Dept. of Phys., Nat. Cheng Kung Univ., Tainan, Taiwan), Y.D.Yao.

Annu. Rep. Inst. Phys. Acad. Sin. (Taiwan), vol.12, p.242- (Dec. 1982). [received: Sept. 1983]

The effect of transition metals on the magnetic properties of Fe-based amorphous alloys has been studied by magnetization measurements and Mossbauer spectroscopy. Magnetization results show that the addition of transition metals such as Mn, Cr, V and Ti to Fe-based alloys decreases the mean magnetic moment per metallic atom drastically. This is attributed to antiferromagnetic coupling between the magnetic moments of iron atoms and those of solute atoms. One of the advantages of Mossbauer effect measurement is the ability to investigate inhomogeneous magnetic character, a characteristic of amorphous magnetic alloys. The authors report their results on studying the influence of Cr and W contents on the isomer shift, hyperfine field distribution, and magnetic anisotropy of amorphous $\text{Fe}_{80-x}\text{Cr}_x\text{B}_{14}\text{Si}_6$ and $\text{Fe}_{80-x}\text{W}_x\text{B}_{14}\text{Si}_6$ alloys. (no refs.)

114759 Mossbauer investigation on $\text{SiO}_2\text{-Fe}_2\text{O}_3$ glasses obtained from gel. M.Guglielmi, A.Maddalena, G.Principi (Istituto di Chimica Industriale, Facoltà di Ingegneria, Padova, Italy).

J. Mater. Sci. Lett. (GB), vol.2, no.9, p.467-70 (Sept. 1983).

The authors studied the influence of Fe concentration on the $\text{Fe}^{2+}/\text{Fe}^{3+}$ ratio in the amorphous $\text{SiO}_2\text{-Fe}_2\text{O}_3$ system, by using the Mossbauer technique to give detailed information on the environment of iron, in whatever structure, and the sol-gel method which enabled the achievement of an alkali-free system in different ox-red conditions. (9 refs.)

114760 A Sn-119 and Fe-57 Mossbauer effect study of the crystalline phase of 7S5. D.G.Todoroff, R.Marande, D.Boyd, D.L.Uhrich (Dept. of Phys., Kent State Univ., Kent, OH, USA).

Mol. Cryst. & Liq. Cryst. (GB), vol.95, no.3-4, p.367-71 (1983).

The Mossbauer effect of Sn-119 and Fe-57 has been used to study solutions of trimethyltin-4-methoxybenzylidene-4'-aminocinnamate (4.3% by weight) and Fe-57 enriched 1-1'-diacetylferrocene (0.2% by weight) in the crystalline phase of the liquid crystalline material 4-n-pentylphenyl-4'-n-heptyloxythiobenzoate (7S5). A pronounced deviation from Debye-like behaviour was observed at 180K in the In (recoil-free fraction) vs. temperature data for the tin-bearing probe molecule. This deviation may be interpreted as due to a crystal-crystal phase transition which has been observed at 183K. For the iron-bearing probe molecule, no deviation from Debye behaviour was found up to 300K. The data of this report support the interpretation that the phase transition is due to a rotation of the 7S5 molecule about the C-S bond. (4 refs.)

114761 Free parameter of spinel structure and Mossbauer lineshift. V.I.Nikolaev, V.S.Rusakov, N.I.Chistyakova (Dept. of General Phys. for Phys. Faculty, Moscow Univ., Moscow, USSR).

Moscow Univ. Phys. Bull. (USA), vol.38, no.1, p.87-9 (1983). Translation of: *Vestn. Mosk. Univ. Ser. 3 (USSR)*, vol.38, no.1, p.74-6 (1983).

The dependence of the Mossbauer lineshift δ in oxygen ferrite-spinels on the free parameter of the structure u is considered. The mutual disposition of the lines for the A and B points in the spectrum depends significantly on the oxygen parameter u . Within the framework of the field theory of ligands, theoretical dependences are obtained for the difference in the shifts $\Delta\delta^{\text{BA}} = \delta^{\text{B}} - \delta^{\text{A}}$ as a function of u , at various values of the lattice parameter a . This difference is expedient for comparison with experimental data, since it does not depend on the choice of radiation source and scarcely depends on a . The available experimental data for ferrite-spinels with Fe^{3+} ions at points A and B agree with the results of the calculations. In particular, the trend of the difference $\Delta\delta^{\text{BA}}$ to sign reversal with rise in u is confirmed. According to the results of the calculations, sign reversal should be observed at $u = u_{\text{cr}} = 0.3845$ for the case when $a = 8.30 \text{ \AA}$. (8 refs.)

114762 Determination of residual austenite by Mossbauer spectrometry. A.Ikhlef, T.Vieira, R.Vilar, G.Cizeron (Lab. de Structure des Matériaux Metalliques, Univ. Paris Sud, Orsay, France).

Mem. & Etud. Sci. Rev. Metall. (France), vol.80, no.7-8, p.377-84 (July-Aug. 1983). In French.

The results obtained by sigma measurement, X-ray diffraction and Mossbauer spectrometry on a spheroidal-graphite cast iron and a high-speed steel show that Mossbauer spectrometry gives a more realistic estimate of the residual austenite content compared with the other methods. (11 refs.)

114763 Mossbauer spectroscopic studies of surface magnetism. T.Shinjo (Inst. for Chem. Res., Kyoto Univ., Uji, Japan).

Oyo Buturi (Japan), vol.52, no.4, p.298-304 (April 1983). In Japanese.

Describes how Mossbauer spectroscopy can be used as a means of studying surface magnetism of ferromagnetic metal, and, especially, shows that a ^{56}Fe layer on which very thin ^{57}Fe is deposited as a probe can serve as a significantly effective specimen for surface magnetism studies. The topical areas include: (1) Mossbauer spectroscopy using inner transition electrons; (2) that using ^{57}Co radiation source nucleus; (3) that using ^{57}Fe absorber; and (4) experimental results for the surface magnetism of an oxide. (56 refs.) K.B.

114764 Comment on 'Mossbauer studies of the 6.2 keV γ -rays of ^{181}Ta in Ta-dichalcogenides'. T.Butz (Phys.-Dept., Tech. Univ. Munchen, Garching, Germany), A.Lerf.

Phys. Lett. A (Netherlands), vol.97A, no.5, p.217-18 (29 Aug. 1983).

For original paper see Eibschutz et al., *ibid.*, vol.93A, p.259 (1983). The reported discrepancy between TDPAC and Mossbauer measurements of the electric field gradient at Ta in 2H-TaS_2 is shown to be an artifact. Combining both results a new value for the 482 keV state quadrupole moment of ^{181}Ta is derived: $Q(5/2) = (+)2.36(5) \text{ b}$. (6 refs.)

114765 Mossbauer study of electrodeposited iron-nickel alloys. J.Jaen (Dept. of Phys. Chem. & Radiology, L. Eotvos Univ., Budapest, Hungary), A.Pashovsky, G.Raichevsky, I.Czako-Nagy, L.Kiss, A.Vertes.

Radiochem. & Radioanal. Lett. (Switzerland), vol.58, no.2, p.111-16 (19 Aug. 1983).

Mossbauer measurements on electrodeposited and cast iron-nickel alloys were carried out in absorption geometry. The average magnetic field of the electrodeposited alloys varies linearly with the nickel concentration in the studied concentration range (59.8-100% Ni) and is somewhat smaller than those of cast alloys of the same concentration. (7 refs.)

114766 Mossbauer spectroscopy on ^{133}Cs as a method to study vacancy migration in metals. E.Verbiest, H.Patyn (Inst. voor Kern-en Stralingsfysika, Univ. of Leuven, Leuven, Belgium).

Point Defects and Defect Interactions in Metals. Proceedings of the Yamada Conference V, Kyoto, Japan, 16-20 Nov. 1981 (Amsterdam, Netherlands: North-Holland 1982), p.485-8

^{133}Cs Mossbauer spectra show which fractions of implanted ^{133}Xe atoms have trapped a certain number of vacancies. Changes of these fractions at certain annealing temperatures are due to migrating defects. This method to study damage recovery, and especially vacancy migration, is illustrated on Mo and Pt. (2 refs.)

114767 Correlated radiation damage induced by heavy ion recoil in cadmium and zinc. S.Hoth, W.Engel, R.Keitel, R.Seelboeck, W.Witthuhn (Phys. Inst., Univ. Erlangen-Nurnberg, Erlangen, Germany).

Point Defects and Defect Interactions in Metals. Proceedings of the Yamada Conference V, Kyoto, Japan, 16-20 Nov. 1981 (Amsterdam, Netherlands: North-Holland 1982), p.815-17

The recoil-induced defect cascades produced after nuclear reactions have been investigated in the systems GeZn and SnCd with the PAD method. The temperature dependence of the fraction of probe nuclei located at unperturbed lattice sites can be explained in terms of trapping and detrapping of defects. The trapped defects are shown to be clusters whose constituents migrate with an activation energy of 0.18(3) eV in Zn and Cd. The impurity-defect complexes dissociate with activation energies of 0.65(4) and 0.75(3) eV in Zn and 0.70(3) eV in Cd. (3 refs.)

Advances in Mossbauer spectroscopy. Applications to physics, chemistry and biology See Entry 111334

A simple experimental technique for very small Mossbauer line shifts using resonance detectors See Entry 111832

Crystal structure and Mossbauer spectrum of vonsenite, 2FeO.FeBO_3 See Entry 113806

Defects in copper studied by PAC between 10K and 800K See Entry 113871

Investigating the distribution of impurity iron atoms in the compounds Ni_3Al , NiAl and Ni_2Al_3 See Entry 113951

Mossbauer study of defect trapping at ^{57}Co in cold worked aluminium See Entry 113959

PAC study of defect trapping at ^{111}In in cold worked aluminium See Entry 113960

A new doping technique for the PAC probes ^{100}Pd and ^{111}In and its application to the study of point defects in BCC metals See Entry 113961

Trapping of interstitials at ^{100}Pd , ^{111}In , and ^{181}Hf -impurities in irradiated cubic metals See Entry 113963

Dose dependence of interstitial trapping at ^{111}In impurities in e^- -irradiated aluminium See Entry 113964

Interactions of defects with Co implanted into Al at 4.2K See Entry 113965

Mossbauer study on Fe-vacancy interaction in aluminium See Entry 113971

Mossbauer analysis on the annealing process of a quenched Al-Sn dilute alloy See Entry 113973

Recovery in electron irradiated aluminium observed by Mossbauer spectroscopy See Entry 113974

Interaction of implanted impurities with extended defect configurations in tungsten single crystal See Entry 113976

Radiation damage in tantalum observed by PAC See Entry 114055

Mossbauer and X-ray structure studies on the phase transition in the Fe(III) dimethylsulfoxide complex See Entry 114160

Metastable phase separation in Au-Fe alloys See Entry 114184

Vacancies in zinc and cadmium produced by proton- and electron-irradiation .. See Entry 114247

Vibrational state and jump frequency of Mossbauer impurity associated with a vacancy in metals See Entry 114273

Interference of the sign of electric field gradient QS-IS correlation in iron compounds See Entry 114505

Magnetic properties and the magnetic phase diagram of the $\text{Cr}_{1-x}\text{Ni}_x\text{S}$ system See Entry 114688

Optical and Mossbauer spectra of manganese-bearing phlogopites: $\text{Fe}_{\text{VI}}^{3+}\text{-Mn}_{\text{VI}}^{2+}$ pair absorption as the origin of reverse pleochroism See Entry 114823

76.90 OTHER TOPICS IN MAGNETIC RESONANCES AND RELAXATION

(inc. muon probe studies)

114768 Muon spin relaxation analysis by trapping model with detrapping. T.Hatano, Y.Suzuki, T.Natsui, M.Doyama (Dept. of Metall. & Materials Sci., Univ. of Tokyo, Tokyo, Japan), Y.J.Uemura, T.Yamazaki, J.H.Brewer.

Point Defects and Defect Interactions in Metals. Proceedings of the Yamada Conference V, Kyoto, Japan, 16-20 Nov. 1981 (Amsterdam, Netherlands: North-Holland 1982), p.274-7

A muon (μ^+) is an unstable particle which has a lifetime of 2.2 μsec . A positron, e^+ , a positive muon, μ^+ and a proton, p^+ are isotopes which have electric charge $+e$ and spin 1/2, and rest masses are $1m_e$, $207m_e$ and $1876m_e$, respectively. A positive muon is emitted from a decayed π^+ meson and the spin direction of the muon is anti-parallel to its momentum direction. Since muon spins are polarized and the muon has quite a large magnetic

moment, they are used as micron magnetic probes for magnetic materials. Furthermore, from the analogy of positron study, muons can be used as non-linear micros prove to lattice defects which trap muons. The muon spin relaxation function including trapping and strapping is discussed. (7 refs.)

77.00 DIELECTRIC PROPERTIES AND MATERIALS

(for conductivity phenomena, see 72.20 and 72.80)

77.20 PERMITTIVITY

114769 On the dielectric theory and computer simulation of water. O.Steinhauser (Inst. fur Theoretische Chem. & Strahlenchem., Univ. Wien, Wien, Austria).

Chem. Phys. (Netherlands), vol.79, no.3, p.465-82 (15 Sept. 1983).

The static dielectric properties of ST2 water are carefully examined by means of a computer-adapted Kirkwood theory. 'Experimental' data are provided by various molecular dynamics simulations involving 216, 500 and 1000 water molecules and corresponding to a variety of boundary conditions. It is shown that the integral of the respective modified T tensor plays the central role in matching different boundary conditions. Thus a unique dielectric constant $\epsilon=82\pm15$ is obtained for a density $\rho=1$ g/cm³ and a temperature $T=120^\circ\text{C}$. Furthermore, it is found that the constitutive relation $\mathbf{P}=[(\epsilon-1)/4\pi]\mathbf{E}$ is already fulfilled in a sample of a few hundred molecules. Finally, R-dependent Kirkwood g factors are discussed, which give a vivid picture, how different boundary conditions influence orientational correlations between water dipoles. (23 refs.)

114770 Effect of Mn doping on the dielectric properties of Ba₂Ti₉O₂₀ ceramics at microwave frequency. S.Nomura, K.Tomaya, K.Kaneta (Dept. of Phys. Electronics, Tokyo Inst. of Technol., Tokyo, Japan).

Jpn. J. Appl. Phys. Part 1 (Japan), vol.22, no.7, p.1125-8 (July 1983).

The effect of Mn doping on the dielectric properties of Ba₂Ti₉O₂₀ ceramics has been investigated at microwave frequency. The dielectric constant and the temperature coefficient are not sensitive to the addition of Mn, while the unloaded Q depends strongly upon it as well as on heat treatment at high temperature. A minute addition of Mn leads to an increase in the Q value. A high value of Q of more than 5200 was obtained at 9 GHz with the addition of 0.5~1.0 mol.% Mn. (9 refs.)

114771 Anisotropy of electric properties in binary cholesteric mixtures. M.Honciuc, C.Motoc, O.Savin (Dept. of Phys., Polytech. Inst., Bucharest, Rumania).

Mol. Cryst. & Liq. Cryst. (GB), vol.95, no.3-4, p.339-50 (1983).

Dielectric permittivity and electric conductivity anisotropies were determined for cholesterol laurate, cholesterol caprilate as well as for their mixtures 25:75%, 50:50% and 75:25% (by weight). Connection between anisotropies of pure substances and their mixtures were found. The mixtures 75:25% and 25:75% have positive conductivities anisotropies within the cholesteric range as for the initial esters; the sign of the dielectric anisotropy is the same as for the prevailing ester. Within the smectic range the dielectric anisotropy is opposite for both mixtures and pure compounds, in accordance to Carr's (1969) hypothesis with reference to the conduction mechanism in smectics. The phase transitions are revealed in most cases by maxima or minima of the dielectric anisotropies. (15 refs.)

114772 Dielectric properties of Ag₃AsS₃ in the region of high ionic conductivity. V.B.Zlokazov, A.N.Babushkin, L.Ya.Kobelev (A.M. Gorki Ural State Univ., Sverdlovsk, USSR).

Sov. Phys.-Solid State (USA), vol.25, no.2, p.324-5 (Feb. 1983). Translation of: *Fiz. Tverd. Tela (USSR)*, vol.25, no.2, p.573-4 (Feb. 1983). [received: Sept. 1983]

Because of the partial dissociation of proustite in a vacuum and in air at 430-470K, it is advisable to investigate its physical properties at high temperatures in a closed system to ensure that the material is in equilibrium with the vapor phase. In order to produce such conditions, the proustite was remelted in an evacuated pyrex ampule with three platinum wire electrodes soldered into the walls. The electrical properties of a polycrystalline proustite specimen were investigated at a frequency of 1592 Hz using an accurate VM484 semiautomatic bridge. Values of the capacitance, electric loss tangent and permittivity were calculated from the volume impedance values. (6 refs.)

114773 Admissible values of permittivity and magnetic permeability of matter. O.V.Dolgov, D.A.Kirzhnits, V.V.Losyakov (P.N. Lebedev Phys. Inst., Acad. of Sci., Moscow, USSR).

Sov. Phys.-JETP (USA), vol.83, no.5, p.1095-102 (Nov. 1982). Translation of: *Zh. Eksp. & Teor. Fiz. (USSR)*, vol.83, no.5, p.1894-907 (Nov. 1982). [received: Sept. 1983]

Results are presented of a systematic investigation of an equilibrium homogeneous and isotropic medium from the viewpoint of its causal properties (the Kramers-Kronig and Leontovich relations) and of its stability to electro-magnetic perturbations. The ranges of permissible values of the permittivity and the magnetic permeability of matter are then found in the static limit and over the entire range of variation of the wave vector. It is shown that the magnetic permeability, unlike the permittivity, cannot be negative; that the lower limit of the magnetic permeability (which coincides with the magnetic permeability of a London superconductor) increases with increasing wave vector and approaches unity, that no order parameter H (magnetic field) can be produced via a phase transition from the state of a stable homogeneous and isotropic medium, and that in this sense no media with spontaneous homogeneous electric field can exist. (16 refs.)

The study of damage profile of ion implanted layer on Si by spectroscopic ellipsometrySee Entry 113946

Measurements of densities and dielectric constants of liquid normal butane from 140 to 300K at pressures to 35 MPaSee Entry 114065

Phase equilibria in Ln₂V₂O₇-Ln₂Ti₂O₇ systems (Ln=Er, Lu)See Entry 114127

Some peculiarities in the spectral characteristics of metal/insulator/metal structures at constant biasesSee Entry 114623

On magneto-photo-electret of sulphur and time-variation of its dielectric constantSee Entry 114774

Studies of Kirkwood-Frohlich's correlation factor and dielectric relaxation in triethylamine-solutionsSee Entry 114776

Effect of the internal bias field on the dielectric characteristics of strontium titanate single crystalsSee Entry 114777

Dielectric relaxation and modulus of V₂O₅-TeO₂ glassesSee Entry 114779

The dielectric properties of lead germanate single crystals having an initial domain structureSee Entry 114780

The dielectric properties of some PbO-based amorphous films prepared by twin-roller methodSee Entry 114784

The effect of dye sorption on electromechanical properties in sodium poly(L-glutamate)See Entry 114788

Birefringence and ferroelectric properties of [Rb_{0.4}(NH₄)_{0.6}]₂SO₄See Entry 114796

Non destructive optical analysis of implanted layers in GaAs by Raman scattering and spectroscopic ellipsometrySee Entry 114871

Optical anisotropy and electrostriction in the anodic oxide of tantalumSee Entry 114941

Plasma enhanced metal-organic chemical vapor deposition of aluminum oxide dielectric film for device applicationsSee Entry 115063

77.30 POLARIZATION AND DEPOLARIZATION EFFECTS

114774 On magneto-photo-electret of sulphur and time-variation of its dielectric constant. A.K.Chatterjee, S.D.Chatterjee (Dept. of Phys., Jadavpur Univ., Calcutta, India).

Indian J. Phys. Part A, vol.57A, no.3, p.208-10 (May 1983).

Nadzhakov (1937) discovered during a study of photo-conduction of polycrystalline sulphur that space charges accumulated in the dielectric, which were retained for a long time after the illumination ceased and the applied electric field removed. An analogous effect has been observed when a thin double-plated and perforated trimmer condenser impregnated with polycrystalline sulphur is illuminated with an incandescent lamp while placed in a magnetic field at room temperature. The induced polarization and subsequent depolarization of the specimen were verified by the measurements of its dielectric constant. (5 refs.)

114775 Polarization character in small ferroelectric particles and the monodomain state conditions. B.N.Rolov, Yu.E.Lorents.

Latv. PSR Zinat. Akad. Vestis Fiz. Teh. Zinat. Ser. (USSR), no.4, p.28-32 (1983). In Russian.

The thermodynamic theory for spontaneous polarization in small ferroelectric particles is carried out. The corresponding model and energy balance for a small ferroelectric particle is considered. An analysis for a monodomain state is carried out and the conditions for this state are obtained. (9 refs.)

114776 Studies of Kirkwood-Frohlich's correlation factor and dielectric relaxation in triethylamine-solutions. S.C.Srivastava (Dept. of Phys., Allahabad Univ., Allahabad, India), R.Sabesan, R.Varadarajan, M.Sargurumoorthy.

Proc. Natl. Acad. Sci. India Sect. A, vol.52, pt.2, p.219-24 (1982). [received: Aug. 1983]

The linear correlation factor of dielectric polarization 'g' is calculated from the Kirkwood-Frohlich relation by measuring the refractive indices for the D-line and the dielectric constants at 300 kHz for pure triethylamine and in dilution with non-interacting solvents. The dielectric relaxation times at the X-band microwave frequency are also measured. The data are obtained in terms of the distribution parameter and the relaxation time of the complexed species in relation to the state of aggregation of the amine. (14 refs.)

114777 Effect of the internal bias field on the dielectric characteristics of strontium titanate single crystals. A.I.Dedyk, N.N.Lebedeva, G.D.Loos (V.I. Ul'yanov Electrotech. Inst., Leningrad, USSR).

Sov. Phys.-Solid State (USA), vol.25, no.2, p.316-17 (Feb. 1983). Translation of: *Fiz. Tverd. Tela (USSR)*, vol.25, no.2, p.559-61 (Feb. 1983). [received: Sept. 1983]

Investigates the nature of the residual polarization and also its effect on the dielectric characteristics of SrTiO₃:e (E), tan δ (E), where E is the external electric bias field. The investigations were carried out on single crystals grown by the Verneuil method, with an impurity concentration (% by weight): Fe=0.005; Cr, Co, Ni, Al, Ng, Ca, Ba—about 0.01; and Mn, Pb—less than 0.0001. All the dielectric measurements were made at a frequency of 1 kHz at 4.2K. (2 refs.)

Electrostatic fields in an ionization chamber electretSee Entry 112895

Solid solutions based on lead barium metaniobateSee Entry 114785

Birefringence and ferroelectric properties of [Rb_{0.4}(NH₄)_{0.6}]₂SO₄See Entry 114796

Free energy of a tetragonal ferroelectric in the region of strong critical fluctuationsSee Entry 114797

77.40 DIELECTRIC LOSS AND RELAXATION

114778 Dipole-phonon coupling and dielectric relaxation. R.Nigmatullin, L.A.Dissado (Chelsea Coll., Univ. of London, London, England).

Chem. Phys. (Netherlands), vol.79, no.3, p.455-63 (15 Sept. 1983).

Equations of motion for the average polarisation are derived from a microscopic approach by use of the local density matrix. A specific form of the dipole-phonon coupling in the memory kernel is investigated and the necessary conditions for the generation of a non-Debye form of response examined. It is shown that these conditions can only be fulfilled by allowing for dipole-induced distortion with the lifetime of the 'photons' determined by the lifetime of the dipole correlation. (24 refs.)

114779 Dielectric relaxation and modulus of V₂O₅-TeO₂ glasses. A.Mansingh, V.K.Dhawan (Dept. of Phys. & Astrophys., Univ. of Delhi, Delhi, India), M.Sayer.

Philos. Mag. B (GB), vol.48, no.3, p.215-36 (Sept. 1983).

The dielectric behaviour of V₂O₅-TeO₂ glasses in the composition region 10 to 80 mol.% V₂O₅ is reported for the temperature region 77 to 500K and the frequency region 0.1 to 100 kHz. The variation of dielectric constant ε' with temperature and frequency in the region where the measured AC conductivity approaches the DC conductivity indicates a bulk dielectric relaxation with a distribution of dielectric relaxation times and in terms of conductivity relaxation using dielectric modulus M* = 1/ε* plots. The d.c. conductivity, dielectric relaxation and conductivity relaxation have the same activation energy of 0.21-0.42 eV for decreasing V₂O₅ content and a frequency factor ν₀ of 5×10¹⁰ Hz. The difference between this value and the 10¹² Hz expected for phonon frequencies is attributed to a tunnelling contribution. The dielectric modulus approach is satisfactory for electronic glasses with respect to the calculation of ε₀ and σ₀, but provides less reliable information on the dielectric relaxation time distribution than would a dielectric analysis. The glass former TeO₂ gives rise to unusually large values for ε₀=40-69 and ε_∞=18-31, and a narrower distribution of relaxation times than the analogous phosphate glasses. The total a.c. conductivity can be clearly separated into three com-

ponents; d.c. conductivity, a dipolar contribution and hopping conduction at low temperatures. (34 refs.)

114780 The dielectric properties of lead germanate single crystals having an initial domain structure. V.Ya.Shur, Yu.A.Popov, A.L.Subbotin (A.M. Gorki Ural State Univ., Sverdlovsk, USSR). *Sov. Phys.-Solid State (USA)*, vol.25, no.2, p.318-19 (Feb. 1983). Translation of: *Fiz. Tverd. Tela (USSR)*, vol.25, no.2, p.564-5 (Feb. 1983). [received: Sept. 1983]

The authors have measured the capacitance and $\tan \delta$ of single-crystal plates of lead germanate having transition domain structures that had different fractions of free domain structures. The fraction of the free domain structure was defined as the ratio of the reversible charges in the transition domain structure and the free domain structure (P/P_{∞}). The specimens were plane-parallel plates 1.2 mm. The value of the reversible charge was found from measurements of the dielectric hysteresis loop at a frequency of 50 Hz. (4 refs.)

Dielectric properties of Ag_3AsS_3 in the region of high ionic conductivity See Entry 114772

Studies of Kirkwood-Frohlich's correlation factor and dielectric relaxation in triethylamine-solutions See Entry 114776

Effect of the internal bias field on the dielectric characteristics of strontium titanate single crystals See Entry 114777

Leakage and breakdown in thin oxide capacitors correlation with decorated stacking faults See Entry 114783

The dielectric properties of some PbO-based amorphous films prepared by twin-roller method See Entry 114784

Ultraviolet A-band absorption in NaCl:Pb^{2+} and clustering of lattice defects See Entry 114887

77.50 DIELECTRIC BREAKDOWN AND SPACE-CHARGE EFFECTS

114781 How electric strength of polyethylene and polystyrene is influenced by residual phenomena caused by ionising radiation and pressure. S.N.Kolesov, I.S.Kolesov.

Elektrichestvo (USSR), no.5, p.72-3 (May 1982). In Russian. Establishes correlation of relationships in variation of super-molecular structure, density and electric strength of industrial specimens subjected to doses of neutron and gamma radiation at various pressures. Heat-treatment reduces the number of micropores and cracks. Polymer residual deformation increases with increase of specific pressure. (7 refs.)

114782 High voltage electric field and space-charge distributions in highly purified water. M.Zahn, T.Takada (High Voltage Res. Lab., MIT, Cambridge, MA, USA).

J. Appl. Phys. (USA), vol.54, no.9, p.4762-75 (Sept. 1983). High voltage Kerr electrooptic field mapping measurements in highly purified water show significant field distortions due to injected positive space charge over the temperature range of 8-25°C using parallel plane stainless steel electrodes stressed to average field strengths up to 150 kV/cm. The net space charge was always positive with density of $\approx 2 \text{ C/m}^3$ which is about 40% of the background value of charge density of thermally generated hydronium and hydroxyl ions. Because measurements only showed a net positive space charge, a unipolar drift dominated conduction model was developed where positive charge would migrate in an ohmic medium. This model predicts the observed propagating charge front, electric field enhancement at the non-charge injecting electrode, and field decrease at the charge injecting electrode. The time of flight of positive charge between electrodes gave an estimate of the positive ion mobility of $\mu \approx 4 \times 10^{-7} \text{ m}^2/(\text{V s})$ which is in between the values of the hydronium ion mobility measured at low voltages and the electrohydrodynamic mobility which accounts for field convection effects due to the Coulombic force putting the fluid into motion. The dielectric relaxation time at $T \approx 8^\circ\text{C}$ ($\tau \approx 320 \text{ } \mu\text{s}$) measured at low voltage was much less than the measured charge transport time between electrodes, $\tau_{\text{mig}} \approx 2 \text{ msec}$, so that the calculated effects of space charge were much less than measured because the charge relaxes quickly as it migrates. It was found that a dielectric relaxation time of $\tau \approx 1.6 \text{ msec}$ would provide a good fit between analysis and experiments. (14 refs.)

114783 Leakage and breakdown in thin oxide capacitors correlation with decorated stacking faults. P.S.D.Lin, R.B.Marcus, T.T.Sheng (Bell Labs., Murray Hill, NJ, USA).

J. Electrochem. Soc. (USA), vol.130, no.9, p.1878-83 (Sept. 1983). Thin oxide MOS capacitors which exhibited high leakage and lowered breakdown strength were studied by a number of methods in order to identify the mechanism responsible for the degradation. Electron beam-induced current (EBIC) studies, Secco etching, transmission electron microscope imaging, and energy dispersive X-ray spectroscopy were all applied to this problem. The results indicated that the defects responsible for the poor dielectric properties are impurity (Cu, Ni, Fe, Zn, Sn)-decorated stacking faults about 1 μ in length, located in silicon near the silicon-silicon dioxide interface. This study establishes that decorated stacking faults degrade the quality of MOS capacitors by increasing capacitor leakage and decreasing breakdown strength. (11 refs.)

Resonant amplification of sound near the spontaneous oscillation threshold of semiconductors under impurity and interband breakdown conditions See Entry 114571

Initial (nonintrinsic) breakdown and defects in the dielectrics of MOS structures based on silicon See Entry 114618

Lowering of the breakdown voltage of silicon dioxide by asperities and at spherical electrodes See Entry 114630

On magneto-photo-electret of sulphur and time-variation of its dielectric constant See Entry 114774

Kerr electro-optic field mapping measurements in water using parallel cylindrical electrodes See Entry 114828

Properties of thermal oxides grown on phosphorus in situ doped polysilicon See Entry 115383

77.55 DIELECTRIC THIN FILMS

114784 The dielectric properties of some PbO-based amorphous films prepared by twin-roller method. H.Nasu, M.Yoshimoto, R.Ota, N.Soga (Dept. of Industrial Chem., Kyoto Univ., Kyoto-shi, Japan).

Yogyo-Kyokai-Shi (Japan), vol.91, no.6, p.303-5 (1983). In Japanese. The glass-forming regions have been determined by a twin-roller method for some PbO-based binary systems which contain no glass-forming oxide SiO_2 or B_2O_3 . The dielectric constant ϵ_s and the dielectric loss $\tan \delta$ were measured at

room temperature in the frequency range 20 Hz \sim 5 MHz for the amorphous films of 80 PbO-20 M_2O_y composition where $\text{M}_2\text{O}_y = \text{Li}_2\text{O}$, CaO, TiO_2 and V_2O_5 . The compositional variations of ϵ_s and $\tan \delta$ were interpreted to be due to be due to the cationic field strength z/r of the additive cations except for the PbO- TiO_2 system, where $\alpha\text{-PbTiO}_3$ -like units of extraordinary high ϵ_s may be formed in the glassy state. (10 refs.)

Domain structure of heteroepitaxial ferroelectric $\text{Ba}_{0.8}\text{Sr}_{0.2}\text{TiO}_3$ films produced by RF cathode sputtering See Entry 114800

Optical anisotropy and electrostriction in the anodic oxide of tantalum See Entry 114941

Plasma enhanced metal-organic chemical vapor deposition of aluminum oxide dielectric film for device applications See Entry 115063

77.60 PIEZOELECTRICITY AND ELECTROSTRICTION

(for piezo-optical effects, see 78.20H)

114785 Solid solutions based on lead barium metaniobate. S.A.Gridnev, N.V.Barmina, N.G.Pavlova, N.N.Parfenova, E.P.Smironova (Voronezh Polytech. Inst., Voronezh, USSR). *Inorg. Mater. (USA)*, vol.18, no.10, p.1399-402 (Oct. 1982). Translation of: *Izv. Akad. Nauk SSSR Neorg. Mater.*, vol.18, no.10, p.1632-5 (Oct. 1982). [received: Sept. 1983]

Solid solutions with the compositions $(1-x-y-z)\text{PbNb}_2\text{O}_6 + x\text{BaNb}_2\text{O}_6 + y\text{Pb}_2\text{Ti}_2\text{O}_6 + z\text{Na}_2\text{Nb}_2\text{O}_6$ with high Curie temperatures (470-600°C) were obtained. Conditions of polarization were worked out, and materials with high values of the piezomodulus $d_{33} = (40-50) \times 10^{-12} \text{ C/N}$ and $d_{31} = 5.3 \times 10^{-12} \text{ C/N}$ were obtained. The investigated system is characterized by a high temperature stability (up to 300°C) of the piezoelectric properties and elastic pliability. The introduction of barium and sodium metaniobates and lead titanate into the ceramic lead metaniobate permits the production of piezomaterials both with high ($Q_m = 300-350$) and with low ($Q_m = 20$) mechanical quality factors. (7 refs.)

114786 Nonlinear electroacoustic equations for piezoelectric powders. J.Pouget, G.A.Maugin (Lab. de Mecanique Theorique, Univ. Pierre-et-Marie-Curie, Paris, France).

J. Acoust. Soc. Am. (USA), vol.74, no.3, p.925-40 (Sept. 1983). A nonlinear theory based on the notion of oriented continuum is presented with a view to describing piezoelectric powders. The generalized kinematics comprehends the macroscopic motion of grains as well as the internal deformation (rotation, stretch) of grains (via a so-called director field) in connection with local electromechanical interactions. A complete set of coupled dynamical electroacoustic equations is deduced from first principles for this class of granular media. Thermodynamical arguments then allow one to construct general constitutive equations that exhibit both thermodynamically reversible and irreversible processes. Of necessity, the theory is first constructed in a fully nonlinear framework. In a second stage, the nonlinear equations are perturbed, by means of a Lagrangian variation, about a free finite initial state in which the directors are randomly oriented. These initial privileged directions provoke a local breaking of the ideal symmetry of the material and there results a nonhomogeneous medium. In addition, in the perturbed equations thus obtained, nonlinear terms related to ponderomotive couples and orientational electromechanical couplings are involved. Among the equations obtained, one governs the internal deformation of grains, which materialize in a microgyration of grains about their center of mass and a microstretch in the direction along which the local electromechanical interactions take place. This work collects all the essential ingredients which are required in a study of physically interesting phenomena such as memory echoes in resonant piezoelectric powders. (40 refs.)

114787 Continuum approach to electroacoustic echoes in piezoelectric powders. J.Pouget, G.A.Maugin (Lab. de Mecanique Theorique, Univ. Pierre et Marie Curie, Paris, France).

J. Acoust. Soc. Am. (USA), vol.74, no.3, p.941-54 (Sept. 1983). Based on an oriented continuum model, a continuum approach for powders made of piezoelectric grains proposed in a previous work is applied to the study of electroacoustic echoes in resonant piezoelectric powders. The nonlinear equations obtained through this approach govern the piezoelectric oscillations and microgyration motion of each grain, as well as the global behavior of the powder and lead to the echo formation. The evaluations of the dynamical echo at 2τ and the memory echo at $T+\tau$ are presented. A memory phenomenon lying in the reorientation of grains due to a ponderomotive couple inside the powder sample is placed in evidence. The global response of the sample consists in summing up all the elementary electric polarizations associated with the piezoelectric oscillations of grains. Then the echoes are caused not only by the nonlinear interaction effects between the deformation of grains and the electric field, but also by a refocalization of collective oscillations which, after a complete dephasing period, gives a coherent signal through the inversion of the phase evolution. This continuum approach presents definite advantages over previous ones. Typical numerical values of parameters involved in this phenomenon as well as physical interpretations are given. (49 refs.)

114788 The effect of dye sorption on electromechanical properties in sodium poly(L-glutamate). Y.Ando, N.Kawabata, K.Nishida (Faculty of Technol., Tokyo Univ. of Agriculture & Technol., Tokyo, Japan).

J. Polym. Sci. Polym. Phys. Ed. (USA), vol.21, no.9, p.1661-5 (Sept. 1983). Piezoelectric constant, Young's elastic modulus, and dielectric constant of undyed and dyed films of poly(L-glutamate) were measured at 10 Hz over the temperature range -120 to 120°C . The temperature of the maximum in $-d'_{14}$ shifts toward higher temperature up to 0.6 mg/g polymer of dye uptake and then shifts toward lower temperature by further dye sorption. The variation of the piezoelectric modulus was interpreted by the change of mobility of impurity ions in the sample. (7 refs.)

114789 Polar glass ceramics—a new family of electroceramic materials: tailoring the piezoelectric and pyroelectric properties. A.Halliyal, A.S.Bhalla, R.E.Newnham (Materials Res. Lab., Pennsylvania State Univ., University Park, PA, USA).

Mater. Res. Bull. (USA), vol.18, no.8, p.1007-19 (Aug. 1983). Grain oriented multicomponent polar glass-ceramics have been prepared by crystallizing the glasses in a temperature gradient. Inexpensive, large area piezoelectric and pyroelectric devices can be fabricated by this method, and by adjusting the composition of the glasses and crystallization conditions, it is possible to tailor the properties to meet device requirements. Based on the growth characteristics and the connectivity pattern of the crystallites, the piezoelectric, pyroelectric and dielectric properties of glass-ceramic composites can be predicted. Two examples discussed in this paper are piezoelectric glass-ceramics which are not pyroelectric, and pyroelectric glass-ceramics which are not piezoelectric. (22 refs.)

114790 On a peculiarity of the piezoeffect in carbonate-cancrinite crystals. I.B.Kobyakov, A.A.Levin, Yu.I.Smolin (Inst. of General & Inorganic Chem., Acad. of Sci., USSR). *Sov. Phys.-JETP (USA)*, vol.83, no.5, p.1112-15 (Nov. 1982). Translation of: *Zh. Eksp. & Teor. Fiz. (USSR)*, vol.83, no.5, p.1924-9 (Nov. 1982). [received: Sept. 1983]
In the course of an X-ray study of the structure of carbonate-cancrinite in an electric field, an anomalously large deformation of the CO₃ ion, located in channels and tightly coupled to the aluminosilico-oxygen framework was observed. A model of the action of the channels on such a lattice characteristic of the piezoeffect has been developed for zeolites. The theoretical value of the piezomodulus $d_{33}=28.3\times10^{-12}$ C/N and the experimental value $d_{15}=-16.5\times10^{-12}$ C/N of carbon cancrinite were found to be higher than the piezomoduli of the strongest linear piezoelectric substances known at present. (12 refs.)

Torsional oscillations of a finite inhomogeneous piezoelectric cylindrical shell See Entry 113343

Polyvinylidene fluoride (PVDF) See Entry 113770

Optical anisotropy and electrostriction in the anodic oxide of tantalum See Entry 114941

Physicochemical aspects of production of ferroelectric ceramics See Entry 115148

Mechanical and electromechanical behaviour of fibre brushes See Entry 115372

77.70 PYROELECTRIC AND ELECTROCALORIC EFFECTS

Advantages of obliquely cut pyroelectric crystals for infrared detectors See Entry 111769

Polyvinylidene fluoride (PVDF) See Entry 113770

Polar glass ceramics—a new family of electroceramic materials: tailoring the piezoelectric and pyroelectric properties See Entry 114789

Ferroelectric and pyroelectric organic materials See Entry 114791

77.80 FERROELECTRICITY AND ANTIFERROELECTRICITY

114791 Ferroelectric and pyroelectric organic materials. V.V.Gagulin, B.A.Chayanov (Sci.-Res. Inst. of Organic Intermediates & Dyestuffs, USSR). *Inorg. Mater. (USA)*, vol.18, no.10, p.1430-4 (Oct. 1982). Translation of: *Izv. Akad. Nauk SSSR Neorg. Mater.*, vol.18, no.10, p.1667-71 (Oct. 1982). [received: Sept. 1983]
The authors have considered and systematized data published in the literature on organic and molecular crystals, liquid crystals, and polymers possessing ferroelectric properties as well as a number of organic materials (asymmetric) which possess pyroelectric properties. (50 refs.)

114792 Ferroelectric fluctuations in KDP and DKDP. R.A.Cowley, H.-J.Bleif, S.R.Andrews, R.J.Nelmes (Dept. of Phys., Univ. of Edinburgh, Edinburgh, Scotland). *Physica B & C (Netherlands)*, vol.120B+C, no.1-3, p.267-9 (May 1983). (Yamada Conference VI on Neutron Scattering in Condensed Matter, Hakone, Japan, 1-4 Sept. 1982).
X-ray scattering measurements have been made of the ferroelectric critical scattering from KDP and DKDP. The results show that the wavevector dependence of the scattering is very similar for KDP and DKDP and is consistent with earlier neutron scattering measurements for DKDP. The atomic displacements in the ferroelectric fluctuations have been determined and it is necessary to take account of the coupling between the ferroelectric fluctuations and a transverse acoustic normal mode. When this is done the atomic motions are found to be consistent with those deduced from recent high-resolution structural measurements in that the K barely moves and the P moves considerably more in DKDP than in KDP. (7 refs.)

Optical second harmonic generation in LiNbO₃ crystals induced by a photovoltaic grating See Entry 113055

Degenerate forward four-wave mixing in LiNbO₃ See Entry 113062

Ferroelectric liquid crystals and their applications See Entry 113732

Crystal-chemical principles of prediction of ferroelectrics and related materials in the case of compounds with $\{[M_2(EO_4)_3]^{P-}\}_{3\infty}$ frameworks See Entry 113820

Hyper-Raman spectra and frequency dependence of soft mode damping in SrTiO₃ See Entry 114118

Incommensurate lattice instability in $[N(CD_3)_4]_2ZnCl_4$ See Entry 114120

Propagation of high-intensity surface acoustic waves in lithium niobate See Entry 114326

The controllable variband structures in a ferroelectric semiconductor See Entry 114432

Photoelasticity of KH₂PO₄, KD₂PO₄, and RbH₂PO₄ See Entry 114824

Optical properties of ferroelectrics with tetragonal potassium-tungsten-bronze in the fundamental absorption region See Entry 114882

Physicochemical aspects of production of ferroelectric ceramics See Entry 115148

77.80B Transitions and Curie point

114793 Study of the ferroelectric phase transition in rubidium hydrogen selenate by high-resolution NMR of ⁷⁷Se. O.V.Rozanov, Yu.N.Moskvich, A.A.Sukhovskii (L.V. Kirenski Inst. of Phys., Acad. of Sci., Krasnoyarsk, USSR). *Sov. Phys.-Solid State (USA)*, vol.25, no.2, p.212-14 (Feb. 1983). Translation of: *Fiz. Tverd. Tela (USSR)*, vol.25, no.2, p.376-80 (Feb. 1983). [received: Sept. 1983]
High-resolution NMR spectra of the rare nuclei ⁷⁷Se were measured in the paraelectric and ferroelectric phases of the rubidium hydrogen selenate crystal. Analysis of the resulting parameters of the magnetic shielding tensors for the selenium nuclei, including the directions of the tensor principal axes, showed that the ferroelectric phase transition in this crystal is due to the ordering of hydrogen on only one of the two types of hydrogen bonds. (17 refs.)

114794 Curie-Weiss law for improper ferroelectric or ferroelastic phase transitions. D.G.Sannikov (Inst. of Crystallography, Acad. of Sci., Moscow, USSR). *Sov. Phys.-Solid State (USA)*, vol.25, no.2, p.249-50 (Feb. 1983). Translation of: *Fiz. Tverd. Tela (USSR)*, vol.25, no.2, p.441-4 (Feb. 1983). [received: Sept. 1983]
It is shown that if two components of the polarization (deformation) vector and of the order parameter transform under different mutually interacting two-dimensional irreducible representations of the symmetry group of the initial crystal phase, then one of the components of the electric susceptibility (mechanical compliance) tensor obeys the Curie-Weiss law in the polar phase. Certain dynamic properties in the neighborhood of such a two-component improper ferroelectric (ferroelastic) phase transition are analyzed. (6 refs.)

114795 On the relation between the dielectric anomalies and the isofrequency dependences of inelastic scattering of light in lithium tantalate crystals. V.S.Gorelik, B.S.Umarov, M.Umarov (P.V. Lebedev Phys. Inst., Acad. of Sci., Moscow, USSR). *Sov. Phys.-Solid State (USA)*, vol.25, no.2, p.279-83 (Feb. 1983). Translation of: *Fiz. Tverd. Tela (USSR)*, vol.25, no.2, p.495-500 (Feb. 1983). [received: Sept. 1983]
This paper reports investigations of the isofrequency temperature dependences of inelastic scattering of light in lithium tantalate crystals. At low frequencies, Ω , sharp changes are observed to occur in the inelastic scattering intensity near the transition temperature. The experimental data obtained are compared with the results of the simplest variant of the theory of light scattering near a phase transition point in crystals. The temperature coefficient of the relaxation time is computed on the basis of the dependences obtained. It is concluded that it is possible to trace a ferroelectric phase transition on the basis of an analysis of isofrequency inelastic scattering. (10 refs.)

114796 Birefringence and ferroelectric properties of $[Rb_x(NH_4)_{1-x}]_2SO_4$. N.R.Ivanov, V.N.Anisimova, L.A.Shuvalov (A.V. Shubnikov Inst. of Crystallography, Acad. of Sci., Moscow, USSR). *Sov. Phys.-Solid State (USA)*, vol.25, no.2, p.296-9 (Feb. 1983). Translation of: *Fiz. Tverd. Tela (USSR)*, vol.25, no.2, p.525-31 (Feb. 1983). [received: Sept. 1983]
The temperature dependences of the birefringence, permittivity, and spontaneous polarization of $[Rb_x(NH_4)_{1-x}]_2SO_4$ mixed crystals with $x=0.4$ were studied, and their behavior near the ferroelectric second-order phase transition at $T_c=-74.5^\circ C$ was analyzed. The paraelectric phase shows anomalies of the permittivity and the birefringence that are not due to phase transitions. The ferroelectric and electrooptic properties are discussed in terms of a two-sublattice phenomenology model. It is shown that a tricritical transition should occur at atmospheric pressure in the $[Rb_x(NH_4)_{1-x}]_2SO_4$ system when $x=0.22\pm0.03$. (19 refs.)

114797 Free energy of a tetragonal ferroelectric in the region of strong critical fluctuations. A.I.Sokolov (V.I. Ulyanov Inst. of Electrical Engng., Leningrad, USSR). *Sov. Phys.-Solid State (USA)*, vol.25, no.2, p.311-13 (Feb. 1983). Translation of: *Fiz. Tverd. Tela (USSR)*, vol.25, no.2, p.552-6 (Feb. 1983). [received: Sept. 1983]
Critical thermodynamics of an 'easy-plane' tetragonal ferroelectric is studied theoretically. The free energies of the orthorhombic and monoclinic ferroelectric phases are determined as functions of the modulus of the order parameter from the summation of ring diagrams. The equations of binodals and over-heating spinodals and also the discontinuities of the spontaneous polarization on these curves, are determined. (6 refs.)

114798 Incommensurate phase in an external field. D.G.Sannikov (Inst. of Crystallography, Acad. of Sci., Moscow, USSR). *Sov. Phys.-Solid State (USA)*, vol.25, no.2, p.352-3 (Feb. 1983). Translation of: *Fiz. Tverd. Tela (USSR)*, vol.25, no.2, p.616-18 (Feb. 1983). [received: Sept. 1983]
The author shows that a transition between soliton states can be achieved by varying only the temperature in a crystal subjected to an external electric field of appropriate symmetry (and under a mechanical stress). He considers the simplest form of the free energy which describes, in particular, initial-incommensurate-commensurate phase transitions in ferroelectric ammonium fluoroberyllate. (3 refs.)

New spontaneous symmetry breaking for the cubic XY model See Entry 111603

Influence of Jahn-Teller impurities on phase transitions See Entry 114125

Thermodynamic theory of phase transitions in solid solutions based on lead metaniobate See Entry 114156

Solid solutions based on lead barium metaniobate See Entry 114785

The influence of thermally activated orientation of the polarization on the electrooptic and elastooptic effects near a diffuse phase transition See Entry 114830

77.80D Domain structure and effects; hysteresis

114799 Stress relaxation in ferroelectric materials. V.C.S.Prasad (Materials Dev. Lab., Bharat Electronics Ltd., Bangalore, India). *Bull. Mater. Sci. (India)*, vol.5, no.1, p.71-7 (March 1983). [received: Sept. 1983]
Stress relaxation takes place in BaTiO₃ type ferroelectric materials due to the motion of non 180° domain boundaries, which are the twin boundaries. The nature of stress relaxation taking place due to plastic deformation in crystalline solids and that due to twin boundaries in ferroelectric materials is discussed. The usefulness of the stress relaxation data for the study of domain wall motions in this type of ferroelectric is pointed out. (20 refs.)

114800 Domain structure of heteroepitaxial ferroelectric Ba_{0.5}Sr_{0.5}TiO₃ films produced by RF cathode sputtering. V.A.Aleshin, V.S.Mukhortov, M.Mukhortov, Yu.I.Golovko, V.I.M.Mukhortov, A.T.Piralo, V.P.Dudkevich, E.G.Fesenko (Sci.-Res. Inst. of Phys., State Univ., Rostov-on-Don, USSR). *Sov. Phys.-Solid State (USA)*, vol.25, no.2, p.350-1 (Feb. 1983). Translation of: *Fiz. Tverd. Tela (USSR)*, vol.25, no.2, p.612-14 (Feb. 1983). [received: Sept. 1983]
The method of Mukhortov et al. (1979) was used to produce films on (100) cleavage planes of MgO crystals (cubic system, $a=4.211\text{ \AA}$), but with a wider variation in the deposition parameters. The fact of epitaxial growth and the relative orientations of the films and substrates were established by X-ray diffraction methods on a DRON 3.0 diffractometer (Cu K α , Fe K α) and in a Lang reflection arrangement (Cu K α). In all cases in which epitaxial growth occurred the authors observed a completely parallel orientation. At room temperature the films were tetragonal, with $(c/a-1)=(5.6\pm0.6)\times10^{-3}$ and with the crystallographic axis c perpendicular to the substrate. In this direction the microdeformations of the second kind, $\Delta c/c$, varied from 0.001 to 0.010 depending on the conditions under which the films were formed, and the

dimensions of the coherent-scattering regions were always larger than 1000 Å, i.e. could not be measured by X-ray methods. (6 refs.)

Polarization character in small ferroelectric particles and the monodomain state conditions See Entry 114775

77.90 OTHER TOPICS IN DIELECTRIC PROPERTIES AND MATERIALS

114801 On the dissociation conductivity of fluid dielectrics. A.I.Zhakin, I.E.Tarapov.

Elektron. Obrab. Mater. (USSR), no.3, p.46-50 (1983). In Russian. English translation in: *Electrochem. Ind. Process. & Biol. (GB)*

The results are given of theoretical studies of relaxation and concentration effects in fluid dielectrics in the presence of dissociation conductivity. It is suggested that ionization of the fluid occurs in consequence of the dissociation of neutrals, the ions thus formed possessing the power to recombine. It is shown that the transient process is characterized by two distinct periods of time: τ_x , the time occupied by the reaction dissociation \rightleftharpoons recombination to reach equilibrium, and τ_d , the time needed for establishment of an equilibrium concentration in the inter-electrode region. Evaluative expressions are obtained for τ_x and τ_d , from which it follows that, for the case of a low degree of dissociation and inter-electrode distances of ~ 1 cm, τ_d is of the order of tens of hours. It is shown that in strongly heterogeneous external fields the ohmic law of conductivity is not obeyed. In the neighborhood of the electrodes only a heterocharge can form, and hence dissociation conductivity cannot be the cause of the development of electroconvective movement. (9 refs.) *A.J.B.*

Thermodynamic and kinetic properties of amorphous dielectrics at low temperatures See Entry 114295

78.00 OPTICAL PROPERTIES AND CONDENSED MATTER SPECTROSCOPY AND OTHER INTERACTIONS OF MATTER WITH PARTICLES AND RADIATION

(for phonon spectra, see 63.)

78.20 OPTICAL PROPERTIES AND MATERIALS

(see also 81.40T Optical properties related to materials treatment; for masers, and lasers see 42.52 and 42.55 respectively)

114802 Differential polarization spectroscopy on single crystals of transition metal complexes. H.P.Jensen (Chem. Dept. A, Tech. Univ. of Denmark, Lyngby, Denmark).

Appl. Spectrosc. Rev. (USA), vol.18, no.3, p.305-27 (1982-1983). [received: Sept. 1983]

The purpose of the review is to solidify the status of the Jones matrix method; to discuss the transformation of the two-dimensional Jones matrix into a corresponding four-dimensional Mueller matrix which can be used in differential polarized absorption spectroscopy based on phase modulation; and to demonstrate the success, power, and limitations of the matrix algebraic methods when used on anisotropic media, especially anisotropic crystals of transition metal complexes. (83 refs.)

114803 Optical properties of small metallic particles in a continuous dielectric medium. A.Liebsch (Inst. fur Festkörperforschung, KFA, Jülich, Jülich, Germany), B.N.J.Persson.

J. Phys. C (GB), vol.16, no.27, p.5375-91 (30 Sept. 1983).

The dielectric function of an inhomogeneous system consisting of small particles in a dielectric host material is investigated using a lattice gas model to describe the topological disorder among the particles. By applying the coherent potential approximation, an effective single-particle polarizability is found, which contains the influence of the local electric fields arising from randomly distributed particles. In the Maxwell-Garnett theory it is assumed that these fields in a random distribution of dipoles are the same as those calculated for a cubic array of dipoles. The disorder is shown to give a substantial red shift of absorption peaks and a comparable blue shift of loss lines. Moreover, absorption as well as loss features are very strongly broadened. These kinds of shifts and enhanced linewidths have been observed experimentally for many systems. A detailed comparison with measured spectra is given for silver particles immersed in a gelatin matrix. (47 refs.)

114804 Properties of semidilute polymer solutions: investigation of an optically labeled three-component system. D.B.Cotts (Polymer Sci. Dept., SRI Internat., Menlo Park, CA, USA).

J. Polym. Sci. Polym. Phys. Ed. (USA), vol.21, no.8, p.1381-8 (Aug. 1983).

A three-component system containing a polymer (2), a good solvent (1) for that polymer, and a second polymer (3) that is compatible with component (2) and isorefractive with the solvent (1) has been studied by static and dynamic light-scattering methods. In concentrated toluene (1) solutions of poly(vinyl methyl ether) (3), where appreciable chain overlap occurs and excluded-volume effects are reduced, polystyrene (2) may be studied in the dilute-solution limit. Consequently, these light-scattering measurements provide an explicit measure of both thermodynamic and hydrodynamic changes that occur as the total polymer concentration is increased from dilute to concentrated solution. Precise numerical coefficients, correct scaling exponents, the radius of gyration, and the effective hydrodynamic radius can be measured directly along with the observation of long-wave single-chain reptation motions and short-range cooperative motions in semidilute and concentrated solutions. (10 refs.)

114805 Influence of solid support sorptive properties on the colour of cholesteric liquid crystals. II. Quantitative results. T.Skoulidakis, M.Koui (Lab. of Phys. Chem. & Appl. Electrochem., Nat. Tech. Univ. of Athens, Athens, Greece).

Mol. Cryst. & Liq. Cryst. (GB), vol.95, no.3-4, p.323-8 (1983).

For pt.I see *ibid.*, vol.61, p.31 (1980). Quantitative measurements (visible diffuse reflectance spectroscopy) at several temperatures on bare metal (Zn, Fe, Cu, Al) surfaces mechanically treated, on chemically and electrolytically prepared ZnO and Fe₂O₃, on electrolytically prepared γ_1 - and γ_2 -Al₂O₃, on copper surfaces electroplated with copper and on electrolytically prepared γ_1 -Al₂O₃ under several current densities, covered with the same mixture of cholesterics as the one used in part I, were carried out. Thus, the results of

the visual observations of the previous work were checked and the following relationship between the reflected wavelength at the peaks (λ) from the examined cholesteric system on γ_1 -Al₂O₃ and on blackened glass (λ') and the physical sorptive abilities of the γ_1 -Al₂O₃ (s') as a function of temperature [$T(K)$] was temporarily established. (27 refs.)

114806 Inhomogeneous and 'lost' optical waves in a bounded anisotropic crystal and supplementary boundary conditions in the theory of additional optical waves. S.I.Pekar, V.I.Pipa (Inst. of Semiconductors, Acad. of Sci., Kiev, Ukrainian SSR).

Sov. Phys.-Solid State (USA), vol.25, no.2, p.206-11 (Feb. 1983). Translation of: *Fiz. Tverd. Tela (USSR)*, vol.25, no.2, p.366-75 (Feb. 1983). [received: Sept. 1983]

It is shown that an inhomogeneous optical wave with complex projections of the wave vector k and $k^2=0$ is important in optical perturbation of a bounded crystal. The amplitude of such a wave can be expressed in terms of the amplitudes of ordinary optical waves in any frequency range of the spectrum. The supplementary boundary conditions are generalized for narrow spectral regions of exciton resonances in which additional optical waves occur. This makes it possible to satisfy the supplementary boundary conditions in the most general case, provided the aforementioned inhomogeneous wave is included. It is also possible to determine the reflection and transmission coefficients of light for the vacuum-crystal interface. The problem can be solved only in the limiting cases of large and small ratios of the width of an exciton band to the longitudinal-transverse splitting. (15 refs.)

114807 The effect of the microscopic structure of metal surfaces on their optical properties. A.M.Brodskii, M.I.Urbakh (Inst. of Electrochem., Acad. of Sci., USSR).

Sov. Phys.-Usp. (USA), vol.25, no.11, p.810-32 (Nov. 1982). Translation of: *Usp. Fiz. Nauk (USSR)*, vol.138, no.3, p.413-53 (Nov. 1982). [received: Sept. 1983]

This review treats the current state of studies on the optical properties of metal surfaces. The authors discuss the use of the theory developed in recent years for describing the results of concrete experiments in modulation spectroscopy of surfaces. They especially examine the dependence of the surface-plasmon spectrum on the microscopic structure of the surface. They describe how one can obtain information from the data of optical measurements on the electronic structure of the surface, and in particular, they discuss the effect of adsorption on this structure. The review of the literature covers the period to the end of 1980. (206 refs.)

Effects of the Abraham ponderomotive force induced by RF and laser light pulses See Entry 113047

Localized systems mechanisms for f-f transition probabilities in lanthanide coordination compounds See Entry 114494

78.20B General theory (for pure homogeneous materials)

114808 Light scattering by free holes in semiconductors with a complex valence band. V.A.Voitenko, I.P.Ipatova, A.V.Subashiev (A.F. Ioffe Physico-techn. Inst., Acad. of Sci., Leningrad, USSR).

JETP Lett. (USA), vol.37, no.7, p.396-400 (5 April 1983). Translation of: *Pis'ma v Zh. Eksp. & Teor. Fiz. (USSR)*, vol.37, no.7, p.334-7 (5 April 1983). [received: Oct. 1983]

A new unscreened mechanism for light scattering by free holes has been found in semiconductors with a valence band of symmetry Γ_8 . This scattering results from fluctuations in the density of the quadrupole moment of the holes. Although heavy holes do the scattering, the mass of the light holes determines the Thomson cross section. (8 refs.)

Localized retarded modes in a ferromagnetic slab See Entry 114722

New quantum form of the equation of the normals for biaxial crystals See Entry 114814

78.20D Optical constants and parameters

114809 Modification of optical properties of GaAs-Ga_{1-x}Al_xAs superlattices due to band mixing. Yia-Chung Chang (Dept. of Phys., Univ. of Illinois, Urbana, IL, USA), J.N.Schulman.

Appl. Phys. Lett. (USA), vol.43, no.6, p.536-8 (15 Sept. 1983).

A theoretical calculation of the optical properties of GaAs-Ga_{1-x}Al_xAs superlattices is presented. The calculation includes the detailed atomic nature of the superlattice electronic states in a realistic tight-binding model. It is found that the mixture of the bulk heavy hole and light hole states in the superlattice wave function substantially affects the optical properties. (20 refs.)

114810 Dynamical conductivity and dielectric function of general semiconductors and of magnetic semiconductors. P.Grosse (I. Phys. Inst., Rheinisch-Westfälischen Tech. Hochschule, Aachen, Germany).

Acta Polytech. Scand. Electr. Eng. Ser. (Finland), no.EL50, p.47-101 (1983). (Proceedings of Helsinki International Summer School on Semiconductors 1982, Espoo, Finland, 14-18 June 1982).

Considers the contribution of conduction electrons and holes to the optical properties of semiconductors and semimetals. These studies lead to more detailed information about the dynamics of 'free electrons' and the related scattering mechanisms than DC-measurements. In principle such information is also available from 'time resolved' transport measurements, but in this case a time resolution < 1 ps would be necessary e.g. to observe the current j as the response to a step of the field E . Another successful method is the study of nonlinear transport and experiments with 'hot electrons'. More efficient than these two transport measurements is the study of the 'dynamical conductivity' $\sigma(\omega)$, which is—roughly speaking—the Fourier-transform of the response function of the time resolved measurements. The experiments carried out with frequencies in the microwave range (1 cm) up to infrared (10 μ m) correspond to a time resolution from 3×10^{-11} s up to 3×10^{-15} s. The author also considers the contribution of electrons, trapped by defects, since they act as very high polarizable centers. A local-field-coupling of these dipoles to the long wavelength, polar optical phonons may explain the dependence of the reststrahlen bands on the magnetic order as found in some magnetic semiconductors. (16 refs.)

114811 Interpretation of the refractive and rotary dispersion of crystalline LiIO₃. M.S.Madhava, C.Satyanarayana (Dept. of Phys., Univ. of Mysore, Mysore, India).

Curr. Sci. (India), vol.52, no.13, p.632-3 (5 July 1983).

Lithium iodate (LiIO₃) belongs to the pyramidal class 6 of the hexagonal system, with space group P6₃ exhibiting high optical activity. Because of their very good optical quality, these crystals have been of considerable interest. Umegaki et al. (1971) have measured the refractive indices for both the ordinary (n_0) and extraordinary (n_e) rays in the spectral range 0.4047 μ to

2.2493 μ to an accuracy of ± 0.0001 in the visible region and ± 0.0003 in the near infrared region. The refractive dispersion can be explained by the Sellmeier-Drude (S-D) type formula. The authors have fitted the experimental data using the three-term S-D formulae. (9 refs.)

114812 Direct intersubband optical absorption of semiconductor thin wire. J.Lee (GTE Labs., Waltham, MA, USA). *J. Appl. Phys. (USA)*, vol.54, no.9, p.5482-4 (Sept. 1983).

The optical absorption due to direct intersubband transitions and including the broadening effects has been calculated by using an electric dipole approximation for a quasi-one-dimensional semiconductor thin wire. Effective mass approximation is adopted to determine the eigenfunctions and energies of the conduction electrons in Schrodinger equation by assuming a two-dimensional infinite potential well. When the electromagnetic wave is polarized in a \hat{z} direction which possesses a size-quantization effect in the thin wire, the selection rule requires that the sum of the quantum numbers of the initial state and final state must be odd integers. AC and DC conductivities, and the absorption line shapes due to collisions are discussed. (18 refs.)

114813 Absorption of picosecond light pulses in semiconductors. S.E.Kumekov, V.I.Perel' (A.F. Ioffe Physicotech. Inst., Acad. of Sci., Leningrad, USSR).

JETP Lett. (USA), vol.37, no.7, p.358-61 (5 April 1983). Translation of: *Pis'ma v Zh. Eksp. & Teor. Fiz. (USSR)*, vol.37, no.7, p.302-5 (5 April 1983). [received: Oct. 1983]

The absorption is calculated for the case in which thermodynamic equilibrium can be reached in the system of free charge carriers during the pulse, but recombination and electron-phonon interactions cannot occur. The analysis is based on Galitskii-Goreslavskii-Elesin quasiparticles. (7 refs.)

114814 New quantum form of the equation of the normals for biaxial crystals. F.I.Fedorov.

J. Appl. Spectrosc. (USA), vol.37, no.6, p.1379-85 (Dec. 1982). Translation of: *Zh. Prikl. Spektrosk. (USSR)*, vol.37, no.6, p.941-9 (Dec. 1982). [received: Sept. 1983]

Theories of the optical properties of biaxial crystals are distinguished by their great complexity in comparison with the corresponding theories for uniaxial crystals, not to mention isotropic media. The main reason for this is the relative complexity of the basic equation describing the laws of plane-wave propagation in biaxial crystals, the so-called equation of the normals. This equation determines the dependence of the refractive indices of the two waves propagating in the crystal with a specified direction of the wave normal (isonormal waves). It was first obtained by Fresnel in the system of principal axes of the dielectric tensor ϵ . This equation reduces to a universal covariant form independent of the choice of coordinate axes. (7 refs.)

114815 Investigation of the refractive indices of LaF₃, CeF₃, PrF₃ and NdF₃. R.Laiho, M.Lakkisto (Wilhuri Phys. Lab., Univ. of Turku, Turku, Finland).

Philos. Mag. B (GB), vol.48, no.2, p.203-7 (Aug. 1983).

Values of the ordinary and extraordinary refractive indices of LaF₃, CeF₃, PrF₃ and NdF₃ single crystals were determined in the visible and the near-ultraviolet regions. The dispersion of the indices was analysed by using a single-effective oscillator model. The energy of the oscillator agrees well with the first strong peaks in the reflectance spectra of these crystals. (12 refs.)

114816 Free-carrier multiphoton laser absorption in magnetic semiconductors. O.A.C.Nunes (Dept. de Fisica, Univ. de Brasilia, Brasilia, Brazil). *Solid State Commun. (USA)*, vol.47, no.11, p.873-5 (Sept. 1983).

The magnon scattering by free carriers in the presence of an intense laser field is discussed. A kinetic equation for electrons is derived from which the multiphoton absorption coefficient is calculated. It is found that for very large fields the absorption coefficient is vanishing small. A physical explanation of this result is also available. (11 refs.)

114817 Comment on the optical absorption edge in a-Si:H. C.B.Roxlo, B.Abeles, C.R.Wronski, G.D.Cody, T.Tiedje (Corporate Res., Exxon Res. & Engng. Co., Linden, NJ, USA).

Solid State Commun. (USA), vol.47, no.12, p.985-7 (Sept. 1983).

The optical absorption edge of undoped amorphous silicon hydride has been measured using optical transmission, photoconductivity, and photothermal deflection spectroscopy. The results obtained by these techniques agree in the exponential edge region. An apparent inconsistency pointed out by Redfield (1982) between the optical absorption edge and the valence band tail density of states as measured by drift mobility is attributed to the nonexponential behavior of the absorption edge above $\alpha \sim 10^3 \text{ cm}^{-1}$. (16 refs.)

114818 Fundamental absorption of test radiation in a semiconductor subjected to the field of a strong electromagnetic wave. S.E.Kumekov (Technol. Inst. of Light & Food Industry, Dzhambul, USSR).

Sov. Phys.-Semicond. (USA), vol.17, no.3, p.273-5 (March 1983). Translation of: *Fiz. & Tekh. Poluprovodn. (USSR)*, vol.17, no.3, p.441-5 (March 1983). [received: Sept. 1983]

A theoretical study is made of the absorption of a weak electromagnetic wave in a semiconductor subjected to a strong electromagnetic field. A general expression is obtained for the absorption coefficient k of the weak test wave and this expression is used to analyze the dependence of k on the method of application and intensity of the strong wave, on the frequencies of the strong and test waves, and on the state of their polarizations. The dependences are essentially different for the abrupt and adiabatic applications of the strong field and they are influenced by the state of saturation. (7 refs.)

114819 Dispersion of the refractive index of light exhibited by Cd_{0.9}Hg_{0.1}-Te epitaxial films. V.G.Sredin.

Sov. Phys.-Semicond. (USA), vol.17, no.3, p.328 (March 1983). Translation of: *Fiz. & Tekh. Poluprovodn. (USSR)*, vol.17, no.3, p.523-4 (March 1983). [received: Sept. 1983]

The author reports the results of a calculation of the dispersion of the refractive index $n(\hbar\omega)$. The calculations were performed for Cd_{0.9}Hg_{0.1}-Te epitaxial films. (7 refs.)

114820 Calculation of optical anisotropy of hydrocarbon chains by the Monte Carlo method. P.G.Khalatur, Yu.G.Papulov, A.S.Pavlov (Kalinin State Univ., Kalinin, USSR).

Theor. & Exp. Chem. (USA), vol.18, no.6, p.683-5 (Nov.-Dec. 1982). Translation of: *Teor. & Eksp. Khim. (USSR)*, vol.18, no.6, p.740-2 (Nov.-Dec. 1982). [received: Sept. 1983]

The optical anisotropy of straight chain hydrocarbons (n-alkanes) present in a solution or in a gaseous phase is a value averaged with respect to all of the possible conformations in the molecule, formed during the rotations around C-C bonds. The main drawback of previous investigations is the neglect of the inherent volume of the molecules, as the result of which, during the conformational changes, the chains could intersect themselves, which in fact does not occur. Meanwhile, it is clear the forbidding of self-intersections should considerably decrease the number of the possible conformations of the chains, and thus influence their optical anisotropy. This fact is taken into account in the authors investigation, in which the results of the calculations of $\langle \gamma^2 \rangle$ for

chains with $n=10-32$ are given within the bounds of the valent-optical scheme by means of the Monte Carlo method. (8 refs.)

Improved differential photocurrent method for measurement of optical-absorption coefficient and minority-carrier diffusion length in a semiconductor See Entry 111703

Low intensity nonlinear refraction in cadmium mercury telluride at 10.6 μm See Entry 113038

Diffusion of iodine into PE and PET See Entry 114263

Thermal nitridation of silicon in nitrogen plasma See Entry 114377

CVD a-Ge and a-Ge:X films: preparation and properties See Entry 114411

Ab initio mixed basis method of band structure calculation: γ -Fe and cubic ZnS electronic structures See Entry 114435

Absorption of light by bound electron-exciton states in two-dimensional molecular crystals See Entry 114451

Admissible values of permittivity and magnetic permeability of matter See Entry 114773

Studies of Kirkwood-Frohlich's correlation factor and dielectric relaxation in triethylamine-solutions See Entry 114776

Linear electrooptic effect in doped KDP crystals See Entry 114827

Optical determination of the electronic characteristics of Nb-Al alloys with the A15 lattice See Entry 114845

Optical properties of leucosapphire at high temperatures. II. Single-crystal properties in the opaque region and properties of the melt See Entry 114846

Infrared properties of quartz fibres and wool See Entry 114847

Optical anisotropy and electrostriction in the anodic oxide of tantalum See Entry 114941

Infrared optical properties of solid monomethyl hydrazine, N₂O₄, and N₂H₄ at cryogenic temperatures See Entry 114942

Linear absorption coefficient of beryllium in the 50-300-Å wavelength range See Entry 114943

In-plane orientation of polyimide See Entry 114944

Anomalies in the dependence of the transmission coefficient of light through thin silver films See Entry 114948

Ellipsometric evaluation of various pretreatments on zircaloy-2 See Entry 115422

The preparation and properties of metallic optically transparent electrodes See Entry 115565

Diffuse transmission and reflection by a thick weakly absorbing layer with close particle packing See Entry 115591

78.20E Optical rotatory power

114821 Pretransitional anomalies in the rotation of the plane of polarization of light in ferroelectric liquid crystals. E.I.Demikhov, V.K.Dolganov, V.M.Filev (Inst. of Solid State Phys., Acad. of Sci., USSR).

JETP Lett. (USA), vol.37, no.7, p.361-5 (5 April 1983). Translation of: *Pis'ma v Zh. Eksp. & Teor. Fiz. (USSR)*, vol.37, no.7, p.305-8 (5 April 1983). [received: Oct. 1983]

It is observed that the sign of the fluctuation contribution to the rotation in the smectic A phase differs from the sign of the rotation in the smectic C* phase and isotropic phase. A theoretical explanation of the observed anomaly is given. (7 refs.)

114822 Propagation of light in cholesteric liquid crystals with frequency dispersion. I.V.Semchenko, A.N.Serdyukov.

J. Appl. Spectrosc. (USA), vol.37, no.5, p.1316-19 (Nov. 1982). Translation of: *Zh. Prikl. Spektrosk. (USSR)*, vol.37, no.5, p.836-9 (Nov. 1982). [received: Sept. 1983]

The authors investigate the effect of dispersion of ϵ on propagation of light along the axis of a cholesteric helix and show that in several cases dispersion can lead to a qualitative change in gyrotropy and Bragg reflection in a cholesteric liquid crystal. (9 refs.)

Nonlinear optical activity See Entry 113041

78.20F Birefringence

(inc. stress birefringence, flow birefringence, etc)

114823 Optical and Mossbauer spectra of manganese-bearing phlogopites: Fe_{1/3}³⁺-Mn_{2/3}²⁺ pair absorption as the origin of reverse pleochroism. G.Smith (Inst. fur Mineralogie und Kristallographie, Tech. Univ. Berlin, Berlin, Germany), U.Halenius, H.Annersten, L.Ackermann.

Am. Mineral. (USA), vol.68, no.7-8, p.759-68 (July-Aug. 1983).

Eight manganese-bearing phlogopites have been studied by means of X-ray powder diffraction, electron microprobe techniques, Mossbauer spectroscopy and single crystal optical absorption spectroscopy. The different types of spectra were measured at room temperature and at liquid nitrogen temperature. The major differences in sample 3d-element chemistry are variations in [Mn²⁺]/[Fe³⁺] and [Fe_{IV}³⁺]/[Fe_{VI}³⁺] ratios. Samples containing Mn_{VI}²⁺ and Fe_{VI}³⁺ are normal pleochroic, while samples containing Mn_{VI}²⁺ and Fe_{IV}³⁺ are reverse pleochroic. These chemical and optical differences are reflected by pronounced variations in the shape and band content of the optical absorption spectra. (31 refs.)

114824 Photoelasticity of KH₂PO₄, KD₂PO₄, and RbH₂PO₄. L.P.Avakyants, D.F.Kiselev, N.V.Perelomova, V.I.Sugrei (M.V. Lomonosov State Univ., Moscow, USSR).

Sov. Phys.-Solid State (USA), vol.25, no.2, p.329-30 (Feb. 1983). Translation of: *Fiz. Tverd. Tela (USSR)*, vol.25, no.2, p.580-2 (Feb. 1983). [received: Sept. 1983]

Ferroelectric crystals of the KDP series are widely used in modern electrooptic and acoustooptic devices. In order to calculate the efficiency of these devices, to study the anisotropy of the elastooptic effect, to determine the contribution of the secondary electrooptic effect, and to solve a number of other problems it is necessary to have the complete matrix of photoelastic constants $P_{\alpha\beta}$, and here it is important to know not only the absolute values but also the signs of all the $P_{\alpha\beta}$. The authors determine the signs and magnitudes of all the $P_{\alpha\beta}$ for KDP, DKDP, and RDP by a Brillouin-scattering method and to study the influence of $P_{(ij)(kl)}$ on the intensity of the Brillouin-scattering. (15 refs.)

Picosecond photoinduced dichroism detected by photothermal deflection See Entry 111776

Chain orientation in polystyrene/poly(2,6-dimethyl-1,4-phenylene oxide) blends See Entry 113769

- Birefringence and ferroelectric properties of $[\text{Rb}_{0.4}(\text{NH}_4)_{0.6}\text{SO}_4]$ See Entry 114796
- The influence of thermally activated orientation of the polarization on the electrooptic and elasto-optic effects near a diffuse phase transition See Entry 114830
- Magnetic fluid's anomalous pseudo-Cotton Mouton effects about 10^7 times larger than that of nitrobenzene See Entry 114831
- Alignment of solutes in stretched polyethylene. Determination of the five second and fourth moments of the orientation distribution of 2-fluoropyrene from polarized fluorescence. Additional evidence for the twisting of weak transition moments by the solvent environment See Entry 114904
- In-plane orientation of polyimide See Entry 114944
- Study of molecular deformation mechanisms in the glassy state. I. Temperature effect on stress-birefringence and strain-birefringence responses of poly(methyl methacrylate) See Entry 115261

78.20H Piezo-, elasto- and acousto-optical effects

- 114825 Properties of light transmission across an ultrasound beam with strong acoustooptical interaction. S.N.Antonov, V.V.Proklov (Inst. of Radio Engng. & Electronics, Acad. of Sci., Moscow, USSR). *Sov. Phys.-Tech. Phys. (USA)*, vol.28, no.2, p.188-90 (Feb. 1983). Translation of: *Zh. Tekh. Fiz. (USSR)*, vol.53, no.2, p.306-10 (Feb. 1983). [received: Sept. 1983]
- The phase change of light passing through a sound wave caused by acoustooptical interaction (zeroth diffraction order) is studied experimentally. Experimental and theoretical data are compared with allowance for the anisotropic character of light diffraction. An experiment is conducted in which acoustooptical interaction is used to tune a Fabry-Perot cavity. (7 refs.)
- Three holes bound to a double acceptor: Be^+ in germanium See Entry 114469
- Photoelasticity of KH_2PO_4 , KD_2PO_4 , and RbH_2PO_4 See Entry 114824
- The influence of thermally activated orientation of the polarization on the electrooptic and elasto-optic effects near a diffuse phase transition See Entry 114830
- Raman spectra of rhombohedral and α -monoclinic selenium under high hydrostatic pressure See Entry 114844
- Brillouin scattering in liquid benzene under high pressure See Entry 114872

78.20J Electro-optical effects

- 114826 Electrochromism for organic materials in polymeric all-solid-state systems. Y.Hirai, C.Tani (Opto-Electronics Res. Labs., NEC Corp., Kanagawa, Japan). *Appl. Phys. Lett. (USA)*, vol.43, no.7, p.704-5 (1 Oct. 1983).
- Reports a new electrochromic polymeric film system consisting of a polymer, an electrochromic (EC) dye which is pyrazoline or tetrahydrofulvalene (TTF), and lithium perchlorate (LiClO_4). The electrochromic cell structure is glass/ITO/polymeric EC film/Au film. The cell using pyrazoline as an EC dye exhibited yellow coloration at 1.0 V and the cell with TTF exhibited red coloration at 3.5 V. These cells exhibited memory. (13 refs.)
- 114827 Linear electrooptic effect in doped KDP crystals. K.B.R.Varma (Dept. of Electrical Engng., Indian Inst. of Technol., Madras, India), K.V.Ramaniah, K.Veerabhadra Rao. *Bull. Mater. Sci. (India)*, vol.5, no.1, p.39-48 (March 1983). [received: Sept. 1983]
- The dispersion of half wave voltages with wave length and temperature of potassium dihydrogen ortho phosphate (KDP) crystals with additives and dopants like borax, nickel phosphate, manganese phosphate, sodium dihydrogen orthophosphate and potassium arsenate were determined. The refractive index for all the above crystals were found by the modified Rayleigh's refractometer method. The linear electrooptic coefficients were calculated at various wavelengths of light. The variation of half wave voltage was also studied as a function of concentration of the dopant. (8 refs.)
- 114828 Kerr electro-optic field mapping measurements in water using parallel cylindrical electrodes. M.Zhan, T.Takada, S.Voldman (Dept. of Electrical Engng. & Computer Sci., MIT, Cambridge, MA, USA). *J. Appl. Phys. (USA)*, vol.54, no.9, p.4749-61 (Sept. 1983).
- An extensive set of Kerr electro-optic field mapping measurements are reported for highly purified water over the temperature range of 8.8-29.5°C. The Kerr constant is independent of temperature over this range and equals $B \approx 3.4 \times 10^{-14}$ m/V². Pulsed high voltages up to 140 kV across parallel cylindrical electrodes with a 1-cm gap are applied on millisecond time scales. For early times, the measured results agree with the space-charge-free electric field distribution while for times greater than 500 μs , there is significant space-charge distortion due to positive charge injection. (4 refs.)
- 114829 Electromodulation spectra of high-resistance p and n GaAs doped with chromium. V.A.Morozova, V.V.Ostrobodova (Dept. of Semiconductor Phys., Moscow Univ., Moscow, USSR). *Moscow Univ. Phys. Bull. (USA)*, vol.38, no.1, p.77-80 (1983). Translation of: *Vestn. Mosk. Univ. Ser. 3 (USSR)*, vol.38, no.1, p.67-9 (1983).
- From the electromodulation spectra of high-resistance p and n GaAs doped with chromium, the ionization energies of the acceptor levels of chromium are determined. They are $\epsilon_{\text{AV}} = 0.61 \pm 0.01$ eV and $\epsilon_{\text{AV}} = 0.870 \pm 0.005$ eV and are independent of the temperature in the range 80-300K. (17 refs.)

- 114830 The influence of thermally activated orientation of the polarization on the electrooptic and elasto-optic effects near a diffuse phase transition. N.N.Krainik, L.S.Kamzina, G.A.Smolenskii (A.F. Ioffe Physicotech. Inst., Acad. of Sci., Leningrad, USSR). *Sov. Phys.-Solid State (USA)*, vol.25, no.2, p.202-6 (Feb. 1983). Translation of: *Fiz. Tverd. Tela (USSR)*, vol.25, no.2, p.359-65 (Feb. 1983). [received: Sept. 1983]
- Results are reported from a study of the electrooptic and elasto-optic effects and the quadratic electrooptic effect under uniaxial compression in lead magneto- and zinconibate-ferroelectrics with a diffuse phase transition—for the case of static stresses and electric fields. These results are compared with those of a model calculation for weakly interacting birefringent polar regions and are discussed in terms of a model in which the diffuse phase transition is due to fluctuations of the composition in the presence of a partially ordered distribution of ions of different valencies in the octahedral positions in the lattice. (30 refs.)

- Coherent image amplification and optical phase conjugation with photorefractive materials See Entry 112959
- Coherent light scattering from ruby dressed with RF photons See Entry 113044

- New liquid crystalline tetrazine derivatives for guest-host displays See Entry 113730
- Ferroelectric liquid crystals and their applications See Entry 113732
- High voltage electric field and space-charge distributions in highly purified water See Entry 114782
- Birefringence and ferroelectric properties of $[\text{Rb}_{0.4}(\text{NH}_4)_{0.6}\text{SO}_4]$ See Entry 114796
- Light scattering by free holes in semiconductors with a complex valence band See Entry 114808

78.20L Magneto-optical effects

- 114831 Magnetic fluid's anomalous pseudo-Cotton Mouton effects about 10^7 times larger than that of nitrobenzene. S.Taketomi. *Jpn. J. Appl. Phys. Part 1 (Japan)*, vol.22, no.7, p.1137-43 (July 1983).
- The magneto-birefringence of magnetic fluid thin films of 12 μm and 25 μm were studied and anomalous phase differences were found when an external magnetic field was applied normal to the direction of light propagation. The order of the phase differences of the films was about 10^7 times larger than that of nitrobenzene, which is known to show a large Cotton-Mouton effect. The author attributes these phenomena theoretically to a rod-like chain formation of the ferrite particles in the magnetic fluid thin films and derives expressions for the phase difference and absorption. There is a definite difference in the H- δ curves between the theory and experiment in the rising gradient near H=0. (13 refs.)
- 114832 Influence of compositional variations in thin solid $\text{Pb}_{1-x}\text{Br}_x$ films on their excitonic spectra. V.V.Mussil, V.K.Miloslavskii, V.Kenig (V.I. Lenin Khar'kov Polytech. Inst., USSR). *Inorg. Mater. (USA)*, vol.18, no.9, p.1350-5 (Sept. 1982). Translation of: *Izv. Akad. Nauk SSSR Neorg. Mater.*, vol.18, no.9, p.1577-82 (Sept. 1982). [received: Sept. 1983]
- Using the Faraday rotation method the authors have studied the exciton spectrum of the hexagonal phase of $\text{Pb}_{1-x}\text{Br}_x$ solid solutions in the region of x values from 0 to 0.2 at 90K. As x increases a frequency shift of the exciton peak is observed, which obeys a linear law for $x \leq 0.10$, along with a change in its shape. It has been shown that the dependence of the exciton peak shape upon composition may not be explained by its broadening in a homogeneous solid solution and is due instead to a nonlinear change in composition over the thickness of the sample. They have calculated the spectral dependence of the Verde constant taking into account parameters which describe a significant concentration variation. (16 refs.)
- 114833 Magnetic circularly polarized luminescence as a probe of ligand fields in the solid state and in solution. D.Foster, F.S.Richardson (Dept. of Chem., Univ. of Virginia, Charlottesville, VA, USA). *J. Less-Common Met. (Switzerland)*, vol.93, no.1, p.236 (1983). (Proceedings of the Sixteenth Rare Earth Research Conference, Tallahassee, FL, USA, 18-21 April 1983).
- Summary form only given, as follows. Magnetic circularly polarized luminescence (MCPL) refers to the differential (spontaneous) emission of left versus right circularly polarized light by luminescent systems placed in a static magnetic field. The MCPL experiment involves the measurement of this differential emission along a direction parallel to the direction of the externally applied magnetic field. The shapes, signs, intensities and splitting patterns of the lines observed in the MCPL spectra of lanthanide 4f-4f transitions are sensitive probes of coordination geometry, lanthanide-ligand interactions and the magnetic properties of the (4f)ⁿ electronic states. Experimental data are reported for a variety of europium(III) systems in crystals and in solution media, and these data are analyzed in terms of ligand structure, coordination geometry and the (4f)ⁿ electronic properties of europium(III). (no refs.)
- 114834 Anomalous field dependence of the Faraday effect in paramagnetic $\text{Gd}_3\text{Ga}_5\text{O}_{12}$ at 4.2K. A.K.Zvezdin, S.V.Koptisk, G.S.Krinchik, R.Z.Levitin, V.A.Lyskov, A.I.Popov (M.V. Lomonosov State Univ., Moscow, USSR). *JETP Lett. (USA)*, vol.37, no.7, p.393-6 (5 April 1983). Translation of: *Pis'ma v Zh. Eksp. & Teor. Fiz. (USSR)*, vol.37, no.7, p.331-4 (5 April 1983). [received: Oct. 1983]
- A nonmonotonic magnetic field dependence of the Faraday effect (Faraday rotation as a function of the magnetic field passes through a maximum) in paramagnetic $\text{Gd}_3\text{Ga}_5\text{O}_{12}$ is observed at 4.2K at a wavelength of 0.47 μm . A theoretical explanation of this effect is given. (4 refs.)
- Linear and circular polarisation modulation for measuring complex magneto-optical rotation. I. Principles and performance See Entry 111742
- Nonlinear magneto-optics in semiconductors See Entry 113036
- Radiative recombination of localized Mott excitons in a strong magnetic field See Entry 114454
- Zeeman spectroscopy of crystal-field transitions of Co-doped InP See Entry 114492
- Nonmagnetic state of cobalt ions in chromium alloys See Entry 114684
- Radiative recombination at Ir^{3+} sites in doped AgBr. Visible luminescence See Entry 114914
- Permeability at optical frequencies See Entry 114947

78.30 INFRARED AND RAMAN SPECTRA AND SCATTERING

- 114835 The study of antimony (V) chloride adducts by vibrational spectroscopy. Y.Gushikem, O.L.Alves (Inst. de Quimica, Univ. Estadual de Campinas, Campinas, Sao Paulo, Brazil). *An. Acad. Bras. Cienc. (Brazil)*, vol.55, no.2, p.179-82 (June 1983).
- The SbO frequencies and the SbO stretching force constants K_{SbO} increase from the POCl_3 complex to the $(\text{Me}_2\text{N})_2\text{PO}$ complex, i.e. in the same order as increase in the donor number of the ligands. An apparent discrepancy is observed for the Cl_2SeO and Me_2SO complexes taking into account their relative position in the donor number scale. In this case the correlation is reasonable considering the approximated model used to calculate the force constants. (14 refs.)
- 114836 A new interpretation of spectral data on $\text{SbCl}_5\text{OSeCl}_2$. O.L.Alves (Inst. de Quimica, Univ. Estadual de Campinas, Sao Paulo, Brazil), Y.Hase. *An. Acad. Bras. Cienc. (Brazil)*, vol.55, no.1, p.27-31 (March 1983). [received: Sept. 1983]
- The laser Raman spectra of $\text{SbCl}_5\text{OSeCl}_2$ have been reexamined in the 850-50 cm^{-1} region for crystalline and molten states. Taking the relative intensity changes of the ligand bands due to the phase transition and the optical activities of the skeletal fundamentals into consideration, a new inter-

pretation of the spectral data is presented for the vibrational band assignments. (14 refs.)

114837 Comment on 'Raman scattering with nanosecond resolution during pulsed laser annealing of silicon'. D.von der Linde, G.Wartmann (Fachbereich Phys., Univ. Essen, Essen, Germany), A.Compaan. *Appl. Phys. Lett. (USA)*, vol.43, no.6, p.613 (15 Sept. 1983). For original paper see von der Linde and Wartmann, *ibid.*, vol.41, p.700 (1982). von der Linde and Wartmann reported time-resolved Raman measurements of the optical phonon population in Si during intense excitation with a 10-ns pulse at 532 nm. The results indicated a phonon temperature in excess of the melting temperature for a UV Raman probe ($\lambda=355$ nm), but a different, much lower temperature for a Raman probe in the visible ($\lambda=532$ nm). The authors show data confirming the supposition that this difference arises from the temperature dependence of the factors which correct for absorption and resonance Raman effects. (5 refs.)

114838 Surface effects of Raman scattering from semi-metal Sb deposited on island Ag films. N.T.Liang (Inst. of Phys., Acad. Sinica, Taipei, Taiwan), T.T.Chen, Hua Chang, Y.C.Chou, Shou-Yih Wang. *Annu. Rep. Inst. Phys. Acad. Sin. (Taiwan)*, vol.12, p.245 (Dec. 1982). [received: Sept. 1983] Enhancement in Raman spectra (115 cm^{-1} and 150 cm^{-1}) of crystalline Sb deposited on island silver films has been observed. The excitation profiles, as well as the dependence of Raman intensity on the thickness of Ag films, were similar to the surface enhanced Raman scattering (SERS) from molecules adsorbed on rough Ag surface. This is the first observation of SERS from crystal vibrational modes rather than the vibrations of individual molecules. (no refs.)

114839 Observations of crystalline and amorphous Sb films by Raman scattering. N.T.Liang (Inst. of Phys., Acad. Sinica, Taipei, Taiwan), Y.C.Chou, Shou-Yih Wang, Hua Chang. *Annu. Rep. Inst. Phys. Acad. Sin. (Taiwan)*, vol.12, p.246 (Dec. 1982). [received: Sept. 1983]

The authors have observed Raman spectra (145 cm^{-1}) of 50–200 Å amorphous Sb films and the crystalline peaks ($115, 150\text{ cm}^{-1}$) of 10–20 Å annealed Sb films. Also observed was the transition to crystal when a silver overlayer was deposited on an amorphous Sb film. This same phenomena was not found for Al overlayers, so that the conjecture of this transition being originated by a temperature effect during deposition was ruled out. The determination of phase change in such thin films via conventional electron diffraction or other methods is very difficult and has not been reported before. (no refs.)

114840 Absorption and surface-enhanced Raman spectra of silver organosols in ethanol. O.Siiman, A.Lepp, M.Kerker (Dept. of Chem., Clarkson Coll. of Technol., Potsdam, NY, USA). *Chem. Phys. Lett. (Netherlands)*, vol.100, no.2, p.163-8 (2 Sept. 1983). Colloidal silver, dispersed in ethanol and stabilized by adsorbed polymer, shows enhanced Raman scattering of the chromophore dabsyl (N-4-dimethylaminoazobenzene-4'-sulfonyl) aspartate, DABS ASP, in the presence of excess base. The requirement of the base appears linked to the adsorption of the dabsyl aspartate by interaction with the polymer and/or promotion of growth and aggregation of the silver particles. The latter conditions are indicated by changes in the absorption spectrum of the sol upon addition of base. The enhancement is comparable to that observed earlier for DABS ASP on colloidal silver in aqueous medium. (35 refs.)

114841 Fermi resonance effect and vibrational intensity in the weak charge-transfer complexes. C.T.Lin, C.A.Caetano, T.D.Z.Atvans (Inst. de Química, Univ. Estadual de Campinas, Campinas, Brazil). *Chem. Phys. Lett. (Netherlands)*, vol.100, no.2, p.169-73 (2 Sept. 1983). Infrared and Raman spectra of naphthalene, tetrachlorophthalic anhydride, tetrabromophthalic anhydride and their respective weak charge-transfer complexes were recorded in solids. The spectral intensities of both donor and acceptor molecules were found to alter drastically upon complexation. The observed intensity changes might be attributed to the removal and formation of the Fermi resonance effect in the complexes. (12 refs.)

114842 Low frequency infrared spectra of copper(II) pyridine N-oxide complexes. A.Malek, J.Fresco (Chem. Dept., McGill Univ., Montreal, Canada). *Chem. Scr. (Sweden)*, vol.22, no.3, p.146-51 (1983). The infrared spectra of 1:1 copper(II) pyridine N-oxide complexes have been recorded and the copper-oxygen vibrational frequencies assigned. These frequencies occur in the same region as that of the corresponding 1:2 complexes. Since the bridging frequencies of the 1:1 complexes occur at higher values than expected, the enhanced bonding could arise in part from superexchange. (33 refs.)

114843 Raman spectroscopic study on molten polyethylene under high pressure. H.Tanaka, T.Takemura (Dept. of Appl. Sci., Kyushu Univ., Fukuoka, Japan). *Jpn. J. Appl. Phys. Part I (Japan)*, vol.22, no.6, p.1001-4 (June 1983). Raman spectral changes of the C-H stretching modes of polyethylene during melting at high pressures up to 5000 kg/cm² were observed in detail and are explained in terms of changes in the intra- and interchain structures. It was found that the peak height ratio $r=(2890)/I(2850)$ in the molten state increases, and the upward shift of the 2890 cm⁻¹ band upon melting decreases with increasing pressures. Several confirmations of the effects of intra- and interchain disordering on the ratio and the upward shift were obtained from other experimental results. It is suggested from these facts that the degree of intrachain regularity in the molten state increases with increasing pressure, and that this should contribute to the formation of extended-chain crystals under high pressure. (18 refs.)

114844 Raman spectra of rhombohedral and α -monoclinic selenium under high hydrostatic pressure. K.Nagata, T.Isikawa, Y.Miyamoto (Dept. of Appl. Phys., Fukuoka Univ., Fukuoka, Japan). *Jpn. J. Appl. Phys. Part I (Japan)*, vol.22, no.7, p.1129-32 (July 1983). The Raman spectra of rhombohedral, α -monoclinic, and trigonal selenium have been measured under high hydrostatic pressures up to about 8 kbar at room temperature. The frequencies of the A₁-type stretching modes in both rhombohedral and α -monoclinic selenium have been observed to decrease with increasing pressure, as has that of trigonal selenium. This indicates that interference between inter- and intramolecular bonding also exists in crystals composed of ring molecules such as Se₆ or Se₈. (16 refs.)

114845 Optical determination of the electronic characteristics of Nb-Al alloys with the A15 lattice. N.D.Kuz'michev, I.S.Levchenko, G.P.Motulevich (P.N. Lebedev Phys. Inst., Acad. of Sci., Moscow, USSR). *Fiz. Met. & Metalloved. (USSR)*, vol.56, no.2, p.266-70 (Aug. 1983). In Russian. English translation in: *Phys. Met. & Metallogr. (GB)* The complex permittivity $\epsilon(\omega)=\epsilon_1(\omega)-i\epsilon_2(\omega)$ was determined for the Nb-Al alloy with the A15 lattice at temperatures 295 and 670K in the spectral range 3.1-0.18 eV. The characteristics of the conduction electrons and of the

three main bands due to interband transitions were determined. An increase in temperature from 295 to 670K increased the conduction electron density by a factor of 1.43 and the effective collision frequency ν by a factor of 1.25. The sum of the values of ω_p^2 for all the bands at 295 and 670K was 140 and 150 eV², which represented 0.39 and 0.42 of Ω_p^2 , respectively (Ω_p is the plasma frequency of all the valence electrons). This indicated the occurrence of important bands due to interband transitions at frequencies in the range $\hbar\omega>3$ eV, where \hbar is the Planck constant divided by 2π . (8 refs.) A.T.

114846 Optical properties of leucosapphire at high temperatures. II. Single-crystal properties in the opaque region and properties of the melt. Yu.K.Lingart, V.A.Petrov, N.A.Tikhonova (Inst. of High Temperatures, Acad. of Sci., USSR). *High Temp. (USSR)*, vol.20, no.6, p.856-62 (Nov.-Dec. 1982). Translation of: *Teplotiz. Vys. Temp. (USSR)*, vol.20, no.6, p.1085-92 (Nov.-Dec. 1982). [received: Sept. 1983]

For pt.I see *ibid.*, vol.20, no.5, p.872 (1982). Experimental data on the indices of absorption and refraction of single-crystal leucosapphire are analyzed over the wavelength interval 6-33 μm at temperatures from room temperature to 1800K. From the collected data in the literature tables of recommended values are presented. The optical properties of molten aluminum oxide are examined. (19 refs.)

114847 Infrared properties of quartz fibres and wool. F.Thiebaud, F.K.Kneubuhl (Solid State Phys. Lab., ETH, Hoenggerberg, Zurich, Switzerland). *Infrared Phys. (GB)*, vol.23, no.3, p.131-48 (May 1983).

This experimental and theoretical study is devoted to the general infrared properties of dielectric fibres and wool with fibre diameters comparable to the infrared wavelengths. Amorphous quartz is used as the fibre material since its bulk infrared dispersion is known, and since it is suitable for the manufacture of thin fibres. Diffuse reflection, extinction and scattering including polarization phenomena of fibres and wools with fibre diameters between 1.8 and 9 μm are measured in the spectral region of 400 to 1400 cm⁻¹. The measured infrared properties of single quartz fibres agree with the theory of Englmann and Rupin (1968). Bulk and surface modes are observed. Thanks to the ideal geometry of the fibres the broadening of modes usually reported for small particles is not observed. The interpretation of the reflectivity spectra of wool is based on the Kubelka-Munk theory. Multiple scattering prevails. The introduction of an empirical factor connecting the ratio of absorption versus the scattering coefficient with the ratio of the efficiency factors for absorption and scattering allows one to predict in first approximation the spectral reflectivity of dielectric wool samples if the diameter distribution function of the fibres and the bulk i.r. dispersion are known. (43 refs.)

114848 Raman spectra of ⁷Li₂SO₄ and ⁶Li₂SO₄. E.Cazzanelli, R.L.Frech (Dept. of Chem., Univ. of Oklahoma, Norman, OK, USA). *J. Chem. Phys. (USA)*, vol.79, no.6, p.2615-20 (15 Sept. 1983). The polarized Raman spectra of single crystal ⁷LiSO₄ and ⁶Li₂SO₄ at room temperature are reported. Symmetry-based vibrational band assignments are given for the external and internal optic modes. Comparison of spectra from the two isotopically substituted crystals identifies higher frequency external modes originating in the lithium ion motion. The interaction of these modes with the intramolecular modes of the sulfate ion is discussed. (25 refs.)

114849 Ammonium ion rotation in ammonium perchlorate as studied by infrared spectroscopy. R.M.Corn, H.L.Strauss (Dept. of Chem., Univ. of California, Berkeley, CA, USA).

J. Chem. Phys. (USA), vol.79, no.6, p.2641-9 (15 Sept. 1983). The infrared spectra of the ND-stretching bands of dilute NH₃D⁺ in NH₄ClO₄ are presented. The spectra are studied over the temperature range from 3K to room temperature. At low temperatures, the NH₃D⁺ is preferentially oriented. The extent of the orientation at a given temperature depends on the deuterium concentration and thus on the concentration of NH₃D⁺ ions. As the temperature is raised, the various ND-stretching bands collapse due to a variety of dephasing processes. At low temperature, the dephasing process is phonon-assisted tunnelling. As the temperature is raised, dephasing is accomplished by interaction among librational states. At still higher temperatures, the bandwidth is due to stochastic motion of the ammonium ions. (34 refs.)

114850 Infrared dephasing and libration motion in liquid methyl iodide. W.G.Rothschild, J.Soussen-Jacob, J.Bessiere, J.Vincent-Geisse (Lab. de Recherches Phys., Univ. Pierre et Marie Curie, Paris, France). *J. Chem. Phys. (USA)*, vol.79, no.6, p.3002-8 (15 Sept. 1983). A theoretical model of vibrational dephasing with motional narrowing by the librational motions of the molecules in their liquid cages is proposed and tested on the infrared ν_6 degenerate fundamental of liquid methyl iodide and perdeutero methyl iodide over a temperature range of -190 to +40°C. The theory, which does not require artificial separation of vibrational and orientational coordinates, is particularly applicable to associated and sterically hindered liquids. (26 refs.)

114851 The electronic structure of f element compounds elucidated by less common spectroscopic methods. H.-D.Amberger (Inst. für Anorganische und Angewandte Chem., Univ. Hamburg, Hamburg, Germany). *J. Less-Common Met. (Switzerland)*, vol.93, no.1, p.235-6 (1983). (Proceedings of the Sixteenth Rare Earth Research Conference, Tallahassee, FL, USA, 18-21 April 1983).

Summary form only given. During the last three decades Koningstein has demonstrated that electronic Raman transitions can often be observed in lanthanide compounds. As the electronic scattering tensor is of gerade parity, electronic Raman transitions are allowed even in centrosymmetric compounds. As no vibronic side bands have yet been observed, the electronic Raman spectra obtained reflect the underlying crystal field splitting patterns directly. The application of this effect to numerous quasi-octahedrally coordinated elpasolites of the type A₂BLnX₆ is reported. (no refs.)

114852 Low-frequency Raman scattering from methylene-oxyethylene-methylene triblock oligomers. T.G.E.Swales, H.H.Teo, R.C.Domszy, K.Viras, T.A.King, C.Booth (Dept. of Chem. & Phys., Univ. of Manchester, Manchester, England).

J. Polym. Sci. Polym. Phys. Ed. (USA), vol.21, no.8, p.1501-11 (Aug. 1983). Low-frequency Raman spectra are reported for monodisperse methylene-oxyethylene-methylene triblock oligomers. Assignments are made to the longitudinal acoustical modes (LAMs) of the oxyethylene block and the methylene block. The results for LAM-1 can be modeled by the vibrations of rods with perturbing forces and masses. The results for LAM-3 are not so readily modeled. (18 refs.)

114853 Raman and infrared spectra of calcium and barium sulphamates. P.Muthusubramanian, A.Sundara Raj (School of Phys., Madurai Kamaraj Univ., Madurai, India). *J. Raman Spectrosc. (GB)*, vol.14, no.4, p.221-4 (Aug. 1983). Raman spectra of a single crystal of calcium sulphamate and polycrystalline barium sulphamate have been recorded at room temperature. Infrared spectra

of polycrystalline calcium and barium sulphamates for the region 20-4000 cm^{-1} are also presented. The assignments made are supported by potential energy distribution calculations. The data show that there is no water of hydration in barium sulphamate. The N-S torsional mode is observed in both the compounds. This has not been found in other sulphamates of this family. The results indicate very weak hydrogen bonding in these crystals. (9 refs.)

114854 The hyper Raman spectra of some chloro- and bromo-methanes and some Group IV tetrachlorides. T.J.Dines, M.J.French, R.J.B.Hall, D.A.Long (School of Chem., Univ. of Bradford, Bradford, England). *J. Raman Spectrosc. (GB)*, vol.14, no.4, p.225-31 (Aug. 1983). The hyper Raman and hyper Raman spectra of the following Group IV halides are reported: the liquids CCl_4 , CHCl_3 , CH_2Cl_2 , CHBr_3 , CH_2Br_2 , CH_3Br , SiCl_4 , GeCl_4 and SnCl_4 and CBr_4 in solution in CCl_4 . Relative hyper Raman and hyper Raman intensities and depolarization ratios have been measured. These are discussed and the intensities compared with those observed in Raman and infrared spectra. (10 refs.)

114855 Temperature dependence of the Raman active B_{3g} torsional mode of sulphamic acid. C.I.Ratcliffe, W.F.Sherman, G.R.Wilkinson (Dept. of Phys., King's Coll., London, England). *J. Raman Spectrosc. (GB)*, vol.14, no.4, p.246-9 (Aug. 1983). The Raman active B_{3g} torsional mode of a single crystal of sulphamic acid has been observed as a function of temperature from liquid nitrogen to room temperature. The frequency decrease and markedly asymmetric broadening with increasing temperature have been characterized and are discussed. (21 refs.)

114856 A Raman study of solubilization of aromatics by non-ionic surfactants. R.P.Cooney (Dept. of Chem., Univ. of Newcastle, Newcastle, Australia), T.W.Healy, C.G.Barracough. *J. Raman Spectrosc. (GB)*, vol.14, no.4, p.250-2 (Aug. 1983). Raman spectra of the aromatic solubilization in the ternary system, non-ionic surfactant aromatic water, are indicative of benzene in a hydrophobic liquid-like environment and of pyridine in a hydrophilic, possibly aqueous environment. The non-ionic surfactants studied were of the alkylphenol- and alkyl-polyoxyethylene type. Addition of traces of water to a solution of Triton X-100 in benzene leads to the appearance of a water spectrum which suggests that 1:1 hydrogen-bond complexes between individual ether groups of the polyoxyethylene chain and water have formed in reversed micelles. (7 refs.)

114857 Vibrational, resonance Raman and electronic spectra of the μ -oxo-bis[pentacyanomanganate(III)] ion. A.H.Jubert, J.A.Espindola, E.L.Varetti, P.J.Aymonino (Facultad de Ciencias Exactas, Univ. Nacional de La Plata, La Plata, Argentina). *J. Raman Spectrosc. (GB)*, vol.14, no.4, p.259-63 (Aug. 1983). The resonance Raman spectra of the polycrystalline substance as well as the polarized infrared spectrum of an ordered array of small monocrystals were obtained for $\text{K}_3[\text{Mn}_2\text{O}(\text{CN})_{10}]\text{CN}$. Several of the bands observed in these spectra as well as in the electronic spectrum of the complex ion are assigned to expected transitions. (15 refs.)

114858 The polarized Raman spectra of CsCdCl_3 single crystals. M.H.Kuok (Dept. of Phys., Nat. Univ. of Singapore, Singapore). *J. Raman Spectrosc. (GB)*, vol.14, no.4, p.264-5 (Aug. 1983). Raman scattering measurements on CsCdCl_3 single crystals have been made at 15K. First- and second-order phonon scattering are observed and the symmetry species of the first-order spectrum have been partly determined by means of polarization studies. (6 refs.)

114859 Vibrational spectra and force constants for trans-sodium hyponitrite. L.-H.Chen, J.Laane (Dept. of Chem., Texas A&M Univ., College Station, TX, USA). *J. Raman Spectrosc. (GB)*, vol.14, no.4, p.284-7 (Aug. 1983). Laser Raman spectra of trans-sodium hyponitrite ($\text{Na}_2\text{N}_2\text{O}_2$) as a solid and in aqueous solution have been recorded, together with its infrared spectrum. Polarization data for the aqueous solution Raman spectra were also determined for the first time. The results confirm the trans structure of the hyponitrite ion and also have led to a new vibrational assignment. Force constant calculations have been carried out and these accurately predict the observed frequency shifts upon isotopic substitution. The potential energy distributions were also determined and these provide a useful picture of the coupling of the vibrational modes. (12 refs.)

114860 Study of uniaxially oriented isotactic polypropylene by the Raman effect: new results. L.D.Cambon, Luu Dang Vinh (Lab. de Spectroscopie Raman, Univ. des Sci. et Tech. du Languedoc, Montpellier, France). *J. Raman Spectrosc. (GB)*, vol.14, no.4, p.291-6 (Aug. 1983). In French. Heat-stretched samples of uniaxially oriented isotactic polypropylene were analysed by polarized Raman scattering. The authors inferred from a close observation of the spectra that lines can be classified into three groups. A theoretical analysis of the elements of derived polarizability tensors was elaborated and a hierarchy between these elements was specified for each group. These results allow the authors to improve and to extend previous assignments of isotactic polypropylene lines. (23 refs.)

114861 Low temperature Raman spectra of dibenzyl; comparison with biphenyl and paraterphenyl. A.Girard, M.Sanquer, G.P.Charbonneau (CNRS, Univ. de Rennes, Rennes, France). *Mol. Cryst. & Liq. Cryst. (GB)*, vol.95, no.3-4, p.237-47 (1983). The Raman spectra of crystal dibenzyl have been recorded from 293 down to 10K. No typical temperature dependence which usually accompanies phase transitions has been observed in frequencies, intensities or background. A comparison is made with biphenyl and paraterphenyl whose evolution of Raman spectra with the temperature looks similar. The very broad bands observed at room temperature result from the superposition of the different modes which appear well separated at 10K. This behaviour is consistent with the large atomic thermal motion observed by X-ray analysis. Vibrational frequencies have been calculated using the intermolecular potential of the atom-atom type in the rigid phenyl approximation and compared with experimental data. (23 refs.)

114862 Polymer deformation studies by time resolved Fourier transform infrared spectroscopy. J.E.Lasch, T.Masaoka, D.J.Burchell, S.L.Hsu (Dept. of Polymer Sci. & Engng., Univ. of Massachusetts, Amherst, MA, USA). *Polym. Bull. (Germany)*, vol.10, no.1-2, p.51-5 (June 1983). The authors have applied a newly developed time resolved Fourier transform infrared spectroscopy to follow microstructural changes in two semicrystalline polymers with time resolution in the order of milliseconds. This is a demonstration of a spectroscopic technique which is capable of measuring structural changes at the segmental level and relating them to macroscopic changes measured by dynamical mechanical spectroscopy. (18 refs.)

114863 Vibrational spectroscopic characterization of rigid rod polymers. IV. Crystalline modifications of poly(p-phenylene terephthalamide). D.Y.Shen, S.E.Molis, S.L.Hsu (Polymer Sci. & Engng. Dept., Univ. of Massachusetts, Amherst, MA, USA). *Polym. Eng. & Sci. (USA)*, vol.23, no.10, p.543-7 (July 1983). For pt.III see Polymer, vol.23, p.969 (1982). Infrared spectroscopy (4000-50 cm^{-1}) was used to characterize the two crystalline modifications of poly(p-phenylene terephthalamide). Polarized studies revealed that hydrogen bonds are oriented primarily perpendicular to the film plane in both forms. It was also found that the crystalline modification coagulated in water could be transformed into the other form by annealing at high temperatures. (23 refs.)

114864 Theory of Raman scattering from molecules adsorbed at semiconductor surfaces. H.Ueba (Dept. of Electronics, Toyama Univ., Toyama, Japan). *Surf. Sci. (Netherlands)*, vol.131, no.2-3, p.328-46 (Sept. 1983). A theory is presented to calculate the Raman polarizability of an adsorbed molecule at a semiconductor surface, where the electronic excitation in the molecule site interacts with excitons (elementary excitations in the semiconductor) through nonradiative energy transfer between them, in an intermediate state in the Raman scattering process. The Raman polarizability thus calculated is found to exhibit a peak at the energy corresponding to a resonant excitation of excitons, thereby suggesting the possibility of surface enhanced Raman scattering on semiconductor surfaces. The mechanism studied here can also give an explanation of a recent observation of the Raman excitation profiles of p-NDMA and p-DMAAB adsorbed on ZnO or TiO_2 , where those profiles were best described by assuming a resonant intermediate state of the exciton transition in the semiconductors. It is also demonstrated that in addition to vibrational Raman scattering, excitonic Raman scattering of adsorbed molecules will occur in the coupled molecule-semiconductor system, where the molecular returns to its ground electronic state by leaving an exciton in the semiconductor. A spectrum of the excitonic Raman scattering is expected to appear in the semiconductor. A spectrum of the excitonic Raman scattering is expected to appear in the background of the vibrational Raman band and to be characterized by the electronic structure of excitons. A desirable experiment is suggested for an examination of the theory. (37 refs.)

114865 Theory of charge transfer excitation in surface enhanced Raman scattering. H.Ueba (Dept. of Electronics, Toyama Univ., Toyama, Japan). *Surf. Sci. (Netherlands)*, vol.131, no.2-3, p.347-66 (Sept. 1983). On the basis of a recently proposed energy diagram of pyridine chemisorbed on Ag, a simple theory is presented to calculate the Raman scattering polarizability of an adsorbed molecule on a metal surface, where charge transfer excitation participates as intermediate state of the Raman process. The charge transfer excitation is assumed to occur from the metal to an unoccupied electron affinity level of the adsorbed molecule. Using a simple version of the Newns-Anderson model (1969) of chemisorption, it is found that the Raman polarizability is substantially enhanced when the frequencies of the incident or Raman scattered photons become resonant with the charge transfer excitations of the coupled system. The degree of enhancement is found to be sensitive to position and broadening of the charge transfer state and also the width of the electronic band of the metal. A broadened Raman line is also expected due to the modified electron-phonon interaction of the adsorbed molecule. (46 refs.)

114866 Surface enhanced Raman scattering from pyridine on copper in UHV. U.Erturk, I.Pockrand, A.Otto (Physik. Inst. III, Univ. Dusseldorf, Dusseldorf, Germany). *Surf. Sci. (Netherlands)*, vol.131, no.2-3, p.367-84 (Sept. 1983). The Raman spectra of pyridine on coldly deposited copper films show two groups of bands: one group originates from pyridine adsorbed at atomically smooth parts of the surface, this signal is enhanced mainly by electromagnetic resonances. The second group originates from pyridine at defect sites—where an additional enhancement of at least 2 orders of magnitude occurs. (56 refs.)

114867 An infra-red reflection absorption study of the adsorption of NO on Pt(111). B.E.Hayden (Fritz-Haber-Inst. Max-Planck-Gesellschaft, Berlin, Germany). *Surf. Sci. (Netherlands)*, vol.131, no.2-3, p.419-32 (Sept. 1983). The adsorption of NO on Pt(111) at 95K has been studied using infrared reflection absorption spectroscopy (IRAS) together with TPD and LEED. As in electron energy loss spectroscopy two vibrations in the NO stretch region are observed in the IRAS spectrum of adsorbed N^{14}O : a peak at 1476-98 cm^{-1} appears at low coverages but completely converts within a rather narrow coverage range ($0.12 > \theta > 0.16$) into a peak at 1700-25 cm^{-1} . The species giving rise to the latter band is associated with $p(2 \times 2)$ LEED pattern, and saturation coverage corresponds to a molecular NO coverage of $\theta = 0.25$. IRAS experiments involving isotopic mixtures of $\text{N}^{14}\text{O}/\text{N}^{15}\text{O}$ indicate that the two NO vibrations are due to bridge and linearly bound species. Two alternative adsorption models recently proposed for this system appear to be incorrect. The mixed isotope experiments have also enabled the dipole and static contributions to the coverage-dependent frequency shift of both species to be separated. The dipole shift, while very small for the bridging species ($< 5 \text{ cm}^{-1}$), is 33 cm^{-1} for the linear species at $\theta = 0.25$. The bridging NO species exhibits a significant positive static shift ($\sim 18 \text{ cm}^{-1}$) while the static shift observed for the linear species is negative ($\sim 13 \text{ cm}^{-1}$). There is evidence that the presence of the linear species on the surface contributes to the static shift of the bridging species in the region in which the two species co-exist. (24 refs.)

114868 Photoabsorption effect in diamagnetic exciton spectra of InSb crystals. S.I.Kokhanovskii, Yu.M.Makushenko, R.P.Seisyan (A.F. Ioffe Physicotech. Inst., Acad. of Sci., Leningrad, USSR). *Sov. Phys.-Semicond. (USA)*, vol.17, no.3, p.312-12 (March 1983). Translation of: *Fiz. & Tekh. Poluprovodn. (USSR)*, vol.17, no.3, p.501-3 (March 1983). [received: Sept. 1983] The authors carried out an experiment designed to detect the photoabsorption in InSb subjected to a magnetic field. Background illumination was provided by an He-Ne laser emitting at $\lambda = 3.39 \mu$, the radiation of which was interrupted at a frequency of $\Omega = 450 \text{ Hz}$. (8 refs.)

114869 Raman scattering in $\text{Bi}_{12}\text{Ti}_{20}$. Yu.G.Zaretskii, G.A.Kurbatov, V.V.Prokofev, Yu.I.Ukhanov, Yu.V.Shmartshev (M.I. Kalinin Polytech. Inst., Leningrad, USSR). *Sov. Phys.-Solid State (USA)*, vol.25, no.2, p.339-4 (Feb. 1983). Translation of: *Fiz. Tverd. Tela (USSR)*, vol.25, no.2, p.596-8 (Feb. 1983). [received: Sept. 1983] The authors have studied the Raman spectra of single-crystal $\text{Bi}_{12}\text{Ti}_{20}$ at $T \approx 80\text{K}$ and $T \approx 10\text{K}$. An attempt was made to calculate the intrinsic vibrational frequencies of the submolecular group $\text{O}_{(2)}\text{Bi}_3$ in $\text{Bi}_{12}\text{Ti}_{20}$ by the method of Babonas et al. (1982). (14 refs.)

- 114870 Raman scattering of light in N activated CdS crystals.** Yu.P.Gnatenko, P.A.Skubenko, A.Kh.Rozhko. *Ukr. Fiz. Zh. (USSR)*, vol.28, no.8, p.1257-8 (Aug. 1983). In Russian. Investigates the Raman scattering spectra of CdS:N crystals at T=300K. The spectra were used to obtain data on the appearance, in the low-frequency region of the spectrum (to 50 cm⁻¹), of oscillations due to the impurity as well as oscillations active in the Jahn-Teller interaction process. (6 refs.) N.G.P.
- 114871 Non destructive optical analysis of implanted layers in GaAs by Raman scattering and spectroscopic ellipsometry.** J.Biellmann, B.Prevot, C.Schwab (Lab. de Spectroscopie et d'Optique du Corps Solide, Strasbourg, France), J.-B.Theeten, M.Erman. Defects in Semiconductors II, Symposium Proceedings, Boston, MA, USA, Nov. 1982 (New York, USA: North-Holland 1983), p.517-22. Non destructive analysis by Raman Scattering (RS) and Spectroscopic Ellipsometry (SE) is demonstrated on B⁺ and Se⁺ shallow implanted GaAs. Qualitative informations are obtained from 1st and 2nd order RS spectra. The former are analysed using the intensity ratio of the TO and LO modes, which defines a lattice potential perfection scale. The SE analysis of the E₁, E₁+Δ₁ structure in the imaginary part of the dielectric function conforms the RS results and its multilayer analysis yields the depth profile of the implanted ions. (8 refs.)
- Rotational Raman interferometric measurement of flame temperatures** See Entry 111687
- Normal-coordinate analysis of retinal isomers and assignments of Raman and infrared bands** See Entry 112707
- Nitrite and nitrate ions as infrared pressure gauges for diamond anvils** See Entry 112734
- Infrared and Raman study of the fast internal motions of non-rigid molecules in condensed state: method of selective deuteration** See Entry 112735
- The Raman spectra and conformational change of simple sodium alkylsulfates and sodium alkylsulfonates in aqueous solution** See Entry 112737
- Raman spectra and vibrational dephasing of methylacetylene** See Entry 112742
- Hybrid four-wave mixing in liquid pyridine** See Entry 113054
- Raman scattering from molten alkali iodides** See Entry 113717
- Competitive equilibria in miscible polymer blends and low molecular weight analogues: a Fourier transform infrared study** See Entry 113724
- Fourier transform infrared studies of poly(vinyl chloride) blends with ethylene co- and terpolymers** See Entry 113725
- Transition metal ions in glasses: network modifiers or quasi-molecular complexes?** See Entry 113748
- Spectroscopic characterization of solvent-induced crystallization of PET** See Entry 113764
- Characterization of lattice disorder in the low-temperature phase of irradiated PTFE by vibrational spectroscopy** See Entry 113768
- Chain orientation in polystyrene/poly(2,6-dimethyl-1,4-phenylene oxide) blends** See Entry 113769
- A critical assessment of the application of FT-IR spectroscopy to the study of crystalline/compatible polymer blends** See Entry 113771
- Crystal structure and vibrational spectra of Pb₂P₂S₆** See Entry 113819
- Crystal chemistry of piezoelectric with a sillenite structure** .. See Entry 113821
- Crystal and molecular structure and IR spectra of 1-hydroxy-4-dibromomethyl-2,2,5,5-tetramethyl- and 4-dibromomethyl-1,2,2,5,5-pentamethyl-3-imidazoline-3-oxide** See Entry 113837
- Structure of salts of arylthioniacycloalkanes with a hydroxy group in the benzene ring. VIII. The crystal structure of 1-(2,5-dihydroxyphenyl)-thanium chloride monohydrate** See Entry 113845
- Measurements of ion-implantation damage in GaP** See Entry 113943
- Correlation of oxygen and recombination centers on a microscale in as-grown Czochralski silicon crystals** See Entry 113954
- Properties of solid potassium cyanide: is the physics of cyanide crystals really chemistry?** See Entry 114101
- Lattice dynamics of solid I₂ under high pressure** See Entry 114102
- Gitterdynamik von Imidazol (Lattice dynamics of Imidazol)** .. See Entry 114110
- Hyper-Raman spectra and frequency dependence of soft mode damping in SrTiO₃** See Entry 114118
- Phase transitions in Pb₃(P_{1-x}As_xO₄)₂: influence of the central peak and flip mode on the Raman scattering of hard modes** See Entry 114159
- Effect of the structural properties of compounds in the system Bi₂O₃-EO₂ (E=Ge, Si) on their dissolution** See Entry 114177
- Carbon and the kinetics of oxygen precipitation in silicon** See Entry 114192
- Oxygen precipitation in silicon—its effects on minority carrier recombination and generation lifetime** See Entry 114194
- Local excitons and effects of their mixing with electronic impurity states in naphthalene** See Entry 114452
- Three holes bound to a double acceptor: Be⁺ in germanium** .. See Entry 114469
- Chalcogenides in silicon** See Entry 114476
- Further interpretation of the spectra of Pr³⁺-LaF₃ and Tm³⁺-LaF₃** See Entry 114496
- Optical and thermal transitions in bismuth silicate** See Entry 114567
- Investigation of the surface of gallium arsenide doped by aluminum recoil atoms** See Entry 114584
- On the relation between the dielectric anomalies and the isofrequency dependences of inelastic scattering of light in lithium tantalate crystals** See Entry 114795
- Comment on the optical absorption edge in a-Si:H** See Entry 114817
- Infrared absorption in proton-irradiated solid deuterium** See Entry 114894
- Infrared-absorption of thermal donors in silicon** See Entry 114897
- Characterization of polycrystalline electrodeposited CdSe photoelectrodes using photoluminescence spectroscopy** See Entry 114902
- Optical probing of silicon-sapphire interface of heteroepitaxial SOS films** See Entry 114940
- Infrared optical properties of solid monomethyl hydrazine, N₂O₄, and N₂H₄ at cryogenic temperatures** See Entry 114942
- LPCVD polycrystalline silicon: growth and physical properties of in-situ phosphorus doped and undoped films** See Entry 115073
- Properties of hot-pressed zirconium pyrovanadate ceramics** ... See Entry 115149

- Thermal behavior of cyclohexaphosphates of certain polyvalent metals (Cu, Co, Ni, Mn, Ba)** See Entry 115523
- Thermal behavior of cyclohexaphosphates of certain polyvalent metals (Cd,Y,Ga)** See Entry 115524
- Proton transfer in complexes of water with hydrogen halides in aprotic solvents** See Entry 115544
- Irreversible loss of adatoms on Ag electrodes during potential cycling determined from surface enhanced Raman intensities** See Entry 115564
- Reaction of trimethylhalosilanes with the silica surface** See Entry 115584

78.35 BRILLOUIN AND RAYLEIGH SCATTERING

- 114872 Brillouin scattering in liquid benzene under high pressure.** A.Asenbaum (Max-Planck-Inst. für Festkörperforschung, Stuttgart, Germany), H.D.Hochheimer. *Z. Naturforsch. Teil A (Germany)*, vol.38A, no.9, p.980-6 (Sept. 1983). Brillouin spectra have been measured in liquid benzene at high pressures up to 1300 bar and at the temperatures 298.15K, 313.15K, 323.15K, and 343.15K. From the experimental spectra the hypersound velocities and the energy relaxation times were determined. The total velocity dispersion v_{ph}^2/v_0^2 due to the relaxation of the vibrational specific heat c_v is found to be nearly density independent in the pressure interval under study. It follows further that the experimentally determined specific heat corresponds to the theoretical value calculated with the vibrational modes of the benzene molecule. The energy relaxation time τ_1 connected with all vibrational modes but the lowest decreases with increasing density at constant temperature, at constant density τ_1 decreases with growing temperature. The relative relaxation rates were used to test the cell model (CM) with movable walls and the collision theory (HS) of Einwohner and Alder (1968). Using a hard sphere diameter derived from experimental transport coefficients the experimental results were predicted better by HS than by CM. (49 refs.)
- Stimulated Brillouin scattering in optical fibers, and wavefront reversal** See Entry 113058
- Studies on dilute solutions of rodlike macroions. I. Light scattering, densitometry, and cryoscopy** See Entry 113719
- Optical investigation of critical behaviour in simple fluids at reduced gravity** See Entry 114131
- Critical fluctuations at the phase transition in benzil** See Entry 114158
- Formation of a liquid crystal phase in the conversion of isotropic solutions of cellulose acetates into the solid state** See Entry 114171
- Observations upon the dynamic structure factor of interacting spherical polyelectrolytes** See Entry 114228
- Photoelasticity of KH₂PO₄, KD₂PO₄, and RbH₂PO₄** See Entry 114824
- The hyper Raman spectra of some chloro- and bromo-methanes and some Group IV tetrachlorides** See Entry 114854
- LPCVD polycrystalline silicon: growth and physical properties of in-situ phosphorus doped and undoped films** See Entry 115073
- Local acoustoelasticity in poly(methyl methacrylate) by Brillouin scattering** See Entry 115235

78.40 VISIBLE AND ULTRAVIOLET SPECTRA

- 114873 Photoacoustic spectra of MoS₂.** K.D.Carlson, D.Hodul (Argonne Nat. Lab., Argonne, IL, USA). *Appl. Opt. (USA)*, vol.22, no.18, p.2893-6 (15 Sept. 1983). The photoacoustic spectra of powdered MoS₂ prepared by particle-size reduction and dilution have been determined and compared with the optical transmittance spectra of single crystals and thin-film deposits. MoS₂ was chosen as a typical representative of the layer-structure transition metal dichalcogenides for which optical properties are important in explaining their unusual structural and transport properties. Reasonably well-resolved photoacoustic spectra were obtained by a layering technique using KCl as a diluent. Analysis of the experiments indicated that the spectral resolution was obtained not by reduction in photoacoustic signal saturation but by the enhancement of diffuse reflectance. (14 refs.)
- 114874 The diffuse reflectance spectra of mono-cadmium and di-cadmium stannates.** F.Golestani-Fard, C.A.Hogarth (Dept. of Phys., Brunel Univ., Uxbridge, England), D.N.Waters. *J. Mater. Sci. Lett. (GB)*, vol.2, no.9, p.505-10 (Sept. 1983). Following the work of A.J. Nozik (1972), the authors measured the spectral dependence of diffuse reflectance and provide evidence of a well-defined fundamental absorption edge which is different for the two materials (CdSnO₃ and Cd₂SnO₄). (10 refs.)
- 114875 The lowest triplet state of tetramethyl-1,3-cyclobutanedithione. I. Single-crystal polarized absorption spectrum.** J.Baiardo, M.Vala (Dept. of Chem., Univ. of Florida, Gainesville, FL, USA), I.Trabjerg. *Chem. Phys. (Netherlands)*, vol.79, no.3, p.391-402 (15 Sept. 1983). The single-crystal polarized absorption spectrum of tetramethyl-1,3-cyclobutanedithione (TMCBNDT) has been measured in the region of the lowest triplet state. All bands are polarized exclusively perpendicular to the tetragonal unit cell c axis. The 0-0 band which lies at 594.3 nm is the most intense feature with active vibrations at 309, 329, 600, 913, and 969 cm⁻¹ of lower intensity. The electronic transition is assigned to ³A_g←A_g (π*) in the D_{2h} molecular point group. Weak, low-frequency vibrations (<100 cm⁻¹) observed near the origin band (and several other vibronic bands) have been analyzed using a model in which the excited triplet and ground electronic states are described by double-minimum potentials (DMPs). The parameters for these states were found by fitting the low-temperature (1.6K) absorption and emission crystal spectra using the Coon, Naugle, and McKenzie (1966) method. A 23 cm⁻¹ potential barrier is found for the ground state and a 95 cm⁻¹ one for the triplet state. (29 refs.)
- 114876 Experimental studies on reflection spectra in monodomain cholesteric liquid crystal cells: total reflection, subsidiary oscillation and its beat or swell structure.** H.Takezoe, Y.Ouchi, M.Hara, A.Fukuda, E.Kuze (Dept. of Textile & Polymeric Materials, Tokyo Inst. of Technol., Tokyo, Japan). *Jpn. J. Appl. Phys. Part 1 (Japan)*, vol.22, no.7, p.1080-91 (July 1983). Many optical properties are studied here in the reflection spectra for monodomain cholesterics of various cell thicknesses at various angles of incidence. It is reported for the first time that left-circularly polarized light incident on a left-handed helix gives rise to a beat structure in the subsidiary oscillation, while right-circularly polarized light causes a swell to be superimposed on the subsidiary oscillation. The beat structure is ascribed to the excitation of two sets of optical eigen modes, each set consisting of two optical eigen modes of slightly different wavelength. The polarization characteristics of the total

reflection band as well as the selective reflection band are also discussed. (18 refs.)

114877 Electronic absorption and emission spectra of binuclear platinum(II) complexes. Characterization of the lowest singlet and triplet excited states of $\text{Pt}_2(\text{H}_2\text{P}_2\text{O}_5)_4^{4-}$. S.F.Rice, H.B.Gray (Arthur Amos Noyes Lab., California Inst. of Technol., Pasadena, CA, USA). *J. Am. Chem. Soc. (USA)*, vol.105, no.14, p.4571-5 (13 July 1983). The low-temperature electronic absorption and emission spectra of single crystals containing a binuclear platinum anion, $\text{Pt}_2(\text{H}_2\text{P}_2\text{O}_5)_4^{4-}$, have been measured and analyzed. Absorption systems in the 450- and 360-nm regions are attributable to transitions to $d\sigma^*p\sigma$ excited states ($^3A_{2g}$ and $^1A_{2g}$, respectively). The Pt-Pt stretching frequency in the $^3A_{2g}$ state (155 cm^{-1}) is much larger than that (110 cm^{-1}) in the ground state (the $^3A_{2g}$ absorption as well as the fluorescence ($^1A_{2u} \rightarrow ^2A_{1g}$) and phosphorescence ($^3A_{2u} \rightarrow ^1A_{1g}$) spectra exhibit Pt-Pt stretching progressions), which accords with the $d\sigma^*p\sigma$ description of the excited state. The Pt-Pt bond is calculated to contract by 0.21 \AA in the $^3A_{2u}$ state (relative to the ground-state value of 2.92 \AA). Measurements of the phosphorescence spectrum of $\text{Ba}_2\text{Pt}_2(\text{H}_2\text{P}_2\text{O}_5)_4$ at low temperatures (8-4.2K) confirm that there are two emitting levels split by 40.9 cm^{-1} (origins at 476.55 and 477.48 nm are assigned to the E_g and A_{1u} spin-orbit components of $^3A_{2u}$). (17 refs.)

114878 Lanthanide hypersensitivity in various solution media. S.A.Davis (Dickinson Coll., Carlisle, PA, USA). *J. Less-Common Met. (Switzerland)*, vol.93, no.1, p.239-40 (1983). (Proceedings of the Sixteenth Rare Earth Research Conference, Tallahassee, FL, USA, 18-21 April 1983). Summary form only given. The absorptive hypersensitive transitions of Nd^{3+} , Ho^{3+} , Er^{3+} and Eu^{3+} are examined under a variety of solution conditions. The hydrated chlorides of these lanthanides were dissolved (equimolar amounts) in various solvents. The solvents used (methanol, ethanol, dimethyl sulfoxide (DMSO), dimethylformamide (DMF) and water) all differ with regard to their dipole moments and polarizability. Each of the absorptive hypersensitive f-f transitions is observed to be composed of a set of crystal field 'bands' which are found to be at the same energies for each transition. As the solvent is changed, the intensities of these bands change. There appears to be a correlation between the increase in the intensity of some of these bands and the increase in polarizability. This is complementary to the observed correlation between the total oscillator strength and the polarizability. (no refs.)

114879 Picosecond dynamics of hot carrier relaxation in highly excited multi-quantum well structures. C.V.Shank, R.L.Fork, R.Yen, J.Shah (Bell Telephone Labs., Holmdel, NJ, USA), B.I.Greene, A.C.Gossard, C.Weisbuch. *Solid State Commun. (USA)*, vol.47, no.12, p.981-3 (Sept. 1983). Dynamics of hot carrier relaxation, exciton screening and subband level renormalization in GaAs-AlGaAs multiple quantum well structures are investigated by time resolved measurements of optical absorption and gain following subpicosecond optical excitation. The cooling rate of the electron hole plasma in these two dimensional structures is approximately the same as for bulk GaAs at comparable photoexcitation density. (6 refs.)

114880 Ni^{2+} pair spectra in the excited orbitally degenerate states. V.Ya.Mitrofanov, A.E.Nikiforov, A.N.Men (Inst. of Metall., Ural Sci. Centre, Sverdlovsk, USSR). *Spectrosc. Lett. (USA)*, vol.16, no.8, p.621-7 (1983). The main features of Ni^{2+} pair spectra in the excited orbitally degenerate nonmagnetic states (1E , 1T_2) caused by the vibronic and exchange interactions are considered. (6 refs.)

114881 Edge absorption and band gap of $\text{CuAl}_x\text{Ga}_{1-x}\text{Se}_2$ solid solutions. I.V.Bodnar, N.L.Gil, A.I.Lukomskii (Inst. of Solid-State & Semiconductor Phys., Acad. of Sci., Minsk, Belorussian SSR). *Sov. Phys.-Semicond. (USA)*, vol.17, no.3, p.333-4 (March 1983). Translation of: *Fiz. i Tekh. Poluprovodn. (USSR)*, vol.17, no.3, p.530-2 (March 1983). [received: Sept. 1983] Ternary semiconductor compounds CuAlSe_2 and CuGaSe_2 crystallize in the chalcopyrite structure. They have attracted attention because of potential applications in nonlinear optics and optoelectronic devices. The optical properties of these compounds have been investigated in the region of the fundamental absorption edge. However, such investigations have not yet been carried out on solid solutions based on these compounds. The authors' aim was to determine the absorption spectra of $\text{CuAl}_x\text{Ga}_{1-x}\text{Se}_2$ solid solutions in the spectral range adjoining directly the fundamental absorption edge, and to determine the nature of the composition dependence of the band gap. (8 refs.)

114882 Optical properties of ferroelectrics with tetragonal potassium-tungsten-bronze in the fundamental absorption region. A.A.Mamedov (Azerbaijani State Univ., Baku, Azerbaijan SSR). *Sov. Phys.-JETP (USA)*, vol.83, no.5, p.1043-9 (Nov. 1982). Translation of: *Zh. Eksp. i Teor. Fiz. (USSR)*, vol.83, no.5, p.1804-15 (Nov. 1982). [received: Sept. 1983] The reflection spectra of ferroelectrics with the structure of tetragonal potassium-tungsten bronze ($\text{Ba}_2\text{Sr}_{1-x}\text{O}_6$ and $\text{Ba}_2\text{NaNb}_2\text{O}_{15}$) are investigated at energies $\hbar\omega=1.0$ to 35 eV . The results are used to calculate the optical function, to propose an interband-transition energy scheme, and to demonstrate the important role of the NbO_6 octahedron in the formation of the band structure of the crystals. (20 refs.)

Production and properties of crystals of complex refractory oxides with perovskite structure See Entry 113776
Growth structure and optical properties of single crystals of rubrene See Entry 113841
Color centers in $\text{K}_2\text{S}_2\text{O}_6$ and $\text{Rb}_2\text{S}_2\text{O}_6$ crystals See Entry 113910
Process study of chemically vapour-deposited SnO_2 ($x \approx 2$) films See Entry 114395
Absorption of light by bound electron-exciton states in two-dimensional molecular crystals See Entry 114451
Zeeman spectroscopy of crystal-field transitions of Co-doped InP See Entry 114492
Mechanism of the photoconductivity of nickel-compensated gallium phosphide See Entry 114565
Influence of solid support sorptive properties on the colour of cholesteric liquid crystals. II. Quantitative results See Entry 114805
Investigation of the refractive indices of LaF_3 , CeF_3 , PrF_3 and NdF_3 See Entry 114815
Comment on the optical absorption edge in α -Si:H See Entry 114817
Optical and Mossbauer spectra of manganese-bearing phlogopites: $\text{Fe}_{1-y}^{3+}\text{-Mn}_{y-1}^{2+}$ pair absorption as the origin of reverse pleochroism See Entry 114823

Absorption and surface-enhanced Raman spectra of silver organosols in ethanol See Entry 114840
Optical determination of the electronic characteristics of Nb-Al alloys with the A15 lattice See Entry 114845
Al-induced enhancement colouration by gamma irradiation in some borate glasses See Entry 114884
Ultraviolet A-band absorption in NaCl:Pb^{2+} and clustering of lattice defects See Entry 114887
Judd-Ofelt parameters and chemical bonding See Entry 114888
Color centers and electron spin resonance in chrysoberyl containing Mn and Ti guest ions See Entry 114890
Absorption spectrum of Cr^{3+} ion doped in lithium ammonium sulphate single crystal See Entry 114895
Optical studies of $\text{In}_x\text{Ga}_{1-x}\text{As-GaAs}$ strained multiquantum well structures See Entry 114898
Spontaneous site reorientation in a mixed molecular crystal: tetracene in benzoic acid See Entry 114903
Luminescence properties and two-photon absorption of Gd^{3+} -doped LaCl_3 See Entry 114906
The optical absorption edge of amorphous thin films of borosilicate glass See Entry 114939
Optical probing of silicon-sapphire interface of heteroepitaxial SOS films See Entry 114940
Abnormal optical absorption of quenched Ag films due to surface roughness See Entry 114946
Detailed absorption, reflectance, and UV photoelectron spectroscopic and theoretical studies of the charge-transfer transitions of CuCl_4^{2-} : correlation of the square-planar and the tetrahedral limits See Entry 115008

78.45 STIMULATED EMISSION

(see also 42.65C in nonlinear optics)

114883 Stimulated Raman emission of coherent phonons by impurities in a crystal. B.Fain (Dept. of Chem., Tel-Aviv Univ., Ramat Aviv., Tel-Aviv, Israel).

J. Appl. Phys. (USA), vol.54, no.9, p.4832-40 (Sept. 1983). The possibility of stimulated emission of coherent phonons by impurities (ions) embedded in a crystal is considered. It is shown that when the ions with homogeneously broadened levels are subjected to an electromagnetic field, the frequency Ω of which is larger than an eigenfrequency of the ion ω_{21} , at the Raman frequency $\omega_0 = \Omega - \omega_{21}$, a coherent stimulated emission of phonons may emerge. The absorption rate of the pumping electromagnetic field has a singularity near the threshold of the phonon self-excitation. (10 refs.)

Cascade laser generation by Er^{3+} ions in YAlO_3 crystals by the scheme $^4S_{3/2} \rightarrow ^4I_{9/2} \rightarrow ^4I_{11/2} \rightarrow ^4I_{13/2}$ See Entry 113002

78.50 IMPURITY AND DEFECT ABSORPTION IN SOLIDS

114884 Al-induced enhancement colouration by gamma irradiation in some borate glasses. A.M.Nassar (Phys. Dept., Nuclear Res. Centre, Cairo, Egypt), M.M.Morsi, M.A.Adawi.

Atomkernenerg. Kerntechnik. (Germany), vol.42, no.2, p.117-19 (1983). Potassium borate and potassium-alumino-borate glasses were prepared and exposed to gamma radiation. Optical transmission studies show that an absorption band is induced at 802-830 nm in binary potassium borate and Al-containing glasses, respectively. The presence of induced bands at 525 and 484 nm is recorded in the latter glasses only. A postulate for the centres responsible for the observed absorption bands is given. The long wavelength band (802-830 nm) is attributed to electron trapped centres on boron atoms co-ordinated with three bridging oxygen atoms and stabilized by alkali ions nearby. The bands at 525 and 484 nm were attributed to trapped hole centers at AlO_4 units. The holes trapped on these units are of different modes. (14 refs.)

114885 Excitation spectrum of neutral and singly ionized beryllium acceptors in germanium. L.T.Ho, J.W.Cross, A.K.Ramdas (Dept. of Phys., Purdue Univ., Lafayette, IN, USA), R.Sauer.

Annu. Rep. Inst. Phys. Acad. Sin. (Taiwan), vol.12, p.240 (Dec. 1982). [received: Sept. 1983] Beryllium, a group II impurity, enters germanium substitutionally, hence it is a double acceptor. Neutral Be^0 binds two holes and the excitation spectrum of $\text{Ge}(\text{Be}^0)$ shows lines with spacings close to those for the other group II impurities Zn and Hg and those recently observed for Mg. The authors have examined the $\text{Ge}(\text{Be}^0)$ with a high resolution Fourier transform spectrometer equipped with a liquid helium cooled bolometer. They have discovered that all the prominent lines are split into doublets with a spacing of 0.09 meV . They interpret this splitting as a consequence of closely spaced $\Gamma_1 + \Gamma_3 + \Gamma_5$ ground states. This ground state multiplicity is due to the double acceptor nature of Be^0 . When beryllium in germanium is suitably compensated it is possible to obtain singly ionized Be^+ , Be^- . The excitation spectrum of $\text{Ge}(\text{Be}^-)$ shows that the spacings of the lines are four times those of the corresponding lines in $\text{Ge}(\text{Be}^0)$. (no refs.)

114886 Excitation spectrum of magnesium acceptors in germanium. L.T.Ho, J.W.Cross, A.K.Ramdas (Dept. of Phys., Purdue Univ., Lafayette, IN, USA).

Annu. Rep. Inst. Phys. Acad. Sin. (Taiwan), vol.12, p.241 (Dec. 1982). [received: Sept. 1983] Magnesium is an interstitial impurity in silicon (Si) with a T_d site symmetry. It exhibits an excitation spectrum characteristic of a shallow, 'He-like' double donor. With a view to exploring the behavior of Mg in germanium (Ge), the authors have diffused it into the pure crystal and examined its excitation spectrum. Ge crystal with the impurities diffused into it is p-type thus strongly indicating that unlike its behavior in Si, Mg is a double acceptor. The excitation spectrum measured on a Fourier transform spectrometer shows excitation lines very similar to that exhibited by $\text{Ge}(\text{Zn})$, $\text{Ge}(\text{Hg})$, and $\text{Ge}(\text{Be})$. The spacings of the lines, G, D, C, B, A, and A' for the various impurities are remarkably close; their relative intensities are also very similar. (no refs.)

114887 Ultraviolet A-band absorption in NaCl:Pb²⁺ and clustering of lattice defects. J.S.Dryden, R.G.Heydon (CSIRO Div. of Appl. Phys., Sydney, NSW, Australia).

J. Phys. C (GB), vol.16, no.27, p.5363-73 (30 Sept. 1983). Changes in the A-band absorption spectrum of NaCl:Pb²⁺, resulting from isothermal aging, have been analysed using information obtained from dielectric relaxation measurements about the state of aggregation of the Pb²⁺ ions and their associated vacancies. Optical absorption has been measured at room and liquid nitrogen temperatures. It is shown that the A band, centred at 4.54 eV for (Pb²⁺-vacancy) pairs, splits into two bands, when clusters of three (Pb²⁺-vacancy) units form during the first stage of aggregation. One band is at the same energy (4.54 eV) and the other at 4.34 eV. In the second stage of aggregation these trimer bands persist with no change in intensity, and two new bands appear at 4.66 eV and 4.34 eV. The significance of these measurements for models of the aggregation process is discussed. (14 refs.)

114888 Judd-Ofelt parameters and chemical bonding. C.K.Jorgensen, R.Reisfeld (Dept. de Chimie Minérale, Analytique et Appliquée, Univ. de Genève, Geneva, Switzerland).

J. Less-Common Met. (Switzerland), vol.93, no.1, p.107-12 (1983). (Proceedings of the Sixteenth Rare Earth Research Conference, Tallahassee, FL, USA, 18-21 April 1983).

The three Judd-Ofelt intensity parameters for erbium(III) are given in 17 different environments. The Ω_2 parameter is strongly affected by covalent chemical bonding. In contrast, the Ω_6 parameter is related to the rigidity of the medium in which the ions are situated. (45 refs.)

114889 Rationalization of the f-f intensity parameters for transitions between crystal field levels of lanthanide ions. M.F.Reid, F.S.Richardson (Dept. of Chem., Univ. of Virginia, Charlottesville, VA, USA).

J. Less-Common Met. (Switzerland), vol.93, no.1, p.113-18 (1983). (Proceedings of the Sixteenth Rare Earth Research Conference, Tallahassee, FL, USA, 18-21 April 1983).

The intensity parameters $A_{\lambda}\bar{\alpha}(r,\lambda)$, which are applied to electric dipole transitions between crystal field levels in lanthanide 4f-4f spectra, are shown to contain much more information regarding intensity mechanisms than do the Ω_{λ} parameters, which are applied to transitions between J multiplets. Within the context of the prevailing electrostatic models for 4f-4f electric dipole intensity, it is shown that the relative contributions of the static-coupling and dynamic-coupling mechanisms to the intensity parameters can be differentiated on the basis of the signs obtained for the various $A_{\lambda}\bar{\alpha}(r,\lambda)$. To illustrate this point, a set of intensity parameters (related to the $A_{\lambda}\bar{\alpha}(r,\lambda)$) are calculated for the Pr³⁺-LaAlO₃ system. The calculated results are then compared with the empirically determined intensity parameters reported for this system, and conclusions are drawn regarding the relative importance of the static-coupling and dynamic-coupling mechanisms. (19 refs.)

114890 Color centers and electron spin resonance in chrysoberyl containing Mn and Ti guest ions. V.P.Solntsev, V.N.Matrosov, E.G.Tsvetkov.

J. Appl. Spectrosc. (USA), vol.37, no.5, p.1319-22 (Nov. 1982). Translation of: *Zh. Prikl. Spektrosk. (USSR)*, vol.37, no.5, p.839-43 (Nov. 1982). [received: Sept. 1983]

The work reported is concerned with a study of the ESR spectra and the optical electronic absorption spectra of Mn and Ti in chrysoberyl with the aim of establishing their valence state, coordination, and possible link with the color of the sample. The ESR lines were measured at a frequency of 9.3 GHz at 300 and 77K. The transmission spectra were recorded in polarized light on an SF-8 spectrophotometer at 300K using disks which had been cut out parallel to the {001}, {010}, and {100} edges. (10 refs.)

114891 Attenuation of optical irradiation by bismuth colloidal colour centres. I.S.Radchenko, Yu.A.Ekmanis.

Latv. PSR Zinat. Akad. Vestis Fiz. Teh. Zinat. Ser. (USSR), no.4, p.10-17 (1983). In Russian.

Calculation results for optical attenuation spectra and scattering of bismuth in the colloidal phase in the matrix of NaCl, KCl, KBr, KI, RbCl are reported. Comparison with experimental data allows the authors to interpret absorption bands of these centres taking into account their structure and shape. (22 refs.)

114892 Fundamental absorption edge of irradiated alkali halides. L.G.Grigor'eva, D.K.Millers.

Latv. PSR Zinat. Akad. Vestis Fiz. Teh. Zinat. Ser. (USSR), no.4, p.60-5 (1983). In Russian.

The fundamental absorption edge and the changes of intrinsic luminescence in NaCl, KCl, KBr and KI crystals irradiated at room temperature have been studied. It is shown that the radiation damage in the form of point defects as well as aggregated defects gives rise to perturbed exciton states. These perturbed exciton states are responsible for changes in the fundamental absorption edge and intrinsic luminescence spectra. The comparison of the fundamental absorption edge irradiated and unirradiated crystals can be used for studying the full annealing of radiation damages. (14 refs.)

114893 Two-photon absorption cross section at F₂⁺ centers of alkali-halide crystals. V.F.Kamalov, Yu.P.Svirko (Dept. of General Phys. & Wave Processes, Moscow Univ., Moscow, USSR).

Moscow Univ. Phys. Bull. (USA), vol.38, no.1, p.43-6 (1983). Translation of: *Vestn. Mosk. Univ. Ser. 3 (USSR)*, vol.38, no.1, p.38-41 (1983).

The nonlinear optical susceptibilities of F₂⁺ centers in alkali-halide crystals are calculated. Values of the energy and dipole moments of transitions determined within the framework of the model of the molecular hydrogen ion allow the two-photon absorption cross section of a series of optical transitions. (9 refs.)

114894 Infrared absorption in proton-irradiated solid deuterium. R.L.Brooks, M.A.Selen, J.L.Hunt, J.R.MacDonald, J.D.Poll (Univ. of Guelph, Guelph, Ontario, Canada), J.C.Waddington.

Phys. Rev. Lett. (USA), vol.51, no.12, p.1077-80 (19 Sept. 1983).

The infrared absorption spectrum of solid D₂ at 4.2K has been studied with the sample irradiated by a 15-MeV proton beam. Three beam-induced spectral features have been observed. Comparison of these features with those previously seen in a sample doped with tritium conclusively establishes the presence and indicates the nature of a radiation-induced absorption process. After turning off the proton beam, these features persist for times of the order of hours; they can be quenched by heating the sample to ~11K. (7 refs.)

114895 Absorption spectrum of Cr³⁺ ion doped in lithium ammonium sulphate single crystal. S.V.J.Lakshman, T.V.Krishna Rao, K.Purandar (Dept. of Phys., SV Univ., Tirupati, India).

Solid State Commun. (USA), vol.47, no.12, p.993-5 (Sept. 1983).

The absorption spectrum of Cr³⁺ ion doped in lithium ammonium sulphate single crystal has been studied both at room (300K) and liquid nitrogen (77K) temperatures. From the nature and position of the observed bands, O_h symmetry is assumed for the ion. The spectroscopic parameters derived for

the ion in the crystal at 77K are D_q=1655 cm⁻¹, B=735 cm⁻¹ and C/B=4.4. (20 refs.)

114896 Spectrum of localized states near the fundamental absorption edge and likely mechanism of compensation of CdTe:Cl crystals. N.V.Agrinskaya, O.A.Matveev (A.F. Ioffe Physicotech. Inst., Acad. of Sci., Leningrad, USSR). *Sov. Phys.-Semicond. (USA)*, vol.17, no.3, p.245-7 (March 1983). Translation of: *Fiz. & Tekh. Poluprovodn. (USSR)*, vol.17, no.3, p.394-7 (March 1983). [received: Sept. 1983]

An investigation was made of the impurity absorption and photoconductivity in the part of the spectrum adjoining the fundamental edge. A distinguishing feature of grown CdTe:Cl crystals subjected to the process of self-purification was the low density of the impurity levels in the region far from the band gap edge, but near the edge of the valence band there were levels due to a high concentration ($\geq 2 \times 10^{16}$ cm⁻³) of acceptor centers with an ionization energy ~0.04 eV. Heat treatment in vacuum at 500°C increased the concentration of acceptors with deeper levels, which were vacancies (V_{Cd}) and complexes (V_{Cd}Cl). The likely compensation mechanism was analyzed and it was concluded that Frenkel pairs formed alongside Cl atoms in the course of self-purification. (7 refs.)

114897 Infrared-absorption of thermal donors in silicon. R.Oeder, P.Wagner (Heliotronic GmbH, Burghausen, Germany).

Defects in Semiconductors II, Symposium Proceedings, Boston, MA, USA, Nov. 1982 (New York, USA: North-Holland 1983), p.171-5

Thermal donors generated in CZ-silicon by annealing at 450°C are investigated by infrared absorption spectroscopy. Up to nine double-donors can be distinguished due to their line spectra characteristic for effective-mass-like donors. Their number and their concentrations depend on the duration of the thermal treatment. The formation of the different donors is ruled by complicated kinetics. (12 refs.)

The role of the state of dispersion of impurity on Z₁-centres in NaCl:Ca²⁺ crystals See Entry 113909

Correlation of oxygen and recombination centers on a microscale in as-grown Czochralski silicon crystals See Entry 113954

Carbon and the kinetics of oxygen precipitation in silicon See Entry 114192

Local excitons and effects of their mixing with electronic impurity states in naphthalene See Entry 114452

Three holes bound to a double acceptor: Be⁺ in germanium See Entry 114469

Chalcogenides in silicon See Entry 114476

Further interpretation of the spectra of Pr³⁺-LaF₃ and Tm³⁺-LaF₃ See Entry 114496

Mechanism of the photoconductivity of nickel-compensated gallium phosphide See Entry 114565

Luminescence properties and two-photon absorption of Gd³⁺-doped LaCl₃ See Entry 114906

78.55 PHOTOLUMINESCENCE

114898 Optical studies of In_xGa_{1-x}As-GaAs strained multiquantum well structures. J.Y.Marzin, E.V.K.Rao (CNET, Bagneux, France).

Appl. Phys. Lett. (USA), vol.43, no.6, p.560-2 (15 Sept. 1983).

The authors present photoluminescence and absorption measurements on molecular beam epitaxy grown strained In_xGa_{1-x}As-GaAs multiquantum well structures. The absorption results are interpreted as excitonic transitions ($n=1$, $n=2$), while the room-temperature luminescence spectrum shows the corresponding subband to subband transitions, and the low-temperature luminescence spectrum exhibits only the $n=1$ excitonic line. (9 refs.)

114899 Radiative lifetime in semiconductors for infrared detection. R.G.Humphreys (Royal Signals & Radar Establ., Malvern, England).

Infrared Phys. (GB), vol.23, no.3, p.171-5 (May 1983).

The radiative lifetime of excess carriers calculated by W. van Roosbroeck and W. Shockley (1954) is re-examined. Due to reabsorption effects, this lifetime is an underestimate of what would be measured in the bulk. It is shown that this extension of the lifetime can be considered as effectively noiseless. The consequences of this for infrared detector operating temperatures are discussed, with the conclusion that the state of the art is much further from the fundamental limit than had been supposed and substantial further improvements are possible. (8 refs.)

114900 Evaluation of spectroscopic parameters for the Pr³⁺ ion in a laser liquid. S.V.J.Lakshman, S.Buddhudu (Dept. of Phys., S.V. Univ., Tirupati, India).

Indian J. Pure & Appl. Phys., vol.21, no.7, p.413-15 (July 1983).

Radiative lifetimes are predicted for the fluorescent ³P₁, ³P₀ and ¹D₂ levels of Pr³⁺ in the laser liquid SeOCl₂. Quantities such as squared reduced matrix elements, electric and magnetic dipole line strengths, total radiative transition probabilities and radiative relaxation rates which are required for lifetime calculations are also reported. (11 refs.)

114901 Improvement of photoluminescence of molecular beam epitaxially grown Ga_xAl_{1-x}In_{1-x-y}As by using an As₂ molecular beam. W.T.Tsang, J.A.Ditzenberger, N.A.Olsson (Bell Labs., Murray Hill, NJ, USA).

IEEE Electron Device Lett. (USA), vol.EDL-4, no.8, p.275-7 (Aug. 1983).

The authors report the use of an As₂ (instead of As₄) beam during molecular beam epitaxial (MBE) growth of Ga_xAl_{1-x}In_{1-x-y}As layers, lattice-matched to InP substrate. They also show that use of the As₂ beam improves the room-temperature photoluminescence intensities of both In_{0.53}Ga_{0.47}As and Ga_{0.39}Al_{0.08}In_{0.53}As epilayers with more significant improvement for the latter. The substrate temperature employed was ~580°C for both. (26 refs.)

114902 Characterization of polycrystalline electrodeposited CdSe photoelectrodes using photoluminescence spectroscopy. R.P.Silberstein, M.Tomkiewicz (Dept. of Phys., Brooklyn Coll., City Univ. of New York, New York, NY, USA).

J. Appl. Phys. (USA), vol.54, no.9, p.5428-35 (Sept. 1983).

The authors have utilized both photoluminescence (PL) and Raman spectroscopy to nondestructively study the surface of polycrystalline electrodeposited CdSe photoelectrodes as a function of surface preparation and aging procedures. The excitation energy dependence of the PL efficiency at 77K, which depends on surface band bending, is consistent with increased concentration of shallow levels in electrodeposited CdSe compared with single crystal material. No PL was observed for unannealed CdSe films; for annealed, unaged films the spectra at 77K were qualitatively similar to those of single crystals in that spectral features could be identified with the A exciton at 1.815 eV and with a donor-acceptor-pair band at 1.70 eV exhibiting photon replicas. The PL and Raman spectra of light-aged electrodes exhibit features which the authors identify with the formation of a surface layer of CdS and the presence of mixed compounds CdS_{1-x}Se_x, which are formed by chemical exchange with the polysulfide electrolyte during light-induced aging. The PL spectra at 4.2K for the unaged and dark-aged electrodes exhibit sharp lines in the vicinity of

1.81 eV which they identify as due to bound-exciton recombination, but which differ in energy from those exhibited by the light-aged film. (21 refs.)

114903 Spontaneous site reorientation in a mixed molecular crystal: tetracene in benzoic acid. H.B.Levinsky, D.A.Wiersma (Dept. of Phys. Chem., Univ. of Groningen, Groningen, Netherlands). *J. Chem. Phys. (USA)*, vol.79, no.6, p.2677-82 (15 Sept. 1983). Absorption and fluorescence spectra of tetracene in a benzoic acid host crystal at 1.5K are presented. The fluorescence zero-phonon line is shifted by more than 800 cm^{-1} to the red of the maximum of the 120 cm^{-1} broad absorption origin. This shift is attributed to a lateral site reorientation of the guest upon excitation, permitted by the difference in size between the tetracene and the benzoic acid dimer it replaces. In addition, other features in the fluorescence spectrum are ascribed to photon tautomerization occurring in the host dimers in the vicinity of the guest. These features disappear upon deuteration of the host acid protons, while the magnitude of the red shift is virtually unchanged. (31 refs.)

114904 Alignment of solutes in stretched polyethylene. Determination of the five second and fourth moments of the orientation distribution of 2-fluoropyrene from polarized fluorescence. Additional evidence for the twisting of weak transition moments by the solvent environment. F.W.Langkilde, M.Gisin, E.W.Thulstrup, J.Michl (Dept. of Chem., Univ. of Utah, Salt Lake City, UT, USA). *J. Phys. Chem. (USA)*, vol.87, no.15, p.2901-11 (21 July 1983). Measurements of linear dichroism and of polarized fluorescence of 2-fluoropyrene (2-F-1) in stretched linear low-density polyethylene (LLDPE) at 77K have been used to evaluate the two independent second moments, $\langle \cos^2 \theta \rangle$ and $\langle \cos^2 \theta \rangle$, as well as the three independent fourth moments, $\langle \cos^4 \theta \rangle$, $\langle \cos^4 \theta \rangle$, and $\langle \cos^4 \theta \rangle$, of the orientation distribution function. The results are used to discuss two previously proposed detailed models for the mechanism of the orientation of aromatics in stretched polyethylene. For pyrene (1) and 2-methylpyrene (2-Me-1), four of the five moments were obtained. In these two molecules the direction of the L_y transition moment does not coincide with the molecular short in-plane y axis, but shows a distribution of orientations within the molecular framework, revealed by a site-selection experiment. On the average, it is inclined approximately 40° and 20° away from the y axis in the two compounds, respectively. This behavior is ascribed to a symmetry-lowering perturbation by the environment, related to the Ham effect. (19 refs.)

114905 Laser-induced emission of $\text{CaF}_2\text{-Tb}^{3+}$ at room and low temperatures. J.Chrysoschoos (Dept. of Chem., Univ. of Toledo, Toledo, OH, USA). *J. Less-Common Met. (Switzerland)*, vol.93, no.1, p.73-80 (1983). (Proceedings of the Sixteenth Rare Earth Research Conference, Tallahassee, FL, USA, 18-21 April 1983). Laser-induced emission spectra of $\text{CaF}_2\text{-Tb}^{3+}$ at room and low temperatures excited via the 4765, 4880 and 4965 Å lines of an argon ion laser consist primarily of two groups of emission lines which are dependent upon both the excitation wavelength and the temperature. Group I is obtained at all excitation wavelengths whereas group II is virtually missing from the emission spectra excited at 4765 Å. Based upon the Stark splitting of the emission spectra recorded and their comparison with appropriate emission spectra of Tb^{3+} in hosts of known symmetry, groups I and II are tentatively assigned to the C_{4v} and C_{3v} sites respectively of Tb^{3+} . (22 refs.)

114906 Luminescence properties and two-photon absorption of Gd^{3+} -doped LaCl_3 . C.Linares, P.Jung, G.Boulon, F.Gaume (Lab. de Physicochimie des Matériaux Luminescents, Univ. de Lyon I, Villeurbanne, France). *J. Less-Common Met. (Switzerland)*, vol.93, no.1, p.89-96 (1983). (Proceedings of the Sixteenth Rare Earth Research Conference, Tallahassee, FL, USA, 18-21 April 1983). A UV tunable dye laser was used to excite selectively the Stark components of the $^4F_{7/2}$ levels of Gd^{3+} in an LaCl_3 host. The results demonstrate the existence of three types of sites in this host, with energy transfer between the Gd^{3+} ions. In addition, an antiStokes emission from the $^6I_{7/2}$ level was observed for which a mechanism is proposed. (13 refs.)

114907 The variation in europium(III) and terbium(III) luminescence lifetimes with concentration in rare earth oxysulphide matrices. Y.Charrere, J.Dexpert-Ghys (Lab. des Elements de Transition dans les Solides, CNRS, Meudon Bellevue, France), M.Leskela, L.Niinisto. *J. Less-Common Met. (Switzerland)*, vol.93, no.1, p.103-5 (1983). (Proceedings of the Sixteenth Rare Earth Research Conference, Tallahassee, FL, USA, 18-21 April 1983). The transient properties of the Eu^{3+} 5D_2 , 5D_1 , 5D_0 emitting levels in oxysulphide matrices at various doping concentrations were analysed under either charge transfer state or direct 5D_1 selective excitation using pulsed laser light. At low Eu^{3+} concentrations the data can be described in terms of the step process $^5D_2 \rightarrow ^5D_1 \rightarrow ^5D_0$. The decrease in the 5D_2 and 5D_1 lifetimes with concentration can be interpreted by cross-relaxation (Eu-Eu) processes, whereas the presence of an (unidentified) impurity in the phosphors is proposed to explain the concentration quenching of 5D_0 . This conclusion is supported by the observation of similar behaviour of Tb^{3+} 5D_4 emission in the same matrices which is attributed to Eu^{3+} ions acting as traps. (3 refs.)

114908 Synthesis and spectroscopic properties of the Sillen phases. O.K.Moune-Minn, L.Albert, P.Caro (Lab. des Elements de Transition dans les Solides, CNRS, Meudon Bellevue, France). *J. Less-Common Met. (Switzerland)*, vol.93, no.1, p.143-50 (1983). (Proceedings of the Sixteenth Rare Earth Research Conference, Tallahassee, FL, USA, 18-21 April 1983). The family of Sillen phases consists of compounds where layers of the quadratic complex cation $(\text{BiO})_2^{2+}$ alternate with layers of perovskite-like structures of the form $\text{A}_{n-1}\text{B}_n\text{O}_{3n+1}$. The authors synthesized compounds with $1 \leq n \leq 5$ containing titanium, niobium or tungsten as the other cations. The fluorescence spectrum of Eu^{3+} embedded in these matrices is very complicated in view of the various point sites occupied by the rare earth. The dye laser selective excitation technique enables three different point sites to be analysed. (15 refs.)

114909 Has the $(\text{LnO})_n^{n+}$ ($\text{Ln} \equiv \text{lanthanide}$) complex cation a spectroscopic 'fingerprint'? P.Porcher, P.Caro (Lab. des Elements de Transition dans les Solides, CNRS, Meudon Bellevue, France). *J. Less-Common Met. (Switzerland)*, vol.93, no.1, p.151-6 (1983). (Proceedings of the Sixteenth Rare Earth Research Conference, Tallahassee, FL, USA, 18-21 April 1983). The spectra of Eu^{3+} -doped oxyhalides, oxymolybdates and oxysulphates are compared. The $(\text{LnO})_n^{n+}$ ($\text{Ln} \equiv \text{lanthanide}$) complex cation not only constitutes the framework of the structure but also appears to characterize the optical spectrum, thus influencing the crystal field parameters derived from the data. (13 refs.)

114910 The terbium-activated rare earth oxysulphide binary systems $(\text{Y}_{1-x}\text{La}_x)_2\text{O}_2\text{S}$, $(\text{Y}_{1-x}\text{Gd}_x)_2\text{O}_2\text{S}$ and $(\text{Gd}_{1-x}\text{La}_x)_2\text{O}_2\text{S}$ and their luminescence properties. Huang Zhu-Po, Xu Geng-Wang (Dept. of Chem., Peking Univ., Beijing, China). *J. Less-Common Met. (Switzerland)*, vol.93, no.1, p.236-7 (1983). (Proceedings of the Sixteenth Rare Earth Research Conference, Tallahassee, FL, USA, 18-21 April 1983). Summary form only given. In a search for new host materials for phosphors, three rare earth oxysulphide binary systems $(\text{Y}_{1-x}\text{La}_x)_2\text{O}_2\text{S}$, $(\text{Y}_{1-x}\text{Gd}_x)_2\text{O}_2\text{S}$ and $(\text{Gd}_{1-x}\text{La}_x)_2\text{O}_2\text{S}$ were investigated. Samples of these systems with various compositions were prepared by sulphidizing the corresponding mixed rare earth oxides at high temperature. The subsolidus phase relations in these pseudobinary systems were determined by lattice parameter measurements. It was found that the diffraction peaks in the middle regions of $(\text{Y}_{1-x}\text{La}_x)_2\text{O}_2\text{S}$ and $(\text{Gd}_{1-x}\text{La}_x)_2\text{O}_2\text{S}$ systems exhibited broadening phenomena as a result of the small crystal size and lattice distortion. The changes in the luminescent brightness, the emission spectrum and the chromaticity coordinates of samples with various host compositions were studied. (no refs.)

114911 Fluorescence spectra, hypersensitivity and lifetimes of the carboxylate and related ligand complexes of the lanthanides in aqueous media. S.P.Sinha (Hahn-Meitner-Inst., Berlin, Germany). *J. Less-Common Met. (Switzerland)*, vol.93, no.1, p.237-8 (1983). (Proceedings of the Sixteenth Rare Earth Research Conference, Tallahassee, FL, USA, 18-21 April 1983). Summary form only given. During the author's studies of the fluorescence spectra of the lanthanides and their complexes in aqueous solution, the anionic tetracarboxylate complexes $[\text{M}(\text{CO}_3)_4]^{5-}$ ($\text{M} \equiv \text{Sm, Eu, Gd, Tb, Dy, Tm}$) have been systematically investigated. Extreme hypersensitivity was observed for the europium complex, where the hypersensitivity factor for the $^5D_0 \rightarrow ^7F_2$ transition is over 100. For other lanthanide tetracarboxylates the hypersensitivity factor varied from 10 to 50. Comparison of the lifetime of the europium(III) aquo ion (110 μs) with that of the isolated $\text{Eu}(\text{H}_2\text{O})_9^{3+}$ ion in a crystal (bromate, 119 μs ; trifluoromethanesulphonate, 102 μs) and the lifetime of the terbium(III) aquo ion (425 μs) with that of crystalline ethylsulphate (410 μs) led the author to conclude that nine-coordinated aquo ions of europium(III) and terbium(III) were present in solution. The eight-coordinated sulphates of europium(III) and terbium(III) have lifetimes of 187 μs and 713 μs respectively. The changes in the fluorescence intensities and the lifetimes of the above-mentioned lanthanides on complexation with ligands like F^- , Cl^- , Br^- , I^- , NO_3^- , SCN^- , CO_3^{2-} , HCOO^- and CH_3COO^- ions have been studied in detail. (2 refs.)

114912 On the trail of bastnasite: a study of the ternary complex (MFCO_3) of europium(III) using a fluorescence lifetime criterion. P.Sinha, P.Moller (Hahn-Meitner-Inst., Berlin, Germany). *J. Less-Common Met. (Switzerland)*, vol.93, no.1, p.238 (1983). (Proceedings of the Sixteenth Rare Earth Research Conference, Tallahassee, FL, USA, 18-21 April 1983). Summary form only given. In connection with studies on lanthanide-carbonate systems, the authors found that an $[\text{M}]/[\text{CO}_3^{2-}]$ ratio of 1/80 is capable of keeping the lanthanides in solution as anionic tetracarboxylate complexes. The lifetimes of $[\text{M}(\text{CO}_3)_4]^{5-}$ complexes ($\text{M} \equiv \text{Sm, Eu, Gd, Tb, Dy, Tm}$) have been studied previously. No energy migration was found to take place from europium to terbium whereas the 5D_4 level of terbium transfers a large part of its excitation energy to the 5D_0 level of europium in a 1:1 mixture of the tetracarboxylate complex. Thus excitation with 380 nm (terbium) radiation gave a lifetime value of 610 μs for terbium (547 nm) and 543 μs for europium (618 nm), whereas excitation with 393 nm (europium) radiation produced lifetime values of less than 8 μs and 479 μs for terbium and europium respectively. These values can be compared with those of the parent complexes: europium, 465 μs ; terbium 1100 μs . The exchange time was calculated from the rise curve to be about 25 μs . The authors used this robust $[\text{Eu}(\text{CO}_3)_4]^{5-}$ complex as a model system to study the interaction between this complex and the F^- ions. (no refs.)

114913 Energy transfer processes between Eu^{3+} and Tb^{3+} in KY_3F_{10} . C.Andraud, A.Vedrine (Univ. de Clermont Ferrand II, Aubiere, France), F.Pelle, B.Blanzat. *J. Less-Common Met. (Switzerland)*, vol.93, no.1, p.239 (1983). (Proceedings of the Sixteenth Rare Earth Research Conference, Tallahassee, FL, USA, 18-21 April 1983). Summary form only given, as follows. The luminescence properties of $\text{KY}_{3(1-x-y)}\text{Eu}_x\text{Tb}_y\text{F}_{10}$ samples ($0 \leq x \leq 15$; $0 \leq y \leq 50$) were investigated at temperatures from 8 to 800K. Two mechanisms of self-quenching between Eu^{3+} ions, which used the 5D_3 , 7F_0 , 5D_2 and 7F_4 levels and the 5D_1 , 7F_0 , 5D_0 and 7F_3 levels, were determined. An energy diffusion process involving 5D_0 and 7F levels of europium was also found. A similar study carried out for terbium luminescence has shown the existence of a self-quenching interaction between 5F_3 , 7D_6 , 5D_4 and 7F_0 levels and an energy diffusion process via the 5D_4 and $^7F_{5,6}$ levels. Two mechanisms for the $\text{Tb}^{3+} \rightarrow \text{Eu}^{3+}$ energy transfer process using (1) the 5D_3 and $^7F_{3,4}$ levels of Tb^{3+} and the 7F_0 and 5D_2 levels of Eu^{3+} and (2) the 5D_4 and $^7F_{4,5}$ levels of Tb^{3+} and the 7F_0 and 5D_0 levels of Eu^{3+} were considered. The luminescence properties of codoped samples showed that at temperatures above 8K only mechanism (2) occurs. Moreover a comparison of the luminescence properties of $\text{KY}_{2.82}\text{Tb}_{0.15}\text{Eu}_{0.03}\text{F}_{10}$, $\text{KY}_{2.73}\text{Tb}_{0.15}\text{Eu}_{0.12}\text{F}_{10}$ and $\text{KY}_{1.44}\text{Tb}_{0.50}\text{Eu}_{0.06}\text{F}_{10}$ indicates a $\text{Eu}^{3+} \rightarrow \text{Tb}^{3+}$ energy transfer phenomenon only at both a high temperature and a high terbium concentration. The proposed mechanism for this process is $\text{Tb}^{3+} (^7F_4) + \text{Eu}^{3+} (^5D_0) \rightarrow \text{Tb}^{3+} (^7F_0) + \text{Tb}^{3+} (^5D_4)$. (no refs.)

114914 Radiative recombination at Ir^{3+} sites in doped AgBr . Visible luminescence. J.P.Sponhower, C.A.Hamer (Res. Labs., Eastman Kodak Co., Rochester, NY, USA). *J. Lumin. (Netherlands)*, vol.28, no.3, p.221-32 (Aug. 1983). Low-temperature photoluminescence spectra of Ir^{3+} -doped AgBr single crystals were obtained. These spectra are highly structured; they show a progression in a low-frequency resonance vibrational mode and the participation of other localised vibrations. A sharp zero-phonon (ZP) line was observed at 1562.9 cm^{-1} . The assignment of this line as the spectral origin of the luminescence band is based upon photoluminescence excitation spectra obtained with a CW dye laser. In crystals doped with ~ 80 molar ppm Ir^{3+} , the linewidth of the ZP line is $\leq 2.0 \text{ cm}^{-1}$. A Zeeman effect on the ZP line was observed. The temperature dependence of the luminescence intensity was obtained. The emission is rapidly quenched with temperature, so that no emission bands are observed above 25K. The results of several experiments suggest that the emission originates at iridium sites in the doped crystal. (23 refs.)

114915 Luminescence of the hydrolysis products of Th(IV). H.G.Brittain (Dept. of Chem., Seton Hall Univ., South Orange, NJ, USA), L.Tsao, D.L.Perry. *J. Lumin. (Netherlands)*, vol.28, no.3, p.257-65 (Aug. 1983). Raising the pH of an aqueous solution of thorium nitrate results in the precipitation of a hydrated thorium oxide. At room temperature this material does not exhibit any emissive properties, but upon cooling to 77K a strong green luminescence can be observed. The emission spectrum is fairly broad, and is characterised by an emission lifetime of 125 μ s. Calcination of the hydrolysis product produces an anhydrous thorium oxide which is not luminescent at any temperature. Through the production of a series of mixed lanthanide/thorium hydrolysis products, it was established that the luminescent species was a clustered thorium compound. Sensitisation of Eu (III) emission by the thorium hydrolysis product was observed. (13 refs.)

114916 Emission spectra in orthorhombic PbCl₂ at low temperature. T.Fujita, K.Soeda, K.Takiyama, M.Nishi (Dept. of Appl. Phys. & Chem., Hiroshima Univ., Higashihiroshima-shi, Japan), T.Hirota. *J. Lumin. (Netherlands)*, vol.28, no.3, p.267-73 (Aug. 1983). The emission spectra and its time decay in PbCl₂ at low temperature are reported. Three emission bands lying at 3.81 (UV), 2.93 (blue) and 2.60 eV are found for the photo-excitation in the intrinsic absorption region at 4.2K. An exponential decay with decay time of 11.4 μ s is observed for the UV emission. For the blue emission two kinds of time decay spectra are observed: a second order process below 10K and an exponential decay above 14K. The mechanisms of these emissions are discussed by taking into account the above results. (10 refs.)

114917 Study of the protoporphyrin luminescence under selective laser excitation. V.I.Rakhovskii (All-Union Centre for Study of Surface and Vacuum Properties, Moscow, USSR), M.N.Sapozhnikov, A.L.Shubin. *J. Lumin. (Netherlands)*, vol.28, no.3, p.301-11 (Aug. 1983). The structural luminescence spectra of protoporphyrin IX solid solutions in ethanol and hydrochloric acid were obtained under selective laser excitation in the region of the inhomogeneously broadened pure electronic and vibronic bands at T=3.8K. The dependence of the excitation selectivity on the excitation frequency was investigated. The vibrational frequencies of protoporphyrin IX were obtained in the ground and excited electronic states when the excitation frequency has been scanned in the region of pure electronic and vibronic bands, respectively. A universal apparatus is described for the investigation of the absorption and luminescence spectra of polyatomic molecules in the temperature range from 3.5 to 300K under the dye laser excitation tunable in the spectral region 265-365 nm, 435-730 nm, detection of spectra in the region 300-900 nm with a polychromator and silicon intensified image detector and processing of the spectral information with an optical spectrum analyser controlled with a microcomputer. (8 refs.)

114918 Site selective excitation of 1-hydronaphthyl radical in irradiated naphthalene crystal. T.Nakayama (Radiation Lab., Univ. of Notre Dame, Notre Dame, IN, USA). *J. Lumin. (Netherlands)*, vol.28, no.3, p.313-17 (Aug. 1983). Fluorescence excitation spectrum of the 1-hydronaphthyl radical is observed by site selective laser excitation. The proposal by Jacobsen et al. (1978) that the origin of the radical is dual is confirmed. (9 refs.)

114919 Time-resolved measurements of photoluminescence in As-S alloy glasses and films evaporated from a-As₂S₃. K.Murayama, G.S.Higashi, M.A.Kastner (Dept. of Phys., MIT, Cambridge, MA, USA). *Philos. Mag. B (GB)*, vol.48, no.3, p.277-88 (Sept. 1983). The excitation-energy dependence of photoluminescence (PL) measurement at short times after 10 ns pulsed excitation and of the spectrally integrated total-light decay (TLD) have been measured for a variety of glasses containing As and S. Measurements are reported for bulk glasses of compositions As₃₅S₆₅, As₄₀S₆₀ and As₄₂S₅₈, as well as for thin films evaporated from bulk a-As₂S₃ which were either measured as prepared, after annealing, or after several hours of optical irradiation. It was found that the short-time (zero-delay) PL spectrum is very sensitive to sample composition and molecular structure. Although only slight variations in the TLD were observed, the zero-delay spectrum changed drastically from sample to sample. Concomitant effects were observed in the quantum efficiency at short times. The results are discussed in terms of some of the current models for the PL mechanism. (17 refs.)

114920 Influence of uniaxial pressure on the impurity photoluminescence band of GaAs:Cu with a maximum near 1.02 eV. T.K.Ashirov, A.A.Gutkin (A.F. Ioffe Physicotech. Inst., Acad. of Sci., Leningrad, USSR). *Sov. Phys.-Semicond. (USA)*, vol.17, no.3, p.258-60 (March 1983). Translation of: *Fiz. & Tekh. Poluprovodn. (USSR)*, vol.17, no.3, p.418-21 (March 1983). [received: Sept. 1983] A wide photoluminescence band of n-type GaAs:Cu with a maximum near 1.02 eV, due to radiative transitions of electrons from the conduction band (or from a shallow level near this band) to a deep-level center, was investigated at temperatures 4.2, 77, and 293K at pressures up to ~3 tonne/cm² applied along the [100], [111], and [110] directions. The polarization dependences of the luminescence under pressure indicated that the centers responsible for the band had the T_d symmetry (for example, a substantial impurity with an undistorted symmetry of the environment consisting of the host atoms). The results obtained at 77 and 293K indicated that the deformation potential constants *b* and *d* of the impurity center responsible for the luminescence were -0.92±0.09 and -2.6±0.2 eV, respectively. (11 refs.)

114921 Investigation of the saturation of the intensity of the $\lambda=1.3 \mu$ luminescence emitted from InGaAsP/InP structures at high rates of excitation. V.P.Chalyi, D.Z.Garbuzov, A.V.Chudinov, V.V.Agaev (A.F. Ioffe Physicotech. Inst., Acad. of Sci., Leningrad, USSR). *Sov. Phys.-Semicond. (USA)*, vol.17, no.3, p.287-9 (March 1983). Translation of: *Fiz. & Tekh. Poluprovodn. (USSR)*, vol.17, no.3, p.464-8 (March 1983). [received: Sept. 1983] An investigation was made of the dependences of the external quantum efficiency of the photoluminescence on the rate of excitation of InGaAsP/InP double heterostructures at various temperatures. It was found that at T≥225K the 'luminescence saturation' effect was observed not only for the luminescence emerging at right angles to the plane of the structure, but for the luminescence propagating parallel to the heterostructure plane. It was established that at T>225K the luminescence intensity saturation was due to a relative reduction in the rate of radiative transitions in the active region of a heterostructure. At low temperatures (T<225K) this luminescence saturation effect was observed only when the luminescence emerged at right angles to the plane of the structure and it was due to changes in the angular and spatial distribution of photons as a result of the appearance and amplification of the superluminescent component of the radiation. (9 refs.)

114922 Photoluminescence of germanium irradiated with ⁶⁰Co γ rays. V.A.Bykovskii, A.V.Mudryi, V.P.Poskrebyshv, V.D.Tkachev (Belorussian Polytech. Inst., Minsk, Belorussian SSR). *Sov. Phys.-Semicond. (USA)*, vol.17, no.3, p.296-9 (March 1983). Translation of: *Fiz. & Tekh. Poluprovodn. (USSR)*, vol.17, no.3, p.479-83 (March 1983). [received: Sept. 1983] An investigation was made of the low-temperature (4.2K) photoluminescence of n- and p-type germanium irradiated with ⁶⁰Co γ rays. Isochronous annealing of crystals up to T=400°C revealed a series of vibronic luminescence bands with strong no-phonon lines in the spectral range 0.50-0.75 eV. The atoms of the main dopants (Sb and Ga) did not occur in the luminescence centers. These centers were assumed to be complexes comprising atoms of residual (accidental) impurities and primary radiation defects. (23 refs.)

114923 Nature of the luminescence lines of heavily doped p-type gallium arsenide under uniaxial deformation. N.S.Averkiev, S.A.Obukhov, A.A.Rogachev, N.A.Rud (A.F. Ioffe Physicotech. Inst., Acad. of Sci., Leningrad, USSR). *Sov. Phys.-Solid State (USA)*, vol.25, no.2, p.193-4 (Feb. 1983). Translation of: *Fiz. Tverd. Tela (USSR)*, vol.25, no.2, p.343-5 (Feb. 1983). [received: Sept. 1983] Luminescence spectra were studied in uniaxially deformed crystals of p-type gallium arsenide ($N_A=2\times 10^{18}$ - 10^{19} cm⁻³). Measurements of the linear polarization of the luminescence showed that the presence of two peaks in the luminescence spectrum is due to the recombination of holes from the valence band split under pressure, with $m_x=-1/2$ and with $m_y=\pm 3/2$. The limiting strain values are calculated for which this splitting affects the luminescence line profile. (4 refs.)

114924 Emission from free and bound excitons in gallium selenide layered crystals. Yu.P.Gnatenko, Z.D.Kovalyuk, P.A.Skubenko, Yu.I.Zhirko (Inst. of Phys., Acad. of Sci., Kiev, Ukrainian SSR). *Sov. Phys.-Solid State (USA)*, vol.25, no.2, p.251-3 (Feb. 1983). Translation of: *Fiz. Tverd. Tela (USSR)*, vol.25, no.2, p.445-9 (Feb. 1983). [received: Sept. 1983] The emission spectra of single crystals of gallium selenide in the ϵ phase containing impurity cobalt atoms in concentrations of 0.001-0.5% are investigated at various temperatures (4.2-35K) in polarized light. It is found that a wide emission band with an energy of 2.031 eV is caused by structural defects in the GaSe crystal, while other wide bands at 2.039 and 2.008 eV are caused by indirect excitonic transitions with emission of TO phonons. Narrow emission lines correspond to the decay of direct excitons bound to various defects and to phonon replicas of these involving phonons of energy 14.5±0.5 meV. The temperature dependence of the doublet structure of the free-exciton emission line is investigated; it is evidently caused by characteristics of the band structure of the GaSe crystal, in particular by the splitting of the valence band by interlayer interactions. (15 refs.)

114925 Kinetics of exciton radiation in fluorite type crystals. A.V.Agafo-nov, P.A.Rodnyi (M.I. Kalinin Polytech. Inst., Leningrad, USSR). *Sov. Phys.-Solid State (USA)*, vol.25, no.2, p.335-6 (Feb. 1983). Translation of: *Fiz. Tverd. Tela (USSR)*, vol.25, no.2, p.589-90 (Feb. 1983). [received: Sept. 1983] The authors have studied the characteristic (excitonic) luminescence of specially purified fluorite-type crystals in the temperature range 5 to 160K. The samples were excited by X-ray pulses of 20 nsec duration as well as a 1 μ sec duration, since, for short (nanosecond) excitation, the amplitude of the long-lived component of the luminescence is very small at low temperatures. In all the crystals studied, CaF₂, SrF₂, and BaF₂, measurements were made of the short-lived component of the characteristic luminescence (the so-called singlet excitons) with a lifetime τ_s of 10 nsec, and the long lived (triplet) component with a lifetime in the microsecond range. (6 refs.)

114926 Photoluminescence study of thermally treated silicon crystals. J.Weber, R.Sauer (Phys. Inst., Univ. Stuttgart, Stuttgart, Germany). Defects in Semiconductors II, Symposium Proceedings, Boston, MA, USA, Nov. 1982 (New York, USA: North-Holland 1983), p.165-9 CZ silicon samples heated to 450°C or higher temperatures for several hours exhibit many sharp photoluminescence lines well below the band edge. The authors study the production of the lines in terms of carbon and oxygen doping and of the heating temperature and duration. First results as to a level scheme of the P(0.7672 eV) line are reported. (15 refs.)

114927 Deep radiative transitions in InP. H.Tamkin, B.V.Dutt (Bell Labs., Murray Hill, NJ, USA). Defects in Semiconductors II, Symposium Proceedings, Boston, MA, USA, Nov. 1982 (New York, USA: North-Holland 1983), p.253-65 Results of a detailed photoluminescence study of deep radiative transitions in InP crystals prepared by bulk and epitaxial techniques with a variety of dopants are reported. In order to understand the origin of the photoluminescence spectra, bulk samples were subjected to isothermal anneals at different partial pressures of phosphorus. Similarly, the LPE wafers were grown with and without phosphorus in the gas stream. The electrical nature of some of the species responsible for the PL emission was inferred by a study of Cd-diffused bulk samples. Based on these experiments the following tentative assignments are proposed. The photoluminescence band at 0.99 eV, common to all samples, is due to emission from a donor-like level related to the P-vacancy-impurity complex. Bands at 1.21 eV and 1.15 eV appear to be due to emission to native acceptor levels associated with the In-vacancy. The 1.08 eV band is attributed to emission to a level involving the complex of the donor (0.99 eV) and acceptor (1.21 eV) species. The relationship between these bands and residual impurities is discussed. A comparison with the work of other investigators tends to support these assignments. (20 refs.)

On the determination of moment of inertia of prolate luminescent molecules See Entry 112696

A well-resolved carbazole excimer emission from a conformationally pure polymer See Entry 112782

Spectroluminescence study of the behavior of organic molecules in a finely porous glass matrix See Entry 112784

Influence of the luminescence saturation effect on the lasing threshold of InGaAsP/InP double heterostructure lasers ($\lambda=1.3 \mu$) at T≥300K See Entry 112996

Streamer discharges in semiconductors in the temperature range 4.2-530K See Entry 113691

Fluorescence study of polymer chain interpenetration and of the rate of phase separation in incompatible polymer blends See Entry 113726

Production and properties of crystals of complex refractory oxides with perovskite structure See Entry 113776

Site symmetry of the metal ion in rare earth oxynitrates doped with europium(II) See Entry 113825

Low-temperature exciton decay with production of defects in KBr and KBr-Cl See Entry 113987

- Thermodynamic and kinetic properties of amorphous dielectrics at low temperatures See Entry 114295
- Detection of exciton luminescence of indium antimonide crystals See Entry 114448
- Polarized luminescence due to localized excitons in $\text{CdS}_{1-x}\text{Se}_x$ solid solutions See Entry 114449
- Local excitons and effects of their mixing with electronic impurity states in naphthalene See Entry 114452
- Emission spectra of electron-hole drops in gallium phosphide See Entry 114453
- Radiative recombination of localized Mott excitons in a strong magnetic field See Entry 114454
- Electrical properties of dislocations and boundaries in semiconductors See Entry 114481
- Zeeman spectroscopy of crystal-field transitions of Co-doped InP See Entry 114492
- Emission spectrum and crystal field parameters of pentanitrateuropate (III) ions See Entry 114501
- Auger recombination in a degenerate electron-hole plasma in InGaAsP solid solutions See Entry 114543
- Photostimulated formation of shallow donors in 'pure' CdS crystals See Entry 114563
- Magnetic circularly polarized luminescence as a probe of ligand fields in the solid state and in solution See Entry 114833
- Electronic absorption and emission spectra of binuclear platinum(II) complexes. Characterization of the lowest singlet and triplet excited states of $\text{Pt}_2(\text{H}_2\text{P}_2\text{O}_5)_4^{4-}$ See Entry 114877
- Judd-Ofelt parameters and chemical bonding See Entry 114888
- Fundamental absorption edge of irradiated alkali halides See Entry 114892
- Production and release of light sums in thin films of activated alkali halides with different crystal structure See Entry 114945
- Growth of $\text{Ga}_{0.47}\text{In}_{0.53}\text{As}$ -InP quantum wells by low pressure metalorganic chemical vapor deposition See Entry 115061
- OMVPE growth of GaInP See Entry 115069
- Enhanced InP substrate protection for LPE growth of InGaAsP DH lasers See Entry 115115
- Thermal decomposition of $\text{Eu}_2(\text{SO}_4)_3 \cdot 8\text{H}_2\text{O}$ studied by high resolution luminescence spectroscopy See Entry 115541
- Mutual influence of wide- and narrow-gap photocells in the operation of multistage n -GaAs- p -AlGaAs- n -AlGaAs heterojunction solar cells See Entry 115649
- Role of the central metal ion and solvent-ligand molecules in the association of metallophorphytins in binary mixtures of solvents See Entry 115726

78.60 OTHER LUMINESCENCE SPECTRA AND RADIATIVE RECOMBINATION

(for photoconduction and photovoltaic effects, see 72.40; for photoluminescence, see 78.55)

- Gamma dosimetry using lyoluminescence of tris (hydroxymethyl) aminomethane See Entry 112446
- Thermal degradation of plastic scintillators See Entry 112573

78.60F Electroluminescence

- 114928 Electroluminescence in ZnS:Mn thin film structures grown with atomic layer epitaxy. R.Tornqvist (Electronic Display Div., Lohja Corp., Espoo, Finland). *Acta Polytech. Scand. Appl. Phys. Ser. (Finland)*, no.Ph140, p.2-34 (1983). Particular emphasis has been given to the excitation and the relaxation processes of the light emitting Mn^{2+} centre in ZnS. Estimations indicate that under operation conditions most of the conduction electrons in the ZnS:Mn layer have a kinetic energy sufficient for impact excitation of the Mn^{2+} centre, and that threshold voltage for the onset of the emission reflects rather free electron generation than the acceleration of electrons up to optical energies. A saturation in the light emission is suggested to arise from an interaction between excited Mn^{2+} centres resulting in nonradiative decay. The experimental results also indicate that the interaction occurs by energy transfer via unexcited Mn^{2+} ions. The aging behaviour of the ZnS:Mn electroluminescence thin film structures is explained in terms of electron trapping at the ZnS:Mn-insulator interfaces. The unique crystalline properties of ZnS:Mn films grown with atomic layer epitaxy are indicated by the presence of fine structure in the emission and the excitation spectra of the Mn^{2+} centre, and by a thin dead layer in the ZnS:Mn film. (32 refs.)
- 114929 Temperature dependent studies of electroluminescence brightness-waves of some rare-earth doped luminors. S.Bhushan, B.R.Kaza (Dept. of Phys., Ravisankar Univ., Raipur, India), A.N.Pandey. *Indian J. Cryog.*, vol.8, no.1, p.32-8 (1983). Brightness-waves (BW) of ZnO:Sm, ZnO:Pr and ZnO:Yb luminors were studied at fixed excitation voltage and frequency from liquid nitrogen temperature (LNT) to room temperature (RT) and above. Due to changes in temperature, for each cycle of the sinusoidal excitation, two primary peaks were observed which always precede the voltage maximum of the exciting field and their positions remained almost fixed with respect to the peak positions of the exciting field. In the case of ZnO:Sm, a secondary peak appears twice in this temperature range. However, for ZnO:Pr, the secondary peak appears only in the alternate primary peaks. The secondary peaks creep forward in the cycle with increase in temperature. No secondary peak was observed for ZnO:Yb but at lower temperatures the height of two consecutive primary peaks are not same and their ratio increases with the rise of temperature and about 255K or above becomes unity. The voltage dependence of electroluminescence (EL) brightness for the systems at RT and LNT satisfied the relation $B=B_0 \exp(-C/V^{1/2})$ which indicates the mechanism of EL excitation to be an acceleration-collision one. The values of the constants B_0 and C at LNT are higher than those at RT and this has been accounted for as due to temperature quenching. The results have been discussed in terms of existing models. (8 refs.)

114930 Low-voltage direct-current electroluminescence in ZnS:RE thin films. F.J.Bryant, A.Krier (Dept. of Phys., Univ. of Hull, Hull, England). *IEEE Proc. 1 (GB)*, vol.130, no.4, p.160-4 (Aug. 1983). Bright direct-current electroluminescence has been obtained in ZnS:Cu:Cl:RE (rare earth) thin films with good maintenance characteristics and efficiency. Different rare-earth elements have been used as dopants, either singly or together, to give devices which exhibit various colour electroluminescence. Brightness/voltage curves were measured as a function of device temperature, and electroluminescence spectra were also recorded. (12 refs.)

114931 Semiconductor electrodes. II. Efficient electroluminescence at ZnS electrode in aqueous electrolytes. F.-R.F.Fan, P.Leempoel, A.J.Bard (Dept. of Chem., Univ. of Texas, Austin, TX, USA). *J. Electrochem. Soc. (USA)*, vol.130, no.9, p.1866-75 (Sept. 1983). Electroluminescence (EL) on ZnS was studied in aqueous solutions containing various redox species. For species able to generate strongly oxidizing intermediates, such as peroxydisulfate or hydrogen peroxide, bright blue luminescence was observed during cathodic polarization at potentials near to or negative of flatband potential (V_{FB}) of ZnS. For solutions containing supporting electrolyte alone at various pH's, no emission was detectable even at potentials 7 V negative of V_{FB} . This suggests that minority carrier (hole) injection is responsible for the initiation of EL. The peak energy of the EL spectrum was much smaller (by 1 eV) than the bandgap of ZnS, suggesting that the radiative recombination is through intermediate luminescent centers. Under steady-state conditions, the EL intensity was proportional to the square of the current, suggesting that EL intensity is dominated by the recombination of electron-hole pairs at luminescent centers. In the early part of a potential pulse (especially the first pulse), the growth behavior of EL intensity was strongly affected by the electron trapping of the empty upper luminescent states. The location of the EL spectra depended on the current density and EL intensity; with increasing EL intensity, a significant blue shift of the emission peak was observed. These results suggest that the overall radiative recombination rate might be limited by electron transfer (through a tunneling mechanism) from the occupied upper luminescent states to the empty lower luminescent states. An EL efficiency of 0.2% can be achieved by operating at a current density of 25 mA/cm². (31 refs.)

114932 A new type of electroluminescent layers with laminar structure. F.Pribyl. *Slaboproudy Obz. (Czechoslovakia)*, vol.44, no.8, p.411-13 (Aug. 1983). In Czech. Discusses the developments of electroluminescent multilayer structures with low-threshold-voltage. The two types of structure described are based on the use of ZnS:Mn/PbTiO₃ (or ZnS:Mn/PLZT) and (Y₂O₃:Eu/ZnS)₃, respectively. Diagrams of these structures together with dependences of luminescence on the excitation voltage at 5 kHz are presented. Practical applicability of multilayer structures are briefly discussed. (3 refs.) E.D.

114933 Effect of chlorine concentration on the spectral characteristics of electroluminescence in ZnS:Cu:Cl phosphor. S.M.Pillai, C.P.G.Vallabhan (Dept. of Phys., Univ. of Cochin, Cochin, India). *Solid State Commun. (USA)*, vol.47, no.11, p.909-11 (Sept. 1983). ZnS:Cu:Cl phosphor prepared under a vacuum firing process is found to give blue electroluminescence with emission peak at 460 nm which remains unaltered with the frequency of the excitation voltage. Addition of excess chlorine in the phosphor gives blue, green and red emission at 460, 520 and 640 nm. The intensity of the blue band decreases and it finally disappears as chlorine concentration is increased. A scheme involving three energy levels attributed to Cu²⁺, Cu⁺ and Cl⁻ centres in ZnS explains the experimental results completely. (8 refs.)

114934 Some characteristics of the electroluminescence emitted by epitaxial Al-Ga-Sb heterostructures. N.S.Zimogorova (A.F. Ioffe Physicotech. Inst., Acad. of Sci., Leningrad, USSR), I.V.Kryachko, I.I.Matkova, L.D.Pramatarova, V.I.Shostka. *Sov. Phys.-Semicond. (USA)*, vol.17, no.3, p.324-6 (March 1983). Translation of: *Fiz. & Tekh. Poluprovodn. (USSR)*, vol.17, no.3, p.517-20 (March 1983). [received: Sept. 1983] The interest in the AlGaSb system originates from the small mismatch of the lattice parameters of the components of the system and from potential practical applications of devices made of materials belonging to this system at wavelengths (1.3-1.6 μ) corresponding to low losses in fiber-optic communication lines. The authors report the results of an experimental study of the electrical properties and luminescence of epitaxial p(n)-GaSb-n(p)-Al_xGa_{1-x}Sb structures (0 $\leq x \leq 0.25$ molar fractions). Heterostructures were formed by the method of liquid epitaxy involving successive crystallization of epitaxial films on p-type GaSb (111) substrates [$p=10^{17} \text{ cm}^{-3}$ or $p=(2-5) \cdot 10^{18} \text{ cm}^{-3}$]. (10 refs.)

Influence of the luminescence saturation effect on the lasing threshold of InGaAsP/InP double heterostructure lasers ($\lambda=1.3 \mu$) at $T \geq 300\text{K}$ See Entry 112996

Studies of electroluminescence in pAlGaAs-pGaAs-nGaAs heterophotocells with distributed parameters See Entry 115651

78.60H Cathodoluminescence, ionoluminescence

- 114935 Method for the analysis of saturation effects of cathodoluminescence in phosphors; applied to Zn₂SiO₄:Mn and Y₃Al₅O₁₂:Tb. D.M.de Leeuw, G.W.'t Hooft (Philips Res. Labs., Eindhoven, Netherlands). *J. Lumin. (Netherlands)*, vol.28, no.3, p.275-300 (Aug. 1983). Saturation of the luminescence of phosphors under stationary cathode-ray excitation is due to activator ground-state depletion and an increased importance of higher order recombination processes at high excitation density. A method based on model considerations is presented to determine the kinetics of the dominating superlinear energy-loss process. The method is illustrated to analyse the saturation of the luminescence of Zn₂SiO₄:Mn and the blue ³D₃-⁵F emission of Y₃Al₅O₁₂:Tb. Quadratic energy-loss processes related to excited activator ions (Mn, Tb) are found. With this result the emitted optical flux under stationary excitation conditions and the rise time and the decay time of the luminescence can be quantitatively interpreted. When activator ground-state depletion occurs excited-state absorption cannot be excluded. (28 refs.)
- 114936 Cathodoluminescence of plasma-grown SiO₂ films. Yu.Ya.Bekeris, M.Kh.Neihtar, V.K.Petrov. *Latv. PSR Zinat. Akad. Vestis Fiz. Teh. Zinat. Ser. (USSR)*, no.4, p.37-40 (1983). In Russian. The cathodoluminescence band dependence on the annealing temperature of plasma-grown SiO₂ films on silicon is studied. The band intensity variations due to annealing temperature are associated with the modification of defect centers in SiO₂ films. (7 refs.)

Photoplastic effects in II-VI crystals See Entry 114077

The terbium-activated rare earth oxysulphide binary systems $(Y_{1-x}La_x)_2O_2S$, $(Y_{1-x}Gd_x)_2O_2S$ and $(Gd_{1-x}La_x)_2O_2S$ and their luminescence properties See Entry 114910

Comments on the physical significance of E^* values for excited sputtered atoms See Entry 114998

78.60K Thermoluminescence

114937 Effect of flux content on thermoluminescence yield of BaS phosphors. R.P.Rao, D.R.Rao (Materials Sci. Centre, Indian Inst. of Technol., Kharagpur, India). *Bull. Mater. Sci. (India)*, vol.5, no.1, p.29-32 (March 1983). [received: Sept. 1983]

BaS phosphors doped with impurities like Cu and Bi were prepared by using NaCl as flux. Thermoluminescence of these samples prepared with different quantities of flux has been studied by exciting them at room temperature with X-rays. The amount of flux for a good thermoluminescence yield has been estimated between 25 to 30% by weight depending upon the type of phosphor. (11 refs.)

114938 Thermoluminescence from extended-chain crystals of polyethylene. T.Hashimoto, K.Ogita, S.Umemoto, T.Sakai (Dept. of Textile & Polymeric Materials, Tokyo Inst. of Technol., Ookayama, Meguro-ku, Tokyo, Japan). *J. Polym. Sci. Polym. Phys. Ed. (USA)*, vol.21, no.8, p.1347-56 (Aug. 1983).

Thermoluminescence (TL) has been observed in γ -irradiated extended-chain crystals of polyethylene above room temperature. The TL curve, which exhibits four peaks at 50, 90, 120 and 140°C, is different from that given by folded-chain crystals, in both shape and intensity. In particular, a shape, strong glow peak is observed at 140°C, corresponding to the melting temperature of the extended-chain crystals. These results are discussed in relation to independent measurements by differential scanning calorimetry and electron spin resonance. (17 refs.)

The role of the state of dispersion of impurity on Z_1 -centres in NaCl:Ca²⁺ crystals See Entry 113909

Detection of minority traps by simultaneous measurement of thermoluminescence and thermally stimulated conductivity See Entry 114535

Production and release of light sums in thin films of activated alkali halides with different crystal structure See Entry 114945

Tunneling afterglow and anomalous fading in dosimetry with CaSO₄:Dy See Entry 115925

78.65 OPTICAL PROPERTIES OF THIN FILMS

114939 The optical absorption edge of amorphous thin films of borosilicate glass. M.Ilyas, C.A.Hogarth (Dept. of Phys., Brunel Univ., Uxbridge, England). *J. Mater. Sci. Lett. (GB)*, vol.2, no.9, p.535-7 (Sept. 1983).

The authors examined how the absorption edge and optical energy gap changed as the composition was varied in mixed films of SiO and B₂O₃. It was found that adding B₂O₃ to SiO increased the optical energy gap and reduced the spin density and thus the density of unpaired electrons on unsatisfied bonds. The band tailing decreased resulting in an increase in the forbidden energy gap. (12 refs.)

114940 Optical probing of silicon-sapphire interface of heteroepitaxial SOS films. J.Lagowski, L.Jastrzebski, G.W.Cullen (RCA Labs., Princeton, NJ, USA). *J. Electrochem. Soc. (USA)*, vol.130, no.8, p.1744-8 (Aug. 1983).

The reflectivity of silicon-on-sapphire in the visible and near infrared spectral range is found to be dependent on the crystalline quality and on the film processing such as thermal annealing and hydrogenation. These findings are quantitatively explained taking into account an amorphous-like character of the silicon-sapphire interface. It is also shown that reflectivity for $h\nu > 2$ eV can be used as a means for probing the crystalline quality of the silicon-sapphire interface. (20 refs.)

114941 Optical anisotropy and electrostriction in the anodic oxide of tantalum. J.L.Ord, W.P.Wang (Dept. of Phys., Univ. of Waterloo, Waterloo, Ontario, Canada). *J. Electrochem. Soc. (USA)*, vol.130, no.9, p.1809-14 (Sept. 1983).

The anodic oxidation of tantalum in sulfuric acid electrolyte is studied using potential stepping transients to study the optical anisotropy of the oxide film under anodizing conditions and the strain induced in the film by changes in the field. The optical measurements are made with a self-nulling ellipsometer, and galvanostatic transients are used to study the changes in low frequency dielectric constant associated with the field-induced refractive index and film thickness changes. Two different analysis techniques are used to determine values for beta, the degree of anisotropy (the ratio between refractive index changes parallel and transverse to the field). The beta values obtained using the two techniques, 1.95 and 2.04, are not greatly different, but the authors regard the 2.04 value as more accurate because the technique used to obtain it is relatively insensitive to common systematic errors. The film thickness increases and the refractive indexes parallel and transverse to the field decrease when the field is applied. Both thickness and index exhibit dependences on field which curve away from the field axis, but the curves are not the parabolas predicted by the theory of electrostriction. The low frequency dielectric constant also decreases when the field is applied, but the charge-discharge cycles exhibit considerable hysteresis, and the dependence on the field is not as clearly defined as it is at optical frequencies. The results of the study of tantalum oxide are compared with the results of studies of the oxides of niobium, tungsten, and molybdenum carried out under similar experimental conditions. The electrostrictive behavior of these oxides and the absence of electrostriction in the anodic oxides of bismuth and zirconium pose a number of questions which theory cannot answer at present. (14 refs.)

114942 Infrared optical properties of solid monomethyl hydrazine, N₂O₄, and N₂H₄ at cryogenic temperatures. J.A.Roux (Univ. of Mississippi, University, MS, USA), B.E.Wood. *J. Opt. Soc. Am. (USA)*, vol.73, no.9, p.1181-8 (Sept. 1983).

To account for and identify the effects of cryocontamination, the infrared complex refractive-index ($\tilde{n} = n - ik$) values of cryofilms of monomethyl hydrazine (MMH), hydrazine (N₂H₄), and nitrogen tetroxide (N₂O₄) were determined for the 500-3700-cm⁻¹ wave-number range. The authors use techniques similar to those described in an earlier paper by Wood et al. (see ibid., vol.72, p.720, 1982) for thin H₂O, CO₂, and NH₃ condensed-gas films. Thin MMH, N₂O₄, and N₂H₄ films from 0.25 to 9.0 μ m thick were formed on a germanium substrate at 20 and 80K in vacuum, and the infrared transmittances were measured by using a Fourier-transform spectrometer. Values of the optical properties (n, k) were derived from the experimental trans-

mittance data by using a nonlinear least-squares method with a thin-film-transmittance analytical model. These optical constants were compared with results obtained with the subtractive Kramers-Kronig technique. These optical properties are important for predicting the performance of contaminated optical components. (13 refs.)

114943 Linear absorption coefficient of beryllium in the 50-300-Å wavelength range. M.A.Barstow, M.Lewis (Dept. of Phys., Univ. of Leicester, Leicester, England), R.Petre. *J. Opt. Soc. Am. (USA)*, vol.73, no.9, p.1220-2 (Sept. 1983).

Transmittance of thin-film filters fabricated for an extreme-UV astronomy sounding-rocket experiment yield values for the linear absorption coefficient of beryllium in the 50-300-Å wavelength range, in which previous measurements are sparse. The inferred values are consistent with the lowest data previously published and may have important consequences for extreme-UV astronomers. (9 refs.)

114944 In-plane orientation of polyimide. T.P.Russell, H.Gugger, J.D.Swales (IBM Res. Lab., San Jose, CA, USA). *J. Polym. Sci. Polym. Phys. Ed. (USA)*, vol.21, no.9, p.1745-56 (Sept. 1983).

As a nondestructive method of evaluation, integrated optics was used to investigate thin films (<8 μ m) of polyamic acid and polyimide as a function of molecular weight, initial imidization temperature, method of imidization, and annealing treatment. Polyamic acid films were found to exhibit a large optical anisotropy, indicating preferential alignment of the long axis of the molecule in the plane of the film. Imidization increased the birefringence of the film by a factor of 2.5 and reduced the film thickness. The only parameter that was found to effect the anisotropy of the films was the method of imidization. Chemical imidization was found to increase the birefringence by a factor of 3, indicative of a higher degree of molecular orientation parallel to the film surface. This effect was not observed in thicker (>25- μ m) films using X-ray diffraction where the orientation function was found to be independent of the method of imidization. (20 refs.)

114945 Production and release of light sums in thin films of activated alkali halides with different crystal structure. L.G.Zaslavskaya, G.K.Vale. *Lav. PSR Zinat. Akad. Vestis Fiz. Teh. Zinat. Ser. (USSR)*, no.4, p.46-52 (1983). In Russian.

Based on experimental investigations of thermoluminescence and kinetics of photostimulated activator luminescence decay in anion exciton absorption bands after X-ray or light excitation of activated alkali halide thin films (~5 mkm) with different structure (mono- and polycrystalline) it has been concluded that more unstable optical and thermal light sums are produced in polycrystalline films. (5 refs.)

114946 Abnormal optical absorption of quenched Ag films due to surface roughness. T.Lopez-Rios, G.Vuye, Y.Borensztein (Lab. d'Optique des Solides, Univ. Pierre et Marie Curie, Paris, France). *Surf. Sci. (Netherlands)*, vol.131, no.1, p.L367-72 (Aug. 1983).

The optical properties of rough Ag films quenched on substrates cooled to 150K are studied by differential reflectivity during annealing to room temperature. An abnormal optical absorption at about 2.5 eV is assigned to surface roughness. (12 refs.)

114947 Permeability at optical frequencies. A.N.Ageev, V.N.Gridnev, O.G.Rutkin, G.A.Smolsenskii (A.F. Ioffe Physicotech. Inst., Acad. of Sci., Leningrad, USSR). *Sov. Phys.-Solid State (USA)*, vol.25, no.2, p.270-1 (Feb. 1983). Translation of: *Fiz. Tverd. Tela (USSR)*, vol.25, no.2, p.478-81 (Feb. 1983). [received: Sept. 1983]

The validity of using the permeability tensor in the analysis of magneto-optic experiments in the phenomenological equations of electrodynamics is discussed. It is shown that in the optical range there is no need to assume the permeability tensor of every substance to be the unit tensor. The influence of this tensor on the waveguide optics properties of a thin magnetic film is examined. An experiment in waveguide optics is proposed which would allow a separate measurement of the off-diagonal components of the permittivity and permeability tensors. (20 refs.)

114948 Anomalies in the dependence of the transmission coefficient of light through thin silver films. A.P.Balashova, B.I.Indrishenok, A.E.Shabel'nikova (Inst. of Radio Engng. & Electronics, Acad. of Sci., USSR). *Sov. Phys.-Solid State (USA)*, vol.25, no.2, p.345-6 (Feb. 1983). Translation of: *Fiz. Tverd. Tela (USSR)*, vol.25, no.2, p.604-7 (Feb. 1983). [received: Sept. 1983]

The authors have observed a room-temperature quantum size effect in thin (less than 100 Å) silver films deposited on indium phosphide single crystals cleaned in an ultrahigh (~10⁻⁹ torr) grease-free vacuum chamber. The light transmission coefficient T_{sub} for the substrate was measured first, and then that for the whole sample as the silver was being deposited. Since indium phosphide begins to transmit light noticeably beginning with wave length $\lambda = 0.9 \mu$, measurements were made in the narrow spectra; range 0.9 < λ < 1.2 μ . They assumed that the transmissivity for the whole sample T_{sample} = T_{sub} T_{Ag}, from which they determined the transmissivity T_{Ag} for the silver film. (4 refs.)

114949 Spectrally selective black tungsten films. L.K.Thomas (Inst. fur Metallforschung-Metallphys. Tech. Univ. Berlin, Berlin, Germany), E.E.Chain.

Proceedings of the 4th European Conference on Chemical Vapour Deposition, Eindhoven, Netherlands, 31 May-2 June 1983 (Eindhoven, Netherlands: Philips Centre Manuf. Technol. 1983), p.130-3

For efficient photothermal solar energy conversion at operation temperatures in excess of 200°C converter surfaces should not only absorb the incident solar radiation but also suppress reradiation losses in the thermal infrared. Such spectrally selective surfaces must therefore demonstrate low reflectance over the solar range and high reflectance in the infrared. Thin films composed of Cr and Cr₂O₃ and of Mo and MoO₂ are being used or have been tested successfully as selective absorbers. Tungsten as the third member of the 6B transition metals group demonstrates greater spectral selectivity than does Cr or Mo. Therefore the authors prepared thin films composed of tungsten and tungsten oxides, which appear black to the eye and which they thus refer to as 'black tungsten films', in order to extend the knowledge obtained for CVD black molybdenum to black tungsten films. (3 refs.)

Ablative optical recording using organic dye-in-polymer thin films: some mechanistic aspects See Entry 112949

Thermal nitridation of silicon in nitrogen plasma See Entry 114377

Process study of chemically vapour-deposited SnO_x (x≈2) films See Entry 114395

CVD a-Ge and a-Ge:X films: preparation and properties See Entry 114411

Indirect and direct formation of polycrystalline silicon during CVD See Entry 114415

- Dispersion of the refractive index of light exhibited by $\text{Cd}_x\text{Hg}_{1-x}\text{Te}$ epitaxial films See Entry 114819
- Surface effects of Raman scattering from semi-metal Sb deposited on island Ag films See Entry 114838
- Picosecond dynamics of hot carrier relaxation in highly excited multi-quantum well structures See Entry 114879
- Improvement of photoluminescence of molecular beam epitaxially grown $\text{Ga}_{1-x}\text{In}_x\text{As}$ by using an As_2 molecular beam See Entry 114901
- Time-resolved measurements of photoluminescence in As-S alloy glasses and films evaporated from $\text{a-As}_2\text{S}_3$ See Entry 114919
- Deep radiative transitions in InP See Entry 114927
- Electroluminescence in ZnS:Mn thin film structures grown with atomic layer epitaxy See Entry 114928
- Low-voltage direct-current electroluminescence in ZnS:RE thin films See Entry 114930
- Cathodoluminescence of plasma-grown SiO_2 films See Entry 114936
- OMVPE growth of GaInP See Entry 115069
- LPCVD polycrystalline silicon: growth and physical properties of in-situ phosphorus doped and undoped films See Entry 115073
- Enhanced InP substrate protection for LPE growth of InGaAsP DH lasers See Entry 115115
- The preparation and properties of metallic optically transparent electrodes See Entry 115565

78.70 OTHER INTERACTIONS OF MATTER WITH PARTICLES AND RADIATION

- 114950 Are crystals birefringent for X-ray frequencies?. E.Zielinska-Rohozinska (Inst. Fizyki Doswiadczalnej, Uniwersytet Warszawski, Warszawa, Poland). *Postepy Fiz. (Poland)*, vol.34, no.3, p.237-48 (1983). In Polish. Polarization phenomena such as birefringence, optical activity and linear dichroism which are possible with visible light can also occur with X-rays with the help of diffracting crystals whereas they are insignificant in the case of simple X-ray transmission. (14 refs.)
- 114951 Inverse UV photoemission. P.O.Nilsson, A.Kovacs (Dept. of Phys., Chalmers Univ. of Technol., Gothenburg, Sweden). *Phys. Scr. (Sweden)*, vol.T4, p.61-4 (1983). (Nordic Conference on Surface Science, Tampere, Finland, 18-20 Aug. 1982). The present status of inverse UV photoemission (bremsstrahlung) spectroscopy is reviewed with regard to theory and experiment. A few examples of recently achieved results are presented. (28 refs.)

78.70B Positron annihilation

(see also 71.65 Positron states)

- 114952 Influence of repeated phase transitions on the annihilation of positrons in brass. P.Hautojarvi, V.S.Mikhaleukov, A.Vehanen, Yu.N.Koval' (Inst. of Metal Phys., Acad. of Sci., Kiev, Ukrainian SSR). *Fiz. Met. & Metalloved. (USSR)*, vol.56, no.2, p.286-9 (Aug. 1983). In Russian. English translation in: *Phys. Met. & Metallogr. (GB)*. A study was made of the changes in the positron lifetime and in the Doppler broadening parameter of an annihilation line as a function of the number of transitions across the martensitic transformation interval in an alloy of copper containing 39.5 mass % of zinc. An analysis of the results based on the positron capture model indicated that 60-70 transition cycles increased the concentration of defects by approximately an order of magnitude and then the accumulation of defects ceased. (5 refs.) A.T.
- 114953 Surface physics with slow positrons. R.M.Nieminen (Dept. of Phys., Univ. of Jyväskylä, Jyväskylä, Finland). *Phys. Scr. (Sweden)*, vol.T4, p.29-33 (1983). (Nordic Conference on Surface Science, Tampere, Finland, 18-20 Aug. 1982). Recent progress in slow beam studies of positron-surface interactions is reviewed. The key physical phenomena are introduced, and the present knowledge of the parameters involved is reviewed. The potential of the slow positron technique for surface science is discussed. (26 refs.)
- 114954 Experimental investigation of positron self-trapping near the vapour-liquid critical point of helium-4. T.-P.Chen, K.F.Canter (Dept. of Phys., Brandeis Univ., Waltham, MA, USA). *Solid State Commun. (USA)*, vol.47, no.11, p.903-7 (Sept. 1983). Positron self-trapping in helium near the vapor-liquid critical point is investigated using the positron annihilation lifetime technique. A 13% decrease in the slowing-down time for positrons to reach the self-trapped state is observed at the critical temperature 5.190K relative to the slowing-down time at 5.200K. (27 refs.)
- 114955 Two-dimensional angular correlation positron studies of defect and defect related problems in metals. A.Alam, R.N.West (School of Math. & Phys., Univ. of East Anglia, Norwich, England). Point Defects and Defect Interactions in Metals. Proceedings of the Yamada Conference V, Kyoto, Japan, 16-20 Nov. 1981 (Amsterdam, Netherlands: North-Holland 1982), p.278-80. The results of some preliminary studies of the utility of the recently developed two-dimensional angular correlation technique in positron defect studies are reported and briefly discussed. (9 refs.)
- 114956 The study of thermal equilibrium defects and melting in indium by two-parameter correlation measurement of positron annihilation. Y.Kishimoto, S.Tanigawa (Inst. of Materials Sci., Univ. of Tsukuba, Ibaraki, Japan). Point Defects and Defect Interactions in Metals. Proceedings of the Yamada Conference V, Kyoto, Japan, 16-20 Nov. 1981 (Amsterdam, Netherlands: North-Holland 1982), p.281-3. Correlation measurements between the positron age at the instant of annihilation and the momentum of the center of mass of the positron-electron pair were carried out in both the solid and liquid states of indium. Direct evidence was obtained that the approximation in the two state trapping model in which the detrapping of positrons from vacancies is neglected is valid in indium. It was found that mean lifetimes decreased upon melting and lifetimes were independent of the momentum in the liquid state. The liquid state of indium is discussed in comparison with that of gallium. (5 refs.)

- 114957 Positron study of a vacancy in graphite. T.Takahashi, M.Shimoto, M.Doyama (Dept. of Materials Sci., Univ. of Tokyo, Tokyo, Japan), T.Iwata. Point Defects and Defect Interactions in Metals. Proceedings of the Yamada Conference V, Kyoto, Japan, 16-20 Nov. 1981 (Amsterdam, Netherlands: North-Holland 1982), p.288-90. Positron techniques are applied to the study of the annealing behavior and electronic structure of a vacancy in highly-oriented pyrolytic graphite. The lifetime of positrons trapped in the vacancies is deduced to be 245 ± 5 ps. The vacancies show mobility around 1200°C. The Doppler-broadened lineshape of annihilation radiation from vacancies is obtained and compared with the results of theoretical calculation. (10 refs.)
- 114958 Positron studies of recovery processes in aluminium and aluminium alloys. R.N.West, A.Alam (School of Math. & Phys., Univ. of East Anglia, Norwich, England). Point Defects and Defect Interactions in Metals. Proceedings of the Yamada Conference V, Kyoto, Japan, 16-20 Nov. 1981 (Amsterdam, Netherlands: North-Holland 1982), p.469-76. A series of Doppler broadening positron studies in neutron-irradiated Al, deformed Al, and quenched Al and low concentration Al alloys is described. Utilization of a simple continuous sample heating technique has enabled the accumulation of a large number of detailed and reproducible recovery curves which provide further evidence concerning the phenomenon of vacancy clustering and the effect of metallic and other impurities on it. (34 refs.)
- 114959 Positron lifetimes in Pb-Ag dilute alloys. Y.Hara, S.Nanao (Inst. of Industrial Sci., Univ. of Tokyo, Tokyo, Japan). Point Defects and Defect Interactions in Metals. Proceedings of the Yamada Conference V, Kyoto, Japan, 16-20 Nov. 1981 (Amsterdam, Netherlands: North-Holland 1982), p.595-8. The positron lifetimes in Pb, Pb-0.015 at.% Ag and Pb-0.17 at.% Ag were measured in an equilibrium state over the temperature range from 300K to 590K. From the temperature dependence of the lifetime parameters, the vacancy formation enthalpy in pure Pb was evaluated to be 0.58 ± 0.06 eV. No definite difference was observed among the lifetime parameters in pure Pb and in Pb-Ag alloys except at the temperatures above 520K where the values of the mean lifetime in Pb-Ag tend to be slightly larger than those in pure Pb. This suggests that the attractive interactions between a silver atom and a vacancy are not intensive. A tentative analysis indicated that the binding energy is below 0.1 eV. (11 refs.)
- 114960 Threshold temperature of positron capture in Cu-Zn vacancies. I.K.MacKenzie, P.J.Schultz (Dept. of Phys., Univ. of Guelph, Guelph, Ontario, Canada). Point Defects and Defect Interactions in Metals. Proceedings of the Yamada Conference V, Kyoto, Japan, 16-20 Nov. 1981 (Amsterdam, Netherlands: North-Holland 1982), p.631-4. Doppler broadening of annihilation gamma rays indicates the threshold temperature T_1 for positron capture in thermally generated vacancies. The dependence of T_1 on alloy concentration is measured for the entire Cu-Zn phase diagram with emphasis on α , β and the mixed ($\alpha+\beta$) phases. (6 refs.)
- 114961 Temperature dependence of positron annihilation parameters in irradiated molybdenum. B.Pagh, H.E.Hansen, B.Nielsen, K.Petersen (Lab. of Appl. Phys., Tech. Univ. of Denmark, Lyngby, Denmark). Point Defects and Defect Interactions in Metals. Proceedings of the Yamada Conference V, Kyoto, Japan, 16-20 Nov. 1981 (Amsterdam, Netherlands: North-Holland 1982), p.691-4. The temperature dependencies of the positron lifetime parameters have been investigated in molybdenum containing vacancies and in molybdenum containing a mixture of vacancy-loops and voids. The results show no temperature dependence of the positron trapping rate at either mono-vacancies or voids in the temperature range from 77K upwards. By using the void response method it was found that at low temperatures the trapping rate of vacancy-loops decreases strongly with temperature. (5 refs.)
- 114962 A positron annihilation study of neutron irradiated titanium. M.Hasegawa (Res. Inst. for Iron, Steel & Other Metals, Tohoku Univ., Oarai, Ibaraki, Japan), S.Koike, M.Hirabayashi, Y.Higashiguchi, E.Kuramoto, K.Kitajima. Point Defects and Defect Interactions in Metals. Proceedings of the Yamada Conference V, Kyoto, Japan, 16-20 Nov. 1981 (Amsterdam, Netherlands: North-Holland 1982), p.695-7. Defects in titanium irradiated with fast neutrons have been studied by measuring lifetime and angular correlation of positron annihilation. Vacancy clusters of microvoids are formed in the specimens irradiated at 80-100°C with the neutron doses of 10^{19} - 10^{20} cm⁻². The formation and dissociation of vacancy clusters or microvoids are sensitive to impurity content in the specimens. (5 refs.)
- 114963 Positron annihilation in molybdenum single crystals irradiated with electrons, neutrons, and α -particles. M.Hasegawa (Res. Inst. for Iron, Steel & Other Metals, Tohoku Univ., Ibaraki, Japan), E.Kuramoto, K.Kitajima, Y.Ohya, K.Abe, S.Morozumi. Point Defects and Defect Interactions in Metals. Proceedings of the Yamada Conference V, Kyoto, Japan, 16-20 Nov. 1981 (Amsterdam, Netherlands: North-Holland 1982), p.876-9. In order to reveal the behavior of vacancy clusters created by irradiation of high energy electrons, neutrons and α -particles, positron lifetime measurements have been performed for high-purity molybdenum. Changes in lifetime parameters depending on the irradiating particles and impurity contents are compared. Annealing processes of the irradiated specimens are also studied. (10 refs.)
- Mobilities of quenched-in defects in NiAl See Entry 113864
- Vacancies in silver: a resistivity and positron annihilation study See Entry 113876
- Submicroscopic vacancy defects in pure and doped gold See Entry 113879
- Vacancy formation in Ni and Ni(Ge) See Entry 113880
- Vacancies in B2(CuCl) type ordered alloys See Entry 113884
- The study of vacancy clustering in deformed metals by positron annihilation See Entry 113898
- A positron lifetime study of vacancy-solute complexes in dilute gold alloys See Entry 113968
- Formation of vacancies in thermal equilibrium in α -range alloys See Entry 113972
- Mobilities of radiation-induced vacancies in Ni₃Al and NiAl studied by positron techniques See Entry 114022
- A study of defect states in neutron-irradiated zirconium using positron annihilation spectroscopy See Entry 114042

78.70C X-ray scattering

114964 Temperature dependence of the X-ray diffuse scattering intensity in V_3Si in the temperature range from 8 to 300K. N.N.Sirota, L.P.Polutchankina, N.S.Orlova (Inst. of Phys. of Solids & Semiconductors, Byelorussian Acad. of Sci., Minsk, Byelorussian SSR). *Cryst. Res. & Technol. (Germany)*, vol.18, no.8, p.1029-34 (1983). Measurements of the diffuse X-ray scattering are performed from the (110) plane in V_3Si single crystal at different temperatures from 300 to 8K. Contours of equal diffuse scattering intensity are drawn over the 440 node in the (001) and (111) sections. The temperature dependence and the anisotropy of the thermal diffuse scattering intensity distribution for this compound are analysed. (15 refs.)

114965 Diffraction effects in the presence of Compton and temperature-diffuse X-ray scattering in mosaic crystals. V.A.Bushnev, A.V.Laushkin, R.N.Kuz'min, N.N.Lobanov (M.V. Lomonosov State Univ., Moscow, USSR). *Sov. Phys.-Solid State (USA)*, vol.25, no.2, p.228-33 (Feb. 1983). Translation of: *Fiz. Tverd. Tela (USSR)*, vol.25, no.2, p.406-15 (Feb. 1983). [received: Sept. 1983] The authors report the results of experimental and theoretical investigations of diffraction effects occurring under inelastic X-ray scattering in mosaic crystals of various degrees of perfection. It is shown that the diffraction of quanta from Compton (CS), Raman, and temperature-diffuse scattering (TDS) in specimens causes interference lines with a fine structure to appear in the angular scattering spectrum. A diffractometric study was made of the profiles of the interference lines from the scattering of Mo K α radiation in LiF single crystals and measurements were made of their widths and their intensities relative to the incoherent background. Within the framework of the theory of secondary extinction the authors give a theoretical explanation of the diffraction effects observed and investigate the dependence of the shape, width, and contrast of the interference lines on the mosaic structure, thickness, reflectivity and scattering geometry of the specimens. The theory is shown to be in satisfactory agreement with the experiment. An anomalous increase in the contrast of the interference lines as the crystal thickness grows is predicted. (21 refs.)

Magnetic Compton scattering with circularly polarised synchrotron radiation .. See Entry 111831

Interstitials and interstitial clusters in fast-neutron irradiated molybdenum by X-ray Huang scattering See Entry 113903

78.70D X-ray absorption and absorption edges

114966 Influence of structural anisotropy on the extended X-ray absorption fine structure at the K edge of polycrystalline cadmium. W.Thulke, P.Rabe (Inst. for Experimentalphys., Univ. Kiel, Kiel, Germany). *J. Phys. C (GB)*, vol.16, no.27, p.L955-60 (30 Sept. 1983). The extended X-ray absorption fine structure at the K edge of polycrystalline cadmium at liquid nitrogen temperature has been measured with X-radiation of a conventional X-ray source. The magnitude of the Fourier transform of the fine structure yields a single maximum which is attributed to the first of two close-lying nearest-neighbour shells alone. The absence of a second-shell contribution due to thermal damping is in good agreement with data obtained from measurements on a cadmium single crystal. (10 refs.)

114967 X-ray spectroscopy contributions to the study of iron oxide mixed valence compounds. Analysis of K absorption fine structure. M.Lenglet, D.Le Calonnec (INSCIR, Faculté des Sci. et Tech., St. Aignan, France), J.Durr, B.Hannoyer, G.Calas, J.Petiau, F.Jeannot. *Mater. Res. Bull. (USA)*, vol.18, no.8, p.935-44 (Aug. 1983). In French. Chemical shifts of $L_{\alpha 1,2}$, $K\beta_{1,3}$, $K\beta_5$ emission bands and X-ray absorption spectra near the K edge have been measured in several iron spinels oxides with the metal in the formal oxidation states +2 and +3. The first high resolution XANES spectra for these materials were performed at the DCI storage ring at LURE, Orsay. Two transitions in the range 15-20 eV above the 1s-3d observed on the derivative XANES spectra are very sensitive to the iron oxidation state. The analysis of the X-ray absorption fine structure in the near edge region and the measurements of the chemical shift of $FeK\beta_5$ are more adapted than Mossbauer effect to disclosing FeII in mixed ferrites. (24 refs.)

114968 L_1 and L_{III} X-ray absorption in dysprosium and location of 4f levels. B.K.Agarwal, V.Balakrishnan (Dept. of Phys., Allahabad Univ., Allahabad, Uttar Pradesh, India). *Phys. Rev. B (USA)*, vol.28, no.5, p.2852-4 (1 Sept. 1983). The L_1 X-ray absorption-edge and near-edge structure in dysprosium are reported along with the first measurement of L_1 extended X-ray-absorption fine structure in metal and compounds. The location of 4f levels is discussed on the basis of the observed near-edge structure in the Dy L_{III} edge. (11 refs.)

114969 Fine structure of ultrasoft X-ray absorption spectra of a number of titanium compounds. A.S.Vinogradov, A.Yu.Dukhnyakov, V.M.Ipatov, A.A.Pavlychev, V.N.Sivkov (A.A. Zhdanov State Univ., Leningrad, USSR). *Sov. Phys.-Solid State (USA)*, vol.25, no.2, p.225-8 (Feb. 1983). Translation of: *Fiz. Tverd. Tela (USSR)*, vol.25, no.2, p.400-5 (Feb. 1983). [received: Sept. 1983] Using an RMS-500 X-ray spectrometer-monochromator, by the method of the quantum yield of the X-ray photoemission effect the authors studied the near-in fine structure in the X-ray absorption spectra of rutile (TiO $_2$) and metallic titanium in the region of the K and $L_{2,3}$ ionization thresholds of oxygen and titanium atoms, respectively. As a result of the joint consideration of the near-in fine structure of the $L_{2,3}$ spectra of titanium in the metal, rutile, and in the earlier investigated coordination compound K $_2$ TiF $_6$ it was found that the main features of these spectra are determined by the spectral distribution of the oscillator strengths for the $2p-3d$, ed transitions in the titanium atomic spectrum, on which are superimposed the neighbourhood effects, manifesting themselves in splitting of the d state, with the magnitude of this splitting increasing with the electronegativity of the surrounding atoms. A marked resemblance is observed between the near-in fine structure of the K spectra of fluorine and oxygen in K $_2$ TiF $_6$ and TiO $_2$. On the basis of this experimental fact as well as the correlation of the energy position of the main details of the near-in fine structure of the spectra of titanium and oxygen in rutile the authors assert that the process of X-ray absorption in the rutile crystal is quasimolecular in character, i.e. the details of the near-in fine structure of all of its spectra are formed mainly by the potential of the first coordination sphere around the titanium atom. (16 refs.)

Photoabsorption study of bonding in some 3d-4f intermetallics and other compounds See Entry 113798

Photon-stimulated desorption from rare earth oxides See Entry 114489

X-ray and photoelectron spectroscopy of light rare earths See Entry 115010

78.70E X-ray emission threshold and fluorescence

114970 Micro-state analysis of iron compounds using the 9th-order FeK α_1 line. H.Fujimori, H.Iba, H.Tsuchiya (Energy Res. Lab., Hitachi Ltd., Ibaraki, Japan). *Jpn. J. Appl. Phys. Part 1 (Japan)*, vol.22, no.6, p.1025-9 (June 1983). The X-ray spectra of 9th-order FeK α_1 (FeK α_1^9), FeL α and FeL β lines were measured for metallic iron, FeO, Fe $_3$ O $_4$, Fe $_2$ O $_3$, FeF $_2$ and FeF $_3$ with an excitation potential of 20 kV using an electron probe microanalyzer (EPMA). The micro-state analysis of these iron compounds using EPMA was greatly improved by observation of the FeK α_1^9 line, because its intensity relative to the FeL α line varied with the chemical state and its peak position became a marker to measure the wavelength shift of the FeL α line ($\Delta L\alpha$). Factors influencing the absorption effect on the measured spectra were evaluated by calculating the absorption correction factors. The wavelength $\Delta L\alpha$ did not exhibit substantial changes in electron binding energy, though it showed correlation with the valency of iron. (16 refs.)

114971 X-ray emission spectra of titanium in TiN $_{0.8}$ and TiN $_{0.8}$ H $_x$. V.V.Nemoshkalenko, V.P.Krivitskii, M.M.Kindrat, B.P.Mamko (Inst. of Metal Phys., Acad. of Sci., USSR). *Inorg. Mater. (USA)*, vol.18, no.9, p.1371-2 (Sept. 1982). Translation of: *Izv. Akad. Nauk SSSR Neorg. Mater.*, vol.18, no.9, p.1596-7 (Sept. 1982). [received: Sept. 1983] The X-ray emission spectra of the components of transition-metal carbides and nitrides demonstrate clearly the energy separation of the electron states involved in directional localized metal-nonmetal bonds M-X and in delocalized metal-type M-M, X bonds. Therefore, these provide good objects for elucidating the interaction of hydrogen atoms with the matrix. The authors present results from X-ray emission spectra in the K $\beta_{2,5}$ and L α bands of titanium in the nitride TiN $_{0.8}$ and the nitrohydride TiN $_{0.8}$ H $_x$; the nitride was hydrogenated to saturation. (3 refs.)

114972 Soft X-ray appearance potential spectroscopy of the lanthanide rare earths. W.E.Harte, P.S.Szczepanek, A.J.Leyendecker (Lab. for Phys. Sci., College Park, MD, USA). *J. Less-Common Met. (Switzerland)*, vol.93, no.1, p.189-200 (1983). (Proceedings of the Sixteenth Rare Earth Research Conference, Tallahassee, FL, USA, 18-21 April 1983). Soft X-ray appearance potential spectroscopy (SXAPS) exploits the sudden changes in the fluorescent yield associated with the thresholds for the electron excitation of core states. Inflections on the yield curve, easily enhanced by differentiation, provide information on the electronic properties of the target material. For the rare earths, the M $_5$, M $_4$ spectra are multi peaked and unusually intense. The excitations are localized involving atomic f levels relatively unaffected by atomic environment. The spectra are attributed to couplings between the incident electron, the excited electron and the resultant hole which leads to a resonant interaction that splits and intensifies the lines. The present status of SXAPS will be presented concentrating on the interpretations given to specific experiments. (52 refs.)

114973 Appearance potential study of the 4f levels of cerium, praseodymium and their oxides. D.Chopra, H.Naraghi (Dept. of Phys., East Texas State Univ., Commerce, TX, USA). *J. Less-Common Met. (Switzerland)*, vol.93, no.1, p.203-12 (1983). (Proceedings of the Sixteenth Rare Earth Research Conference, Tallahassee, FL, USA, 18-21 April 1983). The soft X-ray appearance potential spectra of the M $_4,5$ levels of cerium, praseodymium and their oxides were obtained in the 800-1000 eV energy range using the modulation potential technique. Rare earths, which have the same valence in the metal as in the oxide, are predicted to have localized 4f electrons which are not affected by oxidation. Contrary to this assertion, an effect of oxygen on the spectra of the rare earths, cerium and praseodymium has been recorded. The spectra are interpreted in terms of the atomic-like transitions involving exchange interactions between the 4f electrons and 3d vacancies and are not considered to be a self-convolution of the density of unoccupied 4f states in the above metals. The data are consistent with the trends in localization of the screening orbitals across the lanthanide series. (26 refs.)

114974 Molecular effect of Al K α -X-ray yields from aluminum oxide films for H $^+$ and H $_2^+$ ion bombardments. A.Ootuka, F.Fujimoto, K.Komaki (Coll. of General Education, Univ. of Tokyo, Tokyo, Japan), K.Kawatsura, K.Ozawa, M.Terasawa. *Phys. Lett. A (Netherlands)*, vol.97A, no.5, p.191-03 (29 Aug. 1983). Al K α X-ray spectra for equi-velocity H $^+$ and H $_2^+$ ions of ≈ 0.9 MeV/amu incident on thin aluminum oxide films with thickness 100 and 300 Å were observed. The intensity ratio of the KL 1 satellite line to the KL 0 main one for H $_2^+$ incident on the films of thickness 100 and 300 Å was about 10% and 4% larger than that for incident H $^+$, respectively. (9 refs.)

114975 Incomplete relaxation and plasmon formation in the K emission band of copper. J.Bremer (Norwegian Inst. of Technol., Univ. of Trondheim, Trondheim, Norway). *Solid State Commun. (USA)*, vol.47, no.11, p.881-4 (Sept. 1983). A method of calculating the effect of self-absorption in X-ray emission spectra and which is suitable for non-adiabatic excitation processes is presented. The Fermi-level E_F and the 'true' profile of the electron-excited (20-40 keV) CuK $\beta_{2,5}$ band are determined. A deviation from the calculated one-electron spectrum in the energy interval [-12 eV, -7 eV] below E_F is interpreted as a result of plasmon formation and Auger broadening. A pronounced disagreement is found also in the range [-1 eV, +10 eV]. Above E_F , a part of the intensity may be due to incomplete electron relaxation. (21 refs.)

X-ray spectroscopic investigation of the nature of chemical binding in metal-like titanium carboaluminides of variable composition See Entry 113795

Electronic structure and interparticle interaction in defect cubic oxides of vanadium and titanium See Entry 114443

Electronic structures of sulfide minerals-theory and experiment See Entry 114444

X-ray spectroscopy contributions to the study of iron oxide mixed valence compounds. Analysis of K absorption fine structure See Entry 114967

78.70G Microwave and radiofrequency interactions (exc. resonances)

Generation and detection of millimeter waves by picosecond photoconductivity See Entry 114558

79.00 ELECTRON AND ION EMISSION BY LIQUIDS AND SOLIDS; IMPACT PHENOMENA

79.20 IMPACT PHENOMENA

(inc. electron spectra and sputtering)

114976 Electrification of polymer particles by impact on a metal plate. N.Masui, Y.Murata (Dept. of Electrical Engng., Sci. Univ. of Tokyo, Chiba, Japan).

Jpn. J. Appl. Phys. Part 1 (Japan), vol.22, no.6, p.1057-62 (June 1983). Impact charge and impact area of particles of nylon 66 and PMMA (3.18 mm and 2.19 mm in diameter, respectively) by a single impact on a metal plate (Cr plated brass plate) were measured under various impact speeds v (3.7 m/s~20.3 m/s) and impact angles θ (0° ~ 80°). It was found that both the impact charge and the impact area are functions of the vertical component of the impact speed, $v \cos \theta$, while the horizontal component, $v \sin \theta$, was found to have no effect on them. The impact area is calculated using the theory of plastic-elastic deformation, and the measured values are found to agree well with the calculations. The impact charge density is constant within the range of the experimental conditions examined and is determined only by the combination of materials colliding with each other. (17 refs.)

114977 Quantum features of reflection of relativistic particles by a crystal surface. V.G.Khlabutin, Yu.L.Pivovarov, S.A.Vorobiev (Inst. of Nuclear Phys., Tomsk, USSR).

Phys. Lett. A (Netherlands), vol.97A, no.6, p.249-52 (5 Sept. 1983). A new mechanism of reflection of relativistic particles by a crystal surface at grazing angles is considered. The reflection takes place when the 'transverse' energy value (connected with the particle motion perpendicular to the surface) lies in the forbidden band of the energy spectrum in a one-dimensional periodic potential which is the sum of continuous potentials of crystallographic planes being parallel to the surface. (7 refs.)

Analysis of surfaces and thin filmsSee Entry 114317

79.20D Laser-light impact phenomena

Laser annealing of semiconductorsSee Entry 111333

Emission of melt during laser vaporization of metallic filmsSee Entry 113999

Introduction [laser annealing of semiconductors]See Entry 114001

Crystallization processes [laser annealing of semiconductors]See Entry 114002

Fundamentals of energy deposition [laser annealing of semiconductors]See Entry 114003

Heat flow calculations [laser annealing of semiconductors]See Entry 114004

Surface properties of laser-annealed semiconductorsSee Entry 114321

Study of the protoporphyrin luminescence under selective laser excitationSee Entry 114917

Site selective excitation of 1-hydronaphthyl radical in irradiated naphthalene crystalSee Entry 114918

79.20F Electron impact: Auger emission

114978 Calculated Auger sensitivity factors compared to experimental handbook values. S.Mroczkowski (Midwest Res. Microscopy Inc., Milwaukee, WI, USA), D.Lichtman.

Surf. Sci. (Netherlands), vol.131, no.1, p.159-66 (Aug. 1983). A pseudo-first principles technique for Auger quantisation was used to calculate relative Auger yields. These yields were compared to the experimental sensitivity factors found in the Handbook of Auger Electron Spectroscopy. In cases where pure element standards are readily available, theory agreed quite well with experiment 95% of the time. However, when pure element standards are not available, such as the lanthanide series and the light elements from $Z=7$ to 12, large deviations exist. Plots of the calculated yields for 3, 5 and 10 kV primary beams are superimposed upon the Handbook sensitivity factor graphs and the reasons for the similarities and differences are discussed. (10 refs.)

114979 Angle-resolved Auger electron emission from $\text{LaB}_6(001)$ with and without chemisorbed oxygen. S.A.Chambers, L.W.Swanson (Dept. of Appl. Phys. & Electrical Engng., Oregon Graduate Center, Beaverton, OR, USA).

Surf. Sci. (Netherlands), vol.131, no.2-3, p.385-402 (Sept. 1983). The angular intensity distributions of $\text{La}(\text{M}_5\text{N}_{45}\text{N}_{45})$ and $\text{B}(\text{KL}_1\text{L}_1)$ Auger electrons have been measured as a function of polar and azimuthal angles for clean and oxygen-covered $\text{LaB}_6(001)$. The method used employs a dispersive cylindrical mirror energy analyzer and a two-axis rotation and sample manipulator. Significant structure is observed in both polar and azimuthal profiles and, at least in the case of La Auger emission, can be partially accounted for using a simple scattering model. Polar profiles obtained by this method and those obtained using angle-resolved X-ray photoemission show many similarities. The angular intensity profiles are consistent with a model of the surface in which the La layer is outermost on the polar $\text{LaB}_6(001)$ plane and adsorption of oxygen occurs at both La and B sites. (24 refs.)

114980 Calculation of Auger recombination times in p -type InGaAsP solid solutions. D.Z.Garbuzov, Z.N.Sokolova, V.B.Khalfin (A.F. Ioffe Physicotech. Inst., Acad. of Sci., Leningrad, USSR).

Sov. Phys.-Tech. Phys. (USA), vol.28, no.2, p.193-6 (Feb. 1983). Translation of: *Zh. Tekh. Fiz. (USSR)*, vol.53, no.2, p.315-19 (Feb. 1983). [received: Sept. 1983]

The intergap and impurity Auger recombination times are calculated for a series of p -type InGaAsP solid solutions have the same lattice structure as the InP substrate. The nonradiative transition times are compared with the calculated radiative transition times for solid solutions doped to various degrees by acceptor impurities in order to find how the internal quantum yield depends on the composition, temperature, and hole density. It is found that nonradiative Auger recombination in narrow-gap InGaAsP solid solutions may reduce the internal quantum yield at hole densities as low as $p=10^{17} \text{ cm}^{-3}$. A comparison is made with experimental results on the dependence of the radiation efficiency on the hole density for an $\text{In}_{0.73}\text{Ga}_{0.27}\text{As}_{0.60}\text{P}_{0.40}$ solid solution doped with zinc. (10 refs.)

114981 Surface chemistry of (100) indium phosphide. R.A.Winrow. Univ. Nottingham, England thesis, 1983

The technique of Auger Electron Spectroscopy (AES) has been used to investigate the surface chemistry of epitaxially grown (100) InP produced by the

two most important vapour phase techniques: the $\text{In-H}_2\text{-PCl}_3$ (chloride) process and the $\text{In}(\text{C}_2\text{H}_5)_3\text{-PH}_3$ (alkyl) process. The surface of material in the 'as grown' state from both systems is seen to be nonstoichiometric and oxidised to varying degrees. A mechanism is proposed to account for these effects and for the differences observed between the two types of material. In addition the effects of various chemical treatments upon the surface of both bulk and epitaxially grown (100) InP have been investigated. After chemical treatment and characterisation by AES, samples have been evaporated with silver layers under conditions of ultra high vacuum and the sintered in a nitrogen atmosphere. Subsequent removal of contact material by chemical etching has allowed examination of the InP surface by optical and scanning electron microscopy. A correlation has been obtained between the chemical state of the InP surface prior to metallisation and the subsequent interface behaviour on sintering with the silver contact metallisation. This has led to a better understanding of the processes occurring at the metal semiconductor interface at elevated temperatures, and has provided an explanation for the variable levels of effectiveness observed of silver cathode contacts to InP transferred electron oscillators.

Mechanism and kinetics of radiation-induced segregation in Ni-Si alloysSee Entry 114187

Oxygen adsorption on a cylindrical GaAs single crystal prepared by molecular beam epitaxySee Entry 114341

Ion scattering spectroscopy of $\beta\text{-N}$ and $\beta_3\text{-Co}$ ($\sqrt{2} \times \sqrt{2}$) $\text{R}45^\circ$ structures on $\text{W}(100)$ See Entry 114346

Thermodynamics of xenon adsorption on $\text{Pd(s)}[8(100) \times (110)]$: from steps to multilayersSee Entry 114356

Electron-enhanced CO_2 adsorption and stabilization on aluminum filmsSee Entry 114366

EELS and AES study of epitaxially grown $\text{Pd}(111)$ thin filmsSee Entry 114392

UHV-SEM study of the nucleation and growth of $\text{Ag/W}(110)$ See Entry 114393

The effect of oxygen in cosputtered (titanium+silicon) filmsSee Entry 114401

Investigation of gallium arsenide subjected to an intensive plasma treatmentSee Entry 115003

79.20K Other electron impact phenomena

114982 Influence of film structure on the electron energy loss spectra of GaAs thin films. H.Boudriot, B.Kubier, K.Deus, R.Grundler, E.Kusior (Sektion Phys., Bergakad. Freiberg, Freiberg, Germany).

Cryst. Res. & Technol. (Germany), vol.18, no.8, p.1035-44 (1983). Energy loss measurements of fast electrons on GaAs yielded values for the plasma oscillation, interband transitions and the dielectric function in the region 5-30 eV. The results are discussed in comparison with literature statements. It is dealt especially with the influence of the degree of crystallinity of examined GaAs-films on the energy loss spectrum and the quantities derived from it. (16 refs.)

114983 Excitation of surface plasmons on He-filled cavities in Al. R.Manzke, G.Crecelius (Inst. fur Festkörperforschung, KFA Jülich GmbH, Jülich, Germany), J.Fink.

Phys. Rev. Lett. (USA), vol.51, no.12, p.1095-8 (19 Sept. 1983). Surface plasmon losses excited on spherical, He-filled cavities in Al are studied with use of transmission electron energy-loss spectroscopy. It is found that the excitation energy of the $l=1$ (dipole) surface plasmon mode decreases with increasing He concentration, in line with predictions of an effective-medium theory taking into account the dipole-dipole interactions between bubbles in dense populations, the density dependence of the He dielectric constant, and a density-dependent atomic polarizability of the He in the bubbles. (27 refs.)

114984 Vibrational spectra of coadsorbed CO and H on Ni(100) and Ni(111). G.E.Mitchell, J.L.Gland (Phys. Chem. Dept., General Motors Res. Labs., Warren, MI, USA), J.M.White.

Surf. Sci. (Netherlands), vol.131, no.1, p.167-78 (Aug. 1983). High resolution electron energy loss spectra are reported for coadsorbed hydrogen and carbon monoxide on Ni(100) and Ni(111). On neither surface was there any evidence for either C-H or O-H bonds. On Ni(111) one CO stretching frequency is observed and it does not change significantly in the presence of coadsorbed hydrogen. This is consistent with segregation of CO and H into islands. On Ni(100) the situation is much different; one frequency is observed in the absence of H(a) while three CO stretching frequencies are observed for the coadsorbed layers. These are attributed to on-top, two-fold bridged and four-fold binding of CO to the Ni(110) surface. These results demonstrate significant structure sensitivity for the organization of these coadsorbed species. (24 refs.)

114985 Angular dependence of the electron energy loss spectra of the reconstructed $\text{Si}(001)$ clean surfaces. H.Iwasaki, S.Nakamura (Inst. of Sci. & Industrial Res., Osaka Univ., Osaka, Japan).

Surf. Sci. (Netherlands), vol.131, no.2-3, p.448-54 (Sept. 1983). It is explicitly shown that the asymmetric dimer model of the $\text{Si}(001)2 \times 1$ reconstructed surface proposed by Chadi (1979) should exhibit logarithmic peaks and specific angular dependences in its electron energy loss spectra between the surface dangling bond bands. By comparison with the present experimental result, the authors suggest that the surface consists of microdomains of the asymmetric dimer $c(4 \times 2)$ surface. (11 refs.)

114986 An EELS study of N_2O adsorption of $\text{Pt}(111)$. N.R.Avery (SCIRO Div. of Materials Sci., Univ. of Melbourne, Parkville, Victoria, Australia).

Surf. Sci. (Netherlands), vol.131, no.2-3, p.501-10 (Sept. 1983). At 78K, N_2O adsorbs on a $\text{Pt}(111)$ surface in an end-on configuration through the terminal N atom and inclined at an angle to the surface estimated at 35° . N_2O is a soft Lewis base with adsorption occurring by donor bond formation and without significant back donation into the unoccupied π^* antibonding orbital. Adsorption is accordingly weak with an initial heat of adsorption of $5.6 \text{ kcal mol}^{-1}$ which increased to $6.05 \text{ kcal mol}^{-1}$ at saturation by attractive lateral interactions. No evidence for decomposition was seen. A multilayer state, adsorbed approximately parallel to the surface, desorbed near 86K with a heat of vaporization estimated at $5.24 \text{ kcal mol}^{-1}$. (19 refs.)

Instrument for examining the polarization of low-energy electrons interacting with a solidSee Entry 111822

Electron spectroscopy on adsorption of Cs on transition metalsSee Entry 114344

Characterisation of a low temperature surface phase of CO on Pt [110]See Entry 114345

Electron-enhanced CO₂ adsorption and stabilization on aluminum filmsSee Entry 114366

TEM—electron energy loss spectroscopy study of the diamond particles prepared by the chemical vapour deposition from methaneSee Entry 114379

EELS and AES study of epitaxially grown Pd(111) thin filmsSee Entry 114392

Surface plasmon scattering on flat surfaces at grazing incidenceSee Entry 114462

Surface physics with slow positronsSee Entry 114953

79.20N Atom, molecule, and ion impact

114987 A PIXE-RBS method for measuring partial sputtering yields of stainless steel. M.Tomita, N.Ikuchi, S.Miyagi, M.Sakisaka (Dept. of Nuclear Engng., Kyoto Univ., Kyoto, Japan).
Nucl. Instrum. & Methods Phys. Res. (Netherlands), vol.213, no.2-3, p.469-75 (1 Aug. 1983).
A collector method has been developed for measuring the partial sputtering yields of stainless steel constituents. The sticking probabilities of Cr-, Fe-, and Ni-atoms to a carbon collector are found to be close to unity. By combining a PIXE with an RBS analysis, each quantity of the constituent atoms deposited on the collector surface is micro-quantitatively measured with a good accuracy. When an SS304 plate is exposed to 25 keV He⁺ ions in a vacuum of 10⁻⁶ Torr range, no evident preferential sputtering is found among three constituent elements at a fluence of 4.9×10¹⁹ He/cm². (19 refs.)

114988 Ion induced electron ejection from solids. H.J.Frischkorn, K.O.Groeneveld, D.Hofmann, P.Koschar, R.Latz, J.Schader (Inst. fur Kernphys., J.W. Goethe-Univ., Frankfurt/Main, Germany).
Nucl. Instrum. & Methods Phys. Res. (Netherlands), vol.214, no.1, p.123-8 (1983). (Proceedings of the International Workshop on Cross Sections for Fusion and Other Applications, College Station, TX, USA, 4-6 Nov. 1982).
Electron energy spectra, their angular distribution and their total yield γ give information on electron production mechanisms in energetic (1<E/M<10³ keV/amu) ion-solid interaction. From molecular ion induced total electron yield data the authors report on a novel interference effect of electron density waves in a solid. (29 refs.)

114989 Analytical calculation of energy spectra of keV light particles reflected from solid surfaces. K.Morita (Dept. of Crystalline Materials Sci., Nagoya Univ., Nagoya, Japan).
Jpn. J. Appl. Phys. Part I (Japan), vol.22, no.7, p.112-18 (July 1983).
The energy spectra of keV light particles reflected from solid surface have been calculated within the single collision approximation, taking account of the angular and lateral deviations of the incident beam caused by multiple small-angle collisions. The particle and energy reflection coefficients (R_N and R_E) have also been calculated as a function of the reduced energy (ε₀) in Thomas-Fermi units. It is shown that for various targets, the shape of the energy spectra at given incident and ejection angles depends only on ε₀ and that the values of R_N and R_E are scaled by a universal function of ε₀. Typical values of the calculated reflection coefficients for Au and C together with the energy spectra for Au at normal incidence and for Fe at oblique incidence are shown to agree well with the experimental data on keV H⁺ obtained by the Garching group. (24 refs.)

114990 On the influence of incident energy of protons on chemical erosion of graphite. R.Yamada, K.Sone (JAERI, Ibaraki-ken, Japan).
J. Nucl. Mater. (Netherlands), vol.116, no.2-3, p.200-5 (June 1983).
Calculations of energy dependence of chemical sputtering have been made for 0.1-6 keV protons normally incident on graphite surface. The calculations were based on Erents' model (see *ibid.*, vol.63, p.399, 1976) by taking consideration of surface deposited energy and reflection of protons which are both dependent on the incident energy. The calculated chemical sputtering yields show that they have a maximum value in the vicinity of 1 keV of the incident energy, which is consistent with previous experimental results. (23 refs.)

114991 On the reaction of graphite with atomic hydrogen. Y.Hirooka (Div. of Nuclear Fuel Res., JAERI, Ibaraki, Japan), M.Nagae, T.Sano.
J. Nucl. Mater. (Netherlands), vol.116, no.2-3, p.206-10 (June 1983).
Reaction behaviour of graphite with a molecular/atomic mixture hydrogen beam, produced by a hot W-filament, has been studied in an ultrahigh vacuum system at temperatures between 550 and 800K. Major reaction products have been recognized to be recombined molecular hydrogen and methane. Temperature dependence observed for probability of methane formation suggests apparently negative activation energy for the reaction. It has been implied that molecular hydrogen in the mixture beam may serve as an impurity element to physically adsorb on the graphite surface and hence hinder the reaction due to atomic hydrogen. (23 refs.)

114992 Ion scattering at the surface—elastic and inelastic scattering, and neutralization. Y.Ohtsuki (Dept. of Phys., Waseda Univ., Tokyo, Japan).
J. Vac. Soc. Jpn. (Japan), vol.26, no.2, p.61-8 (1983). In Japanese.
Ion motion caused by potentials on a solid surface has not yet been elucidated, although the motion is a matter of great importance. This paper deals with: (1) local stopping power in inelastic scattering of ion beams; (2) surface plasmon excitations due to motion of valence electrons; (3) wavelet potentials generated when ions go out from a solid surface; (4) ion neutralization by resonance process; and (5) the probability of ion neutralization by Auger process. (17 refs.) K.B.

114993 Ion-induced sputtering. Y.Yamamura (Okayama Univ. of Sci., Okayama, Japan), R.Shimizu, H.Shimizu, N.Itoh.
J. Vac. Soc. Jpn. (Japan), vol.26, no.2, p.69-87 (1983). In Japanese.
Sputtering is the ejection of atoms or groups of atoms from the surface of a solid as the result of heavy-ion impact. The ejected atoms repeat collisions and exhibit collision cascade. This review paper discusses: (1) physics of sputtering, (2) the energy dependency and incident-angle dependency of sputtering, (3) selective sputtering of alloys and compounds, (4) ion enhanced sub-surface segregation, (5) energy and angle distribution of emitted particles, (6) secondary electron emission by ion beam irradiation—kinetic and potential emission, (7) electron enhanced sputtering, (8) chemical sputtering, and (9) measurements of sputtering using a laser resonance excitation method. (59 refs.) K.B.

114994 Low-energy ion scattering. M.Aono (Nat. Inst. for Res. in Inorganic Materials, Ibaraki, Japan).
J. Vac. Soc. Jpn. (Japan), vol.26, no.2, p.136-46 (1983). In Japanese.
The most significant application of low-energy ion scattering analysis (ISS) is the analysis of properties of solid surfaces. This review paper centres around ISS, and is devoted to discussion of: (1) interaction potentials and scattering orbits, (2) neutralization of low-energy ions, (3) impact-collision ion scattering spectroscopy (ICISS), (4) the analysis of surface defect structure using ICISS, (5) the analysis of thermal oscillation amplitude of surface atoms, and

(6) the analysis of two-dimensional space distributions of surface electrons. (19 refs.) K.B.

114995 The effect of an external electric field on the survival of surface-produced negative ions. S.B.Vojvodic (Inst. za Biofiziku Medicinskog Fakulteta, Belgrade, Yugoslavia).
Phys. Lett. A (Netherlands), vol.97A, no.5, p.210-12 (29 Aug. 1983).
Resonant charge exchange between slow atomic particles and a partially coated metal surface, in the presence of a homogeneous electric field, is considered. The survival probabilities are calculated for H⁻ ions, emerging from Cs-coated W and K⁻ coated Ni (110), in the fields of strengths 10⁻⁴, 10⁻³ and 0 au. (13 refs.)

114996 A new observation method of ion-electron emission. M.Soszka, W.Soszka (Inst. of Phys., Jagellonian Univ., Krakow, Poland).
Phys. Lett. A (Netherlands), vol.97A, no.6, p.256-8 (5 Sept. 1983).
The energy spectra of secondary electrons emitted from a molybdenum target in the shape of a wire upon bombardment with 5 keV H³⁺ ions is examined. It is shown that for the grazing angle of ion incidence the structure of the energy spectrum is most sensitive to the target treatment. At such a geometry the ion-electron emission can be used for analysis of the solid surface covered by adsorbed on contaminant particles. (9 refs.)

114997 Reflection of metastable He atoms as ions at surfaces. J.Roussel (Service de Phys. des Atomes et des Surfaces, CENS, Gif-sur-Yvette, France).
Phys. Scr. (Sweden), vol.T4, p.96-9 (1983). (Nordic Conference on Surface Science, Tampere, Finland, 18-20 Aug. 1982).
Scattering in the ionic state of metastable He 2³S and He 2¹S atoms is measured at single crystal surfaces as a function of the work function, lowered by K adsorption. On clean surfaces, the ions cannot be observed. They are again not observed, if the work function is less than the free excited atom ionization energy. A model is proposed, the ion dipole interaction between the He⁺ ion and the adsorbed alkali atom governing the process. Evidence for the conversion of He 2¹S atoms into the He 2³S state is also presented. (19 refs.)

114998 Comments on the physical significance of E* values for excited sputtered atoms. R.F.Garrett, R.J.MacDonald, D.J.O'Conner (Dept. of Phys., Univ. of Newcastle, NSW, Australia).
Surf. Sci. (Netherlands), vol.131, no.1, p.L399-405 (Aug. 1983).
Measurements of parameters associated with the emitted photons from a number of elements have indicated that the kinetic energies of sputtered excited atoms may be of the order of 10²-10³ eV. A recent result of Yu et al. [Phys. Rev. Letters 48 (1982) 427] is in contradiction to those results. The authors argue that the high energy values reported are the result of cascade repopulation of the upper level of the observed transition, distorting the experimental observations. Cascade corrections could reduce the energy values to the order of 10 eV, similar to the most probable energy of secondary ions. (17 refs.)

114999 The velocity dependence of the negatively charged fraction of hydrogen scattered from cesiated tungsten surfaces. J.N.M.van Wunnik, J.J.C.Geerlings, J.Los (FOM-Inst. for Atomic & Molecular Phys., Amsterdam, Netherlands).
Surf. Sci. (Netherlands), vol.131, no.1, p.1-16 (Aug. 1983).
By scattering protons under grazing angles of incidence at a cesiated tungsten (110) surface, the dependence of the scattered H⁻ fraction as a function of the normal and parallel velocity components is measured. The incident energy ranges from 400 to 2000 eV, the angle of incidence is 80° with respect to the surface normal. The experiments are done with a surface which is covered with half a monolayer cesium and a thick layer of cesium, corresponding to work functions of 1.45 and 2.15 eV, respectively. The measurements show a strong dependence on the normal as well as on the parallel velocity component. The normal velocity component dependence can be understood in terms of the probability model. The authors extended this model to incorporate the parallel velocity. The essence of this extension is that the finite velocity of the metal electron is taken into account. (28 refs.)

115000 The scattering of hydrogen from a cesiated tungsten surface. J.N.M.van Wunnik, J.J.C.Geerlings, E.H.A.Granneman, J.Los (FOM-Inst. for Atomic & Molecular Phys., Amsterdam, Netherlands).
Surf. Sci. (Netherlands), vol.131, no.1, p.17-33 (Aug. 1983).
The reflection of protons from a partially cesiated tungsten surface is studied in the energy domain between 100 and 2000 eV and in the angular domain between 75° and 85° with respect to the surface normal. The study is performed by measuring the angular and energy distribution of the scattered negative ions. The reflection can take place along two paths. One path is reflection from the cesium surface layer, the other one is reflection from the tungsten substrate. A dependence of the final charge state on the path is observed. It is inferred that this phenomenon is due to incomplete neutralization of the protons scattered from the cesium layer. The energy loss of the reflected ions cannot be accounted for by using only the binary collision model. Also the electronic stopping of the atoms by the metal electrons is shown to be an important energy loss mechanism. Total conversion measurements of H⁺ to H⁻ combined with the measurements of the negatively charged fraction of the scattered particles yield the particle reflection coefficient as a function of the angle of incidence. These reflection coefficients show that for angles of incidence less than 75° already more than 50% of the particles do not reflect from the surface. Total conversion efficiency measurements with H⁻ ions as primary ions show that the influence of the initial charge state on the total conversion is very small. (13 refs.)

115001 Universal shadow cone expressions for an atom in an ion beam. O.S.Oen (Solid State Div., Oak Ridge Nat. Lab., Oak Ridge, TN, USA).
Surf. Sci. (Netherlands), vol.131, no.2-3, p.L407-11 (Sept. 1983).
Some universal expressions for the classical shadow cone formed behind an atom in an ion beam have been calculated using the Moliere scattering potential and impulse approximation. As a function of a single dimensionless parameter, these universal expressions cover a wide range of ion-target combinations and ion energies. The expressions are easy to program on a hand calculator and are expected to be useful in discussing a wide range of shadow and blocking phenomena. (13 refs.)

115002 Semiclassical trajectory study of He scattering off of LiF(001). R.F.Grote, A.E.Depristo (Dept. of Chem., Iowa State Univ., Ames, IA, USA).
Surf. Sci. (Netherlands), vol.131, no.2-3, p.491-500 (Sept. 1983).
A semiclassical trajectory method is used to study atomic diffraction. This technique allows some dynamical degrees of freedom to be treated classically, while others are described quantum mechanically and couples the two descriptions by enforcing energy conservation. To study the accuracy of the semiclassical method, the authors compare the results to other classical, semiclassical and quantum mechanical solutions of He diffracting from the (001) surface of LiF. (23 refs.)

115003 Investigation of gallium arsenide subjected to an intensive plasma treatment. G.I.Bernotas, A.I.Griginis, L.I.Pranayavichyus, G.V.Skorobogatas (Antanas Snehkus Polytech. Inst., Kaunas, Lithuanian SSR).

Sov. Phys.-Semicond. (USA), vol.17, no.3, p.342-3 (March 1983). Translation of: *Fiz. & Tekh. Poluprovodn. (USSR)*, vol.17, no.3, p.544-5 (March 1983). [received: Sept. 1983]

The authors used electron Auger spectroscopy and electron diffraction (in the reflection configuration) methods to study epitaxial and nonepitaxial samples of n-type gallium arsenide oriented in (100) planes and subjected to treatment in argon, oxygen, and Freon-14 plasmas. The ion current density was varied within the range 0.5-3 mA/cm² and the ion energy within the range 20-1000 eV. The gas pressure in the working chamber was kept within the range 4×10^{-2} – 1×10^{-1} Pa. The ratio of the intensities of the Auger peaks of arsenic and gallium (As/Ga) was 1.0 for epitaxial films and from 0.89 to 0.96 for nonepitaxial films. The ratio As/Ga for the Auger peaks was plotted after 10-min exposure of gallium arsenide to a plasma with an ion current density 1 mA/cm². (3 refs.)

115004 A scattering on an adsorbed layer. IV. Scattering function. N.M.Moskaleva, O.A.Skepko.

Vestn. Leningr. Univ. Ser. Mat. Mekh. & Astron. (USSR), no.3, p.57-63 (July 1983). In Russian.

The problem of scattering on an atom is considered in the framework of hard-sphere theory. The single scattering function is found analytically and the complete scattering indicatrix is estimated by the Monte Carlo method. (3 refs.)

115005 Sputter-induced surface modification in Cu-Ni alloys at elevated temperatures. Y.Ishida (Inst. of Industrial Sci., Univ. of Tokyo, Tokyo, Japan), H.Shimizu, N.Koyama, H.Ichinose.

Point Defects and Defect Interactions in Metals. Proceedings of the Yamada Conference V, Kyoto, Japan, 16-20 Nov. 1981 (Amsterdam, Netherlands: North-Holland 1982), p.958-61

Structural and compositional modifications were investigated in the sputter-damaged surface layer of Cu-Ni alloys at elevated temperatures. A long range depletion of copper was found in the layer beyond the knock-on mixing range. The apparent activation energy of solute diffusion in the layer was 22.6 kJ/mol at 573–723K, suggesting that interstitial type mechanism is operating in the region over 100 nm from the surface. The effect of grain boundary as the enhanced diffusion path was noted at elevated temperatures. (9 refs.)

Proceedings of the International Workshop on Cross Sections for Fusion and Other Applications See Entry 111298

Backscattering coefficients of H, D, and He ions from solids See Entry 111323

CVD coatings in fusion reactor technology See Entry 112442

A molecular beam study of the trapping-desorption of I₂ from a LiF (001) surface See Entry 112769

A comparison of ellipsometer and RBS analysis of implant damage in silicon See Entry 113945

Si-on-sapphire and Si implanted with Zr ions: lattice location, solid phase epitaxial regrowth and electrical properties See Entry 113947

Correlation among secondary ion mass spectrometry, cross-section transmission electron microscopy, and Rutherford backscattering analyses for defect density and depth distribution determination See Entry 113948

Mechanism and kinetics of radiation-induced segregation in Ni-Si alloys See Entry 114187

Diffusion of iodine into PE and PET See Entry 114263

Ion scattering spectroscopy of β -N and β_3 -Co ($\sqrt{2} \times \sqrt{2}$) R45° structures on W{100} See Entry 114346

Rotational state populations of NO molecules scattered from clean and adsorbate-covered Pt (111) surfaces See Entry 115006

Material analysis by means of high energy ion beams See Entry 115600

79.20R Atomic and molecular beam interactions

115006 Rotational state populations of NO molecules scattered from clean and adsorbate-covered Pt (111) surfaces. J.Segner, H.Robota, W.Vielhaber, G.Ertl (Inst. fur Phys. Chemie, Univ. Munchen, Munchen, Germany), F.Frenkel, J.Hager, W.Krieger, H.Walther.

Surf. Sci. (Netherlands), vol.131, no.2-3, p.273-89 (Sept. 1983).

A supersonic beam of NO molecules was scattered from a Pt(111) surface either clean or covered with NO, C, and O. Rotational state populations and angular distributions of the scattered molecules were determined at two incident energies and at different surface temperatures T_s . The rotational distributions obtained are Boltzmann distributions with rotational temperatures T_{rot} . Interaction with the clean and NO-covered Pt surface shows diffuse angular distributions and the independence of T_{rot} on the initial kinetic energy. Full rotational accommodation was found for scattering from the NO-covered ($T_s < 300$ K), only incomplete accommodation at the clean Pt surface ($T_s > 450$ K). Interaction with the C-covered surface results in broad nearly specular scattering lobes and at higher surface temperatures in a constant value of $T_{rot} < T_s$ which depends on the initial kinetic energy. Scattering at the oxygen-covered surface presents an intermediate case: diffusely and specularly scattered fractions are observed. The experimental results are discussed in terms of underlying microscopic scattering processes. (38 refs.)

Semiconductor detector for the selective detection of atomic hydrogen See Entry 112880

79.40 THERMIONIC EMISSION

115007 Work function of Mo(110) in mixed cesium and cesium monoxide vapors. J.-L.Desplat (Rasor Associates Inc., Sunnyvale, CA, USA).

J. Appl. Phys. (USA), vol.54, no.9, p.5494-7 (Sept. 1983).

Electron emission measurements from a Mo(110) emitter are performed in a diode containing both cesium and cesium monoxide vapors over a temperature range from 500 to 1800K. The vapor pressures can be varied independently within a limited range: typical values are 1×10^{-3} and 2×10^{-4} Torr for cesium and Cs₂O, respectively. At temperatures above 1000K, the electron emission is increased by several orders of magnitude over that obtainable with cesium vapor alone by the addition of Cs₂O. This is believed to result from the dissociation of Cs₂O molecules adsorbed on the emitter surface to form an adsorbed oxygen layer. At temperatures below 700K, the work function decreases with temperature to as low as 1.2 eV around 500K. This is interpreted as resulting from multilayer deposition of Cs₂O. Application to thermionic converters is discussed. (17 refs.)

79.60 PHOTOEMISSION AND PHOTOELECTRON SPECTRA

115008 Detailed absorption, reflectance, and UV photoelectron spectroscopic and theoretical studies of the charge-transfer transitions of CuCl₄²⁻: correlation of the square-planar and the tetrahedral limits. S.R.Desjardins, K.W.Penfield, S.L.Cohen (Dept. of Chem., MIT, Cambridge, MA, USA), R.L.Musselman, E.L.Solomon.

J. Am. Chem. Soc. (USA), vol.105, no.14, p.4590-603 (13 July 1983).

Low-temperature (7K) polarized single-crystal absorption and room-temperature polarized specular reflectance spectra have been obtained of the chloride-to-copper charge-transfer region of the three known square-planar salts of CuCl₄²⁻, bis(methanodimethyl) tetrachlorocuprate(II), bis(N-methylphenethylammonium) tetrachlorocuprate(II), and bis(creatinium) tetrachlorocuprate(II) and of the tetragonal monomer, bis(ethylammonium) tetrachlorocuprate(II). These spectra show two intense, x-y polarized, x-y split transitions in the regions 26000-28000 and 37000-39000 cm⁻¹. These bands are assigned to the allowed ²E_g–²B_{1g}(4e_g(π)–3b_{1g}) and ²E_u–²B_{1g}(3e_g(σ)–3b_{1g}) transitions, respectively. In addition, a weaker band is observed between 22000 and 25000 cm⁻¹ and has been assigned to the ²A_{2g}–²B_{1g}(1a_{2g}(nb)–3b_{1g}) transition. These assignments are compared to the results of SCF-Xα-SW ground- and transition-state calculations; although the calculated transition energies are too low and there is overlap of the calculated d-d and charge-transfer manifolds of states, the differences between the calculated energies of the three charge-transfer transitions agree well with those observed experimentally. (35 refs.)

115009 Angle-resolved photoemission study of some first-row transition-metal intercalates of NbS₂ and TaS₂. J.J.Barry, H.P.Hughes (Cavendish Lab., Univ. of Cambridge, Cambridge, England).

J. Phys. C (GB), vol.16, no.27, p.5393-407 (30 Sept. 1983).

Angle-resolved photoemission studies, using synchrotron radiation and UV discharge lamp sources, of the Mn, Fe, Co and Ni intercalates of NbS₂ and TaS₂ support a rigid band description of intercalation, with charge transferred to the host lattice conduction band leaving double ionised intercalant ions between the layers. The host lattice p-d gap is increased by 0.4 eV relative to that measured in earlier work on unintercalated TaS₂, as a result of the charge transfer. Structure seen in photoemission at photon energies ≥ 35 eV may be understood in terms of the many-electron aspects of photoemission from the localised intercalant 3d levels. (25 refs.)

115010 X-ray and photoelectron spectroscopy of light rare earths.

J.C.Fuggle (Inst. fur Festkörperforschung, KFA Jülich, Jülich, Germany).

J. Less-Common Met. (Switzerland), vol.93, no.1, p.159-69 (1983). (Proceedings of the Sixteenth Rare Earth Research Conference, Tallahassee, FL, USA, 18-21 April 1983).

Core level photoelectron spectroscopy, X-ray absorption spectroscopy, bremsstrahlung isochromat spectroscopy and valence band studies are discussed. Particular emphasis is placed on cerium. Correlation effects, multiplet structure, screening effects and the dynamics of the processes involved are illustrated with selected examples. (39 refs.)

115011 The 4f spectral weight in cerium materials—facts and issues.

J.W.Allen (Xerox Palo Alto Res. Center, Palo Alto, CA, USA).

J. Less-Common Met. (Switzerland), vol.93, no.1, p.183-7 (1983). (Proceedings of the Sixteenth Rare Earth Research Conference, Tallahassee, FL, USA, 18-21 April 1983).

Experimental work to determine the spectral weight for 4f electron addition and removal in cerium materials is reviewed briefly, and new inverse photoemission results on CeO₂ and collapsed volume cerium compounds are described. It is pointed out that the tendency for the spectral weight of collapsed volume materials to develop a peak at the Fermi level is implicit in a Kondo picture of their loss of magnetism. (34 refs.)

115012 A multispectroscopic investigation of the electronic structure of luminescent, tetrahedrally coordinated vanadium-oxygen compounds: case of YVO₄. I.M.Curelaru (Dept. of Materials Sci. & Engng., Univ. of Utah, Salt Lake City, UT, USA), E.Suonien, E.Minni, K.-G.Strid, T.Ronnhult.

J. Lumin. (Netherlands), vol.28, no.3, p.241-56 (Aug. 1983).

Photoelectron (XPS) and core ionisation loss (CILS) spectra of YVO₄ have been measured and compared to earlier appearance potential (APS) data on the same compound, literature data on X-ray emission of YVO₄, X-ray emission and absorption of Na₃VO₄, and the energy level diagram of molecular orbitals of the VO₄³⁻ cluster. Strong many-body effects, with participation of a 2p core hole on vanadium atoms, are found to lead to a drastic local perturbation of the outer molecular orbitals of the anionic cluster VO₄³⁻ at the site of the excited vanadium atoms. Identification of the spectroscopic features in XPS on one hand and the edge spectroscopies CILS and APS on the other hand enable determination of an empirical energy level diagram of excited configurations, which is different in different spectroscopies used. As a byproduct of the experiment, data on the excitation of oxygen (within the VO₄³⁻ cluster), yttrium (outside the VO₄³⁻ cluster) and carbon impurity are presented and discussed. (24 refs.)

115013 Diffraction of UV excited photoelectrons by an ordered overlayer. C.G.Larsson, J.Paul, L.Walden (Dept. of Phys., Chalmers Univ. of Technol., Goteborg, Sweden).

Phys. Scr. (Sweden), vol.T4, p.44-6 (1983). (Nordic Conference on Surface Science, Tampere, Finland, 18-20 Aug. 1982).

Angle resolved UV photoemission spectra obtained from Cu(111)-(√3×√3)R30° Xe and Cu(111)-(√3×√3)R30° CO samples are compared with spectra obtained from the clean substrate. Interest is focused on the adsorbate induced changes in the Cu3d band range of initial energies. From the similarity between the spectra observed for the ordered Xe and CO overlayers the authors conclude that the changes are primarily due to diffraction of the photoexcited Cu3d electrons by the adsorbate. This is supported also by calculated photoelectron energy distributions. (19 refs.)

115014 Damping effects in angular-resolved ultraviolet photoemission spectroscopy on Cu(111). B.J.Slagsvold, J.K.Grepstad, P.O.Gartland (Inst. of Experimental Phys., Tech. Univ. of Trondheim, Trondheim, Norway).

Phys. Scr. (Sweden), vol.T4, p.65-70 (1983). (Nordic Conference on Surface Science, Tampere, Finland, 18-20 Aug. 1982).

Previously published photoemission spectra taken at several discrete photon energies from the (111)-surface of copper are analyzed with the purpose of extracting information on the broadening effects involved. In the low energy case (6.40 eV) the effect of surface disorder on the spectral shape of a surface state is explained as the result of a reduced coherence length parallel to the surface, while sensitivity to disorder normal to the surface is the prevailing effect for the bulk transition of the same spectrum. The use of angular instead of frequency tuning is proposed as a feasible alternative to extract electronic lifetimes in favourable cases. Numerical values of inverse lifetimes are derived and found to agree well with the trend in recent measurements of energy dependent inverse lifetimes. Finally, accounting for

the authors' instrumental broadening, the residual k_{\parallel} -dependent width of a dispersive peak is compared with values predicted from the band structure of copper and published lifetimes measured in normal emission. Inhomogeneous damping is proposed as a possible explanation of a deviation seen from the calculated widths as the final state crosses a Brillouin zone boundary. (19 refs.)

115015 Rydberg screening in core level photoemission of ammonia adsorbed on nickel surfaces. K.Hermann, P.S.Bagus (IBM Res. Labs., San Jose, CA, USA).

Phys. Scr. (Sweden), vol.T4, p.113-14 (1983). (Nordic Conference on Surface Science, Tampere, Finland, 18-20 Aug. 1982).

The lowest empty orbitals of the ground state of free ammonia, $4a_1$ and $2e$, are quite diffuse Rydberg-type orbitals. Thus, one might expect that involvement of these orbitals in the final hole states would not lead to additional structure in the N1s core hole photoemission spectra of the adsorbed molecule. Model calculations on NiNH_3 clusters show, however, that in the presence of the N1s core hole Rydberg orbitals can lead to a screening mechanism similar to the one proposed by Schonhammer and Gunnarsson (1977) for adsorbed CO and N_2 . In NiNH_3 the different final states are similar in intensity and are separated by 1-1.5 eV. The XPS data for the NH_3/Ni (110) system show a broad asymmetric N1s peak which, from the present study, can be interpreted as a superposition of at least two peaks stemming from unscreened and Rydberg screened final states of the core hole. (8 refs.)

115016 UV photoemission from sulphur saturated (111), $[6(111)\times(100)]$ and (100) platinum surfaces. T.T.A.Nguyen, R.C.Cinti (Groupe de Transitions de Phases, CNRS, Grenoble, France).

Phys. Scr. (Sweden), vol.T4, p.115-17 (1983). (Nordic Conference on Surface Science, Tampere, Finland, 18-20 Aug. 1982).

Angle-resolved UPS, in the photon energy range of 10.2-40.8 eV, is used to study the adsorption of S on (111), $[6(111)\times(100)]$ and (100) Pt surfaces, in the aim of: (a) determining an eventual influence of the surfaces steps on the electronic character of the adsorption, (b) comparing the chalcogen chemisorption on a large d-band transition metal with previous study on a narrower one, Ni. A saturated S adlayer is much more rapidly formed on the vicinal surface than on its partner (111), but no clear evidence of the role of the surface peculiarity can be deduced from the additional electronic structures given by S adsorption. The UPS spectra are complicated by the mixing of the lower part of the metal d-band with adsorbate derived feature and important structureless extra-emissions. The simplest ones are given by the (100) surface. Two supplementary structures are observed at about 6.5 eV and 2 eV below E_F and attributed respectively to the S 3p orbitals and to the metal states localized by the presence of the adsorbate. These results indicate that the chemisorption bonds of S on Pt and Ni are quite similar. (10 refs.)

115017 Surface core-level shifts for Ge(100)-(2X1). T.Miller, E.Rosenwinkel, T.-C.Chiang (Dept. of Phys., Univ. of Illinois, Urbana, IL, USA).

Solid State Commun. (USA), vol.47, no.11, p.935-8 (Sept. 1983).

Using surface-sensitive photoemission techniques, Ge 3d core-level binding energies for surface atoms of Ge(100)-(2X1) are found to be smaller than the bulk values by 0.41 eV. The surface atoms with shifted core-level binding energies correspond to one full (100) atomic layer. A surface core-exciton resonance is observed in the partial-yield measurements. The empty surface state involved in this excitonic transition, without binding-energy correction, is located at the valence-band maximum. (14 refs.)

115018 Systematics of optical energy gaps and XPS core level satellites in CuO and copper dihalides. S.Hufner (Lab. fur Festkorperphys., ETH Zurich, Honggerberg, Switzerland).

Solid State Commun. (USA), vol.47, no.11, p.943-5 (Sept. 1983).

Using a model of Asada and Sugano (see J. Phys. Soc. Japan, vol.41, p.1291, 1976) a good correlation between the satellites measured in XPS core levels and optical determined energy gaps is found. (21 refs.)

115019 Chlorine adsorption on copper. I. Photoemission from clean Cu(001) and Cu(111) substrates. D.Westphal, A.Goldman (Lab. fur Festorperphys., Univ.-GH-Duisburg, Duisburg, Germany).

Surf. Sci. (Netherlands), vol.131, no.1, p.91-112 (Aug. 1983).

As a first step to an understanding of the atomic chemisorption of Cl on Cu(001) and Cu(111) the authors have studied high-resolution angle and photon-polarization dependent photoelectron spectra of the clean substrate surfaces. They demonstrate that a clear identification of bulk direct transitions, surface state emission and contributions from density of states transitions can be given. In particular they investigated the photoemission spectra from Cu(001) in the Γ XWK bulk mirror plane excited by Ne I, He I, and He II radiation, from Cu(001) in the Γ XUL plane excited by He I radiation, and from Cu(111) along Γ LUX and Γ LKL (He I). The experimental bulk direct transitions are in very good agreement with simple calculations based on Burdick's (1963) initial state band structure and a free electron like final state. (49 refs.)

115020 Chlorine adsorption on copper. II. Photoemission from Cu(001)c(2X2)-Cl and Cu(110)($\sqrt{3}\times\sqrt{3}$)R30°-Cl. D.Westphal, A.Goldmann (Lab. fur Festorperphys., Univ.-GH-Duisburg, Duisburg, Germany).

Surf. Sci. (Netherlands), vol.131, no.1, p.113-38 (Aug. 1983).

For pt.I see *ibid.*, vol.131, no.1, p.92 (1983). The authors have studied high-resolution angle-resolved and photon-polarization dependent photoemission from chlorine adsorbed on Cu(001) and Cu(111). Chlorine forms a c(2X2) saturation overlayer on Cu(001) and adsorbs dissociatively as revealed by LEED and XPS. Several two-dimensional energy bands on Cu(001)c(2X2)-Cl could be identified and their dispersion behaviour along the Γ M and Γ X lines of the surface Brillouin zone, their respective mirror symmetry and their orbital character could be determined. An interpretation of these bands is given in terms of the interaction of the ordered overlayers with particular substrate bulk bands. Besides the appearance of adsorbate-induced two-dimensional bands drastic changes are resolved in the substrate d-band emission region. These can be explained almost exclusively by surface umklapp processes involving reciprocal lattice vectors of the ordered adsorbate mesh. Supplementary studies of the Cu(111) ($\sqrt{3}\times\sqrt{3}$)R30°-Cl system support these ideas. (20 refs.)

115021 Adsorbate band structure of bromine on Pd(111) studied by angle resolved ultraviolet photoemission. D.R.Lloyd (Chem. Dept., Univ. of Dublin, Dublin, Ireland), F.P.Netzer.

Surf. Sci. (Netherlands), vol.131, no.1, p.139-47 (Aug. 1983).

The photoemission spectra from Pd(111) and from the Pd(111)-Br($\sqrt{3}\times\sqrt{3}$)R30° system are reported; some new features for the clean surface are detected and assigned. The principal effect of the Br overlayer on the direct transitions is a general intensity reduction. Three adsorbate derived features are detected; one at 4 eV with no dispersion is probably an adsorbate-induced feature of the metal, and the other two which disperse are assigned as Br $4p_{xy}$ (4.5 eV) and Br $4p_z$ (6 eV) at Γ . (21 refs.)

115022 Photoelectron spectra of silicate glasses containing trivalent cations. Y.Kaneko (Res. & Dev. Dept., Taiko Refractory Co. Ltd., Kitakyushu-shi, Japan), H.Nakamura, M.Yamane, K.Mizoguchi, Y.Suginohara.

Yogyo-Kyokai-Shi (Japan), vol.91, no.7, p.321-4 (1983).

The O1s spectra for glasses in the systems $\text{Na}_2\text{O}-\text{SiO}_2-\text{M}_2\text{O}_3$ ($\text{M}=\text{Al, Ga, In}$ and Y) were measured in order to obtain information about the effect of trivalent cation on the structure of soda-silicate glasses. The spectra indicated that Al_2O_3 and Ga_2O_3 act as network formers, that Y_2O_3 acts as a network modifier, and that In_2O_3 acts as an intermediate oxide. (15 refs.)

115023 Core-level XPS studies of Ce and La intermetallic compounds and their implications for the 4f levels of Ce compounds. J.C.Fuggle, F.U.Hillebrecht, Z.Zolnieriek, R.Lasser, C.Freiburg.

Report JUL-1824, Kernforschungsanlage, Julich, Germany (Jan. 1983), 73 pp.

The 3d core hole X-ray photoelectron spectra (XPS) of approximately 30 intermetallic compounds of La and Ce are reported. Transitions to final states with approximately f^0 , f^1 and f^2 character are observed in some Ce compounds (f^0 and f^1 for La compounds). The results are discussed in terms of the current ideas of the influence of f-counts and f-level hybridization on core level lineshapes. (89 refs.)

Nordic Conference on Surface Science See Entry 111305

Surface properties of laser-annealed semiconductors See Entry 114321

Coadsorption systems with electrochemical relevance: coadsorption of water with oxygen, bromine and sodium on Cu(110) See Entry 114340

Oxidation of Pb monolayers on Cu(100) See Entry 114342

Bromine and iodine adsorption on an Fe(100) surface See Entry 114343

Electron spectroscopy on adsorption of Cs on transition metals See Entry 114344

Characterisation of a low temperature surface phase of CO on Pt {110} See Entry 114345

Ion scattering spectroscopy of $\beta\text{-N}$ and $\beta_3\text{-Co}$ ($\sqrt{2}\times\sqrt{2}$) R45° structures on W{100} See Entry 114346

An XPS study of carbon monoxide and nitric oxide adsorption on platinum (410): unusual dissociation activity See Entry 114353

Adsorption and decomposition of ammonia on W(100): XPS and UPS studies .. See Entry 114355

Site-specific interaction of H_2O with ZnO single-crystal surfaces studied by thermal desorption and UV photoelectron spectroscopy See Entry 114358

Surface and bulk electronic structure of disordered metallic alloys See Entry 114433

Mapping bulk Ge electronic energy bands along Δ using ARPES spectra of the (001) 2×1 surface See Entry 114441

Electronic structures of sulfide minerals—theory and experiment See Entry 114444

Valence instabilities in rare earth systems as revealed by photoemission See Entry 114488

Inverse UV photoemission See Entry 114951

Anodic oxidation of zirconium: Some aspects of the role of foreign ions See Entry 115445

Decomposition of HCOOH on gold studied by XPS and TDS spectroscopies and its behaviour under very low energy electron excitation .. See Entry 115581

Time-resolved photoelectron spectroscopy for the study of dynamic surface species See Entry 115603

79.70 FIELD EMISSION AND FIELD IONIZATION

115024 Stable field electron emission from a tungsten tip under the ultrahigh vacuum of 10^{-10} Pa. C.Oshima, R.Souda, M.Aono, Y.Ishizawa (Nat. Inst. for Res. in Inorganic Materials, Ibaraki, Japan).

Appl. Phys. Lett. (USA), vol.43, no.6, p.611-12 (15 Sept. 1983).

A stable field emission from the tungsten tip with axis in the (110) direction has been found under ultrahigh vacuum of 10^{-10} Pa. The noise of 0.3% under the condition is attributed to the surface migration of impurity atoms and/or tungsten atoms. (6 refs.)

115025 Stable carbide field emitter. H.Adachi, K.Fujii, S.Zaima, Y.Shibata (Dept. of Electronic Engng., Tohoku Univ., Sendai, Japan), C.Oshima, S.Otani, Y.Ishizawa.

Appl. Phys. Lett. (USA), vol.43, no.7, p.702-3 (1 Oct. 1983).

New experimental results of very stable field emitted electrons from TiC single crystal needles are presented. The optimum flashing temperature region for the stable field emission was found. The stability, which is defined by the ratio of current fluctuation to total current, was better than 0.5% at a vacuum of 10^{-7} Pa with total electron emission of 1 μA . (8 refs.)

115026 Comment on 'Temperature dependence of the silicon field evaporation voltage' by G.L. Kellogg. L.Ernst (Kalifornische Inst., Kali und Salz AG, Hannover, Germany).

Surf. Sci. (Netherlands), vol.131, no.2-3, p.L419-20 (Sept. 1983).

For original paper see *ibid.*, vol.124, p.L55 (1982). The author states that the linear relationship between the field evaporation voltage of Si and the temperature, found by Kellogg, may be interpreted by a simple model which involves, on the one hand, the reasonable assumption that the field evaporation rate may be determined by hole density in the space charge layer and on the other hand, previous results concerning the density distribution of surface states. (7 refs.)

115027 Reply to comment on 'Temperature dependence of the silicon field evaporation voltage'. G.L.Kellogg (Sandia Nat. Labs., Albuquerque, NM, USA).

Surf. Sci. (Netherlands), vol.131, no.2-3, p.L421-2 (Sept. 1983).

For original paper see *ibid.*, vol.124, p.L55 (1983), for comment see *ibid.*, vol.131, p.L419 (1983). The Comment by Ernst suggests that the linear relationship between the evaporation field and the temperature of a silicon sample can be explained by assuming that the silicon evaporation rate is limited by the density of holes in the space charge layer. Although this model offers a plausible explanation of the temperature versus voltage relationship, the data presented suggest that the temperature dependence of field evaporation is not strongly influenced by the density of holes. (4 refs.)

115028 Reduced evaporation field by the field induced dipoles of physisorbed He Ne and H_2 . O.Nishikawa (Dept. of Materials Sci. & Engng., Tokyo Inst. of Technol., Yokohama, Japan).

Surf. Sci. (Netherlands), vol.131, no.2-3, p.239-44 (Sept. 1983).

Physisorption of He, Ne and H_2 reduces the evaporation field of Cu, Mo, W and Pt. The observed phenomenon is explained as the result of a reduced potential barrier by the induced dipole potential of the physisorbed gases. The evaporation field of Cu in H_2 is only 68% of that in Ne. The potential

diagram for field evaporation shows that the dipole potential of H_2 reduces the potential barrier more than Ne even at this low evaporation field in H_2 . A crude calculation indicates that the dipole potentials of physisorbed He and Ne are also large enough to reduce the evaporation field of Mo, W and Pt significantly. (18 refs.)

79.80 RESONANCE TUNNELLING

115029 The resonant transmission on new tunnelling theory. D.K.Roy (Dept. of Phys., Indian Inst. of Technol., New Delhi, India), K.N.Rai. *Indian J. Phys. Part A*, vol.57A, no.3, p.190-5 (May 1983). The problem of resonant transmission has been reviewed on new tunnelling theory. An expression for the resonant tunnelling current density has also been derived. (7 refs.)

80.00 CROSS-DISCIPLINARY PHYSICS AND RELATED AREAS OF SCIENCE AND TECHNOLOGY

81.00 MATERIALS SCIENCE

81.10 METHODS OF CRYSTAL GROWTH AND PURIFICATION

(for physics of crystal growth, see 61.50C; for epitaxial growth methods, see 81.15)

Single-crystal fiber [of CsBr] See Entry 113131

81.10B Growth from vapour

115030 Diamond synthesis from gas phase in microwave plasma. M.Kamo, Y.Sato, S.Matsumoto, N.Setaka (Nat. Inst. for Res. in Inorganic Materials, Nihari-gun, Ibaraki, Japan). *J. Cryst. Growth (Netherlands)*, vol.62, no.3, p.642-4 (Aug. 1983). Crystalline diamond predominantly composed of {100} and {111} faces was grown on a non-diamond substrate from a gaseous mixture of hydrogen and methane under microwave glow discharge conditions. (13 refs.)

115031 Gas-phase insertion of fluorine anions (BF_4^- and PF_6^-) in graphite using nitril salts. D.Billaud, A.Chenite (Lab. de Chimie du Solide Mineral, Univ. de Nancy I, Vandoeuvre les Nancy, France). *Mater. Res. Bull. (USA)*, vol.18, no.8, p.1001-6 (Aug. 1983). In French. New intercalation compounds between graphite and nitril/tetrafluoroborates or nitrilhexafluorophosphates have been synthesized using a vapour phase technique. These materials have been characterized by X-ray diffraction, dilatometry, elemental analysis and mass uptake. Room temperature base plane electrical resistivity measurements as a function of the stage shows the high metallic character of these materials. (10 refs.)

Experiments on crystallization of semiconductors aboard Salyut 6-Soyuz orbital complex See Entry 113789

Electron diffraction studies of supersonic jets. V. Low temperature crystalline forms of SF_6 , SeF_6 , and TeF_6 See Entry 113824

Growth structure and optical properties of single crystals of rubrene See Entry 113841

81.10D Growth from solutions

115032 Electrolytic growth, electrical conductivity and magnetic susceptibility of stannous iodide. C.C.Desai, J.L.Rai (Dept. of Phys., Sardar Patel Univ., Gujarat, India).

J. Mater. Sci. Lett. (GB), vol.2, no.9, p.463-6 (Sept. 1983). The authors report their results on electrolytic growth in gels of SnI_2 single crystals up to 12-14 mm in size. Control over growth rate and nucleation centre formation was exercised. The variation of DC electrical conductivity of pellet samples was studied from 60 to 300°C. The activation energy for conduction was estimated. The magnetic susceptibility was found to be -3.238×10^{-6} emu. The negative value indicated diamagnetic material behaviour. (17 refs.)

115033 The flux growth of some transition metal phosphates. B.M.Wanklyn, F.R.Wondre (Clarendon Lab., Univ. of Oxford, Oxford, England), W.Davison, R.Salmon.

J. Mater. Sci. Lett. (GB), vol.2, no.9, p.511-15 (Sept. 1983). The authors report the preparation using the flux method of the following phosphates: $Co_3P_2O_7$, $CoPbP_2O_7$, $FeNaP_2O_7$, $FePb(P_2O_7)_2$, $Fe_3Pb_3(PO_4)_4$, $Fe_3K_3(PO_4)_4$ and $Fe_4Na_8(PO_4)_6O$. X-ray powder diffraction data are also given. (4 refs.)

115034 Preparation of $MnCo_2O_4$ by a wet method and its metal ion distribution. N.Yamamoto, S.Higashi, S.Kawano, N.Achiwa (Dept. of Chem., School of Liberal Arts & Sci., Kyoto Univ., Kyoto, Japan).

J. Mater. Sci. Lett. (GB), vol.2, no.9, p.525-6 (Sept. 1983). The authors report a new preparation method for the cubic spinel $MnCo_2O_4$. The method involves synthesis by direct precipitation from an alkaline water solution containing Co^{2+} and Mn^{2+} cations at low temperature. The method produces remarkable differences in metal ion distribution between A and B sites of the spinel lattice. (4 refs.)

115035 Effect of additives and dopants on the growth of KDP crystals. K.V.Ramanaiah, K.B.R.Varma (Dept. of Phys., PSG Coll. of Technol., Coimbatore, India).

Indian J. Pure & Appl. Phys., vol.21, no.7, p.388-90 (July 1983). The effect of addition of borax, nickel phosphate ($NiPO_4$), manganese phosphate [$Mn_3(PO_4)_2$], sodium dihydrogen orthophosphate (NaH_2PO_4) and potassium arsenate on the growth characteristics and growth habits of KDP crystals at room temperature (25°C) has been studied. Single crystals of KDP with various concentrations of these additives have been grown by the Holden's rotary crystallizer (slow evaporation) technique. The crystals obtained

are of excellent optical quality and of fairly large size. The relative importance of the addition of growth-aiding agents like borax to KDP has been brought out. The presence of the additives and dopants in the grown crystals has been detected by the chemical and the X-ray analyses. (10 refs.)

115036 Effects of ultrasonic waves on crystal growth. Y.Murata, K.Wada, M.Matsuoka (Dept. of Chem. Engng., Tokyo Univ. of Agriculture & Technol., Tokyo, Japan).

J. Cryst. Growth (Netherlands), vol.62, no.3, p.458-64 (Aug. 1983). Effects of ultrasonic waves of the growth of APD crystals were investigated by applying them perpendicularly to the (010) face. The observed growth rates were significantly reduced by the ultrasonic waves with lower frequencies, and higher energy densities, contrary to the increase in volume diffusion rates in the bulk solution. This behavior was considered to be due to the decrease in the concentration of the completely dehydrated growth units on the surface of the growing crystals. (8 refs.)

115037 Growth of KH_2PO_4 crystals at constant temperature and supersaturation. G.M.Loiacono, J.J.Zola, G.Kostecy (Philips Lab., Briarcliff Manor NY, USA).

J. Cryst. Growth (Netherlands), vol.62, no.3, p.545-56 (Aug. 1983). A large (144 liter) three-zone crystallizer system was constructed for growing KH_2PO_4 crystals under conditions of constant temperature and supersaturation. Crystal growth rates exceeding 5 mm day⁻¹ were demonstrated for KH_2PO_4 using seeds measuring 5×5 cm in cross section. (44 refs.)

115038 Crystal growth of NbC by flux method. S.Shimada, T.Koyama, A.Tsunashima, K.Kodaira, T.Matsushita (Dept. of Appl. Chem., Hokkaido Univ., Sapporo, Japan).

J. Cryst. Growth (Netherlands), vol.62, no.3, p.557-60 (Aug. 1983). Single crystals of NbC were grown using Ni metal as a flux at a soaking temperature of 1400°C. Increasing the content of NbC in the Ni melt from 14.8 to 34.5 wt.% leads to a decrease in the maximum crystal size from 1.5 to 0.3 mm. With 20 wt.% NbC, increasing the soaking time to 80 h leads to an increase of the size to 2.0 mm. The golden black crystals have a lattice constant of $a_0 = 4.470$ Å and occur in both columnar and cubic forms, with nearly stoichiometric composition. The grown faces were of the {100} family and the dislocation density on these faces was 3×10^5 /cm². The content of Ni impurity in the crystal was less than 600 ppm. (8 refs.)

115039 Conditions variation and procedural improvement for hydrothermal crystal growth of oxides under highly oxidizing conditions. M.McKelvy, L.Eyring (Dept. of Chem., Arizona State Univ., Tempe, AZ, USA).

J. Cryst. Growth (Netherlands), vol.62, no.3, p.635-8 (Aug. 1983). The hydrothermal technique for the growth of small single crystals of the higher oxides of the rare earths has been investigated with a view toward increasing crystal size and perfection. Conditions such as the substrate: mineralizer ratio, pressure cycling, capsule size and charge concentration, depressurization rate and temperature, thermal gradient and initial and final growth pressure were investigated. (5 refs.)

115040 High-temperature solution properties in the flux systems $RPO_4 \cdot Pb_3P_2O_7$ (R=Dy, Y). W.Eigermann, G.Muller-Vogt (Fakultat fur Phys., Univ. Karlsruhe, Karlsruhe, Germany).

J. Cryst. Growth (Netherlands), vol.62, no.3, p.639-41 (Aug. 1983). Density and surface tension of solutions of $DyPO_4$ and YPO_4 in molten $Pb_3P_2O_7$ have been measured in the temperature range from 1170 to 1470K. (19 refs.)

115041 Flow-induced crystallization by surface growth of polyethylene fibers. J.Rietveld, A.J.McHugh (Dept. of Chem. Engng., Univ. of Illinois, Urbana, IL, USA).

J. Polym. Sci. Polym. Phys. Ed. (USA), vol.21, no.8, p.1513-26 (Aug. 1983). A series of experiments has been carried out investigating several features of the surface growth method for observing longitudinal growth of polyethylene fibers in Couette geometry. Attempts to obtain limiting steady-state take-up rates using a Teflon rotor were hampered by fiber breakage; however, maximum growth rates before breakage were found to be considerably higher than those observed in previous studies. Growth rates were also obtained using a static method, and for the Teflon rotor indicated above a critical concentration a linear growth rate equal to the stirrer velocity with rates essentially independent of temperature. With a silanized glass rotor, the same method gave much lower growth rates at comparable stirrer speeds and temperatures and showed a temperature dependence suggestive of a nucleation-controlled mechanism. The implications of these results for other studies of the mechanisms of growth by the surface method are also discussed. (17 refs.)

Correlation between growth hillocks and dislocations on the {110} faces of flux grown yttrium aluminium garnet See Entry 113777

Some formulae describing spherical and hemispherical diffusion to small crystals in unstirred solutions See Entry 113779

The influence of glycine, according to pH, upon the growth habit of NaCl and KI, in aqueous solution See Entry 113781

In situ observations of the growth behaviour of the {010} face of potassium hydrogen phthalate See Entry 113782

Twin growth of sucrose crystals See Entry 113928

Surface structure change of a crystal in solution See Entry 114307

Behaviour of large-grain polycrystalline n-InP grown by SSD technique See Entry 114551

Crystal growth of A^3B^5 compounds See Entry 115045

An analysis of local flow effects in flow-induced orientation and crystallization See Entry 115184

Crystallization and preliminary X-ray investigation of *Micrococcus* sp. decarboxylase See Entry 115740

81.10F Growth from melts

115042 Spreading resistance of InSb crystals pulled under ultrasonic vibrations. Y.Hayakawa, M.Kumagawa (Res. Inst. of Electronics, Shizuoka Univ., Shizuoka, Japan).

Jpn. J. Appl. Phys. Part 1 (Japan), vol.22, no.6, p.1069 (June 1983). Most large crystals used as substrates are grown by a pulling method, but it is difficult to make added impurities distribute homogeneously because of the occurrence of facet growth. The ultrasonic waves-introduced pulling (UIP) method was proposed as one method of solving this problem, and the effect of vibrations on pulled crystals and on the melt flow was investigated. In this note, the fluctuation of the resistance in a UIP-grown crystal is described in relation to the growth morphology. An ultrasonic vibrations play an effective role in crystal growth, it is concluded that the control of the interface shape by vibrations is important in obtaining crystals with a homogeneous impurity concentration. (4 refs.)

115043 PBN material results in better GaAs crystals, IC device advances. R.L.Finicle (Union Carbide Corp., Lakewood, OH, USA). *Ind. Res./Dev. (USA)*, vol.25, no.6, p.113-16 (June 1983). The author suggests that pyrolytic boron nitride (PBN) boats and crucibles are opening new doors to the growth of better GaAs crystals and to the development of more-advanced and powerful semiconductor devices. The physical and chemical properties of PBN that make this possible are extreme tolerance to thermal shock, impermeability, low outgassing, high purity, and inertness to wetting and attack by molten metals. Thin-film evaporation, molecular beam epitaxy source crucibles, zone refining, microwave assemblies, and high-frequency insulators are a few of the areas where PBN is replacing more-commonly used materials. (no refs.)

115044 Czochralski crystal growth in an axial magnetic field: effects of Joule heating. W.E.Langlois, Ki-Jun Lee (IMB Res. Lab., San Jose, CA, USA). *J. Cryst. Growth (Netherlands)*, vol.62, no.3, p.481-6 (Aug. 1983). The feasibility of using magnetohydrodynamic effects to improve the quality of silicon crystals obtained by Czochralski growth from the melt has been demonstrated by several experimenters. An earlier publication pointed out that certain approximations widely used in liquid metal MHD make it relatively easy to incorporate magnetomotive effects into numerical models for Czochralski flow. Specifically, the low value of the magnetic Reynolds number gives rise to two useful simplifications: the induced magnetic field is negligible and the electric field is irrotational. These lead to the result that the magnetic part of the calculation is diagnostic rather than prognostic. The earlier paper (see W.E. Langlois et al., Proc. 2nd Intern. Conf. on Boundary and Interior Layers, Dublin, p.299-304, 1982) simulated the effect of a strong axial field applied to the melt, under the assumption that Joule heating is negligible. The validity of that assumption is confirmed: except under extremely high fields, Joule heating represents only a miniscule part of the energy budget in magnetic Czochralski growth. Its effect upon the melt circulation can be ignored. (7 refs.)

115045 Crystal growth of A³B⁵ compounds. F.Moravec (Inst. of Radio Engng. & Electronics, Czechoslovak Acad. of Sci., Prague, Czechoslovakia). *TESLA Electron. (Czechoslovakia)*, vol.15, no.4, p.99-104 (Dec. 1982). [received: Sept. 1983] Presents a description of some properties of A³B⁵ compounds. The results achieved in the preparation of GaP and InP bulk crystals are then given. By a practical example of GaP single crystal growth the principle of the liquid encapsulated Czochralski method (LEC) is shown and the basic conditions for crystal growth are specified. Conditions for the growth of A³B⁵ crystals from high-temperature solutions are analyzed. The principle of crystal growth from high-temperature solutions by diffusion of a dissolved compound in a temperature-concentration gradient (SSD method) is explained. The paper concludes with a description of an improved apparatus for the preparation of InP ingots by the SSD method. (18 refs.)

Large crystal sapphire optics	See Entry 113069
Oscillatory convection in a spherical cavity due to G-jitter	See Entry 113444
Growth of Cd ₂ Hg _{1-x} Te: a comparison of some properties with the predictions of two melt growth models	See Entry 113778
Finite analysis of the control of interface shape in Bridgman crystal growth	See Entry 113780
Experiments on crystallization of semiconductors aboard Salyut 6-Soyuz orbital complex	See Entry 113789
X-ray and electron diffraction analysis of GaSe crystals	See Entry 113807
Solidification front dynamics in model systems	See Entry 114147
Periodic crystallization of binary melts under diffusion-controlled mass transfer	See Entry 114149
Directional crystallization of PbTe under microgravity conditions	See Entry 114150
Effect of flux content on thermoluminescence yield of BaS phosphors	See Entry 114937

81.10H Zone melting and zone refining

115046 Preparation of Li₃N single crystal by floating zone technique. K.Nishida, K.Kitahama, S.Kawai (Inst. of Sci. & Industrial Res., Osaka Univ., Osaka, Japan). *J. Cryst. Growth (Netherlands)*, vol.62, no.3, p.475-80 (Aug. 1983). Single crystals of the superionic conductor, Li₃N, have been prepared by a floating zone technique in an infrared imaging furnace. The following peculiar shape transformation of the single crystal is observed. The cross-section of the single crystal at the solid-liquid interface is round. However, it is square at a position about 20 mm below the molten zone. As a result, a single crystal in the shape of a square prism and with dimensions of 9×9×60 mm³ was obtained. Impurity oxygen as well as hydrogen was detected in the crystal, which could possibly enhance the ionic conductivity. The crystal shows the highest ionic conductivity ($\sigma(L_c)=2.0\text{ S m}^{-1}$ at 300K) and the smallest activation energy for Li⁺ ion transport ($E_a=0.15\text{ eV}$) ever known on this material. (14 refs.)

115047 Magnetic field effects on float-zone Si crystal growth. H.Kimura, M.F.Harvey, D.J.O'Connor, G.D.Robertson, G.C.Valley (Hughes Res. Labs., Malibu, CA, USA). *J. Cryst. Growth (Netherlands)*, vol.62, no.3, p.523-31 (Aug. 1983). A transverse magnetic field of 1800 G was applied to the float-zone growth of Ga-doped Si to assess its effects on the distribution of Ga in the crystal. The crystals were grown at a constant average growth rate of 4 mm/min and crystal rotation rates of 12, 6 and 0 rpm. Both application of a magnetic field and rotation of the crystal lead to reduction in the frequency of the fine nonrotational striations. The magnetic field also curtails complex structure ('feathering') in the striations. The application of magnetic field also reduces the amplitude of axial spreading resistance fluctuations at the center of the crystal for rotation rates of 6 and 12 rpm. (5 refs.)

115048 The influence of axial microgravity on the breakage of axisymmetric slender liquid bridges. J.Meseguer (Lab. de Aerodinamica, Univ. Politecnica, Madrid, Spain). *J. Cryst. Growth (Netherlands)*, vol.62, no.3, p.577-86 (Aug. 1983). The dynamics of inviscid, axisymmetric liquid bridges permits a simplified treatment if the bridge is long enough. Under such condition the evolution of the liquid zone is satisfactorily explained through a non-linear one-dimensional model. In the case of breaking, the one-dimensional model fails when the neck radius of the liquid column is close to zero; however, the model allows the calculation of the time variation of the liquid-bridge interface as well as of the fluid velocity field and, because the last part of the evolution is not needed, the overall results such as the breaking time and the volume of each of the two drops resulting after breakage can be calculated.

Numerical results concerning the behavior of cylindrical liquid bridges subjected to a small axial gravitational field are presented. (14 refs.)

115049 The float-zone growth of Ti₃Au and Ti₃Pt. Y.K.Chang (Solid State Div., Oak Ridge Nat. Lab., Oak Ridge, TN, USA). *J. Cryst. Growth (Netherlands)*, vol.62, no.3, p.627-32 (Aug. 1983). The preparation of single crystals of the A15 intermetallic compounds Ti₃Au and Ti₃Pt by an electron-beam float-zone method has been investigated. High quality single crystals of Ti₃Au were grown successfully by using a zoning speed of 12 mm/h under a vacuum of at least 10⁻⁸ Torr. For the case of Ti₃Pt, grains varying from a few mm to over 1 cm with large mosaic spreads were obtained. Ti₃Pt crystals were also grown by means of an RF induction-heating float-zone technique. Surface striations were observed on all of the Ti₃Pt crystals grown. These striations are believed to be a result of melt convection caused by surface tension gradient at the free melt-vapor interface. (9 refs.)

115050 Zone-melting recrystallization of semiconductor films. M.W.Geis, H.I.Smith, B.-Y.Tsaur, J.C.C.Fan, D.J.Silversmith, R.W.Mountain, R.L.Chapman (Lincoln Lab., MIT, Lexington, MA, USA). Laser-Solid Interactions and Transient Thermal Processing of Materials, Boston, MA, USA, 1-4 Nov. 1982 (New York, USA: Elsevier 1983), p.477-89 The use of zone melting recrystallization (ZMR) to prepare large-grain (and in some cases single-crystal) semiconductor films is reviewed, with emphasis on recent work on Si on SiO₂. Encapsulants are generally required to minimize contamination and decomposition, induce a crystalline texture, improve surface morphology and prevent agglomeration. In the case of Si, the solid-liquid interface is faceted, which gives rise to subboundaries. These can be entrained by laterally modulating the temperature through the use of an optical absorber on top of the encapsulant. Control of thermal gradients and in-plane crystallographic orientation are important for reliable entrainment. (37 refs.)

Amounts and character of distribution of impurities in zone-melted single-crystal lanthanum hexaboride	See Entry 113952
--	------------------

81.10J Growth from solid phases
(inc. multiphase diffusion and recrystallisation)

Beam processing of silicon with a scanning CW Hg lamp	See Entry 113989
Beam shaping for CW laser recrystallization of polysilicon films	See Entry 114016
A comparison of CW laser and electron-beam recrystallization of polysilicon in multilayer structures	See Entry 114017
The effects of selectively absorbing dielectric layers and beam shaping on recrystallization and FET characteristics in laser recrystallized silicon on amorphous substrates	See Entry 114019

81.15 METHODS OF THIN FILM DEPOSITION

(inc. epitaxial growth methods; see also 68.55 Thin film growth, structure, and epitaxy)

115051 Plasma-sprayed silicon as a possible base material for the production of low cost solar cells. M.S.Alaee (Dept. of Phys., Brunel Univ., Uxbridge, England), T.Hashemi, C.A.Hogarth. *J. Mater. Sci. Lett. (GB)*, vol.2, no.9, p.490-4 (Sept. 1983). Studies of silicon plasma-sprayed layers with different surface techniques indicated that it is possible to form layers of silicon having desired thicknesses on substrates of various shapes and materials, to be used for the production of low cost solar cells. Electrical measurements of the layers showed them to have suitable electrical properties for photovoltaic purposes. (9 refs.)

115052 Continuous coating with gravity and jet stripping. E.O.Tuck (Appl. Math. Dept., Univ. of Adelaide, Adelaide, Australia). *Phys. Fluids (USA)*, vol.26, no.9, p.2352-8 (Sept. 1983). A thin layer of viscous fluid is transported by a vertical plane surface moving steadily upward under gravity. Some fluid drains downward, a tendency that can be augmented by blowing an air jet upon the layer from the side. An analysis is provided of the possible steady-flow solutions, leading to a relationship between the ultimate layer thickness and the strength of the jet. In order to test stability, a study is made of corresponding unsteady flows, the conclusion being that the stripped flow is stable to perturbations of long wavelength. (15 refs.)

115053 Possibility of melting of silica particles in a plasma jet. A.G.Gnenenko, E.F.Shul'ts (Altai Sci.-Res. Inst. of Machine Construction Technol., USSR). *Sov. Powder Metall. & Met. Ceram. (USA)*, vol.22, no.1, p.24-7 (Jan. 1983). Translation of: *Poroshk. Metall. (USSR)*, vol.22, no.1, p.26-9 (Jan. 1983). [received: Aug. 1983] From the results of calculations and experiments, the authors conclude that in practice silica particles, unlike alumina particles, cannot be melted in argon and ammonia plasma jets of the standard arc plasma units. To obtain good-quality silica coatings, it may be necessary to increase the length of the high-temperature zone, e.g. by using a plasma unit with a laminar plasma jet; employ plasma-forming gases of higher heat content (e.g. hydrogen); or introducing the powder in the cathode region (as is done in the Monolit apparatus). (7 refs.)

Characterization and application of laser induced seeded-lateral epitaxial Si layers on SiO ₂	See Entry 114013
On the substructure of epitaxial (Pb,Sn)Te films grown on KCl cleavage faces	See Entry 114378
New fields of application of plasma spraying in energy technology	See Entry 115443

81.15C Deposition by cathodic sputtering

115054 Control of DC diode sputtering by control electrodes. T.Asamaki, N.Hosokawa (Anelva Corp., Fuchu, Japan), M.Taketani. *Oyo Buturi (Japan)*, vol.52, no.7, p.626-30 (July 1983). In Japanese. A pair of control electrodes between which an AC control voltage can be applied is inserted into the positive column between the target and the substrate holder in order to control the target current of DC diode sputtering systems. By this means the target current can be kept constant within a deviation of $\pm 2\%$ for even such a large pressure change as from 2.7 to 5.3 Pa. This method has been applied to the deposition of Ta films, and electrical properties of the films were investigated. Deposition rates were found to be independent of control voltages. Although specific resistivities and temperature

coefficients of resistance were slightly affected by control voltages, the effect was negligible for the applied voltages between 30 and 130 V. This method is found to be very effective for mass production inline systems combined with a rough pressure control system. (8 refs.)

115055 Structure-hardened amorphous chalcogenide films produced by pulse laser spraying. P.A.Fennich, Yu.Yu.Firtsak, O.V.Luksha, N.M.Erdevdi, V.P.Ivanitskii.

Ukr. Fiz. Zh. (USSR), vol.28, no.8, p.1266-8 (Aug. 1983). In Russian. Chalcogenide semiconductor films in the systems Ge-Se and As-Se were sputtered on NaCl substrates. Their thickness was controlled by an interferometric method using a pulsed He-Ne laser. Structural studies showed that film structures sputtered onto heated substrates differ from those sputtered onto cold substrates. (6 refs.) *V.G.P.*

Properties and structure of carbon excess Ti_xC_{1-x} deposited onto molybdenum by magnetron sputtering See Entry 114397

The effect of oxygen in cosputtered (titanium + silicon) films See Entry 114401

Nb_3Sn -Pb Josephson tunnel junctions using patterned RF sputtered material and RF oxidation See Entry 114645

Metallization of Lavan in a glow discharge See Entry 115379

Sputtered Schottky barrier solar cells on p-type GaAs See Entry 115631

81.15G Vacuum deposition

115056 Some physicochemical problems of vacuum epitaxial growth of ferroelectrics. Yu.Ya.Tomashpol'skii (L.Ya. Karpov Sci.-Res. Physicochem. Inst., Moscow, USSR).

Inorg. Mater. (USA), vol.18, no.10, p.1426-30 (Oct. 1982). Translation of: *Izv. Akad. Nauk SSSR Neorg. Mater.*, vol.18, no.10, p.1662-6 (Oct. 1982). [received: Sept. 1983]

The main problems of the vacuum epitaxy of ferroelectrics are: structural heterogeneity and local nonstoichiometry of the atomic-molecular stream; a complex structural and chemical state of the substrate as a consequence of adsorption of gas molecules, lattice desorption, impurity diffusion to the surface, formation of surface phases; crystallographic misfit of the film and substrate lattices, catalytic activity of the substrate, narrow critical temperature interval of epitaxy. Consideration of these problems and optimization of the epitaxy process make it possible to obtain smooth single-crystal condensates of ferroelectrics with a stoichiometric main layer and a minimal surface layer, as is illustrated in films of complex oxides. (10 refs.)

115057 Computer-aided study of hot wall epitaxy system using a Monte Carlo technique. V.Ramachandran, P.R.Vaya (Centre for Systems & Devices, Indian Inst. of Technol., Madras, India).

J. Appl. Phys. (USA), vol.54, no.9, p.5385-93 (Sept. 1983). Theoretical analysis of PbTe molecular flow in hot wall epitaxy system has been made using a Monte Carlo approach for free molecular flow. Variation in transmission probabilities with the dimensions of the wall have been obtained. These results are applied to get epitaxial growth conditions for PbTe on KCl substrates. It has been observed that at condensation energy $E_c = 1.6$ eV, the substrate temperature range obtained using the present analysis agrees well with the experimental observations. (20 refs.)

115058 The heteroepitaxy of Ge on Si(100) by vacuum evaporation. Y.Ohmachi, T.Nishioka, Y.Shinoda (Musashino Electrical Communication Lab., Nippon Telegraph & Telephone Public Corp., Tokyo, Japan).

J. Appl. Phys. (USA), vol.54, no.9, p.5466-9 (Sept. 1983). High quality Ge epitaxial growth has been attained on Si(100) substrates at relatively low temperatures, 350 and 440°C, by a vacuum evaporation technique. Electrical property and structural quality for the Ge layer were evaluated by Hall measurement, X-ray diffraction, and electron beam diffraction. It is found that the growth layers are p-type and that net acceptor concentration and mobility strongly depend on the layer thickness. Of particular significance is the fact that the acceptor concentration decreases most rapidly and hole mobility remarkably increases with the Ge thickness. The acceptor concentration and the mobility at a point larger than 0.7 μ m from the lattice mismatched interface are 1.6×10^{16} cm⁻³ and 1040 cm²/V sec, respectively. Hole mobility varies as a function of $T^{3/2}$ and $T^{-3/2}$ below and above ~ 100 K. (19 refs.)

115059 Silicon molecular beam epitaxy. Y.Ota (Bell Labs., Reading, PA, USA).

Thin Solid Films (Switzerland), vol.106, no.1-2, p.3-136 (12 Aug. 1983). Considering the recent rapid progress in the technique, it is expected that in the near future silicon MBE will be applied to a much wider range of silicon devices including silicon integrated circuits. The author takes a closer look at the basics of the silicon MBE system design, including such fundamental issues as the essential diagnostic methods for characterizing and monitoring an epitaxial film during its growth, the electrical and crystalline properties, and device applications based on both developments in this laboratory and results obtained by numerous other workers in silicon MBE. The review includes a discussion of germanium MBE techniques needed to grow a high quality germanium epitaxial film. It has been found that germanium MBE requires as careful a process as that employed in silicon MBE. (236 refs.)

115060 The growth of epitaxial $NiSi_2$ single crystals on silicon by the use of template layers. R.T.Tung, J.M.Gibson, J.M.Poate (Bell Labs., Murray Hill, NJ, USA).

Defects in Semiconductors II, Symposium Proceedings, Boston, MA, USA, Nov. 1982 (New York, USA: North-Holland 1983), p.435-9. A novel crystal growth technique for $NiSi_2$ epitaxy is presented which utilizes thin silicide (<60 Å) template layers to pin the subsequent growth under ultrahigh vacuum conditions. Single crystalline $NiSi_2$ films can be grown with either type A or type B orientations on Si(111). Continuous single crystalline $NiSi_2$ is grown on Si(100) with flat interface and uniform thickness. (13 refs.)

Kinetics of structural multiplets during diffusion homogenization of polycrystalline films See Entry 114381

On a relationship between substrate perfection and stacking faults in homoepitaxial silicon See Entry 114391

Process of formation of porous silicon and autoepitaxy on its surface See Entry 114394

Epitaxial InP/fluoride/InP(001) double heterostructures grown by molecular beam epitaxy See Entry 114593

Electronic properties of grain boundaries in GaAs: a study of oriented bicrystals prepared by epitaxial lateral overgrowth See Entry 114629

Improvement of photoluminescence of molecular beam epitaxially grown $Ga_{1-x}Al_xIn_{1-x-y}As$ by using an As_2 molecular beam See Entry 114901

81.15H Chemical vapour deposition

115061 Growth of $Ga_{0.47}In_{0.53}As$ -InP quantum wells by low pressure metal-organic chemical vapor deposition. M.Razeghi, J.P.Hirtz (Lab. Central de Recherches, Thomson-CSF, Orsay, France), U.O.Ziemelis, C.Delalande, B.Etienne, M.Voos.

Appl. Phys. Lett. (USA), vol.43, no.6, p.585-7 (15 Sept. 1983). The authors describe the growth of multiquantum well and single quantum well $Ga_{0.47}In_{0.53}As$ -InP structures by low pressure metalorganic chemical vapor deposition. The multiwell structure consists of 25-, 50-, 100-, and 200-Å quantum wells ($Ga_{0.47}In_{0.53}As$ layers) separated by 500-Å barriers (InP layers). Auger measurements indicate the presence of four distinct wells with abrupt boundaries. Photoluminescence measurements are consistent with the existence of four wells; however, deviations are noted between experimentally determined and theoretically predicted recombination energies. An analogous situation exists for the single (50 and 100 Å) quantum well structures. Possible explanations, including variation of well composition, variation of well thickness, and participation of impurities in the recombination process are suggested. (8 refs.)

115062 $InGa_{1-x}As$ -epitaxy with metalorganic adducts. P.Speier, F.Scholz, K.W.Benz (Phys. Inst., Univ. Stuttgart, Stuttgart, Germany), H.Benz, J.Weidlein.

Electron. Lett. (GB), vol.19, no.18, p.728-9 (1 Sept. 1983). Two metalorganic adducts (trimethylindium-trimethylarsine $(CH_3)_3In-As(CH_3)_3$ and trimethylgallium-trimethylarsine $(CH_3)_3Ga-As(CH_3)_3$) have been used for the epitaxial growth of $InGa_{1-x}As$ on InP and GaAs substrates at normal pressure. Epitaxial layers with net carrier concentrations of $n = 2 \times 10^{16}$ cm⁻³, $\mu_{300K} = 6600$ cm²/V s ($In_{0.53}Ga_{0.47}As/InP$) and $n' = 1 \times 10^{16}$ cm⁻³, $\mu' = 3200$ cm²/V s ($In_{0.2}Ga_{0.8}As/GaAs$) have been grown. (13 refs.)

115063 Plasma enhanced metal-organic chemical vapor deposition of aluminum oxide dielectric film for device applications. K.P.Pande, V.K.R.Nair, D.Gutierrez (Bendix Advanced Technol. Center, Columbia, MD, USA).

J. Appl. Phys. (USA), vol.54, no.9, p.5436-40 (Sept. 1983). Low temperature ($\leq 250^\circ C$) deposition of aluminum oxide gate dielectric film using a new plasma enhanced metal-organic chemical vapor deposition technique is described. With this technique, the substrate was not directly exposed to the plasma which minimizes radiation damage to both the substrate and the film. A DC potential was used to generate the plasma and the deposition of the film was achieved at extremely low plasma power (≤ 2 W) using trimethylaluminum and nitrous oxide reactant sources. The dielectric films were found to have a resistivity of $\sim 10^{14}$ Ω cm, dielectric constant of 7.9 ± 0.2 , and breakdown field $\geq 10^6$ V/cm. A linear dependence of the film growth rate upon TMAI concentration was observed, indicating that the growth process is mass transport limited. Metal-oxide-semiconductor device structures were fabricated both on n-Si and p-InP substrates and the interface properties were evaluated by capacitance-voltage and Auger measurements. Both the devices show sharp interface with a minimum density of states in the range of 8×10^{10} - 10^{11} cm⁻² eV⁻¹ for Si and 4×10^{11} cm⁻² eV⁻¹ for p-InP. (23 refs.)

115064 Enhancement of growth rate due to tin doping in GaAs epilayer grown by low pressure metal-organic chemical vapor deposition. C.Y.Chang, M.K.Lee, Y.K.Su, W.C.Hsu (Dept. of Electrical Engng., Nat. Cheng Kung Univ., Tainan, Taiwan).

J. Appl. Phys. (USA), vol.54, no.9, p.5464-5 (Sept. 1983). Tetraethyltin is used as an n-type dopant in homoepitaxially growing GaAs films from triethylgallium and arsine vapor in a low pressure system. The experimental data show that the growth rate can be enhanced by tin doping. It is found that the deep level transient spectroscopy concentration of the electron trap located at about 0.8 eV below the conduction band is suppressed by Sn doping. Gallium vacancy may be attributed to the trap. A growth model has been proposed, which can be substantiated by the experimental results. (17 refs.)

115065 Tin doping of gallium arsenide by metallic organic chemical vapor deposition (MOCVD). J.D.Parsons, F.G.Krajenbrink (Hughes Res. Labs., Malibu, CA, USA).

J. Electrochem. Soc. (USA), vol.130, no.8, p.1780-1 (Aug. 1983). The authors report the results of a study to determine the feasibility of growing Sn doped GaAs by MOCVD. Tin is a very desirable n-type dopant for MOCVD grown III-V compounds because of its low vapor pressure and low compensation. The most commonly used n-type dopants for MOCVD grown III-V compounds are S, Se and Te. These elements are effective, low compensation dopants; however, they have very high vapor pressures which result in the so called 'memory effect'. As a result, it is not possible to grow epilayers with abrupt high-low doping profiles. The authors have completed a series of experiments in which they determined that: (a) tetramethyltin (TMT) can be used as a Sn source for n-type doping of MOCVD grown GaAs; (b) Sn incorporation can be controlled over a broad range of carrier concentrations; and (c) no surface pile-up of Sn occurs in III-V epilayers grown by atmospheric pressure MOCVD. (2 refs.)

115066 Use of diethylberyllium for metal organic chemical vapor deposition of beryllium-doped gallium arsenide. J.D.Parsons, F.G.Krajenbrink (Hughes Res. Labs., Malibu, CA, USA).

J. Electrochem. Soc. (USA), vol.130, no.8, p.1782-3 (Aug. 1983). A new dopant source [diethylberyllium (DEB)] has been successfully employed to grow Be-doped GaAs epilayers with excellent surface morphology and transport properties. This is the first time that DEB has been used as a Be source for p-type doping of MOCVD-grown GaAs epilayers. Room temperature electrical properties and Hall mobilities of Be doped GaAs epilayers, grown to date, are presented. (2 refs.)

115067 A theoretical study of the low-temperature chemical vapor deposition of SiO_2 films. C.Cobianu, C.Pavelescu (Microelectronica, Bucharest, Rumania).

J. Electrochem. Soc. (USA), vol.130, no.9, p.1888-93 (Sept. 1983). The silicon dioxide deposition on silicon substrates in the SiH_4 - O_2 - N_2 system was investigated in the temperature range from 80° to 400°C on a nozzle-type reactor at atmospheric pressure. An exponential temperature dependence (of Arrhenius type) with a break at 250°C has been observed for the O_2/SiH_4 ratio corresponding to the maximum deposition rate and also for the O_2/SiH_4 ratio corresponding to near-zero deposition rate in the retardation region. Within the bimolecular surface reaction theory (Langmuir-Hinshelwood mechanism), these results are explained, and the break is interpreted as a change in the adsorption mechanism of the reactant gases with temperature. The apparent activation energy of the surface reaction (5.2-6.5 kcal/mol) in the temperature range from 80° to 400°C has been derived from the Arrhenius plot of the maximum deposition rate, in agreement with the above theory. An empirical reaction rate equation has been proposed which, in addition, explains the linear dependence of the maximum deposition rate on silane flow rate at constant O_2/SiH_4 ratio. (16 refs.)

115068 Epitaxial growth of GaAs_{1-x}P_x (0 < x < 0.6) by OM-CVD from ClEt₂GaAsEt₃ complex and diethyl phosphine: HPET₂ as original source of phosphorus. F.Maury, G.Constant (Lab. de Cristallogénie, Reactivité et Protection des Matériaux, Ecole Supérieure de Chimie, Toulouse, France). *J. Cryst. Growth* (Netherlands), vol.62, no.3, p.568-76 (Aug. 1983). In French.

Growth of GaAs_{1-x}P_x epitaxial layers (0 < x < 0.6) on GaAs and Ge substrates has been realized by OM-CVD with ClEt₂GaAsEt₃ and HPET₂ used as element sources for Ga, As and P in the temperature range of 500-650°C. The growth rate strongly depends on the deposition temperature and reaches a maximum at 600°C. The P content of the alloys increases with the HPET₂ molar fraction in the vapor phase but is quite independent of the substrate temperature in the range of 500-600°C. The study of the influence of the parameters shows that the growth mechanism differs from the one which occurs when AsH₃ and PH₃ are used. The good reactivity of HPET₂ is discussed and led the authors to propose this molecule as the phosphorus source in OM-CVD. (18 refs.)

115069 OMVPE growth of GaInP. C.C.Hsu, R.M.Cohen, G.B.Stringfellow (Univ. of Utah, Salt Lake City, UT, USA). *J. Cryst. Growth* (Netherlands), vol.62, no.3, p.648-50 (Aug. 1983).

Excellent photoluminescent quality Ga_{0.5}In_{0.5}P with x ≈ 0.5 has been grown epitaxially on GaAs substrates using OMVPE. The source materials used were trimethylgallium, trimethylindium and phosphine in an H₂ ambient. At the optimum temperature of 625°C and a V/III ratio of 40, high photoluminescence efficiency and narrow half-widths were obtained. (19 refs.)

115070 Epitaxial reactor systems: characteristics, operation, and epitaxy costs. G.W.Cullen, J.F.Corboy, R.Metzl (RCA Labs., Princeton, NJ, USA). *RCA Rev. (USA)*, vol.44, no.2, p.187-216 (June 1983).

Discusses the design and operating characteristics of various homoepitaxial reactor systems for Si deposition now being employed in the semiconductor industry. The parameters available for control of the deposit characteristics, specifically as related to the reactor configurations, are outlined. The current technology of slip control through RF-heated susceptor design is reviewed. The very significant advantages associated with reduced-pressure epitaxial growth are presented. The throughputs and costs involved in each reactor are analyzed. Finally, the authors make some predictions concerning the future trends of development in epitaxial reactor technology. (34 refs.)

115071 An investigation of the factors that influence the deposit/etch balance in a radiant-heated silicon epitaxial reactor. J.F.Corboy, R.Pagliaro (RCA Labs., Princeton, NJ, USA). *RCA Rev. (USA)*, vol.44, no.2, p.231-49 (June 1983).

Discusses the AMC 7900 in the radiant-heated configuration, the thermal gradients normal to the substrate can be minimized. Maintenance of this reactor must be carefully programmed to avoid accumulation of deposits on the reactor bell jar which would attenuate the radiant energy. Despite the drawbacks associated with this approach, this reactor is widely used in the semiconductor industry where deposits with good crystalline perfection are required. Little is to be found in the literature, however, on the impact of the variables of total gas flow, location of the substrate on the susceptor, and susceptor rotation on the local deposition/etch rates and uniformity of the deposit resistivity. To develop an understanding of these factors, the reactor was operated in an experimental mode with no susceptor rotation. The results of this study and the implications with respect to operation of the reactor in the normal rotating-susceptor mode are discussed. (5 refs.)

115072 Double-barrel III-V compound vapor-phase epitaxy systems. G.H.Olsen, T.J.Zamerowski (RCA Labs., Princeton, NJ, USA). *RCA Rev. (USA)*, vol.44, no.2, p.270-86 (June 1983).

A unique system for the growth of III-V compound multilayer structures—without interruption of crystal growth—is described. This system has generated large improvements in the synthesis of long-wavelength optoelectronic devices. A complete 1.3-μm laser structure can be grown in 30 minutes and more than 15 such structures can be grown in a single day. Single layers as thin as 60 Å have been measured. 1.3-μm InGaAsP CW lasers with lasing threshold currents as low as 45 mA and 1.0-1.7-μm InGaAs photodetectors with leakage currents below 10 nA and quantum efficiencies near 80% have been synthesized with the system. (20 refs.)

115073 LPCVD polycrystalline silicon: growth and physical properties of in-situ phosphorus doped and undoped films. G.Harbeke, L.Krausbauer, E.F.Steigmeier, A.E.Widmer (RCA Ltd., Zurich, Switzerland), H.F.Kappert, G.Neugebauer. *RCA Rev. (USA)*, vol.44, no.2, p.287-312 (June 1983).

In this application-oriented study the authors investigate in-situ phosphorus doped LPCVD polysilicon films deposited in the temperature range from 560°C to 640°C and compared the results with those previously obtained on undoped films. X-ray diffraction, TEM, SEM, Raman and elastic light scattering, optical absorption, and reflection, and other techniques were used to obtain information on the grain size, structure, structural perfection, strain, refractive index, surface roughness, and electrical conductivity. They found that to obtain phosphorus doped films of highest quality, deposition in the amorphous form, i.e. at temperatures not exceeding 570°C, is necessary. Of slightly lower quality, but acceptable for less critical applications are films deposited at 580°C ≤ T_d ≤ 620°C. Layers deposited at T_d ≥ 620°C are considered to be of poor quality. (17 refs.)

115074 LPCVD polycrystalline silicon: growth and physical properties of diffusion-doped, ion-implanted, and undoped films. M.T.Duffy, J.T.McGinn, J.M.Shaw, R.T.Smith, R.A.Soltis (RCA Labs., Princeton, NJ, USA), G.Harbeke. *RCA Rev. (USA)*, vol.44, no.2, p.313-25 (June 1983).

The texture and surface smoothness of polycrystalline silicon layers are important in high-density circuits. In this work, amorphous and polycrystalline silicon layers were evaluated with respect to structural, topographical, and electrical properties before and after diffusion doping and ion implantation. Films prepared in the polycrystalline state by LPCVD frequently have a columnar growth structure which is associated with a rough surface. Diffusion-doping with phosphorus promotes grain growth and increases surface roughness. By contrast, films prepared in the amorphous state retain their initial smooth surfaces even after diffusion-doping with phosphorus and subsequent annealing. Amorphous films that are ion-implanted with phosphorus and annealed retain their initial smoothness but reveal inhomogeneity in grain structure from the tops of the films to the bottoms of the films depending upon the depth of the implant. (14 refs.)

115075 A physicomathematical model for the polycrystalline silicon thin film deposition process in a reduced-pressure horizontal reactor. V.G.Kobka, Yu.P.Medvedev, Yu.V.Ushankin. *Sov. Microelectron. (USA)*, vol.12, no.1, p.13-19 (Jan.-Feb. 1983). Translation of: *Mikroelektronika (USSR)*, vol.12, no.1, p.17-23 (Jan.-Feb. 1983). [received: Sept. 1983]

The LPCVD deposition rate dependence on pressure for poly-Si is nonlinear, which can be explained by the effect of adsorption processes. This dependence

is arbitrarily divided into two regions: region 1 is the linear adsorption region and region 2 is the region where adsorption is important. The distribution of the poly-Si thickness over the wafer is determined not only by the total pressure in the reactor, but also by the partial pressure of the reagent, and differs substantially for regions 1 and 2. The depletion of the flow along the reactor leads to a transition of the process from region 2 to region 1 and is accompanied by an increase in the nonuniformity of the poly-Si thickness. The analytical expressions found for deposition rate uniformity G(r) and G(z), for poly-Si give a good description of the experimentally observed regularities. Using the analytical expressions for G(r) and G(z), the authors have optimized the deposition process as a function of the overall gas mixture pressure in the reactor. (12 refs.)

115076 Chemical vapor deposition of group IVB, VB, and VIB elements with nonmetals. A literature review. H.O.McDonald, J.B.Stephenson. *Report IC-8928*, Bur. Mines, Washington, DC, USA (1983), 29 pp.

Reviews the chemical vapor deposition (CVD) literature on the nonmetal binary and ternary compounds of the group IVB, VB and VIB elements, with emphasis directed to the following nonmetals: B, C, N, O, and Si. Each of these binary and selected ternary compounds of the group IVB, VB, and VIB elements are examined as coatings and some of their preparative methods, uses, and properties given. A total of 259 references were found for these compounds of the nine elements. This review was utilized in the Bureau's research to provide abrasion-, erosion-, and corrosion-resistant coatings in order to conserve critical metals and protect various metallic surfaces in metallurgical, mining, and energy conversion systems. (259 refs.)

115077 A systematic approach of the low temperature CVD with organometallic compounds. G.Constant, R.Morancho (Groupe de Recherche, Depots Chimiques A Partir de la Phase Vapeur, ERA, CNRS, Toulouse, France).

Proceedings of the 4th European Conference on Chemical Vapour Deposition, Eindhoven, Netherlands, 31 May-2 June 1983 (Eindhoven, Netherlands: Philips Centre Manuf. Technol. 1983), p.36-43

Some practical rules based on thermal decomposition studies and actual knowledge of the chemical bond, are proposed to guide the choice of an organometallic compound as starting material in an OM CVD process. The mean chemical bond energy between the central atom, which is the element to deposit, and the attached group, gives the approximate reaction temperature; by an electronic modification of the bound carbon or by increasing the stress enthalpy of the substituent the deposition temperature may be lowered. A cooperative elimination of two groups borne by two neighbour atoms is probably a frequent molecular reaction; it takes place at a lower temperature than a radical mechanism and it can be an interesting step when one wants these two elements in the coating. At last amorphous material can be elaborated by OM CVD either by a statistical fragmentation of the different chemical bonds, or by the introduction of organic molecules or atoms group inside an inorganic thin film material. (33 refs.)

115078 Chemical vapor deposition of Si in stagnation point flow. D.B.Graves, K.F.Jensen (Dept. of Chem. Engng. & Materials Sci., Univ. of Minnesota, Minneapolis, MN, USA).

Proceedings of the 4th European Conference on Chemical Vapour Deposition, Eindhoven, Netherlands, 31 May-2 June 1983 (Eindhoven, Netherlands: Philips Centre Manuf. Technol. 1983), p.51-6

A stagnation point flow reactor is presented for the systematic investigation of CVD kinetics over a wide range of conditions. Ideally, stagnation point flow offers a number of attractive features, e.g. the fluid mechanics are relatively simple and well-understood; temperature and chemical species concentration fields vary with axial position, not radius. This configuration may be an effective alternative to the rotating disk because of the absence of natural convective effects; both configurations are ideally one-dimensional. The full power in the method lies in its ability to discriminate between physical transport effects and competing reaction mechanisms thus also allowing identification of kinetic rate constants. The modeling equations are presented and the full set of equations including both gas phase and surface reactions is solved by a Galerkin-finite element technique. Two rival kinetic mechanisms for Si deposition from SiH₄ are used to demonstrate the utility of the method. The effect of pressure and flow on the deposition process is illustrated. (8 refs.)

115079 Low pressure aluminium CVD. R.A.H.Heinecke, M.J.Cooke, R.C.Stern (Standard Telecommunication Labs. Ltd., Harlow, England).

Proceedings of the 4th European Conference on Chemical Vapour Deposition, Eindhoven, Netherlands, 31 May-2 June 1983 (Eindhoven, Netherlands: Philips Centre Manuf. Technol. 1983), p.119-21

Many LPCVD processes are known to be outstanding for their conformal coating properties. The technique has now been applied to the deposition of aluminium-silicon interconnections on silicon integrated circuits. In this presentation the main features of the coatings are highlighted and an outline of the deposition process is given. (no refs.)

115080 CVD-NbC_{1-x}N_y-carbon fiber superconductors. F.Schmaderer, G.Wahl (Brown Boveri, Res. Centre, Heidelberg, Germany), C.H.Dustmann, M.Dietrich.

Proceedings of the 4th European Conference on Chemical Vapour Deposition, Eindhoven, Netherlands, 31 May-2 June 1983 (Eindhoven, Netherlands: Philips Centre Manuf. Technol. 1983), p.148-55

A new promising superconducting material for high field magnets is B₁-niobium-carbonitride. Chemical vapor deposition is chosen as the method of manufacture when using carbon fibres as substrate material due to the high inherent process throwing power. Carbon fibers are promising as a substrate material in a multifiber conductor for coil fabrication because of their high temperature resistance, high elastic modulus, high tensile strength and chemical compatibility with NbC_{1-x}N_y. This concept using carbon fibers together with NbC_{1-x}N_y offers advantages such as—easy handling for coil fabrication, stress and radiation resistance, low costs and reasonable superconducting properties. NbC_{1-x}N_y deposited at atmospheric pressure using a two step process has given B_{c2} values up to 21 T (4.2K) and film thicknesses in the range of 0.05 to 0.5 μm (6). The authors study the influence of low pressure and capacitively coupled plasma activation on nucleation in order to decrease the grain size and consequently increase the critical current J_c. PAN-based carbon fibers type T 300 and M 40 from TORAY with 1000 to 6000 fibers per bundle, each with a diameter of ~7 μm were used. (14 refs.)

115081 Chemical vapor deposition of Nb₃Sn in a fluidized bed. E.Wilfing, F.Holub, E.Horl (Österreichisches Forschungszentrum Seibersdorf GmbH, Inst. für Werkstofftechnologie, Vienna, Austria).

Proceedings of the 4th European Conference on Chemical Vapour Deposition, Eindhoven, Netherlands, 31 May-2 June 1983 (Eindhoven, Netherlands: Philips Centre Manuf. Technol. 1983), p.156-63

The feasibility of a CVD fluidized bed technique for the fabrication of superconductors has been studied using Nb₃Sn as a representative of A 15 type superconductors. Nb₃Sn has been deposited on particles of quartz, copper, molybdenum and on copper wires suspended in a fluidized bed of molybdenum particles by coreduction of NbCl₅ and SnCl₄ with hydrogen. The most

important process variables were deposition temperature and concentration of metal chlorides. The fluidized bed method favors deposition at low temperatures. Nb_2Sn of exact composition and good quality has been deposited with high growth rate at 700°C , while coatings produced at 1100°C consisted practically of niobium only. Among the benefits of the fluidized bed technique are low deposition temperature, good homogeneity and compactness of coating. The small mean crystallite size must be pointed out which should effect the high J_c of the material. (2 refs.)

115082 Kinetics and transport in the CVD of epitaxial silicon. M.L.Hitchman (Dept. of Chem. & Appl. Chem., Univ. of Salford, Salford, England).

Proceedings of the 4th European Conference on Chemical Vapour Deposition, Eindhoven, Netherlands, 31 May-2 June 1983 (Eindhoven, Netherlands: Philips Centre Manuf. Technol. 1983), p.167-74

One of the problems in trying to obtain kinetic information for heterogeneous processes is that often the reaction is occurring under conditions where transport of reactants to the surface is affecting the rate of growth. This is, in fact, the case for silicon epitaxy under the production conditions of $1150-1250^\circ\text{C}$, since in this temperature range the growth rate is dependent on gas flow rate. Therefore in order to obtain a better understanding of the chemistry of the growth process it is necessary to take account of the transport contribution to growth and to separate it out before trying to interpret kinetic parameters and to arrive at a model for the mechanism of deposition. The design of commercial reactors for silicon epitaxy precludes the possibility of a simple analysis of mass transfer characteristics, although attempts have been previously made to quantitatively describe transport controlled deposition in the commonly used barrel and horizontal reactors. The author discusses the rotating disc system, and wall jet and impinging jet systems, as reactor designs which will allow a more tractable solution to the mass transfer problem to be obtained. (28 refs.)

115083 Laser induced chemical vapor deposition of hydrogenated amorphous silicon. R.Bilenchi, I.Gianinoni, M.Musci (CISE SpA, Milano, Italy), R.Murri.

Proceedings of the 4th European Conference on Chemical Vapour Deposition, Eindhoven, Netherlands, 31 May-2 June 1983 (Eindhoven, Netherlands: Philips Centre Manuf. Technol. 1983), p.194-6

The authors have previously published results on a new method of hydrogenated amorphous silicon (a-Si:H) deposition, due to resonant absorption of CW CO_2 laser radiation by silane molecules. In order to enhance the deposited area and to improve the transversal uniformity, the authors now report two different approaches using, a high power excitation source, and laser beam scanning. (no refs.)

115084 Deposit of germanium monocrystalline thin films by chemical vapour transport in a diffusional flow system. F.Langlais, J.C.Launay, M.Pouchard, P.Hagenmuller (Lab. de Chimie du Solide CNRS, Talence, France).

Proceedings of the 4th European Conference on Chemical Vapour Deposition, Eindhoven, Netherlands, 31 May-2 June 1983 (Eindhoven, Netherlands: Philips Centre Manuf. Technol. 1983), p.217-23

A new CVD method has recently been proposed, based on a 'three zone' arrangement (source, deposit and sink) with a forced flow between source and sink. It was applied to congruent and dissociative sublimation for HgI_2 and $\text{Pb}_{1-x}\text{Sn}_x\text{Te}$ respectively. An experimental application of the new 'three zone' method to chemical transport and epitaxy of germanium from its tetraiodide is presented. A fundamental study has been carried out, particular emphasis being laid on the influence of total pressure upon the hydrodynamic transport flow and upon the epitaxy rate. (7 refs.)

115085 Analysis of low pressure CVD processes. K.F.Jensen, D.B.Graves (Dept. of Chem. Engng. & Materials Sci., Univ. of Minnesota, Minneapolis, MN, USA).

Proceedings of the 4th European Conference on Chemical Vapour Deposition, Eindhoven, Netherlands, 31 May-2 June 1983 (Eindhoven, Netherlands: Philips Centre Manuf. Technol. 1983), p.224-9

A detailed mathematical model for the hot wall multiple-disk-in-tube LPCVD reactor is presented. The model gives a detailed description of the physico-chemical processes in the annular region formed by the tube wall and the edges of the wafers as well as those occurring in the spaces between the wafers. The deposition of polycrystalline Si from SiH_4 is considered as a specific example. The model predicts experimental observations and provides quantitative comparisons with experimental data from separate reactor studies. In addition the model allows for optimization of film uniformity. (8 refs.)

115086 Low pressure photosensitized chemical vapour deposition. Equipment and application for SiO_2 depositions below 100°C . R.F.Sarkozy (BTU/Bruce Engng. Corp., North Billerica, MA, USA).

Proceedings of the 4th European Conference on Chemical Vapour Deposition, Eindhoven, Netherlands, 31 May-2 June 1983 (Eindhoven, Netherlands: Philips Centre Manuf. Technol. 1983), p.230-4

The ever increasing complexity in Si wafer processing has generated the need for the deposition on dielectric materials at temperatures far below the $400-900^\circ$ range so routinely used in the past. Insulators over and between multilayer sandwich structures sensitive to alloying, and over narrow and shallow diffusions are now commonplace. The widespread use of $10/1$ step and repeat projection printers has prompted the use of multilayer lithographic technologies for the control of depth of focus and standing wave problems. Pattern delineation in thin film materials is frequently achieved by means of multilayer lift-off techniques. All of the requirements for low temperature dielectrics associated with these and similar processes can be satisfied by depositions at or below a critical temperature defined by the author as the soft bake temperature of photoresists in common use. To fill this need, equipment has been fabricated for the chemical vapour deposition of silicon dioxide utilizing the photosensitized combustion of SiH_4 and O_2 at temperatures below 100°C . The process is named low pressure photosensitized chemical vapour deposition LPPCVD. (6 refs.)

115087 Crystal growth mechanisms of semiconductor $\text{A}^{\text{III}}\text{B}^{\text{V}}$ and $\text{A}^{\text{II}}\text{B}^{\text{V}}$ compounds by metalorganic chemical vapor deposition. V.A.Voronin, V.A.Prochorov, L.S.Plahotnaja, S.K.Chuchmarev.

Proceedings of the 4th European Conference on Chemical Vapour Deposition, Eindhoven, Netherlands, 31 May-2 June 1983 (Eindhoven, Netherlands: Philips Centre Manuf. Technol. 1983), p.235-42

Crystal growth of semiconductors based on metalorganic compounds of non-transition elements is a complex heterogeneous process. Analysis of the probable interaction mechanisms of MO compounds of IIB and IIIA subgroup elements with the hydrides and metals of YA and YIA subgroups is given. The interaction mechanism is represented in the form of a structural topological model (STM), which allows one to account for possible phase and chemical transformations. It has been found that intermediary substance may be formed both in the vapor phase and on the substrate surface. The formed complexes which are superficially active centres, speed up adsorption of

reagents from the vapor phase and later decompose to form a semiconductor compound, methad or ethane. (11 refs.)

115088 LPCVD at quasi high flow. J.Holleman, J.Middelhoek (Dept. of Electrical Engng., Twente Univ. of Technol., Enschede, Netherlands).

Proceedings of the 4th European Conference on Chemical Vapour Deposition, Eindhoven, Netherlands, 31 May-2 June 1983 (Eindhoven, Netherlands: Philips Centre Manuf. Technol. 1983), p.243-56

A new CVD technique is presented. It is especially favourable in the case of the deposition of compound materials. The technique improves the deposition uniformity and reproducibility. The economical use of gaseous reactants is improved by factors of 5-20. The method consists of the manifold repetition of the sequence evacuation, filling and deposition. The filling time of 50 msec is short compared to the deposition period of 1 second. The advantages of the method are demonstrated with the results on the deposition of Si, Si+P, Si+B and SiO_2 . (4 refs.)

115089 GaP and InP films elaborated with the covalent molecules $(\text{Et}_2\text{M}^{\text{III}}-\text{PEt}_2)_3$, $\text{M}^{\text{III}}=\text{Ga, In}$: a possible step in III-V MO-CVD process. F.Maury, M.Combes, G.Constant (Groupe de Recherche, Depots Chimiques a Partir de la Phase Vapeur, Toulouse, France).

Proceedings of the 4th European Conference on Chemical Vapour Deposition, Eindhoven, Netherlands, 31 May-2 June 1983 (Eindhoven, Netherlands: Philips Centre Manuf. Technol. 1983), p.257-64

Growth of polycrystalline GaP layers has been obtained between 650 and 775°C by LP-CVD using the only molecule $(\text{Et}_2\text{Ga}-\text{PEt}_2)_3$ as element source. The compound $(\text{Et}_2\text{In}-\text{PEt}_2)_3$, prepared in situ in the MO-VPE reactor with InEt_3 and HPEt_2 , led to InP epitaxial growth at 550°C . The chemical mechanism discussed in order to explain the results shows that these covalent molecules could be a possible route in the III-V MO-CVD process. (14 refs.)

115090 Epitaxial growth of silicon by CVD in a furnace. H.H.C.de Moor, J.H.L.Hanssen, L.J.Giling, J.Bloem (Dept. of Solid State III, Catholic Univ., Nijmegen, Netherlands).

Proceedings of the 4th European Conference on Chemical Vapour Deposition, Eindhoven, Netherlands, 31 May-2 June 1983 (Eindhoven, Netherlands: Philips Centre Manuf. Technol. 1983), p.278-9

Although epitaxial growth of silicon is a well established technique, there is an increasing demand for growth at lower temperatures in order to obtain sharper pn junctions; for the manufacture of MOS devices and solar cells the costs are of great importance. A solution for both problems is presented. Silicon can be selectively grown on wafers by applying only a very small supersaturation. Under these conditions nucleation difficulties prevent growth on foreign substrates, e.g. quartz or purposely oxidized parts on the silicon slices. To overcome the major problem of depletion a temperature gradient in the direction of the gasflow is applied in such a way that a uniform growth rate can be achieved. (6 refs.)

115091 Chemical vapor infiltration technique. R.Naslain, H.Hannache (Lab. de Chimie du Solide, Univ. de Bordeaux-I, Talence, France), L.Heraud, J.Y.Rossignol, F.Christin, C.Bernard.

Proceedings of the 4th European Conference on Chemical Vapour Deposition, Eindhoven, Netherlands, 31 May-2 June 1983 (Eindhoven, Netherlands: Philips Centre Manuf. Technol. 1983), p.293-304

CVD has been used for a long time mainly to obtain inorganic coatings on the external surface of different kinds of substrate (e.g. hard coatings for cutting tools or sliding parts, high oxidation resistance coatings on alloys, multi-layer thin films for microelectronics components, etc...). More recently, it has been suggested to use the chemical deposition of a solid from a gas mixture to densify porous materials (chemical vapor infiltration, CVI). One of the most important applications of CVI has been the synthesis of carbon-carbon composites, based on the pyrolysis of methane within the pores of a carbon fiber preform, up to almost complete densification. Later on, this process has been extended to the infiltration of other refractory materials such as carbides (SiC , TiC), nitrides (BN) or oxides and it will undoubtedly concern many other materials in the future. It thus appears that CVI will become a method of material synthesis as general as CVD. The authors try to draw the main features of this new technique from the still limited amount of literature data which has been published in this field up to now. (18 refs.)

115092 The CVD of boron nitride from $\text{BF}_3\text{-NH}_3$ mixtures. Application to the synthesis of 2D-C-C/BN composites. H.Hannache, R.Naslain (Lab. de Chimie du Solide, Univ. de Bordeaux-I, Talence, France), C.Bernard, L.Heraud.

Proceedings of the 4th European Conference on Chemical Vapour Deposition, Eindhoven, Netherlands, 31 May-2 June 1983 (Eindhoven, Netherlands: Philips Centre Manuf. Technol. 1983), p.305-12

The aim of the authors' contribution is to show, from a thermodynamic and experimental approach, that BN deposition from $\text{BF}_3\text{-NH}_3$ mixtures can be used to prepare composite materials having a 2D³-carbon fiber skeleton and a C/BN hybrid matrix. Such materials could be used in air, when properly processed, up to $900-1000^\circ\text{C}$. BN can be deposited from different gas mixtures (e.g. $\text{BX}_3\text{-NH}_3$ (with $\text{X}=\text{F, Cl, Br}$), $\text{B}_3\text{N}_3\text{H}_6$ or $\text{B}_3\text{N}_3\text{H}_3\text{Cl}_3$). In the authors' work, $\text{BF}_3\text{-NH}_3$ mixtures were chosen since, according to H.O. Pierson (1975), they lead to well crystallized deposits even at the rather low temperatures required in CVI. (10 refs.)

115093 Low pressure CVD of pyrolytic carbon. C.H.J.van den Brekel (Philips Res. Labs., Eindhoven, Netherlands), B.Lersmacher.

Proceedings of the 4th European Conference on Chemical Vapour Deposition, Eindhoven, Netherlands, 31 May-2 June 1983 (Eindhoven, Netherlands: Philips Centre Manuf. Technol. 1983), p.321-36

The chemical vapour deposition process of pyrolytic carbon from propane in a 'hot-wall' reactor has been studied. A survey of the carbon reaction rate as a function of the input pressure and the deposition temperature is given. The growth rate dependency on the position in the reactor is also reported. The effect of the geometry of the substrate on the growth rate profile is studied by means of the deposition of carbon in capillaries. Growth rate profiles obtained at different experimental conditions are characterized on the basis of the Sherwood number of the process. These measurements allow the characterization of the process as a function of the experimental conditions. (3 refs.)

115094 The effects of reaction parameters on the deposition characteristics in Al_2O_3 CVD. C.Park, J.Kim, J.S.Chun (Dept. of Materials Sci. & Engng., Korea Advanced Inst. of Sci. & Technol., Seoul, Korea).

Proceedings of the 4th European Conference on Chemical Vapour Deposition, Eindhoven, Netherlands, 31 May-2 June 1983 (Eindhoven, Netherlands: Philips Centre Manuf. Technol. 1983), p.401-9

Deposits of aluminium oxides (Al_2O_3) have been formed by a chemical vapor deposition (CVD) technique involving the application of gas mixtures of AlCl_3 , CO_2 and H_2 onto TiN coated cement carbide substrates. The relationships between the deposition rate and various reaction parameters such as the gas flow rate, the deposition temperature, the composition of reactant gases, and the system pressure were studied. The CVD of Al_2O_3 is a thermally activated process and limited by the surface chemical reaction. The apparent activation energy is about 36 Kcal/mol at 50 Torr and decreases with the

increasing system pressure. The dependence of the deposition rate on the reactant gas composition is affected by the variation of the relative contents of the aluminium donor and the oxygen donor. At a low AlCl₃ mole fraction, the deposition rate increases with the AlCl₃ mole fraction; however, at higher AlCl₃ mole fractions, the deposition rate is mainly influenced by the H₂O-forming reaction between CO₂ and H₂. (12 refs.)

115095 Influence of temperature and substrate on Al₂O₃ CVD from AlCl₃/H₂/CO₂ gas mixtures. T.Schmitt, H.Altena, B.Lux (Tech. Univ. Wien, Vienna, Austria).
Proceedings of the 4th European Conference on Chemical Vapour Deposition, Eindhoven, Netherlands, 31 May-2 June 1983 (Eindhoven, Netherlands: Philips Centre Manuf. Technol. 1983), p.421-7
CVD deposition of Al₂O₃ was carried out in a hot-wall reactor with a temperature gradient. Al₂O₃, W, Mo, Fe, Ni, Ni/Cr and Cr were used as substrates. For all experiments high levels of the impurity silicon were present. The experiments showed the influence of the substrate, in the presence of Si, on the crystal morphology resulting at high temperatures (950°-1050°C) where α-Al₂O₃ is formed. At low temperatures unusual crystal morphologies were observed. It became clear from these experiments that the oversaturation existing in the gas mixture has a strong influence on the morphologies of the deposits. The fresh incoming gas mixture gives different morphologies than the gas mixture near the outlet, where high levels of the reaction products CO and HCl are present. The experiments permitted the observation of α-Al₂O₃ growth features similar to those common for Al₂O₃ layers on cemented carbides produced under poorly controlled conditions. (7 refs.)

115096 Deposition and characterization of MO-CVD ZrO₂. L.Ben Dor (Dept. of Inorganic Analytical Chem., Hewbrew Univ., Jerusalem, Israel), A.Elshtein, J.Shappir.
Proceedings of the 4th European Conference on Chemical Vapour Deposition, Eindhoven, Netherlands, 31 May-2 June 1983 (Eindhoven, Netherlands: Philips Centre Manuf. Technol. 1983), p.444-50
ZrO₂ layers obtained by MO-CVD have physical and electronic properties making them suitable for various applications such as discrete capacitors as well as miniature capacitors in VLSI. (5 refs.)

115097 CVD of TiN at the tempering temperature of alloy-steels. W.Hanni, H.E.Hintermann (Lab. Suisse de Recherches Horlogeres, Neuchatel, Switzerland).
Proceedings of the 4th European Conference on Chemical Vapour Deposition, Eindhoven, Netherlands, 31 May-2 June 1983 (Eindhoven, Netherlands: Philips Centre Manuf. Technol. 1983), p.468-73
The deposition of titanium nitride on nitriding and heat-treatment steels, corrosion-resistant ledeburitic and high speed steels (HSS), and, in certain cases, maraging steels has been carried out by the reaction of titanium tetrachloride with ammonia diluted in nitrogen carrier gas. The specimens were coated in a hot-wall reactor where the graphite heating element acts as the reaction chamber or in a hot wall reactor with an ordinary external furnace. To avoid a reaction between the substrate materials and titanium tetrachloride (halide inclusions), special attention is needed when starting the deposition. The titanium nitride layers obtained were hard golden-yellow in colour and bright on polished surfaces. Density and adhesion vary with the deposition temperature and the chloride concentration. Such titanium nitride coatings can be used as functional coatings for friction and wear applications. (6 refs.)

115098 Formation of thin refractory coatings, their properties and fields of application. O.V.Roman, P.A.Vityaz, G.N.Dubrovskaya, L.M.Kirilyuk (Byelorussian Powder Metall. Assoc., Minsk, Byelorussian SSR).
Proceedings of the 4th European Conference on Chemical Vapour Deposition, Eindhoven, Netherlands, 31 May-2 June 1983 (Eindhoven, Netherlands: Philips Centre Manuf. Technol. 1983), p.474-8
The production of TiN coatings by CVD and physical vapour deposition is compared. It is shown that TiN CVD on cutting tools used for processing steels can improve cutting rates by up to 1.4 times and increase the tool life by 1.5 to 2.5 times. (2 refs.)

115099 On the theoretical conditions of deposition of refractory solid solutions: titanium carbonitride. F.Teyssandier (DRET-ETCA, Arcueil, France), M.Ducarroir, C.Bernard.
Proceedings of the 4th European Conference on Chemical Vapour Deposition, Eindhoven, Netherlands, 31 May-2 June 1983 (Eindhoven, Netherlands: Philips Centre Manuf. Technol. 1983), p.509
Summary form only given. The composition of titanium carbonitride deposits generated by an input gas mixture of TiCl₄-CH₄-N₂-H₂ may be thermodynamically predicted if the excess free energy of the ternary solid solutions is known as a function of the temperature and the composition of the solid phase. For titanium carbide the theoretical composition of the solid solution versus the input methane partial pressure is compared with the experimental one of the deposits obtained in a cold wall process. In the case of the titanium nitride system, the deposit domains with isostoechiometric curves are presented at 1400K. Some comparison of theoretical and experimental results is also mentioned. After presentation of the ternary solid solution (TiC_xN_{1-x}) free energy equation, the predicted composition of the vapour deposited materials is discussed. (no refs.)

115100 Industrialisation of titaniumcarbonitride deposition process at moderated temperatures. P.Bonetti, H.Wahl (Bernex Div., Berna AG Olten, Olten, Switzerland).
Proceedings of the 4th European Conference on Chemical Vapour Deposition, Eindhoven, Netherlands, 31 May-2 June 1983 (Eindhoven, Netherlands: Philips Centre Manuf. Technol. 1983), p.510-16
Deals with the scaling-up of a CVD-titaniumcarbonitride coating process using organic nitriles as raw materials. Coating thickness distribution over the reactor volume is discussed in function of nitrile composition, gas mixtures, temperature and residence time. Surface finish is influenced by the nitrile to titanium-tetrachloride ratio and the deposition temperature. In this process adhesion of the coatings is improved at higher temperatures and in the case of steels at temperatures where austenite is stable. (6 refs.)

115101 Effects of the experimental conditions of chemical vapor deposition on TiC/TiN double layer coating. M.S.Kim, J.S.Chun (Dept. of Materials Sci., Korea Advanced Inst. of Sci. & Technol., Seoul, Korea).
Proceedings of the 4th European Conference on Chemical Vapour Deposition, Eindhoven, Netherlands, 31 May-2 June 1983 (Eindhoven, Netherlands: Philips Centre Manuf. Technol. 1983), p.517-30
Deposits of titanium nitride (TiN) were formed on TiC-coated WC-6Co substrates by chemical vapor deposition (CVD) using a TiCl₄, H₂, and N₂ gas mixture. The effects of the deposition temperature, total flow rate of the reactant gases, and the TiCl₄ partial pressure on the deposition rate, preferred orientation, and surface morphology of the TiN deposit were investigated. The controlling mechanism of the TiN deposition reaction and its relationship with the deposition temperature and total flow rate of reactant gases were also investigated. The deposition rate and (220) preferred orientation are increased with an increase in deposition temperature and TiCl₄ partial pressure, and

with a total flow rate of less than 700 cc/min. The particle size of the TiN deposit is reduced with an increase in TiCl₄ partial pressure, and is increased with an increase in deposition temperature and with a total flow rate of less than 700 cc/min. When the total flow rate is larger than 700 cc/min, the deposition rate, (220) preferred orientation, and the particle size of the TiN deposit no longer vary. (15 refs.)

115102 The growth of TiC on iron-carbon substrates by CVD. P.P.J.Ramaekers, F.J.J.van Loo (Lab. of Phys. Chem., Eindhoven Univ. of Technol., Eindhoven, Netherlands).
Proceedings of the 4th European Conference on Chemical Vapour Deposition, Eindhoven, Netherlands, 31 May-2 June 1983 (Eindhoven, Netherlands: Philips Centre Manuf. Technol. 1983), p.546-52
Describes CVD experiments on various iron-carbon substrates with and without carbon supply in the gas phase. From these experiments and from a theoretical consideration the authors try to elucidate the influence of carbon content in the substrate on the kinetics of the growth process. A comparison with diffusion couple experiments is made. All experiments are carried out at a temperature of 1273K. (9 refs.)

Proceedings of the 4th European Conference on Chemical Vapour Deposition .. See Entry 111316
Development of a CVD silica coating for UK advanced gas-cooled nuclear reactor fuel pins See Entry 112351
Study of the OH content of CVD silica glass for optical fibres See Entry 113070
ALPD (axial lateral plasma deposition): a new process for the production of high quality optical fibers See Entry 113154
Optical waveguide manufacturing techniques See Entry 113156
The production of optical fibers and optical fiber cables See Entry 113157
In situ observations of crystal growth processes See Entry 113790
TEM—electron energy loss spectroscopy study of the diamond particles prepared by the chemical vapour deposition from methane See Entry 114379
Properties of molybdenum silicide film deposited by chemical vapor deposition See Entry 114384
Crystallographic orientation and surface morphology of chemical vapor deposited Al₂O₃ See Entry 114385
Si on cubic zirconia See Entry 114388
Simulation of CVD-processes See Entry 114402
Theoretical influence of the deposition conditions on the uniformity of boron carbide coatings See Entry 114404
Modeling of GaAs growth in the MOCVD system See Entry 114406
CVD-deposition of aluminum on nickel-based alloys from AlCl₃/H₂-gas-mixtures See Entry 114407
Chemical vapour deposition of boron on silicon See Entry 114408
Modeling of doping during CVD growth of semiconductor films See Entry 114409
The incorporation of dopants during growth of GaAs by CVD See Entry 114410
CVD a-Ge and a-Ge:X films: preparation and properties See Entry 114411
The mechanism of the growth of InP by MOCVD See Entry 114412
Characterization of thin plasma silicon-nitride layers See Entry 114413
Electrical versus structural properties of polycrystalline silicon deposited by plasma enhanced LPCVD below 550°C See Entry 114414
Indirect and direct formation of polycrystalline silicon during CVD See Entry 114415
Properties of thin polycrystalline silicon films deposited by plasma-assisted CVD See Entry 114416
The effect of reaction condition on the crystallographic orientation and surface morphology of chemical vapor deposited Al₂O₃ See Entry 114419
Growth of α-Al₂O₃ on single- and polycrystalline alumina substrates by CVD .. See Entry 114420
Influence of trace impurities on the formation of α-Al₂O₃ layers by CVD See Entry 114421
Effect of TiCl₄ addition on the structure of chemically vapor-deposited Si₃N₄ .. See Entry 114422
Heat treatments of CVD-coatings on hardmetals See Entry 114425
Formation of whiskers on Al₂O₃ CVD layers See Entry 114428
Thermodynamics and kinetics of the gas phase and pack aluminide coating formation on iron and steel See Entry 115448
The development of CVD oxide coatings for the protection of metal surfaces .. See Entry 115449
Role of CVD in providing wear resistant films See Entry 115450
The decarburization of steel during the CVD of TiC See Entry 115451

81.15J Ion plating and other vapour deposition

115103 Radical species in argon-silane discharges. R.Robertson, D.Hils, H.Chatham, A.Gallagher (Joint Inst. for Lab. Astrophys., Univ. of Colorado, Boulder, CO, USA).
Appl. Phys. Lett. (USA), vol.43, no.6, p.544-6 (15 Sept. 1983).
SiH_n radical densities at the surface of discharges in Ar-SiH₄ mixtures have been measured by low-energy, electron-collisional ionization and mass spectrometer detection of SiH_n⁺. The principal radical seen at the substrate surface of a DC proximity discharge is SiH₃. (11 refs.)

115104 Quantitative ion beam process for the deposition of compound thin films. J.M.E.Harper, J.J.Cuomo, H.T.G.Hentzell (IBM Thomas J. Watson Res. Center, Yorktown Heights, NY, USA).
Appl. Phys. Lett. (USA), vol.43, no.6, p.547-9 (15 Sept. 1983).
The authors describe a quantitative ion beam technique for the deposition of compound thin films. The metal atom flux is supplied by inert ion beam sputtering, and the reactive flux is supplied by a low-energy ion beam directed at the growing film, allowing the fundamental deposition parameters of arrival rates, ion energy, and direction to be measured and controlled. Analysis gives the sputtering yields and incorporation probabilities as a function of film composition, arrival rate ratios, and ion energy. Results are presented for Al films deposited under a range of N₂⁺ ion bombardment (100-500 eV) up to arrival rate ratios exceeding the value needed to form AlN. Nitrogen ions are almost fully incorporated into Al films, and excess N is rejected above the composition N/Al=1. The microstructure is shown to depend on the N/Al arrival rate ratio and the nitrogen ion energy used during deposition. (5 refs.)

115105 Homoeptitaxial growth of ZnTe by horizontal open-tube method. M.Nishio, Y.Nakamura, H.Ogawa (Dept. of Electrical Engng., Saga Univ., Saga, Japan).

Jpn. J. Appl. Phys. Part 1 (Japan), vol.22, no.7, p.1101-5 (July 1983).
The vapor-phase epitaxy of ZnTe was carried out in H_2 , Ar and I_2 gas ambients by the horizontal open-tube method. The depletion rate of the ZnTe source and the growth rate on (110), (111)A and (111)B ZnTe substrates are described here as functions of the carrier gas flow rates, and the molar ratios of I_2 to H_2 and of Ar to H_2 . The values of the depletion rate and the growth rate decreased in the following order: ZnTe- H_2 - I_2 > ZnTe- H_2 > ZnTe-Ar and ZnTe- H_2 - I_2 > ZnTe- H_2 > ZnTe-Ar system, e.g. the depletion rates were 3.0, 3.0 and 2.4 mg/min, and the growth rates were 0.30, 0.24 and 0.18 μ m/min respectively, when the source temperature was kept at 293°C, the substrate temperature at 862°C and the carrier flow rate at 100 ml/min. The surface pattern of the epitaxial layer was strongly influenced by the growth temperature and the surface orientation. (17 refs.)

115106 Low-temperature epitaxial growth of (100) silicon. M.Milosavljevic, C.Jeyens, I.H.Wilson (Univ. of Surrey, Guildford, England).
Electron. Lett. (GB), vol.19, no.17, p.669-71 (18 Aug. 1983).
Epitaxial silicon films have been grown onto as-received and implanted (100) silicon wafers by electron-beam evaporation. A high-temperature treatment to remove native oxide was not employed. Optimum temperatures for epitaxial growth were between 600°C and 700°C. Deposition rates were from 30 to 80 nm/min and the operating pressure was $<5 \times 10^{-7}$ mbar. The Rutherford backscattering spectra of the optimum films have values of χ_{\min} indistinguishable from that of a bulk wafer (3.9%). (7 refs.)

115107 Control of the uniformity of thin films formed by an RF plasma [Josephson technology application]. R.F.Broom, V.Graf, W.Heuberger (IBM Corp., Armonk, NY, USA).
IBM Tech. Disclosure Bull. (USA), vol.26, no.2, p.866-9 (July 1983).
The problem of film uniformity during the formation of nonplanar structures can be significantly reduced by applying a nonuniform magnetic field (providing a field gradient) or by using a modified cathode geometry. This has particular application to edge junction technology employed for Josephson devices. (no refs.)

115108 Deposition rate and structural properties of microcrystalline glow discharge Si:H:Cl films. G.Bruno, P.Capezzuto, F.Cramarossa (Dipt. di Chimica, Univ. di Bari, Bari, Italy).
Thin Solid Films (Switzerland), vol.106, no.3, p.145-52 (19 Aug. 1983).
The deposition rate and the structural properties of Si:H:Cl films produced in $SiCl_4$ - H_2 glow discharges were studied as functions of the substrate temperature, the gas feed composition and the operating pressure. The experiment results were interpreted on the basis of a discharge equilibrium involving both deposition and etching of the film. A close relationship between the deposition rate and the crystallite size is shown. (27 refs.)

1.3 μ m InGaAsP/InP multiquantum-well lasers grown by vapour-phase epitaxy See Entry 113011

Characterization of thin plasma silicon-nitride layers See Entry 114413

Electrical versus structural properties of polycrystalline silicon deposited by plasma enhanced LPCVD below 550°C See Entry 114414

Properties of thin polycrystalline silicon films deposited by plasma-assisted CVD See Entry 114416

pAl_{0.4}Ga_{1-x}As-pGaAs-nGaAs heterostructure concentrator photocells synthesized by liquid-gas-phase epitaxy See Entry 115652

81.15L Deposition from liquid phases (melts and solutions)

115109 Liquid phase epitaxial growth on {111}_A planes of InP. R.A.Logan, C.H.Henry, F.R.Merritt, S.Mahajan (Bell Labs., Murray Hill, NJ, USA).

J. Appl. Phys. (USA), vol.54, no.9, p.5462-3 (Sept. 1983).
Two-step, liquid phase epitaxy is a high yield process without critical steps in the AlGaAs system when used to form buried devices such as buried heterostructure lasers, but similar procedures give a low yield in the InGaAsP system with many short circuited devices. The {111}_A stop-etch plane enables one to etch narrow mesas (≈ 1.5 - μ m wide) to ensure single mode laser operation but regrowth of InP on this plane has a highly nonradiative interface, a characteristic that appears unique to this plane. Studies of the growth morphology correlate the nonradiative behavior with an inability of the initial islands of nucleation so spread laterally to form a continuous layer which gives rise to melt entrapment. (6 refs.)

115110 Electroepitaxial growth of HgCdTe from Te-rich solution. L.Jedral, H.Ruda, P.Becla, J.Lagowski, H.C.Gatos (MIT, Cambridge, MA, USA).

J. Electrochem. Soc. (USA), vol.130, no.7, p.1614-16 (July 1983).
Liquid phase electroepitaxial (LPEE) layers of HgCdTe have been grown from Te-rich solution at 501°C. Growth experiments were performed in a two-zone furnace. A graphite boat with BN slider was placed in the high temperature zone. The lower temperature zone contained a pure Hg reservoir. The mercury pressure over the growth system was controlled by selecting the temperature of this zone and the flow rate of H_2 . A Te-rich solution with the composition $Hg_{0.188}Te_{0.012}Te_{0.800}$ was used. The experimentally determined liquidus temperature for this solution was 501°C, with a mercury reservoir temperature of 294°C at a H_2 flow rate of about 50 cm³/min. (11 refs.)

115111 A highly stable nonaqueous suspension for the electrophoretic deposition of powdered substances. J.Mizuguchi (Res. Center, Sony Corp., Yokohama, Japan), K.Sumi, T.Muchi.

J. Electrochem. Soc. (USA), vol.130, no.9, p.1819-25 (Sept. 1983).
A highly stable nonaqueous suspension for the electrophoretic coating of alumina powders on double helical filaments has been developed. This suspension enables uniform coating in less than a second at a voltage of 300-600 V with an average current density of about 1 mA/cm². The suspension is composed of dispersing powders, acetone, nitrocellulose, and a small amount of the strong base and strong acid. A variety of powders can be anodically deposited uniformly using the same composition. Successful results are obtained for Al₂O₃, (Ba,Sr,Ca)CO₃, MgO, ZnO, TiO₂, SiO₂, SiO, In₂O₃, LaB₆, WC, and CdS powders; for phosphors such as ZnS:Cu,Al, ZnS:Ag, ZnS:Ag,Ag,Al, Y₂O₃:S:Eu, Y₂O₃:Eu, Y₂O₃:Tb, and CaS:Ce; and for metallic powders such as W, Mo, Ni, Al, Zn, and Ru. (17 refs.)

115112 Liquid phase epitaxial growth conditions of lattice-matched Al_{0.48}In_{0.52}As and Al_{0.48}Ga_{0.52}In_{1-x-y}As layers without surface defects. K.Nakajima, T.Tanahashi, S.Komiyama, K.Akita (Semiconductor Materials Lab., Atsugi Labs., Fujitsu Labs. Ltd., Ono, Atsugi, Japan).

J. Electrochem. Soc. (USA), vol.130, no.9, p.1927-33 (Sept. 1983).
The liquid phase epitaxial (LPE) growth conditions for lattice-matched Al_{0.48}In_{0.52}As and Al_{0.48}Ga_{0.52}In_{1-x-y}As layers with various compositions and energy gaps were determined by using the X-ray diffraction and photoluminescence measurements. The epitaxial layers were grown on InP (111)A and (100) substrates. By using these LPE growth conditions, the lattice-matched epitaxial layers can be grown in the energy gap range from 0.8 to 1.44 eV. The Hall measurements unintentionally doped Al_{0.48}In_{0.52}As layers which were grown without using special baking methods were performed at room temperature. The carrier concentration was 4.7×10^{15} and 5.9×10^{15} cm⁻³, and the Hall mobility was 4549 and 4466 cm²/Vsec. The compositional grading in Al_{0.48}Ga_{0.52}In_{1-x-y}As layers was studied by the CuK α rocking curves. It was found that the epitaxial layers with mirror surface were more easily obtained on (111) A InP than on (100) InP. The composition dependence of the growth rate of Al_{0.48}Ga_{0.52}In_{1-x-y}As was studied. The possibility of obtaining heterostructures such as Al_{0.48}Ga_{0.52}In_{1-x-y}As/Al_{0.48}In_{0.52}As and In_{0.52}Ga_{0.48}As/Al_{0.48}In_{0.52}As was also studied. (19 refs.)

115113 In situ electrochemical monitoring and control of oxygen in liquid phase epitaxial growth of GaAs. S.C.Chang, G.Y.Meng, D.A.Stevenson (Dept. of Materials Sci. & Engng., Stanford Univ., Stanford, CA, USA).
J. Cryst. Growth (Netherlands), vol.62, no.3, p.465-74 (Aug. 1983).

An electrochemical method, employing an yttria stabilized zirconia electrolyte, was used to measure and control the oxygen activity in liquid gallium in a vertical liquid phase epitaxial (LPE) growth system for GaAs. A zirconia tube serves both as the container for the Ga(l) solvent and as the electrolyte in an oxygen concentration cell. The rate and extent of deoxygenation of the liquid gallium solvent are reported for three methods of deoxygenation: high temperature annealing in flowing purified hydrogen or argon; use of chemical deoxidizers added to the melt; and electrochemical coulometric titration. In addition, GaAs LPE layers were grown at different measured oxygen activities and the resulting carrier type and concentration related to the oxygen concentration in the gallium solvent. (21 refs.)

115114 Improved meltback procedures for liquid-phase-epitaxial growth of planar and buried heterostructures. B.H.Chin, A.K.Chin, M.A.Digiuseppe, J.A.Lourengo, I.Camilbel (Bell Labs., Murray Hill, NJ, USA).
Defects in Semiconductors II, Symposium Proceedings, Boston, MA, USA, Nov. 1982 (New York, USA: North-Holland 1983), p.277-81

In the liquid phase epitaxy on indium phosphide, the substrate, just prior to the growth of the first epitaxial layer, is commonly etched back with an indium melt to remove any thermally-degraded surface and to ensure uniform and consistent wetting. This procedure, however, often produces defects which degrade both planar and buried heterostructure devices. For planar edge-emitters and lasers, the resulting rippled surface morphology degrades device performance by scattering light. For buried heterostructures, the meltback in the regrowth step leads to indium-rich inclusions. The effects of meltback on material quality are presented, and a new multiple meltback procedure which maintains flat surface morphology and eliminates inclusions is described. (6 refs.)

115115 Enhanced InP substrate protection for LPE growth of InGaAsP DH lasers. P.Besomi, R.B.Wilson, W.R.Wagner, R.J.Nelson (Bell Labs., Murray Hill, NJ, USA).
Defects in Semiconductors II, Symposium Proceedings, Boston, MA, USA, Nov. 1982 (New York, USA: North-Holland 1983), p.289-93

Thermal degradation of InP single crystal substrates prior to LPE growth has been virtually eliminated by using an improved protection technique. The phosphorus partial pressure provided by a Sn-In-P solution localized inside an external chamber surrounding the InP substrate prior to growth prevents thermal damage to the surface. Nomarski contrast photomicrographs, photoluminescence and X-ray diffractometric measurements indicate that InP substrates protected by this method suffer negligible deterioration, in contrast to the results of the more commonly used cover wafer method. (11 refs.)

Mathematical modeling of high-current chromium plating with application of a rotating disk electrode See Entry 114387

Liquid phase epitaxial growth of In_{1-x}Ga_xP_{1-y}As_y on GaAs substrates See Entry 114389

Some characteristics of the electroluminescence emitted by epitaxial Al-Ga-Sb heterostructures See Entry 114934

Chemical deposition of metallic tin upon copper substrates ... See Entry 115432

Electrodeposition of zinc on glassy carbon from ZnCl₂ and ZnBr₂ electrolytes [batteries] See Entry 115629

Al_xGa_{1-x}As/GaAs thin window concentrator solar cells by LPE plus vapour phase diffusion See Entry 115641

Optimization of GaAs photocell properties using a thin Al_xGa_{1-x}As interlayer See Entry 115643

pAl_{0.4}Ga_{1-x}As-pGaAs-nGaAs heterostructure concentrator photocells synthesized by liquid-gas-phase epitaxy See Entry 115652

81.20 OTHER METHODS OF PREPARATION OF MATERIALS

115116 Graphite produced by extrusion of pitch mesophase. J.C.Jenkins, G.M.Jenkins (Dept. of Metall. & Materials Technol., Univ. Coll. of Swansea, Swansea, Wales).

Carbon (GB), vol.21, no.5, p.473-83 (1983).
It is shown that an ideal pitch mesophase can be extruded to form a rod in which the flow anisotropy induced by shear and stretch is preserved. This rod can be coked and graphitized to form a new graphite with prescribed dimensions and structure imposed during extrusion. Optical microscopy, X-ray diffraction and dilatometric analysis served to determine the structural anisotropy of the new coke and the changes taking place during heat treatment. The graphitized product exhibits a highly anisotropic structure and low volume coefficient of thermal expansion similar to premium grade needle coke produced by the delayed coking process. (20 refs.)

115117 Preparation of multialkali antimonide photocathode. R.L.Verma, R.C.Bapna (Laser Section, Bhabha Atomic Res. Centre, Bombay, India).

Indian J. Pure & Appl. Phys., vol.21, no.7, p.422-4 (July 1983).
A method for preparing multialkali photocathode starting with an antimony layer possessing island structure is described. The photocathode thus formed is found to be more sensitive in the near infrared region than that prepared by the conventional method. A reproducible photocathode with average yield of 160 μ A/lm and having long wavelength threshold at 870 nm is obtained. (11 refs.)

115118 Formation of titanium and zirconium carbides with interaction of the oxides with carbon in a low-temperature plasma. G.K.Moisev, S.K.Popov, L.A.Ovchinnikova, N.A.Vatolin (Inst. of Metall., Acad. of Sci., USSR).

Inorg. Mater. (USA), vol.18, no.9, p.1301-4 (Sept. 1982). Translation of: *Izv. Akad. Nauk SSSR Neorg. Mater.*, vol.18, no.9, p.1521-4 (Sept. 1982). [received: Sept. 1983]

Calculations modeling the formation of TiC and ZrC with the interaction of TiO₂ and ZrO₂ with carbon at 1000-4000K in the starting Ar medium and total pressure $9.81 \cdot 10^{-2}$ MPa were performed. It was established that TiC can form at 1500-3400K and ZrC can form at 1900-3800K without appreciable losses of metal in the gas phase. The phase compositions and energy expended in completing the process were determined. Experiments were performed in an (Ar+H₂) plasma on the formation of maximum and minimum carbon-defect TiC_x and ZrC_y from their oxides and carbon at ~3000K within 180 sec. In obtaining maximum defect carbides, oxides were found in the products; in obtaining minimum defect carbides, the phases TiC_{0.975} and TiC_{0.983} are formed with 97-99% transformation. The unit cell parameters were determined. (12 refs.)

115119 Acid orthophosphates and triphosphates of the rare earths. P.P.Mel'nikov, T.A.Butuzova, G.Ya.Pushkina, L.N.Komissarova (M.V. Lomonosov Moscow State Univ., Moscow, USSR).

Inorg. Mater. (USA), vol.18, no.9, p.1333-6 (Sept. 1982). Translation of: *Izv. Akad. Nauk SSSR Neorg. Mater.*, vol.18, no.9, p.1557-60 (Sept. 1982). [received: Sept. 1983]

A cryochemical method has been developed for preparing the acid ortho- and triphosphates of the rare earths. Structural analogies have been established for the compounds discussed with the double phosphates of composition M₃Ln(PO₄)₂. The X-ray diffraction characteristics of the compounds have been determined. (14 refs.)

115120 Synthesis of acid polyphosphates of rare-earth metals and the structure of ErH(PO₃)₄. K.K.Palkina, N.N.Chudinova, C.M.Balagina, S.I.Maksimova, N.T.Chibiskova (N.S. Kurnakov Inst. of General & Inorganic Chem., Acad. of Sci., Moscow, USSR).

Inorg. Mater. (USA), vol.18, no.9, p.1337-41 (Sept. 1982). Translation of: *Izv. Akad. Nauk SSSR Neorg. Mater.*, vol.18, no.9, p.1561-6 (Sept. 1982). [received: Sept. 1983]

Acid polyphosphates of rare-earth metals of the composition LnH(PO₃)₄ (Ln=Sm,Eu,Gd,Tb,Dy,Ho,Er) have been obtained. It has been established that they crystallize in two forms: triclinic (Sm,Eu) and monoclinic (Tb-Er). The change in structure occurs with gadolinium. The structure of the monoclinic form ErH(PO₃)₄ has been studied. It has been shown that the polyphosphate chains in ErH(PO₃)₄ are crystallographically not equivalent. (4 refs.)

115121 Stationary configuration of fibers formed under nonisothermal conditions. A.L.Yarin.

J. Appl. Mech. & Tech. Phys. (USA), vol.23, no.6, p.865-70 (Nov.-Dec. 1982). Translation of: *Zh. Prikl. Mekh. & Tekh. Fiz. (USSR)*, vol.23, no.6, p.139-44 (Nov.-Dec. 1982). [received: Sept. 1983]

Analytic solutions of the stationary problem in fiber molding are obtained under the assumption of large activation energy of the viscous flow. The melt is considered to be shaped to be a Newtonian fluid with viscosity dependent on the temperature according to the Arrhenius law. Such high values of the viscosity correspond to sufficiently low temperatures that flow practically ceases and the material solidifies. The two most widespread technological processes are examined: (1) drawing a fiber from a cylindrical glass blank heated to high temperature, and (2) drawing through a spinneret hole from a tank containing the melt. (9 refs.)

115122 Syntheses and thermal properties of new liquid crystalline materials involving tropolone. T.Uemura, S.Takenaka, S.Kusabayashi (Dept. of Appl. Chem., Osaka Univ., Osaka, Japan), S.Seto.

Mol. Cryst. & Liq. Cryst. (GB), vol.95, no.3-4, p.287-97 (1983). To examine the effect of a tropolone ring system on mesomorphic behaviour, the following 2- and 3-ring compounds have been prepared: R.Ph.X.Ph.OY and R.Ph.CO.O.Ph.X.Ph.OY, where Ph=phenyl; R=C_nH_{2n+1}, C_nH_{2n+1}O; Y=OH, OCH₃; and X=—CH=N—, —N=N—. The 2-ring compounds are non-mesogenic whereas the 3-ring compounds exhibit nematic phases of high stability when R=alkyl or alkoxy, X=—CH=N— or —N=N—, and Y=OH or OCH₃, and an additional smectic phase when R=alkoxy. The nematic phase tends to align homeotropically when placed between two glass plates. (19 refs.)

115123 Skin technology—fundamentals and applications. H.Sprenger (MAN-Neue Technol., Munich, Germany).

Proceedings of the 4th European Symposium on Materials Sciences under Microgravity (ESA SP-191), Madrid, Spain, 5-8 April 1983 (Paris, France: ESA 1983), p.353-8

The Skin Technology provides a valuable means for quality improvement of intricately shaped parts under micro-gravity. The technique is especially suitable for refining multiphase alloys or composites like eutectics, dispersion or whisker reinforced alloys, immiscibles etc. by a melting/solidification process. First experiments have shown that shape stability of skin coated specimens depends mainly on effective compensation of forces introduced by the volume increment during melting and freezing. By use of an expansion container this problem is solved and will be tested in further μ -g experiments. The technology will also find application in cases in which increased heat transfer compared to conventional crucibles is required. Furthermore an advanced version, called Liquid Skin Technology, will allow dynamic supercooling of large volume specimens, and is an alternative to containerless melting. (3 refs.)

Polycrystalline infrared optical fibersSee Entry 113132

81.20E Powder techniques, compaction and sintering

115124 Hydrodynamic pressing of β -alumina components. G.T.Pozdnyakova, O.P.Golubeva, V.M.Levchenko.

Inorg. Mater. (USA), vol.18, no.9, p.1370-1 (Sept. 1982). Translation of: *Izv. Akad. Nauk SSSR Neorg. Mater.*, vol.18, no.9, p.1594-5 (Sept. 1982). [received: Sept. 1983]

Hydrodynamic pressing is used to produce β -alumina parts with elevated density, and this is used along with other methods of pulse pressing in powder metallurgy and is beginning to be used in ceramic production. The method provides high pressures with comparatively low energy consumption and without the use of complicated sealing units. Hydrodynamic pressing is also more productive than the hydrostatic method. The present study was performed with a GDM 20/10-135/190-700 apparatus for hydrodynamic pressing of powders by means of explosive charges. (2 refs.)

115125 The synthesis of densified CMD from Mn-NH₄-carbamate and its discharge properties in ZnCl₂ batteries. I.Tanabe (Technol. Univ. of Nagaoka, Nigata, Japan), N.Miyamoto, H.Kido, Z.Kato, T.Uno.

J. Electrochem. Soc. (USA), vol.129, no.10, p.2372-8 (Oct. 1982). The densification of crude MnO₂ (CMD) from the oxidation of MnCO₃ and its discharge properties were investigated in order to improve the properties of CMD as follows: The chlorate reaction was observed to be quite effective for the densification of CMD. Mn²⁺ adsorbed on the inner surface of the particles of crude MnO₂ reacts with NaClO₃ to form MnO₂, which accumulates on the inner surface. By increasing both the ratio of MnO₂ formed by this reaction to total MnO₂, and decreasing the content of the residual MnCO₃ in the crude MnO₂, the degree of densification of the product was increased. For crude MnO₂ with a lower content of residual MnCO₃, its apparent density, specific surface area, and ion exchange capacity were almost the same as that of EMD when the ratio was about 22%. When the ratio was below 30%, the product appeared to be the amorphous type. Above 34%, the peak of ρ -type MnO₂ was observed. With increasing ratio of MnO₂ formed by the chlorate reaction to total MnO₂, the discharge efficiencies for both wet cells and D-size dry batteries were negligibly decreased up to 22-23%; they were considerably decreased for ratios above 23%. Therefore, the product obtained when the ratio was 22-23% can be regarded as optimum. Its packing capability was the same as that of EMD. For this type of CMD and EMD, the electrolytic solution comprising 32% ZnCl₂ and 1% NH₄Cl can be regarded as optimum. The heavy load discharge properties of this type of CMD were quite similar to those of EMD. Further, the intermittent discharge properties were considerably better than those of EMD. For densified CMD, crushing of the product was desirable to improve the heavyload discharge properties. (13 refs.)

115126 Effect of grain size distribution on sintered density. M.F.Yan (Bell Labs., Murray Hill, NJ, USA), R.M.Cannon, Jr., H.K.Bowen, U.Chowdhry.

Material. Sci. & Eng. (Switzerland), vol.60, no.3, p.275-81 (Sept. 1983). Conditions of pore separation from grain boundaries during sintering are analyzed. It is shown analytically that a minimum intrinsic and solute drag force is required to prevent pore separation. In microstructures with a non-uniform size distribution the minimum dopant concentration is typically 14 times higher than that required in microstructures with a narrow grain size distribution. If the drag force is below the required minimum, pore separation will occur after the compact is sintered to a critical density. In compacts with a narrow grain size distribution, the critical density is about 99.3% of the theoretical density. However, in compacts with a non-uniform size distribution the critical density decreases to about 90.6% of the theoretical density. This analysis shows that it is imperative to maintain a narrow grain size distribution in order to obtain a high sintered density. Sintering data for BaTiO₃, β -Al₂O₃ and ZrO₂ agree with this analysis. (13 refs.)

115127 Cold sintering under high pressure—mechanisms and application. E.Y.Gutmanas (Dept. of Materials Engng., Technion-Israel Inst. Technol., Haifa, Israel).

Powder Metall. Int. (Germany), vol.15, no.3, p.129-32 (Aug. 1983). Plastic flow of powder particles in gradients of high pressure leads to high density, physical contact and chemical bonding of freshly formed surfaces at room temperature, or to cold sintering. Cold sintering of various materials with metallic, ionic and ionic-covalent bonds was observed. Thermal treatments of cold sintered samples at relatively low temperatures compared with those used in sintering show that higher mechanical properties and improved ductility may be obtained on cold sintered samples. Mechanisms of cold sintering are discussed. Possible application of cold sintering for processing of structural parts is considered. (21 refs.)

115128 Densification and change in shape of porous materials during hot pressing under conditions of nonuniform triaxial compression. V.M.Gorokhov, M.S.Koval'chenko, O.V.Roman (Inst. of Materials Sci., Acad. of Sci., Ukrainian SSR).

Sov. Powder Metall. & Met. Ceram. (USA), vol.22, no.1, p.7-11 (Jan. 1983). Translation of: *Poroshk. Metall. (USSR)*, vol.22, no.1, p.8-13 (Jan. 1983). [received: Aug. 1983]

A study is presented, using an approximating model of a linear viscous liquid, of the densification kinetics of a porous body. It is shown that the variation of the density of such a body averaged over its whole volume can be determined directly from the external forces acting on it. An equation is derived describing the densification of a powder material during pressing under conditions of complex loading associated with any pattern of force distribution on its surface. It can be employed for determining the density of a part in free upsetting, pressing in a rigid die, isostatic pressing in a gas, and the like. The plastic change in shape of a porous body under conditions of complex loading is described within the framework of the theory of volume viscous flow by an equation determining the mean value of the deformation tensor at any stage of densification. An equation is proposed for the axial and radial strains in pressing under conditions of nonuniform triaxial compression; it shows that, depending on the lateral-to-axial pressure ratio, the radial deformation of a porous body may take the form of a compressive or tensile strain. (5 refs.)

115129 Initial sintering temperature of ultrafine powders. V.N.Troitskii, A.Z.Rakhmatullina, V.I.Berestenko, S.V.Gurov (Inst. of New Chem. Problems, Acad. of Sci., USSR).

Sov. Powder Metall. & Met. Ceram. (USA), vol.22, no.1, p.12-14 (Jan. 1983). Translation of: *Poroshk. Metall. (USSR)*, vol.22, no.1, p.13-15 (Jan. 1983). [received: Aug. 1983] Determines the initial sintering temperatures of some ultrafine metal, nitride, silicide, and oxide powders under conditions of free filling during vacuum heating and establishes the dependence of these characteristics of the powders on particle size. (3 refs.)

115130 Excess energy stored in the fine powder system. Y.Inomata (Nat. Inst. for Res. in Inorganic Materials, Ibaraki, Japan).

Yogyo-Kyokai-Shi (Japan), vol.91, no.7, p.318-21 (1983). Excess energy stored in a fine crystalline powder system in comparison with large crystal having same structure and composition with the powder was evaluated theoretically. For the system in which the size of particles are larger than ca. 0.1 μ m, the excess energy can be evaluated by the sum of surface energy of powder particles in the system with good approximation. It is not adequate to use Thomson-Freundlich equation for the calculation of the excess energy. The internal pressure of crystalline particle does not increase with decreasing particle size. The pressure, chemical potential and vacancy concentration in the powder particle does not show any gradient caused by the local variation of curvature of the surface and/or interface of the particle. (8 refs.)

- 115131** An analysis of the driving forces in liquid-phase sintering. P.M.Ossi, F.Rossitto (CESNEF, Politecnico di Milano, Milano, Italy), R.Roberti, G.Silva. Proceedings of the 4th European Symposium on Materials Sciences under Microgravity (ESA SP-191), Madrid, Spain, 5-8 April 1983 (Paris, France: ESA 1983), p.343-5.
A study of the first stage of the liquid-phase sintering process is presented, to assess the relevance of the capillary forces in the rearrangement and densification of metallic powders and wires. The force-balance equation is studied to evaluate the various contributions for the different model configurations. The meniscus shapes are evaluated by integrating the Young-Laplace equation. The 'Liquid-phase sintering' experiment to be performed within the ESA Microgravity Programme and included in the TEXUS 8 payload is presented. The aim of the experiment is to obtain a better evidence and quantitative evaluation of the driving forces. (6 refs.)
- UO₂ fuel pellet microstructure modification through impurity additions** See Entry 112328
- Vitrification kinetics of ternary silica-alumina-lime glass powders** See Entry 113755
- Character of impurity distribution in comminuted β -boron crystals** See Entry 113953
- A highly stable nonaqueous suspension for the electrophoretic deposition of powdered substances** See Entry 115111
- Ferromagnetic multifilamentary Fe and Ni wires with high coercive fields produced by powder metallurgy processing** See Entry 115132
- Ferromagnetic multifilamentary composites produced by cold powder metallurgy processing** See Entry 115133
- Liquid phase sintering of tungsten [and optimum mechanical properties]** See Entry 115134
- Hot isostatic pressing of oxide dispersion strengthened superalloy parts** See Entry 115136
- Modern trends in creating sintered antifriction materials** See Entry 115137
- The effect of sintering in hydrogen-nitrogen atmospheres and subsequent aging on the magnetic properties of iron** See Entry 115138
- Heat evolution during the shock pressing of iron powder** See Entry 115139
- Structure and mechanical and corrosion properties of P/M Kh23Ni18 stainless steel** See Entry 115140
- Densification kinetics of chromium carbide and its alloys in hot pressing** See Entry 115141
- Sinterability of alkoxide-derived magnesia** See Entry 115146
- Properties of hot-pressed zirconium pyrovanadate ceramics** See Entry 115149
- Kinetics and mechanism of cluster growth in mixtures of calcia and magnesia** See Entry 115150
- Equipment for the sintering and melting of ceramic materials** See Entry 115151
- Production of metal-carbon system materials with groups IV-V refractory metals** See Entry 115153
- Sintering and electrical resistivity of ZnO-Nb₂O₅ ceramic** See Entry 115155
- Preparation of porous Mg-Al spinel ceramics** See Entry 115156
- Torsional strength of pressureless-sintered silicon nitride** See Entry 115206
- Structure of molybdenum high speed steels after atomization and annealing** See Entry 115228
- Role of molybdenum in sintered steels [tensile properties]** See Entry 115270
- Variational functional for a rigid-plastic porous material** See Entry 115279
- Interfacial segregation and embrittlement in liquid phase sintered tungsten alloys** See Entry 115324
- Microstructure and mechanical strength of aluminum titanate ceramics prepared from synthesized powders** See Entry 115353
- Tensile strength of pressureless-sintered silicon nitride at elevated temperature** See Entry 115354
- Effect of waterglass impregnation upon hardenability of porous sintered steel** See Entry 115431
- Assessment of residual stresses in coatings applied to P/M parts** See Entry 115441
- Determination of the particle-size distributions of powders by mercury porosimetry** See Entry 115467
- Effect of the composition of binding materials on the properties of carbon pastes** See Entry 115509

81.20G Specific metals and alloys (compacts, pseudoalloys)

- 115132** Ferromagnetic multifilamentary Fe and Ni wires with high coercive fields produced by powder metallurgy processing. Y.D.Yao (Inst. of Phys., Acad. Sinica, Taipei, Taiwan), S.Foner. *Appl. Phys. Lett. (USA)*, vol.43, no.7, p.697-9 (1 Oct. 1983).
Powder metallurgy processed multifilamentary Cu-Fe, Cu-Ni, and Nb-Ni ferromagnetic composite wires were fabricated with a relatively high coercive field H_c at room temperature. Compacts of Cu-36 wt.% Fe, Cu-36 wt.% Ni, and Nb-36 wt.% Ni powders were reduced in cross section to produce ferromagnetic multifilamentary materials. Nominal areal reduction ratios of 10^8 for Cu-36 wt.% Fe and 10^4 for Nb-36 wt.% Ni and Cu-36 wt.% Ni resulted in values of $H_c \sim 195$ Oe, 94 Oe, and 77 Oe, respectively. A final 300°C anneal of the Cu-36 wt.% Fe composite gave $H_c \sim 460$ Oe. The average ferromagnetic fiber diameters are estimated to be 100-1000 Å for the Fe fibers and are about 1 μ m for the Ni fibers. (6 refs.)
- 115133** Ferromagnetic multifilamentary composites produced by cold powder metallurgy processing. Y.D.Yao (Inst. of Phys., Acad. Sinica, Taipei, Taiwan), S.Foner. *Annu. Rep. Inst. Phys. Acad. Sin. (Taiwan)*, vol.12, p.18-28 (Dec. 1982). [received: Sept. 1983]
Powder-metallurgy-processed multifilamentary Cu-Fe, Cu-Ni and Nb-Ni ferromagnetic composite wires were fabricated with a relatively high coercive field, H_c , at room temperature. Compacts of Cu-36 wt.% Fe, Cu-36 wt.% Ni and Nb-36 wt.% Ni powders were reduced in cross section to produce ferromagnetic multifilamentary materials. Areal reduction ratios of 10^8 for Cu-36 wt.% Fe and 10^4 for Nb-36 wt.% Ni and Cu-36 wt.% Ni resulted in values of $H_c \sim 195$ Oe, 94 Oe and 77 Oe respectively. A final 300°C anneal of the Cu-36 wt.% Fe composite gave $H_c \sim 460$ Oe. The average ferromagnetic fiber

diameters are estimated to be 100 Å to 1000 Å for the Fe fibers and are about 1 μ m for the Ni fibers. (7 refs.)

- 115134** Liquid phase sintering of tungsten [and optimum mechanical properties]. C.H.Lin, J.H.Jean (Dept. of Materials Sci. & Engng., Nat. Tsing Hua Univ., Hsinchu, Taiwan). *J. Mater. Sci. Lett. (GB)*, vol.2, no.9, p.480-4 (Sept. 1983).
The alloy is prepared by liquid phase sintering. In order to find the optimum mechanical properties the effect of varying the cooling rate and composition of the alloy on the mechanical properties and the fracture of the alloys was examined. (2 refs.)
- 115135** Preparation of rapidly solidified ribbons with second phase particles. P.G.Zielinski, D.G.Ast (Materials Sci. & Engng., Cornell Univ., Ithaca, NY, USA). *J. Mater. Sci. Lett. (GB)*, vol.2, no.9, p.495-8 (Sept. 1983).
The authors describe a new method to prepare metallic glasses containing a distribution of second phase particles. In this process, the particles are added after the liquid alloy is extruded but before it freezes into a ribbon. The method minimizes the contact time between the second phase particle and the liquid and offers the potential of adding a wide variety of particles, since it restricts the opportunities for reaction at the particle matrix interface. (7 refs.)
- 115136** Hot isostatic pressing of oxide dispersion strengthened superalloy parts. R.F.Singer, G.H.Gessinger (Forschungszentrum BBC AG, Baden, Switzerland). *Powder Metall. Int. (Germany)*, vol.15, no.3, p.119-21 (Aug. 1983).
MA6000E powders were consolidated by hot isostatic pressing. MA6000E is a γ' precipitation and oxide dispersion strengthened superalloy. For high temperature applications a coarse grained structure is required. The consolidated material has to be prestrained under certain conditions before it can be successfully grain coarsened by recrystallization. (10 refs.)
- 115137** Modern trends in creating sintered antifriction materials. I.M.Fedorchenko (Inst. of Materials Sci., Acad. of Sci., Kiev, Ukrainian SSR). *Powder Metall. Int. (Germany)*, vol.15, no.3, p.126-8, 132 (Aug. 1983).
Presents ideas on friction mechanism as a dynamical process. The main trends in creating composite sintered antifriction materials are shown. The influence of the phase components of material on the internal stress distribution in the process of work has been considered. Conditions ensuring the optimum internal stress distribution in the material and its optimum wear resistance during functioning are shown. (14 refs.)
- 115138** The effect of sintering in hydrogen-nitrogen atmospheres and subsequent aging on the magnetic properties of iron. K.H.Moyer, M.J.McDermott (Hoeganaes Corp., Riverton, NJ, USA). *Powder Metall. Int. (Germany)*, vol.15, no.3, p.134-8 (Aug. 1983).
The effect of nitrogen on the magnetic properties of iron cores sintered at 1120°C in nitrogen and hydrogen atmospheres is examined. The change in magnetic properties resulting from aging at various times and temperatures is also discussed. Case histories are included which demonstrate how sintering in contaminated production atmospheres causes deterioration of the magnetic properties. An example is also presented which shows that the magnetic properties of contaminated magnetic parts can be restored if the parts are resintered under properly controlled sintering conditions which reduce the carbon, nitrogen, and oxygen contaminants. (2 refs.)
- 115139** Heat evolution during the shock pressing of iron powder. V.F.Reshetnikov, L.I.Svistun, G.G.Serdyuk, Yu.M.Shulyakov (Krasnodar' Polytech. Inst., Acad. of Sci., Ukrainian SSR). *Sov. Powder Metall. & Met. Ceram. (USA)*, vol.22, no.1, p.4-6 (Jan. 1983). Translation of: *Poroshk. Metall. (USSR)*, vol.22, no.1, p.5-7 (Jan. 1983). [received: Aug. 1983]
The temperature of compacts was studied as a function of loading rate and their density. An experiment was carried out by pressing a powder with thermocouples embedded in it and recording the temperature indicated. In the contact zone between the powder and the working surface of the die intense heat evolution took place during shock pressing as a result of sliding and friction. The rise in temperature in this zone may affect the frictional properties of the sliding pair and the welding process, which manifests itself in the formation of metal excrescences on the die walls. In the peripheral layer of the die the heating may give rise to structural changes lowering the hardness of the working surface, which will lead to increased wear of the die. (2 refs.)
- 115140** Structure and mechanical and corrosion properties of P/M Kh23Ni18 stainless steel. I.D.Radomysel'skii, S.G.Napara-Volgina, L.N.Orlova, L.M.Apininskaya, A.K.Grabchak, N.M.Vergeles (Inst. of Materials Sci., Acad. of Sci., Ukrainian SSR). *Sov. Powder Metall. & Met. Ceram. (USA)*, vol.22, no.1, p.39-44 (Jan. 1983). Translation of: *Poroshk. Metall. (USSR)*, vol.22, no.1, p.43-9 (Jan. 1983). [received: Aug. 1983]
It was found that HVP (hot vacuum pressing) and HFPB (hot forging porous blanks) of a prealloyed powder enable high-density Kh23Ni18 stainless steel to be obtained exhibiting good mechanical and corrosion properties. Such steel, when produced by any of the processes investigated, is superior in strength to cast steel; its elongation and corrosion resistance are comparable to or better than those of cast steel only when additional operations of presintering of blanks and diffusional annealing after hot plastic working are employed. For the production of P/M Kh23Ni18 steel and other sintered stainless steels of the austenitic class on an industrial scale the hot-forging method is recommended, since it requires a simpler installation and enables parts of complex configuration to be produced. (5 refs.)
- 115141** Densification kinetics of chromium carbide and its alloys in hot pressing. V.N.Klimenko, V.G.Kayuk, V.A.Maslyuk (Inst. of Materials Sci., Acad. of Sci., Ukrainian SSR). *Sov. Powder Metall. & Met. Ceram. (USA)*, vol.22, no.1, p.60-3 (Jan. 1983). Translation of: *Poroshk. Metall. (USSR)*, vol.22, no.1, p.68-72 (Jan. 1983). [received: Aug. 1983]
A study was made of the densification kinetics in the hot pressing of chromium carbide and its alloys under pressures of 10.8-21.6 MPa at temperatures of 1350-1500°C for Cr₃C₂ and 900-1200°C for KKhN-15 and KKhNF-15 alloys in the isothermal holding time range from 300 to 1500 sec. It was found that increasing the duration of isothermal holding at all the temperatures and pressures investigated increased the relative densities of the materials from 0.65-0.7 at the lowest pressures and temperatures to 0.98-0.99 at the maximum values of these parameters. It is shown that the densification of chromium carbide and its alloys with nickel and nickel-phosphorus binders in hot pressing is described by a generalized equation of volume viscous flow of a porous solid. (8 refs.)

115142 Production of artificial channel insulating matrices and ultrathin metal filaments. V.N.Bogomolov, V.A.Gordeev, Yu.A.Kumzerov, M.I.Marty-nov, A.V.Fokin (A.F. Ioffe Physicotech. Inst., Acad. of Sci., Leningrad, USSR).

Sov. Tech. Phys. Lett. (USA), vol.8, no.11, p.599-600 (Nov. 1982). Translation of: *Pis'ma v Zh. Tekh. Fiz. (USSR)*, vol.8, no.21-22, p.1393-5 (Nov. 1982). [received: Sept. 1983]

The authors synthesized porous matrices from mica ($K_2O \cdot 3Al_2O_3 \cdot 6SiO_2 \cdot 2H_2O$) and fianite (ZrO_2). The densities of these matrices were 2.7 and 6.0 g/cm³, respectively. Ultrathin metal filaments are synthesized by forcing the liquid metal into etched channels. The diameter distribution of the channels is studied by mercury porosimetry. The procedure proposed for synthesizing ultrathin metal filaments by means of synthetic porous insulating matrices extends the list of so-called composite superconductors and makes it possible to study the influence of a photon contact on the value of T_c in metals. (4 refs.)

115143 Preparation of superconducting lead-alloy long filaments by glass-coated melt spinning. T.Goto (Dept of Polymer Technol., Nagoya Inst. of Technol., Nagoya, Japan).

Trans. Jpn. Inst. Met. (Japan), vol.24, no.8, p.595-600 (Aug. 1983). The glass-coated melt spinning of Pb alloy was investigated to produce a superconducting long filament with T_c more than 4.2K. Continuous smooth filaments less than 60 μ m in diameter of Pb, and Pb-Bi, Pb-In and Pb-Sn system alloys, and of $Pb_{84.4}Au_{15.6}$ and In_2Bi alloys were obtained from a molten state at 1450K with various spinning speeds ranging from 0.95 m/s to 7.95 m/s. The Pb system alloy filament obtained was a ductile material with the tensile strength of 40 MPa and elongation of 2.0%. The T_c of the Pb alloy filament did not depend on the sample current density (J_c) less than 3×10^7 A/m², whereas the T_c of the Pb filament depended on the J_c more than 2×10^6 A/m². The maximum T_c at 8.0K was observed for the $Pb_{60.2}Bi_{39.8}$ filament. The enhancement of superconductivity was observed for the $Pb_{70}Sn_{30}$ and $Pb_{65}Sn_{35}$ filaments. (12 refs.)

Character of impurity distribution in comminuted β -boron crystals See Entry 113953

Spreading of Ni-Fe-W melts on polycrystalline tungsten See Entry 114306

Structure of molybdenum high speed steels after atomization and annealing See Entry 115228

Thermal stresses and viscoelastic relaxation in metallic glasses prepared by liquid quenching See Entry 115232

Role of molybdenum in sintered steels [tensile properties] See Entry 115270

Interfacial segregation and embrittlement in liquid phase sintered tungsten alloys See Entry 115324

Influence of melting method on the crack resistance of 42KhMFA steel See Entry 115339

Effect of waterglass impregnation upon hardenability of porous sintered steel See Entry 115431

81.20J Dispersion-, fibre-, and platelet-reinforced metal-based composites

Nature of residual stresses in carbon fibre reinforced 12% silicon aluminium alloy See Entry 114217

Production of artificial channel insulating matrices and ultrathin metal filaments See Entry 115142

81.20L Ceramics and refractories

115144 Siloxanes, silanes, and silazanes in the preparation of ceramics and glasses. R.R.Wills, R.A.Markle, S.P.Mukherjee (Columbus Labs., Battelle, OH, USA).

Am. Ceram. Soc. Bull. (USA), vol.62, no.8, p.904-11, 915 (Aug. 1983). The use of selected organosilicon compounds for the preparation of silicon based ceramic materials is discussed in terms of processing microstructure-property relationships. The mechanisms operative in the formation of gel derived silicate glasses and glass ceramics are reasonably well understood, but this is not true for silicon carbide/nitride based ceramics. The properties of organosilicon precursors and the mechanism of pyrolysis affect the microstructural features of the ceramic. Reaction mechanisms are proposed and the microstructural features and properties of organosilazane derived ceramics discussed. (81 refs.)

115145 Development of zinc oxide varistors. H.S.Kalsi, B.K.Das (Nat. Phys. Lab., New Delhi, India).

Bull. Mater. Sci. (India), vol.5, no.1, p.33-8 (March 1983). [received: Sept. 1983] Grain growth kinetics of ZnO ceramics containing 6% additives of Bi₂O₃, CoO and MnO in equal molar ratios has been studied in the temperature range 1000 to 1350°C. It has been observed that the grain growth data fits the $D^2 = kt$ law and the activation energy computed from the rate constants is 65 kcal/mol. (9 refs.)

115146 Sinterability of alkoxide-derived magnesia. T.Hattori, H.Tatsuo-moto, J.Mohri (Dept. of Industrial & Synthetic Chem., Chiba Univ., Chiba, Japan).

J. Mater. Sci. Lett. (GB), vol.2, no.9, p.503-4 (Sept. 1983). The authors' study showed that the sinterability of magnesia obtained by direct calcination of alkoxide was considerably good. Carbon is believed to have played an important role in the sintering. (9 refs.)

115147 Development of cryochemical processes in oxide piezoceramic technology. Yu.D.Tret'yakov, V.A.Fokin (M.V. Lomonosov Moscow State Univ., Moscow, USSR).

Inorg. Mater. (USA), vol.18, no.10, p.1411-15 (Oct. 1982). Translation of: *Izv. Akad. Nauk SSSR Neorg. Mater.*, vol.18, no.10, p.1645-9 (Oct. 1982). [received: Sept. 1983] The question of employing cryochemical processes in oxide piezoceramic technology is discussed. The processes taking place in solutions of ceramic ingredients treated at low temperatures have been investigated with model substances. The effectiveness of the cryochemical technology as compared with traditional methods of production is illustrated with industrially important ceramic materials based on lead titanate zirconate. (11 refs.)

115148 Physicochemical aspects of production of ferroelectric ceramics. V.V.Klimov, O.S.Didkovskaya, V.V.Prisedskii.

Inorg. Mater. (USA), vol.18, no.10, p.1415-20 (Oct. 1982). Translation of: *Izv. Akad. Nauk SSSR Neorg. Mater.*, vol.18, no.10, p.1650-5 (Oct. 1982). [received: Sept. 1983]

The authors have considered the physicochemical factors which make it possible to vary the properties of ferroelectric and piezoelectric ceramics for spe-

cific purposes: enhancement of the piezo activity in the morphotropic region, composition, structure, structure of the p-T-x phase diagrams, nonstoichiometry, and defects of the crystal structure. (19 refs.)

115149 Properties of hot-pressed zirconium pyrovanadate ceramics. R.C.Buchanan, G.W.Wolter (Dept. of Ceramic Engng., Univ. of Illinois, Urbana, IL, USA).

J. Electrochem. Soc. (USA), vol.130, no.9, p.1905-10 (Sept. 1983). Zirconium pyrovanadate powders prepared from solution precipitation and by solid-state reaction were hot pressed below 800°C. Unit cell parameter and thermal expansion were found to have a negative slope above 150°C, attributed to flexing of the bond angles in the ZrV_2O_7 structure. Thermal expansion coefficient determined was $72 \times 10^{-7}/^\circ C$. Electrical conductivities measured were in the range 10^{-5} - $10^{-6}(\Omega \cdot cm)^{-1}$ at 25°C with activation energy of 0.2 eV. Conduction was determined to be n-type and was attributed to the presence of V^{4+} ions in the hot-pressed ZrV_2O_7 . Infrared transmission was significant in the range 2.5-10 μ m with a maximum (85%) at 7.5 μ m. (15 refs.)

115150 Kinetics and mechanism of cluster growth in mixtures of calcia and magnesia. I.B.Bashir (Dept. of Ceramics, Univ. of Leeds, Leeds, England).

Mater. Sci. & Eng. (Switzerland), vol.60, no.3, p.255-60 (Sept. 1983). The growth of CaO and MgO clusters in dense hot-pressed mixtures of calcia and magnesia was studied. The kinetics observed obeyed a fifth-power law which was expressed in the form $CS^5 - CS_0^5 = Kt$ (where CS is the average cluster size at a time t, CS_0 is the average cluster size at zero time and K is a constant); the mechanism proposed for cluster growth was coalescence by atom diffusion along dislocations. Microstructural evidence showing the presence of dislocations was provided, and a dislocation pipe diffusion coefficient of 6.22×10^{-12} m² s⁻¹ was estimated. Also a dislocation density of 5.2×10^6 cm⁻² agrees well with the value of 10^7 cm⁻² observed for as-fired polycrystalline MgO. (13 refs.)

115151 Equipment for the sintering and melting of ceramic materials. C.Wieja, J.Wieckowski.

Pol. Tech. Rev. (Poland), no.2-3, p.22-3 (1983). The equipment is based on an induction furnace and comprises a graphite crucible lined with a tungsten or molybdenum film. The graphite crucible acting as a heater-susceptor is heated with high frequency currents induced by an exciter coupled with a h.f. generator. The crucible lining makes impossible the reaction between the graphite and the oxides reducing to a minimum the consumption of expensive high-melting metals. (no refs.)

115152 Fine ceramics. H.Okuda.

Solid State Phys. (Japan), vol.18, no.6, p.359-60 (June 1983). In Japanese.

Fine ceramics have been attracting interest recently in many applications for machine parts. The present status of fine ceramics and its trend are described. (no refs.)

115153 Production of metal-carbon system materials with groups IV-V refractory metals. Yu.P.Solodov (All-Union Sci.-Res. Inst. of Electromech., USSR).

Sov. Powder Metall. & Met. Ceram. (USA), vol.22, no.1, p.15-17 (Jan. 1983). Translation of: *Poroshk. Metall. (USSR)*, vol.22, no.1, p.16-18 (Jan. 1983). [received: Aug. 1983] The method described is based on the reduction of appropriate metallic oxides with carbon. A characteristic feature of this method is that the oxide is used in the liquid state and carbon in the form of a carbon-graphite material, a metal-carbon system material forming inside the carbon-graphite material during its infiltration with the liquid oxide. (3 refs.)

115154 Formation of ZnAl₂O₄ in ZnO-Al₂O₃ system accompanied by uneven mixing and composition change. Y.Hukuhara, E.Suzuki, M.Hashiba, E.Miura, Y.Nurishi, T.Hibino (Dept. of Industrial Chem., Gifu Univ., Gifu-shi, Japan).

Yogyo-Kyokai-Shi (Japan), vol.91, no.6, p.281-9 (1983). In Japanese. The mixture of coarse alumina and fine zinc oxide, with different mole fractions of ZnO, X_z , was heated at 1000~1200°C for different times. The rate of ZnAl₂O₄ formation was determined, and also the microstructure was observed. The rate of ZnAl₂O₄ formation increased with the decrease of the composition X_z in the range of $X_z < 0.5$, but its dependence on the composition was not observed in the range of $X_z > 0.5$. The microstructure showed the presence of the agglomerates of sintered ZnO, which resulted in incomplete reaction in the range of $X_z < 0.5$, and consequently, the alumina particles were not able to react with ZnO because of incomplete mixing. The ZnAl₂O₄ layer grew around alumina particles at a rate of formation in parabolic relation with time. The diffusion constant controlling the process was determined from the product layer thickness as 3.59×10^{-15} to 3.16×10^{-13} cm²/s at 1000~1200°C. The temperature dependence of the diffusion constant gave an activation energy of 85.4 kcal/mol. The application of Jander's model to the powder mixture with difference compositions was discussed, and the introduction of three factors to correct the deviation of the practical condition from the Jander's ideal assumption was considered. (25 refs.)

115155 Sintering and electrical resistivity of ZnO-Nb₂O₅ ceramic. K.Hamano, A.Sayano, Z.Nakagawa (Res. Lab. of Engng. Materials, Tokyo Inst. of Technol., Yokohama-shi, Japan).

Yogyo-Kyokai-Shi (Japan), vol.91, no.7, p.309-17 (1983). The sintering behavior and relation between microstructure and electrical resistivity of the sintered bodies were investigated in the system ZnO-Nb₂O₅. ZnO reacted with Nb₂O₅ to form ZnO.Nb₂O₅ and then to form 3ZnO.Nb₂O₅ with increasing temperature, and 3ZnO.Nb₂O₅ melted at the eutectic point of 1297°C in the system 3ZnO.Nb₂O₅-ZnO. Addition of Nb₂O₅ delayed the initial sintering of ZnO (specimens), and the compacts expanded with the melt formation. The wetting of intergranular layer on the ZnO grains of the quenched one was better than that of the one cooled in the furnace with slight variation before and after annealing at 1000°C. Microhardness tests showed that the strength of ZnO-ZnO grain boundary of the quenched body was lower than that of the one cooled in the furnace. Therefore, the difference in the resistivity between the quenched body and the one cooled in the furnace depended on the strength of ZnO-ZnO grain boundaries as well as the wetting of the intergranular layer with a high resistance. (11 refs.)

115156 Preparation of porous Mg-Al spinel ceramics. S.Kanzaki, H.Tabata (Government Industrial Res. Inst., Nagoya, Japan), N.Otsuka, Z.Nakagawa, K.Hamano.

Yogyo-Kyokai-Shi (Japan), vol.91, no.7, p.344-5 (1983). Porous spinel ceramics was prepared from spray pyrolyzed spinel powder. Effects of forming pressure and firing temperature on the bulk density and pore size distribution of the samples were examined. The fired density of the specimens was less than 50% of theoretical density even when fired at 1400°C. The maximum frequency of the pore radius decreased and the pore size distribution became narrower with increasing of forming pressure. The maximum frequency of the pore radius increased with the increasing firing temperature, but the pore size distribution became narrower. A highly porous

spinel ceramics with less than 50% of theoretical density and the maximum frequency of the pore radius ranging from 700 Å to 2000 Å was obtained. (2 refs.)

- UO₂ fuel pellet microstructure modification through impurity additions See Entry 112328
- Vitrification kinetics of ternary silica-alumina-lime glass powders See Entry 113755
- Preparation of MnCo₂O₄ by a wet method and its metal ion distribution See Entry 115034
- Effect of grain size distribution on sintered density See Entry 115126
- Torsional strength of pressureless-sintered silicon nitride See Entry 115206
- Effect of small amounts of tungsten carbide on the strength, creep, and brittle-to-ductile transition temperature of zirconium carbide See Entry 115280
- Microstructure and mechanical strength of aluminum titanate ceramics prepared from synthesized powders See Entry 115353
- Tensile strength of pressureless-sintered silicon nitride at elevated temperature See Entry 115354

81.20N Cermets, ceramic and refractory composites

- The CVD of boron nitride from BF₃-NH₃ mixtures. Application to the synthesis of 2D-C-C/BN composites See Entry 115092
- Volume changes and the technical properties of composites in the spinel-manganese oxide system See Entry 115392

81.20P Glasses

- Mossbauer investigation on SiO₂-Fe₂O₃ glasses obtained from gel See Entry 114759
- The dielectric properties of some PbO-based amorphous films prepared by twin-roller method See Entry 114784
- Preparation of rapidly solidified ribbons with second phase particles See Entry 115135
- Siloxanes, silanes, and silazanes in the preparation of ceramics and glasses See Entry 115144
- Thermal stresses and viscoelastic relaxation in metallic glasses prepared by liquid quenching See Entry 115232

81.20S Polymers

- 115157 The stability of blends of incompatible thermoplastics. B.Maxwell, G.L.Jasso (Dept. of Chem. Engng., Princeton Univ., Princeton, NJ, USA). *Polym. Eng. & Sci. (USA)*, vol.23, no.11, p.614-17 (mid-Aug. 1983). Conventional thermodynamic reasoning would predict that it would be very difficult to melt blend incompatible polymers and that if such blends were made they would be highly unstable and would phase separate upon heating. A method has been developed to melt blend incompatible polymers (such as poly(methylmethacrylate) and polyethylene) to form two continuous interpenetrating phases and that upon prolonged heating the stability of the structure is increased rather than decreased. (6 refs.)
- Elongation rheology of polyolefins and its relation to processability See Entry 114237
- Correlation of morphology, mechanical properties and processing conditions of modified high impact polystyrene See Entry 115290
- Mechanical properties of injection molded blends of poly(ethylene-terephthalate) and poly(amide-6,6) See Entry 115332

81.20T Reinforced polymers and polymer-based composites

- 115158 Vibration-resistant composites intended for damping devices. D.M.Karpinos, I.I.Tuchinskii, A.V.Stupko, L.R.Vishnyakov, Yu.B.Askochenskii (Inst. of Problems of Material Sci., Acad. of Sci., Kiev, Ukrainian SSR). *Strength Mater. (USA)*, vol.14, no.9, p.1281-4 (Sept. 1982). Translation of: *Probl. Prochn. (USSR)*, vol.14, no.9, p.103-5 (Sept. 1982). The authors describe the testing of new wear- and vibration-resistant frictional materials intended for damping devices, and dampers with frictional elements fashioned from new materials. Two groups of composite materials based on a modified phenolformaldehyde oligomer filled with metallic powders with additives of thermoplastic polymers (PEND polyethylene, 32L fluoroplastic, and 42L fluoroplastic) were used as new materials for the frictional elements. (5 refs.)
- 115159 Melt compounding of PVC with ethylene copolymer resins. G.H.Hofmann (Polymer Products Dept., E.I. Du Pont de Nemours & Co., Wilmington, DE, USA). Polymer Alloys III Blends, Blocks, Grafts and Interpenetrating Networks. Proceedings of a Symposium, New York, USA, 23-28 Aug. 1981 (New York, USA: Plenum 1983), p.149-66. Routine procedures used for liquid plasticized PVC are often inadequate to produce homogeneous low gel alloys of PVC/ECR. Melt compounding morphology and rheology were used in analyzing this problem. A Brabender Plasti-Corder technique, used to evaluate the melt compounding of PVC/ECR, showed that standard particle (grain) sized PVC suspension resin produces heterogeneous blends, at shear stresses of 75 kPa or less. The more shear-sensitive large particle PVC suspension resins, however, produce homogeneous blends under these conditions. (15 refs.)
- 115160 The role of the matrix in fibrous composite structures. J.C.Halpin (ASD Engng., Aeronautical Systems Div., Wright-Patterson AFB, OH, USA). Role of the Polymeric Matrix in the Processing and Structural Properties of Composite Materials. Proceedings of a Joint US-Italy Symposium, Capri, Italy, 15-19 June 1981 (New York, USA: Plenum 1983), p.3-17. An overview is provided to advanced composite structural technology and the role played by the matrix material system in this technology. It is concluded that advanced composite technology is a technology whose time has come. Subsonic aircraft application is within the current technological capability. (13 refs.)

115161 Factors affecting the development of new matrix resins for advanced composites. C.E.Browning (Air Force Wright Aeronautical Labs., Wright-Patterson AFB, OH, USA).

Role of the Polymeric Matrix in the Processing and Structural Properties of Composite Materials. Proceedings of a Joint US-Italy Symposium, Capri, Italy, 15-19 June 1981 (New York, USA: Plenum 1983), p.231-43. Discusses the major factors affecting the development of new matrix resins for advanced composites, which include: moisture resistance, toughness, improved processability, and elevated temperature performance. These factors dictate the directions of matrix materials development activities, with the two principal directions being: adapting existing chemistry to new matrix requirements, and developing new chemistry matrices. (7 refs.)

115162 Effects of matrix characteristics in the processing of short fiber composites. L.A.Goettler (Rubber Chem. Div. Monsanto Co., Akron, OH, USA).

Role of the Polymeric Matrix in the Processing and Structural Properties of Composite Materials. Proceedings of a Joint US-Italy Symposium, Capri, Italy, 15-19 June 1981 (New York, USA: Plenum 1983), p.289-318. The role of the matrix on the processing of short fiber composites has been examined with regard to thermoset, thermoplastic, and rubber polymers. The matrix serves as more than a carrier vehicle for the fibers; it imparts its own characteristics upon the reinforced melt: viscosity level, elasticity, stiffness, melt strength, wetting or adhesion characteristics. The wide variations in some of these parameters between the different classes of polymeric matrices dictate applicable processing methods. All are amenable to closed cavity molding, but only the more coherent melts allow free surface forming, as in extrusion and calendaring. (20 refs.)

Role of the Polymeric Matrix in the Processing and Structural Properties of Composite Materials. Proceedings of a Joint US-Italy Symposium See Entry 111312

Polymer-performance on the dimensional stability and the mechanical properties of wood-polymer composites prepared by an electron beam accelerator See Entry 115248

Model plastic-rubber composites from emulsion polymers See Entry 115288

RIM systems from interpenetrating polymer networks See Entry 115291

Internal stresses in fibre reinforced plastics See Entry 115296

Rubber modified matrices See Entry 115360

Effect of the composition of binding materials on the properties of carbon pastes See Entry 115509

81.30 PHASE DIAGRAMS AND MICROSTRUCTURES DEVELOPED BY SOLIDIFICATION AND SOLID-SOLID PHASE TRANSFORMATIONS

(see also 61. Structure of liquids and solids 64.70 Phase equilibria, phase transitions, and critical points)

115163 Computer simulation of a two-dimensional soap froth I. Method and motivation. D.Weaire, J.P.Kermode (Dept. of Phys., Univ. Coll. Dublin, Dublin, Ireland).

Philos. Mag. B (GB), vol.48, no.3, p.245-59 (Sept. 1983). The authors have developed a computer program by means of which a two-dimensional soap froth may be simulated. This system is of interest in connection with theories of grain growth in polycrystalline solids, but only limited and somewhat contradictory experimental statistical data have hitherto been available. The authors present preliminary results for the evolution in time of a froth of 100 cells, with periodic boundary conditions. (13 refs.)

Thermodynamic properties of Th_{0.80}U_{0.20}O_{2+x} solid solution See Entry 112323

UO₂ fuel pellet microstructure modification through impurity additions See Entry 112328

Variation of the glass-forming regions in the B₂O₃-Li₂O system with cooling rate See Entry 113757

Saturation exposure in ferritic stainless steels See Entry 114043

On the energy of interaction in the Si-B system See Entry 114210

Phase composition of aluminium alloys Al-Mn-Li See Entry 115226

81.30B Phase diagrams of metals and alloys

115164 Vapor pressure of dysprosium in the Dy-Pt system. A.I.Zaitsev, Yu.A.Priselkov, An.N.Nesmeyanov (M.V. Lomonosov Moscow State Univ., Moscow, USSR).

High Temp. (USA), vol.20, no.6, p.852-5 (Nov.-Dec. 1982). Translation of: *Teplofiz. Vys. Temp. (USSR)*, vol.20, no.6, p.1081-4 (Nov.-Dec. 1982). [received: Sept. 1983]

Results are presented for the vapor pressure of dysprosium over its alloys with platinum in the concentration interval of 0.62 at.% Pt. The measurements were carried out by an integral variant of the Knudsen effusion method under conditions of ultrahigh oilless vacuum. The temperature dependence of the vapor pressures and the partial thermodynamic functions of dysprosium are calculated from the experimental data. An intermetallic compound is formed in the concentration interval of 48.6-38.0 at.% dysprosium and that the compound Dy₃Pt is absent. (16 refs.)

115165 Investigation of phase equilibria related to fusion reactor materials. I. The ternary system Zr-Al-N. J.C.Schuster (Inst. fur Physikalische Chem., Univ. Wien, Vienna, Austria), J.Bauer, J.Debaigne.

J. Nucl. Mater. (Netherlands), vol.116, no.2-3, p.131-5 (June 1983). Phase equilibria in the ternary system Zr-Al-N are investigated. AlN coexists at 1273K with ZrAl₃, ZrAl₂, Zr₂Al₃, Zr₃AlN and ZrN; at 1573K with ZrAl₃, ZrAl₂ and ZrN. Thus AlN is thermodynamically unstable against zirconium or binary aluminium-zirconium alloys rich in zirconium. Zr₂Al₃ with Mn₂Si₃-type structure is a binary low temperature phase but stabilized by nitrogen solution to higher temperatures. α -zirconium has an extended solubility for aluminum up to the melting region when stabilized by about 2 at.% nitrogen. No other ternary solubilities are observed. The getter characteristics of the Zr-Al-alloy ST 101 for impurity control and hydrogen recycling in fusion reactors are discussed in terms of the phase equilibria within the ternary system. (14 refs.)

115166 Revision of the eutectoid isotherms of the uranium-chromium system. L.R.Chapman (Metals & Ceramics Dept., Union Carbide Corp., Oak Ridge, TN, USA).

J. Nucl. Mater. (Netherlands), vol.116, no.2-3, p.328-31 (June 1983).

Examines previous work on the determination of the eutectoid isotherms. Due to discrepancies in previous work the authors have determined these values to a higher degree of certainty. (7 refs.)

115167 Phase equilibria in nickel rich Ni-Al-Mo and Ni-Al-W alloys. P.Nash, S.Fielding, D.R.F.West (Dept. of Metall. & Materials Sci., Imperial Coll. of Sci. & Technol., London, England).

Met. Sci. (GB), vol.17, no.4, p.192-4 (April 1983). [received: Sept. 1983]

Phase equilibria have been investigated in the Ni rich regions of the Ni-Al-Mo system at 1473K and of the Ni-Al-W system at 1523 and 1273K using electron microprobe analysis, X-ray diffraction, and optical metallography. The phase relationships at 1473 and 1523K are similar in the two systems showing three-phase equilibria of $\gamma + \gamma' + \alpha$ (Mo or W) and $\gamma' + \beta + \alpha$ (Mo or W); no ternary compounds were found in the regions studied. The maximum solubilities of Mo and W in γ' were found to be ~ 6 at.-%. Differences between the present and previous work are reviewed. (20 refs.)

115168 Robust numerical procedure for calculating equilibrium compositions in binary alloy systems. G.R.Luecke, D.M.Bailey, J.F.Smith (Iowa State Univ., Ames, IA, USA).

Met. Sci. (GB), vol.17, no.4, p.195-7 (April 1983). [received: Sept. 1983]

An algorithm for finding common tangents to Gibbs energy functions is presented. The approach differs significantly from those which have been used previously and has the advantage of being very robust in the sense that one can start with a quite rough approximation to the desired solution and still obtain iterative convergence to any required precision to the solution. (16 refs.)

115169 Short-range atomic order in the Fe-Ni system. V.I.Goman'kov, N.I.Nogin, E.V.Kozis.

Russ. Metall. (GB), no.3, p.152-6 (1982). Translation of: *Izv. Akad. Nauk. SSSR Met.*, no.3, p.174-9 (1982).

From the diffusion intensities of neutron scatter on quenched alloys, the temperature and concentration dependences were obtained for the short-range order parameters for five coordination spheres throughout the γ phase. In this way, structural states above the Kurnakov temperature have been established which supplement the phase diagram. The ordering energies have been obtained for three spheres which characterise the atomic interaction potential. (17 refs.)

115170 Influence of alloying with germanium and copper on the conditions of formation of the superconducting compound Nb₃Si. V.M.Pan, V.I.Latyshcheva, O.G.Kulik, A.G.Popov.

Russ. Metall. (GB), no.3, p.167-71 (1982). Translation of: *Izv. Akad. Nauk. SSSR Met.*, no.3, p.191-6 (1982).

Isothermal cross-sections of the Nb-Nb₃Si₃-Nb₃Ge₃ system at 1780, 1800 and 1820°C, were constructed. The compound Nb₃Si with a structure of the Ti₃P type is present in this ternary system at 1800-1820°C in a limited range of compositions. At 1820°C the solubility of silicon in the β -Nb₃Ge increases up to 4 at.% in comparison with lower temperatures. An isothermal cross-section of the Nb-Si-Cu system at 1500°C was constructed and in the niobium-rich range, existence of a new ternary compound with a crystal structure of Nb₃CoSi type was established. In the Nb-Si-Cu system, the compound Nb₃Si is not formed up to a temperature of 1780°C. (15 refs.)

115171 On the thermodynamic properties of Co-Cu melts. V.P.Mintsis, L.Sh.Tsemekhman, B.P.Burylev, V.D.Linev, A.I.Tertichnyy, V.I.Volkov.

Russ. Metall. (GB), no.3, p.171-4 (1982). Translation of: *Izv. Akad. Nauk. SSSR Met.*, no.3, p.196-8 (1982).

1. The equilibrium liquid-vapour was experimentally investigated and activity coefficients at 1793K in the Co-Cu melts were determined. 2. Positive asymmetrical deviations were described by two-member equations of substitution solutions and the concentration dependence of the thermodynamic components of the melts in the Co-Cu system was obtained. (7 refs.)

115172 Examination of alloys of the Pd-Ni-Th system in the palladium-rich region. G.I.Terekhov, S.I.Sinyakova.

Russ. Metall. (GB), no.3, p.189-91 (1982). Translation of: *Izv. Akad. Nauk. SSSR Met.*, no.3, p.211-14 (1982).

The corner of the phase diagram of the Pd-Ni-Th system with the sum of the thorium and nickel contents of up to 12 at.% was constructed by X-ray diffraction, microstructural and thermal analyses. The combined alloying of palladium with thorium and nickel reduces the solubility of thorium in palladium because of an unfavourable change in the volume factor. The large area is occupied by the region of the ($\alpha_1 + \alpha_2$)-solid solutions based on palladium and nickel. Additional alloying of the Pd-Th alloys with nickel increases the size of reduction in their melting point. (4 refs.)

115173 The Zn-Bi-Hg phase diagram. M.V.Nosek, N.M.Atamanova, B.T.Asanova.

Russ. Metall. (GB), no.3, p.192-4 (1982). Translation of: *Izv. Akad. Nauk. SSSR Met.*, no.3, p.215-19 (1982).

The Zn-Bi-Hg phase diagram was constructed and examined using differential thermographic, X-ray phase and microstructural analyses. Three four-phase equilibria were found in the system; two are peritectic: (Zn) + L \rightleftharpoons γ + Bi ($\sim 30^\circ\text{C}$), γ + L \rightleftharpoons β + Bi ($\sim 13^\circ\text{C}$), and one is eutectic: L \rightleftharpoons Bi + β + (Hg) ($\sim 44 \pm 2^\circ\text{C}$). No ternary intermetallic compounds form in the system. (5 refs.)

Concentration and temperature dependences of the magnetic susceptibility of binary alloys of indium with potassium and rubidium See Entry 114678

Strontium as a modifier for aluminium-silicon-copper alloys See Entry 115181

Analysis of the effect of the comparative number of primary crystals on the kinetics of peritectic transformation See Entry 115186

81.30D Phase diagrams of other materials

115174 Thermodynamic study of oxidation of molybdenum sulfides. Jun Soo Kim, Jae Hyun Oh.

J. Korean Inst. Met., vol.21, no.6, p.558-65 (June 1983). In Korean.

Oxidation reactions of molybdenum sulfides have been studied by thermodynamic analysis of the phase diagrams of the molybdenum-sulfur-oxygen system. The results obtained are listed. (18 refs.)

115175 A thermodynamic analysis of the Cu-O system with an associated solution model. R.Schmid (Tech. Univ. Clausthal, Clausthal-Zellerfeld, Germany).

Metall. Trans. B (USA), vol.14B, no.3, p.473-501 (Sept. 1983).

An extension of the associated solution model is developed and applied to the Cu-O liquid phase. Associated species 'Cu₂O' in the liquid solution are assumed, which interact with the surrounding free Cu and O atoms. All thermodynamic properties and the phase diagram calculated from this model

are in good agreement with the experimental information. The success of this mathematical description is, of course, no proof for the physical existence of associated species. A consistent set of thermodynamic data of the various solid, liquid, and gaseous phases is given by this comprehensive evaluation. In addition, linear approximations for the Gibbs energies of reaction of formation and the interaction coefficients are offered. A metastable liquidus of the compound CuO at elevated pressure is predicted, the congruent melting point being 1228°C at $P_{0(2)} = 24.4$ atm (2.47 MPa). (6 refs.)

115176 Predominance area diagrams of the system Co-S-O between 583 and 1148K. N.Jacinto (Univ. of Oruro, Oruro, Bolivia), H.Y.Sohn, M.Nagamori.

Metall. Trans. B (USA), vol.14B, no.3, p.506-9 (Sept. 1983).

Presents new predominance area diagrams of the Co-S-O system in the temperature range 583 to 1148K, including the stability zones of all known cobalt sulfides. (12 refs.)

115177 Influence of pressure on the equilibrium of the melt with graphite, diamond and carbide Mn₇C₃ in the Mn-C system. T.P.Ershova, D.S.Kamenetskaya.

Russ. Metall. (GB), no.3, p.157-61 (1982). Translation of: *Izv. Akad. Nauk. SSSR Met.*, no.3, p.180-4 (1982).

Presents a thermodynamic calculation of graphite, diamond and carbide liquidus in the Mn-C system at pressures up to 100 kbar. The calculated T-P-N_C state diagram on the Mn-C system is illustrated by three isobaric cross-sections ($P = 0.60$ and 100 kbar) as well as by the projections of lines of monovariant equilibria on to the T-P and N_C-P planes. (16 refs.)

115178 Calculation of complex equilibria in ceramic systems. Y.K.Rao, H.G.Lee (Dept. of Mining Metall. & Ceramic Engng., Univ. of Washington, Seattle, WA, USA).

Trans. & J. Br. Ceram. Soc. (GB), vol.82, no.4, p.123-8 (July-Aug. 1983).

Computer-assisted methods for the determination of equilibrium compositions in complex systems are presented. The use of Matrix algebraic techniques to determine the number of linearly independent reactions inherent in a system is demonstrated. An iterative type of method, adapted to a high-speed digital computer, was used to obtain the equilibrium composition. The application of the iterative method is illustrated by suitable examples which include Si-O and Ga-In-As-H-Cl systems. Ordinary calculational methods are used in the analysis of equilibria in the systems Si-C-O and Si-C-N-O. (5 refs.)

115179 A quantitative investigation of phase compositions in magnesia-R₂O₃-silicate systems. IV. A study of commercial magnesia-chrome mixtures. J.D.Dewendra, C.M.Wilson, N.H.Brett (Dept. of Ceramics, Glasses & Polymers, Univ. of Sheffield, Sheffield, England).

Trans. & J. Br. Ceram. Soc. (GB), vol.82, no.4, p.132-6 (July-Aug. 1983).

For pt.III see *ibid.*, vol.82, p.87 (1983). A series of mixtures containing different proportions of a commercial sea-water magnesia and two chrome ores was studied by quenching pressed specimens from temperatures in the range 1400-1700°C and analyzing them by reflected light microscopy and electron probe microanalysis. The volume percentages of the periclase, spinel and liquid phases present in the microstructures were determined by a point-counting method. The results are compared with those previously obtained on synthetic mixtures of similar compositions and phase diagrams relevant to the magnesia-chrome system are reviewed. (7 refs.)

115180 The time-temperature-transformation (TTT) state diagram and cure. J.K.Gillham (Dept. of Chem. Engng., Princeton Univ., Princeton, NJ, USA).

Role of the Polymeric Matrix in the Processing and Structural Properties of Composite Materials. Proceedings of a Joint US-Italy Symposium, Capri, Italy, 15-19 June 1981 (New York, USA: Plenum 1983), p.127-45.

A generalized time-temperature-transformation (TTT) state diagram for the thermosetting process is presented in which the four physical states encountered (i.e. liquid, rubber, ungelled glass and gelled glass) are related to the time and temperature of cure. Gelation and vitrification, as a consequence of quenching morphological development and chemical conversion, respectively, are discussed with respect to the control of material properties. A generalized stress response model for rubber-modified thermoset materials is presented which relates morphology to low and high strain rate behavior. (23 refs.)

Alloys with the Ge_{1-x}Ni_xTe composition See Entry 114126

81.30F Solidification

(see also 64.70D Solid-liquid transitions)

115181 Strontium as a modifier for aluminium-silicon-copper alloys. A.Latkowski.

Arch. Hutn. (Poland), vol.28, no.2, p.187-91 (1983). In English.

An evaluation of the Al-16% Si-10% Sr master alloy in the Al-Si-Cu alloy was made. Addition was convenient and recovery was satisfactory, thus eliminating two of the major problems with sodium modification, namely fume generation and gas porosity and uncertain recovery. In spite of continuous loss of strontium during holding the degree of modification actually improved with holding time. (6 refs.)

115182 Unidirectional growth of dilute Bi-Sb alloys. H.Jamgotchian, B.Billia, L.Capella (Lab. de Phys. Cristalline, Univ. Aix Marseille, Marseille, France).

J. Cryst. Growth (Netherlands), vol.62, no.3, p.539-44 (Aug. 1983).

Observations on the planar and cellular morphologies of the solidification front during upward Bridgman growth of dilute Bi-Sb alloys are reported. Matter transport in the melt is analysed. The importance of averaging of the thermal gradients and of the capillarity term in the Mullins-Sekerka criterion is emphasized. (20 refs.)

115183 Directionally solidified structure and mechanical properties in monovariant Al-Fe-Ni eutectic alloy. Doo Han Kim, Kee Dae Lee, Hyun-Kee Cho.

J. Korean Inst. Met., vol.21, no.6, p.576-83 (June 1983). In Korean.

The variations of microstructure, interphase spacing and mechanical properties in Al-Fe and Al-Fe-Ni eutectic alloys have been investigated over a range of solidification rate from 1.2 to 38 mm/min under the thermal gradient of approximately 80°C/cm. The results obtained are summarized. (17 refs.)

115184 An analysis of local flow effects in flow-induced orientation and crystallization. I.S.Dairanieh, A.J.McHugh (Dept. of Chem. Engng., Univ. of Illinois, Urbana, IL, USA).

J. Polym. Sci. Polym. Phys. Ed. (USA), vol.21, no.8, p.1473-92 (Aug. 1983).

An analysis is presented of the effects of external flow kinematics on the so-called local flow in seeded, flow-induced crystallization and orientation. The flow field around a growing crystal or nucleation seed is modelled by the Stokes flow equations past a prolate ellipsoid of high aspect ratio. Exact solutions for various flow kinematics, worked out elsewhere by the singularity method, are applied to the analysis of local gradients. The results show that along the symmetry axis of the spheroid, the extensional gradients which

result for various free-stream velocity fields are primarily the result of the constant-velocity free-stream component. However, free-stream, extensional flow can significantly enhance the region of such high gradients. Along the symmetry plane of the spheroid, primarily shearing gradients result, with small extensional gradients occurring when the free-stream flow has extensional components. Results of chain extension and birefringence calculations are also presented and discussed. The calculations for Newtonian flow past a prolate ellipsoid can be used to demonstrate the influence of various external flow kinematics on the local gradients and stresses in seeded growth of crystalline fibers. (31 refs.)

115185 The formation of coarse intermetallics in rapidly solidified Al-Co alloys. R.K.Garrett,Jr., T.H.Sanders,Jr. (School of Materials Engng., Purdue Univ., West Lafayette, IN, USA).

Mater. Sci. & Eng. (Switzerland), vol.60, no.3, p.269-74 (Sept. 1983). Rapidly solidified hypereutectic Al-Co alloys cast by melting spinning may contain coarse intermetallic Al_3Co , fine Al_3Co_2 or primary aluminum dendrites with cobalt segregated interdendritically. A metallographic investigation of as-cast ribbons indicated that the volume fraction and size of the intermetallics are determined by the cooling rate and the solute content; decreasing the cooling rate and increasing the solute content tended to increase the fraction of Al_3Co_2 precipitates. The intermetallic Al_3Co_2 does not appear to result from a breakdown of primary aluminum solidification as has been previously proposed but rather from the direct nucleation of Al_3Co_2 from the melt followed by subsequent growth. (8 refs.)

115186 Analysis of the effect of the comparative number of primary crystals on the kinetics of peritectic transformation. I.M.Galushko. *Russ. Metall. (GB)*, no.3, p.145-8 (1982). Translation of: *Izv. Akad. Nauk. SSSR Met.*, no.3, p.168-71 (1982).

The examination of the peritectic solidification of the melts of the Cu-Cd and Cu-Sn peritectic systems showed that the yield of the peritectic reaction (ϵ) decreases with an increase in the comparative amount of the primary crystals (η). This dependence is described by the equation $\epsilon = \kappa(1-\eta)^2$. Coefficient κ depends on the extent of the three-phase contact in peritectic transformation. The difference in the values of ϵ in solidification of the melts with different comparative amounts of the primary crystals is associated with the variation of the mean rate of peritectic transformation in the melts of various compositions. This rate was evaluated on the basis of the ratio of ϵ to the time determined by the width of the plateau corresponding to the peritectic reaction on the solidification thermogram. (11 refs.)

115187 Formation of defects during the solidification of alloys in a two-dimensional region with a short-life internal heat sink. V.A.Zhuravlev, S.P.Bakumenko, G.A.II'in, L.A.Sokolov, N.V.Fedorova. *Russ. Metall. (GB)*, no.3, p.149-51 (1982). Translation of: *Izv. Akad. Nauk. SSSR Met.*, no.3, p.172-3 (1982).

Introducing short-lived internal heat sinks into a two-dimensional solidification region is an effective way to influence the kinetics of melt solidification and the nature of defect (pore) distribution in the growing phase. The presence of short-lived internal heat sinks in the solidification region leads to a rapid development of the two-phase zone and a more uniform distribution of pores in the solid phase (ingot). (1 ref.)

Studies on dilute solutions of rodlike macroions. I. Light scattering, densitometry, and cryoscopy See Entry 113719

Self-diffusion of macromolecules in the crystallization of a polymer from solution See Entry 113758

Spectroscopic characterization of solvent-induced crystallization of PET See Entry 113764

Dissipation-theory treatment of the transition from diffusion-controlled to diffusionless solidification See Entry 114132

Solidification processes in saline solutions See Entry 114135

Localized volume deficiencies as an effect of spherulite growth. I. The two-dimensional case See Entry 114137

Localized volume deficiencies as an effect of spherulite growth. II. The three-dimensional case See Entry 114138

Retardation of spherulitic growth rate in the crystallization of isotactic polystyrene due to the presence of nucleant See Entry 114139

Solidification front dynamics in model systems See Entry 114147

Solidification of Pb-Sn alloys under microgravity conditions See Entry 114148

Flow-induced crystallization by surface growth of polyethylene fibers See Entry 115041

Skin technology—fundamentals and applications See Entry 115123

Preparation of rapidly solidified ribbons with second phase particles See Entry 115135

Thermal stresses and viscoelastic relaxation in metallic glasses prepared by liquid quenching See Entry 115232

Non-equilibrium phases in laser-processed Fe-0.2 wt.% C-20 wt.% Cr alloys .. See Entry 115425

81.30H Constant-composition solid-solid phase transformations: polymorphic, massive, and order-disorder

(see also 64.70K Solid-solid transitions)

115188 Kinetics of a polymorphic transition in an Ag-Zn alloy under the action of γ rays. M.P.Krulikovskaya, L.I.Chirko (Inst. of Phys., Acad. of Sci., Kiev, Ukrainian SSR).

Fiz. Met. & Metalloved. (USSR), vol.56, no.2, p.345-50 (Aug. 1983). In Russian. English translation in: *Phys. Met. & Metallogr. (GB)* A study was made of the influence of γ irradiation at rates up to 4×10^3 R/sec on the kinetics of a $\beta' \rightarrow \zeta$ polymorphic transition in an Ag-Zn alloy. The change in the converted volume of the ζ phase with time as a result of γ irradiation was determined at various temperatures by the electrical resistance method. The results indicated that γ irradiation accelerated the $\beta' \rightarrow \zeta$ process. This was due to an increase in the probability of nucleation of the ζ -phase. Estimates were obtained of the changes (as a result of irradiation) in the probability and energy of formation of nuclei of the ζ -phase and of the energy parameters of the transition. The mechanisms were analysed allowing for the radiation-induced enhancement of the migration of atoms. (11 refs.) A.T.

115189 The cooling behavior of deep penetration welds undergoing austenite-ferrite transformation. M.J.Bibby (Dept. of Mech. & Aeronautical Engng., Carleton Univ., Ottawa, Canada), K.Eastman, J.A.Goldak. *Metall. Trans. B (USA)*, vol.14B, no.3, p.483-6 (Sept. 1983).

Austenite and ferrite-pearlite cooling rate and cooling-time relationships are proposed for deep penetration (electron beam) carbon-manganese and low alloy steel welds. These relationships are based on an analysis of experimental results by the heat transfer methods first suggested by Dorsch (1968), Signes (1972) and recently extended by Gravielle (1973) for the shallow penetration (arc) techniques. The cooling behavior of carbon-manganese and low alloy deep penetration welds is compared to the cooling behavior of equivalent austenitic stainless steel welds where there are no transformation effects. The results are rationalized in terms of the thermal properties of ferrite and austenite. (9 refs.)

Phase transitions, creep, and fission gas behaviour in actinide oxides See Entry 112329

Influence of the quenching temperature on the onset of the $\alpha \rightarrow \gamma$ transition and mechanical properties of maraging steel See Entry 115193

Microstructural stability of γ' strengthened Co-Cr-Ti alloys See Entry 115224

Role of eutectoid transformation and grain size on the creep behaviour of mild steel See Entry 115266

81.30K Martensitic transformations

(see also 64.70K Solid-solid transitions)

115190 Electron microscopic investigation of the growth of martensite platelets. V.M.Schastlivtsev, I.L.Yakovleva, L.N.Romashev (Inst. of Metal Phys., Ural Sci. Centre, Acad. of Sci., Sverdlovsk, USSR).

Fiz. Met. & Metalloved. (USSR), vol.56, no.2, p.271-9 (Aug. 1983). In Russian. English translation in: *Phys. Met. & Metallogr. (GB)* An electron microscopic study was made of the structure of martensite in 52Kh2N23 steel during intermediate stages of formation of lenticular martensite from thin martensite platelets formed under the action of magnetic field pulses. A characteristic dislocation fringe was observed at the beginning of the isothermal treatment around some of the thin martensite plates and its was due to the onset of side growth of these plates. Longer isothermal treatment resulted in the formation of a step-like martensite-austenite interface, which became smooth only on completion of the platelet growth. (9 refs.) A.T.

115191 Mechanism of formation of martensite single crystals as a result of plastic deformation of the alloys based on γ -Mn. E.Z.Vintaikin, S.Yu.Makushev, D.F.Litvin (Inst. of Metall. & Phys. of Metals, Moscow, USSR).

Fiz. Met. & Metalloved. (USSR), vol.56, no.2, p.298-302 (Aug. 1983). In Russian. English translation in: *Phys. Met. & Metallogr. (GB)* X-ray diffraction data were used to plot the pole figures of the tetragonal axes of the original and deformed (by compression along (100)) single crystals of the Mn-18% Cu alloy with a polydomain structure formed as a result of the face-centred cubic-tetragonal transition. It was found that the deformation produced a tetragonal single crystal with axes directed along the cubic axis of the original lattice. A mechanism was proposed according to which the formation of a single crystal was determined by the conditions of accommodation of the deformed twin structure. (7 refs.) A.T.

115192 Structural and phase transition of γ' martensite in binary Cu-Al alloy during deformation. V.V.Martynov, G.P.Martynova, L.G.Khandros (Inst. of Metal Phys., Acad. of Sci., Kiev, Ukrainian SSR).

Fiz. Met. & Metalloved. (USSR), vol.56, no.2, p.303-7 (Aug. 1983). In Russian. English translation in: *Phys. Met. & Metallogr. (GB)* An X-ray diffraction study was made of the structural and phase transitions in single crystals of Cu-13.5 mass % Al with the martensitic point at 180°C. These transitions occurred in the process of deformation at room temperature. The phase transitions occurred under load because the basal plane was oriented suitably for the preferred martensite variant. For different orientations of the stretching axis the deformation was either limited by the process of a reorientation of γ' martensite crystals and led to the formation of a perfect γ' single crystal or gave rise to the $\gamma' \rightarrow \alpha_1'$ phase transition. An α_1' single crystal formed as a result of this phase transition was retained after unloading. (7 refs.) A.T.

115193 Influence of the quenching temperature on the onset of the $\alpha \rightarrow \gamma$ transition and mechanical properties of maraging steel. S.B.Nizhnik, S.P.Doroshenko, G.I.Usikova (Inst. of Mech., Acad. of Sci., Dnepropetrovsk, Ukrainian SSR).

Fiz. Met. & Metalloved. (USSR), vol.56, no.2, p.327-33 (Aug. 1983). In Russian. English translation in: *Phys. Met. & Metallogr. (GB)* X-ray diffraction and direct electron microscopy were used to study the influence of the temperature of quenching of maraging N18K9M5T steel on the onset of the $\alpha \rightarrow \gamma$ transition and the associated changes in the martensite and austenite substructures, and also the influence on the dependences of the morphology and crystal lattice parameter of the converted austenite on its amount. The temperature of the onset of the $\alpha \rightarrow \gamma$ transition decreased and the relaxation of the initial microdistortions of the martensite and austenite lattices became accelerated when the quenching temperature was lowered in the intercritical interval. When the temperature intervals of the $\alpha \rightarrow \gamma$ transition and of the ordering ageing coincided, the converted austenite did not enhance the plasticity of the investigated steel. (9 refs.) A.T.

115194 Shape memory effect in martensitic transformations in TiNi-TiCu alloys. V.N.Tokarev, A.S.Savinov, V.N.Khachin (V.D. Kuznetsov Siberian Physicotech. Inst., Tomsk, USSR).

Fiz. Met. & Metalloved. (USSR), vol.56, no.2, p.340-4 (Aug. 1983). In Russian. English translation in: *Phys. Met. & Metallogr. (GB)* A significant but nonunique change in the parameters of a martensitic transformation and in the shape memory effects were observed when titanium nickelide was alloyed with copper. The replacement of nickel with copper gradually induced two martensitic transitions, B2 \rightarrow B19 and B19 \rightarrow B19', which ensured the optimal conditions for the shape memory effect. These conditions were realized in alloys with 10-12 at.% Cu and 1-3 at.% Fe. (8 refs.) A.T.

115195 Reversion of BCC α' martensite in Fe-Cr-Ni austenitic stainless steels. K.B.Guy, E.P.Butler, D.R.F.West (Engelhard Industries Ltd., Cheshington, England).

Met. Sci. (GB), vol.17, no.4, p.167-76 (April 1983). [received: Sept. 1983] The reverse transformation $\alpha' \rightarrow \gamma$ within two austenitic stainless steels of nominal composition Fe-18Cr-8Ni and Fe-18Cr-12Ni has been studied. A magnetic balance apparatus was used to determine the phase contents after rapid, salt bath heating. Information concerning the structures produced and the mechanisms of the transformation was obtained using transmission electron microscopy examination, including in situ hot stage experiments and

X-ray microanalysis. The results obtained show that the $\alpha'\rightarrow\gamma$ transformation proceeds by both diffusional and shear processes depending upon the heating time and temperature, initially producing austenite having a twinned substructure which recovers into fine subgrains. Diffusion occurs at temperatures between the A_s and A_f to produce the equilibrium austenite and ferrite duplex structure. Further observations on the recrystallisation behaviour, the effect of transformation cycling, and the phenomenon of a magnetic phase 'peak' at $\sim 400^\circ\text{C}$ are also reported, and possible mechanisms operating during these processes are discussed. (33 refs.)

Structural transformations and their precursors	See Entry 114154
Influence of repeated phase transitions on the annihilation of positrons in brass	See Entry 114952
Short-range atomic order in the Fe-Ni system	See Entry 115169
Non-equilibrium phases in laser-processed Fe-0.2 wt.% C-20 wt.% Cr alloys	See Entry 115425
Decomposition of austenitic phase in work hardened steel samples, using hardness measurements	See Entry 115464

81.30M Precipitation

(inc. segregation; see also 64.75 Solubility, segregation and mixing)

115196 Composition of Zr(Cr, Fe)₂-type precipitates in Zircaloy-2 and Zircaloy-4. R.A.Versaci, M.Ipohorski (Dept. de Materiales, Gerencia de Desarrollo, Comision Nacional de Energia Atomica, Buenos Aires, Argentina). *J. Nucl. Mater. (Netherlands)*, vol.116, no.2-3, p.321-3 (June 1983). The results of transmission electron microscopy, electron diffraction and X-ray energy dispersive microanalysis (EDAX) of second-phase particles in Zircaloy-2 and Zircaloy-4 are reported. The chemical composition of the Zr(Cr, Fe)₂-type precipitates were determined, and further information on the stability of their hexagonal structure was obtained. (11 refs.)

115197 The influence of molybdenum on the solubility of phosphorus in α -Fe. S.Suzuki, K.Abiko, H.Kimura (Res. Inst. for Iron, Steel & Other Metals, Tohoku Univ., Sendai, Japan). *Mater. Sci. & Eng. (Switzerland)*, vol.60, no.3, p.L17-21 (Sept. 1983). The authors have re-examined the effect of molybdenum on the solubility of phosphorus in α -Fe and found that the reduction in the phosphorus solubility due to molybdenum is not as large as was found by Kaneko et al. (see J. Jpn. Inst. Met., vol.29, p.166, 1965). The new solubility data are reported. (9 refs.)

115198 Aging behaviour of 18Mn-18Cr high nitrogen austenitic steel for end rings. R.Presser, J.M.Silcock. *Met. Sci. (GB)*, vol.17, no.5, p.241-7 (May 1983). The end windings of electrical generators are held in place by end rings which are heated to over 300°C during the fitting process. A new non-magnetic 18Mn-18Cr-0.6N steel has recently been developed for this application and the possibility of sensitization during service has been investigated. Precipitation of grain boundary nitrides is slow and from observations between 400 and 800°C the extrapolated time at 300°C for 10% of the boundaries of the as-received material to contain precipitates is 10⁵ h. Cellular precipitation occurs at high temperatures but is only detected at 600°C after 32 h. A re-solution treatment for 1 h at 1080°C reduces the subsequent rate of precipitation, whereas prior cold work accelerates precipitation. The precipitates are Cr rich but contain Mn and Fe. Below 700°C only the M₂₃X₆ structure forms, but above 700°C (CrMnFe)₂N is also observed. Both structures coexist for up to 68 h at 800°C. At temperatures above 550°C the rate of precipitation appears to be governed by Cr bulk diffusion. (9 refs.)

115199 Chemical composition of σ phase precipitated in chromium-nickel austenitic steels. J.Barcik, B.Brzycka. *Met. Sci. (GB)*, vol.17, no.5, p.256-60 (May 1983). Using an X-ray microanalyser the chemical composition was determined for σ phase precipitating in type 310 austenitic steels with varying carbon and silicon contents and for type AISI 316 steel stabilized with titanium. It was found that the range of α -phase stability, estimated by average group number, depends on the presence of additional alloying elements. (38 refs.)

115200 Crystalline defects in M₇C₃ carbides. J.P.Mornioli, E.Bauer-Grosse, M.Gantois (Lab. de Genie Metall., Ecole des Mines, Parc de Saurupt, Nancy, France). *Philos. Mag. A (GB)*, vol.48, no.3, p.311-27 (Sept. 1983). M₇C₃ carbides prepared in various conditions have been observed by electron microscopy and diffraction. Examinations of the first-order Laue zone with crystals having the c axis parallel to the electron beam demonstrate that the unit cell describing the structure of these carbides is the orthorhombic cell proposed by Fruchart and Rouault. This cell can be considered as an ordered cell of an average hexagonal cell and can have three orientations at 120° from each other. It contains metal atom tetrahedra whose local environment in prismatic interstices containing carbon atoms is typical and is never destroyed, whatever the conditions of preparation may be. Thus, in primary carbides present in cast irons and steel, the state of crystallization is such that a long-range order of the environment is established: orthorhombic domains are separated by {1100} twins and antiphase boundaries. In Fe₇C₃ carbides, crystallized from amorphous iron-carbon alloys, the local environments are only short-range ordered, and domains and {1120} defects have the same size. Intermediate cases, as seen in ion-plating carbides, are also described. (13 refs.)

115201 The segregation of osmium to grain boundary dislocations in tungsten. H.C.Eaton (Materials Sci. Program, Louisiana State Univ., Baton Rouge, LA, USA), H.Norden. *Scr. Metall. (USA)*, vol.17, no.8, p.1043-6 (Aug. 1983). The field ion microscope and the atom probe are used in an analysis of grain boundary chemistry in tungsten doped with nickel and osmium. The nickel atoms are randomly distributed in the grain boundary plane whereas the osmium is strongly segregated to the core region of a grain boundary dislocation. The differences in behavior of the solute atoms is explained by comparing atomic volumes. (7 refs.)

115202 Precipitation processes in a β -phase Cu-15 at.% Sn shape memory alloy. N.Kuwano, C.M.Wayman (Dept. of Metal. & Mining Engng., Univ. of Illinois, Urbana, IL, USA). *Trans. Jpn. Inst. Met. (Japan)*, vol.24, no.8, p.561-73 (Aug. 1983). β -phase CuSn alloys, like many other β -phase alloys of the noble metals, exhibit various 'extra' reflections in diffraction patterns. The phases which give rise to extra reflections in a quenched Cu-15 at.% Sn shape memory alloy were examined by means of electron microscopy using a dark field imaging technique. The as-quenched alloy was found to consist of a DO₃ matrix containing scattered small particles (designated as the 's'-phase) and another phase which may be identified as a surface phase or a so-called

'surface martensite'. The structure of the s-phase resembles that of an omega phase. In the same alloy annealed at 373K after quenching, coarse precipitates (designated as the 'L-phase') formed. The L-phase forms as four variants in the β -phase each of which takes the shape of a hexagonal platelet, the basal plane of which is parallel to {111} _{β} . After considering the structure of the L-phase it is concluded that the unit cell has the lattice parameters $a=b\approx\sqrt{6}a_\beta$, $c\approx\sqrt{3}a_\beta/2$, and $\gamma=120^\circ$, where a_β is the lattice dimension of the fundamental β -phase parent unit cell. (22 refs.)

115203 Microphase segregation in segmented amine-cured polyurethanes. C.R.Desper, N.S.Schneider (Army Materials & Mech. Res. Center, Organic Materials Lab., Watertown, MA, USA). Polymer Alloys III Blends, Blocks, Grafts and Interpenetrating Networks. Proceedings of a Symposium, New York, USA, 23-28 Aug. 1981 (New York, USA: Plenum 1983), p.233-51. The use of amine curing agents results in a very strong propensity for microphase separation in segmented polyurethanes. The resulting polymers, also denoted as polyurethaneureas, contain urea linkages which promote hard segment aggregation by specific interaction, namely the formation of a three-dimensional hydrogen bonding pattern. The SAXS evidence supports a model of extensive microphase segregation with narrow interphase boundaries, in which the hard segment phases are reasonably pure and the soft segment phases contain varying amounts of dissolved hard segment. The mechanical strength properties are strongly influenced by the state of dispersion of the two phases, and in particular on the relative values of the hard segment phase inhomogeneity length. In a poor material, the hard segments are isolated as microphases with limited lateral dimensions. In better materials the lateral dimensions increase, leading to higher l_H values, with little change in the longitudinal period indicated by the Bragg spacing. (3 refs.)

Polymer Alloys III Blends, Blocks, Grafts and Interpenetrating Networks. Proceedings of a Symposium See Entry 111311

The effect of primary recoil spectrum on radiation induced segregation in nickel-silicon alloys See Entry 114051

Radiation-induced segregation in titanium alloys See Entry 114052

Irradiation-induced segregation in multi-component alloys See Entry 114181

Stability of the radiation-induced γ' phase in 316 stainless steel See Entry 114182

Metastable phase separation in Au-Fe alloys See Entry 114184

Theory of inhomogeneous states of a solid solution in the neighborhood of second-order phase transitions See Entry 114186

A HVEM study of radiation-induced segregation in dilute Ni-Be alloys See Entry 114188

Radiation-induced segregation at internal defect sinks in electron irradiated FCC alloys See Entry 114189

Tweed microstructures. II. In several phases of the Ni-Al system See Entry 114199

Tracer diffusion of P in iron and iron alloys See Entry 114271

The formation of coarse intermetallics in rapidly solidified Al-Co alloys See Entry 115185

Kinetics of a polymorphic transition in an Ag-Zn alloy under the action of γ rays See Entry 115188

Electron microscopic studies on the effect of Sn addition on the ageing characteristics of Al-0.7% Mg₂Si alloy See Entry 115217

Relationship between grain boundary segregation and heat-treatment parameters in an aluminium alloy See Entry 115218

Microstructural stability of γ' strengthened Co-Cr-Ti alloys See Entry 115224

Tempering of cast nickel-aluminium bronze See Entry 115225

Role of eutectoid transformation and grain size on the creep behaviour of mild steel See Entry 115266

Effects of V and Nb additions on high temperature deformation properties of low alloy martensites See Entry 115269

Interfacial segregation and embrittlement in liquid phase sintered tungsten alloys See Entry 115324

Relationships between microstructure and mechanical properties of microduplex $\alpha+(\gamma+\epsilon)$ 6 and 9% Mn steels for cryogenic applications See Entry 115325

Intergranular brittle fracture resistance of 18Kh2N4VA steel after hardening See Entry 115349

Intergranular fracture of a high purity iron due to oxygen ... See Entry 115351

81.40 TREATMENT OF MATERIALS AND ITS EFFECTS ON MICROSTRUCTURES AND PROPERTIES

115204 Effect of loading prehistory on mechanical properties of steel in single-axis extension. A.G.Ivanov, Yu.G.Kashaev, A.I.Korshunov, S.A.Novikov, N.N.Popov, V.A.Ryzhanskii, V.I.Tsytkin. *J. Appl. Mech. & Tech. Phys. (USA)*, vol.23, no.6, p.826-30 (Nov.-Dec. 1982). Translation of: *Zh. Prikl. Mekh. & Tekh. Fiz. (USSR)*, vol.23, no.6, p.98-103 (Nov.-Dec. 1982). [received: Sept. 1983] (11 refs.)

115205 Relationship between processing parameters and mechanical properties of standard test pieces of selected partly crystalline thermoplastics. G.Fienhold, B.Rademacher. *Plaste & Kautsch. (Germany)*, vol.30, no.7, p.390-3 (July 1983). In German. Three high-density polyethylenes and three polypropylenes were examined with regard to the effect of their manufacturing on the characteristic mechanical properties of the material. One of the polypropylenes had been extruded. All the other test pieces were injection mouldings. The injection moulding temperature had the greatest influence on the mechanical characteristics of these plastics. The tool temperature was of comparatively little effect. There is a need for tightening up of the temperature control in the production of test pieces. (16 refs.) *R.S.*

115206 Torsional strength of pressureless-sintered silicon nitride. K.Matsusue, Y.Fujisawa, K.Takahara (Nat. Aerospace Lab., Chofu-shi, Japan). *Yogyo-Kyokai-Shi (Japan)*, vol.91, no.7, p.346-8 (1983). Torsional strength tests of pressureless-sintered silicon nitride were carried out at temperature range from room temperature to 1400°C in air. The torsional strength rapidly decreased at temperatures above 800°C, being 15 percent of room temperature value of 35.6 kg/mm² at 1400°C. Observations of the fracture mode and of the crack propagation on the fracture surfaces were made and discussed. (2 refs.)

115207 Development of design analysis methods for new materials. F.J.Lockett. Report NPL-DMA(A)-66, Nat. Phys. Lab., Teddington, England (May 1983), 21 pp.

Polymers and composites have some mechanical characteristics which are significantly different from those of familiar metallic materials. Consequently, design analysts may have less confidence in these newer materials and in their own ability to design with them. Thus, material selection may be confined to familiar materials, or components may be overdesigned, or failures may occur in service due to faulty design. Essentially, the design analyst requires relevant and credible design data, together with valid calculation methods for predicting and optimising component performance. These methods may involve design formulae or design charts, and the growing use of computer-aided design provides an opportunity for polymers and composites to be handled on an equal basis with other materials. The author examines these factors in the motor vehicle context, identifies present and future needs, surveys the current state of the art, and indicates some relevant recent and ongoing research work. (30 refs.)

Role of the Polymeric Matrix in the Processing and Structural Properties of Composite Materials. Proceedings of a Joint US-Italy Symposium See Entry 113132

Stress analysis of core support post in a very high-temperature reactor See Entry 112334

Design of continuous fiber composite structures See Entry 113291

Unresolved stress analysis problems in Kevlar composite pressure vessels See Entry 113292

Effect of moisture on physical properties of nylon See Entry 113762

A new method of the calculation of the hydrogen trap activation energy in metals See Entry 113855

Saturation exposure in ferritic stainless steels See Entry 114043

The role of the matrix in fibrous composite structures See Entry 115160

Factors affecting the development of new matrix resins for advanced composites See Entry 115161

81.40C Solid solution hardening, precipitation hardening, dispersion hardening

Structure formation in lightly-doped chromium alloys during plastic deformation in the 1400-1450K region See Entry 113802

Softening and hardening induced by point defects and defect clusters in BCC metals See Entry 113900

Preparation of rapidly solidified ribbons with second phase particles See Entry 115135

Hot isostatic pressing of oxide dispersion strengthened superalloy parts See Entry 115136

Shape effect of particles on high-temperature hardness of dispersion-hardened Ni-SiO₂ alloys See Entry 115352

81.40E Cold working, work hardening; annealing, recovery and recrystallisation; textures

115208 Investigation of the influence of thermomechanical treatment on the hardening of AlMgSiCu alloys. S.Stojadinovic (Tech. Inst., Bor, Yugoslavia).

Fiz. Met. & Metalloved. (USSR), vol.56, no.2, p.358-60 (Aug. 1983). In Russian. English translation in: *Phys. Met. & Metallogr. (GB)*

A study was made of the influence of the deformation regime on the hardening of previously aged AlMgSiCu alloys (1.5% Mg₂Si). The hardening was found to depend on the degree of deformation, deformation regime, and copper content. Alloys subjected to a less intense deformation regime, as well as those with high copper concentrations, exhibited stronger hardening. (14 refs.) A.T.

115209 Substructure hardening of polycrystalline niobium. V.M.Netesov, L.A.Chirkina, V.S.Okovits.

Fiz. Met. & Metalloved. (USSR), vol.56, no.2, p.401-3 (Aug. 1983). In Russian. English translation in: *Phys. Met. & Metallogr. (GB)*

High-purity niobium was annealed for 16 h in vacuum at 1150°C. It was then subjected to various rolling and annealing treatments. The dislocation structure was studied by determining the amplitude dependence of the internal friction and the mechanical properties were measured by stretching a sample. The results indicated that a considerable increase in the yield stress could be induced in the as-prepared and previously deformed (by 5%) niobium. The increase was 40 and 100%, respectively, and it was produced by annealing in an elastically stressed state at temperatures below the dislocation recovery stage. Formation of additional boundaries from dislocations was the main hardening mechanism. (6 refs.) A.T.

115210 Effect of cold rolling on the magnetic properties of nonoriented silicon steel. B.H.Hahn, I.S.Park, J.S.Woo.

J. Korean Inst. Met., vol.21, no.6, p.541-7 (June 1983). In Korean.

The effect of cold rolling on the magnetic properties of a nonoriented electrical steel sheet containing 3% silicon was examined by the observation of microstructure and texture analysis. The grain size of each was a maximum when the reduction rate of the second cold rolling was 5% and it gradually reduced as the rate increased. It was thought that grain growth of the second cold rolled specimen occurred by random, abnormal grain growth. In view of the texture of the final product, specimens processed by single cold rolling method had (222) texture, which is unfavorable to magnetic properties, but the ones processed by double cold rolling method had nearly random texture. A specimen subjected to the second cold reduction of 5% thus had the minimum iron-cold loss. (10 refs.)

115211 The use of microscopic and hardness measurement methods in recrystallization studies. C.M.Kamma (Dept. of Mech. Engng., Univ. of Lagos, Lagos, Nigeria), E.Hornbogen.

Mater. Res. Bull. (USA), vol.18, no.8, p.1027-36 (Aug. 1983).

The use of microscopic and hardness measurement methods as effective experimental techniques for recrystallization studies has been investigated. Consideration was given to the production of different starting-point microstructures of varying Fe₃C-particle dispersion, known to be associated with the complications of recrystallization mechanism of second-phase materials. Each of the investigation methods considered was used to study the various aspects of recrystallization phenomenon (recovery, in-situ-recrystallization, particle-controlled subgrain growth, partial recrystallization, grain growth) and the merits and limitations of application are discussed. (11 refs.)

115212 Recrystallization mechanisms in commercial Al-2Mg alloy.

M.A.Zaidi, T.Sheppard.

Met. Sci. (GB), vol.17, no.5, p.219-28 (May 1983).

The mechanism of nucleation of recrystallization is described for material having either a hot worked substructure or a cold work structure. Experiments have been conducted using low and high voltage transmission electron microscopy including in situ observations in the high voltage microscope. Salt bath experiments have been conducted to confirm the results. It is shown that recrystallization of hot worked structures involves subgrain coalescence followed by boundary migration. In the alloy investigated the dissolution of the β phase was important in creating a dislocation free region. The recrystallization of cold worked structures involves the creation of subgrains about the same size as in the parent hot rolled material, dislocation activity to form a medium angle boundary, and the migration of this boundary to form a high angle boundary and the recrystallization nucleus. (13 refs.)

115213 Effect of strain rate on the resistance of metals to plastic deformation. V.A.Persiyantsev, V.V.Fimin.

Russ. Metall. (GB), no.3, p.123-9 (1982). Translation of: *Izv. Akad. Nauk. SSSR Met.*, no.3, p.143-50 (1982).

In deriving the rate of strain-softening under plastic extension with the aim of a more accurate determination of the relaxation rate A the time function $A = \text{pk}^{\text{p}} \text{t}^{-1}$ was used. For the same alloy, according to the test conditions, this function is governed by the value of t, which defines the degree of 'proximity' of the relaxation process in metals to a visco-elastic process, described by the Maxwell equation: $\sigma = \sigma_0 \exp(-K_p t)$. Investigations into relaxation, creep and extension of 1Kh18N9L steel, described in the present paper, confirm that the generalised, or effective, relative relaxation rate A, is, to a large extent, determined by the type of testing. (12 refs.)

115214 Derivation of the through-hardenableity of steels in a fluidised bed. N.N.Varygin, T.V.Merenkova, L.N.Muchkin, O.N.Poddubnaya.

Russ. Metall. (GB), no.3, p.136-8 (1982). Translation of: *Izv. Akad. Nauk. SSSR Met.*, no.3, p.159-61 (1982).

The hardenableity of steels in a fluidised bed depends on the structure of the bed, its temperature and the conditions of fluidisation. Through-hardenableity for 'thin' bodies in a fluidised bed can be predicted by calculation to a sufficient degree of accuracy by using the regular process method. (9 refs.)

115215 Recovery behavior of hydrogen charged 7075-T6 aluminum. M.Mueller, I.M.Bernstein, A.W.Thompson (Dept. of Metall. & Materials Sci., Carnegie-Mellon Univ., Pittsburgh, PA, USA).

Ser. Metall. (USA), vol.17, no.8, p.1039-42 (Aug. 1983).

An investigation was carried out on the recovery behavior of 7075-T6 Al alloy. The ductility decrease observed for specimens tested in laboratory air at slow strain rates is likely due to hydrogen embrittlement by moist air since it does not occur if tests are conducted in vacuum or dried air. Recovery of ductility below a certain strain rate is not influenced by testing in a low pressure hydrogen environment. It is suggested that recovery is due to internal rearrangement of hydrogen at Cr-rich inclusions and at rather large particles, like η and T-phase precipitates in 7075-T6 and 7075-T73 alloys, both of which act as innocuous traps. This behavior should only be evident when testing under conditions of fixed and moderate hydrogen content. The difference in recovery behavior between the tempers UT, T6, T73 observed earlier is attributed to the presence and the size of η and T-particles which reduce by different amounts the hydrogen available to embrittle the material. (21 refs.)

115216 Influence of the degree of preliminary strain on the strain aging of pearlitic casing steel. V.A.Yukanov, S.I.Arkhangel'skii, A.A.Astaf'ev, S.I.Markov (Central Sci.-Res. Inst. for Machine Building Technol., Moscow, USSR).

Strength Mater. (USA), vol.14, no.11, p.1540-4 (Nov. 1982). Translation of: *Probl. Prochn. (USSR)*, vol.14, no.11, p.97-100 (Nov. 1982). [received: Sept. 1983]

The influence of the degree of preliminary strain on artificial strain aging of 15Kh2NMFA pearlitic casing steel was investigated by the internal friction method in combination with mechanical tests. It is concluded that the amount of hardening of 15Kh2NMFA steel in strain aging in the area of small degrees of preliminary strain (up to 6%) is controlled by dislocation-impurity interaction, while in the area of higher degrees ϵ the primary contribution to strengthening is made by the interaction of dislocations. (8 refs.)

Creation of point defects in superconductors. A short review See Entry 113859

Mossbauer study of defect trapping at ⁵⁷Co in cold worked aluminium See Entry 113959

PAC study of defect trapping at ¹¹¹In in cold worked aluminium See Entry 113960

Void-swelling in cold-worked copper during HVEM irradiation See Entry 114023

Differences in saturation of defects between electrons and reactor neutron irradiations at low temperature See Entry 114034

Radiation damage in glassy Pd₈₀Si₂₀ and Cu₅₀Zr₅₀ See Entry 114058

Vacancies in zinc and cadmium produced by proton- and electron-irradiation See Entry 114247

Diffusion of alcohols and relaxation in poly(methyl methacrylate): effect of thermal history See Entry 114267

Properties and structure of carbon excess Ti₂C_{1-x} deposited onto molybdenum by magnetron sputtering See Entry 114397

Magnetomechanical damping of nickel See Entry 114720

Reversion of BCC α' martensite in Fe-Cr-Ni austenitic stainless steels See Entry 115195

Steady state and transient creep of Al at 400K—an analysis in terms of recovery controlled by thermally activated glide See Entry 115254

Work-hardening rates during the high temperature creep of aluminium determined from the instantaneous strain on sudden stress changes See Entry 115265

Large strain plastic deformation of commercially pure nickel See Entry 115267

Work hardening and the stability of deformation in AlZnMg alloys See Entry 115271

The plastic compression of copper cones See Entry 115272

Influence of impurity atoms on the mechanical properties of group Va metals and alloys based on them See Entry 115277

Experimental investigation of laws governing the hardening of initially anisotropic materials See Entry 115281

Effect of cold working and annealing on stress corrosion cracking of AISI 304 stainless steel See Entry 115316

The use of transmission electron microscopy to study the effects of abrasive wear on the matrix structure of a high chromium cast iron ... See Entry 115375

Effect of waterglass impregnation upon hardenability of porous sintered steel ... See Entry 115431

81.40G Other heat and thermomechanical treatments

115217 Electron microscopic studies on the effect of Sn addition on the ageing characteristics of Al-0.7% Mg₂Si alloy. Gouthama, Kishore (Dept. of Metall., Indian Inst. of Sci., Bangalore, India). *Bull. Mater. Sci. (India)*, vol.5, no.1, p.61-70 (March 1983). [received: Sept. 1983]

The effect of trace addition of Sn on the ageing characteristics of Al-0.7% Mg₂Si has been studied by hardness measurements and transmission electron microscopy. The changes observed in the microstructural features have been explained on the basis of the strong interaction existing between Sn atoms and quenched-in vacancies. At aging temperatures below 200°C Sn addition brings about a retardation in the kinetics of GP zone growth whereas at higher ageing temperatures, it aided the precipitate nucleation and growth. The hardness data agree well with the deductions based on observations made on the thin foils. (10 refs.)

115218 Relationship between grain boundary segregation and heat-treatment parameters in an aluminium alloy. F.Pavlyak (Phys. Inst. of Tech. Univ., Budapest, Hungary), T.Churbakova. *J. Mater. Sci. Lett. (GB)*, vol.2, no.9, p.485-9 (Sept. 1983).

The authors investigated oxygen, iron and other dopants segregation on grain boundaries in cast Al-Mg-Si alloy. It was found that the quantity of the inhomogeneities in the grain boundaries decreased with increase of heat duration. Iron and manganese segregation was practically eliminated using a 3 h heat treatment. (11 refs.)

115219 Towards the analysis of magnetothermoelastic effects in metallic specimens during magnetic treatment. V.I.Dresvyannikov, A.A.Ponikarov, S.N.Postnikov.

Elektron. Obrab. Mater. (USSR), no.3, p.36-9 (1983). In Russian. English translation in: *Electrochem. Ind. Process. & Biol. (GB)*

Using as a basis the macroscopic interaction of thermoelectric and electro-magnetic fields, an analysis is made of the effects accompanying the magnetic treatment of metals in a range of weak (with strength up to 10^6 A/m) pulsed magnetic fields. The results of numerical calculations show that mechanical stresses produced by the action of electrodynamic forces do not exceed the yield point of the material. However, the instantaneous interaction of stresses in zones with an abrupt instantaneous plane shift of cross-sections facilitates magnetotriaxial substructural strengthening. (11 refs.) *A.J.B.*

115220 Electron microscopic investigation of structural changes caused by annealing of tungsten wires. G.Radnoci, Yu.A.Skakov (Inst. of Tech. Phys., Hungarian Acad. of Sci., Budapest, Hungary).

Fiz. Met. & Metalloved. (USSR), vol.56, no.2, p.315-21 (Aug. 1983). In Russian. English translation in: *Phys. Met. & Metallogr. (GB)*

Transmission and scanning electron microscopy were used to study thinned sections (foils) and cuts of tungsten wires after deformation and annealing. At the lowest annealing temperatures ($T \geq 1100^\circ\text{C}$) the boundary structure became ordered and dislocations were set in motion producing walls. Below 1700°C there were further changes in the dislocation walls and the diameters of some of the wires increased, but the nature of the fibrous structure was retained. Annealing at 1800 – 2200°C destroyed the fibrous structure producing almost equilibrium grains of 1 – $3 \mu\text{m}$. At higher temperatures a nonuniform grain growth predominated and it produced a structure typical of a nonsagging wire. (19 refs.) *A.T.*

115221 Influence of ageing at room temperature on the changes in volume as a result of tempering of quenched carbon steels. V.A.Korablev, A.P.Shkolenko, A.I.Kabes (Lenin Komsomol Industrial Inst., Tyumen, USSR).

Fiz. Met. & Metalloved. (USSR), vol.56, no.2, p.409-10 (Aug. 1983). In Russian. English translation in: *Phys. Met. & Metallogr. (GB)*

The influence of ageing at room temperature on the volume effects during tempering of 35, U8, and U12 quenched steels was investigated. The carbon content of these steels was 0.36, 0.78, and 1.18%, respectively. The steels were subjected to austenization at 850°C and quenching in 20% solution of NaOH. This was followed by cooling in liquid nitrogen and then ageing at room temperature. The volume effects were studied in the range of tempering at temperatures up to 450°C . The results were interpreted in terms of a redistribution of carbon during tempering and formation of aggregates. (4 refs.) *A.T.*

115222 The effects of cooling rate after controlled rolling on the mechanical properties of HSLA line pipe steels. Tai-Ung Kim, Jae-Eun Kim, Young-Gil Kim.

J. Korean Inst. Met., vol.21, no.2, p.98-104 (Feb. 1983). In Korean. [received: Sept. 1983]

The effects of cooling rates after controlled rolling (CR) on the mechanical properties were investigated for the Mo-Ni-Nb-V type HSLA line pipe steels. The accelerated cooling was carried out after CR in the temperature range from 800°C to 600°C followed by air cooling. Cooling methods employed were air cooling ($1.3^\circ\text{C}/\text{sec}$), compressed air cooling ($4.1^\circ\text{C}/\text{S}$), oil quenching ($9.5^\circ\text{C}/\text{S}$) and water spray cooling ($13.6^\circ\text{C}/\text{S}$). It was found from this work that controlled rolled 0.3%Mo-0.3%Ni type steel exhibited 40% yield strength increments by water spray cooling, while impact energy was not changed greatly. For the conventionally rolled boron containing steel, impact energy at -20°C was increased from about 3 to 17 Kgf.m under water spray cooled condition. (11 refs.)

115223 The effect of hydrogen on reversible and irreversible softening of spheroidized steel. S.X.Xie (Beijing Inst. of Aeronautics & Astronautics, Beijing, China), J.P.Hirth.

Mater. Sci. & Eng. (Switzerland), vol.60, no.3, p.207-12 (Sept. 1983).

Spheroidized AISI 1090 steel was charged with hydrogen at various charging current densities. The effect of hydrogen on the steel was detected by micro-hardness measurements. The charging produced reversible softening below a critical charging current density and irreversible softening above it. The results are discussed in connection with other indications of a critical charging current density and possible mechanisms for softening. (25 refs.)

115224 Microstructural stability of γ' strengthened Co-Cr-Ti alloys. N.-G.Ingesten, R.Warren, M.Dahlen (Dept. of Engng. Metals, Chalmers Univ. of Technol., Goteborg, Sweden).

Met. Sci. (GB), vol.17, no.4, p.159-66 (April 1983). [received: Sept. 1983]

A study has been made of the microstructural stability of various Co-Cr-Ti alloys. The alloy Co-16Cr-5Ti, when solution treated and cooled, forms a microstructure consisting of a homogeneous precipitation of Co_3Ti (γ') particles in an FCC (γ) matrix. This structure remains relatively stable during heat treatment between 600 and 800°C . The addition of 3% Mo to the

alloy causes transformation of the structure in this temperature range both by an FCC—HCP transformation and by discontinuous reprecipitation. The kinetics of these transformations are reported. The addition of 11%Ni to the Mo containing alloy suppresses the FCC—HCP transformation but not the discontinuous transformation. The FCC—HCP transformation, though martensitic in appearance, exhibits thermally activated kinetics. Possible explanations for this are discussed and possible reasons for the enhancement of the discontinuous transformation by Mo are also examined. (19 refs.)

115225 Tempering of cast nickel-aluminium bronze. F.Hasan, G.W.Lorimer, N.Ridley (Dept. of Metall., Univ. of Manchester, Manchester, England).

Met. Sci. (GB), vol.17, no.6, p.289-95 (June 1983).

Microstructural changes associated with the tempering at 675°C of cast nickel-aluminium bronze, of nominal composition (wt.%) Cu-10Al-5Ni-5Fe, have been investigated using optical, electron optical, and microprobe analysis techniques. The tempering treatment resulted in the elimination of the nonequilibrium martensitic phase (retained β), precipitation with the α grains and a coarsening of the as-cast structure. On heating to 675°C the martensite phase, which contained a high density of NiAl precipitates, reconstituted to form the high temperature BCC β phase and, after extended times at 675°C , this phase progressively decomposed into NiAl and α . The precipitates which formed in α grains were based on NiAl and had the B2 structure. These precipitates nucleated as laths either in the α matrix or on the pre-existing particles of Fe_3Al ; the two morphologies exhibited the Kurdjumov-Sachs and the Nishiyama-Wasserman orientation relationships, respectively, with α . (9 refs.)

115226 Phase composition of aluminium alloys Al-Mn-Li. L.V.Tarasenko, N.I.Turkina, G.N.Matveyeva.

Russ. Metall. (GB), no.3, p.185-9 (1982). Translation of: *Izv. Akad. Nauk. SSSR Met.*, no.3, p.207-11 (1982).

The phase composition and structure of alloys Al-(1.3-1.5)% Mn-(2.5-2.9)% Li after casting and homogenisation, as well as after hardening and ageing of various semis, hot extruded strip, hot and cold rolled sheets was studied. Al-Mn-Li alloys are susceptible to the formation of a non-equilibrium manganese intermetallic (Al,Mn) similar to the alloys of the Al-Mn and Al-Cr-Mn systems. After hardening and ageing the Al-Mn-Li alloys with 2.9% Li contain Al_3Li and AlLi phases in addition of MnAl_6 . Due to a thermal treatment in air a mixture of oxides Li_2O and LiAlO_2 is formed on the cold rolled sheets which decreases the tensile strength in comparison with hot rolled sheets. After hardening and ageing of the hot extruded strip it has higher strength due to the effect of working than sheets in which this phenomenon was not observed. (6 refs.)

115227 The mechanical properties and structure of Ti-Al-Zr-Mo alloys.

L.A.Ryabtsev, O.B.Tarasova.

Russ. Metall. (GB), no.3, p.195-8 (1982). Translation of: *Izv. Akad. Nauk. SSSR Met.*, no.3, p.220-3 (1982).

The mechanical properties, at room and elevated temperatures, of Ti-Al-Zr-Mo alloys with a high aluminium (7 wt.%) and zirconium (1 wt.%) contents were studied as functions of the molybdenum content (from 0 to 5%) and of the heat treatment process (annealing and quenching). Introduction of molybdenum into the Ti-7Al-12Zr alloys, up to a content of 3%, increases the ultimate strength at room temperature from 950 to 1200 and the yield limit from 900 to 1150 Mpa (after annealing at 800°C for 1 h and air cooling). Further additions of molybdenum does not bring about an increase in the strength properties of annealed alloys. Over the same range, the ductility properties decrease continuously. The strongest tendency towards an increased strength as a result of quenching is exhibited by an alloy with 5% Mo, the ultimate strength of which reaches 1450 MPa. (4 refs.)

115228 Structure of molybdenum high speed steels after atomization and annealing. A.N.Popandopulo, G.E.Titenskaya (Tulachermest Sci. Production Assoc., USSR).

Sov. Powder Metall. & Met. Ceram. (USA), vol.22, no.1, p.69-73 (Jan. 1983). Translation of: *Poroshk. Metall. (USSR)*, vol.22, no.1, p.77-82 (Jan. 1983). [received: Aug. 1983]

A study was made of the structures and phase compositions of powdered M6F1, M6K8F1, M10F1, and M10F3 molybdenum high-speed steels after atomization and annealing (cooling in a hydrogen stream). Powders were produced by atomization with nitrogen. Annealing was performed for 2 h at 850°C ; the rate of cooling was varied in the range 30 – $50^\circ\text{C}/\text{h}$. Unfractionated powder particles ranging in size from 10 to $600 \mu\text{m}$ were used for investigation. The predominant particle size lay in the range 200 – $250 \mu\text{m}$. The microstructures and phase compositions of the powders were studied in the as-atomized condition and after annealing. X-ray photography of the powders was performed using Fe K_α radiation, with a URS-501M diffractometer. (12 refs.)

115229 Possibility of predicting hardening cracks. V.S.Morganyuk, N.I.Kobasko, V.K.Kharchenko (Inst. of Strength Problems, Acad. of Sci., Kiev, Ukrainian SSR).

Strength Mater. (USA), vol.14, no.9, p.1233-8 (Sept. 1982). Translation of: *Probl. Prochn. (USSR)*, vol.14, no.9, p.63-8 (Sept. 1982).

The authors develop a procedure of strength calculation for engineering components during hardening taking account of phenomena accompanying steel structural transformations. (6 refs.)

115230 Quenching investigations on BCC transition metals. M.Tietze (Max-Planck-Inst. fur Metall., Stuttgart, Germany), S.Takaki, I.A.Schwirtlich, H.Schultz.

Point Defects and Defect Interactions in Metals. Proceedings of the Yamada Conference V, Kyoto, Japan, 16-20 Nov. 1981 (Amsterdam, Netherlands: North-Holland 1982), p.265-7

New observations based on the superfluid helium quenching technique and resistivity measurements are reported for Ta and Ta+C and Ta+C. The results are compared with similar experiments on other BCC metals. (19 refs.)

115231 Quenching secondary defects in austenitic steels containing phosphorus. M.Kikuchi, T.Arai, Y.Yamamoto, H.Takashima, R.Tanaka (Dept. of Metall. Engng., Tokyo Inst. of Technol., Tokyo, Japan).

Point Defects and Defect Interactions in Metals. Proceedings of the Yamada Conference V, Kyoto, Japan, 16-20 Nov. 1981 (Amsterdam, Netherlands: North-Holland 1982), p.733-5

A certain amount of metallic alloying element, such as aluminum, titanium, vanadium, manganese or chromium, need to be added for the formation of quenching secondary defects in a 32 wt pct Ni–0.3 wt pct P austenitic steel. This observation reveals that the metallic alloying element as well as phosphorus plays a significant role in the dislocation loop formation. Direct and interrupted quenching, and two-step and three-step aging including up- and down-quenching were performed in the temperature range between 400 and 900°C , using a 28 wt pct Ni–25 wt pct Cr–2 wt pct Mo–0.3 wt pct P austenitic steel. The latter experiment strongly suggests that the mobility of

the vacancy in this austenitic steel is greatly reduced by forming vacancy-phosphorus-chromium atom complexes. (9 refs.)

- Modelling of fission-gas release from fuel undergoing isothermal heating See Entry 112333
- Determining the characteristics of Ag:LiTaO₃ diffused optical waveguides See Entry 113097
- Defects in quenched and annealed Al-Ge alloys See Entry 113861
- Mobilities of quenched-in defects in NiAl See Entry 113864
- Properties of point defects in FCC metals See Entry 113875
- Vacancies in silver: a resistivity and positron annihilation study See Entry 113876
- Configurations of point defects in neutron-irradiated iron See Entry 113878
- Submicroscopic vacancy defects in pure and doped gold See Entry 113879
- Self-interstitial mobility in a neutron-irradiated austenitic Fe₅₀Cr₁₆Ni₂₅ alloy See Entry 113890
- Agglomerates of interstitial-atoms and vacancies in e⁻-irradiated copper See Entry 113920
- Chlorine redistribution in HCl oxides due to high temperature annealing See Entry 113950
- Strong interaction between vacancy and solute in gold See Entry 113967
- A positron lifetime study of vacancy-solute complexes in dilute gold alloys See Entry 113968
- Interaction and charge transfer between vacancy and solute in dilute aluminium alloys See Entry 113970
- Mossbauer analysis on the annealing process of a quenched Al-Sn dilute alloy See Entry 113973
- Comparison between thermal and laser annealing in ion-implanted silicon See Entry 114021
- Influence of alloy composition on defect production and recovery, in austenitic Fe-Cr-Ni solid solutions electron-irradiated at low temperature See Entry 114032
- Radiation-induced segregation in titanium alloys See Entry 114052
- Solubility of carbon and ageing of Kh15Yu5 type alloys See Entry 114175
- A HVEM study of radiation-induced segregation in dilute Ni-Be alloys See Entry 114188
- Tweed microstructures. II. In several phases of the Ni-Al system See Entry 114199
- Microstructure induced ordering effects in solids See Entry 114200
- Vacancies in zinc and cadmium produced by proton- and electron-irradiation See Entry 114247
- Diffusion of tritium in single crystal Li₂O See Entry 114261
- RF plasma annealing of as-grown defects in the Si/SiO₂ system See Entry 114374
- Heat treatments of CVD-coatings on hardmetals See Entry 114425
- Electronic structure of the alloy Fe₃₀P₁₃C₇ in the liquid, crystalline, and solid amorphous states See Entry 114440
- Quenched-in defects in CW laser irradiated virgin silicon See Entry 114483
- Thermally stimulated current studies on cadmium selenide single crystals heat-treated in selenium vapour See Entry 114534
- Magnetomechanical damping of nickel See Entry 114720
- NMR studies of Ge atoms in quenched f.c.c.-Ge alloys See Entry 114745
- Mossbauer spectroscopy on ¹³³Cs as a method to study vacancy migration in metals See Entry 114766
- Photoluminescence study of thermally treated silicon crystals See Entry 114926
- Positron studies of recovery processes in aluminium and aluminium alloys See Entry 114958
- The effect of sintering in hydrogen-nitrogen atmospheres and subsequent aging on the magnetic properties of iron See Entry 115138
- Examination of alloys of the Pd-Ni-Th system in the palladium-rich region See Entry 115172
- Electron microscopic investigation of the growth of martensite platelets See Entry 115190
- Influence of the quenching temperature on the onset of the α - γ transition and mechanical properties of maraging steel See Entry 115193
- Aging behaviour of 18Mn-18Cr high nitrogen austenitic steel for end rings See Entry 115198
- Investigation of the influence of thermomechanical treatment on the hardening of AlMgSiCu alloys See Entry 115208
- Substructure hardening of polycrystalline niobium See Entry 115209
- Recrystallization mechanisms in commercial Al-2Mg alloy See Entry 115212
- Thermal stresses and viscoelastic relaxation in metallic glasses prepared by liquid quenching See Entry 115232
- Influence of stress cycling on creep behaviour of an Al-Mg alloys under strain ageing conditions See Entry 115253
- Influence of substructure on the mechanical properties of austenitic alloys deformed by warm rolling See Entry 115257
- Properties of two high strength, high temperature, high conductivity copper-base alloys See Entry 115264
- Luder's strain and ductility of ordered Fe-Co-2V and Fe-Co-V-Ni See Entry 115268
- Creep of hardened steel in tempering See Entry 115278
- Effect of texture and grain size on the fracture behaviour of hot rolled Mg, Mg-12.5% Li and Mg-5% Ti alloys See Entry 115300
- Embrittlement of construction steel with bainite structure during tempering See Entry 115308
- Fractographic aspects of cyclic cleavage See Entry 115321
- Interfacial segregation and embrittlement in liquid phase sintered tungsten alloys See Entry 115324
- Relationships between microstructure and mechanical properties of microduplex α -(γ + ϵ) 6 and 9% Mn steels for cryogenic applications See Entry 115325
- Effect of molybdenum on temper brittleness and internal friction behaviour of medium carbon alloy steels See Entry 115326
- High strength sheet steel of medium thickness See Entry 115357

Resistenza a fatica di acciai ad alto limite di snervamento laminati a caldo (Fatigue resistance of high strength hot rolled steels) See Entry 115358

Stress corrosion cracking of aged Al-5Zn-4Mg alloy in 3.5% NaCl solution See Entry 115419

Non-equilibrium phases in laser-processed Fe-0.2 wt. % C-20 wt. % Cr alloys See Entry 115425

81.40J Elasticity and anelasticity

(see also 62.20D Elastic constants, 62.40 Anelasticity, internal friction, and mechanical resonances)

115232 Thermal stresses and viscoelastic relaxation in metallic glasses prepared by liquid quenching. A.R.Yavari, P.Desre (Lab. de Thermodynamique & Phys.-Chimie Metall. ENSEEG, Domaine Univ., Saint Martin d'Heres, France).

J. Mater. Sci. Lett. (GB), vol.2, no.9, p.516-18 (Sept. 1983).

The authors' analysis of experimental data has shown that viscoelastic relaxation (transient creep) similar to that produced by a tensile stress is produced by thermal stresses inherent in the quenching process. (8 refs.)

115233 Elastic constants of fiber-reinforced boron-aluminum: observation and theory. S.K.Datta (Dept. of Mech. Engng., Univ. of Colorado, Boulder, CO, USA), H.M.Ledbetter.

Int. J. Solids & Struct. (GB), vol.19, no.10, p.885-94 (1983).

Elastic constants, both the C_{ij} 's and S_{ij} 's, were measured and calculated for a laminated, uniaxially fiber-reinforced boron-aluminum composite. Three theoretical models were considered: square-array, hexagonal-array, and random-distribution. By combining several existing theoretical studies on randomly distributed fibers, the authors derived relationships for predicting the full set of elastic constants for this model. The random-distribution model agrees best with observation, especially for off-diagonal elastic constants. Considering all nine elastic constants, observation and theory differ on the average by 6%. These discrepancies arise from three sources: experimental error propagation, limited applicability of a transverse-isotropic model to a laminated composite, and elastic anisotropy of boron fibers. (16 refs.)

115234 Dependence of the elastomechanical properties of granular corundum-zirconium refractory materials on their microstructure. I.G.Orlova, A.I.Gudilina (Ukrainian Sci.-Res. Inst. of Refractory Materials, Ukrainian SSR).

Inorg. Mater. (USA), vol.18, no.9, p.1356-8 (Sept. 1982). Translation of: *Izv. Akad. Nauk SSSR Neorg. Mater.*, vol.18, no.9, p.1583-5 (Sept. 1982). [received: Sept. 1983]

The effect of the microstructure of granular corundum-zirconium refractory materials on the elastomechanical properties was studied. The dependence of the tensile strength on the degree of heterogeneity, characterizing the heterogeneity of the material with a maximum with values of $\sim(20-40\%)$ and a decrease in the effective energy of decomposition with an increase in the degree of heterogeneity, was determined. It was found that the tensile strength on bending should be maximally increased while the value of the modulus of normal elasticity should remain unchanged for increasing the overall resistance to decomposition for granular multiphase and microfissured materials. (5 refs.)

115235 Local acoustoelasticity in poly(methyl methacrylate) by Brillouin scattering. B.C.Yap, S.Hichijyo, T.Takemura (Dept. of Appl. Sci., Kyushu Univ., Fukuoka, Japan), K.Matsushige.

J. Appl. Phys. (USA), vol.54, no.9, p.5456-8 (Sept. 1983).

The Brillouin scattering technique was used to study the local mechanical deformation of poly(methyl methacrylate) (PMMA). The extent of local stress concentration could be determined by measuring longitudinal hypersonic velocities in the close vicinity of a circular hole and a sharp single-edge-notch (SEN) in panel PMMA specimens under uniaxial tensile stress. Craze formation in PMMA is also briefly discussed in association with such a local deformation. Present studies demonstrate that the Brillouin scattering technique is a new and effective probe for such an investigation in transparent materials. (6 refs.)

115236 On the measurement of Young's modulus of tubes by propagation of longitudinal waves. F.Povolo (Dto. de Materiales, CNEA, Buenos Aires, Argentina), R.F.Bolmaro.

J. Nucl. Mater. (Netherlands), vol.116, no.2-3, p.166-71 (June 1983).

The equation that describes the propagation of elastic waves has been solved numerically for longitudinal vibrations of tubes and the results are used to calculate Young's modulus for Zircaloy-4 fuel sheathings. The values are compared with the results obtained by using the approximate equations proposed in the literature. The differences observed are less than 0.5% for the fundamental frequency. For the harmonics, however, the numerical solution leads to resonant frequencies that are within 1% of the experimental values and the approximate equations give errors higher than 10%. (15 refs.)

115237 Poisson's ratio in zirconium single crystals. F.Povolo (Comision Nacional de Energia Atomica, Buenos Aires, Argentina), R.E.Bolmaro.

J. Nucl. Mater. (Netherlands), vol.118, no.1, p.78-82 (Aug. 1983).

Poisson's ratio for α -Zr monocrystals has been shown to be strongly dependent on texture and temperature. These data have been compared with results reported for dilute zirconium alloys and several inconsistencies have been pointed out. (9 refs.)

115238 Ab initio calculation of polyethylene deformation including electron correlation effects. S.Suhai (Lehrstuhl fur Theoretische Chem., Friedrich-Alexander-Univ. Erlangen-Nurnberg, Erlangen, Germany).

J. Polym. Sci. Polym. Phys. Ed. (USA), vol.21, no.8, p.1341-6 (Aug. 1983).

The longitudinal acoustic elastic modulus of polyethylene has been calculated with the aid of the ab initio crystal orbital method applying corrections also for electronic correlation effects. The basis set and correlation dependence of the elastic modulus have been investigated. The best theoretical value of 305 GPa of this modulus is in reasonable agreement with the published experimental values. At an elongation of ca. 0.1 the deviation from Hooke's law is found to be substantial. (32 refs.)

115239 Elastic modulus of syntactic foams. L.E.Nielsen.

J. Polym. Sci. Polym. Phys. Ed. (USA), vol.21, no.8, p.1567-8 (Aug. 1983).

A simple method of estimating the shear and Young's moduli of syntactic foams is presented. It is based on the estimation of the apparent modulus of hollow spheres in terms of their inner and outer radii. (5 refs.)

115240 Elastic properties (the stiffness constants, the shear modulus and the dislocation line energy and tension) of Ni-Al solid solutions and of the Nimonic alloy Pe16. H.Pottebohm, G.Neite, E.Nembach (Inst. fur Metallforschung, Univ. Munster, Munster, Germany).

Mater. Sci. & Eng. (Switzerland), vol.60, no.3, p.189-94 (Sept. 1983).

The stiffness constants C_{ik} of the following nickel-base alloys were measured: Ni-Al solid solutions with aluminium contents up to 8 at.%, Nimonic alloy

PE16 and an experimental alloy with the same composition as the matrix of fully precipitated PE16. The temperature range covered is 80-360K. From the stiffnesses C_{ik} a shear modulus and the dislocation line energy and tension are derived. Extrapolation formulae, which describe the temperature and concentration dependences of the elastic parameters are given for the range 0-550K. (19 refs.)

115241 Internal friction study on structural relaxation of a glassy metal $\text{Fe}_{32}\text{Ni}_{36}\text{Cr}_{14}\text{P}_{12}\text{B}_6$. N.Morito (Dept. of Materials Sci. & Engng., Univ. of Pennsylvania, Philadelphia, PA, USA). *Mater. Sci. & Eng. (Switzerland)*, vol.60, no.3, p.261-8 (Sept. 1983). The internal friction of Metglas 2826A ($\text{Fe}_{32}\text{Ni}_{36}\text{Cr}_{14}\text{P}_{12}\text{B}_6$) glassy metal was investigated using a torsion pendulum type of apparatus. The magnitude of the internal friction is reduced by structural relaxation during annealing. It was found that the internal friction reaches, after prolonged annealing, an equilibrium value which depends on temperature. The decay kinetics can be expressed by first-order kinetics with a log-normal distribution of time constants. The activation energy spectrum of the change in the internal friction associated with the structural relaxation of Metglas 2826A alloy was obtained by subtracting the internal friction curve for the fully relaxed material from that for the as-received material. The resulting spectrum has a wide distribution of activation energies from 1.1 to 2.2 eV, with a maximum at about 2.0 eV or higher. (32 refs.)

115242 Strain modulation measurements of stiffening effects in carbon fibers. C.P.Beetz, Jr., G.W.Budd (Phys. Dept., General Motors Res. Labs., Warren, MI, USA). *Rev. Sci. Instrum. (USA)*, vol.54, no.9, p.1222-6 (Sept. 1983). An experimental technique for directly measuring strain-induced stiffening effects in individual carbon fibers has been developed. The technique involves the superposition of a small amplitude oscillating strain ($\Delta\epsilon \sim 10^{-4}$) on a slow linearly increasing strain ($\sim 1.1 \times 10^{-3} \text{ s}^{-1}$). Synchronous detection of the resultant AC component of the measured stress yields a signal proportional to the slope of the stress versus strain curve provided the modulation amplitude is small compared to the ultimate strain at failure (~ 0.005). The experimental arrangement has been designed for use in conjunction with an Instron tensile test apparatus. A novel design for a fiber gripping apparatus which permits direct measurement of the strain is also described. The technique has been applied to carbon fibers produced from two different precursor materials: polyacrylonitrile and mesophase pitch. Fibers from both precursors exhibited strain-induced stiffening. The modulus of the pitch-based fibers increased in proportion to the square root of the strain, whereas that of the PAN-based fibers showed an almost linear increase. (14 refs.)

115243 Fatigue and recovery processes in a multilayer iron-copper composite material. S.L.Revo, V.S.Kopan', V.P.Maiboroda (T.G. Shevchenko Kiev State Univ., Kiev, Ukrainian SSR). *Sov. Powder Metall. & Met. Ceram. (USA)*, vol.22, no.1, p.64-8 (Jan. 1983). Translation of: *Poroshk. Metall. (USSR)*, vol.22, no.1, p.72-7 (Jan. 1983). [received: Aug. 1983] A study was made of the amplitude-dependent internal friction (ADIF) of a sandwich-type MCM consisting of st. 45 (0.45% C) steel and MI copper layers. The composite was produced by thermomechanical working of a steel-copper pseudoalloy with overall reductions of blanks of 70-90%. It was found that in a composite produced from a pseudoalloy by thermomechanical processing the density of microcracks did not grow with decreasing mean layer thickness. The anisotropy of the ADIF indicated that the directions of climb of edge dislocations and of slip of screw dislocations in the MCM were not equivalent. This circumstance must be taken into account when designing parts which are to be made of such materials, because the mechanical properties of sandwich-type composites are linked directly with the density and distribution of dislocations. (5 refs.)

115244 Effect of static tensile stresses on the dissipative properties of copper-aluminum-zinc alloys. V.V.Matveev, B.S.Chaikovskii, D.E.Shpak, G.Ya.Yaroslavskii, S.Yu.Kondrat'ev (Inst. of Strength of Materials, Acad. of Sci., Kiev, Ukrainian SSR). *Strength Mater. (USA)*, vol.14, no.9, p.1271-5 (Sept. 1982). Translation of: *Probl. Prochn. (USSR)*, vol.14, no.9, p.95-8 (Sept. 1982). The authors investigated the effect of static tension on the damping capacity of alloys subjected to flexural vibrations. True vibration decrements were obtained and it was found that the static tensile stresses had a substantial effect on the dissipative properties of the alloys. The degree of this effect was found to depend to a large extent on the chemical composition of the alloy. (11 refs.)

115245 Anisotropy of elastic properties of titanium base α -alloys. R.A.Adamesku, L.P.Andreeva, P.V.Gel'd, E.A.Mityushov, N.D.Reimer (Ural Polytech. Inst., Sverdlovsk, USSR). *Strength Mater. (USA)*, vol.14, no.9, p.1284-7 (Sept. 1982). Translation of: *Probl. Prochn. (USSR)*, vol.14, no.9, p.105-8 (Sept. 1982). A method of calculating the anisotropy of the elastic properties in metals and alloys with a close-packed hexagonal structure in which limitations imposed on the type and character of dispersion of the crystallographic structure are absent has been developed and used. The anisotropy of Young's modulus in titanium α -alloys (within a wide range of deformations) is determined primarily by the crystallographic texture. The role of the interaction between the grains is small. To calculate the anisotropy of Young's modulus in titanium α -alloys, information on the texture obtained by plotting 'to the reflection' from the basal planes is sufficient. (8 refs.)

115246 Analysis of process stresses in two-layer SiC-Si disks. A.S.Tsybenko, A.L.Maistrenko, V.N.Kulakovskii, G.G.Gnesin, Yu.P.Dyban', V.L.Yupko (Kiev Polytech. Inst., Acad. of Sci., Kiev, Ukrainian SSR). *Strength Mater. (USA)*, vol.14, no.11, p.1515-18 (Nov. 1982). Translation of: *Probl. Prochn. (USSR)*, vol.14, no.11, p.76-9 (Nov. 1982). [received: Sept. 1983] The level of residual process stresses and the reasons for crack formation in SiC-Si two-layer discs are investigated. A mathematical model was constructed for the deformation of a disc with cooling from 700°C to room temperature. The finite element method was used in the calculation. (14 refs.)

115247 Influence of the level of stresses on the static Young's modulus of a number of constructional materials. A.F.Voitenko, Yu.D.Skrinipik, H.G.Solov'eva, G.N.Nadezhdin (Inst. of Strength Problems, Acad. of Sci., Kiev, Ukrainian SSR). *Strength Mater. (USA)*, vol.14, no.11, p.1524-6 (Nov. 1982). Translation of: *Probl. Prochn. (USSR)*, vol.14, no.11, p.83-6 (Nov. 1982). [received: Sept. 1983] The results are presented of investigating a number of constructional materials of various classes: the austenitic steel 12Kh18N10T; austenitic steels 03Kh20N16AG6 and 03Kh13AG19; 07Kh16N6 martensitic steel; VT6S titanium alloy; AMtS and AMg6 low strength weldable aluminium alloys. It is concluded that an increase in stresses in a sample to the level at which microplastic deformation occurs leads to a significant reduction in the moduli

of elasticity of the investigated materials. The form and condition of the sample surface plays a definite role in the development of microplastic deformations. (1 ref.)

115248 Polymer-performance on the dimensional stability and the mechanical properties of wood-polymer composites prepared by an electron beam accelerator. T.Handa, I.Seo, T.Ishii, Y.Hashizume (Dept. of Appl. Chem., Sci. Univ. of Tokyo, Tokyo, Japan). Polymer Alloys III Blends, Blocks, Grafts and Interpenetrating Networks. Proceedings of a Symposium, New York, USA, 23-28 Aug. 1981 (New York, USA: Plenum 1983), p.167-90 The state of the art of polymers in wood and their performance were studied for the wood-polymer composites produced by electron beam irradiation. The balance between the enhanced dynamic modulus and the dimensional stability of the products were discussed in relation to the prevention of the formation of fatigue cracks during a long exposure to repeated cycles of humid and dry weather. The particular action of the tight cross-linking bonds in enhancing the mechanical properties as well as the dimensional stability of the products was recognized with regard to the unsaturated polyester WPC. In this regard, an impregnation method in two steps was proposed for producing a polyester WPC fancy veneer with distinguished mechanical properties and dimensional stability. (21 refs.)

115249 Viscoelastic properties of particulate reinforced matrices. C.Migliaresi (Istituto di Principi di Ingegneria Chimica, Univ. di Napoli, Napoli, Italy). Role of the Polymeric Matrix in the Processing and Structural Properties of Composite Materials. Proceedings of a Joint US-Italy Symposium, Capri, Italy, 15-19 June 1981 (New York, USA: Plenum 1983), p.357-68 The viscoelastic behavior of both polystyrene and epoxy resin/glass bead composites has been studied by means of stress relaxation experiments over a wide range of temperatures in the linear viscoelastic region. The glass transition temperature of the thermosetting resin is increased because of the presence of the second phase while no effect has been observed for the thermoplastic matrix. According to the time-temperature superposition principle all the stress relaxation data have been shifted to obtain single master curves at a reference filler content by taking into account the reinforcing effect of the filler and the glass transition temperature of the matrix. (17 refs.)

115250 Reinforced polyester structural foam. G.Carignani, M.Mazzola (Tech. Center, SNIAL Resine Poliestere SpA, Roma, Italy). Role of the Polymeric Matrix in the Processing and Structural Properties of Composite Materials. Proceedings of a Joint US-Italy Symposium, Capri, Italy, 15-19 June 1981 (New York, USA: Plenum 1983), p.453-68 It is concluded that a composite material consisting of three phase components (resin, gas and continuous or long chopped fibers) has the maximum flexural strength and stiffness with minimum weight. It is possible to calculate at the first approximation the elastic modulus of this kind of composite with the quasi-isotropic laminate theory. With polyester foam reinforced with continuous glass fibers it is possible to obtain at the same time high specific flexural stiffness and strength, as well as v.s. the temperature, high thermal insulation and sound deadening, low thermal expansion, good surface appearance, easy and non toxic foaming and molding technology and low cost. (8 refs.)

Effect of shear modulus on the elastic behavior of strongly anisotropic plates ..	See Entry 113305
Device for measuring the loss factor of insulating materials ..	See Entry 113389
Melt rheology of polymer blends: the morphology feedback ..	See Entry 114068
Solubility of carbon and ageing of Kh15Yu5 type alloys	See Entry 114175
Some high-temperature properties of Zircaloy-oxygen alloys	See Entry 114213
Internal friction study on diffusivity on the Cu-SiO ₂ interface	See Entry 114286
Magnetomechanical damping of nickel	See Entry 114720
The effect of dye sorption on electromechanical properties in sodium poly(L-glutamate)	See Entry 114788
Vibration-resistant composites intended for damping devices ..	See Entry 115158
Effect of strain rate on the resistance of metals to plastic deformation	See Entry 115213
Study of molecular deformation mechanisms in the glassy state. I. Temperature effect on stress-birefringence and strain-birefringence responses of poly(methyl methacrylate)	See Entry 115261
RIM systems from interpenetrating polymer networks	See Entry 115291
The mechanical properties and failure modes in reinforced polypropylene	See Entry 115298
Effect of molybdenum on temper brittleness and internal friction behaviour of medium carbon alloy steels	See Entry 115326
Failure of rubber-modified plastic liners	See Entry 115331
Assessment of residual stresses in coatings applied to P/M parts	See Entry 115441

81.40L Deformation, plasticity and creep

(see also 62.20F Deformation and plasticity, 62.20H Creep)

115251 An inelastic finite element model of 4D carbon-carbon composites. L.Delnestre, B.Perez (Soc. Europeenne de Propulsion, Bordeaux, France). *ALAA J. (USA)*, vol.21, no.8, p.1143-9 (Aug. 1983). Sepcarb 4D is a carbon-carbon composite material wherein the reinforcing fibers are bundled in four directions. It is widely and successfully used in integral solid rocket nozzles. An accurate prediction of the material behaviour is difficult, due to the anisotropy and above all to the nonlinear inelasticity of the composite. An elastoplastic finite element model, including homogenized monaxial stiffnesses, is presented. A consistent set of constitutive constants is obtained from test data. The adequacy of the model is demonstrated through comparisons between predicted and measured test results of Sepcarb 4D uniaxial specimens and rings. Results showing the significant influence of the orientation of the 4D reinforcements relative to the applied load are discussed. The model can be extended to an increased number of directional composites and offers new possibilities in the stress analysis of such materials. (8 refs.)

115252 Process of α -relaxation in dense network epoxide polymers obtained under deformation conditions. Yu.K.Glotova, T.I.Ponomareva, V.G.Sheinberg, V.I.Irzhak, B.A.Rozenberg. *Vysokomol. Soedin. Ser. B (USSR)*, vol.25, no.6, p.407-9 (1983). In Russian. A conclusion arrived at from previous work, according to which the deformation of the matrix under the action of the filler is the decisive factor in determining the changes occurring in the structure and properties of dense

network epoxide polymers is studied in more detail, with deformation of the polymer matrix during synthesis by two methods, i.e. direct deformation by bending a polymer plate formed on a metal base, and relaxation of an inclusion previously deformed to a given extent during synthesis of the epoxide polymer matrix. It is suggested that the main factor involved in the relaxation process is chemical flow of the polymer, as was concluded previously in studying the effect of deformation on the structure of a formed cross-linked polymer (see V.I. Irzhak et al., Dok. Akad. Nauk, SSSR, vol.239, no.4, p.876, 1978). (4 refs.) N.S.

115253 Influence of stress cycling on creep behaviour of an Al-Mg alloys under strain ageing conditions. A.G.V.Vladimirova, G.A.Malygin, V.A.Stepanov (A.F. Ioffe Phys.-Tech. Inst., Acad. of Sci., Leningrad, USSR). *Res. Mech. (GB)*, vol.9, no.2, p.65-71 (1983). Low-frequency cyclic loading of Al-0.55 at.%Mg alloy at room temperature with a constant stress amplitude leads to creep rate acceleration due to breakaway of dislocations blocked by impurity atmospheres. (8 refs.)

115254 Steady state and transient creep of Al at 400K—an analysis in terms of recovery controlled by thermally activated glide. W.Blum, H.Schmidt (Inst. für Werkstoffwissenschaften, Friedrich-Alexander-Univ. Erlangen-Nürnberg, Erlangen, Germany). *Res. Mech. (GB)*, vol.9, no.2, p.105-24 (1983). Creep of pure Al has been investigated at 400K. The steady state creep rate $\dot{\epsilon}_s$ (determined by an extrapolation procedure in order to compensate for the effect of necking) varies exponentially with stress σ . In the transient creep range following a stress reduction, the creep rate $\dot{\epsilon}$ goes through a maximum followed by a minimum. This transient is only weakly influenced by static recovery (annealing at test temperature and negligible stress) preceding the transient. The results are interpreted in terms of a model of creep (knitting model) in which recovery is controlled by thermally activated glide of dislocations through subgrain boundaries. The model gives a quantitative description of $\dot{\epsilon}_s(\sigma)$ and correctly predicts the range in which $\dot{\epsilon}$ varies after stress reduction. (18 refs.)

115255 On the mixture rule for strength of fibre reinforced cements. V.Laws (Building Res. Establ., Watford, England). *J. Mater. Sci. Lett. (GB)*, vol.2, no.9, p.527-31 (Sept. 1983). The author suggests how a relationship between bending strength and fibre volume fraction having the appearance of a mixture law can arise although the tensile strength/volume fibre fraction relationship depends on the fibre contribution alone. (11 refs.)

115256 The effect of fast neutron irradiation on the compressive stress-strain relationships of graphite. M.Birch (Springfields Nuclear Power Dev. Labs., UKAEA, Preston, England), D.J.Bacon. *Carbon (GB)*, vol.21, no.5, p.491-6 (1983). A study of the effects of fast neutron irradiation on the mechanical properties of polycrystalline graphite is reported. Irradiation to a maximum dose of 1.14×10^{19} n/cm² at $\sim 50^\circ\text{C}$ increased the Young's modulus by 140%. The linearity of the compressive stress-strain curve increased and the hysteresis losses decreased. The fracture stress doubled, whilst the fracture strain decreased by $\sim 24\%$. Measurements of the total energy absorbed in compression indicated an average increase in the energy required for failure after irradiation. A constant elastic strain to failure criterion was found to be applicable for these irradiation conditions. Upon subsequent thermal annealing the Young's modulus decreased and had almost reached its unirradiated value by 400°C . The fracture stress also decreased towards its unirradiated value and the hysteresis losses increased. (3 refs.)

115257 Influence of substructure on the mechanical properties of austenitic alloys deformed by warm rolling. V.I.Izotov, Yu.G.Virakhovskii, S.Ya.Marusenko (Inst. of Metall. & Phys. of Metals, Moscow, USSR). *Fiz. Met. & Metalloved. (USSR)*, vol.56, no.2, p.372-8 (Aug. 1983). In Russian. English translation in: *Phys. Met. & Metallogr. (GB)*. An investigation was made of the relationship between the substructure and mechanical properties of some austenitic iron alloys differing in respect of the amount of carbon and of carbide-forming elements, as well as in respect of the stacking fault energies. These alloys were subjected to warm rolling. The maximum value of the yield stress after this treatment was achieved for an alloy with a low stacking fault energy because of a high density of thin twins which were formed in this case. (9 refs.) A.T.

115258 Finite plastic strain in annealed mild steel during proportional and non-proportional loading. J.F.Bell (Dept. of Mech., Johns Hopkins Univ., Baltimore, MD, USA). *Int. J. Solids & Struct. (GB)*, vol.19, no.10, p.857-72 (1983). Proportional and non-proportional loading experiments show that the finite strain plastic response of annealed mild steel between the termination of the initial yield and the termination of the ultimate stress closely follows the predictions of an incremental theory of finite plastic strain for which stress and strain components are referred to the original, undeformed reference configuration. Experimental studies of the initial yield domain in terms of dead weight loading of mild steel have shown that the initiation and termination of this region also may be described in terms of the same parabolic generalization. Finally, for annealed mild steel in dead weight loading, the generalized stress at failure is shown to occur on a common von Mises loading surface. (11 refs.)

115259 Elongation minimum and strain rate sensitivity minimum of zircaloy-4. S.I.Hong, W.S.Ryu, C.S.Rim (Div. of Nuclear Fuel Design, Korea Advanced Energy Res. Inst., Chaong-Nam, Korea). *J. Nucl. Mater. (Netherlands)*, vol.116, no.2-3, p.314-16 (June 1983). Annealed Zircaloy sheets were used in experiments to identify the elongation minimum and strain rate sensitivity minimum. The results imply that the elongation minimum is not associated with brittle fracture and that it can be explained in terms of the strain rate sensitivity. (13 refs.)

115260 Plastic deformation of spherical steel shells under internal blast loading. L.N.Aleksandrov, A.G.Ivanov, V.N.Mineev, V.I.Tsyupkin, A.T.Shitov. *J. Appl. Mech. & Tech. Phys. (USA)*, vol.23, no.6, p.831-5 (Nov.-Dec. 1982). Translation of: *Zh. Prikl. Mekh. & Tekh. Fiz. (USSR)*, vol.23, no.6, p.103-8 (Nov.-Dec. 1982). [received: Sept. 1983] The authors present computational and experimental results of research directed toward finding the laws of behaviour of spherical shells of various thicknesses in the region of plastic deformation (up to rupture) under a single internal blast loading. The results show that a simple physical model gives a satisfactory analytic description of the parameters of plastic deformation spherical shells of mild steel under internal symmetric loading by the explosion of a charge of TH 5050. (16 refs.)

115261 Study of molecular deformation mechanisms in the glassy state. I. Temperature effect on stress-birefringence and strain-birefringence responses of poly(methyl methacrylate). S.D.Hong, S.Y.Chung, R.F.Fedors, J.Moacanin (Jet Propulsion Lab., California Inst. of Technol., Pasadena, CA, USA). *J. Polym. Sci. Polym. Phys. Ed. (USA)*, vol.21, no.9, p.1647-60 (Sept. 1983). In order to gain better understanding of the molecular deformation processes occurring in poly(methyl methacrylate), a series of studies was carried out in uniaxial tension on the simultaneous stress and birefringence response in both constant-strain-rate and stress relaxation-experiments. The former covered the temperature range -120 to 75°C and the latter 0 to 90°C . Three deformation mechanisms, i.e. (i) change in intermolecular distance, (ii) distortion of the conformation of the COOCH_3 group from its thermal equilibrium state, and (iii) orientation of main-chain segments, are invoked to interpret the experimental results. It is concluded that, in the temperature range from -120 to 75°C and possibly at higher temperatures as well, the polymer chains deform in the small-strain region by an orientation of those chain segments having lower potential-energy barriers to conformational changes and straining those chain segments having higher potential-energy barriers. Subsequent chain orientation of the already strained segments occur in the higher strain regions. (21 refs.)

115262 Rheo-optical studies on the deformation mechanism of semicrystalline polymers. XIV. Alpha and beta mechanical dispersions of spherulitic high-density polyethylene and the dynamic orientation distribution function of crystallites. K.Fujita, H.Niwa, S.Nomura, H.Kawai (Dept. of Polymer Chem., Faculty of Engng., Kyoto Univ., Kyoto, Japan). *J. Polym. Sci. Polym. Phys. Ed. (USA)*, vol.21, no.9, p.1713-43 (Sept. 1983). The dynamic tensile deformation mechanism of spherulitic high-density polyethylene was investigated by dynamic X-ray diffraction at various temperatures and frequencies in order to assign the α and β mechanical dispersions explicitly. The uniaxial orientation distribution function $g(\xi, 0)$ of the j th crystal plane and its dynamic response $\Delta g(\xi, 0)$ in phase with dynamic strain were observed for the (110), (200), (210) and (020) crystal planes. Then the orientation distribution function $w(\xi, 0, \eta)$ of crystallites (crystal grains) and its dynamic response $\Delta w(\xi, 0, \eta)$, also in phase with the dynamic strain, were determined by a mathematical transformation procedure proposed by Roe and Krigbaum on the basis of the Legendre addition theorem. The temperature and frequency dependences of $\Delta w(\xi, 0, \eta)$, were analyzed in terms of the model parameters for dynamic spherulite deformation, combining affine orientation of crystal lamellae with several types of preferential reorientation of the crystal grains within the orienting lamellae. (44 refs.)

115263 Coble and Harper-Dorn creep in iron at homologous temperatures T/T_m of 0.40-0.54. J.Fiala, J.Novotny, J.Cadek (Inst. of Phys. Metall., Czechoslovak Acad. of Sci., Brno, Czechoslovakia). *Mater. Sci. & Eng. (Switzerland)*, vol.60, no.3, p.195-206 (Sept. 1983). The creep of high purity iron at low stresses (0.1-3.5 MPa) was investigated over a homologous temperature range T/T_m of 0.40-0.54 (where T is the temperature under consideration and T_m is the temperature of the melting point) using the helicoid specimen technique; the mean intercept grain size ranged from 82 to 478 μm . The results obtained enabled the most probable dominant deformation mechanism to be identified as Coble creep (1963) for intercept grain sizes smaller than about 123 μm and Harper-Dorn creep (1957) for intercept grain sizes greater than 123 μm . Coble creep in α -Fe was found to be characterized by Bingham behaviour. The threshold stress increases exponentially with decreasing temperature but does not depend on the mean intercept grain size. Under the experimental conditions considered, Harper-Dorn creep is most probably dislocation core diffusion controlled. It was found that for Harper-Dorn creep in α -Fe there is a threshold stress which increases exponentially with decreasing temperature and does not depend on the mean intercept grain size. (29 refs.)

115264 Properties of two high strength, high temperature, high conductivity copper-base alloys. A.K.Lee, N.J.Grant (Dept. of Materials Sci. & Engng., MIT, Cambridge, MA, USA). *Mater. Sci. & Eng. (Switzerland)*, vol.60, no.3, p.213-23 (Sept. 1983). The properties of two high strength, high temperature, high conductivity ingot-based copper alloys were examined in detail. These are the Cu-0.66 wt.% Mg-0.63 wt.% Cr-0.13 wt.% Zr (M2C) and the Cu-4.94 wt.% Ni-2.40 wt.% Ti materials produced as wrought ingot-based alloys. Tensile tests at 293K and stress rupture tests at 673K were performed. An oxide-dispersed Cu-Zr-Cr alloy produced from fine atomized powders has the same stress rupture properties at 673K as the fully heat-treated wrought M2C alloy, and both are stronger than the wrought Cu-Ni-Ti alloy. The effects of short-time (1 h) annealing to 1223K were examined with the interesting observation that the Cu-Ni-Ti alloy, after loss of hardness due to overaging in the temperature interval 673-1073K, rehardens on heating above 1073K and then cooling, by a resolution and aging process. Combining water quenching from the temperature range 1138-1223K with reaging at 848-873K permitted recovery of the original fully heat-treated room temperature strength and hardness properties to full strength and hardness. (28 refs.)

115265 Work-hardening rates during the high temperature creep of aluminium determined from the instantaneous strain on sudden stress changes. H.Oikawa, M.Nakata, S.Karashima (Dept. of Materials Sci., Tohoku Univ., Sendai, Japan). *Mater. Sci. & Eng. (Switzerland)*, vol.60, no.3, p.247-53 (Sept. 1983). The work-hardening rates during the creep of polycrystalline aluminium were determined from instantaneous plastic strains in stress change tests in the temperature range 455-650K under stresses for which the steady state creep rates lie within the range 5×10^{-7} to $2 \times 10^{-5} \text{ s}^{-1}$. The true work-hardening rates h were estimated by extrapolating the apparent values which were determined from the instantaneous plastic strains occurring during about 0.2 s after the stress increases ranging from 0.1 to 1 MPa. The values of h are of the order of Young's modulus and depend markedly on temperature and stress. The need not only to improve the existing theories of recovery creep but also to extend the present fine structure observations is suggested. (21 refs.)

115266 Role of eutectoid transformation and grain size on the creep behaviour of mild steel. M.R.Nagy, M.M.El-Sayed, A.A.Mohamed (Phys. Dept., Ain Shams Univ., Cairo, Egypt). *Mater. Sci. & Eng. (Switzerland)*, vol.60, no.3, p.113-16 (Sept. 1983). Creep curves were obtained under a constant applied stress σ of 68.7 MN m^{-2} (7 kgf mm^{-2}) for mild steel samples with various grain sizes tested at temperatures between 660 and 750°C (the eutectoid temperature, 723°C , falls into this temperature range). The creep rate showed a maximum at 710°C (i.e. near the eutectoid point) and the peak creep rate increased with increasing grain diameter. This peak was attributed to coarsening and/or dissolution of iron carbide in the vicinity of the eutectoid point. The activation energy for steady state creep in the vicinity of the peak was $268 \pm 4 \text{ kJ mol}^{-1}$. This activation energy was attributed to the decomposition of pearlite. (16 refs.)

115267 Large strain plastic deformation of commercially pure nickel. W.H.Zimmer, S.S.Hecker, D.L.Rohr (Univ. of California/Los Alamos Nat. Lab., Los Alamos, NM, USA), L.E.Murr.

Met. Sci. (GB), vol.17, no.4, p.198-206 (April 1983). [received: Sept. 1983]
Commercially pure nickel was deformed to very large strains by cold rolling. Tensile tests on prestrained sheet were used to establish strain hardening behaviour and residual ductility. The hardening of nickel was found to be peculiar: initial rapid hardening was followed by an apparent plateau, which, in turn, was followed by another stage of rapid hardening at strains larger than 4. The residual elongation dropped precipitously with initial prestrain, levelled off, and then increased again during the final stage of hardening. Nickel rolled to a strain of 6.1 exhibited a remarkable tensile strength of 1400 MN m⁻² with 4% total elongation. Extensive in-plane and limited edge-on transmission electron microscopy was used to examine the evolution of substructure. Dislocation cells formed at strains <0.10 and continued to refine in size with increasing strain. Definite evidence of dynamic recovery was found. The formation of elongated, well defined subgrains appears to coincide with a saturation of hardening in the plateau region. The hardening transition may be caused by the reemergence of original grain boundaries as important structural features at very large strains. (14 refs.)

115268 Luder's strain and ductility of ordered Fe-Co-2V and Fe-Co-V-Ni. C.D.Pitt, R.D.Rawlings (Dept. of Metall. & Materials Sci., Imperial Coll. of Sci. & Technol., London, England).

Met. Sci. (GB), vol.17, no.6, p.261-6 (June 1983).
The effect of thermomechanical treatment on tensile properties has been measured in ordered Fe-Co-2V and Fe-Co-V-Ni alloys containing up to 7.4 wt.% Ni. The aim was to determine the microstructural features affecting the Luder's strain and ductility of these alloys. The dominant microstructural feature was found to be the grain or subgrain size, which was determined by the volume fraction of γ phase present. The extent of the Luder's strain decreased with increasing grain size but the ternary and quaternary alloys showed different grain size dependences. The ductility of all the alloys was proportional to $d^{-1/2}$, where d is the grain, subgrain, or deformation cell size. (19 refs.)

115269 Effects of V and Nb additions on high temperature deformation properties of low alloy martensites. Y.Ohmori, T.Kunitake (Central Res. Labs., Sumitomo Metal Industries Ltd., Amagasaki, Japan).

Met. Sci. (GB), vol.17, no.6, p.267-75 (June 1983).
The effects of microalloying elements such as V and Nb on the high temperature deformation properties of low alloy martensites have been investigated by means of slow strain rate tensile tests at various temperatures. It was confirmed that the precipitations of fine carbonitrides, such as V(C,N) and NbC, are quite effective in reducing the high temperature ductilities. In particular, it has been concluded that the most detrimental effects on ductility arise from the dynamic trapping of the mobile dislocations generated at prior austenite grain boundaries by the simultaneous precipitation of V(C,N) or NbC. The cyclic repetition of such a process would result in strain concentration in the vicinity of prior austenite grain boundaries, and microvoids would form at the cementite/matrix interfaces on these boundaries, leading to intergranular ductile fracture. (37 refs.)

115270 Role of molybdenum in sintered steels [tensile properties]. M.Hamiuddin (Chem. Section, Z.H. Coll. of Engng. & Technol., Aligarh, India).

Powder Metall. Int. (Germany), vol.15, no.3, p.147-50 (Aug. 1983).
The role of molybdenum in PM grade steels is reviewed. Additional experiments are carried out with Fe-O, 45P-(0.4 to 0.8)C-(1 to 4) Mo powder premixes which were compacted at 691 MPa pressure into MPF tensile test bars and sintered at 1120°C and 1200°C for 30 min in dry hydrogen. Ultimate tensile and yield strengths, elongation and linear dimensional change after sintering were determined. Strength properties improved with increasing Mo or C contents and increasing sintering temperature. Ductility increased with increasing sintering temperature but decreased with increasing Mo or C content. The results are supported by microstructural and scanning electron fractography studies and explained on the basis of phase stabilization and diffusion data. (24 refs.)

115271 Work hardening and the stability of deformation in AlZnMg alloys. I.Kovacs, J.Lendvai, T.Ungar, Z.Rajkovits (Inst. for General Phys., Eotvos Univ., Budapest, Hungary).

Philos. Mag. A (GB), vol.48, no.3, p.329-39 (Sept. 1983).
The stress-strain curves of the Al-Zn-Mg alloys investigated consisted of a linear and a parabolic part. The slope of the linear part, unlike that of the parabolic part, was found to be fairly independent of heat treatment, testing temperature and strain rate. The fracture stress of the samples is always smaller than what might be expected on the basis of the classical stability criterion, and this is caused by microcrack formation at grain boundaries. (17 refs.)

115272 The plastic compression of copper cones. M.M.Chaudhri (Cavendish Lab., Univ. of Cambridge, Cambridge, England).

Philos. Mag. A (GB), vol.48, no.3, p.L15-20 (Sept. 1983).
Annealed and unannealed (i.e. work-hardened) cones of included angles in the range 30°-170° of high-conductivity copper have been quasi-statically compressed against a hard transparent surface and their deformation stress measured under load. It was found that for the unannealed cones the deformation stress increased linearly with the cone angle whereas for the annealed cones the deformation stress peaked at a cone angle in the range 60°-90°. The deformation pattern of the cones has also been investigated and found to be quite different in the two types of cone. The deformation stress versus cone angle behaviour has been explained on the mode of deformation of the two types of cone. (10 refs.)

115273 Deformation properties of refractory glass-fiber goods based on mullite-silicate fiber. E.Z.Korol', V.M.Panferov, V.V.Martynenko, E.P.Saenko, A.N.Gaodu, N.V.Pitak (Inst. of Mech., M.V. Lomonosov Moscow State Univ., Moscow, USSR).

Refractories (USA), vol.23, no.11-12, p.594-9 (Nov.-Dec. 1982). Translation of: *Ogneupory (USSR)*, vol.23, no.11, p.41-5 (Nov. 1982).
Studies have been carried out on the deformation characteristics under uniaxial extension and compression of specimens of thermal-insulation refractory glass-fiber tiles type MKRP-340 based on mullite silica fiber in organic binder in the 20-1200°C interval. It was established that the tiles are transversely isotropic, i.e. their mechanical properties remain unchanged with a random rotation relative to the axis perpendicular to the plane of the tile with reflection relative to the plane containing this axis; the anisotropy disappears on heating to 1000-1200°C. It is concluded that the tested tiles can be used as compensation and heat-insulation materials in thermally stressed designs in which compressive stresses are ≤ 0.2 MPa at temperatures up to 1200°C and extension-bend deformation is < 0.005 . The tiles retain their strength when stacked in linings with a curvature > 1.0 m. (4 refs.)

115274 Rheological properties of ShKh15 steel under multistage loading. Polukhin P.I., A.M.Galkin, V.P.Polukhin, S.P.Efimenko, I.M.Gridnev, V.L.Pilyushenko.

Russ. Metall. (GB), no.3, p.119-22 (1982). Translation of: *Izv. Akad. Nauk. SSSR Met.*, no.3, p.139-42 (1982).
An examination was carried out on the resistance to deformation and the plasticity of ShKh15 (NLZ) steel under hot single-stage and multi-stage loading in torsion and compression. Torsion tests were carried out in a torsional plasticity meter. Depending on the temperature and rate of strain conditions of deformation, the amounts of deformation in each of the passes and the durations of the time intervals between loadings, the multi-stage deformation curves may lie below, at the same level or above the curve for continuous loading. (7 refs.)

115275 Influence of silicon on the structure and properties of alloyed compound Ni₃Al. V.P.Buntushkin, K.I.Portnoy, O.D.Melimevker, M.Kh.Levin-skaya, I.V.Romanovich, G.F.Loskutova.

Russ. Metall. (GB), no.3, p.162-5 (1982). Translation of: *Izv. Akad. Nauk. SSSR Met.*, no.3, p.185-9 (1982).
The results of an investigation of the dependence of the structure and properties of alloyed phase Ni₃Al on the amount of introduced silicon, in a concentration within the limits of 0.58-1.4 wt.%, are reported. In the compound Ni₃Al, alloyed with chromium, tungsten, titanium, carbon and close in composition to the γ -phase of heat-resistant nickel alloys, silicon replaces aluminium in the crystal lattice and determines the appearance in the structure of the β -phase on NiAl; thus the transition $\gamma \rightarrow \beta$ shifts towards smaller concentrations of aluminium. Additions of silicon to the compound Ni₃Al in amounts 0.58-1.4%, at 20°C, result in reduced ductility, an increase in its hardness and yield point, and at 1150°C softens the alloyed intermetallic. Silicon has a beneficial influence on the heat resistance of alloyed intermetallic Ni₃Al at 1220°C. (7 refs.)

115276 Effects of stabilization on the elastic to visco-plastic transition in metallic glasses. L.T.Shi, A.S.Argon, H.Y.Kuo (MIT, Cambridge, MA, USA).

Ser. Metall. (USA), vol.17, no.8, p.1014-20 (Aug. 1983).
Experimental data on inelastic deformation in Cu₅₆Zr₄₄ and Pd₈₀Si₂₀ by Argon and Kuo (1980) showed considerable deviations from the proposed theoretical curve of Argon and Shi (1983). Additional creep recovery experiments on Cu₄₀Zr₆₀ ribbons are reported to gain further understanding of the causes of this discrepancy. (11 refs.)

115277 Influence of impurity atoms on the mechanical properties of group Va metals and alloys based on them. V.V.Shirokov, O.I.Eliseeva (G.V. Karpenko Physicomech. Inst., Acad. of Sci., Lvov, Ukrainian SSR).

Sov. Mater. Sci. (USA), vol.18, no.6, p.471-4 (Nov.-Dec. 1982). Translation of: *Fiz.-Khim. Mekh. Mater. (USSR)*, vol.18, no.6, p.16-20 (Nov.-Dec. 1982).
The influence of interstitial and substitutional atoms on the strength characteristics of group Va metals and alloys based on them was investigated. Unalloyed vanadium, niobium, and tantalum, and alloys based on them were used for the experiments. The investigations made showed that under certain conditions (rate of tension and temperature) in group Va metals and alloys based on them, dynamic interaction of the interstitial and substitutional impurity atoms with dislocation occurred, which lead to significant hardening and a reduction in plasticity of the materials. In the area below 650°C interstitial atoms were responsible for the effects of dynamic strain hardening and above 650°C substitutional atoms. (12 refs.)

115278 Creep of hardened steel in tempering. V.A.Likhachev, A.P.Demenkov (A.A. Zhdanov Leningrad State Univ., Leningrad, USSR).

Sov. Mater. Sci. (USA), vol.18, no.6, p.475-8 (Nov.-Dec. 1982). Translation of: *Fiz.-Khim. Mekh. Mater. (USSR)*, vol.18, no.6, p.21-5 (Nov.-Dec. 1982).
The tests were made in different stressed states of the material, including by torsion of thin-walled tubes and under conditions of loading ends of equal cross section with a concentrated tensile force. The error in measuring the strain ϵ was $\sim 3 \times 10^{-3}\%$ and in temperature $t \pm 1^\circ\text{C}$. The rate of heating in tempering was 0.2°C/sec. The stresses and strains were referred to the most heavily loaded outer fiber of the samples, using the theory of elasticity for the calculation. The apparatus was equipped with a device compensating for thermal expansion. The objects of the investigation were various carbon (20, 30, 40, 45, 55, U8, U10, and U12) and alloy (40 Kh, 40 N, and 40 KhN) steels previously subjected to standard (production) hardening cycles. (4 refs.)

115279 Variational functional for a rigid-plastic porous material. A.M.Laptev (Kramatorsk Industrial Inst., USSR).

Sov. Powder Metall. & Met. Ceram. (USA), vol.22, no.1, p.1-3 (Jan. 1983). Translation of: *Poroshk. Metall. (USSR)*, vol.22, no.1, p.1-4 (Jan. 1983). [received: Aug. 1983]
To derive a variational functional with allowance for rate discontinuities, an equation of the virtual powers of a true stressed and kinematically possible strained state is considered. (8 refs.)

115280 Effect of small amounts of tungsten carbide on the strength, creep, and brittle-to-ductile transition temperature of zirconium carbide. B.D.Gurevich, L.B.Nezhevenko, P.V.Zubarev, V.P.Bulychev, N.N.Bragin, V.N.Kruglov, M.A.Fedotov.

Sov. Powder Metall. & Met. Ceram. (USA), vol.22, no.1, p.35-8 (Jan. 1983). Translation of: *Poroshk. Metall. (USSR)*, vol.22, no.1, p.39-42 (Jan. 1983). [received: Aug. 1983]
The starting material was a zirconium carbide powder produced by the carbothermic reduction of ZrO₂ at 1800°C. It was subjected to homogenizing annealing for 1 h at 2100°C under a residual pressure of 1.33×10^{-2} Pa. It is concluded that the use of hard-metal mills for the pretreatment of carbide powders with the aim of increasing to a maximum their sintering activity is permissible when the resultant tungsten content does not exceed 0.5 wt.%. The presence of this amount of tungsten had no effect on the microstructure, lattice constant, substructural characteristics, short-time strength, and creep resistance of zirconium carbide specimens sintered at 2600°C. However, when considering the potentialities and conditions of operation of parts of zirconium carbide containing ~ 0.3 mole % W, it is necessary to bear in mind that the brittle-to-ductile transition temperature of the material was raised some 100°C as a result of the presence of the addition. (10 refs.)

115281 Experimental investigation of laws governing the hardening of initially anisotropic materials. V.V.Kosarchuk, B.I.Koval'chuk, A.A.Lebedev (Inst. of Strength Problems, Acad. of Sci., Kiev, Ukrainian SSR).

Strength Mater. (USA), vol.14, no.9, p.1157-64 (Sept. 1982). Translation of: *Probl. Prochn. (USSR)*, vol.14, no.9, p.3-9 (Sept. 1982).
Using aluminium alloys D16T, AMtS and AMg₃, the authors experimentally investigated the rules of governing the hardening of initially anisotropic metallic materials in order to establish relationships between the parameters that define the shape and size of subsequent yield surfaces, and the level of plastic deformation, and the orientation of the preloading path in stress space. (20 refs.)

115282 Experimental study of the effect of scale and shape of a body on deformation and failure mechanisms of structurally inhomogeneous materials. V.P.Lamashevskii, P.T.Alfimov, A.A.Lebedev (Inst. of Strength Problems, Acad. of Sci., Kiev, Ukrainian SSR).

Strength Mater. (USA), vol.14, no.9, p.1238-43 (Sept. 1982). Translation of: *Probl. Prochn. (USSR)*, vol.14, no.9, p.68-72 (Sept. 1982).

On the basis of data for grey cast iron, the deformation process for quasibrittle materials was found to depend essentially on geometric dimensions of the deformed body, and the greater the deformed volume then the more intense was disintegration, which ultimately affected the value of ultimate strength. The dependence of ultimate strength was satisfactorily described by the statistical theory of strength, and cross-sectional shape did not affect deformation and failure mechanisms for quasibrittle bodies. (12 refs.)

115283 Temperature-time dependence of the cyclic-creep activation energy of heat-resistant alloys. V.P.Golub (Inst. of Mech., Acad. of Sci., Kiev, Ukrainian SSR).

Strength Mater. (USA), vol.14, no.11, p.1466-73 (Nov. 1982). Translation of: *Probl. Prochn. (USSR)*, vol.14, no.11, p.38-45 (Nov. 1982). [received: Sept. 1983]

Determines the activation energy of cyclic creep U_z of heat-resistant nickel alloys in high-cycle loading and evaluates the effect of cycle temperature and stresses on U_z . A cycle of experimental studies were made for cyclic creep within a broad range of temperatures and stresses. The following nickel-based heat-resistant alloys were studied: deformable EI867, and foundry VZhL12U, after the standard heat treatment. The results obtained showed that cyclic creep is based on the mechanism of dislocation limb. (18 refs.)

115284 Study of the high-temperature creep of multilaminar iron/copper and nickel/copper condensates. B.A.Movchan, E.V.Dabizha, R.F.Bansha, R.Nimmagadda (E.O. Paton Inst. of Electric Welding, Kiev, Ukrainian SSR).

Strength Mater. (USA), vol.14, no.11, p.1474-6 (Nov. 1982). Translation of: *Probl. Prochn. (USSR)*, vol.14, no.11, p.45-7 (Nov. 1982). [received: Sept. 1983]

Condensates were used to prepare flat specimens with a working length of 10 mm and working width of 3 mm. The specimens were annealed in a vacuum at 600°C for 1 h before testing. Creep tests were conducted in a vacuum at 600°C in the stress range 20-130 MPa. The microstructure of the original condensates and after the creep tests was studied with a scanning attachment for the JSEM-200 electron microscope. A typical fine two-phase structure was formed in multilaminar condensates with microlayers less than 2-3 μ m thick during high-temperature creep. The dispersed particles of iron or nickel were located in internal volumes of subgrains comprising the copper matrix, characterized by the presence of dislocations with a higher thermal mobility than in pure iron and nickel. (3 refs.)

115285 Influence of alloying on the strength of vanadium. G.G.Maksimovich, E.M.Lyutiy, V.V.Shirokov, I.P.Druzhinina, G.N.Per'kova (Physico-mech. Inst., Acad. of Sci., Kiev, Ukrainian SSR).

Strength Mater. (USA), vol.14, no.11, p.1531-5 (Nov. 1982). Translation of: *Probl. Prochn. (USSR)*, vol.14, no.11, p.89-93 (Nov. 1982). [received: Sept. 1983]

Presents the results of an investigation of the effect of various contents (5-20 wt.%) of titanium, tungsten, chromium, niobium, and tantalum on the strength characteristics of vanadium samples in a wide temperature range (293-1673K). For comparison an alloy of vanadium with 20 wt.% titanium was also tested. It was found that all of the alloying additions tested significantly strengthened the vanadium. (12 refs.)

115286 Experimental examination of the strength of a glass-fiber plastic with longitudinal-transverse reinforcement in the plane stress state. V.I.Kulik, E.V.Meshkov, R.B.Rikards, Z.T.Uptis (Leningrad Inst. of Mech. Engng., Leningrad, USSR).

Strength Mater. (USA), vol.14, no.11, p.1544-50 (Nov. 1982). Translation of: *Probl. Prochn. (USSR)*, vol.14, no.11, p.100-6 (Nov. 1982). [received: Sept. 1983]

The strength of glass-fiber tubular specimens with longitudinal-transverse reinforcement in the plane stress state was examined by means of experiments. The results of the main independent experiments, required for determining the strength properties of the material with the aid of fracture criteria were obtained. Additional experiments were also carried out to verify the reliability of construction of the strength surface. (8 refs.)

115287 Strength of porous net materials in the uniaxial strain state. A.F.Tret'yakov, G.P.Polushkin, A.D.Panov (N.E. Bauman Higher Tech. School, Moscow, USSR).

Strength Mater. (USA), vol.14, no.11, p.1551-6 (Nov. 1982). Translation of: *Probl. Prochn. (USSR)*, vol.14, no.11, p.106-9 (Nov. 1982). [received: Sept. 1983]

A method is proposed of constructing the tensile diagram of the PNM, and the strength and strain anisotropy of a porous sheet with a given type of laying the net layers is examined for the case of the uniaxial strain state. (3 refs.)

115288 Model plastic-rubber composites from emulsion polymers. M.Morton (Inst. of Polymer Sci., Univ. of Akron, Akron, OH, USA), N.K.Agarwal, M.Cizmecioglu.

Polymer Alloys III Blends, Blocks, Grafts and Interpenetrating Networks. Proceedings of a Symposium, New York, USA, 23-28 Aug. 1981 (New York, USA: Plenum 1983), p.1-18

The preparation is described of well-defined dispersions of hard, glassy plastics in SBR vulcanizates and rubber particles in a polystyrene matrix. Both types of composite materials were prepared by blending latex polymers of known particle size, which, upon coagulation, became composites containing the desired particles of plastic 'fillers' for the rubber and rubber particles in the plastic. The effects of filler particle size, rigidity and the filler-rubber adhesion on tensile strength are discussed. (8 refs.)

115289 On the correlation of mechanical properties of high impact polystyrene with its morphology, molecular-weight characteristics and extrusion conditions. V.D.Yenaleyev, V.I.Melnichenko, O.P.Boukunenko, A.N.Shelest, N.M.Tchalaya, Y.I.Yegorova, N.G.Podosyonova (Donetsk State Univ., Donetsk, USSR).

Polymer Alloys III Blends, Blocks, Grafts and Interpenetrating Networks. Proceedings of a Symposium, New York, USA, 23-28 Aug. 1981 (New York, USA: Plenum 1983), p.19-25

An attempt is made to establish, by means of statistical methods, the quantitative correlation between HIPS elongation at break and impact strength and the molecular weight and its distribution of the polystyrene matrix, copolymer and gel quantity, and morphological characteristics. (9 refs.)

115290 Correlation of morphology, mechanical properties and processing conditions of modified high impact polystyrene. V.V.Abramov, V.D.Yenaleyev, M.S.Akutin, N.M.Tchalaya, V.I.Melnichenko, A.N.Shelest (Donetsk State Univ., Donetsk, USSR).

Polymer Alloys III Blends, Blocks, Grafts and Interpenetrating Networks. Proceedings of a Symposium, New York, USA, 23-28 Aug. 1981 (New York, USA: Plenum 1983), p.27-30

Deals with the effect of elastomer addition, introduced into the extrusion process on HIPS morphology and some strength properties. To introduce the elastomer, a single screw extruder was used. The morphology of modified HIPS was studied by electron microscopy, impact strength (according to Charpy, without a notch), elongation at break, and tensile strength. The blending conditions of copolymers A and B with HIPS and their effect on mechanical properties are presented. It is seen that the introduced copolymer greatly affects the impact strength and elongation at break (depending on extrusion conditions). (3 refs.)

115291 RIM systems from interpenetrating polymer networks. R.Pernice, K.C.Frisch, R.Navare (Polymer Inst., Univ. of Detroit, Detroit, MI, USA).

Polymer Alloys III Blends, Blocks, Grafts and Interpenetrating Networks. Proceedings of a Symposium, New York, USA, 23-28 Aug. 1981 (New York, USA: Plenum 1983), p.219-31

Simultaneous interpenetrating polymer networks (SIN-IPNs) based on polyurethane and polyepoxides were synthesized according to the processing conditions of RIM technology. Catalytic systems were selected in order to minimize or avoid formation of any covalent bonds between the epoxy and the polyurethane chains. In this way topological polymer alloys (IPNs) were obtained which exhibited improved physical properties. Both low modulus and high modulus urethane elastomers were used in combination with epoxy resins derived from glycidyl ethers of bisphenol A. In addition, combinations of the latter with novolac epoxy resins were employed together with high modulus urethane elastomers. Maxima in ultimate tensile strength occurred at the ratio of 20/80 of epoxy resin/polyurethane systems. These maxima were interpreted as evidence of a permanent entanglement, between the two different types of polymer networks. A thermoanalytical study using a Rheovibron and DSC was carried out to give further support for the formation of IPNs. (14 refs.)

115292 A stress transfer model for the deformation and failure of polymeric matrices under swelling conditions. D.Cohn, G.Marom (Casali Inst. of Appl. Chem., Hebrew Univ. of Jerusalem, Jerusalem, Israel).

Role of the Polymeric Matrix in the Processing and Structural Properties of Composite Materials. Proceedings of a Joint US-Italy Symposium, Capri, Italy, 15-19 June 1981 (New York, USA: Plenum 1983), p.245-59

It was found that polymers in which the diffusion mechanism was characterized by a sharp advancing boundary between the swollen shell and the core, showed a highly anisotropic swelling response. The anisotropy of the swelling strains was caused by the mechanical constraints exerted mutually by the two regions of the specimen. The swelling stresses developing during the process eventually led to fracture of the polymer specimen. An analytical model which explained the modes of failure of the polymer under the swelling stresses was developed. The proposed approach was based on the general analogy existing between the studied swollen specimens and composite materials. A model for the prediction of the anisotropic hygroelastic response of the swollen systems was also proposed. (12 refs.)

115293 Effect of fiber aspect ratio on ultimate properties of short-fiber composites. J.L.Kardos, E.Masoumy, L.Kacir (Dept. of Chem. Engng., Washington Univ., St. Louis, MO, USA).

Role of the Polymeric Matrix in the Processing and Structural Properties of Composite Materials. Proceedings of a Joint US-Italy Symposium, Capri, Italy, 15-19 June 1981 (New York, USA: Plenum 1983), p.407-23

Even though a ductile epoxy matrix was used, highly oriented short fiber systems were still found to produce nearly linear, brittle-like tensile stress-strain behaviour when tested in the major fiber direction (0°). As the fiber bundle aspect ratio increased, the tensile modulus approached that for a continuous fiber system of the same volume loading, whereas the tensile strength achieved only 59% of the continuous fiber value for the largest aspect ratio studied (557). When the aligned fiber system was tested off-axis, the effect of aspect ratio on modulus became very small at angles exceeding about 15°. (11 refs.)

115294 Dimensional stability of reinforced matrices. A.Apicella, P.Masi, L.Nicodemo, L.Nicolas, S.Piccarolo (Istituto Principi di Ingegneria Chimica, Univ. di Napoli, Napoli, Italy).

Role of the Polymeric Matrix in the Processing and Structural Properties of Composite Materials. Proceedings of a Joint US-Italy Symposium, Capri, Italy, 15-19 June 1981 (New York, USA: Plenum 1983), p.469-79

The effect of draw ratio and glass filler on the recoil kinetics of composite sheets is analyzed. Both amorphous and semicrystalline matrices were used. The recoil of filled polystyrene was largely affected by the presence of filler. In particular the fibers strongly enhanced the dimensional stability of the polystyrene at very low concentration. In contrast the recoil of polypropylene was not influenced by the presence of fillers, at least for the polypropylene studied. (18 refs.)

115295 In situ analysis of the interface. J.L.Koenig, Chwan-hwa Chiang (Dept. of Macromolecular Sci., Case Western Reserve Univ., Cleveland, OH, USA).

Role of the Polymeric Matrix in the Processing and Structural Properties of Composite Materials. Proceedings of a Joint US-Italy Symposium, Capri, Italy, 15-19 June 1981 (New York, USA: Plenum 1983), p.503-16

It is concluded that the great improvement in properties imparted to the fiberglass reinforced composite by traces of appropriate reactive silanes at the interface suggests that an understanding of the molecular structure of the interface might be the key to understanding the mechanical behaviour of composites. The effect of water at the interface of composites is quite complex, depending upon the nature of the polymer system and that of the fibers. Thermosetting resins like epoxy absorb water with swelling and reduction in modulus. Molecular water diffuses readily through the resin phase and attacks the interface of composites. Liquid water can leach soluble materials from the interface and the matrix phase. Silane coupling agents may partially prevent water from attacking the fiber-resin interface. So the strength retention of the silane-treated fibre composite is better than that of non-silane treated fibre composites. (55 refs.)

115296 Internal stresses in fibre reinforced plastics. K.H.G.Ashbee, J.P.Sargent, E.Walter (H.H. Wills Phys. Lab., Univ. of Bristol, Bristol, England).

Role of the Polymeric Matrix in the Processing and Structural Properties of Composite Materials. Proceedings of a Joint US-Italy Symposium, Capri, Italy, 15-19 June 1981 (New York, USA: Plenum 1983), p.517-28

Three experiments are reported. The first two investigate two stages in the development of self-stress during fabrication of a composite and the third investigates the generation of interfacial pockets of osmotic pressure asso-

ciated with the uptake of water. The techniques developed for these experiments include a combination of optical interferometry and thin plate elasticity theory to study cure stresses, the application of oblique incidence polarising optical microscopy to uniquely determine the magnitudes of radial and tangential stresses present in the resin after cooling from the cure temperature, and an analysis of the equilibrium of pressure-filled cavities in order to investigate the phenomenon of loss of load transfer attributable to osmosis during weathering. (6 refs.)

115297 Stress and strength analysis in and around composite inclusions in polymer matrices. A.Pavan (Politecnico di Milano, Milano, Italy). Role of the Polymeric Matrix in the Processing and Structural Properties of Composite Materials. Proceedings of a Joint US-Italy Symposium, Capri, Italy, 15-19 June 1981 (New York, USA: Plenum 1983), p.529-43.

An elementary model is considered for composite inclusions in polymer matrices, and a micromechanical analysis is carried out subject to some simplifying assumptions and based on numerical values applicable to rubbery inclusions containing glassy polymer sub-inclusions. Results of this analysis provide some insight into the effects that the composite particle structure has on stress distribution and craze-yielding. (39 refs.)

CANSWEL-2: A computer model of the creep deformation of Zircaloy cladding under loss-of-coolant accident conditions. Part II. User notes See Entry 112306

Phase transitions, creep, and fission gas behaviour in actinide oxides See Entry 112329

Thermoplastic analysis of a sphere-PAC fuel pin See Entry 112335

Constitutive equations for the creep behaviour of nickel-base alloys for HTR components in the temperature range 1023 - 1273 K See Entry 112341

Contour J-integral in the plastic region See Entry 112362

Examination of the stress state of a helically reinforced composite in shearing See Entry 113364

Small-angle X-ray scattering study of density fluctuation in pressure-densified polystyrene glasses See Entry 113767

Structure formation in lightly-doped chromium alloys during plastic deformation in the 1400-1450K region See Entry 113802

Influence of mechanical stresses on the accumulation of radiation defects in Nb and NbTi See Entry 114040

Direct evidence for stress-enhanced swelling in type 316 stainless steel See Entry 114041

Flow behaviour of nickel irradiated with 15 MeV neutrons and 16 MeV protons See Entry 114049

The characteristic equation for superplastic flow See Entry 114074

Deformation of semibrittle solids See Entry 114075

Laws of the limiting plasticity of metals See Entry 114076

Parameters of mechanical twins emitted by a crack See Entry 114080

A method of creep damage summation based on accumulated strain for the assessment of creep-fatigue endurance See Entry 114081

Investigation of material damage under creep and creep strength See Entry 114082

Polymer deformation studies by time resolved Fourier transform infrared spectroscopy See Entry 114862

Cold sintering under high pressure—mechanisms and application See Entry 115127

Densification and change in shape of porous materials during hot pressing under conditions of nonuniform triaxial compression See Entry 115128

Liquid phase sintering of tungsten [and optimum mechanical properties] See Entry 115134

Structure and mechanical and corrosion properties of P/M Kh23Ni18 stainless steel See Entry 115140

Preparation of superconducting lead-alloy long filaments by glass-coated melt spinning See Entry 115143

Mechanism of formation of martensite single crystals as a result of plastic deformation of the alloys based on γ -Mn See Entry 115191

Structural and phase transition of γ_1 martensite in binary Cu-Al alloy during deformation See Entry 115192

Influence of the quenching temperature on the onset of the α - γ transition and mechanical properties of maraging steel See Entry 115193

Shape memory effect in martensitic transformations in TiNi-TiCu alloys See Entry 115194

Precipitation processes in a β -phase Cu-15 at.% Sn shape memory alloy See Entry 115202

Investigation of the influence of thermomechanical treatment on the hardening of AlMgSiCu alloys See Entry 115208

Substructure hardening of polycrystalline niobium See Entry 115209

Effect of strain rate on the resistance of metals to plastic deformation See Entry 115213

Recovery behavior of hydrogen charged 7075-T6 aluminum See Entry 115215

The effects of cooling rate after controlled rolling on the mechanical properties of HSLA line pipe steels See Entry 115222

The mechanical properties and structure of Ti-Al-Zr-Mo alloys See Entry 115227

Thermal stresses and viscoelastic relaxation in metallic glasses prepared by liquid quenching See Entry 115232

Embrittlement of construction steel with bainite structure during tempering See Entry 115308

The relationship between the physical structure and the microscopic deformation and failure processes of poly(p-phenylene terephthalamide) fibers See Entry 115318

Prediction of stress relaxation and stress relief cracking in SEN testpieces See Entry 115327

Influence of slow strain rate tensile deformation on creep-fatigue endurance of 20Cr-25Ni-Nb stainless steel at 593°C See Entry 115328

Failure of rubber-modified plastic liners See Entry 115331

Embrittlement of chrome-nickel-molybdenum steel after the high-temperature action of hydrogen See Entry 115335

Low-cycle deformation and failure of die steels at service temperatures See Entry 115338

Shape effect of particles on high-temperature hardness of dispersion-hardened Ni-SiO₂ alloys See Entry 115352

Microstructure and mechanical strength of aluminum titanate ceramics prepared from synthesized powders See Entry 115353

Rubber modified matrices See Entry 115360

Characterization of high performance composite matrices See Entry 115361

Creep and fracture initiation in fibre reinforced plastics See Entry 115363

Volume changes and the technical properties of composites in the spinel-manganese oxide system See Entry 115392

A study of the thermo-oxidative process and stability of graphite and glass/PMF polyimide composites See Entry 115394

Environmental aging of epoxy composites See Entry 115395

Effect of surface stresses on ductility and fatigue strength of wear resisting coatings See Entry 115396

Inhomogeneous plastic deformation and its relevance to iodine stress corrosion cracking susceptibility in irradiated Zircaloy-2 tubing See Entry 115418

Predicting the long-term creep of organic-fiber-reinforced plastics See Entry 115472

Relationship between parameters of elastic-wave propagation and rupture-strength characteristics of structural materials See Entry 115473

Plotting stress-strain diagrams by recalculation of the computer diagram See Entry 115477

81.40N Fatigue, embrittlement, and fracture

(inc. hardness; see also 62.20M Fatigue, brittleness, fracture and cracks)

115298 The mechanical properties and failure modes in reinforced polypropylene. Lu Sinien (Inst. of Mech., Chinese Acad. of Sci., China). *Acta Mech. Sin. (China)*, no.3, p.286-92 (1983). In Chinese.

Describes the tension, relaxation behaviour and failure modes in short fibre reinforced PP. The test material is 20% (by weight) glass fibre reinforced chemically coupling polypropylene. The effects of tension speed and temperature on tension strength are shown. The σ_T -log V curves are superimposed by shifting along log V axis to give a master curve of tension strength and shift factors of strength. In the same way, the shift factors of relaxation and the master curve of relaxation are obtained. The log a_T - T curve shows that up to 120°C log a_T follows an approximately linear relation with temperature, which is a simplifying form of W-L-F equation. As a result, it is concluded that from room temperature up to 120°C the principle of time-temperature equivalence is acceptable. The scanning electronic microscope photographs show five typical kinds of failure mode on the tension fracture surface. They are brittle, semi-brittle, ductile (cup-like and layers) and flow mode. The failure mode is greatly affected by test temperature, strain rate and state of stress. (15 refs.)

115299 Discrete spectrum for the strength of Capron fibres. G.M.Bartenev, L.P.Kosareva, A.G.Barteneva.

Vysokomol. Soedin. Ser. B (USSR), vol.25, no.6, p.441-5 (1983). In Russian. Information published since 1960 is discussed in some detail and this leads to the conclusion that the structural discreteness of polymer fibres (Capron) leads to a discrete distribution in the fibre along the lines of microcracks and submicrocracks, which in its turn leads to the existence of a discrete fibre strength spectrum. The discrete dimensions of the microcrack lines obtained by X-ray methods are in agreement with calculations on discrete strength levels. (12 refs.) N.S.

115300 Effect of texture and grain size on the fracture behaviour of hot rolled Mg, Mg-12.5%Li and Mg-5%Ti alloys. G.Sambasiva Rao, Y.V.R.K.Prasad (Dept. of Metall., Indian Inst. of Sci., Bangalore, India). *Res. Mech. (GB)*, vol.9, no.1, p.41-61 (1983).

The dependence of tensile fracture characteristics of hot rolled magnesium, Mg-12.2%Li and Mg-5% Ti alloys, in the temperature range 77-420K, on grain size and texture has been studied. Hot rolled magnesium is found to have a strong basal texture and to undergo intercrystalline fracture at 77K, transcrystalline cleavage at 300 K and ductile failure at 420 K. The brittle fracture stress is grain size dependent and follows a Hall-Petch type relation. The alloys also exhibited a similar relation although the mode of failure has been found to consist of mixed features. The mechanism of crack initiation and mode of failure in hot rolled magnesium have been related to the difficulty of occurrence of basal slip and the ease of occurrence of prismatic slip which are consequences of the texture. The changes observed in the alloys have been attributed to the opposing effects of texture weakening and solid solution strengthening. (21 refs.)

115301 The surface microhardness of nickel alloys cut with a low speed diamond saw. C.E.Price (School of Mech. & Aerospace Engng., Oklahoma State Univ., Stillwater, OK, USA). *Res. Mech. (GB)*, vol.9, no.2, p.125-8 (1983).

Microhardness measurements utilising Vickers DPH impressions were made on a number of Ni alloys after cutting with a low speed diamond saw. They all showed the same type of hardness profile with the hardness level peaking a few microns beneath the surface. (9 refs.)

115302 Fracture, strength and fatigue of filled thermoset composites. S.K.Brown (Dept. of Industrial Sci., Melbourne Univ., Parkville, Australia). *Br. Polym. J. (GB)*, vol.14, no.1, p.1-13 (March 1982).

Flexural strength, impact energy and fatigue resistance are reported for a wide range of filled unsaturated polyester resin composites. Behaviour of these properties is compared with fracture energies reported earlier. Little correlation with the latter is found and reasons for this are discussed. (18 refs.)

115303 Microstructure and thickness effects on fracture in a glass thermoplastic PET injection moulding compound. K.Friedrich (Inst. for Materials Sci., Ruhr-Univ. Bochum, Bochum, Germany). *Plast. & Rubber Process. & Appl. (GB)*, vol.3, no.3, p.255-65 (1983).

Describes the microstructure of injection moulded, short glass fibre reinforced, thermoplastic polyethylene terephthalate plaques as a function of fibre loading and plaque thickness. The influences of the microstructural variations on the fracture mechanical properties of this composite system are measured. The fracture toughness is higher for cracks perpendicular to the main fibre orientation and increases with weight fraction of fibres. Fatigue cracks indicate the same tendency, i.e. their growth rate is low for cracks transverse to the fibres in samples with high fibre loading. Additional effects on fracture mechanical behaviour due to differences in matrix toughness, strength of fibre/matrix bond quality and plaque thickness are also discussed. (14 refs.)

115304 Environmental influences of fatigue damage in glass fibre reinforced polyester. P. Prentice, C.R. Wachnicki, J.C. Radon (Dept. of Mech. Engng., Imperial Coll. of Sci. & Technol., London, England).

Plast. & Rubber Process. & Appl. (GB), vol.3, no.3, p.273-9 (1983). In order to evaluate the influence of the load biaxiality factor, B , and environment on the fatigue behaviour of chopped strand mat glass reinforced polyester, low frequency tensile fatigue tests were performed under constant load conditions on centre notched biaxial test specimens in both air and dilute acid solution. A compliance calibration method was used to give a value of an effective crack length which was used in a fracture mechanics approach to analyse crack propagation data. The Paris law, relating the crack growth rate to the stress intensity factor range, has been found to hold, the value of the exponent decreasing slightly with increasing biaxiality. The value of the exponent for fatigue tests performed in an acid environment was found to be lower, by a factor of at least two, than for the corresponding tests in air. The appearance of the fracture surfaces of specimens from the two test series were found to be different; those tested in air displayed significant fibre pull-out over the whole surface whereas the surface of the slow crack growth region of specimens fatigued in an acid environment showed little sign of fibre pull-out. (12 refs.)

115305 Design for toughness in polymers. IV. The effect of geometry on stable crack propagation in thermoplastics for pressure pipe duties. M.W. Birch, M.D. Taylor, G.P. Marshall (Dept. of Polymer Technol., Manchester Polytech., Manchester, England).

Plast. & Rubber Process. & Appl. (GB), vol.3, no.3, p.281-91 (1983). For p.III see *ibid.*, vol.2, no.4, p.369-79 (1982). The use of fracture mechanics criteria in the design of pipes necessitated a direct measurement of the resistance of material to crack propagation using pre-notched samples. However, the requirement that the stress be restricted to 0.8 of the yield stress for a valid fracture toughness determination results in such large sample sizes in the tougher polymers that the potential usefulness of such tests are severely limited. Previously reported work by the authors on the determination of values of toughness independent of crack length and test configuration has therefore been extended to cover the effect of sample size. It has been shown from bending tests that the conventional minimum width requirement is rather conservative and that a valid initiation fracture toughness may be calculated from results obtained on small samples by the use of a post-yield theory. The influence of sample thickness is shown to be particularly significant in polyethylene due to the presence of large shear lips with their high resistance to crack growth. By using sufficiently thick samples the influence of the shear lips are minimised and it has been possible to produce unstable failure in some grades of PE at room temperature in air. (14 refs.)

115306 Cavitation in high purity aluminium during fatigue at elevated temperatures. P. Yavari, T.G. Langdon (Dept. of Materials Sci. & Mech. Engng., Univ. of Southern California, Los Angeles, CA, USA).

J. Mater. Sci. Lett. (GB), vol.2, no.9, p.522-4 (Sept. 1983). High purity Al was found to exhibit grain boundary cavitation when tested in fatigue at elevated temperatures (573K) although no cavities are formed in this material during high temperature creep. It appeared that the cavities were formed primarily after the grain boundaries had stabilised into the orthogonal grain configuration. (20 refs.)

115307 The impact endurance of polycrystalline graphite. M. Birch, J.E. Brocklehurst (Springfields Nuclear Power Dev. Labs., UKAEA, Preston, England).

Carbon (GB), vol.21, no.5, p.497-10 (1983). Repeated impact tests have been carried out on a wide range of polycrystalline graphites. Two modes of test were employed using centrally impacted rods and discs with the rods supported horizontally at their ends and the discs supported around the circumference. The resulting impact endurance curves for all the different graphites under repeated impacts of constant energy were found to have a substantially common shape in both the disc and the rod tests. The absolute levels of the endurance curves differ considerably and correlate well with other mechanical properties of graphites, in particular the strain energy density at failure in bend. Measurement of impact forces on the single impact failure of graphite rods supports this correlation by showing that the dynamic stresses generated at failure in a single impact are the same as the corresponding static 3-point bend strengths in the same test mode. Measurement of impact forces at energies less than those required to cause failure in a single impact show that the fraction of energy absorbed as specimen strain energy is dependent on specimen size and shape but is not very sensitive to impact energy. A fracture mechanics model based on incremental crack growth and previously used to interpret stress-cycling fatigue data for graphite is proposed to describe also the endurance of polycrystalline graphite under repeated impacts. The model describes available experimental data obtained under both impact and fatigue conditions. On this model, the difference between the two cyclic stressing modes is the rate of crack growth per stress cycle, this being greater under repeated impacts than under fatigue cycles of the same stress amplitude. (6 refs.)

115308 Embrittlement of construction steel with bainite structure during tempering. A.Yu. Kaletin, V.M. Schastlivtsev, N.T. Kareva, M.A. Smirnov (Inst. of Metal Phys., Ural Sci. Centre, Acad. of Sci., Sverdlovsk, USSR).

Fiz. Met. & Metalloved. (USSR), vol.56, no.2, p.366-71 (Aug. 1983). In Russian. English translation in: *Phys. Met. & Metallogr. (GB)*. The reasons for reduction in the impact toughness of tempered 38KhS steel with the bainite structure were investigated. Magnetometric and electron-microscopic methods were used to show that isothermal quenching produced a carbide-free bainite consisting of ferrite and carbon-rich residual austenite. Embrittlement was due to conversion of this residual austenite retained in considerable amounts. The products of conversion were either regions with a pearlite structure formed during tempering or regions with a lath-like martensite structure formed during cooling of the steel after tempering. The influence of high-temperature plastic deformation on the processes of embrittlement of quenched steel during tempering were considered. (7 refs.) A.T.

115309 Fatigue strength of a rotor steel subjected to torsional loading simulating that occurring due to circuit breaker reclosing in an electric power plant. K. Tanaka, S. Matsuoka, F. Kouzu (Nat. Res. Inst. for Metals, Tokyo, Japan).

Fatigue Eng. Mater. & Struct. (GB), vol.6, no.2, p.103-20 (1983). The fatigue strength of notched specimens of a rotor steel was examined under variable torsional loading which simulates turbine-generator oscillations resulting from the high speed reclosing of transmission-line circuit breakers. The local stress-strain response at a notch root was analysed using Neuber's rule and the resulting complex strain sequences applied to smooth specimens. Using the rain flow analysis and the linear summation rule, fatigue lives of the smooth specimens were successfully predicted from constant amplitude fatigue life data in association with the cyclic stress-strain curve obtained by the incremental step method. Experimental crack initiation lives for notched specimens subjected to variable torsional loading were in excellent agreement with the theoretical curves derived from results on smooth specimens. Accord-

ing to the view that fatigue damage is equated to crack length, the propagation life of a mode II crack along the notch root was predicted to be actually coincident with the life to crack initiation at the notch root defined in this study, i.e. the life at the stage of finding a continuous circumferential crack. (22 refs.)

115310 Mixed-mode fracture mechanisms near the fatigue threshold of AISI 316 stainless steel. Gao Hua (Inst. of Mech., Acad. Sinica, Beijing, China), E.R. de los Rios, K.J. Miller.

Fatigue Eng. Mater. & Struct. (GB), vol.6, no.2, p.137-47 (1983). Near threshold, mixed mode (I and II), fatigue crack growth occurs mainly by two mechanisms, coplanar (or shear) mode and branch (or tensile) mode. For a constant ratio of $\Delta K_I/\Delta K_{II}$ the shear mode growth shows a self-arrest character and it would only start again when ΔK_I and ΔK_{II} are increased. Both shear crack growth and the early stages of tensile crack growth are of a crystallographic nature; the fatigue crack proceeds along slip planes or grain boundaries. The appearance of the fracture surfaces suggests that the mechanism of crack extension is by developing slip band microcracks which join up to form a macrocrack. This process is thought to be assisted by the nature of the plastic deformation within the reversed plastic zone where high back stresses are set up by dislocation pile-ups against grain boundaries. The interaction of the crack tip stress field with that of the dislocation pile-ups leads to the formation of slip band microcracks and subsequent crack extension. The change from shear mode to tensile mode growth probably occurs when the maximum tensile stress and the microcrack density in the maximum tensile plane direction attain critical values. (20 refs.)

115311 Fatigue crack propagation in a cast magnesium alloy. Chen Chuan-Yao, Gao Da-Xing (Dept. of Mech., Huazhong Univ. of Sci. & Technol., Wuhan, China).

Fatigue Eng. Mater. & Struct. (GB), vol.6, no.2, p.167-76 (1983). Fatigue crack propagation behaviour in a cast Mg-Al-Zn alloy was examined. The fatigue crack growth rate of the alloy under constant amplitude loading and the threshold resulting from a number of tests are given. Delayed retardation after the application of a single tension overload is explored in detail and described by using the model proposed by Matsuoka and Tanaka. From these observations, it may be seen that the Matsuoka model can be applied to the cast magnesium alloy as well as steels and aluminium alloys. Changes in the extent of retardation and the overload affected zone size with respect to the ratio of peak-to-baseline stress intensity factor range are discussed. Two phenomena, delayed arrest and acceleration in the later stages of retardation are reported. (7 refs.)

115312 Frequency dependence of the high temperature fatigue properties of He-implanted stainless steel. I.S. Batra, H. Ullmaier, K. Sonnenberg (Inst. für Festkörperforschung, Kernforschungsanlage Jülich, Jülich, Germany).

J. Nucl. Mater. (Netherlands), vol.116, no.2-3, p.136-40 (June 1983). The authors have measured the frequency dependence of the number of cycles to failure, N_f , of type 316 stainless steel specimens fatigued at 600°C with a total strain range of 1.2%. Whereas for the helium-free reference material N_f is high and decreases only slightly with decreasing frequency, there is a sharp drop in N_f below a critical frequency, ν_c , for specimens containing 800 ppm He. This behaviour and the value of $\nu_c \approx 3$ Hz is compatible with a theoretical model by Trinkaus (see Scripta Met., vol.15, p.825, 1981) which predicts a change from transgranular to intergranular failure below a critical frequency. This conclusion is substantiated by SEM observations of fracture surfaces and grain boundary bubble structures. (14 refs.)

115313 On the modeling of the high-temperature embrittlement of metals containing helium. H. Trinkaus (Inst. für Festkörperforschung, Kernforschungsanlage Jülich, Jülich, Germany).

J. Nucl. Mater. (Netherlands), vol.118, no.1, p.39-49 (Aug. 1983). Models for premature intergranular fracture of metals in creep tests during He injection and after room temperature He implantation are critically assessed. The creep rupture lifetime and its dependences upon stress, temperature, He generation rate, He concentration and microstructure of the metal are determined by the intrinsic properties of the lifetime-controlling mechanism as well as by the He flux to and the resulting bubble density on the grain boundaries. The He flux on the other hand is controlled by the He generation rate and the bubble density developing within the grains. On the basis of these considerations the differences in the stress and temperature dependences of the lifetimes observed in creep tests during He implantation and after room temperature He implantation are attributed to differences in the bubble nucleation and growth kinetics of the two cases. For creep tests during He injection the approximate agreement between predicted and observed trends in the time to rupture indicate gas driven stable bubble growth up to the stability limit as the life time controlling mechanism. A set of special creep tests to check this indication is suggested. (30 refs.)

115314 Fatigue and overload fracture of carburized steels. T.B. Cameron, D.E. Diesburg (Molybdenum Co., Ann Arbor, MI, USA), K. Kim.

J. Met. (USA), vol.35, no.7, p.37-41 (July 1983). Predictions resulting from a theoretical fracture mechanics model are reviewed and confirmed by experimental fatigue and fracture results from a variety of carburized steels. This comparison emphasizes the unique contribution of molybdenum to the fatigue strength of the carburized part through its role in maintaining case hardenability and a desirable residual stress profile. This analysis also indicates that the use of molybdenum in carburizing steels results in a superior fracture toughness profile and, hence, improved protection against overload-induced failures. (12 refs.)

115315 Rupture and viscosity of lead during spall. V.K. Golubev, S.A. Novikov, Yu.S. Sobolev, N.A. Yukina.

J. Appl. Mech. & Tech. Phys. (USA), vol.23, no.6, p.836-41 (Nov.-Dec. 1982). Translation of: *Zh. Prikl. Mekh. & Tekh. Fiz. (USSR)*, vol.23, no.6, p.148-14 (Nov.-Dec. 1982). [received: Sept. 1983]. Experiments are performed in order to determine the loading levels corresponding to generations of spall microdamage in the material, as are a detailed metallographic analysis of the specimens in order to determine the nature of the rupture, as well as computational estimates of the viscosity of lead under spall rupture conditions. (16 refs.)

115316 Effect of cold working and annealing on stress corrosion cracking of AISI 304 stainless steel. Y.M. Yeon (Dept. of Metall. Engng., Coll. of Engng. Korea Univ., Seoul, Korea), S.I. Kwon.

J. Korean Inst. Met., vol.21, no.2, p.105-11 (Feb. 1983). In Korean. [received: Sept. 1983]. A study was made of the effects of cold working and annealing on the stress corrosion cracking of AISI 304 stainless steel in boiling 42% MgCl₂ solution. When the 60% or 76% of yield stress was applied, the resistance to SCC showed maximum at 30% of cold work. However, when the same load was applied to the annealed specimens after cold working, the resistance to SCC decreased abruptly at 675°C annealing. The fracture mode changed from mixed to intergranular to transgranular as the amount of cold work increased. (12 refs.)

- 115317 Study on the strengthening mechanism by diffusion of temper carbon into ferritic matrix.** S.W.Im, W.Y.Lee, P.W.Shin, J.H.Hong. *J. Korean Inst. Met.*, vol.21, no.6, p.584-91 (June 1983). In Korean. To investigate the effects of hard eye structure on the mechanical properties of BMC (black heart malleable cast iron), a harder second phase was formed around the temper carbon by carbon diffusion. The index, n , in the rate equation for the austenitization (Johnson-Mehl equation) was 1.4. It was found that, although the hardness increased considerably, the impact strength of BMC, having a pearlitic structure surrounding the temper carbon, was inferior to that of BMC not having hard eye structure, but the decrease in the impact strength was not as large as when the tempered martensitic structure was formed. BMC also showed a change from ductile to a brittle mode of fracture with increasing the volume fraction of hard eye structure. (33 refs.)
- 115318 The relationship between the physical structure and the microscopic deformation and failure processes of poly(*p*-phenylene terephthalamide) fibers.** R.J.Morgan, C.O.Prueneda, W.J.Steele (Lawrence Livermore Nat. Lab., Livermore, CA, USA). *J. Polym. Sci. Polym. Phys. Ed. (USA)*, vol.21, no.9, p.1757-83 (Sept. 1983). Relations between the physical structure and the deformation and failure processes of poly(*p*-phenylene terephthalamide) (PPTA) fibers are reported. The effects of the physical processes involved in fiber fabrication, including the crystallization of PPTA-H₂SO₄ dopes under stress, are considered in relation to their effect on the structure of the fiber. The deformation and failure processes together with the structure of the fiber are discussed in the light of fracture-topography studies of fiber-epoxy composite strands, single filaments, HCL-etched and unetched yarns, and transmission optical microscopy studies of stressed and unstressed yarns. In view of these observations, the physical structure of PPTA fibers is discussed in terms of pleated H-bond sheets, the macromolecular chain-end concentration and distribution, and the presence of impurities. The structural parameters that affect the failure processes of these fibers and how such parameters can be modified by service environment conditions are also addressed. (62 refs.)
- 115319 The incipient characteristic tearing energy for an elastomer cross-linked under strain.** R.S.Rivlin (Lehigh Univ., Bethlehem, PA, USA), A.G.Thomas. *J. Polym. Sci. Polym. Phys. Ed. (USA)*, vol.21, no.9, p.1807-14 (Sept. 1983). In a previous paper (see Eng. Fract. Mech., vol.18, p.389, 1983) a two-network model for an elastomer in which crosslinks have been introduced in the strained state, similar to that proposed by Green and Tobolsky (1948) was used to calculate the dependence of the incipient characteristic tearing energy on the number of chain segments in each of the two networks, the number of links in these chain segments, and the deformation at which the crosslinking takes place. The tearing energies were calculated for tearing on planes perpendicular to the principal directions of this deformation. The calculations are extended to cover tearing on a plane with arbitrary orientation. (7 refs.)
- 115320 Mixed-mode crack opening in fatigue.** D.L.Davidson, J.Lankford (Southwest Res. Inst., San Antonio, TX, USA). *Mater. Sci. & Eng. (Switzerland)*, vol.60, no.3, p.225-9 (Sept. 1983). The crack-opening displacements at distances in the range 1-30 μm behind the crack tip were measured in mode I (parallel to the loading axis) and in mode II for the ingot aluminum alloy 7075 in the T651 condition and the similar powder metallurgy aluminum alloy MA-87 using the stereo-imaging technique. A substantial mode II opening was found for both alloys, but for MA-87 the mode II opening exceeded the mode I opening at the crack tip. The crack openings were found to be greater in a very dry environment than in moist air. (10 refs.)
- 115321 Fractographic aspects of cyclic cleavage.** J.I.Dickson, I.Uribe-Perez (Dept. de Genie Metall., Ecole Polytech., Montreal, Quebec, Canada), E.Geckinli. *Mater. Sci. & Eng. (Switzerland)*, vol.60, no.3, p.231-40 (Sept. 1983). A number of aspects of cleavage crack propagation occurring during fatigue were identified from a fractographic study of low cycle fatigue samples of a quenched reinitrogenized mild steel, tested at 20 and 100°C. The most striking aspect was the frequent presence of cyclic cleavage striations, whose visibility increased with an increase in the plasticity accompanying cleavage. Cyclic cleavage results in a locally accelerated crack growth rate and often in a local crack front that proceeds ahead of the macroscopic front. Increasing hindrance to the continuation of cyclic cleavage often results and is responsible for transitions from brittle to semibrittle to ductile striations. This observed continuity between the three types of striation strongly indicates that the first two types of striation correspond to temporary crack arrest sites. (16 refs.)
- 115322 Studies for the interpretation of fatigue behaviour of prime quality chrome nickel stainless steels—presented on wires which for example may be used for orthodontic purposes.** J.Pirs, V.Ciprus. *Mater. Test. (Germany)*, vol.25, no.8, p.271-4 (Aug. 1983). In German. The fracture surfaces of the wires were examined. The wires are produced from Cr-Ni stainless steels and are used in orthodontic practice for holding the active free plate. The wires were broken in fatigue (partly under oxidation influence) and the fracture surfaces examined by a scanning electron microscope. Profiles of the chemical element composition on the surface and beneath the fracture surface were made for a better interpretation of the fracture mode. (2 refs.)
- 115323 A note on the correlation between sulfide inclusion level and fracture toughness of a 12 weight % chromium steel.** V.P.Raghuopathy, R.Vasudevan. *Mater. Test. (Germany)*, vol.25, no.8, p.275 (Aug. 1983). In English. The plane strain fracture toughness K_{IC} of a 12 weight % chromium steel increases with a reduction in sulfur content. The K_{IC} value however tends to saturate at a value around 91.7 MPa $\sqrt{\text{m}}$ corresponding to a sulfur content of about 55 ppm. A further reduction in sulfur level does not appear to improve the K_{IC} value. (10 refs.)
- 115324 Interfacial segregation and embrittlement in liquid phase sintered tungsten alloys.** B.C.Muddle, D.V.Edmonds. *Met. Sci. (GB)*, vol.17, no.5, p.209-18 (May 1983). Auger electron spectroscopy has been used to examine the fracture surfaces of specimens of W-Ni-Cu and W-Ni-Fe particulate composites in both the as-sintered condition and following post-sintering heat treatments. Changes in the levels of impurity contamination on the fracture surfaces and changes in fracture mode detected by scanning electron microscopy have been correlated with changes in toughness determined by comparative impact tests. Changes in microstructure accompanying heat treatments have also been monitored using both quantitative metallography and transmission electron microscopy. Brittle failure of as-sintered, furnace cooled specimens occurs principally by interfacial decohesion and appears to be associated with the presence of an excess concentration of phosphorus, and possibly sulphur, at the interphase boundaries. High temperature solution treatment followed by quenching produces a reduction in the level of segregation, an improvement in the inter-

phase boundary strength, and a resultant improvement in impact resistance. (28 refs.)

- 115325 Relationships between microstructure and mechanical properties of microduplex $\alpha + (\gamma + \epsilon)$ 6 and 9%Mn steels for cryogenic applications.** D.Duchateau, M.Guttman. *Met. Sci. (GB)*, vol.17, no.5, p.229-40 (May 1983). Room temperature tensile properties and low temperature toughness of quenched and doubly tempered 6 and 9%Mn steels were studied for a variety of tempering treatments, and the influence of the various phases present (α tempered martensite, α' and ϵ martensites, and austenite) on the mechanical properties has been established. The intergranular brittleness of the 9%Mn steels is plain temper embrittlement due to P and Mn cosegregation to the former austenite grain boundaries, which can be suppressed by small Mo additions. ϵ martensite is not intrinsically embrittling and the mechanical properties are controlled by the total volume fraction of $(\gamma + \epsilon)$ islands dispersed in the tempered α lath martensitic matrix: the impact transition temperature is lowered and the strain hardening capacity $\sigma_R - \sigma_Y$ increases as $(\gamma + \epsilon)$ increases. These relationships are explained in terms of the morphology of the dispersed phases and of the strain induced phase transformations. (29 refs.)
- 115326 Effect of molybdenum on temper brittleness and internal friction behaviour of medium carbon alloy steels.** T.C.Lei, C.H.Tang, M.Su. *Met. Sci. (GB)*, vol.17, no.5, p.249-55 (May 1983). U-notched impact toughness and internal friction curves were measured for steels 0.4C-2Mn, 0.4C-2Mn-Mo, and 0.4C-Cr, 0.4C-Cr-Ni, 0.4C-Cr-Ni-Mo after different heat treatments. It was found that in these steels temper brittleness always corresponds with the decrease in Koster peak height. The mechanism of the phenomenon has been suggested as being the result of an aging process of α solid solution with precipitation of Fe₃C(N) particles causing 'dead pinning' of dislocations. The effect of molybdenum in diminishing the susceptibility to temper embrittlement may be considered as being due to its high affinity to C,N atoms by which the precipitation processes of the α phase are obstructed. (6 refs.)
- 115327 Prediction of stress relaxation and stress relief cracking in SEN testpieces.** C.A.Hippesley (Dept. of Metall. & Materials Sci., Univ. of Cambridge, Cambridge, England). *Met. Sci. (GB)*, vol.17, no.6, p.277-87 (June 1983). A computer model has been described for the prediction of stress relaxation and stress relief cracking (in coarse grained, heat affected zone microstructure) during the heating period of a simulated post-weld heat treatment in four-point bend single edge notched (SEN) testpieces. Stress relaxation by plastic deformation was calculated from isothermal creep strain rate data. The two main mechanisms of stress relief cracking were considered, i.e. higher temperature, intergranular microvoid coalescence and lower temperature, low ductility, intergranular fracture. Existing theoretical models for 'creep cavitation' were used to estimate crack growth by the intergranular microvoid coalescence mechanism. An experimental relationship between crack propagation rate, stress intensity, and temperature was derived for the estimation of crack growth by the low ductility intergranular fracture mechanism. A comparison was made between the model predictions and experimental results from a recently developed, reheat cracking assessment test which employs SEN specimens. The model was found to predict the major features of stress relaxation and stress relief cracking with reasonable accuracy for three 2.25 Cr-1 Mo steel alloys considered. Practical application of the model to the quantitative assessment of reheat cracking in actual weldments was discussed. (42 refs.)
- 115328 Influence of slow strain rate tensile deformation on creep-fatigue endurance of 20Cr-25Ni-Nb stainless steel at 593°C.** V.B.Livesey, J.Wareing (Springfields Nuclear Power Dev. Labs., UKAEA, Preston, England). *Met. Sci. (GB)*, vol.17, no.6, p.297-303 (June 1983). Tests have been conducted on a 20Cr-25Ni-Nb stabilized stainless steel at 593°C during which a creep component was introduced into the tensile half of a fully plastic fatigue cycle. This was achieved either by the introduction of hold period at the maximum tensile strain of a rapid fatigue cycle or by the reversal of slow strain rate tensile deformation by rapid compressive straining. These cycles result in a significant reduction in fatigue endurance from that obtained during rapid fatigue cycling tests. The present results indicate that the most damaging cycle is one in which slow strain rate tensile deformation is reversed by rapid compressive straining. Here an order of magnitude reduction in life from that in cycles with equal rates of tensile and compressive straining was observed over a wide range of applied strain levels. Detailed metallographic examination of failed specimens has indicated that these life reductions occur because failure takes place by the interaction between a surface nucleated fatigue crack and internal grain boundary creep cavitation. A theoretical model based on this damage mechanism is presented which describes the experimental data obtained from the different cycle shapes. (14 refs.)
- 115329 Mechanical parameters used for the propagation of creep cracks.** D.Francois (Univ. de Technol. de Compiègne, Compiègne, France), K.Dang Van, F.Mudry. *Mem. & Etud. Sci. Rev. Metall. (France)*, vol.80, no.7-8, p.367-76 (July-Aug. 1983). In French. Parameters connected with fracture mechanics are discussed. Special features of stresses and deformations in the neighbourhood of a crack are considered in addition to experimental determination of the cracking rate under creep evaluation of the damaging effect of a defect. (19 refs.)
- 115330 Effect of structure modifying additives on wear resistance and fatigue strength of polyamide 6.** N.Tscholakowa, P.Sobew, A.Nekesow, G.Iwanow, M.Gatewa. *Plaste & Kautsch. (Germany)*, vol.30, no.7, p.406-7 (July 1983). In German. 0.1 wt.% of an hydraulic oil of a kinematic viscosity of 25 to 32 $\times 10^{-6} \text{m}^2/\text{s}$ increased the fatigue strength of polyamide 6. In creep tests the tensile strength was increased from 56.5 to 58.5 MPa. 0.1% was the optimum plasticising concentration. The oil appeared to penetrate into the amorphous parts of the highest polymerised regions of polyamide 6. Increasing the rate of application of tensile stress reduced the Bayley integral criterion which also depended on the oil content of the polymer. With increasing oil content the wear resistance decreased up to a concentration of 0.1%. (5 refs.) R.S.
- 115331 Failure of rubber-modified plastic liners.** Y.W.Mai (Dept. of Mech. Engng., Univ. of Sydney, Sydney, NSW, Australia). *Polym. Eng. & Sci. (USA)*, vol.23, no.10, p.560-6 (July 1983). In order to analyze the failure phenomenon of plastic liners in freezers and refrigerators the mechanical properties of the freon blown polyurethane (PU) foam insulator material and the acrylonitrile-butadiene-styrene (ABS) plastic liner are determined. The properties considered essential for this problem are the elastic modulus, the tensile strength and the fracture toughness over the temperature range -40 to 20°C. By laminating a layer of the polyurethane foam to the ABS liner and depending on the test temperature brittle to semi-brittle fractures are promoted and the maximum load fracture toughness

of the liner material is reduced. The reduction is more severe for notched bend than for single-edge notched tension specimens. Based on these mechanical properties plausible reasons for linear fractures are discussed. (14 refs.)

115332 Mechanical properties of injection molded blends of poly(ethylene-terephthalate) and poly(amide-6,6). M.R.Kamal, M.A.Sahto (Dept. of Chem. Engng., McGill Univ., Montreal, Quebec, Canada), L.A.Utrachi.

Polym. Eng. & Sci. (USA), vol.23, no.11, p.637-41 (mid-Aug. 1983). Data have been obtained regarding the tensile and impact behavior of pure poly(ethylene terephthalate) (PET) and polyamide 6,6 (PA) and blends of PA in PET in concentrations of 5, 10, 25, 30 and 35 percent by weight of PA. The measurements were carried out at -40, 23 and 70°C. Dispersion and sample preparation were carried out in a reciprocating screw injection molding machine. All blends exhibited brittle behavior and low strength, when compared to pure components. Although some enhancement of mechanical properties might be realized by orientation, it is suggested that the observed behavior might be attributed to the low quality of dispersion achievable in the injection molding process. This conclusion is supported by microscopic evidence. (9 refs.)

115333 Effect of bluing on fatigue strength of cold drawn steel wire. T.Hata, H.Usuda, S.Aoki.

Rep. Gov. Ind. Res. Inst. Nagoya (Japan), vol.32, no.5-6, p.117-23 (May-June 1983). In Japanese.

In order to improve the fatigue strength, the bluing of the cold drawn steel wire was undertaken at various temperatures from 250 to 500°C. Instead of the notch, an indentation was given by using a Vickers hardness tester, and then it was subjected to rotating bending fatigue test. The results obtained were as follows: (1) Original specimens had the range of applied load that the fatigue notch factor was nearly 1.0. And the sample wire also had the same range. (2) When the temperature of the bluing was nearly 350°C, the fatigue strength was increased. (2 refs.)

115334 A phenomenological model of embrittlement of metals under conditions of the adsorption action of liquid metal media. I.G.Dmukhovskaya, V.V.Popovich (G.V. Karpenko Physicomech. Inst., Acad. of Sci., Lvov, Ukrainian SSR).

Sov. Mater. Sci. (USA), vol.18, no.6, p.461-7 (Nov.-Dec. 1982). Translation of: *Fiz.-Khim. Mekh. Mater. (USSR)*, vol.18, no.6, p.5-13 (Nov.-Dec. 1982). It is considered how under the influence of a medium on deformation of the surface layer there are created the conditions for the origin and propagation of a brittle crack and how the fracture process itself occurs. (37 refs.)

115335 Embrittlement of chrome-nickel-molybdenum steel after the high-temperature action of hydrogen. V.B.Shepilov, V.I.Kholodnyi, A.M.Belikov, N.K.Meshkov, A.V.Mikhailov (Voronezh Polytech. Inst., USSR).

Sov. Mater. Sci. (USA), vol.18, no.6, p.482-5 (Nov.-Dec. 1982). Translation of: *Fiz.-Khim. Mekh. Mater. (USSR)*, vol.18, no.6, p.28-33 (Nov.-Dec. 1982). The influence of high-temperature gaseous hydrogen impregnation on the strength and plastic characteristics of cast steel containing 0.05% C, 13% Cr, 8% Ni, and 3% Mo was studied. Round samples with a diameter of 5 mm and a working portion length of 25 mm were used. Before testing they were heat-treated by hardening from 1403K with cooling of the container in air for 3 h, cold treatment at 203K for 4 h, and tempering at 773K for 3 h (all twice). Metallographic and X-ray investigations showed that after such a treatment a martensitic structure was formed in the steel. The gaseous hydrogen impregnation was carried out at 793K and pressures of 40 kPa and 70 MPa. Tensile tests were made on an R-20 tensile machine with different strain rates. (13 refs.)

115336 Crack propagation in titanium alloys in a hydrogen atmosphere under constant load. A.V.Fishgoit, B.A.Kolachev (K.E. Tsiolkovskii Moscow Aviation Technol. Inst., Moscow, USSR).

Sov. Mater. Sci. (USA), vol.18, no.6, p.486-91 (Nov.-Dec. 1982). Translation of: *Fiz.-Khim. Mekh. Mater. (USSR)*, vol.18, no.6, p.33-9 (Nov.-Dec. 1982). A physically based model of crack advance in titanium alloys in a hydrogen medium under constant load is developed on the basis of the theory of hydrogen embrittlement caused by internal hydrogen taking into consideration the distribution of stresses at the tip of a crack. (18 refs.)

115337 Influence of internal microstresses in martensite on near-threshold fatigue crack growth. O.N.Romaniv, A.N.Tkach, V.N.Simin'kovich (G.V. Karpenko Physicomech. Inst., Acad. of Sci., Lvov, Ukrainian SSR).

Sov. Mater. Sci. (USA), vol.18, no.6, p.500-5 (Nov.-Dec. 1982). Translation of: *Fiz.-Khim. Mekh. Mater. (USSR)*, vol.18, no.6, p.49-56 (Nov.-Dec. 1982). The investigations were made on 20Kh13 steel, and have shown that the static and cyclic crack resistance of martensite is primarily determined by the level of internal microstresses, decreasing with an increase in them. This is related to the occurrence of cleavage failure in the habitual boundaries of the martensite packets, which are points of localization of the internal microstresses, and to intensification of intergranular crack growth. A reduction in internal microstresses makes it possible to weaken the occurrence at a fatigue crack tip of the hydrogen brittleness of the hardened steel and to create conditions for closing of the crack as a result of formation of oxides, which slows the kinetics of its near-threshold growth in martensite in tests in water or moist air. (19 refs.)

115338 Low-cycle deformation and failure of die steels at service temperatures. V.I.Dobrovolskii, B.P.Kucheryavii, V.V.Pryakhin (Izhevsk Mech. Inst., USSR).

Sov. Mater. Sci. (USA), vol.18, no.6, p.529-31 (Nov.-Dec. 1982). Translation of: *Fiz.-Khim. Mekh. Mater. (USSR)*, vol.18, no.6, p.79-81 (Nov.-Dec. 1982). Investigates the rules of low-cycle deformation and failure of the promising steels 40Kh5MFS and 50KhNMFS and the widely used 50KhNM steel at 600°C, which is characteristic of the surface layers of a die impression in service. Flat samples with a working portion 50 mm long, 10 mm wide, and 5 mm high were subjected to low-cycle tests. The tests were made under conditions of pure bending on a specially developed machine with a symmetric deformation cycle and a frequency of 0.417 Hz. The results presented indicate that 40Kh5MFS steel possesses higher resistance to low-cycle deformation and failure at service temperatures than the widely used 50KhNM steel. In this respect 50KhNMFS steel occupies an intermediate position. (5 refs.)

115339 Influence of melting method on the crack resistance of 42KhMFA steel. A.N.Lipchina, V.I.Povar (Perm Polytech. Inst., USSR).

Sov. Mater. Sci. (USA), vol.18, no.6, p.537-40 (Nov.-Dec. 1982). Translation of: *Fiz.-Khim. Mekh. Mater. (USSR)*, vol.18, no.6, p.86-8 (Nov.-Dec. 1982). The properties of five production heats of 42KhMFA steel were investigated on transverse samples cut from disks from 160-mm square hot-rolled bars and from a 230×125 mm ESR ingot. For a comparison of the properties, the individual characteristics were studied on longitudinal samples. The sample blanks cut from the disks were annealed to 900°C, oil hardened from 870°C, and tempered at 680°C for 2 h. From the data obtained it follows that purging of molten metal with argon together with refining with synthetic slags makes it possible to substantially increase the quality of steel, which is

economically justified, since in crack resistance the steel approaches the very expensive electrosilag remelted. (10 refs.)

115340 Fatigue failure in the grain boundaries in lead and lead alloys. M.A.Bol'shanina, P.A.Kondrat'ev, T.F.Elsukova, M.B.Makogon (V.D. Kuznetsov Physicotech. Inst., Tomsk, USSR).

Strength Mater. (USA), vol.14, no.9, p.1195-201 (Sept. 1982). Translation of: *Probl. Prochn. (USSR)*, vol.14, no.9, p.33-9 (Sept. 1982). An investigation was made of grain boundary failure of lead and lead alloys under cyclic loading, their fatigue characteristics and structural changes in cyclic loading were determined, and the statistics of the number and distribution of cracks by dimensions and their influence on the mechanical strength in different stages of fatigue were studied. (15 refs.)

115341 Delayed fracture of structural alloy E1607A in plane stress. P.A.Pavlov, V.Kh.Bronz (Leningrad Polytech. Inst., Leningrad, USSR).

Strength Mater. (USA), vol.14, no.9, p.1202-5 (Sept. 1982). Translation of: *Probl. Prochn. (USSR)*, vol.14, no.9, p.39-41 (Sept. 1982). The authors studied the fracture laws of nickel-base heat-resistant alloy E1607A in plane stress and under transient loading. The experimental part of the investigation was carried out on a UEM-10TM unit with an attachment which made it possible to test thin-walled tubular specimens under simultaneous tension and torsion. The tensile force and torque could be changed in any ratio, with the transition from one ratio to another being possible after an intervening complete unloading of the specimens. All of the tests were conducted at 700°C. (5 refs.)

115342 Critical size for structural fragments of thermal-shock-resistant refractories. K.K.Strel'ov, G.A.Prantskyvichyus (S.M. Kirov Ural Polytech. Inst., Sverdlovsk, USSR).

Strength Mater. (USA), vol.14, no.9, p.1225-7 (Sept. 1982). Translation of: *Probl. Prochn. (USSR)*, vol.14, no.9, p.57-9 (Sept. 1982). Several simple theoretical methods are suggested for use in determining the critical size of fragment. The critical sizes obtained by these methods are close to the actual sizes. (11 refs.)

115343 Subcritical crack growth in brittle materials in microcracking conditions. S.M.Barinov, Yu.L.Krasulin (A.A. Baikov Inst. of Metall., Moscow, USSR).

Strength Mater. (USA), vol.14, no.9, p.1256-61 (Sept. 1982). Translation of: *Probl. Prochn. (USSR)*, vol.14, no.9, p.84-8 (Sept. 1982). The authors describe the results of investigations into the effects associated with the instantaneous reaction of the system, i.e., with the processes of brittle fracture of the material in the region at the crack tip. Attention is given only to stable subcritical crack propagation leading to the critical state, i.e. spontaneous fracture. This case is of special interest in connection with the problem of increasing the thermal stability of refractory materials. (19 refs.)

115344 Fractographic features of failure of tungsten cermet in the temperature range 20-2000°C. V.A.Stepanenko, A.V.Babak, E.I.Uskov (Inst. of Problems of Strength, Acad. of Sci., Kiev, Ukrainian SSR).

Strength Mater. (USA), vol.14, no.9, p.1262-5 (Sept. 1982). Translation of: *Probl. Prochn. (USSR)*, vol.14, no.9, p.88-90 (Sept. 1982). An attempt was made to analyse qualitatively the crack resistance of tungsten on the basis of the results of electron diffraction examination. It was found that tungsten cermet with the cellular deformation structure was distinguished by the presence of initial defects in the form of sharp micropores and narrow short microcracks. An increase of test temperature resulted in the growth of the initial microcracks. New micropores appeared at 2000°C as a result of the polygonisation stage. (4 refs.)

115345 Calculation of fatigue and life of crack-bearing structural elements under cyclic load. V.T.Troshchenko, P.V.Yasnii, V.V.Pokrovskii (Inst. of Strength Problems, Acad. of Sci., Kiev, Ukrainian SSR).

Strength Mater. (USA), vol.14, no.11, p.1434-9 (Nov. 1982). Translation of: *Probl. Prochn. (USSR)*, vol.14, no.11, p.12-16 (Nov. 1982). [received: Sept. 1983] A method is developed for predicting the life of a crack-bearing specimen under cyclic load with the stage of unsteady crack propagation and the effect of cyclicality on fracture toughness taken into account; the method is based on experimental data concerning the material and on an analysis of crack propagation conditions. The comparison is calculated and experimental data on unsteady crack propagation in a specimen subjected to cantilever bending was carried out on 15Kh2NMFA steel at 183K, and confirmed the correctness of the life calculation method described. (10 refs.)

115346 Fracture toughness of aluminum alloys of the system Al-Mg-Si for cyclic and static loads. V.G.Kudryashov, Yu.K.Shtovba (All-Union Inst. of Light Alloys, USSR).

Strength Mater. (USA), vol.14, no.11, p.1439-43 (Nov. 1982). Translation of: *Probl. Prochn. (USSR)*, vol.14, no.11, p.16-19 (Nov. 1982). [received: Sept. 1983] For the investigation of the fracture toughness of the AVpch, AD33, and AD35 alloys, strip with a 65×200 mm section was pressed. Strip from the AVpch and AD33 alloys was hardened (520°C, 1 h) and aged by a standard process, 165°C, 8 h, and 170°C, 10 h, respectively. The AD35 alloy was aged at 170°C for 10 h after cooling in the press. Regarding the comparison of fracture toughness values obtained in static and cyclic loading, the following was noted. If the cycle symmetry factor R was small (about 0.1) during cyclic fracture of the specimen, then the difference between the K_{IC} and K_{IC}^C values. (6 refs.)

115347 Effect of loading-cycle asymmetry on the crack resistance of structural alloys. P.V.Yasnii, V.V.Pokrovskii, V.T.Kaplunenko, M.V.Avanesov, B.T.Timofeev, G.P.Karlov (Inst. of Strength Problems, Acad. of Sci., Kiev, Ukrainian SSR).

Strength Mater. (USA), vol.14, no.11, p.1456-61 (Nov. 1982). Translation of: *Probl. Prochn. (USSR)*, vol.14, no.11, p.29-34 (Nov. 1982). [received: Sept. 1983] The fatigue crack growth rate (FCR) and fatigue fracture-toughness characteristics of steels 15Kh2NMFA and 15Kh3MA were studied in cantilever bending of flat specimens 25×70×350 mm at frequencies of 0.4 and 25 Hz. The crack resistance of steel 15Kh2NMFA under static and cyclic ($R=0.1-9$ Hz) loading was studied in the off-center tension of flat specimens 150 mm thick. The fatigue fracture toughness K_{IC}^C of steels 15Kh3MA, 15Kh2MFA, and 15Kh2NMFA increased with an increase in positive values of the cycle asymmetry coefficients. For steel 15Kh2NMFA in the range 183-213K and for steel 15Kh3MA at 153K, fracture toughness was roughly the same under symmetrical and nonzero loading conditions. For steel 15Kh2NMFA at 183 and 213K, the critical SIF corresponding to final fracture was not sensitive to a change in the cycle asymmetry coefficient when $R=-1-0.4$. (14 refs.)

115348 Evaluating the limiting states of a steel under combined low-cycle loading and diffusion of sorbed hydrogen. V.V.Litvin, G.N.Tret'yachenko (Inst. of Strength Problems, Acad. of Sci., Kiev, Ukrainian SSR).

Strength Mater. (USA), vol.14, no.11, p.1462-6 (Nov. 1982). Translation of: *Probl. Prochn. (USSR)*, vol.14, no.11, p.35-8 (Nov. 1982). [received: Sept. 1983]

Tubular specimens of steel 20 with an outer diameter of 24 mm, wall thickness of 2 mm, and working length of 45 mm were tested. Electrolytic hydrogenation was done inside the internal cavity of the specimen. The specimen was subjected to elastic-plastic symmetrical tension-compression, with the strain controlled, at a frequency $f=0.033$ Hz and a temperature $T=293$ K on units made originally for low-cycle tests. The distribution of the sorbed hydrogen was determined by means of an electrolytic cell. The experiments showed that the life of steel 20 under low-cycle fatigue was sharply reduced by hydrogen. Hydrogen sorption not only increased stresses in the material under one-time static loading, but also raised the stresses for the entire duration of the fatigue loading. (10 refs.)

115349 Intergranular brittle fracture resistance of 18Kh2N4VA steel after hardening. G.A.Filippov, O.N.Chevskaya (Central Sci. Res. Inst. for Ferrous Metall., Moscow USSR).

Strength Mater. (USA), vol.14, no.11, p.1536-40 (Nov. 1982). Translation of: *Probl. Prochn. (USSR)*, vol.14, no.11, p.93-7 (Nov. 1982). [received: Sept. 1983]

The tendency toward the formation of segregation of antimony atoms in the grain boundaries in austenite was investigated with 18Kh2N4VA steel melted from pure charge materials and containing 0.0005 and 0.007% antimony. The investigation was made in the freshly hardened condition (delay of 15 min) after various hardening cycles. The results of the delayed fracture tests indicated that with a drop in the level of applied stress there was an increase in the time until failure. An increase in antimony content decreased the strength of the steel, the threshold stress, the load below which delayed fracture did not occur, and the time until fracture with the same stress. (19 refs.)

115350 Fracture mechanics of syntactic foam composites. P.G.Krzhechkovskii (Nikolaevsk Shipbuilding Inst., USSR).

Strength Mater. (USA), vol.14, no.11, p.1556-64 (Nov. 1982). Translation of: *Probl. Prochn. (USSR)*, vol.14, no.11, p.110-15 (Nov. 1982). [received: Sept. 1983]

The author proposes a variant of fracture mechanics of the syntactic foam composite based on the combined examination of the strength of the structural constituents of the composite in an arbitrary complicated stress state using the theory of scattered fracture. (22 refs.)

115351 Intergranular fracture of a high purity iron due to oxygen. H.Matsui, H.Kimura (Res. Inst. for Iron, Steel & Other Metals, Tohoku Univ., Sendai, Japan).

Trans. Jpn. Inst. Met. (Japan), vol.24, no.8, p.539-47 (Aug. 1983).

The authors have prepared a high purity iron which in a form of smooth wire does not show intergranular fracture (IGF) at 4.2K by tensile test. Polycrystalline specimens of this iron was doped with oxygen; a thin oxide film was formed on the surface and a concentration (<several mass ppm) of oxygen was dissolved in equilibrium with the oxide. Thereafter, the oxide film was removed and tensile test was performed between 4.2 and 20K. It was found that as the oxygen concentration is increased by increasing the doping temperature (873, 973 and 1073K), the elongation to fracture at 4.2K is decreased. Specimens, which are doped with oxygen at 973 and 1073K and fracture along grain boundaries without any appreciable elongation, are completely ductile at 20K. If well-decarburized and not doped with oxygen, a commercial high purity iron (the Johnson-Matthey iron) is more susceptible to IGF than our high purity iron. The results show that oxygen segregated at grain boundaries weakens the grain boundary cohesion of iron to some extent, but the effect is not so large as considered before. Some previous researches have shown that smooth specimens fracture along grain boundaries by tension at 77K. These results should be interpreted as due to oxide particles or to interactions between oxygen and other impurities, and not due solely to the oxygen segregated at grain boundaries. (25 refs.)

115352 Shape effect of particles on high-temperature hardness of dispersion-hardened Ni-SiO₂ alloys. S.Goto (Graduate School of Engng. Sci., Kyushu Univ., Kasuga, Fukuoka, Japan), K.Mori, H.Yoshinaga.

Trans. Jpn. Inst. Met. (Japan), vol.24, no.8, p.548-60 (Aug. 1983).

In order to investigate the shape effect of the particles on the high-temperature strength of dispersion-hardened alloys, two kinds of nickel alloys with SiO₂ particles of complex and spherical shapes were made by internal oxidation and a heat-treatment after the internal oxidation, respectively. Their strengths were compared by means of hardness test at high temperatures. The Vickers microhardness of the alloy with particles of complex shape was found to be always higher than that of the alloy with particles of spherical shape at all test temperatures from room temperature to 1273K, though the difference in hardness depended on test conditions; for a short loading time only a slight difference was observed, whereas the difference at high temperatures increased gradually with the increase in loading time and approached a final constant value. The dispersion hardening estimated from the final value was in good agreement with the Orowan stress calculated from the dispersion, that is, the final difference between the two alloys can be well explained by the difference in the particle density on a slip plane, and any shape effect on the decrease in high-temperature strength due to the local climb of dislocations around particles was not detected. Creep behaviour of the alloys was estimated from the loading time dependence of the hardness. Both of the stress exponent and the apparent activation energy for the creep were larger in the alloy with complex particles than in the alloy with spherical particles. (25 refs.)

115353 Microstructure and mechanical strength of aluminum titanate ceramics prepared from synthesized powders. Y.Ohya, K.Hamano, Z.Nakagawa (Res. Lab. of Engng. Materials, Tokyo Inst. of Technol., Yokohama-shi, Japan).

Yogyo-Kyokai-Shi (Japan), vol.91, no.6, p.289-97 (1983). In Japanese.

Relations between the microstructure, bending strength and thermal expansion behavior of an aluminum titanate ceramic were investigated. The ceramics were prepared from three kinds of synthesized powders having several grain sizes and various amounts of free corundum. Under crossed nicols field of a polarization microscope, the fired bodies showed domain free structures. The grain size of the titanate of specimens fired at 1500°C for 4 h varied from 2.3 to 7.2 μ m depending on the starting powders. Many cracks were observed on the grain boundaries of bodies which had a grain size larger than 3 μ m, whereas only a few cracks were observed in a body with grain size of 2.3 μ m. In the specimens fired at 1300°C for 2~8 h, their grain sizes were less than 1 μ m, and few cracks were observed on their grain boundaries. The bending strength of the fired bodies increased markedly as their grain sizes decreased below 2.5 μ m. (13 refs.)

115354 Tensile strength of pressureless-sintered silicon nitride at elevated temperature. K.Matsusue, Y.Fujisawa, K.Takahara (Nat. Aerospace Lab., Chofu-shi, Japan).

Yogyo-Kyokai-Shi (Japan), vol.91, no.7, p.325-8 (1983).

Uniaxial tensile strength tests of pressureless-sintered silicon nitride were carried out in air from room temperature up to 1600°C. Three kinds of silicon nitride tested contained Y₂O₃.Al₂O₃, Al₂O₃.MgO or MgO.CeO₂ additives respectively which were used for promoting sintering. The test results showed that the composition of additive influences the strength characteristics of silicon nitride. The tensile strength rapidly decreased above 800°C for materials containing MgO and above some 1000°C for materials with Y₂O₃. At 1300°C, the strength decreased to about 10 percent of the room temperature strength for each case. Observations of the fracture origin and of the crack propagation on the fracture surfaces were made and discussed. (8 refs.)

115355 The K_{IC} values of silicon nitride and zirconia obtained by micro-crack indentation method and single-edge notched beam method. H.Seko (Aisin Seiki Co. Ltd., Kariya-shi, Japan), M.Okada, A.Sawaoka.

Yogyo-Kyokai-Shi (Japan), vol.91, no.7, p.339-43 (1983).

K_{IC} values obtained by the micro-indentation method and the single edge notched beam method were compared for silicon nitride and zirconia ceramics. Results of our measurements demonstrate that K_{IC} values obtained by both methods for silicon nitride and zirconia ceramics corresponded with each other when χ is 0.10. K_{IC} value of partially stabilized zirconia obtained by the single-edge notched beam method decreased upon polishing the surface of the specimen whose opposite surface had a notch. (9 refs.)

115356 Fractographic study of cracks produced by thermal shocks in 20MnMoNi55 and comparable weld material in water environment. K.Torronen, M.Kemppainen, R.Rintamaa.

Report 176, Tech. Res. Centre Finland, Metall. Lab., Espoo (April 1983), 26 pp.

Cracking in the feed water piping system has been found in both PWR and BWR-type nuclear power stations. To avoid this cracking problem and to assure the piping integrity experimental work has been initiated where the crack formation and growth mechanisms are studied under simulated conditions as close as possible to operating conditions. The results of a fractographic study of several cracks produced by thermal loading in 20MnMoNi55 steel and comparable weld material in an aqueous environment are presented. The basic crack growth mechanism is shown to be by mechanical fatigue, but after some crack growth indications of environmentally assisted cyclic crack growth are seen. (6 refs.)

115357 High strength sheet steel of medium thickness. T.F.Gulvin, L.Conway, W.P.Tait.

Report EUR 8007 EN, Comm. European Communities, Luxembourg (1982), 82 pp. Contract 6210.KH/8/801.

Weldability and fracture toughness assessments of welded joints for thirty high strength steels from four European countries are reported. Steel plates in the thickness range 25-76 mm at yield stress levels of (nominally) 420 and 490 N/mm² have been evaluated. In the selected steels, the specified strength levels were achieved by different mechanisms using normalising, controlled rolling, and quenching and tempering routes. From the weldability assessment, a rank order of relative weldability based on the risks of hydrogen cracking in the heat affected zones and solidification cracking in the weld metal was established for the selected steels.

115358 Resistenza a fatica di acciai ad alto limite di snervamento laminati a caldo (Fatigue resistance of high strength hot rolled steels). M.Castagna, G.Pezzuto.

Report EUR 8063 IT, Comm. European Communities, Luxembourg (1982), vi+115 pp. In Italian. Contract 7210.KD/403.

Presents the results concerning the fatigue behaviour of two high strength microalloyed hot rolled steels (8 mm thickness) with strength levels of 500 and 600 MPa respectively. The investigation was carried out with particular reference to use of such steels in the construction of industrial vehicles frames. In view of specific problems, the fatigue behaviour of steels was investigated on notched and welded plates, with constant and variable amplitude tests. Results of variable amplitude fatigue tests simulating a typical service load history have indicated a considerable improvement of fatigue life when a conventional structural steel is replaced by a higher strength microalloyed steel. A computer program was also applied to predict fatigue life of a notched component, subjected to a complex loading history. (16 refs.)

115359 Fracture toughness of poly(methyl methacrylate) blends. R.P.Kusy, W.F.Simmons (Dental Res. Center, Univ. of North Carolina, Chapel Hill, NC, USA).

Polymer Alloys III Blends, Blocks, Grafts and Interpenetrating Networks. Proceedings of a Symposium, New York, USA, 23-28 Aug. 1981 (New York, USA: Plenum 1983), p.71-89.

A series of acrylic blends was prepared from three feedstocks having number average molecular weights (M_n) of 4×10^3 (L), 3×10^4 (M), and 1×10^5 (H). After single-edge-notched tension bars were machined from molded sheets, the fracture surface energy (γ) was determined using the Brown and Srawley equation (1965). When the mean γ was plotted against the blend composition, results showed a different dependence for each binary combination: H/M suggested a linear relationship, while H/L and M/L appeared concave downward and upward, respectively. Further reduction of this data to a molecular weight basis permitted analysis via three general approaches: that a property, $P \propto M_n^{-1}$, that $P \propto \log M_w$, and that $P \propto \log \bar{x}_n$ (where $\bar{x}_n = M_n/M_0$). The first two relationships gave straight line segments for each binary combination and provided interesting parallels with several previous investigators—Sookne, Flory, Nielsen, and Berry. In the second case, moreover, the intersection of the H/L and M/L data lines suggested a common origin, which corresponded to $\gamma = 525$ erg/cm² at $M_w = 26000$ (the entanglement molecular weight, M_e ?). (49 refs.)

115360 Rubber modified matrices. R.Y.Ting (Naval Res. Lab., Orlando, FL, USA).

Role of the Polymeric Matrix in the Processing and Structural Properties of Composite Materials. Proceedings of a Joint US-Italy Symposium, Capri, Italy, 15-19 June 1981 (New York, USA: Plenum 1983), p.171-88.

An experimental study was carried out on epoxy polymers modified by carboxy-terminated butadiene acrylonitriles. It is concluded that rubber-modified polymers exhibit improved fracture toughness over that of the unmodified resin. Whether the liquid and the solid rubber are used alone or in combination, the fracture energy may be increased by orders of magnitude. When these materials are used as matrix resins in composites, the 'toughening' effect is transferred into the composites to enhance their interlaminar fracture energy, flexural fatigue and other off-axis mechanical properties. The rubber-modified resins also offer the additional advantages of high peel strength and controlled flow. Unfortunately, the reduced resin modulus of the rubber-modified matrices will adversely affect composite properties to reduce the interlaminar shear strength, to cause a fast drop-off of strength and

modulus at elevated temperatures, and to lead to a poor wet strength retention. (16 refs.)

115361 Characterization of high performance composite matrices. R.J.Morgan (Lawrence Livermore Nat. Lab., Univ. of California, Livermore, CA, USA).

Role of the Polymeric Matrix in the Processing and Structural Properties of Composite Materials. Proceedings of a Joint US-Italy Symposium, Capri, Italy, 15-19 June 1981 (New York, USA: Plenum 1983), p.207-13
Reviews the fundamental areas of the structure-property relations of composite matrices that are necessary for making meaningful durability predictions. These areas include the chemical and physical structure of epoxies and their modes of deformation and failure. (33 refs.)

115362 Fatigue crack propagation in short-glass-fiber-reinforced nylon 66: effect of frequency. R.W.Lang, J.A.Manson, R.W.Hertzberg (Materials Res. Center, Lehigh Univ., Bethlehem, PA, USA).

Role of the Polymeric Matrix in the Processing and Structural Properties of Composite Materials. Proceedings of a Joint US-Italy Symposium, Capri, Italy, 15-19 June 1981 (New York, USA: Plenum 1983), p.377-96
The fatigue crack propagation response of nylon 66 and composites containing 16 and 31 vol.% short glass fibers was determined at frequencies of 1, 10, 50, and 100 Hz. The sensitivity to frequency was found to depend on glass content and, in the case of the pure matrix, on the value of the stress intensity factor range. (35 refs.)

115363 Creep and fracture initiation in fibre reinforced plastics. J.-F.Jansson, H.Sundstrom (Dept. of Polymer Technol. Royal Inst. of Technol., Stockholm, Sweden).

Role of the Polymeric Matrix in the Processing and Structural Properties of Composite Materials. Proceedings of a Joint US-Italy Symposium, Capri, Italy, 15-19 June 1981 (New York, USA: Plenum 1983), p.397-406
Presents a brief review and analysis of the present state of knowledge and some initial studies concerning the relations between the creep behaviour and creep fracture phenomena in thermoset-based fibre composites with special regard to the fracture initiation. (21 refs.)

115364 Compression fatigue behaviour of notched composite laminates. R.M.Walsh, R.B.Pipes (Center for Composite Materials, Univ. of Delaware, Newark, DE, USA).

Role of the Polymeric Matrix in the Processing and Structural Properties of Composite Materials. Proceedings of a Joint US-Italy Symposium, Capri, Italy, 15-19 June 1981 (New York, USA: Plenum 1983), p.587-606
The influence of compression fatigue on graphite/epoxy laminates containing circular holes of 0.25 inch diameter was investigated. The nature and extent of induced compression fatigue damage was examined and the effects of this damage on the laminate residual failure mechanisms determined. Two modes of compressive failure were found to occur: the diagonal shear and the net compression modes. The mode and direction of failure were dependent upon the nature of the specimen delamination. It was also found that the laminate stacking sequence influenced the intraply crack development in the laminates as well as the failure mode. (11 refs.)

115365 Delamination in graphite-epoxy. D.J.Wilkins (General Dynamics, Fort Worth, TX, USA).

Role of the Polymeric Matrix in the Processing and Structural Properties of Composite Materials. Proceedings of a Joint US-Italy Symposium, Capri, Italy, 15-19 June 1981 (New York, USA: Plenum 1983), p.629-31
Delamination growth is the fundamental issue in the evaluation of laminated composite structures for durability and damage tolerance. When primary composite structures are evaluated originally with respect to durability (fatigue) and damage tolerance (safety), they are judged against the design service usage, and tests are performed to demonstrate their structural integrity. However, after the parts enter service, they are exposed to a variety of operational usages so that techniques are needed to estimate the behaviour of defects as a function of time under changing service conditions. (no refs.)

Polymer Alloys III Blends, Blocks, Grafts and Interpenetrating Networks. Proceedings of a Symposium See Entry 113111

Volume, surface and interface fracture statistics of brittle materials under flexure See Entry 113349

Fracture criteria under creep conditions See Entry 113359

Fracture toughness of high-strength layered plates containing plastic interlayers with a high elastic modulus See Entry 113361

Contour J-integral in the plastic region See Entry 113362

Examination of the stress state of a helically reinforced composite in shearing See Entry 113364

Energy criteria for the brittle fracture of composite materials with initial stresses See Entry 113367

Influence of thickness and temperature on stretched zone size in J_{IC} tests See Entry 113388

Surface modification by ion implantation—effects on fatigue See Entry 113908

Parameters of mechanical twins emitted by a crack See Entry 114080

A method of creep damage summation based on accumulated strain for the assessment of creep-fatigue endurance See Entry 114081

Investigation of material damage under creep and creep strength See Entry 114082

Conditions for cavity growth during slow-fast fatigue See Entry 114083

Dislocation emission from cracks in the presence of liquids See Entry 114085

Tracer diffusion of P in iron and iron alloys See Entry 114271

Properties and structure of carbon excess Ti_2C_{1-x} deposited onto molybdenum by magnetron sputtering See Entry 114397

Liquid phase sintering of tungsten [and optimum mechanical properties] See Entry 115134

Directionally solidified structure and mechanical properties in monovariant Al-Fe-Ni eutectic alloy See Entry 115183

The use of microscopic and hardness measurement methods in recrystallization studies See Entry 115211

Recovery behavior of hydrogen charged 7075-T6 aluminum See Entry 115215

Electron microscopic studies on the effect of Sn addition on the ageing characteristics of Al-0.7% Mg₂Si alloy See Entry 115217

The effect of hydrogen on reversible and irreversible softening of spheroidized steel See Entry 115223

Possibility of predicting hardening cracks See Entry 115229

Fatigue and recovery processes in a multilayer iron-copper composite material See Entry 115243

Analysis of process stresses in two-layer SiC-Si disks See Entry 115246

Polymer-performance on the dimensional stability and the mechanical properties of wood-polymer composites prepared by an electron beam accelerator See Entry 115248

The effect of fast neutron irradiation on the compressive stress-strain relationships of graphite See Entry 115256

Elongation minimum and strain rate sensitivity minimum of zircaloy-4 See Entry 115259

Properties of two high strength, high temperature, high conductivity copper-base alloys See Entry 115264

Effects of V and Nb additions on high temperature deformation properties of low alloy martensites See Entry 115269

Work hardening and the stability of deformation in AlZnMg alloys See Entry 115271

Influence of silicon on the structure and properties of alloyed compound Ni_3Al See Entry 115275

Effect of small amounts of tungsten carbide on the strength, creep, and brittle-to-ductile transition temperature of zirconium carbide See Entry 115280

Experimental study of the effect of scale and shape of a body on deformation and failure mechanisms of structurally inhomogeneous materials See Entry 115282

On the correlation of mechanical properties of high impact polystyrene with its morphology, molecular-weight characteristics and extrusion conditions See Entry 115289

Correlation of morphology, mechanical properties and processing conditions of modified high impact polystyrene See Entry 115290

RIM systems from interpenetrating polymer networks See Entry 115291

A stress transfer model for the deformation and failure of polymeric matrices under swelling conditions See Entry 115292

Stress and strength analysis in and around composite inclusions in polymer matrices See Entry 115297

Electron-microscopical investigations of the structure of the surface layers of titanium carbide after friction at 20-1400°C See Entry 115366

Effects of hardness on the solid particle erosion mechanisms in AISI 1060 steel See Entry 115374

The use of transmission electron microscopy to study the effects of abrasive wear on the matrix structure of a high chromium cast iron See Entry 115375

The long term durability of stressed GRP in acidic environments See Entry 115377

Effect of surface stresses on ductility and fatigue strength of wear resisting coatings See Entry 115396

SiC-coatings as protective layers for carbon fibers and adhesion promoters for superconducting niobium carbonitride See Entry 115398

Stress corrosion cracking of aged Al-5Zn-4Mg alloy in 3.5% NaCl solution See Entry 115419

Problems of the life of constructional materials in nitrogen- and hydrogen-containing media See Entry 115434

An analytical method of evaluating angles in Brookes' formula for effective resolved shear stress on slip systems in crystals See Entry 115453

Decomposition of austenitic phase in work hardened steel samples, using hardness measurements See Entry 115464

Determination of longevity under a two-frequency load (review). I See Entry 115468

Results of an investigation of the service life of heat-resistant materials under repeated static load See Entry 115469

Representation of fatigue damage to a component in terms of reliability theory See Entry 115470

Effect of step duration on the evaluation of the fatigue limit of welded steel structures See Entry 115471

Relationship between parameters of elastic-wave propagation and rupture-strength characteristics of structural materials See Entry 115473

Effect of stored elastic energy on breaking stress See Entry 115476

The measure of fracture toughness of cemented carbide by means of CVD coated layers See Entry 115506

81.40P Friction, lubrication, and wear

(see also 62.20P Tribology)

115366 Electron-microscopical investigations of the structure of the surface layers of titanium carbide after friction at 20-1400°C. A.N.Pilyankevich, V.F.Britun, Yu.G.Tkachenko, V.K.Yulyugin (Inst. of Materials Sci., Acad. of Sci., Ukrainian SSR).

Sov. Powder Metall. & Met. Ceram. (USA), vol.22, no.1, p.56-60 (Jan. 1983). Translation of: *Poroshk. Metall. (USSR)*, vol.22, no.1, p.63-7 (Jan. 1983). [received: Aug. 1983]

An account is given of electron microscopical investigations of the structural changes taking place in the contact zones of TiC specimens during rubbing in a vacuum in the temperature range 20-1400°C. Titanium carbide specimens of composition close to stoichiometric were prepared by pressing a commercially pure TiC powder in metal dies and sintering the resultant compacts in a vacuum. Friction and wear testing was performed in a high-temperature vacuum apparatus. Pairs of identical TiC specimens were rubbed against each other at a mean speed of 0.01 m/sec under a load of 1 MPa in a vacuum corresponding to 5.10^{-3} Pa. The test temperatures were 20, 400, 800, 1200, and 1400°C. The investigation showed that during heating in a vacuum from 20 to 1200°C the coefficient of friction μ and wear rate w of a TiC-TiC pair decreased, but with a further rise in temperature they began to show a tendency to increase. The microhardness of the rubbing surfaces after tests, measured on contact spots, decreased from 28000 at 400°C to 20000 MPa at 1400°C. (6 refs.)

115367 Dry wear studies on glass-fibre-reinforced epoxy composites. R.Ramesh, Kishore (Dept. of Metall., Indian Inst. of Sci., Bangalore, India), R.M.V.G.K.Rao.

Wear (Switzerland), vol.89, no.2, p.131-6 (15 Aug. 1983).
Continuous glass-fibre-reinforced epoxy composites were fabricated and their wear behaviour was studied. A rapid drop in the wear loss occurred with an increase in the sliding speed for the pure epoxy resin while the reinforced sample exhibited a mild decrease, a flat region and then a rise. Optical microscopy examination indicates that the higher wear loss for the composite at higher speeds could be due to loss of glass fibres. The variation in the coefficient of friction, μ , with load and sliding speed was studied. Both the epoxy resin and the composite show a marked dependence of μ on load, which

includes a peak. The pure epoxy resin showed no significant dependence of the coefficient of friction on sliding speed whereas the composite shows a peak value, thereby emphasizing the important role of the reinforcing fibres. (2 refs.)

115368 The effects of erodent composition and shape on the erosion of steel. A.V.Levy, P.Chik (Lawrence Berkeley Lab., Univ. of California, Berkeley, CA, USA).

Wear (Switzerland), vol.89, no.2, p.151-62 (15 Aug. 1983).

The effects of erodent composition, hardness-strength characteristics and shape on the erosion of AISI 1020 carbon steel were determined. Tests were performed at a velocity of 80 m s^{-1} at two angles of impingement ($\alpha=30^\circ$ and 90°). Angularly shaped particles of five compositions were used with Vickers' hardness H_v from 115 to 3000 kgf mm^{-2} . It was determined that the erosion rate increased with increasing particle hardness to a constant rate for particles with $H_v > 700 \text{ kgf mm}^{-2}$. The hardness was a measure of the friability of the particle composition. When the particles were strong enough not to break up on impacting the AISI 1020 steel surface, the erosion rate became constant. It was also determined by using angular and spherical steel erodents that angular particles can result in four times more erosion than spherical particles. (9 refs.)

115369 Comparison of the wear resistance of various grades of cemented carbides that may find application in wood machining. A.-M.Bayoumi, J.A.Bailey, J.S.Stewart (Dept. of Mech. & Aerospace Engng., North Carolina State Univ., Raleigh, NC, USA).

Wear (Switzerland), vol.89, no.2, p.185-200 (15 Aug. 1983).

A laboratory test is described in which specimens of rectangular cemented carbide tool inserts of a standard size are allowed to slide against a rapidly rotating fiberboard disc in either the presence or the absence of a mist spray of a dilute organic acid (tannic acid or acetic acid) to simulate the cutting of green wood and cured wood respectively. It is shown that the worn surfaces of cemented carbide tools used in (field) service are remarkably similar to the worn surfaces of specimens used in the laboratory (simulation) tests. Extensive results are presented that show quantitatively the progressive wear of a wide range of cemented carbides as a function of time for sliding under wet and dry conditions. It is shown that wear depends on the type and amount of binder present in the cemented carbide and on the nature of the environment. Materials with Co-Cr and Ni-Cr binders containing significant amounts of chromium showed the greatest resistance to wear. (19 refs.)

115370 Friction and wear properties of nitrided and N^+ -implanted 17-4 PH stainless steel. G.M.Ecer (Sii Smith Tool Tech. Center, Irvine, CA, USA), S.Wood, D.Boes, J.Schreurs.

Wear (Switzerland), vol.89, no.2, p.201-14 (15 Aug. 1983).

N^+ implantation of thermally nitrided 17-4 PH stainless steel substantially improved friction and wear properties in lubricated sliding wear tests. Some improvement was also obtained by nitriding or by N^+ implantation alone. Auger and surface topography analyses of specimens before wear testing indicated that the improved wear performance may be due in part to the implantation of carbon, and perhaps oxygen, when N^+ was being implanted under a relatively high target chamber pressure and in part by the topographical alteration of the surface in thermal nitriding. (11 refs.)

115371 The effect of surface hardness of carbon steels on scuffing resistance in rolling-sliding contact. Y.Yamamoto (Dept. of Mech. Engng., Kushu Univ., Fukuoka, Japan).

Wear (Switzerland), vol.89, no.2, p.225-34 (15 Aug. 1983).

The effect of surface hardness on scuffing was investigated using a two-disc machine. The changes in the surface conditions, especially surface roughness, surface hardness and the formation of an oxide film, in the running-in process have a marked influence on the scuffing resistance. Therefore a hard disc does not always have a high resistance to scuffing. In this investigation, quenched discs of the highest surface hardness, in which the improvement in surface roughness and the formation of an oxide film are expected to be small, offered the poorest resistance to scuffing. By contrast, annealed discs of lowest hardness, in which a diminished surface roughness and an increased surface hardness caused by the work hardening that necessarily accompanies the formation of an oxide film are expected, exhibited a considerably higher resistance to scuffing. (13 refs.)

115372 Mechanical and electromechanical behaviour of fibre brushes. L.Boyer, G.Fournet (Lab. de Genie Electrique de Paris, Univ. de Paris VI et XI, Gif-sur-Yvette, France).

Wear (Switzerland), vol.89, no.3, p.245-63 (1 Sept. 1983).

Investigations of the mechanics of metal fibres capable of carrying very high currents are presented. The role played by the Laplace force is emphasized. This force appears whenever a fibre carrying a current is subjected to a magnetic field whose direction is different from that of the fibre. The role played by the coefficient of friction is also taken into account. An exact non-linear differential equation is used to describe the problem, i.e. no assumptions are made about the magnitudes of the deflections. When the normal force exerted on the track by the fibre is an increasing function of the Laplace force, it is found that the maximum stress within the fibre has a non-linear dependence on the Laplace force. When the same normal force is a decreasing function of the Laplace force, it is shown that the normal force vanishes for a critical value of the Laplace force. A perturbation method is used to explain the behaviour of the fibre. (20 refs.)

115373 Some aspects of improving abrasive resistance. V.N.Kashcheev (Siberian Phys.-Tech. Inst., Tomsk, USSR).

Wear (Switzerland), vol.89, no.3, p.265-72 (1 Sept. 1983).

A survey of literature on the structural and phase strengthening of alloys and steel is presented. Methods of strengthening such as mechanical riveting and expanding the length of intergrain boundaries do not increase abrasive wear resistance to hard particle attack. Alloying to increase the interatomic bond forces does not increase abrasive wear resistance. Thus there is a close connection between the modulus of normal elasticity of different metals and the wear resistance. The sharp decrease in dislocation mobility at the brittle transition temperature increases abrasive wear resistance. For a high carbon steel the resistance increases by a factor of 2.5. Increased resistance to attack by abrasive particles (by a factor of 2) can be achieved by preliminary friction treatment of the steel surface (especially by dry frictional contact against low carbon steel) because of the complex phase and structural transformations in the material of the surface that is subjected to frictional contact. (12 refs.)

115374 Effects of hardness on the solid particle erosion mechanisms in AISI 1060 steel. Le Khac Hein, P.G.Shewmon (Dept. of Metall. Engng., Ohio State Univ., Columbus, OH, USA).

Wear (Switzerland), vol.89, no.3, p.291-302 (1 Sept. 1983).

The mechanisms of mass loss were studied using impacts of single particles (WC spheres $3/16 \text{ in.}$ in diameter) for a 0.6% C steel (AISI 1060 steel) heat treated to give hardnesses of 12, 45 or 60 HRC. Both oblique and near-normal angles of impact were used. A new foil laminate was developed to measure rebound velocity and angle. Velocities of $100\text{--}200 \text{ m s}^{-1}$ were stu-

died. A measurable mass loss was found only at 200 m s^{-1} . At a hardness of 12 HRC the mode of metal loss involved the loss of shear lips. At 60 HRC the dominant loss mode involves the intersection of adiabatic shear bands (ASBs) and shows a maximum mass loss at near-normal impact. The material with a hardness of 45 HRC shows both modes of mass loss and a maximum mass loss rate at oblique (30°) impact. ASBs on the surface and welding of target material to the impacting ball indicate a high temperature at the surface. However, the material welded to the particle is not a significant fraction of the material lost. (23 refs.)

115375 The use of transmission electron microscopy to study the effects of abrasive wear on the matrix structure of a high chromium cast iron. J.T.H.Pearce (Dept. of Metall., West Bromwich Coll. of Commerce & Technol., Wednesbury, England).

Wear (Switzerland), vol.89, no.3, p.333-44 (1 Sept. 1983).

The wear behaviour of an austenitic high chromium cast iron was investigated under conditions of high stress abrasion using a specimen-on-track test apparatus. The austenite matrix at the wear surfaces of test specimens work hardened during abrasion giving hardness values up to 950 HV but the depth of hardening was seen to be much smaller than that obtained under service conditions. The nature of the work hardening was studied by thin foil transmission electron microscopy. This work has provided evidence of strain-induced martensite formation which is believed to be responsible for the observed increases in hardness. (23 refs.)

Metallurgical surfaces produced by ion implantation See Entry 113940

CVD of TiN at the tempering temperature of alloy-steels See Entry 115097

Formation of thin refractory coatings, their properties and fields of application See Entry 115098

Modern trends in creating sintered antifriction materials See Entry 115137

Vibration-resistant composites intended for damping devices See Entry 115158

Effect of structure modifying additives on wear resistance and fatigue strength of polyamide 6 See Entry 115330

A study of friction and wear resistance of two-layer TiN+Mo vacuum-plasma coatings See Entry 115401

Effecting the corrosion relationship of corroding element-cladding material of ZrNb1 by mechanical surface treatment See Entry 115416

Role of CVD in providing wear resistant films See Entry 115450

81.40R Electrical and magnetic properties (related to treatment conditions)

(see also 72.80 Conductivity of specific semiconductors and insulators, 74.70 Superconducting materials, 75.50 Studies of specific magnetic materials)

The electrical resistivity of GP zones. Temperature dependence See Entry 114510

Change in structure of chromel-alumel thermoelectric transducers used in a medium of natural gas See Entry 114512

Influence of additions on the electrical insulation properties of fused periclase See Entry 114526

Single crystal magnets See Entry 114708

Magnetomechanical damping of nickel See Entry 114720

Energy dissipation due to macroeddy currents with mechanical vibrations See Entry 114721

The effect of sintering in hydrogen-nitrogen atmospheres and subsequent aging on the magnetic properties of iron See Entry 115138

Properties of hot-pressed zirconium pyrovanadate ceramics ... See Entry 115149

81.40T Optical properties (related to treatment conditions)

(see also 78.20 Optical properties and materials)

Determining the characteristics of Ag:LiTaO₃ diffused optical waveguides See Entry 113097

Photoluminescence study of thermally treated silicon crystals See Entry 114926

Properties of hot-pressed zirconium pyrovanadate ceramics ... See Entry 115149

81.60 CORROSION, OXIDATION AND SURFACE TREATMENTS

115376 Thermal stress limitations to laser fire polishing of glasses.

Y.M.Xiao, M.Bass (Univ. of Southern California, Los Angeles, CA, USA).

Appl. Opt. (USA), vol.22, no.18, p.2933-6 (15 Sept. 1983).

The process of laser fire polishing of optical glasses is shown to work very well for materials with small coefficients of thermal expansion. The surfaces of other glasses crack during laser fire polishing or during cool down from an elevated preheat temperature. An analytical model is described and is used to show that, in materials which cannot be laser fire-polished, the thermal-gradient stress resulting from differential expansion exceeds the yield stress. Successful laser fire polishing of fused quartz and Pyrex glasses is reported. (12 refs.)

115377 The long term durability of stressed GRP in acidic environments. F.R.Jones, J.W.Rock, A.R.Wheatley (Dept. of Metall. & Materials Technol., Univ. of Surrey, Guildford, England).

J. Mater. Sci. Lett. (GB), vol.2, no.9, p.519-21 (Sept. 1983).

The authors studied the mode II fracture of an 80°C post-cured, 0° unidirectional polyester laminate after approximately one year half immersed in aqueous H_2SO_4 at constant load. It is found that the long term life in a corrosive environment appears to be controlled by the rate of stress corrosion of the glass-resin interface. (11 refs.)

115378 Considerations on SG insulator failures in operating conditions. L.Egizano, B.Macchiaroli (Univ. di Napoli, Napoli, Italy), P.Giordano Orsini.

Energ. Elettr. (Italy), vol.60, no.3, p.117-21 (March 1983). In English.

Insulators coated with semiconducting glazes, proposed for more compact high voltage transmission lines and for the use in heavily contaminated areas, have shown a poor durability in service. An analysis of the main reasons of the present failures is carried out. The microstructural defects of the insulator glazes and the morphology of their corrosion are examined. Suggestions to improve the manufacturing techniques are proposed. (25 refs.)

115379 Metallization of Lavsan in a glow discharge. I.N.Brovikova, L.V.Bulanova, G.D.Krotova, V.I.Svetlov.

Elektron. Obrab. Mater. (USSR), no.3, p.52-4 (1983). In Russian. English translation in: *Electrochem. Ind. Process. & Biol. (GB)*.

Investigations of the process of metallization of Lavsan by the method of cathodic sputtering were conducted. Data were obtained on the rate of deposition of a nickel coating on the surface of Lavsan in a plasma of helium and residual gases under different conditions of combustion of the glow discharge ($P=10-100$ Pa, $i=2-8$ Ma). It is shown that by the use of cathodic sputtering, coatings of satisfactory quality can be deposited on the surfaces of textile materials at technologically-acceptable rates. (5 refs.) *A.J.B.*

115380 Electroplating of an ultrasonically-activated surface for automatic filling of indentations. H.Coufal, W.Imaino, A.C.Tam (IBM Corp., Armonk, NY, USA).

IBM Tech. Disclosure Bull. (USA), vol.26, no.2, p.837-9 (July 1983).

The present work is concerned with an effect whereby if the whole cathode is ultrasonically activated by appropriate ultrasonic frequencies, automatic focusing of ultrasonic energy occurs in the electrolyte at locations close to indentations; i.e. the cathode surface itself can automatically redistribute the input ultrasonic energy to cause hole-filling without the necessity of directing an energy beam by an external device onto a hole to enhance plating (as in previous experiments). (1 ref.)

115381 Orientation of (100) InGaAsP/InP wafers by HCl chemical etching. L.W.Stulz (Crawford Hill Lab., Bell Labs., Holmdel, NJ, USA), L.A.Coldren.

J. Electrochem. Soc. (USA), vol.130, no.7, p.1628-30 (July 1983).

Presents a very simple method for orienting (100) InP wafers. It does not require X-rays, photomasking or the loss of a significant amount of material. The technique is superior to other orientation techniques, which generally require masking the surface. The edge-to-surface juncture provides a natural nucleation site, and most desirably, it is best to have a mediocre cleave that provides edge striations for a distinctive result. Such results are obtained consistently. Little or no wafer area need be sacrificed, and virtually no additional processing time is spent in this orienting procedure. (10 refs.)

115382 Centrifugal etching: a promising new tool to achieve deep etching results. H.K.Kuiken, R.P.Tijburg (Philips Res. Labs., Eindhoven, Netherlands).

J. Electrochem. Soc. (USA), vol.130, no.8, p.1722-9 (Aug. 1983).

The authors present some theoretical considerations to show that by etching in an enhanced acceleration field, such as can be obtained in a centrifuge, it is possible to circumvent many of the typical objectionable features of some of the traditional etching techniques. The theory is corroborated by a small series of experiments. These clearly indicate that centrifugal etching may yield very low undercutting, large etch rates, and, if proper care is taken, an extremely smooth surface finish. (14 refs.)

115383 Properties of thermal oxides grown on phosphorus in situ doped polysilicon. M.Sternheim, E.Kinsbron, J.Alspector, P.A.Heimann (Bell Labs., Murray Hill, NJ, USA).

J. Electrochem. Soc. (USA), vol.130, no.8, p.1735-40 (Aug. 1983).

The oxidation characteristics and the electrical conductivity and breakdown of thin oxides grown on phosphorus in situ doped polysilicon are reported. Breakdown fields of 8 MV/cm and leakage currents as low as 5×10^{-8} A/cm² at 3.5 MV/cm were measured for 400- to 1200 Å oxides grown thermally at 1000°C in dry O₂ on phosphorus in situ doped films deposited at 600°C. The oxides grown on the 600°C polysilicon films are superior to the oxides grown on the 640°C polysilicon films. The high breakdown fields and low leakage currents are related to the film structure and surface morphology as revealed by SEM and TEM micrographs. (26 refs.)

115384 Cation and anion transport numbers in anodic GaAs oxides. C.W.Fischer, J.D.Canaday (Dept. of Phys., Univ. of Guelph, Guelph, Ontario, Canada).

J. Electrochem. Soc. (USA), vol.130, no.8, p.1740-4 (Aug. 1983).

An Xe¹³⁴ marker atom layer of concentration 2×10^{15} cm⁻² has been implemented into GaAs to a depth of 20 nm. The GaAs containing the Xe¹³⁴ was anodized to various thicknesses, and Rutherford backscattering was used to measure the change in the Xe¹³⁴ marker atom depth relative to the change in oxide thickness. These measurements are used to calculate the cation and anion transport numbers which are 0.18 and 0.82, respectively. A secondary result from backscattering measurements is the oxide bulk stoichiometry and oxide density. The results show a bulk oxide composition of (Ga+As)₂O=2:3, and an oxide density of 4.64 g/cm³. (26 refs.)

115385 Corrosion behavior of SiC/Al metal matrix composites. P.P.Trzaskoma, E.McCafferty (Naval Res. Lab., Washington, DC, USA), C.R.Crowe.

J. Electrochem. Soc. (USA), vol.130, no.9, p.1804-9 (Sept. 1983).

The effect of the SiC phase on the corrosion behavior of SiC/Al metal matrix composites has been studied on 0.1 and 0.6N NaCl, both in the presence and absence of dissolved oxygen. Anodic polarization behavior has been determined, and pitting potentials have been measured for three composite systems: SiC/Al 2024, SiC/Al 6061, and SiC/Al 5456. General corrosion behavior and the effects of anodizing on the corrosion resistance of the composites have been studied by AC impedance techniques. The results show that pitting susceptibility is about the same for the composites and their corresponding alloys, except for Al 2024. In this system, the composite is less resistant to pit initiation than the corresponding wrought aluminum alloy. General corrosion is more significantly affected by the presence of oxygen than by the SiC phase. In the absence of oxygen, corrosion resistance is improved for both the alloys and composites. In addition, the corrosion resistance of the composites can be improved by anodizing. (11 refs.)

115386 The effects of arsenic doping in reactive ion etching of silicon in chlorinated plasmas. G.C.Schwartz, P.M.Schaible (IBM General Technol. Div., East Fishkill Facility, NJ, USA).

J. Electrochem. Soc. (USA), vol.130, no.9, p.1898-1905 (Sept. 1983).

The results of a study of the influence of arsenic doping of silicon and Cl₂ and CCl₄ reactant concentrations on etch rate and etch profile are described. From approximately 10^{16} to 10^{20} As/cm³, the etch is anisotropic and the etch rate does not increase in either Cl₂ or CCl₄ plasmas. At concentrations above 10^{20} As/cm³, mask undercutting occurs and the etch rate rapidly increases (approximately 300% for 1.5×10^{21} As/cm³), although the functional form of the relationship between etch rate and As concentration depends on the reactant, reactant supply, and silicon load. Temperature effects are also described. (10 refs.)

115387 On the formation of planar-etched facets in GaInAsP/InP double heterostructures. L.A.Coldren, K.Furuya, B.I.Miller (Bell Labs., Holmdel, NJ, USA).

J. Electrochem. Soc. (USA), vol.130, no.9, p.1918-26 (Sept. 1983).

Techniques to predict and control the etch wall profile as a mask edge are developed. An understanding of the etch rate vs. substrate orientation angle is

used to predict and experimentally realize desired etched wall profiles on (001) GaInAsP/InP double heterostructure (DH) wafers. The identification and utilization of crystallographic stop etch planes is key to ensuring planar and reproducible etched facets. Fabrication procedures employing wet and dry etching techniques are outlined for either isolated step-etched vertical wall profiles or narrow grooves. (33 refs.)

115388 On the preferential etching of GaAs by H₂SO₄-H₂O₂-H₂O. D.N.MacFadyen (Dept. of Electronic & Electrical Engng., Glasgow Univ., Glasgow, Scotland).

J. Electrochem. Soc. (USA), vol.130, no.9, p.1934-41 (Sept. 1983).

The preferential etching of gallium arsenide in H₂SO₄-H₂O₂-H₂O has been studied. A mechanism for the etching process is discussed drawing on observation by optical and scanning electron microscopy, published results on UHV surface analysis, and surface state models. The etch rates of the revealed planes are related to surface step densities, and the exposure of 'equilibrium' step density surfaces is related to the surface migration lengths of probable reactant species. (18 refs.)

115389 Substrate biasing for plasma etching. T.D.Mantei (Dept. of Electrical & Computer Engng., Univ. of Cincinnati, Cincinnati, OH, USA).

J. Electrochem. Soc. (USA), vol.130, no.9, p.1958-9 (Sept. 1983).

Most plasma etching processes require negative substrate biasing to ensure directional ion bombardment. In many cases, however, it may be desirable to apply an additional separately controllable substrate bias or to establish a substrate bias in a quiescent plasma in which self-bias is negligible. The negative DC substrate bias resulting from the application of an external alternating voltage to a substrate can be accurately predicted by a simple calculation. The results is confirmed by bias measurements in a quiescent plasma. (8 refs.)

115390 Phenomenological model for silicon oxidation in dry oxygen in the presence of HCl. A.I.Ellis, K.M.Gardiner, T.E.Cyr (Solid State Electronics Div., Honeywell Inc., Plymouth, MN, USA).

J. Electrochem. Soc. (USA), vol.130, no.9, p.1970-4 (Sept. 1983).

Thermal oxidation of silicon to form a thin SiO₂ layer is one of the most important processes in VLSI and VHSIC technology. In spite of the pioneering studies of Deal and Grove (1965), the growth of the first several hundred angstroms of oxide has not yet been quantitatively explained. The authors propose a conceptually simple modification of the Deal-Grove model based on the assumption that the oxygen atoms impacting the oxide surface have a definite probability of penetrating to a certain depth. Expressions useful for data analysis and simulation (SUPREM II and III) are given. (13 refs.)

115391 On the study of oxidation kinetics of molybdenite pellets. Jun Soo Kim, Hyun Gun Kim, Jae Hyun Oh.

J. Korean Inst. Met., vol.21, no.6, p.566-75 (June 1983). In Korean.

Oxidation roasting of molybdenite pellets was carried out to study the effect of temperature and oxygen concentration on the oxidation rate. The effect of heat transfer between pellet and surroundings on the reaction rate was also studied by measuring the temperature of the pellet during reaction. The results obtained in these experiments are listed. (27 refs.)

115392 Volume changes and the technical properties of composites in the spinel-manganese oxide system. Yu.D.Kuznetsov, S.A.Suvorov (All-Union Inst. of Refractories, USSR).

Refractories (USA), vol.23, no.11-12, p.584-90 (Nov.-Dec. 1982). Translation of: *Ogneupory (USSR)*, vol.23, no.11, p.33-8 (Nov. 1982).

The volume changes during the oxidation-reduction process of the manganese oxide in the Mg(Al,Cr)₂O₄-Mn₂O₃-Mn₃O₄ system have been studied. It was found that the factors destroying the refractory caused by the oxidation-reduction processes of the manganese oxides appear in composites containing high-chromite spinels. Therefore this study makes it possible to recommend as refractories to be in contact with manganese-type material those in which the spinel part consists of high-alumina spinels. (6 refs.)

115393 Corrosion resistance of materials of the AlN-Si₃N₄ system. A.F.Alekseev, T.S.Bartnitskaya, A.B.Goncharuk, V.A.Lavrenko, E.S.Lugovskaya, A.D.Panasuyuk, P.P.Pikuza, I.I.Timofeeva (Kiev Polytech. Inst., Acad. of Sci., Kiev, Ukrainian SSR).

Sov. Powder Metall. & Met. Ceram. (USA), vol.22, no.1, p.48-50 (Jan. 1983). Translation of: *Poroshk. Metall. (USSR)*, vol.22, no.1, p.53-6 (Jan. 1983). [received: Aug. 1983]

An investigation was carried out into the high-temperature oxidation kinetics of materials of the Si₃N₄-AlN system in oxygen and in air at 800-1400°C. The resultant oxidation products were determined by X-ray phase and petrographic analyses. It was established that the components exert a mutual influence on their oxidation parameters, and that the materials investigated surpass the individual nitrides in oxidation resistance right up to 1400°C. (5 refs.)

115394 A study of the thermo-oxidative process and stability of graphite and glass/PMF polyimide composites. D.A.Scola (United Technol. Res. Center, East Hartford, CT, USA).

Role of the Polymeric Matrix in the Processing and Structural Properties of Composite Materials. Proceedings of a Joint US-Italy Symposium, Capri, Italy, 15-19 June 1981 (New York, USA: Plenum 1983), p.159-69

Composite materials consisting of HTS, HMS T-300, Celion 600 graphite fibers and S-glass fibers in two polyimide matrices, PMR-11 and PMR-15, were subjected to isothermal aging at 316°C in flowing air at two flow rates (100 cc/min and 900 cc/min) for time periods up to 600 hours. The weight losses, shear and flexural properties were determined at room temperature and 316°C. One system, Celion 6000/PMR-15, was selected for study at 335°C in flowing air at 100 cc/min over a 1015 hour period. The oxidation process of this isothermally exposed composite system was followed by optical microscopy and mechanical property measurements. (1 ref.)

115395 Environmental aging of epoxy composites. A.Apicella, L.Nicolais, C.Carfagna (Istituto di Principi di Ingegneria Chimica, Univ. degli Studi di Napoli, Napoli, Italy).

Role of the Polymeric Matrix in the Processing and Structural Properties of Composite Materials. Proceedings of a Joint US-Italy Symposium, Capri, Italy, 15-19 June 1981 (New York, USA: Plenum 1983), p.215-29

Specimens were prepared from Epikote 828 using commercial triethylene-tetramine (TETA) as curing agent. Distilled water was used in sorption experiments. (18 refs.)

115396 Effect of surface stresses on ductility and fatigue strength of wear resisting coatings. K.Roser, H.-P.Kehrer (Siemens AG, Zentrale Fertigungsaufgaben, Munchen, Germany).

Proceedings of the 4th European Conference on Chemical Vapour Deposition, Eindhoven, Netherlands, 31 May-2 June 1983 (Eindhoven, Netherlands: Philips Centre Manuf. Technol. 1983), p.84-90

In order to increase the wear resistance of tools and components, coatings and surface treatments are applied in increasing extent. For this purpose a great variety of layers with different properties are available. In addition to the increased wear resistance, layers also change the mechanical properties of the

parts. However, very little work has been done in this field. The present work is concerned with the effect of wear resistant coatings on ductility and fatigue strength of leaf-springs. These results are completed by X-ray stress measurements in the surface region of the specimens. (12 refs.)

115397 Application of DSL photoetching for defect revealing in epitaxially grown GaAs samples. J.L.Weyher (Dept. of Solid State III, Faculty of Sci., Catholic Univ., Nijmegen, Netherlands).

Proceedings of the 4th European Conference on Chemical Vapour Deposition, Eindhoven, Netherlands, 31 May-2 June 1983 (Eindhoven, Netherlands: Philips Centre Manuf. Technol. 1983), p.273-7

Shows that the DSL (diluted Sirtl-like etchants with laser illumination) method is useful in examining GaAs epitaxial heterostructures. Two types of samples, namely LPE DH laser and VPE FET structures have been subjected to the repeated photoetching and micrography of identical areas. This was done in order to establish: the resolution of the method, the possibility to etch in selective manner layers of different chemical composition and finally the manner in which the defects change during treatment. The mixtures which do not attack GaAs without illumination [10] have been used to reveal defects only within the surface area limited by illumination. (13 refs.)

115398 SiC-coatings as protective layers for carbon fibers and adhesion promoters for superconducting niobium carbonitride. K.Brennfleck, E.Fitzer (Inst. für Chemische, Tech. Univ. Karlsruhe, Karlsruhe, Germany), M.Deitrich.

Proceedings of the 4th European Conference on Chemical Vapour Deposition, Eindhoven, Netherlands, 31 May-2 June 1983 (Eindhoven, Netherlands: Philips Centre Manuf. Technol. 1983), p.370-5

The adhesion between HM-carbon fiber (HM=high modulus) and a niobium carbonitride layer is poor if the deposition temperature is low. During heating up and cooling down crack formation in the layer and spalling of parts of the layer is observed especially with increasing layer thickness (>100 nm), resulting in a decreasing critical current density J_c with increasing layer thickness. Furthermore the reactive hydrogen in the process attacks the surface of the C substrate resulting in a decreased tensile strength of the fiber. With SiC ($\alpha=4.5\cdot10^{-60}C^{-1}$) as interlayer the mentioned adhesion problems are expected to be lowered. The effectiveness of SiC as a protective layer for the carbon fiber and adhesion promoter for the niobium carbonitride has therefore been investigated. (6 refs.)

Thermometric and calorimetric methods in electrochemical and corrosion studies See Entry 111686

Hydrazine usage for corrosion control in PWR plants with powdered resin condensate polishers See Entry 112379

Diffusion and hideout in crevices See Entry 112380

The nature of point defects and their influence on diffusion processes in silicon at high temperatures See Entry 113906

Investigation of defect structure of metal-semiconductor interface in SmS by the method of high-voltage electron microscopy See Entry 113918

Chlorine redistribution in HCl oxides due to high temperature annealing See Entry 113950

Marker experiments for diffusion in the silicide during oxidation of PdSi, Pd₂Si, CoSi₂, and NiSi₂ films on (Si) See Entry 114258

Effects of back-side oxidation of Si substrates on Sb diffusion at front side See Entry 114259

Observation of oxidation-enhanced and -retarded diffusion of antimony in silicon: the behavior of (111) wafers See Entry 114277

Surface relief of crystalline quartz etched in a planar plasma reactor See Entry 114318

Process of formation of porous silicon and autoepitaxy on its surface See Entry 114394

Atom-probe microanalysis and field-ion microscopy of TiC-coatings on cemented carbides See Entry 114405

Two-dimensional surface electrons in semiconducting p-type Hg_{1-x}Cd_xTe with an anodic oxide See Entry 114586

Generation of surface states in MOS structures based on indium antimonide See Entry 114619

Appearance potential study of the 4f levels of cerium, praseodymium and their oxides See Entry 114973

Surface chemistry of (100) indium phosphide See Entry 114981

On the influence of incident energy of protons on chemical erosion of graphite See Entry 114990

Plasma-sprayed silicon as a possible base material for the production of low cost solar cells See Entry 115051

Continuous coating with gravity and jet stripping See Entry 115052

Deposition rate and structural properties of microcrystalline glow discharge Si:H₂Cl films See Entry 115108

Thermodynamic study of oxidation of molybdenum sulfides See Entry 115174

Environmental influences of fatigue damage in glass fibre reinforced polyester See Entry 115304

Electrolytical corrosion behaviour of iron-, nickel- and cobalt-base metallic glasses See Entry 115404

Thermodynamic stability of complex oxides in alkali metals See Entry 115573

81.60B Metals and alloys

(inc. stress corrosion cracking; anticorrosion)

115399 Observations on the growth and impact of intermetallic compounds on tin-coated substrates. M.E.Warwick, S.J.Muckett (Internat. Tin Res. Inst., Greenford, England).

Circuit World (GB), vol.9, no.4, p.5-11 (1983).

Tin and solder coatings interact with substrates commonly used in the electronics industry to produce layers of intermetallic compounds at temperatures above and below the melting point of the coatings. Observations on the rates of compound growth at room temperature for durations of up to 12 years are reported and related to the published results for shorter times at higher temperatures. Recent results concerning the effect of intermetallic compound growth on the solderability of coatings and on the strength of soldered joints are presented. In both cases it is apparent that retarding the rate of compound growth could be useful and the use of barrier layers for this purpose is considered. (13 refs.)

115400 Mass decrement examination of construction materials during chemical cleaning of equipment with hydrofluoric acid. J.Gemza, M.Kowalczewski.

Energetyka (Poland), vol.37, no.4, p.162-4 (April 1983). In Polish. [received: Sept. 1983]

The paper presents the methods and results of mass decrement examination during chemical cleaning with hydrofluoric acid of some tens of steel grades used for power plant equipment. The suitability of the M-B inhibitor for chemical cleaning of all examined grades of steel has been stated. Optimum physical and chemical parameters for the chemical cleaning process with hydrofluoric acid have been determined (bath temperature, acid concentration, flow speed of the solution). (no refs.)

115401 A study of friction and wear resistance of two-layer TiN+Mo vacuum-plasma coatings. V.M.Matsevityi, B.A.Polyanin, M.S.Borushko, L.M.Romanova.

Elektron. Obrab. Mater. (USSR), no.3, p.29-33 (1983). In Russian. English translation in: *Electrochem. Ind. Process. & Biol. (GB)*

An examination is made of some results of a study of the frictional characteristics and wear resistance of single-layer TiN and two-layer TiN+Mo vacuum-plasma coatings with different levels of surface roughness. The wear tests were conducted on a friction machine in an environment of aviation spirit ($t=60^{\circ}C$) using the plane-cylinder arrangement with a speed of slip of 1 m/s. The control specimen was a cylinder or quenched steel Kh12M. It was found that, independently of coating composition or surface roughness, the value of the coefficient of friction was within the limits 0.11-0.13. The TiN+Mo coatings by comparison with those of TiN gave lower values of friction coefficient under low loads, and higher values of bulk wear. (1 ref.) *A.J.B.*

115402 The protection against corrosion of low-voltage heavy-duty fuse contacts. M.Altenhuber.

Elektrotech. Z. ETZ (Germany), vol.104, no.14, p.708-10 (July 1983). In German.

Tin, silver, or nickel deposits are generally used on the lower contacts and contact blades of low-voltage heavy-duty fuses as a protection against corrosion. The requirements of these contact surfaces are low contact resistance, ability to resist corrosion, long life in deleterious atmospheres, safety in extreme thermal conditions, and high mechanical strength of the surface layer. Investigations with nickel show that over an extended period the growth of oxide had little effect on the contact resistance even in strongly corrosive surroundings, the results with tin were similar. The susceptibility to corrosion of silver surfaces in sulphurous atmospheres is well known. Nickel showed the best thermal and mechanical qualities, tin had the lowest mechanical values and there is the danger of the welding together of contacts under extreme current loading. (8 refs.) *A.G.P.*

115403 Scaling of materials for hot gas tubing in an air-cooled solar tower power station under thermal cycling between 623 and 1073K. J.Ebberink, G.Hulmann (Internat. Atomreaktorbau GmbH, Bergisch Gladbach, Germany).

Werkst. & Korros. (Germany), vol.34, no.8, p.385-91 (Aug. 1983). In German.

The corrosion behaviour of two heat resistant alloys X 12 CrNi2521 (1.4845) and X 10NiCrAlTi3220 (1.4876) is studied. These alloys are model alloys for hot air pipes of a gas cooled solar tower power station. The maximum operating temperature is 1073K (solar operation), the minimum is 623K (fossil operation) during cloudy periods and at night. The experimental simulation device for cyclic temperature exposure between 623K and 1073K is described and experimental results are discussed. After 7000 cycles with the temperature gradient of <7K/s growth, composition and adherence of corrosion layers on the materials are determined. The post examinations of the exposed specimens show the better corrosion behaviour of X 12CrNi2521 not only after isothermal exposure at 1073K but also after thermal cyclic exposure between 623 and 1073K. (8 refs.)

115404 Electrolytical corrosion behaviour of iron-, nickel- and cobalt-base metallic glasses. U.Linker, W.Plieth (Inst. für physikalische Chem., Freien Univ. Berlin, Berlin, Germany).

Werkst. & Korros. (Germany), vol.34, no.8, p.391-7 (Aug. 1983). In German.

The corrosion behaviour of the three amorphous metals Fe₄₀Ni₄₀B₂₀, Ni₇₈Si₈B₁₄ and Co₃₈Ni₁₀Fe₃Si₁B₁₆ was investigated in 0.5 M sulfuric acid and in a boric acid/borax buffer solution. Cyclic voltammograms of the three alloys were measured between hydrogen and oxygen evolution. In case a passive region occurred the corrosion rate in this region was increased by two or three orders of magnitude. Otherwise a potential region with small net current density was observed between hydrogen evolution and active dissolution. This is explained by inhibition of the cathodic partial current density of the hydrogen evolution reaction. All three materials showed increased susceptibility to local corrosion. (21 refs.)

115405 Rust formation on iron—a model. H.Worch, W.Forker, D.Rahner (Tech. Univ. Dresden, Dresden, Germany).

Werkst. & Korros. (Germany), vol.34, no.8, p.402-10 (Aug. 1983). In German.

A model is presented on the basis of which the phenomenological variety of rusting can be reduced to a few basic processes. The first step of the formation of rust results in the transfer reaction of iron(II)-ions from the metal surface into the adherent boundary layer, the ions being surrounded there by water molecules or hydroxide ions. Here or after their diffusion into the adherent electrolyte solution they are oxidized to Fe(III)-ions by oxygen or other oxidants, eventually also electrochemically. The nuclei of the structures of FeOOH modifications develop from hydrogen bonded iron hydroxo- and/or -aquo-complexes by transposition of the iron ions and water loss. If only Fe(III)-ions participate in the nucleation process, then the stable oxides or oxyhydroxides in relation to the solution are formed. The metastable structures result from simultaneous participation of Fe(II)- and Fe(III)-ions. (42 refs.)

115406 Results of apparent atomic oxygen reactions on Ag, C, and Os exposed during the shuttle STS-4 orbits. P.N.Peters, R.C.Linton, E.R.Miller (Space Sci. Lab., NASA/Marshall Space Flight Center, Huntsville, AL, USA).

Geophys. Res. Lett. (USA), vol.10, no.7, p.569-71 (July 1983).

Films selected for anticipated reaction with atomic oxygen, namely carbon, silver, and osmium, were exposed during the Shuttle STS-4 mission. A silver film 225 ± 5 nm thick was converted to a transparent blue-green interference film 355 ± 5 nm thick. Both carbon and osmium films 10-30 nm thick apparently formed volatile oxides and disappeared, except where well shielded. A calculated total of approximately 7×10^{19} oxygen atoms per cm² struck the surfaces, which could have removed on the order of 3 μ m of material if only 10% reacted. The absence of apparent effects on adjacent thin and thick gold films is offered as evidence that sputtering is not responsible. (18 refs.)

115407 Continuous hot dip plating process for improved anticorrosion steel strips. K.Nishimura, K.Katayama, T.Kimura, T.Yamaguchi (Ichikawa Works, Nissin Steel Co. Ltd., Tokyo, Japan). *Hitachi Rev. (Japan)*, vol.32, no.2, p.77-82 (April 1983). [received: Aug. 1983]

Improved anticorrosive technology for continuous hot dip plated steel strips has been realized in actual production. Metal plating of uniform thickness has been achieved for steel strips by preventing strip oscillations and levelling bowed strips that are produced at the gas wiping process. Also, a technique has been developed for producing hot dip one-side aluminized steel strips that are superior in anticorrosion to galvanized steel strips. These technologies are significant for improving anticorrosion characteristics of steel strips. (3 refs.)

115408 Cast alloy resists corrosion by hot acids and oxidizing agents. F.G.Hodge (Cabot Corp., Kokomo, IN, USA).

Ind. Res./Dev. (USA), vol.25, no.7, p.82-5 (July 1983). Describes the development of Ni-based C-4C alloy which features high resistance to corrosion as cast, without having to be wrought. Properties of this alloy are tabulated and its practical application in manufacturing Du Pont pumps is described. (no refs.)

115409 Diffusion-coupled active dissolution in the localized corrosion of stainless steels. R.C.Newman, H.S.Isaacs (Corrosion Sci. Group, Brookhaven Nat. Lab., Upton, NY, USA).

J. Electrochem. Soc. (USA), vol.130, no.7, p.1621-4 (July 1983). Examines the anodic dissolution of stainless steels in environments relevant to localized corrosion in neutral chloride solutions. There is a maximum active dissolution rate, for a given potential, which is not associated with the most concentrated localized environment. This observation seems to be significant with respect to the stability of localized corrosion in these alloys. Results of this kind are capable of explaining the existence of a critical pit solution, a protection potential against pitting, multiple steady states, low frequency electrochemical noise and differences between open circuit and potentiostatic behavior. (12 refs.)

115410 The dealloying of a Cu-8.90% Al solid solution. M.J.Pryor (Metals Res. Labs., Olin Corp., New Haven, CT, USA).

J. Electrochem. Soc. (USA), vol.130, no.7, p.1625-7 (July 1983). Mass balance experiments on the dealloying of Cu-Al solid solution were carried out in 0.5 M NaCl solution at 25°C at potentials ranging from +0.50 to -0.50 V_{SHE}. There is substantial and effective dealloying of the CuAl solid solution starting at a potential of 0.00 V with the selectivity of dealloying (i.e. the enhancement of solute concentration found in the total corrosion product), increasing as the potential is depressed to -0.50 V. The experiments confirm the widely held view that Cu-Al solid solutions are somewhat more resistant to dealloying than Cu-Zn solid solutions. (10 refs.)

115411 Corrosion by alternating current: polarization of mild steel in neutral electrolytes. D.-T.Chin, P.Sachdev (Dept. of Chem. Engng., Clarkson Coll. of Technol., Potsdam, NY, USA).

J. Electrochem. Soc. (USA), vol.130, no.8, p.1714-18 (Aug. 1983). The authors' laboratory had previously undertaken a series of investigations of the effect of AC on the corrosion of metals. Sixty cycles sinusoidal AC was superimposed onto an oxygen diffusion cell, and the measurement of corrosion current was compared to the actual weight loss of the specimens in soil. It was found that sinusoidal AC enhanced the corrosion of aluminium, copper, mild steel, and a 50-50% tin-lead alloy. At high AC levels, severe pitting corrosion occurred on copper and mild steel specimens. Subsequent polarization measurements for mild steel in a neutral sodium sulfate solution revealed that sinusoidal AC enhanced the corrosion current, shifted the corrosion potential toward the negative direction, and destroyed the passivity of mild steel at the passive potentials. The effect was similar to the addition of chloride ions to sulfate solutions. In the present work, the polarisation measurement has been extended to neutral sodium chlorate, sodium nitrate, and sodium perchlorate solutions. Anions can exert profound influence on the passivation mechanism. (8 refs.)

115412 Oxidation of Cu₃Sn and Cu₆Sn₅ films in room air from 175° to 250°C. H.G.Tompkins, J.E.Bennett, J.A.Augis, T.M.Paskowski (Bell Labs., Columbus, OH, USA).

J. Electrochem. Soc. (USA), vol.130, no.8, p.1758-62 (Aug. 1983). Stoichiometric single-phase samples of Cu₃Sn and Cu₆Sn₅ were fabricated by sputter deposition. These were subsequently heated in air for various time and temperatures. For most of the time-temperature combinations, the resulting film was tens of angstroms thick and primarily an Sn oxide containing some copper. The film growth can be described kinetically with a logarithmic rate law. For the higher temperatures for longer times, when the Cu-to-Sn ratio in the center of the oxide film reached about 1:1, the film growth mechanism changed. This resulted in films several hundreds of angstroms thick which were primarily copper oxide. (28 refs.)

115413 Surface enrichment of nitrogen during passivation of a highly resistant stainless steel. Y.C.Lu, R.Bandy, C.R.Clayton, R.C.Newman (Brookhaven Nat. Lab., Upton, NY, USA).

J. Electrochem. Soc. (USA), vol.130, no.8, p.1774-6 (Aug. 1983). A stainless steel with 0.44 wt.% N and 6.1 wt.% Mo has been shown to have exceptional resistance to localized corrosion. This resistance is superior to that of commercial alloys based on Fe-Cr-Ni-Mo, and at least equal to that of more expensive Ni-Mo-Cr alloys. The alloy also represents a significant improvement on laboratory materials with somewhat lower N or Mo concentrations. The authors have analyzed the surface of the alloy after passivation, and have obtained evidence for a surface enrichment of N. The role of Mo remains obscure. (7 refs.)

115414 Reactive ion etching of copper films. G.C.Schwartz, P.M.Schaible (IBM, East Fishkill Facility, Hopewell Junction, NY, USA).

J. Electrochem. Soc. (USA), vol.130, no.8, p.1777-9 (Aug. 1983). The authors have demonstrated that it is feasible to reactively ion etch (RIE) copper films. The etch rate is about an order of magnitude higher than the sputter etch rate. There is no undercut of an inert mask and the patterns formed have vertical sidewalls. (2 refs.)

115415 Anodic protection of mild steel in sulphuric acid. T.P.Sastry, V.V.Rao (Dept. of Chem., SV Regional Coll. of Engng. & Technol., Surat, India).

J. Indian Inst. Sci., vol.64, no.1, p.61-9 (Jan. 1983). [received: Sept. 1983] Corrosion of mild steel in dilute sulphuric acid can be controlled to an acceptable level by anodic protection. Analysis of potentiostatic polarization curves for mild steel in sulphuric acid of different concentrations and at different temperatures reveals the parameters necessary for application of anodic protection to this system. A comparison of the corrosion rates of the unprotected and the anodically protected mild steel is made. The efficiency of anodic protection in controlling corrosion is determined: protection efficiencies in most of the cases are a very high order (99%). (17 refs.)

115416 Effecting the corrosion relationship of corroding element-cladding material of ZrNb1 by mechanical surface treatment. G.Naumann (Zentralinstitut für Kernforschung Rossendorf, Bereich, Dresden, Germany).

J. Nucl. Mater. (Netherlands), vol.116, no.2-3, p.147-56 (June 1983). In German.

The reactivity of the outer surface of cladding material of the alloy Zr-1% Nb is significantly increased above the well-known state of chemically or electrochemically polished specimens by abrasive surface treatments. Out-of-reactor oxidation in water resulted in heterogeneous oxide films on liquid honed and belt ground samples. An effect of intensity of mechanical treatment on the degree of the surface reactivity increase was found in voltammetric and potentiostatic investigations. The change of surface activity is due to different electronic conduction of the oxide film. The results are explained on the basis of Thiessen's tribochemical model (1966). Increased reactivity is a consequence of tribochemical reactions including the interacting materials, molecules of sorption layers, and the surrounding atmospheric milieu. The production and distribution of intermetallic reaction products are supposed to play an important role in this process. The forces of mechanical loading determine the induced excess energy, which controls both probability and selection of the tribochemical reactions. (29 refs.)

115417 A new gas equilibration method for the measurement of carbon potential: carbon potential in austenitic 316 stainless steel at 1000°C. M.Handa, I.Takahashi, T.Tsukuda, T.Iwai (Div. of Nuclear Fuel Res., JAERI, Ibaraki-ken, Japan).

J. Nucl. Mater. (Netherlands), vol.116, no.2-3, p.178-83 (June 1983). A new method for the determination and control of the carbon potential of a sample material using CH₄/H₂ gas equilibration was developed. The carbon potential of the sample could be controlled in a wide range with an accuracy of about ±0.1 kcal/mol by adopting several kinds of reference mixtures, in which the temperature of the reference material, metal/metal-carbide mixture set, was changed. The carbon potential in austenitic 316 stainless steel at 1000°C was measured successfully by this method. (19 refs.)

115418 Inhomogeneous plastic deformation and its relevance to iodine stress corrosion cracking susceptibility in irradiated Zircaloy-2 tubing. T.Onchi (Central Res. Inst. of Electric Power Industry, Iwato-Kita, Komae-shi, Tokyo, Japan), H.Kayano, Y.Higashiguchi.

J. Nucl. Mater. (Netherlands), vol.116, no.2-3, p.211-18 (June 1983). Evidence from tensile tests on specimens derived from Zircaloy-2 tubing of current 8×8 BWR type design and irradiated to 3.2×10¹⁹ and 3.0×10²⁰ n/cm² (E>1 MeV) showed that inhomogeneous plastic deformation occurred in the temperature range 300-350°C for the higher neutron fluence, but not for the lower one. Dislocation channelings were also identified by transmission electron microscopy for the specimen irradiated to the higher fluence and strained at around 320°C, but not for the lower fluence. On the basis of the results, an attempt was made to explain the influence of neutron irradiation on the iodine stress corrosion cracking (SCC) susceptibility of Zircaloy tubing, suggesting that a drastic increase of SCC susceptibility at neutron fluences above 10²⁰ n/cm², hypothesized by Lunde and Videm, could be successfully interpreted in terms of the occurrence of dislocation channels. (18 refs.)

115419 Stress corrosion cracking of aged Al-5Zn-4Mg alloy in 3.5% NaCl solution. P.Gopalan (Dev. Group, Hindustan Aeronautics Ltd., Bangalore, India), T.S.Panchapagesan, Kishore, E.S.Dwarakadasa.

J. Electrochem. Soc. India, vol.32, no.1, p.17-21 (Jan. 1983). [received: Sept. 1983]

Specimens of high strength Al-5Zn-4Mg alloy have been subjected to dynamic SCC under constant strain rate tensile loading in 3.5% NaCl solution. Alloys tested in peak aged and overaged conditions reveal that the resistance to SCC improves as the specimen is overaged. The effect of strain rate is significant at low values. Fractures in presence of corrodent, exhibit apparently brittle failures, often obscured by corrosion products. Microstructure of the alloy (studied by TEM) is found to closely control the SCC behaviour. An attempt has been made to correlate the SCC behaviour with structure. A hydrogen embrittlement model of cracking has been used to explain the observed fractographic features. (15 refs.)

115420 Inhibitive action of some amines towards corrosion of 70/30 brass in sulphuric acid. Pushpa Gupta (Inst. of Tech., Banaras Hindu Univ., Varanasi, India), R.S.Chaudhary, T.K.G.Namboodhiri, B.Prakash, B.B.Prasad.

J. Electrochem. Soc. India, vol.32, no.1, p.27-31 (Jan. 1983). [received: Sept. 1983]

Effect of aniline, o-nitroaniline, p-nitroaniline, o-chloroaniline, p-chloroaniline, dibenzyl amine, N-butyl amine, and triethyl amine on corrosion of 70/30 brass in 1% H₂SO₄ solution has been investigated by weight loss, solution analysis and potentiostatic techniques. All the inhibitors studied show poor efficiency and are anodic inhibitors. Aniline, p-nitroaniline, triethyl amine and N-butyl amine have been found to be effective for decreasing the dezincification rate of 70/30 brass in 1% H₂SO₄ solution. The cause of obtaining poor inhibition efficiency with these compounds has been explained on the basis of molecular structures. (12 refs.)

115421 Determination of corrosion rates in high purity water employing coulometric method. K.S.Rajagopalan, N.Krithivasan, S.Thangathirupathy, M.E.K.Janki (Central Electrochem. Res. Inst., Karaikudi, India).

J. Electrochem. Soc. India, vol.32, no.1, p.34-40 (Jan. 1983). [received: Sept. 1983]

The coulometric method was successfully applied to rapid evaluation of metal corrosion rate in solution where a known amount of charge was supplied to a test piece and the potential decay curve recorded was analysed to obtain the corrosion rate. This method avoids some of the essential shortcomings of the polarisation resistance method. Experiments in hydrochloric as well as sulphuric acids of different concentrations with carbon steel yielded corrosion rates comparable with other methods. The method could be successfully applied for the determination of corrosion rates of carbon steel in double distilled water and the results compared very well with weight loss measurements. The influence of the presence of anions like chloride and sulphate at ppm levels was also studied. (10 refs.)

115422 Ellipsometric evaluation of various pretreatments on zircaloy-2. S.V.Phadnis, P.K.Chauhan, H.S.Gadiyar (Metal Div., Bhabha Atomic Res. Centre, Bombay, India).

J. Electrochem. Soc. India, vol.32, no.1, p.41-6 (Jan. 1983). [received: Sept. 1983]

The oxide films developed on zircaloy-2 as a result of various pretreatments, namely (i) mechanical polishing, (ii) etching in HF-HNO₃ solution, (iii) anodization in 1.0% H₂SO₄ at 45 volts, (iv) anodization in 1.0% KOH at 45 volts, and (v) oxidation in 1500 psi steam at 400°C for 10 minutes have been studied for their refractive indices and thicknesses by ellipsometry. The real part 'n' of refractive indices n(1-ik) of all the films was found to be 2.0±0.6, while absorption coefficient 'k' varied. The absorption coefficient for the film formed after anodization in KOH was 0.24 while on those after other pretreatments was in range (0.02-0.06). Thicknesses of films on etched and

mechanically polished zircaloy-2 were 37.3 Å and 55 Å respectively while those of anodized in H_2SO_4 , KOH and oxidised in steam were 1906.3 Å, 691.5 Å and 447.7 Å respectively. An attempt has been made to correlate these film properties with the long term corrosion behaviour of zircaloy-2 in high temperature water. (12 refs.)

115423 Benzotriazole as an inhibitor to corrosion of mild steel in sulphuric acid. P.N.Giriya Shankar, K.I.Vasu. *J. Electrochem. Soc. India*, vol.32, no.1, p.47-51 (Jan. 1983). [received: Sept. 1983]

Corrosion of mild steel in sulphuric acid media was studied by galvanostatic polarization technique. Benzotriazole at concentrations up to 25 mM was found to be a better inhibitor in 1N H_2SO_4 than in 2N H_2SO_4 . A plot of percentage area covered by the inhibitor against the inhibitor concentration reveals that benzotriazole absorbs according to Temkin's rule in 1N H_2SO_4 , while the absorption of the inhibitor in 2N H_2SO_4 follows the Langmuir isotherm. (9 refs.)

115424 A typical and short case study on the effect of pollution on corrosion. E.Elayaperumal. *J. Electrochem. Soc. India*, vol.32, no.1, p.65-6 (Jan. 1983). [received: Sept. 1983]

An engineering fabrication plant has been storing structural steels successfully in an open-yard in the plant of 2 or 3 decades. But in the last few years unacceptable corrosion has been noticed in the steel stored in the open yard. Corrosion has been occurring in spite of application of a certain paint. The unusual corrosion has been ascribed to the several new industries which have come up during the past few years in and around the plant. The emission for these industries not only pollute the air but also lead to corrosion of the structural steels in the neighbouring areas. The air in these surroundings contains corrosive ingredients. The earlier used paint system apparently is not designed to withstand corrosion by these industrial pollutants. The following principal coating resins are considered suitable for the above purposes: 1. Alkyds, 2. Vinyis, 3. Epoxy, and 4. Zinc-rich. (no refs.)

115425 Non-equilibrium phases in laser-processed Fe-0.2 wt.% C-20 wt.% Cr alloys. P.A.Molian (Dept. of Mech. Engng., Iowa State Univ., Ames, IA, USA), W.E.Wood.

Mater. Sci. & Eng. (Switzerland), vol.60, no.3, p.241-5 (Sept. 1983). The microstructures and microhardness of laser-processed Fe-0.2 wt.% C-20 wt.% Cr alloys were investigated as a function of melt depth in single and multiple (overlapping) laser passes. The single-laser-pass alloys exhibited duplex austenite-ferrite structures with no evidence of carbide precipitation. Melt depths of up to 600 µm did not influence this microstructure. The multiple-laser-pass alloys consisted of lath martensite-ferrite structures in deep (about 600 µm) penetration melts and austenite-ferrite structures in shallow (about 120 µm) penetration melts. The transformation of austenite to martensite in multiple-laser-pass alloys, observed only in deep penetration melts, was explained as due to the effects of tempering temperature, time and quench rate obtained during subsequent laser passes. Conventional furnace heat treatments of single-laser-pass alloys substantiated these conclusions. (1 ref.)

115426 Influence of an increase in phosphorus content on the corrosion resistance of austenitic stainless steels type Z 2 CND 17-12. J.C.Charbonnier, T.Jossic, B.Thomas (Inst. de Recherches de la Siderurgie Francaise, St. Germain-en-Laye, France). *Mem. & Etud. Sci. Rev. Metall. (France)*, vol.80, no.7-8, p.349-53 (July-Aug. 1983). In French.

Results of tests carried out on four laboratory castings, each of 25 kg, with P contents varying between 0.001 and 0.040 wt.% are presented. Factors considered include intercrystalline corrosion, pitting corrosion, cavity corrosion and electrochemical behaviour in acid environment. (4 refs.)

115427 Observations of nodule growth during the oxidation of pure binary iron-aluminum alloys. P.Tomaszewicz, G.R.Wallwork (School of Metall., Univ. of New South Wales, Kensington, NSW, Australia).

Oxid. Met. (USA), vol.19, no.5-6, p.165-85 (June 1983). Oxidation studies were carried out in oxygen at 800°C, on a series of pure binary iron-based alloys with between 1.9 and 9.8 wt.% aluminum. The results are presented in conjunction with the existing literature and these permit the development of a classification of scale morphologies based on alloy composition. Alloys with less than 2.4 wt.% aluminum form bulky stratified scales composed of Fe_2O_3 and Fe_3O_4 with FeAl_2O_4 and Al_2O_3 at the scale-metal interface. Alloys with between 2.4 and 6.9 wt.% form an external alloy substrate. Only alloys with greater than 6.9 wt.% aluminum form completely protective Al_2O_3 scales. Models based on oxide nucleation are presented for the growth of bulky scales and also the iron oxide nodules. (23 refs.)

115428 Effect of sulfur dioxide on the oxidation of thin films of tin. C.I.Muneera, S.Varghese (Dept. of Phys., Univ. of Kerala, Kerala, India), V.Unnikrishnan Nayar.

Oxid. Met. (USA), vol.19, no.5-6, p.187-99 (June 1983). The oxidation of thin films of tin in SO_2 -air atmospheres containing 10%, 20%, 30%, 40%, 50%, and 60% SO_2 have been investigated at room temperature. Reaction kinetics were studied by the variation in resistance of thin films and growth patterns by metallography. Addition of SO_2 causes an increase in the oxidation rate of thin films of tin. Probable reactions at lower and higher percentages of SO_2 have been discussed. (28 refs.)

115429 Acidic and basic fluxing of Ni-base superalloys in a 90Na₂SO₄-10K₂SO₄ melt at 1173K. W.T.Wu (Inst. of Metal Res., Acad. Sinica, Shenyang, China), A.Rahmel, M.Schorr.

Oxid. Met. (USA), vol.19, no.5-6, p.201-29 (June 1983). The influence of the electrode potential on the corrosion behavior of a series of Ni-base superalloys has been investigated in a (mole %) 90Na₂SO₄-10K₂SO₄ melt at 1173K. Acidic fluxing occurs at positive potentials and basic fluxing at negative potentials. A protective scale is formed in an intermediate (neutral) potential range on high chromium-containing alloys such as IN-738LC, IN-939, IN-597, and IN-657. The breakthrough potentials for acidic and basic fluxing depend on the composition of the alloy. Alloys with low chromium contents such as IN-100 and IN-713 LC do not form stable protective scales at any potential. Numerous sulfide phases have been identified in the scale and subscale, depending on potential, severity of attack, and material composition. NaCrS₂ only forms under basic fluxing conditions. Its presence can therefore be considered as an indication that basic fluxing conditions have existed. (16 refs.)

115430 Influence of the mechanical pretreatment of the surfaces on the adhesive strength of steel-grey cast iron joints. P.Fahrenschon. *Plaste & Kautsch. (Germany)*, vol.30, no.7, p.403-5 (July 1983). In German. For milled rails with an adhering harder strip the surface roughness of the two adhering components is of less significance than their metallographic structure, with regard to their shear strength. (11 refs.) R.S.

115431 Effect of waterglass impregnation upon hardenability of porous sintered steel. H.-J.Maurer, W.Bodden (Schunk & Ebe GmbH, Giessen, Germany).

Powder Metall. Int. (Germany), vol.15, no.3, p.122-5 (Aug. 1983). Various sintered steels with densities between 5.9 Mg/m³ and 7.4 Mg/m³ were tested after impregnation with liquid waterglass subsequent to sintering. A special hardening method is used to expel the crystal water from the waterglass. The hardened waterglass now affects the pores of the sintered steel part in such a way that diffusion of the hardening gases into the part is very much limited. Thus it becomes possible to apply a hard layer that is strictly limited to the surface areas of sintered steel parts of a density from 6.5 Mg/m³ upwards. The special advantage of this method is, in addition to maintaining a tough core, that very limited dimensional changes occur in the sintered parts. (5 refs.)

115432 Chemical deposition of metallic tin upon copper substrates. G.F.Paus, R.C.V.Piatti, J.J.Podesta (Instituto de Investigaciones Fisicoquimicas Teoricas y Aplicadas (INIFTA), Argentina), La Plata.

Rev. Teleg. Electron. (Argentina), vol.71, no.837, p.59-60 (Jan.-Feb. 1983). In Spanish.

Reports work on the auto deposition of metallic Sn on Cu substrates (copper-clad plastic laminates, printed circuit boards) by immersing them in solutions of SnCl_2 , HCl, $\text{H}_2\text{N.CSNH}_2$ and NaH_2PO_2 in distilled water at temperatures between 30° and 90°C for periods between 5 and 120 minutes. The results of salt spray, weathering and humidity tests upon the samples are given, showing that the method provides coatings of good corrosion resistance, solderability and appearance. Similar experiments were made with autodeposition of acid nickel, alkaline nickel and gold. (no refs.) C.J.O.G.

115433 Structure of the oxide films of VT14 alloy formed in treatment in air at 850°C. G.G.Maksimovich, V.N.Fedirko, A.T.Lizun, L.A.Bunin (G.V. Karpenko Physicochem. Inst., Acad. of Sci., Lvov, Ukrainian SSR).

Sov. Mater. Sci. (USA), vol.18, no.6, p.468-70 (Nov.-Dec. 1982). Translation of: *Fiz.-Khim. Mekh. Mater. (USSR)*, vol.18, no.6, p.13-16 (Nov.-Dec. 1982). Investigates the influence of alloying elements on the structure of the scale on VT14 alloy after treatment in air at 850°C with hold times of 1, 5, and 10 h. A 1-h hold at 850°C created a scale primarily of TiO_2 rutile and Al_2O_3 oxide, and the Al_2O_3 layer was located at the gas-scale interface. With an increase in hold time to 10 h, according to micro-X-ray spectral analysis, TiO_2 oxide and Al_2O_3 oxide located at the surface with MoO_3 and V_2O_5 oxides uniformly distributed over the whole volume became dominant in the structure of the scale. Therefore, in the formation on VT14 alloy at 850°C of a lamellar scale of complex composition all of the alloying elements participate. (9 refs.)

115434 Problems of the life of constructional materials in nitrogen and hydrogen-containing media. A.L.Bichuya (G.V. Karpenko Physicochem. Inst., Acad. of Sci., Lvov, Ukrainian SSR).

Sov. Mater. Sci. (USA), vol.18, no.6, p.479-81 (Nov.-Dec. 1982). Translation of: *Fiz.-Khim. Mekh. Mater. (USSR)*, vol.18, no.6, p.25-8 (Nov.-Dec. 1982). An analysis is made of those factors which influence the high-temperature life of constructional materials in nitrogen and hydrogen containing media, particularly in ammonia. It is concluded that the observed reduction in life may occur as a result of corrosion damage related to nitriding, and also of hydrogen embrittlement occurring as the result of penetration of hydrogen formed in dissociation of the adsorbed gaseous phase on the metal being deformed. (13 refs.)

115435 Local corrosion of martensitic stainless steel in a medium containing chloride ions and hydrogen sulfide. I.I.Vasilenko, M.F.Alekseenko, G.D.Levitskaya, A.I.Radkevich, Z.N.Mukhina (G.V. Karpenko Physicochem. Inst., Acad. of Sci., Lvov, Ukrainian SSR).

Sov. Mater. Sci. (USA), vol.18, no.6, p.491-4 (Nov.-Dec. 1982). Translation of: *Fiz.-Khim. Mekh. Mater. (USSR)*, vol.18, no.6, p.39-42 (Nov.-Dec. 1982). A quantitative analysis was made of the products of H_2S corrosion of a martensitic stainless steel, making it possible to determine the rate of solution of the individual alloying elements as well as the steel as a whole. Steel 15Kh12N2MVFBa hardened from 1020°C and tempered 660°C was investigated. The corrosion rate of the steel was found to be 8 mg/(m².h). Iron, chromium and nickel were found in the solution in the ratio 18.8:13.4:1. Ions of the carbide-forming elements were not found. It therefore follows that carbide-forming elements may be used as alloying elements without loss of corrosion resistance. (13 refs.)

115436 Some problems of investigation of the cyclic crack resistance of materials in liquid media. V.V.Panasnyuk, L.V.Ratyeh, I.N.Dmytrakh (G.V. Karpenko Physicochem. Inst., Acad. of Sci., Lvov, Ukrainian SSR).

Sov. Mater. Sci. (USA), vol.18, no.6, p.494-9 (Nov.-Dec. 1982). Translation of: *Fiz.-Khim. Mekh. Mater. (USSR)*, vol.18, no.6, p.42-9 (Nov.-Dec. 1982). Within the limits of problems of fracture mechanics new approaches and methods of determining the cyclic crack resistance of materials under conditions of the action of liquid corrosive media are discussed and certain results obtained using these methods are presented. Cyclic crack resistance tests on 20SF steel in 3% NaCl solution were carried out using the method described. (31 refs.)

115437 Inhibitors for the protection of steel from acid corrosion at high temperature and pressure. A.K.Mindyuk, N.A.Kravchuk, O.A.Sirotyuk, V.F.Malakhov (G.V. Karpenko Physicochem. Inst., Acad. of Sci., Lvov, Ukrainian SSR).

Sov. Mater. Sci. (USA), vol.18, no.6, p.518-21 (Nov.-Dec. 1982). Translation of: *Fiz.-Khim. Mekh. Mater. (USSR)*, vol.18, no.6, p.69-72 (Nov.-Dec. 1982). Presents the results of investigations of the corrosion of steel (steel of strength group D) in 12% HCl solution and of its protection by KhOSP-10, KhOSP-N, and KhOSP-A inhibitors at temperatures of 100, 120, 140, and 160°C and a pressure of 30 MPa for 3 h. The 25 mm diameter×2 mm samples were cut from casing pipe. The samples were placed in the high-pressure chamber of a special unit with an electric heater and the electric heaters of the high-pressure chamber and the working solution preliminary heating chamber were turned on simultaneously. After heating to 90°C the medium was pumped from the preliminary heating chamber into the high-pressure chamber, where it was heated to the necessary temperature and was subjected to pressure with the help of a manual press. After holding at the established conditions for 3 h, the electric heater was turned off, the pressure was reduced by the manifold, the samples were removed, and they were cleaned and weighed. The error in weighing was 0.1 mg with a sample weight of about 5.6 g each. The test data was averaged for two to four samples. (7 refs.)

115438 High-temperature salt corrosion cracking of titanium alloy semifinished products. V.S.Sinyavskii, V.V.Usova, S.I.Lunina, S.A.Kushakevich, E.A.Makhmutova, Z.K.Khanina.

Sov. Mater. Sci. (USA), vol.18, no.6, p.521-4 (Nov.-Dec. 1982). Translation of: *Fiz.-Khim. Mekh. Mater. (USSR)*, vol.18, no.6, p.72-5 (Nov.-Dec. 1982). The high temperature NaCl corrosion cracking of the Ti alloys VT-20, VT6, VT14 and OT4-1 was investigated on tensile samples. The influence of the

form of the semifinished product, the anisotropy of the corrosion-mechanical properties, and heat treatment on the resistance of the alloys to corrosion cracking were studied. It is concluded that the sensitivity of the alloys to corrosion cracking may be judged indirectly from the change in mechanical properties. (11 refs.)

115439 Optimization of the parameters of obtaining noncarbide-forming coatings. V.I.Korshun (Dnepropetrovsk Chemicotechnol. Inst., Ukrainian SSR).

Sov. Mater. Sci. (USA), vol.18, no.6, p.525-6 (Nov.-Dec. 1982). Translation of: *Fiz.-Khim. Mekh. Mater. (USSR)*, vol.18, no.6, p.75-7 (Nov.-Dec. 1982). A method is developed for the computer calculation of the optimum depth of the decarburized zone, and times of decarburization and coating application on steel. (9 refs.)

115440 Production of bimetallic contact elements by a diffusion impregnation method. M.S.Goikhan (G.V. Karpenko Physicomech. Inst., Acad. of Sci., Lvov, Ukrainian SSR).

Sov. Mater. Sci. (USA), vol.18, no.6, p.527-9 (Nov.-Dec. 1982). Translation of: *Fiz.-Khim. Mekh. Mater. (USSR)*, vol.18, no.6, p.77-9 (Nov.-Dec. 1982). The method of diffusion impregnation of copper in molten sodium containing silver and alloying elements was used to produce bimetal electrical contact elements capable of successfully competing with those produced by hot pressing and rolling. (4 refs.)

115441 Assessment of residual stresses in coatings applied to P/M parts. S.S.Ermakov, A.M.Shmakov, V.M.Studentsov, A.I.Neumoin (Leningrad Polytech. Inst., Leningrad, USSR).

Sov. Powder Metall. & Met. Ceram. (USA), vol.22, no.1, p.17-20 (Jan. 1983). Translation of: *Poroshk. Metall. (USSR)*, vol.22, no.1, p.19-21 (Jan. 1983). [received: Aug. 1983] A study was made of the physicomechanical characteristics of coatings applied to sintered materials and of the properties of such coating/basis systems. It is concluded that by varying the composition of the coating, the density of the base material, and the coating-to-base thickness ratio, it is possible to improve the elastic properties of parts and ensure a favourable distribution of residual stresses in the coating. (10 refs.)

115442 Anodic oxidation of iron and cathodic reduction of the anodic film: a review. J.L.Delplancke (Metall.-Electrochimie, Univ. Libre de Bruxelles, Brussels, Belgium).

Surf. Technol. (Switzerland), vol.20, no.1, p.71-81 (Sept. 1983). The different theoretical models used to describe the electrochemical behaviour of iron in the two most studied electrolytes (a borate buffer solution and a sulphate solution) and the study of the cathodic reduction of the anodic film in a borate buffer solution are dealt with in this review. (80 refs.)

115443 New fields of application of plasma spraying in energy technology. P.C.Wolf.

Waerme (Germany), vol.89, no.3, p.42-5 (June 1983). In German. Describes vacuum plasma spraying as a surface protection technique for boilers, gas turbine blades and other equipment subject to corrosion, erosion and wear. The process is computer controlled. The spraying material is Metco 444 (73.5% Ni with Cr, Al, Mo, Fe), or WC/Co, NiCr, CrC, or (for gas temperatures of over 1200°C) CoCr or NiCoCr alloy. (7 refs.) J.S.

115444 Mechanism of adherence of porcelain enamels—adhering factors of enamels on extra low carbon steels. F.Imoto (Faculty of Engng., Shizuoka Univ., Hamamatsu-shi, Japan), K.Matsudo, T.Shimomura, T.Kurokawa. *Yogyo-Kyokai-Shi (Japan)*, vol.91, no.6, p.272-80 (1983). In Japanese.

Experiments have been carried out to understand the effects of several factors on the adherence of enamels. The microstructure of the steel-enamel interface of the fired enamel was also investigated. It is confirmed that enameling steel (extra low carbon rimmed steel) containing 0.023% copper is suitable for the base of the direct-on enamel and also provides good adherence to the regular ground cast enamels. It is shown that the pretreatment is effective in most cases. Concentration profiles of iron across the steel-enamel interface show simple decreasing curves in all cases. There is no correlation between such a profile and the adherence index of the specimen. An 'interlocking' structure was observed in the steel-enamel interface. During the firing process, the thickness of this structure increased probably by the action of local electric cells on the steel surface whose cathodes are composed of 'smut' (pickling residue) and precipitates from nickel flashing or adherence-promoting agents. As the thick structure develops, the adherence index increased. (11 refs.)

115445 Anodic oxidation of zirconium: Some aspects of the role of foreign ions. C.Panagopoulos.

Univ. Nottingham, England thesis, 1983
The galvanostatic anodization of zirconium in various solutions was studied. The oxide growth kinetics was found to depend upon the nature of the electrolyte. The electric field of zirconium anodization in alkaline solutions was found to decrease with increasing pH of the electrolyte for similar anodizing conditions, i.e. applied current density, temperature and formation voltage. The oxide composition examined by XPS technique was shown to vary with the anodizing conditions. In particular, the oxidation state and the distribution profile of the electrolyte anion in the oxide were clearly determined by the nature of the anion. The breakdown voltage of growing zirconium oxide was fundamentally dependent upon the anodizing conditions, i.e. applied current density, temperature and concentration and nature of the electrolyte. However, the mechanism of oxide breakdown was thought to be determined by several factors; internal stress in the oxide, electron space charge and chemical, electronic and thermal events taking place at the oxide-solution interface. The temperature rise during zirconium anodization increased with increasing applied current density. Finally, the series capacitance and resistance of zirconium oxide in contact with alkaline solutions were found to be a linear function of $\log f$ at a limited range of measuring frequency.

115446 Carbide precipitation in nickel-base model alloys and its influence on the ductility and fracture behaviour at room temperature. K.P.Mohr, H.Schuster, H.Nickel.

Report JUL-1845, Kernforschungsanlage, Julich, Germany (May 1983), 98 pp.

The influence of carburization with internal carbide formation on the room temperature tensile properties was determined for nickel-base model alloys of different compositions. The relationship between carbide volume fraction and the loss of ductility was systematically investigated. The embrittlement was found to be severe for volume fractions greater than about 0.03 if the carbides were formed principally on grain and twin boundaries. Cracks were propagated unhindered in the continuous, grain boundary carbide films formed in alloys containing Cr or Mo and caused intergranular fracture with rupture elongations of similar magnitude to that of the carbide phase itself. Grain boundary carbide precipitates which were not continuous led to less severe ductility loss. (83 refs.)

115447 Intergranular stress corrosion cracking of Ni-Cr-Fe Alloy 600 tubes in PWR primary water - Review and assessment for model development. Y.S.Garud, T.L.Gerber.

Report EPRI-NP-3057, Electr. Power Res. Inst., Palo Alto, CA, USA (May 1983), 80 pp.

Available from Research Report Center, Box 50490, Palo Alto, CA 94303, USA.

A review and assessment of primary-side intergranular stress corrosion cracking (IGSCC) of Ni-Cr-Fe Alloy 600 tubes and related experimental observations are summarized, and the need for a quantitative model to predict the IGSCC is established. A promising approach to quantitative model development is presented, and the analytic-experimental work needed for the model development is suggested. Recommendations for collection of field data from steam generator operation to supplement the model development and its implementation are included.

115448 Thermodynamics and kinetics of the gas phase and pack aluminide coating formation on iron and steel. B.Nciri, L.Vandenbulcke (Univ. of Orleans, Orleans, France).

Proceedings of the 4th European Conference on Chemical Vapour Deposition, Eindhoven, Netherlands, 31 May-2 June 1983 (Eindhoven, Netherlands: Philips Centre Manuf. Technol. 1983), p.141-7

The pack aluminization process of nickel and nickel-base alloys have been extensively studied and used to form protective coatings which extend the life of superalloys in the oxidation, corrosion and erosion environment encountered in gas turbines. On iron and steel, this process has been less studied, but such aluminide or chromaluminide coatings should prevent corrosion in an aggressive chemical environment at mid-temperature (700-800°C), in a sulfur atmosphere for example. The gas-solid diffusion model which includes the multi-component equilibria of the gaseous phase with the pack and the substrate, permits the authors to point out the influence of the relative rates of gas transport and solid-state diffusion on the pack-aluminization process. The surface composition of the coatings and their growth rate depend on the temperature and the aluminium activity in the pack, for a given activator. Fairly good agreement is obtained between the theoretical study and the experimental results in the pack. Theoretical predictions for deposition in the gas phase, on substrates out of contact with the pack, can be qualitatively deduced. (6 refs.)

115449 The development of CVD oxide coatings for the protection of metal surfaces. J.T.K.Clark, A.I.Foster, M.L.Sims, M.A.M.Swidzinski, D.Young (BP Res. Centre, British Petroleum Co. plc, Sunbury-on-Thames, England).

Proceedings of the 4th European Conference on Chemical Vapour Deposition, Eindhoven, Netherlands, 31 May-2 June 1983 (Eindhoven, Netherlands: Philips Centre Manuf. Technol. 1983), p.385-94

Describes the development of a new type of surface coating for metallic substrates, based on relatively low temperature CVD processes. As resistance to chemical attack was a prime requirement, non-reactive oxides were chosen as the coating. Limitations in the heat treatments to which many steel/alloy components can be subjected have necessitated the development of two coatings. These are: titania (TiO₂) deposited at 300-400°C; usable up to ≈500°C; and silica (SiO₂) deposited at 600-800°C; usable up to ≈1000°C. Titania coating was developed initially to impart titanium-like corrosion resistance to lower grade metals such as mild (carbon) and low alloy steels. It is the inert and impervious surface oxide (TiO₂) that provides titanium metal with its corrosion resistance. Silica coating was developed as an inert diffusion barrier to prevent gas phase attack of steel surfaces used at high temperatures. (14 refs.)

115450 Role of CVD in providing wear resistant films. H.E.Hintermann (Lab. Suisse de Recherches Horlogeres, Neuchatel, Switzerland).

Proceedings of the 4th European Conference on Chemical Vapour Deposition, Eindhoven, Netherlands, 31 May-2 June 1983 (Eindhoven, Netherlands: Philips Centre Manuf. Technol. 1983), p.467

Summary form only given. The adhesion, or rather the mechanical properties of the coating/substrate composite, is characterized using the scratch test method. A compilation of friction and wear data from pin-on-disk experiments are reported on TiC, TiN, Cr₂C₃, SiC, Al₂O₃, in dry and humid air. Furthermore the results of some studies on the effect of CVD coatings on the load carrying capacity of the (partial) elastohydrodynamic lubricant film and the boundary lubricant film, applying the IRG transition diagram for lubricated steel point contacts, are reported. Finally the usefulness and feasibility of TiC coated bearing elements in (i) oil lubricated high speed ball bearings in gyros, and (ii) unlubricated slow moving ball bearings at elevated temperature in vacuum or inert atmosphere (He) are demonstrated. (no refs.)

115451 The decarburization of steel during the CVD of TiC. P.J.M.van der Straten, M.M.Michorius, G.Verspui (Philips Centre for Mfg. Technol., Eindhoven, Netherlands).

Proceedings of the 4th European Conference on Chemical Vapour Deposition, Eindhoven, Netherlands, 31 May-2 June 1983 (Eindhoven, Netherlands: Philips Centre Manuf. Technol. 1983), p.553-67

When TiC is deposited on carbon-containing steels using H₂, CH₄ and TiCl₄ containing gas mixtures, the carbon of the TiC layer originates from the CH₄ gas as well as from the steel substrate itself. The contribution of carbon from the steel dominates when the carbon activity in the steel is relatively high. In thin sections and especially in the case of small substrate dimensions severe decarburization may occur, resulting in a loss of hardness of the steel and a decreasing growth rate of TiC. These problems can be diminished by a carburizing treatment before the CVD procedure, by using a high CH₄/TiCl₄ ratio during the deposition of TiC and by employing steels which suffer less from decarburization. (14 refs.)

Calculation of carburization profiles in stainless steel components in a liquid sodium environment See Entry 112315

Weld residual stress redistribution near growing cracks See Entry 112339

Oxidation of Ni-Cr experimental alloys and the effectiveness of the oxide as a barrier against carburization in high-temperature reactor primary circuit helium See Entry 112343

Development of a CVD silica coating for UK advanced gas-cooled nuclear reactor fuel pins See Entry 112351

Secondary water chemistry at Millstone 2 See Entry 112386

Implementation of boric acid in the field - Indian Point Unit 3 plant See Entry 112390

Shape control of non-metallic inclusions in Al-deoxidized steel by calcium treatment See Entry 113728

Vacancy clustering during oxidation of nickel, magnesium, and zinc See Entry 113874

Metallurgical surfaces produced by ion implantation See Entry 113940

Peculiarities of spectral emission of titanium during high-temperature oxidation See Entry 114220

Electron-enhanced CO₂ adsorption and stabilization on aluminum films See Entry 114366
 Heat treatments of CVD-coatings on hardmetals See Entry 114425
 Electrical conductivity of Cr₂O₃ doped with La₂O₃, Y₂O₃ and NiO See Entry 114529
 Inelastic electron tunneling spectroscopy on ultrahigh vacuum prepared tunnel junctions See Entry 114620
 Mossbauer study of electrodeposited iron-nickel alloys See Entry 114765
 Optical anisotropy and electrostriction in the anodic oxide of tantalum See Entry 114941
 Possibility of melting of silica particles in a plasma jet See Entry 115053
 Chemical vapor deposition of group IVB, VB, and VIB elements with nonmetals. A literature review See Entry 115076
 CVD of TiN at the tempering temperature of alloy-steels See Entry 115097
 Formation of thin refractory coatings, their properties and fields of application See Entry 115098
 Industrialisation of titaniumcarbonitride deposition process at moderated temperatures See Entry 115100
 Structure and mechanical and corrosion properties of P/M Kh23N18 stainless steel See Entry 115140
 Fatigue and overload fracture of carburized steels See Entry 115314
 Effect of cold working and annealing on stress corrosion cracking of AISI 304 stainless steel See Entry 115316
 A phenomenological model of embrittlement of metals under conditions of the adsorption action of liquid metal media See Entry 115334
 Fractographic study of cracks produced by thermal shocks in 20MnMoNi55 and comparable weld material in water environment See Entry 115356
 Friction and wear properties of nitrided and N⁺-implanted 17-4 PH stainless steel See Entry 115370
 The effect of surface hardness of carbon steels on scuffing resistance in rolling-sliding contact See Entry 115371
 Determination of the polarization resistance from impedance measurements See Entry 115459
 Absorber surfaces and durability of solar heat collectors See Entry 115700

81.70 MATERIALS TESTING

(inc. sample preparation for examination, metallographic techniques, ion and electron microprobe techniques, Auger and photoelectron techniques, defectoscopy; for measurement in the mechanics of solids and rheology, see 46.30R)

115452 The coefficient of reflection of ultrasonic waves from an adhesive bond interface. A.Pilarski (Inst. of Fundamental Technol. Res., Polish Acad. of Sci., Warsaw, Poland).
Arch. Acoust. (Poland), vol.8, no.1, p.41-53 (1983).
 Reports on an attempt to explain the existence of a relation between the reflection coefficient and mechanical strength of an adhesive bond, based on a model of a bond with finite rigidity. On the basis of formulae derived, a correlation relation was determined from experimental results between the modulus of the pressure reflection coefficient of a plane ultrasonic wave incident normal to the interface of an adhesive bond of lucite with epoxy resin, and the tensile strength of the bond. (9 refs.)
 115453 An analytical method of evaluating angles in Brookes' formula for effective resolved shear stress on slip systems in crystals. V.P.Bhatt, C.F.Desai, R.C.Shah (Phys. Dept., MS Univ. of Baroda, Baroda, India).
Res. Mech. (GB), vol.9, no.1, p.35-40 (1983).
 A simple relation has been evolved for the analytical evaluation of indenter-orientation dependent angular variables in Brookes' formula for the effective resolved shear stress on a slip system of a crystal produced by a hardness-indenter. Its merits over the stereographic method are considered. (1 ref.)
 115454 Automated time-of-flight studies of the defect detection trial plates 1 and 2. G.J.Curtis, B.M.Hawker (Materials Phys. Div., AERE, Harwell, England).
Br. J. Non-Destr. Test. (GB), vol.25, no.5, p.240-8 (Sept. 1983).
 The defect detection trials provided a definitive test of the ultrasonic time-of-flight technique when instrumented into a multi-probe automated detection and sizing system. The specific problem tackled was the examination of a simulated PWR vessel girth weld, austenitically clad and containing deliberately implanted defects. The design and function of the time-of-flight scanner is described. Its detection and sizing capability is examined. (13 refs.)
 115455 CEBG inspection of plates 1 and 2 in UKAEA defect detection trials. K.J.Bowker, J.M.Coffey, D.J.Hanstock, R.C.Owen, J.M.Wrigley (Sci. Services Dept., CEBG, Manchester, England).
Br. J. Non-Destr. Test. (GB), vol.25, no.5, p.249-55 (Sept. 1983).
 Summarises the CEBG's participation in the UKAEA 'Defect Detection Trials' exercise in which four large test specimens, modelling parts of a PWR pressure vessel and containing deliberately introduced defects, were examined by ultrasonic methods. The CEBG, in collaboration with Babcock Power Ltd., inspected Plates 1 and 2, which modelled the main seam welds. The inspection procedure and the equipment used are outlined, taking one particular defect for illustration. A notable aspect of the procedure is that it employs only essentially conventional ultrasonic techniques. The plates have now been partially sectioned to give more detailed information on the defects although full destructive examination has yet to take place and the authors compare the ultrasonic results with the best estimates for the defects actually present. (2 refs.)
 115456 An in-service inspection method: the use of focused probes for the detection and sizing in DDT plates 1 and 2. A.M.Birac (French Atomic Energy Commission, Paris, France), G.Cattiaux, P.Morisseau, G.Pincemaille, R.Saglio.
Br. J. Non-Destr. Test. (GB), vol.25, no.5, p.258-62 (Sept. 1983).
 As part of the UKAEA defect detection trial programme to evaluate the nondestructive testing methods used during the in-service inspection (ISI) of PWR vessels, CEA-STA-SCND performed an ultrasonic examination of two test-plates. Each plate was bisected across its full width by a full-thickness butt-weld in which calibrated defects of various natures, dimensions, orientations had been inserted. It was required that the implementation of control, the equipment and the subsequent data analysis represent as nearly as possible the French procedure in force during the pre-service and in-service inspection of a PWR vessel. To evaluate the influence of examiners on the results, the examinations have been carried out twice by two independent terms. (8 refs.)

115457 Beam spread variations with change of angle. B.Watson (Wells-Krautkramer Ltd., Letchworth, England).
Br. J. Non-Destr. Test. (GB), vol.25, no.5, p.263-4 (Sept. 1983).
 An apparent anomaly in beam spread charts of angle probes with constant parameters is discussed. It is recommended that for the US pulse reflection method of inspection, the reflected mode calculations and beam shapes should be preferred. (1 ref.)
 115458 Application of novel techniques of medical imaging to the nondestructive analysis of carbon-carbon composite materials. N.More, B.Basse-Cathalinat, C.Baquey, F.Lacroix, D.Ducassou (Centre d'Elaboration et d'Experimentation de Matériaux et Systemes Implantables, INSERM, Bordeaux, France).
Nucl. Instrum. & Methods Phys. Res. (Netherlands), vol.214, no.2-3, p.531-6 (1 Sept. 1983).
 Rigorous control of all stages of the fabrication of a composite material is vital. It is best if this control uses nondestructive methods, so allowing the same item to be studied during the different stages of its manufacture. Much research has already been done to perfect such investigations in medicine, so providing a minimum of trauma to the patient. Most of these medical applications use radioactive isotopes. The authors describe the application of currently available techniques, employed in nuclear medicine for the analysis of the density and porosity of carbon-carbon composite materials. Two most powerful medical techniques are applied to measure variations of density of a composite material. These are transmission computed tomography using X-rays and the absorption of photons. The quantitative measurement of porosity can be derived from a scintigraphic technique which allows a detailed noninvasive study of the interior of the composite and the spatial variation of porosity at every stage of its fabrication. For each type of investigation, the principle of the method, a description of the apparatus and several examples of results obtained are presented. The advantages and limitations of these techniques which complement those currently available are discussed, together with future possibilities for nondestructive control of industrial processes. It is likely that their proven success in medicine will be extended to the other fields described. (11 refs.)
 115459 Determination of the polarization resistance from impedance measurements. F.Mansfeld, M.W.Kendig.
Werkst. & Korros. (Germany), vol.34, no.8, p.397-401 (Aug. 1983).
 Four different methods for determining the polarization resistance R_p^{ac} from impedance data are discussed. These methods are suitable for online corrosion monitoring. Their use is illustrated for iron in tapwater and in neutral, aerated Na₂SO₄ containing various inhibitors. R_p^{ac}-values obtained with the CIRFIT-method are compared with R_p^{dc} which is obtained from a linear sweep through E_{corr}. The integration method has the advantage of computation speed. (15 refs.)
 115460 Specimen size dependence of low frequency fatigue tests in high-pressure hydrogen. B.Roebeck (Div. of Materials Applications, NPL, Teddington, England).
Fatigue Eng. Mater. & Struct. (GB), vol.6, no.2, p.177-88 (1983).
 Fatigue data required for estimates of cracked component lifetimes are conventionally obtained by cyclic loading of specimens manufactured to a specific geometry. Crack growth in the specimen results in an increase in the stress intensity factor range and crack growth curves are calculated from the variation of crack length with time. An environmental fatigue study of the effect of high pressure hydrogen on the low cycle fatigue of a medium strength steel has shown that, due to effects of elapsed time in the environment and effects of specimen size, in certain circumstances this procedure may not yield geometry-independent results which can be applied with confidence to cracked components. It is concluded that to obtain useful crack growth data in cases where fracture is influenced by diffusion or other strongly time dependent processes might require a modified approach to fracture mechanics testing procedures. (14 refs.)
 115461 Stress activated Raman scattering and microcrack detection. M.Ciftan (Phys. Dept., Duke Univ., Durham, NC, USA), R.G.Brown, E.Saibel.
Int. J. Eng. Sci. (GB), vol.21, no.11, p.1285-93 (1983).
 A new technique for the detection of microcrack precursors and for the study of the dynamics of crack propagation is proposed. The technique uses laser Raman scattering off of adsorbed surface species to detect microcrack precursors via variations in the Raman spectrum associated with the stresses localized within such precursors. The authors give extensive theoretical justification and detail several approaches designed to substantiate the plausibility of the technique proposed. This technique can become a valuable tool for the detection of microcrack precursors as well as studies of phenomena including adsorption, catalysis, adhesion, wear and the dynamics of stress-corrosion cracking. (23 refs.)
 115462 Affecting the comparison with an index-value by the choice of the evaluation method for variable tests of random samples. G.Loschau.
Mater. Test. (Germany), vol.25, no.8, p.276-9 (Aug. 1983). In English.
 To unify and clarify the valuation of variable tests common treatments of test results are initially summarized. Based on this, an exemplary presentation of different usual quality specifications follows in a gradual order of the decision intensity. Therefore the judgement strength of the required index-value with respect to the choice of the evaluation method is illustrated by selected numerical examples. (13 refs.)
 115463 Non-destructive measurement of plastic anisotropy of sheets by ultrasonics. K.Goebbels, H.J.Salzburger.
Mater. Test. (Germany), vol.25, no.8, p.279-81 (Aug. 1983). In German.
 With two ultrasonic probes whose distance is fixed, the time of travel of surface waves has been measured as a function of the direction of rolling of the sheet. 13 cold- and hot-rolled samples were examined. For sheet of less than 3 mm thickness only orientated waves give some indication of plastic anisotropy with regard to the angle between the direction of wave propagation and that of rolling of the sheet. (11 refs.) R.S.
 115464 Decomposition of austenitic phase in work hardened steel samples, using hardness measurements. H.Reimers.
Mater. Test. (Germany), vol.25, no.8, p.267-70 (Aug. 1983). In German.
 Describes measurements of hardness on fatigue tested steel samples over distances up to 20 millimeters, in order to track austenitic/martensitic transitions away from the fracture line. Comparisons between intentional and work hardened samples are presented and the use of X-ray crystallographic methods is mentioned. Sample preparation and properties are described in detail. (2 refs.) G.M.E.
 115465 Gel electrode imaging of fatigue cracks in titanium. W.J.Baxter (Phys. Dept., General Motors Res. Labs., Warren, MI, USA).
Scr. Metall. (USA), vol.17, no.8, p.1023-6 (Aug. 1983).
 The initial experiments on aluminum alloys demonstrated that the gel electrode is very sensitive: fatigue cracks as short as 10 μm in length were detected, while fatigue deformation was detected and measured earlier than

1% of the fatigue life (Baxter, 1982). It is shown that the technique offers a similar sensitivity for the detection and imaging of fatigue cracks in titanium. The images are clearly visible, particularly with the aid of a pocket magnifier, while closer examination of the image with a low power (50X) optical microscope reveals detailed information on secondary cracking, as well as the presence of small microcracks ahead of the tip of the main crack. Direct comparison of the gel electrode image with scanning electron microscope images of the specimen itself, shows that cracks as short as 20 μm in length are detectable. (4 refs.)

115466 An analytical description of fatigue failure curves by portions. S.Ya.Yarema, L.S.Mel'nychuk, B.A.Popov (G.V. Karpenko Physicomech. Inst., Acad. of Sci., Lvov, Ukrainian SSR). *Sov. Mater. Sci. (USA)*, vol.18, no.6, p.506-8 (Nov.-Dec. 1982). Translation of: *Fiz.-Khim. Mekh. Mater. (USSR)*, vol.18, no.6, p.56-8 (Nov.-Dec. 1982). Proposes an approach to constructing model (kinetic equations) of fatigue crack growth the parameters of which are convenient to interpret as characteristics of the fatigue crack resistance of a material. (6 refs.)

115467 Determination of the particle-size distributions of powders by mercury porosimetry. V.S.Pugin, P.A.Kornienko, N.P.Pavlenko (Inst. of Materials Sci., Acad. of Sci., Ukrainian SSR). *Sov. Powder Metall. & Met. Ceram. (USA)*, vol.22, no.1, p.30-2 (Jan. 1983). Translation of: *Poroshk. Metall. (USSR)*, vol.22, no.1, p.33-5 (Jan. 1983). [received: Aug. 1983] Examines the possibility of determining the particle-size distributions of powders by mercury porosimetry, using integral curves of pore-size and volume distribution in porous bodies formed by loosely poured powders. (4 refs.)

115468 Determination of longevity under a two-frequency load (review). I. V.I.Trufiyakov, V.S.Koval'chuk (E.O. Paton Inst. of Electric Welding, Acad. of Sci., Kiev, Ukrainian SSR). *Strength Mater. (USA)*, vol.14, no.9, p.1165-72 (Sept. 1982). Translation of: *Probl. Prochn. (USSR)*, vol.14, no.9, p.9-15 (Sept. 1982). (37 refs.)

115469 Results of an investigation of the service life of heat-resistant materials under repeated static load. L.P.Lozitskii, A.N.Vetrov, V.A.Ivanenko (Inst. of Mech. Engng. Problems, Acad. of Sci., Kiev, Ukrainian SSR). *Strength Mater. (USA)*, vol.14, no.9, p.1173-8 (Sept. 1982). Translation of: *Probl. Prochn. (USSR)*, vol.14, no.9, p.15-20 (Sept. 1982). The authors describe the results obtained in testing steels for the length of life under a repeated static load on a device adjusted for automatic load application. The specimens were tested with cyclic synchronisation of temperature and mechanical load. (5 refs.)

115470 Representation of fatigue damage to a component in terms of reliability theory. A.E.Bozhko (Inst. of Mech. Engng. Problems, Acad. of Sci., Kharkov, Ukrainian SSR). *Strength Mater. (USA)*, vol.14, no.9, p.1179-82 (Sept. 1982). Translation of: *Probl. Prochn. (USSR)*, vol.14, no.9, p.20-3 (Sept. 1982). The author shows that it is possible to determine, on the basis of reliability theory, the degree of damage to an article and its service life, using the corresponding characteristics of the structural elements of which the article consists. (3 refs.)

115471 Effect of step duration on the evaluation of the fatigue limit of welded steel structures. F.P.Udodov, E.M.Moskaleva, V.M.Gnezdilov. *Strength Mater. (USA)*, vol.14, no.9, p.1183-9 (Sept. 1982). Translation of: *Probl. Prochn. (USSR)*, vol.14, no.9, p.23-8 (Sept. 1982). Investigations were conducted into the effect of step duration on the evaluation of the fatigue limit of flat specimens and welded beams using the fracture criterion i.e. the passage of the crack through the entire thickness of the plate. (12 refs.)

115472 Predicting the long-term creep of organic-fiber-reinforced plastics. E.A.Sokolov, R.D.Maksimov (Inst. of Polymer Mech., Acad. of Sci., Riga, Latvian SSR). *Strength Mater. (USA)*, vol.14, no.9, p.1209-13 (Sept. 1982). Translation of: *Probl. Prochn. (USSR)*, vol.14, no.9, p.45-8 (Sept. 1982). The authors studied the problem of predicting the creep of a unidirectional organic fiber reinforced plastic from the results of tests at high-temperature. It was found that the results of accelerated temperature tests in tension could be used for this purpose. (17 refs.)

115473 Relationship between parameters of elastic-wave propagation and rupture-strength characteristics of structural materials. B.A.Konyukhov, B.S.Perel'man, A.L.Uglov, V.I.Unylov. *Strength Mater. (USA)*, vol.14, no.9, p.1214-17 (Sept. 1982). Translation of: *Probl. Prochn. (USSR)*, vol.14, no.9, p.49-51 (Sept. 1982). The authors examined the problem of constructing a scalar estimate of the rupture strength of materials using acoustic measurements. Appropriate empirical findings are presented, it is found that acoustic methods make it possible to construct algorithms to evaluate the amount of damage sustained by a material subjected to long-term constant loads and to determine the remaining life of a test specimen or structural element at any moment of time. (5 refs.)

115474 Selection of ceramic material specimen dimensions for thermal stability tests. Ya.L.Grushevskii (Inst. of Strength Problems, Acad. of Sci., Kiev, Ukrainian SSR). *Strength Mater. (USA)*, vol.14, no.9, p.1228-32 (Sept. 1982). Translation of: *Probl. Prochn. (USSR)*, vol.14, no.9, p.59-63 (Sept. 1982). The author considers a possible approach to the selection of absolute dimensions of a hollow cylindrical specimen and its thermal loading schedule. Strict modeling in specimens of the thermal stress state for ceramic structures is not generally accomplished since there is not always geometric similarity. Therefore it is possible to limit the selection of radii and heating rate of a specimen at which changes in temperature and thermal stresses with time over its outer surface will be close to that occurring in the structure being considered. In order to solve the problem posed it is necessary to determine the value of the greatest level of tensile stresses which it is possible to realize by thermal loading of a specimen made of the test material. (9 refs.)

115475 Determination of fracture-toughness characteristics under a pulsed loading. G.V.Stepanov, V.A.Makovei (Inst. of Strength Problems, Acad. of Sci., Kiev, Ukrainian SSR). *Strength Mater. (USA)*, vol.14, no.9, p.1252-6 (Sept. 1982). Translation of: *Probl. Prochn. (USSR)*, vol.14, no.9, p.80-4 (Sept. 1982). The results of mechanical tests of materials, including data derived from fracture-toughness tests, are used for a computed estimate of the serviceability of design elements under operating conditions. The operating reliability of designs fashioned from materials with cracks or cracklike defects that are present in the initial material or that form during service is estimated from fracture-toughness characteristics. (10 refs.)

115476 Effect of stored elastic energy on breaking stress. A.I.Korshunov, V.P.Vashchenkov.

Strength Mater. (USA), vol.14, no.9, p.1265-8 (Sept. 1982). Translation of: *Probl. Prochn. (USSR)*, vol.14, no.9, p.91-2 (Sept. 1982). The authors' experiments have shown that the pliability of the specimen-machine system, and thus also the stored elastic energies, does not affect the breaking stress in static loading on condition that similarity in mechanical loading is ensured. The effect of the stored elastic energy on the breaking stress is apparently connected with the difference in the loading rate in tests with different pliability. (12 refs.)

115477 Plotting stress-strain diagrams by recalculation of the computer diagram. A.I.Korshunov, T.N.Kravchenko, O.M.Savel'eva. *Strength Mater. (USA)*, vol.14, no.9, p.1268-71 (Sept. 1982). Translation of: *Probl. Prochn. (USSR)*, vol.14, no.9, p.93-5 (Sept. 1982). The authors show how it is most promising and advantageous to obtain stress-strain diagrams by recalculation of computer diagrams which represent the dependence of an axial tensile load P applied to the specimen on the strain $\Delta\epsilon$ of the system specimen-machine. The essence of the recalculation consists in extracting the strain of the specimen alone from the total strain of the system specimen-machine. (7 refs.)

115478 Determination of certain elastic characteristics of materials with the use of parabolic interpolation of strain curves. Yu.D.Skripnik (Inst. of Strength Problems, Acad. of Sci., Kiev, Ukrainian SSR). *Strength Mater. (USA)*, vol.14, no.11, p.1527-31 (Nov. 1982). Translation of: *Probl. Prochn. (USSR)*, vol.14, no.11, p.86-9 (Nov. 1982). [received: Sept. 1983]

On the basis of approximation of the initial portion of the strain curve by a quadratic parabola an equation is proposed for determining the modulus of normal elasticity of materials using as the original data the two experimental points ($\epsilon_1/2, \sigma(\epsilon_1/2)$) and ($\epsilon_1, \sigma(\epsilon_1)$). The coefficient of loss of strength, which together with the modulus of normal elasticity is responsible for the strain curve in the interval up to the elastic limit and makes it possible to calculate the tangential and secant moduli at any point of this interval, that is, at practically any stresses used in structure, is proposed as a characteristic of the material. It is shown that the proportional limit σ_{pr} is determined by the modulus of normal elasticity E and the coefficient of loss of strength P . (3 refs.)

115479 Software for automatic loading controls in strength testing. V.I.Litvak, V.M.Gal'perin. *Strength Mater. (USA)*, vol.14, no.11, p.1569-73 (Nov. 1982). Translation of: *Probl. Prochn. (USSR)*, vol.14, no.11, p.120-4 (Nov. 1982). [received: Sept. 1983]

The following may be said regarding the realization of special software (SSW). (1) This software system can be used for automatic load controls (ALC) of multiple units even without the time-sharing facilities available with modern computers. However, the performance is considerably improved by time sharing in conjunction with the basic software. The SSW is then to be considered as a target program for the computer. (2) Implementation of the SSW requires a large memory volume. Overlay structures provide the best means of organizing memory loading with allowance for the speeds of the various memories. The best computers for the purpose are the SM control ones, e.g. the SM-4 in extended form (with disks and tapes). (3) The modules, apart from the monitor segments, are written in a high-level language such as FORTRAN IV, which makes the program simple to understand. The information exchange with the operator is performed in interactive mode with set phrases. (6 refs.)

115480 Acoustic emission in the deformation of concrete (review). G.B.Muravin, G.S.Pavlovskaya, A.D.Likhod'ko (All-Union Sci.-Res. Inst. for Transport Construction, Moscow, USSR). *Sov. J. Nondestr. Test. (USA)*, vol.18, no.12, p.925-34 (Dec. 1982). Translation of: *Defektoskopiya (USSR)*, vol.18, no.12, p.3-13 (Dec. 1982). [received: Sept. 1983]

Works devoted to the study of the acoustic emission of concrete and to investigation of the possibility of its practical use for nondestructive testing of reinforced concrete structures are considered. (46 refs.)

115481 Consideration of certain acoustic-emission characteristics in large thick-walled high-pressure vessels. V.M.Geller, M.B.Gitis, V.N.Sosedov (All-Union Sci.-Res. Inst. of Nondestructive Testing, Kishinev, USSR). *Sov. J. Nondestr. Test. (USA)*, vol.18, no.12, p.934-8 (Dec. 1982). Translation of: *Defektoskopiya (USSR)*, vol.18, no.12, p.13-17 (Dec. 1982). [received: Sept. 1983]

Two forces are discussed as an analog for an acoustic-emission source during the formation of microcracks in the thick walls of high-pressure vessels. The use of directional receivers for Rayleigh waves is shown to be advisable in some cases. (8 refs.)

115482 Higher stiffness for the vibratory system of an acoustic durometer. V.A.Prikhod'ko, D.A.Tursunov (Donets Sci.-Res. Inst. of Ferrous Metall., Donetsk, Ukrainian SSR). *Sov. J. Nondestr. Test. (USA)*, vol.18, no.12, p.950-3 (Dec. 1982). Translation of: *Defektoskopiya (USSR)*, vol.18, no.12, p.30-3 (Dec. 1982). [received: Sept. 1983]

It is shown to be advisable, theoretically, to improve the stiffness of the vibratory system of an acoustic durometer by changing from a resonance-sensitive element in the form of a thin uniform rod to one having a variable cross-section. (6 refs.)

115483 Influence of magnetomechanical damping on resonance electromagnetic-acoustic conversion in ferromagnets. R.S.II'yasov, V.A.Komarov (Inst. of Metal Phys., Acad. of Sci., USSR). *Sov. J. Nondestr. Test. (USA)*, vol.18, no.12, p.954-7 (Dec. 1982). Translation of: *Defektoskopiya (USSR)*, vol.18, no.12, p.34-8 (Dec. 1982). [received: Sept. 1983]

The variation of the logarithmic decrement of elastic oscillations as a result of magnetoelastic losses is investigated in connection with resonance electromagnetic-acoustic (EMA) conversion in silicon-iron single-crystal samples cut in different crystallographic directions. It is shown that this effect has an appreciable influence on the curves of the EMA signal amplitude as a function of the polarizing field. (4 refs.)

115484 Conversion of zero-order Lamb-wave modes into an electromagnetic field in ferromagnetic metals. V.A.Komarov, R.S.II'yasov, N.I.Shakshin (Inst. of Metal Phys., Acad. of Sci., USSR). *Sov. J. Nondestr. Test. (USA)*, vol.18, no.12, p.958-64 (Dec. 1982). Translation of: *Defektoskopiya (USSR)*, vol.18, no.12, p.38-45 (Dec. 1982). [received: Sept. 1983]

The electromagnetic field produced in air over a conducting ferromagnetic plate, of infinite extent in both dimensions in the plane and polarized by a magnetic field, from traveling and standing zero-order Lamb modes (modes s_0 and a_0) is calculated, along with the magnetic fluxes of the electromagnetic field in the plate from the same modes. It is shown that overlay sensors are

best recommended for obtaining information in terms of the magnetoelastic constants. (17 refs.)

115485 Ultrasonic inspection of the structure of G13FL steel parts. A.E.Ivanskii, Yu.P.Bashkirov, E.B.Dobreitsin, A.M.Lyubimov (F.E. Dzerzhinskii Ural Car building Plant, USSR). *Sov. J. Nondestr. Test. (USA)*, vol.18, no.12, p.965-6 (Dec. 1982). Translation of: *Defektoskopiya (USSR)*, vol.18, no.12, p.46-7 (Dec. 1982). [received: Sept. 1983]

G13FL steel, which is characterized by comparatively low thermal conductivity, a high alloy content, and a quite high linear solidification rate, is distinguished by an increased tendency toward columnar crystallization, which has a significant detrimental effect on its service properties. For inspection of structure the authors have tested an ultrasonic method based on the fact that in steels attenuation of ultrasonic oscillations is determined by their dispersion at the boundaries of grains and structural constituents. It was established that within the limits of a single part the degree of columnar structure may vary significantly. This was taken into consideration in developing an inspection procedure during production. (6 refs.)

115486 Sensitivity of X-ray computer tomography in the inspection of thin layers, glued joints, cracks, laminations, and coatings. E.I.Vainberg. *Sov. J. Nondestr. Test. (USA)*, vol.18, no.12, p.969-73 (Dec. 1982). Translation of: *Defektoskopiya (USSR)*, vol.18, no.12, p.49-54 (Dec. 1982). [received: Sept. 1983]

Investigates the nonlinear effects arising in the inspection of multilayered structures by the method of X-ray computer tomography. Analytical relationships are obtained for calculating the sensitivity of inspection in dependence on the geometry and contrast of flaws and on the thickness of the inspected section. Experimental results are presented. (4 refs.)

115487 Effectiveness of intensifying screens in a mosaic semiconductor transducer, and the aperture characteristics of sensors. V.S.Melikhov, I.M.Rubinovich (Sci. Res. Inst. of Electronic Introscopy, Tomsk, USSR). *Sov. J. Nondestr. Test. (USA)*, vol.18, no.12, p.974-9 (Dec. 1982). Translation of: *Defektoskopiya (USSR)*, vol.18, no.12, p.54-60 (Dec. 1982). [received: Sept. 1983]

Presents the results of the theoretical evaluation of the front, rear, and lateral intensifying screens in the mosaic semiconductor transducer of a betatron introscope. It is shown that with a silicon layer 1 cm thick and a dose of 100 R/min ahead of the beam trap, the use of these screens makes it possible to attain a sensitivity of 1.1% when the steel is 30 cm thick. The aperture characteristics of the sensors are calculated, and this makes it possible to evaluate the possible degree of improvement of the detectability of flaws by the method of aperture correction. (7 refs.)

115488 Automatic device for establishing the specified regime of X-ray flaw detectors and frequency doubler for electronic stopwatch. S.I.Korneev, P.S.Shchukin.

Sov. J. Nondestr. Test. (USA), vol.18, no.12, p.980-1 (Dec. 1982). Translation of: *Defektoskopiya (USSR)*, vol.18, no.12, p.60-1 (Dec. 1982). [received: Sept. 1983]

The portable X-ray apparatus RUP-150/300-10 is used for examining materials and products under conditions of plant or departmental X-ray flaw detection laboratories. An operator requires at least 10 or 15 min to establish the specified regime of the X-ray apparatus. The scale division of the electromechanical time relay in the apparatus is 15 sec. Apparatus with short exposure times (5-20 sec) cannot therefore be used. The suggested improvement provides broader possibilities of using the apparatus. For this purpose the apparatus was provided with a device permitting automatic control of the voltage on the anode of the X-ray tube, and a doubler of the industrial frequency of the mains for starting the electronically counting frequency meter measuring the exposure time. (no refs.)

115489 Magnetic, electrical, and mechanical properties of 12KhN3A and 12Kh2N4A steels and of case-hardened layers on them. I.A.Kuznetsov, N.M.Skripova (A.M. Gor'kii State Univ., Ural'sk, USSR). *Sov. J. Nondestr. Test. (USA)*, vol.18, no.12, p.985-90 (Dec. 1982). Translation of: *Defektoskopiya (USSR)*, vol.18, no.12, p.65-71 (Dec. 1982). [received: Sept. 1983]

Investigations were conducted into the magnetic, electrical, thermo-electrical, and mechanical properties of case-hardening steels 12KhN3A and 12Kh2N4A and of case hardened layers on them, saturated to various degrees with carbon, in relation to the quenching and tempering temperatures. The conditions of the nondestructive measurement of the thickness and hardness of the case-hardened layer on components by measuring the electromagnetic properties were examined. (6 refs.)

115490 Magnetic inspection of the hardness of steel ShKh15 pipes. O.S.Kononov, R.M.Brusentsova, A.A.Tovpinets, V.I.Roitman (Nikopol'sk Southern Pipe Plant of the 50th Anniversary of the Great October Socialist Revolution, USSR).

Sov. J. Nondestr. Test. (USA), vol.18, no.12, p.999-1000 (Dec. 1982). Translation of: *Defektoskopiya (USSR)*, vol.18, no.12, p.80-1 (Dec. 1982). [received: Sept. 1983]

Presents a method of nondestructive hardness inspection involving coercive force meters. In order to use the magnetic method for inspection of mechanical properties of a material it is necessary to determine experimentally in advance the correlations between these parameters and the readings of the coercive force meter. (4 refs.)

115491 Changes in the strain energy and the surface structure generated during the rotatory bending fatigue test for smooth and notched carbon steel specimens. C.Minamisawa, Y.Ishi-da (Dept. of Mech. Engng., Nat. Defense Acad., Yokosuka, Japan).

Sci. & Eng. Rep. Natl. Def. Acad. (Jpn.) (Japan), vol.20, no.2, p.145-57 (June 1982). In Japanese. [received: Aug. 1983]

Deals with the changes in the strain energy and in the surface structure generated during rotatory bending fatigue tests for two kinds of carbon steel specimens with smooth surfaces and different diameters and for the other two kinds of specimens different radii of circumferential notches. If the plastic strain energy accumulation is plotted against the number of cycles on a log-log paper, four nodal points appear as dividing the process of fatigue in five stages. The several microcracks such as the intrusions appear at the fourth nodal point, therefore the authors suggest that the machine parts corresponding to the specimen ought to be replaced by a new one at the fourth nodal point in order to prevent a fracture accident. (9 refs.)

115492 A torsion testing machine for measurement of shear strength of foam. N.J.Baldwin.

Report MRL-TN-469, Defence Sci. & Technol. Organ., Mater. Res. Labs., Melbourne, Vic., Australia (Dec. 1982), 12 pp.

A torsion machine has been developed to measure shear strength and shear modulus of foam. The machine is compact, portable, easy to use and is an essential link in quality assurance of foam core material for the Australian Minehunter Catamaran.

115493 Influence of magnetization on eddy current inspection of ferromagnetic tubes. V.Kelha, R.Peltonen.

Report 183, Tech. Res. Centre Finland, Instrum. Lab., Espoo (May 1983), 31 pp.

The eddy current method is commonly used for inspecting metal tubes during manufacture. Inservice inspection, however, has been limited to testing of non-ferromagnetic tubes due to the inherent magnetic noise. It has been shown that even mild steel tubes, if magnetically saturated, can be satisfactorily inspected using the eddy current method. By using a laboratory electromagnet and a magnetizing field 2.4 to 360 kA/m, various artificial defects, through holes 0.5 to 2.5 mm in diameter, a conical hole and a groove on the outer surface of the tube, were detected by an internal differential eddy current probe. The signal level and the signal-to-noise ratio increased remarkably with increasing magnetization. (6 refs.)

115494 Acoustic emission: Past experience within ECSC contracts and future trends. M.Mirabile.

Report EUR 7887 EN, Comm. European Communities, Luxembourg (1983), vi+31 pp. Contract 7210-GA/411.

After having introduced the basic elements of acoustic emission as a new NDT method, the survey report deals with mechanical and metallurgical factors affecting materials emissivity, location technique and accuracy, and possible future applications according to the presently available results. It is emphasized that the materials emissivities may be compared only when specimen geometry and test temperature are the same. It is further recognized that a three-point bend specimen and a temperature near the fracture appearance transition temperature (FATT) are the most suitable conditions for promoting a high AE activity. Differences in the tendency of several steels to release elastic energy, are attributed to the different microstructural parameters controlling yield strength and FATT. Thus, the role of pearlite colony size in ferritic-pearlite steels, and that of carbide size and distribution in quenched and tempered steels are discussed, together with the effect of second-phase non-metallic inclusions. In addition to the mechanical and metallurgical factors the several fracture mechanisms are also considered as sources of different AE activities. Brittle and ductile failure under monotonic load generate AE energy pulses which can be quantitatively correlated with the applied load and length of present cracks. (50 refs.)

115495 Operation of the EPRI nondestructive evaluation center. Annual report - 1982. T.A.Nemzek, R.M.Stone, P.L.Schoenecke, F.V.Ammirato, F.L.Becker, M.Behravesh, S.D.Brown, D.E.MacDonald, G.L.Pherigo, G.H.Wilson, III.

Report EPRI-NP-2985, Electr. Power Res. Inst., Palo Alto, CA, USA (April 1983), 114 pp.

Available from Research Report Center, Box 50490, Palo Alto, CA 94303, USA.

Describes a project to design, construct, organize and operate the EPRI Non-destructive Evaluation (NDE) Center, a dedicated facility for providing field-qualified NDE equipment, procedures, and personnel training to the electric utility industry. The entire scope of this work is presented, with major emphasis placed on the activities in 1982, the facility's first full year of operation.

115496 Steam generator U-bend eddy-current NDE. S.Brown.

Report EPRI-NP-3010, Electr. Power Res. Inst., Palo Alto, CA, USA (April 1983), 80 pp.

Available from Research Report Center, Box 50490, Palo Alto, CA 94303, USA.

Details are provided of a study that evaluated an eddy-current bobbin coil method for estimating the ovality of row 1 U-bend opposite-side transitions and conventional bobbin coil and alternate pancake array probe eddy-current inspection methods to detect primary-side cracking in Westinghouse Series 51 row 1 U-bends. Tests results corroborate earlier results, which found no discernible correlation between the eddy-current inspection signal and tube ovality. The pancake array coil proved superior to the conventional bobbin coil probe for U-bend crack detection.

115497 A high accuracy micro hardness tester. Yang Di, Yang Hwi-Quei, Yang Gwei Gien (Mech. Div., Nat. Inst. of Metrology, Beijing, China).

Technological and Methodological Advances in Measurement. Acta IMEKO 1982. Proceedings of the 9th IMEKO Congress of the International Measurement Confederation, Berlin, Germany, 24-28 May 1982 (Amsterdam, Netherlands: North-Holland 1983), p.563-9

A high accuracy micro hardness tester was developed successfully in 1979 as a national micro hardness reference scale for loading, load duration and unload. The measuring microscope used in this tester is possessed of unique measuring model and higher magnification than conventional tester to assure the aim accuracy. The tester possesses very good rigidity and fashion. The hardness accuracy of the tester is $\pm 1.0-3.0\%$ when load is 1000-5 ogf. (no refs.)

115498 Neutron radiography facility using ^{252}Cf neutron source.

N.D.Tyufyakov (All-Union Res. Inst. of Radiation Engng., Moscow, USSR). *Neutron Radiography*. Proceedings of the First World Conference, San Diego, CA, USA, 7-10 Dec. 1981 (Dordrecht, Netherlands: Reidel 1983), p.673-80

The paper represents the layout and description of the transportable neutron radiography facility using ^{252}Cf neutron source as well as the results of the optimization studies of the radiation head parameters. The effects of the moderator sizes and neutron energy spectra for a number of the radionuclide neutron sources on the spatial distribution of slow neutrons in the moderator are discussed. The experiments were carried out using sources of such types as ^{252}Cf , $^{238}\text{PuBe}$, ^{238}PuB , $^{238}\text{PuLiF}$. The author discusses the form of the ^{252}Cf neutron source that allows one to attain the maximum slow neutrons flux in the neutron beam obtained from the radiation head. (7 refs.)

115499 Neutron and gamma simultaneous radiography using a ^{252}Cf isotopic neutron source. N.Wada (JAERI, Ibaraki-ken, Japan), T.Yasui, Y.Yoshida.

Neutron Radiography. Proceedings of the First World Conference, San Diego, CA, USA, 7-10 Dec. 1981 (Dordrecht, Netherlands: Reidel 1983), p.681-8

In the ^{252}Cf -based thermal neutron radiography, a thermal neutron beam always contains some gamma radiation. Attempts are made to obtain neutron and gamma radiographs simultaneously. A combination of scintillator and film, showing a superior gamma-discrimination is used as a thermal neutron image recorder. A combination of lead foil and film, insensitive to thermal neutrons, is used as a gamma image recorder. These recorders are held together in a single cassette and are exposed at the same time. Successful neutron and gamma radiographs which might aid interpretation of the radiographic images are obtained. On the basis of the study, a mobil neutron radiography equipment capable of using 1 mg of ^{252}Cf is designed and fabricated, with which the practical effectiveness of the new technique is being evaluated. (2 refs.)

115500 Application of neutron radiation inspection at the Pantex Plant. J.P.Cassidy (Mason & Hanger, Silas Mason Co. Inc., Amarillo, TX, USA). Neutron Radiography. Proceedings of the First World Conference, San Diego, CA, USA, 7-10 Dec. 1981 (Dordrecht, Netherlands: Reidel 1983), p.707-16. A neutron radiographic capability has been established at the Pantex Plant in Amarillo, Texas. A 3 MeV Van de Graaf accelerator is employed as the neutron source. Neutron radiation inspection techniques have been developed to detect and observe discontinuities in explosive materials encased in aluminum, lead, steel and combinations of these casement materials. These data demonstrate that the capability exists for obtaining satisfactory neutron radiographs of many explosive-loaded components. Additional work will be performed in order to further determine applicable capabilities of the 3 MeV Van de Graaf accelerator. (no refs.)

115501 Improvement of efficiency of n,α converters to realize NR with relatively low n flux sources. M.Fantini (Kodak-Pathe Res. Lab., Paris, France). Neutron Radiography. Proceedings of the First World Conference, San Diego, CA, USA, 7-10 Dec. 1981 (Dordrecht, Netherlands: Reidel 1983), p.727-8. The recording of neutronic images on plastic polymer films is carried out via α particles. Boron and lithium are the only n,α conversion elements having a high yield. High yield converters are obtained with layers of elements containing boron or lithium very finely dispersed in a binder. The surface of these screens must be as smooth as possible and be in perfect contact with the image detecting film. The sensitivity to α particles of cellulose nitrate CN 85 films is higher than 95%. It is understood that sensitivity to neutrons can be increased only by using n,α converter screens having a maximum yield. Every effort has been made in order to make neutronography possible from relatively weak sources that can be used in the industry. (no refs.)

115502 Characterization of the matrix glass transition in carbon-epoxy laminates using the CSD test geometry. S.S.Sternstein, P.Yang (Rensselaer Polytech. Inst., Troy, NY, USA). Role of the Polymeric Matrix in the Processing and Structural Properties of Composite Materials. Proceedings of a Joint US-Italy Symposium, Capri, Italy, 15-19 June 1981 (New York, USA: Plenum 1983), p.39-51. A test geometry is described which has several useful attributes: the geometry is very sensitive to matrix behavior; both transient (creep and stress relaxation) and dynamic mechanical tests are readily performed over a wide range of timescales; the test geometry provides viscoelastic dispersion data which are independent of angular orientation of the sample; consequently sample alignment problems are eliminated; the same test geometry may be used to provide information on delamination strength; relatively small test specimens are required; the test geometry is sufficiently sensitive to matrix changes to allow its use for postcuring, humidity, crosslink density and other matrix change studies. (7 refs.)

115503 On feasibility of accelerated creep measurements in some polymeric materials. A.Franceschini, A.Momo, P.Campagna (Centro Ricerche Fiat SpA, Orbassano, Italy). Role of the Polymeric Matrix in the Processing and Structural Properties of Composite Materials. Proceedings of a Joint US-Italy Symposium, Capri, Italy, 15-19 June 1981 (New York, USA: Plenum 1983), p.369-76. The principle of time-stress equivalence, previously applied in the case of polypropylene and polypropylene toughened with rubber, is successfully applied to an amorphous thermoplastic, polycarbonate: the creep curves at different stress levels can be superimposed in one normalized master curve. A computer program is set up, which in many cases allows the analysis of empirical data. Master curves are also obtained in the case of Sheet Moulding Compounds; but their interpretation and use as a prediction method is not completely developed, because of an odd dependence of the shift factor on the stress. (10 refs.)

115504 An optical technique for measuring fiber orientation in short fiber composites. S.H.McGee, R.L.McCullough (Dept. of Chem. Engng., Univ. of Delaware, Newark, DE, USA). Role of the Polymeric Matrix in the Processing and Structural Properties of Composite Materials. Proceedings of a Joint US-Italy Symposium, Capri, Italy, 15-19 June 1981 (New York, USA: Plenum 1983), p.425-36. A technique for measuring the state of fiber orientation in short fiber composites using a Fraunhofer diffraction apparatus is described. A theoretical analysis is compared to diffraction patterns produced from masks with known state of orientation, and the agreement was found to be excellent. Samples from sheet moulding compounds are analyzed to demonstrate processing induced fiber orientation in the material. (4 refs.)

115505 Consideration on the fatigue damage of specimens used for composite critical components qualification. A.Brivio, G.Parenti, G.Samanni, V.Wagner, C.Zanotti. Role of the Polymeric Matrix in the Processing and Structural Properties of Composite Materials. Proceedings of a Joint US-Italy Symposium, Capri, Italy, 15-19 June 1981 (New York, USA: Plenum 1983), p.607-24. Tests were carried out on glass fibre reinforced epoxy laminates. It is concluded that the described method of fatigue testing is adequate for material qualification and design purposes, because the derived S-N curves are conservative with respect to the true fatigue characteristics of the laminate. The online monitoring of the specimen deformation in the central region, which is a promising extension of the stiffness tests above described, should be useful to show the degradation processes happening outside the end tabs region during fatigue tests. (8 refs.)

115506 The measure of fracture toughness of cemented carbide by means of CVD coated layers. Z.Goffer, R.Porat (Iscar Ltd., Nahariya, Israel). Proceedings of the 4th European Conference on Chemical Vapour Deposition, Eindhoven, Netherlands, 31 May-2 June 1983 (Eindhoven, Netherlands: Philips Centre Manuf. Technol. 1983), p.76-83. When measuring fracture toughness of cemented carbide, the main problem is controlling the precrack length. While measuring transverse rupture strength the tensional stress is applied perpendicular to the crack surface. The mode of crack makes it possible to distinguish fracture toughness. In tests made on samples with a brittle coating, low stress was found to cause a precrack in the coating layer, and this precrack continues as a fracture in the insert body itself. With thicker coatings, the precrack is lengthened and the transverse rupture strength is reduced. Therefore, an applied CVD coating to a standard transverse rupture strength bar makes it possible by measuring the coating thickness to determine the length of the precrack. Experiments were made with straight cemented carbide (WC+Co) and with multi-carbides (WC+TiC+TaC+NbC+Co). Fracture toughness of cemented carbides is a function of their composition and the mean-free-path (mfp) of the binder. Comparing the fracture toughness values against mfp shows two family types, as does examination of the short rod samples by TerraTek fractometer. (8 refs.)

1st European Conference on Cineradiography with Photons or Particles	See Entry 111300
Thermometric and calorimetric methods in electrochemical and corrosion studies	See Entry 111886
Differential measuring instrument of magnetic characteristics	See Entry 111713
Widening the range of constant magnetic fields which can be measured with impedance-type ferroprobe transducers	See Entry 111714
Advances in the infrared microscopy of electronic materials	See Entry 111761
Interference film microscopy for metal phase identification	See Entry 111763
Applications of high voltage electron microscopy in materials science	See Entry 111819
Some applications of cineradiography to gas turbines	See Entry 111836
System of conversational image processing with two independent control-operator boards	See Entry 111841
Flash X-ray generator at high energy: GREC	See Entry 111842
PHERMEX—pulsed high energy radiographic machine emitting X-rays	See Entry 111843
Image converter tubes for radiology and neutronography used in nondestructive testing	See Entry 111847
A new accelerator-based neutron radiography system	See Entry 111860
Optimisation of etching conditions and shortening of the etching time of cellulose nitrate films	See Entry 111861
Effect of pre-exposure of films on radiographic sensitivity	See Entry 112365
Hodoscope cineradiography of nuclear fuel destruction experiments	See Entry 112368
Survey of cineradiographic techniques applied to nuclear reactor safety experiments	See Entry 112369
MIRENE, a mini-nuclear reactor for neutronography—data and applications	See Entry 112370
Underwater neutron radiography facility utilizing small neutron generator	See Entry 112392
How good is nitrocellulose film for neutron radiography?	See Entry 112393
Californium-252 as a source of subthermal neutrons	See Entry 112521
Radiography with fast neutrons by a plastic detector	See Entry 112569
Studies on high-tensile proof tests of optical fibers	See Entry 113120
Analysis of the elastic field of ultrasonic waves scattered by a cylindrical cavity	See Entry 113172
Applications of acoustic microscopy in the semiconductor industry	See Entry 113234
Acoustic microscopy in materials science	See Entry 113237
An edge-cracked mode II fracture specimen	See Entry 113381
Thermoelectric method for studying stresses in plates weakened by holes	See Entry 113391
Prediction of stress relaxation and stress relief cracking in SEN testpieces	See Entry 115327
The K_{IC} values of silicon nitride and zirconia obtained by micro-crack indentation method and single-edge notched beam method	See Entry 115355
Multiwavelength analyzer for the determination of diffusion lengths	See Entry 115653
Quantitative microfocal radiography in medicine, biological research, and the quality control industry	See Entry 115906

81.90 OTHER TOPICS IN MATERIALS SCIENCE

115507 Drying of porous granular materials. A.Hallstrom, R.Wimmerstedt (Dept. of Chem. Engng., Lund Univ., Lund, Sweden). *Chem. Eng. Sci. (GB)*, vol.38, no.9, p.1507-16 (1983). Drying characteristics have been measured for two types of granular compound fertilizer and for granular mono calcium phosphate. Air was forced through a fixed bed, and the humidity of the air leaving the bed was analysed by means of an infrared photometer. All results confirm the assumption of vapour diffusion as the rate determining mechanism. Experiments with varying temperature and air humidity show that the dependence of the drying rate on those parameters may be calculated from the sorption isotherms. These were measured for all three materials. Experiments also show that the drying rate is inversely proportional to the granule radius squared. A shrinking core model was successfully used for predicting the drying behaviour of two of the materials. For the third materials the drying rate fell rapidly, and the shrinking core mode was used with a correction function. (13 refs.)

115508 Metallurgy of interfaces in hardmetal/metal diffusion bonds. E.A.Almond (NPL, Teddington, England), A.M.Cottenden, M.G.Gee. *Met. Sci. (GB)*, vol.17, no.4, p.153-8 (April 1983). [received: Sept. 1983] A study has been made of the metallurgical reactions that control the diffusion bonding of WC-Co hardmetal butt-joints interlayered with Ni, Co, and steel at 1300°C. Vapour transport appears to make a significant contribution to the growth of the bonded regions during the early stages of the process, and the rates of growth are in reasonable agreement with predictions from sintering theories for single component systems. The chemical reactions that occur at the bond interface with Co and steel interlayers are sensitive to differences in the C contents of the interlayers and of the hardmetal binder phase. With low C interlayers the hardmetal near the interface is transformed to an η phase structure. (19 refs.)

115509 Effect of the composition of binding materials on the properties of carbon pastes. T.S.Zamazan, Z.A.Mikhalkuk, A.G.Khoruzhii (Ukrainian Sci.-Res. Inst. of Refractories, Ukrainian SSR). *Refractories (USA)*, vol.23, no.11-12, p.591-3 (Nov.-Dec. 1982). Translation of: *Ogneupory (USSR)*, vol.23, no.11, p.38-41 (Nov. 1982). The effect of a sinter with a softening temperature of $\geq 200^\circ\text{C}$ on the adhesion properties of the paste was studied. It is established that the addition of 8% of such a sinter to a carbon paste at a preparation temperature of $\geq 130^\circ\text{C}$ increases the ultimate shear strength of the join by more than 50% (from 4.0 to 6.4 MPa). The controlling effect of a carboniferous sinter with a softening temperature of $\geq 200^\circ\text{C}$ on the viscosity of a carbon paste prepared and applied at a temperature of 80°C is shown. A carbon paste which does not run out from the vertical joints of the lining of blast furnaces and containing 4-6% of carboniferous sinter with a softening temperature of 200-300°C or more has been developed. (3 refs.)

115510 Adhesives in the electrical and electronic industries—a competitive ‘fix’. I.De Iorio, F.Rossi.
Tecnol. Elett. (Italy), no.4, p.84-8 (April 1983). In Italian. [received: Sept. 1983]
Epoxies and cyanoacrylics are the two most widely used forms of industrial adhesive, with anaerobics and urethanes of more limited application. The physical properties and the surface preparation necessary for these adhesives are described. Some illustrative examples lead to the conclusion that further advances in adhesive techniques may be expected. (no refs.) *M.P.R.*

115511 ‘Adhesion of metals’ experiment simulation and ground-based reference tests results. F.Rossitto (CESNEF, Politecnico di Milano, Milano, Italy), P.G.Sona, G.Grugini, G.Ghersini.
Proceedings of the 4th European Symposium on Materials Sciences under Microgravity (ESA SP-191), Madrid, Spain, 5-8 April 1983 (Paris, France: ESA 1983), p.347-51
The IES340 experiment ‘Adhesion of metals’ is reviewed and the status of the UHV Chamber facility is presented. The phenomenological model used in the computer simulation is discussed together with ground reference test results. The method for extracting the value of the surface energy per unit surface area from the experimental data is also presented. (1 ref.)

Pore size distribution in porous silicon studied by adsorption isotherms See Entry 114333

Results of apparent atomic oxygen reactions on Ag, C, and Os exposed during the shuttle STS-4 orbits See Entry 115406

Influence of the mechanical pretreatment of the surfaces on the adhesive strength of steel-grey cast iron joints See Entry 115430

82.00 PHYSICAL CHEMISTRY

82.20 CHEMICAL KINETICS

115512 Dissipative structures in 1D and 2D chemically reacting systems. P.Nandapurkar, V.Hlavacek (Dept. of Chem. Engng., State Univ. of New York, Buffalo, NY, USA).
Z. Naturforsch. Teil A (Germany), vol.38A, no.9, p.963-73 (Sept. 1983).
A transient analysis of the 1D and 2D reaction-diffusion equations associated with the model reaction of Prigogine and Lefever (1968) (Brusselator model), including diffusion of the initial (substrate) component, has been performed. For low system lengths and for fixed boundary conditions, the steady state low amplitude solutions are unstable. For zero flux boundary conditions a multiplicity of symmetric solutions with the same wave number may exist, the majority of them being unstable. The diffusion of initial components induce relaxation oscillations in space both for fixed as well as zero flux boundary conditions. The amplitude of the oscillation increases as the diffusion coefficient of the initial component decreases. For conditions of relaxation oscillations the spatial profiles result in single or multiple propagating fronts. High system lengths (or low diffusion coefficient of intermediate components), for both zero flux and periodic boundary conditions, may give rise to a multipeak incoherent wave pattern. For periodic boundary conditions a multiplicity of waves has been observed. Numerical simulation of the 2D-spatial structures reveal certain similarities between the 1D and 2D cases. (16 refs.)

115513 Calculation of product distributions by perturbation of the transition state. E.Pollak (Chem. Phys. Dept., Weizmann Inst. of Sci., Rehovot, Israel), P.Pechukas.
J. Chem. Phys. (USA), vol.79, no.6, p.2814-21 (15 Sept. 1983).
Two algorithms are presented for a direct determination of the boundary between reactive and unreactive portions of phase space in collinear collisions. These algorithms provide a fast and highly accurate determination of classical reactant and product distributions. Since boundary trajectories originate at variational transition states, this method provides new insight to an old problem: the relationship between product and reactant state distributions and the transition state of a chemical reaction. (23 refs.)

115514 Comments on two treatments of symmetry rules in chemical reactions. H.Metiu (Dept. of Chem., Univ. of California, Santa Barbara, CA, USA), G.C.Schatz, J.Ross.
J. Chem. Phys. (USA), vol.79, no.6, p.2854-6 (15 Sept. 1983).
In the paper the authors compare a recently presented approach to the determination of symmetry rules for chemical reactions based on adiabatic electronic states (Deguchi, 1982) to earlier work in which a quasideadibatic representation was used. The adiabatic approach is shown not to lead directly to Woodward-Hoffmann symmetry rules, and a number of the conclusions of the adiabatic work are shown to be incorrect and inconsistent. An indirect approach for deriving the Woodward-Hoffman rules in the adiabatic representation is presented which uses the connection between the adiabatic and quasideadibatic representations to relate barrier height to the quasideadibatic electronic matrix elements. (15 refs.)

115515 Indeterminacy in kinetic-model parameters due to non-Hamiltonian structure of the multipath linear reaction graph. V.A.Evstigneev, G.S.Yablonskii (Inst. of Catalysis, Acad. of Sci., Novosibirsk, USSR).
Theor. & Exp. Chem. (USA), vol.18, no.6, p.632-6 (Nov.-Dec. 1982). Translation of: *Teor. & Eksp. Khim. (USSR)*, vol.18, no.6, p.688-94 (Nov.-Dec. 1982). [received: Sept. 1983]
The authors examine the scope for determining all the parameters in a kinetic model. They consider a complex catalytic reaction occurring by a multipath linear mechanism in which all stages are reversible. The reaction mechanisms for the intermediate substances are then represented by a linear scheme, while the corresponding stationary kinetic model is a system of linear algebraic equations (it is assumed that the concentrations of the observable substances are constant). They also assume that all the elementary reactions are of different types. They then show that even in this idealized case one can have a situation where not all the parameters can be determined. (8 refs.)

A new method of the calculation of the hydrogen trap activation energy in metals See Entry 113855

On the study of oxidation kinetics of molybdenite pellets See Entry 115391

Kinetics and detection of F(2P) atoms in a discharge flow system See Entry 115520

The reaction of hydrogen atoms with silyl radicals; the decomposition pathways of chemically activated silanes See Entry 115521

Simulation of amplitude behaviour in the Ag⁺ perturbed excitable Belousov-Zhabotinsky reaction by the Oregonator model See Entry 115522

The self conversion of liquid ortho-hydrogen See Entry 115526

Reactions of energetic tritium atoms with ethyl fluoride over an extensive pressure range See Entry 115531

Reaction velocities and the affinity decay rate See Entry 115536

Second order rate constants for intramolecular conversions: application to gas-phase NMR relaxation times See Entry 115537

Electronic structure and chemical conversions of peroxides. II. MINDO/3 calculations of reaction mechanism in noncatalytic epoxidation of olefins by hydroperoxides See Entry 115542

Influence of electronic structure of a cation-radical skeleton, the nature of the anion attached to it, and the nature of the medium on reaction kinetics of one-electron oxidation of triphenylantimony by cation radicals of substituted triphenylamines See Entry 115546

Effect of diameter on the burning rate of polystyrene See Entry 115557

Laboratory measurements of the association rate coefficients of NO⁺, O₂⁺, N⁺, and N₂⁺ ions with N₂ and CO₂ at temperatures between 100K and 400K See Entry 116330

82.20K Potential energy surfaces for chemical reactions
(see also 31.70F -in atomic and molecular physics, 34.20 Intermolecular forces, 34.50L Atomic and molecular beam studies)

On the origin of the dynamical differences between the Tang and Dalgarno-Henry-Roberts potentials for rigid rotor H₂-H collisions See Entry 112840

82.20M Nonequilibrium kinetics

Observations of order and chaos in nonlinear systems See Entry 111564

Oscillations and chaos in chemical systems See Entry 111567

Experimental studies of bifurcations leading to chaos in the Belousov-Zhabotinsky reaction See Entry 111568

82.30 SPECIFIC CHEMICAL REACTIONS; REACTION MECHANISMS

115516 Evidence for stereoselectivity in the copper (2⁺)-valine system. N.Al-Ani, A.Olin (Dept of Inorganic & Phys. Pharmaceutical Chem., Univ. of Uppsala, Uppsala, Sweden).
Chem. Scr. (Sweden), vol.22, no.3, p.105-7 (1983).
The complex formation between Cu²⁺ and D-valine, L-valine and (L+D)-valine has been investigated by potentiometric methods with respect to stereoselectivity. By carrying out identical experiments, except for the kind of ligand, a small but significant difference could be established between the extent of complexation with optically active ligand and racemate. From this difference the equilibrium constant for the reaction Cu(L-valine)₂+Cu(D-valine)₂⇌2Cu(L-valine) (D-valine) was found to 3.8. Hence the formation of the mixed complex is slightly disfavoured compared to the statistical case, where the constant is 4. (8 refs.)

115517 Reactions of α, β-unsaturated cyclic ketones with thioureas and ammonium thiocyanate. J.Mirek, T.A.Holak (Inst. of Chem., Jagiellonian Univ., Krakow, Poland).
Chem. Scr. (Sweden), vol.22, no.3, p.133-5 (1983).
2-(α-hydroxybenzyl)-cyclohexanone reacts with NH₄SCN yielding 4-phenyl-3,4,5,6,7-hexahydro-2(1H)-quinazolinethione. Mono- and di-benzylidene-cyclopentanones (cyclohexanones) in the base catalyzed reaction with thiourea gave the derivatives of 1,3,4,5,6,7-hexahydro-2H-cyclopentapyrimidine-2-thiones and 3,4,5,6,7,8-hexahydro-2(1H)-quinazolinethiones respectively, while benzylthiourea and dibenzyl-idencyclohexanone produced an oxo-quinazoline. In the reaction of 2-arylidene-5-alkylidencyclopentanones with thiourea with C-4 alkyl derivatives of 7-(arylmethylene)-1,3,4,5,6,7-hexahydro-2H-cyclopenta-pyrimidine-2-thiones are obtained. (14 refs.)

115518 Proton affinity. R.Ponec, J.Kucera (Inst. of Chem. Process Fundamentals, Czechoslovak Acad. of Sci., Prague, Czechoslovakia).
Chem. Scr. (Sweden), vol.22, no.3, p.152-4 (1983).
A method of decomposition of protonation energy based on the Longuet-Higgins theory of proton affinity was proposed. This method, representing an alternative to Morokuma's (1976) decomposition scheme, was applied on the CNDO level to the detailed analysis of proton affinity in a series of aliphatic amines. (6 refs.)

115519 Search for the laser-induced crossed beam reaction of excited I₂ (B¹Π) with Hg. M.M.Oprysko, F.J.Aoiz, R.B.Bernstein, M.A.McMahan (Dept. of Chem., Columbia Univ., New York, NY, USA).
Chem. Phys. (Netherlands), vol.79, no.3, p.341-50 (15 Sept. 1983).
A search for the laser-induced crossed beam reaction I₂^{*}+Hg→Hgl+I has been conducted at total energies ≤4 eV (translational energies ≤2.5 eV). The I₂ molecules are prepared in the B(3Π_{0g}) state within the scattering region via 514.5 nm Ar⁺ laser excitation. The fraction of I₂^{*} molecules in the I₂ beam was ≈4×10⁻³. No significant yield of Hgl in excess of that from the ground-state reaction was detected over the entire range of scattering angles. The experiment yields an upper limit for the ratio of the cross section for the excited-state reaction relative to that of the ground state, estimated to be ≤0.5 at a total energy of 3.9 eV. Assuming 'backward' (rebound) scattering for the excited-state reaction, this upper bound is reduced to ≤0.04. (27 refs.)

115520 Kinetics and detection of F(2P) atoms in a discharge flow system. M.A.A.Clyne, A.Hodgson (Dept. of Chem., Queen Mary Coll., London, England).
Chem. Phys. (Netherlands), vol.79, no.3, p.351-60 (15 Sept. 1983).
A new technique for the detection of F(2P) atoms in a discharge flow system is described. The fast reaction F+Br₂→BrF+Br has been used, in the presence of excess Br₂, to rapidly convert the F atoms to BrF. The BrF is then detected by laser-induced fluorescence, excited on the 5-0 or 7-0 band-heads of the B³Π(0⁺)-X²Σ⁺ transition using a pulsed, tunable dye laser. Using this sensitive spectroscopic marker technique, concentrations of F(2P)≥3×10⁹ cm⁻³ can be detected. This method has been used to measure the rates of reaction of F(2P) atoms with CH₄ and CHF₃ under pseudo-first order conditions with [Reagent]≫[F]. The following rate constants were obtained at 298K and 1 Torr pressure (in cm³ molecule⁻¹ s⁻¹ with errors quoted at 1σ), in good agreement with the literature values: k₂=(6.6±0.4)×10⁻¹¹ for the reaction F+CH₄→HF+CH₃ and k₃=(1.5±0.1)×10⁻¹³ for the reaction F+CHF₃→HF+CF₃. (30 refs.)

115521 The reaction of hydrogen atoms with silyl radicals; the decomposition pathways of chemically activated silanes. K.Worsdorfer, B.Reimann, P.Potzinger (Max-Planck-Inst. fur Strahlenchem., Mulheim, Germany). *Z. Naturforsch. Teil A (Germany)*, vol.38A, no.8, p.896-908 (Aug. 1983). The reactions of hydrogen atoms with silane and the methylated silanes—with the exception of tetramethylsilane—have been investigated in a fast flow reactor. Under the experimental conditions hydrogen abstraction from the Si-H bond is followed by combination of hydrogen atoms with the corresponding silyl radicals. The molecules formed in this way are activated by about 375 kJ/mol of vibrational energy. Two decomposition channels have been unequivocally identified, namely the elimination of molecular hydrogen and of methane, both the substrate under formation of the respective silylenes. In a subsequent step, silylene inserts into the substrate activated molecule competes with decomposition and dominates the kinetics in the case of trimethylsilane. With methyl- and dimethyl-silane, methyl radicals are observed as an additional reaction product. On the basis of RRKM calculations it is unlikely that they originate from a direct decomposition of the activated molecules. Absolute values for the room temperature rate constants of the abstraction reactions are given; for $H + CH_3SiH_3$, Arrhenius parameters have been determined. (32 refs.)

115522 Simulation of amplitude behaviour in the Ag^+ perturbed excitable Belousov-Zhabotinsky reaction by the Oregonator model. P.Ruoff (Dept. of Chem., Univ. of Oslo, Oslo, Norway). *Z. Naturforsch. Teil A (Germany)*, vol.38A, no.9, p.974-9 (Sept. 1983). Potentiometric measurements with platinum and silver electrodes of Ag^+ induced oscillations in the oxygen-inhibited excitable Belousov-Zhabotinsky system are reported. Calculations based on the Oregonator model lead to the conclusion that the platinum electrode's potential is composed of two contributions, the $Ce(III)/Ce(IV)$ redox couple which dominates at low Ag^+ flow rates and the contribution of $HBrO_2$, $HOBr$ and BrO_2 which dominates at higher Ag^+ addition rates. (27 refs.)

115523 Thermal behavior of cyclohexaphosphates of certain polyvalent metals (Cu, Co, Ni, Mn, Ba). E.V.Lazarevski, L.V.Kubasova, N.N.Chudinova, I.V.Tananaev (N.S. Kurnakov Inst. of General & Inorganic Chem., Acad. of Sci., USSR). *Inorg. Mater. (USA)*, vol.18, no.9, p.1322-7 (Sept. 1982). Translation of: *Izv. Akad. Nauk SSSR Neorg. Mater.*, vol.18, no.9, p.1544-9 (Sept. 1982). [received: Sept. 1983]

The thermal conversions of hydrates of Cu, Co, Ni, Mn, and Ba cyclohexaphosphates with composition $M_3P_6O_{18} \cdot nH_2O$ were studied by the methods of thermogravimetry, X-ray phase analysis, paper chromatography, and IR spectroscopy. It was shown that dehydration is accompanied by hydrolytic decomposition of the circular anion and intermediate liberation of diphosphates $M_2P_2O_7$ and free phosphoric acid, which interact at 450-600°C, forming cyclotetraphosphates $M_4P_4O_{12}$. (10 refs.)

115524 Thermal behavior of cyclohexaphosphates of certain polyvalent metals (Cd, V, Ga). E.V.Lazarevski, L.V.Kubasova, N.N.Chudinova, I.V.Tananaev (N.S. Kurnakov Inst. of General & Inorganic Chem., Acad. of Sci., USSR). *Inorg. Mater. (USA)*, vol.18, no.9, p.1327-33 (Sept. 1982). Translation of: *Izv. Akad. Nauk SSSR Neorg. Mater.*, vol.18, no.9, p.1550-6 (Sept. 1982). [received: Sept. 1983]

It was established that the thermal dehydration of cadmium and yttrium cyclohexaphosphates leads to the formation of anhydrous polyphosphates. (7 refs.)

115525 The effect of metal π -complexation on the properties of organic molecules and ions. W.E.Watts (Dept. of Chem., New Univ. of Ulster, Coleraine, N Ireland). *Indian J. Phys. Part B*, vol.57B, no.3, p.4-6 (June 1983). The authors study the change in reactivity on π -attachment of transition metals to cyclobutadiene, cyclopentadienyl, benzene and cycloheptatrienyl. (no refs.)

115526 The self conversion of liquid ortho-hydrogen. R.Stevenson (Phys. Dept., McGill Univ., Montreal, Canada). *Indian J. Cryog.*, vol.6, no.4, p.196-8 (1981).

At 300K hydrogen has an equilibrium composition of 25% of the para- and 75% of the ortho-modification. At the temperature of liquid hydrogen, the equilibrium concentration is greater than 99% para-, but unless a catalyst is used liquid hydrogen initially retains its room temperature composition and undergoes a slow conversion from the ortho- to the para-form with a time constant of 3.29 days. The mechanism which causes the conversion from the ortho- to the para-form has been obscure. There appears to be a basic law underlying all chemical reactions, namely that a chemical reaction takes place in the frame of reference of the molecule involved rather than in the laboratory frame of reference. With that in mind, it is noted that hydrogen in solution undergoes rotational and translational motion in the quadrupolar electric fields of the carbon disulphide molecules and the octupolar fields of the carbon tetrachloride and hence sees a relativistic magnetic field of the order of VE/c^2 , where V is the velocity of a proton of the hydrogen, E is the internal local field of the liquid, and c is the velocity of light. An estimation for the conversion reaction in liquid hydrogen is attempted. The excess concentration of the para- or ortho-modifications decays according to $\exp(-ct)$, where c is the rate constant of the reaction. For liquid ortho-hydrogen, $c = 3.52 \times 10^{-6} \text{ sec}^{-1}$, which is comparable to the rate constants in the other diamagnetic liquids. (7 refs.)

115527 The 1,2 hydrogen shift as an accompaniment to ring closure and opening: ab initio MO study of thermal rearrangements on the C_2H_3N potential energy hypersurface. L.L.Lohr, Jr., M.Hanamura, K.Morokuma (Dept. of Chem., Univ. of Michigan, Ann Arbor, MI, USA). *J. Am. Chem. Soc. (USA)*, vol.105, no.17, p.5541-7 (24 Aug. 1983).

Ab initio electronic structure calculations employing both 4-31G and DZP (double- ζ plus polarization) basis sets have been made for equilibrium geometries and transition states involved in thermal rearrangements on the C_2H_3N potential energy hypersurface. The principal rearrangements studied are those involving vinyl nitrene, 2H-azirine, methyl isocyanide, and acetonitrile. From the computed energies of stationary points and from the pathways connecting these points, several conclusions are drawn. First, singlet vinyl nitrene, although possessing a nonplanar equilibrium geometry, can undergo a ring closure with only a modest activation energy to form 2H-azirine. Second, the combined 1,2 hydrogen shift and ring opening required to form acetonitrile from 2H-azirine proceeds optimally but indirectly via methyl isocyanide as an intermediate. Thus hydrogen transfer precedes C-N bond breakage, necessitating a subsequent ring closure and reopening. Third, although no direct pathway leading from 2H-azirine to acetonitrile was located, there is a higher energy but direct pathway leading to acetonitrile from an excited singlet state of vinyl nitrene. (39 refs.)

115528 Ab initio CI study of chemical reactions of singlet and triplet NH radicals. T.Fueno, V.Bonacic-Koutecky, J.Koutecky (Inst. fur Phys. Chem., Freie Univ. Berlin, Berlin, Germany).

J. Am. Chem. Soc. (USA), vol.105, no.17, p.5547-57 (24 Aug. 1983). Reactions of the NH radical in its low electronic states ($^2\Sigma^-$, $^4\Delta$, $^1\Sigma^+$, and $^3\Pi$) with hydrogen and ethylene have been investigated by the multireference double-excitation (MRD) CI method employing mainly the 4-31G basis set. The 4-31G** basis set has been utilized for special points of interest. The relative energies of these low-lying states calculated by this method are in satisfactory agreement with the experimental data. The insertion of $NH(^3\Pi)$ into H_2 is predicted to proceed maintaining the planar (C_{2v}) symmetric structure with an extremely low-energy barrier. $NH(^4\Delta)$ inserts into hydrogen and cyclo-adds to ethylene with no barrier at all. The minimum-energy path for the addition of $NH(^3\Sigma^-)$ to ethylene has been searched for. The activation barrier height is calculated to be not larger than 24 kcal/mol. The CH_2CH_2NH radical has various local energy minima, among which the face-to-face (FF) singlet diradical is the most stable. Cyclization of the singlet FF diradical to form the ground-state aziridine has virtually no energy barrier. The singlet and triplet diradical states in the face-to-edge (FE) conformation are correlated with the first excited singlet (S_1) and the lowest triplet (T_1) state of aziridine, respectively. Implications of these results are discussed in comparing the reactivities of CH_2 and O as isoelectronic homologues of NH. (34 refs.)

115529 Ionization potentials, electron affinities, and molecular orbitals of 2-substituted norbornadienes. Theory of 1,2 and homo-1,4 carbene cycloaddition selectivities. K.N.Houk, N.G.Rondan, M.N.Paddon-Row, C.W.Jefford, Phan Thanh Huy, P.D.Burrow, K.D.Jordon (Dept. of Chem., Univ. of Pittsburgh, Pittsburgh, PA, USA). *J. Am. Chem. Soc. (USA)*, vol.105, no.17, p.5563-9 (24 Aug. 1983).

The ionization potentials, electron affinities, and π orbital shapes of 2-substituted norbornadienes have been determined by photoelectron spectroscopy, electron-transmission spectroscopy, and ab initio molecular orbital calculations, respectively. The deductions made about the electronic structures of 2-methoxy-, (trimethylsiloxy)-, chloro-, cyano-, (methoxycarbonyl)-, and phenylnorbornadienes permit a detailed interpretation of the reactivities and selectivities observed experimentally in carbene cycloadditions to these molecules. A substituent at C-2 of norbornadiene not only affects the 2-3 π bond but also influences the 5-6 π bond due to through-space interactions between π orbitals. The orbital energy changes and polarization induced by 2-substituents provide a compelling rationale of the variations in 1,2 and homo-1,4 cycloadditions of carbenes to these species, and confirm the electrophilic nature of both of these cycloadditions. (35 refs.)

115530 Electrochemical and spectral characterization of iron mono- and dinitrosyl porphyrins. D.Lancon, K.M.Kadish (Dept. of Chem., Univ. of Houston, Houston, TX, USA). *J. Am. Chem. Soc. (USA)*, vol.105, no.17, p.5610-17 (24 Aug. 1983).

The electrochemistry of (TPP)Fe^{II}(NO) and (OEP)Fe^{II}(NO) was investigated in nine nonaqueous solvents. In weakly binding solvents, such as dichloromethane or benzonitrile, five diffusion-controlled electron-transfer reactions were observed. Three of these reactions were oxidations. The remaining two reactions involved reversible electroreductions, either at the Fe(II) center or at the porphyrin ring. In strongly binding solvents, such as Me_2SO or pyridine, similar redox reactions were observed, but a number of chemical reactions were coupled to the electron-transfer steps. Formation of dinitrosyl complexes from either the unnitrosylated or mononitrosyl Fe(II) and Fe(III) complexes was characterized, and several stability constants measured. Finally, competitive ligation between different solvents and NO as axial ligand in each solvent system was studied along the series of oxidized, neutral, and reduced complexes. (39 refs.)

115531 Reactions of energetic tritium atoms with ethyl fluoride over an extensive pressure range. Y.-N.Tang, E.-C.Wu, J.W.Anderton, R.R.Clark (Dept. of Chem., Texas A&M Univ., College Station, TX, USA). *J. Chem. Phys. (USA)*, vol.79, no.5, p.2181-9 (1 Sept. 1983).

Recoil tritium reactions with ethyl fluoride have been studied over a pressure range of six orders of magnitude. The results show that subsequent to T-for-H substitution, the fraction of collisionally stabilized C_2H_4TF ranges from 0.05 at 10^{-2} Torr to 0.91 in the liquid. The low pressure results indicate that 95% of the C_2H_4TF molecules being formed possess an excitation energy of 65 kcal mol⁻¹ or higher. The high pressure and liquid phase studies suggest that about 15% of the excited molecules have energies distributed in a very long and narrow tail at the high energy end. (41 refs.)

115532 Three-body association reactions of NO^+ and O_2^+ with N_2 . C.V.Speller, M.Fitaire, A.M.Pointu (Lab. de Phys. des Gaz des Plasmas, Univ. Paris-Sud, Orsay, France). *J. Chem. Phys. (USA)*, vol.79, no.5, p.2190-9 (1 Sept. 1983).

The cluster ions $NO^+(N_2)_n$, $n \leq 5$, and $O_2^+(N_2)_n$, $n \leq 6$ were observed in a N_2-O_2 gas mixture irradiated by a particles. The temperature dependence of equilibrium constants K for association reactions $X^+(N_2)_{n-1} + 2N_2 \rightleftharpoons X^+(N_2)_n + N_2$, $X = NO, O_2$, was determined using high-pressure mass spectrometry. With $X = NO$, the enthalpies and entropies of clustering ($-\Delta H^\circ$, kcal/mol; $-\Delta S^\circ$, cal/mol K) are found to be (4.4; 13.3) and (3.9; 12.6) for $n=1$ and 2, respectively. Estimation of K at 204K yields 1.1×10^{-2} ($\pm 30\%$) Torr⁻¹ for $n=3$ and $\sim 4 \times 10^{-3}$ Torr⁻¹ for $n=4$. For $X = O_2$, the ($-\Delta H^\circ$, $-\Delta S^\circ$) values, for $n=1,2,3$ are (5.20; 15.8), (4.3; 3.8), and (3.46; 12.1), respectively. The value of K ($n=4$) is estimated to be $\sim 4 \times 10^{-2}$ Torr⁻¹ at 184K, and $\sim 7 \times 10^{-3}$ Torr⁻¹ at 204K; for $n=5$, K is $\sim 1 \times 10^{-2}$ Torr⁻¹ at 184K. The results for $n=1$ are compared with previously reported measurements. (31 refs.)

115533 Temperature dependence of associative detachment reactions. A.A.Viggiano, J.F.Paulson (Air Force Geophys. Lab., Hanscom AFB, MA, USA). *J. Chem. Phys. (USA)*, vol.79, no.5, p.2241-5 (1 Sept. 1983).

The temperature dependences of the rate coefficients for the associative detachment reactions $O^- + NO$, $S^- + CO$, and $S^- + O_2$ have been measured. All rate coefficients varied as $T^{-0.74 \pm 0.1}$. In addition, the rate coefficients and branching ratios for the reactions $O^- + C_2H_2$ and $O^- + C_2H_4$ have also been studied as a function of temperature. Both reactions were found to have a large associative detachment channel over the entire temperature range 140-494K. (35 refs.)

115534 The reaction $H_2 + D_2 \rightleftharpoons 2HD$. A long history of erroneous interpretation of shock tube results. A.Lifshitz, M.Bidani, H.F.Carroll (Dept. of Phys. Chem., Hebrew Univ., Jerusalem, Israel). *J. Chem. Phys. (USA)*, vol.79, no.6, p.2742-7 (15 Sept. 1983).

An ultraclean 2 in. i.d. single pulse shock tube coupled to an atomic resonance absorption system was constructed in order to determine hydrogen atom concentration by Lyman- α absorption. The tube was baked to 300°C and pumped down to $\sim 10^{-7}$ Torr. Ultrapure argon could be shock heated to $\sim 2500K$ with no spurious H atom absorption. The system was constructed in order to study the kinetic of chemical reactions which are strongly catalyzed

by H atoms, under the conditions where no such atoms are present. Specifically, the role of H atoms in the $H_2 + D_2 \rightarrow 2HD$ exchange reaction was studied. Mixtures of hydrogen and deuterium diluted in argon were shock heated to 1375-1760K; samples were then taken from the tube and analyzed mass spectrometrically for the ratio $[HD]/[D_2]$. 1400K was the highest temperature at which no spurious H atom absorption was observed in a shocked mixture of 1% H_2 -1% D_2 . At 1400K, under the conditions of no absorption, no, or $\leq 1\%$ HD conversion was obtained. At higher temperatures Lyman- α absorption was detected and more HD conversion was observed. A comparison between these results and results obtained previously in conventional systems suggests that the high HD conversion observed in the past was caused by hydrogen atoms generated from impurities. The existence of a molecular mechanism in the H_2 - D_2 exchange reaction is highly doubtful. (28 refs.)

115535 Thermally induced nucleation. I. A new way to obtain activation energies for unimolecular reactions. J.L.Katz, J.G.Ruggiero, Jr. (Dept. of Chem. Engng., Johns Hopkins Univ., Baltimore, MD, USA), R.Patch, D.Warren, F.H.Ebetino. *J. Chem. Phys. (USA)*, vol.79, no.6, p.2763-70 (15 Sept. 1983).

Thermal diffusion cloud chambers have been used to study a variety of physical chemical phenomena, particularly homogeneous nucleation. A new and potentially valuable application of the diffusion cloud chamber—the monitoring of thermally allowed reactions—is presented. It is shown that a low concentration of benzocyclobutenol dissolved in nonane will induce temperature dependent nucleation. At constant temperature the rate of nucleation decays exponentially over time. Exponential decay constants obtained from rates of nucleation, when plotted in Arrhenius fashion, give an activation energy of 31 kcal/mol—the same value reported for the racemization of a chiral benzocyclobutenol derivative. (46 refs.)

115536 Reaction velocities and the affinity decay rate. M.Garfinkle (Dept. of Materials Engng., Drexel Univ., Philadelphia, PA, USA). *J. Chem. Phys. (USA)*, vol.79, no.6, p.2779-85 (15 Sept. 1983).

Reaction velocities are calculated for several chemical reactions with diverse mechanisms from thermodynamic considerations alone. These are compared to reaction velocities computed in the conventional manner from mechanistic considerations. The comparisons indicate that a linear phenomenological relationship between chemical affinity and reaction velocity cannot be justified and that there exists a basic compatibility between the thermodynamic and the mechanistic approach to reaction kinetics. (23 refs.)

115537 Second order rate constants for intramolecular conversions: application to gas-phase NMR relaxation times. S.H.Bauer, K.I.Lazaar (Dept. of Chem., Cornell Univ., Ithaca, NY, USA). *J. Chem. Phys. (USA)*, vol.79, no.6, p.2808-13 (15 Sept. 1983).

The usually quoted expression for the second order rate constant, for a unimolecular reaction at the low pressure limit, is valid only for strictly irreversible processes. Its application to isomerization reactions (which are to some extent reversible) is demonstrably in error; corrected expressions have been published. Attention is directed to intra molecular conversions over low barriers, for which the inappropriateness of the unidirectional expression becomes obvious. For such isomerizations the authors propose a model which incorporates only operationally observable states, so that an essential conceptual ambiguity is avoided. Use of this model is illustrated for the syn-anti conversions of methyl nitrite, derived from a gas phase NMR coalescence curve (M_c/T_c). The present data suggest that during isomerization the alkyl nitrites may not be completely ergodic on a time scale of 10^{-9} s. A regional phase-space model is proposed which has the appropriate formalism to account for this behavior. (27 refs.)

115538 Product distributions in the reactions of excited noble-gas atoms with hydrogen-containing compounds. J.Balamuta, M.F.Golde, Yueh-Se Ho (Dept. of Chem., Univ. of Pittsburgh, Pittsburgh, PA, USA). *J. Chem. Phys. (USA)*, vol.79, no.6, p.2822-30 (15 Sept. 1983).

Dissociation and ionization of small H-containing molecules following energy transfer from electronically excited ($^3P_{0,2}$) states of Ar, Kr, and Xe have been studied in discharge-flow systems using the atomic resonance fluorescence and the saturation ion-current techniques. Chemi-ionization is observed in all reactions in which Penning ionization is exothermic, but molecular dissociation is the major channel in all cases. Elimination of H atoms is strongly favored over both loss of H_2 and cleavage of central bonds of larger molecules, in contrast to the known vacuum-UV photochemistry of several of the molecules. When strongly exothermic, elimination of two H atoms in a single reactive event is a major and, in some cases, the dominant channel. (32 refs.)

115539 Investigation of various ways of forming CsH by irradiating a Cs+H₂ mixture with laser light. J.P.Visticot, M.Ferray, J.Loizingot, B.Sayer (Inst. de Recherche Fondamentale, CENS, Gif-sur-Yvette, France). *J. Chem. Phys. (USA)*, vol.79, no.6, p.2839-47 (15 Sept. 1983).

A detailed study of the formation of CsH by the laser photoexcitation of cesium atoms is presented. It is shown that, under the authors' experimental conditions, CsH can be formed not only from the Cs(7P) state but also from the Cs(6D) state and that the 6D level appears to be even more efficient than the 7P level. CsH formation has also been observed when rubidium impurities present in the medium are photoexcited. In this situation, excitation transfer from excited Rb atoms to Cs atoms is not sufficient to explain the observed rate of CsH formation; consequently most of the CsH appears to be formed in an indirect process requiring no excited Cs atom and perhaps involving vibrationally excited H_2 molecules. (20 refs.)

115540 A multiconfigurational self-consistent field study of the D_{2h} dissociation of excited-state ethylene. D.Feller, E.R.Davidson (Dept. of Chem., Univ. of Washington, Seattle, WA, USA). *J. Phys. Chem. (USA)*, vol.87, no.15, p.2721-2 (21 July 1983).

A semiquantitative potential curve is calculated for the D_{2h} dissociation of the first excited 1A_g state of ethylene to two 1A_1 methylenes. Contrary to previous work, the Rydberg nature of the excited 1A_g state is found to lead to a stable ethylene minimum and a barrier to dissociation. (13 refs.)

115541 Thermal decomposition of $Eu_2(SO_4)_3 \cdot 8H_2O$ studied by high resolution luminescence spectroscopy. H.G.Brittain (Dept. of Chem., Seton Hall Univ., South Orange, NJ, USA). *J. Less-Common Met. (Switzerland)*, vol.93, no.1, p.97-102 (1983). (Proceedings of the Sixteenth Rare Earth Research Conference, Tallahassee, FL, USA, 18-21 April 1983).

The thermal decomposition of hydrated europium sulfate was monitored by high resolution photoluminescence studies of the decomposition products. By application of the luminescence method, information can be gleaned from the fine structure within the europium(III) bands regarding the number of europium(III) species existing in the sample. In addition, some idea of the site symmetry of the emitting europium(III) species can be deduced from a detailed analysis of the spectra. Examination of the luminescence spectra revealed that dehydration of the europium(III) sulfate yields a multitude of hydrated intermediates, and these eventually form a well-defined anhydrous sulfate. The data indicate the presence of a hitherto unsuspected intermediate

$Eu_2O(SO_4)_2$ in the decomposition of the anhydrous $Eu_2(SO_4)_3$ to a well-defined $Eu_2O_2SO_4$ end product. (7 refs.)

115542 Electronic structure and chemical conversions of peroxides. II. MINDO/3 calculations of reaction mechanism in noncatalytic epoxidation of olefins by hydroperoxides. V.N.Kokorev, N.N.Vyshinskii, V.P.Maslennikov, I.A.Abroniin, G.M.Zhidomirov, Yu.A.Aleksandrov (Sci.-Res. Inst. of Chem., N.I. Lobachevskii Gor'kii State Univ., Gorkii, USSR). *J. Struct. Chem. (USA)*, vol.23, no.6, p.830-7 (Nov.-Dec. 1982). Translation of: *Zh. Strukt. Khim. (USSR)*, vol.23, no.6, p.13-21 (Nov.-Dec. 1982). [received: Sept. 1983]

By the SCF MO LCAO method in the MINDO/3 valence approximation with variation of all independent variables, the initial compounds, transition states (TS) and products have been calculated for a series of reactions of noncatalytic epoxidation of olefins by hydroperoxides. The geometric and electronic characteristics of the TSs, as determined by the procedure of McIver and Komornicki (1972), showed that the reaction proceeded through a concerted mechanism with an asymmetric, highly polar TS. The MINDO/3-calculated values of the activation energies, are in good agreement with the available experimental values. The calculations show that in the initial phase of the epoxidation reaction, the formation of a labile prereaction olefin-hydroperoxide intermediate is possible. (22 refs.)

115543 Different nature of outer-sphere complex formation between chloroform and bis-(N-phenyl-salicylaldimine)/Cu(II) and its adduct with pyridine. E.P.Talzi, V.M.Nekipelov, N.V.Kozyrev, K.I.Zamaraev (Inst. of Catalysis, Acad. of Sci., USSR). *J. Struct. Chem. (USA)*, vol.23, no.6, p.956-8 (Nov.-Dec. 1982). Translation of: *Zh. Strukt. Khim. (USSR)*, vol.23, no.6, p.158-60 (Nov.-Dec. 1982). [received: Sept. 1983]

The coordination of $CHCl_3$ to $Cu(Salim)_2$ and $Cu(Salim)_2Py$ at $25^\circ C$ has been studied using NMR. It was found that, in the complexes with $Cu(Salim)_2$, the $CHCl_3$ molecules are arranged out of the plane of the chelate while, with $Cu(Salim)_2Py$, chloroform also forms equatorial outer-sphere complexes. The results are explained by the fact that the planar structure of the chelate is distorted during the axial coordination of pyridine as a result of which the formation of hydrogen bonds between the oxygen atoms of the complex and the hydrogen atoms of the $CHCl_3$ molecules becomes possible. (14 refs.)

115544 Proton transfer in complexes of water with hydrogen halides in aprotic solvents. A.A.Pankov, V.Yu.Borovkov, V.B.Kazanskii. *J. Appl. Spectrosc. (USA)*, vol.37, no.5, p.1306-8 (Nov. 1982). Translation of: *Zh. Prikl. Spektrosk. (USSR)*, vol.37, no.5, p.824-7 (Nov. 1982). [received: Sept. 1983]

For a study of the protonation of water in the absence of specific solvation the authors undertook an IR spectroscopic investigation of complexes of water with strong mineral acids HCl and HBr in aprotic solvents. (8 refs.)

115545 Dissociation of Cn^+ into atomic excited states after acceleration in a tandem accelerator. H.G.Berry (Phys. Div., Argonne Nat. Lab., Argonne, IL, USA), L.Engstrom, R.Hellborg, S.Huldt, C.Jupen, A.Trigueiros, I.Martinon. *Phys. Lett. A (Netherlands)*, vol.97A, no.5, p.187-90 (29 Aug. 1983).

A Cn^+ beam produced by stripping Cn^- in the terminal of a Pelletron Tandem accelerator was dissociated in a thin carbon foil. Optical observations of ultraviolet transitions C III-C IV and IV-N V showed intensity variations as a function of foil thickness. The results indicate an enhancement of population to the neighboring partner projectile for some but not all excited states. (13 refs.)

115546 Influence of electronic structure of a cation-radical skeleton, the nature of the anion attached to it, and the nature of the medium on reaction kinetics of one-electron oxidation of triphenylantimony by cation radicals of substituted triphenylamines. V.G.Koshechko, V.E.Titov, V.D.Pokhodenko (L.V. Pisarzhevskii Inst. of Phys. Chem., Acad. of Sci., Kiev, Ukrainian SSR). *Theor. & Exp. Chem. (USA)*, vol.18, no.6, p.648-53 (Nov.-Dec. 1982). Translation of: *Teor. & Eksp. Khim. (USSR)*, vol.18, no.6, p.705-10 (Nov.-Dec. 1982). [received: Sept. 1983]

In the case of reactions of this type it was interesting to find the factors influencing the reactivity of the cation radicals. In the present work, therefore, the authors studied by the spectrophotometric method the influence of the electronic structure of the cation-radical skeleton of the radical-oxidant, the nature of the anion attached to it, and the nature of the medium on the kinetic parameters of the oxidation of triphenylantimony (Ph_3Sb) by cation radicals of substituted triphenylamines. (20 refs.)

115547 Theoretical investigation of the cyclodimerization of acetylene and the stability of Hartree-Fock solutions. M.N.Glukhovtsev, B.Ya.Simkin, I.A.Yudilevich (Rostov State Univ., Rostov, USSR). *Theor. & Exp. Chem. (USA)*, vol.18, no.6, p.669-72 (Nov.-Dec. 1982). Translation of: *Teor. & Eksp. Khim. (USSR)*, vol.18, no.6, p.726-9 (Nov.-Dec. 1982). [received: Sept. 1983]

An analysis of the stability of the Hartree-Fock (HF) solutions can serve as a basis for the classification of organic reactions and is used as a comparatively simple method for the determination of the type of a given reaction. However, up to the present time, actual calculations have only been carried out in the case of model reactions using idealized geometry and a hypothetical reaction pathway. Meanwhile, variation of all the degrees of freedom in the reaction process can even change the qualitative conclusions. The aim of the work was to carry out a theoretical investigation of the cyclodimerization of acetylene by calculation of the minimum energy reaction path using the MINDO/3 method with variation of all the internal geometric parameters and to analyze the stability of the solutions which were obtained. (18 refs.)

115548 Correlation diagrams of states for certain 'forbidden' reactions. Yu.V.Mitrenin (Tomsk Polytech. Inst., Tomsk, USSR). *Theor. & Exp. Chem. (USA)*, vol.18, no.6, p.692-6 (Nov.-Dec. 1982). Translation of: *Teor. & Eksp. Khim. (USSR)*, vol.18, no.6, p.750-4 (Nov.-Dec. 1982). [received: Sept. 1983]

Correlation diagrams of states (CDS) were constructed and potential barriers (PB) were estimated for several 'forbidden' reactions, including those whose 'forbiddances' are usually not revealed from the CD of the molecular orbitals. By 'forbiddance' is usually meant a high potential barrier due to quasi-intersection of potential energy surfaces (PES). These PB's can be both high and low, and, therefore, the terminology of 'forbiddance' in some cases does not reflect the essence of the matter. Therefore, the numerical estimate of PB is better. Since the CD's of molecular orbitals do not give an unambiguous possibility for constructing the CDS and do not reveal all the types of quasi-intersections, it is necessary to search for direct methods of constructing the CDS. The authors used the possibilities of the valence bond (VB) method for this purpose. (11 refs.)

Observations of order and chaos in nonlinear systems See Entry 111564
Oscillations and chaos in chemical systems See Entry 111567

- Experimental studies of bifurcations leading to chaos in the Belousov-Zhabotinsky reaction See Entry 111568
- Reactive scattering cell for atomic hydrogen and deuterium .. See Entry 111689
- Ab initio investigation of intramolecular rearrangements and nature of barriers in SH_6 and SF_6 molecules See Entry 112640
- Structure of protonated forms of coumarin and its hydroxy derivatives See Entry 112641
- Nitric oxide vibrational excitation from the $\text{N}(^4\text{S}) + \text{O}_2$ reaction See Entry 112699
- Light-induced isomerization and photochemical transformation of methylformate in an Argon matrix. Vibrational frequencies, force field, and normal coordinate analysis of trans-methylformate See Entry 112725
- Raman spectra of Cl_3^+ and Br_3^+ at 12K produced from the reaction of HCl or HBr with NO_2 See Entry 112741
- Fluorescence of trans-4-cyano-4'-dimethylaminostilbene; no evidence for a TICT state See Entry 112774
- Permutational analysis and tunnelling effects in XeF_6 See Entry 112794
- Vaporisation of tungsten bronzes. II. Sodium and potassium tungsten bronzes .. See Entry 114151
- Conductivity of magnesium valerate solutions in binary liquid mixtures See Entry 114227
- An XPS study of carbon monoxide and nitric oxide adsorption on platinum (410): unusual dissociation activity See Entry 114353
- Adsorption and decomposition of ammonia on W(100): XPS and UPS studies .. See Entry 114355
- The influence of the hydrogen reduction process on the electrical properties of $\text{In}_2\text{O}_3/\text{Sn}$ thin films See Entry 114628
- Carbon-13 line shape study of two-site exchange in solid dimethyl sulfone See Entry 114748
- Luminescence of the hydrolysis products of Th(IV) See Entry 114915
- Production of metal-carbon system materials with groups IV-V refractory metals See Entry 115153
- Dissipative structures in 1D and 2D chemically reacting systems See Entry 115512
- Indeterminacy in kinetic-model parameters due to non-Hamiltonian structure of the multipath linear reaction graph See Entry 115515
- Beam-gas study of chemiluminescent reactions of Sn, Ge, and Si with F_2 See Entry 115560
- Pulse-radiolytic investigation of CS_2 reduction See Entry 115570
- Role of the central metal ion and solvent-ligand molecules in the association of metallophorphytins in binary mixtures of solvents See Entry 115726
- Laboratory measurements of the association rate coefficients of NO^+ , O_2^+ , N^+ , and N_2^+ ions with N_2 and CO_2 at temperatures between 100K and 400K See Entry 116330

82.35 POLYMER REACTIONS AND POLYMERIZATION

- 115549 The gamma ray-induced crosslinking of polyacrylamide in the solid state. G.Burillo (Univ. Nacional Autonoma de Mexico, Mexico City, Mexico), T.Ogawa. *J. Polym. Sci. Polym. Lett. Ed. (USA)*, vol.21, no.8, p.615-20 (Aug. 1983). Although there are many studies on the radiation-induced crosslinking of polymers, very little has been reported on the crosslinking of polyacrylamide. Previously, the authors studied the gamma ray-induced gelation of aqueous solution of polyacrylamide and reported that the molecular weight is a very important factor for crosslinking, and later they reported that the water content in the polymer is an important factor for crosslinking in the solid state. In order to obtain more information on the mechanism of crosslinking and to obtain basic data for the optimum conditions for gel formation, the gamma ray irradiation of polyacrylamide was carried out under various conditions, and the results are reported. (8 refs.)
- Electrically conductive thermoplastic elastomer/polyacetylene blends See Entry 114513
- Polymer films on electrodes. XIII. Incorporation of catalysts into electronically conductive polymers: iron phthalocyanine in polypyrrole See Entry 115561

82.40 CHEMICAL KINETICS AND REACTIONS: SPECIAL REGIMES

- 115550 Fluorescence measurements of OH in a turbulent flame. M.Azzazy, J.W.Daily (Univ. of California, Berkeley, CA, USA). *AIAA J. (USA)*, vol.21, no.8, p.1100-6 (Aug. 1983). Laser-induced fluorescence spectroscopy has been used to measure OH concentration probability density functions (PDFs) in a turbulent premixed flame. The methane-air flame is stabilized on a rod flame holder located downstream of a turbulence producing grid. Measurements in both the streamwise and transverse directions have been made for a variety of flow conditions. The PDFs display a single peaked behaviour throughout the flame, with the broadest structure in the center of the flame. A simple limit analysis shows that the observed behaviour of the PDF is consistent with expected behaviour for an intermediate radical specie over the range of flame, optical, and turbulence length scales present in the experiment. (8 refs.)
- 115551 Acoustic signature from flames as a combustion diagnostic tool. M.K.Ramachandra, W.C.Strahle (Georgia Inst. of Technol., Atlanta, GA, USA). *AIAA J. (USA)*, vol.21, no.8, p.1107-14 (Aug. 1983). A nonintrusive acoustic technique has been developed to obtain the fluctuating heat release rate distribution in open premixed turbulent flames. Propane-air flames of equivalence ratio 0.6, 0.8, and 1.0 with a 16.4 mm diam burner and a 11.55 m/s mean flow speed have been employed. The flame sound pressures in the near field were measured in an anechoic chamber. With the acoustic spectra and the input, the heat release rate spectral information was obtained by numerically using an augmented Glearkin method to solve a Fredholm integral equation of the first kind. Computed results have been qualitatively verified by C_2 emission studies. The experimentally observed correspondence between mean and RMS C_2 emission intensity implies that the shape of the mean heat release distribution can, in principle, be deduced by the acoustic technique. (15 refs.)

- 115552 Structure and extinction of convective diffusion flames with general Lewis numbers. S.H.Chung, C.K.Law (Dept. of Mech. & Nuclear Engng., Northwestern Univ., Evanston, IL, USA). *Combust. & Flame (USA)*, vol.52, no.1, p.59-79 (Aug. 1983). The structure and extinction of quasi-one-dimensional diffusion flames with general Lewis numbers for both fuel and oxidiser are analysed using large activation energy asymptotics for the model problems of spherically symmetric droplet combustion, counterflow combustion, and stagnation point combustion over a condensed fuel. General matching and jump conditions up to the first order of expansion are derived. It is shown that by suitably redefining certain parameters the structure equations for all cases can be brought to the same form as that of Linan (1974) so that his numerically generated extinction Damkohler number correlation can be readily used. Combining this with the authors' own numerical result of the reactant leakage correlation, the extinguishability of a given system can be assessed. The present extinction criterion with general Lewis numbers also provides improved accuracy in the determination of overall kinetic constants through correlation of experimental extinction data. (16 refs.)
- 115553 The visible shape and size of a turbulent hydrocarbon jet diffusion flame in a cross-wind. G.T.Kalghatgi (Shell Res. Ltd., Res. Centre, Chester, England). *Combust. & Flame (USA)*, vol.52, no.1, p.91-106 (Aug. 1983). The results of an extensive wind-tunnel study into the shapes and sizes of hydrocarbon jet diffusion flames in a horizontal cross-wind are presented. The shape of a turbulent diffusion flame in a cross-wind can be described by the frustum of a cone, which, in turn, can be defined by five different parameters of shape. When the burner axis is normal to the wind, each shape parameter can be related to the burner diameter, the burner exit velocity, the cross-wind speed, and the density of the burner gas by one equation. When the burner axis is not normal to the wind, the experimental results still follow an identifiable pattern and can be used to estimate flame shapes and sizes. (13 refs.)
- 115554 Diagnostic possibilities on the basis of premixed flame noise levels. G.Petela, R.Petela (Inst. Tech. Cieplnej, Politech. Slaska, Gliwice, Poland). *Combust. & Flame (USA)*, vol.52, no.2, p.137-47 (Sept. 1983). On the basis of an assumed turbulent premixed gaseous flame model a useful formula is derived for the flame noise intensity, which is considered as an effect of combustion intensity fluctuations and flame zone turbulence. The observed similarity between the change in the flame noise spectrum amplitude and the energy release rate suggests the possibility of a diagnostic interpretation of the noise in terms of combustion intensity. This information becomes less clear, however, when the flame turbulence is strongly developed. The mutual relation between combustion intensity, flame zone turbulence, and amplitude of noise spectrum components suggests an analogy with the basic diagnostic formula. (28 refs.)
- 115555 Transient catalytic combustion on a flat plate. A.Fakheri, R.O.Buckius (Dept. of Mech. & Industrial Engng., Univ. of Illinois, Urbana, IL, USA). *Combust. & Flame (USA)*, vol.52, no.2, p.169-84 (Sept. 1983). The transient two-dimensional heterogeneous combustion of fuel on a catalytic flat plate is studied. The solutions are obtained for the three different wall boundary conditions of an isothermal, a perfectly conducting plate, and an adiabatic plate. The laminar boundary layer equations are transformed, and the resulting equations are solved numerically. Equations are nondimensionalized to make the results as general as possible. For a perfectly conducting plate, a universal approach is used which shows the solution of the transport equations to be single valued and that the multiple solutions are caused only by the form of the rate expression. General solutions are found for an isothermal plate which are applicable to any first order reaction or a fuel lean mixture with second order reaction. Solutions for an adiabatic plate show a high temperature region is formed down the plate which moves up. Ignition delay time and ignition distance are found to have the same dependence on the flow and kinetic parameters, except that the ignition delay time does not depend on the free-stream velocity. The results are obtained for CO as well as H_2 oxidations. (18 refs.)
- 115556 Inhibition of acetaldehyde cool flames. J.C.Jones, B.F.Gray (School of Chem., Macquarie Univ., North Ryde, NSW, Australia). *Combust. & Flame (USA)*, vol.52, no.2, p.211-13 (Sept. 1983). Recent studies of the cool flame behaviour of acetaldehyde-oxygen mixtures have all used the continuous stirred tank reactor, thus enabling the observation of limit cycles, multistability, repeated ignitions, and so on. Although a number of studies have dealt with the extinction or inhibition of normal (hot) flames by additives the relevance of the latter to the inhibition of the onset of combustion is not clear. The authors report results obtained with a variety of inhibitors on both the cool flame limits and the heat release rates in the steady (nonoscillatory) slow combustion reaction. (5 refs.)
- 115557 Effect of diameter on the burning rate of polystyrene. K.Kishore, K.Mohandas (Dept. of Inorganic & Phys. Chem., Indian Inst. of Sci., Bangalore, India), I.Spilda. *Combust. & Flame (USA)*, vol.52, no.2, p.215-16 (Sept. 1983). The myriad of test methods used to determine the burning rates of polymeric materials generally overlooks the effect of the size of the samples. Each of the test methods insists on a particular geometry for the test specimen, and this leads to a wide variation in the area of burning surface from one test to another. The authors have studied the influence of rod diameter on the rate of burning of polystyrene (PS). (7 refs.)
- 115558 Toxicologic and physicochemical characterization of high-temperature combustion emissions. E.R.Kirchner, P.F.Dunn, C.B.Reed (Argonne Nat. Lab., Argonne, IL, USA). *Aerosol Sci. & Technol. (USA)*, vol.2, no.3, p.398-400 (1983). Particles and combustion gases produced by two different high-temperature combustors, which burned pulverized coal and a No.2 fuel oil-fly ash slurry, respectively, at adiabatic flame temperatures greater than 2400K, were characterized. Effluent samples were taken at locations along the product gas stream and within the stack. Measurements of the particle size distributions, number concentrations, and gas species concentrations were made. The toxicity and mutagenicity of the effluent particles were determined. A large number of submicrometer particles were found in both cases of high-temperature combustion. The product emissions differed significantly in their particle size distribution and final chemical composition from those of conventional combustion systems having lower combustion temperatures. (18 refs.)
- 115559 Resonant electron scattering by metastable nitrogen. I.Cadez (Cooperative Inst. for Res. in Environmental Sci., Univ. of Colorado, Boulder, CO, USA). *Planet. & Space Sci. (GB)*, vol.31, no.8, p.843-8 (Aug. 1983). The resonant electron impact quenching of metastable molecules might be important for understanding the phenomena in the upper atmosphere. In order to obtain information about the relative importance of this scattering event the resonant cross sections for electron scattering by metastable nitrogen

in the $A^3\Sigma_u^+$ state are calculated using the 'boomerang' model and quenching rates for this state are evaluated for the altitudes of 130, 170 and 210 km. (12 refs.)

Rubens flame tube demonstration: a closer look at the flamesSee Entry 111360

Rotational Raman interferometric measurement of flame temperaturesSee Entry 111687

The ignition and burning behaviour of sodium metal in air ...See Entry 112401

A study on sodium spray combustionSee Entry 112408

Hydrogen phenomena in PWR degraded core accidentsSee Entry 112421

Flame velocity for the onset of detonationSee Entry 113473

An approximate solution for diffusion and reaction in a non-ideal tubular reactorSee Entry 113520

Momentum implications for buoyant diffusion flamesSee Entry 113548

Fire flame radiationSee Entry 113559

Experimental investigation of absorption coefficient of cesium resonance doublets in a plasma of combustion productsSee Entry 113660

Phase separation of phosphonated polystyrenes in the solid state. IV. Influence of this phenomenon on their flame retardancy properties [ESCA observations] ..See Entry 115602

A theoretical study of the height distribution of sodium in the mesosphereSee Entry 116234

Laboratory measurements of the association rate coefficients of NO^+ , O_2^+ , N^+ , and N_2^+ ions with N_2 and CO_2 at temperatures between 100K and 400KSee Entry 116330

82.40T Chemiluminescence and chemical laser kinetics
(see also 42.55K Chemical lasers; 78.60P Chemiluminescence)

115560 Beam-gas study of chemiluminescent reactions of Sn, Ge, and Si with F_2 . W.J.Rosano, J.M.Parson (Dept. of Chem., Ohio State Univ., Columbus, OH, USA). *J. Chem. Phys. (USA)*, vol.79, no.6, p.2696-709 (15 Sept. 1983). Electronic chemiluminescence (CL) has been observed for the reactions of tin, germanium, and silicon with fluorine utilizing a beam-gas configuration. Only electronic states of the metal monofluorides which are energetically allowed in a single reactive collision of the metal atoms $\text{SnF}(A^2\Sigma^+)$, $\text{GeF}(A^2\Sigma^+)$, and $\text{SiF}(A^2\Sigma^+, A^2\Sigma^-)$ have been observed, in contrast with the results of previous flame studies in which other high lying electronic states have been reported. Pressure and temperature variations of the CL indicate a first-order dependence with respect to metal and fluorine. Simulation of the $A^2\Sigma^+-X^2\Pi$ systems has been obtained by nonlinear least-squares fit of the experimental spectra. Vibrational populations of the $A^2\Sigma^+$ states are found to be inverted, with the appearance of double maxima. Adiabatic correlation, with respect to overall electronic symmetries of the reactants and products, indicates all reactant surfaces lead to ground-state products. However, molecular orbital arguments indicate the presence of one diabatic surface connecting reactants and electronically excited products. (64 refs.)

Temperature requirements and corrosion rates in combustion driven hydrogen fluoride supersonic diffusion lasersSee Entry 112986

Simple model for base pressure effects in source flow chemical lasersSee Entry 112987

82.45 ELECTROCHEMISTRY AND ELECTROPHORESIS
(see also 66.10 Ionic conduction in liquids; for electro-osmosis, see 82.65)

115561 Polymer films on electrodes. XIII. Incorporation of catalysts into electronically conductive polymers: iron phthalocyanine in polypyrrole. R.A.Bull, F.-R.Fan, A.J.Bard (Dept. of Chem., Univ. of Texas, Austin, TX, USA). *J. Electrochem. Soc. (USA)*, vol.130, no.7, p.1636-8 (July 1983). Tetrasulfonated iron phthalocyanines (FePcS) can be incorporated into electronically conducting polypyrrole by electrochemical polymerization of pyrrole in the presence of FePcS. The FePcS modified glassy carbon electrodes catalyzed the reduction of O_2 at potentials 250 to 800 mV less negative than at bare glassy carbon or at polypyrrole-coated glassy carbon not containing FePcS. Rotating ring-disk experiments indicated some hydrogen peroxide formation at most pHs. However, at high pH essentially exclusive reduction of O_2 to H_2O was observed at potentials 250 mV less negative than at a non-catalyzed electrode. (13 refs.)

115562 Influence of halide ions, mainly iodide ions upon the kinetics of anodic oxidation of zirconium in 0.1 M potassium tartrate. A.N.Chary (Dept. of Chem., Osmania Univ., Hyderabad, India), Ch.Anjaneyula, K.S.Sastry. *J. Electrochem. Soc. India*, vol.32, no.1, p.32-3 (Jan. 1983). [received: Sept. 1983] The influence of halide ions on the kinetics of anodic oxide film formation on zirconium in 0.1 M potassium tartrate have been studied at a constant current density of 8 mA/cm² and at room temperature. At higher concentration of halide ions (≥ 0.1 M) there is no film formation and deleterious effects are observed. However there is a film formation and improvement in the kinetics of anodic oxidation at lower concentrations (0.001 M) of halide ions. In the presence of iodide ions the kinetics give interesting results. (10 refs.)

115563 Photoelectrochemical properties and optical quenching of photocurrent in $\text{Bi}_{12}\text{SiO}_{20}$ single crystals. K.Kochev, K.Tzvetkova, M.Gospodinov (Central Lab. of Solar Energy & New Energy Sources, Bulgarian Acad. of Sci., Bulgaria). *Mater. Res. Bull. (USA)*, vol.18, no.8, p.915-19 (Aug. 1983). The photoelectrochemical properties of reduced $\text{Bi}_{12}\text{SiO}_{20}$ (BSO) single crystals have been investigated for the first time. The flatband potential determined from the C-V measurements is $U_{fb} \approx 0.9$ V vs. SCE. The photosensitivity is observed up to 0.5 μm in the visible range of the spectrum. The optical quenching of the photocurrent in the BSO-electrolyte-Pt cell has been investigated. This effect appears for wavelengths in the range 0575+1.1 μm . From the infrared threshold of the spectrum, it was defined that the sensitizing centres of the BSO crystals are located at 11 eV above the valence band. (8 refs.)

115564 Irreversible loss of adatoms on Ag electrodes during potential cycling determined from surface enhanced Raman intensities. J.F.Owen, T.T.Chen, R.K.Chang (Center for Laser Diagnostics, Yale Univ., New Haven, CT, USA), B.L.Laube. *Surf. Sci. (Netherlands)*, vol.131, no.1, p.195-220 (Aug. 1983). Surface enhanced Raman scattering of adsorbates ($\text{Ag}^0\text{-Cl}^-$, H_2O and pyridine) on Ag electrodes in 1M KCl and 1M $\text{KCl}+0.05\text{M}$ pyridine electrolytes was monitored continuously with an optical multichannel analyzer system as the electrode potential was cycled over various ranges within nonfaradic regions of the oxidation-reduction cycle. A systematic investigation was performed of the potential dependence of SERS of pyridine in 1M $\text{KX}+0.05\text{M}$ pyridine electrolytes, where $\text{X}=\text{F}, \text{Cl}, \text{Br}$ and I . Since the surface coverage of the adsorbates is reversible with potential cycling within a potential range, it was possible to determine potential dependences of the irreversible loss in the SERS enhancement factor which occurs as the electrode potential is ramped toward the potential of zero charge (PZC). The results provide strong support for the role of adatoms on the electrode surface in the overall enhancement mechanism. There is evidence that the strongly bound adsorbates immobilize the adatoms at positive potentials but allow the adatoms to migrate and become lost at surface defects as the potential approaches the PZC where the adsorbates are less tightly bound. (34 refs.)

115565 The preparation and properties of metallic optically transparent electrodes. L.J.J.Janssen (Dept. of Chem. Tech., Eindhoven Univ. of Technol., Eindhoven, Netherlands), A.T.Kuhn. *Surf. Technol. (Switzerland)*, vol.20, no.1, p.41-9 (Sept. 1983). The uses of optically transparent electrodes (OTEs) are briefly discussed together with the different types of OTE. The review is focused on metallic OTEs and a survey of the various types, their means of preparation and their optical and electrical properties is included. (22 refs.)

Extended Abstracts from the 164th Electrochemical Society Technical MeetingSee Entry 111317

On the limiting law solution of the cylindrical Poisson-Boltzmann equation for polyelectrolytesSee Entry 111613

Thermometric and calorimetric methods in electrochemical and corrosion studiesSee Entry 111686

A new design and experimental testing of a carbon monoxide sensorSee Entry 111700

The investigation of image formation in a large-area solid state X-ray receptor with electrophoretic displaySee Entry 111850

Coadsorption systems with electrochemical relevance: coadsorption of water with oxygen, bromine and sodium on $\text{Cu}(110)$ See Entry 114340

Semiconductor electrodes. LI. Efficient electroluminescence at ZnS electrode in aqueous electrolytesSee Entry 114931

Diffusion-coupled active dissolution in the localized corrosion of stainless steelsSee Entry 115409

Influence of an increase in phosphorus content on the corrosion resistance of austenitic stainless steels type Z 2 CND 17-12See Entry 115426

Anodic oxidation of iron and cathodic reduction of the anodic film: a review ...See Entry 115442

Electrochemical and spectral characterization of iron mono- and dinitrosyl porphyrinsSee Entry 115530

Reactions at the anode during storage of partially discharged Li/SO_2 cellsSee Entry 115627

82.50 PHOTOCHEMISTRY AND RADIATION CHEMISTRY
(see also 33.50 Fluorescence, phosphorescence; radiationless transitions)

115566 Time resolved photoacoustic spectroscopy applied to properties of picosecond transients. L.J.Rothberg, M.Bernstein, K.S.Peters (Dept. of Chem., Harvard Univ., Cambridge, MA, USA). *J. Chem. Phys. (USA)*, vol.79, no.6, p.2569-76 (15 Sept. 1983). Time resolved photoacoustic spectroscopy represents a promising new approach to the study of time resolved absorption with picosecond time resolution. The sensitivity of photoacoustic detection permits investigation of dilute and fluorescent samples which are difficult to study by conventional flash photolysis. Theory shows that quantitative measurements of important transient properties and new insights into photochemical and photophysical dynamics can be obtained by measuring heat deposition as a function of probe fluence. Experimental determinations of absorption and stimulated emission cross sections, and lower limits for rates of nonradiative relaxation of highly excited states, are presented. (16 refs.)

115567 Relative quantum yield of $\text{I}^*(^2\text{P}_{1/2})$ in the tunable laser UV photodissociation of $\text{i-C}_3\text{F}_7\text{I}$ and $\text{n-C}_3\text{F}_7\text{I}$: effect of temperature and exciplex emission. J.E.Smedley, S.R.Leone (Dept. of Chem., Univ. of Colorado, Boulder, CO, USA). *J. Chem. Phys. (USA)*, vol.79, no.6, p.2687-95 (15 Sept. 1983). Wavelength-specific relative quantum yields of I^* from pulsed laser photodissociation of $\text{i-C}_3\text{F}_7\text{I}$ and $\text{n-C}_3\text{F}_7\text{I}$ in the range 265-336 nm are determined by measuring the time-resolved infrared emission ($\lambda=1.135 \mu\text{m}$) from the atomic $\text{I}(^2\text{P}_{1/2} \rightarrow ^2\text{P}_{3/2})$ transition. The quantum yields of I^* from $\text{i-C}_3\text{F}_7\text{I}$ and $\text{n-C}_3\text{F}_7\text{I}$ are constant and appear to be unity from 265-298 nm but decrease to 0.57 and 0.40, respectively, at 336 nm. The lower quantum yields suggest the existence of two distinct bands in this region of the absorption continua. To determine the quantum yields a correction is made for enhanced emission due to formation of exciplexes between I^* and the parent (i- or $\text{n-C}_3\text{F}_7\text{I}$) species. The exciplex emission increases linearly with parent gas pressure, but decreases with increasing temperature. For both molecules the integrated absorption in the long wavelength region (>290 nm) increases substantially with temperature, while at selected wavelengths the quantum yields are found to remain constant with temperature. The results are discussed in terms of the development of solar-pumped iodine lasers. (34 refs.)

115568 Laser flash photolysis of benzene. VIII. Formation of hot benzene from the S_2 state and its collisional deactivation. N.Nakashima, K.Yoshihara (Inst. for Molecular Sci., Okazaki, Japan). *J. Chem. Phys. (USA)*, vol.79, no.6, p.2727-35 (15 Sept. 1983). Time-resolved absorption spectra of gaseous benzene have been observed in the time range from 0 to 4 μs with an ArF laser (193 nm) as an excitation source, which pumps the S_2 state. The absorption strength in the transient spectrum observed immediately after excitation with a 10 ns pulse decreases monotonically from 210 to 290 nm. This spectrum is postulated to be due to $\text{B}^*(\text{S}_0)$ (a hot benzene with internal energy 624 kJ/mol). The transient spectrum can be simulated as part of the $\text{S}_3(^1\text{E}_{1g}) \rightarrow \text{S}_0$ transition at 3390K on the basis of the Sulzer-Wieland model. The agreement between calculated

and observed molar extinction coefficients of $B^{**}(S_0)$ indicates that the yield of internal conversion from S_2 to $B^{**}(S_0)$ is close to unity. Deactivation processes have been detected from $B^{**}(S_0)$ to a thermal equilibrium state in inert gas baths. The time profile of absorption intensity due to collisional deactivation is nonexponential and depends upon observing wavelength, being faster at longer wavelength. The deactivation processes are explained in terms of a simple energy transfer model, which assumes that the removal energy per collision depends on the internal energy of the hot molecule. Internal conversion from S_2 to $B^{**}(S_0)$ is suggested to be the initial step in the photochemical reactions of gaseous benzene. The absorption spectrum and collisional deactivation processes following excitation with a KrF laser (248 nm), which pumps the S_1 state, have been analyzed in the same way. (27 refs.)

115569 The mechanism of the cross linking of poly(vinyl alcohol) by ammonium dichromate with UV-light. L.Grimm, K.-J.Hilke, E.Scharrer (Philips GmbH, Aachen, Germany). *J. Electrochem. Soc. (USA)*, vol.130, no.8, p.1767-71 (Aug. 1983). The phosphor raster of color TV screens is produced by the exposure of photosensitive coats to ultraviolet light. On the basis of existing papers and the authors' own experiments, a model is presented showing the mechanism of the photosensitive reaction between poly(vinyl alcohol), ammonium dichromate, and water. A complex redox reaction takes place between the three components, leading to chromium (III) ions and poly(vinyl alcohol) cleavage products with terminal carboxyl groups. There is interaction to chelate complexes, thus resulting in a three-dimensional poly(vinyl alcohol) network insoluble in water. (28 refs.)

115570 Pulse-radiolytic investigation of CS_2 reduction. O.Brede, R.Mehner, E.Hoyer (Zentralinst. für Isotopen- und Strahlenforschung, Akad. der Wissenschaften, Leipzig, Germany). *Radiochem. & Radioanal. Lett. (Switzerland)*, vol.58, no.2, p.117-28 (19 Aug. 1983). In aqueous solution of *t*-butanol (4.3 molar) e_{aq}^- reacts with CS_2 with a rate constant of $3.3 \times 10^9 \text{ dm}^3 \text{ mol}^{-1} \text{ s}^{-1}$ forming $CS_2^{\cdot -}$. The carbon disulfide radical anion has an optical absorption spectrum with peaks at $\lambda = 275 \text{ nm}$ ($\epsilon = 2 \times 10^4 \text{ dm}^3 \text{ mol}^{-1} \text{ cm}^{-1}$) and $\lambda = 330\text{-}340 \text{ nm}$ ($\epsilon = 8 \times 10^3 \text{ dm}^3 \text{ mol}^{-1} \text{ cm}^{-1}$). In acidic solution $CS_2^{\cdot -}$ is protonated to CS_2H^{\cdot} with $k_5 = 1.3 \times 10^9 \text{ dm}^3 \text{ mol}^{-1} \text{ s}^{-1}$ which has an absorption spectrum peaking at $\lambda = 320 \text{ nm}$ ($\epsilon = 10^4 \text{ dm}^3 \text{ mol}^{-1} \text{ cm}^{-1}$). $CS_2^{\cdot -}$ reacts with oxygen with $k_6 = 1.9 \times 10^9 \text{ dm}^3 \text{ mol}^{-1} \text{ s}^{-1}$. (9 refs.)

115571 Mass spectrometric study of the volatile products from the radiolysis of polyethylene. E.G.Stetsenko, T.Z.Kolmaz, G.N.P'yankov, B.G.Mischanchuk, I.P.Samchenko, M.M.Aleksankin (L.V. Pisarzhevskii Inst. of Phys. Chem., Acad. of Sci., Kiev, Ukrainian SSR). *Theor. & Exp. Chem. (USA)*, vol.18, no.6, p.696-9 (Nov.-Dec. 1982). Translation of: *Teor. & Eksp. Khim. (USSR)*, vol.18, no.6, p.754-7 (Nov.-Dec. 1982). [received: Sept. 1983] The purpose of the investigation is to examine the mechanism of polymer degradation. During the manufacture of products, air bubbles are formed in the bulk of the polymer. Atmospheric oxygen gradually oxidizes molecules located on the internal surface of the bubbles, so that the surface becomes coated by oxygen-containing functional groups viz. hydroxyl carboxyl hydroperoxyl, etc. These parts of the polymer molecules would seem to be more liable to degradation involving the detachment of the terminal fragments than the hydrocarbon chains. The active particles having oxygen-containing functional groups which are formed during degradation have the possibility of escaping into the gas phase where their secondary reactions also take place. If the reactions (e.g., radical recombination) are exothermic, then microheating of adjacent parts of the polymer occurs and their volume increases as a result of the increase in temperature and pressure within the bubbles. The amount of oxygen in the bubbles is small, but it is the initiator of the breakdown of the polymer. With the detachment of an active particle e.g., the oxygen-containing radical CH_2OH^{\cdot} , a radical site remains on the surface which would appear to be capable of further reactions. A strong argument in favor of the above hypothesis would be the detection of oxygen-containing compounds in the composition of the volatile radiolytic products. For this purpose the authors used field mass spectroscopy, which enables trace amounts of a component to be identified in a sample. They analyzed the products evolved on heating polyethylene to 70-80°C. (5 refs.)

Agfapan 25, 100 and 400 See Entry 111791
Nascent NO vibrational distribution from 2485 Å NO_2 photodissociation See Entry 112700

Light-induced isomerization and photochemical transformation of methylformate in an Argon matrix. Vibrational frequencies, force field, and normal coordinate analysis of trans-methylformate See Entry 112725

Study of elementary photophysical and photochemical processes in organic molecules using the optoacoustical effect See Entry 113251

Investigation of various ways of forming CsH by irradiating a Cs+H₂ mixture with laser light See Entry 115539

Photoelectrochemical properties and optical quenching of photocurrent in $Bi_{1-x}SiO_{20}$ single crystals See Entry 115563

Electronic excitation in electron bombardment enhancement of chemical reactions See Entry 115577

Role of the central metal ion and solvent-ligand molecules in the association of metallophophytins in binary mixtures of solvents See Entry 115726

On the photodecomposition of $ClONO_2$ in the middle ultraviolet See Entry 116201

82.55 RADIOCHEMISTRY

115572 Cage effect in recoil studies. K.Berci. Report KFKI-1983-91, Hungarian Acad. Sci., Budapest (1983), 16 pp. The role of the cage effect is one of the most discussed questions of hot atom chemistry in condensed organic systems. So far no direct evidence is available for assessing the exact contribution of thermal recombinations occurring in the liquid cage to the stabilization processes of recoil atoms. However, some conclusions can be drawn from experimental observations concerning the influence on product yield of hot atom recoil spectra, the effects of density, phase and long range order of the medium as well as from comparing systems providing cage walls of different chemical reactivities towards the recoil atom. Recent developments in this field are reviewed primarily based on the investigations of recoil halogen reactions in aliphatic and aromatic hydrocarbons and their haloderivatives. (37 refs.)

82.60 CHEMICAL THERMODYNAMICS

(see also 05.70 Thermodynamics)

115573 Thermodynamic stability of complex oxides in alkali metals. M.N.Ivanovskii, V.A.Morozov, A.L.Shimkevich, B.A.Shmatko. *High Temp. (USA)*, vol.20, no.6, p.867-70 (Nov.-Dec. 1982). Translation of: *Teplofiz. Vys. Temp. (USSR)*, vol.20, no.6, p.1098-101 (Nov.-Dec. 1982). [received: Sept. 1983]

The temperature dependence of the thermodynamic potential of oxygen impurities in a Na-K eutectic circulating in a stainless steel loop is investigated by the EMF method. It is established that on heating this dependence reveals an anomalous transition of the melt from a state of saturation of the oxygen impurities to a state corresponding to the thermodynamic potential of a $NaCrO_3$ phase, and vice-versa on cooling. A model is proposed which explains this phenomenon by a second-order phase transition between crystalline modifications of complex oxides of the Na-K melt. (12 refs.)

115574 Heats of formation and ionization potentials of some α -aminoalkyl radicals. T.J.Burkey, A.L.Castelano, D.Griller (Div. of Chem., Nat. Res. Council of Canada, Ottawa, Ontario, Canada), F.D.Lossing. *J. Am. Chem. Soc. (USA)*, vol.105, no.14, p.4701-3 (13 July 1983). Heats of formation and ionization potentials of α -aminoalkyl radicals, $R_2NCR_2^{\cdot}$, were derived from measurements of the appearance energies for the fragmentations of a series of ethylenediamines. Stabilization energies, E_s , are high and increase with increasing C- or N-alkylation; the converse applies to ionization potentials, IP. For example, in the case of $H_2NC(Me)_2$, $E_s = 17 \text{ kcal mol}^{-1}$ and $IP = 5.4 \text{ eV}$. (31 refs.)

115575 The standard molar enthalpies of formation of $I^-(aq)$ and $HI(g)$ at 298.15K. C.E.Vanderzee, M.E.Sprengel (Dept. of Chem., Univ. of Nebraska, Lincoln, NE, USA). *J. Chem. Thermodyn. (GB)*, vol.15, no.9, p.869-79 (Sept. 1983).

The enthalpy of reaction of $Cl_2(g)$ with $HI(aq)$ and auxiliary enthalpies of mixing of $HCl(aq)$ with $(I_2 + 14.4 HI)$ solutions were measured by solution calorimetry. The results were combined with auxiliary data from the literature to yield the standard molar enthalpy of formation $\Delta_f H_m^\circ(I^-, aq, 298.15K) = -(56.62 \pm 0.14) \text{ kJ mol}^{-1}$. Values from other calorimetric studies, gas-phase equilibria, and e.m.f. studies were reviewed and recalculated. From consideration of all of the values, our recommended values are: $\Delta_f H_m^\circ(I^-, aq, 298.15K) = -(56750 \pm 70) \text{ J mol}^{-1}$; $\Delta_f H_m^\circ(HI, g, 298.15K) = (26500 \pm 70) \text{ J mol}^{-1}$. (37 refs.)

115576 Rate of nucleation of a constant-composition compound in an alloy. D.E.Temkin (Central Sci.-Res. Inst. of Ferrous Metall., USSR). *Sov. Phys.-Crystallogr. (USA)*, vol.28, no.2, p.140-2 (March-April 1983). Translation of: *Kristallografiya (USSR)*, vol.28, no.2, p.240-3 (March-April 1983). [received: Sept. 1983] The author finds the stationary rate of nucleation of a constant-composition compound in a dilute supersaturated solution. The coefficient of diffusion of the clusters in the space of dimensions (necessary in order to calculate the nucleation rate) is obtained from the known relation between this coefficient and the macroscopic growth rate of a nucleus (crystal seed). In the description of growth, account is taken of diffusion in the initial phase and of the kinetics of the chemical reaction at the interphase boundary. (10 refs.)

Critical fluctuations in a thermochemical instability. I. Mean field description See Entry 111558

Enthalpies of solution of some uni-univalent electrolytes in hexamethylphosphoramide at 298.15K See Entry 114183

Carbon-13 line shape study of two-site exchange in solid dimethyl sulfone See Entry 114748

Evidence for stereoselectivity in the copper (2⁺)-valine system See Entry 115516

Simulation of amplitude behaviour in the Ag^+ perturbed excitable Belousov-Zhabotinsky reaction by the Oregonator model See Entry 115522

82.65 SURFACE PROCESSES

115577 Electronic excitation in electron bombardment enhancement of chemical reactions. C.I.H.Ashby (Sandia Nat. Labs., Albuquerque, NM, USA). *Appl. Phys. Lett. (USA)*, vol.43, no.6, p.609-11 (15 Sept. 1983).

The role of electronic excitation in the electron bombardment enhancement of surface reactivity of graphite with hydrogen has been identified. The correlation between the electron and photon enhanced reactivities of a graphite surface is consistent with electrons exciting the 4.8-eV Π -valence to Π^* -conduction transition responsible for photoenhanced reactivity. An electron impact study has shown that low-energy electrons excite the same low-energy transitions observed in optical studies. Secondary electrons produced by electron bombardment are of appropriate energies to excite these transitions. Similar processes are expected to be operative in other chemical systems exhibiting photoenhanced reactivity. (12 refs.)

115578 Langevin analysis of the diffusion model for surface chemical reactions. D.L.Freeman, J.D.Doll (Los Alamos Nat. Lab., Univ. of California, Los Alamos, NM, USA). *J. Chem. Phys. (USA)*, vol.79, no.5, p.2343-50 (1 Sept. 1983).

An analysis is presented of the magnitude of some of the potential sources of error in a recently developed diffusion model of surface chemical reactions. Using single absorber Langevin simulations, comparisons are made between the diffusion equation model and the Fokker-Planck equation for the rates of diffusion controlled surface chemical reactions. The diffusion equation is found to predict rates in good agreement with the Fokker-Planck equation for physical values of the diffusion constant. For unphysically large diffusion constants, the rates predicted by the diffusion equation are found to be in error. By employing multiple absorber Langevin simulations errors in the single absorber approximation used in the diffusion model of surface reactions are examined. The single absorber model is found to be accurate for weakly bound adsorbates. For strongly bound adsorbates rate expressions derived from a two-dimensional model are found to be appropriate. The relative rates of Eley-Rideal and Langmuir-Hinshelwood mechanisms are also studied by multiple absorber Langevin simulations. The ratios of the Eley-Rideal to the Langmuir-Hinshelwood rate is found to be in good agreement with the predictions of the diffusion equation model for physically reasonable diffusion constants. The time dependent solution to be the diffusion equation considered in a previous publication is given in an appendix. (15 refs.)

115579 The role of metal-zeolite interactions in indirect liquefaction catalysis. V.U.S.Rao (Pittsburgh Energy Technol. Center, USDOE, Pittsburgh, PA, USA).

Phys. Scr. (Sweden), vol.T4, p.71-8 (1983). (Nordic Conference on Surface Science, Tampere, Finland, 18-20 Aug. 1982).

The conversion of synthesis gas ($\text{CO} + \text{H}_2$) to gasoline range ($\text{C}_5\text{-C}_{11}$) hydrocarbons can be performed with bifunctional catalysts containing the medium pore zeolite ZSM-5 and a Group VIII element such as Fe or Co. The ZSM-5 has pore openings about 5.5 Å in diameter, and its shape-selective action restricts the product molecules to $\leq \text{C}_{11}$. In the case of Fe-ZSM-5 catalysts, the catalytic behaviour of the following preparations have been compared with each other: Impregnation using (a) metal nitrate solutions and (b) the carbonyl $\text{Fe}_2(\text{CO})_{12}$. Infrared studies on adsorbed pyridine showed that cobalt-ZSM-5 catalysts prepared by nitrate solution impregnation contain significantly decreased Brønsted acidity with concomitant increase in Lewis acidity. The information obtained from magnetic and spectroscopic studies regarding the interaction of the metal component with the zeolite is related to the catalytic activity of the bifunctional catalysts. In particular, methods of identifying metal species within and outside the zeolite pores are discussed. (26 refs.)

115580 Trajectory approach to the hydrogen evolution reaction. S.Holloway (Inst. für Theoretische Phys., Freien Univ. Berlin, Berlin, Germany), J.W.Gadzuk.

Phys. Scr. (Sweden), vol.T4, p.98-91 (1983). (Nordic Conference on Surface Science, Tampere, Finland, 18-20 Aug. 1982).

A classical trajectory analysis for the discharge reaction step in the hydrogen evolution reaction is presented. The construction of an adiabatic potential energy surface is discussed with emphasis on the solvent motion and the charge transfer process. Corrections to absolute rate theory reaction probabilities arising from dynamical effects are presented as a function of applied potential. (17 refs.)

115581 Decomposition of HCOOH on gold studied by XPS and TDS spectroscopies and its behaviour under very low energy electron excitation. M.Chtaib, J.P.Delrue, R.Caudano (Lab. de Spectroscopie Electronique, IRIS, FNDP, Namur, Belgium).

Phys. Scr. (Sweden), vol.T4, p.133-7 (1983). (Nordic Conference on Surface Science, Tampere, Finland, 18-20 Aug. 1982).

XPS and TDS have been jointly used to study the adsorption at low temperature (110K) and the thermal decomposition of formic acid on a polycrystalline gold surface. When increasing progressively the temperature from 110K, XPS measurements reveal changes in the binding energy of C 1s and O 1s lines suggesting the evolution of molecular HCOOH to a formate ion which readily decomposes to H_2 and CO_2 products at approximately 190K. Additional results of the evolution of the XPS C_{1s} and O_{1s} lines of formic acid under the impact of a low energy electron beam (≤ 5 eV) are presented. They suggest that the electrons help to remove the acid hydrogen of the molecule leading to the formate. (5 refs.)

115582 Gas permeability of polyacetylenes with bulky substituents. T.Higashimura, T.Masuda (Dept. of Polymer Chem., Kyoto Univ., Kyoto, Japan), M.Okada.

Polym. Bull. (Germany), vol.10, no.1-2, p.114-17 (June 1983).

In search of new materials for oxygen-enrichment membranes, high polymers of acetylenes with bulky substituents were synthesized with Mo- or Ta-based catalysts, and their permeability coefficients to oxygen (P_{O_2}), nitrogen (P_{N_2}), and carbon dioxide were determined at 25°C. Polymer membranes of the aliphatic acetylenes were highly permeable to oxygen. Polymers of the aromatic acetylenes were less oxygen-permeable, giving P_{O_2} in the order of 10^{-10} , slightly larger than that for polystyrene. (12 refs.)

115583 Gas permeation through composite two-layer systems and the graphical solution. N.Kishimoto, T.Tanabe, H.Yoshida (Nat. Res. Inst. for Metals, Tsukuba Labs., Ibaraki, Japan).

Thin Solid Films (Switzerland), vol.106, no.3, p.225-38 (19 Aug. 1983).

The gas permeation behaviour in a two-layer composite material has been investigated. When a thin layer has a diffusion time comparable with that of the other layer in the two-layer system, the gas permeability for the system cannot be expressed as a simple function of the diffusivity and the solubility. In order to derive the diffusivity of the surface layer from the diffusion behaviour of the composite material, the authors employed a graphical method and the concept of an 'almost characteristic' parameter for diffusion in the two-layer composite material. They also take into account the discontinuity in the solubility at the interface between the two layers. After the theoretical analysis is described, application to the permeation of hydrogen through oxidized metals is discussed. (5 refs.)

115584 Reaction of trimethylhalosilanes with the silica surface. V.A.Tertykh, L.A.Belyakova, A.M.Varvarin, L.A.Lazukina, V.P.Kukhar' (L.V. Pisarzhevskii Inst. of Phys. Chem., Acad. of Sci., Ukrainian SSR). *Theor. & Exp. Chem. (USA)*, vol.18, no.6, p.661-5 (Nov.-Dec. 1982). Translation of: *Teor. & Eksp. Khim. (USSR)*, vol.18, no.6, p.717-22 (Nov.-Dec. 1982). [received: Sept. 1983]

The authors present experimental data on the study of the conditions of the title reactions, and the mechanism of the reaction of trimethylbromo- and trimethyliodosilanes with active centers on the silica surface. (18 refs.)

Nordic Conference on Surface Science See Entry 111305

A molecular beam study of the trapping-desorption of I_2 from a LiF (001) surface See Entry 112769

Studies of the temperature dependence of gas adsorption data on graphite and boron nitride in terms of the partially mobile adsorption model See Entry 114331

On the physisorption interaction of H_2 with Cu-metal See Entry 114337

On the surface reaction of hydrogen with FeTi See Entry 114339

Coadsorption systems with electrochemical relevance: coadsorption of water with oxygen, bromine and sodium on Cu(110) See Entry 114340

Oxygen adsorption on a cylindrical GaAs single crystal prepared by molecular beam epitaxy See Entry 114341

Oxidation of Pb monolayers on Cu(100) See Entry 114342

Bromine and iodine adsorption on an Fe(100) surface See Entry 114343

Electron spectroscopy on adsorption of Cs on transition metals See Entry 114344

Characterisation of a low temperature surface phase of CO on Pt {110} See Entry 114345

Ion scattering spectroscopy of $\beta\text{-N}$ and $\beta_3\text{-Co}$ ($\sqrt{2} \times \sqrt{2}$) $\text{R}45^\circ$ structures on W{100} See Entry 114346

Photon stimulated desorption of ions from water and methanol adsorbed on a Ti(0001) surface See Entry 114347

ESD spectra during adsorption at 300K and thermal desorption of $\text{H}_2/\text{W}(\text{poly})$ See Entry 114348

An XPS study of carbon monoxide and nitric oxide adsorption on platinum (410): unusual dissociation activity See Entry 114353

Adsorption and decomposition of ammonia on W(100): XPS and UPS studies See Entry 114355

Site-specific interaction of H_2O with ZnO single-crystal surfaces studied by thermal desorption and UV photoelectron spectroscopy See Entry 114358

Interactions of sulfur with nickel surfaces: adsorption, diffusion and desorption See Entry 114365

Adsorption of mixtures of methane and krypton on CaA zeolite. II. Analysis of the experimental data using Freundlich- and D dubinin-Radushkevich-type equations derived by assuming similar heterogeneity parameters for single-gas adsorption See Entry 114369

The formation of filamentous carbon from decomposition of acetylene over vanadium and molybdenum See Entry 114427

Rydberg screening in core level photoemission of ammonia adsorbed on nickel surfaces See Entry 115015

UV photoemission from sulphur saturated (111), $[6(111) \times (100)]$ and (100) platinum surfaces See Entry 115016

Rust formation on iron—a model See Entry 115405

Results of apparent atomic oxygen reactions on Ag, C, and Os exposed during the shuttle STS-4 orbits See Entry 115406

Indeterminacy in kinetic-model parameters due to non-Hamiltonian structure of the multipath linear reaction graph See Entry 115515

Transient catalytic combustion on a flat plate See Entry 115555

Polymer films on electrodes. XIII. Incorporation of catalysts into electronically conductive polymers: iron phthalocyanine in polypyrrole See Entry 115561

Phase separation of phosphonated polystyrenes in the solid state. IV. Influence of this phenomenon on their flame retardancy properties [ESCA observations] See Entry 115602

Time-resolved photoelectron spectroscopy for the study of dynamic surface species See Entry 115603

Surface physics and biological phenomena See Entry 115729

82.70 DISPERSE SYSTEMS

(for flow behaviour, see 47.55K)

115585 Particle wall loss rates in vessels. J.C.Crump, R.C.Flagan, J.H.Seinfeld (Dept. of Chem. Engng., California Inst. of Technol., Pasadena, CA, USA).

Aerosol Sci. & Technol. (USA), vol.2, no.3, p.303-9 (1983).

Aerosol particle wall loss rates were determined experimentally in a spherical continuous stirred tank reactor. The particle size and mixing rate dependences agree with the theoretical results of Crump and Seinfeld (1981) in which the particle loss coefficient β is related to particle diffusivity D , particle settling velocity v , the coefficient of the eddy diffusivity k_e was found to be proportional to the $3/2$ power of the volumetric flow rate, in accordance with theoretical expectations. Results of a similar nature may be expected to hold in vessels of arbitrary shape. (8 refs.)

115586 Simulation of condensation aerosol growth by condensation and evaporation. T.H.Tsang, J.R.Brock (Chem. Engng. Dept., Univ. of Texas, Austin, TX, USA).

Aerosol Sci. & Technol. (USA), vol.2, no.3, p.311-20 (1983).

A new numerical method is reported for the solution of the condensation-evaporation equation, a first-order hyperbolic equation. The solution and properties of the nonlinear integrodifferential equation arising when the mass of the condensing vapor is conserved are discussed. For aerosol evolution in the conserved case there develops an asymptotic regime analogous to the asymptotic behaviour found for the coagulation process. (27 refs.)

115587 Factors affecting the collision of aerosol particles with small water drops. K.H.Leong, K.V.Beard, J.J.Stukel, P.K.Hopke (Univ. of Illinois, Urbana, IL, USA).

Aerosol Sci. & Technol. (USA), vol.2, no.3, p.341-9 (1983).

The factors influencing the collision of aerosol particles with small water drops at low collision efficiencies are examined. The gravitational force and velocity slip of air on the drop surface affect the collision efficiency in the range of values of 10^{-4} - 10^{-2} . The efficacies of the different computational models are compared for ratios of particle radius to drop radius of less than 0.1. The accuracy of the numerical scheme in the trajectory model can be verified by comparing the efficiencies obtained of submicrometer particles with the convective-diffusion model. (22 refs.)

115588 Comparative size distribution measurements on chain aggregates. G.Kasper, D.T.Shaw (Lab. for Power & Environmental Studies, State Univ. of New York, Buffalo, NY, USA).

Aerosol Sci. & Technol. (USA), vol.2, no.3, p.369-81 (1983).

Size distribution measurements of polydisperse iron oxide chain aggregates (600-1300 Å thick with aspect ratios up to 700) were made and compared, using an aerosol centrifuge, a cascade impactor, and an electrical aerosol analyzer, with supporting data from electron microscopy. Number and volume frequency distributions are compared and analyzed on the basis of means and widths only. Appropriate conversions between aerodynamic and mobility equivalent diameters are made. Preferred particle orientation due to flow field and electrostatic field is taken into account. An estimate for the increase of average charge per fiber over that of spheres is given for the EAA's diffusion charger. (15 refs.)

115589 Theoretical study of equilibrium bipolar charge distribution on nonuniform primary straight chain aggregate aerosols. Hsu-Chi Yeh, Yung-Sung Cheng (Inhalation Toxicology Res. Inst., Lovelace Biomedical & Environmental Res. Inst., Albuquerque, NM, USA).

Aerosol Sci. & Technol. (USA), vol.2, no.3, p.383-8 (1983).

A general theory describing the equilibrium bipolar charge distribution for straight chain aggregate aerosols consisting of primary spheres of different diameters was derived from a theory previously developed for linear chain aggregate of uniform spheres. The present theory is based on the assumptions that (1) the individual primary particles of a straight chain aggregate are charged independently, (2) the probability that a particular primary particle has acquired q elementary charges is governed by the Gaussian distribution predicted by Boltzmann's law, based on particle size; and (3) the resultant charge of a straight chain aggregate is the algebraic sum of the charges carried by the constituent primary spheres. The present theory can be stated as follows: The equilibrium bipolar charge distribution of straight chain aggregate aerosols with nonuniform primary spheres can be expressed by

Boltzmann's law with an equivalent diameter such that $d_{el} = \sum_{i=1}^n d_i$. The limitations imposed by the assumptions are also discussed. (14 refs.)

115590 Time-resolved studies of fluorescence quenching in a water-in-oil microemulsion. N.J.Bridge, P.D.I.Fletcher (Univ. Chem. Lab., Univ. of Kent, Canterbury, England).

J. Chem. Soc. Faraday Trans. 1 (GB), vol.79, pt.9, p.2161-9 (Sept. 1983).

Nanosecond time-resolved spectrofluorimetry has been used to study the kinetics of quenching of acridinium-ion fluorescence by Co^{2+} and Br^- ions in a water-in-oil microemulsion stabilised by AOT [sodium 1,4-bis(2-ethylhexyl)-sulphosuccinate]. Analysis of the fluorescence decay curves leads to the determination of the aggregation number of the water droplets and the second-order rate constants for quenching in the dispersed water phase, both as functions of the water-to-surfactant mole ratio, W_0 . Quenching by both Br^- and Co^{2+} ions is impeded, relative to the diffusion-controlled process in aqueous solutions of high ionic strength, but the rate constant for Co^{2+} quenching increases with W_0 , whereas that for Br^- decreases. This behaviour can be explained in terms of the distribution of ions and the variation of microviscosity within the reverse micelle. (16 refs.)

115591 Diffuse transmission and reflection by a thick weakly absorbing layer with close particle packing. G.S.Dubova, A.Ya.Khairullina.

J. Appl. Spectrosc. (USA), vol.37, no.5, p.1313-16 (Nov. 1982). Translation of: *Zh. Prikl. Spektrosk. (USSR)*, vol.37, no.5, p.832-6 (Nov. 1982).

[received: Sept. 1983]

The authors consider the coefficients of diffuse reflection and transmission in relation to packing density for large weakly absorbing soft particles such as erythrocytes, chloroplasts, and dispersion filters in the region of the transmission band, etc. The results given have been obtained for erythrocytes with various specimens differing in size, particle shape, and optical constants, and therefore they are applicable to media with analogous characteristics. (23 refs.)

115592 Measurement of sedimentation potential generated in aqueous electrolyte solutions of alkali halides. H.Hirakawa, T.Takeishi (Faculty of Engng., Kagoshima Univ., Kagoshima, Japan).

Oyo Buturi (Japan), vol.52, no.7, p.619-25 (July 1983). In Japanese.

A sedimentation-potential-generating apparatus has been improved to realize precise measurement. From the theoretical discussion, it is found that the total mass of the moving parts consisting of a sample solution, its measuring container, a copper electromagnetic shield made in the form of a thin cylinder, a connecting rod, and the intrinsic mass of the moving parts must be decreased, and that the mass of the sample solution should be equal to the total mass of the remaining moving parts. Therefore, the apparatus is so designed that the shield is divided into two parts, a moving shield and fixed one whereby the total shield mass is lightened, and the measuring container is also lightened. The apparatus has been applied to measure the sedimentation potentials of twenty alkali halide solutions. The results show that the rate of change of the sedimentation coefficient due to atomic weight is approximately proportional to the transport number. (11 refs.)

Dynamic theory of suspensions with Brownian effects See Entry 111594

Sample-size determination in the certification of suspensions of monodisperse particles See Entry 111856

Recent progresses in the applications of nuclear magnetic resonance to the conformations and dynamics of flexible molecules in solution See Entry 112754

Coherent detection of scattered light from submicron aerosols See Entry 112938

Diffusional transport of nonspherical aerosol particles See Entry 113491

Motion and precipitation of a cloud of hot particles See Entry 113494

Relaxation processes in aerosol streams with polydisperse particle phase See Entry 113496

An experimental and analytical investigation of the particle loss mechanism in a circular flow for laser anemometry See Entry 113523

Adjustable isokinetic sampling horn See Entry 113531

Conductivity of magnesium valerate solutions in binary liquid mixtures See Entry 114227

Absorption and surface-enhanced Raman spectra of silver organosols in ethanol See Entry 114840

A highly stable nonaqueous suspension for the electrophoretic deposition of powdered substances See Entry 115111

Computer simulation of a two-dimensional soap froth I. Method and motivation See Entry 115163

Airborne detection of acidic sulfate aerosol using an ATR impactor See Entry 115711

Organic and elemental composition of airborne particulate matter in Beijing, spring 1981 See Entry 115712

Measurement of the time variational behaviours of aerosols based on size distribution See Entry 115716

82.80 CHEMICAL ANALYSIS AND RELATED PHYSICAL METHODS OF ANALYSIS

115593 X-ray fluorescence analysis of Fe, Mn, Cr and V in natural silicate crystals. O.L.Dias, A.R.Pereira Leite Albuquerque, S.Isotani (Inst. de Fisica, Univ. de Sao Paulo, Sao Paulo, Brazil).

An. Acad. Bras. Cienc. (Brazil), vol.55, no.2, p.173-8 (June 1983).

Concentrations of Fe, Mn, Cr and V were determined in samples of beryl, topaz, tourmaline and spodumene by measuring the first order K_α fluorescence lines. The intensity of these lines were calibrated by using beryl as the standard matrix. The matrices were prepared in the form of pressed pellets with 4:1 mixture of beryl and boric acid, where transition metal oxides were added. (10 refs.)

115594 An atomic spectroscopy bibliography for January-June 1983.

D.M.Lawrence (Perkin-Elmer Corp., Norwalk, CT, USA).

At. Spectrosc. (USA), vol.4, no.4, p.118-49 (July-Aug. 1983). (599 refs.)

115595 Simultaneous recording of analyte and background absorbance from the Perkin-Elmer Model 5000 spectrometer using the Model 3600 Data Station. M.T.C.de Loos-Vollebregt, R.A.M.Oosterling, F.B.Boudewijn, L.de Galan (Lab. voor Analytische Scheikunde, Tech. Hogeschool Delft, Delft, Netherlands).

At. Spectrosc. (USA), vol.4, no.4, p.160-2 (July-Aug. 1983).

The system described in the present paper is a simple, inexpensive extension of the possibilities of the Perkin-Elmer Model 5000. The simultaneous plot of background absorption and the total absorbance signal or the background-corrected atomic absorbance signal is very helpful to the analyst during development of a temperature program for the analysis of complex samples. The authors have developed additional hardware and software to transfer the AA and BG signals simultaneously to the Data Station. Background correction is performed in the Data Station to yield AA-BG. A plot of any two out of the three signals can be obtained within one run. (5 refs.)

115596 Techniques in surface microscopy and analysis. J.M.Walls (Dept. of Phys., Loughborough Univ. of Technol., Loughborough, England).

Proc. SPIE Int. Soc. Opt. Eng. (USA), vol.368, p.28 (1983). [received: Sept. 1983] (SPIE Proceedings on Microscopy Techniques and Capabilities, London, England, 21-22 Sept. 1982).

Summary form only given, as follows. A number of techniques are now available for the characterization of solid surfaces. The scanning electron microscope has firmly established its role in industry and elsewhere for routing high resolution studies of surface structure and topography and the addition of energy dispersive X-ray (EDX) analysis provides the technique with a powerful and complementary method of elemental analysis. More recently, techniques such as the scanning Auger microprobe (SAM), X-ray photoelectron spectroscopy (XPS or ESCA), and secondary ion mass spectrometry (SIMS) have become available which combine spatial resolution (of varying utility) with an ability to determine the composition of the outermost atomic layers (with varying precision and sensitivity). The remarkable depth resolution of these methods may also be exploited when used with surface sectioning techniques (such as sputter-etching) to provide composition-depth profiles. The author aims to introduce the principles and analytical procedures of these techniques and to illustrate their areas of application with examples of commercial importance in materials characterization, failure analysis, quality assurance and production problem solving. (no refs.)

115597 Analytical capabilities of transmission electron microscope (TEM) systems. P.Hagemann, M.N.Thompson (Philips, Sci. & Industrial Equipment Div., Electron Optics Applications Lab., Eindhoven, Netherlands).

Proc. SPIE Int. Soc. Opt. Eng. (USA), vol.368, p.29-34 (1983). [received: Sept. 1983] (SPIE Proceedings on Microscopy Techniques and Capabilities, London, England, 21-22 Sept. 1982).

Lists the principle sources of information in electron microscopy which become available due to the electron specimen interaction. The authors further describe the main electron optical and detector components and indicate how special operation modes of a transmission electron microscope based analytical system are obtained. Finally some of the possible applications are demonstrated on stainless steel and palladium catalyst specimens. (no refs.)

115598 Laser instrumentation: analytical uses are growing. B.Spadaro.

InTech (USA), vol.30, no.7, p.59-62 (July 1983).

Ability to sense chemical and physical variables without direct contact or sampling has been an incentive for developing laser-based instrumentation. Systems are now widely employed for composition analysis—including pollution monitoring and particle determining—as well as for temperature and pressure measurement. (23 refs.)

115599 Determination of the concentration distribution of admixture from ratemeter response by continuous analysis. P.Habrman (Vysoka Skola Banska, Ostrava, Czechoslovakia).

Jad. Energ. (Czechoslovakia), vol.29, no.8-9, p.294-7 (Aug.-Sept. 1983). In Slovenian.

A comparison of ratemeter and counter response by using Z-transformation is given. The method is demonstrated by determination of tin in tungsten by means of continuous X-ray spectrometric analysis. (5 refs.)

115600 Material analysis by means of high energy ion beams. F.Fujimoto (Coll. of General Education, Univ. of Tokyo, Tokyo, Japan).

J. Vac. Soc. Jpn. (Japan), vol.26, no.2, p.120-35 (1983). In Japanese.

Outlines physical analyses using hundreds or more keV energy generated from an accelerator, including discussion of ion backscattering, channelling and blocking phenomena, the determination of impurity atom location, lattice defects and their density measurements, the study of surface structure using high-energy ion beams, the detection of light atoms, ion-excited X-ray generation, and particle-induced X-ray emission analysis. (32 refs.) K.B.

115601 Statistical analysis of some gas chromatography measurements.

K.Kafadar, K.R.Eberhardt (NBS, Washington, DC, USA).

J. Res. Natl. Bur. Stand. (USA), vol.88, no.1, p.37-46 (Jan.-Feb. 1983). [received: Sept. 1983]

The National Bureau of Standards has certified Standard Reference Materials (SRMs) for the concentration of polychlorinated biphenyls (PCBs) in hydrocarbon matrices (transformer and motor oils). The certification of these SRMs involved measurements of extremely small concentrations of PCBs made by gas chromatography. Despite the high accuracy of the measurement technique, the correlated data cannot be analyzed in a routine independent manner. A linear model for the measurements is described; its complexity encourages the use of simpler exploratory methods which reveal unexpected features and point the way towards obtaining valid statistical summaries of the data. (2 refs.)

115602 Phase separation of phosphonated polystyrenes in the solid state. IV. Influence of this phenomenon on their flame retardancy properties [ESCA observations]. A.Chiotis, G.Clouet, J.Brossas (Centre de Recherches sur les Macromolécules, Univ. Louis Pasteur, Strasbourg, France), L.Hilaire.

Polym. Bull. (Germany), vol.10, no.1-2, p.101-4 (June 1983).

The authors point out, using the ESCA method, that the repartition of phosphorus atoms of phosphonated telechelic polystyrenes in the solid state, is not homogeneous. On the other hand, a correlation is established between the P/C ratio in a thin superficial layer of the polymer and flammability data. (9 refs.)

115603 Time-resolved photoelectron spectroscopy for the study of dynamic surface species. F.Steinbach, J.Schutte (Inst. für Phys. Chem., Univ. Hamburg, Hamburg, Germany).

Rev. Sci. Instrum. (USA), vol.54, no.9, p.1169-74 (Sept. 1983).

The principle and experimental setup of time-resolved photoelectron spectroscopy are outlined. In comparison to conventional molecular beam relaxation spectroscopy a reaction channel is analyzed not only at the end but prior to the end. In at least three points time-resolved photoelectron spectroscopy is superior to photoelectron spectroscopic experiments under static and direct current adsorption conditions; (1) a general increase in detection power of transient adsorbates and contaminations; (2) the possibility to discriminate by individual relaxation time between species that cannot be resolved in their binding energy; and (3) a significant simplification of the mathematical formalism in comparison to conventional molecular beam relaxation spectroscopy and a more straightforward understanding of the results, in particular the chemical identification of transient species. This is illustrated with time-resolved UV-photoelectron spectra of intermediate adsorbed carbon in the catalytic decomposition of methanol on iron and with time-resolved X-ray photoelectron spectra of intermediate adsorbed oxygen in adsorption and catalysis of methanol/oxygen mixtures on iron. (26 refs.)

115604 Simple apparatus for concentration determinations in binary-gas mixtures. J.S.Brooks, R.B.Hallock (Dept. of Phys. & Astron., Univ. of Massachusetts, Amherst, MA, USA). *Rev. Sci. Instrum. (USA)*, vol.54, no.9, p.1199-201 (Sept. 1983).

A sound resonator is described which allows concentration measurements in binary-gas mixtures. The apparatus is particularly useful for relative measurements between a mixture and a pure gas. (6 refs.)

115605 U and Th analysis of LSI constituent materials—SIMS analysis using highly concentrated separation methods. N.Honma (Technol. Div., NTT, Tokyo, Japan), S.Kurosawa, I.Kawashima. *Rev. Electr. Commun. Lab. (Japan)*, vol.30, no.3, p.503-10 (May 1982). [received: Aug. 1983]

Quantitative analytical methods for U and Th were investigated with high sensitivity. U and Th contents were analyzed in about 30 different kinds of LSI constituent materials. It was found that materials which included relatively high U and Th concentration were alumina ceramics (100 ppb~1 ppm), plastic packages (10 ppb~5 ppm) and Mo metal (100 ppb). Other materials contained less than 10 ppb U and Th. Based on analytical results, LSI constituent materials purification methods were discussed. (7 refs.)

115606 Chromatographic-mass spectrometric study of antitumor preparations (oxazaphosphorines) using electron impact and chemical ionization. Yu.P.Reva, F.A.Medvedev (All-Union Sci. Res., Inst. of Hygiene & Toxicology of Pesticides, Polymers, & Plastics, Kiev, Ukrainian SSR). *Theor. & Exp. Chem. (USA)*, vol.18, no.6, p.699-702 (Nov.-Dec. 1982). Translation of: *Teor. & Eksp. Khim. (USSR)*, vol.18, no.6, p.757-60 (Nov.-Dec. 1982). [received: Sept. 1983]

One of the most refined methods of analyzing organic compounds is by chromatography-mass spectrometry, which possesses a high sensitivity and selectivity which is particularly important in the study of pharmacokinetics and the metabolism of medical preparations. The oxazaphosphorines—cyclophosphamide (CP) (2-bis(2-chloroethyl)amino)tetrahydro-2H-1,3,2-oxazaphosphorine 2-oxide) (a), isophosphamide (b), and triphosphamide (c)—are applied in clinical chemotherapy for the medical treatment of malignant neoplasms and as immunodepressants. In order to elucidate the mechanism of the action of CP, it is necessary to know the character of its distribution in the organs, tissues, and subcellular structures. With the object of developing a chromatographic-mass spectrometric method of determining CP as the trifluoroacetate (TFACP), the fragmentation of TFACP by electron impact and by chemical ionization has been studied. (5 refs.)

115607 Quantitative electron probe analysis: problems and solutions. T.Kitazawa, H.Shuman, A.P.Somlyo (Pennsylvania Muscle Inst., Univ. of Pennsylvania, Philadelphia, PA, USA). *Ultramicroscopy (Netherlands)*, vol.11, no.4, p.251-61 (1983).

Quantitative electron probe microanalysis of thin films was evaluated with a series of sulfur-containing proteins, and a method is given for correcting errors due to changes in detector calibration (centroid position and resolution). The correlation coefficient between the results of electron probe analysis and the stoichiometric concentrations of sulfur was 0.998. Shifts in detector calibration that affect particularly elements having overlapping peaks are shown to be correctable by including the first and second derivative of the characteristic peak in the multiple least squares fitting routine used to determine the number of characteristic X-rays in the spectrum. This method allows the accurate measurement of low concentrations of Ca in the presence of high concentrations of K normally encountered in biological specimens. A systematic small error in the quantitation of Na is reported and shown to be due to digital filtering of this region of the continuum that has a relatively high curvature; methods for correction are proposed. (24 refs.)

115608 Development of an automatic sample-changer and control instrumentation for isotope-source neutron-activation analysis. A.H.Andeweg, J.I.W.Watterson.

Report M53, Council for Miner. Technol., Randburg, S. Africa (15 March 1983), 34 pp.

An automatic sample-changer was developed at the Council for Mineral Technology for use in isotope-source neutron-activation analysis. Tests show that the sample-changer can transfer a sample of up to 3 kg in mass over a distance of 3 m within 5 s. In addition, instrumentation in the form of a three-stage sequential timer was developed to control the sequence of irradiation transfer and analysis. (1 ref.)

Determination of limits for a linear regression or calibration curve See Entry 111623

Accuracy in analytical spectrophotometry See Entry 111784

Analysis of insulating materials by negative ionmicroprobe ... See Entry 111801

Plasma source mass spectrometry See Entry 111803

Analysis of radioactive waste solutions by atomic absorption spectrometry with electrothermal atomization See Entry 112317

Primary-side deposits on PWR steam generator tubes See Entry 112381

An automatic gamma spectrometer for activation analysis See Entry 112527

Semiempirical studies of core electron binding energies. X. The SCC-MO calculations on some purines See Entry 112628

Semiconductor detector for the selective detection of atomic hydrogen See Entry 112880

Experimental investigation of absorption coefficient of cesium resonance doublets in a plasma of combustion products See Entry 113660

Direct hydrogen profile determination in TiO₂ after electrochemical treatment See Entry 113949

Comparisons of the nuclear reactions ¹⁸O(p, α)¹⁵N and ¹⁶O(d, α)¹⁴N to study the oxygen effects in Pt silicide formation See Entry 114285

Analysis of surfaces and thin films See Entry 114317

TEM—electron energy loss spectroscopy study of the diamond particles prepared by the chemical vapour deposition from methane See Entry 114379

Micro-state analysis of iron compounds using the 9th-order FeKα₁ line See Entry 114970

A PIXE-RBS method for measuring partial sputtering yields of stainless steel See Entry 114987

Thermal decomposition of Eu₂(SO₄)₃·8H₂O studied by high resolution luminescence spectroscopy See Entry 115541

Fluorescence measurements of OH in a turbulent flame See Entry 115550

Mass spectrometric study of the volatile products from the radiolysis of polyethylene See Entry 115571

Organic and elemental composition of airborne particulate matter in Beijing, spring 1981 See Entry 115712

Measurement of the time variational behaviours of aerosols based on size distribution See Entry 115716

Flame ionisation detector for analyzing the concentration of total hydrocarbons in automobile exhaust gases See Entry 115717

The spectral shape and the components of the background in in vivo neutron capture prompt gamma ray analysis [of human beings] See Entry 115905

Methodology for the analysis of peroxyacetyl nitrate (PAN) in the unpolluted atmosphere See Entry 116285

An approach to ICP analysis of geological samples See Entry 116288

86.00 ENERGY RESEARCH AND ENVIRONMENTAL SCIENCE

86.10 ENERGY RESOURCES AND THEIR UTILISATION

(inc. economic aspects; for nuclear engineering and nuclear power studies, see 28.00)

115609 Alternative energy resources.

Regul. & Mando Autom. (Spain), vol.17, no.130, p.48-9 (July-Aug. 1983). In Spanish.

Reports on the current position of research into alternative energy resources, with special reference to work in the UK. The JET project at Culham is expected to be put into service in June 1984 and by 1990 to demonstrate whether energy from nuclear fusion is a practical proposition; in any case it is unlikely to make any impact upon the world energy situation before the middle of the 21st century. The British CEBG has installed a 200 kVA wind generator at Carmarthen Bay; a machine of several thousand kVA is projected for 1985 and a farm of similar machines, possibly off-shore, for 1990. It reports experiments on geothermal energy in hot rocks Cornwall, where 80°C is reached at 2000 m, and on a project for drilling to 6000 m and a temperature of 200-220°C. (no refs.) *C.J.O.G.*

86.10D Wind energy

115610 Wind energy inventory for European North of USSR. V.A.Minin, I.P.Stepanov.

Power Eng. (J. Acad. Sci. USSR) (USA), vol.21, no.1, p.98-105 (1983). Translation of: *Izv. Akad. Nauk SSSR Energ. & Transp.*, vol.21, no.1, p.106-14 (1983).

A refined method is presented for calculating the aerological and energy characteristics of wind. Ten-year series of eight standard observations of wind speed at 164 meteorological stations have been processed and the results used to give the basic elements of the wind energy inventory for the European North of the USSR. The areas most promising from the viewpoint of utilization of wind energy are indicated and the wind energy resources estimated. (12 refs.)

86.10F Tidal and flow energy

(inc. water-wave energy)

115611 Tidal power reviewed. E.M.Wilson (Dept. of Civil Engng., Univ. of Salford, Salford, England).

Int. Water Power & Dam Constr. (GB), vol.35, no.9, p.13-16 (Sept. 1983).

Despite regular rises in the cost of oil and coal, and despite continued opposition to the construction of nuclear powerplants, the development of tidal power projects had, until recently, hardly advanced since La Rance was commissioned. However, the completion of Annapolis Royal this year may now lead to a general resurgence of interest and perhaps construction. Details of this pilot power plant are presented and a review of tidal power and its possibilities is presented. (no refs.)

115612 Operation and control of a 2 GW wave-energy scheme. H.W.Whittington, J.R.Jordan (Dept. of Electrical Engng., School of Engng., Edinburgh, Scotland).

IEE Proc. A (GB), vol.130, no.6, p.340-9 (Sept. 1983).

The potential for sea-wave-energy exploitation is high in waters around the UK. Generating stations would typically be 2000 MW in rating, about 30 km long and be situated 10-15 km offshore, the energy being transmitted as electricity in submarine power cables. For such developments to be economic, a high degree of plant availability is necessary so that the maximum amount of energy can be converted and transmitted ashore. An approach is described which bases control, operating and maintenance around comprehensive condition monitoring of generating plant. Details are given of how information from such instrumentation can be used not only for health monitoring of plant, but also as an aid to operation and to scheduling and design of maintenance procedures. (11 refs.)

The experimental and theoretical evaluation of a twin-flap wave-energy absorbing device See Entry 115702

86.10K Solar energy

115613 Heat-accumulation systems for solar power plants. R.B.Akhmedov, M.E.Voronkov, V.A.Pozharnov, V.M.Chakhovskii (G.M. Krzhizhanovskii State Sci. Res. Power Inst., USSR).

Appl. Sol. Energy (USA), vol.18, no.4, p.17-22 (1982). Translation of: *Geliotekhnika (USSR)*, vol.18, no.4, p.16-19 (1982). [received: Aug. 1983]

The principal types of heat accumulators for solar power plants are considered. Energy-accumulation systems with supply-water, steam-water, and phase-transition accumulators are described. A number of chemical reactors for accumulation of solar power are given. (8 refs.)

115614 Heat pipe for parabolocylindrical solar installation. I.I.Kokhova, V.Ya.Sasin, A.A.Borodkin, S.F.Ergashev (G.M. Krzhizhanovskii State Sci. Res. Power Inst., USSR).

Appl. Sol. Energy (USA), vol.18, no.4, p.23-9 (1982). Translation of: *Geliotekhnika (USSR)*, vol.18, no.4, p.21-6 (1982). [received: Aug. 1983]

The authors describe an experimental study of a full-scale heat pipe with an operating temperature of 300°C, intended for use in parabolocylindrical solar installations. (11 refs.)

115615 Technology of fabrication of concentrators from wedge-shaped mirror-glass elements. G.Ya.Umarov, D.N.Alavutdinov, A.Abdurazizov, A.Abdullaev, A.K.Alimov (S.V. Starodubtsev Physicotech. Inst., Acad. of Sci., Uzbek SSR).

Appl. Sol. Energy (USA), vol.18, no.4, p.30-2 (1982). Translation of: *Geliotekhnika (USSR)*, vol.18, no.4, p.26-8 (1982). [received: Aug. 1983]
It is reported that temperatures on the order of 1400K can be obtained in the focal spot by using the concentrator described. (2 refs.)

115616 Mathematical analysis of the performance of cylindrical-parabolic solar concentrators. A.J.Al-Khalili (Dept. of Electrical Engng., Concordia Univ., Montreal, Quebec, Canada), R.A.Al-Ashoor.

Appl. Energy (GB), vol.15, no.1, p.43-55 (1983).
Attention is devoted to the application of cylindrical-parabolic solar concentrators in the intermediate temperature range for which wide receivers are used. Suitable indices that describe the performance of the concentrator are defined and evaluated. The effect of each individual parameter on total concentrator performance is investigated. The results of the analysis are presented as a set of graphs which can be used easily when designing parabolic concentrators. (3 refs.)

115617 Solar energy: a short and medium-term myth. F.Sardinha.

Electr. Energ.-Electron. (Portugal), no.189, p.286-98 (July 1983). In Portuguese.
The aim of the paper is to present a brief, but justified, economic study of solar energy utilization, with its impracticalities being clearly pointed out. (7 refs.)

115618 Training leads to good solar installations. T.V.McLaughlin, H.T.Roman (Public Service Electric & Gas Co., Newark, NJ, USA).

Electr. World (USA), vol.197, no.2, p.97-8 (Feb. 1983).
Solar water heating installation deficiencies uncovered in prior demonstration projects are avoided by a training facility run by a utility to teach contractors proper installation techniques. The contractors install two types of solar water heaters sold by the utility as part of a solar-water-heater promotion program. (no refs.)

115619 Solar and wind energy for water pumping. A.Fritzsche, K.Speidel (Dornier System GmbH, Friedrichshafen, Germany).

Naturwissenschaften (Germany), vol.70, no.8, p.396-402 (Aug. 1983). In German.
Water pumping by means of wind and solar energy becomes more and more attractive by reason of increasing energy prices. Water supply for remote villages especially in developing countries needs hydraulic energy of about 1 to 50 kWh per day. The use of renewable energies like solar and wind seems to be technically successful and has a good chance to be competitive with conventional energy sources like diesel or electricity in regions with mean wind speeds above 4-5 m/s or high insolation of about 5 kWh/day annual average. (7 refs.)

115620 Active solar energy systems—possibilities of application. A.Arata (Univ. Tecnica Federico Santa Maria, Valparaiso, Chile).

Scientia (Chile), vol.46, no.156-157, p.6-11 (Jan.-Dec. 1981). In Spanish. [received: Sept. 1983]
The economic possibility of using active solar energy systems as a solution to the present energy problems is explored. The characteristics of solar energy are outlined and alternatives to solar energy are briefly discussed. The characteristics of indirect solar energy systems are described and compared with those of traditional heating systems. The economic viability of solar energy systems are discussed and the conclusion is reached that solar energy can be considered as an alternative to traditional heating systems only for low temperature heating, at least in the short term. (no refs.) *S.M.H.*

115621 Experimental study of solar energy use for air heating by means of integral structural elements of a building. P.Sarmiento (Univ. Tecnica Federico Santa Maria, Valparaiso, Chile).

Scientia (Chile), vol.46, no.156-157, p.12-18 (Jan.-Dec. 1981). In Spanish. [received: Sept. 1983]
A study is made of the behaviour of a heating system integral with the construction of a building. It is designed on the basis of information obtained from previous research made by the author. The system is described and technical and economic conclusions are presented. (3 refs.) *S.M.H.*

115622 Utility impacts assessment of residential passive solar systems. R.A.Wood, M.D.Siegel.

Report EPRI-EM-3092-SY, Electr. Power. Res. Inst., Palo Alto, CA, USA (March 1983), 44 pp.
Available from Res. Rep. Center (RRC), Box 50490, Palo Alto, CA 94303, USA.

Summarizes a project undertaken to provide the electric utility industry with a tool to use in analyzing the advantages and disadvantages of passive solar residential construction within a service area. The methodology created to accomplish this is discussed as well as the results of tests conducted in cooperation with seven participating utilities.

Scaling of materials for hot gas tubing in an air-cooled solar tower power station under thermal cycling between 623 and 1073K See Entry 115403

Investigations of thermochemical energy storage with sulfuric oxides See Entry 115664

Heating of a laboratory hall by means of a soil heat pump combined with unshielded solar collectors See Entry 115676

Heat-engineering design method for a passive solar heating system (steady state) See Entry 115685

Recent advances in natural-circulation, solar-energy water heater designs See Entry 115693

Effect of a thermal trap on the performance of a solar sand collector See Entry 115694

Solar radiation intensity and its use in parabolic collectors See Entry 115696

Investigations on active and passive systems of solar energy utilisation in a manufacturing bay See Entry 115697

Investigation of the spectral composition of solar radiation under conditions prevailing at Tashkent See Entry 116169

86.30 ENERGY CONVERSION

Extended Abstracts from the 164th Electrochemical Society Technical Meeting See Entry 111317

86.30D Electrochemical conversion: general (for superionic conductors, see 66.30H)

115623 Research in progress: batteries made of plastics. J.Lund.

Eltek. Aktuell Elektron. (Sweden), vol.26, no.13, p.58-60 (Sept. 1983). In Swedish.
Describes research at present in progress at the Royal Technical University of Stockholm, Sweden, into plastics based storage batteries. The article describes the characteristics of polyacetylene, doping techniques, porous films and electric current limitation. The article concludes with details of the funding of the project. (no refs.) *H.J.P.*

86.30E Primary cells

115624 Lithium and alkaline portable power. R.Forsyth (Duracell (UK), Crawley Ltd., England).

Commun. Int. (GB), vol.10, no.8, p.72 (Aug. 1983).
The power source for portable equipment has always presented an important design problem in that conflict arises between making the pack smaller and yet getting more power from it. Some of the recent development such as the Flat-Pak alkaline battery and the lithium battery type LO26SX are considered. (no refs.)

115625 Zinc electrode morphology in alkaline solutions. II. Study of alternating charging current modulation on pasted zinc battery electrodes. J.McBreen, E.Gannon (Dept. of Energy & Environment Brookhaven Nat. Lab., Upton, NY, USA), D.-T.Chin, R.Sethi.

J. Electrochem. Soc. (USA), vol.130, no.8, p.1641-5 (Aug. 1983).
For pt.I see ibid., vol.129, p.2677 (1982). The dependence of the faradaic conductance and the morphology of pasted zinc electrodes on the charging method has been investigated. The charging methods included DC (3-125 mA-cm²) and DC (3-125 mA-cm²) with superimposed square waves of AC of various amplitudes and frequencies (0.1-5000 Hz). In the case of DC charging, the faradaic conductance goes through a maximum at ~75 mA-cm². The decrease in the faradaic conductance at higher current densities (100 mA-cm²) is related to the formation of dense zinc deposits on the electrode surface. At low DC (<30 mA-cm²), superimposition of AC promotes growth of zinc close to the current collector and results in small amounts of dispersed hexagonal zinc deposits on the current collector. Except where dense deposits are formed at high current density, the remainder of the zinc deposit has a very fine structure. Pulsed charging at low current densities (<30 mA-cm²) is beneficial in that it increases the electrode faradaic conductance and promotes growth of the zinc deposit close to the current collector. The relaxation time for the double layer in pasted zinc electrodes is ~50 msec. This indicates that the optimum frequency for pulsed charging is between 1 and 10 Hz. (22 refs.)

The synthesis of densified CMD from Mn-NH₄-carbamate and its discharge properties in ZnCl₂ batteries See Entry 115125

86.30F Secondary cells

115626 Capacity of encapsulated lead batteries grows. W.Liander.

Eltek. Aktuell Elektron. (Sweden), vol.26, no.13, p.62-3 (Sept. 1983). In Swedish.
Describes a range of maintenance-free Pb batteries manufactured by Sonenschen of West Germany. The article covers batteries with a capacity of up to 1350 Ah, and discusses various plate alloys, the Dryfit 600 battery, including a version for use in conjunction with solar cells and design of battery rooms. (no refs.) *H.J.P.*

115627 Reactions at the anode during storage of partially discharged Li/SO₂ cells. K.M.Abraham, L.Pitts (EIC Labs. Inc., Newton, MA, USA).

J. Electrochem. Soc. (USA), vol.130, no.7, p.1618-20 (July 1983).
Although the Li/LiBr, CH₃CN/SO₂ cell is one of the most advanced among the nonaqueous Li cells, concerns of safety have precluded it from being widely accepted. Partially discharged and stored Li/SO₂ cells and batteries have a greater propensity for safety hazards, especially in use under harsh conditions such as high current pulses, temporary short-circuits and overdischarges. In an effort to understand the underlying chemistry the authors have analyzed cells which had been stored for about one year at room temperature after a partial discharge corresponding to ~50% of their rated capacity. Because of the great concern in the user community for the safety of partially discharged and stored Li/SO₂ cells, the authors communicate some of their preliminary analytical results obtained from these cells. They believe that the results have considerable practical relevance. (10 refs.)

115628 Statistical analysis of lithium iron sulfide status cell cycle life and failure mode. E.C.Gay, J.E.Battles, W.E.Miller (Chem. Technol. Div., Argonne Nat. Lab., Argonne, IL, USA).

J. Electrochem. Soc. (USA), vol.130, no.8, p.1646-50 (Aug. 1983).
Groups of 12 or more identical Li-alloy/FeS cells fabricated by Eagle-Picher Industries Incorporated and Gould Incorporated were operated at Argonne National Laboratory in the status cell test program to obtain data for statistical analysis of cell cycle life and failure modes. The cells were full-size electric vehicle battery cells (150-350 A-hr capacity) and were cycled at the 4 hr discharge rate and 8 hr charge rate. The end of life was defined as a 20% loss of capacity or a decrease in the coulombic efficiency to less than 95%. Seventy-four cells (6 groups of identical cells) were cycle life tested, and the results were analyzed statistically. The ultimate goal of this analysis was to predict cell and battery reliability. Testing of groups of identical cells also provided a means of identifying common failure modes which were eliminated by cell design changes. Mean time to failure for the cell group, and corrective actions are discussed. (5 refs.)

115629 Electrodeposition of zinc on glassy carbon from ZnCl₂ and ZnBr₂ electrolytes [batteries]. J.McBreen, E.Gannon (Dept. of Energy & Environment, Brookhaven Nat. Lab., Upton, NY, USA).

J. Electrochem. Soc. (USA), vol.130, no.8, p.1667-70 (Aug. 1983).
The initial stages of the electrocrystallization of zinc from 3M ZnCl₂ and 3M ZnBr₂ on glassy carbon has been investigated using cyclic voltammetry, the potential step method, and scanning electron microscopy. Particular care was taken to ensure electrolyte purity and to eliminate resistance effects in the measurements. The nucleation overvoltage in 3M ZnCl₂ was ~17 and ~12 mV in 3M ZnBr₂. In 3M ZnCl₂, the current transients from the potential step measurements could be fitted to a simple model that assumes instantaneous nucleation followed by growth of three dimensional centers under kinetic control. A similar mechanism is operative for 3M ZnBr₂ at low overvoltages. At higher overvoltages, the current transient is governed by mixed kinetic and diffusion control and cannot be fitted to a simple model. The lower nucleation overvoltage and the faster kinetics in 3M ZnBr₂ is correlated

with the lower stability constants for the zinc bromide complexes. Erroneous results are obtained when resistance effects are not accounted for. (31 refs.)

86.30G Fuel cells

115630 A 50 kW phosphoric-acid fuel-cell power system. K.Kishida, E.Nishiyama, I.Hirata, Y.Hamasaki.
Mitsubishi Denki Giho (Japan), vol.57, no.5, p.28-32 (1983). In Japanese.
Their unique principle of operation is the basis for expectations that fuel cells will emerge as the basis of a new power-generation system. As one link in the development of a multi-megawatt phosphoric-acid fuel-cell power system, Mitsubishi Electric has designed, manufactured, and operated a 50 kW system to study dynamic characteristics and optimize design. The article reports on the system configuration and the initial operating results in terms of a discussion of the characteristics of the electrical cell, fuel processor, inverter, and the overall system. (3 refs.)

86.30J Photoelectric conversion: solar cells and arrays

115631 Sputtered Schottky barrier solar cells on p-type GaAs. M.E.Edweeb, E.J.Charlson, E.M.Charlson (Electrical Engng. Dept., Univ. of Missouri, Columbia, MO, USA).
Appl. Phys. Lett. (USA), vol.43, no.6, p.572-4 (15 Sept. 1983).
Schottky barrier solar cells have been produced on single crystal p-type GaAs by sputtering gold to form the barrier. The rectifying action for the gold sputtered p-type device is unique to the method since normal thermal evaporated gold onto p-type produced Ohmic contacts. The opposite behavior was observed for n-type GaAs. Barrier heights have been measured for both p-type (sputtered) and n-type (thermal) diodes using current-voltage and capacitance-voltage methods and are 0.90 and 0.95 eV, respectively. The power conversion efficiencies without AR coatings have values of 6.56% (p) and 5.58% (n). Deep level transient spectroscopy has been used to identify the trap center concentrations and energy levels for both diodes to account for the relatively large dark currents in the p-type (sputtered) diodes. (15 refs.)

115632 Deep level impurities and current collection in CdS/CdTe thin-film solar cells. L.C.Isett (Res. Labs., Eastman Kodak Co., Rochester, NY, USA).
Appl. Phys. Lett. (USA), vol.43, no.6, p.577-9 (15 Sept. 1983).
Current collection in thin-film CdS/CdTe solar cells prepared by close-spaced sublimation is limited to the depletion region. The width of the depletion region is altered by minority-carrier trapping under light bias. The deep levels responsible for this phenomenon have been identified by deep level transient spectroscopy (DLTS). Heat treatment at 373K changes the energy distribution of the deep levels. Heat treatment with illumination produces an energy level distribution greatly different from that produced by heat treatment without illumination. The observed photocapacitance changes are understood in terms of the emission rates measured in DLTS. (10 refs.)

115633 Wavelength-selective absorption enhancement in thin-film solar cells. Ping Sheng, A.N.Bloch, R.S.Stepleman (Exxon Res. & Engng. Co., Linden, NJ, USA).
Appl. Phys. Lett. (USA), vol.43, no.6, p.579-81 (15 Sept. 1983).
The authors present the general principle of wavelength-selective enhancement of absorption in thin-film solar cells by a periodic grating substrate. By exact numerical calculation they demonstrate that substantial short-circuit current gains are realizable in thin-film amorphous silicon ($a\text{-SiH}_x$) solar cells. In particular, for a 0.5- μm -thick $a\text{-SiH}_x$ solar cell, optimal texturing of an Ag substrate to form a one-dimensional reflective grating can yield a 2-mA/cm² enhancement over the flat substrate case. For a two-dimensional cross-hatched grating substrate the enhancement is estimated to be 3.5-4 mA/cm². (8 refs.)

115634 New types of high efficiency solar cells based on a-Si. Y.Hamakawa, K.Fujimoto, K.Okuda, Y.Kashima, S.Nonomura, H.Okamoto (Faculty of Engng. Sci., Osaka Univ., Osaka, Japan).
Appl. Phys. Lett. (USA), vol.43, no.7, p.644-6 (1 Oct. 1983).
Three types of new structure a-Si solar cells having more than 9% efficiency are presented. The first one has a high optical reflection back electrode metal alloyed with optically transparent n-type $\mu\text{-Si}$ deposited on the conventional glass substrate a-SiC/a-Si heterojunction solar cell. The second type structure is an inverted p-i-n solar cell having Ag/TiO_2 /a-Si metal-insulator-semiconductor type back surface electrode which more efficiently collects longer wavelength photocarriers just above the band edge. The third structure demonstrated here has a-Si/polycrystalline tandem junction to pick up the energy of longer wavelength photons passing through the front side of the a-Si solar cell. All key technologies proposed here are practical and offer more promised real alternatives for the fabrication of high efficiency a-Si solar cells. (18 refs.)

115635 Heterojunction formation in (CdZnS)/CuInSe₂ ternary solar cells. R.K.Ahrenkiel, L.L.Kazmerski, R.J.Matson, C.Osterwald, T.P.Massopust (Solar Energy Res. Inst., Golden, CO, USA), R.A.Mickelsen, W.S.Chen.
Appl. Phys. Lett. (USA), vol.43, no.7, p.658-60 (1 Oct. 1983).
The electrical properties of (CdZnS)/CuInSe₂ solar cells have been investigated by combining electron beam induced current measurements and capacitance-voltage measurements on the same device. In the as-grown device, the CuInSe₂ is lightly doped n type. After baking to about 225°C in vacuum, the CuInSe₂ converts to p type forming the heterojunction. Oxygen does not appear to be necessary for type conversion to occur. (12 refs.)

115636 High-efficiency Si solar cells by beam processing. R.T.Young (Helionetics Inc., San Diego, CA, USA), G.A.van der Leeden, R.L.Sandstrom, R.F.Wood, R.D.Westbrook.
Appl. Phys. Lett. (USA), vol.43, no.7, p.666-8 (1 Oct. 1983).
Utilizing two recently developed beam processing techniques, i.e. gas discharge implantation and XeCl excimer laser annealing p-n junction silicon solar cells with total area (~2 cm²) AM1 efficiencies as high as 16.5% have been made. These cells are of a particularly simple structure, fabricated without any sophisticated processing steps, and subjected to no high-temperature treatment. (11 refs.)

115637 Solar converters based on degenerate semiconductor-semiconductor p-n heterojunctions. S.Yu.Pavelets (Inst. of Semiconductors, Acad. of Sci., Ukrainian SSR).
Appl. Sol. Energy (USA), vol.18, no.4, p.1-4 (1982). Translation of: *Geliotekhnika (USSR)*, vol.18, no.4, p.3-5 (1982). [received: Aug. 1983]
It is reported that the use of strongly degenerate copper chalcogenide Cu_{1-x}S as the p component in HJ is the most efficient method of creating barrier structures based on polycrystalline layers. (10 refs.)

115638 Photoconverters based on InP-CdS heterostructure. E.S.Baleka, E.V.Gilan, L.V.Gorchak, A.D.Kotoroga, A.G.Cheban (Sci. Res. Inst. of Current Sources, Kishinev, Moldavian SSR).
Appl. Sol. Energy (USA), vol.18, no.4, p.5-7 (1982). Translation of: *Geliotekhnika (USSR)*, vol.18, no.4, p.5-7 (1982). [received: Aug. 1983]
Reports the findings of studies of photoconverters based on p-InP-n-CdS heterostructure with a useful area of up to 2 cm². (6 refs.)

115639 Solar elements based on polycrystalline cadmium telluride. S.A.Azimov, Sh.A.Mirsagatov, S.A.Muzafarova (S.V. Starodubtsev Physicochem. Inst., Acad. of Sci., Uzbek SSR).
Appl. Sol. Energy (USA), vol.18, no.4, p.8-12 (1982). Translation of: *Geliotekhnika (USSR)*, vol.18, no.4, p.7-11 (1982). [received: Aug. 1983]
It is shown that ITO is a suitable material for creating p-n heterojunctions based on cadmium telluride. (6 refs.)

115640 Production and some properties of photoelements based on layers of polycrystalline silicon. M.S.Saidov, Z.N.Alad'ina, R.Aliev, V.P.Chirva (U.A. Arifov Inst. of Electronics, Acad. of Sci., Uzbek SSR).
Appl. Sol. Energy (USA), vol.18, no.4, p.13-16 (1982). Translation of: *Geliotekhnika (USSR)*, vol.18, no.4, p.12-15 (1982). [received: Aug. 1983]
The authors describe production conditions for layers of n-type polycrystalline silicon with a small-grain structure, as well as measurements of parameters of photoelements based on such layers, with a p⁺-n junction created by ion implantation of boron. (6 refs.)

115641 Al_xGa_{1-x}As/GaAs thin window concentrator solar cells by LPE plus vapour phase diffusion. R.Romero (Havana Univ., Havana, Cuba), O.V.Sulima.
Cryst. Res. & Technol. (Germany), vol.18, no.8, p.1053-7 (1983).
Zinc diffusion from the vapour phase on a previously grown LPE Al_xGa_{1-x}As/nGaAs sample is discussed for thin window concentrator solar cell manufacture. A high cell shunt resistance and a low series resistance are achieved together with improved optical parameters via an impressed electric field in the emitter. Dark current components are rather low and 21.8% conversion efficiency is measured at AM 1.3. When the photogenerated short circuit current density is 8 A.cm⁻², the fill factor is 0.77 and open circuit voltage is 1140 mV. (14 refs.)

115642 Electro-optical sensors used for inspection and quality control of solar panels. R.W.Paulson, H.Decker, J.Hodor, J.Barney (Lockheed Missiles & Space Co. Inc., Sunnyvale, CA, USA).
Proc. SPIE Int. Soc. Opt. Eng. (USA), vol.360, p.228-36 (1982). [received: July 1983] (Robotics and Industrial Inspection, San Diego, CA, USA, 24-27 Aug. 1982).
Electro-optical sensors are moving rapidly forward in assisting in the fabrication of large solar arrays. Solar power requirements for space missions are increasing and reusable arrays would be most desirable. The technology developed over the past few years is now being applied to fabricate very large light folding reusable arrays. Inspection and quality control are most important. Three areas of sensor applications, and in some cases automation, are described in the paper. The first deals with perhaps the most critical item in fabricating an array, that is, the bonding of the individual solar cells to the circuit. Soldering has been used on many arrays reliably in the past, but for these very light arrays welding is most practical. Although laser welds have been made, parallel gap electronic welding is most popular. The problem has been in getting a physically strong and good electrical bond each time. Sensors and automation have solved this problem and will be discussed. An infrared microscope has in the past proved useful in failure analysis, bonding techniques development and engineering, but always has been restricted to what could be placed on a microscope stage. A new videoized remote sensing infrared microscope that can be on a full solar array panel is described. Lastly, a robot bubble inspection system is shown. (1 ref.)

115643 Optimization of GaAs photocell properties using a thin Al_xGa_{1-x}As interlayer. J.Safrankova, P.Kordos.
Elektrotech. Cas. (Czechoslovakia), vol.34, no.5, p.318-26 (1983). In Slovak.
The possibilities of GaAs photocell parameters optimization are investigated using a thin Al_xGa_{1-x}As interlayer. Theoretical it is shown that the Au-(n)AlGaAs-(n)GaAs structures with the AlGaAs interlayer of certain properties show an increase of the open-circuit voltage U_{oc} and of the efficiency, respectively, in comparison with simple Au-(n)GaAs structures. Results are experimentally confirmed on the structures prepared by isothermal liquid phase epitaxy. An enhancement of U_{oc} by 55 to 65% has been achieved on structures with 100 nm thick compositional graded Al_xGa_{1-x}As interlayer without change in the short-circuit current value I_{sc} . (9 refs.)

115644 A note on the correct evaluation of junction capacitance of a solar cell. S.Deb, M.K.Mukherjee, K.Maitra, B.Ghosh, B.K.Panigrahi (Dept. of Electronics & Telecommunication Engng., Jadavpur Univ., Calcutta, India).
Int. J. Electron. (GB), vol.55, no.3, p.449-55 (Sept. 1983).
In the fabrication of low-cost solar cells one has often to contend with finite series and shunt resistances. These tend to give misleading values of the junction capacitance as measured with an ordinary bridge. The problem is discussed analytically and graphically plots are given for determination of the true values from the measured ones. Practical use of these plots is discussed and illustrated with the help of experiments on thin-film Cu₂S-CdS solar cells. (5 refs.)

115645 Photovoltaics in action.
Int. Power Generation (GB), vol.6, no.6, p.34-6 (July-Aug. 1983).
Electricity generated directly from sunlight is contributing to the economic and social development of many Third World Countries. Photovoltaic systems have been found to be reliable, trouble-free and economical alternative sources of energy where utility grid power is unavailable, or where the cost of extending power lines has proven prohibitive. A major developer, manufacturer and international supplier of the photovoltaic equipment that converts sunlight directly into electricity is Solar Power Corporation of Woburn, Massachusetts, which is an affiliate of Exxon Corporation. Photovoltaic cells, placed in modules and arranged in arrays—combined with power control devices and energy storage—provide reliable electrical power in remote locations not readily accessible to commercial power lines, or operating and maintenance personnel. (no refs.)

115646 Theoretical analysis of solar cells based on graded band-gap structures. G.Sassi (Dipartimento di Fisica, Univ. degli Studi, Milano, Italy).
J. Appl. Phys. (USA), vol.54, no.9, p.5421-7 (Sept. 1983).
The performance of p-n graded energy gap solar cells has been calculated for Ga_{1-x}Al_xAs structures present in either the front region, the base, or both. The graded gap structure in the base is assumed to exist with a high energy gap gradient next to the junction or with a low one along a large portion of the base itself. All the possible configurations in which the built-in fields aid the minority carrier collection are analyzed with a practical theoretical model. The results indicate that the best cell has a high energy gap gradient in the front region and a low energy gap gradient in a large region of the base. This is due to an inverse window effect occurring in the base if the energy gap

variation in it is too high. The optimum junction depths for the various configurations are determined as well, and it is shown how the value of these depths is not a critical parameter, as it can vary widely with little influence on the conversion efficiency of the devices. Finally, the results are analyzed versus the surface recombination velocity S and it appears that these graded energy gap structures are suitable only for $S \gg 10^4$ cm/sec. (14 refs.)

115647 Study of deep-level defects and annealing effects in undoped and Sn-doped GaAs solar cells irradiated by one-MeV electrons. S.S.Li, W.L.Wang (Univ. of Florida, Gainesville, FL, USA), R.Y.Loo, W.P.Rahilly. *Solid-State Electron. (GB)*, vol.26, no.9, p.835-40 (Sept. 1983).

DLTS and C-V techniques have been employed to determine the defect energy levels and density, carrier capture cross sections, lifetimes and diffusion lengths in the Sn-doped and the undoped GaAs solar cells irradiated by one-MeV electrons under different electron fluences (10^{14} to 10^{16} cm $^{-2}$), fluxes (2×10^9 , 4×10^{10} e/cm 2 -s), and annealing conditions ($150 \leq T \leq 230^\circ\text{C}$). The results show that density of both electron and hole traps will in general increase with increasing electron fluence and flux, and decrease with increasing annealing temperature and annealing time. Some distinct difference in defect spectrum was observed in the undoped and the Sn-doped GaAs solar cells studied. The low temperature thermal annealing and the recombination enhanced annealing processes are found to be very effective in reducing the density of deep-level defects induced by one-MeV electrons. (9 refs.)

115648 An EBIC equation for solar cells. K.L.Luke (Dept. of Phys. Astron., California State Univ., Long Beach, CA, USA), O.von Roos. *Solid-State Electron. (GB)*, vol.26, no.9, p.901-6 (Sept. 1983).

When an electron beam of a scanning electron microscope (SEM) impinges on an n-p junction, the generation of electron-hole pairs by impact ionization causes a characteristic short circuit current I_{SC} to flow. The I_{SC} , i.e. EBIC (electron beam induced current) depends strongly on the configuration used to investigate the cell's response. The authors consider the case where the plane of the junction is perpendicular to the surface. An EBIC equation amenable to numerical computations is derived as a function of cell thickness, source depth, surface recombination velocity, diffusion length, and distance of the junction to the beam-cell interaction point for a cell with an ohmic contact at its back surface. It is shown that the EBIC equation presented here is more general and easier to use than those previously reported. The effects of source depth, ohmic contact, and diffusion length on the normalized EBIC characteristic are discussed. (7 refs.)

115649 Mutual influence of wide- and narrow-gap photocells in the operation of multistage n-GaAs-p-AlGaAs-n-AlGaAs heterojunction solar cells. A.M.Allakhverdiev, Yu.M.Zadranov, V.D.Rumyantsev (A.F. Ioffe Physicotech. Inst., Acad. of Sci., Leningrad, USSR). *Sov. Phys.-Semicond. (USA)*, vol.17, no.3, p.276-7 (March 1983). Translation of: *Fiz. & Tekh. Poluprovodn. (USSR)*, vol.17, no.3, p.446-8 (March 1983). [received: Sept. 1983]

An investigation was made of the load current-voltage characteristics of the component photocells in monolithic two-stage n-p-n AlGaAs heterojunction solar energy converters. It was found that the luminescence, which appeared in the wide-gap photocell because of the shunting of the load by the p-n junction, increased the rate of excitation of the narrow-gap photocell. Moreover, spreading of the current over the shared p-type region gave rise to an additional voltage drop which governed the dependence of the form of the load current-voltage characteristics of one of the photocells on the flow of the current in the other photocell. (5 refs.)

115650 Investigation of complementary p-n-p and n-p-n solar cell stages. V.M.Andreev, O.O.Ivent'eva, E.P.Romanova, V.S.Yuferev (A.F. Ioffe Physicotech. Inst., Acad. of Sci., Leningrad, USSR). *Sov. Phys.-Tech. Phys. (USA)*, vol.28, no.2, p.196-8 (Feb. 1983). Translation of: *Zh. Tekh. Fiz. (USSR)*, vol.53, no.2, p.320-4 (Feb. 1983). [received: Sept. 1983]

Theoretical and experimental test results are reported for solar cell stages with complementary p-n-p and n-p-n heterostructures. Calculations reveal that efficiencies of 40-45% are attainable in such photocells. The parameters of the heterostructures corresponding to equal currents in the different stages are calculated, so that complementary pairs of photocells can be combined in a battery. GaAs-AlAs heterostructures were used to fabricate p-n-p and n-p-n solar cell stages, and the calculated parameters have been confirmed by test results. (11 refs.)

115651 Studies of electroluminescence in pAlGaAs-pGaAs-nGaAs heterophotocells with distributed parameters. Kh.K.Aripov, N.S.Koroleva, V.R.Larionov, T.A.Nuller, V.D.Rumyantsev (A.F. Ioffe Physicotech. Inst., Acad. of Sci., Leningrad, USSR).

Sov. Phys.-Tech. Phys. (USA), vol.28, no.2, p.202-4 (Feb. 1983). Translation of: *Zh. Tekh. Fiz. (USSR)*, vol.53, no.2, p.329-32 (Feb. 1983). [received: Sept. 1983]

Electroluminescence techniques for studying defects and internal resistive losses are illustrated using pAlGaAs-pGaAs-nGaAs heterophotocells which convert unconcentrated sunlight into electricity. A laboratory technique for testing heterophotocells is proposed which involves measuring the photocurrent I_{ph} when the cell is illuminated by simulated low-intensity sunlight (in order to find the absolute photosensitivity of the p-n junction) and observing the spatial electroluminescence intensity distribution at the normal working current while simultaneously measuring the forward voltage over the cell. (7 refs.)

115652 pAlGa $_{1-x}$ As-pGaAs-nGaAs heterostructure concentrator photocells synthesized by liquid-gas-phase epitaxy. A.M.Allakhverdiev, V.M.Andreev, I.I.Mokan, R.Romero, O.V.Sulima, B.S.Yavich.

Sov. Tech. Phys. Lett. (USA), vol.8, no.11, p.575-7 (Nov. 1982). Translation of: *Pisma v Zh. Tekh. Fiz. (USSR)*, vol.8, no.21-22, p.1335-9 (Nov. 1982). [received: Sept. 1983]

Heterostructure photocells were fabricated by a method involving fabrication of an n-type GaAs layer by liquid-phase epitaxy, growth of a wide-gap Al $_x$ Ga $_{1-x}$ As layer by gas-phase epitaxy with metal-organic compounds, and formation of a p-n junction by zinc diffusion from the vapor phase. These photocells combine the advantages of liquid- and gas-phase epitaxy. They raise the possibility that this hybrid technique may find widespread use in large-scale manufacture of solar batteries. (7 refs.)

115653 Multiwavelength analyzer for the determination of diffusion lengths. G.E.Davis, M.Jansen (Electrical Sci. & Engng. Dept., Univ. of California, Los Angeles, CA, USA).

Sol. Cells (Switzerland), vol.9, no.4, p.269-80 (Sept. 1983).

A new method for the non-destructive determination of diffusion lengths in the base region of solar cells is described. The method involves the measurement of the short-circuit current produced when the cell is illuminated at two different wavelengths. Only the relative powers (illumination) need be determined. The light source provides alternately one wavelength and then the other. This is accomplished through the use of two light-emitting diodes driven by the opposite phases of a square wave. The difference and the sum of the solar cell short-circuit currents are measured and can be used to

determine the diffusion length. The energy can easily be focused to a small spot and the diffusion length as a function of position can be determined by a scanning technique. Using this method, Motorola ribbon-to-ribbon polycrystalline Si solar cells were analyzed. The average value of the diffusion length agreed well with the surface photovoltage diffusion length measurements. In addition, the multiwavelength analyzer showed spatial variations of more than an order of magnitude in diffusion length across given samples. (9 refs.)

115654 Photovoltaic properties of In/trans-polyacetylene/Electrodag + 502 Schottky barrier cells. J.Kanicki, E.Vander Donckt, S.Boue (Collectif de Chimie Organique Phys., Univ. Libre de Bruxelles, Brussels, Belgium).

Sol. Cells (Switzerland), vol.9, no.4, p.281-8 (Sept. 1983).

The electrical properties of In/trans-polyacetylene/Electrodag + 502 Schottky barrier cells were examined in the dark and under monochromatic and white light irradiation. The experiments were performed between -77 and $+110^\circ\text{C}$. The In/trans-polyacetylene contact is strongly blocking. The photocurrent is proportional to the light intensity and the open-circuit photovoltage is an exponential function of light intensity. Owing to the low quantum yield for carrier production and collection, the fraction of light energy transformed into electrical energy is rather low (about 0.025%) under white light illumination. (13 refs.)

115655 Measurement of the open-circuit photovoltage decay in a silicon solar cell. M.K.Madan, V.K.Tewary (Birla Inst. of Technol. & Sci., Pilani, India).

Sol. Cells (Switzerland), vol.9, no.4, p.289-93 (Sept. 1983).

Experimental results are presented for the open-circuit photovoltage decay in a Si p-n junction solar cell for monochromatic light of five different wavelengths and for composite light. Analysis of the results in terms of the existing theories gives a reasonable estimate of the minority carrier lifetime and other material parameters of the solar cell. (6 refs.)

115656 Quality factors of solar cell arrays. M.Shechter (School of Engng., Tel Aviv Univ., Tel Aviv, Israel), J.Appelbaum, G.Yekutieli.

Sol. Cells (Switzerland), vol.9, no.4, p.295-309 (Sept. 1983).

Solar cells are aggregated in series and parallel combinations into an array to produce desired voltage and power levels. The solar cells are non-identical in their parameters; therefore the array power output is lower than the power output of the individual cells operating separately. The quality of the array is reduced as a result of larger dispersions in the cell parameters. Therefore, measures of the array quality are important for the design and analysis of photovoltaic systems. Three quality factors are defined and derived analytically for the array: the array matching factor AMF, the relative power loss RPL and the array curve fill factor CCF $_a$. (2 refs.)

115657 AlGaAs/GaAs cascade solar cell computer modeling under high solar concentration. M.F.Lamorte (Res. Triangle Inst., Research Triangle Park, NC, USA), D.H.Abbott.

Sol. Cells (Switzerland), vol.9, no.4, p.311-26 (Sept. 1983).

A computer modeling program was used to study a two-junction AlGaAs/cascade solar cell under air mass 1.5 spectral conditions, up to 500 suns solar concentration and in a temperature range 300-600K. The cascade structure used in the study is one of a number that are currently under development. Computer modeling results are graphically presented showing the behavior of the efficiency, photovoltage, photocurrent density and forward current density under the combined influence of high solar concentration and temperature. In addition, normalized temperature coefficients, current mismatch parameters, and the power utilization ratio are determined and their behavior discussed. The major conclusions drawn from the study are that the band gap combination of this structure is very nearly optimum for operation in the 450-550K temperature range and that the normalized temperature coefficient of efficiency improves significantly with increasing solar concentration. (23 refs.)

115658 Rooftop photovoltaic arrays: electric shock and fire health hazards. P.D.Moskowitz, E.A.Coveney, S.Rabinowitz, J.I.Barancik (Dept. of Energy & Environment, Brookhaven Nat. Lab., Upton, NY, USA).

Sol. Cells (Switzerland), vol.9, no.4, p.327-36 (Sept. 1983).

Electric shocks and fires represent two different ways for rooftop photovoltaic energy systems to affect public health adversely during installation, operation or removal. Analysis of a US Department of Energy residential application demonstration project suggests that the voltage generated by six modules connected in series could be sufficient to cause ventricular fibrillation and possibly death. Extrapolation of these results to future installations is limited by lack of failure mode data for various designs representing state-of-the-art module and rooftop applications. Two causes of fire include (i) electrical fires from short circuits and (ii) spontaneous combustion from heat build-up in dead air space. Crude upper-boundary estimates for fire-related risk are less than one reportable fire and less than 10^{-2} deaths per year per 10 MW $_p$ cumulative installed capacity. Although the marginal risk to society from these hazards may be low, the potential risk to exposed individuals is high. Continued evaluation of safeguard effectiveness merits further consideration. (20 refs.)

115659 Grating solar cells: an experimental comparison of alternative structures. D.J.Thomson, H.C.Card (Dept. of Electrical Engng., Univ. of Manitoba, Winnipeg, Manitoba, Canada).

Sol. Cells (Switzerland), vol.9, no.4, p.337-44 (Sept. 1983).

An experimental investigation of majority carrier grating solar cells, as originally proposed by Green, has been made and a comparison is drawn with minority carrier cells fabricated and tested under identical conditions. The collecting junctions between the metal grid and the silicon represent 'peaked' Schottky barriers in the majority carrier devices. Active area efficiencies for air mass 1 solar illumination (both simulated and natural sunlight) are 11.4% and 14.0% respectively for majority and minority carrier cells of about 1 cm 2 area on crystalline silicon. Spectral response data are also presented, and further comparisons are made with cast polycrystalline Si grating solar cells and with commercial diffused p-n junction solar cells. (15 refs.)

115660 The effective lifetime in semicrystalline silicon. S.C.Jain (Solid State Phys. Lab., Delhi, India), R.Janssens, G.Cheek, P.Depauw, R.Mertens, R.Van Overstraeten.

Sol. Cells (Switzerland), vol.9, no.4, p.345-52 (Sept. 1983).

The short-circuit current density J_{sc} and dark saturation current density J_0 in a semicrystalline Si solar cell are given by infinite series. If $S_{eff}W/2D_n$ (where S_{eff} is the effective recombination velocity at the grain boundary, W the grain width and D_n the diffusion constant) is small the minority carrier profile can be described as a part of a cosine curve. In this case, the series is rapidly convergent and the concept of an effective lifetime τ_{eff} can be used. The boundary condition at the junction has an important influence on the carrier profile and makes the series for J_{sc} more rapidly convergent than the series for J_0 . In general, therefore, a semicrystalline silicon solar cell cannot be described by one single τ_{eff} except when $S_{eff}W/2D_n$ is small and both series are rapidly convergent. Variations in S_{eff} with illumination make the boundary conditions at the grain boundary non-linear. The solutions obtained in the paper are valid (1) when S_{eff} is so large that the recombination current is

insensitive to S_{eff} and (2) at high illumination intensities where variations in S_{eff} with illumination are small. For other illumination intensities the problem cannot be solved analytically. (8 refs.)

115661 The significance of interference effects in thin film $\text{Cu}_2\text{S}/\text{CdS}$ solar cells. C.Van De Walle, P.De Visschere (Lab. voor Elektronica, Ghent, Belgium).

Sol. Cells (Switzerland), vol.9, no.4, p.353-8 (Sept. 1983).

The generation rate of electron-hole pairs in the Cu_2S layer of a thin film $\text{Cu}_2\text{S}/\text{CdS}$ solar cell is calculated according to a semicoherent model. In this model the coherent addition of light waves is strictly limited to the Cu_2S layer. In contrast with the results of a fully coherent model, in which coherent addition is assumed throughout the whole structure, the interference effects have no significant influence on the photocurrent. (7 refs.)

115662 Point-contact silicon solar cells. R.M.Swanson.

Report EPRI-AP-2859, Electr. Power Res. Inst., Palo Alto, CA, USA (May 1983), 120 pp.

Available from Res. Rep.Center (RRC), Box 50490, Palo Alto, CA 94303, USA.

Describes a new type of silicon photovoltaic cell called the point-contact cell. A discussion of the new cell is provided as well as an analysis of the modeling results and a comparison of the theory and experiment. Necessary future cell development is discussed. The appendixes include the modeling approach, photogeneration in point-contact cells, series resistance cell optimization and design, and limit calculations.

Bases and applications of the induced resonance absorption. I See Entry 112925

Effect of pulse duration on the annealing of ion implanted silicon with a XeCl excimer laser and solar cells See Entry 114010

Pulsed excimer laser (308 nm) annealing of ion implanted silicon and solar cell fabrication See Entry 114011

Plasma-sprayed silicon as a possible base material for the production of low cost solar cells See Entry 115051

Solar and wind energy for water pumping See Entry 115619

86.30K Photoelectrochemical conversion

115663 A one-volt p-InP/n-CdSe regenerative photoelectrochemical cell. P.G.P.Ang, A.F.Sammells (Eltron Res. Inc., Naperville, IL, USA).

J. Electrochem. Soc. (USA), vol.130, no.8, p.1784-6 (Aug. 1983).

The authors report on a two-photoelectrode regenerative PEC cell which has shown a combined photovoltage in excess of one volt. The cell consists of n-CdSe as the photoanode and p-InP as the photocathode in an aqueous sulfide/polysulfide electrolyte. All work reported here is with single-crystal materials. (24 refs.)

Characterization of polycrystalline electrodeposited CdSe photoelectrodes using photoluminescence spectroscopy See Entry 114902

86.30L Electrodynamics and magnetohydrodynamic conversion

(see also 52.75 Plasma devices and applications)

Cathode spots and erosion of metal electrodes in channel of an open-cycle MHD generator See Entry 113669

86.30Q Chemical energy conversion

(for electrochemical conversion, see 86.30D; for photoelectrochemical conversion, see 86.30K)

115664 Investigations of thermochemical energy storage with sulfuric oxides. O.A.Leiyeh.

Report JUL-1847, Kernforschungsanlage, Jülich, Germany (May 1983), 156 pp. In German.

The thermochemical storage system using reversible chemical reactions seems to be attractive especially for solar energy. In this study a system using the catalytic decomposition/recombination of sulphuric oxides has been investigated for electricity production in small plants. The decomposition reaction of SO_3 is used to gather the solar energy concentrated by a field of parabolic dishes. The exothermal recombination of SO_2 and O_2 provides the energy, which can be used to generate steam required for electricity production. Two concepts have been studied and optimized. The first one using a gas turbine showed a small efficiency because of the high amount of energy needed for compressing the gases. The second concept using a steam turbine was optimized for different system parameters and showed an efficiency of about 35% for the whole energy storage system and electricity production. The energy stored during 8 hours of daylight operation is sufficient to meet electricity production demands around the clock. An economical evaluation of the system showed that the system is still not competitive with other electricity producing systems such as diesel generators which are presently being used in isolated rural areas. The material problems involved in this special process remain still to be solved. (66 refs.)

86.30R Thermal energy conversion (heat engines and heat pumps)

115665 Use of the earth heat for the heating of a signal cabin. W.Eggert, G.Grossohmichen.

Eisenbahntechnik (Germany), vol.31, no.6, p.237-8 (June 1983). In German. The construction and the function of a test plant of the German State Railway is described, which is used for the heating of the signal cabin with push button geographical circuitry 'Biesdorfer Kreuz'. The test plant works with two small-heat pumps type WW 12. Thereby the possibility is shown to substitute the electric direct heating by a heat pump plant. Favourable energetic effects may be reached by the application of microelectronic control. (1 ref.)

115666 Simulation of the heating process of a building with an earth-collector heat pump. V.Eberhard, W.Kast (Tech. Hochschule Darmstadt, Darmstadt, Germany).

HLH (Heiz. Luftung Klimatech. Haustech.) (Germany), vol.34, no.8, p.320-1 (Aug. 1983). In German.

In connection with work in progress on the energy consumption of various heating systems, a numerical simulation is described for a building heated from a heat pump supplying a hot water, floating heat store and feeding hot

water to radiators. The results of the calculations on the earth collector are given and discussed. (no refs.) P.G.R.

115667 Fluorocarbon turbine utilizing waste heat of hot water. An application to a heat pump system. T.Nakanishi, S.Inoue, K.Yoshikawa, T.Kato, H.Yanagi, H.Shimoda, H.Araki, M.Ohsone.

Hitachi Zosen Tech. Rev. (Japan), vol.44, no.1, p.19-28 (March 1983). In Japanese.

Much attention has been given to the development of a heat and power recovery system using organic fluid from low temperature waste heat. For this study, a turbine using refrigerant R-114 was constructed and applied to drive a compressor in a compression type heat pump system as a means of recovering power from low temperature (70°C) waste water. (1) The results obtained show satisfactory turbine performance with maximum output of 116 kW and internal efficiency of 85%. (2) The turbine speed control system with an electronic governor and adjustable stator blades shows good characteristics with relatively high efficiency over the wide operating speed. (3) The design procedure proved itself reliable in the shaft-sealing, rotor-vibration and other mechanical performance areas. (4) In the heat pump system, efficient operation was obtained using the turbine speed control for partial load of the heat pump. (6 refs.)

115668 van't Hoff-van der Waals osmotic pressure and energy transformers. C.Zener (Carnegie-Mellon Univ., Pittsburgh, PA, USA), W.Levenson.

Proc. Natl. Acad. Sci. USA, vol.80, no.14, p.4577-9 (July 1983).

The authors find the van't Hoff relations between osmotic pressure, freezing point depression, and boiling point elevation provide a clue on how, by using salt solutions, one may lower the cost of extracting power from low-grade heat sources. In particular, the ratio of 7 between the heat of evaporation and the heat of freezing of pure water suggests a chemical system that raises 7-fold the temperature difference between heat source and heat sink, while decreasing by the same factor the heat flux. Heat exchangers dominate the cost of heat engines operating upon low-grade heat. Their area for a fixed power output is inversely proportional to the available temperature differential. Herein lies the potential for a great cost reduction. The authors show that the simple van der Waals concept of a gas of hard elastic spheres suffices to understand the colligative properties of salt solutions, at least up to the concentration of the eutectic composition. This concept enables them to physically interpret the thermodynamic processes during the concentration of salt solutions by evaporation and during the mixing of ice and solid salt hydrates at their eutectic temperature. (8 refs.)

115669 A single screw high performance heat pump. B.Zimmern, E.Kallmann (Omphale SA, Puteaux, France).

Proceedings of Four Contractors' Meetings on Heat Pumps (EUR 8077 EN), Brussels, Belgium, 28-29 April & 12-13 May 1982 (Luxembourg: Comm. European Communities 1982), p.40-50

In order to build a heat-only air-water heat pump, for the heating of a medium size collective housing, a single screw compressor with 25-30 kW shaft power is being designed and tested. Such heat pumps, possibly complemented by a conventional combustion or resistor heating for the coldest days, can bring significant energy savings in regions with temperate climates, as in most countries of the EEC. A first set of unsuccessful tests have been run in 1980 with the PC compressor structure initially contemplated; early 1981, a more conventional design, the CP type, has proven to have the potential required provided a number of specific improvements are implemented. The compressor uses an injection of condensed refrigerant as a sealing and a cooling media. It is equipped with a continuous capacity control system, used in such a way that efficiency can be improved from full load down to half load by means of an 'economiser'. The first results obtained at Omphale are shown, pending complete counter-check through Electricite de France in their Testing Laboratories. They show that there is a good probability to reach the technical and economic targets set for the contract. (no refs.)

115670 Improving domestic heat pumps capacity control. H.Martin-Neuville, M.Reybillet, J.P.Patureau (Bertin & Cie Energetics Div., Plaisir, France).

Proceedings of Four Contractors' Meetings on Heat Pumps (EUR 8077 EN), Brussels, Belgium, 28-29 April & 12-13 May 1982 (Luxembourg: Comm. European Communities 1982), p.51-67

The work carried out so far under the present contract has been primarily devoted to setting up a versatile, fully instrumented test bench with the following essential features: sophisticated data acquisition using a minicomputer SILEX. Programs have been developed to allow acquisition, storage and processing of 32 parameters at frequencies up to 500 Hz. Fast phenomena (on/off cycles, house temperature regulation) over long periods of time can thus be properly analyzed, simulation of a typical house heating system thus reproducing in a controllable manner the thermal interaction between heat pump, radiator heat distribution system, house and climatic environment. This feature allows one to investigate various types of regulation with the aim of improving the match between heat pump and house. Along this line, preliminary tests using condensing temperature control suggest a significant improvement over standard house temperature regulation (13% and 21% gain on average COP at 7°C and 15°C outside air temperature, respectively). (no refs.)

115671 Optimized operation of a frozen air heat exchanger by using a microcomputer controlled expansion valve. R.Pleiningner, M.Kuhn (Inst. für Umweltschutz, Univ. Dortmund, Dortmund, Germany).

Proceedings of Four Contractors' Meetings on Heat Pumps (EUR 8077 EN), Brussels, Belgium, 28-29 April & 12-13 May 1982 (Luxembourg: Comm. European Communities 1982), p.68-82

Herein the first results of operating a frozen air heat exchanger as a part of a monovalent heat pump system (air water) controlled by a microcomputer are presented. We will be reporting about the operation of a microcomputer controlled expansion valve, which allows any superheating temperature in all positions of operation of the stable range. The important parameters of the optimization of the evaporator operation are the superheating temperature, the fan operation/air flow rate and the defrosting procedure. The various air flow rates (adjusted by varying the r.p.m. of the fan), have only little importance to the coefficient of performance. But down to air temperatures of 1.5°C it is possible to defrost the evaporator only by the fan, which is highly interesting in terms of energy conservation. A new criterion tested in practical operation for initiating the defrost procedure by using a calculated/estimated heat transfer coefficient is presented. (7 refs.)

115672 Heat pumps for heat recovery from paper dryers, producing process steam from the dryer exhaust air. D.L.Hodgett, W.Friedel (Bat-telle-Inst. e.V., Frankfurt am Main, Germany).

Proceedings of Four Contractors' Meetings on Heat Pumps (EUR 8077 EN), Brussels, Belgium, 28-29 April & 12-13 May 1982 (Luxembourg: Comm. European Communities 1982), p.165-80

The work carried out during the first six months of the project was concerned with the development of heat pump and heat transformer concepts and of a computer code capable of modelling all of those, using $H_2O/LiBr$ as working pair. Subroutines for humid air and water/steam for simulation of the heat source and sink were also completed and the specification of paper hood operating conditions to be used as a reference system for assessment of the possible systems was agreed with the industrial sponsor. Finally a preliminary comparison of the possible systems was made based on the thermodynamic performance for a reference paper machine. (6 refs.)

115673 Development of an absorption heat pump for industrial application. J.Berghmans (Katholieke Univ, Leuven, Leuven, Belgium).

Proceedings of Four Contractors' Meetings on Heat Pumps (EUR 8077 EN), Brussels, Belgium, 28-29 April & 12-13 May 1982 (Luxembourg: Comm. European Communities 1982), p.181-3

A feasibility study is undertaken for the development of absorption heat pumps for industrial application. This study includes a search for suitable working pairs and the design of heat pump components. Where necessary missing fluid properties are determined experimentally. In the design phase considerable attention is given to the development of accurate component models and the application of techniques enhancing heat transfer. (6 refs.)

115674 Earth as a storage medium and a heatsource for heatpump. M.Fordsmann (European Heatpump Consultors Ltd., Charlottenlund, Denmark).

Proceedings of Four Contractors' Meetings on Heat Pumps (EUR 8077 EN), Brussels, Belgium, 28-29 April & 12-13 May 1982 (Luxembourg: Comm. European Communities 1982), p.214-28

The system which is being studied both in theory and in practice consists of a heat accumulator with vertical pipes, an unshielded solar collector of small size, and a heatpump, that will both heat and cool the house. The dimensioning work is concluded, and the construction work is being carried out. The air/water heat pump for the domestic water has been installed. (2 refs.)

115675 Investigation into a complete earth to water heat pump system in a single family dwelling focussing on the application of a vertical subsoil heat exchanger. J.W.J.Bouma, A.D.Koppenol, H.van der Ree (TNO-MT, Apeldoorn, Netherlands).

Proceedings of Four Contractors' Meetings on Heat Pumps (EUR 8077 EN), Brussels, Belgium, 28-29 April & 12-13 May 1982 (Luxembourg: Comm. European Communities 1982), p.229-41

The heat pump system involved operates in the bivalent-parallel mode. The dwelling is fitted with a floor heating system. The previously developed computerised predictive method for heat extraction from the soil and heat pump performance has been applied for the design of the subsoil heat exchanger. Calculations have been performed for seven tubes with a length of 10 m, 15 m and 20 m respectively in relation to the actual heating demand of the dwelling. Preliminary results show that 20 m-tubes yield higher SPF's, whereas in the case of 10 m-tubes the quasi-stationary state of the earth in a natural manner is obtained quicker. (10 refs.)

115676 Heating of a laboratory hall by means of a soil heat pump combined with unshielded solar collectors. J.M.De Hoe, B.Geeraert.

Proceedings of Four Contractors' Meetings on Heat Pumps (EUR 8077 EN), Brussels, Belgium, 28-29 April & 12-13 May 1982 (Luxembourg: Comm. European Communities 1982), p.242-69

Experimental results of a 500 m² laboratory hall heated during the season 1980/81 by three soil heat pumps using only 620 m² soil surface for the double layer horizontal pipe heat exchanger buried at low depth (0.6 m and 1.2 m). The energy demand has been lowered to 45% of the demand in case of resistance heating. Experimental results correspond to predicted ones. (7 refs.)

115677 Domestic heat pump with deep hole ground source evaporator. J.R.Goulburn, J.Fearon (Dept. of Mech. & Industrial Engng., Queen's Univ., Belfast, N Ireland).

Proceedings of Four Contractors' Meetings on Heat Pumps (EUR 8077 EN), Brussels, Belgium, 28-29 April & 12-13 May 1982 (Luxembourg: Comm. European Communities 1982), p.270-83

A programme of ground source heat pump investigations commenced in 1974. Initially, horizontal coils at a moderate depth were installed and results similar to other investigators obtained. Large ground areas were required for significant outputs, and this led to the next stage, where vertical coils were experimented with on a small scale. The performance of these coils was encouraging, and led to the design and installation of a ground source heat pump of 8.9 kW output which required a moderate ground area. This heat pump was installed in a house on the university site, and its performance and the thermal behaviour of the soil measured. Throughout the ground coil experiments described the refrigerant has been directly evaporated in the ground (i.e. no secondary medium was used). Co-operation with a Company called Roots led to installations and experiments with diesel engine driven ground source heat pumps of 50 kW output, using waste heat recovery from the diesel engines. These units are intended to be used in the first instance in horticultural applications. (no refs.)

115678 Design and development of absorption heat pumps. I.E.Smith, C.O.B.Carey, G.F.Smith (School of Mech. Engng., Cranfield Inst. of Technol., Cranfield, England).

Proceedings of Four Contractors' Meetings on Heat Pumps (EUR 8077 EN), Brussels, Belgium, 28-29 April & 12-13 May 1982 (Luxembourg: Comm. European Communities 1982), p.285-96

Investigations and measurements have been carried out concerning the vapour pressure, viscosity, density, thermal conductivity, solubility and thermal stability of solutions of lithium bromide and zinc bromide in 2:1 molar ratio in methanol over more extended temperature ranges than have hitherto been reported, suitable for a heat pump operating at an evaporator temperature of -10°C and an absorber temperature of 70°C . An experimental test rig consisting of an evaporator and adiabatic packed bed adsorber has been successfully operated delivering 250 W at a temperature of 74°C with the methanol evaporating at -10°C . At a temperature of 190°C the methanol-bromide mixture has been found to be unacceptably unstable, with two moles of methanol undergoing dehydration to produce one mole of dimethyl ether. This product behaves as a non-condensable gas in the system and reduces its capacity to an unacceptably low level. A 3 kW, absorption heat pump has been fabricated out of industrial glassware and when fully instrumented and thermally insulated will be used to measure the performance of candidate working fluids and absorbents. (3 refs.)

115679 Compression heat pumps operating with non-azeotropic fluid mixtures. Cl.Ramet, A.Rojey, H.Baglione, L.Reigne, J.Durandet (Inst. Francais du Petrole, Rueil-Malmaison, France).

Proceedings of Four Contractors' Meetings on Heat Pumps (EUR 8077 EN), Brussels, Belgium, 28-29 April & 12-13 May 1982 (Luxembourg: Comm. European Communities 1982), p.297-311

Non azeotropic fluid mixtures in compression heat pumps applied to space heating make it possible to improve the coefficient of performance and/or to increase the thermal capacity, by using specific optimized mixtures for each of these two cases. The report describes the basic principles of the advantages of using fluid mixtures, the IFP experimental work and the application of mixtures to commercial Leroy-Somer heat pumps. In the development step, priority was given to the increase in the thermal capacity, without any change in the layout of the heat pump. The obtained capacity increase reached 28% for water-to-water units and 24% for air-to-water units, with a maintained or even improved COP. These results are encouraging, because they enable a substantial cost reduction of about 10% of the heat pumps. (no refs.)

115680 Absorption-resorption heat pump for space heating investigation of solute-solvent pairs. J.Cheron, A.Rojey, J.Durandet (Inst. Francais du Petrole, Rueil-Malmaison, France).

Proceedings of Four Contractors' Meetings on Heat Pumps (EUR 8077 EN), Brussels, Belgium, 28-29 April & 12-13 May 1982 (Luxembourg: Comm. European Communities 1982), p.312-27

Absorption-resorption cycles widen the range of solute-solvent pairs to be used in heat pumps for space heating. Non toxic, inexpensive, non-flammable and easily available fluids have been studied. CO_2 appears to be a good fluid because of its properties. Many solvents are able to absorb CO_2 . Results are described and show that some additional experimental data are needed for the investigation of solute-solvent pairs better suited for space heating. Thermodynamic models have been developed for the simulation of solute-solvent pairs, and good prediction has been demonstrated even for enthalpic values. A test loop (1 kW at the generator) is under construction. (9 refs.)

115681 Development of a periodically working absorption heat pump. H.B.Grabenhenrich, K.F.Knoche (Lehrstuhl für Tech. Thermodynamik, RWTH Aachen, Aachen, Germany).

Proceedings of Four Contractors' Meetings on Heat Pumps (EUR 8077 EN), Brussels, Belgium, 28-29 April & 12-13 May 1982 (Luxembourg: Comm. European Communities 1982), p.328-33 In German.

In periodically operating heat pumps the generation, condensation and evaporation of the vapour occur at different times. This method which has been abandoned in the absorption cooling is rather favorable for absorption heating processes because a solution pump can be completely avoided and also the control of such a device is rather simple. Heat transfer in the absorber is the most critical step in periodically working absorption heat pumps. First results on heat transfer coefficients are presented. (no refs.)

115682 Thermoelectric exhaust air/water heat pump for space heating. P.Dubois, R.Ravelet, M.Berthet (Lab. de Marcoussis, Generale d'Electricite, Marcoussis, France).

Proceedings of Four Contractors' Meetings on Heat Pumps (EUR 8077 EN), Brussels, Belgium, 28-29 April & 12-13 May 1982 (Luxembourg: Comm. European Communities 1982), p.334-46

The reported work on thermoelectric heat pumps has been conducted on extracted air/water pumps for space heating. It includes: sintering of thermoelectrical pellets, design, fabrication and test of a column with 34 pellets, design and cost studies of a pump for space heating of a well insulated dwelling; computation of energy savings. (no refs.)

115683 Systematic construction and development of an economical; low loss and controllable solvent pump for absorption heat pumps. K.-H.Schrader (Stiebel Eltron GmbH & Co., Holzminden, Germany).

Proceedings of Four Contractors' Meetings on Heat Pumps (EUR 8077 EN), Brussels, Belgium, 28-29 April & 12-13 May 1982 (Luxembourg: Comm. European Communities 1982), p.347-60

Suitable solvent pumps for absorption heat pumps are available on the market only in the form of expensive piston-membrane types. The testing of alternative types available on the market brought to light the problems of shaft seals and the resistance of well-known elastomers to the materials used. The best pumping properties were observed with annular gear pumps, whereby the annular gear pump of a particular hydraulic pump manufacturer was most convincing with regard to smooth running, dimensions and volumetric efficiency. The project will now be continued in cooperation with this firm and a further specialist firm for electric motors. In the medium term, an intermediary solution consisting of annular gear pumps with slide ring seals and flanged, reversible electric motor has been realised. In the long term, development is taking place in the direction of fully hermetic systems in a single housing, using a reversible, slotted tube motor. (14 refs.)

115684 The development of a directly fired heat pump for domestic and light commercial application. D.T.G.Strong (Glynwed Group Services Ltd., Shirley, Solihull, England).

Proceedings of Four Contractors' Meetings on Heat Pumps (EUR 8077 EN), Brussels, Belgium, 28-29 April & 12-13 May 1982 (Luxembourg: Comm. European Communities 1982), p.375-89

A prototype gas fired heat pump has been produced based upon the use of a miniature turbomachine operating on a Rankine/Rankine Cycle. Problems and experience gained with the laboratory prototypes are identified with particular reference to the following: high speed gas bearings, differential thermal expansion, test rig and instrumentation, feed pump and working fluid. Current work associated with optimising the gas bearings, turbo-compressor, feed pump and control system are outlined together with an indication of the future development plan. (no refs.)

Proceedings of Four Contractors' Meetings on Heat Pumps (EUR 8077 EN) ... See Entry 111313

Temperature conditions of the refrigerating chamber of an adsorption solar refrigerator See Entry 115686

Experimental study of the operation of a domestic continuous-operation solar refrigerator See Entry 115687

86.30S Photothermal conversion

115685 Heat-engineering design method for a passive solar heating system (steady state). R.R.Avezov, K.B.Babakulov (S.V. Starodubtsev Physicotech. Inst., Acad. of Sci., Uzbek SSR).

Appl. Sol. Energy (USA), vol.18, no.4, p.33-9 (1982). Translation of: *Geliotekhnika (USSR)*, vol.18, no.4, p.29-34 (1982). [received: Aug. 1983] The balance equations for individual surfaces and volumes and for the structure as a whole are set up and solved. The theoretical data are compared with experiment. (8 refs.)

115686 Temperature conditions of the refrigerating chamber of an adsorption solar refrigerator. B.M.Achilov, V.V.Chugunkov (S. Ordzhonikidze Bukhara State Pedagogical Inst., USSR). *Appl. Sol. Energy (USA)*, vol.18, no.4, p.40-4 (1982). Translation of: *Geliotekhnika (USSR)*, vol.18, no.4, p.34-8 (1982). [received: Aug. 1983] The authors describe a method of calculating the nonsteady temperature conditions for the chamber of a solar refrigerator. (3 refs.)

115687 Experimental study of the operation of a domestic continuous-operation solar refrigerator. N.Ch.Dursunov (V.V. Kuibyshev Samarkand Cooperative Inst., USSR). *Appl. Sol. Energy (USA)*, vol.18, no.4, p.45-7 (1982). Translation of: *Geliotekhnika (USSR)*, vol.18, no.4, p.38-40 (1982). [received: Aug. 1983] (4 refs.)

115688 Full-scale tests of a solar hothouse with subsurface irrigation and heat accumulation. A.B.Vardiashvili, M.Muradov, E.Khasanov, A.A.Vardiashvili, A.Temurkhanov (Kh. Alimdzhan Karshinsk State Pedagogical Inst., USSR). *Appl. Sol. Energy (USA)*, vol.18, no.4, p.48-51 (1982). Translation of: *Geliotekhnika (USSR)*, vol.18, no.4, p.40-3 (1982). [received: Aug. 1983] The authors consider a combined solar hothouse/dryer with subsurface irrigation and with a heat accumulator. It is established that, when the moisture content of the soil is raised, there is an increase in its heat conduction and intensified heat transfer from the air to the soil. (5 refs.)

115689 Antireflection coatings for metallized surfaces of solar elements and thermal collectors. M.M.Koltun, I.P.Gavrilova (All Union Sci. Res. Inst. of Current Sources, USSR). *Appl. Sol. Energy (USA)*, vol.18, no.4, p.52-7 (1982). Translation of: *Geliotekhnika (USSR)*, vol.18, no.4, p.44-8 (1982). [received: Aug. 1983] It is shown that, of the metals considered, only Ni has favorable values of the optical constants such that a zero minimum coefficient of reflection can be obtained by using antireflection coatings. (1 ref.)

115690 Engineering method of calculating solar radiation and radiation absorbed by a collector. M.D.Rabinovich (Regional Sci. Res. & Design Inst. of Standard & Experimental Planning, Kiev, Ukrainian SSR). *Appl. Sol. Energy (USA)*, vol.18, no.4, p.71-6 (1982). Translation of: *Geliotekhnika (USSR)*, vol.18, no.4, p.59-64 (1982). [received: Aug. 1983] The author presents computer calculations of the spatial characteristics of flat solar-energy collectors, and a procedure for utilizing them in calculations. Calculations and a procedure are given for optimal arrangement of collectors on a plane. (11 refs.)

115691 Solar lemon-growing facility with heat accumulator. Ch.Sh.Tursunov, M.Khasanova, T.Sodikov (S. Ordzhonikidze Bukhara State Pedagogical Inst., USSR). *Appl. Sol. Energy (USA)*, vol.18, no.4, p.77-9 (1982). Translation of: *Geliotekhnika (USSR)*, vol.18, no.4, p.65-6 (1982). [received: Aug. 1983] It is shown that large-scale lemon-growing facilities heated by solar energy can be constructed in the southern regions of Central Asia. (no refs.)

115692 Method of calculating incoming radiation in shed-type block hothouses. Yu.N.Yakubov, A.Imamkulov (S. Ordzhonikidze Bukhara State Pedagogical Inst., USSR). *Appl. Sol. Energy (USA)*, vol.18, no.4, p.80-5 (1982). Translation of: *Geliotekhnika (USSR)*, vol.18, no.4, p.67-70 (1982). [received: Aug. 1983] The authors derive analytic expressions for determining the mutual shadowing factors and incoming radiation for shed-type block hothouses. (3 refs.)

115693 Recent advances in natural-circulation, solar-energy water heater designs. B.Norton, S.D.Probert (School of Mech. Engng., Cranfield Inst. of Technol., Bedford, England). *Appl. Energy (GB)*, vol.15, no.1, p.15-42 (1983). Details are given of mathematical simulations and experimental determinations of system performance. Various methods of successfully incorporating a thermosyphon solar-energy water heater into a building are discussed. Recent approaches to the design of compact and indirect types are also described. The viability and acceptability of systems in several countries are reported. (97 refs.)

115694 Effect of a thermal trap on the performance of a solar sand collector. N.K.Dhiman, G.N.Tiwari (Centre of Energy Studies, Indian Inst. of Technol., New Delhi, India). *Appl. Energy (GB)*, vol.15, no.1, p.57-69 (1983). The effects of different parameters—e.g the thickness of the trap material, the flow rate of the water and the depth of the heat-retrieval plane—on the water temperature have been investigated. A comparison of the present system with a conventional solar sand collector was also made. (7 refs.)

115695 Conductive heat transfer in salt gradient stabilized solar ponds. A.K.S.Thakur (Dept. of Phys., Univ. of Sokoto, Sokoto, Nigeria). *Int. Commun. Heat & Mass Transfer (GB)*, vol.10, no.4, p.335-40 (July-Aug. 1983). Deals with heat transfer in salt gradient solar ponds. Spatial variations in thermal properties have been considered and the resulting one dimensional heat conduction equation with a source term, is solved explicitly to obtain a closed form mathematical expression for temperature distribution in the non-convected zone present analysis is not restricted to any one typical profile in thermal properties. (14 refs.)

115696 Solar radiation intensity and its use in parabolic collectors. J.Giman. *Elektrotech. Cas. (Czechoslovakia)*, vol.34, no.5, p.359-69 (1983). In Slovak. The following parameters which affect the effectiveness of solar conversion systems in Czechoslovak conditions are dealt with: solar radiation intensity; the length of insolation in Czechoslovakia based on meteorological records; geometrical parameters of the parabolic collectors, and the nominal and dynamic effectiveness of the collector systems. It is concluded that solar power is an effective source of energy for domestic space and water heating as well as for various industrial applications. (6 refs.) *E.D.*

115697 Investigations on active and passive systems of solar energy utilisation in a manufacturing bay. N.Schadler, W.Kast (Tech. Hochschule Darmstadt, Darmstadt, Germany). *HLH (Heiz. Luftung Klimatch. Haustech.) (Germany)*, vol.34, no.8, p.321-2 (Aug. 1983). In German. The investigations were carried out on a solar heating installation in an industrial assembly bay in Darmstadt comprising an active system incorporating four air collectors with roof mounted absorbers, ducting system and heat stores, and a passive system consisting of a transparent surface on part of the south facing wall. The brief experience gained so far suggests that the calculated contribution of 44% by the solar system to the energy requirement over a heating period will be achieved. (no refs.) *P.G.R.*

115698 Selective solar absorption of chemically etched aluminum-silicon films. G.A.Niklasson, H.G.Craighead (Bell Labs., Holmdel, NJ, USA). *J. Appl. Phys. (USA)*, vol.54, no.9, p.5488-90 (Sept. 1983). Electron-beam evaporated aluminum-silicon composites were chemically etched in a NaOH solution. This treatment produced a textured surface with high solar absorptance and low thermal emittance. The optical properties were qualitatively described by a graded refractive index model. (28 refs.)

115699 Comparison of collector performance measured in a solar simulator. H.Hettinger. *Report EUR 8347 EN*, Comm. European Communities, Luxembourg (1983), 13 pp. The thermal performance of a solar collector is characterized by its instantaneous efficiency in various working conditions. This efficiency curve can be obtained outdoor or using solar simulators. In outdoor measurements, the test conditions have to be restricted in order that the influence on the collector performance of meteorological factors (wind, solar irradiance, sky temperature, angle of incidence, ambient temperature, humidity, etc.) remain within a known limit. As a result of these restrictions, outdoor tests take often much time to complete and the reproducibility of the results is very problematic. For a comparison of collector efficiencies it is important to make tests under both steady state and repeatable operating conditions. This is possible using a light simulator in a climatic chamber. During the last two years, a great number of collector performance measurements have been performed using the solar simulator LS-1 in the CCR Ispra. In this report, a short description of theory and experiment is given, along with the results of thermal efficiency measurements with a selection of 38 solar collectors of 13 different manufacturers. The collectors under investigation are all single glassed liquid heating flat plate collectors which are conceived for domestic hot water production.

115700 Absorber surfaces and durability of solar heat collectors. W.Bogaerts, A.Van Haute, M.Pacolet. *Report EUR 8353 EN*, Comm. European Communities, Luxembourg (1983), 70 pp. Commercially or potentially available selective and nonselective absorber surfaces for solar heat collectors are reviewed and the state-of-the-art of solar collector corrosion processes is outlined. The review of available published literature has indicated that lack of quantitative information exists at the present time relative to corrosion of collector surfaces. Available information (mostly qualitative) on durability aspects and corrosion of solar receiver surfaces is described to indicate potential corrosion problem areas and corrosion prevention possibilities. An outline of appropriate durability tests is presented. (177 refs.)

Bases and applications of the induced resonance absorption. I See Entry 112925

Thermal emissivities of films on substrates See Entry 113068

Spectrally selective black tungsten films See Entry 114949

Mathematical analysis of the performance of cylindrical-parabolic solar concentrators See Entry 115616

Active solar energy systems—possibilities of application See Entry 115620

86.30Z Other topics

115701 Fundamental research on multi-hull-type floating wave energy converter. M.Kobayashi, H.Nakagawa, N.Matsubara. *Mitsui Zosen Tech. Rev. (Japan)*, no.118, p.52-62 (April 1983). In Japanese. The author propose a new multi-hull-type floating wave energy converter which consists of multi-floating bodies with asymmetrical cross section and connecting bars. Wave energy absorption by this converter is induced from the relative motions between the floating bodies and the connecting bars in waves. The method to calculate the hydrodynamic forces and moments on each floating body was developed by using the Okusu method, and the equation of motions of floating bodies and connecting bars in waves was derived. For the twin-hull-type wave energy converter which consists of two Salter-Duck floats and a connecting bar, theoretical calculations by this method and model experiments were carried out. It is found that the results obtained by the present method are in good agreement with the ones by model experiments. The twin-hull-type will give more stable wave energy absorption than the single-hull-type. (14 refs.)

115702 The experimental and theoretical evaluation of a twin-flap wave-energy absorbing device. R.M.Scher, A.W.Troesch (Dept. of Naval Architecture & Marine Engng., Univ. of Michigan, Ann Arbor, MI, USA), G.Zhou. *Ocean Eng. (GB)*, vol.10, no.5, p.325-45 (1983). A series of model experiments with a twin-flap wave-energy absorbing device is described, and the results compared with numerical predictions based on theoretical work reported by Srokosz and Evans (1979). Measurements were made of absorption efficiency, flap motion responses, and total flap forces (mooring forces), all with the supporting structure held fixed, with normal wave encounter. Both 2-D and finite-length flap experiments were conducted. Generally, fair agreement is obtained between theory and experiments. Maximum efficiencies approaching 100% (as predicted analytically) were confirmed by experiments. Some conclusions are drawn with regard to a twin-flap power generating system. (9 refs.)

Utility impacts assessment of residential passive solar systems See Entry 115622

Full-scale tests of a solar hothouse with subsurface irrigation and heat accumulation See Entry 115688

Solar lemon-growing facility with heat accumulator See Entry 115691

Method of calculating incoming radiation in shed-type block hothouses See Entry 115692

86.40 ENERGY STORAGE (SECONDARY ENERGY)

86.40F Storage in thermal energy

Simulation of the heating process of a building with an earth-collector heat pump See Entry 115666

Recent advances in natural-circulation, solar-energy water heater designs See Entry 115693

Effect of a thermal trap on the performance of a solar sand collector See Entry 115694

Investigations on active and passive systems of solar energy utilisation in a manufacturing bay See Entry 115697

86.40K Hydrogen storage and technology

Model calculations for the thermodynamic equilibria in intermetallics in La-Ni under hydrogen See Entry 114129

86.70 ENVIRONMENTAL SCIENCE

(see also 87.60R Radioactive pollution; for oceanographic aspects, see 92.10; for hydrological aspects see 92.40; for meteorological aspects see 92.60)

86.70C Soil

115703 Determination of concentrations of selected radionuclides in surface soil in the US. T.E.Myrick, B.A.Berven, F.F.Haywood (Oak Ridge Nat. Lab., Oak Ridge, TN, USA).

Health Phys. (GB), vol.45, no.3, p.631-42 (Sept. 1983).

Background radionuclide concentrations in surface soil across the US have been measured by the Oak Ridge National Laboratory (ORNL). These measurements have been made as part of the ORNL program of radiological surveillance at inactive uranium mills and sites formerly utilized during Manhattan Engineer District and early Atomic Energy Commission projects. The background soil sampling program involved determination of ^{226}Ra , ^{232}Th and ^{238}U concentrations in surface soil samples for comparative purposes to determine the extent of contamination present at the survey sites and surrounding off-site areas. The sampling program to date has provided background information at 356 locations in 33 states. The nationwide average concentrations of ^{226}Ra , ^{232}Th and ^{238}U in surface soil were determined to be 1.1, 0.98 and 1.0 pCi/g, respectively. This paper summarizes the results of these background measurements and provides a brief analysis of regional differences and similarities in data values. (9 refs.)

Kornyezeti dozisztentzas helyszini meghatározása Ge(Li)-spektrometriával. A korszerű (Environmental dose rate in situ determination by Ge(Li)-spectrometry See Entry 115715

^{90}Sr and ^{137}Cs in soil and biota of fallout areas in southern Nevada and Utah See Entry 115936

86.70E Water

115704 Hydrocarbons in water, sediment and mussels from the southern Baltic Sea. R.Law (Fisheries Lab., Min. of Agriculture, Fisheries & Food, Burnham on Crouch, England), E.Andrulewicz.

Mar. Pollut. Bull. (GB), vol.14, no.8, p.289-93 (Aug. 1983).

Samples of water, sediment and mussels (*Mytilus edulis*) from the southern Baltic Sea have been analysed for total hydrocarbons by fluorescence spectroscopy and capillary gas chromatography. The sediment and mussel samples have also been analysed for specific aliphatic and aromatic hydrocarbons by computerized capillary gas chromatography-mass spectrometry. The highest hydrocarbon concentrations in all samples occurred either inshore (particularly in Gdansk Bay) or in deep offshore basins where fine sediment accumulates. (9 refs.)

115705 Evaluation of ocean pollution (experience of the United Nations Program in the West African region). A.G.Rozanov (Shirshov Inst. of Oceanology, Acad. of Sci., Moscow, USSR).

Oceanology (USA), vol.22, no.4, p.434-7 (1982). Translation of: *Okeanologiya (USSR)*, vol.22, no.4 (1982). [received: Aug. 1983]

Industrial pollution of the Atlantic Ocean off the coast of West Africa was evaluated by UN experts under a project instituted in 1980 on the request of the countries of that region. The procedure used in the project included direct gathering of information from industrial plants about the type of output and the quantity of pollutants discharged into the ocean. Simultaneously, the status of the facilities for the treatment and disposal of hazardous wastes and the prospects for industrial development in terms of its environmental effects are evaluated. The results obtained show that in several West African countries there exist specific coastal areas, sometimes of very large size, in which the present levels of pollutants discharge into the ocean may create an environmental hazard. (11 refs.)

115706 Water quality measurement by observing aquatic animals on mountain streams near Shinshin-so Hut, Doshisha University, 1982. N.Kobayashi (Biological Lab., Doshisha Univ., Kyoto, Japan).

Sci. & Eng. Rev. Doshisha Univ. (Japan), vol.24, no.1, p.29-40 (May 1983). In Japanese.

The biological water quality measurement on mountain streams was carried out in May and November 1982, as a part of investigations upon natural environment around Shinshin-so Hut, Doshisha University. Investigated sites were both rapids and pools on an upper (slow stream), a mid- (few stream) and a down- (rapid stream) streams. Bottom samples were collected in the quadrat (50 cm×50 cm) at the depths of 2-3 cm in May and of 7-10 cm in November. Then, invertebrates were gathered with the naked eye from the bottom samples. The polluted degrees of these water samples were measured by the modified Beck-Tsuda biotic index α method. The measurement showed that the indexes were low (somewhat clean) in spring and high (clean) in autumn generally. The conditions of the collection may have also affected the variation. (17 refs.)

115707 Pollution levels in some Nigerian rivers. P.A.Oluwande, M.K.C.Sridhar, A.O.Bammeke, A.O.Okubadejo (Dept. of Preventive & Social Medicine, Coll. of Medicine, Univ. of Ibadan, Ibadan, Nigeria).

Water Res. (GB), vol.17, no.9, p.957-63 (1983).

Surveys of five rivers in a hot-humid zone of a tropical country (Nigeria) were carried out over 3 years by obtaining samples for physical, chemical and bacteriological analyses. The main characteristics monitored were temperature, turbidity, total, dissolved and suspended solids, pH, dissolved oxygen, BOD, ammonia-nitrogen and the coliform counts. The main characteristics of the liquid waste being discharged into the rivers are determined. (22 refs.)

115708 Factors affecting the concentrations of cadmium, zinc, copper and lead in the sediments of the Vesdre River. C.Houba, J.Remacle (Univ. of Liege, Dept. of Botany, Liege, Belgium), D.Dubois, J.Thorez.

Water Res. (GB), vol.17, no.10, p.1281-6 (1983).

The main factors influencing Cd, Zn, Cu and Pb concentrations in the sediments of the highly polluted Vesdre River (eastern Belgium) are investigated. Only negative correlations are demonstrated between the clay content and heavy metals. The composition of the clay minerals could partially explain this paradox. However, the pretreatment of the minerals might influence the geochemical data obtained from analysis. Iron-hydroxides and phosphates seem to be the main sinks for Pb, Cd and Zn whereas organic components might play a less important role. (24 refs.)

Low-level waste disposal site performance assessment with the RQ/PQ computer program See Entry 112348

Results of environmental radioactivity measurements in the Member States of the European Community for air - deposition - water - milk 1981 See Entry 112458

Biological elimination rates of radioisotopes by mallards contaminated at a liquid radioactive waste disposal area See Entry 115937

Environmental radon and cancer correlations in Maine See Entry 115942

86.70G Atmosphere

115709 The New Jersey project on Airborne Toxic Elements and Organic Substances (ATEOS): A summary of the 1981 summer and 1982 winter studies. P.J.Lioy, J.M.Daisey (Inst. of Environmental Medicine, New York Univ. Medical Center, New York, NY, USA), T.Atherholt, J.Bozzelli, F.Darack, R.Fisher, A.Greenberg, R.Harkov, B.Kebbekus, T.J.Kneip, J.Louis, G.McGarrity, L.McGeorge, N.M.Reiss.

J. Air Pollut. Control Assoc. (USA), vol.33, no.7, p.649-57 (July 1983).

An overview of the purpose, design, and results of the summer 1981 and winter 1982 ATEOS studies is presented. The purpose of the study is to characterize the atmospheric environment at selected population centers in New Jersey, with a special emphasis on airborne species that may pose a human health hazard. The author discusses the seasonal variability in the concentrations, the relative composition of the aerosol at these sites, and the relationships to the sources of the measured airborne pollutants. (26 refs.)

115710 Regional air quality in the Four Corners study region.

D.H.Nochumson (Los Alamos Nat. Lab., Los Alamos, NM, USA).

J. Air Pollut. Control Assoc. (USA), vol.33, no.7, p.670-7 (July 1983).

The results from the regional air quality analysis for the Four Corners Study are discussed. This study was one of five regional studies conducted for the National Commission on Air Quality. Potential regional air quality impacts are evaluated through the year 1995 for alternative energy scenarios under current and alternative regulatory policies. The alternative regulatory policies include emission fees, technology standards, emission ceilings, and prevention of significant deterioration class elimination. The alternatives are compared in terms of their impacts on regional visibility and on the ambient concentrations of SO_2 , SO_4 , and primary fine particulates. The fate of the pollutants is estimated. (19 refs.)

115711 Airborne detection of acidic sulfate aerosol using an ATR impactor. S.A.Johnson, R.Kumar, P.T.Cunningham (Chem. Technol. Div., Argonne Nat. Lab., Argonne, IL, USA).

Aerosol Sci. & Technol. (USA), vol.2, no.3, p.401-5 (1983).

As a first step in determining how aerosol acidity varies with altitude, studies were conducted using a new instrument called an ATR impactor installed aboard the Battelle Pacific Northwest Laboratory's DC-3 aircraft. This instrument combines collection of the aerosol by inertial impaction with infrared spectroscopic analysis by the highly sensitive ATR technique. Results from several series of flights have revealed the occurrence of acidic sulfate aloft, while simultaneously collected ground-level samples contained only neutral ammonium sulfate. Acidic sulfate was detected in aerosol samples collected on four of the five flights conducted in the Chicago area during the spring of 1981. (11 refs.)

115712 Organic and elemental composition of airborne particulate matter in Beijing, spring 1981. J.M.Daisey, T.J.Kneip (New York Univ. Medical Center, Inst. of Environmental Medicine, New York, NY, USA), Wang Ming-xing, Ren Li-xin, Lu Wei-xiu.

Aerosol Sci. & Technol. (USA), vol.2, no.3, p.407-15 (1983).

Selected samples of total suspended particulate matter (TSP) collected in Beijing, China, in March and April 1981 were analyzed for trace elements, extractable particulate organic matter (POM), polycyclic aromatic hydrocarbons, alkylating agents and sulfate. Both the concentration and composition of these aerosol species differed substantially from that of New York City. Concentrations of TSP, Fe, Mn, SO_4^{2-} , POM, alkylating agents, and PAH ranged from a factor of 2 to an order of magnitude higher than those typically seen in New York City and other eastern US cities. Concentrations of benzol(a)pyrene ranged from 2.2 to 31 ng/m³, as compared to the 1980-1981 wintertime average of 0.5 ng/m³ for New York City. Sulfate and organics together constituted only about 13% of the total aerosol mass in Beijing in contrast to the 25%-35% seen in New York City. The greatest proportion of TSP in Beijing appears to originate from windblown dust and coal fly ash, as evidenced by the concentrations of Mn and Fe which were observed. Coal burning for space heating may contribute as much as 200-400 $\mu\text{g}/\text{m}^3$ of the TSP. (18 refs.)

115713 Negative ions—their effect on air pollution. T.S.Ganesh (Digitronics, Bangalore, India).

J. Electrochem. Soc. India, vol.32, no.1, p.105-6 (Jan. 1983). [received: Sept. 1983]

The role of positive and negative ions in the environment is discussed. The use of negative ions as a means of reducing air pollution is recommended. (6 refs.)

Hot particles from nuclear atmospheric test of October 1980 See Entry 112445

Summary report on development of an integral model of a radioactive jet [from a reactor accident] See Entry 112448

Release of gaseous tritium during reprocessing See Entry 112455

Results of environmental radioactivity measurements in the Member States of the European Community for air - deposition - water - milk 1981 See Entry 112458

A typical and short case study on the effect of pollution on corrosion See Entry 115424

Measurement of the time variational behaviours of aerosols based on size distribution See Entry 115716

Flame ionisation detector for analyzing the concentration of total hydrocarbons in automobile exhaust gases See Entry 115717

Indoor radon measurements in New Jersey, New York and Pennsylvania See Entry 115934

Indoor radiation exposures from ^{222}Rn and its daughters: a view of the issue See Entry 115938

Background atmospheric ^{222}Rn concentrations outdoors and indoors: a review See Entry 115939

Airborne radionuclides and radiation in buildings: a review See Entry 115940

Radon daughter exposures in the UK See Entry 115941

Indoor radon progeny exposure in the Florida phosphate mining region: a review See Entry 115943

- Radon concentrations and infiltration rates measured in conventional and energy-efficient houses See Entry 115944
- Indoor radon levels in the northeastern US: effects of energy-efficiency in homes See Entry 115945
- Radon and radon daughter measurements in solar buildings .. See Entry 115946
- Results of indoor radon measurements using the Track Etch method See Entry 115947
- Integrated radon data from dwellings in Maine and Texas See Entry 115948
- Study of radon daughter concentrations in Polk and Hillsborough counties See Entry 115949
- Controlled studies of human health effects of short-term inhalation of atmospheric pollutants See Entry 115993
- Investigation of the spectral composition of solar radiation under conditions prevailing at Tashkent See Entry 116169
- Plume dispersion in a nocturnal drainage wind See Entry 116170
- Measurements of sulfur in gases and particles during sixteen months in the Ohio River Valley See Entry 116171
- Mesoscale air pollution dispersion modelling See Entry 116172
- Modelling of long-range transport of sulphur over Europe: a two-year model run and some model experiments See Entry 116173
- Anatomy of an episode of high sulfate concentration at Whiteface Mountain, New York See Entry 116174
- The relationship of sulfur emissions to sulfate in precipitation. II. Gas phase processes See Entry 116175
- The pH and ionic composition of stratiform cloud water See Entry 116176
- Electron microscopy of acidic aerosols collected over the northeastern United States See Entry 116178
- World-wide ambient measurements of peroxyacetyl nitrate (PAN) and implications for plant injury See Entry 116179
- The mechanism of sulfate aerosol formation: chemical and sulfur isotopic evidence See Entry 116202
- Tropospheric oxalate See Entry 116203
- Simultaneous detection of FC-11, FC-12 and FC-22, through 8 to 13 micrometers IR solar observations from the ground See Entry 116204
- Variations of the nearground aerosol particle size distribution See Entry 116211
- The atmospheric aerosol system: an overview See Entry 116261
- Apportioning light extinction coefficients to chemical species in atmospheric aerosol See Entry 116269
- Water channel simulation of the atmospheric boundary layer See Entry 116284

86.70L Measurement techniques in environmental science

- 115714** Optical remote monitoring of CH₄ gas using low-loss optical fiber link and InGaAsP light-emitting diode in 1.33- μ m region. K.Chan, H.Ito, H.Inaba (Res. Inst. of Electrical Communication, Tohoku Univ., Sendai, Japan). *Appl. Phys. Lett. (USA)*, vol.43, no.7, p.634-6 (1 Oct. 1983). Purely optical remote monitoring of low-level CH₄ gas is realized for the first time by the method employing a 2-km long-distance, low-loss silica optical fiber link and a compact absorption cell in conjunction with a high radiant InGaAsP light-emitting diode (LED) at 1.33 μ m. Based on the present experiment, the detection limit of CH₄ in air was confirmed to be approximately 2000 ppm, i.e. 4% of the lower explosion limit of CH₄. This result supports the conclusion that the fully optical remote sensing system incorporating ultralow loss optical fiber networks and near infrared LEDs or laser diodes can be extensively used for the detection and surveillance of various inflammable and/or explosive gases in industrial and mining complexes as well as in residential areas. (12 refs.)
- 115715** Kornyezeti dozisintenzitas helyszini meghatarozasa Ge(Li)-spektrometriával. A módszer (Environmental dose rate in situ determination by Ge(Li)-spectrometry. P.Zombori, I.Nemeth, A.Andrasi. Report KFKI-1983-44, Hungarian Acad. Sci., Budapest (1983), 42 pp. In Hungarian. The methods of in situ determination of the environmental dose rate by Ge(Li) spectrometry are discussed. The author reports on the calibration of the Ge(Li) spectrometer available for in situ measurement. The measurements and calculations on the energy and direction dependence of the sensitivity of the given detector are discussed. On the basis of this study the radioactive concentrations of the natural and manmade radionuclides in the soil and the resulted dose rates can be determined by the calibrated measuring system belong to the Paks Nuclear Power Station. (11 refs.)
- 115716** Measurement of the time variational behaviours of aerosols based on size distribution. Y.Matsuo (Faculty of Sci. & Technol., Keio Univ., Tokyo, Japan). Technological and Methodological Advances in Measurement. Acta IMEKO 1982. Proceedings of the 9th IMEKO Congress of the International Measurement Confederation, Berlin, Germany, 24-28 May 1982 (Amsterdam, Netherlands: North-Holland 1983), p.377-86 vol.2. Presents a new measurement method of time variational processes of environmental aerosols on the basis of bimodal size distribution model. Collected samples were also analyzed by proton induced X-ray emission analysis (abbreviated: PIXE) for twelve elements. The following field experimental results have been obtained: there exist great differences in behaviour between coarse-sized particles and fine ones bordered at 2 μ m in diameter even in hourly short time duration; fine particles are closely related to the behaviours of gaseous air pollutants; and some fine-sized trace elements have traceability of the combustion sources under the head wind condition. (10 refs.)
- 115717** Flame ionisation detector for analyzing the concentration of total hydrocarbons in automobile exhaust gases. A.Kroncisen, J.Staab (Hartmann und Braun AG, Frankfurt/Main, Germany). Technological and Methodological Advances in Measurement. Acta IMEKO 1982. Proceedings of the 9th IMEKO Congress of the International Measurement Confederation, Berlin, Germany, 24-28 May 1982 (Amsterdam, Netherlands: North-Holland 1983), p.395-404 vol.2. Flame ionisation detectors (FID) are sensitive to carbon in hydrocarbons (HC). FID whose essential elements are standardizable and which ensures the reduction of the uncertainties of the HC-measurements to approximately $\pm 2\%$ for measurement of the total hydrocarbons in automobile exhaust is proposed. (12 refs.)

- Particle size analysis by automated optical microscopy See Entry 111764
- Fluid flow control for the intermittent extended aeration process See Entry 113524
- Laser instrumentation: analytical uses are growing See Entry 115598

86.70Z Other topics

- 115718** An examination of the environmental half-time for radionuclides deposited on vegetation. C.W.Miller, F.O.Hoffman (Health & Safety Res. Div., Oak Ridge Nat. Lab., Oak Ridge, TN, USA). *Health Phys. (GB)*, vol.45, no.3, p.731-44 (Sept. 1983). After radionuclides are deposited on vegetation, environmental removal processes combine with radioactive decay to reduce the quantity of initial contamination. The time in which one-half of the radioactivity is removed from vegetation by environmental processes alone is referred to as the environmental half-time, T_w . For long-lived radionuclides, the dose to man via ingestion of contaminated terrestrial foods may be directly influenced by values of T_w , provided that environmental removal processes dominate root uptake and time is sufficiently long between initial exposure of vegetation and harvest. Values of T_w reported in the literature for various radionuclides and methods of deposition are examined. Factors affecting the variability of T_w are related in part of the physicochemical form of the depositing substance, vegetation type and growth form, climate, season, and experimental procedure. For growing vegetation, values of T_w are generally lower than those reported for dormant vegetation. (53 refs.)
- Dose-rate conversion factors for external exposure to photons and electrons See Entry 115928

87.00 BIOPHYSICS, MEDICAL PHYSICS, AND BIOMEDICAL ENGINEERING

87.10 GENERAL, THEORETICAL, AND MATHEMATICAL BIOPHYSICS

(inc. logic of biosystems, quantum biology, and relevant aspects of thermodynamics, information theory, cybernetics, and bionics)

- 115719** Flow analysis sensitivities for models of energy or material flow. R.W.Bosserman (Systems Sci. Inst., Univ. of Louisville, Louisville, KY, USA). *Bull. Math. Biol. (GB)*, vol.45, no.5, p.807-26 (1983). Sensitivity analyses have been used to examine the flow structure of two hypothetical ecosystem models. These analyses have results which relate to important aspects of ecosystem theory. Cycles are shown to increase the sensitivity of the network, while increased throughflow is shown to decrease the sensitivity. Such results indicate that several factors can be modified to decrease the sensitivity of ecosystems to environmental stress. (37 refs.)
- 115720** A mathematical model for estimation of infarct size from serum creatine phosphokinase. F.H.Schmidt (Dept. of Anatomy, Emory Univ., Atlanta, GA, USA). *Comput. & Biomed. Res. (USA)*, vol.16, no.4, p.357-66 (Aug. 1983). A mathematical model for kinetics of creatine phosphokinase (CK) after myocardial infarct is presented. The transport of CK from the infarct to the distribution space is modeled by a gamma variate. CK is released from the distribution space by a first-order process. The model permits simultaneous estimation of the disappearance rate parameter K_D , the integrated appearance function, and the baseline from a set of observations of serum CK concentration. (12 refs.)
- 115721** Thermodynamics of evolution. I. Thermodynamics of dissipative structures. G.Bourceanu, G.Maftei, S.Chirita (Inst. Politehnic, Iasi, Rumania). *Stud. & Cercet. Fiz. (Rumania)*, vol.35, no.8, p.690-714 (1983). In Rumanian. The series of papers about 'Thermodynamics of Evolution' are intended to present the whole theory of the Brussels School, founded by Professor Prigogine on the evolution of prebiotic systems. The first paper 'Thermodynamics of dissipative structures' examines entropy production into open systems, the theorem of minimum entropy production and the stability criterion of nonequilibrium steady states. In the second part of this paper, examples of dissipative structures from hydrodynamics, optics, chemistry and biology are discussed. Finally, evidence is produced to prove that dissipative structures are a general phenomenon in nature. (30 refs.)
- 115722** Thermodynamics of evolution. II. Chemical and biological oscillations and instabilities. G.Maftei, G.Bourceanu, S.Chirita (Inst. Politehnic, Iasi, Rumania), V.Felea. *Stud. & Cercet. Fiz. (Rumania)*, vol.35, no.8, p.715-43 (1983). In Rumanian. For pt.I see ibid., vol.35, no.8, p.690 (1983). Analyses the chemical oscillations and instabilities by means of nonlinear thermodynamics and the theory of differential nonlinear equations by studying the stability of the steady state solutions. In the second part, the paper analyses the conservative oscillations of Lotka-Volterra type and a set of chemical reactions studied experimentally by Belousov and Zhabotinskii, which admit oscillations of limit cycle type. In the last part a set of reactions has been analysed, suggested by the authors, which includes selfcatalytic and cross-catalytic reactions. Since the reactions are produced between molecular species with selfcatalytic properties (of replication), a fidelity factor, ϵ , was introduced, $\epsilon \in (0,1)$. (37 refs.)

- Thermodynamic approach to biomass distribution in ecological systems See Entry 115757
- Mathematical model of the velocity field external to a tank-treading red cell See Entry 115766
- The dynamics of symmetric nets See Entry 115776
- Mathematical structure of bio-electrical impedance obtained from linear functional point of view See Entry 115780
- Feature extractions for pattern recognition of body surface isopotential maps [in ECGs] See Entry 115781
- Identification of human oculomotor system for quantitative diagnostics of eye muscle diseases See Entry 115784

87.15 MOLECULAR BIOPHYSICS

(see also 36.20 Macromolecules and polymer molecules)

115723 Study of the parameters of the fluorescent spectra of probes in model conditions [biomembrane application]. V.M.Boitsov (Min. of Health, Moscow, USSR).

Biophysics (GB), vol.27, no.5, p.824-9 (1982). Translation of: *Biofizika (USSR)*, vol.27, no.5, p.786-90 (1982). [received: Sept. 1983]

An expression is given for describing the fluorescence spectra of 1-anilino-naphthalene-8-sulphonate and N-phenyl-1-naphthylamine in solvents of different polarity and viscosity which allows one to isolate the homogeneous and inhomogeneous components of the spectra. It is shown that the position of the centre of inhomogeneous widening characterizes better the hydrophobicity of the surroundings than the position of the maximum of the spectrum. A link has been established between the parameters of inhomogeneous widening and the viscosity of the solvent. (10 refs.)

115724 Analysis of the thermodynamic characteristics of the interaction of high potential cytochrome with a bacteriochlorophyll dimer at the reaction centres of the chromatophores of *Ectothiorhodospira shaposhnikovii*. V.P.Shinkarev, A.A.Kononenko, A.B.Rubin (Biology Faculty, Lomonosov State Univ., Moscow, USSR).

Biophysics (GB), vol.27, no.5, p.872-6 (1982). Translation of: *Biofizika (USSR)*, vol.27, no.5, p.832-6 (1982). [received: Sept. 1983]

Analyses the kinetics of the dark reduction of cytochrome c_H ($E_7 = 290$ mV) after its photo-induced oxidation in the chromatophores of *E. shaposhnikovii* at 110-210K. A relation is derived describing the process of dark reduction of the cytochrome and allowing one to determine the value of the free energy of electron transport between the cytochrome and the dimer of bacteriochlorophyll of the reaction centre (BChl)₂. Change in the free energy obtained by linear extrapolation to room temperature agrees with the value determined from the results of direct potentiometric titration of the photo-induced redox conversions of c_H and (BChl)₂. (11 refs.)

115725 Lanthanide ions as fluorescent probes for the nucleotides. G.W.Mushrush, G.Yonuschot (Dept. of Chem., George Mason Univ., Fairfax, VA, USA).

J. Lumin. (Netherlands), vol.28, no.3, p.233-9 (Aug. 1983).

The lanthanide ions reacted with the nucleotides to form a complex in which the lanthanides served as sensitive fluorescent probes. By selectively exciting the nucleotide, the quantum efficiency of narrow-line lanthanide ion fluorescence can be calculated. Quantum efficiency values of 0.19 to 0.01 and 0.14 to 0.01 were obtained for Tb³⁺ and Eu³⁺ respectively. For Dy³⁺ and Sm³⁺ the values were too low to measure accurately for most nucleotides. The binding of the lanthanides to the nucleotides can be reversed by prolonged dialysis against cheating agents. Between pH 3 and pH 7 the complex precipitates and approaches a maximum of lanthanide ion fluorescence at pH 5.5. (9 refs.)

115726 Role of the central metal ion and solvent-ligand molecules in the association of metallophosphorylins in binary mixtures of solvents. E.I.Zen'kevich, M.V.Sarzhhevskaya, T.V.Vitovtseva.

J. Appl. Spectrosc. (USA), vol.37, no.5, p.1301-5 (Nov. 1982). Translation of: *Zh. Prikl. Spektrosk. (USSR)*, vol.37, no.5, p.818-23 (Nov. 1982). [received: Sept. 1983]

The purpose of the authors' work was a spectral-fluorescence investigation of the principles of formation of stable long-wave associates of metallophosphorylins, possessing various active side substituents, in binary solutions when the center of the pigment molecule is substituted by ions of various metals, as well as when the donor-acceptor properties of the solvent-ligand molecules are varied. Of the metalloderivatives, the following were studied: Zn, Mg, Cd, Cu, and Pd-phosphorylins *a* and *b*, chlorin *e*₆, and rhodin *g*₇. (9 refs.)

115727 Computer simulation of the dynamics of hydrated protein crystals and its comparison with X-ray data. W.F.van Gunsteren, H.J.C.Berendsen (Dept. of Chem., Univ. of Groningen, Groningen, Netherlands), J.Hermans, W.G.J.Hol, J.P.M.Postma.

Proc. Natl. Acad. Sci. USA, vol.80, no.14, p.4315-19 (July 1983).

The structure and dynamics of the full unit cell of a protein (bovine pancreatic trypsin inhibitor) containing 4 protein molecules and 560 water molecules have been simulated by using the molecular dynamics method. The obtained structure, atom positional fluctuations, and structure factors are compared with X-ray values. A way of calculating the motional contributions to structure factors is proposed. (35 refs.)

115728 New view of lipid bilayer dynamics from ²H and ¹³C NMR relaxation time measurements. M.F.Brown, A.A.Ribeiro, G.D.Williams (Dept. of Chem., Univ. of Virginia, Charlottesville, VA, USA).

Proc. Natl. Acad. Sci. USA, vol.80, no.14, p.4325-9 (July 1983).

Natural abundance ¹³C spin-lattice (*T*₁) relaxation time measurements are reported for unilamellar vesicles of 1,2-dipalmitoylphosphatidylcholine in the liquid crystalline phase, at various magnetic field strengths. The results are compared to previous ²H *T*₁ studies of multilamellar dispersions. For both the ¹³C and ²H *T*₁ studies, a dramatic frequency dependence of the relaxation was observed. At superconducting magnetic field strengths (4.23-11.7 tesla), plots of the ¹³C *T*₁⁻¹ relaxation rates as a function of acyl chain segment position clearly reveal the characteristic 'plateau' signature of the liquid crystalline phase, as found previously from ²H NMR studies. The dependence of *T*₁⁻¹ on ordering, determined previously from ²H NMR, and the *T*₁⁻¹ dependence on frequency, determined from both ¹³C and ²H NMR studies, suggest that a unified picture of the bilayer molecular dynamics can be provided by a simple relaxation law of the form *T*₁⁻¹ ≈ *Aτ*₁ + *BSC*_H⁻² ω₀^{-1/2}. In the above expression, *A* and *B* are constants, *SC*_H (= *S*_{C-D}) is the bond segmental order parameter, and ω₀ is the nuclear Larmor frequency. (41 refs.)

115729 Surface physics and biological phenomena. I.Lundstrom (Dept. of Phys. & Measurement Technol., Linköping Univ., Linköping, Sweden).

Phys. Scr. (Sweden), vol.T4, p.5-13 (1983). (Nordic Conference on Surface Science, Tampere, Finland, 18-20 Aug. 1982).

Connections between surface physics and biology are discussed. Special attention is paid to protein adsorption on solid surfaces, with relevance to biocompatibility and surface oriented diagnostic methods. Simple models for denaturation of proteins and interaction between antigens and antibodies on surfaces are developed. Some surface oriented biological phenomena are described. It is suggested that electrostatic interaction may be a general cause of changes in the physical properties of excitable membranes. The paper is phenomenological and leaves out a thorough discussion of the use of surface analytical tools on biological phenomena. (33 refs.)

A molecular vision of the world See Entry 112620

Bound-water in biomolecules: a Monte Carlo simulation of the bifurcated hydrogen bond in violuric acid monohydrate See Entry 112803

Energetic approach to the packing of α-helices. I. Equivalent helices See Entry 115736

Absence of the effect of a magnetic field on the dissolving of oxygen in aqueous solutions See Entry 115741

Molecular mechanism of sodium conductance changes in nerve: the role of electron transfer and energy migration See Entry 115775

87.15B Structure, configuration, conformation, and active sites at the biomolecular level

115730 Computer representation of molecular surfaces. N.L.Max (Lawrence Livermore Nat. Lab., Livermore, CA, USA).

IEEE Comput. Graphics & Appl. (USA), vol.3, no.5, p.21-9 (Aug. 1983).

Describes how the recent proliferation of algorithms that produce vector or raster drawings of space-filling models has advanced one's understanding of the 3-D structure of molecules. (26 refs.)

115731 Structure of polylysine-DNA complexes. A.T.Khachatryan, V.A.Ter-Nikogosyan, S.M.Akopyan, M.G.Galustyan, M.A.Novosel (Inst. of Experimental Biology, Acad. of Sci., Erevan, USSR).

Biophysics (GB), vol.27, no.5, p.804-8 (1982). Translation of: *Biofizika (USSR)*, vol.27, no.5, p.768-71 (1982). [received: Sept. 1983]

The methods of nuclease digestion and electron microscopy have been used to study the poly-L-lysine+DNA complexes of phage T₂ obtained by direct mixing. On digestion of the complexes by micrococcal nuclease, nuclease-resistant structures were detected containing DNA fragments with a length of ~300, ~600 and ~1200 base pairs. The electron photomicrographs revealed structures outwardly resembling nucleosomes. (6 refs.)

115732 Heterogeneity of the structure of histone dimers (H2A-H2B). S.N.Khrapunov, A.F.Protas, G.D.Berdyshev (Shevchenko State Univ., Kiev, Ukrainian SSR).

Biophysics (GB), vol.27, no.5, p.829-33 (1982). Translation of: *Biofizika (USSR)*, vol.27, no.5, p.791-4 (1982). [received: Sept. 1983]

It has been established that at pH 7.4 and 100 mM NaCl only about one-third of the histone dimers (H2A-H2B) is able to bind the fluorescent probe-1-anilino-naphthalene-8-sulphonate. The binding constant is equal to 2.2·10⁴ M⁻¹. The heterogeneity of the structure of the histone dimers (H2A-H2B) may be of great genetic importance and together with other factors may determine the structural changes of the protein core of the nucleosomes and the nucleosome itself. (16 refs.)

115733 Structure of bacteriophage T7. Small-angle X-ray and neutron scattering study. G.Ronto (Inst. of Biophys., Medical Univ., Budapest, Hungary), M.M.Agamalyan, G.M.Drabkin, L.A.Feigin, Y.M.Lvov.

Biophys. J. (USA), vol.43, no.3, p.309-14 (Sept. 1983).

Small-angle X-ray and neutron scattering techniques were applied to bacteriophage T7 solutions at different scattering densities. Scattering curves determined under a variety of experimental conditions were used to derive a set of parameters characterizing the shape, size, and weight of the whole phage particle and of its DNA and protein components. The T7 head has an icosahedral shape with an edge of 37.7±0.5 nm, a volume of (12.0±1.0)×10⁴ nm³, and a small tail amounting to 6-7% of the head volume. The intraphage DNA region is most probably a hollow sphere. The best fit to the data was obtained with a model in which the hollow sphere filled with a protein core with a diameter of 24 nm. The average degree of swelling (i.e. the ratio of the hydrated to the dry volume) of the particle is 2.3; the degree of swelling of the DNA component is higher, 3.2, and that of the protein part is lower, 1.2. (36 refs.)

115734 X-ray structure analysis of thin filaments of a molluscan smooth muscle in the living relaxed state. Y.Tajima, K.Kamiya, T.Seto (Dept. of Phys., Tokyo Metropolitan Univ., Tokyo, Japan).

Biophys. J. (USA), vol.43, no.3, p.335-43 (Sept. 1983).

In the small-angle X-ray diffraction pattern of the living relaxed anterior byssus retractor muscle of *Mytilus edulis*, the thin filaments showed the following features. The 59.8-Å reflection was much stronger and a little farther from the meridian than the 51.9-Å reflection, although they are both contributions of the first-order Bessel function and are comparable with each other in the height from the equator. The 381-Å reflection, given by the second-order Bessel function, was weaker than the 59.8-Å reflection by more than the difference between the peak values of the first- and second-order Bessel functions, and was not so distant radially from the latter as estimated from the amount of peak shift brought about by the alteration of the Bessel order. A model of the thin filament was made on the basis of inverse Fourier transformation of the scattering amplitude, and the above features were explained by the characteristic shape of actin shown in this model. The actin subunits are elongated along the genetic left-hand helix with a pitch of 59.8 Å, and are bonded together along the genetic helix in the inner part of the filament. (29 refs.)

115735 The theory and practice of distance geometry. T.F.Havel (Group in Biophys., Univ. of California, Berkeley, CA, USA), I.D.Kuntz, G.M.Crippen.

Bull. Math. Biol. (GB), vol.45, no.5, p.665-720 (1983).

The mathematics of distance geometry constitutes the basis of a group of algorithms for revealing the structural consequences of diverse forms of information about a macromolecule's conformation. These algorithms are of proven utility in the analysis of experimental conformational data. This paper presents the basic theorems of distance geometry in Euclidean space and gives formal proofs of the correctness and, where possible, of the complexity of these algorithms. The implications of distance geometry for the energy minimization of macromolecules are also discussed. (46 refs.)

115736 Energetic approach to the packing of α-helices. I. Equivalent helices. K.-C.Chou, G.Nemethy, H.A.Scheraga (Baker Lab. of Chem., Cornell Univ., Ithaca, NY, USA).

J. Phys. Chem. (USA), vol.87, no.15, p.2869-81 (21 July 1983).

A mathematical framework has been developed for generating interacting α-helices and for calculating and minimizing the interaction energy between α-helices. Computations were carried out on a system of two equivalent right-handed α-helices, each having the structure CH₃CO-(L-Ala)₁₀-NHCH₃. Ten low-energy packing arrangements were found. The three lowest-energy arrangements, occurring within an energy interval of 1.8 kcal/mol, are nearly antiparallel with orientational torsion angles of -154, 170, and 146°, in order of increasing energy. The other seven arrangements, with energies of 3.3-5.3 kcal/mol above that of the most stable structure, have a variety of orientational torsion angles. The major contribution to the intermolecular energy arises from nonbonded interactions, with a minor contribution from the electrostatic interactions. The latter tend to favor an antiparallel arrangement of two α-helices that are located side by side. This is one of the reasons why the packing with an orientational torsion angle of -154° has the lowest energy among the computed packings. This packing arrangement is observed frequently in globular proteins. In all minimum-energy structures, the two helices are closely packed, with the side-chain CH₃ groups of one helix inter-

calated between those of the other helix. This is indicated by the small distance of closest approach (6.7-7.7 Å) of the helix axes. This distance is about 4 Å less than twice the distance of the van der Waals surface of the methyl groups from the helix axis. While most of the computed packing arrangements are similar to some packings derived in other studies on the basis of geometrical considerations of packing, the latter by itself cannot determine the order of stability of the various arrangements. Some geometrically feasible packing arrangements are of high energy; on the other hand, some low-energy arrangements could not be found from geometrical considerations alone. These results show the importance of energy calculations for studying packing. (25 refs.)

115737 Interior turns in globular proteins. G.D.Rose, W.B.Young (Dept. of Biological Chem., Pennsylvania State Univ., Hershey, PA, USA), L.M.Gierasch.

Nature (GB), vol.304, no.5927, p.654-7 (18 Aug. 1983).

Reverse turns are specific sites in proteins at which the polypeptide chain changes its overall direction. This category of secondary structure enables the chain to turn a corner, and its frequent occurrence is the geometric basis for the ultimate globular shape of the protein. The authors have searched proteins of known structure and find that, on occasion, a turn may be buried within the hydrophobic interior of the molecule. In every instance of a buried turn, one or more solvent molecules were also found in a hydrogen-bonded complex with main-chain atoms of the turn residues. These bound water molecules appear to function as an integral part of the protein structure. (29 refs.)

115738 Maximum-entropy calculation of the electron density at 4 Å resolution of Pfl filamentous bacteriophage. R.K.Bryan, M.Bansal, W.Folkhard, C.Nave, D.A.Marvin (European Molecular Biology Lab., Heidelberg, Germany).

Proc. Natl. Acad. Sci. USA, vol.80, no.15, p.4728-31 (Aug. 1983).

A 4 Å electron-density map of Pfl filamentous bacterial virus has been calculated from X-ray fiber diffraction data by using the maximum-entropy method. This method produces a map that is free of features due to noise in the data and enables incomplete isomorphous-derivative phase information to be supplemented by information about the nature of the solution. The map shows gently curved (banana-shaped) rods of density about 70 Å long, oriented roughly parallel to the virion axis but slewing by about 1/6th turn while running from a radius of 28 Å to one of 13 Å. Within these rods, there is a helical periodicity with a pitch of 5 to 6 Å. The authors interpret these rods to be the helical subunits of the virion. The position of strongly diffracted intensity on the X-ray fiber pattern shows that the basic helix of the virion is right handed and that neighboring nearly parallel protein helices cross one another in an unusual negative sense. (36 refs.)

115739 Spectroscopic and structural properties of metallo-proteins. M.Bacci (Istituto di Ricerca sulle Onde Elettromagnetiche, CNR, Firenze, Italy).

Riv. Nuovo Cimento (Italy), vol.5, ser.3, no.12, p.1-45 (1982). [received: Sept. 1983]

The author outlines the electronic structures of some biologically significant metal ions in several limit geometries and the resulting spectroscopic behaviour with emphasis to electronic absorption, electron spin resonance (ESR), magnetic circular dichroism (MCD), Mossbauer spectra and magnetic susceptibility. The role of the vibronic coupling and tunnelling in biological systems is considered and a critical survey of the so far reported experimental results and theoretical interpretations is given. (202 refs.)

115740 Crystallization and preliminary X-ray investigation of *Micrococcus sp.* decarboxylase. G.N.Tishchenko, I.P.Kuranova, N.V.Konareva, N.A.Gonchar, I.I.Votrin, B.K.Vainshtein (Inst. of Crystallography, Acad. of Sci., USSR).

Sov. Phys.-Crystallogr. (USA), vol.28, no.2, p.179-81 (March-April 1983). Translation of: *Kristallografiya (USSR)*, vol.28, no.2, p.306-9 (March-April 1983). [received: Sept. 1983]

By isothermal distillation of the solvent vapor and ultracentrifugation the authors have obtained crystals of histidinedecarboxylase (HDC) from *Micrococcus sp. n.*, suitable for X-ray diffraction, in the form of short hexagonal prisms measuring 0.5×0.5×0.3 mm. X-ray diffraction revealed two crystalline modifications—hexagonal and rhombohedral, representing two-layer and three-layer packing of molecular trimers. The shape and size of the trimers and the individual protein molecules are determined. The trimer is an oblate ellipsoid of revolution with semiaxes of 53.75 and 44.2 Å and axial ratios of 1:1.082; the monomer is a prolate ellipsoid of revolution with semiaxes of 50.0 and 78.8 Å and axial ratios of 1:1.16. (22 refs.)

Normal-coordinate analysis of retinal isomers and assignments of Raman and infrared bandsSee Entry 112707

Bound-water in biomolecules: a Monte Carlo simulation of the bifurcated hydrogen bond in violuric acid monohydrateSee Entry 112803

Thermal denaturing of collagen in solution and fibrilsSee Entry 115756

Epitaxial crystallization of alkane chain lipids for electron diffraction analysisSee Entry 115986

87.15M Interactions with radiations at the biomolecular level

115741 Absence of the effect of a magnetic field on the dissolving of oxygen in aqueous solutions. T.V.Ushakova, V.A.Livshits, A.N.Kuznetsov (Res. Inst. for Biological Testing of Chem. Compounds, Kupavna, USSR).

Biophysics (GB), vol.27, no.5, p.793-7 (1982). Translation of: *Biofizika (USSR)*, vol.27, no.5, p.757-61 (1982). [received: Sept. 1983]

To verify a number of experimental studies the authors have examined the effect of a permanent magnetic field on the solubility and rate of dissolving oxygen in water and 0.1 N NaCl solution. It is shown that the solubility and rate of dissolving of oxygen in water and in aqueous solution of an electrolyte in these systems do not change in magnetic fields of the order 0.1 T, which fully matches theoretical notions and makes it impossible to regard the direct influence of the magnetic field on the molecules of paramagnetic oxygen as one of the possible mechanisms of action of a magnetic field on biological systems. (10 refs.)

115742 Magnetic proton relaxation of aqueous solutions of ribonuclease in the temperature region of intramolecular fusion. Yu.G.Sharimanov, R.Grosescu, G.M.Mrevlishvili (Inst. of Phys., Tbilisi, USSR).

Biophysics (GB), vol.27, no.5, p.809-13 (1982). Translation of: *Biofizika (USSR)*, vol.27, no.5, p.772-5 (1982). [received: Sept. 1983]

The thermal denaturing of ribonuclease at n.m.r. frequencies 22, 75 and 90 MHz has been studied by the method of proton magnetic relaxation. It has been established that the character of proton relaxation in solutions of denatured macromolecules is determined by the slow exchange $\tau_M \sim 10^{-2}-10^{-3}$ sec with the molecules of 'rigidly bound' water and the solvent as a whole. (10 refs.)

115743 Photophysical processes in the molecules of retinoids related to visual chromophores. S.L.Bondarev, M.V.Bel'kov, K.I.Salokhiddinov, P.N.Dyl'ko (Inst. of Phys., Acad. of Sci., Minsk, Belorussian SSR).

Biophysics (GB), vol.27, no.5, p.813-17 (1982). Translation of: *Biofizika (USSR)*, vol.27, no.5, p.776-9 (1982). [received: Sept. 1983]

Methods of luminescence, pulse fluorimetry and laser photolysis have shown that at 293K in the molecules of retinoids related to the visual chromophores, retinals, the bulk (≥ 90 per cent) of the excitation energy is deactivated by the non-photophysical route. As intermediate state through which the excitation energy is degraded the authors postulate the A_2^* state. With fall in the temperature of the solution from 293 to 85K the quantum yield of fluorescence of the retinoids increases 10-500 times. The $(\pi\pi^*)$ state takes part in the photophysical processes of retinal in 'dry' non-polar solvents. (17 refs.)

115744 Picosecond kinetic absorption and fluorescence studies of bovine rhodopsin with a fixed 11-ene. J.Buchert, V.Stefancic, A.G.Doukas, R.R.Alfano, R.H.Callender, J.Pande (Phys. Dept., City Coll., City Univ. of New York, New York, NY, USA), H.Akita, V.Balogh-Nair, K.Nakanishi.

Biophys. J. (USA), vol.43, no.3, p.279-83 (Sept. 1983).

A synthetic retinal having a fixed 11-cis geometry has been used to prepare a nonbleachable analogue of bovine rhodopsin. Marked differences in the picosecond absorption and fluorescence behavior of this analogue at room temperature, compared with that of natural rhodopsin, were observed. This not only indicates that the 11-cis to trans isomerization of the retinal moiety is the crucial primary event in the photolysis of rhodopsin, but also it establishes that this isomerization must occur on the picosecond time scale or faster. (18 refs.)

115745 Neutron diffraction analysis of cytochrome b_5 reconstituted in deuterated lipid multilayers. E.P.Gogol, D.M.Engelman (Dept. of Molecular Biophys. & Biochem., Yale Univ., New Haven, CT, USA), G.Zaccari.

Biophys. J. (USA), vol.43, no.3, p.285-92 (Sept. 1983).

Cytochrome b_5 was reconstituted with a highly deuterated phospholipid to form ordered multilayers consisting of repeated centrosymmetric pairs of asymmetric lipid-protein bilayers. Lamellar neutron diffraction data were collected to ~ 29 Å resolution, and have been interpreted using models for the interaction of the membrane-binding domain of cytochrome b_5 with the lipid bilayer. A range of different models was examined, and those in which the protein penetrates well into the bilayer, possibly spanning it, are favored. (41 refs.)

115746 Quenching-resolved emission anisotropy studies with single and multiptryptophan-containing proteins. M.Eftink (Dept. of Chem., Univ. of Mississippi, University, MS, USA).

Biophys. J. (USA), vol.43, no.3, p.323-34 (Sept. 1983).

Measurements of the anisotropy of protein fluorescence as a function of an added collisional quencher, such as acrylamide, are used to construct Perrin plots. For single tryptophan containing proteins, such plots yield an apparent rotational correlation time for the depolarization process, which, in most cases, is approximately the value expected for Brownian rotation of the entire protein. Apparent limiting fluorescence anisotropy values, which range from 0.20 to 0.32 for the proteins studied, are also obtained from the Perrin plots. The lower values for the limiting anisotropy found for some proteins are interpreted as indicating the existence of relatively rapid, limited (within a cone of angle $0^\circ-30^\circ$) motion of the tryptophan side chains that is independent of the overall rotation of the protein. Examples of the use of this fluorescence technique to study protein conformational changes are presented. Because multiptryptophan-containing proteins have certain tryptophans that are accessible to solute quencher and others that are inaccessible, this method can be used to determine the steady state anisotropy of each class of tryptophan residues. (57 refs.)

115747 Photon and fluorescence correlation spectroscopy and light scattering of eye-lens proteins at moderate concentrations. C.Andries, W.Guedens, J.Clauwaert (Dept. of Cell Biology, Univ. Instelling Antwerpen, Wilrijk, Belgium), H.Geerts.

Biophys. J. (USA), vol.43, no.3, p.345-54 (Sept. 1983).

The bovine eye-lens protein, α_1 -crystallin, has been studied with photon correlation spectroscopy to obtain the mutual diffusion coefficient, D_m , with fluorescence correlation spectroscopy to determine the tracer diffusion coefficient, D_T , and with light scattering to get the isothermal osmotic compressibility $(\delta\pi/\delta c)_{P,T}$. The concentration dependence of D_m , D_T , and $(\delta\pi/\delta c)_{P,T}$ up to a volume fraction ϕ of the protein of 2.5×10^{-2} has been interpreted on the basis of four different interaction potentials: (a) an extended hard-sphere potential; (b) a shielded Coulomb potential; (c) a shielded Coulomb interaction where the effect of counterions is included; (d) a simple mixed potential. The three parameters D_m , D_T , and $(\delta\pi/\delta c)_{P,T}$ have also been combined in the generalized Stokes-Einstein equation, $D_m = [(\delta\pi/\delta c)_{P,T} \cdot (1-\phi) \cdot (D_T)] / (k_B \cdot T)$. The results indicate that, in the case that photon correlation spectroscopy gives the mutual diffusion coefficient D_m , the applicability of the Stokes-Einstein equation can be questioned; or that, when one assumes the Stokes-Einstein equation to be valid, there is significant discrepancy between the result of photon correlation spectroscopy and D_m . (52 refs.)

115748 Fluorescent tandem phycobiliprotein conjugates. Emission wavelength shifting by energy transfer. A.N.Glazer, L.Stryer (Dept. of Microbiology & Immunology, Univ. of California, Berkeley, CA, USA).

Biophys. J. (USA), vol.43, no.3, p.383-6 (Sept. 1983).

A fluorescent tandem phycobiliprotein conjugate with a large Stokes shift was prepared by the covalent attachment of phycoerythrin to allophycocyanin. The efficiency of energy transfer from phycoerythrin to allophycocyanin in this disulfide-linked conjugate was 90%. A distinctive feature of this phycoerythrin-allophycocyanin conjugate is the wide separation between the intense absorption maximum of phycoerythrin ($\epsilon = 2.4 \times 10^6 \text{ cm}^{-1} \text{ M}^{-1}$ at 545 nm) and the fluorescence emission maximum of allophycocyanin (660 nm). Energy transfer from a donor to a covalently attached acceptor can be used to adjust the magnitude of the Stokes shift. Tandem phycobiliprotein conjugates can be used to advantage in fluorescence-activated cell sorting, fluorescence microscopy, and fluorescence immunoassay analyses. (9 refs.)

115749 Raman spectral studies of bleomycin A_2 and related structural fragments: a probe for bleomycin-DNA interactions. T.B.Freedman, F.S.Santillo, C.G.Zimba, L.A.Nafie, J.C.Dabrowiak (Dept. of Chem., Syracuse Univ., Syracuse, New York, USA).

J. Raman Spectrosc. (GB), vol.14, no.4, p.266-70 (Aug. 1983).

Raman spectra have been obtained for bleomycin A_2 and selected fragments. Virtually all of the features in the bleomycin Raman spectrum can be attributed to the preresonance enhanced vibrational transitions of the 2,4'-bithiazole moiety as determined by comparison to the Raman spectra of bithiazole fragments. The Raman spectrum of bleomycin is dominated by a very intense band at 1542 cm^{-1} that can be approximately assigned as a bithiazole ring stretching mode. This feature may serve as a probe of bithiazole environment in bleomycin-DNA interactions. (26 refs.)

115750 Pulsed laser induced vibrational resonance Raman scattering of chlorophyll *a* dimers. A.de Wilton, L.V.Haley, J.A.Koningstein (Dept. of Chem., Carleton Univ., Ottawa, Ontario, Canada).

J. Raman Spectrosc. (GB), vol.14, no.4, p.288-90 (Aug. 1983). The pulsed laser induced Raman spectrum of dry chlorophyll *a* (Chl *a*) in hexane is reported. This sample is excited with a wavelength which is in resonance with an absorption band of the Chl *a* dimer at 432 nm. The observed resonance Raman excitation profile for several Raman bands shows that two electronic origins of the dimer are located at 434.1 and 435.4 nm and these are assigned to a pair of pseudo exciton levels. Features of this excitation profile are used to discuss the observed Raman spectra. (6 refs.)

115751 NMR study of slowly exchanging imino protons in yeast tRNA^{Asp}. N.Figueroa (Groupe de Biophys., Ecole Polytech., Palaiseau, France), G.Keith, J.-L.Leroy, P.Plateau, S.Roy, M.Gueron.

Proc. Natl. Acad. Sci. USA, vol.80, no.14, p.4330-3 (July 1983). The authors have monitored the exchange of imino and amino protons by NMR after quick transfer of yeast tRNA^{Asp} in ²H₂O solvent. When the concentration of exchange-catalyzing buffer is not too high, one imino proton exchanges considerably more slowly than any other (e.g., 100 hr versus 4 hr for the second-slowest imino proton at 18°C in 15 mM Mg). This provides excellent conditions for identification, by the nuclear Overhauser effect, of the slowest exchanging proton, which the authors show to be the imino proton of the U-8-A-14 reverse Hoogsteen tertiary-structure base pair; other slowly exchanging protons are identified as imino protons from A-U-11 and G-Ψ-13. In preliminary experiments, the authors find that the exchange of these protons is catalyzed by cacodylate or Tris buffer. The lifetimes of two other imino protons, ca. 10 min at 28°C, are buffer independent. Slowly exchanging amino protons have also been observed. Correlation with the exchange of the uracil-8 imino proton suggests that they may be from adenine-14. (21 refs.)

115752 Carbon-13 nuclear magnetic resonance spectroscopy of some biologically active imidazoles. A.A.Al-Badr (Dept. of Pharmaceutical Chem., King Saud Univ., Riyadh, Saudi Arabia).

Spectrosc. Lett. (USA), vol.16, no.8, p.613-19 (1983). Carbon-13 NMR Spectral studies of imidazole and several of its derivatives have been undertaken, using chemical shift relationship, signal multiplicity and chemical shift additivity principles. The effect of the substitution, at all positions, on the chemical shift of the imidazole carbons is discussed. (8 refs.)

115753 Light induced anisotropy of bacteriorhodopsin. N.M.Burykin, N.N.Vsevolodov, T.V.Dyukova, E.Ya.Korchemskaia, M.S.Soskin, V.B.Taranenko.

Ukr. Fiz. Zh. (USSR), vol.28, no.8, p.1269-70 (Aug. 1983). In Russian. Investigates refraction induced by linearly polarised He-Ne laser radiation in 'Biochrome' films. Biochrome films are bacteriorhodopsin in a polymer matrix. The bacteriorhodopsin was obtained from purple membranes of Halobacterium halobium. (5 refs.) V.G.P.

Normal-coordinate analysis of retinal isomers and assignments of Raman and infrared bands See Entry 112707

Site selective rare earth spectroscopy in proteins See Entry 112886

New view of lipid bilayer dynamics from ²H and ¹³C NMR relaxation time measurements See Entry 115728

Structure of bacteriophage T7. Small-angle X-ray and neutron scattering study See Entry 115733

X-ray structure analysis of thin filaments of a molluscan smooth muscle in the living relaxed state See Entry 115734

Diode array versus photomultiplier for measuring the UV-excited resonance Raman spectra of enzyme-substrate transients See Entry 115985

Epitaxial crystallization of alkane chain lipids for electron diffraction analysis See Entry 115986

A low-cost microcomputer-based data acquisition and analysis system for an electron spin resonance spectrometer: data handling of dilute spin labeled nucleic acids See Entry 115987

87.16 BIOTHERMICS

115754 Radiosensitizing and cytotoxic effects of hyperthermia on various biological systems. Radiosensitizing and cytotoxic effect of hyperthermia on mouse leukemia La cells. L.V.Shtein, A.G.Konoplyannikov (Sci. Res. Inst. of Medical Radiology, Acad. of Medical Sci., Obninsk, USSR).

Radiobiologiya (USSR), vol.23, no.4, p.489-92 (1983). In Russian. When mouse leukemia cell suspensions were subjected to heating the survival rate of animals decreased exponentially with increasing time of heating. It is shown that an increase of temperature of 1°C in the range 40-45°C is equivalent to a decrease in the heating time by a factor of ~2. The hyperthermia-induced increase in the radiosensitivity of leukemia cells was dependent upon the medium in which the heating was performed. (17 refs.)

115755 The effect of elevated temperature on the vasculature of mouse jejunum. P.Falk (Medical Res. Council Cyclotron Unit, Hammersmith Hospital, London, England).

Br. J. Radiol. (GB), vol.56, no.661, p.41-9 (Jan. 1983). [received: Sept. 1983]. Both local and lower-body heating were employed, using a hot water bath; heating time was kept constant at 1 hour, bath temperatures ranging from 40.0°C to 43.0°C. Animals were sacrificed after heating, the erythrocytes were stained with benzidine and H₂O₂ and the blood vessels revealed by mounting in a clearing resin. The earliest damage seen was the disappearance of capillaries, followed by loss of progressively larger vessels. Loss is interpreted as destruction, not merely as interruption of blood flow. A gradient of sensitivity occurs from the inner layer of the jejunum to the outer, the threshold heating temperature required to produce vascular damage being lowest at the inside. Neither temperature gradient nor early release of gastric juice from the stomach appear responsible for this differential response. The mean length of intact venous tree was employed as a parameter for assessing the damage. (24 refs.)

115756 Thermal denaturing of collagen in solution and fibrils. G.I.Tsereteli (Phys. Faculty, Zhdanov State Univ., Leningrad, USSR).

Biophysics (GB), vol.27, no.5, p.817-23 (1982). Translation of: *Biofizika (USSR)*, vol.27, no.5, p.780-5 (1982). [received: Sept. 1983]. Differential scanning calorimetry using rates of heating in the range 0.3 to 25°C/min has been employed to investigate the thermal denaturing of rat skin collagen in the fibrils and aqueous solutions of different concentrations (0.2-98 per cent). It was found that the thermal effect of denaturing in solutions with a concentration above 10 per cent closely depends on the rate of heating: the thermal effect is greater the higher the rate of heating. On slow heating the enthalpy of denaturing H_d is minimal and depends very little on the rate of heating. In collagen fibrils and also in dilute solution the dependence of H_d on ν_H is not observed. In this case the value of H_d (20±2

cal/g) agrees with the value obtained in concentrated solutions on rapid heating and well agrees with the published findings. It is shown that fall in the value H_d in concentrated solutions with fall in the rate of heating is a manifestation of the exothermal process of post-denaturing aggregation of protein. (11 refs.)

115757 Thermodynamic approach to biomass distribution in ecological systems. D.Lurie, J.Valls, J.Wagensberg (Dept. Termodologia, Univ. de Barcelona, Barcelona, Spain).

Bull. Math. Biol. (GB), vol.45, no.5, p.869-72 (1983). In the derivation of the biomass distribution function for an ecological population critical use is made of an energetic constraint on the maximization of biomass diversity. The nature of this constraint is explored in detail using Kleiber's (1932) relation $\sigma(m) = cm^\gamma$ between animal metabolic rate $\sigma(m)$ and body weight m in conjunction with the Prigogine-Wiame (1946) thermodynamic paradigm for specific entropy production in biological stationary states. These two inputs fix the energetic constraint on the maximization of biomass diversity to be the constancy of the mean metabolic rate of the ecosystem. The resulting biomass distribution function is tested against observational data. (4 refs.)

115758 'Prompt' heat shock proteins: Translationally regulated synthesis of new proteins associated with the nuclear matrix-intermediate filaments as an early response to heat shock. T.Reiter, S.Penman (Dept. of Biology, MIT, Cambridge, MA, USA).

Proc. Natl. Acad. Sci. USA, vol.80, no.15, p.4737-41 (Aug. 1983). The response of mammalian cells, such as HeLa cells, to prolonged exposure to increased temperature (termed heat shock) has been well characterized. In these studies new mRNA is synthesized for several proteins whose translation is best seen after a return to 37°C. The authors show here another response to increased temperature of a distinctively different character. A set of at least 50 newly detectable proteins, exclusively associated with the nuclear matrix-intermediate filament (NM-IF) fraction, is synthesized immediately upon exposure to high temperature. These are of very low abundance or nonexistent in the unstressed cell and none appear to correspond to the 'classic' heat shock proteins produced after new transcription. Prior treatment with actinomycin D has little effect on these 'prompt' proteins, and they appear to be made from preexisting mRNAs that are activated at the increased temperature. The protein synthesis in the soluble, cytoskeletal, and chromatin fractions is strongly reduced by the increased temperature, while the labeling of the prompt proteins associated with NM-IF complex rapidly rises severalfold above that in control cells. Additionally these results suggest that the four cell fractions are not arbitrary cell divisions; rather they represent physiologically significant compartments in the cell. (28 refs.)

AC calorimeter for liquid including suspension of biological materials See Entry 111685

Analysis of the thermodynamic characteristics of the interaction of high potential cytochrome with a bacteriochlorophyll dimer at the reaction centres of the chromatophores of Ectothiorhodospira shaposhnikovii See Entry 115724

Magnetic proton relaxation of aqueous solutions of ribonuclease in the temperature region of intramolecular fusion See Entry 115742

Electrical discontinuity of tissue substitute models at 27.12 MHz See Entry 115772

Fluorescence of the leaves of higher plants at raised temperatures See Entry 115828

Teratogenicity of 27.12-MHz radiation in rats is related to duration of hyperthermic exposure See Entry 115833

Mathematical model of a simultaneous combined action of ionizing radiation and hyperthermia See Entry 115845

Comparison of the effects of radiation and hyperthermia on prenatal retardation of brain growth of guinea-pigs See Entry 115860

Comparative influence of hyperthermia and ionizing radiation on cycle and mitosis lengths in EMT6 mouse tumour cells See Entry 115869

Hyperthermia in a differentiating murine erythroleukemia cell line: cell killing by heat and radiation See Entry 115870

Effect of prolonged heating on the thermal enhancement ratio in X-irradiated murine intestine See Entry 115871

A microwave radiometer for medical applications See Entry 115896

Computer calculations of a one-dimensional model, useful in the application of hyperthermia See Entry 115899

The basics of cryosurgery See Entry 115970

Development of a cryo-probe suitable for gynaecological applications See Entry 115973

Hyperthermia, hypothermia See Entry 115975

87.20 MEMBRANE BIOPHYSICS

115759 Conductivity of bilayer lipid membranes of phosphatidic acid with phasic transition induced by temperature and pH. V.F.Antonov, A.N.Vasserman, A.A.Mol'nar, E.T.Kozhomkulov, L.Linke (Second Pirogov Medical Inst., Moscow, USSR).

Biophysics (GB), vol.27, no.5, p.862-7 (1982). Translation of: *Biofizika (USSR)*, vol.27, no.5, p.822-6 (1982). [received: Sept. 1983]. The authors have studied the conductivity of bilayer lipid membranes formed from synthetic phosphatidic acid and its thio analogues. It is shown that the conductivity of the bilayer membranes abruptly changes in the temperature region of the phasic transition. The temperature of the conductivity jump falls with shift in pH from the acid to the alkaline region. The amplitude of the jump may reach 1.5 to 2 orders. The jump may also be obtained at a constant temperature by changing the pH of the medium. It is assumed that the observed conductivity jumps may determine the phenomena of thermo- and chemo-reception in biological membranes. (16 refs.)

115760 Voltage-dependent K conductance at the apical membrane of Necturus gallbladder. J.F.Garcia-Diaz, W.Nagel, A.Essig (Dept. of Physiology, Boston Univ. School of Medicine, Boston, MA, USA).

Biophys. J. (USA), vol.43, no.3, p.269-78 (Sept. 1983). The epithelial and cellular effects of clamping the transepithelial potential (V_t , mucosa reference) have been investigated in the Necturus gallbladder. Following initial equilibration at short circuit, tissue conductance g_t was 4.1 ± 1.2 (SD) mS/cm², the apical potential V_a was -76 ± 8 mV, and the apical fractional voltage on brief voltage perturbation ($f_a = \Delta V_a / \Delta V_t$, reflecting the ratio of apical membrane to transcellular resistance) was 0.72 ± 0.11 (21 gallbladders, 34 impalements). On clamping V_t at positive values, V_a depolarized and f_a decreased; at the same time g_t decreased. Clamping V_t at negative values produced converse effects. All of the above changes were related directly to the magnitude of the clamping potential V_t and were

reversed on return to the short circuit state. Effects of V_i on f_o are not due to changes in the extracellular pathway resistances (which, however, contribute to g_i). Furthermore, the effects of V_i on f_o were abolished by the mucosal application of TEA or Ba, or acidification of the mucosal solution. Thus, these experiments disclose the presence of a voltage-dependent apical K conductance that increases with apical membrane depolarization. (50 refs.)

115761 Diffusion in lipid bilayers containing barriers. A.A.Rigos, D.F.Calef, J.M.Deutch (Dept. of Chem., MIT, Cambridge, MA, USA). *Biophys. J. (USA)*, vol.43, no.3, p.315-21 (Sept. 1983). In epithelial cells, a barrier or tight junction restricts the diffusion of lipid probes from the apical to the basolateral side of the outer membrane bilayer. This phenomenon is studied theoretically with the diffusion equation on planar and spherical surfaces. Two models for the tight junction are considered: a penetrable barrier embedded in a monolayer and an impenetrable obstacle in the outer membrane of a bilayer that must be bypassed by flip-flopping between inner and outer membranes. The rate of passing from one side of the cell to the other is calculated for each of these models under steady state conditions. The results are compared with recent fluorescent photobleaching recovery experiments. The theoretical interpretation indicates that it would be difficult to distinguish experimentally between the flip-flop case and the barrier crossing case. Assuming a flip-flop model, large differences in the magnitude of the flip-flop rates of probes are necessary to explain the experimental results as suggested by Dragsten et al. (Nature, vol.294, p.718-22, 1981). (15 refs.)

115762 Gating of ion channels made by a diphtheria toxin fragment in phospholipid bilayer membranes. S.Misler (Dept. of Physiology & Biophys., Albert Einstein Coll. of Medicine, New York, NY, USA). *Proc. Natl. Acad. Sci. USA*, vol.80, no.14, p.4320-4 (July 1983). B45, a fragment containing the major hydrophobic region of diphtheria toxin, increases the conductance of thin lipid membranes by forming ion-conducting channels that are gated by transmembrane voltage, V_m , and the bath pH. Single-channel currents show 'bursting' behavior in the form of rapid transitions between a closed and an open conductance level. The average duration of a current 'burst', as well as the total time a channel is actually open within a burst, decreases with increasing V_m . Analysis of these data suggests that, over a range of V_m , increases in the rate constants for transitions from the open to the closed states largely account for the decline in macroscopic conductance with increasing V_m . Increases in rate constants for transitions from a closed to an open conductance state are more likely to account for the increase in macroscopic conductance with increasing bath pH. (12 refs.)

Study of the parameters of the fluorescent spectra of probes in model conditions [biomembrane application] See Entry 115723

New view of lipid bilayer dynamics from ^2H and ^{13}C NMR relaxation time measurements See Entry 115728

Neutron diffraction analysis of cytochrome b_5 reconstituted in deuterated lipid multilayers See Entry 115745

Light induced anisotropy of bacteriorhodopsin See Entry 115753

Dependence of the structural lability of the outer membrane of liver mitochondria on the age and sex of rats See Entry 115764

Increased membrane permeability to chloride in Duchenne muscular dystrophy fibroblasts and its relationship to muscle function See Entry 115771

Effect of 8-methoxypsoralen and ultraviolet radiation on the electrical stability of liposome membranes See Entry 115862

Effect of gamma radiation on enzymatic activity and sulphhydryl groups of human erythrocyte membrane See Entry 115872

Effect of adenine nucleotides and gamma radiation on the transport of TEM-POL across the erythrocyte membrane See Entry 115873

The effect of ionizing radiation on tryptophan fluorescence of thymocyte and erythrocyte plasma membranes See Entry 115874

87.25 CELLULAR BIOPHYSICS

115763 Optical characteristics of individual plant elements and plant canopies grown under radiation regimes of different spectral composition and intensity. A.A.Tikhomirov, F.Ya.Sidko (Biophys. Inst., Acad. of Sci., Krasnoyarsk, USSR). *Appl. Opt. (USA)*, vol.22, no.18, p.2874-81 (15 Sept. 1983). The character of the interaction of radiation with the elements of plant canopies determines the light conditions for their photosynthesis and hence for the formation of the final yield. Investigation of the dependence of the optical properties of canopies on the irradiation conditions makes it necessary to know the variability of the optical properties of both individual phytoelements and whole canopies. If the distribution of radiation within a canopy and the character of transformation of the spectral composition of the radiation penetrating the canopy are known, the efficiency of assimilation of radiant energy can be more accurately estimated. Obtaining such information may be helpful in selecting optimum radiation conditions for canopies of a different structure. This paper examines certain optical characteristics of canopies having different optical densities and their individual phytoelements as well as several characteristics of the radiation field in canopies during their prolonged growth while illuminated with radiant fluxes of different intensities and spectral compositions of photosynthetically active radiation. (17 refs.)

115764 Dependence of the structural lability of the outer membrane of liver mitochondria on the age and sex of rats. V.V.Lemeshko (Gorkii State Univ., Kharkov, Ukrainian SSR). *Biophysics (GB)*, vol.27, no.5, p.877-81 (1982). Translation of: *Biofizika (USSR)*, vol.27, no.5, p.837-40 (1982). [received: Sept. 1983] The experiments reported show that with age the structural lability of the outer membrane of the liver mitochondria of male rats evaluated from hypotonic treatment of the organelles increases. In old age the strength of the outer membrane of the mitochondria in the males is considerably less than in the females. (10 refs.)

115765 Simultaneous measurements of proton motive force, ΔpH , membrane potential, and H^+/O ratios in intact *Escherichia coli*. O.H.Setty, R.W.Hendler, R.I.Shrager (Lab. of Appl. Studies, Div. of Computer Res. & Technol., National Inst. of Health, Bethesda, MD, USA). *Biophys. J. (USA)*, vol.43, no.3, p.371-81 (Sept. 1983). An instrument is described that enables the simultaneous monitoring of proton motive force (PMF), membrane potential ($\Delta\psi$), the ΔpH across a membrane, oxidase activity, proton movements, and H^+/O ratios. The authors have studied the relationship existing among these parameters of energy transduction as a critical condition is changed during an experiment. The major findings described include (a) In the pH range of 4.5 to 7.5, increasing the external pH causes an increase in $\Delta\psi$, internal pH, and oxidase activity, a decrease in H^+/O ratio, and a peak-plateau in PMF from pH 5.5 to 6.6 where ΔpH is converted to $\Delta\psi$. (b) An increase in $[\text{K}^+]$ from 1 to 100 mM,

in the presence of 0.5 μM valinomycin, causes the conversion of $\Delta\psi$ to ΔpH , a gradual decline in PMF and an increase in H^+/O ratio, internal pH, and oxidase activity. (28 refs.)

115766 Mathematical model of the velocity field external to a tank-treading red cell. S.P.Sutera, R.Tran Son Tay (Mech. Engng. Dept., Washington Univ., St. Louis, MO, USA). *Biorheology (GB)*, vol.20, no.3, p.267-82 (1983). The velocity field external to a stationary ellipsoidal particle with continuously rotating surface motion driven by a surrounding shear flow is calculated. The configuration is intended to model the so-called 'tank-treading' behavior of mammalian erythrocytes (red cells) when suspended in shear flow. The boundary-value problem posed is based on the model developed by Keller and Skalak (1982) and is solved by adapting Jeffrey's general solution (1922) for the Stokes flow about a rigid, freely rotating ellipsoid immersed in an unbounded viscous flow. Streamlines and velocity profiles in the plane of symmetry are obtained by numerical computations. The flow pattern reveals two free stagnation points near the ends of the particle and the streamlines branching from these points delineate a region of closed streamlines surrounding the particle and two recirculating wakes extending to infinity both upstream and downstream of the particle. The presence of the wakes suggests a mechanism for enhanced diffusion of smaller solute particles in the surrounding fluid. (17 refs.)

115767 The motion of close-packed red blood cells in shear flow. T.W.Secomb, T.M.Fischer, R.Skalak (Dept. of Physiology, Univ. of Arizona, Tucson, AZ, USA). *Biorheology (GB)*, vol.20, no.3, p.283-94 (1983). Experimental and theoretical results are presented concerning the motion of close-packed red blood cell suspensions subjected to steady simple shear flow. The behavior of the suspension was observed microscopically using a cone-and-plate rheoscope. At moderate and high shear rates the cells show a fairly orderly arrangement, each appearing polygonal in the field of view. An idealized theoretical model for the suspension is developed, in which each cell is a 14-sided polyhedron of varying shape, but with constant surface area and volume. Tank-treading motion of the membrane is predicted, and an approximation to the motion is calculated which is consistent with the known mechanical properties of the membrane. It is shown that considerably more energy is dissipated in the membrane than in the cytoplasm during tank-treading. (16 refs.)

115768 Indices of filterability of red blood cell suspensions. R.Skalak (Dept. of Civil Engng. & Engng. Mech., Columbia Univ., New York, NY, USA), M.Hanss, S.Chien. *Biorheology (GB)*, vol.20, no.3, p.311-16 (1983). A number of different experimental techniques have been devised in recent years to use microsieving as a test of the filterability of suspensions of red blood cells. Various indices have been proposed to express the results of these tests. In the present paper a correlation is made of the intrinsic increase in resistance at the level of a single pore in the filter to the macroscopically observed pressure and flow through the entire filter. Further it is shown how a number of different tests may be used to derive the same index. The results apply only to situations in which there is no plugging of pores. (14 refs.)

Spectroscopy by photothermal radiometry See Entry 111774

Analysis of the thermodynamic characteristics of the interaction of high potential cytochrome with a bacteriochlorophyll dimer at the reaction centres of the chromatophores of *Ectothiorhodospira shaposhnikovii* See Entry 115724

Radiosensitizing and cytotoxic effects of hyperthermia on various biological systems. Radiosensitizing and cytotoxic effect of hyperthermia on mouse leukosis La cells See Entry 115754

'Prompt' heat shock proteins: Translationally regulated synthesis of new proteins associated with the nuclear matrix-intermediate filaments as an early response to heat shock See Entry 115758

The bulk rheology of close-packed red blood cells in shear flow See Entry 115816

Effect of constant magnetic field (CMF) and γ -radiation on hereditary structures of somatic cells. Combined effect of CMF and γ -radiation on human lymphocytes in vitro See Entry 115826

Suppression of T-lymphocyte cytotoxicity following exposure to sinusoidally amplitude-modulated fields See Entry 115834

Effect of microwave radiation on cell immunity in conditions of chronic exposure See Entry 115835

Damages to superhelical structures of nuclear DNA induced by γ -rays and heavy ions See Entry 115839

Enhancement of biological effectiveness of low-energy quantum radiation. Microdosimetric basis for a selective action of ionizing radiation on the chromosomal material of cells See Entry 115840

Radiation damage and recovery of mouse T-cells. Dynamics of suppressor cells after the effect of radiation See Entry 115841

Influence of duration of fixation on the yield of chromosome aberrations in human lymphocyte culture exposed to γ -radiation at different mitotic cycle stages See Entry 115842

Influence of dose-rate and dose fractionation on radiation damage to bone marrow cells forming granulocyte-macrophagal colonies in diffusion chambers (CFUdc) See Entry 115843

Radiosensitivity of bone marrow and spleen CFUdc in mice γ -irradiated in different oxygenation conditions See Entry 115844

Migration of lymphocytes within the internally irradiated body. Effect of internal γ -irradiation on migrating capacity of splenic lymphocytes labeled with ^{51}Cr See Entry 115846

Lymphocyte migration under conditions of incorporated irradiation. Effect of incorporated β -irradiation on spleen lymphocyte migration in CBA mice See Entry 115847

Effect of X-radiation on histones and DNA in nuclei of rat bone marrow and liver See Entry 115850

Electric conductivity of liver cells as a function of dose at early times after γ -irradiation See Entry 115851

Radiosensitivity of homopoietic stroma precursors from long-term bone marrow culture See Entry 115852

Age-related changes in postirradiation recovery of blood system See Entry 115853

On the mechanisms of a change in the coloration of garden rose mutants See Entry 115857

Relative efficiencies of three ultraviolet radiation wavelengths for cell killing and transformation in mouse cells in vitro See Entry 115866

- Measurement of lymphoblastogenic activity from thorium workers See Entry 115867
- Comparative influence of hyperthermia and ionizing radiation on cycle and mitosis lengths in EMT6 mouse tumour cells See Entry 115869
- Hyperthermia in a differentiating murine erythroleukemia cell line: cell killing by heat and radiation See Entry 115870
- Effect of gamma radiation on enzymatic activity and sulphhydryl groups of human erythrocyte membrane See Entry 115872
- The effect of ionizing radiation on tryptophan fluorescence of thymocyte and erythrocyte plasma membranes See Entry 115874
- Intrinsic resistance to the lethal effects of X-irradiation in insect and arachnid cells See Entry 115877
- Determination of left-ventricular volume from first-pass kinetics of labeled red cells See Entry 115912
- Conductimetric method of determining the hematocrit value of blood See Entry 115965

87.25D Biological transport; cellular and subcellular transmembrane physics

- 115769 Evaluation of the probability of penetration of paramagnetic ions into the cells by the NMR pulse method.** A.Anisimov, A.S.Yevaretskov (Kazan Inst. of Biology, Kazan, USSR). *Biophysics (GB)*, vol.27, no.5, p.858-62 (1982). Translation of: *Biofizika (USSR)*, vol.27, no.5, p.818-21 (1982). [received: Sept. 1983]
- To evaluate the probability of the penetration of paramagnetic ions into the cells in investigations of water exchange through the cell membranes the authors propose measurements of the time of transverse relaxation of the intracellular water in conditions of pulse radiofrequency saturation of longitudinal magnetization. (3 refs.)
- 115770 On oxygen diffusion in a spherical cell with Michaelis-Menten oxygen uptake kinetics.** P.Hiltmann, P.Lory (Inst. fur Math., Tech. Univ. Munchen, Munchen, Germany). *Bull. Math. Biol. (GB)*, vol.45, no.5, p.661-4 (1983).
- Demonstrates that there is one and only one solution to a non-linear singular two-point boundary-value problem which describes oxygen diffusion in a spherical cell. Previous authors have calculated numerical results that differ substantially. Numerical computations using the multiple shooting method support the results of McElwain (1978). (8 refs.)
- 115771 Increased membrane permeability to chloride in Duchenne muscular dystrophy fibroblasts and its relationship to muscle function.** C.N.Pato, M.H.Davis, M.J.Doughty, S.H.Bryant, E.Gruenstein (Depts. of Biological Chem., Pharmacology & Cell Biophys., Coll. of Medicine, Univ. of Cincinnati, Cincinnati, OH, USA). *Proc. Natl. Acad. Sci. USA*, vol.80, no.15, p.4732-6 (Aug. 1983).
- Previous studies have suggested an abnormality in Cl^- metabolism in Duchenne muscular dystrophy (DMD) fibroblasts. In order to further characterize this abnormality, the authors have studied $^{36}\text{Cl}^-$ distribution and permeability in 11 DMD and 12 normal fibroblast lines. Under steady-state conditions Cl^- efflux in fibroblasts is observed to be biphasic, revealing the presence of two major subcellular compartments. Each compartment contains approximately half of the cellular Cl^- . The faster of the two observed efflux components is significantly higher in DMD than in control fibroblasts ($P < 0.001$). To determine the results of a similar increase in Cl^- permeability on skeletal muscle action potentials, the authors have simulated the effects of increased Cl^- conductance on muscle by using a computer model. Effects on the simulated action potential include lower rates of membrane depolarization, lower overpotential, longer duration, and lower input resistance. These effects are similar to those actually observed in DMD muscle. (24 refs.)
- Diffusion in lipid bilayers containing barriers See Entry 115761
- Gating of ion channels made by a diphtheria toxin fragment in phospholipid bilayer membranes See Entry 115762
- Fluctuation and linear analysis of Na-current kinetics in squid axon See Entry 115774
- Transient transport across the blood-retina barrier See Entry 115783
- Effect of adenine nucleotides and gamma radiation on the transport of TEM-POL across the erythrocyte membrane See Entry 115873

87.30 BIOPHYSICS OF NEUROPHYSIOLOGICAL PROCESSES

(exc. perception processes and speech)

- 115772 Electrical discontinuity of tissue substitute models at 27.12 MHz.** J.F.Lehmann, J.A.McDougall, A.W.Guy, C.-K.Chou, P.C.Esselman, C.G.Warren (Dept. of Rehabilitation Medicine, School of Medicine, Univ. of Washington, Seattle, WA, USA). *Bioelectromagnetics (USA)*, vol.4, no.3, p.257-65 (1983).
- Tissue-substitute models consisting of layers of synthetic, electrically equivalent subcutaneous fat, muscle, and bone shaped in conformation with the normal anatomy are used for rapid determination of distribution of temperature and specific absorption rate throughout the tissues when exposed to electromagnetic radiation. The surfaces of the bisected models are approximated during a short exposure period, then separated and scanned with a thermograph. A method was developed to eliminate the electrical discontinuity at the bisected surfaces while alloying separation and subsequent thermographic scanning. A thin layer of silk screen wetted with propylene glycol saturated with sodium chloride was used at the fat interface and a 0.9% sodium chloride solution was used to wet the screen at the muscle interface to eliminate electrical discontinuity during exposure to 27.12-MHz diathermy. Tests showed that in the presence of an electrical discontinuity the heating pattern was grossly distorted. With the method used, the electrical discontinuity is minimized and the subsequent thermographic scanning reveals that the heating pattern is equivalent to that of an intact model. (9 refs.)
- 115773 Absorption of calcium by the squid nerve trunks as a function of the frequency of rhythmic excitation.** G.V.Maksimov, N.V.Kaverina, S.N.Orlov, O.R.Kol's (Biology Faculty, Lomonosov State Univ., Moscow, USSR). *Biophysics (GB)*, vol.27, no.5, p.881-4 (1982). Translation of: *Biofizika (USSR)*, vol.27, no.5, p.841-3 (1982). [received: Sept. 1983]
- It has been established that the uptake of ^{45}Ca by squid axons increases on excitation and depends on the frequency of rhythmic stimulation. The maximum uptake of Ca occurs for excitation rhythms of 10 and 30 pulse/sec. In conditions of moderate loads the intensity of Ca uptake is determined by the frequency of stimulation and not by the number of pulses travelling along the

nerve. The link between the intensity of uptake of Ca and the functioning of the Na- and Ca-channels is discussed. (5 refs.)

- 115774 Fluctuation and linear analysis of Na-current kinetics in squid axon.** H.M.Fishman, H.R.Leuchtag, L.E.Moore (Dept. of Physiology & Biophys., Univ. of Texas Medical Branch, Galveston, TX, USA). *Biophys. J. (USA)*, vol.43, no.3, p.293-307 (Sept. 1983).
- The power spectrum of current fluctuations and the complex admittance of squid axon were determined in the frequency range 12.5 to 5000 Hz during membrane voltage clamps to the same potentials in the same axon during internal perfusion with cesium. The complex admittance was determined rapidly and with high resolution by a fast Fourier transform computation of the current response, acquired after a steady state was attained, to a synthesized signal with predetermined spectral characteristics superposed as a continuous, repetitive, small perturbation on step voltage clamps. Linear conduction parameters were estimated directly from admittance data by fitting an admittance model, derived from the linearized Hodgkin-Huxley equations modified by replacing the membrane capacitance with a 'constant-phase-angle' capacitance, to the data. The constant phase angle obtained was $\sim 81^\circ$. At depolarizations the phase of the admittance was 180° , and the real part of the impedance locus was in the left-half complex plane for frequencies below 1 kHz, which indicates a steady-state negative Na conductance. (39 refs.)
- 115775 Molecular mechanism of sodium conductance changes in nerve: the role of electron transfer and energy migration.** C.-Y.Lee (Dept. of Chem., Univ. of Houston, Houston, TX, USA). *Bull. Math. Biol. (GB)*, vol.45, no.5, p.759-80 (1983).
- Shows that the Na conductance changes can be explained quantitatively, based on the following assumptions: (1) there exist in nerve membranes electron transfer (ET) complexes and traps, (2) there is energy migration among them. The gating mechanism is explained in physical terms. Its mathematical expression differs from the Hodgkin-Huxley equations, but resembles the Hoyt formulation. In the present model, the physical parameters for the squid axon can be estimated from currently available experimental data. The density of the ET complexes is on the order of $10^3/\mu\text{m}^2$, and the density of the traps is $10^3/\mu\text{m}^2$. The magnitude of the energy transfer rate between ET complexes is about $10^6/\text{sec}$ at large depolarization and decreases with decreasing depolarizations, as does the Na inactivation rate. The energy gap between the two stable states of the transfer electron in the ET complex is estimated to be around 0.1 eV, which is approximately the same as that for photosynthetic systems. (55 refs.)
- 115776 The dynamics of symmetric nets.** A.Muir, M.W.Warner (City Univ., London, England). *Bull. Math. Biol. (GB)*, vol.45, no.5, p.781-92 (1983).
- The role of symmetry in simplifying the theory of complex neural systems is argued. When the structural symmetries of a network are expressed as an isomorphism group, implications emerge for the dynamics. Various qualitative possibilities concerning stability of uniform motion in homogeneous nets are discussed and an approach to neural hierarchies is outlined. (25 refs.)
- 115777 The influence of unipolar pulse currents on human body.** V.Klimova. *Elektrotech. Obz. (Czechoslovakia)*, vol.72, no.7, p.369-70 (July 1983). In Czech.
- Discusses the effects of fault pulse currents which can arise in electronic instrumentation on heart failure (fibrillation) in relation to the IEC standards. Various types of pulses are considered, namely square pulse, sinusoidal pulse and capacitor discharge pulse. Characteristic variables determined on the basis of studies of the threshold of perceptibility and the threshold of pain are discussed. (1 ref.) E.D.
- 115778 Hopf bifurcation to repetitive activity in nerve.** J.Rinzel (Nat. Inst. of Arthritis, Diabetes, Digestive & Kidney Diseases, Nat. Inst. of Health, Bethesda, MD, USA). *SIAM J. Appl. Math. (USA)*, vol.43, no.4, p.907-22 (Aug. 1983).
- Various nerve axons and other excitable systems exhibit repetitive activity (e.g. trains of propagated impulses) in response to a spatially localized, time-independent stimulus. If the stimulus is too weak, or in some cases too strong, one finds rather a spatially nonuniform, steady response which attenuates with distance from the input site. The authors consider these stimulus-response properties for a qualitative model of nerve conduction, the FitzHugh-Nagumo (parabolic partial differential) equations. For each stimulus amplitude there is a unique steady state solution. At critical stimulus values this steady solution loses stability and a branch of time periodic (spatially nonuniform) solutions appears via Hopf bifurcation. The authors associate this with the onset of repetitive activity. They derive analytic bifurcation formulae and evaluate these for the case of a cubic nonlinearity to determine regions in parameter space where the steady solution is unstable. They interpret physiologically the effect of stimulus form: either voltage or current input, and either spatially localized or spatially uniform stimulus. (11 refs.)
- 115779 A neural network model for the mechanism of feature extraction—a self-organizing network with feedback inhibition.** S.Miyake, K.Fukushima (NHK Broadcasting Sci. Res. Labs., Tokyo, Japan). *Trans. Inst. Electron. & Commun. Eng. Jpn. Part A (Japan)*, vol.J66A, no.6, p.500-7 (June 1983). In Japanese.
- Proposes a self-organizing multilayered neural network model which has modifiable inhibitory feedback connections together with the conventional feed forward connections. If a feature which is already familiar to the network is given to the receptive field of a cell, the cell responds, and consequently the responses of its presynaptic cells are suppressed receiving feedback inhibition. On the contrary, to an unfamiliar feature, the presynaptic cells do not change their responses because of no feedback inhibition. Since the synapses from the presynaptic cells which yield large sustained outputs grow, the cells for detecting novel features quickly develop, and the network acquires a favorable pattern-selectivity. (5 refs.)
- 115780 Mathematical structure of bio-electrical impedance obtained from linear functional point of view.** T.Yamamoto, Y.Yamamoto, E.Mizufune (School of Engng., Okayama Univ., Okayama, Japan). *Trans. Inst. Electron. & Commun. Eng. Jpn. Sect. E (Japan)*, vol.E66, no.6, p.352-8 (June 1983).
- From circle to circle correspondence in mapping theory of the linear function $Z=(ah+b)/(ch+d)$, it is known that Z also describes a circle when its variable h describes a circle or a straight line. From this point of view, the linear functional expression of bioelectrical impedance having a circular locus is discussed in detail. As a result, it became clear that three types h_0 , h_1 and h_2 exist of the variable h and the characteristics of bio-impedance expressions for each of h_0 , h_1 and h_2 are as follows. For the expression by h_0 : (1) a polarization impedance having a constant phase angle appears; (2) the most original equation of bio-impedance can be proposed; (3) the linear or non-linear bio-impedance can be deduced from this original equation; (4) the equivalent circuits satisfying Cole-Cole's circular arc are of two types. For the expressions by h_1 and h_2 : (1) these expressions correspond to the expression using the combination in group theory of the linear function; (2) taking

account of combination, countless equivalent circuits satisfying Cole-Cole's circular arc exist. (10 refs.)

115781 Feature extractions for pattern recognition of body surface isopotential maps [in ECGs]. N.Akamatsu (Faculty of Engng., Tokushima Univ., Tokushima, Japan), S.Ishibashi. *Trans. Inst. Electron. & Commun. Eng. Jpn. Sect. E (Japan)*, vol.E66, no.6, p.403-4 (June 1983). Defines three parameters for feature extraction of body surface isopotential maps. It was found that these parameters marked different characteristics according to the different patterns of the maps. (3 refs.)

Conductivity of bilayer lipid membranes of phosphatidic acid with phasic transition induced by temperature and pH See Entry 115759

Voltage-dependent K conductance at the apical membrane of Necturus gall-bladder See Entry 115760

Gating of ion channels made by a diphtheria toxin fragment in phospholipid bilayer membranes See Entry 115762

Simultaneous measurements of proton motive force, ΔpH, membrane potential, and H⁺/O ratios in intact Escherichia coli See Entry 115765

Behavioral detection of 60-Hz electric fields by rats See Entry 115825

Electric conductivity of liver cells as a function of dose at early times after γ-irradiation See Entry 115851

Effect of 8-methoxypsoralen and ultraviolet radiation on the electrical stability of liposome membranes See Entry 115862

Non-invasive recording of human His-bundle activity using a newly designed device aided by a microcomputer See Entry 115951

Electrocardiography See Entry 115957

The recent trend of biomedical signal processing research See Entry 115958

Information structure analysis of body surface potential maps See Entry 115959

Development of a real-time monitoring system of spatial ST vector See Entry 115960

A computerized analysis system of masticatory electromyograph with silent period See Entry 115964

Development of a microprocessor-based ECG signal processing method See Entry 115966

Aspects of standardisation and validation of automatic ECG interpreting systems See Entry 115967

The stereotrode: a new technique for simultaneous isolation of several single units in the central nervous system from multiple unit records See Entry 115990

A comparison of the selectivities of microelectrodes incorporating the Orion and Corning liquid ion exchangers for potassium over sodium See Entry 115991

87.32 PHYSIOLOGICAL OPTICS, VISION

Photon and fluorescence correlation spectroscopy and light scattering of eye-lens proteins at moderate concentrations See Entry 115747

Influence of intraocular scattered light on lightness-scaling experiments See Entry 115782

Light sources for fluorescein fluorophotometry See Entry 115893

Optimum conditions for protecting the eyes from solar radiation in vision correction See Entry 115933

87.32C Anatomy and optics of the eye

115782 Influence of intraocular scattered light on lightness-scaling experiments. W.A.Stiehl, J.J.McCann, R.L.Savoy (Vision Res. Lab., Polaroid Corp., Cambridge, MA, USA). *J. Opt. Soc. Am. (USA)*, vol.73, no.9, p.1143-8 (Sept. 1983). Following Munsell's bisection procedure (see *ibid.*, vol.23, p.394, 1933) the authors established a nine-step gray scale in which each step is an equal increment in lightness. The authors calculated retinal illuminances after intraocular scatter by using the point-spread function of Vos et al. (see *Vision Res.*, vol.16, p.215, 1976). After this correction for intraocular scatter, the authors find a logarithmic relationship between retinal illuminance and achromatic lightness scales that are determined by the bisection method. Additional bisection experiments with a series of different backgrounds corroborate this result. The authors find that lightness depends linearly on the logarithm of scatter-corrected retinal illuminance, with different slopes for backgrounds of different lightness. This study also highlights the importance of using scatter-corrected illuminance in any quantitative model of lightness. (19 refs.)

87.32E Physiology of the eye; nerve structure and function

115783 Transient transport across the blood-retina barrier. J.Larsen (Math.-Tech. Inst., Charlottenlund, Denmark), H.Lund-Andersen, B.Krogsaa. *Bull. Math. Biol. (GB)*, vol.45, no.5, p.749-58 (1983). A mathematical model of the transport of fluorescein across the blood-retina barrier in the transient state and the subsequent diffusion of fluorescein in the vitreous body is presented. The function of the barrier is lumped in a single parameter—the permeability. The sensitivity of this parameter due to changes in the other parameters of the model is given. This establishes the foundation for the quantitative assessment of the barrier function through vitreous fluorophotometry. (14 refs.)

115784 Identification of human oculomotor system for quantitative diagnostics of eye muscle diseases. H.Helmle, G.Jahn, J.Bille (Inst. fur Angewandte Phys., Univ. Heidelberg, Heidelberg, Germany). *Comput. Biol. & Med. (GB)*, vol.13, no.3, p.189-204 (1983). Various discrete parameter estimation methods are explained and applied to the eye muscle model of Collins (1975). Their effectiveness and accuracy are studied. Comparing saccadic eye movements to the motions of a fixation target data for parameter estimation are provided. As a first application, saccades of a subject with a Duane-Syndrome are evaluated. (13 refs.)

115785 Neural mechanisms of pattern vision in the monkey. III. The neurobehavioural basis. S.Yaginuma (Dept. of Behavioral Physiology, Tokyo Metropolitan Inst. for Neurosci., Fuchu, Japan). *J. Inst. Electron. & Commun. Eng. Jpn. (Japan)*, vol.66, no.3, p.241-6 (March 1983). In Japanese. For pt.II see *ibid.*, vol.66, no.2, p.173 (1983). Pattern recognition consists of identifying through sensory systems the two-dimensional shape and feature of objects in an environment. On the basis of neurobehavioural findings from monkeys, central-nervous development in perceptual and understanding processes in making pattern recognition is discussed in this review paper. The article contains: (1) the inferotemporal cortex as a pattern recognition center, (2) dual nervous functions for completing pattern recognition, (3) the output area to the pattern recognition center, (4) the functional interaction between pattern-recognition systems and reception systems, and (5) the role of nervous function of spatial positioning and information selection actions in feature establishment processes. (38 refs.) *K.B.*

115786 Interactions among converging sensory inputs in the superior colliculus. M.A.Meredith, B.E.Stein (Medical Coll. of Virginia, Richmond, VA, USA). *Science (USA)*, vol.221, no.4608, p.389-91 (22 July 1983).

The responses of superior colliculus cells to a given sensory stimulus were influenced by the presence or absence of other sensory cues. By pooling sensory inputs, many superior colliculus cells seem to amplify the effects of subtle environmental cues in certain conditions, whereas in others, responses to normally effective stimuli can be blocked. The observations illustrate the dynamic, interactive nature of the multisensory inputs which characterize the deeper laminae of the superior colliculus. (5 refs.)

115787 Signal transfer among retinal neurons. M.Sakuranaga (Dept. of Phys., Nippon Medical School, Tokyo, Japan), K.-I.Naka. Identification and System Parameter Estimation 1982. Proceedings of the Sixth IFAC Symposium, Washington, DC, USA, 7-11 June 1982 (Oxford, England: Pergamon 1983), p.481-4 vol.1

A new branch of neurophysiology is introduced and discussed where emphasis is placed on the temporal and spatial characteristics of signal processing in a complex circuitry of the nervous system. The generalized methodology based on the Volterra/Wiener approach is stressed to provide a valuable means by which signal transformation is interpreted. Basic concepts are outlined on which the signal transmission within a vertebrate retina is analyzed. Four kinds of mode are elucidated for the signal transfer in the vertebrate retina. (11 refs.)

115788 Spatiotemporal nonlinear analysis of frog horizontal cells. M.C.Citron (Children's Hospital of Los Angeles, Los Angeles, CA, USA), T.E.Ogden, R.B.Melton.

Identification and System Parameter Estimation 1982. Proceedings of the Sixth IFAC Symposium, Washington, DC, USA, 7-11 June 1982 (Oxford, England: Pergamon 1983), p.485-8 vol.1

Describes the shapes of horizontal cell receptive fields in the frog retina were determined using a retinotopic mapping technique based on a 16×16 spatial array of stimuli. Fields derived from first order kernel magnitude were sometimes circular but more often elliptical. Morphologic studies of Golgi stained horizontal cells showed most to be elliptical with a nonrandom orientation tending to orthogonality. It is suggested that this feature makes unlikely an explanation of field eccentricity based on cell alignment. It is noted that cell axons tend to cross the retina in a line and may function as an extended dendrite to provide the eccentric and elliptical receptive fields. (15 refs.)

115789 The contrast gain control and feedback within the retina. R.Shapley (Rockefeller Univ., New York, NY, USA).

Identification and System Parameter Estimation 1982. Proceedings of the Sixth IFAC Symposium, Washington, DC, USA, 7-11 June 1982 (Oxford, England: Pergamon 1983), p.489-94 vol.1

The retina of the cat contains a contrast gain control which measures the average contrast over a wide area of the retina and adjusts the dynamics of retinal signal processing. This mechanism is a feedback mechanism. It seems to be a nonlinear feedback which modulates the gain-bandwidth product of linear feedbacks within the retina. The existence and properties of the contrast gain control have been discovered by applying techniques of nonlinear systems analysis to the study of the retina. (9 refs.)

Analysis of Helmholtz-Hering illusion by multiple channel model See Entry 115794

Mathematical model for vestibulo-ocular reflex See Entry 115812

87.32L Light detection; adaptation and discrimination

115790 Spectral consequences of photoreceptor sampling in the rhesus retina. J.I.Yellott,Jr. (School of Social Sci., Univ. of California, Irvine, CA, USA).

Science (USA), vol.221, no.4608, p.382-5 (22 July 1983). Optical transforms were used to compute the power spectra of rhesus cones treated as arrays of image sampling points. Spectra were obtained for the central fovea, parafovea, periphery, and far periphery. All were consistent with a novel spatial sampling principle that introduces minimal noise for spatial frequencies below the Nyquist limits implied by local receptor densities, while frequencies above the nominal Nyquist limits are not converted into conspicuous moire patterns, but instead are scattered into broadband noise. This sampling scheme allows the visual system to escape aliasing distortion despite a large mismatch between retinal image bandwidth and the Nyquist limits implied by extrafoveal cone densities. (11 refs.)

Photophysical processes in the molecules of retinoids related to visual chromophores See Entry 115743

Picosecond kinetic absorption and fluorescence studies of bovine rhodopsin with a fixed 11-ene See Entry 115744

An analog-digital feedback system for measuring photoreceptor properties with an equal response method See Entry 115989

87.32N Colour detection; adaptation and discrimination

115791 Consequences of spatial sampling by a human photoreceptor mosaic. D.R.Williams, R.Collier (Center for Visual Sci., Univ. of Rochester, Rochester, NY, USA).

Science (USA), vol.221, no.4608, p.385-7 (22 July 1983). The short wavelength color mechanism in the human visual system can distinguish gratings from uniform fields of the same average radiance at spatial frequencies that are twice as high as the highest at which it can resolve bars in the grating. This discrimination above the resolution limit is associated with a splotchy or mottled appearance of the grating similar to two-dimensional noise. The most plausible explanation for the mottled pattern is

that it is a moire pattern produced by aliasing (spatial undersampling) by an irregular and sparse mosaic of short wavelength cones. (15 refs.)

115792 Human information processing and color displays. J.Durrett, C.Zwiener (Center for Automated Systems in Education, Southwest Texas State Univ., San Marcos, TX, USA). Southcon/81 Conference Record, Atlanta, GA, USA, 13-15 Jan. 1981 (El Segundo, CA, USA: Electron. Conventions 1981), p.12-1/1-7. The authors review the existing literature on the influence of color on human information processing as it relates to the use of color displays. The authors then discuss current research efforts at the Centre for Automated Systems in Education (CASE) directed at the empirical study of color displays. This entails the validation and evaluation of hardware, software and courseware systems used in interactive automated systems. Further, CASE investigates the human factors of using such automated systems. The CASE development effort is directed at applying the results of empirical research to automated system use and design to produce optimal human interaction. (18 refs.)

87.32S Psychophysics of vision, visual perception, binocular vision

115793 Hidden information in early visual processing. H.K.Nishihara (Artificial Intelligence Lab., MIT, Cambridge, MA, USA). *Proc. SPIE Int. Soc. Opt. Eng. (USA)*, vol.360, p.76-87 (1982). [received: July 1983] (Robotics and Industrial Inspection, San Diego, CA, USA, 24-27 Aug. 1982). A definition of scale-specific structure follows from the work of Marr and Poggio (1979) on zero-crossings in gaussian-bandpass-filtered images. This paper presents several examples which illustrate the potential value of scale-specific structure for recognition, inspection, and correspondence related tasks. The suitability of the approach for practical systems is discussed, and a recent result suggesting the importance of this 'hidden' information to human stereo vision is presented.

115794 Analysis of Helmholtz-Hering illusion by multiple channel model. T.Morita, K.Fujii (Dept. of Electrical Engng., Osaka Univ., Osaka, Japan), A.Matsuoka. *Jpn. J. Med. Electron. & Biol. Eng. (Japan)*, vol.21, no.2, p.87-92 (April 1983). In Japanese. [received: Sept. 1983] Geometric illusions closely relate to the excellent functions of the human visual system. The authors formerly analyzed typical illusions by a lateral inhibition model assuming that the geometric illusions originated from interactions of neuronal activities in the visual system. They now propose a new model to interpret illusions on the basis of the assumption that the illusions were caused by multiple spatial frequency channels, the existence of which has been proposed in both physiological and psychological visual science. Taking the Helmholtz-Hering illusion as an example, the authors analyze the kinds of channel that produce illusions. It is shown that the new model is effective for the interpretation of the Helmholtz-Hering illusion, and that this illusion originates mainly from the channels having a 1-octave bandwidth and a central frequency of about half of the fundamental frequency of the illusional figure. It will be possible to analyze more complex illusions by this model in the near future. (9 refs.)

115795 Attenuation of Mach bands by adjacent stimuli. F.Ratliff, N.Milkman, N.Rennett (Rockefeller Univ., New York, NY, USA). *Proc. Natl. Acad. Sci. USA*, vol.80, no.14, p.4554-8 (July 1983). Pronounced bright and dark bands are seen at the bright and dark edges of half-shadows and similar distributions of illumination. These are the so-called Mach bands. A pair of vertical Mach bands was generated with a ramp pattern in the central strip of a horizontal tripartite oscilloscope display. This pattern consisted of two uniform fields (one of low luminance, one of high luminance) joined by a gradient of uniform slope. The upper and lower strips were uniform throughout. A coupled pair of pointers could be displayed in these two strips and adjusted by the observer to match the apparent location and width of either of the Mach bands in the central strip. Insertion of a vertical bar in the central strip nearby and on either side of the ramp attenuates the corresponding Mach band. The closer the bar is to the Mach band, the stronger the attenuation. The attenuation is nearly independent of the sign of the contrast of the bar, but it does depend upon the magnitude and sharpness of the contrast. Also, the attenuation is independent of the width of the bar; a narrow line is as effective as a broad bar of the same contrast. No net luminance change is required; a bipolar stimulus with equal parts above and below the mean is as effective as a monopolar stimulus. These results point to two competing physiological mechanisms with different spatial sensitivities—one that generates Mach bands and one that attenuates them. (25 refs.)

Neural mechanisms of pattern vision in the monkey. III. The neurobehavioural basis See Entry 115785
Human information processing and color displays See Entry 115792

87.34 AUDITION

115796 Remote masker summation and background noise limits for industrial monitoring audiometry. K.Keen, R.Waugh (Nat. Acoustic Labs., Sydney, NSW, Australia). *Aust. J. Audiol. (Australia)*, vol.4, no.2, p.33-9 (Nov. 1982). [received: Sept. 1983] The levels of ten noise bands in the range 125-3150 Hz that just mask a 3 kHz test tone were determined experimentally for 20 normal hearing subjects. Summation of these remote maskers appears to follow a 6 dB per doubling of maskers rule. Subjects with hearing impairment at 3 kHz but normal hearing at lower frequencies tend to suffer less masking than normal hearing subjects. These results are used to derive maximum permissible background noise levels for the performance of industrial monitoring audiometry for test frequencies restricted to the 3-6 kHz range. (16 refs.)

115797 The validity of aided thresholds. J.Macrae (Nat. Acoustic Labs., Sydney, NSW, Australia). *Aust. J. Audiol. (Australia)*, vol.4, no.2, p.48-54 (Nov. 1982). [received: Sept. 1983] Two procedures have been suggested for checking the validity of aided thresholds. The first consists of varying the gain of the hearing aid and observing whether the aided thresholds change or not. If they do not change, they are considered invalid. The second consists of measuring the equivalent input noise levels of the aid and applying corrections to them to estimate the invalid aided threshold levels. The finding that invalid aided thresholds improve when the gain of an aid is increased and worsen when the gain is reduced indicated that at least the first procedure would have to be modified. The effects of amplified ambient testroom noise, earmould venting and the internal noise output of a hearing aid on aided threshold levels were therefore calculated

with the aim of evaluating and improving both procedures. Both were improved but the improved version of the first procedure does not work if there is a significant amount of masking from amplified ambient noise or at frequencies below the vent cutoff frequency when venting is used. The improved version of the second procedure works under all conditions and is therefore the better of the two to use. (7 refs.)

115798 An investigation of the auditory brain stem response in subjects with high frequency cochlear hearing loss. A.R.Marshall (Dept. of Otolaryngology, Royal Victorian Eye & Ear Hospital, East Melbourne, Victoria, Australia). *Aust. J. Audiol. (Australia)*, vol.5, no.1, p.11-18 (May 1983). Auditory brain stem responses were obtained from 10 subjects with high frequency cochlear hearing loss. The relationship between audiometric threshold and response latency was investigated, as well as the effect on the response waveforms of increasing the stimulus repetition rate. Results indicated the importance of the 1 to 8 kHz audiometric contour in determining the presence of the responses and their latencies. In addition, it appeared that the adaptation observed with increased stimulus presentation rates is largely a peripheral process. Methods of analysing response waveforms to aid in the differentiation of cochlear and retrocochlear lesions were investigated. Several procedures involving examination of interaural wave latency differences at both slow and fast presentation rates were devised in an attempt to eliminate false positive retrocochlear findings. (27 refs.)

115799 6-kHz notch in noise-induced hearing loss. D.Y.Chung (Workers' Compensation Board of British Columbia, Richmond, BC, Canada). *Can. Acoust./Acoust. Can. (Canada)*, vol.11, no.4, p.17-23 (Oct. 1983). Audiograms from 49711 workers exposed to industrial noise over 85 dB(A) and with no obvious ear pathology were analyzed by sex and age. It was found that the configuration of the mean audiograms shows a notch at 6 kHz instead of 4 kHz reported in previous studies. When the mean audiograms were corrected for presbycusis, the notch shifted from 6 kHz to 4 kHz only for the age groups over 45 years. The reasons for the difference between results of previous studies and this study are discussed. (7 refs.)

115800 Suggested formulae for calculating auditory-filter bandwidths and excitation patterns. B.C.J.Moore, B.R.Glasberg (Dept. of Experimental Psychology, Univ. of Cambridge, Cambridge, England). *J. Acoust. Soc. Am. (USA)*, vol.74, no.3, p.750-3 (Sept. 1983). Recent estimates of auditory-filter shape are used to derive a simple formula relating the equivalent rectangular bandwidth (ERB) of the auditory filter to center frequency. The value of the auditory-filter bandwidth continues to decrease as center frequency decreases below 500 Hz. A formula is also given relating ERB-rate to frequency. Finally, a method is described for calculating excitation patterns from filter shapes. (23 refs.)

115801 Suppression in simultaneous masking. H.Fastl, M.Bechly (Inst. of Electroacoustics, Tech. Univ., Munich, Germany). *J. Acoust. Soc. Am. (USA)*, vol.74, no.3, p.754-7 (Sept. 1983). Suppression, i.e. the decrease of masked threshold caused by the addition of a second masker M2 to a first masker M1, is measured for the case of simultaneous masking. The magnitude of suppression decreases with increasing test tone duration; pulsed maskers elicit somewhat more suppression than continuous maskers. In comparison to suppression effects obtained in nonsimultaneous masking (post-masking, pulsation threshold) suppression in simultaneous masking is considerably smaller and was found only at the lower slopes of the two maskers. Suppression in simultaneous masking would not be predicted by those models of suppression which require nonsimultaneous presentation of maskers and test sound. (34 refs.)

115802 Broadband masking noise and behavioral pure tone thresholds in cats. J.A.Costalupes (Dept. of Biomedical Engng., Johns Hopkins Univ. School of Medicine, Baltimore, MD, USA). *J. Acoust. Soc. Am. (USA)*, vol.74, no.3, p.758-64 (Sept. 1983). The threshold for detection of pure tones in broadband noise was determined for three cats using an auditory reaction time procedure. Critical ratio is defined as the ratio of the signal power at the masked threshold for detection to the spectrum level of the noise. Critical ratios were obtained for 250-, 500-Hz, and 1-, 2-, 4-, 8-, and 16-kHz tones over a wide range of noise intensities. Results indicate that critical ratios increase with the frequency of the tone stimulus. At frequencies below 4 kHz, critical ratios remain constant at moderate and high noise intensities. For frequencies above 4 kHz, critical ratios increase as the level of the masking noise is raised from moderate to high levels. The difference between low- and high-frequency behavior of the level dependence of critical ratios is considered in terms of two possible mechanisms: (1) different mechanisms may be involved in the encoding of low- and high-frequency information by the nervous system or (2) the difference in level dependence may be due to attenuation by the action of the middle ear muscles at high sound levels. (25 refs.)

115803 Time course of adaptation and recovery of channels selectively sensitive to frequency and amplitude modulation. B.W.Tansley, J.B.Suffield (Psychology Dept., Carleton Univ., Ottawa, Ontario, Canada). *J. Acoust. Soc. Am. (USA)*, vol.74, no.3, p.765-75 (Sept. 1983). In a series of experiments the authors investigated the time course of adaptation and recovery of channels in the human auditory system selectively sensitive to frequency and amplitude modulation (FM and AM). They determined the rate of loss of sensitivity to modulation using sinusoidal frequency or amplitude modulation (SFM or SAM) of a 50 dB SL, 500-Hz pure tone carrier over a 30-min period. Adaptation stimuli were modulated at ten times the preadaptation modulation detection threshold, as determined immediately before the 30-min adaptation session. Modulation rates investigated were 2, 4, 8, 16, and 32 Hz. Long exposure to SFM always elevated thresholds for detection of SFM more than this exposure elevated thresholds for detection of SAM. Similarly, adapting to SAM always elevated SAM detection thresholds more than SFM thresholds. Loss of sensitivity during adaptation was relatively slow; asymptotic loss of modulation sensitivity took 20 to 30 min. The recovery of modulation sensitivity after cessation of the modulation component of the adapting stimulus was determined in a second experiment. Recovery was found to be rapid; most of the recovery occurred within the first 60 sec. Their evidence suggests that there exist two types of modulation-sensitive channels in the human auditory system—one selectively sensitive to amplitude modulation and the other to frequency modulation. They appear to have similar time courses for adaptation and for recovery. (18 refs.)

115804 Performance of hearing-impaired listeners under various types of amplitude compression. I.V.Nabelek (Dept. of Audiology & Speech Pathology, Univ. of Tennessee, Knoxville, TN, USA). *J. Acoust. Soc. Am. (USA)*, vol.74, no.3, p.776-91 (Sept. 1983). Speech perception by subjects with sensorineural hearing impairment was studied using various types of short-term (syllabic) amplitude compression. Average speech level was approximately constant. In quiet, a single-channel wide-band compression (WBC) with compression ratio equal to 10, attack time 10 ms and release time 90 ms produced significantly higher scores than a three-channel multiband compression (MBC) or no compression when a non-

sense syllable test (City University of New York) was used. The scores under MBC, WBC, or no compression were not significantly different when the modified rhyme test (MRT) was used. But when overshoots caused by compression were clipped, the MRT scores improved significantly. The influence of MBC on reverberant speech and of WBC on noisy speech were tested with the MRT. Reverberation reduced the scores, and this reduction was the same with compression as without. Noise added to speech before compression also reduced the scores, but the reduction was larger with compression than without. When noise was added after compression, an improvement was observed when WBC had a compression ratio of about 5, attack time 1 ms, and release time 30 ms. Other compression modes (e.g., with high-frequency pre-emphasis) did not show an improvement. The results indicate that WBC with a compression ratio around 5, attack time shorter than 3 ms, and release time between 30 and 90 ms can be beneficial if signal-to-noise ratio is large, or, if in a noisy or reverberant environment, the effects of noise or reverberation are eliminated by using listening systems. (40 refs.)

115805 Acoustically evoked radial current densities in scala tympani. W.E.Brownell, P.B.Manis, M.Zidanic, G.A.Spirou (Dept. of Neuroscience & Surgery, Univ. of Florida, Gainesville, FL, USA). *J. Acoust. Soc. Am. (USA)*, vol.74, no.3, p.792-800 (Sept. 1983). The authors have developed a method for measuring current density within the fluid spaces of the cochlea and report the existence of stimulus evoked radial currents in scala tympani of the guinea pig cochlea. The spatial distribution of electrical potentials in scala tympani was measured along a radial path parallel to the basilar membrane. Click evoked potentials were recorded at successive points separated by a fixed increment as the electrode was either advanced from the spiral ligament or withdrawn from a position near the modiolus. Potential differences were found to exist between recording points and gradients were calculated from the evoked potential measurements. Evoked potential gradients are observed at the same position along the path of the electrode both on advancing and on withdrawing the electrode. The largest potential gradients are located beneath the organ of Corti. Condensation and rarefaction clicks produce radial currents in opposite directions at a given location along the electrode's path. The magnitude and spatial distribution of radial currents is a function of stimulus intensity. Potential gradients of small magnitude are observed at locations other than below the organ of Corti in some penetrations. Control experiments suggest the smaller gradients are artifactual and may result from displacement of the spiral ligament by the recording electrode. The locations, magnitude, and direction of intracochlear ionic flow relate directly to the mechano-electrical transduction process in the organ of Corti. (43 refs.)

115806 Suppression of auditory nerve responses. II. Suppression threshold and growth, iso-suppression contours. E.Javel, J.McGee, E.J.Walsh, G.R.Farley, M.P.Gorga (Boys Town Nat. Inst. for Communication Disorders in Children, Omaha, NE, USA). *J. Acoust. Soc. Am. (USA)*, vol.74, no.3, p.801-13 (Sept. 1983). For pt.I see *ibid.*, vol.69, p.1735 (1981). Two-tone 'synchrony suppression' was studied in responses of single auditory nerve fibers recorded from anesthetized cats. Suppression thresholds for suppressor tones set to a fiber's characteristic frequency (CF) were approximately equal to discharge rate thresholds for CF tones. Suppression thresholds above and below CF were usually lower than the corresponding discharge rate thresholds. However, at all frequencies studied (including CF), suppression thresholds were higher than the corresponding thresholds for discharge synchronization. Across fibers, rates of suppression growth for suppressors at CF were greatest in low-CF fibers and least in high-CF fibers, and there was a systematic decrease in suppression growth rate at CF as CF increased. Within fibers, rates of suppression growth above CF were typically less than at CF, and slopes were monotonically decreasing functions of frequency. Within-fiber rates of suppression growth below CF were variable, but they usually were greater than rates of growth at CF. Iso-suppression contours (frequencies and intensities producing criterion amounts of suppression) indicated that tones near CF are the most potent suppressors at near-threshold intensities, and that the frequency producing the most suppression usually shifts downward as the amount of suppression increases. These data support the notion that synchrony suppression arises primarily as a passive consequence of hair cell activation. (36 refs.)

115807 A model of pitch discrimination process of the human auditory system. S.Kitamori (Numazu Tech. Coll., Numazu, Japan). *Trans. Inst. Electron. & Commun. Eng. Jpn. Part A (Japan)*, vol.J66A, no.7, p.592-5 (July 1983). In Japanese. Investigates a transitional characteristic of pitch discrimination in the human auditory system. A model of the temporal change process of the probability distribution on the psychological continuum of a brief tonal signal is proposed. The computed values of the proportion of correct responses fit the results of the psychological experiment quite well. (9 refs.)

Interactions among converging sensory inputs in the superior colliculus See Entry 115786

Local cerebral blood flow increases during auditory and emotional processing in the conscious rat See Entry 115819

The effects of infrasound on human health See Entry 115830

The effect of loud sound and traffic noise on the vestibular system See Entry 115832

Formalization of choice for parameters of an acoustic stimulus in a small automatic facility to examine and diagnose the functional status of an auditory analyzer See Entry 115885

Bone-conduction receiver with an extended frequency range for measuring the threshold of audibility See Entry 115886

The selection of modulation waveform for frequency modulated sound field stimuli See Entry 115887

Acoustic notch filters for hearing aids See Entry 115888

Standardized function test for audiometers in the audiological prophylaxis as part of occupational medicine in accordance with principle 20 See Entry 115889

87.36 SPEECH (see also 43.70 Speech communication)

115808 Equivalency of lossless *n*-tubes. L.J.Bonder (Inst. of Phonetic Sci., Univ. of Amsterdam, Amsterdam, Holland). *Acustica (Germany)*, vol.53, no.4, p.193-200 (Aug. 1983). The inverse problem of the lossless speech production model does not have a unique solution, for a continuous set of tubes exists that have the same formant frequencies. This phenomenon is known in literature as articulatory compensation. In this paper the authors describe a method with which one can compute the continuous set of *n*-tubes that have the same formants. It follows that the problem can be handled analytically up to 10-tubes. They

illustrate their analytic method on the basis of 4-tubes. It turns out that the values of the shape parameters of the tubes are restricted to certain intervals. Consequently, for some vowel sounds the corresponding 4-tube configurations must show particular shape characteristics, in spite of the articulatory compensation. (10 refs.)

115809 Changing the shape of lossless *n*-tubes. L.J.Bonder (Inst. of Phonetic Sci., Univ. of Amsterdam, Amsterdam, Holland). *Acustica (Germany)*, vol.53, no.4, p.201-11 (Aug. 1983). The author investigates analytically the acoustical effects of small changes of the shape of lossless *n*-tubes. They derive, by means of a decomposition method, general formant shift formulae for *n*-tubes. This method is not based on the use of eigenfunctions, but on the geometrical interpretation of the *n*-tube formula in the formant space. They give some examples of classes of changes of tube shape with their acoustical effects in the F₁, F₂-plane. (13 refs.)

115810 Multidimensional analysis of alaryngeal voice quality. S.Imai-zumi, S.Boku (Dept. of Otolaryngology, Kinki Univ. School of Medicine, Osaka, Japan), Y.Koike, F.Ohta. *J. Acoust. Soc. Jpn. (E) (Japan)*, vol.4, no.3, p.139-48 (July 1983). Investigates and acoustically defines some of the perceptual parameters which characterize alaryngeal voice quality. Twenty voice samples of vowel /e/ were recorded from 16 alaryngeal and four normal speakers, and were paired, randomized and presented to 20 listeners with normal hearing. The listeners rated the dissimilarities of all combinations of the voices, and these dissimilarities were analyzed by a nonmetric multidimensional scaling method called SMACOF. Five acoustical measures and 21 psychoacoustical ratings were made for each vowel, and these provided the interpretation for the SMACOF solution. The results indicate that at least two dimensions are necessary to describe the alaryngeal voice quality. One is connected with the listeners' preferences for the voices and differentiates the alaryngeal voices from the normal ones. This dimension correlates with the fundamental frequency and the relative spectral level of the high frequency components. Another dimension indicates the abnormalities peculiar to the voices produced with artificial larynges and differentiates them from the normal and esophageal voices. It correlates positively with periodicity in the excitation signal waveform and negatively with aperiodicity in the pitch or in the amplitude. These results suggest some direction toward the enhancement of the alaryngeal voice quality. (20 refs.)

Optical probe for narrow sound field See Entry 113223

Performance of hearing-impaired listeners under various types of amplitude compression See Entry 115804

Comparative study of linear prediction parameters for quantification and monitoring of dysphonic voices See Entry 115963

87.38 MECHANO- AND CHEMIO-CEPTIONS (inc. biosonic generation, detection and guidance)

115811 Range ambiguity and pulse interval jitter in the bottlenose dolphin. J.Kadane, R.Penner (Hawaii Lab., Naval Ocean Systems Center, Kailua, HI, USA). *J. Acoust. Soc. Am. (USA)*, vol.74, no.3, p.1059-61 (Sept. 1983).

A common problem of pulse-mode sonar systems which utilize range gating is the range ambiguity caused by echoes from objects at multiple distances returning simultaneously. Research conducted at the Naval Ocean Systems Center, Oahu, Hawaii, investigating bottlenose dolphin echolocation indicate that there is adequate varying of consecutive interpulse intervals (jittering of the repetition rate) to eliminate range ambiguity and range-ambiguous interference in this biological sonar system. (8 refs.)

115812 Mathematical model for vestibulo-ocular reflex. Z.Si-lan (Faculty of Basic Medical Sci., Beijing Medical Coll., Beijing, China), Y.Li-shen, L.Ke-qui, Q.Gao-xi. Identification and System Parameter Estimation 1982. Proceedings of the Sixth IFAC Symposium, Washington, DC, USA, 7-11 June 1982 (Oxford, England: Pergamon 1983), p.307-11 vol.1

A mathematical model for the vestibulo-ocular reflex based on the knowledge of physiology and anatomy is given. The authors describe how it was applied to certain patients who suffered from vestibular diseases examined by various vestibular tests and to normal subjects who revealed different types of vestibular function. According to their post rotational electronystagmography examination, their model parameters can be examined and their traditional parameters can be obtained by system identification and direct measurement respectively. With these parameters, one can establish some discriminant functions from the data of the subjects examined. These discriminant functions can be applied to clinical diagnosis of vestibular diseases and classification of normal vestibular function. (5 refs.)

Correlation between the vestibular analyzer and individual radiosensitivity of rabbits exposed to a dose of 150 Gy See Entry 115855

87.40 BIOMAGNETISM (inc. magnetocardiography)

115813 Future of biomagnetism. M.Kotami. *Jpn. J. Med. Electron. & Biol. Eng. (Japan)*, vol.20, no.7, p.595-6 (Dec. 1982). In Japanese. [received: July 1983]

The heart, brain, arms and lungs generate weak magnetic fields. By measuring these fields diagnoses can be made. To measure the field, a flux-gate type gauss meter or a SQUID gauss meter is used. The minimum measurable flux density of SQUID gauss meters is as low as 10⁻¹¹ T. Recently, in order to obtain further magnetic-field information, mapping techniques to produce cardiac, pulmonary and cerebral magnetograms have been developed. These are briefly summarized in this paper. (11 refs.) K.B.

New view of lipid bilayer dynamics from ²H and ¹³C NMR relaxation time measurements See Entry 115728

Magnetic proton relaxation of aqueous solutions of ribonuclease in the temperature region of intramolecular fusion See Entry 115742

NMR study of slowly exchanging imino protons in yeast tRNA^{Asp} See Entry 115751

Evaluation of the probability of penetration of paramagnetic ions into the cells by the NMR pulse method See Entry 115769

Effect of constant magnetic field (CMF) and γ -radiation on hereditary structures of somatic cells. Combined effect of CMF and γ -radiation on human lymphocytes in vitro See Entry 115826

Synergistic effect of γ -radiation and constant magnetic field See Entry 115849

87.45 BIOMECHANICS, BIORHEOLOGY, BIOLOGICAL FLUID DYNAMICS

115814 Microcontinuum approach to the pulsatile flow in tubes with and without longitudinal vibration [blood flow application]. S.Parvatham (Univ. of Agricultural Sci., Bangalore, India), R.Devanathan. *Bull. Math. Biol. (GB)*, vol.45, no.5, p.721-37 (1983).

A fully developed pulsatile flow in a circular rigid tube is analysed by a microcontinuum approach. Solutions for radial variation of axial velocity and cell rotational velocity across the tube are obtained using the momentum integral method. Simplified forms of the solutions are presented for the relevant physiological data. Marked deviations in the results are observed when compared to a Newtonian fluid model. It is interesting to see that there is sufficient reduction in the mass flow rate, phase lag and friction due to the micropolar character of the fluid. (21 refs.)

115815 Effects of periodic accelerations on blood flow in arteries. V.K.Sud (Dept. of Biophys., All India Inst. of Medical Sci., New Delhi, India), H.E.Von Gierke, I.Kaleps, H.L.Oestreicher. *Bull. Math. Biol. (GB)*, vol.45, no.5, p.857-67 (1983).

Discusses the flow of blood in large arteries under the influence of linear periodic acceleration. The governing equations and boundary conditions are established and analytical solutions for the velocity, fluid acceleration, bulk flow and shear stress are obtained. The results for these physical quantities are computed for the case of an artery the size of a normal human aorta. It is found that the flow field variables are directly proportional to the external accelerating force. The behaviour of the velocity profile along the radial distance at different stages of times at fixed applied acceleration is also shown. (8 refs.)

115816 The bulk rheology of close-packed red blood cells in shear flow. T.W.Secomb (Dept. of Physiology, Univ. of Arizona, Tucson, AZ, USA), S.Chien, K.-M.Jan, R.Skalak. *Biorheology (GB)*, vol.20, no.3, p.295-309 (1983).

A theoretical analysis is made of the dynamical behavior and bulk rheology of close-packed red blood cell suspensions subjected to simple shear flow. The model for the polyhedral cell shapes and tank-treading membrane motion developed in a companion paper (see *ibid.*, vol.20, no.3, p.283-94, 1983) is used. The flow in the thin lubricating plasma layers between cells is analyzed taking into account the mechanical properties of the membrane at the corner regions of sharp membrane curvature. This leads to predictions for the apparent viscosity as a function of hematocrit and shear rate. Good agreement with experimental results is obtained at moderate and high shear rates (above 20 s^{-1}). At lower shear rates, a rapid rise in apparent viscosity has been found experimentally, and the mechanisms leading to this behavior are examined. (12 refs.)

115817 Human blood oscillating axially in a tube. P.D.Richardson, S.Lazzara (Center for Biomedical Engng., Brown Univ., Providence, RI, USA).

Biorheology (GB), vol.20, no.3, p.317-26 (1983). Experiments were performed to study the rheological response of human blood at hematocrit ratios of 0 to 0.45 in axial oscillatory flow in a tube of uniform bore. Three principal regimes of flow were identified, depending on the amplitude of oscillation. At the highest amplitudes (and therefore the largest range of shear rates in the blood) there was turbulent motion and the friction coefficient increased in proportion to the square of the hematocrit. At small amplitudes the friction decreased with increase in amplitude, the rate of decrease increasing with hematocrit. At intermediate amplitudes the friction increased in proportion to the square of the hematocrit. Glutaraldehyde fixation of the red cells caused increase in the friction, and reduced the rate of decrease of friction with amplitude at small amplitudes. With a stenosis of very modest degree and span the friction in normal blood increased disproportionately, and a small blind hole in the lumen of the stenosis caused additional and disproportionate increase in friction. (11 refs.)

115818 Effect of microrheology of blood on the apparent flow instability in a rotational viscometer. Liao Fu-lung, L.Dintenfass (Kanematsu Memorial Inst., Sydney, Australia).

Biorheology (GB), vol.20, no.3, p.327-42 (1983). Flow instability (formation of vortices and a concurrent increase in the apparent viscosity) was studied in the rotational rhombospheroid viscometer of 3° , 5° and 10° gaps over a range of speeds from 10 to 300 RPM. Comparisons between different blood systems were carried out mainly at 250 RPM. Experiments were carried out on blood samples obtained directly from human subjects, or from the Blood Bank, or from horses. Reconstituted suspensions of red cells in albumin or dextran were also used. Apparent flow instability was found to be not solely a function of blood viscosity, but a multiple function of many viscosity factors or blood subphases, including instability-decreasing factors such as haematocrit and aggregation of red cells; and instability-increasing factors such as rigidity of red cells; and thus specific to and characteristic of individual blood samples. (19 refs.)

115819 Local cerebral blood flow increases during auditory and emotional processing in the conscious rat. J.E.LeDoux, M.E.Thompson, C.Iadecola, L.W.Tucker, D.J.Reis. *Science (USA)*, vol.221, no.4610, p.576-8 (5 Aug. 1983).

Local cerebral blood flow was measured in rats by the ^{14}C -labeled iodoantipyrine technique with quantitative autoradiography during the processing of environmental stimuli. Presentation of a tone increased blood flow in the auditory but not the visual pathway. When the animal had previously been conditioned to fear the tone, blood flow additionally increased in the hypothalamus and amygdala. Local cerebral blood flow can thus be used to detect patterns of cerebral excitation associated with transient (30- to 40-second) mental events in experimental animals. (23 refs.)

115820 Nonparametric modeling of respiratory mechanics and gas exchange. V.Z.Marmarelis, S.M.Yamashiro (Dept. of Biomedical & Electrical Engng., Univ. of Southern California, Los Angeles, CA, USA).

Identification and System Parameter Estimation 1982. Proceedings of the Sixth IFAC Symposium, Washington, DC, USA, 7-11 June 1982 (Oxford, England: Pergamon 1983), p.675-80 vol.1

A nonparametric method of modeling respiratory mechanics and gas exchange is presented and compared to existing parametric methods. The nonparametric approach is based on Wiener's theory of nonlinear system identification by use of white-noise test inputs. The sought nonparametric models have the form of nonlinear functional relations between tracheal pressure and flow (in the study of respiratory mechanics), and between tracheal flow and PCO_2 (in the study of gas exchange). The motivation for this modeling study is provided by the recent emergence of high-frequency ventilation as a useful clinical tool. The obtained results increase one's understanding of the quantitative relations between these physiological variables, and allow optimization studies that may lead to improved clinical applications. (20 refs.)

115821 Parameter identification and adaptive control for blood pressure. B.K.Walker (Dept. of Aeronautics & Astronautics, MIT, Cambridge, MA, USA), T.-L.Chia, K.S.Stern, P.G.Katona.

Identification and System Parameter Estimation 1982. Proceedings of the Sixth IFAC Symposium, Washington, DC, USA, 7-11 June 1982 (Oxford, England: Pergamon 1983), p.1413-18 vol.2

The online identification of the defining parameters and the closed-loop adaptive control of the blood pressure response of anesthetized dogs to the infusion rate of a vasoactive drug is considered. The response of mean arterial pressure to the infusion rate of sodium nitroprusside is modelled as a single-input single-output ARMAX process with known delay. Recursive least squares and maximum likelihood techniques are employed for parameter estimation and closed loop control is provided by a minimum variance algorithm. Simulation results and animal experiments indicate that the behavior of the various adaptive controllers is predicted well by theoretical considerations and that the closed loop performance is excellent. (16 refs.)

115822 Online estimation of lung parameters using multiple gases. D.M.Wiberg, J.W.Bellville (Dept. of System Sci. & Anesthesia, Univ. of California, Los Angeles, CA, USA).

Identification and System Parameter Estimation 1982. Proceedings of the Sixth IFAC Symposium, Washington, DC, USA, 7-11 June 1982 (Oxford, England: Pergamon 1983), p.1419-24 vol.2

A noninvasive multiple gas method is used to obtain dynamic estimates of lung blood perfusion, dead space, lung blood distribution, and lung ventilation/perfusion ratios. Shunt can also be estimated if arterial oxygen partial pressure is measured invasively. The estimates are for use in the operating room and intensive care unit, as a measure of cardiopulmonary state. The extended Kalman filter as modified by Lung and Wiberg computes the estimates from gas measurements at the mouth. Multiple inputs and outputs make the estimation complex. (25 refs.)

115823 Modelling of respiratory patterns in the neonatal period. S.Sjöberg (Dept. of Appl. Electronics, Chalmers Univ. of Technol., Gothenburg, Sweden).

Identification and System Parameter Estimation 1982. Proceedings of the Sixth IFAC Symposium, Washington, DC, USA, 7-11 June 1982 (Oxford, England: Pergamon 1983), p.1425-9 vol.2

The evaluation and monitoring of respiratory function is of special importance in the neonatal period. One way to describe so-called respiratory patterns, characteristics of spontaneous breathing, of newborn infants in a more formal way than is normally done today is presented. It is possible to monitor either air flow or lung volume as a function of time and consider this signal as a realization of a random process. The problem of recognizing different respiratory patterns can be formulated as a problem of identification and detection of random processes. Based on some considerations of properties of the respiratory system and observations of lung volume variation, a simple model of respiratory patterns is proposed, and some aspects of the estimation of the model's parameters are discussed. (6 refs.)

115824 A model-based adaptive blood pressure controller. J.B.Slate, L.C.Sheppard (Dept. of Surgery & Biomedical Engng., Univ. of Alabama, Birmingham, AL, USA).

Identification and System Parameter Estimation 1982. Proceedings of the Sixth IFAC Symposium, Washington, DC, USA, 7-11 June 1982 (Oxford, England: Pergamon 1983), p.1437-42 vol.2

Sodium nitroprusside is a fast-acting drug used to reduce blood pressure in hospitalized patients. A wide range of circulatory system responses to the drug is observed. For design of a controller for clinical use, a model of the system related to arterial pressure and its response to nitroprusside was developed and patient-care practices were analyzed. An adaptive, multiple-mode, multirate sampled-data controller was designed using model-based techniques and implemented with a microcomputer system. Simulation results were verified by experiments in the animal laboratory. Results from clinical evaluations with postsurgical patients were superior to the performance of previous automated infusion systems. (7 refs.)

More bicycle physics See Entry 111373

Mathematical model of the velocity field external to a tank-treading red cell See Entry 115766

The motion of close-packed red blood cells in shear flow See Entry 115767

Indices of filterability of red blood cell suspensions See Entry 115768

Measurement of blood flow See Entry 115880

Method of investigating muscle tone See Entry 115952

Foil electret transducer for blood pressure monitoring See Entry 115955

A digital system for rheoencephalography See Entry 115968

Transducer system for absolute intravascular angiotomy See Entry 115969

Evaluation of intra-aortic counterpulsation with an assisted circulation See Entry 115972

Studies on the loadability of the bone/cement interface in joint replacement See Entry 115976

87.50 BIOLOGICAL EFFECTS OF RADIATIONS

(inc. effects of fields)

115825 Behavioral detection of 60-Hz electric fields by rats. S.Stern, V.G.Laties (Dept. of Radiation Biology & Biophys., Univ. of Rochester, Rochester, NY, USA), C.V.Stancampiano, C.Cox, J.O.de Lorge.

Bioelectromagnetics (USA), vol.4, no.3, p.215-47 (1983). Rats partially deprived of food were trained individually to press a lever in the presence of a vertical, 60-Hz electric field and not to press in its absence.

Correct detections that occurred during brief, 3- or 4-s trials occasionally produced a food pellet. The probability of detecting the field was found to increase as field strength increased. The threshold of detection, i.e. the field strength required for detections at a probability of 0.5 after correction for errors, was generally between 4 and 10 kV/m. The range of field strengths between almost zero and almost 100% correctness of detection was approximately 8 kV/m. A logistic function provided a good description of the increase in the detection probability with increasing field strength. These performances occurred reliably in 19 rats, some of which were studied for 2 years. Control procedures showed that the behavior required that the rat be in the electric field; the behavior was not controlled by any of several potentially confounding variables. (37 refs.)

115826 Effect of constant magnetic field (CMF) and γ -radiation on hereditary structures of somatic cells. Combined effect of CMF and γ -radiation on human lymphocytes in vitro. M.Mileva, B.Ivanov, M.Bulanova, T.Pantev (Inst. of Roentgenology & Radiobiology, Sofia, Bulgaria). *Radiobiologiya (USSR)*, vol.23, no.4, p.562-5 (1983). In Russian. Samples of human whole blood were exposed in a CMF (field induction, 0.3 T) for 15, 30, 45, 60, 75, 90, 120, 150, 180, 240, 300 or 360 min. 15 min following exposure, the samples were γ -irradiated with a dose of 0.0516 C/kg (^{137}Cs) at a dose rate of 1.95 A/kg. The following chromosome aberrations were scored: deletions, dicentric, rings, and symmetrical exchanges. Exposure of the blood in a CMF for 15 to 360 min decreased radiation damage to cells as compared with unexposed irradiated samples. The extension of time from 15 to 180 min increased the effect, the smallest amount of chromosome damage being scored at 170-180 min. A 2.8-fold, 3-fold and 3.5-fold decrease was registered in the number of aberrant cells, deletions and dicentric, respectively. With increasing time of exposure (240 min), the radiomodifying effect started decreasing, and with 300-360 min exposure it was the same as that observed at 15-45 min. (9 refs.)

Synergistic effect of γ -radiation and constant magnetic field See Entry 115849

Contribution of γ -radiation to the dose absorbed, and some radiation effects in a radiation field $p(50\text{ MeV})\rightarrow\text{Be}$ See Entry 115923

87.50B Interactions of biosystems with radiations

115827 Experimental determination of whole body average specific absorption rate (SAR) of mice exposed to 200-400 MHz CW. S.V.Marshall, R.F.Brown (Dept. of Electrical Engng., Univ. of Missouri-Rolla, Rolla, MO, USA). *Bioelectromagnetics (USA)*, vol.4, no.3, p.267-79 (1983). A maximum of six live mice, mouse cadavers, prolate spheroids molded from muscle-equivalent tissue, or saline-filled culture flasks, were exposed to continuous wave radiation in a TEM cell at frequencies between 200 and 400 MHz. Whole-body average specific absorption rate (SAR) was determined from power meter measurements of incident, reflected, and transmitted powers. The SARs for both live mice and cadavers were approximately twice that for the prolate spheroid models, and when housed in Plexiglas restraining cages, about $2^{1/2}$ times greater. An error multiplying factor is identified that quantitatively expresses how SAR data obtained by the three-power-meter method becomes progressively more noisy as the irradiation frequency is lowered or as the TEM cell cross section is increased. (6 refs.)

115828 Fluorescence of the leaves of higher plants at raised temperatures. Ye.A.Kuznetsova (Phys. Faculty of Lomonosov State Univ., Moscow, USSR). *Biophysics (GB)*, vol.27, no.5, p.849-52 (1982). Translation of: *Biofizika (USSR)*, vol.27, no.5, p.809-11 (1982). [received: Sept. 1983] The temperature dependence of fluorescence ($\lambda\approx 630\text{-}760\text{ nm}$) of the leaves of gymnosperm plants in the state of winter rest and in the spring to summer period, and also green and etiolated leaves of angiosperm plants at different stages of development at 20-95°C has been studied. At $\sim 60^\circ$ the intensity of fluorescence rises like an avalanche, more strongly the younger the leaf of the angiosperm. In the leaves of gymnosperms an intense alavanache-like process is observed only in the winter-spring period. (13 refs.)

115829 An iterative extended boundary condition method for solving the absorption characteristics of lossy dielectric objects of large aspect ratios. A.Lakhtakia, M.F.Iskander, C.H.Durney (Dept. of Electrical Engng., Univ. of Utah, Salt Lake City, UT, USA). *IEEE Trans. Microwave Theory & Tech. (USA)*, vol.MTT-31, no.8, p.640-7 (Aug. 1983). The recently developed iterative extended boundary condition method (IEBCM) has been used to compute the internal fields induced in homogeneous, axisymmetric, lossy dielectric objects of large aspect ratios when exposed to incident planewave radiation. Calculations were made for both the E - and k -polarization cases. The computed results for a prolate spheroidal model of an average man are found to be accurate for frequencies up to 300 MHz, while the use of the popular EBCM was found to be essentially restricted to frequencies less than 70 MHz for these models and exposure conditions. The applicability of the IEBCM to composite bodies has also been examined by studying the irradiation of a capped cylindrical object. This composite object was first partitioned into several overlapping spherical subregions, and, alternatively, into two spherical subregions overlapping with a central cylindrical subregion. (42 refs.)

Electrical discontinuity of tissue substitute models at 27.12 MHz See Entry 115772

87.50C Bioacoustics (sonic and ultrasonic effects on living matter)

115830 The effects of infrasound on human health. S.E.Birnie, F.L.Hall, S.M.Taylor (Dept. of Geography, McMaster Univ., Hamilton, Ontario, Canada). *Can. Acoust./Acoust. Can. (Canada)*, vol.11, no.4, p.46-55 (Oct. 1983). Infrasound is defined as sound with a frequency less than 20 Hz. It is produced by both natural and man-made sources, although very high levels of infrasound must be artificially produced. A number of early papers suggested that infrasound may produce very serious adverse effects on human functioning such as the impairment of task performance, including driving. This paper assesses the literature published since those early reports. Auditory, physiological, and performance effects are discussed. The more recent studies show much less severe effects than those suggested in the first studies. Methodological considerations indicate that the recent studies are much more reliable than the earliest reports. (22 refs.)

115831 Involvement of ultrasonically induced cavitation in the production of hind limb paralysis of the mouse neonate. L.A.Frizzell, C.S.Lee, P.D.Ashenbach, M.J.Borrelli, R.S.Morimoto, F.Dunn (Bioacoustics Res. Lab., Univ. of Illinois, Urbana, IL, USA). *J. Acoust. Soc. Am. (USA)*, vol.74, no.3, p.1062-5 (Sept. 1983). The exposure conditions which produce hind limb paralysis in 10%, 50%, and 90% of mouse neonate specimens exposed to 1-MHz ultrasound at 10°C and at 1- and 16-atm hydrostatic pressure were determined for the intensity range 86-289 W/cm². The change in the exposure duration for 50% of the specimens paralyzed resulting from pressurization to 16 atm was negligible at 86 and 144 W/cm² but was almost a factor of 2 increase at 289 W/cm². Pressurization suppressed the observed half-harmonic received signal at all intensities. These results suggest that cavitation may influence the production of the hind limb paralysis produced in the neonate at 1 atm at 289 W/cm². (12 refs.)

115832 The effect of loud sound and traffic noise on the vestibular system. S.Spellenberg. *KeP- & Hangtech. (Hungary)*, vol.29, no.4, p.111-12 (Aug. 1983). Loud sound e.g. traffic noise can induce nystagmus and vertigo 113-123 dB ISO pure tone has been produced in 5 sec and 86 dB(A) fluctuating traffic noise in 30 minutes in an open sound space, while the behaviour of the vestibular apparatus has been registered on the electronystagmogram (ENG). The examinations have been done with patients with operated and nonoperated otosclerosis, patients with sensorineural defects, patients of chronic otitis and with normal ears. ENG changes were found in 45% of the patients with sensorineural hearing loss but none of the normal hearing patients. The series of examinations show that the intensive pure tone, or, long noise can damage the perifical or the central component of the vestibular system and can cause vertigo. (9 refs.)

6-kHz notch in noise-induced hearing loss See Entry 115799

87.50E Bio-optics (effects of microwaves, light, laser and other electromagnetic waves)

115833 Teratogenicity of 27.12-MHz radiation in rats is related to duration of hyperthermic exposure. J.M.Lary, D.L.Conover, P.H.Johnson, J.R.Burg (Div. of Biomedical & Behavioral Sci., Nat. Inst. for Occupational Safety & Health, Cincinnati, OH, USA). *Bioelectromagnetics (USA)*, vol.4, no.3, p.249-55 (1983). Five groups of pregnant Sprague-Dawley rats were either sham exposed or were irradiated in a 27.12-MHz radiofrequency (RF) field at 55 A/m and 300 V/m on gestation day 9. The absorbed power (approximately 11 W/kg) caused a relatively rapid increase in the rat's colonic temperature. Rats in group I were sham irradiated for 2.5 h at 0 A/m, 0 V/m. In group II RF irradiation was terminated after the rat's colonic temperature reached 41.0°C. In group III the 41.0°C temperature was maintained an additional 2 h by manually varying the incident field strength. In group IV irradiation was terminated after the rat's colonic temperature reached 42.0°C. In group V the 42.0°C temperature was maintained an additional 15 min by varying the field strength. At both temperatures the teratogenic and embryotoxic effects of the RF-induced hyperthermia increased as the exposure duration increased, but the increase was especially noticeable at 42.0°C. The results indicate that the teratogenic and embryotoxic effects of RF-induced hyperthermia are related to both the temperature of the dam during exposure and the length of time the dam's temperature remains elevated. (12 refs.)

115834 Suppression of T-lymphocyte cytotoxicity following exposure to sinusoidally amplitude-modulated fields. D.B.Lyle (Div. of Biomedical Sci., Univ. of California, Riverside, CA, USA), P.Schechter, W.A.Adey, R.L.Lundak. *Bioelectromagnetics (USA)*, vol.4, no.3, p.281-92 (1983). Significant inhibition of allogeneic cytotoxicity of the target cell MPC-11 by the murine cytotoxic T-lymphocyte line CTL-L1 was observed when the 4-h cytotoxicity assay was conducted in the presence of a 450-MHz field sinusoidally amplitude-modulated at 60 Hz. Exposure of the effector cells to the field prior to adding them to the target cells in the cytolytic assay resulted in a similar inhibition, suggesting a direct interaction of the field with the cytolytic T lymphocyte. The inhibition was preferentially expressed during the early allogeneic recognition phase. Field-exposed cytolytic cells recovered their full cytolytic capacity in 12.5 h. A differential susceptibility was observed with modulation frequencies from 0 to 100 Hz. Peak suppression occurred at 60 Hz modulation, with progressively smaller effects at 40, 16, and 3 Hz. The unmodulated carrier wave did not affect the cytotoxicity. Effects with 80- and 100-Hz modulation were smaller than at 60 Hz. These results demonstrate an inhibitory but recoverable effect by certain amplitude modulations of weak nonionizing radiation upon the cell-mediated cytolytic immune response. (34 refs.)

115835 Effect of microwave radiation on cell immunity in conditions of chronic exposure. M.G.Shandala, G.I.Vinogradov, M.I.Rudnev, S.F.Rudakova (A.N. Marzhev Sci. Res. Inst. of General & Communal Hygiene, Kiev, Ukrainian SSR). *Radiobiologiya (USSR)*, vol.23, no.4, p.544-6 (1983). In Russian. CBA male mice and albino mongrel rats were exposed to microwave radiation (2375 MHz) of various intensities for 1 to 3 months. The T-system immunity status was studied in vivo and in vitro. Substantial changes were revealed in the cell immunity system, resulting from the long-term action of microwaves of a non-thermal intensity. Latent lesions manifested with functional loads. (6 refs.)

115836 Extremely low frequency electromagnetic emissions from video display terminals and other devices. M.A.Stuchly, D.W.Lecuyer, R.D.Mann (Non-ionizing Radiation Section, Radiation Protection Bur., Health & Welfare Canada, Ottawa, Ontario, Canada). *Health Phys. (GB)*, vol.45, no.3, p.713-22 (Sept. 1983). Video display terminals (VDTs) are in widespread use and can be found in practically every modern office. Assessment of possible health effects of electromagnetic emissions from these devices is necessary. The intensity of the magnetic field and the frequency spectrum of the emissions at extremely low frequencies (ELF) (5-500 Hz) were measured for a few VDTs and compared with the background field intensities and emissions from other devices. The emissions in the frequency range investigated are of such low intensities that they are very unlikely to have any biological effects, let alone represent a health hazard. (39 refs.)

115837 Infrared contact coagulation. A new therapy for solid tumors. C.Lersch, C.Hammer, O.Ganghoff, W.Brendel, G.Nath (Inst. fur Chirurgische Forschung, Klinikum Grosshadern, Munchen, Germany). *Naturwissenschaften (Germany)*, vol.70, no.8, p.416-7 (Aug. 1983). Infrared contact coagulation (ICC) has been applied so far mainly for blood stanching during operations of parenchymatous organs and to the treatment of hemorrhoids, diseases of the cervix uteri and hemangiomas. The effect of ICC on solid animal tumors has now been evaluated in mice, hamsters and rats. The device used produces infrared radiation from a 250-W Wolfram halogen lamp. The rays are focused by a gold-plated reflector. Adherence of the tissue is prevented by a sapphire monocrystal cooled in iced water before use. The emitted energy (about 1200 J in 10 s) is mainly concentrated at a depth of 2-3 mm. Most of the animals with solid tumors can be cured by ICC. BCG has an additional but no significant effect. On this tumor therapy, BCG alone did not cure any animal. Hints are given that there is a T-cell-dependent immune response against tumor cells after ICC (Winn assay, monitoring of spleen, lymphocytes). This stimulation of the immune system by ICC has to be investigated intensively before ICC is applied in humans for therapy of solid tumors and metastases. (4 refs.)

115838 New results on the prevention of hazards due to electromagnetic fields in the vicinity of high-power. M.Dahme (Inst. für Rundfunktech., München, Germany). *Rundfunktech. Mitt. (Germany)*, vol.27, no.4, p.164-70 (July-Aug. 1983). In German.

As sections of electromagnetic compatibility (EMC), two problem areas of hazards due to electromagnetic fields are discussed. The basis of a biophysical nerve-irritation and heat-effect concept as well as limiting values derived therefrom of hazards to persons due to RF fields are indicated. With a view to the prevention of hazards from the unintended ignition of explosive mixtures by RF fields, some results of calculations on antenna theory are put forward, by means of which the decoupling of energy from the field may be estimated. Limiting values are given for the maximum power that can be taken from the field, such that, if those values are respected, the ignition of explosive mixtures may be considered to be impossible. (6 refs.)

Rooftop photovoltaic arrays: electric shock and fire health hazards See Entry 115658

87.50G Ionizing radiations (u.v., X-ray, gamma-ray; particle radiation effects)

115839 Damages to superhelical structures of nuclear DNA induced by γ -rays and heavy ions. Kh.Abel, G.Erzgraber, K.Langrok (Joint Inst. of Nuclear Res., Dubna, USSR).

Radiobiologiya (USSR), vol.23, no.4, p.435-8 (1983). In Russian. Chinese hamster cells (V79-4), human lymphocytes and mouse ascites cells were exposed to γ -rays and heavy ions (^4He and ^{12}C). Sedimentation of complexes containing DNA was studied after cell lysis by centrifugation in a neutral sucrose gradient. The distinctions noted after irradiation with γ -rays and heavy ions are consistent with the idea of the superhelical organization of DNA into discrete and membrane-bound compact units. According to the estimates made the diameter of these complexes was $\sim 0.2 \mu\text{m}$ and DNA content, about 2×10^9 dalton. (9 refs.)

115840 Enhancement of biological effectiveness of low-energy quantum radiation. Microdosimetric basis for a selective action of ionizing radiation on the chromosomal material of cells. V.F.Stepanenko, T.A.Norets, A.N.Dedenkov (Sci. Res. Inst. of Medical Radiology, Acad. of Medical Sci., Obninsk, USSR).

Radiobiologiya (USSR), vol.23, no.4, p.439-43 (1983). In Russian. Microdosimetric data are presented indicating the possibility of a selective action of ionizing radiation on the chromosomal material of cells from the low-energy electrons and photoelectrons formed, as the result of the photoeffect, on the incorporated or native atoms inside DNA upon irradiation with low-energy quantum radiation ('X-activating' effect). A presumed biological effectiveness of the 'X-activating' effect on B-16 melanocarcinoma, with bromine and iodine incorporated into the DNA molecule, was estimated. (14 refs.)

115841 Radiation damage and recovery of mouse T-cells. Dynamics of suppressor cells after the effect of radiation. A.A.Yarilin, E.F.Polushkina (Sci. Res. Inst. of Medical Radiology, Acad. of Medical Sci., Obninsk, USSR).

Radiobiologiya (USSR), vol.23, no.4, p.454-7 (1983). In Russian. Suppressor and helper T-cells precursors, similar in radiosensitivity ($D_0 = 2.16$ and 2.25 , respectively), are restored almost synchronously and reach a normal level by the end of the 2nd month after irradiation. Suppressor macrophage precursors remain intact at doses of up to 7 Gy; one month after irradiation their level decreases, perhaps because of the death of the radiosensitive precursors. The suppressors damage is one of the factors decelerating the reverse development of the immune response after irradiation. (13 refs.)

115842 Influence of duration of fixation on the yield of chromosome aberrations in human lymphocyte culture exposed to γ -radiation at different mitotic cycle stages. A.V.Sevan'kaev, B.A.Bogatyykh, V.A.Lychev (Sci. Res. Inst. of Medical Radiology, Acad. of Medical Sci., Obninsk, USSR).

Radiobiologiya (USSR), vol.23, no.4, p.471-5 (1983). In Russian. A comparative study was made of the yield of chromosome aberrations in a human lymphocyte culture exposed to ^{60}Co - γ -rays (2 Gy) at different mitotic cycle stages, the cells being fixed after 52 and 60 hr. It was shown that with the latter fixation time (60 hr) the frequency of chromosome aberrations after irradiation in G_1 stage was substantially lower than that with the former one (52 hr) and vice versa, it was higher after irradiation in S and G_2 stages. The authors discuss the probable causes of the distinctions observed. (19 refs.)

115843 Influence of dose-rate and dose fractionation on radiation damage to bone marrow cells forming granulocyte-macrophage colonies in diffusion chambers (CFUdc). V.P.Kaplan, A.I.Kolesnikova, A.G.Konoplyannikov (Sci. Res. Inst. of Medical Radiology, Acad. of Medical Sci., Obninsk, USSR).

Radiobiologiya (USSR), vol.23, no.4, p.476-9 (1983). In Russian. The ability of CFUdc to repair radiation-induced lesions in the irradiated body was studied by the methods of dose fractionation and dose-rate reduction. When the dose-rate was decreased from 1-0.5 Gy/min to 0.02 Gy/min, the mean lethal dose per cell increased from 1.35 to 1.93 Gy. With fractionation of the dose, the known picture of repair of sublethal radiation lesions was obtained, the second survival peak being insignificant. The authors discuss the possible causes of the distinctions in the repair parameters of CFUdc obtained by the two methods. (15 refs.)

115844 Radiosensitivity of bone marrow and spleen CFUdc in mice γ -irradiated in different oxygenation conditions. V.P.Kaplan, A.I.Kolesnikova, A.G.Konoplyannikov, N.I.Michanskaya, L.A.Lepikhina (Sci. Res. Inst. of Medical Radiology, Acad. of Medical Sci., Obninsk, USSR).

Radiobiologiya (USSR), vol.23, no.4, p.480-3 (1983). In Russian. After exposure in vitro and in situ CFUdc of CBA mouse bone marrow and spleen were characterised by comparable parameters of radiosensitivity and oxygen-dependent modification: the values of D_0 for bone marrow and spleen cells were 1.31 and 1.35 Gy (in vitro) and 1.36 and 1.37 Gy (in situ), and the values of the oxygen effect were 2.3 and 2.5, respectively. (8 refs.)

115845 Mathematical model of a simultaneous combined action of ionizing radiation and hyperthermia. V.P.Komarov, V.G.Petin (Sci. Res. Inst. of Medical Radiology, Acad. of Medical Sci., Obninsk, USSR).

Radiobiologiya (USSR), vol.23, no.4, p.484-8 (1983). In Russian. A mathematical model is proposed suggesting that the synergistic action of a combination of ionizing radiation and hyperthermia is substantiated by additional lethal damages arising from the interaction of 'sub-lesions' induced by both agents. The model describes quantitatively the synergism of the combined action of the agents used and predicts the maximal value of the synergistic effect and conditions in which it can be achieved. (9 refs.)

115846 Migration of lymphocytes within the internally irradiated body. Effect of internal γ -irradiation on migrating capacity of splenic lymphocytes labeled with ^{51}Cr . Yu.N.Anokhin, T.A.Norets, A.A.Yarilin, V.F.Stepanenko (Sci. Res. Inst. of Medical Radiology, Acad. of Medical Sci., Obninsk, USSR).

Radiobiologiya (USSR), vol.23, no.4, p.493-6 (1983). In Russian. In experiments on CBA mice it was shown that migration of ^{51}Cr -labeled spleen lymphocytes, injected intravenously, to lymph nodes of intact recipients was suppressed 6-24 months after the administration of a radiopharmaceutical preparation of selenium-75-selenomethionine in a quantity giving doses of 1 Gy and 1.5 Gy to the whole body and lymphoid organs, respectively. Migration of labeled lymphocytes to the liver, kidneys and lungs, as well as their retention in the circulating blood, were increased. As the result of the migration disorders the specific affinity of lymphocytes for peripheral lymphoid tissue decreased. (14 refs.)

115847 Lymphocyte migration under conditions of incorporated irradiation. Effect of incorporated β -irradiation on spleen lymphocyte migration in CBA mice. Yu.N.Anokhin, T.A.Norets, A.A.Yarilin, V.F.Stepanenko (Sci. Res. Inst. of Medical Radiology, Acad. of Medical Sci., Obninsk, USSR).

Radiobiologiya (USSR), vol.23, no.4, p.497-500 (1983). In Russian. The syngenic transfer system was used to study migration of ^{51}Cr -labelled spleen lymphocytes in mice after incorporation of the β -emitter, ^{75}Se -methionine. Migration of ^{51}Cr -labelled lymphocytes to lymph nodes was stably decreased, and to liver, kidneys and lungs increased. The lymphocyte migration impairment was associated with the influence of β -radiation on both the migratory properties of cells and the factors of their microenvironment responsible for lymphocyte migration within the mouse body. No distinctions were observed in the character and manifestation of disturbances of lymphocyte migration after the injection of ^{75}Se -methionine and the γ -emitter, ^{75}Se -selenomethionine. (10 refs.)

115848 Influence of ^{131}I on the osteosarcomogenic effectiveness of ^{90}Sr . V.N.Strel'tsova, V.I.Shelesnova, S.V.Stepanov (Inst. of Biophys., Min. of Health, Moscow, USSR).

Radiobiologiya (USSR), vol.23, no.4, p.501-4 (1983). In Russian. Submits the results of estimation of the osteosarcomogenic effectiveness of ^{90}Sr in a combination with ^{131}I incorporated prior to or after the administration of ^{90}Sr . It was demonstrated that the incidence of osteosarcomas increased in rats who received ^{131}I a week after the administration of ^{90}Sr . (3 refs.)

115849 Synergistic effect of γ -radiation and constant magnetic field. A.M.Kuzin, S.E.Nizkyii (Inst. of Biological Phys., Acad. of Sci., Pushchino, USSR).

Radiobiologiya (USSR), vol.23, no.4, p.510-12 (1983). In Russian. In experiments on *Glicina* Max. L., VNIIS-1 series, it was shown that exposure of seeds to a stable magnetic field (2950 E) 5-20 min after 2 Gy irradiation stabilized and enhanced the stimulatory effect of ionizing radiation. (1 ref.)

115850 Effect of X-radiation on histones and DNA in nuclei of rat bone marrow and liver. Yu.Shyuliova, E.Mishurova (Dept. of General Biology, P.J. Safarik Univ., Kosice, Czechoslovakia).

Radiobiologiya (USSR), vol.23, no.4, p.513-16 (1983). In Russian. A study was made of a change in a total concentration of histones and DNA and a relative content of individual histone fractions in the isolated nuclei of bone marrow and liver of rats 3 h to 14 days following X-irradiation with different doses. A considerable decrease in the concentration of histones and DNA in the nuclei and a change in the relative content of individual histone fractions were observed in the bone marrow. In the liver, these changes were less pronounced. (16 refs.)

115851 Electric conductivity of liver cells as a function of dose at early times after γ -irradiation. B.I.Polivoda (Sci. Res. Inst. of Medical Radiology, Acad. of Medical Sci., Obninsk, USSR).

Radiobiologiya (USSR), vol.23, no.4, p.519-21 (1983). In Russian. The dependence of electroconductivity and electric capacity of isolated liver cells, irradiated in vitro, upon radiation dose (within 100 Gy) was described by an extreme curve characterized by the presence of a 'critical' dose (25 Gy) at which the effect was maximum. The kinetics of changes in the electric parameters, which were measured at early times following irradiation (up to 4 h), has an opposite direction. The possibility is discussed that peroxidation and repair processes in membrane lipids are involved in the effects observed. (8 refs.)

115852 Radiosensitivity of hemopoietic stroma precursors from long-term bone marrow culture. O.A.Gurevich, I.L.Chertkov (Central Inst. of Haematology & Blood Transfusion, Min. of Health, Moscow, USSR).

Radiobiologiya (USSR), vol.23, no.4, p.521-3 (1983). In Russian. Radiosensitivity of hemopoietic stroma precursors from a long-term bone marrow culture was measured by implantation of the adherent cell layer under the renal capsule of syngeneic mice. D_0 was 4.86 ± 0.15 Gy and n was 2.4, i.e. the radiosensitivity of cultured cells was nearly the same as that of stromal precursors from fresh bone marrow. (4 refs.)

115853 Age-related changes in postirradiation recovery of blood system. O.I.Belousova, M.I.Fedotova (Inst. of Biophys., Ministry of Health, Moscow, USSR).

Radiobiologiya (USSR), vol.23, no.4, p.530-4 (1983). In Russian. Reports a study on hybrid (CBA \times C57B1) F_1 mice of ages of 17 and 27 months who had been irradiated with a dose of 4 Gy. It was shown that the postirradiation recovery of haemopoiesis in old mice was the same as in the young (2-3-month-old) mice, and in some respects (for instance, granulocytic and erythroid cells of the bone marrow, and CFUc) the recovery was even more active exhibiting a period of a pronounced hyperregeneration. (9 refs.)

115854 Prediction of modification of acute radiation affection of dogs with red bone marrow being partially shielded. V.L.Gozenbuck, I.B.Keirim-Markus (Inst. of Biophys., Ministry of Health, Moscow, USSR).

Radiobiologiya (USSR), vol.23, no.4, p.546-9 (1983). In Russian. It was shown that shielding of a relatively small area of the bone marrow during acute total-body irradiation of dogs permitted one to obtain a prognosticated constant increase in the survival rate within a wide range of doses exceeding the minimal absolutely lethal ones. (4 refs.)

115855 Correlation between the vestibular analyzer and individual radiosensitivity of rabbits exposed to a dose of 150 Gy. A.Yu.Grigor'ev, V.S.Stepanov (Inst. of Biophys., Ministry of Health, Moscow, USSR).

Radiobiologiya (USSR), vol.23, no.4, p.549-51 (1983). In Russian. The authors have revealed a relationship between the original functional state of the vestibular analyzer of rabbits and their individual radiosensitivity. The coefficient of correlation between the vestibular analyzer sensitivity threshold and the life expectancy after exposure to γ -rays from an electron linear accelerator (7.6 MeV, 150 Gy) was 0.505. (8 refs.)

115856 Physical work capacity of rats after the effect of ionizing radiation. N.I.Arlashchenko, D.Ya.Oparina, V.I.Shein. *Radiobiologiya (USSR)*, vol.23, no.4, p.551-3 (1983). In Russian.

An increase in irradiation dose from 2.5 to 15 Gy was found to lead to a progressive diminution of the dynamic and static physical work capacity of animals. (7 refs.)

115857 On the mechanisms of a change in the coloration of garden rose mutants. K.I.Zykov, Z.K.Klimenko (State Nikitsky Botanical Gardens, USSR).

Radiobiologiya (USSR), vol.23, no.4, p.553-8 (1983). In Russian.

When induced and spontaneous mutations occur in the vegetative reproduction organs of garden roses their coloration changes mainly in heterozygous varieties due to the loss or inactivation of the dominant genes and the phenotypic expression of the recessive ones. The effect of γ -radiation on the vegetative reproduction organs may be an adequate method to use for the genetic analysis of varieties with unknown genotypes. (10 refs.)

115858 Effects of nonuniform distribution of the radiation energy absorbed among elements of the population. A.K.Valeev (B.P. Konstantinov, Leningrad Inst. of Nuclear Phys., Acad. of Sci., Gatchina, USSR).

Radiobiologiya (USSR), vol.23, no.4, p.568-73 (1983). In Russian.

The reaction of a particular element of the population, when this element has absorbed some portion of ionizing radiation energy, and the response of the whole population to a given radiation dose are discussed. Functions of the element reaction are supposed to be increasing or decreasing. Formulae have been obtained describing a correlation between the element reaction as a function of the radiation energy absorbed and the response of the whole population as a function of the radiation dose absorbed. (6 refs.)

115859 Bleomycin and radiation-induced lung damage in mice. C.H.Collis, J.D.Down, A.E.Pearson, G.G.Steel (Radiotherapy Res. Unit, Inst. of Cancer Res., Sutton, England).

Br. J. Radiol. (GB), vol.56, no.661, p.21-6 (Jan. 1983). [received: Sept. 1983] Bleomycin-induced lung damage was assessed using both a functional endpoint and mortality. The extent of lung damage was found to depend on the schedule, mode of administration and dose of the drug. Greater damage occurred following twice-weekly administration than when the same dose was given as a single injection. Intravenous administration resulted in greater damage than intraperitoneal administration. When bleomycin was given with thoracic irradiation lung damage occurred earlier and at lower radiation doses than with radiation alone. Similar responses were obtained whether bleomycin was given four weeks before, or four weeks after irradiation. Thus although there was enhanced damage from the combined treatment, there was no evidence of a time-dependent interaction. (30 refs.)

115860 Comparison of the effects of radiation and hyperthermia on prenatal retardation of brain growth of guinea-pigs. R.A.Wanner, M.J.Edwards (Dept. of Veterinary Clinical Studies, Univ. of Sydney, Sydney, Australia).

Br. J. Radiol. (GB), vol.56, no.661, p.33-9 (Jan. 1983). [received: Sept. 1983] On day 21 of pregnancy guinea-pigs were exposed to hyperthermia or γ -radiation. The effects on prenatal growth and especially brain growth of offspring were compared. Doses of 0.04-0.99 Gy of radiation produced a dose-dependent and irreversible reduction of brain weight in the offspring, but had little effect on body weight. Treatment with hyperthermia resulting in maternal temperatures of 41.8-43.9°C after exposure in a heated incubator for an hour also produced a dose-related microcephaly in the offspring. Comparison of the two agents showed that a dose increment of 0.525 Gy of radiation produced a deficit in brain weight equivalent to an elevation of 1°C in maternal temperature. Using this guinea-pig brain weight assay system a threshold was detected of between 0.05 and 0.10 Gy for retardation of brain growth. (18 refs.)

115861 Inhibition and recovery of the iodine uptake function of rat thyroids after 18 MeV proton irradiation in vivo. B.Mukherjee (Inst. für Strahlungs- und Kernphys., Tech. Univ. Berlin, Berlin, Germany).

Br. J. Radiol. (GB), vol.56, no.661, p.67-8 (Jan. 1983). [received: Sept. 1983] The effects of 18 MeV protons (directly ionising radiation) on the iodine uptake kinetics of rat thyroid glands irradiated in vivo are reported. It was found that a single proton dose of 5.7 Gy in vivo had no effect on the proliferative capacity of the highly differentiated thyroid cells, as the gland masses of the irradiated groups remained unchanged. On the other hand the maximum uptake and the biological half life of ^{131}I in the thyroids of the irradiated group were reduced relative to those of the control group by 55% and 35% respectively. Nevertheless almost a complete recovery of the impairment of these thyroid functions occurred after a rest period of six days. It is therefore important to study the time-dependent recovery processes of the (radio) iodine uptake and retention functions of rat thyroids for various types of irradiation at different dose levels and rest periods. (3 refs.)

115862 Effect of 8-methoxypsoralen and ultraviolet radiation on the electrical stability of liposome membranes. O.M.Parnev, L.N.Bezdetnaya, A.Ya.Potapenko, Yu.A.Vladimirov (Second Pirogov Medical Inst., Moscow, USSR).

Biophysica (GB), vol.27, no.5, p.889-93 (1982). Translation of: *Biofizika (USSR)*, vol.27, no.5, p.848-50 (1982). [received: Sept. 1983]

It is shown that irradiation with near ultraviolet reduces the electrical strength of liposome membranes. The presence of 8-methoxypsoralen on irradiation enhances the effects. Vacuum treatment of the sample or addition of α -tocopherol during irradiation inhibits the fall in electrical strength. It is assumed that 8-methoxypsoralen reduces the electrical stability of the liposome membranes by photosensitizing lipid oxidation. (13 refs.)

115863 Dose-effect relationships for early response to total body irradiation. H.Smith (Nat. Radiological Protection Board, Chilton, Didcot, England).

J. Soc. Radiol. Prot. (GB), vol.3, no.3, p.5-10 (Autumn 1983).

In this review, dose-response relationships are recommended that are considered reasonable for estimating the range of early consequences following the release of radioactive material in a major nuclear accident. The limited human data on the effects of brief exposure to radiation that are used as the basis of this assessment are discussed and estimates made of the frequency of prodromal effects and early death relative to dose. The influence of protracting the dose and of the application of simple treatment are also discussed. (35 refs.)

115864 Discounting in assessment of future radiation effects. B.L.Cohen (Dept. of Phys., Univ. of Pittsburgh, Pittsburgh, PA, USA).

Health Phys. (GB), vol.45, no.3, p.687-97 (Sept. 1983).

There is a question as to whether cancer fatalities to be experienced in the distant future as a result of radioactivity produced today should be treated on a par with those experienced now, or whether there should be discounting in analogy with accounting principles for money to be spent in the future. It is shown that recent trends in cancer cure rates justify about an 0.7% per yr discounting. Other rationales for discounting are developed. Money can and always will be usable for saving lives; setting up a trust fund for future

generations to use for this purpose is much more cost-effective than spending money now to reduce their exposure to radiation. The history of interest rates over the past 5000 yr indicates that at least 3% real annual interest can be expected. It may not be necessary to actually set up a trust fund as its purpose is largely accomplished by the decrease in the public debt when money is not spent. The trust fund approach is mathematically equivalent to discounting lives lost in the far future at 3% per yr. As an alternative to the trust fund, money can be invested in biomedical research. (13 refs.)

115865 Simulated responses to lognormally distributed continuous low radiation doses. J.G.Szekely, K.A.Perry, A.Petkau (Whiteshell Nuclear Res. Establ., AECL Res. Co., Pinawa, Manitoba, Canada).

Health Phys. (GB), vol.45, no.3, p.699-711 (Sept. 1983).

Three previously reported equations, expressing response as a function of both dose and dose rate, for low LET radiation were used to compute distributions of response to continuous, low-level, lognormally distributed doses for populations of variable size up to 5000. The simulations show that, when the response is inversely dependent on dose rate, the mean of the response distribution can either increase or decrease with increasing exposure to radiation, depending on whether or not the dose-dependent term is the dominant one in an equation. In one equation, which defines the response as conjugated hydroperoxide formation in irradiated membranes, the magnitude of the dose-dependent term is reduced the most by superoxide dismutase, an enzymic inhibitor of free radical processes. This results in the means of response distributions decreasing with increasing dose from continuous, low-level radiation. (13 refs.)

115866 Relative efficiencies of three ultraviolet radiation wavelengths for cell killing and transformation in mouse cells in vitro. D.Papadopoulos, B.Muel, R.Latarjet (Inst. Curie Biologie, Paris, France).

Int. J. Radiat. Biol. (GB), vol.44, no.3, p.241-9 (Sept. 1983).

C3H 10 T 1/2 clone 8 mouse cells were irradiated in vitro with three UV wavelengths 280, 254, and 230 nm. Two effects were investigated, survival and malignant transformation, and the relative efficiencies were determined for the three radiations. For transformation, these efficiencies were: 280 nm: 3.9; 254 nm: 5.1; 230 nm: 2.3 (transformations produced by 5 J m⁻² of UV for 1000 surviving cells). For cell killing the efficiencies were, in relative units, 34, 100, and 50 respectively. These efficiencies are in agreement with the hypothesis that the main chromophore for both effects is the nucleic acid, and not the protein moiety of the genome. This conclusion agrees with that previously reached by other investigators, but the present results obtained with the short wavelength 230 nm provide an especially strong new argument. (17 refs.)

115867 Measurement of lymphoblastogenic activity from thorium workers.

C.S.Serio, C.B.Henning, R.E.Toohy, E.L.Lloyd (Radiological & Environmental Res. Div., Center for Human Radiobiology, Argonne Nat. Lab., Argonne, IL, USA).

Int. J. Radiat. Biol. (GB), vol.44, no.3, p.251-6 (Sept. 1983).

Mitogenic stimulation of peripheral blood lymphocyte cultures obtained from 36 thorium workers was studied to determine whether the response of these cells was affected by the individuals' occupational exposure to alpha irradiation. The standard assay involved incubating 2×10^5 lymphocytes per test well for 72 hours in the presence of phytohemagglutinin (PHA), concanavalin A or pokeweed mitogen (PWM). The results showed that there was a significant decrease in lymphocyte responsiveness of former thorium workers grouped by decade of life when compared with controls of the same decade of life for each mitogen tested with the exceptions of PHA in the 41-50 age group and the PWM in the 51-60 age group. The authors are unable to correlate the decreased response observed with the measured body burdens, external gamma exposure, or thoron exhalation rates in these thorium cases. However, other occupational exposures (i.e. various chemicals used in processing thorium) cannot be eliminated as a possible cause. (26 refs.)

115868 Comparative effects of exposure to high-energy electrons and gamma radiation on active avoidance behaviour. W.A.Hunt (Behavioral Sci. Dept., Armed Forces Radiobiology Res. Inst., Bethesda, MD, USA).

Int. J. Radiat. Biol. (GB), vol.44, no.3, p.257-60 (Sept. 1983).

The effects of two types of ionizing radiation was examined on active avoidance behaviour. Male Sprague-Dawley rats were trained to avoid footshock by jumping onto a retractable ledge. When irradiated with high-energy electrons or gamma photons, their performance was degraded in a dose-dependent manner. However, electrons were 1.6 times as effective as gamma photons with ED₅₀s of 62 and 102 Gy, respectively. All animals recovered with 24 min for all doses used. The data suggest that different types of ionizing radiation may not be equivalent when assessing their effect on behaviour. (9 refs.)

115869 Comparative influence of hyperthermia and ionizing radiation on cycle and mitosis lengths in EMT6 mouse tumour cells. M.C.D'Hooghe, D.Hemon, E.P.Malaisie (Inst. de Recherches sur le Cancer, Lille, France).

Int. J. Radiat. Biol. (GB), vol.44, no.3, p.267-74 (Sept. 1983).

With exponentially growing EMT6 mouse tumour cells in vitro, the authors have compared the effects of a dose of ionizing radiation and different temperature-time combinations on the lengths of the cell cycle and of mitosis using time-lapse cinematography on individual cells. The radiation dose and various temperature-time combinations all produced 50 per cent lethality. The hyperthermia treatments between 42 and 45°C all cause a mitosis delay (MD) which was greater than that induced by ionizing radiation. The MD was greater with increasing temperature. In contrast, hyperthermia also induced a mitosis lengthening (ML) but this was only of the same order of magnitude as radioinduced ML. The results argue in favour of different mechanisms underlying thermoinduced MD and ML. (24 refs.)

115870 Hyperthermia in a differentiating murine erythroleukemia cell line: cell killing by heat and radiation. G.P.Raaphorst, E.I.Azzam, J.Borsa, M.Einspinner (Medical Biophys. Branch, Atomic Energy of Canada Ltd., Whiteshell Nuclear Res. Establ., Pinawa, Manitoba, Canada).

Int. J. Radiat. Biol. (GB), vol.44, no.3, p.275-83 (Sept. 1983).

The survival response of Friend erythroleukemia cells (a differentiating cell system) to heat and radiation has been examined. The Friend erythroleukemia cells (FELC) were more heat and radiation sensitive than V79 cells, and the heat and radiation survival curves possessed shoulders, showing the ability of the cells to accumulate sublethal damage. Thermal tolerance was expressed after prolonged heating at 41.0-42.0°C. Thermal radiosensitization by heating at 42.0 or 45.0°C was greatest for simultaneous heat and radiation treatments, and recovery occurred when the cells were incubated at 37°C between the heat and radiation or radiation and heat treatments. Arrhenius analysis of the FELC heat survival data showed that the curve for thermal inactivation possessed a break at about 43.0°C and that the thermal inactivation energies above and below the breakpoint were comparable to those for V79 cells and other cell lines reported in the literature. (30 refs.)

115871 Effect of prolonged heating on the thermal enhancement ratio in X-irradiated murine intestine. J.C.L. Marigold, S.P. Hume (MRC Cyclotron Unit, Hammersmith Hospital, London, England).

Int. J. Radiat. Biol. (GB), vol.44, no.3, p.285-91 (Sept. 1983).
When the jejunum in mice was heated for 20-180 min at temperatures between 40.3 and 42.3°C, followed immediately by X-irradiation, the thermal enhancement ratio (TER) for crypt survival increased and then tended to decline with longer heating times. At the higher temperatures, the TER was higher and the peak value was reached with shorter heating times. The decline in TER with longer heating times may be due to the development of thermotolerance. (27 refs.)

115872 Effect of gamma radiation on enzymatic activity and sulphhydryl groups of human erythrocyte membrane. D. Palecz, W. Leyko (Dept. of Biophys., Inst. of Biochem. & Biophys., Univ. of Lodz, Lodz, Poland).

Int. J. Radiat. Biol. (GB), vol.44, no.3, p.293-9 (Sept. 1983).
The effect of ionizing radiation on human erythrocyte ghost membranes was studied by following changes in membrane -SH groups and activities of four membrane bound enzymes: $\text{Na}^+\text{K}^+\text{Mg}^{2+}$ ATP-ase, $\text{Mg}^{2+}\text{Ca}^{2+}$ ATP-ase, Na^+K^+ ATP-ase, and AChE. Irradiation with up to 100 Gy gamma rays produced a significant decrease in the activity of ATP-ase and an increase in AChE activity. At higher radiation doses a marked decrease in the activities of all the enzymes was observed. A correlation between radiation-induced perturbations in enzyme activities and changes in membrane -SH groups was found. (22 refs.)

115873 Effect of adenine nucleotides and gamma radiation on the transport of TEMPOL across the erythrocyte membrane. Z. Jozwiak, K. Gwozdziński, Z. Heszner (Dept. of Biophys., Inst. of Biochem. & Biophys., Univ. of Lodz, Lodz, Poland).

Int. J. Radiat. Biol. (GB), vol.44, no.3, p.301-5 (Sept. 1983).
The experiments reported show that external adenine compounds bring about changes in the transport of hydrophilic molecules across control and irradiated bovine erythrocyte membranes. Changes in the transport induced by incubation of erythrocytes with nucleotides depend on the type of nucleotide and its concentration. The range of nucleotide concentrations over which the stimulatory effect on the transport occurs is established. (16 refs.)

115874 The effect of ionizing radiation on tryptophan fluorescence of thymocyte and erythrocyte plasma membranes. B.S. Fomenko, I.E. Dovgii, I.G. Akoev (Inst. of Biological Phys., Acad. of Sci., Pushchino, USSR).

Int. J. Radiat. Biol. (GB), vol.44, no.3, p.307-11 (Sept. 1983).
The effect of ionizing radiation on tryptophan fluorescence of thymocyte and erythrocyte plasma membrane preparations was studied. The intensity of tryptophan fluorescence decreased after applying radiation doses up to 15 Gy. The radiosensitivity of thymocyte membranes appeared to be higher than that of the erythrocyte ghosts. Tryptophan radiolysis did not significantly contribute to the effects of radiation. The fraction of tryptophan residues accessible for quenching by I^- decreased from 0.87 in the untreated membranes to 0.63 and 0.49 in membranes after doses of 10 and 250 Gy, respectively. The effective quenching constant and the tryptophan fluorescence polarization increased after irradiation. The mechanisms producing these radiation-induced changes are discussed. (14 refs.)

115875 Radiotoxicity of thallium-201 in mouse testes: inadequacy of conventional dosimetry. D.V. Rao, G.F. Govelitz, K.S.R. Sastry (Univ. of Medicine & Dentistry of New Jersey, Newark, NJ, USA).

J. Nucl. Med. (USA), vol.24, no.2, p.145-53 (Feb. 1983). [received: Sept. 1983]
When Tl-201 is concentrated in mouse testes, the low-energy Auger electrons following its electron-capture decay are found to be much more effective in causing loss of testicular weight and reduction of sperm heads than the energetic beta particles from similarly distributed Tl-204. These results are contrary to expectations based on conventional dosimetry of tissue-incorporated radionuclides, and point to possible underestimation of risks by the currently adopted dosimetric procedures, especially in the case of radionuclides decaying by electron capture and internal conversion. (39 refs.)

115876 'Biological dosimetry' of radionuclides and radiation hazards. M.E. Gauden (Health Sci. Center, Univ. of Texas, Dallas, TX, USA).

J. Nucl. Med. (USA), vol.24, no.2, p.160-4 (Feb. 1983). [received: Sept. 1983]
This discussion on the radiobiology of radionuclides deals mainly with spermatogenic effects in mice testes. The author considers: extrapolation of data on the mouse to man; the accumulation of radionuclides in the germinal epithelium; a test for detecting the effects of small amounts of radionuclides; mutations and surviving spermatogonia. (35 refs.)

115877 Intrinsic resistance to the lethal effects of X-irradiation in insect and arachnid cells. T.M. Koval (Dept. of Radiation Therapy & Nuclear Medicine, Hahnemann Medical Coll., Philadelphia, PA, USA).

Proc. Natl. Acad. Sci. USA, vol.80, no.15, p.4752-5 (Aug. 1983).
Twelve cell lines representing 10 genera of three orders (Diptera, Lepidoptera, and Orthoptera) of the class Insecta and one cell line (Acarina) from the class Arachnida were examined to discern their sensitivity to the lethal effects of X-irradiation. Radiosensitivity was measured by a combination of colony formation and population growth curve techniques. Each of these arthropod cell lines is significantly more radioresistant than mammalian cells, though the degree of resistance varies greatly with order. Dipteran cells are 3 to 9 times and lepidopteran cells 52 to 104 times more radioresistant than mammalian cells. Orthopteran and acarine cells are intermediate in radiosensitivity between dipteran and lepidopteran cells. These cells, especially the lepidopteran, should be valuable in determining the molecular nature of repair mechanisms that result in resistance to ionizing radiation. (25 refs.)

115878 How cells respond to ionising radiation. M.J. Ashwood-Smith (Dept. of Biology, Univ. of Victoria, Victoria, British Columbia, Canada).

Phys. Bull. (GB), vol.34, no.9, p.384-6 (Sept. 1983).
The main biological target for ionising radiation is the deoxyribonucleic acid (DNA) of the cell's nucleus; the radiation breaks the phosphate diester backbone of the double-stranded helical DNA molecule. Breaks in one of the two strands (single-strand breaks) are readily produced by X- and gamma rays. If two separate single-stranded breaks are formed on each of the two strands, and if they are nearly opposite, then the resulting double-stranded breaks are invariably lethal. While such damage through accidental exposure can be highly detrimental, this effect of the radiation can also be extremely beneficial when it is channelled specifically towards such structures as tumours. The author discusses the various factors that influence the effect ionising radiation has on any cell and thus how to tailor it to our needs. (4 refs.)

115879 Model for the accumulation of cases of pulmonary malignancy in time when dose is accumulated in time. C.G. Stewart.

Report AECL-7155, Atomic Energy Canada Ltd., Chalk River, Ont. (May 1983), 13 pp.
These notes are directed primarily at the formulation of the accumulation of resulting cases of pulmonary malignancy with time when a dose of ionizing

radiation (e.g. from airborne short-lived daughters of Rn-222) is protracted in time and when the accumulation of tumours from receipt of the dose occurs after an induction-latent period. The model developed is quite general in that it will allow for the incorporation of the receipt of dose as functions of time, dose-response functions, and functions of time for the accumulation of tumours following and resulting from the receipt of a dose of ionizing radiation. (13 refs.)

Transactions of the 4th International Meeting on Radiation Processing See Entry 111308

Effect of constant magnetic field (CMF) and γ -radiation on hereditary structures of somatic cells. Combined effect of CMF and γ -radiation on human lymphocytes in vitro See Entry 115826

Contribution of γ -radiation to the dose absorbed, and some radiation effects in a radiation field p(50 MeV)-Be See Entry 115923

Environmental radon and cancer correlations in Maine See Entry 115942

Effect of the radiation factor on operator activity See Entry 115950

87.60 MEDICAL AND BIOMEDICAL USES OF FIELDS, RADIATIONS, AND RADIOACTIVITY (see also 28.80 Nuclear radiation technology, including shielding)

115880 Measurement of blood flow. S. Yoshimura, H. Furuhashi, K. Kodaira.

Jpn. J. Med. Electron. & Biol. Eng. (Japan), vol.20, no.7, p.519-21 (Dec. 1982). In Japanese. [received: July 1983]

The methods used for blood flow instrumentation are classified into invasive and noninvasive. The former includes laser Doppler techniques and catheter electromagnetic blood-flowmeters; and radioisotope techniques, plethysmograph techniques, thermography and ultrasonic Doppler techniques fall under the noninvasive method. This paper gives a brief description of these techniques and outlines typical blood flow instrumentation is reviewed. The diagnostic significance of blood flow measurements is reviewed. (no refs.) K.B.

115881 Image processing for medicine. M. Onoe.

Jpn. J. Med. Electron. & Biol. Eng. (Japan), vol.20, no.7, p.532-5 (Dec. 1982). In Japanese. [received: July 1983]

Typical medical images are surface patterns, microscope images, electron-microscope images, X-ray images, radioisotope images, NMR images, ultrasound images, endoscope images and fundus-camera images. This paper reviews their features from the standpoint of clinical application. CT scanning has been applied not only to X-ray imaging but also to radioisotope imaging and NMR imaging; furthermore, ultrasound CT, microwave CT, etc. are being developed successively. Digital radiography (DR) can image only blood vessels. DR equipment comprises X-ray apparatus, a video camera, and a digital computer. (no refs.) K.B.

115882 A method of comparing the areas under receiver operating characteristic curves derived from the same cases. J.A. Hanley, B.J. McNeil.

Radiology (USA), vol.148, no.3, p.839-43 (Sept. 1983).

Receiver operating characteristic (ROC) curves are used to describe and compare the performance of diagnostic technology and diagnostic algorithms. This paper refines the statistical comparison of the areas under two ROC curves derived from the same set of patients by taking into account the correlation between the areas that is induced by the paired nature of the data. The correspondence between the area under an ROC curve and the Wilcoxon statistic is used and underlying Gaussian distributions (binormal) are assumed to provide a table that converts the observed correlations in paired ratings of images into a correlation between the two ROC areas. This between-area correlation can be used to reduce the standard error (uncertainty) about the observed difference in areas. This correction for pairing, analogous to that used in the paired t-test, can produce a considerable increase in the statistical sensitivity (power) of the comparison. For studies involving multiple readers, this method provides a measure of a component of the sampling variation that is otherwise difficult to obtain. (10 refs.)

1st European Conference on Cineradiography with Photons or Particles See Entry 111300

87.60B Sonic and ultrasonic radiation

115883 Detectability of gas bubbles in blood by the ultrasonic method. L. Filipczynski (Inst. of Fundamental Technol. Res., Polish Acad. of Sci., Warsaw, Poland).

Arch. Acoust. (Poland), vol.8, no.1, p.11-29 (1983).
The reflection of a plane ultrasonic wave from a gas bubble in the blood was considered quantitatively in the range $ka \leq 1$ (a is the radius of the bubble, $k = 2\pi/\lambda$ and λ is the wavelength). Taking as an example the elbow vein (vena basilica), the losses in a signal caused by electroacoustical transducing, attenuation of the wave in tissues, reflection of the wave from the bubble and divergence of the reflected wave were evaluated using a typical ultrasonic Doppler device with a frequency of 8 MHz. The present calculation procedure permits the determination in a specific anatomic case of the level of signals scattered by blood, the level of electronic noise and also the determination of the detectability of gas bubbles in blood caused, for example, by the decompression of divers or by the caisson disease. In the case of the pulmonary artery, using a frequency of 5 MHz, radii of detectable gas bubbles greater than 70 μm were obtained. (20 refs.)

115884 Ultrasonic characterization of tissues in cardiology. L. Filipczynski (Inst. of Fundamental Technol. Res., Polish Acad. of Sci., Warsaw, Poland).

Arch. Acoust. (Poland), vol.8, no.1, p.83-94 (1983).

In order to analyse the possibility of the determination of the properties of soft tissues using ultrasonic (noninvasive) methods, a review was made of the basic physical properties characterizing acoustic wave propagation in these tissues (propagation velocity, attenuation, scattering). In a discussion of the results of 'in vitro' investigations, it was shown that investigations of backscattering can be very significant for cardiological applications; the heart muscle with scars caused by an infarct is characterized by an increased proportion of collagen-rich connective tissue which has the value of the backscattering coefficient greater by a factor of some dozens than that of normal muscle. This is related to the higher echographic visualizability of collagen than other soft tissues and suggests the practical possibility of noninvasive distinguishing of the regions of the muscle with scars caused by the infarct from normal muscle. This possibility was confirmed by 'in vivo' investigations performed on dogs by the method of grey level histograms obtained from ultrasonograms of dog's hearts. (17 refs.)

115885 Formalization of choice for parameters of an acoustic stimulus in a small automatic facility to examine and diagnose the functional status of an auditory analyzer. E.I.Podgornyi, E.A.Bakai (A.I. Kolomiichenko Kiev Sci. Res. Inst. of Otolaryngology, Kiev, Ukrainian SSR). *Biomed. Eng. (USA)*, vol.16, no.6, p.179-83 (Nov.-Dec. 1982). Translation of: *Med. Tekh. (USSR)*, vol.16, no.6, p.10-14 (Nov.-Dec. 1982). A method is presented for choosing the parameters of the stimulus produced by the acoustic channel of a small automatic facility for examining and diagnosing the functional status of the auditory system. By a concrete example of equipment design, the advantages of the method are demonstrated. (12 refs.)

115886 Bone-conduction receiver with an extended frequency range for measuring the threshold of audibility. B.M.Sagalovich, F.V.Bednin (Moscow Sci. Res. Inst. for Ear, Throat & Nose, Moscow, USSR). *Biomed. Eng. (USA)*, vol.16, no.6, p.183-6 (Nov.-Dec. 1982). Translation of: *Med. Tekh. (USSR)*, vol.16, no.6, p.14-18 (Nov.-Dec. 1982). A piezoelectric transducer type of bone-conduction receiver is described. By means of this receiver thresholds of audibility can be measured over a range from 250 Hz to 20 kHz. This receiver opens up new possibilities for the early diagnosis of hearing disorders for people having various forms of deafness. (14 refs.)

115887 The selection of modulation waveform for frequency modulated sound field stimuli. H.Dillon, G.Walker (Nat. Acoustic Labs., Sydney, NSW, Australia). *Aust. J. Audiol. (Australia)*, vol.4, no.2, p.56-61 (Nov. 1982). [received: Sept. 1983]

Frequency modulated (FM) tones are used in sound field audiometry in order to avoid problems caused by standing waves. To provide uniform sound fields and be sufficiently frequency specific, the FM stimulus should possess a uniform distribution of energy within the frequency limits set by its bandwidth, and a very rapid fall off of energy outside these limits. This paper compares several practical modulation waveforms with regard to how well they meet these constraints. The modulation waveform affects the spectral characteristics both within the signal band and outside it. Sinusoidal modulation provides very steep skirts at the band edges but somewhat non-uniform energy distribution within the band. Triangular and ramp modulation improves uniformity within the band at the expense of shallower skirt slopes. Square wave modulation provides neither uniform energy distribution within the band nor steep skirt slopes. The skirt slope is required to be steeper than the maximum audiogram slope likely to be encountered. Both sinusoidal and triangular modulation meet this requirement but triangular modulation is preferred because of its more uniform energy distribution within the band. Square wave and ramp modulation are not suitable for use in audiometric warble tone generators. (5 refs.)

115888 Acoustic notch filters for hearing aids. J.Macrae (Nat. Acoustic Labs., Sydney, NSW, Australia). *Aust. J. Audiol. (Australia)*, vol.4, no.2, p.71-6 (Nov. 1982). [received: Sept. 1983]

Hearing losses with normal hearing in a narrow band centred on one of the higher frequencies should be fitted with hearing aids which contain a notch filter centred on the region of good hearing. A closed branch tube or a Helmholtz resonator incorporated into the sound channel of the hearing aid will act as an acoustic notch filter. Equations are given for calculating appropriate dimensions and damping for a branch tube or Helmholtz resonator from the centre frequency, bandwidth and depth of the required notch in the hearing aid response. Measurements revealed that the actual effects of a closed branch tube or Helmholtz resonator differ slightly from the calculated effects, as a result of the acoustical interaction of the branch tube or resonator with other components of the sound channel, but allowance can be made for the discrepancies. The branch tube is preferable to the Helmholtz resonator for notches at the higher frequencies, while the Helmholtz resonator is the better to use for notches at the lower frequencies. (2 refs.)

115889 Standardized function test for audiometers in the audiological prophylaxis as part of occupational medicine in accordance with principle 20. B.H.Pfeiffer. *Audiol. Akust. (Germany)*, vol.22, no.5, p.150-8 (Sept.-Oct. 1983). In German, English.

The following topics in the title subject are considered: purpose and application; the minimum program for audiometer function tests; subjective audiometer checking by the user; additional tests of air-conduction equipment; checking the bone-conduction system. (12 refs.)

115890 Effect of half-wavelength membranes on the axial resolution of real-time ultrasonic scanners. J.Ophir, P.A.Narayana (Dept. of Radiology, Univ. of Texas Medical School, Houston, TX, USA).

J. Acoust. Soc. Am. (USA), vol.74, no.3, p.687-90 (Sept. 1983). The effect of interposing a half-wavelength membrane between the transducer and the load in mechanically sectioned ultrasonic scanners was investigated. In particular, the effects of impedance mismatch and detuning on broadband spectra were theoretically and experimentally studied. These studies indicate that for certain common cases, a bandwidth reduction of 20%-30% can be anticipated, resulting in a proportional decrease in the axial resolution. (8 refs.)

115891 Electronic sector-scanning crosssectional echocardiograph, model SSH-40A. S.Sato, T.Ito (Toshiba Corp., Kawasaki, Japan).

Toshiba Rev. (Int. Ed.) (Japan), no.143, p.27-30 (Spring 1983). This equipment is a cardiac sector and linear electronic scanning ultrasound diagnostic system. It incorporates a newly developed high frequency phase array probe and a microcomputerized multifunctional digital scan processor (DSP). By virtue of the DSP, ultrasound echoes can be directly converted into TV signals, thus allowing tomographic images to be displayed on a TV monitor. In addition, a combination of a tomographic image and up to two channels of M-mode waveforms can be displayed simultaneously on the same screen. If a doppler unit is added into the configuration, a combination of tomographic image, M-mode and doppler information can be displayed. Basic ventricular function calculations are made possible by measuring diastolic and systolic parameters on the displayed cardiac image. Dual cardiac synchronization and slow-motion triggering on the tomographic image facilitate heart movement observations at any cardiac phase. (3 refs.)

115892 Three-dimensional imaging in ultrasound. J.F.Greenleaf (Dept. of Physiology & Biophys., Mayo Found., Rochester, MN, USA).

Proceedings of the Fifteenth Hawaii International Conference on System Sciences 1982, Honolulu, HI, USA, 6-8 Jan. 1982 (HI, USA: Hawaii Int. Conference Syst. Sci. 1982), p.425-34 vol.2

Ultrasonic three-dimensional images are accomplished by 'stacking' B-scan tomograms or ultrasonic CAT scans with a computer algorithm for subsequent perspective or sectional display. Perspective images of surfaces representing Doppler measurements of fluid velocity are illustrated in combination with iso-velocity contours for flows through a flexible tube in vitro. Iso-speed contours calculated from a dynamically moving epicardial surface

are mapped onto the heart surface illustrating the combination of quantitative parametric data with a qualitative surface display. The efficacy of three-dimensional displays for increasing the information density and comprehensibility of ultrasonic data sets is discussed. (13 refs.)

Foil electret transducer for blood pressure monitoringSee Entry 115955

Comparative study of linear prediction parameters for quantification and monitoring of dysphonic voicesSee Entry 115963

87.60D Electric and magnetic fields (d.c. and pulsed)

Future of biomagnetismSee Entry 115813

87.60G Laser beams, microwaves, and other electromagnetic waves

(inc. NMR; for X-rays and gamma-rays, see 87.60J)

115893 Light sources for fluorescein fluorophotometry. J.W.McLaren, R.F.Brubaker (Ophthalmology Dept., Mayo Found., Rochester, MN, USA).

Appl. Opt. (USA), vol.22, no.18, p.2897-905 (15 Sept. 1983). Seven light sources were considered as excitation sources for ocular fluorescein fluorophotometry: tungsten, xenon flash, the continuous high pressure short arc lamps of xenon, xenon zinc iodide and mercury, and argon and He-Cd lasers. Each source was evaluated on the basis of its spectral match to the fluorescein absorption spectrum and dissimilarity to the ocular blue light hazard function. Light from the argon laser was found to be most suitable while light from the mercury arc and He-Cd laser was least. Each source was also evaluated on the basis of irradiance available at the cornea when used with a Zeiss slit lamp that had been converted to an ocular fluorophotometer. (19 refs.)

115894 Methods of proportioning the quantity and density of laser radiation for therapeutic action. V.I.Pronin, G.F.Fedotkin, V.F.Evmenov. *Med. Radiol. (USSR)*, vol.28, no.5, p.72-4 (May 1983). In Russian.

The use of medical laser installation 'Impulse-I' allows control of quantity and density of laser radiation for therapeutic treatment of neoplasms of the skin, with reduction of time to $2/3$ without damage to the quality of radiation. The method of proportioning quantity and density is simple, accurate and reliable, and makes the work of the doctor easier. (4 refs.) *D.E.P.*

115895 Medical NMR spectroscopy and introscopy: progress and prospects. A.F.Tsy', G.A.Zedgenidze, O.N.Denisenko, O.V.Nestaiko, V.I.Slesarev.

Med. Radiol. (USSR), vol.28, no.6, p.86-94 (June 1983). In Russian. Describes results from NMR spectroscopy on normal and on pathological tissue. Basic principles of NMR introscopy are given, followed by use in clinical practice. Results of X-ray computed tomography and NMR tomography on brain and infarcted liver are compared. (52 refs.) *D.E.P.*

115896 A microwave radiometer for medical applications. S.Osterrieder, G.Schaller (Inst. fur Hochfrequenztech., Univ. Erlangen-Nurnberg, Erlangen, Germany).

Frequenz (Germany), vol.37, no.1, p.7-12 (Jan. 1983). In German. [received: Aug. 1983]

A microwave radiometer for the determination of the temperatures of the human body is presented. Starting from known procedures, a method is described in which an output signal is obtained which is proportional to the temperature of the object being measured and independent of mismatches of the antenna. Simultaneously, as a measure of the match of the antenna, a second signal is obtained which is independent of temperature. After a short description of the apparatus some results are given; with the 4 GHz radiometer a resolution better than 0.1K for the temperature at a response time smaller than 0.5 s could be achieved. (4 refs.)

115897 The biomedical laser. Y.Sakurai.

Jpn. J. Med. Electron. & Biol. Eng. (Japan), vol.20, no.7, p.546-50 (Dec. 1982). In Japanese. [received: July 1983]

Applications of laser to medical instrumentation include lighting, spectrometry, laser interferometry, laser Doppler blood-flow measurements, stimulation threshold-value measurements, laser holography, laser flow microphotometry, cytofluorometry, and speckle patterning. For applications to therapy there are three methods: (1) stimulating the tissue of the body using continuous or pulsed milliwatt laser beams; (2) selectively destroying particular tissue using weak laser beams and special chemical substances; and (3) evaporating or excising tissue with high-energy laser beams. These are summarized in this review paper. (76 refs.) *K.B.*

115898 Ruby laser system with kaleidoscope for nevus treatment. T.Matozaki, M.Suzuki (Medical Equipment Div., Toshiba Corp., Tokyo, Japan), R.Tanino.

Jpn. J. Med. Electron. & Biol. Eng. (Japan), vol.21, no.2, p.114-20 (April 1983). In Japanese. [received: Sept. 1983]

Ruby laser radiation is effective in treating pigmented skin tumors, such as melanomas and nevus. The conventional ruby laser unit, however, is limited in practical use due to its uneven beam distribution over the target area. To overcome this problem the authors have developed a new ruby laser system utilizing a kaleidoscope as the application head. The spatial uniformity of the kaleidoscope output as well as its efficiency varies depending on the kaleidoscope length, reflection ratio, the incident beam spread angle, incident position, etc. Therefore, the kaleidoscope has excellent characteristics for the authors' purposes, when these parameters are set to proper values. The prototype model has an output energy of 20~40 J/cm² over a 10² mm irradiated area. The pulse interval is 1 msec. The spatial uniformity of the output intensity on the kaleidoscope output surface was found to be below 12%, which is close to simulated data. (8 refs.)

115899 Computer calculations of a one-dimensional model, useful in the application of hyperthermia. M.van-Sliedregt (Delft Univ. of Technol., Delft, Netherlands).

Microwave J. (USA), vol.26, no.6, p.113-26 (June 1983).

Discusses the development of a radiator suited for 27 MHz, consisting of a water-filled ridged waveguide, in which over a part of the cross-section (7x24 cm) the greatest power density is used. This has enabled the construction of an EM radiator for direct contact with the body. Using this 27 MHz radiator, a one-dimensional model has been developed for computing the temperature distribution as a function of place and time in the abdomen of a patient with a deep-seated tumor. The characteristics of this model are described. (7 refs.)

115900 Nuclear magnetic resonance: a gray scale model for head images. R.T.Droege, S.N.Wiener, M.S.Rzeszotarski, G.N.Holland, I.R.Young (Mount Sinai Medical Center, Cleveland, OH, USA).

Radiology (USA), vol.148, no.3, p.763-71 (Sept. 1983).

The gray scale of nuclear magnetic resonance (NMR) head images is explained in terms of tissue and machine parameters. Tissue parameters considered here include the spin-lattice relaxation time, the spin-spin relaxation time, and the proton density. Machine parameters include the pulse sequence (saturation recovery, inversion recovery, or spin echo), the repetition time, and the delay time. The ability of the operator to alter the NMR gray scale predictability is examined by computer simulation. The simulation computes NMR pixel values for a selected combination of tissue and machine parameters. The computed values are compared with those extracted from clinical NMR images. The agreement between simulation and clinical pixel values implies that the operator can use the machine parameters to alter the NMR gray scale, and thereby control contrast, appropriate to the diagnostic requirements. The extent to which the NMR gray scale can be predictably controlled is illustrated through graphs, simulated contrast displays, and representative NMR images. (8 refs.)

115901 NMR zeugmatographic imaging in medicine. P.C.Lauterbur (Dept. of Chem. & Radiology, State Univ. of New York, Stony Brook, NY, USA).

Proceedings of the Fifteenth Hawaii International Conference on System Sciences 1982, Honolulu, HI, USA, 6-8 Jan. 1982 (HI, USA: Hawaii Int. Conference Syst. Sci. 1982), p.435-9 vol.2

The history of the application of nuclear magnetic resonance techniques to biology and medicine is outlined, and the fundamental principles and certain techniques of nuclear magnetic resonance zeugmatographic imaging are described, with emphasis on true three-dimensional reconstruction methods. (22 refs.)

Infrared contact coagulation. A new therapy for solid tumors See Entry 115837

Recent advances in medical imaging See Entry 115914

Computed radiography utilizing scanning laser stimulated luminescence See Entry 115918

87.60J Corpuscular radiation and radioisotopes

(inc. X-rays and gamma-rays)

115902 The prospects of instrumentation in medical radiology and problems of clinical dosimetry. E.A.Zherbin.

Med. Radiol. (USSR), vol.28, no.6, p.3-5 (June 1983). In Russian.

There is a rapid increase in technical provisions for medical diagnostics and treatment of illnesses. Medical radiology is at present the most engineered branch of practical public health. (3 refs.) D.E.P.

115903 Special purpose CT-system for quantitative bone evaluations in the appendicular skeleton. B.Stebler, P.Rueggsegger (Inst. für Biomedizinische Tech., Univ. Zurich, Zurich, Switzerland).

Biomed. Tech. (Germany), vol.28, no.9, p.196-205 (Sept. 1983). In German.

Presents a computed tomography system which has been specially developed to determine the bone density of human extremities. High precision and low radiation dose were the primary goals of the development. It is with respect to these aspects that the authors describe the system, including mechanical construction, X-ray generation and detection, data-acquisition and processing, and evaluation of the CT-images. The system is based on a second-generation translation/rotation scanner. It is controlled by a microcomputer, which on the one hand ensures interactivity between user and system, and on the other permits high flexibility in the adjustment of system parameters to the given measuring conditions. Fast slave processors permit on-line image reconstruction, and thus the immediate availability of the measurement. The computed CT-images are stored in a digital display memory and visualized on a commercial TV monitor. The quantitative evaluation of trabecular and cortical bone is done off-line after completing the investigation. (10 refs.)

115904 Analysis of a camera based SPECT system. J.W.Beck (Bell Labs., Whippany, NJ, USA).

Nucl. Instrum. & Methods Phys. Res. (Netherlands), vol.213, no.2-3, p.415-36 (1 Aug. 1983).

A Monte Carlo computer simulation has been developed to study the emission and transport of gamma radiation through tissue phantoms. The unique features of this research include the development of computed tomographic geometry particular to the SPECT simulation, application of variance reduction techniques, and development of an energy dependent weighting function that reduces the degrading effects of scatter and attenuation while decreasing the measurement time for a given diagnostic study. In addition, the computer simulation is used to illustrate and evaluate other methods of improving image quality. (41 refs.)

115905 The spectral shape and the components of the background in vivo neutron capture prompt gamma ray analysis [of human beings]. D.Vartsky, K.J.Ellis, L.Wielopolski, S.H.Cohn (Medical Res. Centre, Brookhaven Nat. Lab., Upton, NY, USA).

Nucl. Instrum. & Methods Phys. Res. (Netherlands), vol.213, no.2-3, p.437-46 (1 Aug. 1983).

The shape of the background spectrum and the different contributions to the background in vivo neutrons capture prompt gamma ray analysis have been studied using a ²²⁵Cf neutron source. Since the source of background and its contribution varies for different energy regions, the detector shielding and the facility construction materials may be different for each analysed element. Limits of detection for in vivo measurement of Hg, Ca and N were determined. (21 refs.)

115906 Quantitative microfocal radiography in medicine, biological research, and the quality control industry. J.C.Buckland-Wright (Dept. of Anatomy, Guy's Hospital Medical School, London, England).

Proc. SPIE Int. Soc. Opt. Eng. (USA), vol.368, p.9-16 (1983). [received: Sept. 1983] (SPIE Proceedings on Microscopy Techniques and Capabilities, London, England, 21-22 Sept. 1982).

The microfocal X-ray units have an extremely small X-ray source (5-15 μ m diameter) achieved by focusing an electron beam onto the side of a solid target. High resolution magnification radiographs are obtained by placing the object close to the source and the recording surface at some distance away. The advantages of this type of X-ray are described as well as its applications in industry, biomedical research and medicine. The high resolution and magnification of the radiographs enable precise measurements to be carried out. (14 refs.)

115907 Automatic rib detection in chest radiographs. P.De Souza (IBM UK Sci. Centre, Winchester, England).

Comput. Vision, Graphics & Image Process. (USA), vol.23, no.2, p.129-61 (Aug. 1983).

A detailed algorithm is presented for automatic detection of posterior (dorsal) ribs in posterior/anterior chest radiographs. It is entirely automatic and includes algorithms for locating the lung fields and the lung boundary. Written in PL/I for an IBM 3031, it requires about 8 sec to process a 400×400 digitised full chest radiograph which is significantly faster than previously published results. The reason for the efficiency can be attributed to the fact that no two-dimensional image processing is performed; it works instead by locating the ribs on a small set of one-dimensional sections taken through the lung fields. Curves are then fitted through these locations to represent the rib edges. The detection of anterior (ventral) ribs is also discussed. (15 refs.)

115908 A new angiographic equipment with indirect 100-mm film exposure combined with digital subtraction unit (DSA): first clinical results. K.Feldt-Rasmussen, J.Praestholm, G.Niepel (Radiological Dept., Bispebjerg Hospital, Copenhagen, Denmark).

Electromedica (Germany), vol.51, no.3, p.86-92 (1983).

COMPATIX A, first as a prototype and then in operation as a serial product since February 1980, has, in the meantime, completed a substantial trial period. A total of 228 angiographies taken during the test period showed that this compact examination unit based on a 100-mm film indirect imaging technique with a SIRECON 33 N triplex was very versatile in angiography, for both general purpose and peripheral studies. The stepwise movable intensifier/X-ray tube combination obviously invited the mounting of the ANGIOTRON for the digital subtraction alternative. From June 1982, to January 1983 of a total of 922 patients examined with COMPATIX A 218 underwent digital subtraction either intravenously or intraarterially, supplementary to arteriography, with convincing results. (8 refs.)

115909 A universal angiographic set-up for any special investigation—practical experience and remarks. E.R.Briggs, A.G.Martin, G.Haufe (Haemodynamic Dept., Hospital Italiano, Mendoza, Argentina).

Electromedica (Germany), vol.51, no.3, p.92-6 (1983).

In 1980, the haemodynamic department of the Hospital Italiano in Mendoza, Argentina, a town of about one million inhabitants located 1100 kilometres to the west of Buenos Aires, was faced with a decision regarding the purchase of a new angiographic set-up. Since, on the one hand, the spatial and dimensional possibilities were limited while, on the other, the medical requirements were extremely high and wide-ranging, the authors needed a set-up that would cover all aspects of angiography without any restrictions. They made their choice in favour of a system concept which, on the basis of the selection and combination of the individual components permitted without restriction the performance of general haemodynamic examinations, cardangiography and coronary angiography, cerebral and visceral angiography and also the visualization of the peripheral blood vessels. (4 refs.)

115910 20 years of experience with the orthopantomograph. U.Hirschfelder (Polyclinic for Orthodontics, Univ. Hospital Erlangen-Nuremberg, Erlangen-Nuremberg, Germany).

Electromedica (Germany), vol.51, no.3, p.110-14 (1983).

The orthopantomograph provides an excellent radiological survey of the entire upper and lower jaws and dentition, including the ascending branch of the mandible and the temporo-mandibular joint on a single radiograph. As a result, it has become an indispensable aid for the establishment of findings and the planning of treatment in the field of orthodontics. After 20 years of experience with this radiographic procedure in the Polyclinic for Orthodontics of the University Hospital, Erlangen-Nuremberg, the indication of the orthopantomogram, in particular in this specialized field, is presented and discussed with respect to its economics. (25 refs.)

115911 Factors affecting radiation exposure and radiographic image contrast in urology. W.A.Wiatrowski (Audie L. Murphy Memorial Veterans Hospital, San Antonio, TX, USA), D.T.Kopp, D.W.Jordan, F.Barragan.

Health Phys. (GB), vol.45, no.3, p.599-605 (Sept. 1983).

An evaluation of certain radiographic factors affecting patient exposure during urography is made. Factors considered included selection of tube kilovoltage, total beam filtration and film-screen combination. The effect on image quality is considered. Experimental results suggest specific actions which would result in decreased patient exposure without compromising the quality of the examination. (8 refs.)

115912 Determination of left-ventricular volume from first-pass kinetics of labeled red cells. M.D.Harpen, R.L.Dubuisson, G.B.Head, III, L.F.Parmley, T.B.Jones, A.E.Robinson (Univ. of South Alabama Medical Center, Mobile, AL, USA).

J. Nucl. Med. (USA), vol.24, no.2, p.98-103 (Feb. 1983). [received: Sept. 1983]

A mathematical model is presented for the dynamics of a bolus of technetium-99m-labeled red blood cells through the left ventricle. It is used to correct for attenuation the count rate observed over the left ventricle during a conventional gated blood-pool study. The left-ventricular volumes are calculated from the corrected count rates and expressed as a percentage of total blood volume, or in absolute terms if a blood sample is obtained. The procedure was applied to a number of patients with nonvalvular cardiac disease. Cardiac volumes determined by the method were found to correlate well ($r=0.98$) with those determined by contrast left ventriculography. The method is simple, requires no special equipment, and can be applied with existing computer software. (18 refs.)

115913 Nuclear medicine. M.Iio.

Jpn. J. Med. Electron. & Biol. Eng. (Japan), vol.20, no.7, p.525-6 (Dec. 1982). In Japanese. [received: July 1983]

Continued resolution improvement has caused gamma-ray cameras to still dominate imaging applications in the field of nuclear medicine. In conjunction with these cameras, single-photon emission computed tomography (SPECT) enables one to obtain three-dimensional information from gamma rays. Future nuclear medicine may go towards the development of finer-pixel imaging, of drugs for use in SPECT, of selective radiotherapeutic treatment of tumours, and the utilization of polyclonal and monoclonal antibodies. (no refs.) K.B.

115914 Recent advances in medical imaging. T.A.Iinuma.

Jpn. J. Med. Electron. & Biol. Eng. (Japan), vol.20, no.7, p.527-31 (Dec. 1982). In Japanese. [received: July 1983]

According to the X-ray beam shape used, digital X-ray imaging can be classified as follows: (1) digital cone beam imaging, digital radiography and digital fluorography, which use cone beams; (2) digital fan beam scannography using fan beams; and (3) digital pencil beam scannography using pencil beams. The most developed imaging method is cone-beam imaging. Digital subtraction angiography (DSA) has achieved clinical importance in X-ray imaging practice. The technique is noninvasive because it involves only a venous injection, and thus allows angiography on an outpatient basis. DSA equipment can provide coronary images. Nuclear magnetic resonance diagnos-

tic imaging applications have reached the clinical evaluation stage. (9 refs.) K.B.

115915 Cancer and radiotherapy. VI. Present status of radiation therapy. H.Tsunemoto. *Jpn. J. Med. Electron. & Biol. Eng. (Japan)*, vol.21, no.1, p.36-47 (Feb. 1983). In Japanese.
For pt.V see ibid., vol.20, no.4, p.256, 1982. It has been known a long time that highly oxygenated cells can be easily destroyed by radiation. This is of particular importance for hypoxic tumor cells. This paper attempts to describe the present technology of radiotherapy and examines its future possibilities. The optical areas discussed include: (1) irradiation methods in radiotherapy; (2) clinical practice for laryngeal cancer, glioblastoma multiforme, esophagus cancer, digestive cancer, cervical cancer and radiation-resistant cancer; (3) the use of X-ray CT in planning for cancer treatment; and (4) some clinical trials for radiotherapy. (58 refs.) K.B.

115916 Three-dimensional reconstruction and display of coronary arteries obtained from coronary cineangiograms. M.Kaneko, M.Onoe (Inst. of Industrial Sci., Univ. of Tokyo, Tokyo, Japan), J.-I.Fujii, T.Aizawa, K.Kato. *Jpn. J. Med. Electron. & Biol. Eng. (Japan)*, vol.21, no.2, p.73-9 (April 1983). In Japanese. [received: Sept. 1983]
Digital image processing techniques are applied to the extraction of three-dimensional (3-D) information on coronary arteries from mutually orthogonal cineangiograms (e.g. RAO 30 degrees and LAO 60 degrees). Both cineangiograms are of the same scale factor and carefully registered in space. The registration in time is done by determining the end-diastole phase and the end-systole phase on the cineangiograms. The registration of left and right coronary arteries (LCA and RCA) is done by detecting a small intentional leak of contrast material so as to show both entrances of LCA and RCA. Corresponding points in RAO and LAO images are selected on a display and their 3-D coordinates are calculated. The 3-D structures of coronary arteries are approximated by lines which connect points thus obtained. Its view from any direction can be displayed. Branches are color coded to make the identification easy. A 16 mm film and a video tape are used to show the rotation of the 3-D structure around an arbitrary-axis. Stereoscopic pairs of arteries are also presented. These display techniques are quite effective in understanding the 3-D structure of coronary arteries. (5 refs.)

115917 Physical aspects of radiation therapy using fast electrons. W.Binder (Univ. Wien, Wien, Austria). *Roentgenpraxis (Germany)*, vol.36, no.6, p.210-17 (June 1983). In German.
There are at present three types of apparatus used in medicine for generating high energy electrons, i.e. the linear accelerator, the Betatron, and the Microtron. Depending on the original energy, an electron impinging on matter causes various effects, such as ionization, excitation, etc. These effects are schematically illustrated. Electrons of over 100 eV energy emitted as a result of ionization are delta particles, which according to the bicomponent theory by Wideroe, are responsible for biological changes in the tissue. The application of fast electrons in radiation treatment of tumors and the physical effects of such treatment are extensively discussed. The problem of suitable doses of energy applied and absorbed by the subject is dealt with and attention is drawn to problems which could arise as a result of inhomogeneities in the irradiated matter. (9 refs.) G.R.S.

115918 Computed radiography utilizing scanning laser stimulated luminescence. M.Sonoda, M.Takano, J.Miyahara, H.Kato. *Radiology (USA)*, vol.148, no.3, p.833-8 (Sept. 1983).
A new system of computed radiography that is based on new concepts and the latest computer technologies has been developed. This system eliminates the drawbacks of conventional screen-film radiography. The basis principle of the system is the conversion of the X-ray energy pattern into digital signals utilizing scanning laser stimulated luminescence. (7 refs.)

115919 Reconstruction algorithms for nonstandard CT scanner designs. G.T.Herman (Dept. of Radiology, Univ. of Pennsylvania, Philadelphia, PA, USA).
Proceedings of the Fifteenth Hawaii International Conference on System Sciences 1982, Honolulu, HI, USA, 6-8 Jan. 1982 (HI, USA: Hawaii Int. Conference Syst. Sci. 1982), p.410-19 vol.2
Data collected by a CT scanner provide estimates of line integrals of the X-ray attenuation distribution in a cross-section of the human body. The lines along which integrals are collected are determined by the positions of the source-detector pairs during the data collection. Since only the lines are important (and not the positions of the source and the detector on the line) essentially the same data may be collected by scanners of very different design. This article illustrates that in certain situations the problem of reconstruction from data collected by a CT scanner of a new (and nonstandard) design can be 'reduced' to the problem of reconstruction from data collected by a CT scanner for which the problem has already been solved. The 'reduction' involves identifying values of free parameters in the old design (such as the radius of the circle in which the source rotates) which would make the geometry of data collection essentially identical to that of the proposed new design. Since reconstruction algorithms for the old design already exist, they can be applied without any change to the data collected by the new scanner. In other words, the problem of finding a reconstruction algorithm for a non-standard mode of data collection can sometimes be solved by describing a (virtual) machine of standard design whose reconstruction algorithms are immediately applicable to the data collected by the nonstandard machine. The method is demonstrated on a recently proposed concept for transforming a radiotherapy simulator into a CT scanner. (10 refs.)

115920 Positron emission tomography (PET). M.M.Ter-Pogossian (Edward Mallinckrodt Inst. of Radiology, Washington Univ. School of Medicine, St. Louis, MO, USA).
Proceedings of the Fifteenth Hawaii International Conference on System Sciences 1982, Honolulu, HI, USA, 6-8 Jan. 1982 (HI, USA: Hawaii Int. Conference Syst. Sci. 1982), p.420-4 vol.2
Positron emission tomography, often referred to by its acronym 'PET', is an emerging radiologic modality which yields transverse tomographic images of functioning organs in the human body. The image forming variable in PET is the spatial distribution of a positron-emitting radionuclide which is systemically administered to the patient under study incorporated into a selected radioactively labelled compound. The premise which provides the foundation for the usefulness of PET is that any form of physiological activity results from, or is accompanied by, biochemical changes and that pathology is characterised by the divergence of such biochemical changes from the norm. The goal of PET is to study in vivo, regionally, and noninvasively biochemical processes essential to the normal function of human organs with the purpose of understanding better the relationship between their function and the biochemical processes upon which these functions depend and to extend this knowledge to the understanding and diagnosis of pathology. (7 refs.)

Image converter tubes for radiology and neutronography used in nondestructive testing	See Entry 111847
Radiography with fast neutrons by a plastic detector	See Entry 112569
Application of novel techniques of medical imaging to the nondestructive analysis of carbon-carbon composite materials	See Entry 115458
Dosimetry of X-ray and gamma-ray beams for radiation therapy in the energy range 10 keV to 50 MeV. Recommendation of the National Council on Radiation Protection and Measurement. NRC Report No.69. Washington, USA	See Entry 115921
Experiment in the use of thermoluminescent dosimeter IKS-A in therapeutic practice	See Entry 115922
Three-dimensional beam scanning for proton therapy	See Entry 115924
Methods of treatment planning for therapy with irregular fields—a comparison of two methods of dose computation	See Entry 115926
Concentrations of radon and its progeny in the rooms of Polish spas	See Entry 115931
Computer graphics and an interactive stereotactic system for CT-aided neurosurgery	See Entry 115971

87.60M Radiation dosimetry

115921 Dosimetry of X-ray and gamma-ray beams for radiation therapy in the energy range 10 keV to 50 MeV. Recommendation of the National Council on Radiation Protection and Measurement. NRC Report No.69. Washington, USA. M.Sh.Vainberg. <i>Med. Radiol. (USSR)</i> , vol.28, no.5, p.66-70 (May 1983). In Russian. The content of Report 69 is as follows. A summary is given of the most important radiation quantities and dosimetric methods. Brief information is presented on national (or primary standards) of radiation units and measurement systems from the USA National Bureau of Standards. Secondary standards of radiation units and the work of regional calibrating laboratories are dealt with. Instruments used for routine measurements on radiation apparatus and sources of ionising radiation. Material which is very valuable for practical work in radiation therapy is presented. Errors in determining absorption doses are discussed. It is concluded that Report 69 may serve as a prototype for creation of similar instruction manuals for USSR standards in the field of radiation therapy. (4 refs.) D.E.P.	
115922 Experiment in the use of thermoluminescent dosimeter IKS-A in therapeutic practice. I.A.Karpova. <i>Med. Radiol. (USSR)</i> , vol.28, no.5, p.75-7 (May 1983). In Russian. The thermoluminescent dosimeter IKS-A allows determination, with accuracy of 10%, of skin doses during irradiation of patients. Dose fields can be determined at 3-8 mm distances from the axis of the source, permitting determination of the degree of unevenness of irradiation of tissues next to the source. One can determine the position of the source for intracavitary phantom irradiation, which leads to more accurate calculation of doses. IKS-A instruments should be used more widely in oncological clinics, and their repair and testing should be organised on a wider scale. (4 refs.) D.E.P.	
115923 Contribution of γ-radiation to the dose absorbed, and some radiation effects in a radiation field p(50 MeV)—Be. V.N.Bukanov, Yu.F.Kataevsky, V.M.Indyk, E.E.Chebotaev, N.A.Tkachenko (R.E. Kavetsky Inst. of Oncology Problems, Acad. of Sci., Kiev, Ukrainian SSR). <i>Radiobiologiya (USSR)</i> , vol.23, no.4, p.565-8 (1983). In Russian. The contribution of γ -radiation to the total dose absorbed in the radiation field formed during 50 MeV proton bombardment of a beryllium target has been determined. A study was made of the biological effectiveness of the action of mixed γ /neutron-radiation on albino mongrel and inbred (C57 black) female mice. (6 refs.)	
115924 Three-dimensional beam scanning for proton therapy. T.Kanai, K.Kawachi, H.Matsuzawa (Div. of Phys., Nat. Inst. of Radiological Sci., Chiba-shi, Japan), T.Inada. <i>Nucl. Instrum. & Methods Phys. Res. (Netherlands)</i> , vol.214, no.2-3, p.491-6 (1 Sept. 1983). An important goal of radiation therapy is to localize the dose in the target volume. The favorable properties of proton beams, such as a well-determined range and straight penetration through tissues, have been used to develop a three-dimensional beam scanning method. This system consists of a two-dimensional beam scanning system and an energy degrader of variable thickness which are both controlled by a beam monitor that is connected to a minicomputer. A typically conformed dose distribution with the three-dimensional beam scanning system was measured by a specially designed multiwire ionization chamber. The results have shown that the system works satisfactorily and considerably reduces the radiation dose outside the target volume. (9 refs.)	
115925 Tunneling afterglow and anomalous fading in dosimetry with $\text{CaSO}_4\text{:Dy}$. R.Visocekas, M.Ouchene (Lab. d'Optique de la Matière Condensée, Univ. Pierre et Marie Curie, Paris, France), B.Gallois. <i>Nucl. Instrum. & Methods Phys. Res. (Netherlands)</i> , vol.214, no.2-3, p.553-5 (1 Sept. 1983). In irradiated $\text{CaSO}_4\text{:Dy}$ a low temperature tunneling afterglow is observed. This causes some anomalous fading of the stored thermoluminescence, which is evaluated to be negligible in dosimetry. (13 refs.)	
115926 Methods of treatment planning for therapy with irregular fields—a comparison of two methods of dose computation. G.H.Hartmann, H.Scharfenberg, W.Schlegel, R.Thieme (German Cancer Res. Center Heidelberg, Heidelberg, Germany). <i>Electromedica (Germany)</i> , vol.51, no.3, p.107-10 (1983). The treatment planning system, SIDOS, incorporates a method, suggested by Wrede (1972), for calculating the dose in irregular fields. Later, a method described by Clarkson (1941), has also become available for use with this system. The results of dose computation using these methods are compared with direct measurements made at various points in a mantle field. The investigations showed that the computations carried out with the method described by Clarkson resulted in an improvement in the unblocked area. Here, deviations from the measured doses varied between -3% and +1%, while figures of between -3% and +6% were found with the method suggested by Wrede. (9 refs.)	
115927 Recent muon fluence measurements at Fermilab. J.D.Cossairt (Fermilab., Batavia, IL, USA). <i>Health Phys. (GB)</i> , vol.45, no.3, p.651-8 (Sept. 1983). Muon fields at Fermilab were measured during 1980-1 using a Mobile Environmental Radiation Laboratory (MERL). During the spring of 1980, measurements were made with the accelerator operating at 350 GeV; in the spring of 1981, measurements were made at 400 GeV. The measurements were used to obtain an understanding of muon dose-equivalent rates at various locations both on and off the Fermilab site. These were found to be less	

than 1 mrem/yr at any given location. The data indicate that more severe problems may be encountered during operations of the 1000 GeV accelerator presently being installed. (8 refs.)

115928 Dose-rate conversion factors for external exposure to photons and electrons. D.C.Kocher (Health & Safety Res. Div., Oak Ridge Nat. Lab., Oak Ridge, TN, USA).

Health Phys. (GB), vol.45, no.3, p.665-86 (Sept. 1983).

Dose-rate conversion factors for external exposure to photons and electrons have been calculated for approx. 500 radionuclides of potential importance in environmental radiological assessments. The three exposure modes considered are immersion in contaminated air, immersion in contaminated water, and irradiation at a height of 1 m above a contaminated ground surface. For each exposure mode, the source region is assumed to be effectively semi-infinite or infinite in extent with uniform radionuclide concentration. The dose-rate factors then give external dose-equivalent rates per unit radionuclide concentration in air, in water or on the ground surface. The results are tabulated in this paper in the form of effective dose-rate factors based on the definition of the effective dose equivalent given in ICRP Publication 26 (1977). The effective dose-rate factors are obtained from photon dose-rate factors for 23 separate body organs and electron dose-rate factors for skin calculated with the revised DOSFACTER computer code. In addition to presenting the dose-rate factor equations and the tabulated results, this paper emphasizes the assumptions underlying the calculations for each exposure mode, differences between the organ dose-rate factors for photons used here and those used previously with the original version of the DOSFACTER code Kocher, 1980, and limitations inherent in application of the idealized external dose-rate factors to realistic environmental radiological assessments. (41 refs.)

115929 Statistical procedures for assignments of upper bounds for radiation doses to an unbadged individual in a group for which some individuals are badged. R.C.Grimson, L.A.Kammerman (Dept. of Biostatistics, Univ. of North Carolina, Chapel Hill, NC, USA), J.Soukup.

Health Phys. (GB), vol.45, no.3, p.723-9 (Sept. 1983).

Consider a group of individuals exposed to radiation for an interval of time such as units of military personnel during nuclear weapons tests three and four decades ago. Often, dosimetry information is known for several, but not all, individuals of that group. A nonparametric procedure is described that gives probability-based, upper-bound estimates of doses for an unbadged individual (within the group) for whom dose information is required; such information is useful in litigation. The method is illustrated by an application to a Navy unit. (18 refs.)

115930 Radiation exposure of the respiratory tract and associated carcinogenic risk due to inhaled radon daughters. F.Steinhauser, W.Hofmann, E.Pohl, J.Pohl-Ruling (Div. of Biophys., Univ. of Salzburg, Salzburg, Austria).

Health Phys. (GB), vol.45, no.2, p.331-7 (Aug. 1983).

The atmospheric content of radon and its decay products contributes significantly to the radiation exposure of man even in the normal environment. The risk for lung cancer induction associated with normal exposure to natural radionuclides is assessed in Salzburg, Austria. Altogether more than a thousand rooms have been investigated by using combined radon grab-sampling methods together with continuous measurements of radon and daughters at different control stations. Dose calculations were carried out for 729 demographically selected test persons, considering individual differences in age, sex and life-style and atmospheric nuclide concentrations at different sites. Using a specially developed age-dependent lung model, the dose frequency distribution of the absorbed dose to the basal cells of the bronchial epithelium could be evaluated for the population of Salzburg. Dose modifications caused by anatomical and physiological variabilities as well as microdosimetric considerations of the stochastic events during energy deposition result in a significantly increased dispersion of the dose histogram. (15 refs.)

115931 Concentrations of radon and its progeny in the rooms of Polish spas. W.Chruscielowski, T.Domanski, W.Orzechowski (Inst. of Occupational Medicine, Lodz, Poland).

Health Phys. (GB), vol.45, no.2, p.421-4 (Aug. 1983).

Radon concentrations and radon-daughter exposures of workers have been determined in three Polish spas where radon is used as a therapeutic agent. A wide range of values for both parameters was observed during the late 1970s, with some exposures above the annual limit of 3.5 WLM, particularly among technical personnel at a spa using uranium ore as a source. A downward trend in these exposures in recent years reflects the effect of improved practices. (9 refs.)

Gamma dosimetry using lyoluminescence of tris (hydroxymethyl) aminomethane See Entry 112446

Experience in the use of lapel air samplers at AWRE See Entry 112447

SARTEMP2 - A computer program to calculate power and temperatures in a transport flask during a criticality accident See Entry 112456

Neutron response of several fission track detectors worn on the body See Entry 112457

Progress report programme. Radiation protection 1982 See Entry 112459

The neutron sensitivity of a Geiger-Muller counter between 0.5 and 8 MeV See Entry 112571

Kornyezi doziszintenzitas helyszini meghatározása Ge(Li)-spektrometriával. A módszer (Environmental dose rate in situ determination by Ge(Li)-spectrometry See Entry 115715

Electric conductivity of liver cells as a function of dose at early times after γ -irradiation See Entry 115851

Effects of nonuniform distribution of the radiation energy absorbed among elements of the population See Entry 115858

Dose-effect relationships for early response to total body irradiation See Entry 115863

Simulated responses to lognormally distributed continuous low radiation doses See Entry 115865

Radiotoxicity of thallium-201 in mouse testes: inadequacy of conventional dosimetry See Entry 115875

'Biological dosimetry' of radionuclides and radiation hazards See Entry 115876

The prospects of instrumentation in medical radiology and problems of clinical dosimetry See Entry 115902

Factors affecting radiation exposure and radiographic image contrast in urology See Entry 115911

Radon daughter exposures in the UK See Entry 115941

Radon concentrations and infiltration rates measured in conventional and energy-efficient houses See Entry 115944

Indoor radon levels in the northeastern US: effects of energy-efficiency in homes See Entry 115945

Radon and radon daughter measurements in solar buildings See Entry 115946

Results of indoor radon measurements using the Track Etch method See Entry 115947

Integrated radon data from dwellings in Maine and Texas See Entry 115948

Study of radon daughter concentrations in Polk and Hillsborough counties See Entry 115949

87.60P Radiation protection

(inc. radiation monitoring)

115932 RF radiation hazards—measurement and evaluation. A.Schwartz (Narda Microwave Corp., Hauppauge, NY, USA).

R.F. Des. (USA), vol.6, no.4, p.12-22 (July-Aug. 1983).

Discusses the standard (C95.1-1982) that recognizes the physical phenomena which impact exposure level by providing a frequency dependent Radio Frequency Protection Guide, and by explicitly requiring the separate determination of both electric and magnetic field strength in near field situations. A large number of emitters previously exempt have now been included. Below 300 MHz, separate electric and magnetic field measurements should be made. Above 300 MHz, electric field measurements alone are normally adequate. For multiple signal situations where the signals occupy frequency intervals with different RFPG levels there are sensors which automatically incorporate the frequency dependence of the RFPG into their readings. (no refs.)

115933 Optimum conditions for protecting the eyes from solar radiation in vision correction. Kh.M.Kaiyumov (Medoborudovanie Cooperative, Moscow, USSR).

Biomed. Eng. (USA), vol.16, no.6, p.206-9 (Nov.-Dec. 1982). Translation of: *Med. Tekh. (USSR)*, vol.16, no.6, p.39-42 (Nov.-Dec. 1982).

The performance of protective correcting lenses under laboratory conditions was estimated by means of a special instrument with interchangeable filters. A number of conclusions are drawn which should be useful to those designing and making protective spectacles. (1 ref.)

115934 Indoor radon measurements in New Jersey, New York and Pennsylvania. A.C.George (Environmental Measurements Lab., US DOE, New York, NY, USA), J.Eng.

Health Phys. (GB), vol.45, no.2, p.397-400 (Aug. 1983).

The distribution of ^{222}Rn concentrations in 33 buildings near Canonsburg, PA, Lewiston, NY and Middlesex, NJ was investigated over a 2-yr period. One or 2 week-long time-integrated measurements of radon concentration, repeated several times during the study period, were obtained in the living and working areas of the buildings. Average air concentrations of radon, measured over the study period, varied from 0.32 to 4.5 pCi/l. among the buildings, but in only one building did the annual radon concentration exceed the US Nuclear Regulatory Commission's limit of 3 pCi/l. for continuous exposure in uncontrolled areas. (3 refs.)

Organisation of inspection of radioactive waste by the public health services See Entry 112337

Plans for safeguarding the population with respect to nuclear power stations See Entry 112452

Inter-ministerial nuclear security exercises See Entry 112453

Results of environmental radioactivity measurements in the Member States of the European Community for air - deposition - water - milk 1981 See Entry 112458

Progress report programme. Radiation protection 1982 See Entry 112459

Radiation exposure of the respiratory tract and associated carcinogenic risk due to inhaled radon daughters See Entry 115930

Indoor radiation exposures from ^{222}Rn and its daughters: a view of the issue See Entry 115938

Airborne radionuclides and radiation in buildings: a review See Entry 115940

Environmental radon and cancer correlations in Maine See Entry 115942

Indoor radon progeny exposure in the Florida phosphate mining region: a review See Entry 115943

87.60R Radioactive pollution

(see also 86.70 Environmental science)

115935 Levels of ^{234}U , ^{238}U and ^{230}Th in excreta of uranium mill crushermen. D.R.Fisher, P.O.Jackson, G.G.Brodaczynski, R.I.Scherpelz (Radiological Sci. Dept., Battelle Pacific Northwest Lab., Richland, WA, USA).

Health Phys. (GB), vol.45, no.3, p.617-29 (Sept. 1983).

Describes a research program to measure uranium and thorium levels in excreta of uranium mill crushermen who are routinely exposed to airborne uranium ore dust. The purpose of this work was to determine whether ^{230}Th was preferentially retained in the body over either ^{234}U or ^{238}U . Urine and fecal samples were obtained from 14 active crushermen with long histories of exposure to uranium ore dust, plus four retired crushermen and three control individuals for comparison. Radiochemical procedures were used to separate out the uranium and thorium fractions which were then electroplated on stainless steel discs and assayed by α spectrometry. Significantly greater activity levels of ^{234}U and ^{238}U were measured in both urine and fecal samples obtained from uranium mill crushermen, indicating that uranium in the inhaled ore dust was cleared from the body with a shorter biological half-time than the daughter product ^{230}Th . The measurements also indicated that uranium and thorium separate in vivo and have distinctly different metabolic pathways and transfer rates in the body. (6 refs.)

115936 ^{90}Sr and ^{137}Cs in soil and biota of fallout areas in southern Nevada and Utah. E.M.Romney, R.G.Lindberg, J.E.Kinnear, R.A.Wood (Lab. of Biomedical & Environmental Sci., Univ. of California, Los Angeles, CA, USA).

Health Phys. (GB), vol.45, no.3, p.643-50 (Sept. 1983).

Measurements of ^{90}Sr and ^{137}Cs in soil, vegetation and small mammals were made periodically at sites in southern Nevada and Utah that were contaminated by radioactive fallout from nuclear detonations at the Nevada Test Site as well as from global sources. Results from a survey in 1980 indicate that both of these fallout-derived radionuclides have remained primarily within the top 5-cm layer of undisturbed soil in these arid land areas. Trace amounts of ^{90}Sr and ^{137}Cs were measured in soil and biota samples. The ^{90}Sr concentrations in jackrabbit and rodent bone samples in 1980 varied within the range of 2-8 pCi/g ash (equivalent to 0.4-1.6 pCi/g wet bone or 5-20 pCi/g Ca). The ^{137}Cs concentrations in muscle-tissue samples were generally less than 1.5 pCi/g ash (less than 0.045 pCi/g wet muscle). Comparisons of data obtained periodically since the early 1950s show that measured concentrations of ^{90}Sr

in bone tissues have been highly variable in trace amounts, and that the concentration attenuation appears to be following radioactive decay of this radionuclide. (30 refs.)

115937 Biological elimination rates of radioisotopes by mallards contaminated at a liquid radioactive waste disposal area. D.K.Halford, O.D.Markham (Radiological & Environmental Sci. Lab., US Dept. of Energy, Idaho Falls, ID, USA), G.C.White.

Health Phys. (GB), vol.45, no.3, p.745-56 (Sept. 1983).
The biological elimination of nine γ -emitting radioisotopes was studied in mallards (*Anas platyrhynchos*) which were released onto liquid radioactive waste ponds in southeastern Idaho. After 68, 75 or 145 days, the ducks were removed from the contaminated environment and placed in metabolic cages. Whole-body and feces-urine counts were made for 51 days and then the ducks were sacrificed and dissected for tissue analyses. The biological elimination of radioisotopes were fitted to two compartment models using nonlinear least squares estimation. Fecal-urine data substantiated two-compartment elimination of all radionuclides. Biological half-lives in mallards were 10 days (^{131}I), 22 days (^{140}Ba), 86 days (^{51}Cr), 32 days (^{58}Co), 26 days (^{75}Se), 67 days (^{65}Zn), 10 days (^{134}Cs), 67 days (^{60}Co) and 11 days (^{137}Cs). Contaminated waterfowl would receive most of the internal dose in the first month after leaving the contaminated environment indicating that long-term doses would be inconsequential. (28 refs.)

115938 Indoor radiation exposures from ^{222}Rn and its daughters: a view of the issue. A.V.Nero (Lawrence Berkeley Lab., Univ. of California, Berkeley, CA, USA).

Health Phys. (GB), vol.45, no.2, p.277-88 (Aug. 1983).
Exposure to ^{222}Rn daughters indoors can result in significant risk to the general public, particularly those living in homes with much higher than average concentrations. The author reviews what is known about indoor concentrations, associated risks, and the effect of measures to save energy by reducing ventilation rates, using US housing as an example. The author concludes that, by employing appropriate control measures in homes having unacceptably high concentrations, the average exposure (and therefore risk) of the general public can remain at its present level, or even decrease, despite programs to save energy by tightening homes. (29 refs.)

115939 Background atmospheric ^{222}Rn concentrations outdoors and indoors: a review. T.F.Gesell (Univ. of Texas Health Sci. Center, Houston, TX, USA).

Health Phys. (GB), vol.45, no.2, p.289-302 (Aug. 1983).
The sources of outdoor and indoor atmospheric radon are examined. The variation of outdoor atmospheric radon with time of day, time of year, altitude and geographic location is quantitatively assessed. Average values of outdoor atmospheric radon concentrations are examined and it is estimated that the mean value for normal areas of the contiguous United States lies in the range of 100-400 pCi/m³ and is probably about 250 pCi/m³. Values for Alaska and Hawaii are an order of magnitude lower. Indoor atmospheric radon concentrations are found to vary with time of day, geographic location and story above ground. (54 refs.)

115940 Airborne radionuclides and radiation in buildings: a review. A.V.Nero (Lawrence Berkeley Lab., Univ. of California, Berkeley, CA, USA).

Health Phys. (GB), vol.45, no.2, p.303-22 (Aug. 1983).
Reviews the literature on sources and measurement of natural airborne radionuclides and radiation in buildings. The author briefly reviews control measures and suggests areas for further research. The major emphasis is given to ^{222}Rn and its daughters, since they typically cause the largest organ dose to the general population, most of which arises from indoor exposures. The indoor radiation field from radionuclides fixed in building materials and soil is also given substantial treatment. (85 refs.)

115941 Radon daughter exposures in the UK. K.D.Cliff, A.D.Wrixon, B.M.R.Green, J.C.H.Miles (Nat. Radiological Protection Board, Chilton, Didcot, England).

Health Phys. (GB), vol.45, no.2, p.323-30 (Aug. 1983).
Exposure due to the inhalation of the short-lived daughters of ^{222}Rn is the single largest contributor to the exposure of the UK population. A survey of dwellings situated largely in the centres of population indicates an annual exposure of 0.16 WLM, on the average. On the basis of current knowledge this is equivalent to an annual effective dose equivalent of 800 μSv . This compares with the overall average of the effective dose equivalent from natural radiation of almost 1900 μSv in a year. The distribution of exposures to the short-lived daughters of ^{222}Rn is markedly skew and indicates that some dwellings support concentrations of these daughters leading to exposures in excess of 1 WLM in a year. The areas of the UK in which exposures above this level are most likely to occur are regions with enhanced uranium mineralisation. These areas are sparsely populated and high exposures here do not significantly affect the overall average exposure in one predominantly igneous region is reported. (36 refs.)

115942 Environmental radon and cancer correlations in Maine. C.T.Hess, C.V.Weiffenbach, S.A.Norton (Univ. of Maine, Orono, ME, USA).

Health Phys. (GB), vol.45, no.2, p.339-48 (Aug. 1983).
The distribution of ^{222}Rn has been measured in the sixteen counties of Maine, USA by liquid scintillation counting of water samples from more than two thousand public and private wells. Three hundred and fifty of these wells have been characterized for geology and hydrology. Airborne radon has been measured in seventy houses with grab samples and in eighteen houses for 5-7 days each with continuously recording diffusion-electrostatic radon detectors. Concentrations of radon in water ranged from 20 to 180000 pCi/l. Granite areas yielded the highest average levels ($\bar{x}=22100$ pCi/l., $n=136$), with considerably intra-granite variation. Metasedimentary rocks yielded levels characteristic of the lithology for metamorphic grades ranging from chlorite to andalusite. Sillimanite and higher-grade rocks yielded higher ^{222}Rn levels, probably due to the intrusion of uranium-bearing pegmatites in these terranes. Airborne ^{222}Rn in homes ranged from 0.05 to 210 pCi/l. At the high end of this range, doses will exceed recommended industrial limits. In some homes only a small fraction of the airborne ^{222}Rn was due to the water supply. (23 refs.)

115943 Indoor radon progeny exposure in the Florida phosphate mining region: a review. C.E.Roessler, G.S.Roessler, W.E.Bolch (Coll. of Engng., Univ. of Florida, Gainesville, FL, USA).

Health Phys. (GB), vol.45, no.2, p.389-96 (Aug. 1983).
Reviews the data generated in studies of land radioactivity and indoor airborne radon progeny associated with mined and reclaimed phosphate lands in Florida. Highest indoor radon progeny levels are associated with the slab-on-grade type of construction. Concentrations exceeding 0.03 WL are associated with overburden soils, deposits and fill, while concentrations up to about 0.03 WL are associated with tailings. The lower limit for distinguishing increases above non-enhanced natural concentrations is on the order of 0.01-0.02 WL. Results of this study show that about 25% of the land produced by present methods of mining and reclamation practices would require restric-

tions on the type of construction or would require special construction methods. It is projected that with modification of mining and tailings disposal practices, virtually all of the land produced by mining and reclamation would be satisfactory for unrestricted construction use. (6 refs.)

115944 Radon concentrations and infiltration rates measured in conventional and energy-efficient houses. A.V.Nero, M.L.Boegel, C.D.Hollowell, J.G.Ingersoll, W.W.Nazaroff (Lawrence Berkeley Lab., Univ. of California, Berkeley, CA, USA).

Health Phys. (GB), vol.45, no.2, p.401-5 (Aug. 1983).
To elucidate any connection between high radon concentrations and low-infiltration houses, the authors have concurrently measured the ^{222}Rn concentration and the infiltration rate in US houses. Three housing surveys have been undertaken: one in 'energy-efficient' houses located throughout the US and two in 'conventional' houses in the San Francisco area and in Maryland. In each of the groups surveyed, no clear correlation was observed between ^{222}Rn concentrations and infiltration rate, although each parameter varied over a wide range. Infiltration rates for the entire sample, numbering 98 houses, ranged between 0.02 and 1.6 air changes per hr, and ^{222}Rn concentrations ranged from 0.1 to 27 pCi/l. It appears that the major cause of the observed differences in ^{222}Rn concentration is variation from one house to another in the rate at which ^{222}Rn enters houses from its sources. (10 refs.)

115945 Indoor radon levels in the northeastern US: effects of energy-efficiency in homes. R.L.Fleischer, A.Mogro-Campero, L.G.Turner (General Electric Res. & Dev. Center, Schenectady, NY, USA).

Health Phys. (GB), vol.45, no.2, p.407-12 (Aug. 1983).
The expectation of elevated ^{222}Rn levels in modern homes that have low air interchange rates with the out-of-doors causes the authors to survey both solar and conventional homes in northeastern New York State. The solar homes as a group have three times the ^{222}Rn levels of the conventional homes, and specific problems exist that are introduced or exaggerated by modern construction. For example the highest two levels of radon in the solar homes give radiation doses over 30 yr that are known to produce lung cancer in 1% of uranium miners. Summer readings in more than half of the cases are different from winter ones by a factor of two or more, so that year-round measurements are necessary for precise dosimetry. The track etching technique is ideally suited for such measurements. (9 refs.)

115946 Radon and radon daughter measurements in solar buildings. A.C.George, E.O.Knutson, H.Franklin (Environmental Measurements Lab., US DOE, New York, NY, USA).

Health Phys. (GB), vol.45, no.2, p.413-20 (Aug. 1983).
Measurements of radon and radon daughters in 11 buildings in five states, using active or passive solar heating, showed no significant excess in concentrations over the levels measured in buildings with conventional heating systems. Radon levels in two buildings using rock storage in their active solar systems exceeded the US Nuclear Regulatory Commission's limit of 3 pCi/l. for continuous exposure in uncontrolled areas. In the remainder of the buildings, radon concentrations were found to be at levels considered to be normal. It appears that the slightly elevated indoor radon concentrations result from the local geological formations and from the tightening of the buildings rather than as a result of the solar heating technology. (15 refs.)

115947 Results of indoor radon measurements using the Track Etch method. H.W.Alter, R.A.Oswald (Terradex Corp., Walnut Creek, CA, USA).

Health Phys. (GB), vol.45, no.2, p.425-8 (Aug. 1983).
Summarizes the (rather startling) results of numerous indoor radon measurements made in the US, Canada and Sweden over the past year by means of Track Etch monitors. (12 refs.)

115948 Integrated radon data from dwellings in Maine and Texas. H.M.Prichard, T.F.Gesell (Univ. of Texas School of Public Health, Houston, TX, USA), C.T.Hess, C.Weiffenbach, P.Nyberg.

Health Phys. (GB), vol.45, no.2, p.428-32 (Aug. 1983).
Presents a preliminary analysis of surveys of ^{222}Rn in dwellings made in the summer and fall of 1980 in Houston, TX, and in the late fall and winter of 1980-1 in several communities in central Maine. Approximately 100 dwellings were surveyed in each area during the season when houses are most likely to be closed for the purpose of temperature control. The primary objectives of the surveys were to develop baseline data on the distribution of indoor radon concentrations in the two areas, to determine the extent of spatial variations within dwellings, to add to the understanding of source mechanisms and to evaluate the utility and practicality of a number of air sampling strategies. (6 refs.)

115949 Study of radon daughter concentrations in Polk and Hillsborough counties. W.B.Johnson, P.G.Bailey (Radiological Health Services, Dept. of Health, Orlando, FL, USA).

Health Phys. (GB), vol.45, no.2, p.432-5 (Aug. 1983).
Because U decay series are present in Florida phosphate ore deposits, structures built on reclaimed phosphate land have high Rn daughter levels. Measurements were made of γ exposure rates and working levels inside homes built on undisturbed-nonmineralized, undisturbed-mineralized and reclaimed land in Polk and Hillsborough counties. Track-etch and thermoluminescent dosimeters were deployed in homes. It was found that the average excess dose equivalent resulting from reclaimed land was below the NCRP limit but that the annual average excess exposure from Rn daughter inhalation on reclaimed land was more than 5 times the national average dose and a significant number of individuals receive lung doses which exceed NCRP recommended limits. (5 refs.)

Summary report on development of an integral model of a radioactive jet [from a reactor accident] See Entry 112448

Release of gaseous tritium during reprocessing See Entry 112455

Results of environmental radioactivity measurements in the Member States of the European Community for air - deposition - water - milk 1981 See Entry 112458

Progress report programme. Radiation protection 1982 See Entry 112459

Determination of concentrations of selected radionuclides in surface soil in the US See Entry 115703

Kornyezeti dozisztentitas helyszini meghatarozasa Ge(Li)-spektrometriaval. A modszert (Environmental dose rate in situ determination by Ge(Li)-spectrometry) See Entry 115715

An examination of the environmental half-time for radionuclides deposited on vegetation See Entry 115718

Radiation exposure of the respiratory tract and associated carcinogenic risk due to inhaled radon daughters See Entry 115930

Concentrations of radon and its progeny in the rooms of Polish spas See Entry 115931

Indoor radon measurements in New Jersey, New York and Pennsylvania See Entry 115934

87.65 AEROSPACE BIOPHYSICS AND MEDICAL PHYSICS (EFFECTS OF ACCELERATIONS, WEIGHTLESSNESS AND ENVIRONMENT)

(see also 94.80 Aerospace facilities and techniques; space research)

115950 Effect of the radiation factor on operator activity. B.I.Davydov, V.V.Antipov, I.B.Ushakov.

Cosmic Res. (USA), vol.20, no.6, p.660-70 (Nov.-Dec. 1982). Translation of: *Kosm. Issled. (USSR)*, vol.20, no.6, p.928-40 (Nov.-Dec. 1982). [received: Sept. 1983]

Reviews papers on radiation psychophysiology. An evaluation of the psychophysiological possibilities for an irradiated person is given based on clinical observational data. Special attention has been allotted to an analysis of the behavioral effects for irradiated monkeys according to such tests as: irradiation and the retention of discrimination skills, the transfer of skills into new situations, delayed reactions, attention, manipulations with objects, etc. The dose and time laws governing these effects have been evaluated for dependence on the conditions of irradiation. The authors arrive at the conclusion that damage to a cosmonaut's operator activity can occur only at very high irradiation doses, the probability for the occurrence of which is extremely small even for very prolonged flights. (47 refs.)

87.70 BIOMEDICAL ENGINEERING

115951 Non-invasive recording of human His-bundle activity using a newly designed device aided by a microcomputer. Quan Wei Lun, Ou Yang Jing Zheng.

Biomed. Tech. (Germany), vol.28, no.9, p.188-91 (Sept. 1983). In German. Describes a newly designed device for recording His-Purkinje activity in humans from the surface of the body, using signal averaging. The principal components of the equipment are a microcomputer and a special trigger circuit controlling the data flow. The method has proved to be extremely effective, even in the case of a complete AV-block. (7 refs.)

115952 Method of investigating muscle tone. A.A.Uten'kin, N.N.Kalinina, G.V.D'yachkova (Khirkiz Sci. Res. Inst. of Experimental & Clinical Orthopedics & Traumatology, USSR).

Biomed. Eng. (USA), vol.16, no.6, p.199-201 (Nov.-Dec. 1982). Translation of: *Med. Tekh. (USSR)*, vol.16, no.6, p.31-3 (Nov.-Dec. 1982).

Muscle tone is one of the principal parameters of muscle function. Instruments for measuring tone (myotonometers) differ in design and principle of action. An indicator of pointer type, with limits of measurement 0-10 mm and with a scale division of 0.01 mm (State Standard 577-68) is often used as the measuring element of the tonometer. This paper describes an analysis of the method of using the pointer-type indicator for myotonometry and gives the experimental basis for a scale of units for the measurement of muscle tone. (2 refs.)

115953 Biomedical telemetry: the formative years. R.S.MacKay (Boston Univ., Boston, MA, USA).

IEEE Eng. Med. & Biol. Mag. (USA), vol.2, no.1, p.11-17 (March 1983). [received: Sept. 1983]

The descriptions and examples presented suggest that, although it is not absolutely clear when biomedical telemetry started, the formative years are still in progress and are limited only by the imagination of the investigators using new technologies as they evolve. (32 refs.)

115954 Overview of biomedical telemetry techniques. D.C.Jeutter (Marquette Univ., Milwaukee, WI, USA).

IEEE Eng. Med. & Biol. Mag. (USA), vol.2, no.1, p.17-24 (March 1983). [received: Sept. 1983]

Biomedical telemetry has been around for about 30 years and has become a useful tool for obtaining restraint-free physiological data from a broad spectrum of animal species and of monitoring setting. The techniques described for biotelemetry circuit design and construction are now well established and it seems likely that future development will be in the further miniaturization and integration of biotelemetry and transducers, improved power sources, and improved packaging. (7 refs.)

115955 Foil electret transducer for blood pressure monitoring. J.E.West, I.J.Busch-Vishniac (Acoustics Res. Dept., Bell Labs., Murray Hill, NJ, USA), G.A.Harshfield, T.G.Pickering.

J. Acoust. Soc. Am. (USA), vol.74, no.3, p.680-6 (Sept. 1983).

A foil electret microphone for use under the cuff of an automatic blood pressure monitoring system is described. The transducer is designed to operate with relatively flat sensitivity over a static pressure range of 40 to 250 mm Hg (5.33×10^4 to 3.33×10^5 dyn/cm²). The new electret microphone differs from conventional microphones used for airborne sound reception in two ways: (1) the diaphragm thickness is 50 μ m rather than the typical 12.5 or 25 μ m, and (2) the backplate contains a set of annular ridges spaced at 4 mm rather than the typical 7-10 mm. This microphone offers three advantages over the piezoelectric microphone now in use: (1) greater tolerance in positioning the microphone over the brachial artery, (2) nearly 20-dB higher sensitivity and signal-to-noise ratio, and (3) the ability to obtain measurements with the microphone placed midway between the elbow and shoulder. Tests of the new foil electret microphone in conjunction with the automatic blood pressure monitoring system indicate that the automatic and conventional measurements of systolic and diastolic blood pressure agree to within 5 mm Hg at least 90% of the time. In addition, the electret microphone is able to obtain automatic measurements on subjects with a wider range of ages and sizes. (15 refs.)

115956 Transducers. T.Togawa.

Jpn. J. Med. Electron. & Biol. Eng. (Japan), vol.20, no.7, p.516-18 (Dec. 1982). In Japanese. [received: July 1983]

Many attempts to develop new versions of transducers for biomedical applications have been made according to the need for more safety, long term instrumentation, suitability for signal processing, manageability, and productivity. This paper reviews recent advances in transducers for measuring pressure inside living organisms; in electromagnetic flowmeters, ultrasonic Doppler flowmeters, laser Doppler flowmeters, thermal flowmeters and plethysmographs for blood flow or velocity measurement; in transducers for body-surface strain and stress instrumentation; and in biochemical instrumentation transducers. (39 refs.) K.B.

115957 Electrocardiography. M.Okajima.

Jpn. J. Med. Electron. & Biol. Eng. (Japan), vol.20, no.7, p.522-4 (Dec. 1982). In Japanese. [received: July 1983]

It has been known for many years that a measurable amount of electric current is associated with activity of the heart. Inferring cardiac electrophysiological details from potentials measured on the body surface has flourished remarkably today. Widespread utilization of computers has led to significant advances in electrocardiography. An image recognition algorithm for electrocardiogram waves is now being developed. Automated routine elec-

trocardiogram diagnoses are top in popularity. Today's electrocardiographs are progressing from analog recording to digital recording. (no refs.) K.B.

115958 The recent trend of biomedical signal processing research. S.Kikawa, Y.Saitoh.

Jpn. J. Med. Electron. & Biol. Eng. (Japan), vol.20, no.7, p.536-40 (Dec. 1982). In Japanese. [received: July 1983]

Considerable research has been done on bioelectric signal processing, and a number of review papers has been written concerning it. In this paper, a brief outline is given of the signal processing research. Processing of electrocardiographic data has well been developed and includes data reduction, rhythm spectrum analysis and digital filtering. The analysis of brain waves has been carried out using predictive filters, autoregressive models, etc. For analyzing neural pulse waves, the nearest neighbor method and template matching method have been proposed. One of the central themes in myoelectric signal processing has been the search for optimal estimation applied to electromyography. (81 refs.) K.B.

115959 Information structure analysis of body surface potential maps. H.Tanaka, K.Hirayanagi, K.Yajima (Inst. of Medical Electronics, School of Medicine, Univ. of Tokyo, Tokyo, Japan), T.Furukawa.

Jpn. J. Med. Electron. & Biol. Eng. (Japan), vol.21, no.2, p.106-13 (April 1983). In Japanese. [received: Sept. 1983]

The information structure of body surface potential distributions has been analyzed according to the concepts of the Karhunen-Loeve transform and of information entropy. As a result of the Karhunen-Loeve transform, 10 components were extracted as the effective information patterns and their accumulated contribution rate was found to be 96.0%. The first three components resembled dipolar patterns and the other seven components showed complicated patterns. From entropy analysis, the simple information amount at each lead reached the maximum at 3.41 bits on the left precordial field. The specific information amount at each lead, free from the effect of correlation with the other leads, showed positive values only in the limited region of the left precordial field. The information amounts of all the leads totaled 10.33 bits. Based on the results of the information amount distribution, the authors propose a 3-electrode system which reduces the redundancy of the 96-electrode system. The 30-electrode system could explain 97% of the 96-channel body surface potentials. (15 refs.)

115960 Development of a real-time monitoring system of spatial ST vector. A.Kuroiwa, T.Fukumoto (Dept. of Internal Medicine, Univ. of Occupational & Environmental Health, Kitakyushu, Japan), Y.Senda.

Jpn. J. Med. Electron. & Biol. Eng. (Japan), vol.21, no.2, p.121-4 (April 1983). In Japanese. [received: Sept. 1983]

A real-time continuous monitoring system for the ST-segment of the electrocardiogram has been developed at the authors' laboratory. This system calculates a spatial ST magnitude and two angles (azimuth and elevation) from three-channel Frank electrocardiograms using the following formulae with a microcomputer: spatial ST magnitude = $\sqrt{(ST(X)^2 + ST(Y)^2 + ST(Z)^2)}$, azimuth = $\tan^{-1} ST(Z)/ST(X)$, elevation = $\tan^{-1} ST(Y)/\sqrt{(ST(X)^2 + ST(Z)^2)}$. The data obtained are displayed on a CRT display system (4 channels) and a penwriting recorder (6 channels) simultaneously. This system could record changes of spatial ST magnitude on experimental coronary artery occlusion. It is concluded that this system will be useful for non-invasive monitoring of myocardial ischemia or injury in intensive care units. (9 refs.)

115961 Human factors approach to medical instrument design. J.Kreifeldt (Dept. of Engng. Design, Tufts Univ., Medford, MA, USA).

Electro/82 Conference Record, Boston, MA, USA, 25-27 May 1982 (El Segundo, CA, USA: Electron. Conventions 1982), p.3-3/1-4

The approach is given and illustrated from several different areas. Basically, designing medical instruments for direct use by operators is essentially the same as designing consumer products. The most important feature of the process is the early and intensive involvement of human factors in the design process since human factors engineering is an integral rather than supplementary part of the design process. The user-tool-task systems forms the framework for the human factors design of medical instruments. As with any other area of design or engineering, proficiency with the approach comes with practice. (1 ref.)

Biomedical engineering course development for health care delivery See Entry 111338

The selection of modulation waveform for frequency modulated sound field stimuli See Entry 115887

Standardized function test for audiometers in the audiological prophylaxis as part of occupational medicine in accordance with principle 20 See Entry 115889

Light sources for fluorescein fluorophotometry See Entry 115893

A microwave radiometer for medical applications See Entry 115896

The prospects of instrumentation in medical radiology and problems of clinical dosimetry See Entry 115902

The spectral shape and the components of the background in vivo neutron capture prompt gamma ray analysis [of human beings] See Entry 115905

87.70E Diagnostic methods and instrumentation

(see also 87.60 Medical and biomedical uses of fields, radiations and radioactivity)

115962 A method of estimating biosignal stability. A.A.Smerdov, V.K.Gorelik (REMA Organization, L'vov, Ukrainian SSR).

Biomed. Eng. (USA), vol.16, no.6, p.194-9 (Nov.-Dec. 1982). Translation of: *Med. Tekh. (USSR)*, vol.16, no.6, p.26-31 (Nov.-Dec. 1982).

One is frequently restricted to analyzing a unique (measurable) data-bearing signal in medical diagnosis in relation to state evaluation for a complicated and inaccessible object. A mathematical analysis of biosignal stability is given based on state diagnosis. This enables automated analysis of the signal to be made. The method proposed has a high noise immunity. (2 refs.)

115963 Comparative study of linear prediction parameters for quantification and monitoring of dysphonic voices. C.Hernandez, S.Fejoo, J.E.Arias, M.A.Bernal.

IEE Proc. A (GB), vol.130, no.6, p.336-9 (Sept. 1983).

Linear prediction parameters have been used to study the vocal changes accompanying a case of laryngitis, the aim being to quantify the vocal degeneration so as to monitor the progress of the laryngeal dysfunction. The effectiveness for this purpose of a number of parameters (predictor coefficients, autocorrelation function, area coefficients, long-area ratios, PARCOR coefficients and cepstrum) and metrics (the Euclidean and Itakura distances and the crosscorrelation function) are compared and discussed. Of the parameters used the most intrinsically sensitive (as measured by the Kullback divergence) are the PARCOR coefficients. However, when a metric is introduced to measure the deviation from normal vocal performance, the combina-

tions producing the best results seem to be the Itakura distance applied to the predictor and autocorrelation coefficients and the crosscorrelation of the cepstral coefficients, both of which appear capable of registering changes in the patient's vocal condition which might pass unnoticed in a conventional noninvasive examination. The way seems to be open towards effective quantification of voice deformation for the diagnosis and treatment of laryngeal disorders. (11 refs.)

115964 A computerized analysis system of masticatory electromyograph with silent period. T.Kiryu, Y.Saito (Dept. of Information Engng., Niigata Univ., Niigata, Japan), T.Yamaga, K.Ishioka. *Jpn. J. Med. Electron. & Biol. Eng. (Japan)*, vol.21, no.2, p.93-9 (April 1983). In Japanese. [received: Sept. 1983]

A computerized analysis system for the masticatory muscles has been developed. The silent period (SP), which observed in masticatory muscles shortly after tooth contact during tapping movements or after chin tap during clenching, has been determined because of its diagnostic value for TMJ dysfunction. This system has the following characteristics: (1) it is suitable for a dental clinic, (2) it enables automated objective measurements of the SP parameters, and (3) it enables the easy data processing for statistical analyses. In order to measure the SP parameters, the threshold level technique and the peak to peak technique are common. However, since these techniques have some disadvantages, a new technique, 'activity changing curve' technique, has been developed. The activity changing curve is independent of the amplitude of the EMG and shows a marked increase at the onset or the termination of the SP. Thus this technique indicates the SP parameters more clearly and more objectively than the other methods. (23 refs.)

115965 Conductimetric method of determining the hematocrit value of blood. P.S.Neelakantaswamy, K.F.Aspar, A.Rajaratnam (Dept. of Phys., Nat. Univ. of Singapore, Singapore), N.P.Das. *Rev. Sci. Instrum. (USA)*, vol.54, no.9, p.1186-90 (Sept. 1983).

A simple conductimetric method for measuring the hematocrit value of blood is described. Using a conventional electronic conductivity meter having a two-electrode cell, the conductivity between the electrodes dipped in a diluted sample of the blood is measured and related quantitatively to the strength of suspended erythrocytes (that is, to the hematocrit value) in the test suspension. The extent of diluting the sample prior to the measurement is optimally determined on the basis of theoretical considerations. The merits of this instrumentation in terms of simplicity, economy, and linearity are compared with those of conventional methods of hematocrit determination. Possibilities of improving the present method by using inductive-type conductivity meters and/or by using VHF (very high frequency) resonant circuit sensors are suggested. Relevant theoretical considerations and experimental results are presented. (17 refs.)

115966 Development of a microprocessor-based ECG signal processing method. J.K.Choudhury, S.N.Bhattacharyya, A.Rakshit (Electrical Engng. Dept., Jadavpur Univ., Calcutta, India), A.Chattopadhyay.

Technological and Methodological Advances in Measurement. Acta IMEKO 1982. Proceedings of the 9th IMEKO Congress of the International Measurement Confederation, Berlin, Germany, 24-28 May 1982 (Amsterdam, Netherlands: North-Holland 1983), p.417-27 vol.2

Describes two microprocessor based algorithms for ECG signal monitoring and spectrum analysis. The resulting system which is relatively limited in scope, is considered to be useful for the medicare of cardiac patients particularly in economically underdeveloped countries. (3 refs.)

115967 Aspects of standardisation and validation of automatic ECG interpreting systems. D.Neubert, U.Tepfner, R.Schliel (Phys.-Tech. Bundesanstalt, Inst. Berlin, Berlin, Germany).

Technological and Methodological Advances in Measurement. Acta IMEKO 1982. Proceedings of the 9th IMEKO Congress of the International Measurement Confederation, Berlin, Germany, 24-28 May 1982 (Amsterdam, Netherlands: North-Holland 1983), p.429-41 vol.2

Automatic ECG-interpretation by computers is on the verge of becoming a helpful tool in cardiological diagnostics. Aspects of standardization and validation of computerized ECG-interpreting systems are discussed. Especially, it is argued that standardization cannot be achieved purely by majority rule, but must be based on scientific reasoning. For the purpose of validation of interpreting systems a dedicated storage device containing a library of representative ECG-source signals is proposed as a materialized standard. The independent validation of the diagnostic meaning of the source signals is a necessary requirement. (21 refs.)

115968 A digital system for rheoencephalography. C.De Rooij, B.R.Cleine (Dept. of Electrical Engng., Twente Univ. of Technol., Enschede, Netherlands).

Technological and Methodological Advances in Measurement. Acta IMEKO 1982. Proceedings of the 9th IMEKO Congress of the International Measurement Confederation, Berlin, Germany, 24-28 May 1982 (Amsterdam, Netherlands: North-Holland 1983), p.443-52 vol.2

Presents an on-line biomedical measuring and processing system for the measurement of electrical impedance fluctuations of the human brains, which is considered to be a good indication of the blood velocity fluctuations. The method used is patient-friendly, noninvasive and requires neither adjustments nor balancing. To gain an overall accuracy of 10% the most important noise- and error sources are analysed. The digital processing of the signal and the determination of the most important parameters as well as the statistical calculations are described. (4 refs.)

115969 Transducer system for absolute intravascular angiometry. B.Szucs, J.Sandor, E.Monos (Dept. of Automation, Tech. Univ. of Budapest, Budapest, Hungary).

Technological and Methodological Advances in Measurement. Acta IMEKO 1982. Proceedings of the 9th IMEKO Congress of the International Measurement Confederation, Berlin, Germany, 24-28 May 1982 (Amsterdam, Netherlands: North-Holland 1983), p.473-7

Deals with a transducer system for in vivo measurement of intravascular diameter changes in the range of 2 and 20 mm. A resilient lens-shaped absolute angiometer loop is introduced via an angiographic catheter as a sensor into the target blood vessel. The electromotive force induced in the sensor loop is processed by a newly developed transducer system for measurement and recording the diameter changes in the frequency range between 0 and 30 Hz. The frequency and output power of the driving circuit are optimized according to sensitivity and physiological requirements. (4 refs.)

Computer-generated holograms in biology and medicineSee Entry 112958

Mathematical model for vestibulo-ocular reflexSee Entry 115812

Future of biomagnetismSee Entry 115813

Measurement of blood flowSee Entry 115880

Image processing for medicineSee Entry 115881

A method of comparing the areas under receiver operating characteristic curves derived from the same casesSee Entry 115882

Formalization of choice for parameters of an acoustic stimulus in a small automatic facility to examine and diagnose the functional status of an auditory analyzerSee Entry 115885

Bone-conduction receiver with an extended frequency range for measuring the threshold of audibilitySee Entry 115886

Effect of half-wavelength membranes on the axial resolution of real-time ultrasonic scannersSee Entry 115890

Electronic sector-scanning crosssectional echocardiograph, model SSH-40ASee Entry 115891

Medical NMR spectroscopy and introscopy: progress and prospectsSee Entry 115895

Nuclear magnetic resonance: a gray scale model for head imagesSee Entry 115900

Special purpose CT-system for quantitative bone evaluations in the appendicular skeletonSee Entry 115903

Analysis of a camera based SPECT systemSee Entry 115904

Quantitative microfocus radiography in medicine, biological research, and the quality control industrySee Entry 115906

Automatic rib detection in chest radiographsSee Entry 115907

A new angiographic equipment with indirect 100-mm film exposure combined with digital subtraction unit (DSA): first clinical resultsSee Entry 115908

A universal angiographic set-up for any special investigation—practical experience and remarksSee Entry 115909

20 years of experience with the orthopantomographSee Entry 115910

Factors affecting radiation exposure and radiographic image contrast in urologySee Entry 115911

Determination of left-ventricular volume from first-pass kinetics of labeled red cellsSee Entry 115912

Nuclear medicineSee Entry 115913

Recent advances in medical imagingSee Entry 115914

Three-dimensional reconstruction and display of coronary arteries obtained from coronary cineangiogramsSee Entry 115916

Computed radiography utilizing scanning laser stimulated luminescenceSee Entry 115918

Reconstruction algorithms for nonstandard CT scanner designsSee Entry 115919

Positron emission tomography (PET)See Entry 115920

Safety and reliability in medical equipment and systemsSee Entry 115974

87.70G Patient care and treatment

115970 The basics of cryosurgery. R.Rzasa.

ASTM Stand. News (USA), vol.11, no.7, p.28-9 (July 1983).

A cryosurgical medical instrument is a surgical tool that can be applied in the fields of dermatology, gynecology, proctology, ophthalmology, neurosurgery, orthopedics, and urology. Tissue destruction without bleeding or scarring, minimal use of anaesthesia, and reduced hospitalization are some of cryosurgery's highlights. The destruction of tissue by cryosurgery occurs when the tissue is adequately frozen below -20°C . Below this temperature protein denaturation and cellular death occur. Following the freeze procedure, swelling occurs and the body begins to reject the dead tissue. After a brief period of time, this dead tissue sloughs off leaving clean, healthy tissue with no stitch marks and minimal scattering. The development of standards for cryosurgical instruments is discussed. (no refs.)

115971 Computer graphics and an interactive stereotactic system for CT-aided neurosurgery. M.L.Rhodes, W.V.Glenn, Jr., Y.-M.Azzawi (Multi-Planar Diagnostic Imaging Inc., Torrance, CA, USA), R.S.Howland, D.L.Hibbard.

IEEE Comput. Graphics & Appl. (USA), vol.3, no.5, p.31-7 (Aug. 1983).

Using digital CT image data transformed to a patient-frame coordinate system, neurosurgeons can simulate, plan, and execute their procedures with submillimeter precision—all in the CT suite. (14 refs.)

115972 Evaluation of intra-aortic counterpulsation with an assisted circulation. V.E.Tolpekin, G.G.Amosov, S.I.Shchukin, G.L.Khodzhshvili (Res. Inst. of Transplantation & Artificial Organs, Min. of Health, Moscow, USSR).

Biomed. Eng. (USA), vol.16, no.6, p.201-4 (Nov.-Dec. 1982). Translation of: *Med. Tekh. (USSR)*, vol.16, no.6, p.33-6 (Nov.-Dec. 1982).

Dog experiments and a case history are described. It is concluded that the addition of an internal work index to the external work index in the criterion of efficacy enables the time course of changes in energy consumption of the heart during assisted circulation to be estimated objectively. Also, the addition of an equivalent of the coronary blood flow, calculated on the basis of hemodynamic parameters, into the criterion of efficacy of intraaortic counterpulsation enables the state of myocardial bioenergetics to be reflected more completely; the mean intra-aortic diastolic pressure can be used as such a parameter. (7 refs.)

115973 Development of a cryo-probe suitable for gynaecological applications. N.G.Shah, V.M.Mehta (Dept. Obstetrics & Gynaecology, Sheth K.M. School of Post-graduate Medicine & Res., Ahmedabad, India), G.H.Shah. *Indian J. Cryog.*, vol.8, no.1, p.57-63 (1983).

In India, cryo-surgery has never gained momentum because of the price of the instrument. Even though, two or three Indian manufacturers have now introduced different types of cryo-probes, their price is still in the range of few thousand rupees. This project to develop a cheap and dependable cryo-probe was undertaken so that the cryo-probe can become a useful tool in day-to-day practice of each and every gynaecologist. (8 refs.)

115974 Safety and reliability in medical equipment and systems. M.Saito. *Jpn. J. Med. Electron. & Biol. Eng. (Japan)*, vol.20, no.7, p.557-8 (Dec. 1982). In Japanese. [received: July 1983]

Medical treatment is evaluated in three aspects: safety, reliability and clinical availability. Safety and reliability are most important. Low-frequency current, electromagnetic waves, light, radiant ray, acoustic waves, ultrasonic waves, heat, etc. are used as the physical energy in medical treatment. The effects of these energies on living organisms should be managed quantitatively for safety. Faulty operation of medical treatment equipment and malfunction of diagnostic equipment can cause the patient to be endangered. Reliability is related directly to safety. National standards for the reliability and safety of medical equipment should be established. (no refs.) K.B.

115975 Hyperthermia, hypothermia. M.Kikuchi. *Jpn. J. Med. Electron. & Biol. Eng. (Japan)*, vol.20, no.7, p.600-1 (Dec. 1982). In Japanese. [received: July 1983]
Hyperthermia and hypothermia in medical treatment are briefly summarized. Hyperthermia devices may be increasingly used as part of cancer therapeutic treatment; they can damage tumor cells. Hypothermia may be applied as a new method for storing internal organs for transplantation. Hyperthermia and hypothermia techniques will play an important role in medical therapy. The topical areas discussed in this paper include: (1) cancer therapy by hyperthermia, (2) orthopedic operation using hypothermia, and (3) cryosurgery and after-freeze immunity. (17 refs.) *K.B.*

Studies for the interpretation of fatigue behaviour of prime quality chrome nickel stainless steels—presented on wires which for example may be used for orthodontic purposes See Entry 115322

Methods of proportioning the quantity and density of laser radiation for therapeutic action See Entry 115894

The biomedical laser See Entry 115897

Ruby laser system with kaleidoscope for nevus treatment See Entry 115898

Computer calculations of a one-dimensional model, useful in the application of hyperthermia See Entry 115899

Nuclear medicine See Entry 115913

Cancer and radiotherapy. VI. Present status of radiation therapy See Entry 115915

Physical aspects of radiation therapy using fast electrons See Entry 115917

Dosimetry of X-ray and gamma-ray beams for radiation therapy in the energy range 10 keV to 50 MeV. Recommendation of the National Council on Radiation Protection and Measurement. NCRP Report No.69. Washington, USA See Entry 115921

Experiment in the use of the thermoluminescent dosimeter IKS-A in therapeutic practice See Entry 115922

Three-dimensional beam scanning for proton therapy See Entry 115924

Methods of treatment planning for therapy with irregular fields—a comparison of two methods of dose computation See Entry 115926

87.70J Prosthetics and other practical applications

115976 Studies on the loadability of the bone/cement interface in joint replacement. D.Gebauer (Orthopädische Klinik, Univ. München, München, Germany), H.Hager, S.Breier.

Biomed. Tech. (Germany), vol.28, no.9, p.192-5 (Sept. 1983). In German.
Mechanical overloading of the bone/cement interface is often discussed as the cause of loosening cemented artificial joints. Experimental studies on the loadability of the interface were performed under various types of pressure and shear loading, and their combinations under static and dynamic, in particular impact, conditions. The results confirm the problem of impact loads for the long-term stability of endoprostheses. (2 refs.)

115977 Inductive dynamic transducer for an electrically driven extracorporeal blood circulator. V.A.Artamonov, V.M.Dement'ev, A.I.Skorospehkin (V.V. Kuibyshev Polytech. Inst., Kuibyshev, USSR).

Biomed. Eng. (USA), vol.16, no.6, p.204-6 (Nov.-Dec. 1982). Translation of: *Med. Tekh. (USSR)*, vol.16, no.6, p.37-9 (Nov.-Dec. 1982).

An inductive dynamic transducer has the advantages of small mass and size, high reliability, and long service life. An apparatus has been developed for extracorporeal blood circulation. It is an integrated design with an inductive dynamic transducer and a pump. The transducer, which is mounted in a housing, comprises an exciting winding enveloped within magnetic circuits (types 600NN and 2000MI ferrites) and a cylindrical moving element made of copper that is connected with the piston of the pump and a diaphragm spring in one subassembly. Located between the side walls of the housing and the piston is a flexible diaphragm made of a thin, nonstretching spindle-shaped film. The end surface of the piston is a cone with exponential elements. Such a design provides a smooth variation in the velocity for the input and output of the blood, i.e. an eddy-free flow with minimal hydraulic resistance, thereby reducing the traumatization of the blood's constituents. (3 refs.)

115978 Artificial organs. K.Atsumi.

Jpn. J. Med. Electron. & Biol. Eng. (Japan), vol.20, no.7, p.541-5 (Dec. 1982). In Japanese. [received: July 1983]

Reviews recent technological development in artificial organs. The topical areas include: (1) the classification of artificial organs; (2) the historical aspect of artificial organs; (3) activity of the artificial internal organ society in each country; (4) clinical evaluation of artificial organs; (6) operating costs; (7) typical applications; (8) new technologies; and (9) development processes. (no refs.) *K.B.*

115979 Development of sensors to be used in orthopaedic implants. T.Yamamuro.

Jpn. J. Med. Electron. & Biol. Eng. (Japan), vol.20, no.7, p.574-5 (Dec. 1982). In Japanese. [received: July 1983]

In orthopaedic implant treatment, a suitable sensor is required to detect and control stress applied to the artificial os or joint implanted into the patient. Although the orthopaedic implant material used has passed an in-vitro fatigue failure test under cyclic load, the in-vitro test condition differs from the in-vivo behaviour. This paper deals with the detection of displacement of the interface between a living organism and implanted material, the detection of stress in orthopaedic implant, and the control of implanted material. (no refs.) *K.B.*

115980 Sensory prosthesis. T.Ifikube.

Jpn. J. Med. Electron. & Biol. Eng. (Japan), vol.20, no.7, p.597-9 (Dec. 1982). In Japanese. [received: July 1983]

Most of the themes in the study of sensory prostheses are common to those in pattern recognition and robotics studies. For sensory prostheses there are three practicable methods: (1) aiding the disabled through cutaneous sensation to electrical signals into which characters, images or sounds are converted, such as optical-to-tactile image conversion; (2) aiding the blind through auditory sense or the deaf through visual sensation, e.g. ultrasound glasses and sound-response typewriters; and (3) aiding the disabled by means of electrical stimulation of the visual or auditory nerve, e.g. artificial internal ears. These methods are briefly outlined in this paper. (15 refs.) *K.B.*

115981 Measurement of spatial forces by the 'matrix'-method [prosthetics application]. G.Bergmann, J.Siraky, A.Rohlmann, R.Koelbel (Dept. of Orthopaedics, Free Univ. of Berlin, Berlin, Germany).

Technological and Methodological Advances in Measurement. Acta IMEKO 1982. Proceedings of the 9th IMEKO Congress of the International Measurement Confederation, Berlin, Germany, 24-28 May 1982 (Amsterdam, Netherlands: North-Holland 1983), p.463-72 vol.2

Transducers for the measurement of spatial forces are mostly constructed by using conventional strain gauge technique. They require at least the application of six strain gauges, arranged in three independent bridge circuits. The matrix-method, however, reduces the necessary expenditure to three single SG. It requires additional digital equipment but enables construction of extremely small transducers and is much more accurate than the usual method. The matrix-method was used for the construction of artificial hip joints in animal experiments. (5 refs.)

October 8, 1958—first pacemaker implantation: a milestone in medical history See Entry 111386

The validity of aided thresholds See Entry 115797

Acoustic notch filters for hearing aids See Entry 115888

Optimum conditions for protecting the eyes from solar radiation in vision correction See Entry 115933

87.80 BIOPHYSICAL INSTRUMENTATION AND TECHNIQUES

115982 Soft X-ray imaging microscopy using zone plates and nonsynchrotron sources. R.J.Rosser (Blackett Lab., Imperial Coll. London, London, England).

Proc. SPIE Int. Soc. Opt. Eng. (USA), vol.368, p.17-20 (1983). [received: Sept. 1983] (SPIE Proceedings on Microscopy Techniques and Capabilities, London, England, 21-22 Sept. 1982).

The resolution of hydrated biological specimens by soft X-ray microscopy is considered. This is set by damage to the specimen caused by secondary electrons and free radicals. Using synchrotron radiation the limit would be about 10 nm. By using short lived (~1 ns) sources as produced by a laser generated plasma, the Rayleigh limit of 2.3 nm should be possible. (10 refs.)

115983 Wildlife biotelemetry. F.M.Long (Univ. of Wyoming, Laramie, WY, USA), R.W.Weeks.

IEEE Eng. Med. & Biol. Mag. (USA), vol.2, no.1, p.42-6 (March 1983). [received: Sept. 1983]

A brief review is given. Telemetry has become a valuable tool for studying wildlife in its native habitat. With telemetry, a biologist can monitor animals in the dark, in rough terrain, in water, underground, or in the air. He can monitor heart rate as a measure of stress or as an indication of metabolic rate. Movement can be correlated with feeding, stress, or other activity. The electronics and circuitry used in telemetry systems for wildlife studies have probably reached a mature state, with modifications mostly being the results of new technologies rather than bringing new fundamental ideas to the design. Thus, the improvement of telemetry systems will likely depend on improvements in sensors, in packaging, and in overall system reliability. (13 refs.)

115984 Bioelectrodes. T.Matsuo.

Jpn. J. Med. Electron. & Biol. Eng. (Japan), vol.20, no.7, p.513-15 (Dec. 1982). In Japanese. [received: July 1983]

Practical electrodes attached to living organisms to measure bioelectric phenomena or supply electrical energy to the body can be classified under four main divisions: (1) electrodes for inducing bioelectric phenomena; (2) stimulating electrodes; (3) electrodes for measuring bioimpedance; and electrodes as chemical sensors. This paper briefly describes surface-attached electrodes, microelectrodes, multielectrode arrays, and electrodes serving as chemical sensors. (14 refs.) *K.B.*

115985 Diode array versus photomultiplier for measuring the UV-excited resonance Raman spectra of enzyme-substrate transients. P.R.Carey, L.R.S.Cartier (Div. of Biological Sci., Nat. Res. Council of Canada, Ottawa, Ontario, Canada).

J. Raman Spectrosc. (GB), vol.14, no.4, p.271-5 (Aug. 1983).

The construction of a multiplex system for recording the resonance Raman (RR) spectra of enzyme-substrate complexes in the near-UV region is described. The instrument is based on commercially available components consisting of a 2 W UV krypton ion laser, a triple spectrograph (in which the first two monochromators act as a zero dispersion, variable bandpass filter) and an intensified diode array. The performance of this system is compared with that of a double monochromator with a photomultiplier as a detector. The enzyme-substrate systems chosen as examples for the comparison offer a difficult experimental challenge because they evolve rapidly and have poor optical homogeneity. In addition, a simple apparatus is described for recording the RR spectra of enzyme-substrate complexes in cryosolvents at temperatures as low as -50°C. (8 refs.)

115986 Epitaxial crystallization of alkane chain lipids for electron diffraction analysis. D.L.Dorset, W.A.Pangborn (Electron Diffraction Dept., Medical Foundation of Buffalo Inc., Buffalo, NY, USA), A.J.Hancock.

J. Biochem. & Biophys. Methods (Netherlands), vol.8, no.1, p.29-40 (Aug. 1983).

Thin microcrystals of a wide variety of polymethylene chain materials, including *n*-alkanes, linear waxes, glycerides, a detergent, phospholipids and phospholipid analogs based on cyclopentane-1,2,3-triol, were epitaxially grown on naphthalene to give an orientation with long chain axes parallel to the best developed crystal face. These crystals, which represent a different orientation than those grown from solution, facilitate ab initio quantitative crystal structure analysis from electron diffraction intensity data from the projection yielding the most crystallographic information. (40 refs.)

115987 A low-cost microcomputer-based data acquisition and analysis system for an electron spin resonance spectrometer: data handling of dilute spin labeled nucleic acids. J.C.Ireland, J.A.Willett, A.M.Bobst (Dept. of Chem., Univ. of Cincinnati, Cincinnati, OH, USA).

J. Biochem. & Biophys. Methods (Netherlands), vol.8, no.1, p.49-56 (Aug. 1983).

Describes the construction of an inexpensive and reliable data acquisition system for a Varian E-line Century Series ESR spectrometer utilizing an Apple II Plus microcomputer. All necessary hardware is readily available and used without modification. A BASIC program for routine collection, display, plotting and disk storage of experimental data has been written and subsequently compiled into machine code for high speed operation. The interface offers distinct advantages in spectral resolution as well as instrument control. An example of signal enhancement via computer controlled time averaging is presented for a spin labeled DNA experiment. The technique has recently been applied to studies of relative binding affinities of gene-32 protein for various spin-labeled polynucleotides. (16 refs.)

115988 A simplified method for the estimation of individual amino acid radioactivity in plasma samples. P.Roca, A.Palou (Dept. de Bioquímica, Univ. de la Ciutat de Mallorca, Mallorca, Spain), M.Alemay. *J. Biochem. & Biophys. Methods (Netherlands)*, vol.8, no.1, p.63-7 (Aug. 1983).
A method is presented for the quantitative estimation of the individual amino acid radioactivity in biological samples. The material is deproteinized with cold acetone, and, after acetone evaporation, is passed through a column containing 1 g of Amberlite XAD-2, then eluted with 10% ethanol. The samples are derivatized with Sanger's reagent (alkaline 1-fluoro-2,4-dinitrobenzene) and passed again through the Amberlite XAD-2 column; the 10% ethanol eluate is now discarded and the DNP-amino acids eluted with acetone. Aliquots are used for TLC chromatography on Silicagel plates; the spots are identified, cut away and their radioactivity estimated. The actual recovery of radioactivity in the spots is about 86-92% of the initial radioactivity. No contamination with radioactive glucose, lactate, pyruvate or glycerol has been observed. (10 refs.)

115989 An analog-digital feedback system for measuring photoreceptor properties with an equal response method. J.G.J.Smakman, B.A.Pijpker (Lab. voor Algemene Natuurkunde, Biophys. Dept., Univ. of Groningen, Groningen, Netherlands). *J. Neurosci. Methods (Netherlands)*, vol.8, no.4, p.365-73 (Aug. 1983).
Describes a feedback system in which a neutral density wedge automatically controls the light flux applied to a photoreceptor, so that an intracellular recorded response is held constant. The authors describe a 'differential sampler' that subtracts the photoreceptors dark response from the light response induced by a chopped light source. The resulting signal drives the feedback system. The response time of the feedback system can be adjusted with a 'digital integrator' to match a range of variable conditions that occur in different experiments. (7 refs.)

115990 The stereotrode: a new technique for simultaneous isolation of several single units in the central nervous system from multiple unit records. B.L.McNaughton (Dept. of Psychology, Univ. of Colorado, Boulder, CO, USA), J.O'Keefe, C.A.Barnes. *J. Neurosci. Methods (Netherlands)*, vol.8, no.4, p.391-7 (Aug. 1983).
A new method is described for the recording and discrimination of extracellular action potentials in CNS regions with high cellular packing density or where there is intrinsic variation in action potential amplitude during burst discharge. The method is based on the principle that cells with different ratios of distances from two electrode tips will have different spike-amplitude ratios when recorded on two channels. The two channel amplitude ratio will remain constant regardless of intrinsic variation in the absolute amplitude of the signals. The method has been applied to the rat hippocampal formation, from which up to 5 units have been simultaneously isolated. The construction of the electrodes is simple, relatively fast, and reliable, and their low tip impedances result in excellent signal to noise characteristics. (9 refs.)

115991 A comparison of the selectivities of microelectrodes incorporating the Orion and Corning liquid ion exchangers for potassium over sodium. P.J.Laming, M.B.A.Djamgoz (Dept. of Pure & Appl. Biology, Imperial Coll., London, England). *J. Neurosci. Methods (Netherlands)*, vol.8, no.4, p.399-402 (Aug. 1983).
The K^+ : Na^+ selectivities of double-barrelled microelectrodes employing either of two commercially available liquid ion exchangers for K^+ (Corning 477317 and Orion) have been measured using several calibration methods. Microelectrodes employing the Orion exchanger were found to be much less selective than those based on Corning 477317. (8 refs.)

115992 Schlieren optical imaging of weak objects. T.Von Zglinicki (Abteilung fur Elektronenmikroskopie am Pathologischen, Inst. der Charite, Berlin, Germany), S.Heymann. *Micron (GB)*, vol.14, no.2, p.109-18 (1983).
It is shown that with the aid of a schlieren optical mode in real electron microscopes, the amplitude contrast of weak objects can be enhanced up to twofold in comparison with the bright-field mode, if a part of the unscattered beam strikes the objective aperture. This remains true also in the case of thicker objects imaged (for example, unstained sections of biological matter). Furthermore, evidence is given for the existence of an optimum schlieren image in the transition range between strict schlieren optics and conventional bright-field microscopy. Such images are characterized by high amplitude contrast without significant distortion. Theory and experiment are shown to be in good agreement. As an application, unstained nucleosomes have been investigated schlieren-optically. Model calculations show that the 'hole' in their centre, which has been demonstrated from dark field images, is probably not due to a structural void (cavity), but is a consequence of the lower density of the protein core as compared with DNA. (26 refs.)

Advances in Mossbauer spectroscopy. Applications to physics, chemistry and biology See Entry 111334

AC calorimeter for liquid including suspension of biological materials See Entry 111685

Holography applied to stereomicroscopy See Entry 111762

Spectroscopy by photothermal radiometry See Entry 111774

Application to bio-organic compounds [ion physics] See Entry 111802

Fiber optic scattering monitor for application on bulk biological tissue, paper, and plastic See Entry 113103

Quantitative electron probe analysis: problems and solutions See Entry 115607

Quantitative microfocal radiography in medicine, biological research, and the quality control industry See Entry 115906

Biomedical telemetry: the formative years See Entry 115953

Overview of biomedical telemetry techniques See Entry 115954

Conductimetric method of determining the hematocrit value of blood See Entry 115965

87.90 OTHER TOPICS IN BIOPHYSICS, MEDICAL PHYSICS, AND BIOMEDICAL ENGINEERING

115993 Controlled studies of human health effects of short-term inhalation of atmospheric pollutants. J.D.Hackney. **Report EPRI-EA-3125**, Electr. Power Res. Inst., Palo Alto, CA, USA (1983), 116 pp.
Available from Res. Rep. Center (RRC), Box 50490, Palo Alto, CA 94303, USA.
The results of three years of research into the effects of inhaled air pollutants on human volunteers are presented. The pollutants studied include ammonium nitrate aerosols, mixed SO_2 and NO_2 , and sulfate salts of several trace metals

used singly and in combination with gaseous pollutants. Physiological responses during actual exposures are compared to responses during sham exposures.

Bifurcation and chaos in a periodically stimulated cardiac oscillator See Entry 111569

Origin of Espanola Island and the age of terrestrial life on the Galapagos Islands See Entry 116088

90.00 GEOPHYSICS, ASTRONOMY AND ASTROPHYSICS

91.00 SOLID EARTH GEOPHYSICS

91.10 GEODESY AND GRAVITY
(for relations of gravity observations to tectonics and isostasy, see 91.45 Physics of plate tectonics)

115994 Orbital rates of Earth satellites at resonances to test the accuracy of Earth gravity field models. J.Klokocnik (Astron. Inst., Czechoslovak Acad. of Sci., Ondrejov, Czechoslovakia). *Celestial Mech. (Netherlands)*, vol.30, no.4, p.407-22 (Aug. 1983).
Differences among the Earth gravity field models, which were (in Klokocnik and Pospisilova, 1981) expressed as dispersions of the relevant lumped geopotential coefficients, are transformed to the differences in variations of orbital quantities. Theoretical formulae, the Lagrange (planetary) equations, describing the orbital rates near resonances due to the geopotential, are derived in a simple and unified form. They are then applied to estimate the orbital uncertainty as a function of Earth models differences. The first set of the Earth models (set I) consists of 11 models from the decade 1970-80 of greatly varying quality; the set II contains several recent models; the author presents a test (for the 13th- to 15th-order) based on standard deviations of the lumped values of GEM 10B, which were estimated by means of independent resonant data (in Klokocnik, 1982). (25 refs.)

115995 Collocations and thirtieth order resonant harmonics. J.Kostecky (Res. Inst. of Geodesy, Topography & Cartography, Geodetical Obs., Pecny, Ondrejov, Czechoslovakia), J.Klokocnik. *Planet. & Space Sci. (GB)*, vol.31, no.8, p.829-41 (Aug. 1983).
The method of collocations (LSC) is compared with traditional least-squares adjustments, (LSA) for determining the values of the individual harmonic coefficients in the expansion for the Earth's gravitational potential from the lumped geopotential coefficients of order 30. The computations are based on data from King-Hele and Walker (1982), where the 30th-order harmonic coefficients were determined from the lumped values by means of the usual least-squares method. The authors take into account the correlation coefficients among the lumped coefficients; Four groups of runs performed: from LSA (similar to that in King-Hele and Walker, 1982) to as general an LSC as possible. The resulting harmonic coefficients are compared mutually, with the resonant solution by King-Hele and Walker (1982), with the older trials (Kostecky and Klokocnik, 1979) and with the comprehensive Earth models (GEM 10 B(C), 'Rapp 77' and GRIM 3). (13 refs.)

115996 Variations in the Earth's rotation. J.B.Merriam (Dept. of Earth Sci., Memorial Univ. of Newfoundland, St. John's, Newfoundland, Canada). *Sci. Prog. (GB)*, vol.68, no.271, p.387-401 (Autumn 1983).
The author discusses the variations in the Earth's rotation, and measurements of the phenomenon since the seventeenth century. (24 refs.)

115997 Equivalent solutions of the inverse three-dimensional gravimetry problem for a class of polynomial densities. P.I.Balk (Computational Center, Acad. of Sci., Irkutsk, USSR). *Sov. Geol. & Geophys. (USA)*, vol.23, no.5, p.88-96 (1982). Translation of: *Geol. & Geofiz. (USSR)*, vol.23, no.5, p.98-107 (1982).
It is shown that the inverse linear problem does not have a unique solution for a class of field sources with polynomial density and piecewise-analytic mass-carrier boundary consisting of planes and second-order algebraic surfaces. Sufficiently broad model families are identified in which the inverse problem has unique solutions, and examples of families of equivalent distributions are constructed. The study was carried out with the aid of a computerized analysis of theoretical problems in gravimetry. (10 refs.)

115998 A high resolution gravimetric geoid for Europe and bordering marine areas. W.Torge, G.Weber, H.-G.Wenzel. *Z. Vermessungswes. (Germany)*, vol.108, no.8, p.321-31 (Aug. 1983). In German.
A high resolution gravimetric geoid has been determined in the area $30^\circ < \phi < 73^\circ$ and $-30^\circ < \lambda < 46^\circ$ in a $12'$ by $20'$ grid covering Europe, the North Sea, Baltic Sea, Mediterranean Sea, and parts of the North Atlantic Ocean. The computation has been carried out by least squares spectral combination using closed integral formulas, combining 104000 mean $6'$ by $10'$ free air gravity anomalies 12000 mean 1° by 1° free air gravity anomalies and the spherical harmonic model GEM9 complete to degree and order 20. The precision of the computed geoid heights has been estimated at ± 1 m. (27 refs.)

115999 Movements of the fracture zone and the seismic activity under the fracture zone—based on the observations at Abuyama. Y.Umeda, J.Yamazaki (Faculty of Sci., Kyoto Univ., Kyoto, Japan). *Zisin. J. Seismol. Soc. Jpn. (Japan)*, vol.36, no.1, p.43-51 (March 1983). [received: Sept. 1983]
The movements of the fracture zone (strike $N20^\circ E$, dip angle $20^\circ W$ and thickness 1 m) in the observational vault at Abuyama Seismological Observatory have been monitored by two extensometers crossing this zone. The movements of this zone are analyzed with special reference to the temporal variation of activity of small earthquakes and microearthquakes occurring under the fracture zone. (5 refs.)

A combined analysis of the gravitational and magnetic anomalies for the detection of magnetically active rock complexes in the basement of the West Siberian plate See Entry 116015

Study of Iwasaki earthquake swarm in Aomori Prefecture. II. Seismic activity and crustal movement See Entry 116038

Relation of summit deformation to East Rift Zone eruptions on Kilauea volcano, Hawaii See Entry 116055

Combined interpretation of magnetic and gravitational fields based on calculations of the pseudogravitational field See Entry 116311

A computer-controlled tachymetric surveying system for the supervision of kinematic events without observers See Entry 116313

On the possibility of seasonal corrections while adjusting coordinates of stars ..
..... See Entry 116490

91.25 GEOMAGNETISM AND PALAEOMAGNETISM; GEOELECTRICITY

116000 The interpretation of magnetotelluric and electrical sounding's data by modified generalized inverse matrix. Chen Ming-Sheng, Chen Le-Shou (Beijing Graduate School, Wuhan Coll. of Geology, China), Wang Tian-Sheng, Bai Gai-Xian.

Acta Geophys. Sin. (China), vol.26, no.4, p.390-400 (July 1983). In Chinese. English translation in: *Acta Geophys. Sin. (USA)*

The essential theory of inversion with a generalized inverse matrix is systematically explained. Several practical problems in the inversion of MTS and electrical sounding (ES) curves using generalized inverse matrix have been studied and solved. Good results have been obtained and demonstrated. Moreover, some relationships are explored, so that interpretation can be improved. (5 refs.)

116001 Paleomagnetism of the Paleocene Ghost Rocks Formation, Prince William terrane, Alaska. P.W.Plumley (Earth Sci., Univ. of California, Santa Cruz, CA, USA), R.S.Coe, T.Byrne.

Tectonics (USA), vol.2, no.3, p.295-314 (June 1983). It is suggested that, despite the lack of evidence for a major Tertiary suture zone between the Prince William terrane and central Alaska, the Prince William and perhaps adjacent terranes may have lain substantially south of their present position in the Early Tertiary. (45 refs.)

116002 Rapid diffusion of the poloidal geomagnetic field through the weakly conducting mantle: a perturbation solution. E.R.Benton, K.A.Whaler (Dept. of Astro-Geophys., Univ. of Colorado, Boulder, CO, USA).

Geophys. J. R. Astron. Soc. (GB), vol.75, no.1, p.77-100 (Oct. 1983). A systematic regular perturbation procedure is developed to account for weak mantle conduction as unsteady electromagnetic fields are extrapolated downward from the Earth's surface to the core-mantle boundary. The mantle is treated as a radially symmetric conductor of highly variable conductivity. The unique poloidal-toroidal decomposition of a magnetic vector potential leads first to three-dimensional and then, after spherical harmonic analysis, to one-dimensional linear diffusion equations for the two defining scalar functions. Emphasis is placed on a regular perturbation solution to the inverse poloidal diffusion problem, for the case where diffusion through the mantle is rapid on the time-scale for changes in forcing at the core-mantle boundary. The perturbation theory is evaluated with reference to a range of proposed conductivity profiles and two geomagnetic field models. It is found that uncertainty in the conductivity is at present less important than errors in the field models, and that the first-order corrections to the main field and secular variation at the core surface are likely to be negligible and small, respectively. (31 refs.)

116003 Inversion of the electromagnetic induction problem using Parker's algorithms were both precise and practical data. R.J.Jady, G.A.Paterson (Dept. of Math., Univ. of Exeter, Exeter, England), K.A.Whaler.

Geophys. J. R. Astron. Soc. (GB), vol.75, no.1, p.125-42 (Oct. 1983). An important contribution to the theory of inversion of the electromagnetic induction problem has been made by Parker (1980, 1982). A numerical procedure for implementing the theory has been described by Parker & Whaler (1981). The physical interpretation of the resulting conductivity models is difficult because of the wide range of acceptable solutions generated by the method. This is a consequence of the inherent non-uniqueness associated with a finite dataset. Before applying the algorithms to practical data, the authors have examined their performance using analytic datasets derived from simple conductivity distributions. The results of using the methods on both precise and real Dst data are shown. The storm data suggest that the upper mantle has low conductivity overall to a depth between 650 and 700 km, followed by a rise to about 0.1 S m^{-1} and a further sharp increase at about 1000 km, which is close to the penetration depth for these data. (9 refs.)

116004 Palaeomagnetism of Palaeozoic rocks from the Cabo de Penas, Asturias, Spain. H.Perroud (Univ. de Rennes 1, Rennes, France).

Geophys. J. R. Astron. Soc. (GB), vol.75, no.1, p.201-15 (Oct. 1983). Ordovician volcanic samples of the Cabo de Penas area yielded a primary remanent magnetization ($D=202^\circ$, $I=78^\circ$, $\alpha_{95}=6^\circ$) which is partially or entirely overprinted by a Late Palaeozoic remagnetization. Late Devonian-Early Carboniferous sedimentary samples reveal a pre- or syntectonic Carboniferous remanent magnetization similar to the secondary one of the volcanic samples. A soft post-tectonic component appears also in few samples, for which a Late Carboniferous age is inferred. Comparison of the Carboniferous remanent magnetizations and structural parameters suggest that in a late stage of the deformation, the sites have undergone minor rotations around a vertical axis. A 'strike correction' is therefore proposed to take such an effect into account. The average of the corrected mean-site directions is considered to be a good approximation of the Early or Middle Carboniferous palaeomagnetic direction in Asturias. (28 refs.)

116005 Palaeomagnetism of NW Scotland syenites in relation to local and regional tectonics. H.B.Turnell, J.C.Briden (Dept. of Earth Sci., Univ. of Leeds, Leeds, England).

Geophys. J. R. Astron. Soc. (GB), vol.75, no.1, p.217-34 (Oct. 1983). A detailed thermal demagnetization study has been carried out on a number of syenitic intrusions from north of the Great Glen Fault in Scotland. Multi-component remanences of normal and reversed polarity have been recognized. These define a series of palaeomagnetic poles from which an Ordovician to Silurian apparent polar wander path for northern Scotland is deduced. Comparison of this apparent polar wander path with the established path for Britain throws new light on the sequence of thrusting and magmatic activity in the NW Highlands and precludes large-scale ($\geq 1500 \text{ km}$) movement along the Great Glen Fault later than the Ordovician. The data are consistent with the suggestion that Britain was among a set of intracratonic microplates which underwent complicated, distinct movements throughout the Caledonian orogeny. (28 refs.)

116006 Palaeomagnetism of late Precambrian-Cambrian volcanics and intrusives from the Armorican Massif, France. R.Perigo, van der Voo (Dept. of Geological Sci., Univ. of Michigan, Ann Arbor, MI, USA), B.Auvray, N.Bonhomme.

Geophys. J. R. Astron. Soc. (GB), vol.75, no.1, p.235-60 (Oct. 1983). Samples of the keratophyre tufts of Treguier ($640 \pm 12 \text{ Myr}$) of the Upper Brioverian series, and the microgranite dykes of Loguivy ($548 \pm 24 \text{ Myr}$) have been collected from the north coast of Brittany, France. The samples were progressively demagnetized with AF and, predominantly, thermal methods. Blocking temperatures, coercivities and acquisition of isothermal remanent magnetization (IRM) indicate that the keratophyre remanence, is variably carried in magnetite, hematite, or occasionally in both. After removal of a soft viscous component, two stable palaeomagnetic directions were found, one in magnetite, the other in hematite. The characteristic magnetite direction ($T_b=300-580^\circ\text{C}$) is a prefoling primary thermoremanent magnetization (TRM) which after structural correction has a mean declination/inclination of $217.9^\circ/-30.4^\circ$. The younger hematite component has a mean in situ direction of $320.4^\circ/+20.3^\circ$. The microgranite natural remanent magnetization intensity distribution is distinctly bimodal, forming high and low intensity groups. (70 refs.)

116007 Singular solutions to Maxwells equations and their significance for geomagnetic induction. D.Wolf (Dept. of Phys., Univ. of Toronto, Toronto, Ontario, Canada).

Geophys. J. R. Astron. Soc. (GB), vol.75, no.1, p.279-83 (Oct. 1983). In geomagnetism the interpretation of induction anomalies has frequently encountered difficulties. Sometimes the problems may be overcome if channelled currents are taken into account. This idea was introduced by Japanese workers to explain the characteristics of the Central Japan anomaly in a consistent manner (Rikitake 1959). But whereas their channelling models showed some resemblance to electrical circuits, later work has usually considered the three-dimensionality of the problem. Dyck and Garland (1969) correctly pointed out that current channelling would always be presented unless: (1) the source fields are local or (2) the conductivity of the host rocks is vanishing. For the real Earth neither condition applies rigorously. Any serious interpretation of induction anomalies must consider their frequency response. In this article the low-frequency limit of the response of several model conductors is discussed. The general conclusion is that for configurations adequate to the Earth the solutions are incompatible with excessively large anomalous fields at points sufficiently removed from conductivity contrasts. (12 refs.)

116008 Internal and external components of the 60-yr variations in the geomagnetic field. Yu.D.Kalinin, T.S.Rozanova (L.V. Kirenskii Inst. of Phys., Acad. of Sci., USSR).

Geomagn. & Aeron. (USA), vol.22, no.3, p.395-6 (1982). Translation of: *Geomagn. & Aeron. (USSR)*, vol.22, no.3 (1982). [received: Sept. 1983] The amplitude of the internal component of the 60-yr variations in the geomagnetic field is approximately five times the amplitude of the external component. Some possible consequences are discussed. (8 refs.)

116009 Palaeomagnetic evaluation of the orocline hypothesis in the Central and Southern Appalachians. A.Y.Schwartz, R.Van der Voo (Dept. of Geological Sci., Univ. of Michigan, Ann Arbor, MI, USA).

Geophys. Res. Lett. (USA), vol.10, no.7, p.505-8 (July 1983). The axial traces of the major Appalachian folds change azimuthal direction from a NE-SW orientation to a N-S orientation in the area of the Pennsylvania Salient and swing back to a NE-SW orientation in the vicinity of the Virginia Reentrant. All available palaeomagnetic data from the folded Appalachians have been examined to test the Appalachian orocline hypothesis. Pre-deformational site-mean directions from suitable studies were rotated by the amount required to bring the strike of the sampled beds into coincidence with an average trend of the Central and Southern Appalachians (N35E). A comparison of clustering of site-means before and after this correction, reveals that in all cases unbending of the arc causes site-mean directions to disperse. This dispersal demonstrates that the curvature of the Appalachian orogen is to a very large degree a primary feature rather than a feature which resulted from the bending of initially straight fold axes. (18 refs.)

116010 Reduction of the vertical magnetic anomalies to the magnetic pole and the estimation of the parameters used in the reduction, based on the Poisson's relation. K.Kis.

Magy. Geofiz. (Hungary), vol.24, no.3, p.81-96 (1983). In Hungarian. The maxima and minima of the magnetic anomalies are mainly influenced by the direction of the magnetic polarisation. In order to get rid of this influence the reduction to the magnetic pole can be derived without reference to the Poisson's relation. The derived transfer function is valid in the case of the homogeneous polarisation. The transfer function of the reduction to the magnetic pole has a finite discontinuity at the origin of the coordinate system. For the elimination of this finite discontinuity an appropriate truncating function is suggested. The unknown value of the parameters of the reduction are calculated by optimisation based on the Poisson's relation. The suggested procedure is illustrated by model calculations and a field example. (21 refs.)

116011 Non-recurrent geomagnetic disturbances from high-speed streams. M.S.Bobrov (Astron. Council, Acad. of Sci., Moscow, USSR).

Planet. & Space Sci. (GB), vol.31, no.8, p.865-70 (Aug. 1983). It is shown that at any phase of solar activity cycle the Earth is circumflown mainly by high-speed solar wind streams (M-streams). The attention is called to the fact that M-streams cause not only the well-known recurrent geomagnetic disturbances (at the declining phase of solar cycle) but also numerous non-recurrent disturbances (at all the other phases). The intensity and duration of a typical non-recurrent M-disturbance are less than those of a recurrent one. (9 refs.)

116012 Worldwide features of the strength of recurrent geomagnetic activity. G.K.Rangarajan, A.Bhattacharyya (Indian Inst. of Geomagnetism, Bombay, India).

Proc. Indian Acad. Sci. Earth & Planet. Sci., vol.92, no.1, p.5-13 (March 1983). [received: Sept. 1983]

Variation of the strength of recurrent geomagnetic activity, which occurs just before a sunspot minimum, with local time is studied for a network of observatories covering different latitude and longitude zones. For this purpose, hourly averages of horizontal intensity for each UT hour for 173 days, which are totally free of disturbances due to solar transients, have been subjected to spectral analysis. Well-defined spectral peaks associated with periodicities of 28, 14 and 9 days were present in almost all the spectra. (18 refs.)

116013 Analytical representation of spatial and temporal variations of the geomagnetic field in the Indian region. B.R.Arora, V.H.Badshah, B.P.Singh (Indian Inst. of Geomagnetism, Bombay, India), M.G.Arur, P.S.Bains, Jeevan Lal.

Proc. Indian Acad. Sci. Earth & Planet. Sci., vol.92, no.1, p.15-30 (March 1983). [received: Sept. 1983]

The magnetic measurements of declination (D), and horizontal (H) and vertical (Z) components of the Earth's magnetic field, collected from ground

surveys between 1962 and 1966, are used to develop an analytical model of geomagnetic field variations over India for the epoch 1965. In order to reflect spatial features with wavelengths of approximately 1000 km, a sixth degree polynomial as a function of differential latitude and longitude is calculated by the method of least squares. The values of the field at common repeat stations recorded between 1962 and 1974 are used to determine the secular variation and its spatial dependence. (20 refs.)

116014 An episode of steep geomagnetic inclination 120000 years ago. K.L.Verosub (Dept. of Geology, Univ. of California, Davis, CA, USA). *Science (USA)*, vol.221, no.4608, p.359-61 (22 July 1983). The mean inclinations of three sections of 120000-year-old fine-grained sediments from northern California range from 62° to 66°. These inclinations are significantly steeper than the inclination of the geocentric axial dipole at this site. Because these sediments have probably recorded an actual episode of steep inclination lasting several thousand years, they provide new insights into the significance of mean inclinations shallower than the geocentric axial dipole. Such inclinations are characteristic of fine-grained sediments younger than 35000 years. The results raise questions about the time-averaged geomagnetic field and about the determination of plate motions from paleomagnetic data. (15 refs.)

116015 A combined analysis of the gravitational and magnetic anomalies for the detection of magnetically active rock complexes in the basement of the West Siberian plate. T.L.Zakharova, L.A.Sharlovskaya (Inst. of Geology & Geophys., Acad. of Sci., Novosibirsk, USSR). *Sov. Geol. & Geophys. (USA)*, vol.23, no.5, p.59-66 (1982). Translation of: *Geol. & Geofiz. (USSR)*, vol.23, no.5, p.67-75 (1982). Presents the results of a geologic interpretation of the gravitational and magnetic anomalies in the Ob'-Irtys' region of the West Siberian plate. On the basis of a quantitative estimate of Poisson's areal coefficient and the anomalous magnetic field, transformed by the differentiated method at the level of the basement, the distribution of magnetically active rock complexes and the metallogeny associated with them is suggested. (18 refs.)

116016 A geological and paleomagnetic study of the Hyblean volcanic rocks, Sicily. M.Grasso, F.Lentini (Istituto di Scienze della Terra, Univ. of Catania, Catania, Italy), A.E.M.Nairn, L.Vigliotti. *Tectonophysics (Netherlands)*, vol.98, no.3-4, p.271-95 (1983). The geological and paleomagnetic study of the Hyblean volcanic rocks in southeastern Sicily permits the following conclusions: (1) The Upper Cretaceous volcanics are considerably more extensive than earlier studies indicated. Their magnetization is identical to that of the better known outcrops around Capo Passero. Of the two new age dates reported, one is younger than any so far reported. (2) The Upper Tortonian flows are normally magnetized, suggesting a correlation of the Carlentini Formation with magnetic interval 7. The flows at the top of the Tellaro Formation are also normally magnetized and are tentatively correlated with the Carlentini Formation flows. Shorter reversed intervals within interval 7 may be represented by two less well-dated flows. (3) The lowest Pliocene flows have an adequate stratigraphic control and their magnetization is consistent with the extrusion of the pillow lavas during the Mammoth event. (4) The geomagnetic pole positions are consistent with that of the African plate during the Cretaceous, and a European plate location during both Pliocene and Miocene time.

116017 Paleomagnetic investigations in the Thuringer Forest (GDR). H.J.Mauritsch, K.Rother (Dept. of Geophys., Mining Univ. Leoben, Leoben, Austria). *Tectonophysics (Netherlands)*, vol.99, no.1, p.63-72 (1983). In the Thuringer Forest, the whole 'Rotliegendes' is well exposed, and was chosen as the starting place for a Permian traverse via Czechoslovakia, Austria into Italy. Rock magnetic experiments established haematite as main carrier of the NRM, except a few localities, where magnetite was found to present. Sediments and volcanities show consistent ChRM directions. The comparison with KrS's (1978) compilation proves a good Permian pole position.

116018 Magnetic anomalies on and around the Bonin Rise. T.Matsumoto, Y.Tomoda (Ocean Res. Inst., Univ. of Tokyo, Tokyo, Japan). *Zisin. J. Seismol. Soc. Jpn. (Japan)*, vol.36, no.1, p.77-82 (March 1983). In Japanese. [received: Sept. 1983] Magnetic data obtained in and around the Bonin region are compiled. The magnetic anomaly of the Bonin Rise shows that the rise was produced at about 19°N in latitude. The distribution of the differential magnetic anomalies indicates extension of the subbottom structure of the Bonin Rise onto the landward region of the Bonon Trench at this area. (7 refs.)

Study of Iwasaki earthquake swarm in Aomori Prefecture. II. Seismic activity and crustal movement	See Entry 116038
Further thermochronometric unravelling of the age and palaeomagnetic record of the southwest Grenville Province	See Entry 116040
Determining the components of the magnetic field of a vehicle	See Entry 116292
Calculation of well log apparent resistivities by discrete convolution	See Entry 116296
An EM field modelling unit for geophysical prospecting problems	See Entry 116299
Classification capability and resolving power of the method of transients in searches for kimberlites	See Entry 116310
Combined interpretation of magnetic and gravitational fields based on calculations of the pseudogravitational field	See Entry 116311
Experimentation d'un systeme de sondage en a source controlee, en prospection miniere (Experiments with an EM sounding system with a controlled source in mineral prospecting)	See Entry 116314
Distribution of meteor heights and sunrise	See Entry 116322
Reconstruction of the three-dimensional current system from variations in the ground-level magnetic field for sloping lines of force	See Entry 116353
Heliomagnetic cycle in geomagnetic activity	See Entry 116383

91.30 SEISMOLOGY

116019 P-wave velocity structure of the upper mantle in northern China. Zhao Zhu (Seismological Bur. of Sichuan Province, China). *Acta Geophys. Sin. (China)*, vol.26, no.4, p.341-54 (July 1983). In Chinese. English translation in: *Acta Geophys. Sin. (USA)* The data of 140 earthquakes recorded at different azimuths from the Beijing network are used. By using both the smoothing method and $dT/d\Delta$ method, the slowness curves of P-waves are obtained. By incorporating the travel-time and slowness data, continuous travel-time curves can be obtained. A simple formula is derived and used to invert the initial velocity models. The average velocity model shows that a shallow low velocity zone begins near 60 km in

depth: two abrupt increases in velocity from 360 to 420 km and from 660 to 680 km are also obtained; a possible minor zone of high-velocity gradient near 500 km is detected. (12 refs.)

116020 Direct and indirect aftershocks. Lu Yuan-Zhong, Wu Pei-Zhi, Shen Jian-Wen (Seismological Bur. of Anhui Province, China). *Acta Geophys. Sin. (China)*, vol.26, no.4, p.355-65 (July 1983). In Chinese. English translation in: *Acta Geophys. Sin. (USA)* Aftershock sequences of 25 large earthquakes, $M \geq 6$, which occurred in China since the $M=7.2$ Xingtai earthquake of 1966, are analyzed. It is found that in these sequences a great number of aftershocks followed the mainshocks in two or three days. The frequencies of these aftershocks decreased rapidly and exhibited a time decay law different from that governing the later aftershocks. These early aftershocks governed the temporal variation of the later aftershocks and had already roughly sketched out the aftershock regions. Based on these characteristics, aftershocks are considered to be of two kinds; direct aftershocks and indirect aftershocks. (4 refs.)

116021 A splitting-up method for solution of higher-order migration equation by finite-difference scheme. Ma Zai-Tian. *Acta Geophys. Sin. (China)*, vol.26, no.4, p.377-89 (July 1983). In Chinese. English translation in: *Acta Geophys. Sin. (USA)* The lower-order migration equations, second-order and third-order migration equations (i.e. first and second approximations of wave equation), are used to seismic migration practice. They are not accurate enough to migrate the events with steep dips. In order to obtain more accurate migrated seismic data, the higher-order migration equation must be used. For this purpose the author has developed a splitting-up method which is a general algorithm for solving the higher-order migration equations (including third-order equation and over) by a finite-difference scheme. The theory of this method is described and some practical experiments are shown. (7 refs.)

116022 Microearthquake activity of Derbendikhan dam area. S.A.Alsinawi (Dept. of Geology, Coll. of Sci., Univ. of Baghdad, Baghdad, Iraq), B.S.Ayar. *Iraqi J. Sci.*, vol.22, no.4, p.570-88 (1981). [received: Aug. 1983] Microearthquake activity was monitored during the period from January 1978 to March 1978. 1900 hours were recorded continuously from which 1550 hours were analysed. The rate of microearthquake occurrence, spatial distribution, fluctuation of seismic activity with duration of recording, relation between the number of microearthquakes and their duration. Poisson's distribution, frequency distribution of the maximum trace amplitude, the relation between magnitude, energy and intensity of events, and the predominant frequency were determined from statistical and Fourier analysis. (12 refs.)

116023 Amplitude spectra for some earthquakes recorded in Iraq. S.A.Alsinawi (Dept. of Geology, Coll. of Sci., Univ. of Baghdad, Baghdad, Iraq), H.J.Al-Shukri. *Iraqi J. Sci.*, vol.22, no.4, p.589-612 (1981). [received: Aug. 1983] Amplitude spectra were studied for 38 earthquakes recorded at 10 different sites in Iraq. These spectra were obtained from 10 seconds of the recorded events starting just before the P-onset. These earthquakes were recorded by a 3-component short period seismograph. The spectral characteristics indicate that the predominant frequencies of the analysed earthquakes fall in the range of 0.23-3.5 Hz. The decrease in the energy of the seismic waves as the frequency increases reaches a value of about 35% of the relative amplitude at 3.5 Hz. (11 refs.)

116024 A lithospheric seismic refraction profile in the western North Atlantic Ocean. R.B.Whitmarsh (Inst. of Oceanographic Sci., Wormley, England), C.E.Keen, L.Steinmetz, J.Tomblin, R.B.Whitmarsh, M.Donegan, R.C.Lilwall, B.D.Loncarevic, B.Nichols, J.Shepherd, J.Shepherd. *Geophys. J. R. Astron. Soc. (GB)*, vol.75, no.1, p.23-69 (Oct. 1983). A study of the seismic velocity structure of the subcrustal oceanic lithosphere was conducted in the Western North Atlantic north of the Lesser Antilles, where the age of the lithosphere is 80-95 Ma. A 1000 km long north-south array of 18 ocean-bottom seismographs (OBS), spaced at 60 km intervals, recorded arrivals from explosions at ranges up to 800 km and arrivals from earthquakes in the northern Caribbean region at ranges up to 1400 km. Analysis of the travel-time and amplitude data from the explosions provided the velocity structure down to about 65 km below sea-level. (90 refs.)

116025 Long-term premonitory seismicity patterns in Italy. M.Caputo (Accademia Nazionale dei Lincei, Roma, Italy), R.Console, A.M.Gabrielov, V.I.Keilis-Borok, T.V.Sidorenko. *Geophys. J. R. Astron. Soc. (GB)*, vol.75, no.1, p.71-5 (Oct. 1983). The clustering of earthquakes as a premonition to a strong earthquake in the same region is defined as pattern BG, which is a generalization of patterns B ('burst of aftershocks') and S ('swarm'), described previously (Caputo et al.; Keilis-Borok et al.); five out of the seven strongest earthquakes in Italy ($M \geq 6.3$, 1900-1980) are preceded by pattern BG within 5 yr; and eight out of 11 patterns BG are followed by a strong earthquake within 5 yr; the last pattern BG (1979 November 11) was diagnosed in advance of the Irpinia earthquake of 1980 November 23 ($M=6.5$). The statistical significance of pattern BG cannot be tested with the data on Italy alone. (9 refs.)

116026 Calculation of complete theoretical seismograms in vertically varying media using collocation methods. P.Spudich (US Geological Survey, Menlo Park, CA, USA), U.Ascher. *Geophys. J. R. Astron. Soc. (GB)*, vol.75, no.1, p.101-24 (Oct. 1983). Presents a method for calculating complete theoretical seismograms in Earth models whose velocity, density and attenuation profiles are arbitrary piecewise-continuous functions of depth only. A form of attenuation valid for low loss situations is included by allowing the seismic velocities to be complex, and frequency is also allowed to be complex to avoid wrap-around problems in the time-domain seismograms. Solutions for the stress-displacement vectors in the medium are expanded in terms of orthogonal cylindrical functions. A seismic source is applied at the Earth's surface and a radiation condition is applied at depth. The resulting two-point boundary value problem for the expansion coefficients is solved by a collocation technique which works best for those cases that other methods, e.g. propagator matrices, work most poorly, i.e. highly evanescent solutions. Solutions for the expansion coefficients are obtained in the depth, frequency and horizontal wavenumber domain. Phase velocity filtering may be affected at this point by restricting the portion of the frequency-wavenumber plane in which solutions are sought. (20 refs.)

116027 A study of the 1980 summer seismic sequence in the Magnesia region of Central Greece. B.C.Papazachos, D.G.Panagiotopoulos, T.M.Tsapanos (Geophys. Lab., Univ. of Thessaloniki, Thessaloniki, Greece), D.M.Mountrakis, G.Ch.Dimopoulos. *Geophys. J. R. Astron. Soc. (GB)*, vol.75, no.1, p.155-68 (Oct. 1983). Properties of the seismic sequence (foreshocks and aftershocks) of the 1980 July 9, ($M=6.5$) earthquake in the Magnesia region of Central Greece are investigated. Fault plane solutions of the three major shocks of the sequence, distribution of epicentres, geological data and field observations show that the seismic fault is a normal trending ENE-WSW and dipping SSE. Evidence

that its dip angle decreases with depth is presented. The parameter b , in the frequency-magnitude relation, was found equal to 0.84 for the foreshocks and equal to 1.28 for the aftershocks, while the decay parameter p of the time distribution of the aftershock frequency was found equal to 0.72. The frequency of foreshocks, which started on July 4, increased till July 6 but after that decreased till the occurrence of the main shock, while their average magnitude decreased continuously between July 4 and 9. A striking similarity between the focal properties of shocks of this sequence and of shocks of two other sequences which occurred in 1978 and 1981 in the back-arc. Aegean area is attributed to tensional forces acting in this area since the middle Pleistocene. (19 refs.)

116028 Synthesis of complete *SH* seismograms. S.F.Ingate, G.Bock (Res. School of Earth Sci., Australian Nat. Univ., Canberra, Australia), R.Kind. *Geophys. J. R. Astron. Soc. (GB)*, vol.75, no.1, p.261-74 (Oct. 1983). A method for calculation of theoretical *SH*-waves in a laterally homogeneous layered medium is presented. The *SH* wave trains are complete, i.e. they include surface waves as well as body waves. The *SH* displacements are calculated for two point sources, a single horizontal force and a shear dislocation of arbitrary orientation, both buried in the layered half-space. Numerical problems are discussed. The correctness of the method is ascertained by its ability to reproduce complete synthetic *SH* seismograms published elsewhere in the literature. Several examples demonstrate that this method is well suited for crustal studies as well as for teleseismic studies of the upper and lower mantle. (28 refs.)

116029 An alternative method for fault-plane solutions from a single station. S.F.Ingate (Res. School of Earth Sci., Australian Nat. Univ., Canberra, Australia). *Geophys. Res. Lett. (USA)*, vol.10, no.7, p.497-9 (July 1983). An alternative to the method of Langston (1982) for determining fault-plane solutions from a single 3-component seismic station is proposed. The method calculates synthetic *P* and *SH* seismograms for three basic orientations of a shear dislocation embedded in a plane layered Earth model, and uses least-squares to minimise the error between the observed data and a linear sum of the synthetic seismograms. The result is five trigonometric functions of fault strike θ , fault dip δ , and rake of the slip vector λ . When applied to the Borrego Mountain event of 9 April 1968, the method provides a solution which is in close agreement with well-constrained studies of the main shock. (7 refs.)

116030 T-phases from an earthquake swarm on the Mid-Atlantic Ridge at 31.6°N. T.M.Brocher (Hawaii Inst. of Geophys., Univ. of Hawaii, Honolulu, HI, USA). *Mar. Geophys. Res. (Netherlands)*, vol.6, no.1, p.39-49 (1983). An ocean bottom seismometer array on the Nova Scotia shelf edge recorded T-phases from an earthquake swarm on the mid-Atlantic ridge at about 31.6°N in June 1975. The swarm occurred along a segment of the ridge that ruptured similarly 17 yr previously. From 1964 to mid-1979 the worldwide network recorded three other earthquake swarms along this segment of the Mid-Atlantic Ridge (MAR). A sparse network of sensors in the SOFAR channel, having a lower magnitude threshold, might provide a better means of monitoring the seismicity of both short-length transforms and ridge crests along the MAR than does the worldwide seismic network. (25 refs.)

116031 A standard format for storage and exchange of natural and explosive-source seismic data: the ROSE format. S.L.Latraille, L.M.Dorman (Hawaii Inst. of Geophys., Univ. of Hawaii, Honolulu, HI, USA). *Mar. Geophys. Res. (Netherlands)*, vol.6, no.1, p.99-105 (1983). The ROSE experiment (Ewing and Meyer, 1982) involved the participation of much of the US marine seismic community. Prior to that experiment, wide consultation was made and much effort was expended in the intercomparison of instruments and in the establishment of a uniform, yet flexible, data exchange format. Results of the instrument intercomparison were reported earlier (Sutton et al., 1981) and the data exchange format is described. The participating institutions have provided their data to a central exchange facility at the University of Hawaii where the data are catalogued and distributed. The authors hope that the use of this format for the exchange of data from other experiments will reduce the time spent on work of a housekeeping nature, time which is irretrievably lost to the pursuit of scientific goals. (3 refs.)

116032 Scattering of seismic waves by the broken edge of a flat boundary. A.M.Aizenberg (Inst. of Geology & Geophys., Acad. of Sci., USSR). *Sov. Geol. & Geophys. (USA)*, vol.23, no.5, p.74-82 (1982). Translation of: *Geol. & Geofiz. (USSR)*, vol.23, no.5, p.83-92 (1982). The scattering of seismic waves by the broken edge of a flat boundary is investigated on the basis of the Huygens-Fresnel principle (secondary sources). The scattered field is represented by the superposition of three types of waves: a geometrical wave (reflected or refracted), the diffracted wave, and the wave from a corner point on the broken edge. It is shown that the results obtained in this way are equivalent to the description of this phenomenon within the framework of the theory of edge waves (Young's principle). (15 refs.)

116033 The seismology of Greece. M.Bath (Seismological Section, Uppsala, Sweden). *Tectonophysics (Netherlands)*, vol.98, no.3-4, p.165-208 (1983). A review and a bibliography are given of the seismological literature for the area of Greece in the period from 1950 up to the present time. The aim is to incorporate all aspects of seismology, starting with instrumental installations, passing on to earthquake catalogues, statistics and effects, and ending up with structural properties and seismotectonics. The purpose is to provide a service to every geophysicist who has an interest in this tectonically complex area and particularly to the numerous researchers engaged in geophysical expeditions to Greece.

116034 The occurrence of large earthquakes in South Italy. M.Caputo (Inst. of Phys., Univ. of Rome, Rome, Italy). *Tectonophysics (Netherlands)*, vol.99, no.1, p.73-83 (1983). An analysis of the data in the catalogues of Italian earthquakes indicates that large earthquakes which occur in the area of radius of about 140 km centered in the Straits of Messina occur in sequences. Each sequence is generally formed by two events and covers an average time window of 10 years. The last four sequences occurred in the time windows 1783-1891, 1818-1823, 1865-1870, 1905-1908 and are separated by about 40 years indicating that in that area there is now a gap in the time domain. The analysis of the data in the catalogue for the region between the latitudes 39°N and 41°50'N indicates that in the region the large earthquakes occurred in 13 sequences. Each sequence is formed by 3 events in average and covers an average time window of 7 years. This indicates that, after the earthquake of Nov. 1980, which occurred after a gap of 67 years, other moderately large earthquakes may be expected.

116035 Long-term prediction of earthquakes in western Honshu, Japan. H.Miki (Faculty of Sci., Kyoto Univ., Kyoto, Japan). *Zisin. J. Seismol. Soc. Jpn. (Japan)*, vol.36, no.1, p.1-11 (March 1983). In Japanese. [received: Sept. 1983] Great earthquakes along the Nankai Trough did not occur at random but occur quasi-periodically. The time intervals of their recent occurrences are 90-150 years. As the most recent past earthquakes were the Tonankai earthquake in 1944 and the Nankai earthquake in 1946, about the first third of this time interval has lapsed. If the seismicity in the coming second term is the same as that in the past term, the possibility of the occurrence of an earthquake is 50%. (16 refs.)

116036 Scaling of rupture size. II. On time and space distributions and magnitude-frequency distribution of swarm. Y.Iio (Faculty of Sci., Kyoto Univ., Kyoto, Japan). *Zisin. J. Seismol. Soc. Jpn. (Japan)*, vol.36, no.1, p.13-21 (March 1983). In Japanese. [received: Sept. 1983] For pt. I see *ibid.*, vol.35, no.2, p.183-93 (1982). The time and space distributions and b -values of the micro-fractures in mines and acoustic emissions were investigated and compared with those of earthquake swarms. (33 refs.)

116037 Focal distribution of earthquakes in relation to major geological tectonic lines in Shikoku, Japan. K.Okano (Dept. of Phys., Kochi Univ., Kochi, Japan), S.Kimura, T.Konomi. *Zisin. J. Seismol. Soc. Jpn. (Japan)*, vol.36, no.1, p.23-9 (March 1983). In Japanese. [received: Sept. 1983] Shikoku Island is divided into four zones of different geological nature by three major faults called the Median-, the Mikabu-, and the Butsuzo-Tectonic Lines, respectively. It has become obvious from the precise examination of the focal distribution of earthquakes that the four zones are characterized not only by geological features but by seismological ones: there exist aseismic zones along the three tectonic lines and the deepest levels of seismically active regions in the crust are discontinuous across the tectonic lines. (10 refs.)

116038 Study of Iwasaki earthquake swarm in Aomori Prefecture. II. Seismic activity and crustal movement. T.Sato, S.Horiuchi, S.Hori, T.Satoh, K.Kusunose, E.Murakami, K.Tachibana, H.Ishii, A.Takagi (Faculty of Sci., Tohoku Univ., Ibaraki, Japan), T.Sato. *Zisin. J. Seismol. Soc. Jpn. (Japan)*, vol.36, no.1, p.63-75 (March 1983). In Japanese. [received: Sept. 1983] For pt. I see *ibid.*, vol.34, no.1, p.81-93 (1981). An earthquake swarm with the largest event of magnitude 4.3 occurred in and near Iwasaki, on the west coast of Aomori Prefecture, NE Honshu, Japan, between September 1978 and January 1979. The authors present the results of measurements of hypocentral locations, focal mechanisms, fault plane solutions and the total seismic energy liberated. Large anomalies in the total geomagnetic field were observed in the epicentral region. No abnormal variations were detected by a tiltmeter located about 9 km from the swarm region. The results of distance measurements and levelling surveys are discussed: the crustal movements observed could not be explained by a simple elastic deformation model. (21 refs.)

Movements of the fracture zone and the seismic activity under the fracture zone—based on the observations at Abuyama See Entry 115999

A marine seismic refraction study of the Santa Barbara Channel, California See Entry 116043

The Long Valley/Mono Basin volcanic complex in eastern California: status of present knowledge and future research needs See Entry 116056

The underthrusting movement of the Western Pacific Plate and the deep focus earthquake zone or northeast China See Entry 116059

Fault slip beyond a barrier on a transform plate boundary See Entry 116064

Characteristics of distributions of thermal stress and stress due to phase change in the descending plate beneath Island Arc See Entry 116072

Evidence for correlation of ultrasonic attenuation and fluid permeability in very low porosity water-saturated rocks See Entry 116081

Dynamic processes during slip of stick-slip as an earthquake fault model See Entry 116084

The long period seismograph type 763 See Entry 116287

Calibration of long-period seismic channels See Entry 116303

Fast seismic ray tracing See Entry 116309

Inverse problems for reflection seismograms See Entry 116316

Extraction of seismic profiles for one-dimensional nonhomogeneous media using the impulse response model See Entry 116317

Review of some exact methods for the solution of the one-dimensional inverse problems See Entry 116318

Difference methods for solving one-dimensional inverse problems See Entry 116319

Maximum-likelihood as applied to seismic inversion problems See Entry 116320

Some results on the three-dimensional geophysical inverse problem See Entry 116321

91.35 EARTH'S INTERIOR STRUCTURE AND PROPERTIES

116039 The characteristics of geophysical field and the distribution and formation of oil- and gas-bearing basin in eastern China. Teng Ji-Wen, Wang Qian-Shen, Liu Yuan-Long, Wei Si-Yu (Inst. of Geophys., Acad. Sinica, Beijing, China). *Acta Geophys. Sin. (China)*, vol.26, no.4, p.319-30 (July 1983). In Chinese. English translation in: *Acta Geophys. Sin. (USA)* Based on the crust and upper mantle structures on both sides of the Tangcheng-Lujiang fault system in the epicontinental region of Eastern China, as well as on the characteristics of the geophysical fields the authors discuss the relation between these characteristics and the distribution of a series of rift valley oil- and gas-bearing basins, as well as the sedimentation and evolution of these basins. The conclusions are that, all these basins are distributed in uplifted regions of the upper mantle and that there exist anomalies of geophysical fields as well as anomalous crust and upper mantle structures. In these basins, there are Meso-Cenozoic thick sediments, with favourable conditions for the formation and accumulation of petroleum. The formation of these basins is directly connected with the motion of the Pacific and Eurasian plates and is restricted by the movement of the material in the deep mantle. (12 refs.)

- 116040 Further thermochronometric unravelling of the age and palaeomagnetic record of the southwest Grenville Province.** M.Lopez-Martinez, D.York (Dept. of Phys., Univ. of Toronto, Toronto, Canada). *Can. J. Earth Sci. (Canada)*, vol.20, no.6, p.953-60 (1983). The Cordova gabbro in the Hastings Basin of the southwestern Grenville Province has been studied thermochronometrically to see if the anomalous C magnetic pole was actually acquired prior to 1200 Ma ago. Resetting of the plagioclase argon clock very strongly indicates that, in fact, the C pole was acquired during a mild Siluro-Ordovician event and does not record the existence of a pre-Grenville small ocean between a Grenville plate and Interior Laurentia. Such a hypothesised mild event is consistent with the magnetic, isotopic, and fluid inclusion record. (17 refs.)
- 116041 Marathon dikes: Rb-Sr and K-Ar geochronology of ultrabasic lamprophyres from the vicinity of McKellar Harbour, northwestern Ontario, Canada.** R.G.Platt, R.H.Mitchell (Dept. of Geology, Lakehead Univ., Thunder Bay, Canada), P.M.Holm. *Can. J. Earth Sci. (Canada)*, vol.20, no.6, p.961-7 (1983). Discusses the Rb/Sr and K/Ar geochronology of a set of ultramafic lamprophyres located in the vicinity of McKellar Harbour (48°48'N, 86°44'W) some 40 km west of Marathon. (24 refs.)
- 116042 Apatite fission-track dating of erosion in the eastern Andes, Bolivia.** S.T.Crough (Dept. of Geosci., Purdue Univ., West Lafayette, IN, USA). *Earth & Planet. Sci. Lett. (Netherlands)*, vol.64, no.3, p.396-7 (Sept. 1983). Three samples from a Triassic-age batholith in the eastern Andes northeast of La Paz, Bolivia, yield apatite fission-track ages of 11-13 Ma. Interpreting these young ages as due to uplift and erosion requires approximately 2.5-5.0 km of erosion in the past 12 Ma, an amount which is consistent with the known geology and which is typical of many active mountain ranges. (7 refs.)
- 116043 A marine seismic refraction study of the Santa Barbara Channel, California.** G.J.Crandall, B.P.Luyendyk, M.S.Reichle, W.A.Prothero (Dept. of Geological Sci., Univ. of California, Santa Barbara, CA, USA). *Mar. Geophys. Res. (Netherlands)*, vol.6, no.1, p.15-37 (1983). Seismic data from a 186 km-long refraction profile in the Santa Barbara Channel are interpreted using several velocity inversion techniques. Data were obtained during two cruises in 1978 and 1979. Seismic arrivals from fifty explosions of between 1 and 300 lb of TNT were recorded by two ocean bottom seismometers, four permanent ocean bottom stations (University of Southern California), and much of the United States Geological Survey/California Institute of Technology Southern California seismic network. Travel-time inversion is discussed. The velocity structure determined by these methods suggests that the channel has a sedimentary fill of from 4 to 7 km and a layer of mafic plus ultramafic rock 14 to 17 km thick. The greatest thicknesses of sediments are restricted to east of Point Conception. The velocity data also suggest that the Franciscan formation may not be present beneath the channel. Rather, the crust may represent a thickened portion of the Coast Range ophiolite. (43 refs.)
- 116044 Ion microprobe identification of 4100-4200 Myr-old terrestrial zircons.** D.O.Froude, T.R.Ireland, P.D.Kinny, I.S.Williams, W.Compton (Res. School of Earth Sci., Australian Nat. Univ., Canberra, Australia), I.R.Williams, J.S.Myers. *Nature (GB)*, vol.304, no.5927, p.616-18 (18 Aug. 1983). Reports the existence of detrital zircons from Western Australia which are far older than any known terrestrial rocks. They are from quartzites at Mt. Narryer, a locality which has created interest because of the nearby occurrence of 3630 ± 40 Myr orthogneisses. The older zircons were discovered during reconnaissance U-Pb age determinations of zircon concentrates from Archaean metasediments, using the ion microprobe SHRIMP at the Australian National University. These determinations are being made specifically to search for zircons having ages in the interval 3800-4500 Myr, a period unrepresented so far by reliable terrestrial age determinations. Grain-by-grain measurements of one particular concentrate revealed four zircons having near-concordant U-Pb ages between 4100 and 4200 Myr, in striking contrast to most grains whose ages are ~3750 and ~3500 Myr. These results show that pre-3800 Myr silica-saturated rocks were indeed present on the Earth's crust. (7 refs.)
- 116045 Some features of the evolution of the shelf zones of the globe during Mesozoic-Cenozoic time.** Ye.N.Nevesskiy (Shirshov Inst. of Oceanology, Acad. of Sci., Moscow, USSR). *Oceanology (USA)*, vol.22, no.1, p.40-9 (1982). Translation of: *Okeanologiya (USSR)*, vol.22, no.1 (1982). [received: Aug. 1983] The theory of plate tectonics is used to analyze the possible influence of continental drift and other global factors on the evolution of the shelf zones of the Earth during Mesozoic-Cenozoic time. The author compares paleogeographic maps, with maps for the corresponding time, reflecting the movement of the continents. The evolution of the shelves under conditions of unstable tectonic, hydrodynamic, and climatic environments, which determined the main features of sedimentational process, and the structure and composition of the shelf sediments, is traced. Maps of the likely distribution of Mesozoic-Cenozoic sedimentary associations of different lithologies on the present shelves are presented. (29 refs.)
- 116046 On the relation between the deep subsurface structure of the Baikal and Red Sea rifts and the lateral movements of lithospheric plates.** Ye.G.Mirlin, N.Yu.Bocharova (Shirshov Inst. of Oceanology, Acad. of Sci., Moscow, USSR). *Oceanology (USA)*, vol.22, no.4, p.438-43 (1982). Translation of: *Okeanologiya (USSR)*, vol.22, no.4 (1982). [received: Aug. 1983] The relationship between the height of ascent of mantle material and the total separation of continental plates in a rift zone is analyzed on the examples of the Baikal and the Red Sea rifts. All the available geologic and geophysical data is taken into account in preparing sections showing the structure of both rifts at depth. It is shown that the subsurface structure of the Red Sea rift differs from that of the Baikal rift in the greater height to which the mantle material rises and in the formation of a crust of the oceanic type. The differences are assumed to be due to the different stages of development of the two rifts. A comparative analysis is made of other rift zones with similar plate separations. (22 refs.)
- 116047 The dynamic Earth.** R.Siever. *Sci. Am. (USA)*, vol.249, no.3, p.30-9 (Sept. 1983). A general account is given of the Earth's history throughout geological time. The structure of the Earth's interior is described and plate tectonic processes are explained. The author discusses the other geologic processes that influence the shape and form of the Earth. These processes include the hydrologic cycle and volcanic activity. (no refs.)
- 116048 The Earth's core.** R.Jeanloz. *Sci. Am. (USA)*, vol.249, no.3, p.40-9 (Sept. 1983). A general account is given of the structure and properties of the Earth's core. The article describes how seismology is used to study the interior structure.

Dynamo models of the geomagnetic field are considered. These dynamo models require convection processes to occur in the core. The chemical composition of the core and its accretional history are described. (no refs.)

- 116049 The Earth's mantle.** D.P.McKenzie. *Sci. Am. (USA)*, vol.249, no.3, p.50-62 (Sept. 1983). A general account is given of the structure, chemical composition and tectonic convection processes occurring in the Earth's mantle. (no refs.)
- 116050 The oceanic crust.** J.Francheteau. *Sci. Am. (USA)*, vol.249, no.3, p.86-98 (Sept. 1983). Oceanic crust is created from mantle material at midocean ridges, it slowly spreads out to be consumed at subduction zones located at the junction with the continents or at island arcs. This article gives a general account of this plate tectonic process. The article also describes the detailed structure of the oceanic crust describing the transform faults, geology and gravity field. The results of seismic surveys and deep-sea sonar studies are also described. Details are given of sediment core studies and studies of ocean bottom rocks and submarine surveys. (no refs.)
- 116051 The continental crust.** B.C.Burchfiel. *Sci. Am. (USA)*, vol.249, no.3, p.86-98 (Sept. 1983). The article provides an overview of the continental crust describing its geology and the tectonic processes that have shaped it. Several examples are used to describe these processes. These areas are the Basin and Range Province in the USA, the Dead Sea rift system, the Pannonian Basin and the Australasia-Solomon Sea area. (no refs.)
- 116052 A model of thermal conduction in the Earth's crust in the Okhotomorskii region.** N.A.Volkova. *Sov. Geol. & Geophys. (USA)*, vol.23, no.5, p.83-7 (1982). Translation of: *Geol. & Geofiz. (USSR)*, vol.23, no.5, p.92-7 (1982). A thermal-conduction model is proposed for the Earth's crust in the Okhotomorskii region. It is based on the results of experimental and theoretical studies. It is concluded that the thermophysical properties of the Earth's crust are highly inhomogeneous in the horizontal direction in this region. (8 refs.)
- 116053 Cataclastic rocks of the San Gabriel fault—an expression of deformation at deeper crustal levels in the San Andreas fault zone.** J.L.Anderson, R.H.Osborne (Dept. of Geological Sci., Univ. of Southern California, Los Angeles, CA, USA), D.F.Palmer. *Tectonophysics (Netherlands)*, vol.98, no.3-4, p.209-51 (1983). The San Gabriel fault, a deeply eroded late Oligocene to middle Pliocene precursor to the San Andreas, was chosen for petrologic study to provide information regarding intrafault material representative of deeper crustal levels. Cataclastic rocks exposed along the present trace of the San Andreas in this area are exclusively a variety of fault gouge that is essentially a rock flour with a quartz, feldspar, biotite, chlorite, amphibole, epidote, and Fe-Ti oxide mineralogy representing the milled-down equivalent of the original rock. Likewise, fault gouge and associated breccia are common along the San Gabriel fault, but only where the zone of cataclasis is several tens of meters wide. At several localities, the zone is extremely narrow (several centimeters), and the cataclastic rock type is cataclasite, a dark, aphanitic, and highly comminuted and indurated rock. The San Gabriel cataclastic rocks also show more mineralogical changes.
- 116054 Geochronological and structural study of Tertiary and Quaternary dikes in southern France and Sardinia: an example of the utilization of dike swarms as paleostress indicators.** G.Feraud, R.Campredon (Lab. de Geologie et Geochemie, ERA, Nice, France). *Tectonophysics (Netherlands)*, vol.98, no.3-4, p.297-325 (1983). Ancient dikes swarms which are datable by geochronological methods can be used as paleostress indicators. This study defines criteria by which suitable dike swarms can be selected. This paper deals with Tertiary and Quaternary dike swarms of the French and Sardinian peri-Alpine platform. The results of geochronological and structural analysis show that the general trends of dikes (ranging from NW-SE to N-S) intruded during the last 8 Ma on the border of Massif Central and in Languedoc parallel the general trajectories of the present stress field (plane $\sigma_1\sigma_2$) as deduced from in situ measurements and from focal mechanism determination of earthquakes.
- Movements of the fracture zone and the seismic activity under the fracture zone—based on the observations at Abuyama** See Entry 115999
- Rapid diffusion of the poloidal geomagnetic field through the weakly conducting mantle: a perturbation solution** See Entry 116002
- Paleomagnetic evaluation of the orocline hypothesis in the Central and Southern Appalachians** See Entry 116009
- A geological and paleomagnetic study of the Hyblean volcanic rocks, Sicily** See Entry 116016
- Paleomagnetic investigations in the Thuringer Forest (GDR)** See Entry 116017
- Magnetic anomalies on and around the Bonin Rise** See Entry 116018
- P-wave velocity structure of the upper mantle in northern China** See Entry 116019
- A lithospheric seismic refraction profile in the western North Atlantic Ocean** See Entry 116024
- Focal distribution of earthquakes in relation to major geological tectonic lines in Shikoku, Japan** See Entry 116037
- The Long Valley/Mono Basin volcanic complex in eastern California: status of present knowledge and future research needs** See Entry 116056
- The Mesozoic magmatism of the Aldan shield as an indicator of its tectonic regime** See Entry 116058
- The underthrusting movement of the Western Pacific Plate and the deep focus earthquake zone or northeast China** See Entry 116059
- The Snake Range decollement: an exhumed mid-Tertiary ductile-brittle transition** See Entry 116061
- Tectonic stresses in the lithosphere** See Entry 116063
- Tectonics of ridge-transform intersections at the Kane fracture zone** See Entry 116066
- Changing stress field in the middle segment of the Tan-Lu fault zone, eastern China** See Entry 116067
- The reliability of asymmetric c-axis fabrics of quartz to determine sense of vorticity** See Entry 116069
- Analogue models of folds above a wrench fault** See Entry 116071
- Characteristics of distributions of thermal stress and stress due to phase change in the descending plate beneath Island Arc** See Entry 116072
- ²²⁶Ra and ²²²Rn contents of Galapagos Rift hydrothermal waters—the importance of low-temperature interactions with crustal rocks** See Entry 116073
- Intense hydrothermal activity at the axis of the East Pacific Rise near 13°N: submersible witnesses the growth of sulfide chimney** See Entry 116074

- New data on the structure of Ampere SeamountSee Entry 116075
- Ninigi and Godaigo seamounts: twins of the Emperor Chain by multi-beam sonarSee Entry 116078
- Dynamic compression of diopside and salite to 200 GPaSee Entry 116080
- Nd-Sr systematics of the Setouchi volcanic rocks, southwest Japan: a clue to the origin of orogenic andesiteSee Entry 116085
- Rb-Sr, Sm-Nd, K-Ca, O, and H isotopic study of Cretaceous-Tertiary boundary sediments, Caravaca, Spain: evidence for an oceanic impact siteSee Entry 116086
- Possible origin of K-rich volcanic rocks from Virunga, East Africa, by metasomatism of continental crustal material: Pb, Nd and Sr isotopic evidenceSee Entry 116087
- An approach to ICP analysis of geological samplesSee Entry 116288
- Silica standardization: a discriminant technique applied to a volcanic arc systemSee Entry 116289
- Quantitative determination of Al_2O_3 content in bauxite drill holes by neutron activation logSee Entry 116297
- From qualitative to quantitative magnetic anisotropy analysis: the prospect of finite strain calibrationSee Entry 116312
- A second-order correlation approximation for thermal conductivity and Prandtl number of free turbulenceSee Entry 116461

91.40 VOLCANOLOGY

- 116055** Relation of summit deformation to East Rift Zone eruptions on Kilauea volcano, Hawaii. D.Epp (Hawaii Inst. of Geophys., Univ. of Hawaii, Honolulu, HI, USA), R.W.Decker, A.T.Okamura. *Geophys. Res. Lett. (USA)*, vol.10, no.7, p.493-6 (July 1983). An inverse relationship exists between the summit deflation of Kilauea, as recorded by summit tilt, and the elevation of associated eruptive vents on the East Rift Zone. This relationship implies that East Rift eruptions drain the summit magma reservoir to pressure levels that are dependent on the elevation of the eruptive vents. (11 refs.)
- 116056** The Long Valley/Mono Basin volcanic complex in eastern California: status of present knowledge and future research needs. J.F.Hernance (Dept. of Geological Sci., Brown Univ., Providence, RI, USA). *Rev. Geophys. & Space Phys. (USA)*, vol.21, no.7, p.1545-65 (Aug. 1983). The Long Valley-Mono Basin volcanic complex in eastern California is a major silicic system which is considered to be still potentially active. The complex is associated with a well developed convective hydrothermal system and with hot spring activity at the surface. Recent earthquakes and tectonic deformation, and the reactivation of fumaroles, indicate that a potential volcanic hazard exists for the southwest segment of Long Valley caldera. The author recommends a programme of drilling to 2-3 km depth, coupled with surface field studies, to understand the nature of the inferred high-temperature hydrothermal reservoir and how it is linked to a possible magma body at depth. (69 refs.)
- 116057** ^{14}C age of volcanic ash flow at Danan Island Somma of Krakatau Volcano, Indonesia. T.Yokoyama (Dept. of Earth Sci., Doshisha Univ., Kyoto, Japan), O.Yamada, S.Nishimura. *Sci. & Eng. Rev. Doshisha Univ. (Japan)*, vol.24, no.1, p.78-82 (May 1983). In Japanese.
- The radiocarbon age of the wood sample, obtained from the outcrop of ash flow at Danan Island, Krakatau Volcano was measured. This volcano locates between Sumatra and Jawa Islands, Indonesia, and is very famous for the most disastrous eruption in 1983. Obtained ^{14}C age is 190 ± 25 B.P. This age indicates the Early Caldera Stage or the Second Stage. It was clarified that the actual activity of Krakatau Volcano is very young. (8 refs.)
- 116058** The Mesozoic magmatism of the Aldan shield as an indicator of its tectonic regime. E.P.Maksimov (Central Combined Specialized Thematic Expedition, Yakutsk, USSR). *Sov. Geol. & Geophys. (USA)*, vol.23, no.5, p.9-14 (1982). Translation of: *Geol. & Geofiz. (USSR)*, vol.23, no.5, p.11-18 (1982).
- The Mesozoic association of potassic-alkalic basites is extensively developed on the Aldan shield of the Siberian platform. The arched-block structure of the region and the antitropic direction of the magmatic process indicate a rift-forming regime of its tectonic development during the Mesozoic. Moreover the alkalic magmatism is linked through subalkalic monzonite-syenites within a single lateral series to calcic-alkalic granitoid magmatism. The lateral zonality, which also extends to the Stanovoi orogenic region, results from the formation of a Benioff zone during the Late Jurassic and Early Cretaceous. (16 refs.)
- Ninigi and Godaigo seamounts: twins of the Emperor Chain by multi-beam sonarSee Entry 116078
- Nd-Sr systematics of the Setouchi volcanic rocks, southwest Japan: a clue to the origin of orogenic andesiteSee Entry 116085
- Possible origin of K-rich volcanic rocks from Virunga, East Africa, by metasomatism of continental crustal material: Pb, Nd and Sr isotopic evidenceSee Entry 116087
- Origin of Espanola Island and the age of terrestrial life on the Galapagos IslandsSee Entry 116088
- Silica standardization: a discriminant technique applied to a volcanic arc systemSee Entry 116289

91.45 PHYSICS OF PLATE TECTONICS

- 116059** The underthrusting movement of the Western Pacific Plate and the deep focus earthquake zone or northeast China. Zhang Li-Min (Inst. of Geophys., Acad. Sinica, China), Tang Xiao-Ming. *Acta Geophys. Sin. (China)*, vol.26, no.4, p.331-40 (July 1983). In Chinese. English translation in: *Acta Geophys. Sin. (USA)*
- In the Huichuen region of northeast China, there is a deep focus earthquake zone, the depth of which reaches as deep as 600 km. As seen from the projection of the focal profile, it is the result of underthrusting of the Western Pacific Plate. The angle of the thrusting plate with the horizontal is about 26° . The authors set up a plate underthrusting model to calculate the temperature distribution within the thrusting plate at various depths, taking the thermal conduction between the mantle material and the lithospheric plate into account. The calculation shows that the plate reaches the Huichuen region, at the depth of 600 km the temperature at its center is about $1200^\circ C$, which is much lower than that of the mantle around it. So it is possible to form elastic fractures and thus generate deep earthquakes. The focal mechanism solutions of earthquakes in this region are discussed. (7 refs.)

116060 Isostatic adjustments in a full glacial sea. J.England (Dept. Geography, Univ. of Alberta, Edmonton, Canada). *Can. J. Earth Sci. (Canada)*, vol.20, no.6, p.895-917 (1983).

During the last glaciation an ice-free corridor existed between the northeast Ellesmere Island and northwest Greenland ice sheets. This corridor constituted a peripheral depression in which the marine limit marks the uppermost extent of a full glacial sea. Relative sea-level curves from the full glacial sea confirm previous morphostratigraphic and glaciostatic evidence for limited ice extent during the last glaciation. These curves also document the history of glacial unloading and the form of the relative sea-level curve that one would theoretically expect in the peripheral depression. These relative sea-level curves are discussed in relation to other paleoclimatic changes and the deglacial history of northwest Greenland. (64 refs.)

116061 The Snake Range decollement: an exhumed mid-Tertiary ductile-brittle transition. E.L.Miller, P.B.Gans, J.Garing (Dept. of Geology, Stanford Univ., Stanford, CA, USA). *Tectonics (USA)*, vol.2, no.3, p.239-63 (June 1983).

Focuses on the age, three-dimensional extent, and tectonic significance of the northern Snake Range decollement in east-central Nevada. (58 refs.)

116062 Paleogene evolution of the Kodiak Islands, Alaska: consequences of ridge-trench interaction in a more southerly latitude. J.C.Moore (Center for Coastal Marine Studies, Univ. of California, Santa Cruz, CA, USA), T.Byrne, P.W.Plumley, M.Reid, H.Gibbons, R.S.Coe. *Tectonics (USA)*, vol.2, no.3, p.265-93 (June 1983).

Outlines a geological and paleomagnetic case for the interaction of a spreading center with a subduction zone bordering one of the displaced terranes of southern Alaska. An accretionary complex bordering southern Alaska landward of the modern Aleutian Trench is investigated. The structural geology, petrology, geochemistry and paleomagnetism of igneous and sedimentary rocks formed prior, during and after the Paleocene igneous activity in the Kodiak Islands has been investigated. (111 refs.)

116063 Tectonic stresses in the lithosphere. L.Fleitout, C.Froidevaux (Lab. de Geophys. et Geodynamique Interne, Univ. Paris-Sud, Orsay, France). *Tectonics (USA)*, vol.2, no.3, p.315-24 (June 1983).

Analyzes the effect of both boundary and internal forces on the lithospheric stress pattern and shows that both contributions are of comparable magnitude. The presence of internal sources makes the problem three-dimensional. However, it can be reduced to a two-dimensional plane stress formulation, where the edge forces are expressed by the 'non-hydrostatic stresses' and the basal shear is increased by the addition of a term proportional to the gradient of the mean vertical stress. (32 refs.)

116064 Fault slip beyond a barrier on a transform plate boundary. M.Bonafede, E.Boschi, M.Dragoni (Dipartimento di Fisica, Univ. di Bologna, Bologna, Italy). *Geophys. J. R. Astron. Soc. (GB)*, vol.75, no.1, p.143-53 (Oct. 1983).

A strike-slip plate boundary is considered with nonuniform strength. Depth-dependent slip on the fault is assumed to occur aseismically in the lower fault section, in response to a basal shear stress, and seismically in the brittle upper section. The upper fault section acts as a friction decreases in the proximity of the Earth's surface, brittle fracture may occur beyond the barrier. It is found that, when friction in the uppermost fault section exceeds the applied shear stress, fault slip occurs there with a smaller amplitude than at larger depth. This may explain the discrepancies, which have been sometimes reported, between fault offsets observed at the Earth's surface and fault offsets inferred from seismograms by using simpler dislocation models. (44 refs.)

116065 Thermoelastic bending of the lithosphere: implications for basin subsidence. B.G.Bills (Jet Propulsion Lab., California Inst. of Technol., Pasadena, CA, USA). *Geophys. J. R. Astron. Soc. (GB)*, vol.75, no.1, p.169-200 (Oct. 1983).

Thermoelastic stresses are capable of producing significant lithospheric deflection. A systematic approach to modelling this effect is presented, in which the lithosphere is presumed to behave as a thin, elastic (or viscoelastic) plate on a fluid substrate, and lateral variations in basal heat flow induce both vertical buoyant loads and thermoelastic bending moments. The amount of uplift or subsidence produced by a given heat source depends on a number of factors, including the strength, duration and lateral extent of the thermal anomaly, and the thickness, density, rigidity and viscosity of the plate. The mechanical response of the plate is characterized by two distinct length scales (one for shearing, the other for bending) and the deformation produced depends critically on the scaled width of the heat source. The plate acts as a low pass spatial filter in response to thermal loads, but has a narrow band pass filter response to applied moments. The temporal response to an abrupt change in basal temperature or heat flow also depends on the ratio of the thermal diffusion time for the plate versus the viscoelastic relaxation time of the material. (71 refs.)

116066 Tectonics of ridge-transform intersections at the Kane fracture zone. J.A.Karson, H.J.B.Dick (Dept. Geology & Geophys., Woods Hole Oceanographic Instn., Woods Hole, MA, USA). *Mar. Geophys. Res. (Netherlands)*, vol.6, no.1, p.51-98 (1983).

The Kane Transform offsets spreading-center segments of the Mid-Atlantic Ridge by about 150 km at $24^\circ N$ latitude. In terms of its first-order morphological, geological, and geophysical characteristics it appears to be typical of long-offset (>100 km), slow-slipping (2 cm yr^{-1}) ridge-ridge transform faults. High-resolution geological observations were made from deep-towed ANGUS photographs and the manned submersible ALVIN at the ridge-transform intersections and indicate similar relationships in these two regions. These data indicate that over a distance of about 20 km as the spreading axes approach the fracture zone, the two flanks of each ridge axis behave in very different ways. These are discussed. (78 refs.)

116067 Changing stress field in the middle segment of the Tan-Lu fault zone, eastern China. Lu Huaifu, Yu Hongnian, Ding Youwen, Zhang Qinglong (Dept. of Geology, Nanjing Univ., Nanjing, China). *Tectonophysics (Netherlands)*, vol.98, no.3-4, p.253-70 (1983).

The Tan-Lu active fault zone is an important tectonic boundary in east China. Minor structures associated with the fault show that the nature of displacement on the middle segment of the fault zone has changed in consecutive episodes since the Cretaceous: normal faulting during the Cretaceous, sinistral strike-slip and reverse faulting at the end of the Cretaceous or in the early Tertiary, and dextral strike-slip and reverse faulting from the late Tertiary to the present. The regional orientation of the maximum principal compressive stress, based upon the statistical study of minor shear fracture orientation, is 6° , $S52^\circ W$ in the late Tertiary to Quaternary. This stress field may be related to the collision between India and Tibet and the microspreading of the Japan Sea.

116068 Continental uplift, compensation and shunting during trench-spreading center collision. P.E.Damon (Dept. of Geosci., Univ. of Arizona, Tucson, AZ, USA).

Tectonophysics (Netherlands), vol.99, no.1, p.T1-8 (1983).

A model for continental uplift at a convergent margin (Damon, 1979) is further developed. The model assumes the necessity of isostatic compensation of the subducted lithospheric plate. It predicts a continental declivity that reaches its maximum uplift and extent at the time of trench-spreading center collision. As a result of the passage of the subducted plate eastward the region of maximum uplift increases and migrates eastward behind the eastward migrating declivity. The 'gang plank' from the Front Range to the Mississippi River is the most obvious modern expression of the continental declivity whereas the Great Basin is an expression of the area of maximum uplift lowered somewhat by extension and crustal thinning. Compensation takes place by transfer of asthenosphere to the base of continental lithosphere.

116069 The reliability of asymmetric c-axis fabrics of quartz to determine sense of vorticity. C.W.Passchier (Dept. of Geology, Univ. Coll. of Swansea, Swansea, Wales).

Tectonophysics (Netherlands), vol.99, no.1, p.T9-18 (1983).

Asymmetric c-axis fabrics of quartz are convergent margin (Damon, 1979) is further developed. The model assumes the necessity of isostatic compensation of the subducted lithospheric plate. It predicts a continental declivity that reaches its maximum uplift and extent at the time of trench-spreading center collision. As a result of the passage of the subducted plate eastward the region of maximum uplift increases and migrates eastward behind the eastward migrating declivity. The 'gang plank' from the Front Range to the Mississippi River is the most obvious modern expression of the continental declivity whereas the Great Basin is an expression of the area of maximum uplift lowered somewhat by extension and crustal thinning. Compensation takes place by transfer of asthenosphere to the base of continental lithosphere.

116070 Oceans, continents and orogens. J.H.Brunn (Univ. of Paris, Paris, France).

Tectonophysics (Netherlands), vol.99, no.1, p.1-29 (1983).

The processes related to subduction and mountain building are discussed, and some new models and notions are proposed. At all known epochs, the Earth's surface comprised essentially migrating plates and large belts where the lithosphere is mobilised, so that subductions and crustal resorption occur in complex structural patterns. Through time, these orogens start as island arcs and evolve into folded ranges. The formation and location of island-arc belts is shown to be related to the obliquity between rifts and continental margins. It is suggested that the energy output (heat flow) varies with the pressure exerted by the top (elastic) lithosphere upon the underlying mantle. A compression tends to be established between the inner flow and tectonic stress, as the latter brings about pressure variations through uplift-subsidence couples. These may therefore be related to the generation of paired metamorphic belts.

116071 Analogue models of folds above a wrench fault. F.Odonne, P.Vialon (Inst. de Recherches Interdisciplinaires de Geologie et de Mecanique, Domaine Univ. de Grenoble, France).

Tectonophysics (Netherlands), vol.99, no.1, p.31-46 (1983).

Describes the experimental deformation of models made with sheets of parafin wax simulating a bedded cover resting on a basement wrench fault. During the experiments, 'en echelon' folds appear in the cover. As a result of early fault motion, folds first appear at heterogeneities in the bedding and with axes at about 45° to the trace of the wrench fault. Further fault displacement causes a bulk rotation of fold axes towards parallelism with the basement wrench fault, and a resulting curvature of fold axes at larger fault displacement. Folding affects an area which tends to quickly stabilize in width, since folding weakens the sheared cover and subsequent deformation is concentrated in it. Axial surfaces of folds are initially upright, then tend to become inclined with an external vergence, forming a fan centered on the basement wrench fault. Deeper layer-deformation, close to the basement, involves fold reorientations that are greater than in the upper layers.

116072 Characteristics of distributions of thermal stress and stress due to phase change in the descending plate beneath Island Arc. K.Goto, H.Hamaguchi (Geophysical Inst., Tohoku Univ., Ibaraki, Japan).

Zisin. J. Seismol. Soc. Jpn. (Japan), vol.36, no.1, p.31-41 (March 1983). In Japanese. [received: Sept. 1983]

Studies on double-planed intermediate seismic zones beneath some island arcs reveal that the earthquakes have two different types of focal mechanism solutions: down-dip compression and down-dip extension. This feature is important for studies of the stress distribution in the descending plate, and several stress sources are proposed. The authors calculate the distributions of thermal stress and the stress due to the olivine-spinel phase change in the descending plate. (33 refs.)

Metallogeny and Tectonics of the North American Cordillera GAC/MAC/CGU Symposium See Entry 111299

Movements of the fracture zone and the seismic activity under the fracture zone—based on the observations at Abuyama See Entry 115999

Palaeomagnetism of Palaeozoic rocks from the Cabo de Penas, Asturias, Spain See Entry 116004

Palaeomagnetism of NW Scotland syenites in relation to local and regional tectonics See Entry 116005

Palaeomagnetic evaluation of the orocline hypothesis in the Central and Southern Appalachians See Entry 116009

The seismology of Greece See Entry 116033

Focal distribution of earthquakes in relation to major geological tectonic lines in Shikoku, Japan See Entry 116037

Study of Iwasaki earthquake swarm in Aomori Prefecture. II. Seismic activity and crustal movement See Entry 116038

Some features of the evolution of the shelf zones of the globe during Mesozoic-Cenozoic time See Entry 116045

On the relation between the deep subsurface structure of the Baikal and Red Sea rifts and the lateral movements of lithospheric plates See Entry 116046

The dynamic Earth See Entry 116047

The Earth's mantle See Entry 116049

The oceanic crust See Entry 116050

The continental crust See Entry 116051

Cataclastic rocks of the San Gabriel fault—an expression of deformation at deeper crustal levels in the San Andreas fault zone See Entry 116053

Geochronological and structural study of Tertiary and Quaternary dikes in southern France and Sardinia: an example of the utilization of dike swarms as palaeostress indicators See Entry 116054

The Long Valley/Mono Basin volcanic complex in eastern California: status of present knowledge and future research needs See Entry 116056

The Mesozoic magmatism of the Aldan shield as an indicator of its tectonic regime See Entry 116058

Ninigi and Godaigo seamounts: twins of the Emperor Chain by multi-beam sonar See Entry 116078

91.50 MARINE GEOLOGY AND GEOPHYSICS

116073 ²²⁶Ra and ²²²Rn contents of Galapagos Rift hydrothermal waters—the importance of low-temperature interactions with crustal rocks. J.Dymond, R.Cobler, L.Gordon (School of Oceanography, Oregon State Univ., Corvallis, OR, USA), P.Biscaye, G.Mathieu.

Earth & Planet. Sci. Lett. (Netherlands), vol.64, no.3, p.417-29 (Sept. 1983). Hydrothermal waters collected by 'Alvin' from the Galapagos Spreading Center are enriched in ²²²Rn by factors of 50-200 over bottom waters. The ²²⁶Ra in the same samples, however, is enriched by less than a factor of four over bottom waters. Enrichments of ²²²Rn result primarily from α-recoil from rock surfaces while ²²⁶Ra enrichments are dominantly produced by high-temperature alteration of cooling ridge volcanics. The data extrapolate to bottom water temperatures and compositions, demonstrating the importance of seawater mixing. The ²²²Rn/²²⁶Ra value appears to be a sensitive indicator of low-temperature crustal interaction. (19 refs.)

116074 Intense hydrothermal activity at the axis of the East Pacific Rise near 13°N: submersible witnesses the growth of sulfide chimney. R.Hekinian (Centre Océanologique de Bretagne, Brest, France), J.Francheteau, V.Renard, R.D.Ballard, P.Choukroune, J.L.Cheminee, F.Albarede, J.F.Minster, J.L.Charlou, J.C.Marty, J.Bouleuge.

Mar. Geophys. Res. (Netherlands), vol.6, no.1, p.1-14 (1983).

A submersible study of the East Pacific Rise near 12°5'N led to the discovery of intense hydrothermal activity. Twenty four sites with active vents and sixty inactive hydrothermal deposits were found within a narrow graben averaging about 300 m in width along a 20 km long segment of the ridge crest. From both deep towed camera stations and manned submersible observations, the average spacing between the ridge axis hydrothermal deposits is discussed. Detailed investigations of one active site enabled the authors to witness the growth of an active chimney. The hydrothermal deposits found on both the ridge axis and on the seamount are similar in composition. Chemical studies conducted on the venting fluids showed the concentration of the dissolved major metal ions (Fe, Mn, and Zn). (23 refs.)

116075 New data on the structure of Ampere Seamount. V.M.Litvin, V.V.Matveyenko, E.L.Onishchenko, M.V.Rudenko, A.M.Sagalevich (Shirshov Inst. of Oceanology, Acad. of Sci., Moscow, USSR).

Oceanology (USA), vol.22, no.1, p.62-4 (1982). Translation of: *Okeanologiya (USSR)*, vol.22, no.1 (1982). [received: Aug. 1983]

The Ampere Seamount was studied with the aid of the Pisces manned submersible craft and the Zvuk-4m towed device. The seamount consists of volcanic rocks, including trachytes. The latter outcrop in the form of narrow, linear ridges. On the summit of the seamount, there are conglomerates dissected by deep scours, and cavernous limestones. (8 refs.)

116076 Geologic mapping of the summit of Afanasiy Nikitin Seamount from the Zvuk-4 towed submersible. N.A.Rimskiy-Korsakov, A.A.Shreyder (Shirshov Inst. of Oceanology, Acad. of Sci., Moscow, USSR).

Oceanology (USA), vol.22, no.4, p.489-92 (1982). Translation of: *Okeanologiya (USSR)*, vol.22, no.4 (1982). [received: Aug. 1983]

The Zvuk-4 towed submersible, carrying a bilateral side-scanning sonar (SSS), a precision echo sounder, an acoustic profiler (AP), and a photographic system was used in a geologic and morphological survey of the summit of the Afanasiy Nikitin Seamount on the twenty-fifth cruise of the R/V Dmitriy Mendeleev in the Indian Ocean. The authors identify and map three types of seafloor. Layered sand, solid rock lightly covered with a sandy material, and solid rock devoid of sediment. The photographic survey, the visual examination of the bottom, and the taking of samples in the area under study using the Pisces manned submersible suggest that the solid rock is limestone covered with manganese crusts. (1 ref.)

116077 The benthic boundary layer and sediment transport. A.R.M.Nowell (School of Oceanography, Univ. of Washington, Seattle, WA, USA).

Rev. Geophys. & Space Phys. (USA), vol.21, no.5, p.1181-92 (June 1983). Recent research by US workers into the dynamics and sedimentation processes of the BBL are reviewed. The viscous sublayer and logarithmic layer are described. The similarity variables which are used to scale the flow are reviewed. The effects of internal waves and the structure of the mixed layer are covered in this review. Both laboratory experiments and sediment transport models are also described. (137 refs.)

116078 Ninigi and Godaigo seamounts: twins of the Emperor Chain by multi-beam sonar. N.C.Smoot (US Naval Oceanographic Office, NSTL Station, MS, USA).

Tectonophysics (Netherlands), vol.98, no.3-4, p.T1-5 (1983).

Bathymetry is shown for two heretofore unknown seamounts in the Emperor Chain: Ninigi and Godaigo seamounts. They were discovered by the US Naval Oceanographic Office and named by the author. Very accurate bathymetry and positioning allows a clarification of previous mid-chain bathymetric charts and an explanation of hot spot multiple conduit flow.

Hydrocarbons in water, sediment and mussels from the southern Baltic Sea See Entry 115704

Magnetic anomalies on and around the Bonin Rise See Entry 116018

Some features of the evolution of the shelf zones of the globe during Mesozoic-Cenozoic time See Entry 116045

The oceanic crust See Entry 116050

The incidence of internal waves onto a thin submerged barrier See Entry 116096

Experimental studies of low-frequency waterborne and sediment-borne acoustic wave propagation on a continental shelf See Entry 116101

Paleoceanography: global ocean evolution See Entry 116145

The ocean See Entry 116150

Evaluation of the climatic zonality of the Indian Ocean during Pliocene time from deep-sea drilling data See Entry 116268

Chemical and isotopic study of extraterrestrial particles from the ocean floor See Entry 116554

91.60 PHYSICAL PROPERTIES OF ROCKS AND MINERALS

116079 Stress corrosion and acoustic emission during tensile crack propagation in Whin Sill dolerite and other basic rocks. P.G.Meredith, B.K.Atkinson (Geology Dept., Imperial Coll. of Sci. & Technol., London, England).

Geophys. J. R. Astron. Soc. (GB), vol.75, no.1, p.1-21 (Oct. 1983).

Double torsion tests in ambient air and liquid water have been used to establish critical stress intensity factors (K_{Ic}) and stress intensity factor (K_I)-crack velocity (v) diagrams for propagation of single tensile cracks in Whin Sill

dolerite and Ralston Intrusive. K_{Ic} for Whin Sill dolerite was $3.28 \text{ MN m}^{-3/2}$ and for Ralston Intrusive was $2.58 \text{ MN m}^{-3/2}$. No stress corrosion limit was encountered. Acoustic response was monitored during experiments on Whin Sill dolerite which spanned a velocity range from 5×10^{-4} to $5 \times 10^{-9} \text{ m s}^{-1}$. The rate of acoustic emission was an indirect measure of crack velocity. The slopes of K_{Ic} diagrams and K_{Ic} -acoustic emission rate diagrams had similar slopes of c. 30 in double logarithmic coordinate frames. The activation enthalpy for dolerite between 20° and 75°C was determined. A discussion is given of these results in terms of their implications for earthquake mechanisms. (38 refs.)

116080 Dynamic compression of diopside and salite to 200 GPa. B.Svendsen, T.J.Ahrens (Seismological Lab., California Inst. of Technol., Pasadena, CA, USA).

Geophys. Res. Lett. (USA), vol.10, no.7, p.501-4 (July 1983). New Hugoniot data on single crystal diopside, $\text{CaMgSi}_2\text{O}_6$ (Di), suggest that transformation to a high-pressure thermomechanical state begins at ~50 GPa and is complete above 100 GPa, in agreement with other pyroxenes and silicates of geophysical interest. Comparison of the new high pressure phase (HPP) data for Di and salite, $\text{CaMg}_{0.82}\text{Fe}_{0.18}\text{Si}_2\text{O}_6$ (Sa) with appropriate mixed oxide and perovskite models implies compatibility between either model and the data. Conversely, least-squares fits to the HPP Di data favour lower ($3.6\text{--}3.9 \text{ Mg/m}^3$) values of zero-pressure, room-temperature density than the models ($4.0\text{--}4.1 \text{ Mg/m}^3$). This may represent the influence of multiple transition processes (e.g. polymorphism and Fe^{2+} high-low spin) as a function of Fe content across the Di-Hd series. The new HPP Sa data closely parallel ($\approx 0.1 \text{ Mg/m}^3$ less dense) the lower mantle density profile from ~90 GPa to 136 GPa. The results are consistent with the speculations of Jeanloz and Ahrens on the possibility of significant Ca in the lower mantle. (41 refs.)

116081 Evidence for correlation of ultrasonic attenuation and fluid permeability in very low porosity water-saturated rocks. J.G.Berryman, B.P.Bonner, R.C.Y.Chin (Lawrence Livermore Nat. Lab., Livermore, CA, USA).

Geophys. Res. Lett. (USA), vol.10, no.7, p.595-8 (July 1983). The measured amplitude A of ultrasonic pulses in intact and fractured samples of water-saturated gabbro and granite is observed to decrease as the permeability κ increases according to the proportionality $A \propto \kappa^{-1/2}$. This relation is predicted by Biot's theory of elastic waves in fluid-saturated porous media and, therefore, suggests that Biot's attenuation mechanism may play a significant role in low porosity materials at ultrasonic frequencies. The evidence is not conclusive. The limited data set studied is also consistent with correlations of the form $A \propto \kappa^{-\epsilon}$ where $0.2 < \epsilon < 0.6$. Nevertheless, the observed correlations may still provide a means for monitoring changes in permeability of low-porosity underground repositories of radioactive waste. (10 refs.)

116082 Influence of the type of thermodynamic approximation on the description of the dynamic compressibility of multicomponent media. S.V.Bobrovskii, V.M.Gogolev, V.P.Lozhkina.

J. Appl. Mech. & Tech. Phys. (USA), vol.23, no.6, p.811-16 (Nov.-Dec. 1982). Translation of: *Zh. Prikl. Mekh. & Tekh. Fiz. (USSR)*, vol.23, no.6, p.83-7 (Nov.-Dec. 1982). [received: Sept. 1983]

The authors consider the degree of disparity between the limiting approximations in shock compressions and isentropic stress relief and they investigate the conditions under which they yield either close or sharply different mechanical parameters of the state of the medium. The solution of these problems will provide a basis for considering the application of a particular thermodynamic approximation to various practical problems involving multicomponent soils. (7 refs.)

116083 Compression, nonstoichiometry and bulk viscosity of wüstite. R.Jeanloz (Dept. of Geology & Geophys., Univ. of California, Berkeley, CA, USA), R.M.Hazen.

Nature (GB), vol.304, no.5927, p.620-2 (18 Aug. 1983). Wüstite (Fe_{1-x}O) is a complex oxide that is invariably non-stoichiometric ($0.04 \leq x \leq 0.12$). Point defects associated with this nonstoichiometry are clustered and result in a modulated crystal structure that has been extensively studied, but is not well understood. Many of the properties of these compounds, such as chemical diffusivity, electrical conductivity and magnetic transitions seem to be significantly affected by the nonstoichiometry and resulting ordering of defects. The authors summarise new and existing data on the elasticity of wüstite; these data indicate virtually no correlation between the bulk modulus and stoichiometry. There appears, however, to be a systematic difference between static and dynamic measurements. This behaviour suggests the presence of a frequency dependence to the bulk modulus that can be ascribed formally to a finite bulk viscosity of Fe_{1-x}O . (30 refs.)

116084 Dynamic processes during slip of stick-slip as an earthquake fault model. M.Ohnaka (Earthquake Res. Inst., Univ. of Tokyo, Tokyo, Japan), K.Yamamoto, Y.Kuwahara, T.Hirasawa.

Zisin. J. Seismol. Soc. Jpn. (Japan), vol.36, no.1, p.53-62 (March 1983). In Japanese. [received: Sept. 1983]

Dynamic strain and displacement during stick-slip in Tsukuba granite have been measured at different locations in the neighborhood of a fault, and typical strain and displacement records are presented. A local stress concentration resulting in strain change is observed near the fault prior to the onset of foreship, and this premonitory strain change and the onset of foreship, often accompanied by foreshocks, propagate slowly along the fault. If this occurs along natural faults, it can be a promising premonitory effect for earthquake prediction. (15 refs.)

Interference film microscopy for metal phase identification ...See Entry 111763

Palaeomagnetism of late Precambrian-Cambrian volcanics and intrusives from the Armorican Massif, FranceSee Entry 116006

A combined analysis of the gravitational and magnetic anomalies for the detection of magnetically active rock complexes in the basement of the West Siberian plateSee Entry 116015

Scaling of rupture size. II. On time and space distributions and magnitude-frequency distribution of swarmSee Entry 116036

A model of thermal conduction in the Earth's crust in the Okhotomorskii regionSee Entry 116052

The reliability of asymmetric c-axis fabrics of quartz to determine sense of vorticitySee Entry 116069

Characteristics of distributions of thermal stress and stress due to phase change in the descending plate beneath Island ArcSee Entry 116072

An approach to ICP analysis of geological samplesSee Entry 116288

From qualitative to quantitative magnetic anisotropy analysis: the prospect of finite strain calibrationSee Entry 116312

91.65 GEOPHYSICAL ASPECTS OF GEOLOGY, MINERALOGY AND PETROLOGY

116085 Nd-Sr systematics of the Setouchi volcanic rocks, southwest Japan: a clue to the origin of orogenic andesite. K.Ishizaka, R.W.Carlson (Dept. of Terrestrial Magnetism, Carnegie Instn. of Washington, Washington, DC, USA).

Earth & Planet. Sci. Lett. (Netherlands), vol.64, no.3, p.327-40 (Sept. 1983). Twenty-three volcanic rocks from the Setouchi volcanic belt, southwest Japan, were analyzed for Nd and Sr isotopic compositions for the purpose of examining the genetic relationships among the basalt, high-magnesium andesite and evolved porphyritic andesite. The andesites have higher $^{87}\text{Sr}/^{86}\text{Sr}$ and lower $^{143}\text{Nd}/^{144}\text{Nd}$ than the basalts. This result confirms earlier conclusions that the andesites cannot be fractionation products of basaltic magma but that the andesitic and basaltic magmas were generated independently. On the basis of melting experiments it is inferred that there is an isotopically stratified mantle beneath southwest Japan. (41 refs.)

116086 Rb-Sr, Sm-Nd, K-Ca, O, and H isotopic study of Cretaceous-Tertiary boundary sediments, Caravaca, Spain: evidence for an oceanic impact site. D.J.DePaolo, F.T.Kyte, B.D.Marshall (Dept. of Earth & Space Sci., Univ. of California, Los Angeles, CA, USA), J.R.O'Neil, J.Smit.

Earth & Planet. Sci. Lett. (Netherlands), vol.64, no.3, p.356-73 (Sept. 1983). Isotopic ratios and trace element abundances were measured on samples of Ir-enriched clay at the Cretaceous-Tertiary boundary, and in carbonate and marl from 5 cm below and 3 cm above the boundary. The data indicate that most of the clay material was derived from a terrestrial source with relatively low $^{87}\text{Sr}/^{86}\text{Sr}$ and high $^{143}\text{Nd}/^{144}\text{Nd}$ ratios. The isotopic evidence for foreign terrestrial detritus in the boundary clay, the low rare earth element concentrations and high Ni concentration support the hypothesis of a terminal Cretaceous asteroidal impact that produced a global layer of fallout. The data are most easily explained if the impact site was on oceanic crust, and if a substantial fraction of the fallout was derived from relatively deep within the lithosphere (>3 km). (60 refs.)

116087 Possible origin of K-rich volcanic rocks from Virunga, East Africa, by metasomatism of continental crustal material: Pb, Nd and Sr isotopic evidence. R.Vollmer, M.J.Norry (Dept. of Earth Sci., Leeds Univ., Leeds, England).

Earth & Planet. Sci. Lett. (Netherlands), vol.64, no.3, p.374-86 (Sept. 1983). The isotopic compositions of Sr, Nd and Pb together with the abundances of Rb, Sr, U and Pb have been determined for mafic and felsic potassic alkaline rocks from the young Virunga volcanic field in the western branch of the East African rift system. Excellent correlations of $^{87}\text{Sr}/^{86}\text{Sr}$ with Rb/Sr, 1/Sr and $^{207}\text{Pb}/^{206}\text{Pb}$ for Sabinyo rocks suggest these to be members of a hybrid magma series. However, the nearly uniform Pb compositions for this series points to radiogenic growth of ^{87}Sr in the magma source region following an event which homogenized the isotopic compositions but not Rb/Sr. The Rb-Sr age derived from the erupted Sabinyo isochron-mixing line is consistent with the ~500 Myr Pb-Pb age from Nyiragongo. (35 refs.)

116088 Origin of Espanola Island and the age of terrestrial life on the Galapagos Islands. M.L.Hall.

Science (USA), vol.221, no.4610, p.545-7 (5 Aug. 1983). Geological studies of Espanola (Hood) Island, Galapagos, Ecuador, indicate that the island had a subaerial rather than a submarine origin. Because the younger lava flows are dated at 3 million years. Espanola has apparently existed as an island for at least that long. Thus terrestrial life may have existed or arrived on the Galapagos Islands at least 3 million years ago, more than twice as long as had been assumed. (25 refs.)

More light on the U clanSee Entry 112321

An episode of steep geomagnetic inclination 120000 years agoSee Entry 116014

A combined analysis of the gravitational and magnetic anomalies for the detection of magnetically active rock complexes in the basement of the West Siberian plateSee Entry 116015

Focal distribution of earthquakes in relation to major geological tectonic lines in Shikoku, JapanSee Entry 116037

Apatite fission-track dating of erosion in the eastern Andes, BoliviaSee Entry 116042

The Mesozoic magmatism of the Aldan shield as an indicator of its tectonic regimeSee Entry 116058

The reliability of asymmetric c-axis fabrics of quartz to determine sense of vorticitySee Entry 116069

Characteristics of distributions of thermal stress and stress due to phase change in the descending plate beneath Island ArcSee Entry 116072

Evidence for correlation of ultrasonic attenuation and fluid permeability in very low porosity water-saturated rocksSee Entry 116081

Indonesia's Asahan hydro project. IISee Entry 116157

An approach to ICP analysis of geological samplesSee Entry 116288

Silica standardization: a discriminant technique applied to a volcanic arc systemSee Entry 116289

Classification capability and resolving power of the method of transients in searches for kimberlitesSee Entry 116310

91.90 OTHER TOPICS IN SOLID EARTH GEOPHYSICS

116089 The Vredefort dome in South Africa. Crater of a gigantic meteorite or a terrestrial gas explosion?. W.Schreyer (Inst. fur Mineralogie, Ruhr-Univ., Bochum, Germany).

Naturwissenschaften (Germany), vol.70, no.8, p.388-95 (Aug. 1983). In German.

A meteorite impact origin of the Vredefort structure is in conflict with the results of recent geological, petrological, and fluid-inclusion studies. They indicate that the shock event was preceded by domal uplift and static thermal metamorphism within the dome rising to temperatures above 900°C in the central region now exposed. Here heating has also continued after the shock and caused strong annealing recrystallization and nearly complete obliteration of the shock features in the former lower crustal granulites. High-density CO_2 fluid inclusions are still aligned along shock-induced planar elements in quartz despite complete post-shock recrystallization of this mineral. Fluid pressures of 2-4 kbar at the time of trapping, that is shortly after the shock catastrophe, are not compatible with a near-surface cause of the shock by meteorite impact but may point to a deep-seated gas explosion that occurred as one episodic event during the long-term tectonic and thermal evolution of the dome. However, difficulties still exist to explain the high intensity of the

shock and its pervasive character through internal terrestrial mechanisms. (45 refs.)

Apatite fission-track dating of erosion in the eastern Andes, Bolivia See Entry 116042

Rb-Sr, Sm-Nd, K-Ca, O, and H isotopic study of Cretaceous-Tertiary boundary sediments, Caravaca, Spain: evidence for an oceanic impact site See Entry 116086

Paleoceanography: global ocean evolution See Entry 116145

Image resolution in microwave radiometry See Entry 116280

Microwave radiometric features of vegetated surfaces See Entry 116281

92.00 HYDROSPHERIC AND ATMOSPHERIC GEOPHYSICS

(for marine geology and geophysics, see 91.50)

92.10 PHYSICS OF THE OCEANS

(see also 43.30 Underwater sound)

116090 Wind dependence of underwater ambient noise. B.R.Kerman (Boundary Layer Res. Div., Atmospheric Environment Service, Downsview, Ontario, Canada), D.L.Evans, D.R.Watts, D.Halpern. *Boundary-Layer Meteorol. (Netherlands)*, vol.26, no.2, p.105-13 (June 1983). Sound generated underwater by wind waves displays two sensitivities to wind speed depending on whether the waves are breaking. A historical review is presented of several experimental studies over the years, as well as new results obtained at a relatively quiet, deep equatorial Pacific site. The duration of the experiment, the multiple high frequency bands as well as the desirable acoustic attributes of the site are useful in establishing the wind sensitivity, and its variability. The results are compared to a recent theoretical model of sound generation by oscillating bubbles in breaking waves. (19 refs.)

116091 The role of sea surface temperature in large-scale air-sea interactions. S.J.S.Khalsa (Cooperative Inst. for Res. in Environmental Sci., Univ. of Colorado, Boulder, CO, USA). *Mon. Weather Rev. (USA)*, vol.11, no.5, p.954-66 (May 1983).

Data from the 1972-73 El Nino event are used to study relationships between sea surface temperature (SST), surface wind, surface heat fluxes and rainfall in the tropical Pacific east of the dateline. It is found that the maximum in SST anomaly is not correlated spatially or temporally in any consistent manner with the sum of latent and sensible heat fluxes ($Q_E + Q_S$) or rainfall as estimated from highly reflective cloud. Varying anomalies in wind speed and sea-air temperature and humidity differences all influence the $Q_E + Q_S$ anomaly in ways which may be unrelated to the SST anomaly. Implications to modeling efforts which equate SST anomalies with diabatic heating anomalies are discussed. (36 refs.)

116092 ^{224}Ra , ^{228}Ra , and ^{226}Ra in Winyah Bay and Delaware Bay. R.J.Elsinger, W.S.Moore (Geology Dept., Univ. of South Carolina, Columbia, SC, USA).

Earth & Planet. Sci. Lett. (Netherlands), vol.64, no.3, p.430-6 (Sept. 1983). The first ^{224}Ra ($t_{1/2}=3.64$ days) measurements from mixing zones of estuarine systems are presented for the Pee Dee River-Winyah Bay and Delaware Bay estuaries. High-resolution gamma-ray spectrometry was used to determine ^{224}Ra , ^{228}Ra ($t_{1/2}=5.7$ years), and ^{226}Ra ($t_{1/2}=1622$ years) activity ratios. In Delaware Bay ^{224}Ra concentrations were nearly constant over the 2.5% to 15% salinity range where two turbidity maximum zones are located. Samples collected on the ebb and flood tide from a salt marsh along Delaware Bay have a 5-fold increase in ^{224}Ra from flood to ebb and 3- and 2-fold increases for ^{228}Ra and ^{226}Ra respectively. (15 refs.)

116093 Reduction of thermohaline circulation during deglaciation: the effect on atmospheric radiocarbon and CO_2 . R.S.Keir (Scripps Instn. of Oceanography, Univ. of California, La Jolla, CA, USA).

Earth & Planet. Sci. Lett. (Netherlands), vol.64, no.3, p.445-56 (Sept. 1983). A two-box ocean reservoir model is employed to examine the combined effects of vertical ocean circulation, organic matter extraction and cosmic ray production on the $^{14}\text{C}/^{12}\text{C}$ in the atmosphere, ocean and sediment ratio. If the vertical ocean circulation decreased by 50% during the maximum rate of deglaciation, the atmospheric $^{14}\text{C}/^{12}\text{C}$ would have increased concurrently by 10% relative to the pre-bomb present. Further, if cosmic ray production of ^{14}C was 50% greater than at present at about 7800 years BP, a double maximum of 10% occurs. This result is similar to the variation of $^{14}\text{C}/^{12}\text{C}$ over the last 10000 years calculated from ^{14}C dates on the varved Lake of the Clouds. (37 refs.)

116094 An observation of the surface circulation in a Gulf Stream frontal perturbation. F.M.Vukovich, G.A.Maul (Research Triangle Inst., Res. Triangle Park, NC, USA).

Geophys. Res. Lett. (USA), vol.10, no.7, p.591-4 (July 1983). In the period of 3-16 June 1979, a satellite-tracked, free-drifting buoy passed through a Gulf Stream frontal perturbation and was entrained into a warm filament on the shoreward side of the perturbation. Significant speed convergence noted as the buoy passed through the perturbation and approached the counterclockwise turn into the warm filament, the buoy drifted to the southwest at speeds of about 0.1 to 0.3 m/sec. Eventually, the buoy drifted out of the filament and went westward in an apparent response to wind-induced surface drift. (17 refs.)

116095 Barotropic instability of weakly non-parallel zonal flows. L.-O.Merkine (Dept. of Math., Technion-Israel Inst. of Technol., Haifa, Israel), R.Balgovind.

Geophys. & Astrophys. Fluid Dyn. (GB), vol.25, no.3, p.157-90 (1983). The barotropic instability of weakly non-parallel zonal flows with localized intense shear regions is investigated numerically. The numerical integrations of the linear stability problem reveal the existence of unstable localized wave packets whose spatial structure and eigenfrequencies depend on two parameters which measure the degree of supercriticality and the zonal length-scale of the shear region. The structure of the instability is determined by conditions that ensure the decay of the wave packet at infinity and the transition from long to short waves across a turning point (critical layer) region which is controlled by non-parallel effects. (20 refs.)

116096 The incidence of internal waves onto a thin submerged barrier. L.F.Clovis, H.G.Pinsent (Math. Dept., Chelsea Coll., London Univ., London, England).

Geophys. & Astrophys. Fluid Dyn. (GB), vol.25, no.3, p.191-212 (1983). The problem of oblique incidence of internal ocean waves on a thin submerged ocean barrier is considered when the ocean has exponential density

stratification. A Wiener-Hopf approach is used combined with numerical evaluation of series. Results for the reflected energy are obtained and reveal a complex dependence on incidence and barrier height. Application of this model to waves incident on the Mid-Atlantic Ridge suggests that the ridge almost isolates first mode energy on one side of the ocean from the other side. In certain circumstances there is a surprising appearance of 'barrier' waves. These waves are closely confined to the barrier and propagate along it. (5 refs.)

116097 Contour dynamics method in the model problems on the ocean topographical cyclogenesis. V.F.Kozlov.

Izv. Akad. Nauk SSSR Fiz. Atmos. & Okeana, vol.19, no.8, p.845-54 (Aug. 1983). In Russian. English translation in: *Izv. Acad. Sci. USSR Atmos. & Oceanic Phys. (USA)*

The contour dynamics method presented by Zabusky et al. (1979) is extended to the problems on cyclogenesis in rapidly rotating homogeneous fluid flows above an uneven bottom. The calculation algorithm involves the spline approximation of the contour parametric equations and the systematic rearrangement of the markers for their uniform distribution. Examples are presented. (8 refs.)

116098 Stability of wind waves at weak wind. K.D.Ruvinskii, G.I.Freidman.

Izv. Akad. Nauk SSSR Fiz. Atmos. & Okeana, vol.19, no.8, p.855-9 (Aug. 1983). In Russian. English translation in: *Izv. Acad. Sci. USSR Atmos. & Oceanic Phys. (USA)*

The stability of stationary waves excited by a weak wind is considered assuming that their amplitude is restricted by capillary-gravity waves (ripples). It is shown that account of the dispersion of nonlinear damping can lead to the instability of stationary wind waves in that region of parameters where they are stable disregarding the decrement dispersion (threshold wave number is in this region). (7 refs.)

116099 Vertical structure of currents and hydrological elements in central region of the Red Sea. V.M.Kushnir, Yu.N.Koltakov, S.Yu.Zakharov.

Izv. Akad. Nauk SSSR Fiz. Atmos. & Okeana, vol.19, no.8, p.860-7 (Aug. 1983). In Russian. English translation in: *Izv. Acad. Sci. USSR Atmos. & Oceanic Phys. (USA)*

Studies results of experimental researches on the vertical structure of currents, sound velocity, temperature, salinity and density carried out with the help of current velocity profiler and CTD-probe. It is found that maxima in spectra of vertical wave numbers with wavelengths equal to 20-25 m are conditioned by gravitation-inertial waves with the frequency differing by 6-7% from inertial one. It is shown that speed drops in gravitation-inertial waves can be a cause of local hydrodynamic instability. (15 refs.)

116100 The space-time structure of internal inertia-gravity and topographical waves in the sea with frequency close to the inertial one. A.S.Blatov, V.A.Ivanov.

Izv. Akad. Nauk SSSR Fiz. Atmos. & Okeana, vol.19, no.8, p.868-77 (Aug. 1983). In Russian. English translation in: *Izv. Acad. Sci. USSR Atmos. & Oceanic Phys. (USA)*

Spectral space-time analysis of current and hydrological data shows the existence in the inertial frequency band of different wave motions at the same density stratification: inertial-gravity and topographic waves. These waves are distinguished in space structure and origin. Wave parameters obtained are in good agreement to theory. (20 refs.)

116101 Experimental studies of low-frequency waterborne and sediment-borne acoustic wave propagation on a continental shelf. T.M.Brocher, B.T.Iwatake, D.A.Lindwall (Hawaii Inst. of Geophys., Univ. of Hawaii, Honolulu, HI, USA).

J. Acoust. Soc. Am. (USA), vol.74, no.3, p.960-72 (Sept. 1983).

The loss rates for propagation of 5- to 40-Hz acoustic normal modes recorded on a shallow, sandy bottom off Nova Scotia were found to be strongly dependent on the azimuth and range of propagation. Beyond a certain range the propagation loss rates for signals just below the nominal cutoff frequency (calculated assuming a range-independent acoustic medium) differed only insignificantly from those just above the nominal cutoff, suggesting that propagation of signals at long ranges below cutoff may not be less efficient than those slightly above cutoff. Although it is commonly thought that scattering, conversion to shear waves, and surface wave generation are important causes of acoustic wave attenuation at low frequencies, our data indicate that nearly all loss arises from sediment attenuation. These results are of general interest because the near seafloor geology of many continental shelves is similar. The authors are less certain of the reasons for the lack of success in modeling the observed propagation loss using the parabolic approximation for frequencies well above the cutoff frequency. They do know that the spatial variation of the sound velocity, density, and thickness of the water column was not measured in sufficient detail during the experiment. More reasonable fits to the observed propagation loss at lower frequencies suggest that the parabolic approximation was not the major source of modeling error. (34 refs.)

116102 Investigation of chemical sound absorption in seawater. IV. R.H.Mellen, D.G.Browning (Naval Underwater Systems Center, New London, CT, USA), V.P.Simmons.

J. Acoust. Soc. Am. (USA), vol.74, no.3, p.987-93 (Sept. 1983).

For pt.III see *ibid.*, vol.70, p.143 (1981). The low-frequency boric acid relaxation mechanism in seawater has been identified as an acid-base exchange between the $\text{B}(\text{OH})_3/\text{B}(\text{OH})_4^-$ and $\text{HCO}_3^-/\text{CO}_3^{2-}$ equilibria. Ion pairing with Ca^{2+} is also involved and a coupled-system model is proposed. Supporting experimental data for the CO_2 exchange mechanism are presented. Similar exchanges with ammonia and silicic acid are also investigated. (9 refs.)

116103 On equatorial dynamics, mixed layer physics and sea surface temperature. P.S.Schopf (Goddard Lab. for Atmospheric Sci., NASA/Goddard Space Flight Center, Greenbelt, MD, USA), M.A.Cane.

J. Phys. Oceanogr. (USA), vol.13, no.6, p.917-35 (June 1983).

Describes a new numerical model designed to study the interactions between hydrodynamics and thermodynamics in the upper ocean. The model incorporates both primitive equation dynamics and a parameterization of mixed layer physics. There is a consistent treatment of mixed layer structure for all physical processes. In order to study interplay between dynamics and mixed layer physics in the equatorial ocean, the authors carry out a series of numerical experiments with simple patterns of wind stress and surface heating. In some cases stratification and/or mixed layer physics are suppressed. (30 refs.)

116104 On equatorial waves and El Nino. I. Influence of initial states on wave-induced currents and warming. P.S.Schopf (Goddard Lab. for Atmospheric Sci., NASA/Goddard Space Flight Center, Greenbelt, MD, USA), D.E.Harrison.

J. Phys. Oceanogr. (USA), vol.13, no.6, p.936-48 (June 1983).

Presents results from three numerical model experiments designed to study the thermal and hydrodynamical changes associated with downwelling Kelvin wave passage and east coastal reflection along and near the equator. The

model employs primitive equation dynamics in two active layers and a full thermodynamics equation, so that sea surface temperature, thermocline displacement and sea level are each independently predicted. Wind and thermal forcing are used. The surface layer is a slab mixed layer using Kraus and Turner-style bulk physics. Kelvin waves are excited by introducing a westerly wind anomaly in the western part of the basin, and the temperature and current changes caused by the waves are studied as the wave fronts propagate through the circulation forced by three different mean wind fields: no mean winds, southerly mean winds and easterly mean winds. (16 refs.)

116105 Internal wave wake of a moving storm. I. Scales, energy budget and observations. J.F.Price (Woods Hole Oceanographic Inst., Woods Hole, MA, USA).

J. Phys. Oceanogr. (USA), vol.13, no.6, p.949-65 (June 1983).

The ocean's baroclinic response to a steadily moving storm is analyzed using a numerical model for an inviscid, multi-layered fluid. The author gives detailed account of the response to a rapidly moving hurricane. A central theme is the coupling between wind-forcing, the surface mixed layer, and the thermocline. The baroclinic response is made up of a geostrophic component and a three-dimensional wake of inertial-internal waves which is emphasized. These waves initially have large horizontal spatial scales set directly by the storm. An important qualitative result is that the vertical penetration scale is large compared to the thermocline thickness. Measurements made by buoy EB-10 in the wake of Hurricane-Eloise provide a semi-quantitative check on the model results. (38 refs.)

116106 A statistical model of vertical shear from Moored current meters. D.Rubenstein, F.Newman (Sci. Applications Inc., McLean, VA, USA), W.Grabowski.

J. Phys. Oceanogr. (USA), vol.13, no.6, p.966-71 (June 1983).

Derives a statistical model of shear to predict how measurements of mean-square shear vary with stratification and with vertical separation Δz between moored current meters. The model is based on a simplified version of the vertical wavenumber-shear spectrum proposed by Garrett et al. (1981). The authors compare the model predictions with shear derived from current meter measurements in the seasonal thermocline, from the MILE-1 mooring. The comparison is favorable and provides one with a framework for evaluating the vertical length scales of shear from current meter time series. (9 refs.)

116107 Radiating barotropic instability. L.D.Talley (School of Oceanography, Oregon State Univ., Corvallis, OR, USA).

J. Phys. Oceanogr. (USA), vol.13, no.6, p.972-87 (June 1983).

The linear stability of zonal, parallel shear flow on a beta-plane is discussed. While the localized shear region supports unstable waves, the far-field can support Rossby waves because of the ambient potential-vorticity gradient. An infinite zonal flow with a continuous cross-stream velocity gradient is approximated with segments of uniform flow, joined together by segments of uniform potential vorticity. This simplification allows an exact dispersion relation to be found. There are two classes of linearly unstable solutions. One type is trapped to the source of energy and has large growth rates. The second type is weaker instabilities which excite Rossby waves in the far-field: the influence of these weaker instabilities extends far beyond that of the most unstable waves. (19 refs.)

116108 A multi-limit mixed-layer entrainment formulation. J.W.Deardorff (Dept. of Atmospheric Sci., Oregon State Univ., Corvallis, OR, USA).

J. Phys. Oceanogr. (USA), vol.13, no.6, p.988-1002 (June 1983).

The second-moment equations for buoyancy flux and density-fluctuation variance in the entrainment zone of a mixed layer are combined to yield an entrainment rate (w_e) dependence having the nature of Turner's relation (1973). That is, $w_e q^{-1}$ is seen as a function solely of an interfacial Richardson number (Ri_i) involving q , where q^2 is twice the interfacial turbulence kinetic energy (TKE). The TKE equation in the entrainment layer is then utilized to evaluate Ri_i so that w_e can be obtained. This procedure allows the TKE equation to be solved past the point at which the interfacial-shear bulk Richardson number, Ri_b , becomes critical, and into the more unstable regime beyond where the experiment of Ellison and Turner (1959) can give guidance. The present entrainment results are shown as a function of the various Richardson numbers: Ri_i , Ri_b based on the friction velocity, and Ri_s based on the convective velocity scale, for values of each ranging from near zero to 1000. Comparison is made with previous results. (73 refs.)

116109 The generation and propagation of sea level variability along the Pacific coast of Mexico. D.B.Enfield, J.S.Allen (School of Oceanography, Oregon State Univ., Corvallis, OR, USA).

J. Phys. Oceanogr. (USA), vol.13, no.6, p.1012-33 (June 1983).

Case history analysis, cross spectra and multiple regression analysis are used in a study of low-pass filtered sea level records from the Pacific mainland coast of Mexico in 1971 and 1973-5. The authors focus on several aspects of the variability of Mexico that are complementary to the study of Christensen et al. (1983): (1) examination of individual, large amplitude events; (2) documentation of how the propagating variability is generated; (3) frequency domain analysis of the sea level fluctuations; and (4) consideration of the seasonality of the propagating variability and its forcing. Following a summary of the data used, the occurrence of tropical storms and their relation to individual sea level events are discussed and the statistical evidence for forcing is presented. The observed characteristics of alongshore propagation are then examined through spectral analytical techniques and compared with those expected from history. (35 refs.)

116110 The mean and seasonal circulation off southwest Nova Scotia. P.C.Smith (Atlantic Oceanographic Lab., Bedford Inst. of Oceanography, Dartmouth, Nova Scotia, Canada).

J. Phys. Oceanogr. (USA), vol.13, no.6, p.1034-54 (June 1983).

Long-term measurements off southwest Nova Scotia and the mean circulation are discussed. The gyre circulation appears permanent but the coastal current and upwelling exhibit annual variations of the same order as the means. Strong seasonal cycles are found in the salinity and density fields at Cape Sable which appear to be controlled both by buoyancy input from the coastal current and local mixing effects. A linear diagnostic model indicates that the primary dynamical balance for the circulation is between a longshore pressure gradient and longshore mean density and stratification gradients which have summer maxima. The 'centrifugal upwelling' hypothesis fails and the main driving force for Cape Sable upwelling appears to be the longshore density variations maintained by tidal mixing. (31 refs.)

116111 Blocking of steady circulation by coastal geometry. U.Unluata, T.Oguz, E.Ozsoy (Inst. of Marine Sci., Middle East Tech. Univ., Icel, Turkey).

J. Phys. Oceanogr. (USA), vol.13, no.6, p.1055-62 (June 1983).

Along the southern Turkish continental shelf the intensity of the observed mean flow has a considerable degree of variability. The relatively strong currents along the straight portion of the coast is reduced significantly in the nearshore region upon encountering irregularities in the form of bays and headlands. As a possible explanation of such blockage by coastal irregularities, a linear, homogeneous, wind-stress free model is presented incorporating

the constraints of topographic steering and linear bottom friction. Solutions are given for an idealized case of an abrupt indentation on a straight coast adjoining a linearly deepening shelf. The directional preference of blocking and the applicability of boundary layer approximations are discussed. Numerical solutions are obtained for the realistic bathymetry and coastal configuration along the southern Turkish continental shelf. The concepts developed are applied to the observed blocking features. (15 refs.)

116112 Formation of eddies and transverse currents in a two-layer channel of variable bottom with application to the lower St. Lawrence estuary. Heung-Jae Lie (Korea Advanced Inst. of Sci. & Technol., Seoul, Korea), M.El-Sabbh.

J. Phys. Oceanogr. (USA), vol.13, no.6, p.1063-75 (June 1983).

Baroclinic shelf waves and Kelvin waves in a two-layer channel of variable bottom are discussed using a simple numerical model. Two different propagation directions are shown to be possible, analogous to the existence of shelf waves and trench waves in an ocean bounded by a coast with a trench, described by Mysak et al. (1979). The eigenfunctions of baroclinic shelf wave modes are quite different from the barotropic eigenfunctions: that is, each of the baroclinic modes shows a pattern similar to the first mode with the exception of small scale structures near the coast. The model also shows the formation of a series of eddies with alternating rotation senses accompanied by transverse currents between two successive eddies. (27 refs.)

116113 Low-pass filters to suppress inertial and tidal frequencies. R.O.R.Y.Thompson (Div. of Oceanography, CSIRO Marine Labs., Hobart, Australia).

J. Phys. Oceanogr. (USA), vol.13, no.6, p.1077-83 (June 1983).

A systematic way is given to design digital filters which allow clear separation of signals with periods of a few days from noise of higher frequency, particularly tidal and inertial. Several examples are given which pass little high-frequency power and none at the principal tidal frequencies. The Lanczos-cosine filter passes too much energy near diurnal frequencies, the Godin filter is better but not optimal. A longer filter is recommended, with flat low-frequency response, a sharp cut-off and very low noise. For current meter records containing inertial motions, it appears desirable to design a filter which specifically suppresses the local inertial frequency. (6 refs.)

116114 Water waves, nonlinear Schrodinger equations and their solutions. D.H.Peregrine (School of Maths., Univ. of Bristol, Bristol, England).

J. Aust. Math. Soc. Ser. B (Australia), vol.25, pt.1, p.16-43 (July 1983).

Equations governing modulations of weakly nonlinear water waves are described. The modulations are coupled with wave-induced mean flows except in the case of water deeper than the modulation length scale. Equations suitable for water depths of the order the modulation length scale are deduced from those derived by Davey and Stewartson (1974) and Dysthe (1979). A number of cases in which these equations reduce to a one-dimensional nonlinear Schrodinger (NLS) equation are enumerated. Several analytical solutions of NLS equations are presented, with discussion of some of their implications for describing the propagation of water waves. Some of the solutions have not been presented in detail, or in convenient form before. One is new, a 'rational' solution describing an 'amplitude peak' which is isolated in spacetime. (24 refs.)

116115 Scattering analysis and synthesis of wave trains. R.J.Sobey (Dept. of Civil & Systems Engng., James Cook Univ., Townsville, Queensland, Australia), E.J.Colman.

J. Aust. Math. Soc. Ser. B (Australia), vol.25, pt.1, p.44-63 (July 1983).

The Zakharov-Shabat scattering transform is an exact solution technique for the nonlinear Schrodinger equation, which describes the time evolution of weakly nonlinear wave trains. Envelope soliton and uniform wave train solutions of the nonlinear Schrodinger equation are separable in scattering transform space. The scattering transform is a potential analysis and synthesis technique for natural wave trains. Discrete versions of the direct and inverse scattering transform are presented, together with proven algorithms for their numerical computation from typical ocean wave records. The consequences of discrete resolution are considered. (19 refs.)

116116 The generation of surface waves by an intense cyclone. F.Viera, V.T.Buchwald (School of Maths., Univ. of New South Wales, Kensington, NSW, Australia).

J. Aust. Math. Soc. Ser. B (Australia), vol.25, pt.1, p.64-83 (July 1983).

Assuming a travelling oscillating pressure source model, this paper sets out to investigate the observation of surface gravity waves generated by a cyclone moving with constant speed v . It is shown that when the source frequency is near the critical resonant value $g/4v$, large amplitude waves may be generated. There is some agreement with observations of waves from cyclone Pam of February, 1974. (7 refs.)

116117 Surface-wave interaction with a deeply submerged circular duct. J.W.Miles (Univ. of California, La Jolla, CA, USA).

J. Aust. Math. Soc. Ser. B (Australia), vol.25, pt.1, p.84-93 (July 1983).

The interaction of a surface wave of angular frequency ω with a deeply submerged, vertical, open-mouthed, circular duct of radius a is considered. The resulting boundary-value problem is solved by the Wiener-Hopf technique. The pressure-amplification factor (the ratio of the complex amplitude of the pressure in the depths of the duct to that of the incident wave in the plane of the mouth) is determined in closed form as a function of the dimensionless wave number $K = \omega a/g$. (6 refs.)

116118 Interaction of internal waves in a continuous thermocline model. N.T.Hung, S.A.Maslowe (Dept. of Maths., McGill Univ., Montreal, Quebec, Canada).

J. Aust. Math. Soc. Ser. B (Australia), vol.25, pt.1, p.94-109 (July 1983).

Weak nonlinear interactions are studied for systems of internal waves when the Brunt-Vaisala frequency is proportional to $\text{sech}^2 z$, where $z=0$ is the centre of the thermocline. Explicit results expressed in terms of gamma functions have been obtained for the interaction coefficients appearing in the amplitude evolution equations. The cases considered include resonant triads as well as second and third harmonic resonance. In the non-resonant situation, the Stokes frequency correction due to finite-amplitude effects have been computed and the extension to wave packets is outlined. Finally, the effect of a mean shear on resonant interactions is discussed. (17 refs.)

116119 The anti-cyclonic shear wave: a new geophysical wave. R.L.Hughes (Australian Numerical Meteorology Res. Center, Melbourne, Victoria, Australia).

J. Aust. Math. Soc. Ser. B (Australia), vol.25, pt.1, p.110-26 (July 1983).

A new type of first baroclinic mode wave which propagates on an anti-cyclonic vorticity field is identified. It is of the vorticity class of waves which contains Rossby waves amongst others. This anti-cyclonic shear wave is produced by pressure variations distorting the vertical stratification in such a manner that the associated vortex stretching generates the velocity variation required for Bernoulli compatibility with the initial pressure variation. The wave travels at a speed characteristic of particles within the undisturbed shear flow and is a low frequency and low wavenumber wave. In the present study

this wave is considered in the presence of a weak anti-cyclonic shear. (6 refs.)

116120 The baroclinic instability of the large-scale ocean circulation. A.V.Frolov (Hydrometeorological Center, Moscow, USSR). *Oceanology (USA)*, vol.22, no.1, p.1-5 (1982). Translation of: *Okeanologiya (USSR)*, vol.22, no.1 (1982). [received: Aug. 1983]
The problem of the baroclinic instability of large-scale currents in the main ocean thermocline is considered. The necessary conditions for the amplification of small synoptic perturbations are presented. The stability of the subtropical anticyclonic gyres (beyond the western boundary layer), described in terms of particular solutions of the nonlinear equations for the 'advective' thermocline, is examined in detail. (7 refs.)

116121 Theory of the equatorial undercurrent. D.D.Mallik (Univ. of Calcutta, Calcutta, India). *Oceanology (USA)*, vol.22, no.1, p.6-10 (1982). Translation of: *Okeanologiya (USSR)*, vol.22, no.1 (1982). [received: Aug. 1983]
An analytic model of the equatorial undercurrent is presented. The calculated maximum velocity was $127 \text{ cm} \cdot \text{sec}^{-1}$ at a depth of 86 meters. These values, and also features of the temperature field such as the eastward rise of the isotherms and the depression of the thermocline at the equator, are in good agreement with observations. (5 refs.)

116122 Evolution of synoptic disturbances deduced from measurements in the north-central Atlantic. V.I.Byshev, Yu.A.Ivanov, V.G.Kort (Shirshov Inst. of Oceanology, Acad. of Sci., Moscow, USSR). *Oceanology (USA)*, vol.22, no.1, p.11-14 (1982). Translation of: *Okeanologiya (USSR)*, vol.22, no.1 (1982). [received: Aug. 1983]
The evolution of synoptic disturbances in the ocean is examined on the basis of measurements made southwest of the Azores. The synoptic disturbances observed are shown to propagate toward the west-southwest and to dissipate quite rapidly. The hydrodynamic instability of topographic eddies may be the reason for the high energy of the synoptic disturbances. (3 refs.)

116123 The seasonal variability of the Lomonosov Current. V.A.Bubnov (Shirshov Inst. of Oceanology, Acad. of Sci., Kaliningrad, USSR). *Oceanology (USA)*, vol.22, no.1, p.15-18 (1982). Translation of: *Okeanologiya (USSR)*, vol.22, no.1 (1982). [received: Aug. 1983]
The response of the ocean to the seasonally varying winds is analyzed on the basis of data gathered in an equatorial study area during FGGE in 1979. It is shown that the strengthening of the southeasterly trade wind from spring to summer in the northern hemisphere induces a significant increase of the zonal pressure gradient along the equator, which in turn intensifies the flow in the Lomonosov current. This suggests that on a seasonal time scale, the ocean in the equatorial region is in dynamic quasi-equilibrium with the controlling trade winds. (7 refs.)

116124 Estimation of the small-scale turbulence level from its empirical dependence on the Richardson number. V.D.Pozdynin (Shirshov Inst. of Oceanology, Acad. of Sci., Moscow, USSR). *Oceanology (USA)*, vol.22, no.1, p.19-22 (1982). Translation of: *Okeanologiya (USSR)*, vol.22, no.1 (1982). [received: Aug. 1983]
Analyzes the empirical dependence of the r.m.s. turbulence level on the Richardson number, derived from simultaneous measurements of small-scale fluctuations of current velocity, its vertical gradients and the vertical water density gradients. An algorithm for computing the distribution of the r.m.s. turbulence level-Richardson number relation in the equatorial current system of the Central Pacific is suggested. (11 refs.)

116125 Isotropy of inertial and semi-diurnal tidal motions in the ocean. N.N.Golenko (Shirshov Inst. of Oceanology, Acad. of Sci., Kaliningrad, USSR). *Oceanology (USA)*, vol.22, no.1, p.23-8 (1982). Translation of: *Okeanologiya (USSR)*, vol.22, no.1 (1982). [received: Aug. 1983]
The spatial structure of the horizontal components of the velocity of the semi-diurnal tidal and inertial oscillations is investigated by analysis of their mean statistical hodographs. The semi-diurnal tidal oscillations in the POLY-GON-70 and TROPX-74 areas are anisotropic, with a prevailing south-to-north propagation. The anisotropy of the semi-diurnal tidal oscillations in the POLYMODE area is less pronounced, but exhibits two or more probable directions. The inertial oscillations turned out to be isotropic in all regions examined. (8 refs.)

116126 An investigation of low-frequency short-wave motions in the ocean. V.M.Kamenkovich, T.B.Tsybaveva (Shirshov Inst. of Oceanology, Acad. of Sci., Moscow, USSR). *Oceanology (USA)*, vol.22, no.4, p.391-5 (1982). Translation of: *Okeanologiya (USSR)*, vol.22, no.4 (1982). [received: Aug. 1983]
Presents an analysis of the eigenmotions of a stratified fluid layer of constant depth on a rotating sphere, assuming a complete rather than an approximate equation for the Coriolis force. A general asymptotic method is proposed for surface short-wave motions. Local dispersion relations are constructed for surface gravity and internal waves. The applicability of the Ω -plane approximation for description of these waves is demonstrated. The effect of the horizontal component of the Earth's angular rotation rate is investigated. (4 refs.)

116127 Statistical estimates of the Antarctic circumpolar current in the Pacific Ocean. A.M.Gritsenko (Shirshov Inst. of Oceanology, Acad. of Sci., Moscow, USSR). *Oceanology (USA)*, vol.22, no.4, p.409-12 (1982). Translation of: *Okeanologiya (USSR)*, vol.22, no.4 (1982). [received: Aug. 1983]
A two-dimensional empirical probability function was used in a statistical study of the mean multiyear circulation of the Antarctic circumpolar current. In order to study the variability of this current with depth, the circulation at standard depths is correlated with that of the surface. It is concluded that there is no continuous westward flow at depth. (5 refs.)

116128 Mediterranean water in the central Atlantic. Ye.A.Plakhin, V.G.Smirnov (Shirshov Inst. of Oceanology, Acad. of Sci., Moscow, USSR). *Oceanology (USA)*, vol.22, no.4, p.417-19 (1982). Translation of: *Okeanologiya (USSR)*, vol.22, no.4 (1982). [received: Aug. 1983]
Thermohalinity probe measurements of the Mediterranean water along its path of propagation to the central Atlantic area analyzed, and its stability parameters are calculated. The authors find practically untransformed Mediterranean water in the central Atlantic, a finding which has been confirmed by more recent measurements. (6 refs.)

116129 The near-surface dynamics of coastal upwelling. K.H.Brink (Woods Hole Oceanographic Inst., Woods Hole, MA, USA). *Prog. Oceanogr. (GB)*, vol.12, no.3, p.223-57 (1983).
An attempt is made to examine some observational and theoretical aspects of upper ocean dynamics in regions of strong coastal upwelling. 'Upper ocean' is roughly defined as about the upper 10-30 m of water column for most systems. First, the basic surface Ekman and mixed layers are discussed, including some of the modifications due to upwelling. Next, coastal upwelling fronts and their associated circulation are treated. Finally, areas of strongly

three-dimensional upwelling are classified and discussed. Horizontal advection of heat and momentum appear to be generally important for the near-surface dynamics of coastal upwelling, and these phenomena make realistic theoretical treatments especially difficult. (66 refs.)

116130 Coastal upwelling in the California Current system. A.Huyer (School of Oceanography, Oregon State Univ., Corvallis, OR, USA). *Prog. Oceanogr. (GB)*, vol.12, no.3, p.259-84 (1983).
Coastal upwelling in the California Current system has been the subject of large scale studies off California and Baja California, and of small scale studies off Oregon. Recent studies of the winds along the entire coast from 25°N to 50°N indicate that there are significant alongshore variations in the strength of coastal upwelling, which are reflected in the observed temperature distribution. Active upwelling appears to be restricted to a narrow coastal band (about 10-25 km wide) along the entire coast, but the region influenced by coastal upwelling may be much wider. Intensive observations of the upwelling zone during summer off Oregon show the presence of a southward coastal jet at the surface, a mean vertical shear, a poleward undercurrent along the bottom, and persistently sloping isopycnals over the continental shelf; most of the upwelling there occurs during relatively short periods (several days long) of upwelling-favorable winds. (79 refs.)

116131 The physical environment of the Peruvian upwelling system. K.H.Brink (Woods Hole Oceanographic Inst., Woods Hole, MA, USA), D.Halpern, A.Huyer, R.L.Smith. *Prog. Oceanogr. (GB)*, vol.12, no.3, p.285-305 (1983).
Four important phenomena are discussed: wind-driven upwelling, the poleward undercurrent, surface mixed layer deepening, and low-frequency coastal-trapped waves. The coastal winds were invariably favorable for coastal upwelling, even during the 1976 El Nino. The agreement between the offshore transport in the relatively shallow (30 m) surface layer and the Ekman transport, deduced from the local wind, was good for both the mean and variable state. The agreement with the deeper onshore transport was less good, consistent with the marked three-dimensionality and spatial variability of the upwelling. (35 refs.)

116132 The upwelling area off Northwest Africa—a description of phenomena related to coastal upwelling. E.Mittelstaedt (Deutsches Hydrographisches Inst., Hamburg, Germany). *Prog. Oceanogr. (GB)*, vol.12, no.3, p.307-31 (1983).
Presents a brief review of the oceanography along the upwelling coast of Northwest Africa. The description contains information on: seasonal variations of large-scale winds, ocean circulation and some gross features of the hydrography, characteristic meso-scale patterns of currents during the upwelling season between 16°N and 26°N , air- and water-temperature differences during upwelling season, diurnal and semi-diurnal variations of temperature, atmospheric pressure, wind and current, regional peculiarities: canyons and the Banc d'Arguin. (65 refs.)

116133 The Benguela upwelling area. G.Nelson, L.Hutchings (Sea Fisheries Res. Inst., Cape Town, S Africa). *Prog. Oceanogr. (GB)*, vol.12, no.3, p.333-56 (1983).
The authors provide a description of the coastal upwelling occurring in the South Atlantic off the South African coast. In particular the authors describe the macroscale features of the Benguela system, the meteorology of the area and finally they provide a review of mesoscale upwelling processes. (58 refs.)

116134 Monsoon response of the Somali Current and associated upwelling. F.Schott (Rosenstiel School of Marine & Atmospheric Sci., Univ. of Miami, Miami, FL, USA). *Prog. Oceanogr. (GB)*, vol.12, no.3, p.357-81 (1983).
The Somali Current typically develops in different phases in response to the onset of the summer monsoon. Each of these phases exists quasistationary for some time ranging from weeks to months. There periods of rather constant circulation patterns are separated by periods of rapid transition. The authors provide a detailed description of these development phases. (39 refs.)

116135 An overview of the physical oceanography report. A.Leetmaa (Atlantic Oceanographic & Meteorological Labs., NOAA, Miami, FL, USA). *Rev. Geophys. & Space Phys. (USA)*, vol.21, no.5, p.1105-7 (June 1983).
To a great extent, this US physical oceanographic report to IUGG (1978-1982) focuses on advances made in large-scale oceanography. Reviews are presented for the areas of equatorial oceanography, subtropical gyre studies, polar oceanography, mid-latitude variability and oceanic heat flux. The last topic is a common thread that runs through all of the reviews since there is the realization that the ocean is an essential element in determining the climate of the Earth. (no refs.)

116136 Mid-latitude mesoscale variability. W.J.Schmitz, Jr. (Woods Hole Oceanographic Inst., Woods Hole, MA, USA), W.R.Holland, J.F.Price. *Rev. Geophys. & Space Phys. (USA)*, vol.21, no.5, p.1109-19 (June 1983).
Mesoscale ocean circulation phenomena are reviewed. Over the last few years, a promising zero-order description and rationalisation of the mesoscale field has become available. That is, eddy energy is largest near strong flows (intensification not only in western boundary currents, but along their mid-latitude open-ocean extension), roughly as indicated by gyre-scale numerical models where eddies develop as a result of instability processes in the mid-latitude jet and recirculation regimes, and then propagate into the ocean interior. The authors' point of view is that mesoscale eddies drive recirculations but do not play a crucial role in the dynamics of the mean flow in the ocean interior. In addition, the fluctuating response to forcing by variable winds may now be widely perceived as forming the horizontally homogeneous background signal in subtropical gyres. The time-dependent field associated with thermohaline flows at abyssal depths also has a special character. (134 refs.)

116137 Subsurface subtropical gyre of the North Atlantic and Pacific oceans. H.Stommel (Dept. of Phys. Oceanography, Woods Hole Oceanographic Inst., Woods Hole, MA, USA). *Rev. Geophys. & Space Phys. (USA)*, vol.21, no.5, p.1119-23 (June 1983).
In this review attention is restricted to studies of the structure of subtropical gyres (i) in the North Atlantic and Pacific, (ii) between the bottom of the mixed layer and about 1500 metres depth, (iii) between 15°N and 35°N , (iv) in the open ocean eastward of the Gulf Stream and Kuroshio Current and high-energy eddy regions. Work published since 1978 or later by American workers is reviewed. (69 refs.)

116138 Polar oceanography. A.L.Gordon (Lamont-Doherty Geological Obs., Columbia Univ., Palisades, NY, USA). *Rev. Geophys. & Space Phys. (USA)*, vol.21, no.5, p.1124-31 (June 1983).
Oceanographic progress pertaining to polar waters for the 1979-82 period is briefly presented within three research areas: Southern Ocean; Arctic; and ocean-ice interaction, after a discussion of general review articles and atlases. A conclusion is added which presents the author's view of future research direction in a general sense. Emphasis is placed on published US work, though key non US publications are included. The bibliography contains articles not cited in the text. This article is not meant to be a complete synthesis of research, but rather to provide a list of publications with an

associated narrative of the recent US polar oceanographic research. (122 refs.)

116139 Poleward heat transport by the ocean. K.Bryan (Geophys. Fluid Dynamics Lab., NOAA, Princeton, NJ, USA). *Rev. Geophys. & Space Phys. (USA)*, vol.21, no.5, p.1131-7 (June 1983). Reviews poleward heat transport and its relation to the thermohaline circulation of the World Ocean. A perceived need for a better understanding of the Earth's climate have given an impetus to studies of the ocean's role in the global heat balance. Oceanographers have a new appreciation of the existing hydrographic and geochemical data base, and ambitious plans are being made to measure new sections in all the major oceans. It is best to consider ocean heat transport in the context of fresh water, oxygen, silica and other geochemical transports. From the standpoint of climate, however, heat transport is of primary interest. To keep the scope of this review within manageable limits, attention will be restricted to this one aspect of a broader ocean transport problem. Research over the last four years has brought about some important changes in outlook. (40 refs.)

116140 Equatorial oceanography. M.A.Cane (Dept. of Meteorology & Phys. Oceanography, MIT, Cambridge, MA, USA), E.S.Sarachik. *Rev. Geophys. & Space Phys. (USA)*, vol.21, no.5, p.1137-48 (June 1983). Interest and activity in the equatorial oceans (defined arbitrarily as that part of the ocean within ten degrees of the equator) have undergone a remarkable expansion in the last four years. The previous IUGG report (O'Brien, 1979) listed about one hundred references—the present one lists over two hundred and fifty. Among the many reasons for this growth, a primary one is the realisation of the rapid nature of equatorial responses. The vanishing of the Coriolis parameter in the presence of density stratification means that the ocean can respond strongly to basinwide winds on the climatically important, and observationally accessible, annual and interannual time scales. This realisation has taken hold as the result of an interplay among theory, modelling and observation. (243 refs.)

116141 Physical oceanography of continental shelves. J.S.Allen (School of Oceanography, Oregon State Univ., Corvallis, OR, USA), R.C.Beardsley, J.O.Blanton, W.C.Boicourt, B.Butman, L.K.Coachman, A.Huyer, T.H.Kinder, T.C.Royer, J.D.Schumacher, R.L.Smith, W.Sturges, C.D.Winant. *Rev. Geophys. & Space Phys. (USA)*, vol.21, no.5, p.1149-81 (June 1983). Knowledge of the physical oceanography of continental shelves has increased tremendously in recent years, primarily as a result of new current and hydrographic measurements made in locations where no comparable measurements existed previously. Recent work in this field is reviewed in this article. In general, observations from geographically distinct continental shelves have shown that the nature of the flow may vary considerably from region to region. Although some characteristics, such as the response of currents to wind forcing, are common to many shelves, the relative importance of various physical processes in influencing the shelf flow field frequently is different. In the last several years, the scientific literature on shelf studies has expanded rapidly, with that for separate regions, to some extent, developing independently because of the variable role played by different physical effects. (526 refs.)

116142 Small-scale physics of the ocean. D.R.Caldwell (School of Oceanography, Oregon State Univ., Corvallis, OR, USA). *Rev. Geophys. & Space Phys. (USA)*, vol.21, no.5, p.1192-205 (June 1983). Recent progress in the study of fine structure and microstructure phenomena in the oceans is reviewed. Turbulence, internal wave and salt-finger phenomena are discussed. Surface mixing layers are also reviewed. Instrumentation and measurement techniques are described and a bibliography of recent work is provided. (211 refs.)

116143 Internal waves in the ocean: a review. M.D.Levine (School of Oceanography, Oregon State Univ., Corvallis, OR, USA). *Rev. Geophys. & Space Phys. (USA)*, vol.21, no.5, p.1206-16 (June 1983). This review documents the advances in knowledge of the oceanic internal wave field during the past four years. Emphasis is placed on studies that deal most directly with the measurement and modelling of internal waves as they exist in the ocean. Progress has come by realising that specific physical processes might behave differently when embedded in the complex, omnipresent sea of internal waves. To understand fully the dynamics of the internal wave field requires knowledge of the simultaneous interactions of the internal waves with other oceanic phenomena as well as with themselves. This report is not meant to be a comprehensive overview of internal waves. The focus is on topics that have been discussed most actively in the literature; subjects that may be important, but have not received recent attention, are omitted. The reference list is intended to be a comprehensive compilation of papers published since 1979. (232 refs.)

116144 Advances in satellite oceanography. O.B.Brown (Rosenstiel School of Marine & Atmospheric Sci., Univ. of Miami, Miami, FL, USA), R.E.Cheney. *Rev. Geophys. & Space Phys. (USA)*, vol.21, no.5, p.1216-30 (June 1983). Progress has been made in the past four years by US scientists in the development and application of active and passive satellite remote sensing techniques to the study of oceanic processes. This report summarises technical advances and recent applications. Major advances have been made in developing and applying quantitative measurements from active and passive satellite based sensor systems launched in the late 1970s and that proven methodologies now exist to observe sea surface temperature, ocean elevation, ocean colour, surface wind stress and waves, and to locate free drifting buoy data collection platforms. Many of the advances in technique and application have occurred using sensors which were experimental, i.e. not part of an operational satellite observing system. Consequently future geophysical application and development of advanced techniques to enhance understanding of the ocean will probably be limited in the next five years by data availability rather than knowledge of how to apply given satellite observations. (503 refs.)

116145 Paleooceanography: global ocean evolution. J.P.Kennett (Graduate School of Oceanography, Univ. of Rhode Island, Kingston, RI, USA). *Rev. Geophys. & Space Phys. (USA)*, vol.21, no.5, p.1258-74 (June 1983). Paleooceanography is concerned with the development of oceanic circulation through geologic time. This is a multifaceted and integrated endeavour since none of the subdisciplines is easily separated from the others. The field includes the history and effects of bottom, intermediate and surface circulation patterns, planktonic and benthonic biogeographic development and rates of organic evolution, the history of biogenic productivity and dissolution and their effect on sediment distribution and the consequences of sea level change. Paleooceanography was largely born of the Deep Sea Drilling Project (DSDP) and continues to be nourished by it. Because problems are of global scope, the appetite for new sediment core material is large, and is being supplied by numerous expeditions of DSDP. This article is a brief overview of a number of advances that have occurred in paleooceanography and related fields during the period from 1979 to 1982. (426 refs.)

116146 Models of the oceanic internal wave field. D.J.Olbers (Max-Planck-Inst. fur Meteorologie, Hamburg, Germany). *Rev. Geophys. & Space Phys. (USA)*, vol.21, no.7, p.1567-606 (Aug. 1983). This review presents kinematical models of the wave field in terms of vertically progressive waves (WKB waves) as well as standing modes. Some importance is attributed to critical layer effects. Spectral models have been successfully developed for the wave field in the main thermocline. Several methods of separating the internal wave contribution from turbulence and other contaminations in observations have been proposed. This problem is of particular relevance in the transition region between waves and small-scale turbulence at small vertical wavelengths. The search for dynamical relations between the wave field and environmental conditions is described. (170 refs.)

The group velocity of normal modes See Entry 113183

Cyclic gravity waves in deep water See Entry 113458

Destabilization of an initially stable shear flow by internal waves See Entry 113460

Isostatic adjustments in a full glacial sea See Entry 116060

The benthic boundary layer and sediment transport See Entry 116077

Marine chemistry and paleoceanography in the United States—1978-82—an overview See Entry 116147

Global temperature variations in the troposphere and stratosphere, 1958-1982 See Entry 116187

A comparison of different sea level pressure analysis fields in the east Greenland Sea See Entry 116239

Stationary waves forced by topography in a vertically sheared, stratified, rotating fluid See Entry 116240

Evaluation of the climatic zonality of the Indian Ocean during Pliocene time from deep-sea drilling data See Entry 116268

Influence of the dimensions of a sensor on estimates of the turbulent energy dissipation rate in the ocean See Entry 116300

A method for calculating dispersion relations and eigenfunctions for internal waves in the ocean from field data See Entry 116301

92.20 INTERDISCIPLINARY ASPECTS OF OCEANOGRAPHY

116147 Marine chemistry and paleoceanography in the United States—1978-82—an overview. D.R.Schink (Dept. of Oceanography, Texas A&M Univ., College Station, TX, USA).

Rev. Geophys. & Space Phys. (USA), vol.21, no.5, p.1231-2 (June 1983). A brief review is given of recent oceanographic research performed by American workers during the last four years. The various research programs studying chemical oceanography and paleoceanography are described. These programs include: Transient Tracers in the Ocean (TTO), Sea/Air Exchange (SEAREX), Manganese Nodule Program (MANOP), Coastal Upwelling Ecosystems Analysis (CUEA), Particle Flux Intercalibration (PARFLUX), Sub-seabed Disposal, Warm Core Rings, Spectral Mapping (SPECMAP), and Cenozoic Paleooceanography (CENOP). The author describes various trends in oceanographic research. Theoretical modelling work as well as experimental work is reviewed. (no refs.)

116148 Advances in marine chemistry 1979-82. W.J.Jenkins (Woods Hole Oceanographic Inst., Woods Hole, MA, USA), J.M.Edmond.

Rev. Geophys. & Space Phys. (USA), vol.21, no.5, p.1233-45 (June 1983). These four years saw advances in many areas. Further developments in sampling and analytical techniques have opened new avenues of exploration for trace elements and particulate matter. The impact of the GEOSECS expedition was further felt in the field of marine chemistry as the results were still being published. A major field effort occurred as a follow-on to the GEOSECS work (TTO), and intensive sampling was performed in the newly discovered submarine hydrothermal vent fields. An important and unresolved controversy has arisen regarding the ability to measure 'preformed' CO₂ in the seawater system. In many respects the field of marine chemistry appears to be gaining a momentum spurred by both improvements in analytic techniques and an increasing social and economic relevance. (386 refs.)

116149 Review of marine organic geochemistry. R.B.Gagosian (Dept. of Chem., Woods Hole Oceanographic Inst., Woods Hole, MA, USA).

Rev. Geophys. & Space Phys. (USA), vol.21, no.5, p.1245-58 (June 1983). Over the past four years the field of marine organic geochemistry has expanded in many directions. In order to cover the major areas of this expansion in a review of the type presented, several major topic areas have been selected focusing on the processes responsible for the transport and transformation of organic material. They include: (1) the atmosphere over the oceans and the air/sea interface; (2) dissolved material in seawater; (3) particulate material as it is transported vertically through the water column; (4) recent marine sediments, as well as (5) transformation reactions; (6) metal-organic interactions including adsorption/desorption processes in the ocean, and (7) selected subjects in new areas of research. (591 refs.)

116150 The ocean. W.S.Broecker.

Sci. Am. (USA), vol.249, no.3, p.100-12 (Sept. 1983). The author provides a comprehensive account of all the processes that influence the chemical composition of seawater. These processes include the marine biological processes and the carbon cycle, the input of volcanic and erosion products to the oceans and the loss of chemicals to marine sediments. Emphasis is placed on the supply, reactions and loss of dissolved oxygen, calcium, phosphate, CO₂, carbonate ion and bicarbonate ion. (no refs.)

Fluid flow control for the intermittent extended aeration process See Entry 113524

The characteristics of salt fingers in a variety of fluid systems, including stellar interiors, liquid metals, oceans, and magmas See Entry 114232

Hydrocarbons in water, sediment and mussels from the southern Baltic Sea See Entry 115704

²²⁴Ra, ²²⁸Ra, and ²²⁶Ra in Winyah Bay and Delaware Bay .. See Entry 116092

Reduction of thermohaline circulation during deglaciation: the effect on atmospheric radiocarbon and CO₂ See Entry 116093

Investigation of chemical sound absorption in seawater. IV .. See Entry 116102

Evaluation of the climatic zonality of the Indian Ocean during Pliocene time from deep-sea drilling data See Entry 116268

92.40 HYDROLOGY AND GLACIOLOGY

116151 A Fortran (IV) program for the evaluation of hydraulic geometry parameters of river channels. N.A.Al-Ansari (Dept. of Geology, Coll. of Sci., Univ. of Baghdad, Baghdad, Iraq), M.H.Al-Jabbari, J.McManus, D.McDonald.

Iraqi J. Sci., vol.22, no.4, p.613-22 (1981). [received: Aug. 1983]

A computer program was developed to facilitate calculation of bed load budget in natural rivers by providing essential data for selected indirect methods. The program evaluates the cross sectional area, hydraulic radius, wetted perimeter and mean depth for given depth increments. In addition the above variables are plotting against elevation in a selected reach with the equations used for the plottings. (1 ref.)

116152 Hydrologic flood routing. R.J.Heggen (Dept. of Civil Engng., Univ. of New Mexico, Albuquerque, NM, USA). *CoED (USA)*, vol.2, no.4, p.8-11 (July-Aug. 1983).

Whereas students in introductory engineering hydrology should be exposed to computerized analyses, HEC-1 and other large models are generally too slow for interactive demonstration and unduly complex for student practice. Hydrologic routing through a multiple channel and/or reservoir system having known or predicted inflow hydrographs at upstream locations can be solved with a computer program much smaller, quicker, and easier to run than HEC-1. This paper documents a short classroom-oriented BASIC program which routes stream flow through a system of channels and reservoirs. Reach hydrographs are computed by the Muskingum method and reservoir hydrographs are calculated by the Puls procedure. Program data requirements consist of input hydrographs for the top reaches, Muskingum time constant and weighting values for channels, stage-discharge-storage coordinates for reservoirs, and a sequential listing of reach confluences. The program is suited for analyses of open channel conveyance systems, flood detention reservoirs, and combinations of the two. Having mastered this program, students are better prepared for the sophisticated practice-oriented packages they may later encounter. (no refs.)

116153 A model study of the short-term climatic and hydrologic effects of sudden snow-cover removal. T.-C.Yeh, R.T.Wetherald, S.Manabe (Geophys. Fluid Dynamics Lab./NOAA, Princeton Univ., Princeton, NJ, USA). *Mon. Weather Rev. (USA)*, vol.11, no.5, p.1013-24 (May 1983).

Describes the results from a set of numerical experiments which stimulate the effect of a large scale removal of snow cover in middle and high latitudes during the early spring season. This is done through use of a simplified general circulation model with a limited computational domain and idealized geography. It is found that removal of snow cover reduces the water available to the soil through snowmelt and decreases soil moisture in this region during the following seasons. Furthermore, it also reduces surface albedo in this region and increases absorption of insolation by the ground surface. This, in turn, heats the ground surface and allows more evaporation to occur. The removal of snow cover also affects the thermal and dynamical structure of the atmosphere. (13 refs.)

116154 Slope hydrology as influenced by thawing of the active layer. Resolute, N.W.T.. Ming-ko Woo, P.Steer (Dept. of Geography, McMaster Univ., Hamilton, Canada).

Can. J. Earth Sci. (Canada), vol.20, no.6, p.978-86 (1983).

Discusses the role played by the thawing of the active layer on the hydrology of slopes in permafrost terrains. Results from this study will have applications in streamflow forecasting and in construction projects that require a knowledge of slope drainage. (11 refs.)

116155 Operational flood routing for hydroelectric plants. M.Mimikou (Civil Engng. Dept., Tech. Univ. of Athens, Athens, Greece).

Int. Water Power & Dam Constr. (GB), vol.35, no.9, p.24-7 (Sept. 1983).

Hydraulic flood routing models need geomorphological, hydrologic and hydraulic field information from the stream-watershed system where they are applied. The spatial and temporal variability and the limited variability of this field information for most of natural streams are the main reasons for application difficulties and inaccuracies of the hydraulic flood routing models. The stochastic model presented for transferring flood streamflows with lateral inflows overcomes all these difficulties and has been used successfully in the design and the operation of hydroelectric plants. (8 refs.)

116156 The behaviour of silt-laden current. II. W.H.Graf (Lab. d'hydraulique, Ecole Polytech. Federale, Lausanne, Switzerland).

Int. Water Power & Dam Constr. (GB), vol.35, no.9, p.33-8 (Sept. 1983).

For pt.1, see *ibid.*, vol.35, no.4, p.45 (1983). Continuing his examination of the mechanics of reservoir sedimentation, the author examines the characteristics of those currents which carry sediment into existing bodies of water. A better understanding of their behaviour, it is argued, would improve the techniques of reservoir control. (32 refs.)

116157 Indonesia's Asahan hydro project. II. I.Miyachi, K.Miyake.

Int. Water Power & Dam Constr. (GB), vol.35, no.9, p.46-53 (Sept. 1983).

For pt.1 see *ibid.*, vol.35, no.8, p.59 (1983). Gives details of the area's hydrology, topography and geology and explains how these factors, among others, determined the form of the scheme. Also describes the execution of the project, and how the various problems during construction were overcome. (no refs.)

116158 Verification and correction of BKF-precipitation forecasts for the use in a runoff model. R.Dreissigacker, H.Fleer (Univ. Hannover, Hannover, Germany).

Meteorol. Rundsch. (Germany), vol.36, no.4, p.169-80 (Aug. 1983). In German.

The Germany Weather Service computes quantitative precipitation forecasts and publishes them in the form of charts with plotted isohyets. In the view of an application to flood forecasting in the Leine-river basin the forecast data are compared with two area-averaged observation data sets: one for an orographically undisturbed region in Schleswig-Holstein, and the other one for the Leine-river basin which is influenced by mountainous regions. The influence of orography in the Leine-river basin is investigated by analysing the correlations separately for various wind direction forecasts. (13 refs.)

116159 Oxygen isotope ratios in German groundwater. H.Forstel, H.Hutzen (Inst. of Radioagronomy, KFA Julich, Julich, Germany).

Nature (GB), vol.304, no.5927, p.614-16 (18 Aug. 1983).

The natural variation in the $^{18}\text{O}/^{16}\text{O}$ ratio in precipitation has a characteristic global pattern corresponding to the worldwide distribution of the local mean annual temperature. This global pattern is not, however, sensitive enough to predict the local $^{18}\text{O}/^{16}\text{O}$ ratio in precipitation. A survey of groundwater throughout the FRG was obtained from about 900 samples of the municipal water supply. Using a multicorrelation study the authors demonstrate that both distance from the coast and height above sea level determine the local $^{18}\text{O}/^{16}\text{O}$ ratio, and that this ratio generally decreases from the northern coast towards the southern mountainous region. The geographical variation in the

$^{18}\text{O}/^{16}\text{O}$ ratio may serve as a basis for palaeoclimatological, plant-physiological and food analytical applications. (10 refs.)

116160 A model for predicting currents in stratified basins. M.A.Akopyan, Yu.L.Demin (Shirshov Inst. of Oceanography, Acad. of Sci., Moscow, USSR).

Oceanology (USA), vol.22, no.4, p.404-8 (1982). Translation of: *Okeanologiya (USSR)*, vol.22, no.4 (1982). [received: Aug. 1983]

Describes a prognostic model for currents in stratified basins, based on simple equations of motion and the equation for the surface of the basin. Using this model the authors calculate currents and water temperatures for Lake Sevan using a computational grid with spacings of 1 km. The results are compared to observational data. (12 refs.)

116161 Extraction of the synoptic component from hydrology survey data. O.P.Nikitin (Shirshov Inst. of Oceanology, Acad. of Sci., Moscow, USSR).

Oceanology (USA), vol.22, no.4, p.413-16 (1982). Translation of: *Okeanologiya (USSR)*, vol.22, no.4 (1982). [received: Aug. 1983]

A procedure for extracting the synoptic component of the field of any scalar hydrophysical quantity from the corresponding data of a unified hydrological survey is described. The procedure consists of a series of successive least-square approximations for the field of the desired components by surfaces derived from polynomials orthonormalized over the given set of points of the hydrological survey. Conditions which must be satisfied by the extracting surface are derived. (5 refs.)

116162 Quantitative estimation of groundwater potentiality and rainfall infiltration in a typical crystalline environment. B.H.Briz-Kishore (Centre of Exploration Geophys., Osmania Univ., Hyderabad, India).

Proc. Indian Acad. Sci. Earth & Planet. Sci., vol.92, no.1, p.63-71 (March 1983). [received: Sept. 1983]

A sophisticated method of measuring water levels is adopted to determine the groundwater potentialities in a typical weathered and fractured environment. The frequency of the rainfall is shown to have a direct bearing on recharging the groundwater system. The Thiessen polygon method is used to determine the weighted average of the rainfall over the basin area to estimate the groundwater infiltration rates. The long term average infiltration is established as 15% of the total rainfall. (8 refs.)

116163 Regionalization of water quality in the Upper Fraser River basin, British Columbia. P.H.Whitfield (Water Quality Branch, Inland Waters Directorate, Environment Canada, Vancouver, BC, Canada).

Water Res. (GB), vol.17, no.9, p.1153-66 (1983).

Uniformity of water quality in the Upper Fraser River basin is examined using cluster analysis. Substantial variations in water quality exist within the basin. These differences are largely related to the geology of the watersheds. Differences in water quality are more pronounced among the tributaries than along the mainstream of the Fraser River. The mainstem of the river could be considered to have three distinct reaches where water quality properties were relatively constant. Cluster analysis was a useful technique for establishing similarities and differences for both the tributaries and the mainstem stations. Some limitations of water quality data and the methods used are discussed. (19 refs.)

116164 Parameter identification of compartmental models—case of hydrologic rainfall-runoff models. S.Sorooshian (Dept. of Systems Engng. & Civil Engng., Case Western Reserve Univ., Cleveland, OH, USA).

Identification and System Parameter Estimation 1982. Proceedings of the Sixth IFAC Symposium, Washington, DC, USA, 7-11 June 1982 (Oxford, England: Pergamon 1983), p.1565-70 vol.2

Addresses some of the difficulties associated with the parameter identification of hydrologic rainfall-runoff models ('compartmental' type) which simulate the dynamic response of watersheds. The presence of threshold (jump) parameters results in a nonexplicit structural equation for the model and consequently estimation techniques that do not require gradient evaluations are commonly employed. In this case the choice of the estimation criterion becomes a critical factor. It is shown that by using maximum likelihood estimators which take into account some of the stochastic properties of the rainfall-runoff process, better parameters and more reliable forecasts can be obtained. Some of the problems needing further research are also presented. (12 refs.)

116165 Optimal estimation of the average areal rainfall over a basin and optimal selection of rain-gauge locations. B.Lorent, G.Bastin, C.Duque, M.Gevers (Louvain Univ., Louvain-la-Neuve, Belgium).

Identification and System Parameter Estimation 1982. Proceedings of the Sixth IFAC Symposium, Washington, DC, USA, 7-11 June 1982 (Oxford, England: Pergamon 1983), p.1571-6 vol.2

Using a linear minimum variance unbiased estimation procedure for the estimation of spatially distributed random variables (called 'Kriging' by geostatisticians) the authors solve the following problems: estimate the average areal rainfall over a catchment area from measurements in a few rain-gauges; and find the measurement locations that will give the most accurate estimate of this areal rainfall. Furthermore they show that the estimated areal rainfall depends only on the location of the rain-gauges, and that one can find the measurement locations leading to the smallest estimation error variance. (6 refs.)

116166 Contemporary stochastic approach to water resources systems: the ARMP and feature prediction models. O.Ibidapo-Obe (Faculty of Engng., Univ. of Lagos, Lagos, Nigeria).

Identification and System Parameter Estimation 1982. Proceedings of the Sixth IFAC Symposium, Washington, DC, USA, 7-11 June 1982 (Oxford, England: Pergamon 1983), p.1583-7

An autoregressive model with Markovian parameters (ARMP) and a feature prediction scheme (FPM) are developed. The ARMP is physically based and adaptive in its implementation thus taking into consideration the inherent periodicities in hydrological time series. The FPM is motivated by the current inability to provide a suitable and sufficiently comprehensive yet simplified mathematical hydrological model. It is based on pattern analysis and is such that a system dynamic feature is identified using a priori data which can subsequently be used to simulate the missing data and forecast future hydrological parameter. The ARMP and FPM provide efficient alternatives to some other existing models which are not, in general, applicable to all classes of hydrological problems (perennial droughts and storm surges). It also affords an added advantage as a result of the ability of the schemes to forecast in real-time. A comparative analysis of the two techniques are undertaken using the discharge record data from the River Nile at Aswan Dam from 1870-1945. It is further proposed that in order to enhance the over-all performance of the prediction scheme, the FPM may be used as an input (training data) to the ARMP. (9 refs.)

- Low-level waste disposal site performance assessment with the RQ/PQ computer program See Entry 112348
- Water quality measurement by observing aquatic animals on mountain streams near Shinshin-so Hut, Doshisha University, 1982 See Entry 115706
- Pollution levels in some Nigerian rivers See Entry 115707
- Factors affecting the concentrations of cadmium, zinc, copper and lead in the sediments of the Vesdre River See Entry 115708
- The Long Valley/Mono Basin volcanic complex in eastern California: status of present knowledge and future research needs See Entry 116056
- Isostatic adjustments in a full glacial sea See Entry 116060
- Evidence for correlation of ultrasonic attenuation and fluid permeability in very low porosity water-saturated rocks See Entry 116081
- ^{224}Ra , ^{228}Ra , and ^{226}Ra in Winyah Bay and Delaware Bay .. See Entry 116092
- Reduction of thermohaline circulation during deglaciation: the effect on atmospheric radiocarbon and CO_2 See Entry 116093
- Microwave radiometric features of vegetated surfaces See Entry 116281

92.60 METEOROLOGY

(see also 43.28 Aerodynamics and atmospheric sound)

- 116167 A model for rain attenuation prediction in single and site diversity Earth-satellite links.** C.Capsoni, E.Matriciani (Dipartimento di Elettronica, Politecnico di Milano, Milano, Italy). *Alta Freq. (Italy)*, vol.52, no.3, p.215-17 (May-June 1983). (4th Italian National Meeting on Applied Electromagnetics, Florence, Italy, 4-6 Oct. 1982).
- Site diversity systems are foreseen for Earth-to-satellite links operating at frequencies above 10 GHz in localities with high rain-induced attenuation. An analytical model for the rainrate statistical process is developed using radar derived information on the rain structure collected at Spino d'Adda in the framework of the SIRIO experiment. The procedure for estimating rain attenuation in both single and site diversity systems is outlined in a general formulation which makes it applicable to different situations. The model gives results very similar to experimental ones. (6 refs.)
- 116168 Clear air scintillation in electromagnetic line-of-sight propagation at 35 GHz.** P.Basili, P.Ciotti, G.D'Auria (Dipartimento di Elettronica, Univ. di Roma, Roma, Italy), D.Solimini. *Alta Freq. (Italy)*, vol.52, no.3, p.221-3 (May-June 1983). (4th Italian National Meeting on Applied Electromagnetics, Florence, Italy, 4-6 Oct. 1982).
- Scintillation of millimetre waves propagating in the atmosphere is considered from the theoretical point of view and practical formulas and diagrams are given. An experiment has been carried out at 34.8 GHz and some results are reported. The general properties of amplitude spectra with respect to the statistical fluctuations of refractivity are presented and their relationships with the covariance functions and with the relevant meteorological parameters are illustrated. (11 refs.)
- 116169 Investigation of the spectral composition of solar radiation under conditions prevailing at Tashkent.** B.Z.Mavashev, Yu.Z.Mavashev (S.V. Starodubtsev Physicotech. Inst., Acad. of Sci., Uzbek SSR). *Appl. Sol. Energy (USA)*, vol.18, no.4, p.68-70 (1982). Translation of: *Geliotekhnika (USSR)*, vol.18, no.4, p.57-9 (1982). [received: Aug. 1983]
- The authors describe the variability of the distribution of solar radiation over certain portions of the spectrum, in relation of the time of day, season, meteorological conditions, and pollution of the ground layer of the atmosphere. (4 refs.)
- 116170 Plume dispersion in a nocturnal drainage wind.** S.Barr, T.G.Kyle, W.E.Clements, W.Sedlacek (Los Alamos Nat. Lab., Los Alamos, NM, USA). *Atmos. Environ. (GB)*, vol.17, no.8, p.1423-9 (1983).
- A series of tracer experiments were conducted under nocturnal drainage wind conditions in a complex terrain setting in the Piceance Basin of western Colorado. Concurrent meteorological information including profiles of wind and temperature as well as gross turbulence fluctuations from fixed 2-m stations provided the basis to test plume growth and dilution prescriptions for this moderately complex site. Plume parameters exhibited slightly greater diffusion than would be indicated by simple stability-based prediction methods or the gross turbulence indicators. Two terrain-related mechanisms appear to contribute to the development of the plume: these two mechanisms are described. (13 refs.)
- 116171 Measurements of sulfur in gases and particles during sixteen months in the Ohio River Valley.** R.W.Shaw, Jr., R.J.Paur (Office of Res. & Dev., US Environmental Protection Agency, Research Triangle Park, NC, USA). *Atmos. Environ. (GB)*, vol.17, no.8, p.1431-8 (1983).
- During the period May 1980-August 1981, air quality measurements were made at three rural sites in the Ohio River Valley. Monthly averages of O_3 , NO_2 and gaseous and particulate sulfur were quite uniform from site to site and showed a strong annual pattern: NO_2 and gas phase sulfur were highest in winter; while O_3 and particulate sulfur were highest in summer. The ratio of particulate sulfur to gaseous sulfur varied from less than 0.1 in winter to nearly 1 in summer. (22 refs.)
- 116172 Mesoscale air pollution dispersion modelling.** H.Van Dop, B.J.De Haan (Royal Netherlands Meteorological Inst., De Bilt, Netherlands). *Atmos. Environ. (GB)*, vol.17, no.8, p.1449-56 (1983).
- An air pollution model is developed which describes the transport of pollutants on a scale of $500 \times 500 \text{ km}^2$. This corresponds with episodes of a few days. In the model a detailed description is given of the vertical diffusion processes under different stability conditions. Also much effort is put into the determination of the horizontal mean wind field, which is strongly non-homogeneous and non-stationary on the above space- and timescales. The transport equation is numerically solved. For the advective part a pseudo-spectral scheme was applied. The vertical diffusion is treated with a Crank-Nicolson scheme. Dry deposition is included in the model in a way which accounts for the chemical properties of pollutant and soil. Wet deposition and chemical transport are included by simple linear decay terms. The model is tested in a complex source area (Netherlands and surrounding countries), during a fair weather episode on 29 and 30 May 1978. (18 refs.)
- 116173 Modelling of long-range transport of sulphur over Europe: a two-year model run and some model experiments.** A.Eliassen, J.Saltbones (Norwegian Meteorological Inst., Oslo, Norway). *Atmos. Environ. (GB)*, vol.17, no.8, p.1457-73 (1983).
- The long-range transport of sulphur over Europe is quantified using a simple trajectory model with constant mixing height. Results from a model run covering a two-year period shows that average concentrations of sulphur dioxide and particulate sulphate are predicted reasonably well. The calculations

confirm that, in most countries in Europe, the deposition of sulphur due to foreign sources represents an important contribution to the total deposition. Seasonal concentration variations are not well predicted with this simple model. The model experiments show that improvements are gained in this respect when a variable mixing height is introduced. (17 refs.)

- 116174 Anatomy of an episode of high sulfate concentration at Whiteface Mountain, New York.** V.A.Dutkiewicz, J.A.Halstead, P.P.Parekh, A.Khan, L.Husain (Center for Labs. & Res., New York State Dept. of Health, Albany, NY, USA). *Atmos. Environ. (GB)*, vol.17, no.8, p.1475-82 (1983).
- Concentrations of seven metals and sulfate in aerosols collected at Whiteface Mountain, New York, were measured continuously in 6-h intervals for 2 weeks in June 1979. Thirteen consecutive samples showed high episodic concentrations of sulfate, Fe, Al and, to a lesser extent, Zn, Pb, K, Mg and Ca. The trajectories for the period of elevated $[\text{SO}_4^{2-}]$ passed through the mid-western United States and entered New York State from the southwest. The trajectories for the time periods of low $[\text{SO}_4^{2-}]$ before and after the episode entered New York from the north. This relationship between high concentrations and the surface-air trajectories suggests that in this particular episode SO_4^{2-} and metals may have been transported from the Midwest. (20 refs.)

- 116175 The relationship of sulfur emissions to sulfate in precipitation. II. Gas phase processes.** M.Oppenheimer (Environmental Defense Fund Inc., New York, NY, USA). *Atmos. Environ. (GB)*, vol.17, no.8, p.1489-95 (1983).
- For pt.1 see *ibid.*, vol.17, p.451-60 (1982). A climatological box model is applied to wet deposition of sulfur in eastern North America using the extreme assumption that all wet-deposited sulfates originate in sulfate aerosol. The measured sulfate in precipitation during 1977-1979 constrains the probability that an SO_2 molecule emitted in the eastern United States is oxidized before deposition or outflow from the region to values greater than 0.5 and more likely near 1.0. This result implies that uniform SO_2 emission reductions will produce nearly proportional reductions in wet sulfates originating in those emissions and deposited on land. The amount of wet sulfate deposition is demonstrated to constrain the mean scale of transport along air parcel trajectories for the precursor of wet sulfur, whether SO_2 or sulfate aerosol, to values greater than 900 km. (30 refs.)

- 116176 The pH and ionic composition of stratiform cloud water.** R.A.Castillo, J.E.Justo (Atmospheric Sci. Res. Center, State Univ. of New York, Albany, NY, USA), E.McLaren. *Atmos. Environ. (GB)*, vol.17, no.8, p.1497-505 (1983).
- Over 50 cloud water samples were collected during five comprehensive case studies of the water chemistry of stratiform clouds at Whiteface Mountain, New York. The water samples were analyzed for pH, conductivity and ions of sodium, potassium, magnesium, calcium, ammonium, sulfate, chloride and nitrate. Trajectory analyses and cloud condensation nucleus concentrations at 0.5% confirmed that the air masses in all five of these cases represented continental air that was relatively clean (low aerosol concentration) for the northeastern United States. The major ions related to cloud water pH were found to be sulfate, nitrate, potassium, ammonium and calcium. The results revealed a mean pH=3.6 for all collected cloud samples. The low pH values are related to a normal background of nitrate ions found in the rural continental air masses plus sulfate ions largely from the industrial emissions of the midwestern United States. (21 refs.)

- 116177 Aerosol composition at Chacaltaya, Bolivia, as determined by size-fractionated sampling.** F.Adams, P.Van Espen (Dept. of Chem., Univ. of Antwerp, Wilrijk, Belgium), W.Maenhaut. *Atmos. Environ. (GB)*, vol.17, no.8, p.1521-36 (1983).
- Thirty four cascade impactor samples were collected between September 1977 and November 1978 at Chacaltaya, Bolivia. The concentrations of 25 elements were measured for the six impaction stages of each sample by means of energy-dispersive X-ray fluorescence and proton-induced X-ray emission analysis. The results indicated that most elements are predominantly associated with a unimodal coarse particle soil dust dispersion component. Also chlorine and the alkali and alkaline earth elements belong to this group. The anomalously enriched elements (S, Br and the heavy metals Cu, Zn, Ga, As, Se, Pb and Bi) showed a bimodal size distribution. Correlation coefficient calculations and principal component analysis indicated the presence in the submicrometer aerosol mode of an important component, containing S, K, Zn, As and Br, which may originate from biomass burning. (43 refs.)

- 116178 Electron microscopy of acidic aerosols collected over the northeastern United States.** R.J.Ferek (Dept. of Oceanography, Florida State Univ., Tallahassee, FL, USA), A.L.Lazrus, J.W.Winchester. *Atmos. Environ. (GB)*, vol.17, no.8, p.1545-61 (1983).
- As part of the acid precipitation experiment (APEX) conducted in the northeastern US, aerosols were collected from an aircraft in different seasons, locations and meteorological conditions. Particles were impacted on electron microscope grids for morphological analysis and thin-film chemical tests for sulfate and nitrate. Under most conditions the accumulation mode aerosols ($c. 0.1\text{-}1.0 \mu\text{m}$ diameter) collected in the boundary layer were composed of sulfate particles of uniform composition (i.e. an internally mixed aerosol), indicating that individual particle composition could be inferred from bulk measurements. Externally mixed aerosols (i.e. assemblages of different kinds of particles) were found to exist near certain sources (e.g. power plants), in urban plumes, and near fair weather cumulus clouds. Direct evidence of rapid oxidation of SO_2 to H_2SO_4 in cloud droplets was obtained in samples collected near clouds in northern New York and central Illinois, and this represents a potentially major pathway for SO_2 oxidation in the lower troposphere. (22 refs.)

- 116179 World-wide ambient measurements of peroxyacetyl nitrate (PAN) and implications for plant injury.** P.J.Temple, O.C.Taylor (Dept. of Botany & Plant Sci., Univ. of California, Riverside, CA, USA). *Atmos. Environ. (GB)*, vol.17, no.8, p.1583-7 (1983).
- Peroxyacetyl nitrate (PAN) is a major phytotoxic component of the photochemical oxidant complex in southern California. Based on ambient air sampling at Riverside, California, in 1980, and published reports of PAN concentrations from other parts of the world, PAN concentrations in southern California appear to be five or ten times higher than those reported from eastern North America, western Europe, or Japan. Potentially phytotoxic episodes, defined herein as $\text{PAN} > 15 \text{ ppb}$ for 4 h during the a.m. period or $> 25 \text{ ppb}$ for 4 h in the p.m. period occurred 27 times in Riverside, California, in 1980. PAN normally averages 1 ppb or less outside of southern California, and because of this low concentration, PAN by itself does not appear to be a major cause of photochemical oxidant injury to vegetation in those regions. (38 refs.)

116180 Estimating the zero-plane displacement for tall vegetation using a mass conservation method. L.C.B.Molion, C.J.Moore (Inst. of Hydrology, Wallingford, England).

Boundary-Layer Meteorol. (Netherlands), vol.26, no.2, p.115-25 (June 1983). This note describes estimation of the zero-plane displacement derived from experimental windspeed measurements above an 18 m pine forest and an 8-9 m savannah using a 'mass conservation technique' mentioned by Tajchman (1981). The results obtained using this analysis exhibit a lack of sensitivity to experimental errors which is in marked contrast to those commonly obtained over tall vegetation using more conventional least-square analyses. The consistency in the results allows an investigation of the windspeed dependence of the aerodynamic properties of the mean horizontal airflow over tall vegetation, and permits consideration of the effect of experimental errors on such dependence. (17 refs.)

116181 Tracer experiments with turbulently dispersed air ions. P.B.Storebo, T.Bjorvatten, K.Honnashagen, A.Lillegraven (Norwegian Defence Res. Establ., Kjeller, Norway), C.D.Jones, C.J.P.van Buijtenen. *Boundary-Layer Meteorol. (Netherlands)*, vol.26, no.2, p.127-39 (June 1983). Unipolar air ions released into the wind constitute a tracer which can be measured with high resolution. An ion source produces a cloud with homogeneous charge density, insensitive to source strength, dependent on time since formation only. It is well suited for tracing concentration changes due to turbulence, less suited for cloud size tracing. A tight array of 8 sensors has been used to examine turbulently dispersed ions. High-resolution records are presented and discussed. The highest concentrations measured could be undiluted source material. The frequency distribution within a plume did not differ from that in a multitude of puffs. The distribution seems to be log-normal with a geometric standard deviation of about 2.45. The time resolution used corresponds to volume resolutions of 40, 225, and 650 cm³. Sample size had no apparent effect. (7 refs.)

116182 Wave and turbulence structure in a disturbed nocturnal inversion. Lu Nai-Ping (Inst. of Atmospheric Phys., Acad. Sinica, Beijing, China), W.D.Neff, J.C.Kaimal.

Boundary-Layer Meteorol. (Netherlands), vol.26, no.2, p.141-55 (June 1983). Acoustic sounder and tower data obtained at the Boulder Atmospheric Observatory are used to examine several features of the wave and turbulence structure associated with a disturbed nocturnal inversion. General features, including mean fields and Richardson number, for the case selected for this study are presented. Spectral analysis of the tower data reveals a separation of energy into wavelike and turbulent fluctuations. Analysis of the heat flux, however, shows upward counter-gradient fluxes in the vicinity of a low-level jet and near the top of the inversion. The major contribution to the upward heat flux occurs at frequencies that would normally be considered characteristic of waves. In some cases, the upward flux is associated with a phase shift between vertical velocity w and fluctuating temperature θ different from the quadrature relation that would be expected of internal waves. (18 refs.)

116183 A study of multiple stable layers in the nocturnal lower atmosphere. Li Xing-Sheng (Inst. of Atmospheric Phys., Acad. Sinica, Beijing, China), J.E.Gaynor, J.C.Kaimal.

Boundary-Layer Meteorol. (Netherlands), vol.26, no.2, p.157-68 (June 1983). The structure of nocturnal inversions in the first 300 m of the atmosphere is analyzed using observational data from the Boulder Atmospheric Observatory from March through June 1981. The temperature profiles show more than one inversion layer 41 of the time during the observational period. The vertical distributions of wind speed and moisture also show evidence of stratification during these multiple-layer events. The relation between the radiative cooling rate in time and height, including moisture, and the vertical structure of the multiple layers is calculated. The vertical distribution of eddy kinetic energy and the turbulent vertical fluxes of heat and momentum are also calculated. Turbulent structure in the elevated inversion layers is more complicated than that in the single-layer, stable nocturnal boundary layer. The total heat budget for a multiple-layer case is calculated, and turbulent cooling is found to be negligible relative to radiative cooling and to horizontal advection and/or horizontal divergence of heat flux. (21 refs.)

116184 A simple model of neutrally stratified boundary-layer flow over real terrain incorporating wavenumber-dependent scaling. P.A.Taylor, J.L.Walmsley (Boundary Layer Res. Div., Atmospheric Environment Service, Downsview, Ontario, Canada), J.R.Salmon.

Boundary-Layer Meteorol. (Netherlands), vol.26, no.2, p.169-89 (June 1983). The authors' experience in applying earlier versions of a model of boundary-layer flow over low hills to real terrain (see Walmsley et al., 1982) has led to the development of a new version which is designated MS3DJH/3. The main improvements are the use of terrain-dependent length and velocity scales and the blending of inner and outer layer results into a single 'universally valid' solution for the velocity perturbation field. MS3DJH/3 was carefully calibrated against alternative computations of flow over idealized two-dimensional terrain features using more detailed models prior to its application to real, three-dimensional terrain. It still provides high spatial resolution with low computing cost and is applicable to flow over terrain features with horizontal scales from 10 m to 10 km. (8 refs.)

116185 A suggested refinement for O'Brien's convective boundary layer eddy exchange coefficient formulation. R.A.Pielke (Dept. of Atmospheric Sci., Colorado State Univ., Fort Collins, CO, USA), H.A.Panofsky, M.Segal. *Boundary-Layer Meteorol. (Netherlands)*, vol.26, no.2, p.191-5 (June 1983). With observational data collected and interpreted by Crane et al. (1977), the adequacy of the O'Brien polynomial to represent the exchange profile of heat and pollution in a convective boundary layer is examined and a refinement suggested. Also, it is shown that the height of the surface layer, $h=0.04 z_i$, developed by Blackadar and Tennekes (1968) for a neutrally stratified boundary layer (with $z_i=0.25 u_*^2/f$) appears to be equally valid for the convective boundary layer where z_i , defined as the top of the mixed layer, is used. (13 refs.)

116186 Seasonal variation of wind direction fluctuations vs. Pasquill stabilities in complex terrain. Y.Sadurham, K.P.R.Vittal Murthy (Nat. Inst. of Oceanography, Dona Paula, Goa, India).

Boundary-Layer Meteorol. (Netherlands), vol.26, no.2, p.197-202 (June 1983). The authors have studied the seasonal variation of σ_θ (the standard deviation of wind direction fluctuations) vs. Pasquill stabilities over complex terrain. It is found that the values of σ_θ are quite high in the month of April in contrast with other months. Values are also high when compared with those estimated over flat terrain and at a coastal site. (13 refs.)

116187 Global temperature variations in the troposphere and stratosphere, 1958-1982. J.K.Angell, J.Korshover (Air Resources Labs., NOAA, Rockville, MD, USA).

Mon. Weather Rev. (USA), vol.11, no.5, p.901-21 (May 1983). A network of 63 well-distributed radiosonde stations is used to estimate mean-annual temperature variations at the surface and for 85-30 kPa (850-300 mb), 30-10 kPa, 10-5 kPa, 10-3 kPa, and surface-10 kPa layers for five climate zones both hemispheres, and the world for the interval 1958-81. There

is evidence for an 0.3°C decrease in Northern Hemisphere surface temperature following the Agung eruption in 1963, as well as at least a 1.0°C temperature increase in the low stratosphere of the tropics, but no convincing evidence that the eruptions of Fuego in 1974 or St.Helens in 1980 affected either tropospheric or stratospheric temperatures. Between 1958 and 1981, the correlation between sea-surface temperature in the equatorial eastern Pacific and global temperature for the surface-10 kPa layer, is discussed. (39 refs.)

116188 The large-scale circulation and heat sources over the Tibetan Plateau and surrounding areas during the early summer of 1979. I. Precipitation and kinematic analyses. Huibang Luo, Michio Yanai (Dept. of Atmospheric Sci., Univ. of California, Los Angeles, CA, USA).

Mon. Weather Rev. (USA), vol.11, no.5, p.922-44 (May 1983). The time evolution of the large-scale precipitation, low-level (850 mb) wind, moisture and vertical motion fields over the Tibetan Plateau and surrounding areas during a 40-day period from late May to early July 1979 is studied based on the objectively analyzed FGGE Level II-b data set. During this period the general circulation over East Asia undergoes a distinct change characterizing the onset of the summer monsoon circulation. The Tibetan Plateau exerts profound orographic and thermal influences upon the low-level wind field. Detailed examinations of daily values of the areal mean vertical p -velocity, mixing ratio and rainfall are made for four heat source regions (the western Plateau and adjacent areas, the eastern Plateau, the Yangzi River, the Assam-Bengal region) as a preliminary to the discussion of heating mechanisms operating in these regions. (49 refs.)

116189 On the relative motion of binary tropical cyclones. K.Dong (Central Meteorological Bur., Acad. of Meteorological Sci., Beijing, China), C.J.Neumann.

Mon. Weather Rev. (USA), vol.11, no.5, p.945-53 (May 1983). The interaction between spatially proximate (binary) tropical cyclones is such that relative rotation in the counterclockwise sense and decreasing separation distance between the two storm centers can be expected. This is referred to as the Fujiwhara effect. The author analyzes this effect for 43 binary tropical cyclone systems which occurred over the western North Pacific, 1949-78. It is shown that most demonstrated mutual interaction according to Fujiwhara expectations. However, there were notable apparent exceptions. Further analysis of these exceptional cases shows that environmental currents in which the storms were embedded has a significant effect on relative motion and masked the Fujiwhara effect. Additionally, it was found that storms exhibiting behavior most in accordance with Fujiwhara expectations were located in or near the Intertropical Convergence Zone. (13 refs.)

116190 Variability of the Indian summer monsoon and tropical circulation features. D.A.Mooley, B.Parthasarathy (Indian Inst. of Tropical Meteorology, Pune, India).

Mon. Weather Rev. (USA), vol.11, no.5, p.967-78 (May 1983). The Indian economy is very closely linked with the variable performance of the summer monsoon. The incidence of dry and wet conditions over the country is examined for the period 1871-1978 by examining the normal monsoon rainfall and its variability over the region by means of the Index of Dryness over India (IDI) and the Index of Wetness over India (IWI). These are respectively defined as the country's percentage area characterized by dry and wet conditions. These series are found to be homogeneous, random, highly variable and positively skewed. The year in which IDI (IWI) exceeds the mean by more than two times the mean deviation from the mean is taken as a year of large-scale drought (flood). The IDI and IWI show consistently significant correlation with the Southern Oscillation Index and with sea surface temperature anomalies of the equatorial eastern Pacific for the concurrent and succeeding seasons. (55 refs.)

116191 Monitoring tropical-cyclone intensity using environmental wind fields derived from short-interval satellite images. E.Rodgers (Goddard Space Flight Center, NASA, Greenbelt, MD, USA), R.C.Gentry.

Mon. Weather Rev. (USA), vol.11, no.5, p.979-96 (May 1983). Rapid-scan visible images from the Visible Infrared Spin Scan Radiometer (VISSR) sensor on board SMS-2 and GOES-1 are used to derive high-resolution upper and lower tropospheric environmental wind fields around three western Atlantic tropical cyclones (Caroline, August 1975; Anita, August and September 1977; and Ella, September 1978). These wind fields are used to derive the local change of the net relative angular momentum (RAM) upper and lower tropospheric areal mean relative vorticity and their difference, and the storm's transverse circulation. The local change of the storm's net RAM is investigated for the purpose of predicting future storm intensification while the areal mean relative vorticity and transverse circulation are investigated to better understand how the storm's environmental circulation affects its intensification. (38 refs.)

116192 A convergence analysis of a numerical method for solving the balance equation. S.J.Bijlsma, R.J.Hoogendoorn (Royal Netherlands Meteorological Inst., De Bilt, Netherlands).

Mon. Weather Rev. (USA), vol.11, no.5, p.997-1001 (May 1983). The convergence of an iterative method for solving the nonlinear balance equation is analyzed. It is shown that this iterative method, originally proposed by Miyakoda (1958) and Shuman (1957) is convergent if a sufficiently accurate initial approximation is used and if the successive iterates satisfy the ellipticity condition. Otherwise the method may be divergent. Experimental results are presented. (6 refs.)

116193 Limitations of some common lateral boundary schemes used in regional NWP models. H.C.Davies (Lab. Atmospheric Phys., ETH, Zurich, Switzerland).

Mon. Weather Rev. (USA), vol.11, no.5, p.1002-12 (May 1983). A brief critical assessment is presented of several lateral boundary schemes currently employed in regional weather prediction models. Simple flow models are used to determine the nature and cause of the primary shortcomings of each of the considered schemes. An awareness of these deficiencies can prove helpful in the implementation and further refinement of these schemes, and also in the interpretation of the resulting prediction errors. (40 refs.)

116194 A cyclone/anticyclone couplet over North America: an example of anticyclone evolution. J.S.Boyle, L.F.Boisart (Dept. of Atmospheric Sci., State Univ. of New York, Albany, NY, USA).

Mon. Weather Rev. (USA), vol.11, no.5, p.1025-45 (May 1983). A detailed case study is made of a cyclone/anticyclone couplet over North America during early winter, 11-18 November 1969. The anticyclone was the dominant member of the couplet in this case. Objective analyses of the wind and mass fields are carried out in both the isobaric and isentropic coordinate systems. Calculated quantities which are discussed include quasi-geostrophic vertical velocity and height tendency, potential vorticity, and quasi-Lagrangian kinetic energy budgets. The movement of the cold, polar anticyclone out of its source region in Alaska southeastward to the Gulf of Mexico is seen to be thermally steered. The mechanism by which the cold air dome associated with the anticyclone moves southward intact is explained from two complementary perspectives. One viewpoint is that of asymmetries in the jet stream about the long wave trough with a jet streak to the west of the cold dome. The other is

that a maximum in potential vorticity located above the coldest air will prevent the dome from subsiding. (37 refs.)

116195 Duration of convective events related to visible cloud, convergence, radar and rain gage parameters in south Florida. R.L.Holle, A.I.Watson (Environmental Res. Labs., NOAA, Boulder, CO, USA). *Mon. Weather Rev. (USA)*, vol.11, no.5, p.1046-51 (May 1983). The time interval between initiation of surface convergence and the subsequent response of visible cloud growth to this convergence is examined for nine cases of convection that occurred over the FACE 1973 and 1975 mesonetworks in south Florida. Clouds ranged in size from small echoes with a few towers to merged lines or large clusters of towers, but they met a series of observational criteria that specified them as belonging to a similar set of clouds, and were not representative of the entire range of clouds in the area. Visible clouds first formed 10 to 55 min after the associated surface convergence began, and grew rapidly upward 20 to 100 min after convergence started. This highly variable response can be understood better by taking into account the duration of the cloud, which is defined as the time from first surface convergence to complete dissipation. The same nine cases are examined as were chosen initially for the visible cloud study. (9 refs.)

116196 Analysis of nighttime drainage winds in Boulder, Colorado during 1980. B.W.Hootman, W.Blumen (Dept. of Astro-Geophys., Univ. of Colorado, Boulder, CO, USA). *Mon. Weather Rev. (USA)*, vol.11, no.5, p.1052-61 (May 1983). Characteristics of nighttime drainage winds that occurred along the eastern slope of the Rocky Mountains around Boulder, Colorado during the calendar year 1980 are examined. The data used for this study were acquired from the Boulder Wind Network (BWN) and from the Boulder Atmospheric Observatory (BAO). Data were available almost continuously from BWN and less frequently from BAO. BAO is a 300 m tower, instrumented at eight levels, but only surface wind observations are obtained from BWN. However, the combination of BWN and BAO observations represents a relatively unique set of wind data for the examination of drainage flows. Criteria for the identification of drainage winds are used to isolate events that are relatively free from external influences. Eighteen drainage wind events are identified, and some climatological features of the wind regime are established. In addition, the vertical structure of the flow associated with one event that reached the tower is examined in detail. Descriptions of the features of this flow and physical interpretations are presented. (10 refs.)

116197 The orographic modulation of pre-warm-front precipitation in southern New England. R.E.Passarelli, Jr., H.Boehm (Dept. of Meteorology & Phys. Oceanography, MIT, Cambridge, MA, USA). *Mon. Weather Rev. (USA)*, vol.11, no.5, p.1062-70 (May 1983). Topographic forcing over the hills and small mountains of southern New England plays an important role in determining the distribution of pre-warm-front precipitation from winter cyclones. Upslope regions receive 20-60% more precipitation than do nearby downslope or coastal regions. Both the intensity and duration of precipitation contribute to the positive upslope anomalies. The magnitude of the upslope anomalies, the details of the precipitation intensity distributions at proximal upslope and downslope gauges, and the results of simple models indicate that precipitation scavenging in orographic clouds can explain the orographic enhancement. Also, the existence of a positive precipitation anomaly over the coastal plain suggests that frictional convergence may be generating weak, but persistent vertical motions. (12 refs.)

116198 Atlantic hurricane season of 1982. G.B.Clark (Nat. Hurricane Center, NOAA, Miami, FL, USA). *Mon. Weather Rev. (USA)*, vol.11, no.5, p.1071-9 (May 1983). Five named tropical cyclones and one subtropical cyclone were tracked during 1982 in the Atlantic-Caribbean-Gulf of Mexico region. There were no land-falling hurricanes. (3 refs.)

116199 Eastern North Pacific tropical cyclones of 1982. E.B.Gunther, R.L.Cross, R.A.Wagoner (Eastern Pacific Hurricane Center, NOAA, Redwood City, CA, USA). *Mon. Weather Rev. (USA)*, vol.11, no.5, p.1080-101 (May 1983). Discusses the important features of the 1982 seasons. These include positions, velocities and maximum wind speeds. (1 ref.)

116200 Swedish Meteorological and Hydrological Institute (SMHI) invests in new technology: better weather forecasts using radar and microwaves. R.Carlsson. *Elek. Aktuell Elektron. (Sweden)*, vol.26, no.13, p.6-9 (Sept. 1983). In Swedish. Describes a new project proposed by SMHI for improving forecasts by using meteorological radar, laser technology and measurement of atmospheric microwave radiation. The article covers microwave measurement of humidity and temperature, obsolescence of weather balloons, microwave measurements, data comparison and meteorological radar. (no refs.) H.J.P.

116201 On the photodecomposition of CIONO₂ in the middle ultraviolet. H.-D.Knauth, R.N.Schindler (Inst. fur Phys. Chem., Univ. Kiel, Kiel, Germany). *Z. Naturforsch. Teil A (Germany)*, vol.38A, no.8, p.893-5 (Aug. 1983). Photodecomposition of gaseous CIONO₂ was investigated in a static system at wavelengths 265 nm and 313 nm. From the quantitative determination of the products O₂, N₂O₅, and ClO¹⁵NO₂ formed, and from Φ(-CIONO₂) it is concluded that the predominant primary step is CIONO₂ + hν → Cl + NO₃(3). (11 refs.)

116202 The mechanism of sulfate aerosol formation: chemical and sulfur isotopic evidence. E.S.Saltzman (Div. of Marine Geology & Geophys., Univ. of Miami, Miami, FL, USA), G.W.Brass, D.A.Price. *Geophys. Res. Lett. (USA)*, vol.10, no.7, p.513-16 (July 1983). In order to study the mechanism of aerosol sulfate formation, weekly samples of SO₂ and aerosol SO₄²⁻ were collected at Hubbard Brook Experimental Forest, West Thornton, New Hampshire from July to December, 1980. Samples were analysed for concentration and sulfur isotopes (δ³⁴S). Late summer-early fall samples are characterised by high, variable SO₄²⁻ levels and low SO₂ levels, while late fall-early winter samples exhibit low SO₄²⁻ and high SO₂ levels. These trends suggest that the oxidation rate varies seasonally, with faster oxidation during warmer months. The sulfur isotopic fractionation between aerosol SO₄²⁻ and SO₂ is intermediate between that expected from homogeneous and heterogeneous reactions, indicating that both processes can be important. The isotopic data suggest that homogeneous oxidation reactions are more important than solution reactions, particularly during warm months. (14 refs.)

116203 Tropospheric oxalate. R.B.Norton, J.M.Roberts (Aeronomy Lab./NOAA/ERL, Boulder, CO, USA), B.J.Huebert. *Geophys. Res. Lett. (USA)*, vol.10, no.7, p.517-20 (July 1983). The existence of oxalate (COO)₂²⁻ in tropospheric aerosols and in precipitation has been demonstrated using ion chromatography. Mixing ratios have been observed up to 50 pptv in air samples and 0.3 ppm in precipitation.

Correlation of airborne oxalate with airborne nitrate suggests a pollution source. (13 refs.)

116204 Simultaneous detection of FC-11, FC-12 and FC-22, through 8 to 13 micrometers IR solar observations from the ground. R.Zander (Inst. of Astrophys., Univ. of Liege, Liege-Ougree, Belgium), G.M.Stokes, J.W.Brault. *Geophys. Res. Lett. (USA)*, vol.10, no.7, p.521-4 (July 1983). High-resolution solar observations covering the 8 to 13 μm atmospheric window are now being carried out routinely at the Kitt Peak National Observatory (KPNO), Tucson, Arizona, using a 1 meter-path difference Fourier transform spectrometer. Such observations allow the simultaneous measurement of a large number of trace gases. Preliminary results for the three most important fluorocarbons, FC-11, FC-12 and FC-22 are reported. These results, in the form of average mixing ratios, show the potential and illustrate the performance of the Kitt Peak interferometer for this application. (25 refs.)

116205 Centimeter wave propagation experiments using the beacon signals of CS and BSE satellites. H.Fukuchi, T.Kozu, K.Nakamura, J.Awaka, H.Inomata (Kashima Branch, Radio Res. Labs., Ibaraki, Japan), Y.Otsu. *IEEE Trans. Antennas & Propag. (USA)*, vol.AP-31, no.4, p.603-13 (July 1983).

The wave propagation experiments using Japanese geostationary satellites CS (20/30 GHz) and BSE (12/14 GHz) satellites have been performed at the Kashima earth station of the Radio Research Laboratories (RRL). Cumulative rain attenuation and cross-polarization discrimination (XPD) statistics are given for the period of three years at 11.7 GHz (vertical polarization) and for the period of four years at 19.5 GHz (circular polarization) and for the period of four years at 19.5 GHz (circular polarization). It is shown that the yearly rainfall rate and attenuation distributions are well approximated by log-normal distributions, and the XPD distribution is well approximated by a normal distribution. Monthly and time-of-day variation of the attenuation and XPD distributions are presented. Duration statistics of attenuation and XPD are presented and characterized. Other characteristics in the wave propagation, such as effective path length, frequency dependence of attenuation, and joint statistics of attenuation and XPD are derived and discussed. Rainfall events are classified into three rainfall types, 'stratus', 'cumulus', and 'others' using measurements of the radar reflectivity factor along the satellite-to-earth path, and the dependence of XPD characteristics on the rainfall type is also presented and discussed. Some prediction methods of calculating attenuation and XPD statistics are applied to the data obtained in these experiments and the predicted results are compared with the measured ones. It is found that some corrections are needed when the XPD statistics are predicted from the attenuation statistics using the theoretical relation between XPD and attenuation. (24 refs.)

116206 A comparative study of scintillation analysis over two line-of-sight paths at 6.7 GHz and 7.6 GHz. N.Sengupta, M.K.Das Gupta (Inst. of Radio Phys. & Electronics, Univ. of Calcutta, Calcutta, India), B.M.Reddy, H.N.Dutta, S.K.Sarkar. *IEEE Trans. Antennas & Propag. (USA)*, vol.AP-31, no.4, p.620-4 (July 1983).

A comparison of the signal intensity fluctuations or scintillation of signal level, observed over two line-of-sight links is presented. These links are situated over Calcutta, DumDum-Andul (6.7 GHz) and Delhi, Delhi-Sonepat (7.6 GHz). The study reveals departures, in the occurrence and variation of the scintillation over the Calcutta path as compared with the path over Delhi. This deviation has been attributed to the large variation in humidity which exists in the coastal region, and also which plays a major role in microwave propagation in the troposphere. (11 refs.)

116207 Radio propagation beyond the horizon observed at 1 and 3 GHz compared with predicted reflections from random rough layers. L.Hoglund (Nat. Defence Res. Inst., Linköping, Sweden). *IEEE Trans. Antennas & Propag. (USA)*, vol.AP-31, no.4, p.631-5 (July 1983).

Measurements from the scaled tropospheric scatter links at 1 and 3 GHz Stockholm-Mora have given unexpected results. As a rule, the variation in received signal level in decibels of the half-hour median is three times higher at the lower frequency than at the higher frequency for comparatively low signal levels, whereas for high signal levels it is almost only the signal level at the higher frequency that shows variations. The measurements are compared with the theory of reflections from random rough layers with a linear refractive index step Δn and a length L, which is shorter than the Fresnel zone and shorter than the glistening surface. The theory is in very good agreement with the measurements. (6 refs.)

116208 Spectral density of millimeter wave amplitude scintillations in an absorption region. F.C.Medeiros Eilho (Dept. of Electronic & Electrical Engng., Univ. Coll. London, London, England), D.A.R.Jayasuriya, R.S.Cole, C.G.Helmis. *IEEE Trans. Antennas & Propag. (USA)*, vol.AP-31, no.4, p.672-6 (July 1983).

A detailed theory including the effect of water vapor fluctuations for the spectral density of the log amplitude scintillations of a radio wave propagating in an absorption medium is presented. The scintillation spectra obtained from links at 55.5 and 36.1 GHz on a common 4.1 km path are given together with the relevant meteorological data. Results show that the lower corner frequency predicted by Ott and Thompson, for the enhancement of the scintillations in an absorption region, is a good approximation. (13 refs.)

116209 On parameters determining the frequency of tropical cyclone genesis. V.N.Ivanov, A.P.Khain. *Izv. Akad. Nauk SSSR Fiz. Atmos. & Okeana*, vol.19, no.8, p.787-95 (Aug. 1983). In Russian. English translation in: *Izv. Acad. Sci. USSR Atmos. & Oceanic Phys. (USA)*

Climatological tropical cyclone genesis parameters by Gray (1968, 1975, 1981) are critically analyzed. New parameters and a criterion function of seasonal genesis frequency are proposed. A satisfactory agreement between predicted and observed seasonal cyclone frequency is obtained. (13 refs.)

116210 The nonlinear wave-train evolution in the background of weakly unstable stratified shear flow. N.N.Romonova, V.Yu.Tseitlin. *Izv. Akad. Nauk SSSR Fiz. Atmos. & Okeana*, vol.19, no.8, p.796-807 (Aug. 1983). In Russian. English translation in: *Izv. Acad. Sci. USSR Atmos. & Oceanic Phys. (USA)*

Weakly nonlinear phenomena which occur when the shear flow of an ideal incompressible fluid loses its stability are considered. The nonlinear evolution equation for the amplitude of the wave-train formed by nearly neutral modes is obtained and it is shown that the nonlinear term in this equation is purely imaginary so the nonlinearity results only in a frequency shift. (15 refs.)

- 116211 Variations of the nearground aerosol particle size distribution.** D.M.Metreveli, G.I.Gorchakov, S.O.Lomadze, G.V.Rosenberg. *Izv. Akad. Nauk SSSR Fiz. Atmos. & Okeana*, vol.19, no.8, p.807-12 (Aug. 1983). In Russian. English translation in: *Izv. Acad. Sci. USSR Atmos. & Oceanic Phys. (USA)*.
The submicron fractions of atmospheric aerosol particle size distributions are measured for Tajikistan and Moscow, urban and rural regions. The variations due to different meteorological and geographical conditions are discussed. The histograms of particle concentration in size ranges 0.2-0.3 and 0.8-0.9 microns are presented. (11 refs.)
- 116212 Large-scale energy transformations in the high latitudes of the Northern Hemisphere.** E.C.Kung, S.E.Masters (Dept. of Atmospheric Sci., Univ. of Missouri, Columbia, MO, USA), J.A.M.Corte-Real. *J. Atmos. Sci. (USA)*, vol.40, no.5, p.1061-72 (May 1983).
The kinetic energy balance and kinetic energy sources are studied for high latitudes north of 55°N with twice daily upper air observations during a seven-year period from 1973 to 1979. Energy variables are presented for 5° latitudinal zones from 55 to 75°N and for the polar cap north of 75°N. Spatial distributions of important energy variables are also presented. The flux convergence of potential energy from the source in lower latitudes is identified as the single major source of kinetic energy in higher latitudes. The contribution of the baroclinic conversion is minor. (19 refs.)
- 116213 On the theory of the long-term variability of the atmosphere.** J.Egger, H.-D.Schilling (Meteorologisches Inst., Univ. Munchen, Munchen, Germany). *J. Atmos. Sci. (USA)*, vol.40, no.5, p.1073-85 (May 1983).
Much of the atmosphere's long-term variability is contained in the planetary modes with zonal wavenumber $m \leq 5$. It is proposed that a considerable fraction of this variability is induced by the nonlinear interaction of synoptic-scale modes ($m > 5$) with the planetary-scale modes. To test this hypothesis, the synoptic-scale forcing of the planetary-scale 500 mb streamfunction is determined from data. The response of the planetary motions to this forcing is calculated within the framework of the linear barotropic vorticity equation on the sphere and for β -plane flow. The power spectra and the low-frequency variance of the induced planetary-scale motions are presented. (13 refs.)
- 116214 Space-time spectral analyses of Northern Hemisphere geopotential heights.** P.Speth, R.A.Madden (Nat. Center for Atmospheric Res., Boulder, CO, USA). *J. Atmos. Sci. (USA)*, vol.40, no.5, p.1086-100 (May 1983).
A space-time spectral analysis of a long time series of observed geopotential heights for each season at several levels and latitudes of the Northern Hemisphere is performed as part of a continuing investigation of large-scale traveling waves. The data set that is analyzed consists of the first six zonal wavenumbers. A discussion emphasizes westward traveling wave 1 with periods near 16 and 5 days which the authors argue are consistent with external Rossby waves. An additional outstanding feature is an eastward propagating wave 6 which may result from baroclinic instability. (53 refs.)
- 116215 A diagnostic study of the forcing of the Ferrel cell by eddies, with latent heat effects included.** G.Salustri, P.H.Stone (Dept. of Meteorology & Phys. Oceanography, MIT, Cambridge, MA, USA). *J. Atmos. Sci. (USA)*, vol.40, no.5, p.1101-9 (May 1983).
A diagnostic study of the forcing of the Ferrel cell by eddy fluxes in the Northern Hemisphere is carried out. The quasi-geostrophic omega equation, and Oort and Rasmusson's (1971) data set are used. The effects of condensation associated with the large-scale motions are introduced to the omega equation by using the quasi-geostrophic moisture conservation equation. Thus the dry static stability is replaced by a moist static stability and the forcing of the Ferrel cell by eddy latent heat fluxes as well as sensible heat and momentum fluxes is included. Both effects tend to enhance the forcing of the Ferrel cell. The numerical analysis indicates that the effects are small in January, but in July the maximum vertical velocities are enhanced by ~30%. (12 refs.)
- 116216 The effect of the interference of traveling and stationary waves on time variations of the large-scale circulation.** R.A.Madden (Nat. Center for Atmospheric Res., Boulder, CO, USA). *J. Atmos. Sci. (USA)*, vol.40, no.5, p.1110-25 (May 1983).
It is hypothesized that the interference of stationary and traveling waves of the same longitudinal scale can cause some of the observed time variations in the large-scale circulation. To explore this hypothesis the eight-winter average structure of a regularly occurring, westward propagating disturbance which was earlier (Madden, 1978) called the '16-day wave' is further documented. Energy quantities are calculated as this 16-day wave moves in and out of phase with the stationary or time-mean wave. Eddy heat and momentum transports associated with energy conversions have phase relationships between pressure levels that can be approximately predicted by a simple linear superposition of the observed stationary waves and traveling external Rossby waves. In further support of the hypothesis, cross-spectral results determined from independent data show a reasonable agreement with these predictions. (47 refs.)
- 116217 Interactions between orographically and thermally forced planetary waves.** K.E.Trenberth (Dept. of Atmospheric Sci., Univ. of Illinois, Urbana, IL, USA). *J. Atmos. Sci. (USA)*, vol.40, no.5, p.1126-53 (May 1983).
A comprehensive analysis is made of the atmospheric planetary wave response to orographic and thermal forcing in midlatitudes using a simple model. Vertical heating profiles with maxima at the surface and in the mid-troposphere are considered. The model is quasi-geostrophic on a beta-plane, and has a constant zonal mean basic-state wind. With these simplifications it is possible to obtain complete analytic solutions, not only for the wave response with and without Ekman pumping, but also for the secondary effects of the waves on the zonal mean flow. The presence of diabatic heating in the waves results in significant non-zero Eliassen-Palm fluxes and violates conditions for non-acceleration of the zonal mean flow, both for propagating and trapped waves. The potential vorticity transport or, alternatively, the Eliassen-Palm flux divergence is shown to be directly related to the vertical heating profile. It is the interaction between orographic and thermally forced waves that is mainly responsible for changes in the zonal mean flow, and the results therefore strongly depend upon the relative phase of the thermal and orographic forcing. (57 refs.)
- 116218 A moist baroclinic model for monsoonal mid-tropospheric cyclogenesis.** M.Mak (Dept. of Atmospheric Sci., Univ. of Illinois, Urbana, IL, USA). *J. Atmos. Sci. (USA)*, vol.40, no.5, p.1154-62 (May 1983).
Investigates the effects of condensational heating on the formation of a monsoonal mid-tropospheric cyclone (MTC) by applying the heating parameterization of Mak (1982) to the dynamic model of Brode and Mak (1978) except that the beta-effect is also included. It is found that the observed basic baroclinic flow with turning provides a dynamic framework conducive for a MTC-like disturbance to interact with the embedded moist

convection. The joint processes give rise to an unstable disturbance that has a large but finite growth rate and an intermediate length scale. The key structural features of the observed MTC are reproduced in the most unstable model disturbance. The main influence of the beta-effect is on the phase speed of the model disturbance. In the presence of condensational heating, the beta-effect only has a secondary influence on the growth rate. To understand whether or not the instability results might be strongly controlled by the low-level basic shears, the results computed with or without the latter are compared. (10 refs.)

- 116219 The behavior of stationary waves and the summer monsoon.** B.-D.Lin (Dept. of Atmospheric Sci., Univ. of Washington, Seattle, WA, USA). *J. Atmos. Sci. (USA)*, vol.40, no.5, p.1163-77 (May 1983).
A linear primitive equation model has been used to simulate the behavior of summer stationary waves in the Northern Hemisphere. The role of different forcing mechanisms for the summer stationary waves is compared. It is found that latent heating plays the dominant role for the formation and maintenance of the summer monsoon circulation in the subtropics, but in high latitudes, where advective processes become more important topography and sensible heat flux from the surface produce more realistic surface wave patterns than does the latent heating. The performance of the model for different latitude domains is discussed in some detail. The effects of the mean wind structure on the behavior of stationary waves, especially on horizontal propagation, are examined. (30 refs.)
- 116220 Absolute barotropic instability and monsoon depressions.** R.S.Lindzen, B.Farrell (Center for Earth & Planetary Phys., Harvard Univ., Cambridge, MA, USA), A.J.Rosenthal. *J. Atmos. Sci. (USA)*, vol.40, no.5, p.1178-84 (May 1983).
Approaches the barotropic instability of mean zonal flows over the Bay of Bengal for the months of June, July and August from the perspective of pulse asymptotics rather than most rapidly growing normal modes. (24 refs.)
- 116221 The mesoscale and microscale structure and organization of clouds and precipitation in midlatitude cyclones. VIII. A model for the 'seeder-feeder' process in warm-frontal rainbands.** S.A.Rutledge, P.V.Hobbs (Dept. of Atmospheric Sci., Univ. of Washington, Seattle, WA, USA). *J. Atmos. Sci. (USA)*, vol.40, no.5, p.1185-206 (May 1983).
For pt.VII see *ibid.*, vol.40, no.3, p.559-79 (1983). Previous field studies have indicated that warm-frontal rainbands form when ice particles from a 'seeder' cloud grow as they fall through a lower-level 'feeder' cloud. The authors present results from a parameterized numerical model of the growth processes that can lead to the enhancement of precipitation in a 'seeder-feeder' type situation. The model is applied to two types of warm-frontal rainbands. In the first (Type 1 situation) the vertical air motions are typical of those associated with slow, widespread lifting in the vicinity of warm fronts. In the second (Type 2 situation) the vertical air motions are stronger, and more characteristic of the mesoscale. (41 refs.)
- 116222 Bounds on the growth of perturbations to non-parallel steady flow on the barotropic beta plane.** R.T.Pierrehumbert (Dept. of Meteorology & Phys. Oceanography, MIT, Cambridge, MA, USA). *J. Atmos. Sci. (USA)*, vol.40, no.5, p.1207-17 (May 1983).
Based on considerations of the perturbation enstrophy and energy equations, the author derives a general family of bounds on the growth rates of perturbations to non-parallel (vortex-like or wave-like) flow on the barotropic beta-plane, allowing for the effects of forcing, Ekman friction, and topography. The family of bounds generalizes Arnold's stability criterion. A number of specific applications of the family of bounds are explored. In particular, the formulas are used to demonstrate that the growth rate of the perturbations must vanish if the perturbation length-scale approaches zero or infinity. The distinction between transient and sustained growth of perturbation energy is discussed in light of the results. It is suggested that the bounds are most useful for estimating transient growth rates. (11 refs.)
- 116223 The kinematics of orographic airflow during Sierra storms.** J.D.Marwitz (Dept. of Atmospheric Sci., Univ. of Wyoming, Laramie, WY, USA). *J. Atmos. Sci. (USA)*, vol.40, no.5, p.1218-27 (May 1983).
Two case studies of the kinematics of the airflow over the Sierra barrier are presented. The observations consisted of rawinsondes and single Doppler RHI and velocity azimuth display (VAD) analysis of PPI scans. The RHI scans were made orthogonal to the nearly two-dimensional Sierra barrier. The cloud in the first case study contained a strong stable layer at 0°C while the second storm was highly unstable. The radar bright band and soundings near the radar indicated that an ~250 m thick 0°C isothermal layer was present in response to the diabatic process of melting. When the bright band was impinging upon the barrier, the associated 0°C isothermal layer was inferred to expand until it finally reached the ground. At that point it was ~1 km in depth. Direct thermodynamic soundings are presented for a similar situation which agrees with the modified soundings inferred for this study. The resulting effects on the airflow and precipitation are discussed. (17 refs.)
- 116224 A laboratory experiment on the dynamics of the land and sea breeze.** S.Mitsumoto, H.Ueda (Nat. Inst. for Environmental Studies, Ibaraki, Japan), H.Ozoe. *J. Atmos. Sci. (USA)*, vol.40, no.5, p.1228-40 (May 1983).
The land and sea breeze (LSB) circulation was simulated in a laboratory using a temperature controlled water tank. Flow visualization by tellurium and phenolphthalein and velocity measurement by laser-Doppler velocimeter were carried out in addition to temperature measurements. From similarity considerations, the simulated flow pattern is shown to have good correspondence with that in the atmosphere. It is shown that the overall features of the LSB flow pattern consist of a closed circulating motion caused by the periodically changing horizontal temperature difference between the land and the sea, and several kinds of small scale motions induced by the periodic variation of the land surface temperature itself. (27 refs.)
- 116225 Theoretical experiments on cumulus dynamics.** L.R.Koenig, F.W.Murray (Rand Corp., Santa Monica, CA, USA). *J. Atmos. Sci. (USA)*, vol.40, no.5, p.1241-56 (May 1983).
The sensitivity of a two-dimensional cloud model to changes in microphysical characteristics is examined using two soundings. The dynamical evolution of clouds having relatively warm bases is controlled more by rapidity of the production of liquid-phase precipitation than by the differences in the concentration of ice particles. There is little change in the dynamical properties of the relatively cold-base clouds with changes in either liquid or ice phases. A study of the components of the forces causing evolution of the clouds indicated that the net force acting at a given location was often quite small compared to several individual components of the force. Anything causing these individual forces to move relative to one another will make changes in the net force and alter the dynamical properties of the cloud. (17 refs.)

116226 A numerical simulation of winter cumulus electrification. I. Shallow cloud. T.Takahashi (Dept. of Meteorology, Univ. of Hawaii, Hilo, HI, USA).

J. Atmos. Sci. (USA), vol.40, no.5, p.1257-80 (May 1983).

The development of electricity in a shallow wintertime cumulus is studied using an axisymmetric cloud model containing both microphysical and electrical charge separation processes during graupel formation. The charge separation mechanisms considered included ion induction, ion diffusion, polarization and riming electrification. An unexpected result was that polarization did not intensify cloud electrification. Instead, riming electrification appears to be the principal charge separation process acting to intensify cloud electricity. (60 refs.)

116227 Effects of growth temperatures and surface roughness on crystal orientation of ice accreted in a dry regime. L.Levi, F.Prodi (Istituto FIS-BAT-CNR, Bologna, Italy).

J. Atmos. Sci. (USA), vol.40, no.5, p.1281-99 (May 1983).

The dependence of crystal orientation on air and deposit temperatures in ice accreted in the dry growth regime is re-examined by producing accretions over a wide range of these temperatures and critically examining the structural aspects of the deposits, such as surface roughness. It is shown that the variation in the preferred c -axis orientation with the air and deposit temperatures during growth is an intrinsic effect of the freezing mode of ice, rather than an effect of surface roughness. The $F(\phi)$ distributions of the angle ϕ between the accretion radius and the crystal c -axis, and those of its component angles $F(\eta)$ and $F(\theta)$, are obtained. (19 refs.)

116228 Observations of liquid water in orographic clouds over Elk Mountain. M.K.Politovich, G.Vali (Dept. of Atmospheric Sci., Univ. of Wyoming, Laramie, WY, USA).

J. Atmos. Sci. (USA), vol.40, no.5, p.1300-12 (May 1983).

The relatively simple orographic clouds forming in winter over Elk Mountain, Wyoming, provided useful opportunities for field studies of cloud formation and of ice crystal development. The observations of cloud droplet populations, spanning a range of five consecutive years, are summarized. Data are presented which describe the climatology of the cloud droplet spectra. Selected cases are described in detail to illuminate the processes at work and to allow comparisons with theoretical predictions. Droplet concentrations are mostly around 300 cm^{-3} in accordance with the weak updrafts of the clouds and with the mid-continental, unpolluted cloud condensation nucleus concentrations prevailing in the region. (19 refs.)

116229 On the aerosol particle size distribution spectrum in Alaskan air mass systems: Arctic haze and non-haze episodes. G.E.Shaw (Geophys. Inst., Univ. of Alaska, Fairbanks, AK, USA).

J. Atmos. Sci. (USA), vol.40, no.5, p.1313-20 (May 1983).

Aerosols in central Alaskan winter air mass systems are classified according to size by diffusive separation and light-scattering spectrometry. Particles entering central Alaska from the Pacific Marine environment had number concentrations ranging from 300 to 2000 cm^{-3} and unimodal size spectra, with maximum in number concentration near $1 \times 10^{-6}\text{ cm}$ radius. Air masses entering Alaska from the Eurasian Arctic possessed a factor of two smaller aerosol number concentrations than Pacific Marine systems but contained a factor of two greater particle volume loading within the fine particle radius range $\sim 5 \times 10^{-7} < r < 1 \times 10^{-5}\text{ cm}$. The particles in Eurasian Arctic air masses were bimodally distributed, with maxima in the particle size spectra near $r = 3 \times 10^{-7}$ and $5 \times 10^{-6}\text{ cm}$. Sulfur was the predominant element in all cases studied. A particle depleted region was present in the size spectra obtained for Eurasian Arctic air masses. The deficiency of particles in the 10^{-6} cm radius range is interpreted. (24 refs.)

116230 Troposphere-stratosphere (surface-55 km) monthly winter general circulation statistics for the Northern Hemisphere—four year averages. M.A.Geller (NASA/Goddard Space Flight Center, Greenbelt, MD, USA), M.-F.Wu, M.E.Gelman.

J. Atmos. Sci. (USA), vol.40, no.5, p.1334-52 (May 1983).

Monthly mean Northern Hemisphere general circulation statistics are presented for the four-year average December, January and February months of the winters 1978-9 through 1981-2. These calculations start with daily maps for eighteen pressure levels between 1000 and 0.4 mb of Northern Hemisphere temperature at 1200 GMT that are supplied by NOAA/NMC. Geopotential height and geostrophic wind are constructed using the hydrostatic and geostrophic relationships, respectively. Fields presented are zonally averaged temperature, mean zonal wind, and amplitude and phase of planetary waves with zonal wavenumbers 1-3. Diagnostic quantities, such as the northward fluxes of heat and eastward momentum by standing and transient eddies along with their wavenumber decomposition and Eliassen-Palm flux propagation vectors and divergences by the standing and transient eddies along with their wavenumber decomposition, are also given. The results are compared with those of several other works. (27 refs.)

116231 Asymmetries of the upper stratospheric ozone distribution between two hemispheres. K.Maeda, D.F.Heath (NASA/Goddard Space Flight Center, Greenbelt, MD, USA).

J. Atmos. Sci. (USA), vol.40, no.5, p.1353-9 (May 1983).

Based on the Nimbus-7 solar backscattered UV-radiation data which are free from the instrumental background noise (dark-current) produced by magnetospheric particles, it is found that the southern winter hemispheric ozone densities in the upper stratosphere are nearly 20% higher than their counterparts in the Northern Hemisphere. This is in significant contrast to the well-known hemispheric asymmetry of the total ozone content which is higher in the northern hemispheric winter than in the southern hemispheric winter. Comparisons of those findings with the previously obtained similar results from the Nimbus-4 backscattered UV radiation (BUV) experiment manifest that the dark-current effect on the latter was negligible. Therefore, using the stratospheric temperature which was observed by means of the selective chopper radiometer simultaneously with the BUV experiments on the Nimbus-4 for 1970 and 1972, the cause of these asymmetries due to the temperature dependent photochemistry is examined. (21 refs.)

116232 Hurricane Allen and island obstacles. H.F.Hawkins (Cooperative Inst. for Marine & Atmospheric Studies, Univ. of Miami, Coral Gables, FL, USA).

J. Atmos. Sci. (USA), vol.40, no.5, p.1360-1 (May 1983).

The first significant filling of Hurricane Allen coincided with its encroachment on Haiti, Jamaica and eastern Cuba. It is suggested that the filling was due to the interruption offered to its circulation by the mountainous terrain. The accompanying secondary wind maximum may have contributed to, or have been coincidental with, the weakening observed. (2 refs.)

116233 Occurrence probability of solar-geomagnetic-weather relations. B.R.Arora (Indian Inst. of Geomagnetism, Bombay, India).

J. Atmos. & Terr. Phys. (GB), vol.45, no.8-9, p.569-72 (Aug.-Sept. 1983).

Relationships of the vorticity area index (VAI) and the geomagnetic activity (Ap) to solar magnetic sector boundary passage (SBP) are examined in terms of the probability of occurrence of these associations with individual SBP.

The results reveal that the probability of occurrence of the characteristic variation in the VAI in relation to the SBP is comparable to the well-established association between Ap and SBP. It is further shown that the sector related effects on VAI are completely independent of the nature of transient changes in the geomagnetic activity accompanying the SBP. (12 refs.)

116234 A theoretical study of the height distribution of sodium in the mesosphere. L.Thomas (Dept. of Phys., Univ. Coll. of Wales, Aberystwyth, Wales), M.C.Isherwood, M.R.Bowman.

J. Atmos. & Terr. Phys. (GB), vol.45, no.8-9, p.587-94 (Aug.-Sept. 1983).

Time-dependent solutions of the diffusion and continuity equations for oxygen-hydrogen and sodium constituents are used to examine the characteristics of the height distribution of sodium atoms. Account is taken of recent experimental data on relevant chemical and photochemical processes. Particular attention is paid to the processes which determine the peak altitude of the layer, the slope of the height distribution above the peak, and the diurnal variation of the layer, as revealed by measurements using various techniques. (44 refs.)

116235 Intensity fluctuations due to a deeply modulated phase screen. I. Theory. B.J.Uscinski, C.Macaskill (Dept. of Appl. Math. & Theoretical Phys., Univ. of Cambridge, Cambridge, England).

J. Atmos. & Terr. Phys. (GB), vol.45, no.8-9, p.595-605 (Aug.-Sept. 1983).

Analytical expressions are found for the intensity fluctuation spectrum due to a deeply modulated phase screen that are valid over the whole range of spatial frequencies including previously neglected transition regions. A screen with a Gaussian phase spectrum is considered, as well as screens with two different types of power-law spectra. The results illustrate the basic differences that exist in the intensity fluctuations for the different types of screen. It is shown that the low frequency part of the intensity fluctuation spectrum must be included to obtain the correct form of the limiting spectrum and scintillation index. (12 refs.)

116236 Intensity fluctuations due to a deeply modulated phase screen. II. Results. C.Macaskill, B.J.Uscinski (Dept. of Appl. Math. & Theoretical Phys., Univ. of Cambridge, Cambridge, England).

J. Atmos. & Terr. Phys. (GB), vol.45, no.8-9, p.607-15 (Aug.-Sept. 1983).

For pt.I see *ibid.*, vol.45, no.8/9, p.595-605 (1983). Detailed numerical results are presented for the spatial frequency spectra of intensity fluctuations for three representative types of one dimensional phase screen. Only deeply modulated screens are considered and comparison is made with analytical approximations. The role of the inner scale is discussed and shown to be significant in the case of a screen with an exponential correlation function. The effect of allowing the outer scale to become very large is also considered. (12 refs.)

116237 Determination of excessive absorption by atmospheric water vapour at 22.235 GHz. C.K.Bhattacharya, G.S.Uppal, M.K.Raina, V.Dubey (Radio Sci. Div., Nat. Phys. Lab., New Delhi, India).

J. Atmos. & Terr. Phys. (GB), vol.45, no.8-9, p.617-20 (Aug.-Sept. 1983).

A theoretical estimation of zenith attenuation at 22.235 GHz using radio-sonde data is presented. It is computed by dividing the atmosphere into thirteen layers and summing the contribution of attenuation from each layer. The attenuation of each layer has been computed by using line-by-line summation. The zenith attenuation is compared with that observed by a radiometer operating at 22.235 GHz. The radiometer observations are found to be 7-18% higher than the values computed by the radio-sonde data. This excessive absorption by water vapour is suggested to be due to clusters present in the water vapour phase in the Earth's atmosphere. (16 refs.)

116238 Estimation of low-frequency wind stress fluctuations over the open ocean. K.R.Thompson, R.F.Marsden (Dept. of Oceanography, Dalhousie Univ., Halifax, Nova Scotia, Canada), D.G.Wright.

J. Phys. Oceanogr. (USA), vol.13, no.6, p.1003-11 (June 1983).

A simple, approximate formula for mean wind stress is given in terms of the mean and variance of the wind fluctuations over the averaging period. The formula is tested using 3 h wind observations from eight North Atlantic Ocean Weather Ships. Mean wind stress is calculated (1) by vector averaging the 3 h wind stresses, and (2) by applying the approximate formula. For an averaging period of 4 months the two methods agree to within $\pm 0.025\text{ Pa}$, 95% of the time. A straightforward method is described for the estimation of vector mean wind and variance fields, and thus mean stress fields, over the open ocean. To check the method, the long-term stress field of the North Atlantic, and the seasonal Sverdrup transport across 31°N , are computed and compared with the values given by Willebrand (1978), and Bunker and Leetma (1978). The zonally integrated Sverdrup transport across 45°N is also calculated. (15 refs.)

116239 A comparison of different sea level pressure analysis fields in the east Greenland Sea. W.B.Tucker,III. (US Army Cold Regions Res. & Engng. Lab., Hanover, NH, USA).

J. Phys. Oceanogr. (USA), vol.13, no.6, p.1084-8 (June 1983).

Geostrophic wind fields, used to drive a numerical sea ice model, are calculated from three sources of sea-level pressure. The pressures obtained from the National Weather Service's operational analysis system, which are also included as part of the level III-A FGGE data set, yield erroneously high winds concentrated in a narrow band adjacent to the Greenland coast and, consequently, lead to unrealistic model results. Other pressure fields obtained from (1) an independent optimal analysis that merged pressure data from Arctic FGGE buoys with high latitude land stations and from (2) manual digitization of the NWS hand-analyzed Northern Hemisphere surface charts agree well and do not exhibit these high winds. The extreme pressure gradient parallel to Greenland results partially from the pressure reduction procedure used to obtain the sea level pressures from the terrain-following sigma coordinate system. An associated problem may be that the NWS data filtering procedure sees the rapid elevation change of eastern Greenland as a discontinuity. (7 refs.)

116240 Stationary waves forced by topography in a vertically sheared, stratified, rotating fluid. C.B.Fandry, R.L.Hughes, L.M.Leslie (Australian Numerical Meteorology Res. Centre, Melbourne, Victoria, Australia).

J. Aust. Math. Soc. Ser. B (Australia), vol.25, pt.1, p.127-44 (July 1983).

The effect of an isolated topographic bump in a two-layer fluid on a β -plane is investigated. An analytical solution is derived in terms of the appropriate Green's function for arbitrary topography of finite horizontal extent. It is found that the disturbances generated by the bump are composed of two fundamental modes which may be wavelike or evanescent. The wavelike modes are topographically induced Rossby waves which occur only when there is eastward flow in at least one of the layers. These waves are always confined to the downstream (eastward) side of the bump. Whereas previous studies of this type have concentrated on eastward flow over topography, the theory has been extended here to include a wide range of vertically sheared flows. Particularly important is the case of low level westward flow combined with upper level eastward flow, as it has direct application, for example, to

the summertime atmospheric circulation over the subtropical regions of the continental land masses. (15 refs.)

116241 Possible improvements in meteorology for aircraft navigation. M.Bisiaux, M.E.Cox, D.A.Forrester, J.T.Storey. *J. Navig. (GB)*, vol.36, no.1, p.54-63 (Jan. 1983). The studies described indicate the feasibility of improving the quality of meteorological forecast data, both for airborne flight management systems (FMS) and ATC purposes, based on the use of aircraft measurements of wind and temperature. Two-way communications could most effectively be supported by SSR Mode-S, the implementation of which should commence in Europe in the early 1990s. This timescale should enable all data source validation, system refinement, planning and implementation to take place in an efficient manner. The improvements envisaged should yield many benefits to ATC, aircraft operators and the meteorological services and thus facilitate an 'overall-system' approach to the more efficient operation and control of air traffic. (9 refs.)

116242 A synoptic case-study using a numerical model. E.McCallum, Jr., J.R.Grant (Meteorological Office Coll., Shinfield Park, England), B.W.Golding.

Meteorol. Mag. (GB), vol.112, no.1334, p.275-88 (Sept. 1983). Conventional analysis is supplemented by results from a numerical model to give increased understanding of the airflow through a system causing an area of extensive frontal rain over England on 22 June 1982. (9 refs.)

116243 An analysis of noctilucent cloud over western Europe during the period 1966 to 1982. D.A.R.Simmons, D.H.McIntosh.

Meteorol. Mag. (GB), vol.112, no.1334, p.289-98 (Sept. 1983). A statistical analysis of noctilucent cloud observations received at the Edinburgh Data Centre from 1966 to 1982 shows a somewhat higher elevation for the upper border of the clouds than has been previously suggested. The range in solar depression over which the clouds were visible and their distribution in latitudes are more restricted than in earlier surveys. The median date for peak frequency of occurrence of the clouds is found to be 4 July. An inverse relationship between annual sunspot number and corresponding frequency of noctilucent cloud occurrence is suggested but not definitely confirmed. (6 refs.)

116244 Spectra of nascent wind waves. G.E.Kononkova, K.V.Pokazeev (Dept. of Phys. of Sea & Inland Water Bodies, Moscow Univ., Moscow, USSR).

Moscow Univ. Phys. Bull. (USA), vol.38, no.1, p.16-20 (1983). Translation of: *Vestn. Mosk. Univ. Ser. 3 (USSR)*, vol.38, no.1, p.16-19 (1983).

The spectra of wind undulation with startup distances of less than 4 m and dynamic velocities of 35 to 90 cm/sec are considered. The difference in the dependence of the spectra on the dynamic velocity and frequency under these conditions in comparison with the spectra of wave disturbance at large distances is explained by the action of drift flow. (7 refs.)

116245 Some periodicities of atmospheric circulation. A.Kh.Khrgian, E.D.Astakhova (Dept. of Atmospheric Phys., Moscow Univ., Moscow, USSR).

Moscow Univ. Phys. Bull. (USA), vol.38, no.1, p.66-71 (1983). Translation of: *Vestn. Mosk. Univ. Ser. 3 (USSR)*, vol.38, no.1, p.57-62 (1983).

On the basis of generalization of much statistical material, the periodicity of atmospheric circulation is studied in various regions of the terrestrial globe at three basic isobaric surfaces (10, 30, and 500 mbar). Zonal circulation varies with a period of 27 days at the 10- and 30-mbar levels and with a period of 25 days at all the levels investigated. An attempt is made to explain a series of the results obtained on the basis of the hypothesis of solar action on the atmospheric circulation and also taking account of the superposition of oscillations. (18 refs.)

116246 Remarks on the numerical forecast of the blizzard situation in Mid-Europe at the turn of the year 1978/79—a case study. P.Emmrich.

Meteorol. Rundsch. (Germany), vol.36, no.4, p.180-9 (Aug. 1983). In German.

The remarkable large-scale development of the atmospheric circulation in Mid-Europe at the turn of the year 1978-9 leading to a blizzard situation with a snow disaster in northern Germany is briefly described. Some important aspects concerning the judgement of numerical field forecasts are discussed from the forecaster's point of view. (6 refs.)

116247 Interpretation of NOAA 7 information for the Mediterranean on 7.10.1981 between 1220 and 1225 GMT. G.Beratung.

Meteorol. Rundsch. (Germany), vol.36, no.4, p.189-95 (Aug. 1983). In German.

The interception facility of AVHRR-data of weather-satellites of the NOAA-series at the German Military Geophysical Office at Traben-Trarbach has been used for a mesoscale-case study based on pictures of NOAA 7 in channels 2, 3 and 4 on 7.10.1981, between 1220-1225 GMT. Channel 2 gives the cloudiness, channel 4 with regard to the black-body-temperature gives the height of the clouds. The signal of channel 3 is made up of two components: the black-body-temperature and the reflected energy of the Sun. It helps to fix the geographic location of the cloudlayers. One problem is the distortion of the radiance caused by thin layers over thick clouds or the ocean surface. In this case study it appears as if a thin hazelayer (seen in channel 2 and partly 3) over the Aegean, Ionian, and Tyrrhenian Sea obstructs the calculation of exact sea surface temperatures. (1 ref.)

116248 3K cosmic microwave background radiation and the rotational levels of the atmospheric H₂O molecule. S.Chakravarty, H.L.Duorah (Dept. of Phys., Gauhati Univ., Gauhati, India).

Proc. Natl. Acad. Sci. India Sect. A, vol.52, pt.2, p.232-44 (1982). [received: Aug. 1983]

The effect of 3K cosmic microwave background radiation on the molecular constituent, H₂O, of the Earth's atmosphere is studied. The transitions among the rotational levels of H₂O, which take part in the absorption of this radiation, are obtained. Earth's motion through the microwave background results in the Doppler-shift of the spectral lines. The absorption coefficient for these lines are then calculated to study the radiation transfer of the 3K background both in emission and absorption. It is found that both emission and absorption are equally important, though absorption is found to exceed the emission slightly, for all the lines under consideration. It is suggested that the atmospheric emission lines need to be subtracted from observed radiation to determine microwave background emission. (10 refs.)

116249 Stratospheric negative ions—detailed height profiles. A.A.Vigiano, H.Schlager, F.Arnold (Max-Planck-Inst. für Kernphys., Heidelberg, Germany).

Planet. & Space Sci. (GB), vol.31, no.8, p.813-20 (Aug. 1983).

Balloon-borne mass spectrometers with extended mass range have been flown during controlled descents. This gives detailed height profiles of stratospheric negative ions between 15 and 34 km. The main ion families are HSO₄⁻ (H₂SO₄)_n (HNO₃)_n and NO₃⁻ (HNO₃)_n. Information concerning trace gases is obtained as well as an assessment of the problems of ion fragmenta-

tion and contamination. The data are used to derive information concerning the rate of H₂SO₄ clustering. (24 refs.)

116250 Solar cycle and equatorial stratopause temperature. K.Mohanakumar, S.Devanarayanan (Dept. of Phys., Univ. of Kerala, Trivandrum, India).

Proc. Indian Acad. Sci. Earth & Planet. Sci., vol.92, no.1, p.31-6 (March 1983). [received: Sept. 1983]

Variations in solar activity and their effect on the temperature of the stratopause are studied. Monthly mean stratopause temperatures during 1969-1976 and departures from the monthly mean determined for four equatorial rocket launching stations, viz. Ascension Island, Kwajalein, Fort Sherman, and Thumba, are statistically compared with sunspot numbers. (9 refs.)

116251 A method for estimating rain attenuation and site diversity effect on earth-satellite links for global use. K.Morita (Electrical Communication Labs., NTT, Tokyo, Japan).

Rev. Electr. Commun. Lab. (Japan), vol.30, no.4, p.676-85 (July 1982). [received: Aug. 1983]

Proposes a simple method for estimating rain attenuation and site diversity effects on earth-satellite links, respectively, from correction factor K_p for the uniform rain rate of each of two slant propagation paths and the simultaneous probability of rain attenuation occurrences over these two paths. Two parameters for the estimation—0°C layer height and the lognormal rain rate distribution—are presented for various parts of the world. Numerical investigations show that satisfactory estimates can be obtained by the method. (13 refs.)

116252 Progress in cloud physics 1979-1982. J.Hallett (Atmospheric Sci. Centre, Desert Res. Inst., Reno, NV, USA).

Rev. Geophys. & Space Phys. (USA), vol.21, no.5, p.965-84 (June 1983).

This review looks at many subjects and techniques. Topics are described beginning with the small and going to the large and then examining the implication of the large-scale phenomena on the small scale. Progress in Cloud Physics is made through laboratory studies, through numerical simulation, and through field observation, aided by new instruments and computers for data handling and reduction. Most important, however, is the birth and development of ideas, occurring on a somewhat random basis, arguably unrelated to the apparent magnitude of effort, but often depending on fortuitous circumstances of discovery and technology development. In particular this review considers atmospheric aerosol, nucleation, droplet growth, convective cloud mixing, ice crystal growth, hail, precipitation, optical and radar properties, electrification, cloud modelling, weather systems and instrumentation and techniques. (454 refs.)

116253 Cloud electrification. R.Lhermitte (Rosenstiel School of Marine & Atmospheric Sci., Univ. of Miami, Miami, FL, USA), E.Williams.

Rev. Geophys. & Space Phys. (USA), vol.21, no.5, p.984-92 (June 1983).

This article describes theories of cloud electrification, radar reflectivity and motion fields of storms, thunderstorm electric fields, lightning; VHF emissions; corona current and electrical processes in the atmospheres of other planets. (112 refs.)

116254 Lightning. M.A.Uman (Dept. of Electrical Engng., Univ. of Florida, Gainesville, FL, USA).

Rev. Geophys. & Space Phys. (USA), vol.21, no.5, p.992-7 (June 1983).

The research on lightning performed in the USA in the period 1976 to 1982 is reviewed. Much of the work reviewed was performed as part of the Thunderstorm Research International Program (TRIP). All aspects of lightning research are discussed. These areas are: (1) phenomenology of lightning; (2) locations of charges associated with various lightning processes; (3) characteristics of lightning electric and magnetic fields; (4) lightning theory and modelling; (5) lightning location by RF techniques; (6) optical measurements; (7) thunder, and (8) unusual lightning. (138 refs.)

116255 The dynamics of large scale atmospheric motions. J.R.Holton (Dept. of Atmospheric Sci., Univ. of Washington, Seattle, WA, USA).

Rev. Geophys. & Space Phys. (USA), vol.21, no.5, p.1021-7 (June 1983).

Dynamic meteorology is the study of atmospheric motions associated with weather and climate. During the past four years there have been a number of exciting developments in the dynamics of synoptic and planetary scale motions. Many of these are related to various aspects of short term atmospheric variability both internally and externally generated. A number of studies have gone beyond the traditional perturbation approach in which disturbances are imposed on a zonally symmetric basic state. Significant progress has been made in understanding the dynamics of the quasistationary zonally asymmetric flow and its control of the transient circulations. This review focuses on the progress made in the understanding of synoptic and planetary scale motions in the troposphere. (117 refs.)

116256 Mesoscale meteorology. K.Emanuel, F.Sanders (Dept. of Meteorology & Phys. Oceanography, MIT, Cambridge, MA, USA).

Rev. Geophys. & Space Phys. (USA), vol.21, no.5, p.1027-42 (June 1983).

Recent research in mesoscale meteorology is reviewed. The authors define what they mean by the mesoscale and go on to review a selected number of topics. These topics include organised convective systems, severe thunderstorms, mesoscale structures within extratropical cyclones, small-scale cyclones, mesoscale wave generation and propagation, thermally forced circulations, orographic circulations, mesoscale turbulence and finally regional scale numerical modelling. (291 refs.)

116257 Atmospheric boundary layers. L.Mahrt (Dept. of Atmospheric Sci., Oregon State Univ., Corvallis, OR, USA).

Rev. Geophys. & Space Phys. (USA), vol.21, no.5, p.1042-8 (June 1983).

This review addresses only fundamental aspects of the physics of the boundary layer and excludes research related to instrumentation, specific applied areas of boundary layer research, and interactions with larger-scale circulations. Some aspects of the boundary layer will be treated very briefly or included only in the reference lists while other topics, which have been omitted in past reviews, will be covered in more depth. Topics described include mixed-layer growth, surface momentum and heat fluxes, surface moisture flux, stability stratified boundary layers, cold air drainage and transitional periods. (217 refs.)

116258 Polar meteorology and climatology 1979-1982. E.Robinson (Coll. of Engng., Washington State Univ., Pullman, WA, USA).

Rev. Geophys. & Space Phys. (USA), vol.21, no.5, p.1048-64 (June 1983).

Recent progress in the study of polar region atmospheric processes is reviewed. The review is divided into four sections on instrumentation, climatology, synoptic studies and precipitation and atmospheric chemistry. (291 refs.)

116259 Progress in weather modification research: 1979-1982. R.A.Dirks (Atmospheric Sci. Div., NSF, Washington, DC, USA).

Rev. Geophys. & Space Phys. (USA), vol.21, no.5, p.1065-76 (June 1983).

This review considers only research which has direct bearing on weather modification. The review of inadvertent weather modification is limited to short term effects due to man which occur only in limited meteorological

conditions and occur over local and regional geographic scales. These somewhat arbitrary bounds distinguish it from climate modification. This review examines a wide range of topics and techniques. Topics are chosen along traditional lines of research beginning with advances in understanding weather modification concepts related to specific cloud and precipitation types, followed by a review of advances in modification and observational technology, design and evaluation techniques, societal impacts of weather modification and, finally, a discussion of the future directions for weather modification research. (181 refs.)

116260 Advances in short term climate prediction. T.P.Barnett, R.C.J.Somerville (Scripps Inst. of Oceanography, Univ. of California, La Jolla, CA, USA).

Rev. Geophys. & Space Phys. (USA), vol.21, no.5, p.1096-102 (June 1983). Dynamical and several empirical and statistical approaches to short term climate prediction are surveyed. General circulation models have displayed considerable potential for this application. Physical/synoptic and purely statistical methods have been intensively developed and tested in recent years. Important problems have been recognised in areas such as predictability, forecast verification and evaluation, and combining supplementary approaches to prediction. (84 refs.)

116261 The atmospheric aerosol system: an overview. J.M.Prospiero (Div. of Marine & Atmospheric Chem., Univ. of Miami, Miami, FL, USA), R.J.Charlson, V.Mohnen, R.Jaenicke, A.C.Delany, J.Moyers, W.Zoller, K.Rahn.

Rev. Geophys. & Space Phys. (USA), vol.21, no.7, p.1607-29 (Aug. 1983). The authors discuss work on atmospheric aerosols that illustrates the complex nature of the aerosol chemical and physical system, and suggest strategies for future research. A major conclusion is that man has had a great impact on the global budgets of certain species, especially sulfur and nitrogen, that play a dominant role in the atmospheric aerosol system. However, at present there is no evidence linking anthropogenic activities with a persistent increase in aerosol concentrations on a global scale. (242 refs.)

116262 Propagation experiment at 140 GHz through simulated rainfall.

T.Manabe, T.Ihara, K.Kitamura, Y.Imai, K.Tohma, Y.Furuhama. *Rev. Radio Res. Lab. (Japan)*, vol.28, no.147, p.541-51 (Sept. 1982). In Japanese. [received: Sept. 1983]

Measurements of rainfall attenuation of a millimeter wave at 140 GHz were conducted through simulated rain using a large scale rainfall installation. Using this installation, rainfalls with different drop-size distributions were realized without varying the rainfall rate. It was experimentally verified that the rainfall attenuation at the millimeter wave band is strongly affected by the raindrop size measurements of the attenuation and the rainfall rate was proposed. This method was applied to the experimental results. The inferred drop-size distribution showed fairly good agreement with those measured directly. The polarization dependence of attenuation and the depolarization were also measured. The effects of raindrop distortion from spherical shapes were found to be too small to be detected by the experimental system. (20 refs.)

116263 The atmosphere. A.P.Ingersoll.

Sci. Am. (USA), vol.249, no.3, p.114-30 (Sept. 1983).

A summary is given of the present state of knowledge about the Earth's atmosphere. The heat balance and optical properties of the atmosphere are described. A large part of the article describes the large scale circulation of the atmosphere and the attempts by meteorologists to make computer models of this circulation. Climate modelling and weather forecasting are also considered. (no refs.)

116264 Improved atmospheric path-length correction by a dual-frequency microwave radiometer. T.Ojima (Radio Res. Labs., Koganei, Japan). *Trans. Inst. Electron. & Commun. Eng. Jpn. Sect. E (Japan)*, vol.E66, no.7, p.427-34 (July 1983).

Water vapor excess path-length (WVEP) in atmosphere, in spite of its much smaller average value than a dry air component which is stable, makes larger seasonal and diurnal variations. An estimation algorithm for WVEP is improved for less errors even in large opacity of the atmosphere and the multi-algorithm program (MAP), together with the Wu-algorithm of JPL in CalTech, is applied to make the least estimation error. A limitation of the MAP is also discussed. The differential emission measurement (DEM) is also applied to WVEP estimation in order to reduce additional errors due to measurement errors of antenna temperature, which can make them a half through one tenth of those by other algorithms. The experimental results gave proof of the effectiveness of the DEM. (19 refs.)

116265 Diurnal variation of rainfall at Nandi Airport, Fiji. S.K.Sharma (Fiji Meteorological Service, Nandi Airport, Fiji). *Weather (GB)*, vol.38, no.8, p.231-9 (Aug. 1983).

Studies the diurnal variation of tropical rainfall on a coastal station based on data from Nandi Airport (17°45'S, 177°27'E, 16 metres), situated on the western, leeward side of Viti Levu. Viti Levu has an area of 10 384 km² and is the largest island in Fiji, from a group of over 300 islands. The extent of orographic effect is noteworthy on this island, since about one-third of Viti Levu lies above 300 metres. (11 refs.)

116266 On the temporal variance of stratospheric trace gas concentrations. D.H.Ehhalt, E.P.Roth, U.Schmidt. *Report JUL-1836*, Kernforschungsanlage, Julich, Germany (March 1983), 44 pp.

The relative variances in stratospheric observations of long-lived trace gases, CH₄, N₂O, CF₃Cl₂, CFC1₃, show large differences. These differences are greatly reduced when the local mean standard deviation is normalized to the local vertical gradient. This ratio, called 'equivalent displacement height' exhibits a characteristic vertical profile which is very similar for all the long-lived trace gases as well as for O₃. With the help of this ratio it is demonstrated that the variances are essentially due to natural causes, i.e. transport. Using the mixing length hypothesis a theoretical expression for the equivalent displacement height is derived. (16 refs.)

116267 Application of nonlinear identification to long range weather prediction. P.M.Toldalgi, R.K.Mehra (Sci. Systems, Inc., Cambridge, MA, USA).

Identification and System Parameter Estimation 1982. Proceedings of the Sixth IFAC Symposium, Washington, DC, USA, 7-11 June 1982 (Oxford, England: Pergamon 1983), p.515-20 vol.1

Discusses the problem of long range weather prediction using the Group Method of Data Handling, in which nonlinear time series models are constructed and trained on the weather data. The research reported involves the reduction and preliminary analysis of hemispheric 700-maps. (21 refs.)

Self-study manual on optical radiation measurements: Part III - Applications, chapter 1. Measurement of solar terrestrial spectral irradiance in the ozone cut-off regionSee Entry 111383

Supersonic stabilization of a tangential shear in a thin atmosphereSee Entry 113416

Measurement of the time variational behaviours of aerosols based on size distributionSee Entry 115716

Wind dependence of underwater ambient noiseSee Entry 116090

The role of sea surface temperature in large-scale air-sea interactionsSee Entry 116091

Reduction of thermohaline circulation during deglaciation: the effect on atmospheric radiocarbon and CO₂See Entry 116093

Barotropic instability of weakly non-parallel zonal flowsSee Entry 116095

Internal wave wake of a moving storm. I. Scales, energy budget and observationsSee Entry 116105

The generation of surface waves by an intense cycloneSee Entry 116116

The seasonal variability of the Lomonosov CurrentSee Entry 116123

Verification and correction of BKF-precipitation forecasts for the use in a runoff modelSee Entry 116158

Apportioning light extinction coefficients to chemical species in atmospheric aerosolSee Entry 116269

Spatial and temporal variability of the tropospheric aerosol absorption coefficient in the spectral region 0.4-2.2 micronsSee Entry 116272

Finite exposure time, astronomical speckle transfer functionSee Entry 116274

Propagation of thermal radiation in the presence of random refraction of rays in a medium with a fluctuating dielectric constantSee Entry 116276

Atmospheric radiation: 1975-1983See Entry 116277

The Global Atmospheric Research Program: 1979-82See Entry 116279

OH PepsiosSee Entry 116283

Water channel simulation of the atmospheric boundary layerSee Entry 116284

Methodology for the analysis of peroxyacetyl nitrate (PAN) in the unpolluted atmosphereSee Entry 116285

On the dynamic range of resonance spectrophoneSee Entry 116293

HF Doppler measurements of mesospheric gravity wave momentum fluxesSee Entry 116294

Radio transillumination of the atmosphere by artificial and natural sourcesSee Entry 116304

Advances in remote sensing of the atmosphereSee Entry 116305

Radar-acoustic probing of randomly oriented air flowsSee Entry 116306

On the extraction of tidal information from measurements covering a fraction of a daySee Entry 116327

92.60S Climatology

116268 Evaluation of the climatic zonality of the Indian Ocean during Pliocene time from deep-sea drilling data. Ye.V.Ivanova, M.S.Barash (Shirshov Inst. of Oceanology, Acad. of Sci., Moscow, USSR).

Oceanology (USA), vol.22, no.1, p.50-6 (1982). Translation of: *Okeanologiya (USSR)*, vol.22, no.1 (1982). [received: Aug. 1983]

Semi-quantitative data on the distribution of planktic forams in early, middle, and late Pliocene sediments of the Indian Ocean, published in reports on deep-sea drilling, are reduced to a single point scale and to percentages. On this basis, the authors determine the types and subtypes of thanatocoenoses of the planktic forams and reconstruct the position of the corresponding climatic zones. The authors find that during Pliocene time there was a gradual drop of the temperature of the surface layer of water in the Indian Ocean. (33 refs.)

Isostatic adjustments in a full glacial seaSee Entry 116060

Reduction of thermohaline circulation during deglaciation: the effect on atmospheric radiocarbon and CO₂See Entry 116093

A model study of the short-term climatic and hydrologic effects of sudden snow-cover removalSee Entry 116153

Variability of the Indian summer monsoon and tropical circulation featuresSee Entry 116190

Polar meteorology and climatology 1979-1982See Entry 116258

Advances in short term climate predictionSee Entry 116260

92.65 ATMOSPHERIC OPTICS

(see also 42.00 Optics)

116269 Apportioning light extinction coefficients to chemical species in atmospheric aerosol. H.Hasan, T.G.Dzubay (Environmental Sci. Res. Lab., US Environmental Protection Agency, Research Triangle Park, NC, USA). *Atmos. Environ. (GB)*, vol.17, no.8, p.1573-81 (1983).

A 1978 Denver aerosol data set has been analyzed by a variety of methods for determining light scattering and extinction coefficients per unit mass concentration for specific chemical species in fine particles (<2.5 µm diameter). Multiple regression of light scattering coefficient versus chemical species concentrations was used to determine scattering to mass concentration ratios and their related uncertainties for specific chemical species, and the results are compared with those reported by previous investigators. Differences in the scattering to mass concentration ratios for all the major species in the aerosol except ammonium sulfate were found to be statistically insignificant. Light scattering and absorption coefficients were apportioned by chemical species for an external mixture using a published equation and for an internal mixture using equations that the authors derived. (32 refs.)

116270 Surface illuminance and albedo of a planetary atmosphere with nearly conservative scattering. Zh.M.Dlugach, E.G.Yanovitskii.

Izv. Akad. Nauk SSSR Fiz. Atmos. & Okeana, vol.19, no.8, p.813-23 (Aug. 1983). In Russian. English translation in: *Izv. Acad. Sci. USSR Atmos. & Oceanic Phys. (USA)*

A plane homogeneous atmosphere of an arbitrary thickness with anisotropic scattering is considered. It is shown that in a nearly conservative case the plane albedo and illuminance of the surface are expressed by two functions at the conservative case. For calculation of complete amount of radiant energy absorbed by column of atmosphere of the unit section an additional function is needed. The tables of these functions for the Rayleigh and the Henyey-Greenstein phase functions are given for wide region of the values of the optical thickness. (7 refs.)

116271 Statistical method for calculation of molecular absorption. Yu.S.Makushkin, A.A.Mitsel', K.M.Firsov.
Izv. Akad. Nauk SSSR Fiz. Atmos. & Okeana, vol.19, no.8, p.824-30 (Aug. 1983). In Russian. English translation in: *Izv. Acad. Sci. USSR Atmos. & Oceanic Phys. (USA)*
Statistical forecast of molecular absorption characteristics according to the known value of the absorption coefficient near the Earth's surface is suggested. The correlation matrix of the optical thickness using the statistical information on humidity and temperature is calculated for the wavelength $\lambda=10.6\text{ }\mu\text{m}$. In conclusion the diagrams are given which allow to estimate effectively the optical thickness and transparency. (12 refs.)

116272 Spatial and temporal variability of the tropospheric aerosol absorption coefficient in the spectral region 0.4-2.2 microns. L.I.Chapurskii.
Izv. Akad. Nauk SSSR Fiz. Atmos. & Okeana, vol.19, no.8, p.831-8 (Aug. 1983). In Russian. English translation in: *Izv. Acad. Sci. USSR Atmos. & Oceanic Phys. (USA)*
Data are obtained on radiation fluxes in different atmospheric layers and various climatic zones, air masses and seasons. Data on spectral behaviour of mean values of the aerosol absorption coefficients are presented for altitude layers from 0.3-0.6 to 6.1-9 km. The data agree with published results of aircraft, aerostat and ground-based measurements of aerosol attenuation and absorption. Attention is paid to the spectral behaviour of these values which have a repeating maximum of absorption near 1.25 microns. The maximum may be connected with various particles of natural and anothropogenic origin. (22 refs.)

116273 Investigations of atmospheric spectroscopy. V.E.Zuev.
J. Appl. Spectrosc. (USA), vol.37, no.6, p.1362-78 (Dec. 1982). Translation of: *Zh. Prikl. Spektrosk. (USSR)*, vol.37, no.6, p.923-41 (Dec. 1982). [received: Sept. 1983]
Investigations of atmospheric spectroscopy are of interest from the standpoint of the study of the fundamental laws of intermolecular and intramolecular interactions and in connection with the enormous practical needs to have data on the parameters of lines and the absorption coefficients and functions of atmospheric gases. The latter are especially important for a quantitative estimate of the energy losses of laser radiation in the atmosphere due to its absorption by gaseous components as well as due to the widespread development of a research front in spectroscopic methods of laser sounding of the atmosphere. The article is devoted to an exposition of the principal results of investigations with special emphasis on results obtained recently. (25 refs.)

116274 Finite exposure time, astronomical speckle transfer function. R.Barakat (Div. of Appl. Sci., Harvard Univ., Cambridge, MA, USA), P.Nisenson.
Opt. Acta (GB), vol.30, no.10, p.1405-16 (Oct. 1983).
The effects of finite exposure time (used to record astronomical speckle data) on the speckle transfer function are shown to be highly dependent on the details of the atmospheric turbulence in the optical path as well as on the deterministic wavefront aberrations of the optical system. Both Taylor turbulence, where a frozen layer or layers are convected across the aperture, and Mintzer turbulence, where the turbulence is boiling and stationary, are taken into account. Computations have been made for some typical cases of the time integrated speckle transfer function for various combinations of Taylor and Mintzer turbulence with focused and defocused optical systems. (18 refs.)

116275 Amplification of the mean intensity of backscattering in a turbulent atmosphere. S.S.Kashkarov (Inst. of Atmospheric Phys., Acad. of Sci., USSR).
Radiophys. & Quantum Electron. (USA), vol.26, no.1, p.36-40 (Jan. 1983). Translation of: *Izv. VUZ Radiofiz. (USSR)*, vol.26, no.1, p.44-8 (Jan. 1983). [received: Sept. 1983]
Describes an experimental study of the backscattering of optical radiation from a 'rough' scatterer over paths near the ground having lengths of 650 and 1300 m. The author investigates the dependence of backscatter amplification of the size of fluctuations in the radiation incident on the scatterer and on the direction of scattering. The ratios between the backscatter amplification and characteristics of the intensity fluctuations of the radiation at the scatterer are in agreement with theoretical predictions. (12 refs.)

116276 Propagation of thermal radiation in the presence of random refraction of rays in a medium with a fluctuating dielectric constant. A.N.Reznik.
Radio Eng. & Electron. Phys. (USA), vol.27, no.11, p.81-6 (Nov. 1982). Translation of: *Radiotekh. & Elektron. (USSR)*, vol.27, no.11, p.2156-62 (Nov. 1982). [received: Sept. 1983]
Transfer of thermal radiation in a randomly inhomogeneous medium is examined with a consideration of random refraction of rays. Expressions are derived for the average value and the variance of the brightness temperature of the characteristic radiation of a planar layer. It is shown that in terms of external radiation an inhomogeneous layer is a filter of low spatial frequencies and the transfer function of the layer is derived. The derived effects are estimated for conditions existing in the atmosphere and in the ionosphere of the Earth. (9 refs.)

116277 Atmospheric radiation: 1975-1983. W.Wiscombe (Dept. of Appl. Sci., New York Univ., New York, NY, USA).
Rev. Geophys. & Space Phys. (USA), vol.21, no.5, p.997-1021 (June 1983).
Recent progress in the field of atmospheric radiation is reviewed. Topics discussed include the greenhouse effect due to trace gases, molecular spectra, cloud radiation, Earth radiation budget, aerosol radiation, single and multiple scattering, surface reflectivity and measurement techniques. (1407 refs.)

116278 Krakatoa sunsets. J.Austin (Sci. Museum, London, England).
Weather (GB), vol.38, no.8, p.226-31 (Aug. 1983).
The major eruption of Krakatoa took place on 27 August 1883 and huge quantities of dust and water vapour were ejected into the stratosphere. The quantities involved, especially for water vapour, are not accurately known. A succession of optical phenomena then followed: coloured Suns, twilight glows, Bishop's Ring and noctilucent clouds in that approximate order. It seems that all of these, with the possible exception of noctilucent clouds, were attributable to optically active particles of size $0.5\text{ }\mu\text{m}$, situated in the stratosphere. The feature which changed with time was the amount of background haze due to larger optically neutral particles. Thus the coloured Suns were only seen in extremely murky conditions, while the Bishop's Ring was best seen on clear days or from the top of a mountain. There is no record of both being seen at exactly the same time. (9 refs.)

Self-study manual on optical radiation measurements: Part III - Applications, chapter 1. Measurement of solar terrestrial spectral irradiance in the ozone cut-off regionSee Entry 111383

Analysis of the absorption spectrum of heavy water vapor near 1.06 μm See Entry 112731

Investigation of the spectral composition of solar radiation under conditions prevailing at TashkentSee Entry 116169

Simultaneous detection of FC-11, FC-12 and FC-22, through 8 to 13 micrometers IR solar observations from the groundSee Entry 116204

Intensity fluctuations due to a deeply modulated phase screen. I. TheorySee Entry 116235

Intensity fluctuations due to a deeply modulated phase screen. II. ResultsSee Entry 116236

Determination of excessive absorption by atmospheric water vapour at 22.235 GHzSee Entry 116237

Northern skies. Britain's new telescopes in the Canary IslandsSee Entry 116471

On the instrumental and atmospheric stray-light for solar observationsSee Entry 116478

92.90 OTHER TOPICS IN HYDROSPHERIC AND ATMOSPHERIC GEOPHYSICS

Adiabatic lapse rates of planet atmospheresSee Entry 111368

Paleoceanography: global ocean evolutionSee Entry 116145

93.00 GEOPHYSICAL OBSERVATIONS, INSTRUMENTATION, AND TECHNIQUES

93.30 INFORMATION RELATED TO GEOGRAPHICAL REGIONS

Hot particles from nuclear atmospheric test of October 1980See Entry 112445

Hydrocarbons in water, sediment and mussels from the southern Baltic SeaSee Entry 115704

Evaluation of ocean pollution (experience of the United Nations Program in the West African region)See Entry 115705

Water quality measurement by observing aquatic animals on mountain streams near Shinshin-so Hut, Doshisha University, 1982See Entry 115706

Pollution levels in some Nigerian riversSee Entry 115707

Factors affecting the concentrations of cadmium, zinc, copper and lead in the sediments of the Vedre RiverSee Entry 115708

The New Jersey project on Airborne Toxic Elements and Organic Substances (ATEOS): A summary of the 1981 summer and 1982 winter studiesSee Entry 115709

Organic and elemental composition of airborne particulate matter in Beijing, spring 1981See Entry 115712

Background atmospheric ^{222}Rn concentrations outdoors and indoors: a reviewSee Entry 115939

Radon daughter exposures in the UKSee Entry 115941

Environmental radon and cancer correlations in MaineSee Entry 115942

Indoor radon progeny exposure in the Florida phosphate mining region: a reviewSee Entry 115943

Radon concentrations and infiltration rates measured in conventional and energy-efficient housesSee Entry 115944

Indoor radon levels in the northeastern US: effects of energy-efficiency in homesSee Entry 115945

Radon and radon daughter measurements in solar buildingsSee Entry 115946

Results of indoor radon measurements using the Track Etch methodSee Entry 115947

Integrated radon data from dwellings in Maine and TexasSee Entry 115948

Study of radon daughter concentrations in Polk and Hillsborough countiesSee Entry 115949

A high resolution gravimetric geoid for Europe and bordering marine areasSee Entry 115998

Movements of the fracture zone and the seismic activity under the fracture zone—based on the observations at AbuyamaSee Entry 115999

Paleomagnetism of the Paleocene Ghost Rocks Formation, Prince William terrane, AlaskaSee Entry 116001

Palaеomagnetism of Palaeozoic rocks from the Cabo de Penas, Asturias, SpainSee Entry 116004

Palaеomagnetism of NW Scotland syenites in relation to local and regional tectonicsSee Entry 116005

Palaеomagnetism of late Precambrian-Cambrian volcanics and intrusives from the Armorican Massif, FranceSee Entry 116006

Paleomagnetic evaluation of the orocline hypothesis in the Central and Southern AppalachiansSee Entry 116009

Analytical representation of spatial and temporal variations of the geomagnetic field in the Indian regionSee Entry 116013

An episode of steep geomagnetic inclination 120000 years agoSee Entry 116014

A combined analysis of the gravitational and magnetic anomalies for the detection of magnetically active rock complexes in the basement of the West Siberian plateSee Entry 116015

A geological and paleomagnetic study of the Hyblean volcanic rocks, SicilySee Entry 116016

Paleomagnetic investigations in the Thuringer Forest (GDR)See Entry 116017

Magnetic anomalies on and around the Bonin RiseSee Entry 116018

P-wave velocity structure of the upper mantle in northern ChinaSee Entry 116019

Direct and indirect aftershocksSee Entry 116020

Microearthquake activity of Derbendikhan dam areaSee Entry 116022

Amplitude spectra for some earthquakes recorded in IraqSee Entry 116023

A lithospheric seismic refraction profile in the western North Atlantic OceanSee Entry 116024

- Long-term premonitory seismicity patterns in Italy See Entry 116025
- A study of the 1980 summer seismic sequence in the Magnesia region of Central Greece See Entry 116027
- T-phases from an earthquake swarm on the Mid-Atlantic Ridge at 31.6°N See Entry 116030
- The seismology of Greece See Entry 116033
- The occurrence of large earthquakes in South Italy See Entry 116034
- Long-term prediction of earthquakes in western Honshu, Japan See Entry 116035
- Scaling of rupture size. II. On time and space distributions and magnitude-frequency distribution of swarm See Entry 116036
- Focal distribution of earthquakes in relation to major geological tectonic lines in Shikoku, Japan See Entry 116037
- Study of Iwasaki earthquake swarm in Aomori Prefecture. II. Seismic activity and crustal movement See Entry 116038
- The characteristics of geophysical field and the distribution and formation of oil- and gas-bearing basin in eastern China See Entry 116039
- Further thermochronometric unravelling of the age and palaeomagnetic record of the southwest Grenville Province See Entry 116040
- Marathon dikes: Rb-Sr and K-Ar geochronology of ultrabasic lamprophyres from the vicinity of McKellar Harbour, northwestern Ontario, Canada See Entry 116041
- Apatite fission-track dating of erosion in the eastern Andes, Bolivia See Entry 116042
- A marine seismic refraction study of the Santa Barbara Channel, California See Entry 116043
- Ion microprobe identification of 4100-4200 Myr-old terrestrial zircons See Entry 116044
- On the relation between the deep subsurface structure of the Baikal and Red Sea rifts and the lateral movements of lithospheric plates See Entry 116046
- A model of thermal conduction in the Earth's crust in the Okhotomorskii region See Entry 116052
- Cataclastic rocks of the San Gabriel fault—an expression of deformation at deeper crustal levels in the San Andreas fault zone See Entry 116053
- Geochronological and structural study of Tertiary and Quaternary dikes in southern France and Sardinia: an example of the utilization of dike swarms as paleostress indicators See Entry 116054
- Relation of summit deformation to East Rift Zone eruptions on Kilauea volcano, Hawaii See Entry 116055
- The Long Valley/Mono Basin volcanic complex in eastern California: status of present knowledge and future research needs See Entry 116056
- ¹⁴C age of volcanic ash flow at Danan Island Somma of Krakatau Volcano, Indonesia See Entry 116057
- The Mesozoic magmatism of the Aldan shield as an indicator of its tectonic regime See Entry 116058
- The underthrusting movement of the Western Pacific Plate and the deep focus earthquake zone or northeast China See Entry 116059
- The Snake Range decollement: an exhumed mid-Tertiary ductile-brittle transition See Entry 116061
- Paleogene evolution of the Kodiak Islands, Alaska: consequences of ridge-trench interaction in a more southerly latitude See Entry 116062
- Tectonics of ridge-transform intersections at the Kane fracture zone See Entry 116066
- Changing stress field in the middle segment of the Tan-Lu fault zone, eastern China See Entry 116067
- ²²⁶Ra and ²²²Rn contents of Galapagos Rift hydrothermal waters—the importance of low-temperature interactions with crustal rocks See Entry 116073
- Intense hydrothermal activity at the axis of the East Pacific Rise near 13°N: submersible witnesses the growth of sulfide chimney See Entry 116074
- New data on the structure of Ampere Seamount See Entry 116075
- Geologic mapping of the summit of Afanasy Nikitin Seamount from the Zvuk-4 towed submersible See Entry 116076
- Ninigi and Godaigo seamounts: twins of the Emperor Chain by multi-beam sonar See Entry 116078
- Stress corrosion and acoustic emission during tensile crack propagation in Whin Sill dolomite and other basic rocks See Entry 116079
- Nd-Sr systematics of the Setouchi volcanic rocks, southwest Japan: a clue to the origin of orogenic andesite See Entry 116085
- Rb-Sr, Sm-Nd, K-Ca, O, and H isotopic study of Cretaceous-Tertiary boundary sediments, Caravaca, Spain: evidence for an oceanic impact site See Entry 116086
- Possible origin of K-rich volcanic rocks from Virunga, East Africa, by metasomatism of continental crustal material: Pb, Nd and Sr isotopic evidence See Entry 116087
- Origin of Espanola Island and the age of terrestrial life on the Galapagos Islands See Entry 116088
- The Vredefort dome in South Africa. Crater of a gigantic meteorite or a terrestrial gas explosion? See Entry 116089
- Wind dependence of underwater ambient noise See Entry 116090
- The role of sea surface temperature in large-scale air-sea interactions See Entry 116091
- ²²⁴Ra, ²²⁸Ra, and ²²⁶Ra in Winyah Bay and Delaware Bay See Entry 116092
- An observation of the surface circulation in a Gulf Stream frontal perturbation See Entry 116094
- The incidence of internal waves onto a thin submerged barrier See Entry 116096
- Vertical structure of currents and hydrological elements in central region of the Red Sea See Entry 116099
- On equatorial waves and El Nino. I. Influence of initial states on wave-induced currents and warming See Entry 116104
- The generation and propagation of sea level variability along the Pacific coast of Mexico See Entry 116109
- The mean and seasonal circulation off southwest Nova Scotia See Entry 116110
- Blocking of steady circulation by coastal geometry See Entry 116111
- Formation of eddies and transverse currents in a two-layer channel of variable bottom with application to the lower St. Lawrence estuary See Entry 116112
- The generation of surface waves by an intense cyclone See Entry 116116
- Theory of the equatorial undercurrent See Entry 116121
- Evolution of synoptic disturbances deduced from measurements in the north-central Atlantic See Entry 116122
- The seasonal variability of the Lomonosov Current See Entry 116123
- Isotropy of inertial and semi-diurnal tidal motions in the ocean See Entry 116125
- Statistical estimates of the Antarctic circumpolar current in the Pacific Ocean See Entry 116127
- Mediterranean water in the central Atlantic See Entry 116128
- Coastal upwelling in the California Current system See Entry 116130
- The physical environment of the Peruvian upwelling system See Entry 116131
- The upwelling area off Northwest Africa—a description of phenomena related to coastal upwelling See Entry 116132
- The Benguela upwelling area See Entry 116133
- Monsoon response of the Somali Current and associated upwelling See Entry 116134
- Subsurface subtropical gyre of the North Atlantic and Pacific oceans See Entry 116137
- Slope hydrology as influenced by thawing of the active layer, Resolute, N.W.T. See Entry 116154
- Verification and correction of BKF-precipitation forecasts for the use in a runoff model See Entry 116158
- Oxygen isotope ratios in German groundwater See Entry 116159
- A model for predicting currents in stratified basins See Entry 116160
- Regionalization of water quality in the Upper Fraser River basin, British Columbia See Entry 116163
- Plume dispersion in a nocturnal drainage wind See Entry 116170
- Measurements of sulfur in gases and particles during sixteen months in the Ohio River Valley See Entry 116171
- Mesoscale air pollution dispersion modelling See Entry 116172
- Modelling of long-range transport of sulphur over Europe: a two-year model run and some model experiments See Entry 116173
- Anatomy of an episode of high sulfate concentration at Whiteface Mountain, New York See Entry 116174
- The relationship of sulfur emissions to sulfate in precipitation. II. Gas phase processes See Entry 116175
- The pH and ionic composition of stratiform cloud water See Entry 116176
- Aerosol composition at Chacaltaya, Bolivia, as determined by size-fractionated sampling See Entry 116177
- Electron microscopy of acidic aerosols collected over the northeastern United States See Entry 116178
- World-wide ambient measurements of peroxyacetyl nitrate (PAN) and implications for plant injury See Entry 116179
- Estimating the zero-plane displacement for tall vegetation using a mass conservation method See Entry 116180
- Tracer experiments with turbulently dispersed air ions See Entry 116181
- Wave and turbulence structure in a disturbed nocturnal inversion See Entry 116182
- A study of multiple stable layers in the nocturnal lower atmosphere See Entry 116183
- Seasonal variation of wind direction fluctuations vs. Pasquill stabilities in complex terrain See Entry 116186
- The large-scale circulation and heat sources over the Tibetan Plateau and surrounding areas during the early summer of 1979. I. Precipitation and kinematic analyses See Entry 116188
- On the relative motion of binary tropical cyclones See Entry 116189
- Variability of the Indian summer monsoon and tropical circulation features See Entry 116190
- Monitoring tropical-cyclone intensity using environmental wind fields derived from short-interval satellite images See Entry 116191
- A cyclone/anticyclone couplet over North America: an example of anticyclone evolution See Entry 116194
- Duration of convective events related to visible cloud, convergence, radar and rain gage parameters in south Florida See Entry 116195
- Analysis of nighttime drainage winds in Boulder, Colorado during 1980 See Entry 116196
- The orographic modulation of pre-warm-front precipitation in southern New England See Entry 116197
- Atlantic hurricane season of 1982 See Entry 116198
- Eastern North Pacific tropical cyclones of 1982 See Entry 116199
- The mechanism of sulfate aerosol formation: chemical and sulfur isotopic evidence See Entry 116202
- Tropospheric oxalate See Entry 116203
- Simultaneous detection of FC-11, FC-12 and FC-22, through 8 to 13 micrometers IR solar observations from the ground See Entry 116204
- Variations of the nearground aerosol particle size distribution See Entry 116211
- Absolute barotropic instability and monsoon depressions See Entry 116220
- The kinematics of orographic airflow during Sierra storms See Entry 116223
- Observations of liquid water in orographic clouds over Elk Mountain See Entry 116228
- On the aerosol particle size distribution spectrum in Alaskan air mass systems: Arctic haze and non-haze episodes See Entry 116229
- Hurricane Allen and island obstacles See Entry 116232
- Determination of excessive absorption by atmospheric water vapour at 22.235 GHz See Entry 116237
- Estimation of low-frequency wind stress fluctuations over the open ocean See Entry 116238
- A comparison of different sea level pressure analysis fields in the east Greenland Sea See Entry 116239
- A synoptic case-study using a numerical model See Entry 116242
- An analysis of noctilucent cloud over western Europe during the period 1966 to 1982 See Entry 116243

- Remarks on the numerical forecast of the blizzard situation in Mid-Europe at the turn of the year 1978/79—a case study See Entry 116246
- Interpretation of NOAA 7 information for the Mediterranean on 7.10.1981 between 1220 and 1225 GMT See Entry 116247
- Polar meteorology and climatology 1979-1982 See Entry 116258
- Diurnal variation of rainfall at Nandi Airport, Fiji See Entry 116265
- Evaluation of the climatic zonality of the Indian Ocean during Pliocene time from deep-sea drilling data See Entry 116268
- Apportioning light extinction coefficients to chemical species in atmospheric aerosol See Entry 116269
- Methodology for the analysis of peroxyacetyl nitrate (PAN) in the unpolluted atmosphere See Entry 116285
- The type 81 system for direction finding of whistler observations in Beijing See Entry 116286
- Silica standardization: a discriminant technique applied to a volcanic arc system See Entry 116289
- Northern skies. Britain's new telescopes in the Canary Islands See Entry 116471
- Occultation of 14 Piscium by (51) Nemausa See Entry 116515
- Terrestrial age of an Antarctic meteorite by thermoluminescence technique See Entry 116555

93.55 INTERNATIONAL ORGANIZATIONS, NATIONAL AND INTERNATIONAL PROGRAMS

- 116279 The Global Atmospheric Research Program: 1979-82.** J.S.Fein, P.L.Stephens (Atmospheric Sci. Div., NSF, Washington, DC, USA), K.S.Loughran. *Rev. Geophys. & Space Phys. (USA)*, vol.21, no.5, p.1076-96 (June 1983). Discusses the activities of the Global Atmospheric Research Program (GARP) during 1979-82. The period 1979-82 was one of extraordinary activity. Several major field programs were completed: the Global Weather Experiment (also known as FCGE, the First GARP Global Experiment) with its regional subprograms, the Monsoon Experiment (MONEX) and the West African Monsoon Experiment (WAMEX), and the last of the GARP field programs, the Alpine Experiment (ALPEX). These experiments are described and some of the preliminary results are reported, the GATE research results for the last four years are also summarised. (791 refs.)
- Marine chemistry and paleoceanography in the United States—1978-82—an overview** See Entry 116147

93.65 DATA ACQUISITION AND STORAGE

- A computer-controlled tachymetric surveying system for the supervision of kinematic events without observers** See Entry 116313

93.85 INSTRUMENTATION AND TECHNIQUES FOR GEOPHYSICAL RESEARCH

- 116280 Image resolution in microwave radiometry.** G.D'Auria, D.Solimini (Dipartimento di Elettronica, Univ. di Roma, Roma, Italy). *Alta Freq. (Italy)*, vol.52, no.3, p.227-9 (May-June 1983). (4th Italian National Meeting on Applied Electromagnetics, Florence, Italy, 4-6 Oct. 1982). The effects of atmospheric opacity and antenna characteristics on the resolving capability of microwave radiometers are examined. Limits of resolution for temperature, emissivity and spatial extent are found. Under simplifying assumptions it is found that the transmittance of the atmosphere is the relevant parameter for determining the resolving capability of the radiometer. Therefore this parameter has been calculated on the basis of climatological data obtained from the Italian Air Force at Fiumicino Airport and the results for the limits of resolution are reported for the bands of frequency at 35 and 90 GHz. (6 refs.)
- 116281 Microwave radiometric features of vegetated surfaces.** F.Benincasa, G.Fasano, S.Paloscia, P.Pampaloni, G.Zipoli (IATA, CNR, Firenze, Italy). *Alta Freq. (Italy)*, vol.52, no.3, p.230-2 (May-June 1983). (4th Italian National Meeting on Applied Electromagnetics, Florence, Italy, 4-6 Oct. 1982). Microwave emission of soil and vegetation depends on the physical conditions of the medium. Due to the high value of the water dielectric constant with respect to that of dry soil and vegetation, detected microwave radiation may be used to evaluate soil moisture and plant water content. Radiometer data at 9.8 and 36.6 GHz of corn have been correlated with 'in situ' measured physical parameters of soil and vegetation. A strong correlation between the brightness and physical temperature of crop has been found, moreover daily emissivity variations are small, but clearly correlated with the humidity of air at the top of vegetation. (13 refs.)
- 116282 Lidar remote-sensing: fluorescence and differential reflectance experiments.** P.Burlamacchi, G.Cecchi, P.Mazzinghi (IEQ-CNR, Firenze, Italy), L.Pantani, I.Pippi. *Alta Freq. (Italy)*, vol.52, no.3, p.233-5 (May-June 1983). (4th Italian National Meeting on Applied Electromagnetics, Florence, Italy, 4-6 Oct. 1982). Experiments were carried on Lidar applications to the remote sensing of land and sea. A laboratory experiment was done on Lidar fluorosensing of oil films on sea water. Four different wavelengths were tested and films of thickness as low as 0.01 μm were detected. The ability of a two wavelength Lidar in the signature of topographical targets by means of their reflectance spectra was also investigated. (5 refs.)

- 116283 OH Pepsios.** C.R.Burnett, E.B.Burnett (Florida Atlantic Univ., Boca Raton, FL, USA). *Appl. Opt. (USA)*, vol.22, no.18, p.2887-92 (15 Sept. 1983). An ultraviolet spectrometer of Pepsios design has been constructed and used for measurements of the vertical column abundance of atmospheric hydroxyl. Ground-based observations are made of the spectroscopic absorption of sunlight by OH at 3081.7 Å. The measurements are of relevance to the problem of stratospheric ozone. The spectrometer is a series arrangement of four pressure-scanned Fabry-Perot etalons with vernier spacer ratios. The spectral resolution of 0.06 cm^{-1} permits the identification and measurements of the sharp absorption feature from cool terrestrial OH against the solar background. The observations from Fritz Peak Observatory, Colorado, are presently contributing to a new data base on this atmospheric trace constitu-

ent which should be of importance in the understanding of middle atmospheric photochemical processes. (25 refs.)

- 116284 Water channel simulation of the atmospheric boundary layer.** S.C.Cheah, J.W.Cleaver, A.Millward (Dept. of Mech. Engng., Univ. of Liverpool, Liverpool, England). *Atmos. Environ. (GB)*, vol.17, no.8, p.1439-48 (1983). As part of a programme of work designed to assess the feasibility of modelling the dispersion of heavy plumes in a water channel it has been necessary to develop artificially structured shear layers which attempt to simulate atmospheric conditions. For a variety of reasons the choice of simulation is similar to that developed by Counihan (1969) and consists of a rough surface preceded by a castellated barrier and a number of profiled vorticity generators. Mean velocity and turbulence distributions, together with turbulent spectra and integral length scales, compared favourably with boundary layers modelled in wind tunnels and with full scale experiments in rural surroundings. (22 refs.)

- 116285 Methodology for the analysis of peroxyacetyl nitrate (PAN) in the unpolluted atmosphere.** H.B.Singh, L.J.Salas (Atmospheric Sci. Center, SRI Internat., Menlo Park, CA, USA). *Atmos. Environ. (GB)*, vol.17, no.8, p.1507-16 (1983). A light weight electron capture gas chromatograph has been laboratory- and field-tested to conduct surface and airborne PAN measurements in the unpolluted troposphere. A dynamic calibration system based on $\text{CH}_3\text{CHO}/\text{NO}_2/\text{Cl}_2$ photolysis studies by Gay et al. (1976) was constructed and successfully tested. PAN was cryogenically preconcentrated prior to analysis. A sensitivity of 5 parts per trillion (ppt) and an overall accuracy of $\pm 20\%$ is estimated. PAN measurements at a marine Pacific site, and aboard an aircraft, show that PAN is always present at a concentration range of 10-100 ppt, although concentrations as high as 400 ppt were measured at an altitude of 4.6 km over the Pacific Ocean. (32 refs.)

- 116286 The type 81 system for direction finding of whistler observations in Beijing.** *Acta Geophys. Sin. (China)*, vol.26, no.4, p.309-18 (July 1983). In Chinese. English translation in: *Acta Geophys. Sin. (USA)* The principle of whistler observation, its instrumentation, and some observations in Beijing are described. Preliminary analyses of the data obtained on March 11, 1982 in Beijing show that the mean angle of incidence of the whistlers is 13° , its azimuth is 32° , and the mean field strength is 270 $\mu\text{V}/\text{m}$. (8 refs.)

- 116287 The long period seismograph type 763.** Qin Chao-Zhi, Wang Ming, Yang Ye-Yu, Zhang Wei-Qing, Duan Ming-Chu (Inst. of Geophys., State Seismological Bur., China). *Acta Geophys. Sin. (China)*, vol.26, no.4, p.366-76 (July 1983). In Chinese. English translation in: *Acta Geophys. Sin. (USA)* A matched three-component long period seismograph with galvanometer recording is described. The response of such a system is designed in accordance with that of the long period seismography at WWSSN. Many data had been obtained with this type of instruments operating in BJI, MDJ, WMQ, SSE, TIA stations. The records indicate that type 763 LP seismography have contributed to seismological research and internal structure of the Earth by providing increased sensitivity in period range longer than 50 sec. No other seismographs cover this period range in China. (11 refs.)

- 116288 An approach to ICP analysis of geological samples.** B.Casetta (Perkin-Elmer Italiana SpA, Padua, Italy), A.Giaretta, G.Rampazzo. *At. Spectrosc. (USA)*, vol.4, no.4, p.152-4 (July-Aug. 1983). The authors evaluate the Inductively Coupled Plasma (ICP) technique in geological analysis for precision and accuracy, real time for setup of analytical protocol, and real time for routine running of samples. In a pool of six rock samples, including the international standard BCR1, the determination of six elements (Ba, Er, Eu, La, Y, Zr) was chosen as a basis for evaluation of the ICP technique. (6 refs.)

- 116289 Silica standardization: a discriminant technique applied to a volcanic arc system.** P.C.Ragland, M.J.Defant (Dept. of Geology, Florida State Univ., Tallahassee, FL, USA). *Earth & Planet. Sci. Lett. (Netherlands)*, vol.64, no.3, p.387-95 (Sept. 1983). A classic tholeiitic, calc-alkaline, and shoshonitic island-arc sequence has developed in western Luzon, the Philippines as a result of subduction defined by an eastward-dipping Benioff zone. A simple technique of standardizing the data allows chemical concentrations to be recast to 'andesite equivalent' compositions. Based on the excellent linear correlations that exist between SiO_2 and other elements, individual analyses were standardized to 55% SiO_2 by projecting parallel to least-squares regression lines. Results of the analysis of valiance indicate that at the 99% confidence level 20 to 27 chemical variates discriminate between at least two of the three geographically distinct magma series. (24 refs.)

- 116290 Remote reconnaissance: methods of observation, picture analysis, examples. II.** R.Fiedler, H.Helbig, G.Kritikos, D.Kubler, H.van der Piepen. *Elektronik (Germany)*, vol.32, no.13, p.69-73 (1 July 1983). In German. For pt.I see *ibid.*, no.12, p.85 (1983). Discusses geometric distortion of surface pictures from aircraft or satellites, and correction methods based on system parameters and comparison with reference pictures. Mapping, overlay, and computer aided mosaicing techniques for composite picture generation are described and illustrated. Principles of spectral signature application in classification algorithms for surface features are explained. The greatest application of picture processing has been in remote Earth reconnaissance including resource and environment monitoring. The methods however apply in other fields such as medicine, buildings, engineering and automation. (no refs.) H.V.H.

- 116291 Structure of the perturbed zone near a large charged photoemitting object.** A.M.Moskalenko (Inst. of Terrestrial Magnetism, Ionosphere & Radio Wave Propagation, Acad. of Sci., USSR). *Geomagn. & Aeron. (USA)*, vol.22, no.3, p.314-18 (1982). Translation of: *Geomagn. & Aeron. (USSR)*, vol.22, no.3 (1982). [received: Sept. 1983] The electric field and the plasma structure near a charged spherical object are studied. It is assumed that electrons are photoemitted from the sunlit part of the object's surface. The radius of the object is assumed small in comparison with the mean free path of the particles but large in comparison with the plasma Debye length. The photocurrent is treated as a perturbation. Analytic expressions are derived for the distributions of the electric field and of the densities of ions, electrons, and photoelectrons. A detailed study is made of the case in which the electric field has only a slight effect on the photoelectron density distribution. (7 refs.)

- 116292 Determining the components of the magnetic field of a vehicle.** V.A.Blednov (Inst. of Terrestrial Magnetism, Ionosphere & Radio Wave Propagation, Acad. of Sci., USSR). *Geomagn. & Aeron. (USA)*, vol.22, no.3, p.397-9 (1982). Translation of: *Geomagn. & Aeron. (USSR)*, vol.22, no.3 (1982). [received: Sept. 1983]
A procedure is described for determining the components of the magnetic field of a vehicle from on-board vector measurements. The components are grouped as certain vector quantities. The accuracy with which they are determined does not depend on the accuracy with which the direction of the geomagnetic meridian is found. (3 refs.)
- 116293 On the dynamic range of resonance spectrophone.** Yu.G.Toporkov. *Izv. Akad. Nauk SSSR Fiz. Atmos. & Okeana*, vol.19, no.8, p.839-44 (Aug. 1983). In Russian. English translation in: *Izv. Acad. Sci. USSR Atmos. & Oceanic Phys. (USA)*
The problem of estimating a resonance spectrophone dynamic range in an integral form as a function of particle size spectra of the investigated aerosol medium is considered. A minimum possible (the far-infrared region) dynamic range is analytically determined for Junge size distribution. The numerical calculation of real ranges for the visible region ($\lambda=0.51 \mu\text{m}$) is performed. (8 refs.)
- 116294 HF Doppler measurements of mesospheric gravity wave momentum fluxes.** R.A.Vincent, I.M.Reid (Dept. of Phys., Univ. of Adelaide, Adelaide, Australia). *J. Atmos. Sci. (USA)*, vol.40, no.5, p.1321-33 (May 1983).
Recent theoretical studies have emphasized the probable importance of internal gravity waves in balancing the momentum budget of the mesosphere. The authors propose a method by which the vertical flux of horizontal momentum can be measured by ground based radars. The method uses two or more radar beams each offset from the vertical to measure the atmospheric motions by the Doppler technique. Provided there is horizontal homogeneity, the momentum flux is proportional to the difference of the variances of the Doppler velocities measured in each beam. The flux convergence and, hence, the associated body force acting on the atmosphere can be inferred by measuring the flux as a function of height. It is shown that mean wind components can also be measured by this method and, under certain circumstances, so can the horizontal wavelengths and phase velocities of the internal waves. Observations of the vertical flux of zonal momentum made with this technique using an HF radar located near Adelaide, Australia (35°S, 138°E) in May 1981 are discussed. (27 refs.)
- 116295 A VHF radar antenna for the measurement of incoherent scattered radiation from the ionosphere.** G.Schroer, T.Hagfors, P.-S.Kildal. *Mikrowellen Mag. (Germany)*, vol.8, no.5, p.545-6, 548-51 (Oct. 1982). [received: Aug. 1983]
A parabolic cylinder antenna with a $120 \times 40 \text{ m}$ aperture has been developed for observing scattered radiation from the ionosphere plasma at a frequency of 224 MHz. By an arrangement whereby the primary radiator lies outside the radiation field of the antenna (offset feed system) and other measures a gain of 43.6 dB was achieved corresponding to an efficiency of 64%. The antenna radiates northwards and can be swung up to 90° in the meridian plane. It is made of four 30 m sections which can either be moved together or independently. The primary feed comprises 128 crossed dipoles. By changing their relative phases electrical beam swinging of $\pm 21.3^\circ$ about the meridian plane can be achieved. The HF divide network for feeding the crossed dipoles is designed for a transmitted power of 375 kW continuous and 3 MV peak power for each orthogonal polarisation. (8 refs.) *J.R.B.*
- 116296 Calculation of well log apparent resistivities by discrete convolution.** D.Drahoš. *Magy. Geofiz. (Hungary)*, vol.24, no.3, p.97-110 (1983). In Hungarian.
Deals with the numerical solution of the electrical direct problem of well logging by applying the discrete convolution method. The discrete convolution method is effective in the numerical solution of linear integral transforms. The method is described briefly and its accuracy is illustrated by calculating such an integral transform the output function of which is known analytically. Formulae are derived to calculate the apparent resistivities of normal, lateral and laterolog arrangements. The results calculated by discrete convolution show good agreement with those calculated earlier by L.M. Alpin. (10 refs.)
- 116297 Quantitative determination of Al_2O_3 content in bauxite drill holes by neutron activation log.** I.Balogh, J.Horvath. *Magy. Geofiz. (Hungary)*, vol.24, no.3, p.111-18 (1983). In Hungarian.
Presents a complex solution for basic equation of the neutron activation logging. This solution considers the effects of the hole diameter, the nuclear parameters of the measuring environment, and the technical parameters of the continuous logging, simultaneously. The theoretical calculations have been controlled by experimental measurements. As a result of theoretical and experimental works the authors have elaborated a quantitative aluminium content interpretation system. In its practical use it was found that the average deviation from the laboratory data was 3.5 $\text{Al}_2\text{O}_3\%$ referring to a 1 metre interval. (6 refs.)
- 116298 Two-wavelength lidars. Target identification through a differential reflectance technique.** L.Pantani, I.Pippi (Istituto di Ricerca sulle Onde Elettromagnetiche, CNR, Florence, Italy). *Opt. Acta (GB)*, vol.30, no.10, p.1473-81 (Oct. 1983).
The ability of a two-wavelength lidar in the identification of natural and artificial targets is discussed. The analysis is carried out on the basis of target spectral reflectance and taking into account the atmospheric extinction at the two laser wavelengths. Preliminary results performed with a two-wavelength (0.532 and $1.064 \mu\text{m}$) Nd-YAG lidar are reported. (10 refs.)
- 116299 An EM field modelling unit for geophysical prospecting problems.** V.I.Gordienko, N.D.Pechenyak, V.P.Ubogii, E.V.Yaroshevskii. *Otbor & Peredacha Inf. (USSR)*, no.67, p.47-51 (1983). In Russian.
Presents details of design and evaluation of a unit for the modelling of EM field, for application to problems of geophysical prospecting by harmonic fields. The features of the unit are high accuracy, repeatability of measured results, suitability for automatic processing of amplitude/phase and impedance/admittance data and suitability for application to a wide range of problems of geophysical prospecting on land and sea, using dipole profiling and long cable methods. (11 refs.) *Z.F.V.*
- 116300 Influence of the dimensions of a sensor on estimates of the turbulent energy dissipation rate in the ocean.** V.M.Zhurbas, V.N.Nabatov (Shirshov Inst. of Oceanology, Acad. of Sci., Moscow, USSR). *Oceanology (USA)*, vol.22, no.1, p.111-14 (1982). Translation of: *Okeanologiya (USSR)*, vol.22, no.1 (1982). [received: Aug. 1983]
Field measurement data are used to analyze the influence of the dimensions of the sensitive element of a conductive magnetohydrodynamic anemometer (CMA) on estimates of the turbulent energy dissipation rate ϵ in the ocean. It is found that for CMA variants used in oceanologic studies ϵ is underestimated by a factor of 2-3 due to the finiteness of the sensor dimensions. An empirical estimate of the CMA spectral characteristics obtained from the field measurement data is presented. (8 refs.)
- 116301 A method for calculating dispersion relations and eigenfunctions for internal waves in the ocean from field data.** V.A.Gritsenko, V.P.Krasitskiy (Shirshov Inst. of Oceanology, Acad. of Sci., Moscow, USSR). *Oceanology (USA)*, vol.22, no.4, p.400-3 (1982). Translation of: *Okeanologiya (USSR)*, vol.22, no.4 (1982). [received: Aug. 1983]
A finite-difference method is suggested for solving the boundary-value problem for the amplitudes of the vertical modes of internal waves. This method uses actual field measurements of the density profile. The method is based on a direct solution of the characteristic equation for the matrix of the corresponding finite-difference equations. An example of the calculation is given. (9 refs.)
- 116302 Computers in geophysical well-logging units.** R.M.Babaev. *Prib. & Sist. Upr. (USSR)*, no.7, p.15-17 (1983). In Russian. English translation in: *Sov. J. Instrum. & Control (GB)*
Special measuring devices used for geophysical well-logging and their adaptability for computer control are examined. Special microprocessors are used to process the information from the digging level which may be distorted by dispersive cable characteristics. Special modulation/demodulation schemes are suggested which should facilitate faithful reproduction of data after the A/D conversion. Block diagrams of several proposed systems are illustrated and discussed. (5 refs.) *J.K.S.*
- 116303 Calibration of long-period seismic channels.** J.Rasson, F.De Meyer. *Publ. Inst. R. Meteorol. Belg. Ser. A (Belgium)*, no.110, p.7-50 (1983).
Earthquake signals, as they are recorded on the seismogram, are deformed by the various systems they pass through after having been issued at the focus. Two main such systems can purposely be distinguished: the Earth and the seismometer. If one is to gain knowledge of the Earth deforming system or the signal generating focus or both, it is best that they be the only unknowns: since the seismometer is easily accessible for measurement (contrary to the Earth), it is worth designing an experiment giving as complete as possible a description of the instrument signal deforming action. Such an experiment, called a calibration, is discussed. (17 refs.)
- 116304 Radio transillumination of the atmosphere by artificial and natural sources.** M.A.Kolosov, A.G.Pavel'yev. *Radio Eng. & Electron. Phys. (USA)*, vol.27, no.12, p.30-7 (Dec. 1982). Translation of: *Radiotekh. & Elektron. (USSR)*, vol.27, no.12, p.2310-17 (Dec. 1982). [received: Sept. 1983]
A new procedure for transillumination of the atmosphere of the Earth by artificial and natural sources is examined. It is shown that measurements of amplitude and frequency characteristics of signals radiated by sources observed at low elevation angles enable one to calculate the angle of refraction and its derivative as functions of the impact parameter. When the accuracy of measurement is sufficiently high, one can reconstruct the profile of the refractive index and of its gradient as functions of altitude with the help of an analytic solution of the inverse problem, which also possesses a regularizing property. (10 refs.)
- 116305 Advances in remote sensing of the atmosphere.** K.S.Gage, B.B.Balsley (Aeronomy Lab., NOAA, Boulder, CO, USA). *Rev. Geophys. & Space Phys. (USA)*, vol.21, no.5, p.955-65 (June 1983).
The present review emphasises US contributions in the AD 1979 to 1983 period to techniques of atmospheric remote sensing. Both ground-based and satellite methods are described. Passive radiometric methods and active (lidar and radar methods) are included in this survey. Specific atmospheric variables for which techniques are described include humidity, precipitated water, cloud cover, rainfall, wind and chemical composition. Weather radar and clear air radar methods are also described. (312 refs.)
- 116306 Radar-acoustic probing of randomly oriented air flows.** I.V.Korytsev. *Radiotekhnika, Kharkov (USSR)*, no.61, p.57-9 (1982). In Russian. [received: Aug. 1983]
A multi-positional radar-acoustic probing method designed for determining the three velocity components of an air flow and the temperature of the atmosphere with a high space-time resolution is considered. An analysis is made of the measurement errors with three sloping and one vertical path for probing the same spatial region. (1 ref.) *L.M.H.*
- 116307 Equipment, procedure and some results relating to measurements of luminance temperature of water in liquid and solid phase in millimeter wave band.** A.S.Levda, I.Kh.Vakser, Yu.I.Malyshenko. *Radiotekhnika, Kharkov (USSR)*, no.61, p.77-81 (1982). In Russian. [received: Aug. 1983]
A study is made of the units and components of the radiometers which have been developed with sensitivities of 1 and 0.5K (with a time constant of 1 sec) at wavelengths of 3 and 8 mm and of the device for measuring the emissive properties of specimens of the Earth's mantle given differing angles of incidence. The results of measurements of the luminance temperature of water, snow and ice at these wavelengths are presented and shown to be of interest for the development of the remote radio-physical method. (4 refs.) *L.M.H.*
- 116308 Highly accurate inversion methods for three-dimensional stratified media.** M.Lahlou, J.K.Cohen, N.Bleistein (Dept. of Math., Univ. of Denver, Denver, CO, USA). *SIAM J. Appl. Math. (USA)*, vol.43, no.4, p.726-58 (Aug. 1983).
Describes two highly accurate velocity inversion methods for three-dimensional isovelocity stratified media. The first one is a Born-type perturbation method based on an asymptotic, implicit Green's function, while the second one is based on the Kirchhoff representation of the reflected field. It is shown that, given a band-limited reflected signal resulting from one backscatter experiment, both methods can be used in a recursive manner to accurately reconstruct the unknown velocity profile. They are tested on both synthetic and real data sets. The tests on synthetic data demonstrate higher accuracy than has been the case for previous methods in the literature. In the most extreme test, synthetics with 10 layers and velocity variation on the order of 200% were used and extremely accurate inversion was achieved. (51 refs.)
- 116309 Fast seismic ray tracing.** H.B.Keller (Appl. Math., California Inst. of Technol., Pasadena, CA, USA), D.J.Perozzi. *SIAM J. Appl. Math. (USA)*, vol.43, no.4, p.981-91 (Aug. 1983).
New methods for the fast, accurate and efficient calculation of large classes of seismic rays joining two points x_s and x_r in very general two-dimensional configurations are presented. The medium is piecewise homogenous with arbitrary interfaces separating regions of different elastic properties (i.e. differing wave speeds c_p and c_s). In general there are 2^{N+1} rays joining x_s to x_r while making contact with N interfaces. The authors methods find essentially all such rays for a given N by using continuation or homotopy methods on the wave speeds to solve the ray equations determined by Snell's law. In addition travel times, ray amplitudes and caustic locations are obtained.

When several receiver positions $X_R^{(i)}$ are to be included, as in a gather, the authors' techniques easily yield all the rays for the entire gather by employing continuation in the receiver location. (5 refs.)

116310 Classification capability and resolving power of the method of transients in searches for kimberlites. L.A.Tabarovskii, G.B.Itskovich (Inst. of Geology & Geophys., Acad. of Sci., Novosibirsk, USSR). *Sov. Geol. & Geophys. (USA)*, vol.23, no.5, p.50-8 (1982). Translation of: *Geol. & Geofiz. (USSR)*, vol.23, no.5, p.56-66 (1982). The solution of the direct problem of the field due to a vertical magnetic dipole above a half-space containing a cylindrical inhomogeneity is used to investigate the classification capability of different components of a nonstationary field in the case of a geoelectric section characterizing the presence of a kimberlite pipe. The resolving power of different systems relying on the method of transients is estimated in relation to determinations of the size and conductivity of the pipe. A method is proposed for determining a generalized electromagnetic parameter. (6 refs.)

116311 Combined interpretation of magnetic and gravitational fields based on calculations of the pseudogravitational field. I.D.Savinskii, G.I.Rossmann, V.V.Grushina, V.L.Briskin, E.I.Kulikova, Yu.A.Filipchenko. *Sov. Geol. & Geophys. (USA)*, vol.23, no.5, p.67-73 (1982). Translation of: *Geol. & Geofiz. (USSR)*, vol.23, no.5, p.75-83 (1982). The transformation of three-dimensional magnetic fields into the pseudogravitational field is discussed as a possible technique for geophysical exploration. Maps of such fields are reproduced for a region containing a volcano-tectonic depression. When the pseudogravitational and gravitational fields are analyzed together, this provides a new basis for the combined interpretation of magnetic and gravity data because the perturbing effects of anomalies vary in the same way for the two fields. Compilation of the correlation coefficients between the values of these fields in a 'sliding window' shows that there is good correspondence between regions of weak correlation and ore mineralization zones. (10 refs.)

116312 From qualitative to quantitative magnetic anisotropy analysis: the prospect of finite strain calibration. B.Henry, L.Daly (Lab. de Tectonophys., Paris, France). *Tectonophysics (Netherlands)*, vol.98, no.3-4, p.327-36 (1983). A method of separating low field, susceptibility anisotropies due to ferrimagnetics and the matrix, proposed hitherto in cases where the principal axis of these two components are merged, is generalized in cases where the axes are distinct. The method consists of analysing, in specimens close in the same sample, anisotropies, the differences of which are due to the variation of respective percentages of the two components, although the strain rate remains constant. One thus uses the cause which itself renders global anisotropy unusable. A first application is presented, where a control using the anisotropy of isothermal remanent magnetization allows the validity of the method to be tested. A discussion of the choice of the best ellipsoid, relative either to the matrix or to the ferrimagnetics, to give the best indication of relative finite strain rate, is opened.

116313 A computer-controlled tachymetric surveying system for the supervision of kinematic events without observers. H.Kahmen, H.Suhre. *Z. Vermessungswes. (Germany)*, vol.108, no.8, p.345-51 (Aug. 1983). In German. The development of an automatic computer-controlled tachometer system is described. The system provides automatic monitoring of an array of slowly moving control points for deformation measurements, manages the recording of the data and computes the displacements. Only the initial pointing of a reference point requires an operator. (1 ref.)

116314 Experimentation d'un système de sondage en source contrôlée, en prospection minière (Experiments with an EM sounding system with a controlled source in mineral prospecting). J.Mosnier. *Report EUR 8258 FR*, Comm. European Communities, Luxembourg (1983), iv+46 pp. In French. Contract 082-79-4/MPPF. Discusses a new type of electromagnetic receiver. The device was constructed for prospecting for conductive ores. It has a very high sensitivity and it is protected against interference noise by means of a double frequency change, amplification at a fixed frequency (30 Hz) and phase detection. In order to get a reference signal for the detector, the author uses either a radiotelemetric link, or two synchronous independent clocks. The device has been used for the detection of an ore of copper sulphide near 'La Porte aux Moines' in French Brittany. The author has also measured the electric and magnetic fields, produced by an artificial source at a variable frequency in the band 100 Hz-6000 Hz.

116315 A solid-state compass with microprocessor controlled data acquisition. K.Williams (Univ. of Santa Clara, Santa Clara, CA, USA). *Wescon/82 Conference Record*, Anaheim, CA, USA, 14-16 Sept. 1982 (El Segundo, CA, USA: Electron. Conventions 1982), p.SS-3/1-5. Describes the design and fabrication of a solid-state compass. The compass uses two high-sensitivity Hall-effect sensors oriented at right angles to each other to determine direction by sensing the Earth's magnetic field. The analog signals from the Hall-effect devices are digitized and stored under microprocessor control. Finally, the data are transmitted using ASCII code to an appropriate computer for processing and display. A small, single-board computer was used. (5 refs.)

116316 Inverse problems for reflection seismograms. E.A.Robinson (Dept. of Theoretical & Appl. Mech., Cornell Univ., Ithaca, NY, USA). Identification and System Parameter Estimation 1982. Proceedings of the Sixth IFAC Symposium, Washington, DC, USA, 7-11 June 1982 (Oxford, England: Pergamon 1983), p.939-44 vol.2. The purpose of seismic migration is to find the coordinate of inaccessible subsurface points by use of seismic reflection measurements taken on the Earth's surface. The three most popular conventional migration methods are the finite difference method, the Kirchhoff method, and the frequency wavenumber method. They are each based on a stratified model, that is a two-dimensional model in which all the interfaces encountered by propagating waves must be horizontal. Such a model is called a 1 1/2 dimensional (1.5D) model, because a true two-dimensional model would allow dipping interfaces. As a justification for the use of 1.5D wave equation migration on seismic data, in the paper the author proposes the random reflector-dip hypothesis. This statistical justification is the only reason the conventional migration methods give satisfactory results on actual seismic data. (11 refs.)

116317 Extraction of seismic profiles for one-dimensional nonhomogeneous media using the impulse response model. W.J.Vetter (Faculty of Engng. & Appl. Sci., Memorial Univ. of Newfoundland, St. John's, Newfoundland, Canada). Identification and System Parameter Estimation 1982. Proceedings of the Sixth IFAC Symposium, Washington, DC, USA, 7-11 June 1982 (Oxford, England: Pergamon 1983), p.945-50 vol.2. The time domain response for a horizontally stratified lossless acoustic medium, for normal incidence plane wave pulse type excitation, is detailed as

a response summation by order of reflection. Specialized to mathematical stratification in terms of layerwise homogeneous medium components having equal propagation delays, and considered in the limit of layer shrinkage to the continuum, the response becomes the solution of the wave equation for a vertically nonhomogeneous medium having independent segmentwise continuous profile functions of density and elastic constant, or equivalently of propagation velocity and characteristic acoustic impedance. A recursive procedure for efficient numerical generation of the response multiples is detailed. This analytical time response solution complements and extends the insight on the wave propagation phenomenon. The details in the solution structure point to the salient features in the reflectance profile or characteristic acoustic impedance profile estimation problem. (23 refs.)

116318 Review of some exact methods for the solution of the one-dimensional inverse problems. F.Santosa (Dept. of Theoretical & Appl. Mech., Cornell Univ., Ithaca, NY, USA). Identification and System Parameter Estimation 1982. Proceedings of the Sixth IFAC Symposium, Washington, DC, USA, 7-11 June 1982 (Oxford, England: Pergamon 1983), p.951-6 vol.2. The inverse problem in geophysics is the determination of the inhomogeneous structure of an elastic medium from experimental observations. The author reviews the Gelfand-Levitán and the Marchenko methods for the solution of the related quantum inverse problem. In these approaches, as well as in the methods for the geophysical problem, the author discusses how the desired information is recovered from the solution of certain integral equations. Next, the construction of a computational scheme for the inversion of geophysical data based on one of the methods is considered. Further it is shown that the resulting algorithm is stable under small perturbations to the data. Finally the inversion scheme is demonstrated by inverting noiseless and noise-corrupted synthetic seismograms. (11 refs.)

116319 Difference methods for solving one-dimensional inverse problems. K.P.Bube, R.Burridge (Dept. of Math., Univ. of California, Los Angeles, CA, USA). Identification and System Parameter Estimation 1982. Proceedings of the Sixth IFAC Symposium, Washington, DC, USA, 7-11 June 1982 (Oxford, England: Pergamon 1983), p.957-61 vol.2. Considers the one-dimensional inverse problem of reflection seismology. An impulsive plane wave in pressure is applied to a horizontally homogeneous elastic half space and the ensuing particle velocity is measured at the surface. The characteristic impedance is recovered as a function of travel time. Several methods of solution of this inverse problem require the construction of an auxiliary solution of the differential equations with a wave front, and the impedance is recovered using the theory of propagation of singularities. The use of difference schemes to construct this auxiliary solution leads to fast algorithms to solve this inverse problem. Fast recursive algorithms for solving discrete integral equations, which are Toeplitz linear systems, can be identified with difference schemes. A downward continuation algorithm developed by the authors which uses difference schemes is also presented. (9 refs.)

116320 Maximum-likelihood as applied to seismic inversion problems. J.M.Mendel (Dept. of Electrical Engng., Univ. of Southern California, Los Angeles, CA, USA). Identification and System Parameter Estimation 1982. Proceedings of the Sixth IFAC Symposium, Washington, DC, USA, 7-11 June 1982 (Oxford, England: Pergamon 1983), p.963-6 vol.2. Surveys work on maximum-likelihood as applied to seismic inversion problems performed by the USC Geo-Signal Processing Program. The author describes work on maximum-likelihood deconvolution, maximum-likelihood wavelet estimation and deconvolution, maximum-likelihood normal incidence inversion, and normal-incidence geo-optimal deconvolution. (14 refs.)

116321 Some results on the three-dimensional geophysical inverse problem. M.T.Silvia (Dept. of Electrical Engng., Univ. of Tulsa, Tulsa, OK, USA). Identification and System Parameter Estimation 1982. Proceedings of the Sixth IFAC Symposium, Washington, DC, USA, 7-11 June 1982 (Oxford, England: Pergamon 1983), p.967-73 vol.2. In geophysical signal processing, the basic problem is to identify the spatially-variant parameters of the wave equation which governs the propagation of seismic waves. In one dimension (1-D), this problem has several analytic solutions, which are accompanied by the 1-D concepts of deconvolution and wavelet processing. In the paper, the author discusses the identification of the three-dimensional (3-D) acoustic wave equation and explains how the ideas of deconvolution and wavelet processing can be extended to three dimensions. (15 refs.)

Holography applied to stereomicroscopy	See Entry 111762
Interference film microscopy for metal phase identification	See Entry 111763
Measurement of the time variational behaviours of aerosols based on size distribution	See Entry 115716
Collocations and thirtieth order resonant harmonics	See Entry 115995
Equivalent solutions of the inverse three-dimensional gravimetry problem for a class of polynomial densities	See Entry 115997
The interpretation of magnetotelluric and electrical sounding's data by modified generalized inverse matrix	See Entry 116000
Inversion of the electromagnetic induction problem using Parker's algorithms were both precise and practical data	See Entry 116003
A splitting-up method for solution of higher-order migration equation by finite-difference scheme	See Entry 116021
An alternative method for fault-plane solutions from a single station	See Entry 116029
Scattering of seismic waves by the broken edge of a flat boundary	See Entry 116032
The seismology of Greece	See Entry 116033
Long-term prediction of earthquakes in western Honshu, Japan	See Entry 116035
The reliability of asymmetric c-axis fabrics of quartz to determine sense of vorticity	See Entry 116069
Dynamic processes during slip of stick-slip as an earthquake fault model	See Entry 116084
A statistical model of vertical shear from Moored current meters	See Entry 116106
Advances in satellite oceanography	See Entry 116144
Optimal estimation of the average areal rainfall over a basin and optimal selection of rain-gauge locations	See Entry 116165
Estimating the zero-plane displacement for tall vegetation using a mass conservation method	See Entry 116180

- Estimation of low-frequency wind stress fluctuations over the open ocean See Entry 116238
- Progress in cloud physics 1979-1982 See Entry 116252
- Polar meteorology and climatology 1979-1982 See Entry 116258
- On the extraction of tidal information from measurements covering a fraction of a day See Entry 116327
- Ionospheric investigations using Sirio VHF beacon See Entry 116339
- A microwave scanning radiometer for Marine Observation Satellite-1 See Entry 116426

94.00 AERONOMY AND SPACE PHYSICS

94.10 PHYSICS OF THE NEUTRAL ATMOSPHERE

(for planets, see 96.30)

- 116322** Distribution of meteor heights and sunrise. V.Purubcan (Astron. Inst., Slovak Acad. of Sci., Bratislava, Czechoslovakia), G.Cevolani. *Bull. Astron. Inst. Czech. (Czechoslovakia)*, vol.34, no.4, p.213-19 (July 1983).

The echo heights of 6921 sporadic meteors, determined by an interferometric height-finding system of the Budrio (44.5°N, 11.65°E) meteor radar in April-September 1978 during a 15-hour interval around sunrise, are analysed. No correlation in the variation of the mean height with the geomagnetic K_p index is found; mean sporadic heights exhibit a clear correlation with the elevation angle of the Earth's apex. The observed mean height seasonal variation at three times of the day (0^h, 6^h, 12^h) can almost entirely be accounted for by the position of the apex. Mean height with respect to local sunrise at 90 km shows a variation in a range of 92.4 km, with a minimum just after sunrise and a maximum about 4-5 hours after sunrise. (20 refs.)

- 116323** A possible mechanism for the excitation of mid-latitude internal gravity waves in the upper ionosphere. O.N.Savina (Gor'kii State Univ., Gor'kii, USSR).

Geomagn. & Aeron. (USA), vol.22, no.3, p.329-31 (1982). Translation of: *Geomagn. & Aeron. (USSR)*, vol.22, no.3, p.361-4 (1982). [received: Sept. 1983]

The possible excitation of internal gravity waves by turbulent velocity fluctuations near the turbopause is analyzed. The conditions under which the waves will reach the upper ionosphere are studied. An expression is derived for the vertical component of the energy flux. With strong wind shear in the turbopause vicinity, the existence of semitransparent sporadic E layers may be accompanied by the excitation of intermediate-scale moving perturbations. (11 refs.)

- 116324** Temperature inversion in the thermosphere. A.G.Kolesnik, S.S.Kololev, S.G.Pasynikov (Siberian Physicotech. Inst., USSR).

Geomagn. & Aeron. (USA), vol.22, no.3, p.361-4 (1982). Translation of: *Geomagn. & Aeron. (USSR)*, vol.22, no.3 (1982). [received: Sept. 1983]

The previously proposed mechanism for cooling of the lower thermosphere, which produces regions with opposite formed dependence of T_n on $F_{10.7}$, is analyzed based on a one-dimensional model combining the effects of the composition and temperature at altitudes of 80 to 300 km. It is shown that the mechanism for vertical transport of mass and heat by turbulence and macroscopic motions can generate regions with a temperature inversion of up to 30% and a composition inversion of up to 20%. (10 refs.)

- 116325** Latitude dependence of disturbances of thermospheric winds. A.A.Namgaladze, L.P.Zakharov, V.M.Smertin (Inst. of Terrestrial Magnetism, Ionosphere & Radio Wave Propagation, Acad. of Sci., USSR).

Geomagn. & Aeron. (USA), vol.22, no.3, p.365-7 (1982). Translation of: *Geomagn. & Aeron. (USSR)*, vol.22, no.3 (1982). [received: Sept. 1983]

It is shown that in the latitude band of 45 to 65° disturbances of the meridional velocity of thermospheric winds induced by geomagnetic activity constitute 25 to 250 m/sec at $K_p=6$ when calculated from the Jacchia-1977 neutral atmosphere model, and 150-350 m/sec in a self-consistent calculation of disturbances in the temperature, density, and winds in the thermosphere. Such winds cause positive ionosphere disturbances, compensating or exceeding the negative effects of changes in the neutral composition at $k_p \geq 6$, suggesting that the latter could not produce negative ionospheric storms. (8 refs.)

- 116326** Geocoronal imaging with Dynamics Explorer: a first look. R.L.Rairden, L.A.Frank, J.D.Craven (Dept. of Phys. & Astron., Univ. of Iowa, Iowa City, IA, USA).

Geophys. Res. Lett. (USA), vol.10, no.7, p.533-6 (July 1983).

The ultraviolet photometer of the University of Iowa spin-scan auroral imaging instrumentation on board Dynamics Explorer 1 has returned numerous hydrogen Lyman alpha images of the geocorona from altitudes of 570 km to 23300 km. Attempts were made to fit these observations with a spherically symmetric isothermal Chamberlain model of the exosphere using numerical solutions to the radiative transfer equation. The removal of a substantial portion of the satellite component at higher altitudes was necessary to obtain the required functional dependence of hydrogen density with radial distance. The optimum fit utilizes a Chamberlain model of temperature 1050°K, with exobase r_c at 1.094 R_E (600 km altitude), exobase density of 40000 cm⁻³, and a satellite critical level r_{cs} equal to 3.5 r_c . (14 refs.)

- 116327** On the extraction of tidal information from measurements covering a fraction of a day. D.J.Crary, J.M.Forbes (Dept. of Phys., Boston Coll., Chestnut Hill, MA, USA).

Geophys. Res. Lett. (USA), vol.10, no.7, p.580-2 (July 1983).

The errors incurred by extracting tidal information from data covering only a fraction of a day are investigated quantitatively as a function of fit span and tidal period. Assuming a noise component in the observational data with standard deviation σ , errors in the diurnal and semidiurnal Fourier components equal to σ occur at fit spans of 15.5 and 13.5 hours, respectively, for hourly data points. Errors increase at an exponential rate for shorter fit spans. Assuming nominal values of tidal amplitudes and standard deviations applicable to 12 hours of daytime mesopause region winds that might be obtained from MST radar measurements, it is shown that data is required at approximately 5-minute intervals to determine with acceptable accuracy tidal Fourier components from a single day's measurements. Alternatively, one to three weeks of daytime data at 30-minute intervals would enable determination of diurnal and semidiurnal components to roughly the same accuracy. (5 refs.)

- 116328** Simultaneous observations of the quasi 2-day wave in the northern and southern hemispheres. R.L.Craig, R.A.Vincent (Dept. of Phys., Univ. of Adelaide, Adelaide, Australia), S.P.Kingsley, H.G.Muller.

J. Atmos. & Terr. Phys. (GB), vol.45, no.8-9, p.539-41 (Aug.-Sept. 1983).

Observations of winds in the mesosphere and lower thermosphere made in July and August 1980 at Sheffield (53°N, 2°W), Townsville (19°S, 147°E) and Adelaide (35°S, 138°E) are compared. A quasi 2-day oscillation is evident in both the Sheffield and Townsville data, which suggests a significant cross-equatorial leakage of the wave from the summer to the winter hemisphere. A mean period of near 50 h and a vertical wavelength of about 50 km are found. (11 refs.)

- 116329** Upper atmosphere wind observations of waves and tides with the UNH Meteor Radar System at Durham 43°N (1977, 1978 and 1979). R.R.Clark (Electrical and Computer Engng. Dept., Univ. of New Hampshire, Durham, NH, USA).

J. Atmos. & Terr. Phys. (GB), vol.45, no.8-9, p.621-7 (Aug.-Sept. 1983).

Meteor wind data obtained during the years 1977-1979 have been processed to obtain prevailing 12 h, 24 h, and pseudo 2 day components. Monthly wind values at various heights show regularity for the semidiurnal tide in both amplitudes and phase. The average properties of the semidiurnal tide agree well with classical tidal theory. There is considerable energy present in the diurnal and pseudo 2 day components; their amplitudes and phases are quite irregular. During the summer, the meridional component is equatorward at all levels (4-12 m s⁻¹) and the zonal component is eastward at all levels (15-30 m s⁻¹). (19 refs.)

- 116330** Laboratory measurements of the association rate coefficients of NO⁺, O₂⁺, N⁺, and N₂⁺ ions with N₂ and CO₂ at temperatures between 100K and 400K. S.Dheandhanoo, R.Johnsen (Dept. of Phys. & Astron., Univ. of Pittsburgh, Pittsburgh, PA, USA).

Planet. & Space Sci. (GB), vol.31, no.8, p.933-8 (Aug. 1983).

Rate coefficients for the association reactions of NO⁺ ions with N₂ and CO₂, O₂⁺ with N₂, and N⁺ and N₂⁺ with N₂ have been determined as a function of gas temperature in a laboratory experiment employing a variable-temperature drift-tube apparatus. The measured rate coefficients are fitted to power laws of the form $k=C(T/300)^x$ where the exponents x range from 2.2 to 4.3. The strong temperature dependence observed in the case of the reaction of NO⁺ with N₂ ($x=4.3$) supports the thesis by Arnold et al. (1979) that the temperature variability of D-region ion densities is a result of this reaction step in the ion clustering sequence. (15 refs.)

- 116331** Intensity of variations of the source of internal gravity waves and the ionospheric response during the substorm of September 18, 1974. T.V.Gaivoronskaya, G.F.Deminova, L.A.Yudovich (Inst. of Terrestrial Magnetism, Ionosphere & Radio-Wave Propagation, Acad. of Sci., USSR).

Radiophys. & Quantum Electron. (USA), vol.26, no.1, p.4-8 (Jan. 1983). Translation of: *Izv. VUZ Radiofiz. (USSR)*, vol.26, no.1, p.7-11 (Jan. 1983). [received: Sept. 1983]

The location of the auroral electrojets is determined and the geomagnetic field variations with quasiperiods of 20-25 and 40-45 min along a chain of stations in the auroral region during the substorm are isolated by the methods of spectral analysis. The intensity distribution of the variations along the auroral oval allows one to identify the source of internal gravity waves (IGW) with the entire western electrojet. The spectral analysis of geomagnetic and ionospheric data makes it possible to connect the variations of electrojets with the properties of IGW generated by them. (6 refs.)

- 116332** A thermal mechanism for the escape of neutral hydrogen from the Earth's atmosphere. M.I.Pudovkin, I.V.Golovchanskaya (Leningrad State Univ., Leningrad, USSR).

Sol. Syst. Res. (USA), vol.17, no.1, p.36-42 (Jan.-March 1983). Translation of: *Astron. Vestn. (USSR)*, vol.17, no.1, p.49-55 (Jan.-March 1983). [received: Sept. 1983]

The thermal escape rate has been calculated for neutral hydrogen atoms from the present atmosphere of the Earth. It is shown that at $T_{\infty}=1000K$ the disappearing flux of hydrogen atoms amounts of 3.4×10^8 atoms/cm².sec and is found to be in good agreement with data on the rates of the appearance of atomic hydrogen in the Earth's atmosphere. (31 refs.)

- Results of apparent atomic oxygen reactions on Ag, C, and Os exposed during the shuttle STS-4 orbits See Entry 115406

- Resonant electron scattering by metastable nitrogen See Entry 115559

- A theoretical study of the height distribution of sodium in the mesosphere See Entry 116234

- Propagation of thermal radiation in the presence of random refraction of rays in a medium with a fluctuating dielectric constant See Entry 116276

- HF Doppler measurements of mesospheric gravity wave momentum fluxes See Entry 116294

- Investigation of the relation between perturbations of the altitude of the E_s layer and the intensity of nighttime luminescence at [OI] 557.7 nm See Entry 116333

- Nature of wave variations in nighttime hydroxyl-ion emission in the upper atmosphere See Entry 116334

- Measurement of the OH rotational temperature at Mawson, East Antarctica .. See Entry 116335

- A study of global structures of the ionosphere using modelling methods See Entry 116375

- Motion of a man-made satellite in the Earth's atmosphere represented by spherical harmonic functions See Entry 116421

94.10Q Airglow and nightglow

- 116333** Investigation of the relation between perturbations of the altitude of the E_s layer and the intensity of nighttime luminescence at [OI] 557.7 nm. T.A.Gorbunova, N.Yu.Kuznetsova, G.M.Shved (Univ. of Leningrad, Leningrad, USSR).

Geomagn. & Aeron. (USA), vol.22, no.3, p.357-60 (1982). Translation of: *Geomagn. & Aeron. (USSR)*, vol.22, no.3 (1982). [received: Sept. 1983]

Measurements of the altitude of the E_s layer and the intensity of luminescence at [OI] 557.7 nm, obtained in Ashkhabad, are compared by two methods: comparison of temporal spectra and comparison of departures from the average values. The velocities of propagation of dynamic disturbances in the lower thermosphere are: upward 1-6 km.h⁻¹ and downward 2-5 km.h⁻¹. (13 refs.)

116334 Nature of wave variations in nighttime hydroxyl-ion emission in the upper atmosphere. I.M.Gavrilov, V.A.Yudin (Leningrad Univ., Leningrad, USSR). *Geomagn. & Aeron. (USA)*, vol.22, no.3, p.368-71 (1982). Translation of: *Geomagn. & Aeron. (USSR)*, vol.22, no.3 (1982). [received: Sept. 1983]
Equations for estimates of amplitudes and phases of wave variations in the intensity of the nighttime emission of OH⁺ are obtained. These are derived within the linear theory of IGW assuming the oxygen-hydrogen model for formation of vibrationally excited hydroxyl ion OH⁺ at altitudes of 70-100 km. Theoretical and experimental estimates of the ratio of the amplitudes η and phase differences Δt of oscillations in the emission intensity and temperature, generated upon the passage of the wave, coincide in order of magnitude. (16 refs.)

116335 Measurement of the OH rotational temperature at Mawson, East Antarctica. L.C.Stubbs, J.S.Boyd, F.R.Bond (Antarctic Div., Dept. of Sci. & Technol., Kingston, Tasmania, Australia). *Planet. & Space Sci. (GB)*, vol.31, no.8, p.923-32 (Aug. 1983).
Measurements of the hydroxyl rotational temperature for the (8,3) Meinel band are reported for observations made at Mawson, East Antarctica (67°36'S, 62°53'E) over the austral winter of 1979. Mean values of the rotational temperature are given for 54 nights. The average value lies in the range 160-170K. The measured temperatures appear lower than those that have been reported at similar latitudes in the Northern Hemisphere. A gradual decrease in the value of the temperature throughout the course of the evening is the only diurnal trend observed. There is little evidence for any impulsive heating associated with auroral activity. (36 refs.)

94.10S Aurora

116336 Ground-based observations of subauroral energetic-electron arcs. R.Vondrak, S.Harris, S.Mende (Space Sci. Lab., Lockheed Palo Alto Res. Lab., Palo Alto, CA, USA). *Geophys. Res. Lett. (USA)*, vol.10, no.7, p.557-60 (July 1983).
On March 1, 1981 the spatial distributions of ionisation and luminosity were monitored at Chatanika, Alaska, with the incoherent-scatter radar, an all-sky television system, and meridian scanning photometers. The radar detected discrete regions of enhanced E-region ionisation at subauroral latitudes, more than 3° equatorward of the diffuse aurora. The high-resolution all-sky television measurements at 427.8 nm showed that the luminosity pattern resembles multiple auroral arcs; they are narrow in latitudinal width and they extend from horizon to horizon in an east-west direction. These observations indicate the existence of a subauroral source of electron precipitation that is both narrow in latitude and extended in longitude. (15 refs.)

116337 Ionospheric characteristics of a detached arc in the evening-sector trough. R.R.Vondrak (Space Sci. Lab., Lockheed Palo Alto Res. Lab., Palo Alto, CA, USA), J.S.Murphree, C.D.Anger, D.D.Wallis. *Geophys. Res. Lett. (USA)*, vol.10, no.7, p.561-4 (July 1983).
Simultaneous measurements by the ISIS-2 satellite and the Chatanika incoherent-scatter radar have been used to identify the ionospheric characteristics of a detached arc in the evening-sector trough region. On 26 February 1977 at 0737 UT, the ISIS-2 Auroral Scanning Photometer detected a detached arc at 65° north geomagnetic latitude that extended from approximately 1900 MLT to 2100 MLT. The arc was about 2° wide in latitude and was separated by about 3° from the equatorward edge of the diffuse aurora. The ratio of observed emission intensity at 557.7 nm to that at 391.4 nm was low, indicating a fairly hard electron distribution. The ISIS-2 Energetic Particle Detector observed energetic electron precipitation (E>40 keV) in the detached arc. The Chatanika radar found that the detached arc consisted of several narrow ionisation enhancements, with peak E-region electron densities of about $1 \times 10^5 \text{ cm}^{-3}$ at 95 km altitude. The persistent spatial pattern suggests the presence of an energetic electron precipitation mechanism that is periodic in latitude and extended in longitude. (12 refs.)

116338 Apparent electrostatic ion cyclotron waves in the diffuse aurora. E.A.Bering (Phys. Dept., Univ. of Houston, Houston, TX, USA). *Geophys. Res. Lett. (USA)*, vol.10, no.8, p.647-50 (1983). (American Geophysical Union Chapman Conference on Waves in Magnetospheric Plasma, Kona Coast, HI, USA, 7-11 Feb. 1983).
Emissions that have properties consistent with electrostatic ion cyclotron (EIC) waves have been observed at low altitude in the diffuse aurora by a sounding rocket payload. Peaks were observed in the power spectrum of the electric field near the hydrogen and oxygen ion cyclotron frequencies. Doppler shift and polarization analyses have been performed using EIC wave parameters derived from linear theory. (12 refs.)

Simultaneous geomagnetic and radio auroral observations See Entry 116362

Electron precipitation equatorward of the auroral oval and the mantle aurora in the midday sector See Entry 116370

Notes on the auroral electrojet indices See Entry 116374

PIC magnetic pulsations and variations of the ionospheric electric field and conductivity See Entry 116406

94.20 PHYSICS OF THE IONOSPHERE
(for planets, see 96.30)

116339 Ionospheric investigations using Sirio VHF beacon. P.Spalla, E.Capannini, L.Ciraola, R.Ragionieri (Istituto di Ricerca Sulle Onde Elettromagnetiche, CNR, Firenze, Italy). *Alta Freq. (Italy)*, vol.52, no.3, p.218-20 (May-June 1983). (4th Italian National Meeting on Applied Electromagnetics, Florence, Italy, 4-6 Oct. 1982).
Some results are reported concerning ionospheric measurements carried out at Istituto di Ricerca sulle Onde Elettromagnetiche (IROE), Firenze, Italy, using the VHF beacon of the SIRIO satellite. Total electron content (TEC) determinations were obtained by measuring Faraday rotation with a circular component polarimeter. Details are presented concerning the method used to solve the π ambiguity, relating the TEC to other independent ionospheric data from a nearby ionosonde. A simple method to determine the polarization at the satellite is presented. TEC profiles of over 1200 days and their monthly median values were obtained. This allowed inference of some preliminary results concerning the statistics of TEC behaviour during the 21st solar cycle. (8 refs.)

116340 Horizontal gradients and correlation coefficients in total electron content of the ionosphere. Huang Tian-Xi (Wuhan Inst. of Phys., Acad. Sinica, China). *Acta Geophys. Sin. (China)*, vol.26, no.4, p.301-8 (July 1983). In Chinese. English translation in: *Acta Geophys. Sin. (USA)*
The horizontal distribution and space correlation of TEC observed in Western Europe under quiet solar conditions during phase II of synchronous beacon

satellite ATS-6 when it was repositioned at 35°E over Eastern Africa are analysed. The latitudinal and longitudinal gradients, their diurnal variations and seasonal characteristics are dealt with. (13 refs.)

116341 The ionosphere at low and equatorial latitudes at a height of 500 km during magnetospheric-ionospheric disturbances in 1977 (September to December): data from Kosmos-900 satellite. G.L.Gdalevich, I.S.Vsekhsvyatskaya, V.D.Ozerov, T.N.Soboleva. *Cosmic Res. (USA)*, vol.20, no.6, p.616-24 (Nov.-Dec. 1982). Translation of: *Kosm. Issled. (USSR)*, vol.20, no.6, p.872-80 (Nov.-Dec. 1982). [received: Sept. 1983]
Kosmos-900 data on changes in charged particle densities at different phases of development of geomagnetic storms are used to analyze how magnetoionospheric disturbances affect the ionosphere at low and equatorial latitudes. (25 refs.)

116342 Ion kinetics, minor neutrals, and excited constituents in the D-region with an excess of ionization. I. Statement of the problem and a general schematic of the processes involved. S.I.Kozlov, V.A.Vlaskov, N.V.Smirnova. *Cosmic Res. (USA)*, vol.20, no.6, p.624-33 (Nov.-Dec. 1982). Translation of: *Kosm. Issled. (USSR)*, vol.20, no.6, p.881-91 (Nov.-Dec. 1982). [received: Sept. 1983]
On the basis of a critical analysis of published data, the authors have selected a general schematic of the processes involved, with appropriate values for the reaction rate constants. The authors consider in detail the difficulties which arise in connection with solving the large system of differential equations of chemical kinetics. A one-dimensional approach is suggested. (37 refs.)

116343 Determination of the electron content of the plasmasphere using coherent signals from the ATS-6 satellite recorded in the city of Neustrelitz. N.Yakovski, Kh.-G.Kugland. *Cosmic Res. (USA)*, vol.20, no.6, p.633-9 (Nov.-Dec. 1982). Translation of: *Kosm. Issled. (USSR)*, vol.20, no.6, p.892-9 (Nov.-Dec. 1982). [received: Sept. 1983]
Discusses the problems and methods of determining the integrated electron density in the plasmasphere by receiving radio waves from ATS-6. (19 refs.)

116344 Natural waves excited in the ionospheric plasma by an intense radio wave. V.V.Vas'kov, A.V.Gurevich (Inst. of Terrestrial Magnetism, Ionosphere & Radio Wave Propagation, Acad. of Sci., USSR). *Geomagn. & Aeron. (USA)*, vol.22, no.3, p.309-13 (1982). Translation of: *Geomagn. & Aeron. (USSR)*, vol.22, no.3 (1982). [received: Sept. 1983]
A study is made of the behavior of trapped natural waves in a magnetized plasma (the z mode) which are excited in the ionosphere when an ordinary radio wave is scattered by small-scale, approximately steady-state inhomogeneities which are stretched out along the magnetic field. The propagation of the z mode from the excitation point to the region of the plasma resonance, the absorption of this mode, and its scattering by ionospheric inhomogeneities are studied. The z-mode energy flux in the region of the plasma resonance is determined. (6 refs.)

116345 Nature of the geophysical invariance in the lower part of the ionospheric F region. G.S.Ivanov-Kholdnyy, Yu.K.Kalinin (Inst. of Appl. Geophys., State Committee on Hydrometeorology, USSR). *Geomagn. & Aeron. (USA)*, vol.22, no.3, p.319-22 (1982). Translation of: *Geomagn. & Aeron. (USSR)*, vol.22, no.3 (1982). [received: Sept. 1983]
The geophysical-invariance properties established previously for the lower part of the ionospheric F region, which are manifested in a determinate variability of the parameters of the exponential electron density profiles approximating the experimental data, are explained as a consequence of aeronic processes which give rise to steeply and gently sloping density profiles. A superposition of such profiles in the height interval 15-300 km can explain the basic features of the experimental profiles of the electron density which have been obtained for the quiet and moderately disturbed ionosphere. (2 refs.)

116346 Calculation of the spatial and temporal distribution of the ionization maximum in the polar F₂ layer. A.S.Besprozvannaya, T.M.Krupitskaya, L.N.Makarova, V.M.Uvarov, K.E.Chernin, A.V.Shirochkov (Arctic & Antarctic Inst., State Committee on Hydrometeorology, USSR). *Geomagn. & Aeron. (USA)*, vol.22, no.3, p.323-8 (1982). Translation of: *Geomagn. & Aeron. (USSR)*, vol.22, no.3 (1982). [received: Sept. 1983]
A new model is offered for the spatial and temporal distribution of the ionization in the high-latitude F layer. This model was developed through a solution of the time-varying, one-dimensional continuity equation along a convection path. The structure of the convection paths is determined from a numerical model of the large-scale electric-field distribution which agrees with direct measurements. The calculated results are compared with experimental data. (13 refs.)

116347 Mathematical model for ionosphere-plasmasphere interactions. V.M.Polyakov, M.A.Koyen, L.D.Ryazanova, I.M.Sidorov, G.V.Khazanov (Inst. of Appl. Phys., Irkutsk State Univ., Irkutsk, USSR). *Geomagn. & Aeron. (USA)*, vol.22, no.3, p.332-6 (1982). Translation of: *Geomagn. & Aeron. (USSR)*, vol.22, no.3 (1982). [received: Sept. 1983]
An attempt is made to construct a self-consistent model for the ionosphere which does not depend on the choice of upper boundary conditions and which incorporates the interaction of the charged component of the ionospheric plasma with the neutral component. An effort is made to correctly take into account the heating sources which produce superthermal electrons from thermal electrons and the contribution of small neutral components to the energy balance in the ionosphere. (20 refs.)

116348 Frequency dependence of statistical properties of a decameter-band signal. I.S.Vsekhsvyatskaya, E.Z.Gorshkova (Inst. of Terrestrial Magnetism, Ionosphere & Radio Wave Propagation, Acad. of Sci., USSR). *Geomagn. & Aeron. (USA)*, vol.22, no.3, p.340-2 (1982). Translation of: *Geomagn. & Aeron. (USSR)*, vol.22, no.3 (1982). [received: Sept. 1983]
The frequency dependences of the statistical properties of a decameter-band signal, obtained by multifrequency oblique sounding along a radio path with length D=3000 km, are discussed. The frequency dependences of the energy scattering parameter β in the case of inhomogeneities with different scales and skewness and kurtosis coefficients on the depth of penetration of the wave into the ionosphere layer are derived. (6 refs.)

116349 Variations of the Doppler shift in frequency, angles of arrival and lateral deflections of short-wave signals at sunrise. M.F.Bayuklina, A.V.Dokuchayeva (Acad. of Sci., Kazakh SSR). *Geomagn. & Aeron. (USA)*, vol.22, no.3, p.343-6 (1982). Translation of: *Geomagn. & Aeron. (USSR)*, vol.22, no.3 (1982). [received: Sept. 1983]
A model experiment for purposes of study of the variations in the Doppler frequency shift f_d , the angles of arrival ϕ , and the lateral deflections β of a shortwave signal on single-hop mid-latitude paths in a three dimensionally inhomogeneous two-layer ionosphere at sunrise was performed. The time dependences of f_d , ϕ , and β were devised for paths with different orientation. The azimuthal asymmetry in these dependences is discussed. (7 refs.)

116350 Long-range propagation of radio waves from an emitter located in the ionosphere. S.M.Yefimuk, B.E.Lyanoy, V.A.Pakhotin (Univ. of Kaliningrad, Kaliningrad, USSR).

Geomagn. & Aeron. (USA), vol.22, no.3, p.347-9 (1982). Translation of: *Geomagn. & Aeron. (USSR)*, vol.22, no.3 (1982). [received: Sept. 1983]
Results of experimental investigations of long-range propagation of radio waves with the emitter situated in the ionosphere wave channel are presented. The possibility of selecting the direction of the probable reception of long range signals from the values of the gradients of the critical frequencies at the point of reception is demonstrated. The inapplicability of a selection criterion for optimum directions with the emitter situated in the ionospheric wave channel is demonstrated. (4 refs.)

116351 Investigation of the requirements on three-dimensional laminar models of the ionosphere in problems of propagation of shortwave radio waves. Yu.I.Nadezhnikov, M.A.Nikitin, V.G.Tokar' (State Univ. Kaliningrad, Kaliningrad, USSR).

Geomagn. & Aeron. (USA), vol.22, no.3, p.350-3 (1982). Translation of: *Geomagn. & Aeron. (USSR)*, vol.22, no.3 (1982). [received: Sept. 1983]
The general requirements imposed on the three-dimensional laminar models of the ionosphere in problems of propagation of shortwave radio waves are determined. The requirements are supported by specific calculations of paths for different conditions. (2 refs.)

116352 Heating of the cold geomagnetospheric plasma. I.V.Kovalevskiy (Inst. of Terrestrial Magnetism, Ionosphere & Radio Wave Propagation, Acad. of Sci., USSR).

Geomagn. & Aeron. (USA), vol.22, no.3, p.376-9 (1982). Translation of: *Geomagn. & Aeron. (USSR)*, vol.22, no.3 (1982). [received: Sept. 1983]
The energy characteristics of the plasma with energies from a few electron volts to hundreds of electron volts which have been observed in the outer plasmasphere and in the plasma trough can be explained in terms of a heating of the cold plasmaspheric plasma by an induced scattering of longitudinal ion cyclotron waves by cold ions and a Landau damping of oblique waves by thermal electrons. (10 refs.)

116353 Reconstruction of the three-dimensional current system from variations in the ground-level magnetic field for sloping lines of force. N.I.Gershenzon, A.L.Krylov (Inst. of Earth Phys., Acad. of Sci., USSR).

Geomagn. & Aeron. (USA), vol.22, no.3, p.384-7 (1982). Translation of: *Geomagn. & Aeron. (USSR)*, vol.22, no.3 (1982). [received: Sept. 1983]
Analytical solutions are derived for determining the variations in the magnetic field produced by the three-dimensional current system and for the inverse problem of reconstructing the electric field from the variations in the ground-level magnetic field. The calculations are carried out for the case of sloping lines of force and for a uniform ionospheric conductivity. For structures which are stretched out in the latitudinal direction the effect of the inclination angle I is minimized and take the form of a change proportional to $1/\sin I$ in the integral conductivity. In general, the inclination can have an arbitrarily large effect, even for small deviations of the magnetic field from the vertical. For this reason, the conventional approach of ignoring the sloping lines of force at high latitudes is not always justified. (9 refs.)

116354 Electric field behavior in various substorm phases according to balloon measurements. T.V.Kozelova, M.I.Pudovkin, I.A.Zhulin, L.L.Lazutin (Polar Geophys. Inst., Acad. of Sci., USSR).

Geomagn. & Aeron. (USA), vol.22, no.3, p.388-91 (1982). Translation of: *Geomagn. & Aeron. (USSR)*, vol.22, no.3 (1982). [received: Sept. 1983]
Electric field distributions in the ionosphere are constructed for various phases of a substorm from measurements of the field E on high-altitude balloons in the SAMBO-79 experiment. (16 refs.)

116355 Equatorial disturbance dynamo electric fields. B.G.Fejer, M.F.Larsen, D.T.Farley (School of Electrical Engng., Cornell Univ., Ithaca, NY, USA).

Geophys. Res. Lett. (USA), vol.10, no.7, p.537-40 (July 1983).
F-region vertical drift data from Jicamarca, Peru, show that equatorial east-west electric fields are sometimes perturbed 16-24 hours after the onset of geomagnetic storms. These disturbance dynamo electric fields, which must be caused primarily by the action of neutral winds at low and middle latitudes, decrease and sometimes even reverse the quiet time electric field pattern during both daytime and nighttime. The long delay excludes the possibility that gravity waves are responsible and suggests that the thermospheric circulation is disturbed. The data also show that after some storms there are no such delayed disturbances, a fact which may be due to the longitudinal structure of the disturbances at high latitudes and/or that only very strong storms can produce major thermospheric perturbations that extend to middle and low latitudes. (14 refs.)

116356 Ionospheric conditions affecting the evolution of equatorial plasma depletions. D.N.Anderson, M.Mendillo (Dept. of Astron., Boston Univ., Boston, MA, USA).

Geophys. Res. Lett. (USA), vol.10, no.7, p.541-4 (July 1983).
Model studies have been carried out to specify the ionospheric conditions and electrodynamical processes required to describe the geometry of westward tilting and bifurcating equatorial plasma depletions inferred from airglow imaging measurements taken on Ascension Island in early 1981. The results indicate that if the westward tilts are to be associated with eastward plasma drifts that decrease with altitude above the F peak, this shear must be set up by a zonal wind pattern of decreasing speed at increasing distances from the equator. Below the peak, calculations of flux tube integrated Pedersen conductivity, including both E and F region contributions, are in agreement with the simulations of Zalesak et al. (1982) that show bifurcated depletions to be associated with a mild gradient in the bottomside conductivity profile. (20 refs.)

116357 Characteristics of two types of beam plasma discharge in a laboratory experiment. R.W.Boswell, P.J.Kellogg (Res. School of Phys. Sci., Australian Nat. Univ., Canberra, Australia).

Geophys. Res. Lett. (USA), vol.10, no.7, p.565-8 (July 1983).
Experiments on the Beam Plasma Discharge (BPD) using an electron beam traveling along a magnetic field have been carried out in a large volume laboratory vacuum chamber. Two different types of BPD have been observed, and scaling laws for varying neutral gas pressure, axial magnetic field, interaction length and electron flux, deduced. The second type of BPD occurs when the beam current is increased well above the threshold for the first type. The transition from the first type to the second, like the ignition of the first, is distinguished by abrupt changes of luminosity, discharge diameter, and wave emission signature. (9 refs.)

116358 Photometric evidence of electron precipitation induced by first hop whistlers. J.H.Doolittle, D.L.Carpenter (STAR Lab., Stanford Univ., Stanford, CA, USA).

Geophys. Res. Lett. (USA), vol.10, no.8, p.611-14 (1983). (American Geophysical Union Chapman Conference on Waves in Magnetospheric Plasma, Kona Coast, HI, USA, 7-11 Feb. 1983).
Electron precipitation events induced by discrete VLF whistler mode waves have previously been detected by photometers at Siple Station, Antarctica. This paper presents the first observations of ionospheric optical emissions correlated with VLF waves at the conjugate location, near Roberval, Quebec. (11 refs.)

116359 The modulated precipitation of radiation belt electrons by controlled signals from VLF transmitters. W.L.Imhof, J.B.Reagen, H.D.Voss, E.E.Gaines, D.W.Datlowe, J.Mobilia (Lockheed Palo Alto Res. Lab., Palo Alto, CA, USA), J.A.Helliwell, U.S.Inan, J.Katsufurakis, R.G.Joier.

Geophys. Res. Lett. (USA), vol.10, no.8, p.615-18 (1983). (American Geophysical Union Chapman Conference on Waves in Magnetospheric Plasma, Kona Coast, HI, USA, 7-11 Feb. 1983).
Reports the detection of the precipitation of radiation belt electrons by the controlled injection of signals from the US Navy VLF transmitters at Cutler, Maine (NAA) or at Annapolis, Maryland (NSS) modulated in a 3s ON/2s OFF format. During each of these events the fluxes of precipitating electrons were observed repeatedly to display a characteristic time behavior with respect to the transmitter modulation: a relatively slow rate of increase after start of the ON period leading to a maximum about 2 seconds later. Details of this consistent pattern and the statistics of occurrence of modulation events are presented along with comparisons of the absolute fluxes of precipitating electrons observed during normal transmitter operation with those recorded when one of the transmitters was modulated. (11 refs.)

116360 The mass dependence of wave particle interactions as observed with the ISEE-1 energetic ion mass spectrometer. R.D.Sharp, W.Lennartsson, W.K.Peterson, E.Ungstrup (Lockheed Palo Alto Res. Lab., Palo Alto, CA, USA).

Geophys. Res. Lett. (USA), vol.10, no.8, p.651-4 (1983). (American Geophysical Union Chapman Conference on Waves in Magnetospheric Plasma, Kona Coast, HI, USA, 7-11 Feb. 1983).
Simultaneous measurements of the O^+ and H^+ distributions from two transverse acceleration events in the high altitude auroral ionosphere are presented. The data were acquired from the energetic ion mass spectrometer on the ISEE-1 satellite, in the dusk sector, on auroral field lines ($L \approx 8.9$), at geocentric radial distances of $\sim 3 R_E$. Temporal and/or spatial fluctuations during the measurement cycle resulted in some scatter of the data points, but the transverse velocity distributions are reasonably well represented by Maxwellians at energies in the few hundred eV range. The transverse temperatures were about 60 eV in both cases and no O^+ significant differences were observed between the temperatures of the O^+ and H^+ . The flux intensities of the two ion species were also generally comparable. (28 refs.)

116361 Reflection of MHD-waves in the Pc 4-5 period range at ionospheres with non-uniform conductivity distributions. K.H.Glassmeier (Inst. fur Geophys., Univ. Munster, Munster, Germany).

Geophys. Res. Lett. (USA), vol.10, no.8, p.678-81 (1983). (American Geophysical Union Chapman Conference on Waves in Magnetospheric Plasma, Kona Coast, HI, USA, 7-11 Feb. 1983).
A theoretical model is proposed which describes the influence of non-uniform ionospheric conductivity distributions on ULF-pulsations. The assumption is made that the field-aligned currents carried out by the wave-field are closed by polarisation currents in the magnetosphere and by the irrotational part of the ionospheric currents. Current continuity at the magnetosphere-ionosphere boundary provides for a differential equation for the reflected electric field for arbitrary non-uniform conductivity distributions. A solution of the equation for two simple but realistic conductivity and electric field distributions shows that anomalies in the reflected electric field can occur which are confined to the conductivity gradient region. Under certain conditions also double peak electric field disturbances have been obtained. (9 refs.)

116362 Simultaneous geomagnetic and radio auroral observations. C.Haldoupis (Inst. of Phys., Univ. of Oslo, Oslo, Norway), E.Nielsen.

J. Atmos. & Terr. Phys. (GB), vol.45, no.8-9, p.543-56 (Aug.-Sept. 1983).
A correlative study was carried out using ground magnetometer data and STARE radar auroral data from an ionospheric region above the magnetometer station. The observations are from a reasonably disturbed period which covers the evening, midnight and morning sectors. A close relationships was found to exist between the long period geomagnetic and backscatter amplitude variations which are mainly controlled by conductivity modifications in the E-region. The irregular P_1 pulsation activity is positively related to enhancements in backscatter intensity. It is suggested that the major source of irregular P_1 -noise is the auroral Hall current perturbed by electron density fluctuations. (21 refs.)

116363 Annual and semiannual periodicities in NmF_2 in the African sector. M.C.Isherwood, L.B.Kolawole (Dept. of Phys., Univ. of Ife, Ile-Ife, Nigeria).

J. Atmos. & Terr. Phys. (GB), vol.45, no.8-9, p.557-62 (Aug.-Sept. 1983).
The annual and semiannual periodicities in amplitude and phase of NmF_2 have been computed for eleven stations in the African sector. The computations are for the sunspot maximum years of 1958 and 1968 and the solar minimum of 1964. Four patterns of diurnal behaviour in NmF_2 are discerned for different dip latitudes. The annual amplitude component is small in all sectors at low dip latitudes; however, at higher latitudes it is much larger in the northern hemisphere than the southern hemisphere at sunspot maximum. The annual phase occurs generally in December/January whilst the semiannual phase is in October/April. (11 refs.)

116364 Experimental results on satellite scintillations due to field-aligned irregularities at mid-latitudes. K.Sinno, H.Minakoshi (Radio Res. Labs., Tokyo, Japan).

J. Atmos. & Terr. Phys. (GB), vol.45, no.8-9, p.563-7 (Aug.-Sept. 1983).
Experiments using multi-station networks receiving signals from the VHF beacon of a geostationary satellite have been carried out in order to clarify the geometrical factor involved in ionospheric intensity scintillations due to field-aligned irregularities. The characteristics of scintillation observed in the daytime agree with the theoretical value expected for weak diffractive scattering by ionospheric irregularities with an elongation of 10 along the geomagnetic field. However, those in the night-time show much marked enhancement along the field-line due to strong refractive scattering by irregularities having the same elongation. (17 refs.)

116365 Determination of the latitude of Sq focus and its relation to the electrojet variations. M.Rajaram (Indian Inst. of Geomagnetism, Bombay, India).

J. Atmos. & Terr. Phys. (GB), vol.45, no.8-9, p.573-8 (Aug.-Sept. 1983).
The latitude of the Sq focus is determined analytically using the method of natural orthogonal components Geomagnetic data along the 75°E meridian

have been used. The day-to-day variations of the latitude of the Sq focus thus determined are very highly correlated with the electrojet enhancements. The strength of the normal Sq field and the electrojet field are not correlated. It appears that as the Sq focus moves towards the equator the entire current pattern bodily moves equatorwards with an increased current concentration in the electrojet region. (21 refs.)

116366 The accuracy of simple methods for determining the height of the maximum electron concentration of the F2-layer from scaled ionospheric characteristics. J.R.Dudeney (British Antarctic Survey, NERC, Cambridge, England).

J. Atmos. & Terr. Phys. (GB), vol.45, no.8-9, p.629-40 (Aug.-Sept. 1983). Techniques for estimating hmF_2 for $M(3000)F_2$ are reviewed with particular stress put upon those in which the effects of underlying ionization are accounted for by a correction (ΔM) to $M(3000)F_2$, formulated in terms of the ratio foF_2/foE . The factors considered are the dependence upon ymF_2 , the importance of the underlying layer shape (in particular the significance of the F_1 -ledge), and the influence of the geomagnetic field. It is demonstrated that the correction technique relies upon ymF_2 being a direct polynomial function of hmF_2 . (14 refs.)

116367 A scattering theory of VHF transequatorial propagation. J.A.Ferguson (Naval Ocean Systems Center, San Diego, CA, USA), H.G.Booker.

J. Atmos. & Terr. Phys. (GB), vol.45, no.8-9, p.641-57 (Aug.-Sept. 1983). Transequatorial propagation in the VHF band can occur when the ionosphere does not support such propagation by refraction. The phenomenon is closely associated with the scattering phenomenon known as spread-F. A model of scattering from long curve irregularities, aligned along the Earth's magnetic field, is developed. The theory leads to the conclusion that single partial reflections from field-aligned irregularities are all that are required to explain observations of VHF transequatorial propagation, and that multiple total reflections in a field-aligned duct are not needed. (27 refs.)

116368 Dynamics of artificial plasma clouds in 'Spolokh' experiments: movement pattern. N.I.Dzubenko (Phys. Dept., Kiev State Univ., Kiev, USSR), A.P.Zhilinsky, I.A.Zhulin, I.S.Ivchenko, A.A.Molotai, V.A.Rozhinsky, Yu.Ya.Ruzhin, V.S.Skomarovskiy, L.D.Tsandin.

Planet. & Space Sci. (GB), vol.31, no.8, p.849-58 (Aug. 1983). The data on space location and movement of the high-density ($n_e \gg n_b$) barium clouds injected at midlatitudes during the 'Spolokh-1' and 'Spolokh-2' shaped-charge experiments in the ionosphere are presented. At the initial stage, the neutral and ionized components move together at a speed of the neutral wind. An outflow of ions in the form of a stratified tail was also observed. Its movement is interpreted. (17 refs.)

116369 Auroral beam/plasma interaction observed directly. M.P.Gough (School of Math. & Phys. Sci., Univ. of Sussex, Brighton, England), A.Urban.

Planet. & Space Sci. (GB), vol.31, no.8, p.875-83 (Aug. 1983). On 9 December 1981 rocket borne energetic electron spectrometers measured energy spectra over a stable auroral arc. An associated microprocessor accurately timed the electron detection pulses to calculate auto-correlation functions for each of 16 energy levels between 300 eV and 19 keV. The observation provides the most direct measurement of the auroral beam/ionospheric plasma interaction to date. It provides hard experimental evidence to support the theories which have previously predicted that a major wave-particle interaction responsible for the evolution of the auroral distribution function occurs at heights where the upper hybrid frequency equals twice the local electron gyrofrequency. (23 refs.)

116370 Electron precipitation equatorward of the auroral oval and the mantle aurora in the midday sector. C.-I.Meng (Appl. Phys. Lab., Johns Hopkins Univ., Laurel, MD, USA), S.-I.Akasofu.

Planet. & Space Sci. (GB), vol.31, no.8, p.889-99 (Aug. 1983). In the midday sector, the hard electron precipitation and the associated patchy aurora at geomagnetic latitude $\sim 65^\circ$ are the only auroral features (≤ 20 keV) located equatorward of the dayside auroral oval during intense and moderately disturbed geomagnetic conditions. The authors identify the patchy luminosity in the midday and late morning sectors as the active mantle aurora. The precipitating electrons reside mostly at energies greater than several keV with an energy flux of ≥ 0.1 erg $\text{cm}^{-2} \text{s}^{-1} \text{sr}^{-1}$ during geomagnetic active periods. This hard precipitation occurs in a region which is asymmetric in LT with respect to the noon meridian. The region extends from the morning sector to only early afternoon (13-14 MLT) along the geomagnetic latitude circle of about $65-70^\circ$. (27 refs.)

116371 Intense night-time equatorial radio scintillations by sporadic E layers. R.G.Rastogi (Indian Inst. of Geomagnetism, Bombay, India).

Proc. Indian Acad. Sci. Earth & Planet. Sci., vol.92, no.1, p.37-43 (March 1983). [received: Sept. 1983] Almost saturated scintillations of radio beacons from geostationary satellites received at an equatorial station during the night have been shown to occur even during complete absence of spread F on the vertical incidence ionograms at the same location. These scintillation events were observed when the ionograms showed the blanketing type of sporadic E layers simultaneously at different heights. It is suggested that strong equatorial radio wave scintillations during the night-time are caused by multiple scattering between different levels of large plasma density gradients in the F or sometimes in the E regions of the ionosphere. (21 refs.)

116372 Indices of equatorial electrojet and counter-electrojet in the Indian region: evolution of the indices and their authenticity. B.N.Bhargava, B.R.Arora, N.S.Sastri (Indian Inst. of Geomagnetism, Bombay, India).

Proc. Indian Acad. Sci. Earth & Planet. Sci., vol.92, no.1, p.45-55 (March 1983). [received: Sept. 1983] Indices based on the difference in the horizontal field strength between a station under the electrojet axis (Trivandrum) and a station outside the jet influence (Alibag) can be used to characterize each day of the year. The distribution of monthly, seasonal and annual electrojet and counter-electrojet frequencies at Trivandrum during the 20-year period 1959-78 is examined. (27 refs.)

116373 Attenuation of high-frequency radio waves in the low-ionosphere at high latitudes when the ionosphere is artificially perturbed by powerful radio emission. S.I.Martynenko, V.A.Misyura, L.A.Piven', V.G.Simov, L.F.Chernogor, A.S.Shemet.

Radiophys. & Quantum Electron. (USA), vol.26, no.1, p.1-4 (Jan. 1983). Translation of: *Izv. VUZ Radiofiz. (USSR)*, vol.26, no.1, p.3-6 (Jan. 1983). [received: Sept. 1983]

The authors have discovered a significant (up to 60% and more) attenuation of the intensity of high frequency probe signals received from the low night-time ionosphere at high altitudes. The reason for the attenuation is that the ionosphere is being influenced by powerful shortwave radio emission. The experiment was performed in the region of the city of Monchegorsk during February-March, 1978. (4 refs.)

116374 Notes on the auroral electrojet indices. Y.Kamide (NOAA Space Environment Lab., Boulder, CO, USA).

Rev. Geophys. & Space Phys. (USA), vol.21, no.7, p.1647-56 (Aug. 1983). The authors examined the limitations of the auroral electrojet indices as an accurate quantitative measure of the auroral electrojets and of magnetospheric substorms. Such limitations should be kept in mind in studying individual substorms, the correlation with solar wind parameters, etc., particularly because the accuracy of the AE index decreases for $AE < \sim 250$ nT. A few suggestions are made to improve the present indices, which can be implemented efficiently when digital outputs become available from all the observatories contributing to the electrojet indices. (48 refs.)

116375 A study of global structures of the ionosphere using modelling methods. T.Tanaka.

Rev. Radio Res. Lab. (Japan), vol.28, no.147, p.521-40 (Sept. 1982). In Japanese. [received: Sept. 1983]

Diurnal variations of the thermosphere and the ionosphere are calculated by solving simultaneous time-dependent continuity equations for O^+ , H^+ , O_2^+ and NO^+ ions, equations of motion for ions and neutrals, the heat conduction equations for electrons and ions, and photoelectron transport equations. Equations are solved in the region from 120 km altitude to the equatorial plane along the field line, therefore coupling processes between the ionosphere and the protonosphere are taken into account. In addition, microprocesses controlling the energy flow in the thermosphere are treated precisely to evaluate the heating efficiency of EUV radiations. It is shown that the results calculated for the structure of the ionosphere based on MSIS (mass spectrometer and incoherent scatter data) atmospheric model show good agreements with observations. (35 refs.)

116376 A new solar index which leads to improved foF2 predictions using the CCIR Atlas. R.Y.Liu, P.A.Smith, J.W.King (Rutherford Appleton Lab., Chilton, England).

Telecommun. J. (Engl. Ed.) (Switzerland), vol.50, no.8, p.408-14 (Aug. 1983). A new index of solar activity which leads to more accurate ionospheric F2-layer critical frequency predictions, and which is intended for use with the 'CCIR Atlas of ionospheric characteristics', has been developed. An explanation of this new index, the 'global effective sunspot number', is presented together with results which indicate the extent to which the predictions of monthly median F2-layer critical frequencies are improved when it is used. (6 refs.)

Two-dimensional problem of the formation of a disturbed zone in the vicinity of a plate when a supersonic rarefied plasma flows over it See Entry 113584

Filamentation instability in magneto plasmas See Entry 113591

Construction of a high density plasma device for microwave-plasma interaction experiment See Entry 113671

Intensity fluctuations due to a deeply modulated phase screen. I. Theory See Entry 116235

Intensity fluctuations due to a deeply modulated phase screen. II. Results See Entry 116236

Propagation of thermal radiation in the presence of random refraction of rays in a medium with a fluctuating dielectric constant See Entry 116276

The type 81 system for direction finding of whistler observations in Beijing See Entry 116286

Structure of the perturbed zone near a large charged photoemitting object See Entry 116291

Determining the components of the magnetic field of a vehicle See Entry 116292

A possible mechanism for the excitation of mid-latitude internal gravity waves in the upper ionosphere See Entry 116323

Latitude dependence of disturbances of thermospheric winds See Entry 116325

Laboratory measurements of the association rate coefficients of NO^+ , O_2^+ , N^+ , and N_2^+ ions with N_2 and CO_2 at temperatures between 100K and 400K See Entry 116330

Intensity of variations of the source of internal gravity waves and the ionospheric response during the substorm of September 18, 1974 See Entry 116331

Investigation of the relation between perturbations of the altitude of the E_s layer and the intensity of nighttime luminescence at [01] 557.7 nm See Entry 116333

Ground-based observations of subauroral energetic-electron arcs See Entry 116336

Ionospheric characteristics of a detached arc in the evening-sector trough See Entry 116337

Apparent electrostatic ion cyclotron waves in the diffuse aurora See Entry 116338

Heating of heavy ions on auroral field lines See Entry 116389

Ion acceleration in the supauroral region: a Monte Carlo model See Entry 116391

Pc 1 pearl-electron interactions on the $L=4.2$ magnetic shell See Entry 116396

Experimental modelling of satellite wakes in auroral arcs See Entry 116405

PiC magnetic pulsations and variations of the ionospheric electric field and conductivity See Entry 116406

94.30 PHYSICS OF THE MAGNETOSPHERE

(for planets, see 96.30)

116377 Trapping and loss boundaries for particles in the external radiation belt due to the magnetospheric magnetic field. V.A.Sergeev, N.A.Tsyganenko. *Cosmic Res. (USA)*, vol.20, no.6, p.612-16 (Nov.-Dec. 1982). Translation of: *Kosm. Issled. (USSR)*, vol.20, no.6, p.866-71 (Nov.-Dec. 1982). [received: Sept. 1983]

A model of the quiet magnetospheric magnetic field is used to calculate the drift shells and rates of loss of high energy particles owing to pitch-angle scattering of particles crossing the equatorial current sheet on the night side. Numerical calculations of the magnitude of the angular scattering are presented. Losses in the external closed drift shells have a characteristic time ~ 1 h for high energy electrons and much longer for protons. (17 refs.)

- 116378** Positions of sources of sporadic radio emission in the frequency range 0.7-2.3 MHz, observed from the Elektron-2 and Elektron-4 satellites. G.M.Artem'eva, N.A.Mityakov, V.V.Pisareva, A.F.Tarasov. *Cosmic Res. (USA)*, vol.20, no.6, p.645-9 (Nov.-Dec. 1982). Translation of: *Kosm. Issled. (USSR)*, vol.20, no.6, p.907-12 (Nov.-Dec. 1982). [received: Sept. 1983]
The space-time distribution of the intensity of sporadic radio emission of the Earth's magnetosphere in the frequency range 0.7-2.3 MHz is investigated. Radio emission sources are located on the nightside hemisphere at geocentric distances $R \sim (2-6)R_E$ and invariant latitudes $\sim 60-75^\circ S$. On the dayside hemisphere the radio emission sources are more often located in the region of the dayside polar cusp, and an indistinct maximum at 1110 kHz is also noted at invariant latitudes $66-76^\circ S$ and $R \sim (5-8)R_E$. (10 refs.)
- 116379** Charged-particle acceleration at a tangential discontinuity in the hydrodynamic velocity of a plasma in space. E.G.Berezhko (Inst. of Space Phys. Res. & Aeronomy, Acad. of Sci., USSR). *Geomagn. & Aeron. (USA)*, vol.22, no.3, p.303-5 (1982). Translation of: *Geomagn. & Aeron. (USSR)*, vol.22, no.3 (1982). [received: Sept. 1983]
As charged particles are scattered by inhomogeneities of the magnetic field in a collisionless plasma, and as they repeatedly cross a tangential discontinuity in the hydrodynamic velocity of the plasma, they can acquire energy. An expression is derived for the rate at which energy is acquired. The steady-state energy distribution of the accelerated particles is derived. This acceleration mechanism may be important in shaping the energy distributions of the particles in the plasma sheet in the earth's magnetosphere. (7 refs.)
- 116380** Motion of fast particles in the geomagnetic field. E.V.Gorchakov, V.I.Severinov, M.V.Ternovskaya (Inst. of Nuclear Phys., Moscow State Univ., Moscow, USSR). *Geomagn. & Aeron. (USA)*, vol.22, no.3, p.306-8 (1982). Translation of: *Geomagn. & Aeron. (USSR)*, vol.22, no.3 (1982). [received: Sept. 1983]
Certain aspects of the motion of fast charged particles, for which the adiabatic approximation does not hold, in a dipole field are examined. The study is based on an analysis of numerically calculated proton paths. This path analysis yields estimates of the energies at which the bounce points of particles injected from low altitudes can lie above the injection point. (6 refs.)
- 116381** Relation between the Alfvén velocity and phase delays in a one-dimensionally inhomogeneous plasma. M.B.Gokhberg, A.L.Krylov, A.E.Lifshits (Inst. of Phys. of Earth, Acad. of Sci., USSR). *Geomagn. & Aeron. (USA)*, vol.22, no.3, p.337-9 (1982). Translation of: *Geomagn. & Aeron. (USSR)*, vol.22, no.3 (1982). [received: Sept. 1983]
Equations that describe the relation between the Alfvén velocity and phase delays are derived. An equation that permits solving the inverse problem and finding the Alfvén velocity from the known phase delays is obtained. (6 refs.)
- 116382** Interpolation equation for whistlers. A.V.Gul'yel'mi (Inst. of Phys. of Earth, Acad. of Sci., USSR). *Geomagn. & Aeron. (USA)*, vol.22, no.3, p.354-6 (1982). Translation of: *Geomagn. & Aeron. (USSR)*, vol.22, no.3 (1982). [received: Sept. 1983]
An interpolation equation is derived for whistlers. It describes the behavior of the dispersion curve over a wide range of frequencies ($0 < \omega < \Omega_e \Omega_i$) and the entire range of angles of propagation ($0 \leq \theta \leq \pi/2$). The equation is used to estimate the parameters of the trajectory of unchanneled whistlers in the meridional plane of the magnetosphere. (11 refs.)
- 116383** Helio-magnetic cycle in geomagnetic activity. N.S.Zaretskiy (Inst. of Space Phys. & Aeronomy, Acad. of Sci., USSR). *Geomagn. & Aeron. (USA)*, vol.22, no.3, p.372-5 (1982). Translation of: *Geomagn. & Aeron. (USSR)*, vol.22, no.3 (1982). [received: Sept. 1983]
The differential relations between the levels of geomagnetic activity during the even and odd eleven year solar cycles are analyzed on the basis of long time series of various characteristics of this activity. It is shown that the 22-year variation in the disturbance of the Earth's magnetic field is present in all phases of the sunspot-generating cycle. The helio-magnetic cycle of the integral amplitude of the activity is decomposed into two components with approximately opposite phases, corresponding to moderate and (very) large disturbances. (15 refs.)
- 116384** Electric field in the magnetospheric tail at various geomagnetic activity levels and at various strengths of E_y in the solar wind. M.I.Pudovkin, V.V.Osipov, M.A.Shukhtina, S.A.Zaytseva (Inst. of Phys., Leningrad State Univ., Leningrad, USSR). *Geomagn. & Aeron. (USA)*, vol.22, no.3, p.380-3 (1982). Translation of: *Geomagn. & Aeron. (USSR)*, vol.22, no.3 (1982). [received: Sept. 1983]
The large-scale electric field in the inner tail of the magnetosphere is evaluated from the time by which the variations in the AE index lag behind those in the interplanetary electric field. The electric field in the tail increases with increasing magnetic activity. The electric field of the solar wind penetrates at essentially full strength into the magnetosphere during a strong magnetic disturbance, while under magnetically quiet conditions it is substantially weakened. (13 refs.)
- 116385** Properties of the convective flow of magnetospheric plasma. I.M.Alekseyeva (Inst. of Nuclear Phys., Moscow State Univ., Moscow, USSR). *Geomagn. & Aeron. (USA)*, vol.22, no.3, p.392-4 (1982). Translation of: *Geomagn. & Aeron. (USSR)*, vol.22, no.3 (1982). [received: Sept. 1983]
A possible Hall-effect mechanism is discussed for the magnetohydrodynamic instability of a convective flow in the magnetosphere. The ohmic conductivity of the magnetospheric plasma is estimated to be $\sim 3 \times 10^3 \text{ s}^{-1}$. (15 refs.)
- 116386** Modeling of interactions of artificially released lithium with the Earth's bow shock. R.B.Decker, A.T.Y.Lui, S.M.Krimigis (Appl. Phys. Lab., Johns Hopkins Univ., Laurel, MD, USA). *Geophys. Res. Lett. (USA)*, vol.10, no.7, p.525-8 (July 1983).
A numerical simulation is used to predict the interaction between the Earth's bow shock and lithium to be released in the solar wind during the Active Magnetospheric Particle Tracer Explorers program in 1984. Based on the simulation results for a release near the subsolar point, it is recommended that a favorable release condition is when the garden-hose angle of the interplanetary magnetic field exceeds about 60 to 70° so that the transmission of Li^+ ions through the bow shock is optimized. The model also predicts that the Li^+ is 'shock-drift' accelerated at the bow shock. The energy gain of Li^+ ions is on the average less for the transmitted particles (below a factor of about 4) than for the reflected particles (below a factor of about 16). (12 refs.)
- 116387** Shape of the magnetosphere. C.C.Wu (Dept. of Phys., Univ. of California, Los Angeles, CA, USA). *Geophys. Res. Lett. (USA)*, vol.10, no.7, p.545-8 (July 1983).
The shape of the magnetosphere has been studied by using a global MHD model of the magnetosphere. It is found that MHD and the Chapman-Ferraro models agree in total magnetopause current distributions, but that the MHD model presents a very different physical picture from that of the Chapman-Ferraro model. In the MHD model with $B_{IMF}=0$ or northward, the cusp

is not exposed directly to the solar wind because the dayside magnetic field lines drape around the nightside magnetosphere. Furthermore, in the MHD model a current sheet exists above the cusp region. (10 refs.)

- 116388** On the injection boundary model and dispersing ion signatures at near-geosynchronous altitudes. R.J.Strangeway, R.G.Johnson (Lockheed Palo Alto Res. Lab., Palo Alto, CA, USA). *Geophys. Res. Lett. (USA)*, vol.10, no.7, p.549-52 (July 1983).
A simple particle drift model is used to investigate the applicability of the injection boundary concept to the ion dispersion event observed on March 22 (day 81), 1979. The model consists of a dipole magnetic field with a uniform cross-tail electric field plus a corotation field. A full spectrum of particles from 100 eV to 32 keV is injected at the $K_p=6$ —Mauk and McIlwain injection boundary at the time of substorm onset on this day (1100 UT). A new approach is presented for displaying the model-produced ion drift trajectories to make the large scale spatial characteristics of the evolving energy distributions easier to envision and to facilitate the comparison of the model results with experimental observations. (12 refs.)
- 116389** Heating of heavy ions on auroral field lines. K.-I.Nishikawa, H.Okuda (Plasma Phys. Lab., Princeton Univ., Princeton, NJ, USA), A.Hasegawa. *Geophys. Res. Lett. (USA)*, vol.10, no.7, p.553-6 (July 1983).
Heating of heavy ions is studied in the presence of a large amplitude hydrogen cyclotron wave. A three wave decay process, in which a large amplitude pump hydrogen cyclotron wave decays into a daughter hydrogen cyclotron wave and a low frequency oxygen cyclotron wave, is studied theoretically and by numerical simulations. The numerical simulations show a decay instability resulting in strong heating of both the oxygen ions and the hydrogen ions. In particular, the high energy tail of the oxygen ions is observed in the perpendicular distribution. (18 refs.)
- 116390** The relationship of total Birkeland currents to the merging electric field. P.F.Bythrow, T.A.Potemra (Appl. Phys. Lab., Johns Hopkins Univ., Laurel, MD, USA). *Geophys. Res. Lett. (USA)*, vol.10, no.7, p.573-6 (July 1983).
The Sun-synchronous orbit of the MAGSAT spacecraft has provided a new means to study the temporal response of large-scale Birkeland currents to variations in interplanetary parameters. The authors examined magnetic field data from 32 MAGSAT crossings of the northern auroral zone selected from 6 days in November and December, 1979. On each day at least 5 consecutive orbits were studied. The objectives of this study were to examine variations in the gross features of magnetic field disturbances observed on consecutive MAGSAT orbits, to investigate their relationship to interplanetary quantities, to estimate the total Birkeland current magnitude and correlate this current with various IMF parameters, and to study the relationship between the total Birkeland current and the inferred merging electric field E_M . (23 refs.)
- 116391** Ion acceleration in the supauroral region: a Monte Carlo model. J.M.Retterer (Space Data Analysis Lab., Boston Coll., Chestnut Hill, MA, USA), T.Chang, J.R.Jasperse. *Geophys. Res. Lett. (USA)*, vol.10, no.7, p.583-6 (July 1983).
The acceleration of ions and the formation of ion conics in the supauroral region is studied using a model which includes the effects of wave-particle interaction, the inhomogeneous geomagnetic field, and field-aligned potential drops. Particle acceleration by interaction with turbulence is treated as a random process in a simplified way using a Monte Carlo technique. Applying the model to ion acceleration by lower-hybrid turbulence between 1000 and 5000 km, it was found that the observed amplitudes of the waves are sufficient to accelerate ions to the energies often found in conics. (20 refs.)
- 116392** Electron acceleration by Landau resonance with whistler mode wave packets. D.A.Gurnett, L.A.Reinleitner (Dept. of Phys. & Astron., Univ. of Iowa, Iowa City, IA, USA). *Geophys. Res. Lett. (USA)*, vol.10, no.8, p.603-6 (1983). (American Geophysical Union Chapman Conference on Waves in Magnetospheric Plasma, Kona Coast, HI, USA, 7-11 Feb. 1983).
Observations of electrostatic waves associated with whistler mode chorus emissions provide evidence that electrons are being trapped by Landau resonance interactions with the chorus. The trapping, acceleration and escape of electrons in Landau resonance with a whistler mode wave packet are discussed. It is shown that acceleration can occur by both inhomogeneous and dispersive effects. The maximum energy gained is controlled by the points where trapping and escape occur. Large energy changes are possible if the frequency of the wave packet or the magnetic field strength increases between the trapping and escape points. Various trapping and escape mechanisms are discussed. (15 refs.)
- 116393** Computer simulation studies of VLF triggered emissions deformation of distribution function by trapping and detrappping. H.Matsumoto (Radio Atmospheric Sci. Center, Kyoto Univ., Kyoto, Japan), Y.Omura. *Geophys. Res. Lett. (USA)*, vol.10, no.8, p.607-10 (1983). (American Geophysical Union Chapman Conference on Waves in Magnetospheric Plasma, Kona Coast, HI, USA, 7-11 Feb. 1983).
A simulation study of VLF triggered emissions has been carried out in order to investigate quantitative changes of the velocity distribution function of resonant electrons caused by a combined action of nonlinear phase-trapping and geomagnetic inhomogeneity. It is a counterpart of the analytic theory proposed by Roux and Pellat (1978). (10 refs.)
- 116394** Observations of VLF transmitter-induced depletions of inner zone electrons. A.L.Vampola (Space Sci. Lab., Aerospace Corp., Los Angeles, CA, USA). *Geophys. Res. Lett. (USA)*, vol.10, no.8, p.619-22 (1983). (American Geophysical Union Chapman Conference on Waves in Magnetospheric Plasma, Kona Coast, HI, USA, 7-11 Feb. 1983).
Examines the relative rates of pitch-angle diffusion versus radial diffusion for electrons in the interval $2 > L > 1.5$. The result is that pitch-angle diffusion lifetimes due to interactions with the VLF waves are much shorter than the radial diffusion rate. Thus, the outer edge of the inner zone is controlled by, and is probably the result of, interactions with waves from ground-based VLF transmitters. (10 refs.)
- 116395** Observations on GEOS-1 of whistler mode turbulence generated by a ground-based VLF transmitter. T.Neubert (Danish Space Res. Inst., Lyngby, Denmark), F.Lefeuve, M.Parrot, N.Cornilleau-Wehrin. *Geophys. Res. Lett. (USA)*, vol.10, no.8, p.623-6 (1983). (American Geophysical Union Chapman Conference on Waves in Magnetospheric Plasma, Kona Coast, HI, USA, 7-11 Feb. 1983).
Signals from the NLK Jim Creek transmitter in Alaska at 18.60 and 18.65 kHz have been observed on GEOS-1. Data for one pass over Alaska on June 11, 1977, are presented. The peak amplitude of the signals is $\sim 5 \text{ pT}$ (0.6 mV/m), which is received when the satellite is close to exact conjugacy at 7500 km altitude. While the weaker signals received at some distance from conjugacy behave as expected from linear theory, the stronger signals received

closer to conjugacy have features which indicate that some non-linear process is active. (13 refs.)

116396 **Pc 1 pearl-electron interactions on the L=4.2 magnetic shell.** R.L.Arnoldy, R.L.Kaufmann (Space Sci. Center, Univ. of New Hampshire, Durham, NH, USA), L.J.Cahill, S.B.Mende. *Geophys. Res. Lett. (USA)*, vol.10, no.8, p.627-30 (1983). (American Geophysical Union Chapman Conference on Waves in Magnetospheric Plasma, Kona Coast, HI, USA, 7-11 Feb. 1983). A number of examples of auroral light bursts correlated with Pc 1 'pearl' wave packets have been recorded at Siple, Antarctica (L=4.2). The events are unique in that an individual light burst occurs at Siple not when the wave packet is recorded at Siple but rather when the wave is measured to be at the conjugate point over Roberval, Quebec. Although one can fit the observations to a model where ions are precipitated from an interaction region near the equator via cyclotron resonance, the number of ions required to produce the light and the above mentioned light burst-ULF wave phase relationship both make the precipitation of electrons a more plausible interpretation. (11 refs.)

116397 **Frequency gap formation in electromagnetic cyclotron wave distributions.** B.H.Mauk (Appl. Phys. Lab., Johns Hopkins Univ., Laurel, MD, USA). *Geophys. Res. Lett. (USA)*, vol.10, no.8, p.635-8 (1983). (American Geophysical Union Chapman Conference on Waves in Magnetospheric Plasma, Kona Coast, HI, USA, 7-11 Feb. 1983). Addresses in detail the structure of the gap near the helium cyclotron frequency observed within the statistical distribution of the frequencies of electromagnetic cyclotron waves encountered at synchronous altitudes. It is shown that, at most, two-thirds of the gap (the high frequency portion) results from linear dispersion effects. It is suggested that at least one-third of the gap (the low frequency portion) results from nonlinear, off-resonant absorption of the waves by means of near cyclotron resonance with singly charged helium ions. (13 refs.)

116398 **Drift boundaries and ULF wave generation near noon at geostationary orbit.** A.Korth, G.Kremser (Max-Planck-Inst. fur Aeronomie, Katlenburg Lindau, Germany), A.Roux, S.Perraut, J.-A.Sauvaud, J.-M.Bosqued, A.Pedersen, B.Aparicio. *Geophys. Res. Lett. (USA)*, vol.10, no.8, p.639-42 (1983). (American Geophysical Union Chapman Conference on Waves in Magnetospheric Plasma, Kona Coast, HI, USA, 7-11 Feb. 1983). Coordinated observations on board GEOS 2 of energetic particles (20 to 400 keV), plasma particles (300 eV to 20 keV), DC electric fields and ULF waves (0.2 to 10 Hz) at geostationary orbit reveal several occasions on which sharp increases in particle flux occurred near 1400 LT without any appreciable energy dispersion for ions at 90° pitch angle. The global electric field establishes boundaries that particles of given adiabatic invariants cannot penetrate. A change or reversal of the electric field moves these boundaries so as to permit their observation at GEOS 2. The waves may be compressional drift waves destabilized by plasma pressure gradients. The relationship between waves and gradients is discussed in detail for the event that occurred on August 17, 1978. (16 refs.)

116399 **Generation of Alfvén-ion cyclotron waves on auroral field lines in the presence of heavy ions.** R.L.Lysak (School of Phys. & Astron., Univ. of Minnesota, Minneapolis, MN, USA), M.A.Temerin. *Geophys. Res. Lett. (USA)*, vol.10, no.8, p.643-6 (1983). (American Geophysical Union Chapman Conference on Waves in Magnetospheric Plasma, Kona Coast, HI, USA, 7-11 Feb. 1983). Discusses the excitation of Alfvén-ion cyclotron waves in the presence of heavy ion species. The dispersion and growth of these waves in the presence of an electron beam are discussed. Wave spectra are computed using the local approximation and their dependence on various parameters is discussed. Finally, generation of ELF waves by the electron beam process is compared with the generation of the better known VLF hiss. (13 refs.)

116400 **Transfer of pulsation-related wave activity across the magnetopause observations of corresponding spectra by ISEE-1 and ISEE-2.** E.W.Greenstadi (Space Sci. Dept., TRW/STG, Redondo Beach, CA, USA), M.M.Mellott, R.L.McPherron, C.T.Russell, H.J.Singer, D.J.Knecht. *Geophys. Res. Lett. (USA)*, vol.10, no.8, p.659-62 (1983). (American Geophysical Union Chapman Conference on Waves in Magnetospheric Plasma, Kona Coast, HI, USA, 7-11 Feb. 1983). A comparison of power spectra of magnetic field data from ISEE-1 and -2 recorded simultaneously on both sides of the magnetopause shows that the power level inside the magnetosphere varies with the power level outside in the magnetosheath and suggests that the same frequencies are enhanced on the two sides of the boundary. Power levels are two to three orders of magnitude lower inside than outside the magnetosphere, indicating that wave energy is transmitted inside from the sheath, through a locally stable magnetopause. (16 refs.)

116401 **The rate of occurrence of dayside Pc 3,4 pulsations: the L-value dependence of the IMF cone angle effect.** C.T.Russell, J.G.Luhmann (Inst. of Geophys. & Planetary Phys., Univ. of California, Los Angeles, CA, USA), T.J.Odera, W.F.Stuart. *Geophys. Res. Lett. (USA)*, vol.10, no.8, p.663-6 (1983). (American Geophysical Union Chapman Conference on Waves in Magnetospheric Plasma, Kona Coast, HI, USA, 7-11 Feb. 1983). The normalized rate of occurrence of dayside Pc 3,4 pulsations from L=2.4 to 4.3 has a strong enhancement for low cone angles of the interplanetary magnetic field. When the angle of the IMF to the Earth-Sun-line is 15° or less the occurrence rate is 7-8 times the average rate at L=2.4 to 2.8 and 2.2 to 3.5 times the average rate at L=4 to 4.3. These waves disappear when the IMF is nearly at right angles to the Sun-Earth-line. The streamline geometry and its connection to the foreshock region is illustrated for a variety of IMF orientations using a simple approximation to the magnetosheath flow field. (33 refs.)

116402 **Plasma drift measurements with the electron beam experiment on GEOS-2 during long period pulsations on April 7, 1979.** H.Junginger, O.H.Bauer, G.Haerendel, F.Melzner (Max-Planck-Inst. fur Extraterrestrische Phys., Garching, Germany), B.Higel, E.Amata. *Geophys. Res. Lett. (USA)*, vol.10, no.8, p.667-70 (1983). (American Geophysical Union Chapman Conference on Waves in Magnetospheric Plasma, Kona Coast, HI, USA, 7-11 Feb. 1983). Illustrates the significance of sensitive electric field measurements inside the magnetosphere for the interpretation of long period magnetospheric pulsations. The electric field data presented have been measured by the electron beam experiment S-329, on ESA's geostationary satellite GEOS-2. The experiment measures the drift of 1.2 keV electrons injected by an electron gun perpendicular to the magnetic field. Drift velocities between 1 and 50 km/sec can be detected. (17 refs.)

116403 **Remote determination of the outer radial limit of stormtime Pc 5 wave occurrence using geosynchronous satellites.** J.N.Barfield, C.S.Lin (Dept. of Space Sci., Southwest Res. Inst., San Antonio, TX, USA). *Geophys. Res. Lett. (USA)*, vol.10, no.8, p.671-3 (1983). (American Geophysical Union Chapman Conference on Waves in Magnetospheric Plasma, Kona Coast, HI, USA, 7-11 Feb. 1983). Magnetic field data from the geostationary satellites GOES 2 and GOES 3 have shown the characteristics of stormtime Pc 5 waves to vary dramatically with local magnetic field inclination angle. To investigate this effect, data from GOES 2 and GOES 3 for the twelve-month period March 1979-February 1980 have been scanned. 105 Pc 5 events were observed at GOES 3, and 28 events at GOES 2. Using the GOES 3 Pc 5 events as a control set, the dependence of GOES 2 Pc 5 occurrence on the local magnetic field inclination angle is investigated. Further, using a simple partial ring current model to produce field distortion at GOES 2, the equivalent L value of GOES 2 is determined for each 10-minute interval during which Pc 5 waves were observed at both satellites. (4 refs.)

116404 **New observations of plasma vortices and insights into their interpretation.** E.W.Hones, J.Birn, S.J.Bame (Los Alamos Nat. Lab., Univ. of California, Los Alamos, NM, USA), C.T.Russell. *Geophys. Res. Lett. (USA)*, vol.10, no.8, p.674-7 (1983). (American Geophysical Union Chapman Conference on Waves in Magnetospheric Plasma, Kona Coast, HI, USA, 7-11 Feb. 1983).

Two- and three-dimensional plasma measurements and three-dimensional magnetic field measurements made with the ISEE 1 and 2 satellites during sixteen plasma vortex occurrences in the magnetotail plasma sheet are used to develop a fuller description of the vortex phenomenon. The phase and energy propagation properties of the vortex waves are studied. (9 refs.)

116405 **Experimental modelling of satellite wakes in auroral arcs.** N.Wild (JAYCOR, San Diego, CA, USA), R.L.Stenzel, W.Gekelman. *Geophys. Res. Lett. (USA)*, vol.10, no.8, p.682-5 (1983). (American Geophysical Union Chapman Conference on Waves in Magnetospheric Plasma, Kona Coast, HI, USA, 7-11 Feb. 1983). Preliminary measurements have been made in a large laboratory discharge device configured to simulate plasma wake phenomena. A large relative electron drift impinging on a nonconducting disc gives rise to a perturbed density structure downstream, as well as a reflected beam of electrons upstream. Velocity distribution measurements were made using a novel analyzer with angular resolution. (18 refs.)

116406 **PiC magnetic pulsations and variations of the ionospheric electric field and conductivity.** J.Leinonen, J.Kangas (Dept. of Phys., Univ. of Oulu, Oulu, Finland), A.V.Kustov, G.S.Stepanov, M.V.Uspensky. *J. Atmos. & Terr. Phys. (GB)*, vol.45, no.8-9, p.579-85 (Aug.-Sept. 1983). The sources of PiC magnetic pulsations are investigated by using ground-based geomagnetic and radar auroral data. It is shown that one part of the magnetic pulsation intensity is due to electric field variations in the ionosphere whereas another part originates in conductivity variations. It is also shown that pulsations of radar auroral intensity are correlated with conductivity variations. (28 refs.)

116407 **The evolution of pearls in the Earth's magnetosphere.** V.A.Mazur, A.S.Potapov (Siberian Inst. of Terrestrial Magnetism, Ionosphere & Radio Wave Propagation, Acad. of Sci., Irkutsk, USSR). *Planet. & Space Sci. (GB)*, vol.31, no.8, p.859-63 (Aug. 1983). Propagation and amplification of the pearls are analysed, with diffusion of wave trains in the k-space taken into account. The competition between the instability-induced amplification and the diffusion determines the values of magnetospheric parameters at which the appearance of pearls is possible. Diffusion is particularly large under conditions of a thin plasmopause and generation of pearls there is hindered or is not possible at all. (12 refs.)

116408 **The viscous-like magnetospheric convection and the length of the Earth's magnetotail.** P.Oberc (Astron. Inst., Univ. of Bonn, Bonn, Germany). *Planet. & Space Sci. (GB)*, vol.31, no.8, p.885-8 (Aug. 1983). An estimate of an upper bound on the length of the Earth's magnetotail is made under the assumptions that (1) the flux of open magnetic field lines in the polar caps never vanishes, and (2) the annihilation of the open field line flux is extremely low during magnetically quiet periods. These two basic assumptions are discussed and justified. It is found that the tail may be as long as 6000 Re (0.25 AU) after a prolonged quiet time period. On the other hand, the length of the shortest tail, which would result from a sequence of strong magnetospheric substorms, is estimated to be ~600 Re. These events are thus capable of shortening the tail by an order of magnitude. (19 refs.)

116409 **On the ring current energy injection rate.** L.C.Lee, G.Corrick, S.-I.Akasofu (Geophys. Inst., Univ. of Alaska, Fairbanks, AK, USA). *Planet. & Space Sci. (GB)*, vol.31, no.8, p.901-11 (Aug. 1983). Assuming that the formation of the ring current belt is a direct consequence of an enhanced cross-tail electric field and hence of an enhanced convection, the authors calculate the total ring current kinetic energy and the ring current energy injection rate as a function of the cross-tail electric field; the cross-tail electric field is assumed to have a step function-like increase. The loss of ring current particles due to recombination and charge-exchange is assumed to be distributed over the whole ring current region. (13 refs.)

116410 **Propagation characteristics of hydromagnetic waves in a cold plasma mixed with a hot plasma and right-hand polarized Pc 1 and Pc 5.** T.Namikawa, H.Hamabata, Y.Hosoya (Dept. of Phys., Osaka City Univ., Osaka, Japan), S.Matsushita. *Planet. & Space Sci. (GB)*, vol.31, no.8, p.913-21 (Aug. 1983). Propagation characteristics of hydromagnetic waves in a cold plasma mixed with a hot plasma under a uniform static magnetic field are investigated. The existence of cold plasma seriously affects the polarization properties of the waves. The results are applied to the interpretation of Pc 1 and Pc 5 with right-hand polarizations guided along the geomagnetic field line. (20 refs.)

116411 **On the effect of oblique disturbances on Kelvin-Helmholtz instability at magnetospheric boundary layers and in solar wind.** V.V.Mishin, A.G.Morozov (Siberian Inst. of Terrestrial Magnetism, Ionosphere & Radio Wave Propagation, Acad. of Sci., Irkutsk, USSR). *Planet. & Space Sci. (GB)*, vol.31, no.8, p.821-8 (Aug. 1983). Discusses the Kelvin-Helmholtz instability in the indissipative plasma with an external magnetic field. A detailed analysis is made of the results known from the approximation of a tangential discontinuity. The finiteness of the interface thickness effect is considered numerically at the arbitrary distribution of the density, velocity and magnetic field vectors inside this shear layer. The influence of plasma compressibility with an arbitrarily varying magnetic field is investigated. A comparison is made of the instability period on discontinuities in the solar wind, and at magnetospheric and plasmaspheric boundaries, with the range of geomagnetic pulsations. (18 refs.)

American Geophysical Union Chapman Conference on Waves in Magnetospheric Plasma See Entry 111303
Filamentation instability in magneto plasmas See Entry 113591

Structure of perpendicular shocks in collisionless plasma See Entry 113614

Non-recurrent geomagnetic disturbances from high-speed streams See Entry 116011

Occurrence probability of solar-geomagnetic-weather relations See Entry 116233

The type 81 system for direction finding of whistler observations in Beijing See Entry 116286

Structure of the perturbed zone near a large charged photoemitting object See Entry 116291

Intensity of variations of the source of internal gravity waves and the ionospheric response during the substorm of September 18, 1974 See Entry 116331

Apparent electrostatic ion cyclotron waves in the diffuse aurora See Entry 116338

The ionosphere at low and equatorial latitudes at a height of 500 km during magnetospheric-ionospheric disturbances in 1977 (September to December): data from Kosmos-900 satellite See Entry 116341

Determination of the electron content of the plasmasphere using coherent signals from the ATS-6 satellite recorded in the city of Neustrelitz See Entry 116343

Mathematical model for ionosphere-plasmasphere interactions See Entry 116347

Heating of the cold geomagnetospheric plasma See Entry 116352

Reconstruction of the three-dimensional current system from variations in the ground-level magnetic field for sloping lines of force See Entry 116353

Photometric evidence of electron precipitation induced by first hop whistlers See Entry 116358

The modulated precipitation of radiation belt electrons by controlled signals from VLF transmitters See Entry 116359

Reflection of MHD-waves in the Pc 4-5 period range at ionospheres with non-uniform conductivity distributions See Entry 116361

Simultaneous geomagnetic and radio auroral observations See Entry 116362

Notes on the auroral electrojet indices See Entry 116374

The relationships between disappearing solar filaments, coronal mass ejections, and geomagnetic activity See Entry 116625

94.40 COSMIC RAYS

Workshop on Positron-Electron Pairs in Astrophysics See Entry 111296

94.40C Origin and propagation outside the solar system

116412 Cosmic ray acceleration in supernova blast waves. H.Moraal, W.I.Axford (Max-Planck-Inst. fur Aeronomie, Katlenburg-Lindau, Germany). *Astron. & Astrophys. (Germany)*, vol.125, no.2, pt.1, p.204-16 (Sept. 1983). The solution of the test particle approximation of diffusive shock acceleration in plane, steady shocks with homogeneous up-and downstream media is used to determine cosmic ray spectra produced over the lifetime of an evolving blast wave of a supernova remnant. Adiabatic cooling and acceleration time cutoff effects are included in this solution and it is shown that very early strong shocks contribute negligibly to the resulting spectra. Injection of $T \approx 500$ eV particles at the shock produces power laws up to at least 3×10^{12} eV. These power law spectra are at least as hard as the source spectra typically used in Leaky Box propagation calculations. (23 refs.)

116413 The maximum energy of cosmic rays accelerated by supernova shocks. P.O.Lagage, C.J.Cesarsky (Service d'Astrophys., CENS, Gif-sur-Yvette, France). *Astron. & Astrophys. (Germany)*, vol.125, no.2, pt.1, p.249-57 (Sept. 1983). Evaluates the maximum energy E_{\max} that particles subjected to the process of diffusive shock acceleration can acquire during the lifetime of a supernova remnant. The rate of acceleration depends on the particle diffusion coefficient, which is determined by the level of hydromagnetic wave energy present at a scale comparable to the particle Larmor radius. The authors study the variations of the diffusion coefficient as a function of momentum, space, and time. (47 refs.)

Upper limit for mediation of baryon decay by slow magnetic monopoles See Entry 116416

Energy spectra of the cosmic gamma-ray bursts See Entry 116876

Positrons from gamma bursts See Entry 116882

94.40E Interplanetary propagation and effects

Solar wind disturbances in the outer heliosphere, caused by six successive solar flares from the same active region See Entry 116420

94.40H Energetic solar particles and photons

116414 Implications of high-energy neutron observations from solar flares. R.Ramaty (Lab. for High Energy Astrophys., NASA Goddard Space Flight Center, Greenbelt, MD, USA), R.J.Murphy, B.Kozlovsky, R.E.Lingenfelter. *Astrophys. J. Lett. Ed. (USA)*, vol.273, no.1, pt.2, p.L41-5 (1 Oct. 1983). The time-dependent flux of high-energy neutrons discovered from the solar flare of 1980 June 21 provides a new technique for determining the total number and energy spectrum of accelerated protons and nuclei at the Sun. The implications of these observations on gamma-ray emission, relativistic electron spectrum and number, proton and electron energy contents, and the location of the interaction region are also examined. (27 refs.)

Solar γ -ray lines See Entry 116564

High energy particle acceleration in solar flares—observational evidence See Entry 116590

Gamma-ray lines and neutrons from solar flares See Entry 116591

Characteristics of gamma-ray line flares as observed in hard X-ray emissions and other phenomena See Entry 116592

On the storage of high-energy protons in the solar corona: the cyclotron instability See Entry 116621

94.40K Solar modulation and geophysical effects

Upper limit for mediation of baryon decay by slow magnetic monopoles See Entry 116416

Solar wind disturbances in the outer heliosphere, caused by six successive solar flares from the same active region See Entry 116420

94.40L Composition and energy spectra

116415 Measurement of the relative composition of the cosmic-ray iron group with Lexan polycarbonate. M.Casas, C.Biaxeras, A.Vidal-Quadras, M.Ortega, F.Fernandez (Dept. de Fisica Fundamental, Univ. Autonoma de Barcelona, Barcelona, Spain). *Astrophys. & Space Sci. (Netherlands)*, vol.94, no.2, p.371-81 (Aug. 1983). Relative abundances for the VH group ($20 \leq Z \leq 28$) at energies $E \leq 600$ MeV nucl^{-1} have been measured by means of the plastic detector Lexan. The stack was exposed to cosmic rays during a 82 hr balloon flight from Sioux Falls (South Dakota) at an average altitude equivalent to 4 g cm^{-2} of residual atmosphere. A total number of 1058 events have been analyzed, out of which 675 have been unambiguously identified. In spite of the poor mass resolution, a high abundance of ^{54}Fe indicates a nonstellar origin for cosmic iron. (39 refs.)

Cosmic ray acceleration in supernova blast waves See Entry 116412

Implications of high-energy neutron observations from solar flares See Entry 116414

Gamma-ray lines and neutrons from solar flares See Entry 116591

Energy spectra of very high energy γ -rays from the Crab and Vela pulsars See Entry 116723

Energy spectra of the cosmic gamma-ray bursts See Entry 116876

94.40R High-energy interactions

116416 Upper limit for mediation of baryon decay by slow magnetic monopoles. N.A.Porter, J.Clear, D.J.Fegan, G.C.MacNeill (Dept. of Phys., Univ. Coll., Dublin, Ireland), K.Gibbs, T.C.Weekes. *Nature (GB)*, vol.304, no.5927, p.606-7 (18 Aug. 1983). Rubakov (1981) and Callan (1983) have pointed out that grand unified theory magnetic monopoles will mediate the decay of baryons, and find that the cross-section for the process should be in the strong interaction region. Others find a smaller cross-section but agree that the process will occur. Severe constraints on the density of these monopoles in the Galaxy can be deduced from astrophysical arguments, but it is possible that local clustering due to the Sun may produce a greater density at the Earth, particularly for particles with $\beta < 10^{-4}$. Using an atmospheric Cerenkov detector the authors describe how to set a limit to the flux of monopoles on the Earth's surface at these low velocities. (15 refs.)

94.60 INTERPLANETARY SPACE

(see also 96.60 Solar physics)

116417 Theoretical non-Maxwellian particle velocity distribution functions for spherically symmetric solar wind-like plasma systems and consequences. S.Superman (Space Environment Lab., NOAA, Boulder, CO, USA), I.Weiss, M.Dryer. *Astrophys. J. (USA)*, vol.273, no.1, pt.1, p.363-73 (1 Oct. 1983). The authors consider spherically symmetric solar wind-like situations in which each plasma component, a (electrons, protons, alpha particles, etc.), is adequately described by the first seven moments of the velocity distribution function, f_a . For such situations a variational principle is used in order to derive the most probable velocity distribution function for each component a , f_a . (15 refs.)

116418 Observations of the solar wind with high time resolution. G.N.Zastenker, Yu.I.Ermolaev, S.Pinter, Z.Nemecsek, Ya.Shafrankova, A.B.Belikova, A.V.Leibov, V.I.Prokhorenko, A.E.Stefanovich, A.G.Bedrikov, B.T.Karimov. *Cosmic Res. (USA)*, vol.20, no.6, p.640-5 (Nov.-Dec. 1982). Translation of: *Kosm. Issled. (USSR)*, vol.20, no.6, p.900-6 (Nov.-Dec. 1982). [received: Sept. 1983]. Describes the methods and first results of high rates of measurement of the solar wind using the Soviet-Czechoslovakian plasma spectrometer 'Monitor'. (8 refs.)

116419 Upstream electron oscillations and ion overshoot at an interplanetary shock wave. D.W.Potter, G.K.Parks (Univ. of Washington, Seattle, WA, USA). *Geophys. Res. Lett. (USA)*, vol.10, no.7, p.529-32 (July 1983). During the passage of a large interplanetary shock on 13 October 1981, the ISEE-1 and -2 spacecraft were in the solar wind outside of the upstream region of the bow shock. The high time resolution data of the University of California particle instruments pinpointed the expected electron spikes as occurring just before the magnetic ramp. In addition, two features that occur at this shock have not been observed before: (1) electron oscillations associated with low frequency waves upstream of the shock and (2) sharp 'overshoot' (~ 1 sec) in the ion fluxes that occur right after the magnetic ramp. The interplanetary shock exhibits many of the same characteristics that are observed at the Earth's bow shock. (11 refs.)

116420 Solar wind disturbances in the outer heliosphere, caused by six successive solar flares from the same active region. S.-I.Akasofu, K.Hakamada (Geophys. Inst., Univ. of Alaska, Fairbanks, AK, USA). *Geophys. Res. Lett. (USA)*, vol.10, no.7, p.577-9 (July 1983). Solar wind disturbances caused by six hypothetical flares from the same active region are traced out to about 15 au, using a simple, empirical modeling method developed by Hakamada and Akasofu [1982]. This method provides a first order construction, temporal and spatial, of flare-induced shocks and their multiple interactions with each other, as well as with the corotating interaction regions. The results are discussed in connection with recent cosmic ray observations by space probes. (19 refs.)

Backscattering cascade of beam modes off ambient density fluctuations See Entry 113600

Occurrence probability of solar-geomagnetic-weather relations See Entry 116233

Electric field in the magnetospheric tail at various geomagnetic activity levels and at various strengths of E_y in the solar wind See Entry 116384

Modeling of interactions of artificially released lithium with the Earth's bow shock See Entry 116386

- The relationship of total Birkeland currents to the merging electric field See Entry 116390
- The viscous-like magnetospheric convection and the length of the Earth's magnetotail See Entry 116408
- On the effect of oblique disturbances on Kelvin-Helmholtz instability at magnetospheric boundary layers and in solar wind See Entry 116411
- Dependence of MHD turbulence spectra on the velocity field-magnetic field correlation See Entry 116446
- Motion of dust particles in cometary atmospheres See Entry 116550
- Preferred longitudes of sunset groups and high-speed solar wind streams: evidence for a 'solar memory' See Entry 116597
- Frequency splitting in stria bursts: possible roles of low-frequency waves See Entry 116622

94.80 AEROSPACE FACILITIES AND TECHNIQUES; SPACE RESEARCH

(see also 87.65 Aerospace biophysics and medical physics)

- 116421** Motion of a man-made satellite in the Earth's atmosphere represented by spherical harmonic functions. M.Vyuktilova (Astron. Obs., Valasske Mezirici, Czechoslovakia). *Bull. Astron. Inst. Czech. (Czechoslovakia)*, vol.34, no.4, p.245-51 (July 1983).
Describes a special simplified model of the upper atmosphere which is based on the development of the density value in a specific layer into spherical harmonic functions and its application to computing the changes of orbital elements. The analytical theory is elaborated using the averaging method to remove the short-period terms. The theory is used to compute the perturbations of the orbital elements of the INTERKOSMOS 17 satellite. The results are compared to those computed using another theory (King-Hele) and also to the observed values of the changes of the orbital elements. (11 refs.)
- 116422** Algorithm for estimating the parameters of relative motion of two satellites with a complete set of measurements. A.A.Bermishev, A.F.Bragazin, I.P.Shmyglevskii, P.I.Smolkina. *Cosmic Res. (USA)*, vol.20, no.6, p.581-8 (Nov.-Dec. 1982). Translation of: *Kosm. Issled. (USSR)*, vol.20, no.6, p.828-36 (Nov.-Dec. 1982). [received: Sept. 1983].
A suboptimal algorithm for estimating the relative motion of two satellites along nearly circular orbits with complete set of measurements is examined. The orbit of the passive satellite is assumed to be known. The orbital parameters of the active satellite are estimated. The problems of stability of the algorithm, its smoothing properties, and noise stability are examined. Results of modeling are presented. (7 refs.)
- 116423** Radiative heat exchange in the vicinity of the critical point of a blunt body with an intensely vaporizing surface in a three-dimensional hypersonic stream of a hydrogen-helium mixture [planetary atmosphere entry]. E.A.Gershbein, V.D.Gol'din, G.A.Tirskii. *Cosmic Res. (USA)*, vol.20, no.6, p.606-12 (Nov.-Dec. 1982). Translation of: *Kosm. Issled. (USSR)*, vol.20, no.6, p.859-65 (Nov.-Dec. 1982). [received: Sept. 1983].
The three-dimensional flow over a blunt body of a hypersonic stream of selectively emitting and absorbing gas consisting of hydrogen and helium is analyzed with allowance for the strong injection of gaseous products of disintegration of the body. A solution of the problem is obtained in the vicinity of the critical point in an inviscid formulation with allowance for equilibrium reactions taking place in the gas stream. Both the emission in the continuous spectrum and spectral lines are taken into account in calculating the emission. The radiant fluxes are analyzed as functions of the ratios of radii of principal curvature of the body at the critical point and the conditions in the oncoming stream. (12 refs.)
- 116424** The IUE mission. P.Benvenuti (ESTEC Astron. Div., ESA-IUE Obs., Madrid, Spain). *Mem. Soc. Astron. Ital. (Italy)*, vol.54, no.2, p.359-71 (1983).
The IUE mission is reviewed after five years of successful operations. In particular the present status of the spacecraft, of the scientific instrumentation, of the image-processing software and of the data archive are discussed. A short description of the main activities at the European IUE Observatory is also given. (14 refs.)
- 116425** The promise of the Space Telescope. B.J.Bok (Univ. of Arizona, Tucson, AZ, USA). *Mercury (USA)*, vol.12, no.3, p.66-75 (May-June 1983).
Discusses the main characteristics of the Space Telescope. The main instrumentation is described together with the impact of this telescope on astronomy. (no refs.)
- 116426** A microwave scanning radiometer for Marine Observation Satellite-1. Y.Ishizawa, T.Imatani. *Mitsubishi Denki Gihō (Japan)*, vol.57, no.5, p.53-8 (1983). In Japanese.
A microwave scanning radiometer (MSR) will be carried into orbit in 1986 by Marine Observation Satellite-1 (MOS-1). This MSR is a remote sensing device designed for satellite-based measurement of weak microwave radiation from the Earth's atmosphere and surface. Measurement data from basic tests performed by the MSR will be used to determine marine atmospheric moisture and water-vapor levels, marine-ice distribution, snowpack size, and other physical quantities. The article discusses the principles of microwave radiometric observation, describes the MSR design and main operating characteristics, and reports on the results of development testing based on an engineering model. (1 ref.)
- 116427** Scientists gain a foothold in space. P.Marsh. *New Sci. (GB)*, vol.99, no.1376, p.874-9 (22 Sept. 1983).
Discusses the prospects for the Spacelab missions. Some of the experiments to be performed are discussed together with economic factors. (no refs.)
- Results of apparent atomic oxygen reactions on Ag, C, and Os exposed during the shuttle STS-4 orbits See Entry 115406
- Orbital rates of Earth satellites at resonances to test the accuracy of Earth gravity field models See Entry 115994
- Determining the components of the magnetic field of a vehicle See Entry 116292
- Experimental results on satellite scintillations due to field-aligned irregularities at mid-latitudes See Entry 116364
- A noncanonical analytic solution to the J_2 perturbed two-body problem See Entry 116430
- An analytic solution for the J_2 perturbed equatorial orbit See Entry 116431
- Helium-II application in space cooling systems See Entry 116475

- Galileo Jupiter probe Atmosphere Structure Instrument See Entry 116480
- Planetary Soil Water Analyzer (PSWA) prototype See Entry 116486

95.00 FUNDAMENTAL ASTRONOMY AND ASTROPHYSICS, INSTRUMENTATION AND TECHNIQUES AND ASTRONOMICAL OBSERVATIONS

95.10 FUNDAMENTAL ASTRONOMY

- 116428** A faint star astrometric grid for the galactic center. R.Vanderspek, G.R.Ricker (Center for Space Res., MIT, Cambridge, MA, USA). *Astron. J. (USA)*, vol.88, no.8, p.1264-8 (Aug. 1983).
Presents results of an astrometric analysis of stars in the direction of the galactic center. The absolute coordinates of 19 stars within $2'$ of the galactic center were calculated in a 12-parameter least-squares fit. The epoch 1958.3 and epoch 1976.3 coordinates as well as the calculated proper motions and epoch 1950.0 coordinates are given. The RMS error of the epoch 1958.3 and epoch 1976.3 coordinates is $\sim 0.4''$. (15 refs.)
- On the possibility of seasonal corrections while adjusting coordinates of stars See Entry 116490
- New double stars (18th series) discovered at Nice See Entry 116493
- The Danjon limit of lunar visibility: a re-examination See Entry 116498
- Analysis of lunar occultations. V. Grazing occultations 1964-1977 See Entry 116499
- 1983 RB See Entry 116513
- 1983 RD See Entry 116514
- Occultation of 14 Piscium by (51) Nemausa See Entry 116515
- Observations of Jupiter with the astrolabe of the CERGA Observatory (February 1980-May 1981) See Entry 116517
- The structure of Neptune's upper atmosphere: the stellar occultation of 24 May 1981 See Entry 116527
- Calculations of comet orbits from observations of 1980/81 See Entry 116534
- Comet Shoemaker (1983p) See Entry 116536
- Periodic Comet Arend (1983q) See Entry 116540
- Periodic Comet Harrington-Abell (1983r) See Entry 116541
- Periodic Comet Wild 2 (1983s) See Entry 116542
- Comet Kowal (1983t) See Entry 116543
- Comet Cernis (1983i) See Entry 116544
- Periodic Comet IRAS (1983j) See Entry 116545
- Analysis of solar observations made with the CERGA astrolabe See Entry 116562
- On influence of the magnitude equation in proper motions of stars on the determination of some astronomical constants See Entry 116646
- Micrometric measurements of binary stars (first list) See Entry 116755
- Arcsecond positions for milliarcsecond VLBI nuclei of extragalactic radio sources. II. 207 sources See Entry 116814
- The galactic nucleus See Entry 116850
- High precision astrometry via very-long-baseline radio interferometry: estimate of the angular separation between the quasars 1038+528A and B See Entry 116870

95.10C Celestial mechanics

(for dynamics and kinematics of stellar systems, see 98.10)

- 116429** Symmetric rectilinear periodic orbits of three bodies. P.C.Kam-meyer (Vitro Labs. Div., Automation Industries Inc., Silver Spring, MD, USA). *Celestial Mech. (Netherlands)*, vol.30, no.4, p.329-42 (Aug. 1983).
The existence of families of symmetric periodic orbits in the rectilinear three body problem with the middle mass much larger than the masses on the outside is rigorously established. A number of these families are continued numerically and their stability properties as orbits of the planar general problem of three bodies are studied. (6 refs.)
- 116430** A noncanonical analytic solution to the J_2 perturbed two-body problem. D.J.Jezewski (NASA, Lyndon B. Johnson Space Centre, Houston, TX, USA). *Celestial Mech. (Netherlands)*, vol.30, no.4, p.343-61 (Aug. 1983).
The motion of a satellite subject to an inverse-square gravitational force of attraction and a perturbation due to the Earth's oblateness as the J_2 term is analyzed, and a uniform, analytic solution correct to first-order in J_2 is obtained using a noncanonical approach. The basis for the solution is the transformation and uncoupling of the differential equations for the model. The resulting solution is expressed in terms of elementary functions of the independent variable (the 'true anomaly'), and is of a compact and simple form. Numerical results are comparable to existing solutions. (10 refs.)
- 116431** An analytic solution for the J_2 perturbed equatorial orbit. D.J.Jezewski (NASA, Lyndon B. Johnson Space Center, Houston, TX, USA). *Celestial Mech. (Netherlands)*, vol.30, no.4, p.363-71 (Aug. 1983).
An analytic solution for the J_2 perturbed equatorial orbit is obtained in terms of elliptic functions and integrals. The necessary equations for computing the position and velocity vectors, and the time are given in terms of known functions. The perturbed periaapsis and apoaapsis distances are determined from the roots of a characteristic cubic. (12 refs.)
- 116432** Theory of the Trojan asteroids. IV. B.Garfinkel (Yale Univ. Obs., New Haven, CT, USA). *Celestial Mech. (Netherlands)*, vol.30, no.4, p.373-83 (Aug. 1983).
For pt.III see *ibid.*, vol.22, no.3, p.267-87 (1980). In a previous publication (1977) the author has constructed a family \mathcal{A} of long-periodic orbits in the Trojan case of the restricted problems of three bodies. The author constructs the domain \mathcal{D} of the analytical solution of the problem of the motion, excluding the vicinity of the critical divisor which vanishes at the exact commensurability of the natural frequencies ω_1 and ω_2 . (9 refs.)

116433 Three-dimensional regions of stability about the triangular equilibrium points. A.L. Whipple (Univ. of Texas, Austin, TX, USA). *Celestial Mech. (Netherlands)*, vol.30, no.4, p.385-94 (Aug. 1983).

Within the context of the restricted problem of three bodies, an analytic upper bound on the three-dimensional regions of stability about the triangular equilibrium points is derived for general initial velocity limits and a wide class of bounding regions. This upper bound is illustrated and compared to numerical investigations for two bounding regions using the Earth-Moon mass ratio. (11 refs.)

116434 Existence of the solution of Szebehely's equation in three dimensions using a two-parametric family of orbits. F.Varadi, B.Erdi (Dept. of Astron., Eotvos Univ., Budapest, Hungary).

Celestial Mech. (Netherlands), vol.30, no.4, p.395-405 (Aug. 1983). The three-dimensional inverse problem is investigated. A quasi-linear system of partial differential equations is derived for the determination of the potential. The solution of this system is studied by a method of differential geometry. A necessary condition for the solution is derived and the determination of the potential is reduced to algebraic equations written in vectorial form. A few examples are also given. (13 refs.)

116435 A method for constructing families of spatial periodic orbits in the Hill problem. M.L.Lidov.

Cosmic Res. (USA), vol.20, no.6, p.547-64 (Nov.-Dec. 1982). Translation of: *Kosm. Issled. (USSR)*, vol.20, no.6, p.787-807 (Nov.-Dec. 1982). [received: Sept. 1983]

Describes a method for establishing and constructing symmetric periodic orbits of the family L_0 using the invariance properties of the variational equations with respect to certain linear transformations. All the canonical linear variable transformations, which do not change the equations of the Hill problem, are determined. The problem of stability is based on the calculation of the eigenvalues of the monodromy matrix. (5 refs.)

116436 The angular momentum of celestial bodies and the fundamental dimensionless constants of nature. V.De Sabbata, M.Gasperini (Istituto di Fisica, Univ. di Ferrara, Ferrara, Italy).

Lett. Nuovo Cimento (Italy), vol.38, ser.2, no.3, p.93-5 (17 Sept. 1983). A possible connection is suggested between two empirical astrophysical laws concerning the angular momentum of celestial bodies. It is shown that both relations seem to indicate that the fine-structure constant α is the typical dimensionless parameter not only of atomic physics, but also of gravitational physics. (7 refs.)

A transformation method of non-Hamiltonian system and its application See Entry 111425

Orbital rates of Earth satellites at resonances to test the accuracy of Earth gravity field models See Entry 115994

Motion of a man-made satellite in the Earth's atmosphere represented by spherical harmonic functions See Entry 116421

Algorithm for estimating the parameters of relative motion of two satellites with a complete set of measurements See Entry 116422

Additive remarks to the problem of Mercury's motion of the perihelion See Entry 116502

A new system of orbital elements of Saturn's satellites See Entry 116524

The obliquity of Pluto See Entry 116526

Entwined and parallel bundled orbits as alternative models for narrow planetary ringlets See Entry 116529

Distribution of cometary binding energies based on the assumption of steady state See Entry 116547

European Network fireballs photographed in 1977 See Entry 116551

95.30 FUNDAMENTAL ASPECTS OF ASTROPHYSICS

116437 Ambipolar diffusion in self-gravitating isothermal layers. F.H.Shu.

Astrophys. J. (USA), vol.273, no.1, pt.1, p.202-13 (1 Oct. 1983). The author formulates and solves the problem of the drift of magnetic field and ions embedded in a self-gravitating layer of neutral isothermal gas under the assumptions of quasi-magnetohydrostatic equilibrium and local ionization equilibrium. When Lagrangian coordinates referred to the neutral gas are introduced, it is found that the problem can be reduced to a nonlinear diffusion equation for the magnetic field. The shape-invariant solution for the problem is then sought and found. The results are interpreted physically, and possible implications for the problem of star formation are discussed. (25 refs.)

116438 On the propagation of acoustic waves in a radiating fluid. D.Mihalas, B.W.Mihalas (High Altitude Obs., Nat. Center for Atmospheric Res., Boulder, CO, USA).

Astrophys. J. (USA), vol.273, no.1, pt.1, p.355-62 (1 Oct. 1983). Previous discussions of the propagation of acoustic disturbances in a radiating fluid are extended by taking into account the time-dependence and dynamical behavior of the radiation field using the correct Lagrangian radiation energy and momentum equations (in the Eddington approximation). The analysis yields a much more complete, consistent, and physically satisfying picture than hitherto available. (12 refs.)

116439 Monodeuterated methane in the outer solar system. I. Spectroscopic analysis of the bands at 1.55 and 1.95 microns. B.L.Lutz (Planetary Res. Center, Lowell Obs., Flagstaff, AZ, USA), C.de Bergh, J.P.Maillard.

Astrophys. J. (USA), vol.273, no.1, pt.1, p.397-409 (1 Oct. 1983). The analysis of the near-infrared spectrum of monodeuterated methane (CH_3D) near 6400 cm^{-1} and 5100 cm^{-1} is presented. Three new parallel bands which have locally perturbed upper states connecting with the ground state are identified, and approximate rotational constants are derived. The band centered near 6425 cm^{-1} and the 9613 cm^{-1} band previously analyzed by Lutz, Daney, and Ramsay (1978) are found to form an apparent vibrational progression with the ν_2 fundamental at 2200 cm^{-1} , and vibrational assignments of $3\nu_2$ and $5\nu_2$, respectively, are proposed. Detailed comparison of the rotational constants of the states involved is shown to support these assignments. (20 refs.)

116440 Relativistic reductions for radiointerferometric observables. A.M.Finkelstein, V.Ja.Kreinovich, S.N.Pandey (Special Astrophys. Obs., Acad. of Sci., Leningrad, USSR).

Astrophys. & Space Sci. (Netherlands), vol.94, no.2, p.233-47 (Aug. 1983). The special and general relativistic corrections for the basic radiointerferometric observables—time-delay and fringe frequency—are studied with an accuracy of the order of 4×10^{-10} ('post-Newtonian approximation'). (8 refs.)

116441 Effect of rotation on magnetogravitational instability of finite conducting gas in presence of suspended particles. R.K.Chajlani, P.Purohit (School of Studies in Phys., Vikram Univ., Ujjain, India).

Astrophys. & Space Sci. (Netherlands), vol.94, no.2, p.425-36 (Aug. 1983). The effect of rotation on the self-gravitational instability of an infinite homogeneous magnetised gas-particle medium in the presence of suspended particles is investigated. The conductivity of the medium is assumed to be finite. The equations of the problem are linearized and the general dispersion relation is obtained. The rotation is assumed to be along two directions and separate dispersion relations for each case are obtained. The dispersion relation for propagation parallel and perpendicular to the uniform magnetic field along with rotation is derived. (13 refs.)

116442 Magnesium II line formation: the contribution of high atomic levels to the resonance lines. P.Lemaire, P.Gouttebroze (Lab. de Phys. Stellaire & Planetaire, Verrieres-le-Buisson, France).

Astron. & Astrophys. (Germany), vol.125, no.2, pt.1, p.241-5 (Sept. 1983). Different atomic models for the Mg^+ ion are used in line profile computations in order to evaluate their consequences for the modelling of solar and stellar atmospheres. The cores of the h and k lines (280.3 , 279.6 nm) appear to be practically insensitive to the number of levels used in the profile computations. They are not affected either by a fluorescence mechanism induced by H I L β . However, a careful treatment of the blended wings of the resonance doublet appears to be necessary for atmospheric diagnostics using the subordinate (279.1 and 279.9 nm) lines. The cores and the near wings of h and k are strongly sensitive to the atmospheric model from the higher part of the photosphere to the upper part of the chromospheric plateau. (19 refs.)

116443 Propagation of Alfvén waves in an isothermal atmosphere when the displacement current is not neglected. B.Leroy (Dept. d'Astrophys. Fondamentale, Obs. de Paris, Meudon, France).

Astron. & Astrophys. (Germany), vol.125, no.2, pt.1, p.371-4 (Sept. 1983). If the solar atmosphere is modelled by a medium with a (possibly piece-wise) exponentially decreasing density, permeated by a uniform magnetic field, for MHD waves with a period ranging between a few seconds and several hours the WKBJ approximation is nowhere valid. Consequently, the concept of a travelling wave is no longer meaningful and difficulties arise concerning the boundary condition that there be no incoming wave from infinity. In the past, these have been circumvented by confining arbitrarily the inhomogeneous medium to a region of finite extension. The author proposes an alternative solution devoid of this free parameter; it simply consists in not discarding the displacement current in Maxwell's equations. (15 refs.)

116444 A class of self-similar astrophysical explosions. M.Nepveu (Astron. Inst., Univ. Bonn, Bonn, Germany).

Astron. & Astrophys. (Germany), vol.125, no.2, pt.1, p.375-7 (Sept. 1983). A class of gasdynamical explosions is presented in which the flows are continuously heated. The heating is produced by obstacles in the flow. The results of the calculations are applied to some features of galaxy cluster heating. (9 refs.)

116445 Determination of stellar neutron-capture rates for radioactive nuclei with the aid of β -delayed neutron emission. K.-L.Kratz, W.Ziegert (Inst. fur Kernchem., Univ. Mainz, Mainz, Germany), W.Hillebrandt, F.-K.Thielemann.

Astron. & Astrophys. (Germany), vol.125, no.2, pt.1, p.381-7 (Sept. 1983). Demonstrates that the decay mode of β -delayed neutron emission can, in principle, be considered as the inverse process to neutron capture. This decay mode may reveal level parameters of neutron emitting states which can serve in two ways to predict neutron capture rates for unstable isotopes of astrophysical interest. (a) For medium and heavy mass nuclei, where due to the high level density the capture rate is not dominated by single resonances, information on the density and quantum numbers of states populated in Gamow-Teller β -decay yields a lower limit of the neutron capture cross section. (b) For nuclides near closed shells, in particular for light-mass nuclei, individual neutron-capture resonances may dominate the total cross section. (26 refs.)

116446 Dependence of MHD turbulence spectra on the velocity field-magnetic field correlation. R.Grappin (Obs. de Meudon, Meudon, France), A.Pouquet, J.Leorat.

Astron. & Astrophys. (Germany), vol.126, no.1, pt.2, p.51-8 (Sept. 1983). Steady-state MHD turbulence with non-zero velocity \mathbf{v} -magnetic field \mathbf{b} correlation is studied using both a two-point turbulence closure and phenomenological arguments. It is found that equilibrium spectra have power laws which may strongly depart from the $3/2$ law derived by Kraichnan (1965) in the uncorrelated case. This departure stems from the broken symmetry between the two fields $\mathbf{z}^{\pm} = \mathbf{v} \pm \mathbf{b}$ when the correlation is non-zero. For strong correlations, the spectral index for the total energy spectrum may lie anywhere between $3/2$ and 3 , depending on the correlation level whose maximum is determined by the molecular dissipation coefficients. (9 refs.)

116447 Dielectronic recombination at low temperatures. H.Nussbaumer (Inst. of Astron., ETH Zentrum, Zurich, Switzerland), P.J.Storey.

Astron. & Astrophys. (Germany), vol.126, no.1, pt.2, p.75-9 (Sept. 1983). Total dielectronic recombination coefficients are calculated for all ions of C, N and O for which the recombining ion has $n=2$ valence electrons in the temperature range 10^3 to $6 \times 10^4\text{ K}$. The coefficients are fitted to a convenient function of temperature. The dielectronic recombination coefficients are greater than those for direct radiative recombination in most of the cases considered over the main part of the temperature range. (15 refs.)

116448 Fundamental processes in pair plasmas. A.P.Lightman (Harvard-Smithsonian Center for Astrophys., Cambridge, MA, USA).

AIP Conf. Proc. (USA), no.101, p.359-67 (1983). (Workshop on Positron-Electron Pairs in Astrophysics, Greenbelt, MD, USA, Jan. 1983). Reviews the various processes that produce and destroy electron-positron pairs, and then compares the timescales of these processes to thermalization, accretion, and cooling timescales. The author next considers the various radiation spectra produced by relativistic, thermal plasmas. Finally, he reviews recent results for the equilibria available to finite, thermal relativistic plasmas with and without embedded magnetic fields. Such plasmas, in steady state, have maximum temperatures, luminosities, and field strengths—useful diagnostics for interpreting quasars and active galaxies. (19 refs.)

116449 Temporal evolution of electron-positron plasmas. W.Brinkmann (Max-Planck-Inst. fur Phys. und Astrophys., Inst. fur Extraterrestrische Phys., Garching, Germany).

AIP Conf. Proc. (USA), no.101, p.368-72 (1983). (Workshop on Positron-Electron Pairs in Astrophysics, Greenbelt, MD, USA, Jan. 1983). Pair annihilation processes do not influence the temporal evolution of non-relativistic e^-e^+ -plasmas to a large degree. This is mainly due to the short thermalization time scale and the fact that the nonrelativistic annihilation cross section is nearly energy-independent. Nevertheless, the emitted spectrum might differ at first drastically from a thermal equilibrium form and observations of the annihilation radiation with high temporal and spectral resolution

gives valuable information about the state of the system. If the plasma contains protons at a different temperature, the pair component evolves as quasi Maxwellian on a much longer time scale ($\tau_{\text{e.m.}}/m_e$) towards total thermal equilibrium. In relativistic plasmas where the energy dependence of all cross sections is much more pronounced things will be different, but the strongest influence on the evolution of the plasma is expected from Compton scattering of the annihilation photons on the pairs. (15 refs.)

116450 Pair production in thermal plasmas: a computer model. S.Stepney (Inst. of Astron., Univ. of Cambridge, Cambridge, England). *AIP Conf. Proc. (USA)*, no.101, p.373-6 (1983). (Workshop on Positron-Electron Pairs in Astrophysics, Greenbelt, MD, USA, Jan. 1983). A computer code has been developed to follow the processes of electron-positron pair production, annihilation, bremsstrahlung and Comptonization in a slab of mildly relativistic thermal plasma. The resulting equilibrium solutions are compared with the semi-analytic calculations of Svensson (1982). (7 refs.)

116451 Monte Carlo calculations of pair annihilation and its inverse. P.D.Noerdlinger (Los Alamos Nat. Lab., Appl. Theoretical Phys. Div., Los Alamos, NM, USA). *AIP Conf. Proc. (USA)*, no.101, p.377-81 (1983). (Workshop on Positron-Electron Pairs in Astrophysics, Greenbelt, MD, USA, Jan. 1983). The reaction rates and product energy spectra were evaluated by Monte Carlo methods for the processes of electron positron pair annihilation and the inverse (pair production by the collision of gamma rays) in a relativistic, low density plasma. The results were applied to study the collision of isotropic power law spectra of pairs or gamma rays, respectively, as a model for processes of interest in winds from active galactic or QSO nuclei. As emphasized by Cavallo and Rees (1978), the annihilation spectra favored photons with a strong peak around the electron rest mass; extended tails persisted, however, with slope about 80% that of the incident particle spectra. In the case of pair production by gamma ray collision, the resulting pair spectra had much broader peaks near 5 to 10 electron rest masses, rather insensitive to the form of the photon spectra. If the two processes feed each other repeatedly, as expected in a wind flow, one expects substantial degradation of the emergent gamma ray spectrum toward the 0.5-1.0 MeV region. (4 refs.)

116452 The particle and photon spectrum of an optically thick relativistic wind. L.J.Caroff (NASA Ames Res. Center, Moffett Field, CA, USA), J.A.Eilek, P.D.Noerdlinger. *AIP Conf. Proc. (USA)*, no.101, p.382-6 (1983). (Workshop on Positron-Electron Pairs in Astrophysics, Greenbelt, MD, USA, Jan. 1983). Compact astrophysical sources of energetic particles and photons are somewhat optically thick to particle-particle, particle-photon and photon-photon interactions. These interactions include pair production and annihilation, Compton and inverse Compton scattering, and electron-electron collisions (including bremsstrahlung). The authors present preliminary results from a calculation in which they evaluate the modulation of an initial source spectrum by these processes in an expanding relativistic electron-photon wind. (7 refs.)

116453 Pair production and annihilation in strong magnetic fields. J.K.Daugherty (Univ. of North Carolina, Asheville, NC, USA), A.K.Harding. *AIP Conf. Proc. (USA)*, no.101, p.387-99 (1983). (Workshop on Positron-Electron Pairs in Astrophysics, Greenbelt, MD, USA, Jan. 1983). Electromagnetic phenomena occurring in the presence of strong magnetic fields are currently of great interest in high-energy astrophysics. In particular, the process of pair production by single photons in the presence of fields of order 10^{12} Gauss is of importance in cascade models of pulsar gamma ray emission, and may also become significant in theories of other radiation phenomena whose sources may be neutron stars (e.g. gamma ray bursts). In addition to pair production, the inverse process of pair annihilation is greatly affected by the presence of superstrong magnetic fields. The most significant departures from annihilation processes in free space are a reduction in the total rate for annihilation into two photons, a broadening of the familiar 511-keV line for annihilation at rest, and the possibility for annihilation into a single photon (which dominates the two-photon annihilation for $B > 10^{13}$ Gauss). The physics of these pair conversion processes, which is reviewed briefly, can become quite complex in the teragauss regime, and can involve calculations which are technically difficult to incorporate into models of emission mechanisms in neutron star magnetospheres. However, recent theoretical work, especially in the case of pair annihilation, also suggests potential techniques for more direct measurements of field strengths near the stellar surfaces. (21 refs.)

116454 Equilibrium pair density in a relativistic plasma with magnetic fields. F.Takahara (Tokyo Astron. Obs., Univ. of Tokyo, Nagano, Japan), M.Kusunose. *AIP Conf. Proc. (USA)*, no.101, p.400-4 (1983). (Workshop on Positron-Electron Pairs in Astrophysics, Greenbelt, MD, USA, Jan. 1983). Equilibrium e^+e^- pair density in an optically thin relativistic plasma with magnetic fields is numerically calculated. The authors examine how the properties of a plasma are affected by hard photons produced by the multiple inverse Compton scatterings of synchrotron photons. The effect of magnetic fields, i.e. copious production of synchrotron photons, turns out to be significant even if the energy density of magnetic fields is below the equipartition value by several orders of magnitude. Both maximum temperature attainable and allowable maximum thickness of a plasma are shown to decrease rapidly with the increase of magnetic fields. (6 refs.)

116455 Annihilation lines from confined plasmas. P.W.Guilbert (Joint Inst. for Lab. Astrophys., Univ. of Colorado, Boulder, CO, USA). *AIP Conf. Proc. (USA)*, no.101, p.405-10 (1983). (Workshop on Positron-Electron Pairs in Astrophysics, Greenbelt, MD, USA, Jan. 1983). The author investigates confined electron positron pair plasmas produced by the two photon process and by the magnetic single photon process. Two photon pair production is shown to be incapable of producing an annihilation line, however, sufficiently large magnetic fields cause single photon pair production which can give large luminosities in the annihilation line. (6 refs.)

116456 Electron-positron pair annihilation and creation in superstrong magnetic fields. G.Wunner, H.Herold, H.Ruder (Lehrstuhl für Theoretische Astrophys., Univ. Tübingen, Tübingen, Germany). *AIP Conf. Proc. (USA)*, no.101, p.411-15 (1983). (Workshop on Positron-Electron Pairs in Astrophysics, Greenbelt, MD, USA, Jan. 1983). The paper reviews the results obtained so far in recalculating the processes of one-photon and two-photon pair annihilation and creation in strong magnetic fields ($B \sim 10^{11}$ - 10^{13} G, as are characteristic of neutron stars), with special emphasis being laid on annihilation. (5 refs.)

116457 Comparison of photon-photon and photon-magnetic field pair production rates. M.L.Burns, A.K.Harding (NASA/Goddard Space Flight Center, Greenbelt, MD, USA). *AIP Conf. Proc. (USA)*, no.101, p.416-20 (1983). (Workshop on Positron-Electron Pairs in Astrophysics, Greenbelt, MD, USA, Jan. 1983). Neutron stars have been proposed as the site of gamma-ray burst activity and the copious supply of MeV photons admits the possibility of electron-positron pair production. It the neutron star magnetic field is sufficiently intense ($>10^{12}$ G), both photon-photon (2γ) and photon-magnetic field (1γ) pair production should be important mechanisms. Rates for the two processes have been calculated using a Maxwellian distribution for the photons. The ratio of 1γ to 2γ pair production rates has been obtained as a function of photon temperature and magnetic field strength. (6 refs.)

116458 Conditions for stimulated-annihilation in a degenerate e^-e^+ fluid at the surface of pulsars. C.M.Varma (Bell Labs., Murray Hill, NJ, USA). *AIP Conf. Proc. (USA)*, no.101, p.421-7 (1983). (Workshop on Positron-Electron Pairs in Astrophysics, Greenbelt, MD, USA, Jan. 1983). Electrons and positrons in the large magnetic fields at the surface of pulsars condense into rod shaped droplets. The conditions for stimulated annihilation in such droplets are examined. The motivation for this investigation are the observation of Leventhal et al. (1977) of very narrow γ -ray lines emanating from the Crab nebula. (11 refs.)

116459 The production of spinless hadron pairs via virtual photon exchange in uniform magnetic fields. D.White (Dept. of Phys., Roosevelt Univ., Chicago, IL, USA). *AIP Conf. Proc. (USA)*, no.101, p.444-7 (1983). (Workshop on Positron-Electron Pairs in Astrophysics, Greenbelt, MD, USA, Jan. 1983). The method involved in bridging the gap between production of lepton pairs (as per the Kallen virtual photon formalism) and production of spinless hadron pairs is outlined. Some results associated with transitions to the ground state are displayed. (8 refs.)

116460 $^{12}\text{CH}_3\text{D}$ rovibrational intensities and the Jovian D/H ratio. C.Chackerian, Jr. (Space Sci. Div., NASA Ames Res. Center, Moffett Field, CA, USA). *Astrophys. J. Lett. Ed. (USA)*, vol.273, no.1, pt.2, p.L47-9 (1 Oct. 1983). Presents a tabulation of line intensities for the ν_2 band of CH_3D which have absolute accuracies of $\pm 3\%$. These intensities are used to interpret some of the previous Jovian D/H determinations. (11 refs.)

116461 A second-order correlation approximation for thermal conductivity and Prandtl number of free turbulence. K.-O.Eschrich, G.Rudiger (Zentralinst. für Astrophys., Akad. der Wissenschaften, Potsdam, Germany). *Astron. Nachr. (Germany)*, vol.304, no.4, p.171-80 (1983). The authors determine the dependence of the scalar thermal eddy conductivity (χ_T) on the spectral function of the turbulence and the microscopic conductivity (χ). The profile $\chi_T(\chi)$ is strongly dependent on the shape of the frequency spectrum of the velocity fluctuations. Very small molecular diffusivities generally lead to a turbulent Prandtl number of 0.4, whereas for large diffusivities the turbulent Prandtl number varies inversely with the molecular Prandtl number. The effective Prandtl number of the Sun is found to be $\text{Pr}_{\text{eff}} < 0.3$; and that of the small-scale motions in the outer core of the Earth is $\text{Pr}_{\text{eff}} = 0.4$. (31 refs.)

116462 Fourier spectroscopy of the $^{12}\text{C}_2$, $^{13}\text{C}_2$, and $^{12}\text{C}^{13}\text{C}$ (0-0) Swann bands. C.Amiot (Lab. de Phys. Moléculaire et d'Optique Atmosphérique, CNRS, Orsay, France). *Astrophys. J. Suppl. Ser. (USA)*, vol.52, no.3, p.329-40 (July 1983). The (O-O) band of the C_2 Swann electronic system $d^3\Pi_g \rightarrow a^3\Pi_u$ has been recorded by Fourier spectroscopy. The three isotopic species $^{12}\text{C}_2$, $^{13}\text{C}_2$, and $^{12}\text{C}^{13}\text{C}$ were investigated. The observed wavenumbers were reduced to molecular parameters using a nonlinear least-squares fitting procedure. Well-known perturbations at $N'=47$ and $N'=51$ are again observed in the $^{12}\text{C}_2$ $d^3\Pi_g$ ($v=0$) level. Perturbations of the same kind are present in the $^{13}\text{C}_2$ spectrum at $N'=34$ and $N'=44, 48, 52$. The $^{12}\text{C}^{13}\text{C}$ spectrum exhibits in the observed spectral range a unique perturbation for $N'=41$. (25 refs.)

116463 A simple kinetic model of a multi-particle cloud. P.Hadrava (Astron. Inst., Czechoslovak Acad. of Sci., Ondrejov, Czechoslovakia). *Bull. Astron. Inst. Czech. (Czechoslovakia)*, vol.34, no.4, p.234-41 (July 1983). A simple method for modelling the evolution of a cloud of particles is given. This method, based on the assumption of a Gaussian distribution function, enables one to treat the shape, velocity gradient and the stress tensor of the cloud. Two analytical solutions are given as examples. The first one, corresponding to moving groups of stars, shows focusing by galactic potential. The second one, appropriate to viscous gaseous discs (for example around a binary component), leads to a different form of expansion (a thick ring or flat disc) and to oscillation frequencies within the limits of an optically thick or thin ring, respectively. (6 refs.)

116464 The existence of a black hole due to condensation of matter. R.Schoen (Dept. of Maths., Univ. of California, Berkeley, CA, USA), S.-T.Yau. *Commun. Math. Phys. (Germany)*, vol.90, no.4, p.575-9 (1983). When enough matter is condensed in a small region, gravitational effects will be strong enough to cause collapse and a black hole will be formed. The authors formulate and prove here such a statement in the language of general relativity. (5 refs.)

116465 On the dynamics of a thin spherically symmetric radiating shell, its classical model, and relativistic effects. M.Castagnino (CONICET, Univ. Nacional de Rosario, Rosario, Argentina), N.Umerez. *Gen. Relativ. & Gravitation (USA)*, vol.15, no.7, p.625-34 (July 1983). A general relativity model of nova and supernova explosions is studied and improved. Its classical limit is found, and the magnitude of the velocity and mass necessary to detect relativistic effects are computed. (6 refs.)

116466 Reynolds stresses and differential rotation. III. Zonal momentum fluxes in rapidly rotating stars. G.Rudiger (Akad. der Wissenschaften, Astrophys. Obs. Potsdam, Potsdam, Germany). *Geophys. & Astrophys. Fluid Dyn. (GB)*, vol.25, no.3, p.213-33 (1983). For pt.II see ibid., vol.21, no.1 and 2, p.1-25 (1982). The author considers the influence of the Coriolis force on given turbulence models. For solar applications it is found that the basic rotation must be assumed to be neither too slow nor too rapid in order to allow a non-trivial expansion of the non-diffusive zonal momentum fluxes. Two different turbulence fields provide the desired latitudinal profiles but give different radial rotation laws: turbulence with a dominant horizontal (vertical) intensity always yields equatorial acceleration as well as the observed horizontal Reynolds stresses in connection with radial superrotation, $\partial\Omega/\partial r > 0$ (subrotation, $\partial\Omega/\partial r < 0$). In both cases the turbulent cells must be rather flat. (25 refs.)

116467 Numerical fits to important rates in high temperature astrophysical plasmas. S.Stepney (Inst. of Astron., Univ. of Cambridge, Cambridge, England), P.W.Guilbert.
Mon. Not. R. Astron. Soc. (GB), vol.204, no.3, p.1269-77 (Sept. 1983).
The authors give simple but accurate numerical fits to various two-body rates in relativistic thermal plasmas, in the temperature range $kT_e \sim 50$ keV-1 MeV. The processes discussed are bremsstrahlung, Coulomb heating and electron-positron pair production and annihilation. In particular the authors present a fit to the thermal electron-electron bremsstrahlung spectrum which is accurate to better than 5 per cent. The results are suitable for semi-analytic or computer modelling of hot plasmas. (16 refs.)

116468 Ca XVII line ratios in solar flares. P.L.Dufton (Dept. of Pure & Appl. Phys., Queen's Univ. of Belfast, N Ireland), A.E.Kingston, J.G.Doyle, K.G.Widing.
Mon. Not. R. Astron. Soc. (GB), vol.205, no.1, p.81-90 (Oct. 1983).
New electron impact collision rates are presented for transitions between the 10 lowest states of Ca XVII. These data are then used to predict Ca XVII level populations and emission-line intensity ratios for electron densities and temperatures appropriate to solar flares. A comparison is made with observations obtained with the NRL spectroheliograph aboard Skylab. (38 refs.)

116469 The evolution of viscous discs. IV. Stream penetration effects. G.T.Bath, A.C.Edwards, V.J.Mantle (Dept. of Astrophys., Univ. of Oxford, Oxford, England).
Mon. Not. R. Astron. Soc. (GB), vol.205, no.1, p.171-85 (Oct. 1983).
For pt.III see ibid., vol.201, no.1, p.345-55 (1982). The interaction between the mass transfer stream and a circularized accretion disc is described in terms of a general transport equation including sources of mass and angular momentum from the stream. The stream stripping process associated with disc penetration is parameterized in terms of the impact momentum of disc material. The anisotropic radiation pattern generated by the stream/disc interaction is discussed. Evidence is presented that suggests the superhumps are not a disc phenomenon, but are due to asymmetric structure on a non-synchronously rotating red component. (15 refs.)

116470 The expansion of a plasma into a vacuum: basic phenomena and processes and applications to space plasma physics. U.Samir (Space Phys. Res. Lab., Univ. of Michigan, Ann Arbor, MI, USA), K.H.Wright,Jr., N.H.Stone.
Rev. Geophys. & Space Phys. (USA), vol.21, no.7, p.1631-46 (Aug. 1983).
The authors call attention to basic phenomena and physical processes involved in the expansion of a plasma into a vacuum, or the expansion of a plasma into a more tenuous plasma, in particular the fact that upon expansion ions are accelerated and reach energies well above their thermal energy. Also, in the process of the expansion a rarefaction wave propagates into the ambient plasma, an ion front moves into the expansion volume, and discontinuities in plasma parameters occur. The physical processes which cause the above phenomena are discussed, and their possible applications are described. (89 refs.)

Workshop on Positron-Electron Pairs in Astrophysics See Entry 111296

Galactic lens See Entry 111366

On the global geometry of the Stephani universe See Entry 111510

A rotating mass embedded in an Einstein-Godel universe See Entry 111513

Non-Einsteinian gravitational Lagrangians assuring cosmological solutions without collapse See Entry 111514

Absorber theory for the Einstein equations in the first approximation See Entry 111518

Remote quantum mechanical detection of gravitational radiation See Entry 111522

Material and electromagnetic sources of the Kerr-Newman geometry See Entry 111523

A bimetric Machian approach to gravitation See Entry 111524

Emission of relativistic particles in a strong gravitational field See Entry 111531

Elimination of unitarily nonequivalent vacua in supersymmetric grand unified theories by gravity See Entry 111922

Search for neutrino masses and oscillations See Entry 111940

An upper limit on neutrino electric dipole moments See Entry 112002

Hyperfine structure measurements for lines of astrophysical interest in Mn I See Entry 112680

An ab initio SCF study on the stability and structure of $H_2CN^+ \cdot nN_2$ clusters See Entry 112891

The gravitational instability of a rotating plasma in the presence of finite Larmor radius, Hall currents and suspended particles See Entry 113582

Backscattering cascade of beam modes off ambient density fluctuations See Entry 113600

Nonlinear periodic solutions for the isothermal magnetostatic atmosphere See Entry 113601

Upper limit for mediation of baryon decay by slow magnetic monopoles See Entry 116416

Theoretical non-Maxwellian particle velocity distribution functions for spherically symmetric solar wind-like plasma systems and consequences See Entry 116417

Parametric detector as a tunable antenna for continuous gravitational radiation See Entry 116485

Reflection of light by a multilayered planetary atmosphere See Entry 116501

Electromagnetic ion-cyclotron instability in the multi-ion Jovian magnetosphere See Entry 116519

Photolysis of methane and the ionosphere of Uranus See Entry 116528

The atmosphere of a dirty-clathrate cometary nucleus: a two-phase, multifluid model See Entry 116531

Infrared fluorescence of molecules in comets: the general synthetic spectrum See Entry 116533

Comments on the solar neutrino problem See Entry 116557

On a possible mechanism of quasi-periodic pulses of the quiet Sun decametric radio emission See Entry 116570

On the relation of local sources of centimeter solar radioemission with noise storms based on the RATAN-600 observations See Entry 116571

Asymmetries in Stokes profiles of magnetic lines: a linear analysis in terms of velocity gradients See Entry 116611

Calculation or coronal line intensities for boron-like ions See Entry 116612

Transient brightenings of interconnecting loops. III. Interpretation See Entry 116616

Magnetic stability of coronal arcades relevant to two-ribbon flares See Entry 116617

Magnetic equilibrium in coronal arcades See Entry 116618

On the storage of high-energy protons in the solar corona: the cyclotron instability See Entry 116621

Frequency splitting in stria bursts: possible roles of low-frequency waves See Entry 116622

The pulsar P/P distribution and the postulated solar companion See Entry 116627

The formation of emission lines in the expanding chromospheres of luminous cool stars. I. The importance of atmospheric extension and partial redistribution effects See Entry 116629

Effect of excited states on thermonuclear reaction rates See Entry 116631

Broadband linear polarization from magnetized stellar atmospheres. II. The influence of damping on net spectral line polarization See Entry 116640

Vibrating-dust spheres in the Reissner-Nordstrom metric See Entry 116643

Stellar collapse without singularities? See Entry 116644

Matter transfer by MHD waves in stellar atmospheres See Entry 116645

Neutrino emission from a hot, dense, plane-parallel atmosphere in hydrostatic equilibrium. III. The three-flavored atmosphere See Entry 116706

Do filaments form at the time of supernova explosions? See Entry 116707

Softening effects in the equation of state and influence of general relativity on the outcome of stellar collapse See Entry 116708

Similarity solutions for explosions in radiating stars with time-dependent energy and idealized magnetic field See Entry 116713

Electron positron pairs in radio pulsars See Entry 116724

Pair production near threshold in pulsar magnetic fields See Entry 116725

The pulsar oblique rotator: numerical solution of an illustrative problem See Entry 116728

Pulsar electrodynamics: cylindrical model and radio and gamma-ray radiation See Entry 116729

Gravitational radiation reaction in the binary pulsar and the quadrupole-formula controversy See Entry 116731

Resonant free-free emission from electrons in magnetic polar regions of accreting neutron stars See Entry 116733

Black hole electromagnetic fields and negative energy states for charged particles See Entry 116734

Rotating black hole in asymptotic de Sitter space: perturbation of the space-time with spin fields See Entry 116738

Radio emission from AM Herculis: the quiescent component and an outburst See Entry 116740

The effect of low-velocity, low-mass intruders (collisionless gas) on the dynamical evolution of a binary system See Entry 116743

Digital analysis of narrow-band imagery of the Cygnus Loop See Entry 116778

Semianalytical treatment of the hydrodynamics of supernova remnants during the snowplow phase See Entry 116779

Hydrogen and helium ionization structure of gaseous nebulae See Entry 116783

Tentative detection of the CS^+ molecular ion in diffuse interstellar clouds See Entry 116784

Neutrino-gaseous 'Pancakes' and the problem of hidden mass See Entry 116861

An optical test for the distance of gamma-ray burst sources See Entry 116873

Detection of an extended soft X-ray source H 2326-79 in the southern sky See Entry 116874

Emission model of gamma-ray bursts See Entry 116880

Criteria for gas action in astrophysical sources See Entry 116884

Pair production and non-thermal radio stars See Entry 116885

Plane symmetric vacuum Bianchi type I cosmological model in Brans-Dicke theory See Entry 116890

On the statistical distribution of massive fermions and bosons in a Friedmann Universe See Entry 116893

Constraints on neutrino-dominated cosmologies from large-scale streaming motion See Entry 116894

The cosmological problem as initial value problem on the observer's past light cone: observations See Entry 116895

Bianchi-I universes of the Brans-Dicke theory for the vacuum See Entry 116896

Neutrinos in cosmology See Entry 116897

Spatially homogeneous and anisotropic cosmological solution in Brans-Dicke theory See Entry 116898

Cosmic censorship and curvature growth See Entry 116899

Proto-galactic perturbations See Entry 116900

The cosmological constant and classical tests of general relativity See Entry 116901

Monopoles in the inflationary Universe See Entry 116902

Modeling in chaotic relativity See Entry 116903

Homogeneity of Riemannian space-times of Godel type See Entry 116906

New model of the metagalaxy See Entry 116908

Viscosity and the monopole density of the Universe See Entry 116909

95.45 OBSERVATORIES

116471 Northern skies. Britain's new telescopes in the Canary Islands. P.Murdin.
Phys. Bull. (GB), vol.34, no.9, p.377-9 (Sept. 1983).
This year (1983) sees the rebirth of Britain's largest astronomical telescope, the 2.5 m Isaac Newton Telescope, at its new observatory on the island of La Palma in the Canaries. Dismantled in 1979 from its dome at the site of the Royal Greenwich Observatory near Herstmonceux in Sussex, the telescope has been renovated by its original builders, Grubb-Parsons in Newcastle, and re-erected at a height of 2400 m in the Observatorio del Roque de los Muchachos. It will be joined quickly by a 1 m reflecting telescope. In 1984, the Carlsberg Automatic Transit Circle, in which Britain has an equal share

with Denmark, will begin operation and in 1986 the largest of the telescopes already planned for the mountain top will be completed, the 4.2 m William Herschel Telescope. Two telescopes belonging to Sweden are already at work on La Palma, and other European countries are contemplating erection of telescopes in the observatorio. (no refs.)

95.55 ASTRONOMICAL INSTRUMENTS

116472 An imaging gas scintillation proportional counter for use in X-ray astronomy. C.J.Hailey, W.H.-M.Ku, M.H.Vartanian (Dept. of Astron. & Phys., Columbia Univ., New York, NY, USA). *Nucl. Instrum. & Methods Phys. Res. (Netherlands)*, vol.213, no.2-3, p.397-410 (1 Aug. 1983).

An imaging gas scintillation proportional counter (GSPC) has been constructed for use in X-ray astronomy. The IGSPC consists of a gas scintillation proportional counter (GSPC) with a 1 μ m polypropylene window coupled to a multiwire proportional counter (MWPC) via a calcium fluoride window. The MWPC, filled with a mixture of argon, methane, and tetrakis (dimethylamino) ethylene, detects the UV photons emitted by the xenon gas in the GSPC. The measured energy resolution is 17.0% (FWHM) and 8.0% (FWHM) at 1.5 keV and 5.9 keV, respectively. The measured position resolution is 1.9 mm (FWHM) and 0.9 mm (FWHM) at 1.5 and 5.9 keV, respectively. The authors also discuss possible astrophysical observations which can be performed with an IGSPC at the focal plane of a grazing incidence telescope. (41 refs.)

116473 A proportional counter with one dimensional position sensitivity for image scanning in the soft X-ray region. K.H.Stephán, M.Henne (Max-Planck-Inst. für Extraterrestrische Phys., Garching bei München, Germany). *Nucl. Instrum. & Methods Phys. Res. (Netherlands)*, vol.213, no.2-3, p.411-14 (1 Aug. 1983).

A device is described to measure spatial intensity distributions of images of the soft X-ray region by means of a proportional counter which has positional sensitivity capability in one dimension. Collection, reduction and storing of the data are controlled by a desktop computer with specially written software to provide data transfer from a multichannel analyser. The measuring unit is used in a long beam X-ray testing facility to study the features of rocket and satellite borne instrumentation under simulated outer space conditions in the laboratory. (7 refs.)

116474 Design and performance of a one square meter proportional counter system for hard X-ray astronomy. A.Bazzano, L.Boccacini, C.D.La Padula, M.Mastropietro, R.Patriarca, F.Polcaro, P.Ubertini, R.K.Manchanda (Istituto di Astrofisica Spaziale, CNR, Rome, Italy).

Nucl. Instrum. & Methods Phys. Res. (Netherlands), vol.214, no.2-3, p.481-90 (1 Sept. 1983).

A versatile balloon-borne hard X-ray experiment with a very large area (≈ 1.1 m²) and high spectral resolution has been developed for the study of the hard X-ray sources in the energy range 20-180 keV. The telescope consists of four multiwire proportional chambers (MWPC) that have a geometrical sensitive area of 2700 cm² each. The detector system has a sensitivity of $\sim 10^{-3}$ photons cm⁻² s⁻¹ keV⁻¹ during a typical balloon observation. A background rate of $\sim 3 \times 10^{-4}$ counts cm⁻² s⁻¹ keV⁻¹ was observed in the operative energy range at 2.4 gm/cm² ceiling altitude and geographic latitude of 38°N. The design details, fabrication and flight performance of the instrument are briefly discussed with reference to the effectiveness of background reduction and other test parameters. (19 refs.)

116475 Helium-II application in space cooling systems. G.Klippling (Fachbereich Phys., Freie Univ. Berlin, Berlin, Germany). *Indian J. Cryog.*, vol.6, no.4, p.147-53 (1981).

The cooling of IR telescopes requires temperatures below 2K for long term missions. Therefore He-II cooling systems are to be developed which provide a favourable relation between cooling power and the amount of coolant, uniform temperature distribution and the advantage of the special properties of He-II. A most important part of such a cooling system is the phase separator which must work reliably under zero g conditions. A number of interesting problems of He-II physics are to be solved in connection with these developments. (10 refs.)

116476 The Couder telescope-better than the Schmidt?. R.V.Willstop (Inst. of Astron., Obs., Cambridge, England). *Mon. Not. R. Astron. Soc. (GB)*, vol.204, no.3, p.99P-103 (Sept. 1983).

The optical quality of the Couder telescope is examined, and it is shown that with small modifications to the original design it is comparable with, or better than, the Schmidt camera. (9 refs.)

116477 Low-noise MM-wave receivers with quasioptical inputs [for radioastronomical observations]. P.Zimmerman (Jet Propulsion Lab., Pasadena, CA, USA).

Mikrowellen Mag. (Germany), vol.8, no.5, p.552-6 (Oct. 1982). [received: Aug. 1983]

Describes two systems with cooled Schottky-barrier-diode mixers at 183 GHz and 230 GHz, which have been used for observations of molecular line emission in galactic objects. Low loss coupling of signal- and local-oscillator-frequencies was provided at 183 GHz through a folded Fabry-Perot-Resonator and at 230 GHz through a Mach-Zehnder-Diplexer. System noise temperatures of 750K (DSB) at 183 GHz and 260K (DSB) at 230 GHz were measured. The decrease in system noise temperature at the higher frequency is mainly due to improvements in diode- and FET-technology over the years 1978 to 1981. (11 refs.)

116478 On the instrumental and atmospheric stray-light for solar observations. W.Mattig (Kiepenheuer-Inst. für Sonnenphys., Freiburg, Germany). *Sol. Phys. (Netherlands)*, vol.87, no.1, p.187-93 (Aug. 1983).

From aureole measurements made with the 40 cm-Vacuum-Telescope at Izana (Tenerife) in the wavelength region 417 nm < λ < 785 nm and from a comparison with other aureole measurements it is concluded that: (a) within one solar radius from the limb, the aureole is mostly of instrumental origin; (b) beyond that distance, the contribution of atmospheric stray-light becomes noticeable; (c) the atmospheric contribution to the aureole intensity is, under good conditions at mountain stations, a very slowly decreasing function, and amounts to some 10^{-3} of the solar disk intensity. A procedure is given to separate the variable atmospheric component of the stray-light from the constant instrumental one. (2 refs.)

116479 The Mount Wilson magnetograph. R.Howard, J.E.Boyden, D.H.Bruning, M.K.Clark, H.W.Crist, B.J.Labonte (Mount Wilson & Las Campanas Obs., Carnegie Inst. of Washington, Pasadena, CA, USA).

Sol. Phys. (Netherlands), vol.87, no.1, p.195-203 (Aug. 1983). Alterations to the Mount Wilson Observatory solar magnetograph were made during 1981. The present state of the instrument, including the spectrograph, is described. The magnetic and Doppler velocity signals and the setup procedure for the magnetogram observation are discussed. The advantages of the new system are described. (7 refs.)

116480 Galileo Jupiter probe Atmosphere Structure Instrument. J.R.Padilla (Martin Marietta Corp., Denver, CO, USA).

ITC/USA/82. International Telemetering Conference, San Diego, CA, USA, 28-30 Sept. 1982 (Woodland Hills, CA, USA: Int. Found. Telemetering 1982), p.711-18

The scientific objective is to define the profiles of the Jovian atmospheric static and dynamic state properties over a wide altitude range. The acceleration measurement system provides data on probe deceleration and velocity from early entry through descent. Associated pressure and temperature data will help to define density, atmospheric turbulence and the radial distance of the probe from the center of Jupiter. The accelerometers are of the pendulous mass-displacement type which operate in an oil fluid medium. Each accelerometer is accompanied with a set of hybrid electronics which converts pendulum mass-displacement into volts per g. Four ranges are possible for each axial accelerometer and three ranges for the lateral accelerometers. (3 refs.)

The promise of the Space Telescope See Entry 116425

Northern skies. Britain's new telescopes in the Canary Islands See Entry 116471

IUE data reduction See Entry 116487

95.65 AUXILIARY AND RECORDING INSTRUMENTS

116481 Near-infrared photopolarimeter for astronomical observations. T.Sajo (Lab. of Cosmic Phys. & Relative Technol., Nat. Res. Council of Italy, Milan, Italy).

Infrared Phys. (GB), vol.23, no.3, p.125-30 (May 1983).

The construction of a near-infrared (1.9-2.5 μ m) photopolarimeter for linear polarization analysis and corresponding testing is described. Details of the polarimetric components are shown. A description is given of the manufacture and features of a mica sheet half-wave phase retarder, which allows the rotation of the polarization plane of incident radiation in front of an analyzer. Observations of radiation from the planet Mars and a few standard unpolarized stars, utilizing the bent Cassegrain-type reflector (1.37 m dia) of the Merate Observatory, are reported. The interpretation of measurements, in terms of the extraction of information on polarization percentages from experimental curves, is obtained by means of an analytical treatment which involves the behaviour of the incident light passing through the instrumental components. (11 refs.)

116482 Four-centimeter traveling-wave maser with high amplitude and phase stability [radioastronomy application]. Ya.L.Shamfarov, A.I.Stetsenko, S.K.Kondrashin (Radiophys. & Electronics Inst., Acad. of Sci., Kharkov, Ukrainian SSR).

Instrum. & Exp. Tech. (USA), vol.25, no.5, pt.1, p.1157-9 (Sept.-Oct. 1982). Translation of: *Prib. & Tekh. Eksp. (USSR)*, vol.25, no.5, p.104-7 (Sept.-Oct. 1982). [received: Sept. 1983]

A traveling-wave maser for the 4 cm wavelength range with high amplitude and phase stability is described. The device is intended for use in the receiver system of a radioastronomical interferometer. Measures taken to eliminate amplitude and phase instability sources are described. Phase and amplitude noise produced by passage of gas bubbles through the electric field region of the retarding structure is eliminated. Phase instability over the course of 45 min is $\pm 0.03^\circ$, with gain varying over the same time by $\leq \pm 0.03$ dB. (5 refs.)

116483 Electronographic polarimetry: the Durham polarimeter. S.M.Scarrott, R.F.Warren-Smith, W.S.Pallister, D.J.Axon (Phys. Dept., Univ. of Durham, Durham, England), R.G.Bingham.

Mon. Not. R. Astron. Soc. (GB), vol.204, no.3, p.1163-77 (Sept. 1983).

An imaging polarimeter has been constructed for use with a McMullan electronographic camera and is designed to suit a telescope with an $f/15$ focus. The polarimeter enables linear optical polarization to be measured in a 40-mm diameter image with a spatial resolution limited by atmospheric 'seeing'. The method is independent of variations in background sky brightness and polarization and in atmospheric transparency. The optical system is suitable for use with other types of area detector such as CCD cameras. (21 refs.)

116484 High precision spectropolarimetry of stars and planets. I. The ROE spectropolarimeter. R.D.Wolstencroft, W.A.Cormack, J.W.Campbell (Royal Obs., Edinburgh, Scotland), R.J.Smith.

Mon. Not. R. Astron. Soc. (GB), vol.205, no.1, p.23-38 (Oct. 1983).

A spectropolarimeter is described which is capable of measuring linear and circular polarization between 3000 and 8000 Å at a resolution of between 5 and 400 Å. Narrow-band observations of unpolarized stars are presented which demonstrate that the instrumental polarization is very small (≤ 0.01 per cent). (9 refs.)

Use of BPS-75+'Elektronika-100I' scanning-measuring system for analysis of photographs from wide-gap chambers See Entry 112576

95.70 OTHER INSTRUMENTATION AND TECHNIQUES

(inc. clocks, frequency standards)

116485 Parametric detector as a tunable antenna for continuous gravitational radiation. F.Bordoni, F.Fulgini (Istituto di Fisica dello Spazio Interplanetario, CNR, Frascati, Italy).

Phys. Rev. D (USA), vol.28, no.6, p.1285-90 (15 Sept. 1983).

A way of using Weber-type antennas as tunable detectors of gravitational radiation from pulsars is described. Preliminary laboratory tests on the feasibility of such an instrument give encouraging results. (6 refs.)

116486 Planetary Soil Water Analyzer (PSWA) prototype. W.F.Cashin (Ball Aerospace Systems Div., Huntington Beach, CA, USA), D.M.Anderson. ITC/USA/82. International Telemetering Conference, San Diego, CA, USA, 28-30 Sept. 1982 (Woodland Hills, CA, USA: Int. Found. Telemetering 1982), p.701-8

The use of differential scanning calorimetry is advantageous in determining water content of soil samples. The basic idea is to use two matched ovens, one with a soil sample included. The average temperature of the ovens is forced to track a desired programmed temperature (normally a slow ramp) with one control loop, while a second control loop forces the oven temperatures to be equal, even during a transition. The power necessary to keep the temperatures equal is monitored, containing information as to the transition energy, and thus the water content at programmed water transition temperatures. This approach uses the microprocessor to close both of the loops, taking oven sensor temperatures as an input, and providing power duty cycles as outputs. In actuality, two microprocessors are used—a slave to accumulate and process sensor information, and a master to generate the loop control, output data control, and temperature program control. The PSWA perfor-

mance is compared with that of a state-of-the-art commercial instrument using analog loop control. (8 refs.)

Design and performance of a one square meter proportional counter system for hard X-ray astronomySee Entry 116474

95.75 TECHNIQUES OF OBSERVATION AND REDUCTION

116487 IUE data reduction. C.Morossi, G.Sedmak (Oservatorio Astron. di Trieste, Trieste, Italy). *Mem. Soc. Astron. Ital. (Italy)*, vol.54, no.2, p.373-84 (1983).

IUE data reduction is examined with regard to the present and future importance of IUE astronomy in the UV range of evaluating the standard IUE-SIPS (spectral image processing system) procedure and the alternative Italian procedures. The IUESIPS version presently available for high and low spectral resolution modes is described. (21 refs.)

116488 Galactic profiles and the point spread function. G.F.R.Ellis, L.Lawrence, G.B.Brundrit. *Mon. Notes Astron. Soc. South Afr. (S. Africa)*, vol.41, no.11-12, p.107-17 (Dec. 1982).

Because of point-spread effects, the photographic image of a galaxy is significantly different from the 'true' image that would be obtained on a screen near the galaxy. The authors point out how this resolves a paradox concerning the visibility of distant galaxies, and give a simple model that may be used to estimate such point-spread effects. In particular, the authors obtain a simple analytic formula for estimating the averaging effect of the point-spread function on the image profile. (6 refs.)

116489 Effects of photon noise on speckle image reconstruction with the Knox-Thompson algorithm. P.Nisenson (Harvard-Smithsonian Center for Astrophys., Harvard Univ., Cambridge, MA, USA), C.Papaliolios. *Opt. Commun. (Netherlands)*, vol.47, no.2, p.91-6 (15 Aug. 1983). An analysis of the effects of photon noise on astronomical speckle image reconstruction using the Knox-Thompson algorithm (1974) is presented. It is shown that the quantities resulting from the speckle average are biased, but that the biases are easily estimated and compensated. Calculations are also made of the convergence rate for the speckle average as a function of the source brightness. An illustration of the effects of photon noise on the image recovery process is included. (11 refs.)

116490 On the possibility of seasonal corrections while adjusting coordinates of stars. V.L.Gorshkov. *Pis'ma v Astron. Zh. (USSR)*, vol.9, no.8, p.500-3 (1983). In Russian. English translation in: *Sov. Astron. Lett. (USA)* A modification for the chain adjustment of the coordinates of stars is proposed, which makes it possible to correct instrumental and refraction errors if they are linear night trends. The method is tested for group as well as for nongroup observations. The advantages of the method are demonstrated using Pulkovo time service observations. (10 refs.)

Relativistic reductions for radiointerferometric observablesSee Entry 116440
Four-centimeter traveling-wave maser with high amplitude and phase stability [radioastronomy application]See Entry 116482
Electronographic polarimetry: the Durham polarimeterSee Entry 116483
Solar-flared prognostication by the empirical-statistical approachSee Entry 116569
The formation of emission lines in the expanding chromospheres of luminous cool stars. I. The importance of atmospheric extension and partial redistribution effectsSee Entry 116629
The temperature of central stars of planetary nebulae: the energy-balance methodSee Entry 116651
Tracing the gas in galaxiesSee Entry 116809
An optical test for the distance of gamma-ray burst sourcesSee Entry 116873

95.80 ASTRONOMICAL OBSERVATIONS (LISTED BY TECHNIQUES OF OBSERVATION)

95.80D Radio and radar

A catalog of high accuracy circular polarization measurementsSee Entry 116494
Variability of carbon monoxide in the Mars atmosphereSee Entry 116508
Radio observations of Comet 1983dSee Entry 116532
On the relation of local sources of centimeter solar radioemission with noise storms based on the RATAN-600 observationsSee Entry 116571
Power spectrum of brightness temperature fluctuations derived from solar eclipse observations at 2.8 GHzSee Entry 116572
Source characteristics of main and post-burst-increase phases of solar bursts at 17 GHzSee Entry 116623
Observations on the slowly varying component of solar radio emission at decameter wavelengthsSee Entry 116624
The disc-like envelopes around young stars seen in the maser linesSee Entry 116658
On the correlation between H α line intensity and SiO maser emission of the long-period variable χ cygniSee Entry 116702
The effect of nulls on the drifting subpulses in PSR 0809+74See Entry 116718
Radio emission from AM Herculis: the quiescent component and an outburstSee Entry 116740
A search for neutral hydrogen near nine globular clustersSee Entry 116772
Isotopic fractionation and mass motion in giant molecular cloudsSee Entry 116776
The temperature of molecular gas in the galactic center regionSee Entry 116781
Far-infrared and CO observations of Cep F: implications for star formation in Cepheus OB3See Entry 116782
The magnetic field of the NGC 2024 molecular cloud: detection of OH line Zeeman splittingSee Entry 116785
A comparison of high resolution optical and radio observations of W3See Entry 116787
Ammonia absorption toward W3(OH): 0.3'' resolution maps in the (2,2) lineSee Entry 116790

Formaldehyde, cold neutral hydrogen and dust distribution in a globular filament in TaurusSee Entry 116792
The detection of butadiynyl (C $_4$ H) in absorption against Cassiopeia ASee Entry 116793
Regions of low molecular column density near the galactic planeSee Entry 116795
CS J=5-4 observations of galactic molecular cloudsSee Entry 116797
Ammonia observations of the Herbig-Haro objects HH 24-27See Entry 116801
Observations of H $_2$ O maser emission in the Large Magellanic CloudSee Entry 116803
Determination of the angular size of the H $_2$ O maser outburst region in Orion KL defined by a linearly polarized emissionSee Entry 116806
Neutral hydrogen absorption in Mrk 6, NGC 3810, 1506+34, and NGC 1068See Entry 116811
Arcsecond positions for milliarcsecond VLBI nuclei of extragalactic radio sources. II. 207 sourcesSee Entry 116814
The trivariate (radio, optical, X-ray) luminosity function of cD galaxies. I. New Westerbork observations of 22 cD galaxies and Einstein observations of A 1918 and A 2317See Entry 116818
Discovery of a large intergalactic H I cloud in the M96 groupSee Entry 116839
VLA radio continuum observations of the edge-on spiral galaxy NGC 3079See Entry 116841
The Hydra I cluster of galaxies. II. First results from H I-observationsSee Entry 116862
The Ursa Major supercluster. II. A statistical analysis of the radio surveySee Entry 116866
31.4 GHz flux density measurements of a complete sample of sources from the 5-GHz SS surveySee Entry 116868
Flux density and linear polarization measurements of variable radio sources at λ 900 mm (33.5 GHz)See Entry 116869
High precision astrometry via very-long-baseline radio interferometry: estimate of the angular separation between the quasars 1038+528A and BSee Entry 116870
A VLBI search for compact components in extended high redshift quasarsSee Entry 116872
Low-frequency measurement of the spectrum of the cosmic background radiationSee Entry 116889

95.80G Far infrared (bolometric, photoconductive)

CO $_2$ altimetry of the Memnonia Fossae-Margaritifer Sinus region by the Mars-5 probeSee Entry 116507
Observations of asteroids in the 3- to 4- μ m regionSee Entry 116512
Results of astrophysical investigations of asteroids (survey). IISee Entry 116516
Comparison of coronal holes observed in soft X-ray and He I 10830 \AA spectroheliogramsSee Entry 116600
On the T Tauri nature of the variable star BM ChaSee Entry 116650
An infrared study of the eclipsing dwarf nova U GeminorumSee Entry 116692
Simultaneous infrared and optical photometry of cataclysmic variablesSee Entry 116696
Infrared photometry of HD 101065See Entry 116701
Infrared study of the Crab pulsar: the 'shoulder' pulse and the 3.45 micron pulse profileSee Entry 116715
Infrared photometry of the RS CVn binaries. III. JHK light curves of UV PscSee Entry 116753
Far-infrared and CO observations of Cep F: implications for star formation in Cepheus OB3See Entry 116782
Infrared objects near H $_2$ O masers in regions of active star formation. III. Evolutionary phases deduced from IR recombination line and other dataSee Entry 116789
3 μ m spectroscopy of IRS 7 towards the Galactic CentreSee Entry 116802
Luminous molecular hydrogen emission in the galaxy system NGC 3690-IC 694See Entry 116843
High-resolution images of the galactic centreSee Entry 116849
The galactic nucleusSee Entry 116850
Central distribution of the near-infrared colours in two early-type spiralsSee Entry 116852

95.80J Photographic region (near infrared, visible, and normal ultraviolet)

Near-infrared photopolarimeter for astronomical observationsSee Entry 116481
High precision spectropolarimetry of stars and planets. I. The ROE spectropolarimeterSee Entry 116484
Second catalogue of H α line profiles in 55 Be star spectraSee Entry 116491
New double stars (18th series) discovered at NiceSee Entry 116493
A photoelectric UBV catalogue of 610 stars in PuppisSee Entry 116495
Spectroscopy of molecular oxygen in the atmospheres of Venus and MarsSee Entry 116505
Photoelectric photometry of asteroids 45, 120, 776, 804, 814, and 1982DVSee Entry 116511
1983 RBSee Entry 116513
1983 RDSee Entry 116514
Occultation of 14 Piscium by (51) NemausaSee Entry 116515
Results of astrophysical investigations of asteroids (survey). IISee Entry 116516
Observations of Jupiter with the astrolabe of the CERGA Observatory (February 1980-May 1981)See Entry 116517
High precision spectropolarimetry of stars and planets. II. Spectropolarimetry of Jupiter and SaturnSee Entry 116522

Speckle interferometry observations of Pluto's moon CharonSee Entry 116525

The disappearance of OH from Comet P/EnckeSee Entry 116535

Comet Shoemaker (1983p)See Entry 116536

Comet Cernis (1983l)See Entry 116537

Periodic Comet IRAS (1983j)See Entry 116538

Periodic Comet Tempel 2 (1982d)See Entry 116539

Periodic Comet Arend (1983q)See Entry 116540

Periodic Comet Harrington-Abell (1983r)See Entry 116541

Periodic Comet Wild 2 (1983s)See Entry 116542

Comet Kowal (1983t)See Entry 116543

Periodic Comet Kopff (1982k)See Entry 116546

Temporal variations of the absolute magnitude of Halley's cometSee Entry 116548

Photospheric faculae. III. Intensity, and magnetic field mapping of a typical element of the photospheric networkSee Entry 116559

Solar rotation 1947-1981—determined from sunspot dataSee Entry 116560

The study of umbral flashes in the umbrae of two sunspotsSee Entry 116596

Magnetic canopies in unipolar regionsSee Entry 116598

Line profile analysis of an active region corona observed successively at the east and west limbSee Entry 116601

The H α -cyclonic spectra of a flare loop system on 1981 April 27See Entry 116607

Low-*I* 5-min oscillation observationsSee Entry 116610

The characteristic size and brightness of facular points in the quiet photosphereSee Entry 116613

Kinematics of solar prominencesSee Entry 116615

The emerging magnetic flux and the elementary eruptive phenomenonSee Entry 116619

The relationships between disappearing solar filaments, coronal mass ejections, and geomagnetic activitySee Entry 116625

Objective-prism discoveries in the northern sky. ISee Entry 116632

Narrow-band photometry of G and K stars near the North Galactic PoleSee Entry 116641

Radial velocities for early type stars in six galactic regionsSee Entry 116642

The extreme LMC supergiant HD 38489: an optical and ultraviolet studySee Entry 116647

The reddening, metal abundance, and luminosity of high-luminosity G-type starsSee Entry 116649

On the T Tauri nature of the variable star BM ChaSee Entry 116650

Recent photometry of the central star of NGC 2346See Entry 116653

Visible and UV observations of the giant early-type members of the Large Magellanic CloudSee Entry 116654

Cessation of the 63 second periodicity in the light curve of V533 HerculisSee Entry 116659

PI Gruis: molecular identifications and spectral classificationSee Entry 116662

Photometric search for Ap-stars in open clusters. IV. NGC 2287, Cr 121, NGC 2422 and supplementary measurements in NGC 1662 and NGC 2516See Entry 116667

The runaway Wolf-Rayet star HD 143414: evidence for a low-mass companionSee Entry 116668

Study of the variability of the delta Scuti stars. VI. Pulsational behaviour of HR 1392 (69 Tau)See Entry 116670

Study of the variability of the delta Scuti stars. VII. The problem of stability and monop periodicity in 20 CVnSee Entry 116671

Absolute measurements of flux in the continuum of galactic Wolf-Rayet stars: comparison with main-sequence OB starsSee Entry 116672

HR 981—a new USPCSee Entry 116673

On the pulsation of HD 201601See Entry 116674

B and V photometry of the southern RS CVn candidate HD 196818See Entry 116675

On some remarkable pulsation properties of the high-latitude F-type supergiantsSee Entry 116676

Optical behavior of EZ PegasiSee Entry 116677

HR 5=ADS 61: a new variable starSee Entry 116678

Photometry of FK ComaeSee Entry 116679

Search for ultra short period variations in Epsilon OctantisSee Entry 116681

Magnetometric measurements of the carbon star Y CVnSee Entry 116682

PU VulpeculaeSee Entry 116684

R Coronae BorealisSee Entry 116685

U AquariiSee Entry 116686

GK PerseiSee Entry 116687

Novalike variable in LibraSee Entry 116688

Possible novaeSee Entry 116689

Possible optical bursterSee Entry 116690

The discovery of 13.72-min oscillations in the cool magnetic Ap star HD 217522See Entry 116694

Frequency analysis of the rapidly oscillating Ap star HR 1217 (HD 24712)See Entry 116695

Simultaneous infrared and optical photometry of cataclysmic variablesSee Entry 116696

On the correlation between H α line intensity and SiO maser emission of the long-period variable χ cygniSee Entry 116702

Frequency of novae in M33See Entry 116703

Variation of the profile of H α line in the spectrum of DH PegasiSee Entry 116704

Optical variability of PU Vulpeculae (nova-like Kuwano's object 1979) in 1982See Entry 116705

BV photometry of the supernova 1982 in NGC 2268See Entry 116709

Supernova in faint spiral galaxySee Entry 116710

Possible supernova in NGC 7418See Entry 116711

The F-type eclipsing binaries ZZ Bootis, CW Eridani, and BK PegasiSee Entry 116741

SS Bootis: a totally eclipsing binary of the RS CVn typeSee Entry 116742

The possible long-period eclipsing binary BM EriSee Entry 116746

Photometric observations. Is HZ Herculis getting darker?See Entry 116748

Photometric observations and elements of the eclipsing binary TT HerculisSee Entry 116749

The light curve changes of VW CepheiSee Entry 116751

A photometric study of the eclipsing binary V478 CygniSee Entry 116754

Micrometric measurements of binary stars (first list)See Entry 116755

Photoelectric minima of eclipsing binariesSee Entry 116756

Eclipse timings of 31 CygniSee Entry 116757

Spectroscopic observations of the cool eclipsing X-ray binary HD 155638See Entry 116758

A 0538—66See Entry 116759

The chemical composition of distant globular clusters: are there any metal-poor clusters?See Entry 116765

On the intrinsic width and luminosity function of the M92 main sequenceSee Entry 116766

The globular cluster NGC 6638See Entry 116768

The WN4.5 component of HD 219460 in the open cluster Markarian 50See Entry 116769

Variable stars in NGC 6397See Entry 116771

Ellipticity variations within some globular clusters of the Galaxy and the Magellanic CloudsSee Entry 116773

VLW photometry of the open cluster NGC 2516See Entry 116774

The chemical composition of stars in globular clustersSee Entry 116775

The abundance of carbon in planetary nebulaeSee Entry 116777

Digital analysis of narrow-band imagery of the Cygnus LoopSee Entry 116778

Spectrophotometry of the optical emission from RCW 103 and Milne 23See Entry 116780

Diffuse light near zeta Orionis and the Horsehead nebula, and anomalous extinction of HD 37903, as measured with the ANSSee Entry 116786

A comparison of high resolution optical and radio observations of W3See Entry 116787

The Rosette nebula. I. An absolutely calibrated photoelectric H α surface photometrySee Entry 116794

Optical polarization in the bipolar nebula associated with LkH α 208See Entry 116799

Ring nebulae associated with WR stars: stellar wind or stellar ejecta?See Entry 116807

Optical spectroscopy of the radio-loud nuclei of spiral galaxies: starbursts or monsters?See Entry 116810

On the distance to M33 determined from magnitude corrections to Hubble's original Cepheid photometrySee Entry 116813

ESO 438-G 9: a Seyfert galaxy with unusual propertiesSee Entry 116820

Upper limits to O III λ 5592 and [Ni IX] λ 4594 in Seyfert galaxiesSee Entry 116844

Standard photometric diameters of galaxiesSee Entry 116845

High-resolution optical observations of NGC 3379. II. On the derivation of the East-West profileSee Entry 116846

An H α [N II] survey of the nuclei of a complete sample of spiral galaxiesSee Entry 116847

The reddening of radio elliptical galaxiesSee Entry 116848

The galactic nucleusSee Entry 116850

The high-ionization optical spectrum of the Seyfert galaxy Tololo 0109—383See Entry 116851

Redshifts of five extragalactic radio sourcesSee Entry 116853

Slippery evidence on the Galaxy's invisible heavy haloSee Entry 116854

Six quasars near the jets of NGC 1097See Entry 116855

Is the polarisation of NGC 1068 evidence for a non-thermal source?See Entry 116860

Poor evidence of merging in loose galaxy groupsSee Entry 116864

The evolution of galaxies in clusters. III. Photometry of 17 intermediate redshift clustersSee Entry 116865

Identification of a blue object with a newly detected X-ray sourceSee Entry 116867

95.80M Space ultraviolet

Fluid motions in the solar chromosphere-corona transition region. IV. Mass motions over sunspot umbraeSee Entry 116556

The extreme LMC supergiant HD 38489: an optical and ultraviolet studySee Entry 116647

Visible and UV observations of the giant early-type members of the Large Magellanic CloudSee Entry 116654

Far ultraviolet observations of Population IISee Entry 116655

Late type stars [IUE observations]See Entry 116657

The dust envelope of the Herbig Ae star, AB AurSee Entry 116665

The ultraviolet variability of the symbiotic star HBV 475See Entry 116666

Molecules in celestial objects. IV. IUE observation of CO lines towards Be stars with low reddeningSee Entry 116691

IUE observations of cataclysmic variablesSee Entry 116697

New results on symbiotic stars [IUE observations]See Entry 116698

Solar-like activity phenomena in starsSee Entry 116699

Chemically peculiar stars [IUE observations]See Entry 116700

[IUE observations]See Entry 116712

The BUSS spectrum of β LyraeSee Entry 116750

HZ Her: the nature and origin of the emission linesSee Entry 116760

Ultraviolet observations of binary X-ray sourcesSee Entry 116763

Diffuse light near zeta Orionis and the Horsehead nebula, and anomalous extinction of HD 37903, as measured with the ANSSee Entry 116786

IUE observations of stars in the M8 nebula See Entry 116798
Planetary nebulae: IUE results See Entry 116804
H II regions [IUE observations] See Entry 116805
ESO 438-G 9: a Seyfert galaxy with unusual properties See Entry 116820
Active galactic nuclei: IUE results on continuum, emission and absorption lines See Entry 116857
Far ultraviolet observations of BL Lac objects See Entry 116858
The UV spectrum of elliptical galaxies See Entry 116859

95.80N X-ray

Time variations of hard X-ray bursts observed with the solar X-ray Telescope aboard Hinotori (with a movie) See Entry 116584
Computed magnetic field structure of the flares observed by the Hinotori hard X-ray telescope See Entry 116585
Spatial structure of high energy photon sources in solar flares See Entry 116587
Observations of fine time structure in solar flare hard X-ray bursts See Entry 116588
Comparison of coronal holes observed in soft X-ray and He I 10830 Å spectroheliograms See Entry 116600
The trivariate (radio, optical, X-ray) luminosity function of cD galaxies. I. New Westerbork observations of 22 cD galaxies and Einstein observations of A 1918 and A 2317 See Entry 116818
Einstein observations of NGC 4438: dynamical ablation of gas in the Virgo Cluster See Entry 116840
Six quasars near the jets of NGC 1097 See Entry 116855
Detection of an extended soft X-ray source H 2326-79 in the southern sky See Entry 116874

95.80Q gamma-ray and elementary particle

Implications of high-energy neutron observations from solar flares See Entry 116414
Positron annihilation radiation from solar flares See Entry 116565
COS-B upper limits on gamma-ray emission from radio pulsars See Entry 116722
Energy spectra of very high energy γ -rays from the Crab and Vela pulsars See Entry 116723
Ultra high energy gamma rays from Cygnus X-3 See Entry 116747
Upper limits to the annihilation radiation luminosity of Centaurus A See Entry 116836
Energy spectra of the cosmic gamma-ray bursts See Entry 116876
Fine time resolution spectral analysis of the 1978 November 4 and 19 gamma-ray bursts See Entry 116877
Upper limits on narrow annihilation lines in gamma-ray bursts See Entry 116878
The quest for elusive Geminga: a unique object proposed as the counterpart of 2CG 195+04 See Entry 116883

95.80S Other (inc. gravitational radiation, magnetograms, etc)

Stratosphere of Venus according to the data of the accelerometer measurements of the Venera-11 and Venera-12 spacecraft See Entry 116503

95.85 CATALOGUES, ATLASES ETC

116491 Second catalogue of H α line profiles in 55 Be star spectra. Y.Andrillat (Obs. de Haute Provence, Saint-Michael-l'Observatoire, France). *Astron. & Astrophys. Suppl. Ser. (France)*, vol.53, no.3, p.319-38 (Sept. 1983). In French.
For first catalogue, entitled 'Study of H α profile in 72 Be stars', see *ibid.*, vol.48, no.1, p.93-136 (1983). Presents the second catalogue of H α line profiles in 55 Be star spectra. With those published in the first catalogue, (Andrillat and Fehrenbach 1982) the sample now comprises 127 stars. It is found that the H α emission is so strong that in most cases (64%) the underlying photospheric absorption line is not visible. A central absorption is detected in the H α emission line for 73% of the stars; this absorption feature presents a large diversity of aspects. The width measured at half maximum of emission intensity is correlated with the rotational velocity of the star. The extension of the line wings is correlated with the spectral type and with the rotational velocity of the star. (15 refs.)
116492 Galaxies rotation curves: a catalogue. G.C.Baiesi-Pillastrini, G.G.C.Palumbo, G.Vetolani. *Astron. & Astrophys. Suppl. Ser. (France)*, vol.53, no.3, p.373-81 (Sept. 1983).
The catalogue contains all bibliographical information pertaining to rotation curves of external galaxies which have appeared in the astronomical literature up to December 1981. Information about 271 galaxies is given from 332 papers. (334 refs.)
116493 New double stars (18th series) discovered at Nice. P.Couteau (Obs. de Nice, Nice, France). *Astron. & Astrophys. Suppl. Ser. (France)*, vol.53, no.3, p.441-4 (Sept. 1983). In French.
For 17th series see *ibid.*, vol.48, no.3, p.443-7 (1982). Presents a list of 150 close visual binaries discovered at the 50 cm and the 74 cm refractors. (3 refs.)
116494 A catalog of high accuracy circular polarization measurements. K.W.Weiler (Div. of Astron. Sci., Nat. Sci. Found., Washington, DC, USA), I.de Pater. *Astrophys. J. Suppl. Ser. (USA)*, vol.52, no.3, p.293-327 (July 1983).
An attempt has been made to collect into one catalog all high accuracy circular polarization measurements of the nonthermal synchrotron radiation from nonstellar, extra-solar system radio sources published by early 1982. 'High accuracy' has been defined for this purpose as a quoted standard error of better than 0.1%. For those sources having measurements in the catalog at at least three different frequencies, the spectrum of the circular polarization is plotted. For those having measurements at at least four different times at any one frequency, the time dependence is plotted. Whenever total intensity and

linear polarization measurements were published concurrently with the circular polarization results, these are included in the catalog. (68 refs.)
116495 A photoelectric *UBV* catalogue of 610 stars in Puppis. B.C.Reed, M.P.FitzGerald (Dept. of Phys., Univ. of Waterloo, Waterloo, Ontario, Canada). *Mon. Not. R. Astron. Soc. (GB)*, vol.205, no.1, p.241-64 (Oct. 1983).
Presents a catalogue of photoelectric *UBV* photometry and some spectral types for 610 stars in a field in Puppis centred at (*l*,*b*)=(245°, 0°). This catalogue reports results taken from the literature, as well as observations recently obtained by the authors, all reduced to a homogeneous *UBV* system. (27 refs.)

95.90 OTHER TOPICS IN ASTRONOMY AND ASTROPHYSICS

116496 If they are here, where are they? Observational and search considerations. R.A.Freitas,Jr. (Xenology Res. Inst., Sacramento, CA, USA). *Icarus (USA)*, vol.55, no.2, p.337-43 (Aug. 1983).
Discusses observational considerations in a search for extraterrestrial intelligence (SETI) program to detect extraterrestrial messenger probes in the Solar System. Observable artifacts will most likely be found in a search space consisting of geocentric, selenocentric, Earth-Moon libration, and Earth-Moon halo orbits, which may be searched to a limiting artifact size of 1-10 m(*p*_v=0.1) using existing or foreseeable instrumentation. (57 refs.)
Proceedings of the Eighteenth General Assembly of the IAU See Entry 111314
Finite exposure time, astronomical speckle transfer function See Entry 116274

96.00 SOLAR SYSTEM

96.10 GENERAL, SOLAR NEBULA, AND COSMOGONY

Evolution of the surface of Mars See Entry 116510
Distribution of cometary binding energies based on the assumption of steady state See Entry 116547

96.20 MOON

116497 The direct planetary perturbations of the rotation of the Moon. I.Pesek (Astron. Obs., Tech. Univ., Praha, Czechoslovakia). *Bull. Astron. Inst. Czech. (Czechoslovakia)*, vol.34, no.4, p.242-4 (July 1983).
Direct planetary perturbations of lunar rotation are derived. (5 refs.)
116498 The Danjon limit of lunar visibility: a re-examination. M.Ilyas. *J. R. Astron. Soc. Can. (Canada)*, vol.77, no.4, p.214-19 (Aug. 1983).
It is found that the correct value of the Danjon's limiting elongation for lunar visibility is close to 10.5°C. The limit provides only a general guide, not sufficient for calendrical purposes. (13 refs.)
116499 Analysis of lunar occultations. V. Grazing occultations 1964-1977. G.M.Appleby, L.V.Morrison (Royal Greenwich Obs., Hailsham, England). *Mon. Not. R. Astron. Soc. (GB)*, vol.205, no.1, p.57-65 (Oct. 1983).
For pt.IV see *ibid.*, 1982, no.3, p.1119-25 (1982). Observations of 800 grazing occultations of stars at the polar regions of the Moon, which occurred in the years 1964-77, are analysed for corrections to Watt's (1963) charts of the lunar profile, systematic errors in the analytical lunar ephemeris *j*=2, and for the correction to the zero point of right ascension in the FK4 catalogue. (15 refs.)
116500 Lunar magnetism, polar displacements and primeval satellites in the Earth-Moon system. S.K.Runcorn (Inst. of Lunar & Planetary Sci., Univ. of Newcastle upon Tyne, Newcastle upon Tyne, England). *Nature (GB)*, vol.304, no.5927, p.589-96 (18 Aug. 1983).
The discovery that rocks of the lunar crust possess remanent magnetism is a surprising result in view of the fact that the present Moon does not exhibit a magnetic field, nor was there once evidence of an iron core in which one could be generated. This review looks at the concept of lunar palaeomagnetism and discusses its implications for lunar science as a whole. (86 refs.)

96.30 PLANETS AND SATELLITES

(*exc. the Moon; for celestial mechanics, see 95.10; for Earth as an astronomical body, see 91. Geophysics*)

116501 Reflection of light by a multilayered planetary atmosphere. Zh.M.Dlugach (Primary Astron. Obs., Acad. of Sci., Kiev, Ukrainian SSR). *Sol. Syst. Res. (USA)*, vol.17, no.1, p.14-19 (Jan.-March 1983). Translation of: *Astron. Vestn. (USSR)*, vol.17, no.1, p.20-6 (Jan.-March 1983). [received: Sept. 1983]
A layer addition method is presented that is modified for multilayer media. Some numerical results for two-layer atmospheres are given, which can be useful in interpretation of planetary observational data. (9 refs.)
Adiabatic lapse rates of planet atmospheres See Entry 111368
Surface illuminance and albedo of a planetary atmosphere with nearly conservative scattering See Entry 116270
Planetary Soil Water Analyzer (PSWA) prototype See Entry 116486
The direct planetary perturbations of the rotation of the Moon See Entry 116497

96.30D Mercury

116502 Additive remarks to the problem of Mercury's motion of the perihelion. V.E.R.Bagge (Inst. fur Reine und Angewandte Kernphys., Christian-Albrechts-Univ., Kiel, Germany). *Atomkernenerg. Kerntechnik. (Germany)*, vol.42, no.2, p.130-4 (1983). In German.
It is shown that the value for the secular motion of Mercury's perihelion received by the numerical solution of the Newtonian equation of motion at very fine intervals for the steps of integration is sustained always. In these calculations the relativistic change of mass at varying velocity is taken in

account not only at the acceleration term but also at the gravitational force between the Sun and the moving planet. The numerical calculations have been confirmed by two completely different programs, one formulated in cartesian coordinates the other one in polar coordinates; the two results are exactly the same. (no refs.)

96.30E Venus

116503 Stratosphere of Venus according to the data of the accelerometer measurements of the Venera-11 and Venera-12 spacecraft. V.S.Avduevskii, V.V.Semenchenko, G.R.Uspenskii, Z.P.Cheremukhina.

Cosmic Res. (USA), vol.20, no.6, p.649-55 (Nov.-Dec. 1982). Translation of: *Kosm. Issled. (USSR)*, vol.20, no.6, p.913-20 (Nov.-Dec. 1982). [received: Sept. 1983]

A description is given of the instrumentation onboard the Venera-11 and Venera-12 spacecraft. The measurement results and the procedure for their analysis are given. The altitude distributions of the pressure, density, and temperature of the stratosphere are constructed. (11 refs.)

116504 Magnetic field fluctuations in the Venus magnetosheath. J.G.Luhmann, M.Tatraliyay, C.T.Russell, D.Winterhalter (Inst. of Geophys. & Planetary Phys., Univ. of California, Los Angeles, CA, USA).

Geophys. Res. Lett. (USA), vol.10, no.8, p.655-8 (1983). (American Geophysical Union Chapman Conference on Waves in Magnetospheric Plasma, Kona Coast, HI, USA, 7-11 Feb. 1983).

Using a model for the convection pattern of the shocked solar wind flow around Venus, Pioneer Venus observations of ultra-low-frequency (~10-40 s period) magnetic field fluctuations in the magnetosheath have been traced along streamlines to the region of the quasi-parallel bow shock. The periods and polarizations of the sinusoidal fluctuations are similar to those observed upstream of the quasi-parallel bow shock, where streaming superthermal particles are believed to produce MHD waves by a beam-plasma instability. The results suggest that both disturbances at the ionopause at Venus and the Earth's magnetopause may be caused by convection of turbulent magnetic fields from the subsolar bow shock, when the interplanetary field direction produces a quasi-parallel shock there. (17 refs.)

116505 Spectroscopy of molecular oxygen in the atmospheres of Venus and Mars. J.T.Trauger, J.I.Lunine (Div. of Geological & Planetary Sci., California Inst. of Technol., Pasadena, CA, USA).

Icarus (USA), vol.55, no.2, p.272-81 (Aug. 1983).

The abundances of molecular oxygen in the atmospheres of Venus and Mars are sensitive to fundamental photochemical processes. A new upper limit is reported for the molecular oxygen mixing ratio ($O_2/CO_2 < 3 \times 10^{-7}$) in the integrated column above the visible cloud tops of Venus, based on spectroscopic observations carried out in early spring, 1982. During the same observing period, an O_2 column abundance of 8.5 cm-am for the atmosphere of Mars was measured, slightly below the O_2 abundances measured a decade earlier. (34 refs.)

116506 Fluctuations of frequency and phase of radio waves propagating through the atmosphere of Venus. A.I.Yefinov, V.M.Razmanov, T.S.Timofeyeva, O.I.Yakovlev.

Radio Eng. & Electron. Phys. (USA), vol.27, no.12, p.38-41 (Dec. 1982). Translation of: *Radioelektr. & Elektron. (USSR)*, vol.27, no.12, p.2318-22 (Dec. 1982). [received: Sept. 1983]

Experimental data, gathered during radio sounding of the Venus atmosphere by the Venera-10 probe, are used to analyze the effect of atmospheric inhomogeneities of that planet on fluctuations of frequency and phase of radio waves. An analysis of the data obtained indicates that, just as in the case of amplitude fluctuations, the frequency and phase fluctuations increase when the beam axis passes at a distance of 58-60 km above the Venus surface and are attenuated at the altitude of 54-56 km. The external scale of turbulence of the Venus atmosphere, equal to 4.5-6 km, is determined from the obtained experimental data for the upper turbulence region, localized near the altitude of 60 kilometers. (7 refs.)

96.30G Mars

116507 CO₂ altimetry of the Memnonia Fossae-Margaritifer Sinus region by the Mars-5 probe. L.V.Zasova, V.M.Zubkova, V.S.Zhegulev, L.V.Ksanfomaliti, V.I.Moroz, E.V.Petrova.

Cosmic Res. (USA), vol.20, no.6, p.655-9 (Nov.-Dec. 1982). Translation of: *Kosm. Issled. (USSR)*, vol.20, no.6, p.921-7 (Nov.-Dec. 1982). [received: Sept. 1983]

The relief of Mars is studied along a line extending south from the rift valley Marineris Valles. The measurements were made in a complex experiment including studies of the thermal properties of the soil, the structure of the surface, its photometric characteristics, and the relief. CO₂-altimetry was used in the latter study. The measurements were made in 1974 onboard the Mars-5 probe. Changes in altitude of up to 6 km over a baseline of 50 km were seen (Claritas Fossae). The regions of the Holden-Hale craters and the Nirgal Vallis are extended areas of low elevation. (15 refs.)

116508 Variability of carbon monoxide in the Mars atmosphere. R.T.Clancy, D.O.Muhleman, B.M.Jakosky (Div. of Geological & Planetary Sci., California Inst. of Technol., Pasadena, CA, USA).

Icarus (USA), vol.55, no.2, p.282-301 (Aug. 1983).

In January of 1982 the authors measured a microwave spectrum of CO in the Martian atmosphere utilizing the rotational J=1-2 transition of CO. The authors analyze data and reanalyze the microwave spectra of Kakar, Waters, and Wilson (1977) and Good and Schloerb (1981) in order to constrain estimates of the temporal variability of CO abundance in the Martian atmosphere. Values of CO column density are given. The most recent estimate of CO column density from the 1967 infrared spectra of Connes, Connes, and Maillard (1969), is discussed. The large uncertainties given for the microwave measurements are due primarily to uncertainty in the difference between the continuum brightness temperature and atmospheric temperatures of Mars. The authors calculate the variation among the observations of the continuum (surface) brightness temperature of Mars, which is primarily a function of the observed aspect of Mars. The authors also consider variability of global atmospheric temperatures among the observations, particularly the effects of global dust storms and the ellipticity of the orbit of Mars. (40 refs.)

116509 Martian great dust storms: interpretive axially symmetric models. E.K.Schneider (Center for Earth & Planetary Phys., Harvard Univ., Cambridge, MA, USA).

Icarus (USA), vol.55, no.2, p.302-31 (Aug. 1983).

The simplified theory of steady, nearly inviscid, thermally forced axially symmetric atmospheric motions developed by Schneider (1977) is applied to the study of the problem of the Martian great dust storms. A highly idealized calculation of the atmospheric response to heating concentrated in a small latitude band is carried out. Qualitatively different local and global response

regimes are identified. As the heating is increased from zero, some critical value is reached at which the response jumps from local to global. It is suggested that this transition from local to global response may be related to the observed explosive growth of great dust storms. The steady axially symmetric Martian response to solar forcing is examined. Modification to the solar forced response due to an added latitudinally localized heat source is briefly discussed. Implications of the dynamical model for the dependence of the occurrence of great dust storms on orbital parameters are remarked on. (26 refs.)

116510 Evolution of the surface of Mars. A.J.Connell, M.M.Woolfson (Phys. Dept., Univ. of York, Heslington, England).

Mon. Not. R. Astron. Soc. (GB), vol.204, no.3, p.1221-30 (Sept. 1983).

Various models of the Martian crust, differing in the amount of water content, are evaluated in terms of a satellite origin for the planet. It is shown that the hemispherical asymmetry of the planet, in particular the low elevation and smoothness of the northern plain can be accounted for by the abrasion of material from the northern crust by projectiles from a planetary collision. An estimate of ~2.8 km is found for the centre-of-mass centre-of-figure offset which agrees quite well with observation. (18 refs.)

Near-infrared photopolarimeter for astronomical observations See Entry 116481

Spectroscopy of molecular oxygen in the atmospheres of Venus and Mars See Entry 116505

96.30H Asteroids

116511 Photoelectric photometry of asteroids 45, 120, 776, 804, 814, and 1982DV. H.Debhogne (Obs. Royal de Belgique, Bruxelles, Belgium), G.De Sanctis, V.Zappala.

Icarus (USA), vol.55, no.2, p.236-44 (Aug. 1983).

Photoelectric lightcurves of six asteroids, observed at the ESO 50-cm photometric telescope, are presented. 45 Eugenia, observed for pole determination program, showed a small amplitude of light variation. For 120 Lachesis, no period of rotation was deduced from three observing nights; it is probably longer than 20 hr. 776 Berbericia was observed again to eliminate the ambiguity between 23^h and 15.3^h periods, as pointed out by Schober (1979). The longer period is ruled out, but the authors suggest a very plausible shorter period of 7.762^h, implying, at least at this opposition, one maximum and one minimum per cycle. A similar ambiguity is present for 804 Hispania also. The period could be either 14.84^h or 7.42^h. For 814 Tauris a long period of 35.8 hr is found, confirming the tendency of dark asteroids of intermediate size to rotate more slowly than larger ones. Finally a single-night lightcurve of the fast-moving object 1982DV is presented. (18 refs.)

116512 Observations of asteroids in the 3- to 4-μm region. N.Eaton (Astron. Dept., Univ. of Leicester, Leicester, England), S.F.Green, R.S.McCheyne, A.J.Meadows, G.J.Veeder.

Icarus (USA), vol.55, no.2, p.245-9 (Aug. 1983).

Spectra of eleven asteroids (1, 2, 8, 10, 15, 16, 22, 83, 386, 433, 471) have been obtained in the 3- to 4-μm region. Of these, only Ceres and Pallas have previously been observed in this wavelength region. Spectra of the S- and M-type asteroids are generally featureless, but 8 Flora may be an exception. None of the three new C-type spectra show significant absorption. (11 refs.)

116513 1983 RB. C.Shoemaker, C.M.Bardwell.

I.A.U. Circ. (USA), no.3861, 1 pp. (14 Sept. 1983).

Reports the discovery of a 15th-magnitude fast-moving asteroidal object in Aquarius. Precise positions are reported for the period 1983 September 7 to 12. Orbital elements are given, together with an ephemeris for the period 1983 September 13 to October 13 at five-day intervals: the object is an Amor-type asteroid. (no refs.)

116514 1983 RD. R.S.Dunbar, A.Harris, C.S.Shoemaker, B.G.Marsden.

I.A.U. Circ. (USA), no.3862, 1 pp. (14 Sept. 1983).

Reports the discovery of a 12th-magnitude fast-moving asteroidal object in Pegasus. Precise and semi-accurate positions are reported for the period 1983 September 7 to 13. Tentative orbital elements are given, together with an ephemeris for the period 1983 September 13 to 23 at one-day intervals: the object is an Amor-type asteroid. (no refs.)

116515 Occultation of 14 Piscium by (51) Nemausa. D.W.Dunham.

I.A.U. Circ. (USA), no.3869, 1 pp. (23 Sept. 1983).

It is reported that this occultation, on 1983 September 11, was observed throughout the southeastern United States. The northern limit was defined by an observation of a 2.3 s occultation at Yorktown, Virginia. The longest reported chord (13.5 s), observed in central North Carolina, corresponds to a diameter of 160 km for Nemausa. The southernmost positive observation, at Greenville, North Carolina, was of an 8.2 s occultation. No well-established secondary occultations were observed. (no refs.)

116516 Results of astrophysical investigations of asteroids (survey). II. D.F.Lupishko, I.N.Bel'skaya (A.M. Gor'ki State Univ., Kharkov, Ukrainian SSR).

Sol. Syst. Res. (USA), vol.17, no.1, p.1-13 (Jan.-March 1983). Translation of: *Astron. Vestn. (USSR)*, vol.17, no.1, p.5-19 (Jan.-March 1983). [received: Sept. 1983]

For pt.I see *Astron. Vestn.*, vol.16, no.4, p.195-208 (1982) and *Solar System research*, vol.16, no.4, p.153-64 (1983). The results of polarimetric, spectrophotometric and radiometric investigations of asteroids are presented, and the principal problems for future investigations are briefly formulated. (50 refs.)

Rb-Sr, Sm-Nd, K-Ca, O, and H isotopic study of Cretaceous-Tertiary boundary sediments, Caravaca, Spain: evidence for an oceanic impact site See Entry 116086

Theory of the Trojan asteroids. IV See Entry 116432

96.30K Jupiter

116517 Observations of Jupiter with the astrolabe of the CERGA Observatory (February 1980-May 1981). G.Vigouroux, G.Dudognon, P.Granes, F.Mignard, J.Pham-Van (CERGA, Grasse, France).

Astron. & Astrophys. Suppl. Ser. (France), vol.53, no.3, p.361-2 (Sept. 1983). In French.

Contains the results of the third Jupiter campaign with the CERGA astrolabe. Because of the low declination of this planet (10° to 1°) it was only observed at 45° of elevation: 41 east and west transits were recorded. The table gives the dates, the zenith distance residuals, the corrections for defective illumination as usual and the indication of the observer and of the reference groups. (4 refs.)

116518 Ion cyclotron waves in the Io plasma torus: polarization reversal of whistler mode noise. D.A.Gurnett, C.K.Goertz (Dept. of Phys. & Astron., Univ. of Iowa, Iowa City, IA, USA). *Geophys. Res. Lett. (USA)*, vol.10, no.7, p.587-90 (July 1983). Because of the presence of multiple ion species in the Io plasma torus whistler mode noise can be converted to ion cyclotron waves via a polarization reversal process at the local crossover frequency. Using whistler mode intensity measurements in the Jovian magnetosphere from Voyager 1 the authors estimate the pitch-angle diffusion rates that would occur if the noise is converted to ion cyclotron waves. Typical pitch-angle diffusion coefficients range from $D_{\alpha\alpha} \approx 10^{-6} \text{ sec}^{-1}$ for protons resonating near the equator to $D_{\alpha\alpha} \approx 10^{-4} \text{ sec}^{-1}$ for 10 keV O^+ ions resonating at high latitudes. Although complete bounce averaged diffusion coefficients have not yet been computed, preliminary estimates indicate that the energetic ion precipitation caused by these waves may be able to account for the EUV auroral emissions at the foot of the torus field lines. (19 refs.)

116519 Electromagnetic ion-cyclotron instability in the multi-ion Jovian magnetosphere. R.M.Thorne, J.Moses (Dept. of Atmospheric Sci., Univ. of California, Los Angeles, CA, USA). *Geophys. Res. Lett. (USA)*, vol.10, no.8, p.631-4 (1983). (American Geophysical Union Chapman Conference on Waves in Magnetospheric Plasma, Kona Coast, HI, USA, 7-11 Feb. 1983). Propagation characteristics of electromagnetic ion-cyclotron waves are extremely sensitive to the relative composition of thermal ions: this can consequently control the instability properties of resonant energetic ions in the Jovian magnetosphere. The dominance of heavy ions in the Io plasma torus will suppress ion-cyclotron instability near the equatorial plane. Wave growth, however, can still occur away from the equator in the region where thermal hydrogen is expected to predominate. A theoretical assessment of the convective L-mode gain indicates that Voyager 1 did not enter the preferred region of instability. Evidence for instability may nevertheless be available since oblique ion-cyclotron waves are expected to experience a natural polarization reversal to the R-mode which is able to propagate from high latitudes to the equator. (25 refs.)

116520 Two classes of volcanic plumes on Io. A.S.McEwen, L.A.Soderblom (US Geological Survey, Flagstaff, AZ, USA). *Icarus (USA)*, vol.55, no.2, p.191-217 (Aug. 1983). The authors discuss the eruptions of Pele and Surt. The authors describe the discovery of yet another large eruption, from the caldera named Aten Patera, that also occurred between the two encounters, this time in the south polar region, and with surface changes almost identical to those at Surt. The recognition of the strong similarity of scale and appearance of the deposits from these three large plume eruptions led the authors to investigate the possible existence of discrete classes of volcanic plumes on Io. Evidently, Pele, Surt, and Aten Patera represent a class of plume eruptions that are larger and shorter lived than a second class of smaller plumes. Albedos and colors of source regions and plume deposits, along with evidence for sizes, durations, and temperatures, suggest that there are, in fact, two distinct and very different types of volcanic plumes. The authors present the results of the analysis and examine proposed models for Io's volcanism in the context of the two classes. (44 refs.)

116521 On the detectability of H_2S in Jupiter. B.Bezard (Lab. d'Astron. Infrarouge, Obs. de Meudon, Meudon, France), A.Marten, J.P.Baluteau, D.Gautier, J.-M.Flaud, C.Camy-Peyret. *Icarus (USA)*, vol.55, no.2, p.259-71 (Aug. 1983). The influence of hydrogen sulfide, a still-undetected key molecule for the Jovian atmospheric chemistry in the infrared spectrum, is investigated. Synthetic spectra including various vertical distribution profiles of H_2S are computed and compared with observational data for Jupiter in the 2- to 15-cm^{-1} and 1160- to 1200-cm^{-1} spectral ranges. No firm conclusion about the presence of H_2S can be drawn from the latter spectral region because of large uncertainties in gaseous opacities. In the microwave range, H_2S is found to be a possible candidate to explain the measurements. Constraints to its vertical distribution which would imply a significant supersaturation in the troposphere are derived. Physical and chemical processes involving H_2S in the atmosphere are discussed in the light of this hypothesis. (40 refs.)

116522 High precision spectropolarimetry of stars and planets. II. Spectropolarimetry of Jupiter and Saturn. R.J.Smith (Dept. of Astron., Univ. of Edinburgh, Edinburgh, Scotland), R.D.Wolstencroft. *Mon. Not. R. Astron. Soc. (GB)*, vol.205, no.1, p.39-55 (Oct. 1983). For pt.1 see ibid., vol.205, no.1, p.23-38 (1983). A rise in the linear polarization detected from the integrated disc of Jupiter across the 7270 Å methane band is confirmed. The effect is also shown to be present across the same band for Saturn. A large enhancement in the circular polarization of Saturn at phase angle 2.7° has been seen, and its remarkable wavelength dependence studied. These observations provide useful constraints for the more sophisticated models that are clearly needed for the atmospheres of these planets. (23 refs.)

Backscattering cascade of beam modes off ambient density fluctuations See Entry 113600

Monodeuterated methane in the outer solar system. I. Spectroscopic analysis of the bands at 1.55 and 1.95 microns See Entry 116439

$^{12}CH_3D$ rovibrational intensities and the Jovian D/H ratio ... See Entry 116460

Galileo Jupiter probe Atmosphere Structure Instrument See Entry 116480

Velocities of ejection of comets by Jupiter and Saturn See Entry 116549

96.30M Saturn

116523 Tidal dissipation in small viscoelastic ice moons: the case of Enceladus. J.P.Poirier, L.Boloh, P.Chambon (Inst. de Phys. du Globe, Univ. Paris VI, Paris, France). *Icarus (USA)*, vol.55, no.2, p.218-30 (Aug. 1983). Tidal dissipation is investigated in a viscoelastic homogeneous sphere having the orbital and physical characteristics of the icy inner satellite of Saturn, Enceladus. The dissipated power is calculated for Kelvin-Voigt and Maxwell rheologies, whose dissipation function can be expressed in terms of viscosity. Expressions for the dissipated power as a function of viscosity is calculated in both cases and compared to the expression found for a lossy elastic body. A physical law relating viscosity of water ice to temperature and grain size is introduced and the feedback between dissipated power and temperature is investigated. (15 refs.)

116524 A new system of orbital elements of Saturn's satellites. I.G.Chugunov. *Pis'ma v Astron. Zh. (USSR)*, vol.9, no.8, p.508-12 (1983). In Russian. English translation in: *Sov. Astron. Lett. (USA)* Elements of the orbits of Saturn I-VI are given, based on 285000 measurements covering the period 1682-1981. The correlation matrix is analysed. (7 refs.)

An ab initio SCF study on the stability and structure of $H_2CN^+ \cdot nN_2$ clusters See Entry 112891

Monodeuterated methane in the outer solar system. I. Spectroscopic analysis of the bands at 1.55 and 1.95 microns See Entry 116439

High precision spectropolarimetry of stars and planets. II. Spectropolarimetry of Jupiter and Saturn See Entry 116522

Entwined and parallel bundled orbits as alternative models for narrow planetary ringlets See Entry 116529

Velocities of ejection of comets by Jupiter and Saturn See Entry 116549

96.30T Other planets

116525 Speckle interferometry observations of Pluto's moon Charon. N.Hetterich, G.Weigelt (Phys. Inst., Univ. Erlangen, Erlangen, Germany). *Astron. & Astrophys. (Germany)*, vol.125, no.2, pt.1, p.246-8 (Sept. 1983). Performs photon-counting speckle interferometry of Pluto and its moon Charon. 12000 speckle interferograms were recorded in two different nights with the 1.5 m Danish telescope at the European Southern Observatory, Chile. (12 refs.)

116526 The obliquity of Pluto. A.R.Dobrovolskis, A.W.Harris (Jet Propulsion Lab., California Inst. of Technol., Pasadena, CA, USA). *Icarus (USA)*, vol.55, no.2, p.231-5 (Aug. 1983). Pluto's obliquity (the angle between its spin axis and orbit normal) varies between $\sim 102^\circ$ and $\sim 126^\circ$ over a period of about 3 million years. These oscillations are nearly sinusoidal and quite stable, leading to only modest changes in the isolation regime. Thus, Pluto's rotation has been slightly retrograde ever since its current orbit and rotation rate were established. (15 refs.)

116527 The structure of Neptune's upper atmosphere: the stellar occultation of 24 May 1981. R.G.French (Dept. of Earth & Planetary Sci., MIT, Cambridge, MA, USA), J.H.Elias, D.J.Mink, J.L.Elliott. *Icarus (USA)*, vol.55, no.2, p.332-6 (Aug. 1983). Observations of the 24 May 1981 occultation of an uncatalogued star by Neptune made at the Cerro Tololo Inter-American Observatory are analyzed to yield temperature profiles of Neptune's upper atmosphere for number densities near $5 \times 10^{13} \text{ cm}^{-3}$. The mean temperatures at immersion (latitude 56°) and emersion (latitude 16°) obtained by numerical inversion were $140 \pm 10\text{K}$ and $154 \pm 10\text{K}$, respectively. The immersion and emersion profiles are remarkably similar in overall shape, suggestive of global atmospheric layering. From the astrometry of the event, precise relative positions of Neptune and the occulted star are obtained. (15 refs.)

116528 Photolysis of methane and the ionosphere of Uranus. S.K.Atreya, J.J.Ponthieu (Dept. of Atmospheric & Oceanic Sci., Univ. of Michigan, Ann Arbor, MI, USA). *Planet. & Space Sci. (GB)*, vol.31, no.8, p.939-44 (Aug. 1983). Photochemical calculations for Uranus predict an extensive region of condensation of acetylene, ethane and methane in the vicinity of the temperature inversion layer. This could explain why ethane was not detected on Uranus, unlike Neptune which has a much warmer inversion layer. Subsequent snow-out of the condensibles is expected to result in reduced visibility in the troposphere. Ionospheric calculations for the equatorial region to be probed by Voyager, indicate peak electron concentrations on the order of $5 \times 10^4 \text{ cm}^{-3}$ if dynamical effects are important. Upper limit to the electron peak is $3 \times 10^4 \text{ cm}^{-3}$. Exospheric temperatures are discussed. (26 refs.)

116529 Entwined and parallel bundled orbits as alternative models for narrow planetary ringlets. R.Eshleman (Stanford Univ., Stanford, CA, USA). *Science (USA)*, vol.221, no.4608, p.361-4 (22 July 1983). Particle orbits can be bundled in two different ways to produce narrow, Uranus-type ringlets. The usual assumption is that they are packed in a parallel manner in a structure that is essentially only two-dimensional. The alternative of a bundle of entwined orbits produces a three-dimensional structure of potentially large protected areal density. The two models might be discriminated observationally by differences in the motion of the line of intersection of the orbital and equatorial planes, and by the predicted radial reversal (entwined) or nonreversal (parallel) of features in occultation signatures taken at certain longitudes. (12 refs.)

Monodeuterated methane in the outer solar system. I. Spectroscopic analysis of the bands at 1.55 and 1.95 microns See Entry 116439

96.50 OTHER OBJECTS IN THE PLANETARY SYSTEM

96.50D Interplanetary matter, magnetic and electric fields

(inc. gegenschein and zodiacal light; see also 94.60 Interplanetary space)

116530 Out of ecliptic zodiacal cloud profile. A.Mujica, G.Lopez, F.Sanchez (Inst. de Astrofisica de Canarias, CSIC, Univ. de La Laguna, Tenerife, Spain). *Planet. & Space Sci. (GB)*, vol.31, no.8, p.871-3 (Aug. 1983). In a previous paper, Mujica et al. (1980), the optical homogeneity of the medium in the ecliptic plane was established calculating, for the ecliptic, the density and scattering functions. Starting with these results, the authors attempt to find the zodiacal cloud shape out of the ecliptic. (5 refs.)

Motion of dust particles in cometary atmospheres See Entry 116550

96.50G Comets

116531 The atmosphere of a dirty-clathrate cometary nucleus: a two-phase, multifluid model. M.L.Marconi, D.A.Mendis (Dept. of Electrical Engng. & Computer Sci., Univ. of California, San Diego, CA, USA). *Astrophys. J. (USA)*, vol.273, no.1, pt.1, p.381-96 (1 Oct. 1983). A self-consistent, transonic, multifluid solution of the dynamical and thermal structure of a dusty gas atmosphere of a dirty-clathrate cometary nucleus is

presented. While the heavy neutral and ion species are treated as a single fluid in the collision-dominated region, the photo-produced hydrogen is treated separately. It is assumed to be composed of a thermalized component and a prethermal component which gradually thermalizes by elastic collisions with the heavier species. Also, the photoelectrons are considered as a separate fluid. The thermal profile of the atmosphere is entirely different from those predicted by earlier models. (42 refs.)

116532 Radio observations of Comet 1983d. W.J.Altenhoff, W.Batrla, W.K.Huchtmeier, J.Schmidt, P.Stumpff, M.Walmsley (Max-Planck-Inst. für Radioastron., Bonn, Germany).

Astron. & Astrophys. (Germany), vol.125, no.2, pt.1, p.L19-22 (Sept. 1983). Radio continuum and spectral line observations of Comet 1983d (Iras-Araki-Alcock) have been made using the Effelsberg 100-m telescope at a wavelength of 1.3 cm. A continuum point source of strength 9 mJy was detected at the time of perigee (May 11), and this emission persisted throughout the next day. The authors have probably detected both the NH_3 (3,3) and H_2O (6_16-5_23) lines from the comet. The derived ammonia production rate of $6 \cdot 10^{26} \text{ s}^{-1}$ suggests that NH_3 forms roughly six percent of the gases sublimating from the cometary nucleus. (4 refs.)

116533 Infrared fluorescence of molecules in comets: the general synthetic spectrum. J.Crovisier, T.Encrenaz (Obs. de Paris-Meudon, Meudon, France). *Astron. & Astrophys. (Germany)*, vol.126, no.1, pt.2, p.170-82 (Sept. 1983). Medium infrared is a spectral range suitable for the study of parent molecules in cometary atmospheres. In order to prepare infrared observations of comets from the Earth or from fly-by probes, the authors list 130 vibration-rotation bands of 20 possible parent molecules, and consider their plausible excitation mechanisms. Band emission may occur through excitation by direct solar radiation field, by solar radiation reflected or scattered by the dust or nucleus, by thermal radiation of the dust or nucleus; collisions may also provide thermal excitation. The authors show that the main emission process is expected to be resonant fluorescence of the fundamental vibrational bands by direct solar excitation. The authors compute synthetic spectra in the range 2.5-16 μ . (47 refs.)

116534 Calculations of comet orbits from observations of 1980/81. L.Buffoni, A.Manara, M.Scardia (Osservatorio Astron. di Brera, Milano, Italy).

Astron. Nachr. (Germany), vol.304, no.4, p.189-93 (1983). From observations published in Smithsonian Astrophysical Observatory and the Minor Planet Circulars, corrected orbits of 26 comets have been calculated. (6 refs.)

116535 The disappearance of OH from Comet P/Encke. M.F.A'Hearn (Univ. of Maryland, College Park, MD, USA), R.L.Millis, D.T.Thompson. *Icarus (USA)*, vol.55, no.2, p.250-8 (Aug. 1983).

Photoelectric observations of comet P/Encke during its 1980 apparition are combined with other published data to relate molecular production rates to the visual lightcurve. In addition to a substantial asymmetry about perihelion which is already well known, there are shorter-term variations in specific molecules which have not been duplicated by models. The most dramatic of these fluctuations is a rapid decrease by more than a factor of 3 in the production of OH at 0.75 AU preperihelion. (16 refs.)

116536 Comet Shoemaker (1983p). C.Shoemaker.

I.A.U. Circ. (USA), no.3863, 1 pp. (14 Sept. 1983). Reports the discovery of a 16th-magnitude comet in Pegasus. Two precise positions are reported for the epoch 1983 September 7. (no refs.)

116537 Comet Cernis (1983l). J.Bortle, C.E.Spratt, C.S.Morris.

I.A.U. Circ. (USA), no.3863, 1 pp. (14 Sept. 1983). Presents total visual magnitude estimates for the period 1983 September 4 to 9. (no refs.)

116538 Periodic Comet IRAS (1983j). C.E.Spratt, C.S.Morris, J.Bortle.

I.A.U. Circ. (USA), no.3863, 1 pp. (14 Sept. 1983). Presents total visual magnitude estimates for the period 1983 August 20 to September 9. (no refs.)

116539 Periodic Comet Tempel 2 (1982d). C.E.Spratt, J.E.Bortle, C.S.Morris.

I.A.U. Circ. (USA), no.3863, 1 pp. (14 Sept. 1983). Reports total visual magnitude estimates for the period 1983 August 13 to September 9. (no refs.)

116540 Periodic Comet Arend (1983q). J.Gibson.

I.A.U. Circ. (USA), no.3867, 1 pp. (23 Sept. 1983). Reports the recovery of this comet as a 20th-magnitude object in Lynx. Two precise positions are given for 1983 September 16 and 17. (2 refs.)

116541 Periodic Comet Harrington-Abell (1983r). J.Gibson.

I.A.U. Circ. (USA), no.3867, 1 pp. (23 Sept. 1983). Reports the recovery of this comet as a 20th-magnitude object in Gemini. Two precise positions are reported for 1983 September 17 and 18. (2 refs.)

116542 Periodic Comet Wild 2 (1983s). J.Gibson.

I.A.U. Circ. (USA), no.3867, 1 pp. (23 Sept. 1983). Reports the recovery of this comet as a 20th-magnitude object in Taurus. A single precise position is reported for the epoch 1983 September 18. (2 refs.)

116543 Comet Kowal (1983t). C.T.Kowal, B.G.Marsden.

I.A.U. Circ. (USA), no.3868, 1 pp. (23 Sept. 1983). Reports the discovery of a 16th-magnitude comet in Libra. Precise positions are given for the period 1983 May 8 to 15. Parabolic and elliptical orbital elements have been determined: it is quite probable that the object is a short-period comet, but the orbit is completely indeterminate. Three ephemerides are presented for the period 1983 June 15 to October 13, at ten-day intervals. (no refs.)

116544 Comet Cernis (1983l). B.G.Marsden.

I.A.U. Circ. (USA), no.3869, 1 pp. (23 Sept. 1983). Presents an ephemeris for the period 1983 September 23 to 1984 January 1 at ten-day intervals. (1 ref.)

116545 Periodic Comet IRAS (1983j). B.G.Marsden.

I.A.U. Circ. (USA), no.3870, 1 pp. (23 Sept. 1983). Presents an ephemeris for the period 1983 September 23 to 1984 January 1, at ten-day intervals. (1 ref.)

116546 Periodic Comet Kopff (1982k). C.E.Spratt, J.E.Bortle, C.S.Morris.

I.A.U. Circ. (USA), no.3870, 1 pp. (23 Sept. 1983). Reports total visual magnitude estimates for the period 1983 August 2 to September 9. (no refs.)

116547 Distribution of cometary binding energies based on the assumption of steady state. S.Yabushita (Dept. of Appl. Maths. & Phys., Kyoto Univ., Kyoto, Japan).

Mon. Not. R. Astron. Soc. (GB), vol.204, no.3, p.1185-91 (Sept. 1983). Long-period comets are continually expelled from the Solar System by planetary perturbations, so that the cometary population can be in a steady state if

the loss of observable comets is compensated by the injection of new comets. An integral equation derived on the steady-state assumption is adopted and analytical solutions thereof are compared with observational data. It is shown that there is a considerable excess of new comets in Oort's sense in accordance with an earlier result obtained by Everhart (1979). It is further shown that cometary decay is inadequate to account for the discrepancy. (12 refs.)

116548 Temporal variations of the absolute magnitude of Halley's comet. D.W.Hughes (Dept. of Phys., Univ. of Sheffield, Sheffield, England).

Mon. Not. R. Astron. Soc. (GB), vol.204, no.3, p.1291-5 (Sept. 1983). The variation of the absolute magnitude H_0 of Halley's comet, 1910 II, as a function of the apparition number, A , ($1910 \equiv -1$) is given by $H_0 = (6.028 \pm 0.329) + (0.0205 \pm 0.0210)A$. The comet was about 0.5 ± 0.5 mag brighter 2000 years ago and is losing about 2.3 ± 2.3 per cent of its mass at each apparition. (7 refs.)

116549 Velocities of ejection of comets by Jupiter and Saturn. M.A.Mamedov (Yu. Mamedaliev Astrophys. Obs., Shemakhinsk, USSR).

Sol. Syst. Res. (USA), vol.17, no.1, p.33-5 (Jan.-March 1983). Translation of: *Astron. Vestn. (USSR)*, vol.17, no.1, p.45-8 (Jan.-March 1983). [received: Sept. 1983]

The velocity of the ejection of a small body into a heliocentric orbit from any of the major planets is considered in general form. The distribution for aperiodic comets is obtained. (2 refs.)

116550 Motion of dust particles in cometary atmospheres. A.Korosmezey, I.Yusupov.

Report KFKI-1983-67, Hungarian Acad. Sci., Budapest (1983), 9 pp.

The motion of dust particles in a cometary coma is examined. The dust grains are assumed to be accelerated initially by the outstreaming gas up to a certain velocity and then to move solely under the influence of the light pressure of the Sun. Calculations are made according to Mie's theory to determine the maximal cometocentric distance in the sunward direction and the dust density distribution, for dust particles of several materials of various grain size. (14 refs.)

96.50K Meteors, showers and meteoroids

116551 European Network fireballs photographed in 1977. Z.Cepelach, J.Bocek, M.Novakova-Jezkova (Astron. Inst., Czechoslovak Acad. of Sci., Ondrejov, Czechoslovakia), V.Porubcan, T.Kirsten, J.Kiko.

Bull. Astron. Inst. Czech. (Czechoslovakia), vol.34, no.4, p.195-212 (July 1983).

Geometric, dynamic, photometric, and orbital data on all 29 fireballs photographed within the European Network in the year 1977 are given. In two cases, meteorite impacts are predicted and their impact points and areas given. A few remarks on the measuring and reduction procedures are included, especially on the problem of standard deviations of computed velocities. (18 refs.)

116552 Correction of meteor radiants for zenith attraction. G.V.Andreev (Tomsk Univ. Sci.-Res. Inst. for Appl. Math. & Mech., Tomsk, USSR).

Sol. Syst. Res. (USA), vol.17, no.1, p.43-5 (Jan.-March 1983). Translation of: *Astron. Vestn. (USSR)*, vol.17, no.1, p.56-9 (Jan.-March 1983). [received: Sept. 1983]

A general formula is given for the zenith attraction of meteor radiants which is valid for all meteor zenith distances. The accuracy of the Schiaparelli formula used previously is evaluated. It is shown that it is quite accurate for fast meteors, and may give errors of several degrees for slow ones. (2 refs.)

Distribution of meteor heights and sunrise See Entry 116322

Upper atmosphere wind observations of waves and tides with the UNH Meteor Radar System at Durham 43°N (1977, 1978 and 1979) See Entry 116329

96.50M Meteorites, micrometeorites

116553 Fission track age and cooling rate of the Marjalahti pallasite. P.Pellias, C.Perron, G.Crozaz (Lab. de Mineralogie du Museum, Paris, France), V.P.Perelygin, S.G.Stetsenko.

Earth & Planet. Sci. Lett. (Netherlands), vol.64, no.3, p.319-26 (Sept. 1983). Nuclear tracks were studied in olivine and merrillite from the Marjalahti pallasite. The merrillite contains an important fission contribution due mainly to the spontaneous decay of now extinct ^{244}Pu . The U contents of 29 merrillite grains range from 60 to 140 ppb (median value: 85 ppb). Assuming a reasonable fractionation temperature of $\sim 1750\text{K}$ for the pre-pallasitic material, a lower limit of $\sim 5 \text{ K/Myr}$ is obtained for the cooling rate, in strong contrast with the previous metallographic result ($\sim 0.5 \text{ K/Myr}$). This disagreement, together with those observed in the case of mesosiderites, strengthens the need for a revision of the metallographic method of retracing the cooling histories of meteorites. (35 refs.)

116554 Chemical and isotopic study of extraterrestrial particles from the ocean floor. D.A.Papanastassiou, G.J.Wasserburg, D.E.Brownlee (California Inst. of Technol., Pasadena, CA, USA).

Earth & Planet. Sci. Lett. (Netherlands), vol.64, no.3, p.341-55 (Sept. 1983). The authors report chemical, mineralogical and Rb-Sr data on deep-sea spherules and on particles from an Antarctic Ocean core in which an excess Ir content has been identified. The $^{87}\text{Sr}/^{86}\text{Sr}$ compositions and the Sr concentrations are in the range observed for the majority of chondritic meteorites. Extreme depletion of Rb relative to the chondritic abundance is found in the deep-sea spherules. These data support the inference that the deep-sea spherules are produced by the ablation or heating of meteoroids in the Earth's atmosphere. Most terrestrial sources for the deep-sea spherules can be excluded, based on the chemical composition and on the Sr isotopic composition. The results on vesicular, Ir-rich particles from the Antarctic Ocean core are also discussed. (46 refs.)

116555 Terrestrial age of an Antarctic meteorite by thermoluminescence technique. K.Ninagawa (Dept. of Appl. Phys., Okayama Univ. of Sci., Okayama, Japan), S.Miono, M.Yoshida, N.Takooka.

Lett. Nuovo Cimento (Italy), vol.38, ser.2, no.2, p.33-6 (10 Sept. 1983).

The authors have determined the terrestrial age of an Antarctic meteorite by measuring the terrestrial growth of thermoluminescence (TL) on the meteorite surface. The TL technique employed for the determination of the terrestrial age so far is based on natural fading of the TL intensity acquired during cosmic-ray exposure in space. The meteorite acquires a high intensity of TL in space by cosmic-ray bombardment. Once it falls on the Earth, the cosmic-ray irradiation decreases and the environmental temperature becomes higher comparatively, however. Therefore, the fading of TL is enhanced and overwhelms the growth. The terrestrial age has been estimated from the magnitude of fading at the inner position of meteorite. (5 refs.)

Rb-Sr, Sm-Nd, K-Ca, O, and H isotopic study of Cretaceous-Tertiary boundary sediments, Caravaca, Spain: evidence for an oceanic impact site See Entry 116086

96.60 SOLAR PHYSICS

116556 Fluid motions in the solar chromosphere-corona transition region. IV. Mass motions over sunspot umbrae. J.B.Gurman, R.G.Athay (SMM Experiment Operations Facility, Goddard Space Flight Center, Greenbelt, MD, USA).

Astrophys. J. (USA), vol.273, no.1, pt.1, p.374-80 (1 Oct. 1983). For pt.III see *ibid.*, vol.269, no.2, pt.1, p.706-14 (1983). Doppler velocity measurements in the C IV resonance line $\lambda 1548.19$ have been obtained over the umbrae of eight sunspots with the ultraviolet spectrometer and polarimeter (UVSP) on the Solar Maximum Mission. The velocity bandpass of these observations is approximately $\pm 30 \text{ km s}^{-1}$, and their spatial resolution is $3'' \times 3''$. Although a few individual resolution elements display flow velocities $\sim \pm 15 \text{ km s}^{-1}$ relative to the quiet network, the mean upflow is $(1.2 \pm 5.6) \text{ km s}^{-1}$ when averaged over all the resolution elements. Means over individual umbrae frequently show smaller variances, which is evidence for a real distribution of umbral transition region velocity fields. Two possible explanations for the smaller nonthermal broadening of the sunspot C IV line are examined. (31 refs.)

116557 Comments on the solar neutrino problem. R.Opher (Inst. Astron. e Geofisico, Univ. de Sao Paulo, Sao Paulo, Brazil).

Astron. & Astrophys. (Germany), vol.125, no.2, pt.1, p.L9-11 (Sept. 1983). Suggests that electrons of energy $E \sim 7 \text{ keV}$ (responsible for the opacity) gain energy from the electrons of energy $E \sim \text{keV}$ (electrons of greater density which produce plasma excitations) by means of the interaction with plasma excitations. Electrons $E \sim \text{keV}$ interact only with plasma excitations of wave number $0.7 \leq k/k_D \leq 1$ while electrons $E \sim 7 \text{ keV}$ interact only with plasma excitations $0.25 \leq k/k_D \leq 1$. Only the plasma excitations $0.7 \leq k/k_D \leq 1$ are common to both groups of electrons. The author suggests that the most likely explanation of the solar neutrino problem is the strong electron interaction with the plasma at the centre of the Sun. Due to this interaction, the group of electrons above the threshold for plasma excitation share their energy among themselves such that a distorted Maxwellian distribution results. Electrons $E \sim \text{keV}$ transfer energy to electrons $E \sim 7 \text{ keV}$, distorting the electron distribution in the Sun sufficient to resolve the solar neutrino problem. (8 refs.)

116558 Solar diameter measurements. F.Laclaire (Centre d'Etudes & Recherches Geodynamiques & Astron., Grasse, France).

Astron. & Astrophys. (Germany), vol.125, no.2, pt.1, p.200-3 (Sept. 1983). In French.

Since 1975 Sun observations have been regularly made at CERGA Observatory with an astrolabe with the purpose of improving the Earth's orbit around the Sun. The accuracy of the results leads the author to investigate whether this type of observation could contribute to determine the value of the Sun's radius. The principle of the procedure used involves determining this parameter from the difference between the crossing times of two successive edges by the same almucaantar. The use of reflector prisms makes it possible to observe at three different zenithal distances, allowing one to cover at CERGA the apparent orbit for a period of about 8 to 9 months. For all the measurements made between 1975 and 1982 (totalling 842 Sun crossings) the author obtains the following mean value of the radius reduced to one astronomical unit: $959.37'' \pm 0.02''$. During the period 1978 to 1982, a cycle of about 900 d is detected, reaching an amplitude of $0.5''$. (17 refs.)

116559 Photospheric faculae. III. Intensity, and magnetic field mapping of a typical element of the photospheric network. H.Daras-Papamargaritis (Center for Astron., Athens, Greece), S.Koutchmy.

Astron. & Astrophys. (Germany), vol.125, no.2, pt.1, p.280-6 (Sept. 1983). For pt.II see *ibid.*, vol.67, no.1, p.93-102 (1978). Studies a typical quiet Sun magnetic network element. Without introducing any correction, high spatial resolution spectra ($\approx 0.75''$) of two Fe I lines (5576 and 6302.5 Å), simultaneous CA II K and white-light slit-jaw pictures as well as spectroheliograms in H_α and Mg b₁—0.4 Å of a typical quiet region of the solar photosphere were analyzed in order: to map the intensity, the velocity field and the magnetic field of a typical element of this region; to study the underlying solar granulation, which seems to have a lower contrast; and to get from H_α filtergrams the fibril structure around the rosette, where the magnetic field is supposed to be dispersed. Finally the magnetic flux of a large region of the quiet Sun using Mg b₁ 0.4 Å spectroheliograms is estimated. (19 refs.)

116560 Solar rotation 1947-1981—determined from sunspot data.

G.Lustig (Sonnenobs. Kanzelhoehe, Univ. Graz, Graz, Austria). *Astron. & Astrophys. (Germany)*, vol.125, no.2, pt.1, p.355-8 (Sept. 1983). Positions of sunspots between 1947 and 1981 as observed at the Solar-Observatory Kanzelhoehe are used to determine the differential rotation of the Sun. Whereas equatorial velocities increased, the gradient of the differential rotation decreased during this period. Further, velocities at the equator during solar-minimum years are greater than in the neighbouring maxima. The rotational behavior during the various spot cycles is examined. (24 refs.)

116561 Calculation of stellar structure. III. Solar models that satisfy the necessary conditions for a unique solution to the stellar structure equations. C.A.Rouse (General Atomic Co., San Diego, CA, USA).

Astron. & Astrophys. (Germany), vol.126, no.1, pt.2, p.102-10 (Sept. 1983). For pt.II see *Progress in High Temperature Physics and Chemistry*, vol.4, (Pergamon) p.139 (1971). A series of provisional solar models are calculated that satisfy the necessary conditions for a unique solution to the stellar structure equations (Rouse, 1975). The models are qualitatively consistent with the solar neutrino experiment results through the magnitude of the central temperature ($\sim 14 \times 10^6 \text{ K}$) or its variation near the center. A fundamental modification of one basic standard model assumption is that each helium nucleus is not assumed to stay at the same radius where it is produced. The most important fundamental consequence of this preliminary study is that in order not to arbitrarily reduce the opacity in such a manner, it is deduced that the Sun has a small high- Z iron-like core with a mass of about $0.005 M_\odot$ in a radius of about $0.05 R_\odot$. Various periods of oscillation calculated for each model are discussed. (47 refs.)

116562 Analysis of solar observations made with the CERGA astrolabe.

M.Bougard (Univ. de Paris XI, Sceaux, France), F.Chollet, F.Laclaire. *Astron. & Astrophys. (Germany)*, vol.126, no.1, pt.2, p.161-9 (Sept. 1983). In French.

Describes the method of analysis of solar observations made at the CERGA Observatory and gives the results obtained during the campaigns of 1978, 1979 and 1980. The observational residuals are expressed as functions of corrections to zenith distance, and to solar right ascension, declination and semi-diameter. Several relations obtained by observations of upper and lower sides of the Sun during some east and west transits, are solved by least squares method to give the unknowns $\Delta\alpha$, $\Delta z + \Delta d \cos S$ and Δd . Corrections of the main parameters of the solar orbit are made. (19 refs.)

116563 The MHD Kelvin-Helmholtz instability in the solar photosphere. I.C.Rae (Dept. of Appl. Math., Univ. of St. Andrews, St. Andrews, Scotland).

Astron. & Astrophys. (Germany), vol.126, no.1, pt.2, p.209-15 (Sept. 1983). Recent studies indicate the possibility of MHD surface and body wave propagation along magnetic structures in the solar atmosphere. Observations indicate the existence of guided flows in these structures. Under certain flow and plasma conditions, the surface and body waves become unstable, possibly leading to secondary wave propagation and microturbulence. The study of this (Kelvin-Helmholtz) instability under solar conditions is therefore important. The author surveys the relevant published literature for planar geometries. (80 refs.)

116564 Solar γ -ray lines. D.J.Forrest (Univ. of New Hampshire, Durham, NH, USA).

AIP Conf. Proc. (USA), no.101, p.3-14 (1983). (Workshop on Positron-Electron Pairs in Astrophysics, Greenbelt, MD, USA, Jan. 1983). The Gamma Ray Spectrometer on the Solar Maximum Mission satellite has observed emissions produced by nuclear reactions in over 20 separate solar flares. The observed intensity from different flares of some of these emissions ranges over a factor of 100 and the time scale for their production ranges from 10 s pulses, to complete events lasting over 1000 s. The emissions include narrow and broadened prompt γ -ray lines from numerous isotopes (from ^7Li to ^{56}Fe and cover the energy range 0.431 MeV (^7Be) to 7.12 MeV (^{16}O). The instrument has also observed emissions at energies greater than 10 MeV from the decay of π^0 mesons, from electron bremsstrahlung, and from the direct observation of $> 10^2$ MeV solar neutrons. The intensity, temporal and spectral properties of these emissions are reviewed from the point of view that solar flares represent an astrophysical particle acceleration site. (28 refs.)

116565 Positron annihilation radiation from solar flares. G.H.Share (Naval Res. Lab., E.O. Hulburt Center for Space Res., Washington, DC, USA), E.L.Chupp, D.J.Forrest, E.Rieger.

AIP Conf. Proc. (USA), no.101, p.15-20 (1983). (Workshop on Positron-Electron Pairs in Astrophysics, Greenbelt, MD, USA, Jan. 1983). Positron annihilation radiation has been observed from the 21 June 1980 and 3 June 1982 flares by the gamma-ray spectrometer on the Solar Maximum Mission satellite. The observed 0.511 MeV line fluences from the flares were $14.6 \pm 3.3 \text{ } \gamma/\text{cm}^2$ and $103 \pm 8 \text{ } \gamma/\text{cm}^2$, respectively. Measurement of the line width allows the authors to set an upper limit to the temperature in the annihilation region of $3 \times 10^6 \text{ K}$. The time dependence of the 0.511 MeV line during the 21 June 1980 flare is consistent with Ramaty et al.'s (1983) calculations¹ for positrons created in the decay of radioactive nuclei. The time dependence of 0.511 MeV line for the 3 June 1982 flare is more complex and requires more detailed study. (12 refs.)

116566 How does the magnetic field of an usual active region develop? V.Bumba (Astron. Inst., Czechoslovak Acad. of Sci., Ondrejov, Czechoslovakia).

Bull. Astron. Inst. Czech. (Czechoslovakia), vol.34, no.4, p.219-29 (July 1983).

Using more than 160 'qualitative' magnetic maps in series of 36 new regions, the author describes the standard features of the morphological development of a usual active region's magnetic field in connection with the formation of its sunspot group. The author derives a pattern of magnetic field distribution for small and large active regions in their several evolutionary stages. He finds not only signs of the influence of solar differential rotation on the shape of the magnetic field, but also indications of other dynamical forces acting on the active region as the photospheric matter flows around it. New observational facts concerning the role of the magnetic singularity in the active region's 'centre' (centre of magnetic activity), lying in the middle part of the group at the magnetic boundary, are demonstrated. (9 refs.)

116567 Frequency dependent characteristics of solar impulsive radio bursts. T.K.Das, M.K.Das Gupta (Centre of Advanced Study in Radio Phys. & Electronics, Calcutta, India).

Bull. Astron. Inst. Czech. (Czechoslovakia), vol.34, no.4, p.229-33 (July 1983).

An investigation is made of the impulsive radio bursts observed in the frequency range 0.245-35 GHz. Important results obtained are (i) simple 1 type with intensities 0-10 f.u. and simple 2 type with intensities 10-500 f.u. are more predominant in the frequency ranges 1.415-4.995 GHz and 4.995-8.8 GHz, respectively; (ii) with maxima around 2.7 GHz and 4 GHz for the first and second types respectively, the durations of the radio bursts decrease gradually both towards lower and higher frequencies; (iii) as regards occurrences, the first type dominates in the southern solar hemisphere peaking around 8.8 GHz, whereas the second type favours the north and with no well-defined maximum in any frequency; (iv) both types prefer the eastern hemisphere, the peak occurrences being around 8.8 GHz and 5 GHz for the two successive types, respectively; (v) the spectra of impulsive radio bursts are generally inverted U-type with the maximum emission intensity between 5 and 15 GHz. (30 refs.)

116568 Solar irradiance modulation by active regions from 1969 through 1981. D.V.Hoyt, J.A.Eddy (High Altitude Obs., Nat. Centre for Atmospheric Res., Boulder, CO, USA).

Geophys. Res. Lett. (USA), vol.10, no.7, p.509-12 (July 1983). Recent satellite measurements of the solar total irradiance (S) indicate that on time scales of days to months the solar constant varies by a few tenths of a percent. The predominant part of these variations can be explained by blocking of the upward solar flux by sunspots. The observations are consistent with current theoretical models of energy storage in which the energy blocked by the sunspots is temporarily stored in the convective zone. The authors present modelled solar constant variations on a day by day basis selected from model calculations for the period 1874 through 1981. Because neither faculae nor bright rings about sunspots balance the net blocking by sunspots, there is a net eleven year modulation in irradiance with a relative depression of as much as 0.07% for the period 1969-1981. (23 refs.)

116569 Solar-flared prognostication by the empirical-statistical approach.

P.A.Stahl. *J. R. Astron. Soc. Can. (Canada)*, vol.77, no.4, p.203-13 (Aug. 1983).

Social emphasis is placed on factors affecting one particular technique, multiple regression. The points made are illustrated by way of example, as applied to ex post facto predictions of solar flares. It is concluded that the elucidation of a flare 'trigger', with its correspondent pre-flare recognition, is indispensable to the further refinement of empirical-statistical schemes. (15 refs.)

116570 On a possible mechanism of quasi-periodic pulses of the quiet Sun decametric radio emission. B.N.Levin, S.D.Snegirev.

Pis'ma v Astron. Zh. (USSR), vol.9, no.8, p.490-4 (1983). In Russian. English translation in: *Sov. Astron. Lett. (USA)*.

The observed fluctuations of the decametric, radio emission of the quiet Sun are interpreted on the basis of the plasma mechanism of generation. These

fluctuations may be caused by modulation of the optical depth of the radio source due to propagation of the sound wave packet through the corona. (6 refs.)

116571 On the relation of local sources of centimeter solar radioemission with noise storms based on the RATAN-600 observations. T.A.Bravova, G.B.Gel'freikh, A.A.Gnedzilov. *Pis'ma v Astron. Zh. (USSR)*, vol.9, no.8, p.495-9 (1983). In Russian. English translation in: *Sov. Astron. Lett. (USA)*. The RATAN-600 observations of local sources of the solar radioemission S-component in the range of 2-4 cm are compared with data on noise storms at 169 and 204 MHz. It is found that intensification of noise storms at 169 and 204 MHz. It is found that intensification of noise storms was closely connected with an increase the cyclotron component of local sources. Noise storm appearances were preceded by an increase of the magnetic field in the corona above the spot from 1800 to 2500 Oe. (6 refs.)

116572 Power spectrum of brightness temperature fluctuations derived from solar eclipse observations at 2.8 GHz. S.K.Alurkar, S.S.Degaonkar, R.V.Bhonsle (Phys. Res. Lab., Ahmedabad, India). *Proc. Indian Acad. Sci. Earth & Planet. Sci.*, vol.92, no.1, p.57-61 (March 1983). [received: Sept. 1983] Reports on the maximum entropy method power spectrum analysis of brightness temperature fluctuations observed at 2.8 GHz during the total solar eclipse of 16 February 1980. The observed periodicities range from 3.5 min to 64 min. These periodicities may arise due to spatial and/or temporal variations in the solar radio emission. The observed periodicities imply presence of scale sizes ranging from 70000 to 600000 km assuming that the brightness fluctuations arise because of spatial variation only. On the other hand, if these fluctuations are due to temporal variation, the observed periodicities correspond well to predicted modes of solar global oscillations. (5 refs.)

116573 Late phase gradual enhancements in microwaves and hard X-rays of the 6 November 1980 flare. K.Kai, H.Nakajima, T.Kosugi (Tokyo Astronomical Obs., Univ. of Tokyo, Tokyo, Japan), S.R.Kane. *Sol. Phys. (Netherlands)*, vol.86, no.1-2, p.231-6 (1983). (Proceedings of the US-Japan Seminar on Recent Advances in the Understanding of Solar Flares, Tokyo, Japan, 5-8 Oct. 1982). Gradual enhancements which repeatedly appeared 20-50 min after the onset of an impulsive burst were observed in microwaves and hard X-rays. The observed characteristics of the gradual enhancements are (i) the similarity of time profiles in both the frequency range of 17 GHz to 160 MHz and the energy range of 40 to ~400 keV, (ii) the low peak frequency of the microwave spectrum (~4 GHz), and (iii) the flat X-ray spectrum with the power-law exponent of ~1.7. It is suggested that the radio and X-ray gradual enhancements are due to a single population of energetic electrons which extend high in the corona (at least 1.4×10^5 km). (11 refs.)

116574 Hard X-ray dynamic spectrum of flares observed by Hinotori. N.Nitta, T.Takakura (Dept. of Astron., Univ. of Tokyo, Tokyo, Japan), K.Ohki, M.Yoshimori. *Sol. Phys. (Netherlands)*, vol.86, no.1-2, p.241-6 (1983). (Proceedings of the US-Japan Seminar on Recent Advances in the Understanding of Solar Flares, Tokyo, Japan, 5-8 Oct. 1982). Time variations of the hard X-ray spectrum in solar flares are observed by the hard X-ray spectrometer aboard the Hinotori satellite. With a new presentation of the dynamic spectrum the authors study the differences between impulsive and gradual hard X-ray bursts. In the impulsive events a 'bent' spectrum up to some hundred keV persists at least until the main peak. In the gradual events, on the other hand, a power-law spectrum augmented by a low-energy excess is dominant.

116575 A flare model deduced from Hinotori and millimeterwave interferometer observations. K.Kawabata, H.Ogawa, I.Suzuki (Dept. of Phys. & Astrophys., Nagoya Univ., Nagoya, Japan). *Sol. Phys. (Netherlands)*, vol.86, no.1-2, p.247-52 (1983). (Proceedings of the US-Japan Seminar on Recent Advances in the Understanding of Solar Flares, Tokyo, Japan, 5-8 Oct. 1982). The γ -ray and white-light flare of 13 May, 1981 is used for a study of spatial distributions of energetic electrons and high-temperature plasma. (6 refs.)

116576 Relation between hard X-ray spectra and electron energy spectra. I.Suzuki, K.Kawabata (Dept. of Phys. & Astrophys., Nagoya Univ., Nagoya, Japan). *Sol. Phys. (Netherlands)*, vol.86, no.1-2, p.253-7 (1983). (Proceedings of the US-Japan Seminar on Recent Advances in the Understanding of Solar Flares, Tokyo, Japan, 5-8 Oct. 1982). The relationship between hard X-ray spectra and energetic spectra in solar X-ray bursts is investigated, and a simplified cross-section for Bremsstrahlung which is applicable to the region of mildly relativistic energies is proposed. Using the proposed cross section, the authors solve an integral equation to obtain the electron energy spectrum. The validity of the proposed cross-section is checked by comparing the spectrum calculated by the exact Bethe-Heitler formula. (7 refs.)

116577 A comparison of high-energy events in the quiet Sun with solar flares. G.E.Brueckner (E.O. Hulbert Center for Space Res., Naval Res. Lab., Washington, DC, USA). *Sol. Phys. (Netherlands)*, vol.86, no.1-2, p.259-65 (1983). (Proceedings of the US-Japan Seminar on Recent Advances in the Understanding of Solar Flares, Tokyo, Japan, 5-8 Oct. 1982). Observations of high-speed coronal clouds (OSO-7), flare ejecta (Skylab) and high-energy jets are compared. It is possible that the same physical mechanism—an expanding loop—which is responsible for the high speed jets (400 km sec^{-1} , 2.5×10^{26} ergs) can also account for the high-speed coronal clouds (1300 km sec^{-1} , 4×10^{30} ergs), which were correlated with a flare-connected spray. Field strength of 15 gauss and 2500 gauss are required for the jets and the sprays, respectively. (7 refs.)

116578 Pre- and post-flare X-ray variations in active regions. Z.Svestka, A.Schadee (Space Res. Lab., Astronomical Inst., Utrecht, Netherlands). *Sol. Phys. (Netherlands)*, vol.86, no.1-2, p.267-77 (1983). (Proceedings of the US-Japan Seminar on Recent Advances in the Understanding of Solar Flares, Tokyo, Japan, 5-8 Oct. 1982). Extremely low background noise of the HXIS experiment aboard the SMM made it possible to detect >3.5 keV X-ray emissions from nonflaring active regions which are 10^3 - 10^4 times weaker than the X-ray flux from flares. Short-lived X-ray bursts and long-lived X-ray enhancements of various intensities seem to characterize active regions in different phases of their development. After major two ribbon-flares, giant X-ray arches are seen in the corona, slowly decaying for many hours after the flare end. Associated with these arches appear to be quasi-periodic flare-like variations of purely coronal nature. (7 refs.)

116579 Imaging of impulsive solar flare phenomena. A.Duijveman, P.Hoynig (Astronomical Inst., Space Res. Lab., Utrecht, Netherlands). *Sol. Phys. (Netherlands)*, vol.86, no.1-2, p.279-88 (1983). (Proceedings of the US-Japan Seminar on Recent Advances in the Understanding of Solar Flares, Tokyo, Japan, 5-8 Oct. 1982). Reviews some advances in the understanding of impulsive solar flare phenomena obtained through new hard X-ray and radio imaging instruments (the Solar Maximum Mission and Hinotori satellites, the VLA and VLBI). (31 refs.)

116580 Temperature structure of spatially resolved hard X-ray flares. G.M.Simnett (Dept. of Space Res., Univ. of Birmingham, Birmingham, England). *Sol. Phys. (Netherlands)*, vol.86, no.1-2, p.289-99 (1983). (Proceedings of the US-Japan Seminar on Recent Advances in the Understanding of Solar Flares, Tokyo, Japan, 5-8 Oct. 1982). High resolution X-ray images are used to study the temperature structure and evolution of two spatially resolved, but compact, solar flares. Both flares developed within a magnetic loop whose footpoints were separated by typically 15000 km, and involved primary energy release at one footpoint. This was followed by transfer of chromospheric material into and around the loop. The flares involved total energies differing by over an order of magnitude, and they follow different evolutionary paths because of this. (5 refs.)

116581 General aspects of hard X-ray flares observed by Hinotori: gradual burst and impulsive burst. K.Ohki (Tokyo Astronomical Obs., Tokyo, Japan), T.Takakura, S.Tsuneta, N.Nitta. *Sol. Phys. (Netherlands)*, vol.86, no.1-2, p.301-12 (1983). (Proceedings of the US-Japan Seminar on Recent Advances in the Understanding of Solar Flares, Tokyo, Japan, 5-8 Oct. 1982). Surveys the observational results on five gradual and four impulsive type events from the hard X-ray imaging (SXT) and spectrometer (HXM) instruments on the Hinotori satellite. A set of differences are clearly recognized between the gradual and impulsive type bursts. These are: (1) Hard X-ray images show the existence of a large coronal source for each gradual burst and a wide variety of source structures for impulsive bursts. (2) The source heights of the impulsive bursts appear to be low. (3) All gradual bursts show power-law spectra while impulsive bursts show exponential thermal spectra at least before the maximum phase. (4) Energy-dependent peak delays are observed only in gradual bursts. The authors suggest that two different acceleration and emission mechanisms are involved with these two kinds of hard X-ray bursts. (17 refs.)

116582 Vertical structure of hard X-ray flare. S.Tsuneta, T.Takakura, N.Nitta (Dept. of Astron., Univ. of Tokyo, Tokyo, Japan), K.Ohki, K.Makishima, T.Murakami, M.Oda, Y.Ogawara. *Sol. Phys. (Netherlands)*, vol.86, no.1-2, p.313-21 (1983). (Proceedings of the US-Japan Seminar on Recent Advances in the Understanding of Solar Flares, Tokyo, Japan, 5-8 Oct. 1982). Presents studies of the vertical structure of hard X-ray flares for two contrasting examples. The 1981 May 13 flare contained a coronal hard X-ray source which was located above 50000 km above the photosphere. On the other hand, the 1981 July 20 flare had a chromospheric double source structure in the initial phase. Electrons in this case were able to stream freely from the corona to the chromosphere. (10 refs.)

116583 Hard X-ray images of impulsive bursts. T.Takakura (Dept. of Astron., Univ. of Tokyo, Tokyo, Japan), K.Ohki, S.Tsuneta, N.Nitta. *Sol. Phys. (Netherlands)*, vol.86, no.1-2, p.323-31 (1983). (Proceedings of the US-Japan Seminar on Recent Advances in the Understanding of Solar Flares, Tokyo, Japan, 5-8 Oct. 1982). A morphological study is made for the hard X-ray images (25-50 keV) of nine impulsive bursts observed by Hinotori. Most of them revealed single sources, either extended or compact, during the whole duration of the bursts. The sources of all of four spike bursts in the sample are compact. After the main phase of the impulsive bursts, generally the source size becomes smaller accompanying a shift of position. The X-ray source size is much greater than that of the H α kernel in two events out of three. Four possible explanations for the X-ray source to be single are suggested. (10 refs.)

116584 Time variations of hard X-ray bursts observed with the solar X-ray Telescope aboard Hinotori (with a movie). T.Kosugi (Tokyo Astronomical Obs., Univ. of Tokyo, Tokyo, Japan), S.Tsuneta. *Sol. Phys. (Netherlands)*, vol.86, no.1-2, p.333-8 (1983). (Proceedings of the US-Japan Seminar on Recent Advances in the Understanding of Solar Flares, Tokyo, Japan, 5-8 Oct. 1982). A new method for synthesizing hard X-ray maps from the raw data of the Solar X-ray Telescope (SXT) aboard Hinotori has been developed. Using this method, five typical SXT events have been analyzed and their images collected in a movie with a time resolution of about 8 s (the half spin period of the satellite). The movie clearly shows that (1) three different classes of bursts, i.e. the gradual thermal burst, the multiple impulsive burst, and the extended outburst, have different structures and show quite different variations from each other, and that (2) the source of the extended outburst is located in the corona above 10^4 km and its shape appears to be a large loop. (14 refs.)

116585 Computed magnetic field structure of the flares observed by the Hinotori hard X-ray telescope. T.Sakurai (Dept. of Astron., Univ. of Tokyo, Tokyo, Japan). *Sol. Phys. (Netherlands)*, vol.86, no.1-2, p.339-44 (1983). (Proceedings of the US-Japan Seminar on Recent Advances in the Understanding of Solar Flares, Tokyo, Japan, 5-8 Oct. 1982). Potential field computations have been carried out to study the location of hard X-ray sources observed by the Hinotori hard X-ray imaging instrument, SXT. Of the two flares studied, the X-ray source of the 1981 May 13 event, a very unusual gradual flare, appears to lie at the top of an arcade of field lines. In the other event, the 1981 October 15 flare, the observed double source structure is not explained implying the existence of nonnegligible electric currents in the flare region. (11 refs.)

116586 Dynamical interpretation of the very hot region appearing at the top of a loop. K.Shibata (Dept. of Earth Sci., Aichi Univ. of Education, Aichi Prefecture, Japan), Y.Uchida, T.Sakurai. *Sol. Phys. (Netherlands)*, vol.86, no.1-2, p.345-51 (1983). (Proceedings of the US-Japan Seminar on Recent Advances in the Understanding of Solar Flares, Tokyo, Japan, 5-8 Oct. 1982). In order to explain the appearance of a hard X-ray source at the top of a loop, a model is presented in which the dynamical effects of the dark filament mass infalling along the loop in association with the 'disruption brusque' plays an important role. The crash of the infalling mass produces high temperature regions in the low corona above the two footpoints of the loop. The up-going shocks, created in the crash and strengthened in the steep density gradient, produce a very high temperature (10^8 K) near the top of the loop. This process in successively higher loops may account for the sources of

gradual hard X-ray bursts appearing at the top of the loop-like structure. (13 refs.)

116587 Spatial structure of high energy photon sources in solar flares. S.R.Kane (Space Sci. Lab., Univ. of California, Berkeley, CA, USA).

Sol. Phys. (Netherlands), vol.86, no.1-2, p.355-65 (1983). (Proceedings of the US-Japan Seminar on Recent Advances in the Understanding of Solar Flares, Tokyo, Japan, 5-8 Oct. 1982).

Stereoscopic observations of high energy (≥ 100 keV) photon emission from five solar flares have been made with the X-ray spectrometers aboard the International Sun Earth Explorer-3 and Pioneer Venus Orbiter spacecraft. The observed altitude structure of the photon source and its dependence on the photon energy and time during a flare are compared with the predictions of thermal and nonthermal models of the hard X-ray source. (19 refs.)

116588 Observations of fine time structure in solar flare hard X-ray bursts. K.Hurly, M.Niel, R.Talon (Centre d'Etude Spatiale des Rayonnements, Toulouse, France), I.V.Estulin, V.Ch.Dolidze.

Sol. Phys. (Netherlands), vol.86, no.1-2, p.367-73 (1983). (Proceedings of the US-Japan Seminar on Recent Advances in the Understanding of Solar Flares, Tokyo, Japan, 5-8 Oct. 1982).

Hard X-ray (≥ 100 keV) time histories of the solar flares which occurred on 1978 December 4 and 1979 February 18 are presented. The first flare was observed by three identical instruments from near-earth orbit (Prognostic 7) and interplanetary space (Venera 11 and 12). Fine time structure is present down to the 55 ms level for the e-folding rise and fall times. These data may be used to localize the emission region by the method of arrival time analysis. (8 refs.)

116589 Gamma-ray observations from Hinotori. M.Yoshimori, K.Okudaira, Y.Hirasima (Dept. of Phys., Rikkyo Univ., Tokyo, Japan), I.Kondo.

Sol. Phys. (Netherlands), vol.86, no.1-2, p.375-82 (1983). (Proceedings of the US-Japan Seminar on Recent Advances in the Understanding of Solar Flares, Tokyo, Japan, 5-8 Oct. 1982).

Some interesting results on gamma-ray line emission and its time profiles observed by Hinotori are presented. Possible explanations of gamma-ray line and hard X-ray emissions for the impulsive and gradual flares are discussed. The relationship between the gamma-ray line emission and acceleration and escape of the solar particles is also studied. (15 refs.)

116590 High energy particle acceleration in solar flares—observational evidence. E.L.Chupp (Univ. of New Hampshire, Durham, NH, USA).

Sol. Phys. (Netherlands), vol.86, no.1-2, p.383-93 (1983). (Proceedings of the US-Japan Seminar on Recent Advances in the Understanding of Solar Flares, Tokyo, Japan, 5-8 Oct. 1982).

Gamma ray and neutron observations made by the SMM Gamma Ray Spectrometer are reviewed. The implication these observations hold for understanding particle acceleration in solar flares are discussed. The data require that both electrons and ions must be accelerated together to relativistic energies and interact with matter in a time scale of seconds. (19 refs.)

116591 Gamma-ray lines and neutrons from solar flares. R.Ramaty, R.J.Murphy (Goddard Space Flight Center, Greenbelt, MD, USA), B.Kozlovsky, R.E.Lingenfelter.

Sol. Phys. (Netherlands), vol.86, no.1-2, p.395-408 (1983). (Proceedings of the US-Japan Seminar on Recent Advances in the Understanding of Solar Flares, Tokyo, Japan, 5-8 Oct. 1982).

Derives the energy spectrum of accelerated protons and nuclei at the site of the June 21, 1980 limb flare by a new technique, using observations of the time-dependent flux of high-energy neutrons at the Earth. The authors find that this energy spectrum is very similar to the energy spectra of 7 disk flares for which the accelerated particle spectra have been previously derived using observations of 4-7 MeV-to-2.223 MeV fluence ratios. The implied spectra for all of these flares are too steep ($\alpha T \approx 0.02$) to produce any significant amount of radiation from π meson decay. The authors suggest that the observed >10 MeV gamma rays from the June 21, 1980 flare are bremsstrahlung of relativistic electrons. (30 refs.)

116592 Characteristics of gamma-ray line flares as observed in hard X-ray emissions and other phenomena. T.Bai (Inst. for Plasma Res., Stanford Univ., Stanford, CA, USA), B.R.Dennis, A.L.Kiplinger, L.E.Orwig, K.J.Frost.

Sol. Phys. (Netherlands), vol.86, no.1-2, p.409-19 (1983). (Proceedings of the US-Japan Seminar on Recent Advances in the Understanding of Solar Flares, Tokyo, Japan, 5-8 Oct. 1982).

Observations of gamma-ray lines from solar flares by SMM demonstrated that energetic protons and heavy ions are accelerated during the impulsive phase. In order to understand the acceleration mechanism for gamma-ray producing protons and heavy ions, the authors study the characteristics of the flares from which gamma-ray lines were observed by SMM. In order to identify the characteristics unique to the gamma-ray line flares, the authors study intense hard X-ray flares with no gamma-ray line emissions. (38 refs.)

116593 Narrow-band decimeter bursts and X-ray emissions—possible evidence of negative absorption or maser effect. S.Enome (Toyokawa Obs., Res. Inst. of Atmospheric, Nagoya Univ., Toyokawa, Japan).

Sol. Phys. (Netherlands), vol.86, no.1-2, p.421-6 (1983). (Proceedings of the US-Japan Seminar on Recent Advances in the Understanding of Solar Flares, Tokyo, Japan, 5-8 Oct. 1982).

Bursts with peculiar time evolution and narrow-band microwave spectra are studied in detail using X-ray data from the satellite HINOTORI and microwave data from Toyokawa Observatory. Discussions are given for emission mechanisms and a burst scenario. (10 refs.)

116594 Particle acceleration in the 1981 April 1 flare. H.Nakajima (Nobeyama Solar Radio Obs. of the Tokyo Astronomical Obs., Univ. of Tokyo, Tokyo, Japan).

Sol. Phys. (Netherlands), vol.86, no.1-2, p.427-32 (1983). (Proceedings of the US-Japan Seminar on Recent Advances in the Understanding of Solar Flares, Tokyo, Japan, 5-8 Oct. 1982).

The large microwave burst of 1981 April 1, which was accompanied by both hard X-ray and γ -ray emissions, has been analyzed to study the acceleration of particles in the impulsive phase. (15 refs.)

116595 The spatial distribution of umbral dots and granules. J.K.Lawrence (Dept. of Phys. & Astron., San Fernando Obs., California State Univ., Northridge, CA, USA).

Sol. Phys. (Netherlands), vol.87, no.1, p.1-5 (Aug. 1983).

A statistical analysis is made of the spatial distribution of umbral dots and photospheric granules. The dots and granules are more evenly spaced than random points, though dots mapped by different observers have different distributions. (12 refs.)

116596 The study of umbral flashes in the umbrae of two sunspots. I.P.Turova, R.B.Teplitskaja, G.V.Kuklin (Siberian Inst. of Terrestrial Magnetism, Ionosphere & Radiowave Propagation, Irkutsk, USSR).

Sol. Phys. (Netherlands), vol.87, no.1, p.7-22 (Aug. 1983).

The results of observations of the umbral flashes in two sunspots are reported. The sunspots differ in their morphological properties (evolution rates and activity levels) and in observation conditions (heliocentric distances). The oscillation parameters of the two sunspots do not coincide. The most significant differences are pronounced in the phase relations and amplitudes of observed oscillations. (20 refs.)

116597 Preferred longitudes of sunspot groups and high-speed solar wind streams: evidence for a 'solar memory'. H.Balthasar, M.Schussler (Univ.-Sternwarte, Göttingen, Germany).

Sol. Phys. (Netherlands), vol.87, no.1, p.23-36 (Aug. 1983).

Correlation analysis of the mean longitude distribution of sunspot groups (taken from the Greenwich Photoheliographic Results) and high-speed wind streams (inferred from the C9 index for geomagnetic disturbances) with the Bartels rotation period $P=27.0$ days shows anticorrelation for individual cycles. In particular, the longitudes of post-maximum stable streams of cycle 18 and 19 are well anticorrelated with the preferred longitudes of sunspot groups during the maximum activity periods of these cycles. This is further analyzed using the daily Zurich sunspot number, R , between 1932 and 1980. The authors conclude that there is a 'solar memory' for preferred longitudes of activity extending at least over one, probably two cycles. (43 refs.)

116598 Magnetic canopies in unipolar regions. H.P.Jones (Lab. for Astron. & Solar Phys., NASA/Goddard Space Flight Center, Greenbelt, MD, USA), R.G.Giovanelli.

Sol. Phys. (Netherlands), vol.87, no.1, p.37-42 (Aug. 1983).

Base-height statistics are presented for magnetic canopies in six unipolar magnetic regions which were observed near the limb with the Kitt Peak Vacuum Telescope and Diode Array Magnetograph during the period 25 April-3 July, 1980. As in earlier studies, extensive areas are found to be covered by low-lying canopies. (5 refs.)

116599 A model of a quiescent prominence on the basis of studying the K Ca⁺ line fine structure. M.S.Gigolashvili (Abastumani Astrophys. Obs., Georgia, USSR), Yu.D.Zhugzhda.

Sol. Phys. (Netherlands), vol.87, no.1, p.43-6 (Aug. 1983).

Constructs a model of a quiescent prominence with nonparallel structural elements, based on a study of the K Ca⁺ line fine structure of two quiescent prominences. The dependences of the radial velocities on the height found for the structural elements making up the prominence gives information on the inner spatial structure of the prominence. The available data suggest an alternative model of quiescent prominences. (5 refs.)

116600 Comparison of coronal holes observed in soft X-ray and He I 10830 Å spectroheliograms. S.W.Kahler, J.M.Davis (American Sci. & Engng. Inc., Fort Washington, Cambridge, MA, USA), J.W.Harvey.

Sol. Phys. (Netherlands), vol.87, no.1, p.47-56 (Aug. 1983).

Compares coronal holes observed in solar soft X-ray images obtained with rocket-borne telescopes during 1974 to 1981 with holes observed on nearly simultaneous 10830 Å maps. The results appear inconsistent with the popular view that the quiet corona is sharply separated into open magnetic field regions consisting of coronal holes and closed field regions consisting of the large scale structure. (25 refs.)

116601 Line profile analysis of an active region corona observed successively at the east and west limb. T.Tsubaki (Dept. of Earth Sci., Shiga Univ., Otsu, Japan).

Sol. Phys. (Netherlands), vol.87, no.1, p.57-63 (Aug. 1983).

A systematic line profile analysis of the Fe XIV $\lambda 5303$ coronal line was carried out for a single active region successively observed both above the east and west solar limb (4, 18 and 19 October, 1974). Cross-correlations of the intensity, temperature and velocity structures among these three sets of observations show that although considerable variations are seen in intensity with accompanying change in temperature, the velocity field can be stable as long as the magnetic field configuration remains stable. It is also pointed out that the standard wavelength of the green line is 5302.81 Å which is somewhat shorter than the currently adopted value of 5302.86 Å, and that a 'general' flow from west to east might exist in this region superimposed on the local velocity field. (6 refs.)

116602 Simple models for magnetic flux tubes. G.W.Simon (Air Force Geophys. Lab., Sacramento Peak Obs., Sunspot, NM, USA), N.O.Weiss, A.H.Nye.

Sol. Phys. (Netherlands), vol.87, no.1, p.65-75 (Aug. 1983).

Known potential field solutions can be used to model the structure of magnetic fields in the solar photosphere. Several two-dimensional and axisymmetric solutions are compared. In the most satisfactory model the vertical component of the field is prescribed on a horizontal plane so as to be uniform within a finite disc and zero outside it. The resulting flux distribution provides a good description of small scale intergranular magnetic fields and of the observed field structure in a pore, but is inadequate for sunspots. (24 refs.)

116603 Wave propagation in intense flux tubes. B.Roberts (Dept. of Appl. Math., Univ. of St. Andrews, St. Andrews, Scotland).

Sol. Phys. (Netherlands), vol.87, no.1, p.77-93 (Aug. 1983).

The nature of non-adiabatic wave propagation in a slender magnetic flux tube is explored. The results of the theory are compared with the observations of Giovanelli et al. (1978). Those observations of tubes in the photosphere-chromosphere show outwardly propagating waves, with periods of 300 s, which take some 19 s to propagate from one level of line formation to another level higher in the atmosphere. In sharp contrast to this is the time of 7 s for a similar disturbance outside the tube to propagate between the same two levels of line formation, estimated to be some 600 km apart in the field-free atmosphere. It is argued that the sharply contrasting propagation times for the tube and its environment is principally due to the elasticity of the tube and its subsequent propensity for propagation. The theory suggests that the observed disturbances are non-adiabatic, acoustic-gravity waves channelled along a magnetic flux tube and modulated by external pressure variations. (22 refs.)

116604 Heating of chromospheric magnetic features by direct current dissipation. S.Hinata (Phys. Dept., Auburn Univ., Auburn, AL, USA).

Sol. Phys. (Netherlands), vol.87, no.1, p.95-101 (Aug. 1983).

It is shown that the direct current dissipation is very unlikely to be the heat source of the coronal loop, because it accompanies an unacceptably high heating rate in the chromospheric portion of the loop. This also suggests that a rather weak current density can supply the heat to small ($R < 10^7$ cm) chromospheric magnetic features. A larger magnetic element may be heated by the direct current dissipation only if the current changes direction within a single element so that the generated magnetic field is sufficiently weak to insure MHD stability. (13 refs.)

116605 Stability of two-dimensional pre-flare structures. K.Schindler, J.Birn, L.Janicke (Ruhr-Univ. Bochum, Bochum, Germany).

Sol. Phys. (Netherlands), vol.87, no.1, p.103-33 (Aug. 1983).

Several theoretical approaches to the problem of the onset of solar flares identify the point of onset as a 'critical' point, where the solution curve turns back. In other theories, a flare occurs at a conventional transition from stability to instability. The present paper provides stability results relevant for both

types of approaches. Restricting the discussion of two-dimensional configurations (e.g. models for two-ribbon flares), stability is discussed in the framework of ideal MHD, resistive MHD and Vlasov theory. Several rather general criteria for stability of the lower part of the solution curve ('minimal solutions') are derived. The results provide support to the concept of flare onset at a critical point. (28 refs.)

116606 On the mass motions and the atmospheric states of moustaches. R.Kitai (Dept. of Astron., Faculty of Sci., Univ. of Kyoto, Kyoto, Japan).

Sol. Phys. (Netherlands), vol.87, no.1, p.135-54 (Aug. 1983). Analyses of broad moustache profiles of Balmer lines and Ca II H and K lines are performed based on spectroscopic observations under good seeing conditions. H α emission profiles are found to consist of three components, i.e. a central absorption, a Gaussian core and a power-law wing. Each of them has a different Doppler shift. From the Doppler shifts, mass motions with velocity of about 6 km s⁻¹ are found to be present in chromospheric levels of moustache atmospheres. Computations of H α emission profiles from a variety of model atmospheres are compared with observed ones leading to the conclusion that a broad H α profile is due to a formation of heated ($\Delta T=1500$ K) and condensed ($\rho/\rho_0=5$) chromospheric layers. (21 refs.)

116607 The Ha-cyclonic spectra of a flare loop system on 1981 April 27. X.M.Gu, B.S.Li, Y.J.Ding, S.C.Li, Z.Li (Yunnan Obs., Acad. Sinica, Yunnan, China).

Sol. Phys. (Netherlands), vol.87, no.1, p.155-64 (Aug. 1983). H α -spectrum-spectroheliographic observations and H α -chromospheric observations of a flare-loop prominence which occurred on the western solar limb on 1981 April 27 have been obtained at Yunnan Observatory. The distribution of the internal and macroscopic motions of the flare loop prominence in time and space in the course of its eruption is derived. The instability of the loop is inferred and discussed. (12 refs.)

116608 Correlation of hard X-ray and type III bursts in solar flares. V.Petrosian, J.Leach (Inst. for Plasma Res., Stanford Univ., Stanford, CA, USA).

Sol. Phys. (Netherlands), vol.87, no.1, p.165-75 (Aug. 1983). The observed correlations between X-ray and type III radio emissions from solar bursts are described by means of a bivariate distribution function. Procedures for determining the form of this distribution are described using data analyzed by Kane (1981). With the help of this distribution a model is constructed to explain the correlation between the X-ray spectral index and the ratio of X-ray to radio intensities. Implications of the model are described. (7 refs.)

116609 A torsional wave model for solar radio pulsations. K.F.Tapping (Herzberg Inst. of Astrophys., Nat. Res. Council, Ottawa, Ontario, Canada).

Sol. Phys. (Netherlands), vol.87, no.1, p.177-86 (Aug. 1983). One of the widely accepted models for solar radio pulsations invokes radial oscillations of a magnetic flux tube. Due to acoustic, radiative damping, this theory does not easily explain the long length of the pulse trains, the large modulation depths or the great stability of the pulse repetition rate often observed. Torsional waves efficiently modulate synchrotron emission, and since they do not undergo radiative damping, can produce stable pulse repetition rates and long pulse trains. (15 refs.)

116610 Low- l 5-min oscillation observations. J.R.Kuhn, M.O'Hanlon (Phys. Dept., Princeton Univ., Princeton, NJ, USA).

Sol. Phys. (Netherlands), vol.87, no.2, p.207-19 (Sept. 1983). Medium resolution CCD-spectrograph observations have been obtained that are suitable for studying long spatial wavelength 5-min oscillations. Evidence is found that at wavelengths of the order of one solar radius the oscillation field is not isotropic. It is also not well described by modes of uniform excitation. The velocity power density per spherical harmonic increases with decreasing l to 1.1×10^3 cm² s⁻² per 3.5×10^{-4} Hz angular frequency bandwidth at $l=4$. These results are inconsistent with the data of Fossat and Ricort (1975), who found a substantially constant modal amplitude at intermediate l values. (20 refs.)

116611 Asymmetries in Stokes profiles of magnetic lines: a linear analysis in terms of velocity gradients. E.Landi Degl'innocenti, M.Landolfi (Astrophys. Obs. of Arcetri, Firenze, Italy).

Sol. Phys. (Netherlands), vol.87, no.2, p.221-31 (Sept. 1983). A linear analysis of the asymmetries in Stokes profiles of magnetic lines is performed. The asymmetries in the linear and circular polarization profiles are characterized by suitable quantities, δQ and δV , strictly related to the observed profiles. The response functions of δQ and δV to velocity fields are introduced and computed for various configurations of the magnetic field vector in a Milne-Eddington atmosphere. Some conclusions are drawn as to the importance of the asymmetries in the Stokes profiles for recovering the velocity gradients from observations. (14 refs.)

116612 Calculation of coronal line intensities for boron-like ions. H.P.Saha, E.Treffitz (Max-Planck-Inst. fur Phys. und Astrophys., Inst. fur Astrophys., Garching, Germany).

Sol. Phys. (Netherlands), vol.87, no.2, p.233-42 (Sept. 1983). New atomic data (Saha and Treffitz, 1982a) have been used to calculate line intensities of S XII for the physical conditions found in the solar corona. They are compared with similar calculations for Si X (Saha and Treffitz, 1982b) and with published work. For the density sensitive intensity ratio I_{227}/I_{1218} the new values give the observed ratio (Malinowski and Heroux, 1973) for an electron density of $\log N_e=8.5$ which is more likely than the density deduced from the values of Flower and Nussbaumer (1975), $\log N_e \leq 7$. (13 refs.)

116613 The characteristic size and brightness of facular points in the quiet photosphere. R.Muller, S.L.Keil (Air Force Geophys. Lab., Sacramento Peak Obs., Sunspot, NM, USA).

Sol. Phys. (Netherlands), vol.87, no.2, p.243-50 (Sept. 1983). Using two very high resolution, white-light plates of the solar granulation, the authors have measured a characteristic size and intensity for facular points. The plates were obtained with the 50 cm refractor at Pic-du-Midi Observatory using a 60 Å bandpass filter center at 5750 Å. After adjustment for atmospheric and instrumental smearing the authors find a characteristic size of 0.22 arc sec and a characteristic intensity of 1.3 to 1.5 times the mean continuum intensity. (9 refs.)

116614 Solar cycle dynamo wave origin of sunspot intensity and X-ray bright point number variation. H.Yoshimura (Dept. of Astron., Univ. of Tokyo, Tokyo, Japan).

Sol. Phys. (Netherlands), vol.87, no.2, p.251-9 (Sept. 1983). A new concept concerning sunspot cooling and X-ray bright point heating is presented. Sunspot and X-ray bright point small scale flux ropes are detached from global scale solar cycle main flux tubes created by the dynamo in the convection zone. The main flux tubes, and the associated roots of small scale ropes, gradually rise to the surface. When the roots are deep in the beginning and maximum phases of the solar cycle, the cooling mechanism works efficiently, sunspots look darker and the number of bright points is small. In the

ending and minimum phases when the roots are shallow, the number of phenomena take place. (31 refs.)

116615 Kinematics of solar prominences. J.L.Ballester (Dept. de Fisica de la Tierra y del Cosmos, Facultad de Ciencias, Univ. de Palma de Mallorca, Baleares, Spain), J.Kleckzek.

Sol. Phys. (Netherlands), vol.87, no.2, p.261-9 (Sept. 1983). Using a 16-mm film recorded by Dunn at Sacramento Peak Observatory with a 15-inch coronagraph, the authors have studied motions of three solar prominences from the kinematic point of view. Three methods proposed earlier (Billings and Pecker, 1954; Palus, 1972; Makhmudov et al., 1980) are applied to three prominences. A new method based on geometrical considerations is introduced. The results of all the four methods are compared and discussed. (19 refs.)

116616 Transient brightenings of interconnecting loops. III. Interpretation. D.S.Spicer (Inst. for Astron., ETH-Center, Zurich, Switzerland), Z.Svestka.

Sol. Phys. (Netherlands), vol.87, no.2, p.271-8 (Sept. 1983). For pt.II see ibid., vol.71, no.2, p.349-59 (1981). The authors present two alternative interpretations of the sudden X-ray brightenings observed in loops that interconnect active regions. They argue that a fast tearing mode may be the cause of brightenings in the young newly formed interconnecting loops, whereas anomalous Joule heating might occur in old loop connections when an external disturbance propagates through them. (13 refs.)

116617 Magnetic stability of coronal arcades relevant to two-ribbon flares. A.W.Hood (Dept. of Math., Napier Coll., Edinburgh, Scotland).

Sol. Phys. (Netherlands), vol.87, no.2, p.279-99 (Sept. 1983). The dense photosphere provides an extremely efficient mechanism, called line-tying, for stabilising coronal magnetic fields. The author studies the ideal MHD stability of cylindrically symmetric arcades, the field structure thought to be present prior to the onset of a large two-ribbon flare. It is found that, when the axis of symmetry lies on the photosphere, a wide range of force-free fields are completely stable to all possible perturbations. Instability will occur if the symmetry axis, assumed to coincide with an active-region filament is too high above the photosphere to benefit from its stabilising influence. (28 refs.)

116618 Magnetic equilibrium in coronal arcades. J.P.Melville, A.W.Hood (Dept. of Math., Napier Coll., Edinburgh, Scotland), E.R.Priest.

Sol. Phys. (Netherlands), vol.87, no.2, p.301-7 (Sept. 1983). An analytical solution to the magnetohydrostatic equations is presented that generalises a solution due to Birn et al. (1978) to include the effect of gravity. There exists two solutions to the same boundary conditions for small base pressures. If the base pressure exceeds a critical value, then 'non-equilibrium' may occur and initiate a two-ribbon flare. (9 refs.)

116619 The emerging magnetic flux and the elementary eruptive phenomenon. Z.Mouradian, M.J.Martres, I.Soru-Escout (Obs. de Paris, Meudon, France).

Sol. Phys. (Netherlands), vol.87, no.2, p.309-28 (Sept. 1983). Observational studies before and during the beginning of the flare were made in H α on a large sample of 'elementary' flares, both on the disk and along the limb of the Sun. The concept of elementary eruptive phenomenon (EEP) is proposed to describe these observational data. The EEP may be considered as the basic element of complex flares. In the inferred scenario, the chromospheric eruptive phenomenon consists of two systems of loops: one cold, the surging arch, $T \approx 10^4$ K; the other hot, the flaring arch, covering a temperature range up to 10^6 K. (44 refs.)

116620 White-light radiation from semi-empirical flare models. L.Dame (Lab. de Phys. Stellaire et Planetaire, Verrieres-le-Buisson, France), L.Cram.

Sol. Phys. (Netherlands), vol.87, no.2, p.329-35 (Sept. 1983). It is shown that some semi-empirical models for solar flares predict a significant flux of visible continuum radiation, due to bound-free radiation from hydrogen atoms and H⁺ ions in the chromospheric flare. The ratio of the emergent intensity in one flare model to that in the quiet Sun is more than 100% at the head of the Balmer continuum for a large flare close to the limb, and 8% at disk centre. The predicted flare spectrum has a relatively strong Balmer jump. The authors compare the theoretical flare continuum with observations and find disagreements in several important respects. (6 refs.)

116621 On the storage of high-energy protons in the solar corona: the cyclotron instability. B.I.Meerson, I.V.Rogachevskii (Inst. of Appl. Geophys., State Committee for Hydrometeorology & Control of the Natural Environment, Moscow, USSR).

Sol. Phys. (Netherlands), vol.87, no.2, p.337-57 (Sept. 1983). The authors consider the problem of long-time storage of high-energy protons, accelerated in the process of a flare, in coronal magnetic traps. From the viewpoint of storage, one of the most important plasma instabilities is the kinetic cyclotron instability of Alfvén waves. The instability is analysed for typical conditions of the solar corona. It is the refraction of Alfvén waves in combination with a drastic decrease of the instability growth rate with an increase of the angle between the wave vector and the stationary magnetic field that leads to the possibility of the long-term storage of flare protons. (19 refs.)

116622 Frequency splitting in stria bursts: possible roles of low-frequency waves. D.B.Melrose (School of Phys., Univ. of Sydney, Sydney, NSW, Australia).

Sol. Phys. (Netherlands), vol.87, no.2, p.359-71 (Sept. 1983). The kinematics of the process $L \pm F \rightarrow L'$ are explored where L represents a parallel Langmuir wave, F represents a low frequency fluctuation and L' represents a secondary Langmuir wave, and the results are used to discuss a possible interpretation of the frequency splitting in stria bursts in terms of the processes $L \pm F \rightarrow L'$, $L' \pm F \rightarrow L$, where l represents a transverse wave, and second harmonic emission due to the processes $L \pm s \rightarrow L'$, $L' \pm s \rightarrow L$, where s represents an ion sound wave. (27 refs.)

116623 Source characteristics of main and post-burst-increase phases of solar bursts at 17 GHz. T.Kosugi, K.Kai, T.Suzuki (Tokyo Astronomical Obs., Tokyo, Japan).

Sol. Phys. (Netherlands), vol.87, no.2, p.373-90 (Sept. 1983). Twenty four solar bursts of peak fluxes above 50 sfu were observed with the 17 GHz interferometer at Nobeyama during the period from 1978 September to 1979 December. The source characteristics and their temporal evolutions are investigated on a statistical basis with high time resolutions up to 0.8 s. A model-fitting technique recently developed by Kosugi (1982) is used to derive both the centroid position and the size (\sim FWHM) of the burst source with an uncertainty of a few arc secs. (24 refs.)

116624 Observations on the slowly varying component of solar radio emission at decameter wavelengths. C.V.Sastry, R.K.Shevgaonkar, M.N.Ramanuja (Indian Inst. of Astrophys., Bangalore, India).

Sol. Phys. (Netherlands), vol.87, no.2, p.391-9 (Sept. 1983). The authors have made two-dimensional maps of the slowly varying component (SVC) of solar radio emission at a frequency of 34.5 MHz with a half

power beam width of 26' and 40'. It is found that a majority of SVC sources have brightness temperatures of the order of $0.5 \times 10^6 \text{ K}$ and half power widths of about $4 R_{\odot}$. The shifts in the positions of the centroids of the SVC sources from the center of the Sun were in the range of 1.5 to $2 R_{\odot}$. These observations can be explained in terms of thermal emission from coronal regions of the enhanced density and temperature. (8 refs.)

116625 The relationships between disappearing solar filaments, coronal mass ejections, and geomagnetic activity. C.S.Wright, L.F.McNamara (Ionospheric Prediction Service, Darlinghurst, NSW, Australia). *Sol. Phys. (Netherlands)*, vol.87, no.2, p.401-17 (Sept. 1983). The relationships between disappearing solar filaments and geomagnetic activity are examined using data obtained between 1974 and 1980. The average level of geomagnetic activity is found to increase after the disappearance of large filaments. The magnitudes of the geomagnetic disturbances depend upon the sizes and, to a lesser extent, upon the darkness of the filaments. The delays between filament disappearances and resulting geomagnetic disturbances are typically 3-6 days, corresponding to Sun-Earth velocities of $580\text{--}290 \text{ km s}^{-1}$. These are consistent with the observed velocities of those coronal mass ejections that are associated with disappearing filaments. (50 refs.)

116626 Static equilibrium of horizontal ring prominence. Wang Zhengzhi, Lin Yuanzhang (Beijing Obs., Acad. Sinica, Beijing, China), Hu Wenrui. *Sci. Sin. (China)*, vol.26, no.7, p.739-52 (July 1983). In 1980 the Beijing Observatory successively observed several rare completely closed ring prominences whose ring plane was approximately parallel to the solar surface with a characteristic life about 1-2 days. The authors discuss the static equilibrium of this kind of horizontal ring plasma under the simultaneous actions of magnetic force, gravity and pressure gradients. Assuming a ring plasma with axisymmetry and rectangular plasma cross-section, and adopting a closed magnetic field boundary condition from the basic equations they obtain the exact zero order general solutions for the magnetic field (force-free field) and density (pressure). They further obtain an eigensolution for the zero order magnetic field and density as well as the first order magnetic field, thus giving a possible distribution of magnetic field and density for the horizontal closed ring prominence. (7 refs.)

Nonlinear periodic solutions for the isothermal magnetostatic atmosphere See Entry 116361

An analysis of noctiluculent cloud over western Europe during the period 1966 to 1982 See Entry 116243

Implications of high-energy neutron observations from solar flares See Entry 116414

Magnesium II line formation: the contribution of high atomic levels to the resonance lines See Entry 116442

Propagation of Alfvén waves in an isothermal atmosphere when the displacement current is not neglected See Entry 116443

A second-order correlation approximation for thermal conductivity and Prandtl number of free turbulence See Entry 116461

Reynolds stresses and differential rotation. III. Zonal momentum fluxes in rapidly rotating stars See Entry 116466

Ca XVII line ratios in solar flares See Entry 116468

96.90 OTHER TOPICS ON THE SOLAR SYSTEM

116627 The pulsar P/P distribution and the postulated solar companion. S.A.Cowling (Dept. of Appl. Maths. & Astron., Univ. Coll., Cardiff, Wales). *Mon. Not. R. Astron. Soc. (GB)*, vol.204, no.3, p.1237-44 (Sept. 1983). Evidence for the existence of a companion object in a closed or open orbit about the Sun is reviewed. It is shown that such an object, postulated by Harrison (1977) in order to explain anomalies in the period derivatives of certain pulsars, would have a high probability of being detected, by the gravitational deflection of light, using the ESA Astrometry Satellite Hipparcos. An analysis of up-to-date pulsar statistics does not appear to support the existence of a companion. An upper limit of $\sim 10^{-8} \text{ ms}^{-2}$ is placed on any Solar System acceleration. (13 refs.)

97.00 STARS

97.10 STELLAR CHARACTERISTICS

116628 Self-regulated star formation in the Galaxy. J.Franco, D.P.Cox (Dept. of Phys., Univ. of Wisconsin, Madison, WI, USA). *Astrophys. J. (USA)*, vol.273, no.1, pt.1, p.243-8 (1 Oct. 1983). The stellar birthrate is obtained under the assumption that the regions of star formation are supported against gravity by winds from low-mass young objects. For winds interacting in the momentum conservation stage, it is found that the rate is correlated with the molecular gas density of the parent fragment as $n^{13/8}$ or $n^{5/8}$, for rates per unit volume or per unit mass, respectively. In particular, the birthrates derived from protostellar rotationally driven winds are in good agreement with the observed star production in the cloud B18. With the aid of the observed properties of the Taurus-Auriga complex, the model is extrapolated to the Galaxy as a whole. (34 refs.)

116629 The formation of emission lines in the expanding chromospheres of luminous cool stars. I. The importance of atmospheric extension and partial redistribution effects. S.A.Drake, J.L.Linsky (Joint Inst. for Lab. Astrophys., Univ. of Colorado, Boulder, CO, USA). *Astrophys. J. (USA)*, vol.273, no.1, pt.1, p.299-308 (1 Oct. 1983). Most late-type luminous stars are losing mass in cool stellar winds. In many red giants the only evidence for mass loss is the presence of a characteristic asymmetry in the strongest ultraviolet resonance lines, such as the Mg II k line. The available methods for treating radiative transfer in such chromospheric lines in an expanding, extended medium are discussed, and the comoving frame method (including partial redistribution) is selected as the most suitable. This technique is outlined in the context of a two-level atom. The difference in the computed line profiles between assuming partial and complete redistribution is illustrated for a wide range of atmospheric and wind parameters. (55 refs.)

116630 Temperature-grid coordinates for treating pulsations in the hydrogen ionization zone. T.Aikawa, N.R.Simon (Dept. of Phys. & Astron., Univ. of Nebraska, Lincoln, NE, USA). *Astrophys. J. (USA)*, vol.273, no.1, pt.1, p.346-54 (1 Oct. 1983). A temperature grid is used for the description of motion in the hydrogen ionization region (HIR). This means zones are labeled by temperature rather than mass. Outside the HIR, the conventional Lagrangian grid is used, with

transitional coordinates at the boundaries. Although the final object is to apply this scheme to the nonlinear periodic integration problem, the authors have first constructed a linear version as a test. It is found that periods and growth rates agree very well with those calculated using pure Lagrangian coordinates, but the temperature grid scheme proves less sensitive to a reduction of zones in the HIR. (16 refs.)

116631 Effect of excited states on thermonuclear reaction rates. D.G.Sargood (School of Phys., Univ. of Melbourne, Parkville, Victoria, Australia). *Aust. J. Phys. (Australia)*, vol.36, no.4, p.583-9 (1983).

Values of the ratio of the thermonuclear reaction rate of a reaction, with target nuclei in a thermal distribution of energy states, to the reaction rate with all target nuclei in their ground states are tabulated for neutron, proton and α -particle induced reactions on the naturally occurring nuclei from ^{20}Ne to ^{70}Zn , at temperatures of 1, 2, 3.5 and $5 \times 10^9 \text{ K}$. The ratios are determined from reaction rates based on statistical model cross sections. (15 refs.)

116632 Objective-prism discoveries in the northern sky. I. W.P.Bidelman (Warner & Swasey Obs., Case Western Reserve Univ., Cleveland, OH, USA).

Astron. J. (USA), vol.88, no.8, p.1182-6 (Aug. 1983). Lists 175 newly recognized peculiar or otherwise interesting northern-hemisphere stars noted in a preliminary inspection of moderate-dispersion objective-prism plates obtained with the new 10° prism of the Burrell Schmidt, located at the Warner and Swasey Observatory's Kitt Peak Station. (10 refs.)

116633 Observationally-based infrared efficiencies and Planck means for circumstellar dust grains. T.Henning, J.Gurtler, J.Dorschner (Univ. Sternwarte Jena, Jena, Germany).

Astrophys. & Space Sci. (Netherlands), vol.94, no.2, p.333-49 (Aug. 1983). The mean relative efficiency factors for absorption of dust grains in the wavelength range from 8 to $22 \mu\text{m}$ are derived from IR spectra of the optically thin dust shells surrounding the O-rich supergiants $\mu \text{ Cep}$, $\alpha \text{ Ori}$, X Her and R Cas. The resulting absorption efficiency curve is extrapolated into the near as well as the far infrared regions. Planck mean efficiency factors are calculated for the temperature range 30 to 1500 K . (37 refs.)

116634 Adiabatic radial pulsations of a composite stellar model. M.Singh, S.R.Agarwal (Dept. of Math., Univ. of Roorkee, Roorkee, India).

Astrophys. & Space Sci. (Netherlands), vol.94, no.2, p.351-9 (Aug. 1983). Small adiabatic radial oscillations of composite models are investigated. The effect of a central condensation $\rho_c/\bar{\rho}$ on the period of pulsation is also examined. It is shown that the second moment of the mass concentration characterizes the periods of pulsations more effectively than the central condensation. (13 refs.)

116635 The equations that govern rotational and tidal perturbations of stellar oscillations. P.Smeyers, L.Martens (Astron. Inst., Katholieke Univ. Leuven, Leuven, Belgium).

Astron. & Astrophys. (Germany), vol.125, no.2, pt.1, p.193-9 (Sept. 1983). Uses a perturbation method to determine linear oscillations in a uniformly rotating star and in a uniformly and synchronously rotating component of a binary system accurate to the second order in the slow angular velocity. In this approximation, one has to deal with a surface perturbation due to the distortion of the star's equilibrium configuration. It is noted that the procedures applied by Simon (1969) for pseudo-radial oscillations and by Smeyers and Denis (1971) for non-radial oscillations allow the distortion of the star's equilibrium surface to be taken into account both by an appropriate transformation of the operator in the vector wave equation and by a parallel transport of the Lagrangian displacement from each point to an associated neighbouring point in a spherical domain. The emphasis is placed on the parallel transport since this part of the procedure has been omitted in the recent investigations of Saio (1981, 1982). The correct equations are established. (17 refs.)

116636 Phase transitions in stellar cores. I. Equilibrium configurations. R.Schaeffer (Service de Phys. Theorique, CENS, Gif-sur-Yvette, France), P.Haensel, L.Zdunik.

Astron. & Astrophys. (Germany), vol.126, no.1, pt.2, p.121-45 (Sept. 1983). The effect of a first order phase transition occurring in the central core of a degenerate star is studied within the Newtonian theory of gravitation. The changes of parameters such as the radius (δR), the moment of inertia (δI) or the energy (δE) during the transition from a one-phase to a two-space star are expressed by means of analytical formulae that are valid for any equation of state. They turn out to be accurate even for moderately large changes of the stellar parameters, typically a sizeable fraction of their initial value. In the limit where the radius r_s of the condensed core made out of the new phase is small, scaling laws ($\delta R, \delta I \sim r_s^3, \delta E \sim r_s^5$) are derived. The stability of the two-phase stars with respect to small radial perturbations is studied, and the properties of polytropic condensed cores are investigated. (17 refs.)

116637 The disk-star boundary layer and its effect on the accretion disk structure. O.Regev (Dept. of Phys., Technion-Israel Inst. of Technol., Haifa, Israel).

Astron. & Astrophys. (Germany), vol.126, no.1, pt.2, p.146-51 (Sept. 1983). The method of matched asymptotic expansions is proposed for a self-consistent calculation of an accretion disk and the disk-accreting star boundary layer. A model of a thin, optically thick, region (c) accretion disk and boundary layer is calculated with the help of the method. The disk in this model is hotter and denser than in the corresponding Shakura and Sunyaev (1973) model. The significance of the model is discussed and the method is proposed for other cases of interest. (10 refs.)

116638 Far ultraviolet colors of B and Be stars. J.Zorec (Inst. d'Astrophys., Paris, France), D.Briot, L.Divan.

Astron. & Astrophys. (Germany), vol.126, no.1, pt.2, p.192-204 (Sept. 1983). A G index, free of interstellar reddening and characterizing the ultraviolet color of the star, is defined by using observations of B and Be stars with the TD-1 satellite. For each luminosity class of normal B stars, a mean sequence of G index, against the spectral type, is obtained. Most of the Be stars show ultraviolet color indices less negative than those of normal B stars but sometimes such color indices are more negative. Be stars are divided into two categories according to the strength of the emission features: the strong Be stars and the weak Be stars. Characteristics of each are discussed. (59 refs.)

116639 Semiconvective diffusion and energy transport. N.Langer, D.Sugimoto, K.J.Fricke (Univ.-Sternwarte Gottingen, Gottingen, Germany).

Astron. & Astrophys. (Germany), vol.126, no.1, pt.2, p.207-8 (Sept. 1983). On the basis of the theories of radiation-driven overstability and non-radial oscillations, an expression is proposed with which semiconvective mixing in stellar interiors may be handled. Deviations from the Schwarzschild as well as from the Ledoux criterion and mixing of chemical elements can then be treated time-dependently by means of a diffusion equation. (9 refs.)

- 116640 Broadband linear polarization from magnetized stellar atmospheres. II. The influence of damping on net spectral line polarization.** G.Calamai, E.Landi Degl'Innocenti (Astrophys. Obs. of Arcetri, Firenze, Italy). *Astron. & Astrophys. Suppl. Ser. (France)*, vol.53, no.3, p.311-18 (Sept. 1983).
For pt.1 see ibid., vol.49, no.4, p.677-85 (1982). The influence of broadening by damping on broadband linear polarization expected from a stellar atmosphere through the mechanism of magnetic intensification is investigated. Numerical tables are presented. (3 refs.)
- 116641 Narrow-band photometry of G and K stars near the North Galactic Pole.** L.Hansen, G.A.Radford (Copenhagen Univ. Obs., Copenhagen, Denmark). *Astron. & Astrophys. Suppl. Ser. (France)*, vol.53, no.3, p.427-31 (Sept. 1983).
Narrow-band photometry of 292 late type stars within 15° of the North Galactic Pole has been obtained in the Copenhagen g, n, k, m, f -system. For most of the stars estimates of the following quantities have been derived: V -magnitude, $R-I$ colour, metal abundance, M_V and a duplicity parameter $res(k)$. (12 refs.)
- 116642 Radial velocities for early type stars in six galactic regions.** N.Zentis (Stockholm Obs., Saltsjobaden, Sweden). *Astron. & Astrophys. Suppl. Ser. (France)*, vol.53, no.3, p.445-53 (Sept. 1983).
Coude spectroscopy has been carried out for 353 stars of spectral types B0-A0 and V magnitudes between 6.5^m and 10.8^m , selected in six regions (three northern and three southern) close to the galactic plane at the galactic longitudes 135° , 175° , 315° and 350° . The radial velocities were obtained by cross-correlating each spectrogram with a reference spectrogram giving an internal error of 1.4 km/s. (6 refs.)
- 116643 Vibrating-dust spheres in the Reissner-Nordstrom metric.** F.de Felice (Internat. School for Advanced Studies, SISSA, Trieste, Italy), Yu Yunqiang. *Nuovo Cimento B (Italy)*, vol.76B, ser.2, no.1, p.28-34 (11 July 1983).
The authors consider the collapse of a charged dust sphere with a charge Q larger than the mass M (both in geometrized units). They show that the outcome of collapse is most likely a stable, vibrating configuration. The period of the vibrations is of the order of 10^{-4} s for masses of the order of a solar mass. Optically such an object shows a quasi-steady red-shift which can be very large when Q is close to M . (3 refs.)
- 116644 Stellar collapse without singularities?.** T.A.Roman (Dept. of Phys., Syracuse Univ., Syracuse, NY, USA), P.G.Bergman. *Phys. Rev. D (USA)*, vol.28, no.6, p.1265-77 (15 Sept. 1983).
For the singularity theorems of Hawking and Penrose to hold, the stress-energy tensor of matter must satisfy certain restrictions. A model is developed representing the interior of a collapsing, spherically symmetric cloud of matter, which is everywhere free of singularities, due to a relaxation of the so-called 'weak energy condition'. The regions of the model in which the condition must be violated, and the properties of matter and energy which result, are determined. The indications are that, at least in spherically symmetric cases involving very large masses, the energy condition must be violated in a region where the density is no larger than normal matter densities, which seems physically implausible. Hence suspending the energy conditions may not be a reasonable approach to the avoidance of singularities. (17 refs.)
- 116645 Matter transfer by MHD waves in stellar atmospheres.** E.A.Rudenchik. *Pis'ma v Astron. Zh. (USSR)*, vol.9, no.8, p.504-7 (1983). In Russian. English translation in: *Sov. Astron. Lett. (USA)*
It is shown, that fast MHD waves can transfer significant amounts of matter together with the frozen magnetic field through a stratified atmosphere. For a wave propagating through an atmosphere with a strong horizontal magnetic field an increase is found in the acoustic flow. (4 refs.)
- 116646 On influence of the magnitude equation in proper motions of stars on the determination of some astronomical constants.** V.V.Vityazev. *Vestn. Leningr. Univ. Ser. Mat. Mekh. & Astron. (USSR)*, no.3, p.75-81 (July 1983). In Russian.
Provided that the systematic errors in the proper motions are represented by means of spherical functions analytical expressions showing the influence of different harmonics on the determination of the solar motion, galactic rotation and precession corrections are derived. These results are generalized to consider the dependence of systematic errors on the magnitude equation. It is shown that the discovered magnitude equation for the proper motions of FK4 stars has only a small influence on the results for galactic rotation and precession determination. (8 refs.)
- The characteristics of salt fingers in a variety of fluid systems, including stellar interiors, liquid metals, oceans, and magmas See Entry 114232
- A faint star astrometric grid for the galactic center See Entry 116428
- Ambipolar diffusion in self-gravitating isothermal layers See Entry 116437
- Magnesium II line formation: the contribution of high atomic levels to the resonance lines See Entry 116442
- Determination of stellar neutron-capture rates for radioactive nuclei with the aid of β -delayed neutron emission See Entry 116445
- A second-order correlation approximation for thermal conductivity and Prandtl number of free turbulence See Entry 116461
- A simple kinetic model of a multi-particle cloud See Entry 116463
- Reynolds stresses and differential rotation. III. Zonal momentum fluxes in rapidly rotating stars See Entry 116466
- The evolution of viscous discs. IV. Stream penetration effects See Entry 116469
- High precision spectropolarimetry of stars and planets. I. The ROE spectropolarimeter See Entry 116484
- Parametric detector as a tunable antenna for continuous gravitational radiation See Entry 116485
- Second catalogue of $H\alpha$ line profiles in 55 Be star spectra See Entry 116491
- A photoelectric UBV catalogue of 610 stars in Puppis See Entry 116495
- Calculation of stellar structure. III. Solar models that satisfy the necessary conditions for a unique solution to the stellar structure equations See Entry 116561
- The pulsar P/\dot{P} distribution and the postulated solar companion See Entry 116627
- The extreme LMC supergiant HD 38489: an optical and ultraviolet study See Entry 116647
- Collapse and explosion of white dwarfs. I. Precollapse evolution See Entry 116648

- The reddening, metal abundance, and luminosity of high-luminosity G-type stars See Entry 116649
- On the T Tauri nature of the variable star BM Cha See Entry 116650
- The temperature of central stars of planetary nebulae: the energy-balance method See Entry 116651
- The detection limits in ground based measurements of stellar microvariability See Entry 116652
- Recent photometry of the central star of NGC 2346 See Entry 116653
- Visible and UV observations of the giant early-type members of the Large Magellanic Cloud See Entry 116654
- Far ultraviolet observations of Population II See Entry 116655
- Some aspects of the velocity fields in early-type stars See Entry 116656
- Late type stars [IUE observations] See Entry 116657
- The disc-like envelopes around young stars seen in the maser lines See Entry 116658
- Cessation of the 63 second periodicity in the light curve of V533 Herculis See Entry 116659
- The outbursts of symbiotic novae See Entry 116660
- Mixing by shear instabilities in differentially rotating inhomogeneous stars with application to accreting white dwarf models for novae See Entry 116661
- PI Gruis: molecular identifications and spectral classification See Entry 116662
- Star-planet systems as progenitors of cataclysmic binaries: tidal effects See Entry 116663
- Superoutbursts: a general phenomenon in dwarf novae See Entry 116664
- The dust envelope of the Herbig Ae star, AB Aur See Entry 116665
- The ultraviolet variability of the symbiotic star HBV 475 See Entry 116666
- Photometric search for Ap-stars in open clusters. IV. NGC 2287, Cr 121, NGC 2422 and supplementary measurements in NGC 1662 and NGC 2516 See Entry 116667
- The runaway Wolf-Rayet star HD 143414: evidence for a low-mass companion See Entry 116668
- Far ultraviolet colors of β Cephei stars See Entry 116669
- Study of the variability of the delta Scuti stars. VI. Pulsational behaviour of HR 1392 (69 Tau) See Entry 116670
- Study of the variability of the delta Scuti stars. VII. The problem of stability and monopiodicity in 20 CVn See Entry 116671
- Absolute measurements of flux in the continuum of galactic Wolf-Rayet stars: comparison with main-sequence OB stars See Entry 116672
- HR 981—a new USPC See Entry 116673
- On the pulsation of HD 201601 See Entry 116674
- B and V photometry of the southern RS CVn candidate HD 196818 See Entry 116675
- On some remarkable pulsation properties of the high-latitude F-type supergiants See Entry 116676
- Optical behavior of EZ Pegasi See Entry 116677
- HR 5=ADS 61: a new variable star See Entry 116678
- Photometry of FK Comae See Entry 116679
- On delta Scuti stars in open clusters See Entry 116680
- Search for ultra short period variations in Epsilon Octantis See Entry 116681
- Magnetometric measurements of the carbon star Y CVn See Entry 116682
- V436 Cen revisited See Entry 116683
- PU Vulpeculae See Entry 116684
- R Coronae Borealis See Entry 116685
- U Aquarii See Entry 116686
- GK Persei See Entry 116687
- Novalike variable in Libra See Entry 116688
- Possible novae See Entry 116689
- Possible optical burster See Entry 116690
- Molecules in celestial objects. IV. IUE observation of CO lines towards Be stars with low reddening See Entry 116691
- An infrared study of the eclipsing dwarf nova U Geminorum See Entry 116692
- On the secular variation of amplitudes in double-mode Cepheids See Entry 116693
- The discovery of 13.72-min oscillations in the cool magnetic Ap star HD 217522 See Entry 116694
- Frequency analysis of the rapidly oscillating Ap star HR 1217 (HD 24712) See Entry 116695
- Simultaneous infrared and optical photometry of cataclysmic variables See Entry 116696
- Solar-like activity phenomena in stars See Entry 116699
- Chemically peculiar stars [IUE observations] See Entry 116700
- Infrared photometry of HD 101065 See Entry 116701
- On the correlation between $H\alpha$ line intensity and SiO maser emission of the long-period variable χ Cygni See Entry 116702
- Variation of the profile of $H\alpha$ line in the spectrum of DH Pegasi See Entry 116704
- Optical variability of PU Vulpeculae (nova-like Kuwano's object 1979) in 1982 See Entry 116705
- Neutrino emission from a hot, dense, plane-parallel atmosphere in hydrostatic equilibrium. III. The three-flavored atmosphere See Entry 116706
- Do filaments form at the time of supernova explosions? See Entry 116707
- Softening effects in the equation of state and influence of general relativity on the outcome of stellar collapse See Entry 116708
- BV photometry of the supernova 1982 in NGC 2268 See Entry 116709
- Supernova in faint spiral galaxy See Entry 116710
- Possible supernova in NGC 7418 See Entry 116711
- Similarity solutions for explosions in radiating stars with time-dependent energy and idealized magnetic field See Entry 116713
- On the two possible progenitors of type I super nova See Entry 116714
- Infrared study of the Crab pulsar: the 'shoulder' pulse and the 3.45 micron pulse profile See Entry 116715

General track of pulsar evolution	See Entry 116716
Discovery of a millisecond pulsar	See Entry 116719
Properties of the Crab pulsar inferred from the phase-averaged spectrum	See Entry 116721
COS-B upper limits on gamma-ray emission from radio pulsars	See Entry 116722
Pair production near threshold in pulsar magnetic fields	See Entry 116725
Polarization mode coupling in radio pulsars	See Entry 116726
Pulsar gamma-ray lines from quarkonium systems	See Entry 116727
The pulsar oblique rotator: numerical solution of an illustrative problem	See Entry 116728
Pulsar electrodynamics: cylindrical model and radio and gamma-ray radiation	See Entry 116729
The evolution of radio pulsars	See Entry 116730
Gravitational radiation reaction in the binary pulsar and the quadrupole-formula controversy	See Entry 116731
Phase transitions in dense stars	See Entry 116732
Radio emission from AM Herculis: the quiescent component and an outburst	See Entry 116740
The F-type eclipsing binaries ZZ Bootis, CW Eridani, and BK Pegasi	See Entry 116741
SS Bootis: a totally eclipsing binary of the RS CVn type	See Entry 116742
The effect of low-velocity, low-mass intruders (collisionless gas) on the dynamical evolution of a binary system	See Entry 116743
The multiple system β Sco and the age of the Upper Scorpius complex	See Entry 116744
Mass transfer in close binary systems: original and remnant masses	See Entry 116745
The possible long-period eclipsing binary BM Eri	See Entry 116746
Ultra high energy gamma rays from Cygnus X-3	See Entry 116747
Photometric observations. Is HZ Herculis getting darker?	See Entry 116748
Photometric observations and elements of the eclipsing binary TT Herculis	See Entry 116749
The BUSS spectrum of β Lyrae	See Entry 116750
The light curve changes of VW Cephei	See Entry 116751
A study of ultraviolet spectra of ζ Aur/VV Cep systems. III. Atlas of theoretical curves of growth	See Entry 116752
Infrared photometry of the RS CVn binaries. III. JHK light curves of UV Psc	See Entry 116753
A photometric study of the eclipsing binary V478 Cygni	See Entry 116754
Photoelectric minima of eclipsing binaries	See Entry 116756
Eclipse timings of 31 Cygni	See Entry 116757
Spectroscopic observations of the cool eclipsing X-ray binary HD 155638	See Entry 116758
A 0538-66	See Entry 116759
HZ Her: the nature and origin of the emission lines	See Entry 116760
A model for A 0538-66: the fast flaring pulsar	See Entry 116761
Analytic treatment of polarization by arbitrary scattering mechanisms in circumstellar envelopes. II. Binary stars	See Entry 116762
Ultraviolet observations of binary X-ray sources	See Entry 116763
Magnetic focusing in the Sco X-1 radio source	See Entry 116764
The chemical composition of distant globular clusters: are there any metal-poor clusters?	See Entry 116765
On the intrinsic width and luminosity function of the M92 main sequence	See Entry 116766
On the age of M92 and M15	See Entry 116767
The globular cluster NGC 6638	See Entry 116768
The WN4.5 component of HD 219460 in the open cluster Markarian 50	See Entry 116769
VBLUW photometry of the open cluster NGC 2516	See Entry 116774
The chemical composition of stars in globular clusters	See Entry 116775
Far-infrared and CO observations of Cep F: implications for star formation in Cepheus OB3	See Entry 116782
Diffuse light near zeta Orionis and the Horsehead nebula, and anomalous extinction of HD 37903, as measured with the ANS	See Entry 116786
Infrared objects near H ₂ O masers in regions of active star formation. III. Evolutionary phases deduced from IR recombination line and other data	See Entry 116789
CS J=5-4 observations of galactic molecular clouds	See Entry 116797
IUE observations of stars in the M8 nebula	See Entry 116798
Optical polarization in the bipolar nebula associated with LkH α 208	See Entry 116799
Hydrodynamic models of Herbig-Haro objects	See Entry 116800
3 μ m spectroscopy of IRS 7 towards the Galactic Centre	See Entry 116802
Ring nebulae associated with WR stars: stellar wind or stellar ejecta?	See Entry 116807
A survey of H α emission in normal galaxies	See Entry 116812
On the distance to M33 determined from magnitude corrections to Hubble's original Cepheid photometry	See Entry 116813
Chemical evolution of the galactic halo. II. Enrichment in primary elements	See Entry 116816
Positrons from supernovae and the origin of the galactic center positron annihilation radiation	See Entry 116831
Positron production by a hot, young pulsar	See Entry 116833
Luminous molecular hydrogen emission in the galaxy system NGC 3690-IC 694	See Entry 116843
High-resolution images of the galactic centre	See Entry 116849
Central distribution of the near-infrared colours in two early-type spirals	See Entry 116852
Slippery evidence on the Galaxy's invisible heavy halo	See Entry 116854
An optical test for the distance of gamma-ray burst sources	See Entry 116873
Gamma ray bursts	See Entry 116875

Theories of gamma-ray bursts	See Entry 116879
A fireball model for the March 25, 1978 gamma ray burst ..	See Entry 116881

97.20 NORMAL STARS (BY CLASS): GENERAL OR INDIVIDUAL

- 116647 The extreme LMC supergiant HD 38489: an optical and ultraviolet study.** S.N.Shore, N.Sanduleak (Warner & Swasey Obs., Dept. of Astron., Case Western Reserve Univ., Cleveland, OH, USA). *Astrophys. J. (USA)*, vol.273, no.1, pt.1, p.177-86 (1 Oct. 1983). This investigation combines near-infrared, optical, and ultraviolet observations covering λ 1200-7000 to study the extremely luminous B star HD 38489=S134. The star is found to be an evolved B star with $T_{\text{eff}} \approx 25000\text{K}$, $M \sim 80\text{-}90 M_{\odot}$, and $R \sim 70 R_{\odot}$. Estimates of mass loss suggest $\dot{M} \approx 10^{-5} M_{\odot} \text{ yr}^{-1}$, comparable to galactic stars. Similarity is shown to stars of the Hubble-Sandage class and to several transition-type stars. A nitrogen enhancement of a factor of 6-20 is suggested, and model envelope derived. (52 refs.)
- 116648 Collapse and explosion of white dwarfs. I. Precollapse evolution.** J.Isern, J.Labay, M.Hernanz, R.Canal (Dept. de Física de la Tierra y del Cosmos, Univ. de Barcelona, Barcelona, Spain). *Astrophys. J. (USA)*, vol.273, no.1, pt.1, p.320-9 (1 Oct. 1983). The long-term evolution of accreting carbon-oxygen white dwarfs in close binary systems is considered. Depending on the time of onset of mass accretion, thermonuclear ignition happens when the star's center is either in the fluid or in the solid phase. In the last case, burning propagation should be slow, and previous carbon-oxygen separation is likely. It is shown that by considering different degrees of chemical separation (associated with different cooling times) diverse outcomes are possible: total collapse for maximum separation and off-center ignitions for partial chemical differentiation. The off-center ignitions might provide a mechanism for Type I supernova outbursts. (68 refs.)
- 116649 The reddening, metal abundance, and luminosity of high-luminosity G-type stars.** O.J.Eggen (Cerro Tololo Inter-American Obs., La Serena, Chile). *Astron. J. (USA)*, vol.88, no.8, p.1187-98 (Aug. 1983). Photometry of some 100 G-type bright giants and supergiants is discussed. The sample is less than half of the observed 'G'-type supergiants, but the remaining majority are actually F-type stars with heavy line blanketing and they will be discussed elsewhere. The abundance parameters of this sample of stars indicate values of [Fe/H] between about +0.6 dex and the solar value, using a preliminary calibration of the photometric indices. The luminosities are derived from previously calibrated photometric results and are in reasonably good agreement with spectroscopically assigned luminosity classes. The few long-period Cepheids that are not heavily blanketed F-type stars give reddening values in agreement with current results from other methods of analyses. The supergiants show no obvious gradients in the galactic distribution of abundances and those nearest the Sun range from very overabundant ([Fe/H] $\sim +0.3$ dex), for members of the Local Association (Pleiades Group), to near solar abundance. A small sample of LMC supergiants shows nearly the same range in metal abundance as the galactic stars and gives a modulus for the LMC of $18.3 \pm 0.20(\sigma)$ mag. (22 refs.)
- 116650 On the T Tauri nature of the variable star BM Cha.** J.Krautter (Max-Planck-Inst. für Extraterrestrische Phys., Garching bei München, Germany), M.Mouchet. *Astron. & Astrophys. (Germany)*, vol.125, no.2, pt.1, p.378-80 (Sept. 1983). The variable star BM Cha has been shown to be a T Tauri star. Unusually strong variations of the Fe II emission lines on a time scale of one day were found. (13 refs.)
- 116651 The temperature of central stars of planetary nebulae: the energy-balance method.** A.Preite-Martinez, S.R.Pottasch (Kapteyn Astron. Inst., Groningen, Netherlands). *Astron. & Astrophys. (Germany)*, vol.126, no.1, pt.2, p.31-44 (Sept. 1983). The authors present a method for determining the color temperature of the ionizing continuum of the central star photoionizing a surrounding nebula. The method is based on the assumption that energy balance holds in the photoionized nebula. A simple analytical expression is derived for the energy-balance temperature T_{EB} of the central stars of low excitation nebulae and T_{EB} is found for a sample of 51 planetary nebulae. A good consistency is found between the computed T_{EB} and Zanstra temperature. The authors also predict the apparent visual magnitude of central stars not yet observed or only marginally detected. (51 refs.)
- 116652 The detection limits in ground based measurements of stellar microvariability.** F.-L.Deubner, J.Isserstedt (Inst. für Astron. & Astrophys., Univ. Würzburg, Würzburg, Germany). *Astron. & Astrophys. (Germany)*, vol.126, no.1, pt.2, p.216-19 (Sept. 1983). With photoelectric photometry in the VBLUW system the authors tried to detect short period brightness fluctuations in solar-like stars. Although the result of this experiment is negative, the RMS noise level per frequency band of ca. 2.5×10^{-5} mag in the data appears low enough to encourage the ground-based search for low-l p -mode oscillations in F-type main sequence stars. (13 refs.)
- 116653 Recent photometry of the central star of NGC 2346.** L.Kohoutek (Hamburg Obs., Hamburg, Germany). *Mon. Not. R. Astron. Soc. (GB)*, vol.204, no.3, p.93P-7 (Sept. 1983). The light curve of the variable central star of NGC 2346 has been observed in 1983 January and shows substantial changes compared with 1982. The end of 1981 November is estimated as being the beginning of the present eclipsing behaviour with photometric period $P=15.957$ day. The slope of the (V , $B-V$) relation is interpreted as the ratio $R=6.6$ of total to selective extinction which may arise in a dust cloud moving from the planetary nucleus. (12 refs.)
- 116654 Visible and UV observations of the giant early-type members of the Large Magellanic Cloud.** K.Nandy, G.I.Thompson (Royal Obs., Edinburgh, Scotland), D.H.Morgan, A.J.Willis, R.Wilson, L.Houziaux. *Mon. Not. R. Astron. Soc. (GB)*, vol.205, no.1, p.231-9 (Oct. 1983). Visible and UV observations of a sample of LMC members with $V > 14$ mag are presented. The sample contains an O9 V star and B0-B3 giants. Their flux distributions in the IUE range are found to be the same as those of galactic giants. The effective temperatures and radii of the LMC members are determined by comparison with models. (22 refs.)
- 116655 Far ultraviolet observations of Population II.** V.Caloi (Istituto di Astrofisica Spaziale, Frascati, Italy), V.Castellani. *Mem. Soc. Astron. Ital. (Italy)*, vol.54, no.2, p.419-41 (1983). Far UV observations of galactic and extragalactic Population II objects are reported and the relevance of this type of information for the understanding of stellar and galactic evolution is discussed. (30 refs.)

- 116656** Some aspects of the velocity fields in early-type stars. M.L.Franco, R.Stalio (Osservatorio Astron. di Trieste, Trieste, Italy). *Mem. Soc. Astron. Ital. (Italy)*, vol.54, no.2, p.537-52 (1983). Considers the structure and dynamics of the outer atmospheric layers of early-type stars and the interaction of these layers with the interstellar medium. (30 refs.)
- 116657** Late type stars [IUE observations]. S.Catalano (Istituto di Astron., Univ. di Catania, Catania, Italy). *Mem. Soc. Astron. Ital. (Italy)*, vol.54, no.2, p.553-69 (1983). The study of the outer atmospheres of cool stars, achieved with IUE observations are reviewed. The main results are summarized. The main widely accepted result that is emerging from IUE observations of cool stars is that magnetic fields control the structure and energy balance of the outer atmospheres of stars later than A7-F0. (50 refs.)
- 116658** The disc-like envelopes around young stars seen in the maser lines. V.P.Grinin, S.A.Grigor'ev. *Pis'ma v Astron. Zh. (USSR)*, vol.9, no.8, p.463-8 (1983). In Russian. English translation in: *Sov. Astron. Lett. (USA)*
The observational profiles of the SiO and H₂O maser lines in sources connected with star formation regions are analysed on the basis of theoretical profiles corresponding to different stages of axial-symmetric collapse. A number of sources whose profiles have special features typical of accretion motions and of quasi-Keplerian rotation are selected. Since the objects are young it is supposed that these stars are in the early phases of forming either protoplanetary discs or disc-like envelopes connected with the origin of binary systems. (23 refs.)
- Second catalogue of H α line profiles in 55 Be star spectra** ...See Entry 116491
- Occultation of 14 Piscium by (51) Nemausa**See Entry 116515
- Self-regulated star formation in the Galaxy**See Entry 116628
- The formation of emission lines in the expanding chromospheres of luminous cool stars. I. The importance of atmospheric extension and partial redistribution effects**See Entry 116629
- Observationally-based infrared efficiencies and Planck means for circumstellar dust grains**See Entry 116633
- Narrow-band photometry of G and K stars near the North Galactic Pole**See Entry 116641
- Radial velocities for early type stars in six galactic regions** ...See Entry 116642
- Cessation of the 63 second periodicity in the light curve of V533 Herculis**See Entry 116659
- The outbursts of symbiotic novae**See Entry 116660
- Mixing by shear instabilities in differentially rotating inhomogeneous stars with application to accreting white dwarf models for novae**See Entry 116661
- PI Gruis: molecular identifications and spectral classification**See Entry 116662
- Star-planet systems as progenitors of cataclysmic binaries: tidal effects**See Entry 116663
- Superoutbursts: a general phenomenon in dwarf novae**See Entry 116664
- The dust envelope of the Herbig Ae star, AB Aur**See Entry 116665
- The ultraviolet variability of the symbiotic star HBV 475**See Entry 116666
- Far ultraviolet colors of β Cephei stars**See Entry 116669
- Study of the variability of the delta Scuti stars. VI. Pulsational behaviour of HR 1392 (69 Tau)**See Entry 116670
- Study of the variability of the delta Scuti stars. VII. The problem of stability and monopiodicity in 20 CVn**See Entry 116671
- HR 981—a new USPC**See Entry 116673
- B and V photometry of the southern RS CVn candidate HD 196818**See Entry 116675
- On some remarkable pulsation properties of the high-latitude F-type supergiants**See Entry 116676
- Optical behavior of EZ Pegasi**See Entry 116677
- HR 5=ADS 61: a new variable star**See Entry 116678
- Photometry of FK Comae**See Entry 116679
- Search for ultra short period variations in Epsilon Octantis** ...See Entry 116681
- Magnetometric measurements of the carbon star Y CVn**See Entry 116682
- PU Vulpeculae**See Entry 116684
- R Coronae Borealis**See Entry 116685
- Possible optical burster**See Entry 116690
- An infrared study of the eclipsing dwarf nova U Geminorum**See Entry 116692
- New results on symbiotic stars [IUE observations]**See Entry 116698
- On the correlation between H α line intensity and SiO maser emission of the long-period variable χ cygni**See Entry 116702
- Variation of the profile of H α line in the spectrum of DH Pegasi**See Entry 116704
- Optical variability of PU Vulpeculae (nova-like Kuwano's object 1979) in 1982**See Entry 116705
- On the two possible progenitors of type I super nova**See Entry 116714
- Radio emission from AM Herculis: the quiescent component and an outburst** ...See Entry 116740
- Photometric observations and elements of the eclipsing binary TT Herculis**See Entry 116749
- The light curve changes of VW Cephei**See Entry 116751
- A study of ultraviolet spectra of ζ Aur/VV Cep systems. III. Atlas of theoretical curves of growth**See Entry 116752
- A photometric study of the eclipsing binary V478 Cygni**See Entry 116754
- Eclipse timings of 31 Cygni**See Entry 116757
- Spectroscopic observations of the cool eclipsing X-ray binary HD 155638**See Entry 116758
- The chemical composition of distant globular clusters: are there any metal-poor clusters?**See Entry 116765
- The globular cluster NGC 6638**See Entry 116768
- Variable stars in NGC 6397**See Entry 116771
- The chemical composition of stars in globular clusters**See Entry 116775
- IUE observations of stars in the M8 nebula**See Entry 116798
- Optical polarization in the bipolar nebula associated with LkH α 208**See Entry 116799

- Hydrodynamic models of Herbig-Haro objects**See Entry 116800
- Ammonia observations of the Herbig-Haro objects HH 24-27**See Entry 116801
- 3 μ m spectroscopy of IRS 7 towards the Galactic Centre**See Entry 116802
- On the distance to M33 determined from magnitude corrections to Hubble's original Cepheid photometry**See Entry 116813
- Chemical evolution of the galactic halo. II. Enrichment in primary elements**See Entry 116816
- High-resolution images of the galactic centre**See Entry 116849
- Slippery evidence on the Galaxy's invisible heavy halo**See Entry 116854

97.30 VARIABLE AND PECULIAR STARS (inc. novae)

- 116659** Cessation of the 63 second periodicity in the light curve of V533 Herculis. E.L.Robinson, R.E.Nather (McDonald Obs., Dept. of Astron., Univ. of Texas, Austin, TX, USA). *Astrophys. J. (USA)*, vol.273, no.1, pt.1, p.255-60 (1 Oct. 1983). In 1978 and 1980 the old nova V533 Her had a 63.6 s periodic variation in its light curve. The authors present high-speed photometry of V533 Her obtained in 1982. Although mass transfer and accretion are still taking place, the 63.6 s periodicity has disappeared. The available data on V533 Her now cast serious doubt on the magnetic rotator model for the periodicity. It is shown that the 63.6 s periodicity in V533 Her was similar to periodicities in the cataclysmic variable WZ Sge. The authors suggest that V533 Her should more properly be classified as a WZ Sge star, not a DQ Her star. (26 refs.)
- 116660** The outbursts of symbiotic novae. S.J.Kenyon, J.W.Truran (Dept. of Astron., Univ. of Illinois, Urbana, IL, USA). *Astrophys. J. (USA)*, vol.273, no.1, pt.1, p.280-8 (1 Oct. 1983). Discusses possible conditions under which thermonuclear burning episodes in the hydrogen-rich envelopes of accreting white dwarfs give rise to outbursts similar in nature to those observed in the symbiotic stars AG Peg, RT Ser, RR Tel, AS 239, V1016 Cyg, V1329 Cyg, and HM Sge. In principle, thermonuclear runaways involving low-luminosity white dwarfs accreting matter at low rates produce configurations that evolve into A-F supergiants at maximum visual light and which resemble the outbursts of RR Tel, RT Ser, and AG Peg. Very weak, nondegenerate hydrogen shell flashes on white dwarfs accreting matter at high rates may explain the outbursts in V1016 Cyg, V1329 Cyg, and HM Sge. (59 refs.)
- 116661** Mixing by shear instabilities in differentially rotating inhomogeneous stars with application to accreting white dwarf models for novae. J.MacDonald (Dept. of Astron., Univ. of Illinois, Urbana-Champaign, IL, USA). *Astrophys. J. (USA)*, vol.273, no.1, pt.1, p.289-98 (1 Oct. 1983). The problem of how shear instabilities redistribute matter and angular momentum accreted by a star from a disk is considered. Necessary conditions for stability of the star to nonaxisymmetric perturbations are derived by use of the short wavelength approximation. By considering growth rates, it is shown that freshly accreted material rapidly takes up a quasi-spherical distribution due to dynamical instabilities. However, mixing inward toward the stellar interior occurs on a thermal time scale or longer. The application of these results to accreting white dwarf models of classical novae is discussed. (25 refs.)
- 116662** PI Gruis: molecular identifications and spectral classification. P.S.Murty (Indian Inst. of Astrophys., Kodaikanal, India). *Astrophys. & Space Sci. (Netherlands)*, vol.94, no.2, p.295-305 (Aug. 1983). Identifications of the molecular absorption feature in the visible spectrum of the S star pi Gruis are presented. Moderate dispersion spectrum of π^1 Gru covering the region 5800-7300 Å, demonstrates the presence of a multitude of molecular bands. Wavelength measures of well over 150 red-degraded band heads are listed. Nearly 80% of the observed features are identified with the ZrO, LaO, YO, and CeO molecules. Many molecular bands due to ZrO, YO, and CeO are reported identified for the first time. Neither TiO molecular features nor any Ba compounds are detectable. (64 refs.)
- 116663** Star-planet systems as progenitors of cataclysmic binaries: tidal effects. M.Livio, N.Soker (Dept. of Phys., Technion-Israel Inst. of Technol., Haifa, Israel). *Astron. & Astrophys. (Germany)*, vol.125, no.2, pt.1, p.L12-15 (Sept. 1983). The evolution of a star-planet system is calculated at a stage in which a planet accretes from a red giant star's wind. Tidal interaction is included. For initial separations larger than a certain critical value, the separation is found to increase, while for smaller initial separations a tidally induced spiralling-in ensues. A second (smaller) critical initial separation is found to exist. For initial separations smaller than this second critical value, the planet manages to penetrate the giant's envelope before the latter is lost via the stellar wind. It is suggested that the spiralling-in process combined with accretion inside the giant's envelope, as calculated by Livio and Soker (1983), can lead to the formation of low-mass cataclysmic binaries. (16 refs.)
- 116664** Superoutbursts: a general phenomenon in dwarf novae. J.van Paradijs (Astronomical Inst. 'Anton Pannekoek', Univ. of Amsterdam, Amsterdam, Netherlands). *Astron. & Astrophys. (Germany)*, vol.125, no.2, pt.1, p.L16-18 (Sept. 1983). The occurrence of a bimodal distribution of outburst durations is a general property of dwarf novae. The intrinsic duration of the long outbursts is not correlated with the orbital period; that of short outbursts tends to increase with orbital period. The impressive contrast between the short and long outbursts in SU UMa type systems is a consequence of this, in combination with the positive correlation between the decay time of the outbursts and the orbital period (Bailey relation). Thus the restriction of the term 'superoutburst' to short-orbital-period systems is misleading. (7 refs.)
- 116665** The dust envelope of the Herbig Ae star, AB Aur. C.Catala (DESPA, Obs. de Paris-Meudon, Meudon, France). *Astron. & Astrophys. (Germany)*, vol.125, no.2, pt.1, p.313-19 (Sept. 1983). Ultraviolet low resolution observations of a Herbig Ae star, AB Aur, when compared with a theoretical energy distribution for the same spectral type, show the existence of an anomalous extinction, which is believed to be due to a circumstellar dust envelope surrounding the star. The study of this anomalous extinction can be used to determine the properties of the grains responsible for it. These properties can then be tested by comparing a computed infrared energy distribution with infrared calibrated observations. (56 refs.)
- 116666** The ultraviolet variability of the symbiotic star HBV 475. H.Nussbaumer, W.Schmutz (Inst. of Astron., Zurich, Switzerland). *Astron. & Astrophys. (Germany)*, vol.126, no.1, pt.2, p.59-69 (Sept. 1983). The authors present evidence for the binary nature of the symbiotic star HBV 475 (=V1329 Cyg). Changes in line and continuum fluxes, observed in the far ultraviolet (1200 Å-3200 Å), are consistent with the 950^d period found

from the visual luminosity variations. Periodicity and amplitudes found in the wavelength shifts, indicate a size of the binary system of $\approx 2 \times 10^{14}$ cm. The emission lines originate in a radiatively ionized gas with $10^6 < N_e [\text{cm}^{-3}] < 10^7$ and $T_e < 15000\text{K}$. Evidence has been discussed for a hot outer envelope around the whole system. (40 refs.)

116667 Photometric search for Ap-stars in open clusters. IV. NGC 2287, Cr 121, NGC 2422 and supplementary measurements in NGC 1662 and NGC 2516. H.M.Maitzen (Inst. fur Astron., Univ. Wien, Wien, Austria), H.J.Wood.

Astron. & Astrophys. (Germany), vol.126, no.1, pt.2, p.80-5 (Sept. 1983). For pt.III entitled 'A photoelectric investigation of Ap-stars in open clusters', see *ibid.*, vol.115, no.2, p.275-9 (1982). The authors have continued the search for Ap-stars in open clusters with the photoelectric peculiarity index Δa (Maitzen, 1976) and found NGC 2287-56, NGC 2422-P3, NGC 1662-4 to be CP2-stars as members in their respective clusters. HD 51088 which is also peculiar according to its Δa -value, may be a member of one of the two very young star concentrations previously called Cr 121. There is only a small probability that HD 49333 is a member of NGC 2287. It is a CP4 (=He weak) star with a Δa significant for peculiarity. (33 refs.)

116668 The runaway Wolf-Rayet star HD 143414: evidence for a low-mass companion. J.Isserstedt, A.F.J.Moffat, V.S.Niemela (Inst. fur Astron. & Astrophys., Univ. Wurzburg, Wurzburg, Germany). *Astron. & Astrophys. (Germany)*, vol.126, no.1, pt.2, p.183-91 (Sept. 1983). Extensive photoelectric photometry and photographic spectroscopy reveal HD 143414 to be a single-line binary with a 7.690-d orbit. The mass function is low, $0.007 M_\odot$. This leads to a mass for the companion star of $\sim 2.8 M_\odot$, assuming the WN6 component to have a mass of $40 M_\odot$ and the orbital inclination to be 60° . Its large displacement from the galactic plane ($z = -44$ pc) and its high peculiar radial velocity (-107 km s^{-1} in excess of differential galactic rotation) suggest that HD 143414 is a runaway. This is likely the result of a recoil after a supernova explosion of the original primary, which would have occurred $< 5 \times 10^6$ yr ago near the galactic plane. (29 refs.)

116669 Far ultraviolet colors of β Cephei stars. J.Zorec (Inst. d'Astrophys., Paris, France), D.Briot, L.Divan. *Astron. & Astrophys. (Germany)*, vol.126, no.1, pt.2, p.205-6 (Sept. 1983). Studies the ultraviolet colors of β Cephei-type stars using a G index independent of a mean interstellar reddening. The G index characterizes the ultraviolet energy distribution of the stars in the range $\lambda\lambda$ 1460-2740 Å. The β Cephei stars have ultraviolet colors which correspond to those of normal B stars having the same spectral type and luminosity class, that is, colors of normal B stars between those of luminosity classes IV and V and those of luminosity class III. However, the G index of σ Sco is quite different from that of normal stars. It identifies an abnormal energy distribution, interpreted up to now as due to a peculiar interstellar absorption law. (10 refs.)

116670 Study of the variability of the delta Scuti stars. VI. Pulsational behaviour of HR 1392 (69 Tau). M.Bossi, G.Guerrero, L.Mantegazza, M.Scardia (Osservatorio Astron. di Brera, Merate, Italy). *Astron. & Astrophys. Suppl. Ser. (France)*, vol.53, no.3, p.395-7 (Sept. 1983). Photoelectric observations of the delta Scuti star 69 Tau are presented. The analysis of the light curves shows a single sinusoidal component over the detectability threshold. The observed frequency does not agree with the fundamental pulsation mode. The small observed amplitude is probably connected with the high rotational velocity. However the presence in the same region of the HR diagram of monopulsating delta Scuti stars involving pulsational energies which differ by orders of magnitude, remains an open problem. (15 refs.)

116671 Study of the variability of the delta Scuti stars. VII. The problem of stability and monopulsation in 20 CVn. M.Bossi, G.Guerrero, L.Mantegazza, M.Scardia (Osservatorio Astron. di Brera, Merate, Italy). *Astron. & Astrophys. Suppl. Ser. (France)*, vol.53, no.3, p.399-402 (Sept. 1983).

For pt.VI see *ibid.*, vol.53, no.3, p.395-97 (1983). The long term stability of the delta Scuti star 20 CVn is established from the results of 17 hours of observations obtained in 1982. However the presence of a second pulsation mode is suspected although this star has so far been considered as a monopulsator. The small pulsational amplitude, like that of many other similar variable stars, still needs an exhaustive explanation. In this case, it may be connected with the excitation of several high order modes, which would be photometrically undetectable, and/or with a possible peculiar metallicity. (19 refs.)

116672 Absolute measurements of flux in the continuum of galactic Wolf-Rayet stars: comparison with main-sequence OB stars. Hua Chon-Trung, Woo Jong-Ok (Lab. d'Astron. Spatiale, Marseille, France), Nguyen Huu-Doan. *Astron. & Astrophys. Suppl. Ser. (France)*, vol.53, no.3, p.407-17 (Sept. 1983). In French.

The authors present absolute measurements of the flux emitted in the visible continua of some galactic Wolf-Rayet stars, carried out by means of a two-channel scanner. The dereddened fluxes are combined with IUE and ANS of Kurucz (1979) in order to derive the effective temperatures and angular diameters of the programme stars. The authors then compute $\log L/L_\odot$ and thereby locate the WR stars in the HR diagram: the WR stars are cooler than the ZAMS, and the WN7, WN8 types appear more luminous than the other subclasses. (38 refs.)

116673 HR 981—a new USPC. T.T.Moon, D.W.Coates, L.Halprin, K.Thompson (Dept. of Phys., Monash Univ., Clayton, Victoria, Australia).

Inf. Bull. Variable Stars (Hungary), no.2383, p.1-4 (15 Aug. 1983). The authors report V-band photometry of the visual binary star HR 981 (=HD 20313; F0 II) during 1981 and 1982. Light variations are found with an amplitude of about 0.02 magnitudes, and with periods of 0.065 and 0.041 days. The period ratio (0.63 ± 0.03) indicates pulsation in the fundamental mode and the second overtone. This interpretation is consistent with the PLC relation for ultra-short-period Cepheids. It is concluded that the variable star is the primary component of the visual binary (HR 981A), since HR 981B is too late in spectral type to be an ultra-short-period Cepheid. (3 refs.)

116674 On the pulsation of HD 201601. W.W.Weiss (Inst. fur Astron., Wien, Austria).

Inf. Bull. Variable Stars (Hungary), no.2384, p.1-2 (15 Aug. 1983). The author reports photometric observations of the rapidly oscillating Ap star γ Equulei (=HR 8097=HD 201601) between 9 and 11 July 1983. Light variations with an amplitude of about 0.8 mmag and a frequency of 0.079/min were observed on all three nights. (4 refs.)

116675 B and V photometry of the southern RS CVn candidate HD 196818. J.L.Innis, D.W.Coates, S.W.B.Dieters, T.T.Moon, K.Thompson (Dept. of Phys., Monash Univ., Clayton, Victoria, Australia).

Inf. Bull. Variable Stars (Hungary), no.2386, p.1-4 (18 Aug. 1983). The authors report photoelectric BV photometry of HD 196818 (K0 IIIp), alias BV 893, between August 1982 and July 1983. Small-amplitude light

variations ($\Delta V \sim 0.3$ mag.) have been observed; the photometric period is estimated to be 20.31 days. The light curve resembles a 'sawtooth' wave, with an almost linear rise and fall. The light variations are consistent with the presence of cool active regions on the surface of the star. (5 refs.)

116676 On some remarkable pulsation properties of the high-latitude F-type supergiants. D.D.Sasselov (Dept. of Astron., Univ. of Sofia, Sofia, Bulgaria).

Inf. Bull. Variable Stars (Hungary), no.2387, p.1-3 (18 Aug. 1983). The author describes a class of variable F-type supergiant stars, designated UU Herculis stars, which occur far above the galactic plane and which are distinguished by unusual photometric behaviour. These stars show at least two distinct alternating pulsational modes, with periods between 40 and 90 days, and switch from one mode to the other; UU Herculis itself has three modes, with periods of 71, 80 and 90 days. Another common phenomenon among these stars is that their pulsations may cease abruptly, and the star may remain constant for a couple of months before beginning to pulsate again. Five stars of this class have been identified, namely UU Herculis, 89 Herculis, BL Telescopii (F), HD 161796 and HD 112374; they are interpreted as luminous passive Population I stars pulsating in nonradial modes. (9 refs.)

116677 Optical behavior of EZ Pegasi. S.K.Pope (American Assoc. of Variable Star Observers, Cambridge, MA, USA).

Inf. Bull. Variable Stars (Hungary), no.2388, p.1-4 (19 Aug. 1983). The author reports observations of the unique, possibly cataclysmic, variable star EZ Pegasi. Spectroscopic observations between October 1971 and January 1972 showed normal G5 V spectra in the blue region, except that H δ appeared as a very broad, weak absorption line with possible core emission; spectra in the visual region revealed short term fluctuations in the intensity of the H α emission. Visual magnitude estimates for the star are reported, and a light curve for the period 1972 to 1982 is presented; the brightness of the star is found to be essentially constant. (3 refs.)

116678 HR 5=ADS 61: a new variable star. O.H.Brettman (Braeside-Midwest Obs., Huntley, IL, USA), R.E.Fried, W.M.Duvall, D.S.Hall, C.H.Poe, J.S.Shaw.

Inf. Bull. Variable Stars (Hungary), no.2389, p.1-3 (22 Aug. 1983). The authors report differential photoelectric photometry of the visual binary star HR 5 (=HD 123=ADS 61: dG4+dG8) during 1981 and 1982. The star is found to be variable ($\Delta V \sim 0.2$ mag.), with a period of 1.0819 days; the amplitude of the variation increases by a factor of 3 from the infrared to the ultraviolet. It is not known which component of the binary is variable, and the mechanism of the light variations is uncertain; the authors tentatively attribute them to the rapid rotation of an unevenly-spotted star or to the existence of a short-period spectroscopic binary in the system. (1 ref.)

116679 Photometry of FK Comae. E.Bohusz, A.Udalski (Warsaw Univ. Obs., Warsaw, Poland).

Inf. Bull. Variable Stars (Hungary), no.2390, p.1-3 (25 Aug. 1983). The authors report BV photometry of the rapidly-rotating giant star FK Comae Berenice (BD+24°2592) during May and June 1982. The light curve is similar to that found by Rucinski (1981). The phase found for maximum light (0.4 to 0.5) suggests that the region of the star responsible for the light variations did not move on the stellar surface during the period 1974 to 1982. (2 refs.)

116680 On delta Scuti stars in open clusters. M.Breger (Inst. for Astron., Wien, Austria).

Inf. Bull. Variable Stars (Hungary), no.2393, p.1-4 (30 Aug. 1983). The observational correlations for delta Scuti stars in clusters reported by Frolov and Irkaev (1982) between average period and cluster age, as well as average absolute magnitude and age, are examined. These correlations are shown to be a natural consequence of the systematically different color-magnitude diagrams for clusters of different ages, and the existence of a period-luminosity-colour relation for delta Scuti stars. (8 refs.)

116681 Search for ultra short period variations in Epsilon Octantis. T.T.Moon, D.W.Coates, J.L.Innis, K.Thompson (Dept. of Phys., Monash Univ., Clayton, Victoria, Australia).

Inf. Bull. Variable Stars (Hungary), no.2394, p.1-3 (1 Sept. 1983). The authors report photoelectric photometry of the semiregular variable star ϵ Octantis (=HR 8481=HD 210967; M5 III) between May and July 1983. The star faded in V-light by about 0.5 mag. from May 18 to June 17, with a corresponding change of about 0.1 mag. in B-V; it is deduced that the temperature of the star decreased from about 3890 to 3760K in this time. A search on July 18 for light variations attributable to ultrashort period oscillations was unsuccessful; no such variations were observed to a limit of ± 0.005 mag. (3 refs.)

116682 Magnetometric measurements of the carbon star Y CVn. M.Vetesk (Dept. of Astron., Brno Univ., Brno, Czechoslovakia).

Inf. Bull. Variable Stars (Hungary), no.2395, p.1 (2 Sept. 1983). The author reports measurements of Zeeman spectra of the N-type carbon star Y Canum Venaticorum. No magnetic field was detected; the mean value of the magnetic induction was found to be $B = 0.005 \pm 0.010$ Tesla. (no refs.)

116683 V436 Cen revisited. B.Warner (Dept. of Astron., Univ. of Cape Town, Cape Town, S Africa).

Inf. Bull. Variable Stars (Hungary), no.2397, p.1-3 (5 Sept. 1983). The author discusses the observation by Semenik (1980) of an increasing superhump period in the SU Ursae Majoris star V436 Centauri during the supermaximum of May 1978. It is suggested that the superhumps observed towards the end of this outburst were 'late superhumps', similar to those observed in VW Hydri, which have periods similar to those of normal superhumps but which are displaced 0.5P in phase with respect to them; and that as a result the superhump elements found by Semenik have been distorted. It is concluded that the superhumps of V436 Cen have an apparently decreasing period, similar to those of the other SU Ursae Majoris stars. (6 refs.)

116684 PU Vulpeculae. A.Purgathofer, A.Schnell. *I.A.U. Circ. (USA)*, no.3859, 1 pp. (14 Sept. 1983).

The authors report spectroscopic observations of PU Vulpeculae during July and September 1983. The star has a late F-type spectrum of luminosity class I. Observations between 4 and 8 September 1983 show H α and H β only in emission; O III 501 nm and O II 373 nm emission lines are also present. In addition the star has been brightening in the U-band since around July 5, at a rate between 0.004 and 0.03 mag/day. (no refs.)

116685 R Coronae Borealis. K.Hirosawa, K.Meday, M.Verdenet, J.Shanklin, C.Hurless, G.Chaple, L.Hiett, C.E.Spratt, C.Scovill, J.Bortle. *I.A.U. Circ. (USA)*, no.3859, 1 pp. (14 Sept. 1983).

Visual magnitude estimates are reported for the period 1983 August 26 to September 9. (no refs.)

116686 U Aquarii. *I.A.U. Circ. (USA)*, no.3859, 1 pp. (14 Sept. 1983).

Visual magnitude estimates are reported for 1983 August 21 and September 5: the star is recovering from its recent short, shallow minimum. (no refs.)

116687 GK Persei. C.E.Spratt.*I.A.U. Circ. (USA)*, no.3861, 1 pp. (14 Sept. 1983).

Visual magnitude estimates are reported for 1983 September 5 and 6. (no refs.)

116688 Novalike variable in Libra. B.E.J.Pagel, M.M.Phillips.*I.A.U. Circ. (USA)*, no.3863, 1 pp. (14 Sept. 1983).The authors report that a low-dispersion spectrogram obtained on 1983 September 1 showed strong H γ , H β and H α emission. The apparent visual continuum magnitude estimated from this spectrum was 14.1. (2 refs.)**116689 Possible novae. W.Liller, E.P.Aksenov.***I.A.U. Circ. (USA)*, no.3869, 1 pp. (23 Sept. 1983).It is reported that a possible nova has been discovered in Norma at $\alpha=16^h09^m51.0^s$, $\delta=-52^\circ11'32''$ (equinox 1950.0). The object was detected at magnitude 9.4 on 1983 September 19 but must have been fainter than magnitude 11.5 on September 10. In addition it is reported that a possible nova has been discovered in Triangulum at $\alpha=2^h42^m$, $\delta=+33^\circ19'$ (equinox 1950.0). The object was observed at $m_{pg}=15.0$ on 1983 September 11. (no refs.)**116690 Possible optical burster. S.Djorgovski.***I.A.U. Circ. (USA)*, no.3870, 1 pp. (23 Sept. 1983).Spectroscopic observations on 1983 September 11 have shown that the candidate object at $\alpha=00^h54^m50.10^s$, $\delta=-01^\circ38'06.7''$ (equinox 1950.0) proposed by Klemola (1983) for the possible optical burster found by Popovic (1982) is a normal galactic star. (2 refs.)**116691 Molecules in celestial objects. IV. IUE observation of CO lines towards Be stars with low reddening. S.P.Tarafdar (Tata Inst. of Fundamental Res., Bombay, India).***Mon. Not. R. Astron. Soc. (GB)*, vol.204, no.3, p.1081-9 (Sept. 1983).For pt.III see *ibid.*, vol.200, no.2, p.431-44 (1982). IUE spectra of two Be stars with small colour excesses are presented to show the presence of a number of absorption lines due to the A-X transition of ^{12}CO and ^{13}CO is shown that ^{12}CO towards Be stars comes from a region where the density of molecular hydrogen is large compared to that towards non-Be stars. As a high density of molecular hydrogen is favoured in the high density circumstellar material, it is suggested that the observed CO towards Be stars is circumstellar in origin. This suggestion is supported by the presence of absorption from excited $^2P_{3/2}$ level of Si II. (26 refs.)**116692 An infrared study of the eclipsing dwarf nova U Geminorum.**

G.Berriman (Div. of Phys., Maths. & Astron., California Inst. of Technol., Pasadena, CA, USA), D.H.Beattie, I.Gatley, T.J.Lee, S.W.Mochnecki, P.Szkody.

Mon. Not. R. Astron. Soc. (GB), vol.204, no.3, p.1105-15 (Sept. 1983).

Presents broadband infrared photometry (J, H, K) of the cataclysmic binary system U Geminorum throughout two orbital cycles, one series of data was obtained several days before an outburst, and a second series when the system had returned almost to quiescence from the same outburst. In quiescence, the red star, an M4-M5.5 dwarf, supplies most of the infrared luminosity of the system. The quiescent light curves are the tidally induced ellipsoidal variations of the red dwarf. The amplitude of the light curves is such that the red dwarf must fill, or nearly fill, its Roche lobe. (33 refs.)

116693 On the secular variation of amplitudes in double-mode Cepheids.

T.Aikawa (Dept. of Phys. & Astron., Univ. of Nebraska, Lincoln, NE, USA).

Mon. Not. R. Astron. Soc. (GB), vol.204, no.3, p.1193-202 (Sept. 1983).

Under the assumption that the resonant interactions among the fundamental, the first overtone and the third overtone radial modes cause the phenomenon of double periodicity of double-mode Cepheids, the secular variation of amplitudes is investigated theoretically. The magnitudes and period of the secular variation are determined in terms of mode-coupling constants. The possibility of alternate appearance of single and double periodicity in the vicinity of the resonance is suggested. (28 refs.)

116694 The discovery of 13.72-min oscillations in the cool magnetic Ap star HD 217522. D.W.Kurtz (Dept. of Astron., Univ. of Cape Town, Rondebosch, S Africa).*Mon. Not. R. Astron. Soc. (GB)*, vol.205, no.1, p.3-10 (Oct. 1983).Announces the discovery of oscillations with a period near 13.72 min in the cool magnetic Ap star HD 217522. The author presents 97 hr of high-speed photometric observations obtained on 18 nights spread over a time span of 74 days in 1982. The amplitude of the oscillations in HD 217522 is variable from night to night and also on a longer time-scale. A frequency analysis of the data identifies the principal frequency of oscillation to be $4.37435 \pm 0.00014 \text{ hr}^{-1}$. This star is the seventh member of the class of rapidly oscillating Ap stars. (9 refs.)**116695 Frequency analysis of the rapidly oscillating Ap star HR 1217 (HD 24712). D.W.Kurtz, J.Seeman (Dept. of Astron., Univ. of Cape Town, Rondebosch, S Africa).***Mon. Not. R. Astron. Soc. (GB)*, vol.205, no.1, p.11-22 (Oct. 1983).

High speed photometric observations of HR 1217 have been obtained during 119 hr on 18 nights in 1981. On five of these nights contemporaneous observations were obtained at the South African Astronomical Observatory and Cerro Tololo Inter-American Observatory which greatly reduce the severe daily aliasing problem in the frequency analysis of this star. A frequency analysis of three nights of data at the phase of pulsation amplitude maximum reveals six nearly uniformly spaced frequencies which the authors suggest are associated with six consecutive overtones of pulsation. From the frequency ratios the authors estimate the overtones of the pulsations. (12 refs.)

116696 Simultaneous infrared and optical photometry of cataclysmic variables. M.R.Sherrington, R.F.Jameson (Astron. Dept., Univ. of Leicester, Leicester, England).*Mon. Not. R. Astron. Soc. (GB)*, vol.205, no.1, p.265-73 (Oct. 1983).

Simultaneous infrared and optical photometry of 22 cataclysmic variables was obtained at the 1.5-m infrared flux collector at the Cabezon Observatory, Tenerife, in order to study the relative contributions of the disc and secondary across a wide wavelength range. The results allow one to estimate the spectral types of the secondaries and the distances of eight of the systems. (15 refs.)

116697 IUE observations of cataclysmic variables. P.L.Selvelli (Obs. Nacional de Brazil, Rio de Janeiro, Brazil), M.Hack.*Mem. Soc. Astron. Ital. (Italy)*, vol.54, no.2, p.467-91 (1983).

Illustrates the results of IUE observations of novae and old novae, recurrent novae, dwarf novae and nova-like variables. (71 refs.)

116698 New results on symbiotic stars [IUE observations]. G.B.Baratta (Osservatorio Astron., Roma, Italy), R.Viotti.*Mem. Soc. Astron. Ital. (Italy)*, vol.54, no.2, p.493-509 (1983).

A considerable amount of new results on symbiotic stars has been obtained during the first five years of operation of the IUE satellite. The authors review the UV properties of these stars, in particular the hot continuum, and the emission line intensities and profiles as a diagnostic of the physical processes which take place in their emitting regions. The various problems related to the symbiotic phenomenon such as stellar winds, accretion, Roche lobe

overflow, and the nature and IR variability of the cool star are also discussed. (52 refs.)

116699 Solar-like activity phenomena in stars. M.Rodono (Istituto di Astron., Univ. di Catania, Catania, Italy).*Mem. Soc. Astron. Ital. (Italy)*, vol.54, no.2, p.571-83 (1983).

The significant impact of the international ultraviolet explorer (IUE) in the study of stellar variability is presented. Specifically, the key role played by IUE observations in the stellar activity is emphasized. Variability phenomena, due to flares and surface inhomogeneities occurring in the atmospheres of cool stars and systems, are remarkably similar to the solar ones, but develop under rather different physical conditions. This provides a powerful tool in investigating the physical structure and evolution of stellar atmospheres. The potentially wide scientific benefit of the study of solar-like activity in stars has yet to be fully exploited. (30 refs.)

116700 Chemically peculiar stars [IUE observations]. F.Castelli (Osservatorio Astron. di Trieste, Trieste, Italy).*Mem. Soc. Astron. Ital. (Italy)*, vol.54, no.2, p.585-99 (1983).On a first, rough inspection, the IUE files appear to include numerous observations of all classes of chemically peculiar stars. However, a more careful inspection of the data and of the results so far obtained shows that this material is not sufficient to clarify the many unsolved problems regarding chemically peculiar stars. In order to derive reliable T_{eff} , $\log g$ values from the observed flux distribution of chemically peculiar stars, both corrections on IUE data of higher quality than those made at present at VILSPA and ad hoc models calculated with the proper abundance values for these stars are needed. Studies of variability of chemically peculiar stars carried out with IUE data are very scanty; they require a lot of observations at different epochs and accurate reduction procedures are essential. IUE observations on variability have confirmed previous results obtained from ground observations. New information on the line spectrum and the discovery of highly excited ions and multiple structures point up the need to make a thorough study of these problems. (45 refs.)**116701 Infrared photometry of HD 101065. I.S.Glass.***Mon. Notes Astron. Soc. South Afr. (S. Africa)*, vol.41, no.11-12, p.117-18 (Dec. 1982).

JHK photometry of Przybylski's star, HD 101065 is presented. The apparent colours are similar to those of FO dwarfs. (5 refs.)

116702 On the correlation between H α line intensity and SiO maser emission of the long-period variable χ cygni. T.E.Derviz.*Pis'ma v Astron. Zh. (USSR)*, vol.9, no.8, p.461-2 (1983). In Russian.English translation in: *Sov. Astron. Lett. (USA)*The results of 1975 and 1978-79 observations of the H α emission line in the spectrum of χ Cyg are given. Comparison of the data with the observations of the SiO maser line ($J=2-1$, $v=1$) by Wolff and Carlsson (1982) suggests a correlation between the intensities of the H α and SiO lines. (5 refs.)**116703 Frequency of novae in M33. A.S.Sharov.***Pis'ma v Astron. Zh. (USSR)*, vol.9, no.8, p.478-81 (1983). In Russian.English translation in: *Sov. Astron. Lett. (USA)*

It is shown that the frequency of novae in M33 is about one or possibly two per year. (19 refs.)

116704 Variation of the profile of H α line in the spectrum of DH Pegasi. G.A.Garbulov.*Pis'ma v Astron. Zh. (USSR)*, vol.9, no.8, p.482-5 (1983). In Russian.English translation in: *Sov. Astron. Lett. (USA)*Splitting of the H α line and emission in the line core were discovered in the spectrum of the RRc-type pulsating variable DH Peg. These phenomena are attributed to the existence of a shock wave in the atmosphere of this star. An anomalous shortward displacement of the H α line at light minimum is noted. (8 refs.)**116705 Optical variability of PU Vulpeculae (nova-like Kuwano's object 1979) in 1982. E.A.Kolotilov.***Pis'ma v Astron. Zh. (USSR)*, vol.9, no.8, p.486-9 (1983). In Russian.English translation in: *Sov. Astron. Lett. (USA)*Results of photoelectric UVB observations of PU Vul made in March 1982-January 1983 are presented. During this period the star remained in the state of maximum brightness ($V \approx 8.50^m$) which started in the autumn of 1981. The observed small variations of brightness did not reveal the presence of periodicity which was characteristic of the star in the 1979 maximum. A small increase of V magnitude and a significant decrease of $U-B$ and $B-V$ colours were recorded in October 1982. Spectral observations indicate that these changes resulted from an increase in the temperature of the star. (16 refs.)

On the dynamics of a thin spherically symmetric radiating shell, its classical model, and relativistic effects See Entry 116465

Second catalogue of H α line profiles in 55 Be star spectra See Entry 116491

Temperature-grid coordinates for treating pulsations in the hydrogen ionization zone See Entry 116630

Far ultraviolet colors of B and Be stars See Entry 116638

The extreme LMC supergiant HD 38489: an optical and ultraviolet study See Entry 116647

On the T Tauri nature of the variable star BM Cha See Entry 116650

The detection limits in ground based measurements of stellar microvariability See Entry 116652

Radio emission from AM Herculis: the quiescent component and an outburst See Entry 116740

SS Bootis: a totally eclipsing binary of the RS CVn type See Entry 116742

Infrared photometry of the RS CVn binaries. III. JHK light curves of UV Psc See Entry 116753

Spectroscopic observations of the cool eclipsing X-ray binary HD 155638 See Entry 116758

A 0538-66 See Entry 116759

A model for A 0538-66: the fast flaring pulsar See Entry 116761

The WN4.5 component of HD 219460 in the open cluster Markarian 50 See Entry 116769

Variable stars in NGC 6397 See Entry 116771

VBLW photometry of the open cluster NGC 2516 See Entry 116774

Ring nebulae associated with WR stars: stellar wind or stellar ejecta? See Entry 116807

On the distance to M33 determined from magnitude corrections to Hubble's original Cepheid photometry See Entry 116813

Slippery evidence on the Galaxy's invisible heavy halo See Entry 116854

97.60 LATE STAGES OF STELLAR EVOLUTION

(inc. black holes)

97.60B Supernovae

116706 Neutrino emission from a hot, dense, plane-parallel atmosphere in hydrostatic equilibrium. III. The three-flavored atmosphere. P.J.Schinder, S.L.Shapiro (Center for Radiophys. & Space Res., Cornell Univ., Ithaca, NY, USA).

Astrophys. J. (USA), vol.273, no.1, pt.1, p.330-45 (1 Oct. 1983). For pt.II see *Astrophys. J. Suppl. Ser.*, vol.50, no.1, p.23-38 (1982). The authors continue their investigation of plane-parallel neutrino atmospheres in hydrostatic equilibrium by relaxing one of the assumptions made in paper I and allowing transport by all three flavors of neutrinos; electron, μ , and τ . As in paper I, it is assumed that the gas through which the neutrinos flow consists of free, nondegenerate, nonrelativistic nucleons, extreme relativistic positrons and electrons of arbitrary degeneracy, and photons. It is found that the three-flavored atmospheres are cooler and denser than the corresponding electron-flavored atmospheres. (6 refs.)

116707 Do filaments form at the time of supernova explosions? R.Bandiera (European Southern Obs., Garching bei Munchen, Germany), F.Pacini, M.Salvati.

Astron. & Astrophys. (Germany), vol.126, no.1, pt.2, p.7-9 (Sept. 1983). The authors consider the evidence that, at least in the case of the Crab Nebula filaments are formed much before a substantial interaction with the interstellar medium has taken place. It is suggested that in supernovae with a central pulsar the envelope is fragmented shortly after the explosion because of a Rayleigh-Taylor instability. The emission from a pulsar-powered bubble would then become visible, in agreement with the radio supernova phenomenon. (14 refs.)

116708 Softening effects in the equation of state and influence of general relativity on the outcome of stellar collapse. B.Kampfer (Zentralinst. fur Kernforschung, Acad. der Wissenschaften Rossendorf, Germany).

Astron. Nachr. (Germany), vol.304, no.4, p.167-70 (1983). The hydrodynamical evolution of a collapsing stellar core is followed to test the influence of general relativity and of softening effects in the equation of states. The general relativistic treatment of the collapse does not show any spectacular deviation from the Newtonian treatment. In particular there is no indication within the standard scenario for potential barrier penetration and continued collapse to a black hole. In the case of strong electron capture during the collapse the nuclear matter equation of state is of importance. A softening according to a phase transition below the bounce density is found to reduce the shock strength, but the shock is strong enough to cause the usual blowing-off. (25 refs.)

116709 BV photometry of the supernova 1982 in NGC 2268. R.Cadonau, C.Trefzger.

Inf. Bull. Variable Stars (Hungary), no.2382, p.1-3 (12 Aug. 1983). The authors report photographic BV photometry and a light curve for this supernova, covering the period 1982 February 27 to May 14. BV magnitudes are also given for a sequence of comparison stars surrounding the supernova. (3 refs.)

116710 Supernova in faint spiral galaxy. J.Maza.

I.A.U. Circ. (USA), no.3859, 1 pp. (14 Sept. 1983). Reports the discovery on 1983 July 12 of an 18th-magnitude supernova 4" east and 18" south of the nucleus of a faint spiral galaxy at $\alpha=0^h15.6^m$, $\delta=-37^\circ59'$ (equinox 1950.0), in Sculptor. Photographic magnitude estimates are reported for 1983 July 12 and September 6. (no refs.)

116711 Possible supernova in NGC 7418. J.Maza.

I.A.U. Circ. (USA), no.3867, 1 pp. (23 Sept. 1983). Reports the discovery on 1983 September 3 of a 15th-magnitude possible supernova $11''$ west and $52''$ south of the nucleus of the Sc-type galaxy NGC 7418 ($\alpha=22^h53.8^m$, $\delta=-37^\circ18'$, equinox 1950.0) in Grus. (no refs.)

116712 [IUE observations]. N.Panagia (Istituto di Radioastron., CNR, Bologna, Italy).

Mem. Soc. Astron. Ital. (Italy), vol.54, no.2, p.443-52 (1983). The results of IUE observations of supernovae are reviewed and discussed. A comparison with the spectral properties at other frequencies is also presented. (29 refs.)

116713 Similarity solutions for explosions in radiating stars with time-dependent energy and idealized magnetic field. B.G.Verma, J.P.Vishwakarma, V.Sharan (Dept. of Maths., Univ. of Gorakhpur, Gorakhpur, India).

Nuovo Cimento B (Italy), vol.76B, ser.2, no.1, p.62-72 (11 July 1983). A stellar model in which density in the undisturbed conducting-gas medium is assumed to obey a power law is considered. Similarity solutions for central explosion in radiating stars have been obtained under the assumption of isothermal-shock conditions. For the existence on self-similar character, the authors have assumed that both radiation pressure and energy are negligible. The results of numerical calculations for different models are illustrated through graphs. Moreover, a comparative study has been made between the results in ordinary gasdynamics and those obtained in magnetogasdynamics. (10 refs.)

116714 On the two possible progenitors of type I super nova. I.S.Shklovskii.

Pis'ma v Astron. Zh. (USSR), vol.9, no.8, p.474-7 (1983). In Russian. English translation in: *Sov. Astron. Lett. (USA)*. It is concluded from the observational data that there are two classes of stars outbursting as type I supernovae: relatively massive ($M\sim 3-6 M_\odot$) young ($T<10^9$ years) stars, and white dwarf components of low-mass binary systems with ages of $\sim 10^{10}$ years. The identical spectral and photometric characteristics of the two kinds of SN I imply the identity of the exploding nuclei of evolved stars. This is only possible if the mass of the nucleus of an evolved relatively massive star slightly exceeds the Chandrasekhar limit. (9 refs.)

On the dynamics of a thin spherically symmetric radiating shell, its classical model, and relativistic effects See Entry 116465

Collapse and explosion of white dwarfs. I. Precollapse evolution See Entry 116648

Positrons from supernovae and the origin of the galactic center positron annihilation radiation See Entry 116831

97.60G Pulsars

116715 Infrared study of the Crab pulsar: the 'shoulder' pulse and the 3.45 micron pulse profile. J.Middleditch, C.Pennypacker, M.S.Burns.

Astrophys. J. (USA), vol.273, no.1, pt.1, p.261-6 (1 Oct. 1983). Infrared measurements of the Crab pulsar with the NASA IRTF 3.0 m telescope show that the spectrum of the main pulse turns downward for

wavelengths longer than $3 \mu\text{m}$. The 'shoulder' pulse discovered by Penny-packer (1981) is measured in the 0.9-2.4 μm region, but disappears at 3.5 μm . This pulse rises from 0 to 20% of the height of the main pulse within 1 to 2 ms after the main pulse peak and decays with a 4 to 5 ms time constant. Excess infrared flux also appears after the interpulse. The main peak itself may be narrower at 3.45 μm than in the optical to 2.2 μm band. (10 refs.)

116716 General track of pulsar evolution. O.H.Guseinov, I.M.Yusifov (Phys. Inst., Acad. of Sci., Baku, Azerbaidzhan, SSR).

Astrophys. & Space Sci. (Netherlands), vol.94, no.2, p.249-52 (Aug. 1983). It is shown that large nulling, small luminosity and a large value of polarization angle variation are, together, a good indication of a pulsar's old age. Selection effects connected with the discovery of pulsars are analyzed. The general track of pulsar evolution, along which the diagram of pulsar emission and the angle between the magnetic and rotation axes decrease, is found. (7 refs.)

116717 Radio pulsars: intensity, polarization, and rotation fluctuations. J.M.Cordes (NAIC & Cornell Univ., Ithaca, NY, USA).

AIP Conf. Proc. (USA), no.101, p.98-112 (1983). (Workshop on Positron-Electron Pairs in Astrophysics, Greenbelt, MD, USA, Jan. 1983). In this review of radio emission phenomena emphasis is given to observables that may constrain the particle content in pulsar magnetospheres. These include intensity variations within single pulses (time scales from 1 μs to tens of milliseconds); pulse-to-pulse variations (one period to years) which are both 'continuous' (drifts of subpulse features through pulse phase and other quasi-periodic and aperiodic variations) and 'discontinuous' (pulse nulling, average pulse shape changes, changes in drift rates); polarization transitions between orthogonal modes; relationship of drifting subpulses to nulling; constraints on emission altitudes; and rotation noise due to internal and magnetospheric torque fluctuations. (54 refs.)

116718 The effect of nulls on the drifting subpulses in PSR 0809+74. A.V.Filipenko, A.C.S.Readhead, M.S.Ewing (Dept. of Astron., California Inst. of Technol., Pasadena, CA, USA).

AIP Conf. Proc. (USA), no.101, p.113-17 (1983). (Workshop on Positron-Electron Pairs in Astrophysics, Greenbelt, MD, USA, Jan. 1983). The manner in which nulls affect the drifting subpulses of PSR 0809+74 has been investigated. Immediately following a null, subpulses reappear at approximately the longitudes expected for subpulses in the first nulled pulse, as previously reported. The higher quality of the new data, however, has made it possible to demonstrate that the 'phase memory' is not perfect; there is a small systematic phase shift in the direction of normal drift. This result is probably inconsistent with the hypothesis that during a null, electron-positron pair production in the polar gap is absent and local 'hot spots' identify the regions over which discharges last occurred. On the other hand, if nulling is the manifestation of temporally steady discharge within discrete regions in the polar gap, a slight phase shift is expected, but the observations do not confirm the prediction that its magnitude should be proportional to null length. In addition, this scenario has difficulty explaining the abnormally slow subpulse drift following long nulls and the absence of radio radiation during nulls associated with large phase shifts. (10 refs.)

116719 Discovery of a millisecond pulsar. S.R.Kulkarni (Dept. of Astron., Univ. of California, Berkeley, CA, USA).

AIP Conf. Proc. (USA), no.101, p.118-28 (1983). (Workshop on Positron-Electron Pairs in Astrophysics, Greenbelt, MD, USA, Jan. 1983). The authors have discovered a pulsar with a period of about 1.556 milliseconds. The discovery of the pulsar has cleared up the mystery surrounding the enigmatic source, 4C 21.53. An exposition of the history of the search process, results from the timing program, the pulse waveform, the distance and the origin of the pulsar are discussed. (33 refs.)

116720 High energy observations of pulsars. G.Kanbach (Max-Planck-Inst. fur Phys. und Astrophys., Inst. fur Extraterrestrische Phys., Garching, Germany).

AIP Conf. Proc. (USA), no.101, p.129-40 (1983). (Workshop on Positron-Electron Pairs in Astrophysics, Greenbelt, MD, USA, Jan. 1983). High energy emissions have so far only been definitely observed from two pulsars: Crab (PSR 0531+21) and Vela (PSR 0833-45). In these sources, however, the luminosity at gamma-ray energies surpasses the radio luminosity by approximately 10^6 which demonstrates the basic importance of this emission for the pulsar radiation budget. Deep observations performed with the COS-B instrument in the 0.1 to 1 GeV gamma-ray energy range have revealed several previously unknown details. The Vela pulsar gamma-ray spectrum changes with light-curve phase such that the second peak of emission exhibits a harder spectrum than the first peak. In the Crab pulsar a secular change of the relative strength of the two peaks of emission has been detected with high probability in the course of observations spread over 5 years. It is remarkable that concurrent observations of the X-ray (2-12 keV) pulse profile of Crab do not show this variation. The search for gamma-ray emission from further radio pulsars has up to now been inconclusive. From the estimated flux limits it is however possible to derive limits to the contribution of pulsars to the high energy luminosity of the Galaxy. It is expected that the next generation of telescopes on board the Gamma Ray Observatory will discern several more gamma-ray pulsars. (33 refs.)

116721 Properties of the Crab pulsar inferred from the phase-averaged spectrum. F.K.Knight (Naval Res. Lab., E.O. Hulbert Center for Space Res., Washington, DC, USA).

AIP Conf. Proc. (USA), no.101, p.141-6 (1983). (Workshop on Positron-Electron Pairs in Astrophysics, Greenbelt, MD, USA, Jan. 1983). The Crab pulsar emission can be described adequately by using the phase-averaged spectrum, which is continuous from the near infrared to the γ -ray range. Using most of the published observations over this energy range, a power law fit to the emission requires at least two power laws with a break of 0.74 ± 0.02 in spectral index at 39 ± 3 keV. If this emission is synchrotron radiation, then the emitting electron spectrum is continuous over about five decades and has a break of ~ 1.5 in spectral index at $\gamma = E/mc^2 = 1900 \pm 200$ (10^6 gauss/B) $^{1/2}$. With $B_\perp = 10^6$ gauss, the electrons emitting in the infrared have $\gamma = 10$. Because a fit with three power laws has approximately the same χ^2 , a gradual turnover is consistent with the data, as one would expect from synchrotron emission. (20 refs.)

116722 COS-B upper limits on gamma-ray emission from radio pulsars. R.Buccheri (IFCAI-CNR, Palermo, Italy).

AIP Conf. Proc. (USA), no.101, p.147-51 (1983). (Workshop on Positron-Electron Pairs in Astrophysics, Greenbelt, MD, USA, Jan. 1983). Reports on the results of a search for pulsed gamma-ray emission from old radio pulsars in the COS-B data in the energy range 50 MeV to 2 GeV. The analysis has been done by using either pulsar parameters obtained in simultaneous radio and gamma-ray observations or parameters which could be reliably derived by interpolation from radio observations spanning the COS-B observations. (16 refs.)

116723 Energy spectra of very high energy γ -rays from the Crab and Vela pulsars. S.K.Gupta, P.V.Ramana Murthy, B.V.Sreekantan, S.C.Tonwar, P.R.Viswanath (Tata Inst. of Fundamental Res., Bombay, India). *AIP Conf. Proc. (USA)*, no.101, p.157-62 (1983). (Workshop on Positron-Electron Pairs in Astrophysics, Greenbelt, MD, USA, Jan. 1983).

Using the atmospheric Cerenkov radiation technique the authors have observed pulsed emission of very high energy, $E_{\gamma} \geq 10^{12}$ eV, γ -rays from the Crab and Vela pulsars. Ooty Cerenkov telescope composed of 18 reflectors has been used in the 'distributed mode' for these observations during early 1981. In this mode the arrival direction of individual showers has been measured to an accuracy $\sim 0.3^\circ$ which has made possible a more reliable estimation of the γ -ray energy thresholds in the direction of these two pulsars. Observations on the Crab pulsar show evidence of sporadic emission with significant variability of the pulsed flux over periods as short as tens of minutes. The measured pulsed flux of $2.2 \pm 0.5 \times 10^{-11}$ ph. $\text{cm}^{-2} \text{s}^{-1}$ at energies $> 9 \times 10^{11}$ eV during the active phase agrees well with the extrapolation of the Cos-B spectra $2.9 \times 10^{-11} \text{ GeV}^{-1.17} \text{ ph. cm}^{-2} \text{s}^{-1}$, both in amplitude and spectral slope. The time averaged flux is however considerably smaller. On the other hand the time averaged pulsed flux of $1.0 \pm 0.4 \times 10^{-11} \text{ ph. cm}^{-2} \text{s}^{-1}$ at energies $> 2.3 \times 10^{12}$ eV for the Vela pulsar is about two orders of magnitude smaller than the extrapolated value from the Cos-B spectrum, $1.8 \times 10^{-7} \text{ E}_{\text{GeV}}^{-1.11} \text{ ph. cm}^{-2} \text{s}^{-1}$. Also the energy spectrum for the Vela pulsar at energies $\sim 2.5 \times 10^{12}$ eV with a slope of -2.2 ± 0.2 is much steeper than at lower energies. These observations suggest significant differences between γ -ray emission from these two pulsars. (9 refs.)

116724 Electron positron pairs in radio pulsars. J.Arons (Astron. Dept., Univ. of California, Berkeley, CA, USA). *AIP Conf. Proc. (USA)*, no.101, p.163-93 (1983). (Workshop on Positron-Electron Pairs in Astrophysics, Greenbelt, MD, USA, Jan. 1983). Outlines the role of electron-positron pairs in some theoretical models of the magnetospheres of radio pulsars. While there is little direct evidence for the presence of pairs in the form of an observed recombination line, their formation leads to many promising features in theories of the electrodynamics and plasma physics of these objects' magnetospheric structure and for the interpretation of the observed photon emissions, both from pulsars themselves and from the surrounding interstellar medium. (128 refs.)

116725 Pair production near threshold in pulsar magnetic fields. A.K.Harding (NASA/Goddard Space Flight Center, Greenbelt, MD, USA), J.K.Daugherty. *AIP Conf. Proc. (USA)*, no.101, p.194-8 (1983). (Workshop on Positron-Electron Pairs in Astrophysics, Greenbelt, MD, USA, Jan. 1983). In pulsar polar cap models, curvature radiation γ -rays produce e^+e^- pairs in the strong magnetic fields near the surface of the neutron star. While these γ -rays have energies $E_{\gamma} \gg mc^2$, they also propagate at very small angles to the field, such that the threshold condition, $E_{\gamma} > 2 mc^2/\sin\theta$ is just barely satisfied when they pair produce. Threshold effects on the pair production attenuation coefficient, which are due to the discreteness of the e^+e^- Landau states, must therefore be considered when computing the mean free paths of curvature radiation photons in pulsar magnetic fields. These effects, which are not incorporated in the asymptotic expression for the attenuation coefficient, have some interesting consequences for pulsar models. Since pair production is suppressed near threshold, the photon mean free paths are longer than previously thought. In magnetic fields $\geq 6 \times 10^{12}$ G, the pairs tend to be produced in the ground state Landau level and will not synchrotron radiate. Since synchrotron radiation is an essential ingredient in the electromagnetic cascades which produce low energy pairs above the acceleration region, pulsars with very high magnetic fields may not produce many pairs. (8 refs.)

116726 Polarization mode coupling in radio pulsars. D.R.Stinebring (Nat. Radio Astron. Obs., Charlottesville, VA, USA), J.M.Cordes. *AIP Conf. Proc. (USA)*, no.101, p.199-203 (1983). (Workshop on Positron-Electron Pairs in Astrophysics, Greenbelt, MD, USA, Jan. 1983). Mode coupling (polarization limiting) has been proposed as an explanation for the orthogonally polarized radiation (OPR) observed from pulsars. Using a simplified magnetospheric model the authors show that it cannot account for the presence of circular polarization in the OPR phenomenon. Mode coupling occurs much closer to the star than the point at which the normal modes of the plasma become significantly elliptically polarized. (11 refs.)

116727 Pulsar gamma-ray lines from quarkonium systems. G.Kanbach (Inst. fur Extraterrestrische Phys., Max-Planck-Inst. fur Phys. und Astrophys., Garching, Germany), R.Schlickeiser. *AIP Conf. Proc. (USA)*, no.101, p.204-10 (1983). (Workshop on Positron-Electron Pairs in Astrophysics, Greenbelt, MD, USA, Jan. 1983). Excited states of heavy quark-antiquark systems (quarkonium) might be created by colliding e^-e^+ beams in the magnetospheres of gamma-ray pulsars. The authors investigate the hypothesis that radiative transitions to the ground state, in particular of charmonium, may lead to observable fluxes of gamma-ray lines in the 120-450 MeV range and compare the estimates to the continuum flux expected from curvature radiation. If the particle density in the source volumes is high enough the lines could be resolvable with the next generation of high-energy gamma-ray telescopes (Gamma Ray Observatory). (20 refs.)

116728 The pulsar oblique rotator: numerical solution of an illustrative problem. V.G.Endean (Dept. of Engng., Univ. of Durham, Durham, England).

Mon. Not. R. Astron. Soc. (GB), vol.204, no.3, p.1067-79 (Sept. 1983). A series solution of the force-free pulsar magnetosphere equations inside the velocity-of-light cylinder and excluding conduction current along the field lines, is developed. Computer-generated field line plots for the fully oblique rotator are presented. These illustrate the topology of the closed field line, open field line and vacuum regions which contains some unexpected features. Implications for pulse emission theories are briefly discussed. (22 refs.)

116729 Pulsar electrodynamics: cylindrical model and radio and gamma-ray radiation. A.A.da Costa (Dept. of Astron., Univ. of Manchester, Manchester, England). *Mon. Not. R. Astron. Soc. (GB)*, vol.204, no.3, p.1125-44 (Sept. 1983). Magnetospheres of pulsars contain charged particles. The motion of electrons and positrons in a simplified cylindrical model is discussed for pulsars with three different periods. It will be shown that this motion near the region $E=cB$ provides not only a mechanism for the production of incoherent radiation at gamma-ray frequencies but also the basis to explain the radio emission. A single region to explain the radiation in both frequency domains is supported by observations of the Crab Pulsar. (27 refs.)

116730 The evolution of radio pulsars. B.N.Candy, D.G.Blair (Dept. of Phys., Univ. of Western Australia, Nedlands, Australia). *Mon. Not. R. Astron. Soc. (GB)*, vol.205, no.1, p.281-4 (Oct. 1983). Considers a model for the evolution of radio pulsars which incorporates decay of the emission-cone angle and alignment of the emission cone with the spin axis. This model predicts that decay of the emission-cone angle dominates for the youngest pulsars, producing a decrease in the observed pulsewidth. Align-

ment of the emission cone dominates for the oldest pulsars, producing a rapid increase in the observed pulsewidth. The authors show that radio pulsars do indeed have a dependence of pulsewidth on characteristic age which is in good agreement with this model. The results suggest that the emission cone aligns on a time-scale $\approx 10^7$ yr. (8 refs.)

116731 Gravitational radiation reaction in the binary pulsar and the quadrupole-formula controversy. T.Damour (Groupe d'Astrophys. Relativiste, Obs. de Paris-Meudon, Meudon, France). *Phys. Rev. Lett. (USA)*, vol.51, no.12, p.1019-21 (19 Sept. 1983). The evolution of the orbit of a binary pulsar under the action of gravitational radiation reaction is calculated. No approximation is made of weak gravity inside the individual stars; the details of the orbital motion are given directly (to order c^{-5} and G^3). The calculation reveals no acceleration of the center of mass of the system, and a secular decrease of the time of return to periastron. The quantitative results agree both with the well-known 'quadrupole formula' and with observations. (12 refs.)

Conditions for stimulated-annihilation in a degenerate e^-e^+ fluid at the surface of pulsars See Entry 116458

The production of spinless hadron pairs via virtual photon exchange in uniform magnetic fields See Entry 116459

Parametric detector as a tunable antenna for continuous gravitational radiation See Entry 116485

The pulsar P/P distribution and the postulated solar companion See Entry 116627

Do filaments form at the time of supernova explosions? See Entry 116707

Positron production by a hot, young pulsar See Entry 116833

97.60J Neutron stars

116732 Phase transitions in dense stars. J.Diaz Alonso (Groupe d'Astrophys. Relativiste, Obs. de Paris, Meudon, France).

Astron. & Astrophys. (Germany), vol.125, no.2, pt.1, p.287-301 (Sept. 1983). In order to analyze the effects of first-order phase transitions of dense matter on the structure and collapse of dense stars, a simple analytically-solvable model is proposed. The model shows the existence of two kinds of stable spherically-symmetric equilibrium configurations: the one-phase configurations with a central pressure which is lower than the phase-transition pressure, and the two-phase (mixed) configurations with a dense-phase core and a diluted-phase envelope. The stability of the static configurations is analyzed. Some (eventually observable) parameters characterizing the collapse such as the characteristic time of collapse, the energy release and the small-oscillation frequencies near the final equilibrium configuration are estimated. (22 refs.)

116733 Resonant free-free emission from electrons in magnetic polar regions of accreting neutron stars. R.Lieu (Dept. of Phys., Univ. of Calgary, Calgary, Alberta, Canada).

AIP Conf. Proc. (USA), no.101, p.438-43 (1983). (Workshop on Positron-Electron Pairs in Astrophysics, Greenbelt, MD, USA, Jan. 1983). Near the magnetic polar cap of an accreting neutron star, emission of photons at cyclotron resonance is accompanied with the transition of electrons between Landau levels as a result of free-free collisions with ions. In quantum electrodynamics, the resonance condition is satisfied whenever the energy denominators of the two possible time orderings in electron free-free emission become singular. In the absence of motion along the magnetic field, both singularities occur near the cyclotron frequency. If there is a definite longitudinal momentum due to bulk motion of the accreting plasma, the singularities for forward and backward scattering can occur at different frequencies. Moreover, the frequencies are dependent on the pitch angle of photon emission. For a given line-of-sight direction, this is a line splitting effect, the observability of which depends on the degree of Comptonization and the plasma temperature. (2 refs.)

Comparison of photon-photon and photon-magnetic field pair production rates See Entry 116457

Do filaments form at the time of supernova explosions? See Entry 116707

Photometric observations. Is HZ Herculis getting darker? See Entry 116748

HZ Her: the nature and origin of the emission lines See Entry 116760

A model for A 0538-66: the fast flaring pulsar See Entry 116761

Gamma ray bursts See Entry 116875

Theories of gamma-ray bursts See Entry 116879

A fireball model for the March 25, 1978 gamma ray burst See Entry 116881

97.60L Black holes

116734 Black hole electromagnetic fields and negative energy states for charged particles. A.R.Prasanna (Max-Planck-Inst. fur Astrophys., Garching, München, Germany).

Astron. & Astrophys. (Germany), vol.126, no.1, pt.2, p.111-14 (Sept. 1983). Compares two kinds of electromagnetic fields of a black hole space-time between (i) the field due to a Kerr-Newmann black hole and that of (ii) the field due to current rings outside the event horizon of an uncharged black hole. Further, the author considers the effective potentials for charged particles in both fields and finds that a potential well with stable negative energy states occurs in the latter case, whereas in the former the negative energy states occur only for capture orbits. (6 refs.)

116735 Electron-positron processes and spectral evolution in black hole accretion disk dynamo models for AGN sources of the cosmic X-ray and gamma ray backgrounds. D.Leiter (Lab. for High Energy Astrophys., NASA Goddard Space Flight Center, Greenbelt, MD, USA).

AIP Conf. Proc. (USA), no.101, p.337-42 (1983). (Workshop on Positron-Electron Pairs in Astrophysics, Greenbelt, MD, USA, Jan. 1983). The author discusses a black hole accretion disk dynamo model for active galactic nuclei (AGN) sources of the cosmic X-ray and gamma ray backgrounds which involves both thermal and nonthermal accretion disk processes around $\geq 10^8 M_\odot$ Kerr black holes. Before black hole spin-up to the Kerr metric state, the large value of the compactness parameter $> 10^{30}$ erg/cm-sec associated with the $L/L_{\text{Edd}} \leq 1$ luminosity ratio in precursor active galaxies (PAG) suppresses all nonthermal emission mechanisms. In this PAG state the resulting emission is predominantly thermal and is due to comptonization of soft photons by an electron-positron plasma, generated within the hot accretion disk region by $\gamma + \gamma \rightarrow e^+e^-$ processes in the transrelativistic regime. While the underlying plasma in the PAG accretion disk hot inner region may be optically thin initially, the overall effect of the copious $\gamma + \gamma \rightarrow e^+e^-$ generated electron-positron plasma is to push the overall optical depth to $\tau \geq 1$. (16 refs.)

116736 High energy spectrum of spherically accreting black holes. P.Meszaros (Harvard-Smithsonian Center for Astrophys., Cambridge, MA, USA), J.P.Ostriker.
AIP Conf. Proc. (USA), no.101, p.348-52 (1983). (Workshop on Positron-Electron Pairs in Astrophysics, Greenbelt, MD, USA, Jan. 1983).
Spherically accreting black holes may sustain strong collisionless shocks, downstream of which the fluid approximation is not valid. The proton-electron Coulomb exchange provides for the downstream matter diffusion into the hole. Energy conversion efficiencies upward of 10-30% are obtained, with most of the luminosity in hard X-rays and γ -rays. The authors discuss the whole spectrum and its application for radio-quiet QSOs and galactic X- and γ -ray sources. (11 refs.)

116737 Hot accretion disks and γ -ray cosmic sources. M.Kafatos (George Mason Univ., Fairfax, VA, USA), J.A.Eilek.
AIP Conf. Proc. (USA), no.101, p.354-8 (1983). (Workshop on Positron-Electron Pairs in Astrophysics, Greenbelt, MD, USA, Jan. 1983).
Hot accretion disks around rotating black holes produce copious amounts of X-rays, γ -rays and e^+e^- pairs. These complexized models with an energy flux spectral index of the X-ray spectrum ~ 1 are optically thick to $\gamma\gamma$ pair production. The resultant high energy spectrum steepens above a few MeV. The few γ -ray spectra of active galactic nuclei that are available show this steepening as well as the γ -ray diffuse background. The same processes that take place in a hot accretion disk around a supermassive black hole at the center of an active nucleus also operate in a hot accretion disk around a stellar mass black hole. The authors examine the implications for the two galactic sources Cygnus X-1 and particularly the positron source at the galactic nucleus. (19 refs.)

116738 Rotating black hole in asymptotic de Sitter space: perturbation of the space-time with spin fields. U.Khanal (Dept. of Phys., Tribhuvan Univ., Kirtipur, Nepal).
Phys. Rev. D (USA), vol.28, no.6, p.1291-7 (15 Sept. 1983).
The Newman-Penrose formalism is used to work with gravitational, electromagnetic, and Dirac field perturbations of the Kerr-de Sitter space. It is shown that the resulting equations are separable, and the radial parts (for the massless fields) combine into a master equation resembling that of Teukolsky. This master equation includes the Teukolsky equation and the equation arising from the de Sitter-Schwarzschild Universe, and can be reduced to these cases under appropriate limiting conditions. Finally, the radial parts of the electromagnetic and neutrino fields are transformed to the form of the one-dimensional barrier-penetration equation. (12 refs.)

116739 Black holes. W.Israel (Dept. of Appl. Math., Univ. of Cape Town, Rondebosch, South Africa).
Sci. Prog. (GB), vol.68, no.271, p.333-63 (Autumn 1983).
A review of black holes is presented. The author follows roughly the historical evolution of the theories, beginning with the 1930s work by Chandrasekhar, Landau and Oppenheimer on the inevitability of collapse for sufficiently heavy cold stars, and culminating with an account of the unsuspected connections between thermodynamics, quantum theory and gravitation revealed by Hawking's celebrated discovery that black holes evaporate thermally by a quantum tunnelling process. (58 refs.)

Emission of relativistic particles in a strong gravitational field	See Entry 111531
The existence of a black hole due to condensation of matter	See Entry 116464
Softening effects in the equation of state and influence of general relativity on the outcome of stellar collapse	See Entry 116708
Electron/positron/gamma ray beams in cosmic radio sources	See Entry 116837

97.80 BINARY AND MULTIPLE STARS
(inc. extrasolar planetary systems)

116740 Radio emission from AM Herculis: the quiescent component and an outburst. G.A.Dulk, T.S.Bastian (Dept. of Astro-Geophys., Univ. of Colorado, Boulder, CO, USA), G.Chanmugam.
Astrophys. J. (USA), vol.273, no.1, pt.1, p.249-54 (1 Oct. 1983).
The Very Large Array was used to search for radio emission from AM Herculis type binaries. The detection of 4.9 GHz radio emission from AM Her was verified. Upper limits of about 0.2 mJy (3 σ) for the 4.9 GHz radiation from VV Pup, EF Eri, PG 1550+191, CW 1103+254, and AN UMa were also obtained. A remarkable outburst of radiation from AM Her at 4.9 GHz was also detected. It is suggested that electrons with energies of ~ 500 keV trapped in the magnetosphere of the white dwarf can account for the quiescent emission of AM Her. The outburst is probably due to an electron-cyclotron maser which operates near the surface of the red-dwarf companion. (28 refs.)

116741 The F-type eclipsing binaries ZZ Bootis, CW Eridani, and BK Pegasi. D.M.Popper (Dept. of Astron., Univ. of California, Los Angeles, CA, USA).
Astron. J. (USA), vol.88, no.8, p.1242-56 (Aug. 1983).
Spectrographic orbits of these three double-lined binaries are determined from spectrograms obtained at the Lick Observatory. The photometric observations of ZZ Boo by McNamara et al. and of CW Eri by Chen are reanalyzed, and revised properties of the components are derived. The properties of the most definitive F-type stars are shown in the mass-radius, mass-luminosity, and color-magnitude planes, along with zero-age relations. The components of the three systems analyzed are among the more evolved binaries having both components in the state of core hydrogen burning. (27 refs.)

116742 SS Bootis: a totally eclipsing binary of the RS CVn type. J.W.Wilson (Dyer Obs., Vanderbilt Univ., Nashville, TN, USA), S.D.Hall, G.W.Henry, C.A.Vaucher, J.L.Africano.
Astron. J. (USA), vol.88, no.8, p.1257-63 (Aug. 1983).
Six years of photoelectric photometry, from 1976 to 1981, are presented. The distortion wave has varied in amplitude from 0.05^m to 0.20^m, with no apparent pattern; one change in 1980, from 0.05^m to 0.10^m, occurred within three months. In 1980 to 1981 the wave migration, which a few years before had been towards increasing orbital phase and quite rapid, appears to have stopped. Between 1976 and 1981 the mean brightness outside eclipse has increased by 0.075^m in V. From the rectified light curve a new time of midprimary eclipse is found to be JD(hel.) = 2444332.0335 \pm 0.0005^d. Solutions of the primary eclipse data, rectified for starspots as well as for ellipticity and reflection, yield $L_1(V) = 0.4163 \pm 0.0006$, $L_1(B) = 0.5000 \pm 0.0009$, $r_1 = 0.064 \pm 0.002$, $r_c = 0.160 \pm 0.001$, and $i = 88.8^\circ \pm 0.3^\circ$. Using values of $M \sin^2 i = 1.00 M_\odot$ for each star, the authors $M_h = 1.00 M_\odot$, $M_c = 1.00 M_\odot$, $R_h = 1.31 R_\odot$. (22 refs.)

116743 The effect of low-velocity, low-mass intruders (collisionless gas) on the dynamical evolution of a binary system. J.G.Hills (Theoretical Div., Los Alamos Nat. Lab., Los Alamos, NM, USA).
Astron. J. (USA), vol.88, no.8, p.1269-83 (Aug. 1983).
More than 20000 computer-simulated encounters between low-mass (compared to the binary components) intruders and binary systems are made. These calculations are made in the important (and difficult) limit where the intruder velocity is small compared to the orbital velocity of the binary. The dependence of the encounters on orbital eccentricity, on the mass ratios of the binary components, and on the impact parameter is found. These encounters increase the binding energy of the binary. At zero impact parameter, the average increase in the binding energy is proportional to the square of the binary orbital eccentricity. However, the increase in the binding energy decreases much faster with increasing impact parameter as the eccentricity increases. The net result is that the total cross section for increasing the binding energy of a binary through encounters with low-mass intruders is independent of the orbital eccentricity of the binary. The average increase in the binding energy per encounter is directly proportional to the mass of the intruder. (14 refs.)

116744 The multiple system β Sco and the age of the Upper Scorpius complex. M.A.Giannuzzi (Osservatorio Astron. di Roma, Roma, Italy).
Astron. & Astrophys. (Germany), vol.125, no.2, pt.1, p.302-7 (Sept. 1983).
Physical quantities for the massive components of β Sco A, the brightest member of the multiple system β Sco, are calculated on the basis of the spectroscopic orbit elements and of the photometric measurements carried out when the system underwent occultations. The age of the system is determined by using Stother's (1972) evolutionary models. The stars of the Upper Scorpius complex (to which β Sco belongs), that are earlier than ($B - V_0 = -0.20$, agree with the same value of the age (log t ranging from 6.7 and 6.8, t in years), but later stars appear to be older. An analysis of the various data used supports the value of 170 pc as the mean distance to Upper Scorpius. (34 refs.)

116745 Mass transfer in close binary systems: original and remnant masses. G.Giuricin, F.Mardirossian, M.Mezzetti (Osservatorio Astron., Trieste, Italy).
Astron. & Astrophys. (Germany), vol.125, no.2, pt.1, p.388-90 (Sept. 1983).
The comparison of the masses of numerous Algol binaries (and a few Wolf-Rayet systems) with some new relevant theoretical predictions, in which the influence of overshooting in stellar interiors is considered, appears to reconfirm that usual mass transfer computations cannot satisfactorily account for the observed masses of the post-mass exchange (case B) remnants. (15 refs.)

116746 The possible long-period eclipsing binary BM Eri. P.Ahlin, A.Sundman (Stockholms Obs., Saltsjobaden, Sweden).
Astron. & Astrophys. (Germany), vol.125, no.2, pt.1, p.391-3 (Sept. 1983).
BM Eri, an M giant which had a drop in brightness of about 0.8 in photographic magnitude in 1944 and is suspected to be a long period eclipsing binary, has been observed for radial velocity (-1.4 km s⁻¹) and spectral type and luminosity (M6 III, $M_V = -2.5$). The absolute magnitude is determined from the Wilson-Bappu effect. No secondary spectrum is observed. The star cannot be confirmed to be an eclipsing binary, but possible periods are discussed. Because of the long period of the object the observations are described in more detail than would normally be necessary. (21 refs.)

116747 Ultra high energy gamma rays from Cygnus X-3. J.C.Dowthwaite, A.I.Gibson, A.B.Harrison, I.W.Kirkman, A.P.Lotts, J.H.Macrae, K.J.Orford, K.E.Turver, M.Walmsley (Dept. of Phys., Univ. of Durham, Durham, England).
Astron. & Astrophys. (Germany), vol.126, no.1, pt.2, p.1-6 (Sept. 1983).
Results of two years of observation of Cygnus X-3 using the Dugway gamma ray telescopes are presented. The suggested variability of ultra high energy (UHE) gamma ray intensity on a time scale of 4.8 h is investigated. Evidence for a 4.8 h modulation was obtained from drift scan observations indicating that UHE gamma rays of energy > 1300 GeV are emitted with an average peak strength of about 2×10^{-10} cm⁻² s⁻¹, with the maximum in gamma rays coinciding with the X-ray maximum. A 34d variation in the strength of the 4.8 h maximum, as already noted in X-rays, has been observed in UHE gamma rays. (25 refs.)

116748 Photometric observations. Is HZ Herculis getting darker? H.-C.Thomas (Max-Planck-Inst. fur Phys. & Astrophys., Garching, Munchen, Germany), J.Africano, A.J.Delgado, H.U.Schmidt.
Astron. & Astrophys. (Germany), vol.126, no.1, pt.2, p.45-50 (Sept. 1983).
New photometric measurements of HZ Her in the B-filter are presented and analyzed, together with some of the older observations, for their dependence on orbital phase and phase in the 35^d-cycle. It is shown that conclusions can be drawn for turn-on times, light curve asymmetries, and brightness variations of this source. (17 refs.)

116749 Photometric observations and elements of the eclipsing binary TT Herculis. K.K.Kwee, A.M.van Genderen (Leiden Obs., Leiden, Netherlands).
Astron. & Astrophys. (Germany), vol.126, no.1, pt.2, p.94-101 (Sept. 1983).
Photoelectric observations in yellow and blue light (UBV system) made in 1962 and 1963 of the β Lyrae type eclipsing binary TT Her are presented and discussed. The period appears to be variable. Photometric and absolute dimensions are determined and discussed. (24 refs.)

116750 The BUSS spectrum of β Lyrae. M.Hack, J.Sahade (Astron. Obs., Trieste, Italy), C.de Jager, Y.Kondo.
Astron. & Astrophys. (Germany), vol.126, no.1, pt.2, p.115-20 (Sept. 1983).
The spectrum of β Lyrae taken with the Balloon-borne ultraviolet Stellar Spectrograph experiment in May, 1976, at phase 0.61 p, has disclosed the presence of N II emission and has provided evidence for about the same location, in the outer envelope of the system, of the layers responsible for the resonance Mg II doublet emissions and for the 'narrow' H α emission. Three sets of absorption lines, P Cygni profiles of Fe III and broad Beals type III emissions of Mg II, are also present. (20 refs.)

116751 The light curve changes of VW Cephei. I.Kotarska, Z.Glownia (Inst. of Phys., Silesian Univ., Katowice, Poland).
Astron. Nachr. (Germany), vol.304, no.4, p.181-8 (1983).
A long series of photoelectric observations of the W UMa type eclipsing binary VW Cephei collected since 1952 is discussed. The so-called Kwee effect is examined—regarding the heights of maxima and the depths of minima—in order to detect periodicities in the light curve changes. The frequency analysis reveals periodicities only in small homogeneous observational domains, but the power spectrum (in the sense of a discrete Fourier transform) of all the observations is very complicated for exact interpretation. The light curve changes are much larger than the possible errors, but they have lost their periodic character in the whole of the time interval under discussion. (27 refs.)

116752 A study of ultraviolet spectra of ζ Aur/VV Cep systems. III. Atlas of theoretical curves of growth. K.Hempe (Univ. Hamburg, Hamburg, Germany). *Astron. & Astrophys. Suppl. Ser. (France)*, vol.53, no.3, p.339-46 (Sept. 1983).
An atlas of theoretical curves of growth calculated for pure absorption lines formed in the winds of the cool component of ζ Aur/VV Cep systems is presented. The envelope structure is characterized by the wind velocity which has been assumed to be constant, the dimensions of the system and the atomic parameters of the line under study. The phase dependence of equivalent widths and the effect of different velocity laws are discussed. Observed UV absorption lines such as those of Fe II multiplet 9 can be used to determine wind velocities, stochastic velocities and mass loss rates from the calculated curves of growth. (6 refs.)

116753 Infrared photometry of the RS CVn binaries. III. *JHK* light curves of UV Psc. E.Antonopoulou (Royal Obs. of Edinburgh, Edinburgh, Scotland). *Astron. & Astrophys. Suppl. Ser. (France)*, vol.53, no.3, p.347-9 (Sept. 1983).
For pt.II see *ibid.*, vol.52, no.3, p.381-2 (1983). *JHK* light curves of the RS CVn binary UV Psc are presented. A detailed analysis of the light curves is published separately. (3 refs.)

116754 A photometric study of the eclipsing binary V478 Cygni. C.Sezer (Ege Univ. Obs., Izmir, Turkey), N.Gudur, O.Gulmen, H.Sengonca. *Astron. & Astrophys. Suppl. Ser. (France)*, vol.53, no.3, p.363-72 (Sept. 1983).
Nearly 1100 new photoelectric observations of the photometrically neglected eclipsing binary V478 Cygni in blue and yellow colours are presented. The improved light elements are calculated from the new photoelectric minima. The light curves were analyzed using Wood's (1972) model simulation program WINK. The system was found to be a detached binary. (14 refs.)

116755 Micrometric measurements of binary stars (first list). M.Scardia (Osservatorio Astron. di Brera, Merate, Italy). *Astron. & Astrophys. Suppl. Ser. (France)*, vol.53, no.3, p.433-40 (Sept. 1983). In French.
The results of 167 micrometric measurements of 48 binaries, obtained at Brera-Merate Observatory with a 23 cm refractor during the period September 1982-February 1983, are given. 85 measurements of 30 systems that were found in the archives of 'Urania' of the association of amateur astronomers of Genoa are also given. These measurements were made during the period 1935-1937 with the Salmoiraghi, refractor of 156 mm diameter by the Genoese amateur Ugo Mantelli. (8 refs.)

116756 Photoelectric minima of eclipsing binaries. E.Pohl (Nurnberg Obs., Nurnberg, Germany), E.Hamzaoglu, N.Gudur, C.Ibanoglu. *Inf. Bull. Variable Stars (Hungary)*, no.2385, p.1-6 (18 Aug. 1983).
The authors report photoelectric times of minima, mostly obtained during 1982, for 30 eclipsing binary stars. (no refs.)

116757 Eclipse timings of 31 Cygni. P.C.Schmidtke (Kitt Peak Nat. Obs., Tucson, AZ, USA), R.E.Fried, J.L.Hopkins, R.E.Stencel. *Inf. Bull. Variable Stars (Hungary)*, no.2392, p.1-2 (26 Aug. 1983).
The authors report photoelectric UVB observations of the total eclipse of 31 Cygni during 1982. The time of mid-eclipse is given, together with the times t_{50} when 50% of the light of the secondary is transmitted at ingress and egress. The mean duration of the eclipse is found to be 64.03 days in U and 62.94 days in B. The mean orbital period, from 1962 to 1982, is 3784.34 days. (3 refs.)

116758 Spectroscopic observations of the cool eclipsing X-ray binary HD 155638. D.M.Popper (Dept. of Astron., Univ. of California, Los Angeles, CA, USA). *Inf. Bull. Variable Stars (Hungary)*, no.2396, p.1-4 (5 Sept. 1983).
The author describes spectroscopic observations of HD 155638 (G8 IV+F?). The velocity amplitudes are found to be 46 km/s for the cooler star and about 50 km/s for the hotter star. The masses and radii are $1.3 M_{\odot}$ and $1.2 M_{\odot}$, and $8.2 R_{\odot}$ and $2.5 R_{\odot}$. These results suggest that HD 155638 may be considered as an RS Canum Venaticorum system intermediated between typical double-lined systems (e.g. RS CVn) and single-lined systems such as λ And. Some discrepancies between these results and the photometry of Bloomer et al. (1983) are discussed. (3 refs.)

116759 A 0538-66. S.Tjemkes. *I.A.U. Circ. (USA)*; no.3870, 1 pp. (23 Sept. 1983).
Reports photometric observations of the LMC recurrent transient X-ray source A 0538-66 during the optical outburst of August to September 1983. It is found that the difference in brightness between on and off states exceeds 1 magnitude, and that on 1983 September 12, during the decay of the outburst, the object was of magnitude 14.5. (2 refs.)

116760 HZ Her: the nature and origin of the emission lines. I.D.Howarth, B.Wilson (Dept. of Phys. & Astron., Univ. Coll. London, London, England). *Mon. Not. R. Astron. Soc. (GB)*, vol.204, no.3, p.1091-104 (Sept. 1983).
High- and low-dispersion IUE spectroscopy of the HZ Her/Her X-1 system is used to investigate the line spectrum. Velocity arguments discredit the classical sites of emission (primary's X-ray heated photosphere, accretion stream and disc) but support an origin in discrete blobs of material orbiting at the rim of the accretion disc. Analysis of the line intensity data suggests $T_e \approx 10^4$ K, $n_e \approx 10^{13.3}$ cm $^{-3}$ in the blobs. It is argued that these blobs can be identified with the material responsible for X-ray dips. (34 refs.)

116761 A model for A 0538-66: the fast flaring pulsar. L.Maraschi, R.Traversini, A.Treves (Dipartimento di Fisica, Univ. di Milano, Milano, Italy). *Mon. Not. R. Astron. Soc. (GB)*, vol.204, no.3, p.1179-84 (Sept. 1983).
A model of A 0538-66, where the X-ray and optical outbursts are associated with impulsive accretion on to a neutron star, is explored. The critical density for the onset of accretion on to a fast pulsar is discussed. The region emitting optical outbursts is substantially larger than the accretion disc and its mass greatly exceeds that of an ordinary Be envelope. The optical outbursts may be due to X-ray reprocessing in the primary's envelope and/or to cooling of an expanding shell accelerated by the X-ray burst. (22 refs.)

116762 Analytic treatment of polarization by arbitrary scattering mechanisms in circumstellar envelopes. II. Binary stars. J.F.L.Simmons (Dept. of Astron., Univ. of Glasgow, Glasgow, Scotland). *Mon. Not. R. Astron. Soc. (GB)*, vol.205, no.1, p.153-70 (Oct. 1983).
For pt.I see *ibid.*, vol.200, no.1, p.91-113 (1982). Extends the treatment given in Paper I of the linear polarization produced by scattering in circumstellar envelopes of arbitrary form to corotating envelopes of binary stars. As in Paper I the scattering mechanism assumed is very general, the only assumption being that it is spherically symmetric. Series expressions are derived for the Fourier components of the variable linear polarization, and the results of Brown, McLean & Emslie (1978) for Thomson scattering are re-derived as a special case. The author illustrates the results by considering Mie scattering

in envelopes of specified geometry. The inverse problem, that of determining the density distribution of scatterers, the scattering mechanism and the inclination of the binary axis, is briefly discussed. (12 refs.)

116763 Ultraviolet observations of binary X-ray sources. L.Maraschi (Dipartimento di Fisica, Univ. di Milano, Milano, Italy), E.G.Tanzi, A.Treves. *Mem. Soc. Astron. Ital. (Italy)*, vol.54, no.2, p.453-66 (1983).
Considers low mass X-ray binaries and UV observations in relation to visible and IR studies of line emitting regions and accretion disks. (28 refs.)

116764 Magnetic focusing in the Sco X-1 radio source. A.Achterberg, R.D.Blandford, P.Goldreich (Theoretical Astrophys., California Inst. of Technol., Pasadena, CA, USA). *Nature (GB)*, vol.304, no.5927, p.607-9 (18 Aug. 1983).
There has been much theoretical discussion of the confinement of the radio jets associated with extragalactic radio sources. There are now several examples of sources where the minimum pressure inferred in the jets appears to exceed the external gas pressure, which suggests that magnetic pinching may be playing an important part in the confinement. The authors argue that the results necessitate magnetic focusing and that this also strengthens the case for magnetic focusing in the extragalactic sources. (11 refs.)

New double stars (18th series) discovered at Nice See Entry 116493

The equations that govern rotational and tidal perturbations of stellar oscillations See Entry 116635

Narrow-band photometry of G and K stars near the North Galactic Pole See Entry 116641

Collapse and explosion of white dwarfs. I. Precollapse evolution See Entry 116648

Recent photometry of the central star of NGC 2346 See Entry 116653

The disc-like envelopes around young stars seen in the maser lines See Entry 116658

Cessation of the 63 second periodicity in the light curve of V533 Herculis See Entry 116659

The outbursts of symbiotic novae See Entry 116660

Star-planet systems as progenitors of cataclysmic binaries: tidal effects See Entry 116663

Superoutbursts: a general phenomenon in dwarf novae See Entry 116664

The ultraviolet variability of the symbiotic star HBV 475 See Entry 116666

The runaway Wolf-Rayet star HD 143414: evidence for a low-mass companion See Entry 116668

HR 981—a new USPC See Entry 116673

B and V photometry of the southern RS CVn candidate HD 196818 See Entry 116675

Optical behavior of EZ Pegasi See Entry 116677

HR 5=ADS 61: a new variable star See Entry 116678

V436 Cen revisited See Entry 116683

PU Vulpeculae See Entry 116684

GK Persei See Entry 116687

An infrared study of the eclipsing dwarf nova U Geminorum See Entry 116692

Simultaneous infrared and optical photometry of cataclysmic variables See Entry 116696

IUE observations of cataclysmic variables See Entry 116697

Optical variability of PU Vulpeculae (nova-like Kuwano's object 1979) in 1982 See Entry 116705

On the two possible progenitors of type I super nova See Entry 116714

Gravitational radiation reaction in the binary pulsar and the quadrupole-formula controversy See Entry 116731

97.90 OTHER TOPICS IN STELLAR ASTRONOMY

BV photometry of the supernova 1982 in NGC 2268 See Entry 116709

The globular cluster NGC 6638 See Entry 116768

Space distribution of stars in the southern Milky Way. III. A region in Centaurus-Crux See Entry 116815

98.00 STELLAR SYSTEMS; GALACTIC AND EXTRAGALACTIC OBJECTS AND SYSTEMS; THE UNIVERSE

98.10 STELLAR DYNAMICS

A simple kinetic model of a multi-particle cloud See Entry 116463

The tensor virial theorem for subsystems See Entry 116822

98.20 STELLAR CLUSTERS AND ASSOCIATIONS

116765 The chemical composition of distant globular clusters: are there any metal-poor clusters?. C.A.Pilachowski (Kitt Peak Nat. Obs., Tucson, AZ, USA), G.D.Bothun, E.W.Olszewski, A.Odell. *Astrophys. J. (USA)*, vol.273, no.1, pt.1, p.187-94 (1 Oct. 1983).
The authors report echelle spectroscopy of giants in the distant clusters NGC 4147, M53, NGC 5466, and NGC 6229. Abundances are determined from model atmosphere analyses of the equivalent widths of the metal lines. The analyses yield [Fe/H] values in the range of -1.3 to -1.9. These values are moderately high for clusters at these galactocentric distances ($R \sim 20$ kpc). In particular, these data argue against the existence of a strong metallicity gradient in the halo. These data may also suggest that the cluster system of the Galaxy predates the formation of the bulge and halo system. (40 refs.)

116766 On the intrinsic width and luminosity function of the M92 main sequence. A.Sandage, B.Katem (Mount Wilson & Las Campanas Obs., Carnegie Inst. of Washington, Pasadena, CA, USA). *Astron. J. (USA)*, vol.88, no.8, p.1146-58 (Aug. 1983).
Measurements of B and V magnitudes of ~ 475 identified stars in the magnitude interval $18.0 \leq V \leq 22.0$ are given. They occupy an area ~ 35 square arcminutes located $\sim 8'$ north of the center of M92. The measurements were

made on seven Hale 5-m reflector plates in each of two colors, relative to a faint photoelectric sequence determined earlier. The measuring errors, determined from the deviations from the mean values, are listed for each star so as to test if the observed width of the main sequence is due to measuring errors alone. The resulting distribution of errors is used to predict the observed width of the MS. Comparison with the observations shows that the intrinsic width could be zero, with an upper limit of $\sigma(B-V) \approx 0.02$ mag. Comparison with theoretical evolutionary models by Vandenberg shows that this gives an upper limit for the variation of the helium abundance star-to-star, to be $\sigma(\delta Y) \leq 0.1$. As in M15, the variation of the metal abundance is not well measured by the sharpness of the M92 main sequence because the metal abundance at $Z = 10^{-4}$ is too low. The luminosity function, obtained from the present data, is compared with that determined earlier by Taylor, by Hartwick, by van den Bergh, and with Fukuoka and Simoda, with good agreement. The evidence favors that $\phi(M_V)$ flattens fainter than $M_V \approx +6$ as predicted in some dynamical models, due to loss of loss mass stars. (25 refs.)

116767 On the age of M92 and M15. A.Sandage (Mount Wilson & Las Campanas Obs. Carnegie Inst. of Washington, Pasadena, CA, USA). *Astron. J. (USA)*, vol.88, no.8, p.1159-65 (Aug. 1983). Comparison of Vandenberg's isochrones for globular clusters with the photometry of many main-sequence stars in M92 and M15 gives an age $T = 18 \pm 2 \times 10^9$ years for both clusters, using a vertical fit to the turn-off luminosity, together with distance moduli found from the period-color-luminosity relation of their RR Lyrae stars. Comparison of the systematics of the composite CM diagram for clusters of different metallicity with that predicted from Vandenberg's isochrones, all for $T = 18 \times 10^9$ years, shows good agreement. Justification of the adopted zero-point value of $M_V(RR, M92) = +0.63$ is made by comparing the main sequences of M92, M3, and M5 with that defined by 11 field subdwarfs whose metallicities lie between $[Fe/H]$ of -2.2 and -1.2 for which adequate astrometric distances exist. (36 refs.)

116768 The globular cluster NGC 6638. G.Alcaino, W.Liller (Inst. Isaac Newton, Ministerio de Educacion de Chile, Santiago, Chile). *Astron. J. (USA)*, vol.88, no.8, p.1166-74 (Aug. 1983). Presents photographic photometry for 219 stars in the previously unstudied globular cluster NGC 6638, as well as for 187 stars in two neighboring zones equal in area to that measured for the cluster. A Pickering-Racine wedge has been used with the CTIO 1-m Yale telescope and the Las Campanas 2.5-m du Pont telescope to extend the limit of the photoelectric sequence from $V \sim 15.7$ to $V \sim 18.9$. Giant branch members, difficult to pick out due to the abundance of field stars, appear to define a steep sequence. A stubby red horizontal branch is well outlined by a group of 13 stars at $V_{HB} = 16.5 \pm 0.2$ within the narrow color range $0.92 < B-V < 1.06$, and 13 blue stars with $0.27 < B-V < 0.76$ populate a blue horizontal branch. Assuming the horizontal branch absolute magnitude $M_{VHB} = +0.6$ and the interstellar reddening $E(B-V) = 0.40$, the authors find NGC 6638 to be 8.7 ± 0.5 kpc from the Sun and 1.7 kpc from the galactic center. (20 refs.)

116769 The WN4.5 component of HD 219460 in the open cluster Markarian 50. D.G.Turner (Dept. of Phys. & Astron., Laurentian Univ., Sudbury, Ontario, Canada), A.F.J.Moffat, R.Lamontagne, H.M.Maitzen. *Astron. J. (USA)*, vol.88, no.8, p.1199-1209 (Aug. 1983). The open cluster Markarian 50 is reinvestigated using photoelectric *UBV* photometry, resulting in a newly determined distance of 3.55 ± 0.20 kpc, an age of $\sim 7(\pm 2) \times 10^6$ yr, and a space reddening for HD 219460 of $E_{B-V} = 0.90 \pm 0.01$. As delineated by star counts, the cluster is small and very poorly populated, with nuclear and coronal radii of 1.75 arcmin (1.8 pc) and 3.5 arcmin (3.6 pc), respectively. The optical components of HD 219460 are identified as a possibly variable WN4.5 star and a brighter B1 II companion, with luminosities of $M_V = -4.85$ ($M_V = -4.92$) and $M_V = -5.05$, respectively. Both stars appear to be single on the basis of new radial velocity data obtained for them over a three year time span, and seem certain to be cluster members. The location of the WR star in the cluster H-R diagram is, in fact, consistent with evolution with a high rate of mass loss from a star of initially $\sim 30 M_\odot$. The cluster and WR star are probably physically associated with portions of the surrounding H II region Sharpless 157, despite the fact that this produces a discrepancy with previously published radial velocity data for Markarian 50 members. (27 refs.)

116770 Cool neutral hydrogen in the direction of an anonymous OB association. T.M.Bania (Dept. of Astron., Boston Univ., Boston, MA, USA). *Astron. J. (USA)*, vol.88, no.8, p.1222-27 (Aug. 1983). H I self-absorption is seen in the direction $l = 55.6^\circ$ probably physically associated with an anonymous OB association which has the Cepheid GY Sagittae as a member. The cool H I is in two clouds at least 15 pc in diameter located 3.25 kpc from the Sun. If their temperature is ~ 50 K, the cloud masses are $\sim 10^3 M_\odot$. The neutral atomic hydrogen clouds are probably warm envelopes surrounding cold molecular cloud cores because CO observations in this region show two molecular clouds nearly coincident with the absorbing H I gas. Since the OB association is only $\sim 10^7$ years old, these clouds are likely to be part of the original cloud complex from which the stellar cluster formed. The H I clouds are part of the larger Arcicob survey of self-absorption which suggests that many of the Arcicob clouds are associated with heretofore unidentified star clusters. Even if this is generally not the case, the Arcicob objects have accurate kinematic distances and thus provide a new sample of cool H I clouds whose thermodynamic properties can be studied. (21 refs.)

116771 Variable stars in NGC 6397. H.M.H.El-Worfalli, E.Budding (Dept. of Astron., Univ. of Manchester, Manchester, England). *Astrophys. & Space Sci. (Netherlands)*, vol.94, no.2, p.253-72 (Aug. 1983). Thirty-four deep sky plates of NGC 6397 taken from AAO, UKSTU and SAAO sources were examined with the aim of checking parameters of (three) known variables in the cluster, and also to discover new and generally fainter (main-sequence) variables. The search methods have included various visual and automated procedures, a comparison of which provides another aspect of the present work. At least two faint variables have been identified. A number of other candidates for genuine stellar variability are presented. (32 refs.)

116772 A search for neutral hydrogen near nine globular clusters. M.Birkinshaw (Mullard Radio Astron. Obs., Cavendish Lab., Cambridge, England), P.T.P.Ho, B.Baud. *Astron. & Astrophys. (Germany)*, vol.125, no.2, pt.1, p.271-5 (Sept. 1983). A search for neutral hydrogen in emission or absorption near nine globular clusters has been made and limits to the masses of neutral hydrogen towards eight are presented. A large mass of H I lies near M56, a part of this may be associated with the cluster. (21 refs.)

116773 Ellipticity variations within some globular clusters of the Galaxy and the Magellanic Clouds. E.H.Geyer (Obs. Hoher List, Univ. Bonn, Daun, Germany), U.Hopp, B.Nelles. *Astron. & Astrophys. (Germany)*, vol.125, no.2, pt.1, p.359-67 (Sept. 1983). The apparent flattening-variations of 20 galactic- and four Magellanic Cloud globular clusters have been investigated by means of the Agfa-Contourfilm

technique and an objective reduction method on plates obtained with telescopes of different f -ratios and scales. It is shown that in reality an individual isodensity contour can be approximated by an ellipse with an accuracy of only ± 0.05 for the axis ratio, and, as to be expected, the position angle of the major axis becomes more and more indefinite for $b/a > 0.92$. (23 refs.)

116774 VBLUW photometry of the open cluster NGC 2516. J.N.Verschoor, A.M.van Genderen (Leiden Obs., Leiden, Netherlands). *Astron. & Astrophys. Suppl. Ser. (France)*, vol.53, no.3, p.419-25 (Sept. 1983).

VBLUW photometry of the young open cluster NGC 2516 is presented and discussed. Temperatures and gravities for most of the stars and reddenings for nearly all stars could be determined. The reddening and the distance are in good agreement with the results of other references. (25 refs.)

116775 The chemical composition of stars in globular clusters. C.A.Pilachowski (Kitt Peak Nat. Obs., Tucson, AZ, USA), C.Snedden, G.Wallerstein. *Astrophys. J. Suppl. Ser. (USA)*, vol.52, no.3, p.241-87 (July 1983). The authors present detailed analyses for stars in seven globular clusters, bringing the total number of globular clusters analyzed using high resolution spectroscopy and model atmospheres to 23. Equivalent-width data published by other investigators for some clusters have been reanalyzed to derive abundances on a uniform scale. Values of $[Fe/H]$ range from -2.2 (NGC 6397) to -0.9 (NGC 362). Abundance ratios of various elements relative to iron are significantly different from their solar ratios. The α elements represented largely by calcium and titanium, are substantially enhanced in most clusters, with values of $[\alpha/H]$ ranging from -0.45 (NGC 362) to -1.8 (NGC 6397). (141 refs.)

Photometric search for Ap-stars in open clusters. IV. NGC 2287, Cr 121, NGC 2422 and supplementary measurements in NGC 1662 and NGC 2516 See Entry 116667

Study of the variability of the delta Scuti stars. VI. Pulsational behaviour of HR 1392 (69 Tau) See Entry 116670

On delta Scuti stars in open clusters See Entry 116680

The multiple system β Sco and the age of the Upper Scorpius complex See Entry 116744

Far-infrared and CO observations of Cep F: implications for star formation in Cepheus OB3 See Entry 116782

98.40 INTERSTELLAR MATTER; AND NEBULAE

116776 Isotopic fractionation and mass motion in giant molecular clouds. A.A.Penzias (Bell Labs., Murray Hill, NJ, USA).

Astrophys. J. (USA), vol.273, no.1, pt.1, p.195-201 (1 Oct. 1983). Millimeter-wave rotation spectra of the $^{12}C^{16}O$, $^{13}C^{16}O$, and $^{12}C^{18}O$ isotopes of carbon monoxide were mapped in two giant molecular clouds in the Galaxy, NGC 2264 and W3(OH). The data were used to derive $^{13}C^{16}O/^{12}C^{16}O$ abundance ratios as a function of velocity, as well as position, in these sources. Two key features emerge from these observations. First, carbon-13 isotopic abundance determinations, particularly those involving carbon monoxide, are more subject to chemical enhancement effects than had been previously realized. Second, there is a suggestive association between velocity wings and cloud edges. This latter feature fits predictions of cloud evolution models involving large-scale radial motion. (18 refs.)

116777 The abundance of carbon in planetary nebulae. H.B.French (Dept. of Phys. & Astron., Univ. of Oklahoma, Norman, OK, USA). *Astrophys. J. (USA)*, vol.273, no.1, pt.1, p.214-18 (1 Oct. 1983). New photoelectric observations of the C II $\lambda 4267$, C III $\lambda 4647$, 4650, 4651, and C IV $\lambda 4659$ recombination lines have been obtained for 14 bright planetary nebulae and used to derive carbon abundances for these objects. The results indicate that carbon was enhanced in the progenitor by a factor of about 2 at the time of planetary nebula ejection presumably from the dredge-up of newly synthesized triple- α carbon. It appears that C/O ≥ 1 , indicating that the progenitor was a carbon star at that time. Planetary nebulae may be important contributors to galactic carbon enrichment, perhaps equaling or exceeding supernovae in this respect. (44 refs.)

116778 Digital analysis of narrow-band imagery of the Cygnus Loop. J.J.Hester (Rice Univ., Houston, TX, USA), R.A.R.Parker, R.J.Dufour.

Astrophys. J. (USA), vol.273, no.1, pt.1, p.219-42 (1 Oct. 1983). Digital analysis of narrow passband direct imagery of a field in the southeast part of the Cygnus Loop SNR is presented. Calibrated surface brightness and spectral line ratio maps involving emission from six different ionic species are shown. Features present in surface brightness maps are not generally apparent as features in line ratio maps. Differences in the morphologies of the remnant as viewed in different emission lines and gradients in spectral line ratios are interpreted as a continuous transition with distance behind the blast wave from nonsteady flow shocks with velocities ≥ 130 km s $^{-1}$ to steady flow shocks with velocities ≈ 60 km s $^{-1}$. (36 refs.)

116779 Semianalytical treatment of the hydrodynamics of supernova remnants during the snowplow phase. B.Gaffet (Section d'Astrophys., CENS, Gif-sur-Yvette, France).

Astrophys. J. (USA), vol.273, no.1, pt.1, p.267-79 (1 Oct. 1983). The author presents a semianalytical solution for the hydrodynamical evolution of a supernova remnant during the snowplow phase, making the following idealizations or approximations. First, remembering that, according to the standard model, cooling occurs only near the outer edge of the remnant, near the neutral shell, it is assumed that adiabaticity holds throughout most of the volume of the hot interior. The outer regions where radiative cooling is important, on either side of the neutral shell, are treated by means of Bernoulli's theorem. The first-order solution does not give good results, so a second-order expansion of the solution was undertaken. (19 refs.)

116780 Spectrophotometry of the optical emission from RCW 103 and Milne 23. M.T.Ruiz (Dept. de Astron., Univ. de Chile, Santiago, Chile).

Astron. J. (USA), vol.88, no.8, p.1210-21 (Aug. 1983). Spectrograms of five different filaments in RCW 103 and three filaments in Milne 23 were obtained using a SIT Vidicon tube at the 1.5-m and 4-m telescopes of CTIO. The region between 3700 Å and 7400 Å was covered with overlapping spectra. In RCW 103 the observed H_α/H_β ratio indicates variations in the visual absorption of up to 1.5 mag for different filaments. The minimum value found is 4.4 mag, implying a distance of 6.5 kpc from the Sun and a galactocentric distance of 4 kpc. Comparison of observed line ratios with models gives temperatures of about 10 4 K and densities between 10 cm $^{-3}$ and 100 cm $^{-3}$. An overabundance of nitrogen by a factor of 2 is found that can be explained as due to a galactic abundance gradient. The observed H_α/H_β ratios obtained for the filaments of Milne 23 imply a visual absorption of about 0.5 mag. Line ratios suggest densities about 5 cm $^{-3}$ and temperatures over 2.5 $\times 10^4$ K. (21 refs.)

116781 The temperature of molecular gas in the galactic center region. M.Morris, N.Polish (Astron. Dept., Columbia Univ., New York, NY, USA), B.Zuckerman, N.Kaifu.

Astron. J. (USA), vol.88, no.8, p.1228-35 (Aug. 1983).

The (1,1), (2,2), and (3,3) inversion lines of NH_3 were observed with a 5.3' telescope beam at 1.3 cm wavelength along a portion of the galactic plane centered on the galactic nucleus. The maps of antenna temperature in the longitude-velocity plane are used to construct maps of line intensity ratios. An analytical expression is derived which relates the gas kinetic temperature to the line ratios under the assumption of large opacity in the inversion lines. This relationship is (1) insensitive to assumptions about the collision rates and the magnitude of the opacity, and (2) in the temperature range of interest, similar to the relationship derived assuming optical thinness. It is therefore argued that the maps of line ratios can be used to derive an approximate kinetic temperature for the molecular gas, independent of assumptions about opacity. The implied temperatures are relatively high (30-60K) and roughly uniform over several hundred parsecs. A number of heating mechanisms which might account for these characteristics are examined. The authors cannot decide on the basis of presently available data which mechanism, if any, is dominant. (31 refs.)

116782 Far-infrared and CO observations of Cep F: implications for star formation in Cepheus OB3. A.I.Sargent (Owens Valley Radio Obs., California Inst. of Technol., Pasadena, CA, USA), R.J.van Duinen, H.L.Nordh, C.V.M.Fridlund, J.W.G.Aalders, D.Beintema.

Astron. J. (USA), vol.88, no.8, p.1236-41 (Aug. 1983).

Observations at 80- μm and 130- μm have revealed a source of far-infrared emission in the Cep F portion of the Cepheus OB3 molecular cloud. Molecular line measurements of this region, at the CO $J=1-0$ line frequency, have led to the discovery of two CO maxima. One of these coincides with the new far-infrared source. The other is at least as intense as Cep B, until now considered to be the hottest part of the cloud. There is some evidence to suggest that a second far-infrared source is associated with this hotspot. If the far-infrared emission results from the presence of embedded protostars, their location, relative to the OB association stars and to the other active region, Cep A, requires a reexamination of how stars form in the Cepheus OB3 association. (27 refs.)

116783 Hydrogen and helium ionization structure of gaseous nebulae.

E.Oliva (Osservatorio Astrofisico di Arcetri, Firenze, Italy), N.Panagia.

Astrophys. & Space Sci. (Netherlands), vol.94, no.2, p.437-61 (Aug. 1983).

Discusses the ionization equilibrium of hydrogen and helium in a nebula with an arbitrary gas density distribution. Considering the spectral characteristics of hot stars, a power law is found to provide a good approximation to the Lyman continuum spectrum for stars with $T_{\text{eff}} \leq 100000\text{K}$. With this simplification the ionization equilibrium equation is analytically solved first for a pure hydrogen nebula, then for the general case of a nebula containing H, He and heavy elements. A simple and quite general formula for the determination of the size and the emission of the He^+ zone is obtained. Finally, the ionization equilibrium $\text{He}^{++}-\text{He}^+$ is considered. (13 refs.)

116784 Tentative detection of the CS^+ molecular ion in diffuse interstellar clouds. R.Ferlet (LPSP, Verrieres-le-Buisson, France), E.Roueff, M.Horani, J.Rostas.

Astron. & Astrophys. (Germany), vol.125, no.2, pt.1, p.L5-8 (Sept. 1983).

Suggests the discovery of the CS^+ molecular ion observed in absorption in the diffuse interstellar clouds on the ζ Oph and δ Sco lines of sight. Synthetic spectra seem to favour a rotational excitation of the (3,0) band of the $\text{A}^{11}_{1/2}-\text{X}^2\Sigma^+$ transition by the cosmological radiation background. This is the first sulphur-bearing molecule detected in diffuse clouds. (24 refs.)

116785 The magnetic field of the NGC 2024 molecular cloud: detection of OH line Zeeman splitting. R.M.Crutchfield, I.Kazes (Dept. de Radioastron., Obs. de Paris-Meudon, Meudon, France).

Astron. & Astrophys. (Germany), vol.125, no.2, pt.1, p.L23-6 (Sept. 1983).

Zeeman splitting of the main lines of OH in absorption has been detected for the first time. The derived magnetic field for a clump in the NGC 2024 molecular cloud is -38 ± 1 microgauss. (10 refs.)

116786 Diffuse light near zeta Orionis and the Horsehead nebula, and anomalous extinction of HD 37903, as measured with the ANS. K.S.de Boer (Astron. Inst. Tubingen, Tubingen, Germany).

Astron. & Astrophys. (Germany), vol.125, no.2, pt.1, p.258-64 (Sept. 1983).

The light of ζ Ori, reflected by the diffuse interstellar medium to the SSE of this star, was measured with the UV-instrument onboard of the ANS. The diffuse light is bluer than the light of the stars. Possible contributions of emission by the gas are discussed. The gradient of the surface brightness in this region in front of the dark cloud L 1630 is steeper than the gradients reported from the OAO-2 and TD1 satellites, indicating a complicated geometry for the scattering material. The normalised surface brightness is small and is interpreted. The extinction of HD 37903 in L 1630 is found to be anomalous. (37 refs.)

116787 A comparison of high resolution optical and radio observations of W3. H.R.Dickel (Astron. Dept., Univ. of Illinois, Urbana, IL, USA), R.H.Harten, T.R.Gull.

Astron. & Astrophys. (Germany), vol.125, no.2, pt.1, p.320-32 (Sept. 1983).

High resolution maps of the W3 complex are presented for radio continuum and selected optical emission lines. These maps are used to derive the visual extinction, the excitation and evolutionary state of the component H II regions. Three main ionized gas structures are identified: (1) a large diffuse H II region in the east which is the most evolved and least obscured H II region; (2) a southern complex of H II regions; and (3) a northern complex of young, compact H II regions which are still embedded in the W3 molecular core. These three regions represent different stages in the process of H II-blisters formation at the edge of the molecular cloud. The observed distribution of dust is compared with ionized and atomic hydrogen, and several molecules in W3. Detailed structure of the W3A source is presented which is interpreted as W3A being in the earliest stage of the 'Champagne' phenomena. (46 refs.)

116788 Special perturbations of rotating isothermal gas clouds with constant rotational velocity. F.Schmitz (Inst. fur Theoretische Astrophys., Univ. Heidelberg, Heidelberg, Germany).

Astron. & Astrophys. (Germany), vol.125, no.2, pt.1, p.333-7 (Sept. 1983).

A class of special perturbations of stationary rotating and self-gravitating gaseous clouds with constant rotational velocity and constant temperature is studied. The perturbations are isothermal and are connected with displacements only in the direction of the rotation axis. A perturbation equation which can be separated is presented. The radial dependence of the perturbed variables is a simple closed expression, the angular dependence is given by an ordinary second order differential equation. The perturbed configurations show the asymptotic features of the regular solutions of the isothermal gas sphere. The relevance for the stability of the equilibrium state is discussed, and applications to the formation of the planetary system are considered. (10 refs.)

116789 Infrared objects near H_2O masers in regions of active star formation. III. Evolutionary phases deduced from IR recombination line and other data. A.F.M.Moorwood (European Southern Obs., Garching bei Munchen, Germany), P.Salinari.

Astron. & Astrophys. (Germany), vol.125, no.2, pt.1, p.342-54 (Sept. 1983).

For pt.II see *ibid.*, vol.102, no.2, p.197-206 (1981). Spectroscopy of Br γ (2.17 μm), Pf γ (3.74 μm) and Br α (4.05 μm) hydrogen recombination line emission together with 2-20 μm photometry, continuously variable filter spectroscopy around 10 μm and 10 μm slit scans are used to define more precisely the nature of several compact infrared objects detected in systematic 3.6 μm surveys of H_2O masers. (65 refs.)

116790 Ammonia absorption toward W3(OH): 0.3' resolution maps in the (2,2) line. S.Guilloteau (Groupe d'Astrophys., Univ. Sci. et Medicale de Grenoble, Saint Martin d'Heres, France), M.T.Stier, D.Downs.

Astron. & Astrophys. (Germany), vol.126, no.1, pt.2, p.10-15 (Sept. 1983).

The authors present line maps of the ammonia (2,2) inversion line in absorption against the continuum source W3(OH), made with a spatial resolution of $0.26'' \times 0.26''$. The ammonia cloud covers the western part of the continuum source, coinciding with the OH masers in front of the continuum. Evidence for velocity and line width gradients within the NH_3 cloud has also been found. The cloud is clumpy, with some structure probably on scales down to $0.2''$ or less. The sharp edges of the opacity maps at the boundary of the H II region suggest that the cloud extends further, presumably as far as the OH masers. (22 refs.)

116791 The fraction of the sky screened by local diffuse dust clouds.

J.Knude (Copenhagen Univ. Obs., Copenhagen, Denmark).

Astron. & Astrophys. (Germany), vol.126, no.1, pt.2, p.89-93 (Sept. 1983).

An estimate of the interstellar cloud cover as a function of distance is presented. This estimate is based on detailed observations of local diffuse clouds in samples of the sky over all galactic latitudes and covering in total, $\sim 5\%$ of the celestial sphere. The spatial frequency of clouds observed in the distance interval from 50 to 150 pc may be evaluated. The fraction of sky covered by diffused dust clouds closer than the distance D , $CF(D)$, is evaluated. The coverage function $CF(D)$ is found to obey a power law. $CF(D) = -1.7777 + 0.4568 \ln(D(\text{pc})) \sim \ln(D^{1/2}/6)$. (11 refs.)

116792 Formaldehyde, cold neutral hydrogen and dust distribution in a globular filament in Taurus. W.G.Poppel (Inst. Argentino de Radioastron. & Obs. Astron., Univ. de La Plata, La Plata, Argentina), K.Rohlf, W.Celnik.

Astron. & Astrophys. (Germany), vol.126, no.1, pt.2, p.152-60 (Sept. 1983).

The distribution of the 4.83 GHz absorption line of the I_{10-11} rotational transition of formaldehyde H_2CO and of the 1420 MHz self-absorption of cold neutral hydrogen have been measured for the globular filament GF 16 in Taurus with the 100 m telescope at Effelsberg. A total of 128 positions spaced on an irregular grid with $\sim 4'$ spacing have been measured in formaldehyde. For the same area the self-absorption of cold neutral hydrogen was measured too. The whole region turns out to be rather quiescent with no noticeable streaming motions. For several individual globules D , E , C_4 , C_3+C_2 estimates of the total mass is derived. (50 refs.)

116793 The detection of butadiynyl (C_4H) in absorption against Cassiopeia A. M.B.Bell, P.A.Feldman, H.E.Matthews (Herzberg Inst. of Astrophys., Nat. Res. Council of Canada, Ottawa, Ontario, Canada).

Astrophys. J. Lett. Ed. (USA), vol.273, no.1, pt.2, p.135-9 (1 Oct. 1983).

Observations of the $N=1-0$ transition of the butadiynyl radical, C_4H , in absorption against Cas A are reported. The inferred column density of C_4H is $10^{12}-10^{13} \text{ cm}^{-2}$ in the Orion arm, and this is high enough to be of potential significance vis-a-vis the carriers of the diffuse interstellar bands. (30 refs.)

116794 The Rosette nebula. I. An absolutely calibrated photoelectric H α surface photometry. W.E.Celnik (Astron. Inst., Ruhr-Univ. Bochum, Bochum, Germany).

Astron. & Astrophys. Suppl. Ser. (France), vol.53, no.3, p.403-6 (Sept. 1983).

The brightness distribution of the $\text{H}\alpha$ emission line in the Rosette nebula has been measured for an area of $2.4'' \times 2.4''$ using the Bochum 61 cm telescope at ESO/La Silla equipped with a photoelectric photometer. An interference filter with 10 \AA bandwidth was used to exclude both [NII] lines at $\lambda\lambda 6548, 6584 \text{ \AA}$. The map, which has an angular resolution of 4.75 arcmin, was constructed from 76 scans measured with a stationary telescope; the intensity scale was calibrated using stars with absolutely calibrated continuum. In this, the detailed shape of the stellar $\text{H}\alpha$ absorption line was taken into account using both high resolution coude spectra and photoelectric scanner measurements. (15 refs.)

116795 Regions of low molecular column density near the galactic plane.

F.Verter, G.R.Knapp (Princeton Univ. Obs., Princeton, NJ, USA), A.A.Stark, R.W.Wilson.

Astrophys. J. Suppl. Ser. (USA), vol.52, no.3, p.289-92 (July 1983).

A partial survey of the first quadrant of the galactic plane in the ^{12}CO $J=1-0$ transition has been searched of emission-free positions. Over 100 directions at low galactic latitude have been found which have no molecular clouds along the line of sight. The antenna temperature in these directions is $< 0.5 \text{ K}$ for all galactic velocities implying $\text{N}(\text{H}_2) < 1 \times 10^{21} \text{ cm}^{-2}$ and $A_v < 1.5 \text{ mag}$. These directions may be used to study distant visual objects or as 'off' positions for radio and infrared spectroscopy. (2 refs.)

116796 Magnetic field lines in the Galaxy (Review of the interstellar magnetic field). J.P.Vallee (Section d'Astron., Inst. Herzberg d'Astrophys., Ottawa, Ontario, Canada).

J. R. Astron. Soc. Can. (Canada), vol.77, no.4, p.177-202 (Aug. 1983). In French.

A review of the interstellar magnetic field is given. The principle contributor to the present knowledge of the geometry of the interstellar magnetic field has been the observed angle of the linear polarization of the radio and optical radiations reaching the Earth. In particular, such optical observations in 1949 afforded the first proof of the existence of the interstellar magnetic field, while such radio observations since 1963 have revealed the various components of the interstellar magnetic field. The interaction of the interstellar magnetic field on the interstellar plasma and the observed percentage of the linear polarization of the radio and optical radiations reaching the Earth, are discussed. (116 refs.)

116797 CS $J=5-4$ observations of galactic molecular clouds. G.J.White, J.P.Phillips, K.J.Richardson, R.F.Frost, G.D.Watt, J.E.Beckman (Phys. Dept., Queen Mary Coll., Univ. of London, London, England), J.H.Davis.

Mon. Not. R. Astron. Soc. (GB), vol.204, no.3, p.1117-23 (Sept. 1983).

Observations are reported of a sample of six regions of star formation in the $J=5-4$ rotational transition of CS at 244 GHz. In combination with published results at lower frequencies, the authors show the $J=5-4$ line temperatures for OMC-1, M17 SW, W3(OH) and Ori B to be consistent with constant density large velocity gradient models, indicating typical abundances $X(\text{dV/dr}) \sim 4 \times 10^{-10} \text{ km}^{-1} \text{ s pc}$, and H_2 number densities $\sim 10^5 \text{ cm}^{-3}$. For two clouds, W51 and DR21(OH), however, the results may indi-

cate the need for substantial levels of CS thermalization, suggesting in turn high source densities and beam dilutions. (11 refs.)

116798 IUE observations of stars in the M8 nebula. B.Y.Welsh (Dept. of Phys. & Astron., Univ. Coll. London, London, England). *Mon. Not. R. Astron. Soc. (GB)*, vol.204, no.3, p.1203-19 (Sept. 1983). The early-type stars HD 164794, 164816, 164906 and 165052 belonging to the M8 nebula have been observed at high resolution using the IUE satellite. High velocity interstellar absorption components have been detected in each star's spectra at velocities of -32 and -53 km s^{-1} . A line profile fitting analysis has been carried out on all the UV interstellar lines to determine cloud component column densities and subsequently to determine the physical condition and chemical abundance of the associated interstellar gas. It is proposed that the stellar wind energy from the star HD 164794 (9 Sgr) may be sufficient to produce the high velocity gas motions. (41 refs.)

116799 Optical polarization in the bipolar nebula associated with LkH α 208. J.V.Shurt, R.F.Warren-Smith, S.M.Scarrott (Phys. Dept., Univ. of Durham, Durham, England). *Mon. Not. R. Astron. Soc. (GB)*, vol.204, no.3, p.1257-61 (Sept. 1983). Optical polarization data are presented for the archetypal premain-sequence bipolar nebula illuminated by LkH α 208. The data lead to an interpretation whereby the major axis of the nebula is close to the plane of the sky and the circumstellar ring is very extensive in the radial direction and partially obscures one of the lobes. The mass of the ring is estimated to be $0.3 M_{\odot}$. (9 refs.)

116800 Hydrodynamic models of Herbig-Haro objects. M.T.Sandford, II, R.W.Whitaker (Los Alamos Nat. Lab., Univ. of California, Los Alamos, NM, USA). *Mon. Not. R. Astron. Soc. (GB)*, vol.205, no.1, p.105-121 (Oct. 1983). Two-dimensional cylindrical hydrodynamic models of neutral and collisionally ionized stellar wind-cloudlet interactions are calculated as possible models for HH objects. For neutral winds, shocks propagate into the cloudlet and its shape is distorted and displaced in the direction of the wind. For hot ionized winds interacting with spherical mass concentrations a bow shock is formed, but the highest temperatures and largest ionization fraction occurs on the lee side of the cloudlet. Winds interacting with a neutral globule imbedded near the ionized surface of an elongated cloud are also discussed. (18 refs.)

116801 Ammonia observations of the Herbig-Haro objects HH 24-27. N.Matthews, L.T.Little (Electronics Labs., Univ. of Kent, Canterbury, England). *Mon. Not. R. Astron. Soc. (GB)*, vol.205, no.1, p.123-30 (Oct. 1983). The region centred on HH 25 has been mapped in the $J=1, K=1$ inversion line of ammonia, with spatial and velocity resolutions of 2.2 arcmin and 0.43 km s^{-1} respectively. The ammonia emission covers the known centres of activity HH 24-26, including the recently observed bipolar CO outflows. Its spatial distribution relative to the outflows probably implies a disc structure (of mass $\sim 70\text{-}210 M_{\odot}$), with the bipolar outflow perpendicular to the faces of the disc. The derived particle density is discussed. The abundance ratio of ammonia is estimated. (29 refs.)

116802 3 μm spectroscopy of IRS 7 towards the Galactic Centre. T.J.Jones (Dept. of Astron., Univ. of Minnesota, Minneapolis, MN, USA), A.R.Hyland, D.A.Allen. *Mon. Not. R. Astron. Soc. (GB)*, vol.205, no.1, p.187-90 (Oct. 1983). Intermediate and low resolution spectra of IRS 7 from $3.0\text{-}3.6 \mu\text{m}$ are presented. Sharp absorption features previously reported at 3.192 and $3.295 \mu\text{m}$ are not confirmed. The overall broad absorption characteristics and the presence of a shallow feature in the red wing of the broad $3.4 \mu\text{m}$ absorption are confirmed. This shallow feature is resolved, $\sim 0.036 \mu\text{m}$ wide with an equivalent width of $30 \pm 10 \text{ \AA}$ and centred at $3.489 \pm 0.005 \mu\text{m}$. (11 refs.)

116803 Observations of H $_2$ O maser emission in the Large Magellanic Cloud. J.B.Whiteoak, K.J.Wellington, D.L.Jauncey, F.F.Gardner, J.R.Forster, J.L.Caswell, R.A.Batchelor (Div. of Radiophys., CSIRO, Epping, NSW, Australia). *Mon. Not. R. Astron. Soc. (GB)*, vol.205, no.1, p.275-9 (Oct. 1983). A search for H $_2$ O maser emission towards 10 continuum sources in the Large Magellanic Cloud was made with the Parkes radio telescope (beamwidth 1.7 arcmin). Maser emission was detected near three H II regions, including the 30 Doradus nebula the positions of the main features are estimated with an accuracy of ± 15 arcsec. The maser luminosities are comparable to the typical value of H $_2$ O masers in galactic H II regions. Upper intensity limits for maser emission in the remaining sources were 0.5 Jy . In contrast with previous observations, no emission was detected near N159. (9 refs.)

116804 Planetary nebulae: IUE results. M.Cerruti-sola, M.Perinotto (Osservatorio Astrofisico di Arcetri, Firenze, Italy). *Mem. Soc. Astron. Ital. (Italy)*, vol.54, no.2, p.511-27 (1983). The IUE satellite has provided important information on both the nebulae and the central stars. For the nebulae the advances concern: (a) the density and temperature profiles across the nebula, (b) the nebular continuum, (c) the ionization structure, (d) the chemical composition and (e) the nebular dust. For the central stars: (a) the mass loss phenomenon from fast winds, (b) the determination of the temperature of the nuclei and therefore an improvement of their HR diagram, and possibly (c) the chemical composition of the stellar surface layers. (54 refs.)

116805 H II regions [IUE observations]. P.Patriarchi, M.Perinotto (Osservatorio Astrofisico di Arcetri, Firenze, Italy). *Mem. Soc. Astron. Ital. (Italy)*, vol.54, no.2, p.529-36 (1983). The IUE satellite has observed relatively few galactic and extragalactic H II regions because of the faintness of these sources. However, important results have been obtained in relation to chemical abundances in zones of recent star formation, the nature and amount of dust associated with gas in such zones, and the dynamical interaction of violent stellar winds. (29 refs.)

116806 Determination of the angular size of the H $_2$ O maser outburst region in Orion KL defined by a linearly polarized emission. L.I.Matveenko, A.M.Romanov, L.R.Kogan, I.G.Moiseev, R.L.Sorochenko, V.V.Timofeev. *Pis'ma v Astron. Zh. (USSR)*, vol.9, no.8, p.456-60 (1983). In Russian. English translation in: *Sov. Astron. Lett. (USA)*. The angular size of a region of linearly polarised emission observed in the Orion Kleinmann-Low nebula has been measured by the Simeiz-Pushchino radiointerferometer. The radial velocity of the outburst region is $+8 \text{ km/s}$. The radiation in the central part of the line profile comes from an elliptical region with axes of 0.75 and $1.0 \times 10^{13} \text{ cm}$. The higher-frequency radiation is related to a larger region. The degree of linear polarisation is in the range $0.5 < p < 0.7$: the polarised radio source is 1.5 to 2.0 times smaller than the unpolarised sources. (5 refs.)

116807 Ring nebulae associated with WR stars: stellar wind or stellar ejecta? T.A.Lozinkaya. *Pis'ma v Astron. Zh. (USSR)*, vol.9, no.8, p.469-73 (1983). In Russian. English translation in: *Sov. Astron. Lett. (USA)*. The statistics of Wolf-Rayet stars associated with H II regions (including ring nebulae) are presented. 29% of Wolf-Rayet stars (40% of early-type WN stars, 30% of late-type WN stars, and 17% of WC stars) are shown to be associated with ring nebulae. The data do not confirm the origin of ring nebulae due solely to sweeping of the interstellar gas by the stellar wind. A shell ejection is likely to precede the stellar wind stage. Some reasons for the fact that strong stellar winds do not necessarily from ring nebulae are discussed. (13 refs.)

116808 The determination of cloud masses and dust characteristics from submillimetre thermal emission. R.H.Hildebrand (Dept. of Astron. & Astrophys., Univ. of Chicago, Chicago, IL, USA). *Q. J. R. Astron. Soc. (GB)*, vol.24, no.3, p.267-82 (Sept. 1983). Reviews the principles by which the dust masses and total masses of interstellar clouds and certain characteristics of interstellar dust grains can be derived from observations of far-infrared and submillimetre thermal emission. To the extent possible, the discussion is independent of particular grain models. (41 refs.)

116809 Tracing the gas in galaxies. W.C.Keel (Kitt Peak Nat. Obs., Tucson, AZ, USA). *Sky & Telesc. (USA)*, vol.66, no.3, p.206-10 (Sept. 1983). The author describes optical methods of observing the distribution of interstellar gas in galaxies, based on the use of narrow-band filters that transmit only at the wavelengths of emission lines. These observations have shown that ionised gas is present in the nuclei of normal spiral galaxies and active galaxies (e.g. Seyfert galaxies and radio galaxies). The line-emitting gas forms relatively cool (10000 to 12000 K) dense clouds and filaments embedded in a hot, tenuous galactic wind. Systems of filaments also occur in active galaxies, particularly in the dominant central galaxies of rich clusters (e.g. M87 and NGC 1275), where they form vast networks more than 10 kpc in diameter. Finally, emission-line jets have been observed in a few active galaxies, notably in the Seyfert galaxy NGC 4151. (no refs.)

Nonlinear periodic solutions for the isothermal magnetostatic atmosphere	See Entry 113601
Cosmic ray acceleration in supernova blast waves	See Entry 116412
The maximum energy of cosmic rays accelerated by supernova shocks	See Entry 116413
Ambipolar diffusion in self-gravitating isothermal layers	See Entry 116437
Self-regulated star formation in the Galaxy	See Entry 116628
The temperature of central stars of planetary nebulae: the energy-balance method	See Entry 116651
Recent photometry of the central star of NGC 2346	See Entry 116653
The ultraviolet variability of the symbiotic star HBV 475	See Entry 116666
Do filaments form at the time of supernova explosions?	See Entry 116707
The effect of low-velocity, low-mass intruders (collisionless gas) on the dynamical evolution of a binary system	See Entry 116743
Cool neutral hydrogen in the direction of an anonymous OB association	See Entry 116770
A search for neutral hydrogen near nine globular clusters	See Entry 116772
VLW photometry of the open cluster NGC 2516	See Entry 116774
Optical spectroscopy of the radio-loud nuclei of spiral galaxies: starbursts or monsters?	See Entry 116810
Neutral hydrogen absorption in Mrk 6, NGC 3810, 1506+34, and NGC 1068	See Entry 116811
Estimated energy and momentum input to the interstellar medium for several external galaxies	See Entry 116821
Discovery of a large intergalactic H I cloud in the M96 group	See Entry 116839
Einstein observations of NGC 4438: dynamical ablation of gas in the Virgo Cluster	See Entry 116840
Luminous molecular hydrogen emission in the galaxy system NGC 3690-IC 694	See Entry 116843
An H α [N II] survey of the nuclei of a complete sample of spiral galaxies	See Entry 116847
The reddening of radio elliptical galaxies	See Entry 116848
The high-ionization optical spectrum of the Seyfert galaxy Tololo 0109-383 ..	See Entry 116851
Central distribution of the near-infrared colours in two early-type spirals	See Entry 116852
Slippery evidence on the Galaxy's invisible heavy halo	See Entry 116854
The galactic extinction towards Maffei 1	See Entry 116856
Detection of an extended soft X-ray source H 2326-79 in the southern sky	See Entry 116874

98.50 THE GALAXY, EXTRAGALACTIC OBJECTS AND SYSTEMS

116810 Optical spectroscopy of the radio-loud nuclei of spiral galaxies: starbursts or monsters? T.M.Heckman (Astron. Program, Univ. of Maryland, College Park, MD, USA), W.Van Breugel, G.K.Miley, H.R.Butcher. *Astron. J. (USA)*, vol.88, no.8, p.1077-87 (Aug. 1983). Presents optical spectroscopic data pertaining to the physical state, kinematics, and spatial extent of the emission-line gas near the radio-loud nuclei of spiral galaxies. These data are combined with published optical, radio, and infrared data to evaluate the suggestions by Condon et al. (1982) that the nuclear radio emission in this class of galaxy is produced by multiple supernova remnants generated as a consequence of a nuclear starburst. As a whole, the radio-loud nuclei have stronger emission lines than radio-quiet nuclei of galaxies of similar Hubble/de Vaucouleurs type. This emission-line gas is generally at least as spatially extended as the radio continuum emission. However, the authors find that only about $1/3$ of the spiral galaxies examined have optical spectroscopic properties consistent with those of 'extranuclear starbursts' (i.e. giant H II regions). The majority of the nuclei seem to require a form of energy input to the ionized gas which is 'harder' than the Lyman continuum radiation of OB stars, as their emission-line spectra are of the Seyfert or Liner variety. The nuclei with H II region spectra are distinct from the nuclei with Seyfert spectra in terms of radio morphology and radio spectral index, and tend to occur in spiral galaxies of much later Hubble type

than do the Seyfert or Liner nuclei (Sc vs. Sa). Moreover, the most luminous nuclear radio sources in the sample ($P_{1400\text{ MHz}} \geq 10^{22}$ Watts Hz^{-1} Sr^{-1}) are not associated with H II region nuclei. The authors summarize evidence that the putative nuclear starbursts must differ significantly from extranuclear starbursts. (74 refs.)

116811 Neutral hydrogen absorption in Mrk 6, NGC 3810, 1506+34, and NGC 1068. W.A.Baan (Dept. of Astron., Pennsylvania State Univ., University Park, PA, USA), A.D.Haschick.

Astron. J. (USA), vol.88, no.8, p.1088-93 (Aug. 1983). H I absorption has been reported in NGC 1068 and NGC 3810. The absorbing material in NGC 1068 has a low column density and is positioned in front of the compact nuclear source. Absorption in NGC 3810 occurs across a large fraction of the extended (4') radio source. Velocity offsets in NGC 3810 are due to disk rotation of the absorbing gas. Interpreting the features in these galaxies in terms of H I holes is considered implausible. H I absorption spectra are presented for Mrk 6 and a high resolution spectrum is given for 1506+34, suggesting the presence of distinct components in the 1506+34 absorption feature. (29 refs.)

116812 A survey of H α emission in normal galaxies. R.C.Kennicutt (Dept. of Astron., Univ. of Minnesota, Minneapolis, MN, USA), S.M.Kent.

Astron. J. (USA), vol.88, no.8, p.1094-1107 (Aug. 1983). Presents the combined results of photometric and spectrophotometric surveys of H α emission in 200 field and Virgo cluster galaxies. In most spiral galaxies the emission is dominated by normal disk H II regions, and consequently the integrated Balmer flux of a galaxy can be used as a quantitative index of its current OB star formation rate. Uncertainties due to instrumental effects, nuclear emission, [N II] emission, and extinction by dust are evaluated. The integrated emission of a galaxy is strongly correlated with its Hubble type and color, confirming the earlier conclusions of Cohen. Emission among galaxies of a given type varies greatly, however, and in most cases is due to a real dispersion in star formation activity. This activity is only weakly correlated with galaxy luminosity or H I content, suggesting that some other parameter is more important. (46 refs.)

116813 On the distance to M33 determined from magnitude corrections to Hubble's original Cepheid photometry. A.Sandage (Mount Wilson & Las Campanas Obs., Carnegie Inst. of Washington, Pasadena, CA, USA).

Astron. J. (USA), vol.88, no.8, p.1108-25 (Aug. 1983). New photoelectric photometry in Selected Area 45, and transfers from a faint photoelectric sequence adjacent to the south-preceding arm in M33 are made to the comparison stars for Hubble's Cepheids in M33. Progressive magnitude corrections are required to Hubble's M33 scales, reaching 2.8 mag at the limit of the Mount Wilson 2.5-m Hooker reflector. Hubble's Cepheid light curves are corrected to the B photoelectric system, and new photometric parameters are given for 35 of his variables. The P-L relation agrees in zero point to within 0.2 mag of the P-L relation from independent data by Sandage and Carlson for 12 new Cepheids in an outlying region of M33. Application of an adopted absolute P-L relation, calibrated by Martin, Warren, and Feast, to these data gives an apparent blue modulus of $(m-M)_{M33}^{AB} = 25.35$, which is 0.67 mag fainter than a previously adopted value, and represents a factor of 4.2 increase of Hubble's earliest distance. Three consequences of this larger apparent distance modulus are (1) the mean absolute magnitude of the first three brightest red supergiants is $M_{(V(3))}^{\max} = -8.7$ rather than ~ -8.0 in M33, complicating but not destroying use of red supergiants as distance indicators, (2) the mean absolute magnitude of the two brightest blue irregular supergiant variables is $M_{(B(2))} = -9.95$, which is close to the value for the brightest known supergiants in the galaxy, and (3) the absolute magnitude of M33 itself is brighter than heretofore assumed. (45 refs.)

116814 Arcsecond positions for milliarcsecond VLBI nuclei of extragalactic radio sources. II. 207 sources. D.D.Morabito, R.A.Preston, M.A.Slade (Jet Propulsion Lab., California Inst. of Technol., Pasadena, CA, USA), D.L.Jauncey, G.D.Nicolson.

Astron. J. (USA), vol.88, no.8, p.1138-45 (Aug. 1983). For pt.I see *ibid.*, vol.87, no.3, p.517-27 (1982). VLBI measurements of time delay and fringe frequency at 2.29 GHz on baselines of $\sim 10^5$ km are used to determine the positions of the milliarcsecond nuclei in 207 extragalactic radio sources. Estimated accuracies generally range from $\sim 0.1''$ to $\sim 1.0''$ in both right ascension and declination, with all sources having uncertainties $< 4''$ in both coordinates. The observed sources are part of an all-sky VLBI catalog of milliarcsecond radio sources. Arcsecond positions have now been determined for 752 of these sources. (12 refs.)

116815 Space distribution of stars in the southern Milky Way. III. A region in Centaurus-Crux. S.W.McCuskey (Warner & Swasey Obs., Case Western Reserve Univ., Cleveland, OH, USA).

Astron. J. (USA), vol.88, no.8, p.1175-81 (Aug. 1983). The space density at various distances of stars of several spectral-type groupings is determined in a 20-square-degree area centered on $l=298^\circ$, $b=+1^\circ$ from objective-prism and photometric data on approximately 8000 stars of common spectral types and 158 OB stars. A rather pronounced maximum in the numbers of B8-A1 stars and G-K giants as well is found at a distance of about 350 parsecs; there is also some indication of a maximum in the OB-star distribution at a distance of the order of 2500 kpc. A sharp decrease in the numbers of later-type dwarfs with increasing distance from the Sun is found, though the data are reliable for only a few hundred parsecs or so. This is the final contribution by the author to a long-term project started in 1945 to evaluate star density and luminosity function variations in the Milky Way plane. (21 refs.)

116816 Chemical evolution of the galactic halo. II. Enrichment in primary elements. M.Busso (Osservatorio Astron. di Torino, Pino Torinese, Italy), R.Gallino.

Astrophys. & Space Sci. (Netherlands), vol.94, no.2, p.273-89 (Aug. 1983). For pt.I see *ibid.*, vol.90, no.2, p.277-98 (1983). The chemical enrichment in the galactic halo is studied with particular attention to the overabundances of O and light elements with respect to Fe shown by metal poor stars. Some representative nucleosynthesis pictures for stars of both Population I and Population II are considered and their yields are compared with observations of relative abundances in the Sun and in the halo, to identify the possible reasons of the observed compositional differences. (59 refs.)

116817 Determination of physical parameters in extragalactic radio jets from large scale, small amplitude oscillations. A.Ferrari, E.Trussani, L.Zaninetti (Istituto di Fisica Generale, Univ. di Torino, Torino, Italy).

Astron. & Astrophys. (Germany), vol.125, no.2, pt.1, p.179-86 (Sept. 1983). Discusses the interpretation of large scale, small amplitude morphologies in jets (the so-called wiggles and knots) in terms of MHD Kelvin-Helmholtz instability in cylindrical supersonic flows. Theoretical growth rates and perturbation wavelengths are compared with observations of a VLA sample of well analysed jets. This model allows one to estimate the physical parameters of the jet plasma. Limits and approximations of the model are indicated. (31 refs.)

116818 The trivariate (radio, optical, X-ray) luminosity function of cD galaxies. I. New Westerbork observations of 22 cD galaxies and Einstein observations of A 1918 and A 2317. W.Bijleveld (Sterrewacht Leiden, Leiden, Netherlands), E.A.Valentijn.

Astron. & Astrophys. (Germany), vol.125, no.2, pt.1, p.217-22 (Sept. 1983). Radio observations with the Westerbork Synthesis Radio Telescope at 1412 MHz continuum of 22 cD galaxies and Einstein Observatory X-ray observations of two cDs are reported. Six cDs are detected at 1412 MHz, while both the cD galaxies that have been surveyed in the X-ray band have been detected. The centres of the two detected X-ray sources coincide with the optical centres of the cD galaxies. This again shows the existence of a special class of X-ray sources associated with cD galaxies. (32 refs.)

116819 The trivariate (radio, optical, X-ray) luminosity function of cD galaxies. II. The fuelling of radio sources. E.A.Valentijn (European Southern Obs., Garching bei Munchen, Germany).

Astron. & Astrophys. (Germany), vol.125, no.2, pt.1, p.223-40 (Sept. 1983). For pt.I see *ibid.*, vol.125, no.2, p.217-22 (1983). In order to test the hypothesis that radio sources in elliptical galaxies are fuelled by a fraction of accreted X-ray gas, a sample of 81 cD galaxies in clusters and 23 cD galaxies in poor groups is studied. Various subsamples are defined according to the origin of the cD galaxy classification (optically, radio or X-ray selected). A catalogue is presented, listing the measured optical, radio and X-ray luminosities from various origins, but all transformed to a uniform and homogeneous system: optical M_V (38 kpc metric diameter), radio $P_{1.4}$ (1.4 GHz monochromatic total radio power) and L_X (1 Mpc metric diameter 0.5-3.0 keV X-ray band). The three luminosity parameters are investigated for cross-correlations by studying power-power plots and by analysing how the integral radio luminosity function, expressed in fractions of radio detections ($F(>P_{1.4})$), depend on M_V and L_X . The physical origins of the relations between cluster richness R , L_X , M_V , and $P_{1.4}$ are discussed in detail. (65 refs.)

116820 ESO 438-G 9: a Seyfert galaxy with unusual properties. W.Koltschyn, K.J.Fricke (Univ. Gottingen, Gottingen, Germany).

Astron. & Astrophys. (Germany), vol.125, no.2, pt.1, p.276-9 (Sept. 1983). Discusses optical and UV spectroscopic data of the 1.5 Seyfert galaxy ESO 438-G 9 found from a survey of barred galaxies. Its spectrum shows strong Fe II emission. A very steep continuum gradient in the UV is reflected in the absence of higher ionisation lines. A double absorption feature is present shortward of the H α and H β emission line centres at relative velocities 2500 and 3500 km s^{-1} . This Seyfert galaxy is a member of a cluster of galaxies. (17 refs.)

116821 Estimated energy and momentum input to the interstellar medium for several external galaxies. I.Tarrab (Inst. d'Astrophys., Paris, France).

Astron. & Astrophys. (Germany), vol.125, no.2, pt.1, p.308-12 (Sept. 1983). Estimates the input of kinetic energy from stellar winds and supernovae explosions in several galaxies (LMC, SMC, NGC 6822, IC 1613, and M33) for comparison with the solar neighbourhood where a similar estimate has been made by Abbott (1982). The radiative energy and momentum input to the interstellar gas is also estimated. The amount of kinetic energy per unit mass of gas varies widely from galaxy to galaxy and is shown to be correlated with the presence of interstellar bubbles visible on H α photographs of these objects. (44 refs.)

116822 The tensor virial theorem for subsystems. P.Brosche (Obs. Hoher List, Univ.-Sternwarte Bonn, Daun, Germany), R.Caimmi, L.Secco.

Astron. & Astrophys. (Germany), vol.125, no.2, pt.1, p.338-41 (Sept. 1983). An extension of the tensor virial theorem for subsystems is formulated. The new terms are evaluated for the special case of two homogeneous oblate spheroids, one lying completely within the other. A possible application to elliptical galaxies is given. (8 refs.)

116823 Rotation curves and masses of galaxies. J.Lequeux (Obs. de Marseille, Marseille, France).

Astron. & Astrophys. (Germany), vol.125, no.2, pt.1, p.394-5 (Sept. 1983). The determination of the mass $M(R)$ of a spiral galaxy interior to a radius R where the rotation velocity $V(R)$ has been measured is discussed. It is shown that in spiral galaxies $M(R)$ is almost certainly in the range (0.6 to 1.0) $RV^2(R)/G$. The value $M(R) = RV^2(R)/G$ might be the most appropriate at all radii in the case of galaxies with a massive halo. (8 refs.)

116824 Galactic gamma radiation: the contribution from discrete sources. B.P.Houston, A.W.Wolfendale (Dept. of Phys., Univ. of Durham, Durham, England).

Astron. & Astrophys. (Germany), vol.126, no.1, pt.2, p.22-30 (Sept. 1983). The contribution to the galactic gamma-ray emission from discrete sources is currently based on the analysis of the COS B data, i.e. the 2CG catalogue, which indicates the presence of 25 'sources' (actually localised peaks of emission). A check on this catalogue has been made by adopting the earlier SAS II data and using the cross-correlation technique developed by the COS B group. Many of the 2CG peaks have been confirmed, but there is evidence that many of the 'sources' in the catalogue could be extended regions of enhanced emission, unresolved by the detectors. (27 refs.)

116825 Observations of annihilation radiation from the galactic center region. C.J.MacCallum (Sandia Nat. Labs., Albuquerque, NM, USA), M.Leventhal.

AIP Conf. Proc. (USA), no.101, p.211-29 (1983). (Workshop on Positron-Electron Pairs in Astrophysics, Greenbelt, MD, USA, Jan. 1983). The experiments that have demonstrated variability of the 511 keV positron annihilation line from the galactic center region are reviewed. The simplest history consistent with all (but one) of the eleven measurements is that of a narrow (< 2.5 keV FWHM), unredshifted ($dE < 25$ keV) line, which was constant in intensity ($(1.6 \pm 0.1) \times 10^{-3}$ ph cm^{-2} s^{-1} at Earth) from before 1970 until the beginning of 1980, when it dropped to zero in less than a year. The limited evidence for detection of the continuum expected from the three-photon decay of orthopositronium is evaluated, with particular attention to the possibility of simulation by atmospheric scattering. The question of possible correlation between variations in the inverse-power-law galactic center continuum and the strength of the 511 keV annihilation line is discussed; the evidence is inconclusive. (26 refs.)

116826 The gamma-ray spectrum of the galactic-center region. G.R.Riegler, J.C.Ling, W.A.Mahoney, W.A.Wheaton, A.S.Jacobson (Jet Propulsion Lab., California Inst. of Technol., Pasadena, CA, USA).

AIP Conf. Proc. (USA), no.101, p.230-6 (1983). (Workshop on Positron-Electron Pairs in Astrophysics, Greenbelt, MD, USA, Jan. 1983). The HEAO-3 high resolution gamma-ray spectrometer observed the galactic center region in fall 1979 and in the spring of 1980. Variation of the positron annihilation line at 511 keV has been reported previously. The fall 1979 observations show a significant high-energy continuum at energies above 511 keV. The intensity of a possible positronium triplet-state continuum is found to be less than that expected for direct positron annihilation and positronium decay in an ionized, warm ($T \leq 10^5$ K) plasma; depending on assumption for the shape of the high-energy continuum spectrum, positronium fractions bet-

ween 0.0 and 0.75 (at 90% statistical confidence level) are consistent with the observations. (18 refs.)

116827 Effects of line width and spatial extent on measurements of the 0.51 MeV galactic center line. P.P.Dunphy, E.L.Chupp, D.J.Forrest (Univ. of New Hampshire, Durham, NH, USA). *AIP Conf. Proc. (USA)*, no.101, p.237-41 (1983). (Workshop on Positron-Electron Pairs in Astrophysics, Greenbelt, MD, USA, Jan. 1983). Over the past 15 years, a number of measurements have been made of positron-electron annihilation radiation from the galactic center region. The results after 1979 show a significant decrease in measured flux intensity from that previously observed with the same instruments. This is probably due to time variations; however, the contributions of a spatially extended and/or energy-broadened component should also be considered. The entire data set is consistent with a time variable point source plus a distribution along the galactic disk. There is no strong evidence for a component broadened in energy. (11 refs.)

116828 Low-temperature positron annihilation. R.J.Drachman (Lab. for Astron. & Solar Phys., NASA/Goddard Space Flight Center, Greenbelt, MD, USA). *AIP Conf. Proc. (USA)*, no.101, p.242-52 (1983). (Workshop on Positron-Electron Pairs in Astrophysics, Greenbelt, MD, USA, Jan. 1983). For a satisfactory understanding of astrophysical annihilation radiation, especially that observed from the galactic center direction, the interaction of positrons with the ambient medium must be carefully investigated. Although hot, ionized regions may be important sources of annihilation radiation, in this report the author examines the processes occurring in low-temperature neutral hydrogen gas. The goal is to set limits on conditions in the annihilation region by using the predictions of atomic theory compared with the observed γ -ray line width, continuum strength and time dependence. (23 refs.)

116829 'Gamma-gun' in the center of the Galaxy. N.S.Kardashev, I.D.Novikov, A.G.Polnarev, B.E.Stern (Space Res. Inst., Acad. of Sci., Moscow, USSR). *AIP Conf. Proc. (USA)*, no.101, p.253-66 (1983). (Workshop on Positron-Electron Pairs in Astrophysics, Greenbelt, MD, USA, Jan. 1983). The authors discuss a model of physical processes that occur in the center of the Galaxy and cause the emission of the 511 keV annihilation γ -line and of a continuous γ -spectrum. The hypothesis is that electron positron pairs whose annihilation produces the observed γ -line are formed when a gas-cloud target is irradiated by a directed beam of hard (~ 100 MeV) γ -quanta. A model is developed that shows how a γ -beam (gamma-gun) forms near a supermassive rotating black-hole surrounded by a gaseous accretion disk with a magnetic field. The results of numerical simulations are compared with observational data. (40 refs.)

116830 The origin of the galactic center annihilation radiation. R.E.Lingenfelter (Center for Astrophys. & Space Sci., Univ. of California, La Jolla, CA, USA), R.Ramaty. *AIP Conf. Proc. (USA)*, no.101, p.267-72 (1983). (Workshop on Positron-Electron Pairs in Astrophysics, Greenbelt, MD, USA, Jan. 1983). Observations of the e^+e^- annihilation radiation from the galactic center suggest that something truly extraordinary is occurring there. The authors review the observations of this intense, time-varying, 0.511 MeV emission and discuss the implications of these and other recent observations on the positron production process, the annihilation region and the fundamental nature of the galactic center source. (28 refs.)

116831 Positrons from supernovae and the origin of the galactic center positron annihilation radiation. S.A.Colgate (Los Alamos Nat. Lab., Los Alamos, NM, USA). *AIP Conf. Proc. (USA)*, no.101, p.273-80 (1983). (Workshop on Positron-Electron Pairs in Astrophysics, Greenbelt, MD, USA, Jan. 1983). The emission of positrons from supernova ejecta is discussed in terms of the galactic center annihilation radiation. The positrons from the radioactive sequences ^{56}Ni — ^{56}Co — ^{56}Fe are the most numerous source from supernova. Only Type I supernova will allow a significant fraction to escape the expanding ejecta. For a neutron star model of a Type I SN a fraction 4×10^{-3} of the escaped positron is enough to create the observed several year fluctuation of the annihilation radiation. The likelihood of this model is discussed in terms of other astrophysical evidence as well as the type I SN light curve. (21 refs.)

116832 An electron-positron jet model for the galactic center. M.L.Burns (NASA/Goddard Space Flight Center, Greenbelt, MD, USA). *AIP Conf. Proc. (USA)*, no.101, p.281-6 (1983). (Workshop on Positron-Electron Pairs in Astrophysics, Greenbelt, MD, USA, Jan. 1983). High energy observations of the galactic center on the subparsec scale seem to be consistent with electron-positron production in the form of relativistic jets. These jets could be produced by a $\sim 10^6 M_\odot$ black hole dynamo transporting pairs away from the massive core. An electromagnetic cascade shower would develop first from ambient soft photons and then non-linearly; the shower using itself as a scattering medium. This is suited to producing, cooling and transporting pairs to the observed annihilation region. It is possible the center of our galaxy is a miniature version of more powerful active galactic nuclei that exhibit jet activity. (15 refs.)

116833 Positron production by a hot, young pulsar. K.Brecher, A.Mastichiadis (Dept. of Astron., Boston Univ., Boston, MA, USA). *AIP Conf. Proc. (USA)*, no.101, p.287-90 (1983). (Workshop on Positron-Electron Pairs in Astrophysics, Greenbelt, MD, USA, Jan. 1983). The authors consider a way of positron production in pulsars: pair production from electron-photon collisions. They show that this process must be the dominant one for a young pulsar when its surface temperature is around 10⁸ K. They apply this model to the observed positron flux coming from the galactic center and show that a pulsar with parameters close to those of the Crab at birth can explain, in principle, the flux. (10 refs.)

116834 X-rays and gamma-rays from active galaxies. J.L.Matteson (Center for Astrophys. & Space Sci., Univ. of California, La Jolla, CA, USA). *AIP Conf. Proc. (USA)*, no.101, p.292-302 (1983). (Workshop on Positron-Electron Pairs in Astrophysics, Greenbelt, MD, USA, Jan. 1983). Photon-photon pair production in active galaxies is considered and the concept of the annihilation efficiency, the efficiency for the conversion of >511 keV continuum luminosity into positron annihilation luminosity, is introduced. Equations that give a source's annihilation luminosity and 511 keV flux as a function of its size, continuum luminosity and distance are developed. These are applied to the available X-ray and gamma-ray data on active galaxies in order to make specific predictions. Efficiencies as high as >6 percent and fluxes up to 8×10^{-4} ph/cm²-sec result. While the latter are below present limits, they are within the reach of advanced instruments now in development. (38 refs.)

116835 Are mildly active galaxies sources of e^\pm annihilation radiation? A.P.Marscher, K.Brecher (Dept. of Astron., Boston Univ., Boston, MA, USA), W.A.Wheaton, J.C.Ling. *AIP Conf. Proc. (USA)*, no.101, p.303-8 (1983). (Workshop on Positron-Electron Pairs in Astrophysics, Greenbelt, MD, USA, Jan. 1983). The authors propose 7 galaxies of various types, within an order of magnitude of the galactic center, as possible sources of positrons. They present a relation between these galaxies and the variation in electron-positron 511 keV annihilation radiation. (19 refs.)

116836 Upper limits to the annihilation radiation luminosity of Centaurus A. N.Gehrels, T.L.Cline, W.S.Paciesas, B.J.Teegarden, J.Tueller (NASA/Goddard Space Flight Center, Greenbelt, MD, USA). *AIP Conf. Proc. (USA)*, no.101, p.309-13 (1983). (Workshop on Positron-Electron Pairs in Astrophysics, Greenbelt, MD, USA, Jan. 1983). A high-resolution observation of the active nucleus galaxy Centaurus A (NGC 5128) was made by the GSFC low energy gamma-ray spectrometer (LEGS) during a balloon flight on 1981 November 19. The measured spectrum between 70 and 500 keV is well presented by a power law of the form $1.05 \times 10^{-4} (E/100 \text{ keV})^{-1.59} \text{ ph cm}^{-2} \text{ s}^{-1}$ with no breaks or line features observed. The 98% confidence (2 σ) flux upper limit for a narrow (<3 keV) 511-keV positron annihilation line is $9.9 \times 10^{-4} \text{ ph cm}^{-2} \text{ s}^{-1}$. Using this upper limit, the ratio of the narrow-line annihilation radiation luminosity to the integral ≥ 511 keV luminosity is estimated to be <0.09 (2 σ upper limit). This is compared with the measured value for the galactic center in the Fall of 1979 of 0.10-0.13, indicating a difference in the emission regions in the nuclei of the two galaxies. (16 refs.)

116837 Electron/positron/gamma ray beams in cosmic radio sources. R.V.E.Lovelace, C.B.Ruchi (Cornell Univ., Ithaca, NY, USA). *AIP Conf. Proc. (USA)*, no.101, p.314-31 (1983). (Workshop on Positron-Electron Pairs in Astrophysics, Greenbelt, MD, USA, Jan. 1983). Further study has been made of an electrodynamic model for the origin of the beams which are thought to power extra-galactic double radio sources. In this model the rotating magnetized accretion disk of a massive black hole acts as a unipolar induction dynamo. Energy and angular momentum of the infalling matter of the disk is extracted electromagnetically and propagated outward along the $\pm z$ axes initially as the Poynting flux of a relativistic space-charge flow. An analysis of the space charge flow is made utilizing the analogy with laboratory high-voltage, magnetically insulated transmission lines. The magnetic insulation is predicted to undergo electrical breakdown at a distance $\sim z_p$ providing a termination for the transmission line. At the termination the Poynting flux is transformed into particle kinetic energy. The remaining fraction of the energy is directed outward, and under appropriate conditions it gives rise to electromagnetic cascade showers. The showers result in collimated, $\pm z$ directed beams of electrons, positrons, and gamma rays. The relevant shower equations of Burns and Lovelace have been integrated numerically to determine the ratio of the energy in the gamma rays to the energy in the electrons and positrons for different physical conditions. The electron-positron beams are eventually stopped and scattered in pitch angle by the ram pressure of an external medium. Synchrotron radiation of the scattered electrons and positrons produces the observed radio lobes. (50 refs.)

116838 Compactness and pair production in active galactic nuclei. M.Salvati (European Southern Obs., Garching, Germany), A.Cavaliere, E.Costa, E.Massaro. *AIP Conf. Proc. (USA)*, no.101, p.332-6 (1983). (Workshop on Positron-Electron Pairs in Astrophysics, Greenbelt, MD, USA, Jan. 1983). Barring relativistic bulk motions, the continuum emitted by AGNs implies very compact sources. The authors find that the compactness parameter $k=L_c/R$ cannot, especially in the X-ray band, exceed a level interestingly close to the current data. In sources driven by high energy electrons, the main limitation is associated with pair production by heavily absorbed, inverse-Compton gamma-rays. (13 refs.)

116839 Discovery of a large intergalactic H I cloud in the M96 group. S.E.Schneider (Nat. Astron. & Ionosphere Center, Cornell Univ., Ithaca, NY, USA), G.Helou, E.E.Salpeter, Y.Terzian. *Astrophys. J. Lett. Ed. (USA)*, vol.273, no.1, pt.2, p.L1-5 (1 Oct. 1983). The authors report the discovery of an intergalactic H I cloud, found in the western part of the Leo group of galaxies, using the Arecibo 21 cm system. The cloud has a systemic radial velocity of about 960 km s⁻¹. The emission is found mainly in a region approximately 100 kpc long by 30 kpc wide midway between M96 and M105. The nominal H I mass of the whole cloud is about $10^9 M_\odot$. However, because of the low rate of collisional excitation, M_{HI} may be substantially underestimated for this cloud. The velocity structure of the cloud gives an indicative gravitational mass of at least $2 \times 10^{10} M_\odot$. (25 refs.)

116840 Einstein observations of NGC 4438: dynamical ablation of gas in the Virgo Cluster. C.Kotanyi (European Southern Obs., Garching, Germany), J.H.van Gorkom, R.D.Ekers. *Astrophys. J. Lett. Ed. (USA)*, vol.273, no.1, pt.2, p.L7-9 (1 Oct. 1983). High-resolution observations are presented of the X-ray emission of the peculiar galaxy NGC 4438 in the center of the Virgo Cluster. The observations, made with the HRI on the Einstein Observatory show a compact source (size $\leq 10''$) near the center of the galaxy with a luminosity $L_x = 1.5 \times 10^{39} \text{ ergs s}^{-1}$ (0.1-2 keV) and an extended region of emission about 3 kpc in size and with a luminosity $L_x = 3 \times 10^{39} \text{ ergs s}^{-1}$ situated asymmetrically to the NW of the galaxy. The asymmetry is similar to the asymmetry in the radio emission and could be due to ram-pressure sweeping of the interstellar gas from the disk of the galaxy. (16 refs.)

116841 VLA radio continuum observations of the edge-on spiral galaxy NGC 3079. N.Duric, E.R.Seaquist (Dept. of Astron., Univ. of Toronto, Toronto, Ontario, Canada), P.C.Crane, R.C.Bignell, L.E.Davis. *Astrophys. J. Lett. Ed. (USA)*, vol.273, no.1, pt.2, p.L11-15 (1 Oct. 1983). Radio continuum VLA maps of the edge-on spiral galaxy NGC 3079 are presented at 1.4 and 4.9 GHz. Extensions of emission along the minor axis are resolved at 4.9 GHz into lobes and bridges. The eastern component consists of a highly polarized ring-shaped lobe connected by a thin bridge to the central region of the galaxy and has an integrated flux density of 70 mJy at 1.4 GHz. The western component has an incomplete lobe, also connected to the center of the galaxy by a thin bridge and has a flux density of 90 mJy at 1.4 GHz. At 4.9 GHz, a nuclear point source (size <100 pc at a distance of 24 Mpc) has a flux density of 87 mJy. (15 refs.)

116842 The bend in the correlation function: the surviving imprint of adiabatic perturbations? A.L.Melott (Dept. of Phys. & Astron., Univ. of Pittsburgh, Pittsburgh, PA, USA). *Astrophys. J. Lett. Ed. (USA)*, vol.273, no.1, pt.2, p.L21-5 (1 Oct. 1983). Results are presented from numerical analysis of a two-dimensional simulation of the clustering of collisionless particles. The initial perturbation spectrum was cut off to simulate damping (as in the adiabatic theory of galaxy formation). The two-point correlation function was driven to a power law at small scales and remained small at large scales during nonlinear 'pancaking'.

There were small ($\sim 10^{-1}$) imprints of large-scale power in the form of bumps in the covariance function. During nonlinear evolution, these bumps were found to cause a downward bend in the correlation function, as observed in sky surveys. If the primordial spectral index was 0 or 1, anticorrelation was found just outside this bend. (23 refs.)

116843 Luminous molecular hydrogen emission in the galaxy system NGC 3690-IC 694. J.Fischer (E.O. Hulbert Center for Space Res., Naval Res. Lab., Washington, DC, USA), M.Simon, J.Benson, P.M.Solomon. *Astrophys. J. Lett. Ed. (USA)*, vol.273, no.1, pt.2, p.L27-30 (1 Oct. 1983). The authors report the detection of line emission of vibrationally excited H_2 from the galaxy system NGC 3690-IC 694. The line emission is distributed within the system. The total observed luminosity in the H_2 $v=1-0$ S(1) line alone is approximately $1.5 \times 10^7 L_\odot$. The authors also detected Br γ line emission from the system; its observed luminosity indicates that at least 4×10^{34} ionizing photons per second are required to maintain ionization of the H II. The H_2 is probably heated by shocks, and the mass of hot H_2 exceeds $2 \times 10^4 M_\odot$. (25 refs.)

116844 Upper limits to O III $\lambda 5592$ and [Ni IX] $\lambda 4594$ in Seyfert galaxies. D.E.Osterbrock (Inst. for Advanced Study, Princeton, NJ, USA), O.Dahari, J.O.Ekberg. *Astrophys. J. Lett. Ed. (USA)*, vol.273, no.1, pt.2, p.L31-4 (1 Oct. 1983). Observational upper limits are given to the strengths of the undetected emission lines O III $\lambda 5592$ and [Ni IX] $\lambda 4594$ in several well-observed Seyfert galaxies. The $\lambda 5592$ upper limits show that the O III charge-exchange process does not contribute appreciably to the observed strength of $\lambda 4363$ and thus does not appreciably modify the [O III] intensity ratio from which the temperature in the O^{++} zone is derived. The $\lambda 4594$ upper limits are consistent with 'normal' abundance ratios Ni:Fe ≈ 0.1 in these objects, but would not be consistent with Ni:Fe ≈ 1 . (19 refs.)

116845 Standard photometric diameters of galaxies. P.Fouque (Obs. de Meudon, DERADN, Meudon, France), G.Paturel. *Astron. & Astrophys. Suppl. Ser. (France)*, vol.53, no.3, p.351-9 (Sept. 1983). A sample of mean standard major axis diameters and axis ratios at 25 mag.arcsec $^{-2}$ and 26.5 mag. arcsec $^{-2}$ brightness levels for 237 galaxies has been built from new measurements and from a compilation in the literature. Only the best data are kept according to the results of intercomparisons in order to give a good reference sample of mean diameters. This sample will be used to reduce visual apparent diameters given in large catalogs to a homogeneous system. (18 refs.)

116846 High-resolution optical observations of NGC 3379. II. On the derivation of the East-West profile. J.-L.Nieto (Observatoires du Pic-du-Midi et de Toulouse, Bagneres-de-Bigorre, France). *Astron. & Astrophys. Suppl. Ser. (France)*, vol.53, no.3, p.383-93 (Sept. 1983). For pt.I see *ibid.*, vol.53, no.2, p.247-53 (1983). Presents high-resolution observations (FWHM $\sim 0.5''$ - $1.0''$) of the luminosity standard NGC 3379 obtained with the CHF telescope, and new regular-resolution data. The problems related to photography at high resolution are discussed. The consistency and accuracy of the new material are checked against previous data analysed in paper I (Nieto, 1983). Following the method of de Vaucouleurs and Capaccioli (1979), the composite high-resolution East-West profile of NGC 3379 is derived. (19 refs.)

116847 An H α [N II] survey of the nuclei of a complete sample of spiral galaxies. W.C.Keel (Lick Obs., Univ. of California, Santa Cruz, CA, USA). *Astrophys. J. Suppl. Ser. (USA)*, vol.52, no.3, p.229-39 (July 1983). New spectrophotometry of the nuclei of an optically complete sample of 93 spiral galaxies brighter than integrated magnitude $B_T=12.0$ is presented. All the nuclei exhibit emission lines. These are divided into those produced by stellar photoionization (H II regions) and low-ionization emission regions. In addition, five Seyfert nuclei occur in this sample, including one (NGC 4941) not previously identified. Relations between nuclear luminosity and emission-line luminosity, and between the character of the emission spectrum and line luminosity, are presented. (25 refs.)

116848 The reddening of radio elliptical galaxies. W.B.Sparks (Dept. of Appl. Maths. & Astron., Univ. Coll., Cardiff, Wales). *Mon. Not. R. Astron. Soc. (GB)*, vol.204, no.3, p.1049-66 (Sept. 1983). The photometric properties of radio-emitting and radio-quiet elliptical galaxies are compared. A statistically significant reddening of the radio ellipticals is evident for galaxies of a given optical luminosity. There is also evidence that radio ellipticals display less scatter in their colours. The reddening is interpreted as being due to extinction by dust within the radio ellipticals, requiring $\sim 10^6 M_\odot$ of gas. This supports the idea that a high gas content and nuclear activity are related, and may be accommodated within the framework of galactic wind models. (51 refs.)

116849 High-resolution images of the galactic centre. D.A.Allen (Anglo-Australian Obs., Epping, NSW, Australia), A.R.Hyland, T.J.Jones. *Mon. Not. R. Astron. Soc. (GB)*, vol.204, no.3, p.1145-52 (Sept. 1983). The authors present grey-scale images of the central 45 arcsec 2 region around the galactic centre at 2.2 μ m. The region is resolved into a great number of point sources whose distribution peaks strongly on the nonthermal radio source. The surface brightness distribution appears cusped. If this represents an isothermal spherical distribution of stars, then its innermost core must be smaller than that of any globular cluster, and very much smaller than that of M31. Alternatively, a large, compact mass lies within the central 2 arcsec. The luminosity function of the point sources is steeper than that of the old disc population. (27 refs.)

116850 The galactic nucleus. J.W.V.Storey, D.A.Allen (Anglo-Australian Obs., Epping, NSW, Australia). *Mon. Not. R. Astron. Soc. (GB)*, vol.204, no.3, p.1153-61 (Sept. 1983). The authors have observed the immediate vicinity of the galactic centre at optical and infrared wavelengths, and present images at 1.0, 1.2 and 2.2 μ m. A detailed map is given of the Brackett γ emission in the region, together with some measurements of the CO absorption at 2.3 μ m. By relating all positional measurements to the Perth catalogue, the authors locate the optical, infrared and radio data to a relative accuracy of 0.4 arcsec. (34 refs.)

116851 The high-ionization optical spectrum of the Seyfert galaxy Tololo 0109-383. R.A.E.Fosbury (Royal Greenwich Obs., Hailsham, England), A.E.Sansom. *Mon. Not. R. Astron. Soc. (GB)*, vol.204, no.3, p.1231-6 (Sept. 1983). Optical emission line intensity measurements are presented of the high-ionization Seyfert galaxy T 0109-383. Using the transauroral to nebular ratios of [O II] and [S II], the extinction to the forbidden line region is found to be $A_v=1.6$ mag. The reddening corrected [Fe VII] spectrum indicates a temperature and an electron density in the high-ionization zone of $<3.5 \times 10^4$ K and 2×10^6 cm $^{-3}$ respectively. While this supports the notion that the higher ions are photoionized in Seyfert galaxies, a significantly higher assumed value of the extinction ($A_v > 2$ mag) to the high-ionization

zone would be consistent with an [Fe VII] temperature of $\sim 10^5$ K and collisional ionization. (20 refs.)

116852 Central distribution of the near-infrared colours in two early-type spirals. T.J.Jones, A.R.Hyland (Mount Stromlo & Siding Spring Obs., Res. School of Phys. Sci., Australian Nat. Univ., Canberra, Australia), I.Gatley. *Mon. Not. R. Astron. Soc. (GB)*, vol.204, no.3, p.1263-7 (Sept. 1983). Point J-K colours at a number of positions in the galaxies NGC 7814 and 5746 are presented. The variation of colour with position is strongly correlated with the location of the optically visible disc component in both galaxies. This supports the conclusion of Griensmith, Hyland and Jones (1982) that the UVK and JHK colours for early-type spirals (with colours different from ellipticals) are due to contamination of the pure bulge light by a young dusty disc component. (6 refs.)

116853 Redshifts of five extragalactic radio sources. P.J.Warner, J.M.Riley, S.A.Eales, A.J.B.Downes, J.E.Baldwin (Mullard Radio Astron. Obs., Cambridge, England). *Mon. Not. R. Astron. Soc. (GB)*, vol.204, no.3, p.1279-83 (Sept. 1983). Redshifts have been measured for five optical objects associated with extragalactic radio sources. They are 0.1047, 0.1204, 0.0837 and 0.0600 for the radio galaxies 0908+37, 1141+37, 1227+11 and 1739+17 respectively and 0.2842 for the quasar 1255+37. (11 refs.)

116854 Slippery evidence on the Galaxy's invisible heavy halo. D.Lyndén-Bell (Inst. of Astron., Obs., Cambridge, England), R.D.Cannon, P.J.Godwin. *Mon. Not. R. Astron. Soc. (GB)*, vol.204, no.3, p.87P-92P (Sept. 1983). New measurements have been made of the velocities of carbon stars in the Carina and other dwarf galaxies, and of the planetary nebula in Fornax. Carina, previously thought to be the Galaxy's fastest moving satellite, is shown instead to be moving very slowly. The new result for Carina combined with the revised velocity of Sculptor (and a new distance reported for Palomar 1) removes some of the evidence for a heavy halo. The best modern data on all the nine satellites of the Galaxy now yield a total mass out to about 100 kpc of $(2.6 \pm 0.8) \times 10^{11} M_\odot$. (28 refs.)

116855 Six quasars near the jets of NGC 1097. R.D.Wolstencroft (Royal Obs., Edinburgh, Scotland), W.H.-M.Ku, H.C.Arps, S.M.Scarrott. *Mon. Not. R. Astron. Soc. (GB)*, vol.205, no.1, p.67-80 (Oct. 1983). Six quasars have been discovered in a 0.43 deg 2 field surrounding NGC 1097. The quasars are grouped in a small area of the field: five of the quasars lie within the area defined by the jets emanating from the galaxy. Four of the quasars are clearly detected in a deep X-ray map of the field. The probability of finding such an unusual configuration is discussed. (32 refs.)

116856 The galactic extinction towards Maffei 1. R.J.Buta, M.L.McCall (Dept. of Astron. & McDonald Obs., Univ. of Texas, TX, USA). *Mon. Not. R. Astron. Soc. (GB)*, vol.205, no.1, p.131-52 (Oct. 1983). The extinction of Maffei 1 has been measured by two new techniques. First, BV aperture photometry has been performed to obtain the colour excess from standard aperture-colour relations for early-type galaxies. Secondly, millimetre and radio observations of galactic CO and H I are used to calculate the total hydrogen column density along the line-of-sight, and thereby estimate the colour excess from the local dust-to-gas ratio. After consideration of all extinction measurements to date, it is concluded that $A_v=5.1 \pm 0.2$ mag. The isophotal diameter and the corrected apparent visual magnitude are estimated making Maffei 1 one of the biggest and brightest galaxies in the sky. The distance is found, indicating that Maffei 1 is probably associated with the Ursa Major-Camelopardalis cloud, not the Local Group. (45 refs.)

116857 Active galactic nuclei: IUE results on continuum, emission and absorption lines. G.C.Perola (Istituto Astron., Univ. di Roma, Roma, Italy). *Mem. Soc. Astron. Ital. (Italy)*, vol.54, no.2, p.385-97 (1983). Concentrates on results obtained with IUE concerning the continuum, emission and absorption lines. The reddening correction, the UV continuum and UV lines are discussed. (59 refs.)

116858 Far ultraviolet observations of BL Lac objects. L.Maraschi (Dipartimento di Fisica, Univ. di Milano, Milano, Italy), E.G.Tanzi, A.Treves. *Mem. Soc. Astron. Ital. (Italy)*, vol.54, no.2, p.399-413 (1983). These objects are discussed first with special regard to the overall energy distribution. The two cases of recorded UV observations are summarized, and some general considerations on the 'average spectrum' are advanced. (51 refs.)

116859 The UV spectrum of elliptical galaxies. F.Bertola, M.Capaccioli (Istituto di Astron., Univ. di Padova, Padova, Italy). *Mem. Soc. Astron. Ital. (Italy)*, vol.54, no.2, p.415-17 (1983). Examines IUE spatial and spectral resolution of the flux forming the so-called UV rising branch of E galaxies. (7 refs.)

116860 Is the polarisation of NGC 1068 evidence for a non-thermal source? I.S.McLean (Royal Obs., Univ. of Edinburgh, Edinburgh, Scotland), C.Aspin, S.R.Heathcote, M.J.McCaughrean. *Nature (GB)*, vol.304, no.5927, p.609-11 (18 Aug. 1983). Unresolved questions concern the nature and relationship of the sources of the excess flux seen in the UV and IR, their connection with the collimated jets apparent in high-resolution radio maps and their association with the extended region responsible for the broad emission lines. A further question is the location of any dust and its role in modifying the optical and UV spectrum. The authors report observations with two high-resolution optical spectropolarimeters which throw new light on these questions. The authors conclude that dilution by starlight modifies the polarisation to an extent not previously appreciated. In fact, the polarisation of the non-stellar flux in the optical and near IR is approximately independent of wavelength with a direction orthogonal to that of the radio jets. (33 refs.)

116861 Neutrino-gaseous 'Pancakes' and the problem of hidden mass. A.G.Doroshkevich. *Pis'ma v Astron. Zh. (USSR)*, vol.9, no.8, p.451-5 (1983). In Russian. English translation in: *Sov. Astron. Lett. (USA)*. Taking into account the peculiar velocities of neutrinos the gaseous component is shown to dominate in the central part of a cosmological 'pancake'. Therefore fragmentation of a gaseous 'pancake' and later clustering of the fragments into galaxies and groups of galaxies are determined by velocity distribution and self-gravity of the gaseous component. The hidden mass is formed by capture of neutrinos by clustering clouds. The formation of clusters of galaxies is connected with perturbations embracing the entire neutrino gaseous 'pancake'. (22 refs.)

Galactic lens	See Entry 111366
Galactic profiles and the point spread function	See Entry 116488
Galaxies rotation curves: a catalogue	See Entry 116492
Self-regulated star formation in the Galaxy	See Entry 116628

Narrow-band photometry of G and K stars near the North Galactic Pole See Entry 116641

Radial velocities for early type stars in six galactic regions ..See Entry 116642

The extreme LMC supergiant HD 38489: an optical and ultraviolet study See Entry 116647

Visible and UV observations of the giant early-type members of the Large Magellanic Cloud See Entry 116654

Frequency of novae in M33 See Entry 116703

Supernova in faint spiral galaxy See Entry 116710

Possible supernova in NGC 7418 See Entry 116711

Electron-positron processes and spectral evolution in black hole accretion disk dynamo models for AGN sources of the cosmic X-ray and gamma ray backgrounds See Entry 116735

Hot accretion disks and γ -ray cosmic sources See Entry 116737

The effect of low-velocity, low-mass intruders (collisionless gas) on the dynamical evolution of a binary system See Entry 116743

A 0538-66 See Entry 116759

A model for A 0538-66: the fast flaring pulsar See Entry 116761

The chemical composition of distant globular clusters: are there any metal-poor clusters? See Entry 116765

Ellipticity variations within some globular clusters of the Galaxy and the Magellanic Clouds See Entry 116773

The temperature of molecular gas in the galactic center region See Entry 116781

The fraction of the sky screened by local diffuse dust clouds See Entry 116791

Regions of low molecular column density near the galactic plane See Entry 116795

Observations of H₂O maser emission in the Large Magellanic Cloud See Entry 116803

Tracing the gas in galaxies See Entry 116809

The Hydra I cluster of galaxies. II. First results from H I-observations See Entry 116862

Poor evidence of merging in loose galaxy groups See Entry 116864

The evolution of galaxies in clusters. III. Photometry of 17 intermediate redshift clusters See Entry 116865

The Ursa Major supercluster. II. A statistical analysis of the radio survey See Entry 116866

Flux density and linear polarization measurements of variable radio sources at λ 900 mm (33.5 GHz) See Entry 116869

Magnitude and redshift distributions of QSOs See Entry 116871

Fragmentation of the Universe See Entry 116892

Constraints on neutrino-dominated cosmologies from large-scale streaming motion See Entry 116894

The cosmological problem as initial value problem on the observer's past light cone: observations See Entry 116895

Proto-galactic perturbations See Entry 116900

New model of the metagalaxy See Entry 116908

98.50K Groups, clusters, superclusters

116862 The Hydra I cluster of galaxies. II. First results from H I-observations. O.G.Richter, W.K.Huchtmeier (Max-Planck-Inst. fur Radioastron., Bonn, Germany). *Astron. & Astrophys. (Germany)*, vol.125, no.2, pt.1, p.187-92 (Sept. 1983). For pt.1 see ibid., vol.111, no.1, p.193-200 (1982). H I 21 cm-line observations of 42 galaxies in the field of the Hydra I (=Abell 1060) cluster are presented. 17 galaxies have been detected, raising the number of known redshifts in the area of the Hydra I cluster to 96. Although the authors detected only a few galaxies, they find evidence for an increase of the H I-deficiency factor radially inwards to the centre of the cluster. The distance modulus of the Hydra I cluster relative to the Virgo cluster from the (blue magnitude) Tully-Fisher relation ($2.68^m \pm 0.21^m$) is in agreement with other determinations and with the value based on the ratio of cluster redshifts ($2.61^m \pm 0.15^m$). Thus a constraint to the infall velocity of the Local Group toward the Virgo cluster is given to values less than 350 km s⁻¹. (34 refs.)

116863 Galaxy groups: correlations between luminosities, velocity dispersions, and virial radii. M.Mezzetti, G.Giuricin, M.L.Malagnini, F.Mardirossian (Osservatorio Astron. di Trieste, Trieste, Italy). *Astron. & Astrophys. (Germany)*, vol.125, no.2, pt.1, p.368-70 (Sept. 1983). Considers selection and contamination effects in a subsample of 49 groups extracted from the new, three-dimensional, catalogue of groups of galaxies made by Huchra and Geller (1982). It is possible to subdivide the groups into two sets: those (20) having the logarithm of the recession velocity smaller than 3.2, and the others with log W>3.2 (29). The nearer groups are little affected by selection effects and contain only a moderate fraction of interlopers (which is almost constant with the distance) while the opposite holds for the farther groups. The latter subsample of groups adds 'noise' when the correlations between the logarithms of the virial parameters are evaluated, and one is thus led to regard as reliable only the estimates based on the nearer groups. The most significant correlation turns out to be the one between the logarithms of the total luminosity and the velocity dispersion. (9 refs.)

116864 Poor evidence of merging in loose galaxy groups. F.Mardirossian, G.Giuricin, M.Mezzetti (Osservatorio Astron. di Trieste, Trieste, Italy). *Astron. & Astrophys. (Germany)*, vol.126, no.1, pt.2, p.86-8 (Sept. 1983). By examining a sample extracted from Huchra and Geller's (1982) catalogue of galaxy groups, poor evidence is found of galactic cannibalism. In particular, the correlations of the magnitude difference between the two brightest members of each group with group compactness or dynamical times turn out not to be significant. (11 refs.)

116865 The evolution of galaxies in clusters. III. Photometry of 17 intermediate redshift clusters. H.Butcher (Kitt Peak Nat. Obs., Tucson, AZ, USA), A.Oemler,Jr., D.C.Wells. *Astrophys. J. Suppl. Ser. (USA)*, vol.52, no.3, p.183-228 (July 1983). For pt.II see *Astrophys. J.*, vol.226, no.2, pt.1, p.559-65 (1978). The authors present photometry in two bands of 17 rich clusters of galaxies with redshifts between 0.17 and 0.39. Fifteen of the clusters were studied on *J* and *F* (or in case *N*) plates taken at the prime focus on the KPNO and CTIO 4 m telescopes. Two clusters were observed in *V* and *R* with the KPNO video-camera on the 2.1 m telescope. Photometry extends to, typically, a red magni-

tude of 22 mag, although there is some incompleteness near the limit. From internal error indicators, the colors are estimated to be accurate to, typically, 0.13 mag at a red magnitude of 21. (17 refs.)

116866 The Ursa Major supercluster. II. A statistical analysis of the radio survey. N.J.Schuch (Mullard Radio Astron. Obs., Cambridge, England). *Mon. Not. R. Astron. Soc. (GB)*, vol.204, no.3, p.1245-56 (Sept. 1983). For pt.1 see ibid., vol.196, no.2, p.695-704 (1981). A statistical analysis of the 5C 10 radio survey of the Ursa Major supercluster is used to derive estimates for the radio luminosity distribution of the central cluster (Abell 1318) and the whole supercluster. Galaxies within the supercluster only form about 12 per cent of the total number of radio sources, and only 3 per cent of the galaxies were detected. The overall radio source counts and spectral-index distribution are compatible with previous 5C surveys, but there is a significant difference between the spectral-index distribution and that found for more intense sources. This difference has implications for the radio source counts. (20 refs.)

A class of self-similar astrophysical explosions See Entry 116444

The trivariate (radio, optical, X-ray) luminosity function of cD galaxies. I. New Westerbork observations of 22 cD galaxies and Einstein observations of A 1918 and A 2317 See Entry 116818

The trivariate (radio, optical, X-ray) luminosity function of cD galaxies. II. The fuelling of radio sources See Entry 116819

Discovery of a large intergalactic H I cloud in the M96 group See Entry 116839

Einstein observations of NGC 4438: dynamical ablation of gas in the Virgo Cluster See Entry 116840

The bend in the correlation function: the surviving imprint of adiabatic perturbations? See Entry 116842

Neutrino-gaseous 'Pancakes' and the problem of hidden mass See Entry 116861

Constraints on neutrino-dominated cosmologies from large-scale streaming motion See Entry 116894

98.70 OTHER OBJECTS AND BACKGROUND RADIATIONS OF UNKNOWN ORIGIN AND DISTANCES (for pulsars, see 97.60G)

116867 Identification of a blue object with a newly detected X-ray source. E.H.Geyer, M.Hoffmann (Obs. Hoher List, Univ. Sternwarte Bonn, Daun, Germany). *Astrophys. & Space Sci. (Netherlands)*, vol.94, no.2, p.291-3 (Aug. 1983). A blue object was identified on POSS prints. Its position coincides with an X-ray source (α 15^h07^m01^s, σ +40°18'7") found by the HEAO-B satellite. (2 refs.)

98.70D Discrete radio sources

116868 31.4 GHz flux density measurements of a complete sample of sources from the 5-GHz S5 survey. B.J.Geldzahler (E.O. Hulburt Center for Space Res., Naval Res. Lab., Washington, DC, USA), H.Kuhr. *Astron. J. (USA)*, vol.88, no.8, p.1126-32 (Aug. 1983). Measurements at 31.4-GHz (9.5-mm) are presented for the complete sample of 66 radio sources with declinations greater than +70° and 5-GHz flux densities greater than 0.5 Jy. About half the sources have the flat radio spectra characteristic of objects with compact components radiating most strongly in the mid-centimeter wavelength range, and about one third show evidence of very compact components ($\theta \leq 0.0001''$) radiating at short centimeter wavelengths regardless of morphological type. The median spectral index of all the sources, the quasars alone, and the galaxies alone tends to flatten with increasing frequency for steep spectrum sources, whereas a steepening was found with increasing frequency for the flat spectrum sources. (16 refs.)

116869 Flux density and linear polarization measurements of variable radio sources at λ 900 mm (33.5 GHz). A.M.Flett, C.Henderson. *Mon. Not. R. Astron. Soc. (GB)*, vol.204, no.3, p.1285-9 (Sept. 1983). Measurements of the flux densities of 12 extragalactic sources at λ 9 mm throughout 1980 June to 1982 March are presented. This period includes the decay of the 1980 outburst of BL Lac. Measurements of the integrated linear polarization of the stronger sources are also given and compared with those of other observers. (17 refs.)

A catalog of high accuracy circular polarization measurements See Entry 116494

The disc-like envelopes around young stars seen in the maser lines See Entry 116658

On the correlation between H α line intensity and SiO maser emission of the long-period variable χ cygni See Entry 116702

Do filaments form at the time of supernova explosions? See Entry 116707

Radio emission from AM Herculis: the quiescent component and an outburst ... See Entry 116740

Magnetic focusing in the Sco X-1 radio source See Entry 116764

Isotopic fractionation and mass motion in giant molecular clouds See Entry 116776

Spectrophotometry of the optical emission from RCW 103 and Milne 23 See Entry 116780

Ammonia absorption toward W3(OH): 0.3'' resolution maps in the (2,2) line See Entry 116790

The detection of butadiynyl (C₄H) in absorption against Cassiopeia A See Entry 116793

Regions of low molecular column density near the galactic plane See Entry 116795

CS *J*=5-4 observations of galactic molecular clouds See Entry 116797

Observations of H₂O maser emission in the Large Magellanic Cloud See Entry 116803

Determination of the angular size of the H₂O maser outburst region in Orion KL defined by a linearly polarized emission See Entry 116806

The determination of cloud masses and dust characteristics from submillimetre thermal emission See Entry 116808

Tracing the gas in galaxies See Entry 116809

- Optical spectroscopy of the radio-loud nuclei of spiral galaxies: starbursts or monsters? See Entry 116810
- Neutral hydrogen absorption in Mrk 6, NGC 3810, 1506+34, and NGC 1068 See Entry 116811
- Arcsecond positions for milliarcsecond VLBI nuclei of extragalactic radio sources. II. 207 sources See Entry 116814
- Determination of physical parameters in extragalactic radio jets from large scale, small amplitude oscillations See Entry 116817
- The trivariate (radio, optical, X-ray) luminosity function of cD galaxies. I. New Westerbork observations of 22 cD galaxies and Einstein observations of A 1918 and A 2317 See Entry 116818
- The trivariate (radio, optical, X-ray) luminosity function of cD galaxies. II. The fuelling of radio sources See Entry 116819
- Upper limits to the annihilation radiation luminosity of Centaurus A See Entry 116836
- Electron/positron/gamma ray beams in cosmic radio sources See Entry 116837
- Discovery of a large intergalactic H I cloud in the M96 group See Entry 116839
- Einstein observations of NGC 4438: dynamical ablation of gas in the Virgo Cluster See Entry 116840
- VLA radio continuum observations of the edge-on spiral galaxy NGC 3079 See Entry 116841
- The reddening of radio elliptical galaxies See Entry 116848
- The galactic nucleus See Entry 116850
- Redshifts of five extragalactic radio sources See Entry 116853
- Is the polarisation of NGC 1068 evidence for a non-thermal source? See Entry 116860
- The Hydra I cluster of galaxies. II. First results from H I-observations See Entry 116862
- The Ursa Major supercluster. II. A statistical analysis of the radio survey See Entry 116866
- A VLBI search for compact components in extended high redshift quasars See Entry 116872
- Pair production and non-thermal radio stars See Entry 116885

98.70J Quasars

- 116870 High precision astrometry via very-long-baseline radio interferometry: estimate of the angular separation between the quasars 1038+528A and B. J.M.Marcaide, I.I.Shapiro (MIT, Cambridge, MA, USA). *Astron. J. (USA)*, vol.88, no.8, p.1133-7 (Aug. 1983).
- Dual-wavelength VLBI observations with the Mark III system of the two radio quasars 1038+528A and B yield the following relative positions for the epoch 17 March 1981 (1950.0 coordinate system): $\Delta\alpha_{B-A} = 2.1205009'' \pm 0.0000002''$; $\Delta\delta_{B-A} = 27.429228'' \pm 0.000003''$ ($\lambda 3.6$ cm); $\Delta\alpha_{B-A} = 2.1204408'' \pm 0.0000006''$; $\Delta\delta_{B-A} = 27.428622'' \pm 0.000009''$ ($\lambda 13$ cm). The statistical standard errors represent fractional uncertainties of about 1 and 3 parts in 10^7 for $\lambda 3.6$ and $\lambda 13$ cm, respectively. The position of the brightest CLEAN component is chosen as the reference in each source at each wavelength. The difference found in the separations of these points at the two wavelengths, about $0.0008''$, is statistically very significant and probably represents the effect of wavelength-dependent opacity in the quasar 1038+528A (Marcaide and Shapiro 1983); plasma refraction contributes negligibly. Earlier, lower precision observations of these sources at these two wavelengths yield relative positions consistent with those from the March 1981 epoch. (8 refs.)
- 116871 Magnitude and redshift distributions of QSOs. D.Basu (Dept. of Phys., Univ. of the West Indies, St. Augustine, Trinidad). *Astrophys. & Space Sci. (Netherlands)*, vol.94, no.2, p.463-8 (Aug. 1983).
- The peak in the distribution of apparent magnitude (V) of QSOs at 18.0 can be explained by loss of QSOs for $V \leq 18.0$ arising out of selection effects due to the availability of search lines necessary for the determination of redshifts and due to the misidentification of QSOs as main-sequence stars. For $V > 18.0$, the number of objects seem to fall off as they become progressively fainter and detection efficiency goes down. The present analysis also shows that a strong correlation exists between apparent magnitude and redshift of QSOs indicating redshifts are of cosmological origin. (6 refs.)
- 116872 A VLBI search for compact components in extended high redshift quasars. P.D.Barthel (Sterrewacht Leiden, Leiden, Netherlands). *Astron. & Astrophys. (Germany)*, vol.126, no.1, pt.2, p.16-21 (Sept. 1983).
- Sensitive 21 cm VLBI observations of components in extended high-redshift quasars have been made with the European network. In most sources in the sample, compact (< 1 kpc) components of varying complexity were detected; these components account for a substantial fraction of the total source flux density. Identification with hot spots in the radio lobes was possible in most cases. Some ultracompact hot spots were detected with energy densities of the order of 10^{-6} erg/cm³. Two kpc-size double sources at redshifts of 1.875 and 2.594 have been found. Correlations between 'compactness' and other parameters are briefly discussed, as well as cosmological implications. (38 refs.)
- High energy spectrum of spherically accreting black holes ... See Entry 116736
- Redshifts of five extragalactic radio sources See Entry 116853
- Six quasars near the jets of NGC 1097 See Entry 116855
- Apparent superluminal velocities due to the curvature of space See Entry 116891

98.70L IR sources

(see also 98.40 in nebulae)

- Infrared study of the Crab pulsar: the 'shoulder' pulse and the 3.45 micron pulse profile See Entry 116715
- 3 μ m spectroscopy of IRS 7 towards the Galactic Centre See Entry 116802
- Luminous molecular hydrogen emission in the galaxy system NGC 3690-IC 694 See Entry 116843
- High-resolution images of the galactic centre See Entry 116849
- The galactic nucleus See Entry 116850

98.70Q X-ray and gamma-ray sources

- 116873 An optical test for the distance of gamma-ray burst sources. M.C.Jennings (Inst. of Geophys. & Planetary Phys., Univ. of California, Riverside, CA, USA). *Astrophys. J. (USA)*, vol.273, no.1, pt.1, p.309-19 (1 Oct. 1983).
- The possibility of observable H α produced by gamma-ray burst optical radiation reacting with a neutral hydrogen ambient medium is investigated. The ionization structure surrounding galactic bursts is determined by the hydrogen ionizing luminosity, L_1 , and geometric dilution when the ambient number density, N_H , is ≤ 15 cm⁻³. A model describing the H α fluence is derived and evaluated for representative L_1 and N_H . Optical bursts are classified into three groups based on the production of H α flux within (group 1), in the vicinity of (group 2), or beyond (group 3) the total ionization zone radius, R_1 . Analytic expressions estimate R_2 or its lower limit for group 1 and R_3 and N_H for groups 2 and 3. (24 refs.)
- 116874 Detection of an extended soft X-ray source H 2326-79 in the southern sky. P.C.Agrawal (Tata Inst. of Fundamental Res., Bombay, India), G.R.Riegler, K.P.Singh. *Astron. & Astrophys. (Germany)*, vol.126, no.1, pt.2, p.70-4 (Sept. 1983).
- Reports the detection of a new extended soft X-ray source H 2326-79 with the low energy detectors of the HEAO-1 A-2 experiment. The source has an angular size of $\sim 2.5''$ and is centered at RA(1950)=23^h26^m. Decl.(1950)=-79°24'. The observed energy flux, seen mainly in the 0.18-0.4 keV band, is about 2.6×10^{-11} erg cm⁻² s⁻¹. The source spectrum fits well with either an exponential model or with a Raymond Smith plasma model; the best fit values of temperature and hydrogen column density for the two models being: $T = 8 \times 10^5$ K and $N_H = 2 \times 10^{20}$ cm⁻² and $T = 6.3 \times 10^5$ K and $N_H = 1.6 \times 10^{20}$ cm⁻². (34 refs.)
- 116875 Gamma ray bursts. K.Hurley (Centre d'Etude Spatiale des Rayonnements, Toulouse, France). *AIP Conf. Proc. (USA)*, no.101, p.21-35 (1983). (Workshop on Positron-Electron Pairs in Astrophysics, Greenbelt, MD, USA, Jan. 1983).
- The time histories, size spectrum, spatial distribution, and repetition rates of gamma ray bursts are reviewed briefly. Evidence for a neutron star origin for gamma ray bursts may be found in many of these aspects of bursters. New results from optical searches are described. Substantial progress has been made recently in the optical identification of the 1978 November 19 burst. (57 refs.)
- 116876 Energy spectra of the cosmic gamma-ray bursts. E.P.Mazets, S.V.Golenetskii, Yu.A.Guryan, R.L.Aptekar, V.N.Ilyinskii, V.N.Panov (A.F. Ioffe Phys.-Tech. Inst., Leningrad, USSR). *AIP Conf. Proc. (USA)*, no.101, p.36-53 (1983). (Workshop on Positron-Electron Pairs in Astrophysics, Greenbelt, MD, USA, Jan. 1983).
- Preliminary results of a spectroscopic study of gamma bursts in the KONUS experiment on Venera 13 and 14 are surveyed. A brief description is given of the new instrumentation and data treatment procedure used. The characteristics of continuous spectra and of the absorption and emission features are considered. Evidence is presented for a fast spectral variability and a strong positive correlation between the hardness of the spectrum and gamma-ray intensity which suggests that the instantaneous values of the source luminosity are determined by the temperature in the emitting region. (22 refs.)
- 116877 Fine time resolution spectral analysis of the 1978 November 4 and 19 gamma-ray bursts. C.Barat (Centre d'Etude Spatiale des Rayonnements, Toulouse, France). *AIP Conf. Proc. (USA)*, no.101, p.54-8 (1983). (Workshop on Positron-Electron Pairs in Astrophysics, Greenbelt, MD, USA, Jan. 1983).
- The French SIGNE experiments aboard the Soviet Venera probes allow a spectral analysis with a time resolution of 250 ms. From a study of the intense 1978 November 4 and 19 gamma-ray bursts, evidence is presented for (a) a significant evolution in the continuum spectra, (b) the appearance on a time scale of several hundred ms of spectral features such as emission lines around 400 keV, absorption lines ($E < 200$ keV), and a high energy cutoff ($E > 1$ MeV). (9 refs.)
- 116878 Upper limits on narrow annihilation lines in gamma-ray bursts. P.L.Nolan, G.H.Share (Naval Res. Lab., E.O. Hulburt Center for Space Res., Washington, DC, USA), D.J.Forrest, E.L.Chupp, S.Matz, E.Rieger. *AIP Conf. Proc. (USA)*, no.101, p.59-63 (1983). (Workshop on Positron-Electron Pairs in Astrophysics, Greenbelt, MD, USA, Jan. 1983).
- The SMM gamma ray experiment has observed 60 gamma-ray bursts from March 1980 to August 1982. Details of one burst are illustrated. There is weak evidence for a broadened spectral feature early in the burst which was also detected by the Konus experiment. The detailed search was limited to narrow lines (< 70 keV FWHM) near 500 keV; the authors find none in any of the bursts. This absence contrasts with the reported detection of several broader features. The authors discuss the implications for the physical conditions in the annihilation region. (11 refs.)
- 116879 Theories of gamma-ray bursts. Katz, J.I. (Washington Univ., St. Louis, MO, USA). *AIP Conf. Proc. (USA)*, no.101, p.65-75 (1983). (Workshop on Positron-Electron Pairs in Astrophysics, Greenbelt, MD, USA, Jan. 1983).
- Gamma ray bursts have remained an enigma for a decade. This is attributable to the difficulty of obtaining accurate positions, the low duty cycle of burst sources which prevents planned observations, and their low mean power which rules out arguments based on gross energetics. Several lines of evidence now point to an origin in neutron star magnetospheres. The evidence includes spectral features interpreted as cyclotron and gravitationally redshifted annihilation lines, and temporal periodicity interpreted as rotation. The reason for the outbursts remains as much a mystery as when they were first discovered. It is unclear whether gamma ray bursters are located in binary stars, or whether this is incidental or essential to their activity. It is not known if there is any evolutionary connection or physical resemblance between gamma ray bursters and pulsars or accretional X-ray sources. The author discusses some of the problems which arise in constructing models for gamma ray bursters, with particular attention to the event of March 5, 1979, physical processes at high energy density, and the role of electron-positron pairs in producing line and continuum radiation. (21 refs.)
- 116880 Emission model of gamma-ray bursts. E.P.Liang (Lawrence Livermore Nat. Lab., Univ. of California, Livermore, CA, USA). *AIP Conf. Proc. (USA)*, no.101, p.76-88 (1983). (Workshop on Positron-Electron Pairs in Astrophysics, Greenbelt, MD, USA, Jan. 1983).
- Reviews the emission mechanisms of cosmic gamma-ray bursts. In particular, the thermal synchrotron model is discussed in detail as the most viable mechanism for the majority of the continuum emission. Within this framework various information about the source region can be extracted. The picture that emerges is that of a hot ($kT = 2-1.0$ mc²), thin sheet of dense pair-dominated plasma emitting via cyclo-synchrotron radiation in a strong magnetic field ($B \sim 10^{11}$ to 10^{12} gauss). Speculations on the origin and struc-

ture of this sheet are attempted. The author briefly discusses the problem of high-energy photons above pair production threshold escaping from the source. (26 refs.)

116881 A fireball model for the March 25, 1978 gamma ray burst. G.J.Hueter, R.E.Lingenfelter (Center for Astrophys. & Space Sci., Univ. of California, La Jolla, CA, USA). *AIP Conf. Proc. (USA)*, no.101, p.89-93 (1983). (Workshop on Positron-Electron Pairs in Astrophysics, Greenbelt, MD, USA, Jan. 1983). Suggests that the bulk of the gamma ray emission in the March 25, 1978 burst comes from a fireball of photons and e^+ pairs expanding from a jet off the polar cap of a neutron star and that the duration of the burst is defined by the expansion and dissipation times of the fireball. This model enables one to determine the total energy, $\sim 10^{39}$ ergs, and the distance, ~ 1 kpc, of the burst and should be applicable to a large class of gamma ray bursts. (12 refs.)

116882 Positrons from gamma bursts. S.A.Colgate, A.G.Petschek (Univ. of California, Los Alamos Nat. Lab., Los Alamos, NM, USA). *AIP Conf. Proc. (USA)*, no.101, p.94-7 (1983). (Workshop on Positron-Electron Pairs in Astrophysics, Greenbelt, MD, USA, Jan. 1983). The authors propose that the mechanism for the production of the hard spectrum of photons observed in the typical gamma burst is associated with the charge separation and electron-photon heating of Eddington limited accretion onto a neutron star. The charge separation occurs because of the radiation stress on the electrons and the gravitational stress on the ions and amounts to some 100 to 1000 volts cm^{-1} depending upon whether the accreting matter is dynamically decelerated by radiation or is accreted in quasistatic, steady flow. A positron produced in pair formation by the high energy part of the photon spectrum will be accelerated by both the radiation stress and the electrostatic field. Since for electrons these two stresses are equal and opposite, a positron will attain an energy significantly greater than the purely radiation driven free expansion limit where for these conditions $(1-\beta^2)^{0.5} = \gamma_{rel} \approx [(m_e MG/r)/(m_e c^2)]^{1/2} \approx 4$. This value of γ_{rel} is near the threshold for pair production on additional in-falling matter. Only electrostatic acceleration can produce significantly greater velocities. Hence the number of positrons produced will be much less than the number of high energy photons, but may contribute to the limitation of the photon heating by shorting out the electric field. (9 refs.)

116883 The quest for elusive Geminga: a unique object proposed as the counterpart of 2CG 195+04. P.A.Caraveo, G.F.Bignami (Istituto di Fisica Cosmica del CNR Milano, Milano, Italy), R.C.Lamb. *AIP Conf. Proc. (USA)*, no.101, p.152-6 (1983). (Workshop on Positron-Electron Pairs in Astrophysics, Greenbelt, MD, USA, Jan. 1983). Geminga is the brightest unidentified source in the COS-B catalogue, second only to the Vela pulsar PSR 0833-45, with a flux limit of 5×10^{-6} photons $(>100 \text{ MeV})/cm^2 \cdot s$, $\sim 2.4 \times 10^{-9}$ ergs $cm^{-2} \cdot s$ in the interval 50 MeV-3 GeV. The source, discovered during the SAS-2 mission, was repeatedly observed by COS-B. No long term variability was found. Short term variability was also actively sought, with no convincing success. The long observation times devoted by COS-B to Geminga, coupled with the relatively hard spectrum of the source allow for a positional accuracy unusually high for current γ -ray astronomy: the error box, centered at $l=195.1^\circ$ and $b=4.2^\circ$, has a radius of ~ 24 arcmins. The complete γ -ray error box could thus be contained in a single Einstein IPC field, providing a unique opportunity for in-depth search in the keV region. The several sources found were investigated at radio and optical wavelengths, leading to some identifications. (18 refs.)

116884 Criteria for grasar action in astrophysical sources. J.M.McKinley, R.Ramaty (Lab. for High Energy Astrophys., NASA/Goddard Space Flight Center, Greenbelt, MD, USA). *AIP Conf. Proc. (USA)*, no.101, p.428-32 (1983). (Workshop on Positron-Electron Pairs in Astrophysics, Greenbelt, MD, USA, Jan. 1983). The theory of gamma-ray amplification through stimulated annihilation radiation (grasar) was developed by Ramaty, McKinley and Jones (1982). For gamma-ray bursts similar to the March 5, 1979 burst, an observed annihilation line of width <0.03 MeV would imply a grasar source. The minimum pair density needed for the onset of grasar action is $\sim 10^{30} \text{ cm}^{-3}$ and the peak of the grasar line, without a gravitational redshift, is at <0.5 MeV. (8 refs.)

116885 Pair production and non-thermal radio stars. W.T.Vestrand (Nat. Radio Astron. Obs., Charlottesville, VA, USA). *AIP Conf. Proc. (USA)*, no.101, p.433-7 (1983). (Workshop on Positron-Electron Pairs in Astrophysics, Greenbelt, MD, USA, Jan. 1983). The generation of relativistic electrons and positrons in thermal material surrounding a γ -ray source is examined. This in situ generation of particles can resolve many of the problems associated with the quiescent emission from non-thermal radio stars. The most luminous radio star, Cyg X-3, is used as a paradigm throughout. (15 refs.)

116886 Gamma-ray astronomy. A.W.Wolfendale (Dept. of Phys., Univ. of Durham, Durham, England). *Q. J. R. Astron. Soc. (GB)*, vol.24, no.3, p.226-45 (Sept. 1983). Discusses the discovery of cosmic γ -rays and their methods of production. Galactic gamma-rays in the middle energy range, extragalactic gamma ray emission and possible future projects are discussed. (48 refs.)

Workshop on Positron-Electron Pairs in Astrophysics See Entry 111296
Comparison of photon-photon and photon-magnetic field pair production rates See Entry 116457

Conditions for stimulated-annihilation in a degenerate e^-e^+ fluid at the surface of pulsars See Entry 116458

Numerical fits to important rates in high temperature astrophysical plasmas See Entry 116467

High energy observations of pulsars See Entry 116720

Pulsar gamma-ray lines from quarkonium systems See Entry 116727

Pulsar electrodynamics: cylindrical model and radio and gamma-ray radiation See Entry 116729

Electron-positron processes and spectral evolution in black hole accretion disk dynamo models for AGN sources of the cosmic X-ray and gamma ray backgrounds See Entry 116735

High energy spectrum of spherically accreting black holes ... See Entry 116736

Hot accretion disks and γ -ray cosmic sources See Entry 116737

SS Bootis: a totally eclipsing binary of the RS CVn type See Entry 116742

Ultra high energy gamma rays from Cygnus X-3 See Entry 116747

Spectroscopic observations of the cool eclipsing X-ray binary HD 155638 See Entry 116758

Spectrophotometry of the optical emission from RCW 103 and Milne 23 See Entry 116780

The trivariate (radio, optical, X-ray) luminosity function of cD galaxies. I. New Westerbork observations of 22 cD galaxies and Einstein observations of A 1918 and A 2317 See Entry 116818

The trivariate (radio, optical, X-ray) luminosity function of cD galaxies. II. The fuelling of radio sources See Entry 116819

Galactic gamma radiation: the contribution from discrete sources See Entry 116824

Observations of annihilation radiation from the galactic center region See Entry 116825

The gamma-ray spectrum of the galactic-center region See Entry 116826

Effects of line width and spatial extent on measurements of the 0.51 MeV galactic center line See Entry 116827

Low-temperature positron annihilation See Entry 116828

'Gamma-gun' in the center of the Galaxy See Entry 116829

The origin of the galactic center annihilation radiation See Entry 116830

Positrons from supernovae and the origin of the galactic center positron annihilation radiation See Entry 116831

An electron-positron jet model for the galactic center See Entry 116832

Positron production by a hot, young pulsar See Entry 116833

X-rays and gamma-rays from active galaxies See Entry 116834

Are mildly active galaxies sources of e^\pm annihilation radiation? See Entry 116835

Upper limits to the annihilation radiation luminosity of Centaurus A See Entry 116836

Electron/positron/gamma ray beams in cosmic radio sources See Entry 116837

Compactness and pair production in active galactic nuclei See Entry 116838

Einstein observations of NGC 4438: dynamical ablation of gas in the Virgo Cluster See Entry 116840

Six quasars near the jets of NGC 1097 See Entry 116855

The galactic extinction towards Maffei 1 See Entry 116856

The Hydra I cluster of galaxies. II. First results from H I-observations See Entry 116862

Identification of a blue object with a newly detected X-ray source See Entry 116867

98.70V Background radiations

116887 e^+e^- annihilation and the cosmic X-ray background. D.Kazanas, R.A.Shafer (NASA/Goddard Space Flight Center, Greenbelt, MD, USA). *AIP Conf. Proc. (USA)*, no.101, p.343-7 (1983). (Workshop on Positron-Electron Pairs in Astrophysics, Greenbelt, MD, USA, Jan. 1983). The possibility that the processes responsible for the cosmic X-ray background (CXB) would also produce an e^-e^+ annihilation feature is examined. Under the assumption that these processes are thermal, the absence of a strong e^-e^+ annihilation feature places constraints on the compactness (L/R ratio) of these sources. Observations favor sources of small compactness ratio. (13 refs.)

116888 Massive neutrinos and the anisotropy of the cosmic microwave background radiation. M.Szymanski, M.Jaroszynski (Warsaw Univ. Obs., Warszawa, Poland). *Mon. Not. R. Astron. Soc. (GB)*, vol.205, no.1, p.91-104 (Oct. 1983). The growth of primordial adiabatic density perturbations in a Universe model containing massive neutrinos is investigated in the linear approximation. The final spectra of perturbations are computed for the initial amplitudes obeying power laws: $|\delta|^2 \sim k^n$. The resulting spectra are not amplitude-modulated by an oscillatory function. The mass distribution auto-correlation function is also calculated. The comparison of the above characteristics of matter distribution with observations suggests that the initial spectrum of perturbations should be steep. These results are in agreement with those of Peebles (1982). The anisotropy of the relic radiation is predicted. (24 refs.)

116889 Low-frequency measurement of the spectrum of the cosmic background radiation. G.F.Smoot, G.De Amici, S.D.Friedman, C.Witebsky (Lawrence Berkeley Lab., Univ. of California, Berkeley, CA, USA), N.Mandolesi, R.B.Partridge, G.Sironi, L.Danese, G.De Zotti. *Phys. Rev. Lett. (USA)*, vol.51, no.12, p.1099-102 (19 Sept. 1983). Measurements have been made of the cosmic-background-radiation spectrum at five wavelengths (0.33, 0.9, 3, 6.3, and 12 cm) with use of radiometers with wavelength-scaled corrugated-horn antennas having very low sidelobes. A single large-mouth (0.7-m-diameter) liquid-helium-cooled absolute reference load was used for all five radiometers. The results of the observations are consistent with previous measurements and represent a significant improvement in accuracy at low frequencies. (14 refs.)

3K cosmic microwave background radiation and the rotational levels of the atmospheric H₂O molecule See Entry 116248

Electron-positron processes and spectral evolution in black hole accretion disk dynamo models for AGN sources of the cosmic X-ray and gamma ray backgrounds See Entry 116735

Galactic gamma radiation: the contribution from discrete sources See Entry 116824

98.80 COSMOLOGY

(for observational cosmology, see 98.70V; for origin and evolution of galaxy, see 98.50)

116890 Plane symmetric vacuum Bianchi type I cosmological model in Brans-Dicke theory. Shri Ram (Appl. Math. Section, Inst. of Technol., Banaras Hindu Univ., Varanasi, India). *Astrophys. & Space Sci. (Netherlands)*, vol.94, no.2, p.307-10 (Aug. 1983). Presents an exact solution of the vacuum Brans-Dicke field equations for the metric tensor of a spatially homogeneous and anisotropic cosmological model. The kasner metric is shown as a special case. Some physical properties of the model are discussed. (5 refs.)

116891 Apparent superluminal velocities due to the curvature of space. J.Soucek (Astron. Society, Czechoslovak Acad. of Sci., Prague, Czechoslovakia). *Astrophys. & Space Sci. (Netherlands)*, vol.94, no.2, p.319-31 (Aug. 1983). Shows that it is important where the observer is located in the curved space of the Universe and that this positioning objectively determines the optical properties of curved space recorded by the observer usually associated with the properties of the observed objects. There may be many phenomena of this

category, one of which can be the superluminal velocities of assumed object components. The author carefully distinguishes between objective reality of objects in curved space on the one hand and the shape of distorted notion which, on the other hand, the observer inside his curved space must necessarily form. A model of a spherical surface, locally Euclidean, immersed in Euclidean three-dimensional space is adopted as the objective reality and for the distorted notion the term 'distorted shape' is adopted for unrealistic properties which prove to be objective as an optical illusion. (38 refs.)

116892 Fragmentation of the Universe. W.K.Brown, R.R.Karpp (Los Alamos Nat. Lab., Los Alamos, NM, USA), D.E.Grady. *Astrophys. & Space Sci. (Netherlands)*, vol.94, no.2, p.401-12 (Aug. 1983). Tests the hypothesis that the Universe underwent a single fragmentation event, separating into protogalactic volumes at a relatively early stage after the Big Bang. Assuming that the present total luminosity of each galaxy is proportional to its mass, the authors plot the number and mass distribution of a thousand nearby galaxies just as in an analysis of fragments from a laboratory high-explosive experiment. The results are consistent with the single-fragmentation hypothesis. (23 refs.)

116893 On the statistical distribution of massive fermions and bosons in a Friedmann Universe. R.Ruffini, D.J.Song, L.Stella (Istituto di Fisica 'G. Marconi', Univ. di Roma, Roma, Italy). *Astron. & Astrophys. (Germany)*, vol.125, no.2, pt.1, p.265-70 (Sept. 1983). The distribution function of massive Fermi and Bose particles in an expanding Universe is considered as well as some associated thermodynamic quantities, pressure and energy density. These considerations are then applied to cosmological neutrinos. A new limit is derived for the degeneracy of a cosmological gas of massive neutrinos. (24 refs.)

116894 Constraints on neutrino-dominated cosmologies from large-scale streaming motion. N.Kaiser (Dept. of Astron., Univ. of California, Berkeley, CA, USA). *Astrophys. J. Lett. Ed. (USA)*, vol.273, no.1, pt.2, p.L17-20 (1 Oct. 1983).

The streaming motion due to long-wavelength density perturbations is calculated for neutrino-dominated cosmological models. The predictions of the models are compared with the observed motion, relative to the background radiation of a region surrounding the Galaxy with an effective diameter of approximately $50 h^{-1}$ Mpc. If the velocity of this region is typical, then the primary structure ('pancakes') can only just be forming at the present; and the short-wavelength cutoff, which sets the scale of the structures, is limited to be approximately 12 Mpc. (21 refs.)

116895 The cosmological problem as initial value problem on the observer's past light cone: observations. G.Dautcourt (Zentralinst. fur Astrophys., Akad. der Wissenschaften, Potsdam-Babelsberg, Germany).

Astron. Nachr. (Germany), vol.304, no.4, p.153-61 (1983). In a previous paper (Dautcourt 1982) it was shown how cosmological models can be characterized by few initial data on the observer's past light cone. Part of the inner geometry of the past cone as well as some matter variables taken on the cone determine a world model uniquely within the past light cone. Since the initial data to some degree enter the relations between observable quantities such as redshift, luminosity, angular diameter, number counts, distortion parameters and background radiation intensity, it might be possible to determine the required initial data from observations. This problem is discussed. (30 refs.)

116896 Bianchi-I universes of the Brans-Dicke theory for the vacuum. U.Dyllong (Zentralinst. fur Astrophys., Akad. der Wissenschaften, Potsdam, Germany).

Astron. Nachr. (Germany), vol.304, no.4, p.163-6 (1983). In German. The field equations of the Brans-Dicke theory are solved for a vacuum with the aid of a space-time metric of Bianchi-I type. Two solutions are found. One of them corresponds to a generalisation of the flat de Sitter universe. The other solution represents the Kasner variant of the Brans-Dicke theory. (7 refs.)

116897 Neutrinos in cosmology. R.J.Tayler (Astron. Centre, Univ. of Sussex, Brighton, England).

Europhys. News (Switzerland), vol.14, no.7, p.1-3 (July 1983). Gives a broad outline of the principal aspects of the standard big bang theory as it involves neutrinos. Outside these are non standard versions containing degenerate neutrinos or a non-zero cosmological constant, the possible role of grand unified theories of elementary particles in providing the initial conditions, and the influence of what are at present hypothetical particles such as the gravitino and photino. (no refs.)

116898 Spatially homogeneous and anisotropic cosmological solution in Brans-Dicke theory. Shri Ram (Inst. of Technol., Banaras Hindu Univ., Varanasi, India).

Gen. Relativ. & Gravitation (USA), vol.15, no.7, p.635-40 (July 1983). An exact solution of the vacuum Brans-Dicke field equations has been obtained for the metric tensor of a spatially homogeneous and anisotropic Bianchi type-I cosmological model. The Kasner metric is shown to be a special case. Some physical properties of the model have been discussed. (11 refs.)

116899 Cosmic censorship and curvature growth. R.P.A.C.Newman (Dept. of Appl. Maths., Queen Mary Coll., London, England).

Gen. Relativ. & Gravitation (USA), vol.15, no.7, p.641-53 (July 1983). A censorship theorem is established concerning space-times which are weakly asymptotically simple and empty according to a new definition. Future asymptotic predictability is shown to be a consequence of a criterion which bounds components of the Riemann tensor from below near locally naked singularities of a certain type. (11 refs.)

116900 Proto-galactic perturbations. R.I.Epstein (Nordita, Copenhagen, Denmark).

Mon. Not. R. Astron. Soc. (GB), vol.205, no.1, p.207-29 (Oct. 1983). In the gravitational instability picture of galaxy formation, the precursor of a galaxy or a cluster of galaxies is a region with a significantly perturbed mean density or velocity field. This region may, and generally does, have considerable substructure. To relate the early perturbations to the currently observable structures it is necessary to distinguish between perturbations which merge with other perturbations and those, more encompassing ones, which form galaxies by themselves. The latter can be thought of as 'isolated' fluctuations. The relationship between isolated fluctuations and current observations is discussed in general terms. One of the main focuses is the computation of the mass spectra of 'extremal mass' fluctuations for a Poisson distribution of point masses. The spectra of isolated fluctuations can be derived from the spectra of extremal fluctuations when the dynamics of small perturbations in a uniform background is determined. (9 refs.)

116901 The cosmological constant and classical tests of general relativity. J.N.Islam (Dept. of Math., City Univ. London, London, England). *Phys. Lett. A (Netherlands)*, vol.97A, no.6, p.239-41 (5 Sept. 1983). An upper limit of 10^{-42} cm^{-2} is placed on the absolute value of the cosmological constant by comparing with the prediction of the perihelion shift of

Mercury. It is shown that the bending of starlight near the sun gives no limit on the cosmological constant since the equation for a null geodesic takes the same form with or without the cosmological constant. (4 refs.)

116902 Monopoles in the inflationary Universe. I.G.Moss (School of Phys., Univ. of Newcastle upon Tyne, Newcastle upon Tyne, England). *Phys. Lett. B (Netherlands)*, vol.128B, no.6, p.385-8 (8 Sept. 1983). Exponential expansion of the very early Universe caused by the vacuum energy of a metastable phase provides an attractive solution to the monopole problem. However, fluctuations in the Higgs field can still lead to appreciable monopole production. In the SU(5) grand unified theory their density depends on the gauge coupling constant g and can give important information about the parameters of the theory. (21 refs.)

116903 Modeling in chaotic relativity. A.Zardecki (Theoretical Div., Los Alamos Nat. Lab., Los Alamos, NM, USA).

Phys. Rev. D (USA), vol.28, no.6, p.1235-42 (15 Sept. 1983). The chaotic behaviour of solutions to Einstein's equations has recently been studied by Barrow within the framework of the dynamical systems theory. Barrow's program of gravitational turbulence is implemented in part by considering the solutions of type VII₀ and IX as well as some intermediate types. Quantitative measures of chaos, such as the power spectrum and Lyapunov characteristic exponent, are computed. By converting the equations of motion for the cosmic scale factors to stochastic Langevin's equations, the Mixmaster cosmology in the presence of driving noise terms is investigated. Possible sources of noise can be attributed to an imperfect cancellation of the effective vacuum energy density and the energy density associated with the Higgs field. An ensemble average over random trajectories leads to the suppression of chaotic behavior for type-IX cosmology. (25 refs.)

116904 Coherent scalar-field oscillations in an expensive Universe. M.S.Turner (Astron. & Astrophys. Center, Univ. of Chicago, Chicago, IL, USA).

Phys. Rev. D (USA), vol.28, no.6, p.1243-7 (15 Sept. 1983). Motivated by the cosmological importance of coherent (classical), scalar-field oscillations in the context of the invisible axion and the new inflationary-Universe scenario, the author analyzes in general, the classical evolution of a scalar field in an isotropic and homogeneous cosmology. For a scalar potential of the form $V(\phi) = a\phi^n$ the energy density of the scalar-field oscillations decreases as $R^{-6n/(n+2)}$ when the oscillations are rapid compared to the expansion rate (R = cosmic scalar factor). The author investigates the effect of higher-order terms in the potential perturbatively, and analyzes the decay of the coherent field oscillations due to quantum particle creation. (14 refs.)

116905 Preferred anisotropies of the Universe. F.H.Busse (Dept. of Earth & Space Sci., Univ. of California, Los Angeles, CA, USA).

Phys. Rev. D (USA), vol.28, no.6, p.1248-50 (15 Sept. 1983). The problem of bifurcation from an isotropic Universe is considered. It is shown that the degeneracy of bifurcating solutions is in part removed by nonlinear effects. In particular, preferred solutions are obtained in the limits of low and high values of n where n denotes the degree of the hyperspherical harmonics describing the bifurcating solution. (8 refs.)

116906 Homogeneity of Riemannian space-times of Godel type. M.J.Reboucas, J.Tiomno (Centro Brasileiro de Pesquisas Fisicas, Rio de Janeiro, Brazil).

Phys. Rev. D (USA), vol.28, no.6, p.1251-64 (15 Sept. 1983). The conditions for space-time homogeneities of a Riemannian manifold with a Godel-type metric are examined. The Raychaudhuri-Thakurta necessary conditions for space-time homogeneity are shown to be also sufficient and to lead to five linearly independent Killing vectors. These vector fields are exhibited for the most general case and their algebra is examined. The irreducible set of isotometrically independent space-time-homogeneous Godel type metrics is shown to be given, in cylindrical coordinates, by $d\bar{s}^2 = [dt + (4\Omega/m^2)\sinh^2(mr/2)d\phi]^2 - (1/m^2)\sinh^2(mr)d\phi^2 - dr^2 - dz^2$, where Ω is the vorticity and $-\infty \leq M^2 \leq +\infty$, $m^2 = 2\Omega^2$ corresponding to the Godel metric. Sources of Einstein's equations leading to these metrics as solutions are examined, and it is shown that the inclusion of a scalar field extends the previously known region of solutions $-\infty \leq m^2 \leq 2\Omega$ to $-\infty \leq m^2 \leq 4\Omega^2$. The problem of ambiguity of physical sources of the same metric and that of violation of causality in Godel-type space-time-homogeneous universes are examined. In the case $m^2 = 4\Omega^2$, the authors obtained the first exact Godel-type solution of Einstein's equations describing a completely causal space-time-homogeneous rotating universe. (16 refs.)

116907 Feynman propagator in a linearly expanding Universe. E.Calzetta (Inst. de Astron. y Fisica del Espacio, Buenos Aires, Argentina), M.Castagnino.

Phys. Rev. D (USA), vol.28, no.6, p.1298-307 (15 Sept. 1983). It is demonstrated that three reasonable physical criteria yield a unique Feynman propagator in a linearly expanding Robertson-Walker Universe. (24 refs.)

116908 New model of the metagalaxy. A.Meszaros.

Report KFKI-1983-68, Hungarian Acad. Sci., Budapest (1983), 22 pp. The known physical laws do not exclude the existence of anticollapsing bodies in nature (anticollapse is a gravitational collapse with time reversal). It is shown that the metagalaxy, i.e. the observed part of the Universe, may in the first approximation be the interior of a giant anticollapsing body having a boundary beyond the particle horizon. This is the 'anticollapse model' of the metagalaxy. The advantage of this model follows from the fact that some anisotropies in the metagalaxy are already considered in the first approximation. Theoretical considerations show that the anticollapse model is better than the usual Friedmann model. (19 refs.)

116909 Viscosity and the monopole density of the Universe. L.Diosi, B.Keszthelyi, B.Lukacs, G.Paal.

Report KFKI-1983-77, Hungarian Acad. Sci., Budapest (1983), 9 pp. It is shown that GUT monopoles with energy about 10^{16} GeV might themselves solve the so-called monopole problem of GUT cosmologies by their unavoidable viscosity, which may lead to a quasi-inflationary scenario even without appeal to a 'false vacuum'. (23 refs.)

On the global geometry of the Stephani universe See Entry 111510

A rotating mass embedded in an Einstein-Godel universe See Entry 111513

Non-Einsteinian gravitational Lagrangians assuring cosmological solutions without collapse See Entry 111514

Absorber theory for the Einstein equations in the first approximation See Entry 111518

A bimetric Machian approach to gravitation See Entry 111524

Chaotic inflation See Entry 111528

Domain walls. II. Baryon-number generation See Entry 111915

Elimination of unitarily nonequivalent vacua in supersymmetric grand unified theories by gravity See Entry 111922

An upper limit on neutrino electric dipole moments See Entry 112002

Rotating black hole in asymptotic de Sitter space: perturbation of the space-time with spin fieldsSee Entry 116738

The bend in the correlation function: the surviving imprint of adiabatic perturbations? See Entry 116842

Neutrino-gaseous 'Pancakes' and the problem of hidden massSee Entry 116861

Massive neutrinos and the anisotropy of the cosmic microwave background radiation See Entry 116888

Author index

- +Aalders, J.W.G. 116782
 Aaron, R. + 111973
 Aarts, E.H.L. + 112237
 +Aarts, E.H.L. 112232
 Ababou, N. + 114414
 Abakumov, V.N. + 114000
 +Abbey, F. 112419
 +Abbott, D.H. 115657
 Abbott, S. + 112474
 +Abdrimov, K. 114565
 +Abduazizov, A. 115615
 +Abdul Jalil, M.A. 111727
 +Abdullaev, A. 115615
 +Abdullaev, G.B. 114524
 Abdullaev, A.G. + 114623
 Abdullaev, A.G. + 114396
 +Abdullaev, K.I. 114623
 Abdurakhimov, A.A. + 114569
 +Abe, H. 113900
 +Abe, H. 113357
 +Abe, K. 114963
 +Abe, K. 112235
 Abe, T. + 113905
 Abel, Kh. + 115839
 +Abela, R. 112884
 +Abelard, P. 113858
 +Abeles, B. 114817
 Aben, Kh.K. 113302
 Abi-Ghanem, G.V. + 114136
 +Abiko, K. 115197
 Ablekov, V.K. + 113076
 Ablekov, V.K. + 113545
 Ablyazov, N.N. + 114450
 Abouaf, M. + 113316
 +Abouzeid, M.A. 112219
 Abraham, K.M. + 115627
 Abrahams, K. (ed.) 111295
 +Abrahams, M.S. 114541
 +Abraimov, V.V. 114078
 +Abram, R.A. 114591
 Abramov, V.V. + 115290
 +Abramovich, H. 111435
 +Abrams, G.S. 112011
 Abramski, K.M. 112980
 +Abronin, I.A. 115542
 +Abu-Zaid, G.A. 112397
 Abushady, Y. 112316
 +Accorsi, C.A. 113928
 +Achenbach, J.D. 113161
 Achilov, B.M. + 115686
 +Achiwa, N. 115034
 Achterberg, A. + 116764
 +Achterberg, O. 112015
 Ackermann, G.K. + 113939
 +Ackermann, L. 114823
 Adachi, G.-Y. + 112780
 Adachi, H. + 115025
 +Adachi, H. 114354
 +Adachi, M. 112117
 Adamashvili, G.T. + 113181
 Adamesku, R.A. + 115245
 Adams, A.J. 111349
 Adams, D.L. + 114309
 Adams, F. + 116177
 +Adams, F.M. 113988
 Adams, M.J. 112993
 +Adawi, M.A. 114884
 Adelberger, E.G. 112065
 Ader, J.P. 111488
 Ader, J.P. + 111910
 +Adey, W.A. 115834
 +Adiels, L. 112544
 +Adler, D. 114485
 +Adler, L. 113161
 +Adriaenssens, G.J. 114486
 Aeshin, A.I. + 114474
 +Afanas'ev, A.M. 114668
 Affleck, I. + 111913
 +Africano, J. 116748
 +Africano, J.L. 116742
 +Agaev, V.V. 114921
 +Agaev, V.V. Trukan, M.K. 112996
 Agafonov, A.V. + 114925
 Agafonov, V. + 113828
 +Agamalyan, M.M. 115733
 Agarwal, A.K. + 113112
 Agarwal, B.K. + 114968
 Agarwal, M.K. + 113916
 +Agarwal, N.K. 115288
 +Agarwal, S.R. 116634
 Ageev, A.N. + 114947
 +Agladze, K.I. 113466
 Agranovich, V.M. + 114582
 +Agrawal, H.B. 112875
 Agrawal, H.L. + 113512
 Agrawal, P.C. + 116874
 Agrinskaya, N.V. + 114896
 Aguilera-Navarro, V.C. + 114123
 A'Hearn, M.F. + 116535
 Ahlin, P. + 116746
 +Ahmad, M. 112562
 +Ahmed, H. 114029
 +Ahmed, M. 113940
 Ahrenkiel, R.K. + 115635
 Ahrenkiel, R.K. + 114608
 +Ahrens, T.J. 116080
 Ai-Lien Jung + 114485
 Aidun, J. + 114447
 +Aifantis, E.C. 111616
 Aikawa, T. 116693
 Aikawa, T. + 116630
 +Aina, O. 114480
 +Aita, K. 112522
 Aivazov, M.I. + 114487
 Aivazov, M.I. + 114663
 +Aizawa, T. 115916
 Aizenberg, A.M. 116032
 +Ajika, N. 113891
 +Ajika, N. 113892
 +Akaiishi, K. 113622
 Akamatsu, N. + 115781
 +Akao, Y. 113152
 Akasofu, S.-I. + 116420
 +Akasofu, S.-I. 116409
 +Akasofu, S.-I. 116370
 +Akasofu, S.-I. 112912
 +Akazaki, M. 113664
 Akesson, T. + 112024
 Akhiezer, I.A. 114689
 Akhmedov, R.B. + 115613
 +Akhter, P. 114393
 +Akiba, M. 111815
 Akimov, P.I. + 112904
 +Akinci, G. 111602
 +Akita, H. 115744
 +Akita, K. 115112
 Akkermans, J.M. 112165
 +Akoef, I.G. 115874
 Akopyan, M.A. + 116160
 +Akopyan, S.M. 115731
 +Aksenov, E.P. 116689
 Aksenov, E.T. + 113085
 Aksenov, V.L. + 114107
 Akulenko, L.D. + 113269
 +Akutin, M.S. 115290
 Al Najjar, A.A. + 114222
 +Al-Amili, M.A. 112189
 Al-Ani, N. + 115516
 Al-Ansari, N.A. + 116151
 +Al-Ashoor, R.A. 115616
 Al-Badr, A.A. 115752
 +Al-Jabbari, M.H. 116151
 +Al-Janabi, T.J. 112189
 Al-Khalili, A.J. + 115616
 Al-Najar, A.A. + 111700
 +Al-Shukri, H.J. 116023
 Al-Zhen Chang see Chang Al-Zhen
 +Alad'ina, Z.N. 115640
 Alae, M.S. + 115051
 Alam, A. + 114955
 +Alam, A. 114958
 +Alasia, F. 113540
 +Alavutdinov, D.N. 115615
 Albano, A.M. + 114749
 +Albarede, F. 116074
 +Albert, L. 114908
 Alberty, W.J. + 114607
 +Albrecht, R. 112113
 Albrow, M.G. + 112549
 +Albrow, M.G. 112024
 Albuquerque, A.R. Pereira Leite see Pereira Leite Albuquerque, A.R.
 Alcaino, G. + 116768
 Alcantara, M.R. + 113736
 Aldazabal, G. + 111887
 +Aldebert, P. 113154
 +Aldred, A.T. 114649
 Aldrich, P.D. + 112764
 +Aldridge, B.G. 111341
 Alekhin, A.D. 113552
 +Aleksan, R. 112016
 Aleksandrov, A.S. + 114456
 +Aleksandrov, K.S. 113822
 Aleksandrov, L.N. + 115260
 +Aleksandrov, S.B. 113841
 Aleksandrov, V.M. + 113274
 +Aleksandrov, Yu. A. 115542
 +Aleksandrovich, S.V. 114487
 +Aleksandrovich, S.V. 114663
 +Aleksankin, M.M. 115571
 +Aleksenko, M.F. 115435
 Alekseev, A.F. + 115393
 +Aleksiev, A.G. + 111714
 Alekseev, Yu.K. + 112917
 Alekseyeva, I.M. 116385
 +Alemany, M. 115988
 +Alencastro, R.B. 112871
 Aleshin, N.P. + 113172
 Aleshin, V.A. + 114800
 Alestig, G. + 114015
 +Alexander, G. 112015
 Alexander, J.C. + 111446
 +Alexander, J.M. 112291
 +Alexander, T.K. 112547
 +Alexandrova, S. 114374
 Alexiades, V. + 111616
 +Alfano, R.R. 113000
 +Alfano, R.R. 115744
 +Alferov, A.V. 112402
 Alferov, D.F. + 113004
 +Alfimov, P.T. 115282
 +Ali, S. 114236
 +Ali, S. 112235
 +Alicka, M. 112773
 Alicki, R. + 112773
 Alidzhanov, M.A. + 114524
 Alidzhanov, M.A. + 114126
 +Aliiev, A.N. 111531
 Aliiev, F.G. + 114669
 +Aliiev, F.M. 114546
 +Aliiev, R. 115640
 Alikakos, N.D. 111614
 +Alimov, A.K. 115615
 Alizon, J. + 114753
 +Allaart, K. (ed.) 111295
 Allakhverdiev, A.M. + 115652
 Allakhverdiev, A.M. + 115649
 +Alle, N. 113727
 Allen, D.A. + 116849
 +Allen, D.A. 116802
 +Allen, D.A. 116850
 Allen, G.C. + 114373
 Allen, J.S. + 116141
 +Allen, J.S. 116109
 Allen, J.W. 115011
 +Allen, S.L. 113641
 Allen, S.M. + 113155
 Allia, P. + 114712
 Allinger, N.L. + 112672
 +Allison, J. 111990
 +Allison, J. 112012
 Allmen, M.F. von see von Allmen, M.F.
 +Allnatt, A.R. 114240
 Allred, D.D. + 114411
 +Almehed, S. 112024
 Almeida, A.M. Ozorio de see Ozorio de Almeida, A.M.
 +Almeida, F. 112015
 Almlof, J. + 112632
 Almond, E.A. + 115508
 +Aloisi, G. 114303
 Alonso, J.A. + 111983
 Alonso, J. Diaz see Diaz Alonso, J.
 Alport, M.J. + 113604
 Al'shits, V.I. + 114090
 Alsinawi, S.A. + 116023
 Alsinawi, S.A. + 116022
 +Alspector, J. 115383
 Altena, H. + 114428
 Altena, H. + 114420
 Altena, H. + 114421
 +Altena, H. 115095
 Altenhoff, W.J. + 116532
 Altenhuber, M. 115402
 Alter, H.W. + 115947
 Altman, C. 113077
 Altman, W. + 111442
 Altmann, S.L. 112625
 +Altona, C. 112750
 +Altona, C. 112751
 +Altukhov, V. 113018
 Alurkar, S.K. + 116572
 +Alvarez-Estrada, R.F. 113088
 +Alves, M.A.F. 112689
 Alves, O.L. + 114836
 +Alves, O.L. 114835
 +Amata, E. 116402
 Amatuni, L.E. + 114648
 Ambardar, A. 111338
 Amberger, H.-D. 114851
 +Ambrosino, M., Jr. 112387
 Ambrosio, M. + 112595
 +Amelinckx, S. 111659
 +Ametani, A. 111402
 Amici, G. De see De Amici, G.
 +Amidei, D. 112011
 Amiot, C. 116462
 +Ammirato, F.V. 115495
 +Amosov, G.G. 115972
 +Amouric, M. 114071
 Amsler, C. + 112030
 +Amusia, M.Ya. 112690
 +Amus'ya, M.Ya. 112859
 +Anantaraman, N. 112158
 Anantharaman, V. + 112778
 Anantharaman, V. + 112779
 Anazawa, N. 111814
 Andel, H.W.H. van see van Andel, H.W.H.
 +Andersen, F.E. 113727
 +Andersen, J.N. 114309
 +Andersen, N.H. 114250
 +Anderson, B.D. 112562
 +Anderson, D.M. 116486
 Anderson, D.N. + 116356
 Anderson, D.V. 111398
 Anderson, D.V. 111399
 Anderson, D.V. + 111397
 +Anderson, D.V. 111396
 Anderson, J.L. 111876
 Anderson, J.L. + 116053
 Anderson, L. + 112256
 +Anderson, L. 112257
 +Anderson, M.R. 112181
 +Anderson, R.A. 113635
 +Anderson, R.E. 112149
 +Anderson, W.A. 114528
 +Anderton, J.W. 115531
 Andeweg, A.H. + 115608
 Ando, S. + 113228
 Ando, Y. 113203
 Ando, Y. + 114788
 +Andrasi, A. 115715
 Andraud, C. + 114913
 Andreeschchev, E.A. + 112573
 +Andreev, A.A. 113776
 +Andreev, D.A. 113361
 Andreev, E.A. + 112605
 Andreev, G.V. 116552
 Andreev, S.P. + 114556
 Andreev, V.M. + 115650
 +Andreev, V.M. 115652
 +Andreeva, L.I. 111767
 +Andreeva, L.P. 115245
 +Andrejschiff, W. 112236
 Andresen, P. + 112842
 +Andrews, H.R. 112033
 Andrews, P.L. + 113592
 Andrews, P.L. + 113593
 +Andrews, S.R. 114792
 Andries, C. + 115747
 Andrikanis, L.I. + 112919
 Andriat, Y. 116491
 Andronenko, S.I. + 114666
 +Andruliewicz, E. 115704
 Ang, P.G.P. + 115663
 Angell, J.K. + 116187
 +Angelopoulos, M.G. 112495
 Angelov, A.K. + 113097
 Angelov, S. + 114677
 +Anger, C.D. 116337
 Angert, N. 112467
 Anghinolfi, M. + 112198
 +Ania, F. 113760
 +Anikin, V.F. 113839
 Anis, M.K. + 113807
 Anisimov, A. + 115769
 Anisimova, N.P. + 114627
 +Anisimova, V.N. 114796
 Anisovich, V.V. + 111966
 +Anisatov, A.T. 113822
 +Anjaneyula, Ch. 115562
 Anklam, T.M. + 112411
 +Annersten, H. 114823
 Annunziata, M. + 112585
 Anokhin, Yu.N. + 115846
 Anokhin, Yu.N. + 115847
 +Ansaldò, E.J. 112176
 +Ansaldò, E.J. 112175
 +Anseau, M.R. 113755
 Anshakov, O.M. + 112537
 Antal, J.J. 112521
 +Antartiss, A.D. 111440
 +Anthony, A.M. 113741
 Antic-Fidancev, E. + 114497
 +Antipenko, B.M. 112998
 Antipin, M.Yu. + 113852
 Antipov, G.N. + 112514
 Antipov, S.V. + 113417
 +Antipov, V.V. 115950
 +Antipov, S.S. 111446
 Antonopoulou, E. 116753
 +Antonov, A.A. 111823
 +Antonov, A.V. 111713
 Antonov, S.N. + 114825
 +Antonov, V.A. 113938
 Antonov, V.F. + 115759
 Antonov-Romanovskii, V.V. 111610
 +Antonova, L.M. 114381
 +Antonsen, T.M., Jr. 113590
 Antreasyan, A. + 112989
 Anttila, R. + 112724
 Antunes, O.A.C. + 112871
 Aoi, F.J. + 112771
 +Aoi, F.J. 115519
 Aoki, K. + 112082
 +Aoki, S. 115333
 +Aoki, S. 111811
 +Aoki, Y. 112213
 +Aoki, Y. 112223
 Aono, M. 114994
 +Aono, M. 115024
 +Aono, Y. 113900
 +Aparicio, B. 116398
 +Apel, W.-D. 112016
 Apicella, A. + 115294
 Apicella, A. + 115395
 +Apininskaya, L.M. 115140
 Apostol, M. 114515
 +Apostolis, Th. 112755
 +Appelbaum, J. 115656
 Appleby, G.M. + 116499
 +Appleton, B.R. 113945
 +Appleton, B.R. 114005
 +Aprehmanian, A. 112100
 +Aptekar, R.L. 116876
 +Aquilano, D. 113928
 +Arafat, E.S. 111683
 Arai, R. + 112550
 +Arai, S. 112862
 +Arai, S. 113008
 +Arai, S. 112466
 +Arai, T. 115231
 +Arajs, S. 114507
 Arakelyan, S.M. + 113064
 +Araki, H. 115667
 +Araki, H. 114397
 +Araki, T. 113804
 Arata, A. 115620
 Arata, Y. 111837

- + Aratono, Y. 114260
 Arbabi, F. 113298
 + Arcan, M. 113381
 Arce, R. + 114642
 Archibald, I.W. + 114591
 + Ardisson, G. 112072
 Ardisson-Marsol, C. + 112072
 + Arditty, H.J. 113101
 Aref'eva, I.Ya. 111909
 Arens, R. 111466
 Areshv, I.P. + 111759
 + Argon, A.S. 115276
 + Arias, J.E. 115963
 Arima, A. 112098
 Arima, A. 112116
 + Arima, A. 112293
 + Arimura, Y. 112437
 Aripov, Kh.K. + 115651
 Arkad'ev, V.A. + 111499
 + Arkhangel'skii, S.I. 115216
 Arlashchenko, N.I. + 115856
 Armand, S.A. + 113035
 Armstrong, D.D. 112464
 + Armstrong, R.L. 111687
 Armstrong, T. + 112020
 Arnaud, J. 112994
 Arnell, S.E. + 112292
 Arnison, G. + 112031
 + Arnold, F. 116249
 Arnold, M. + 114590
 Arnold, R.C. 113012
 + Arnold, W. 112187
 + Arnold, W. 112188
 Arnol'dy, R.L. + 116396
 Aron, M. 113300
 Arons, J. 116724
 Arora, B.R. 116233
 Arora, B.R. + 116013
 + Arora, B.R. 116372
 + Arp, H.C. 116855
 Arsayev, I.Ye. 112906
 + Arsenault, H.H. 112944
 Artamonov, V.A. + 115977
 Artemenko, S.N. + 114595
 Artem'eva, G.M. + 116378
 Arter, W. 113441
 + Arur, M.G. 116013
 + Arutunyan, A.M. 113055
 Arutyunyan, R.A. 113359
 Arutyunyan, V.M. 114547
 Arve, P. + 112045
 + Aryacinejad, R. 112112
 Arzamastseva, G.V. + 114718
 + Arzoumanian, E. 113430
 + Asahi, K. 112278
 Asamaki, T. + 115054
 Asano, K. + 112437
 + Asanova, B.T. 115173
 + Aschenbach, P.D. 115831
 + Ascher, U. 116026
 Aschhoff, H.-G. 112359
 Asenbaum, A. + 114872
 + Ash, W.W. 111992
 + Ashaks, Ya.V. 113838
 Ashbee, K.H.G. + 115296
 Ashby, C.I.H. 115577
 Ashirov, T.K. + 114920
 + Ashton, C.J. 112800
 Ashton, G. 111790
 Ashton, G. 111791
 Ashwood-Smith, M.J. 115878
 + Askochenskii, Yu.B. 115158
 + Aspar, K.F. 115965
 + Aspin, C. 116860
 + Ast, D. 113931
 + Ast, D.G. 115135
 + Astaf'ev, A.A. 115216
 + Astakhova, E.D. 116245
 Astanin, V.V. + 111665
 + Astbury, A. 112031
 Atabek, O. + 111486
 + Atamanova, N.M. 115173
 Atanasov, V.B. + 113653
 + Athas, B. 111958
 + Athay, R.G. 116556
 + Atherholt, T. 115709
 Atherton, N.M. + 114737
 + Atherton, P.S. 112790
 + Atkinson, B.K. 116079
 Atkinson, D. 111939
 Atluri, S.N. 113294
 + Atluri, S.N. 111443
 + Atovmyan, L.O. 114160
 Atreya, S.K. + 116528
 Atsumi, K. 115978
 Attia, M. + 113083
 + Atvars, T.D.Z. 114841
 + Atwater, H. 114475
 Aub, M.R. + 111352
 + Aubert, B. 112031
 Aubry, S. 111577
 Aubry, S. + 111608
 + Aucouturier, J. 111844
 Audit, Ph. 113877
 Audouard, A. + 114035
 + Augis, J.A. 115412
 + August, R.A. 112217
 Augustinovicz, F. + 113239
 Aune, B. + 112472
 + Aupoix, B. 113430
 + Austin, I.G. 114756
 Austin, J. 116278
 Auston, D.H. + 114558
 + Auvray, B. 116006
 + Auzel, F. 112723
 Avakants, L.P. + 114824
 + Avanesov, M.V. 115347
 + Avchukhov, V.D. 112189
 Avdonina, N.B. + 112690
 Avdonina, N.B. + 112859
 Avduvskii, V.S. + 116503
 + Averbach, B.L. 114319
 Averbach, R.S. + 114051
 + Averbach, R.S. 114187
 Averin, S.A. + 112576
 Averkiev, N.S. + 114923
 + Averous, M. 114574
 Avery, N.R. 114986
 Avevov, R.R. + 115685
 + Avignant, D. 114753
 + Avishai, Y. 111550
 + Awaka, J. 116205
 + Axford, W.I. 116412
 + Axon, D.J. 116483
 + Ayar, B.S. 116022
 Ayers, R.D. 111353
 + Aymonino, P.J. 114857
 + Ayrault, G. 114052
 + Ayres, R.L. 112480
 Aysto, J. + 112131
 Azcarraga, J.A. de 115550
see de Azcarraga, J.A.
 Azheganov, A.S. + 111716
 Azimov, S.A. + 115639
 Aziz, M.J. 114132
 + Azizov, Sh.B. 114623
 Azuma, K. + 111777
 + Azumi, M. 113647
 + Azzam, E.I. 115870
 Azzam, R.M.A. 112929
 + Azzawi, Y.-M. 115971
 Azzazy, M. + 115550
 Baan, W.A. + 116811
 Babaev, R.M. 116302
 + Babaev, Yu.N. 113076
 + Babaev, Yu.N. 113545
 + Babak, A.V. 115344
 + Babakulov, K.B. 115685
 + Babcock, C.D. 113375
 Babich, A.A. + 111935
 Babkin, E.V. + 114683
 + Babu, R. 113577
 + Babushkin, A.N. 114772
 + Bacci, C. 112031
 Bacci, M. 115739
 + Bachheimer, J.P. 114215
 + Back, B.B. 112255
 Back, N.L. + 112199
 + Backenstoss, G. 112544
 + Backer, A. 112015
 + Bacon, D.J. 115256
 Badalyan, A.G. + 113910
 Badre, A. + 112448
 + Badshah, V.H. 116013
 Badurek, G. + 111490
 Badzagua, T.Sh. + 113953
 + Baerends, E.J. 112637
 Baeri, P. + 114004
 Bagge, V.E.R. 116502
 + Baghdadli, M. 114028
 + Bagiev, V.E. 114471
 + Baglione, H. 115679
 Bagnaia, P. + 112022
 Bagus, P.S. + 112666
 + Bagus, P.S. 115015
 Bahuguna, R.D. + 112940
 Bai, T. + 116592
 + Bai Gai-Xian 116000
 Baiardo, J. + 114503
 Baiardo, J. + 114875
 Baier, R. + 112027
 Baiasi-Pillastrini, G.C. + 116492
 + Bailey, D.M. 115168
 Bailey, J. 112885
 + Bailey, J.A. 115369
 + Bailey, P.G. 115949
 Bailey, R. + 112540
 Baillif, R. + 114744
 + Bains, P.S. 116013
 + Bak, P. 114349
 + Bakai, E.A. 115885
 Bakeev, A.A. + 113031
 Baker, R. + 112347
 Baker, R.T.K. + 114427
 + Baker, W.A., Jr. 114676
 Bakhyshov, A.E. + 114471
 + Bakonyi, I. 114754
 Bakos, J.S. + 113621
 + Bakumenko, S.P. 115187
 Balabanyan, G.O. 112978
 + Balagina, C.M. 115120
 Balakirev, M.K. + 114326
 Balakireva, V.B. + 114573
 + Balakrishnan, V. 114968
 Balamuta, J. + 115538
 Balantekin, A.B. + 112095
 + Balantsev, S.K. 114096
 + Balaraman, V. 112363
 Balashova, A.P. + 114948
 Balasubramanian, K. 112646
 Balasubramanian, K. 112809
 + Balasubramanian, N. 113293
 Balberg, I. + 114579
 Balbinot, R. + 115159
 + Baldwin, A.R. 112562
 + Baldwin, J.E. 116853
 Baldwin, N.J. 115492
 Baleka, E.S. + 115638
 Balfour, W.J. + 112745
 + Balgovind, R. 116095
 Baliga, B.J. + 114536
 + Baliga, B.J. 114480
 + Balk, P. 114406
 Balk, P.I. 115997
 + Balkare, Yu.I. 114571
 + Ball, A.H. 111990
 + Ball, A.H. 112012
 + Ball, C.J. 111854
 + Ballard, R.D. 116074
 Ballester, J.L. + 116615
 Balling, L.C. + 112636
 + Ballman, A.A. 114254
 Balluffi, R.W. + 113929
 + Balluffi, R.W. 113863
 Balogh, I. + 116297
 + Balogh-Nair, V. 115474
 + Balsley, B.B. 116305
 + Balta Calleja, F.J. 114539
 + Balta Calleja, F.J. 113760
 Balthasar, H. + 116597
 + Baluteau, J.P. 116521
 + Bame, S.J. 116404
 + Bamford, G. 111990
 + Bamford, G. 112012
 + Bammeke, A.O. 115707
 Banaschek, J. 112309
 + Bancroft, G.M. 112786
 + Band, H.R. 111992
 Bandiera, R. + 116707
 + Bando, H. 112105
 + Bandy, R. 115413
 + Banerjee, B.K. 113801
 + Banerjee, K. 113442
 + Banerjee, M.B. + 113442
 + Banerjee, P.P. + 113465
 + Banerjee, S. + 113992
 + Bange, K. 114340
 Bania, T.M. 116770
 + Bankoff, S.G. 112410
 Banks-Sills, L. + 113381
 + Banner, M. 112022
 Banos, J.O. + 114077
 + Banovetz, L.M. 114637
 + Bansal, J.L. 113585
 + Bansal, M. 115738
 + Bansha, R.F. 115284
 Bansil, A. + 114433
 Banwell, T. + 114611
 + Bapna, R.C. 115117
 + Baquay, C. 115458
 Barakat, R. 112939
 Barakat, R. + 116274
 + Barancik, J.I. 115658
 Baranov, N.V. + 114671
 + Baranov, P.G. 114755
 + Baranov, V.I. 112713
 Baranov, V.Yu. + 113681
 + Baranovskii, V.I. 112655
 + Baranowski, J. 114491
 Baras, F. + 111557
 + Barash, M.S. 116268
 Barar, C. 116877
 Baratta, G.B. + 116698
 + Barbarino, G.C. 112595
 Barbaro-Galtieri, A. + 112542
 + Bata, G.L. 113238
 + Barbee, D.B. 111479
 + Barber, M.N. 114028
 Barbier, D. + 114030
 Barbier, D. + 114030
 + Barbu, A. 113995
 Barcik, J. + 115199
 + Bard, A.J. 115561
 + Bard, A.J. 114931
 + Bard, A.J. 114606
 + Bardadin-Otwinowska, M. 112028
 Bardeen, W.A. + 111899
 + Bardwell, C.M. 116513
 + Bare, S.R. 114345
 Barefield, J.E., II. + 112776
 Bareket, N. 111730
 + Barel, A. 111708
 Barfield, J.N. + 116403
 + Barfuss, H. 113030
 Barinov, S.M. + 115343
 Barkai, D. + 111866
 Barker, F.C. 112201
 + Barker, J.H. 112261
 Barkich, J.L. + 112379
 + Barla, K. 114333
 + Barlow, A.J. 111738
 + Barlow, A.J. 113119
 + Barlow, R. 111990
 + Barlow, R. 112012
 + Barmin, I.V. 114148
 + Barmin, S.M. 114690
 Barmina, N.V. + 114382
 + Barmina, N.V. 114785
 + Barnard, A.J. 113666
 + Barnes, C.A. 115990
 Barnes, C.E. + 114464
 Barnes, C.W. + 113573
 Barnes, T. + 112009
 Barnes, T. + 111971
 Barnett, C.F. 113639
 Barnett, T.P. + 116260
 + Barney, J. 115642
 + Barnham, K.W.J. 112028
 Barny, P. Le 115465
see Le Barny, P.
 + Baron, M.H. 112744
 Baroni, G. + 112559
 + Baronnnet, A. 114071
 Barr, S. + 116170
 Barr, S.M. 111923
 + Barraclough, C.G. 114856
 + Barraclough, K.G. 114027
 + Barragan, F. 115911
 Barranco, M.P.M. + 112103
 + Barreiro, F. 112015
 + Barrero, A. 113580
 + Barrett, B.R. 112095
 + Barrett, P.J. 113604
 + Barrette, J. 112259
 + Barrot, A. 113229
 Barry, J.J. + 115009
 Bars, I. + 111532
 Barstow, M.A. + 114943
 + Barsuk, V.A. 112575
 Bartel, W. + 111990
 Bartel, W. + 112012
 + Bartell, L.S. 113824
 Bartels, G. 111386
 + Bartelt, H. 112956
 Bartenev, G.M. + 115299
 + Barteneva, A.G. 115299
 Barthel, P.D. 116872
 + Barthels, H. 112383
 Bartlett, A.A. 111374
 + Bartlett, P.N. 114607
 + Bartnitskaya, T.S. 115393
 + Bartolotti, L.J. 112616
 + Barton, D.S. 112476
 + Barton, J.P. 111858
 + Bartos, D.J. 111690
 Bartur, M. + 114258
 + Barut, A.O. 112617
 Bar'yakhtar, V.G. + 114691
 + Barykina, L.R. 113845
 + Barz, H. 114635
 + Basehore, K.L. 112312
 Bash, V.Ya. 113391
 + Basha, A.M. 112121
 Bashir, I.B. 115150
 + Bashkirov, Yu.P. 115485
 + Bashmakov, Yu.A. 113004
 Basili, P. + 116168
 Baskakov, A.N. + 113079
 + Baskakov, S.I. 112904
 + Baskova, K.A. 112189
 + Basmanov, I.N. 114394
 + Bass, M. 115376
 + Basse-Cathalinat, B. 115458
 Bassi, P. + 111743
 Bastard, G. 114596
 + Bastian, T.S. 116740
 + Bastin, G. 116165
 Basu, B. + 114173
 Basu, D. 116871
 + Basu, M. 112856
 Basu, P.K. + 114518
 + Basu, S. 114551
 + Basu, G.L. 114069
 + Batalin, G.I. 113705
 + Batchelor, R.A. 116803
 + Bates, J.L. 114213
 Bath, G.T. + 116469
 Bath, M. 116033
 Batishche, S.A. + 113060
 + Batley, R. 112024
 Batra, A.K. 112572
 Batra, I.S. + 115312
 + Batrla, W. 116532
 Batson, P.E. 114462
 + Battaglia, P.J. 112379
 + Batteh, J.H. 112987
 + Battiston, R. 112022
 + Battles, J.E. 115628
 + Battut, J.P. 114753
 + Batur, V.P. 114134
 + Baubillier, M. 112020
 + Baud, B. 116772
 + Bauer, G. 112031
 Bauer, G.S. 112491
 + Bauer, J. 115165
 + Bauer, O.H. 116402
 + Bauer, R.K. 111783
 Bauer, R.S. + 114598
 Bauer, S.H. + 115537
 Bauer, W. + 112506
 + Bauer-Grosse, E. 115200
 Baumann, W. 112873
 Baumard, J.F. + 113858
 + Baumgart, H. 112188
 Baur, G. + 112220
 + Baur, G. 112163
 + Baur, G. 112827
 + Bauschlicher, C.W., Jr. 112666
 Baxter, W.J. 115465
 + Bayazitoglu, Y. 113259
 + Bayer, C. 113656
 + Bayliss, M.A. 111786
 Bayoumi, A.-M. + 115369
 Bayoumi, M.A. + 112397
 Bayuklina, M.F. + 116349
 Bazarov, I.P. + 111543
 Bazdenkov, S.V. + 113416
 + Bazhan, A.N. 114666
 + Bazik, N.G. 114610
 + Bazin, C. 112516
 + Bazzacco, D. 112109
 Bazzano, A. + 116474
 + Beadle, N.J. 112549
 + Bean, J.C. 114399
 Beard, B.C. + 113950
 + Beard, K.V. 115587
 + Beardsley, R.C. 116141
 Beatham, N. + 112305
 + Beattie, D.H. 116692
 + Beattie, D.R.H. 112373
 Beatty, M.F. 113270
 Beaudry, R. 112336
 Becchetti, F.D. + 112289
 + Becerra, C.C. 114664
 + Bechly, M. 115801
 Beck, J.W. 115904
 Becker, C. + 112543
 + Becker, F.L. 115495
 + Becker, J.A. 112066
 + Becker, L. 111990
 + Becker, L. 112012
 Becker, R. + 113819
 Becker, R.L. + 112831
 Becker, U. + 112566
 + Beckman, J.E. 116797
 + Beckmann, P.A. 114749
 + Becla, P. 115110
 Bedanov, V.M. + 114144
 Bedbenov, V.S. + 112536
 + Beddin, F.V. 115886
 + Bedrikov, A.G. 116418
 + Beebe, E.D. 113997
 Beek, G. van 115110
see van Beek, G.
 Beeler, J.R., Jr. 111332
 Beeley, P.A. + 112286
 + Beene, J.R. 112049
 + Beene, J.R. 112261
 + Beene, J.R. 112059
 Beere, W. 114083
 Beers, A.M. + 114415
 Beetz, C.P., Jr. + 115242
 Beg, M.A.B. 111945
 + Begova, Z.S. 114521
 Behm, H. 113811
 + Behraves, M. 115495
 Behrend, H.J. + 112016
 + Behrens, M.A. 113604
 + Beintema, D. 116782
 Bekeris, Yu.Ya. + 114936
 Bel, L. 111430
 + Belan, V.N. 114127
 Belau, E. + 112554
 Belen'kii, A.Ya. 113745
 Beletskii, I.P. + 112659
 + Belikov, A.M. 115335
 + Belikova, A.B. 116418
 Belinsky, B.P. 113175
 + Bel'kov, M.V. 115743
 + Bell, A. 111990
 + Bell, A. 112012
 Bell, J.F. 115258
 Bell, M.B. + 116793
 + Bella, G. 112015
 + Bellini, V. 112510
 Bellomo, G. + 112489
 Bellomo, N. + 113544
 + Bellville, J.W. 115822
 Belo, M. Da Cunha 115822
see Da Cunha Belo, M.
 + Belokurova, I.N. 113789
 + Belonogov, E.K. 114380
 + Belostotskii, A.L. 114326
 Belousova, O.I. + 115853
 + Belov, A.G. 113786
 Belov, G.Ya. 113260
 Belov, K.P. + 114687

- +Belov, N.V.113844
+Belov, N.V.113830
+Belov, N.V.113842
+Belov, N.V.113843
+Belov, N.V.113829
+Belov, N.V.113792
Belov, S.V. +114096
+Belovintsev, K.A.113004
+Bel'skaya, I.N.116516
+Bel'skii, V.K.113841
+Beltran, D.114699
Beltzer, A.I.113168
Belyaev, V.A. +112843
+Belyaev, V.A.112604
Belyaev, V.N. +112878
+Belyakov, V.K.114256
+Belyakova, L.A.115584
Ben Dor, L. +115096
Ben-Aryeh, Y. +112971
+Benary, O.112024
Bencini, A. +112652
Bender, D. +112176
+Bender, H.111659
Bender, O. +113886
+Benedek, R.113990
+Benedek, R.114033
Benedek, S.112399
Benedictis, S.De
.....see De Benedictis, S.
+Bengtson, A.112679
Bengtsson, T.112047
Benichou, J.L. +112553
Benincasa, F. +116281
Bennani, A.Lahmam
.....see Lahmam Bennani, A.
Bennetch, J.I. +113543
Bennett, D.P. +113459
+Bennett, J.E.115412
Bennett, M.J. +112351
+Beno, M.A.114637
+Bensinger, J.112550
+Benson, J.113665
+Benson, J.116843
+Benson, S.W.112644
Benton, E.R. +116002
Benton, J.L. +114477
Benvenuti, P.116424
+Ben'yamin, M.114471
+Benz, H.115062
+Benz, K.W.115062
Benza, V. +112970
Beratung, G.116247
Berchiesi, G. +114066
+Berdyshev, G.D.115732
Berei, K.115572
+Berendsen, H.J.C.115727
Berens, P.H. +112647
+Berestenko, V.I.115129
Berezhiani, Z.G.111924
Berezhkin, V.I.114567
Berezhko, E.G.116379
Berezhnitskii, L.T. +113358
Berezhnitskii, L.T. +113363
Berezin, A.A.114466
+Berezovskaya, M.M.113570
Berezovskii, E.L. +113570
Berg, G.P.A. +112076
+Berg, G.P.A.112528
+Berg, H.112187
+Berg, H.112188
Berg, R.Van
.....see Van Berg, R.
+Bergamini, R.111519
Berger, C. +112015
Bergh, C.de
.....see de Bergh, C.
Bergh, L.C.van den
.....see van den Bergh, L.C.
Berghmans, J.115673
+Bergman, P.G.116644
Bergmann, C.A. +112381
Bergmann, G. +115981
+Bergquist, J.C.113057
Bergqvist, I. +112159
+Bergstrom, I.112544
Bering, E.A.116338
Berk, H.A. +113643
Berk, H.L. +113597
+Berk, H.L.113599
Berliner, R. +112526
Berman, G.P. +111583
Berman, R.H. +113610
Bermishev, A.A. +116422
+Bernabeu, J.112191
+Bernal, I.113835
+Bernal, M.A.115963
Bernard, C. +111959
+Bernard, C.115092
+Bernard, C.115091
+Bernard, C.113070
+Bernard, C.115099
Bernhardi, K. +111321
Bernotas, G.I. +115003
+Bernstein, E.R.114158
+Bernstein, I.M.115215
+Bernstein, M.115566
+Bernstein, R.B.112771
+Bernstein, R.B.115519
Berre, M.Le
.....see Le Berre, M.
Berriel, L.R. +112941
Berriman, G. +116692
+Berry, G.C.113719
Berry, H.G. +115545
Berry, M.V. +111496
Berryman, J.G. +116081
+Berst, J.D.112587
+Bersuker, I.B.112671
+Bersuker, I.B.112708
+Berstel, E.114347
+Berthet, M.115682
+Berthier, B.112259
Bertola, F. +116859
+Bertolasi, V.111369
Bertolotti, M. +111634
+Bertolotti, M.113983
+Bertrand, F.E.112153
+Bertsch, G.F.112073
+Berven, B.A.115703
+Bescos, J.112941
Besley, L.M.111680
Besomi, P. +115115
Besprozannaya, A.S. +116346
+Bessiere, J.114850
Bessling, H.113523
Bessonov, A.F. +113243
+Bessonov, E.G.113004
Bestmann, G. +112716
Bethke, K.111667
+Bethke, S.111990
+Bethke, S.112012
Betremieux, P.111841
+Betrencourt-Sürnemann, K.112724
Betts, R.R. +112156
+Betz, P.112060
+Beusch, W.112020
Beuzekom, A.A.van
.....see van Beuzekom, A.A.
Beveren, E.van
.....see van Beveren, E.
+Bevov, R.K.113681
Beyer, O. +113744
Beyer, R.P.114206
Beyer, R.P. +111682
Beyers, R. +114401
Beysens, D.114130
+Bezaguet, A.112031
Bezard, B. +116521
+Bezdetnaya, L.N.115862
Bezhanov, K.A.113474
Beznosikov, B.V. +113822
+Bhagia, L.J.114079
Bhakta, J.C. +113603
+Bhalla, A.S.114789
Bhanumathi, R. +114235
+Bhar, G.C.114293
Bhargava, B.N. +116372
+Bhargava, S.C. (ed.)111334
Bhatt, A.P. +114528
Bhatt, V.P. +115453
Bhattacharya, C.K. +116237
+Bhattacharya, R.112057
Bhattacharya, S. +112143
+Bhattacharyya, A.116012
+Bhattacharyya, S.N.115966
+Bhonsle, B.R.113254
+Bhonsle, R.V.116572
Bhushan, S. +114929
+Bixareras, C.116415
Bibby, M.J. +115189
Bichuya, A.L.115434
+Bichuya, A.L.113304
+Bidani, M.115534
+Biddle, D.112782
Bidelman, W.P.116632
Biegelsen, D.K.113742
Biegelsen, D.K. +114018
+Biegelsen, D.K.114612
+Bielinski, J.W.112991
Biellmann, J. +114871
Bieren, K.Von
.....see Von Bieren, K.
+Biero, H.111842
Biet, M.113135
+Bignami, G.F.116883
+Bignell, R.C.116841
Bijleveld, W. +116818
Bijlsma, S.J. +116192
Bilenchi, R. +115083
Bilenko, D.I. +111642
Billaud, D. +115031
+Bille, J.115784
+Billet, M.L.112957
+Billia, B.115182
+Billon, D.113656
Bills, B.G.116065
Billey, M. +113826
+Bilpuch, E.G.112157
Bin-Yao Jiang
.....see Jiang Bin-Yao
+Binaghi, E.112585
Bindal, V.N. +113230
Binder, W.115917
+Binenbaum, N.114579
+Bingham, R.G.116483
Binkley, J.S. +112635
Binnig, G. +114312
Binon, F. +112556
Birac, A.M. +115456
+Biradar, A.M.114625
Birch, K.G. +111752
Birch, M. +115256
Birch, M. +115307
Birch, M.W. +115305
+Birch, R.D.113109
+Birch, R.D.113119
+Birdsall, C.K.113589
Birge, R.R. +112876
+Birkelund, J.R.112249
Birkshaw, M. +116772
+Birman, J.L.111603
+Birn, J.116404
+Birn, J.116605
Birnie, S.E. +115830
Biro, T.S. +112266
Biryulin, P.V. +111768
+Biscaye, P.116073
+Bischel, W.K.112700
+Bischke, S.D.114366
Bishop, A.R. +111578
Bishop, C.M. +111890
Bishop, D.M. +112704
Bisiaux, M. +116241
+Bismayer, U.114159
Bissing, G.112846
+Bisyarin, V.P.113035
Bitterwolf, E. +112060
Bityurin, N.M. +114218
+Biyushkin, V.N.113700
+Bizot, J.C.112030
+Bjorkholm, J.E.113997
+Bjornholm, S.112058
+Bjornholm, S.112046
+Bjorvatten, T.116181
+Black, T.D.114676
+Black, W.M.113003
+Blackman, G.S.114637
Blagojevic, M. +115130
+Blair, D.G.116730
+Blak, A.R.114731
Blake, D.M.111839
+Blanch, H.F.111368
+Bland, L.C.112219
+Blandford, R.D.116764
Blankenship, M.G.113156
+Blanton, J.O.116141
+Blanzat, B.114913
Blaszczyzyn, M. +114365
+Blaszczyzyn, R.114365
Blatov, A.S. +116100
Blednov, V.A.116292
+Bleidis, Ya.Ya.112865
+Bleidis, Ya.Ya.113838
+Bleif, H.-J.114792
+Bleistein, N.116308
+Blevins, L.R.113429
+Blitzer, L.D.114639
+Bloch, A.N.115633
+Bloch, P.112022
+Blocker, C.A.112011
+Bloom, J.114415
+Bloem, J.115090
Bloem, J. (ed.)111316
+Blomqvist, J.112044
+Bloodworth, I.J.112020
+Bloom, S.D.112128
Blosse, A. +114021
Blow, K.J. +114468
Blum, P. +112544
Blum, W. +115254
+Blume, H.T.111992
+Blumen, W.116196
Blyholder, G. +114364
Boal, T.J. +112170
Boardman, A.D. +113039
+Bobkowski, R.112684
Bobovich, Ya.S. +112743
Bobrov, A.V. +112793
Bobrov, M.S.116011
Bobrovskii, A.N. +113081
Bobrovskii, S.V. +116082
+Bobst, A.M.115987
+Boca, G.112020
+Boccacini, L.116474
+Bocek, J.116551
+Bocharova, N.Yu.116046
+Bocian, D.F.112876
Bock, C. +112648
+Bock, G.116028
+Bock, R.112031
+Bock, R.112267
Bock, R.K.112613
Bocko, M.F. +111537
Bocquet, J.-L.114281
+Bocquet, J.-L.113995
+Bodak, O.I.113833
+Bodden, W.115431
+Bodnar, I.V. +114881
Boedeker, R.R.111337
+Boegel, M.L.115944
+Boehme, H.116197
+Boehnlein, A.J.113115
Boer, K.S.de
.....see de Boer, K.S.
Boer, R.de
.....see de Boer, R.
Boer, W.de
.....see de Boer, W.
+Boerner, H.112550
+Boes, D.115370
+Boesten, L.112015
Bogaerts, W. +115700
Bogan, Yu.A.113305
+Bogatov, Yu.E.114127
+Bogatykh, B.A.115842
Bogatyeva, I.V. +111758
+Bogdanov, A.N.114691
+Bogdanov, N.S.114564
+Boggild, H.112024
Bogoljubsky, M.Yu. +112021
Bogolyubov, N.N., Jr. +111551
Bogomolov, V.N. +115142
Bogoslovskii, G.Yu.111527
Bogoslovskii, S.A. +114675
Boheim, J. +114361
+Bohlen, H.G.112539
+Böhme, D.112992
Bohne, W. +112270
+Böhne, W.112273
+Böhne, W.112272
+Bohringer, T.112554
Bohusz, E. +116679
Boiarchenko, S.I. +113331
+Boicourt, W.C.116141
Boiko, B.B. +113040
+Bois, D.114483
Boitsov, V.M.115723
Bok, B.J.116425
+Boku, S.115810
Bol, A. +111809
+Bolch, W.E.115943
Boldyrev, A.I. +112640
+Bolmaro, R.E.115237
+Bolmaro, R.F.115236
+Boloh, L.116523
Boloni, P.111647
+Bolotnik, N.N.113269
Bolotnyuk, A.L. +113242
Bol'shanina, M.A. +115340
Boman, M. +114408
+Bomben, K.D.112762
Bomchil, G. +114333
Bomsdorf, H. +112761
+Bona, J.L.113459
Bonaccorsi, R. +112804
+Bonacic-Koutecky, V.115528
Bonafede, M. +116064
+Bonaforte, S.D.112548
+Bonaudi, F.112022
Bonch-Bruevich, A.M. +113251
+Bonchev, D.114330
+Bond, F.R.116335
Bondar, A.G. +113325
+Bondar, I.A.114666
+Bondar, V.I.113842
+Bondar, V.I.113843
+Bondarenko, V.P.114394
Bondarev, S.L. +115743
Bonder, L.J.115808
Bonder, L.J.115809
+Bonesini, M.112020
Bonetti, P. +115100
Bonetti, R. +112164
Bonetti, R. +112135
+Bonetti, R.112233
+Bonhommet, N.116006
+Bonner, B.P.116081
+Bonnier, B.111910
Bonzon, L.L.112403
Booi, H.C. +113395
+Booker, H.G.116367
+Boon, M.H.114430
+Boon, P.J.112757
Booth, A.J. +112680
+Booth, C.114852
+Bordi, S.114303
Bordon, F. +116485
+Borensztein, Y.114946
+Borensztein, Y.114344
+Borer, K.112022
+Borg, R.J.114184
+Borggreen, J.112058
+Borggreen, J.112046
Borghi, R. +113521
+Borghini, M.112022
Borisenco, V.E.114278
Borisenco, V.E. +114253
Borisovich, N.A. +112733
Boriskin, A.I. +111805
+Borison, E.V.113144
+Borison, V.T.114440
Borisova, L.D. +114550
+Borland, R.S.112307
Borodin, L.V. +111710
Borodin, V.A. +114686
+Borodkin, A.A.115614
+Borovkov, V.Yu.115544
+Borrelli, M.J.115831
+Borsa, J.115870
Borsboom, P.C.F. +113103
Borshch, S.A. +112671
Bortle, J. +116537
+Bortle, J.116685
+Bortle, J.116538
+Bortle, J.E.116539
+Bortle, J.E.116546
+Bortolotto, D.112020
Bortz, J.C. +111726
+Boreshko, M.S.115401
+Bosart, L.F.116194
Bosch, J.J.ten
.....see ten Bosch, J.J.
+Boschi, E.116064
+Boschitz, E.112285
+Bose, D.N.114551
+Bose, T.K.111705
Bosi, L.112654
+Bosqued, J.-M.116398
Bosserman, R.W.115719
Bossi, M. +116670
Bossi, M. +116671
Bossi, R.H. +111858
Boswell, R.W. +116357
+Botthun, G.D.116765
+Botner, O.112024
Botschwin, P. +112705
Bottvinnik, I.E. +112974
Boucher, D. +113154
+Bouchez, J.112016
+Boudewijn, F.B.115595
+Boudrie, R.L.112283
+Boudrie, R.L.112149
Boudriot, H. +114982
+Boue, S.115654
Bougard, M. +116562
+Bouix, J.113070
+Boukunen, O.P.115289
+Boulegue, J.116074
+Boulon, G.114906
Bouma, J.W.J. +115675
+Bountis, T.111609
+Bourbin, Y.113101
Bourceanu, G. +115721
+Bourceanu, G.115722
+Bourgeois, J.C.114021
+Bousquet, C.112789
Boux, J.-C.111568
+Bowcock, T.J.V.112031
Bowden, A.L. +114707
+Bowden, C.M.112966
+Bowdery, C.111990
+Bowdery, C.112012
+Bowen, H.K.115126
Bower, R.D. +112799
Bowers, J.E. +113126
+Bowers, R.G.114696
Bowker, K.J. +115455
+Bowman, M.K.114724
+Bowman, M.R.116234
+Boyarski, A.M.112011
+Boyd, D.114760
+Boyd, D.A.113665
Boyd, J.N. +112893
+Boyd, J.S.116335
+Boyd, T.J.112482
+Boyden, J.E.116479
Boye, C.A. +112924
Boyer, L. +115372
Boyle, J.S. +116194
Bozhko, A.E.115470
+Bozowski, S.114579
+Bozakov, L.114670
+Bazzelli, J.115709
+Braam, J.M.114637
Bracher, R.J.111840
Bracher, R.J.111846
Brack, M. +112094
+Bradley, D.J.113026
+Bradley, E.R.114049
Bradley, J.S.113192
+Bragazin, A.F.116422
Brager, H.R. +114182
+Bragin, N.N.115280
Brand, J.C.D. +112712
+Brandelik, A.112506
Brandt, D.112847
Brandt, N.B. +113786
+Brandt, N.B.114669
+Brandt, S.112015
+Brannen, E.112979
Bras, N. +112789
+Brass, G.W.116202
+Bratman, V.L.112974
Bratova, T.A. +116571
+Brault, J.W.116204
Braun, O.M. +114357
+Bravman, J.114288
Brearley, I.R. +112333
+Brecher, K. +116833
+Brecher, K.116835
+Brechignac, P.113686
+Brede, O. +115570
Bregier, M.116680
+Breidenbach, M.112011
+Breier, S.115976
Brekel, C.H.J.van den
.....see van den Brekel, C.H.J.

- Bremer, J. 112405
 Bremer, J. 114975
 Brenci, M. + 111674
 + Brendel, C. 112273
 + Brendel, W. 115837
 Brener, E.A. + 113787
 Brener, E.A. + 113788
 + Brenig, W. 114361
 Brenk, H.D. + 112454
 Brennleek, K. + 115398
 Brentano, P. von
 see von Brentano, P.
 Breton, M. + 113533
 + Brett, N.H. 115179
 Brettman, O.H. + 116678
 Breuer, H. + 112249
 Breugel, W. Van
 see Van Breugel, W.
 + Breuker, H. 112024
 + Brewer, J.H. 114768
 Brezhnev, A.L. + 111451
 + Briden, J.C. 116005
 Bridge, N.J. + 115590
 + Brient, J.C. 112020
 Briggs, E.R. + 115909
 Briggs, G.A.D. + 113237
 + Brill, D. 113171
 + Brill, M.H. 111736
 + Brilliantov, N.V. 112823
 Brink, K.H. 116129
 Brink, K.H. 116131
 Brinkmann, W. 116449
 + Brinkmeyer, E. 113030
 + Brinson, H.F. 113384
 + Briot, D. 116638
 + Briot, D. 116669
 + Briskin, V.L. 116311
 Bristow, D.J. + 112786
 Brittain, H.G. 115541
 Brittain, H.G. + 114915
 + Britun, V.F. 115366
 Brivio, A. + 115505
 Brivio, G.P. + 114367
 Brixner, L.H. + 113818
 Briz-Kishore, B.H. 116162
 + Broadway, J.A. 112610
 Brocas, J. + 112794
 Brocher, T.M. 116030
 Brocher, T.M. + 116101
 + Brock, J.R. 115586
 Brock, L.M. 113912
 Brockerhoff, P. + 112310
 + Brocklehurst, J.E. 115307
 Brockman, R.A. 111408
 + Brockmann, R. 112267
 + Brockner, W. 113819
 + Brodaczynski, G.G.
 115935
 + Brodeur, P. 113618
 Brodskii, A.M. + 114807
 + Brody, H. 112024
 Broeck, C. Van den
 see Van den Broeck, C.
 Broecker, W.S. 116150
 Broglia, R.A. 112042
 + Broglia, R.A. 112240
 + Brokman, A. 113929
 Bron, V.A. + 114526
 + Brondi, A. 112120
 + Bronz, V.Kh. 115341
 Brooks, E. III + 111958
 Brooks, J.S. + 115604
 Brooks, J.S. + 111711
 Brooks, R.E. 113204
 Brooks, R.L. + 114894
 Broom, R.F. + 115107
 Brosche, P. + 116822
 Brossa, F. 112442
 + Brossas, J. 115602
 Brovchenko, I.V. + 114452
 Brovikova, I.N. + 115379
 + Brown, B.A. 112127
 Brown, D.S. + 111753
 + Brown, G.R. 114139
 + Brown, G.S. 113039
 + Brown, K.L. 112528
 + Brown, M.D. 112829
 + Brown, M.D. 114535
 Brown, M.F. + 115728
 Brown, O.B. + 116144
 + Brown, R.F. 115827
 Brown, R.G. + 113526
 + Brown, R.G. 115461
 + Brown, R.W. 113459
 Brown, S. 115496
 + Brown, S.D. 115495
 Brown, S.K. 115302
 Brown, W.K. + 116892
 Brownell, W.E. + 115805
 Browning, C.E. 115161
 + Browning, D.G. 116102
 + Brownlee, D.E. 116554
 + Brubaker, R.F. 115893
 Brucher, H. + 112455
 + Bruckner, W. 112256
 + Bruckner, W. 112257
 + Brudnyi, S.R. 113274
 Brueckner, G.E. 116577
 + Brundrit, G.B. 116488
 + Brunel, L. 114414
 Brunelle, E.J. + 113328
 + Bruning, D. 114261
 + Bruning, D.H. 116479
 Brunn, J.H. 116070
 Bruno, G. + 115108
 Brunson, G.S. 112598
 Bruschi, M. + 111392
 + Brusentsova, R.M. 115490
 Bruskov, V.A. + 113833
 Bruzzese, R. + 112984
 Bryan, K. 116139
 Bryan, R.K. + 115738
 Bryant, F.J. + 114930
 Bryant, P.J. 113458
 + Bryant, S.H. 115771
 + Bryngdahl, O. 112950
 + Brysgalov, V.V. 112021
 Brytov, I.A. + 113795
 + Bryukhanov, A.S. 111805
 Brzezinski, B. + 112730
 + Brzycka, B. 115199
 Bubak, M. + 112361
 Bube, K.P. + 116319
 Bubnov, V.A. 116123
 + Bucaro, J.A. 113125
 Bucchini, R. 116722
 Buchanan, R.C. + 115149
 + Buchanan, R.C. 113747
 + Bucher, E. 114162
 Buchert, J. + 113000
 Buchert, J. + 115744
 Buchet, J. + 111842
 + Buchet, J. 111844
 Buchstab, V. 112602
 Buchwald, G. + 112251
 + Buchwald, G. 112263
 + Buchwald, V.T. 116116
 Buck, P. + 112085
 + Buckius, R.O. 115555
 Buckland-Wright, J.C.
 115906
 + Buckley, L.P. 112349
 + Buckley, S.N. 114023
 + Budd, G.W. 115242
 + Buddhudu, S. 114900
 + Budding, E. 116771
 Budick, B. 112123
 Budinsky, N. + 111609
 Budkin, L.A. + 113046
 + Budnikov, S.S. 112708
 + Budzyska, K. 114628
 Buevich, Yu.A. + 114301
 Buffoni, L. + 116534
 + Bugaev, A.S. 114571
 Bugaev, S.P. + 112513
 Buhl, L.L. 113089
 Buhr, W. + 111350
 + Buhrer, W. 114107
 Buijtenen, C.J.P. van
 see van Buijtenen, C.J.P.
 Buishvili, L.L. + 114725
 + Buishvili, L.L. 113181
 + Bukach, N.I. 111767
 Bukanov, V.N. + 115923
 Bukhshtab, M.A. 111734
 + Bukowski, M.S.T.
 114447
 Bulakh, B.M. 113799
 + Bulanova, L.V. 115379
 + Bulanova, M. 115826
 + Bules, S. 114471
 Bulgadaev, S.A. 111868
 Bulgarovskaya, I.V. +
 113841
 Bull, R.A. + 115561
 Bullock, F.W. + 111934
 Bullough, R. + 114036
 Bullough, R.K. + 113048
 + Bulow, M. 114369
 + Buluychev, V.P. 115280
 Bumba, V. 116566
 Bunde, R. 112435
 Bungener, A. + 112555
 + Bunin, L.A. 115433
 + Bunina, N.S. 112919
 Bunker, Ph.R. + 112621
 + Bunell, L.R. + 114213
 + Buntun, R.A.J. 113717
 Buntushkin, V.P. + 115275
 Bunzli, J.-C.G. + 113825
 Bunzli, J.-C.G. + 114501
 Burakov, V.S. + 113661
 + Burakov, V.S. 113060
 + Burchell, D.J. 114862
 Burchfiel, B.C. 116051
 Burde, G.I. + 113394
 + Burde, T.M. 113394
 Burdina, V.I. 113793
 Burenin, A.V. + 112728
 + Burg, J.R. 115833
 + Burger, C.P. 113383
 + Burger, J. 112015
 Burger, W.R. + 114416
 Burgess, D.D. + 112531
 + Burgess, D.D. 113648
 Burgess, P.H. 112568
 Burillo, G. + 115549
 + Burkard, A. 112060
 + Burkart, D. 112015
 + Burke, D.L. 112011
 Burke, R.W. + 111784
 + Burkert, V. 112024
 Burkett, H. + 113150
 Burkey, T.J. + 115574
 Burkitt, T. 111870
 Burkow, A.T. + 114168
 + Burkow, V.V. 112594
 Burlamacchi, P. + 116282
 Burlaw, E.J. + 111687
 + Burman, R.L. 112007
 + Burnell, E.E. 112763
 Burnett, C.R. + 116283
 + Burnett, E.B. 116283
 Burnett, S.M. + 112785
 + Burns, A. 112020
 Burns, M.L. 116832
 Burns, M.L. + 116457
 + Burns, M.S. 116715
 Burns, W.K. + 113124
 + Burrige, R. 116319
 + Burrow, P.D. 115529
 + Bursas, C.A. 113090
 Burshtein, A.I. + 112736
 Burton, B. 114074
 + Buryak, N.I. 113952
 Burykin, N.M. + 115753
 + Burylev, B.P. 115171
 + Busch-Vishniac, I.J.
 115955
 + Buschhorn, G. 112016
 + Buschmann, J. 112114
 + Busek, K. 112277
 Bushueva, G.V. + 113913
 Bushvev, V.A. + 114965
 Busico, V. + 114249
 Busse, F.H. 116905
 + Busse, J. 114055
 + Bussey, P.J. 112015
 Busso, M. + 116816
 Buta, R.J. + 116856
 Butcher, H. + 116865
 + Butcher, H.R. 116810
 + Butikova, I.K. 113832
 + Butler, E.P. 115195
 + Butler, S.R. 113950
 + Butman, B. 116141
 + Butsman, M.P. 114443
 Butt, R. + 113964
 + Butt, R. 113961
 + Butt, R. 113963
 + Butuzova, T.A. 115119
 Butz, T. + 114764
 Buzdin, A.I. + 114638
 Buz'ko, A.M. + 114713
 Byakov, V.M. + 112882
 Byakov, V.M. + 112883
 Bykov, A.D. + 112731
 Bykovskii, V.A. + 114922
 + Bykovskii, Yu.A. 111805
 + Byrd, R.C. 112202
 + Byrne, P.F. 113944
 + Byrne, T. 116062
 + Byrne, T. 116001
 Byshev, V.I. + 116122
 Bystritskii, V.M. + 112486
 Bystrom, K. 112657
 Bythrow, P.F. + 116390
 Byung Chan Eu. 113481
 + Cachard, A. 114028
 + Cadek, J. 115263
 Cadez, I. 115559
 Cadonau, R. + 116709
 + Caetano, C.A. 114841
 Caffisch, R. + 111594
 + Cahill, L.J. 116396
 Cailliau, R. + 112612
 + Caimmi, R. 116822
 Calamai, G. + 116640
 + Calarese, W. 113424
 + Calas, G. 114967
 Calder, I.D. + 114012
 Caldwell, D.R. 116142
 Caldwell, J. + 112894
 Calef, D.F. 111599
 + Calef, D.F. 115761
 + Cales, B. 114216
 + Callebaut, D.K. 113418
 Calleja, F.J. Balta
 see Balta Calleja, F.J.
 + Callender, R.H. 115744
 Caloi, V. + 116655
 Calonnec, D.Lc
 see Le Calonnec, D.
 Calucci, G. 111942
 + Calvetti, M. 112031
 Calvo, M.L. + 113088
 Calzetta, E. + 116907
 + Cambier, F. 113755
 Cambon, L.D. + 114860
 Cameron, T.B. + 115314
 + Caminati, W. 112717
 + Camlibel, I. 115114
 + Campagna, P. 115503
 + Campbell, E.J. 112764
 + Campbell, E.J. 112765
 + Campbell, E.M. 113635
 Campbell, J.C. + 113090
 + Campbell, J.W. 116484
 Campbell, P.M. + 114480
 Campbell, S.A. + 114650
 + Campisano, S.U. 114004
 Campo, J. Gomez del
 see Gomez del Campo, J.
 + Campredon, R. 116054
 + Camy-Peyret, C. 116521
 + Canaday, J.D. 115384
 + Canal, R. 116648
 Candy, B.N. + 116730
 Cane, M.A. + 116140
 + Cane, M.A. 116103
 + Cannon, R.D. 116854
 + Cannon, R.M., Jr. 115126
 + Canter, K.F. 114954
 Cantile, J. 111803
 + Capaccioli, M. 116859
 + Capannini, E. 116339
 + Capell, M. 112566
 + Capella, L. 115182
 + Capezuto, P. 115108
 + Capitelli, M. 113686
 + Caplan, P.J. 114612
 + Caplar, R. 112277
 Capper, P. + 113778
 Capsoni, C. + 116167
 Caputo, M. 116034
 Caputo, M. + 116025
 Caraveo, P.A. + 116883
 Carballo, F.J. + 111359
 + Card, H.C. 115659
 + Carey, C.O.B. 115678
 Carey, P.R. + 115985
 + Carfagna, C. 115395
 Carignani, G. + 115250
 + Carithers, W. 112542
 Carla, M. + 114303
 Carlfors, J. + 114224
 + Carlson, C.D. 114637
 + Carlson, F.M. 113780
 + Carlson, J.B. 112066
 Carlson, K.D. + 114873
 + Carlson, R.R. 112253
 Carlson, R.W. + 112360
 + Carlson, R.W. 116085
 + Carlsson, J.-O. 114408
 Carlsson, R. 116200
 Carlsson, T. + 113737
 Carnall, W.T. + 114496
 + Carne, A. 111808
 + Carneiro, K. 114637
 + Carneseccchi, G. 112016
 + Carney, J.N. 112020
 + Caro, P. 114497
 + Caro, P. 114908
 + Caro, P. 114909
 Caroff, L.J. + 116452
 Carolan, P.G. + 113689
 + Carpenter, B. 112612
 + Carpenter, D.L. 116358
 Carpenter, J.M. + 112525
 Carpenter, R.W. + 114195
 Carpenter G.J.C. + 114042
 + Carrazza, J. 112819
 + Carreras, B.A. 113578
 Carrico, E.E. 111643
 + Carrington, M.E. 114749
 + Carroll, H.F. 115534
 Carstensen, E.L. + 113238
 + Carter, A.A. 112024
 + Carter, A.A. 112549
 Carter, C.B. + 113923
 Carter, J. + 112273
 + Carter, J.R. 112024
 + Carter, J.R. 112549
 + Cartier, L.R.S. 115985
 + Cartwright, S.L. 112015
 Carvalho, H.F. De
 see De Carvalho, H.F.
 Carvalho, M.M.G. de
 see de Carvalho, M.M.G.
 Casartelli, M. 111559
 Casas, M. + 116415
 + Case, D.A. 112653
 + Case, S.K. 112960
 + Case, S.K. 112956
 Casetta, B. + 116288
 Cashin, W.F. + 116486
 + Cass, T.R. 114016
 Cassidy, J.P. 115500
 + Casson, A.L. 112562
 + Casson, W. 112562
 Castagna, M. + 115358
 Castagnino, M. + 116465
 + Castagnino, M. 116907
 Castagnolo, M. + 114183
 + Castelhan, A.L. 115574
 + Castellani, V. 116655
 + Castellano, M. 112595
 Castelli, F. 116700
 Casten, R.F. + 112100
 Castillo, R.A. + 116176
 + Castro, E.A. 112706
 + Caswell, J.L. 116803
 Catala, C. 116665
 Catalano, S. 116657
 + Cathles, L.M. 112356
 + Cattiaux, G. 115456
 + Catz, P. 112031
 + Caudano, R. 115581
 Cauvin, R. + 114283
 + Cauvin, R. 113995
 + Cavagnat, D. 112735
 Cavallier, C. + 113655
 + Cavaliere, A. 116838
 + Cavallo, J. 113665
 + Cavanaugh, D.B. 112983
 Cavenett, B.C. + 114756
 Cazzanelli, E. + 114848
 + Cazzoli, G. 112727
 Cea, P. + 111975
 + Cecchet, G. 112020
 + Cecchi, G. 116282
 + Cecil, P. 112024
 + Cecil, P.C. 112549
 + Cecil, R.A. 112562
 Celenza, L.S. + 112141
 Celmaster, W. + 111872
 + Celnik, W. 116792
 Celnik, W.E. 116794
 + Cennini, P. 112031
 + Centro, S. 112031
 Cepelcha, Z. + 116551
 + Ceradini, F. 112031
 Cernia, E. + 112889
 + Cerny, J. 112449
 Cerri, C. + 112551
 Cerruti-sola, M. + 116804
 Cesar, C.L. + 114292
 + Cesarsky, C.J. 116413
 + Cevenini, F. 112595
 + Cevolani, G. 116322
 + Cha, D. 112073
 Chachaty, C. + 112754
 Chackerian, C., Jr. 116460
 + Chad, R.D. 113937
 + Chad, S. + 111936
 Chadwick, D. + 114342
 + Chadwick, G.B. 111992
 Chahine, R. + 111705
 Chai, H. + 113375
 + Chaikovskii, B.S. 115244
 + Chain, E.E. 114949
 Chajlani, R.K. + 116441
 Chakarvarti, S.K. + 112565
 + Chakhovskii, V.M. 116133
 Chakrabarti, J. 111950
 Chakrabarty, D.R. + 112063
 Chakrabarty, K. + 113823
 + Chakraborty, B. 114336
 Chakraborty, K.G. 114658
 + Chakravarty, N. 112877
 Chakravarty, S. + 116248
 + Chakravorty, S.J. 111322
 Chalmers, J.S. 112086
 Chalyi, V.P. + 114921
 + Chalyi, V.P. 112996
 Chambers, F.W. + 113486
 Chambers, S.A. + 114979
 Chambless, D.A. + 112610
 + Chambon, P. 116523
 Chambrier, A. De
 see De Chambrier, A.
 Chan, A.K.F. + 113562
 + Chan, I. 114195
 Chan, K. + 115714
 Chan Eu Byung
 see Byung Chan Eu
 Chandna, O.P. + 113451
 + Chandra, S. 113798
 + Chandrasekhar, J. 112645
 + Chandrasekhar, P.
 114534
 Chanfray, G. + 112151
 Chang, C.Y. + 115064
 + Chang, C.Y. 112015
 Chang, E.S. 112676
 Chang, J. + 113657
 + Chang, R.K. 115564
 Chang, S.C. + 115113
 Chang, S.L. + 114219
 + Chang, S.T. 114612
 + Chang, T. 116391
 Chang, Y.F. + 111422
 Chang, Y.K. 115049
 + Chang Al-Zhen. 113054
 Chang Chia-Nan
 see Chia-Nan Chang
 Chang Hua. see Hua Chang
 Chang Hui-Chi
 see Jon-Chi Chang
 Chang Li. see Li Chang
 Chang On-Kok
 see On-Kok Chang
 Chang Qianshun. 111498
 Chang Shaw Jiin
 see Jiin Chang Shaw
 Chang Yia-Chung
 see Yia-Chung Chang

- Chang-guo Lu 112469
 see Lu Chang-guo
 + Chang-Sing Hwang 112469
 + Chanmugam, G. 116740
 Channabasappa, M.N. + 113506
 Chantre, A. + 114483
 + Chantre, A. 114030
 + Chao, Y.J. 111636
 Chao Kuang-Tn 112004
 Chao-Zhi Qin 114587
 see Qin Chao-Zhi
 + Chaple, G. 116685
 Chapman, D.M.F. + 113183
 Chapman, L.R. 115166
 + Chapman, R.L. 115050
 Chapoy, L.L. + 112782
 + Chapuran, T. 112035
 Chapurskii, L.I. 116272
 Charap, J.M. + 111516
 + Charbonneau, G.P. 114861
 Charbonnier, J.C. + 115426
 + Charity, R.J. 112244
 + Charkin, O.P. 112640
 + Charlou, J.L. 116074
 + Charlson, E.J. 115631
 + Charlson, E.M. 115631
 + Charlson, R.J. 116261
 Charrreire, Y. + 114907
 Chary, A.N. + 115562
 Chasman, R.R. 112056
 + Chason, M.K. 113880
 Chatelet, M. + 112816
 + Chatham, H. 115103
 Chatterjee, A. + 112166
 Chatterjee, A.K. + 114774
 Chatterjee, E. + 113702
 + Chatterjee, M. 112286
 Chatterjee, P. + 114632
 + Chatterjee, S. 114632
 + Chatterjee, S.D. 114774
 Chattopadhyay, A. + 113339
 + Chattopadhyay, A. 115966
 + Chaudhari, P. 112578
 + Chaudhary, R.S. 115420
 Chaudhuri, M.M. 115272
 Chaudhuri, S. + 114467
 + Chauhan, H.S. 113798
 + Chauhan, P.K. 115422
 + Chausssat, C. 114414
 Chavel, P. 112947
 + Chavez, E. 112259
 + Chayanov, B.A. 114791
 + Chayanov, B.A. 112868
 + Chayanov, B.A. 113847
 Cheah, S.C. + 116284
 + Cheban, A.G. 115638
 + Chebotarev, A.M. 115545
 + Chebotarev, E.E. 115923
 Chee-seng Lim 115660
 + Cheek, G. 115660
 Chekhlov, A.N. 113699
 Chekhlov, A.N. + 113834
 + Chelnokov, B.I. 113348
 + Chelnokov, V.A. 113926
 + Chemine, J.L. 116074
 + Chen, C.R. 112538
 Chen, H.T. + 112087
 + Chen, H.T. 112097
 Chen, I.-W. 114181
 Chen, L.-H. + 114859
 Chen, L.-H. + 112741
 + Chen, M. 112566
 Chen, T.-P. + 114954
 + Chen, T.T. 114838
 + Chen, T.T. 115564
 + Chen, W.S. 115635
 + Chen, Y.S. 112045
 Chen Ching-Shang 115311
 see Ching-Shang Chen
 Chen Chuan-Yao + 113276
 Chen Guodong 113276
 Chen Hsuan 115736
 see Hsuan Chen
 Chen Jiunn Chuu 112581
 see Jiunn Chuu Chen
 + Chen Le-jun 116000
 + Chen Le-Shou 116000
 Chen Lien-Wen 114594
 see Lien-Wen Chen
 Chen Ming-Sheng + 116000
 + Chen Ning Yang 112019
 + Chen Xian-neng 112581
 Chen Yingting + 11538
 Chen Yu-Jiuan 114485
 see Yu-Jiuan Chen
 + Chen-Hsi Lin. 114485
 + Cheney, R.E. 116144
 + Cheng, C.Z. 113643
 Cheng, L.J. + 114279
 + Cheng, L.J. 114482
 Cheng, R.K. + 113425
 + Cheng, Y.S. 112955
 Cheng Yung-Sung 115931
 see Yung-Sung Cheng
 + Chenite, A. 115031
 + Chenot, J.L. 113316
 + Chensky, E.V. 114432
 + Cheremukhina, Z.P. 116503
 + Cherenkov, P.A. 113004
 Cherin, A.H. + 113117
 Chern, R.T. + 114335
 + Chernika, I.M. 113263
 + Chernin, K.E. 116346
 + Chernogor, L.F. 116373
 + Chernopiskii, D.I. 113283
 + Chernov, A.S. 114587
 + Chernov, I.A. 111451
 Chernov, S.P. + 113042
 Chernova, N.I. + 114231
 Chernyak, V.Ya. 114455
 + Chernyakov, A.L. 114305
 + Chernykh, V.A. 113097
 Cheron, J. + 115680
 + Chertkov, I.L. 115852
 + Chesnokov, S.M. 112513
 Chesnoy, J. 112821
 + Cheung, L.M. 112704
 + Cheung, N.W. 113944
 + Chevskaya, O.N. 115349
 + Chew, N.G. 114133
 + Chi, C.C. 112578
 + Chia, T.-L. 115821
 Chia-Nan Chang + 114098
 Chia-Nan Chang + 114100
 + Chia-Nan Chang 114099
 Chiang, H.C. + 112092
 + Chiang, S.W. 114019
 + Chiang, T.-C. 115017
 Chiang Chun 115261
 see Chun Chiang
 Chiang Chwan-hwa 112609
 see Chwan-hwa Chiang
 + Chiba, K. 112609
 + Chiba, Y. 112484
 + Chibiskova, N.T. 115120
 + Chien, S. 115816
 + Chien, S. 115768
 Chien Lai-Chen 113805
 see Lai-Chen Chien
 + Chihara, K. 113805
 + Chik, P. 115368
 + Chikawa, J. 113905
 + Chin, A.K. 115114
 Chin, B.H. + 115114
 Chin, D.-T. + 115411
 + Chin, D.-T. 115625
 Chin, L.-Y. + 113780
 + Chin, R.C.Y. 116081
 + Chin, T.S. 112648
 + Ching-Shang Chen 113450
 + Chinowsky, W. 112011
 Chiotis, A. + 115602
 + Chirita, S. 115721
 + Chirita, S. 115722
 + Chirkin, N.M. 111824
 + Chirkina, L.A. 115209
 + Chirko, L.I. 115188
 + Chirkov, L.E. 114089
 + Chirva, V.P. 115640
 Chisholm, I. 111797
 + Chistyakov, I.G. 113439
 + Chistyakov, R.R. 113654
 + Chistyakov, N.I. 114761
 + Chivers, R.C. 113230
 Chizhik, S.P. + 114116
 + Chizhikova, Z.A. 112783
 + Chludzinski, J.J. 114427
 + Cho, A.Y. 114588
 Cho Hyun-Kee 115721
 see Hyun-Kee Cho
 + Chollet, F. 116562
 + Chollet, J.-C. 112022
 Chon-Trung Hua 114761
 see Hua Chon-Trung
 + Chong, K.P. 111413
 Chong-sheng Li 114973
 see Li Chong-sheng
 Chopra, D. + 114973
 + Chou, C.-K. 115772
 Chou, K.-C. + 115736
 + Chou, L.T. 114758
 Chou, T.S. + 112019
 + Chou, Y.C. 114838
 + Chou, Y.C. 114839
 + Choudhury, A.N.M.M. 114594
 Choudhury, J.K. + 115966
 + Choukroune, P. 116074
 + Chowdhry, U. 115126
 + Chowdhury, P. 112058
 Choy, C.L. + 114214
 + Christiansen, J.J. 112726
 Christiansen, P.A. 112665
 + Christiansen, P.J. 113605
 + Christie, W.H. 114011
 + Christie, W.H. 114010
 + Christin, F. 115091
 Christov, C.V. + 112134
 Chrusciewski, W. + 115931
 Chrysochoos, J. 114905
 + Chrysochoos, J. 112778
 + Chrysochoos, J. 112779
 Chtaib, M. + 115581
 Chu, H.S. + 112890
 + Chu, S.-G. 113719
 Chu, Y.Y. + 112129
 Chu Guo 113448
 see Guo Chu
 Chu Yuenrei 113448
 Chuan-Yao Chen 112537
 see Chen Chuan-Yao
 Chuang I-Ssuer 114210
 see I-Ssuer Chuang
 Chubinidze, T.A. + 115087
 + Chuchmarev, S.K. 112537
 + Chudakov, V.A. 114921
 + Chudinov, A.V. 114669
 + Chudinova, N.N. 115523
 + Chudinova, N.N. 115524
 + Chudinova, N.N. 115120
 Chuen-hua Jiang 115686
 see Jiang Chuen-hua
 + Chugunov, V.V. 116524
 Chugunov, I.G. 114124
 Chui, S.T. 114458
 Chuiko, G.P. 113786
 + Chukichev, M.V. 115101
 + Chun, J.S. 114419
 + Chun, J.S. 115094
 + Chun, J.S. 114385
 Chun Chiang 114572
 Chung, D.Y. 115799
 Chung, S.H. + 115552
 + Chung, S.U. 112024
 + Chung, S.-U. 112549
 + Chung, S.Y. 112561
 + Chung, Y.H. 112058
 + Chuntunov, K.A. 114678
 + Chuong, C.J. 112377
 Chupp, E.L. 116590
 + Chupp, E.L. 116827
 + Chupp, E.L. 116878
 + Chupp, E.L. 116565
 + Churbakova, T. 115218
 Church, D.A. 112844
 Chutov, Yu.I. + 113684
 Chuu Chen Jiunn 112031
 see Jiunn Chuu Chen
 + Chwan-hwa Chiang 115295
 + Chwastowski, J. 112028
 Chyba, T.H. 111361
 + Chyi, J.J. 114395
 + Chyi-Jang Shiau 113487
 Ciaccio, A. Di 114155
 see Di Ciaccio, A.
 + Ciach, R. 113676
 Ciccon, G. 115461
 Ciftan, M. + 113540
 Cignolo, C. + 112804
 + Cimraglia, R. 115016
 + Cinti, R.C. 116168
 + Ciotti, P. 115322
 + Ciprus, V. 116339
 + Ciriola, L. 112506
 Citron, M.C. + 115788
 + Cittolin, S. 112031
 Civitarese, O. + 112104
 + Cizeron, G. 114762
 + Cizmecioglu, M. 115288
 Claassen, W.A.P. + 114413
 Claes, J. + 113976
 + Claesson, G. 112162
 Claesson, S. + 114236
 + Claeys, C. 111659
 Clair, G. 116508
 see le Clair, G.
 Clancy, R.T. + 112022
 Clark, B.C. + 112203
 Clark, G.B. 116198
 Clark, J.T.K. + 115449
 + Clark, M.K. 116479
 Clark, N.J. + 114151
 + Clark, R.B. 111341
 Clark, R.R. 116329
 + Clark, R.R. 115531
 Clark, T. 112649
 Clark, T. + 112645
 + Clarke, D. 111990
 + Clarke, D. 112012
 Clary, D.C. + 112818
 + Clausen, K. 112188
 + Clausnitzer, G. 114250
 + Clausnitzer, G. 112187
 + Clauwaert, J. 115747
 Claverie, P. 112619
 + Clayton, C.R. 115413
 + Clear, J. 116416
 + Clearwater, S.H. 111992
 Cleary, J.G. + 112380
 + Cleaver, J.W. 116284
 Clechet, P. + 113949
 + Cleine, B.R. 115968
 + Cleland, J.W. 114011
 + Cleland, W.E. 112024
 Clement, H. 112067
 Clementi, E. + 112808
 + Clements, W.E. 116170
 + Clendenin, J.E. 112471
 + Clerc, H.-G. 112133
 Cleveland, B.T. 112601
 Cleymans, J. + 111943
 Cliff, K.D. + 115941
 + Cliff, K.D. 112608
 Clifton, J.A.G. 111792
 + Cline, D. 112031
 + Cline, H.E. 113942
 + Cline, J.G. 113429
 + Cline, T.L. 116836
 + Close, F.E. 111971
 + Close, F.E. 112009
 Close, L.G., Jr. + 114750
 Cloth, P. + 112492
 + Clout, G. 115602
 + Clough, P.N. 112419
 Clovis, L.F. + 116096
 Clyne, M.A.A. + 115520
 + Coachman, L.K. 116141
 + Coates, D.W. 116675
 + Coates, D.W. 116673
 + Coates, D.W. 116681
 Cobb, W.R. + 112307
 Cobianu, C. + 115067
 + Cobler, R. 116073
 + Cochet, C. 112031
 + Cochran, D.R.F. 112007
 + Cockayne, B. 114492
 + Cockerill, D. 112024
 + Cockerill, D.J.A. 112549
 + Cody, G.D. 114817
 + Coe, R.S. 116062
 + Coe, R.S. 116001
 + Coffey, J.M. 115455
 + Coghlan, W.A. 113994
 Cognola, G. + 111467
 Cohen, B.L. 115864
 Cohen, D.S. + 114238
 Cohen, J. 114577
 Cohen, J. + 112177
 + Cohen, J.K. 116308
 + Cohen, R.M. 115069
 + Cohen, S.L. 115008
 Cohn, D. + 115292
 + Cohn, S.H. 115905
 + Cohn, S.H. 112517
 + Colas, J. 112031
 + Colas, P. 112016
 Colbourn, E.A. + 113862
 + Colditz, R. 112697
 Coldren, L.A. + 115387
 + Coldren, L.A. 115381
 Cole, J.D. 113182
 + Cole, J.H. 113125
 + Cole, R.S. 116208
 Coleman, J.W. + 113632
 Coleman, M.M. + 113771
 Colgate, S.A. 116831
 Colgate, S.A. + 116882
 + Collier, R. 115791
 + Collinson, C.D. 111509
 Collis, C.H. + 115859
 Collocott, S.J. 111681
 + Colman, E.J. 116115
 Colombant, D.G. + 113625
 + Colombant, D.G. 113580
 + Colombar, C. 114420
 + Colombar, C. 114421
 + Colombar, C. 114428
 + Colombo, L. 112164
 + Colvin, G. 112124
 + Combes, M. 115089
 + Comfort, J.R. 112196
 Common, A.K. 111991
 + Compaan, A. 114837
 + Compton, W. 116044
 + Compton, D.A.C. 112738
 Comsa, G. + 111491
 + Conde, A. 113743
 + Conde, C.F. 113743
 Connell, A.J. + 116510
 + Connell, G.A.N. 112948
 Connerade, J.P. 112677
 + Connor, W.M. 112387
 + Conover, D.L. 115833
 Conradi, M.S. 114752
 + Console, R. 116025
 Constant, G. + 115077
 + Constant, G. 115068
 + Constant, G. 115089
 + Conta, C. 112022
 Contopoulos, G. 111420
 + Conway, L. 115357
 + Cook, R.D. 111434
 + Cooke, M.J. 115079
 + Coombes, R.W. 111992
 + Coon, D.D. 114467
 Cooney, R.P. + 114856
 + Cooper, G.S. 113039
 + Cooper, M.J. 111831
 + Copeland, J.A. 113090
 Copenhaver, C. 113579
 Coppa, G. + 113099
 Coppa, G. + 113114
 Coppa, G. + 113106
 Coppa, G. + 112296
 + Coppalle, A. 113559
 Corbel, C. + 113879
 + Corbelli, G. 112717
 + Corbett, J.W. 114190
 + Corbett, J.W. (ed.) 111315
 Corboy, J.F. + 115071
 + Corboy, J.F. 115070
 + Corden, M. 112031
 Cordery, R. + 111886
 Cordes, J.M. 116717
 + Cordes, J.M. 116726
 + Cordier, A. 112016
 + Cords, D. 111990
 + Cords, D. 112012
 Corey, G.C. + 112814
 + Cormack, W.A. 116484
 Corn, R.M. + 114849
 + Cornilleau-Wehrin, N. 116395
 + Cornish, B. 113988
 + Coronado, E. 114699
 + Corrick, G. 116409
 Corrievau, F. + 111999
 + Corte-Real, J.A.M. 116212
 + Corvisiero, P. 112198
 Cossairt, J.D. 115927
 Cossart-Magos, C. 112674
 Costa, A.A. da 116838
 + Costa, E. 112020
 + Costa, G. 112020
 + Costa, P.R.R. 112871
 Costalupes, J.A. 115802
 Costello, J. + 113226
 + Cottenden, A.M. 115508
 Cotts, D.B. 114804
 Coufal, H. + 115380
 Couillet, P.H. + 115193
 Cousins, J.M. + 113554
 Cousteix, J. + 113430
 Coutau, P. 116493
 Coutinho, F.A.B. + 111489
 Couture, P. + 113646
 + Coveney, E.A. 115658
 + Cowlam, N. 113753
 + Cowley, J.M. 114320
 Cowley, R.A. + 114792
 Cowley, R.A. + 113753
 Cowling, S.A. 116627
 + Cox, C. 115825
 + Cox, D.P. 116628
 + Cox, M.E. 116241
 + Cozzika, G. 112016
 + Crabi, G. 112317
 + Crabtree, G.W. 114650
 Craig, R.L. + 116328
 + Craighead, H.G. 115698
 Craik, A.D.D. 113454
 + Cram, L. 116620
 + Cramarossa, F. 115108
 + Cramarossa, F. 113686
 + Cramer, J.G. 112199
 Crandall, D.H. 112855
 Crandall, G.J. + 116043
 Crane, L.J. 113414
 + Crane, P.C. 116841
 Crary, D.J. + 116327
 Crasemann, J.H. + 114738
 + Craven, J.D. 116326
 Crawford, F.S. 111348
 Crawley, G.M. + 112158
 + Creelley, G.M. 112200
 + Creelley, G.M. 114983
 Cremers, T.L. + 113814
 Cremers, T.L. + 113813
 + Creutz, M. 111866
 Crew, G.B. + 113598
 Crewe, A.V. 111827
 Cribrier, S. + 113045
 + Criegee, L. 112015
 + Crippen, G.M. 115735
 + Crist, H. 116479
 Crivelli Visconti 113291
 + Crocker, M.J. 113194
 Cromer, D.T. + 113809
 + Cromer, D.T. 113800
 Cross, J.B. + 112769
 + Cross, J.W. 114885
 + Cross, J.W. 114886
 + Cross, R.L. 116199
 + Crosswhite, H. 114496
 Crough, S.T. 116042
 Crovisier, J. + 116533
 + Crowe, C.R. 115385
 Crowley-Milling, M.C. 112523
 + Crozaz, G. 116553
 Crump, J.C. + 115585
 Crutcher, R.M. + 116785
 Crutchfield, J.P. + 111575
 Cruz, C.R. de la 113087
 see de la Cruz, C.R.
 Cruz, F. de la 112274
 see de la Cruz, F.
 + Csernai, L.P. 112263
 + Csernai, L.P. 112014
 Csikor, F. + 113087
 Cui Xiang-zong 112581
 Cullen, G.W. + 115070

- +Cullen, G.W. 114940
 Cullis, A.G. 113709
 +Cullis, A.G. 114133
 Cumbera, F.L. + 113743
 Cunha Belo, M.Da
 + see Da Cunha Belo, M.
 +Cunningham, P.T. 115711
 Cunsolo, A. + 112148
 Cuomo, J.J. + 112512
 +Cuomo, J.J. 115104
 Cuperman, S. + 116147
 Curelaru, I.M. + 115012
 Curro, J.J. + 113767
 +Curtin, M.S. 112127
 Curtis, G.J. + 115454
 Cuta, J.M. + 112313
 +Cuta, J.M. 112312
 +Cutler, R.I. 112480
 Cuvellier, J. + 112812
 +Cybulska, E.W. 112247
 Cycon, H.L. 111493
 +Cyshi, O. 112229
 +Cyr, T.E. 115390
 +Cyvin, B.N. 112695
 Cyvin, S.J. + 112695
 +Czabalay, L. 113239
 +Czako-Nagy, I. 114765
 Czarnecki, P. + 111704
 Czyzyk, M.T. + 114435
- da Costa, A.A. 116729
 +Da Cunha Belo, M. 113890
 +Da Hsuan Feng 112096
 Da-Xing Gao.
 + see Gao Da-Xing
 +Dabizha, E.V. 115284
 +Dabrowiak, J.C. 115749
 +Dacal, A. 112267
 +Dadashev, I.Sh. 114126
 Dadashyan, K.Yu. + 111905
 Dae Lee Kee.
 + see Kee Dae Lee
 Dae Soo Kim 113261
 Daeron, P.Y.Le
 + see Le Daeron, P.Y.
 +Dagan, S. 112024
 Dagg, I.R. + 112790
 +D'Agostini, G. 112016
 +d'Agostino, R. 113686
 +Dahari, O. 116844
 +Dahl, I. 113737
 +Dahl-Jensen, E. 112024
 +Dahl-Jensen, I. 112024
 +Dahlen, M. 115224
 Dahme, M. 115838
 +Daily, J.W. 115550
 Daimon, H. + 112852
 +Dainton, J.B. 112015
 Dairanieh, I.S. + 115184
 +Daiser, S. 114356
 Daisey, J.M. + 115712
 +Daisey, J.M. 115709
 Dakin, J.P. 113104
 Dakshinamurthy, P. +
 113500
 +Daley, H.M. 112586
 +Dallman, D. 112031
 +Dally, J.W. 113352
 Dalton, B.J. 112626
 +Daly, L. 116312
 +Daly, P.J. 112036
 +Daly, P.J. 112058
 Dam, J.W.Van
 + see Van Dam, J.W.
 +Dam, P. 112024
 +Damask, A.C. 114525
 Dame, L. + 116620
 +Damerell, C.J.S. 112540
 +Damgaard, G. 112024
 Damiani, D. + 112717
 Damon, P.E. 116068
 Damour, T. 116731
 Danby, G. 112638
 Danby, G. + 112639
 +Dandekar, D.P. 114203
 +Danese, L. 116889
 +Danesh, P. 114318
 +Dang Van, K. 115329
 Dang Vinh Luu
 + see Luu Dang Vinh
 +Dange, S.P. 112287
 Daniel, M. + 111938
 +Daniel, M. 111936
 Danielsen, P. + 113100
 +Danil'chenko, V.P. 111758
 Danilenko, V.A. + 113478
 +Danilov, A.V. 111716
 Danno, T. + 114334
 Daoust, H. + 114202
 +Darack, F. 115709
 Daras-Papamargaritis, H. +
 116559
- +Darbin, S.D. 113064
 +Dargeiko, M.M. 113640
 +Darrulat, P. 112022
 +Das, B.K. 115145
 Das, G. 114251
 +Das, N.P. 115965
 Das, P.K. + 113836
 Das, T.K. + 116567
 +Das Gupta, M.K. 116567
 +Das Gupta, M.K. 116206
 Dashuk, P.N. + 114423
 +Dass, S.C. 114011
 Dassiog, G. + 111464
 +Datlowe, D.W. 116359
 Datta, S. + 112838
 Datta, S.K. + 115233
 +Datta, S.K. 113162
 Datta, T. + 112287
 Datzoff, A.B. 111465
 +Dau, D. 112031
 Daubechies, I. 111546
 Daubechies, I. + 111474
 Daudel, R. 112620
 Daugherty, J.K. + 116453
 +Daugherty, J.K. 116725
 +Daum, H.J. 112015
 D'Auria, G. + 116280
 +D'Auria, G. 116168
 Dautcourt, G. 116895
 +Dautet, H. 112286
 David, M. 111459
 Davids, C.N. + 112126
 +Davids, C.N. 112071
 Davidson, D.L. + 115320
 +Davidson, E.R. 115540
 +Davidson, E.R. 112792
 Davidyuk, G.E. + 114564
 +Davier, M. 112016
 +Davies, E.J. 114707
 Davies, G. + 113235
 Davies, H.C. 116193
 +Davies, R. 112169
 Davis, G.E. + 115653
 +Davis, J.H. 116797
 +Davis, J.M. 116600
 +Davis, L.E. 116841
 +Davis, M.H. 115771
 +Davis, R.L. 111854
 Davis, S.A. 114878
 +Davis, W. 111860
 +Davison, W. 115033
 Davydenko, V.I. + 111816
 Davydov, B.I. + 115950
 Davydov, V.A. 112933
 Davydov, V.N. + 114619
 Davydov, V.S. 113335
 +Dawson, B. 113734
 +Dawson, W.K. 112288
 +Day, C. 112542
 +Dayras, R.A. 112254
 +Dazord, J. 113070
 +De, R.K. 113339
 de Almeida, A.M.Ozorio. see
 Ozorio de Almeida, A.M.
 +De Amici, G. 116889
 de Azcarra, J.A. + 111896
 De Benedictis, S. + 113686
 +de Bergh, C. 116439
 de Boer, K.S. 116786
 de Boer, R. + 113311
 +de Boer, W. 112016
 +De Carvalho, H.F. 111985
 de Carvalho, M.M.G. +
 114574
 De Chambrier, A. + 113630
 de Deus, J.Dias.
 + see Dias de Deus, J.
 de Felice, F. + 116643
 +De Fouquet, C. 114071
 +de Galan, L. 115595
 De Gregorio, S. + 111449
 +de Haan, B.J. 116172
 De Hoe, J.M. + 115676
 De Iorio, I. + 115510
 +de Jager, C. 116750
 +De Jeu, W.H. 114067
 +de Jong, M.S. 112463
 +de Keijser, T.H. 114403
 De Kumar, D. 114729
 de la Cruz, C.R. 111381
 +de la Cruz, F. 114642
 +de la Vaissiere, C. 112011
 +de Lange, C.A. 112637
 +de Lange, C.A. 112763
 de Leeuw, D.M. + 114935
 de Leeuw, F.A.A.M. +
 112750
 de Leeuw, F.A.A.M. +
 112751
 +De Lima, E.P. 112689
 +de Llano, M. 114123
 de Loos-Vollebregt,
 M.T.C. + 115595
 +de Lorge, J.O. 115825
 +de los Rios, E.R. 115310
 +de Meijer, R.J. 112237
 +De Melo, M.V.M.C. 113736
- +De Meyer, F. 116303
 de Moor, H.H.C. + 115090
 +de Moor, H.H.C. 114410
 +de Oliveira, A.M. 111442
 De Palma, M. + 112008
 +de Pater, I. 116494
 De Paula, R.P. + 113125
 +de Pujo, P. 112812
 +De Renzi, R. 112535
 De Rooij, C. + 115968
 De Sabbata, V. + 116436
 De Sanctis, E. + 112510
 +De Sanctis, G. 116511
 +De Sangro, R. 111992
 +de Segovia, J.L. 114348
 +de Socio, L.M. 113544
 De Souza, P. 115907
 de Torquat, C. 112415
 +de Viron, F. 111971
 +De Visschere, P. 115661
 De Volpi, A. 112368
 De Volpi, A. 112369
 de Waal, S.A. 112321
 De Walle, C.Van.
 + see Van De Walle, C.
 de Wilton, A. + 115750
 De Yoreo, J.J. + 114294
 +De Zotti, G. 116889
 Deacon, C.G. + 113874
 +Deacon, D.A.G. 112516
 Dean, P.J. 114465
 +Dean, P.J. 114492
 +Dearborn, J.R. 114237
 Deardorff, J.W. 116108
 Dearnley, R. + 111708
 Deb, S. + 115644
 +DeBeer, M. 112031
 Debehogne, H. + 116511
 +DeBenedictis, E. 111958
 Debieire, J.-M. + 116101
 Debroux, M.-H. + 111739
 +Debuigne, J. 115165
 +Decker, H. 115642
 Decker, R.B. + 116386
 +Decker, R.W. 116055
 +Declercq, G. 116659
 Decman, D.J. + 112066
 +Decoste, R. 113576
 +Decroisette, M. 113656
 +Dedegkaev, T.T. 114550
 +Dedenkov, A.N. 115840
 Dedyk, A.I. + 114777
 +Defant, M.J. 116289
 +DeGaonkar, S.S. 116572
 Degl'Innocenti, E.Landi.
 + see Landi Degl'Innocenti,
 E.
 Degtyarev, L.S. + 112656
 +Degtyarev, S.A. 113530
 +Degtyareva, I.N. 113845
 +Deguchi, Y. 113897
 +Dehne, Ch. 112015
 +Dehnard, D. 112283
 Deicher, M. + 113871
 +Deicher, M. 114055
 +Deigraf, V.D. 114721
 +Deitrich, M. 115398
 Dekhtyar', A.S. + 113327
 del Campo, J.Gomez.
 + see Gomez del Campo, J.
 +del Rio, J. 114123
 +Delalande, C. 115061
 +Delany, A.C. 116261
 Delaroche, J.P. + 112202
 +DeLaunay, B. 112120
 Delaunay, M. + 112498
 +Delchev, I.I. 112134
 +Delfino, M.C. 111992
 +Delgado, A.J. 116748
 Delhez, R. + 114403
 +Delic, G. 112084
 +Della Monica, M. 114183
 +Della Negra, M. 112031
 Delneste, L. + 115251
 +Delorme, J. 112151
 Delph, T.J. 113313
 Delplanche, J.L. 115442
 +Delrue, J.P. 115581
 +Delyagina, N.I. 113852
 +DeMeijer, R.J. 112232
 +Demenkov, A.P. 115278
 +Demenskii, G.K. 114204
 Dement'ev, A.I. 112642
 +Dement'ev, V.M. 115977
 +DeMeo, N.L., Jr. 113094
 +Demer, L.J. 114195
 +Demidov, A.M. 112189
 Demidova, G.N. + 114618
 Demikhov, E.I. + 114821
 +Demin, Yu.L. 116160
 +Deminova, G.F. 116331
 +Demma, G. 113714
 +Demmer, D.R.M. 111771
 +Demoulin, M. 112031
 +Demus, D. 113730
 +Dem'yanets, Yu.N. 113718
 den Bergh, L.C.Van
 + see van den Bergh, L.C.
- den Brekel, C.H.J.van.
 + see van den Brekel, C.H.J.
 den Broeck, C.Van
 + see Van den Broeck, C.
 Dence, J.B. 111370
 +Denegri, D. 112031
 +Deneuille, A. 114414
 Deng Shi-tao.
 + see Shi-tao Deng
 Denis, M. 111931
 +Denisenko, O.N. 115895
 +Denisov, G.G. 112974
 +Denisov, S.P. 112551
 Denisov, V.N. + 114118
 +Denisova, L.Ya. 113746
 +Denisyuk, I.T. 113358
 +Dennis, B.R. 116592
 Dennis, R.B. + 113036
 +Dental, A.G. 113090
 Denteneer, P.J.H. + 111556
 Denus, S. + 113637
 Deopura, B.L. + 113762
 DePaolo, D.J. + 116086
 +Depauw, P. 115660
 +Depinna, S.P. 114756
 +Deprick, B. 113781
 +DePristo, A.E. 112818
 +DePristo, A.E. 115002
 +Deputatova, L.V. 113660
 Der Hoek, B.Van.
 + see Van Der Hoek, B.
 der Lans, J.van
 + see van der Lans, J.
 der Leeden, G.A.van. see van
 der Leeden, G.A.
 der Linde, D.von. see von der
 Linde, D.
 der Meer, W.van
 + see van der Meer, W.
 der Piepen, H.van.
 + see van der Piepen, H.
 der Plaats, G.van.
 + see van der Plaats, G.
 der Ree, H.van
 + see van der Ree, H.
 der Straten, P.J.M.van.
 + see van der Straten, P.J.M.
 der Voo, R.Van. see Van der
 Voo, R.
 der Voo van. see van der Voo
 der Werf, S.Y.van
 + see van der Werf, S.Y.
 Derendiaev, N.V. + 113268
 +Derikum, K. 112015
 +Derno, M. 113701
 Derviz, T.E. 116702
 +Deryagin, A.V. 114671
 +Deryugin, L.N. 113243
 Derzhavina, A.I. 113472
 Desai, C.C. + 115032
 +Desai, C.F. 115453
 +Deshpande, U.D. 112712
 +Desimone, D.M. 113923
 Desjardins, S.R. + 115008
 Desper, C.R. + 115203
 Desplat, J.-L. 115007
 +Despres, M. 112603
 +Desre, P. 115232
 Deubner, F.-L. + 116652
 Deus, J.Dias de.
 + see Dias de Deus, J.
 +Deus, K. 114982
 +Deutsch, J.M. 115761
 +Deuter, A. 112015
 Deutsch, C. 113564
 Deutz, J.W. + 111438
 +Devanarayanan, S. 116250
 +Devanathan, R. 115814
 +Devarajan, V. 114159
 +Devenish, R.C.E. 111934
 DeVolpi, A. 112391
 +Devyatkov, L.I. 113786
 +Dewald, A. 112109
 Dewendra, J.D. + 115179
 Dexpert-Ghys, J. + 112723
 +Dexpert-Ghys, J. 114907
 Dey, S. + 111452
 Dey, S.S. + 113293
 Dhaliwal, R.S. + 113377
 Dhar, A. 111882
 +Dhawan, V.K. 114779
 Dheandhanoo, S. + 116330
 Dhilly, G. + 112603
 Dhiman, N.K. + 115694
 D'Hoker, E. 111470
 D'Hooghe, M.C. + 115869
 +Di Ciccio, A. 112031
 +Di Lella, L. 112022
 +Di Liberto, S. 112559
 Di Nardo, M. + 112152
 +Di Toro, M. 112152
 +di Vita, P. 113099
 +Di Vita, P. 113106
 +Di Vita, P. 113114
 Di Yang. see Yang Di
 +Diana, E. 114024
 Dias, O.L. + 115593
 Dias de Deus, J. + 111955
 Diaz Alonso, J. 116732
- +DiBitonto, D. 112031
 +Dick, H.J.B. 116066
 Dick, R.D. 111838
 Dick, R.D. 111843
 Dickel, H.R. + 116787
 Dickens, J.K. 112110
 Dickens, J.K. 112192
 Dickinson, R.D. + 114676
 Dickson, J.I. + 115321
 Dicus, D.A. + 112010
 Dicus, D.A. + 112000
 +Didenko, A.N. 112486
 Didenkulov, I.N. 114570
 +Didkovskaya, O.S. 115148
 +Dieckmann, A. 111990
 +Dieckmann, A. 112012
 Diehl, J. + 113966
 +Diehl, J. 113878
 +Diehlmann, K. 112015
 Dien Tap Ngo. see Ngo Dien
 Tap
 +Dieperink, A.E.L. 112702
 +Dieperink, A.E.L. (ed.)
 111295
 Dierksen, G.H.F. + 112634
 +Diesburg, D.E. 115314
 +Dieterle, W.E. 112011
 +Dieters, S.W.B. 116675
 +Dietrich, G. 111990
 +Dietrich, G. 112012
 +Dietrich, M. 115080
 +Diguseppe, M.A. 115114
 +DiGregorio, D. 112254
 +Diikov, L.K. 114627
 +Dikanov, S.A. 112759
 Dikshtein, I.E. + 114186
 +D'Illario, L. 112889
 Diligenti, A. + 114621
 Dillon, H. + 115887
 +Dillon, J.B. 112011
 +Dilmanian, F.A. 112049
 +Dilmanian, F.A. 112261
 +Dilmanian, F.A. 112059
 Dimitrov, C. + 113890
 +Dimitrov, C. 114032
 Dimitrov, O. + 114032
 +Dimitrov, O. 113890
 +Dimopoulos, G.Ch. 116027
 +Dimov, G.I. 111816
 Din, A.M. + 111891
 Din, A.M.Shams El.
 + see Shams El Din, A.M.
 +Dine, M. 111913
 Dines, T.J. + 114854
 +Dines-Hansen, J. 112022
 +Ding, Y.J. 116607
 +Ding Youwen 116067
 +Dinh, Q.V. 113403
 +Dinhut, J.F. 113883
 +Dintenfass, L. 115818
 Dinur, U. + 112775
 Dionysiou, D. 112911
 Diosi, L. + 111620
 Diosi, L. + 116909
 +D'Ippolito, D.A. 113644
 +Dirk, E.H. 113561
 Dirks, R.A. 116259
 +DiSalvo, F.J. 114639
 +Dissado, L.A. 114778
 +Distler, G.I. 113935
 Ditlevsen, O. 113312
 +Ditzenberger, J.A. 114901
 +Divan, L. 116638
 +Divan, L. 116669
 Dixit, L. + 112692
 Dixon, G.S. + 114104
 +Djalali, C. 112158
 +Djamozi, M.B.A. 115991
 Djorgovski, S. 116690
 Djurle, S. 112346
 Dlouha, M. + 111855
 Dlugach, Zh.M. 116501
 Dlugach, Zh.M. + 116270
 +Dmitriev, A.P. 113485
 Dmitriev, A.V. + 114557
 +Dmitriev, M.F. 113076
 Dmowski, W. 114703
 Dmukhovskaya, I.G. +
 115334
 +Dmytrakh, I.N. 115436
 Doan, N.V. 113896
 +Doan-Kim-Son 113440
 +Dobiasch, H. 112197
 +Dobreshtin, E.B. 115485
 +Dobrikov, V.N. 112591
 Dobrovol'skii, V.I. + 115338
 Dobrovol'skii, A.R. + 116526
 +Dobrzynski, L. 112031
 Dock-Chool Lee + 113677
 +Doi, K. 113752
 +Doi, S. 112392
 +Dokuchayeva, A.V. 116349
 +Dolganov, V.K. 114821
 +Dolgov, O.V. + 114773
 +Dolidze, V.Ch. 116588
 +Dolino, G. 114215
 D'Olivera, A.B. + 111985

- + Doll, J.D. 115578
 + Doll, J.D. 114368
 + Dolya, S.N. + 112515
 + Domanski, T. 115931
 + Domarus, J.C. 112393
 + Domany, E. 114695
 + Domszy, R.C. 114852
 + Donahue, T.J. 114416
 + Donckt, E. Vander
 see Vander Donckt, E.
 + Donegan, M. 116024
 + Dong, K. + 116189
 + Dong-Ha Kim 113677
 + Dongcai Liang
 see Liang Dongcai
 + Donnelly, J.P. + 113094
 + Donnelly, T.W. 112179
 + D'Onofrio, A. 112120
 + Donskov, S.V. 112556
 + Doo Han Kim + 115183
 + Doolittle, J.H. + 116358
 + Doong Ji-Liang.. see Ji-Liang
 + Doong
 see Van Dop, H.
 + Dop, H. Van
 see Van Dop, H.
 + Dor, L. Ben... see Ben Dor, L.
 + Dorfan, J.M. 112011
 + Dorfl, G. + 112532
 + Dorman, L.M. 116031
 + Doroshenko, S.P. 115193
 + Doroshev, V.D. 114686
 + Doroshkevich, A.G. 116861
 + Dorsaz, P.-A. 112022
 + Dorschner, J. 116633
 + Dorset, D.L. + 115986
 + Dorsey, J. 111668
 + Doss, P.L. 112389
 + Dost, S. 111453
 + Doughty, M.J. 115771
 + Douglas, M.A. + 112722
 + Douglass, D.H. 111537
 + Doukas, A.G. 115744
 + Dousson, S. 112498
 + Dovgii, I.E. 115874
 + Dovlete, C. 112445
 + Dovletov, K.O. 114524
 + Dowben, P.A. + 114343
 + Dowell, J.D. 112031
 + Down, J.D. 115859
 + Downes, A.J.B. 116853
 + Downes, D. 116790
 + Downing, K.H. 114026
 + Douthwaite, J.C. + 116747
 + Doyama, M. + 113887
 + Doyama, M. 113978
 + Doyama, M. 114273
 + Doyama, M. 114768
 + Doyama, M. 114022
 + Doyama, M. 114957
 + Doyama, M. 113864
 + Doyle, J.G. 116468
 + Drabkin, G.M. 115733
 + Drachman, R.J. 116828
 + Dracoulis, G.D. 112244
 + Drager, K. 114732
 + Dragoni, M. 116064
 + Dragos, L. + 113482
 + Drahos, D. 116296
 + Drake, D.M. 112567
 + Drake, D.M. 112153
 + Drake, J.F. + 113590
 + Drake, S.A. + 116629
 + Draper, T. 111959
 + Drechsler, W. 111525
 + Dreeben, A. + 114391
 + Dreiden, G.V. + 113485
 + Dreiding, A. 112622
 + Dreiding, A.S. 112623
 + Dreissgacker, R. + 116158
 + Dreizler, H. 112716
 + Dreizler, H. 112761
 + Dreizler, H. 112715
 + Dreizler, H. 112872
 + Drela, I. + 114387
 + Dress, A. + 112622
 + Dressler, K. 112703
 + Dresvyannikov, V.I. +
 115219
 + Drevall, V.E. + 113392
 + Drewel, M. + 111782
 + Drillon, M. + 114699
 + Droeg, R.T. + 115900
 + Drouillard, R.F. 112460
 + Drowley, C.I. + 114014
 + Drowley, C.I. 114016
 + Drowly, C.I. + 114017
 + Druinskii, E.I. + 114740
 + Druk, R.V. + 114512
 + Drumheller, J.E. 114248
 + Drummond, P.D. 112930
 + Druyanov, B.A. 113320
 + Druzhinina, I.P. 115285
 + Dryden, J.S. + 114887
 + Dryer, M. 116417
 + Drykin, V.G. 114307
 + Du Plessis, J. + 114315
 + Du Wen-fu 112520
 + Du Wen-ming-Chu 112687
 + Dube, G.S. 113442
 + Dubey, K.S. 114519
 + Dubey, V. 116237
 + Dubinin, M.N. 111944
 + Dubler, E. + 113808
 + Dubois, D. 115708
 + Dubois, P. + 115682
 + Dubova, G.S. + 115591
 + Dubrovin, M.M. + 112604
 + Dubrovina, M.M. 112843
 + Dubrovskaya, G.N.
 115098
 + Dubrovskii, G.B. 114446
 + Dubuissou, R.L. 115912
 + Ducaroir, M. 115099
 + Ducassou, D. 115458
 + Duch, W. + 112766
 + Duchateau, D. + 115325
 + Duclos, J. 112007
 + Ducourtieux, J.-L. 111552
 + Ducros, Y. 112016
 + Duda, C.R. 111766
 + Dudash, N.S. 114427
 + Dudderar, T.D. + 113115
 + Dudderar, T.D. + 113385
 + Dudek, J. + 112048
 + Dudeney, J.R. 116366
 + Dudkevich, V.P. 114800
 + Dudnik, R.A. + 113190
 + Dudogon, G. 116517
 + Duerdth, I.P. 111990
 + Duerdth, I.P. 112012
 + Duff, K.J. + 113791
 + Duffy, J. 112158
 + Duffy, J. 112200
 + Duffy, M.T. + 115074
 + Dufour, R.J. 116778
 + Dufton, P.L. + 116468
 + Dugay, M. + 114434
 + Duguet, A. + 112857
 + Duhamel, E. + 112569
 + Duijveman, A. + 116579
 + Duinen, R.J. van
 see van Duinen, R.J.
 + Duke, P.J. 111849
 + Dukhnyakov, A. Yu.
 114969
 + Dulk, G.A. + 116740
 + Dullemond, C. 111967
 + Dumanis, A. 113387
 + Dumont, H. 112120
 + Dunbar, I.H. 112419
 + Dunbar, R.S. + 116514
 + Duncan, G. + 113213
 + Duncan, M.J. 111957
 + Duncan, W.D. + 112487
 + Duneman, D.C. 111721
 + Dunham, D.W. 116515
 + Dunlavy, D. 114608
 + Dunn, F. 115831
 + Dunn, M.R. 111751
 + Dunn, P.F. 115558
 + Dunning, F.B. 112988
 + Dunning-Davies, J. 111618
 + Dunphy, P.P. + 116827
 + Duorah, H.L. 116248
 + Dupre, J. 112724
 + Dupree, T.H. 113611
 + Dupree, T.H. 113610
 + Dupuis, J. 114753
 + Dupuis, R.D. + 113013
 + Duque, C. 116165
 + Duquesnoy, A.J. 113219
 + Durachenko, A.M. 114148
 + Durand, M. 112242
 + Durand, J. 115680
 + Durand, J. 115679
 + Duren, R. 112842
 + Duric, N. + 116841
 + Durkee, G.C. 112428
 + Durney, C.H. 115829
 + Durr, J. 114967
 + Durrett, J. + 115792
 + Durshimbetov, K. + 114554
 + Dursunov, N.Ch. 115687
 + Duruissea, J.P. + 111514
 + Dustmann, C.H. 115080
 + Duteil, P. 112556
 + Dutkiewicz, V.A. + 116174
 + Dutt, B.V. 114927
 + Dutta, H.N. 116206
 + Dutta Roy, S.K. 114205
 + Dutton, R.W. 114255
 + Duvall, W.M. 116678
 + Duvaux, Y. 112338
 + Duyar, A. + 113498
 + Dvoyashkin, N.K. 113758
 + Dvoyashkin, N.K. 114221
 + Dvurechenskii, A.V. +
 113958
 + Dwarakadasa, E.S. 115419
 + D'yachkova, G.V. 115952
 + Dyakin, V.V. + 114716
 + Dyban', Yu.P. 114216
 + Dybdal, K. + 112035
 + Dyer, M.J. 112700
 + Dyke, M. Van... see Van Dyke,
 M.
 + Dyl'ko, P.N. 115743
 + Dyllong, U. 116896
 + Dymond, J. + 116073
 + Dyukova, T.V. 115753
 + Dzhamanov, S. 113866
 + Dzubay, T.G. 116269
 + Dzubenko, N.I. + 116368
 + Eales, A.T. 112342
 + Eales, S.A. 116853
 + Eargle, J. 113200
 + Earle, E.D. 112507
 + Early, T.A. 114741
 + Eary, L.E. + 112356
 + Easa, S.I. + 112810
 + Easterday, H.T. 114042
 + Eastman, K. 115189
 + Eaton, G.H. + 111808
 + Eaton, H.C. + 115201
 + Eaton, M.W. 112011
 + Eaton, N. + 116512
 + Eave, S. 113443
 + Ebberink, J. + 115403
 + Eberhard, V. + 115666
 + Eberhardt, K.R. 115601
 + Eberle, E. 111482
 + Ebert, E. 113939
 + Ebetino, F.H. 115535
 + Ebner, C. 114350
 + Eby, R.E. 114011
 + Ecer, G.M. + 115370
 + Eckardt, V. + 112541
 + Eckelmann, H. 113427
 + Ecker, A. + 114147
 + Eckerle, K.L. + 111781
 + Ecklund, S.D. 112471
 + Economy, J. 113734
 + Eddy, J.A. 116568
 + Eden, J.G. 112982
 + Edmond, J.M. 116148
 + Edmonds, D.V. 115324
 + Edwards, A. 111834
 + Edwards, A.C. 116469
 + Edwards, C.M. 111720
 + Edwards, M.J. 115860
 + Edwards, P.L. + 113185
 + Edweeb, M.E. + 115631
 + Efimenko, S.P. 115274
 + Efros, A.L. 114450
 + Efthimion, P.C. 113003
 + Eftink, M. 115746
 + Egawa, C. + 114355
 + Egelstaff, P.A. 113721
 + Egely, G. 112424
 + Egely, G. + 113497
 + Eggen, O.J. 116649
 + Egger, J. + 116213
 + Egger, J. 111999
 + Eggert, K. 112031
 + Eggert, W. + 115665
 + Egizano, L. + 115378
 + Egorov, E.A. 114526
 + Egorov, Yu.P. 112714
 + Egorov, Yu.P. 112753
 + Ehhlalt, D.H. + 116266
 + Ehle, R. 114480
 + Ehrhart, P. + 113920
 + Ehrhart, P. 114051
 + Ehrhart, P. 113886
 + Ehringer, H. (ed.) 111313
 + Ehrlich, P. 114528
 + Eichler, R. 111990
 + Eickhoff, W. + 113030
 + Eidelman, S. 112024
 + Eigermann, W. + 115040
 + Eijk, B. Van... see Van Eijk, B.
 + Eilam, G. 112013
 + Eilek, J.A. 116452
 + Eilek, J.A. 116737
 + Eilho, F.C. Medeiros
 see Medeiros Eilho, F.C.
 + Einspinner, M. 115870
 + Eisele, H. + 113015
 + Eisenberg, J.M. 112177
 + Eisenberg, J.M. 112284
 + Eisenhandler, E. 112031
 + Eisler, P. + 112530
 + Eissa, M. 113374
 + Ejiri, H. 112218
 + Ekberg, J.O. 116844
 + Ekers, R.D. 116840
 + Ekimov, A.E. 113190
 + Ekmanis, Yu.A. 114891
 + El Din, A.M. Shams
 see Shams El Din, A.M.
 + El Hamamsy, M. + 114525
 + El Mekawey, F. 114231
 + El-Konsol, S. + 112121
 + El-Sabb, M.I. 116112
 + El-Sayed, A.A. 112121
 + El-Sayed, M.H. 115266
 + El-Wafay, H.M.H. +
 116771
 + Elayaperumal, E. 115424
 + Elbek, B. 111387
 + Elcombe, M.M. 111854
 + Elcrat, A.R. + 113404
 + Elderfield, D. + 114693
 + Elenin, G.G. 113415
 + Elesin, V.F. 114456
 + Elfstrom, S. + 112558
 + Elghobashi, S.E. + 113428
 + Elias, J.H. 116527
 + Eliassen, A. + 116173
 + Eliseeva, O.I. 115277
 + Elizarov, A.I. + 114586
 + Eller, P.G. 113813
 + Eller, P.G. 113814
 + Ellerbroek, B. + 111728
 + Ellerbroek, B.L. 111731
 + Elliman, R.G. 114390
 + Elliott, J.L. 116527
 + Elliott, C.R. + 111761
 + Ellis, A.I. + 115390
 + Ellis, D.D. 113183
 + Ellis, G.F.R. + 116488
 + Ellis, K.J. 115905
 + Ellis, N. 112031
 + Ellison, F.O. 112631
 + Elnahwy, S.A. 114525
 + Elsen, E. 111990
 + Elsen, E. 112012
 + Elstein, A. 115096
 + Elsing, R.J. + 116092
 + Eliskova, T.F. 115340
 + Ellwell, D. 113777
 + Elwyn, A.J. 112126
 + Emanuel, K. + 116256
 + Emberger, B. 114563
 + Emkey, W.L. 113095
 + Emmling, H. 112058
 + Emmrich, P. 116246
 + Empson, T.R. 111762
 + En-chiu Wu.. see Wu En-chiu
 + Enckevort, W.J.P. van
 see van Enckevort, W.J.P.
 + Enckevort, W.J.P. van
 see Van Enckevort, W.J.P.
 + Encrenaz, T. 116533
 + Endean, V.G. 116728
 + Endo, T. + 113044
 + Endo, Y. 112718
 + Endoh, A. 113025
 + Endoh, H. 113891
 + Endoh, Y. 114109
 + Endoh, Y. 114163
 + Enfield, D.B. + 116109
 + Eng, J. 115934
 + Engdahl, A. + 112720
 + Enge, W. 112570
 + Engel, W. 114767
 + Engel, W. 114247
 + Engeland, T. 112075
 + Engelke, R. 113468
 + Engelman, D.M. 115745
 + Enger, R.C. + 112960
 + England, J. 116060
 + England, J.B.A. + 112557
 + England, P.J. + 113932
 + Engler, J. 112016
 + English, C.A. 114056
 + English, R.L. 112540
 + Engman, S. + 113080
 + Engster, C. 112589
 + Engstrom, L. 115545
 + Ennis, P.J. 112341
 + Enome, S. 116593
 + Ensign, P.W. + 112017
 + Enter, A.C.D. van
 see van Enter, A.C.D.
 + Epifanov, V.P. 114086
 + Epp, D. + 116055
 + Epstein, I.R. 111567
 + Epstein, L. 111429
 + Epstein, R.I. 116900
 + Eramzhan, R.A. + 112171
 + Erdevi, N.M. 115055
 + Erdi, B. 116434
 + Eremeev, A.V. 112865
 + Eremenko, V.M. 111805
 + Ergashev, S.F. 115614
 + Erhard, P. 112031
 + Erikson, D.O. 112271
 + Eriksson, L.J. + 113197
 + Eriksson, M. 112504
 + Eriksson, M. 112505
 + Eringen, A.C. 111445
 + Ermakov, S.M. 111590
 + Ermakov, S.S. + 115441
 + Erman, B. 112739
 + Erman, M. 114871
 + Ermenko, O.N. 113851
 + Ermolaev, Yu.I. 116418
 + Ernst, H. 112246
 + Ernst, L. 115026
 + Ernst, M.H. 111556
 + Ernst, R.R. 111715
 + Erokhin, A.I. + 113063
 + Ershov, A.V. 114127
 + Ershova, T.P. + 115177
 + Ertl, G. 114356
 + Ertl, G. 115006
 + Erturk, U. + 114866
 + Erzgraeber, G. 115839
 + Esayan, S.K. + 113055
 + Eschbach, R. + 112950
 + Eschrich, K.-O. + 116461
 + Escherick, P. 112740
 + Eshleman, R. 116529
 + Eskola, K. 112131
 + Eskreys, A. 112015
 + Espen, P. Van
 see Van Espen, P.
 + Espindola, J.A. 114857
 + Esplin, M.P. + 112729
 + Esselman, P.C. 115772
 + Essig, A. 115760
 + Este, G.O. + 112815
 + Estrin, Y. + 114241
 + Estulin, I.V. 116588
 + Eswaran, M.A. 112063
 + Etchegut, P. 114216
 + Etienne, B. 115061
 + Ettenberg, M.I. 113485
 + Etters, R.D. 114102
 + Eu Byung Chan
 see Byung Chan Eu
 + Evangelista, C. 112020
 + Evans, C.A., Jr. 113948
 + Evans, D.L. 116090
 + Evans, W.M. 112024
 + Evans, W.M. 112549
 + Evers, G. 113112
 + Evmenov, V.F. 115894
 + Evard, D. 111485
 + Evseev, B.A. 114487
 + Evseev, B.A. 114663
 + Evstigneev, A.A. 111800
 + Evstigneev, V.A. + 115515
 + Ewaraye, A.O. 114536
 + Ewert, S. 114620
 + Ewing, M.S. 116718
 + Eyre, B.L. + 114056
 + Eyring, L. 115039
 + Eysseric, P. 111514
 + Ezra, G.S. 112624
 + Faber, S.R. 112036
 + Fabian, W. + 112661
 + Fabjan, C.W. 112024
 + Fabre, C. 114434
 + Fabrikant, V.I. + 113376
 + Faegri, K., Jr. 112632
 + Faessler, A. 112050
 + Fahey, P. + 114255
 + Fahrenschoen, P. 115430
 + Fain, B. 114883
 + Fair, R.B. 114275
 + Fairweather, G. 113435
 + Faissner, H. + 112006
 + Faissner, H. + 112005
 + Faissner, H. 112031
 + Fakheri, A. + 115555
 + Falciari, R. 111674
 + Falciglia, F. + 111483
 + Falconer, J.L. + 114366
 + Falicov, L.M. 114469
 + Falk, P. 115755
 + Fallavier, M. 113949
 + Fallone, B.G. + 112895
 + Falls, A.H. 111829
 + Fan, F.-R. 115561
 + Fan, F.-R.F. + 114931
 + Fan, G.-Y. 112277
 + Fan, J.C.C. 115050
 + Fan, J.C.C. 114629
 + Fandry, C.B. + 116240
 + Fanning, M.W. + 112427
 + Fanning, M.W. 112378
 + Fantini, M. 115501
 + Fantini, M. + 111861
 + Fantone, S.D. 112952
 + Fantone, S.D. 112953
 + Faria, R.B. 112871
 + Farley, D.T. 116355
 + Farley, G.R. 115806
 + Farmer, J.D. + 111573
 + Farrant, D.B. 112002
 + Farrell, B. 116220
 + Farwell, R.S. + 111877
 + Fasano, G. 116281
 + Fastl, H. + 115801
 + Fastow, R. 114054
 + Fau, C. 114574
 + Faucher, M. + 114493
 + Faucher, M. 114495
 + Faust, H.R. 112106
 + Faust, H.R. + 112524
 + Favenne, J.-M. + 112394
 + Favre, F. + 113010
 + Favuzzi, C. 112008
 + Fawcett, B.C. 111325
 + Fawcett, B.C. 111326
 + Fayard, L. 112022
 + Fazy, A. 112562
 + Fazio, M.V. 112482
 + Fearon, J. 115677

- Feder, R. 114311
 + Fedik, I.I. 111678
 + Fedirko, V.N. 115433
 Fedorchenko, I.M. 115137
 + Fedorenko, S.G. 112736
 + Fedoriv, R.F. 111737
 + Fedorov, A.V. 114562
 + Fedorov, F.I. 114814
 + Fedorov, F.I. 111935
 + Fedorov, V.A. 114080
 + Fedorova, E.L. 114381
 + Fedorova, N.V. 115187
 + Fedors, R.F. 115261
 + Fedotkin, G.F. 115894
 + Fedotov, M.A. 115280
 + Fedotova, M.I. 115853
 + Fedyukhin, L.A. 114326
 + Fegan, D.J. 116416
 + Fehf, D.L. 113657
 + Fehlmann, J. 112566
 + Fehrenbach, C., Jr. 112880
 + Feidenhans'l, R. 114352
 Feigenbaum, M.J. 115165
 + Feigerle, C.S. 112785
 + Feigin, L.A. 115733
 + Feigin, L.A. 111503
 + Feijoo, S. 115963
 + Feile, R. 114174
 Feilitzsch, F. von
 + see von Feilitzsch, F. 116279
 + Feizollahi, F. 112347
 Fejer, B.G. + 116355
 + Fejes, P.L. 114194
 + Feld, M.S. 111344
 Fel'd, Ya.N. 112907
 + Feldman, G.J. 112011
 + Feldman, P.A. 116793
 + Feldmeier, H. 112085
 + Feldmeier, H. 112273
 Feldt-Rasmussen, K. + 115908
 + Felea, V. 115722
 Felice, F. de. see de Felice, F.
 Feller, D. + 115540
 + Felst, R. 111990
 + Felst, R. 112012
 + Felsteiner, J. 112971
 Feng, S. + 113176
 Feng, S. + 113177
 Feng Da Hsuan
 + see Da Hsuan Feng
 Feng Zhensheng 113379
 + Fennell, L.E. 114018
 + Fennell, L.E. 114475
 + Fenner, H. 112016
 Fennich, P.A. + 115055
 Feraud, G. + 116054
 Ferek, R.J. + 116178
 Ferguson, A.I. + 111776
 Ferguson, A.I. + 111785
 Ferguson, A.I. + 111775
 Ferguson, J.A. + 116367
 + Ferguson, R.E. 112377
 + Ferguson, R.L. 112261
 + Ferland, P. 114202
 Ferlet, R. + 116784
 Fernandez, E. + 111992
 + Fernandez, F. 116415
 + Fernandez, F.M. 112706
 + Fernando Perez, J. 111489
 + Ferrante, G.A. 113094
 + Ferrante, M.J. 111682
 Ferrara, S. + 111918
 Ferrari, A. + 116817
 + Ferrari, A. 111634
 + Ferray, M. 112812
 + Ferray, M. 115539
 + Fesenko, E.G. 114800
 + Fesser, K. 111578
 Fessler, H. + 113374
 + Feth, L.L. 113214
 + Fetscher, W. 111999
 + Fevral'skikh, T.M. 112728
 Fiala, J. + 115263
 + Fialkov, Yu.A. 112753
 + Fichler, R. 112012
 + Ficht, D. 112470
 Fidler, S. + 113195
 Fiedler, R. + 116290
 + Fiedorowicz, H. 113637
 + Field, J.H. 112016
 + Fielding, H.W. 112288
 + Fielding, S. 115167
 Fields, C.A. + 112232
 + Fields, C.A. 112289
 Fienhold, G. + 115205
 Fiero, I.B. 112314
 Fiero, I.B. + 112340
 Fiero, I.B. + 112308
 + Figari, G. 112643
 Figueroa, N. + 115751
 Fiks, V.B. 114517
 + Filev, V.M. 114821
 + Filges, D. 112492
 Filho, J. Mendes
 + see Mendes Filho, J.
 Filimonov, A.V. 111709
 + Filin, Yu.N. 113776
 + Filipchenko, Yu.A. 116311
 Filipezynski, L. 115883
 Filipezynski, L. 115884
 Filippenko, A.V. + 116718
 + Filippone, B.W. 112126
 + Filippov, B.V. 111823
 Filippov, G.A. + 115349
 + Filippov, G.A. 113955
 + Filippov, V.N. 113667
 Filippov, V.V. 114091
 Filippova, S.E. + 114204
 Fillaux, F. + 112744
 + Filo, A.J. 112190
 + Fimin, V.V. 115213
 + Finch, A. 111990
 + Finch, A. 112012
 + Fincke, M. 112031
 Findenegg, G.H. 114371
 Findlay, D.J.S. 112596
 + Findlay, R.H. 112662
 + Findley, D.J.S. 112170
 + Finetti, M. 114611
 Finicle, R.L. 115043
 + Fink, J. 114983
 + Fink, J.K. 112329
 Finkelstein, A.M. + 116440
 Finlayson, T.R. 114154
 + Finokhin, V.I. 114692
 Fintinaru, N. + 111671
 + Firsov, K.M. 116271
 + Firtsak, Yu.Yu. 115055
 Fischer, C.W. + 115384
 + Fischer, D. 113525
 Fischer, J. + 113665
 Fischer, J. + 116843
 + Fischer, P. 114744
 + Fischer, T.M. 115767
 Fisenko, V.V. + 112402
 + Fish, G.I. 114714
 Fisher, D.R. + 115935
 + Fisher, L.M. 114587
 + Fisher, M.E. 114304
 + Fisher, R. 115709
 Fishgoit, A.V. + 115336
 Fishman, H.M. + 115774
 + Fitaire, M. 115532
 + Fitzer, E. 115398
 Fitzgerald, J.E. 113292
 + FitzGerald, M.P. 116495
 + Flagan, R.C. 115585
 + Flanagan, H.L. 112672
 Flato, M. + 111988
 + Flaud, J.-M. 116521
 + Flecher, G. 114165
 + Fleer, H. 116158
 Fleischer, R.L. + 115945
 + Fleischman, L.S. 114557
 Fleitout, L. + 116063
 + Fleming, R.J. 114537
 + Flerov, V.N. 114295
 + Fletcher, P.D.I. 115590
 Fletcher, S. 113779
 Flett, A.M. + 116869
 + Fleuret, N. 113655
 + Flodstrom, S.A. 114347
 Floersheim, P. + 112623
 + Flolo, L.H. 112015
 Flora, C. + 113534
 Flores, F. + 113868
 + Flores, F. 114583
 + Florian, R.J. 112294
 + Florkowski, J. 113248
 Flory, C.A. 111901
 + Flory, P.J. 112739
 + Flouquet, J. 114674
 + Flower, D.R. 112639
 + Floyd, C.E. 112202
 + Flugge, G. 112016
 Flurry, R.L., Jr. 111395
 + Fluss, M.J. 113880
 Fogedby, H.C. + 114702
 + Fokin, A.V. 115142
 + Fokin, V.A. 115147
 + Fokina, N.P. 114725
 + Folds, I.B. 113621
 Foley, J.T. + 111727
 + Folkhard, W. 115738
 Fomenko, B.S. + 115874
 + Fomenko, V.I. 111707
 Fomin, N.V. 114445
 + Foner, S. 115132
 + Foner, S. 115133
 + Fong, K. 113666
 + Fonstad, C.G. 114594
 + Fontaine, G. 112031
 + Fontaneto, M.G. 112585
 + Foote, J.H. 113641
 Forbes, C.E. 114730
 + Forbes, J.M. 116327
 + Ford, A.L. 112831
 + Ford, J.L.C., Jr. 112254
 + Ford, W.T. 111992
 Fordsmand, M. 115674
 + Forgacs, G. 111620
 + Forgham, J.L. 112923
 + Fork, R.L. 114879
 + Forker, W. 115405
 + Forman, R.G. 113350
 + Fornes, R.E. 114750
 Forrest, D.J. 116564
 + Forrest, D.J. 116827
 + Forrest, D.J. 116878
 + Forrest, D.J. 116565
 + Forrest, S.R. 114593
 + Forrester, D.A. 116241
 Forstel, H. + 116159
 + Forster, A. 112529
 + Forster, J.R. 116803
 Forsyth, R. 115624
 + Fortes, M. 114123
 Fortov, V.E. 113633
 + Fortov, V.E. 113569
 + Fortune, H.T. 112070
 + Fortune, H.T. 112219
 + Fortune, H.T. 112275
 Fosbury, R.A.E. + 116851
 + Fossan, D.B. 112035
 + Foster, A.I. 112351
 + Foster, A.I. 115449
 + Foster, C.C. 112209
 + Foster, C.C. 112196
 Foster, D. + 114833
 + Foster, F. 111990
 + Foster, F. 112012
 + Foti, A. 112148
 Foti, G. + 114398
 Foulkes, E.J. 114272
 Fouque, P. + 116845
 Fouquet, C. De
 + see De Fouquet, C.
 + Fournet, G. 115372
 + Fournier, D. 112016
 + Fournier, G. 111842
 + Foux, A. 114578
 Fowler, A.C. + 113405
 + Fox, G. 111958
 Fradkov, A.I. + 111656
 Frahm, C.P. 111355
 Franceschini, A. + 115503
 Francheteau, J. 116050
 + Francheteau, J. 116074
 Francioni, W.M. 112462
 Franco, J. + 116628
 Franco, M.L. + 116656
 Francois, D. + 115329
 + Frandsen, P. 112024
 + Franey, M.A. 112283
 Frank, J.S. + 112007
 + Frank, L.A. 116326
 Frank, W. 113869
 + Frank, W. 113706
 + Franke, G. 112015
 + Frankel, S. 112024
 + Frankenberg, R. 112679
 + Franklin, H. 115946
 Franklin, J.C. + 112460
 + Franklin, M.E.B. 112011
 + Fransson, K. 112544
 Franz, J.R. + 111341
 + Fraternali, M. 112022
 + Frati, W. 112024
 + Fraunheim, Th. 114107
 + Frazier, G. 113150
 + Frech, R.L. 114848
 + Freeburn, H.R. 112308
 Freed, C. + 112991
 Freedman, T.B. + 115749
 Freeman, D.L. + 115578
 Freeman, W.S. + 112246
 Freger, G.E. 113364
 + Freiburg, C. 115023
 Freidberg, J.P. + 113644
 + Freidman, G.I. 116098
 + Friessleben, H. 112089
 Freitas, R.A., Jr. 116496
 + Frekers, D. 112058
 French, H.B. 116777
 French, J.B. 112091
 + French, M.J. 114854
 French, R.G. + 116527
 + Frenckho, V.S. 114512
 + Frenkel, F. 115006
 + Frenzel, E. 112006
 + Fresco, J. 114842
 + Freund, H.P. 113003
 + Frey, R. 112031
 Friar, J.L. + 112078
 Friberg, A.T. + 112930
 Friberg, A.T. + 112935
 Fricke, B. + 112686
 + Fricke, K.J. 116820
 + Fricke, K.J. 116639
 + Friedlund, C.V.M. 116782
 + Fried, R.E. 116678
 + Fried, R.E. 116757
 + Friedel, W. 115672
 + Friedland, S.S. 112958
 Friedman, E. 112281
 + Friedman, E. 112114
 + Friedman, M.H. 111973
 + Friedman, S.D. 116889
 Friedman, W.A. + 112195
 Friedrich, H. + 112258
 Friedrich, K. 115303
 + Fries, D.C. 112016
 + Friesel, D. 112200
 + Frisch, H.L. 111620
 + Frisch, H.L. 114262
 + Frisch, K.C. 115291
 + Frisch, K.C. (ed.) 111311
 Frischkorn, H.J. + 114988
 Fritzsche, H.-G. + 114330
 Fritzsche, A. + 115619
 Fritzsche, H. 113738
 Frizzell, L.A. + 115831
 + Froberger, J.P. 112587
 Frobrich, P. + 112242
 + Frobrich, P. 112270
 Frohberg, G. + 113882
 Frohlich, H. + 112395
 + Froidevaux, C. 116063
 + Froidevaux, D. 112022
 + Frolov, A.M. 113545
 Frolov, A.V. 116120
 + Frolov, A.V. 113076
 Frolov, P. + 111484
 + Frolov, Yu.L. 113846
 + Fronsdaal, C. 111988
 + Frost, K.J. 116592
 + Frost, R.F. 116797
 Froude, D.O. + 116044
 Froyland, J. 111423
 + Fruhauf, J. 114590
 + Fruhwirth, R. 112031
 + Fu, X.-Y. 112629
 Fu Ke-Jian. see Ke-Jian Fu
 Fu Zhengmin + 114170
 Fu-lung Liao
 + see Liao Fu-lung
 Fuchs, A. + 113022
 Fuchs, G. + 113673
 Fueno, T. + 115528
 + Fues, W. 112016
 + Fuess, H. 114165
 Fuggle, J.C. 115010
 Fuggle, J.C. + 115023
 + Fugmitto, R. 114172
 + Fujihira, H. 113535
 + Fujii, J.-I. 115916
 + Fujii, K. 115025
 + Fujii, K. 115794
 + Fujikawa, T. 114529
 Fujimori, H. + 114970
 + Fujimoto, F. 114974
 + Fujimoto, K. 115634
 Fujimoto, T. + 113687
 + Fujimura, Y. 112767
 Fujino, T. + 112354
 + Fujioka, M. 112235
 + Fujisawa, Y. 115206
 + Fujisawa, Y. 115354
 + Fujishita, H. 114164
 + Fujishita, H. 114633
 + Fujita, F.E. 114061
 Fujita, H. 112760
 + Fujita, H. 113615
 + Fujita, J. 113567
 Fujita, K. + 115262
 + Fujita, M. 112609
 + Fujita, S. 114377
 Fujita, T. + 114916
 + Fujita, Y. 112207
 + Fujita, Y. 112210
 + Fujita, Y. 112212
 + Fujitsuka, M. 114397
 Fujiwara, M. + 112207
 + Fujiwara, M. 112210
 + Fujiwara, M. 112212
 + Fujiwara, T. 113978
 Fujimoto, F. 115600
 + Fukada, H. 113028
 + Fukada, M. 112227
 + Fukakusa, S. 112372
 + Fukamichi, K. 114509
 + Fukano, Y. 113857
 Fukuchi, H. + 116205
 + Fukuda, A. 114876
 + Fukuda, K. 113687
 + Fukuda, K. 112325
 + Fukuda, T. 112160
 + Fukuda, Y. 114757
 + Fukugita, M. 111874
 + Fukumoto, S. 112485
 + Fukumoto, T. 115960
 Fukunaga, T. + 113751
 + Fukunaga, T. 113749
 + Fukushima, K. 115779
 Fukushima, S. + 112327
 + Fukushima, T. 112466
 + Fukushima, Y. 112550
 + Fukushima, Y. 112230
 + Fukutomi, M. 114397
 + Fukuyama, T. 113250
 + Fulachier, L. 113430
 + Fuligni, F. 116485
 + Fulton, B.R. 112557
 + Fumagalli, G. 112022
 Fumoto, H. + 112352
 Funahashi, S. + 114106
 + Funato, Y. 113650
 Fung, B.M. 112748
 Fung, W.Y.P. + 114499
 Funnell, W.R.J. 111409
 + Furman, V.I. 112659
 Furmanova, N.G. + 113844
 + Furuhashi, Y. 116262
 + Furuhashi, Y. 111641
 + Furuhashi, H. 115880
 Furiu, S. 113221
 + Furukawa, K. 113970
 + Furukawa, K. 112208
 + Furukawa, K. 113968
 + Furukawa, S. 114376
 + Furukawa, S. 113241
 + Furukawa, T. 113748
 + Furukawa, T. 115959
 + Furuya, K. 115387
 + Fusco, F.A. 114749
 Fushchich, V.I. + 111902
 Fushchich, W.I. + 111879
 + Gaafar, S.A. 112121
 Gaarde, C. 112154
 Gaardhoje, J.J. + 112049
 + Gagliardi, R.M. 116025
 + Gabuniya, D.L. 113953
 + Gadiyak, G.V. 114144
 + Gadiyar, H.S. 115422
 Gadre, S.R. + 111322
 + Gadzhiev, N.N. 112793
 + Gadzuk, J.W. 115580
 Gaffet, B. 116779
 Gage, K.S. + 116305
 Gagliardi, R.M. 111722
 Gagosian, R.B. 116149
 Gagulin, V.V. + 114791
 + Gahinet, M.-E. 112337
 Gai, P.L. 114197
 Gai-Xian Bai
 + see Bai Gai-Xian
 + Gaidot, A. 112016
 + Gaillard, J.-M. 112022
 + Gaines, E.E. 116359
 Gaivoronskaya, T.V. + 116331
 + Gakhramanov, N.F. 114546
 Gal, I.J. + 114140
 Galam, S. + 111603
 Galan, L.de. see de Galan, L.
 Galanin, M.D. + 112783
 + Galasun, A.P. 113952
 Galdi, G.P. + 111447
 + Gales, S. 112200
 Galeski, A. + 114137
 Galeski, A. + 114138
 Galfi, I. 111795
 Galich, N.E. 113047
 + Galkin, A.A. 114691
 + Galkin, A.M. 115274
 Galkina, O.S. + 114705
 + Gallagher, A. 115103
 + Gallagher, N.C. 112951
 + Gallagher, W. 112470
 Gallagher, W.J. 112479
 + Gallino, R. 116816
 + Gallois, B. 115925
 + Galonsky, A. 112158
 Galperin, A. 112301
 + Gal'perin, V.M. 115479
 + Gal'tsov, D.V. 111531
 Galunov, N.Z. + 112574
 + Galushka, A.P. 114564
 Galushko, I.M. 115186
 + Galushko, V.A. 114691
 + Galustyan, M.G. 115731
 + Gambhir, Y.K. 112250
 + Gamby, D. 113384
 + Gamberding, K. 112016
 Ganapol'skii, E.M. + 114726
 Ganesh, T.S. 115713
 + Ganey, G.S. 112590
 + Gangadharaiyah, T. 113452
 + Ganghoff, O. 115837
 + Ganin, E.V. 113839
 Ganin, Yu.G. + 113839
 Ganne, J.P. + 113872
 + Gannon, E. 115625
 + Gannon, E. 115629
 Ganoulis, N. 111864
 + Gans, P.B. 116061
 + Gantois, M. 115200
 + Gao Da-Xing 115311
 Gao Hua + 115310
 + Gao Zheng 113054
 + Gao-xi, Q. 115812
 + Gaodu, A.N. 115273
 Garbuzov, D.Z. + 112996
 + Garbuzov, D.Z. + 114980
 + Garbuzov, D.Z. 114921
 Garbuzov, G.A. 116704
 Garcia, D. + 114495
 + Garcia, D. 114493
 Garcia-Diaz, J.F. + 115760
 Garcilazo, H. + 112079
 + Garde, A.M. 112308
 + Gardiner, K.M. 115390
 + Gardner, F.F. 116803
 + Gardner, J.H. 115880

- Gardner, K. + 113037
 + Garetz, B.A. 112840
 Garfinkel, B. 116432
 Garfinkle, M. 115536
 Garg, K.B. + 113798
 Garguichevich, G.G. 113255
 + Garing, J. 116061
 + Garmash, Yu.V. 114617
 + Garner, F.A. 114182
 Garpman, S. + 112162
 Garrett, G.S. + 113186
 Garrett, J.D. 112039
 + Garrett, J.D. 112049
 + Garrett, J.D. 112112
 Garrett, R.F. + 114998
 Garrett, R.K., Jr. + 115185
 + Gartland, P.O. 115014
 + Gartner, N. 112468
 Garton, A. 113724
 + Garuccio, A. 111483
 Garud, Y.S. + 115447
 + Garvey, J. 112031
 + Gasch, A. 113049
 + Gascon, J. 112547
 Gaspar, Z. 113306
 + Gasperin, M. 113810
 + Gasperini, M. 116436
 + Gaspero, M. 112015
 Gass, A.S. + 112591
 + Gast, T. 111670
 + Gast, W. 112109
 + Gatewa, M. 115330
 Gatilov, Yu.V. + 113837
 + Gatley, I. 116692
 + Gatley, I. 116852
 + Gatos, H.C. 115110
 + Gatos, H.C. 113954
 + Gatteschi, D. 112652
 + Gauger, E. 113129
 Gaudien, M.E. 115876
 + Gaume, F. 114906
 Gaunaud, G.C. + 113171
 Gaunt, P. 114704
 + Gautier, D. 116521
 + Gavaleshko, N.P. 114544
 Gavrilenko, G.D. 113334
 + Gavrilin, N.I. 114618
 Gavrilov, I.M. + 116334
 + Gavrilova, I.P. 115689
 Gavroglou, K. 111997
 Gay, E.C. + 115628
 Gay, R.R. + 112345
 Gay, T.J. 111741
 + Gaylord, T.K. 112927
 + Gaynor, J.L. 116183
 Gdalevich, G.L. + 116341
 Gebauer, D. + 115976
 + Geckinli, E. 115321
 + Ged, P. 111739
 + Gee, M.G. 115508
 + Geer, S. 112031
 + Geeraert, B. 115676
 + Geerlings, J.J.C. 114999
 + Geerlings, J.J.C. 115000
 + Geerts, H. 115747
 + Geesaman, D.F. 112246
 Gehrels, N. + 116836
 + Geier, R. 112468
 Geiger, L.C. + 111475
 Geis, M.W. + 115050
 + Gejji, S.P. 111322
 + Gekelman, W. 116405
 + Gelberg, A. 112109
 + Gel'd, I.V. 114690
 + Gel'd, P.V. 115245
 Geldzahler, B.J. + 116868
 + Gel'fand, B.E. 113493
 + Gel'freikh, G.B. 116571
 Geller, M.A. + 116230
 + Geller, R. 112498
 Geller, V.M. + 115481
 + Gelman, M.E. 116230
 Gel'mont, B.L. + 114543
 + Gelpey, J.C. 114594
 Gemza, J. + 115400
 Genderen, A.M. van
 see van Genderen, A.M.
 Gendlin, E.T. + 111504
 + Genet, M. 114500
 Geng-Wang Xu
 see Xu Geng-Wang
 Genkin, L.V. + 113308
 + Genkin, V.N. 114218
 + Gensch, U. 112021
 + Gensch, U. 112028
 + Gentry, R.C. 116191
 + Genzel, H. 112015
 George, A.C. + 115934
 George, A.C. + 115946
 + George, C. 113262
 + George, E.A. 111491
 George, O.D. 113342
 + George, P. 112648
 + George, R. 112016
 + George, T.F. 112841
 + George, T.L. 112335
 + George, T.L. 112312
 + Georges, R. 114699
 Geramb, H.V. von
 see von Geramb, H.V.
 Gerard, J.-M. + 111952
 Gerasimenko, N.N. +
 114383
 Gerasimov, Yu.M. +
 113935
 + Gerbar, T.L. 115447
 + Gerber, Ch. 114312
 + Gerber, H.-J. 111999
 + Gerberon, J.M. 112370
 + Gerck, E.C. 111985
 + Gergel, B. 112394
 + Gerke, Ch. 112015
 + Gerlic, E. 112200
 Germer, R. 113674
 Gershbein, E.A. +
 116423
 Gershenson, E.M. +
 114472
 Gershenson, N.I. +
 116353
 Gershikov, A.G. 112854
 Gersten, A. 112018
 + Gerstenkorn, S. 112711
 Gervais, J.-L. + 111501
 Gesell, T.F. 115939
 + Gesell, T.F. 115948
 + Gesi, K. 114120
 + Gessinger, G.H. 115136
 + Gettner, M.W. 111992
 + Geus, J.W. 114141
 + Gevers, M. 116165
 Geyer, E.H. + 116867
 Geyer, E.H. + 116773
 + Ghersini, G. 115511
 + Ghesquiere, C. 112031
 + Ghez, P. 112031
 + Ghidini, B. 112020
 Ghoniem, N.M. + 114060
 + Ghorai, S.K. 114205
 + Ghosh, A.S. 112856
 + Ghosh, B. 115644
 + Ghosh, D.K. 114293
 Ghosh, J.K. + 112365
 + Giacobino, E. 113045
 + Gianinoni, I. 115083
 Giannuzzi, M.A. 116744
 + Giansiracusa, G. 112152
 + Giaretta, A. 116288
 + Gibbon, J.D. 113405
 + Gibbons, H. 116062
 + Gibbons, J. 113989
 Gibbons, J.F. + 114006
 + Gibbs, K. 116416
 + Gibbs, W.R. 112282
 Giberson, K.W. + 112988
 Giberti, G. + 112062
 + Giboni, K. 112031
 + Gibson, A.I. 116747
 + Gibson, B.F. 112078
 Gibson, J. 116540
 Gibson, J. 116541
 Gibson, J. 116542
 Gibson, J.M. + 114322
 + Gibson, J.M. 115060
 + Gibson, M. 112024
 + Gibson, M.D. 112549
 + Gibson, W.R. 112031
 + Gidal, G. 112011
 Gien Yang Gwei
 see Yang Gwei Gien
 + Gierach, L.M. 115737
 Gierke, H.E. Von
 see Von Gierke, H.E.
 Giese, E. 113102
 Giffon, M. + 111982
 + Gignac, W.J. 114441
 Gigolashvili, M.S. +
 116599
 + Gil', B.I. 114512
 + Gil', N.L. 114881
 + Gil, S. 112255
 + Gilan, E.V. 115638
 + Gilbert, J.A. 113115
 + Gilbert, R.D. 114750
 Gilblom, D.L. 113225
 Gilboud, H.B. 112836
 + Gildemeister, O. 112022
 Giling, L.J. + 114410
 + Giling, L.J. + 114417
 + Giling, L.J. 115090
 Gilinski, I.A. + 114680
 + Gill, M.E. 113526
 + Gillespie, P.A. 112350
 Gillham, J.K. 115180
 Gilli, G. + 111369
 + Gillman, A.R. 112540
 Gilmore, C.M. + 113388
 Gilmore, R. + 112096
 + Gils, H.J. 112114
 Gilyarov, V.L. + 114117
 Giman, J. 115696
 + Ginnerich, K.A. 112664
 + Ginobbi, P. 112559
 + Ginnob, B.J. 114277
 Gionis, V. + 114172
 + Giordano Orsini, P.
 115378
 + Giorgini, B. 111519
 + Giovannelli, R.G. 116598
 Girard, A. + 114861
 + Giraud-Heraud, Y.
 112031
 Girija Shankar, P.N. +
 115423
 + Girtler, P. 112028
 + Gisin, M. 114904
 + Gitis, M.B. 115481
 Giulietti, A. + 113663
 + Giulietti, D. 113663
 + Giuricin, G. + 116745
 + Giuricin, G. 116864
 + Giuricin, G. 116863
 + Givernaud, A. 112031
 G.J.C. Carpenter
 see Carpenter G.J.C.
 + Gladd, N.T. 113590
 + Gladikh, N.T. 114116
 Gladkov, L.L. 112879
 + Gladney, L. 112011
 + Gladushchak, V.I. 113060
 + Gladyshevskii, E.I. 113833
 + Gland, J.L. 114984
 + Glasberg, B.R. 115800
 Glass, I.S. 116701
 Glass, L. + 111569
 + Glasser, R.G. 112015
 + Glassmeier, K.H. 116361
 + Glatz, F. 112060
 Glaudemans, P.W.M.
 112090
 Glazer, A.N. + 115748
 Glazman, R.E. 114302
 + Glendinning, I. 111990
 + Glendinning, I. 112012
 + Glenn, W.V., Jr. 115971
 Glikman, B.F. 113502
 + Glinenko, L.K. 114394
 Gliner, E. 111520
 + Globus, T.R. 114627
 + Glodeanu, F. 112330
 + Gloski, D.M. 112345
 Glotova, Yu.K. + 115252
 Glowinski, R. + 113403
 + Glowina, Z. 116751
 Gluck, M. 111989
 Gluck, M. 111993
 + Gludkin, O.P. 114618
 Glukhovtsev, M.N. +
 115547
 + Gmitro, M. 112171
 + Gnat, Y. 112015
 Gnatenko, Yu.P. + 114924
 Gnatenko, Yu.P. + 114870
 Gnatenko, A.G. + 115053
 + Gnesin, G.G. 115246
 + Gnezdilov, A.A. 116571
 + Gnezdilov, V.M. 115471
 + Gobbi, A. 112089
 Gobbur, S.G. 112588
 Gochev, I.G. 114682
 + Goddard, W.A., III
 114359
 + Goderre, G.P. 111992
 + Godwin, P.J. 116854
 Goebels, K. + 115463
 Goeler, E. von
 see von Goeler, E.
 + Goerlach, U. 112024
 + Goertz, C.K. 116518
 Goettler, L.A. 115162
 Goffer, Z. + 115506
 + Goggi, V.G. 112022
 Gogol, E.P. + 115745
 + Gogolev, V.M. 116082
 Gohil, P. + 113648
 Gokhman, M.S. 115440
 Gokhberg, M.B. + 116381
 + Gold, M.S. 112011
 Gold, S.H. + 113003
 Goldaev, V.S. 113680
 + Goldak, J.A. 115189
 + Goldberg, M. 112016
 + Golde, M.F. 115538
 + Goldhaber, G. 112011
 + Gold'vin, D. 116423
 + Golding, B.W. 116242
 + Golding, L.J. 112011
 + Goldman, A. 115019
 Gold'man, E.I. + 114603
 + Goldman, M.V. 113600
 + Goldmann, A. 115020
 Goldoni, R. 111524
 + Goldreich, P. 116764
 + Goldschmidt, V.W.
 113486
 Goldschmidt, Y.Y. 114654
 + Goldschmidt-Clermont, Y.
 112028
 + Goldstein, C. 114491
 Golecki, I. + 113947
 + Golecki, I. 114388
 + Golenetskii, S.V. 116876
 Golenko, N.N. 116125
 Golestani-Fard, F. + 114874
 + Golosovskii, I.V. 114675
 + Golovchanskaya, I.V.
 116332
 Golovitskii, A.P. + 112981
 Golovko, V.A. 114166
 + Golovko, Yu.I. 114800
 + Gol'tsev, V.Yu. 113662
 Golub, V.P. 115283
 Golubev, V.K. + 115315
 + Golubeva, O.P. 115124
 Goman'kov, V.I. + 115169
 + Gomes, A.O.S. 113143
 Gomez del Campo, J. +
 112248
 + Gomez del Campo, J.
 112254
 Gomez-Reino, C. + 112932
 Gomez-Reino, C. + 112922
 + Gonchar, N.A. 115740
 Goncharenko, A.M. 113151
 + Goncharuk, A.B. 115393
 + Gonidec, A. 112031
 + Gonsalves, R.A. 111724
 Gonzales, D. 111927
 Gonzales-Cuesta, M. +
 112407
 + Gonzalez, A. 114153
 Gonzalez, F. + 114348
 + Gonzalez-Arroyo, A.
 111887
 + Goodman, A.L. 112101
 Goodman, A.M. + 114540
 Goodman, J. + 112413
 + Goodman, L.A. 114540
 + Goodman, R.K. 113641
 + Goodrick, M.J. 112549
 Gopalan, P. + 115419
 Gorbacheva, O.B. + 111606
 Gorbatiy, Yu.E. + 113718
 Gorbunova, T.A. + 116333
 Gorbunova, T.V. + 113705
 + Gorchak, L.V. 115638
 Gorchakov, E.V. + 116380
 + Gorchakov, G.I. 116211
 + Gordeev, I.V. 114709
 + Gordeev, V.A. 115142
 Gordienko, V.I. + 116299
 Gordon, A.L. 116138
 Gordon, H. + 113668
 + Gordon, H. 112024
 + Gordon, L. 116073
 Gordov, A.N. + 111678
 + Gorelik, V.K. 115962
 Gorelik, V.S. + 114795
 + Goremychkin, E.A.
 114107
 Gorev, M.V. 114167
 + Gorga, M.P. 115806
 + Goria, R. 113540
 Gorina, I.I. + 113439
 Goringe, M.J. 111819
 Gorkom, J.H. van
 see van Gorkom, J.H.
 + Gorkunov, E.S. 111713
 + Gorlei, P.N. 114544
 + Gorler, G.P. 114291
 + Gorlov, Yu.I. 112659
 + Gorner, H. 112774
 + Gornik, E. 114602
 + Gorobchenko, V.D.
 114668
 Gorobets, Yu.I. + 114692
 Gorokhov, V.M. + 115128
 Gorokhova, N.A. + 114175
 + Gorse, C. 113686
 Gorshkov, V.L. 116490
 + Gorshkova, E.Z. 116348
 Gortel, Z.W. + 114351
 Gortz, W. + 112877
 + Goryaga, A.N. 114687
 Gosele, U. + 113906
 Gosele, U. + 114478
 + Gospodinov, M. 115563
 + Gossard, A.C. 114879
 + Gossenberger, H.F.
 114540
 + Gostoli, C. 114267
 + Goto, C. 113687
 Goto, K. + 116072
 Goto, N. + 113152
 Goto, S. + 115352
 + Goto, S. 113645
 Goto, T. 115143
 Gott, Yu.V. + 113654
 Gottgens, R. + 112028
 + Gottschalk, B. 111992
 Gottschling, G.S. + 114152
 + Gottstein, G. 114241
 + Gouanere, M. 112556
 Gough, M.P. + 116369
 Goulburn, J.R. + 115677
 Gour, S.N. + 114227
 + Gourley, P.L. 113943
 Gouthama + 115217
 + Gouttebroze, P. 116442
 + Govelitz, G.F. 115875
 Govindarajan, S. + 113319
 Govor, L.I. + 112189
 + Govorun, E.Ya. 112937
 Gowda, B.T. + 112644
 Gozenbuck, V.L. + 115854
 + Grabchak, A.K. 115140
 Grabenhenrich, H.B. +
 115681
 + Grabisch, K. 112270
 + Grabisch, K. 112273
 + Grabisch, K. 112272
 + Grabowski, W. 116106
 + Grabowski, Z.W. 112058
 Gradov, O.M. + 113617
 + Grady, D.E. 116892
 + Graebner, G. 112251
 + Graebner, G. 112263
 + Graf, F. 112506
 + Graf, V. 115107
 Graf, W.H. 116156
 + Graindorge, P. 113101
 Gramsberger, E.F. + 114067
 + Granan, L. 114146
 + Granatstein, V.L. 113003
 + Grand, D. 112448
 + Grandt, A.F., Jr. 113387
 Graneau, P. 112897
 + Granes, P. 116517
 Granitskii, L.V. + 111767
 + Granneman, E.H.A.
 115000
 + Grant, D.M. 114748
 + Grant, E.R. 112802
 + Grant, J.R. 116242
 + Grant, M.W. 112348
 + Grant, N.J. 115264
 Grappin, R. + 116446
 Grassberger, P. 111561
 Grassberger, P. 111562
 Grasso, M. + 116016
 Gratton, R. + 113638
 Graves, D.B. + 115078
 + Graves, D.B. 115085
 Graw, G. + 112067
 + Gray, B.F. 115556
 + Gray, H.B. 114877
 + Grayer, G. 112031
 Grebogi, C. + 111574
 Grech, E. + 112749
 + Green, A.E.S. 111383
 + Green, B.M.R. 115941
 Green, J.E. 111598
 + Green, S.F. 116512
 Green, W.J. + 112373
 + Greenberg, A. 115709
 + Greene, B.I. 114879
 + Greene, J.M. 111422
 + Greenfield, M.B. 112232
 Greenleaf, J.F. 115892
 Greenslade, T.B., Jr. 111373
 Greenspan, E. + 112431
 Greenstadt, E.W. + 116400
 + Greer, D.L. 114637
 Gregorio, S. De
 see De Gregorio, S.
 + Greim, L. 112569
 + Grein, F. 112815
 + Greiner, A. 112259
 + Greiner, W. 112251
 + Greiner, W. 112263
 + Grepstad, J.K. 115014
 Grest, G.S. + 114701
 + Gribkovskii, V.P. 113691
 Gribov, L.A. + 112713
 Grider, D.E. + 114340
 + Gridnev, I.M. 115274
 + Gridnev, K.A. 112140
 Gridnev, S.A. + 114785
 + Gridnev, V.N. 114947
 Gridunova, G.V. + 112868
 Gridunova, G.V. + 113847
 + Griem, H.T. 113923
 + Grier, B.H. 114164
 + Grier, B.H. 114633
 Griffiths, M. + 114037
 + Grigoris, A.I. 115003
 Grigor'chuk, N.I. 114451
 Grigor'ev, A.Yu. + 115855
 Grigor'ev, I.A. + 112759
 + Grigor'ev, I.A. 113837
 + Grigor'ev, I.A. 116658
 Grigor'eva, L.G. + 114892
 + Grigor'yeva, L.K. 114116
 + Grillakis, M. 111464
 + Griller, D. 115574
 + Grimley, T.B. 114367
 Grimm, L. + 115569
 Grimm, L. + 111701
 Grimmeiss, H.G. + 114476
 Grimson, R.C. + 115929
 + Grindhammer, G. 112016
 Grinin, V.P. + 116658
 Gritsenko, A.M. 116127
 Gritsenko, V.A. + 116301
 + Grivaz, J.F. 112016
 + Groeneveld, K.O. 114988
 Groening, H. + 112061
 + Groessl, M. 114424
 + Gronsky, R. 113708
 Gronvold, F. + 114207
 + Groom, D.E. 111992
 + Groscup, R. 115742
 Gross, D.H.E. 112269
 + Gross, E.E. 112153
 + Gross, R.J. 113498
 Grosse, P. 114810
 + Grosse-Wiesmann, P.
 112016
 Grosser, B. 113075

- +Grossetete, B. 112016
 +Grossohmichen, C. 115665
 +Groth, H. 112687
 +Grote, H. 112022
 +Grote, R.F. + 115002
 Grovenor, C. + 114323
 Grub, R. + 113982
 +Grubel, G. 113871
 Gruen, H. + 112774
 +Gruenstein, E. 115771
 +Grugni, G. 115511
 Gruhn, H.-H. 113201
 Gruhn, H.-H. 113202
 +Grundevik, P. 112686
 +Grundler, R. 114982
 Gruner, G. 114514
 +Grunhau, S. J. 112015
 +Grunze, M. 114343
 +Gruppen, C. 112015
 Grushevskii, Ya.L. 115474
 +Grushina, V.V. 116311
 Gryaznov, V.K. + 113569
 +Grynberg, G. 113045
 Gu, X.M. + 116607
 Gu Meng-Ping + 112511
 Guang-lie Li see Li Guang-lie
 Guangzu Zhang see Zhang Guangzu
 +Guazzoni, P. 112585
 +Gubankov, V.N. 114648
 +Gubanov, V.A. 114443
 Gubarev, V.F. + 113640
 +Gubbins, K.E. 113713
 Guckel, H. 111673
 Guckenheimer, J. 111570
 +Gudilina, A.I. 115234
 +Gudimetla, V.S.R. 113074
 Gudladt, H.-J. + 114244
 +Gudladt, H.-J. 114274
 +Gudur, N. 116756
 +Gudur, N. 116754
 +Guedens, W. 115747
 Guen, D.Le. see Le Guen, D.
 Guenthard, H.H. 112673
 +Gueron, M. 115751
 +Guerrero, G. 116670
 +Guerrero, G. 116671
 +Guevara, M.R. 111569
 +Gugger, H. 114944
 Guggi, D. + 114261
 Guglielmi, M. + 114759
 +Guha, S.N. 112688
 Gui-shan Zhang see Zhang Gui-shan
 Guichon, P.A.M. 112003
 +Guigas, R. 112544
 Guilbert, P.W. 116455
 +Guilbert, P.W. 116467
 +Guillot, C. 114344
 Guillot, M.W. + 113386
 Guilleoteau, S. + 116790
 +Guimaraes, D.M.C. 114159
 +Guimpel, J. 114642
 +Guin, R. 112287
 +Guix, R. 113525
 +Guketlov, Kh.M. 114328
 +Gulenko, V.A. 114381
 +Gull, T.R. 116787
 +Gulmen, O. 116754
 Gulvin, T.F. + 115357
 +Gulyaev, Yu.V. 114571
 Gul'ye'l'mi, A.V. 116382
 Gun Kim Hyun see Hyun Gun Kim
 +Gunder, O.A. 112574
 +Gunderson, B. 112016
 Gunsteren, W.F.van see van Gunsteren, W.F.
 Gunter, P. 112959
 Gunther, E.B. + 116199
 Guo, R.M. + 113310
 Guo Chu + 113054
 Guo-Hui Zhu see Zhu Guo-Hui
 Guocan Ling see Ling Guocan
 Guodong Chen see Chen Guodong
 +Gupta, A.K. 114622
 +Gupta, A.K. 114646
 +Gupta, A.K. 111693
 +Gupta, A.P. 111417
 +Gupta, A.S. 113480
 Gupta, A.Sen see Sen Gupta, A.
 Gupta, M. 111972
 Gupta, M.K.Das see Das Gupta, M.K.
 +Gupta, M.R. 113603
 +Gupta, P.L. 112692
 +Gupta, R. 111886
 +Gupta, R.B. 112692
 Gupta, S.K. + 116723
 +Gupta, S.K. 112166
 Gupta, S.P.Sen see Sen Gupta, S.P.
 Gupta, S.S. + 112901
 Gupta Pushpa see Pushpa Gupta
 +Gurevich, A.V. 116344
 Gurevich, A.V. + 114641
 Gurevich, B.D. + 115280
 Gurevich, O.A. + 115872
 Gurija, G.T. + 111487
 +Gurinovich, V.I. 112537
 Gurman, J.B. + 116556
 Gurnett, D.A. + 116518
 Gurnett, D.A. + 116392
 +Gurov, S.V. 115129
 Gursel, Y. 111511
 Gursey, F. + 111925
 +Gurtler, J. 116633
 Gurtovoi, K.G. + 114679
 +Gurvich, L.V. 112878
 +Guryan, Yu.A. 116876
 Gusakovskaya, I.G. + 114160
 +Guseinov, A.G. 114546
 Guseinov, O.H. + 116716
 Gushikem, Y. + 114835
 +Gust, P.P. 112202
 +Gustafson, D. 113533
 +Gustafson, T.K. 114613
 Gustav, K. + 112697
 +Gustavsson, S. 112468
 Gutbrod, F. + 111884
 +Gutierrez, D. 115063
 +Gutkin, A.A. 114920
 Gutkin, E. + 111595
 Gutmanas, E.Y. 115127
 +Guttman, M. 115325
 Gutzwiller, M.C. 111494
 +Guy, A.W. 115772
 Guy, K.B. + 115195
 +Guymont, M. 113828
 Guz', A.N. 113365
 Guz, A.N. 113367
 Gwei Gien Yang see Yang Gwei Gien
 +Gwozdziński, K. 115873
 +Gyimesi, J. 114400
 Gyulai, J. + 114054
 +Gyulai, J. 114400
 Ha, T.-K. + 112891
 Haan, B.J.De see De Haan, B.J.
 +Habitz, P. 112808
 Habrman, P. 115599
 Habs, D. + 112113
 Hack, M. + 116750
 +Hack, M. 116697
 +Hacker, U. 112528
 Hackney, J.D. 115993
 Haddad, G.N. + 112860
 +Haddow, J.B. 113341
 Hadrava, P. 116463
 +Haegel, N.M. 114469
 +Haegi, H. 112622
 +Haegi, H.R. 112623
 +Haensel, P. 116636
 +Haerendel, G. 116402
 Haeringen, H.van see van Haeringen, H.
 Haesner, B. + 112197
 Hagekyriakou, J. + 114537
 +Hagemann, G.B. 112049
 +Hagemann, G.B. 112112
 Hagemann, P. + 115597
 +Hagenmuller, P. 115084
 +Hager, H. 115976
 +Hager, J. 115006
 +Hagfors, T. 116295
 +Hahn, B. 112022
 Hahn, B.H. + 115210
 +Hahn, G. 112658
 Hahne, A. + 114226
 +Haidt, D. 111990
 +Haidt, D. 112012
 Haigh, J. + 114412
 +Haight, R.C. 112125
 Hailey, C.J. + 116472
 Hairie, A. + 111357
 +Haikins, J. 112016
 +Hakamada, K. 116420
 +Hakansson, A. 112159
 Hakemi, H. 114230
 +Haken, H. 112977
 +Halbach, K. 112528
 Halbert, M.L. + 112261
 +Halbert, M.L. 112049
 +Halbert, M.L. 112059
 +Halbwachs, M. 113962
 Halderon, D. + 112172
 Haldoupis, C. + 116362
 +Halenius, U. 114823
 Hales, R. 114081
 +Haley, L.V. 115750
 Halford, D.K. + 115937
 +Hall, D.S. 116678
 +Hall, F.L. 115830
 Hall, L.S. 111419
 Hall, M.L. 116088
 +Hall, R.J.B. 114854
 +Hall, S.D. 116742
 Hall, S.F. + 112421
 Haller, E.E. + 114469
 Hallett, J. 116252
 Halliyal, A. + 114789
 +Hallowell, R.B. 115604
 Hallstrom, A. + 115507
 +Halpern, D. 116131
 +Halpern, D. 116090
 Halpern, P.O. 112453
 Halpin, J.C. 115160
 +Halpin, L. 116673
 +Halstead, J.A. 116174
 +Hama, S. 112203
 Hama, Y. + 112023
 +Hama, Y. 111982
 +Hamabata, H. 116410
 +Hamaguchi, H. 116072
 Hamakawa, Y. + 115634
 Hamamoto, I. 112038
 Hamamoto, S. 111911
 +Hamamoto, T. 113968
 Hamamsy, M.El see El Hamamsy, M.
 Hamano, K. + 115155
 +Hamano, K. 115156
 +Hamano, K. 115353
 +Hamasaki, Y. 115630
 +Hamer, C.A. 114914
 Hamiuddin, M. 115270
 +Hamaren, E. 112075
 +Hammer, B. 114424
 +Hammer, C. 115837
 +Hammer, D.A. 113014
 +Hammond, J.K. 113193
 +Hamon, O. 112016
 +Hamzaoglu, E. 116756
 Han, S.H. + 112410
 Han Kim Doo see Doo Han Kim
 +Hanada, Y. 114143
 +Hanamura, M. 115527
 +Hanawa, T. 114313
 +Hancock, A.J. 115986
 Handa, M. + 115417
 +Handa, M. 112327
 Handa, T. + 115248
 Hang Nian-Ning. 111455
 Hankey, W.L. + 113424
 Hanley, J.A. + 115882
 +Hanna, G.J. 114366
 Hannache, H. 115092
 +Hannache, H. 115091
 +Hannay, J.H. 111496
 +Hannemann, M. 112992
 +Hanni, H. 112022
 Hanni, W. + 115097
 +Hannoyer, B. 114967
 Hansen, G. + 112032
 +Hansen, H.E. 114961
 Hansen, J.C. + 113245
 +Hansen, J.E. 112668
 +Hansen, J.R. 112022
 +Hansen, K.H. 112024
 Hansen, L. + 116641
 +Hansen, P. 112022
 +Hansen, W.L. 114469
 +Hansl-Kozanecka, T. 112031
 +Hanson, D.M. 114347
 Hanson, D.W. 111729
 Hanson, F.E. + 112983
 +Hanson, G. 112011
 +Hans, M. 115768
 +Hanssen, J.H.L. 115090
 Hanssen, K.-J. 112918
 +Hanstock, D.J. 115455
 Hanxin Zhang see Zhang Hanxin
 +Happe, A. 111630
 Hara, M. + 112912
 +Hara, M. 114876
 Hara, Y. + 114959
 +Harada, H. 113905
 +Harada, Y. 112839
 Haraux, A. 111458
 Harbeke, G. + 115073
 +Harbeke, G. 115074
 +Harder, Ch. 112990
 Harding, A.K. + 116725
 +Harding, A.K. 116457
 +Harding, A.K. 116453
 +Hardt, A. 112528
 +Hareesh, T.V. 113351
 +Hargreaves, R. 112305
 +Hargrove, C.K. 112007
 +Haribabu, V. 113909
 +Harkov, R. 115709
 Harpen, M.D. + 115912
 Harper, J.M.E. + 115104
 +Harris, A. 116514
 +Harris, A.W. 116526
 Harris, J. + 114337
 +Harris, J.W. 112267
 +Harris, S. 116336
 +Harrison, A.B. 116747
 +Harrison, D.E. 116104
 Harrison, H.B. + 113988
 +Harrison, H.R. 114070
 Harrison, J.G. 112615
 Harrison, M.F.A. + 112441
 +Harrop, L.P. 112420
 +Harshfield, G.A. 115955
 Hart, H. 111663
 Harte, W.E. + 114972
 +Harten, R.H. 116787
 +Hartman, R.L. 113013
 Hartmann, G.H. + 115926
 Hartmann, H.-J. + 113065
 +Hartmann, K. 112270
 +Hartmann, K. 112455
 Haruyama, O. + 114511
 +Harvey, G.T. 113148
 +Harvey, J. 112589
 Harvey, J.E. + 112923
 +Harvey, J.W. 116600
 Harvey, K.C. + 112880
 +Harvey, M.F. 115047
 Hasan, F. + 115225
 Hasan, H. + 116269
 +Haschick, A.D. 116811
 +Hase, Y. 114836
 +Hasegawa, A. 116389
 Hasegawa, M. + 114962
 Hasegawa, M. + 114963
 +Hasegawa, R. 114754
 Hasegawa, S. + 111703
 Hasegawa, T. + 113163
 +Hasegawa, T. 111648
 +Hasenfratz, P. 111884
 +Hashemi, T. 115051
 +Hashi, T. 114757
 +Hashiba, M. 115154
 +Hashimoto, E. 113897
 Hashimoto, H. + 113891
 +Hashimoto, H. 113894
 +Hashimoto, H. 113892
 +Hashimoto, K. 112213
 +Hashimoto, K. 112228
 +Hashimoto, K. 112223
 Hashimoto, M. + 114273
 Hashimoto, M. + 113978
 Hashimoto, T. + 114938
 +Hashizume, Y. 115248
 +Hasiguti, R.R. 113991
 +Hasinoff, M. 112544
 +Hasiza, M.L. 112122
 +Hassam, A.B. 113590
 Hassan, M.I. 113399
 +Hassan, S.S. 113048
 Hasselbeck, M. + 113017
 +Hasselberg, G. 113574
 +Hasselberg, G. 113575
 Haste, T.J. 112306
 Haste, T.J. 112417
 Hastings, D.E. 113571
 Hastings, J.D. 111859
 Hata, T. + 115333
 +Hata, T. 111389
 +Hatanaka, K. 112210
 +Hatanaka, K. 112224
 +Hatanaka, K. 112051
 +Hatanaka, K. 112229
 +Hatanaka, K. 112216
 +Hatanaka, K. 112225
 Hatano, T. + 114768
 +Hatano, Y. 112862
 +Hatta, I. 111685
 Hattori, T. + 115146
 +Hattori, T. 112466
 +Hattula, J. 112059
 Hauck, R. + 113001
 Haucke, H. + 114299
 Hauducoeur, A. + 111844
 Hauducoeur, A. + 113525
 +Haufe, G. 115909
 +Haug, E. 111321
 +Hauge, R.H. 112722
 Haugen, P.R. + 112956
 Haus, H.A. + 112913
 +Hausman, R.F., Jr. 112128
 Hauser, O. + 112033
 Hauser, O. + 112547
 Haute, A.Van see Van Haute, A.
 Hautojarvi, P. + 114952
 +Hautojarvi, P. 113876
 Havel, T.F. + 115735
 +Haw, J.F. 114741
 +Hawker, B.M. 115454
 +Hawkins, B.L. 114741
 Hawkins, H.F. 116232
 +Hawkins, W.G. 114018
 +Hawthorne, J.R. 113388
 +Hayakawa, S.I. 112207
 +Hayakawa, S.I. 112211
 +Hayakawa, S.I. 112212
 Hayakawa, Y. + 115042
 +Hayamizu, K. 114747
 Hayashi, K. + 112325
 +Hayashi, K. 112550
 +Hayashi, M. 112872
 +Hayashi, N. 113751
 Hayashi, S. + 114747
 +Hayashi, S. 114422
 +Hayashibe, S. 112235
 Hayden, B.E. 114867
 Hayes, M. 114317
 +Hayes, R.E. 114608
 +Hayes, W. 114492
 +Haynes, W.J. 112031
 Haynes, W.M. 114065
 Haynes, W.M. + 113550
 Hayns, M.R. + 112419
 +Haywood, F.F. 115703
 +Hazeltine, R.D. 113566
 +Hazen, R.M. 116083
 +Hazi, A.U. 112675
 +Head, G.B., III 115912
 +Head, J. 114364
 +Healy, T.W. 114856
 +Heath, D.F. 116231
 +Heathcote, S.R. 116860
 +Heck, B. 112024
 +Hecker, R. 112492
 +Hecker, S.S. 115267
 Heckman, T.M. + 116810
 +Hedberg, V. 112024
 +Hedegard, P. 114702
 Heel, M.Van see Van Heel, M.
 +Heeringa, W. 112197
 Hefter, E.F. + 112140
 Heggen, R.J. 116152
 Hehenkamp, T. 113972
 +Heidinger, F. 112060
 +Heidsiek, H. 113888
 +Heimann, P.A. 115383
 Hein, D. + 112396
 Hein Le Khac see Le Khac Hein
 Heinecke, R.A.H. + 115079
 +Heinlein, W.E. 113111
 +Heinrigs, W. 112005
 +Heinrigs, W. 112006
 Heins, C.P. + 111410
 +Heintze, J. 111990
 +Heintze, J. 112012
 +Heinzelmann, G. 111990
 +Heinzelmann, G. 112012
 Heisel, F. + 112770
 Hekinian, R. + 116074
 +Helbig, H. 116290
 Heldt, J. + 112682
 +Helfand, E. 112887
 +Hellborg, R. 115545
 +Hellenbrand, K.H. 111990
 +Hellenbrand, K.H. 112012
 Heller, E.J. 111495
 +Helliwell, R.A. 116359
 +Helmis, C.G. 116208
 Helmle, H. + 115784
 +Helmolt, U.v. 112113
 +Helmrich, H. 113499
 +Helms, C.R. 114372
 +Helou, G. 116839
 Helppi, H. + 112036
 +Helppi, H. 112058
 +Helszer, Z. 115873
 +Heltzley, B.K. 111992
 Hemmati, H. + 113057
 Hemmen, J.L.van see van Hemmen, J.L.
 +Hemmi, M. 112484
 +Hemon, D. 115869
 Hempe, K. 116752
 +Hemphill, R. 114613
 +Hender, T.C. 113578
 +Henderson, C. 116869
 +Hendler, R.W. 115765
 +Hendriks, M. 114403
 Henjeler, A. + 114405
 Henley, E.M. + 112080
 +Henne, M. 116473
 +Hennrich, W. 112113
 +Henning, C.B. 115867
 Henning, T. + 116633
 +Henning, W. 112246
 +Hennrich, H.J. 112113
 Henon, M. + 111421
 Henriksen, M. 113296
 +Henriquez, A. 112075
 Henry, B. + 116312
 Henry, B.R. + 112738
 +Henry, C.H. 115109
 +Henry, G.W. 116742
 Henry, J.F. + 114153
 +Hensley, D.C. 112049
 +Hensley, D.C. 112261
 +Hensley, D.C. 112059
 Hentschel, H.G.E. + 111589
 +Hentzell, H.T.G. 115104
 +Hepp, V. 112015
 +Heraud, L. 115092
 +Heraud, L. 115091
 Herbst, J.F. 113797
 +Herino, R. 114333
 +Heritage, J. 111857
 Herm, R.R. + 112699
 Herman, G.T. 115919
 Herman, M.F. 111478
 Hermance, J.F. 116056

Hermann, K. +	115015	+Hirth, J.P.	115223	Hong, S.I. +	115259	+Huang, H.-C.W.	113863	+Ichimiya, K.	114143
+Hermans, J.	115727	+Hirtz, J.P.	115061	Hongnian Yu	see Yu Hongnian	+Huang, L.	113017	Ichimura, M. +	112115
+Hermanska, J.	112449	Hishinuma, A. +	114045	+Honjo, Y.	112357	Huang, T. +	114157	+Ichinose, H.	115005
+Hermansson, B.	113134	Hitchcock, D.A. +	113566	+Honma, A.	112031	Huang Tao +	111977	+Ichinose, T.	113536
Hermes, G. +	113701	Hitchman, M.L.	115082	Honma, N. +	115605	Huang Tian-Xi	116340	Ievlev, V.M. +	114380
Hernandez, C. +	115963	+Hitomi, Y.	112437	+Honma, T.	112466	Huang Zhu-Po +	114910	+Ievlev, V.M.	114382
+Hernanz, M.	116648	+Hjorth, S.A.	112292	+Honnashagen, K.	116181	+Hubbelling, L.	112554	Ifukube, T.	115980
+Herold, H.	116456	Hlasnik, I. +	114651	+Hons, Z. +	112119	+Huber, J.R.	112725	+Igaki, K.	114522
+Herps, H.	111640	+Hlavacek, V.	115512	+Hontebeyrie, M.	111910	+Huber, M.K.	112623	+Igarashi, Z.	112485
+Herrick, C.C.	113813	+Ho, H.	112277	Hood, A.W.	116617	+Huchtmeier, W.K.	116532	Igata, N. +	114057
Herrmann, Ka. +	112992	+Ho, J.C.	114203	+Hood, A.W.	116618	+Huchtmeier, W.K.	116862	Igloi, F. +	116112
+Herskind, B.	112049	Ho, L.T. +	114886	Hoof, G.W. +	116618	+Huebert, B.J.	116203	Igloi, F. +	116105
+Herskind, B.	112112	Ho, L.T. +	114885	see 't Hooft, G.W.		Huei Peng	see Peng Huei	+Igolkina, L.S.	113802
Hertz, J.A. +	114700	Ho, L.T. +	114203	+Hoogendoorn, R.J.	116192	+Huerre, P.	113419	+Ihara, T.	116262
+Hertzberg, R.W.	115362	+Ho, P.T.P.	116772	+Hooper, J.	112024	+Hueter, G.J. +	116881	+Ihara, T.	11641
+Hertzberger, L.O.	112031	Ho Jeon Seung	see Seung Ho Jeon	+Hoopes, R.H.	113197	Hufner, S.	115018	+Ihle, R.R.	11426
+Herve, A.	112553	+Ho Yu-kun	112142	Hootman, B.W. +	116196	Hughes, D.W.	116548	+Iida, H.	112213
Hervieu, M. +	113856	Ho Yueh-Se	see Yueh-Se Ho	+Hopke, P.K.	115587	+Hughes, G.	111990	+Iida, H.	112221
Hervieu, M. +	113933	+Hoath, S.D.	112557	+Hopkins, J.L.	116757	+Hughes, G.	112012	+Iida, H.	11222
Hess, C.T. +	115942	+Hoobbs, P.V.	116221	+Hopkins, R.G.	112447	+Hughes, H.P.	115009	Iinuma, T.A.	115914
+Hess, C.T.	115948	+Hochheimer, H.D.	114872	+Hopp, G.	112016	Hughes, R.L.	116119	Iio, M.	115913
Hess, J.P. +	113387	+Hochheimer, H.D.	114162	+Hopp, U.	116773	+Hughes, R.L.	116240	Iio, Y.	116036
Hester, J.J. +	116778	Hockman, G.M.	113246	Hora, H.	112434	+Hughes, T.J.R.	111444	Iizumi, M. +	114120
Hetterich, N. +	116525	+Hockney, R.W.	113754	+Horani, M.	116784	+Hughes, V.W.	112007	+Iizumi, M.	114106
Hettinger, H.	115699	Hodge, F.G.	115408	+Horen, D.J.	112153	+Hugi, M.	112241	+Iizumi, M.	114109
+Heuberger, W.	115107	+Hodges, C.	112031	+Hori, S.	116038	Hugon, P.L. +	114661	+Ikawa, K.	112325
+Heuer, R.D.	111990	Hodges, C.H. +	113188	+Hori, Y.	111389	Hui, D. +	113337	Ikebata, Y. +	112215
+Heuer, R.D.	112012	Hodgett, D.L. +	115672	+Horie, A.	111811	Huibang Luo +	116188	+Ikeda, K.	112052
Heung-Jac Lie +	116112	+Hodgson, A.	115520	+Horiike, H.	111815	Huijser, P.H. +	114131	+Ikeda, K.	112105
+Hewett, C.A.	114054	+Hodor, J.	115642	+Horiuchi, H.	112082	+Huizenga, J.R.	112249	+Ikeda, M.	113149
Heyder, J. +	113491	+Hodul, D.	114873	+Horiuchi, S.	116038	Hukuhara, Y. +	115154	+Ikeda, S.	113749
+Heydon, R.G.	114887	Hoe, J.M.De	see De Hoe, J.M.	+Hori, E.	115081	+Huld, S.	115545	Ikeda, T. +	11737
+Heyen, M.	114409	Hoek, A. van	see van Hoek, A.	+Horn, D.	112035	Hull, C.M.	111505	+Ikegami, H.	112207
+Heyen, M.	114406	Hoek, B. van Der	see Van Der Hoek, B.	+Hornbogen, E.	115211	+Hull, G.W., Jr.	114639	+Ikegami, H.	112212
+Heym, A.	113630	Hoenen, F.	112584	+Hornemann, U.	114094	+Hulmann, G.	115403	+Ikegami, K.	112485
+Heymann, S.	115992	Hoeschen, D.	111851	+Horodyski, T. +	114628	+Hults, M.	112682	+Ikegaya, K.	113189
+Heyng, H.W.	112113	Hoeff, D. +	111706	+Hornby, P.G. +	111479	+Humanic, T.J.	112246	Ikeuchi, M. +	112899
+Hiibard, D.L.	115971	+Hoffman, F.O.	115	+Hornemann, U.	114094	+Hume, S.P.	115871	Ikeya, M.	112450
+Hibino, T.	115154	+Hoffman, G.W.	112203	+Horodyski, T. +	114628	Humphreys, R.G.	114899	+Ikazawa, E.	112484
+Hicks, H.R.	113578	+Hoffmann, D.	112031	+Hornby, P.G. +	111479	Humphries, S., Jr. +	112469	Ikhlaf, A. +	114762
+Hicks, K.H.	112289	+Hoffmann, H.	112031	+Hornby, P.G. +	111479	+Hundhausen, A.J.	113601	+Iksanova, S.V.	112714
Hicks, T.J.	114685	+Hoffmann, M.	116867	+Hornby, P.G. +	111479	Hung, N.T. +	116118	+Ikuchi, N.	114987
+Hiddleston, J.	112024	+Hoffmann, D.	114988	+Hornby, P.G. +	111479	Hunger, W. +	112570	Ikuta, N. +	114708
+Hiddleston, J.	112549	+Hoffmann, F.	113630	+Hornby, P.G. +	111479	+Hungerbuhler, V.	112022	+Ilett, C.	113237
+Hietl, L.	116685	Hofmann, G.H.	115159	+Hornby, P.G. +	111479	+Hunt, J.L.	114894	+Iliev, K.	113785
+Higashi, A.	113881	+Hofmann, H.	112290	+Hornby, P.G. +	111479	Hunt, W.A.	115868	+Il'in, G.A.	115187
+Higashi, G.S.	114919	+Hofmann, P. +	114345	+Hornby, P.G. +	111479	Hunter, J.K. +	113396	+Il'in, L.A. +	113326
+Higashi, S.	115034	+Hofmann, W.	115930	+Hornby, P.G. +	111479	Huntington, H.B.	114290	+Il'inets, A.M. +	113830
+Higashiguchi, Y.	114962	+Hofmann, W.	115930	+Hornby, P.G. +	111479	+Hurless, C.	116685	+Ilijinov, A.S. +	112186
+Higashiguchi, Y.	115418	+Hofmann, F.	113630	+Hornby, P.G. +	111479	Hurley, K.	116875	Illy, H.	111336
Higashimura, T. +	115582	Hofmann, G.H.	115159	+Hornby, P.G. +	111479	+Hurlimann, W.	112076	Ilyas, M.	116498
Higbie, J.	111366	+Hofmann, H.	112290	+Hornby, P.G. +	111479	+Hurlimann, W.	112528	Ilyas, M. +	114939
+Higel, B.	116402	Hofmann, P. +	114345	+Hornby, P.G. +	111479	Hurly, K. +	116588	+Il'yasov, R.S. +	115488
+Higuchi, H.	114259	+Hofmann, W.	115930	+Hornby, P.G. +	111479	Hurni, J.-P. +	111533	+Il'yasov, R.S.	115484
+Hijikata, T.	114389	+Hoftiezer, J.	112285	+Hornby, P.G. +	111479	+Hurst, R.B.	111992	+Il'yinskii, V.N.	116876
Hiki, Y. +	113975	+Hogan, D.C.	112984	+Hornby, P.G. +	111479	Husain, D. +	112681	+Ilyukhin, V.V.	113830
+Hilaire, L.	115602	+Hogarth, C.A.	115051	+Hornby, P.G. +	111479	+Husain, L.	116174	+Ilyukhin, V.V.	113842
Hildebrand, R.H.	116808	+Hogarth, C.A.	114874	+Hornby, P.G. +	111479	+Hussein, M.S.	112135	+Ilyukhin, V.V.	113843
+Hildenbrand, K.D.	112089	+Hogarth, C.A.	114939	+Hornby, P.G. +	111479	+Hutchings, L.	116133	+Ilyukhin, V.V.	113829
+Hildingsson, L.	112558	Hoglund, L.	116207	+Hornby, P.G. +	111479	+Hutiray, G.	114516	+Ilyukhin, V.V.	113792
+Hilgemeier, M.	112502	+Hoheisel, C.	113744	+Hornby, P.G. +	111479	+Hutka, P.	114631	Im, S.W. +	115317
+Hilke, H.J.	112024	Hojan, E. +	113248	+Hornby, P.G. +	111479	Hutson, J.M. +	112800	Imai, K. +	112224
+Hilke, K.J.	115569	Hojman, R. +	111469	+Hornby, P.G. +	111479	Huttel, E. +	112188	Imai, K. +	113189
Hill, C.	114009	+Hojman, S.	111469	+Hornby, P.G. +	111479	Huttel, E. +	112187	+Imai, Y.	116262
+Hill, J.R.	113038	+Hol, W.G.J.	115727	+Hornby, P.G. +	111479	+Hutzen, H.	116159	+Imaino, W.	115380
Hill, R.A. +	112740	+Holak, T.A.	115517	+Hornby, P.G. +	111479	Huu-Doan Nguyen	see Nguyen Huu-Doan	Imazumi, S. +	115810
Hillair, J. +	113876	Holburn, D.M.	111633	+Hornby, P.G. +	111479	see Phan Thanh Huy		Imazumi, S. +	11685
+Hillebrandt, W.	116445	+Holder, M.	112555	+Hornby, P.G. +	111479	Huyer, A.	116130	+Imamkulov, A.	115692
+Hillebrecht, F.U.	115023	Holdom, B.	111915	+Hornby, P.G. +	111479	+Huyer, A.	116141	+Imanishi, A.	112609
Hillel, A.J.	114510	+Holdom, G.N.	115900	+Hornby, P.G. +	111479	+Huyer, A.	116131	+Imanishi, S.	112207
Hillman, R.E. +	113214	+Holland, W.R.	116136	+Hornby, P.G. +	111479	+Huyer, A.	116131	+Imanishi, S.	112212
Hills, J.G.	116743	Holle, R.L. +	116195	+Hornby, P.G. +	111479	Hwang, H.J. +	111666	+Imase, M.	113149
+Hils, D.	115103	Holle, W.G.Von	see Von Holle, W.G.	+Hornby, P.G. +	111479	Hwang, R.R. +	113487	+Imatani, T.	116422
+Hilscher, D.	112249	see Von Holle, W.G.		+Hornby, P.G. +	111479	Hwang, R.R. +	113489	Imhof, W.L. +	116359
Hiltmann, P. +	115770	+Hollebeek, R.J.	112011	+Hornby, P.G. +	111479	Hwang, R.R. +	113490	+Imme, G.	112148
+Himel, T.	112022	Hollebein, M.L.A.von	see von Hollebein, M.L.A.	+Hornby, P.G. +	111479	Hwang, R.R. +	113421	Imoto, F. +	115444
+Himes, V.L.	114491	Hollebein, M.L.A.	115088	+Hornby, P.G. +	111479	Hwang Chang-Sing	see Chang-Sing Hwang	+In Joon Oh.	113716
+Himmele, G.	112113	Holleman, J. +	115088	+Hornby, P.G. +	111479	see Chang-Sing Hwang		+In-shieh Kung	113432
Hinata, S.	116604	+Hollenstein, H.	112725	+Hornby, P.G. +	111479	Hwi-Quei Yang	see Yang Hwi-Quei	+Inaba, H.	115714
+Hinde, D.J.	112244	+Hollinger, F.	113001	+Hornby, P.G. +	111479	+Hyakutake, M.	112146	+Inaba, R.	111770
Hingmann, R. +	112133	Holloway, S. +	115880	+Hornby, P.G. +	111479	+Hyland, A.R.	116849	+Inaba, S.	112550
+Hinken, J.H.	111701	+Holloway, S. +	115880	+Hornby, P.G. +	111479	+Hyland, A.R.	116802	+Inada, K.	113121
Hintermann, H.E.	115450	+Holloway, S. +	115880	+Hornby, P.G. +	111479	+Hyland, A.R.	116802	+Inada, T.	115924
+Hintermann, H.E.	115097	+Holloway, S. +	115880	+Hornby, P.G. +	111479	+Hyland, A.R.	116802	+Inan, U.S.	116359
Hippsey, C.A.	115327	+Holloway, S. +	115880	+Hornby, P.G. +	111479	Hynne, F.	113553	Inawashiro, S. +	114655
+Hira, H.	113970	+Holloway, S. +	115880	+Hornby, P.G. +	111479	+Hyun Gun Kim.	115391	Indebetouw, G.	112954
+Hirabayashi, M.	114962	+Holloway, S. +	115880	+Hornby, P.G. +	111479	Hyun Oh Jae	see Jae Hyun Oh	+Indosov, V.O.	113390
+Hirai, H.	112609	+Holloway, S. +	115880	+Hornby, P.G. +	111479	see Jae Hyun Oh		+Indrischenok, B.I.	114948
Hirai, T. +	114422	+Holm, A.	112049	+Hornby, P.G. +	111479	+Hyun-Kee Cho	115183	+Indyk, V.M.	115923
Hirai, Y. +	114826	Holm, D.D.	113518	+Hornby, P.G. +	111479			Infeld, E.	113461
Hirakawa, H. +	115592	Holm, D.D. +	113517	+Hornby, P.G. +	111479			Ingate, S.F.	116029
+Hirakawa, H.	111661	+Holm, P.M.	116041	+Hornby, P.G. +	111479			Ingate, S.F. +	116028
Hirano, T.	113695	+Holm, U.	113139	+Hornby, P.G. +	111479			+Ingebrechtsen, F.	112075
+Hirao, Y.	112466	+Holmen, G.	114015	+Hornby, P.G. +	111479			Ingersoll, A.P.	116263
+Hirasawa, T.	116084	Holmes, J.A. +	113578	+Hornby, P.G. +	111479			+Ingersoll, J.G.	115944
+Hirasima, Y.	116589	Holmes, J.F. +	113074	+Hornby, P.G. +	111479			Ingensten, N.-G. +	115224
+Hirata, I.	115630	+Holmes, N.C.	113635	+Hornby, P.G. +	111479			+Ingles, A.	114183
Hirata, S. +	113731	Holmes, P. +	111571	+Hornby, P.G. +	111479			+Ingli, A.D.	114665
+Hirayama, H.	113061	Holohan, A.M. +	113020	+Hornby, P.G. +	111479			+Ingoldsby, T.C.	111342
+Hirayanagi, K.	115959	Holt, R.S. +	111831	+Hornby, P.G. +	111479			+Inkson, J.C.	114468
Hirone, M. +	113174	+Holthuisen, D.J.	112031	+Hornby, P.G. +	111479			+Innes, W.R.	112011
Hirooka, Y. +	114991	Holtz, T. +	113476	+Hornby, P.G. +	111479			Innis, J.L. +	116675
Hirosawa, K. +	116685	+Holtzberg, F.	114674	+Hornby, P.G. +	111479			+Innis, J.L.	116681
+Hirose, N.	113535	+Holub, F.	115081	+Hornby, P.G. +	111479			+Inomata, H.	116205
+Hirota, E.	112718	+Holzhauer, E.	113652	+Hornby, P.G. +	111479			Inomata, T. +	113473
+Hirota, J.	112211	+Homentcovschi, D.	113482	+Hornby, P.G. +	111479			Inomata, Y.	115130
+Hirota, J.I.	112227	+Homer, R.J.	112031	+Hornby, P.G. +	111479			+Inoue, H.	111777
+Hirota, T.	114916	+Homma, M.	114708	+Hornby, P.G. +	111479			+Inoue, M.	112161
Hirschfelder, U.	115910	Honciu, M. +	114771	+Hornby, P.G. +	111479				

- +Inoue, N. 113163
 +Inoue, N. 111648
 +Inoue, N. 114191
 +Inoue, N. 111811
 Inoue, S. + 114384
 +Inoue, S. 115667
 Inoue, T. + 112214
 +Inoue, T. 112484
 +Ioffe, V.A. 114666
 +Ilogansen, L.V. 113096
 +Ionov, A.P. 114553
 +Ionov, S.N. 113834
 Iorio, I. De. *see* De Iorio, I.
 +Iosilevskii, I.L. 113569
 +Ipatov, V.M. 114969
 +Ipatova, L.P. 114808
 +Iphorski, M. 115196
 Ireland, J.C. + 115987
 +Ireland, T.R. 116044
 +Iriyama, H. 113898
 +Ironsde, C.N. 111776
 Irvine, P.A. + 112739
 +Irzhak, V.I. 115252
 +Isaacs, H.S. 115409
 Isenberg, A. + 113730
 Iseri, Y. + 112226
 +Iseri, Y. 112230
 Isern, J. + 116648
 Isett, L.C. 115632
 Isherwood, M.C. + 113633
 +Isherwood, M.C. 116234
 +Ishi-da, Y. 115491
 Ishibashi, K. + 114376
 +Ishibashi, S. 115781
 +Ishida, K. 113169
 +Ishida, N. 112609
 Ishida, Y. + 115005
 +Ishida, Y. 113978
 +Ishida, Y. 114273
 +Ishida, Y. 113122
 +Ishida, Y. 113137
 +Ishida, Y. 113973
 +Ishida, Y. 113974
 +Ishihara, N. 112550
 +Ishii, H. 116038
 +Ishii, N. 114735
 +Ishii, S.I. 113250
 +Ishii, T. 115248
 Ishii, T.K. 115432
 Ishikawa, J. + 111813
 Ishikawa, K. + 111969
 +Ishikawa, K. 114334
 +Ishikawa, M. 112228
 +Ishikawa, T. 113735
 Ishimasa, T. + 113857
 +Ishimatsu, T. 112235
 +Ishimura, T. 113645
 +Ishino, S. 113993
 +Ishioka, K. 115964
 Ishioka, S. + 114245
 Ishitani, T. 111812
 Ishizaka, K. + 116085
 Ishizaki, Y. + 112211
 Ishizawa, Y. + 116426
 +Ishizawa, Y. 115025
 +Ishizawa, Y. 115024
 +Ishwar, B. 111418
 Isichenko, M.B. + 113623
 Ishihara, A. + 114459
 +Isikawa, T. 114844
 Iskandar, M. + 113725
 +Iskander, M.F. 115829
 Iskhakov, R.S. + 114714
 Islam, J.N. 116901
 +Islam, M.N. 112913
 +Isotani, S. 115593
 +Isotani, S. 114731
 Isoya, A. + 112522
 +Isoya, A. 112214
 +Isoya, J. 114724
 +Isozaki, T. 112414
 Israel, R. + 113492
 Israel, W. 116739
 Isserstedt, J. + 116668
 +Isserstedt, J. 116652
 +Isshiki, M. 114522
 +Itahashi, T. 112207
 +Itahashi, T. 112229
 +Itano, A. 112466
 +Itikawa, Y. 111323
 +Ito, H. 115714
 +Ito, H. 113645
 Ito, K. + 113969
 +Ito, K. 114214
 +Ito, R. 111323
 +Ito, T. 115891
 Ito, Y. 114736
 +Ito, Y. 113645
 +Ito, Y. 112861
 Itoh, K. + 113631
 Itoh, N. + 113911
 +Itoh, N. 111323
 +Itoh, N. 114993
 +Itoh, S.-I. 113631
 +Itoh, T. 113881
 +Itskovich, G.B. 116310
 Itzykson, C. + 111871
 Iudice, N. Lo 111871
see Lo Iudice, N.
- +Iura, K. 112235
 +Ivanchenko, V.M. 111805
 +Ivanenko, V.A. 115469
 +Ivanitskii, V.P. 115055
 Ivannikov, A.N. + 113240
 +Ivanov, A.F. 113636
 Ivanov, A.G. + 115204
 +Ivanov, A.G. 115260
 Ivanov, A.V. + 113678
 +Ivanov, B. 115826
 Ivanov, N.R. + 114796
 +Ivanov, R.M. 112590
 Ivanov, V.A. + 112824
 +Ivanov, V.A. 116100
 +Ivanov, V.K. 114217
 Ivanov, V.N. + 116209
 +Ivanov, V.N. 111624
 Ivanov, V.V. + 114508
 +Ivanov, Yu.A. 116122
 Ivanov-Kholodnyy, G.S. + 116345
 Ivanov-Omskii, V.I. + 114448
 Ivanova, N.V. + 112655
 Ivanova, Ye.V. + 116268
 Ivanovskii, A.L. + 114443
 Ivanovskii, M.N. + 115573
 Ivanskii, A.E. + 115485
 +Ivchenko, I.S. 113638
 +Ivchenko, V.I. 113795
 +Ivent'eva, O.O. 115650
 +Ivochkin, Yu.P. 113529
 +Iwai, T. 115417
 Iwaki, M. 114308
 +Iwamoto, I. 113671
 +Iwamoto, K. 112160
 Iwanaga, H. + 113927
 +Iwanow, G. 115330
 Iwao, S. 111912
 Iwasaki, H. + 114316
 Iwasaki, H. + 114985
 +Iwasaki, M. 112758
 +Iwasaki, Y. 112211
 +Iwase, A. 114061
 +Iwata, T. 114296
 +Iwata, T. 114061
 +Iwata, T. 114957
 +Iwatake, B.T. 116101
 +Iyengar, P.K. (ed.). 111334
 +Iyengar, R. 113157
 Izotov, V.I. + 115257
 +Izui, K. 113893
 +Izumoto, T. 112115
 +Izovchikov, A.B. 113570
- Jaanimagi, P.A. + 111852
 Jaaskelainen, M. + 112059
 +Jaaskelainen, M. 112049
 +Jaaskelainen, M. 112261
 +Jaber, M. 112744
 Jaccodine, R. 114276
 +Jaccodine, R.J. 114193
 +Jacholkowska, A. 112028
 Jacinto, N. + 115176
 +Jack, M.A. 113213
 +Jackson, K. 111752
 +Jackson, P.O. 115935
 +Jackson, R.H. 113003
 Jacob, M. (ed.). 111319
 Jacobi, A., Jr. 112322
 +Jacobi, K. 114358
 Jacobs, E.L. + 112548
 +Jacobs, U. 112015
 +Jacobson, A.S. 116826
 +Jacquot, B. 112498
 Jacucci, G. + 115448
 +Jacucci, G. 113860
 Jady, R.J. + 116003
 +Jae Hyun Oh 115174
 +Jae Hyun Oh 115391
 +Jae-Eun Kim 115222
 Jaen, J. + 114765
 +Jaenicke, R. 116261
 Jager, C. de. *see* de Jager, C.
 +Jager, D. 113049
 +Jahn, G. 115784
 Jain, S.C. + 115660
 Jain, V.K. 114728
 Jain, V.K. + 113605
 Jaklevic, J.M. + 112564
 Jakobsson, B. 112268
 +Jakosky, B.M. 116508
 Jalil, M.A. Abdul 111771
see Abdul Jalil, M.A.
 James, D.R. + 114771
 James, M.B. + 112471
 +Jameson, R.F. 116696
 Jamgotchian, H. + 115182
 +Jan, K.-M. 115816
 +Jang, L.Y. 114758
 Jang Shain-Way 111871
see Shain-Way Jang
 +Jani, P. 111634
- +Janicke, L. 116605
 +Jank, W. 112031
 +Janki, M.E.K. 115421
 Janseen, L.J.J. + 115565
 +Jansen, R. 115653
 +Janssens, M. 115660
 +Janssens, R.V.F. 112058
 Jansson, J.-F. + 115363
 +Janta, J. 113087
 +Janzen, E. 114476
 +Jarczyk, L. 112241
 +Jargocki, C.P. 111973
 +Jarkskog, G. 112024
 Jarlborg, T. + 114431
 +Jaroneic, M. 114331
 Jaronec, M. + 114369
 +Jaros, J.A. 112011
 +Jaroszynski, M. 116888
 +Jarzynski, J. 113185
 Jaske, C.E. 113354
 +Jasperse, J.R. 116391
 +Jasso, G.L. 115157
 +Jastrzebski, L. 114940
 Jata, K.V. + 113908
 +Jauncey, D.L. 116814
 +Jauncey, D.L. 116803
 Javel, E. + 115806
 +Jayasuriya, D.A.R. 116208
 +Jaywant, S.M. 112712
 +Jean, J.H. 115134
 Jeanloz, R. 116048
 Jeanloz, R. + 116083
 +Jeannot, F. 114967
 +Jeavons, A.P. 112535
 Jedral, L. + 115110
 +Jeevan Lal 116013
 +Jefford, C.W. 115529
 +Jeffreys, P. 112024
 Jegering, R. 111793
 +Jele, V.G. 111832
 +Jellison, G.E., Jr. 114011
 Jena, S.N. + 111987
 Jeng Shian-Woei 115116
see Shian-Woei Jeng
 +Jenkins, G.M. 115116
 Jenkins, J.C. + 115116
 +Jenkins, J.J. 113215
 Jenkins, R.B. + 114264
 Jenkins, W.J. + 116148
 +Jenni, P. 112022
 Jennings, M.C. 116873
 +Jennings, P.J. 114363
 Jensen, A.S. + 112290
 +Jensen, A.S. 112032
 +Jensen, D.E. 113554
 Jensen, H.P. 114802
 Jensen, K.F. + 115085
 +Jensen, K.F. 115078
 +Jensen, S.J.K. 114349
 Jensen, V.O. 112440
 Jentsch, D. + 113817
 Jeon Seung Ho 115116
see Seung Ho Jeon
 +Jerabek, J. 111855
 Jergel, M. + 114631
 +Jerrestam, D. 112558
 +Jesser, W.A. 113543
 Jesus, A.P. + 112828
 Jetten, L.A.M.J. + 113782
 Jetten, L.A.M.J. + 113790
 Jeu, W.H. De. *see* De Jeu, W.H.
 Jeutter, D.C. 115954
 +Jewulski, J. 112361
 +Jeyens, C. 115106
 +Jeys, T.H. 112988
 Jezewski, D.J. 116430
 Jezewski, D.J. 116431
 Jha, S. + 112247
 +Ji-Liang Doong 113329
 Ji-min Wu. *see* Wu Ji-min
 Ji-Wen Teng 115174
see Teng Ji-Wen
 Jian-feng Liu 115174
see Liu Jian-feng
 Jian-guo Shen 115174
see Shen Jian-guo
 Jian-Lin Mi. *see* Mi Jian-Lin
 Jian-Wen Shen 115174
see Shen Jian-Wen
 Jiang Bin-Yao + 112500
 +Jiang Chuen-hua 112581
 Jiin Chang Shaw + 111862
 J.I. Katz. *see* Katz, J.I.
 Jin Li 114485
 Jin-Shen Luo 114485
 Jin-Zhi Xia. *see* Xia Jin-Zhi
 Jindal, V.K. + 114108
 Jing Zheng Ou Yang. *see* Ou Yang
 +Jing 115174
 +Jing-xian Lu 115174
see Lu Jing-xian
 +Jiunn Chuu Chen 111862
 +Justo, J.E. 116176
 +Job, B.E. 112715
 +Johansson, K.E. 112553
 +John, J. 111860
 +Johnsen, R. 116330
- +Johnsen, R.M. 114223
 +Johnson, A. 112292
 +Johnson, A.D. 112011
 Johnson, B.M. 112845
 +Johnson, D.L. 113176
 +Johnson, D.L. 113177
 Johnson, F.D. + 113427
 +Johnson, G.E. 112949
 +Johnson, J.R. 111992
 +Johnson, K.F. 111999
 +Johnson, K.J. 112542
 Johnson, K.L. 113314
 Johnson, N.M. + 114612
 Johnson, N.M. + 114475
 +Johnson, N.M. 114018
 Johnson, P.D. + 112509
 +Johnson, P.H. 115833
 +Johnson, R.G. 116388
 Johnson, S.A. + 115711
 Johnson, S.M. + 113930
 +Johnson, S.T. 113988
 +Johnson, T.L. 113215
 Johnson, W.B. + 115949
 +Johnson, W.L. 113756
 +Johnson, W.W. 111537
 Johnston, M.G. 111655
 Johnston, W.D., Jr. 113915
 +Johnston, W.D., Jr. 114593
 +Joiner, R.G. 116359
 +Jon, G.C. 112234
 Jon-Chi Chang + 112963
 Jon-Chi Chang + 112964
 +Jonathan, J.M.C. 113083
 +Jones, A.R. 113562
 +Jones, C.D. 116181
 +Jones, C.L. 113778
 Jones, D.T.L. + 112571
 Jones, E.W. + 112447
 Jones, F.R. + 115377
 Jones, H.P. + 116598
 Jones, J.C. + 115556
 +Jones, J.D. 113429
 +Jones, K.W. 112578
 +Jones, P.G. 113817
 +Jones, R. 111754
 Jones, R.H. + 114049
 Jones, R.H. + 111629
 +Jones, R.H. 111628
 +Jones, R.T. 112507
 +Jones, R.W. 112799
 +Jones, T.B. 115912
 Jones, T.J. + 116802
 Jones, T.J. + 116852
 +Jones, T.J. 116849
 Jones, W.B. 112999
 Jong, M.S. de. *see* de Jong, M.S.
 Jong-Ok Woo 115116
see Woo Jong-Ok
 Joon Oh In. *see* In Joon Oh
 +Jopson, H. 114513
 +Jorat, G. 112031
 +Jordan, D.W. 115911
 +Jordan, J.R. 115612
 +Jordon, K.D. 115529
 Jorgensen, C.K. + 114888
 +Jorgensen, L. 113297
 +Jorgensen, P. 112807
 Joshi, D.P. + 114548
 +Joshi, M.C. 114552
 Joshi, S.V. + 114552
 +Jossic, T. 115426
 +Joswig, H. 112842
 +Jourdain, J.C. 112158
 +Journé, V. 112016
 +Joussot, J.C. 114035
 +Jouze, B. 113630
 Jozwiak, Z. + 115873
 Jubert, A.H. + 114857
 Jug, K. + 112658
 Julg, A. + 113781
 +Julian, G.M. 112247
 +Julien, R. 112043
 +Jumonji, H. 111652
 Jun Soo Kim + 115391
 Jun Soo Kim + 115174
 +Jung, P. 114906
 Jung Ai-Lien. *see* Ai-Lien Jung
 +Junge, H. 112015
 +Jungerman, R.L. 113126
 Junginger, H. + 116402
 Jungman, A. + 113161
 +Jupen, C. 115545
 +Juraszek, D. 113656
 +Jury, J.W. 112599
 +Jury, J.W. 112217
 Jusino, B.J. 112390
 +Jyoti, B.G. 113629
- +Kabes, A.I. 115221
 +Kable, S.H. 112822
 +Kac, M. 111595
 +Kachanov, V.A. 112556
 +Kachi, S. 113132
 +Kachurin, G.A. 113941
 +Kacir, L. 115293
 Kadane, J. + 115811
 +Kader, H. 112067
 +Kadish, K.M. 115530
 +Kado, H. 111990
 +Kado, H. 112012
 +Kadota, K. 113567
 +Kadota, Y. 112210
 +Kadota, Y. 112051
 +Kadyk, J.A. 112011
 Kafadar, K. + 115601
 +Kafadar, K. 111781
 Kafatos, M. + 116737
 +Kagawa, Y. 113174
 Kahana, S. + 112259
 Kahane, A. + 113032
 Kahler, S.W. + 116600
 Kahmen, H. + 116313
 +Kahn, D. 112451
 Kai, K. + 113749
 Kai, K. + 116573
 +Kai, K. 113751
 +Kai, K. 116623
 +Kaidanov, A.I. 113999
 +Kaifu, N. 116781
 +Kailas, S. 112143
 +Kaimal, J.C. 116183
 +Kaimal, J.C. 116182
 Kaiser, A.B. 114563
 +Kaiser, H. 111491
 Kaiser, N. 116894
 Kaiyumov, Kh.M. 115933
 Kajwadkar, A.P. + 111477
 Kajwadkar, A.P. + 112864
 +Kakazei, N.G. 113953
 +Kako, M. 113645
 +Kakusho, O. 113209
 Kalasinsky, V.F. + 112742
 Kalbermann, G. + 112284
 +Kalenki, J. 112749
 +Kaleps, I. 115815
 Kaletnik, A.Yu. + 115308
 Kalghatgi, G.T. 115553
 +Kalinin, A.E. 113845
 Kalinin, V.B. + 113794
 Kalinin, V.B. + 113820
 Kalinin, Yu.D. + 116008
 +Kalinin, Yu.K. 116345
 +Kalinin, Yu.V. 114627
 +Kalinina, N.N. 115952
 +Kalinkin, I.P. 114176
 +Kalinovsky, A. 112024
 Kalitetskii, N.I. + 111780
 +Kallmann, E. 115669
 +Kalmus, P.I.P. 112031
 Kalsi, H.S. + 115145
 +Kalus, J. 114108
 +Kalvius, G.M. 112529
 +Kamakura, K. 112609
 Kamal, M.R. + 115332
 +Kamalov, G.L. 113839
 +Kamalov, S.S. 112171
 Kamalov, V.F. + 114893
 Kamata, M. 111928
 Kambara, H. + 111802
 +Kambara, T. 112484
 Kamenetskias, Yu. + 115484
 +Kamenetskaya, D.S. 115177
 Kamenkovich, V.M. + 116126
 Kamide, Y. 113074
 Kamigaki, N. + 113897
 Kamimura, M. + 112230
 +Kamin, S. 111615
 Kaminishi, K. + 112185
 +Kamino, T. 113889
 +Kamins, T.I. 114014
 +Kamins, T.I. 114016
 Kaminskii, A.A. 113002
 +Kaminskii, V.F. 113848
 +Kaminskii, V.F. 113854
 +Kamiya, K. 115734
 Kamma, C.M. + 115211
 +Kammerman, L.A. 115929
 Kammeyer, P.C. 116429
 +Kammuri, T. 112279
 +Kammuri, T. (ed.). 111309
 Kamo, M. + 115030
 Kamon, T. + 112545
 Kamper, B. 116708
 Kamran, N. + 115058
 +Kamys, B. 112241
 +Kamzina, L.S. 114830
 Kanai, T. + 115924
 Kanaun, S.K. 111436
 Kanaya, K. + 112892
 +Kanazawa, I. 113861
 +Kanazawa, I. 114745
 Kanbach, G. 116720
 Kanbach, G. + 116727
 +Kanbe, H. 114594
 Kane, M.J. + 114492

- Kane, S.R.116587
 + Kane, S.R.116573
 + Kaneda, R.111632
 Kaneiwa, S. +114389
 Kaneko, M. +115916
 + Kaneko, M.114377
 + Kaneko, T.114509
 Kaneko, Y. +115022
 Kanematsu, K. +111402
 + Kaneta, K.114770
 + Kangas, J.116406
 Kanicki, J. +115654
 + Kano, K.111410
 Kanstad, S.O. +111774
 Kant, R.113356
 + Kantele, J.112043
 + Kantele, J.112111
 + Kanzaki, J.111990
 + Kanzaki, J.112012
 Kanzaki, S. +115156
 Kao, C.K.111330
 + Kapitza, H.112015
 Kaplan, I.G. +112583
 Kaplan, M. +112271
 Kaplan, V.P. +115843
 Kaplan, V.P. +115844
 Kaplun, V.A. +112909
 + Kaplunenko, V.T.115347
 + Kapon, E.116007
 + Kapon, E.113009
 + Kapor, D.111612
 + Kappert, H.F.115073
 + Kapral, R.113043
 + Kaptsevich, V.M.114096
 + Kapusta, F.112016
 + Karagiozova, St.114677
 + Karamov, A.G.113938
 Karapetian, A.V.113267
 + Karashima, S.115265
 + Karavaev, V.G.113786
 Kardashev, N.S. +116829
 Kardos, J.L. +115293
 + Kareva, N.T.115308
 Kargin, Yu.F. +113821
 + Karimaki, V.112031
 + Karimov, B.T.116418
 Karkheck, J. +113542
 Karlhede, A. +115106
 + Karnaukhov, A.M.114623
 Karney, C.F.F.111588
 + Karthaler, H.P.113917
 + Karolewski, M.A.114342
 Karpinos, D.M. +115158
 + Karplus, M.112653
 Karpova, I.A.115922
 + Karpov, R.R.116892
 Karson, J.A. +116066
 + Kartenko, N.F.113776
 + Karunasiri, R.P.G.114467
 + Karyakin, E.N.112728
 + Karzov, G.P.115347
 Kasagi, J. +112200
 Kasahara, Y. +111770
 Kase, M. +112484
 + Kashaev, Yu.G.115204
 Kashcheev, V.N.114657
 Kashcheev, V.N.115373
 + Kashaeva, T.N.112714
 + Kashima, N.111746
 + Kashima, Y.115634
 Kashkarov, S.S.116275
 + Kashnikov, B.P.113958
 + Kashy, E.112200
 + Kasir, F.A.114505
 + Kaspar, H.111999
 + Kaspar, H.112007
 + Kasperek, V.113825
 Kasperek, W. +113652
 Kasper, G. +115588
 + Kassam, S.A.113206
 + Kast, W.115666
 + Kast, W.115697
 Kasten, W. +112715
 + Kastenbergh, W.E.112407
 + Kastner, M.A.114919
 + Kat, D.113217
 + Kataev, B.S.112865
 + Kataevsky, Yu.F.115923
 + Katano, S.114109
 + Kataria, N.D.114622
 + Kataria, N.D.114646
 + Kataria, N.D.111693
 + Katayama, I.112076
 + Katayama, I.112207
 + Katayama, I. (ed.)111309
 + Katayama, K.115407
 + Katem, B.116766
 Kato, H. +111389
 + Kato, H.115918
 + Kato, K.115916
 + Kato, N.112277
 Kato, S. +112051
 + Kato, S.112210
 + Kato, S.112211
 + Kato, S.112225
 + Kato, S.112227
 + Kato, T.115667
 + Kato, T.113979
 + Kato, T.112485
 + Kato, Y.113122
 + Kato, Y.113011
 + Kato, Z.115125
 + Katoch, D.C.113442
 + Katoh, Y.114644
 + Katona, P.G.115821
 + Katona, T.112422
 + Katori, K.112207
 + Katori, K.112212
 + Katsube, K.112235
 + Katsufraakis, J.116359
 + Katsumata, I.111810
 Katsuta, H. +114180
 + Katsuyama, Y.113137
 + Katsuyuba, O.A.111656
 Katz, J. +113007
 Katz, J. +113009
 Katz, J.L. +115535
 + Katz, W.113942
 Katz, J.I.116879
 + Kaufman, H.R.112512
 + Kaufman, S.B.112126
 Kaufmann, H.-J. +114078
 + Kaufmann, R.L.116396
 Kaufmann, W.B. +112282
 + Kaup, U.112109
 + Kavalero, G.I.111624
 + Kavanagh, K.114054
 + Kaverina, N.V.115773
 + Kawabata, K.116576
 + Kawabata, N.114788
 Kawabe, R. +112408
 + Kawachi, K.115924
 Kawaguchi, H. +113005
 + Kawai, M.115262
 + Kawai, H.112226
 + Kawai, S.115046
 Kawakami, T. +113029
 + Kawakami, Y.113645
 + Kawamoto, T.111990
 + Kawamoto, T.112012
 Kawamura, N. +112235
 Kawamura, T. +113622
 + Kawano, S.115034
 Kawasaki, S. +112478
 + Kawashima, I.115605
 + Kawata, K.112780
 Kawata, S. +113628
 + Kawatsura, K.114974
 Kawbata, K. +116575
 Kawohl, B.113400
 Kawski, A.112696
 Kay, K.G.111547
 + Kay, P.112324
 + Kayano, H.115418
 + Kayano, H.114043
 + Kaye, H.S.111992
 + Kayuk, V.G.115141
 Kayuk, Ya.F. +113287
 + Kaza, B.R.114929
 + Kazakov, S.V.114231
 Kazanas, D. +116887
 + Kazanova, N.P.111642
 + Kazanskii, V.B.115544
 Kazantsev, Yu.I. +111718
 + Kazaryan, A.R.111551
 + Kazes, I.116785
 + Kazmerski, L.L.115635
 + Ke-Jian Fu.112802
 + Ke-qui, L.115812
 + Kebekus, B.115709
 + Kechouane, M.114030
 + Kechouane, M.114483
 Kedro, M.114289
 + Kee Dae Lee.115183
 Keel, W.C.116809
 Keel, W.C.116847
 + Keeler, R.112031
 + Keen, C.E.116024
 Keen, K. +115796
 + Keer, L.M.113376
 Keyges, A.111796
 + Kehrer, H.-P.115396
 Keijsers, T.H. de
 + Keijsers, T.H. de
 + Keil, S.L.116613
 + Keilis-Borok, V.I.116025
 + Keilmann, F.114542
 Keinigs, R.K.113612
 + Keinonen, J.112033
 Keir, R.S.116093
 + Keirim-Markus, I.B.115854
 + Keitel, R.114767
 + Keitel, R.114247
 Keiter, R.L.111367
 + Keith, G.115751
 + Kelarev, V.V.114671
 Kelha, V. +115493
 + Keller, D.112931
 Keller, H.B. +116309
 + Keller, J.G.112133
 + Keller, R.113630
 + Kello, V.112634
 Kellogg, G.L.115027
 + Kellogg, P.J.116357
 + Kellogg, R.G.112015
 Kelly, J.M.112418
 + Kelly, J.M.112312
 + Kelly, W.H.111340
 Kemeny, T. +114146
 + Kemme, A.A.113838
 + Kemmer, J.112554
 + Kemppainen, M.115356
 + Kendig, M.W.115459
 + Kenig, V.114832
 Kennedy, M.A. +114139
 Kennedy, T.C. +112335
 Kennett, J.P.116145
 Kennicutt, R.C. +116812
 Kenny, L.C. +111764
 + Kent, S.M.116812
 + Kenyon, I.112031
 Kenyon, S.J. +116660
 + Kerek, A.112544
 + Kerker, M.114840
 Kerman, B.R. +116090
 + Kermod, J.P.115163
 + Kern, Th.112060
 + Kernal, A.112031
 Kernel, G. +112589
 Kerner, B.S. +113690
 + Kerner, R.115154
 + Kesler, Ya.A.114709
 + Kessel, P.G.111434
 + Kessler, G.112024
 + Kestner, G.113918
 + Kesztelyi, B.116097
 + Ketterson, J.B.114650
 + Keyes, T.111540
 Khabibullaev, P.K. +113866
 Khac Hein Le.
 + Khac Hein Le.
 + Khachin, V.N.115194
 + Khain, A.P.116209
 + Khairullina, A.Ya.115591
 Khalatur, P.G. +114820
 + Khalifin, V.B.114980
 + Khalifin, V.B.114543
 + Khalileev, P.A.111714
 + Khalilov, Sh.S.114432
 Khalilov, V.R.112968
 Khallaf, S.A.E.112238
 Khalsa, S.J.S.116091
 + Khan, A.113828
 + Khan, A.116174
 + Khan, A.112190
 + Khan, A.H.113511
 Khan, R.U. +114601
 Khan Malek, C. +114500
 Khanal, U.116738
 + Khanchich, O.A.114171
 + Khandros, L.G.115192
 + Khanin, V.A.114178
 + Khanina, Z.K.115438
 + Khanna, S.K.113756
 Khapchava, Yu.P. +113698
 + Khapchava, L.I.113844
 Kharchenko, V.A.114454
 + Kharchenko, V.K.115229
 Khar'kov, E.I. +114506
 + Khasanov, E.115688
 + Khasanova, M.115691
 + Khattak, C.P.113069
 + Khavin, B.S.113739
 + Khazanov, G.V.116347
 Khenven, A.R. +113504
 + Khetrapal, C.L.114742
 Khil'chevskii, V.V. +114721
 Khlabin, V.G. +114977
 + Khlébopros, R.G.114714
 + Khlöpin, A.N.112843
 + Khodzhashvili, G.L.115972
 + Kholev, S.R.113683
 + Kholmetskii, A.L.112537
 + Kholodnyi, V.I.115335
 + Khomenko, S.V.113681
 + Khomutinina, A.D.114526
 Khondker, A.N. +114530
 Khoo, I.C. +113733
 Khoo, T.L. +112058
 + Khoo, T.L.112036
 + Khoruzhii, A.G.115509
 + Khoruzhii, S.S.111905
 + Khrantsov, V.A.113910
 + Khranovskii, V.A.112753
 Khrapunov, S.N. +115732
 Khragian, A.Kh. +116245
 + Khuri-Yakub, B.T.113126
 + Ki-Jun Lee.115044
 + Kiang, G.C.112208
 + Kiang, G.C.112234
 + Kiang, L.L.112234
 + Kido, H.115125
 Kidson, G.V.113985
 + Kiefer, J.114425
 + Kieffer, J.112816
 Kienle, W. +113706
 + Kiesling, C.112016
 Kieu, T.D. +113581
 Kihara, M. +111652
 Kihara, N. +111794
 + Kihara, R.112483
 Kikkawa, S. +115958
 + Kiko, J.116551
 Kikuchi, K. +112334
 Kikuchi, M.115975
 Kikuchi, M. +115231
 + Kikuchi, M.112235
 + Kikuchi, T.112325
 Kikuchi, Y. +112409
 + Kikuta, S.113752
 Kilaas, R. +113708
 + Kildal, P.-S.116295
 + Kildir, M.112271
 + Kilin, S.F.112573
 Killean, K.P. +112982
 + Killian, T.112024
 + Killner, I.112612
 + Kim, C.115314
 Kim, C.J.111749
 + Kim, D.M.114530
 + Kim, J.114419
 + Kim, J.115094
 + Kim, J.-G.114385
 Kim, K.S. +113728
 Kim, M.S. +115101
 Kim Dae Soo.
 + Kim Dae Soo.
 Kim Dong-Ha.
 + Kim Dong-Ha.
 Kim Doo Han.
 + Kim Doo Han.
 Kim Hyun Gun.
 + Kim Hyun Gun.
 Kim Jae-Eun.
 + Kim Jae-Eun.
 Kim Jun Soo.
 + Kim Jun Soo.
 Kim Tai-Ung.
 + Kim Tai-Ung.
 Kim Young-Gil.
 + Kim Young-Gil.
 Kim Young-Il.
 + Kim Young-Il.
 Kimel'fel'd, Ya.M.112793
 Kimura, H. +115047
 + Kimura, H.115351
 + Kimura, H.115197
 Kimura, K. +112777
 Kimura, M. +113132
 + Kimura, S.116037
 + Kimura, T.112995
 + Kimura, T.115407
 + Kimura, T.113149
 + Kimura, T.113092
 Kimura, Y.112235
 + Kind, R.116028
 + Kinder, T.H.116141
 + Kindrat, M.M.114971
 + King, B.T.112015
 King, D.A.114310
 + King, D.A.114345
 + King, D.A.114346
 + King, J.W.116376
 + King, M.M.112092
 + King, N.S.P.112149
 + King, T.A.114852
 King, W.E. +113990
 King, W.E. +114033
 + Kingsley, S.P.116328
 Kingston, A.E. +112858
 + Kingston, A.E.116468
 + Kinkead, A.K.113003
 + Kinnear, J.E.115936
 + Kinnunen, R.112031
 + Kinny, P.D.116044
 + Kino, G.S.113126
 Kino, T. +113873
 + Kino, T.113975
 + Kino, T.113897
 Kinoshita, C. +113889
 Kinoshita, C. +113902
 + Kinoshita, C.114038
 Kinra, V.K. +113344
 + Kinsbron, E.115383
 + Kinser, D.L.114733
 + Kinson, J.B.112020
 + Kiplinger, A.L.116592
 Kirby, S.111675
 Kircheva, P.P.112768
 Kircheva, P.P. +112801
 Kirchner, E.R. +115558
 Kirejczyk, J.113484
 + Kirillov, V.V.113669
 + Kiriluk, K.V.114396
 + Kirilyuk, L.M.115098
 + Kiritani, M.113971
 + Kiritani, M.114061
 + Kiritani, M.113934
 + Kirkbride, R.112305
 + Kirkman, I.W.116747
 + Kirov, S.A.114681
 Kirsanov, V.V. +112651
 + Kirschbaum, E.114225
 + Kirsten, T.116551
 Kiryu, T. +115964
 + Kirzhnits, D.A.114773
 Kis, K.116010
 Kiselev, A.P.113345
 + Kiselev, D.F.114824
 + Kiseleva, S.G.112021
 Kishida, K. +115630
 Kishimoto, N. +115583
 + Kishimoto, T.112218
 Kishimoto, Y. +114956
 + Kishore.115419
 + Kishore.115217
 + Kishore.115367
 Kishore, K. +115557
 Kisker, E.112916
 + Kiss, L.114765
 Kissel, L. +111320
 + Kisslinger, L.S.112080
 + Kitagawa, K.113894
 + Kitagawa, K.113895
 Kitagawa, M.112606
 Kitagawara, Y. +112617
 + Kitahama, K.115046
 Kitai, R.116606
 Kitajima, K.114059
 Kitajima, K. +113900
 + Kitajima, K.114962
 + Kitajima, K.114963
 + Kitajima, K.114039
 + Kitajima, K.113980
 Kitajima, S. +113650
 + Kitajima, S.113902
 + Kitajima, S.114038
 Kitamori, S.115807
 + Kitamura, J.113536
 + Kitamura, K.116262
 + Kitamura, K.111641
 + Kitamura, T.113371
 Kitayama, K. +113122
 Kitazawa, T. +115607
 Kitowski, J.112364
 Kittaka, T. +114047
 Kittl, P.113349
 + Kiyose, R.112352
 + Kjellsson, L.114405
 Kjems, J.K. +114250
 + Kjems, J.K.114174
 + Klages, H.O.112197
 + Klanner, R.112554
 Klapisch, R.112026
 Klamunzer, S. +114058
 + Klamunzer, S.113961
 + Klaus, R.F.113187
 Kleban, P. +111602
 + Kleczek, J.116615
 Klee, K.-D. +113282
 + Klein, B.113825
 + Klein, B.114501
 + Klein, B.M.114436
 Klein, M.L. +114101
 Klein, N. +114630
 + Klein, W.111350
 + Klement, T.113018
 + Klemm, R.A.114700
 Klemperer, D. (ed.)111311
 Klepser, Ya.Ya. +114269
 Kleppinger, E.W. +112194
 Kleva, R.G. +112518
 + Klewe-Nebenius, H.112524
 + Klewe-Nebenius, H.112114
 Klim, B.P. +111737
 Klimenko, V.N. +115141
 + Klimenko, Z.K.115857
 Klimkova, V.115777
 + Klimov, A.I.112513
 Klimov, V.V. +115148
 + Klimova, A.Yu.113910
 Klinger, D.J. +114304
 Klinker, T. +111607
 Klipping, G.116475
 Klipping, G. +111692
 Klobukowski, M.112678
 Klokocnik, J.115994
 + Klokocnik, J.115995
 + Klovning, A.112015
 Kluberger-Stern, H. +111873
 Klug, D.D. +112734
 + Kluge, W.112532
 + Klygin, A.V.113530
 + Knapp, G.R.116795
 + Knapp, G.R.114649
 Knapp, J.A. +114031
 + Knauss, W.G.113375
 Knauth, H.-D. +116201
 + Knecht, D.J.116400
 + Kneip, T.J.115712
 + Kneip, T.J.115709
 + Kneubühl, F.K.114847
 + Knies, G.112015
 + Knight, A.E.W.112822
 Knight, C.A.113783
 + Knight, D.G.112815
 Knight, F.K.116721
 + Knobloch, J.A. (ed.)111313
 Knoblauch, G. +113136
 + Knobler, C.M.114128
 + Knoche, K.F.115681
 Knoll, J.112265
 + Knorr, K.114174
 Knude, J.116791
 + Knudson, J.M.112562
 + Knunyants, I.L.113852
 + Knupfer, W.112176

- +Knupfer, W. 112174
+Knutson, E.O. 115946
+Ko, C.M. 112115
+Koabayshi, S. + 112995
+Koba, K. 112609
+Kobashi, K. + 114102
+Kobasho, N.I. 115229
+Kobayashi, A.S. 113290
+Kobayashi, F. 112325
+Kobayashi, H. 111696
+Kobayashi, H. 113137
+Kobayashi, K. 112522
+Kobayashi, K. 111735
+Kobayashi, K. 113011
+Kobayashi, M. + 115701
+Kobayashi, N. 115706
+Kobayashi, R. 115356
+Kobayashi, S. 111735
+Kobayashi, S. 112225
+Kobayashi, T. 111990
+Kobayashi, T. 112012
+Kobelev, L.Ya. 114772
+Koberstein, J.T. + 113763
+Kobiyama, M. 114046
+Kobka, V.G. + 115075
+Kobriniski, M.N. 111966
+Kobyakov, I.B. + 114790
+Kocevar, P. 114531
+Koch, H. 112544
+Koch, J.E. 112413
+Kocher, D.C. 115928
+Kocher, D.G. 111733
+Kochev, K. + 115563
+Kochsiek, M. + 111650
+Kochubei, A.D. + 111536
+Kock-Yee Law + 112949
+Koda, M. 114286
+Kodaïra, K. 115038
+Kodaïre, K. 115880
+Koehler, J.S. 113887
+Koehler, W.C. 114673
+Koelbel, R. 115981
+Koening, J.L. + 115295
+Koening, J.L. 113764
+Koening, L.R. + 116225
+Kofod-Hansen, O. 112022
+Kogan, L.R. 116806
+Kohe, T. 112470
+Kohl, W. 113888
+Kohli, J.M. 112028
+Kohmoto, T. + 114257
+Kohnlein, D. + 114746
+Kohn, T. 112117
+Kohoutek, L. 116653
+Kohriki, T. 112550
+Koike, K. 111946
+Koike, M. + 113970
+Koike, S. 114962
+Koike, Y. 115810
+Koima, M. 114245
+Kok, L.P. 112081
+Kokame, J. + 112609
+Kokhanovskii, S.I. + 114868
+Kokhanovskii, S.I. 114448
+Kokhova, I.I. + 115614
+Kokorev, V.N. + 115542
+Kokoszka, G.F. + 114491
+Kolachev, B.A. 115336
+Kolawole, L.B. 116363
+Kolb, B. 112113
+Kolchin, O.P. 114306
+Kol'chugin, B.D. 112974
+Kolesnik, A.G. + 116324
+Kolesnikov, Yu.B. + 113426
+Kolesnikova, A.I. 115843
+Kolesnikova, A.I. 115844
+Kolesov, I.S. 114781
+Kolesov, S.N. + 114781
+Koletsnichenko, L.L. 114506
+Kolopoulos, C.J. 111750
+Kollatschny, W. + 116820
+Kollberg, E. 114588
+Kolmanovskii, V.B. 113308
+Kolmaz, T.Z. 115571
+Kololev, S.S. 116324
+Kolomeiko, E.P. 114610
+Koloso, M.A. + 116304
+Koloso, M.A. 113035
+Kolotilov, E.A. 116705
+Kolovsky, A.R. 111583
+Kolpakov, A.G. 111437
+Kol's, O.R. 115773
+Koltakov, Yu.N. 116099
+Koltik, E.D. + 111707
+Koltun, M.M. + 115689
+Kolyadin, S.A. 113076
+Koma, A. 114050
+Komaki, K. 114974
+Komamiya, S. 111990
+Komamiya, S. 112012
+Komarov, V.A. + 115484
+Komarov, V.A. 115483
+Komarov, V.P. + 115845
+Komatsu, M. 113805
+Komissarova, I.I. + 113667
+Komissarova, L.N. 115119
+Komiya, S. 115112
+Komiya, A. 112910
+Komoda, S. + 112183
+Komotskiy, V.A. 113243
+Konareva, N.V. 115740
+Kondilenko, V. + 113062
+Kondo, I. 116589
+Kondo, K. 112545
+Kondo, M. 112437
+Kondo, M. 112210
+Kondo, M. 112051
+Kondo, M. 112229
+Kondo, T. 113922
+Kondo, Y. 116750
+Kondorskii, E.I. + 114684
+Kondow, T. 112852
+Kondow, T. 114106
+Kondrashin, S.K. 116482
+Kondrashova, A.S. 114526
+Kondratenko, A.N. 113583
+Kondratenko, A.N. 113606
+Kondrat'ev, P.A. 115340
+Kondrat'ev, S.Yu. 115244
+Kondratiev, V.A. + 111448
+Konigstein, J.A. 115750
+Konishi, S. 114180
+Konishi, S. 114751
+Konno, H. 112299
+Kono, H. + 114111
+Konomi, T. 116037
+Kononenko, A.A. 115724
+Kononenko, W. + 112552
+Kononova, G.E. + 116244
+Konoplyannikov, A.G. 115843
+Konoplyannikov, A.G. 115844
+Konoplyannikov, A.G. 115754
+Kononov, O.S. + 115490
+Konstantinov, Yu.S. 111719
+Konyukhov, B.A. + 115473
+Koonin, S.E. 111550
+Koontz, A.S. 112313
+Koontz, A.S. 112312
+Kopan', V.S. 115243
+Kopina, I.V. 112574
+Kopp, D.T. 115911
+Koppel, L.N. 113658
+Koppenol, A.D. 115675
+Koppitz, B. 112015
+Koppitz, B. 112555
+Koptsik, V.A. 114834
+Koptsik, S.A. + 113703
+Korabiev, V.A. + 115221
+Korchenskaya, E.Ya. 115753
+Kordas, G. + 114733
+Kordos, P. 115643
+Korec, J. + 114409
+Korec, J. 114406
+Korneev, S.I. + 115488
+Korner, A. + 113917
+Kornienko, P.A. 115467
+Kornilov, L.N. 113035
+Kornuta, P.P. 112714
+Korobkov, N.N. + 111799
+Korol', E.Z. + 115273
+Korolev, A.P. + 114080
+Koroleva, L.I. + 114709
+Koroleva, N.S. 115651
+Korol'kov, D.V. 112708
+Korolyuk, O.V. 113684
+Koros, W.J. 114335
+Korosemzev, A. + 116550
+Korovin, S.K. 114618
+Korp, J.D. + 113835
+Korpel, A. 113465
+Korsah, J.K. + 112533
+Korshover, J. 116187
+Korshun, V.I. 115439
+Korshunov, A.I. + 115477
+Korshunov, A.I. + 115476
+Korshunov, A.I. 115204
+Korshunov, F.P. + 114025
+Korsunskaya, N.E. 114563
+Kort, V.G. 116122
+Kortelahti, M. 112058
+Korth, A. + 116398
+Kortov, S.V. 114690
+Korytsev, I.V. 116306
+Kosa Somogyi, I. 113138
+Kosarchuk, V.V. + 115281
+Kosareva, L.P. 115299
+Koschar, P. 114988
+Kosevich, A.M. + 114112
+Koshchenko, A.V. 113739
+Koshechko, V.G. + 115546
+Koshiba, M. 111990
+Koshiba, M. 112012
+Kosov, A.V. 114177
+Kost, J. + 115078
+Kostecky, G. 115037
+Kostecky, J. + 115995
+Kostienco, A.I. 112917
+Kostina, K.I. 114684
+Kostkowski, H.J. + 111383
+Kostoff, R.N. 112436
+Kostomarov, D.P. 113670
+Kostov, L.K. + 112236
+Kostromina, L.P. 114526
+Kostrukova, M.O. + 114694
+Kosugi, T. + 116623
+Kosugi, T. + 116584
+Kosugi, T. 113975
+Kosugi, T. 116573
+Kotami, M. 115813
+Kotanyi, C. + 116840
+Kotarska, I. + 116751
+Kotlikov, E.N. 111780
+Kotoroga, A.D. 115638
+Kotova, A.I. 112021
+Kotova, L.B. 113327
+Kotthaus, R. 112016
+Kotlyukov, M.V. 113243
+Kotz, U. 112554
+Kouchi, N. 112862
+Koui, M. 114805
+Kounnas, C. + 111929
+Kourou, N.I. 114211
+Koutchmy, S. 116559
+Koutecky, J. 115528
+Kouvel, J.S. 114649
+Kouzu, F. 115309
+Kovacs, A. 114951
+Kovacs, F. 112016
+Kovacs, I. + 115271
+Koval', K.P. 114683
+Koval, T.M. 115877
+Koval', Yu.N. 114952
+Koval'chenko, M.S. 115128
+Koval'chuk, B.I. 114075
+Koval'chuk, B.I. 115281
+Koval'chuk, V.S. 115468
+Koval'chuk, Yu.V. 114000
+Kovalenko, E.V. + 113307
+Kovalev, A.V. 113952
+Kovalevskiy, I.V. 116352
+Kovalyuk, Z.D. 114924
+Kovrizhnykh, A.M. 114073
+Kovyzin, Yu.A. 111714
+Kowal, C.T. + 116543
+Kowalczyk, M. 115400
+Kowalski, S.J. 113311
+Kownacki, J. 112046
+Koyama, A. 113991
+Koyama, N. 115005
+Koyama, T. 115038
+Koyanagi, K. + 113061
+Koyen, M. 116347
+Kozaneki, W. 112031
+Kozelova, T.V. + 116354
+Kozhomkulov, E.T. 115759
+Kozis, E.V. 115169
+Kozlov, S.I. + 116342
+Kozlov, V.A. + 114739
+Kozlov, V.F. 116097
+Kozlovsky, B. 116414
+Kozlovsky, B. 116591
+Kozma, R. + 112422
+Kozu, T. 116205
+Kozuka, T. 111632
+Kozyrev, N.V. 115543
+Kraichinskii, A.N. + 113867
+Krainik, N.N. + 114830
+Kraizman, I.L. + 114156
+Krajenbrink, F.G. 115065
+Krajenbrink, F.G. 115066
+Kramer, H.H. + 111654
+Kramer, H.M. 112534
+Krammen, M.A. 112308
+Krane, K.S. 112597
+Krasavin, I.A. 113849
+Krasinski, A. 111510
+Krasitskiy, V.P. 116301
+Kraski, K. 112015
+Krasnikov, N.V. + 111968
+Krasnokutsky, N. 112551
+Krasnov, K.S. 112878
+Krasny, M.W. 112028
+Krasulin, Yu.L. 115343
+Kratz, K.-L. + 116445
+Krausbauer, L. 115073
+Krause, H.H. 112187
+Kraushaar, J.J. 112149
+Krausz, F. 111872
+Krautter, J. + 116650
+Kravchenko, A.F. 114554
+Kravchenko, I.I. 111856
+Kravchenko, I.T. 112909
+Kravchenko, S.A. 111707
+Kravchenko, T.N. 115477
+Kravchuk, N.A. 115437
+Krautsov, D.N. 113840
+Krautsov, V.E. 114582
+Krehbiel, H. 111990
+Krehbiel, H. 112012
+Kreinfeldt, J. 115961
+Kreinovich, V.Ja. 116440
+Krekelberg, A. + 114064
+Krekhtunov, V.M. + 112903
+Kremer, K. 111611
+Kremlev, M.M. 112753
+Kremser, G. 116398
+Krenn, H. 111787
+Krentsis, R.P. 114690
+Kreuzer, H.J. 114351
+Kricheldorf, H.R. 113765
+Krieger, W. 115006
>Kriegsmann, G.A. + 111463
>Kriegsmann, G.A. 111497
>Krier, A. 114930
>Krigbaum, W.R. + 113735
>Krimigis, S.M. 116386
>Krinchik, G.S. 114834
>Krinsky, V.I. + 113466
>Krischker, P. + 111670
>Krischker, P. + 111664
>Krishan, K. 114200
>Krishna Rao, T.V. 114895
>Krishnamma, B. 114534
>Krishnan, M. 113613
>Krishnapur, P.P. + 111702
>Krishnaswamy, R. + 113409
>Krithivasan, N. 115421
>Kritikos, G. 116290
>Krivitskiy, V.P. 114971
>Krivonos, Yu.G. 113640
>Krivtsov, M.G. 113368
>Krizan, P. 112589
>Kroeger, R. 112024
>Kroger, F.A. 113907
>Krogh, J.von .see von Krogh, J.
+Krogas, B. 115783
>Krompiewski, S. 114662
>Kroneisen, A. + 115717
>Kronmuller, H. 114711
>Kroth, R. 112113
>Krotova, G.D. 115379
>Krucke, B. 113730
>Kruger, A. 112497
>Kruger, M. 112015
>Kruglov, V.N. 115280
>Krulikovskaya, M.P. + 115188
>Krull, O. + 111630
>Krupa, J.C. 114500
>Krupitskaya, T.M. 116346
>Krupnikov, E.S. 114396
>Kruse, U. 112016
>Krustev, V.P. 114521
>Kruzhaev, V.V. 114586
>Kruzhalov, V.A. 112981
>Kryachko, I.V. 114934
>Krylov, A.L. 116353
>Krylov, A.L. 116381
>Kryn, D. 112031
>Kryskov, V.A. 113333
>Kryszyewski, M. 114539
>Krzehchovskii, P.G. 115350
>Ksanfomaliti, L.V. 116507
>Kshatriya, J.D. 113916
>Ku, H.C. 114635
>Ku, W.H.-M. 116472
>Ku, W.H.-M. 116855
>Ku, W.T. 114758
>Kuang-Tn Chao .see Chao Kuang-Tn
+Kubacek, L. 111621
>Kubackova, L. + 111621
>Kubasova, L.V. 115523
>Kubasova, L.V. 115524
>Kubenko, V.D. + 113495
>Kubicki, J. 114387
>Kubier, B. 114982
>Kubler, D. 116290
>Kubo, J. + 111922
>Kubo, K. 112206
>Kubo, T. 112484
>Kuboi, O. 114626
>Kubono, S. 112211
>Kubono, S. 112227
>Kubota, C. 112485
>Kubota, C. 113735
>Kubota, Y. 112478
>Kubsch, M. 112532
>Kucera, J. 115518
>Kucerovsky, Z. + 112979
>Kuchel, F.M. + 111757
>Kucheryavii, B.P. 115338
>Kuchitsu, K. 112852
>Kuchler, G. + 112174
>Kudinov, V.M. 113478
>Kudinov, V.M. 113470
>Kudo, Y. 112215
>Kudryashov, V.G. + 115346
>Kudryavtsev, S.V. + 114715
>Kudyakov, V.Ya. 111710
>Kugland, Kh.-G. 116343
>Kugo, T. + 111534
>Kuhl, J. 114542
>Kuhn, A.T. + 111686
>Kuhn, A.T. 115565
>Kuhn, D. 112028
>Kuhn, J.R. + 116610
>Kuhn, M. 115671
>Kuhn, W. 112246
>Kuhn, W. 112058
>Kuhr, H. 116868
>Kuiken, H.K. + 115382
+Kuiper, A.E.T. 114413
>Kujal, J. 112304
>Kujawska, T. 113232
+Kukhar', V.P. 115584
+Kukharev, A.V. 113085
+Kukita, Y. 112406
+Kuklin, G.V. 116596
+Kuklin, R.N. 114116
+Kuklin, V.M. 113583
+Kuklin, V.M. 113606
+Kukolich, S.G. 112764
+Kulakovskii, V.N. 115246
>Kulgein, N.G. 112943
+Kulic, M.L. 114638
+Kulik, A.V. 112556
+Kulik, O.G. 115170
>Kulik, V.I. + 115286
+Kulikov, V.N. 113694
+Kulikova, E.I. 116311
+Kulka, K. 112024
>Kulkarni, S.R. 116719
+Kulkarni, U.D. 113992
>Kulke, B. + 112483
+Kumabe, I. 112146
+Kumagai, N. 113091
+Kumagawa, M. 115042
+Kumar, A. 113230
>Kumar, D.De .see De Kumar, D.
+Kumar, N. 113519
+Kumar, P. 112692
+Kumar, R. 115711
+Kumar, U. 114227
>Kumari, M. + 113410
>Kumasaka, K. + 114710
>Kumekov, S.E. 114818
>Kumekov, S.E. + 114813
>Kumikov, V.K. 114329
+Kumpulainen, J. 112043
>Kumykov, V.K. + 114328
+Kumzerov, Yu.A. 115142
+Kundrat, N.M. 113363
>Kung, E.C. + 116212
>Kung In-shieh .see In-shieh Kung
>Kunin, I.A. 111318
+Kunitake, T. 115269
>Kuno, K. 113189
>Kunold, W. + 112884
+Kunovsky, J. 112404
+Kunszt, Z. 115884
+Kuntz, I.D. 115735
+Kunwar, A.C. 114742
>Kunz, J. + 112093
+Kunz, J. 112173
>Kunze, J. + 114743
+Kunzmann, H. 111650
+Kuo, C.S. 111683
+Kuo, H.Y. 115276
>Kuo, S.P. + 113591
+Kuo, T.T.S. 111981
>Kuok, M.H. 114858
>Kupersmidt, B.A. 111582
+Kupersmidt, B.A. 113517
+Kupka, H. 112710
>Kuprievich, V.A. 112669
>Kuraev, A.A. + 113023
>Kuramoto, E. + 114039
+Kuramoto, E. 114962
+Kuramoto, E. 114963
+Kuramoto, E. 113900
+Kuramoto, E. 113980
+Kuramoto, T. 111534
+Kuranawa, I.P. 115740
+Kurasawa, H. 112150
+Kurasawa, T. 114044
+Kurata, M. 114268
+Kurbanov, Sh.E. 113528
+Kurbatov, A.M. 111551
+Kurbatov, G.A. 114869
>Kurita, G. + 113647
+Kurmaev, E.Z. 114443
>Kurobori, T. + 113016
>Kuroda, K. + 111661
>Kuroiwa, A. + 115960
+Kurokawa, T. 115444
+Kurosawa, S. 115605
>Kurova, I.A. + 114566
+Kurpin, V.A. 113570
>Kurtz, D.W. 116694
>Kurtz, D.W. + 116695
+Kurz, U. 114261
+Kusabayashi, S. 115122
+Kushakevich, S.A. 115438
+Kushakevich, Yu.P. 112573
+Kushch, L.A. 113848
+Kushnerik, S.A. 112547
>Kushnir, N.Ya. + 114544
>Kushnir, V.M. + 116099
+Kusior, E. 114982
+Kusunose, M. 116454
+Kuster, H. 112016
+Kustov, A.V. 116406
+Kusunose, K. 116038
>Kusy, R.P. + 115359
+Kuts, V.N. 112593
+Kutshnada, M. 113889
+Kutshinov, V.I. 111935

- Kuwabara, H. + 113222
 + Kuwabara, K. 113371
 + Kuwahara, Y. 116084
 Kuwano, N. + 115202
 + Kuzakov, A.K. 111821
 + Kuze, E. 114876
 Kuzele, M.V. + 113672
 Kuzemsky, A.L. + 114442
 Kuzin, A.M. + 115849
 + Kuzin, E.A. 113058
 Kuz'michev, N.D. + 114845
 Kuz'michev, V.M. + 112937
 + Kuz'min, E.A. 113792
 + Kuz'min, E.A. 113850
 + Kuz'min, N.L. 113926
 + Kuz'min, R.N. 114965
 + Kuz'min, V.A. 114604
 Kuz'mina, L.G. + 113840
 + Kuz'minykh, A.I. 114709
 + Kuznetsov, A.F. 113775
 + Kuznetsov, A.N. 115741
 + Kuznetsov, G.F. 113698
 Kuznetsov, I.A. + 115489
 Kuznetsov, N.M. + 113493
 Kuznetsov, Yu.D. + 115392
 Kuznetsov, Yu.V. + 112488
 + Kuznetsova, N.Yu. 116333
 Kuznetsova, Ye.A. 115828
 + Kvale, T.J. 111689
 + Kvasil, J. 112119
 + Kwan, J. 113666
 Kwee, K.K. + 116749
 + Kwok, H.S. 113017
 + Kwon, O.Y. 113073
 + Kwon, S.I. 115316
 Kyker, G.C., Jr. 111362
 + Kyle, T.G. 116170
 + Kyte, F.T. 116086
- la Cruz, C.R.de
 see de la Cruz, C.R.
 la Cruz, F.de
 see de la Cruz, F.
 + La Padula, C.D. 116474
 la Vaissiere, C.de
 see de la Vaissiere, C.
 Laak, F.A.Van
 see Van Laak, F.A.
 + Laane, J. 112741
 + Laane, J. 114859
 + Labay, J. 116648
 Labbe, A.Toro
 see Toro Labbe, A.
 + Labbe, J.C. 113826
 + Labonte, B.J. 116479
 Labunov, V.A. + 114394
 + Lacava, F. 112031
 Lachaine, A.R. + 111363
 Lachambre, J.L. + 113576
 + Lackas, W. 112015
 Laclaire, F. 116558
 + Laclaire, F. 116562
 + Lacroix, F. 115458
 Lagage, P.O. + 116413
 + Lagarde, A. 113384
 Lage, A.L.V.S. + 113143
 Lagowski, J. + 114940
 + Lagowski, J. 115110
 + Lagowski, J. 113954
 + Lagu, R.K. 113093
 + Lagutin, A.S. 114679
 Lahlou, M. + 116308
 + Lahmam Bennani, A. 112857
 + Lai Yuan-fen 112581
 Lai-Chen Chien + 113450
 Lai-chen Chien + 113432
 Laiho, R. + 114815
 + Lakh, V.I. 114512
 Lakhtakia, A. + 115829
 Lakiza, V.D. + 113420
 + Lakiza, V.D. 113495
 + Lakkistro, M. 114815
 Lakshman, S.V.J. + 114900
 Lakshman, S.V.J. + 114895
 + Lakshminarayana, V. 112691
 Lal Jeevan see Jeevan Lal
 Lal, B.B. + 112688
 Lam, C.S. 111894
 Lam, C.S. + 112025
 Lam, K.-S. + 112841
 Lam, S.T. + 112288
 Lamarra, A. 111385
 Lamashevskii, V.P. + 115282
 + Lamb, R.C. 116883
 Lambert, R.P. + 112599
 Laming, P.J. + 115991
 + Lamond, S. 113940
 + Lamontagne, R. 116769
 Lamorte, M.F. + 115657
 + Lancaster, H. 112475
 + Lancman, H. 112561
 Lancon, D. + 115530
 + Lancon, E. 112022
 Land, D.J. + 112829
 Landa, P.S. + 111591
 Landau, R.H. 112881
 Landi Degl'Innocenti, E. + 116611
 + Landi Degl'Innocenti, E. 116640
 + Landolfi, M. 116611
 Landsberg, P.T. 111358
 Landsberg, P.T. + 114541
 + Landsberg, P.T. 112975
 Landuyt, J.Van
 see Van Landuyt, J.
 Lanford, O.E. 111572
 + Lang, J. 112241
 + Lang, R. 113011
 Lang, R.W. + 115362
 Lang Shain-Way
 see Shain-Way Lang
 Langanke, K. + 112243
 + Langanke, K. 112258
 Langbein, D. 113444
 + Langdon, T.G. 115306
 Lange, C.A.de see de Lange, C.A.
 Langer, N. + 116639
 + Langeset, B. 113982
 Langkilde, F.W. + 114904
 Langlais, F. + 115084
 Langlois, P. 112900
 Langlois, W.E. + 115044
 + Langrok, K. 115839
 + Lanier, R.G. 112066
 + Lanier, R.G. 112125
 + Lanford, A.J. 112011
 + Lankford, J. 115320
 Lans, J.van der
 see van der Lans, J.
 + Lapierre, F. 114674
 + Laplanche, F. 112016
 Laptev, A.M. 115279
 + Laptev, I.D. 111805
 Lardner, R.W. 113340
 + Larionov, V.P. 113678
 + Larionov, V.P. 115651
 Larkin, A.I. + 111481
 + Larkina, T.I. 114160
 + Laroche, C. 113443
 + Larrea, E. 112922
 + Larrea, E. 112932
 Larsen, A.Nylandsted
 see Nylandsted Larsen, A.
 Larsen, J. + 115783
 + Larsen, M.F. 116355
 + Larsen, R.R. 112011
 + Larson, A.C. 113800
 Larson, B.C. + 113919
 Larsson, C.G. + 115013
 Larsson, M. + 112788
 Lary, J.M. + 115833
 Lasch, J.E. + 114862
 Lascombe, J. + 112735
 Lassailly, Y. + 114674
 + Lassegues, J.C. 112735
 + Lasser, R. 115023
 Lassnig, R. + 114602
 Laszewski, R.M. 112501
 + Latariet, R. 115866
 + Latics, V.G. 115825
 Latkowski, A. 115181
 + LaTourette, R.A. 113205
 Latraille, S.L. + 116031
 + Lattanzi, F. 112727
 + Latysheva, V.A. + 114185
 + Latysheva, V.I. 115170
 + Latz, R. 114988
 + Lau, K.H. 111992
 Lau, K.Y. + 112990
 + Lau, S.S. 114611
 + Lau, S.S. 114008
 + Laube, B.L. 115564
 + Lauberau, A. 113065
 + Lauderale, J.G. + 112675
 Laughlin, C. 112667
 + Laugier, A. 114028
 + Laugier, A. 114030
 + Laugier, J.-P. 112031
 + Launay, J.C. 115084
 + Launder, B.E. 113428
 Launspach, J. + 113656
 Laurenzi, B.J. 112701
 + Laushkin, A.V. 114965
 + Lauterborn, W. 111607
 Lauterborn, P.C. 115901
 + Lauzier, J. 113899
 + Lavagne, Y. 112016
 Laval, P. 111450
 + Lavine, T.L. 111992
 + Lavrenko, V.A. 115393
 Lavrinenko-Ometinskaya, E.D. + 114370
 + Law, C.K. 115552
 Law, R. + 115704
 Law Kock-Yee
 see Kock-Yee Law
- Lawitzky, G. 111512
 Lawrence, D.M. 115594
 + Lawrence, G. 112924
 + Lawrence, G. 113072
 Lawrence, J.K. 116595
 + Lawrence, L. 116488
 Laws, V. 115255
 Layman, J.W. 111339
 + Lazaar, K.I. 115537
 Lazarevski, E.V. + 115523
 Lazarevski, E.V. + 115524
 + Lazorenko, V.I. 113952
 + Lazoryak, B.I. 113794
 + Lazus, A.L. 116178
 + Lazukina, L.A. 115584
 + Lazutin, E.V. 112488
 + Lazutin, L.L. 116354
 + Lazzara, S. 115817
 + Lazzarini, A. 112255
 + Le Barny, P. 114172
 Le Berre, M. + 113066
 + Le Calonnec, D. 114967
 + le Clair, G. 113618
 + Le Daeron, P.Y. 111608
 + Le Guen, D. 113010
 Le Khac Hein + 115374
 + Le Roy, R.J. 112800
 + Le Roy, R.J. 112711
 Le-jun Chen
 see Chen Le-jun
 Le-Shou Chen
 see Chen Le-Shou
 + Leach, J. 116608
 + Leander, G.A. 112045
 + Lebedev, A.A. 115281
 + Lebedev, A.A. 115282
 + Lebedev, S.V. 114508
 + Lebedev, Yu.G. 114716
 + Lebedeva, N.L. 112878
 + Lebedeva, N.N. 114777
 + Lebl, A. 114428
 + Leblans, P. 113935
 + Leblud, C. 113755
 + Lebo, C. 112562
 + Lecante, J. 114344
 Lechner, H. 113532
 + LeClaire, B. 112011
 Lecoq, J. + 112587
 + Lecoq, P. 112553
 + Lecuyer, D.W. 115836
 + Leebetter, H.M. 115233
 LeDoux, J.E. + 115819
 + Leduc, M. 113015
 Lee, A.K. + 115264
 + Lee, C.C. + 113719
 + Lee, C.S. 115831
 Lee, C.-Y. 115775
 Lee, D.H. + 112425
 + Lee, H.G. 115178
 + Lee, I.Y. 112049
 Lee, J. 114812
 + Lee, J.K.P. 112286
 + Lee, J.K.P. 112507
 + Lee, J.-Y. 113855
 + Lee, J.-Y. 114257
 + Lee, K.I. + 114513
 + Lee, K.Y. + 113855
 + Lee, L.C. + 116409
 + Lee, M. 111328
 + Lee, M.K. 115064
 + Lee, S.M. 112293
 + Lee, S.Y. + 112099
 + Lee, S.Y. + 111492
 + Lee, S.Y. + 112097
 + Lee, S.Y. 112087
 + Lee, S.Y. 112092
 + Lee, T.C. 114484
 + Lee, T.J. 116692
 + Lee, W.J. 113728
 + Lee, W.Y. 115317
 Lee Dock-Chool
 see Dock-Chool Lee
 Lee Hoyun see Hoyun Lee
 Lee Huan see Huan Lee
 Lee Kee Dae
 see Kee Dae Lee
 Lee Ki-Jun see Ki-Jun Lee
 Leeden, G.A.van der
 see Leeden, G.A.
 + Leedy, R.E. 111992
 + Leempoel, P. 114931
 Leen, T.K. + 111522
 + Lees, J.-P. 112031
 Leetmaa, J. + 116135
 Leeuw, D.M.de
 see de Leeuw, D.M.
 Leeuw, F.A.A.M.de
 see de Leeuw, F.A.A.M.
 + Lefebvre, R. 111486
 + Lefevre, F. 116395
 + Lefevre, H.C. + 113101
 + Leffers, J. 112290
 + Leffers, T. + 114023
 Legeay, V. + 113158
 + Legnini, D.G. 113880
 Leguista, F.F. 113173
 Legold, S. 114652
 Lehmann, G. + 114731
 + Lehmann, H. 112031
 Lehmann, J.F. + 115772
 + Lehmann, R. 112060
 Lehnig, M. + 112755
 + Lehr, H. 112270
 + Lehr, H. 112273
 + Lehr, H. 112272
 Lei, T.C. + 115326
 + Leibow, A.V. 116418
 Leibowitz, L. + 112329
 + Leigh, J.R. 112244
 Leinonen, J. + 116406
 Leiser, G. + 113765
 + Leissa, A.W. 113337
 + Leite, S.C.P. 112689
 Leite
 Albuquerque
 A.R.Pereira
 see Pereira Leite Albuquerque
 A.R.
 Leiter, D. 116735
 Leiyeh, O.A. 115664
 + Leja, E. 114628
 + Lele, M.V. 111702
 + Leleux, P. 111809
 Lella, L.Di. see Di Lella, L.
 Lemaire, P. + 116442
 + Lemaire-Blaise, M. 114497
 + Lemanov, V.V. 113055
 Lemeshko, V.V. 115764
 + Lemke, J. 111504
 + Lendvai, J. 115271
 Lenglet, M. + 114967
 + Lennartsson, W. 116360
 + Lennert, P. 111990
 + Lennert, P. 112012
 + Lenti, V. 112020
 + Lentini, F. 116016
 Leo, M. + 111401
 + Leo, R.A. 111401
 + Leone, S.R. 115567
 Leong, K.H. + 115587
 + Leoni, M. 112703
 + Leonidou, D.J. 112495
 Leonov, M.Ya. + 113321
 Leont'ev, A.I. + 113263
 + Leorat, J. 116446
 + Lepekina, L.A. 115844
 + Lepkov, A.A. 113775
 + Lepp, A. 114840
 Lequeux, J. 116823
 + Lerf, A. 114764
 Leriche, A. + 113755
 Lerner, N.B. + 112915
 Leroy, B. 116443
 + Leroy, J. 112472
 + Leroy, J.-L. 115751
 Leroy, M. 112896
 Leroy, M.M. 113614
 Lersch, C. + 115837
 + Lersmacher, B. 115093
 + LeSar, R. 113809
 + LeSar, R. 113800
 + Leskela, M. 114907
 + Leskova, T.A. 114582
 + Leslie, L.M. 116240
 Lettau, H. + 112539
 + Leuchs, R. 112031
 + Leuchtig, H.R. 115774
 Levchenko, E.B. + 114305
 + Levchenko, I.S. 114845
 + Levchenko, V.M. 115124
 + Levda, A.S. + 116307
 + Levenson, W. 115668
 + Leventhal, M. 116825
 + Leveque, A. 112031
 Levi, L. + 116227
 + Levi, M. 112011
 + Levin, A.A. 114790
 + Levin, B.N. + 116570
 + Levine, M.D. 116143
 + Levine, R.D. 112702
 + Levine, R.Y. 111897
 + Levinskaya, M.Kh. 115275
 + Levinsky, H.B. + 114903
 + Levinson, M. 114477
 + Levit, S. 112095
 + Levitin, R.Z. 114834
 + Levitskaya, G.D. 115435
 + Levitsky, M.S. 112021
 + Levitt, M.H. + 111715
 + Levy, A.V. + 115368
 + Lew, P.W. + 114372
 + Lewendel, B. 112015
 Lewins, J.D. 112362
 + Lewis, A.J. 114201
 + Lewis, M. 114943
 + Lewis, R.W. 111744
 + Leyendecker, A.J. 114972
 + Leyko, W. 115872
 + Lezheiko, L.V. 114383
 Lhermitte, R. + 116253
 + Li, B.S. 116607
 Li, G.P. + 114470
 + Li, S.C. 116607
 + Li, S.S. + 115647
 + Li, Z. 116607
 + Li Chang 114100
 Li Chong-sheng + 11916
- Li Guang-lie + 111981
 + Li Jin 112581
 + Li Pei-qin 112581
 + Li Wenxiu 114170
 + Li Wenxuan 113449
 Li Xing-Sheng + 116183
 Li Yajun see Yajun Li
 Li-bo Sun see Sun Li-bo
 Li-Min Zhang
 see Zhang Li-Min
 + Li-shen, Y. 115812
 Li-xin Ren see Ren Li-xin
 Liander, W. 115626
 Liang, E.P. 116880
 Liang, N.T. + 114838
 Liang, N.T. + 114839
 + Liang Dongcai 114170
 Liang Yunmin 113380
 Liao Fu-lung + 115818
 Libhaber, A. + 113443
 Liberto, S.Di. see Di Liberto, S.
 + Lichtman, D. 114978
 Lidov, M.L. 116435
 Lie Heung-Jae
 see Heung-Jae Lie
 Lieb, E.H. 111539
 + Lieb, E.H. 111474
 Liebsch, A. + 114803
 + Liebsch, A. 114337
 Liegener, C.-M. 112796
 Liehr, M. + 114620
 Lien, C.-D. + 114285
 Lien-Wen Chen + 113329
 Liepinya, V.E. + 114220
 + Lierl, H. 112016
 Lieser, G. 113766
 + Lietti, A. 113630
 Lieu, R. 116733
 + Lifshits, A.E. 116381
 Lifshitz, A. + 115534
 Lightman, A.P. 116448
 Likal'ter, A.A. 113556
 + Likar, A. 112159
 Likhachev, V.A. + 115278
 + Likhod'ko, A.D. 115480
 + Liljestrand, R. 112153
 + Lillgren, A. 116181
 Liller, W. + 116589
 + Liller, W. 116768
 + Lillstoll, E. 112015
 + Lilwall, R.C. 116024
 + Lim, T.K. 111364
 Lim Chee-seng 113370
 + Lima, C. 112050
 + Lima, C.A.S. 112969
 Lima, E.P.De
 see De Lima, E.P.
 Lima, M.B.S. + 112969
 Lima, N.P. + 114722
 Lin, B.-D. 116219
 + Lin, C. 113051
 Lin, C.H. + 115134
 + Lin, C.P. 114724
 + Lin, C.S. 116403
 Lin, C.T. + 114841
 + Lin, E.K. 112099
 + Lin, E.K. 112234
 + Lin, H.C. 113930
 Lin, I.-H. + 114084
 Lin, I.-H. + 114085
 + Lin, L. 112087
 + Lin, L. 112097
 + Lin, M.S. 114395
 Lin, P.S.D. + 114783
 Lin, S.-B. + 113764
 Lin, S.H. + 112767
 + Lin, S.H. 114111
 Lin, S.T. + 114758
 + Lin, S.T. 114507
 Lin Chen-Hsi
 see Chen-Hsi Lin
 Lin Liu see Liu Lin
 + Lin Yuanzhang 116626
 Lin-Chung, P.J. 114479
 Linares, C. + 114906
 Lind, D.A. + 112209
 + Lindberg, R.G. 115936
 + Lindblad, T. 112292
 + Lindblad, T. 112558
 + Lindblad, T. 112049
 + Lindblom, P. 113080
 Linde, A.D. 111528
 Linde, D.von der see von der Linde, D.
 + Lindgren, I. 112686
 Lindgren, L.J. + 112505
 Lindgren, L.J. + 112504
 + Lindholm, A. 112159
 + Lindsay, J. 112024
 + Lindsay, W.T., Jr. 112380
 + Lindsey, C. 113007
 + Lindsey, C. 113009
 + Lindstrom, E.R. 112480
 + Lindstrom, J. 114428
 + Lindstrom, U. 111506
 + Lindwall, D.A. 116101
 Lindzen, R.S. + 116220
 + Lineberger, W.C. 112785

- +Linev, V.D. 115171
+Ling, J.C. 116835
+Ling, J.C. 116826
Ling Guocan 113447
Lingart, Yu.K. + 114846
Lingenfelter, R.E. + 116830
+Lingenfelter, R.E. 116881
+Lingenfelter, R.E. 116414
+Lingenfelter, R.E. 116591
+Linglin, D. 112031
Linhart, J.G. 112443
Link, K.H. 114110
+Linke, L. 115759
Linker, U. + 115404
Linsheng Lu see Lu Linsheng
+Linsky, J.L. 116629
+Lintern, A.L. 112540
+Linton, R.C. 115406
+Liotta, R.J. 112044
Lioy, P.J. + 115709
+Lipatov, Yu.S. 113761
Lipchina, A.N. + 115339
+Lipko, A.L. 114545
+Lipnik, P. 111809
+Lipovskii, A.A. 113085
Lipson, J. + 113148
+Lisanti, J. 112153
Lisicki, E. + 112684
Lisitsa, M.P. 113041
+Lisovskii, F.V. 114718
+Lissauer, D. 112024
+Lister, J.B. 113630
Litniewski, J. 113231
+Little, L.T. 116801
+Little, T.S. 112742
Litvak, V.I. + 115479
Litvin, D.B. 114327
+Litvin, D.F. 115191
Litvin, V.M. + 116075
Litvin, V.V. + 115348
Liu, H.C. + 113885
Liu, R.Y. + 116376
Liu, W.-K. + 113560
Liu, Y.S. + 113942
+Liu, Y.S. 114019
Liu Jian-feng + 112142
Liu Lin + 111425
+Liu Yuan-Long. 116039
Liu Zhe-ming 111895
+Liuukonen, E. 112075
+Livan, M. 112022
Livesey, V.B. + 115328
+Livingston, R. 111697
Livio, M. + 116663
+Livshits, M.A. 111487
+Livshits, V.A. 115741
+Lizun, A.T. 115433
Llano, M.de. see de Llano, M.
Lloyd, D.R. + 115021
+Lloyd, E.L. 115867
+Lloyd, M.L. 113937
+Lo, W. 112991
+Lo Iudice, N. 112062
+Lobanov, N.N. 114965
+Lobkova, N.A. 113326
Lobkovskaya, R.M. + 113851
Lobkovskaya, R.M. + 113853
+Loboda, L.I. 112641
Loc Vu Tien see Vu Tien Loc
+Locci, E. 112031
Lockett, F.J. 115207
+Lockyer, N. 112011
+Loebinger, F.K. 111990
+Loebinger, F.K. 112012
+Loesing, D.M. 114637
+Loeffler, H. 114155
+Logan, D.R.G. 112271
Logan, R.A. + 115109
+Loh, E.C. 111992
Lohr, L.L., Jr. + 115527
Loiacono, G.M. + 115037
Loidi, A. + 114174
Lokoshchenko, A.M. 114082
+Lomadze, S.O. 116211
Lombard, R.J. 112193
+Lombardi, J.R. 113054
+Lombardo, U. 112152
+Lomdahl, P.S. 111578
+Loncarevic, B.D. 116024
+London, G. 112016
Lone, M.A. + 112507
+Lone, M.A. 112547
+Long, D.A. 114854
Long, F.M. + 115983
+Long, S.H. 113220
Lonngren, K.E. 113602
+Lonngrén, K.E. 113465
Loo, F.J.J.van. see van Loo, F.J.J.
+Loo, R.Y. 115647
+Loos, G.D. 114777
Loos-Vollebregt, M.T.C.de. see de Loos-Vollebregt, M.T.C.
+Lopasov, V.P. 112731
+Lopatinskii, I.E. 114512
+Lopes, J.S. 112828
Lopez, C.A. 111523
+Lopez, G. 116530
Lopez-Martinez, M. + 116040
Lopez-Rios, T. + 114946
Lorent, B. + 116165
+Lorents, Yu.E. 114775
+Loretto, M.H. 113874
+Loretto, M.H. 114037
Lorge, J.O.de. see de Lorge, J.O.
+Lorimer, G.W. 115225
+Lorstad, B. 112024
+Lory, P. 115770
+Los, J. 114999
+Los, J. 115000
los Rios, E.R.de. see de los Rios, E.R.
Loschau, G. 115462
+Loskutova, E.A. 114619
+Loskutova, G.F. 115275
+Losing, F.D. 115574
+Losyakov, V.V. 114773
Lotem, H. 111778
+Lotts, A.P. 116747
Lou, J.C. + 114395
Loubriel, G. + 114489
+Loucatos, S. 112022
+Loughran, K.S. 116279
Louis, E. + 114583
+Louis, J. 115709
+Lourenco, J.A. 115114
+Lourtioz, J.-M. 112985
Lovas, I. + 114053
+Love, D.J.G. 112112
Love, W.G. 112205
Lovelace, R.V.E. + 116837
Low, B.C. + 113601
+Low, K.S. 112161
+Lowell, S. 111639
Lowndes, D.H. + 114011
+Lozhkina, V.P. 116082
+Lozingot, J. 115539
Lozinskaya, T.A. 116807
Lozitskii, L.P. + 115469
+Lozovik, Yu.E. 114144
Lu, Y.C. + 115413
+Lu Chang-guo 112580
+Lu Chang-guo 112581
Lu Hua-fu + 116067
+Lu Jing-xian 111962
+Lu Jing-xian 111963
+Lu Linsheng 113483
Lu Nai-Ping + 116182
Lu Sinien 115298
+Lu Ting. 113462
+Lu Wei-da 112581
+Lu Wei-xiu 115712
Lu Yuan-Zhong + 116020
Luan Hua see Hua Luan
+Lubenets, S.V. 114078
+Luc, P. 112711
+Lucasson, A. 113962
+Lucasson, P. 113962
+Lucchesi, M. 113663
+Lucherini, V. 112510
Lucke, K. + 113888
+Lucke, K. 114241
Ludicke, F. 111637
+Ludlam, T. 112024
Ludolf, W.S. + 113129
Ludvigsen, M. + 111515
Ludwig, D. 111406
Luecke, G.R. + 115168
+Luers, D. 112016
+Lugovskaya, E.S. 115393
+Lugovskii, A.P. 112732
Luhmann, J.G. + 116504
+Luhmann, J.G. 116401
+Luhrens, W. 112015
+Lui, A.T.Y. 116386
Lukacs, B. + 112274
Lukacs, B. + 111521
+Lukacs, B. 111620
+Lukacs, B. 116909
Luke, K.L. + 115648
+Lukens, H.R., Jr. 111860
+Lukierski, J. 111896
+Lukomskii, A.I. 114881
+Luksha, O.V. 115055
Lumbroso, H. + 112874
Lun Quan Wei see Quan Wei Lun
+Lund, I. 112162
Lund, J. 115623
+Lund-Andersen, H. 115783
+Lundak, R.L. 115834
Lundstrom, I. 115729
Lunelli, B. + 112727
+Lunina, S.I. 115438
+Lunine, J.I. 116505
Luo, J. + 113946
Luo Huibang see Huibang Luo
Luo Jin-Shen see Jin-Shen Luo
Luo Zhengming 112432
+Luontama, M. 112043
+Luontama, M. 112111
+Lupin, V.A. 113322
Lupishko, D.F. + 116516
Lurie, D. + 115757
+Lurie, J.B. 112769
+Lurie, N. 111860
+Lusis, A.P. 114269
Lustig, G. 116560
+Luth, V. 112011
+Luthra, A.K. + 113206
Lutz, B.L. + 116439
+Lutz, G. 112554
+Lutz, O. 114746
+Luu Dang Vinh. 114860
Lux, B. 114418
+Lux, B. 114420
+Lux, B. 114421
+Lux, B. 114428
+Lux, B. 115095
+Lyudnydyk, B.P. 116043
Luyten, P. + 113418
+Luz, Z. 114229
+Lvov, Y.M. 115733
+Lvova, I.V. 114684
+Lwin, T. 112530
+Lyakhov, D.M. 113504
+Lyalyuk, D.F. 113283
Lyamshev, L.M. + 113348
+Lyanov, B.E. 116350
+Lychev, V.A. 115842
+Lyerla, J.R., Jr. 113734
Lyle, D.B. + 115834
+Lynch, H.L. 111992
+Lynch, J.F. 113207
+Lynch, V.E. 113578
+Lynch, W.G. 112195
Lynden-Bell, D. + 116854
+Lynen, U. 112089
Lyngaee-Jorgensen, J. 113723
Lyngaee-Jorgensen, J. + 113727
Lysak, R.L. + 116399
+Lyskov, V.A. 114834
+Lyubimov, A.M. 115485
+Lyubimov, V.N. 114090
+Lyubin, V.M. 114423
+Lyubopytova, E.V. 114383
+Lyutyi, E.M. 115285
Ma Zai-Tian 116021
+Maby, E.W. 114475
+Mc Marr, P.J. 113946
McAbee, T.L. 112834
+MacAdam, K.B. 112683
McAlister, S.P. + 114665
McArthur, A.D. 112388
Macaskill, C. + 116236
+Macaskill, C. 116235
+McAtee, J.L., Jr. 114236
+Macbeth, A.A. 111990
+Macbeth, A.A. 112012
+Macbeth, P.J. 112348
McBrayer, J.D. + 114288
McBreen, J. + 115629
McBreen, J. + 115625
+McCaferly, E. 115385
+McCaffrey, B.J. 113548
+McCall, M.L. 116856
MacCallum, C.J. + 116825
MacCallum, E., Jr. + 116242
+McCann, H. 111990
+McCann, H. 112012
+McCann, J.J. 115782
McCartin, B.J. 113397
+McCarty, R.D. 113550
+McCaskey, J.S. + 114325
+McCaughrean, M.J. 116860
McCausland, I. 111431
+Macchiesney, J.B. 113123
+McCheyney, R.S. 116512
Macchiarella, G. + 113247
+Macchiarelli, B. 115378
+McClain, B. 114384
McClelland, B.J. 112746
+McClelland, R.W. 114629
+McClintock, P.V.E. 111563
+McCourt, F.R. 112814
+McCourt, F.R. 113560
+McCubbin, N.A. 112024
+McCubbin, N.A. 112549
+McCullough, R.L. 115504
+McCurdy, C.W. 112675
McCuskey, S.W. 116815
McDaniel, F.D. 112832
+McDaniels, D.K. 112153
+McDermott, M.J. 115138
Macdonald, A.L. 111346
+McDonald, D. 116151
+MacDonald, D.E. 115495
McDonald, H.O. + 115076
+McDonald, I.R. 114101
MacDonald, J. 116661
+MacDonald, J.R. 114894
McDonald, K.T. + 112580
+MacDonald, R.J. 114998
+McDonald, R.J. 112271
+McDougall, J.A. 115772
McDowell, H.K. + 114368
+MacDowell, S.W. 111532
+McEllistrem, M.T. 112190
McEwen, A.S. + 116520
MacFadyen, D.N. 115388
+McGarrity, G. 115709
+McGee, J. 115806
McGee, S.H. + 115504
+McGeorge, L. 115709
+McGill, R. 112474
+McGinn, J.T. 115074
+McGinness, M.J. 113405
MacGowan, D. 113565
+McGrath, J.E. 113725
+McGrath, J.F. 112438
+McGrory, J.B. 112219
+Macht, M.-P. 114244
+Macht, M.-P. 114274
+McHugh, A.J. 115184
+McHugh, A.J. 115041
Maciel, G.E. + 114741
+Macinnes, D.A. 112333
+McIntosh, D.H. 116243
+McKay, D.R. 114741
Mackay, R.S. 111579
MacKay, R.S. 115953
+McKee, B.T.A. 114042
McKelvey, M. + 115039
McKenzie, D.P. 116049
+MacKenzie, H.A. 113036
MacKenzie, I.K. + 114960
+MacKenzie, J. 112421
+MacKenzie, J. 111860
Mackenzie, N.D. + 114698
McKenzie-Wilson, R.B. 112473
McKinley, J.M. + 116884
MacKinnon, A. 114457
+Mackrodt, W.C. 113862
+McLaren, E. 116176
McLaren, J.W. + 115893
McLaughlin, T.V. + 115618
McLean, I.S. + 116860
+McMahan, M.A. 115519
+McMahon, T. 112031
+McManus, J. 116151
McMillan, G.B. + 114029
+McMullan, D. 111830
+McMurray, R.E., Jr. 114469
+McMurray, W.R. 112571
+McNair, R.E. 111344
+McNamara, L.F. 116625
McNaughton, B.L. + 115990
+McNaughton, J. 112021
+McNaughton, J. 112028
+McNeil, B.J. 115882
+McNeill, G.C. 116416
+McPherron, R.L. 116400
+Macq, P. 111809
Macrae, J. 115797
Macrae, J. 115888
+Macrae, J.H. 116747
Macrander, A.T. + 111826
+McWilliams, R.A. 111772
Madan, M.K. + 115655
Maday, Y. + 113406
+Maddalena, A. 114759
+Madden, N.W. 112564
Madden, R.A. 116216
+Madden, R.A. 116214
Maderbacher, F. 111676
Mader, R. + 112562
+Mader, T.E. 114365
+Mader, T.E. 114347
Madhava, M.S. + 114811
+Madsen, B. 112022
Maeda, A. + 114575
+Maeda, A. 112327
+Maeda, K. + 116231
+Maeda, K. 112208
+Maeda, K. 114077
+Maeda, M. 114384
+Maenhaut, W. 116177
+Maeno, Y. 114299
Maeta, H. 113903
+Maeta, H. 114047
Maftai, G. + 115722
+Maftai, G. 115721
+Maggi, G. 112008
+Magiera, A. 112241
+Magnanini, R. 112535
+Magnasco, V. 112643
+Mahajan, S. 115109
Mahajan, S. (ed.) 111315
Mahajan, S.M. + 113594
+Mahajan, S.M. 113566
Mahalakshmi, C.V. 113438
Mahan, J.R. + 113429
Maharana, J. 111883
Mahaux, C. 112053
Mahaux, C. + 112088
Maher, A. + 111434
+Maher, F.J. 111817
+Mahler, H.J. 111999
Mahmoud, S.A. + 114720
+Mahoney, W.A. 116826
Mahrt, L. 116257
Mai, Y.W. 115331
+Maiani, L. 111918
+Maiboroda, V.P. 115243
Maiella, G. + 111885
+Maier, K.H. 112066
+Maier, M. 112267
+Maier, P. 113982
+Maillard, J.P. 116439
Maino, G. + 112068
Mair, S.L. 114121
+Maury, C. 113876
+Maistrenko, A.I. 115246
+Maiti, H.S. 114173
+Maitra, K. 115644
Maitzen, H.M. + 116667
+Maitzen, H.M. 116769
Major, B. + 114155
+Majumder, D. 113603
Mak, A.A. + 112998
+Mak, H.-B. 114263
Mak, M. 116218
+Makarenko, V.G. 114565
+Makarov, V.P. 113935
+Makarova, L.N. 116346
Makhankov, V.G. 111903
Makhmutov, F.A. + 114256
+Makhmutova, E.A. 115438
Makhviladze, G.M. + 113494
+Makishima, A. 112117
+Makishima, K. 116582
Maklakov, A.I. + 113758
Maklakov, A.I. + 114221
+Makogon, M.B. 115340
+Makovei, V.A. 115475
+Makovetskii, D.N. 114726
Makovetskii, G.I. + 114688
Maksic, Z.B. + 112628
Maksimenco, V.P. 113285
Maksimov, E.P. 116058
Maksimov, G.V. + 115773
+Maksimov, R.D. 115472
Maksimov, S.B. + 113322
+Maksimova, L.V. 113322
+Maksimova, S.I. 115120
Maksimovich, G.G. + 115433
Maksimovich, G.G. + 115285
+Makushenko, Yu.M. 114868
+Makushev, S.Yu. 115191
Makushkin, Yu.S. + 116271
+Makushkin, Yu.S. 112731
+Malacara, D. 112940
+Malagnini, M.L. 116863
+Malaise, E.P. 115869
+Malakhov, V.F. 115437
+Malarski, Z. 112749
Malek, A. + 114842
Malek, C.Khan. see Khan Malek, C.
+Malek Mansour, M. 111557
Malfliet, R. + 112252
+Malfliet, R.A.R.L. 112237
+Malkin, B.Z. 114666
Mal'kov, A.S. 111806
Mallik, D.D. 116121
+Mallik, U. 112016
Malomed, B.A. 111461
Malomed, B.A. 111587
+Malosse, J.-J. 112031
Malov, V.V. + 113096
+Malta, C.P. 111489
Maluendes, S.A. + 112706
+Malvicini, G. 113524
+Malugin, G.A. 115253
+Malysenko, Yu.I. 116307
+Malyutin, V.I. 114715
Mamedov, A.A. 114882
Mamedov, M.A. 116549
+Mamko, B.P. 114971
Man Wang see Wang Man
+Manabe, S. 116153
Manabe, T. + 116262
+Manabe, T. 111641
+Manara, A. 116534
Manasevich, H.M. + 114388
+Manchanda, R.K. 116474
Mandel, P. + 113043
Mandel, P. + 113021
Mandelbrot, B.B. 111576
+Mandelli, L. 112020
Mandjukov, I.G. + 111832
+Mandjukova, B.V. 111832
+Mandl, F. 112028

- + Mandolesi, N.116889
Mangiavacchi, C. + ...113679
+ Manheimer, W.113580
+ Manheimer, W.M.113625
Mani, H.S. +112029
+ Mani, P.112022
+ Manilov, V.A.113802
+ Manin, V.N.114256
+ Manis, P.B.115805
+ Mankevich, V.N.114301
+ Mann, L.G.112066
+ Mann, R.D.115836
+ Manninen, M.114336
Mannone, F.112344
+ Manokhin, S.P.111823
Mansfeld, F. +115459
Mansingh, A. +114779
+ Manson, J.A.115362
+ Mansoulie, B.112022
Mansour, M. Malek
..... see Malek Mansour, M.
+ Mansouri, I.114753
Mansur, L.K. +113994
+ Mansur, L.K.114060
+ Mansur, L.K.114045
Mansuripur, M. +112948
+ Mansvetova, E.G.114718
+ Mantegazza, L.116670
+ Mantegazza, L.116671
Mantei, T.D.115389
Mantena, N.R.113142
+ Manthorpe, S.A.114023
+ Mantica, P.112585
+ Mantle, V.J.116469
Mantovani, G. +113928
+ Mantovani, G.C.112022
Manzanares, C. +112819
+ Manzhirou, A.V.113307
Manzke, R. +114983
+ Mapelli, L.112022
+ Marande, R.114760
Maraschi, L. +116763
Maraschi, L. +116858
Maraschi, L. +116761
Marcaide, J.M. +116870
+ March, N.H.113868
+ March, N.H.114325
+ Marchenko, I.G.114025
Marconi, M.L. +116531
+ Marcus, R.B.114783
+ Marczewski, A.W.114331
Mardirossian, F. +116864
+ Mardirossian, F.116745
+ Mardirossian, F.116863
+ Margalit, S.113007
+ Margalit, S.113009
Margaret, F.J. +112054
Margolies, S. +112840
+ Margrave, J.L.112722
Marigold, J.C.L. +115871
Marihal, B.N. +113629
Marilleau, J.111835
+ Mar'in, A.A.113821
+ Marini, A.111992
Markeev, A.P.113266
+ Markevich, I.V.114563
+ Markham, O.D.115937
+ Markiewicz, T.112031
+ Markin, Yu.V.114603
+ Markina, A.I.113669
+ Markle, R.A.115144
+ Markou, A.112024
+ Markov, S.I.115216
+ Markova, N.V.111832
+ Marks, S.114192
+ Markytan, M.112028
Marmarelis, V.Z. +115820
Marmur, I.Ya. +114562
+ Marom, G.115292
+ Marquez, R.113743
Marr, P.J. Mc. see Mc Marr, P.J.
Marscher, A.P. +116835
Marsden, B.G.116544
Marsden, B.G.116545
+ Marsden, B.G.116514
+ Marsden, B.G.116543
Marsden, J. +113455
+ Marsden, R.F.116238
Marsh, P.116427
Marshall, A.R.115798
+ Marshall, B.D.116086
Marshall, G.F. +113153
Marshall, G.L.113710
+ Marshall, G.P.115305
+ Marshall, J.M.114486
+ Marshall, R.111990
+ Marshall, R.112012
Marshall, S.V. +115827
+ Mart, P.L.114151
+ Martelet, A.113949
+ Marten, A.116521
+ Martens, L.116635
+ Martin, A.G.115909
+ Martin, E.R.112480
Martin, G. +113995
Martin, G. +113860
+ Martin, G.114283
Martin, J.C.112650
+ Martin, M.112539
Martin, P.P.111869
+ Martin, R.J.114254
Martin, S.A. +112528
+ Martin, S.A.112076
Martin-Neuville, H. +115670
+ Martini, G.113540
+ Martinson, I.115545
+ Martens, M.J.116619
Martuscelly, E. +113714
+ Martz, J.C.116074
+ Marty, N.112158
Martynenko, S.I. +116373
+ Martynenko, V.V.115273
+ Martynov, M.I.115142
Martynov, V.V. +115192
+ Martynova, G.P.115192
Martynyuk, A.A. +111426
Maruani, J. +112627
Maruani, J. (ed.)111310
+ Maruhn, J.A.112251
+ Maruhn, J.A.112263
+ Marusenko, S.Ya.115257
Marushchak, V.A. +114504
+ Marusin, V.V.111798
+ Maruyama, T.111992
+ Marvakov, D.I.114442
+ Marvin, D.A.115738
Marwitz, J.D.116223
Marzin, J.Y. +114898
Masaki, N. +114044
+ Masaoka, T.114862
Mascarenhas, S. +112803
Mascheck, H.-J.113423
+ Masden, B.F.113578
+ Masel, R.I.114353
Mashenko, V.A. +112732
Mashimo, T. +114093
+ Mashinskaya, G.P.113759
Mashovets, T.V. +113986
+ Masi, P.115294
+ Masiello, P.J.112377
+ Maslennikov, V.P.115542
Maslov, V.P. +111545
+ Maslowe, S.A.116118
+ Maslyuk, V.A.115141
Mason, S.F.114494
+ Masoni, S.114267
+ Masoumy, E.115293
Massalski, J.M.111625
+ Massaro, E.116838
Massie, N.A.111732
Massie, N.A. +111751
+ Masson, J.112394
+ Massopust, T.P.115635
+ Masters, S.E.116212
+ Masterson, T.G.112209
+ Masterson, T.G.112149
+ Mastichiadis, A.116833
+ Mastropietro, M.116474
+ Masuda, K.113977
+ Masuda, T.115582
Masui, N. +114976
+ Masumoto, T.114509
+ Masutomi, O.112522
Matal, O. +112404
+ Matcha, R.L.112795
+ Mateev, E.S.113653
+ Matera, M.113051
+ Mathelitsch, L.112079
Mathews, G.J. +112128
Mathews, G.J. +112125
Mathews, H.-G. +112497
Mathie, E.L. +112285
+ Mathieu, G.116073
Mathur, V.K. +114535
+ Matkova, I.I.114934
+ Matkovits, I.111671
Matkovsky, B.J. +111592
Matoba, M. +112146
Matozaki, T. +115898
+ Matricciani, E.116167
+ Matrosov, V.N.114890
Matsevityi, V.M. +115401
+ Matson, R.J.115635
+ Matsubara, N.115701
Matsuda, S.111930
+ Matsudo, K.115444
Matsueda, H. +114319
Matsui, H. +115351
Matsui, J.112997
+ Matsui, L.Yu.114506
Matsui, Y. +114379
+ Matsuki, S.112210
+ Matsuki, S.112051
Matsumoto, G. +112392
Matsumoto, H. +116393
Matsumoto, S. +111696
+ Matsumoto, S.115030
+ Matsumoto, S.114379
+ Matsumoto, S.114377
Matsumoto, T. +116018
+ Matsumura, H.111990
+ Matsumura, H.112012
+ Matsunaga, T.113257
Matsuo, K. +112888
Matsuo, T.115984
Matsuo, T. +114751
Matsuo, Y.115716
+ Matsuoaka, A.115794
Matsuoka, C.111403
+ Matsuoka, M.115036
Matsuoka, N. +112229
+ Matsuoka, N.112210
+ Matsuoka, N.112224
+ Matsuoka, N.112051
+ Matsuoka, N.112225
+ Matsuoka, S.115309
Matsuoka, T.112412
Matsuse, T. +112293
+ Matsushige, K.115235
+ Matsushita, K.114745
+ Matsushita, S.116410
Matsushita, T. +111553
+ Matsushita, T.115038
Matsusue, K. +115206
Matsusue, K. +115354
+ Matsuura, T.K.113534
Matsuyama, T. +114271
+ Matsuzawa, H.115924
Matsuzawa, K. +111648
+ Matsuzawa, K.113163
+ Mattar, F.113066
Mattar, F.P. +112966
Matteson, J.L.116834
Matteuzzi, C. +112011
+ Matthews, D.L.113658
+ Matthews, H.E.116793
Matthews, N. +116801
Mattig, W.116478
+ Mattiuz, U.112317
Mattsson, A.111845
+ Mattsson, S.112292
+ Matushko, V.L.112186
+ Matuskova, N.112216
Matveenko, A.V.112139
Matveenko, L.I. +116806
+ Matveev, O.A.114896
Matveev, V.V.112752
Matveev, V.V. +115244
+ Matveyenkov, V.V.116075
+ Matveyeva, G.A.115226
+ Matvienko, A.N.113952
Matvienko, Yu.G. +113362
+ Matz, S.116878
+ Maugin, G.A.114786
+ Maugin, G.A.114787
Mauk, B.H.116397
+ Maul, G.A.116094
Maurer, H.-J. +115431
Maurer, R.J. +112837
+ Maurin, G.112031
Mauritsch, H.J. +116017
Maurone, P.A. +111364
Maurone, P.A. +111365
+ Maurus, U.112015
Maury, F. +115089
Maury, F. +115068
Maury, F. +113962
+ Mauze, G.R.114262
Mavashov, B.Z. +116169
+ Mavashov, Yu.Z.116169
+ Mavrin, B.N.114118
+ Mavrodineanu, R.111784
Mavrogenes, G. +112470
+ Mavroides, J.G.114629
Max, N.L.115730
+ Maxeiner, C.112015
+ Maxeiner, H.112015
+ Maxfield, S.J.112015
Maxwell, B. +115157
May, P.G. +113052
Maybury, R. +112586
Mayer, F.J. +112438
+ Mayer, J.W.114054
+ Mayer, J.W.114001
+ Mayer, J.W. (ed.)111333
Mayes, P.J.D.113279
+ Maynald, D.113656
Mayya, Y.S. +111555
Maza, J.116710
Maza, J.116711
Mazets, E.P. +116876
+ Mazov, L.S.114739
Mazumdar, P.S. +112856
Mazur, V.A. +116407
+ Mazzinghi, P.116282
+ Mazzola, M.115250
+ Mead, W.C.113635
+ Meadows, A.J.116512
+ Mclewski, R.114365
+ Meday, K.116685
+ Meddi, F.112559
Medeiros Eilho, F.C. +116208
Medhi, K.C.112698
+ Medved, S.A.112551
+ Medvedev, F.A.115606
Medvedev, N.N. +113729
+ Medvedev, Yu.P.115075
+ Mee, J.E.114388
Meer, W. van der
..... see van der Meer, W.
Meerson, B.I. +116621
+ Meggitt, B.T.111761
Mehedinteanu, S. +112330
+ Mehnert, R.115570
Mehra, M. +113756
+ Mehra, R.K.116267
Mehta, S.K. +112446
+ Mehta, V.M.115973
+ Meier, K.111990
+ Meier, K.112012
Meijer, R.J. de
..... see de Meijer, R.J.
+ Meisingset, K.K.114207
Meisner, G.P. +114635
+ Meissburger, J.112076
+ Meissburger, J.112528
Meisser, C.113538
+ Meissner, M.114294
Mekawey, F. El
..... see El Mekawey, F.
+ Mekenyan, O.114330
Melekh, B.T. +113776
Melekhov, L.Z. +114678
Melichar, F.112355
+ Melikhov, O.I.113494
Melikhov, V.S. +115487
+ Melikov, M.Z.112919
+ Melimevker, O.D.115275
+ Melkadze, R.G.114116
Melle, H.112934
Mellen, R.H. +116102
+ Mellinger, G.B.114213
+ Mello, P.A.112135
+ Mellott, M.M.116400
+ Melled, A.J.114365
+ Melnichenko, V.I.115290
+ Melnichenko, V.I.115289
+ Mel' nichok, L.S.115466
+ Mel'nikov, A.P.114472
Mel'nikov, P.P. +115119
+ Mel'nikov, V.K.114220
Mel'nikova, O.N. +113509
Melo, M.V.M.C. de
..... see de Melo, M.V.M.C.
Melone, S. +112297
Melott, A.L.116842
Melrose, D.B.116622
+ Melton, R.B.115788
Melville, J.P. +116618
Melz, B.113264
+ Melzner, F.116402
+ Men, A.N.114880
Menaglia, F. +113983
+ Mende, S.116336
+ Mende, S.B.116396
Mendel, J.M.116320
+ Mendes Filho, J.114292
+ Mendiburu, J.-P.112031
+ Mendillo, M.116356
+ Mendis, D.A.116531
Meng, C.-I. +116370
+ Meng, G.Y.115113
+ Meng, R.L.114162
Meng-Ping Gu
..... see Gu Meng-Ping
+ Mengel, M.114360
Mengoli, M. +113586
+ Menke, K.114542
+ Mensch, W.113966
Men'shov, I.S.113477
Menyuk, C.R.113588
+ Menzenhauer, P.112319
Mercer, J. +111540
+ Mercer, R.L.112203
Meredith, M.A. +115786
Meredith, P.G. +116079
+ Merenkova, T.V.115214
+ Merkel, B.112022
+ Merkens, W.114064
Merkle, L.-O. +116095
+ Merkle, K.L.114033
+ Merkt, U.114738
+ Mermaz, M.C.112259
+ Mermikides, M.112022
+ Merrell, G.B.112348
Merrett, G.J. +112350
Merriam, J.B.115996
+ Merritt, F.R.115109
+ Mertens, R.115660
+ Merz, E.112352
+ Merz, F.112067
Meseguer, J.115048
+ Meserve, R.111711
+ Meshalkin, S.S.113831
+ Meshi, M.114033
+ Meshkov, E.V.115286
+ Meshkov, N.K.115335
+ Meshkovskii, I.K.112784
+ Messelt, S.112131
+ Messner, R.L.111992
+ Mestdagh, J.M.112812
+ Mestechkin, M.M.112670
Meszaros, A.116908
Meszaros, P. +116736
+ Metag, V.112113
+ Methfessel, M.S. +114430
Metiu, H. +115514
+ Metiveli, B.113406
+ Metreveli, D.M. +116211
+ Mettler, S.C.113117
Metzdorf, J.111742
Metzger, R.M. +111683
+ Metzl, R.115070
Metzner, H. +113961
+ Metzner, H.113963
Meuresch, S.112444
Meurice, Y.111976
Meyer, F. de
..... see De Meyer, F.
+ Meyer, H.112015
+ Meyer, H.J.112015
Meyer, J. +111541
+ Meyer, J.112015
+ Meyer, J.M.112587
+ Meyer, M.112544
+ Meyer, M.112285
+ Meyer, O.A.111992
Meyer, R.E.113412
+ Meyers, C.111910
+ Mezentseva, L.P.114666
Mezzetti, M. +116863
+ Mezzetti, M.116745
+ Mezzetti, M.116864
+ Mi Jian-Lin112511
+ Michael, D.113828
Michaelides, E.E. +112374
+ Michaelis, E.G.112589
+ Michalowski, S.J.111992
+ Michanskaya, N.I.115844
+ Michel, J.113772
+ Michelato, P.112585
+ Michels, A.C.114131
+ Michelsen, U.112015
+ Michette, A.G.113078
Michiel, H. +114486
+ Michikami, O.114644
+ Michio Yanai116188
+ Michl, J.114904
+ Michl, J.114748
+ Michorius, M.M.115451
+ Michotte, D.112556
+ Mickelsen, R.A.115635
+ Middelhoeck, J.115088
Middleditch, J. +116715
Middleton, R.112503
+ Middttun, G.112075
Miecznik, P.114097
+ Miehe, J.A.112770
+ Mighell, A.D.114491
Migliarese, C.115249
Mignaco, J.A. +111949
+ Mignard, F.116517
+ Mignerey, A.C.112249
Mignerot, J.-G.113191
+ Mihalas, B.W.116438
Mihalas, D. +116438
Mihaly, G. +114516
+ Mihalý, L.114516
+ Mikhkhe'lov, V.113018
+ Mikhailov, A.V.115335
+ Mikhailov, M.G.114318
+ Mikhailov, V.S.112551
+ Mikhailov, Yu.V.112556
+ Mikhail'chuk, Z.A.115509
+ Mikhalevich, V.S.114952
Mikheev, M.N. +111713
Miki, H.116035
Miklavcic, M.113402
+ Miklayev, P.G.113361
Miksis, M.J. +113462
+ Mikuz, M.112589
Miles, J.C.H. +112608
+ Miles, J.C.H.115941
Miles, J.W.116117
Milet, C. +112331
Mileva, M. +115826
+ Mileý, G.K.116810
+ Milkman, N.115795
+ Millan, M.113743
+ Miller, A.113038
Miller, A.J.113234
+ Miller, B.I.115387
Miller, C.W. +115718
Miller, E.L. +116061
+ Miller, E.R.115406
+ Miller, G.A.112080
+ Miller, K.J.115310
+ Miller, R.F.112411
+ Miller, R.H.112471
Miller, T. +115017
+ Miller, W.E.115628
+ Miller, W.H.112533
+ Millers, D.K.114892
+ Mills, R.L.116535
+ Milloy, H.B.112860
Mills, A.P., Jr. +114580
+ Mills, H.E.111990
+ Mills, H.E.112012
+ Mills, R.L.113809
+ Mills, R.L.113800
+ Millward, A.116284
Milosavljevic, M. +115106
+ Miloslavskii, V.K.114832
Mimikou, M.116155
Mimura, Y.113131
Min-Guang Zhao111526
+ Minakoshi, H.116364
+ Minakov, V.N.113802
+ Minakova, R.V.114306
+ Minami, M.111877
Minamisawa, C. +115491

- + Minamisono, T. 112278
 + Minard, M.-N. 112031
 + Minato, A. 112408
 + Minato, K. 112325
 + Minato, T. 113645
 + Minde, R. 113871
 + Mindyuk, A.K. + 115437
 + Mineev, V.N. 115260
 + Minemoto, T. + 112961
 + Ming Wang. *see* Wang Ming
 + Ming-Chu Duan.
 see Duan Ming-Chu
 + Ming-ko Woo + 116154
 + Ming-Sheng Chen.
 see Chen Ming-Sheng
 + Ming-xing Wang.
 see Wang Ming-xing
 + Mingay, D.W. 112239
 + Minier, C. 113899
 + Minier, C. 113876
 + Minin, V.A. + 115610
 + Mink, D.J. 116527
 + Min'kov, G.M. 114586
 + Minni, E. 115012
 + Minowa, M. 111990
 + Minowa, M. 112012
 + Minowa, T. 114708
 + Minster, J.F. 116074
 + Mints, R.G. 114641
 + Mints, V.P. 115171
 + Mintz, J.M. 113984
 + Mintz, S.L. 112178
 + Mioduchowski, A. 113341
 + Miono, S. 116555
 + Mirabile, M. 115494
 + Miranda, L.C.M. 111773
 + Miranda, L.C.M. 114292
 + Miranda, L.C.M. 112969
 + Miranda, R. + 114356
 + Mirek, J. + 115517
 + Mirlin, Ye.G. + 116046
 + Mirochnik, V.L. + 113955
 + Mironenko, V.R. 113063
 + Mirsaev, I.F. + 114719
 + Mirsaetov, Sh.A. 115639
 + Mirzaa, M.C. 112190
 + Misawa, M. 113750
 + Mischanchuk, B.G.
 115571
 + Mishima, T. 113061
 + Mishin, V.V. + 116411
 + Mishina, T. 114757
 + Mishnev, A.F. + 112865
 + Mishurova, E. 115850
 + Misler, S. 115762
 + Misyura, V.A. 116373
 + Mitasov, M.A. 113837
 + Mitchell, E.W.J. 113717
 + Mitchell, G.E. + 114984
 + Mitchell, G.E. 112157
 + Mitchell, L.W. 112181
 + Mitchell, R.H. 116041
 + Mitchell, T.E. 113885
 + Mitchell, T.E. 114188
 + Mito, I. 113011
 + Mitra, A.N. + 111996
 + Mitra, G.B. + 113697
 + Mitra, S.K. + 113754
 + Mitra, S.S. + 114205
 + Mitrenin, Yu.V. 115548
 + Mitrofanov, V.P. 111536
 + Mitrofanov, V.Ya. + 114880
 + Mitsel', A.A. 116271
 + Mitsuk, V.E. 113694
 + Mitsumoto, S. + 116224
 + Mitsunaga, Y. + 113137
 + Mittal, R. 112122
 + Mittelstaedt, E. 116132
 + Mittendorfer, J. 112028
 + Mityakov, N.A. 116378
 + Mityugov, V.V. 113046
 + Mityushov, E.A. 115245
 + Miura, E. 115154
 + Miura, K. 112211
 + Miura, K. 112208
 + Miyachi, I. + 116157
 + Miyagi, S. 114987
 + Miyahara, A. 113622
 + Miyahara, A. 112478
 + Miyahara, J. 115918
 + Miyajima, Y. 113120
 + Miyake, K. 116157
 + Miyake, S. + 115779
 + Miyake, S. 113567
 + Miyama, Y. + 112279
 + Miyamoto, H. 111777
 + Miyamoto, M. + 113121
 + Miyamoto, N. 115125
 + Miyamoto, Y. 114844
 + Miyao, M. + 114013
 + Miyasaka, K. 114334
 + Miyashita, T. 113133
 + Miyazaki, E. + 114354
 + Miyazaki, N. 112414
 + Miyazaki, Y. 113152
 + Miyazawa, T. 114143
 + Miyazawa, Y. 112484
 + Miyoshi, S. 111811
 + Mizobuchi, A. 112466
 + Mizoguchi, K. 115022
 + Mizoguchi, R. + 111735
 + Mizoguchi, Y. 114047
 + Mizota, T. + 113805
 + Mizurukhin, L.V. 113867
 + Mizufune, E. 115780
 + Mizuguchi, F. 113338
 + Mizuguchi, J. + 115111
 + Mizukami, K. 111439
 + Mizuno, K. 113975
 + Mizuo, S. + 114259
 + Mizutani, K. 113249
 + Mjornmark, U. 112024
 + Mkrtchyan, V.S. 114487
 + Mnatsakanov, T.T.
 114604
 + Moacanin, J. 115261
 + Mobilia, J. 116359
 + Mochacki, S.W. 116692
 + Moeller, E. + 112257
 + Moeller, E. 112256
 + Moeller, R.P. 113124
 + Moffat, A.F.J. 116668
 + Moffat, A.F.J. 116769
 + Mogil'ner, L.Yu. 113172
 + Mogro-Campero, A.
 115945
 + Mohamed, A.A. 115266
 + Mohammadi, M. 112031
 + Mohanakumar, K. + 116250
 + Mohandas, K. 115557
 + Moharam, M.G. + 112927
 + Mohanen, V. 116261
 + Mohr, D.L. 112480
 + Mohr, G.A. + 111720
 + Mohr, K.P. + 115446
 + Mohri, J. 115146
 + Moiseev, A.M. 112021
 + Moiseev, G.K. + 115118
 + Moiseev, I.G. 116806
 + Moiseyev, V.V. + 111745
 + Moiseyev, A.M. 112028
 + Mojzis, M. 111622
 + Mojzis, M. 111662
 + Mokan, I.I. 115652
 + Molian, P.A. + 115425
 + Molinari, V.G. 113586
 + Molion, L.C.B. + 116180
 + Molis, S.E. 114863
 + Moller, P. 114912
 + Moller, P.J. 114339
 + Moller, R. 112024
 + Mollerud, R. 112022
 + Mol'nar, A.A. 115759
 + Molodkin, A.K. + 114127
 + Molotai, A.A. 116368
 + Molvich, A.W. 113641
 + Molzon, W. 112024
 + Momo, A. 115503
 + Monastireva, N.I. 114306
 + Mongan, T.R. 111978
 + Monica, M. Della.
 see Della Monica, M.
 + Moniz, E.J. 112083
 + Monod, P. 114431
 + Monos, E. 115969
 + Monson, P.A. + 113713
 + Montaldi, E. 112970
 + Montanes, J.L. 113580
 + Montemayor, R. + 111917
 + Montgomery, S.D. 112313
 + Montoneri, E. 112874
 + Montvay, I. 111884
 + Moodenbaugh, A.R.
 114164
 + Moodenbaugh, A.R.
 114633
 + Moodie, T.B. + 113341
 + Moody, K.J. 112061
 + Mooley, D.A. + 116190
 + Moon, H.T. + 113419
 + Moon, T.T. + 116673
 + Moon, T.T. + 116681
 + Moon, T.T. 116675
 + Moor, H.H.C.de.
 see de Moor, H.H.C.
 + Moore, B.C.J. + 115800
 + Moore, C.E. 111331
 + Moore, C.J. 116180
 + Moore, D.A. 112351
 + Moore, E.P. 113818
 + Moore, J.C. + 116062
 + Moore, L.E. 115774
 + Moore, P.B. + 113804
 + Moore, R.B. 112507
 + Moore, W.S. 116092
 + Moorwood, A.F.M. +
 116789
 + Moose, P.H. + 113187
 + Mooraal, H. + 116412
 + Morabito, D.D. + 116814
 + Morancho, R. 115077
 + Moravec, F. 115045
 + Morawetz, C.S. + 111497
 + Morawetz, H. 113726
 + Mordyuk, V.S. 114185
 + More, N. + 115458
 + Morel, A. 111873
 + Morel, B. 111533
 + Moreno, D. 111380
 + Moreno, M. 111917
 + Morgan, D.H. 116654
 + Morgan, J.A. + 112002
 + Morgan, K. 112031
 + Morgan, P.D. 113630
 + Morgan, R.J. 115361
 + Morgan, R.J. + 115318
 + Morganyuk, V.S. + 115229
 + Morgenstern, H. + 112272
 + Morgenstern, H. 112270
 + Morgenstern, H. 112273
 + Mori, A. 112206
 + Mori, H. + 113671
 + Mori, K. 115352
 + Mori, K. 113619
 + Mori, T. 114286
 + Mori, Y. 112485
 + Moriarty, K.J.M. 111866
 + Moricca, M. 112031
 + Morimoto, R.S. 115831
 + Morinaga, H. 112468
 + Morinaka, A. + 113071
 + Morinobu, S. 112207
 + Morinobu, S. 112212
 + Morishita, Y. 113921
 + Morisseau, P. 115456
 + Morita, K. 114989
 + Morita, K. 116251
 + Morita, K. + 114239
 + Morita, K. 111323
 + Morita, N. 113091
 + Morita, S. 113659
 + Morita, T. + 115794
 + Morito, N. 115241
 + Moriwaiki, T. 113473
 + Morlet, M. 112158
 + Morniroli, J.P. + 115200
 + Moro, R. + 112120
 + Morokuma, K. 115527
 + Moromisato, J.H. 111992
 + Moroshin, R.N. 113547
 + Morossi, C. + 116487
 + Moroz, V.I. 116507
 + Morozov, A.G. 116411
 + Morozov, I.I. 111816
 + Morozov, V.A. 115573
 + Morozova, V.A. + 114829
 + Morozumi, S. 114963
 + Morris, C.L. 112283
 + Morris, C.L. 112149
 + Morris, C.S. 116537
 + Morris, C.S. 116539
 + Morris, C.S. 116546
 + Morris, E.C. + 113549
 + Morris, M. + 116781
 + Morrison, D. 111728
 + Morrison, D.O. 112028
 + Morrison, L.V. 116499
 + Morsi, M.M. 114884
 + Mortari, G. Piano.
 see Piano Mortari, G.
 + Mortensen, O.S. 112738
 + Morton, M. + 115288
 + Moscinski, J. 112361
 + Mosel, U. 112093
 + Mosel, U. 112101
 + Mosel, U. 112173
 + Moseley, M.E. + 114229
 + Moser, P. 113879
 + Moser, U. 112007
 + Moses, D.J. 112271
 + Moses, J. 116519
 + Moshchalkov, V.V.
 114669
 + Moshchalkov, V.V.
 113786
 + Moshe, M. 111899
 + Moshkalev, S.A. 113060
 + Moshkalev, S.A. 113661
 + Moskalenko, A.M. 116291
 + Moskalenko, V.I. 114127
 + Moskaleva, E.M. 115471
 + Moskaleva, N.M. + 115004
 + Moskowitz, P.D. + 115658
 + Moskvich, Yu.N. 114793
 + Moslehi, M. 114255
 + Mosnier, A. 112472
 + Mosnier, J. 116314
 + Moss, D.B. + 112822
 + Moss, F. 111563
 + Moss, I.G. 116902
 + Mostinski, I.L. 113263
 + Mostovnikov, V.A. 113060
 + Mostow, M.A. + 111865
 + Motoba, T. 112105
 + Motobayashi, T. 112218
 + Motobayashi, T. 112216
 + Motoc, C. 114771
 + Motoc, I. 112661
 + Motulevich, G.P. 114845
 + Motz, H. 112695
 + Mouchet, M. 116650
 + Moudy, L.A. 114388
 + Moun, G. 112526
 + Moune-Minn, O.K. +
 114908
 + Mountain, R.W. 115050
 + Mountrakis, D.M. 116027
 + Moura, J.M.F. 113210
 + Mouradian, Z. + 116619
 + Mousty, F. 112317
 + Movchan, B.A. + 115284
 + Moyer, K.H. + 115138
 + Moyer, M.D. 114018
 + Moyer, M.D. 114475
 + Moyer, M.D. 114612
 + Moyers, J. 116261
 + Mozharovskii, N.S. +
 114088
 + Mrazek, R.V. 111682
 + Mrevlishvili, G.M. 115742
 + Mroczkowski, S. + 114978
 + Muchi, T. 115111
 + Muchkin, L.N. 115214
 + Muckett, S.J. 115399
 + Muddle, B.C. + 115324
 + Mudry, F. 115329
 + Mudryi, A.V. 114922
 + Muel, B. 115866
 + Mueller, F.M. 114435
 + Mueller, F.M. 114430
 + Mueller, M. + 115215
 + Muentner, S.E. 111751
 + Muhle, E. 114107
 + Muhleman, D.O. 116508
 + Muhlans, K. + 112101
 + Muir, A. + 115776
 + Muir, P.H. + 113435
 + Muirhead, E.G. 112170
 + Muirhead, H. 112031
 + Mujica, A. + 116530
 + Mukai, T. + 114188
 + Mukai, T. 113902
 + Mukai, T. 113885
 + Mukhametzyanov, F.Kh.
 113672
 + Mukhametzyanov, R.E.
 112825
 + Mukherjee, B. 115861
 + Mukherjee, M. 113836
 + Mukherjee, M.K. 115644
 + Mukherjee, P. + 112057
 + Mukherjee, P.S. 113697
 + Mukherjee, S.C. 112838
 + Mukherjee, S.N. + 112168
 + Mukherjee, S.P. 111452
 + Mukherjee, S.P. 115144
 + Mukhina, Z.N. 115435
 + Mukhopadhyay, S. 111617
 + Mukhortov, M. 114800
 + Mukhortov, Vas.M.
 114800
 + Mukhortov, V.I.M. 114800
 + Muller, E.M. 112101
 + Muller, F. 112031
 + Muller, H. 112016
 + Muller, H. 112015
 + Muller, H.G. 113960
 + Muller, H.G. 113964
 + Muller, H.G. 116328
 + Muller, H.G. 113963
 + Muller, M. 114062
 + Muller, M. 112590
 + Muller, R. 113258
 + Muller, R. + 116613
 + Muller, R. 112241
 + Muller, R.P. + 112725
 + Muller, T. + 113111
 + Muller, W.F. 114094
 + Muller-Vogt, G. 115040
 + Munera, C.I. + 115428
 + Muntz, E.P. 113476
 + Muradov, M. 115688
 + Murakami, E. 116038
 + Murakami, H. + 114745
 + Murakami, H. + 113861
 + Murakami, H. 114047
 + Murakami, T. 116582
 + Muramoto, T. 113044
 + Muraoka, K. 113664
 + Murata, Y. + 115036
 + Murata, Y. 114976
 + Muratova, L.A. 113833
 + Muravin, G.B. + 115480
 + Murayama, K. + 114919
 + Murayama, N. 113770
 + Murdin, P. 116471
 + Murgai, A. 113451
 + Muroga, T. + 113993
 + Muroo, Y. 114038
 + Murphree, J.S. 116337
 + Murphy, K. 112202
 + Murphy, M.J. + 112071
 + Murphy, P.G. 111990
 + Murphy, P.G. 112012
 + Murphy, P.K. + 112951
 + Murphy, R.J. 116414
 + Murphy, R.J. 116591
 + Murphy, S.M. + 114024
 + Murphy, W.F. 112738
 + Murr, L.E. 115267
 + Murray, F.W. 116225
 + Murray, L.A. 111672
 + Murri, R. 115083
 + Murthy, K.P.R.Vittal.
 see Vittal Murthy, K.P.R.
 + Murthy, N.Srinivasa.
 see Srinivasa Murthy, N.
 + Murthy, P.V.Ramana.
 see Ramana Murthy, P.V.
 + Murty, M.V.R.K. + 111755
 + Murty, P.S. 116662
 + Muscat, J.P. 114362
 + Musci, M. 115083
 + Mushrush, G.W. + 115725
 + Musselman, R.L. 115008
 + Musser, J.A. 112546
 + Mussil, V.V. + 114832
 + Musso, G.F. + 112643
 + Musto, R. + 111888
 + Muta, T. 111389
 + Muthusubramanian, P. +
 114853
 + Mutka, H. 114636
 + Mutoh, H. 112839
 + Muzafarova, S.A. 115639
 + Muzikante, I.Ya. + 114538
 + Myalitsin, L.A. 113636
 + Myers, D.R. + 113943
 + Myers, J.S. 116044
 + Myl'nikov, G.D. 113081
 + Myl'nikov, G.D. 113059
 + Myl'nikov, M.Yu. 114218
 + Mynick, H.E. 113572
 + Myrick, T.E. + 115703
 + Mytsyk, I.A. 112593
 + Na, T.Y. 113480
 + Nabatov, V.N. 116300
 + Nabelek, I.V. 115804
 + Naberukhin, Yu.I. 113729
 + Nadezhdin, G.N. 115247
 + Nadezhnikov, Yu.I. +
 116351
 + Naem, A.A. 114012
 + Nafie, L.A. 115749
 + Nag, B.R. 114518
 + Nagae, M. 114991
 + Nagai, H. + 114529
 + Nagamachi, S. 112051
 + Nagamiya, S. 112256
 + Nagamiya, S. 112257
 + Nagamori, M. 115176
 + Nagano, K. 112213
 + Nagano, K. 112223
 + Nagasubramanian, G. +
 114606
 + Nagata, A. 113651
 + Nagata, K. + 114844
 + Nagata, K. 115309
 + Nagatomo, K. 111471
 + Nagayama, K. 114093
 + Nagel, W. 115760
 + Nagesha Rao, N. + 113616
 + Naghi, P.M. + 113275
 + Nagi Reddy, K. 113916
 + Nagpaul, K.K. 112565
 + Nagraba, S. 113637
 + Naguib, H.H. 114012
 + Nagy, M.E. 112397
 + Nagy, M.R. + 115266
 + Nahory, R.E. 114254
 + Nai-Ping Lu.
 see Lu Nai-Ping
 + Naik, I.K. 113086
 + Nair, V.K.R. 115063
 + Nairn, A.E.M. 116016
 + Naito, M. 114575
 + Naito, S. 114355
 + Najar, A.A.Al. *see* Al Najar, A.A.
 + Naka, K.-I. 115787
 + Nakagawa, H. 115701
 + Nakagawa, K. 114077
 + Nakagawa, K. 113108
 + Nakagawa, M. 114034
 + Nakagawa, T. 112211
 + Nakagawa, T. 112208
 + Nakagawa, Z. 115155
 + Nakagawa, Z. 115156
 + Nakagawa, Z. 115353
 + Nakai, K. + 114038
 + Nakai, Y. + 114105
 + Nakajima, H. 116594
 + Nakajima, H. 114245
 + Nakajima, H. 116573
 + Nakajima, K. + 115112
 + Nakajima, T. 112767
 + Nakamura, A. 113178
 + Nakamura, A. 113179
 + Nakamura, A. 113170
 + Nakamura, F. + 113884
 + Nakamura, F. 113970
 + Nakamura, H. + 114377
 + Nakamura, H. 112522
 + Nakamura, H. 115022
 + Nakamura, K. 116205
 + Nakamura, K.-I. + 113770
 + Nakamura, M. 112225

- +Nakamura, S. 112550
 +Nakamura, S. 114316
 +Nakamura, S. 114985
 Nakamura, T. + 113178
 Nakamura, T. + 113179
 +Nakamura, T. 114384
 +Nakamura, Y. 115105
 +Nakane, Y. 114459
 +Nakanishi, K. 115744
 Nakanishi, T. + 115667
 +Nakanishi, T. 112466
 +Nakano, K. 112147
 +Nakano, M. 112230
 Nakashima, M. + 114260
 Nakashima, N. + 115568
 Nakashima, S. + 114615
 +Nakashima, T. 112522
 +Nakata, H. 113257
 +Nakata, M. 115265
 +Nakau, T. 113911
 Nakayama, I. + 113170
 +Nakayama, S. 112160
 Nakayama, T. 114918
 Nakazawa, M. 113128
 Namatame, I. + 112406
 +Nambodhiri, T.K.G. 115420
 Namgaladze, A.A. + 116325
 Namikawa, T. + 116410
 +Nanao, S. 114959
 Nandapurkar, P. + 115512
 +Nandi, A.K. 112031
 +Nandi, S. 112010
 Nandy, K. + 116654
 +Nanopoulos, D.V. 111929
 +Napara-Volgina, S.G. 115140
 +Napartovich, A.P. 113681
 +Napoly, O. 111873
 +Nappi, E. 112008
 +Naraghi, H. 114973
 Narasimha, R. 113422
 Narayan, J. 114020
 +Narayan, J. 114011
 +Narayan, J. 114010
 +Narayan Reddy, P. 111660
 +Narayana, P.A. 115890
 Narayankhedkar, K.G. 111691
 +Narayankhedkar, K.G. 111694
 Nardo, M.Di. *see* Di Nardo, M.
 +Nardulli, G. 111975
 +Narici, L. 111537
 Narita, S.-I. 114605
 +Narkis, M. 114578
 +Naroska, B. 111990
 +Naroska, B. 112012
 +Nash, F.R. 113013
 Nash, P. + 115167
 Nashif, A.D. 113198
 Naslain, R. + 115091
 +Naslain, R. 115092
 Nason, D. 113784
 Nassar, A.M. + 114884
 Nasu, H. + 114784
 Nasu, S. + 113971
 +Nasu, S. 114261
 +Nasu, S. 114044
 +Nasyrov, A.N. 114095
 Natanson, G.A. 112709
 Natarajan, A. + 112805
 Natarajan, G. + 111684
 +Nath, G. 113409
 +Nath, G. 113410
 +Nath, G. 115837
 +Nather, R.E. 116659
 +Natsui, T. 114768
 +Natsume, H. 112354
 Nauka, K. + 113954
 Naumann, G. 115416
 +Naumann, L. 112031
 +Naumenkov, P.A. 113661
 +Naumov, N.I. 112551
 +Naumov, S.N. 113242
 Naundorf, V. + 114274
 +Naundorf, V. 114244
 +Navach, F. 112020
 +Navare, R. 115291
 +Navarra, F.S. 112023
 +Navasardyan, G.V. 112576
 +Nave, C. 115738
 +Naya, E. 113904
 +Nayak, I.V. 113506
 Nayar, V.Unnikrishnan
 ... *see* Unnikrishnan Nayar, V.
 +Nazar, F.M. 113807
 +Nazarewicz, W. 112048
 Nazarkin, A.V. + 112976
 Nazarov, W.W. 112607
 +Nazaroff, W.W. 115944
 +Nazaroff, W.W. 111658
 Nazarov, S.A. 113369
 +Nazarov, V.G. 114256
 Nciri, B. + 115448
 Neelakantaswamy, P.S. + 115965
 Neergard, K. 112041
 +Nefedov, A.P. 113660
 +Nefedov, E.I. 113023
 +Nefedov, I.M. 114739
 +Neff, W.D. 116182
 +Negele, J.W. 112167
 Negra, M.Della
 ... *see* Della Negra, M.
 +Neihart, M.Kh. 114936
 +Neilson, G.C. 112288
 Neilson, G.W. 113720
 +Neite, G. 115240
 +Nekesow, A. 115330
 +Nekipelov, V.M. 115543
 +Nelander, B. 112720
 +Nelin, C.J. 112666
 +Nelles, B. 116773
 +Nelmes, R.J. 114792
 +Nelson, A.H. 112112
 Nelson, C. + 113748
 Nelson, G. + 116133
 +Nelson, G. 112530
 +Nelson, J.E. 111516
 Nelson, J.G. + 114441
 Nelson, J.H. 111376
 +Nelson, M.E. 112011
 +Nelson, R.J. 115115
 +Nelyubov, A.I. 111390
 Neman, R.L. 111375
 +Nembach, E. 115240
 Nemchinskii, V.A. 113692
 Nemchinskii, V.A. 113693
 +Nemechek, Z. 116418
 +Nemeth, I. 115715
 +Nemethy, G. 115736
 +Nemethy, P. 112007
 +Nemets, O.F. 112591
 Nemish, Yu.N. + 113283
 Nemoshkalenko, V.V. + 114971
 Nemzek, T.A. + 115495
 +Neov, S. 114670
 Neporent, B.S. + 113056
 Nepveu, M. 116444
 Nero, A.V. 115938
 Nero, A.V. 115940
 Nero, A.V. + 115944
 +Neruda, O. 112449
 +Nesheva, D. 114563
 +Neshpor, V.S. 113795
 +Neskoromnyi, V.N. 111551
 +Nesmeyanov, An.N. 115164
 +Nestaiko, O.V. 115895
 Nesterenko, V.A. + 111961
 Nettore, V.M. + 115209
 +Netzer, F.P. 115021
 Neubert, D. + 115967
 Neubert, T. + 116395
 Neudeck, G.W. + 114484
 +Neugebauer, E. 112554
 +Neugebauer, G. 115073
 +Neuimin, A.D. 114573
 +Neuman, V. 113154
 +Neumann, B. 112015
 +Neumann, C.J. 116189
 +Neumann, J.P. 113865
 +Neumann, W.P. 112755
 +Neumoin, A.I. 115441
 +Nevanlinna, O. 114630
 Nevesskiy, Ye.N. 116045
 +Neveu, A. 111501
 +Nevins, W.M. 113589
 +Nevskii, N.N. 113830
 +Nevskii, N.N. 113829
 Newman, B.G. 113445
 Newman, D.J. 114498
 +Newman, D.J. 114499
 +Newman, E.T. 111508
 +Newman, F. 116106
 Newman, R.C. + 115409
 +Newman, R.C. 115413
 Newman, R.N. 112401
 Newman, R.P.A.C. 116899
 +Newnham, R.E. 114789
 +Newton, J.O. 112244
 +Newton, M. 111958
 +Nezhevenko, L.B. 115280
 +Nezlin, M.V. 113417
 Ng, A. + 113666
 +Ng, K.K. 111981
 Ng, L.C. + 113205
 +Ng, T.T. 113425
 Nghi Nguyen Thanh
 ... *see* Nguyen Thanh Nghi
 +Ngo, C. 112103
 +Ngo, H. 112088
 +Ngo Dien Tap. 114378
 +Nguyen, M.T. 112891
 Nguyen, T.T.A. + 115016
 +Nguyen, V.V. 114136
 +Nguyen Huu-Doan. 116672
 +Nguyen Thanh Nghi. 114149
 +Nguyen Thanh Nghi. 114150
 Nian-Ning Hang
 ... *see* Hang Nian-Ning
 +Nichols, B. 116024
 Nichols, J.S. + 111721
 +Nickel, H. 115446
 +Nickel, H. 112341
 +Nickel, H. 112343
 +Nicklow, R.M. 114104
 +Nicodemi, F. 111888
 +Nicodemo, L. 115294
 +Nicolai, A. 113673
 +Nicolais, L. 115294
 +Nicolais, L. 115395
 +Nicolais, L. (ed.) 111312
 +Nicolle, R. 112033
 +Nicolet, M.A. 114611
 +Nicolet, M.A. 114258
 +Nicolet, M.A. 114285
 +Nicolis, G. 111557
 +Nicolson, G.D. 116814
 Niede, G.E.Von
 ... *see* Von Niede, G.E.
 +Niederreiter, H. 111352
 +Niel, M. 116588
 +Nielsen, B. 114961
 +Nielsen, B.S. 112024
 +Nielsen, E. 116362
 +Nielsen, H.B. 114309
 Nielsen, L.E. 115239
 Niemann, B. + 111848
 +Niemi, V.S. 116668
 Nieminen, R.M. 114953
 +Nieminen, R.M. 114336
 +Nieminen, R.M. 114581
 +Niepel, G. 115908
 Nieto, J.-L. 116846
 +Niewiarowicz, M. 113248
 +Nigam, K.D.P. 113520
 Nigam, K.M. + 113520
 Nigmatullin, B.I. + 113528
 Nigmatullin, R. + 114778
 Nihura, T. + 114296
 +Niinisto, L. 114907
 +Nikiforov, A.E. 114880
 +Nikiforova, T.V. 114168
 +Nikitin, A.G. 111902
 +Nikitin, M.A. 116351
 Nikitin, O.P. 116161
 +Nikitin, V.V. 111713
 Nikityuk, V.A. 113284
 +Nikkinen, L. 112507
 Niklasson, G.A. + 115698
 +Nikolaev, P.N. 111543
 Nikolaev, V.I. + 114761
 Nikolaev, V.S. 113662
 +Nikolaeva, T.G. 114627
 +Nikolaiko, A.S. 112593
 +Nikolic, I.A. 111530
 +Nikolov, V. + 113785
 +Nikolova, L. 112962
 Nildebrandt, J. 113006
 Nilles, H.P. 111951
 +Nilles, H.P. 111952
 +Nilson, J.A. 114011
 +Nilsson, A. 112024
 +Nilsson, B. 112022
 +Nilsson, L. 112159
 Nilsson, P.O. + 114951
 +Nimmagadda, R. 115284
 Ninagawa, K. + 116555
 +Ninane, A. 111809
 +Ninburg, O.P. 111799
 Ning Yang Chen
 ... *see* Chen Ning Yang
 Nisenson, P. + 116489
 +Nisenson, P. 116274
 +Nishi, K. 113011
 +Nishi, M. 114916
 Nishida, K. + 115046
 +Nishida, K. 114788
 Nishida, T. + 113893
 Nishihara, H.K. 115793
 +Nishihara, S. 112208
 +Nishikawa, K. 113257
 Nishikawa, K.-I. + 116389
 Nishikawa, M. 112439
 Nishikawa, O. 111825
 Nishikawa, O. 115028
 Nishimura, K. + 115407
 +Nishimura, S. 116057
 +Nishinari, K. 113393
 Nishio, M. + 115105
 Nishioka, H. 112276
 +Nishioka, T. 115058
 +Nishiyama, E. 115630
 +Nisimura, K. 112224
 Niskanen, J.A. 112132
 +Nissen-Meyer, S. 112256
 +Nissen-Meyer, S. 112257
 Nitta, A. + 113371
 Nitta, N. + 116574
 +Nitta, N. 116581
 +Nitta, N. 116583
 +Nitta, N. 116582
 +Niu, K. 113628
 +Niwa, H. 115262
 Nix, J.Rayford
 ... *see* Rayford Nix, J.
 Nizhnik, S.B. + 115193
 +Nizkyii, S.E. 115849
 Nobuyoshi, T. + 113091
 Nochumson, D.H. 115710
 +Noda, K. 114261
 +Noda, K. 114044
 +Noda, K. 114751
 Noda, Y. + 114109
 +Noda, Y. 114163
 +Nodulman, L. 112545
 +Noel, P. 113576
 Noerdlinger, P.D. 116451
 +Noerdlinger, P.D. 116452
 +Nogin, N.I. 115169
 Noguera, S. + 112191
 +Nojiri, Y. 112278
 +Nolan, P. 112049
 Nolan, P.J. + 112112
 Nolan, P.L. + 116878
 Nolte, E. + 112468
 Nolte, L.-P. + 113281
 Nomura, M. 111698
 Nomura, M. 112137
 +Nomura, M. 112212
 Nomura, S. + 114770
 +Nomura, S. 115262
 +Nonami, T. 112961
 +Nonomura, S. 115634
 Norbeck, E. + 112253
 +Norbert, S. 112060
 +Norden, P.-E. 111774
 +Norden, H. 115201
 +Norden, H. 114405
 +Nordh, H.L. 116782
 Nordine, P.C. 112986
 +Nordman, J.E. 114645
 +Norets, T.A. 115846
 +Norets, T.A. 115847
 +Norets, T.A. 115840
 +Norlin, L.O. 112535
 +Noro, T. 112210
 +Noro, T. 112051
 +Noro, T. 112225
 Norris, D.I.R. + 112324
 +Norris, J.R. 114724
 Norros, L. + 112384
 +Norry, M.J. 116087
 +Norskov, J.K. 114336
 +Norton, A. 112031
 Norton, B. + 115693
 Norton, R.B. + 116203
 +Norton, S.A. 115942
 Nosek, M.V. + 115173
 Nosenko, A.D. 113180
 Nosova, G.I. + 113925
 Notz, D. 112490
 Noumach, M. + 112218
 +Nour, E.M. 112741
 Nous, M.H. 111880
 Nous, M.H. 111881
 +Novakova-Jezkova, M. 116551
 +Novikov, I.D. 116829
 +Novikov, I.I. 111678
 Novikov, N.P. + 113746
 +Novikov, S.A. 115315
 +Novikov, S.A. 115204
 Novikov, Yu.A. 112592
 +Novikov, Yu.A. 112488
 +Novikova, N.N. 113746
 +Novosel, M.A. 115731
 +Novotny, J. 115263
 +Novotny, M.A. 111886
 Nowell, A.R.M. 116077
 Nowinski, J.L. 113309
 +Nozaki, M. 111990
 +Nozaki, M. 112012
 +Nozaki, T. 111990
 +Nozaki, T. 112012
 Nuaimi, A.L. 111627
 +Nuller, T.A. 115651
 Nunes, O.A.C. 114816
 Nunome, K. + 112758
 +Nureki, S. 112185
 +Nurishi, Y. 115154
 Nurdinov, N.R. + 114453
 +Nurdinov, N.R. 113786
 Nussbaum, A. 114600
 Nussbaumer, H. + 116666
 Nussbaumer, H. + 116447
 +Nyberg, J. 112292
 +Nyberg, P. 115948
 +Nye, A.H. 116602
 +Nylandsted Larsen, A. 114253
 Nystrom, B. + 114223
 +Nystrom, B. 114224
 +Oberlack, H. 112016
 +Obermann, W. 112826
 +Obolenskii, E.A. 113795
 Obraztsov, I.F. + 111390
 O'Brien, K. + 112611
 +O'Brien, S. 114412
 +O'Bryan, C.L. 112946
 +Obukhov, S.A. 114923
 Obukhov, S.P. 114145
 Ochmann, F. 114640
 +O'Connor, D.J. 114998
 +O'Connor, D.J. 115047
 +Oda, H. 113895
 +Oda, M. 116582
 +Oda, N. 112862
 Odaka, K. + 111874
 +Odaka, S. 111990
 +Odaka, S. 112012
 Odani, H. + 114268
 Oddershede, J. + 112633
 +Odell, A. 116765
 +Oden, J.T. 113373
 +Odera, M. 112484
 +Odera, T.J. 116401
 Odier, P. + 114216
 Odiq, T. 111613
 Odone, F. + 116071
 +Oudoulo, S. 113062
 Oeder, R. + 114897
 Oehrlein, G.S. 113957
 Oehrlein, G.S. + 114190
 +Oemler, A., Jr. 116865
 Oen, O.S. 115001
 Oertzen, W.von
 ... *see* von Oertzen, W.
 +Oesterle, E. 113214
 Oesterreicher, H. 114129
 +Oestreicher, H.L. 115815
 +Ofitserov, M.M. 112974
 +Oganov, G.A. 112536
 Ogasawara, H. + 112371
 +Ogasawara, M. 113608
 +Ogata, H. 112160
 Ogata, H. (ed.) 111309
 +Ogawa, H. 116575
 +Ogawa, H. 115105
 +Ogawa, H. 112225
 Ogawa, K. 112069
 +Ogawa, K. 112550
 +Ogawa, M. 112609
 +Ogawa, T. 115549
 +Ogawara, Y. 116582
 +Ogden, T.E. 115788
 Ogilvie, J.F. 112693
 +Ogilvie, J.F. 112806
 +Ogino, K. 112210
 +Ogino, K. 112051
 +Ogino, Y. 114268
 +Ogita, K. 114938
 +Ogorodnikov, V.P. 113529
 +Ogurtsov, I.Ya. 112671
 +Oguz, T. 116111
 Oh In Joon
 ... *see* In Joon Oh
 Oh Jae Hyun
 ... *see* Jae Hyun Oh
 +O'Hanlon, M. 116610
 +Ohara, Y. 111815
 +Ohashi, M. 113122
 Ohba, R. 113223
 Ohde, R.N. + 113216
 Ohga, J. 113252
 +Ohgushi, K. 113222
 Ohi, S. + 113645
 +Ohki, K. + 116581
 +Ohki, K. 116574
 +Ohki, K. 116583
 +Ohki, K. 116582
 +Ohkura, M. 114013
 Ohmachi, Y. + 115058
 +Ohmichi, T. 112327
 Ohmori, Y. + 115269
 +Ohmori, Y. 113053
 Ohnabe, H. + 113338
 Ohnaka, M. + 116084
 Ohnishi, T. + 114589
 +Ohno, H. 114751
 Ohno, K. + 114735
 Ohno, K. + 112839
 Ohnuki, S. + 114189
 +Ohnuki, S. 113979
 +Ohnuma, H. 112208
 +Ohson, M. 115667
 +Ohta, F. 115810
 +Ohta, Y. 112972
 +Ohtani, F. 112229
 +Ohtani, F. 112218
 Ohtsu, M. + 113028
 +Ohtsu, Y. 113969
 Ohtsuki, Y. 114992
 +Ohwada, K. 114615
 Ohya, Y. + 115353
 +Ohya, Y. 114963
 Oikawa, H. 114270
 Oikawa, H. + 115265
 +Oikawa, S. 113071
 Ojima, T. 116264
 +Okabayashi, H. 112737
 +Okada, K. 112210
 +Okada, K. 112051
 +Obama, M. 112437
 Obenhuber, T. + 115259
 Ober, P. 116408

- +Okada, K. 112218
 +Okada, K. 113149
 +Okada, K. 112160
 +Okada, M. 115582
 +Okada, M. 114708
 +Okada, M. 115355
 +Okada, M. 114397
 +Okada, M. 113645
 Okajima, M. 115957
 +Okamoto, H. 115634
 +Okamoto, K. 111738
 Okamoto, P.R. + 114187
 +Okamoto, Y. 112334
 +Okamura, A.T. 116055
 Okamura, Y. + 114240
 Okano, K. + 116037
 +Okano, K. 111811
 +Okawa, M. 111887
 +Okazaki, A. 112507
 +Okazaki, S. 113473
 +O'Keefe, J. 115990
 +O'Keefe, M.A. 113707
 +Okenko, A.P. 113955
 +Okley, A.L. 114210
 +Okoshi, T. 112963
 +Okoshi, T. 112964
 +Okovitz, V.S. 115209
 +Okrent, D. 112407
 +Oksengorn, B. 112816
 +Oksman, Ya.A. 114562
 +Okubadejo, A.O. 115707
 +Okubo, K. 112392
 Okuda, H. 115152
 +Okuda, H. 116389
 +Okuda, K. 115634
 +Okudaira, K. 116589
 +Okumura, Y. 111815
 Olavarria, R. + 113524
 Olbers, D.J. 116146
 Olbrich, G. + 112710
 +Oldekoop, W. 112398
 +O'Leary, J.R. 111411
 +Oleinik, O.A. 111448
 +Olesk, A.O. 114627
 Olevskii, S.S. + 113739
 +Olier, R. 113949
 +Olin, A. 115516
 +Olinger, B. 111697
 Oliva, E. + 116783
 Olive, D.I. + 111596
 Oliveira, A.M. de
 see de Oliveira, A.M.
 +Oliveira, F.A. 114722
 +Olivier, P. 112553
 +Olmi, A. 112089
 +Olness, R.J. 113635
 Olsen, G.H. + 115072
 +Olsen, J.M. 112015
 +Olsen, L.H. 112024
 Olsen, O.H. + 114647
 Olson, R.E. 112835
 +Olsson, G. 112686
 +Olsson, J. 111990
 +Olsson, J. 112012
 Olsson, M.G. 111920
 +Olsson, N. 112159
 +Olsson, N.A. 113024
 +Olsson, N.A. 114901
 +Olsson, T. 112686
 +Olzowski, E.W. 116765
 Oluwande, P.A. + 115707
 +Olynyk, K. 111959
 O'Malley, R.E., Jr. 111424
 +Omata, K. 112609
 +Omenetto, N. 112317
 +Omeriti, E. 111548
 +Omura, Y. 116393
 On-Kok Chang. 111371
 Onchi, T. + 115418
 Omega, R.J. + 112294
 +O'Neil, J.R. 116086
 +O'Neill, A.E. 114749
 +Onions, C. 112022
 +Onishchenko, E.L. 116075
 +Onishi, K. 112899
 +Ono, F. 114047
 +Ono, K. 113873
 +Ono, K. 114710
 +Onodera, H. 115589
 Onoe, M. 115881
 +Onoc, M. 115916
 +Onuchic, J.N. 112803
 +Oommen, I.K. 112446
 +Oosterling, R.A.M.
 115595
 Ootuka, A. + 114974
 +Oparina, D.Ya. 115856
 +Ophel, T.R. 112557
 Opher, R. 116557
 Ophir, J. + 115890
 Oppenheimer, M. 116175
 Oprysko, M.M. + 115519
 +Oprysko, M.M. 112771
 Orbons, P.J. + 113539
 Ord, J.L. + 114941
 +Oren, Y. 112024
 Oreshkin, P.T. + 114617
 +Orford, K.J. 116747
 Orihara, H. + 112208
 +Orito, S. 111990
 +Orito, S. 112012
 +Ortiz, M.E. 112267
 +Orkin-Lecourtois, A.
 112031
 +Orlov, S.N. 115773
 Orlova, I.G. + 115234
 +Orlova, L.N. 115140
 +Orlova, N.S. 114964
 +Ormont, N.N. 114566
 +Orsini, J. 114491
 Orsini, P. Giordano
 see Giordano Orsini, P.
 Ort, W.J. 111669
 Ortega, J.M. + 112516
 +Ortega, M. 116415
 +Orwig, L.E. 116592
 Orzechowski, T.J. +
 113641
 +Orzechowski, W. 115931
 Orzechovskaya, O.P.
 113303
 +Osadchuk, L.A. 113636
 +Osaka, J. 114191
 +Osborne, R.H. 116053
 Oset, E. + 111324
 +Oshikubo, T. 112609
 Oshima, C. + 115024
 +Oshima, C. 115025
 +Oshio, T. 111810
 Osin, A.V. + 112914
 +Osipov, V.V. 113690
 +Osipov, V.V. 116384
 +Osipov, V.V. 113529
 Osipova, L.V. + 114667
 +Osiv, P.N. 113360
 Osman, A. 112077
 Osman, A. 112222
 Ossi, P.M. + 115131
 +Ost-semin, A.A. 113322
 +Ostapenko, N.I. 114452
 Osterbrock, D.E. + 116844
 Osterrieder, S. + 115896
 +Osterwald, C. 115635
 Osthoff, W. + 112341
 Ostlund, S. + 115886
 +Ostriker, J.P. 116736
 +Ostroborodova, V.V.
 114829
 Ostroumov, P.N. + 113627
 +Ostrovskaya, G.V. 113667
 +Ostrovskii, Yu.I. 113485
 +Ostrovsky, L.A. 111606
 +O'Sullivan, M.S. 113032
 +Oswald, H.R. 113808
 +Oswald, R.A. 115947
 +Ota, K. 111811
 Ota, R. + 113757
 +Ota, R. 114784
 Ota, Y. 115059
 +Otani, S. 115025
 +Otani, S. 114050
 +Otsu, Y. 116205
 +Otsuka, K. 113005
 +Otsuka, N. 115156
 +Ott, E. 111573
 +Ott, E. 111574
 +Ott, E. 112518
 +Otterlund, I. 112162
 +Otto, A. 114866
 Otto, S. + 111875
 +Otto, S. 111958
 Ottosen, N.S. 113318
 +Ou Yang Jing Zheng.
 115951
 +Ouchene, M. 115925
 +Ouchi, K. 112354
 +Ouchi, Y. 114876
 +Oumba, M.T. 113827
 +Oura, K. 114313
 +Ovchinnikov, V.E. 113704
 +Ovchinnikov, Yu.N.
 111502
 +Panferov, V.M. 115273
 +Pangborn, W.A. 115986
 +Panigrahi, B.K. 115644
 Panin, A.I. 111394
 Panissod, P. + 114754
 +Panjkov, A.A. 111817
 Pankov, A.A. + 115544
 +Panofsky, H.A. 116185
 +Panov, A.D. 115287
 +Panov, V.I. 113958
 +Panov, V.N. 116876
 +Pansart, J.P. 112016
 Pantani, L. + 116298
 +Pantani, L. 116282
 Pantchev, B.G. + 114318
 Pantel, R. 114597
 +Panteleymonov, L.A.
 114667
 +Pantev, T. 115826
 +Paoli, V.R. 113736
 +Paolucci, G. 114340
 +Paoluzzi, L. 112031
 Papadopoulos, D. + 115866
 Papadopoulos, P.G. 111433
 +Papaev, A.Yu. 113703
 +Papaliolios, C. 116489
 Papanastassiou, D.A. +
 116554
 +Paal, G. 116909
 Pacher, O. + 114425
 +Paciesas, W.S. 116836
 +Pacini, F. 116707
 +Packard, N.H. 111575
 +Pacolet, M. 115700
 +Paddon-Row, M.N.
 115529
 Paderno, Yu.B. + 113952
 Padilla, J.R. 116480
 Padula, C.D. La
 see La Padula, C.D.
 Pagel, B.E.J. + 116688
 Pagh, B. + 114961
 +Pagliaro, R. 115071
 +Paiano, G. 111975
 Pailwal, K.K. 113212
 +Pairsuwan, W. 112562
 Pajewski, W. + 114324
 Pakeva, S.V. + 114521
 +Pakhotin, V.A. 116350
 +Pakkanen, A. 112058
 +Pal, B.B. 114601
 +Palamarchuk, B.I. 113470
 +Palano, A. 112020
 Palecz, D. + 115872
 Palfalvi, J. 112457
 +Pal'guev, S.F. 114573
 +Paligoric, I. 114140
 +Palkin, A.M. 114554
 Palkina, K.K. + 115120
 Pal'ko, L.S. 113407
 +Palla, P. 112804
 +Pallister, W.S. 116483
 Palma, A. 112797
 Palma, M. De. *see De Palma,*
 M.
 +Palmen, J. 113395
 +Palmer, A.J. 112971
 +Palmer, C.H. 111748
 +Palmer, D.F. 116053
 Palmer, M.H. + 112662
 Palmer, N.R. + 114346
 +Palmore, J.J. 113456
 +Palmstrom, C.J. 114054
 +Paloscia, S. 116281
 Palosz, B. 113812
 +Palou, A. 115988
 +Palumbo, G.G.C. 116492
 +Palvadeau, P. 114672
 +Pamela, J. 112016
 +Pampaloni, P. 116281
 Pan, V.M. + 115170
 Panagia, N. 116712
 +Panagia, N. 116783
 +Panagiotopoulos, D.G.
 116027
 Panagopoulos, C. 115445
 +Panakkal, J.P. 112365
 +Panasyuk, A.D. 115393
 Panasyuk, V.V. + 115436
 +Panchapagesan, T.S.
 115419
 Pancheri, G. + 111960
 +Pande, J. 115744
 Pande, K.P. + 115063
 +Pandey, A.N. 114929
 +Pandey, K.S. 113475
 +Pandey, L.N. 112168
 +Pandey, S.N. 116440
 Pandya, J.R. + 114079
 +Pancitzi, S.M. + 111502
 +Panferov, V.M. 115273
 +Pangborn, W.A. 115986
 +Panigrahi, B.K. 115644
 Panin, A.I. 111394
 Panissod, P. + 114754
 +Panjkov, A.A. 111817
 Pankov, A.A. + 115544
 +Panofsky, H.A. 116185
 +Panov, A.D. 115287
 +Panov, V.I. 113958
 +Panov, V.N. 116876
 +Pansart, J.P. 112016
 Pantani, L. + 116298
 +Pantani, L. 116282
 Pantchev, B.G. + 114318
 Pantel, R. 114597
 +Panteleymonov, L.A.
 114667
 +Pantev, T. 115826
 +Paoli, V.R. 113736
 +Paolucci, G. 114340
 +Paoluzzi, L. 112031
 Papadopoulos, D. + 115866
 Papadopoulos, P.G. 111433
 +Papaev, A.Yu. 113703
 +Papaliolios, C. 116489
 Papanastassiou, D.A. +
 116554
 +Papanicolaou, G.C.
 111594
 Papazachos, B.C. + 116027
 +Pape, K.H. 112015
 +Papeschi, G. 114303
 +Pappalardo, G. 112148
 +Pappalardo, G.C. 112874
 +Pappalardo, L. 111483
 Pappas, P.T. 111468
 +Papulov, Yu.G. 114820
 +Paquet, D. 114661
 Paradijs, J. van
 see van Paradijs, J.
 +Parekh, P.P. 116174
 +Parenti, G. 115505
 +Parfenieva, L.S. 114550
 +Parfenova, N.N. 114785
 +Parga, N. 111887
 +Parikh, S. 112374
 +Parisi, G. + 111948
 Park, C. + 114419
 Park, C. + 115094
 Park, C.N. + 114257
 Park, C.S. + 114385
 +Park, G.S. 114264
 +Park, I.S. 115210
 Park, J.T. + 111689
 Park, J.Y. + 113863
 Park, Y.O. + 114353
 Park Sang-Hyun
 see Sang-Hyun Park
 +Parker, K.J. 113238
 +Parker, L. 111522
 +Parker, R.A.R. 116778
 +Parks, C.C. 114489
 +Parks, E.K. 112798
 +Parks, G.K. 116419
 +Parks, H.G. 113942
 +Parks, H.G. 114019
 +Parks, L. 111860
 +Parmar, P.H. + 111694
 +Parmley, L.F. 115912
 Parnes, R. 113280
 Parnev, O.M. + 115862
 Parr, R.G. + 112616
 +Parrot, M. 116395
 +Parrou, G. 112022
 Parry, G. + 113038
 +Parson, J.M. 115560
 Parsons, J.D. + 115065
 Parsons, J.D. + 115066
 +Parsons, R.W. 112790
 +Partch, R. 115535
 +Parthasaradhi, K. 112691
 +Parthasarathy, B. 116190
 +Partridge, R.B. 116889
 +Parusnikov, B.V. 113849
 Parvathamma, S. + 115814
 Pasa, G.I. 113299
 +Pashovsky, A. 114765
 +Pasini, D. 113666
 Pask, C. + 113107
 Paskhin, V.M. + 113253
 +Paskowski, T.M. 115412
 +Pasquinucci, A. 112585
 +Passamonti, P. 114066
 Passarelli, R.E., Jr. +
 116197
 Passarino, G. 111956
 Passchier, C.W. 116069
 Passoja, A. + 112043
 Passoja, A. + 112111
 +Pastore, F. 112022
 +Pastushenko, S.N. 113951
 +Pasynikov, S.G. 116324
 +Patalakha, D.I. 112021
 +Patalakha, D.I. 112028
 Patel, M.D. + 111513
 Patel, S.M. + 114625
 Pater, I.de. *see de Pater, I.*
 +Paternoster, G. 112595
 +Paterson, G.A. 116003
 Patete, A.R. + 113865
 Pato, C.N. + 115771
 +Patramanskii, B.V. 111714
 +Patriarca, R. 116474
 Patriarchi, P. + 116805
 +Patricell, S. 112595
 +Patrick, J.F. 112011
 Patron, M.A. 111343
 +Patrikijew, A. + 114331
 Patterson, K.E. + 112987
 +Pattyn, H. 113965
 +Pattyn, H. 114766
 +Patureau, J.P. 115670
 +Paturel, G. 116845
 +Paul, A. 114173
 +Paul, D.McK. 113753
 Paul, H. + 112826
 +Paul, J. 115013
 Paula, R.P. De. *see De Paula,*
 R.P.
 +Paulson, J.F. 115533
 Paulson, R.W. + 115642
 Paulson, W.M. + 113945
 +Paur, R.J. 116171
 Paus, G.F. + 115432
 +Paus, H.J. 113015
 +Paus, F. 112031
 Pavan, A. 115297
 +Pavelescu, C. 115067
 Pavelets, S.Yu. 115637
 +Pavel'yev, A.G. 116304
 Pavio, A.M. 111456
 +Pavlenko, A.V. 113085
 +Pavlenko, N.P. 115467
 +Pavlenko, V.F. 111390
 +Pavlopoulos, P. 112544
 +Pavlov, A.S. 114820
 Pavlov, P.A. + 115341
 Pavlova, L.M. + 113938
 +Pavlova, N.G. 114785
 +Pavlovskaya, G.S. 115480
 +Pavlovskii, V.S. 113495
 Pavlyak, F. + 115218
 +Pavlychev, A.A. 114969
 +Pawlowicz, W. 113637
 +Payne, D.N. 111738
 +Payne, D.N. 113109
 +Payne, D.N. 113119
 +Payne, G.L. 112078
 Payne, R.C. 113199
 +Pazis, D. 112623
 Pchelkin, I.A. + 111822
 +Peacock, N.J. 113630
 +Pearce, C.W. 114193
 +Pearce, E.J. 113778
 +Pearce, G.F. 111990
 +Pearce, G.F. 112012
 Pearce, J.T.H. 115375
 +Pearl, W.L. 112386
 +Pearson, A.E. 115859
 +Pearson, R.B. 111871
 +Pecharskii, V.K. 113833
 +Pechenyak, N.D. 116299
 +Pechukas, P. 115513
 Peck, E.R. 112920
 +Pediccord, K.L. 112335
 +Pedersen, A. 116398
 Pedersen, A.S. + 114339
 Pedersen, H.M. + 112936
 Pedersen, J. + 112046
 +Pedersen, J. 112058
 Pedersen, P. + 113297
 +Pedersen, T. 112719
 +Pedrazzini, G.J. 112837
 +Peercy, P.S. 113943
 Pegg, I.L. + 114128
 Pei-qin Li. *see Li Pei-qin*
 Pei-ying Zhao. *see Zhao Pei-ying*
 Pei-Zhi Wu. *see Wu Pei-Zhi*
 +Peigneux, J.P. 112556
 Pekar, S.I. + 114806
 +Pelce, J. 112416
 +Pella, P.J. 112562
 Pellas, P. + 116553
 +Pelle, F. 114913
 Pellerin, P. + 112337
 +Pelte, D. 112113
 +Peltonen, R. 115493
 +Pelykh, N.A. 113495
 +Pelzl, G. 113730
 +Penarrocha, J.A. 111938
 Pender, L.F. + 114263
 Peneva, I.H. + 113583
 +Penfield, K.W. 115008
 Peng Hui. 111535
 Penin, N.A. 114592
 +Penman, S. 115758
 +Penneman, R.A. 113813
 +Penneman, R.A. 113814
 +Penner, R. 115811
 +Penner, S. 112480
 Pennycook, S.J. + 111830
 +Pennypacker, C. 116715
 +Pensil, S. 112497
 +Penzes, W.B. 111756
 Penzias, A.A. 116776
 +Pepler, W. 112319
 +Perchanok, T.M. 112981
 Percus, J.K. + 113712
 Perdikis, C. 113436
 +Perdikis, C. 113501
 +Perederii, L.I. 113938
 +Perederii, V.D. 113321
 Peregrine, D.H. 116114
 +Peregudov, A.S. 113840
 Peregudov, V.N. + 114668
 +Pereira Leite Albuquerque,
 A.R. 115593
 +Perkalina, Z.B. 113910
 +Perel', V.I. 114813
 +Perel'man, B.S. 115473
 +Perelomova, N.V. 114824
 +Perelomova, N.V. 114089
 +Perelygin, A.I. 114617
 +Perelygin, V.P. 116553
 +Perepetchko, I.I. 113759
 Pereverzev, E.S. 114087
 +Perez, B. 115251
 Perez, J. Fernando
 see Fernando Perez, J.
 +Perez, M.V. 112922
 +Perez, R. 111569
 +Periaux, J. 113403
 Perigo, R. + 116006
 +Perini, A. 113860

- + Perini, L. 112020
 + Perinotto, M. 116804
 + Perinotto, M. 116805
 + Perjes, Z. 111521
 + Perkampus, H.-H. 112877
 + Perkins, F.W. 113592
 + Perkins, F.W. 113593
 + Per'kova, G.N. 115285
 + Perl, M.L. 112011
 + Perlin, E.Yu. 114562
 + Perlmutter, R.J. + 112958
 + Perlov, G. + 111829
 + Perly, B. 112754
 + Permogorov, S.A. 114449
 + Pernice, R. + 115291
 + Perola, G.C. 116857
 + Perone, D.W. 112381
 + Perouze, J.J. 113316
 + Perozzi, D.J. 116309
 + Perraudin, C. 111844
 + Perraut, S. 116398
 + Perrin, M. 112587
 + Perron, C. 116553
 + Perroud, H. 116004
 + Perry, A.J. + 114424
 + Perry, D.L. 114915
 + Perry, K.A. 115865
 + Persiyansev, V.A. + 115213
 + Persson, B.N.J. 114803
 + Peruzzi, I. 111992
 + Pesek, I. 116497
 + Peshev, P. 113785
 + Pesl, R. + 112114
 + Pessa, M. 114433
 + Petela, G. + 115554
 + Petela, R. 115554
 + Peter, M. 114431
 + Petermann, K. 113113
 + Peters, J. + 111645
 + Peters, K.S. 115566
 + Peters, L.K. 114153
 + Peters, P.C. 111345
 + Peters, P.N. + 115406
 + Petersen, A. 111990
 + Petersen, A. 112012
 + Petersen, K. 114961
 + Peterson, B.A. + 113165
 + Peterson, R.J. 112064
 + Peterson, R.J. 112289
 + Peterson, R.J. 112232
 + Peterson, R.J. 112149
 + Peterson, T.W. 112938
 + Peterson, W.K. 116360
 + Petersson, B. 111873
 + Peterstrom, S. 114015
 + Petiau, J. 114967
 + Petin, V.G. 115845
 + Petit, D.R. + 112938
 + Petkau, A. 115865
 + Petkov, I.J. 112134
 + Petrakis, L. 114741
 + Petranovskii, V.P. 113832
 + Petrauskas, G. 114584
 + Petre, R. 114943
 + Petrella, G. 114183
 + Petrenko, V.F. 114555
 + Petreza, S. 112559
 + Petronzio, R. 111948
 + Petrosian, V. + 116608
 + Petrov, A.E. 114634
 + Petrov, B.I. 113850
 + Petrov, K. 114677
 + Petrov, M.P. + 113058
 + Petrov, N.S. 113040
 + Petrov, N.S. 112967
 + Petrov, V.A. 114117
 + Petrov, V.A. 114846
 + Petrov, V.I. 112743
 + Petrov, V.K. 114936
 + Petrova, E.V. 116507
 + Petry, W. 113959
 + Petschek, A.G. 116882
 + Pettitt, B.M. + 112795
 + Pettorino, R. 111888
 + Petuchov, V.R. 112882
 + Petuchov, V.R. 112883
 + Pestvov, A.B. 113776
 + Pezzuto, G. 115358
 + Pfeiffer, B.H. 115889
 + Pfeiffer, L. 114580
 + Pfister, J.C. 114333
 + Phadnis, S.V. + 115422
 + Pham, V.H. 113524
 + Pham-Van, J. 116517
 + Phan Thanh Huy. 115529
 + Pherigo, G.L. 115495
 + Philipp, B. 114743
 + Phillips, G.D.J. 114228
 + Phillipp, F. + 114246
 + Phillips, J.P. 116797
 + Phillips, M.M. 116688
 + Phillips, P. + 112792
 + Phillips, W.J. 112787
 + Philpott, R.J. 112172
 + Piani Mortari, G. 112031
 + Pianti, R.C.V. 115432
 + Piccari, L. 113983
 + Piccarolo, S. 115294
 + Piccolo, M. 111992
 + Pickering, T.G. 115955
 + Pickett, P.T. 112811
 + Pickett, W.E. + 114436
 + Picconi, C. 112331
 + Picraux, S.T. 114031
 + Piel, W.F., Jr. 112035
 + Pielke, R.A. + 116185
 + Pielorz, J. 112015
 + Piepen, H. van der
 + see van der Piepen, H.
 + Pierce, W.G. + 111690
 + Pierre, F. 112016
 + Pierrehumbert, R.T. 116222
 + Pietarinen, E. 112031
 + Pigozzi, G. 112317
 + Pipker, B.A. 115989
 + Pikhitelev, A.I. 113046
 + Pikna, M. 112577
 + Pikul', V.V. 113288
 + Pikuza, P.P. 115393
 + Pilachowski, C.A. + 116765
 + Pilachowski, C.A. + 116775
 + Pilarski, A. 115452
 + Pilate, P. 113755
 + Pillai, S.M. + 114933
 + Pilyankevich, A.N. + 115366
 + Pilyushenko, V.L. 115274
 + Pimenta, M. 111955
 + Pimental, I.R. 112828
 + Pimentel, L.O. 115222
 + Pimia, M. 112031
 + Pincemaille, G. 115456
 + Ping Sheng + 115633
 + Pini, R. + 113051
 + Pinizzotto, R.F. + 114192
 + Pinsent, H.G. 116096
 + Pinter, S. 116418
 + Pinto, A.C. 112871
 + Pintus, S.M. 114383
 + Pionkowski, J.A. 114411
 + Piotrowska, E. 114137
 + Piotrowska, E. 114138
 + Piotrowicz, V.A. 113689
 + Piotrowska, J. 114369
 + Pipa, V.I. 114806
 + Pipes, R.B. 115364
 + P.I. Polukhin
 + see Polukhin P.I.
 + Pippi, I. 116282
 + Pippi, I. 116298
 + Piragino, G. 112186
 + Piralo, A.T. 114800
 + Pires, E.B. + 113373
 + Piriz, A.R. 113638
 + Pirogov, A.N. 114671
 + Pirs, J. + 115322
 + Pisarev, V.S. + 113390
 + Pisareva, V.V. 116378
 + Pitak, N.V. 115273
 + Pitkanen, V. 112527
 + Pitt, C.D. + 115268
 + Pitts, L. 115627
 + Pitzer, K.S. 113557
 + Piven', L.A. 116373
 + Pivovarov, A.A. 111968
 + Pivovarov, Yu.L. 114977
 + Pizzio, F. 113586
 + Plaats, G. van der
 + see van der Plaats, G.
 + Placci, A. 112031
 + Plachkova, S.K. 114521
 + Plachotnaja, L.S. 115087
 + Plakhin, Ye.A. + 116128
 + Plakhtii, V.P. 114675
 + Plans, J. + 114539
 + Plaschko, P. 113488
 + Plasil, F. 112049
 + Plastino, A. 114123
 + Plastino, A. 112104
 + Plateau, P. 115751
 + Platt, R.G. + 116041
 + Platzman, P.M. 114580
 + Plechkins, E.S. + 114634
 + Pleibel, W. 113123
 + Pleininger, R. + 115671
 + Plessas, W. 112081
 + Plessis, J. du
 + see du Plessis, J.
 + Plieith, W. 115404
 + Plochocki, A.P. 114068
 + Plotow-Besch, H. 112022
 + Plowiec, R. 114066
 + Plumley, P.W. + 116001
 + Plumley, P.W. 116062
 + Plyashkevich, V.Yu. 111404
 + Poate, J.M. + 114399
 + Poate, J.M. + 114001
 + Poate, J.M. 114322
 + Poate, J.M. 115060
 + Poate, J.M. (ed.) 111333
 + Pobo, L.G. 112798
 + Pochelon, A. 113630
 + Pockrand, I. 114866
 + Pocsik, G. 112014
 + Poddar, R.S. + 112363
 + Poddubnaya, O.N. 115214
 + Podesta, J.J. 115432
 + Podgornyi, E.I. + 115885
 + Podgornyyk, S.M. + 114211
 + Podgorsak, E.B. 112895
 + Podil'chuk, V.D. 111426
 + Podini, P. 112535
 + Podievskikh, N.A. 114587
 + Podobedov, V.B. 114118
 + Podolinsky, V.V. + 114307
 + Podosyonova, N.G. 115289
 + Poe, C.H. 116678
 + Poerschke, R. + 114287
 + Poggiosi, L. 112016
 + Pogrebkov, A.K. 111499
 + Pogrebnyak, V.A. 114112
 + Pogutse, O.P. 113416
 + Pohl, E. + 116756
 + Pohl, E. 115930
 + Pohl, R.O. 114294
 + Pohl-Ruling, J. 115930
 + Pohlack, H. 112925
 + Poindexter, E.H. 114612
 + Pointu, A.M. 115532
 + Poirier, J.P. + 116523
 + Pokatilov, V.S. 114502
 + Pokazeev, K.V. 116404
 + Pokhodenko, V.D. 112656
 + Pokhodenko, V.D. 115546
 + Pokropivnyi, V.V. + 113956
 + Pokrovskii, L.N. 113347
 + Pokrovskii, V.V. 115345
 + Pokrovskii, V.V. 115347
 + Polansky, O.E. 114437
 + Polansky, O.E. 112661
 + Polcaro, F. 116474
 + Policarpo, A.J.P.L. 112689
 + Polish, N. 116781
 + Politch, J. 112971
 + Politovich, M.K. + 116228
 + Polivanov, M.K. 111499
 + Polivoda, B.I. 115851
 + Poll, J.D. 114894
 + Pollak, E. + 115513
 + Pollak, R.A. 114488
 + Pollard, C.J. + 114027
 + Pollaro, G. + 112240
 + Polnarev, A.G. 116829
 + Polonskii, V.S. 113263
 + Polovnikov, S.A. 112551
 + Poluktov, I.A. 112976
 + Polukhin, V.P. 115274
 + Polukhin P.I. + 115274
 + Polushkin, G.P. 115287
 + Polushkina, E.F. 115841
 + Polutshankina, L.P. 114964
 + Polvado, R.O. 112015
 + Polverel, M. 112022
 + Polyak, F.D. 112865
 + Polyakov, V.M. + 116347
 + Polyakov, Yu.A. + 113530
 + Polyakova, I.N. + 113849
 + Polyakova, N.A. 113925
 + Polyani, B.A. 115401
 + Polyanayana, V.P. 111642
 + Polyanyski, N.V. 112583
 + Polyanyski, O.L. 112728
 + Pomar, C. 112044
 + Pomortseva, L.I. 114604
 + Ponce, F.A. + 114196
 + Ponce, R. + 115518
 + Ponikarov, A.A. 115219
 + Ponomarev, V.I. 114160
 + Ponomareva, T.I. 115252
 + Pons, Y. 112020
 + Ponthieu, J.J. 116528
 + Popandopulo, A.N. + 115228
 + Pope, J.M. 112328
 + Pope, S.K. 116677
 + Popenoe, C.H. 111383
 + Popov, A.G. 115170
 + Popov, A.I. 114834
 + Popov, B.A. 115466
 + Popov, B.E. 114217
 + Popov, I.Yu. + 111980
 + Popov, N.N. 115204
 + Popov, S.K. 115118
 + Popov, V.N. + 113437
 + Popov, V.V. 113775
 + Popov, Yu.A. 114780
 + Popovich, V.V. 115334
 + Poppe, M. 112015
 + Poppel, W.G. + 116792
 + Popper, D.M. 116741
 + Popper, D.M. 116758
 + Popytak, W. 114387
 + Porat, R. 115506
 + Porcher, P. + 114909
 + Porcher, P. 114501
 + Porras-Montenegro, N. 114490
 + Porte, J.P. 112031
 + Porter, B.F. + 111340
 + Porter, D.L. + 114041
 + Porter, N.A. + 116416
 + Porter, R.S. 114214
 + Porter, R.S. 113769
 + Portnoi, E.L. 114000
 + Portnoi, K.I. 115275
 + Porubcan, V. 116551
 + Poskrebyshev, V.P. 114922
 + Pospelov, L.A. 111758
 + Possin, G.E. + 114019
 + Possin, G.E. 113942
 + Post, J.E. 114426
 + Post, R.S. 113632
 + Postma, J.P.M. 115727
 + Postnikov, S.N. 115219
 + Potapenko, A.Ya. 115862
 + Potapenko, S.Yu. + 114624
 + Potapov, A.S. 116407
 + Potapov, V.T. 111745
 + Potemkin, V.V. 114713
 + Potemra, T.A. 116390
 + Potenza, M. 113114
 + Poth, H. 112544
 + Pothier, J. 112553
 + Pottasch, S.R. 116651
 + Pottebohm, H. + 115240
 + Potter, D.I. + 113940
 + Potter, D.W. + 116419
 + Potzel, W. 112529
 + Potzinger, P. 115521
 + Pouchard, M. 115084
 + Pouget, J. + 114786
 + Pouget, J. + 114787
 + Poughon, F. 112254
 + Pouppou, R. 114229
 + Pouquet, A. 116446
 + Pourbaix, E. 113521
 + Pourre, J.L. 111844
 + Povar, V.I. 115339
 + Povolo, F. + 115237
 + Povolo, F. + 115236
 + Powell, I. 112921
 + Pozdnyakova, G.T. + 115124
 + Pozdynin, V.D. 116124
 + Pozharnov, V.A. 115613
 + Prade, H. 112236
 + Pradervand, G.-O. 114501
 + Pradhan, R.M. 111818
 + Praestholm, J. 115908
 + Prakash, B. 115420
 + Prakash, S. 112287
 + Pramanik, D. + 114048
 + Pramatara, L.D. 114934
 + Prantskyavichyus, G.A. 115342
 + Pranyavichyus, L.I. 115003
 + Prasad, B.B. 115420
 + Prasad, C. + 114147
 + Prasad, J.B. + 114243
 + Prasad, M. + 114622
 + Prasad, M. + 114646
 + Prasad, M. 111693
 + Prasad, M.A. + 112851
 + Prasad, V.C.S. 114799
 + Prasad, Y.V.R.K. 115300
 + Prasanna, A.R. 116734
 + Pratt, R.H. 111320
 + Predazzi, E. 111982
 + Preite-Martinez, A. + 116651
 + Prentice, P. + 115304
 + Prepost, R. 111992
 + Preskitt, C. 111860
 + Presser, R. + 115198
 + Pressler, S. 111350
 + Preston, J. 113735
 + Preston, R.A. 116814
 + Preussger, A. 112005
 + Preussger, A. 112006
 + Prevot, B. 114871
 + Pribyl, F. 114932
 + Price, C.E. 115301
 + Price, D.A. 116202
 + Price, J.F. 116105
 + Price, J.F. 116136
 + Prichard, H.M. + 115948
 + Priest, E.R. 116618
 + Prigogine, I. + 113262
 + Prikhod'ko, V.A. + 115482
 + Prikril, I. + 113522
 + Prima, N.A. 114461
 + Primkulov, M.T. 114171
 + Principi, G. 114759
 + Prisedskii, V.V. 115148
 + Priselkov, Yu.A. 115164
 + Prishchepov, A.S. 111740
 + Pritchard, T.W. 112549
 + Probert, S.D. 115693
 + Proccaccia, I. 111589
 + Proch, D. 112506
 + Prochorov, V.A. 115087
 + Prodi, F. 116227
 + Prokhorenko, V.I. 116418
 + Prokhorov, A.M. 113097
 + Proklov, V.V. 114825
 + Prokof'ev, V.K. 113082
 + Prokof'ev, V.V. 114869
 + Prokofeva, L.V. 114550
 + Prokoshkin, Yu.D. 112556
 + Pronin, V.I. + 115894
 + Pronin, V.N. 114687
 + Prospero, J.M. + 112621
 + Prosser, F.W. 112246
 + Prosychev, I. 114584
 + Protas, A.F. 115732
 + Prothero, W.A. 116043
 + Protopopova, L.F. 112656
 + Prouza, Z. + 112449
 + Provenzano, V. 113388
 + Provost, J. 111357
 + Prtinidhi, M. 111783
 + Prunedea, C.O. 115318
 + Prunty, S.L. 113020
 + Prutton, M. 111335
 + Pryakhin, V.V. 115338
 + Pryor, M.J. 115410
 + Pshenichnyi, S.A. 112605
 + Puchta, H. 112049
 + Puchta, H. 112261
 + Puchta, H. 112059
 + Pudovkin, M.I. + 116332
 + Pudovkin, M.I. + 116384
 + Pudovkin, M.I. 116354
 + Pugh, D.J. 111752
 + Pugh, H.G. 112267
 + Pugin, V.S. + 115467
 + Pujo, P.de. see de Pujo, P.
 + Pulay, P. 112614
 + Puliti, P. 112297
 + Pullen, D.A.W. + 111836
 + Purandar, K. 114895
 + Purgathofer, A. + 116684
 + Puro, A.E. 113271
 + Purohit, P. 116441
 + Purubcan, V. + 116322
 + Purushotham, G. 113516
 + Purushotham, G. + 113453
 + Pusep, A.Yu. 112736
 + Pusey, P.N. 111782
 + Pushkina, G.Ya. 115119
 + Pushkina, M.A. 111804
 + Pushpa Gupta + 115420
 + Puska, M.J. + 114581
 + Puska, M.J. + 114336
 + Pustynskii, L.N. + 113683
 + Putilin, V.V. 114092
 + Putkey, T.A. + 112386
 + Putlit, G. zu
 + see zu Putlit, G.
 + Putz, N. + 114406
 + P'yankov, G.N. 115571
 + Pyn'ko, V.G. 114683
 + Pyrkyn, Yu.G. 113509
 + Qi-xing Shen
 + see Shen Qi-xing
 + Qian Zhu-Ming 112511
 + Qian-Shen Wang
 + see Wang Qian-Shen
 + Qianruo Shen
 + see Shen Qianruo
 + Qianshun Chang
 + see Chang Qianshun
 + Qin Chao-Zhi + 116287
 + Qing Wang
 + see Wang Qing
 + Qinglong Zhang
 + see Zhang Qinglong
 + Qizhao Zhou
 + see Zhou Qizhao
 + Quan Wei Lun + 115951
 + Quarles, C.A. 111320
 + Quarton, M. + 113827
 + Que You-kuen 112581
 + Queisser, H.J. 114481
 + Quelch, M.J.T. 113778
 + Quercigh, E. 112020
 + Quere, Y. + 113859
 + Quere, Y. 113872
 + Quested, P.N. 111763
 + Quigley, T.M. 114036
 + Quinones, D.F. + 112339
 + Quiros, M. 111929
 + Quoc, L.V. + 111411
 + Raaphorst, G.P. + 115870
 + Rabach, G. 113679
 + Rabe, P. 114966
 + Rabin, J.M. 111867
 + Rabinovich, M.D. 115690
 + Rabinovich, M.S. 113672
 + Rabinovich, R.I. 114472
 + Rabinowitz, S. 115658
 + Rabolt, J.F. 113768
 + Rachmatov, O.I. 114150
 + Raciti, G. 112148
 + Radchenko, I.S. + 114891
 + Radelaar, S. 114403
 + Rademacher, B. 115205
 + Rademacher, E. 112031
 + Radford, G.A. 116641
 + Radford, K.C. + 112328
 + Radkevich, A.I. 115435

- Radnoczi, G. + 115220
 Radomysel'skii, I.D. + 115140
 + Radon, J.C. 115304
 Radousky, H.B. + 114649
 Raduta, A.A. + 112050
 Radyushkin, A.V. 111964
 + Radyushkin, A.V. 111961
 + Radzhus, V.D.R. 114634
 Radzievskii, V.N. 113620
 Rae, I.C. 115663
 + Raeva, I.S. 114526
 Raevskii, O.A. + 112870
 + Raevskii, V.Ya. 114716
 + Raff, L.M. 112813
 + Rafilipomanana, C. 112735
 + Raghava Rao, A. 112691
 + Raghavacharyulu, I.V. 111941
 Raghupathy, V.P. + 115323
 + Ragionieri, R. 116339
 Ragland, P.C. + 116289
 + Ragnarsson, I. 112047
 + Ragni, A. 111743
 + Ragnisco, O. 111392
 + Ragoowansi, N.L. 112063
 Rague Schleyer, P. von 115323
 ... see von Rague Schleyer, P.
 + Ragulskis, K. 111644
 + Rahilly, W.P. 115647
 Rahman, M. 113457
 + Rahmel, A. 115429
 + Rahn, K. 116261
 + Rahner, D. 115405
 Rai, A. + 113475
 + Rai, J.L. 115032
 Rai, J.N. 112721
 + Rai, K.N. 115029
 + Raich, J.C. 114158
 + Raich, U. 112544
 + Raichevsky, G. 114765
 + Raikh, M.E. 114450
 + Raina, M.K. 116237
 + Raine, C. 112015
 Raine, K.W. + 111763
 Raiden, R.L. + 116326
 Raj, A. Sundara. see Sundara Raj, A.
 Raj, R. + 112034
 Raj, V.V. 113503
 Raja Reddy, D. + 114534
 Rajagopal, K.R. + 113480
 Rajagopalan, K.S. + 115421
 + Rajanandam, K.S. 113500
 Rajaram, M. 116365
 + Rajaratnam, A. 115965
 Rajaratnam, N. + 113452
 + Rajauria, A.K. 112875
 + Rajkovits, Z. 115271
 + Rakhmatullina, A. Z. 115129
 Rakhovski, V.I. + 114917
 + Rakshit, A. 115966
 + Ram, P.C. 113512
 + Ram, R.S. 112745
 Ram Shri. see Shri Ram
 + Rama Reddy, K. 111660
 Ramachandra, M.K. + 115551
 + Ramachandramurthy, C.V. 113500
 + Ramachandran, R. 112029
 Ramachandran, V. + 115057
 Ramaekers, P.P.J. + 115102
 + Raman, R. 113068
 + Ramana Murthy, P.V. 116723
 Ramana Reddy, S.V.S. + 112691
 Ramanaiiah, K.V. + 115035
 + Ramanaiiah, K.V. 114827
 + Ramanathan, R. 111996
 + Ramanuja, M.N. 116624
 Ramaswamy, V. + 113093
 Ramaty, R. + 116414
 Ramaty, R. + 116591
 + Ramaty, R. 116830
 + Ramaty, R. 116884
 Ramavataram, S. 111329
 Rambidi, N.G. 112866
 + Rambidi, N.G. 111821
 + Ramdas, A.K. 114885
 + Ramdas, A.K. 114886
 Ramesh, R. + 115367
 Ramet, C.I. + 115679
 + Ramirez, B.I. 112795
 + Ramos, J.J. 113598
 + Rampans, A. Yu. 114538
 + Rampazzo, G. 116288
 + Rand, D. 111586
 + Randa, J. 112017
 + Randeria, M. 111958
 + Randeria, M. 111875
 + Randoll, H. 112016
 Randrup, J. 112136
 Rangacharyulu, C. + 112175
 + Rangacharyulu, C. 112176
 + Rangarajan, G. 111692
 Rangarajan, G.K. + 116012
 + Ranieri, A. 112008
 Ranke, W. 114341
 + Rankin, G.W. 113451
 + Ransdell, J. 112031
 + Ranta, J. 112384
 Rao, A. Raghava. see Raghava Rao, A.
 + Rao, D.R. 114937
 Rao, D.V. + 115875
 + Rao, E.V.K. 114898
 Rao, G. Sambasiva. see Sambasiva Rao, G.
 Rao, K. Veerabhadra. see Veerabhadra Rao, K.
 + Rao, M.L. 113909
 + Rao, M.N. 112247
 Rao, N. Nagesha. see Nagesha Rao, N.
 + Rao, R.M.V.G.K. 115367
 Rao, R.P. + 114937
 Rao, T.V. Krishna. see Krishna Rao, T.V.
 Rao, V.U.S. 115579
 + Rao, V.V. 115415
 Rao, Y.K. + 115178
 + Rapaport, J. 112196
 Raptis, A. + 113501
 Raptis, A. + 113515
 Raptis, A. + 113510
 Raptis, C. + 113717
 + Rapuano, F. 111948
 + Rasheed, M.A. 113453
 Rashleigh, S.C. 113118
 + Rasskazov, A.O. 113325
 Rasson, J. + 116303
 Rastogi, R.G. 116371
 + Rasuvaev, E.A. 112551
 Ratcliffe, C.I. + 114855
 Ratliff, F. + 115795
 Rattee, I.D. + 114266
 + Ratych, L.V. 115436
 + Ratzingler, U. 112468
 + Rau, T.F. 113843
 Rau, V.G. + 113842
 Rau, V.G. + 113843
 + Rauch, H. 111490
 + Rauckham, M.R. 113789
 + Raupach, F. 112015
 + Raut, V. 112507
 + Raveau, B. 113856
 + Raveau, B. 113933
 + Ravelet, R. 115682
 + Ravetto, P. 112296
 + Ravrik, M.S. 113304
 Rawitscher, G.H. + 112084
 + Rawlings, R.D. 115268
 + Ray, A. 112255
 + Ray, L. 112203
 + Ray, P.S. 111943
 + Ray, S. 113836
 Raychaudhuri, A.K. + 111507
 + Raychowdhury, P.N. 112893
 + Rayford Nix, J. 112169
 + Raymond, R.S. 112289
 + Raymond, R.S. 112232
 + Raymond, R.S. 112209
 + Raymond, R.S. 112149
 + Razdobarin, G.T. 113060
 + Razdobarin, G.T. 113661
 Razeghi, M. + 115061
 + Razgonyayev, V.K. 113242
 + Razmanov, V.M. 116506
 + Razumova, T.K. 113251
 + Read, A.L., Jr. 111992
 + Read, W.G. 112764
 + Read, W.G. 112765
 Reader, J. + 112685
 + Readhead, A.C.S. 116718
 + Reading, D.H. 111808
 + Reading, J.F. 112831
 + Reagen, J.B. 116359
 + Reaugh, J.E. 112339
 Rebane, K.K. 112791
 + Rebel, H. 112524
 + Rebel, H. 112114
 Rebenko, A.L. 113568
 Reboucas, M.J. + 116906
 + Reckagel, E. 113871
 + Redd, E. 111689
 + Reddy, B.M. 116206
 Reddy, D. Raja. see Raja Reddy, D.
 Reddy, K.C. 113398
 Reddy, K.N. + 113909
 Reddy, K. Nagi. see Nagi Reddy, K.
 Reddy, K. Rama. see Rama Reddy, K.
 + Reddy, K.V. 114243
 Reddy, P.A. 113467
 Reddy, P. Narayan. see Narayan Reddy, P.
 Reddy, P. Yadagiri. see Yadagiri Reddy, P.
 Reddy, S.V.S. Ramana. see Ramana Reddy, S.V.S.
 + Redekopp, L.G. 113419
 + Redondo, A. 114359
 + Redwine, R.P. 112007
 Ree, F.H. 114179
 Ree, H. van der. see van der Ree, H.
 Ree Talkyue. see Talkyue Ree
 + Reece, R.K. 112476
 Reed, B.C. + 116495
 + Reed, C.B. 115558
 Reed, K.W. + 111443
 Reeder, R.J. + 113803
 + Reese, J.M. 113164
 Regel, L.L. + 114148
 Regel, L.L. + 114149
 Regel, L.L. + 114150
 Regev, O. 116637
 Reginato, L. 112465
 + Regnault, J.C. 111761
 + Rehm, K.E. 112126
 + Rehn, L.E. 114051
 + Rehn, L.E. 114187
 Reich, A. + 114407
 + Reichl, H. 111666
 + Reichle, M.S. 116043
 + Reid, I.M. 116294
 + Reid, M. 116062
 Reid, M.F. + 114889
 + Reif, P.-D. 111630
 + Reif, R. 114416
 + Reigne, L. 115679
 + Reikhsfel'd, V.O. 112660
 Reilly, N.R. 111604
 + Reimann, B. 115521
 + Reimer, N.D. 115245
 + Reimer, V.A. 114671
 Reimers, H. 115464
 Rein, D. 111932
 + Reinlechner, L.A. 116392
 + Reis, D.J. 115819
 + Reischle, R. 114888
 + Reiss, E.L. 111463
 Reiss, H.R. 112130
 + Reiss, N.M. 115709
 Reiter, T. + 115758
 + Reith, T.M. 114372
 + Reithler, H. 112031
 Rektstad, J. + 112075
 + Remacle, J. 115708
 + Ren Li-xin. 115712
 + Renard, G. 111861
 + Renard, V. 116074
 Renardy, M. 113479
 Renardy, M. + 112977
 Renault, C. + 113440
 + Renfordt, R.E. 112267
 + Renneboog, J. 111708
 + Rennett, N. 115795
 + Rentzsch, S. 114058
 Renzi, R. De. see De Renzi, R.
 + Repellin, J.-P. 112022
 + Repko, W.W. 112010
 + Repnow, R. 112113
 + Repond, J. 112544
 + Repp, B.H. 113217
 Reshetnikov, V.F. + 115139
 + Ressayre, E. 113066
 Retterer, J.M. + 116391
 + Rettig, D. 112326
 + Retz, A. 112528
 Reva, Yu. P. + 115606
 Revesz, P. + 114400
 Revo, S.L. + 115243
 Revokator, O.P. + 112823
 + Revol, J.-P. 112031
 + Reybillet, M. 115670
 Reznik, A.N. 116276
 + Reznitskii, A.N. 114449
 + Reznitskii, L.A. 114204
 + Rhee, K.T. 114219
 Rhodes, M.L. + 115971
 + Ribas, R.V. 112247
 Ribaut, M. 113446
 Ribeirete, M.M.F. + 112689
 + Ribeiro, A.A. 115728
 + Rizzo, G. 112198
 Rice, S.F. + 114877
 Rice, T.M. 114463
 + Rice, W.W. 112776
 + Rich, J. 112031
 + Rich, K. 111992
 + Rich, P.J. 113117
 Richard, J.M. + 111986
 + Richardson, A. 113760
 + Richardson, F.S. 114833
 + Richardson, F.S. 114889
 + Richardson, K.J. 116797
 + Richardson, M.C. 111852
 Richardson, P.D. + 115817
 + Richert, J. 111550
 Richter, A. 112155
 + Richter, A. 112176
 + Richter, A. 112273
 + Richter, A. 112174
 + Richter, B. 112544
 + Richter, B. 112011
 Richter, H.J. + 112428
 Richter, J. + 114225
 + Richter, J. 114226
 + Richter, J. 114064
 Richter, O.-G. + 116862
 + Ricker, G.R. 116428
 + Ridley, N. 115225
 + Riebsell, M. 112554
 Rieder, K.H. + 114314
 Riedinger, L.L. 112040
 + Riedle, K. 112396
 + Rieger, E. 116878
 + Rieger, E. 116565
 + Rieger, H. 112983
 Riegler, G.R. + 116826
 + Riegler, G.R. 116874
 + Rieseberg, H. 111990
 + Rieseberg, H. 112012
 Rietveld, J. + 115041
 Rifflet, J.C. + 113741
 + Righini, G.C. 113098
 Rigos, A.A. + 115761
 + Rijken, T.A. 111967
 + Rijssenbeek, M. 112031
 + Rikards, R.B. 115286
 + Rikus, L. 112147
 + Riley, J.M. 116853
 Riley, S.J. + 112798
 + Rille, E. 111689
 + Rime, C.S. 115259
 + Rimini, E. 114398
 Rimkus, W. 111646
 + Rimoldi, A. 112022
 Rimskiy-Korsakov, N.A. + 116076
 Ring-Ting Xu. see Xu Ring-Ting
 Ringwood, A.E. 112320
 + Rintamaa, R. 115356
 Rinzel, J. 115778
 Rio, J. del. see del Rio, J.
 + Rionero, S. 111447
 Rios, E.R. de los. see de los Rios, E.R.
 + Ripoché, P. 113154
 + Ristinen, R.A. 112289
 + Ristinen, R.A. 112149
 Ritchie, B.G. 112280
 + Ritson, D.M. 111992
 + Ritzman, R.L. 112429
 + Rivetti, A. 113540
 Riviere, J.P. + 113883
 Rivlin, R.S. + 115319
 + Rivoal, M. 112016
 + Riwan, R. 114344
 Robb, A.W. + 111658
 Roberson, N.R. + 112567
 + Roberson, N.R. 112217
 + Robert, A. 113576
 + Robert, H. 114753
 + Roberti, R. 115131
 Roberts, A.J. 113464
 Roberts, B. 116603
 + Roberts, C. 112031
 Roberts, D. 111356
 + Roberts, J.M. 116203
 Roberts, K.J. + 113777
 + Roberts, R. 113161
 + Robertson, G.D. 115047
 Robertson, I.M. + 114198
 Robertson, I.M. + 114199
 Robertson, J. 114439
 Robertson, R. + 115103
 + Robeson, L.M. 113725
 + Robey, S.W. 114441
 Robinett, R.W. 111377
 + Robinson, A.E. 115912
 Robinson, A.H. + 113541
 + Robinson, A.H. 111858
 Robinson, E. 116258
 Robinson, E.A. 116316
 Robinson, E.L. + 116659
 Robinson, L.J. 111635
 Robinson, S.R. 111725
 + Robota, H. 115006
 + Robrock, K.-H. 114187
 + Robson, J.M. 112507
 Roca, P. + 115988
 + Roca, V. 112120
 + Rochon, P. 111363
 + Rock, J.W. 115377
 Roddy, C.J. 111378
 Rodgers, E. + 116191
 + Rodionov, V.K. 113417
 + Rodionov, V.N. 111921
 + Roditi, I. 111949
 + Rodnyi, P.A. 114925
 Rodono, M. 116699
 + Roe, R.J. 113767
 Roebuck, B. 115460
 + Roemer, J. 112381
 Roessler, C.E. + 115943
 + Roessler, G.S. 115943
 Roetschi, H. 111679
 + Rogachev, A.A. 114923
 + Rogachevskii, I.V. 116621
 + Rogers, J.D. 112247
 Rogers, V.C. + 112348
 Rogister, A. + 113575
 Rogister, A. + 113574
 Rogovskii, B. 113366
 + Rohlf, J. 112031
 + Rohlf, K. 116792
 + Rohlmann, A. 115981
 + Rohr, D.L. 115267
 + Rohrer, H. 114312
 + Roitman, V.I. 115490
 + Rojey, A. 115680
 + Rojey, A. 115679
 + Rojo, O. 114123
 + Rokhlina, E.M. 113840
 Rolfes, R.G. + 112683
 + Rolfs, C. 112502
 Rolov, B.N. 114161
 Rolov, B.N. + 114775
 + Roman, H.T. 115618
 Roman, O.V. + 115098
 + Roman, O.V. 115128
 Roman, T.A. + 116644
 Romanenko, E.A. + 112714
 Romanov, O.N. + 115337
 + Romano, G. 112559
 + Romano, M. 112120
 + Romanov, A.M. 116806
 Romanov, N.G. + 114755
 Romanov, O.V. 114616
 + Romanova, E.P. 115650
 + Romanova, L.M. 115401
 + Romanova, M.V. 114550
 + Romanovich, I.V. 115275
 + Romashchenko, Yu.N. 113795
 + Romashev, L.N. 115190
 + Romer, J.G.M. 112076
 + Romer, J.G.M. 112528
 Romero, R. + 115641
 + Romero, R. 115652
 Romney, E.M. + 115936
 Romonova, N.N. + 116210
 + Ronami, G.N. 113786
 + Rondan, N.G. 115529
 Ronen, Y. 112302
 Rong Sheng. 113514
 + Ronga, F. 111992
 + Ronn, A.M. 113555
 + Ronnhult, T. 115012
 Ronto, G. + 115733
 + Rood, A.P. 111764
 Rooij, C. De. see De Rooij, C.
 Roos, O. von. see von Roos, O.
 + Roose, U. 112570
 + Roosen, R. 112553
 Roosmalen, O.S. van. see van Roosmalen, O.S.
 + Ropke, H. 112060
 Rosano, W.J. + 115560
 Rose, G.D. + 115737
 + Rosel, F. 112220
 + Rosel, F. 112163
 + Rosel, F. 112827
 + Rosemeier, R.G. 113930
 Rosen, A. + 111435
 + Rosen, A. 112686
 Rosenau, P. 113595
 Rosenau, P. + 111615
 + Rosenberg, A. 112971
 + Rosenberg, G.V. 116211
 + Rosenberg, L.J. 111992
 + Rosenberg, R.J. 112527
 + Rosenbluth, M.N. 113597
 + Rosenbluth, M.N. 113643
 + Rosenbluth, M.N. 113599
 + Rosencranz, R., Jr. 113350
 + Rosenthal, A.J. 116220
 + Rosenwinkel, E. 115017
 Roser, K. + 115396
 + Rosner, D.E. 113492
 + Ross, D.W. 113594
 + Ross, G.G. 111937
 + Ross, J. 115514
 + Ross, R.T. 112028
 + Rossat-Mignod, J. 114672
 + Rosset, L. 112024
 Rosser, R.J. 115982
 + Rossi, E. 113714
 + Rossi, F. 115510
 Rossi, G. + 112317
 + Rossi, P. 112031
 + Rossi, P. 111885
 + Rossi, U. 113106
 + Rossi, U. 113114
 + Rossignol, J.Y. 115091
 Rossitto, F. + 115511
 + Rossitto, F. 115131
 + Rossman, G.I. 116311
 + Rossner, H. 112539
 + Rosso, E. 112024
 Rossouw, C.J. + 111817
 + Rost, M. 112015
 + Rostaing, M. 113655
 + Rostas, J. 116784
 + Rosylakow, G.V. 111816
 + Roth, E.P. 116266
 + Roth, H.A. 112292

- Roth, P. +113496
+ Roth, S.114542
Rothberg, L.J. +115566
+ Rothe, D.E.114010
Rothe, P.H. +112378
+ Rothe, P.H.112427
+ Rothenberg, A.112022
+ Rother, K.116017
+ Rothman, L.S.112729
Rothschild, W.G. +114850
+ Rotondo, P.L.112308
+ Rots, M.113976
+ Rotter, H.112236
Rouanet, H.112452
+ Rouault, M.112857
+ Roueff, E.116784
Rouff, M. +114298
+ Rougeot, H.111847
+ Roulit, G.113826
Rouse, C.A.116561
+ Roussarie, A.112022
Roussel, J.114997
Roussis, P.P.114265
+ Roux, A.116398
+ Roux, J.113229
Roux, J.A. +114942
Roux, J.-C. +111585
+ Rouxel, R.112603
+ Rowe, D.S.112312
+ Rowe, J.M.114294
+ Rowe, P.111990
+ Rowe, P.112012
+ Rowson, P.C.112011
Roxlo, C.B. +114817
Roy, D.K. +115029
Roy, J.N. +114551
+ Roy, K.112838
+ Roy, P.R.112365
Roy, R.J. Le
see Le Roy, R.J.
+ Roy, S.115751
Roy, S.K. Dutta
see Dutta Roy, S.K.
+ Roy, S.M.111891
+ Roybal, L.114608
+ Royer, T.C.116141
Rozanov, A.G.115705
Rozanov, O.V. +114793
+ Rozanova, T.S.116008
+ Rozenberg, B.A.115252
Rozgonyi, G.A. +114193
+ Rozhansky, V.A.116368
+ Rozhdestvenskaya, I.V.
113831
+ Rozhin, F.V.113240
+ Rozhko, A.Kh.114870
+ Rozman, I.M.112573
Rozvany, G.I.N. +113277
+ Rozvany, G.I.N.113278
Rubanovskii, V.N.113265
+ Rubbia, C.112031
+ rubbo, M.113928
Rubenstein, D. +116106
+ Rubin, A.B.115724
+ Rubimovich, I.M.115487
+ Rubins, R.S.114676
Rubinsky, B.114135
+ Ruchti, C.B.116837
+ Ruckl, R.112027
+ Rud, N.112033
+ Rud, N.A.114923
Rud', Yu.V. +114561
+ Rud', Yu.V.114569
+ Ruda, H.115110
+ Rudakov, K.N.114088
+ Rudakova, S.F.115835
Rudenchik, E.A.116645
+ Rudenko, M.V.116075
+ Ruder, H.116456
+ Rudge, A.112024
Rudiger, G.116466
+ Rudiger, G.116461
+ Rudnev, M.I.115835
Rudnitskii, E.N. +113361
+ Rudolph, D.111848
+ Rudy, Z.112241
Rueda, D.R. +113760
+ Rueggesser, P.115903
Ruelle, D.111566
+ Ruette, F.114364
Ruffini, R. +116893
+ Ruggiero, J.G., Jr.115535
+ Ruhl, F.113107
+ Ruhl, F.113110
+ Ruhl, F.113127
Ruijgrok, T.W. +111926
Ruiz, M.T.116780
+ Rukhadze, A.A.113672
+ Rullier-Albenque, F.
113859
+ Rummyantsev, V.D.115649
+ Rummyantsev, V.D.115651
Runcorn, S.K.116500
+ Runt, J.P.113771
+ Ruoff, A.L.114157
Ruoff, P.115522
Rupert, V.C. +113658
+ Rupnik, K.112628
+ Rusakov, V.S.114761
+ Rush, J.J.114294
Rushchitskii, Ya. Ya.113286
+ Rushton, M.111959
Rusov, V.D. +112575
Russell, C.T. +116401
+ Russell, C.T.116400
+ Russell, C.T.116404
+ Russell, C.T.116504
Russell, D.A. +113600
+ Russell, J.L., Jr.112360
Russell, T.P. +114944
+ Russo, G.112152
Russo, V. +113098
+ Rustigi, M.L.112034
+ Rusticelli, F.112297
+ Rusu, C.112794
+ Rut, O.E.114586
Rutkevich, I.M.113607
+ Rutkin, O.G.114947
Rutledge, S.A. +116221
Ruvinskii, K.D. +116098
+ Ruzhin, Yu. Ya.116368
+ Ryabov, A.V.113918
Ryabova, N.A. +113587
+ Ryabtsev, A.112685
Ryabtsev, L.A. +115227
Ryadno, A.A.113505
+ Ryan, R.R.113800
+ Ryazanov, L.D.116347
+ Rybalov, S.V.112514
+ Rybnicek, J.112404
Ryde, H.112264
Rydstrom, L. +112044
+ Rymden, R.114224
+ Ryndalev, S.V.111718
+ Rytus, N.N.114168
+ Ryu, W.S.115259
+ Ryzhanskii, V.A.115204
Rzasa, R.115970
+ Rzeszotarski, M.S.115900
+ Saito, T.112210
+ Saito, T.112224
+ Saito, T.112051
+ Saito, T.112229
+ Saito, T.112216
+ Saito, Y.115964
+ Saitoh, Y.115958
Sajo, T.116481
+ Sajot, G.112031
Saka, H. +113922
Saka, M. +113357
+ Sakaguchi, A.112227
Sakaguchi, H.112204
+ Sakaguchi, H.112224
+ Sakaguchi, H.112225
+ Sakaguchi, S.112408
Sakai, H. +112216
Sakai, M. +114386
+ Sakai, T.114938
Sakai, Y. +111810
Sakairi, H. +113991
+ Sakakibara, S.111922
+ Sakakibara, M.112899
+ Sakalas, A.114584
Sakamoto, H. +112225
+ Sakamoto, H.112213
+ Sakamoto, H.112223
+ Sakamoto, M.112375
Sakamoto, T.112928
+ Sakano, T.111695
+ Sakharova, I.I.113732
+ Sakhenko, V.P.114156
+ Sakisaka, M.114987
+ Sakkena, M.D.112747
+ Sakuma, T.112375
+ Sakuraba, I.113061
+ Sakurada, Y.112466
+ Sakuragi, Y.112230
Sakurai, K.112366
Sakurai, T.116585
+ Sakurai, T.116586
Sakurai, Y.115897
Sakurai, Y. +113169
Sakurana, G. M. +115787
+ Salaeu, F.M.114095
Salama, M.112184
+ Salas, L.J.116285
Saldana, J.J.111388
Saleh, N.A. +114519
Salerno, J.P. +114629
+ Salerno, M.114647
+ Salete, M.112689
+ Salib, E.H.113791
+ Salimbeni, R.113051
+ Salinari, P.116789
Salje, E. +114159
+ Salmon, J.R.116184
+ Salmon, R.115033
+ Salokhiddinov, K.I.
115743
+ Salour, M.M.113022
+ Salpeter, E.E.116839
+ Saltbones, J.116173
Saltzman, E.S. +116202
Salustri, G. +116215
Salvati, M. +116838
+ Salvati, M.116707
+ Salvini, G.112031
+ Salvini, G.112031
+ Salzburger, H.J.115463
+ Salzmann, M.111999
+ Samanni, G.115505
+ Samanta, C.112057
Samanta, L.K. +114293
+ Samara, G.A.114464
Sambasiva Rao, G. +
115300
+ Samchenko, I.P.115571
+ Samedov, S.R.114471
Samir, U. +116470
+ Sann, D.112005
+ Sann, D.112006
+ Sannells, A.F.115663
+ Samoilenko, Yu.I.113640
+ Samoilenov, S.S.114440
+ Samuel, A.G.113217
+ Samuelsen, M.R.114647
+ Sanchez, F.116530
+ Sanchez-Gomez, J.L.
111983
+ Sanchez-Velasco, E.
111359
Sanctis, E. De
see De Sanctis, E.
Sanctis, G. De
see De Sanctis, G.
Sandage, A.116767
Sandage, A.116813
Sandage, A. +116766
+ Sandalov, V.M.113268
+ Sandell, A.112504
+ Sandels, E.G.111808
+ Sanders, E.S.114335
+ Sanders, F.116256
+ Sanders, T.H., Jr.115185
Sandford, M.T., II +116800
+ Sandler, M.S.113253
Sandomirskii, P.A. +113831
Sandomirskii, V.B. +114432
+ Sandor, J.115969
+ Sandoval, A.112267
+ Sandstrom, R.L.114010
+ Sandstrom, R.L.115636
+ Sanduleak, N.116647
+ Sanford, N.M.113032
+ Sang, H.W.114598
+ Sang-Hyun Park113677
Sangro, R. De
see De Sangro, R.
+ Sanin, K.V.114569
+ Sanitarov, V.A.114176
+ Sankaranarayanan, V.
111692
Sankawa, I. +111746
Sankhla, V.D. +113585
Sanmartin, J.R. +113580
+ Sann, H.112089
+ Sanna, R.112611
Sannikov, D.G.114794
Sannikov, D.G.114798
+ Sano, T.114991
+ Sanokawa, K.112334
+ Sanquer, M.114861
+ Sansom, A.E.116851
Santilli, R.M.111428
+ Santillo, F.S.115749
+ Santisteban, A.112941
Santosa, F.116318
+ Santry, D.C.112507
+ Sanzone, M.112198
+ Sapozhnikov, M.N.
114917
+ Sarachik, E.S.116140
+ Sarantites, D.G.112049
+ Sarantites, D.G.112261
+ Sarantites, D.G.112059
+ Saratov, I.E.112660
+ Sarbeev, V.D.112514
Sardinha, F.115617
Sargent, A.I. +116782
+ Sargent, J.P.115296
Sargood, D.G.116631
+ Sargood, D.G.112181
+ Sargurumoorthy, M.
114776
Sarkadi, L.112830
Sarkar, M.111833
+ Sarkar, S.K.116206
Sarkozy, R.F.115086
Sarlet, W.111416
Sarma, K. Venkateswara
see Venkateswara Sarma, K.
Sarmiento, P.115621
Saro, S. +112577
Sarrak, V.I. +113924
+ Sarrak, V.I.114175
+ Sarrak, V.I.113955
Sarti, G.C. +114267
+ Sartor, I.112871
Sartre, A. +113070
+ Sarzhetskaya, M.V.
115726
+ Sasaki, A.114377
+ Sasaki, F.113241
+ Sasaki, K.112817
Sasaki, S. +114061
Sasaki, Y. +113053
+ Sasin, Y. Ya.115614
+ Sass, J.112031
+ Sass, J.K.114340
+ Sass, V.P.112753
Sassa, K. +113959
+ Sassa, K.113974
Sasselov, D.D.116676
Sassi, G.115646
+ Sastri, N.S.116372
Sastry, C.V. +116624
+ Sastry, C.V.111984
+ Sastry, K.S.115562
+ Sastry, K.S.R.115875
Sastry, T.P. +115415
+ Satake, T.111746
+ Satani, A.M.114624
+ Satchler, G.R.112248
+ Sathiyamurthy, N.112840
Sato, A. +113977
+ Sato, A.111990
+ Sato, A.112012
Sato, M. +114164
Sato, M. +114633
Sato, S. +115891
+ Sato, S.114057
Sato, T. +116038
+ Sato, T.116038
+ Sato, Y.113687
+ Sato, Y.115030
+ Sato Turtelli, R.114712
Satoh, S. +114522
+ Satoh, T.116038
Satten, R.A.114103
+ Satyanarayana, C.114811
+ Saudraix, J.112031
+ Sauer, R.114885
+ Sauer, R.114926
+ Saukov, A.I.113636
+ Saunders, R.D.111383
+ Sauneuf, R.113655
+ Saunier, N.112148
+ Saupe, A.114742
+ Sauvage, G.112022
+ Sauvaud, J.-A.116398
Savchenko, M.A. +114643
Savchenko, V.G.113323
Savel'ev, P.A. +113508
+ Savel'ev, P.A.113256
+ Savel'eva, O.M.115477
+ Savin, O.114771
Savina, O.N.116323
Savinskii, I.D. +116311
+ Savoy, R.L.115782
+ Savoy-Navarro, A.112031
Savruk, M.P. +113360
+ Savvatimskii, A.I.114508
+ Savvinov, A.S.115194
+ Sawai, T.114057
+ Sawan, M.E.112397
+ Sawaoka, A.114093
+ Sawaoka, A.115355
+ Sawochka, S.G.112386
+ Saxena, S.G.113798
+ Saxton, W.O.113707
+ Sayano, A.115155
Sayasov, Yu.S.113558
+ Sayer, B.115539
+ Sayer, M.114779
Sayers, C.M.113167
Scalera, G.C.111400
+ Scappini, F.112717
Scardia, M.116755
+ Scardia, M.116670
+ Scardia, M.116671
+ Scardia, M.116534
+ Scarfone, L.M.114527
+ Scarr, J.M.112015
Scarrott, S.M. +116483
+ Scarrott, S.M.116799
+ Scarrott, S.M.116855
+ Schaad, T.112011
Schaahe, H.F. +114201
+ Schacher, J.112022
Schachinger, H.113141
+ Schacht, P.112016
+ Schachte, M.-J.112016
+ Schadee, A.116578
+ Schader, J.114988
Schadler, N. +115697
Schaeffer, R. +116636
Schaffer, H. +114094
+ Schaffer, H.113819
Schaffer, O.112423
+ Schaille, P.M.115386
+ Schaille, P.M.115414
+ Schaller, G.115896
+ Scharf, B.112775
+ Scharfenberg, H.115926
+ Scharrer, E.115569
Schastlivtsev, V.M. +
115190
+ Schastlivtsev, V.M.
115308
Schattschneider, P.114063
+ Schatz, G.C.111475
+ Schatz, G.C.115514
+ Schatzel, K.113102
Schaub, B. +114695
+ Schechter, P.115834
+ Scheef, F.111999
+ Scheffel, R.113888
+ Scheggi, A.M.111674
+ Scheggi, A.M.113983
+ Scheler, G.114743
+ Schellman, H.112011
Schemm, J.B. +111747
Schenk, M. +114378
Scher, R.M. +115702
+ Scheraga, H.A.115736
+ Scherpelz, R.I.115935
+ Scherzer, R.112570
+ Scheuch, G.113491
+ Schick, G.A.112876
Schickentanz, D.113105
+ Schiemenz, P.112067
+ Schierholz, G.111969
Schiferl, D. +113800
Schiferl, D. +111697
+ Schiffer, J.P.112126
+ Schiffer, J.P.112246
+ Schifferl, D.113809
+ Schifino, J.112681
+ Schilling, H.-D.116213
Schilling, M. +112679
Schilling, T.112358
Schinder, P.J. +116706
Schindler, K. +116605
+ Schindler, R.112024
+ Schindler, R.N.116201
Schink, D.R.116147
+ Schinzel, D.112031
+ Schlager, H.116249
+ Schlatter, D.112011
+ Schlegel, W.115926
Schleyer, P. von Rague
see von Rague Schleyer, P.
+ Schlickeiser, R.116727
+ Schlieff, R.115967
+ Schlingmann, H.113499

- Schmaderer, F. + 115080
+ Schmahl, G. 111848
+ Schmalz, G. 112197
+ Schneider, T. 111757
Schmid, C. 111933
Schmid, F. + 113069
Schmid, R. 115175
+ Schmidt, D. 112015
Schmidt, F.H. 115720
+ Schmidt, G. 112016
+ Schmidt, G. 113591
+ Schmidt, H. 115254
+ Schmidt, H.U. 116748
+ Schmidt, J. 116532
+ Schmidt, K.-H. 112133
+ Schmidt, U. 116266
Schmidt-Nielsen, A. 113218
+ Schmidt-Ott, W.-D. 112055
Schmidtke, P.C. + 116757
+ Schmiedekamp, A. 112648
Schmitt, R.W. 114232
Schmitt, T. + 115095
Schmitz, D. 113389
Schmitz, F. 116788
Schmitz, W.J., Jr. + 116136
Schmucker, R.F. + 114527
+ Schmutz, W. 116666
+ Schneekloth, U. 111990
+ Schneekloth, U. 112012
+ Schneider, C. 112060
Schneider, E.K. 116509
+ Schneider, H. 112016
+ Schneider, H.G. 114590
Schneider, H.R. + 112475
Schneider, J. 114734
+ Schneider, M. 112884
Schneider, M.V. + 114588
+ Schneider, N.S. 115203
Schneider, S.E. + 116839
+ Schnell, A. 116684
+ Schober, H.R. 111438
Schoen, R. + 116464
+ Schoenecke, P.L. 115495
Scholl, E. + 112975
+ Schollmeier, W. 112468
+ Scholz, F. 115062
+ Scholz, R. 113875
+ Schonbacher, H. 113982
+ Schonfeld, B. 113920
+ Schoonman, J. 114250
Schopf, P.S. + 116103
Schopf, P.S. + 116104
+ Schorr, M. 115429
Schott, F. 116134
+ Schouler, M.C. 113070
Schouten, J.A. + 113551
Schrauder, K.-H. 115683
Schram, D.C. + 113618
Schreckenbach, K. + 112124
+ Schreurs, J. 115370
Schrewe, U.J. + 112055
Schreyer, W. 116089
+ Schriber, S.O. 112477
+ Schriener, G. 112273
+ Schroder, V. 112016
+ Schroder, W.U. 112488
+ Schroeder, L. 112256
+ Schroeder, L. 112257
+ Schroeder, L.S. 112267
Schroger, G. + 116295
+ Schrofel, J. 113087
+ Schroter, B. 114743
+ Schroter, J. 115141
Schuch, N.J. 116866
+ Schugerl, K. 113499
+ Schuh, A. 112173
+ Schujko, A. 114391
Schule, W. 113870
Schule, W. 114282
Schule, W. + 113875
+ Schulman, J.N. 114809
+ Schult, O.W.B. 112528
+ Schultz, H. 115230
+ Schultz, M.E. 113115
+ Schultz, P.J. 114960
+ Schultz, T. 113195
+ Schultz-DuBois, E.O. 113102
Schulze, G.E.W. 114122
+ Schumacher, G. 114058
+ Schumacher, J.D. 116141
Schumann, S. + 112398
Schurenkramer, M. + 112383
+ Schurmann, B. 112252
+ Schuss, Z. 111592
+ Schussler, M. 116597
+ Schuster, H. 115446
+ Schuster, H. 112341
+ Schuster, H. 112343
Schuster, J.C. + 115165
+ Schutte, J. 115603
+ Schwab, C. 114871
+ Schwalm, D. 112113
Schwandt, P. 112144
Schwartz, A. 115932
Schwartz, A.Y. + 116009
Schwartz, G.C. + 115386
Schwartz, G.C. + 115414
+ Schwarz, G. 113765
+ Schwarz, P. 112197
+ Schwarzmann, E. 113817
Schwebe, A.H. + 113555
Schweiger, W. + 112081
Schweiss, B.P. + 114165
+ Schwirlich, I.A. 115230
+ Schwitters, R.F. 112011
Scola, D.A. 115394
+ Scoles, G. 112815
+ Scoppola, E. 111449
+ Scott, A. 114024
+ Scott, D.M. 114611
+ Scott, J.F. 114118
+ Scott, M.E. 114749
Scott, P.J. 111765
+ Scott, R.L. 114128
Scott, T.A. 111379
+ Scott, W. 112031
+ Scovill, C. 116685
+ Seaborg, G.T. 112061
Seager, C.H. 114549
+ Seale, W.A. 112247
+ Seale, E.R. 116841
+ Searle, T.M. 114756
+ Sears, F.M. 113123
+ Sebald, P. 112705
Sebastian, D.H. + 114237
+ Sebestyen, A. 111521
+ Secco, L. 116822
+ Sechi, G. 112585
+ Sechi-Zorn, B. 112015
+ Sechkaev, A.V. 112784
Secomb, T.W. + 115816
Secomb, T.W. + 115767
+ Sedlacek, W. 116170
+ Sedmak, G. 116487
Seeböck, R. + 114247
+ Seeböck, R. 114767
+ Seebrunner, H.J. 112554
+ Seeman, J. 116695
Seestrom-Morris, S.J. + 112283
+ Seferis, J.C. 112890
Seferis, J.C. (ed.) 111312
Sefidvash, F. 112400
Segal, D. 113642
+ Segal, G.A. 112766
+ Segal, I.E. 111502
+ Segal, M. 116185
Seggern, H. von 115006
Segner, J. + 115006
Segovia, J.L. de 113714
+ Segre, A.L. 113714
+ Seiberg, N. 111913
+ Seibt, E.W. 114651
+ Seichert, N. 112067
+ Seidman, D.N. 114048
Seifritz, W. 112496
+ Seiger, A. 113706
+ Seiler, P.G. 112566
+ Seinfeld, J.H. 115585
+ Seisyan, R.P. 114448
+ Seisyan, R.P. 114868
+ Seitz, C. 111958
+ Seki, E. 112375
+ Seki, S. 111802
+ Sekine, T. 114386
+ Sekiya, T. 112183
Seko, H. + 115355
+ Selen, M.A. 114894
Selin, A.A. + 114134
+ Selin, A.A. 114178
+ Selin, V.V. 113938
Selker, T. 112945
+ Selove, W. 112552
+ Selvaraj, A. 113826
Selvelli, P.L. + 116697
+ Semary, M.A. 114720
Semchenko, I.V. + 114822
+ Semchenko, V.V. 116503
+ Semenov, M.Yu. 112575
Semenov, S.G. + 112660
Semenov, V.A. 113584
+ Semenov, V.V. 113060
+ Semenov, V.V. 113661
+ Semenova, I.Yu. 113729
+ Semichastnova, Z.M. 111767
+ Semmler, W. 113964
+ Semmler, W. 113961
+ Semmler, W. 113963
Sen, D. 111893
Sen, D. 111953
+ Sen, K. 114548
Sen Gupta, A. + 113801
+ Sen Gupta, S.P. 113823
+ Sen Gupta, S.P. 113702
Sen Zhang see Zhang Sen
Senchenkov, I.K. 113324
+ Sendu, Y. 115960
+ Sengonca, H. 116754
+ Sengupta, A.K. 113762
Sengupta, D. + 113685
Sengupta, N. + 116206
+ Sengupta, S. 112446
+ Sengupta, S.N. 113685
+ Senina, R.V. 114687
Senjanovic, I. 111412
+ Seo, I. 115248
+ Serafini, L. 112489
Serby, M.R. + 111756
+ Serdyuk, G.G. 115139
+ Serdyuk, O.V. 113627
+ Serdyuk, V.V. 114560
+ Serdyukov, A.N. 114822
Sergeev, A.G. 111405
+ Sergeev, M.S. 113739
Sergeev, V.A. + 116377
+ Sergiampietri, F. 112551
+ Serginov, M. 114569
Serikov, S.V. 113315
+ Serio, C.S. + 115867
+ Serkov, A.T. 114171
+ Sermund, G. 112570
+ Serot, B.D. 112203
+ Serov, A.V. 113004
+ Serra, A. 113983
Serre, J. 112618
+ Serre, J. (ed.) 111310
+ Seshakumari, C. 111660
+ Setaka, N. 115030
+ Setaka, N. 114379
+ Sethi, R. 115625
+ Sethna, J. 111586
+ Seto, S. 115122
+ Seto, T. 115734
+ Setser, D.W. 112820
Setty, O.H. + 115765
Seung Ho Jeon + 113716
Sevan'kaev, A.V. + 115842
Sevast'yanov, A.A. + 114690
Sevenhuijsen, P.J. 113382
+ Severinov, V.I. 116380
Sevier, M.E. + 112181
Sevryugin, V.A. + 111717
Sezan, M.I. + 112942
Sezer, C. + 116754
+ Seznec, R. 113158
+ Sgarbi, C. 112559
Shabanova, I.N. + 114440
+ Shabel'nikova, A.E. 114948
+ Shablovskii, A.V. 114688
Shadlesky, P.S. 113431
+ Shafer, R.A. 116887
+ Shafizade, R.B. 114396
+ Shafrankova, Ya. 116418
Shah, A.H. + 113162
+ Shah, A.J. 114079
+ Shah, G.H. 115973
+ Shah, J. 114879
Shah, N.G. + 115973
+ Shah, R.C. 115453
+ Shah, R.R. 114530
+ Shah, T.P. 112031
Shahin, F. + 112233
+ Shain-Way Jang 113489
+ Shain-Way Lang 113490
+ Shakhovtsov, V.I. 113867
+ Shakin, C.M. 112141
+ Shakhshin, N.I. 115484
+ Shalashov, V.F. 114705
+ Shallis, M.J. 112680
+ Shalnikov, A.Sh. 113935
+ Shambrum, W.D. 111992
Shamfarov, Ya.L. + 116482
+ Shams El Din, A.M. 111686
Shandala, M.G. + 115835
Shang-Chen Wei 115824
+ Shang-Chen Wei 115824
Shani, G. 112182
Shank, C.V. + 114879
Shankar, P.N. Girija 112875
+ Shanklin, J. 116685
+ Shannon, J.M. 114029
+ Shapin, S.M. 112728
Shapira, D. + 112254
+ Shapiro, A.B. 113853
Shapiro, D.A. 113408
+ Shapiro, G. 112256
+ Shapiro, G. 112257
+ Shapiro, I.I. 116870
+ Shapiro, S.L. 116706
Shapley, R. 115789
+ Shappir, J. 115096
+ Sharafat, S. 114060
+ Sharafutdinov, R.G. 112863
+ Sharan, V. 116713
Share, G.H. + 116565
+ Share, G.H. 116878
Sharimanov, Yu.G. + 115742
+ Sharlovskaya, L.A. 116015
Sharma, A.K. + 114523
Sharma, B.B. + 114742
Sharma, K.C. 113582
+ Sharma, L.K. 111477
+ Sharma, L.K. 112864
Sharma, N.D. + 114505
+ Sharma, S. 111984
Sharma, S.K. 116265
Sharov, A.S. 116703
Sharp, R.D. + 116360
+ Sharpe, W.N., Jr. 113386
Sharshakov, I.M. + 114092
+ Sharshunov, A.G. 114383
Shastry, C.S. + 112250
Shatz, M.P. 111970
Shaulov, A. 111769
+ Shaw, D.E. 111347
+ Shaw, D.T. 115588
Shaw, G.E. 116229
+ Shaw, J.M. 115074
+ Shaw, J.S. 116678
Shaw, P.M. 112456
Shaw, R.W., Jr. + 116171
Shaw Jiin Chang 113786
+ see Jiin Chang Shaw
+ Shchedrin, B.M. 111503
+ Shchedrin, B.M. 113704
+ Shcheglov, I.M. 114680
+ Shchepinov, V.P. 113390
+ Shcherbatova, T.D. 113786
+ Shchukin, G.I. 112759
+ Shchukin, P.S. 115488
+ Shchukin, S.I. 115972
Shea, J.A. + 112765
Shearer, M. 111457
Shechter, M. + 115656
+ Shedova, E.N. 113667
+ Shein, V.I. 115856
+ Sheinbaum, J. 111469
+ Sheinberg, V.G. 115252
+ Sheinina, E.V. 113050
+ Sheldon, P. 114608
+ Sheldon, P.D. 112011
+ Sheldrick, G.M. 113817
+ Shelesnova, V.I. 115848
+ Shelest, A.N. 115290
+ Shelest, A.N. 115289
Shelevoi, K.D. + 112594
+ Sheline, R.K. 112066
+ Shelyag, V.K. 114096
+ Shemet, A.S. 116373
Shen, D.Y. + 114863
+ Shen, I.R. 113064
Shen, M.C. 113469
+ Shen Jian-guo 111954
+ Shen Jian-Wen 116020
Shen Qi-xing + 111962
Shen Qi-xing + 111963
Shen Qianruo 111414
Shen Wen-qing 112538
+ Sheng, T.T. 114783
Sheng Ping see Ping Sheng
Sheng Rong see Rong Sheng
Sheng-Hua Ye 112233
+ see Ye Sheng-Hua
Shenker, S.J. 111580
+ Shenoy, A.V. 114234
Shenpan Zhang 112145
+ see Zhang Shenpan
Shepard, J.R. 112145
+ Shepard, S. 113733
+ Shepelev, A.V. 113042
+ Shepelev, Yu.F. 113832
Shepelyansky, D.L. 111584
+ Shepherd, J. 116024
+ Shepherd, J. 116024
Shepilov, V.B. + 115335
Sheppard, C.J.R. 111760
+ Sheppard, J.C. 112471
+ Sheppard, L.C. 115824
+ Sheppard, T. 115212
+ Sher, E.S. 114095
+ Sheridan, J. 112715
+ Sherman, N.K. 112599
+ Sherman, W.F. 114855
+ Sherrington, D. 114693
Sherrington, M.R. + 116696
Shestakov, A.I. + 111396
+ Shestakov, A.I. 111397
+ Shestakov, V.P. 111807
+ Shestopalov, V.P. 112908
+ Shevchenko, V.A. 112605
+ Shevgaonkar, R.K. 116624
Shevkunov, S.V. + 113563
+ Shewmon, P.G. 115374
Shi, L.T. + 115276
Shi-ke Hu see Hu Shi-ke
+ Shi-tao Deng 111446
+ Shian-Woei Jeng 113421
+ Shiau, B.S. 113421
Shiau Chyi-Jang 113536
+ Shiba, K. 112323
Shibaeva, R.P. + 113854
Shibaeva, R.P. + 113848
+ Shibaeva, R.P. 113851
+ Shibaeva, R.P. 113853
Shibata, K. + 116586
+ Shibata, N. 113927
+ Shibata, T. 112218
+ Shibata, T. 112216
+ Shibata, Y. 115025
+ Shibatomi, A. 114589
Shibuya, K. + 112772
+ Shichijyo, S. 115235
+ Shieh, J.H. 114395
Shields, J.E. + 111639
+ Shigemasa, Y. 112409
Shigenaka, N. + 114286
Shikama, T. + 114397
+ Shilov, V.B. 113056
+ Shilov, V.V. 113761
Shim, I. + 112664
+ Shim, J.D. 113728
+ Shima, K. 113969
Shimada, S. + 115038
+ Shimizu, A. 112229
+ Shimizu, A. 112216
Shimizu, F.O. + 112817
+ Shimizu, H. 115005
+ Shimizu, H. 112051
+ Shimizu, H. 114239
+ Shimizu, H. 114993
+ Shimizu, K. 113608
Shimizu, N. + 113149
+ Shimizu, R. 114993
+ Shimizu, T. 112545
+ Shimizu, T. 114745
+ Shimkevich, A.L. 115573
+ Shimoda, H. 115667
+ Shimoda, T. 112160
+ Shimoda, Y. 112406
Shimomura, R. + 114143
+ Shimomura, T. 115444
+ Shimomura, T. 111735
Shimomura, Y. + 113894
Shimomura, Y. + 113904
Shimomura, Y. + 113895
Shimotomai, M. + 114022
+ Shimotomai, M. 114957
+ Shimotomai, M. 113864
+ Shimoura, S. 112227
+ Shin, P.W. 115317
Shinjo, T. 114763
Shinkarev, V.P. + 115724
+ Shinno, H. 114397
+ Shino, M. 112892
+ Shinoda, Y. 115058
+ Shinohara, C. 112892
Shinomoto, S. 111542
+ Shinta, I. 113898
+ Shintani, Y. 114143
+ Shiokawa, J. 112780
+ Shiomos, C. 111365
+ Shirai, H. 111794
Shirai, Y. + 113968
+ Shirakawa, H. 114724
Shirakawa, K. 113317
Shirakawa, K. + 114509
+ Shiratori, T. 112323
+ Shirley, D.A. 114441
+ Shirobokov, M.I. 111713
+ Shirochikov, A.V. 116346
Shirokov, V.V. + 115277
+ Shirokov, V.V. 115285
+ Shiroyama, K. 113132
+ Shitov, A.T. 115260
Shivakumar, V. + 113350
Shkitin, V.A. + 114089
+ Shklover, V.E. 112868
+ Shklover, V.E. 113847
+ Shklovskii, B.I. 114553
Shklovskii, I.S. 116714
+ Shklyar, D.R. 113587
+ Shkolenko, A.P. 115221
+ Shkvarunets, A.G. 113672
Shlimak, I.S. + 114553
Shlyakhter, A.I. 112353
+ Shmakov, A.M. 115441
+ Shmartsev, Yu.V. 114869
+ Shmatko, B.A. 115573
+ Shmyglevskii, I.P. 116422
+ Shneider, V.E. 114169
+ Shnider, S. 111865
Shoemaker, C. 116536
Shoemaker, C. + 116513
+ Shoemaker, C.S. 116514
+ Shohet, J.L. 113597
+ Shohoji, M.C.B. 114737
+ Shoji, F. 114313
+ Shoji, K. 114529
+ Shonija, V.M. 112573
Shore, S.N. + 116647
+ Short, K.T. 113988
Short, R.W. + 113688
+ Shostka, V.I. 114934
+ Shou-Yih Wang 114838
+ Shou-Yih Wang 114839
Showler, R.E. 113401
+ Shpak, D.E. 115244
Shpak, E.V. 112499
+ Shpak, M.T. 114452
+ Shrager, R.I. 115765
+ Shreider, E.Ya. 113060
+ Shreter, U. 113007
+ Shreyder, A.A. 116076
Shri Ram 116890
Shri Ram 116898
+ Shrier, A. 111569
Shriner, J.F., Jr. + 112157

- Shtein, L.V. + 115754
 + Shtelen, W.M. 111879
 + Shtovba, Yu.K. 115346
 Shu, F.H. 116437
 Shubaly, M.R. + 112463
 + Shubin, A.L. 114917
 Shubotenko, S.A. + 111800
 + Shukhtina, M.A. 116384
 Shukla, A. + 113352
 Shukla, G.C. 111391
 + Shukla, G.C. 112810
 + Shukla, P.K. 113616
 + Shukla, R.P. 111755
 + Shukurov, T. 112733
 + Shulepov, V.I. 114217
 + Shul'ts, E.F. 115053
 + Shulyakov, Yu.M. 115139
 Shumaker, J.B. 111382
 + Shuman, H. 115607
 + Shuman, V.B. 114604
 Shur, V.Ya. + 114780
 + Shurygin, V.A. 113654
 + Shuto, Y. 113108
 + Shuvalov, L.A. 114796
 + Shuvalov, R.S. 112551
 + Shved, G.M. 116333
 + Shvedov, A.A. 112591
 Shvets, R.N. + 113304
 Shyam, R. + 112163
 + Shyam, R. 112220
 Shyu, C.M. + 114482
 + Shyu, C.M. 114279
 Shyuliova, Yu. + 115850
 Si-lan, Z. + 115812
 Si-Yu Wei, see Wei Si-Yu
 + Sibbett, W. 113052
 + Sibilia, C. 111634
 + Siciliano, E.R. 112149
 Sick, I. 112180
 + Sidko, F.Ya. 115763
 + Sidman, D.N. 111826
 + Sidorenko, T.V. 116025
 + Sidorov, I.M. 116347
 + Sidorov, N.I. 111688
 Sidzhimov, B. + 114670
 + Siedle, A.R. 114491
 + Siefert, E. 112395
 + Siefert, J. 112060
 + Siegbahn, E.M. 112788
 + Siegel, D. 113404
 + Siegel, M.D. 115622
 + Siegel, R.W. 113863
 + Siegel, R.W. 113880
 Siegel, W. 111914
 + Siegerist, F. 112623
 + Siegert, G. 112102
 + Siegrist, J.L. 112022
 Sielemann, R. + 113963
 + Sielemann, R. 113961
 + Siemens, P.J. 112115
 + Siemens, P.J. 112290
 + Sierk, A.J. 112169
 Siever, R. 116047
 + Siggia, E. 111586
 Siggia, E.D. 111581
 + Sigmon, T.W. 114006
 + Sigmon, T.W. 114288
 + Sigmon, T.W. 113948
 Siiman, O. + 114840
 + Silaev, A.N. 113654
 Silberstein, R.P. + 114902
 + Silcock, J.M. 115198
 + Silin'sh, E.A. 114538
 Silva, A.T.e see e Silva, A.T.
 + Silva, G. 115131
 + Silversmith, D.J. 115050
 Silvia, M.T. 116321
 + Simeonov, S.D. 112801
 + Simin'kovich, V.N. 115337
 + Simkin, B.Ya. 115547
 Simmons, D.A.R. + 116243
 Simmons, J.F.L. 116762
 + Simmons, V.P. 116102
 + Simmons, W.F. 115359
 Simmetts, G.M. 116580
 + Simmonds, A.J. 114427
 Simon, G.W. + 116602
 + Simon, M. 116843
 + Simon, N.R. 116630
 + Simon, R.S. 112113
 + Simonen, T.C. 113641
 + Simonetto, A. 112585
 + Simonov, Yu.A. 113839
 + Simons, D.G. 112829
 Simons, J. + 112807
 + Simons, L.M. 112884
 Simopoulos, S.E. + 112495
 + Simov, V.G. 113473
 + Simoyi, R.H. 111585
 Simpson, J.R. + 113123
 Simpson, M.J. + 113078
 + Sims, M.L. 115449
 + Sinclair, C.K. 112471
 + Sinclair, R. 114401
 + Sinclair, R. 114284
 + Sindt, H. 112016
 + Singer, H.J. 116400
 + Singer, M. 111919
 Singer, R.F. + 115136
 + Singh, A.J. 114551
 Singh, A.K. 113513
 Singh, A.K. + 113519
 + Singh, A.K. 113515
 Singh, B. + 111327
 + Singh, B. 114523
 + Singh, B.M. 113377
 + Singh, B.N. 114023
 + Singh, B.P. 116013
 + Singh, C.P. 112001
 Singh, H.B. + 116285
 Singh, K. + 112122
 + Singh, K.P. 116874
 Singh, M. + 116634
 Singh, M. + 112747
 Singh, S.N. + 113577
 + Singh, V. 113512
 + Singheiser, L. 114407
 + Singovsky, A.V. 112556
 Sinha, P. + 114912
 Sinha, S.P. 114911
 Sinien Lu, see Lu Sinien
 + Sinita, L.N. 112731
 + Sinnaeve, J. 112608
 Sinno, K. + 116364
 + Sinyaev, A.Ya. 113346
 + Sinyakova, S.I. 115172
 Sinyavskii, V.S. + 115438
 + Siraky, J. 115981
 + Sironi, G. 116889
 Sirota, N.N. + 114964
 Sirotnik, O.S. + 114332
 + Sirotiyuk, O.A. 115437
 + Sit'ko, S.P. 112605
 + Sivash, V.G. 114526
 Sivashinsky, G.I. 114142
 + Sivkov, V.N. 114969
 + Sixel, P. 112028
 + Sizova, N.L. 113439
 + Sizova, O.V. 112655
 Sjoberg, S. 115823
 + Sjoreen, T.P. 112153
 + Skaali, B. 112075
 + Skakov, Yu.A. 115220
 Skalak, R. + 115768
 + Skalak, R. 115767
 + Skalak, R. 115816
 + Skard, J.A. 112015
 + Skarzshinsky, V.D. 111484
 + Skensved, P. 112033
 + Skepko, O.A. 115004
 + Skepstedt, O. 112292
 + Skillcorn, I.O. 112015
 + Skipetrova, L.A. 114687
 + Skirida, V.D. 111717
 + Skobov, V.G. 114587
 + Skogsmo, J. 114405
 + Skolnick, M.S. 114492
 + Skomarovsky, V.S. 116368
 + Skopyuk, M.I. 112605
 + Skorikov, V.M. 113821
 + Skorobogatov, G. 114584
 + Skorobogatov, G.V. 115003
 + Skorospeshkin, A.I. 115977
 + Skoryukin, V.E. 114569
 + Skoryukin, V.E. 114561
 Skouliditis, T. + 114805
 + Skrinjar, M. 111612
 Skripnik, Yu.D. 115478
 + Skripnik, Yu.D. 115247
 + Skripova, N.M. 115489
 + Skubenko, P.A. 114870
 + Skubenko, P.A. 114924
 Skudnov, V.A. 114076
 + Skuja, A. 112015
 Skvor, Z. 113244
 + Slade, M.A. 116814
 + Sladec, R.J. 114070
 + Slagle, O.D. 112329
 Slagsvold, B.J. + 115014
 Slanger, T.G. + 112700
 Slate, J.B. + 115824
 Slavnov, A.A. 111974
 Slavyanov, E.V. + 113700
 + Slemrod, M. 113396
 + Slepyan, A.Ya. 113023
 + Slepyan, G.Ya. 113023
 + Slesarev, V.I. 115895
 + Sletten, G. 112049
 + Sletten, G. 112058
 + Sletten, G. 112046
 + Sluchanko, N.E. 114669
 + Slusher, R.E. 113649
 + Slusher, R.E. 113034
 Slutskii, M.E. + 111804
 Smakman, G.J.G. + 116663
 + Smallman, R.E. 113874
 + Smallman, R.E. 114037
 Smedley, J.E. + 115567
 Smedskjaer, L.C. + 113880
 Smerdov, A.A. + 115962
 + Smerlin, V.M. 116325
 Smeyers, P. + 116635
 Smid, H. + 112668
 + Smidt, F.A., Jr. 113388
 + Smirnitkii, V.B. 114000
 + Smirnov, A.M. 111719
 Smirnov, B.I. + 113926
 Smirnov, B.I. + 113918
 Smirnov, B.M. 113546
 + Smirnov, I.A. 114550
 + Smirnov, I.A. 113918
 + Smirnov, L.S. 114474
 + Smirnov, M.A. 115308
 + Smirnov, M.V. 111710
 + Smirnov, O.P. 114675
 + Smirnov, V.A. 114448
 + Smirnov, V.G. 116128
 + Smirnova, E.P. 114785
 + Smirnova, N.N. 114585
 + Smirnova, N.V. 116342
 + Smirnova, V.B. 114472
 + Smit, J. 116086
 Smith, B.L. + 113220
 Smith, C.W. + 114297
 Smith, D. 113774
 Smith, D. 114212
 + Smith, D. 112031
 + Smith, D.B. 112683
 Smith, D.J. + 113707
 Smith, D.L. 114559
 + Smith, D.L.E. 112447
 Smith, G. + 114823
 + Smith, G. 114323
 Smith, G.A. 112426
 + Smith, G.B. 113226
 + Smith, G.F. 115678
 + Smith, G.R. 112285
 Smith, H. 115863
 + Smith, H.I. 115050
 Smith, I.E. + 115678
 Smith, J. + 114697
 + Smith, J.F. 115168
 + Smith, J.G. 111992
 + Smith, K.M. 112015
 + Smith, N.V. 112509
 Smith, P. 112650
 + Smith, P.A. 116376
 Smith, P.C. 116110
 + Smith, P.J. 112112
 + Smith, P.R. 114558
 Smith, R.J. + 116522
 + Smith, R.J. 116484
 + Smith, R.L. 116141
 + Smith, R.L. 116131
 + Smith, R.T. 115074
 Smith, R.W. + 111762
 + Smithgall, B.F. 112946
 + Smithsonian, M.J. 112275
 + Smolenskii, G.A. 114947
 + Smolenskii, G.A. 114830
 Smolin, Yu.I. + 113832
 + Smolin, Yu.I. 114790
 + Smolkin, P.I. 116422
 Smoot, G.F. + 116889
 Smoot, N.C. 116078
 + Smyth, D.M. 113858
 + Smyth, M.J. 111753
 Smythe, J. + 115363
 + Sneden, C. 116775
 + Snegirev, S.D. 116570
 + Snell, A.H. 112254
 + Snezhkin, E.N. 113417
 Snider, D.R. 111472
 Snijders, J.G. + 112763
 Snijders, J.G. + 112637
 Snitko, V. + 111644
 + Snively, L.O. 114248
 Snow, L.D. + 112756
 Snyder, A. + 111994
 Snyder, A.W. + 113110
 Snyder, A.W. + 113127
 + So, S. 114266
 + Soares, O.D.D. 113143
 + Sobczyk, L. 112749
 + Sobel'man, I.I. 112976
 + Sobew, P. 115330
 Sobey, R.J. + 116115
 + Sobolenko, D.N. 113059
 + Sobolev, A.P. 113031
 + Sobolev, Yu.S. 115315
 + Soboleva, L.V. 113844
 + Soboleva, T.N. 116341
 Socio, L.M.de see de Socio, L.M.
 + Soderblom, L.A. 116520
 + Sodikov, T. 115691
 + Sodja, J. 112471
 + Soeda, K. 114916
 + Soga, N. 114784
 + Soga, N. 113757
 Sohlstrom, H. + 113139
 + Sohma, J. 114735
 + Sohn, H.Y. 115176
 + Soker, N. 116663
 Sokolov, A.A. + 111531
 Sokolov, A.I. 114797
 Sokolov, E.A. + 115472
 + Sokolov, I.A. 114000
 + Sokolov, L.A. 115187
 + Sokolov, V.I. 114675
 Sokolova, I.V. + 112641
 + Sokolova, Z.N. 114980
 + Sokolova, Z.N. 114543
 + Sokolovskaya, T.G. 114694
 + Sokolovskiy, A.A. 111745
 + Soldati, R. 111467
 Soldatov, E.A. + 113792
 + Soliani, G. 111401
 + Solimini, D. 116168
 + Solimini, D. 116280
 + Solntsev, V.A. 112914
 Solntsev, V.P. + 114890
 Solodov, Yu.P. 115153
 + Solombrino, L. 111401
 + Solomon, E.I. 115008
 + Solomon, P.M. 116843
 + Solov'eva, H.G. 115247
 + Solov'eva, L.P. 113704
 + Soltani, P. 113930
 + Soltis, R.A. 115074
 Sol'tsas, R.Kh. + 114169
 Solum, M.S. + 114748
 + Solyom, J. 111605
 + Solyom, J. 111612
 + Soman, S.D. 112446
 + Somasundaram, S. 112805
 + Sameda, C.G. 111743
 + Somekh, M.G. 113237
 + Somerville, R.C.J. 116260
 + Somlyo, A.P. 115607
 Somogyi, I.Kosa see Kosa Somogyi, I.
 Son Tay, R.Tran see Tran Son Tay, R.
 + Sona, P.G. 115511
 + Sone, K. 114990
 + Song, D.J. 116893
 + Sonnenberg, K. 115312
 + Sonnenberg, K. 113920
 Sonoc, S. + 112445
 Sonoda, M. + 115918
 Sonoda, Y. + 113664
 Sontag, H. + 112781
 Sontum, S.F. + 112653
 Soo Kim Dae see Dae Soo Kim
 Soo Kim Jun see Jun Soo Kim
 Sorensen, G.O. + 112719
 + Sorita, K. 112780
 + Sorochenko, R.L. 116806
 + Sorokin, V.N. 114487
 Sorooshian, S. 116164
 + Soru-Escut, I. 116619
 + Sorvin, V.M. 112488
 + Sosodov, V.N. 115481
 + Soskin, M. 113062
 + Soskin, M.S. 115753
 Soszka, M. + 114996
 + Soszka, W. 114996
 + Sottini, S. 113098
 Soucek, J. 116891
 + Souda, R. 115024
 Soudek, I. 111712
 Soukiasian, P. + 114344
 + Soukoulis, C.M. 114701
 + Soukup, J. 115929
 + Soussens-Jacob, J. 114850
 South, H.M. + 111748
 Southwick, R. 111653
 Souza, P.De see De Souza, P.
 Spadaro, B. 115598
 Spaepen, F. + 114002
 Spagna, G.F., Jr. 111360
 Spalla, P. + 116339
 + Spamer, E. 112176
 + Spamer, E. 112174
 Sparks, W.B. 116848
 + Sparling, G.A.J. 111521
 + Specht, H.J. 112113
 Spedden, S.E. 113531
 + Speidel, K. 115619
 Speier, P. + 115062
 + Speight, J.D. 114027
 Spellenberg, S. 115832
 Speller, C.V. + 115532
 Speranzini, R.A. + 112349
 Sperling, L.H. + 113772
 Speth, P. + 116214
 Spicer, D.S. + 116616
 + Spiegel, E.A. 111593
 + Spilda, I. 115557
 Spiller, G.D.T. + 114393
 + Spinelli, P. 112008
 Spiridonov, V.P. 112853
 + Spiro, A.G. 113056
 + Spiro, M. 112031
 + Spirou, G.A. 115805
 + Spitzer, H. 112015
 + Spitznagel, G.W. 112645
 + Spol'nik, A.I. 114740
 Spong, D.A. + 113599
 Spoonhower, J.P. + 114914
 + Sprangle, P. 112518
 Spratt, C.E. 116687
 Spratt, C.E. + 116539
 Spratt, C.E. + 116546
 Spratt, C.E. + 116538
 + Spratt, C.E. 116537
 + Spratt, C.E. 116685
 + Sprengel, M.E. 115575
 Sprenger, H. 115123
 SPudich, P. + 116026
 + Spurney, F. 112449
 + Squarcia, S. 112028
 Sredin, V.G. 114819
 + Sreekantan, B.V. 116723
 + Sridhar, M.K.C. 115707
 Sridharan, K. 113301
 Srinath, L.S. + 113351
 + Srinivasa Murthy, N. 113351
 + Srinivasan, R. 111692
 Srinivasan, S.R. 112315
 Srivastava, A.K. + 111418
 + Srivastava, Y.K. (ed.) 111334
 + Srivastava, R.C. 113511
 Srivastava, S.C. + 114776
 + Srivastava, V.K. 113520
 + Srivastava, Y.N. 111960
 Sromicki, J. + 112241
 Staa, R.van. see van Staa, R.
 + Staab, J. 115717
 + Stademann, R. 112243
 + Stadenyuk, B.I. 111678
 + Stager, C.V. 112033
 + Stagi, M. 114621
 Stahel, D. + 112703
 + Stahelin, P. 112555
 Stahl, P.A. 116569
 Stahl, W. + 112872
 + Stalio, R. 116656
 Stallard, W.A. + 113026
 + Stamberger, J. 114425
 + Stamnes, J.J. 112936
 + Stamp, M.F. 113630
 + Stancampiano, C.V. 115825
 + Stanev, N. 114670
 + Stanish, M.J. 113155
 + Stanishevskii, L.S. 112732
 + Stanley, E.A. 114238
 + Stanovnik, A. 112589
 + Stansfield, B.L. 113646
 + Stansfield, S.E. 113459
 Stapp, H.P. 111900
 + Stares, E.J. 112608
 + Starikova, Z.A. 113849
 + Stark, A.A. 116795
 + Stark, H. 112942
 + Starke, E.A., Jr. 113908
 Starke, K. 111384
 + Starobogatov, I.O. 113251
 + Starostin, I.A. 114560
 Startsev, O.V. + 113759
 + Startseva, L.T. 113759
 + Stary, F. 112236
 + Stas', V.F. 114474
 Stauffer, C.C. + 112389
 + Stausebach, D. 112310
 + Staveley-Smith, L. 113235
 Stebler, B. + 115903
 Stechemesser, H. 112494
 + Steel, G.G. 115859
 + Steele, J.W. 112438
 + Steele, W.J. 115318
 + Steer, P. 116154
 + Steer, R.P. 111771
 + Stefancic, V. 115744
 Stefanou, G.D. 113295
 + Stefanovich, A.E. 116418
 + Stefanovich, S.Yu. 113794
 + Stefanovich, S.Yu. 113820
 + Steffen, B. 113673
 + Steffen, P. 111990
 + Steffen, P. 112012
 + Steffen, W. 112174
 + Steffens, E. 112277
 + Steigmeier, E.F. 115073
 + Steil, H. 113701
 + Stein, B.E. 115786
 + Stein, R.S. 113763
 Steinbach, F. + 115603
 + Steinbichler, H. 114291
 + Steiner, H. 112256
 + Steiner, H. 112257
 + Steiner, H.M. 112022
 + Steinfink, H. 113806
 Steinhilber, D.W. 111354
 Steinhilber, O. 114769
 Steinhilber, F. + 115930
 + Steinmetz, L. 116024
 + Stenolfson, R.S. 113596
 + Stell, G. 113542
 + Stella, B. 112015
 + Stella, L. 116893
 + Stelson, P.H. 112254
 Stelzer, J.F. 112493
 + Stencil, R.E. 116757
 + Stenflo, L. 113617
 Stensgaard, I. + 114352
 + Stenzel, R.L. 116405
 + Stepanenko, N.P. 113346
 Stepanenko, V.A. + 115344
 + Stepanenko, V.A. 112591
 Stepanenko, V.F. + 115840
 + Stepanenko, V.F. 115846
 + Stepanenko, V.F. 115847

- +Stepanov, B.M. 111767
+Stepanov, G.S. 116406
Stepanov, G.V. + 115475
+Stepanov, G.V. 116665
+Stepanov, I.P. 115610
+Stepanov, S.V. 115848
+Stepanov, V.A. 115253
+Stepanov, V.S. 115855
+Stepanova, M.N. 114504
Stephan, K.H. + 116473
+Stephanovitch, A.V. 116463
Stephens, F.S. 112037
+Stephens, K. 111990
+Stephens, K. 120112
+Stephens, P.L. 116279
+Stephenson, J.B. 115076
Stepina, N.P. + 113941
+Stepleman, R.S. 115633
Stepney, S. 116450
Stepney, S. + 116467
+Stern, B.E. 116829
+Stern, K.S. 115821
+Stern, R.C. 115079
Stern, S. + 115825
Stern, S.A. 111351
Stern, S.A. + 114262
Sternheim, M. + 115383
+Sternheimer, D. 111988
Sternstein, S.S. + 115502
+Stetsenko, A.I. 116482
Stetsenko, E.G. + 115571
+Stetsenko, S.G. 116553
+Stevens, A.E. 112785
+Stevens, K.N. 113216
+Stevenson, D.A. 115113
Stevenson, J.D. + 112546
Stevenson, R. 115526
Stewart, A.M. 114723
Stewart, C.G. 115879
Stewart, C.W. + 112312
+Stewart, C.W. 112313
+Stewart, J.S. 115369
Stewart, P.A.E. + 111857
+Stewart, P.A.E. 111836
Stickler, D.C. 113184
Stiehl, M.A. + 115782
+Stier, M.T. 116790
+Stika, K.M. 114279
Stillinger, F.H. + 117115
+Stimpfl, G. 112022
Stineberg, D.R. + 116726
+Stirling, W.G. 113753
+Stobbs, W.M. 113707
Stock, K.D. 111638
Stock, R. + 112267
Stockbauer, R. + 114347
+Stocker, F. 112022
Stocker, H. + 112263
+Stocker, H. 112251
+Stocker, W. 112094
+Stockmayer, W.H. 112888
+Stoffl, W. 112066
+Stoffler, W. 112270
+Stoffler, W. 112272
+Stoicheff, B.P. 113032
Stojadinovic, S. 115208
+Stokes, G.M. 116204
Stokes, J. + 111860
+Stokstad, R.G. 112254
Stolen, R.H. 113116
+Stolen, R.H. 113123
+Stolt, K. 114353
Stommel, H. 116137
+Stone, N.H. 116470
+Stone, P.H. 116215
+Stone, R.M. 115495
+Storchak, N.A. 113802
Storebo, P.B. + 116181
+Storey, J.T. 116241
Storey, J.W.V. + 116850
+Storey, P.J. 116447
+Stoughair, J.D. 113459
+Stoyanov, D.A. 112551
Strachan, J.D. + 111626
+Strachan, J.D. 113573
+Strachman, Z. 112020
+Strack, B. 112242
+Strahle, W.C. 115551
+Strait, J. 112011
Strange, W. + 113215
Strangeway, R.J. + 116388
Straten, P.J.M. van der
... see van der Straten, P.J.M.
Stratonovich, R.L. + 112898
+Stratonovich, R.L. 111591
+Strauss, H.L. 114849
+Strauss, J. 112031
Street, R.A. + 114533
+Streets, J. 112031
+Strelko, V.V. 114370
+Strelkov, P.S. 113672
Strelou, K.K. + 115342
Strel'tsova, V.N. + 115848
+Streptov, A.V. 111980
+Strid, K.-G. 115012
+Stringfellow, G.B. 115069
Strobl, G.R. 114113
+Stroebele, H. 112267
+Strogatz, S.H. 111460
Strong, D.T.G. 115684
+Stroot, J.P. 112556
+Strottman, D. 111324
+Struble, G.L. 112066
+Struchkov, Yu.T. 113852
+Struchkov, Yu.T. 112868
+Struchkov, Yu.T. 113847
+Struchkov, Yu.T. 113840
+Struchkov, Yu.T. 113842
+Struchkov, Yu.T. 113843
+Struchkov, Yu.T. 113845
+Struchkov, Yu.T. 113846
+Struchkov, Yu.T. 113850
+Stryer, L. 115748
+Strzalkowski, A. 112241
+Strzelecka, H. 114172
+Stuart, W.F. 116401
Stubbs, L.C. + 116335
Stuchly, M.A. + 115836
+Studentin, A.I. 111921
+Studentov, V.M. 115441
+Stuhl, F. 112772
Stuhmiller, J.H. + 112377
+Stukel, J.J. 115587
Stultz, T. 113989
Stulz, L.W. + 115381
+Stumpf, H. 113281
+Stumpf, P. 116532
+Stupko, A.V. 115158
+Stupperich, K. 112015
+Sturges, W. 116141
+Sturm, J. 113989
Sturman, B.I. 114568
+Stus', N.M. 114585
+Styecz, B. 112076
+Styrikovich, M.A. 113263
+Styris, D.L. 114049
+Su, M. 115326
Su, W.P. 114438
+Su, Y.K. 115064
+Subashiev, A.V. 114808
+Subashiev, V.K. 111759
+Subbotin, A.L. 114780
+Subrahmanyam, V. 113500
+Subramanian, P.R. 112263
+Subramanyam, S.V. 111702
Sud, V.K. + 115815
+Sudnik, M.V. 113853
+Sudol, J. 112526
Suehiro, M. + 113934
+Suehiro, T. 112211
+Suehiro, T. 112227
+Suematsu, Y. 113008
+Suetsugu, Y. 113664
+Suffert, M. 112544
+Suffield, J.B. 115803
Sugano, T. 114614
Suganuma, K. + 114043
+Sugarbaker, E. 112209
+Sugarman, M.D. 113220
Sugaya, R. 113624
Sugerman, A. 114609
+Sugimoto, D. 116639
+Sugino, Y. 115022
+Sugitani, M. 112227
+Sugiyama, T. 112228
+Sugrei, V.I. 114824
Suhai, S. 115238
+Suhr, H. 116313
+Suizt, T. 113671
+Sukegawa, T. 111703
+Sukharev, V.I. 114242
Sukhinin, G.I. + 112863
+Sukhomlinov, V.S. 112824
Sukhorukov, A.P. + 113067
+Sukhovich, E.P. 113426
+Sukhovskii, A.A. 114793
+Sulima, O.V. 115652
+Sulima, O.V. 115641
+Sullivan, B.J. 112699
+Sullivan, J.C. 114637
+Sullivan, M. 112024
+Sulwinski, L. 113637
+Sul'zhenko, P.S. 114603
+Sumi, K. 115111
+Sumida, S. 111746
+Sumini, M. 112296
Sumino, K. 113981
+Summers, H.P. 113668
+Summhammer, J. 111490
+Sumorok, K. 112031
+Sumpf, B. 112992
+Sun Li-bo. 112519
Sun Xiangfu + 112109
+Sundara Raj, A. 114853
+Sundararajan, V. 113319
Sunden, B. 113433
Sundermeyer, K. 111878
+Sundman, A. 116746
+Sundstrom, H. 115363
+Sun, I. 114611
+Sun, I. 113947
+Suonien, E. 115012
Surko, C.M. + 113649
+Surma, M. 111704
+Susman, S. 114294
+Suszycki, L. 112028
Sutera, S.P. + 115766
+Suto, H. 114271
Sutton, M.A. + 111636
+Suvorov, S.A. 115392
+Suvorova, S.O. 114175
+Suvorova, S.O. 113924
+Suzuki, E. 115154
Suzuki, F. + 113241
Suzuki, H. 114300
Suzuki, I. + 116576
+Suzuki, I. 116575
+Suzuki, K. 113751
+Suzuki, K. 111685
+Suzuki, K. 113749
+Suzuki, K. 113750
+Suzuki, M. 113473
+Suzuki, M. 115898
Suzuki, S. + 115197
+Suzuki, S. 114589
Suzuki, T. 112108
Suzuki, T. + 112117
+Suzuki, T. 116623
+Suzuki, Y. 114768
+Suzuoki, A. 112408
+Suzuki, A. 112371
+Svane, A. 114702
Svendsen, B. + 116080
Svergun, D.I. + 111503
+Sveshnikov, B.V. 113253
Sveshnikova, E.I. 113336
Svestka, Z. + 116578
+Svestka, Z. 116616
+Svetlichnyi, P.N. 112591
+Svetlov, V.I. 115379
+Sviridov, V.A. 112515
+Sviridov, V.A. 111745
+Svirko, Yu.P. 114893
+Svistun, L.I. 115139
Svitin, A.P. + 112708
+Swain, D.M. 111751
+Swalen, J.D. 114944
Swales, T.G.E. + 114852
Swallow, W.H. + 111623
+Swanson, L.W. 114979
Swanson, R.M. 115662
+Swanson, R.M. 114288
Swantner, W. + 113072
+Swantner, W. 112924
+Swedlow, J.L. 113310
+Swensen, L.W. 112153
Swenson, R.J. 111476
+Swidzinski, M.A.M. 112351
+Swidzinski, M.A.M. 115449
+Swift, P.V.D. 111890
Swinnea, J.S. + 113806
+Swinnett, D. 112425
Swinney, H.L. 111564
+Swinney, H.L. 111585
Swisterski, W. + 113355
+Sy, W.N.-C. 113581
Symons, F.W. 113208
Symons, M.C.R. + 112757
+Sy'rev, N.E. 114681
+Syromyatnikov, V.N. 114671
+Szabo, A. 111554
+Szalewski, M. 114324
+Szczekowski, M. 112028
+Szczepanek, P.S. 114972
Szczerski, R. 112303
+Szecsenyi-Meszaros, K. 114140
+Szecsi, L. 112506
Szekely, J.G. + 115865
Szekeres, A. + 114374
+Szokody, P. 116692
+Szoncs, F. 112031
Szucs, B. + 115969
+Szudy, J. 112684
Szymanski, M. + 116888
+Szymanski, Z. 112048
+t Hooft, G.W. 114935
Ta-You Wu 111473
Tabarovskii, L.A. + 116310
+Tabata, H. 115156
Tabata, T. + 111323
Tabatabaie-Alavi, K. + 114594
+Tabor, M. 111422
+Tachibana, K. 116038
+Tachikawa, E. 114260
+Taczanowski, S. 112431
Taddeucci, T.N. + 112196
Tagirov, V.I. + 114546
+Tagirov, V.I. 114471
Tagishi, Y. + 112228
+Tagishi, Y. 112213
+Tagishi, Y. 112223
Tai, I. + 112375
+Tai Tsun Wu 111926
Tai-Ung Kim + 115222
Tai-xuan Yan
... see Yan Tai-xuan
Tairrov, M.M. 113987
+Tain, J.L. 112076
+Tait, R.J. 113341
+Tait, W.P. 115357
+Taiuti, M. 112198
Tajima, Y. + 115734
+Takada, K. 112522
+Takada, T. 114782
+Takada, T. 114828
+Takagi, A. 116038
+Takagi, A. 112485
Takagi, F. 111965
+Takagi, M. 114384
+Takagi, T. 111813
Takahara, F. + 116454
+Takahara, K. 115206
+Takahara, K. 115354
Takahashi, H. + 113979
+Takahashi, H. 114189
+Takahashi, I. 115417
Takahashi, K. + 115355
+Takahashi, K.I. 113250
Takahashi, N. + 112862
Takahashi, N. + 112277
+Takahashi, N. 112278
Takahashi, T. 116226
Takahashi, T. + 114957
Takahashi, T. + 113752
Takai, Y. + 113892
+Takai, Y. 113891
+Takai, Y. 113894
+Takaki, S. 115230
Takakura, T. + 116583
+Takakura, T. 116574
+Takakura, T. 116581
+Takakura, T. 116582
+Takamiya, K. 112892
Takamura, J. 113967
+Takamura, J. 113970
+Takamura, J. 113884
+Takamura, J. 113968
Takamura, S. + 114046
+Takanaka, M. 112466
+Takano, M. 112609
+Takano, M. 115918
Takasaki, E. + 112485
+Takasaki, F. 112550
+Takashima, H. 115231
+Takata, M.L. 114041
+Takeda, H. 111990
+Takeda, H. 112012
+Takeda, T. 113647
Takei, M. + 112223
+Takei, M. 112213
+Takei, M. 112228
+Takeishi, T. 115592
+Takemura, T. 114843
+Takemura, T. 115235
+Takenaka, S. 115122
+Takenaka, T. 114389
+Takenaka, T. 112485
+Takeris, S.Ya. 114269
+Takeshita, H. 114044
+Takeshita, I. 112406
+Takeshita, T. 111990
+Takeshita, T. 112012
+Takeshita, T. 113968
+Taketani, H. 112117
+Taketani, M. 115054
Taketomi, S. 114831
+Takeuchi, N. 113016
Takeuchi, S. + 114077
+Takeyama, H. 113209
+Takeyama, T. 114189
+Takeyama, T. 113979
Takezoe, H. + 114876
+Takigawa, N. 111492
+Takimoto, K. 112227
+Takiyama, K. 114916
+Tako, T. 113731
+Tako, T. 113028
+Tako, T. 113027
+Takoaka, N. 116555
Talanov, V.M. 113796
+Talkyue Ree 113716
+Tallet, A. 113066
Talley, L.D. 116107
+Talmon, Y. 111829
+Talon, R. 116588
+Taluts, G.G. 114719
+Talybov, V.M. 113661
Talzi, E.P. + 115543
+Tam, A.C. 115380
+Tamaru, K. 114355
+Tamborini, M. 112020
Tamkin, H. + 114927
+Tamminga, Y. 114413
Tamura, H. 111801
Tamura, S. 111699
+Tamura, S. 112161
Tan, T.Y. + 114277
+Tan, T.Y. 113906
+Tan, T.Y. 114478
Tanabe, I. + 115125
Tanabe, K. + 114644
+Tanabe, T. 115583
+Tanahashi, T. 115112
+Tanaka, A. 111703
+Tanaka, A. 114422
Tanaka, H. + 115959
Tanaka, H. + 114050
Tanaka, H. + 114843
+Tanaka, H. 112223
Tanaka, K. + 115309
Tanaka, K.H. + 112278
Tanaka, M. + 112160
+Tanaka, R. 115231
Tanaka, S. + 111815
+Tanaka, S. 114575
+Tanaka, S. 114050
Tanaka, T. 116375
+Tananaev, I.V. 115523
+Tananaev, I.V. 115524
+Tang, C.H. 115326
Tang, H.H.K. + 112167
Tang, J. + 114724
Tang, T.-H. + 112629
Tang, Y.-N. + 115531
+Tang Xiao-Ming 116059
+Tanglis, E. 113171
Tanguy, P. + 112416
+Tanguy, P. 112500
+Tani, C. 114826
+Tanifuji, T. 114261
+Tanifuji, T. 114044
+Tanigawa, M. 114757
Tanigawa, S. + 113898
+Tanigawa, S. 113969
+Tanigawa, S. 114956
Tanimoto, M. + 112718
Tanimoto, M. + 112726
Tanimura, O. + 112245
+Tanino, R. 115898
Tanisho, S. + 112357
Taniuchi, T. + 113130
Taniwaki, M. + 113973
+Taniwaki, M. 113974
+Taniyo, M. 113645
Tansley, B.W. + 115803
+Tanzi, E.G. 116763
+Tanzi, E.G. 116858
+Tao, C. 112031
Tao Huang. see Huang Tao
+Taoka, T. 111820
Tap Ngo Dien. see Ngo Dien
Tap
Tapping, K.F. 116609
Tarafdar, S.P. 116691
+Taranenko, V.B. 115753
+Tarapov, I.E. 114801
+Taras, P. 112033
Tarascon, J.M. + 114639
Tarasenko, L.V. + 115226
+Tarasenko, N.V. 113060
+Tarasenko, N.V. 113661
+Tarasenko, T.N. 114686
+Tarasenko, V.V. 114186
+Tarasov, A.F. 116378
Tarasova, L.S. + 114177
+Tarasova, O.B. 115227
Tarbeev, Yu.V. 111631
+Tarbox, E.J. 113109
Tariyal, B.K. + 113157
+Tarr, A.W. 112738
Tarrab, I. 116821
Tartter, V.C. + 113217
+Taskinen, P. 112131
+Tasumi, M. 112707
+Tata, X. 112010
Tateda, M. + 113092
+Tatallay, M. 116504
+Tatsumoto, H. 115146
Tatum, K.E. 113471
+Taure, L.F. 114538
+Tauscher, L. 112544
+Tavernier, S.P.K. 112553
+Tavkhelidze, N.N. 111968
+Taxil, P. 111986
Tay, R. Tran Son
... see Tran Son Tay, R.
+Tayal, S.S. 112858
Tayler, R.J. 116897
+Taylor, B.A. 111785
Taylor, C. + 111898
+Taylor, C.L. 113153
+Taylor, H. 112807
+Taylor, M.D. 115305
+Taylor, O.C. 116179
Taylor, P.A. + 116184
+Taylor, R.A. 111775
+Taylor, S.M. 115830
Taylor, T.R. 111947
+Taylor, W.L. 112811
+Tchalaya, N.M. 115290
+Tchalaya, N.M. 115289
Tedeschi, R. + 112535
+Teegarden, B.J. 116836
+Teffteller, S. 113195
+Teiger, J. 112022
+Teiwani, M.J. 114297
+Tejedor, C. 114583
Tel, T. 111560
+Tel, T. 114053

- +Telegina, I.V.113786
+Telepa, V.T.114691
Tell, B. +113997
+Temerin, M.A.116399
Temkin, D.E.115576
+Temkin, D.E.113787
+Temkin, D.E.113788
Temple, P.J. +116179
+Temurkhanov, A.115688
+ten Bosch, J.J.113103
Teng Ji-Wen +116039
+Teo, H.H.114852
+Teper, M.111969
+Teplitzkaja, R.B.116596
+Teplitz, V.L.112000
+Teplov, I.B.112107
+Teplov, O.A.114204
+Teppner, U.115967
+Ter-Nikogosyan, V.A.115731
Ter-Pogossian, M.M.115920
+Teramoto, Y.113770
+Terasaka, T.111553
+Terasawa, M.114974
+Terekhin, A.S.114096
Terekhov, G.I. +115172
Ternov, I.M. +111921
+Ternovskaya, M.V.116380
+Terrasi, F.112120
+Tertichnyy, A.I.115171
Tertykh, V.A. +115584
+Tervo, R.J.112531
+Terzian, Y.116839
+Teschke, C.D.112578
Teske, K. +112326
Teshlenko, V.V.114473
Tessler, A. +111444
+Tetreault, D.J.113610
+Tewari, D.P.112901
+Tewary, V.K.115655
Teyssandier, F. +115099
+Thacher, P.D.112548
+Thakoor, A.P.113756
Thakur, A. +113068
Thakur, A.K.S.115695
+Thangathirupathy, S.115421
Thanh Huy Phan
..... see Phan Thanh Huy
Thanh Nghi Nguyen
..... see Nguyen Thanh Nghi
+Thawani, P.T.113197
+Theeten, J.-B.114871
Theimer, O. +113561
+Theis, J.112251
+Theis, J.112263
Theocaris, P.S.113372
+Theodosiou, G.E.112552
+Thibault, L.R.113385
Thiebaud, F. +114847
Thiele, U. +112343
+Thielemann, F.-K.116445
+Thielen, K.113496
+Thieme, R.115926
+Thiessen, H.A.112283
+Thode, L.E.113626
+Thomas, A.G.115319
+Thomas, B.115426
Thomas, G.J. +113984
Thomas, H.-C. +116748
+Thomas, J.P.113949
Thomas, K. +112169
Thomas, L. +116234
Thomas, L.K. +114949
+Thomas, M.E.114401
Thomas, N.114115
Thomas, P.114520
Thomas, R.G. +112420
+Thompson, A.W.115215
+Thompson, B.J.111726
+Thompson, C.J.114655
+Thompson, D.L.112813
+Thompson, D.T.116535
+Thompson, G.112031
+Thompson, G.I.116654
+Thompson, K.116675
+Thompson, K.116673
+Thompson, K.116681
Thompson, K.R. +116238
+Thompson, M.E.115819
+Thompson, M.J.114533
+Thompson, M.N.115597
+Thompson, M.O.114054
Thompson, R.O.R.Y.116113
Thompson, W., Jr. +113164
Thomson, D.J. +115659
+Thomson, J.C.112015
+Thomson, R.114084
+Thomson, R.114085
+Thorez, J.115708
+Thorne, L.R.112635
Thorne, R.M. +116519
Thorson, W.R.112848
+Thorsteinsen, T.F.112075
+Thorsteinson, G.112024
Thosar, B.V. (ed.)111334
Thulke, W. +114966
+Thulstrup, E.W.114904
Thunen, J.G. +113073
Thurgate, S.M. +114363
+Thurn, G.111664
Thurzo, G.113196
Thylwe, K.-E.111979
Tian-Min Wang +113864
Tian-Sheng Wang
..... see Wang
Tian-Sheng
Tian-Xi Huang
..... see Huang
Tian-Xi
+Tiedje, T.114817
+Tiee, J.J.112776
+Tiernsma-Thoone, G.113395
+Tien, P.K.114254
Tien Loc Vu
..... see Vu
Tien Loc
+Tier, C.111592
Tietze, M. +115230
Tijges, C.P. +114248
+Tijburg, R.P.115382
Tikhomirov, A.A. +115763
+Tikhonova, N.A.114846
+Tikhonravov, A.V.113079
+Tilley, D.R.112217
+Tilley, R.J.D.113932
+Timakova, G.P.114381
Timchenko, I.N. +114585
+Timm, U.112015
+Timmer, J.112031
+Timofeev, B.T.115347
+Timofeev, E.I.113493
+Timofeev, V.V.116806
+Timofeeva, I.I.115393
+Timofeyeva, T.S.116506
Ting, R.Y.115360
Ting Lu
..... see Lu
Ting Lu
+Tingwell, C.I.W.112181
Tinin, M.V.112902
Tinoco, I., Jr. +112931
Tinsley, J.R. +112153
+Tinti, D.S.112762
+Tiomno, J.116906
Tipping, R.H. +112806
+Tirozzi, B.111449
+Tirskii, G.A.116423
Tishchenko, G.N. +115740
+Tishchenko, G.N.112869
+Titchomb, S.113950
+Titenskaya, G.E.115228
+Titkov, A.N.114504
+Titov, V.E.115546
+Tiwari, G.N.115694
Tiwari, K.P. +112001
Tiwari, T.N. +111984
+Tiziani, H.J.111757
Tjermkes, S.116759
+Tjon, J.A.111926
+Tjotta, J.N.113186
+Tjotta, S.113186
+Tkach, A.N.115337
+Tkachenko, N.A.115923
+Tkachenko, S.V.114556
+Tkachenko, Yu.G.115366
+Tkachev, V.D.114922
+Tobin, J.G.114441
Toda, K. +113249
+Toda, K.113527
Toda, M.111454
Toda, S.113330
+Todd, D.M.112112
Todoroff, D.G. +114760
Todorov, T.112962
Togawa, T.115956
+Tohei, T.112211
Tohma, K. +111641
+Tohma, K.116262
Tohmori, Y. +113008
Tohsaki-Suzuki, A. +112052
+Tokar, V.G.116351
+Tokarev, A.T.114185
Tokarev, V.F.111907
+Tokarev, V.I.111780
Tokarev, V.N. +115194
+Tokarskii, V.P.112515
Toki, H. +112073
+Tokuda, N.112466
Tokue, I. +112861
+Tokuyama, T.114013
Toldalgi, P.M. +116267
Tolmachev, S.M.112867
+Tolmachev, S.T.114706
Tolpearev, R.G. +113144
Tolpekin, V.E. +115972
+Tolstikhina, A.L.113739
+Tolstopyatenko, A.V.112898
Tolstoy, I.113166
+Tomaneek, D.114343
Tomar, V.S. +111693
+Tomar, V.S.114622
+Tomar, V.S.114646
Tomashpol'skii, Yu.Ya.115056
+Tomasi, E.112103
+Tomasi, J.112804
Tomaszewicz, P. +115427
+Tomaya, K.114770
+Tomblin, J.116024
+Tomonitsu, H.113752
Tomita, M. +114987
+Tomkiewicz, M.114902
Tomoda, T. +112372
+Tomoda, Y.116018
+Tomokiyo, K.112780
+Tomova, N.112962
+Tomozawa, Y.111897
Tompkins, H.G. +115412
+Tonakanov, O.S.113240
Tonomura, A.111828
Tonomura, A.114717
+Tonoyan, I.G.113739
+Tonuma, T.112484
+Tonwar, S.C.116723
+Toohy, R.E.115867
Topchyay, L.S.114040
Toporkov, Yu.G.116293
+Torbohm, G.112686
Torge, W. +115998
+Toriumi, H.113735
+Toriyama, K.112758
Tornqvist, R.114928
Toro, M.Di.
..... see Di Toro, M.
+Toro Labbe, A.112627
Torquat, C.
..... see de Torquat, C.
Torrone, K. +115356
+Torti, R.P.113632
+Tosheva, V.V.112402
+Tossell, J.A.114444
Tostevin, J.A.112221
+Toth, A.112014
+Totsuka, Y.111990
+Totsuka, Y.112012
Tougui, A. +113384
+Toulemonde, M.114414
Touratier, M.113159
Tourenne, C.J.111619
+Toussaint, H.-N.113136
+Tovpinets, A.A.115490
+Townes, B.M.112507
+Toyokura, N.114384
+Trabjerg, I.114875
+Tracey, J.E.113632
+Trachtman, M.112648
+Trahern, C.G.111994
Trainor, R.J. +113635
Trakhtenberg, L.I. +114295
+Tran, C.113725
+Tran Son Tay, R.115766
+Trappeniers, N.J.114131
+Trappeniers, N.J.113551
+Trasi, M.S.112363
Trauger, J.T. +116505
Trautmann, D. +112827
+Trautmann, D.112220
+Trautmann, D.112163
+Traversini, R.116761
+Treffitz, E.116612
Trefilov, V.I. +113802
+Trefzger, C.116709
Trenberth, K.E.116217
+Trepakov, V.A.113776
+Tret'yachenko, G.N.115348
Tret'yakov, A.F. +115287
+Tret'yakov, S.G.114452
Tret'yakov, Yu.D. +115147
+Treves, A.116761
+Treves, A.116763
+Treves, A.116858
Trias, A. +114659
Trietley, H.L.111677
+Trigari, S.113098
+Trigueiros, A.115545
+Trilling, G.H.112011
Trinhammer, O.111892
Trinkaus, H.115313
+Tripati, T.111987
+Trippe, A.P.111860
+Troesch, A.W.115702
+Trofimov, V.A.113067
Troitskii, V.N. +115129
Tromp, J.W. +112711
Troshchenko, V.T. +115345
Trostel, R.111549
+Troster, D.112544
Troudert, T. +115344
+Trout, J.R.111623
+Trubitsina, N.V.114684
+Trubnikov, A.S.113417
+True, W.W.112149
Truett, W.L. +111786
Trufiyakov, V.I. +115468
+Trullinger, S.E.111578
Truong, S. +112070
+Truran, J.W.116660
+Trussoni, E.116817
Tryon, P.V. +111628
+Tryon, P.V.111629
Trzaskoma, P.P. +115385
+Tsai, H.L.114195
+Tsai, S.F.112087
+Tsai, S.H.112097
Tsang, T.H. +115586
Tsang, W.T. +114901
Tsang, W.T. +113024
+Tsao, L.114915
Tsao, Y.H. +113193
+Tsapanos, T.M.116027
+Tsapenko, A.S.113420
+Tsarev, O.M.114487
+Tsarev, O.M.114663
+Tsaryuk, D.A.112909
+Tsaur, B.-Y.115050
+Tscheslog, E.112031
Tscholakowa, N. +115330
Tse Wan-Sun
..... see Wan-Sun Tse
+Tseitlin, V.Yu.116210
+Tsemekhan, L.Sh.115171
+Tsengin, L.D.116368
Tsereteli, G.I.115756
+Tskhin, B.G.112915
Tsimring, L.Sh.113460
+Tsimring, Sh.E.112973
+Tsioukin, Yu.N.114211
+Tsirolin, Yu.A.112574
Tsiulyanu, D.I. +114610
+Tskhai, V.A.112651
Tsong, T.T.114338
Tsubaki, T.116601
Tsuchida, H. +113027
+Tsuchida, H.113028
Tsuchida, K. +113567
+Tsuchiya, H.114970
Tsuchiya, T. +115554
+Tsuei, C.C.112578
Tsuge, H. +114645
+Tsujimoto, Y.113130
+Tsukada, M.114354
Tsukruk, V.V. +113761
+Tsukuda, T.115417
+Tsumigi, Y.113861
Tsun Wu Tai
..... see Tai
Tsun Wu
+Tsunashima, A.115038
+Tsunematsu, T.113647
Tsunemoto, H.115915
Tsuneta, S. +116582
+Tsuneta, S.115854
+Tsuneta, S.116581
+Tsuneta, S.116583
Tsunoda, K. +111820
+Tsunoda, Y.114105
Tsuruta, K. +113675
+Tsumishima, H.113008
+Tsvetkov, E.G.114890
Tsvetkov, E.I. +111624
+Tsvetkov, E.N.112870
+Tsvetkov, Yu.D.112759
Tsy, A.F. +115895
+Tsybaneva, T.B.116126
Tsybenko, A.S. +115246
+Tsyganenko, N.A.116377
+Tsygkin, V.I.115260
+Tsygkin, V.I.115204
Tu, C.W. +114593
+Tuchinskii, L.I.115158
+Tuchkova, E.A.113999
Tuck, E.O.115052
+Tucker, L.W.115819
+Tucker, M.O.112332
Tucker, W.B., III.116239
+Tueller, J.116836
+Tully, J.A.113668
Tung, R.T. +115060
+Tung, R.T.114322
+Tungate, G.112202
+Tuominiemi, J.112031
+Turban, L.111601
+Turkna, N.I.115226
+Turkner, K.-H.111706
+Turnbull, D.114002
Turnell, H.B. +116005
Turner, D.G. +116769
Turner, D.J.114233
+Turner, J.W.111557
+Turner, L.G.115945
Turner, M.S.116904
+Turner, R.E.113635
+Turok, N.111596
Turova, I.P. +116596
+Turovsev, A.V.113096
Tursunov, Ch.Sh. +115691
+Tursunov, D.A.115482
Turtelli, R.Sato
..... see Sato
Turtelli, R.114139
+Turver, K.E.116747
Turygin, A.Yu.111517
Turygin, A.Yu.111518
Tvergaard, V.113332
Twersky, V.111462
+Twin, P.J.112112
+Tylka, A.J.112015
Tyufiyakov, N.D.115498
+Tyulin, V.A.112903
+Tze, C.-H.111925
+Tzivanidis, G.113510
+Tzvetkova, K.115563
+Uberall, H.113171
+Ubertini, P.116474
+Ubogii, V.P.116299
+Uchida, K.114044
+Uchida, N.113122
+Uchida, T.111811
+Uchida, Y.116586
+Uchikura, M.114268
Udagawa, T. +112161
+Udalski, A.116679
Udodov, F.P. +115471
Ueba, H.114864
Ueba, H.114865
+Ueda, K.116224
+Ueda, K.112817
Ueda, N. +112466
+Uehara, S.115134
Uemura, T. +115122
+Uemura, Y.J.114768
Ueno, M. +113750
Ueno, T. +113250
+Uetani, Y.113687
+Ufimtsev, E.V.114217
+Ufimtsev, M.V.111657
Ugajin, M. +112323
+Uglov, A.L.115473
+Uhrich, D.L.114760
+Uhleinn, C.114492
+Ukai, K.112609
+Ukhanov, Yu.I.114869
+Ulbright, J.112187
+Ulenikov, O.N.112731
+Ullmaier, H.115312
+Ullmann, H.112326
Ullmann, J.L. +112149
+Ullmann, J.L.112289
+Ullmann, J.L.112232
+Ullrich, D.F.113507
+Ulmer, R.114746
Um, G.S. +112946
Uman, M.A.116254
+Umantsev, P.G.111799
+Umapathy, K.G.113506
+Umarov, B.S.114795
Umarov, G.Ya. +115615
+Umarov, M.114795
+Umarova, I.O.112870
Umbach, H.113537
Umeda, Y. +115999
+Umamoto, S.114938
+Umerez, N.116465
Umeyama, S. +113974
+Umeyama, S.113973
+Umezawa, K.113211
Underwood, K. +111750
+Ungar, T.115271
+Ungrecht, E.112241
Ungryn, J. +112477
+Ungstrup, E.116360
Unluata, U. +116111
+Unnikrishnan, K.112851
+Unnikrishnan Nayar, V.115428
+Unno, Y.112550
+Uno, T.115125
+Unrau, U.113112
+Unylov, V.I.115473
Upatnieks, J.113140
+Upitis, Z.T.115286
+Uppal, G.S.116237
Urabe, H. +113527
Urabe, S. +112972
Uramoto, J.113634
+Urbakh, M.I.114807
+Urban, A.116369
Urban, K.113996
Urban, K. +113901
+Urban, K.113992
+Urban, K.114246
+Urbie-Perez, I.115321
+Urusova, B.I.114705
Uryupin, S.A.112850
Uscinski, B.J. +116235
+Uscinski, B.J.116236
+Ushakov, I.B.115950
Ushakova, T.V. +115741
+Ushankin, Yu.V.115075
+Ushigami, Y.113752
+Usikova, G.I.115193
+Uskov, E.I.115344
+Usova, V.V.115438
+Uspenskiy, G.R.116503
+Uspenskiy, M.V.116406
+Usuda, H.115333
Usyukina, N.I.111908
Uten'kin, A.A. +115952
Utracki, L.A.113722
Utracki, L.A. +114069
+Utracki, L.A.115332
+Uvarov, V.M.116346

- + Vagabova, L.K. 114126
 Vagner, V. + 115190
 + Vaidya, P.C. 115131
 Vainberg, E.I. 115486
 Vainberg, M.Sh. 115921
 + Vainshtein, B.K. 115740
 Vainshtein, L.A. 114576
 Vaissiere, C. de la
 see de la Vaissiere, C.
 + Vajda, P. 113962
 Vakarov, B.S. + 114560
 Vakhlaeva, L.F. + 113333
 Vakhnenko, V.A. + 113470
 + Vakser, I.Kh. 116307
 + Vala, M. 114503
 + Vala, M. 114875
 + Valbusa, U. 112815
 + Vale, G.K. 114945
 Valeev, A.K. 115858
 + Valenta, H. 114225
 Valente, E.J. + 113824
 Valentijn, E.A. 116819
 + Valentijn, E.A. 116818
 Valentini, M.A. + 112886
 + Vali, G. 116228
 Valiullin, A.Kh. 113289
 + Valkenburg, W.G.J.N.
 114413
 + Valkuns, L.L. 114452
 + Vallabhan, C.P.G. 114933
 Valle, J.W.F. + 111919
 Vallee, J.P. 116796
 + Valley, G.C. 115047
 Valley, J.F. + 113034
 + Vallieres, M. 112096
 + Valls, J. 115757
 + Valone, S.M. 114368
 + Valyanskaya, T.V. 114675
 Vampola, A.L. 116394
 Van, K.Dang. *see* Dang Van, K.
 + van Andel, H.W.H.
 113618
 + van Beek, G. 112553
 + Van Berg, R. 112552
 + van Beuzekom, A.A.
 112751
 van Beveren, E. + 111967
 + Van Breugel, W. 116810
 + van Buijtenen, C.J.P.
 116181
 + Van Dam, J.W. 113643
 + Van Dam, J.W. 113599
 Van De Walle, C. + 115661
 + van den Bergh, L.C.
 113551
 van den Brekel, C.H.J. +
 115093
 Van den Broeck, C. 111558
 + Van Der Hoek, B. 113782
 + van der Lans, J. 112024
 + van der Leeden, G.A.
 114010
 + van der Leeden, G.A.
 115636
 + van der Meer, W. 112637
 + van der Piepen, H. 116290
 van der Plaats, G. + 111640
 + van der Ree, H. 115675
 van der Straten, P.J.M. +
 115451
 + van der Voo, R. 116006
 + Van der Voo, R. 116009
 + van der Werf, S.Y.
 112237
 Van Dop, H. + 116172
 + van Duinen, R.J. 116782
 Van Dyke, M. 113413
 + Van Eijk, B. 112031
 + Van Enckevort, W.J.P.
 113782
 + van Enckevort, W.J.P.
 113790
 van Enter, A.C.D. + 111600
 + Van Espen, P. 116177
 + van Genderen, A.M.
 116749
 + van Genderen, A.M.
 116774
 + van Gorkom, J.H. 116840
 van Gunsteren, W.F. +
 115727
 + van Haeringen, H. 112081
 + Van Haute, A. 115700
 Van Heel, M. 113696
 + van Hemmen, J.L. 111600
 van Hoek, A. + 113033
 + Van Laak, F.A. 113539
 + Van Landuyt, J. 111659
 + van Loo, F.J.J. 115102
 + Van Overstraeten, R.
 115660
 + Van Overstraeten, R.
 116569
 van Paradis, J. 116664
 van Roosmalen, O.S. +
 112702
 van Saarloos, W. + 113740
 + van Staa, R. 112015
 + van Staa, R. 112555
 Van Wunnik, J.N.M. +
 115000
 van Wunnik, J.N.M. +
 114999
 van-Sliedregt, M. 115899
 Vanden-Broeck, J.-M.
 113463
 Vandenbosch, R. + 112255
 Vandenbulcke, L. 114404
 + Vandenbulcke, L. 115448
 + Vander Donckt, E. 115654
 Vanderspek, R. + 116428
 Vanderzee, C.E. + 115575
 Vanhellemont, J. + 111659
 + Vanherck, P. 111645
 + Vanin, J.A. 113736
 Vanisovich, V.V. 111432
 Vankar, V.D. + 114392
 Vankov, I.D. + 112590
 Vanska, L. + 112527
 + Vanyukova, N.V. 113938
 Vanzani, V. 112138
 + Vanzo, L. 111467
 + Varadan, V.K. 113165
 + Varadan, V.V. 113165
 + Varadarajan, R. 114776
 Varadi, F. + 116434
 + Varcaccio, G. 112062
 Vardiashvili, A.A. 115688
 Vardiashvili, A.B. +
 111393
 Varea, V.R. 111739
 + Varelle, A. 112973
 Varentsov, V.A. + 114857
 + Varet, J.C. 112562
 + Vargas, H. 114292
 + Varghese, S. 115428
 + Varker, C. 114195
 Varker, C.J. + 114194
 Varma, C.M. 116458
 Varma, K.B.R. + 114827
 + Varma, K.B.R. 115035
 + Varma, R.K. 113616
 + Varma, R.P. 114227
 + Varnell, D.F. 113771
 Varnham, M.P. + 111738
 Varnham, M.P. + 113119
 Varnham, M.P. + 113109
 + Varoquaux, E. 114298
 + Vartanian, M.H. 116472
 Vartsy, D. + 115905
 + Vartsy, D. 112517
 + Varvarin, A.M. 115584
 + Varvarovsky, F. 112404
 + Vary, J.P. 112054
 Varygin, N.N. + 115214
 + Vaselli, M. 113663
 + Vashchenkov, V.P. 115476
 Vasilenko, I.I. + 115435
 + Vasil'ev, E.A. 114688
 Vasil'eva, I.A. + 113660
 Vas'ko, F.T. + 114461
 Vas'kov, V.V. + 116344
 + Vasserman, A.N. 115759
 Vassilev, Y.T. 113998
 + Vasu, K.I. 115423
 + Vasudevan, R. 115323
 Vateva, E. + 114563
 + Vatolin, N.A. 115118
 + Vaucher, C.A. 116742
 Vaudin, M. + 113931
 Vaughan, D.J. + 114444
 + Vaughan, J.M. 113037
 + Vause, C.A. 113711
 + Vaya, P.R. 115057
 Vaz, E.G.L.R. + 111509
 Vaz, L.C. + 112291
 Vebien, D.R. + 114426
 + Vedam, K. 113946
 + Vedani, A. 113808
 Vedenov, A.A. + 113059
 + Vedernikov, M.V. 114168
 + Vedernikov, V.V. 111823
 + Vedha-Nayagam, M.
 113435
 + Vedrine, A. 114913
 + Veeder, G.J. 116512
 + Veerabhadra Rao, K.
 114827
 + Vehanen, A. 114952
 + Vehanen, A. 113876
 Veiko, V.P. + 113999
 + Veillet, J.-J. 112016
 Veliev, E.I. + 112908
 + Vella, E. 112024
 + Venables, J.A. 114393
 Veniaminov, N.N. + 111821
 + Venien, J.P. 114672
 + Venikov, A.A. 112594
 Venkateswara Sarma, K.
 113443
 + Ventura, A. 112068
 Verat, M. + 111847
 Verbiest, E. + 113965
 Verbiest, E. + 114766
 Verbin, S.Yu. + 114449
 + Vercesi, V. 112022
 + Verdenet, M. 116685
 + Veremei, V.V. 112908
 Verfondern, K. 112382
 + Vergeles, N.M. 115140
 + Vergnes, M. 112111
 + Verma, A. 113762
 Verma, B.G. + 113511
 Verma, B.G. + 116713
 Verma, R.L. + 115117
 + Vermeulen, D. 112133
 Verosub, K.L. 116014
 + Verrall, R.E. 111771
 Versaci, R.A. + 115196
 Verschoor, J.N. + 116774
 + Verspui, G. 115451
 + Verspui, G. (*ed.*) 111316
 + Versteegen, P.L. 112307
 Verter, F. + 116795
 + Vertes, A. 114765
 Vervisch, P. + 113559
 + Veseli, A. 112628
 + Veselova, G.V. 112576
 + Vest, C.M. 113522
 + Vest, C.M. 111747
 Vestrand, W.T. 116885
 Vetesnik, M. 116682
 + Vetrov, A.N. 115469
 + Vetrov, V.A. 114755
 Vetter, W.J. 116317
 + Vettier, C. 114674
 + Vettolani, G. 116492
 + Vialle, J.-P. 112031
 + Vialon, P. 116071
 + Vianna, S.S. + 114664
 + Vick, B. + 113507
 + Vickers, J.A.G. 111515
 + Vidal-Quadras, A. 116415
 + Videau, H. 112542
 + Vieira, T. 114762
 + Vielhaber, W. 115006
 + Viera, F. + 116116
 + Vierinen, K. 112131
 + Vigdorovich, V.N. + 114178
 + Vigdorovich, V.N. 114134
 + Viggars, D.A. 111327
 + Viggiano, A.A. + 115533
 + Viggiano, A.A. + 116249
 + Vighlene, S.S. 113227
 + Vigiotti, L. 116016
 + Vigouroux, G. + 116517
 + Vijayalakshamma, S.K.
 114235
 + Vikhain, V.S. 114125
 + Vikram, C.S. + 112957
 + Vilar, R. 114762
 + Viljoen, P.E. 114315
 + Vill, A. + 113018
 + Vinai, F. 114712
 + Vinas, X. 112103
 + Vincent, R.A. + 116294
 + Vincent, R.A. 116328
 + Vincent-Geisse, J. 114850
 Vinh Luu Dang
 see Luu Dang Vinh
 + Vinogradov, A.A. 113528
 + Vinogradov, A.S. + 114969
 + Vinogradov, G.I. 115835
 + Vinogradov, G.V. 113392
 + Vinogradov, S.S. 112905
 + Vinogradov, V.A. 113528
 + Vinogradov, Yu.K. + 111688
 + Vintaikin, E.Z. + 115191
 + Viola, G. 113247
 + Viola, V.E. 112249
 + Violet, C.E. + 114184
 + Viotti, R. 116698
 + Virakhovskii, Yu.G.
 115257
 + Viras, K. 114852
 + Viron, F. *de* *see* de Viron, F.
 + Visconti Crivelli
 see Crivelli Visconti
 + Vishnyakov, L.R. 115158
 + Vishwakarma, G.P. 116713
 + Viskov, A.S. + 114217
 + Viscoekas, R. + 115925
 + Visschere, P. *de*
 see de Visschere, P.
 + Visser, A.J.W.G. 113033
 + Visticot, J.P. + 115539
 + Vistin', L.K. + 113084
 + Vistin', L.K. + 113732
 + Viswanath, D.S. 111684
 + Viswanath, P.R. 116723
 + Viswanathan, R. + 112813
 + Vita, P. *di* *see* di Vita, P.
 + Vita, P. *di* *see* di Vita, P.
 + Vitali, C. 114066
 + Vitovskii, N.A. 113986
 + Vitovtseva, T.V. 115726
 + Vittal Murthy, K.P.R.
 116186
 + Vityaz', P.A. 114096
 + Vityaz, P.A. 115098
 + Vityazev, V.V. 116646
 + Vityuk, V.Ya. + 114176
 + Vivian, R. 112317
 + Vladimirov, V.S. + 111544
 + Vladimirov, Yu.A. 115862
 Vladimirova, A.G.V. +
 115253
 + Vlahov, J.P. 114442
 + Vlaskov, V.A. 116342
 Vlasov, N.M. + 114072
 Vlasov, S.N. + 113050
 + Vlasova, M.V. 113953
 + Vliet, A.E. + 112502
 + Vodop'yanova, L.S.
 114306
 Vogel, P. 111940
 + Vogl, G. 114058
 + Vogl, G. 113959
 + Vogt, H. 112028
 + Vogt, K.J. 112454
 + Voigt, R. 111860
 + Voitenko, A.F. + 115247
 + Voitenko, V.A. 114808
 + Voitenko, V.L. 114306
 + Voitoich, V.P. 111779
 + Vojvodic, S.B. 114995
 + Vokes, R.A. 112477
 + Vokhmyanin, A.P. 114671
 + Voldman, S. 114828
 + Volenko, V.V. + 113636
 + Volkenshtein, N.V.
 114211
 + Volkov, A.B. 112974
 + Volkov, A.F. 114595
 + Volkov, A.S. + 114545
 + Volkov, V.I. 115171
 + Volkova, N.A. 116052
 + Volkovitski, P.E. 111966
 + Volksen, W. + 113734
 + Voller, V.R. 114208
 + Vollmer, R. + 116087
 + Volodarskii, L.B. 113837
 + Volodarskii, L.B. 112759
 + Volokitin, A.I. 114357
 + Voloshin, A.S. + 113383
 + Voloshin, I.F. + 114587
 + Volovich, I.V. 111906
 + Volovich, I.V. 111544
 Volpi, A. *de* *see* De Volpi, A.
 + Volubuev, M.I. 111768
 von Allmen, M.F. 114003
 von Allmen, M.F. + 114008
 + Von Bieren, K. 112923
 + von Brentano, P. 112109
 von der Linde, D. + 114837
 + von Feilitzsch, F. 112124
 von Geramb, H.V. + 112147
 + Von Gierke, H.E. 115815
 + von Goeler, E. 111992
 Von Holle, W.G. + 111772
 + von Holleben, M.L.A.
 112871
 + von Krogh, J. 111990
 + von Krogh, J. 112012
 + Von Nieda, G.E. 112380
 + von Oertzen, W. 112539
 + von Rague Schleyer, P.
 112645
 + von Roos, O. 115648
 + von Seggern, H. 111654
 Von Zglinicki, T. + 115992
 + Vondrak, R. + 116336
 + Vondrak, R.R. + 116337
 + Vongsarnpigoon, L.
 113275
 Voo, R. Van der. *see* Van der Voo, R.
 Voo van der. *see* van der Voo, R.
 + Voos, R.W. 114392
 + Voos, M. 115061
 Vorob'ev, P.A. 114460
 Vorob'ev, V.M. 113272
 + Vorob'ev, V.M. + 113606
 + Vorobiev, S.A. 114977
 + Voronin, V.A. + 115087
 + Voronkov, M.E. 115613
 + Vorontsov-Vel'aminov, P.N. 113563
 + Voroshen', V.I. + 111824
 + Voskresenskii, Yu.S. +
 113256
 + Voskresenskii, Yu.S.
 113508
 + Voss, H.D. 116359
 + Votrin, I.I. 115740
 + Vovk, A.B. 112189
 + Vozzhennikov, V.M.
 113841
 + Vrana, J. 112031
 + Vratislav, S. 111855
 + Vrbik, J. 113377
 + Vsekhsvyatskaya, I.S. +
 116348
 + Vsekhsvyatskaya, I.S.
 116341
 + Vsevolodov, N.N. 115753
 + Vu, B.Q. 113344
 + Vu Tien Loc. 114216
 + Vuillemin, V. 112031
 + Vukovich, F.M. + 116094
 + Vuorinen, S. 114375
 + Vuye, G. 114946
 + Vykutlova, M. 116421
 + Vyshinskii, N.N. 115542
 + Vysikailo, F.I. 113681
 Vyzulin, S.A. + 114681
 Waal, S.A. *de* *see* de Waal, S.A.
 + Wachnicki, C.R. 115304
 Wada, K. + 114191
 + Wada, K. 115036
 Wada, N. + 115499
 + Waddington, J.C. 114894
 + Waelbroeck, F. 113574
 + Wagensberg, J. 115757
 + Wagner, A. 111990
 + Wagner, A. 112012
 + Wagner, J. 113015
 + Wagner, P. 114897
 + Wagner, V. 115505
 + Wagner, W. 114051
 + Wagner, W. 112015
 + Wagner, W. 114287
 + Wagner, W.R. 115115
 + Wagoner, R.A. 116199
 Wahl, G. 114402
 + Wahl, G. 114407
 + Wahl, G. 115080
 + Wahl, H. 115100
 + Wahl, H.D. 112031
 + Wahl, W. 112113
 + Wahlstrom, B. 112384
 + Wakai, M. 112051
 + Wakai, M. 112160
 Wakamatsu, A. + 113608
 + Wakao, N. 112357
 + Wakayama, N. 112372
 + Wald, H.B. 111992
 + Waldoet, G.L. 112451
 + Walenta, A.H. 112580
 Walker, B.K. + 115821
 + Walker, D.H. 112419
 + Walker, G. 115887
 Walker, H.C., Jr. + 112787
 Walker, J.S. + 113711
 Walker, P.M. 112074
 + Walker, R.D. 112305
 Walker, R.P. 112508
 + Wallace, D.M. 112447
 + Wallden, L. 115013
 Walle, C. Van De.
 see Van De Walle, C.
 + Wallerstein, G. 116775
 + Wallis, D.D. 116337
 Wallner, E.P. 111723
 Walls, J.M. 115596
 + Wallwork, G.R. 115427
 + Walmsley, J.L. 116184
 + Walmsley, M. 116532
 + Walmsley, M. 116747
 + Waloschek, P. 112015
 + Walsh, E.J. 115806
 Walsh, R.M. + 115364
 + Walter, E. 115296
 + Walter, H. 111692
 Walter, K.-H. 112318
 + Walter, R.L. 112202
 + Walters, R.T. 112776
 + Walther, H. 115006
 Wan-Sun Tse + 114099
 + Wan-Sun Tse. 114098
 + Wan-Sun Tse. 114100
 + Wandelt, K. 114356
 Wanders, K. + 114291
 Wang, C.-M. + 113278
 + Wang, C.-M. 113277
 Wang, C.W. + 112234
 + Wang, C.W. 112099
 + Wang, J.T. 112756
 + Wang, K.L. 114470
 + Wang, K.L. 114482
 Wang, L.H. + 113769
 Wang, M.E. + 113194
 Wang, S. 113019
 + Wang, S. 112989
 + Wang, S.L. 113541
 Wang, S.W. + 112367
 + Wang, T.-M. 114022
 + Wang, W.L. 115647
 + Wang, W.P. 114941
 Wang, Z. + 114052
 Wang Man + 112581
 + Wang Ming. 116287
 + Wang Ming-xing. 115712
 + Wang Qian-Shen. 116039
 + Wang Qing. 111538
 Wang Shou-Yih
 see Shou-Yih Wang
 Wang Tian-Min
 see Tian-Min Wang
 + Wang Tian-Sheng. 116000
 Wang Yuan-ling. 112481
 Wang Zhengzhi + 116626
 Wankhed, P.C. + 113254
 Wanklyn, B.M. + 115033

- Wanner, R.A. + 115860
 + Warabisako, T. 114013
 + Warburton, E.K. 112035
 Ward, B.F.L. 111995
 Ward, D. + 112244
 + Ward, D. 112033
 + Ward, I.M. 113760
 + Ward, J.F. 111383
 Ware, W.R. + 111783
 + Wareing, J. 115328
 + Warming, P. 111990
 + Warming, P. 112012
 Warner, B. 116683
 + Warner, D.D. 112100
 + Warner, M.W. 115776
 Warner, P.J. + 116853
 + Warren, C.G. 115772
 + Warren, D. 115535
 + Warren, R. 115224
 + Warren-Smith, R.F. 116483
 + Warren-Smith, R.F. 116799
 + Wartmann, G. 114837
 Warwick, M.E. + 115399
 Waschull, W. 112295
 + Washburn, J. 113944
 Waskowska, A. 113815
 + Wassel, A.T. 112429
 + Wasserburg, G.J. 116554
 Wastberg, S. 113353
 + Waszczak, J.V. 114639
 Watanabe, S. 111529
 + Watanabe, H. 113650
 + Watanabe, H. 114044
 + Watanabe, H. 114751
 + Watanabe, J. 113735
 Watanabe, K. + 113921
 + Watanabe, M. 113025
 + Watanabe, N. 112525
 + Watanabe, N. 113751
 + Watanabe, N. 113749
 Watanabe, S. + 113025
 + Watanabe, S. 114731
 + Watanabe, S.-I. 112609
 + Watanabe, T. 111703
 + Watanabe, Y. 111990
 + Watanabe, Y. 112012
 Watase, M. + 113393
 + Watase, Y. 112550
 + Waters, D.N. 114874
 + Watkins, P. 112031
 + Watson, A.I. 116195
 Watson, B. 115457
 Watson, D.L. + 112219
 Watson, D.L. + 112275
 + Watson, J.W. 112562
 + Watson, R.L. 112837
 + Watt, G.D. 116797
 + Watterson, J.I.W. 115608
 + Watts, D.R. 116090
 + Watts, S.J. 112540
 Watts, W.E. 112630
 Watts, W.E. 115525
 + Waugh, R. 115796
 + Waurick, G. 112553
 + Wayman, C.M. 115202
 + Wayman, C.M. 114198
 + Wayman, C.M. 114199
 + Waysand, G. 112563
 Wazen, P. + 112985
 Weaire, D. + 115163
 Webber, H.C. + 114133
 Weber, E.R. + 113936
 + Weber, E.W. 112679
 + Weber, G. 111990
 + Weber, G. 112012
 + Weber, G. 115998
 + Weber, H. 113001
 Weber, J. + 114926
 + Weber, R. 112781
 Weber, T.A. + 112887
 + Weber, T.A. 113715
 Wedding, B. + 113049
 Wedler, G. + 114360
 + Weekes, T.C. 116416
 + Weeks, J.D. 113740
 + Weeks, R.A. 114733
 + Weeks, R.W. 115983
 Wei Lun Quan
 see Quan Wei Lun
 + Wei Shang-Chen 112965
 + Wei Si-Yu 116039
 Wei Zhonglei + 113449
 Wei Zhu see Zhu Wei
 Wei-da Lu see Lu Wei-da
 Wei-Qing Zhang
 see Zhang Wei-Qing
 Wei-xiu Lu see Lu Wei-xiu
 + Weibel, E. 114312
 + Weidberg, A.R. 112022
 Weidinger, A. + 114055
 + Weidlein, J. 115062
 + Weidner, V.R. 111781
 + Weiffenbach, C. 115948
 + Weiffenbach, C.V. 115942
 + Weigelt, G. 116525
 + Weiguny, A. 112243
 + Weihs, W. 112543
 + Weil, J.L. 112190
 Weiler, K.W. + 116494
 + Weihhammer, P. 112554
 + Weinig, A. 112497
 + Weinstein, A. 113455
 + Weinstein, R. 111992
 + Weisbuch, C. 114879
 Weise, L. 112298
 + Weisman, J. 112367
 + Weiss, A. 114165
 + Weiss, I. 116417
 + Weiss, J. 111422
 + Weiss, M. 114373
 + Weiss, N.O. 116602
 Weiss, W.W. 116674
 + Welch, G.E. 112015
 + Weller, A. 112277
 + Weller, H.R. 112217
 Weller, M. + 113878
 + Weller, M. 113966
 + Wellington, K.J. 116803
 + Wells, D.C. 116865
 + Wells, M. 112680
 Welsh, B.Y. 116798
 Weltner, K. 113378
 Wen-fu Du see Du Wen-fu
 Wen-ging Shen
 see Shen Wen-ging
 + Wender, S.A. 112567
 + Wendrock, G. 114155
 + Wenig, S. 112541
 + Wenk, H.-R. 113803
 Wenrui Hu see Hu Wenrui
 Wenxiu Li see Li Wenxiu
 Wenxuan Li
 see Li Wenxuan
 Wenzel, A.R. 113160
 + Wenzel, H.-G. 115998
 + Wenzel, W.A. 112542
 Werf, S.Y. van der
 see van der Werf, S.Y.
 Werner, A. + 114162
 + Werner, S.A. 111491
 + West, D.R.F. 115195
 + West, D.R.F. 115167
 West, G. 112300
 West, G. + 111736
 West, J.E. + 115955
 + West, P.C. 111918
 + West, P.D. 111752
 West, R.M. (ed.) 111314
 West, R.N. + 114958
 + West, R.N. 114955
 + Westbrook, R.D. 114011
 + Westbrook, R.D. 115636
 + Westenberg, L. 112292
 + Westerfeldt, C.R. 112157
 Westfall, G.D. 112262
 Westphal, D. + 115019
 Westphal, D. + 115020
 + Wetherald, R.T. 116153
 + Wever, H. 113882
 + Wexler, S. 112798
 + Weygand, D.P. 112549
 Weyher, J.L. 115397
 + Whaler, K.A. 116002
 + Whaler, K.A. 116003
 + Whalley, E. 112734
 + Whately, K.M. 112157
 + Wheatley, A.R. 115377
 + Wheaton, W.A. 116835
 + Wheaton, W.A. 116826
 + Wheeler, B.L. 114606
 Whetten, R.L. + 112802
 Whipple, A.L. 116433
 + Whitaker, R.W. 116800
 White, C.W. + 114005
 + White, C.W. 113945
 + White, C.W. 114321
 White, D. 116459
 + White, G.C. 115937
 White, G.J. + 116797
 + White, J. 114037
 + White, J.M. 114984
 + White, M. 112566
 + White, P.S. 113245
 White, R.J. + 112332
 + White, R.M. 112125
 + White, W.B. 113748
 Whiteaway, J.E.A. 114599
 Whiteley, S.R. + 114613
 Whiteoak, J.B. + 116803
 + Whitfield, J.D. 114194
 Whitfield, P.H. 116163
 + Whitley, D. 111571
 Whitmarsh, R.B. + 116024
 + Whitmarsh, R.B. 116024
 + Whitson, M.E., Jr. 112699
 + Whittaker, J.B. 111990
 + Whittaker, J.B. 112012
 Whittmore, A.S. 111407
 Whittington, H.W. + 115612
 Whyman, G.E. + 112670
 + Wiatrowski, E. 112553
 Wiatrowski, W.A. + 115911
 + Wibelmann, C. 112695
 Wiberg, D.M. + 115822
 + Wichert, Th. 113871
 + Wickens, F.J. 112540
 Wickramasinghe, H.K.
 113233
 + Widing, K.G. 116468
 + Widmaier, J.M. 113772
 + Widmer, A.E. 115073
 + Widom, B. 114304
 + Wieckowski, J. 115151
 Wiedenmann, A. + 114672
 + Wiedersich, H. 114052
 + Wiegand, C.E. 112564
 Wieja, C. + 115151
 Wielopolski, L. + 112517
 + Wielopolski, L. 115905
 + Wielunski, L. 114285
 + Wiener, S.N. 115900
 + Wiersma, D.A. 114903
 + Wieseemann, K. 111321
 + Wiffl, N. 113936
 + Wikne, J. 112075
 + Wilcke, W.W. 112249
 + Wilczynski, A. 113637
 + Wilczynski, J. 112197
 Wild, N. + 116405
 + Wild, R.K. 114373
 Widental, B.H. + 112127
 Wiley, L.G. + 113014
 Wilfing, E. + 115081
 Wilk, S.R. + 111344
 Wilkins, D.J. 115365
 Wilkinson, D. + 111597
 + Wilkinson, G.R. 114855
 Wilks, G. 113411
 Will, H. + 112319
 + Willemssen, J.F. 111597
 + Willett, J.A. 115987
 Williams, D.E.G. + 114114
 Williams, D.R. + 115791
 + Williams, E. 116253
 + Williams, E.A. 113688
 + Williams, F. 112756
 Williams, G.A. 111789
 + Williams, G.D. 115728
 + Williams, G.O. 113712
 + Williams, G.P. 112487
 + Williams, I.R. 116044
 + Williams, I.S. 116044
 Williams, J.M. + 114637
 Williams, J.S. 114007
 Williams, J.S. + 114390
 + Williams, J.S. 113988
 Williams, K. 116315
 + Williams, O.R. 112553
 + Williams, R.J. 112663
 + Williams, R.S. 114441
 + Williams, S.G. 111731
 Williams, T.A. 113224
 Williamson, J. 113145
 Williamson, J. 113146
 Williamson, J. 113147
 + Williamson, J. 112024
 + Willis, A. 112158
 + Willis, A.J. 116654
 + Willis, S.E. 112007
 + Willis, W.J. 112024
 Willoughby, A.F.W. 114252
 Wills, R.R. + 115144
 Willstrop, R.V. 116476
 + Wilsch, H. 114314
 + Wilson, B. 116760
 + Wilson, C.M. 115179
 Wilson, E.M. 115611
 + Wilson, G.H., III. 115495
 + Wilson, I.H. 115106
 + Wilson, J. 112031
 + Wilson, J. 111860
 Wilson, J.M. + 111342
 Wilson, J.W. + 116742
 + Wilson, K.R. 112647
 Wilson, M.A. + 112480
 + Wilson, R. 112031
 + Wilson, R. 116654
 + Wilson, R.B. 115115
 Wilson, R.G. + 113948
 + Wilson, R.W. 116795
 + Wilson, S.R. 113945
 + Wilson, S.R. 114005
 Wilton, A.de see de Wilton, A.
 Wimmel, H.K. 111427
 + Wimmerstedt, R. 115507
 + Winant, C.D. 116141
 + Winchester, J.W. 116178
 Winfree, A.T. + 111460
 + Winik, M. 112024
 + Winnewisser, G. 112726
 Winrow, R.A. 114981
 Winter, G. 112118
 + Winter, G.G. 112015
 Winterberg, F. 112433
 Winterberg, F. 112461
 + Winterhalter, D. 116504
 Winther, A. 112260
 + Winther, A. 112240
 + Wintle, H.J. 114263
 + Wippert, D. 113499
 + Wirth, K. 112623
 Wirz, P. 111651
 Wiscombe, W. 116277
 + Wisdom, J. 111421
 + Wiser, D.E. 111992
 Wisgerhof, E. + 114141
 Wisniak, J. 114209
 + Wisshak, K. 112524
 Witalis, E.A. 113609
 + Witebsky, C. 116889
 Witkover, R.L. + 112476
 + Witt, A.F. 114629
 Witt, M. 111441
 + Witten, T.R. 112562
 + Witthuhn, W. 114767
 + Witthuhn, W. 114247
 Wittmann, K. + 113499
 + Wittzel, W. 112024
 Wohlfarth, E.P. 114660
 + Wohner, H.-J. 114152
 Wolf, D. 116007
 + Wolf, E. 112935
 + Wolf, G.H. 113673
 + Wolf, K.L. 112249
 + Wolf, K.L. 112267
 Wolf, P.C. 115443
 + Wolf, R. 112245
 Wolfe, C.R. + 112387
 Wolfendale, A.W. 116886
 + Wolfendale, A.W. 116824
 + Wolff, L.R. (ed.) 111316
 + Wollenberger, H. 114244
 + Wollenberger, H. 114274
 + Wollenberger, H. 114287
 + Wolnikowski, J. 112684
 + Wolowski, J. 113637
 + Wolski, R. 112277
 Wolstencroft, R.D. + 116484
 Wolstencroft, R.D. + 116855
 + Wolstencroft, R.D. 116522
 + Wolter, G.W. 115149
 + Wondre, F.R. 115033
 + Wong, A.K. 111636
 Wong, J.S. 111788
 + Wong, K.C. 113162
 + Woo, J.S. 115210
 + Woo Jong-Ok 116672
 Woo Ming-ko
 see Ming-ko Woo
 + Wood, B.E. 114942
 + Wood, C.E.C. 113923
 + Wood, E.L. 114041
 + Wood, G.J. 113707
 + Wood, H.J. 116667
 + Wood, J.L. 112096
 Wood, R.A. + 115622
 + Wood, R.A. 115936
 + Wood, R.F. 114011
 + Wood, R.F. 115636
 + Wood, S. 115370
 + Wood, W.E. 115425
 + Woodhouse, J. 113188
 + Woodward, R. 112049
 + Woodward, R. 112261
 + Woodward, R. 112059
 Woodworth, J.G. + 112217
 + Woody, C. 112024
 Wooff, C. 112600
 + Woolfson, M.M. 116510
 Worch, H. + 115405
 Worsdorfer, K. + 115521
 + Worsell, M.F. 112020
 Woyanovich, F. 114429
 + Wriedt, H. 111990
 + Wriedt, H. 112012
 + Wriggers, P. 113282
 Wright, C.S. + 116625
 + Wright, D.G. 116238
 + Wright, J.C. 112886
 + Wright, J.G. 113157
 + Wright, J.J. 112636
 Wright, J.S. + 112663
 + Wright, K.H., Jr. 116470
 + Wright, P.R.S. 112028
 + Wrigley, J.M. 115455
 + Wrixon, A.D. 115941
 + Wroblewski, A. 113355
 + Wronski, C.R. 114817
 Wu, C.C. 116387
 + Wu, E.-C. 115531
 + Wu, M.-F. 116230
 Wu, N. + 111731
 + Wu, P.T. 112253
 Wu, T. + 115429
 Wu En-chiu + 112089
 + Wu Ji-min 111962
 + Wu Ji-min 111963
 + Wu Pei-Zhi 116020
 Wu Ta-You see Ta-You Wu
 Wu Tai Tsun
 see Tai Tsun Wu
 Wu Yong-Shi 111863
 + Wulz, C. 112031
 Wunderlich, F.J. + 111347
 Wunner, G. + 116456
 Wunnik, J.N.M. van
 see van Wunnik, J.N.M.
 Wunnik, J.N.M. van
 see Van Wunnik, J.N.M.
 + Wurrier, B. 113154
 + Wurm, P. 112277
 Wust, E. + 112173
 + Wust, J. 112884
 + Wyant, J.C. 111750
 Wyatt, A.F.G. 113236
 Wykes, C. + 111754
 + Wylie, A. 112554
 + Wylie, R.G. 113549
 + Xi Yao 114485
 + Xia Jin-Zhi 112500
 + Xia Xiao-mi 112581
 Xian-neng Chen
 see Chen Xian-neng
 Xiang-zong Cui
 see Cui Xiang-zong
 Xiangfu Sun
 see Sun Xiangfu
 Xiao, Y.M. + 115376
 Xiao-mi Xia
 see Xia Xiao-mi
 Xiao-Ming Tang
 see Tang Xiao-Ming
 + Xie, L.Z. 114613
 Xie, S.X. + 115223
 + Xie, Y.G. 112031
 + Xie Yicheng 111977
 Xing-Sheng Li
 see Li Xing-Sheng
 + Xu Geng-Wang 114910
 + Xu Ring-Ting 112965
 + Xue, S.T. 112015
 + Ya-Wen Yang 114485
 Yabe, M. + 112206
 + Yablonskii, G.P. 113691
 + Yablonskii, G.S. 115515
 Yabushita, S. 116547
 Yabuuchi, Y. + 114313
 Yacoby, Y. + 114542
 Yadagiri Reddy, P. + 111660
 + Yaffe, L. 112286
 + Yagi, E. 113991
 + Yagi, K. 112213
 + Yagi, K. 112223
 Yaginuma, S. 115785
 Yagnik, S.K. 114280
 + Yagodka, V.V. 113956
 + Yagola, G.K. 111718
 + Yagubskii, E.B. 113848
 + Yagupol'skii, L.M. 112753
 Yagura, S. + 113615
 Yagzhev, V.V. + 111798
 Yaihiro, M. 112231
 + Yaihiro, M. 112230
 + Yajima, K. 115959
 Yajun Li 112926
 + Yakhsahtova, E.M. 113913
 + Yakovenko, S.S. 113084
 + Yakovenko, S.S. 113732
 + Yakovkin, I.B. 113242
 + Yakovlev, E.B. 113999
 + Yakovlev, O.I. 116506
 + Yakovlev, V.I. 113031
 + Yakovlev, V.V. 113390
 + Yakovleva, I.L. 115190
 Yakovski, N. + 116343
 Yakubov, Yu.N. + 115692
 + Yakushin, G.V. 113683
 Yamada, K. 112694
 + Yamada, K. 112726
 Yamada, M. + 114254
 + Yamada, N. 112117
 + Yamada, O. 116057
 Yamada, R. + 114990
 + Yamada, S. 111990
 + Yamada, S. 112012
 + Yamada, S. 112466
 Yamada, T. + 112105
 + Yamada, T. 111777
 Yamada, Y. + 114163
 + Yamada, Y. 111389
 + Yamaga, T. 115964
 + Yamagata, T. 112160
 + Yamagishi, H. 112372
 + Yamaguchi, H. 114511
 + Yamaguchi, H. 113921
 + Yamaguchi, K. 113228
 + Yamaguchi, M. 113011
 Yamaguchi, S. + 113619
 + Yamaguchi, T. 113927
 + Yamaguchi, T. 115407
 + Yamakawa, K. 113895
 + Yamakawa, S. 113108
 Yamaki, H. + 112430
 Yamamoto, F. + 113108
 + Yamamoto, H. 111641

- + Yamamoto, H. 112430
 + Yamamoto, K. 112478
 + Yamamoto, K. 116084
 + Yamamoto, M. 111826
 Yamamoto, N. + 115034
 + Yamamoto, N. 113970
 + Yamamoto, O. 114747
 + Yamamoto, R. 113978
 + Yamamoto, R. 114273
 Yamamoto, T. + 111632
 Yamamoto, T. + 115780
 + Yamamoto, T. 111389
 Yamamoto, Y. 115371
 + Yamamoto, Y. 115231
 + Yamamoto, Y. 115780
 Yamamura, Y. + 114993
 Yamamuro, T. 115979
 + Yamane, M. 115022
 + Yamashiro, S.M. 115820
 + Yamashita, A. 112545
 Yamashita, K. 112311
 + Yamashita, S. 112372
 Yamashita, T. + 114284
 + Yamashita, T. 112354
 + Yamashita, T. 112912
 + Yamashita, T. 114196
 + Yamauchi, R. 113121
 Yamaya, T. + 112227
 + Yamazaki, H. 113071
 + Yamazaki, J. 115999
 Yamazaki, T. + 112212
 + Yamazaki, T. 112207
 + Yamazaki, T. 114768
 + Yamazaki, Y. 114386
 Yan, M.F. + 115126
 Yan Tai-xuan + 112519
 + Yanagi, H. 115667
 Yanagida, M. + 113209
 + Yanagisawa, C. 111990
 + Yanagisawa, C. 112012
 Yanai Michio see Michio Yanai
 Yanase, T. + 113011
 Yang, H. + 114070
 Yang, H.Y. + 111413
 + Yang, J.J. 114388
 Yang, K.H. 111850
 + Yang, P. 115502
 Yang Chen Ning see Chen Ning Yang
 Yang Di + 115497
 + Yang Gwei Gien 115497
 + Yang Hwi-Qui 115497
 Yang Jing Zheng Ou see Ou Yang
 Yang Jing Zheng see Ou Yang
 Yang Ya-Wen see Ya-Wen Yang
 + Yang Ye-Yu 116287
 + Yan'kov, G.C. 113437
 + Yan'kov, V.V. 113623
 + Yano, M. 113675
 + Yano, S. 114389
 Yano, T. + 112414
 + Yanokura, M. 112484
 + Yanovitskii, E.G. 116270
 + Yanovskii, A.I. 113845
 + Yanovskii, A.I. 113846
 + Yanushkevich, K.I. 114688
 Yao, Y.D. + 114507
 Yao, Y.D. + 115132
 Yao, Y.D. + 115133
 + Yao, Y.D. 114758
 Yao Xi see Xi Yao
 Yap, B.C. + 115235
 Yarema, S.Ya. + 115466
 Yariilin, A.A. + 115841
 + Yariilin, A.A. 115846
 + Yariilin, A.A. 115847
 Yarin, A.L. 115121
 + Yariv, A. 113007
 + Yariv, A. 113009
 + Yariv, A. 112990
 + Yaroshevskii, E.V. 116299
 + Yaroslavskii, G.Ya. 115244
 + Yashina, A.N. 113046
 Yasnii, P.V. + 115347
 + Yasnii, P.V. 115345
 + Yasnitskii, R.I. 114669
 + Yasue, M. 112609
 + Yasui, T. 115499
 Yates, S.W. + 112190
 + Yates, S.W. 112194
 Yatsenko, N.A. 113682
 + Yatsenko, S.P. 114678
 + Yatsimirskii, K.B. 112659
 Yatsu, K. + 111811
 + Yau, S.-T. 116464
 Yavari, A.R. + 115232
 Yavari, P. + 115306
 + Yavich, B.S. 115652
 + Ye, C.H. 112566
 Ye Sheng-Hua + 112965
 Ye-Yu Yang see Yang Ye-Yu
 + Yee, K. 112566
 Yefimuk, S.M. + 116350
 Yefinov, A.I. + 116506
 + Yefremenko, V.V. 113035
 + Yegorova, Y.I. 115289
 Yeh, T.-C. + 116153
 + Yeh, T.R. 112561
 Yeh Hsu-Chi see Hsu-Chi Yeh
 + Yekutieli, G. 115656
 Yellott, J.I., Jr. 115790
 + Yelton, J.M. 112011
 + Yen, R. 114879
 Yenalyev, V.D. + 115289
 + Yenalyev, V.D. 115290
 + Yeo, J.K. 113772
 + Yeomans, J. 114697
 Yeon, Y.M. + 115316
 + Yeung, P.S. 112025
 + Yevaretskov, A.S. 115769
 Yevick, D. + 113134
 + Yevick, D. 113100
 Yia-Chung Chang + 114809
 Yicheng Xie see Xie Yicheng
 Yingtian Chen see Chen Yingtian
 + Yndurain, F. 114659
 + Yoder, N.R. 112480
 + Yokobori, T. 112334
 + Yokobori, T. 112334
 + Yokomizo, Y. 111695
 + Yokoshima, I. 113029
 + Yokota, Y. 113891
 + Yokoyama, N. 114589
 + Yokoyama, S. 113535
 Yokoyama, T. + 116057
 Yong-Shi Wu see Wu Yong-Shi
 + Yonuschot, G. 115725
 + Yoo, K.C. 113930
 + Yoon, J.K. 113728
 Yoreo, J.J. De see De Yoreo, J.J.
 + York, D. 116040
 York, R.W. + 112811
 + Yorke, J.A. 111573
 + Yorke, J.A. 111574
 + Yoshida, H. 114180
 + Yoshida, H. 115583
 + Yoshida, H. 114751
 + Yoshida, H. 113904
 + Yoshida, H. 113974
 + Yoshida, M. 116555
 Yoshida, N. + 113980
 + Yoshida, N. 114039
 + Yoshida, N. 113934
 + Yoshida, N. 113901
 Yoshida, S. + 113257
 + Yoshida, S. 114511
 + Yoshida, S. 113921
 + Yoshida, T. 112737
 + Yoshida, T. 112224
 + Yoshida, Y. 115499
 Yoshihara, A. + 114158
 + Yoshihara, K. 115568
 + Yoshiie, T. 113927
 + Yoshikado, S. 113671
 + Yoshikawa, K. 115667
 Yoshimori, M. + 116589
 + Yoshimori, M. 116574
 + Yoshimoto, M. 114784
 Yoshimura, H. 116614
 Yoshimura, S. + 115880
 + Yoshinaga, H. 115352
 + Yosoi, M. 112224
 You-kuen Que see Que You-kuen
 + Youl, S. 112530
 + Young, A.P. 114698
 + Young, D. 115449
 + Young, F.W., Jr. 113919
 + Young, G.R. 112261
 + Young, I.R. 115900
 + Young, L.M. 112480
 Young, R.T. + 114010
 Young, R.T. + 115636
 + Young, W.B. 115737
 + Young-Gil Kim 115222
 + Young-II Kim 113677
 + Youred, R. 112474
 + Yousef, A.S. 112121
 Yousif, B.Y. + 114696
 Youwen Ding see Ding Youwen
 + Yu, J.H.-Y. 112377
 + Yu, L.L. 112288
 + Yu, M.Y. 113616
 + Yu Hongnian 116067
 + Yu Hongqiang 116643
 + Yu Zechu 113483
 Yu-Juan Chen + 113589
 Yu-kun Ho see Ho Yu-kun
 Yuan-fen Lai see Lai Yuan-fen
 Yuan-ling Wang see Wang Yuan-ling
 Yuan-Long Liu see Liu Yuan-Long
 Yuan-Neng Hsu + 112944
 Yuan-Zhong Lu see Lu Yuan-Zhong
 Yuanzhang Lin see Lin Yuanzhang
 + Yuasa, K. 112160
 Yucel, A. + 113259
 + Yudilevich, I.A. 115547
 + Yudin, V.A. 116334
 + Yudin, V.V. 114381
 Yudin, L.A. + 114381
 + Yudovich, L.A. 116331
 + Yudson, V.I. 113063
 + Yuh-Se Ho 115538
 Yuenrei Chu see Chu Yuenrei
 + Yuferev, V.S. 115650
 Yufit, D.S. + 113846
 Yufit, D.S. + 113845
 + Yui, R. 114335
 Yukanov, V.A. + 115216
 Yukawa, T. + 112150
 + Yukina, N.A. 115315
 + Yuldashev, Sh.U. 114448
 + Yulyugin, V.K. 115366
 + Yung-Sung Cheng 115589
 Yunmin Liang see Liang Yunmin
 + Yunovich, A.B. 113786
 + Yunovich, A.E. 114453
 Yungqiang Yu see Yu Yungqiang
 Yunusov, V.Yu. + 114171
 Yupko, V.L. + 114306
 + Yupko, V.L. 115246
 Yurchenko, V.M. + 112753
 Yushin, N.K. + 114095
 + Yusifov, I.M. 116716
 + Yusupov, I. 116550
 Yuuki, K. + 111695
 + Yvert, M. 112031
 + Yvon, K. 114744
 + Zabbarov, A. 111644
 Zabolotnyi, V.A. + 113704
 + Zaccai, G. 115745
 Zaccane, H. 112022
 + Zachara, M. 112015
 + Zadiranos, Yu.M. 115649
 + Zafiratos, C.D. 112209
 + Zafiratos, C.D. 112208
 + Zag, W. 113901
 + Zaginailov, G.I. 113583
 + Zagromski, S. 112114
 Zahn, M. + 114782
 Zai-Tian Ma see Ma Zai-Tian
 Zaidi, M.A. + 115212
 + Zaidins, C.S. 112289
 Zaikin, P.N. + 111657
 + Zaima, S. 115025
 + Zainulin, Yu.G. 114443
 + Zaiser, C. 112011
 Zaitsev, A.I. + 115164
 + Zaitsev, A.V. 114648
 + Zajc, W.A. 112024
 Zak, A.R. + 111440
 Zakharov, K.L. + 111719
 Zakharov, L.N. + 113850
 + Zakharov, L.P. 116325
 + Zakharov, S.Yu. 116099
 Zakharov, V.E. 111500
 Zakharova, A.A. + 114571
 Zakharova, T.L. + 116015
 + Zakhovaiko, A.A. 114088
 + Zakrzewski, J.A. 112022
 Zakrzhevskii, A.G. 113273
 + Zakzhevskii, V.E. 112640
 + Zaleskaya, G.A. 112733
 Zalewski, E.F. + 111766
 Zalkind, V.I. + 113669
 Zaltsev, S.I. 113914
 + Zamaraev, K.I. 115543
 Zamazan, T.S. + 115509
 + Zamerowski, T.J. 115072
 Zander, R. + 116204
 + Zaninetti, L. 116817
 + Zankl, G. 111626
 + Zannotti, C. 115505
 + Zappala, V. 116511
 Zardecki, A. 116903
 Zaretskii, A.V. + 114555
 Zaretskii, Yu.G. + 114869
 Zaretskii, N.S. 116383
 Zarin, A.S. + 113694
 + Zaslavsky, H. 113730
 Zashkvara, V.V. + 111807
 Zaslavskaya, L.G. + 114945
 Zasova, L.V. + 116507
 Zastenker, G.N. + 116418
 + Zavlshko, N.N. 114176
 + Zavrtanik, D. 112589
 Zav'yalov, O.I. 111904
 + Zaytseva, S.A. 116384
 + Zborovskii, B.I. 114443
 + Zdarko, R.W. 111992
 Zdesenko, Yu.G. + 112593
 + Zdonik, L. 116636
 Zdzieborski, J.H.G. + 112451
 + Ze, F. 113635
 + Zebik, B. 112241
 + Zech, G. 112543
 + Zech, G. 112015
 Zechu Yu see Yu Zechu
 + Zedgenidze, G.A. 115895
 Zedler, A. 113773
 + Zegers, P. (ed.) 111313
 + Zeghlache, H. 113021
 Zehner, D.M. + 114321
 + Zeidman, B. 112246
 Zeiri, Y. + 114359
 + Zeintz, B. 112197
 Zelenkov, I.A. + 113951
 + Zelenova, O.V. 114000
 Zelenskaya, N.S. + 112107
 + Zell, K.O. 112109
 + Zeller, W. 112022
 + Zemb, T. 112754
 Zetskii, V.I. + 112784
 Zemskov, V.S. + 113789
 Zener, C. + 115668
 + Zenin, E.I. 111714
 Zen'kevich, E.I. + 115726
 Zentelis, N. 116642
 + Zephata, A.G. 112589
 + Zerbini, S. 111467
 + Zesch, J. 114533
 + Zetta, L. 112585
 Zeyen, C.M.E. 114119
 Zeyen, C.M.E. + 114215
 + Zeyen, C.M.E. 114674
 Zglinicki, T. Von see Von Zglinicki, T.
 Zhakin, A.I. + 114801
 + Zhakupov, Sh.R. 114678
 Zhan, M. + 114828
 Zhang, H.X. + 112561
 + Zhang Guangzu 111853
 Zhang Gui-shan + 112582
 Zhang Hanxin + 113483
 + Zhang Huan-qiao 112582
 Zhang Li-Min + 116059
 + Zhang Qinglong 116067
 Zhang Sen + 111853
 + Zhang Shenpan 114225
 + Zhang Wei-Qing 116287
 Zhao Min-Guang see Min-Guang Zhao
 + Zhao Pei-ying 111962
 + Zhao Pei-ying 111963
 Zhao Zhu 116019
 Zhavoronkov, V.I. + 111823
 + Zhdan, A.G. 114603
 + Zhdanov, G.S. 113786
 Zhe-ming Liu see Liu Zhe-ming
 + Zhegulev, V.S. 116507
 Zheng Gao see Gao Zheng
 Zheng Ou Yang Jing see Ou Yang
 Zhengmin Fu see Fu Zhengmin
 Zhengming Luo see Luo Zhengming
 Zhengzhi Wang see Wang Zhengzhi
 Zhensheng Feng see Feng Zhensheng
 + Zhenzhurist, I.A. 114332
 Zherbin, E.A. 115902
 + Zhidomirov, G.M. 115542
 Zhilina, V.G. + 113529
 + Zhilinsky, A.P. 116368
 + Zhirko, Yu.I. 114924
 Zhonglei Wei see Wei Zhonglei
 + Zhou, G. 115702
 + Zhou, M.L. 112129
 Zhou Qizhao 111415
 + Zhu Guo-Hui 112511
 Zhu Wei + 111954
 Zhu Zhao see Zhao Zhu
 Zhu-Ming Qian see Qian Zhu-Ming
 Zhu-Po Huang see Huang Zhu-Po
 Zhubaev, N.Zh. + 113346
 + Zhugzhda, Yu.D. 116599
 Zhukhlistova, N.E. + 112869
 + Zhukov, L.L. 114175
 + Zhukovskii, A.P. 113287
 + Zhulin, I.A. 116368
 + Zhulina, I.A. 116354
 Zhuravlev, V.A. + 115187
 + Zhuravlev, V.A. 114440
 Zhurbas, V.M. + 116300
 + Zhuruli, M.A. 114210
 + Zidanic, M. 115805
 + Ziebeck, K.R.A. 114114
 + Ziegert, W. 116445
 Ziegler, J.F. + 112578
 Zielinska-Rohozinska, E. 114950
 + Zielinski, M. 114539
 Zielinski, P.G. + 115135
 + Zielinski, W. 112028
 + Ziemelis, U.O. 115061
 + Zilm, K.W. 114748
 + Zimanyi, J. 112266
 + Zimba, C.G. 115749
 Zimin, A.B. + 112967
 + Zimin, G.P. 111656
 + Zimmer, E. 112352
 Zimmer, W.H. + 115267
 Zimmerer, R.W. 111372
 + Zimmerman, G.O. 111711
 Zimmermann, P. 116477
 + Zimmermann, W. 112015
 Zimmern, B. + 115669
 Zimogorova, N.S. + 114934
 Zinn, W. 114656
 + Zioc, K.O.H. 112589
 + Zioutas, K. 112544
 + Zipoli, G. 116281
 + Zirath, H. 114588
 + Zisman, M.S. 112271
 + Zisserman, A. 112894
 + Zito, G. 112020
 + Zitoun, R. 112020
 Zlokazov, V.B. + 114772
 Znojil, M. 111480
 + Zoboli, M. 111743
 Zochowski, A. + 111439
 + Zola, J.J. 115037
 + Zoller, W. 116261
 + Zolnierke, Z. 115023
 + Zolotov, E.M. 113097
 Zombori, P. + 115715
 + Zomorodian, M. 112028
 Zorabedian, P. + 114016
 Zorec, J. + 116638
 Zorec, J. + 116669
 + Zorn, G.T. 112015
 + Zorro, R. 112159
 Zotov, V.S. + 114242
 Zotti, G. De see De Zotti, G.
 + Zsigrai, I.J. 114140
 zu Putlitz, G. + 112102
 + Zubarev, P.V. 115280
 + Zubarev, P.V. 114072
 + Zubenko, V.V. 113786
 + Zuber, J.B. 111871
 + Zubits, Yu.E. 113802
 + Zubbkova, V.M. 116507
 + Zubov, L.M. 113331
 Zubrilov, A.S. + 114604
 Zubrinskii, V.V. + 113691
 + Zucchiatti, A. 112198
 + Zuckerman, B. 116781
 Zuev, V.E. 116273
 + Zuev, V.E. 112731
 Zukauskas, A. 113434
 + Zundel, G. 112730
 + Zurcher, P. 114598
 + Zurfluh, E. 112031
 Zusman, L.D. 112849
 + Zverev, L.P. 114586
 Zvezdin, A.K. + 114834
 + Zviadadze, M.D. 113181
 + Zvonok, A.M. 112732
 + Zweibel, E.G. 113601
 Zwickler, G. + 114358
 + Zwiener, C. 115792
 + Zyczkowski, M. 113355
 Zykov, K.I. + 115857
 + Zyryanov, G.K. 111822

BIBLIOGRAPHY INDEX

- Acoustic emission, (50 refs.).....115494
Active galactic nuclei, (59 refs.).....116857
Airborne radionuclides and radiation in buildings, (85 refs.).....115940
alpha contaminated wastes, management and disposal, (138 refs.).....112344
Amplitude equations for systems with competing instabilities, (72 refs.).....111593
Applications of laser annealing of semiconductors, (130 refs.).....114009
Asteroids, (50 refs.).....116516
Atmosphere large scale circulation, (117 refs.).....116255
Atmosphere remote sensing advances, (312 refs.).....116305
Atmospheric aerosol system, (242 refs.).....116261
Atmospheric boundary layers, (217 refs.).....116257
Atmospheric radiation, (1407 refs.).....116277
Atomic spectroscopy bibliography for January-June 1983, (599 refs.).....115594
Background atmospheric ^{222}Rn concentrations, (54 refs.).....115939
Beam-gas study of chemiluminescent reactions of Sn, Ge, and Si with F_2 , (64 refs.).....115560
Biomedical lasers, (76 refs.).....115897
Biomedical signal processing, (81 refs.).....115958
BL Lacertae-type objects, (51 refs.).....116858
Black holes, (58 refs.).....116739
Cancer and radiotherapy, (58 refs.).....115915
Cataclysmic variable stars, (71 refs.).....116697
Chemical vapour deposition of group IVB, VB, and VIB elements with non-metals, (259 refs.).....115076
Clean and adsorbate-induced surface phase transitions on $\text{W}\{100\}$, (73 refs.).....114310
Climate prediction, (84 refs.).....116260
Cloud electrification, (112 refs.).....116253
Cloud physics, (454 refs.).....116252
Collapse and explosion of white dwarfs, (68 refs.).....116648
Collective acceleration of ions in straight relativistic electron beams, (115 refs.).....112486
Cool stars chromospheres, (55 refs.).....116629
Cretaceous-Tertiary boundary sediments, (60 refs.).....116086
Differential polarization spectroscopy on single crystals of transition metal complexes, (83 refs.).....114802
Dynamic methods in plasma physics, (240 refs.).....113633
Electrical properties of dislocations and boundaries in semiconductors, (95 refs.).....114481
Electron positron pairs in radio pulsars, (128 refs.).....116724
Electronic transport in tetrahedral amorphous semiconductors, (92 refs.).....114520
Energy deposition during laser annealing of semiconductors, (50 refs.).....114003
Environmental half-time for radionuclides deposited on vegetation, (53 refs.).....115718
Epitaxy by pulsed annealing of ion-implanted silicon, (69 refs.).....114398
Epitaxy of deposited Si, (81 refs.).....114399
Extraterrestrial messenger probes in Solar System, (57 refs.).....116496
Ferroelectric and pyroelectric organic materials, (50 refs.).....114791
Fibre optic gyroscopes, (34 refs.).....113101
Fission fragment angular distributions from continuum states, (120 refs.).....112291
Fission gas release model, (55 refs.).....112332
Galaxies rotation curves, (334 refs.).....116492
Gamma ray bursters, (57 refs.).....116875
Gd, rare earth ion recoiling and high-spin states, (53 refs.).....112033
Generation of coherent far-infrared radiation using lasers, (234 refs.).....113059
Glacioisostasy, (64 refs.).....116060
Global Atmospheric Research Program, (791 refs.).....116279
Globular cluster stars, (141 refs.).....116775
Greece.....116033
Group theory of nonrigid molecules, (81 refs.).....112809
Hard inclusive processes in QCD, (131 refs.).....111964
Highly accurate inversion methods for three-dimensional stratified media, (51 refs.).....116308
Infrasound effects on human health, (22 refs.).....115830
Interstellar magnetic field, (116 refs.).....116796
Ion-induced sputtering, (59 refs.).....114993
Ion sources, (65 refs.).....111812
Large-angle scattering of 1p-shell nuclei, (51 refs.).....112241
Laser and electron beam annealing of compound semiconductors, (80 refs.).....114007
Late-type stars, (50 refs.).....116657
Lattice diffusion of substitutional elements in iron and iron-base solid solutions. A critical review, (248 refs.).....114270
Lepton spectroscopy, (560 refs.).....111934
Lightning, (138 refs.).....116254
Long Valley/Mono Basin volcanic complex, (69 refs.).....116056
Lorenz equations, real and complex, relevance to physical systems, (70 refs.).....113405
Lunar palaeomagnetism, (86 refs.).....116500
Magnetic ordering phenomena in rare earth semiconductors, (71 refs.).....114656
Marine sediment transport, (137 refs.).....116077
Medical NMR spectroscopy and microscopy, (52 refs.).....115895
Metal surfaces, microscopic structure effect on optical properties, (206 refs.).....114807
Meteorology and climatology of polar regions, (291 refs.).....116258
Meteorology at mesoscale, (291 refs.).....116256
Microstructure and topography of laser annealed semiconductors, (126 refs.).....113709
Molecular mechanics with an array processor, (66 refs.).....112647
Molecular mechanism of Na conductance changes in nerve, (55 refs.).....115775
Mossbauer spectroscopic studies of surface magnetism, (56 refs.).....114763
MRD-CI potential surfaces using balanced basis sets, (51 refs.).....112663
Na metal, ignition and burning behaviour in air, (87 refs.).....112401
Negative ion sources, (54 refs.).....111813
 NH_4Cl particle nucleation and growth dynamics, (52 refs.).....114153
Noncrystalline semiconductors, (59 refs.).....113738
Nonempirical calculations of molecular characteristics, (62 refs.).....112642
Nonlinear and frequency-dependent transport phenomena in low-dimensional conductors, (98 refs.).....114514
Nonlinear systems, orders and chaos, (101 refs.).....111564
Nonlinear waves: from hydrodynamics to plasma theory, (80 refs.).....113461
Nuclear data sheets for $A=153$, (203 refs.).....111328
Nuclear data sheets for $A=79$, (153 refs.).....111327
Nuclear data sheets, references for January-April 1983, (506 refs.).....111329
Nucleon energy in nucleus, (81 refs.).....112053
Ocean chemistry, recent research, (386 refs.).....116148
Ocean fine structure and microstructure, (211 refs.).....116142
Ocean internal waves, (232 refs.).....116143
Ocean mesoscale circulation, (134 refs.).....116136
Oceanic internal wave field, (170 refs.).....116146
Oceanic subsurface tropical gyres, (69 refs.).....116137
Oceanographic remote sensing, (503 refs.).....116144
Oceanography of continental shelf areas, (526 refs.).....116141
Oceanography of equatorial regions, (243 refs.).....116140
Oceanography of polar regions, (122 refs.).....116138
Oceans, organic chemistry, (591 refs.).....116149
Optical fibre sensors: principles and applications, (32 refs.).....113104
Optical image processing in coherent and incoherent light, (52 refs.).....112947
Oxygen clustering and effect on electrical behaviour in silicon, (102 refs.).....114190
Palaeo-oceanography, (426 refs.).....116145
Phase polarisation laser spectroscopy, (78 refs.).....111779
Photon and fluorescence correlation spectroscopy and light scattering of eye-lens proteins at moderate concentrations, (52 refs.).....115747
Photosphere MHD instability, (80 refs.).....116563
Planetary nebulae, (54 refs.).....116804
Planetary nebulae nuclei, (51 refs.).....116651
Plasma expansion into vacuum, (89 refs.).....116470
Point defect thermodynamics of semiconductors, (196 refs.).....113907
Polarisation effects in single-mode fibres, (81 refs.).....113118
Polymer blend melt flow, (87 refs.).....113722
Post-critical heat flux heat transfer in reactors, (71 refs.).....112367
Preparation of ceramics and glasses from organosilicon compounds, (81 refs.).....115144
PWR primary coolant, analytical and sampling problems, (178 refs.).....111336
Quenching-resolved emission anisotropy studies with single and multiphoton-containing proteins, (57 refs.).....115746
Radio elliptical galaxies, (51 refs.).....116848
Radio pulsars, (54 refs.).....116717
Radio sources circular polarisation, (68 refs.).....116494
radioactive jet from reactor accident, integral model, (61 refs.).....112448
Rotation barriers in molecules with lone pairs, bond orbital calculations, (54 refs.).....112643
Si:Zn structures, physical properties and functional possibilities, (69 refs.).....114547
Silicon molecular beam epitaxy, (236 refs.).....115059
Solar filaments, (50 refs.).....116625
Solid phase regrowth of semiconductors, (70 refs.).....114006
Soliton experiments in plasmas, (309 refs.).....113602
Solitons and numerical experiments, (142 refs.).....111903
Solubility of H_2 -He mixtures in fluid phases to 1 GPa, (56 refs.).....114179
Spectroscopic and structural properties of metallo-proteins, (202 refs.).....115739
Splitting up schemes for solving hyperbolic and parabolic nonlinear problems, (60 refs.).....111450
Stopping power for heavy ions in low energy region, (53 refs.).....112606
Surfaces and thin films, (353 refs.).....114317
Symbiotic novae, (59 refs.).....116660
Symbiotic stars, (52 refs.).....116698
Symmetries of Maxwell and Dirac equations, (64 refs.).....111902
Thermometric and calorimetric methods in electrochemical and corrosion studies, (66 refs.).....111686
Thermosyphon domestic solar energy water heaters, (97 refs.).....115693
Transition metal impurities in silicon, (55 refs.).....113936
Turbulence, (131 refs.).....113422
UV two photon spectroscopy of benzene, (65 refs.).....112802
Vibrational band intensities of hydrocarbons, (275 refs.).....112692
Vibrational energy relaxation of highly compressed gaseous H_2 and N_2 , (57 refs.).....112816
Voltage-dependent K conductance at the apical membrane of *Necturus* gall-bladder, (50 refs.).....115760
Wave optics and Fresnel's theory of diffraction, (58 refs.).....111388
Weather modification, (181 refs.).....116259
 $X\alpha$ multiple scattering calculations on iron (ii) porphine, (51 refs.).....112653

BOOK INDEX

- Advances in Mossbauer spectroscopy. Applications to physics, chemistry and biology;** *B.V.Thosar, P.K.Iyengar, J.K.Srivastava, S.C.Bhargava (editor/s)*, [Amsterdam, Netherlands: Elsevier 1983] 111334
Elastic media with microstructure II. Three-dimensional models; *I.A.Kunin*, [Berlin, Germany: Springer-Verlag 1983] 111318
Laser annealing of semiconductors; *J.M.Poate, J.W.Mayer (editor/s)*, [London, England: Academic Press 1982] 111333 (introductory abstract), 113709, 114001-9, 114321, 114398-9

- Optical fiber systems: Technology, design, and applications;** *C.K.Kao*, [New York, USA: McGraw-Hill 1982] 111330
Perturbative quantum chromodynamics; *M.Jacob (editor/s)*, [Amsterdam, Netherlands: North-Holland 1982] 111319
Radiation effects computer experiments; *J.R.Beeler Jr.*, [Amsterdam, Netherlands: North-Holland 1982] 111332
Surface physics. Second edition; *M.Prutton*, [Oxford, England: Clarendon 1983] 111335

CONFERENCE INDEX

- 1982 CERN School of Computing**; Zinal, Valais, Switzerland, 29 Aug.-11 Sept. 1982, [Geneva, Switzerland: CERN 1983] 112490, 112523
- Accelerator engineering and technology**; Santa Fe, NM, USA, 21-23 March 1983, [Aug. 1983] 112463-85, 112511
- Acoustics, speech and signal processing, 1982**; Paris, France, 3-5 May 1982, (*IEEE*) [New York, USA: IEEE 1982] 112394, 112310
- Application systems development**; Nurnberg, Germany, 22-24 March 1983, *H.J.Schneider (editor/s)*, [Stuttgart, Germany: B.G. Teubner 1983] 112612-13
- Applied electromagnetics**; Florence, Italy, 4-6 Oct. 1982, [May-June 1983] 111674, 111743, 113098-9, 116167-8, 116280-2, 116339
- Chemical vapour deposition**; Eindhoven, Netherlands, 31 May-2 June 1983, *J.Bloem, G.Verspu, L.R.Wolff (editor/s)*, [Eindhoven, Netherlands: Philips Centre Manuf. Technol. 1983] 111316 (introductory abstract), 112351, 112442, 113070, 113790, 114375, 114402-22, 114424-5, 114428, 114949, 115077-102, 115396-8, 115448-51, 115506
- Cineradiography with photons or particles**; Paris, France, 18-21 May 1981, (*CEA*) [1983] 111300 (introductory abstract), 111835-47, 112319, 112368-70, 112569-70, 113525, 113655-8, 113674
- Composite materials**; Capri, Italy, 15-19 June 1981, *J.C.Seferis, L.Nicolas (editor/s)*, [New York, USA: Plenum 1983] 111312 (introductory abstract), 112890, 113291-2, 113372, 115160-2, 115180, 115249-50, 115292-7, 115360-5, 115394-5, 115502-5
- Consumer electronics**; Des Plaines, IL, USA, 8-10 June 1983, (*IEEE*) [1983] 111695, 111794, 113150
- Cross sections for fusion and other applications**; College Station, TX, USA, 4-6 Nov. 1982, [1983] 111298 (introductory abstract), 112826-37, 112844-8, 112855, 113639, 114988
- Defects in semiconductors**; Boston, MA, USA, Nov. 1982, *S.Mahajan, J.W.Corbett (editor/s)*, [New York, USA: North-Holland 1983] 111315 (introductory abstract), 112997, 113742, 113905-7, 113915, 113923, 113930-1, 113936, 113943-7, 113954, 113981, 114020-1, 114077, 114190-6, 114201, 114251-2, 114275-9, 114284, 114322-3, 114400-1, 114476-83, 114549, 114611, 114629, 114734, 114871, 114897, 114926-7, 115060, 115114-15
- Electro '82**; Boston, MA, USA, 25-27 May 1982, [El Segundo, CA, USA: Electron. Conventions 1982] 111672-3, 113224-7, 115961
- Electrochemical Society technical meeting**; Washington, DC, USA, 9-14 Oct. 1983, [Pennington, NJ, USA: Electrochem. Soc. 1983] 111317 (introductory abstract)
- Fifteenth Hawaii International Conference on System Sciences 1982**; Honolulu, HI, USA, 6-8 Jan. 1982, (*Univ. Hawaii; Univ. Southwestern Louisiana; W.Riddle, K.Thurber, P.Keen, R.H.Sprague Jr., B.Shriver, T.M.Walker, R.R.Grams (editor/s)*, [HI, USA: Hawaii Int. Conference Syst. Sci. 1982] 115892, 115901, 115919-20
- Heat pumps**; Brussels, Belgium, 28-29 April & 12-13 May 1982, *H.Ehringer, P.Zegers, G.Hoyaux, J.A.Knobbout (editor/s)*, [Luxembourg: Comm. European Communities 1982] 111313 (introductory abstract), 115669-84
- IAU General Assembly 1982 Patras meeting proceedings**; Patras, Greece, 17-26 Aug. 1982, (*IAU*) *R.M.West (editor/s)*, [Dordrecht, Netherlands: Reidel 1983] 111314 (introductory abstract)
- Identification and system parameter identification**; Washington, DC, USA, 7-11 June 1982, (*IFAC*) *G.A.Bekey, G.N.Saridis (editor/s)*, [Oxford, England: Pergamon 1983] 115787-9, 115812, 115820-4, 116164-6, 116267, 116316-21
- Instrumentation in the mining and metallurgy industries**; Denver, CO, USA, 5-7 May 1982, *D.J.Spottiswood, D.H.Davis (editor/s)*, [Research Triangle Park, NC, USA: ISA 1982] 112460
- ITC/USA 82**; San Diego, CA, USA, 28-30 Sept. 1982, [*Int. Found. Telemetering*] [Woodland Hills, CA, USA: Int. Found. Telemetering 1982] 116480, 116486
- Laser-solid interactions and transient thermal processing of materials**; Boston, MA, USA, 1-4 Nov. 1982, (*US DOE*) *J.Narayan, W.L.Brown, R.A.Lemons (editor/s)*, [New York, USA: Elsevier 1983] 113942, 113988-9, 114010-19, 114027-31, 114054, 114475, 114530, 115050
- Light ion reaction mechanisms**; Osaka, Japan, 16-20 May 1983, *H.Ogata, T.Kammuri, I.Katayama (editor/s)*, [Osaka, Japan: Osaka University 1983] 111309 (introductory abstract), 112051-2, 112067, 112076, 112082, 112084, 112105, 112115-17, 112137-9, 112144-7, 112158-60, 112163, 112204-18, 112223-32, 112237, 112275-9, 112293, 112522
- Magnetosphere waves**; Kona Coast, HI, USA, 7-11 Feb. 1983, [1983] 111303 (introductory abstract), 116338, 116358-61, 116392-405, 116504, 116519
- Materials sciences under microgravity**; Madrid, Spain, 5-8 April 1983, (*ESA; UPM; ELGRA; COSPAR*) [Paris, France: ESA 1983] 113444, 113789, 114130-1, 114147-50, 114233, 114291, 114371, 115123, 115131, 115511
- Measurement methods and technology**; Berlin, Germany, 24-28 May 1982, *K.Havrilla, J.Solt, T.Kemeny (editor/s)*, [Amsterdam, Netherlands: North-Holland 1983] 111624, 111630-1, 111644-7, 111650, 111666-71, 111707-8, 112965, 113139, 113223, 113244, 113538-40, 115497, 115716-17, 115966-9, 115981
- Metallogeny and tectonics of North American Cordillera**; Calgary, Alta., Canada, 13 May 1981, [1983] 111299 (introductory abstract)
- Microscopy techniques and capabilities**; London, England, 21-22 Sept. 1982, (*IOP; IEE*) [1983] 111302 (introductory abstract), 111633, 111760-5, 111819, 111848-9, 113233-7, 115596-7, 115906, 115982
- Neutron radiography**; San Diego, CA, USA, 7-10 Dec. 1981, (*ASTM; American Soc. Nondestructive Testing; British Inst. Nondestructive Testing*) *J.P.Barton, P.Von Der Hardt (editor/s)*, [Dordrecht, Netherlands: Reidel 1983] 111857-61, 112391-3, 112521, 113541, 115498-501
- Neutron scattering in condensed matter**; Hakone, Japan, 1-4 Sept. 1982, [May 1983] 113720-1, 113749-53, 114105-9, 114114, 114119-20, 114163-5, 114215, 114250, 114459, 114792
- Nuclear physics**; Fuglso, Denmark, 16-20 Aug. 1982, (*NORDITA; Danish Natural Sci. Res. Council; Niels Bohr Inst*) [1983] 111306 (introductory abstract), 111387, 112026, 112037-49, 112058-9, 112064, 112074-5, 112088, 112111-13, 112131-2, 112136, 112154-6, 112162, 112260-9, 112290, 112292, 112440
- OPTICS 82, ECOSA 82**; Edinburgh, Scotland, 7-10 Sept. 1982, (*SPIE*) [1983] 111634-5, 111752-4, 111774-6, 111785, 112947, 112959, 112966, 113036-9, 113048, 113066, 113088, 113101-4, 113153-4, 113526, 113937, 113983
- Order in chaos**; Los Alamos, NM, USA, 24-28 May 1982, [May 1983] 111307 (introductory abstract), 111494-5, 111564-82, 113405, 113419, 113443, 113455-6, 113517, 114297, 114299
- Point defects and defect interactions in metals**; Kyoto, Japan, 16-20 Nov. 1981, *J.-I.Takamura, M.Doyama, M.Kiritani (editor/s)*, [Amsterdam, Netherlands: North-Holland 1982] 113706, 113859-60, 113868-904, 113919-22, 113934, 113959-80, 113990-6, 114032-9, 114046-7, 114055-61, 114187-9, 114200, 114241, 114246-7, 114273-4, 114281-3, 114287, 114290, 114296, 114300, 114511, 114745, 114766-8, 114955-63, 115005, 115230-1
- Polymer alloys**; New York, USA, 23-28 Aug. 1981, (*American Chem. Soc*) *D.Klempner, K.C.Frisch (editor/s)*, [New York, USA: Plenum 1983] 111311 (introductory abstract), 113727, 113771-2, 114069, 115159, 115203, 115248, 115288-91, 115359
- Positron-electron pairs in astrophysics**; Greenbelt, MD, USA, Jan. 1983, [1983] 111296 (introductory abstract), 116448-59, 116564-5, 116717-27, 116733, 116735-7, 116825-38, 116875-85, 116887
- Radiation processing**; Dubrovnik, Yugoslavia, 4-8 Oct. 1982, [1983] 111308 (introductory abstract)
- Radionuclide metrology**; Geel, Belgium, 16-17 May 1983, [1983] 112603
- Rare earth research**; Tallahassee, FL, USA, 18-21 April 1983, [1983] 111304 (introductory abstract), 112677, 112723, 112778-80, 113797-8, 113825, 114103, 114436, 114488-9, 114493-501, 114652, 114673, 114833, 114851, 114878, 114888-9, 114905-13, 114972-3, 115010-11, 115541
- Robotics and industrial inspection**; San Diego, CA, USA, 24-27 Aug. 1982, [1982] 112945, 115642, 115793
- Semiconductors 1982**; Espoo, Finland, 14-18 June 1982, [1983] 111297 (introductory abstract), 113738, 114520, 114531, 114614, 114656, 114661, 114810
- Solar flares**; Tokyo, Japan, 5-8 Oct. 1982, (*Japan Soc. Promotion of Sci.; U.S. Nat. Sci. Found*) [1983] 116573-94
- Southcon '81**; Atlanta, GA, USA, 13-15 Jan. 1981, [El Segundo, CA, USA: Electron. Conventions 1981] 113156-7, 115792
- Surface science**; Tampere, Finland, 18-20 Aug. 1982, [1983] 111305 (introductory abstract), 114309-11, 114337-48, 114433, 114581, 114951, 114953, 114997, 115013-16, 115579-81, 115729
- Symmetries and properties of non-rigid molecules**; Paris, France, 1-7 July 1983, (*CNRS; Direction de la Recherche du Ministere Educ. Nat*) *J.Marumani, J.Serre (editor/s)*, [Amsterdam, Netherlands: Elsevier 1983] 111310 (introductory abstract), 111395, 112618-27, 112673-4, 112709, 112719, 112735, 112744, 112754, 112794, 112809
- Symmetries in nuclear structure**; Dronten, Netherlands, 16-28 Aug. 1982, (*NATO; Netherlands' Min. Educ. & Sci.; Found. Physica; Netherlands' Phys. Soc*) *K.Abrahams, K.Allaart, A.E.L.Dieperink (editor/s)*, [New York, USA: Plenum Press 1983] 111295 (introductory abstract), 111939-40, 112053, 112065, 112083, 112090-1, 112098, 112179-80, 112885
- Wavefront Sensing**; San Diego, CA, USA, 24-25 Aug. 1982, [1983] 111301 (introductory abstract), 111722-33, 111744, 111749-51, 112923-4, 112946, 113072-3
- Wescon '82**; Anaheim, CA, USA, 14-16 Sept. 1982, [El Segundo, CA, USA: Electron. Conventions 1982] 113019, 116315

CORPORATE AUTHOR INDEX

Atomic Energy Canada Ltd., Chalk River, Ont.

- Model for the accumulation of cases of pulmonary malignancy in time when dose is accumulated in time, AECL-7155, 115879
- Nuclear fuel waste disposal: Long-term stability analysis, AECL-6820, 112350
- Reactor physics and economic aspects of the CANDU reactor system, AECL-7615, 112376
- Summary of methods for conditioning and immobilizing ion-exchange resins, AECL-7976, 112349
- Bur. Mines, Washington, DC, USA**
- Chemical vapor deposition of group IVB, VB, and VIB elements with non-metals. A literature review, IC-8928, 115076
- Central Res. Inst. Electr. Power Ind., Tokyo, Japan**
- Finite element model simulation of creep crack growth in low-ductility material, E281005, 113371

Comm. European Communities, Luxembourg

- Absorber surfaces and durability of solar heat collectors, EUR 8353 EN, 115700
- Acoustic emission: Past experience within ECSC contracts and future trends, EUR 7887 EN, 115494
- Comparison of collector performance measured in a solar simulator, EUR 8347 EN, 115699
- Experimentation d'un systeme de sondage en a source controlee, en prospection miniere (Experiments with an EM sounding system with a controlled source in mineral prospecting), EUR 8258 FR, 116314
- High strength sheet steel of medium thickness, EUR 8007 EN, 115357
- Management and disposal of alpha-contaminated wastes. A survey of current practices, strategies and R & D activities in some EC countries and the USA, EUR 8574 EN, 112344
- Progress report programme. Radiation protection 1982, EUR 8486 DE/EN/FR, 112459

- Resistenza a fatica di acciai ad alto limite di snervamento laminati a caldo (Fatigue resistance of high strength hot rolled steels), EUR 8063 IT. 115358
- Results of a quality assurance exercise for radon and radon decay product measurements, EUR 8629 EN. 112608
- Results of environmental radioactivity measurements in the Member States of the European Community for air - deposition - water - milk 1981, EUR 8308 DA/DE/EN/FR/IT/NL. 112458
- Council for Miner. Technol., Randburg, S. Africa**
- Development of an automatic sample-changer and control instrumentation for isotope-source neutron-activation analysis, M53. 115608
- Defence Sci. & Technol. Organ., Mater. Res. Labs., Melbourne, Vic., Australia**
- A torsion testing machine for measurement of shear strength of foam, MRL-TN-469. 115492
- Electr. Power Res. Inst., Palo Alto, CA, USA**
- Assessment of SPEAR-FCODE-BETA for fuel licensing, EPRI-NP-2939. 112308
- BWR spray nozzle performance in steam environment, EPRI-NP-3119. 112428
- Condensate polisher resin leakage quantification and resin transport studies, EPRI-NP-2981. 112389
- Controlled studies of human health effects of short-term inhalation of atmospheric pollutants, EPRI-EA-3125. 115993
- Diffusion and hideout in crevices, EPRI-NP-2979. 112380
- Estimate of primary-system temperatures in severe reactor accidents, EPRI-NP-3120. 112429
- Evaluation of critical flow for supercritical steam-water, EPRI-NP-3086. 112425
- Evaluation of steam generator fluid mixing during layup, EPRI-NP-2993. 112388
- Evaluation of techniques to predict flow-induced tube vibration in a preheat steam generator, EPRI-NP-2986. 112377
- Hydrazine usage for corrosion control in PWR plants with powdered resin condensate polishers, EPRI-NP-2969. 112379
- Implementation of boric acid in the field - Indian Point Unit 3 plant, EPRI-NP-3066. 112390
- In-plant low-level radwaste technology needs, EPRI-NP-3117. 112347
- Intergranular stress corrosion cracking of Ni-Cr-Fe Alloy 600 tubes in PWR primary water - Review and assessment for model development, EPRI-NP-3057. 115447
- Licensing applications and requirements of an ideal steady-state fuel performance code, EPRI-NP-2940. 112340
- Low-level waste disposal site performance assessment with the RQ/PQ computer program, EPRI-NP-2664. 112348
- On-line use of chelants in nuclear steam generators - Feasibility study, EPRI-NP-2973. 112387
- Operation of the EPRI nondestructive evaluation center. Annual report - 1982, EPRI-NP-2985. 115495
- Point-contact silicon solar cells, EPRI-AP-2859. 115662
- Primary-side deposits on PWR steam generator tubes, EPRI-NP-2968. 112381
- Secondary water chemistry at Millstone 2, EPRI-NP-2974. 112386
- SIMULATE-E: A nodal core analysis program for light-water reactors. Computer code user's manual, EPRI-NP-2792-CCM. 112307
- SPEAR-FCODE-GAMMA functional specifications, EPRI-NP-2941. 112314
- Steam generator U-bend eddy-current NDE, EPRI-NP-3010. 115496
- Studs vik over-ramp project, EPRI-NP-3007. 112346
- Testing and evaluation of on-line leak sealing methods, EPRI-NP-3111. 112426
- Thermal mixing in a model cold leg and downcomer at low flow rates, EPRI-NP-2935. 112378
- Transient cooldown in a model cold leg and downcomer, EPRI-NP-3118. 112427
- Use of base isolation and energy-absorbing restrainers for the seismic protection of a large power plant component, EPRI-NP-2918. 112418
- Utility impacts assessment of residential passive solar systems, EPRI-EM-3092-SY. 115622
- Verification of the GFLOW computer code using experimental data from the Maine Yankee spent-fuel storage pool, EPRI-NP-3097. 112345
- VIPRE-01: A thermal-hydraulic analysis code for reactor cores. Vol.I: Mathematical modeling, EPRI-NP-2511-CCM. 112312
- VIPRE-01: A thermal-hydraulic analysis code for reactor cores. Vol.II: User's manual, EPRI-NP-2511-CCM. 112313
- Weld residual stress redistribution near growing cracks, EPRI-NP-2964. 112339
- Hungarian Acad. Sci., Budapest**
- Bubble growth in variable pressure fields, KFKI-1983-72. 112424
- Cage effect in recoil studies, KFKI-1983-91. 115572
- Critical behaviour of a quantum spin problem with three-spin coupling, KFKI-1983-62. 111612
- Evaluation of kinetic parameters from non-isothermal experiments: Application to crystallization kinetics, KFKI-1983-73. 114146
- Fényvezető üvegcsalak a tavkozlesben (Light propagation in optical fibres), KFKI-1983-75. 113138
- Környezeti dózisintenzitás helyszíni meghatározása Ge(Li)-spektrometriával. A módszer (Environmental dose rate in situ determination by Ge(Li)-spectrometry, KFKI-1983-44. 115715
- Lectures on the inverse scattering method, KFKI-1983-71. 111500
- Local boron environment in $\text{Ni}_{100-x}\text{B}_x$ metallic glasses: A NMR study, KFKI-1983-57. 114754
- Macroscopic coherence length of charge-density waves in orthorhombic TaS_3 , KFKI-1983-52. 114516
- Metricization of thermodynamic state space and the renormalization group, KFKI-1983-53. 111620
- Motion of dust particles in cometary atmospheres, KFKI-1983-67. 116550
- Neutron response of several fission track detectors worn on the body, KFKI-1983-65. 112457
- New model of the metagalaxy, KFKI-1983-68. 116908
- Pattern formation in metallic glasses induced by helium ion implantation, KFKI-1983-82. 114053
- Probing phase transitions via energetic nuclear collisions, KFKI-1983-76. 112274
- Recent bibliography on analytical and sampling problems of a PWR primary coolant. Supplement II, KFKI-1983-81. 111336
- Self-focusing in laser produced spark, KFKI-1983-50. 113621
- Stationary vacuum fields with a conformally flat three-space III. The conformal condition, KFKI-1983-31. 111521
- Study of momentum transfer in two-fluid formulation of two-phase flow, KFKI-1983-84. 113497
- Theoretical analysis of hydrogen concentration distribution and acoustic field in Na-water steam generator in presence of micro-leak, KFKI-1983-60. 112422
- Viscosity and the monopole density of the Universe, KFKI-1983-77. 116909
- Ist. Naz. Fis. Nucl., Bari, Italy**
- Measurement, parametrization and fast simulation of hadronic showers in lead, INFN/AE-83/4. 112008
- Ist. Naz. Fis. Nucl., Milan, Italy**
- SCAMPI - A FORTRAN program simulating charge and mass particle identification, INFN/BE-83/1. 112585
- Study of the magnetic forces acting on the trim coils, for the Milan superconducting cyclotron, INFN/TC-83/7. 112489
- Ist. Naz. Fis. Nucl., Naples, Italy**
- Fast and low-cost discriminator and shaper, INFN/TC-83/8. 112595
- Kernforschungsanlage, Jülich, Germany**
- Anomalous impurity transport in plasmas, JUL-1846. 113575
- Berechnungsmethoden und Analysen zum dynamischen Verhalten von Kraftwerksanlagen mit Hochtemperaturreaktor (Computation methods and analyses on the dynamic behaviour of power plants with high temperature gas cooled reactors), JUL-1841. 112309
- Carbide precipitation in nickel-base model alloys and its influence on the ductility and fracture behaviour at room temperature, JUL-1845. 115446
- Constitutive equations for the creep behaviour of nickel-base alloys for HTR components in the temperature range 1023 - 1273 K, JUL-1843. 112341
- Core-level XPS studies of Ce and La intermetallic compounds and their implications for the 4f levels of Ce compounds, JUL-1824. 115023
- Der Einfluss von Wasserstoff auf die Supraleitung von Nichtübergangsmetallen (The influence of hydrogen on the superconductivity of non-transition metals), JUL-1849. 114640
- Experimental investigation for the thermohydraulics of packed beds in the comparison with the computer code THERMIX-2D: The investigation of the dispersive heat transfer examined by a cold gasstream, JUL-1839. 112383
- Experimental investigations of actinide release from coated fuel particles for high-temperature reactors, JUL-1833. 112342
- First investigations on a wrapped fibre blanket insulation with massive spacers consisting of carbon fibre composite, JUL-1840. 112310
- Gitterdynamik von Imidazol (Lattice dynamics of Imidazol), JUL-1850. 114110
- Investigation of the behaviour of TRISO coated UO_2 -kernels in the head-end burning and experimental determination of the radioactive contents of irradiated particles, JUL-1857. 112359
- Investigations of thermochemical energy storage with sulfuric oxides, JUL-1847. 115664
- Möglichkeiten der Spaltstoffzeugung für Hochtemperatur-Reaktoren im Verbundsystem von Hochtemperatur-Reaktor und Fusionsreaktor (Facilities for producing fissile fuel for high temperature gas-cooled reactors in a symbiotic fission-fusion system), JUL-1827. 112444
- Neutron physical and thermohydraulic investigations on the fissile fuel production with spallation neutrons, JUL-1835. 112358
- Neutron spectra unfolding from measured detector activations. The computer programme SAND-MX2, JUL-1837. 112298
- New HTR conception for a modular system with block-fuel elements and its comparison with an HTR with ball-shaped fuel shaped elements, JUL-1842. 112311
- Numerische Untersuchung der 3-dimensionalen stationären Temperatur- und Stromungsverteilung im Core eines Kugelhafen-Hochtemperaturreaktors (Numerical investigation of the 3-dimensional steady-state temperature - and flow-distribution in a pebble bed high temperature reactor core), JUL-1826. 112382
- On the temporal variance of stratospheric trace gas concentrations, JUL-1836. 116266
- Optimierung sphärischer Ionisationskammern für die Neutronendiagnostik an Tokamakanlagen (Optimisation of spherical ionisation chambers for neutron diagnostics in Tokamaks), JUL-1848. 112584
- Oxidation of Ni-Cr experimental alloys and the effectiveness of the oxide as a barrier against carburization in high-temperature reactor primary circuit helium, JUL-1790. 112343
- Quantifizierende Bemerkungen zur Frage der Konservativität der 'Allgemeinen Berechnungsgrundlagen' (Quantified remarks on the question of the conservation of general calculation inputs), JUL-1821. 112454
- Release of gaseous tritium during reprocessing, JUL-1838. 112455
- Resonant helical magnetic limiter, JUL-1820. 113673
- Transport properties of drift waves, JUL-1829. 113574
- Two-group criticality models for safety analysis considerations, JUL-1856. 112423
- Untersuchungen zur statistischen Mechanik von linearen Polymeren unter verschiedenen physikalischen Bedingungen (Investigation of the statistical mechanics of linear polymer molecules under various physical conditions), JUL-1832. 111611
- Nagoya Univ., Japan**
- Dissipative trapped ion instability in PLT and INTOR, IPPJ-635. 113608
- Numerical simulations for intense light-ion beam propagation in channel under influence of plasma inertia, IPPJ-627. 113628
- Plasma equilibrium and field diffusion during current rise phase of STP-2 screw pinch tokamak, IPPJ-594. 113651
- Simple method of sheet plasma production in lower pressure, IPPJ-628. 113634
- Wall material characteristics in reacting plasma modelling, IPPJ-592. 113622
- Nat. Bur. Stand., Washington, DC, USA**
- Accuracy in analytical spectrophotometry, NBS-SP-260-81. 111784
- NBS reactor: Summary of activities July 1981 through June 1982, NBS-TN-1178. 112385
- Selected tables of atomic spectra. Atomic energy levels and multiplet table. O IV. Data derived from the analyses of optical spectra, NSRDS-NBS-3-3ect.10. 111331
- Self-study manual on optical radiation measurements: Part III - Applications, chapter 1. Measurement of solar terrestrial spectral irradiance in the ozone cut-off region, NBS-TN-910-5. 111383
- Self-study manual on optical radiation measurements: Part I - Concepts, chapter 10. Introduction to coherence in radiometry, NBS-TN-910-6. 111382
- Three guises of generation-recombination noise, NBS-TN-1173. 114577

Nat. Phys. Lab., Teddington, England

Development of design analysis methods for new materials, NPL-DMA(A)-66. 115207

Effect on the measurement of aircraft noise of reflections from the ground, Ac 102. 113199

Rutherford Appleton Lab., Chilton, Oxon., England

Chiral Lagrangian calculation of nucleon decay modes induced by $d = 5$ supersymmetric operators, RL-83-056. 111936

Lepton number violation with quasi-Dirac neutrinos, RL-83-018. 111919

Measurements of hyperon semileptonic decays at the CERN super proton synchrotron IV tests of the Cabibbo model, RL-83-054. 111998

Photoproduction of hermaphrodite baryons, RL-83-020. 112009

Reconstruction of data for an experiment using multi-gap spark chambers with six-camera optics, RL-82-085. 112586

$SU_3 \times SU_2 \times U_1$ next to leading corrections for proton decay in SU_5 model, RL-83-042. 111938

Towards a realistic SUGRA-GUT, RL-83-060. 111937

Tech. Res. Centre Finland, Electr. Eng. Lab., Espoo

Assessment of control rooms of nuclear power plants, 184. 112384

Tech. Res. Centre Finland, Instrum. Lab., Espoo

Influence of magnetization on eddy current inspection of ferromagnetic tubes, 183. 115493

Tech. Res. Centre Finland, Metall. Lab., Espoo

Fractographic study of cracks produced by thermal shocks in 20MnMoNi55 and comparable weld material in water environment, 176. 115356

The Second Experimental Div., Inst. of High Energy Phys., Acad. Sinica, Peking, China

Research on some characteristics and improvements of a 70 cm streamer chamber, . 112579

UKAEA, Culcheth, Lancs., England

Hydrogen phenomena in PWR degraded core accidents, SRD R 271. 112421

SARTEMP2 - A computer program to calculate power and temperatures in a transport flask during a criticality accident, SRD R 266. 112456

Seismic response analysis with liquid-structure interaction, SRD R 259. 112420

Technical basis of 'spectral source terms' for assessing uncertainties in fission product release during accidents in PWRs with special reference to Sizewell-B, SRD R 256. 112419

UKAEA, Culham, Abingdon, Oxon., England

Calculation of spectrum line emission from plasmas, CLM-R 229. 113668

Predicted behaviour of the single-null divertor of INTOR, CLM-R 226. 112441

UKAEA, Risley, Lancs., England

CANSWEL-2: A computer model of the creep deformation of Zircaloy cladding under loss-of-coolant accident conditions. Part II. User notes, ND-R-814 (S) Part 2. 112306

Comparison of measured fission gas releases for Windscale AGR fuel irradiated above 18 GWd/tU with those predicted using the computer code MINIPAT D, ND-R-803(W). 112305

A study using the MABEL-2C code of the effects of pellet and cladding asymmetries on PWR fuel rod deformation under conditions relevant to the NRU MT-3 ballooning experiment, ND-R-876 (S). 112417

SUPPLEMENTARY LIST OF JOURNALS

Account. Mag. (GB)

Accountant's Magazine Published for the Institute of Chartered Accountants of Scotland by The Accountant's Publishing Co. Ltd., 27 Queen Street, Edinburgh EH2 1LA, Scotland

Acta Phys. Hung. (Hungary) - (APAHAQ)

Acta Physica Hungarica Formerly: *Acta Phys. Acad. Sci. Hung. (Hungary)* Akademiai Kiado, Publishing House of the Hungarian Academy of Sciences, H-1054 Budapest, Alkotmany U. 21, Hungary

BPICS Control (GB)

BPICS Control British Production and Inventory Control Society, 3 The Square, Sawbridgeworth, Herts, England

Circuits Syst. & Signal Process. (USA)

Circuits, Systems, and Signal Processing Birkhauser Boston Inc., 380 Green Street, Cambridge, MA 02139, USA

Database & Network J. (GB)

Database and Network Journal Formerly: *Database J. (GB)* A.P. Publications Ltd., 322 St. John Street, London EC1V 4QH, England

Earth-Oriented Appl. Space Technol. (GB)

Earth-Oriented Applications of Space Technology Formerly: *Adv. Earth Oriented Appl. Space Technol. (GB)* Pergamon Press Ltd., Headington Hill Hall, Oxford OX3 0BW, England

Health & Soc. Serv. J. (GB) - (HSSJBH)

Health & Social Service Journal Hospital and Social Service Publications Ltd., 4 Little Essex Street, London WC2R 3LF, England

Impact: Off. Autom. (USA)

Impact: Office Automation Formerly: *Impact: Inf. Technol. (USA)* Administrative Management Society, Maryland Road, Willow Grove, PA 19090, USA

Laser Focus/Electro-Opt. (USA)

Laser Focus/Electro-Optics PennWell Publishing Co., Advanced Technology Group, 119 Russell Street, Littleton, MA 01460, USA. Formed by merger of Laser Focus (USA) and Electro-Opt. (USA)

Libr. Retr. & Libr. Autom. (USA) - (IRLAAQ)

Library Retrieval & Library Automation Lomond Publications Inc., P.O.Box 88, Mt. Airy, MD 21771, USA

Manage. Focus (USA)

Management Focus Peat, Marwick, Mitchell & Co., 345 Park Avenue, New York, NY 10154, USA

Micron & Microsc. Acta (GB)

Micron and Microscopica Acta Formerly: *Micron (GB)* Pergamon Press Ltd., Headington Hill Hall, Oxford OX3 0BW, England

Mikrocomput. Z. (Germany)

Mikrocomputer Zeitschrift Franzis-Verlag GmbH, Karlstrasse 37, 8000 Munchen 2, Germany

Nondestr. Test. Commun. (GB)

Nondestructive Testing Communications Gordon and Breach Science Publishers Ltd., 42 William IV Street, London WC2N 4DE, England

Pers. Comput. (USA) - (PLCMDL)

Personal Computing Benwill Publishing Corp., 1050 Commonwealth Avenue, Boston, MA 02215, USA

Rec. AT&T Bell Lab. (USA)

Record AT&T Bell Laboratories Formerly: *Bell Lab. Rec. (USA)* Bell Telephone Laboratories Inc., 600 Mountain Avenue, Murray Hill, NJ 07974, USA

Technol. & Sci. Inf. (GB)

Technology and Science of Informatics [Translation of: *Tech. & Sci. Inf. (France)*] North Oxford Academic Publishing Co. Ltd., 242 Banbury Road, Oxford OX2 7DR, England

Trans. ASME. J. Mech. Transm. & Autom. Des. (USA)

Transactions of the ASME. Journal of Mechanisms, Transmissions, and Automation in Design American Society of Mechanical Engineers, United Engineering Center, 345 East 47th Street, New York, NY 10017, USA. Supersedes in part: *Trans. ASME. J. Mech. Des. (USA)*

Trans. ASME. J. Vib. Acoust. Stress & Reliab. Des. (USA)

Transactions of the ASME. Journal of Vibration, Acoustics, Stress, and Reliability in Design American Society of Mechanical Engineers, United Engineering Center, 345 East 47th Street, New York, NY 10017, USA. Supersedes in part: *Trans. ASME. J. Mech. Des. (USA)*

articles from
literature you
do not hold ?

BOSTON SPA

Can help you

Over 54000 current periodicals available*

Most of the papers listed in INSPEC services
are held at the British Library Lending Division (BLLD)

REQUESTS DEALT WITH IN 48 HOURS*

Write for further information to:

The Director General
The British Library Lending Division
Boston Spa
Wetherby
West Yorkshire LS23 7BQ
U.K.
Telephone 0937 843434

*Photocopies of papers are available for research or private study to organisations in the UK registered as users of the BLLD. Where individuals in the UK do not belong to an organisation registered with the BLLD they should apply via their public library. In case of difficulty please contact the BLLD.

All requests from outside the UK should be made via the BLLD Overseas Photocopy Service.

COMPUTER AND CONTROL ABSTRACTS

A Complete information Service in Computer Science and Control Engineering

Coverage

Over 40,000 references are included each year. These are selected by scanning over 3,000 journals and the proceedings of over 1,000 conferences. In addition coverage is given of books, reports and dissertations.

What Information is Included?

Each reference in CCA includes the following information:

Title of paper

All authors' names and affiliation of first author

Source of paper (eg name of journal, volume and issue number, page numbers and date of publication)

100-150 word abstract.

Ease of use

Careful classifying and indexing of entries puts information at your fingertips. References are classified under 250 headings, allowing you to go straight to the information of most interest to you. (A summary of the classification appears in every issue).

These six separate indexes are included in each issue:

Subject guide

Author index

Bibliography index

Book index

Conference index

Corporate author index

The above indexes are cumulated at six-monthly intervals.

The author and subject indexes are also cumulated at four-yearly intervals*.

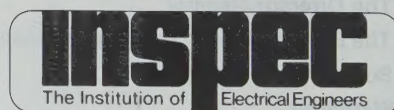
Do You Have Access to This Important Journal?

Does your library or information service provide you with access to this important journal? If not, ask your librarian to contact INSPEC for a free sample and subscription details or write to us direct.

(*four year cumulative indexes not included in annual subscription price)

INSPEC Marketing Department
IEE
Station House
Nightingale Road
Hitchin
Herts SG5 1RJ England
Tel: (0462) 53331
Telex: 825962 IEE G

INSPEC
IEEE Service Center
445 Hoes Lane
Piscataway
NJ 08854
USA
Tel: 201 981 0060
Telex: 833233 IEEE P WAY



ABSTRACTS AND CURRENT PAPERS JOURNALS
SUBSCRIPTION PRICES 1983

	USA \$	UK £	ROW £	JAPAN ¥
PHYSICS ABSTRACTS (PA)	1350	540	690	462,300
2nd and subsequent copies	560	300	300	201,000
ELECTRICAL & ELECTRONICS ABSTRACTS (EEA)	1000	460	560	375,200
COMPUTER & CONTROL ABSTRACTS (CCA)	610	285	350	234,500
PA/EEA/CCA COMBINED SUBSCRIPTION	2650	1120	1430	958,100
EEA/CCA COMBINED SUBSCRIPTION	1460	650	830	556,100
CURRENT PAPERS IN PHYSICS				
Member rate	78	38	38	—
Non-Member rate	170	98	98	65,000
CURRENT PAPERS IN ELECTRICAL & ELECTRONICS ENGINEERING				
Member rate	78	38	38	—
Non-Member rate	145	80	80	53,600
CURRENT PAPERS ON COMPUTERS & CONTROL				
Member rate	78	38	38	—
Non-Member rate	145	80	80	53,600
KEY ABSTRACTS				
Member rate*	38	19	19	—
Non-Member rate	80	36	36	24,100
KEY ABSTRACTS EMI/PMI COMBINED	—	60	60	40,200
All Key Abstracts combined				
Member rate	250	125	125	—
Non-Member rate	580	275	275	184,200

*The Key Abstracts Member rate is available to Members of the IEE and IEEE only.

CUMULATIVE INDEXES

Cumulative indexes are available for *Physics Abstracts*, *Electrical & Electronics Abstracts* and *Computer & Control Abstracts*, for both authors and subjects. These cumulations generally cover a period of four years, with the exception of *Computer & Control Abstracts* where the initial volume covered the period 1966-68. The table below shows the prices and periods for the two types of cumulative index.

	PHYSICS ABSTRACTS		ELECTRICAL & ELECTRONICS ABSTRACTS		COMPUTER & CONTROL ABSTRACTS	
	Subject	Author	Subject	Author	Subject	Author
	£	£	£	£	£	£
1955-59	20	20	15	20	—	—
1960-64	40	17	20	12	—	—
1965-68	60	25	35	20	—	—
1969-72	—	—	72	64	48	30
1973-76	600	300	250	150	150	75
1977-80	770	450	380	250	250	120
1966-68	—	—	—	—	15	

For US\$ and Yen prices please contact the appropriate address below

ORDERING PROCEDURE

THE AMERICAS

North (including Canada), Central and South

All orders from the above areas, and orders from members of Institute of Electrical and Electronics Engineers Inc. anywhere in the world, should be sent to Fulfillment Manager, Institute of Electrical & Electronics Engineers Inc., 445 Hoes Lane, Piscataway, N.J. 08854, USA. Telephone (201) 981 0060

日本のお客様にご案内申し上げます

日本国内に於ける INSPEC の購入価格はすべて円建てとなっております。また刊行物はすべて航空便で配達されます。INSPEC 刊行物の価格、その他についてのお問い合わせは最寄の支店取扱専門店または輸入総代理店株式会社・エス・エシテック・カンパニー 〒105 東京都港区新橋1-13-12、TEL 03 (502) 6471 までご連絡ください。

REMAINDER OF THE WORLD

All remaining subscriptions should be sent to INSPEC Marketing Department, P O Box 26, Hitchin, Herts SG5 7RS, England. Telephone Hitchin 53331, Telex 825962, Telegrams IEE G.

OTHER INSPEC SERVICES

SDI

(Selective Dissemination of Information.) This is a service individually tailored to the requirements and interests of the engineer or research worker. Details of information relevant to the interest profile of the individual subscriber are selected from the data being processed for the INSPEC database. Information is dispatched weekly on 150 mm x 100 mm (6" x 4") cards.

TOPICS

This is an SDI service based on standard profiles. There are over 70 subjects covering high-activity areas of research and development. This is an inexpensive card service designed to alert engineers and researchers to the availability of literature within their subject area.

MAGNETIC TAPES

Tapes containing all the information included in the INSPEC publications are issued twice monthly. They enable the larger research and development organisations to produce their own internal information and current-awareness services.

Summary Classification

The full classification and contents are given at the front of the journal, followed by an **Alphabetical Index** to the subjects covered

00.00 General

- 01.00 Communication, Education, History and Philosophy
- 02.00 Mathematical Methods in Physics
- 03.00 Classical and Quantum Physics; Mechanics and Fields
- 04.00 Relativity and Gravitation
- 05.00 Statistical Physics and Thermodynamics
- 06.00 Measurement Science, General Laboratory Techniques, and Instrumentation Systems
- 07.00 Specific Instrumentation and Techniques of General Use in Physics

10.00 The Physics of Elementary Particles and Fields

- 11.00 General Theory of Fields and Particles
- 12.00 Specific Theories and Interaction Models; Particle Systematics
- 13.00 Specific Reactions and Phenomenology
- 14.00 Properties of Specific Particles and Resonances

20.00 Nuclear Physics

- 21.00 Nuclear Structure
- 23.00 Radioactivity and Electromagnetic Transitions
- 24.00 Nuclear Reactions and Scattering: General
- 25.00 Nuclear Reactions and Scattering: Specific Reactions
- 27.00 Properties of Specific Nuclei listed by Mass Ranges
- 28.00 Nuclear Engineering and Nuclear Power Studies
- 29.00 Experimental Methods and Instrumentation for Elementary-Particle and Nuclear Physics

30.00 Atomic and Molecular Physics

- 31.00 Theory of Atoms and Molecules
- 32.00 Atomic Spectra and Interactions with Photons
- 33.00 Molecular Spectra and Interactions with Photons
- 34.00 Atomic and Molecular Collision Processes and Interactions
- 35.00 Properties of Atoms and Molecules; Instruments and Techniques
- 36.00 Studies of Special Atoms and Molecules

40.00 Classical Areas of Phenomenology

- 41.00 Electricity and Magnetism; Fields and Charged Particles
- 42.00 Optics
- 43.00 Acoustics
- 44.00 Heat Flow, Thermal and Thermodynamic Processes
- 46.00 Mechanics, Elasticity, Rheology
- 47.00 Fluid Dynamics

50.00 Fluids, Plasmas and Electric Discharges

- 51.00 Kinetic and Transport Theory of Fluids; Physical Properties of Gases
- 52.00 The Physics of Plasmas and Electric Discharges

60.00 Condensed Matter: Structure, Thermal and Mechanical Properties

- 61.00 Structure of Liquids and Solids; Crystallography
- 62.00 Mechanical and Acoustic Properties of Condensed Matter
- 63.00 Lattice Dynamics and Crystal Statistics
- 64.00 Equations of State, Phase Equilibria, and Phase Transitions
- 65.00 Thermal Properties of Condensed Matter
- 66.00 Transport Properties of Condensed Matter (Nonelectronic)
- 67.00 Quantum Fluids and Solids; Liquid and Solid Helium
- 68.00 Surfaces and Interfaces; Thin Films and Whiskers

70.00 Condensed Matter: Electronic Structure, Electrical, Magnetic, and Optical Properties

- 71.00 Electron States
- 72.00 Electronic Transport in Condensed Matter
- 73.00 Electronic Structure and Electrical Properties of Surfaces, Interfaces, and Thin Films
- 74.00 Superconductivity
- 75.00 Magnetic Properties and Materials
- 76.00 Magnetic Resonances and Relaxation in Condensed Matter; Mossbauer Effect
- 77.00 Dielectric Properties and Materials
- 78.00 Optical Properties and Condensed Matter Spectroscopy and other Interactions of Matter with Particles and Radiation
- 79.00 Electron and Ion Emission by Liquids and Solids; Impact Phenomena

80.00 Cross-Disciplinary Physics and Related Areas of Science and Technology

- 81.00 Materials Science
- 82.00 Physical Chemistry
- 86.00 Energy Research and Environmental Science
- 87.00 Biophysics, Medical Physics, and Biomedical Engineering

90.00 Geophysics, Astronomy and Astrophysics

- 91.00 Solid Earth Geophysics
- 92.00 Hydrospheric and Atmospheric Geophysics
- 93.00 Geophysical Observations, Instrumentation, and Techniques
- 94.00 Aeronomy and Space Physics
- 95.00 Fundamental Astronomy and Astrophysics, Instrumentation and Techniques and Astronomical Observations
- 96.00 Solar System
- 97.00 Stars
- 98.00 Stellar Systems; Galactic and Extragalactic Objects and Systems; The Universe